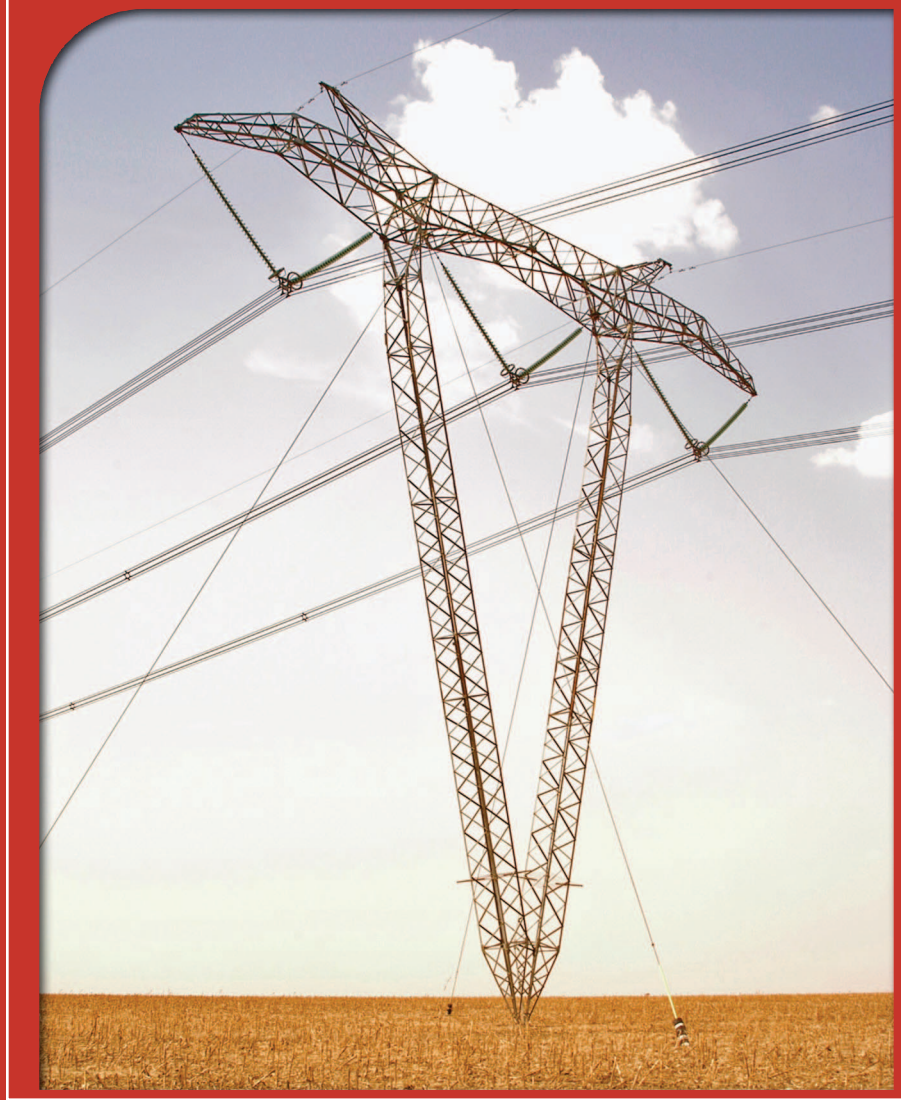
EPRI | ELECTRIC POWER RESEARCH INSTITUTE

EPRI AC Transmission Line Reference Book—200 kV and Above, Third Edition



EPRI AC Transmission Line Reference Book—200 kV and Above, Third Edition

1011974

Final Report, December 2005

EPRI Project Manager
R. Lings

ELECTRIC POWER RESEARCH INSTITUTE
3420 Hillview Avenue, Palo Alto, California 94304-1395 ▪ PO Box 10412, Palo Alto, California 94303-0813 ▪ USA
800.313.3774 ▪ 650.855.2121 ▪ askepri@epri.com ▪ www.epri.com

DISCLAIMER OF WARRANTIES AND LIMITATION OF LIABILITIES

THIS DOCUMENT WAS PREPARED BY THE ORGANIZATION(S) NAMED BELOW AS AN ACCOUNT OF WORK SPONSORED OR COSPONSORED BY THE ELECTRIC POWER RESEARCH INSTITUTE, INC. (EPRI). NEITHER EPRI, ANY MEMBER OF EPRI, ANY COSPONSOR, THE ORGANIZATION(S) BELOW, NOR ANY PERSON ACTING ON BEHALF OF ANY OF THEM:

(A) MAKES ANY WARRANTY OR REPRESENTATION WHATSOEVER, EXPRESS OR IMPLIED, (I) WITH RESPECT TO THE USE OF ANY INFORMATION, APPARATUS, METHOD, PROCESS, OR SIMILAR ITEM DISCLOSED IN THIS DOCUMENT, INCLUDING MERCHANTABILITY AND FITNESS FOR A PARTICULAR PURPOSE, OR (II) THAT SUCH USE DOES NOT INFRINGE ON OR INTERFERE WITH PRIVATELY OWNED RIGHTS, INCLUDING ANY PARTY'S INTELLECTUAL PROPERTY, OR (III) THAT THIS DOCUMENT IS SUITABLE TO ANY PARTICULAR USER'S CIRCUMSTANCE; OR

(B) ASSUMES RESPONSIBILITY FOR ANY DAMAGES OR OTHER LIABILITY WHATSOEVER (INCLUDING ANY CONSEQUENTIAL DAMAGES, EVEN IF EPRI OR ANY EPRI REPRESENTATIVE HAS BEEN ADVISED OF THE POSSIBILITY OF SUCH DAMAGES) RESULTING FROM YOUR SELECTION OR USE OF THIS DOCUMENT OR ANY INFORMATION, APPARATUS, METHOD, PROCESS, OR SIMILAR ITEM DISCLOSED IN THIS DOCUMENT.

ORGANIZATION(S) THAT PREPARED THIS DOCUMENT

Electric Power Research Institute

ORDERING INFORMATION

Requests for copies of this report should be directed to EPRI Orders and Conferences, 1355 Willow Way, Suite 278, Concord, CA 94520, (800) 313-3774, press 2 or internally x5379, (925) 609-9169, (925) 609-1310 (fax).

Electric Power Research Institute and EPRI are registered service marks of the Electric Power Research Institute, Inc.

Copyright © 2005 Electric Power Research Institute, Inc. All rights reserved.

CITATIONS

This report was prepared by

Electric Power Research Institute (EPRI)
3420 Hillview Avenue
Palo Alto, CA 94304

Principal Investigator
R. Lings

The authors of each chapter of this book are listed with the chapters. This report describes research sponsored by EPRI.

The report is a corporate document that should be cited in the literature in the following manner:

EPRI AC Transmission Line Reference Book—200 kV and Above, Third Edition. EPRI, Palo Alto, CA: 2005. 1011974.

Cover photo of Eskom 765-kV guyed-V structure courtesy of Eskom. Cover design by Jay Canale, Enertech Consultants.

PRODUCT DESCRIPTION

This report is an updated edition of the longtime industry standard EPRI *Transmission Line Reference Book*, or the "Red Book," which was last issued in 1987. Publication of this new edition is the culmination of three years of research by a global team of experts. The report includes the latest information on research, technology, and materials and represents a significant contribution to the global industry of electric power transmission.

Results & Findings

This new edition of the Red Book preserves the style and depth of previous editions while including the latest information on topics associated with the design of high-voltage transmission lines. Accordingly, eleven chapters in the previous edition of the book have been extensively updated. The new edition also adds four new chapters—Chapters 12 through 15—on shared use of rights-of-way, inspection and maintenance concerns, voltage upgrading, and experience with lines above 700 kV. These new chapters reflect both changing concerns over the past 15 years as well as the availability of experience in line design, operation, and maintenance.

In addition to the revised text, the new edition of the Red Book also includes 50 applets, which are small software programs, or stand-alone calculation modules. These applets enable users to make specific calculations for transmission-line design parameters and include associated example and design features.

Challenges & Objectives

Since publication of the last edition of the Red Book in 1987, theories and technologies related to transmission line design have advanced, and the Red Book had fallen behind. As a result, it was necessary to upgrade the book.

Updating the Red Book was undertaken with several objectives:

- Preserve the style of previous editions.
- Present the science and technology in the same depth as earlier editions.
- Maintain focus on the electrical design and performance of transmission lines.
- Expand the international quality of the presentation to include international practices, technology, sources of information, and use of units.
- Direct the presentation to line designers and engineers and assume at least two years of university training in mathematics and physics.
- Take advantage of advances in electronic media, including integration of software routines and incorporation of video and tutorial material.

- Add a glossary and index.

Applications, Values & Use

The Red Book has been recognized for some 25 years as the worldwide industry standard for transmission line design. The latest update represents a significant advance on the previous edition and will provide an essential resource for all utilities involved in line design.

EPRI Perspective

The EPRI report, *Transmission Line Reference Book, 345 kV and Above* (EL-2500-R1), was originally printed with a red cover and quickly became known in the industry simply as the "Red Book." The book had its origins in the 1960s when General Electric established the Lenox Laboratory in Lenox, Massachusetts, to experiment with transmission lines on the order of 1 MV. Known as Project UHV, the Lenox Laboratory site designed and tested transmission lines at ultra high voltages. The Red Book was written essentially as the final report for Project UHV. The first edition was published in 1975, the second in 1982, and the second revised edition was issued in 1987.

Approach

While the original edition was essentially a final report to a research project, the approach used to write it and present the information has proved to be very successful. Each chapter in the book is a refereed paper on a specific topic. The chapters are not intended to be a complete thesis on a subject; a comprehensive list of references is provided at the end of each chapter if readers need more detailed information.

Keywords

AC
Electric field
High voltage
Insulators
Lightning
Magnetic field
Switching surge
Transmission
Transmission line design
Transmission system
Insulation coordination

Authors and Reviewers

Project Manager
Raymond Lings

Editorial Committee
Raymond Lings
Luciano E. Zaffanella
Jan P. Reynders
Jonas Weisel

Chapter 1: Transmission Systems

Authors: Jan P. Reynders, Raymond Lings, Robert G. Stephen, Lori A. Nielsen, Andrew C. Ludwig
Reviewer: Luciano E. Zaffanella

Chapter 2: Electrical Characteristics of Conductor Configurations and Circuits

Authors: Dale A. Douglass, James R. Stewart, Bernie Clairmont
Reviewers: Sven Hoffmann, Vic Morgan, and Robert G. Stephen

Chapter 3: Insulation Design

Authors: Nicholas C. Abi-Samra, Ian Grant
Reviewers: Jan P. Reynders, Luciano E. Zaffanella, William A. Chisholm, Andrew Phillips, and Christiaan S. Engelbrecht

Chapter 4: Insulation for Power Frequency Voltage

Authors: Andrew Phillips, Christiaan S. Engelbrecht
Contributor: William A.Chisholm
Reviewers: Ray Houlgate and John Kuffel

Chapter 5: Switching Surge Performance

Authors: Luciano E. Zaffanella
Reviewer: John M. Van Coller

Note: Brief profiles of the authors appear at the start of each chapter.

Chapter 6: Lightning and Grounding

Authors: William A. Chisholm, John G. Anderson
Reviewer: Mat Darveniza

Chapter 7: Electric and Magnetic Fields

Author: Luciano E. Zaffanella
Reviewers: Jan P. Reynders and James R. Stewart

Chapter 8: Corona and Gap Discharge Phenomena

Author: P. Sarma Maruvada
Reviewers: Jan P. Reynders and Giao N. Trinh

Chapter 9: Electromagnetic Interference

Authors: Robert G. Olsen, Vernon L. Chartier
Reviewers: P. Sarma Maruvada and Tony Britten

Chapter 10: Audible Noise

Authors: Tony Britten, Vernon L. Chartier, Luciano E. Zaffanella

Chapter 11: Corona Loss and Ozone

Author: P. Sarma Maruvada
Reviewer: Vernon L. Chartier

Chapter 12: Shared Use of the Right-of-Way

Authors: Robert G. Olsen, T. Dan Bracken
Reviewers: James R. Stewart and Monty W. Tuominen
Contributors: Paul Wong and Richard Harness

Chapter 13: Considerations for Inspection and Maintainability

Authors: Andrew Stewart, George Gela
Contributors: Andrew Phillips, Gail Carney, Fabio Bologna, George Watt, John K. Chan, Lance Powell, Kurt Bell, Robert Kluge, John Peckinpaugh, Cal Stripling, Terry S. Eagar, Alan Holloman, Bill Hewitt, and J. A. Tony Gillespie

Chapter 14: Voltage Upgrading of Existing Transmission Lines

Authors: Dale A. Douglass, James R. Stewart
Reviewers: Anand Goel and Jerry Reding

Chapter 15: Transmission Lines Above 700 kV

Authors: Vernon L. Chartier, P. Sarma Maruvada
Reviewers: J. P. Gingras, A. Dutil, H. Létourneau, L. Allard, J. M. Gagnon, J. C. Carrière, D. Bouchard, M. Hamel, L. Vo Van, M. Lavoie, D. Goulet, Y. Deshaies, Eric Engdahl, Ed Schnell, Viktor Rashkes, Jose Antonio Delgado Garcia, Javier Tarazona Gomez, Jose Antonio Pardinas, Carlos Garcia Cuestas, Joaquin Oliveira Da Silva, Paulo Cesar Vaz Esmeraldo, Ben Shperling, Peter S. Muench, Tony Britten, Fabio Bologna, Dave Cretchley, Dzevad Muftic, Logan Pillay, Riaz Vajeth, R. P. Singh, R. N. Nayak, M. Krishnakumar, Rajiv Gandhi, Dong Il-Lee, and Chang-Hyo Oh.

Acknowledgments

EPRI wishes to acknowledge the funders of this reference book, who made possible the generation and publication of this latest edition.

Alabama Electric Cooperative, Inc.

American Electric Power Service Corporation (AEP)

American Transmission Company (ATC)

Anchorage Municipal Light & Power (ML&P)

Arkansas Electric Cooperative Corporation

Bonneville Power Administration (BPA)

California Dept. of Water Resources

CenterPoint Energy, Inc.

Central Hudson Gas & Electric Corporation

City Public Service, San Antonio

Consolidated Edison Company of New York, Inc. (ConEd)

Constellation Energy Group, Inc.

CVG Electrificación del Caroní, C.A. (CVG EDELCA)

Dairyland Power Cooperative

Dominion Resources, Inc.

East Kentucky Power Cooperative, Inc. (EKPC)

Electricity Generating Authority of Thailand (EGAT)

Entergy Services, Inc.

ESB Networks

Eskom

Golden Valley Electric Association, Inc.

Grant County Public Utility District

Great River Energy

Hawaiian Electric Company, Inc. (HECO)

Hetch Hetchy Water & Power

Hoosier Energy Rural Electric Cooperative, Inc.

Hydro One Networks, Inc.

Jacksonville Electric Authority (JEA)

Kansas City Power & Light Company (KCP&L)

Lincoln Electric System

Lower Colorado River Authority (LCRA)

Manitoba Hydro-Electric Board

MidAmerican Energy Holdings Company

National Grid Company PLC (NGT)

Nebraska Public Power District (NPPD)

New York Power Authority (NYPA)

Northeast Utilities (NU)

Omaha Public Power District (OPPD)

Power Grid Corporation of India Limited (PGCIL)

Powerlink Queensland

Public Service Company of New Mexico (PNM)

Public Service Electric & Gas Company (PSE&G)

Richmond Power & Light

Salt River Project (SRP)

San Diego Gas & Electric Company (SDG&E)

South Carolina Electric & Gas Company

Sunflower Electric Power Corporation

Tri-State G&T Association, Inc.

TXU Electric Delivery Company

Western Area Power Administration (WAPA)

Foreword

In 2001, the Electric Power Research Institute (EPRI), with technical and financial support from the global transmission industry, decided to redraft and reissue the internationally renowned handbook entitled "Transmission Line Reference Book: 345 kV and Above." Because of the red cover of previous editions, the book has become affectionately known as the "EPRI Red Book." The cover of this new edition preserves the tradition.

The origin of the Red Book dates back more than three decades. In 1968, the Edison Electric Institute published the EHV Transmission Line Reference Book, a design handbook for U.S. electric utilities. The book was based on the results of many years of research sponsored by General Electric and the industry at what was then Project EHV in Pittsfield, Massachusetts. This research evolved around the design and development of EHV transmission from 345 to 735 kV, the latter being the maximum expected ac transmission voltage in North America for several years to come.

However, before the book was published, AEP (American Electric Power Service Corporation) in April 1966 (The Wall Street Journal, Wednesday, April 27, 1966) announced plans to build 1050 miles of 765-kV transmission in five states. In making this decision, AEP had the benefit of the research conducted at both Project EHV and The Apple Grove 750-kV Project, which was a joint project of AEP and Westinghouse. The impetus for lines operating at even higher voltages resulted in plans in the early 1970s to construct facilities where research above 1000 kV (UHV) could be conducted. The drive to UHV voltages led to a number of large collaborative research efforts under the banner of Project UHV (a successor of Project EHV). These efforts culminated in the EPRI handbook, published in 1975. A second edition of this handbook was published in 1982, and the second edition revised was issued in 1987.

Early on in the latest revision of the Red Book, we made a number of decisions. Today the majority of new and existing transmission is in the range of 200 to 400 kV. As a result, we decided to select a "region-neutral" voltage, rather than list a voltage limit for the book that matched either a "standard" within North America (i.e., 230 or 345 kV) or a "standard" European voltage (220, 275, or 400 kV). The level of 200 kV was considered appropriate because it addresses the issue above and incorporates the 220- and 230-kV series of lines. We also decided to include the term "ac" in the title. There is a growing trend again towards HVDC (High-Voltage Direct Current), and the intention is to differentiate this book from books covering "dc".

In drafting this new edition, we paid particular attention to the needs of utilities and students. The following is considered the audience profile:

- Experienced line designers who need to confirm design parameters, select technology, optimize designs, defend decisions, and understand non-routine design topics.
- Students of line engineering with college or third-year engineering calculus and physics.
- Utilities that have the need to preserve institutional knowledge.
- Other users, including public utility commissions, lawyers, and the public-at-large. (While the book is not written for this audience, it is recognized that this latter audience will turn to this resource for guidance.)

The new edition has the following attributes:

- Technical Depth. Every attempt was made to keep the same technical depth as previous editions. It was clear that the format of previous editions resonated well with the intended audience. Chapters do not attempt to replace the many handbooks and texts dedicated to each topic.
- International Developments. The focus of the book was expanded to include developments outside of the United States. There was a conscious effort to find an international author or reviewer for each chapter. Further, there was a very clear effort to make sure the book was truly international in its content. Extensive use was made of IEC, CIGRE, and international experts to complement the existing North American content.
- Self-Contained Chapters. Each chapter is self-contained, having its own appendices, references, and applets. However, it was recognized that making the chapter boundaries very steep would result in duplication within the handbook, so some compromise in terms of cross-referencing was necessary.

- References. Each chapter contains a very comprehensive and updated list of references. Readers of the previous editions have regularly turned to the reference list at the end of each chapter for guidance. The new edition preserves this capability.
- Applets. Where appropriate, the design theory is translated into software code and included with the handbook in the form of "applets." These are software applications with very useful help files, simple input and output screens, and the ability to export results to spreadsheets, graphs, etc. The new book contains some 51 applets covering many of the chapters. The inclusion of applets will make it considerably easier to review and exercise the theory. The inclusion of graphing allows the reader to see precise results as well as trends. The addition of applets to this edition of the book will, in our mind, add considerable value and expand the use of this book.

The new edition of the book rearranges the chapters to better align with the design process. The book is organized into themes with a "foundation" chapter at the start of each theme and specialized chapters behind the foundation. It was also decided to include new chapters focused on understanding how lines designed using previous editions of the Red Book have stood the test of time. In addition, chapters are included that attempt to close the feedback loop from actual field experience back to the designer.

As a result, the revised edition includes three general themes:

- **Insulation Coordination.** This theme spans Chapters 3 to 6, and covers general insulation coordination, power frequency insulation, switching, and lightning and grounding
- **Corona and Field Effects.** This theme spans Chapters 7 to 11, and covers corona and its effects (corona loss, audible noise, and high-frequency electromagnetic interference) and the effects of power frequency electric and magnetic fields.
- **Application.** This theme spans Chapters 12 to 15, and includes right-of-way management, designing for inspection and maintenance, voltage upgrading, and the field performance of lines designed to operate above 700 kV. This theme is a new addition to the book.

As regards application, Chapter 15 is a particularly unique chapter. This chapter pulls together the theory in the Red Book and shows how life was breathed into this theory. The authors surveyed some 10 utilities from around the globe that have transmission lines above 700 kV. The chapter starts with a history and EHV and UHV transmission research and then completes a design review of each line—covering the reasons why the technology was chosen, the approach to the design, and the operation and maintenance experience.

At the time of writing this third edition, two countries have lines over 1000 kV (Russia and Japan). However, both networks are presently operated at 500 kV. Eskom (South Africa) will, quite rightly, argue that its operating 765-kV line at high altitude is "equivalent" to a 1000-kV line at sea level. The Foreword to the previous edition of the Red Book noted "no upper limit to ac transmission voltages is apparent." While the dream of "no upper limit to ac transmission" has yet to materialize, developing regions around the globe (China, in particular) are considering UHV (1000 kV and above) transmission—the driver being the transmission of bulk power over long distances from inexpensive hydro-generation to load centers. It is predicted that we will again see lines operating above 1000 kV. In the United States, AEP has just been awarded a license to extend its existing 765-kV network. It took 10 years to secure the license. While the notion of ever-increasing transmission voltage may have been lost in the 1980s and 1990s, it appears set to make a rebound in the 21st century.

The new edition also contains a number of useful additions:

- **Glossary.** A glossary is provided that draws off both the IEEE and the IEC.
- **Base Cases.** To help demonstrate the theory, a large number of bases cases are provided. These base cases are loaded into the applets. The base cases help the reader exercise the theory and also gauge the technical limits of various line design parameters.
- **Index.** Previous editions of the book did not contain an index. While each chapter is self contained, the index helps readers find the right information across the entire handbook.
- **Harmonized Technical Units.** The focus is on SI units. While this is not always possible since many historical results are in English units, every attempt has been made to harmonize technical units used. An applet that allows conversion of units is provided.

It is important that we recognize a number of key individuals who played pivotal roles in bringing this new edition to life: Standing head-and-shoulders above the rest, Luciano Zaffanella was a technical powerhouse. His contribution—both on individual chapters and the overall handbook—was phenomenal. His leadership and experience shines through in every chapter. His ability to translate complex theory into a simple applet is unique. This book stands testimony to Luciano's leadership in high-voltage power

transmission. The editorial team was complemented with Professor Jan Reynders of the University of the Witwatersrand, South Africa and key advisor to Eskom and CIGRE. Jan's role was to present the "European" approach to transmission-line design. Finally, the text was edited and laid out under the expert guidance of Jonas Weisel. Jonas worked wonders with the large number of contributors and established a very high editorial and publishing standard. He was assisted by Lee Lehrman, who laid out the pages and redrew many of the illustrations.

Each author is recognized at the start of each chapter with a picture and short biography. The reviewers and the authors are also recognized on a specific "Authors and Reviewers" page. The team was particularly privileged to be able to draw on John Anderson. Well into his eighties, John is someone to marvel at and a real inspiration to all. Having been associated with Lenox for "countless-years," John brought considerable insight and energy to this edition. Chapter 6 on lightning, for the first time, captures his extensive knowledge and experience in one place.

This book would not have been possible without the technical and financial support of utilities from around the globe. A page of "Acknowledgments" recognizes those who funded the third edition.

Finally, on a personal level, the regular semi-annual meeting of the authors will, I am sure, remain in the memory of all participants for the rest of our lives. The extremes of Lenox, Massachusetts in midwinter and then again in midsummer each year for four years is something to be experienced. The idea of pulling together over 25 experts from around the globe into one room for three days to debate the structure of each chapter conjures up an image of "mind-numbing intellectual debates." These fears were totally unfounded. The debates were very spirited, very constructive—with every author making a point of helping the other. The process of constructing the contents page, debating where information should reside, and the inevitable trading of text between chapters was an absolute pleasure to facilitate. It would be fair to say that every author left the project having learned something from his peers. Solid friendships were either made or rekindled during the four years of this project.

In every engineer's life there are those events that leave a lasting impression. This book marks such an event for many associated with this monumental effort. Finally, it is the wish of all participants that this new edition will spur a renewed interest in high-voltage transmission—ultimately leading to a new generation of transmission-line engineers.

Raymond J Lings
EPRI
Palo Alto, California

Contents

Symbols **S-1**

Chapter 1 **Transmission Systems**

1.1 INTRODUCTION 1-3
Background 1-3
Transmission System Characteristics 1-4
Industry Trends Affecting Line Design 1-5
Feedback of Experience 1-6
Organization of this Chapter 1-6

1.2 ELECTRICAL DESIGN 1-6
Voltage, Impedance and Power Limit 1-6
Standing Waves 1-8
Transients 1-8

1.3 ENVIRONMENTAL CONSIDERATIONS 1-8
The Impact of a Line on the Environment 1-8
The Impact of the Environment on a Line 1-9

1.4 TRENDS IN THE ELECTRICITY SUPPLY INDUSTRY 1-10
Generation 1-10
Transmission 1-11
Distribution 1-14
Overall Impact 1-15

1.5 FUTURE DIRECTION OF THE ELECTRICITY SUPPLY INDUSTRY 1-15
Technical Strategies 1-15
Specific Issues to be Addressed 1-16

1.6 LEGISLATIVE AND REGULATORY ISSUES 1-17
Introduction 1-17
Examples of Inadequate Planning 1-18
Regulatory Framework and Process for Transmission-Line Permitting 1-19
Primary Issues for Transmission-Line Permitting 1-23
New or Expanding Issues 1-28

1.7 COMPARISON OF THE THIRD EDITION OF THE REFERENCE BOOK TO THE SECOND EDITION 1-28

1.8 CONCLUSION 1-31

REFERENCES 1-33

Chapter 2 **Electrical Characteristics of Conductor Configurations and Circuits**

2.1 INTRODUCTION 2-2

2.2 BARE CONDUCTORS FOR OVERHEAD TRANSMISSION LINES 2-2
Conductor Materials 2-3
Areas and Diameter 2-4
Weight and Rated Strength 2-4
Electrical Resistance 2-4
GMR of Stranded Conductors 2-7
Inductive and Capacitive Reactance "to One Meter (Foot)" 2-7
Annealing of Aluminum Stranded Conductors 2-8
Sag Tension of Overhead Lines 2-9
Thermal Rating (Ampacity) of Bare Conductor 2-10
Transient Thermal Ratings 2-11

2.3 CONDUCTOR SURFACE GRADIENTS 2-12
Introduction and Overview 2-12
Single Conductor 2-14
Multiple Conductors 2-15
Conductor Bundling 2-18
Toroidal Shielding Electrodes (Corona Rings) 2-19
Variation of Surface Gradient with Design Parameters—Applets and Examples 2-20

2.4 BASIC TRANSMISSION LINE IMPEDANCE AND ADMITTANCE PARAMETERS 2-21
Introduction 2-21
Positive Sequence Inductive Reactance 2-22
Positive Sequence Capacitive Reactance 2-24
Surge Impedance and Surge Impedance Loading 2-25

2.5 GENERAL TRANSMISSION-LINE PARAMETERS 2-26
Capacitive (Electric Field) Unbalance 2-26
Single-Circuit Inductive (Magnetic Field) Unbalance 2-28
Unbalance in Parallel Double-Circuit Untransposed Lines 2-30

2.6 INDUCED VOLTAGES ON PARALLEL CONDUCTORS 2-31
Electric Field Induction on the De-Energized Circuit 2-31
Magnetic Field Induction on the De-Energized Circuit 2-32

Appendix 2.1 ELECTRICAL AND MECHANICAL CHARACTERISTICS OF CONDUCTORS 2-33

REFERENCES 2-42

Chapter 3 **Insulation Design**

3.1 INTRODUCTION 3-2
Definition 3-2
Design Factors for Transmission Lines 3-2
Critical Factors versus Stress Type 3-2
Design Optimization 3-2
Calculation Methodology 3-3
Typical Performance Criteria and Design Clearances 3-3
Applets 3-4
Summary 3-5
Layout of this Chapter 3-5

3.2 VOLTAGE AND ENVIRONMENTAL STRESSES ON TRANSMISSION LINES 3-5
Introduction 3-5
Lightning 3-6
Switching Surges 3-9
Temporary Overvoltages 3-14
Environmental Stress 3-17
Summary 3-18

3.3 INSULATION STRENGTH 3-19
Introduction 3-19
Lightning Impulse Strength 3-19
Switching Impulse Strength 3-21
Power Frequency Strength 3-22
Effect of Weather Conditions 3-25
Summary 3-26

3.4 OVERVOLTAGE CONTROL 3-27
Introduction 3-27
Control of Lightning Overvoltages 3-27
Control of Switching Surges 3-32
Control of Power Frequency Stress Caused by Insulator Contamination 3-36
Summary 3-38

3.5 ELECTRIC SAFETY CODE REQUIREMENTS 3-38
Introduction 3-38
National Electric Safety Code (NESC 2002) Clearance Requirements 3-38
Summary 3-42

3.6 COORDINATION OF DESIGN REQUIREMENTS 3-42
Introduction 3-42
Insulation Coordination Analysis Methods 3-43
Lightning Performance of Transmission Lines 3-44
Switching Surge Performance of Transmission Lines 3-46
Power Frequency Performance of Transmission Lines 3-47
Consolidation of Design Requirements 3-49
Alternate Method for Line Design: Storm Outage Rate 3-50
Summary 3-50

3.7 ECONOMIC CONSIDERATIONS 3-51
Introduction 3-51
Insulation Coordination and Cost 3-51
Line Component Costs 3-53
Cost Sensitivities 3-53
Independent Cost Items 3-54
Base Line Costs 3-54
Cost Analysis Methods 3-54
Summary 3-54

Appendix 3.1 INSULATION COORDINATION ANALYSIS TOOLS 3-55

Appendix 3.2 SURGE ARRESTER APPLICATIONS ON TRANSMISSION SYSTEMS: STATION AND LINE ARRESTERS 3-60

Appendix 3.3 INSULATION COORDINATION METHODOLOGIES 3-69

Appendix 3.4 APPLICATION OF INSULATION COORDINATION ACCORDING TO IEC 71-2 INSULATION COORDINATION APPLICATION GUIDE 3-77

REFERENCES 3-81

BIBLIOGRAPHY 3-85

Chapter 4 **Insulation for Power Frequency Voltage**

4.1 INTRODUCTION 4-2

4.2 INSULATOR TECHNOLOGY 4-3
Historical Perspective 4-3
General Insulator Terms and Classification 4-5
Hydrophobicity 4-9
Components of Ceramic and Glass Insulators 4-11
Components of Polymer Insulators 4-12

4.3 THE MECHANISM OF CONTAMINATION FLASHOVER 4-17
Introduction 4-17
Buildup of Contaminants on Insulator Surfaces 4-18
Wetting Processes 4-21
Discharge Activity and Development of Flashover 4-23

4.4 LONG-TERM PERFORMANCE OF INSULATORS 4-27
Causes of Degradation and Damage 4-27
Porcelain and Glass Insulators 4-28
Polymer Insulators 4-30

4.5 LABORATORY TESTING 4-38
Introduction 4-38
Test Methods to Determine the Long-Term Performance of Insulators (Aging Tests) 4-38
Contamination Flashover Tests 4-42

4.6 ELECTRICAL PERFORMANCE OF INSULATORS AND AIR GAPS UNDER AC VOLTAGE 4-47
Introduction 4-47
Dry and Wet AC Flashover Strength of Air Gaps and Insulators 4-47
Contamination Flashover Performance of Insulators 4-49
Glass and Porcelain Insulators 4-50
Polymer Insulators 4-54
Resistive Glaze Insulators 4-56

4.7 PERFORMANCE OF INSULATORS IN FREEZING CONDITIONS 4-57
Introduction 4-57
Clean- and Cold-Fog Test Results 4-58
Icing Test Results 4-58
Snow Test Results 4-61

4.8 INSULATION DESIGN 4-61
Introduction 4-61
Characterizing the Environment and its Severity 4-62
Choice of Material 4-67
Flashover Probability of Contaminated Insulators 4-74
The Insulator Dimensioning Process 4-75

4.9 ELECTRIC FIELD ON INSULATORS AND GRADING RINGS 4-81
E-Field Distribution on Polymer Insulators 4-81
E-Field Distribution on Glass and Porcelain Insulator Strings 4-90
Appendix 4.1 INSULATOR TYPES REFERRED TO IN THIS CHAPTER 4-92
REFERENCES 4-93

Chapter 5 **Switching Surge Performance**
5.1 INTRODUCTION 5-2
5.2 PRINCIPAL VARIABLES IN SWITCHING SURGE FLASHOVER 5-3
Switching Surges and Switching Impulses 5-3
Switching Impulse Polarity 5-4
Switching Impulse Waveshape 5-4
Influence of Geometry on Switching Impulse Strength 5-6
Meteorological Influence on Switching Impulse Strength 5-7
Statistical Fluctuations in Switching Impulse Strength 5-7
5.3 FLASHOVER MECHANISM 5-7
5.4 SWITCHING IMPULSE TESTING TECHNIQUES 5-10
Switching Impulse Generators, Test Circuits, Test Objects 5-10
Test Methods 5-12
5.5 SWITCHING IMPULSE STRENGTH OF SIMPLE AIR GAPS 5-13
Rod-Plane 5-13
Vertical Rod-Rod 5-14
Horizontal Rod-Rod 5-15
Sphere-Plane 5-16
5.6 SWITCHING IMPULSE STRENGTH OF LINE INSULATION 5-16
Tower Window 5-16
Outside Phase 5-19
Insulator Strings 5-19
Conductor-to-Tower Leg 5-20
Conductor-to-Grounded Objects at Midspan 5-20
Anomalous Flashovers 5-20
5.7 SWITCHING IMPULSE STRENGTH OF STATION INSULATION 5-21
Introduction 5-21
Horizontal Insulator Strings 5-21
Station Post Insulators 5-21
5.8 PHASE-TO-PHASE SWITCHING SURGE STRENGTH 5-22
Introduction 5-22
Phase-to-Phase Strength for a Horizontal Rod-Rod 5-24
Phase-to-Phase Strength of the Air Gap Between Conductors 5-25
Phase-to-Phase Strength of Other Insulation Geometries 5-26
Phase-to-Phase Insulation Stress 5-26
Design of Phase-to-Phase Gap Length 5-26
5.9 VARIATION OF FLASHOVER PROBABILITY WITH VOLTAGE 5-27
Withstand Voltage Level 5-28
5.10 EFFECT OF WAVESHAPE ON SWITCHING IMPULSE STRENGTH 5-28
5.11 EFFECT OF AIR DENSITY AND HUMIDITY ON SWITCHING IMPULSE STRENGTH: CORRECTION TO STANDARD CONDITIONS 5-29
Introduction 5-29
Standard Air Density and Humidity Conditions 5-29
Effect of Air Density 5-29
Effect of Humidity 5-31
5.12 EFFECT OF RAIN AND OTHER WET WEATHER CONDITIONS ON SWITCHING IMPULSE STRENGTH 5-32
Air Gaps and Clean Insulators 5-32
Switching Impulse Strength of Contaminated Insulators 5-33
5.13 RISK OF FAILURE OF PHASE-TO-GROUND INSULATION 5-34
Introduction 5-34
Distribution of Switching Surges on Transmission Lines 5-34
Parameters Affecting Risk of Failure Caused by Switching Surges 5-34
Simplified Design Procedure 5-35
5.14 CONSIDERATION OF SWITCHING SURGES DURING LIVE-LINE MAINTENANCE 5-37
Introduction 5-37
Minimum Number of Insulators to Withstand Switching Surges 5-38
Performance of Portable Protective Gaps 5-38
Effect of Floating Objects 5-39
Appendix 5.1 COMPUTATION OF THE SWING ANGLE DISTRIBUTION 5-40
Appendix 5.2 MODEL FOR THE CALCULATION OF SWITCHING IMPULSE STRENGTH OF AIR GAPS 5-41
REFERENCES 5-44

Chapter 6 **Lightning and Grounding**
6.1 INTRODUCTION 6-2
Historical Context 6-2
Lightning Protection of Transmission Lines 6-2
Simulation of Lightning on Transmission Lines 6-2
Capital Cost of Lightning Protection for Transmission Systems 6-3
Benchmark: Cost of Avoided Momentary Outages 6-4
Organization and Contents of the Chapter 6-5
6.2 THE LIGHTNING FLASH 6-6
Cloud Electrification 6-6
The Stroke Mechanism—Negative Downward Leaders 6-7
The Stroke Mechanism—Upward Positive Leaders 6-8
The Stroke Mechanism—Positive Flashes 6-9
Charge and Voltage 6-9
Leader Diameter, Visibility, and Branching 6-9

Structure and Progression of the Positive Upward Connecting Leader 6-10
First Return Stroke Waveshapes 6-11
First Negative Return Stroke Parameter Distributions 6-14
Positive Return Stroke Parameter Distributions 6-16
Subsequent Stroke Parameters 6-17
Electromagnetic Fields from Return Strokes 6-19
Upward Flashes from Tall Structures 6-19
Experience on 60–140 m Towers 6-20
Winter Lightning 6-20
Arc Damage from Flash Charge 6-21

6.3 REGIONAL LIGHTNING FLASH STATISTICS AND DATA 6-22
Isokeraunic Maps, OTD Measurements, and Lightning Flash Counters 6-23
General Observations 6-26
The North American Lightning Detection Network 6-29
Inter-comparison of Lightning Detection Methods 6-31

6.4 SURGE IMPEDANCE AND CORONA EFFECTS 6-31
Surge Impedance of Single Wires and Bundles 6-32
Surge Impedance of Towers 6-37
Calculation of Insulator Voltage and Lightning Performance 6-45

6.5 INSULATION STRENGTH FOR LIGHTNING IMPULSES 6-45
Volt-Time Curve Penetration Algorithm, Evaluated at Span Reflection Time 6-46
The Disruptive Effect (DE) Algorithm, Typically for Faster-Front Flashover/Puncture 6-46
The Leader Progression Model, Typically Evaluated for Several Span Reflection Times 6-47
Insulator Puncture Strength 6-48

6.6 SHIELDING FAILURE CALCULATIONS 6-48
The Shielding Failure Process 6-49
Uncovered Areas in the Shielding Failure Models 6-50
Recommended Strike Distance Equations 6-50
Perfect Shielding 6-51
The Method of Maximum Heights 6-51
Cascading Flashovers 6-52
Transmitted Stress to Terminals 6-52
Calculation Procedures 6-52
Simplified Models 6-53

6.7 INITIATION OF BACKFLASHOVERS 6-55
The Backflashover Process 6-55
Dynamic Models for Electrical Insulation Strength 6-56
Calculation Procedures 6-57
Digital Models for Backflashover 6-57
Applet Descriptions 6-59

6.8 INITIATION OF INDUCED FLASHOVERS 6-60
Induction from EM Fields of the Lightning Flash 6-60
Simplified Model for Induced Overvoltages 6-60
Protection against Induced Flashovers 6-61
Importance for Subtransmission and Underbuilt Distribution 6-61

6.9 INITIATION OF MIDSPAN FLASHOVERS 6-62
The Failure Mechanism 6-62
Corona Coupling at Midspan 6-62
Current Injection into Phase Conductors 6-63
Tower Flashovers Caused by Midspan Strokes 6-63
Cascading Flashovers at Adjacent Structures 6-63
Rules for Midspan Spacing 6-63
Importance for Subtransmission and Underbuilt Distribution 6-64

6.10 TRANSMISSION-LINE GROUNDING 6-64
Mechanical Integrity 6-64
Guy Anchors for Additional Strength 6-64
Corrosion and End-of-Life Aspects 6-64
Steady-State Tower Potentials 6-65
Earth Resistivity—Its Importance and Measurement 6-69
Influence on Dielectric Strength of Soils 6-69
Vertical and Horizontal Layering 6-69
Measurement Techniques and Typical Results of Field Tests 6-70
Capacitance, Electrolytic and Dielectric Effects 6-70
Dynamics of Ground Resistance (Applets L-1 and L-3) 6-71
Nonlinear Dynamics of Ground Rods 6-71
The Liew-Darveniza Calculation of Rod Dynamic Resistances 6-71
Use of the Korsuncev Criterial Curve 6-72
Metal Tower and Reinforced Concrete Foundations 6-73
Radial and Continuous Counterpoise 6-74
Recommendations for Line Flashover Calculations 6-74
Step, Touch and Transferred Potentials 6-75
Coordination With Safe Body Withstand Levels 6-77
Calculation of Surface Potentials Using L-6 Applet 6-77

Appendix 6.1 THEORY OF THE DISRUPTIVE EFFECT ALGORITHM 6-79

Appendix 6.2 ELECTROMAGNETIC FIELDS FROM LIGHTNING 6-80

REFERENCES 6-83

Chapter 7 **Electric and Magnetic Fields**

7.1 INTRODUCTION 7-2

7.2 BASIC ELECTRIC AND MAGNETIC FIELD PRINCIPLES 7-3
EMF: Electric and Magnetic Fields 7-3
Phasors and Vectors 7-4
Electric Field 7-4
Magnetic Fields 7-7

7.3 CALCULATION OF ELECTRIC FIELDS 7-11
General Method for Transmission Lines 7-11
Lateral Profile of Electric Field at Ground Level 7-14
Maximum Electric Field at Ground – Generalized Curves 7-15
Effect of Line Parameters 7-16
Electric Field of Double-Circuit Lines 7-17
Electric Field in Substations 7-18

7.4 CALCULATION OF MAGNETIC FIELDS 7-19
General Method for Transmission Lines 7-19
Example Calculation 7-21
Calculation of Magnetic Field from Power Lines Using Simple Equations 7-21
Calculation of Magnetic Field from Sets of Conductors in Three Dimensions 7-22

7.5 MEASUREMENT OF ELECTRIC FIELDS 7-25
Techniques for Measuring the Unperturbed Electric Field 7-25

Measurement of the Electric Field on a Boundary Surface 7-28
Measurement of the Space Potential 7-29

7.6 MEASUREMENT OF MAGNETIC FIELDS 7-30
Magnetic Field Meters 7-30
Measurement of Magnetic Field from Power Lines 7-31
Waveform Capture Instrumentation 7-32

7.7 COMPARISON BETWEEN HV TRANSMISSION-LINE AND COMMON ENVIRONMENT ELECTRIC AND MAGNETIC FIELDS 7-32

7.8 ELECTRIC FIELD INDUCTION IN OBJECTS 7-34
Introduction 7-34
Electrical Parameters of Objects with Different Shapes 7-35
Accuracy Expected in Calculating Short-Circuit Currents 7-40
Electric Field Induction in Long Objects in a Nonuniform Electric Field 7-41
Impedance of Vehicles to Ground 7-42

7.9 MAGNETIC FIELD INDUCTION IN OBJECTS 7-44
Short-Circuit Currents and Open-Circuit Voltages of Sets of Conductors Parallel to Transmission Lines 7-44
Shield Wire Currents 7-46

7.10 RESPONSE OF PEOPLE TO TRANSMISSION-LINE FIELDS 7-47
Induced Currents and Their Distribution 7-47
Field Enhancement on the Surface of the Body 7-48
Currents Induced by Spark Discharges 7-49
Transient Currents Induced by Switching Surges 7-51
People Response to Short-Term Exposure to Electric Field 7-51

7.11 BIOLOGICAL EFFECTS OF ELECTRIC FIELDS 7-57

7.12 CURRENTS INDUCED IN THE HUMAN BODY BY TRANSMISSION LINE MAGNETIC FIELDS AND A COMPARISON WITH THOSE INDUCED BY ELECTRIC FIELDS 7-57

7.13 BIOLOGICAL EFFECTS OF MAGNETIC FIELDS 7-58

7.14 FUEL IGNITION 7-59
Fuel Ignition Caused by Spark Discharges 7-59
Corona-Induced Fuel Ignition 7-61

7.15 EFFECTS OF HIGH-INTENSITY ELECTRIC FIELDS 7-62
Wood Pole Burning 7-62
Dead Tree Burning 7-62
Tree Tip Damage 7-63
Corona on Grounded Objects 7-63

7.16 METHODS FOR REDUCING TRANSMISSION-LINE ELECTRIC FIELDS 7-64
Introduction—Passive and Active Shielding 7-64
Shielding by a Horizontal Grid of Grounded Wires 7-65
Shielding By a Vertical Grid of Grounded Wires 7-66
Shield Wire Mesh 7-67
Shielding by Objects 7-67
Effect of Underbuilt Lines on Electric Field (Active Shielding) 7-69

7.17 METHODS FOR REDUCING TRANSMISSION-LINE MAGNETIC FIELDS 7-70
Line Design for Low Magnetic Field 7-70
Optimization of Line Parameters 7-70
Line Compaction 7-73
Split-Phase Lines 7-76
Passive Shielding of Transmission Line Magnetic Field Using Cancellation Loops 7-78
Example of Cancellation Loops Applied to a 345-kV Corridor 7-88
Fourth-Wire Scheme 7-92

Appendix 7.1 CALCULATION OF FIELD ELLIPSE PARAMETERS 7-93

Appendix 7.2 USE OF TWO-DIMENSIONAL DIPOLES AND QUADRUPOLES FOR CALCULATING TRANSMISSION-LINE MAGNETIC FIELDS 7-95

Appendix 7.3 STANDARDS AND GUIDELINES 7-99

Appendix 7.4 MONITOR JITTER CAUSED BY TRANSMISSION-LINE MAGNETIC FIELDS 7-103

Appendix 7.5 MAGNETIC INDUCTION WITH RESISTIVE GROUND RETURN 7-107

Appendix 7.6 ELECTRIC FIELD CALCULATIONS FOR THREE-DIMENSIONAL GEOMETRY 7-109

REFERENCES 7-113

Chapter 8 **Corona and Gap Discharge Phenomena**

8.1 INTRODUCTION 8-2

8.2 MECHANISM OF CORONA DISCHARGES 8-2
Basic Discharge Physics 8-2
Discharges in Uniform Fields 8-5
Discharges in Nonuniform Fields 8-6
Modes of Corona Discharge 8-7

8.3 GAP DISCHARGES 8-12

8.4 CORONA ONSET ON CONDUCTORS AND HARDWARE 8-14
Conductors 8-14
Hardware 8-16

8.5 CORONA EFFECTS 8-17
Corona Loss 8-17
Electromagnetic Interference 8-18
Audible Noise 8-19
Ozone and NO_X 8-19
Light Emission 8-20
Electrical Wind and Corona-Induced Vibrations 8-20
Other Effects 8-20

8.6 FACTORS INFLUENCING CORONA PERFORMANCE 8-21
Fair Weather Corona Sources 8-21
Conductor Surface Conditions 8-21
Influence of Water on Conductors 8-22
Influence of Weather Conditions 8-22
Influence of Conductor Heating 8-23
Statistical Consideration of Corona Performance 8-23

8.7 GENERATION QUANTITIES OF CORONA EFFECTS 8-24
General Principles of Corona Testing 8-24
Generated Corona Loss 8-25
Radio Noise Excitation Function 8-26
Generated Acoustic Power Density 8-28
8.8 CORONA ATTENUATION OF POWER SYSTEM OVERVOLTAGES 8-28
Lightning Overvoltages 8-29
Switching Overvoltages 8-30
Temporary Overvoltages 8-32
Appendix 8.1 GUIDELINES FOR CORONA TESTING OF HARDWARE 8-33
Appendix 8.2 CURRENTS INDUCED BY MOVING CHARGED PARTICLES 8-37
REFERENCES 8-38

Chapter 9 **Electromagnetic Interference**
9.1 INTRODUCTION 9-2
9.2 CHARACTERISTICS OF TRANSMISSION-LINE EMI 9-4
EMI Due to Conductor Corona 9-4
EMI Due to Hardware Corona 9-8
Gap Discharge EMI 9-9
9.3 DESIGN CONSIDERATIONS AND EMI GUIDELINES AND LIMITS 9-10
EMI Tolerability Criteria 9-10
Design Guidelines and Limits 9-15
9.4 MEASUREMENT OF EMI 9-16
EMI Instrumentation 9-17
Weighting Circuits 9-17
Meter Response – Bandwidth and Pulse Repetition Rate 9-19
Actual Band-Pass Characteristics 9-22
Antenna Systems 9-23
Measurement of Transmission-line EMI 9-24
Pre-construction, Pre-energization and Post-energization Measurements 9-25
9.5 CALCULATION OF EMI FROM CONDUCTOR CORONA BELOW 30 MHZ 9-27
Philosophy of Modeling 9-27
Analytical Methods 9-29
Empirical Methods 9-45
9.6 CALCULATION OF EMI FROM CONDUCTOR CORONA ABOVE 30 MHZ 9-46
Introduction 9-46
Analytical Methods 9-47
Empirical Methods 9-49
Calculation of TVI – Low VHF Band 9-51
9.7 PASSIVE INTERFERENCE 9-51
AM Broadcast Reradiation 9-51
TV Broadcast Reradiation 9-54
Appendix 9.1 CALCULATION OF CORONA-INDUCED CURRENT ON PHASE CONDUCTORS 9-55
Appendix 9.2 STATISTICAL AVERAGES 9-64
Appendix 9.3 EVALUATION OF INVERSE SPATIAL TRANSFORMS 9-64
Appendix 9.4 APPROXIMATIONS FOR Fey, Fhx, AND Fez 9-66
Appendix 9.5 GROUND CONDUCTIVITY 9-69
REFERENCES 9-70

Chapter 10 **Audible Noise**
10.1 INTRODUCTION 10-2
10.2 CHARACTERISTICS OF TRANSMISSION-LINE NOISE 10-2
10.3 AUDIBLE NOISE AS A DESIGN FACTOR 10-4
Effect of Weather Conditions and Load Current 10-5
Effect of Line Geometry and Conductor Surface Conditions 10-8
Audible Noise from Insulators and Fittings 10-9
10.4 CALCULATION OF TRANSMISSION-LINE AUDIBLE NOISE 10-10
Introduction 10-10
Generation and Propagation of Audible Noise 10-11
Calculation of A-Weighted Audible Noise-Levels in Rain 10-15
Audible Noise in Fair Weather 10-17
Influence of Tower, Sag, and Ground Wires 10-19
Effect of Rain Rate 10-20
Effect of Conductor Aging 10-21
Effect of Altitude above Sea Level 10-23
Effect of Bundle Orientation 10-23
Comparison of Audible-Noise Calculation Methods with Measured Data (Rain) 10-24
Generation and Calculation of Hum 10-24
10.5 MEASUREMENT OF AUDIBLE NOISE 10-27
Sound Pressure, Sound-Pressure Level, the Decibel 10-27
Weighted Sound Level 10-28
Statistical Descriptors 10-28
Leq, Ldn and CNEL 10-28
Instrumentation 10-28
Measurements 10-29
10.6 ASSESSING THE IMPACT OF TRANSMISSION-LINE AUDIBLE NOISE—AUDIBLE-NOISE REGULATIONS 10-30
Noise Evaluation Studies 10-30
Noise Ordinances—United States 10-31
Case Study: Example of Limits Based on Any One Hour 10-33
Case Study: Example of Limits Based on Some Variation of the EPA “Levels Document” 10-33
Case Study: Example of Limits Based on South African Noise Code 10-36
10.7 AUDIBLE-NOISE REDUCTION TECHNIQUES 10-37
Introduction 10-37
Bundle Geometry Optimization 10-37
Other Techniques of Audible Noise Reduction 10-40

Appendix 10.1 ADJUSTMENT OF MEASURED AUDIBLE-NOISE LEVELS TO ACCOUNT FOR AMBIENT NOISE INTRUSIONS 10-43

Appendix 10.2 AMBIENT NOISE DURING RAIN 10-44

REFERENCES 10-46

Chapter 11 **Corona Loss and Ozone**

11.1 INTRODUCTION 11-2

11.2 PHYSICAL MECHANISM OF CORONA LOSS 11-3

11.3 MEASUREMENT OF CORONA LOSS 11-4

11.4 CORONA LOSS IN FAIR WEATHER 11-6

11.5 CORONA LOSS IN FOUL WEATHER 11-9
Corona Losses in Rain 11-9
Corona Losses in Snow, Ice, and Hoarfrost 11-13
Influence of Conductor Heating 11-14

11.6 EFFECT OF ALTITUDE ON CORONA LOSS 11-14

11.7 EVALUATION OF CORONA LOSS 11-15

11.8 INFLUENCE OF CORONA LOSSES ON LINE DESIGN 11-16

11.9 OZONE AND NO_X 11-18
Mechanism of Generation 11-18
Rates of Generation 11-18
Ozone Dispersion from Transmission Lines 11-18
Ozone Levels Near Transmission Lines 11-19
Standards for Ambient Ozone Levels 11-20

REFERENCES 11-21

Chapter 12 **Shared Use of the Right-of-Way**

12.1 INTRODUCTION 12-2
Background 12-2
EMC Regulations, Standards and Guidelines 12-2
Elements of EMC 12-2
Electric Power Transmission-Line Sources 12-3
Coupling Paths 12-4
Receptors 12-5
Organization and Contents of the Chapter 12-5

12.2 INTERFERENCE WITH THE OPERATION OF RAILROADS 12-6
Background 12-6
Introduction to Coupling Mechanisms between Power Lines and Railroads 12-7
Electric-Field (Capacitive) Induction 12-7
Magnetic-Field (Inductive) Induction 12-8
Conductive (Resistive) Induction 12-9
Common and Differential Modes 12-9
Coupling between Common and Differential Modes 12-10
Overview of Railroad Signaling 12-10
Abnormal Operation of Railroad Equipment 12-10
Damage to Railroad Equipment 12-10
Personnel Safety Considerations (Steady-State Operation) 12-11
Personnel Safety Considerations (Fault Conditions) 12-11
"Rules of Thumb" of Railroad Signals and AC Interference 12-11

12.3 INTERFERENCE WITH THE OPERATION OF PIPELINES 12-12
Background 12-12
Electric-Field Induction 12-12
Magnetic-Field Induction 12-13
Conductive Coupling 12-17
Damage to Pipelines 12-17
Personnel Safety 12-18

12.4 INTERFERENCE WITH THE OPERATION OF POWER LINE COMMUNICATION SYSTEMS 12-19
Power Line Carrier 12-19
High-Speed Communications 12-19

12.5 INTERFERENCE WITH THE OPERATION OF OPTICAL FIBER COMMUNICATIONS 12-21
Introduction 12-21
Comparison of OPGW, ADSS, and WRAP 12-21
Experience with WRAP 12-22
OPGW EMC Issues 12-22
ADSS EMC Issues 12-24

12.6 CONSEQUENCES OF INSTALLING COMMUNICATION SYSTEM ANTENNAS ON TRANSMISSION-LINE TOWERS 12-26
Introduction 12-26
Influence of the Power Line on the Antenna 12-26
Issues Relating to Grounding and Low-Voltage Feeds 12-27
Exposure to RF Electromagnetic Fields 12-27

12.7 INTERFERENCE WITH THE OPERATION OF SYSTEMS FOR WARNING AIRCRAFT 12-29
Introduction 12-29
Warning Lights 12-29
Airway Marking Balls 12-29

12.8 INTERFERENCE WITH THE OPERATION OF TELEPHONE SYSTEMS 12-29
Telephone Lines 12-29
Cordless Phones 12-30
Cell Phones 12-30

12.9 CONSEQUENCES OF INSTALLING DISTRIBUTION LINES UNDER TRANSMISSION LINES 12-31

12.10 INTERFERENCE WITH THE OPERATION OF RADIO NAVIGATION SYSTEMS 12-32
LORAN-C 12-32
Instrument Landing Systems (ILS) 12-32
Global Positioning System (GPS) 12-33
Differential Global Positioning System (DGPS) 12-34

12.11 INTERFERENCE WITH THE OPERATION OF COMMUNICATION RECEIVERS 12-36

12.12 IMPACTS ON AGRICULTURAL OPERATIONS NEAR TRANSMISSION LINES 12-36
Introduction 12-36
Operation of Irrigation Equipment 12-37
Interference with Cornering Guidance Systems 12-37

12.13 USE OF VEHICLES AND LARGE EQUIPMENT NEAR TRANSMISSION LINES 12-38
Introduction 12-38

Induced Currents from Vehicles 12-39
Spark Discharges (Induced Voltages) from Vehicles 12-40
Fuel Ignition 12-40
Parking Lots 12-40

12.14 IMPACTS ON BUILDINGS NEAR TRANSMISSION LINES 12-41

12.15 IMPACTS ON PUBLIC USE OF RIGHTS-OF-WAY 12-42
Introduction 12-42
Exposure Guidelines for the General Public 12-42
Nuisance Shocks 12-43
Open-Space Uses of the Right-of-Way 12-44

12.16 AVIAN INTERACTIONS WITH TRANSMISSION LINES 12-45
Introduction 12-45
Bird Electrocutions 12-45
Bird Collisions 12-45
Nesting Issues—Structural 12-46
Nesting Issues—Electrical 12-46
Nesting Issues—Legal 12-47
Nesting Issues—Liability 12-47
Bird Pollution 12-47
Bird Streamers 12-48
Other Bird Issues 12-48

REFERENCES 12-49

Chapter 13 **Considerations for Inspection and Maintainability**

13.1 INTRODUCTION 13-3

13.2 DESIGNING FOR INSPECTION AND MAINTAINABILITY 13-3
Introduction 13-3
Background 13-4
Designing for Durability and Longevity 13-14
Design Examples 13-45

13.3 OPTIMIZING THE DESIGN FOR EFFECTIVE LIVE WORKING 13-48
Introduction 13-48
Brief Overview of Live Working (LW) 13-49
Design and Construction Aspects Important to LW 13-54
Low-Cost-Impact Design Modifications That Help Facilitate LW 13-63
High-Cost-Impact Design Modifications That Help Facilitate LW 13-64
Examples and Lessons Learned 13-64
Determining Whether a Line is Maintainable Using LW Methods 13-68

REFERENCES 13-70

Chapter 14 **Voltage Upgrading of Existing Transmission Lines**

14.1 INTRODUCTION 14-2

14.2 SYSTEM LEVEL STUDY OF POWER FLOW NEED AND VOLTAGE STRATEGY 14-4
Reactance Limits, Stability, and Surge Impedance Loading 14-5
Voltage Drop 14-7
Thermal Uprating 14-8

14.3 ASSESSING ELECTRICAL FEASIBILITY 14-9
Data Gathering 14-10
Review of Line Design 14-10
Electrical Clearances and Right-of-Way 14-10
Review of Electrical Design Criteria 14-11
Insulation and Conductor to Structure Clearances 14-12
Corona and Field Effects 14-13
Grounding and Bonding 14-14
Other Issues 14-14

14.4 ASSESSING MECHANICAL FEASIBILITY 14-15
Mechanical Data Gathering 14-16
Review of Original Structure Loads 14-16
Sag-tension Calculations 14-17
Hardware/Connectors 14-19
Insulator Strength 14-19
Structure Phase Geometry 14-19
Shield Wires 14-19
Right-of-Way 14-19
Wind and Ice-Induced Conductor Motions 14-20

14.5 EVALUATION OF PRESENT LINE CONDITION 14-20
Physical Examination 14-21
Historical Damage Report Examination 14-23

14.6 DETAILED ENGINEERING DESIGN FOR VOLTAGE UPGRADING 14-24
Detailed Review of Criteria Applied to Upgrading 14-25
Power Frequency Insulation 14-25
Switching Surge 14-26
Corona and Field Effects 14-27
Lightning 14-28
Structural Analysis and Reinforcement 14-29
Detailed Economic Review 14-29
Maintenance and Minimum Approach Distance Requirements 14-29
Conductor Motion 14-29
Laboratory Tests of Prototype Upgraded Structure 14-30

14.7 EXAMPLES OF VOLTAGE UPGRADES 14-30
Example 1: 115 to 230 kV Voltage Upgrading 14-30
Example 2: 230 to 345 kV Voltage Upgrading 14-31
Example 3: 300 to 420 kV Voltage Upgrading 14-32
Example 4: 230 to 500 kV Voltage Upgrading 14-34

REFERENCES 14-36

Chapter 15 **Transmission Lines Above 700 kV**

15.1 INTRODUCTION 15-3

15.2 RESEARCH TO DEVELOP TRANSMISSION SYSTEMS ABOVE 700 KV 15-3
Introduction 15-3
Research to Develop 800-kV Systems 15-4
Research to Develop Transmission Systems Above 1000 kV 15-5

15.3 CASE STUDIES OF TRANSMISSION LINES ABOVE 700 KV 15-7

15.4 HYDRO-QUÉBEC 735-KV LINES IN CANADA 15-8
System Planning 15-8
Electrical Design 15-10
Mechanical and Tower Design 15-11
Operation and Maintenance 15-13

15.5 AMERICAN ELECTRIC POWER SERVICE CORPORATION (AEP) 765-KV SYSTEM IN THE U.S. 15-14
System Planning 15-14
Electrical Design 15-15
Mechanical and Tower Design 15-16
Operation and Maintenance 15-17

15.6 RUSSIAN 750-KV AND 1150-KV LINES 15-19
System Planning 15-20
Electrical Design 15-20
Mechanical and Tower Design 15-22
Operation and Maintenance 15-23

15.7 EDELCA 765-KV LINES IN VENEZUELA 15-24
System Planning 15-25
Electrical Design 15-25
Mechanical and Tower Design 15-26
Operation and Maintenance 15-28

15.8 FURNAS 750-KV LINES IN BRAZIL 15-28
System Planning 15-28
Electrical Design 15-29
Mechanical and Tower Design 15-30
Operation and Maintenance 15-30

15.9 NEW YORK POWER AUTHORITY (NYPA) 765-KV SYSTEM IN THE U.S. 15-32
System Planning 15-32
Electrical Design 15-33
Mechanical and Tower Design 15-33
Operation and Maintenance 15-33

15.10 ESKOM 765-KV LINES IN SOUTH AFRICA 15-35
System Planning 15-35
Electrical Design 15-36
Mechanical and Tower Design 15-37
Operation and Maintenance 15-39

15.11 765-KV TRANSMISSION LINES IN INDIA 15-40
System Planning 15-41
Electrical Design 15-41
Mechanical and Tower Design 15-42
Operation and Maintenance 15-42

15.12 KOREA ELECTRIC POWER CORPORATION (KEPCO) 765-KV SYSTEM IN SOUTH KOREA 15-43
System Planning 15-43
Electrical Design 15-43
Mechanical and Tower Design 15-46
Operation and Maintenance 15-47

15.13 TOKYO ELECTRIC POWER COMPANY (TEPCO) 1000-KV LINES IN JAPAN 15-49
System Planning 15-49
Electrical Design 15-50
Mechanical and Tower Design 15-51
Operation and Maintenance 15-53

15.14 SUMMARY 15-53

Appendix 15.1 SURVEY QUESTIONNAIRE 15-58

REFERENCES 15-60

BIBLIOGRAPHY 15-62

Appendix 1 **Base Case Line Configurations** **A1-1**

Appendix 2 **Applets** **A2-1**

Glossary **G-1**

Index **I-1**

Symbols

Symbol	Quantity
A	Generated acoustic power (dBA)
A	Surface areas (m^2)
A *(or Alt if A used for another quantity in equation)*	Altitude above sea level (m)
A,B,C	Phasing
B	Magnetic flux density (mG)
c	Velocity of light
C	Capacitance (F)
d	Subconductor diameter (cm)
d_b	Bundle diameter (cm)
d_{eq}	Equivalent diameter of a bundle (cm)
D	Distance conductor-to-measuring point
D	Dissipation factor
$D_{subscript}$	Distances between phases (m)
$D'_{subscript}$	Distance to images
E	Electric field away from conductors (kV/m)
E_{av}	Average surface gradient of a subconductor (kV/m)
E_c	Corona onset gradient (kV/cm)
E_m	Maximum surface gradient of a subconductor (kV/m)
E_{max}	Conductor surface gradient (average of max of subconductor gradients) (kV/m)
f	Frequency (Hz)
GMD	Geometric Mean Diameter
GMR	Geometric Mean Radius
GMR_B	Geometric Mean Radius (bundle)
GMR_C	Geometric Mean Radius (subconductor)
h	Humidity
H	Magnetic field strength (A/m)

Symbol	Quantity
H	Conductor height above ground (m)
I	Current (A)
J	Power Density
J	Current Density
L	Inductance
L_{50}	50% exceedance level
L_5	5% exceedance level
L_{seg}	Length of a segment (m)
log	Base 10
ln	Base e (Natural log)
m	Conductor surface irregularity factor
n	Number of subconductors in a bundle
N	Number of elements
p	Pressure
p	Barometric pressure
P	Power loss (W/m)
P	Potential coefficients (1/F or m/F)
q *(instantaneous value)*	Line Charge (C/m)
Q *(phasor magnitude)*	Line Charge (C/m)
r	Conductor radius
r_b	Bundle radius (cm)
r_{eq}	Radius of equivalent zero potential cylinder
r_{eq}	Equivalent radius of a bundle (cm)
r_s	Average radius of space charge
R	Resistance (Ω)
RR	Rain rate (mm/h)
s	Subconductor spacing (cm)
t	Time (s)
t	Time interval (s)

Symbol	Quantity
T	Temperature
v	Speed of wave (m/s)
V	Voltage (kV)
V_{sp}	Space potential (kV)
W	Energy
X	Reactance
X_a	Inductive reactance at 1-foot spacing
X'_a	Capacitive reactance at 1-foot spacing
Y	Admittance
Z	Impedance
Z_o	Surge impedance
x,y,z	Orthogonal coordinates
α	Phase angle

Symbol	Quantity
β	Phase angle
δ	Air density (Kg/m^3)
δ	Loss angle
δ_i	Image depth (m)
δ_r	Relative air density
ε	Permittivity (F/m)
γ	Phase angle
Γ	Radio noise excitation (or generation function)
μ	Permeability (H/m)
μ	Ion mobility (m/s per V/m)
ρ	Resistivity (m)
σ	Surface charge density (C/m^2)
σ	Standard deviation

CHAPTER 1

Transmission Systems

Jan P. Reynders—University of the Witwatersrand
Raymond Lings—EPRI
Robert G. Stephen—Eskom
Lori A. Nielsen—EDM International, Inc.
Andrew C. Ludwig—ENSR International

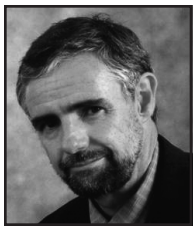
This chapter provides a broad introduction to power transmission. It describes the evolution of transmission from the late 19th century to developments in the early 21st century. The chapter also introduces the topic of line permitting. While not directly applicable to the electrical design of a transmission line, line permitting today is seen as the single largest hurdle to the expansion of the global transmission system.



Jan P. Reynders has been a researcher and academic in the field of electrical engineering since 1964. He has been active as a specialist on working groups in CIGRE since 1978, all largely in the field of insulation and insulation coordination. He has served on the Administrative Council and the Technical Committee of CIGRE, as well as being the National Member on Study Committees 15 and 33. On the academic level, he served as head of the Department of Electrical Engineering and as Dean of the Faculty of Engineering at the University of the Witwatersrand. He had two terms as a member of the University Council. Along with his masters and doctoral students, he has published 170 journal and conference papers on various aspects of electrical power and engineering education. Jan is a Registered Professional Engineer in South Africa, and has been appointed as a consultant to a wide variety of organizations both in South Africa and elsewhere in the world.



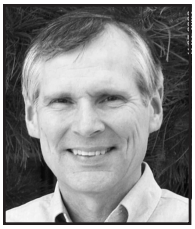
Raymond Lings is the Area Manager for Transmission and Substations within the Science and Technology Development Division of EPRI. In his present duties, Lings is responsible for the management and execution of EPRI's research in overhead and underground transmission, substations, increased transmission capacity, EMC (electromagnetic compatibility), energy storage for T & D applications, and applications of superconductivity. Lings joined EPRI in 1998 as a project manager in substations. Prior to joining EPRI, he was the Research Operations Manager at Eskom, South Africa, where he worked for 11 years, starting as an Engineer-in-Training and rising to Manager of Electrical Research and then to Research Operations Manager covering research in distribution, transmission, and generation. As Manager of Electrical Research, he managed Eskom's extensive electrical laboratories. Lings is a senior member of the IEEE and is a registered professional engineer in South Africa. He is the author or co-author of more than 15 publications in the field of transmission and distribution, with the majority of his publications covering electronic domestic metering. As EPRI project manager for this edition of the Reference Book, Lings led the editorial committee, and had overall management responsibility for the new edition. He has also represented South Africa and the United States on an IEC Working Group on the reliability of metering. Lings holds a number of degrees including a Masters Degree in Electrical Engineering (MSc) and a Masters of Business Administration (MBA).



Robert G. Stephen has been actively involved in line design and line optimization since 1985. He has led the design and project engineering team in Eskom, the South African utility, and has introduced optimization processes for line designs that have resulted in large cost reductions. He specializes in thermal rating of lines, and was instrumental in drafting the CIGRE documents on steady-state determination of conductor temperature as well as probabilistic rating. Stephen has authored a number of local and international papers on the subject. For 9 years he was chairman of CIGRE SC B2 -12 dealing with electrical aspects of overhead lines. He received the Technical Committee award for CIGRE in 1996, served as Special Reporter for SC B2 in the same year, and was chairman of CIGRE SC B2 (Overhead lines) from 2000 to 2004. He is an honorary member of CIGRE and a fellow of the South African Institute of Electrical Engineers.



Lori Nielsen with EDM International, Inc. has more than 18 years experience managing and coordinating environmental permitting, biological studies, mitigation plans, and monitoring programs in the United States. Her focus has been on permitting and compliance for projects subject to national, state, local, and tribal regulatory review. Ms. Nielsen has provided technical expertise on, or managed, over 55 Environmental Assessments (EAs) and Environmental Impact Statements (EISs), including routing and siting studies for generation and transmission projects, permit review and authorization for projects on public lands, and regulatory compliance for sensitive biological resources. In addition to these federal reviews, she was involved with five solar energy generating projects over eight years with the state permitting review in the western Mojave Desert of California. She works closely with a range of utilities, including investor owned, municipalities, federal, public, and the Rural Utilities Service Electric Cooperatives. As a senior wildlife biologist, Ms. Nielsen is also involved in permitting review and compliance for a number of environmental regulations pertaining to power line siting, construction, and operation, encompassing over 40 biological reviews and problem resolution for electric utilities under the United States Endangered Species Act and International Migratory Bird Treaty Act.



Drew Ludwig has been with ENSR International in Fort Collins, Colorado for the past 28 years, and has 32 years total experience in environmental analysis and report preparation for capital development projects, including transmission lines and power plants. He has been involved in transmission line, pipeline, and generating station siting analysis since beginning his career with Commonwealth Associates in 1973 and has worked on numerous projects in the eastern and western United States and Canada, including nuclear, coal-fired, and gas turbine power plants and high-voltage electric transmission lines from 69-kV to 765-kV. These projects have required the preparation of EAs and EISs for the Rural Utilities Service (and its predecessor the Rural Electrification Administration), as well as the Department of Energy, Bureau of Land Management, and National Park Service. In total, Mr. Ludwig has participated in the preparation of more than 40 EAs and EISs in both technical and management roles. His transmission-line experience includes testimony on environmental issues before the Wyoming Public Service Commission and New York Public Service Commission.

1.1 INTRODUCTION

1.1.1 Background

This chapter introduces the subject of transmission-line design through a brief, high-level overview of fundamental concepts and industry issues bearing on the role of line design.

Given the requirement of the electricity system for precisely balancing supply and demand while rapidly and reliably delivering electromagnetic energy across thousands of miles, it is not surprising that the system is often described as the most complex machine ever built. It is also arguably the most influential machine of the last century. In fact, the U.S. National Academy of Engineering voted electrification as the number-one engineering achievement of the 20th century due to its impact on the course of industrialization and its contribution to the quality of life in innumerable applications (Constable and Somerville 2003).

Modern society is dependent on the ready availability of energy and communication, both of which are indispensable for economic growth and sustainability. Electricity plays a vital role in providing these two resources. Electrical generation and transmission systems take natural energy sources in their raw, and often difficult-to-use, state and deliver power in a highly controllable, clean, and usable form to wherever it is needed. Electrical power is converted into heat, light, and mechanical energy. It provides the power for mass transport systems; it makes audible and visual communication as well as data transmission possible with amazing speed and efficiency. Industry, business, banking, education, medical facilities, and family life are all dependent on the availability of low-cost, highly reliable electricity.

Despite its ubiquity, electricity is generally taken for granted by most users—at least until there is a widespread outage, when the central critical role of electricity in modern economies is demonstrated. This was evidenced by the blackout of August 14, 2003, in the northeast United States and Canada, the largest blackout in North American history. In just a few days, this outage affected 40 million people across eight U.S states and 10 million people in Canada—a third of that country's population. It involved more than 250 power plants and 62,000 MW of power, closed 12 airports, disrupted water and communications systems, and resulted in $6 billion of economic losses in goods and services (U. S. DOE 2003, 2004; U. S.–Canada Power System Outage Task Force 2003). Where electricity is unavailable or costly, many of the resources needed in society remain primitive, economic growth is hampered, health services and education remain problematic, and transportation grinds to a halt.

Transmission lines are the means whereby the electrical energy is transported from the source of generation to the places of use. Distances involved can be very long, and the lines may traverse a variety of environments. The lines must be capable of operating reliably in all the environmental conditions that they experience and should have as low an impact as possible on these environments.

Power lines have been in existence for almost 120 years, as illustrated in Table 1.1-1. In the U.S. in the early 1880s, Thomas Alva Edison and his team established the first power company in New York City and designed a small but complete electrical system based on direct current (dc). A few years later George Westinghouse established a rival company, and after purchasing patents from Nikola Tesla, began building electrical systems with alternating current (ac).

Initially, the electrical grid in North America primarily consisted of small, isolated, locally operated networks serving urban centers. However, beginning in the 1930s, and intensifying in the 1950s and 1960s, there evolved a large, interconnected system of interstate transmission lines linking many different electrical systems. Large generation plants were built to take advantage of economies of scale, and transmission lines with increasingly higher voltages were constructed to allow the bulk delivery of power over great distances. Figure 1.1-1 shows the rise in maximum operating transmission voltages over the years.

From these humble beginnings, the North American grid today contains more than 200,000 miles (322,000 km) of high-voltage lines operating above 230 kV and serving over 120 million consumers and nearly 300 million people. The U.S. electricity delivery system—which consists of the grid and the downstream distribution system—is a $360 billion asset.

Worldwide, there are now dc lines operating up to ±533 kV and ac lines that have been designed and operated up to 1200 kV (as described in Chapter 15). These lines traverse distances of 1500 km or more.

These achievements have been realized with the constant dynamic of reducing cost, improving reliability, and mini-

Table 1.1-1 First Electrical Power Lines (Glover and Sarma 2002)

	ac/dc	Length (km)	Voltage (kV)	Date	Location
First line	dc	50	2.4	1882	Germany
First single-phase line	ac	21	4	1889	Oregon, USA
First three-phase line	ac	179	12	1891	Germany

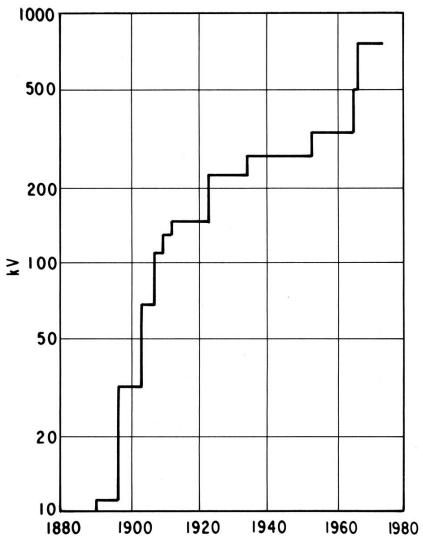


Figure 1.1-1 Highest ac transmission voltages in North America (EPRI 1982).

mizing environmental impact. There is a constant evolution in design to address these requirements. Modern guyed structures have contributed to the compaction of lines, and this has resulted in reductions in cost, improvements in performance, and lower levels of environmental impact. Structures and their foundations, the electric and magnetic fields produced by the voltage and current, and audible and radio interference produced by corona must all conform to demanding requirements. The challenge facing the designer is to design a cost-effective and reliable line within the bounds set by the performance and regulatory requirements.

1.1.2 Transmission System Characteristics

Around the world, the underlying principles governing operation of transmission systems are generally similar. From country to country, the differences lie in design specifications and margins of operation.

In addition, there are differences in frequency and standard voltages. As regards frequency, two basic types of power systems are in use around the world. For convenience, they can be referred to as North American-type systems and European-type systems. Most power systems share basic characteristics with one of these two types (see Figure 1.1-2).

North American systems are characterized by 60 Hz as the fundamental frequency, while European systems are characterized by 50 Hz.

Not every country, however, follows strictly "North American" or "European" power system. One example of this is Japan, where the transmission system uses both frequencies, with the northern region of the country operating on



Figure 1.1-2 North American vs. European type power systems, based on 50- and 60-Hz systems throughout the world (*Energy Information Administration and CIA World Fact Book* 2002).

50 Hz, and the southern region operating on 60 Hz (see Figure 1.1-3).

China in 2004 experienced an explosion in new networks and growth. The network was constructed using the latest technologies and included integrated ac transmission and HVDC (see Figure 1.1-4).

For the two main types of power systems, the standard voltages are also different, as shown in Table 1.1-2.

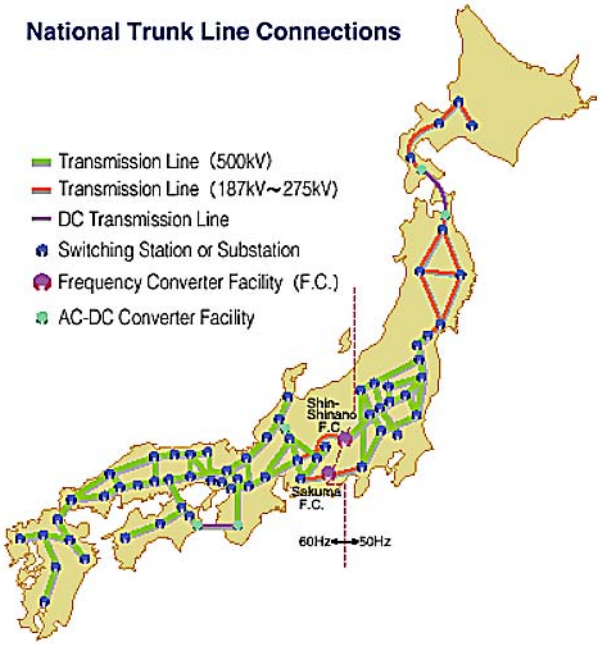


Figure 1.1-3 Japanese transmission system (EPRI 2004).



Figure 1.1-4 Transmission infrastructure in China (EPRI 2004).

The introduction of a new transmission voltage is prompted by the increase in power generation and distribution requirements within a region that cannot be efficiently handled using the existing transmission network. Generally, lower-voltage transmission networks are overlaid by a transmission network with voltages higher by a factor of two to three. In certain areas of North America, 115-161 kV transmission networks are overlaid by 345-kV network, and these by 765-kV networks. In other North America areas, 230-kV networks are overlaid by 500-kV network. Several European systems have 110 kV, 220 kV, and 400 kV (each approximately a factor of two from the next lower voltage).

The title for this edition of the Red Book reflects a clarification of the book's focus and a change from previous editions, as regards transmission system characteristics. Recognizing that most lines are in the voltage range of 230 to 345 kV, it was decided to lower the voltage range of the book. The choice of 200 kV was taken because this level is clearly in the transmission range. In addition, 200 kV is a "country-neutral" threshold. It represents neither the common North American standard of 230 kV nor the European standard of 220 kV. Also, because the Red Book focuses only on ac technology, and since EPRI has a separate handbook on dc technology (*HVDC Transmission Line Reference Handbook*), the term "ac" was added to the book's title.

1.1.3 Industry Trends Affecting Line Design

Starting in the late 1980s, there have been a number of broad electric industry trends that have had a profound impact on transmission-line design today in ways that extend far beyond the concerns of traditional electric design.

Foremost among these trends is the deregulation of the electricity industry in North America and various other parts of the world, and the associated unbundling of generation, transmission, distribution, and retail services. In some cases, the initial effects of deregulation have been a

Table 1.1-2 Standard Voltages

North American Transmission (kV)	European Transmission (kV)
69	60
115	110
138	132
161	220
230	275
345	400
500	
735–765	765
	1100 (not in general use)

lack of coordinated network planning to meet load, rapid increase in wholesale transactions, changes in grid flows and increased grid congestion, and low levels of infrastructure investment.

Other general industry trends in recent years with the potential to affect transmission-line design include increased legal and environmental requirements and high costs of rights-of-way, an aging infrastructure, lack of investment in maintenance, and growing needs for grid security.

Finally, at the time of this writing, a key concern for the industry is the loss of skills—a trend that may or may not be reversed. This loss is evident in the following areas:

- **Staff Reductions.** The focus on deregulation has meant major staff reductions. The uncertainty in the industry has seen the wide-scale loss of deep technical skills, with less attention on the technical and more on the financial operations of the industry (the standard comment being that the company is now run primarily by nonengineering managers).
- **Contracting.** Transmission companies are contracting out more and more of the day-to-day operations. (It is now typical for independent transmission companies with workforces of 300 employees to contract out nearly every day-to-day function.)
- **Hiring.** Since the late 1980's, hiring of graduates has been in decline. This trend has started to change, but in reality the poor job market has meant that potential graduates have turned to other industries for a career. Interestingly, the transmission industry now complains that there are now skilled positions available and that the universities are not producing the required supply of graduates to meet demand.
- **Graduates.** Universities have seen declining graduate numbers (although anecdotal comments indicate that the North American blackout of August 14, 2003, plus the decline in the luster of the "dot-com" industry, has made power engineering a more attractive career path).

The net result of these trends is that the practice of transmission-line design has undergone significant changes in the past 15 years. Accordingly, this edition of the Red Book reflects these changes in the breadth and content of its coverage. More detailed discussion of these trends is found in Sections 1.4 through 1.6.

1.1.4 Feedback of Experience

Another opportunity provided by this new edition of the Red Book is that, since the publication of the previous edition, more than 15 years of experience in line design, operation, and maintenance are available to today's designers. This edition, therefore, intentionally sets out to capture key areas of experience, including use of rights-of-way (servitudes), line maintenance, voltage uprating, and development of lines above 700 kV.

1.1.5 Organization of this Chapter

Section 1.2 reviews several basic concepts of electrical design that are relevant to line design, including voltage, impedance, and power limits, and the effects of standing waves and transients.

Section 1.3 discusses environmental factors pertinent to the design and siting of lines.

Given the profound changes in the electricity supply industry in recent years, Sections 1.4 and 1.5 examine issues related to the current state of the industry and its future direction that have the potential to shape the practice of transmission-line design.

Section 1.6 describes legislative and regulatory issues typically encountered during the siting and construction of new high-voltage transmission lines and ancillary facilities. This latter section provides extended discussion, because in recent years, it has been found that the majority of instances of delay or cancellation of new line projects are due to the permitting process.

Section 1.7 provides a mapping between the second edition and third edition of this Reference Book. Those familiar with the second edition will find this section useful when trying to locate information.

1.2 ELECTRICAL DESIGN

1.2.1 Voltage, Impedance and Power Limit

Some Basic Considerations

Under steady-state balanced ac conditions, a power line can be represented by the simple, Π equivalent-circuit shown in Figure 1.2-1.

In Figure 1.2-1, the subscript "S" on the voltage and current applies to the sending-end and the subscript "R" to the voltage and current at the receiving-end of the line. *R* is the series resistance, *L* the series inductance and *C* is half the

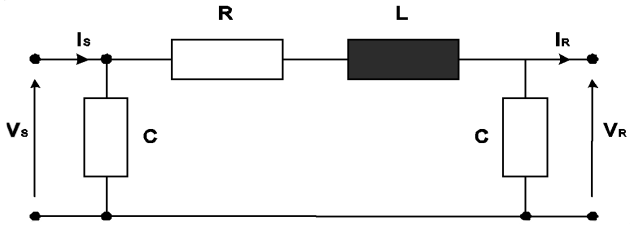


Figure 1.2-1 Π equivalent-circuit for a power line.

total shunt capacitance of the line. Shunt conductance provides a resistive path in parallel with both shunt capacitors. However, since the basic insulation for transmission lines is air, the shunt conductance is assumed to be zero and is ignored.

An analysis of a loaded line shows that, if line losses can be regarded as small in comparison with the power transferred by the line, the maximum power that the line can transmit is given by Equation 1.2-1 (Glover and Sarma 2002; Grainger and Stevenson 1994):

$$P_L = \frac{V_S V_R}{X} \qquad 1.2\text{-}1$$

Where:

P_L is the power limit of the line

V_S and V_R are the rms values of the sending-end and receiving-end voltages, respectively.

X is the series reactance of the line

This simple equation leads us to two very important limits on the performance of a line:

- **Voltage.** The maximum power that a line can transmit is directly proportional to the product of sending- and receiving-end voltages. In most transmission systems, these two voltages are more-or-less the same and hence the power limit is proportional to the square of the system voltage. This is why utilities move to higher voltages as the amount of power to be transmitted increases. The reactance of the line has a logarithmic dependence on the ratio between conductor size and phase spacing. It decreases with conductor size and increases with phase spacing. As the voltage increases, the change in reactance is generally small. Hence, as the system voltage is doubled, the power limit of the line approximately quadruples, provided the line length does not change.

  Increases in voltage require greater phase spacings and more insulation, necessitating wider rights-of-way, or servitudes. However, the relationship is not linear, and the economics of line design as well as the environmental impact are, usually, in favor of increasing the voltage instead of placing additional parallel lines in the same right-of-way. Chapter 15 describes the experiences of ten utilities that have developed transmission lines to operate above 700 kV.
- **Series Reactance.** The power limit is inversely proportional to the series reactance of the line. This reactance is directly related to the phase separation and the dimensions and configuration of the phase conductors as well as the line length (Glover and Sarma 2002, Chapter 4; Grainger and Stevenson 1994, Chapter 4). For a given length of line, the power limit can be increased by reducing the series reactance. This involves a reduction of phase spacing—realizable with compact structures and the use of large conductor bundles. With long lines, it is feasible to "tune out" the series inductance by means of series capacitive compensation. This involves placing series capacitor installations at appropriate positions along the line length and is economically viable for lines of approximately 800 km (500 miles) or longer. Frequently these installations are made at points of transposition.

  The electrical resonance produced by the series arrangement is always below power frequency so that resonance at power and harmonic frequencies will be avoided. Care must be taken to ensure that the resonant frequency chosen does not coincide with mechanical resonances in the generators. Where this has been the case, these subsynchronous resonances have caused severe damage to generators (Glover and Sarma 2002).

In addition, while the Red Book is an ac handbook, it is worth noting that high-voltage direct current (HVDC) is a viable alternative to ac for long-distance transmission because the conversion cost has decreased and reliability has increased. Also, high-capacity dc interties may be used to connect adjacent, asynchronous regions in order to resolve stability problems. Issues of long power transmission, coupled with improvements in converter technologies and increasing concerns about network stability, have meant that HVDC continues to receive consideration as a complementary technology to the existing ac transmission backbone in most countries and regions of the world.

Increasing the Power Transfer Capacity of a Line

The preceding section showed that the power limit of a line can be increased by increasing the operating voltage of the line or by reducing the series reactance of the line, neither of which are trivial issues.

To upgrade the voltage, the insulation to ground and between phases has to be increased. In addition, the conductor surface gradient must to be maintained below certain levels to prevent the generation of audible noise and radio and television interference. Frequently these requirements lead to larger towers and conductors. Voltage upgrading is addressed in Chapter 14, while corona is comprehensively dealt with in Chapters 8-11.

The reduction of series reactance can be addressed by changing the phase spacing and conductor geometries. This topic is addressed in Chapter 2. On long lines, the series reactance is frequently reduced through the installation of series capacitors. Shunt capacitors and inductors are installed on lines to improve voltage stability at the terminations, and this is referred to as shunt compensation. Power Electronics-based Controllers are used in conjunction with the compensation and the system is then referred to as a Flexible AC Transmission System (FACTS). They

are frequently used to provide dynamic compensation and control of line impedance. FACTS technology provides dynamic and flexible transmission compensation, which results in increasing transmission capacity while maintaining operation reliability of transmission grids (Edris 2000). Further information can be found in the book by Glover and Sarma (Glover and Sarma 2002).

The power transfer of a line can also be increased (uprating) by increasing the allowable current (ampacity) in the line, provided the total power remains below the power limit in Equation 1.2-1 and voltage drop criteria are adhered to. This can be achieved by employing probabilistic rating techniques, using real-time monitoring methods, increasing the height of the line above ground (increasing the design temperature of the line), or by changing the conductor on the line. High-temperature, low-sag conductors can operate up to above 200°C while not causing the conductor to sag below the allowable amount. Note that these conductors are not low-resistance conductors but rather low-sag conductors. These issues are addressed in Chapter 2.

1.2.2 Standing Waves

The lumped parameter networks used for representing a transmission line are approximations of a system with distributed resistance, inductance and capacitance. They are adequate for steady-state analysis of the voltages and currents at the terminations. However, if the voltage and current profiles along the length of the line are to be analyzed, the distributed nature of the line components has to be taken into account. This analysis can be found in any good text on transmission line theory or electromagnetics (Guile and Paterson 1977; Kraus 1953) and it shows that electricity is transmitted as a travelling wave. In steady-state ac conditions, this gives rise to a standing wave along the length of the line.

A standing wave is the envelope of the variation of the voltage or current with line length. If the line is terminated in its characteristic impedance, the voltage and current are constant. If the load is different from the characteristic impedance, the standing wave has a sinusoidal-like variation, with the distance between peaks or troughs being half of the power frequency wavelength. The distance from a peak to a trough is a quarter of a wavelength. A quarter of a wavelength is 1500 km at 50 Hz and 1250 km at 60 Hz, and the issue becomes very important when line lengths exceed about 700 km. Under normal operation, on a long radial line, there can be a significant difference in voltage between sending and receiving ends. This is one of the reasons that we have to design for temporary overvoltages, which are limited-duration power frequency voltages that can exceed the maximum ac voltage for which the line is designed. This issue is also discussed in Section 3.2.4 under "Ferranti Effect."

1.2.3 Transients

Lightning and switching operations produce transients that propagate along the line. They experience reflections at the terminations, and depending on the reflection coefficient, there may be an increase or a decrease of the total voltage on the line. The resistance of the line causes attenuation of the travelling waves, and where the transient voltage causes the line to go into corona, there is additional loss and attenuation. The effects of lightning and switching transients on line insulation are discussed in Chapters 5 and 6.

1.3 ENVIRONMENTAL CONSIDERATIONS

1.3.1 The Impact of a Line on the Environment

Visual impact is the most obvious intrusion that a transmission line makes into the environment. There is an onus on designers and surveyors to ensure that line design and routing are as least intrusive as possible, and that the route avoids environmentally-sensitive areas wherever possible (see Figure 1.3-1). Regulatory and legislative issues associated with line characteristics and siting are dealt with in Section 1.6 below.

The impact of a line on wildlife also needs careful consideration. Several bird species find the line structures ideal places for perching and nesting. Utilities have designed ingenious structures to either make the towers undesirable to birds for perching and nesting or have adapted their structures to encourage nesting and perching at positions where there will be no material hindrance to the normal operation of the line (see Figure 1.3-2) (Van Rooyan et al. 2003; Van Rooyan 2004; Vosloo and Van Rooyan 2001). Section 12.16 also addresses bird interactions with transmission lines.



Figure 1.3-1 Environmentally-sensitive transmission line tower structure. Architect: RFR and Gustavson. (Courtesy RTE).

The electric field at the conductor surfaces can cause the generation of corona and audible noise as well as radio and television interference. In addition to the high nuisance value to residents close to the line, the radio frequency noise may render carrier communication on the conductors useless. Chapters 8-11 cover these issues in detail.

Epidemiological studies conducted over the last 30 years have suggested that the electric and magnetic fields associated with power lines may cause childhood cancers. This is a very controversial topic, and despite the fact that medical scientists have not identified a mechanism associated with the field magnitudes typical of power lines, most regulatory bodies have adopted a prudent avoidance or cautious approach by setting appropriate magnitudes at the borders of the right-of-way. In general, permission to build new lines that do not conform to this approach is unlikely to be granted. Chapter 7 addresses the methods of calculating these fields, suggests mitigation methods, and reviews the literature on the health effects.

1.3.2 The Impact of the Environment on a Line

Environmental pollution is the most obvious manner in which the environment influences the performance of a line. Airborne pollution is deposited on the surfaces of the support insulation, and if this becomes conducting through condensation or light rain, a leakage current flows over the insulator surface. This current causes partial drying and local arcing, which can lead to complete flashover of the insulator. On the other hand, strong winds and/or heavy rain can inhibit the deposition of pollution and promote natural cleaning, thereby preventing the formation of a conducting layer on the insulator surfaces. Snow and ice also deposit on insulator surfaces and lead to a deterioration in performance. The design and selection of insulation to suit particular environments are complex issues. Chapter 4 presents the relevant background material, as well as practical approaches to address these issues.



Figure 1.3-2 "Bird guards" on a transmission tower positioned above the insulators (courtesy Eskom).

Ice also accumulates around conductors in severe weather, and the additional mechanical loading can cause towers to collapse. This phenomena caused very serious power outages in Quebec in 1998 (Hydro-Québec TranÉnergie 1998a and 1998b; Milton and Bourque 1999).

Lightning is responsible for very-high-voltage travelling waves on transmission lines. The containment and dissipation of these waves require careful design of the line and the earthing systems. Chapter 6 addresses the theory and modelling of lightning phenomena on power lines, and Chapter 3 suggests practical approaches for the design of lines where lightning is an issue.

The electric strength of air and of insulator surfaces in air varies with air density and hence inversely with altitude. Correction factors have to be applied in the design of insulation for altitudes above approximately 500 m. These factors are discussed for power frequency, lightning and switching voltage waveforms in Chapters 4-6.

Finally the interaction of wildlife, particularly birds, with power lines has to be considered. Many bird species choose to perch and nest on transmission-line towers. Their excreta is conducting and, if it sufficiently bridges the air gap between the line conductor and the tower, an immediate flashover may occur. If their excreta sufficiently pollutes the insulator, a flashover may occur in time. A variety of measures are available to discourage birds from perching on the towers at positions close to the insulators (see Figure 1.3-2), and are discussed further in Section 12.16.

Improving the integration of lines into their operating environment can lead to improved line performance. As shown in Figure 1.3-3, Eskom reported decreases in line faults over a six-year period in the late 1990s and early 2000s. The company attributed this improved performance to—

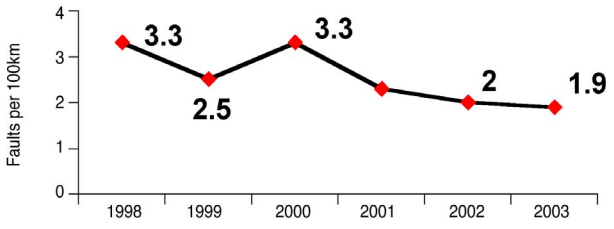


Figure 1.3-3 Line faults on Eskom transmission network showing the reduction as a result of intervention strategies (Naidoo et al. 2004).

among other things—the use of firebreaks for the management of planned fires on the right-of-way (servitude), installation of bird guards, and improved right-of-way maintenance programs (Naidoo et al. 2004).

1.4 TRENDS IN THE ELECTRICITY SUPPLY INDUSTRY

As the electricity supply industry grew in the middle of the twentieth century, it developed as a vertically integrated structure, comprising the major components of generation, transmission, and distribution. Since the late 1980s, however, the industry has undergone a process of deregulation and the associated unbundling of generation, transmission, distribution, and retail services. The drive in recent years has been to restructure the industry as a horizontally integrated industry—with the components of generation, transmission, and distribution being independent industries, and with further subdivisions within each of the component industries.

Deregulation, in turn, has brought about a number of developments, including a lack of coordinated network planning to meet load, rapid increases in wholesale transactions, changes in grid flows and increased grid congestion, and low levels of infrastructure investment.

In addition, in recent years, the industry has also witnessed a number of other important trends, including an aging infrastructure, lack of investment in maintenance, increased legal and environmental requirements and high costs of rights-of-way, and growing needs for grid security.

This section explores these trends by looking at their impacts on the three areas of the electricity supply industry: generation, transmission, and distribution.

1.4.1 Generation

Lack of Coordinated Planning

Under deregulation, the separation of generation and transmission entities into independent companies has had a negative impact on planning. Previously, under the vertically integrated structure, companies owning both generation and transmission could coordinate long-term planning for growth in generation capabilities with investment in transmission capacity. Likewise, companies could coordinate planned outages to conduct maintenance.

Today new generation is permitted to enter the market as desired. Normally transmission companies are not allowed to refuse access to any new generator, irrespective of where they wish to connect to the grid. There is also normally no requirement of the generating company to provide baseload or peaking power or auxiliary services.

In the late 1990s, the trend in the U.S. was to place "peaking" gas turbines at the intersection of natural gas pipelines and the transmission network. The rules of the market encouraged such investments. This generation can be installed and placed in operation within as little as nine months (whereas large coal-fired generation can take some ten years from conception to full generation). In the early 2000s, the rules of the market have matured, and also the price of natural gas has risen to a point where this practice is receiving much tighter review.

The lack of coordinated planning has meant that, in Europe for example, there is no obligation from any company to ensure security of supply. There is a lack of baseload generation due to the long payback periods and high initial cost. The benefits offered to renewable generation have resulted in most generation companies opting for wind generation, so much so that at least 15 GW is planned in Europe over the next few years. This has an adverse effect on grid operation due to the intermittent nature of this energy source.

For transmission company planners, the requirement to accept any generation at any part of the grid (requiring quotes within two weeks) has led to planners spending most of their time preparing quotations for the prospective generators. Grid designs have to be radically altered to allow for the new location of plants never before envisaged.

Load Growth

One effect of deregulation, and the separation of generation and transmission companies, is the decreasing ability to plan to meet loads. For example, in the United States, load growth from 2001 to 2002 was 2.8%, and from 2002 to 2003, it was 1.1% (EEI 2004). As noted below in Section 1.4.2, investment in transmission infrastructure, which is expected to average 0.5% per annum over the next 10 years, will be inadequate to meet this anticipated load.

In addition, the lack of coordinated planning between generation and transmission means that there are fewer capabilities for meeting daily peak loads. Figure 1.4-1 shows a

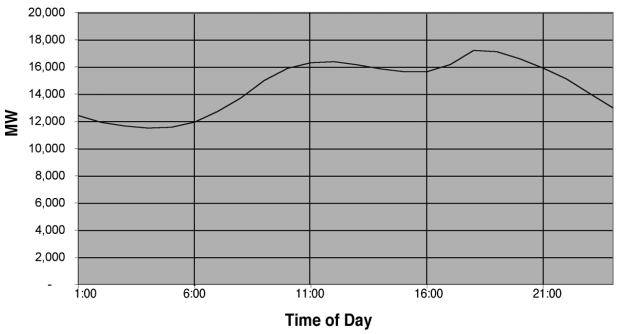


Figure 1.4-1 Typical daily load curve.

typical daily load curve. This is an aggregated load profile for 24 hours for the New England Independent System Operator (ISO) in the U.S. It shows the characteristic two daily peaks and the late-night trough. The best utilization of load would be to flatten the peaks and utilize 100% of line capacity 100% of the time. Previously, generation and transmission facilities were typically planned in unison to meet peak demands. However, with deregulation, and the creation of independent generation and transmission companies, there is no central coordination of measures to control peak load.

Figure 1.4-2 shows load factor as a percentage of the year. Load factor plays a major role in decisions with respect to the voltage of a particular network and also the networks' load-carrying capability. As a result, it is a key factor in the design of a network. Traditionally, load factor could be improved in several ways, including moving generation closer to loads or encouraging customers to change electricity usage patterns through demand-side management. However, under deregulation, generation companies have had little incentive to undertake steps to control load, and transmission companies have no control over the load factor. In an ideal world, the load factor would be flat, with the line running at 100% of load for 100% of the year. Running below 100% of load translates into unused or untapped capacity.

1.4.2 Transmission

Transmission companies are generally strictly regulated, because they are, by nature, monopolies. They plan and maintain networks according to established regulation. Transmission companies have been further divided into wires businesses and system operators, which are normally independent. The system operators are required to ensure that the network is stable under all operating conditions.

Initially, one impact of trading for transmission companies was to cause them to cut operating costs by outsourcing all engineering skills. This outsourcing led to a large reduction in skilled engineers within transmission companies (especially in the U.S.). The trend has since altered with utilities realizing the need to be informed buyers.

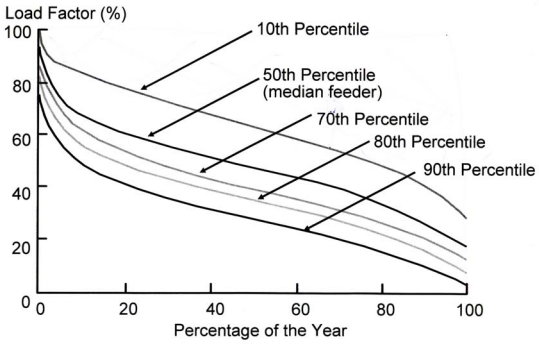


Figure 1.4-2 Feeder load duration estimates.

In North America, ISOs were formed under deregulation to operate the large control regions of the North American Electric Reliability Council (NERC). As of the writing of this book, there is discussion of forming Regional Transmission Operators (RTOs), which would have responsibility for overall system planning and coordination of generation and transmission planning.

Trading Practices

A further complication has been the introduction of traders who purchase from generators and sell to distributors or individual customers. The price traded can vary every 30 minutes, in some cases, and depend on the supply and demand.

Energy industry trading practices have forced system operators to push the networks to extremes never before thought possible. For example, from 1997 to 2001, the transaction volume in several NERC control regions in North America increased by more than 200%. Some large energy companies participated in as many transactions in an hour as they had once conducted in a day (EPRI 2001). This increase in volume is due to the high cost per MW that is realized in times of shortage. Amounts of $10,000 (USD) per MWh in some areas of the world are not uncommon. The high cost leads operators and transmission companies to attempt to increase power flow as much as possible. Attempts to increase power flow, coupled with the lack of skills in the companies, have been linked, in some cases, to blackouts in the U.S., Europe, and South America in recent years—which is discussed below.

One measure of the impact of deregulation—and the associated lack of coordinated network planning—is the current state of Transmission Loading Relief (TLR). As customers and generation companies contract to provide power, they may discover that the transmission network is not able to provide the required transport due to bottlenecks or network congestion. Figure 1.4-3 shows the rising

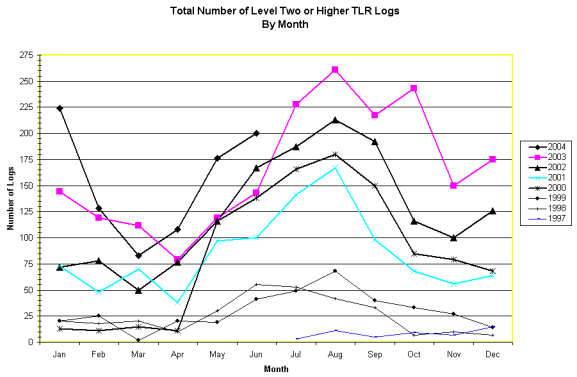


Figure 1.4-3 Transmission Loading Relief calls, Level 2 or higher, in North America, 1997-2004 (NERC 2004).

number of level-two or higher TLRs on the North American grid. This trend reflects the increasing inability of the transmission system, as built today, to accommodate open markets.

Grid Flows

Of major interest is the change in load flows as a result of the changing generation pattern. This change has resulted in some lines being overloaded, and others being under capacity. To deal with overloading, for example, in England, the National Grid first converted their transmission-line conductors from ACSR (Aluminium Conductor Steel Reinforced) to AAAC (All Aluminium Alloy Conductor), and then later to GTACSR (Gapped Thermal resistant Aluminium Conductor Steel Reinforced) conductors.

Figure 1.4-4 illustrates how the changing generation patterns following deregulation of the industry in England have led to a far greater flow from north to south and far less from east to west. The change in flow has resulted in lines running from north to south being overloaded, and lines running from east to west being underutilized. In addition, the rapid change of the generation pattern has meant that the response time that utilities have to deal with the situation has been reduced from approximately 10 to 3 years.

A similar situation occurs on the U.S./Canadian border. Traditionally, the trade has been predominantly in a north-to-south direction, utilizing the Canadian hydroelectric and nuclear generation capabilities. However, on occasion, there have also been significant flows in a south-to-north direction, particularly into Ontario (Barrie et al. 2003).

Investment in Infrastructure

The deregulation of the industry has also meant that now many different companies are owners of transmission grids. These companies are mainly focused on profit and increasing shareholder wealth. Many transmission grids are owned by companies that are not resident in the same country.

The result of these developments is that some transmission companies would rather increase utilization of the current assets, and thereby increase profit, than invest in new assets with long break-even periods and low initial returns.

Also delaying investment in transmission assets are the environmental and legal requirements for obtaining rights-of-way (servitudes), which result in long delays and high costs (see Section 1.6). In Europe, it may take 20 years to obtain the rights to build a transmission line. In the U.S., legal costs can exceed the cost of the line construction. Together with the high public profile (often negative) associated with obtaining the rights to build lines, these factors have resulted in under-investment in transmission networks over the past 20 years. These factors make it more attractive to add new lines in existing corridors, upgrade existing

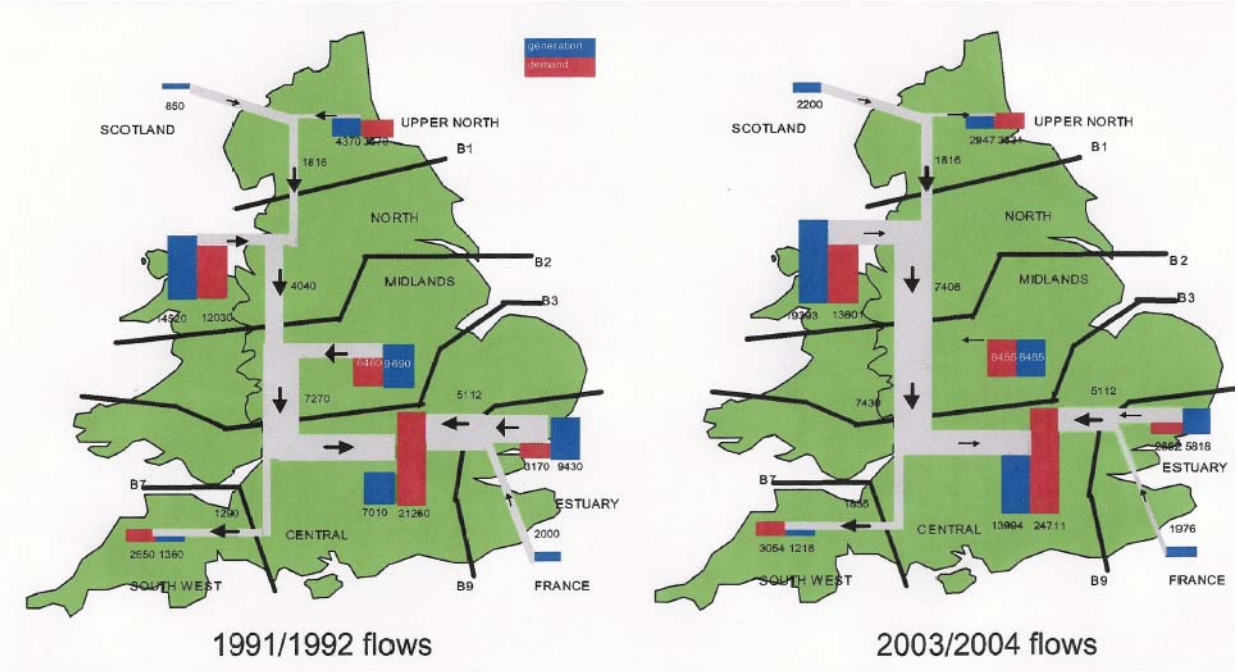


Figure 1.4-4 Changing flows in the UK network (CIGRE 2003).

lines, and even plan converting existing ac lines into dc lines in order to increase power transmission capabilities.

Figure 1.4-5 indicates the levels of capital invested in the U.S. transmission system as a percentage of U.S. electricity revenues. Of note is that the investment in the 1990s was about 12% of revenues, which is less than that experienced in the Great Depression in that country. An upward trend from 2002 to 2020 is envisaged but may not occur.

There are a few large-scale consequences relating to a lack of planned investment in transmission: In many developing countries, investment in transmission infrastructure is not meeting the massive growth in electricity demand (due to large-scale industrialization), and consequently networks are stretched. In addition, in the U.S., for example, from 1988 to 1998, total electricity demand rose by nearly 30%, but the capacity of the nation's transmission network grew by only 15%. Figure 1.4-6 shows the growth of system peak demand compared to the decline in transmission investment in the U.S. during the 1990s. The problem here is not so much a lack of planning, but rather a lack of incentives to investment in new transmission, coupled with a very lengthy and difficult process needed to secure rights-of-way.

For the future, this disparity is expected to increase—with demand anticipated to grow by 20% over the next 10 years, while the transmission system is planned to grow by only 3.5%.

Most developed countries have experienced, and are expecting to see, only limited growth in their transmission systems. For example, Figure 1.4-7 shows actual and projected increases in North American transmission circuit miles over the next 10 years. The per annum average increase in lines is 0.5%. In the U.K., transmission network expansion during the 1990s increased at about 0.5% per year. At the time of the writing of this book, no significant network expansion is being planned in England or Wales (Hoffmann 2004). In Australia, kilometers of transmission lines above 220 kV have grown about 1-2% per year from 1998 to 2002 (Gillespie 2004).

On the other hand, some developing countries are seeing higher levels of expansion. For example, in Thailand, lines above 230 kV grew about 7% in 1998 and 1999 (Booranasantigul 2004). In Brazil, expansion of transmission lines above 230 kV grew by about 17% from 1999 to 2003, and is anticipated to increase by about 19% from 2004 to 2008 (Esmeraldo 2004).

In sum, where there is a disparity between increasing electricity demand and declining investment in the transmission infrastructure, the system is, and will continue to be, inadequate to operate as needed.

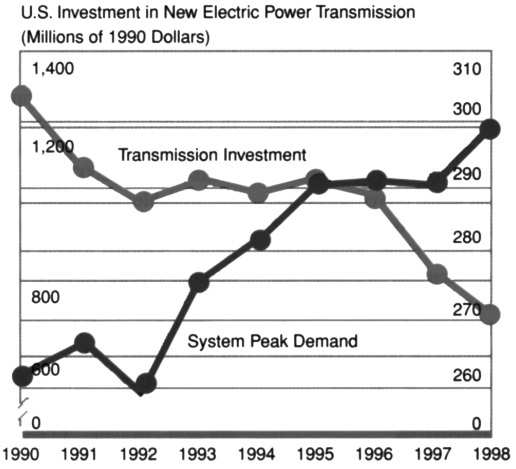


Figure 1.4-6 U.S. investment in new electric power transmission (Shahidehpour 2004).

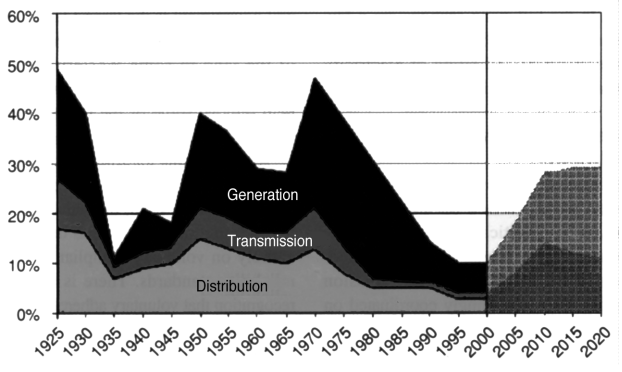


Figure 1.4-5 Capital invested as a percentage of electricity revenues (Shahidehpour 2004).

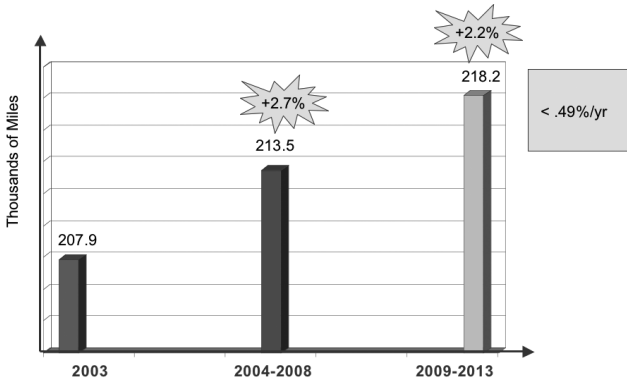


Figure 1.4-7 Projected growth in North American transmission (> 230 kV) (NERC 2004).

One offshoot of the lack of substantial capital investment in new transmission capacity is that some transmission companies, when required to add capacity, are doing so incrementally. This trend has spurred interest in transmission uprating of existing lines, which is described in Chapter 14. A similar situation pertains in Europe and most industrialized countries.

Maintenance

As noted in Section 1.1.1, the major expansion of the transmission network in the U.S. occurred in the 1950s to 1970s. Figure 1.4-8 shows the addition of ac circuit miles during this period. As a result, the bulk of the transmission assets in operation today have been in operation for 35 or more years, and are approaching or have exceeded their typical design life of 40 years.

Given this aging infrastructure, one might expect to see a focus in the industry on life extension of transmission assets. However, in recent years, there has been a steady decline in maintenance spending for transmission systems. Figure 1.4-9 shows the total transmission maintenance dollars spent in the U.S. during the 1990s and through 2002—a decline of about 20.5% over the 11 years. Figure 1.4-10 shows transmission maintenance spending in the U.S. in dollars per MWh sold.

Declining maintenance spending has several important implications. First, obviously, failure to adequately maintain lines, particularly with the current aging infrastructure, may cause a significant deterioration of the reliability of the system. Second, given the decreased levels of maintenance, it is important to design new lines in ways that require less maintenance.

Outages

The loss of transmission line power through an outage indicates the pivotal role that electricity transmission plays in world economies. Figure 1.4-11 provides a snapshot of recent outages around the world. At the time of the writing of this book, the largest blackout in North American history occurred in August 2003 in the Northeast U.S. and Canada. The outage affected approximately 50 million people in eight states and one province, and resulted in $6 billion of economic losses in goods and services ((U. S. DOE 2003, 2004; U. S.–Canada Power System Outage Task Force 2003).

1.4.3 Distribution

The distribution business has been split into two distinct parts, the wires business and the retail business. The wires business, responsible for the design, maintenance and, in some cases, the operation of the network, is normally strictly regulated in a similar manner to the transmission companies'. The retail business offers the customers many different types of product. Customers can choose the

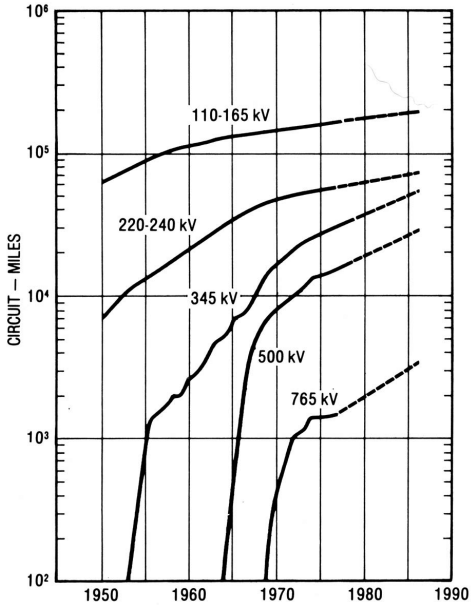


Figure 1.4-8 Circuit miles of overhead ac transmission lines in the United States (EPRI 1982).

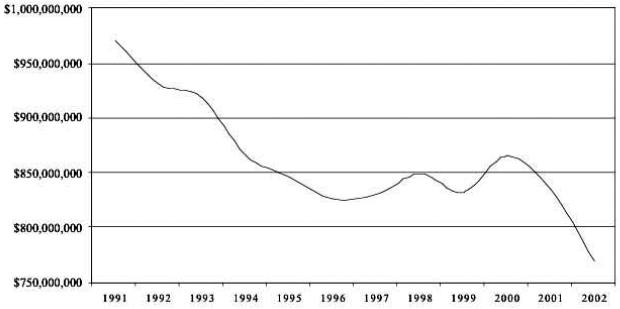


Figure 1.4-9 Transmission maintenance spending in the U.S., in total dollars, adjusted for inflation.

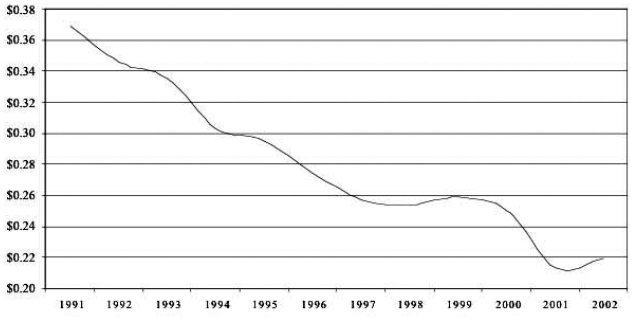


Figure 1.4-10 Transmission maintenance spending in the U.S., in dollars per MWh sold, adjusted for inflation.

retailer that they wish to take supply from depending on their needs. There is large competition between retailers, and this generally results in a lower cost.

The impact of this split on the distribution business was initially similar to the transmission industries with the outsourcing of technical staff. This trend has also begun to change. The advent of the retailers has led to wire companies being required to provide different products. This trend includes varying types of metering having to be used to accommodate the tariff types offered (e.g., Time-of-Use), as well as having to accommodate the different power flows on the network depending on customer response to the tariff options.

1.4.4 Overall Impact

Although much of the impact mentioned above appears to be negative, it is mainly as a result of the wires business not being able to respond rapidly or to fully understand the impact of the deregulation process. However, recent developments have resulted in the industry reviewing certain practices and strategies to counteract the negative effects experienced to date. This includes the initiatives of the U.S. government to increase investment in transmission infrastructure. In time, it is expected that the skills and operating practices will adequately meet the trading and customer requirements of the industry, and result in a more cost reflective service and possibly lower energy cost for customers.

1.5 FUTURE DIRECTION OF THE ELECTRICITY SUPPLY INDUSTRY

In response to the deregulation, organizations such as CIGRE and the IEEE have embarked on specific actions to provide guidance to the electricity supply industry in the face of future challenges.

1.5.1 Technical Strategies

The following strategies have been specifically identified as important fields of research in the future.

Analysis of Re-regulated Industry

This analysis will take place in three areas.

1. **Restructuring and Reliability.** The first area of study is the impact of the electricity supply industry restructuring on network reliability and loading. This realm explores the effect of competitive tariffs on load flows,

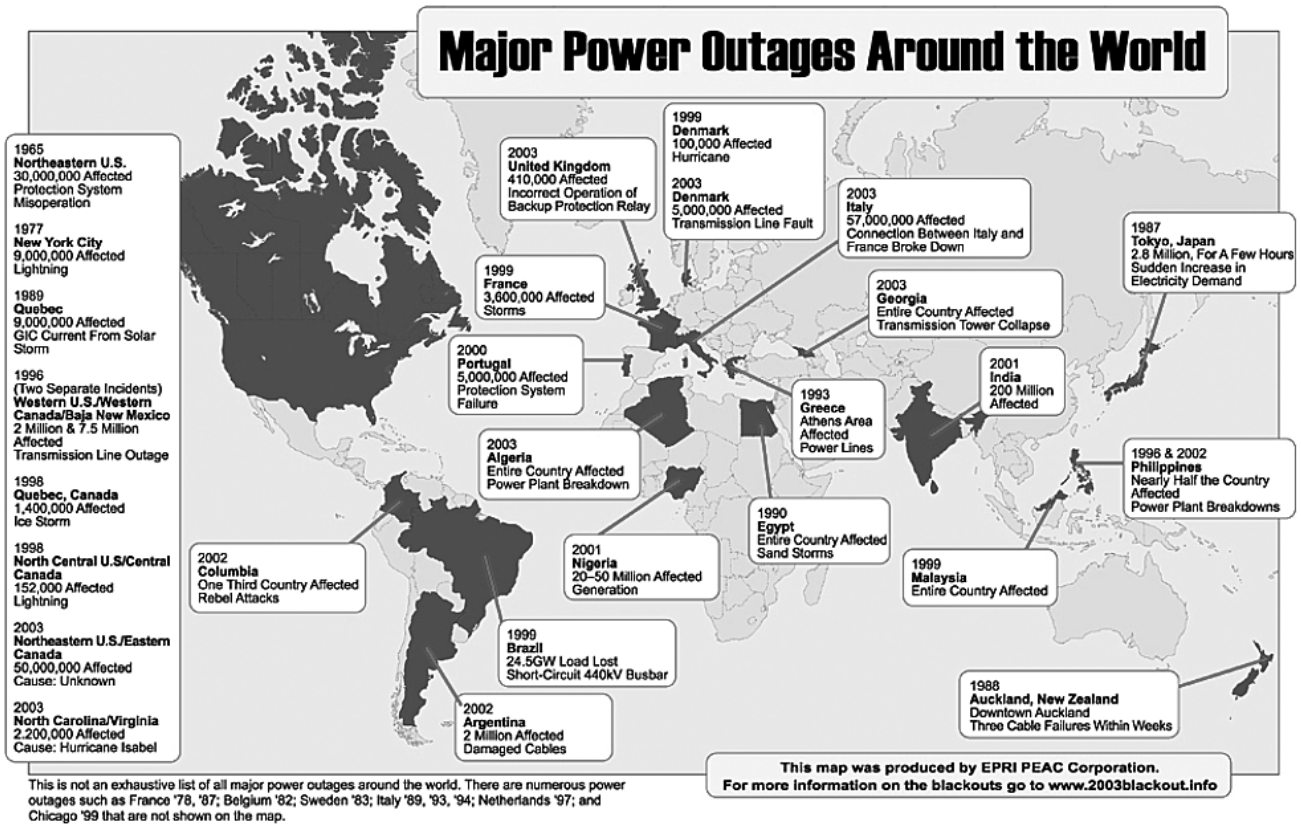


Figure 1.4-11 Major power outages around the world (EPRI 2004).

the resulting increased utilization of assets, as well as the potential catastrophic failures that can result once assets fault under high load transfer conditions. Examples include the blackouts in the Northeast U.S. and Canada, in Denmark, and to a lesser extent in England. This study also includes the need to build large interconnectors in Europe at the transmission level. At present, the inability to build transmission lines has forced the increased focus on cables.

2. **Distributed Generation and Storage.** The second area of study is to investigate the impact of dispersed generation and storage on the electricity supply industry. This area involves the advent of large-scale renewable (mainly wind) generators in Europe and the complexity of managing this type of generation when it becomes more than 20% of the total installed capacity. A further study will be undertaken on the ability of the deregulated environment to ensure security of supply (adequate generation) especially in Europe.
3. **Environmental Impacts.** The third area of study is the analysis of the impact of environmental issues on the industry (EMC, EMF, audible noise, visual impact, material recycling). An example of this study is the requirement to perform life-cycle assessment of each component in the network. This involves, for example in transmission lines, the evaluation of the impact of bauxite mining on the production of aluminium conductors.

1.5.2 Specific Issues to be Addressed

System Development

- There are conflicting needs relating to the electricity market and those of network reliability. The challenge is to meet both needs without jeopardizing one another.
- The other main area of focus is that of security of supply. The rules laid down by regulators and incentives offered by governments will determine the type of generation installed. For example, the large incentives for renewable power have resulted in the late 1990s and early 2000s in many GW of wind power being installed in Northern Europe.
- Electricity trading across many countries and large geographical areas, such as from Russia to England, leads to many challenges relating to the transfer capability of the network as well as system dynamics. This also involves studies related to removing the system congestion caused by power flowing in directions very different from that originally planned.
- There is also a need to determine the best manner in which to meet the need for high generation demand in developing countries.
- The developing countries also have sparse grids and loads remote from the closest supply point. The best method to supply these remote loads will also be studied.

System Operation

- The advent of the electricity trading market beyond geographical boundaries has implied that there is little meaning to the historical national grid. There is a need to ensure processes are in place to maintain optimum operation across national boundaries and to operate on an international basis rather than a national basis.
- The short-term generator shortages brought about by the lack of base generation will need innovative solutions to ensure the quality of supply is maintained.
- Operation of renewable and dispersed generation will require that different types of characteristics be studied.
- At the other end of the market, the customer demands are becoming increasingly severe, especially as customers move into the "digital society."
- The need to integrate the information and communication technology into the operations of the network is another field that will be studied. This field includes the use of the Internet to convey real-time rating data of circuits. Operators will need to determine the optimum level of information that is required to perform successfully.

Technology

- Technology developments will focus on development in materials that could affect breaker, transformer, generator, and even conductor design. These developments should, in turn, lead to components requiring less maintenance.
- The technology relating to control and protection engineering is developing extremely fast. There is also integration between the two areas. These areas need to be managed to ensure the important data and decisions made in real time are not jeopardized.
- The focus on HVDC will be intensified as converter technologies become more reliable and less costly. HVDC offers considerable network stability and security advantages over ac. These advantages have risen in importance as a result of deregulation.
- The new types of technology will also have to consider the environmental impacts at all stages of manufacture. One key driver has been the desire of the public to have transmission networks undergrounded. At this time, the costs of undergrounding are the biggest problem. Further, while the pubic wants an undergrounded system, they are not prepared to pay for it. In the interim, it is predicted that the industry will see new lines being a combination of overhead and underground technologies. This approach brings with it many new challenges—most of them involving changing network impedances and the associated inability of network protection to have complete visibility down the circuit. The transmis-

sion points between overhead and underground transmission also need further refinement.

- Transmission technologies including GIL (Gas-Insulated Lines) and HTSC (High-Temperature Superconducting) systems are starting to make an impact. GIL has been around for some 30 years, with the first systems being installed in 1974 in Germany, spreading a few years later to Japan (Nonjima et al. 1998) and many other parts of the world. The significant advantages of this technology are that the capacity of a line can readily be four times greater than what can be achieved with cable technology (Nonjima et al. 1998) and, because the ducts can be mounted in tunnels or even buried, they are much less intrusive than overhead lines. The proximity of the ducts also means that the electric and magnetic fields are much more confined than is the case with overhead lines. The restriction on their use has largely been related to the fact that the insulating medium is SF_6 (sulfur hexafluoride) and this is costly and is one of the greenhouse gases. Recent developments using mixtures of N_2 with SF_6, in the ratio of 15-20% SF_6 to 85-80% N_2, have proved very successful and are likely to become widely used in the future for special applications (CIGRE 2004b).
- At the time of this writing, EPRI and DOE (U.S. Department of Energy) had just completed a demonstration of an HTSC cable at the Detroit Edison Frisbie Substation. Further, three new HTSC cable demonstrations are presently in various stages of design. With each new pilot, new ground is broken.
- Also at the time of this writing, there is considerable discussion of the "Hydrogen Economy." Predictions are that, in time, energy in the form of hydrogen will be transported to the point-of-use, where it will be converted into either electricity or heat. As this thinking, and the associated technology, matures, it will challenge the traditional ac transmission backbone that presently exists in all countries.

Network Maintenance

- The main focus relating to all components will be the determination of the best method of asset management to minimize maintenance cost. This area will include the accurate assessment of life-cycle costs and life-extension techniques. The key, however, is to make sure that experiences gained during the life assessment and life extension phase make their way back into future designs.
- With the environmental pressures prohibiting lines and other new interconnectors to be built, it is necessary to upgrade or uprate the particular circuit. This upgrading involves condition assessment of the assets, determination of their remaining life, and the capability of the assets to be upgraded.

Technical Training

- With the increased reduction in staff and the retrenchment of skilled experts, it is necessary to focus on retention of existing knowledge, as well as ensuring new developments and solutions to problems are readily accessible to the engineers who remain in the industry.

1.6 LEGISLATIVE AND REGULATORY ISSUES

1.6.1 Introduction

Environmental permitting is increasingly the "critical path" for transmission-line siting, construction, and operation. The siting and permitting of new electrical infrastructure, including generation and transmission projects, can be one of the most challenging and often frustrating assignments that a utility's engineering and environmental personnel may undertake. Changing political climates, expanding environmental issues, increasing public concern and involvement, and established precedence often underlie many environmental review processes. Utilities have a broad range of corporate experience in environmental permitting, with many that have not permitted any significant projects in the last decade and may be unaware of new and changing environmental issues and approaches. For a smooth and streamlined project permitting process, it is imperative that a project applicant (e.g., utility) is informed of what will be specifically required; how the process works; what are the interrelated permitting requirements; and what are the new, upcoming issues.

In the present deregulated environment, it is no longer desirable or possible for utilities to construct lines by expropriating property. In most countries, permission is required from numerous authorities. Public involvement is critical for success. In addition, stringent environmental impact studies also are a prerequisite for approval to construct or (in some cases) modify overhead lines. The time taken to obtain the necessary permits has been increasing over the past two decades. In the United States, project permitting may require up to 10 years. In Europe, it has now extended to 20 years. Typically, this timeline means that the staff who originally plan the line are not involved at the construction phase, so that the process requires strict documentation and ongoing communication. It also is possible that the legal fees and the purchase of the rights-of-way could be in excess of the line itself. These factors limit the effect of line optimization and reduce the advantages of over-design on the line. In this section, the process whereby the line right-of-way and permission to construct are obtained is referred to as the "permitting process."

The permitting process, of course, varies from country to country, and the relevant agencies and applications are not standard in all countries. However, many of the lessons learned and types of agencies involved are common to

many countries and utilities. CIGRE WG14 and WG15 (SC B2) have completed documents on environmental assessments as well as best consulting practices (CIGRE 1999; CIGRE 2004a).

This chapter uses examples from the United States, primarily because the majority of project delays, cancellations, and increased costs for a utility have been attributed to the permitting process. It is assumed that most other countries have parallel processes where some of these examples would apply.

The following sections outline the environmental permitting processes and challenges typically encountered during the siting and construction of a new high-voltage transmission line and ancillary facilities to assist utilities in better understanding and resolving some of the more prominent issues. While each agency and environmental review process may have a unique set of well-defined and discrete steps, the process is fundamentally consistent in function and goals across many of these agencies. Each process typically has four primary steps or phases:

1. The applicant (i.e., utility) contacts the authorizing agency and submits the proposed project information, usually in the form of a permit application, for agency review.
2. The agency performs a preliminary assessment of the project and may request input from other governmental entities and the public.
3. The agency (or third-party contractor) prepares the environmental documentation under an established framework.
4. The agency uses this documentation as a decision-making tool on whether to issue or deny a permit to construct and operate the proposed project.

Understanding the key points of this process is particularly important, given the complexities associated with the applicable regulatory or land management agency review procedures. Further, public acceptance of a project can be integral to minimizing costs and maintaining project schedules.

Regulatory requirements, permitting processes, review procedures, and public participation mechanisms vary by country, state, province, county, and local municipality. Because of this variability, the following procedural discussion, insight, and recommendations applicable to environmental permitting for overhead transmission lines are relatively general. Some specific references to processes required in the United States and Canada are provided as examples to further illustrate these actions.

This section is designed to provide direction specifically to project engineers and managers who are responsible for siting considerations and project planning. It is not intended to be a comprehensive summary for transmission-line siting and permitting, but rather, the following information highlights the regulatory framework and primary issues that may be encountered, so that the utility project manager and/or engineer can effectively interface with his/her environmental staff or consultant and better understand the environmental permitting requirements and ever-evolving "political climates" that often surround environmental issues. Ultimately, the project manager or engineer should have the applicable tools to develop a project-specific plan that incorporates a standard approach to problem resolution, acknowledging the variables associated with different projects and planning scenarios. Because power generation is obviously associated with power transmission, a number of the following discussions on environmental permitting apply to both processes.

Whether permitting a line involving national, international, state, or local entities, it is imperative to maintain a clear approach to communicating and coordinating with the applicable agencies responsible for permitting oversight and project authorization. Developing an appropriate strategy for interagency and intergovernmental coordination and consultation, in addition to public notification and interaction, is often critical to a successful environmental permitting process, and lays the foundation for the entire permitting effort. An environmental permitting strategy should be developed in sufficient detail to be incorporated into an overall estimate of project costs and an overall timeline for project planning, permitting, and construction. The following sections outline and discuss specific permitting requirements, approaches, and suggested methods to streamline these processes, particularly as they relate to proactive communication, coordination, and problem resolution.

1.6.2 Examples of Inadequate Planning

The majority of project delays, cancellations, and cost overruns can be attributed to a few factors, including:

- Not addressing changing and evolving project economics.
- Not allowing sufficient time for project permitting.
- Not following the applicable process or integrating other environmental requirements.
- Not meeting the established "purpose and need" identified for a specific project through either the proposed project or its associated alternatives.
- Not developing a thorough and complete project description for a proposed project.

A few examples of project failures or costly delays are provided to underscore the importance of

1. understanding the applicable environmental permitting process;

2. applying that knowledge to both short- and long-term project planning, in advance;
3. implementing proactive communication, both internally and externally; and
4. developing strategies for problem resolution, when warranted.

Permit Review for an International Interconnection
A proposed transmission line between the United States and Canada required both federal review and a Presidential Permit because of the associated international interconnection. The utility's failure to firmly establish all project components necessary from a systems perspective at the start of the environmental process resulted in the need for a supplemental environmental permitting document and a total of four years to complete the environmental review process. The costs associated with this project delay were "significant."

Authorization by Multiple Agencies
A 200-mile (322-km) transmission line in the United States required certification of need and approval of a route by a state Public Utility Commission. The line also would cross 5000 feet (1524 m) of federal land, necessitating compliance with the United States' National Environmental Policy Act (NEPA) prior to granting a right-of-way (ROW). Both state and federal regulations encourage a consolidated permitting process; however, the parties involved were reluctant to request a ROW from the federal agency prior to the state certificating a route. Because a ROW application was not submitted, there was no "trigger" to bring the federal agency into the state's review process. Thus, the NEPA process was initiated after the state process was completed, adding about 2.5 years to the overall review process.

Substation on Native Tribal Lands
A rural U.S. utility had proceeded with standard environmental permitting processes for a proposed expansion of an existing substation less than 2 acres in size on native tribal lands without checking to determine whether additional permitting review would be required because of the land status. The utility's failure to recognize the additional environmental permitting review process required for facilities located on native tribal lands resulted in a 3-year project delay. In South Africa, although there are no "tribal" lands, there are areas still very much under control of traditional leaders. Some of these leaders respect the formal political structures and others do not. It is essential, as in the case mentioned in the U.S., that permission be obtained from the traditional leader before continuing the line construction.

Transmission-Line Routing
A utility's proposed routing of two parallel, double-circuit 345-kV transmission lines failed to recognize the political sensitivity of a designated nature preserve (e.g., siting constraint) during the corridor analysis phase of the project. This oversight resulted in rerouting of both ROWs with increased costs for eight additional 45-degree turning structures.

Many of these problems can be avoided or minimized by understanding the process and pitfalls that may be encountered and planning accordingly, as discussed below.

1.6.3 Regulatory Framework and Process for Transmission-Line Permitting

The following steps outlined for project permitting delineate not only the basic process, but also integral strategies for each process and how they are typically implemented. The chronology of a specific environmental permitting process can be important; therefore, it may be critical to understand what step depends on another or when these project stages should be initiated.

Initial Permit Planning Process
Strategic Planning

Most utilities conduct early strategic planning as part of their load growth and system capacity management. Once it is determined that a new transmission line is required in the system, preliminary economic feasibility and project design begin. However, strategic planning, as it relates to the environmental permitting process, is often overlooked or viewed as being of secondary importance. Early strategic planning for the project-specific environmental review process can avoid significant effects on a project's schedule, costs, and ultimate success.

One important planning strategy is to become familiar with regulatory and land management requirements for siting on both public and private lands. Although a standard strategic plan may apply to a number of development scenarios, it is important to acknowledge the variables and adopt a flexible, dynamic plan. This approach can greatly aid project planning and environmental permitting review. With the increased difficulty of obtaining ROW on both private and public lands and the overlap of system configuration, facility design, ROW acquisition, and environmental permitting considerations, it is critical to have all four specialties involved in early strategic planning.

Determining Whether an Environmental Permit Process Applies

One of the first steps necessary for new or proposed projects is to determine whether a regulatory review is applicable to that project. A screening process is typically applied to determine whether a project warrants a full environmental review or may be "categorically excluded" from further analysis. Different authorizing agencies have different screening processes or thresholds for environmental review. The key to this step is to initiate early dialog with the responsible agencies to identify what these thresholds

are and to become familiar with the criteria that may apply to this decision.

Route Selection and ROW Siting

Route selection and ROW siting can be complex and controversial, encompassing issues such as land-use conflicts, resource effects, public perception, and interagency coordination and communication. Environmental permitting processes and project-specific needs can be varied and are often confusing, and they differ internationally, nationally, and locally. They also may vary among the same types of projects, depending on project-specific issues and the degree of public participation. These differences can result in a frustrating effort for utilities to understand what is expected, how to proceed, and what are the associated costs and time restrictions. Addressing or avoiding many of these issues or possible problems in ROW siting typically involves understanding the:

- current environmental permitting "climate,"
- repercussions of certain approaches that may be used to site and construct a line, and
- components to subsequently develop and implement a project-specific planning strategy that proactively addresses these issues.

This knowledge aids in developing an effective mechanism to accurately estimate associated siting and line construction costs, and in developing a practicable and logical project schedule.

For large-scale transmission line projects, a routing study or siting analysis is often appropriate to better identify applicable siting constraints and define project-related issues. However, even smaller projects benefit from preliminary route selection, based on a number of site-specific variables. A routing study may either delineate general, broad corridors for transmission-line placement, or it may examine a more site-specific routing network. The appropriate approach typically depends on the length or the ROW (i.e., relative size of the proposed project). Within these corridors or routing alignments, site-specific constraints or opportunities should be identified and mapped. Possible constraints generally range among economic considerations, regional electrical needs and reliability, engineering constraints, land ownership and management, land access issues, environmentally sensitive areas or features, extreme topography or surface cover, land-use restrictions, and environmental justice concerns. Opportunities may include existing linear ROWs, existing public easements, compatible land uses, and topographical features (or lack thereof).

The identification of these objectives, opportunities, or sensitive areas is critical in the advanced project review and planning effort, in order to maintain the estimated project budget and timeline. Project engineering typically examines possible construction and operational options from electrical feasibility, line constructability, and overall economic perspectives; however, examples of specific siting issues that can result in increased costs, if caught unaware, could include ROW alignments crossing or located adjacent to the following:

- Natural areas, wildlife refuges, or environmentally sensitive areas that have been designated with either public or private protection criteria.
- Wetland systems or water bodies, particularly if used by large numbers of resident or migrating birds.
- Unknown, significant archaeological features.
- Sensitive plant or wildlife species' locations or associated habitats.
- Existing residential, commercial, or recreational areas.
- Urban interfaces.
- Agricultural lands.
- Areas planned for future development that may be incompatible with a transmission line.

The relative sensitivity of each resource item identified as a project constraint during the corridor selection process is typically compiled and compared among the alternative corridors and ROW alignments. Different resources have varying sensitivity to the construction, operation, and maintenance activities associated with a transmission-line project. These data may be categorized by specific corridor segment, possibly leading to the identification of other alternative routes, if warranted. Based on these siting constraints and opportunities, an applicant-preferred route is established and evaluated according to the applicable permitting requirements. Land ownership, funding sources, and the regulatory oversight often determine the type and extent of these permitting requirements.

Regulatory Review Process

Role of the Utility or Permit Applicant

New transmission-line construction or rebuild of an existing line generally requires some level of environmental review, which may address a wide range of issues and concerns. The utility responsible for this construction or expansion would be the "applicant" in this process. The utility (or applicant) then would be directly coordinating with the applicable reviewing or authorizing agency for environmental permit application and approval.

Role of the Authorizing Agency

Permitting agencies vary depending on their respective roles (e.g., land management versus regulatory, lead versus cooperating), the type of project proposed, and the applicable permitting process involved. It is vital to understand which agency or other governing entity may be responsible

for the environmental permit review. In addition, knowing when and how to initiate discussions with these agencies is fundamentally important.

Communication between the utility and applicable agencies cannot be overemphasized. Communication, or lack of, is often one of the more critical elements of environmental review. Proactive communication generally results in greater conflict resolution; whereas, uncoordinated processes often result in adversarial situations. Agency communication is discussed in greater detail below.

Because the United States' NEPA process encompasses a number of different types of federal, state, and local agencies that may be involved in moderate to large transmission-line projects, this Act is used as a representative example. For this example, there is always a federal agency responsible for reviewing the project in accordance with a mandatory set of guidelines that apply to earth, biological, and human resources. This agency is referred to as the "lead agency." In larger, more complex projects, there also may be one or more "cooperating agencies" that may be involved with project review.

Whether an agency is a "regulatory" versus a "land management" agency has no direct bearing on the role that an agency fulfills for project review under NEPA. In the United States, examples of "regulatory agencies" that may be involved in transmission-line projects include the Department of Energy (DOE), Rural Utilities Service (RUS), Environmental Protection Agency (EPA), U.S. Army Corps of Engineers (USACE), U.S. Fish and Wildlife Service (USFWS), Federal Aviation Administration (FAA), Federal Highway Administration (FHA), and Bureau of Indian Affairs (BIA). All of these agencies could be involved with a transmission-line project in a regulatory role. Representative "land management agencies" include Bureau of Land Management (BLM), U.S. Army Corps of Engineers (USACE), Bureau of Reclamation (BuRec), U.S. Forest Service, USFWS, and Sovereign Native Tribal Nations. Additionally, federal power marketing agencies are often involved in environmental permitting review of a project, particularly for proposed interconnects.

Any of these regulatory, land management, and oversight agencies may act as a "lead" or "cooperating" agency during an environmental review process. It is important to distinguish which agencies may be associated with a proposed project, what their respective roles may be, and what type of communication process will work the best in order to streamline the permit review.

Public Involvement and Perception

Most utilities have developed a standard approach to public relations, given the typical customer-based needs and demands. However, certain topics associated with transmission-line construction and operation can be volatile and highly emotional. The public's interest in a proposed transmission-line project can greatly differ from that associated with a typical utility–customer relationship.

For many environmental review processes, there is a public input component. The opportunity for the public to participate in the siting and permitting of a transmission-line project may be formal or informal, depending on the process and size of the project. Historically, the public has had a significant role in transmission-line placement. Public knowledge and level of sophistication on environmental issues have greatly increased, and at times, a project's success may largely depend on the level of public involvement. Accordingly, public demands for effective and timely participation in the decision-making processes also have increased.

Key to a successful public review process is

- becoming informed of the associated issues,
- understanding the public process that may apply to specific project types, and
- initiating proactive dialog.

Frustrated citizens, when treated as adversaries, often result in legal appeals and litigation, but acknowledging the public as project participants often establishes more of a working relationship. Ensuring public needs are met may involve public notice, public scoping meetings, and opportunity for public comment on a project. Using the public review process for scoping a project can be a valuable tool for identifying public and agency stakeholders; setting the spatial (geographical) and temporal (time) boundaries of the study; identifying key concerns and issues; delineating available data for the analyses; defining a reasonable range of alternatives; and providing a flexible mechanism for project modifications, if warranted.

Creating a partnership with the public requires more than holding public hearings and providing documentation, however. One tool that often can be advantageous is the use of small, breakout groups during public meetings. These groups, typically led by a utility or agency representative, may:

- allow citizens who are not as likely to speak in a large group the opportunity to voice any concerns;
- minimize the potential for emotional and disrupting outbursts that often are structured to monopolize meeting times;
- categorize issues and concerns in an efficient manner; and
- steer the group toward constructive discussions.

For those environmental review processes that do not require public review or comment, it may benefit the utility and authorizing agency to continue to provide information on the proposed project and make available opportunities for public comment to ensure that partnerships are forged with the surrounding community and interested stakeholders. This approach may avoid or minimize controversy, legal challenges, and increased costs and time.

Environmental Permit Documentation and Report Production

A variety of processes, approaches, and report types apply to the documentation of an environmental permitting process. Typically, this step or project phase is considered a tool or mechanism to document a process or disclose anticipated effects from proposed project implementation. Project documentation can be both internal and external to utility staff.

Project Scope and Alternatives Development

Delineating the project scope is closely associated with defining the project's purpose and need, and directly leads to identifying potential environmental effects from project implementation. An important aspect of many environmental review processes is the development of viable project alternatives that are reviewed parallel in timing and level of detail to the applicant's proposed project. In conjunction with practicable project alternatives, the environmental review process also may require that the "alternatives considered but eliminated from detailed analysis" be delineated. No detailed impact assessment is completed on these unrealistic or improbable alternatives, but they often must be disclosed to demonstrate the range of alternatives that have been examined.

Environmental Review and Impacts Analyses

Integral to a project's environmental review and impacts analyses is identifying and compiling relevant interdisciplinary or resource-specific information that is commensurate with the project scope, the anticipated project effects, and the degree of public concern (i.e., project complexity and level of volatility). When the environmental impact review and analyses are being completed, existing information should be used to the extent possible and appropriate. This approach builds on work already completed, avoids redundancy, minimizes additional project costs and expanded schedule, and provides a coherent and logical record of the analytical and decision-making process. As part of this process, it should be examined whether any existing analyses or other environmental documentation either partially or fully analyzes parallel resource issues that can be applied to the proposed project.

The types of resources examined vary, based on the project type and size, its location or setting, and the regulatory framework required for that area. For some analyses, impact significance thresholds must be identified, such as required for the preparation of an Environmental Assessment (EA) under the federal NEPA process in the United States. In the event that any of these significance thresholds are, or are anticipated to be, exceeded, the permitting review must be then taken to the next level, requiring an expanded Environmental Impact Statement (EIS), which is substantially greater in detail, time required, and associated costs. This example emphasizes the importance of understanding the process prior to initiating the environmental review.

Analyzing and disclosing the environmental consequences of a project are the main components of most environmental review processes. These analyses cover a broad range of topics and resource issues, such as earth resources (e.g., air quality, geology, soils, water quality and quantity, palaeontology, minerals); biological resources (e.g., vegetation, wildlife, sensitive species, wetlands, noxious weeds); and human resources (e.g., socioeconomics, transportation, land use, cultural resources, noise, aesthetics). The intent of the environmental documentation effort is to provide decision-makers and often the public with an objective evaluation of environmental impacts, both beneficial and adverse, that would be anticipated from implementation of the proposed project and reasonable project alternatives.

Cumulative Effects

For some projects, combining what may be individually minor, but cumulatively major, effects of multiple actions over time may result in a significant level of impacts. Analyzing the cumulative effects from a proposed project can be frustrating, confusing, and variable. The confusion and variability often can be attributed to the different approaches followed by different authorizing agencies. Some agencies and review processes require a cumulative assessment; others do not. A standard definition of cumulative impacts is those effects caused by the combination of past, present, and reasonably foreseeable future actions. It is important to note that the impact area, or "domain," varies from resource to resource. For example, a cumulative effects area to be examined for air quality differs greatly from that identified for sensitive plants, which, in turn, differs from that identified for mobile terrestrial wildlife species. A strategy to streamline the cumulative assessment for a project would be to initiate early dialog with the authorizing agencies on the potential cumulative actions to include in the analyses, refine the cumulative effects domains to reasonable and management sizes, and acknowledge that the information should provide the reviewing agencies with a tool to make an informed

decision and not necessarily be a "perfect" and "all-encompassing" analysis of cumulative effects.

Mitigation vs. Committed Environmental Protection Measures

Measures to minimize potential impacts to resources from implementation of a proposed transmission-line project can vary. Most applicants are familiar with "mitigation measures," which are typically developed as part of the environmental review process to minimize short- and long-term effects. Mitigation measures are assembled after the impacts analyses. Another category is the development of "committed protection measures." The applicant or utility commits to implementing these measures as part of the proposed project, and the impacts analyses are conducted with these measures in place. Identifying and applying committed protection measures early in the process, as part of the proposed project, can be advantageous. Although the utility has committed to the costs of implementing certain measures, this approach typically

- reduces the level of impact analysis required,
- streamlines the environmental permitting review and associated schedule,
- minimizes the potential for agency and public opposition, and
- enhances the potential for project authorization.

A common question relative to implementing mitigation measures is whether "monitoring" can apply as mitigation. By definition, monitoring is not a form of mitigation. Monitoring can be used as a tool to determine the need for, or relative effectiveness of, mitigation. Examples may include short-term monitoring (e.g., 2 to 4 years) of noxious weeds along a ROW. Based on the results of monitoring, an agency may determine if additional mitigation is warranted. The disadvantage of developing and implementing a project monitoring plan can be the additional costs, although this is not applicable for all scenarios. The advantages of developing a monitoring plan is it:

- ensures the adequacy of the mitigation measures, which is typically the intent of the plan;
- facilitates the environmental permitting process with the authorizing agency;
- may advance the project schedule; and
- may actually reduce environmental review costs by avoiding the need to answer all unknown questions prior to project implementation in order to gain project approval.

The decision to include a monitoring plan in a permit application is project specific and requires weighing all factors. Where resources are not likely to be appreciably affected in the long term, and there is an opportunity to reclaim or mitigate environmental damage, an adaptive environmental management approach may be appropriate, using monitoring to identify future mitigative measures.

Administrative Procedures and Agency Decision Records

Authorizing agencies issue a decision record following the environmental review of a proposed transmission-line project that requires regulatory oversight. This decision record varies, depending on the regulatory process, applicable agency, and type of project. Decisions can take the form of a permit, an ROW grant, or a certificate of public convenience and necessity, as examples. Ultimately, the decision record determines how the project may or may not proceed and what stipulations would apply to project construction and operation, if authorized. Understanding how a decision can be appealed, what procedural steps are involved in an appeal, and who has standing to appeal a decision is important. Project appeals result in increased costs and timelines for a utility and may ultimately threaten a project proceeding.

Other Legislative Acts and How They Are Integrated

A number of supplementary regulatory Acts often apply to a project's permit review and authorization. Some of this ancillary legislation can be equally as exacting as the overall environmental permitting requirements. Representative examples of this type of legislation that apply directly to transmission-line projects include the United States' Clean Water Act, Endangered Species Act, and National Historic Preservation Act. The Migratory Bird Treaty Act also applies to projects in Canada, the United States, and Mexico. The Endangered Species Act and Migratory Bird Treaty Act are discussed further in Section 12.16.

Once again, strategic planning and communication are key. Knowledge of how additional Acts may apply to a project is essential. For example, the wetlands analysis under the Clean Water Act, the federally listed species' analysis (i.e., Biological Assessment) under the Endangered Species Act, and the archaeological clearances under the National Historic Preservation Act are all powerful legislative requirements that can dramatically affect a project's costs and schedule, if the utility's staff is unaware of what these supplemental reviews entail. Allowing for these types of analyses is discussed in greater detail in Section Primary Issues for Transmission-Line Permitting for primary permitting issues.

1.6.4 Primary Issues for Transmission-Line Permitting

Project Purpose and Need

If a project does not begin with a solid base, credibility can become compromised. The public may assert that there is

no need for a new transmission line. If the utility or applicant has not developed a basic, understandable explanation of the need for the project, it can negatively influence the entire review process. It also may be important to examine potential system alternatives to the line being proposed. This type of analysis is as important for the regulators as it is for the public, because it is typically a component of a facility siting review.

Communication

The importance of open communications and understanding between the utility proposing to build new or expand existing transmission facilities (i.e., the applicant) and the associated regulatory and land management agencies involved in this often complex and mandatory process cannot be overstated. Proactive communication is key among the utility's project managers, design engineers, and environmental staff; technical specialists or other consultants; agency personnel; and the public. Communication affects all components of a utility's strategic plan for line permitting. It is important to understand who is responsible for what task and how the associated processes interrelate. One planning strategy is to develop a communication network among the applicable stakeholders, with a project core team for continuity. The communication network can be developed, using appropriate pathways (both internally and externally) to facilitate information transfer among engineering, environmental, management, and technical resources.

Overcommitted Agency Staff

Timeframes required for environmental permit review and authorization can be long, often because of the increased demands on federal, state, provincial, and local agency staff. Many agencies are understaffed and cannot process the number of regulatory and land management reviews that are proposed within their jurisdiction in a timely manner, often resulting in project delays. Another issue for projects requiring agency permitting review, authorization, and oversight is referred to as the "loss of institutional memory." Rapid personnel turnovers within an agency can result in a change in approach and direction mid-project, sometimes causing project delays or additional costs. As a result, applicants need to proactively plan for insufficient staff availability and changes in agency personnel by using their knowledge of the process and established communication mechanisms to achieve their goals in spite of these barriers. In addition, in planning schedules and budgets, applicants must anticipate delays, expect staffing changes, and plan accordingly.

Interagency Coordination

Approval processes for transmission-line projects typically fall into two general categories: (1) those that review and approve the entire project, and (2) those that are designed to protect a sensitive resource, primarily during facility construction, although some predominant issues associated with transmission-line operation are beginning to emerge. Both types of approvals can occur at varying levels (e.g., federal, state, provincial, county, local), and frequently there is overlapping interest. Federal and state (or provincial) regulatory agencies in a given region have usually developed procedures over the past few decades to integrate their review and approval processes so that they may run concurrently, but it is important to note that these are independent processes. For some projects, through lack of planning and coordination, different regulatory processes may run sequentially, typically extending the project schedule and increasing project costs. Timelines can be complicated further if approvals are also required at the county or local level. Historically, sequential reviews and approvals have had disastrous consequences for a project. It can be critical for a utility applicant to take the lead in developing consultation and coordination among agencies.

Due to staff turnover or the lack of previous transmission-line projects in an area, it should be expected that the applicant's team will have to work with agency personnel who have no understanding or very limited understanding of transmission lines and the unique challenges that they present for design, construction, and operation. These challenges and project impediments can be overcome through an honest and professional effort to educate the agency staff as the project progresses, as emphasized for general communication strategies. Situations still exist where federal, state, and local regulations require different degrees of environmental review for a proposal. It is recommended that a planning meeting be held at the beginning of the environmental permitting process, where all responsible agencies are invited. Each agency's regulatory responsibilities can be reviewed, and a method can be developed to integrate these requirements into a project-specific permitting strategy. An interagency agreement developed at the start of the planning process also can aid in coordinating timelines and resolving disputes. While each agency still requires its unique environmental permit application, the applicant (utility) can develop complete and consistent application documentation with maximum efficiency.

Baseline Information Availability

An environmental review process is based on the review and analysis of interdisciplinary resource information from many fields and sources in order to disclose potential short- and long-term impacts from project implementation, and provide the authorizing agency with a decision-making tool. Problems arise when sufficient data or resource information to make informed impact conclusions are unavailable prior to permit application submittal and review. Different interagency requirements and timelines can result in conflicts, such as the need to obtain sufficient field data for a federal corridor analysis when the local permit-

ting process prevents land access for data collection until a ROW centerline has been delineated.

One approach to mitigate these problems is to develop suitable "environmental indicators" (comparable to economic indicators) to provide more consistent resource information. New tools, such as the use of geographic information systems (GIS), help to provide sufficient resource information and focus the analyses. Finally, communication among the authorizing agencies is vital to resolving disputes regarding approaches to data collection, land access, and chronology of the different environmental permitting timelines, as discussed above for interagency coordination.

Public Perception and Opposition

For a new transmission-line project to be successful, it is also critical for the project applicant to be prepared for the opposition that may be encountered. It should be expected that some members of the public and possibly some regulators may have difficulty accepting a new transmission line, primarily due to the size of the structures involved, the visual intrusion they pose, and the effects of the ROW on property values and land uses. Other issues also may be raised as a means of opposing a project, some of which may have merit and some of which may not. For example, electric and magnetic field (EMF) concerns may be raised for a 69-kV line. Although EMF effects would not typically apply to voltage classes 69 kV or lower, utility personnel must be aware of high-profile and potentially volatile issues and be prepared to discuss these types of issues with the regulatory and land management agencies, organizations, and the public. Regardless of the project team's personal opinion about the issues raised by agency staff or the public, the team must be prepared to respond to the concern in a professional manner and act in an educational role. With the advent of the Internet, opposition groups can organize with surprising speed, and they have access to other groups across the country that are opposing similar projects. These groups should be expected to share issues and information.

A common tactic of opposition groups is to keep raising new issues over an extended period of time in hopes that the project will be cancelled or approval denied. Issues identified by the opposition groups may expand, and addressing the specific concerns can become a "moving target" for a utility. If the applicant is prepared to respond to the range of issues that may be raised in its initial permit application or submittal, delays can be avoided. While most issues will be environmental in nature, many will address other aspects of the project. The environmental staff will need to work closely with the design, engineering, and ROW staff to cover the range of issues. It also can be very helpful if someone with transmission-line construction experience is available to the team. Each project team will have to determine exactly how these issues may apply to the unique geography and design of the line that is being proposed.

The old adage states that "all politics is local," and that can certainly hold true for transmission-line permitting. Local agencies, generally counties, have permitting authority over land use and zoning. A difficulty for local agencies reviewing a proposed transmission line that would cross their jurisdictions is that they may not receive any direct benefit from the line, improved reliability not withstanding. This fact may result in local agencies reflecting the opinions of their constituencies by opposing a project that has substantial regional benefits. Again, an applicant must be sensitive to the perception of disproportionate impacts without benefits, be ready to address the system-wide benefits of the new line, and be prepared to accommodate local concerns to the extent that they are practical. Involving local agencies early in the planning process can have significant benefits in reducing local opposition.

Project Rebuild and Undergrounding New Lines

Agency and public perception of proposed new transmission lines is often that they are unnecessary, that existing lines should be rebuilt versus new lines constructed, or if new lines are warranted, they should be undergrounded. Addressing these issues is closely associated with the discussion for better defining a project's purpose and need. Many recent projects have been rebuilds of lines that were constructed in the 1930s and 1940s. It is common for these projects to increase the voltage class from 69 kV to 115 kV or 230 kV, for example. There may be good design reasons why the existing ROW or ROW width cannot be used for the new project. Paralleling an existing route also may be undesirable for reliability, land-use, or environmental reasons. These design considerations should be clearly explained, with specific references to conditions in the proposed project area or the applicant's service territory. Regulators and the public alike also often request that a line, or portion of a line, be placed underground, assuming that such an installation is as simple as constructing a pipeline. Design limitations, cost implications, and increased environmental effects of underground construction should be identified and communicated among the stakeholders.

Controversial and High-profile Resource Issues

The range of issues and concerns that the public or regulators may raise concerning transmission lines is broad, and a utility should be prepared to deal with those issues that may apply to its proposed project before they are raised. In September 2001, EPRI published Technical Report No. 1005189 titled, *Communicating with the Public About Rights-of-Way: A Practitioner's Guide*. Chapter 4 of this report, "Identifying and Addressing Issues," presents a comprehensive discussion of issues that were identified in

a research survey, in order of their ranking by the respondents. These issues were grouped into four categories dealing with local, regional, and maintenance topics. The reader is encouraged to refer to this technical report for discussion of each of the subjects presented below.

Local Public Issues Associated with ROW Corridors

- Property values.
- Equity/fairness (i.e., those who must live next to the line versus those who benefit).
- Compensations for easements/tax implications.
- Use of eminent domain.
- Impacts of construction (erosion, soil compaction, and mixing).
- Future corridor maintenance (e.g., use of herbicides, tree-trimming).
- Impacts of corridor on agricultural uses.
- Restrictions on use of easements.
- Local zoning/permits.

Local Issues Associated with Power Lines

- Visual impact/aesthetic appearance of the towers/poles.
- Electromagnetic fields.
- Need for the line (e.g., use of conservation or distributed generation instead).
- Impact of the presence of towers/poles on agricultural use.
- Stray voltage/current effects on animals.
- Stray voltage/current effects on humans.
- Electrical safety.
- Electromagnetic interference with equipment.
- Noise.
- Proximity to schools/daycare centers.
- Chemically treated poles.
- Ozone/odor.

Regional Environmental/Cultural Issues

- Impacts on the viewshed (scenic aesthetics).
- River/stream crossings.
- Wetland impacts.
- Impacts on archeological/historic sites.
- Co-location with other facilities (e.g., gas pipelines, railroads).
- Impacts on endangered species.
- Pesticide use.
- Biodiversity/habitat fragmentation.
- Avian interactions.
- Local zoning/permits.
- Environmental justice (relative impact on low-income or minority populations).

Issues Associated with ROW Maintenance

- Too much tree trimming/clearing within ROW.
- Illegal trespass (e.g., snowmobile, ATV use by outside parties).
- Removal/trimming of danger trees outside of ROW.
- Use of herbicides.
- Maintenance and use of access roads/routes (e.g., culverts, stream crossings, fences, gates).
- Method of herbicide application.
- Too little mowing.
- Pole/transformer maintenance (e.g., painting, replacement).
- Too little tree trimming/clearing within ROW.
- Too much mowing.

The following issues can be high-profile concerns associated with transmission-line permitting, and these topics are also often the catalyst for organized project opposition during the permitting review process. The following discussion includes a brief description of these issues and suggested approaches to streamlining a utility's response to them.

EMF

EMF (electric and magnetic fields) effects have been issues in transmission-line permitting for more than 30 years. Millions of dollars have been spent to investigate potential adverse health effects without a universally accepted conclusion on the existence or magnitude of risk presented by exposure to EMF in general and transmission lines in particular. Therefore, this issue is typically raised in opposition to new or upgraded transmission lines. A utility should be prepared to respond to concerns that are raised concerning EMF by both the public and regulators as part of the permitting review process. EPRI's *Electric and Magnetic Field Management Reference Book* presents the current understanding of EMF that can be incorporated into a utility's comprehensive policy statement on EMF. This issue is also discussed in Chapter 7 of this Reference Book.

Endangered Species Act and Other Sensitive Species

On an international level, endangered, threatened, and other sensitive plant and animal species attract some of the greatest attention and regulatory review. Federal, state, provincial, and local laws protect a number of terrestrial and aquatic species and the associated habitats upon which they depend. Undeniably, one of the more stringent endan-

gered species laws is the Endangered Species Act in the United States. This law requires an independent, yet interconnected, review of potential impacts to federally listed species and those proposed for federal listing through another regulatory agency, the U.S. Fish and Wildlife Service. Depending on the type of project, its location, and the species involved, a separate environmental review and associated documentation effort (e.g., Biological Assessment, Biological Opinion) must be completed. This process further supports the recommended approach for interagency communication and increased knowledge of a project. Since the Endangered Species Act maintains a very structured and mandatory process with established timelines, it is beneficial for the utility or applicant to "communicate well and communicate often." This strategy helps to ensure that the sensitive species' permitting review and authorization parallels and is incorporated into the overall permitting review process.

Bird Electrocution and Collision Risk

Bird electrocution is not typically an issue for transmission lines, given the dimensions phase-to-phase and phase-to-ground. However, Section 12.16 of this Reference Book summarizes potential electrocution and collision risks to birds on and near transmission-line structures. Impacts to birds continue to receive a great degree of attention and concern internationally. Permitting agencies are becoming more aware of avian-related issues and may require specific protection measures to minimize future effects. However, one existing problem is the lack of continuity among agencies, even those within the same region. Different agencies are requiring different approaches to making overhead power lines, including transmission, safer for birds. This concern is discussed further in Section 1.6.5 "New or Expanding Issues," in regards to new issues facing utility companies in the environmental permitting realm.

Bird Predation

Predation is the use of transmission-line structures by birds of prey to reduce the species of certain animals below that which would normally be expected. It may be necessary to reduce this effect by installing bird guards on lines that prevent birds of prey using towers as perches. This is a more difficult task than that mentioned previously where the birds are prevented from settling on certain parts of the tower in that the entire tower needs to be fitted with guards. Another point of note is that communication and links with environmentalists are essential.

These points are adequately illustrated by two examples prevalent at the time of writing of this book. For decades the predation of juvenile desert tortoises by the common raven has been problematic in the southwestern United States. The presence of both transmission and distribution lines across the desert habitats supporting the federally threatened desert tortoise has contributed to the overall population decline recorded for this tortoise species, thereby increasing the regulatory pressures on associated utilities in these areas.

More recently, two grouse species are beginning to receive greater scrutiny from federal, state, and local regulatory and management agencies based on the continued decline of sage-grouse populations in the western United States and Canada. These losses are typically attributed to a number of factors, predominantly habitat loss and fragmentation. In addition to surface disturbance and construction activity restrictions for power line corridors near grouse breeding sites (leks), a more recent and expanded concern for the utility industry is that transmission-line structures introduce possible perch sites for avian predators (e.g., golden eagles) near sage-grouse use areas.

Because of this issue, regulatory and land management agencies have recently begun to require perch deterrents on power line structures within a certain distance of active lek sites to try to discourage perching by eagles and other grouse predators. However, presently, there is no consistency among the agencies on this distance, the types of perch deterrents that should be used, or how they should be installed. It is commonly accepted that the scientific evidence is lacking on the determination of adequate distances or buffers between power lines and grouse use areas. Additional evidence is needed to determine whether the proximity of power lines to active sage-grouse use areas may result in increased grouse predation, what this level of this predation may be, if a buffer area is warranted, and what the appropriate buffer size should be. Finally, if perch management is warranted within a specific buffer area, the extent and efficacy of perch deterrents are also unknown

A number of "Working Groups" have been established to review the decline in grouse. One of the proactive strategies currently employed by the western United States' utilities is becoming more involved in these working groups that typically consist of government agencies, grouse researchers, environmental groups, and private citizens. Again, communication and participation are key to ensure that the environmental community is aware of the utility's position, willingness to cooperate, and the respective limitations for certain mitigation approaches.

Invasive and Noxious Weeds

Many parts of the world are experiencing the spread of undesirable plants. Many of these plants are exotic, or not native to a region or continent, and due to the absence of

natural controls, they may spread rapidly. Some plants are toxic to livestock or wildlife, and others are pests in agricultural or developed areas. There is a concern among land owners and managers that the construction of a transmission line will facilitate the spread of invasive or noxious weeds, either through seeds being transported on construction equipment or through weeds becoming established in disturbed areas, such as along access roads, at staging areas, or around structure sites. A utility should be aware of weed issues in the area crossed by its proposed ROW and have a weed control plan prepared that can be included with permit applications.

1.6.5 New or Expanding Issues

Historically, issues associated with siting, permitting, constructing, and operating a transmission line, associated generating facility, and other ancillary components have arisen and evolved. Some of these historical issues have been resolved or at a minimum addressed with standardized plans (e.g., cultural resources), while others continue to be problematic for utility planning and operations (e.g., EMF, land use conflicts, aesthetics).

Many of the new or expanding issues facing utilities today have been mentioned as part of the environmental permitting review information. It is anticipated that the following topics will continue to grow in depth and complexity in the near future:

1. **Generation Siting.** One evolving issue for the electric utility industry is that new generation will be located far from load, necessitating the construction of new transmission lines. As an example, power generation in the United States has always required proximity to fuel (or transportation), cooling water, and transmission, but the implementation and evolution of air quality regulations over the past 35 years continue to push new generation to less densely populated areas. Prevention of Significant Deterioration (PSD) requirements for Class I areas (primarily national parks and designated wilderness) further restrict the siting of new coal-fired power plants, particularly in the western portion of the country. Coupled with the increased difficulty of obtaining regulatory approval and securing ROW on both public and private lands, new transmission projects frequently miss their budget and in-service targets.
2. **Restrictions Near Load Centers.** Parallel to the project siting constraints discussed above, urban and suburban expansions worldwide restrict availability for new ROWs, limiting access to load centers. There are significant land-use issues associated with maintaining capacity and reliability in such areas.
3. **Conflicting Priorities**. Conflicting agency environmental permitting priorities and process chronologies are growing, particularly when combining federal, regional, and local processes.
4. **Necessary Security.** Security presence at public meetings due to increased issue volatility and public emotion is now required in some areas.
5. **Bird Predation.** Grouse predation and bird perch management in the western United States, and the interagency and interregional inconsistencies associated with this issue, will have to rely on extensive and thorough communication processes.
6. **Operational Issues.** Operational issues that pertain to wildlife concerns continue to evolve—e.g., bird streamer effects on high-voltage, steel structures (see Section 12.16).

In summary, an educated and informed approach regarding environmental permitting processes, resource issues, agency and public concerns, and the relative volatility of each will be the greatest aid to a utility's project managers, design engineers, environmental permitting personnel, and public relations staff. Because of the variability of each project, its location, the reviewing and authorizing agencies, and associated issues and concerns, this "education" must occur at the beginning of the project prior to any commitment of resources.

1.7 COMPARISON OF THE THIRD EDITION OF THE REFERENCE BOOK TO THE SECOND EDITION

The *Transmission Line Reference Book* had its origins in the 1960s, when General Electric established the Lenox Laboratory in Lenox, Massachusetts, to experiment with transmission lines on the order of 1 MV. Known as Project UHV, the Lenox Laboratory site designed and tested transmission lines at Ultra High Voltages. While the original edition of the Red Book was essentially a final report to Project UHV, the approach used to write it and present the information has proved to be very successful. Each chapter in the book is a refereed paper on a specific topic. However, over time, the theories and technologies related transmission-line design have advanced, and the Red Book has fallen behind.

This new edition of the Red Book is intended to preserve the style of previous editions and present the science and technology in the same depth as previous editions, while including the latest information on research, technologies, and materials. Accordingly, 10 of the chapters in the previous edition of the book have been extensively updated. Tables 1.7-1 and 1.7-2 show the corresponding chapters in the second and the third editions.

A copy of the second edition of this Reference Book is included on the CD associated with the third edition,

Table 1.7-1 Chapter Organization, Second Edition, *Transmission Line Reference Book: 345 kV and Above*

Chapter No., 2nd Edition	Chapter Title, 2nd Edition	Corresponding Chapter, 3rd Edition	Comments
1	Project UHV: A Transmission Research Facility	——	This chapter is dated and not directly applicable to the process of line design.
2	EHV-UHV Transmission Systems	Chapter 1	The content dealing with sample lines and structures was not carried over into the third edition. This information was considered too narrow and dated.
3	Electrical Characteristics of EHV-UHV Conductor Configurations and Circuits	Chapter 2	Many of the graphs on conductor and conductor bundles were deleted from the third edition and replaced by a software applet. The base cases were pulled out as an appendix in the third edition. Conductor tables and line parameters are now an applet in the third edition.
4	Corona Phenomena on AC Transmission Lines	Chapter 8	This chapter has been considerably enhanced with updated information, and with the support of applets to aid in modelling effects and performing calculations.
5	Radio Noise	Chapter 9	This chapter has been considerably enhanced with updated information, and with the support of applets to aid in modelling effects and performing calculations.
6	Audible Noise	Chapter 10	This chapter has been considerably enhanced with updated information, and with the support of applets to aid in modelling effects and performing calculations.
7	Corona Loss	Chapter 11	This chapter has been considerably enhanced with updated information, and with the support of applets to aid in modelling effects and performing calculations.
8	Field Effects of Overhead Transmission Lines and Stations	Chapter 7	This chapter has been considerably enhanced with updated information, and with the support of applets to aid in modelling effects and performing calculations.
9	Insulation—Design Criteria	Chapter 3	This chapter has been revamped with the focus on insulation co-ordination methodologies including consideration of line economics, the latest system operating experience, and the latest standards.
10	Insulation for Power Frequency Voltage	Chapter 4	This chapter has been totally revised to include developments in insulator materials and designs as well as the latest developments in contamination.
11	Insulation for Switching Surges	Chapter 5	This chapter has been considerably enhanced with updated information, and with the support of applets to aid in modelling effects and performing calculations.
12	Lightning Performance of Transmission Lines	Chapter 6	This chapter has been totally redrafted with considerable new information and supported by applets.
13	Planning and Electrical Design of Transmission Lines	——	Elements of this chapter are included in the relevant chapters within the third edition

Table 1.7-2 Chapter Organization, Third Edition, *AC Transmission Line Reference Book: 200 kV and Above*

Chapter No., 3rd Edition	Chapter Title, 3rd Edition	Corresponding Chapter, 2nd Edition	Comments
1	Transmission Systems	Chapter 2	This chapter introduces the subject of transmission-line design through a brief, high-level overview of fundamental concepts and industry issues bearing on the role of line design.
2	Electrical Characteristics of Conductor Configurations and Circuits	Chapter 3	This chapter reviews information about transmission conductors and the parameters that they influence. Included in the chapter are discussions of the common types of conductor and their characteristics, conductor surface gradients, transmission-line impedance and admittance parameters, types of unbalance, and induced voltages.
3	Insulation Design	Chapter 9	This chapter describes insulation coordination, or how overvoltage and line insulation performance are balanced in a transmission-line design at least cost. Guidance is provided for determining overvoltages (stresses), insulation levels (strengths), and the balance between them to achieve acceptable line performance.
4	Insulation for Power Frequency Voltage	Chapter 10	This chapter discusses transmission line insulator technologies, including ceramic and polymer (nonceramic or composite) insulators. Selection and dimensioning of insulation from a power frequency perspective is discussed from a range of perspectives including contamination performance and life expectancy.
5	Switching Surge Performance	Chapter 11	This chapter discusses the strength of phase-to-ground and phase-to-phase transmission line insulation when subject to switching surges.
6	Lightning and Grounding	Chapter 12	This chapter describes the mechanisms of lightning, the effects of those mechanisms on transmission-line equipment, and methods of mitigation of effects.
7	Electric and Magnetic Fields	Chapter 8	This chapter presents engineering issues related to electric and magnetic fields produced by high-voltage transmission lines and to their effects. It includes methods of calculations and measurements, and evaluations of currents, voltages, and energies induced on objects and assessments of their effects.
8	Corona and Gap Discharge Phenomena	Chapter 4	This chapter describes the basic physical processes involved in corona and gap discharges and their electrical characteristics.
9	Electromagnetic Interference	Chapter 5	This chapter describes the nature of electromagnetic interference produced by corona and gap discharges on high-voltage transmission lines. It outlines in detail the procedures for calculating the EMI due to corona from 100 kHz to 1 GHz produced by any practical line configuration.
10	Audible Noise	Chapter 6	This chapter describes the nature of this acoustic noise produced by corona on high-voltage transmission lines. It includes procedures for calculating the noise produced by any practical line configuration, and methods for measurements and criteria for assessing annoyance or compliance with noise regulations.
11	Corona Loss and Ozone	Chapter 7	This chapter describes the mechanism of generation and techniques for measurement of corona losses on transmission lines. The chapter outlines methods for calculation of corona losses in different weather conditions, as well as calculation of mean annual and maximum corona losses.
12	Shared Use of the Right-of-Way	——	This chapter reviews issues associated with shared uses of transmission-line corridors. Included is a discussion of the basic elements of electromagnetic compatibility and descriptions of 15 planned and incidental uses of the rights-of-way.
13	Considerations for Inspection and Maintainability	——	This chapter provides guidance on designing transmission lines for inspection and maintainability. It includes practical information, learned from experience, on design principles that will promote durability and longevity, and facilitate inspection, condition assessment, and maintenance activities.
14	Voltage Upgrading of Existing Transmission Lines	——	This chapter addresses the process of increasing the operating voltage of an existing transmission line (line upgrading). It includes a summary of items that need to be considered in an upgrading study.
15	Transmission Lines Above 700 kV	——	This chapter provides detailed case studies of nine 700-800 kV lines and two 1000-1200 kV lines. It also includes a brief review of the research and development efforts required for the design and construction of the lines.
Appendix 1	Base Case Line Configurations	——	The bases cases were included in the second edition, but not given the appropriate attention. This appendix allows for easy access to the base cases, which are used to help the reader. The base cases provide a balance between number of cases and diversity.
Appendix 2	Applets	——	This appendix identifies and describes the 50 applets that accompany this book.
	Glossary	——	New addition. The basis of the Glossary was the IEEE Dictionary augmented by definitions used in IEC and CIGRE.
	Index	——	New addition. The index offers a tool for quickly locating information.

thereby allowing the reader to review material in the second edition.

Examples of new information in these chapters are as follows:

- **Conductor Configurations.** The new chapter includes recent advances, international configurations, and configurations of shield wires.
- **Insulation for Power Frequency Design.** The new chapter has been expanded to discuss transmission line insulator technologies, including ceramic and polymer (nonceramic or composite) insulators. Selection and dimensioning of insulation from a power frequency perspective is discussed from a range of perspectives including contamination performance and life expectancy.
- **Lightning Performance.** The new chapter has been extensively rewritten to include information on NLDN, LPATS, FALLS, transmission-line surge arrestors, TFLASH, sizing of shield wires, shielding failure, and tower grounding and impedance issues.
- **Electric and Magnetic Fields.** The focus of this chapter is shifted to acknowledge the change in industry interest from electric fields to magnetic fields. Field mitigation techniques are also discussed in some detail.
- **Corona Phenomena.** This chapter is expanded to include information on corona onset, corona effects, corona and polymer insulators, gap discharges, and space discharges.
- **Radio Noise.** This chapter is expanded to electromagnetic interference (EMI) to cover the wide range of communication systems now in use.
- **Audible Noise.** This chapter is expanded to add information on the impact of conductors and fittings, background hum, increased gradients, correction factors for gradient and altitude, software models from BPA and TLW, noise regulations, and noise measurement and mitigation.

As shown in Table 1.7-2, the new edition also changed the sequence in which these chapters are presented in order to bring forward information on insulation design and stresses (power frequency, switching surge, and lightning), prior to sections on effects (EMF, corona, EMI, and audible noise).

The new edition also adds four new chapters—Chapters 12-15—on shared use of rights-of-way, inspection and maintenance concerns, voltage upgrading, and experience with lines above 700 kV. These new chapters reflect both the changing concerns over the past 15 years as well as the availability of experience in line design, operation, and maintenance.

In addition to the revised text, the new edition of the Red Book also includes applets, which are small software programs, or stand-alone calculation modules, that enable users to make specific calculations for transmission-line design parameters, with associated example and design features. Each applet has transmission-line data input screens, calculation results screens, and help files. The help file contains a sample problem that the user can load directly to calculate results. The user can also enter specific transmission-line information for a particular problem and then calculate specific results for that problem. Transmission-line parameters can also be modified and the result recalculated, thereby illustrating how the change in a particular parameter can affect the calculation results.

More than 50 different applets have been developed, with calculation capabilities related to conductor surface gradients, switching surges, lightning effects, electric and magnetic fields, radio noise and audible noise generation, and corona (see Table 1.7-3). Overall, the inclusion of these applets in the third edition offers users of the Red Book the advantages of software calculation, which were not available to users of the second edition, and enables rapid and accurate comparison of alternatives and understanding of effects.

1.8 CONCLUSION

Transmission lines embody a complex and deliberate balance between costs, energy to be transported, and electrical, mechanical, civil, performance, and environmental tradeoffs. Lines also need to operate within a system that has, in recent years, seen major changes driven by deregulation. Finally, lines are expected to operate for more than 40 years. Consequently, arriving at a "standard" design capable of serving all operating environments is nearly impossible. Considering the expansive system of lines that weave a mesh across the globe, it is hardly surprising that the vast system is considered one of the largest "structures" known to man.

As such a unique system, it is critical that engineers understand the many aspects of line design, construction and operation. The subject is so broad that one book cannot cover all electrical, mechanical, civil, and environmental aspects. This book covers only the electrical factors, but the reader is urged to understand the relationships between the mechanical, civil and electrical aspects that make up the line.

This chapter has endeavored to inform the reader on the basics of the electrical aspects of the line as well as to cover the dynamic environment (legal, social and political) that impacts on the line design engineer at present.

Table 1.7-3 Applets

Chapter No.	Applet No.	Applet Name
2	CC-1	Conductor Surface Gradient (2-D)
2	CC-2	Conductor Surface Gradient (3-D)
2	CC-3	Surface Gradient on Toroidal Corona Shields
2	CC-4	Conductor Tables
2	CC-5	Transmission Line Parameters (Single Circuit)
2	CC-6	Conductor Surface Gradient—Base Case Curves and Effect of Line Parameters
2	CC-7	Induction in Parallel De-Energized Lines
3	IC-1	Insulation Coordination. Comparative Evaluation of Insulation Distance Requirements
3	IC-2	Risk of Failure (Same as S-2)
4	I-1	Insulator ESDD and Parameter Evaluation
4	I-2	Electric Field Distribution for Polymer Insulators—Effect of Dimensions and Location of Corona Ring
4	I-3	Statistical Method for Dimensioning Insulators with Respect to Contamination
5	S-1	Switching Surge Flashover Model
5	S-2	Risk of Failure Calculation for Transmission Line Switching Surges
5	S-3	Calculation of 50% Flashover Voltage and Standard Deviation from a Set of Test Data
6	L-1	Transmission Line Lightning Performance
6	L-2	Stoke Attraction Model
6	L-3	Tower Footing Dynamic Resistance of Vertical Rods
6	L-4	Tower Lightning Flashover Tutorial
6	L-5	Tower Surge Impedance
6	L-6	Step and Touch Potential
7	EMF-1	Field Ellipse
7	EMF-2	Electric Field of Transmission Lines in 2-D
7	EMF-3	Single Conductor Equivalent to a Bundle
7	EMF-4	Electric Field of Transmission Lines in 3-D
7	EMF-5	Electric Field Shielding by Grids of Wires—2D
7	EMF-6	Magnetic Field from Sets of Current Carrying Conductors (2-D)
7	EMF-7	Magnetic Field (3-D)
7	EMF-8	Magnetic Induction in Wires Parallel to Transmission Lines
7	EMF-9	Distant Magnetic Field Equations for Transmission Lines
7	EMF-10	Electric Field Induction on Objects
7	EMF-11	Magnetic Field Reduction Using Cancellation Loops (3-D)
7	EMF-12	Magnetic Field Reduction Using 4th-Wire Scheme
8	Co-1	Corona Inception Gradient
9	RN-1	Electromagnetic Interference up to 30 MHz
9	RN-2	EMI Calculations Using Empirical Methods
9	RN-3	EMI Base Case Curves and Effect of Line Parameters
9	RN-4	Traditional Radio Noise Calculation Method
10	AN-1	Audible Noise of Transmission Lines
10	AN-2	Audible Noise of Transmission Line (3-D)
10	AN-3	Bundle Geometry for Minimum Audible Noise
10	AN-4	Audible Noise, Hum
10	AN-5	Audible Noise—Base Case Curves and Effect of Line Parameters
10	AN-6	Audible Noise vs. Rain Rate
11	CL-1	Transmission Line Corona Loss
11	CL-2	Corona Loss—Base Case Curves and Effect of Line Parameters
11	CL-3	Ozone Concentration near Transmission Lines
13	M-1	Minimum Approach Distance
	G-1	Unit Converter
	G-2	World Map of Ground Flash Density and North American Map of Earth Resistivity
	BC-1	Base Case Line Configurations and Their Performance

REFERENCES

Barrie, D, M. Graham, and C. Marcello. 2003. "Evolution of Canada-United States Interconnections." *Electra.* No. 210. October.

Booranasantigul, V. 2004. Personal communication.

CIGRE. 1999.Working Group 22-14. "High Voltage Overhead Lines: Environmental Concerns, Procedures, Impact and Mitigations." TB-147.

CIGRE. 2003. "UK Transmission and Distribution: An Era of Change." CIGRE Colloquim. Edinburgh.

CIGRE. 2004a. Working Group 22-15. "Environmental Management Plans (EMP) for Activities Associated with Overhead Lines." ER N˚212. February.

CIGRE. 2004b. Task Force D1.03.10. "N_2/SF_6 Mixtures for Gas-Insulated Systems." CIGRE Session 2004. Paper D1-201.

Constable, G. and B. Somerville. 2003. *A Century of Innovation.* National Academies of Engineering. Joseph Henry Press. Washington, D.C.

Edris, A. 2000. "FACTS Technology Development: An Update." *IEEE Power Engineering Review.* Vol. 20. No. 3. March 2000. Page 4-9.

EEI (Edison Electric Institute). 2004. *Statistical Yearbook of the Electric Utility Industry: 2002 Data with Preview 2003 Data.* EEI. Washington, D.C. August.

Energy Information Administration. 2002. *Energy Information Administration and CIA World Fact Book*.

EPRI. 1982. *Transmission Line Reference Book: 345 kV and Above.* Second Edition, Revised.

EPRI 2001. *Assessment Methods and Operating Tools for Grid Reliability.* Report 1001408. April.

EPRI. 2004. "Global T&D System Practices: Executive Overview."

Esmeraldo, P. C. 2004. Personal communication.

Gillespie, T. 2004. Personal communication.

Glover, J. D. and M. S. Sarma. 2002. *Power System Analysis and Design.* Third Edition. Brooks/Cole.

Grainger, J. J. and W. D. Stevenson. 1994. *Power System Analysis.* McGraw-Hill Inc.

Guile, A. E. and W. Paterson. 1977. *Electrical Power Systems.* Volumes 1 and 2. Second Edition. Pergamon Press.

Hoffmann, S. 2004. Personal communication.

Hydro-Québec TranÉnergie. 1998a. "Effets et conséquences sur les lignes de transport de la tempête de verglas survenue du 5 au 9 janvier 1998." Rapport détaillé. Aspect climatique. October.

Hydro-Québec TranÉnergie. 1998b. "Effets et conséquences sur les lignes de transport de la tempête de verglas survenue du 5 au 9 janvier 1998." Rapport détaillé. Diagnostic des Dommages. November.

Kraus, J. D. 1953. *Electromagnetics.* McGraw-Hill.

Milton, J. and A. Bourque. 1999. *A Climatological Account of the January 1998 Ice Storm in Quebec: Scientific Report*. 87 pages. Available from Environment Canada. Atmospheric Sciences and Climate Monitoring Division. 100 Blvd. Alexis-Nihon. Suite 300. Ville Saint-Laurent (Québec). H4M 2N8. ISBN 0-660-17764-1. Cat. No. En57-34/1-1999E.

Naidoo, P., N. L. Diseko, P. Goosen, R. D. Estment, and D. Bhana. 2004. "Transmission Network Planning Design and Asset Management: The Case of Eskom, South Africa." CIGRE 40th General Session. Paris, France. August 29–September 3, 2004.

NERC (North American Electric Reliability Council). 2004. www.nerc.com

Nonjima, T. et al. 1998. "Installation of 275-kV, 3.3 km gas-insulated transmission line for underground large-capacity transmission in Japan." CIGRE Session 1998. Paper 21/23/33-01.

Shahidepoor, M. 2004. "Investing in Expansion." *IEEE Power and Energy Magazine.* January/February. Pp. 14-18.

U. S.–Canada Power System Outage Task Force. 2003. *Interim Report: Causes of the August 14th Blackout in the United States and Canada.* November.

U. S. DOE (Department of Energy). 2003. "Testimony of Jimmy Glofelty." Director. Office of Electric Transmission and Distribution. Before the Subcommittee on Energy. Committee on Science. U. S. House of Representatives. September 25.

U. S. DOE (Department of Energy). 2004. "Fiscal Year 2005 Budget Presentation." Office of Electric Transmission and Distribution. February 2004. Page 3.

Van Rooyen, C. S., Vosloo, H. F., and R. Harness. 2003. "Watch the Birdie!" *IEEE Industry Applications.* September/October 2003. Vol. 9. No 5.

Van Rooyen, C. S. 2004. "The Management of Wildlife Interaction with Overhead Lines." In Pillay T. and S. Bisnath (eds). *The Fundamentals and Practice of Overhead Line Maintenance.* Johannesburg. Crown Publications.

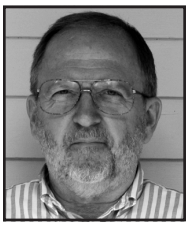
Vosloo, H. F. and C. S. van Rooyen. 2001. "Guarding Against Bird Outages." *Transmission & Distribution World.* April 2001. Vol. 53. No. 4.

CHAPTER 2

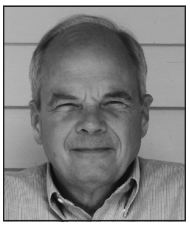
Electrical Characteristics of Conductor Configurations and Circuits

Dale A. Douglass
James Stewart
Bernie Clairmont

This chapter reviews information about transmission conductors and the parameters that they influence. Included in the chapter are discussions of the common types of conductor and their characteristics, conductor surface gradients, transmission-line impedance and admittance parameters, types of unbalance, and induced voltages.



Dr. Dale A. Douglass is a Principal Engineer of Power Delivery Consultants, Inc. based in Niskayuna, New York. He has more than 30 years of experience in transmission line engineering and conductor design, having worked with Power Technologies, Inc., Kaiser Aluminum, and Bell Laboratories. He is presently the Vice Chairman of IEEE's Towers, Poles, and Conductors Subcommittee and the convener of CIGRÉ Working Group B2-12 on Electrical Aspects of Transmission Lines. He has been involved in studies of overhead line sag-tension, high temperature operation, and both current and voltage upgrading of existing lines. In 1996, he was elected a Fellow of the Institute of Electrical and Electronic Engineers for "contributions to understanding the characteristics and applications of overhead power transmission conductors."



Dr. James Stewart is an independent consultant based in Scotia, New York. He has more than 30 years of experience in power systems and transmission lines, having worked for Niagara Mohawk Power Corporation and Power Technologies, Inc. He has been involved in analysis and measurement of transmission line electrical parameters, including research contributions to compact and high phase order transmission line design. He taught circuit analysis at Syracuse University and taught power circuit analysis as part of the PTI Power Technology Course. He was elected a Fellow of the Institute of Electrical and Electronics Engineers in 1987 for "advances in transmission line theory and its reduction to practice through prototype demonstration." He is presently Chairman of the Transmission and Distribution Committee of the IEEE Power Engineering Society.



Bernie Clairmont has been a lead researcher at the EPRI laboratory in Lenox, Massachusetts for 18 years, following a six-year period of teaching physics at a nearby college. His research interests have included the corona and field effects of transmission lines, magnetic field management, application of fiber optics in high-voltage environments, and dynamic rating of overhead lines. He was the Principal Investigator of many EPRI and utility sponsored research projects. He worked on the development of several computer programs that are part of EPRI's workstations, such as the Transmission Line Workstation module for calculating field and corona effects, and authored or coauthored many published papers and EPRI reports, such as the *Magnetic Field Shielding Handbook.* As a Project Manager and Senior Research Engineer, he now leads the EPRI effort in the field of increased power flow of transmission lines.

2.1 INTRODUCTION

Many sizes and types of conductor are used in transmission lines at voltages above 200 kV, although most are at least 25 mm in diameter and are stranded with aluminum wires. This chapter provides information about conductors and the transmission-line parameters that they influence. The information supplied in this chapter is intended to be useful to those using the other chapters of this book and to those simply looking for basic information on transmission conductors.

Section 2.2 describes the various types of conductor that are in widespread use, describing their relative strength, weight per unit length, electrical resistance, and both inductive and capacitive reactance. The sag behavior of conductors under ice, wind, and high electrical loading is discussed as well as the reasons for limiting conductor temperature (annealing and electrical clearance). Thermal rating limits are also mentioned, since such limits are an essential part of line design and system planning.

Conductor surface gradients are explained in Section 2.3. The line's phase spacing and configuration, the number of conductors per phase bundle, and the subconductor diameter are all factors in determining the surface gradient. Applets concerning surface gradient calculations are discussed.

Section 2.4 concerns the calculation of basic line impedance and admittance parameters, the pi electrical equivalent, and the meaning and calculation of surge impedance and surge impedance loading. Examples are presented for typical line geometries.

Although modern power system circuits and their overhead transmission lines are intended for application in a balanced three-phase system, unbalances do occur and can be analyzed as described in Section 2.5. The importance of line "transposition" is discussed.

Section 2.6 concerns electric and magnetic field induction on de-energized circuits. Appropriate mention of applicable applets is included.

Appendix 2.1 includes several examples of conductor data tables for the most common transmission conductors. The conductor database applet allows the user access to types and sizes of transmission conductors.

A number of applets are provided with this book to assist in the calculation of conductor characteristics. These applets include the following:

- Applet CC-1, "Conductor Surface Gradients (2-D)." This applet provides the surface gradients of all the conductors (and subconductors) within a transmission corridor, and presents the results in tabular and graphical forms.
- Applet CC-2, "Conductor Surface Gradient (3-D)." This applet enables users to compute and plot the surface gradient (maximum and average) along a conductor's length. The applet accepts line geometry, voltage, objects, and terrain variation, and will provide surface gradients as a function of longitudinal distance down the line.
- Applet CC-3, "Corona Shield Surface Gradient." This applet computes the maximum surface gradient, as a single number, for toroids (and other simple objects).
- Applet CC-4, "Conductor Data." This applet allows users to access sizes and types of transmission conductors.
- Applet CC-5, "Transmission Line Parameters." This applet computes three-phase transmission-line phase and symmetrical component sequence impedance parameters including the effects of lossy earth.
- Applet CC-6, "Conductor Surface Gradient Base Case Curves and Effect of Line Parameters." This applet accepts base case number and the parameter to be varied, and will produce a plot of surface gradient versus varied parameter. Parameters that can be varied include conductor (or subconductor) diameter, phase spacing, and conductor heights above the ground.
- Applet CC-7, "Induced Voltages on Parallel Lines." This applet computes electric and magnetic field coupling from a three-phase transmission line to parallel wires.

2.2 BARE CONDUCTORS FOR OVERHEAD TRANSMISSION LINES

A wide variety of sizes and types of conductor have been used in transmission lines for voltages of 200 kV and above. In most cases, however, transmission phase conductors are at least 25 mm in diameter, and are stranded with aluminum wires and a stranded steel core for mechanical reinforcement. Because aluminum is highly conductive and the diameter is relatively large, transmission conductors typically have relatively low electrical resistance per unit length. This keeps electrical losses to a minimum.

Conductors used as shield wires are typically stranded with galvanized steel or aluminum-clad steel wires. They are, therefore, both strong and resistant to electrical arc damage. In recent years, shield wire conductors enclosing fiber-optic wires used for communications have come into widespread use.

This section concerns the electrical characteristics (and, to a lesser extent, the mechanical characteristics) of commonly used phase conductors and shield wires for transmission lines at 200 kV and above. The primary

characteristics of concern in these conductors are their electrical resistance as a function of temperature and current, the maximum allowable operating temperature, and the surface gradient as installed.

A variety of aluminum conductors with stranded steel reinforcing cores are available. Product specifications for many of these conductors exist either in IEC 1597-1995 or ASTM Volume 2.03 on Electrical Conductors. The conductors include:

- Aluminum Conductor Steel Reinforced, ACSR or A1/S1 (ASTM B-232 1992), and ACSR/TW (ASTM B-779 1991)
- Self-Damping Conductor, SDC (Livingston 1969; McCulloch et al. 1980; ASTM B-701 1991)
- T2 Conductor, T2/ACSR (Roche and Douglass 1981)
- Aluminum Conductor Steel-Supported, ACSS (Adams 1970; Thrash; 1999; ASTM B-856 1995) and ACSS/TW (ASTM B-857 1995)

The steel core wires used in these various ACSR conductors must all be galvanized GA, GB, or GC (ASTM B-498 1993), aluminized, AZ (ASTM B-341 1993), or aluminum-clad, AW (ASTM B-502 1993) to avoid electrolytic corrosion between steel and aluminum. The thickness of the galvanizing on steel core wires is usually Class A (the tables in Appendix 2.1 are for Class A galvanizing), but heavier zinc layers referred to as Class B and C galvanizing can also be specified when corrosion is severe. Greater thickness of galvanizing results in reduced strength for a given core wire diameter.

In addition to the ACSR family of conductors, conductors stranded entirely of aluminum, entirely of aluminum alloy (aluminum-magnesium-silicon) wires, or made of a combination of aluminum and aluminum alloy wires are available. All are relatively light in weight but more susceptible to loss of tensile strength and excessive creep elongation at temperatures in excess of 100^{o} C. The commonly available all aluminum conductors (ASTM B1 1991; IEC 1089 1991) include:

- All Aluminum Conductor (AAC, AAC/TW, A1)
- All Aluminum Alloy Conductor (AAAC, AAAC/TW, A2 or A3)
- Aluminum Conductor Alloy Reinforced (ACAR, A1/A2 or A1/A3)

Aluminum Conductor Alloy Reinforced conductors have outer layers of 1350-H 19 aluminum strands reinforced with a core of 6201-T81 aluminum alloy. These conductors are typically available with the same resistance as common ACSR conductors. Changing the ratio of 1350-H19 to 6201-T81 strands can vary the strength of ACAR. Common strandings for medium-sized transmission conductors include 30/7, 24/13, and 18/19. These are listed in order of increasing strength.

Special-purpose conductors have been developed and are utilized in many lines. These include:

- Expanded ACSR. These conductors generally use EC-H19 strand with a steel core. Expansion is by open helices of aluminum wire, flexible concentric tubes, or combinations of aluminum wires and fibrous ropes. Since there are no industry standards for these conductors, the data have not been included in this book. They are no longer in widespread use.
- Aluminum Alloy Conductor Steel Reinforced (AACSR [ASTM B-711 1993]). This conductor is used where very high strength is required. Typical applications are in long spans exposed to severe icing and wind loads.
- High-Temperature Conductors. On older lines that have been reconductored, certain high-temperature conductors are used, such as Aluminum Conductor Steel Supported (ACSS [ASTM B856 1995; Thrash 1999] or ACSS/TW [ASTM B857 1995]), "Gapped" ACSR with "Heat-Resistant" Aluminum Alloy (GTACSR [Kotaka et al. 2000; Tunstall et al. 2000]), High Temperature Aluminum reinforced with "Invar" steel (TACIR [Sasaki et al. 1985]), and high-temperature aluminum reinforced with various types of strong, lightweight composites.

Commonly used shield wires include "aluminum-clad-steel conductor" (Alumoweld), high-strength and extra-high-strength steel (EH and EHS), and optical ground wire (OPGW).

Choice of conductor type is primarily driven by mechanical considerations such as maximum ice and wind loads and maximum allowable conductor operating temperature and the corrosiveness of the line environment. Choice of conductor diameter is primarily driven by electrical considerations such as corona-induced radio and TV noise and, to a lesser extent, by electrical losses.

2.2.1 Conductor Materials

Table 2.2-1 summarizes the metal wire materials used in transmission conductors.

Copper wires are almost never used in conductors for high-voltage transmission lines, because the density of copper is three times that of aluminum, whereas its conductivity is less than twice that of aluminum. This makes it unattractive for use where the conductor is self-supporting but makes copper conductors quite attractive for use in high-voltage underground cables.

Table 2.2-1 Mechanical and Electrical Properties of Transmission Conductor Wire Materials

Name (ASTM/ IEC)	Tensile Strength (Ksi/Pa)	Minimum Elongation (%)	ASTM or IEC Specification	Temper	Conductivity (% I.A.C.S.)
1350/A1	24	1.5	B230/ IEC889	H19	61.2
1350	8.5	20	B609	H0	63.0
6201/A3	44-46/ 315-325	3.0	B398 IEC60104	T81	52.5
A2	295	3.5	IEC60104		53.0
Galvanized Steel/S	A-185 B-175 C-165	3.5 3.0 3.0	B498		
High Strength Galvanized Steel	A-205	3.0	B606		
Aluminized Steel (AZ)	160	3.5	B341		9.0
Aluminum-Clad Steel	175	1.5	B502		20.3

Most quantities in the conductor parameter tables of Appendix 2.1 have been calculated from the basic strand dimensions. The following is a summary of the formulae and procedures.

2.2.2 Areas and Diameter

The areas in kcmil and square millimeters are calculated from the strand dimensions. The area of an overhead conductor is typically described in terms of the aluminum area since this is the primary current-carrying conductor component. If the resistance of the conventional galvanized steel core is taken into account, the resistance of an ACSR conductor is reduced by 1 to 2%.

The conductor diameter is determined by the strand geometry. For example, Bluebird conductor is an ACSR with four layers of aluminum over two layers of steel. The steel core diameter is five times the diameter of the 0.0961-in. strand (0.480 in.). The total conductor diameter is then two times the four layers of 0.1602-in. aluminum strand, plus the core diameter, or 1.762 in.

2.2.3 Weight and Rated Strength

The weight and strength of those conductors that are included in Appendix 2.1, and those that may be accessed with Applet CC-4, "Conductor Data," are calculated from the ASTM or IEC manufacturing standards, and are generally consistent with the values in the Aluminum Association handbook (Aluminum Association 1989). The methods of calculation for both weight per unit length and "rated breaking strength" are described in detail in the appropriate ASTM or IEC standards. Essentially, the rated breaking strength (RBS) of stranded conductor is the sum of the strengths of the individual wires allowing for some reduction due to the helical stranding. For ACSR, the tensile "strength" of the steel core is calculated at the maximum elongation of the surrounding aluminum strands (1%), not the maximum elongation of the steel itself.

2.2.4 Electrical Resistance

For a bare, stranded, all-aluminum conductor, the electrical resistance depends on the aluminum conductivity, the lay length of each of the wire layers, the wire diameter, the temperature of the conductor, and the frequency of the electrical current.

The calculation process begins with the conductor's dc resistance. This is found from the strand conductivity, the wire diameter, and a correction factor for the lay length of each of the conductor layers. Since lay length varies with the position of the layer and with the particular manufacturer, correction factors for the helical stranding of the aluminum wires (2% for most transmission conductors) have been given by the American Society for Testing and Materials in Standard B232 (for ACSR), Standard 231 (for AAC), and Standard B524 (for ACAR).

If the lay length is known, then Equation 2.2-1 provides a method for a more exact calculation of the dc resistance of each layer:

$$R_i = \frac{\rho}{A} \cdot \sqrt{1 + \left(\frac{2 \cdot \pi \cdot r_i}{S} \right)^2} \qquad 2.2\text{-}1$$

R_i = Ohms per unit length of the ith layer at the reference temperature, $T_{REF.}$
ρ = Resistivity of aluminum strands at a standard reference temperature, $T_{REF.}$
S = Length of lay in i^{th} layer.
r_i = Stranded conductor radius to middle of i^{th} layer.
A = Area of aluminum strands in i^{th} layer.

The exact total dc conductor resistance, R_{dc}, is the parallel combination of the individual layer resistances, R_i:

$$R_{dc} = \frac{1}{\left(\frac{1}{R_1} + \frac{1}{R_2} + .. \right)} \qquad 2.2\text{-}2$$

This initial estimate of dc resistance must be further corrected for the temperature of the conductor, T_C, and the frequency of the electrical current through it.

DC Resistance as a Function of Temperature

The dc resistance of the conductor at temperatures other than T_{REF} is determined by using Equation 2.2-3 with the appropriate temperature coefficient of resistance, α_{REF}.

$$R_{dc}(T_C) = R_{dc}(T_{REF}) \cdot \left[1 + \alpha_{REF} \cdot \left(T_C - T_{REF}\right)\right] \qquad 2.2\text{-}3$$

where T_{REF} is the reference temperature in degrees Celsius, and T_C is the conductor temperature in degrees Celsius.

The thermal coefficient of resistance varies with wire metal alloy and with the reference temperature. The resistance of aluminum and copper wires increases approximately 3.5 to 4.0% per 10°C. The resistance of galvanized steel wires increases 3.2% and aluminum-clad steel wires about 3.6% per 10°C. The coefficient of resistance decreases as the reference temperature increases, going from 0.00403 for 61.0% I.A.C.S. aluminum at 20°C to 0.00360 at a reference temperature of 50°C.

In recent years, it has become common to reduce the resistance of steel core aluminum conductors (ACSR) by accounting for the conductivity of the galvanized steel wires. Including the conductivity of the steel core reduces the conductor's dc resistance by between 1% and 2% depending on the steel wire area. To do this, the resistance of the core is calculated with an equation like 2.2-1 with a conductivity of 8% I.A.C.S. The core resistance is combined with the aluminum layer resistances in Equation 2.2-2.

In correcting the dc resistance of ACSR, the steel wire resistance of the steel core must be corrected separately for temperature since its thermal coefficient of resistance is only about 2.9% per 10°C.

Adjusting Conductor (AC) Resistance for Frequency

Even after correcting the dc resistance for temperature, the ac resistance of bare stranded transmission conductors is greater than the dc resistance due to skin effect (i.e., the tendency of current density to be higher toward the outside of the conductor than in the middle due to magnetic field effects within). Except for steel-core aluminum conductor with an odd number of aluminum strand layers, the ratio of ac to dc resistance at 25-60 Hz is nearly 1.00 for transmission conductors less than 20 mm in diameter. For larger conductors, the ac/dc resistance ratio increases. The ac/dc resistance ratio for three relatively large all-aluminum conductors as a function of outside diameter is shown in Table 2.2-2.

The correction of ac resistance for skin effect may be accomplished by use of the graph shown in Figure 2.2-1. Note that R_{DC} is in ohms per mile. Other than that, the other dimensions can be SI or U.S. common units.

AC Resistance for 60 Hz Frequency with One- and Three-Layer ACSR

The ratio of ac to dc resistance due to skin effect is not dependent on the current magnitude. For aluminum conductors with a steel-reinforcing core, particularly those with one or three aluminum layers, however, ac resistance is dependent on both frequency and on current magnitude. Table 2.2-3 illustrates the dependence of ac resistance of three-layer 54/7 1033.5 kcmil (524 mm^2) Curlew ACSR (A1/S1) (Aluminum Association 1989).

The increase in effective ac resistance is even greater for single-layer ACSR, as shown in Table 2.2-4 (Aluminum Association 1989).

Complex models, to account for the increase in ac resistance of ACSR conductors, have been developed (Lewis

Table 2.2-2 Increased Resistance due to Skin Effect at 60 Hz (Dwight 1923)

AAC/S1 Conductor	Alum. Area (kcmil/mm^2)	Outside Diameter (in./mm)	R_{DC} @ 20°C [Ω/mi]/Ω/km	R_{AC}/R_{DC}
Arbutus	795/403	1.026/26.1	0.115/0.0713	1.023
Narcissus	1272/645	1.300/33.0	0.0718/0.0446	1.048
Coreopsis	1590/806	1.454/36.9	0.0574/0.0356	1.087

Table 2.2-3 Three Aluminum Layer, 54/7 ACSR Conductor Resistance as a Function of Current

Current – (amps)	Current Density (amps/mm^2)	R_{AC}/R_{DC} Skin Effect @ 60 Hz	R_{AC}/R_{DC} Core Magnetization	R_{AC}/R_{DC} Total
200	0.38	1.025	1.007	1.032
400	0.76	1.025	1.013	1.038
600	1.15	1.025	1.018	1.044
800	1.52	1.025	1.022	1.048
1000	1.91	1.025	1.025	1.051

Table 2.2-4 Single-Layer, 6/1 #4/0 AWG ACSR Conductor Resistance as a Function of Current

Current – (amps)	Current Density (amps/mm^2)	R_{AC}/R_{DC} Skin Effect @ 60 Hz	R_{AC}/R_{DC} Core Magnetization	R_{AC}/R_{DC} Total @ 75°C
100	0.93	1.002	1.057	1.064
200	1.86	1.002	1.166	1.168
300	2.79	1.002	1.196	1.198
400	3.72	1.002	1.186	1.188

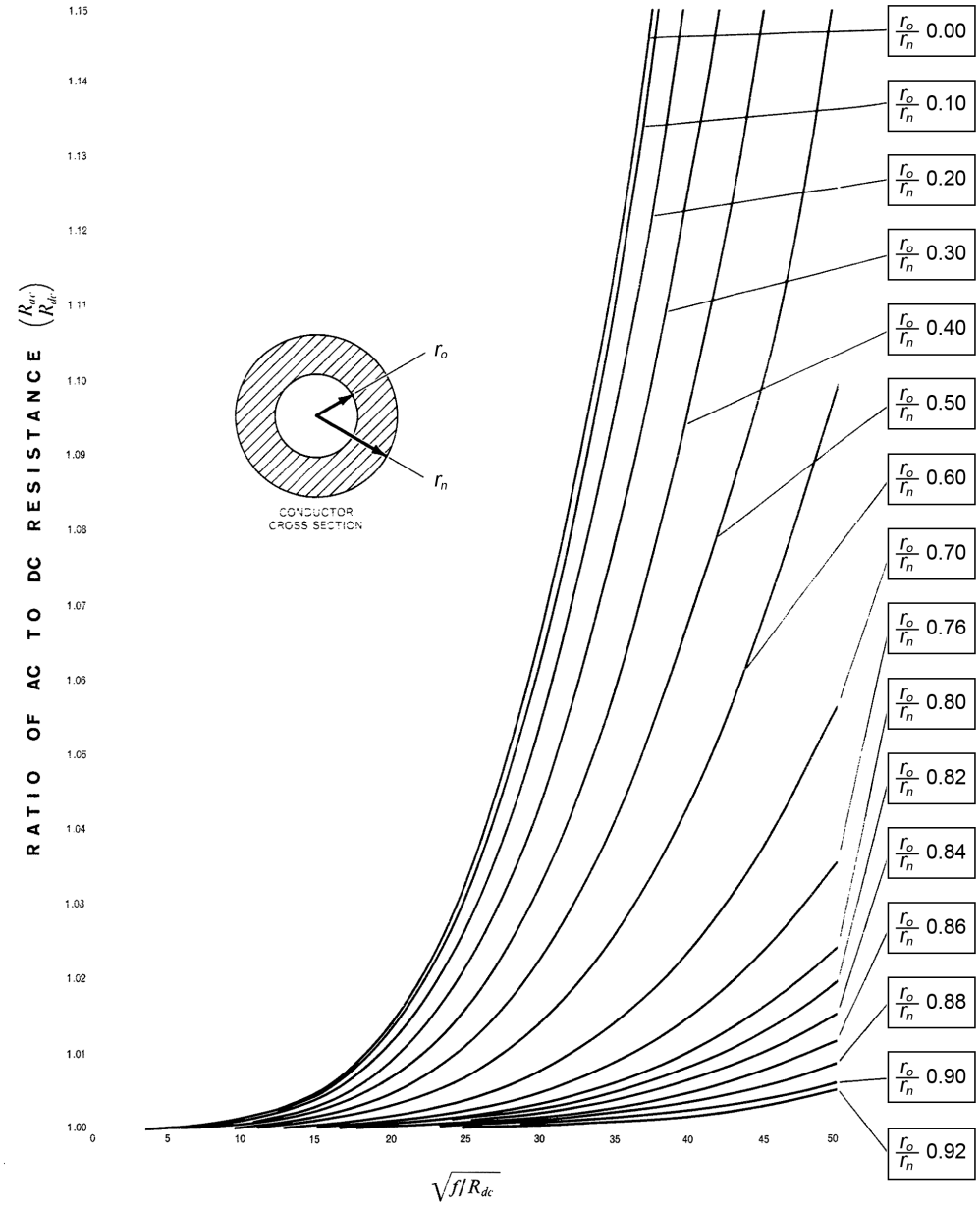


Figure 2.2-1 Skin effect curves for solid round or bare stranded conductor (Dwight 1923).

and Tuttle 1959; Morgan et al. 1997; and Barrett et al. 1986). These models consider the increase in losses due to both iron losses in the core and uneven current densities between the helical aluminum wire layers. The increase in ac resistance due to the steel core depends on both the magnetic properties of the structural steel core wires and the lay lengths of the aluminum wire layers.

Practically speaking, the steel core and the lay lengths are chosen to assure sufficient strength and stiffness, and to assure proper handling characteristics of the composite conductor during tension stringing procedures. As a result, there is a good deal of variation in lay length and magnetic steel wire properties between manufacturers, and it is unlikely that the impact of core magnetization can be known exactly. The phenomenon of core magnetization is still under investigation, and the effects of core magnetization can only be determined in an approximate fashion.

The tables in Appendix 2.1 include ac resistance values for 25°C and 75°C. For single-layer ACSR (6/1, 7/1, 8/1, 12/7), as shown in Table 2.2-4, the resistance shows large changes with current as well as with temperature. For these small conductors, rarely used in transmission lines at 200 kV and above, the resistance values at high temperature must be calculated based on laboratory measurements (Aluminum Company of America 1960). For three-layer ACSR, however, which is commonly used in transmission lines at 200 kV and above, the resistance can be calculated as follows:

- Calculate the resistance at the desired temperature and correct for skin effect, as described in the preceding part of this section.
- Correct for magnetization losses by multiplying the resistance by the core magnetization multiplier shown in Figure 2.2-2.

If the details of the ACSR conductor construction and core magnetic properties are known, the methods suggested by Barrett (Barrett et al. 1986) and Morgan (Morgan et al. 1997) may be used and a more precise estimate of ac resistance obtained. The method outlined in these two papers incorporates a more precise estimate of the core losses and recognizes that the current density in the aluminum wires varies between layers due to mutual inductance rather than skin effect.

2.2.5 GMR of Stranded Conductors

The geometric mean radius (GMR) is the name given the quantity used in calculating the inductive reactance from the conductor dimensions. The GMR for a solid cylindrical nonmagnetic conductor with uniform current density is:

$$\text{GMR} = e^{-1/4} D_s / 2 \cong 0.7788\, R_s \qquad 2.2\text{-}4$$

Where:
D_s = strand diameter
R_s = strand radius

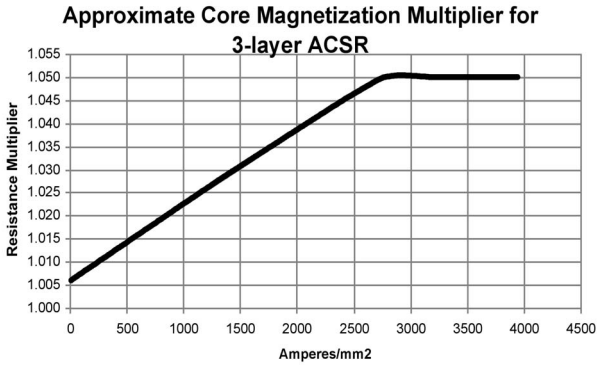


Figure 2.2-2 Core magnetization resistance multiplier for three-layer ACSR (Douglass).

The GMR of a composite conductor (Figure 2.2-3), such as ACSR and AAC, which consists of strands of equal diameter and conductivity regularly spaced in concentric layers, is calculated in the following:

For a single cylindrical conductor with uniform current density (dc, no skin effect), the GMR is

$$\text{GMR} = (e^{-\mu_r/4})r \qquad 2.2\text{-}5$$

Where:
r = radius of the conductor.
μ_r = relative permeability of the conductor (approximately equals 1 for aluminum and copper).
GMR $\cong$ 0.7788r for copper and aluminum

The GMR of transmission conductors is typically equal to between 75% and 80% of the conductor radius. Thus for a stranded conductor that is 28 mm in diameter, the GMR is typically about 21 to 22 mm. The exact value of GMR depends on the numbers of layers of aluminum strands and the presence or absence of a steel core. GMR values are included in the conductor tables of Appendix 2.1 and in Applet CC-4.

The calculation of the GMR for conductors where the strand diameters are sometimes unequal, as in expanded designs or in designs where the conductivity varies, is accomplished with the procedure outlined by Lewis and Tuttle (Lewis and Tuttle 1959).

2.2.6 Inductive and Capacitive Reactance "to One Meter (Foot)"

The positive sequence inductive reactance, X_1, of a three-phase transmission line is a function of both the properties of the individual conductors and the line geometry (as presented in Section 2.4). Many authors have traditionally split the equations for reactance into two parts, so the total reactance becomes the sum of two terms:

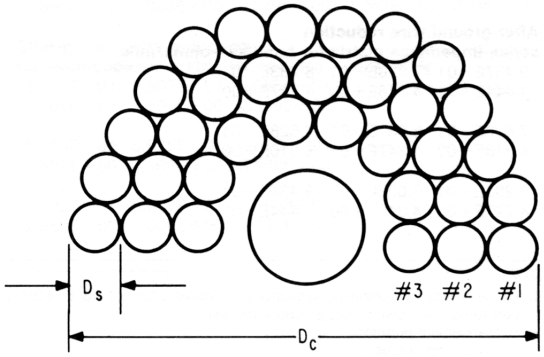


Figure 2.2-3 GMR diagram for an ACSR conductor.

- The reactance of the conductor itself, X_a, called the reactance to one meter in metric units and the reactance to one foot in English units. The reactance to one foot or one meter is a property of the individual conductor. The reactance to one foot is given in the conductor tables in Appendix 2.1.
- The spacing factor term X_d, as described in Section 2.4.

This division into two terms is possible because ln (A/B) = ln (A/1) + ln (1/B), where the number "1" represents 1 meter or 1 foot, depending on the dimensions employed.

A complication arises because different, but equivalent, forms of the equations have been used in different parts of the world. Both give identical answers, but superficially look different. The metric form uses the fundamental physical quantities ω and μ, the frequency, *f*, and the natural logarithm, ln. The English form is traditionally presented with a coefficient *k* that assumes a 60-Hz frequency and uses the logarithm to the base 10, log. Both forms of the equation are given because both are in common use in different parts of the world.

The metric form of the equation for inductive reactance at one-meter spacing in ohms per meter is:

$$X_a = 2\pi f \frac{\mu_0}{2\pi} \ln\left(\frac{1}{GMR}\right) \qquad 2.2\text{-}6$$

Where:
μ_0 = permeability of free space $4\pi \times 10^{-7}$ H/m.
f = frequency in Hz.
GMR = geometric mean radius of the conductor in m.
ln = natural logarithm.

The English form yields inductive reactance at one-foot spacing in ohms per mile as:

$$X_a = k \log\left(\frac{1}{GMR}\right) \qquad 2.2\text{-}7$$

Where:
k = 4.657×10^{-3} *f* = 0.2794 at 60 Hz.
f = frequency in Hz
GMR = geometric mean radius of the conductor in ft.
log = logarithm to the base 10.

The derivation of the positive sequence capacitive reactance follows the same pattern as that of the inductive reactance, allowing for the similar differences of form found in different parts of the world. The positive sequence capacitive reactance, X_{C1}, of a three-phase transmission is given as the sum of the reactance to one meter (foot) term *X*'a and the spacing factor term *X*'d, as described in Section 2.4.

The metric form of the capacitive reactance at 1-m spacing in ohm-meters is:

$$X'_a = \left(\frac{1}{2\pi f}\right) \bullet \left(\frac{1}{2\pi\varepsilon_0}\right) \bullet \ln\left(\frac{1}{r}\right) \qquad 2.2\text{-}8$$

Where:
ε_0 = permittivity of free space 8.854×10^{-12} F/m.
f = frequency in Hz.
r = radius of the conductor in m.
ln = natural logarithm.

In contrast to inductive reactance, where the conductor is characterized by GMR, for capacitive reactance the conductor is characterized by its spatial radius, *r*.

The English form of the capacitive reactance at 1-ft spacing in megohm-miles is:

$$X'_a = k' \log\left(\frac{1}{r}\right) \qquad 2.2\text{-}9$$

Where:
k' = $4.093/f = 0.06822$ at 60 Hz.
f = frequency in Hz.
r = radius of the conductor in ft.
log = logarithm to the base 10.

For background and further information, see one of the standard works.

2.2.7 Annealing of Aluminum Stranded Conductors

Normally overhead transmission lines are designed such that maximum conductor tension under heavy ice and wind loading does not exceed a certain percentage of the conductor's RBS. A significant reduction in the RBS can lead to a tensile failure during subsequent high ice and wind loading events. To avoid this, energized conductors are typically not allowed to operate at a high enough temperature for a long enough period of time to reduce their breaking strength by more than 10% over their expected lifetime.

The ASTM or IEC standards specify the minimum tensile strength of new aluminum and copper wires, which is the stress at which the wire breaks. At temperatures above 75°C, the tensile strength decreases with time. Even for moderately long exposures to temperatures as high as 300°C, however, the tensile strength of galvanized, aluminum-clad, or copper-clad steel wires is not reduced (though the galvanizing may deteriorate). Extended exposure of conductors with little or no steel reinforcing core to temperatures above 75°C can, therefore, lead to tensile failures during high ice and/or wind loading events.

Figure 2.2-4 shows typical tensile strength reduction data for 1350-H19 "EC" hard drawn aluminum wire (Aluminum Association 1989). In general, tensile strength reduction of aluminum wires at temperatures of less than 90°C is considered negligible. At 100°C, the tensile strength of the wire is reduced by 10% after 5000 hours and at 125°C, the tensile strength is reduced 10% after 250 hours.

When compared to copper, aluminum appears to anneal somewhat more slowly.

In applying these curves, the cumulative strength reduction for multiple exposures at the same conductor temperature may be found by simply adding up all the hours and calculating the residual strength. However, for multiple exposures at different conductor temperatures, the calculation process is more complex. To determine the cumulative strength reduction for a series of high-temperature exposures at different temperatures and times, all exposures must be expressed in equivalent time at the highest temperature before adding.

If the hard-drawn aluminum strand is raised to 125°C for 100 hours and then at a later time for 50 hours, then the strength reduction can be calculated for 150 hours at 125°C. With reference to Figure 2.2-4, the remaining strength is then approximately 91%. If the same conductor is raised to 125°C for 100 hours and then at a later time is raised to 150°C for 50 hours, then the following calculation must be performed: Again, with reference to Figure 2.2-4, the remaining strength after 100 hours at 125°C is approximately 93%. This is equivalent to 3 hours at 150°C. After the next 50 hours at 150°C, the remaining strength is equivalent to 53 hours at 150°C, or approximately 85%.

A similar but more accurate estimate of remaining strength can be obtained by using the formulas given in (Harvey 1972). Harvey's paper also considers 6201 aluminum alloy and the change in composite strength of various strandings of ACSR. As shown in his paper, conductors with a relatively large steel reinforcing core are less susceptible to annealing. For example, consider Table 2.2-5.

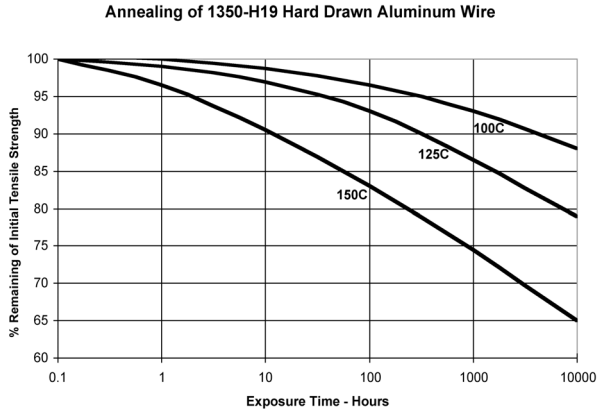


Figure 2.2-4 Annealing of 1350-H19 hard-drawn aluminum wire (Aluminum Association 1989).

The rate of loss of strength also depends on the amount of "cold work" imparted to the wires in drawing them to size from their 3/8-in. rod form. Aluminum wires drawn from rod produced by the Properzi continuous cast process exhibits slower annealing rates than wire drawn from "rolled" rod. Most conductors manufactured in the last 30 years have aluminum strands drawn from Properzi rod.

2.2.8 Sag Tension of Overhead Lines

In the design and maintenance of power transmission lines, the concern of primary importance is public safety. Other than designing the supporting structures such that they remain standing under even the most severe weather conditions, the safety of a line is essentially determined by the position of its energized conductors relative to people, buildings, and vehicles that are nearby. Maintaining minimum distances to nearby objects and people is primarily a matter of limiting the sag of the energized conductors under either high-mechanical load or high-temperature conditions.

In addition to making lines safe, other important constraints are the level of electric and magnetic fields produced (e.g., electric fields increase as the conductor gets closer to the ground), the maximum structure loads during occasional high wind and ice loads, and the maximum temperature at which the energized conductors are allowed to operate. Given standard "worst-case" rating weather conditions, the maximum allowable conductor temperature determines the thermal rating of an existing line.

Figure 2.2-5 is a basic sag-clearance diagram, which illustrates how minimum ground clearance must be maintained under both heavy loading and high-temperature events over the life of both new and re-rated transmission lines. The

Table 2.2-5 Reduction in Conductor Rated Strength (Due to Annealing of Aluminum Strands) as a Function of the Size of Steel Reinforcing Core. All Three Conductors Have an Aluminum Cross-sectional Area of 400 mm^2.

Conductor Type	% Steel by Area	Residual Strength after 1000 hrs@100°C (%)	Residual Strength after 100 hrs @150°C (%)	Residual Strength after 1000 hrs@ 150°C (%)
Arbutus AAC	0	97.7	82.5	75.6
Tern ACSR	6.5% [Type 7]	100	91.1	86.4
Drake ACSR	14.0% [Type 16]	100	98.6	96.0

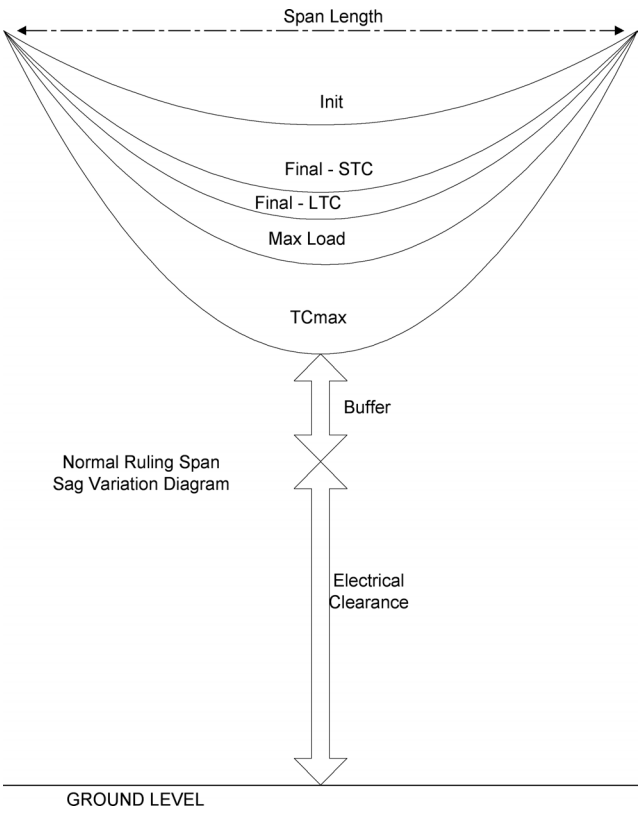


Figure 2.2-5 Sag diagram showing sags for various times and loading conditions.

figure shows ground clearance and line sags under normal, high ice/wind load, and high-temperature conditions for a ruling (or "equivalent") span. Note that the sum of the minimum ground clearance, the buffer, and the sag at maximum temperature is the minimum attachment height, which determines structure height and spacing. In a detailed line design that has many different spans, this sort of sag-clearance calculation must be developed for all spans (Varney 1927; Winkelman 1959).

Definitions of the labels in Figure 2.2-5 are as follows:

- **"Init"** is the initial installed unloaded (with no ice or wind) sag of the conductor. It is typically at a conductor temperature of 10°C to 25°C (50°F to 80°F). This is also typically referred to as the line "ruling span stringing sag."
- **"Final – STC"** is the final sag of the conductor at 15°C (60°F) after an ice/wind-loading event has occurred for a short time—typically an hour. STC stands for "short-time creep."
- **"Final – LTC"** is the final sag of the conductor at 15°C (60°F) after an extended period—typically 10 years—where the conductor simply persists at a conductor temperature of the order of 15°C (59°F) without ice or wind. "LTC" stands for "long-time creep," which occurs even if heavy ice and wind loads never occur.
- **"Max Load"** is the sag of the conductor during the specified maximum ice and wind loading at a reduced temperature—typically –18°C to 0°C (0°F to 32°F). Note that the sag prior to this event is normally assumed to be the Init sag, and the sag after this event is the Final – STC sag.
- **"TCmax"** is the sag of the conductor when its temperature is the maximum for which the line is designed—typically 50°C to 150°C. The final sag at 15°C (60°F), prior to this high-temperature event, is assumed to be the larger of the Final – STC and the Final – LTC sags.

Figure 2.2-5 shows typical behavior of transmission conductors where the sag under maximum ice and wind load conditions is less than that at the maximum temperature. For small or weak conductors experiencing heavy ice loads, this may not be true.

Note that the diagram illustrates the "snapshot" nature of traditional sag-tension calculations. The actual conductor sag position at any time in the life of the line depends on the actual mechanical and electrical load history of the line. If the high load event is more severe or persists for a longer time than assumed in determining the Max Load condition, then the corresponding sag at Max Load and the sag increase will be greater. The use of buffers is required because of such uncertainties.

For transmission conductors made primarily of aluminum strands under tension, sag never stops increasing with both time and high-loading events throughout the life of the line (Harvey 1972). That is, the sag at a given conductor temperature (e.g., 15.5°C, or 60°F) increases steadily over the years after construction. However, with moderate unloaded and loaded conductor tensions (typically 15% and 50% of rated strength), the rate of change in sag with each such event decreases over the life of the line. Thus, if a heavy ice load event occurs 10 years after installation, the permanent increase in sag is much smaller than if it occurred in the first 6 months after construction. Similarly, under everyday unloaded conditions, the rate of change in sag will decrease with time, over the life of the line.

2.2.9 Thermal Rating (Ampacity) of Bare Conductor

The electrical power conductors of overhead transmission lines carry relatively large electrical currents, and are self-supporting and energized at high voltage. As the current flowing through a conductor increases, the conductor's temperature increases, and it elongates. This elongation increases the sag of the conductor between support points, decreasing the clearance to people, ground, other conduc-

tors, buildings, and vehicles under the line. Beyond a certain "maximum allowable" sag, the line may flashover, resulting in either a power supply outage or injury to the public. If the conductor temperature remains high for an extended period of time, the strength of the conductor and tensioned connectors may decrease, resulting in mechanical failure during the next occurrence of ice or high wind loading.

Maximum Conductor Temperature

Modern transmission conductors are typically stranded from aluminum wires with a steel core added where increased strength is required. The temperature limit on all-aluminum or ACSR conductors is based on the maximum sag or maximum loss of strength in the aluminum. Temperature limits for normal ACSR conductors in use today range from 50°C to 150°C (122°F to 302°F). The temperature limit is normally selected at the time the line is designed. The higher this temperature, the higher the thermal capacity of the line, the higher maximum conductor sag, and the higher (or closer) the structures required to maintain ground clearance.

If aluminum or copper conductor temperatures remain high (above 95°C, or 203°F) for an extended period of time, the strength of the conductors and tensioned connectors may decrease, which eventually results in mechanical failure during the next ice or high wind occurrence. Generally, rating durations are kept short if maximum conductor temperatures are high (e.g., 4 hour maximum at 115°C (239°F) and 15 minutes at 125°C (257°F)).

Weather Conditions for Rating Calculation

Traditionally power utilities use fixed "worst-case" weather conditions in order to calculate (static) line ratings using heat balance methods (IEEE 738 1993b). The impact of changes in these weather parameters upon thermal line ratings depends on the specific rating situation. Consider an overhead line with 795 kcmil (402 mm^2 of aluminum), 26/7, "Drake" ACSR conductor, whose static rating is based upon a maximum allowable conductor temperature of 100°C with an air temperature of 40°C, full summer sun, and a wind blowing perpendicular to the conductor axis at 2 ft/sec. The static rating under these conditions is 1000 amp.

Clearly, if the current in this conductor is 1000 amp with the assumed weather conditions, the conductor temperature is 100°C. Table 2.2-6 shows how the conductor temperature is affected by small changes in weather conditions. For example, the conductor temperature drops to 92°C if there is no solar heating. The table also shows how the thermal rating (i.e., the current that yields a temperature of 100°C) changes with small changes in weather.

Note that, with the conductor at a reasonably high temperature and near "worst-case" heat transfer conditions, the overhead line rating and conductor temperature are very sensitive to wind direction, modestly sensitive to changes in wind speed and solar heating, and less affected by small changes in air temperature. Other minor factors are gradual changes in emissivity and absorptivity of the conductor with age and seasonal shifts in solar heating.

How Line Design Temperature Affects Line Ratings

Line design temperature is the maximum allowable conductor temperature for a particular line. As noted previously, for normal conventional ACSR, it varies from 50°C to 150°C. The impact of changes in the line design temperature upon thermal line ratings depends on the specific rating situation, but certain observations are possible.

Until the early 1970s, the National Electric Safety Code (National Electric Safety Code 1997) suggested that minimum electrical clearances were to be met at conductor temperatures up to 120°F (49°C). Line thermal capacity was typically calculated by conductor manufacturers for a conductor temperature of 75°C, a temperature sure to avoid possible annealing problems with aluminum and copper.

In the 1970s, the NESC changed and stated that the electrical clearances listed were to be met at "the maximum conductor temperature for which the line was designed to operate, if greater than 50°C, with no wind displacement" (excerpted from Rule 232.A.2). Thus the maximum allowable conductor temperature used in line rating calculations may vary from 50°C to 200°C according to available ground clearance and consistent with concerns about loss of tensile strength at temperatures above 90°C.

2.2.10 Transient Thermal Ratings

The need for increased thermal capacity in overhead lines is often driven by occasional sharp increases in load after

Table 2.2-6 Variation in Conductor Temperature and Rating with Weather Conditions (for 795 kcmil, 26/7, "Drake" ACSR conductor with a maximum allowable conductor temperature of 100°C, an air temperature of 40°C, full summer sun, and a wind blowing at 2fps perpendicular to the line)

Change in Assumed Weather Conditions	Line Rating @ 100°C (amperes)	Conductor Temperature at 1000 amps	
		(°C)	(°F)
None	1000	100	212
Air temp = 39°C	1010	99	210
No sun	1070	92	198
3ft/sec (0.91m/sec)	1090	90	194
Parallel wind	750	133	271

certain system contingencies. For example, an HV line might only reach high current levels after the loss of an EHV line or a critical generating facility. Since these occasions of high load occur infrequently and may persist for short time periods, it is often useful to consider transient thermal ratings for lines.

The temperature of an overhead power conductor is constantly changing in response to changes in electrical current and weather. With regard to transient rating calculations, however, weather parameters (wind speed and direction, ambient temperature, etc.) are assumed to remain constant; and any change in electrical current is limited to a step change from an initial current, I_i, to a final current, I_f, as illustrated in Figure 2.2-6 (IEEE 738 1993b).

Immediately prior to the current step change, the conductor is assumed to be in thermal equilibrium. That is, the sum of heat generation by ohmic losses and solar heating equals the heat loss by convection and radiation.

Immediately after the current step change, the conductor temperature is unchanged (as are the conductor resistance and the heat loss rate due to convection and radiation), but the rate of heat generation due to ohmic losses has suddenly increased. Therefore, the excess heat goes into heating the conductor to a higher temperature.

As time passes, the conductor temperature increases, yielding higher heat losses due to convection and radiation and somewhat higher ohmic heat generation due to the increased conductor resistance. After several "thermal time constants," the conductor temperature approaches its final steady-state temperature (T_f).

The transient thermal rating of an overhead line is dependent on the duration of the elevated current, the maximum temperature that the conductor is allowed to attain during the rating period, and on the starting temperature of the conductor. For example, with the Drake ACSR that was used for rating calculations previously, the transient ratings for various rating durations, maximum temperatures, and starting temperatures are shown in Table 2.2-7.

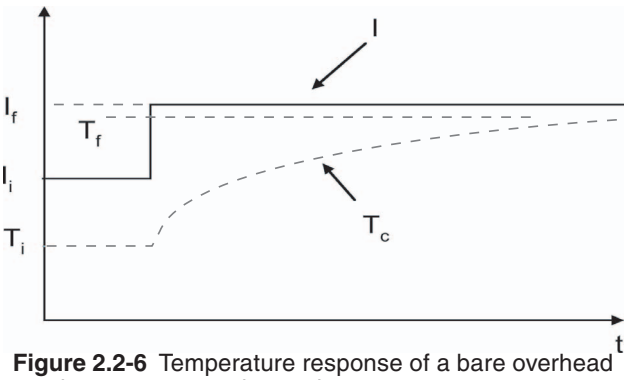


Figure 2.2-6 Temperature response of a bare overhead conductor to a step-change in current.

The advantage in using transient ratings is that the line can be loaded above its continuous rating without violating the constraints on sag clearance or annealing. The drawback is that the load must be reduced to the continuous rating or below within a short time (15 to 30 minutes). See, for example, references (Black and Rehberg 1985; Davidson et al. 1969).

2.3 CONDUCTOR SURFACE GRADIENTS

2.3.1 Introduction and Overview

The electric field at the surface of overhead transmission conductors (and other nearby conductive objects such as hardware, wood poles, trees, etc.) is an important quantity to the transmission engineer because it is the driving force behind all corona activity. As described extensively in Chapter 8, corona activity is the source of audible noise, radio noise, TV interference, ozone production, and some power loss. For HVDC lines, it also produces space charge. (Space charge is also produced by HVAC lines, but it tends to stay in the immediate vicinity of the conductors. There are claims that space charge has been measured downwind of HVAC lines, but the issue remains controversial.) In fact, the magnitude of this electric field is frequently used as a surrogate for the corona-related phenomena.

Because electric field is equal to the *gradient* of the space potential, i.e.,

$$\vec{E} = -\nabla V_{sp} \qquad 2.3\text{-}1$$

the electric field at the surface of conductors (and other objects) is referred to as the *surface gradient*. (The negative sign represents the fact that electric fields, by definition, point in the direction of decreasing potential.)

The exact, actual surface gradient around the periphery of a conductor is complicated by the non-uniformity of the surface caused by conductor stranding and by protrusions such as insects and raindrops. Also, corona itself affects the surface gradient (particularly on HVDC lines).

Table 2.2-7 Transient Ratings versus Rating Duration

Rating Duration (Min.)	Maximum Temperature (°C)	Starting Temperature (°C)	Rating (amps)
continuous	100	N/A	1040
60	100	50	1045
30	100	50	1090 (+ 4.8%)
15	100	50	1230 (+ 18.3%)
15	100	75	1135 (+ 9.1%)

Consequently, it has become standard practice to compute and specify the surface gradient of conductors as though they were smooth cylinders with diameters equal to their nominal diameters, and in a corona free environment. This is sometimes referred to as the *nominal surface gradient*.

The surface gradient of an overhead transmission conductor (or any conductive object) is perpendicular to the conductor everywhere over its surface. For a single conductor in free space (i.e., far from a ground plane), the surface gradient is constant around its periphery, as depicted in Figure 2.3-1.

However, the presence of a ground plane or other conductors causes the magnitude of the surface gradient to vary around the periphery (see Figure 2.3-2). Therefore, the surface gradient cannot be completely specified by a single number. The surface gradient varies around the periphery of a conductor with circular cross section, approximately

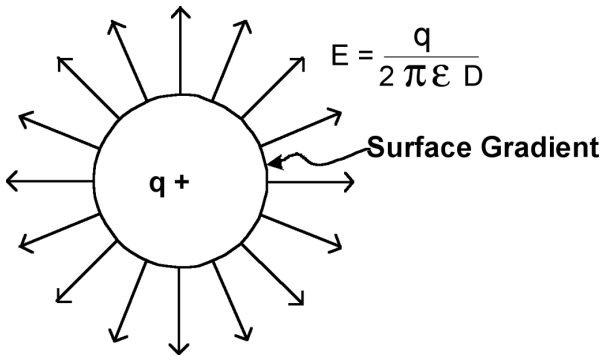


Figure 2.3-1 A positive line charge, q (C/m), and its resulting electric field lines. In general, D is the distance from the line charge, and at the conductor's surface, it is equal to the conductor's radius.

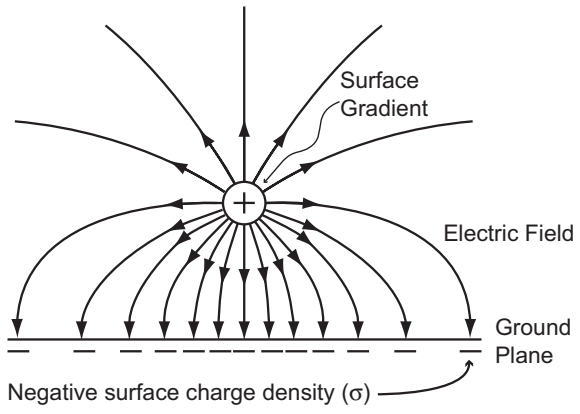


Figure 2.3-2 A positive line charge, q, above a ground plane. Note that a negative surface charge, σ, is induced on the ground plane, which causes the surface gradient to vary around the conductor's periphery.

following a sinusoidal relationship (see Equation 2.3-7). The average and the maximum surface gradients, and the point on the periphery where the surface gradient reaches its maximum value, fully characterize the electric field not only on the conductor surface but also in the immediate vicinity of the conductor where ac corona phenomena take place. The *maximum surface gradient* is the quantity chosen to characterize the corona effects of bundled conductors, together with diameters of the individual conductors, number of conductors in a bundle, and bundle diameter (see Subsection 2.3.4).

For a given conductor, the maximum surface gradient is simply the maximum value of the surface gradient around its periphery. However, for a bundle of two or more subconductors, the individual subconductors may have maximum surface gradients that differ from each other. This situation led an IEEE committee to define surface gradient terminology for bundled conductors as follows (IEEE Standard Definitions):

> *Maximum bundle gradient*: The highest of the maximum surface gradients of the individual subconductors in the bundle. For example, for a three-subconductor bundle with individual maximum surface gradients of 16.5, 16.9, and 17.0 kV/cm, the maximum bundle gradient is 17.0 kV/cm.
>
> *Average-maximum bundle gradient*: The simple arithmetic average of the individual maximum surface gradients of the individual subconductors in the bundle. For example, for a three-subconductor bundle with individual maximum surface gradients of 16.5, 16.9, and 17.0 kV/cm, the average-maximum bundle gradient is 16.8 kV/cm.

In most practical cases, the difference between the maximum bundle gradient and the average-maximum bundle gradient is about 1-4%. It was the practice at Project UHV and in previous editions of this reference book, and is the practice within IEEE, to use the average-maximum bundle gradient to characterize corona effects, and to simply use the term *maximum gradient*, *maximum surface gradient*, or just the term *gradient* in its place.

Various methods of calculating conductor gradients have been developed. An IEEE subcommittee has compared the results of several different methods and in general has found all to give comparable results (IEEE Subcommittee Report). The method discussed below is considered to be very accurate, and is the method used in previous editions of this reference book, in EPRI's Transmission Line Workstation (TLW), and in the applets.

2.3.2 Single Conductor

When a voltage, *V*, is applied to a single overhead conductor, it becomes charged due to the capacitance of the conductor to ground. This charge, *q*, is characterized by the charge-per-length (i.e., C/m) distributed along the conductor. For the commonly used 2-D approximation of the situation (infinitely long, straight conductor running parallel to a ground plane), *q* is constant along the conductor's length. The electric field at all points in space, including at the conductor's surface (the *surface gradient*), is due to this charge, and the induced charge on the ground plane below.

For calculation of the electric field, it can be assumed, to a very high degree of accuracy, that the charge *q* is distributed along a line running down the center of the conductor. Hence, the equivalent problem becomes that of a line charge above a ground plane. This problem is commonly treated in undergraduate textbooks on the subject (Reitz and Milford 1967).

The electric field at a distance *D* from a line charge *q* in free space is given by:

$$E = \frac{q}{2\pi\varepsilon D} \qquad 2.3\text{-}2$$

and is in a direction radially outward from the charge (ε is the permittivity of free space). Figure 2.3-1 shows a line charge *q* (assumed to be positive in polarity) running down the middle of a cylindrical surface coincident with that of the conductor it is representing, and its associated electric field lines emanating from that surface.

When a line charge resides above a ground plane, a surface charge density, σ (C/m^2), is induced on the plane below. The magnitude of the induced surface charge is greatest directly under the overhead line charge, and diminishes off to the sides. This surface charge is opposite in polarity to *q*. The electric field at all points in space is a vector superposition of the electric fields from *q* and from σ. The resulting electric field lines are depicted in Figure 2.3-2.

Solving for the numerical values of the charge densities *q* and σ, and then solving for the corresponding electric fields at points above the ground plane, is relatively difficult. However, a common method used to solve this problem is the *method of images* (Reitz and Milford 1967). In this method, the ground plane is conceptually replaced with a second line charge, -*q*, which is a "mirror image" of *q*. Because of the location of this image charge, every point on the ground plane is equidistant from a positive charge and a negative charge of equal magnitudes. Hence the potential on the plane remains zero, and is, therefore, still a "ground" plane. This concept is depicted in Figure 2.3-3.

As far as all points above the ground plane are concerned, the situations of Figure 2.3-2 and Figure 2.3-3 are identical. However, solving the two-line charge problem of Figure 2.3-3 is much simpler than solving the problem of Figure 2.3-2. Once the magnitude of the charge *q* is determined, Equation 2.3-2 can be used to determine the electric field at all points in space from each of the two charges.

The space potential, V_{sp}, at any point in space at distances D_1 and D_2 from charges *q* and –*q*, respectively, is given by:

$$V_{sp} = \frac{q}{2\pi\varepsilon}\ln\frac{D_2}{D_1} \qquad 2.3\text{-}3$$

If the charge q is placed in the center of the conductor, the points at the conductor surface are only approximately at the same potential. The approximation is acceptable when the conductor diameter is much smaller than the height above ground. In this case, applying Equation 2.3-3 to the surface of a real overhead conductor results in:

$$P = \frac{1}{2\pi\varepsilon}\ln\frac{4H}{D} \qquad 2.3\text{-}4$$

Where:

D = the conductor diameter.
H = height of the conductor above the ground plane (assumed to be large compared to *D*).
V = voltage applied to the conductor.

For a given problem, Equation 2.3-4 can be solved for the charge *q*, and Equation 2.3-2 can then be used to determine

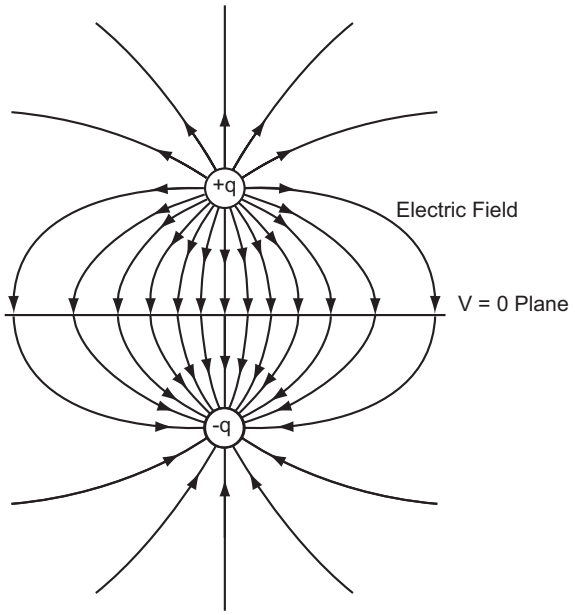


Figure 2.3-3 A positive line charge, *q*, its image, -*q*, and their resultant electric field lines.

the electric field at the conductor's surface—i.e., the surface gradient.

In addition, the ratio of voltage to charge is frequently referred to as the Maxwell potential coefficient, *P*. From Equation 2.3-4:

$$P = \frac{1}{2\pi\varepsilon}\ln\frac{4H}{D} \qquad 2.3\text{-}5$$

This variable has units of m/F, and its inverse is the capacitance-per-length of the conductor to ground (refer to Chapter 7 for greater detail).

As a simple example, consider the case of a single overhead conductor that is 3.42 cm in diameter, located 7.5 m above a level ground, and energized at a system voltage of 230 kV (132 kV to ground).

With Equation 2.3-5, the Maxwell potential coefficient is:

$$P = 1.219\times10^{11}\,\text{m/F}$$

Its inverse is:

$$1/P = 8.205\times10^{-12}\,\text{F/m}$$

This latter term represents the capacitance-per-length of the conductor to ground.

Using Equation 2.3-4 to determine the charge yields:

$$q = 1.09\times10^{-6}\,\text{C/m}$$

This charge is conceptually placed down the middle of the conductor. The magnitude of the electric field produced by this line charge, at a distance away equal to the radius of the conductor, represents the average electric field around the periphery of the conductor (i.e., the *average surface gradient*). With Equation 2.3-2, this average surface gradient is:

$$E_{AVG} = 11.46\ \text{kV/cm}$$

The electric field at any single point around the periphery of the conductor is due to the vector sum of the electric field due to the charge *q*, and its image *-q*. If the radius is much smaller than the height above ground, the contribution of the image charge may be neglected and the gradient may be considered the same all around the periphery. In reality, the surface gradient is maximum at the bottom of the conductor. To calculate the maximum gradient, the line charge must be placed not in the center of the conductor, but at a point just below the center such that the conductor surface under the action of the charge and its image becomes an equipotential. This point is a little below the center by a distance, *x*, such that $(2H\text{-}x)\cdot x = r^2$, (therefore, $x \approx r^2/2H$), where *r* is the conductor radius. This relationship is derived by applying Equation 2.3-6 to the top and bottom of the conductor.

For an example, consider the electric field at the very bottom of the conductor's surface, where the surface gradient is at its maximum around the conductor's periphery (i.e., the *maximum surface gradient*). The situation is illustrated in Figure 2.3-4. The net electric field is, according to Equation 2.3-2:

$$E_{MAX} = \frac{q}{2\pi\varepsilon(r-x)} + \frac{q}{2\pi\varepsilon(2h-r)} = 11.486\ \text{kV/cm}$$

The surface gradient around the periphery of the conductor can be obtained from Applet CC-1. This applet provides plots of surface gradient versus the angle θ (θ being measured counter clockwise from the right-side horizontal as shown in Figure 2.3-4). A corresponding plot of *E* (i.e., surface gradient) versus θ is shown in Figure 2.3-5. Note that the range on the vertical axis in Figure 2.3-5 is very small, and the sinusoidal variation is very small for this case. In some cases, particularly for individual subconductors of a bundle, the peak-to-peak variation can be much larger.

2.3.3 Multiple Conductors

The general method for calculating surface gradients for multiple conductors is similar to that above for a single conductor, although the mathematics becomes tedious and the need for a computer is obvious. The case of multiple conductors includes the conductors of multiple phases (including ground wires), as well as the individual subconductors of conductor bundles (i.e., the method applies to all the individual conductors for a given transmission corridor).

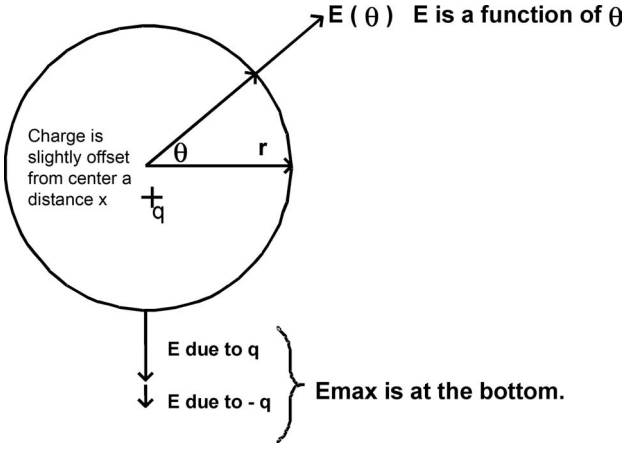


Figure 2.3-4 The surface gradient is a function of position around the conductor's periphery; for a single conductor above a ground plane, the maximum surface gradient is on the bottom.

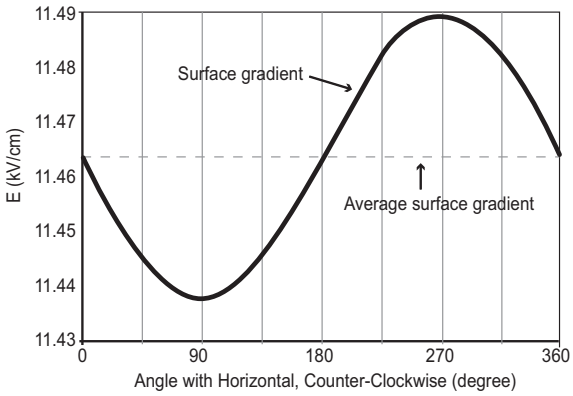


Figure 2.3-5 Surface gradient of a single conductor above a ground plane as a function of position, θ, around its periphery. The maximum surface gradient is at the bottom (θ= 270 degrees).

However, there is one important difference between the simple case of a single overhead conductor, and the case of multiple conductors. In the single-conductor case, a single image charge was required. But for the multiple-conductor case, each conductor requires the introduction of several image charges (this approach is referred to as the method of successive images).

To explain the method, an example is described below in some detail for the simple case of two conductors. The same method can be extended to include any number of conductors. However, it is useful at this point to digress a little to discuss the concept of equipotential surfaces for a pair of parallel line charges that are equal in magnitude and opposite in polarity.

It is a fact, commonly presented in textbooks, that the equipotential surfaces for a pair of parallel line charges, equal in magnitude and opposite in polarity, are cylindrical surfaces, as depicted in Figure 2.3-6 (Reitz and Milford 1967). This figure shows a positive line charge, q, parallel to a second line charge, $-q$, and a few of the resulting cylindrical equipotential surfaces (in fact, the ground plane midway between the two charges can be thought of as the surface of an equipotential cylinder infinite in diameter). The requirement for any of the equipotential surfaces is that the space potential calculated with Equation 2.3-3 remains constant over the surface, which requires that

$$D_1 / D_2 = \text{constant} \qquad 2.3\text{-}6$$

where D_1 and D_2 are the distances from the two line charges.

Each equipotential surface is cylindrical. If the distance between the charges is L, and the center of an equipotential surface is at a distance x from the charge $+q$, the following relations exist (in order to satisfy Equation 2.3-6) between the charge, the radius of the equipotential cylinder, r, and the cylinder potential, V.

$$x \cdot (L + x) = r^2 \qquad 2.3\text{-}6a$$

$$V = \frac{q}{2\pi\varepsilon} \ln \frac{r}{x} \qquad 2.3\text{-}6b$$

This fact is the reason why a line charge and its image can be used to represent an energized conductor for the single-conductor case above. The surface of such a conductor is an equipotential surface (as is the entire surface of any conductor), and it is cylindrical in shape. Therefore, the potential throughout space can be obtained by defining a pair of line charges (plus and minus q) such that the equipotential surface representing the conductor's surface is at the conductor's voltage. Also, it can be shown that the solution for the electric field throughout the region of concern is unique once the potentials at the surfaces of the conductor and ground plane are set (Jackson 1975).

However, when a second conductor is introduced, along with its image, the situation is altered. Now there are four line charges, and the surface of the first conductor is no longer an equipotential surface. However, the problem can

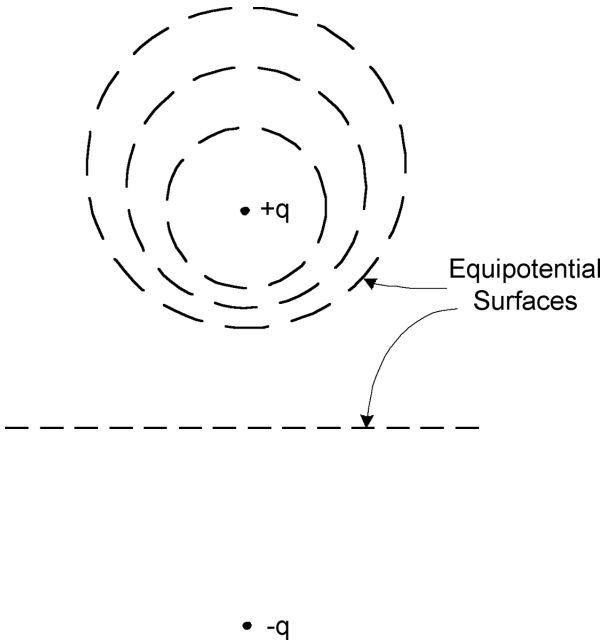


Figure 2.3-6 Two infinitely long parallel line charges of equal magnitude and opposite polarity, q and $-q$, and their resultant cylindrical equipotential surfaces.

be solved using the method of successive images (Maruvada and Janischewskyj 1969). The lack of equipotentiality can be remedied by adding within the surface of the first conductor two more "second-order" images that are equal in magnitude and opposite in polarity to the line charge representing the second conductor and its image, and located such that pairs of line charges hold the surface at equipotential by satisfying Equation 2.3-6. An example of this method is illustrated in Figure 2.3-7, and explained below.

Referring to Figure 2.3-7, two energized parallel conductors, with surfaces labeled S1 and S2, are placed above a ground plane. The linear charge densities along these conductors, q_1 and q_2, respectively, are placed at distances x_1 and x_2 below the centers of the conductors. Their "first-order" images, $-q_1'$ and $-q_2'$, are placed at the respective mirror locations below the ground plane.

The pair of charges, q_1 and $-q_1'$, will cause the surface S1 to be an equipotential. However, the pair of charges, q_2 and $-q_2'$, does not create an equipotential on surface S1. Hence, to maintain the equipotentiality of surface S1, two "second-order" image charges, $-q_2''$ and q_2'', must be introduced. Note that this procedure is allowed because it is consistent with reality. After all, q_2 and its image do exist, and S1 is an equipotential, therefore, q_2 and $-q_2'$, must have images, $-q_2''$ and q_2'', within S1. The positions of the second-order images are such as to satisfy Equation 2.3-6.

Note that the introduction of $-q_2''$ and q_2'' does not change the net charge on S1, since they are equal in magnitude but opposite in polarity, nor does it change the average gradient on the surface S1. It will, however, change the maximum surface gradient on S1 and will not maintain the ground plane and S2 as equipotentials. In order to maintain the ground plane as an equipotential line, images of $-q_2''$ and q_2'' must be placed below the plane. In order to maintain S2 as an equipotential, line images of $-q_2''$ and q_2'' must be placed inside S2. These third-order images will increase the accuracy. Higher-order images may be introduced, and the process can be carried out until the error in the definition of equipotential surfaces becomes negligible. In practice, consideration of second-order images is amply sufficient for transmission-line configurations where the conductors' diameters are significantly smaller than their spacings. This limitation should be considered if

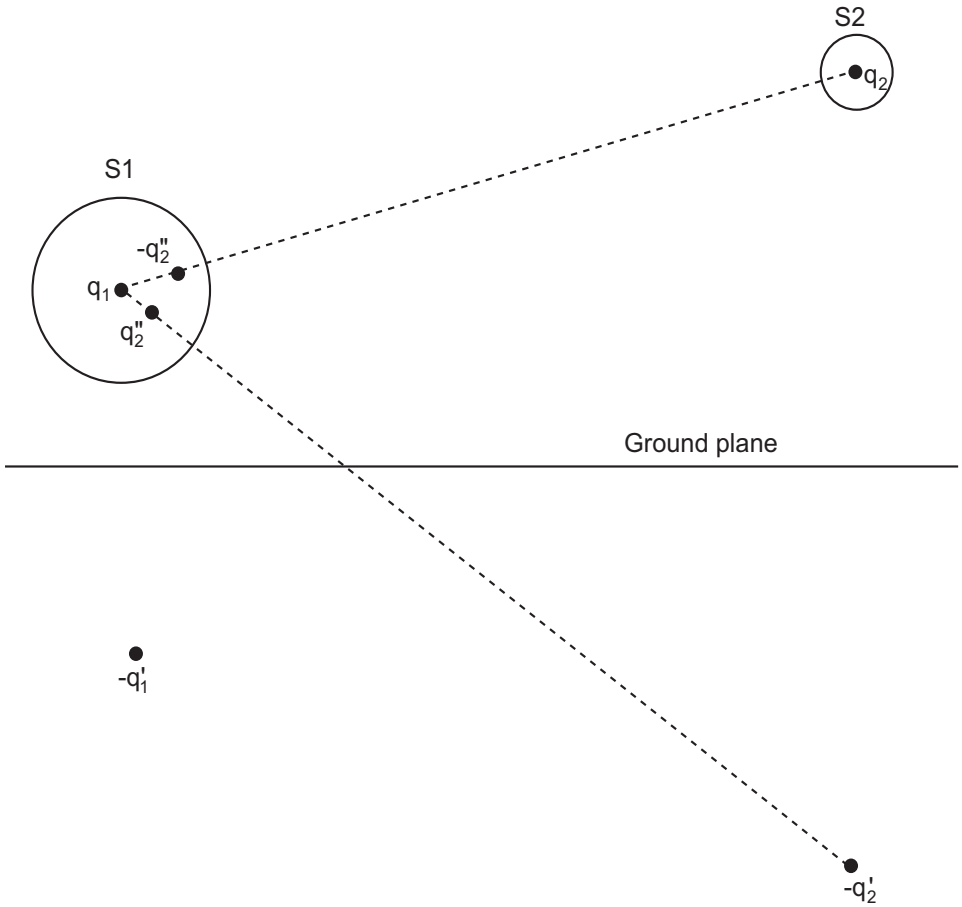


Figure 2.3-7 Two parallel conductors above a ground plane, with surfaces S1 and S2, and all the line charges used to calculate the surface gradient at all points around the periphery of S1.

this technique is applied to unusual conductor configurations with very small spacings.

To summarize, the charge pairs, (q_1, $-q_1'$), (q_2, $-q_2''$), and ($-q_2'$, q_2'') each produce an equipotential on the surface S1. Also, the position of all the images must be such that Equation 2.3-6 is satisfied (can be easily done by applying Equation 2.3-6 to opposite sides of the equipotential cylinder).

The entire procedure outlined above for S1 also holds for S2. In fact, this procedure is extended to include all conductors that may reside within a transmission corridor.

These line charges are conceptual constructs; however, they do represent the capacitive charge that is distributed on the surface of conductors. In the example of Figure 2.3-7, the line charge q_1 represents the magnitude of the capacitive charge and is solely responsible for the average surface gradient around S1. The contributions from all the other charges represent the nonuniform distribution of charge (and, therefore, nonuniform surface gradient) around the periphery of S1 due to the presence of the ground plane and other conductors.

2.3.4 Conductor Bundling

The term *conductor bundle* (sometimes simply referred to as *bundle*) is used above and elsewhere throughout this reference book. Conductor bundling is a common technique used by transmission-line designers to control certain performance parameters, especially for higher voltage lines. A conductor bundle is an assembly of two or more conductors used for a single phase of an overhead transmission line, employing spacers to maintain a predetermined configuration. The individual conductors are called subconductors. Figure 2.3-8 shows a photo of a 500-kV line utilizing conductor bundles of four subconductors each.

Using a conductor bundle increases the effective size of a transmission line's phase without having to use a single larger conductor. A larger phase conductor offers several advantages, along with some obvious disadvantages (cost, weight, wind and ice loading, etc.). These advantages include:

- Greater surge impedance loading (SIL)
- Greater current-carrying capacity
- Lower surface gradient

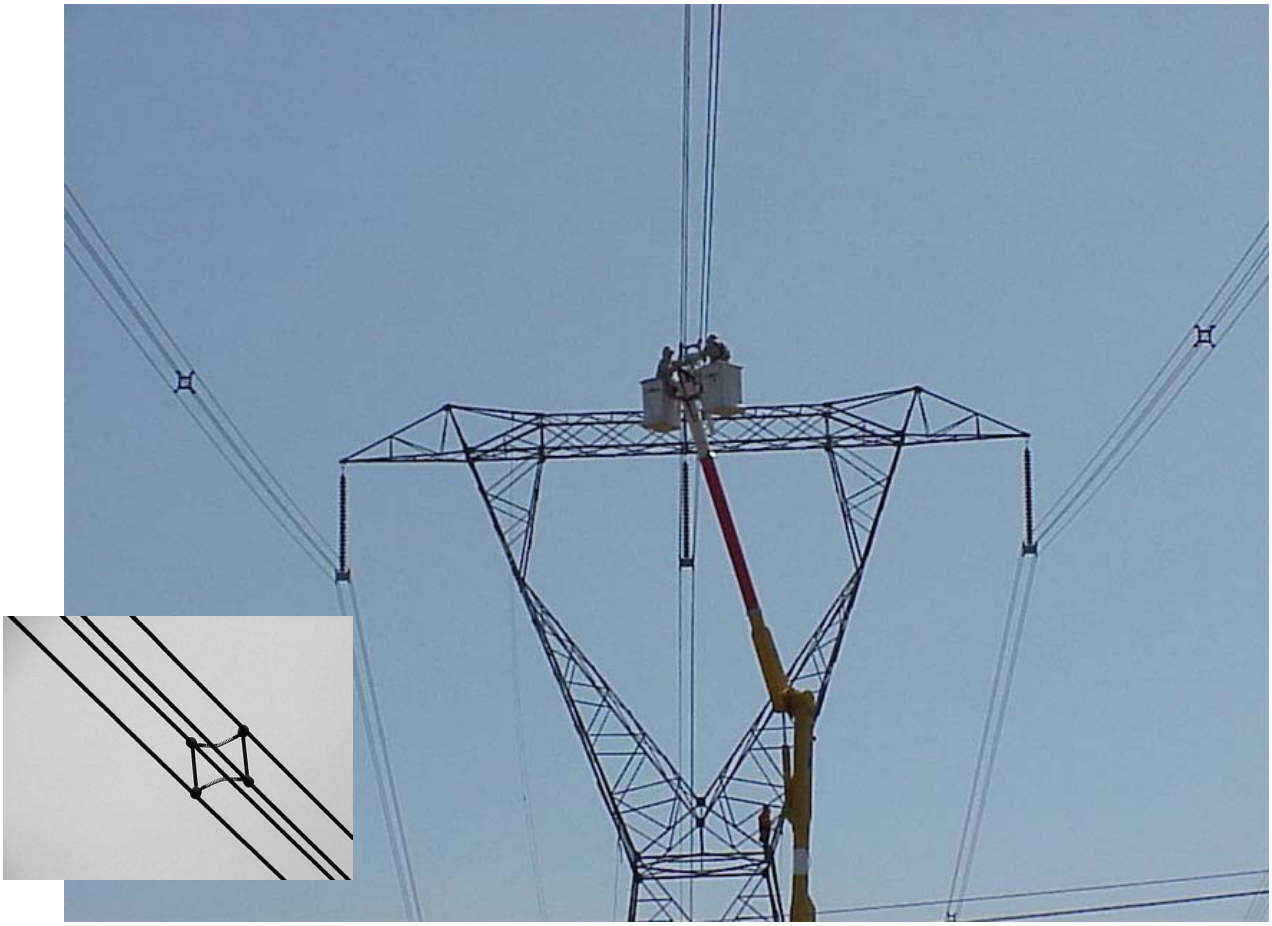


Figure 2.3-8 500-kV line with three four-subconductor bundles (and inset).

Employing conductor bundles can be an effective means for maximizing the advantages relative to the disadvantages, including surface gradients, which is the focus here.

As described above, the subconductors of a conductor bundle each have their own individual surface gradients, which vary around their periphery with the following sinusoidal relationship:

$$E(\theta) = E_{av}\left[1 + \frac{d}{d_b}(n-1)\cos(\theta)\right] \qquad 2.3\text{-}7$$

Where:

E_{av} = average subconductor surface gradient (given by Equation 2.3-2).
d = subconductor diameter.
d_b = bundle diameter (diameter of an imaginary circle on which the subconductors lie).
n = number of subconductors.
θ = angle as defined in Figure 2.3-9.

From Equation 2.3-7, it can be seen that the maximum surface gradient around a subconductor is at $\theta = 0$.

It is an interesting fact that, everything else being the same, the surface gradient depends only on the outside diameter of a conductor (a result deduced from Equations 2.3-2 and 2.3-4). Therefore, a hollow pipe or a solid pipe of the same diameter would have the same surface gradient. Conductor bundling is a useful method for increasing the effective size of a transmission line's phase without increasing the amount of conductor material required. Another tool that has been used in some rare cases is the so-called air-expanded conductor (see Figure 2.3-10). In this case, the diameter of a conductor is increased by leaving voids inside.

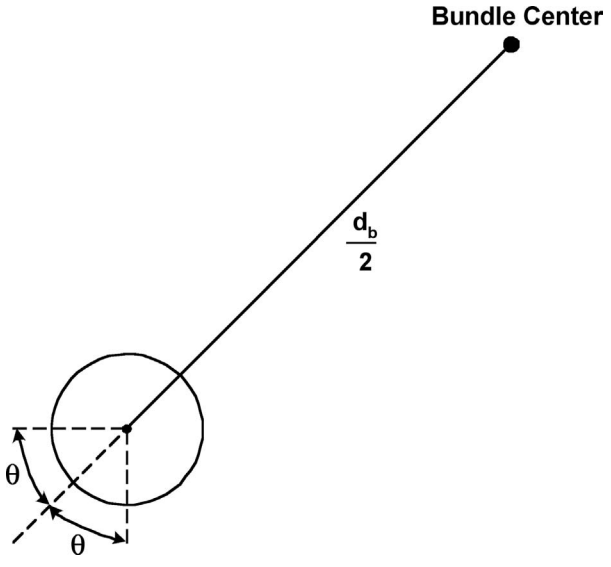


Figure 2.3-9 Definition of terms for a subconductor of a conductor bundle.

2.3.5 Toroidal Shielding Electrodes (Corona Rings)

The analysis of conductor gradients to this point has been limited to collections of long, parallel conductors over a ground plane. At the ends of these conductors, and at the ends of bushings and other station equipment, electrodes in the shape of toroids are often used to lower the surface gradient there. Because these "ends" are relatively "pointed," surface gradients there would be elevated and corona may result. As such, these toroidal electrodes are commonly referred to as corona rings. Figures 2.3-11 and 2.3-12 show photographs of corona rings on station equipment and conductor bundles, respectively.

Although these devices are used to prevent corona on conductors, it is possible for them to be configured such that they experience corona themselves due to their surface



Figure 2.3-10 An air-expanded conductor. This can be used to increase the outside diameter of a conductor without increasing its weight.



Figure 2.3-11 Toroidal corona rings on station equipment.

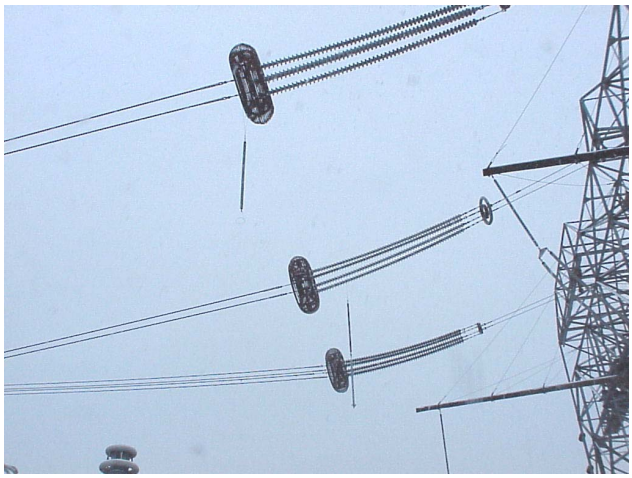


Figure 2.3-12 Toroidal corona rings at the ends of conductor bundles.

gradients. The surface gradient of a toroidal corona ring is characterized by the maximum value on its surface. The maximum surface gradient depends on the voltage applied to the toroid, its size, and its position in space with respect to other objects. Its size is specified by its inner and outer diameters, and its position in space is specified by the location of its center and the orientation of its axis.

Applet CC-3 is for computing the maximum surface gradients on toroids (as single numbers) and other simple objects. Refer to Chapter 8 for discussions on the evaluation of corona performance based on maximum surface gradients.

2.3.6 Variation of Surface Gradient with Design Parameters—Applets and Examples

While the theoretical foundation to calculate surface gradients is quite simple, the need for computer programs can be appreciated. Four applets are included with the reference book to help the user evaluate surface gradients. These applets are named CC-1, CC-2, CC-3, and CC-6. Below are brief descriptions of each of these applets, including examples. The purpose here is not only to introduce the reader to the applets, but also to help the reader understand some of the relationships between surface gradients and transmission-line design parameters.

Applet CC-1: Conductor Surface Gradients (2D)

Applet CC-1 provides the surface gradients of all the conductors (and subconductors) within a transmission corridor, and presents the results in tabular and graphical forms. The graphs are plots of surface gradient versus angle. The angle is defined counterclockwise from the right-side horizontal (see Figure 2.3-4). The conductors can be lone, or part of a bundle. The calculations are performed using the 2D approximation that the conductors are straight, infinitely long, and parallel to each other and the ground plane.

Consider the simple case of a three-phase 230-kV transmission line with single-phase conductors 3.42 cm in diameter, phase spacings of 4.5 m, and a height above ground of 16 m. Figure 2.3-13 shows the graphical result for the center phase conductor provided by Applet CC-1.

This graph clearly shows the sinusoidal nature of the surface gradient around the outside perimeter of the conductor (although the variation is typically very small for single conductor phases). It can be seen that the maximum surface gradient is 14.298 kV/cm, and occurs at the bottom of the conductor, and the minimum surface gradient is 14.268 kV/cm at the top of the conductor. Every conductor or subconductor within a transmission corridor will have its own surface gradient characteristics; however, they all are sinusoidal around the conductor's perimeter.

Applet CC-2: Conductor Surface Gradients (3D)

The surface gradient not only varies around the periphery of a conductor, but it also varies along the length of a conductor due to change in its elevation, change in terrain, change in relative position to other conductors, and the presence of objects. Applet CC-2 lets the user compute and plot the surface gradient (maximum and average) along its length. This applet accepts line geometry, voltage, objects, and terrain variation, and will provide surface gradients as a function of longitudinal distance down the line.

Applet CC-6: Sensitivity Analysis

This applet *accepts base case number*, and the *parameter to be varied*, and will produce a plot of *surface gradient* versus *varied parameter*. Parameters that can be varied include conductor (or subconductor) diameter, phase spacing, and conductor heights above ground. Below are graphical examples for the same 230-kV base case as described above for Applet CC-1.

Figure 2.3-14 shows how the surface gradient of the example varies with diameter of the conductors. It is interesting

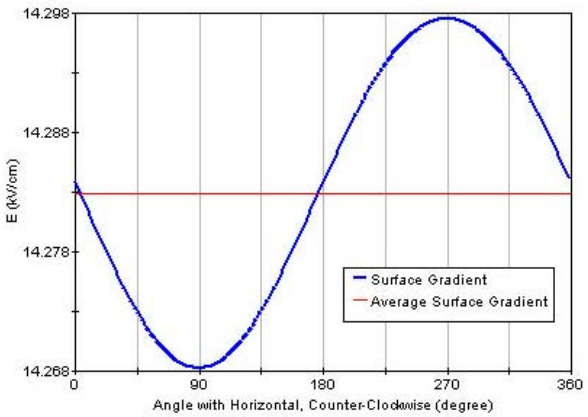


Figure 2.3-13 Plot of surface gradient around the outside perimeter of a conductor, as provided by Applet CC-1.

to note that with a greater size conductor, the net charge on the conductor increases (see Equation 2.3-4) and, therefore, the electric field on the ground increases, but the surface gradient decreases.

Figure 2.3-15 shows how surface gradient of the example varies with phase spacing. As the phase spacing increases, the surface gradient decreases. Note that this is not true if the phases are of the same phase, such as in a double-circuit case.

Applet CC-3: Surface Gradient on Corona Toroidal Shields

Applet CC-3 computes the maximum surface gradient, as a single number, for toroids (and other simple objects). A toroid is specified by its voltage, its inner and outer diameters, the location of its center, and the orientation of its axis (refer to Figure 2.3-16). Refer to Chapter 8 for discussions on the acceptable levels of surface gradient for corona performance.

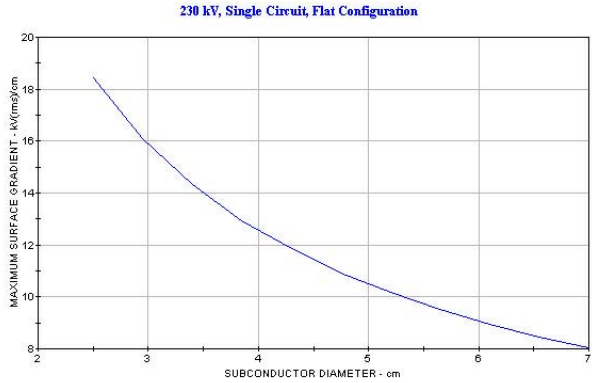


Figure 2.3-14 Plot of surface gradient versus conductor diameter as provided by CC-6.

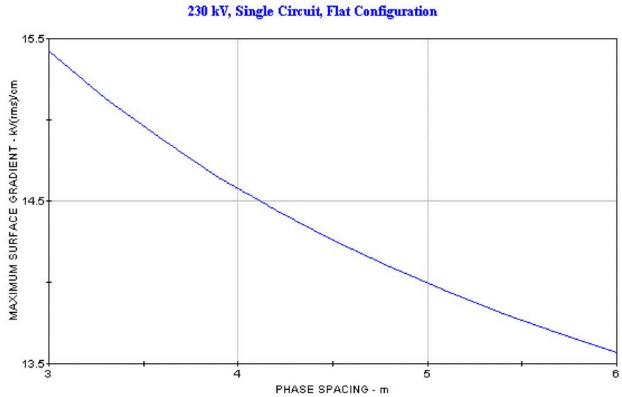


Figure 2.3-15 Plot of surface gradient versus phase spacing as provided by CC-6.

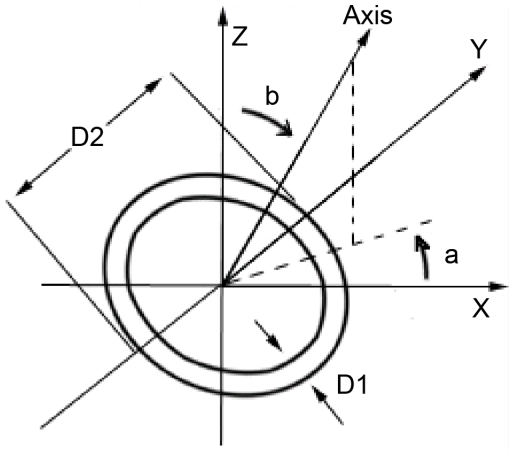


Figure 2.3-16 Depiction of a toroidal corona shield in Applet CC-3.

2.4 BASIC TRANSMISSION LINE IMPEDANCE AND ADMITTANCE PARAMETERS

2.4.1 Introduction

Knowledge of impedance and admittance parameters of transmission lines is essential for power system studies such as power flow, stability and fault investigations. These studies generally rely on a lumped parameter pi equivalent circuit representation for short lines, as given in Figure 2.4-1, where R represents conductor resistance and X_L represents series inductive reactance. Half of the line shunt capacitance C is placed on each side of the circuit, or $2X_C$ on each side.

A complete impedance representation of a three-phase power transmission line requires 3 x 3 complex matrices of self and mutual series and shunt impedances. This level of detail is not necessary for many system analysis purposes. In order to simplify the analytical representation, a matrix transformation has been developed to transform the phase impedances into "symmetrical component" impedances, called positive sequence, negative sequence, and zero sequence. Each sequence network is a single-phase circuit

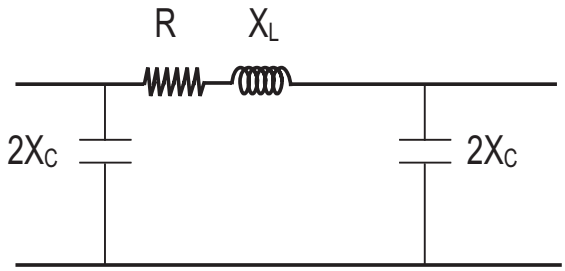


Figure 2.4-1 Pi equivalent circuit for transmission line.

representing certain aspects of the system behavior. Positive sequence values represent the normal steady-state operation of the power system, and are adequate by themselves for many studies when it is sufficient to consider the line to be in balanced, steady-state, three-phase operation. This section presents a brief overview of positive sequence inductive and capacitive reactance of transmission lines. Because balanced phase currents sum to zero, earth return effects are usually negligible in a positive sequence analysis. For a detailed exposition of symmetrical components, see one of the standard texts (Gross 1979; El-Hawry 1983; Grainger and Stevenson 1994).

In order to analyze cases of unbalanced construction or operation, it is usually necessary to know the zero sequence impedance and admittance in addition to the positive sequence. The zero sequence impedance includes the effects of the current return path in the earth. The negative sequence impedance of a passive element, such as a transmission line, is equal to the positive sequence impedance. For some purposes, either a complete matrix of self and mutual phase inductive and capacitive impedances, or a complete matrix of self and mutual sequence inductive and capacitive impedances is required. These additional terms in the inductive reactance matrix include the effects of conducting earth and are addressed in Section 2.5. Ground effects and conductor skin effects are frequency-sensitive. Thus, when knowledge of line parameters for surge propagation or other transient studies is required, it is necessary to determine how the impedance or admittance elements vary with frequency.

Applet CC-5 contains calculations for phase and sequence inductive and capacitive reactances. This section presents a hand calculation method for positive sequence inductive and capacitive reactance for transmission lines with symmetrical phase conductor bundles. Impedances of transmission lines with asymmetrical phase conductor bundles can be calculated with Applet CC-5.

2.4.2 Positive Sequence Inductive Reactance

The positive sequence inductive reactance X_1 of a three-phase transmission line is customarily given as the sum of the reactance-to-one-meter (foot) term X_a and the spacing factor term X_d. The "one-meter" and "one-foot" terms were defined in Section 2.2.6.

The relation between the one-meter (foot) and spacing factor terms is given in Equations 2.4-1 through 2.4-3.

$$X_1 = k \log (\text{GMD} / \text{GMR}) \qquad 2.4\text{-}1$$

Expanding Equation 2.4-1 gives

$$X_1 = k \log (\text{GMD}) + k \log (1 / \text{GMR}) \qquad 2.4\text{-}2$$

$$X_1 = X_d + X_a \qquad 2.4\text{-}3$$

$$X_d = k \log (\text{GMD}) \qquad 2.4\text{-}4$$

$$X_a = k \log (1 / \text{GMR}) \qquad 2.4\text{-}5$$

where in SI units:

k = $2.895 \bullet 10^{-6} f = .0001737$ at 60 Hz.
f = frequency in Hertz.
GMD = geometric mean distance between the phase conductor bundles in meters (Equation 2.4-6).
GMR = geometric mean radius of the phase conductor bundle in meters from Equations 2.4-9 and 2.4-11 for single or bundled conductors.
X_d = inductive reactance spacing factor in ohms per meter (Equation 2.4-4 and Table 2.4-1).
X_a = inductive reactance at one-foot spacing in ohms per meter (Equation (2.4-5).

In English units for use with the conductor tables:

k = $4.657 * 10^{-3} f = 0.2794$ at 60 Hz.
f = frequency in Hertz.
GMD = geometric mean distance between the phase conductor bundles in feet (Equation 2.4-6).
GMR = geometric mean radius of the phase conductor bundle in feet from conductor data tables or Equations 2.4-9 and 2.4-11 for single or bundled conductors.
X_d = inductive reactance spacing factor in ohms per mile (Equation 2.4-4 and Table 2.4-1).
X_a = inductive reactance at one-foot spacing in ohms per mile (Equation 2.3-5).

The geometric mean distance (GMD) is the geometric mean of the distances between the phase conductor bundles

$$\text{GMD} = \sqrt[3]{D_{12} D_{23} D_{31}} \qquad 2.4\text{-}6$$

where D_{12}, D_{23}, and D_{31} are the distances between centers of the three-phase bundles of a three-phase circuit. X_d can then be expanded as:

$$\begin{aligned} X_d &= k \log (\text{GMD}) \\ &= (1/3)(k \log D_{12} + k \log D_{23} + k \log D_{31}) \end{aligned} \qquad 2.4\text{-}7$$

The reactance to one meter (foot) spacing X_a is:

$$X_a = k \log (1 / \text{GMR}) \qquad 2.4\text{-}8$$

where the geometric mean radius (GMR) is the geometric mean radius of the phase conductor bundle. For a single conductor per phase, GMR is given in the conductor data in the tables in Appendix 2.1. For a single cylindrical conductor with uniform current density (dc, no skin effect), the GMR is:

$$GMR = (e^{-\mu_r/4})r \qquad 2.4\text{-}9$$

Where:

r = radius of the conductor.

μ_r = relative permeability of the conductor (approximately equals 1 for aluminum and copper).

$$\text{GMR} \cong 0.7788\, r \quad \text{for copper and aluminum} \qquad 2.4\text{-}10$$

For a symmetrically bundled conductor:

$$\text{GMR}_B \cong [n(\text{GMR}_C)\, r_b^{(n-1)}]^{1/n} \qquad 2.4\text{-}11$$

Where:

n = number of subconductors per phase.

GMR_B = geometric mean radius of the conductor bundle.

GMR_C = geometric mean radius of each subconductor.

r_b = bundle radius.

When the bundle size is described by bundle spacing (the distance between adjacent subconductors of a symmetrical bundle) then:

$$r_b = s / \left[2\sin(\pi / n)\right] \text{ when } n > 1 \qquad 2.4\text{-}12$$

$$r_b = 0 \quad 0^0 = 1 \text{ when } n = 1 \qquad 2.4\text{-}13$$

s = bundle spacing.

Table 2.4-3 shows the effect of conductor bundling on X_a, and consequently on the line series inductive reactance for the same phase geometry (same X_d for each case). For approximately the same total cross section area of aluminum in the conductor bundle, dividing up the aluminum into a greater number of smaller subconductors decreases the line series reactance. This has been a factor in the decision to use a larger number of subconductors per phase in designing long transmission lines.

Conductor resistance from the conductor data tables is vectorially added to the inductive reactance to give the complete positive sequence series impedance.

Table 2.4-1 Inductive Reactance Spacing Factor X_d, at 60 Hz (Ohms per Mile)

ft	0.0	1.0	2.0	3.0	4.0	5.0	6.0	7.0	8.0	9.0
0	-∞	0.0000	0.0841	0.1333	0.1682	0.1953	0.2174	0.2361	0.2523	0.2666
10	0.2794	0.2910	0.3015	0.3112	0.3202	0.3286	0.3364	0.3438	0.3507	0.3573
20	0.3635	0.3694	0.3751	0.3805	0.3856	0.3906	0.3953	0.3999	0.4043	0.4086
30	0.4127	0.4167	0.4205	0.4243	0.4279	0.4314	0.4348	0.4382	0.4414	0.4445
40	0.4476	0.4506	0.4535	0.4564	0.4592	0.4619	0.4646	0.4672	0.4697	0.4722
50	0.4747	0.4771	0.4795	0.4818	0.4840	0.4863	0.4884	0.4906	0.4927	0.4948

Table 2.4-2 Shunt Capacitive Reactance Spacing Factor, X'_d, at 60 Hz (Megohm-Miles)

ft	0.0	1.0	2.0	3.0	4.0	5.0	6.0	7.0	8.0	9.0
0	—	0.0000	0.0205	0.0325	0.0411	0.0477	0.0531	0.0577	0.0616	0.0651
10	0.0682	0.0710	0.0736	0.0760	0.0782	0.0802	0.0821	0.0839	0.0856	0.0872
20	0.0888	0.0902	0.0916	0.0929	0.0942	0.0954	0.0965	0.0976	0.0987	0.0998
30	0.1008	0.1017	0.1027	0.1036	0.1045	0.1053	0.1062	0.1070	0.1078	0.1085
40	0.1093	0.1100	0.1107	0.1114	0.1121	0.1128	0.1134	0.1141	0.1147	0.1153
50	0.1159	0.1165	0.1171	0.1176	0.1182	0.1187	0.1193	0.1198	0.1203	0.1208

Table 2.4-3 Effect of Bundling on Inductive Reactance

No. of Conductors	Total (kcmil)	Conductor Code Name	Bundle Spacing (in.)	Bundle Diameter (in.)	X_a (ohms per mile)	X_d (ohms per mile)	X_L (ohms per mile)	X_L (per unit)
1	2515	Joree	—	—	0.337	0.464	0.801	1.00
2	2544	Pheasant	18	18	0.161	0.464	0.625	0.78
3	2625	Crane	18	20.5	0.099	0.464	0.563	0.70
4	2544	Grosbeak	18	25.5	0.051	0.464	0.515	0.64
6	2392	Ibis	—	36	-0.004	0.464	0.460	0.57
8	2400	Ostrich	—	40	-0.091	0.464	0.373	0.47
12	2539	Penguin	—	50	-0.154	0.464	0.310	0.39
16	2683	Pigeon	—	60	-0.182	0.464	0.282	0.35

Example:
Consider the 345-kV single-circuit flat configuration from the list of cases given in Appendix 2-1. Data for the line are:

- Twin 954 kcmil Cardinal subconductors per phase
- Flat configuration, 7.5 m phase spacing, 12.5 m average conductor height

This simplified calculation ignores the shield wires, which have a negligible effect on positive sequence inductive reactance.

The first step is to calculate the geometric mean distance of the three phases from Equation 2.4-4. $D_{12} = D_{23} = 24.6$ ft and $D_{31} = 49.2$ ft, giving GMD from Equation 2.4-4 = 31.015 ft. From Equation 2.4-5 $X_d = 0.4167$ Ω/mile.

Each phase consists of a bundle of twin Cardinal subconductors of 1.196 in. diameter. From Table A2.1-1 in Appendix 2.1, GMR_C for Cardinal is 0.0404 ft. For a two-subconductor bundle of bundle radius 0.75 ft, the bundle GMR is given by $GMR_B = [(2)(0.0404)(.75)]^{1/2} = 0.2462$ ft. From Equation 2.4-7, $Xa = 0.1701$ Ω/mile.

The positive sequence reactance is given by Equation 2.4-3: $X_1 = X_d + X_a = 0.5868$ Ω/mile.

Applet CC-5 gives the same positive sequence reactance.

2.4.3 Positive Sequence Capacitive Reactance

A development parallel to that for inductive reactance can be given for positive sequence capacitive reactance of a three-phase transmission line is given by:

$$X_c = k' \log (GMD / r) = k' \log (GMD) + k' \log (1/r) = X'_d + X'_a \quad 2.4\text{-}14$$

where in SI units:
k' = $6.588 \bullet 10^9 / f = 109.8 \bullet 10^6$ at 60 Hz.
f = frequency in Hertz.
GMD = geometric mean distance in meters (same value as for inductive reactance).
r = effective radius of the conductor in meters.
X_C is in ohm-meters.

In English units for use with the conductor tables:
k' = $4.093/f = 0.06822$ at 60 Hz.
f = frequency in Hertz.
GMD = geometric mean distance in feet (same value as for inductive reactance)
r = effective radius of the conductor in feet.
X_C is in megohm-miles.

The capacitive reactance spacing factor (values are given in Table 2.4-2):

$$X'_d = k' \log (GMD) \quad 2.4\text{-}15$$

The capacitive reactance at one-meter (foot) spacing is:

$$X'_a = k' \log (1/r) \quad 2.4\text{-}16$$

The effective radius, r_{eq}, for symmetrically bundled conductors is:

$$r_{eq} = (n r r_b^{n-1})^{1/n}$$

Where:
n = number of subconductors per phase.
r = radius of each subconductor.
r_b = bundle radius.

When the bundle size is described by the bundle spacing (the distance between adjacent subconductors of a symmetrical bundle), then;

$$r_b = s / \left[2 \sin(\pi / n)\right] \text{ when n } > 1 \quad 2.4\text{-}17$$

$$r_b = 0 \quad 0^0 = 1 \quad \text{when n} = 1 \quad 2.4\text{-}18$$

s = bundle spacing.

Table 2.4-4 shows the effect of conductor bundling on X'_a, and consequently on the line shunt capacitive reactance for the same phase geometry (same X'_d for each case). For approximately the same total cross-section area of alumi-

Table 2.4-4 Effect of Bundling on Capacitive Reactance

No. of Conductors	Total (kcmil)	Conductor Code Name	Bundle Spacing (in.)	Bundle Diameter (in.)	X'_a (megohms-miles)	X'_d (megohms-miles)	X_c (megohms-miles)	X_c (per unit)
1	2515	Joree	—	—	0.0755	0.1134	0.1889	1.00
2	2544	Pheasant	18	18	0.0363	0.1134	0.1497	0.79
3	2625	Crane	18	20.5	0.0223	0.1134	0.1357	0.72
4	2544	Grosbeak	18	25.5	0.0120	0.1134	0.1254	0.66
6	2392	Ibis	—	36	-0.0020	0.1134	0.1114	0.59
8	2400	Ostrich	—	40	-0.0078	0.1134	0.1057	0.56
12	2539	Penguin	—	50	-0.0168	0.1134	0.0966	0.51
16	2683	Pigeon	—	60	-0.0236	0.1134	0.0898	0.48

num in the conductor bundle, dividing up the aluminum into a greater number of smaller subconductors decreases the line shunt reactance, and increases the line-charging current.

Example:
Consider the same 345-kV single-circuit flat configuration used for calculation of inductive reactance in the previous section. This simplified calculation ignores the effect of shield wires and the ground plane, which have a minor effect on positive sequence capacitive reactance.

The geometric mean distance of the three phases is the same as calculated from Equation 2.4-4 for inductive reactance. $D_{12} = D_{23} = 24.6$ ft and $D_{31} = 49.2$ ft, giving GMD from Equation 2.4-4 = 31.015 ft. From Equation 2.4-12, $X'_d = 0.1018$ megohm-mile.

Each phase consists of a bundle of twin Cardinal subconductors of 1.196 in. diameter. Capacitance calculations use the outer conductor diameter rather than the conductor GMR used for inductance calculations. This is because the electric field is zero inside the conductor, while a nonzero magnetic field exists within the conductor. Thus, the radius to use for capacitance calculation is 0.0498 ft. For a two-subconductor bundle of bundle radius 0.75 ft, the bundle GMR is given by $GMR_B = [(2)(0.0498)(.75)]^{1/2} = 0.2733$ ft. From Equation 2.4-13, $X'a = 0.0384$ megohm-mile.

The positive sequence reactance is given by Equation 2.4-11: $X_{C1} = X'_d + X'_a = 0.1402$ megohm-mile.

Repeating the same calculation with Applet CC-5 (including the shield wires) gives $X_{C1} = 0.137$ megohm-mile, or about 2% less capacitive reactance than the simplified calculation. The difference is due to the effect of the conducting earth and shield wires. Removing the shield wires and moving the phase conductors far from earth gives the same capacitive reactance as the simplified calculation.

2.4.4 Surge Impedance and Surge Impedance Loading

The surge impedance of any transmission line, whether power frequency or radio frequency is:

$$Z_0 = \sqrt{X_L \cdot X_c} \qquad 2.4\text{-}19$$

where X_L and X_c are the inductive and capacitive reactances per unit length, respectively. Surge impedance is thus a parameter determined by the design of the line, since it depends only on the line impedances. When positive sequence inductive and capacitive impedance are used in Equation 2.4-19, the resulting value is the positive sequence surge impedance. Surge impedance is a real number, representing a resistance. Surge impedance is the special case of the more general characteristic impedance, when series resistance and shunt conductance are assumed to be zero (lossless condition). When any line is terminated in its characteristic impedance, the voltage and current are pure forward traveling waves with no reflections at the termination. This is the desired termination condition for radio frequency transmission lines.

"Surge impedance loading" (SIL) is that loading when the transmission line is terminated in a wye-connection of resistors, each resistor having the value of the line surge impedance. This is the case of the line terminated in its own impedance with pure forward traveling waves. In the case of a lossless line, this is the power loading where the reactive power generated by the line capacitance exactly compensates the reactive power absorbed by the line inductance. This equality of capacitive and inductive vars is correct to a good approximation for practical values of conductor resistance.

Positive sequence surge impedance of a power transmission line has long been used as a "rule of thumb" measure of the loadability of the line under practical conditions (Bergen 1986; Gutman 1988). Since the line is a part of a larger power system, surge impedance loading is insufficient by itself to determine a line's rating. However, it is a useful basis of comparison of different line designs and different operating voltages, and serves as a check on the practicality of a given line loading. The use of surge impedance loading in assessing transmission lines is shown in Figure 14.2-1.

For a three-phase line, the surge impedance loading is:

$$\mathrm{SIL}(3\Phi) = (\mathrm{kV}_{LL})^2 / Z_0 \ \mathrm{MW} \qquad 2.4\text{-}20$$

Comparison of the series and shunt impedance values in Tables 2.4-3 and 2.4-4 shows that both series and shunt reactances decrease as the phase conductor material is divided into a greater number of subconductors. This reactance decrease reduces the surge impedance and increases the surge impedance loading as given in Table 2.4-5. For this particular example, dividing the conductor material from a single subconductor to twin-subconductor bundles increases surge impedance loading 27%. Further subdividing into a quad-subconductor bundle increases surge impedance loading 53% compared to a single subconductor per phase.

Table 2.4-5 Effect of Bundling on Surge Impedance

No. of Conductors	Total (kcmil)	Conductor Code Name	Bundle Spacing (in.)	Bundle Diameter (in.)	Surge Impedance (Ohms)	Per Unit Surge Impedance Loading
1	2515	Joree	—	—	389	1.00
2	2544	Pheasant	18	18	306	1.27
3	2625	Crane	18	20.5	276	1.41
4	2544	Grosbeak	18	25.5	254	1.53
6	2392	Ibis	—	36	226	1.72
8	2400	Ostrich	—	40	199	1.96
12	2539	Penguin	—	50	173	2.25
16	2683	Pigeon	—	60	159	2.44

2.5 GENERAL TRANSMISSION-LINE PARAMETERS

In addition to the positive sequence impedance developed in Section 2.4, it is frequently necessary to know the zero sequence impedance and admittance for analysis of faults and unbalanced conditions. For a passive circuit element, such as a transmission line, the positive and negative sequence impedances are equal, leaving positive and zero sequence impedances to be determined. More detailed studies may require either a complete matrix of self and mutual phase inductive and capacitive impedances, or a complete matrix of self and mutual sequence inductive and capacitive impedances. Terms in the inductive reactance matrix include the effects of conducting earth. Ground effects and conductor skin effects are frequency-sensitive. Thus, when knowledge of line parameters for surge propagation or other transient studies is required, it is necessary to determine how the impedance or admittance elements vary with frequency.

A frequent concern is the degree of line impedance unbalance produced by asymmetrical placement of line conductors above the ground plane. This unbalanced condition leads to generation of negative and zero sequence voltages and currents in an otherwise balanced system. These negative and zero sequence voltages and currents may have adverse effects sufficient to require line transposition to balance the line impedances. Generators, motors, shunt reactors, and relay performance may be affected by negative- and zero-sequence values. For example, manufacturers give generators negative sequence current limits, expressed as a percentage of rated current. Exceeding the negative sequence current limit can result in excessive heating of the machine rotor. Mutual coupling in the zero sequence between parallel circuits is a consideration in design of ground fault protection.

Transmission-line impedances can be balanced by line transposition, where the phase conductors occupy different structure positions for different portions of the line length. For example, conductor placement on the structures may be a-b-c for one-third of the line length, b-c-a for one-third of the line length, and c-a-b for the remaining third of the line length. The effect of line transposition on the phase impedance matrix is to make all the diagonal terms equal, and all the off-diagonal terms equal, leaving the self impedance Z_S for all the diagonal terms, and the mutual impedance Z_M for all the off-diagonal terms. Transformation to sequence components results in a diagonal matrix where the diagonal terms are the zero, positive, and negative sequence impedances and all the off-diagonal terms are zero. The sequence networks are decoupled by transposition, and the positive sequence network by itself represents the balanced operating condition with no interaction from the other two sequence networks. For a more detailed exposition, see one of the standard texts (Gross 1979; El-Hawry 1983; Grainger and Stevenson 1994). Development of component transformations as a special case of the general matrix transformation is given in Long and Gelopulos 1982.

The single-circuit series and shunt impedance matrix equations presented in this section are incorporated in Applet CC-5. Applet CC-5 gives both phase impedance and sequence impedance matrices. Another approach to calculation of unbalanced voltages and currents on transmission lines is by use of a phase matrix technique such as the electromagnetic transients program EMTP.

2.5.1 Capacitive (Electric Field) Unbalance

There are two ways to mathematically represent the capacitive (electric field) unbalance. The first is in terms of phase quantities, while the second is in terms of symmetrical components.

Phase Quantities

The capacitance equations in terms of phase voltages and charges in matrix notation are:

$$\begin{bmatrix} V_1 \\ V_2 \\ \cdot \\ \cdot \\ \cdot \\ V_m \end{bmatrix} = \begin{bmatrix} P_{11} & P_{12} & \cdots & P_{1n} \\ P_{21} & P_{22} & \cdots & P_{2n} \\ \cdot & \cdot & & \cdot \\ \cdot & \cdot & & \cdot \\ \cdot & \cdot & & \cdot \\ P_{m1} & P_{m2} & \cdots & P_{mn} \end{bmatrix} \begin{bmatrix} q_1 \\ q_2 \\ \cdot \\ \cdot \\ \cdot \\ q_m \end{bmatrix} \quad 2.5\text{-}1$$

where q is the conductor charge in coulombs per-unit distance, V the conductor potentials in volts with respect to ground, and P the "potential coefficients" defined in Equations. 2.5-2, 2.5-3, 2.5-4, and 2.5-5.

$$P_{mm} = 1.7975 \times 10^{10} \ln(D_{mm'} / r_m) \text{miles / farad} \quad 2.5\text{-}2$$

or

$$P_{mm} = 2.5718 \times 10^{7} \log(D_{mm'} / r_m) \text{miles / farad} \quad 2.5\text{-}3$$

when $m \neq n$

$$P_{mn} = 1.7975 \times 10^{10} \ln(D_{mn'} / D_{mn}) \text{miles / farad} \quad 2.5\text{-}4$$

or

$$P_{mn} = 2.5718 \times 10^{7} \log(D_{mn'} / D_{mn}) \text{miles / farad} \quad 2.5\text{-}5$$

Where:

r_m = radius of each conductor.

D_{mn} = distance between conductors m and n.

$D_{mn'}$ = distance between conductor m and the image conductor n' (See Figure 2.5-1).

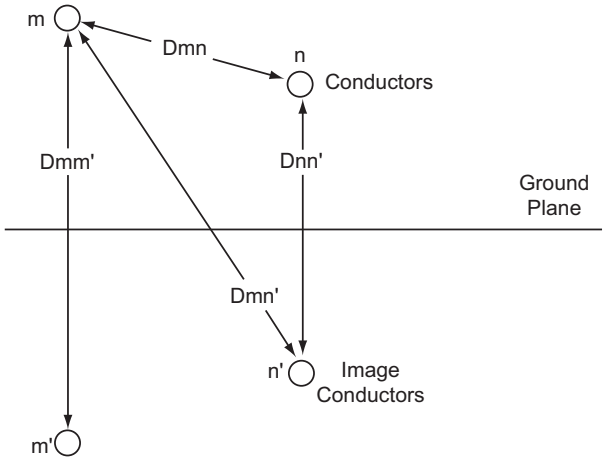


Figure 2.5-1 Conductor and image geometry symbols.

Dimensions for r_m, D_{mn} and $D_{mn'}$ must be in the same units. The notational form of Equation 2.5-1 is:

$$[V] = [P][Q] \quad 2.5\text{-}6$$

In order to calculate the current flow, it is necessary to write Equation 2.5-1 in terms of currents rather than electric charges. First recall that:

$$q_n(t) = Q_{n(\max)} \sin \omega t \quad 2.5\text{-}7$$

and that

$$i_n(t) = d[q_n(t)]dt \quad 2.5\text{-}8$$

Then:

$$i_n(t) = \omega Q_{n(\max)} \cos \omega t = \omega Q_{n(\max)} \sin(\omega t + 90°) \quad 2.5\text{-}9$$

In phasor form, Equation 2.5-9 becomes:

$$I_n = j\omega Q_n \quad \text{or} \quad Q_n = (1 / j\omega) I_n \quad 2.5\text{-}10$$

Thus Equation 2.5-6 can be written as:

$$[V] = (1 / j\omega)[P][I] = [Z][I] \quad 2.5\text{-}11$$

or in expanded form as:

$$\begin{bmatrix} V_1 \\ V_2 \\ \cdot \\ \cdot \\ \cdot \\ V_m \end{bmatrix} = \frac{1}{j\omega} \begin{bmatrix} P_{11} & P_{12} & \cdots & P_{1n} \\ P_{21} & P_{22} & \cdots & P_{2n} \\ \cdot & \cdot & & \cdot \\ \cdot & \cdot & & \cdot \\ \cdot & \cdot & & \cdot \\ P_{m1} & P_{m2} & \cdots & P_{mn} \end{bmatrix} \begin{bmatrix} I_1 \\ I_2 \\ \cdot \\ \cdot \\ \cdot \\ I_m \end{bmatrix} \quad 2.5\text{-}12$$

It is often desirable to determine the currents in terms of the voltages. In this case, premultiply each side of Equation 2.5-12 by Z^{-1} to obtain:

$$I = Z^{-1} V = j\omega P^{-1} V = j\omega C V = Y V \quad 2.5\text{-}13$$

or in expanded form:

$$\begin{bmatrix} I_1 \\ I_2 \\ \cdot \\ \cdot \\ \cdot \\ I_m \end{bmatrix} = j\omega \begin{bmatrix} C_{11} & C_{12} & \cdots & C_{1n} \\ C_{21} & C_{22} & \cdots & C_{2n} \\ \cdot & \cdot & & \cdot \\ \cdot & \cdot & & \cdot \\ \cdot & \cdot & & \cdot \\ C_{m1} & C_{m2} & \cdots & C_{mn} \end{bmatrix} \begin{bmatrix} V_1 \\ V_2 \\ \cdot \\ \cdot \\ \cdot \\ V_m \end{bmatrix} \quad 2.5\text{-}14$$

where the matrix C is called the capacitance matrix, and Y the admittance matrix. It should be noted that each element of the capacitance matrix is an involved expression that cannot be readily determined from physical dimensions. It is best to determine the potential coefficients, P, and then find the capacitance coefficients, C, as the elements of the inverse of the P matrix.

Sequence Quantities

The symmetrical component transformation is a matrix transformation based on the eigenvalue analysis for diagonalization of a matrix. (Long and Gelopulos 1982; Bellman 1960) The usefulness of the symmetrical component transformation is the ease with which it allows understanding of unbalance phenomena. For a three-phase transmission line, the shunt capacitive matrix given in Equation 2.5-13 becomes:

$$\begin{bmatrix} I_0 \\ I_1 \\ I_2 \end{bmatrix} = j\varpi \begin{bmatrix} C_{00} & C_{01} & C_{02} \\ C_{10} & C_{11} & C_{12} \\ C_{20} & C_{21} & C_{22} \end{bmatrix} \begin{bmatrix} V_0 \\ V_1 \\ V_2 \end{bmatrix} \qquad 2.5\text{-}15$$

It is important to keep in mind the different significance of the terms in Equations 2.5-14 and 2.5-15. In the phase impedance matrix of Equation 2.5-14, the off-diagonal terms represent mutual coupling between phases, where a voltage on one phase results in a current in another phase. In the sequence impedance matrix of Equation 2.5-15 the off-diagonal terms represent mutual coupling between *sequences*, or the degree of unbalance in the line impedances.

The significance of off-diagonal terms in the sequence impedance matrix is shown in that, for a perfectly symmetrical or perfectly transposed transmission line, the capacitance matrix is a diagonal matrix with all the off-diagonal terms equal to zero. In this case, a positive sequence voltage results in only a positive sequence current; a negative sequence voltage results in only a negative sequence current; and a zero sequence voltage results in only a zero sequence current. For a normal, untransposed transmission line—for example, a horizontal configuration line above earth—the off-diagonal terms are not zero. The interpretation of off-diagonal terms can be seen by injecting a purely positive sequence voltage into Equation 2.5-14.

$$\begin{bmatrix} I_0 \\ I_1 \\ I_2 \end{bmatrix} = j\varpi \begin{bmatrix} C_{01} \\ C_{11} \\ C_{21} \end{bmatrix} V_1 = j\varpi \begin{bmatrix} C_{00} & C_{01} & C_{02} \\ C_{10} & C_{11} & C_{12} \\ C_{20} & C_{21} & C_{22} \end{bmatrix} \begin{bmatrix} 0 \\ V_1 \\ 0 \end{bmatrix} \qquad 2.5\text{-}16$$

Currents result in all three sequences from a voltage of only one sequence. The three resulting currents are determined by the middle column in the capacitance matrix. A similar analysis can be conducted by injecting pure zero or negative sequence voltages.

An alternative approach to capacitive unbalance is use of three unbalance factors defined as follows (Gross and Weston 1951; Gross and Chin 1968):

1. Ground displacement d_0

$$d_0 = \frac{V_0}{V_{ph}} \qquad 2.5\text{-}17$$

V_0 = voltage from neutral to ground.
V_{ph} = voltage from phase to neutral.

2. Zero sequence unbalance factor d'$_0$

$$d'_0 = \frac{Q_{a0}}{Q_{a1}} = \frac{I'_{a0}}{I'_{a1}} \qquad 2.5\text{-}18$$

Q_{a0} = zero sequence charge.
Q_{a1} = positive sequence charge.
I'_{a0} = zero sequence charging current.
I'_{a1} = positive sequence charging current.

3. Negative sequence unbalance factor d_2

$$d_2 = \frac{Q_{a2}}{Q_{a1}} = \frac{I'_{a2}}{I'_{a1}} \qquad 2.5\text{-}19$$

Q_{a2} = negative sequence charge.
Q_{a1} = positive sequence charge.
I'_{a2} = negative sequence charging current.
I'_{a1} = positive sequence charging current.

2.5.2 Single-Circuit Inductive (Magnetic Field) Unbalance

The inductive unbalance may be presented in terms of phase quantities or in terms of symmetrical components.

Phase Quantities (Carson Form)

The inductive matrix may be calculated by using the equations developed by Carson and modified by Clarke and Calabrese (Carson 1928; Clarke 1943; Calabrese 1959). In matrix form, the equations are:

$$\begin{bmatrix} V_1 \\ V_2 \\ \cdot \\ \cdot \\ \cdot \\ V_m \end{bmatrix} = \begin{bmatrix} Z_{11} & Z_{12} & \cdots & Z_{1n} \\ Z_{21} & Z_{22} & \cdots & Z_{2n} \\ \cdot & \cdot & & \cdot \\ \cdot & \cdot & & \cdot \\ \cdot & \cdot & & \cdot \\ Z_{m1} & Z_{m2} & \cdots & Z_{mn} \end{bmatrix} \begin{bmatrix} I_1 \\ I_2 \\ \cdot \\ \cdot \\ \cdot \\ I_m \end{bmatrix} \qquad 2.5\text{-}20$$

In notational form, Equation 2.5-20 is:

$$[V] = [Z][I] \qquad 2.5\text{-}21$$

when $m = n$,

$$Z_{mm} = R_m + 4\pi\, 10^{-7} f \left[\begin{matrix} j \ln(D_{mm'} / \mathrm{GMR}_m) \\ + \ 2(P + jQ) \end{matrix} \right] \text{ohms / meter} \quad \text{2.5-22}$$

or

$$Z_{mm} = R_m + j0.004657 f \log(D_{mm'} / \mathrm{GMR}_m) + 0.004043 f (P + jQ) \text{ ohms / mile} \quad \text{2.5-23}$$

when $m \neq n$,

$$Z_{mn} = 4\pi\, f\, 10^{-7} \left[\begin{matrix} j \ln(D_{mn'} / D_{mn}) \\ + \ 2(P + jQ) \end{matrix} \right] \text{ohms / meter} \quad \text{2.5-24}$$

or

$$Z_{mn} = j0.004657 f \log(D_{mn'} / D_{mn}) + 0.004043 f (P + jQ) \text{ ohms / mile} \quad \text{2.5-25}$$

Where:

f = frequency, Hertz.

$\mathrm{GMR_m}$ = geometric mean radius for conductor m.

D_{mn} = distance between conductors m and n.

$D_{mm'}$, $D_{mn'}$ = distance between conductors m and image conductor m' or n' (see Figure 2.5-1). The dimensions for $\mathrm{GMR_m}$, D_{mm}, $D_{mm'}$ and $D_{mn'}$ must be in the same units.

R_m = ac resistance of conductor m, ohms/meter, for Equation 2.5-22 and ohms/mile for Equation 2.5-23.

The terms P and Q are defined by the following expressions:

$$P = \frac{\pi}{8} - \frac{1}{3\sqrt{2}} k \cos\theta + \frac{k^2}{16} \cos 2\theta \left(0.6728 + \ln \frac{2}{k} \right) + \frac{k^2}{16} \theta \sin 2\theta + \frac{k^3 \cos 3\theta}{45\sqrt{2}} - \frac{\pi k^4 \cos 4\theta}{1536} \quad \text{2.5-26}$$

$$Q = -0.0386 + \frac{1}{2} \ln \frac{2}{k} + \frac{1}{3\sqrt{2}} k \cos\theta - \frac{\pi k^2}{64} \cos 2\theta + \frac{k^3 \cos 3\theta}{45\sqrt{2}} - \frac{k^4 \theta}{384} \sin 4\theta - \frac{k^4 \cos 4\theta}{384} \times \left(\ln \frac{2}{k} + 1.0895 \right) \quad \text{2.5-27}$$

The terms P and Q have different values for the impedance coefficients Z_{mn}, when $m = n$ and $m \neq n$.

In the case of $m = n$,

$$k = 2.81 \times 10^{-3} D_{mm'} \sqrt{f\rho} \quad \text{2.5-28}$$

$$\theta = 0 \quad \text{2.5-29}$$

In the case of $m \neq n$,

$$k = 2.81 \times 10^{-3} D_{mn'} \sqrt{f / \rho} \quad \text{2.5-30}$$

$$\theta = \arcsin(H_{mn} / D_{mn'}) \quad \text{2.5-31}$$

Where:

f = frequency, Hertz.

ρ = resistivity of earth, ohm meters.

H_{mn} = horizontal distance between conductors m and n in meters.

D_{mn} = image distance for Equation 2.5-30 as shown in Figure 2.5-1 in meters.

The computer calculation of the Z matrix is described by Hesse (Hesse 1963).

Approximating Equations

Electromagnetic calculations have been made with approximating Equations 3.5-32 and 3.5-33 (Westinghouse 1964; Lawrence and Povejsil 1952).

The impedance for $m = n$ is:

$$Z_{mm} = Z'_{mm} + Z_g - 2Z_{mg} \quad \text{2.5-32}$$

and for $m \neq n$ is:

$$Z_{mm} = Z'_{mn} + Z_g - Z_{mg} - Z_{ng} \quad \text{2.5-33}$$

where:

Z'_{mm} = self-impedance of conductor.
= $r_m + j4\pi f 10^{-7} \ln(1/\mathrm{GMR_m})$ ohms/meter.
= $r_m + j4.657 * 10^{-3} f \log(1/\mathrm{GMR_m})$ ohms/mile.

Z'_{mn} = mutual impedance between conductors.
= $j4\pi f 10^{-7} \ln(1/\mathrm{D_{mn}})$ ohms/meter.
= $j4.657 * 10^{-3} f \log(1/\mathrm{D_{mn}})$ ohms/mile.

Z_g = $9.865 * 10^{-7} f + j0$ ohms/meter.
= $0.001588 f + j0$ ohms/mile.

Z_{mg} or

Z_{ng} = mutual impedance between conductor and ground.
= $j2\pi * 10^{-7} f \ln(1/660\sqrt{\rho}/f)$ ohms/meter.
= $j2.3283 * 10^{-3} f \log(1/2160\sqrt{\rho}/f)$ ohms/mile.

r_m = resistance of conductor in ohms/meter or ohms/mile as applicable.

D_{mn} = distance between conductors in meters or feet as applicable.

ρ = resistivity of the earth in ohm meters.

f = frequency in Hertz.

Sequence Quantities

The representation of inductive unbalance in a single-circuit, three-phase system by symmetrical components follows the same procedure as for capacitive unbalance. The series sequence inductive impedance matrix takes the form:

$$\begin{bmatrix} V_0 \\ V_1 \\ V_2 \end{bmatrix} = j\omega \begin{bmatrix} L_{00} & L_{01} & L_{02} \\ L_{10} & L_{11} & L_{12} \\ L_{20} & L_{21} & L_{22} \end{bmatrix} \begin{bmatrix} I_0 \\ I_1 \\ I_2 \end{bmatrix} = \begin{bmatrix} Z_{00} & Z_{01} & Z_{02} \\ Z_{10} & Z_{11} & Z_{12} \\ Z_{20} & Z_{21} & Z_{22} \end{bmatrix} \begin{bmatrix} I_0 \\ I_1 \\ I_2 \end{bmatrix} \quad \text{2.5-34}$$

The series impedance matrix is diagonal for a perfectly symmetrical or perfectly transposed transmission line. For the transposed case, a current of one sequence results in a voltage drop of only that sequence. For an untransposed line, a current of one sequence generally results in voltage drops in all three sequences. As was the case with capacitive unbalance, inductive unbalance can be studied by injecting a current of a single sequence and comparing the voltage drops in the three sequences. Two helpful ratios for looking at inductive unbalance are the zero sequence unbalance ratio, M_0; and the negative sequence unbalance ratio, M_2. The unbalance factors M are defined in percentages as:

$$M_0 = \left| \frac{Z_{01}}{Z_0} \right| \times 100 \quad \text{2.5-35}$$

$$M_2 = \left| \frac{Z_{21}}{Z_1} \right| \times 100 \quad \text{2.5-36}$$

The X_0/X_1 ratio is very useful for assessing fundamental frequency overvoltages on unfaulted phases for single or double line to ground fault conditions (Peterson 1966). A frequently used measure of whether a system is effectively grounded is $X_0/X_1 \leq 3.0$ and $R_0/X_1 \leq 1.0$. For the case of zero resistance and $X_0/X_1 = 3$, a single phase to ground fault on phase A will result in 1.25 per unit phase to ground voltage on phase c. If $X_0/X_1 = \infty$, the phase to ground voltage will rise to phase to phase voltage (1.73 per unit of phase to ground voltage). No system is truly ungrounded, as there is always capacitance to ground resulting in a negative zero sequence reactance. In such a case, the phase to ground voltage can rise above phase to phase voltage. For further details, see Peterson 1966.

Shield wires affect the zero sequence impedance of a transmission line, but have little impact on the positive or negative sequence impedances. This is apparent because zero sequence current flows in a grounded continuous shield wire, but positive and negative currents sum to zero and thus have no contribution to shield wire current. Compared to a line with no shield wires, the presence of a shield wire reduces the zero sequence reactance and increases the zero sequence impedance. The physical explanation for the reduction in reactance is the reduction in flux loop caused by the presence of a return current path in the shield wire that is closer to the phase conductors than the equivalent return current path in the earth. The apparently odd phenomena of the increase in zero sequence resistance is due to the reactance distribution forcing current into the closer, higher-resistance, shield wire path, thus increasing the zero sequence resistance.

2.5.3 Unbalance in Parallel Double-Circuit Untransposed Lines

Unbalance in parallel, double-circuit untransposed lines can be analyzed on a phase impedance matrix basis using one of the available computer programs such as the electromagnetic transients program EMTP. Double-circuit line unbalance can also be analyzed on a symmetrical component basis. A current of a pure single sequence in a single–circuit, untransposed transmission line results in voltage drops in all three sequences. In the case of a double–circuit, untransposed transmission line, a single sequence current in one circuit in general results in voltage drops in all three sequences in *both* lines. As part of the overall system, this voltage drop results in currents of all three sequences in both circuits.

A double circuit line has a 6 x 6 phase impedance matrix consisting of self-impedances of all six conductors and mutual impedances between all combinations of pairs of conductors. In symmetrical components, each circuit has a 3 x 3 sequence impedance matrix for each circuit (Equation 2.5-34), and in addition, there is a mutual sequence impedance matrix relating the two circuits, illustrated by Equation 2.5-37. Notation in Equation 2.5-37 is as follows: $V_{1\text{-}0}$ means zero sequence voltage drop in circuit 1. $I_{2\text{-}0}$ means zero sequence current in circuit 2. For example, a positive sequence current in circuit 2 results in voltage drops in all three sequences in circuit 1. It is important to keep in mind the distinction between the mutual impedances within a circuit and the mutual impedances between circuits, where a sequence current results in voltages of different sequences in both circuits. The zero sequence coupling between circuits is especially important to relay engineers.

$$\begin{bmatrix} V_{1-0} \\ V_{1-1} \\ V_{1-2} \end{bmatrix} = \begin{bmatrix} Z_{00} & Z_{01} & Z_{02} \\ Z_{10} & Z_{11} & Z_{12} \\ Z_{20} & Z_{21} & Z_{22} \end{bmatrix} \begin{bmatrix} I_{2-0} \\ I_{2-1} \\ I_{2-2} \end{bmatrix} \quad \text{2.5-37}$$

The self and mutual phase and sequence impedance matrices can be calculated using available transmission line constants programs. Calculations with a pocket calculator can

be used to estimate the relative degree of unbalance, or appropriate ratios of terms can be used as unbalance factors.

The mutual impedance in the positive sequence has the effect of changing the effective impedance of the individual circuits. For the phasing:

a	a
b	b
c	c

the mutual positive sequence impedances add, slightly increasing the line impedance. This relative phasing is called "superbundle" because conductors at the same electrical phase angle are adjacent.

For the phasing:

a	c
b	b
c	a

the mutual positive sequence impedance subtracts, slightly reducing the line impedance. This relative phasing is called "low reactance" because of this effect.

This discussion has focused only on unbalance as it relates to the transmission circuit itself. Any circuit is part of the overall power system, and thus actual unbalance voltages and currents will be determined by analysis of the whole system. However, investigation of the sequence impedance matrices is a useful exercise in comparing circuits of different designs, and in determining whether transposition is necessary.

2.6 INDUCED VOLTAGES ON PARALLEL CONDUCTORS

A number of situations arise where electric and magnetic field induction into conductors parallel to an energized transmission line is an important consideration. This includes the case of induction to a de-energized conductor of the same circuit. For example, single-pole switching is sometimes used to increase the stability limits of a transmission system. The success of single-pole switching depends on sufficiently small induction (called secondary arc current) to the switched conductor so that the fault arc extinguishes by itself. An excessive secondary arc current may result in continued arc burning and failure of the fault to clear (Lambert et al. 1978). Parallel transmission lines with shunt reactors may exhibit resonance phenomena with one circuit energized and the other de-energized (Chaston 1969; LaForest 1972).

Another example of induction within a circuit is induced circulating current in shield wires. Reduction of shield wire current is sometimes considered as part of reducing circuit power losses. The induction of concern may be to a conductor of a parallel circuit that is de-energized and undergoing some maintenance operation, or the induction may be to some parallel conductor different from the power system, such as telephone circuits, railroad signals, fences or pipelines. These effects fall under environmental effects of transmission lines.

Induction to parallel power transmission lines is an important safety consideration for protection of workers during construction and maintenance operations. Adequate grounding must be provided to protect workers on de-energized lines paralleling operating lines during normal line operation as well as during power system faults. Details of grounding protection are given in IEEE Standards on power line grounding (IEEE 1993a; IEEE 2003).

Induction to parallel conductors is both capacitive (electric field) and inductive (magnetic field). Electric and magnetic field induction and environmental effects on objects near the earth's surface are addressed in Section 7, starting from the physics of electromagnetic fields. In the case of long parallel conductors, it is also possible to calculate induced voltages and currents starting from the point of view of circuit theory. Induction is calculated from series inductive reactance and shunt capacitive admittance matrices. The matrix formulation is given in Sections 2-4 and 2-5. This section extends that development to the parallel conductor induction issue.

The same geometrical and electrical parameters affect the amount of induction as enter an impedance calculation. Among these are phase spacing, circuit spacing, conductor height, and transposition scheme (if any). Circuit loading is a factor, whether the condition is normal operation or fault current. As impedance matrix methods are based on sinusoidal steady-state phasor analysis, steady currents and voltages are assumed for either condition. In each case a matrix is developed relating voltages and currents, and the resulting system of equations is solved to determine the induction.

2.6.1 Electric Field Induction on the De-Energized Circuit

Electric field induction for a double circuit line is calculated from the shunt capacitive admittance Equation 2.5-14 recast in admittance form in Equation 2.6-1 (IEEE 1972; IEEE 1993a). Rows and columns 1,2, and 3 represent the energized circuit; rows and columns 4, 5, and 6 represent the de-energized circuit. Additional rows and columns could be added to represent shield wires. By specifying the line voltages V_1, V_2, and V_3 and setting currents I_4, I_5, and I_6 to zero, solving the resulting set of equations calculates

the induced voltages V_4, V_5, and V_6. The mathematics to do this is programmed into Applet CC-7. If voltages V_4, V_5, and V_6 are set to zero instead of the three currents, short circuit to ground induced on the de-energized conductors can be calculated. The short circuit current gives the secondary arc current for single-pole switching analysis.

$$\begin{bmatrix} I_1 \\ I_2 \\ I_3 \\ I_4 \\ I_5 \\ I_6 \end{bmatrix} = \begin{bmatrix} Y_{11} & Y_{12} & Y_{13} & Y_{14} & Y_{15} & Y_{16} \\ Y_{21} & Y_{22} & Y_{23} & Y_{24} & Y_{25} & Y_{26} \\ Y_{31} & Y_{32} & Y_{33} & Y_{34} & Y_{35} & Y_{36} \\ Y_{41} & Y_{42} & Y_{43} & Y_{44} & Y_{45} & Y_{46} \\ Y_{51} & Y_{52} & Y_{53} & Y_{54} & Y_{55} & Y_{56} \\ Y_{61} & Y_{62} & Y_{63} & Y_{64} & Y_{65} & Y_{66} \end{bmatrix} \begin{bmatrix} V_1 \\ V_2 \\ V_3 \\ V_4 \\ V_5 \\ V_6 \end{bmatrix} \quad \text{2.6-1}$$

As an example of this calculation, consider the base case 345-kV double circuit line. One circuit is energized at a nominal 345 kV, and the other is floating. The three phases of the de-energized circuit rise to 24, 18, and 32 kV.

The induced voltage calculation can be visualized as a capacitive voltage divider consisting of all the self and mutual capacitances relating the six phases. Because all the capacitances are proportional to line length, the induced voltage is independent of the length of the line.

The short circuit to ground calculation can be visualized as a voltage source and a capacitive source impedance to the grounded conductor. Because the source impedance is proportional to line length, the resulting current is also proportional to length. In this example case, the three phases each have induced current of approximately 2 mA per mile.

2.6.2 Magnetic Field Induction on the De-Energized Circuit

Magnetic field induction for a double circuit line is calculated from the series impedance matrix in Equation 2.6-2 (IEEE 1974; IEEE 1993a). As in Equation 2.6-1, rows and columns 1, 2, and 3 represent the energized circuit; rows and columns 4, 5, and 6 represent the de-energized circuit. Additional rows and columns could be added to represent shield wires. By specifying the line currents I_1, I_2, and I_3 and setting currents I_4, I_5, and I_6 to zero, solving the resulting set of equations calculates the induced voltages V_4, V_5, and V_6. The mathematics to do this is programmed into Applet CC-7.

$$\begin{bmatrix} V_1 \\ V_2 \\ V_3 \\ V_4 \\ V_5 \\ V_6 \end{bmatrix} = \begin{bmatrix} Z_{11} & Z_{12} & Z_{13} & Z_{14} & Z_{15} & Z_{16} \\ Z_{21} & Z_{22} & Z_{23} & Z_{24} & Z_{25} & Z_{26} \\ Z_{31} & Z_{32} & Z_{33} & Z_{34} & Z_{35} & Z_{36} \\ Z_{41} & Z_{42} & Z_{43} & Z_{44} & Z_{45} & Z_{46} \\ Z_{51} & Z_{52} & Z_{53} & Z_{54} & Z_{55} & Z_{56} \\ Z_{61} & Z_{62} & Z_{63} & Z_{64} & Z_{65} & Z_{66} \end{bmatrix} \begin{bmatrix} I_1 \\ I_2 \\ I_3 \\ I_4 \\ I_5 \\ I_6 \end{bmatrix} \quad \text{2.6-2}$$

The self and mutual terms in the impedance matrix in Equation 2.6-2 are dimensioned in ohms per unit length. Thus the voltage calculated by Equation 2.6-2 is the longitudinal voltage along the parallel conductor. This voltage is frequently called "longitudinal electromotive force" (LEF), formerly called "longitudinal electric field." If the conductor were grounded at one end, the voltage represents the voltage along the conductor as one moves away from the ground.

As an example of this calculation, consider the same base case 345-kV double circuit line used for the capacitance calculation. One circuit has a specified balanced 1000 ampere current, and the other circuit's phase conductors are floating. Voltages induced in the three phases of the de-energized circuit are approximately 1, 5, and 10 volts per mile. Setting the three currents I_4, I_5, and I_6 to zero instead of the voltages gives the induced currents.

A similar calculation for a 10,000-ampere fault current in phase 1 of the energized circuit gives induced voltages in the three phases of the de-energized circuit of approximately 5 kV per mile. This illustrates the significance of considering fault currents in magnetic field induction problems.

It is possible to combine the electric and magnetic field calculations by developing the ABCD matrix of the six-conductor array and manipulating the resulting equations. More elaborate calculations, including the effects of resistance in the ground connection, can be made using the ABCD matrix approach.

Magnetic field induction causes circulating current in continuous grounded shield wires and can be calculated in the same manner as induced current in parallel circuits. See Chapter 6 and Applet EMF-8 for a fuller description. One consideration in the sizing of shield wires is the ability to carry the portion of fault current that flows in the shield wires (Lambert et al.1978). Some utilities use segmented shield wires and similar approaches as a method of reducing power losses connected with circulating shield wire current (Fakheri et al.1984). System relay engineers generally desire a continuous shield wire path for zero sequence current return.

This page intentionally left blank.

APPENDIX 2.1 ELECTRICAL AND MECHANICAL CHARACTERISTICS OF CONDUCTORS

Table A2.1-1 Electrical Characteristics of Common North American Aluminum Conductors Steel Reinforced (ACSR)

Conductor Name	Stranding Ratio	# of Aluminum Layers	Outside Diameter		Aluminum Crossectional Area		Diameter of OL Strands	# Strands in Outer Layer (OL)	Rdc@25C DC	Rac@25C 60Hz	Rac@75C 60Hz	GMR	Xa	X'a
			inches	mm	kcmil	sq mm	inches		Ohm/mi	Ohm/mi	Ohm/mi	ft	Ohm/mi	Mohm-mi
SWIFT	36/1	3	0.930	23.6	636	322	0.1329	18	0.1459	0.1480	0.1760	0.0300	0.426	0.0964
KINGBIRD	18/1	2	0.940	23.9	636	322	0.1880	12	0.1453	0.1470	0.1750	0.0301	0.425	0.0951
ROOK	24/7	2	0.977	24.8	636	322	0.1628	15	0.1446	0.1460	0.1740	0.0327	0.415	0.0950
GROSBEAK	26/7	2	0.990	25.1	636	322	0.1564	16	0.1440	0.1450	0.1730	0.0335	0.412	0.0944
EGRET	30/19	2	1.019	25.9	636	322	0.1456	18	0.1431	0.1440	0.1720	0.0351	0.406	0.0936
FLAMINGO	24/7	2	1.000	25.4	666.6	338	0.1667	15	0.1379	0.1390	0.1660	0.0335	0.412	0.0942
GANNET	26/7	2	1.014	25.8	666.6	338	0.1601	16	0.1375	0.1390	0.1660	0.0343	0.409	0.0937
CROW	54/7	3	1.036	26.3	715.5	363	0.1151	24	0.1286	0.1280	0.1530	0.0372	0.407	0.0931
STARLING	26/7	2	1.051	26.7	715.5	363	0.1659	16	0.1279	0.1290	0.1540	0.0355	0.405	0.0927
REDWING	30/19	2	1.081	27.5	715.5	363	0.1544	18	0.1273	0.1280	0.1530	0.0372	0.399	0.0919
TERN	45/7	3	1.063	27.0	795	403	0.1329	21	0.1166	0.1190	0.1410	0.0352		
COOT	36/1	3	1.040	26.4	795	403	0.1486	18	0.1167	0.1190	0.1420	0.0335	0.412	0.0932
CUCKOO	24/7	2	1.092	27.7	795	403	0.1820	15	0.1157	0.1170	0.1400	0.0361	0.402	0.0916
CONDOR	54/7	3	1.092	27.7	795	403	0.1213	24	0.1158	0.1170	0.1400	0.0368	0.401	0.0916
DRAKE	26/7	2	1.108	28.1	795	403	0.1749	16	0.1152	0.1170	0.1390	0.0375	0.399	0.0911
SKIMMER	30/7	2	1.140	29.0	795	403	0.1329	18	0.1143	0.1155	0.1379	0.0392	0.393	0.0904
MALLARD	30/19	2	1.140	29.0	795	403	0.1628	18	0.1145	0.1160	0.1380	0.0392	0.393	0.0903
WILLET	45/7	3	1.115	28.3	874.5	443	0.1394	21	0.1060	0.1080	0.1280		0.400	0.0909
CRANE	54/7	3	1.146	29.1	874.5	443	0.1273	24	0.1051	0.1070	0.1270		0.395	0.0901
RUDDY	45/7	3	1.131	28.7	900	456	0.1414	21	0.1031	0.1060	0.1250	0.0374	0.399	0.0905
CANARY	54/7	3	1.162	29.5	900	456	0.1291	24	0.1022	0.1040	0.1240	0.0392	0.393	0.0897
BALDPATE	30/7	2	1.212	30.8	900	456	0.1732	18	0.1011	0.1020	0.1220		0.385	0.0885
CORNCRAKE	20/7	2	1.165	29.6	954	483	0.2184	13	0.0972	0.0994	0.1180	0.0381	0.396	0.0897
RAIL	45/7	3	1.165	29.6	954	483	0.1456	21	0.0972	0.0994	0.1180	0.0385	0.395	0.0896
CARDINAL	54/7	3	1.196	30.4	954	483	0.1329	24	0.0964	0.0983	0.1170	0.0404	0.389	0.0889
REDBIRD	24/7	2	1.196	30.4	954	483	0.1994	15	0.0964	0.0982	0.1170	0.0400	0.390	0.0890
ORTOLAN	45/7	3	1.212	30.8	1033.5	524	0.1515	21	0.0898	0.0922	0.1100	0.0401	0.390	0.0886
CURLEW	54/7	3	1.245	31.6	1033.5	524	0.1383	24	0.0890	0.0910	0.1080	0.0420	0.385	0.0877
BLUEJAY	45/7	3	1.258	32.0	1113	564	0.1573	21	0.0833	0.0859	0.1020	0.0416	0.386	0.0873
FINCH	54/19	3	1.293	32.8	1113	564	0.1436	24	0.0830	0.0851	0.1010	0.0436	0.380	0.0866
BUNTING	45/7	3	1.302	33.1	1192.5	604	0.1628	21	0.0777	0.0805	0.0954	0.0431	0.382	0.0863
GRACKLE	54/19	3	1.338	34.0	1192.5	604	0.1486	24	0.0775	0.0798	0.0947	0.0451	0.376	0.0855
BITTERN	45/7	3	1.345	34.2	1272	645	0.1681	21	0.0729	0.0759	0.0898	0.0445	0.378	0.0854
PHEASANT	54/19	3	1.382	35.1	1272	645	0.1535	24	0.0727	0.0751	0.0890	0.0466	0.372	0.0846
DIPPER	45/7	3	1.386	35.2	1351.5	685	0.1733	21	0.0686	0.0717	0.0848	0.0459	0.374	0.0845
MARTIN	54/19	3	1.424	36.2	1351.5	685	0.1582	24	0.0684	0.0710	0.0840	0.0480	0.368	0.0837
BOBOLINK	45/7	3	1.427	36.2	1431	725	0.1783	21	0.0648	0.0681	0.0804	0.0472	0.371	0.0836
PLOVER	54/19	3	1.465	37.2	1431	725	0.1628	24	0.0646	0.0673	0.0796	0.0494	0.365	0.0828
NUTHATCH	45/7	3	1.465	37.2	1510.5	765	0.1832	21	0.0614	0.0649	0.0765	0.0485	0.367	0.0829
PARROT	54/19	3	1.505	38.2	1510.5	765	0.1672	24	0.0612	0.0641	0.0757	0.0508	0.362	0.0821
LAPWING	45/7	3	1.504	38.2	1590	806	0.1880	21	0.0583	0.0620	0.0729	0.0497	0.364	0.0821
FALCON	54/19	3	1.545	39.2	1590	806	0.1716	24	0.0581	0.0611	0.0721	0.0521	0.358	0.0813
CHUKAR	84/19	4	1.602	40.7	1781	902	0.1456	30	0.0522	0.0561	0.0658	0.0534	0.355	0.0802
BLUEBIRD	84/19	4	1.762	44.8	2156	1092	0.1602	30	0.0431	0.0477	0.0555	0.0588	0.344	0.0774
KIWI	72/7	4	1.735	44.1	2167	1098	0.1735	27	0.0431	0.0484	0.0562	0.0570	0.348	0.0778
THRASHER	76/19	4	1.802	45.8	2312	1172	0.1744	28	0.0404	0.0454	0.0528	0.0595	0.342	0.0767
JOREE	76/19	4	1.880	47.8	2515	1274	0.1819	28	0.0371	0.0425	0.0491	0.0621	0.338	0.0756

Table A2.1-2 Mechanical Characteristics of Common North American Aluminum Conductors Steel Reinforced (ACSR)

Conductor Name	Stranding Ratio	Type Number	# of Aluminum Layers	Outside Diameter		Aluminum Crossectional Area		Total Crossectional Area		Rated Breaking Strength		Total Conductor Weight		Weight of Steel Core (Class A galvanizing)	
				inches	mm	kcmil	sq mm	sq in.	sq mm	lbs	kN	lbs/kft	kg/km	lbs/kft	kg/km
SWIFT	36/1	3	3	0.930	23.6	636	322	0.5133	331.2	13,800	61.4	643.7	957.9	46.8	69.6
KINGBIRD	18/1	6	2	0.940	23.9	636	322	0.5275	340.3	15,700	69.8	690.8	1028.0	93.6	139.3
ROOK	24/7	13	2	0.977	24.8	636	322	0.5643	364.1	22,600	100.5	819.2	1219.1	219.2	326.2
GROSBEAK	26/7	16	2	0.990	25.1	636	322	0.5808	374.7	25,200	112.1	875.2	1302.4	275.3	409.7
EGRET	30/19	23	2	1.019	25.9	636	322	0.6135	395.8	31,500	140.1	988.2	1470.6	386.8	575.6
FLAMINGO	24/7	13	2	1.000	25.4	666.6	338	0.5917	381.7	23,700	105.4	858.9	1278.2	229.8	342.0
GANNET	26/7	16	2	1.014	25.8	666.6	338	0.6086	392.6	26,400	117.4	917.3	1365.1	288.5	429.3
CROW	54/7	13	3	1.036	26.3	715.5	363	0.634	409.0	26,300	117.0	921.0	1370.6	246.5	366.8
STARLING	26/7	16	2	1.051	26.7	715.5	363	0.6535	421.6	28,400	126.3	984.8	1465.5	309.7	460.9
REDWING	30/19	23	2	1.081	27.5	715.5	363	0.6896	444.9	34,600	153.9	1110.0	1651.9	434.0	645.9
TERN	45/7	7	3	1.063	27.0	795	403	0.6674	430.6	22,100	98.3	895.8	1333.1	146.1	217.4
COOT	36/1	3	3	1.040	26.4	795	403	0.6416	413.9	16,800	74.7	804.7	1197.5	58.5	87.1
CUCKOO	24/7	13	2	1.092	27.7	795	403	0.7053	455.0	27,900	124.1	1024.0	1523.9	274.0	407.8
CONDOR	54/7	13	3	1.092	27.7	795	403	0.7049	454.8	28,200	125.4	1024.0	1523.9	274.0	407.8
DRAKE	26/7	16	2	1.108	28.1	795	403	0.7264	468.6	31,500	140.1	1094.0	1628.1	344.0	511.9
SKIMMER	30/7	23	2	1.140	29.0	795	403	0.7702	496.9	38,300	170.4	1244.0	1851.3	493.3	734.1
MALLARD	30/19	23	2	1.140	29.0	795	403	0.7669	494.8	38,400	170.8	1235.0	1837.9	483.0	718.8
WILLET	45/7	7	3	1.115	28.3	874.5	443	0.7347	474.0	25,000	111.2	987.0	1468.8	161.4	240.2
CRANE	54/7	13	3	1.146	29.1	874.5	443	0.7766	501.0	31,400	139.7	1126.0	1675.7	301.2	448.2
RUDDY	45/7	7	3	1.131	28.7	900	456	0.7555	487.4	24,400	108.5	1015.0	1510.5	165.5	246.3
CANARY	54/7	13	3	1.162	29.5	900	456	0.7984	515.1	31,900	141.9	1159.0	1724.8	310.0	461.3
BALDPATE	30/7	23	2	1.212	30.8	900	456	0.8711	562.0	43,300	192.6	1410.0	2098.3	559.1	832.0
CORNCRAKE	20/7	7	2	1.165	29.6	954	483	0.801	516.8	25,600	113.9	1075.0	1599.8	175.5	261.2
RAIL	45/7	7	3	1.165	29.6	954	483	0.801	516.8	25,900	115.2	1076.0	1601.3	176.0	261.9
CARDINAL	54/7	13	3	1.196	30.4	954	483	0.8462	545.9	33,800	150.3	1229.0	1829.0	329.0	489.6
REDBIRD	24/7	13	2	1.196	30.4	954	483	0.8466	546.2	33,500	149.0	1229.0	1829.0	328.7	489.2
ORTOLAN	45/7	7	3	1.212	30.8	1033.5	524	0.8673	559.5	27,700	123.2	1164.0	1732.2	190.0	282.8
CURLEW	54/7	13	3	1.245	31.6	1033.5	524	0.9163	591.2	36,600	162.8	1330.0	1979.3	356.0	529.8
BLUEJAY	45/7	7	3	1.258	32.0	1113	564	0.935	603.2	29,800	132.6	1255.0	1867.6	205.0	305.1
FINCH	54/19	13	3	1.293	32.8	1113	564	0.9854	635.7	39,100	173.9	1431.0	2129.6	376.0	559.6
BUNTING	45/7	7	3	1.302	33.1	1192.5	604	1.001	645.8	32,000	142.3	1344.0	2000.1	219.0	325.9
GRACKLE	54/19	13	3	1.338	34.0	1192.5	604	1.055	680.6	41,900	186.4	1533.0	2281.4	403.0	599.7
BITTERN	45/7	7	3	1.345	34.2	1272	645	1.068	689.0	34,100	151.7	1434.0	2134.0	234.0	348.2
PHEASANT	54/19	13	3	1.382	35.1	1272	645	1.126	726.5	43,600	193.9	1635.0	2433.1	429.0	638.4
DIPPER	45/7	7	3	1.386	35.2	1351.5	685	1.134	731.6	36,200	161.0	1523.0	2266.5	248.0	369.1
MARTIN	54/19	13	3	1.424	36.2	1351.5	685	1.196	771.6	46,300	205.9	1737.0	2584.9	456.0	678.6
BOBOLINK	45/7	7	3	1.427	36.2	1431	725	1.201	774.8	38,300	170.4	1613.0	2400.4	263.0	391.4
PLOVER	54/19	13	3	1.465	37.2	1431	725	1.267	817.4	49,100	218.4	1840.0	2738.2	483.0	718.8
NUTHATCH	45/7	7	3	1.465	37.2	1510.5	765	1.268	818.1	40,100	178.4	1703.0	2534.3	278.0	413.7
PARROT	54/19	13	3	1.505	38.2	1510.5	765	1.336	861.9	51,700	230.0	1940.0	2887.0	509.0	757.5
LAPWING	45/7	7	3	1.504	38.2	1590	806	1.335	861.3	42,200	187.7	1792.0	2666.8	292.0	434.5
FALCON	54/19	13	3	1.545	39.2	1590	806	1.407	907.7	54,500	242.4	2044.0	3041.8	537.0	799.1
CHUKAR	84/19	8	4	1.602	40.7	1781	902	1.513	976.1	51,000	226.8	2075.0	3087.9	387.0	575.9
BLUEBIRD	84/19	8	4	1.762	44.8	2156	1092	1.8309	1181.2	60,300	268.2	2511.0	3736.8	468.0	696.5
KIWI	72/7	4	4	1.735	44.1	2167	1098	1.7758	1145.7	49,800	221.5	2303.0	3427.2	249.0	370.6
THRASHER	76/19	5	4	1.802	45.8	2312	1172	1.9144	1235.1	56,700	252.2	2526.0	3759.1	335.4	499.1
JOREE	76/19	5	4	1.880	47.8	2515	1274	2.0826	1343.6	61,700	274.4	2749.0	4091.0	364.9	543.0

Table A2.1-3 Electrical Characteristics of Common British Standard Aluminum Conductors Steel Reinforced (ACSR)

Conductor Name	Stranding Ratio	# of Aluminum Layers	Outside Diameter		Aluminum Crossectional Area		Diameter of OL Strands	# Strands in Outer Layer (OL)	Rdc@25C DC	Rac@25C 60Hz	Rac@75C 60Hz	GMR	Xa	X'a
			inches	mm	kcmil	sq mm	inches		Ohm/mi	Ohm/mi	Ohm/mi	ft	Ohm/mi	Mohm-mi
COUGAR	18/1	3	0.600	15.2	262	132.8	3.09	12	0.2211	0.2213	0.2656	0.0192	0.2989	0.1768
TIGER	30/7	2	0.651	16.5	262	132.8	2.39	18	0.2174	0.2179	0.2614	0.0224	0.2858	0.1717
DINGO	18/1	3	0.659	16.7	311	157.6	3.33	12	0.1844	0.1850	0.2220	0.0211	0.2902	0.1717
CARACAL	18/1	3	0.711	18.1	367	186.0	3.59	12	0.1588	0.1596	0.1915	0.0228	0.2852	0.1688
WOLF	30/7	2	0.714	18.1	311	157.6	2.59	18	0.1815	0.1819	0.2183	0.0246	0.2790	0.1677
JAGUAR	18/1	3	0.760	19.3	420	212.8	3.86	12	0.1388	0.1396	0.1675	0.0243	0.2852	0.1648
LYNX	30/7	2	0.770	19.6	367	186.0	2.81	18	0.1566	0.1570	0.1884	0.0265	0.2734	0.1638
PANTHER	30/7	2	0.826	21.0	420	212.8	3.03	18	0.1360	0.1361	0.1634	0.0284	0.2684	0.1603
LION	30/7	2	0.875	22.2	467	236.6	3.17	18	0.1210	0.1212	0.1454	0.0301	0.2628	0.1580
BEAR	30/7	2	0.924	23.5	524	265.5	3.38	18	0.1084	0.1089	0.1306	0.0318	0.2599	0.1553
GOAT	30/7	2	1.022	26.0	636	322.3	3.70	18	0.0884	0.0890	0.1068	0.0351	0.2523	0.1506
ANTELOPE	54/7	3	1.053	26.7	742	376.0	2.98	24	0.0774	0.0784	0.0940	0.0360	0.2517	0.1490
BISON	54/7	3	1.062	27.0	753	381.6	3.00	24	0.0762	0.0771	0.0925	0.0363	0.2510	0.1487
SHEEP	30/7	2	1.099	27.9	742	376.0	3.99	18	0.0766	0.0772	0.0927	0.0378	0.2467	0.1469
ZEBRA	54/7	3	1.125	28.6	848	429.7	3.18	24	0.0679	0.0688	0.0826	0.0385	0.2479	0.1458
DEER	30/7	2	1.176	29.9	848	429.7	4.27	18	0.0669	0.0679	0.0814	0.0404	0.2417	0.1438
CAMEL	54/7	3	1.188	30.2	943	477.8	3.36	24	0.0607	0.0619	0.0743	0.0406	0.2423	0.1434
ELK	30/7	2	1.239	31.5	940	476.3	4.50	18	0.0601	0.0610	0.0731	0.0426	0.2380	0.1413
MOOSE	54/7	3	1.251	31.8	1044	529.0	3.51	24	0.0547	0.0560	0.0672	0.0428	0.2392	0.1411

Table A2.1-4 Mechanical Characteristics of Common British Standard Aluminum Conductors Steel Reinforced (ACSR)

Conductor Name	Stranding Ratio	Type Number	# of Aluminum Layers	Outside Diameter		Aluminum Crossectional Area		Total Crossectional Area		Rated Breaking Strength		Total Conductor Weight		Weight of Steel Core (Class A galvanizing)	
				inches	mm	kcmil	sq mm	sq inches	sq mm	lbs	kN	lbs/kft	kg/km	lbs/kft	kg/km
COUGAR	18/1	5	3	0.600	15.2	262	132.8	0.215	138.7	6720	29.9	281	418.2	38.1	56.7
TIGER	30/7	22	2	0.651	16.5	262	132.8	0.2513	162.1	13600	60.5	407	605.7	161.4	240.2
DINGO	18/1	6	3	0.659	16.7	311	157.6	0.26	167.7	8100	36.0	336	500.0	45.5	67.8
CARACAL	18/1	4	3	0.711	18.1	367	186.0	0.301	194.2	9280	41.3	392	583.4	53.1	79.0
WOLF	30/7	24	2	0.714	18.1	311	157.6	0.3023	195.0	16100	71.6	489	727.7	193.9	288.6
JAGUAR	18/1	5	3	0.760	19.3	420	212.8	0.345	222.6	10300	45.8	451	671.2	61.1	90.9
LYNX	30/7	22	2	0.770	19.6	367	186.0	0.3516	226.8	18700	83.2	568	845.3	225.2	335.2
PANTHER	30/7	23	2	0.826	21.0	420	212.8	0.4048	261.2	21400	95.2	655	974.7	259.7	386.5
LION	30/7	24	2	0.875	22.2	467	236.6	0.454	292.9	23400	104.1	734	1092.3	291.1	433.2
BEAR	30/7	23	2	0.924	23.5	524	265.5	0.5062	326.6	26100	116.1	819	1218.8	324.8	483.3
GOAT	30/7	24	2	1.022	26.0	636	322.3	0.6194	399.6	30600	136.1	1002	1491.1	397.3	591.3
ANTELOPE	54/7	13	3	1.053	26.7	742	376.0	0.6558	423.1	26800	119.2	953	1418.2	255.1	379.7
BISON	54/7	13	3	1.062	27.0	753	381.6	0.6673	430.5	27300	121.4	970	1443.5	259.7	386.4
SHEEP	30/7	23	2	1.099	27.9	742	376.0	0.7163	462.1	35100	156.1	1159	1724.8	459.6	684.0
ZEBRA	54/7	12	3	1.125	28.6	848	429.7	0.7485	482.9	29900	133.0	1088	1619.1	291.3	433.4
DEER	30/7	23	2	1.176	29.9	848	429.7	0.8203	529.2	40200	178.8	1328	1976.3	526.6	783.7
CAMEL	54/7	13	3	1.188	30.2	943	477.8	0.8345	538.4	33400	148.6	1213	1805.1	324.7	483.2
ELK	30/7	23	2	1.239	31.5	940	476.3	0.9106	587.5	44600	198.4	1473	2192.1	584.1	869.3
MOOSE	54/7	13	3	1.251	31.8	1044	529.0	0.9254	597.0	37000	164.6	1346	2003.1	360.3	536.2

Table A2.1-5 Electrical Characteristics of Aluminum Conductor Steel Reinforced (ACSS)

Conductor Name	Stranding Ratio	# of Aluminum Layers	Outside Diameter		Aluminum Crossectional Area		Diameter of OL Strands	# Strands in Outer Layer (OL)	Rdc@25C DC	Rac@25C 60Hz	Rac@75C 60Hz	GMR	Xa	X'a
			inches	mm	kcmil	sq mm	inches		Ohm/mi	Ohm/mi	Ohm/mi	ft	Ohm/mi	Mohm-mi
Partridge/ACSS	26/7	2	0.642	16.3	266.8	135.2	0.1013	16	0.3338	0.3343	0.4019	0.0217	0.465	0.1074
Junco/ACSS	30/7	2	0.660	16.8	266.8	135.2	0.0943	18	0.3316	0.3320	0.3991	0.0227	0.459	0.1066
Ostrich/ACSS	26/7	2	0.680	17.3	300.0	152.	0.1074	16	0.2969	0.2974	0.3575	0.0230	0.458	0.1057
WoodCock/ACSS	22/7	2	0.701	17.8	336.4	170.5	0.1237	14	0.2669	0.2677	0.3218	0.0232	0.457	0.1048
Linnet/ACSS	26/7	2	0.720	18.3	336.4	170.5	0.1137	16	0.2648	0.2654	0.3190	0.0243	0.451	0.1040
Oriole/ACSS	30/7	2	0.741	18.8	336.4	170.5	0.1059	18	0.2630	0.2635	0.3167	0.0255	0.445	0.1031
Ptarmigan/ACSS	20/7	2	0.752	19.1	397.5	201.4	0.1410	13	0.2268	0.2277	0.2737	0.0246	0.450	0.1027
Brant/ACSS	24/7	2	0.772	19.6	397.5	201.4	0.1287	15	0.2250	0.2258	0.2714	0.0259	0.444	0.1019
Ibis/ACSS	26/7	2	0.783	19.9	397.5	201.4	0.1236	16	0.2241	0.2248	0.2701	0.0265	0.441	0.1015
Lark/ACSS	30/7	2	0.806	20.5	397.5	201.4	0.1151	18	0.2226	0.2232	0.2681	0.0277	0.435	0.1007
Tailorbird/ACSS	20/7	2	0.824	20.9	477.0	241.7	0.1544	13	0.1890	0.1901	0.2284	0.0270	0.439	0.1000
Flicker/ACSS	24/7	2	0.846	21.5	477.0	241.7	0.1410	15	0.1875	0.1885	0.2264	0.0283	0.433	0.09920
Hawk/ACSS	26/7	2	0.858	21.8	477.0	241.7	0.1354	16	0.1867	0.1876	0.2253	0.0290	0.430	0.09880
Hen/ACSS	30/7	2	0.883	22.4	477.0	241.7	0.1261	18	0.1855	0.1862	0.2236	0.0304	0.424	0.09800
Sapsucker/ACSS	22/7	2	0.901	22.9	556.5	282.	0.1590	14	0.1614	0.1626	0.1952	0.0298	0.426	0.09740
Parakeet/ACSS	24/7	2	0.914	23.2	556.5	282.	0.1523	15	0.1607	0.1618	0.1943	0.0306	0.423	0.09690
Dove/ACSS	26/7	2	0.927	23.5	556.5	282.	0.1463	16	0.1600	0.1610	0.1933	0.0313	0.420	0.09650
Eagle/ACSS	30/7	2	0.953	24.2	556.5	282.	0.1362	18	0.1590	0.1598	0.1919	0.0328	0.415	0.09570
Peacock/ACSS	24/7	2	0.953	24.2	605.0	306.6	0.1588	15	0.1478	0.1490	0.1789	0.0319	0.418	0.09570
Squab/ACSS	26/7	2	0.966	24.5	605.0	306.6	0.1525	16	0.1472	0.1483	0.1780	0.0327	0.415	0.09530
Wood Duck/ACSS	30/7	2	0.994	25.2	605.0	306.6	0.1420	18	0.1463	0.1471	0.1766	0.0342	0.410	0.09440
Teal/ACSS	30/19	2	0.994	25.2	605.0	306.6	0.1420	18	0.1464	0.1472	0.1767	0.0342	0.410	0.09450
Goldfinch/ACSS	22/7	2	0.963	24.5	636.0	322.3	0.1700	14	0.1412	0.1426	0.1711	0.0319	0.418	0.09540
Rook/ACSS	24/7	2	0.977	24.8	636.0	322.3	0.1628	15	0.1406	0.1419	0.1702	0.0327	0.415	0.09500
Grosbeak/ACSS	26/7	2	0.991	25.2	636.0	322.3	0.1564	16	0.1400	0.1412	0.1694	0.0335	0.412	0.09460
Scoter/ACSS	30/7	2	1.019	25.9	636.0	322.3	0.1456	18	0.1391	0.1401	0.1681	0.0351	0.407	0.09370
Egret/ACSS	30/19	2	1.019	25.9	636.0	322.3	0.1456	18	0.1392	0.1402	0.1682	0.0351	0.407	0.09370
Flamingo/ACSS	24/7	2	1.000	25.4	666.6	337.8	0.1667	15	0.1342	0.1355	0.1625	0.0335	0.412	0.09430
Gannet/ACSS	26/7	2	1.014	25.8	666.6	337.8	0.1601	16	0.1336	0.1348	0.1617	0.0343	0.409	0.09390
Stilt/ACSS	24/7	2	1.036	26.3	715.5	362.6	0.1727	15	0.1250	0.1264	0.1516	0.0347	0.408	0.09320
Starling/ACSS	26/7	2	1.051	26.7	715.5	362.6	0.1659	16	0.1245	0.1258	0.1508	0.0355	0.405	0.09280
Redwing/ACSS	30/19	2	1.081	27.5	715.5	362.6	0.1544	18	0.1238	0.1248	0.1497	0.0372	0.399	0.09200
Puffin/ACSS	22/7	2	1.077	27.4	795.0	402.8	0.1901	14	0.1130	0.1147	0.1374	0.0357	0.396	0.09210
Cuckoo/ACSS	24/7	2	1.092	27.7	795.0	402.8	0.1820	15	0.1125	0.1141	0.1367	0.0365	0.402	0.09170
Drake/ACSS	26/7	2	1.108	28.1	795.0	402.8	0.1749	16	0.1120	0.1135	0.1359	0.0375	0.399	0.09120
Macaw/ACSS	42/7	3	1.055	26.8	795.0	402.8	0.1376	20	0.1136	0.1157	0.1385	0.0346	0.408	0.09270
Tern/ACSS	45/7	3	1.063	27.0	795.0	402.8	0.1329	21	0.1134	0.1153	0.1390	0.0352	0.406	0.09250
Condor/ACSS	54/7	3	1.092	27.7	795.0	402.8	0.1213	24	0.1125	0.1141	0.1406	0.0368	0.401	0.09170

Table A2.1-5 Electrical Characteristics of Aluminum Conductor Steel Reinforced (ACSS) (Continued)

Conductor Name	Stranding Ratio	# of Aluminum Layers	Outside Diameter		Aluminum Crossectional Area		Diameter of OL Strands	# Strands in Outer Layer (OL)	Rdc@25C DC	Rac@25C 60Hz	Rac@75C 60Hz	GMR	Xa	X'a
			inches	mm	kcmil	sq mm	inches		Ohm/mi	Ohm/mi	Ohm/mi	ft	Ohm/mi	Mohm-mi
Mallard/ACSS	30/19	2	1.140	29.0	795.0	402.8	0.1628	18	0.1114	0.1125	0.1349	0.0392	0.393	0.09040
Ruddy/ACSS	45/7	3	1.131	28.7	900.0	456.	0.1414	21	0.1002	0.1023	0.1232	0.0374	0.399	0.09060
Canary/ACSS	54/7	3	1.162	29.5	900.0	456.	0.1291	24	0.09938	0.1012	0.1245	0.0392	0.393	0.08980
Corncrake/ACSS	20/7	2	1.165	29.6	954.0	483.4	0.2184	13	0.09448	0.09681	0.1156	0.0381	0.396	0.08970
Redbird/ACSS	24/7	2	1.196	30.4	954.0	483.4	0.1994	15	0.09376	0.09564	0.1144	0.0400	0.391	0.08900
Rail/ACSS	45/7	3	1.165	29.6	954.0	483.4	0.1456	21	0.09448	0.09681	0.1164	0.0385	0.395	0.08970
Towhee/ACSS	48/7	3	1.175	29.8	954.0	483.4	0.1410	22	0.09425	0.09642	0.1152	0.0391	0.393	0.08950
Cardinal/ACSS	54/7	3	1.196	30.4	954.0	483.4	0.1329	24	0.09376	0.09564	0.1176	0.0404	0.390	0.08900
Canvasback/ACSS	30/19	2	1.248	31.7	954.0	483.4	0.1783	18	0.09282	0.09422	0.1128	0.0430	0.382	0.08769
Snowbird/ACSS	42/7	3	1.203	30.6	1033.5	523.7	0.1569	20	0.08741	0.09010	0.1075	0.0395	0.392	0.08879
Ortolan/ACSS	45/7	3	1.212	30.8	1033.5	523.7	0.1515	21	0.08722	0.08973	0.1077	0.0401	0.390	0.08860
Curlew/ACSS	54/7	3	1.245	31.6	1033.5	523.7	0.1383	24	0.08654	0.08859	0.1087	0.0420	0.385	0.08780
Bluejay/ACSS	45/7	3	1.258	32.0	1113.0	564.	0.1573	21	0.08099	0.08368	0.1003	0.0416	0.386	0.08740
Finch/ACSS	54/19	3	1.292	32.8	1113.0	564.	0.1436	24	0.08078	0.08296	0.1017	0.0436	0.380	0.08670
Bunting/ACSS	45/7	3	1.302	33.1	1192.5	604.2	0.1628	21	0.07559	0.07846	0.09394	0.0431	0.382	0.08640
Grackle/ACSS	54/19	3	1.337	34.0	1192.5	604.2	0.1486	24	0.07539	0.07773	0.09511	0.0451	0.376	0.08560
Bittern/ACSS	45/7	3	1.345	34.2	1272.0	644.5	0.1681	21	0.07086	0.07392	0.08836	0.0448	0.378	0.08550
Pheasant/ACSS	54/19	3	1.381	35.1	1272.0	644.5	0.1535	24	0.07068	0.07317	0.08939	0.0466	0.372	0.08470
Dipper/ACSS	45/7	3	1.386	35.2	1351.5	684.8	0.1733	21	0.06669	0.06993	0.08346	0.0459	0.374	0.08460
Martin/ACSS	54/19	3	1.424	36.2	1351.5	684.8	0.1582	24	0.06653	0.06916	0.08436	0.0480	0.368	0.08380
Bobolink/ACSS	45/7	3	1.427	36.2	1431.0	725.1	0.1783	21	0.06299	0.06640	0.07912	0.0472	0.371	0.08370
Plover/ACSS	54/19	3	1.465	37.2	1431.0	725.1	0.1628	24	0.06283	0.06560	0.07989	0.0494	0.365	0.08290
Nuthatch/ACSS	45/7	3	1.466	37.2	1510.0	765.1	0.1832	21	0.05967	0.06326	0.07525	0.0485	0.367	0.08290
Parrot/ACSS	54/19	3	1.505	38.2	1510.0	765.1	0.1672	24	0.05952	0.06245	0.07592	0.0508	0.362	0.08210
Ratite/ACSS	42/7	3	1.492	37.9	1590.0	805.7	0.1946	20	0.05682	0.06083	0.07177	0.0490	0.366	0.08240
Lapwing/ACSS	45/7	3	1.504	38.2	1590.0	805.7	0.1880	21	0.05669	0.06045	0.07178	0.0497	0.364	0.08220
Falcon/ACSS	54/19	3	1.544	39.2	1590.0	805.7	0.1716	24	0.05655	0.05961	0.07235	0.0521	0.359	0.08140
Chukar/ACSS	84/19	4	1.601	40.7	1780.0	901.9	0.1456	30	0.05080	0.05475	0.06447	0.0534	0.355	0.08030
Mockingbird/ACSS	72/7	4	1.681	42.7	2034.5	1030.9	0.1681	27	0.04467	0.04978	0.05812	0.0553	0.351	0.07890
Roadrunner/ACSS	76/19	4	1.700	43.2	2057.0	1042.3	0.1645	28	0.04412	0.04904	0.05729	0.0562	0.349	0.07853
Bluebird/ACSS	84/19	4	1.762	44.8	2156.0	1092.5	0.1602	30	0.04194	0.04661	0.05444	0.0588	0.344	0.07750
Kiwi/ACSS	72/7	4	1.735	44.1	2167.0	1098.	0.1735	27	0.04194	0.04732	0.05508	0.0570	0.348	0.07790
Thrasher/ACSS	76/19	4	1.802	45.8	2312.0	1171.5	0.1744	28	0.03925	0.04467	0.05188	0.0595	0.342	0.07680
Joree/ACSS	76/19	4	1.880	47.8	2515.0	1274.4	0.1819	28	0.03608	0.04188	0.04842	0.0621	0.337	0.07550

Table A2.1-6 Mechanical Characteristics of Aluminum Conductor Steel Reinforced (ACSS)

Conductor Name	Stranding Ratio	Type Number	# of Aluminum Layers	Outside Diameter		Aluminum Crossectional Area		Rated Breaking Strength - HS Steel		Rated Breaking Strength - EHS Steel		Total Conductor Weight		Weight of Steel Core (Class A galvanizing)	
				inches	mm	kcmil	sq mm	lbs	kN	lbs	kN	lbs/kft	kg/km	lbs/kft	kg/km
Partridge/ACSS	26/7	16	2	0.642	16.3	266.8	135.2	8,880	39.5	9,730	43.3	366.9	546.0	115.6	172.0
Junco/ACSS	30/7	23	2	0.660	16.8	266.8	135.2	11,700	52.0	13,000	57.8	416.8	620.3	165.5	246.3
Ostrich/ACSS	26/7	16	2	0.680	17.3	300.0	152.	10,000	44.5	10,900	48.5	412.3	613.6	129.8	193.2
WoodCock/ACSS	22/7	10	2	0.701	17.8	336.4	170.5	7,610	33.9	8,260	36.7	404.9	602.6	87.8	130.7
Linnet/ACSS	26/7	16	2	0.720	18.3	336.4	170.5	11,200	49.8	12,300	54.7	462.1	687.7	145.5	216.5
Oriole/ACSS	30/7	23	2	0.741	18.8	336.4	170.5	14,800	65.8	16,300	72.5	526.4	783.4	208.7	310.6
Ptarmigan/ACSS	20/7	7	2	0.752	19.1	397.5	201.4	7,090	31.5	7,630	33.9	447.7	666.3	73.2	108.9
Brant/ACSS	24/7	13	2	0.772	19.6	397.5	201.4	11,000	48.9	12,100	53.8	511.4	761.1	137.0	203.9
Ibis/ACSS	26/7	16	2	0.783	19.9	397.5	201.4	13,000	57.8	14,200	63.2	546.0	812.5	171.9	255.8
Lark/ACSS	30/7	23	2	0.806	20.5	397.5	201.4	17,500	77.8	19,300	85.8	621.9	925.5	246.6	367.0
Tailorbird/ACSS	20/7	7	2	0.824	20.9	477.0	241.7	8,490	37.8	9,140	40.7	536.7	798.7	87.6	130.4
Flicker/ACSS	24/7	13	2	0.846	21.5	477.0	241.7	13,000	57.8	14,200	63.2	613.9	913.6	164.5	244.8
Hawk/ACSS	26/7	16	2	0.858	21.8	477.0	241.7	15,600	69.4	17,100	76.1	655.4	975.3	206.4	307.2
Hen/ACSS	30/7	23	2	0.883	22.4	477.0	241.7	21,000	93.4	22,700	101.0	746.4	1110.8	296.0	440.5
Sapsucker/ACSS	22/7	10	2	0.901	22.9	556.5	282.	12,600	56.1	13,600	60.5	669.0	995.6	145.1	215.9
Parakeet/ACSS	24/7	13	2	0.914	23.2	556.5	282.	15,200	67.6	16,600	73.8	716.1	1065.7	191.8	285.4
Dove/ACSS	26/7	16	2	0.927	23.5	556.5	282.	18,200	81.0	19,900	88.5	765.2	1138.7	241.0	358.6
Eagle/ACSS	30/7	23	2	0.953	24.2	556.5	282.	24,500	109.0	26,500	117.9	870.8	1295.9	345.3	513.9
Peacock/ACSS	24/7	13	2	0.953	24.2	605.0	306.6	16,500	73.4	18,100	80.5	778.7	1158.8	208.7	310.6
Squab/ACSS	26/7	16	2	0.966	24.5	605.0	306.6	19,700	87.6	21,700	96.5	831.3	1237.1	261.8	389.6
Wood Duck/ACSS	30/7	23	2	0.994	25.2	605.0	306.6	26,100	116.1	28,300	125.9	946.5	1408.5	375.3	558.5
Teal/ACSS	30/19	23	2	0.994	25.2	605.0	306.6	26,600	118.3	29,300	130.3	938.7	1396.9	367.5	546.9
Goldfinch/ACSS	22/7	10	2	0.963	24.5	636.0	322.3	14,100	62.7	15,300	68.1	764.8	1138.1	165.9	246.9
Rook/ACSS	24/7	13	2	0.977	24.8	636.0	322.3	17,300	77.0	19,000	84.5	818.2	1217.6	219.1	326.1
Grosbeak/ACSS	26/7	16	2	0.991	25.2	636.0	322.3	20,700	92.1	22,400	99.6	874.2	1301.0	275.2	409.5
Scoter/ACSS	30/7	23	2	1.019	25.9	636.0	322.3	27,400	121.9	29,700	132.1	995.1	1480.9	394.6	587.2
Egret/ACSS	30/19	23	2	1.019	25.9	636.0	322.3	28,000	124.5	30,900	137.4	987.2	1469.1	386.7	575.5
Flamingo/ACSS	24/7	13	2	1.000	25.4	666.6	337.8	18,200	81.0	19,900	88.5	857.9	1276.7	229.7	341.8
Gannet/ACSS	26/7	26	2	1.014	25.8	666.6	337.8	21,700	96.5	23,400	104.1	916.2	1363.5	288.5	429.3
Stilt/ACSS	24/7	13	2	1.036	26.3	715.5	362.6	19,500	86.7	21,300	94.7	920.8	1370.3	246.6	367.0
Starling/ACSS	26/7	16	2	1.051	26.7	715.5	362.6	23,300	103.6	25,200	112.1	983.7	1463.9	309.7	460.9
Redwing/ACSS	30/19	23	2	1.081	27.5	715.5	362.6	30,800	137.0	34,000	151.2	1109.4	1651.0	434.1	646.0
Puffin/ACSS	22/7	10	2	1.077	27.4	795.0	402.8	17,700	78.7	19,200	85.4	956.4	1423.3	207.6	308.9
Cuckoo/ACSS	24/7	13	2	1.092	27.7	795.0	402.8	21,700	96.5	23,300	103.6	1022.7	1521.9	273.9	407.6
Drake/ACSS	26/7	16	2	1.108	28.1	795.0	402.8	25,900	115.2	28,000	124.5	1093.4	1627.2	344.3	512.4
Macaw/ACSS	42/7	5	3	1.055	26.8	795.0	402.8	11,800	52.5	12,600	56.1	857.6	1276.3	108.6	161.6
Tern/ACSS	45/7	7	3	1.063	27.0	795.0	402.8	14,200	63.2	15,200	67.6	894.7	1331.5	146.1	217.4
Condor/ACSS	54/7	13	3	1.092	27.7	795.0	402.8	21,700	96.5	23,300	103.6	1022.3	1521.4	273.9	407.6
Mallard/ACSS	30/19	23	2	1.140	29.0	795.0	402.8	34,300	152.6	37,900	168.6	1233.9	1836.2	483.2	719.1
Ruddy/ACSS	45/7	7	3	1.131	28.7	900.0	456.	15,800	70.3	17,000	75.6	1012.9	1507.4	165.5	246.3

Table A2.1-6 Mechanical Characteristics of Aluminum Conductor Steel Reinforced (ACSS) (Continued)

Conductor Name	Stranding Ratio	Type Number	# of Aluminum Layers	Outside Diameter		Aluminum Crossectional Area		Rated Breaking Strength - HS Steel		Rated Breaking Strength - EHS Steel		Total Conductor Weight		Weight of Steel Core (Class A galvanizing)	
				inches	mm	kcmil	sq mm	lbs	kN	lbs	kN	lbs/kft	kg/km	lbs/kft	kg/km
Canary/ACSS	54/7	13	3	1.162	29.5	900.0	456.	24,600	109.4	26,400	117.4	1157.9	1723.1	310.2	461.6
Corncrake/ACSS	20/7	7	2	1.165	29.6	954.0	483.4	16,700	74.3	18,000	80.1	1074.0	1598.3	175.5	261.2
Redbird/ACSS	24/7	13	2	1.196	30.4	954.0	483.4	26,000	115.6	28,000	124.5	1227.5	1826.7	328.7	489.2
Rail/ACSS	45/7	7	3	1.165	29.6	954.0	483.4	16,700	74.3	18,000	80.1	1074.0	1598.3	175.5	261.2
Towhee/ACSS	48/7	9	3	1.175	29.8	954.0	483.4	19,700	87.6	21,300	94.7	1122.8	1670.9	224.0	333.3
Cardinal/ACSS	54/7	13	3	1.196	30.4	954.0	483.4	26,000	115.6	28,000	124.5	1227.0	1826.0	328.7	489.2
Canvasback/ACSS	30/19	23	2	1.248	31.7	954.0	483.4	41,100	182.8	45,400	201.9	1480.1	2202.6	579.6	862.5
Snowbird/ACSS	42/7	5	3	1.203	30.6	1033.5	523.7	15,400	68.5	16,500	73.4	1115.4	1659.9	141.5	210.6
Ortolan/ACSS	45/7	7	3	1.212	30.8	1033.5	523.7	18,100	80.5	19,500	86.7	1162.7	1730.3	189.9	282.6
Curlew/ACSS	54/7	13	3	1.245	31.6	1033.5	523.7	28,200	125.4	30,300	134.8	1328.8	1977.5	356	529.8
Bluejay/ACSS	45/7	7	3	1.258	32.0	1113.0	564.	19,500	86.7	21,100	93.9	1253.5	1865.4	204.8	304.8
Finch/ACSS	54/19	13	3	1.292	32.8	1113.0	564.	30,400	135.2	33,200	147.7	1430	2128.1	376.1	559.7
Bunting/ACSS	45/7	7	3	1.302	33.1	1192.5	604.2	20,900	93.0	22,500	100.1	1342.5	1997.9	219.1	326.1
Grackle/ACSS	54/19	13	3	1.337	34.0	1192.5	604.2	32,600	145.0	35,500	157.9	1531.4	2279.0	402.8	599.4
Bittern/ACSS	45/7	7	3	1.345	34.2	1272.0	644.5	22,300	99.2	24,000	106.8	1431.6	2130.5	233.9	348.1
Pheasant/ACSS	54/19	13	3	1.381	35.1	1272.0	644.5	34,100	151.7	37,300	165.9	1633.7	2431.2	429.4	639.0
Dipper/ACSS	45/7	7	3	1.386	35.2	1351.5	684.8	23,700	105.4	25,500	113.4	1521.2	2263.8	248.3	369.5
Martin/ACSS	54/19	13	3	1.424	36.2	1351.5	684.8	36,200	161.0	39,600	176.1	1735	2582.0	455.9	678.5
Bobolink/ACSS	45/7	7	3	1.427	36.2	1431.0	725.1	25,100	111.6	27,000	120.1	1610.6	2396.8	263.1	391.5
Plover/ACSS	54/19	13	3	1.465	37.2	1431.0	725.1	38,400	170.8	41,900	186.4	1837.8	2734.9	483.2	719.1
Nuthatch/ACSS	45/7	7	3	1.466	37.2	1510.0	765.1	26,500	117.9	28,100	125.0	1700	2529.9	277.5	413.0
Parrot/ACSS	54/19	13	3	1.505	38.2	1510.0	765.1	40,500	180.1	44,200	196.6	1938	2884.1	509.2	757.8
Ratite/ACSS	42/7	5	3	1.492	37.9	1590.0	805.7	23,400	104.1	25,000	111.2	1715.6	2553.1	217.5	323.7
Lapwing/ACSS	45/7	7	3	1.504	38.2	1590.0	805.7	27,900	124.1	29,600	131.7	1790.3	2664.3	292.2	434.8
Falcon/ACSS	54/19	13	3	1.544	39.2	1590.0	805.7	42,600	189.5	46,600	207.3	2042	3038.8	537	799.1
Chukar/ACSS	84/19	8	4	1.601	40.7	1780.0	901.9	35,400	157.5	38,200	169.9	2072.1	3083.6	386.7	575.5
Mockingbird/ACSS	72/7	4	4	1.681	42.7	2034.5	1030.9	27,200	121.0	28,900	128.5	2159.6	3213.8	233.9	348.1
Roadrunner/ACSS	76/19	6	4	1.700	43.2	2057.0	1042.3	31,700	141.0	33,900	150.8	2245.1	3341.1	298.6	444.4
Bluebird/ACSS	84/19	8	4	1.762	44.8	2156.0	1092.5	42,100	187.3	45,500	202.4	2507.9	3732.2	467.5	695.7
Kiwi/ACSS	72/7	4	4	1.735	44.1	2167.0	1098.	29,000	129.0	30,800	137.0	2300.6	3423.7	249.2	370.9
Thrasher/ACSS	76/19	6	4	1.802	45.8	2312.0	1171.5	35,600	158.3	38,100	169.5	2523.3	3755.1	335.4	499.1
Joree/ACSS	76/19	6	4	1.880	47.8	2515.0	1274.4	38,700	172.1	41,400	184.1	2745	4085.0	364.9	543.0

Table A2.1-7 Electrical and Mechanical Characteristics of Common North American All Aluminum Conductors (AAC or A1)

Conductor Name	Number of Strands	# of Aluminum Layers	Outside Diameter		Total Crossectional Area			Rated Breaking Strength		Total Conductor Weight		Rdc@25C DC	Rac@25C 60Hz	Rac@75C 60Hz	GMR	Xa	X'a
			inches	mm	kcmil	sq in	sq mm	lbs	kN	lbs/kft	kg/km	Ohm/mi	Ohm/mi	Ohm/mi	ft	Ohm/mi	Mohm-mi
DAISY	7	1	0.5860	14.9	266.8	0.2097	135.3	4830	21.48	250.6	372.9	0.3490	0.3500	0.4190	0.0177	0.4890	0.1100
LAUREL	19	2	0.5930	14.9	266.8	0.2095	135.3	4970	21.48	250.4	372.9	0.3490	0.3500	0.4190	0.0187	0.4830	0.1097
TULIP	19	2	0.6660	16.9	336.4	0.2644	170.6	6150	27.36	316.0	470.3	0.2766	0.2780	0.3320	0.0210	0.4690	0.1062
CANNA	19	2	0.7230	18.4	397.5	0.3124	201.5	7110	31.63	373.4	555.7	0.2340	0.2350	0.2820	0.0228	0.4590	0.1037
COSMOS	19	2	0.7930	20.2	477.0	0.3744	241.5	8360	38.65	447.5	665.8	0.1954	0.1970	0.2350	0.0250	0.4480	0.1010
SYRINGA	37	3	0.7950	20.1	477.0	0.3743	241.5	8690	37.19	447.4	666.0	0.1954	0.1970	0.2350	0.0254	0.4460	0.1010
DAHLIA	19	2	0.8550	21.8	556.5	0.4369	281.8	9750	44.21	522.1	776.8	0.1674	0.1690	0.2020	0.0270	0.4380	0.09880
MISTLETOE	37	3	0.8580	21.7	556.5	0.4368	281.9	9940	43.37	522.0	777.0	0.1674	0.1690	0.2020	0.0275	0.4360	0.09870
ORCHID	37	3	0.9180	23.3	636.0	0.4995	322.3	11400	50.71	596.9	888.3	0.1464	0.1490	0.1770	0.0294	0.4280	0.09670
NASTURTIUM	61	4	0.9750	24.8	715.5	0.5619	362.5	13100	58.27	671.6	999.5	0.1301	0.1330	0.1580	0.0312	0.4200	0.09490
VIOLET	37	3	0.9740	24.7	715.5	0.5622	362.7	12800	56.93	672.0	1000.1	0.1301	0.1330	0.1580	0.0314	0.4210	0.09490
ARBUTUS	37	3	1.0260	30.1	795.0	0.6245	402.8	13900	63.16	746.4	1110.2	0.1170	0.1200	0.1420	0.0328	0.4150	0.09340
LILAC	61	4	1.0280	26.1	795.0	0.6248	402.9	14300	61.83	746.7	1110.8	0.1170	0.1200	0.1420	0.0331	0.4140	0.09330
ANEMONE	37	3	1.0770	27.4	874.5	0.6874	443.5	15000	66.72	821.0	1221.8	0.1064	0.1090	0.1300	0.0344	0.4090	0.09200
CROCUS	61	4	1.0780	27.4	874.5	0.6876	443.6	15800	70.28	821.0	1221.8	0.1064	0.1090	0.1300	0.0347	0.4080	0.09190
GOLDENROD	61	4	1.1260	33.0	954.0	0.7498	483.2	16900	74.28	896.1	1333.4	0.0975	0.1010	0.1200	0.0360	0.4030	0.09060
MAGNOLIA	37	3	1.1240	28.6	954.0	0.7495	483.5	16400	72.95	895.8	1333.1	0.0975	0.1010	0.1190	0.0362	0.4030	0.09070
BLUEBELL	37	3	1.1700	29.8	1033.5	0.8124	524.0	17700	81.40	970.9	1444.4	0.0900	0.0933	0.1110	0.0374	0.3990	0.08950
LARKSPUR	61	4	1.1720	29.7	1033.5	0.8122	524.1	18300	78.73	970.6	1444.9	0.0900	0.0933	0.1110	0.0377	0.3980	0.08950
MARIGOLD	61	4	1.2160	35.6	1113.0	0.8744	563.9	19700	86.74	1045.0	1555.1	0.0836	0.0872	0.1030	0.0391	0.3930	0.08840
HAWTHORN	61	4	1.2580	36.8	1192.5	0.9363	603.9	21100	90.74	1119.0	1665.3	0.0781	0.0819	0.09680	0.0405	0.3890	0.08740
NARCISSUS	61	4	1.3000	33.0	1272.0	0.9990	644.5	22000	97.86	1194.0	1776.9	0.0732	0.0772	0.09110	0.0418	0.3850	0.08640
COLUMBINE	61	4	1.3400	34.0	1351.5	1.0620	685.2	23400	104.1	1269.0	1888.5	0.0688	0.0731	0.08610	0.0431	0.3810	0.08550
CARNATION	61	4	1.3790	35.0	1431.0	1.1240	725.2	24300	108.1	1344.0	2000.1	0.0650	0.0695	0.08170	0.0444	0.3780	0.08460
GLADIOLUS	61	4	1.4170	36.0	1511.0	1.1870	765.8	25600	113.9	1419.0	2111.7	0.0616	0.0663	0.07780	0.0456	0.3750	0.08380
COREOPSIS	61	4	1.4540	42.7	1590.0	1.2500	805.8	27000	123.7	1493.0	2221.8	0.0585	0.0634	0.07430	0.0468	0.3720	0.08310
JESSAMINE	61	4	1.5250	38.7	1750.0	1.3750	887.1	29700	132.1	1643.0	2445.1	0.0532	0.0585	0.06830	0.0490	0.3660	0.08170
COWSLIP	91	5	1.6300	41.4	2000.0	1.5700	1012.9	34200	152.1	1876.0	2791.8	0.0466	0.0525	0.06090	0.0526	0.3570	0.07970
LUPINE	91	5	1.8230	46.3	2500.0	1.9620	1265.8	41800	185.9	2368.0	3524.0	0.0376	0.0446	0.05120	0.0588	0.3440	0.07640
TRILLIUM	127	6	1.9980	50.8	3000.0	2.3560	1520.0	50300	223.7	2844.0	4232.3	0.0313	0.0392	0.04450	0.0646	0.3320	0.07360
BLUEBONNET	127	6	2.1580	54.8	3500.0	2.7490	1773.5	58700	261.1	3350.0	4985.4	0.0271	0.0357	0.04020	0.0697	0.3230	0.07140

REFERENCES

Adams, H.W. 1974. "Steel Supported Aluminum Conductors (SSAC) for Overhead Transmission Lines." *IEEE Transactions on Power Apparatus and Systems*. Vol. PAS-93. No. 5. September/October. Pp. 1700-1705.

Aluminum Association. 1989. *Aluminum Electrical Conductor Handbook*. Third Edition.

Aluminum Company of America. 1960."Resistance and Reactance of Aluminum Conductors." *Alcoa Aluminum Overhead Conductor Engineering Data*. Section 5. Rome Cable Division. Pittsburgh, PA.

ASTM. B856-95. "Standard Specification for Concentric-Lay-Stranded Aluminium Conductors." Coated Steel Supported (ACSS).

ASTM. B857-95. "Standard Specification for Shaped Wire Compact Concentric-Lay-Stranded Aluminium Conductors." Coated Steel Supported (ACSS/TW).

ASTM. B-1 Standard. 1996. *1996 Annual Book of ASTM Standards—Section 2, Nonferrous Metal Products*. Volume 02.03. Electrical Conductors.

ASTM. B701. 2000. "Concentric-Lay-Stranded Self-Damping Aluminum Conductors, Steel Reinforced (ACSR/SD)."

ASTM. B232. 2001. "Concentric-Lay-Stranded Aluminum Conductors, Coated-Steel Reinforced (ACSR)."

ASTM. B498. 2002. "Zinc-Coated (Galvanized) Steel Core Wire for Aluminum Conductors, Steel Reinforced (ACSR)."

ASTM. B502. 2002. "Aluminum-Clad Steel Core Wire for Aluminum Conductors, Aluminum-Clad Steel Reinforced."

ASTM. B779. 2003. "Shaped Wire Compact Concentric-Lay-Stranded Aluminum Conductors, Steel-Reinforced (ACSR/TW)."

Barrett, J.S., O. Nigol, C.J. Fehervari, and R.D. Findlay. 1986. "A New Model of AC Resistance in ACSR Conductors." *IEEE Transactions on Power Delivery.* Vol. 1. No. 2. pp. 198-207.

Bellman, R. 1960. *Introduction to Matrix Analysis.* New York, NY: McGraw-Hill Book Company.

Bergen, A.R. 1986. *Power Systems Analysis*. Englewood Cliffs, NJ: Prentice-Hall, Inc.

Black, W. Z. and R. L. Rehberg. 1985. "Simplified Model for Steady State and Real-Time Ampacity of Overhead Conductors." *IEEE Transactions on Power Apparatus and Systems*. Vol. 104. October. pp. 29-42.

Calabrese, G.O. 1959. *Symmetrical Components*. New York, NY: Ronald. pp. 289-298; 371-380.

Carson, J.R. 1928. "Wave Propagation in Overhead Wires with Ground Return." *Bell System Technical Journal*. Vol. 5. October. Pp. 539-554.

Chaston, N. 1969. "EHV AC Parallel Transmission Line Calculations with Application to the Near Resonance Problem." *IEEE Transactions on Power Apparatus and Systems.* Vol. PAS-88. No. 5. May. Pp. 627-635.

Clarke, E. 1943. *Circuit Analysis of A-C Power Systems.* Vol. 1. New York, NY: John Wiley and Sons. Pp. 373-375; 434-442.

Davidson, G. A. et al.1969. "Short-Time Thermal Ratings for Bare Overhead Conductors." *IEEE Transactions on Power Apparatus and Systems*. Vol. PAS-88. No.3. March.

Douglass, D. A. and L. A. Kirkpatrick. 1985. "AC Resistance of ACSR—Magnetic and Temperature Effects." *IEEE Transactions on Power Apparatus and Systems.* Vol. PAS-104. No. 6. June. pp.1578-1584.

Dwight, H.B. 1923. *Skin Effect in Tubular and Flat Conductors*.

El-Hawry, M.E. 1983. *Electrical Power Systems Design and Analysis*. Reston, VA: Reston Publishing Co.

Fakheri, A.J., A. Nourai, and J. M. Schneider. 1984. "The Open Loop Scheme: An Effective Method of Ground Wire Loss Reduction." IEEE *Transactions on Power Apparatus and Systems.* Vol. PAS-103. No. 12. December. Pp. 3615-3624.

Grainger, J.J. and W.D. Stevenson, Jr. 1994. *Power System Analysis*. New York, NY: McGraw-Hill, Inc.

Gross, C.A. 1979. *Power System Analysis*. New York, NY: John Wiley and Sons.

Gross, E.T.B. and A. H. Weston. 1951 "Transposition of High Voltage Overhead Lines and Elimination of Electrostatic Unbalance to Ground." *AIEE Transactions Power Apparatus and Systems.* Vol. 70. Part II. pp. 1837-1844; *Electrical Engineering*. Vol. 71. pp. 606-607. 1952.

Gross, E.T.B. and W. Chin. 1968. "Electrostatic Unbalance of Untransposed Single Circuit Lines." *IEEE Transactions on Power Apparatus and Systems*. Vol. PAS-87. pp. 24-34.

Gutman, R. 1988. "Application of Line Loadability Concepts to Operating Studies." *IEEE Transactions on Power Systems.* Vol 3. No 4. November. Pp. 1426-1433.

Harvey, J.R. 1972. "Effect of Elevated Temperature Operation on the Strength of Aluminum Conductors." Paper No. T 72 1984. IEEE Winter Meeting. New York, N.Y.

Harvey, J.R. and R.E. Larson. 1972. "Creep Equations of Conductors for Sag-Tension Calculations." IEEE Paper C72 190-2.

Hesse, M.H. 1963. "Electromagnetic and Electrostatic Transmission Line Parameters by Digital Computer." *IEEE Transactions on Power Apparatus and Systems*. Vol. PAS-82. June. Pp. 282-291.

IEC. International Standard 1089-1991 entitled: "Round Wire Concentric Lay Stranded Bare Overhead Conductors." First Edition.

IEEE. *Standard Definitions of Terms Relating to Overhead Power Line Corona and Radio Noise*.

IEEE. 1972. Working Group on Electrostatic Effects of Transmission Lines. "Electrostatic Effects of Overhead Transmission Lines. Part II – Methods of Calculation." *IEEE Transactions on Power Apparatus and Systems.* Vol. PAS-91. No. 2. March/April. Pp. 426-430.

IEEE. 1974. Working Group on Electromagnetic and Electrostatic Effects of Transmission Lines. "Electromagnetic Effects of Overhead Transmission Lines Practical Problems, Safeguards, and Methods of Calculation." *IEEE Transactions on Power Apparatus and Systems.* Vol. PAS-93. No. 3. May/June. Pp. 892-899.

IEEE. 1979. Subcommittee Report: *A Survey of Methods for Calculating Transmission Line Conductor Surface Voltage Gradients.* Paper F79 257-7. Presented at IEEE PES Winter Meeting. New York, NY. February.

IEEE. 1993a. "IEEE Guide to Grounding During the Installation of Overhead Transmission Line Conductors." *IEEE Standard 524a-1993.* IEEE New York.

IEEE. 1993b. "Standard for Calculating the Current-Temperature Relationship of Bare Overhead Conductors." IEEE Std 738-1993. 8 November.

IEEE. 2003. "IEEE Guide for Protective Grounding of Power Lines." *IEEE Standard. 1048-2003.* IEEE New York.

Jackson, J.D. 1975. *Classical Electrodynamics.* New York, NY: John Wiley & Sons, Inc.

Kotaka, S., et al. 2000. "Applications of Gap-Type Small-Sag Conductors for Overhead Transmission Lines." *SEI Technical Review.* No. 50. June.

LaForest, J.J. 1972. "Resonant Voltages on Reactor Compensated Unenergized 765 kV Transmission Line Excited by Nearby Energized 345 kV Line." *IEEE Transactions on Power Apparatus and Systems.* Vol. PAS-91. No. 6. November/December. Pp. 2528-2536.

Lambert, S.R. 1983. "Minimum Shield Wire Size – Fault Current Considerations." *IEEE Transactions on Power Apparatus and Systems.* Vol. PAS-102. No. 3. March. Pp. 572-578.

Lambert, S.R., V. Koschik, C.E. Wood, G. Worner, and R.G. Rocamora. 1978. "Long Line Single-Phase Switching Transients and their Effect on Station Equipment." *IEEE Transactions on Power Apparatus and Systems.* Vol. PAS-97. No. 3. May/June. pp 857-865.

Lawrence, R.F. and D. J. Povejsil. 1952. "Determination of Inductive and Capacitive Unbalance for Untransposed Transmission Lines." *AIEE Transactions Power Apparatus and Systems.* Vol. 71. pp. 547-556. April.

Lewis, W.A. and P.D. Tuttle. 1959. "The Resistance and Reactance of Aluminum Conductors, Steel Reinforced." *AIEE Transactions Power Apparatus and Systems.* Vol. 77. Part III. February. pp. 1189-1215.

Livingston, A.E. 1969. "Self-Damping Conductors for the Control of Aeolian Vibration of Transmission Lines." CEA Paper 70-TR-225. Presented at Calgary, Alberta, Canada meeting. October.

Long, R.W. and D. Gelopulos 1982. "Component Transformations – Eigenvalue Analysis Succinctly Defines Their Relationships." *IEEE Transactions on Power Apparatus and Systems*. Vol PAS-101, No. 10. October. Pp 4055-4063.

Maruvada, P.S. and W. Janischewskyj. 1969. "Electrostatic Field of a System of Parallel Cylindrical Conductors." *IEEE-PAS 88*. July. Pp. 1069-1079.

McCulloch, A.R. et al. 1980 "Ten Years of Progress with Self-Damping Conductor." *IEEE Transactions on Power Apparatus and Systems*. Vol. PAS-99. no.3. May/June.. pp. 998-1011.

Morgan, V.T. 1996. "Effect of Elevated Temperature Operation on the Tensile Strength of Overhead Conductors." *IEEE Transactions on Power Delivery*. Vol. 11. No. 1. January. Pp. 345-351.

Morgan, V.T., B. Zhang, and R.D. Findlay. 1997. "Effect of Magnetic Induction in a Steel-Cored Conductor on Current Distribution, Resistance and Power Loss." *IEEE Transactions on Power Delivery*. Vol. 12. No. 3. pp. 1299-1306.

National Electric Safety Code. 1997. 1997 Edition, C2-1997.

Peterson, H.A. 1966. *Transients in Power Systems*. New York: Dover Publications. pp 2-29.

Reitz, J. and F. Milford. 1967. *Foundations of Electromagnetic Theory.* Reading, MA: Addison-Wesley Publishing Co.

Roche, J.B. and D.A. Douglass. 1981. "Anti-Galloping Potential of a New Twisted Conductor Design." *Proceedings of the Canadian Electrical Association International Symposium on Overhead Conductor Dynamics*. Toronto, Canada. June. pp. 83-98.

Sasaki, S. et al. 1985. "ZTACIR-New Extra-Heat Resistant Galvanized Invar-Reinforced Aluminium Alloy Conductor." *Sumitomo Electric Technical Review*. No. 24. January.

Thrash, F.R. 1999. "ACSS/TW – An Improved Conductor for Upgrading Existing Lines or New Construction." 1999 IEEE T&D Conference. New Orleans, LA. April 11-16.

Tunstall, M.J., S.P. Hoffmann, Derbyshire, and Pyke. 2000. "Maximizing the Ratings of National Grid's Existing Transmission Lines Using High Temperature, Low Sag Conductor." Paper 22-202. CIGRE Session. Paris. August.

Varney, T. 1927. *ACSR Graphic Method for Sag-Tension Calculations*. Alcoa Publication.

Westinghouse. 1964. *Electrical Transmission and Distribution Reference Book*. Fourth Edition. East Pittsburgh, PA: Westinghouse. Pp. 41, 749-752.

Winkelman, P.F. 1959. "Sag-Tension Computations and Field Measurements of Bonneville Power Administration." AIEE Paper 59-900. June.

CHAPTER 3

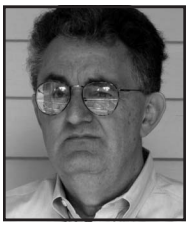
Insulation Design

Nicholas C. Abi-Samra
Ian Grant

This chapter describes insulation coordination, or how overvoltage and line insulation performance are balanced in a transmission-line design. Guidance is provided for determining overvoltages (stresses), insulation levels (strengths), and the balance between them to achieve acceptable line performance.



Nicholas (Nick) C. Abi-Samra is a leading expert and practitioner in transmission line and station insulation coordination. He has conducted numerous lightning and switching surge analysis studies for utilities in the U.S. and other countries. He was instrumental in designing a high-voltage test facility for the study of insulation strength, as well as a facility to collect and analyze contamination on line insulators. Abi-Samra taught Insulation Coordination in graduate-level courses at Carnegie-Mellon, Penn State Universities, and the Westinghouse Advanced School in Power Engineering. He has co-authored more than 50 technical papers for IEEE, IEE, and CIGRE, as well as a number of articles for trade magazines. Presently, as Senior Technical Director of EPRIsolutions, he has the responsibility for a wide range of power system technical issues in transmission and distribution engineering. He is a Registered Professional Engineer in several states in the U.S., and the recipient of more than 10 engineering awards.



Ian Grant has worked in all aspects of transmission-line design for more than 40 years, initially with the Electricity Commission of NSW, Australia, later with GE's HV Laboratories in Pittsfield and Lenox, Mass, Power Technologies, Inc., and most recently as Manager of Special Studies at the Tennessee Valley Authority. He is a co-author of the *EPRI Compact Line Design Book* (the Light Blue Book) and over 40 IEEE, CIGRE, and EPRI publications on transmission-line design, insulation, lightning, and switching surge research. He also developed a number of early computer programs for transmission studies. Ian pioneered use of polymer insulators in compact lines, and helped design and build the first experimental high-phase-order 6 and 12 phase lines. He has chaired and contributed to numerous IEEE and CIGRE committees and working groups. Ian is a Fellow of IEEE and a Distinguished Member of CIGRE.

3.1 INTRODUCTION

The apparent simplicity of a transmission line is, in reality, the result of a sophisticated design process. Tradeoffs are made between performance, which requires withstanding all overvoltages, and the cost of controlling them and providing sufficiently strong insulation. This chapter describes insulation coordination, or how overvoltage and line insulation performance are balanced in a transmission-line design. Insulation coordination addresses critical tower dimensions and insulation, and is based on a mass of experimental data, modeling and calculation techniques, operating and design experience, and economics. Guidance is provided here for determining overvoltages (stresses), insulation levels (strengths), and the balance between them to achieve acceptable line performance. Properly coordinated transmission-line insulation achieves reliability goals at least cost.

3.1.1 Definition

In his seminal book on the subject, Hileman (Hileman 1999) provides a range of definitions of insulation coordination. His simplest definition is perhaps also the most sophisticated: "Insulation coordination is the selection of the insulation strength."

In selecting insulation strength for transmission lines, we consider all the following:

- A transmission line is subject to power frequency voltage and to transient voltages resulting from switching and lightning. These voltages can differ substantially from event to event.
- The strength of air gap clearances and insulation varies with weather and voltage stress characteristics.
- Voltage stress can be controlled by shielding, grounding, and by devices such as surge arresters and breaker resistors.
- The goal of the designer is the optimum combination of insulation, clearances, and voltage control to achieve a reliability target at least cost. As will be pointed out in this chapter, perfect performance is impossible or too costly to achieve.
- Since insulation breakdown is inevitable, provision should be made to ensure that any insulation breakdown is self-restoring.

Good transmission-line insulation coordination is not only important to achieve high reliability of transmission lines, but is also a key element to obtain acceptable mean time between failures (MTBF) for substations. Well-coordinated designs in both lines and substations are crucial to attaining a reliable transmission system at an affordable cost.

3.1.2 Design Factors for Transmission Lines

Transmission-line design requires the following specifications:

- The type of structure—single or multiple circuit, wood or metal, phase geometry
- Airgap clearances, including phase-to-tower, phase-to-phase, and phase-to-ground at midspan
- The amount, type, and configuration of insulators
- Grounding, including paths to ground and grounding resistance
- The number and location of overhead shield wires
- The need for, rating, and location of voltage-limiting devices, such as line surge arresters and breaker insertion resistors
- Possible use of wood in the lightning flashover paths for arc quenching

3.1.3 Critical Factors versus Stress Type

The flashover strength of air gaps and insulators differs depending on whether the voltage stress is power frequency, switching surge, or lightning, and the factors affecting flashover performance differ for each stress type. If the line strength is overdesigned for any one of these factors, the cost is nonoptimal. The insulation for power frequency (or switching surge, or lightning) is overdesigned when the cost of having provided better power frequency (or switching surge or lightning insulation) is greater than the cost of the avoided insulation failures. So the concept of overdesign resides within each type of stress, not in the comparison between stress types. Table 3.1-1 illustrates which design variables are critical for each of the stresses.

3.1.4 Design Optimization

A typical insulation coordination process is shown in Figure 3.1-1.

Table 3.1-1 Parameters Driven By the Different Stresses

	Tower Strike Distance	Surge Arresters	Tower Grounding	Shield Wires	Insulator String Length	Type of Insulators
Power Frequency (Contamination)						
Switching Surge						
Lightning						

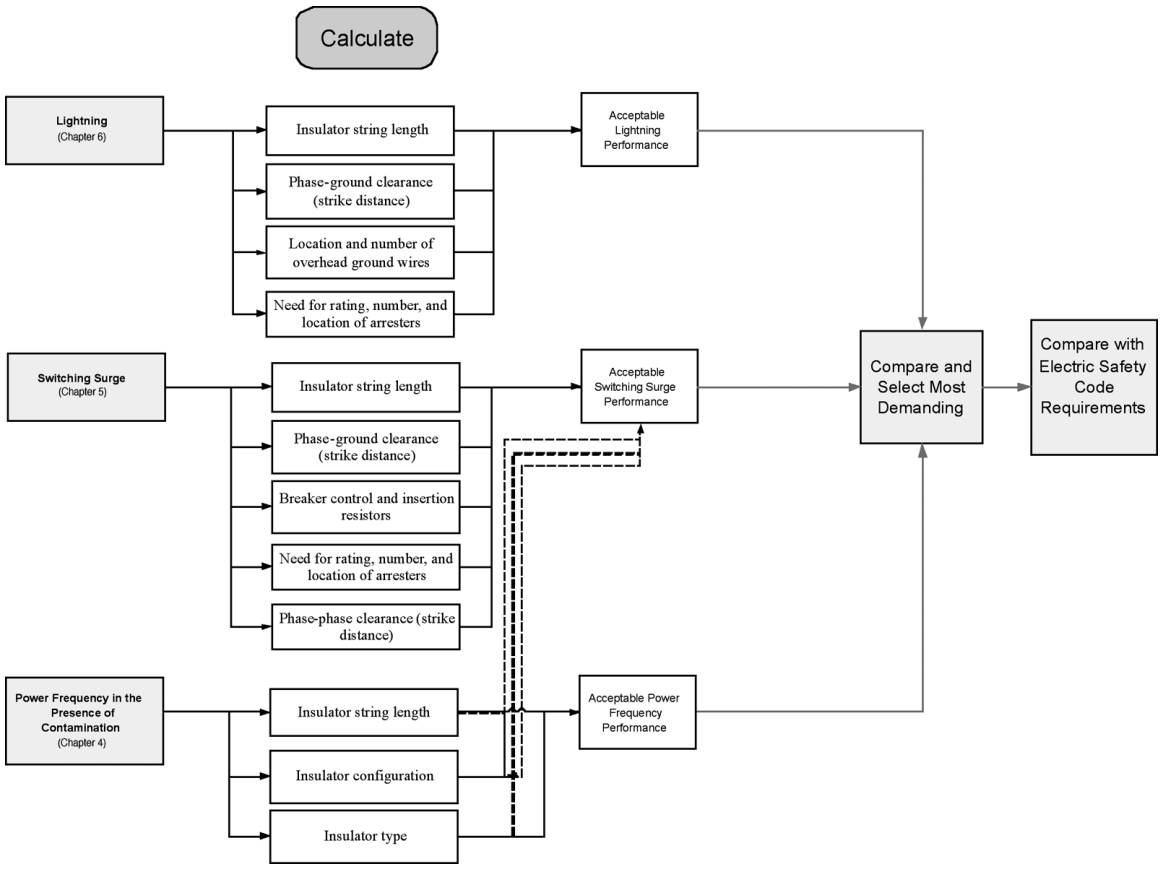


Figure 3.1-1 Insulation coordination process.

3.1.5 Calculation Methodology

This chapter provides designers with details on how to calculate voltage stress, and refers to Chapters 4-6 as appropriate for additional details on the calculation of strength. The process of insulation coordination is illustrated in Figure 3.1-2, showing how the range of stress is related to strength, to arrive at a practical low level of failure.

Two principal methods for coordination are described, deterministic and probabilistic, and reference is given to useful computer tools to help designers. In the simpler deterministic process, the stress and strength curves of Figure 3.1-2 would not overlap but would be separated by a safety margin. The more sophisticated probabilistic process provides a more realistic representation of the overlap of the curves in cost-effective designs. The probabilistic method is used in Applet IC-1 to calculate the risk of line flashover caused by switching surges. The calculation requires knowledge of the probability of overvoltage amplitudes, the strength of all the insulation elements of the line, and the value of the parameters affecting the strength.

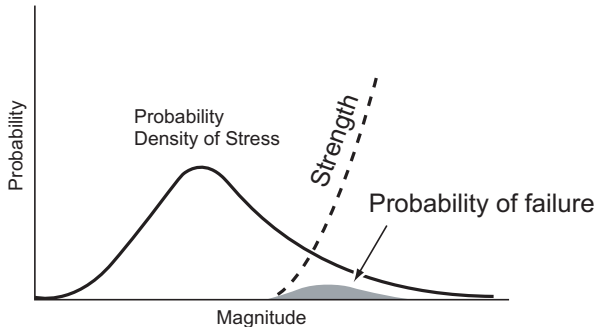


Figure 3.1-2 The balance of stress and strength in insulation coordination.

3.1.6 Typical Performance Criteria and Design Clearances

Today, in the absence of contamination, there is normally no performance criterion for power frequency voltages, such as there is for switching surges and lightning. Power frequency failures may be related to events causing insula-

tor damage, such as gunshots or aging, but, since these events are difficult to assess, it is not possible to derive a performance indicator. If contamination is an issue, a criterion may be set, but more typically the designer attempts to eliminate the problem. For switching surges, performance is specified in terms of flashovers per 100 switching operations, and for lightning, the performance criterion is normally specified as the number of flashovers per 100 km-years. Another criterion for lightning is denoted as the storm outage rate (SOR), which is the number of unsuccessful reclosures per year, obtained by multiplying the lightning flashovers per year by the switching surge flashovers per switching operation. For example, assuming the lightning flashover rate to be two per year, and the switching surge flashover rate to be one per 100 switching operations, the storm outage rate is two per 100 years. Both the storm outage rate and the lightning flashover rate may be important to customer power quality. Figure 3.1-3, derived from (Hileman 1999), illustrates relationships between typical performance criteria and designed strike distance as a function of system voltage.

Applet IC-2 calculates the strike distances required by the different stress types for system voltages from 200 to 1200 kV. Strike distances are calculated with various assumptions regarding acceptable performance criteria.

Although lines are typically designed for switching surge flashover rates between 1 and 10 flashovers per 100 switching operations, switching surge flashovers are extremely rare due to conservative assumptions in the design process. Lightning flashover rates on transmission lines vary with system voltage, and may range from 0.5 for systems exceeding 345 kV to 20 per 100 km-year for lower-voltage systems. Acceptable levels of lightning flashovers for a line are most often determined by soil resistivity and the cost of implementing countermeasures, such as supplemental grounding.

3.1.7 Applets

Two applets are provided with this chapter:

- IC-1: "Insulation Coordination—Comparative Evaluation of Insulation Distance Requirements." The applet compares the strike distances resulting from design specifications regarding power frequency (insulator contamination), switching surges, lightning, and the U.S. National Electrical Safety Code. The user may set the design specifications: contamination level, ceramic or nonceramic insulators, switching surge level, number of towers, admissible switching surge flashover rate, lightning flash density, footing resistance, and admissible lightning flashover rate. The applet shows graphically, for maximum system voltages from 200 to 1200 kV, the

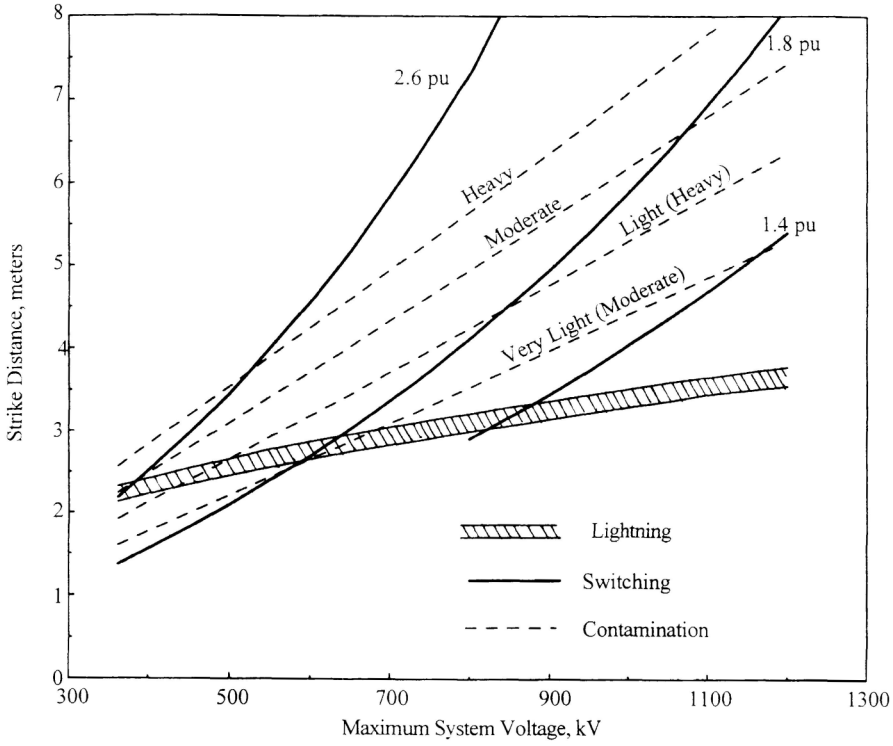


Figure 3.1-3 Comparison of requirements for power frequency, switching, and lightning.

strike distances conductor-to-tower that are required to meet the various specifications.

- IC-2: "Risk of Failure Calculations for Transmission Line Switching Surges." This applet calculates the risk of failure of a transmission line due to switching surges. The risk of failure is defined as the probability of an unwanted flashover of any insulation element of the transmission line when a switching operation is made. The risk of failure may be expressed as expected flashovers per million operations (e.g., 2.64 flashovers every million switching operations) or expected number of operations that result in one flashover (e.g., one flashover every 380,000 switching operations). Only three-phase lines and phase-to-ground flashovers are considered. It is implicitly assumed that the risk of phase-to-phase flashover is much lower. The user must input all the parameters that affect the risk of failure, such as the statistical distribution of the surge amplitudes, the statistical distribution of the surge waveshape, the statistical distribution of the weather conditions, the strength of each insulation element type, and the number of insulation elements for each type. The applet calculates the risk of flashover for the entire line and for each phase and each line section individually. The user may assess the effect of surge waveshape by comparing the results with those obtained if all the surges had critical waveshape.

3.1.8 Summary

The absolute protection of transmission lines against overvoltages is practically impossible. The task of this chapter is to help designers develop transmission lines that combine low risk with economy. No matter what the dictating stress may be, large economic incentives exist to reduce insulator string length and other tower dimensions. In the remainder of the chapter, we review the sources and nature of voltage stress; describe how to design for insulation strength with cross-references to the more detailed chapters on power frequency, switching surge, and lightning insulation design; and provide guidance and examples for optimization.

This chapter demonstrates that, with the use of measures like preinsertion resistors and controlled switching, switching surges do not dominate the design for transmission lines except at 1200 kV. It also shows that a number of measures can be employed to keep lightning flashovers under control, ranging from improving the grounding to employing transmission-line arresters. Finally, with the use of nonceramic (polymer) insulators, and special insulators, flashovers due to contamination can be minimized.

The ultimate goal of line design is that some day the line insulation will be dictated only by the normal power frequency voltage. We are still years away from this, but it can be stated with certainty that major accomplishments in countermeasures over the last 40 years have been achieved.

3.1.9 Layout of this Chapter

Section 3.2 describes the voltage stresses to which a transmission line is subjected and the key parameters that are significant to designers. Section 3.3 defines transmission-line insulation strength. Section 3.4 discusses the countermeasures available to line designers to control for lightning, switching surge, and power frequency under contamination. Section 3.5 illustrates how the requirements of local safety codes can influence transmission-line design (using the U.S. National Electric Safety Code as an example). Section 3.6 reviews the line insulation requirements and explains how they are coordinated. Section 3.7 discusses some of the economic decisions that designers may face during and after the technical tasks are completed.

Appendix 3.1 describes analytical tools available to line designers for use with insulation coordination. Appendix 3.2 identifies different types of surge arresters and their applications for controlling lighting and switching overvoltages. Appendix 3.3 reviews two types of approaches to insulation coordination—a probabilistic and a deterministic method. Appendix 3.4 presents IEC's approach to line insulation coordination.

3.2 VOLTAGE AND ENVIRONMENTAL STRESSES ON TRANSMISSION LINES

3.2.1 Introduction

This section describes the nature of the voltage *stresses* that a transmission line is subjected to, and hence, for which the insulation *strength* (as described in Section 3.3) should be designed. These stresses are caused by power frequency voltage (also known as "service voltage"), and temporary, switching, and lightning overvoltages.

Lightning strokes to transmission structures, phase conductors, or shield wires can cause flashovers that force the line to trip. Switching surges result from energizing and de-energizing of lines, capacitors, reactors, and transformers. Temporary overvoltages, also known as power frequency overvoltages, are caused by faults or are due to the Ferranti Effect (the phenomenon caused by capacitive charging of lines, and by which the steady voltage at the open end of an uncompensated unloaded transmission line is always higher than the voltage at the sending end). Environmental stresses to lines—due to pollution, rain, snow, ice, and temperature affecting the line insulation—are also important, and are covered briefly in this chapter and in detail in Chapter 4 for power frequency voltage and in Chapter 5 for switching overvoltages.

This section provides an overview of voltage stress and the key parameters that are significant to the designer. It covers the voltage stresses in the following order:

- Lightning overvoltages
- Switching surge overvoltages
- Temporary overvoltages
- Environmental stresses

For greater detail, the designer is referred to the chapters on power frequency (Chapter 4), switching surge, (Chapter 5), and lightning (Chapter 6).

3.2.2 Lightning

A detailed discussion of lightning is provided in Chapter 6. The following provides an overview of key issues for the designer. Design applications are discussed in Section 3.3.

Lightning is usually the principal factor in setting transmission insulation levels. Lightning strokes to transmission structures, phase conductors, or shield wires can cause flashovers that force the line to trip. Lightning can damage insulators, shatter wood poles or crossarms, and sever conductor strands, although these are rare occurrences on properly designed lines.

During the 1960s and 1970s, a number of new line designs were developed, including those for higher system voltages. These designs required detailed studies of lightning performance to ensure that appropriate performance was achieved, and years of operation to confirm the design expectations. Today most line construction uses designs or derivative designs for which the lightning performance is understood, so greater confidence can be placed in the study of the effects of design modifications. Typical practice is to refer to standards or expectations for each line type, with the primary parameter for adjustment being the footing resistance. On some lines having high exposure to lightning or where soil resistivity is high, it may also be necessary to address "hot spots" with special measures such as special grounding schemes, line arresters, or underbuilt shield wires. Use of the arc-quenching properties of wood (Darveniza 1980) has been successful on lower voltage lines, but may be difficult to incorporate as a retrofit. Adding insulators may seem a simple way to deal with hot spots, but it is usually impractical since it requires redimensioning and special structures to accommodate the longer insulator strings. Nonceramic insulators can offer an improved performance over glass and porcelain for the same connecting length. Their relatively light weight is also an advantage, and they can, frequently, be used to address "hot spot" problems.

Transmission-line lightning performance is, in the end, simply a matter of economics. At one extreme, a lightly insulated line with no shield wires and no grounding augmentation will have lighter and less costly structures, but will trip out more often during lightning (higher tripout rate). As each ameliorating measure is added—first one shield wire, then another, longer insulator strings and greater phase-ground clearance, basic grounding augmentation, then grounding measurements and special measures, line arresters, and other schemes—there is a tradeoff of cost versus tripout rate. Selection of tripout rates based on cost is, of course, complex, since the cost of an outage is difficult to quantify, and varies widely with time of day and the type of load served; also tripout rates can vary widely from year to year.

Lightning Characteristics

A lightning stroke can be considered as a high-impedance source of current. A stroke to a line structure or shield wire places the line in series with a discharge path between the cloud and ground, and the current passing through the structure raises its potential with respect to ground. The structure potential may increase to the point that a flashover occurs from the (higher-potential) structure to one or more of the (lower-potential) phase conductors. Because of the unusual circumstance of the structure being at a potential higher than the phase conductor, this type of flashover is called "backflashover." If a stroke connects to a phase conductor, then the reverse process may occur: a higher potential is created on the phase conductor than on the structure, and a flashover may occur if the difference in potential is sufficiently high. This type of flashover results from a "shielding failure," which is the failure of the shielding wires to intercept the lightning.

Most lightning strokes terminate on the shield wires at, or close to, the structure, which is the highest point at the end of a span, or on the structure itself. Strokes to the midspan of the conductor or shield wire appear to be less of a factor in line flashover rates than strokes near the support structures.

The strength of line insulation elements, such as insulators and air gaps, is often defined by the lightning impulse 50% flashover voltage, which is the crest voltage of a double-exponential impulse with a standardized waveshape (1.2 μs front time and 50 μs tail time) traditionally used to simulate lightning stress. For the calculation of lightning performance of transmission lines, however, Chapter 6 shows that the waveshape of the stroke current is defined in various ways to reproduce the most important features of the variety of waveshapes seen for actual strokes. Stroke characteristics and the number of strokes per year in a given area can vary widely with location and season as well as from year to year.

Table 3.2-1 Lightning Overvoltages

Source of Lightning Overvoltages	Comments
Flashes to the phase conductors (shielding failure).	Due to lack of shield wires or to inadequate shielding.
Flashes to the grounded line structure (or shield wires), which raises its potential so that it may flash over to a phase conductor (backflashover).	Voltage surges from backflash are usually more severe than those caused by shielding failures.
Flashes to ground in proximity to the line, which induce overvoltages in the phase conductors.	Voltages induced from nearby flashes are generally below 400 kV and pose no threat for lines of 200 kV and above.

Effect of Lightning on a Line

Overvoltage resulting from a lightning stroke develops in three ways, as shown in Table 3.2-1.

The lightning performance of transmission lines over 200 kV is then the sum of the following:

- The Shielding Failure Flashover Rate (SFFOR), and
- The Backflashover Rate (BFR).

Both these flashover rates are directly proportional to the number of lightning flashes to the line. In lightning performance calculations, this is assumed to be proportional to the lightning flash density, typically stated as flashes per square km per year. Statistically, however, it is possible to have high lightning activity, yet low tripout rates, if the lightning does not terminate in the immediate vicinity of the line. This might result from natural shielding, such as where a line is sheltered by trees or higher terrain. Conversely hot spots can occur where a portion of a line is particularly exposed.

Chapter 6 provides details of flash density that can be used by the designer and describes systems that provide real-time information on lightning occurrence. These systems can be useful in identifying "hot spots" where line improvements may be needed.

Effect of Power Frequency Voltage

As the current from a lightning stroke passes through the impedance of a structure, it raises the structure potential relative to ground. Since the phase conductors are insulated from the lightning current and are otherwise oscillating about true ground potential at power frequency, the potential difference across each phase insulator string is affected by the instantaneous value of power frequency voltage at the instant of the stroke, so this affects which phase flashes over first. For example, if the instantaneous value of power frequency voltage on a phase is opposite in polarity to the structure voltage caused by the lightning current, then the potential difference across the insulators is higher, and a backflashover may be more likely to occur on that phase. For shielding failures, the probability of flashover is slightly increased if the instantaneous value of power frequency voltage has the same polarity as the lightning-caused voltage.

While power frequency voltage may determine which phase flashes over first, it may be secondary to other considerations. For example, a design where one phase is higher on the structure than another will result in different instantaneous voltages at each location. These differences may be much greater than differences caused by power frequency voltage.

For shielding failures, the probability of a lightning stroke hitting a phase is theoretically increased slightly when the instantaneous value of the power frequency voltage is of opposite polarity to that of the lightning stroke, because in this case upward streamer generation is facilitated. Section 6.2 shows, however, that the leader potentials are in the range of 20-100 MV so the effect is small. Once a phase is hit, however, the overvoltage is greater if the instantaneous value of the power frequency voltage is of the same polarity and would, therefore, add to the voltage caused by the lightning. The two factors may balance each other and can be ignored. Generally, the effect of power frequency is not considered in the calculations of shielding failure rate.

Finally, some lighting-caused flashovers are self-extinguishing because they occur when the power frequency voltage is near zero and, therefore, may not be sufficient to sustain the arc. For lines with voltages greater than 200 kV, this effect is considered negligible and is not taken into account in the calculations of lightning flashover rates.

Shielding

If a stroke reaches a phase conductor, it creates an overvoltage whose amplitude depends on the stroke current and the surge impedance of the phase. If the stroke current is sufficiently high, the overvoltage exceeds the level that can be withstood by line insulation. In most regions, the frequency of flashovers caused by flashes to phase conductor would be intolerably high, if shield wires were not installed above the phase conductors to intercept lightning strokes. Thus overhead shield wires are customarily used to shield the phase conductors of a transmission line from lightning strokes.

As described in Chapter 6, a lightning leader develops as a series of steps between the cloud and ground. Whether or not a lightning stroke hits a phase conductor is governed by the length of the upward leader from the conductor to the downward leader. Lightning strokes with smaller currents have smaller charges and, therefore, induce shorter upward leaders from the shield wires. With shorter upward leaders, the protection provided by the shield wires is less.

A lightning stroke to a phase conductor injects a current pulse, creating traveling waves of current and voltage emanating from the strike point. The phase-ground voltage stress caused by a stroke to a phase conductor is as shown in Equation 3.2-1.

$$V_c = I_c \times Z_p / 2 \quad \text{3.2-1}$$

Where:

I_c is the stroke current.

Z_p is the surge impedance of the phase conductors, typically between 350 and 600 Ω. With corona, Z_p is typically between 250 and 350 Ω.

If the shielding angle (see Figure 3.4-3) is designed so that lightning strokes with currents greater than the critical current cannot terminate on the phase conductor, the SFFOR should be low but some subsequent strokes will still cause flashovers.

Note that, at midspan, the sag of the phase conductor is usually greater than the sag of the shield wire. Thus the shielding angle will be better at midspan than at the tower.

On some lines, the shield wire is insulated from the tower for communications purposes or to reduce losses from induced currents. These insulators are small and designed to flash over at very low voltages, so for the purposes of lightning protection and insulation design, it can be assumed that the shield wire is connected to the tower.

Design of line shielding is usually considered independently from design for backflash.

Backflash

A lightning stroke terminating at a tower top initially sees the surge impedance of the tower, paralleled by the surge impedances of the shield wires on both sides. Thus the initial (up to 3μs) surge impedance is:

$$Z = Z_{Tower} \,//\, Z_{OHGW} / 2 \quad \text{3.2-2}$$

Where:

Z_{Tower} is the traveling-wave surge impedance of the tower, 100-150 Ω

Z_{OHGW} is the self- and mutual surge impedance of the overhead groundwire in corona, 250-350 Ω.

The initial surge impedance rings down quickly to the footing resistance of the tower, Z_{ground}, in a process described in Section 6.4 and Applet L-5. For the time of main interest in the insulation coordination process, while the tower stands without help from adjacent structures (between 0.2 and 3 μs), the equivalent circuit become:

$$Z = Z_{Ground} \,//\, Z_{OHGW} / 2 \quad \text{3.2-2A}$$

The initial impedance to the stroke is then approximately Z = 75 ohms, falling to about 22 Ω for the case where Z_{Ground} = 25 Ω If a lightning stroke were considered as a current step with a very steep front relative to the tower travel time, a 100-kA stroke would raise the tower voltage to approximately 7.5 MV for about 200 ns (on a 60-m tower), and 2.2 MV thereafter. The phase conductors, connected to a remote source, may be considered at ground potential. Therefore, potentially, all the 2.2 MV would be across the insulation between phase conductors and tower.

However, the voltage across the insulator string is not the full 2.2 MV of the tower. There is strong coupling between the traveling waves on the shield wires and the phase conductors. There are reflections from the footing impedance at the bottom of the tower. There are traveling waves also on the shield wires and reflections and refractions at adjacent towers. In reality, the wavefront of the current is not a step wave, so the voltage does not immediately rise or fall to the 7.5 or 2.2-MV values. Also there is significant loss from the traveling waves due to corona, and as noted above, the instantaneous value of the power frequency voltage adds or subtracts from the total. The insulator strings are located partway down the tower, so the voltage across them is affected by the travel time of the waves up and down the structure. The grounding and soil characteristics provide a dynamic impedance varying as a function of current and time, which affects the reflections of traveling waves from the tower base. As a result, the actual voltage seen across the insulator strings has a peak magnitude considerably less than the theoretical maximum, and a waveshape based on all the above factors. An excellent description of the development of voltages due to traveling waves that serves as the basis of many calculation methods is given in (Bewley 1951), and this work is described in detail in Chapter 6.

Ground flash density establishes the occurrence frequency of voltage stresses but does not affect the magnitude distribution. The factors that affect the lightning overvoltages, leading to backflashovers are in order of sensitivity: insulator length and tower striking distances; the presence of Transmission Line Surge Arresters (TLSAs); tower footing resistance; and the conductor geometry and its effect on coupling between the shield wire and phase conductors. A discussion of insulation strength is provided in Section 3.3, and a discussion of the effects of varying line design parameters to improve lightning performance is given in Section 3.4. A detailed description of how the expected frequency of occurrence of backflashovers is affected by line design parameters and how it can be calculated is included in Chapter 6.

Induced Voltages

The electric and magnetic fields from a lightning stroke to ground close to a line can induce currents and voltages in the various line components. As described in Chapter 6, induced voltages across the insulators are typically less than 400 kV. Induced voltages can be a significant source of tripouts at distribution voltages, but not for transmission voltages covered by this reference book.

Conductor Damage

Although uncommon, conductor damage from lightning on both steel shield wires and aluminum conductors is known to occur. Typically the damage consists of two to three severed strands. As verification that this damage is solely due to the lightning and not to power frequency fault currents, it has been observed on new lines that are not yet energized.

An exception to this phenomenon occurs for covered conductors (or tree wires), where the phase conductor has a layer of insulation intended to protect it against momentary contacts to grounded objects such as trees. Covered conductor has been widely used, but primarily at distribution voltages. Faults caused by lightning can result in power frequency arcs being channeled to a particular point on the conductor through a puncture in the covering, and severing the conductor. Special measures, such as additional hardware, have been proposed to eliminate this problem, but transmission designers are unlikely to use this type of conductor.

Calculation of Lightning Voltage Stress

Lightning voltage stress is calculated using a transmission-line model, typically based on surge impedance, and a probabilistic approach to describe the variable characteristics of lightning. A number of computer programs are designed to calculate lightning-caused voltage stress, as part of the process to determine line lightning performance. A more detailed discussion is provided in Appendix 3.1 in this chapter, and in Chapter 6.

3.2.3 Switching Surges

Switching surges in a power system result from the energizing and de-energizing of lines, capacitors, reactors, and transformers. Energy is stored in the system's electric and magnetic fields, with magnetic energy stored in the inductance of the system and electric energy stored in the capacitance. Energy transfer between a transmission line and the system during a switching operation causes voltage surges.

Switching surges are not normally a determining factor for line voltages below 345 kV. Prior to the advent of 500-kV transmission in the early 1960s, line insulation was solely determined by lightning and power frequency voltage. Switching surges were recognized as important with the advent of 500 kV and higher voltages, and many studies were then made to predict and measure surges and insulation strength.

An idealized representation of a phase-ground switching surge is shown in Figure 3.2-1. Switching surges can have a wide range of waveforms, corresponding to the range of initiating influences. A "typical" waveform could be considered as a 250 x 2500 μs double-exponential, as illustrated in the figure. Switching surges are customarily expressed in per unit of the phase-ground peak steady-state voltage.

The switching operations of greatest concern in lines over 345 kV are:

- Line energization
- Line re-energization with trapped charge on the line
- Load rejection with a circuit breaker opening at the far end of a line, possibly followed by disconnection at the near end
- Transformer switching at no load or with a secondary load of shunt reactors
- Reactor switching

A detailed discussion of switching surge strength is provided in Chapter 5. The following provides an overview of key issues for the designer in considering switching stress on a line.

The Effect of Trapped Charge

If the breaker at the energizing end of an open-circuited line is opened at line charging-current-zero, the line voltage will be at peak and charge will be trapped on the phase conductors. The only path for discharge is leakage over the insulators, which usually have a very high resistance, so discharge can take several minutes. If the line is re-energized while trapped charge remains, it is possible for this to occur with opposite polarities between the supply and line sides of the breaker. A 2 p.u. traveling wave can be doubled at the open-circuit far end of the line, resulting in a 4 p.u. line-to-ground voltage. If the line is long enough to have an appreciable Ferranti effect (see Section 3.2-4), the initial wave may be greater than 2 p.u.

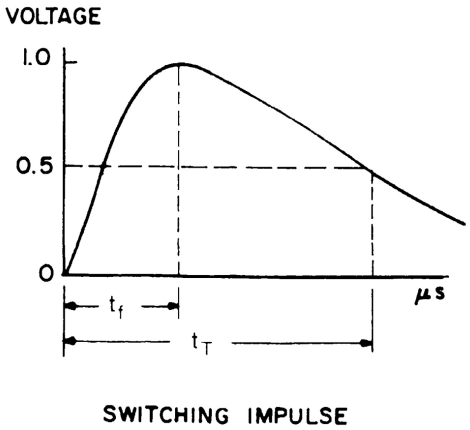


Figure 3.2-1 Idealized surge waveform.

Overvoltages from a Circuit Opening

Switching surges from de-energizing a transmission line are usually of less concern, since the line is in the process of being de-energized anyway. Circuit breakers are controlled to open their contacts at zero instantaneous phase current, but if a nonzero current is interrupted, this will cause a transient that is usually small. The greatest concern for circuit opening is a restrike across the opening contacts, which can initiate a traveling wave to the far end of the line. If the far circuit breaker has already opened, then a voltage doubling can occur as the traveling wave is reflected, with the possibility of further arcing across the breaker contacts. In reality, these voltage surges would be limited, for example by arresters, and the primary concern in this circumstance would be the failure of the breaker.

Circuit Opening with a Fault

A fault on an overhead line is most commonly phase to ground, but other types of fault may occur. Faults can result in high currents and depressed voltages. When the breaker operates to de-energize the line and clear the fault, there may be significant voltage swings—in particular on unfaulted phases. However, since the line is being de-energized, any resulting voltage surges are of little consequence to the line insulation, except when single-phase switching is used.

Variation of Switching Surge Amplitude along a Transmission Line

Unlike lightning, where the most severe voltages occur at a few structures close to the stroke, a switching surge voltage is considered as appearing on all the structures of the line.

The magnitude of the surge varies along the line. This variation is described by the *surge profile*, which gives the relation between the surge magnitude at a point of the line and the surge magnitude at the receiving end—i.e., the end of the line opposite to the location where switching operation takes place. At an unterminated receiving end, a surge propagating along the line reaches its highest value. The switching surge amplitude distribution for a transmission line refers to the receiving end. The surge profile is usually simplified by considering a linear variation of amplitude versus distance. In this case, the surge profile is characterized by the ratio, α, between the surge amplitudes at the sending end, S_S, and at the receiving end, S_R:

$$\alpha = \frac{S_S}{S_R} \qquad 3.2\text{-}3$$

Values of α range between 0.6 and 1.0.

Distribution of Switching Surge Waveshapes

The shape of the switching surges is usually not considered as a variable in line design: all surges are assumed to have the same shape with an equivalent time-to-crest corresponding to the critical wave—i.e., the shape that corresponds to the lowest strength (see Section 5.2.3). This simplification leads to some conservatism in estimates of the risk of failure. It is known that most surges have equivalent times-to-crest much longer than the critical, but quantitative data are scarce. Four distributions of times-to-crest have been reported for 345-kV transmission systems (McElroy and Charkow 1967). The reported times-to-crest were converted into equivalent times-to-crest of double-exponential impulses (see Section 5.2.3). The 50% values and the standard deviations were estimated, and the curves were approximated by Gaussians and plotted as shown in Figure 3.2-2. For these examples, practically all surges have equivalent times-to-crest far greater than those that are critical for the insulation systems of 345-kV transmission lines, which are in the range of 50 to 150 μs.

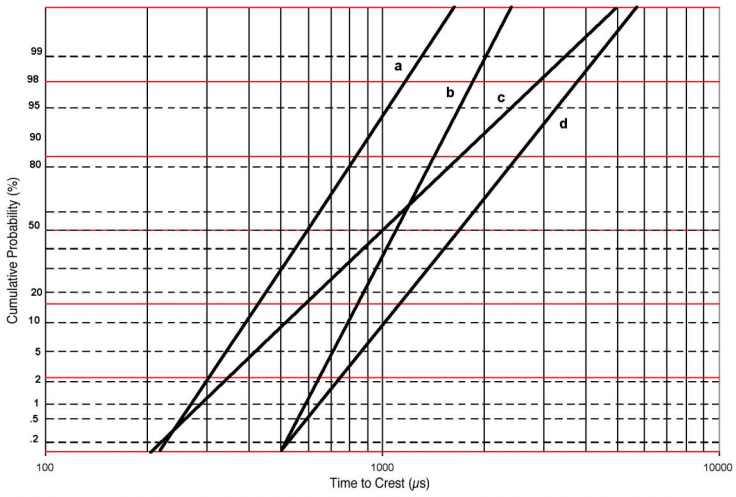


Figure 3.2-2 Distribution of switching surge equivalent times-to-crest recorded on various unterminated configurations of well-developed 345-kV transmission systems (McElroy and Charkow 1967). (a) Receiving end of 100-km line. Source with transformers and two other lines. (b) Receiving end of 100-km line. Source with transformers only and no other lines connected. (c) Receiving end, composite of configurations with line lengths between 100 and 250 km. (d) At 345-kV buses, composite for all configurations.

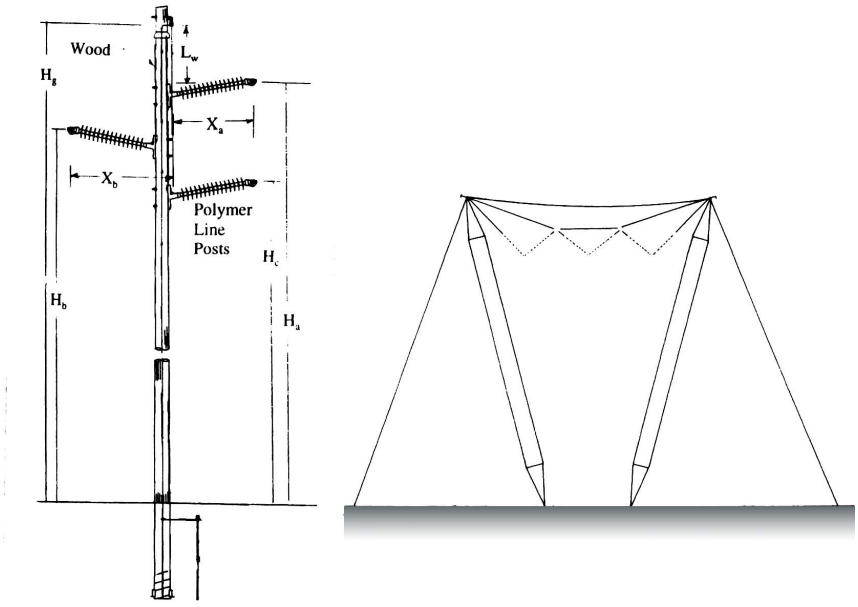


Figure 3.2-3 Examples with phase-to-phase clearances with no grounded member between phases. Left side: vertical configuration with insulator posts. Right side: Chainette.

Phase-to-Phase Switching Surges

Until recently, overhead transmission-line designs were built using structures where the phases were separated by grounded tower members—for example, in a typical H-frame structure. As a result, phase-to-phase spacing was determined as a byproduct of two phase-to-ground clearances. However, in some modern designs, such as the Chainette or where insulator posts are used, as shown in Figure 3.2-3, there may be no grounded member between phases, and the phase-to-phase clearance must be considered.

Phase-to-phase switching surges can be characterized as shown in the idealized waveform in Figure 3.2-4. The phase-to-phase voltage results from the difference between the phase-to-ground voltages. Factors include relative polarity, relative magnitude, and the time difference between crest values (Grant and Paulson 1980).

Distributions of phase-to-phase switching surges can be calculated in just the same way as for phase-to-ground using EMTP or similar programs, although most programs are configured solely for phase-to-ground voltages, and obtaining phase-to-phase values may require extra work. The wider range of variables involved in the waveform makes it more difficult to characterize the surge in a way that can be compared with insulator flashover strength information.

While the peak value of the phase-to-ground surges are often known with a sufficient degree of confidence, there have been only a few data on phase-to-phase switching surges. These data suggest an approximate relation between phase-to-ground and phase-to-phase magnitude (EPRI 1978; CIGRE 1979). This relation may be used to estimate the phase-to-phase surge amplitude distribution. If the 2% or the 50% values of the phase-to-ground surge magnitudes are known, the corresponding 2% or 50% values of the phase-to-phase surge magnitudes may be estimated using the curves of Figure 3.2-5. The figure shows that, although the theoretical maximum of the phase-to-phase surge is twice the maximum of the phase-to-ground surge, this is far from the practical case. The ratio between phase-to-phase and phase-to-ground surges goes from $\sqrt{3}$

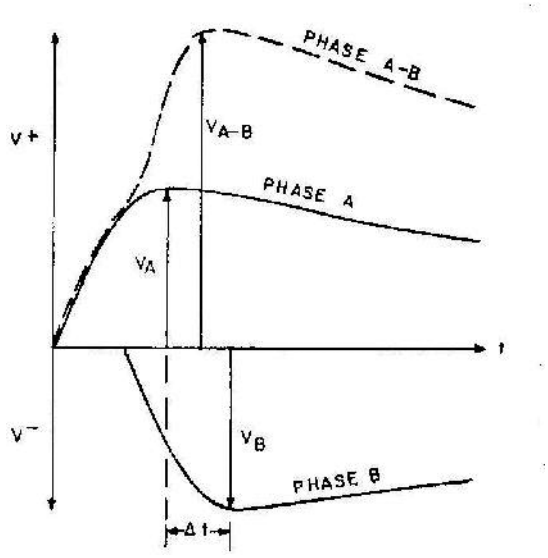


Figure 3.2-4 Idealized phase-to-phase waveform.

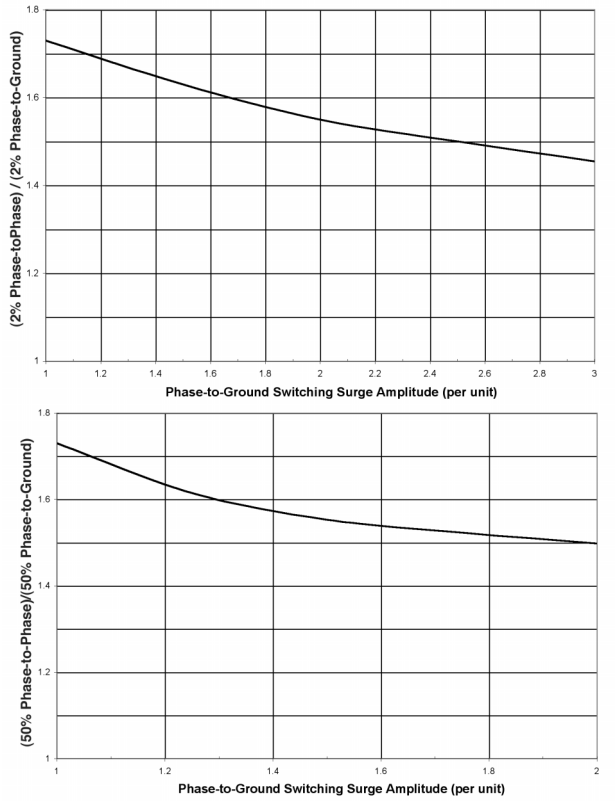


Figure 3.2-5 Approximate relation between phase-to-phase and phase-to-ground switching surge distribution values.

in the steady state (set of three phase-to-ground voltages at power frequency) to less than 1.5 for high-surge values; i.e., when one phase-to-ground surge is high, there is a low probability that another simultaneous phase-to-ground surge is also high and of opposite polarity.

The standard deviation, σ_S, of the phase-to-phase surge amplitude distribution may be estimated from Figure 3.2-6, which represents the average results obtained in a large number of Transient Network Analyzer (TNA) tests (CIGRE 1979). The standard deviation of the switching surge amplitude distribution is important for the design of phase-to-phase distances. It should be noted that, for this purpose, the most important surges are those with the largest amplitudes. The surge amplitude distribution is far from Gaussian in the region of highest surges (see example in Figure 3.2-8) and it would be preferable to consider the equivalent standard deviation obtained interpolating with a Gaussian only the highest surges. The equivalent standard deviation so obtained is much smaller than that reported in Figure 3.2-6.

A much more difficult parameter to obtain from switching surge studies is the value of the ratio, α, between the voltage applied to the negative phase and the phase-to-phase

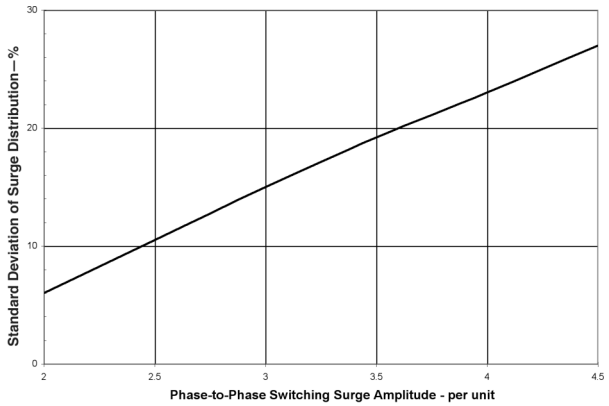


Figure 3.2-6 Standard deviation of the distribution of phase-to-phase switching surge amplitudes versus the 2% phase-to-phase surge amplitude.

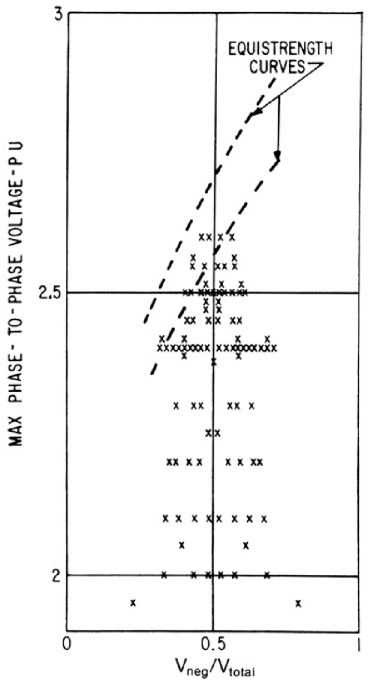


Figure 3.2-7 Example of phase-to-phase crest voltages and corresponding values of $\alpha = V_{neg}/V_{tot}$. One per-unit equals the crest value of line-to-ground voltage.

amplitude at the instant of maximum phase-to-phase surge ($\alpha = V_{neg}/V_{tot}$). An example is shown in Figure 3.2-7, which is representative of cases in which surges are minimized by using breakers with pre-insertion resistors (EPRI 1982). In this example, the maximum phase-to-phase overvoltages are concentrated around $\alpha = 0.5$. Another example that confirms this conclusion can be found in (Cortina et al. 1976).

Because the strength is a function of α, each point of Figure 3.2-7 may be shifted along equi-strength lines having the slope equal to that of the curves showing V_{50} versus α

(see Section 5.8). In such a manner, all the points can be transported on the line for $\alpha = 0.5$. Each surge is now assumed to consist of the combination of equal positive and negative phase-to-ground surges ($\alpha = 0.5$). The statistical distribution of the values so obtained is drawn in Figure 3.2-8 in a log-normal graph. It represents the same stress as the real distribution. An equivalent Gaussian distribution may be obtained by interpolating with a straight line the upper part of the curve, which is the most important for insulation design. This procedure yields the 2% and 50% phase-to-phase surge values and the standard deviation of the surge amplitude distribution that should be used for phase-to-phase distance design. The values applicable to the example of Figure 3.2-7 are:

V_{tot}, 2% = 2.6 per unit.
V_{tot}, 50% = 2.47 per unit.
σ_S = 2.4%.

Calculation of Switching Surge Magnitudes

Switching surge magnitudes were once determined from TNA studies, but today are obtained from digital programs such as EMTP (see Appendix 3.1). Magnitudes can be modeled as a statistical distribution. Early models considered magnitudes as histograms, but today they are typically modeled as continuous functions.

Several examples of switching surge voltage distributions can be found in the literature (CIGRE 1979; Truax et al. 1978; Clerici 1972; CIGRE 1972; CIGRE 1973-2; CIGRE 1974). The region of interest consists in the upper third of the distribution, because only the high-surge values have an impact on the risk of failure. Unfortunately, the upper portion of the distribution is the most difficult to define. Although a majority of switching surge results are reasonably fit by a Gaussian distribution, others have shown better fit to an extreme value or to a bimodal distribution. A reasonable approximation consists of a Gaussian curve that interpolates only the upper third of the switching surge distribution up to a point at which the curve can be truncated. An example of a surge distribution determined with a large number of digital switching simulations and of the truncated Gaussian approximation is shown in Figure 3.2-9. The truncation point depends on the type of distribution, and varies between 2 and 3 standard deviations above the 50% value.

The surge value, S_2, corresponding to 2% probability is considered a good measure of the level of surges in the low probability region, and is defined as the statistical maximum surge. For a Gaussian curve, 2% probability corresponds approximately to the 2.05 standard deviations above the 50% value, $S_2 \approx S_{50}\,(1+2.05 \cdot \sigma_s)$. The statistical maximum surge, S_2, the standard deviation, σ_s, and the value of the probability at the truncation point are needed to characterize the surge distribution. In the example of Figure 3.2-9 S_{50} = 1.47 per unit, S_2 = 1.82 per unit, $\sigma_s = \dfrac{(1.82 - 1.47)/2.05}{1.47} \cdot 100 = 11.6\%$, and the truncation point is set at about 2.1 standard deviations above the 50% value.

There are several data on the statistical maximum switching surges on transmission lines. As transmission-line voltages are increased, and switching surges play a more limiting role in line design, there are more economic incentives to reduce their maximum values using sophisticated surge control techniques. For this reason, the statistical maximum values usually considered in the design of transmission lines decreases with system voltage, as indicated in Table 3.2-2.

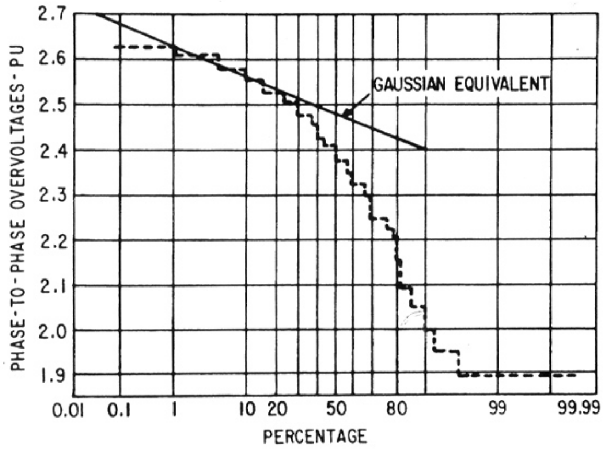


Figure 3.2-8 Distribution of phase-to-phase equivalent (α = 0.5) surge amplitudes for the example of Figure 3.2-7.

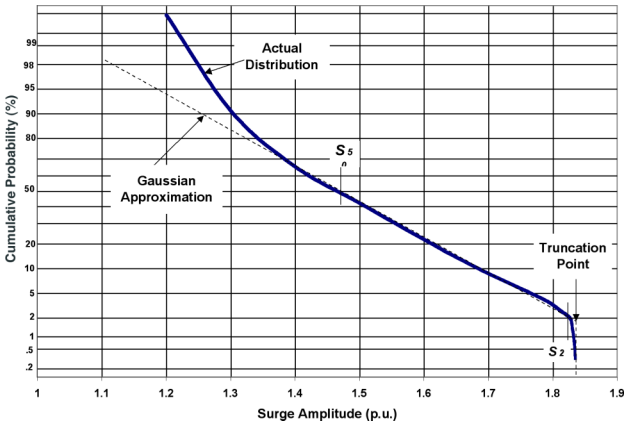


Figure 3.2-9 Example of switching surge amplitude distribution and its approximation with a truncated Gaussian curve.

Table 3.2-2 Practical Values of Statistical Maximum Phase-to-Ground Switching Surge Amplitudes versus System Voltage

Maximum System Voltage (kV)	230	362	550	800	1200
Statistical Maximum (2%) (p.u.)	2.5 2.25 2.0	2.25 2.0 1.75	2.0 1.75	2.0 1.75	2.0 1.75 1.5

The standard deviation of the Gaussian equivalent of the upper portion of the surge distribution varies with the system parameters and configurations, and with the method of interpolation of the actual distribution, especially if the truncation point is not well defined. Most likely values of σ_s are between 10 and 20%.

3.2.4 Temporary Overvoltages

Transmission lines operate continuously at their design voltage (230 kV, 345 kV, etc.), and their voltage is controlled within very narrow bounds, typically no more than ±5%, although ±10% is sometimes used. Line insulation is not normally governed by power frequency, unless the insulation is damaged or degraded, or environmental stresses are significant. Environmental stresses include contamination, ice, snow, fires, bird droppings, and rain, and like the temporary overvoltages, have the effect of reducing the resistance of the insulation to flashover. Allowance for these stresses is described in the later design sections of this Chapter.

Two sources of elevated voltage are considered in the same time domain as power frequency: the Ferranti effect, and the effects of faults.

Ferranti Effect

The steady voltage at the open end of an uncompensated transmission line is always higher than the voltage at the sending end (see Figure 3.2-10). This phenomenon is known as the "Ferranti effect." It occurs because the capacitive charging current flows through the series inductance of the line. The voltage at the sending end, although lower than that at the remote end, is still higher than the one that prevailed when the line was loaded. Overvoltages due to the Ferranti effect are sinusoidal in nature.

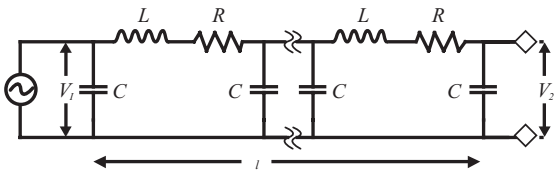


Figure 3.2-10 Typical uncompensated long transmission line.

As shown in Equation 3.2-4, for a typical uncompensated line, the voltage at the open end of the line is approximately (Naidu and Kamaraju 1995):

$$V_2 = \frac{V_1}{l.\cos\beta} \qquad 3.2\text{-}4$$

Where:

V_1 = sending-end voltage.
V_2 = receiving-end voltage, open circuit.
β = phase constant of the line.

$$\approx \left[\frac{(R + j\omega L)(G + j\omega C)}{LC}\right]^{1/2}$$

≈ about 7.2° per 100-km line (4.5° per 100-mile line) at 60 Hz and 6° per 100-km line (3.75° per 100-mile line) at 50 Hz.

Where:

ω = angular frequency.
l = line length.
R = resistance per unit length.
C = capacitance per unit length.
L = inductance per unit length.
G = leakage conductance per unit length.

An approximate solution can be derived simplifying the circuit of Figure 3.2-10 as in Figure 3.2-11. The capacitance is concentrated in the middle of the line. The charging current, I_C, is:

$$I_C \approx j\omega C V_1 = \frac{V_1}{X_C} \qquad 3.2\text{-}5$$

And the voltage

$$V_2 \approx V_1\left[1 - \frac{X_L}{2X_C}\right] \qquad 3.2\text{-}6$$

Where:

X_L = line inductive reactance.
X_C = line capacitive reactance.

This approximate solution is shown in Figure 3.2-11.

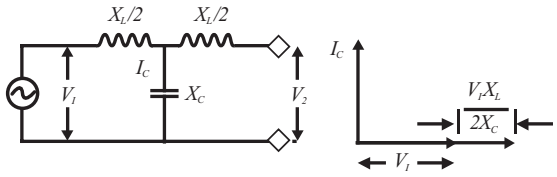


Figure 3.2-11 Transmission-line approximation for Ferranti Effect calculations.

Overvoltage due to the Ferranti effect is more pronounced the longer the line, the higher the line voltage, and the lighter the load at the receiving end. It is one of the most common overvoltages on lines exceeding 345 kV, and unless corrected, may be a concern for the insulation level of relevant components and the selection of the surge arresters. In some cases, the overvoltage due to the Ferranti effect may be higher than the maximum continuous operating voltage of the arresters at the transmission terminals (Petcharaka et al. 1999). In 345-kV systems and above, after a full-load rejection, the phase-to-ground overvoltages may reach 1.5 p.u., or even more when Ferranti or resonance effects occur. Overvoltage durations may be in the order of seconds. Figure 3.2-12 illustrates the receiving-end voltage rise due to Ferranti effects with different voltage level and load conditions.

Design for Ferranti Effect

Because Ferranti effect overvoltages are controlled by line compensation, they are typically considered separately from the main insulation coordination process. Compensation can be achieved with either shunt (inductive, more common) or series (capacitive, sometimes used—e.g., Hydro-Quebec, see below) compensation. Figure 3.2-12, from Diesendorf (Diesendorf 1974), shows the results of shunt and series compensation. Some shunt reactor compensation may be controlled in order to dampen all significant voltage surges and to improve power stability limits. In 500-kV transmission systems, the optimal ratio of controllable to noncontrollable shunt reactors is about 1:3.

In the Hydro-Québec 735-kV transmission system, the length of the two major transmission branches running from Churchill Falls to Québec City and from James Bay generating stations to Montreal is approximately 1000 km

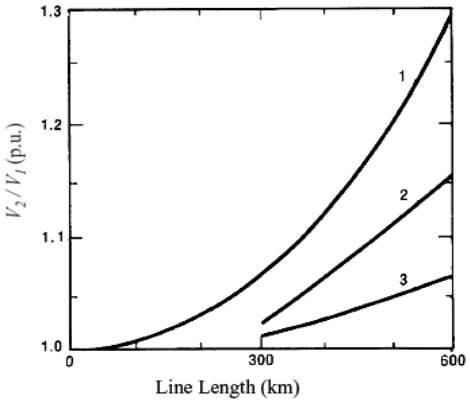


Figure 3.2-12 Effects of line compensation on Ferranti Effect (Diesendorf 1974)
1) No compensation;
2) 50% series capacitor compensation; and
3) 50% series capacitor and 70% shunt reactor compensation

(Bui-Van and Rousseau 2001). Shunt reactors, synchronous condensers, and static VAR compensators were installed on this transmission system. However, after a system separation occurred as a result of a system fault, severe temporary overvoltages due to the Ferranti effect appeared on long unloaded lines connected to generators. In order to control the magnitude and duration of such temporary overvoltages, several measures were also applied including implementation of series-capacitor banks, instantaneous 1.2 p.u. overvoltage protection, and various automatic switching schemes.

Fault-Related Overvoltages

The occurrence of a fault on a transmission system causes both a switching overvoltage and a temporary overvoltage. Temporary overvoltages initiated from faults may persist and stress the insulation until the voltage is removed by switching.

Line fault conditions include single line-to-ground (SLG), double line-to-ground (DLG), three-phase grounded (3ϕG), and three-phase ungrounded (3ϕU) (Colclaser et al. 1970). The most common fault is single line-to-ground, especially on high-voltage lines (Kimbark and Legate 1968). Three-phase faults are very rare, and their likelihood decreases as the system voltage increases. The waveform of fault-initiated overvoltages is generally sinusoidal, and may be described in terms of an rms or a peak value. If the voltage is high enough, there may be saturation effects in transformers, leading to the generation of harmonics and waveform distortion. Under any conditions in which the waveshape is distorted, a description of the voltage in terms of an rms value would be misleading if one were considering insulation. The peak voltage is a better measure of the effects of the voltage on the insulation, but even this may not be very appropriate.

Whenever a fault occurs, a current is suddenly injected into the system from the fault point, and a voltage with equal and opposite polarity to that existing is also suddenly applied to the same point. This will result in traveling waves along both the faulted lines and the electrically adjacent unfaulted lines. The resultant transient voltages are normally damped out within half a cycle similar to switching overvoltages. This initial transient is followed by longer-term voltage changes on the faulted and unfaulted phases until the fault is cleared. The magnitudes of such voltages are influenced by the length of the line, the losses in the conductors, and the ground path.

Switching overvoltage related to faults depends on many factors such as:

- The “stiffness” of the system
- The grounding of the system

- The length of the transmission lines
- The location and parameters of the transformers
- The degree of compensation, and
- The nature of the fault

Overvoltages on Unfaulted Phases

Single line-to-ground faults can cause a significant increase in voltage of the other two phases due to the asymmetry of a system if its neutral is not solidly grounded. Theoretically the magnitude of an overvoltage can reach 2.73 p.u. when the peak of the overvoltage occurs simultaneously with the peak of the power frequency voltage. In practice, it is suppressed by charge reversal of capacitances and lines, and is generally well below 2.7 p.u. It is higher only in exceptional cases in radial lines or widely spread-out systems with floating neutrals or ground fault compensation. Reported values range from 1.45 p.u. for an UHV system (Colclaser et al. 1970) to as high as 2.1 p.u. for 345-kV and above systems. The worst location of a single line-to-ground fault is at the midpoint of a line. The worst termination is zero impedance, which is approximately the situation for a bus having several other lines (Kimbark and Legate 1968; Boonyubol et al. 1970). As the line length increases, the maximum transient overvoltage due to a single line-to-ground fault increases (with a decreasing rate). For example, simulation shows that this overvoltage can range from about 1.9 p.u. for a 50-mile line to about 2.1 p.u. for a 1000-mile line (Boonyubol et al. 1970).

If a healthy phase cannot withstand the overvoltage during a single line-to-ground fault, a double line-to-ground fault will occur. The magnitude of a double line-to-ground fault-initiated transient overvoltage can reach 2.2 p.u., and the resulting transient recovery voltage (TRV) can be as high as 3.8 p.u. for a series-compensated line (Thanassoulis et al. 1975).

Overvoltages on Compensated Lines

Because of transmission-line reactive characteristics, the fault-clearing operation of a breaker can be equivalent to the opening of a capacitive circuit. The resulting overvoltage magnitude can easily reach 1.7 p.u. for a single line-to-ground fault (Colclaser et al. 1970; Thanassoulis et al. 1975) and as high as 2.2 p.u. for a double line-to-ground fault (Kimbark and Legate 1968). If the line is equipped with series or shunt compensation, the fault-clearing phenomena are usually more complex and the overvoltages higher. A series-compensated system can experience high-magnitude overvoltages on unfaulted lines following the fault initiation and subsequent bypassing of series capacitors. Series capacitors can suppress power frequency temporary overvoltages, such as those due to the Ferranti effect, but when there is a fault on a line, the voltage increase across the series capacitors will cause a bypassing operation to protect them. The decay of capacitor-stored energy can produce transients with very high frequency oscillations and high peaks that can reach about 2.0 p.u. The case is particularly serious for long and highly compensated lines. The magnitude of these voltage transients depends on the parameters of the line, the values of system impedance, and the characteristics of series capacitor protective bypass devices. These transients can be minimized by careful selection of the bypass devices.

Effect of System Grounding on Overvoltages

An isolated-neutral system can give rise to dangerous arcing fault overvoltages if the capacitive arc current exceeds 5 to 10 A. An arc initiated by a fault can persist if its current is maintained through the capacitive coupling of the other two healthy phases. When the arc experiences continual extinguishing and restriking, there is a high risk of a very high voltage because of the capacitive nature of the arc current (Bickford and Heaton 1986). These conditions rarely exist in 345-kV and above systems, since most are effectively grounded, but under certain conditions, the grounding of a system may change—for example, if a transformer with a grounded neutral is removed from the system. It is important for insulation design that overvoltages be calculated under the worst possible conditions to identify the highest values that are likely to occur. With the loss of effective grounding, the temporary overvoltages might be high enough to operate surge arresters. The resulting waveforms will be nonsinusoidal, and calculations of insulation performance must allow for this.

Overvoltages from "Short Line" Faults

When a ground fault occurs within a short distance along the transmission line, a triangular wave voltage appears on the line side terminal of the circuit breaker when the fault is cleared (Greenwood 1991). This phenomenon is named as a short line fault or a kilometric fault. The triangular waveform appears also as a component in the transient recovery voltage (TRV) across the circuit breaker. The frequency of the triangular component of voltage is inversely proportional to the travel time along the length of line between the fault and the circuit breaker. The amplitude of this component is directly proportional to the length of the line between the circuit breaker and the location of the fault itself. For faults up to a few kilometers from the circuit breaker, high initial rates of rise of TRV are obtained. These are onerous for the circuit breaker.

Design for Fault-Initiated Overvoltages

Since system insulation must be able to withstand overvoltages caused by faults, it would be prudent to design or use breakers that limit switching overvoltages to less than these values. When breakers operate to clear fault current, a switching overvoltage may occur. This overvoltage magnitude may exceed 1.7 per unit. If the line is equipped with

series or shunt compensation, the resultant transients may be more complex and the overvoltages may be higher. For example, when an unloaded transmission line is exposed to a single or two-phase fault, the circuit breaker at its sending end may open the contacts to interrupt the current. The interruption of current on the unfaulted phases is a case of capacitive switching. Circuit unbalances introduced by the fault also affect the voltage on the unfaulted phases prior to current interruption, causing in most cases a voltage rise on the unfaulted phases. The magnitudes of overvoltages appearing on unfaulted phases depend on fault location, system X_0/X_1 ratio, and fault current magnitude. The overvoltage on the unfaulted phases will be less than 1.4 per unit on effectively grounded systems and 1.73 per unit or greater on ungrounded systems. According to IEEE Standard C62.11 (IEEE 1999), a system is defined as effectively grounded when the highest rms line-to-ground voltage on a sound phase is 80% or less of the normal line-to-line voltage at the fault location. An ungrounded load supplied from the delta winding of a transformer is an example of an ungrounded system. Under certain conditions, the grounding of a system may change—for example, if a transformer with a grounded neutral is removed from the system. It is important for insulation design that the overvoltages be calculated under the worst possible conditions to identify the highest values that are likely to occur. With the loss of effective grounding, temporary overvoltages might be high enough to operate surge arresters. Arresters on a well-grounded system are normally exposed to only low-magnitude temporary overvoltages during a single-line-to-ground fault.

As for Ferranti effects, overvoltages due to faults are typically considered separately from the main insulation coordination process. Accommodation of these overvoltages is achieved through selection of appropriate grounding, breakers, and station arresters.

3.2.5 Environmental Stress

Environmental stresses to lines—due to pollution, rain, snow, ice, and temperature affecting the line insulation—are important. Like temporary overvoltages, they have the effect of reducing the resistance of the insulation to flashover. A brief overview is provided here, and more detailed information in Chapter 4 for power frequency voltage and in Chapter 5 for switching overvoltages.

Sources of Contamination on Line Insulation

Contamination and humidity falling on the insulators produce a conductive film on the surface that causes a surface leakage current that can increase and eventually result in flashover. Many types of contamination may be present along the route of the transmission line, depending upon their source. Table 3.2-3, which is from IEEE Standard 957 (IEEE 1995), details the most common types of contamination. Basically, the types of contamination can be classified into two categories: sea contamination and industrial contamination. Different laboratory tests are used to determine the strength of insulators against these two types of contamination. The severity of sea contamination may be defined by the salinity (amount of salt per unit of water volume) or electrical conductivity of the water used to spray the insulators under tests. Industrial contamination is sometimes expressed by the equivalent salt deposit density (ESDD), which is defined as the equivalent amount of NaCl that, when wet, would yield the same conductivity as the actual contaminant.

The general site severity and its definition from the IEC 60815 Guide (IEC, 1986) are shown in Table 3.3-3 in terms of the ESDD. The amount of salt deposit density that leads to flashovers at line voltage depends mainly on the voltage stress across the insulators and the insulator material. The pollution deposit on the top surfaces of insulators builds up rapidly, but is also effectively cleaned by relatively small amounts of rain.

Icing

Under conditions of moderate icing, it is common for icicles to form on insulator strings. These icicles tend to grow in length, bridging the air gaps between insulator caps or

Table 3.2-3 Typical Sources of Contamination on Line Insulators

Type of Contaminant	Typical Source of Contamination
Sea	
Salt	Coastal areas Salt industries/farms
Industrial	
Cement	Cement plants Construction sites Rock quarries
Dust	
Earth	Plowed fields Earth moving on construction projects
Fertilizers	Fertilizer plants Frequent use of fertilizers in cultivated fields
Metallic	Mining handling processes Mineral-handling processes
Coal	Coal mining Coal-handling plants/thermal plants Coal burning/brick kilns areas
Feedlot	Provender dust and earth dust stirred by animals in large feedlots
Defecation	Roosts in bird areas
Chemical	Wide variety of chemical / process industries, oil refineries, etc.
Smog	Automobile emissions at highway crossings Diesel engine emissions at railway crossings / yards
Smoke	Wild fires Industrial burning Agricultural burning

sheds and shorting out the leakage distance. The combination of pollution accumulation—for example, from road salting—followed by ice or freezing fog accretion, has proved to be particularly severe conditions for insulators in power systems to withstand.

Most troubles have occurred on transmission lines and stations that are located near sources of salt, such as the ocean or urban expressways. With typical road salting levels of 16 tons per lane mile in the winter season for most provinces and states that perform winter maintenance, a location near an expressway is equivalent to a location 1 km from the sea coast.

Rain

Rain may substantially reduce the ac strength of insulators, depending on the rate of rainfall, conductivity of the rainwater and the insulator configuration considered. Typical flashover stress levels on glass and porcelain cap-and-pin insulators lie between 250 and 300 kV per meter of section length during standard wet tests with a low conductivity artificial rain. Figure 3.2-13 shows the wet ac flashover strength of a selection of typical disc insulators.

Birds

Birds resting on or taking off from transmission lines may produce a stream of defecation that contaminates an insulator or even creates a conductive path between a phase and grounded structure component. Other bird-caused problems include nests on transmission structures that include sticks or material that can bridge an insulator.

Bird contamination may cause either direct flashovers or subsequent flashovers in the presence of dew or rain. The problem tends to be regional, depending on the preferred habitat and sources of food of the birds.

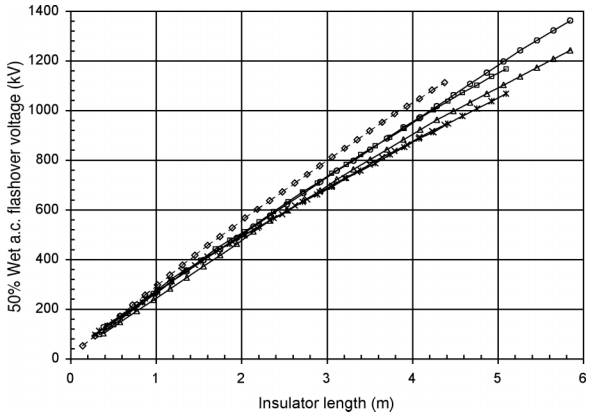


Figure 3.2-13 Wet ac flashover voltage of various shapes of cap-and-pin insulator strings.

3.2.6 Summary

This section described the nature of the voltage stresses that a transmission line is subjected to, and hence, for which the insulation strength should be designed.

Lightning Overvoltages

Lightning strokes to transmission structures, phase conductors, or shield wires can cause flashovers that force the line to trip. On transmission lines covered by this reference book, lightning-related outages are of two kinds: shielding failures or backflashovers. For the calculation of lightning performance of transmission lines, the waveshape of the stroke current is defined in various ways that either try to reproduce the variety of waveshapes of actual strokes or are convenient for carrying out calculations (see Chapter 6). While power frequency voltage may determine which phase flashes over first, it may also be secondary to other considerations.

Design for lightning includes setting the insulation level, line geometry and clearances, shielding, grounding, pole-top arresters, and other self-extinguishing discharge mechanisms, and rearrangements of line phases.

Switching Surge Overvoltages

Switching surges in a power system result from energizing and de-energizing of lines, capacitors, reactors, and transformers. Switching surges from de-energizing a transmission line are usually of less concern from those associated with the energization of lines or the equipment. The greatest concern for circuit opening is a restrike across the opening contacts, which can initiate a traveling wave to the far end of the line.

Distributions of phase-to-phase switching surges can be calculated in just the same way as for phase-to-ground using a transients program, although most programs are configured solely for phase-to-ground voltages, and obtaining phase-to-phase values may require extra work. While the peak value of the phase-to-ground surges is often known with a sufficient degree of confidence, little data is available on phase-to-phase switching surges.

As transmission-line voltages are increased, and switching surges play a more limiting role in line design, there are more economic incentives to reduce their maximum values using more sophisticated surge control techniques. For this reason, the statistical maximum values usually considered in the design of transmission lines decrease with system voltage.

Temporary Overvoltages

Transmission lines operate continuously at their design voltage (230 kV, 345 kV, etc.), and their voltage is controlled within very narrow bounds, typically no more than

+5%, although +10% is sometimes used. Line insulation is not normally governed by power frequency, unless the insulation is damaged or degraded, or contamination is present. However, there are two sources of elevated power frequency voltages. These are the Ferranti effect, and the effects of faults. Overvoltages due to the Ferranti effect are more pronounced the longer the line, the higher the line voltage, and the lighter the load at the receiving end.

Unless corrected, these temporary overvoltages may be a concern for the insulation level of relevant components and the selection of the surge arresters. It is important for insulation design that the temporary overvoltages be calculated under the worst possible conditions to identify the highest values that are likely to occur.

Environmental Stresses

Environmental stresses to lines—due to pollution, rain, snow, ice, and temperature—have the effect of weakening the line insulation, and are considered at the appropriate level together with the worst-case temporary overvoltages, as described above.

Given the voltage stresses, the insulation for the transmission line is specified and coordinated, as discussed in Section 3.3.

3.3 INSULATION STRENGTH

3.3.1 Introduction

This section provides an overview of transmission-line insulation strength and the key parameters that are significant to the line designer. For greater detail, the designer is referred to the chapters on power frequency (Chapter 4), switching surge (Chapter 5), and lightning (Chapter 6).

The line insulation must have enough strength to meet the stresses produced by the overvoltages discussed in Section 3.2. In all cases (lightning, switching, and power frequency), the insulation strength is expressed in terms of a withstand voltage. This voltage is the highest voltage that the insulation can withstand without failure or disruptive discharge, and is a quantity determined by tests conducted under specified conditions with a specified waveshape of the applied voltage. The parameters generally used to characterize the waveshape of a lightning or a switching impulse are polarity; “front time” (variously defined), or time from zero to crest; and “tail time” (variously defined), or time from zero to half value after crest. In particular, this chapter and Chapters 4, 5, and 6 relate the strength of the insulations in terms of a statistical term, V_{50}. V_{50} is the crest value of the impulse wave that, under specified conditions, causes flashover through the surrounding medium on 50% of the applications. It is also known as the *critical flashover voltage* (CFO). The term V_{50} will be used throughout this book.

Since overvoltages may have a wide range of waveshapes, rather than attempting to determine the withstand strength for each of the naturally occurring stresses by test, it is common practice to assign a specific testing waveshape and duration of its application to each category of overvoltage.

The purpose of the lightning impulse test is to evaluate the performance of insulation when exposed to short-duration voltages, principally those produced by lightning. It is performed with a test voltage having a shape of 1.2/50 μs.

The purpose of the switching impulse test is to evaluate the insulation under stresses such as those produced by switching operations. Since switching surges may occur with a variety of waveshapes, it is of particular importance to test the insulation with the waveshape that corresponds to the lowest flashover voltage. The critical waveshape is of positive polarity, and the critical time-to-crest varies from 50 to 500 μs, depending on the length of the gap between the energized electrode and the grounded part of the insulation. The performance of insulation subjected to switching impulses is discussed in Chapter 5. Since the lowest values of V_{50} flashover voltage occur for a positive polarity impulse applied to a rod protruding toward a plane, the strength of this gap geometry is given particular attention.

The purpose of the long-duration, low-frequency test is to determine if the insulation can operate permanently at the maximum system voltage. For internal insulation, the test is concerned with a demonstration of aging, and for external insulation, with the effect of the usual types of contamination. The testing waveshape is 60- or 50-Hz voltage, and the duration of its application may extend from minutes to hours, depending on the test's specific purpose. Tests to determine the effects of contamination, in particular, require the test voltage be maintained for long periods of time. Even though contamination itself may hardly be classified as voltage stress, it certainly is a factor determining insulator withstand. Behavior of insulation under this test is discussed in Chapter 4.

3.3.2 Lightning Impulse Strength

This section briefly summarizes the lightning impulse strength (more detail is available in Section 6.5). It describes the insulation dielectric strength when subjected to the standard lightning waveshape, and explains how to calculate the strength for nonstandard lightning waveshapes.

The lightning impulse strength is proportional to the gap spacing (strike distance in the case of insulators) and depends on polarity. The lowest strength, about 520-560 kV/m, occurs

when the conductor is positive with respect to the tower, such as when a negative stroke hits the tower (backflash). When the conductor is negative with respect to the tower, such as when a negative stroke hits a conductor (shielding failure), the strength is about 600-610 kV/m.

The insulation strength for lightning impulses is normally only available through testing for the standard lightning impulse voltage wave, specified by its rise time and time to half value as 1.2/50 μs. However, this waveshape seldom occurs on the utility system; as noted in Section 6.2, there is no "one" lightning waveshape. Instead a statistical approach is needed to define the stress correctly. Therefore, either some approximations or a mathematical model of the breakdown process are frequently necessary to evaluate the strength of the insulation for nonstandard waveshapes. This is of primary importance in evaluating the insulation strength for surges resulting from a backflash, since the waveshape is nothing like the standard lightning waveshape. In contrast to the switching impulse, the tail or time-to-half-crest value of the lightning impulse usually has a significant influence on the V_{50}. Steep-rising overvoltages with duration that is limited by the distance to adjacent structures can cause less flashovers than indicated by test results obtained with a standard 1.2 x 50 μs voltage wave. From experience, the authors found that on a 345 kV line the calculated lightning outage rate is decreased by a factor between 2 and 3 by using the short-time impulse strength (2 μs).

Strength to Standard Lightning Waveshape: Volt-Time Curve Penetration Algorithm

In the second edition of the Red Book (EPRI 1982), a simple empirical expression was used to describe the flashover process (modeling the dielectric strength for positive polarity as a function of time to flashover) for a standard lightning impulse voltage wave, which is repeated here in Equation 3.3-1.

$$V_{50\%} = L(400 + 710 / t^{0.75}) \qquad 3.3\text{-}1$$

Where:

$V_{50\%}$ is the flashover voltage in kV (the actual voltage at flashover for flashovers occurring before crest and the crest voltage for flashovers occurring after crest).

t is the time to flashover in μs.

L is the insulator length in m.

For wet tower insulation in center or outside phases, approximations of insulation tower requirements for lightning have been recommended by Hileman (Hileman 1999). Hileman recommends a positive-polarity gradient for the $V_{50\%}$ of 560 kV/m for positive polarity and 605 kV/m for negative polarity for air-porcelain insulation. These apply for the porcelain insulator string length as well as strike distance.

Strength for Nonstandard Waveshape

The strength for nonstandard lightning waveshape has been approximated by a number of techniques. Two such techniques are presented here. This strength to nonstandard waveshapes is of primary importance in evaluating the insulation strength for surges resulting from a backflash since the waveshape is very different from the standard lightning waveshape.

The Disruptive Effect (DE) Algorithm, Typically for Faster-Front Flashover/Puncture

A widely used algorithm in digital programs to determine insulator strength to nonstandard lightning waveshape is the Disruptive Effect (DE) Algorithm. This method assumes that a critical voltage, V_0, could be withstood by the insulation even if applied continuously. If the voltage exceeds the critical voltage it acquires a Disruptive Effect which may lead to flashover depending on the magnitude of the voltage and the time above the critical voltage. The DE of a waveshape is evaluated as shown in Equation 3.3-2. As long as the voltage remains above the critical value, the disruptive effect keeps increasing until flashover when DE reaches a fixed critical value, DE_{crit}, which depends on gap configuration and voltage polarity. Different waveshapes may reach the critical DE at different voltages, as shown in Figure 3.3-1.

$$DE = \int_{T_0}^{T_d} (V(t) - V_0)^n dt \qquad 3.3\text{-}2$$

The IEEE Task Force (IEEE 2001) noted that the use of $n = 2.5$, $DE = 10^{10}$, and $V_0 = 300$ kV offers the best match to the volt-time characteristics of porcelain insulators in Equation 3.3-1.

The Leader Progression Model

Another model used to depict lighting insulation strength for nonstandard waveshapes is the leader progression model. CIGRE recommendations for leader propagation modelling, along with the reference volt-time characteris-

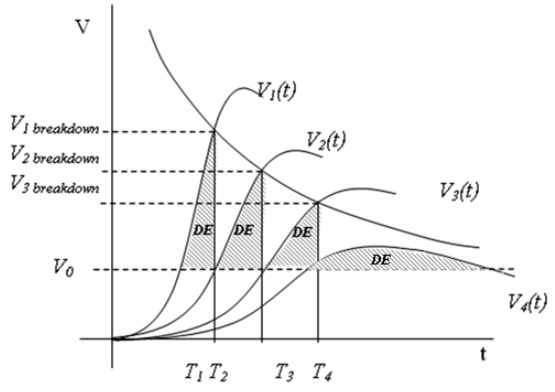


Figure 3.3-1 Disruptive effect for three nonstandard voltage waves.

tic for standard lightning impulse voltage on insulator strings, are shown in Figure 3.3-2. In examining this figure, there are two times of interest in the high-voltage flashover process: t_s, the time to develop streamers across the gap from both electrodes, and t_l, the time for a leader to propagate across the gap.

3.3.3 Switching Impulse Strength

A switching surge on a phase of a transmission line stresses all the insulation elements present on that phase. Insulation elements to be considered are the conductor-to-tower air gaps and insulator strings that are present on that phase. Calculation of the risk of switching surge flashover requires consideration of the parameters that define the surge (stress) and those that define the strength of the insulating elements (see Applet IC-2).

The parameters that define the stress are discussed in Section 3.2. They are:

- The statistical distribution of surge amplitudes at the receiving end. For application to Applet IC-2, this distribution is assumed to be a Gaussian distribution truncated at the upper end, and is defined by the value of:
  - The statistical maximum amplitude, S_2, which is the amplitude exceeded by 2% of all possible surges. This parameter is expressed in per unit of the crest value of the maximum phase-to-ground power frequency voltage.
  - The standard deviation of the surge amplitudes, σ_S. This parameter is expressed as a percentage of the amplitude exceeded 50% of the time, S_{50}.
  - The truncation value, which is the highest possible amplitude. This parameter is expressed by the number, T, of standard deviations above the 50% value.

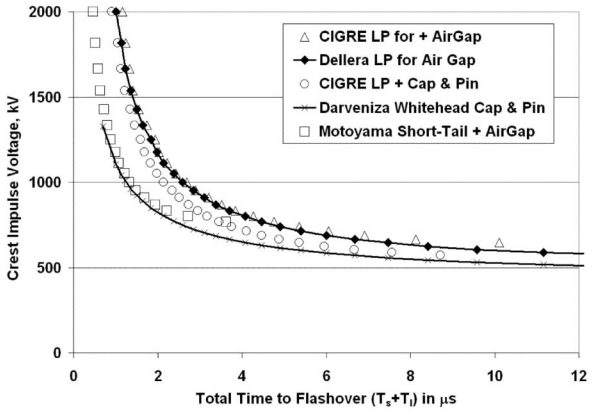


Figure 3.3-2 Comparison of predicted crest flashover voltage for leader progression (LP) models and observed volt-time characteristic of Equation 3.3-1.

- The function describing how the surge amplitude varies from sending to receiving end. Generally, this function is assumed linear. It is then defined by a parameter, α, which is equal to the ratio between sending-end and receiving-end amplitudes.
- The statistical distribution of the equivalent times-to-crest of the surges. The equivalent time-to-crest of a surge is defined in Chapter 5, Section 5.2.3. It is assumed that the distribution of equivalent times-to-crest is independent of the distribution of amplitudes. The distribution of times-to-crest is assumed to be Gaussian, and is defined by the 50% time-to-crest value, T_{50}, and by the standard deviation, σ_T.
- The polarity of the surges. It is assumed that surges may be either positive or negative with equal probability. For practical line insulation elements, the strength with negative polarity surges is significantly greater than that with positive polarity surges, so much so that negative polarity surges may be neglected entirely. The calculated risk of line flashover is divided by two.

The parameters that define the strength are:

- The switching surge strength of each insulating element of the line, defined by:
  - The 50% flashover voltage, V_{50}, corresponding to the critical time-to-crest. This parameter also is expressed in per unit of the crest value of the maximum phase-to-ground power frequency voltage. The value of V_{50} versus gap length is provided in Chapter 5 for a large variety of geometry. For a geometry that is not considered in Chapter 5, V_{50} may be calculated with Applet S1, "Switching Surge Flashover Model."
  - The standard deviation of the flashover probability function, σ_V. This parameter is expressed as a percentage of V_{50}. It is assumed that σ_V is independent of gap geometry and weather conditions. A large number of switching impulse flashover tests performed in several laboratories on transmission-line insulation elements indicates that the best estimate of the standard deviation is $\sigma_V = 4.5\%$. A conservative value of 5% is recommended for risk of flashover calculations.
  - All the parameters that may affect V_{50}. V_{50} depends on altitude above sea level (see Chapter 5, Section 5.11). V_{50} depends on the time-to–crest, and the dependence is a function of gap length (see Chapter 5, Section 5.10). V_{50} is also affected by wet weather, and the dependence is a function of gap length and of insulator strike distance (see Chapter 5, Section 5.12.1). Therefore, altitude, gap length, and insulator strike distance must also be provided (in addition to V_{50} or σ_V) to fully describe the switching surge strength of an insulating element.

Calculation of the risk of flashover of a transmission line due to a switching operation is based on comparing stress to strength. The line design is often uniform along the line. In some cases, however, various considerations may result in different insulation elements for different line sections. For instance, a certain type of tower may be preferable for aesthetic reasons in a populated area, all V-strings may be used in sections with high winds, more massive stronger towers may be used in sections with high icing incidence, different types of insulators may be used in sections with a high level of contamination and humidity, etc. Finally, even when the towers are the same, the insulation elements of each phase vary along the line if the line is transposed. It is, therefore, convenient to divide the line into sections in which there are different sets of insulating elements with all the elements of a set having the same strength and being subjected to the same stress.

Within each section, each phase is considered separately, since the insulating elements of the different phases are different (the phase-to-tower geometry, the height of the phase above ground, or the type of insulators may be different). Line sections must be chosen so that there is no transposition within the section, and the types of towers and the phase arrangements do not vary within the section. In addition, the surge amplitude, the altitude above sea level, and the atmospheric conditions applicable to each insulation element should not be too variable within the section so that they could be reasonably described by the average surge amplitude, the average altitude, and the average atmospheric conditions of the section.

While certain parameters (S_2, σ_S, T, T_{50}, and σ_T) are clearly attributes of the stress, and certain others (V_{50}, σ_V, gap length, insulator strike distance) are clearly attributes of the strength, other parameters that affect the risk of flashover may be considered as attributes of either the stress or the strength. Take, for instance, the effect of atmospheric conditions: temperature, humidity, and air pressure. As they vary, so does V_{50} (see Chapter 5, Section 5.11). The effect of atmospheric conditions would, therefore, appear to be an attribute of the strength. However, since temperature, humidity, and air pressure may be assumed to vary in a similar way for all the insulation elements of a line section, it is more convenient to incorporate their effect into the stress by introducing the *Relative Insulation Stress (RIS*). RIS is defined as the ratio between the flashover voltage in standard atmospheric conditions (760 mm Hg, 20˚C, 11 g/m^3) and that in actual atmospheric conditions. A statistical distribution of RIS may be defined for a specific section or for the entire line.

The calculation of risk of line flashover is made by dividing the stress into a number of "stress situations," and the insulation elements of each section and phase into "sets" in which the elements have the same strength. The probability of flashover is then calculated for each combination of stress situation and insulation set (see Applet IC-2).

Rod-Plane Strength

The lowest values of V_{50} flashover voltage occur for a positive polarity impulse applied to a rod protruding toward a plane.

The 50% flashover voltage of rod-plane gaps is a function of the time-to-crest of the impulse, with the lowest value appearing at the critical time-to-crest (see Figure 5.5-2). Three equations describing this switching surge strength versus the spacing of the rod-plane gap are given in Table 3.3-1. These are plotted in Figure 3.3-3, which is taken from Section 5.5. Note the saturation characteristic of the strength with respect to gap spacing. This is a very important behavior compared to the strength required for lightning, and explains the importance of keeping switching surge overvoltages under check for higher voltages; otherwise, the insulator string length, and hence the tower dimensions, become excessively demanding and expensive. Figure 3.3-4 shows an approximate comparison of the switching impulse (SI) and lightning impulse (LI) strengths (both positive and negative polarity).

Parameters Affecting the Switching Surge Strength

The effect of selected other parameters on the critical flashover voltage, $V_{50\%}$, is presented in Table 3.3-2. These, and other factors, are covered in detail in Section 5.6.

3.3.4 Power Frequency Strength

Line insulators must withstand the maximum system voltage over long periods of time. In addition, they must either withstand or be protected against temporary overvoltages

Table 3.3-1 Common Equations Governing the Switching Surge Strength of the Rod-Plane Gap

Electricité de France (EdF) (Gallet et al. 1975)	CRIEPI (Kishizima et al. 1984)	Rizk 1989 (Rizk 1989)
$V_{50,Rod-Plane} = \dfrac{3400}{1+\dfrac{8}{L}}$ 3.3-3	$V_{50,Rod-Plane} = 1080 \cdot \ln(0.46 \cdot L + 1)$ 3.3-4	$V_{50,Rod-Plane} = \dfrac{1830 + 59 \cdot L}{1+\dfrac{3.89}{L}} + 92$ 3.3-5
$V_{50\%}$ is expressed in kV, and the gap length or strike distance, L, in m. The equations are valid for standard atmospheric conditions of relative air density, δ, and absolute humidity, h: = 1 and h = 11 g/m^3.		

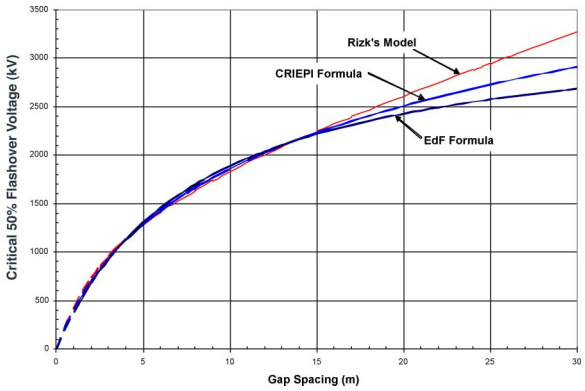


Figure 3.3-3 50% flashover voltage of rod-plane gaps versus gap distance for critical waves and standard atmospheric conditions.

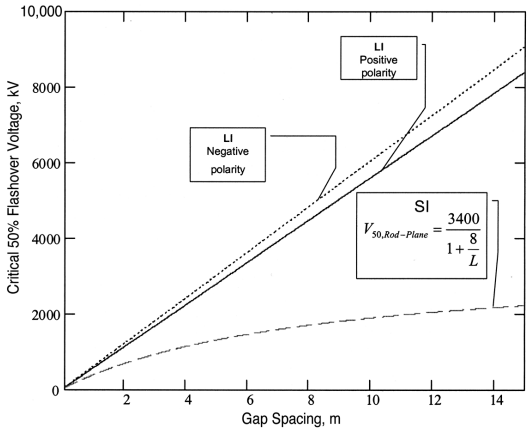


Figure 3.3-4 Comparison of rod-plane for switching impulse (SI) vs. lightning impulse (LI) strengths.

Table 3.3-2 Effect of Different Parameters on Switching Surge Impulse Strength

Parameter	Effect on $V_{50\%}$
Effect of Length of V-Insulators	The 50% flashover voltage is reduced when the gap spacing across the insulators becomes less than the gap spacing conductor-to-tower. The insulator length is generally considerably greater than the gap spacing, and therefore, the presence of V-insulators does not affect the switching impulse strength.
Effect of Atmospheric Conditions	Rain does not affect the switching impulse strength of tower windows, except when the insulator length becomes comparable or less than the gap length. These variables are normally correlated with each other— i.e., high humidity corresponds to low air density. Calculations may be simplified, assuming that they vary randomly within a given range, maintaining a certain correlation with each other. However, they have the same values along the line, with the exception of a systematic variation of relative air density due to altitude, if the altitude varies along the line.
Effect of Window Shape	Whenever the geometry departs significantly from a simple known configuration, reliable strength data can be obtained only by performing switching impulse tests on full-scale models in an outdoor high-voltage laboratory.
Conductor Size	Varying the size of the phase conductors, from single conductors to four-conductor bundles with a bundle diameter of 65 cm, does not affect significantly the flashover strength if the same gap spacing clearance is maintained between conductor and tower.
Outside Phase	In general, the switching impulse strength of outside phase tower gaps with V-insulators is stronger than that of tower windows with the same gap length. The increase in strength depends on the geometry, particularly the dimensions of the tower arm and of the tower body and the horizontal distance to the tower body. If the outside phase conductor has the same distance to the tower arm and to the tower body, and if the tower arm and body have the same width of those of a square window, the outside phase strength is about 6% greater than that of the tower windows for gap spacing less than 5 m. For gap spacing of 7 m or longer, the outside phase strength is only slightly (2~3%) greater of that of the tower window.
Insulator Strings	For positive polarity, the strength in fair weather is the same as the strength of the gap without insulators, provided the insulators are not placed directly along the possible flashover path. V-insulators in a tower window, where flashovers occur from conductor to upper truss, do not affect the tower window strength. The positive dry switching impulse strength is reduced by up to 5% when the insulators are placed along the shortest gap distance, such as vertical insulators in a tower window or in an outside phase, or horizontal insulators in a dead-end structure. For negative polarity, the strength in fair weather is usually much higher than the positive-polarity strength. The negative polarity strength is generally significantly reduced by foul weather. For very light or light contamination, a 10-20% reduction is suggested. In these cases, and if the switching impulse strength becomes a limiting factor in line design, the use of antifog or other special types of insulators is recommended.
Conductor-to-Grounded Objects at Midspan	Minimum clearances of transmission-line conductors to ground are recommended by national standards, such as the National Electrical Safety Code (NESC 2002) in the U.S., which are based, among other factors, on the requirement that the gap between conductor and grounded objects should withstand switching surges with a high degree of reliability.

having a magnitude equal to the short-duration, power frequency overvoltages. Temporary overvoltages are described in Section 3.2.4, and will not be discussed any further here.

Key points of significance to insulator strength under power frequency conditions include:

- Consideration of contaminated performance (if applicable) versus clean conditions.
- Contaminated performance is dependent on the insulator design, including type, profile, material, and dimensions.
- Flashover values are influenced by the type and level of both soluble and nonsoluble contaminants.
- When designing for contaminated conditions, a worst-case assumption is usually made that the contaminant is evenly distributed with critical wetting.

Figures 3.3-5 and 3.3-6 illustrate the withstand contamination performance for both ceramic and polymer insulator types.

Power Frequency Strength Under Clean Conditions

In the absence of contamination, power frequency voltages will not drive the insulation requirements (strike distance) of transmission lines. Flashover from ice bridging will only occur if the ice is contaminated, and hence it will not be covered any further here.

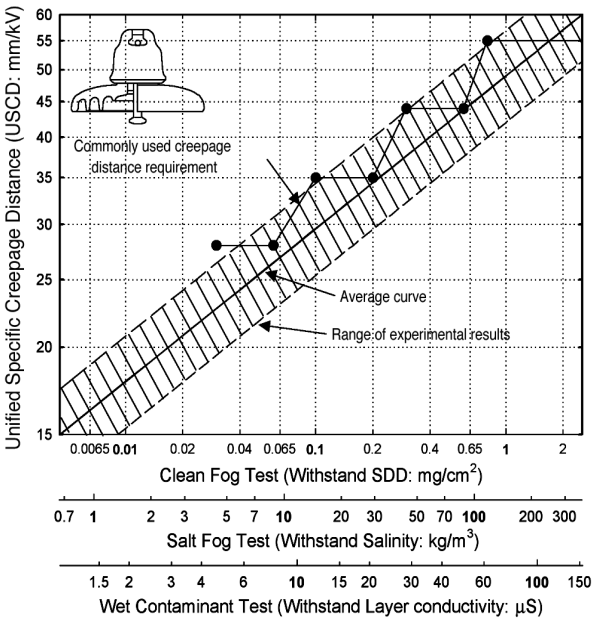


Figure 3.3-5 The withstand ac contamination performance of standard types of disc insulator based on the results from Salt-Fog and the Solid-Layer tests.

The flashover of clean insulators in wet conditions is very similar to that of dry insulators, so no allowance for this is normally made.

Power frequency flashovers at normal operating voltage can occur to ground if there is a fire under the line. This is a common operating consideration in countries where bush fires travel across lines. Flashovers of this type can also occur for gas or oil pipe line accidents.

For tower configurations for which the gap factor, "K", is known (see Section 5.2.4); the ac 50% flashover strength can be estimated from (IEC 1993):

$$V_{a.c.50} = 750(1.35K - 0.35K^2)Ln(1 + 0.55L^{1.2})$$

This equation is valid for gap spacings greater or equal to 2 m. A standard deviation of 2% may be assumed for the ac flashover strengths of air gaps. If the withstand voltage is assumed to be at the 3-σ level, it voltage would be 94% of the 50% flashover voltage (CFO).

Power Frequency Strength Under Contaminated Conditions

When contamination is present, coordination of flashover strength with power frequency voltage stress becomes important, and may even dictate the design of the transmission-line insulation (Table 3.3-3).

Insulation strength in the presence of contamination is dependent on the following factors:

- leakage distance and length,
- profile (sheds, etc.),

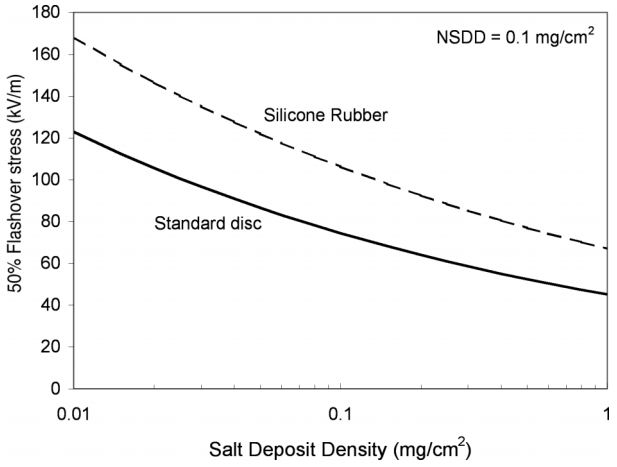


Figure 3.3-6 Comparison of the flashover stress of a hydrophobic silicone rubber insulator to that of a standard shape disc insulator.

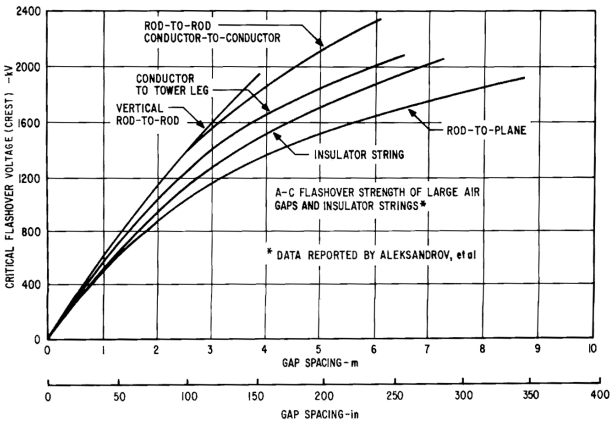


Figure 3.3-7 AC Flashover strength of large air gaps as reported by Aleksandrov (Aleksandrov et al. 1962).

Table 3.3-3 Contamination Site Severity

Site Severity	ESDD, mg/cm²	
	CIGRE	IEEE
None	0.0075—0.015	
Very light	0.015—0.03	0—0.03
Light	0.03— 0.06	0.03—0.06
Average/moderate	0.06—0.12	0.06—0.10
Heavy	0.12—0.24	>0.10
Very heavy	0.24—0.48	
Exceptional	>0.48	

- surface properties (water repellant, etched with age, semiconductive etc.),
- type and level of contaminant, and
- type and amount of wetting (dew, light or heavy rain, etc.).

3.3.5 Effect of Weather Conditions

The vulnerability of exposed insulation to surges and, in the case of lightning, the number of surges themselves, depend greatly on weather conditions. Therefore, weather data must be considered in design procedures.

In general, in the absence of contamination, occurrences of rain, drizzle, fog, snow, and any other type of precipitation do not affect the strength of air gaps, and without some form of precipitation, the presence of contamination alone does not affect the air-gap strength either. However, the combination has low electrical strength. The occurrence of extended periods with high wind or without rain, followed by light precipitation, is an important consideration for line insulation coordination in many areas.

Flashover voltages for air gaps depend on the moisture content and density of the air. Generally, insulation strength increases with absolute humidity, but test results become erratic above 85% relative humidity. Insulation strength decreases with decreasing air density, which is a concern for lines at high elevations. A detailed description of the effects of air density and absolute humidity is given in IEC 60-1 (IEC 1989) for different types of voltage stresses. Therefore, the estimation of the strength can usually be based on the average ambient conditions at the location. For insulators, the possible reduction in the withstand voltage due to snow and ice (0°C, 100% RH), or dew and fog (10-20°C, 100% RH) should be taken into account. Corrections applicable for humidity and ambient temperature variations may cancel each other. The effects of relative air density and absolute humidity are discussed in Section 5.13.

Rain does not affect the switching impulse strength of tower windows, except when the insulator length becomes comparable or less than the gap length. In this case, rain and other wet weather conditions, such as fog, drizzle, wet snow, and high humidity, may, depending on the type of insulators, further reduce the switching impulse strength (see Section 5.12).

The positive polarity switching impulse for most transmission-line insulation systems is not affected by wet weather because flashover paths are in the air, away from insulators. Vertical insulator strings supporting a transmission-line conductor from a tower crossarm may be an exception, especially if the crossarm is slender.

In this case the positive polarity switching impulse strength may be reduced by a few percentages, with a 5% reduction being a reasonably conservative value. The negative polarity strength of insulation systems with insulator strings is significantly affected by wet weather, yet the reduction in negative polarity strength is of little concern regarding line performance, because negative polarity strength in dry conditions is generally much higher than the positive polarity strength.

Conventional insulators designed to sufficient dry arc distance to withstand the power frequency voltage when covered with ice or snow will also generally withstand switching impulses with crest values of at least 2.5 per unit.

Generally, for the transient voltage case and, to some extent, for the 60-Hz case, it is most economical to consider flashovers as noncatastrophic, and to consider a certain number of flashovers of line insulation as tolerable. Likewise, it is more economical to consider a temporary insulator contamination situation as endurable, or a nonzero value of lightning tripout-rate-per-year as allowable. Given that insulation analysis is statistical in nature and that some flashovers may be permitted, it is most appropriate to consider the effects of weather on insulation in a statistical manner.

Figure 3.3-8 describes the effect of weather on the performance of line insulation.

High wind speeds off the ocean increase the contamination level rapidly (something like the third power of wind speed), so annual extreme wind will have an effect on contamination too.

Lightning occurrence increases rapidly as dew point temperature rises above 25°C. This could be a lower limit for the absolute humidity value to be used in RAD corrections.

RAD/RH corrections for impulse may be less important than characterizing the change in standard deviation of flashover strength when RH rises above 85%.

3.3.6 Summary

This section provided an overview of insulation strength and the key parameters that are significant to the designer. As a principle, the line insulation must have enough strength to meet the stresses produced by the overvoltages discussed in Section 3.2.

Insulation strength is expressed in terms of withstand voltage, a quantity determined by tests conducted under specified conditions with specified waveforms, and depends greatly on the waveshape of the applied voltage. The parameters generally used to characterize the waveshape of a lightning or a switching impulse are polarity, "front time" (variously defined) or time from zero to crest, and "tail time" (variously defined) or time from zero to half value after crest.

Transmission-line insulation, being air, is a self-restoring insulation, and hence can be mathematically represented by cumulative Gaussian distribution with a mean ($V_{50\%}$), and a standard deviation σ.

Of the three withstands needed to specify the insulation coordination of a transmission line (lightning, switching, and power frequency), the lightning withstand is characterized by having greater linearity than for the other stress types. The withstand to lightning is dependent on the polarity of the lightning, as well as atmospheric conditions (wet vs. dry)—positive polarity withstand being inferior to that of negative. For quick calculations, recommended gradi-

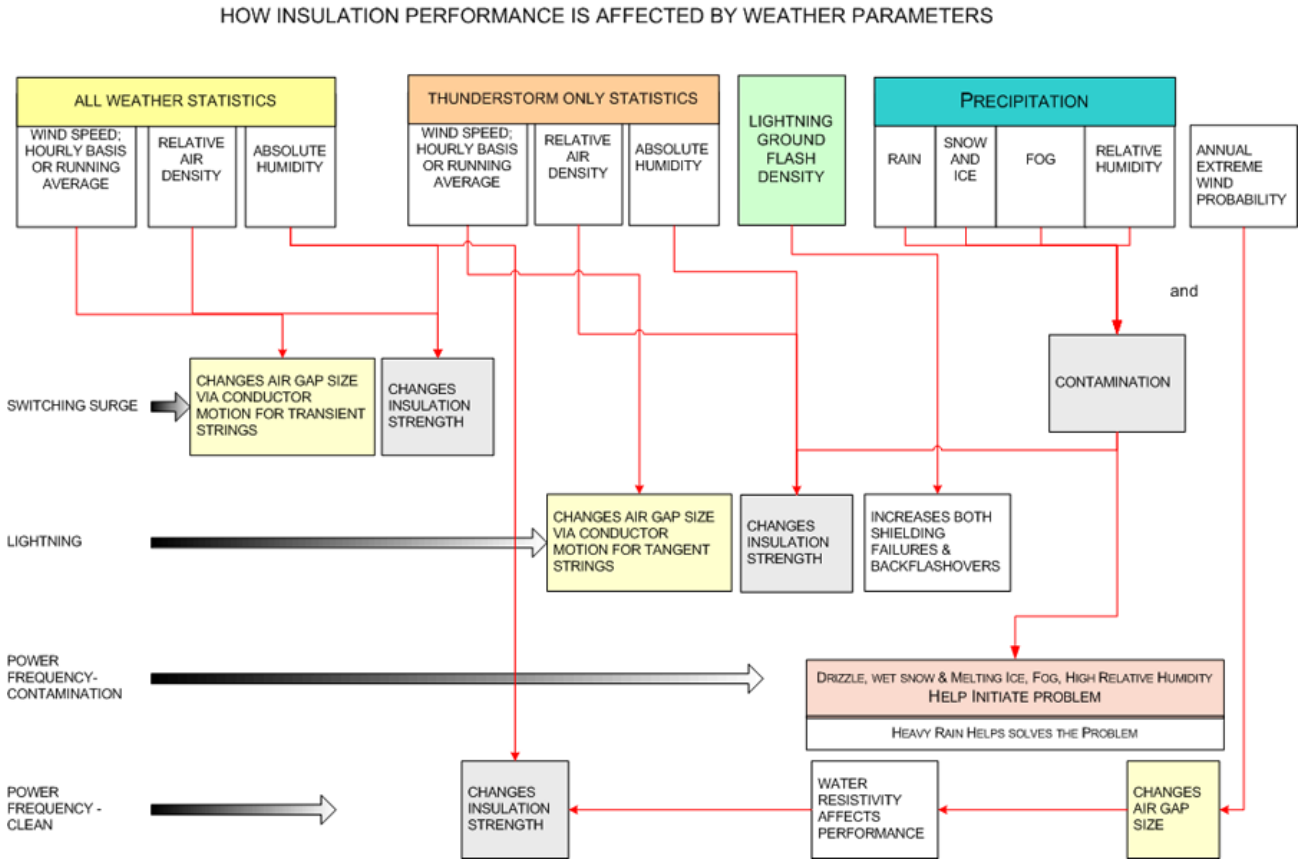


Figure 3.3-8 Effect of weather parameters on insulation performance.

ents are 560 kV/m for the positive polarity Critical Flashover Voltage (+V50%) and 605 kV/m for negative polarity (-V50%). For laboratory tests, the relative standard deviation of lighting impulse strength is about 3%.

The switching surge strength is dependent on many variables, including altitude above sea level, wet weather, gap length, and insulator strike distance.

For switching surges, the calculation of risk of line flashover is made by dividing the stress into a number of "stress situations," and the insulation elements of each section and phase into "sets" in which the elements have the same strength. The probability of flashover is then calculated for each combination of stress situation and insulation set. The lowest values of V_{50} flashover voltage occur for a positive polarity impulse applied to a rod protruding toward a plane. Switching surge strength exhibits a saturation effect with the strike distance. This is a very important behavior compared to the strength required for lightning, and explains the importance of keeping switching surge overvoltages under check for higher voltages; otherwise, the insulator string length, and hence the tower dimensions, become excessively demanding and expensive. Negative polarity switching impulse is sufficiently higher than the positive polarity strength, which is not considered in the insulation coordination. For laboratory tests, the relative standard deviation of switching impulse strength is about 6%.

In the absence of contamination, power frequency voltages do not drive the insulation requirements (strike distance) of transmission lines. When contamination is present on insulator surfaces or in ice layers, protecting for power frequency voltages becomes more important, and may even dictate the design of the transmission-line insulation. For laboratory tests, the relative standard deviation of contamination flashover strength varies from 3 to 10%.

3.4 OVERVOLTAGE CONTROL

3.4.1 Introduction

While the previous sections described the stress on line insulation (overvoltages) and insulation withstand characteristics (the strength), this section describes the ameliorating measures for reducing flashovers from lightning, switching, and power frequency under contamination.

Design for lightning flashovers (associated with shielding failures and backflashovers) includes setting the insulation level, line geometry/clearances, shielding, grounding, and the application of surge arresters. Design for switching surge (typically associated with reclosing on transmission lines) can be achieved through a number of measures, such as strategically placed surge arresters, use of closing resistors, or controlled switching. Designs to withstand the effect of insulator contamination include use of nonstandard ceramic insulators (insulators with longer creepage) or fog-type insulators), use of nonceramic insulators such as polymer insulators, or the use of special insulator surface coatings.

This section describes these countermeasures and others in some detail to provide line designers with an arsenal of solutions to choose from in overall line insulation coordination specification. The objective is to match the stresses with strength, and thereby achieve acceptable reliability of the line at an affordable cost.

3.4.2 Control of Lightning Overvoltages

Design for lightning includes setting the insulation level, line geometry and clearances, shielding, grounding, and transmission line arresters. Typical practice is to set standards for design and construction of each line type, and then address "hot spots" with special measures. Extra effort may be required for lines having high exposure to lightning or where soil resistivity is high.

Chapter 6 provides a detailed discussion on the occurrence and characteristics of lightning. For convenience, the key information is summarized here, to give a context for discussion of insulation coordination design for lightning and other stresses.

Table 3.4-1 and Figure 3.4-1 summarize the lightning overvoltage design options typically considered by utilities for transmission lines.

Figure 3.4-2 summarizes the steps needed for evaluating the lightning performance of existing transmission lines, and finding appropriate measures to support line performance within acceptable standards.

Design for Lightning Protection

One of the most successful ways to estimate the lightning performance of a new transmission circuit is to perform multiple linear regression of the observed performance of nearby lines against the most sensitive parameters. This is especially helpful when comparing lines with similar conductor geometry, tower style, and span length. If such information is not available, the designer must consider the following design variables.

Design Variables and Protection Techniques

The principal parameters available to a line designer to improve lightning performance are structure type, line routing, insulation level, number and placement of shield wires, grounding, and transmission-line surge arresters.

Table 3.4-1 Lightning Overvoltage Design Options

	Shielding Failures	Backflashover Failures	Induced Failures
Root Cause	Small first strokes that terminate on the phase conductor rather than the shield wire.	Large first stroke currents, in combination with high footing resistance and/or high tower surge impedance on tall towers.	Fast-rising (high dI/dt) current in proximity to phase conductors.
Insulation	Does not affect shielding failure flashover rate much, since subsequent strokes follow same path.	Strong effect on backflashover rate.	Transmission lines have >450 kV BIL and are generally immune to induced voltage flashovers.
Add or Move Overhead Groundwires	Moving the shield wires outward will increase their effectiveness. On EHV lines, some shield wires are outside of the phases (negative shielding angle).	Adding more shield wires, above or below the phases, improves electromagnetic coupling and reduces backflashover rate.	Adding more grounded shield wires will reduce the induced voltage.
Improve Grounding	No effect, except on multiple-circuit flashover rates.	Strong effect on backflashover rate.	Induced voltages higher in areas where grounding is difficult.
Install Transmission Line Surge Arresters (TLSA)	Reduces number of shielding failures by limiting voltage across insulator of stricken phase.	Reduces number of backflashovers by limiting voltage on protected phases and improving coupling on unprotected phases.	Clips induced voltage to less that peak flashover level of insulator.

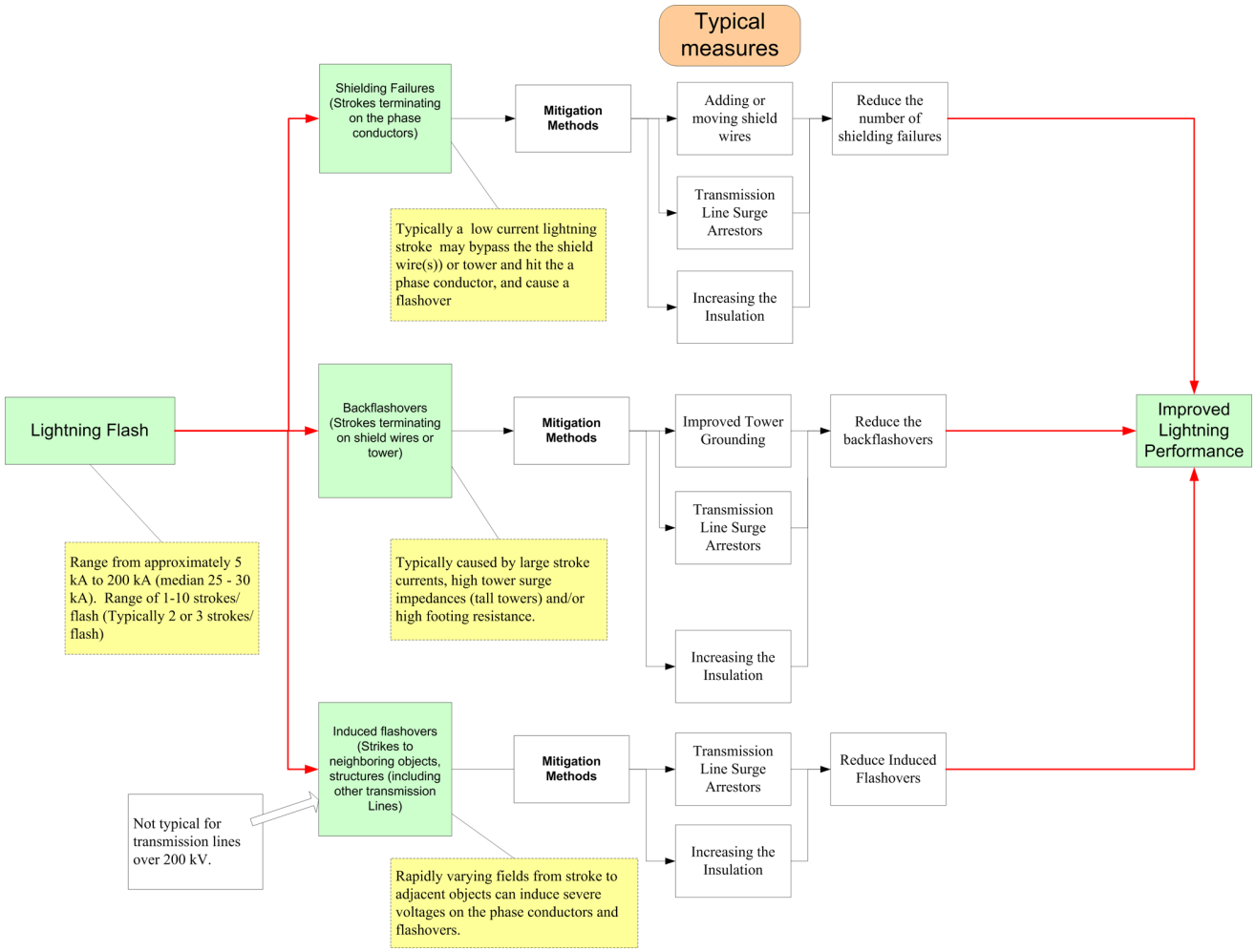


Figure 3.4-1 Lightning overvoltage design options

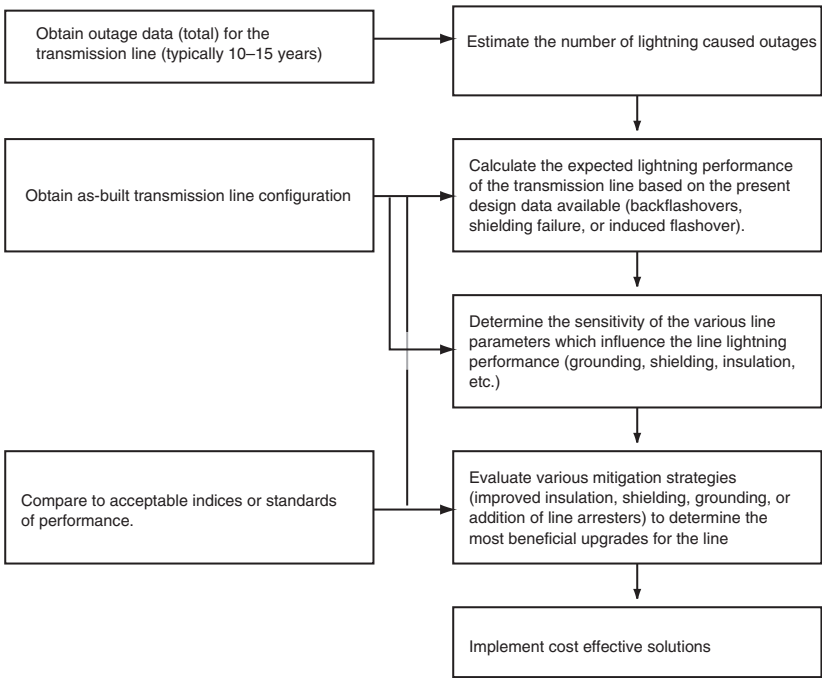


Figure 3.4-2 Lightning performance analysis for existing lines.

Structure Type

It is unlikely that the choice of structure type would be determined exclusively by lightning performance, but some lines have indeed been designed in this way. Key issues in choosing the structure type when considering lightning performance are:

- Steel lattice structures have lower surge impedance than steel poles (or wood poles with grounding downleads).
- Guyed structures have lower surge impedance than free-standing towers.
- Lattice and guyed structures have larger foundation footprints and hence lower footing resistance.
- The strength of steel allows flexibility for placement of shield wires.
- Although rarely used for transmission lines above 200 kV, wood structures offer an ability to use the arc-quenching capabilities of wood members. Unbonded wood crossarms can be used on steel structures to the same end. The wires connecting the shield wires and, in the case of wood crossarms, the ground-end insulator hardware to the tower footing must be kept away from the wood structure.

Line Routing

It is unlikely that a line designer will be able to choose the line route based only on lightning performance or ease of grounding. However, there are benefits from:

- Routes through forested areas, which provide some degree of natural shielding.
- Routes that avoid exposed structures, such as on top of ridges. Fortunately the routing of lines along the side of hills is also consistent with environmental desires to reduce the visual impact. On the other hand, location of structures on hilltops, rather than in valleys, allows longer conductor spans that meet ground clearance requirements, and so reduces the number of structures and the line cost.
- Routes that take some advantage of the tower-to-tower variation in resistivity, by selecting those locations where earth resistivity is lower.

Insulation Level

The length of insulator strings and of air gaps may be increased in order to increase the insulation strength and reduce the flashover rate.

Number and Placement of Shield Wires

Shielding failure is an uncommon cause of transmission-line lightning flashovers, with shield wire effectiveness reaching more than 95% for most new designs. Shield wires are quite successful in intercepting lightning flashes, using design methods that have been extensively studied and developed for more than 50 years. A shielding failure occurs when a flash appears in such a location that it gets by the shield wire protection and strikes a phase conductor. Shielding failures (i.e., lightning hitting a phase conductor rather than a shield wire) are more likely to occur for low-current strokes. For stroke currents above a certain value, I_S, the upward leader starting from the shield wire is always able to intercept the downward leader of a vertical stroke

channel. Even if the stroke current is sufficiently low that its voltage stress on the phase conductor does not exceed the insulation strength, one of the subsequent strokes that follows the same path will likely be large enough to cause a phase-to-tower flashover.

Shielding failure calculations usually assume that stroke leaders advance vertically. This is the least conservative assumption. Leaders approaching the transmission line at an angle from the vertical may cause shielding failures with higher stroke currents. Adding or moving shield wires is one method of improving the lightning performance of a transmission line. A poorly placed shield wire can allow an excessive number of lightning strokes to attach directly to the phase conductors and cause flashovers. Improved shielding reduces the number of shielding failures, and resulting flashovers, on a transmission line. The type and size of the shield wire are not important for lightning performance calculations. Shield wire parameters should be based on the expected mechanical loads for a specific installation.

The principle of so-called "perfect shielding design" is to locate the shield wires so that the value of I_S, the maximum stroke current that can cause a shielding failure, is greater than the value of I_C, the maximum stroke current that, if applied to a phase conductor, can cause a flashover of the line insulation. In practice, lines should usually be designed with a small (0.05 per 100 km per year) shielding failure rate (Hileman 1999) to acknowledge and minimize some of the uncertainties in the calculation process. Figure 3.4-3 defines the shielding angle of transmission lines. For lines above 200 kV, it is common practice for transmission lines to have two shield wires, with shield angles in the range of +30 to -12 degrees. However, to save costs, lines may be built with one shield wire, or even with no shield wires, where weather conditions allow or require it (for example, infrequent lightning or unusually severe icing).

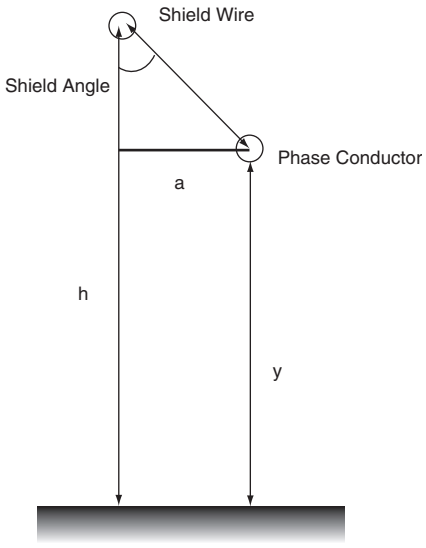


Figure 3.4-3 Definition of the shielding angle.

One of the limitations of the use of "perfect" shielding is that, on average, subsequent strokes tend to follow the same ionized path as the first stroke. For instance, 500-kV line insulators and air gaps may withstand lightning impulses with crest voltages up to 1800 kV or higher. A stroke hitting a phase of a 500-kV line, whose surge impedance in corona is, for example, 300 Ω, may cause a flashover only if any of the stroke currents is greater than I_C =1800/(300 Ω/2) = 12 kA. A shielding failure with first-stroke current $I_S<I_C$ stroke may not cause a flashover but one of the subsequent strokes, each having a 12-kA median, may still cause a flashover. Section 6.6.4 gives more details on this issue. Perfect shielding must also be violated by flashes approaching a line at an angle rather than vertical. One photograph exists of a flash coming in almost horizontal and hitting a phase.

In addition to the number of shield wires, the midspan clearance between shield and phase conductors should be considered. The midspan clearance between a shield wire and a conductor must also withstand the overvoltages caused by lightning. In most cases, the possibility of a flashover from a shield wire to a phase conductor may be ignored because of several mitigating factors:

1. The voltage wave created by a stroke injected in the shield wire at midspan travels toward the two ends of the span, and is reflected at the structures. A significant fraction of it comes back with the opposite polarity, and reduces the voltage at midspan after a time equal to the travel time along the span.
2. The shield wire-to-phase conductor clearance is usually much larger at midspan than at the tower because the shield wire sag is significantly smaller than the phase conductor sag.
3. The voltage wave on the shield wire induces a wave of the same polarity on the phase conductor, which causes a reduction of the voltage between shield wire and conductor. This effect is more significant the closer the phase conductor is to the shield wire.
4. Lightning hits at midspan are less frequent than those at or near the structures because of the lower height at midspan.
5. Predischarge effects (Wagner and Hileman 1963) may reduce the shield wire voltage significantly.

Grounding

Grounding is one of the most effective and cost-effective methods of controlling backflashover performance. Reducing the ground impedance of a tower reduces the voltage developed on the structure when a lightning stroke hits the structure or shield wire. A lower crossarm voltage reduces

the insulation stress during a lightning event and reduces the number of backflashovers for the line. The voltage over the insulator strings is significantly reduced when the first reflected traveling wave returns from the bottom of a well-grounded structure.

There is a large body of publications (see Chapter 6) on measuring soil resistivity and footing impedance. Section 6.10 provides many details and some simplified models for the relationship between soil resistivity, foundation shape and as-built impedance. Some cost-effective methods of reducing footing impedance by addition of combinations of ground rods, counterpoise, and soil treatment are also described. Designers should also consider the effects of high-impulse current from lightning on the soil impedance. At high currents, ionization and breakdowns may occur, effectively reducing the soil resistivity.

High footing impedance, such as in rocky terrains, often coincides with higher exposure to lightning. Even one or two poorly grounded and exposed structures can be the source of very significant increases in tripout rates above design expectations. Detection and remedial measures can include visual inspection of the line, local soil resistivity measurements, footing resistance measurements by disconnecting the ground wires at the tower top, or footing impedance measurements using a portable impulse source. Lightning location network data can also be compared with synchronized time tags of relay records to determine the likely location of a line "hot spot."

Many transmission-line structures have entirely satisfactory footing resistances from the standard foundation, with no augmentation. When additional grounding is required, a few grounding rods combined with horizontal counterpoise connections are often sufficient to reduce footing resistance to a desired level. The depth of the rods and the spread of the augmented grounding can be increased as needed. Although it is not normally a consideration, grounding beyond 60 m (200 ft) from the structure is subject to the law of diminishing returns; beneficial reflections from the grounding do not reach the structure in time to influence the backflashovers. On the other hand, continuous counterpoise reaching from one structure to the next is sometimes used. A "crows-foot" counterpoise or ring electrode is recommended in many areas.

There is a tradeoff between grounding improvement cost and effectiveness that is more difficult to manage than the tradeoffs in other approaches, such as fitting line surge arresters. After a certain level of grounding augmentation is reached, either an elevated probability of flashover is accepted, or other measures such as line-mounted arresters are used.

Changes in grounding have no effect on the shielding failure flashover rates and an indirect effect on induced overvoltages, as detailed in Chapter 6. However, the role of TLSA versus grounding improvements is an important evaluation in the modern insulation coordination process and is described next in detail.

Transmission Line Surge Arresters (TLSAs)

Transmission Line Surge Arresters have been used successfully on many transmission lines to control the lightning-caused overvoltages across insulator strings where high exposure and difficult grounding cause poor lightning performance. The superior life, ruggedness, and physical size of arresters with polymer housings provide a reasonably economic solution that can be retrofitted to lines that fail to meet expectations. Depending on the line voltage, specific problems, and desired performance, arresters may be applied at every structure or periodically at every second or third structure, and in any case, can be limited to the area of concern rather than the whole line. Appendix 3.2 provides details on applying transmission-line surge arresters.

Special Considerations

Multi-Circuit Lines, Unbalanced Insulation, Unsymmetrical Phase Arrangement. For double or multi-circuit structures, in addition to the single-circuit lightning tripout rate, the double-circuit tripout rate is of great concern. Losing one circuit—with the possibility of a single pole of conventional reclosing—may be acceptable, but loss of both circuits simultaneously could have serious consequences. Typically system planners need to know the probability of the loss of two circuits on the same structure or on the same right-of-way.

The double-circuit calculation requires that, after the first flashover has occurred, the calculation model must be modified to allow for the additional paths of currents on the flashed-over phase and the increased (and beneficial) coupling that will occur. Of course, on a perfectly symmetrical double-circuit design, with matching phases at the same heights on the structure, it is possible that simultaneous flashovers will occur on both circuits. If the two circuits have reverse phasing, such as ABC–CAB, one circuit will have a better chance of surviving after a flashover on the other.

Another practice that has been used is to deliberately build one circuit with slightly weaker insulation than the other circuit—the argument being that this circuit will flash over first, and by doing so, will improve the performance of the other circuit. In reality, this practice is more likely to result in significantly worse performance for one circuit and little, if any, improvement for the other circuit, so the practice is not recommended.

High-Phase Order. As discussed under multi-circuit lines, the flashover of one circuit results in a reduction of voltage over the unflashed insulators as a result of increased coupling from the flashed-over phase conductor. For the special case of high-phase order (6 or 12 phase) lines, this effect can provide an essentially lightning-proof design. After one or two phases have flashed over, the remaining phases will be protected, and the line is capable of operating with its remaining phases in an unbalanced mode until the faulted phases have been cleared. A short length of high-phase-order line has been operated on both the Niagara Mohawk and Tennessee Valley Authority (TVA) systems in the U.S.

Multiple Lines on a Right-of-Way. If two lines are on the same right-of-way and they are the same voltage, it is common practice to locate the structures immediately adjacent to each other for aesthetic reasons. This practice creates the possibility that a lightning flash to one line could affect the other. If the tower footings have augmented grounding, it is possible that the bases of the towers are connected below ground level.

Study of this case requires specially adapted software. As a general rule, it is preferable that the footings of adjacent lines not be interconnected, although attenuation, coupling, and other losses make it unlikely that a stroke to one can cause a flashover on both. If footing resistances are high due to poor soil resistivity, it may be practically impossible to keep them separate, in which case other measures such as arresters may be necessary.

3.4.3 Control of Switching Surges

The control of overvoltages due to switching surges is an important requirement for the economic design of transmission systems operating above 200 kV, and a necessity above 400 kV. Finding the most suitable and cost-effective solution depends on the initiating event. Switching overvoltage control strategy is largely dependent on the autoreclose operation requirements for the system.

To review, the switching operations of greatest concern in EHV are:

- Line energization
- Line re-energization with trapped charge on the line
- Load rejection, with a circuit breaker opening at the far end of a line, possibly followed by disconnection at the near end
- Transformer switching at no load or with a secondary load of shunt reactors
- Reactor switching

Energizing overvoltages are controlled by:

- One or multi-stage pre-insertion resistors
- Phased (voltage-controlled) closing of the breaker contacts
- Shunt reactors, or other drainage of the trapped charge before reclosing
- Use of suitably coordinated arresters

Various methods of control have been in use successfully for many years. These methods are described here, along with some new concepts.

Circuit Breakers

When a protective relay detects a fault or other system disturbance on the protected circuit or line, the circuit breaker operates to physically separate current-carrying contacts in each of the three phases by opening the circuit to prevent the continued flow of current. In addition, a circuit breaker is capable of load-current switching.

The major components of a circuit breaker include:

- The interrupters, which open and close one or more sets of current-carrying contacts housed therein
- Operating mechanism (provides the energy necessary to open or close the contacts)
- Arcing control mechanism and interrupting media
- One or more tanks for housing the interrupters
- Bushings
- Mechanical linkage connecting the interrupters and the operating mechanism.

Circuit breakers can differ in the overall configuration of the above components; however, the operation of most circuit breakers is substantially the same. A circuit breaker may include a single-tank assembly, which houses all the interrupters. Alternatively, a separate tank for each interrupter may be provided in a multiple-tank configuration. All circuit breaker switching operations generate closing or opening transients or switching overvoltages (SOVs) in the system as the system adjusts to the new set of operating conditions as a result of the switching operation. This section reviews some of the possible changes to the basic breaker configuration.

Pre-Insertion Closing and Tripping Resistors

Traditionally, the most common measure to reduce energizing transients is the use of pre-insertion resistors (PIRs) or closing resistors. Closing resistors are inserted in series with the line being switched for a short period of time, before closing the main contacts of the breaker, thereby damping the transient overvoltages. Optimum overvoltage control requires correct choice of the resistor value in rela-

tion to the source impedance level, the line length, and the line parameters. Luckily, the magnitude of the resulting overvoltages is not critically sensitive to any of these parameters (see Figure 3.4-4), making it an easier task for the design engineer. Nevertheless, detailed studies are necessary to quantify the value of the resistor (or resistors, if a dual-stage PIR is used), and this should be done under an overall line insulation coordination effort. Although a well-proven technology, breakers equipped with closing resistors inevitably involve relatively complex mechanical constructions. The complex mechanical linkages and an extra set(s) of contacts needed to equip the breaker with preinsertion resistors may present reliability and maintenance concerns. The use of PIRs for transmission-line energization has been a standard requirement on 550-kV systems, particularly on long lines (i.e., > 200 km).

If chosen properly, PIRs in the closing operation of the breakers can drastically reduce the SOVs. Figure 3.4-4 illustrates the reduction effect on SOVs in reclosing and energizing operations on a 500-kV transmission line. Note reclosing SOVs are more severe than those created from energizing the line, due to the residual trapped charge on the line in the case of reclosing.

A number of studies by the authors have shown that the use of PIRs was superior to other countermeasures in the control of SOVs. However, this was highly dependent on the system that was studied. In 500-kV studies performed in the 1980s, it was shown that the use of PIRs to control SOVs under specific system parameters and configurations resulted in the lowest voltage transient levels, compared to some other methods. Additionally, the overvoltage profiles of the lines where PIRs were used were much flatter, compared to those where other solutions were applied. For example, when arresters were used, they exhibited the major part of their control only close to their location, and hence resulted in less flat overvoltage profiles, unless many of them were used.

Today, with the advent of transmission-line arresters, new breaker technologies, and new concepts of applying system protection, other solutions (e.g., those involving strategically located surge arresters) may have equally good results compared to PIR-equipped breakers. For example, in the past decade, a large North American utility has been replacing older breakers equipped with PIRs with resistorless breakers and applying metal-oxide surge arresters (MOSAs) to the opposite end of a number of their 500-kV lines. The new breakers also incorporate staggered closing, where each phase closes about one cycle apart.

Another example can be found at another North American utility, where the desire to eliminate closing resistors led to the adoption of controlled high-speed auto-reclosing on its newest 500-kV lines. Malfunction or misoperation of the control device is mitigated by staggering the close signals to the control device, using special features in the control device itself, and by providing special low-protective-level metal-oxide surge arresters at the line terminals and in the middle of the line.

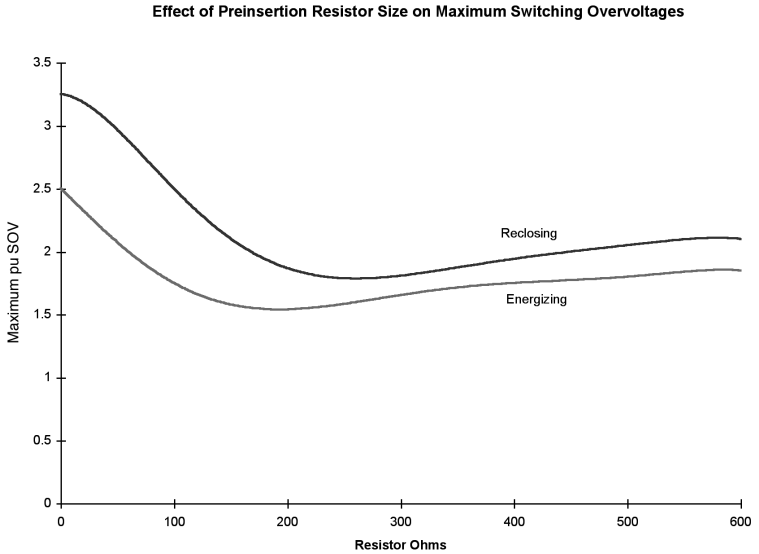


Figure 3.4-4 Effect of breaker preinsertion resistors on maximum switching surge overvoltages.

The preceding shows a trend in the industry that may be more acceptable and applicable at lower-voltage levels, especially with the use of transmission-line arresters.

Controlling Overvoltages from Circuit Opening

Switching surges from de-energizing a transmission line are usually of less concern for the line designer. Ideally, circuit breakers are controlled to open their contacts as the instantaneous phase current passes through zero, but if a nonzero current is interrupted, this interruption will cause a transient that is usually small. The greatest concern for circuit opening is a restrike across the opening contacts, which can initiate a traveling wave to the far end of the line. If the far circuit breaker has already opened, a voltage doubling can occur as the traveling wave is reflected, with the possibility of further arcing across the breaker contacts. In reality, these voltage surges would be limited (for example, by arresters), and the primary concern in this circumstance would be the failure of the breaker, rather than the possibility of a line insulation flashover.

Opening (or tripping) resistors are usually not the same as closing resistors. Insertion of these resistors during the opening of the breaker helps to drain the residual charge on a line and prevent trapped charge voltage. Opening resistors are typically not used on modern SF_6 circuit breakers. Surge arresters can be used across an interrupter to limit reactor-switching transient recovery voltage (IEEE 1993). Surge arresters can be used instead of opening resistors on circuit breakers to reduce trapped charge on shunt capacitors or transmission lines.

In past years, many U.S. utilities used bulk oil circuit breakers for most 230-kV applications. These circuit breakers sometimes had restrikes when switching capacitive current. Hence utilities equipped their breakers with opening resistors (with values > 3000 ohms) to control restrike transients while line dropping and capacitor switching. While the resistors were primarily intended for insertion on opening, some were inserted on both opening and closing, due to the mechanical complexities of the breaker mechanisms. Although such values would not help in reducing SOVs upon closing, their typical insertion of two to three cycles helped to discharge a large percentage of the trapped charge on the unfaulted phases, and hence the resultant SOVs during high-speed reclosing were lower with the use of the resistors. Today utilities are using SF_6 breakers for such applications, and some are applying controlled switching in place of the opening resistors.

Synchronous Switching

All circuit breaker switching operations generate closing or opening transients in the system as the system adjusts to the new set of operating conditions as a result of the switching operation. Synchronization of circuit breaker closing and opening to system voltage and current waveforms can drastically reduce these transients and, in addition, reduce interrupter wear. The most challenging application for synchronous switching is the switching of a de-energized shunt capacitor bank or high-speed reclosing of a long transmission line with trapped charge.

Synchronous switching of breakers in utility transmission systems can offer many benefits for reducing switching-related system problems. Application of synchronous switching in utility systems has been gaining interest and application. Synchronous switching can offer an economical alternative to conventional switching transient reduction methods such as pre-insertion resistors, current limiting reactors, and surge arresters by closing on the appropriate point of the voltage wave across the circuit breaker.

Several issues must be considered for the proper design of a synchronous-closing circuit breaker. These considerations include both system application requirements as well as circuit breaker performance requirements. Traditional circuit breaker technology has suffered from mechanical inaccuracies and lack of repeatability, which has prevented the widespread use of synchronous switching. Modern-day single-pressure SF_6 circuit breakers, when properly designed, can provide reliable and accurate synchronous switching performance for utility transmission systems. These design considerations include considerations for prestrike variations and control strategies for maintaining long-term consistent performance. The advent of single-pressure SF_6 interrupter technology has provided a significant boost to synchronous switching applications in utility transmission systems. Single-pressure SF_6 technology has eliminated the need for multiple-series interrupters, except at the highest transmission voltages. This change has reduced mechanical complexity, and made the application of synchronous switching easier. Among the common applications associated with synchronous switching is the zero-voltage-controlled closing of shunt capacitor banks to minimize the energization transients.

Design Considerations for Synchronous Switching

A simplistic view of synchronous switching would consider a circuit breaker coupled with the necessary control hardware to trigger the operation of the circuit breaker at the appropriate instant. From this simplified perspective, any circuit breaker containing a basic independent pole operation capability could be adapted with controls to provide synchronous switching capability. However, to provide a reliable, long-term solution in utility transmission systems, several special requirements must be considered in the original design of the circuit breaker and control algorithms. These requirements include accounting for the prestrike behavior of the interrupter and accounting for the

effect of operating variables such as temperature and control voltage.

While the concept of synchronous or controlled switching seems simple, cost-effective solutions are not always easy to achieve, primarily due to the high cost of providing the required timing accuracy in a mechanical system. One solution is to use three separate operating mechanisms and corresponding linkages to synchronously control the operation of each pole individually. This solution adds costs and increases the overall size and complexity of the circuit breaker. An advanced way to accomplish this goal is to provide a time shift between the instant of contact in the different phases. This approach requires a prior knowledge of the time required to close and open the interrupter contacts in each of the three phases. Any time differences can be accounted for by an appropriate design of the mechanical linkage. Circuit breakers applied in utility systems are expected to provide consistent performance for 20 or 30 years. Over the circuit breaker's operating life, the circuit breaker operating time can change as a result of mechanical wear.

Other ideas for the application of synchronous switching include: developing the means for continuous monitoring of current (or voltage) waveform on a switched circuit; and providing compensation for variations in operating mechanism stored energy, temperature, and controlled voltage. To account for these slowly changing operating time variations, it is important for the synchronous closing algorithm to allow some kind of feedback and apply correction to the operating parameters.

Surge Arresters

The application of surge arresters (either for lightning or switching surge overvoltage control) has yielded advantages, which have been documented in many technical papers.

Such advantages include:

- Increased reliability of existing lines
- Switching surge overvoltage (SOV) control
- Double-circuit outage reduction
- Compact line design
- Facilitating of line upgrading
- Compatibility between different voltage level lines
- Overvoltage control in the vicinity of HV and EHV substations
- Live working

Arresters can be used very effectively to reduce SOVs, and can be installed either at:

- Substations (the more traditional way to applying surge arresters)
- On the transmission line itself (transmission-line surge arresters, or TLSAs). The arresters can be installed directly on the towers.

Surge arresters dissipate switching surges by absorbing thermal energy. The amount of energy is related to:

- Prospective switching surge magnitude and waveshape (without the surge arresters)
- Circuit topology and impedance
- Arrester voltage-current characteristics
- Number of operations (single/multiple events).

The switching surge duty on metal-oxide arresters applied on overhead transmission lines increases for increased system voltage and increased length of switched line. Typically, transients occurring from high-speed reclosing impose greater duty than energizing. The selected arrester should have an energy capability greater than the energy associated with the expected switching surges on the system. The actual amount of energy discharged by a metal-oxide arrester during a switching surge can be determined through detailed system studies.

Transmission-Line Surge Arresters for SOV Control

A trend in recent years has been to try to find alternatives to the popular PIRs to control SOVs by more active use of arresters. Efficient limitation of the overvoltages along the lines by surge arresters is possible with the introduction of high-energy polymer-housed surge arresters that permit easy installation on the lines. Arresters can be installed directly on the towers. The energy requirements due to switching surges are considerably less for line arresters than for arresters located at the receiving end of the switched line. Hence, protection against switching typically requires one energy class lower for line arresters, than what is used for arresters installed at the substation. Unlike lightning-related applications, where arresters may be installed at consecutive structures, arresters to control switching surges may be needed only at the end of the line and maybe at one or two other points along the line. For switching overvoltage control, TLSAs are usually installed in all phases. The number of line arresters needed is dependent on the length of the line. For shorter lines, installation at the line ends may suffice to control SOVs. For longer lines, arresters may be needed at several locations. Compact lines, or those with upgraded voltage levels, may require line arresters on every tower for one or all phases. System studies show how many are needed, and in what locations. Appendix 3.2 goes into more detail on the application of TLSAs.

For delayed three-phase auto-reclose and high-speed single-phase auto-reclose, MOAs offer a good alternative to PIRs. However, for 550-kV systems, which require three-phase high-speed auto-reclose, the PIR has been the only economic solution, particularly for compact transmission tower designs. Alternatives, such as fitting surge arrester stations at line mid-points, have been proposed in place of PIRs, but could prove more costly. Controlling switching overvoltages by synchronizing the circuit breaker closing operation to a point at voltage zero has been researched for many years, but was inhibited by the available technology. However, with modern circuit breaker designs and electronic controls, the necessary equipment is available to achieve controlled switching.

Special Considerations

Capacitor Switching
Voltage and current transients generated during the energization of shunt capacitor banks have become an increasing concern for the electric utility industry. One concern relates to power quality for voltage-sensitive loads and excessive stresses on power system equipment on the utilization levels. Therefore, utilities have set objectives to reduce the occurrence of transients and to provide a stable power waveform.

Conventional solutions for reducing the transients resulting from shunt capacitor energization include circuit breaker preinsertion devices—for example, resistors or inductors, and fixed devices, such as current-limiting reactors. The maximum shunt capacitor bank energization transients are associated with closing the circuit breaker at the peak of the system voltage waveform, where the greatest difference exists between the bus voltage, which will be at its maximum, and the capacitor bank voltage, which will be at a zero level. Where the closings are not synchronized with respect to the system voltage, the probability of obtaining the maximum energization transients is high. One solution to this problem is to synchronously close the circuit breaker at the instant the system voltage is substantially zero. In this way, the voltages on both sides of the circuit breaker at the instant of closure would be nearly equal, allowing for an effectively "transient-free" energization.

Another major concern of capacitor switching is associated with addressing prestrike considerations of the breakers. During a closing operation, the circuit breaker interrupter contacts come together to close the circuit. The voltage withstand of the interrupter gap decreases from its peak voltage withstand capability (open position) to zero voltage withstand capability (closed position). A slower velocity results in a lower slope of the interrupter voltage withstand characteristic versus time, whereas a faster closing velocity results in a higher slope.

Reactor Compensated Line
Switching operations of shunt reactors are relatively frequent and primarily depend on power network loading. When a shunt-compensated line is switched off from the remote side, the line-side voltage may oscillate with a frequency determined by the line charging capacitance and the shunt reactor inductance with normally weak damping due to low losses in the line. Since the line voltages oscillate with a frequency that differs from the power frequency, the voltages across the open breaker poles show a low-frequency beat phenomena. Switching transients are inversely proportional to the shunt-reactor-rated power.

With regard to its inductive character, switching of shunt-reactor-rated-current-results can jeopardize insulation of the shunt reactor itself and other switchyard elements, and create mechanical stresses.

3.4.4 Control of Power Frequency Stress Caused by Insulator Contamination

The power frequency flashover voltage is considered to be the same for 60 Hz and for 50 Hz.

Contamination is a major criterion for design of transmission-line insulators. Control of power frequency strength of standard ceramic insulators under contamination depends on factors that include choice of insulator type, design, and leakage distance, depending on the type and severity of the contaminant, nature and frequency of the precipitation, and the degree of natural cleaning (see Figure 3.4-5). At this time, the following are the most common solutions adopted by utilities to successfully combat contamination:

- **Increasing the number of discs in the string.** Increasing the number of insulators in a string increases the creepage and dry arc distances, which, in turn, reduce the frequency of flashover due to contamination or ice bridging. However, a decision in this regard may be taken after examining whether adequate electrical clearances are available and ensuring that the angle of the V string would not be disturbed.
- **Using high-leakage insulators.** Insulators such as the fog-type units offer increased leakage distance per unit of insulator length. Leakage-distances-to-dry-arc distance ratios of 2.9 to 4.5 are available.
- **Using polymer insulators.** Over the last three decades, the use of polymer or non-ceramic insulators (NCIs) on transmission lines has become more prevalent. The flashover performance of NCIs in the presence of contamination is considerably superior to that of porcelain insulators. Nonceramic insulator qualities reduce the amount of leakage distance required, as described above. The improvement in terms of the withstand volt-

age per connected length is 40 to 100% (IEEE 1999a), falling to a margin of only 25% in freezing conditions. One concern regarding NCIs compared to porcelain insulators is that they cannot withstand as well the heat produced from leakage current. Chapter 4 of this book deals with NCIs in detail.

- **Silicone coating of the insulators.** Ceramic insulators and bushings may be coated with special electrical-grade silicone coatings or, less effectively, silicone or petroleum greases, to provide a smooth surface that is hydrophobic (beads water) and active (encapsulates surface contamination under a floating layer of low-viscosity oil). Grease coatings must be removed and reapplied periodically to maintain effectiveness. Greasing and silicone-rubber coatings can increase the interval between insulator maintenance activities such as washing. Greasing is not recommended for NCI insulators, but silicone coatings may be appropriate in some applications. The difficulty of application and cleaning/reapplication on transmission lines normally limits this technique to substations.
- **Washing/cleaning of the insulators.** Routine maintenance, such as live line or de-energized high-pressure water washing or dry cleaning, removes contamination and restores insulators to their original insulation strength, thereby preventing flashover. Care should be taken when washing these insulators, and methods developed for porcelain, which often include using high water pressures, may damage NCIs.
- **Insulators with semi-conducting glaze.** Coating the insulators with a thin layer of semiconductive glaze leads to a leakage current that can short out the dry banding activity that occurs under condensation and wetting. With no open arcing, the flashover strength of the contaminated surface is increased. By themselves in clean conditions, insulators with semiconductive glaze do not heat up very much, but they can run at 20 C° above ambient when heavily contaminated. Post-type insulators using semi-conducting glaze have superior contamination performance with in-service experience of more than 25 years. Early semiconducting glaze disc insulators encountered some problems with uneven current density—high at the insulator pins (causing glaze erosion) and low at the edges (reducing effectiveness)—but these problems have been addressed in more recent designs.

Consideration must also be given to the spacing of consecutive sheds/under-ribs, especially on polymer insulators. Other considerations that should be taken into account during the design of the insulator string for contamination include the ability to withstand the electrical stresses imposed and allowance of natural cleaning by rain and wind.

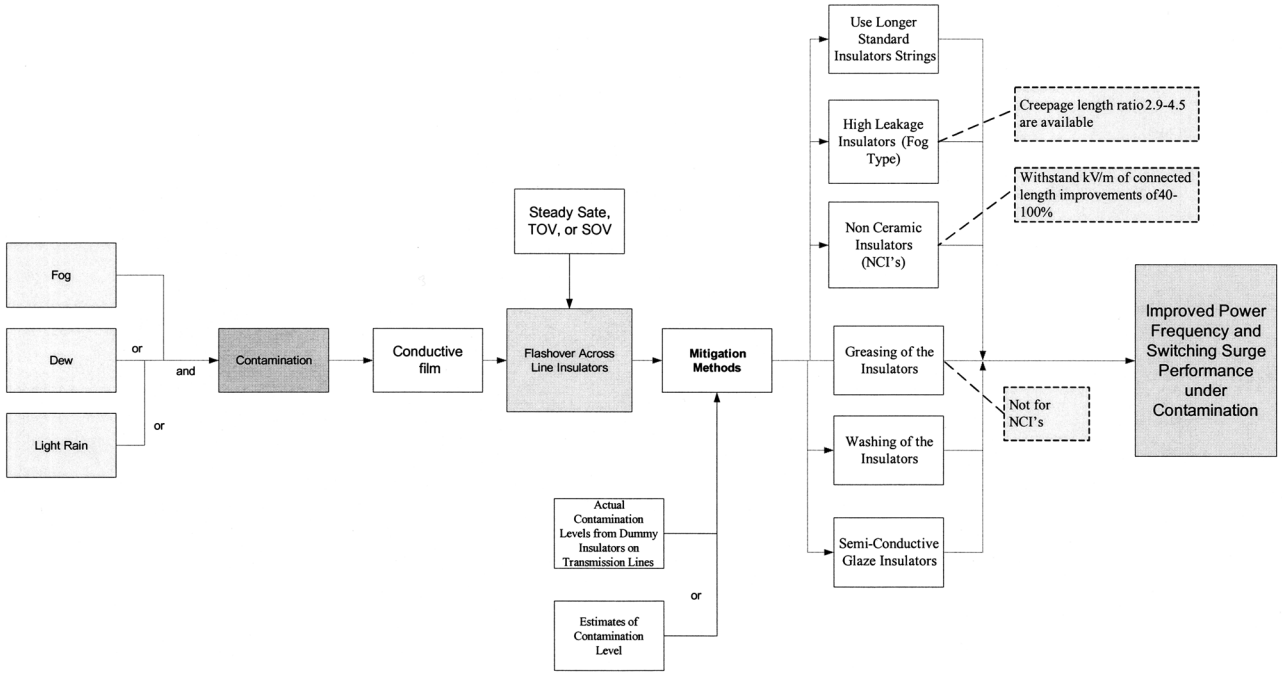


Figure 3.4-5 Power frequency performance under contamination.

3.4.5 Summary

This section provided an overview of some typical methods and design approaches needed to control the voltage stresses on the line insulation due to lightning, switching, and power frequency.

Design for lightning overvoltages includes setting the insulation level, line geometry and clearances, shielding, grounding, and arresters. Solutions for shielding failures and backflashovers are different in many respects, but some common solutions do apply. For example, improving the backflashover rate of an existing line can be accomplished by improving the ground resistance of the towers through supplemental grounding. If improved grounding is not an option, then enhanced lightning performance can be achieved by using transmission surge arresters. The use of surge arresters can also reduce the number of shielding failure flashovers. In many cases, a head start on the design of new lines for lightning overvoltages can be achieved by evaluating the lightning performance of existing transmission lines in the same geographical areas. This information can then be refined or supplemented by studies.

Design for switching overvoltages is an important requirement for the economic design of transmission systems operating above 200 kV, and a necessity above 400 kV. All circuit breaker switching operations generate closing or opening transients or SOVs in the system as the system adjusts to the new set of operating conditions, as a result of the switching operation. Various methods of control have been in use successfully for many years, and finding the most suitable and cost-effective solution for switching surge overvoltages depends on the initiating event. In contrast to lightning overvoltages design, examining the performance of existing lines in the same geographical areas would not be very beneficial in designing new lines, and detailed studies are necessary to quantify the switching overvoltages and the appropriate countermeasures.

The application of surge arresters (either for lightning or switching surge overvoltage control) have yielded advantages, which have been documented in many technical papers.

In the design of line insulation for reducing flashovers due to contamination, many methods can be used. For ceramic insulators, these methods include high-leakage insulator designs or washing/cleaning. Coating insulators with silicon or petroleum grease has been used on transmission lines but the difficulty of application and cleaning/recoating normally limits it to substations. Alternatively, polymer insulators offer improvement in terms of the withstand voltage per connected length of up to 100%.

With Sections 3.2 through 3.4 reviewing the stress, strength, and options available to the line designer for reducing flashovers, Section 3.5 will discuss the National Electric Safety Code (NESC 2002a) as an example of the local or government regulation to which the design has to adhere from the standpoint of public safety.

3.5 ELECTRIC SAFETY CODE REQUIREMENTS

3.5.1 Introduction

The previous sections discussed the voltage stress and the strength of the required line insulation, but nothing was mentioned about the safety of utility field personnel who maintain these lines, or the public who may go under these lines. The safety issue is as important as the technical requirements, and some may argue more important. As a result, designers have to factor safety into the final specification of the line insulation coordination.

In most countries, national electric safety code dictates line clearances; in some countries, even stricter local and state codes may apply. One such code is the National Electric Safety Code (NESC) (NESC 2002a), which is used in the U.S., and also (in full or in part) by other countries. The NESC is the subject of this section.

3.5.2 National Electric Safety Code (NESC 2002) Clearance Requirements

In the United States and certain other countries, the NESC prescribes minimum clearances for transmission lines. The 2002 NESC ANSI C2 has now succeeded the 1997 issue of the Code.

The NESC provides safety requirements for the installation, operation, and maintenance of outdoor communication and electric power facilities. It complements the National Electrical Code (NEC), which provides requirements for indoor facilities. The NESC is mainly concerned with the safety of employees and the public, and is not intended to be a design specification or instruction manual, although in some cases, it may dictate the tower strike distances as well as midspan clearances.

The minimum clearance requirements of the NESC are basically covered in Part 2. Part 2, (Sections 20–27), which deals with Safety Rules for the Installation and Maintenance of Overhead Electric Supply and Communication Lines, is divided into two subparts. Sections 20–23 (Overhead Lines—Clearances) define the organization and location of communication and supply conductors on the overhead facilities, clearances between conductors and structures, and the grounding and arrangement of circuits and associated overhead equipment and hardware. Sections

24–27 (Overhead Lines—Strength and Loading) define various grades of construction and the corresponding storm-loading and strength requirements for them.

In the 2002 edition, the Scope of Part 2 (Overhead Lines) was modified to include appropriate references and rules for personnel approach distances during various construction activities. Sag-related clearances addressing the separation between conductors carried on the same support structure were modified to ensure that adequate clearances are maintained under the worst-case combination of operating temperatures and ice loadings. A new rule was added to specify minimum clearances between supply line cables and communications antennas. Various other clarifications were included throughout Sections 21–23 regarding separations between conductors, equipment, objects, and surfaces. (As a point of reference, Sections 24–27 of Part 2 of the NESC were the subject of the most extensive changes from the earlier editions.)

For transmission lines, the NESC rules pertain to:

1. The midspan clearance to ground for the current-carrying conductors
2. Clearance to the tower: clearance from the current-carrying conductors to the tower body and its components (tower strike distances).

The NESC provides two approaches to calculate the above—a primary and an alternate approach.

Figures 3.5-1 and 3.5-2 describe the general process for calculating these according to the NESC 2002. Further details on the methods and their limitations can be found in this section.

Transmission-Line Midspan Clearance –(Primary Approach)

The lowest clearance of transmission lines from the ground between two towers (midspan clearance) is dictated by the 2002 NESC based on some "reference heights" and on the maximum operating voltage of the line. In some cases, especially for road crossing and voltages of 500 kV or higher, the electric field produced by the line near ground may dictate the ground clearances (see Section 7.8). In fact, the 2002 Code, as was the case in the earlier code, contains the following statement: "For voltages exceeding 98 kV ac to ground, either the clearances shall be increased or the electric field or the effects thereof shall be reduced by other means, as required, to limit the steady state current due to electrostatic effects to 5 mA, rms, if the largest anticipated truck, vehicle, or equipment under the line were short-circuited to ground. The size of the anticipated truck, vehicle, or equipment used to determine these clearances may be less than but need not be greater than that limited by federal, state, or local regulations governing the area under the line. For this determination, the conductors shall be at final unloaded sag at 120˚F (50˚C)."

Reference Heights

Reference heights are shown in Table 3.5-1 (which is extracted from NESC Table 232-1). These heights are divided into several categories, with categories 4 and 5 being the most applicable for the design of transmission lines clearances at midspan.

It must be noted that clearance values for this NESC 2002 edition cannot be directly compared with the 1987, 1990, 1993, or 1997 editions. Vertical clearance values ***appear*** smaller, because sag changes formerly included in these values are now addressed in the application rules.

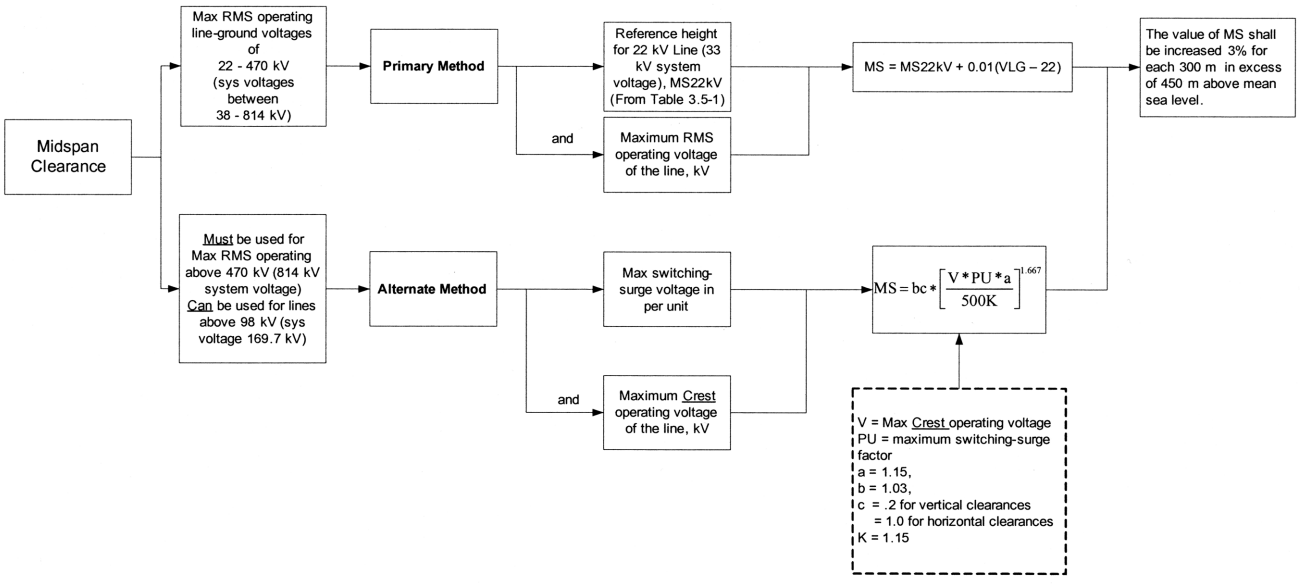


Figure 3.5-1 Determination of the midspan clearance according to NESC 2002.

Horizontal clearance values ***appear*** larger, because wind displacement is now applicable to energized conductors and certain supply cables only; clearances for all other wires, conductors, and cables are shown in the tables under at-rest conditions.

Maximum Operating Voltage

The minimum midspan clearance according to NESC for transmission lines with maximum phase-ground operating voltages between 22 kV and 470 kV (corresponding to maximum phase-phase system voltages between 38 kV and 814 kV) is given by:

$$MS = MS_{22kV} + 0.01\left(V_{LG} - 22\right) \qquad 3.5\text{-}1$$

Where:

MS_{22kV} is the midspan clearance for lines with maximum line-ground voltages greater than 750 V to 22 kV (38-kV system voltage) from Table 3.5-1, fifth column, in meters

V_{LG} is the maximum rms operating voltage of the line, kV.

Clearances must be increased by 3% for each 300 m in excess of 1000 m above sea level to allow for decreasing air density with altitude. The clearance is determined for conductor sags using 50°C or the maximum conductor temperature and 0°C temperature with radial ice and no wind displacement.

For category 4 (other land traversed by vehicles, such as cultivated, grazing, forest, orchard, etc.), the midspan clearance can be calculated as follows:

$$S = MS_{22kV} + 0.01(V_{LG} - 22)$$

For a maximum system voltage of 550 kV (maximum line-ground voltage of 317.5 kV), the midspan clearance is hence:

$$S\ (317.5) = 5.6 + 0.01\ (317.5\text{-}22) = 8.6\ m$$

Table 3.5-2 shows midspan clearances for other voltages for both categories 4 and 5.

Transmission Lines Midspan Clearances (Alternate Approach)

NESC allows an alternate method for determination of midspan clearances for lines with voltages exceeding 98 kV ac to ground or 139 kV dc to ground "with known maximum switching-surge factor." The alternate method usually yields clearances less than those required by the primary method described above. The alternate method must be used for voltages above 470 kV (814-kV system voltage). For voltages exceeding 50 kV, the additional clearance shall be increased 3% for each 300 m (1000 ft) in excess of 1000 m (3300 ft) above mean sea level.

Table 3.5-2 Midspan Clearances Derived by the Primary NESC Approach

Transmission Line Voltage (kV)		Midspan Clearance (m)	
Maximum L-G Voltage	Maximum System Voltage	Category 5	Category 4
140	242	5.6	6.8
209	362	6.3	7.5
318	550	7.4	8.6
461	800	8.8	10.0

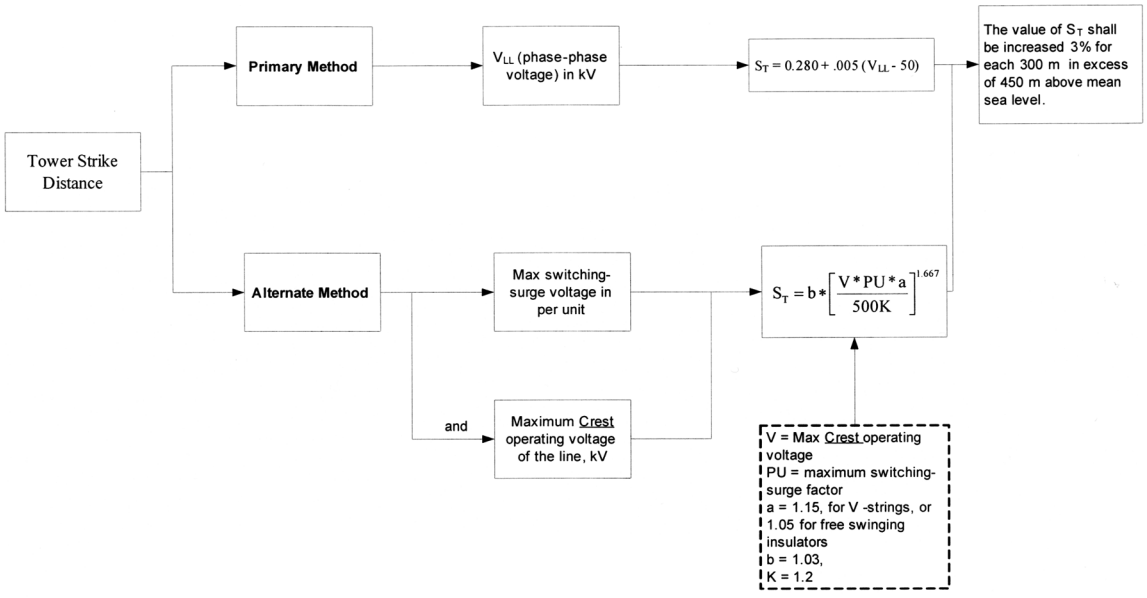


Figure 3.5-2 Determination of the tower strike distance according to NESC 2002.

Using the alternate method, the clearances specified may be reduced for circuits with known switching-surge factors, but shall be not less than the clearance computed by the primary method for a line with maximum line-to-ground voltage of 98 kV (169 kV system voltage).

Using the alternate method, the midspan clearance MS (in meters) shall be computed using Equation 3.5-2.

$$MS = bc * \left[\frac{V * PU * a}{500K} \right]^{1.667} \text{ m} \qquad 3.5\text{-}2$$

Where:

V = maximum ac crest (compared to the rms voltage used for the primary approach) operating voltage to ground or maximum dc operating voltage to ground in kilovolts.

PU = maximum switching-surge factor expressed in per-unit peak voltage to ground and defined as a switching-surge level for circuit breakers corresponding to 98% probability that the maximum switching surge generated per breaker operation does not exceed this surge level, or the maximum anticipated switching-surge level derived by other means, whichever is greater.

a = 1.15, the allowance for three standard deviations.

b = 1.03, the allowance for nonstandard atmospheric conditions.

c = the margin of safety:
1.2 for vertical clearances.
1.0 for horizontal clearances.

K = 1.15, the configuration factor for conductor-to-plane gap.

The value of MS shall be increased 3% for each 300 m (1000 ft) in excess of 450 m (1500 ft) above mean sea level.

Table 3.5-1 Vertical Clearances of Wires, Conductors, and Cables Above Ground, Roadway, Rail, or Water Surfaces (Extracted from Table 232-1 of the NESC 2002)

Nature of Surface Underneath Wires, Conductors, or Cables	Insulated Communication Conductors and Cable; Messengers; Surge-Protection Wires; Grounded Guys; Ungrounded Guys Exposed to 0 to 300 V Neutral Conductors Meeting Rule 230E1; Supply Cables Meeting Rule 230C1 (m)	Noninsulated Communication Conductors; Supply Cables of 0 to 750V Meeting Rules 230C2 or 230C3 (m)	Supply Cables Over 750V Meeting Rules 230C2 or 230C3; Open Supply conductors, 0 to 750V; Ungrounded Guys Exposed to over 300V to 750V (m)	Open supply Conductors, over 750V to 22kV; Ungrounded Guys Exposed to 750V to 22kV (m)	Trolley and Electrified Railroad Contact Conductors and Associated Span or Messenger Wires	
					0 to 750V to Ground (m)	Over 750V to 22kV to Ground (m)
Where wires, conductors, or cables cross over or overhang						
1. Track rails of railroads (except electrified railroads using overhead trolley conductors)	7.2	7.3	7.5	8.1	6.7	6.7
2. Roads, streets, and other areas subject to truck traffic	4.7	4.9	5.0	5.6	5.5	6.1
3. Driveways, parking lots, and alleys	4.7	4.9	5.0	5.6	5.5	6.1
4. Other land traversed by vehicles, such as cultivated, grazing, forest, orchard etc.	4.7	4.9	5.0	5.6	—	—
5. Spaces and ways subject to pedestrians or restricted traffic only	2.9	3.6	3.8	4.4	4.9	5.5

Limit:
The alternate clearance shall be not less than the clearance computed for 98 kV for the "primary" method.

Clearances in Any Direction From Line Conductors to Supports, and to Vertical or Lateral (Tower Strike Distance)
As for the midspan clearance, the NESC gives two ways to calculate the tower strike distance.

Transmission Lines Strike Distances (Primary Approach)
The primary method to calculate the strike distance at the tower can be calculated by Equation 3.5-3 for lines with voltages above 50 kV.

$$S_T = 0.280 + .005\ (V_{LL} - 50) \qquad 3.5\text{-}3$$

Where:
V_{LL} is the phase-phase voltage in kV.

Table 3.5-3 summarizes the strike distances calculated with the primary approach.

Transmission Lines Strike Distances, Fixed Insulators (Alternate Approach)
NESC allows an alternate method for determination strike distances for lines with voltages exceeding 98 kV ac to ground (maximum system voltage of 169.7) or 139 kV dc to ground "with known maximum switching-surge factor." The alternate method usually yields clearances less than those required by the primary method described above. The alternate method must be used for voltages above 470 kV (814-kV system voltage). For voltages exceeding 50 kV, the additional clearance shall be increased 3% for each 300 m (1000 ft) in excess of 1000 m (3300 ft) above mean sea level. With this method, the clearance at the tower (strike distance) is given by Equation 3.5-4:

$$S_T = b * \left[\frac{V * PU * a}{500K} \right]^{1.667} \text{ m} \qquad 3.5\text{-}4$$

Where:
V = maximum ac crest operating voltage to ground or maximum dc operating voltage to ground in kilovolts.
PU = maximum switching-surge factor expressed in per-unit peak voltage to ground and defined as a switching-surge level for circuit breakers corresponding to 98% probability that the maximum switching surge generated per breaker operation does not exceed this surge level, or the maximum anticipated switching-surge level generated by other means, whichever is greater.
a = 1.15, the allowance for three standard deviations with fixed insulator supports, or = 1.05, the allowance for one standard deviation with free-swinging manipulators.
b = 1.03, the allowance for nonstandard atmospheric conditions.
K = 1.2, the configuration factor for a conductor-to-tower window.

Table 3.5-3 Tower Strike Distances (Primary Approach)

Max. System Operating (kV)	Strike Distance (m)
169	0.9
242	1.2
362	1.8
550	2.8
800	4.0

The value of S_T shall be increased 3% for each 300 m (1000 ft) in excess of 450 m (1500 ft) above mean sea level.

The clearance derived from this alternate method (Rule 235E3b) shall not be less than the clearances obtained with the basic method computed for 169 kV ac.

This section does not detail the line working clearances. These clearances have to be factored in the ultimate design of the overall clearances. This topic is covered in Chapter 13.

3.5.3 Summary

This section summarizes some of the requirements and the working clearances of the U.S. National Electric Safety Code (2002) to the clearances at the tower and midspan. These are intended to uphold the safety of utility personnel as well as the general public. If the requirements by the NESC or other applicable codes are enforced, some of the strike distances that may be obtained by the probabilistic design of transmission lines may be exceeded, and hence may dictate the design.

3.6 COORDINATION OF DESIGN REQUIREMENTS

3.6.1 Introduction

This section offers an overview of line insulation coordination. It is where the line insulation is actually "coordinated." The intent here is to present the reader with a stand-alone section that reviews some of the concepts already discussed in this and other chapters, and presents a high-level picture of the challenges that line designers face.

The absolute protection of transmission lines against overvoltages (lightning, switching, and power frequency) is impossible, even with the use of the most conservative approaches. Hence the designer should strive to design transmission lines based on probabilistic methods (when sufficient probabilistic data exist) that combine low risk (not no risk) with economy of design.

Good line insulation coordination is not only important to achieve high reliability of transmission lines, but also is a focal element in station insulation coordination to obtain acceptable mean time between failures (MTBF). Well-coordinated designs in both lines and stations are crucial for attaining a reliable bulk transmission system, and because such designs are probability based, this goal is achieved at an affordable cost. This approach is becoming increasingly important under deregulation.

Line insulation coordination is the specification of all the dimensions or characteristics of the transmission line tower that affect its voltage withstand. These dimensions include:

1. Strike distance, or clearance between the phase conductor and the grounded tower sides and truss
2. Insulator string length (number and type of insulators)
3. Location and number of overhead ground (shield) wires
4. Specification of supplemental tower grounds
5. Phase-phase strike distances
6. Conductor clearances at midspan

The goal behind line insulation coordination is to specify the minimum line insulation for a specific degree of reliability at minimum cost. This specification is determined through:

1. Determining the electrical stress applied to the transmission line.
2. Comparing the stress to the insulation characteristics.
3. Applying ameliorating measures such as surge arresters, shield wires, breaker–closing resistors, etc., when the insulation strength requirements are excessive.
4. Balancing insulation strategy costs and—whenever possible—costs of failures.

3.6.2 Insulation Coordination Analysis Methods

The coordination efforts for lightning, switching overvoltages, and power frequency are essentially independent. Insulation coordination assumes that the magnitude of the overvoltages are known. Concurrently, the electrical insulation characteristics of the transmission lines are also assumed to be known. As a first step, and for a new line, experience on comparable systems and lines may be used in the rationalization of both the system overvoltages and line performance.

The insulation strength of lines for lightning and switching stresses should be chosen on the basis of predicted overvoltages. This determination is then combined with requirements from power frequency and temporary overvoltages. Either a statistical (probabilistic) or a conventional procedure may be used.

A statistical approach is particularly applicable when there is economic incentive for reduction of insulation strength, especially when switching overvoltages are a problem and primarily appropriate to the extra-high and ultra-high voltage. Appendix 3.3 describes in detail the principles of the deterministic and probabilistic approaches.

Statistical Procedure

The statistical procedure allows for some insulation failures to occur, and the procedure attempts to quantify the risk of its failure. A rigorous determination of the probability or risk of failure requires that both the overvoltage stresses and the line insulation strength be described in terms of their respective frequency distributions (see Figure 3.6-1). Simplifications of the rigorous approach are also made and have been applied. In such approximate methods, the statistical lightning or switching overvoltage is so defined that this voltage value, $E2$, has a 2% probability of being exceeded.

Lightning Impulse Strength (LI) and Switching Impulse Strength (SI)

For either Lightning Impulse Strength (LI) or Switching Impulse Strength (SI), tower insulation strengths are typically represented by cumulative Gaussian (normal) distributions. The mean of each distribution is called the Critical Flashover Voltage (CFO) or the $V_{50\%}$. The CFO is, therefore, the voltage where the probability of flashover of the insulation is 50% (the CFO is sometimes referred to as $V_{50\%}$).

Typically the standard deviation for the SI is about 5% of its CFO, and the standard deviation for LI is in the range of 1-2% of its corresponding CFO. For LI, the curve of the CFO as a function of the strike distance is linear, compared to the nonlinear relation for the CFO with strike distance for the SI, as can be seen in Figure 3.6-2. Table 3.6-1 compares the characteristics of lightning and switching impulse strengths. Note that the insulator strength characteristics are defined for standard conditions.

The phase-phase switching impulse insulation strength of transmission lines is a function of the components of the

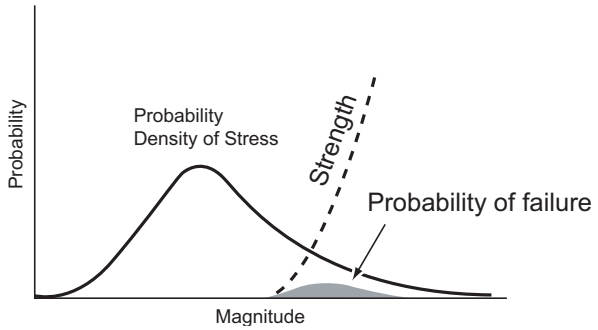


Figure 3.6-1 Statistical procedure for determining insulation failures.

phase-phase switching impulse. Because the switching impulse strength is dependent on the components of the phase-phase switching impulse, both the positive and negative switching overvoltages must be known.

Lightning Overvoltages (LOV)

The approximate distribution of peak magnitude of the lightning current distribution is shown in Figure 3.6-3, based on a relationship formulated by Anderson (EPRI 1982) and adopted by the IEEE/PES Working Group on Estimating the Lightning Performance of Transmission Lines (IEEE 1985). For transmission lines, two regions of the distribution can be viewed: the shielding region, where $I < 20$ kA; and the backflashover region, where $I > 20$ kA. These regions are identified in Figure 3.6-3.

$$P > 0 = \frac{1}{1 + \left(\frac{I_P}{31}\right)^{2.6}} \qquad 3.6\text{-}1$$

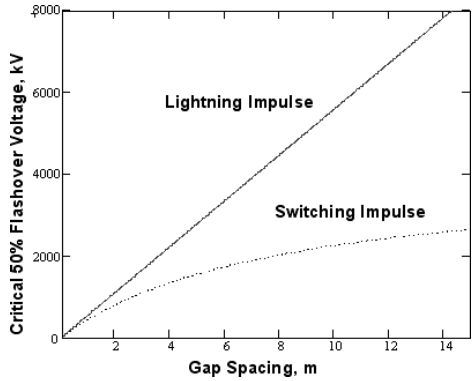


Figure 3.6-2 Comparison of lightning and switching impulse strength.

3.6.3 Lightning Performance of Transmission Lines

For EHV and UHV transmission lines, lightning can produce overvoltages by direct strokes to the shield wires or the phase conductors. Lightning strokes may hit the phase conductors directly, or they may strike the overhead ground (shield) wires.

The lightning performance of transmission lines is the sum of the following:

1. The shielding failure flashover rate (SFFOR), and
2. The backflash rate (BFR).

Both of these flashover rates are linearly dependent on the lightning ground flash density, measured in flashes per square km-year.

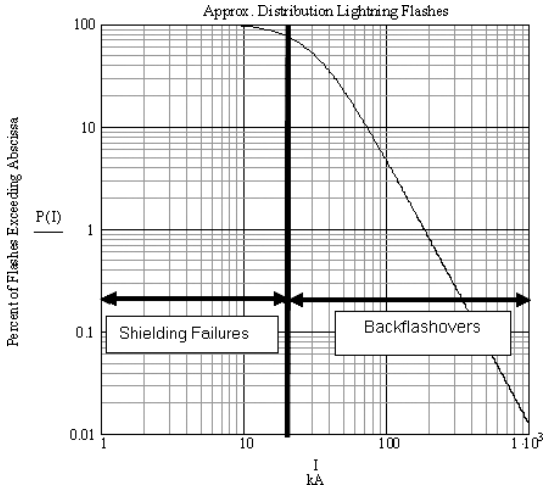


Figure 3.6-3 Cumulative distribution of first negative downward lightning flashes to objects < 60 m (Anderson and Eriksson 1980). (Note the extension of the curve beyond 100 kA is only a "mathematical" fit to the equation. Little actual data exists beyond 100 kA).

Table 3.6-1 Critical Flashover Voltage (CFO) for Lightning and Switching Impulse Strengths under Standard Conditions(1)

Switching Impulse Strength	Lightning Impulse Strength
$V_{50\%,Tower} = 1.2\,\frac{3400}{1 + \frac{8}{L}}$ L is strike distance in meters. Notes: Applies to center phase. @ Standard conditions, V strings. Both dry and wet conditions. Outside phase, increase CFO by 6%.	For positive polarity: 520-560 kV/m (160-170 kV/ft). For negative polarity: 605 kV/m (185 kV/ft). Wet conditions. Either center or outside phases.
1. Standard conditions are defined as follows: • Ambient temperature 20°C. • Air pressure: 760 mm of Hg. • Relative air density of 1. • Absolute humidity: 1.1 grams of water/m³ of air.	

Shielding of Transmission Lines

On a line with overhead shield wires, most of the lightning strokes that terminate on the line hit the shield wire. A shielding failure is defined as a lightning stroke that terminates on a phase conductor. The number of shielding failures calculated for a particular transmission-line model depends on a number of factors. These factors include the line's electromagnetic parameters, the stroke current distribution, and natural shielding from trees, terrain, or buildings. Not all shielding failures result in insulator flashover. A lightning stroke terminating on the phase conductor creates waves of current and charge. These waves develop into voltage waves that, with no surge protection, flash over the insulation in the majority of the cases (e.g., for a conductor with a surge impedance of 400 ohms, a 10 kA stroke can produce 10,000 x 400/2 = 2 MV). If the flashover occurs through the air or across the porcelain insulation, the power arc triggered by the flashover may cause damage, strip insulator sheds, etc. On the other hand, if the flashover occurs through solid insulation, such as a transformer or cable in a substation, permanent damage would result almost all the time. The critical current *Ic* is defined as the lightning stroke current that, when injected into the conductor, results in flashover. The critical current for a particular transmission line can be estimated by:

$$I_C = \frac{2.V_{50\%}}{Z} \qquad 3.6\text{-}2$$

Where:

$V_{50\%}$ = lightning impulse negative polarity critical flashover voltage.

Z = conductor surge impedance.

Shielding Failure Flashover Rate (SFFOR)

The primary aim in the selection of the number and the location of the ground wires is to provide a means of intercepting vertical lightning flashes before they hit the phase conductors—i.e., reducing the probability of shielding failure flashover rate (SFFOR). Hence one shield wire may be adequate in areas of low ground flash density, while two may be needed for areas with higher levels of lightning activity. A practical recommended value for the SFFOR is 0.05 flashovers per 100 km-year.

Even if the shielding angle is set so that lightning flashes with currents greater than the critical current do not terminate on the phase conductor, the SFFOR is not zero because subsequent strokes will follow the same path. The shielding angle is determined for the first stroke of the flash, because this current is thought to have the strongest correlation to the charge on the downward leader. However, even though the first stroke does not result in a flashover, subsequent strokes may have larger currents that can produce flashover. Two primary methods—the IEEE Std 1243-1997 (IEEE 1997b) and CIGRE Technical Bulletin 63 (CIGRE 1991a) methods—are in use to estimate the SFFOR. Calculations with the two methods for the shielding angle values for different tower heights appear to agree for the lower tower heights, but can differ by more than 2:1 for larger heights. As a result, the user has to be cautious when applying either method. The required shielding angle decreases as the ground flash density increases for both methods.

Backflash

A lightning stroke terminating on the overhead ground conductor creates waves of current and voltage, which produce potential differences across the line insulation. If the potentials are in excess to the line insulation strength, flashovers occur. Such an event is referred to as a "backflash," from the tower to the phase conductor, and the number of flashovers per 100 km per year is defined as the backflash rate (BFR). In order of sensitivity the BFR is a function of the insulation strength (length of the insulator string length and strike distance), surge arresters (if used), number of shield wires, tower footing resistance, ground flash density (Ng), span length, tower height, and type of conductors (single bundle) used. As in the case of shielding failures, the backflash event can produce overvoltages that travel to the substations and cause permanent damage in solid insulation. In the case that a low BFR cannot be attained by minimizing the tower footing resistance or other measures, surge arresters can be applied across the insulation.

The BFR of present lines varies significantly with the system voltage; 345- and 500-kV lines often have BFRs in the range of 0.3 to 0.6 flashovers per 100 km-year. The BFR for 138- and 230 kV may be in the range from 0.6 to 2.

As with the SFFOR, the methods of IEEE and CIGRE differ. The IEEE method is more conservative because it makes less allowance for ionization of earth electrodes which is appropriate for large transmission towers.

Improving Performance of Existing Lines

Generally the primary method of improving the flashover rate of an existing design is by use of supplemental grounding, which almost universally consists of a combination of radial counterpoise buried rings, or driven drilled rods. However, in cases where counterpoise cannot be installed because of soil conditions (rock formations), or because towers are on public areas such as roads, improvements in performance may be achieved by doing the following:

- Using transmission line surge arresters
- Increasing the number of insulators and strike distance (overinsulation)
- Chemical treatment of the soil if environmental rules permit.

Effect of Power Frequency Voltage on Lightning Overvoltages

The power frequency voltage, although small in magnitude compared to the surge voltage, is to some extent responsible for determining which phase insulation has the largest voltage and will flashover. Therefore, the voltages across the insulators may be calculated throughout the 360-degree phase rotation, and the flashover rate is determined by averaging these values. Backflashes usually occur on a phase with power frequency voltage that is opposite in polarity to the surge voltage. The maximum longitudinal overvoltage is the difference between the lightning overvoltage on one terminal and the power frequency voltage of opposite polarity on the other terminal of the switching device. For shielding failures, the voltage on the struck phase is random.

3.6.4 Switching Surge Performance of Transmission Lines

Prior to the appearance of 500-kV transmission lines in the early 1960s, little was known about switching overvoltages and switching impulse strengths. Insulation strength was defined only by its lightning impulse and power frequency voltage strengths. With the introduction of 500-kV, switching surges became an important consideration in line insulation design. Analytical studies and field investigations revealed that insulation requirements for switching surges exceeded those required for lightning and power frequency. To overcome such a problem, the breaker design was changed by inserting a resistor in the closing stroke to reduce the switching surges. From that time on, switching overvoltages became an important point in transmission-line design. This section addresses design for switching.

Origins of Switching Surge Overvoltages (SOVs)

The magnitude and waveshape of SOVs vary considerably with the system parameters. Even for the same system configuration, SOVs vary as a function of the characteristics of the breaker (including the characteristics of the breaking media, the mechanical tolerances between the three poles, etc.) and the point-on-wave where the switching operation occurs.

Typically there are three kinds of SOVs:

1. SOVs due to fault initiation
2. SOVs due to fault clearing
3. SOVs due to line energization or reclosing

The important sources of SOVs on EHV and UHV systems are associated with the following events:

1. Line energization, with the line open circuited at the far end or terminated with an unloaded transformer or a shunt reactor
2. Line re-energization, with trapped charge
3. Load rejection
4. Transformer switching at no-load, or with inductive load

Three-phase energization or reclosing of a power line may produce switching overvoltages on all three phases. The overvoltages are dependent on trapped charges left on the phases without fault in the case of high-speed reclosing. In the worst case, each switching operation produces three phase-ground and three phase-phase overvoltages. The magnitudes of the SOVs can be usually be fitted to a probabilistic distribution, often of Gaussian or Extreme value nature. (The variation of the magnitude of the SOVs is due to the point of switching and the electrical and mechanical tolerances of the breaker.) The upper tail of such a distribution is important to quantify in line design, because it is directly compared to the insulation strength. From this comparison, the switching surge outage rate or flashover rate is calculated. Today virtually all EHV and UHV lines are designed using the probabilistic method.

Determining the SOV Probabilistic Distribution

Two methods are in universal use for characterizing the overvoltage probability distribution function: the case-peak method and the phase-peaks method, as described in Table 3.6-2. These methods are used to determine both a phase-ground and phase-phase overvoltage distribution.

The phase-to-phase insulation strength of transmission lines requires determining the distribution of the phase-to-phase overvoltages. Usually only peak (case-peaks or phase-peaks) phase-to-phase voltages are tabulated. A more complete characterization of the phase-to-phase overvoltages also requires the knowledge of the magnitude of the lowest of the two phase-to-ground voltages occurring at the instant of the phase-to-phase peak.

Switching Surge Flashover Rate (SSFOR)

The switching surge flashover rate (SSFOR) of a transmission line is determined by calculating the probability that the stress along the line exceeds the line insulation

Table 3.6-2 Two Methods for Characterizing Switching Overvoltages

Case-Peak Method	Phase-Peaks Method
From each switching operation, the highest crest overvoltage of the three overvoltages is selected, tabulated, and included in the probability distribution. Each switching operation contributes only one value to the overvoltage distribution. This results in the distribution of switching surge overvoltages per each three-phase energization or reclosing operation, and is used to calculate the probability of flashover per three-phase switching operation.	From each switching operation, the crest switching overvoltage on each of the three phases is tabulated and included in the probability distribution. Each operation contributes three crest values to the probability distribution. This results in a per-phase distribution of overvoltages that can be used to calculate a per-phase probability of flashover for the switching operation.

strength. The flashover rate is shown in Equation 3.6-3 (Hileman 1980).

$$SSFOR = \frac{1}{2}\int_{E1}^{EM} f_s(V)\left[1-\prod_{i=1}^{n} q_i\right]dV \qquad 3.6\text{-}3$$

Where:

SSFOR is the flashover rate in terms of flashover per number of switching operations.

$fs(V)$ is the probability density function of the switching overvoltages at the open end of the line.

q_i is the probability of no flashover (withstand) at the i-th tower, which is equal to $(1–p_i)$ where p_i is the probability of flashover corresponding to $\alpha(i)\cdot V$, where $\alpha(i)$ is the ratio between the overvoltage at the i-th tower and the overvoltage at the open end of the line.

n is the number of towers.

$E1$ is the minimum SOV usually set at 1.0 p.u. of crest system line-ground voltage, and Em is the maximum SOV.

The factor $^1/_2$ accounts for the fact that only the positive polarity overvoltages, which are one-half of the total overvoltages, are considered potential cause of a flashover.

The equation may be visualized from Figure 3.6-4. The probability density function at the open end of the line is illustrated in the figure by the solid line, where $E1$ is the minimum SOV usually set at 1.0 p.u. of crest system line-ground voltage and Em is the maximum SOV. The SOV density function may be obtained through the use of a transient computer program with the breakers randomly switched within their pole closing

Acceptable practice is to design for approximately one flashover per 100 switching operations. However, a better design criterion is to consider all switching operations (energization, reclosing with trapped charge, etc.) and the expected number of operations per year. For lines with grounded metal structures between the phase conductors, the phase-to-ground strike distance dictates the SSFOR.

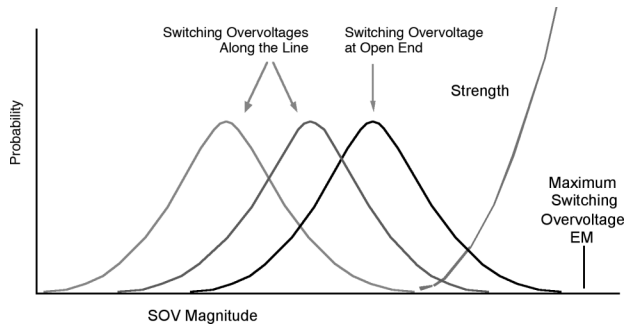


Figure 3.6-4 Switching overvoltages probability densities along a line vs. switching overvoltage strength (Abi-Samra 2000).

For compact line designs where insulators separate phases, the phase-phase strike distance may dictate the design.

3.6.5 Power Frequency Performance of Transmission Lines

The power frequency voltage controls the design of insulator strings in contaminated conditions. The degree of contamination and the associated factors of contamination type and incidence of moisture determines the insulation string design. In addition, the power frequency voltage controls the air clearance between the conductors and the tower when the conductor and insulator string swing in conditions of extreme winds toward the tower or other conductors.

Designs may be obtained by deterministic or statistical methods for power frequency. A detailed description of these alternate methodologies is given in Appendix 3.3.

Design Approach

The power frequency requirements for the design of transmission lines are specified by the creepage distance per kV of line-to-ground voltage (based on the maximum system voltage) needed for contamination. The best known and most reliable method to meet the contamination requirement is to analyze data from existing lines. The thought process here is that if an existing line has a satisfactory 60-Hz performance, its design in terms of creepage cm/kV can be copied for the new line. This is a linear phenomena and it follows that the required creepage/kV is constant regardless of the voltage level of the line. Recommended creepage using standard $5^3/_4$ x10 in. is shown in Table 3.6-4, from IEEE Std 1313.2-1999 (IEEE 1999a).

Contamination decreases the insulators' power frequency voltage strength. The design for the decreased strength can be based on simple historical data, if available, or on a simple deterministic design approach. The deterministic design rule is to set the statistical withstand voltage (V_3) equal to the maximum phase-ground voltage (Em), which includes temporary overvoltages as shown in Equation 3.6-4:

$$V_3 = \mathrm{Em} \qquad 3.6\text{-}4$$

$$V_3 = V_{50\%}\left[1-3\sigma/V_{50\%}\right] \qquad 3.6\text{-}5$$

Where:

$V_{50\%}$ is the power frequency flashover voltage in kV under contaminated conditions.

σ is the standard deviation, and the coefficient of variation,

$\sigma/V_{50\%}$, is assumed to be 10%.

Effect of Contamination on Lightning and Switching Impulse Strengths

Because of the short duration of the impulse, the lightning impulse strength is unaffected by contamination. The decrease in switching impulse strength is a function of the degree of contamination and of the time-to-crest of the

impulse (see Section 5.12.2 for greater details). For heavy contamination and long times-to-crest, the switching surge flashover voltage is not much greater than the crest of the power frequency flashover voltage. The design of insulators for heavy contamination should be based exclusively on withstanding the power frequency voltage with a high degree of reliability, since line re-energization may not be successful.

Insulation Strength—IEEE Recommendations

Table 3.6-3 (IEEE 1999) gives the recommended number of standard insulators in a string for system voltages from 138 kV to 765 kV.

Insulation Strength—IEC Recommendation

It is noted that use of Table 3.6-4 with creepage distance is a useful simplified approach and it does not cover all cases. A more involved dimensioning process is described in Chapter 4.

IEC Standard 60071-2 (IEC 1996) recommends creepage distance for ceramic or glass insulators for different levels of contamination severity, as shown in Table 3.6-4.

Reduction of Airgap due to Wind

For insulator strings not constrained from movement, wind may move the conductor closer to the grounded tower metalwork, thus decreasing the strike distance. The movement can be estimated by calculating the swing angle, with Equation 3.6-6, and as shown in Figure 3.6-5 (from Appendix 5.1).

The swing angle of free-swinging insulator strings is a function of the parameter:

$$K = \frac{D}{W} \cdot \frac{H}{V} \qquad 3.6\text{-}6$$

Where:

D is the diameter of the conductor (mm).

W is the weight per unit of length of the conductor (kg/m).

H is the horizontal span (m).

V is the vertical span (m).

Table 3.6-3 Number of Standard Insulators (146 mm x 254 mm and a leakage distance of 292 mm)

System Voltage (kV)	Number of Standard Units for a Contamination Severity (I-strings/ V-strings)			
	Very Light	Light	Moderate	Heavy
138	6/6	8/7	9/7	11/8
161	7/7	10/8	11/9	13/10
230	11/10	14/12	16/13	19/15
345	16/15	21/17	24/19	29/22
500	25/22	32/27	37/29	44/33
765	36/32	47/39	53/42	64/48

Table 3.6-4 IEC Recommendations for Unified Creepage Distance (revision of IEC 815 1985) (Copyright © 1996, Geneva, Switzerland. www.iec.ch.)

Pollution Level	Examples of Typical Environments	Minimum Unified Specific Creepage Distance (mm/kV)
I Light	• Areas without industries and with low density of houses equipped with heating plants. • Areas with low density of industries or houses, but subjected to frequent winds and/or rainfall. • Agriculture areas. • Mountainous areas. All these areas shall be situated at least 10–20 km from the sea, and shall not be exposed to winds directly from the sea.	28
II Medium	• Areas with industries not producing particularly polluting smoke and/or with average density of houses equipped with heating plants. • Areas with high density of houses and/or industries, but subjected to frequent winds and/or rainfall. • Areas exposed to wind from the sea, but not too close to coasts (at least several kilometers distant).	35
III Heavy	• Areas with high density of industries, and suburbs of large cities with high density of heating plants producing pollution. • Areas close to the sea or in any case exposed to relatively strong winds from the sea.	44
IV Very Heavy	• Areas generally of moderate extent, subjected to conductive dusts and to industrial smoke producing particularly thick conductive deposits. • Areas generally of moderate extent, very close to the coast and exposed to sea spray or to very strong and polluting winds from the sea. • Desert areas, characterized by no rain for long periods, exposed to strong winds carrying sand and salt, and subjected to regular condensation.	55

For high-voltage lines, 60% of the 100-year mean recurrence wind is used. The 100-year wind is the wind speed with a mean recurrence interval of 100 years.

In the presence of wind and the subsequent swinging of the insulators toward the grounded tower downlead or metalwork, the voltage distribution is modified on the individual insulator discs due to the proximity of the grounded members. During power frequency overvoltage conditions, the buildup of voltage across the string is slow (compared to lightning or switching), allowing more time to ionize the air near the surface of the insulator string, with the highest voltage stresses closer to the conductor. These higher-voltage stresses will trigger a flashover at a lower level of voltage than when the string is in the vertical position. The swing of the conductor also has a significant effect on flashover characteristics due to switching surges and lightning because of the higher voltage present on the conductor-end insulator discs, and the proximity to the tower of the conductor. However, it is prudent to assume that the likelihood of having high wind speeds and high SOVs is low, and hence extreme swings are not typically used for switching designs.

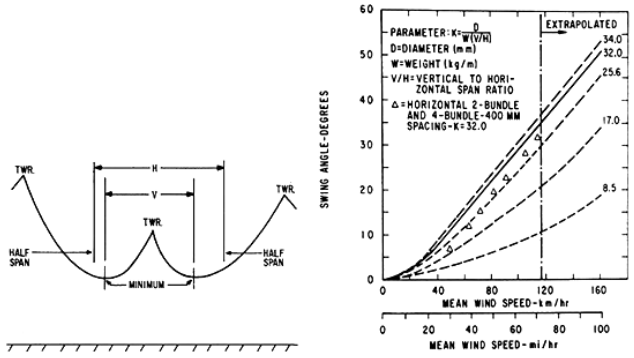


Figure 3.6-5 Swing angle as a function of mean wind speed.

Hence the power frequency design of insulators under wind conditions is done in conditions of extreme winds. However, the wind pressure used for switching surge design is generally assumed to be much lower than for power frequency voltage.

3.6.6 Consolidation of Design Requirements

Hileman (Hileman 1980, 1999) offers a great overview of line design requirements. This is illustrated in Figure 3.6-6. In this figure, the strike distance is shown as a function of maximum system voltage for the three criteria—lightning, switching surge, and power frequency voltage. Table 3.6-5

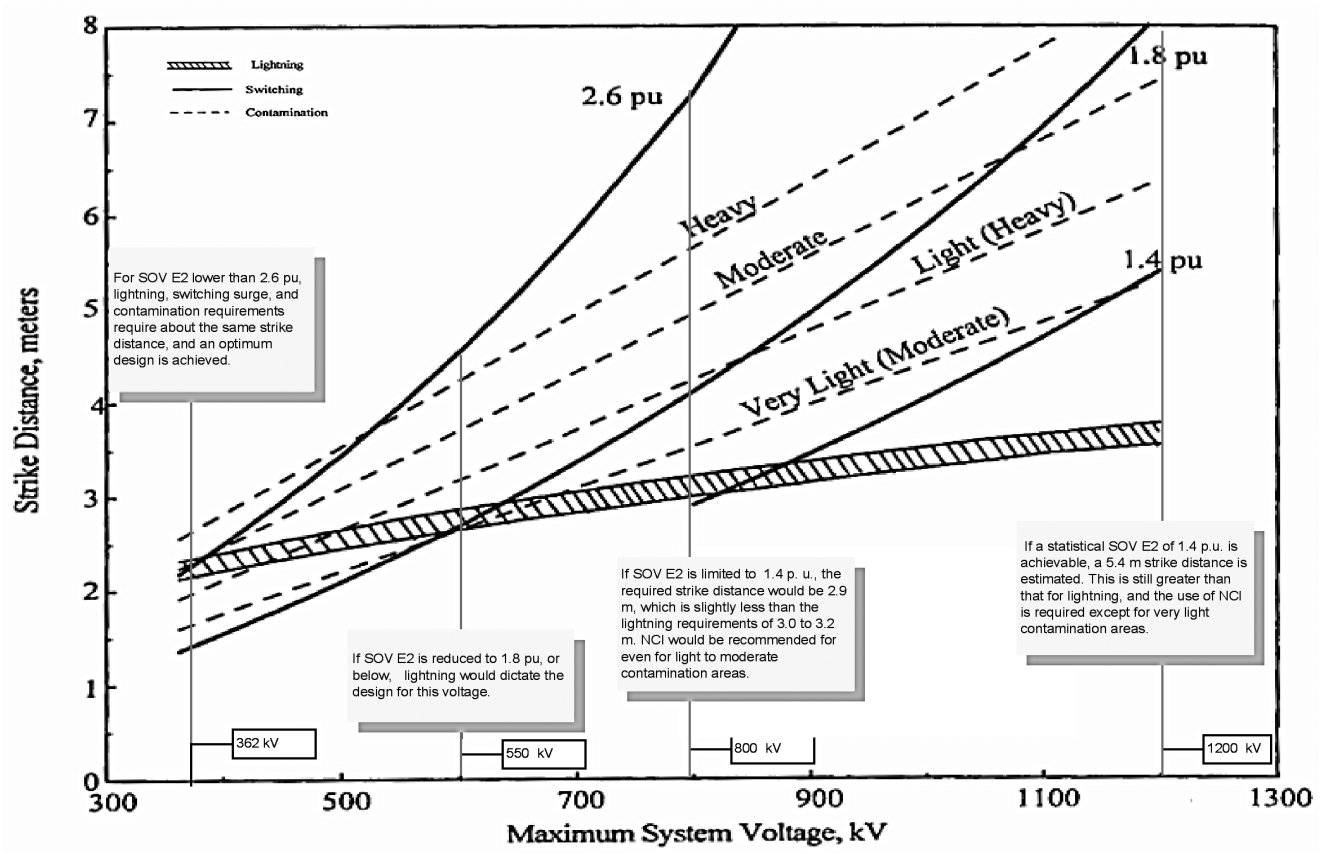


Figure 3.6-6 Comparison of insulation coordination requirements (Hileman 1980, 1999).

Table 3.6-5 Assumptions for Figure 3.6-6

Lightning	• Flashover rate of 0.6 flashover per 100 km-years. • Tower footing resistance of 20 ohms with a soil resistivity of 400 ohm-meters. • The upper portion of the band assumes a ground flash density of 4.0 flashes/km^2-year and the lower portion, 8.0 flashes/km^2-year. Note that the lightning curves are relatively flat, since the lightning requirements should be relatively constant with system voltage. Tower heights increase, and coupling factors decrease with increasing system voltage. These effects, along with the increase in power frequency voltage, combine to produce a gentle increase in the curve.
Switching Surge	Gaussian stress distribution and for statistical overvoltages E_2 of 2.6, 1.8, and 1.4 per unit. (E_2 of 2.6 per unit represents a typical value for high-speed reclosing of breakers without a preinsertion resistor; 1.8 per unit represents a typical value for high-speed reclosing with a single preinsertion resistor; and 1.4 per unit represents a value for a breaker with possibly one or two preinsertion resistors or with controlled closing.). A line with 500 towers is assumed. Each of the curves sweeps sharply upward, portraying the plot of the strike distance as a function of the $V_{50\%}$.
Power Frequency	The power frequency voltage requirements are shown as a function of the IEEE contamination levels of: Very Light 0.03 mg/cm^2, 20 mm/kV Light 0.06 mg/cm^2, 24 mm/kV Moderate 0.10 mg/cm^2, 28 mm/kV Heavy 0.30 mg/cm^2, 32 mm/kV • Use of ceramic 146 x 254 mm insulators in V-strings is assumed.

summarizes the assumptions used to derive the data used for Figure 3.6-6. Refer also to Applet IC-1.

3.6.7 Alternate Method for Line Design: Storm Outage Rate

The performance/reliability criterion for lightning is normally specified as the number of flashovers per 100 km-years. For switching surges, the flashover rate is normally specified in terms of flashovers per number of switching operations. However, the highest magnitude switching surges typically occur when reclosing the line. Such a condition can be caused by a fault associated with lightning. Thus the two separate criteria (lightning and switching) may be combined in one rate known as the Storm Outage Rate in specifying the line reliability.

For transmission lines, lightning flashover rates vary with system voltage, and may range from 0.5 for EHV systems to 20 per 100 km-year for HV systems, although lines are being designed for switching surge flashover rates between 1 and 10 flashovers per 100.

The SSFOR and the lightning LFOR can be combined together to form the storm outage rate (SOR). An outage during a storm may be thought of as having the following scenario:

1. Lightning hits the line and causes a flashover.
2. The flashover causes a fault, leading to the operation of the breaker.
3. After a predetermined time, the breaker recloses, creating a switching overvoltage.
4. The SOV causes a flashover, which brings about another fault.
5. For EHV systems, the breaker reopens and is locked-out, resulting in an outage.

The SOR for the line is essentially obtained by multiplying the lightning flashover rate in units of flashovers per year by the switching surge flashover rate in terms of flashovers per switching operation. For example, assuming the lightning flashover rate to be two per year, and the switching surge flashover rate to be one per 100 switching operations, the storm outage rate is two per 100 years, assuming one reclosing operation per year.

Hileman (Hileman 1980) extends the "logic" of using the SOR to practical terms in determining line insulation coordination: in areas with low-lightning activity, the SSFOR may be selected as high as 0.1, since the probabilities of lightning flashovers are low. Similarly, in the areas of high-lightning activity, the SSFOR may need to be selected very low (i.e., 0.001) for reliable line operation. (The lightning flashover rate [LFOR] is essentially the backflashover rate [BFR] for effectively shielded lines.)

3.6.8 Summary

The absolute protection of transmission lines against overvoltages (lightning, switching, and power frequency) is impossible, even with the use of the most conservative approaches. Hence the designer should strive to design transmission lines based on probabilistic methods that combine low risk (not no risk) with economy of design.

Good line insulation coordination is not only important to achieve high reliability of transmission lines, but also is a focal element in station insulation coordination to obtain acceptable mean time between failures (MTBF). Well-coordinated designs in both lines and stations are crucial for attaining a reliable bulk transmission system, and because such designs are probability based, this goal is achieved at an affordable cost. This approach is becoming increasingly important under deregulation.

Line insulation coordination is the specification of all the dimensions or characteristics of the transmission line tower that affect its voltage withstand. These dimensions include:

1. Strike distance, or clearance between the phase conductor and the grounded tower sides and truss
2. Insulator string length (number and type of insulators)
3. Location and number of overhead ground (shield) wires
4. Specification of supplemental tower grounds
5. Phase-phase strike distances
6. Phase-to-ground clearances at midspan

The goal behind line insulation coordination is to specify the minimum line insulation for a specific degree of reliability at minimum cost. This specification is determined through:

- Determining the electrical stress that is applied to the transmission line.
- Comparing the stress to the insulation characteristics.
- Applying ameliorating measures such as surge arresters, shield wires, breaker-closing resistors, etc., when the insulation strength requirements are excessive.

The consolidation of such requirements is referred to as line insulation coordination. Figure 3.6-7 summarizes a methodology for performing line insulation coordination for lines of various voltages.

3.7 ECONOMIC CONSIDERATIONS

3.7.1 Introduction

Previous sections in this chapter have described the stress on line insulation and how to design lines with appropriate strength to achieve reliability goals. However, an additional important goal for designers is to minimize cost.

Changes in line design affect the line cost. Increased clearances may improve line reliability, but at a higher price. This section attempts to provide some insight into the economic consequences of design changes, and to compare costs of some alternatives such as TLAs versus increased clearance or grounding. However, it is recognized that cost analysis is complex. Costs can vary significantly between different designs, terrains and soil conditions, and atmospheric conditions. Also, cost sensitivities may be considered less important than design standardization. Therefore, this section is primarily an introduction to techniques and options that designers may use.

It should be noted that the tools used for assessing the effects of design changes on line cost are the same as those used for the life-cycle cost analysis of the most appropriate technology, including selection of line voltage, conductor type and size, and whether ac or HVDC. These tools evaluate the present worth of alternatives to provide the optimum design and determine the sensitivity to parameter changes.

3.7.2 Insulation Coordination and Cost

Design of a transmission line includes the following parameters:

- The type of structure—single or multiple circuit, wood or metal, phase geometry
- Airgap clearances, including phase-to-tower, phase-to-phase, and phase-to-ground at midspan
- The amount, type, and configuration of insulators
- Grounding, including paths to ground and grounding resistance
- The number and location of overhead shield wires
- The need for, rating, and location of voltage-limiting devices, such as line surge arresters and breaker insertion resistors
- Possible use of wood in lightning flashover paths for arc quenching

Changes in any of these parameters affect the line cost. In insulation coordination, the goal of the designer is the optimum combination of insulation, clearances, and voltage control to achieve a reliability target at least cost. As an example, increasing the length of the insulator strings requires that the tower height be increased to provide the same conductor-ground clearance at midspan. This additional height not only requires additional steel for the tower, it also increases the overturning moment on the tower and the torsional load in the event of a broken conductor. The taper of the tower may require a larger footprint for a higher structure. The end result is not simply that the tower is higher—the tower, together with its foundation, must also be made stronger. Similar consequences arise from different phase conductor or shield wire size and material; changing conductor tensions; using V strings instead of I strings to reduce conductor swing; designing for different phase-ground, phase-structure, or phase-phase clearances; adding shield wires or changing shielding angles; and different phase geometries. Changing tower heights and loading may result in a different placement or even in a different number of towers spotted along the right-of-way, and use of a different mix from the family of structures (tangent, angle, and deadend types, each with additional subcategories) available. Soil conditions vary along a line, so foundations may differ for the same loading capability. Thus a design change might lie within the capabilities of a particular structure with no changes, while in another location the design change might force the use of a heavier and more expensive choice. Design detailing, or small adjustments in the member location in a design, can also make a disproportionate difference to the strength required for a particular load.

In addition, there are independently costed items that may result from different tower insulation or clearances, such as grounding, line arresters, and breaker resistors.

Optimizing the cost implications of insulation coordination is, therefore, an interactive process. Similar issues are encountered when designing a compact line. However, it is important to consider practical issues and the design process as a whole when adjusting a line design. For short lines, for example, it is usually cheaper to use an overdesigned standard design drawn from stock than to attempt an

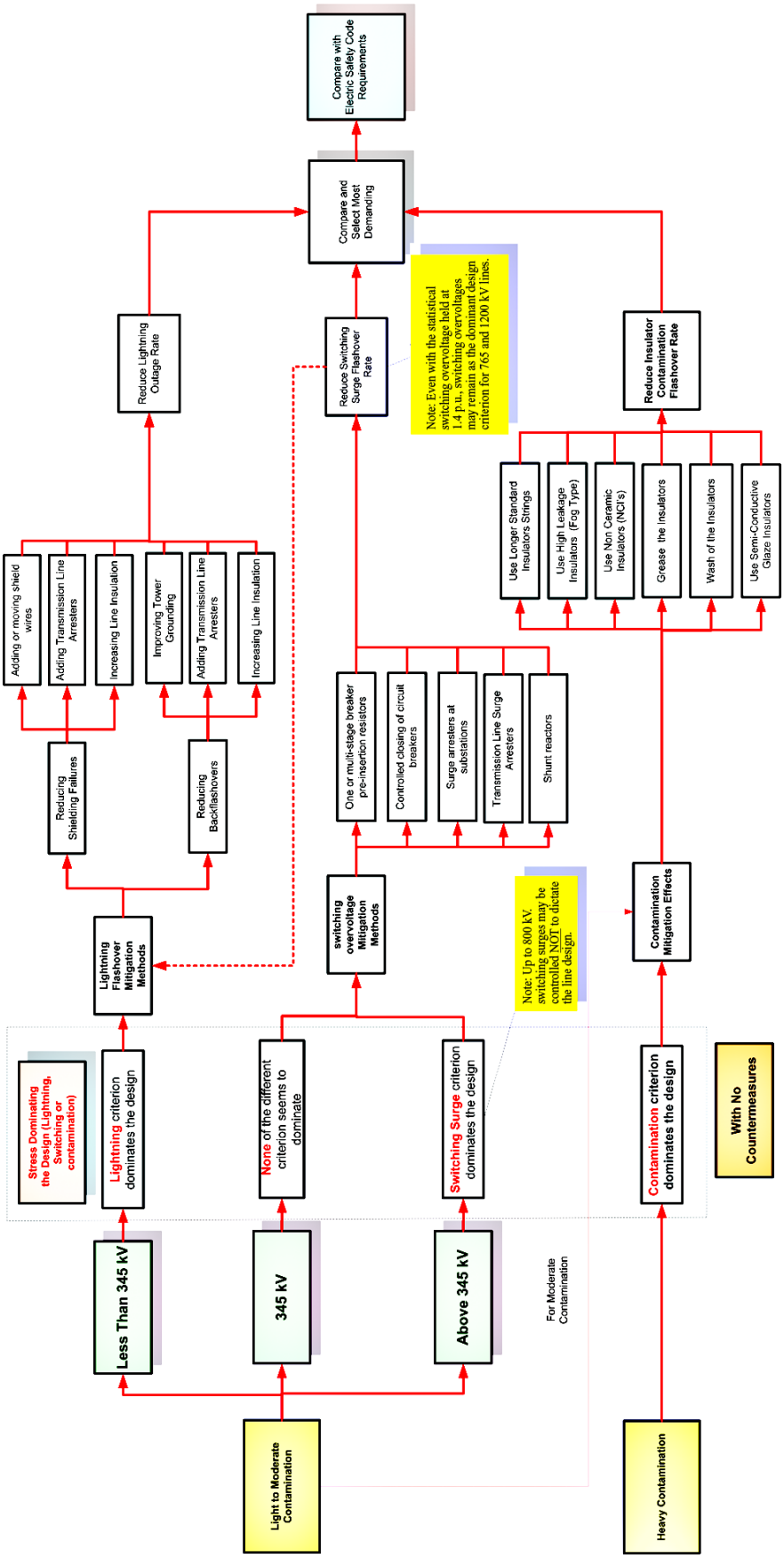


Figure 3.6-7 Line insulation coordination methodology.

optimized design. The advantages of lower cost for an optimized structure are offset by the design and engineering costs, testing, and increased need for spare parts. Smaller clearances may also present difficulties for hot line maintenance. If regional contamination is uncertain, it is less costly to design for one or two extra insulators or for insulators with better performance in contaminated conditions than to wrestle with a continuing contamination problem and hot line washing, greasing, or insulator retrofitting.

Yet another complication is determining the worth of the benefits of improving insulation performance. The consequence of designing for (say) a lower level of switching surge failures can be expressed as a reduction in line tripouts—although, as discussed elsewhere, the precision of predicting actual improvement in performance is limited. But what is the cost of a line tripout? If no load is interrupted, the cost may be negligibly low, but conversely if the tripout triggers a series of consequential events leading to a blackout, the cost may be very high. Chapter 6 explores some possible cost strategies by reverse-engineering some costs of line protection using overhead groundwires. Even if a predictable amount of load is lost, the value of lost electricity sales by the supplier may be very different from the costs of interrupting a critical industrial process, the possibility of civil disturbance, or political or regulatory consequences following loss of confidence in the supplier. In practical terms, sophisticated analysis procedures should sometimes be put aside in favor of simplifying the process.

Nevertheless, considerable savings can result from cost optimization on lines of any significant length, and this section outlines some considerations for a designer in estimating the cost consequences of insulation coordination.

3.7.3 Line Component Costs

Before exploring cost sensitivities, it is useful to consider the magnitudes of the basic components of a line. A broad international survey is provided in (CIGRE 1991b). As an example of the information provided, Table 3.7-1 compares the cost breakdown for lines between 150 and 300 kV, and > 300 kV.

The values in the table are based on international surveys carried out in 1989-90, and may vary with time, geographic location, and specific designs. However, the numbers obtained from the survey are relatively insensitive to differences over a wide range of alternative parameters.

3.7.4 Cost Sensitivities

As noted above, changes in line design parameters are often highly interactive, so it is misleading to consider the cost of a single modification. Each change should be considered for its effect on the total line.

Table 3.7-2 shows some typical values for a 400-kV single-circuit horizontal-phase configuration line (CIGRE 1991b; CIGRE 1991c). As can be seen, the net effect of a change may be partially offset by consequential changes in other parameters. Also, the change in structure cost is itself an incomplete indicator, as there remains the possibility of changes in tower spotting that can be unique as a function of the actual terrain, route angles, etc.

As shown in Table 3.7-1, the structure cost is approximately 36% of the total cost of the line (including only materials and erection), so this additional factor should be applied to arrive at the overall effect on cost.

It should also be noted that in mature transmission systems, new lines are often short and highly constrained by route and permit issues. In extreme examples, a new line may have mostly angle or deadend structures despite their much higher cost, because the route has been selected to go around individual properties rather than cross them, and a short line with the costs of land and permitting included may be 10-20 times costlier per km or mile than the same line in a remote location—levels at which underground cables may be an option.

Table 3.7-1 Summary of Line Component Costs (Values in Percent)

Category	Material	Construction		Conductor	Shield	Insulators	Structure	Foundation
150–300 kV	64.3	35.7		31.6	4.1	8.8	36	19.5
> 300 kV	65	35		31.5	3.5	9.3	36	19.7

Note: Numbers do not include right-of-way or permitting costs.

Table 3.7-2 Cost Sensitivities to Design Changes

Parameter	Change in Parameter	Change in Cost of Structure (%)
Phase - tower clearance	-1%	-0.3
Number of shield wires	2, 1, 0	0, -6.5, -12.9
Shielding angle	20, 10, 0, -10	0, +0.3, +0.7, +1.4
Insulator configuration	I, V	0, -1.4
Insulator string length	+1%	0, +1

3.7.5 Independent Cost Items

As noted above, it is possible to improve line performance with grounding augmentation, line arresters, or circuit breaker insertion resistors. While the need for these items may be a consequence of decisions on the structure parameters, they are applied independently, and are not directly linked with the interaction of structure parameters and costs. Table 3.7-3 illustrates some typical values.

3.7.6 Base Line Costs

Line costs vary as a function of electrical and mechanical loading requirements, terrain, route, soil type and conditions, regional labor and materials costs, design practices and codes, and permitting and environmental requirements. The costs in Table 3.7-4 are "typical" costs only, and do not include significant land or permitting amounts. Line costs can change significantly with mountainous terrain, rocky or marshy soil, and a need for frequent angle structures.

3.7.7 Cost Analysis Methods

Estimation of line costs in sufficient detail for use in insulation coordination considerations can be difficult, since it requires relationships between costs and design parameters that are both highly interactive with other parameters and also not normally available to electrical designers. The most accurate method for determining the cost of a design change to meet insulation coordination requirements is to carry out a ground-up design for the specific line in question. This is normally, of course, lengthy and expensive. More typically, a limited amount of redesign based on typical examples is used.

Table 3.7-3 Typical Costs of Independent Items

Category	230 kV	500 kV	765 kV
Grounding augmentation (note that this varies widely with local conditions)	$900-$1500 per structure	$900-$1500 per structure	Augmentation not normally required
Line arrester	$3400/arrester. Use 1-3 per structure	$9000/arrester—not normally used due to cost	Not used
Breaker resistors	Not normally used	$25-30k per 3-phase breaker	$30-40k per phase

Table 3.7-4 Base Line Costs

Category	230 kV	500 kV	765 kV
Cost per mile	800 k$	1.2 M$	1.4 M$

A useful and versatile tool developed by EPRI is described in (EPRI 1986). The TLOP component of EPRI's TLWorkstation™ uses regression analysis to model the relationship between each member of the tower family with its foundation and cost, and then either combines a tower spotting calculation or a pre-sited design with mechanical loading calculations and conductor characteristics to produce a complete table of structures for the line and thus the total cost. The software includes a limited ability to calculate the effect of tower dimension changes on cost, as input to the regression analysis. Commercial software with similar capabilities is available, such as the PLS-CADD program (Peyrot et al. 1992).

Another useful alternative is supplied in (CIGRE 1991b), based on international surveys of transmission line costs. This reference includes sensitivity analyses of the effects on cost of the principal parameters of interest including conductor tension, structure clearances, and the number and positioning of shield wires. While this data is limited to typical structure types and voltages, it is sufficiently accurate for most design purposes. Similarly (CIGRE 1996) provides cost data on foundations.

The EPRI TFLASH transmission line lightning analysis program includes an optimizing algorithm to search for the least cost to attain a specified transmission line lightning performance or the strategy to gain the maximum lightning performance improvement for a fixed cost. It is frequently the case that the most cost-effective improvement in line lightning performance is not to concentrate on improving the performance of the structure with the highest flashover rate, but to apply the money to the structure that can show the greatest improvement per dollar expended.

3.7.8 Summary

Insulation coordination is the optimum combination of insulation, clearances, and voltage control to achieve a reliability target at least cost. Estimation of the costs of design changes resulting from insulation coordination is complex, but can readily be handled by available software tools and data. However, the line cost optimization may be secondary to use of standard components and designs or to permitting and routing constraints.

APPENDIX 3.1 INSULATION COORDINATION ANALYSIS TOOLS

Introduction

Knowledge of overvoltages for line insulation coordination may be obtained in two ways: by measurement (or past history on similar lines) or by modeling and analysis. Field measurements are the preferred way to obtain data, such as performance for lightning and contamination, but such measurements are not always possible or affordable. There are numerous cases of validation with field measurements.

With the development of modeling and simulation techniques in the last two decades, almost all kinds of transient problems related to insulation coordination can be analyzed. Modeling for line insulation coordination can be performed with a number of tools, which can be grouped into three distinct areas shown below. The order shown also depicts the chronological introduction of such tools in the design of transmission lines:

1. Analog tools—e.g., Transient Network Analyzer
2. Multi-purpose software tools that can be adapted to the calculation of overvoltages—e.g., EMTP
3. Specialized software tools—e.g., EPRI TFlash, which was especially formulated for the sole purpose of calculating the performance of the transmission lines under lightning.

The following sections discuss the above tools. At the present, the dominant method of analyzing insulation coordination is through digital simulation. Digital simulations have always dominated lightning studies due to the range of frequencies involved.

Analog and Hybrid Modeling

Transient Network Analyzers (TNA)

It should be noted that although TNAs are rarely used today, a brief description is helpful to the understanding of the historical evolution of electromagnetic transient simulations, and a number of TNA-developed techniques are being used in the digital simulations.

Basically, the TNA represented scaled models of the actual electrical systems. The models duplicate the electrical response of the actual devices. The various models are physically assembled by the operator and interconnected with wires. The network is then energized in an appropriate way, and measurements are made at the desired points. Conventional TNA modeling was ideal for switching surge and temporary overvoltage calculations, and to a much lesser extent, for lightning studies, due to the required time scaling. Today digital TNAs have been developed and can represent power system components in some cases more accurately than the scale analog components.

Modeling Considerations for the TNA

- **Transmission-Line Modeling.** Transmission lines in the TNA were modeled as lumped-constant ladder networks, called pi, π sections. Each π section would model the resistance, reactance, and line charging of transmission (R, L, C) line segments. A good model would be made of many such sections, and would be able to represent phase transpositions, earth return frequency dependency, variations of line parameters as the line transverses different terrains, and other variations. The number of elements required in the model depends on the amount of traveling wave distortion that may be permitted. The more elements used, the less distortion there is, but at the expense of having to model a smaller system, since the number of elements is limited. This challenge compelled the engineer to become very cognizant of power system behavior, and what needs to be modeled, and what can be equivalenced, and to what degree. (This is somewhat lost with digital simulations, which can model thousands upon thousands of busses and branches. The capabilities of these simulations seem limitless, and hence the need for some decision-making is reduced.) Also, the TNA was the "real-time simulator" and the perfect method to perform a sensitivity analysis on the variables. (Changes were made by the turning of one or two dials, and the consequences were instantly apparent, even faster than digital simulation. It was straightforward, for example, to learn the consequences of changing the rating of a shunt reactor, or selecting a different arrester. Such features made collection of statistical data so cost-effective with TNAs.) On the other hand, analysis of data from earlier TNAs (up to and through the 1970s) used to be time-consuming. In the 1980s, the situation changed dramatically with the introduction of digital computers to control the TNA and to organize and analyze the output.
- **Other Models.** Transformers were generally represented by a network of single-phase units, with one branch representing the magnetizing effects and another representing the impedance between windings. Coupling between phases, either through the core or through a tertiary winding, was accomplished with auxiliary windings. Magnetization and saturation effects could be studied because the magnetizing branches were wound on steel cores that had saturation effects similar to those of real transformers, which made these miniature transformers very expensive. Reactors were represented either by actual air core reactors or by electronic circuits that injected currents into the model circuit of the same amplitude and phase as those in the actual reactors. Surge arresters were modeled by electronic circuits that duplicated the nonlinear resistances and gaps. Circuit breakers and switches were represented by relays that were closed and opened at preselected times by an electronic control device. Generally the relays employed

contacts that were wetted with mercury in order to have low contact resistance and eliminate contact bounce. Opening and closing resistors in actual breakers were represented, but the dynamic arc resistance of the breakers was seldom duplicated.

- **Time Scaling.** Most TNAs were operated with a unity time scale and a unity impedance scale. This means that the TNA operated at the same frequency as the actual system and that impedances (in ohms) on the TNA were the same as on the actual system. Often different time scales were used to fine-tune the electrical lengths of transmission lines or to make a model transformer more closely match the impedance of an actual transformer. This is no longer needed in digital simulations.

Digitized TNA (DTNA)
Although most electrical transient simulations have been taken over by digital models, the digitalized TNA (DTNA) continues to gain attention due to its high speed, quick setup, and reproducibility, aided by parallel processing techniques and state-of-the-art digital signal processors (DSP). DTNAs are also referred to as "real-time digital simulators" (RTDS). RTDS has overcome most of the problems faced by traditional TNAs. The RTDS is currently applied to many areas of development, testing, and studies including:

- Protective relaying schemes
- Integrated protection and control systems
- Control system for HVDC, SVC, synchronous machines, and FACTS devices
- General ac and dc system operations and behavior
- Interaction of ac and dc systems
- Interaction of various electrical installations (e.g., between two HVDC systems)
- Demonstration and training

An RTDS has been developed and is maintained by the Manitoba HVDC Research Centre (Mathur and Wang 1989; McLaren et al. 1991; Durie and Pottle 1993; Pratico and Eitzmann 1994).

General-Purpose Digital Programs
From the 1970s, a number of digital programs have been developed for analysis of transients (Thoren and Carlsson 1970; Ametani 1973). One that is widely used is the Electromagnetic Transients program (EMTP) developed by Dommel and Meyer (Dommel 1969). Other popular programs include: ATP (Alternative Transients Program: the public domain version of the EMTP), PSCAD/EMTDC (Power Systems Computer Aided Design, a Graphical User Interface for the EMTDC—ElectroMagnetic Transients including DC), and the Matlab/Simulink/Power System Toolbox. Most are time-domain programs, which have many features in common, at least with regard to methods of use.

As for the TNA, digital programs use models of actual physical devices. The individual models are interconnected by the user to build a composite model of the system to be studied. While the analog modeling (e.g., TNA) is mainly applied for switching surge and temporary overvoltages—due to the frequency response and model complexities—the digital programs are used for lightning, switching, and temporary overvoltage calculation aspects of line insulation coordination.

Electromagnetic Transients Program (EMTP)
The EMTP is a comprehensive computer program designed to solve electrical transients on power systems, regardless of their nature, as long as the user specifies the correct models and time frames. Its development started in the early 1960s by H. W. Dommel. The program attracted much attention and was widely used by engineers in the United States and elsewhere. Individuals and groups have subsequently adapted, expanded, and generally augmented the techniques, increasing the program's capability. (By 1980, EMTP had become very popular in the electric power industry. For better improvement and maintenance, an EMTP development coordinating group (DCG) was established in 1982. Two years later, EPRI reached an agreement with DCG to take charge of documentation, conduct EMTP validation tests, and add a more user-friendly input processor. In 1996, an EMTP96 version with graphic user interface was released. EPRI/DCG continuously updates the EMTP program to make it more flexible and user-friendly.)

Transient analysis using EMTP can be carried out in circuits with any arbitrary configurations. Transmission lines with distributed parameters, transposed or untransposed, can be included in the network. Losses in such lines are approximately modeled to good effect by lumped resistance. Frequency dependence of line parameters can also be represented, as well as nonlinear resistance (for surge arresters) and nonlinear inductors (for saturable devices). It is also possible to open and close switches to simulate breaker operations, flashovers, etc.

Some of the EMTP operating principles are summarized below:

- The trapezoidal rule of integration is used to solve differential equations of system components in the time domain.
- Nonzero initial conditions can be determined either automatically by a steady-state phasor solution, or they can be entered by the user for simpler components.

- Symmetric or unsymmetric disturbances are allowed, such as faults, lightning surges, and any kind of switching operations including commutation of valves.

Both voltage and current sources are available to model switching and lightning studies. There can be sinusoidal, ramp, or step functions. Alternatively, arbitrary waveforms can be applied from a point-by-point description. Trapped charges can be recognized.

Alternative Transients Program (ATP)
In 1984, Drs. W. Scott Meyer and Tsu-huei Liu, the co-Chairmen of the Canadian/American EMTP User Group, started a derivative program from a copy of BPA's public-domain EMTP, called Alternative Transient Program (ATP). ATP has been developed through international contributions. EPRI/DCG's EMTP and ATP are similar in many ways. For all practical purposes, for line insulation coordination, the ATP can do everything the EMTP can do, and hence no further discussion on this will be made here. There are differences in program interfaces, graphical user interfaces, and ancillary programs.

PSCAD/EMTDC
EMTDC™ stands for ElectroMagnetic Transients including DC. PSCAD™ or Power Systems Computer Aided Design is used as a Graphical User Interface for the EMTDC™. EMTDC was developed by Dennis Woodford in 1975 to study the Manitoba Hydro Nelson River HVDC Power System. The program is now used extensively for many types of power simulation studies including ac, lightning overvoltages, and power electronics.

Specialized Programs
EPRI TFlash
EPRI and EPRIsolutions, under a multi-year project, with the participation of many utilities, have developed a special program, TFlash, exclusively to predict the performance of transmission lines designs for lightning. TFlash uses a traveling wave simulation to calculate voltage and current distributions on power systems. The software provides statistical results for complete coverage of lightning stroke locations and currents. The results can be used to analyze relative performance of different line configurations and to identify problem areas where excessive lightning flashovers may occur along a line. TFlash is used for the evaluation of the lightning performance of new and existing overhead transmission lines, and is also utilized to optimize new designs and improve the performance of new lines. With TFlash, one can study the advantages, tradeoffs, and cost justification of applying various structure, conductor, arrester, and grounding techniques to improve lightning reliability.

The latest version of this program can:

- Create computer models of multiple lines in a single right-of-way (ROW).
- With its automatic optimization function, it can compare specific cost and performance improvements of various options and determine the most cost-effective changes to the line.
- Import lightning stroke data from Fault Analysis and Lightning Locating System (FALLS) to calculate line performance.
- Fly the line with TFlash 4.0's 3-D line model viewer.

Aids to Calculation of Transients
Engineers who perform transient simulations typically spend a disproportionately small amount of time actually running the simulations. The bulk of their time is spent on:

- Obtaining parameters for component models (and benchmarking the component models to confirm proper behaviors), and
- Constructing the overall system model (and benchmarking the overall system model).

Only after the component models and the overall system model have been verified can one confidently proceed to run meaningful simulations.

With digital solution techniques, it is easier to simulate perfect components than actual frequency-dependent components. For example, an actual transmission line has distributed resistance, and it continuously distorts a surge traveling along the line. A transmission line in a time domain digital program could be either lossless or distortionless, but real lines do have losses, and these losses must be accounted for by some means. For a transmission line digital model, the losses may be approximated by breaking the line into two pieces and placing resistances at the middle and two ends of the line. However, when high frequencies or rapid rates of change are involved, such simple means may not be sufficient to prevent spurious results or numerical instabilities. More sophisticated line models with frequency-dependent losses have been developed to address this issue.

Transient phenomena in power systems are caused by switching operations, faults, and lightning strokes. The frequency range of these phenomena extends from dc to several MHz. An accurate simulation of a power system requires an adequate representation of its components, taking into account the frequency of the transients. An acceptable representation of all equipment throughout the complete frequency range is very difficult, and for most components is not practically possible. To solve this problem, the representation of a component can be made by

developing mathematical models that are accurate for a specific frequency range. According to the CIGRE Working Group 33-02, model frequency ranges are classified as four groups, with overlapping between them:

- Group I: Low-frequency oscillations, from 0.1 Hz to 3 kHz
- Group II: Slow-front surges, from 50/60 Hz to 20 kHz
- Group III: Fast-front surges, from 10 kHz to 3 MHz
- Group IV: Very-fast-front surges, from 100 kHz to 50 MHz.

Especially in the high-frequency range, data of stray inductances and capacitances are always required to be taken into account. These data are difficult to calculate precisely, but rough estimates are often sufficient. As a rule of thumb, one may say that the inductance of a conductor is about 1 μH/m. The inductance of a small wire is greater, perhaps 1.5 μH/m, and the inductance of a busbar less, perhaps 0.7 μH/m.

Generally, stray capacitance is more important than stray inductance. Both bushings and transformer windings have considerable capacitance. The capacitance of a bushing is often shown on the nameplate, but if not, it may be estimated from tables given in IEEE C37.011-1994 (IEEE 1994). Usually capacitance is on the order of 300 pF for small or low-voltage bushings and 500 pF for large or high-voltage bushings. Greenwood (Greenwood 1991) gives a more comprehensive discussion of inductances and capacitances to use in the calculation of transients.

In high-frequency transient simulation, a large transformer is usually modeled as a capacitance. The input capacitance may be quite large—5 to 25 nF. This capacitance depends on the type and size of the transformer. It is neither given on nameplates nor routinely measured. IEEE C37.011-1994 gives some information on capacitance as a function of transformer size (IEEE 1994). More precisely, modeling of a large transformer can be simplified according to the frequency range of interest. The CIGRE WG document considers different models for power transformers, distinguishing between studies in which surge transfers are not of interest and those for which these transfers have to be taken into account. For more detail, refer to (Martinez-Velasco 1998; CIGRE 1990; Arturi 1991; Stuehm 1993; Mork 1998).

Example Use of the EMTP for Backflash Design: Modeling Guidelines

The following are some modeling guidelines for performing backflash calculations with the EMTP. Although the information presented in this book generally refers to the EMTP, the modeling requirements are general enough to be equally applicable to the other digital transient programs.

- **Transmission-Line Models.** For backflash studies, the most important model needed to construct is the model of the transmission line. Hence, for such studies, overhead lines are represented by multiphase, distributed parameter, untransposed, and "traveling wave" models. Conductor (phase and shield wire) data and configuration, and physical line and tower configurations are needed to derive "modal" surge impedance and velocities for the transmission lines. Either a frequency-dependent or a constant parameter model can be used. If the constant parameter model is selected, it is recommended to calculate parameters at a frequency of 500 kHz.
- **Line Termination.** Two or three spans must be represented at each side of the strike point or point of impact. A line termination is needed at each side of the above model to avoid unrealistic reflections. This can be achieved by inserting a resistance matrix at each termination whose values equal the line modal surge impedances. This can be also obtained by adding a long enough section, several miles (or kilometers) at each side.
- **Steel Tower Representations.** Steel towers can be represented as a single conductor distributed parameter line terminated at their footing impedances. Tower surge impedance values range from 100 to 300 ohms.
- **Tower Grounding.** A waveshape-dependent, or a frequency-dependent representation, is recommended. If not available, a resistance in the range of 10 to 100 ohms can be used. One difficulty is representing the nonlinear impedance of grounding systems with surge current.
- **Lightning Stroke.** The lightning stroke is typically represented as a current source with negative polarity and a specified waveshape for backflash calculations, as described in Chapter 6. The lightning stroke is not represented by a log-normal current source. Its cumulative probability of occurrence can be represented by a log-normal probability curve; the stroke itself is represented by an infinite impedance current source.
- **Power Frequency Voltage (Initial Conditions).** Phase voltages at the instant of the lightning stroke should be included. One simplified approach used for statistical calculations, is to select phase voltages every 30 or 60 degrees and average the results. More rigorous analysis assumes the phase voltages selects the phase voltages by considering a uniform distribution between 0º and 360º. For a deterministic calculation, worst-case conditions should be determined and used. A value of phase voltage equal to 105% of the crest value of the phase-to-ground voltage and of opposite polarity to the tower voltage can be used as the most conservative number.
- **Insulators.** Insulators are represented as voltage-dependent flashover switches in parallel with capacitors. Every time a flashover is produced, a counter is increased and the flashover rate is updated.

The flowchart in Figure A3.1-1 depicts the process of using the EMTP in doing lightning study for backflash over analysis.

Summary

With the development of modeling and simulation techniques in the last two decades, almost all kinds of transient problems related to insulation coordination can be analyzed. This appendix reviewed some of these tools that can be used by transmission line designers today. Some other tools are also described in several sections in this book, and are not repeated here.

An accurate simulation of a power system requires an adequate representation of its components, taking into account the frequency of the transients. An acceptable representation of all equipment throughout the complete frequency range is very difficult and for most components is not practically possible.

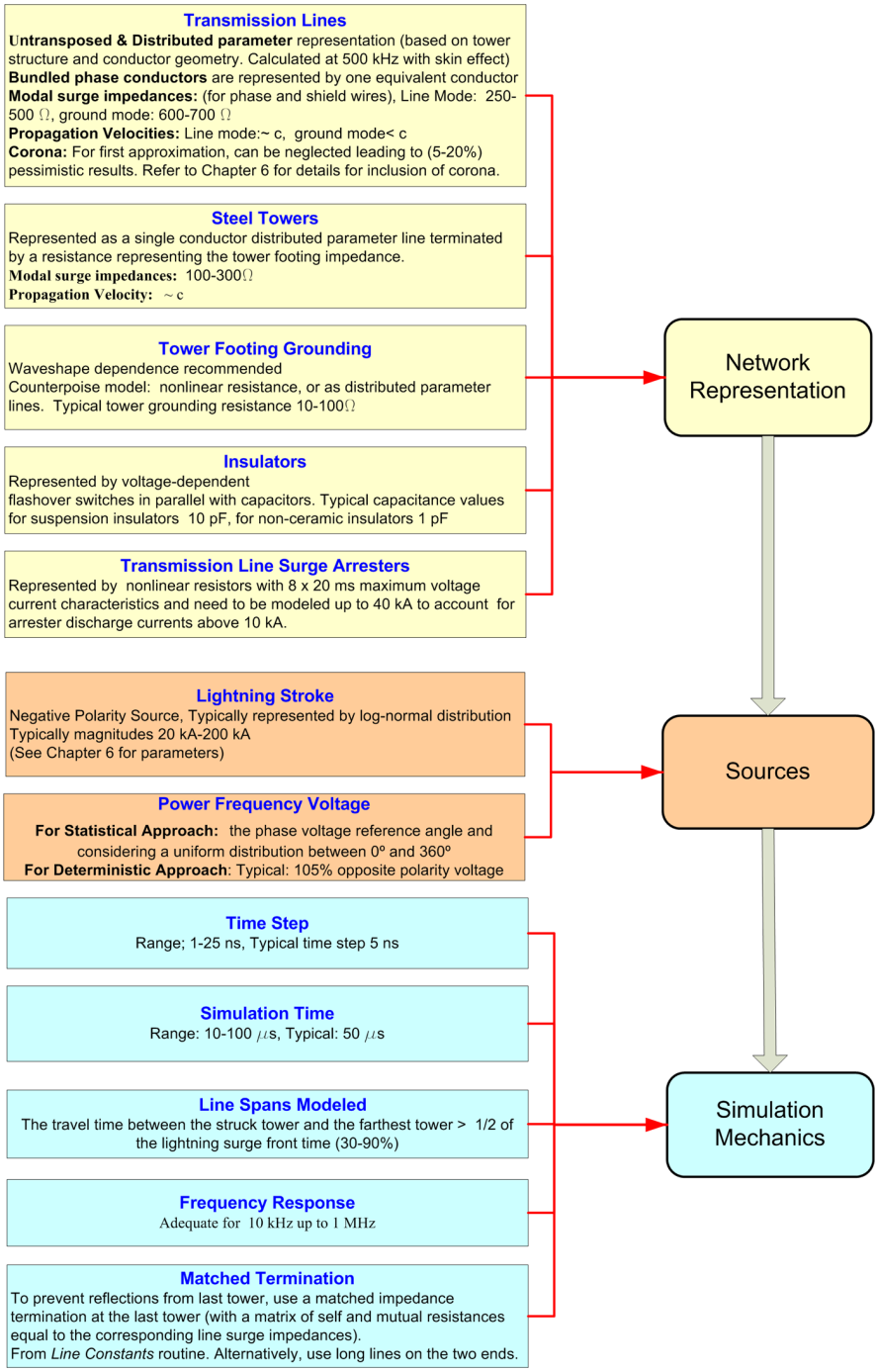


Figure A3.1-1 Backflash analysis using the EMTP.

APPENDIX 3.2 SURGE ARRESTER APPLICATIONS ON TRANSMISSION SYSTEMS: STATION AND LINE ARRESTERS

Introduction

This appendix describes the application of surge arresters on transmission systems. It covers both applications of surge arresters: the more classical applications of surge arresters at substations as well as the applications on the transmission lines themselves, which is gaining in popularity as a countermeasure for reducing lightning as well as switching overvoltages. It is noted here that the two types of arresters are different in construction and energy capabilities. This appendix starts with a description of the different types of station surge arresters, and then it tackles the application to transmission lines and associated considerations.

Station Surge Arresters

The use of modern surge arresters has made possible the reduction of the required basic impulse-insulation levels of much transmission system equipment. The primary function of early arresters was to protect the system insulation from the effects of lightning. Modern arresters not only dissipate lightning-caused surges, but also control other system surges caused by switching or faults. Surge arresters are seldom called upon to dissipate full lightning current, because transmission systems are generally shielded with ground wires, thus reducing the possibility of direct strokes to the phase conductors. (The ground wires are usually connected to earth through the tower structure with ground rods or mats. Ideally, tower footing resistance is kept to minimum practical levels so that lightning currents may be conducted to earth without unduly causing high voltages on the structure. If the tower footing resistance is high, a stroke to the ground wire or tower momentarily raises the tower voltage sufficiently so that an insulator flashes over. A portion of the lightning current then flows onto the phase conductor, and a surge begins to travel along the transmission line. Even a lightning stroke that does not impinge on either ground wires or phase conductors may induce traveling surges on the line. Because induced surges are unimportant for transmission voltage levels above 69 kV, the usual lightning effect that an arrester is intended to dissipate is the surge along the transmission line into the substation.

The modern surge arrester is a metal-oxide surge arrester (MOSA), which has largely replaced the older type silicon carbide arrester that was widely used. The MOSA is fabricated from nonlinear resistance metal-oxide (zinc oxide) materials.

Metal-oxide arresters fall into three categories:

- Gapless Arresters
- Shunt-Gapped Arresters
- Series-Gapped Arresters.

Nonceramic housed gapless arresters have the majority of TLSA market share at transmission voltages below 200 kV, but above this level other topologies offer increasing advantages of cost versus complication. To date, series-gapped arresters have been applied widely at 500 kV, and gapless topologies have been applied in spot applications outside stations at 765 kV. The shunt-gapped topology is described for completeness.

Gapless Arresters

Gapless arresters utilize stacked column(s) of metal-oxide valve elements, as shown in Figure A3.2-1 with the corresponding arrester volt-ampere characteristic. The arrester discharge voltage for a given surge-current magnitude is directly proportional to the height of the valve element stack, and is a function of the rate of rise of the current surge, with higher voltages occurring for faster rates of rise and vice-versa. At the maximum continuous operating voltage (MCOV) of the arrester, the arrester current is usually not more than a few milliamperes (mA), typically less than 10 mA. On the arrival of a surge, the increasing surge current is accompanied by a rise in arrester voltage to a maximum level determined by the volt-ampere characteristic.

Shunt-Gapped Arresters

The discharge voltage of a column or columns of metal-oxide valve elements can be reduced by shunting a portion of the stack as shown in Figure A3.2-2. On the arrival of a surge, the arrester voltage initially increases with increasing surge-current magnitude, according to the volt-ampere characteristics A-B. When the surge current magnitude reaches the B-C region, sparkover of a gap in parallel with a few metal-oxide valve elements occurs. This shunts the surge current around these valve elements, and proportionally lowers the discharge voltage (in the range D-E). For further increases in surge current, the voltage increases according to the characteristic E-F.

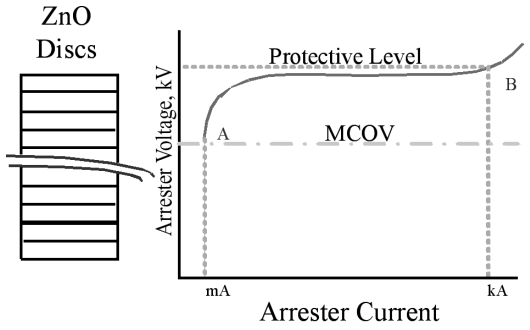


Figure A3.2-1 Gapless metal-oxide surge arrester.

Series-Gapped Arresters

Further reduction of the protective levels of arresters can be achieved by using fewer valve elements in conjunction with series-connected spark gaps as shown in Figure A3.2-3. On the arrival of a surge, the arrester voltage begins to rise (A-B). At a level of current in the vicinity of 1 A (depending on the rate of rise in the range B-C), the gaps spark over, and the arrester voltage is reduced to the discharge voltage of the metal-oxide elements only. For further increase in surge current, the voltage increases according to the characteristic D-E-F (Hileman 1999).

The voltage across the terminals of an arrester depends on two main factors: the magnitude of the current through the arrester and the waveshape of the current. The magnitude of the current is strongly influenced by the impedance of the circuit between the arrester and the source of the surge, as shown in Figure A3.2-4. If the impedance is low—for instance, near a large capacitor bank—the current through the arrester, and hence the voltage across the arrester, may be excessive and may damage the arrester. Because the arrester is in fact a nonlinear circuit element, a direct solution for the current and voltage is not possible.

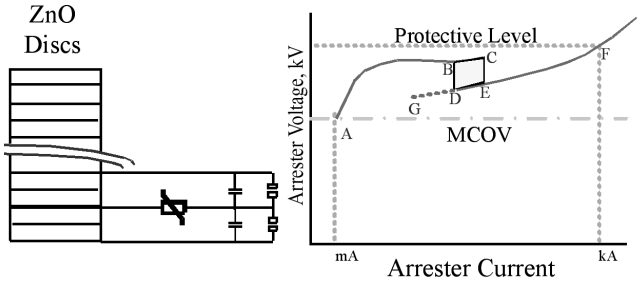


Figure A3.2-2 Shunt-gapped metal-oxide surge arrester.

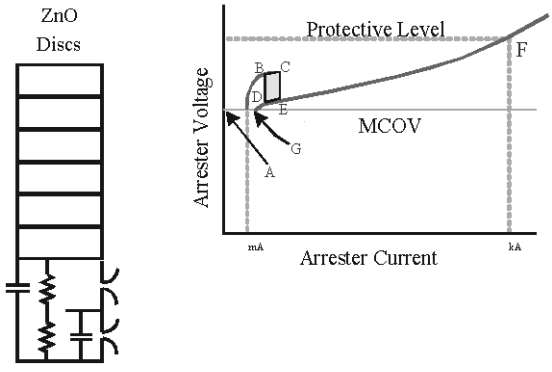
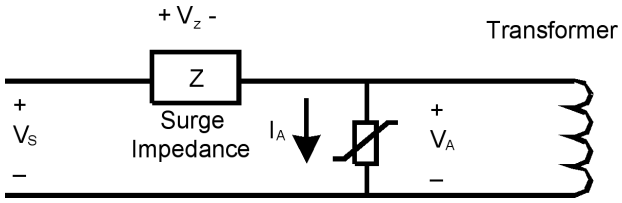


Figure A3.2-3 Series-gapped metal-oxide surge arrester.

As may be seen in Figure A3.2-4, the arrester current depends on V_S, Z, and V_A—the latter being a function of the desired current. This problem may be solved by either iterative or graphical means. Very fast-rising currents of a given magnitude produce higher voltages across the arrester than more slowly rising currents. In part, this is due to the inherent characteristics of the nonlinear resistance material of the arrester. Figure A3.2-5 indicates the magnitude of the voltage rise that may be expected. The values for silicon carbide and metal oxide are each normalized to unity at a time-to-crest of 10 μs because the standard current wave for the testing of arresters crests at 10 μs (IEEE 1999a).

Inductance in series with the arrester also produces higher voltage for fast current waves than for slow current waves. Long ground leads can contribute a significant inductance



V_s = Surge Voltage
V_z = Voltage Across the Surge Impedance of the line
V_A = Protective Level of the Arrester
Z = Surge Impedance of the Line
I_A = Arrester Current
$V_s = V_z + V_A$
$V_S = I_A Z = V_A$

Figure A3.2-4 The role of system impedance on arrester current.

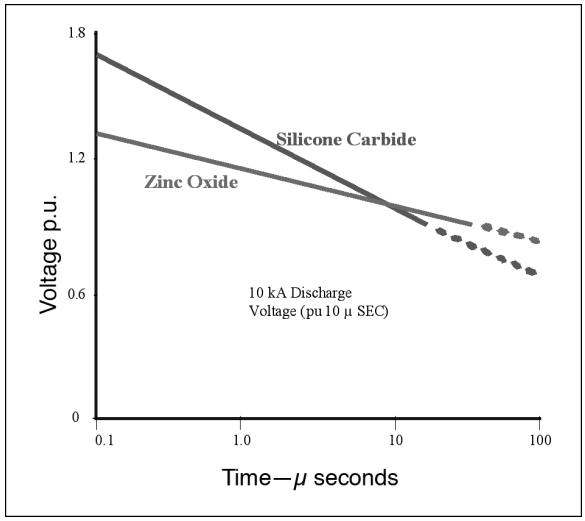


Figure A3.2-5 Effect of rise time on voltage.

so surge currents that rise to crest faster than 10 μs will cause higher voltages of shorter duration than those produced by the standard current test wave. Fortunately, the insulation in most oil-filled equipment such as transformers is able to withstand higher voltages if the duration is short. Some types of insulation, notably SF_6, do not exhibit much rise in insulation strength for voltages of short duration, and therefore arresters must be applied carefully to ensure that proper protection is provided for all types of surges, fast or slow.

Temporary Overvoltages (TOVs)
It is possible to control temporary overvoltages with surge arresters. When a temporary overvoltage occurs on the system—for instance, because of a fault—an arrester may be able to protect the equipment for the short time it takes to operate the applicable breakers. Because arresters cannot withstand high levels of overvoltage indefinitely, the timing of breakers may be of critical importance. Metal-oxide devices have greatly improved capabilities in this regard.

Switching-Surge Overvoltages (SSOVs)
It is possible to use surge arresters to control switching-surge overvoltages along a transmission line and thereby reduce the length of the required insulator strings. An example is shown in Figure A3.2-6 for the switching of a 280-km (175-mile) line having metal-oxide arresters at the receiving end. It is clear that the arresters can reduce the switching overvoltage along the entire line, from a maximum of 2.2 p.u. to 1.8 p.u. If the line can be energized from either end, arresters must be provided at both ends. Also see the section on Transmission Line Arresters below.

Arrester Selection
For a given application, the selection of an appropriate arrester involves considerations of many factors such as:

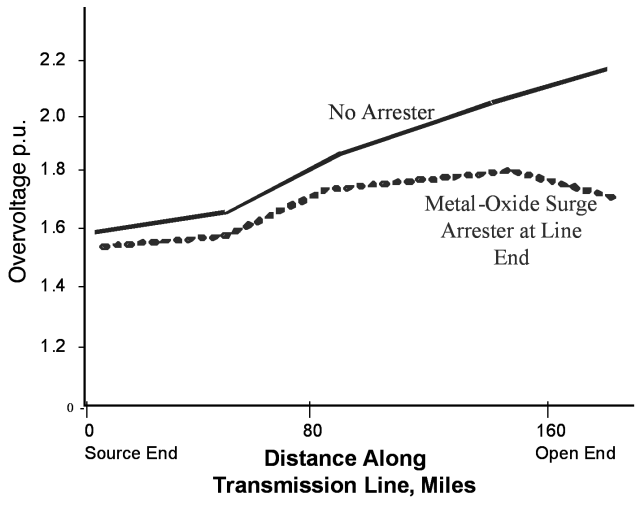


Figure A3.2-6 Typical effect of a surge arrester in controlling switching-surge overvoltages along a line.

- The maximum continuous operating voltage (MCOV) to which the arrester is subjected.
- The protective characteristics of the arrester for lightning and switching impulses
- Temporary overvoltages in the system—that is, durability
- Service conditions under which the arrester is applied.

The flowchart in Figure A3.2-7 explains how surge arresters are selected for substation equipment protection. The reader is also encouraged to refer to IEEE Std C62.22-1997, IEEE Guide for the Application of Metal-Oxide Surge Arresters for Alternating-Current Systems, New York, 1997 (IEEE 1997a). At present, there is no equivalent industry-standard approach for selecting TLSA for transmission lines.

Transmission Line Arresters (TLAs)
Transmission-line insulators may be protected from lightning flashover by overhead shield wires. However, the effectiveness of the shield wire depends on many factors. Prime among these are shield angle and structure ground footing resistance.

Strokes to the shield wire cause surge voltages to be induced in the phase conductors. The magnitude of the induced voltage is a function of the current magnitude, resistance, and geometry. Stroke currents exceeding a critical current value develop sufficient voltage between the structure and the phase conductor to cause an insulator flashover. The phase with the poorest coupling to the shield wire is the most highly stressed and therefore most likely to flash over in most cases. The possibility of a flashover of the line insulation and subsequent service interruption may be significantly reduced through the application of line arresters. Line arresters may also be applied on one circuit of a double-circuit line in order to reduce double-circuit interruptions due to lightning. Line arresters may be installed phase-to-ground, either in parallel with the line insulators or built into the insulators. While the failure rate of these arresters is low, the user should consider the failure mode of the arrester. After failure, the arresters should be disconnected by some form of disconnecting device from the line to allow for successful line reclosing.

The protective level of the line arresters should be greater than the protective levels of the adjacent substation arresters. This precaution reduces the energy absorbed by the line arresters due to switching surges and therefore reduces the possibility of a line arrester failure.

The appropriate location of the surge arresters depends on many factors, including lightning ground stroke density, exposure, span length, conductor geometry, footing resistance, insulation level, and desired line performance goals.

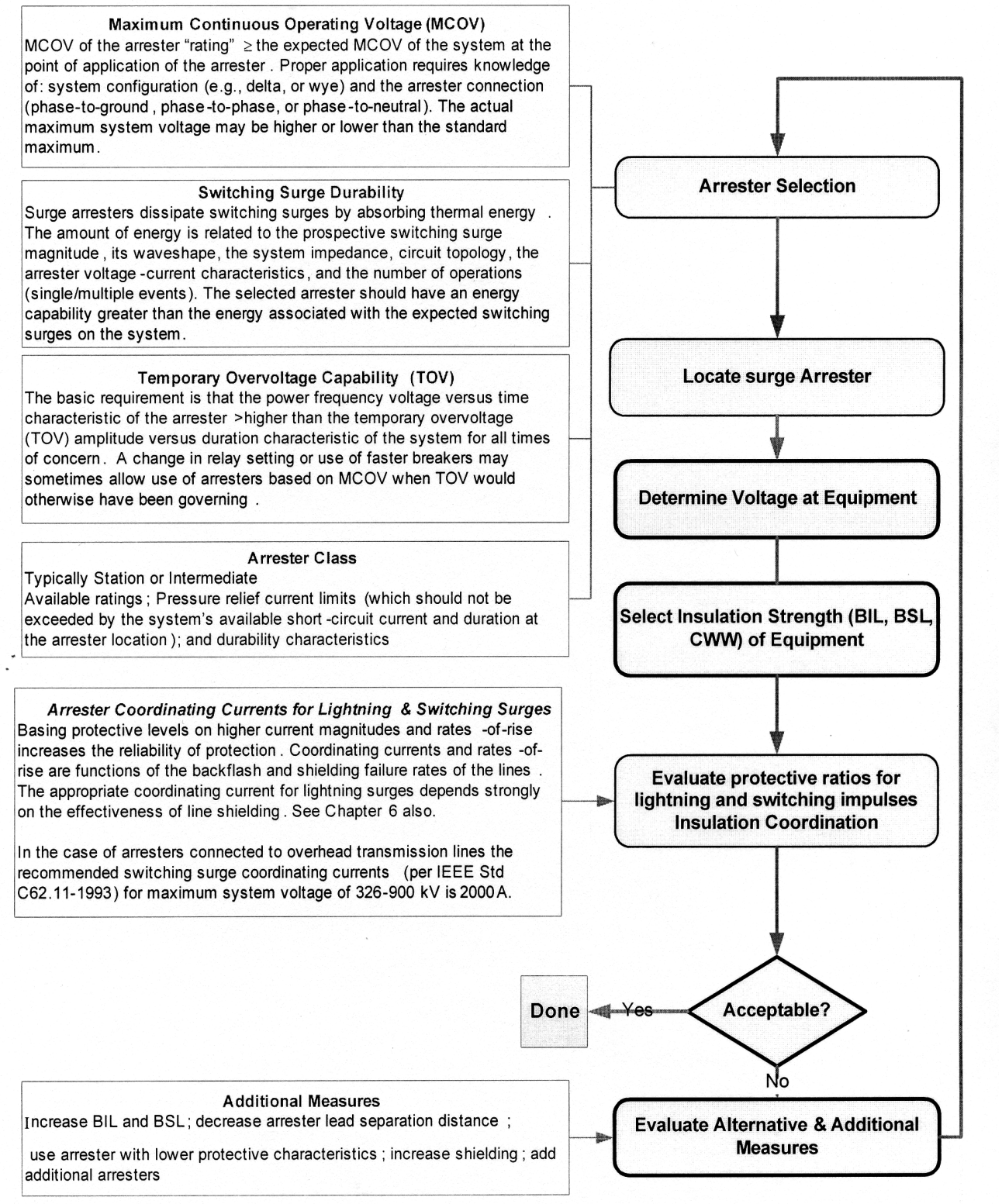


Figure A3.2-7 Flowchart for selection of surge arresters.

In general, the more frequently arresters are installed, the better the performance. Several computer models are available to assist in selecting the location of surge arresters, or the arrester manufacturer may be contacted for a recommendation.

In some cases, arresters are being used successfully in place of shield wires. The user should consider energy, mechanical strength, and weight requirements in developing the system design. The arrester manufacturer should be contacted for recommendations.

Line arresters are now manufactured for application in localities where lightning exposure is high and soil conditions limit installation of counterpoise or other ground electrode configurations. If applied properly, they can be very effective in reducing flashover rates, but if applied improperly, they simply transfer flashovers to structures with no arresters (Shih et al. 1985). They can also serve to inhibit shielding failures on critical spans, but again only if properly applied following the application theory to be described in this section.

Transmission-Line Arresters (TLAs) are now used to address lightning-related phenomena with the intent of improving the reliability of transmission lines. Transmission-line surge arresters also offer an efficient alternative for limitation of switching surges along transmission lines instead of using closing resistors or controlled closing schemes. Line arresters limit maximum lightning voltages across line insulators to values below the flashover value.

Hence the following functions of the systems can be improved by using TLAs:

- Reduction of line-to-ground and line-to-line lightning outage rates
- Reduction of backflashover rate on unshielded transmission lines
- Improved reliability of shielded and unshielded transmission lines
- Upgrading of system voltage on an existing transmission line
- Building new compact transmission lines
- Switching overvoltage control along transmission lines
- Reduction of the need for controlled closing of circuit breakers
- Reduction of the need for preinsertion resistors

Line Arrester Construction

Transmission-line arresters consist of a series of metal-oxide varistor blocks usually encased in a polymer weatherproof shell. The shell is designed to vent high-pressure gasses in case of a failure so as not to scatter fragments over a wide area. The varistor blocks can be substantially smaller than station arrester blocks because the lightning energy is usually shared by several arresters, or distributed along the stricken phase conductor in case of a shielding failure.

Important mechanical issues affect the use of TLAs. The first is the fact that practical TLAs tend to be about 30% longer than the insulators that they are protecting and need to be mounted at an angle to get the extra length. The physical reasons for this are as follows. For a typical lightning surge current of 31 kA, a column of large arrester blocks with 6.4 cm ($2^1/_2$ in.) diameter develops a voltage of about 380 kV/m. To protect a 230-kV insulator with length of 2 m and BIL of 1080 kV, the arrester column would need to be shorter than 2.8 m. However, the arresters have only a limited ability to withstand temporary overvoltage, so the columns are manufactured to be as long as possible. The connection from the transmission line to the arrester is also an area of potential weakness. Most connections incorporate current-limiting protection (see next section) that separate the arrester from the power system in the event of failure. This connection is often made using live-line work methods, which tend to have a wider distribution of installation forces than barehand work. The connection must also tolerate a range of conductor motion and, at the same time, avoid transfer of vibration energy or static forces that could distort the TLA housing and break open seals.

The ability of the TLA to radiate heat without damaging the polymer housing may also be an issue in some applications. Standard test methods for polymer insulators (CEA 1996) include boiling for 100 h in saltwater, followed by steep-front impulse application to establish the integrity of seals. This gives some guidance that the intended steady-state temperature of TLA in nonceramic housings should also be maintained below 100°C, based on existing construction methods.

TLA Failure Modes and Their Implications

Transmission-line surge arresters are relatively complicated components that may be susceptible to a number of long-term failure modes. Also, substitution of TLAs for overhead shield wires may only be practical if a low but nonzero arrester failure rate is used in the design process. Also, TLAs typically fail short rather than open, and need to be disconnected from the line to allow line reclosing. For these reasons, many manufacturers provide fuse-type disconnecting devices that can physically remove the connection from the power system, leaving sufficient distance between the phase conductor and the arrester so that there is no subsequent reduction in electrical insulation strength. (Such devices are placed on the ground terminal of the arrester and connected between the ground terminal and

the ground lead. TLAs mounted directly in the tower or parallel to insulators typically have the disconnector mounted on the high-voltage clamp between the high-voltage terminal and the line clamp. Operation of the disconnector physically separates the arrester ground connection from the failed arrester and gives a visual indication of failure.) With co-ordination between the breaker operation time and the I-t characteristics of the disconnector, the failed arrester does not cause a momentary outage. Disconnect operation can be identified from terminal transients or by visual inspection.

Some manufacturers provide fault-tolerance through the use of a series air gap rather than a fused disconnect. On distribution systems, this practice was well established because it was necessary to protect silicon carbide nonlinear elements from normal power frequency operation. For newer arresters, the improved voltage-current characteristics of metallic oxide elements make this unnecessary, but in some conditions, the series gap gives advantages of lower weight and cost.

Since conductors tend to swing laterally under different wind conditions, for transmission line suspension insulators, it is usually necessary to provide a ring of some sort to maintain a constant series gap. This approach has given satisfactory results in one EHV field trial (Kawamura et al. 1994).

Transmission Line Arrester Energy Capabilities

The surge arrester metallic-oxide elements tend to have higher energy absorption capability under lightning surge conditions than under ac conditions. Ringler et al. (Ringler et al. 1997) reported a mean for three manufacturers of 400-600 Joules / cm^3 at low current, typically from a single hole through the bulk material. When surge currents were increased to typical lightning levels of 35 kA, the arresters were able to absorb between 1600 and 2000 J/cm^3, and failures showed many small pinholes. A typical set of parameters from this test-to-destruction work included:

- Cylindrical block: 3.2 cm radius, 2.3 cm tall, area 32.2 cm^2, volume 74 cm^3
- Average test condition: 8.7 kV at 36.5 kA (318 MW)
- Average test results: 540 μs time to failure, 172 kJ, 2320 J/cm^3

The product of test current and time-to-destruction in experiments with power frequency ac and pulse voltage is remarkably constant for each type of arrester over more than five orders of magnitude. The increase in arrester voltage with higher current nearly exactly compensates for the increase in energy absorption capability. Since the product of arrester current and time is simply the charge, the parameters described in Section 6.2 for positive and negative flash charge will be relevant to the engineering applications below. In routine applications, with long life and multiple exposures to lightning, the energy level that causes a significant change in the arrester voltage-current relationship in terms of the application environment may be more limiting than the ultimate time-to-destruction result. This will be particularly true if there is little margin between the arrester maximum continuous operating voltage (MCOV) and the system overvoltage level.

Arrester manufacturers specify the maximum energy capability of each arrester sold, and experience has shown that some of these ratings are very conservative. Nevertheless, before any application to unshielded lines is evaluated, it is essential that a careful lightning energy analysis be made via computer programs dedicated to the probabilities of arrester failures on lines with no shield wires. The EPRI TFlash program has this capability.

Line Arrester Application Theory

The application of TLA is explained in a simple example, involving three towers (A, B and C) and a simplified transmission line consisting of only one shield wire and one phase conductor. Because of high footing resistance, a lightning flash terminating on the shield wire near the top of tower A will impress transient voltages across the tower A insulator far in excess of the critical flashover voltage. To avoid flashover, a line arrester can be connected across this insulator. Suppose the tower top voltage is 3000 kV, and the arrester limits the insulator voltage to 800 kV. The difference of 3000 kV– 800 kV = 2200 kV is then injected by the arrester onto the phase conductor at tower A. This 2200 kV then travels in both directions along the phase conductor and arrives at tower B. If the footing resistance at tower B is high, the difference between the tower top voltage and phase voltage at B may be sufficiently small, so that no flashover occurs at the tower B insulators, but in the usual case—if tower B insulators are not protected by arresters—they will fail. If arresters are also installed at tower B and the tower B footing resistance is high, the phase transient can still travel to tower C with sufficient magnitude to flash those insulators, unless arresters are present. However, if towers C have a low-footing resistance to conduct the lightning current to ground, the tower top voltage at C will collapse, the arresters will limit the transient voltage leaving towers C to less than the insulator CFO, and arresters will not be required beyond towers C. Low-footing resistance towers C are called “drain towers,” and their function is to dump the energy and to carry the stroke currents to ground through low-resistance paths so that flashovers will not occur beyond them. Between the two drain towers, flashovers can be expected to occur unless arresters are applied. Each drain tower must have low-footing resistance. For short distribution spans, arresters can sometimes be applied on every other support structure, but only after careful analysis using a computer

program written to evaluate all the traveling-wave effects, such as the EPRI TFlash program or an EMTP analysis. For double-circuit applications, arresters applied to one circuit can often reduce the flashovers on the companion circuit by coupling. Applet L-1 does not have capability to evaluate line arrester effectiveness.

To install line arresters without a careful traveling-wave analysis and without knowing the tower footing resistances can often result in little or no benefit for a large expenditure of time and money. Conversely, if problem areas exist where lightning flashovers are frequent, proper installation of line arresters after a careful analysis can be very effective.

For long EHV lines, TLAs usually are located at line ends. In addition, by locating arresters at one or more points along the line (e.g., at the midpoint or the one-third and two-thirds points), switching surge overvoltages and thus line insulation requirements can be limited without preinsertion resistors. Arresters used for this type of application should be designed for high-energy capability. Usually a class 2 or 3 arrester is sufficient, but higher arrester classes may be necessary at the receiving end of a line.

By the application of TLAs there are also possibilities for compacting lines and for upgrading of existing lines. The majority of TLAs presently used in North America are gapless metal-oxide arresters in polymeric housings, although there may be some that have gaps and/or porcelain housings. Polymer-housed high-energy transmission line surge arresters suitable for switching surge control are available for all EHV system levels up to and including 800 kV. The energy requirements for TLAs due to switching surges are considerably less for line arresters than for arresters located at the receiving end of the switched line. Figures A3.2-8 and A3.2-9, respectively, show the applications of gapless and gapped surge arresters on 275-kV lines at Eskom. In the case of Figure A3.2-9, the gapped arrester application, note the use of counterweights to keep the arrester in its proper placement. The gap is selected so that it does not flash over under switching surges. This means that, in the event of surge arrester failure, it is still possible to switch the line back (with the faulty arrester still present).

Figure A3.2-10 (Stenström and Mobedjina 1998) illustrates that, with a reasonable number of arresters, it would be possible to obtain an average overvoltage (2% value) of approximately 2 p.u. along an entire 100-km 550-kV line.

Application Considerations of TLAs

TLAs can help reduce the number of backflashovers and shielding failure flashovers on a transmission line. To a lesser extent, they are also used to reduce switching surge overvoltages. Table A3.2-1 discusses some common applications of TLAs.

Effects of Tower Footing Ground Resistance on TLAs

For shielded lines with no line arresters, the lower the ground resistance, the better the backflash performance. On the other hand, when TLAs are applied, a lower ground resistance in some cases may worsen the lightning performance, as explained here. When a lightning stroke terminates on the phase conductor due to a shielding failure (or the lack of the shield wire) most of the current will discharge to ground through the nearest TLA. Adjacent arresters, on adjacent towers, will discharge some amount of the energy based on the span length. The sharing is more pronounced on the slower tail of the surge where more of the energy is concentrated. The energy sharing is affected by

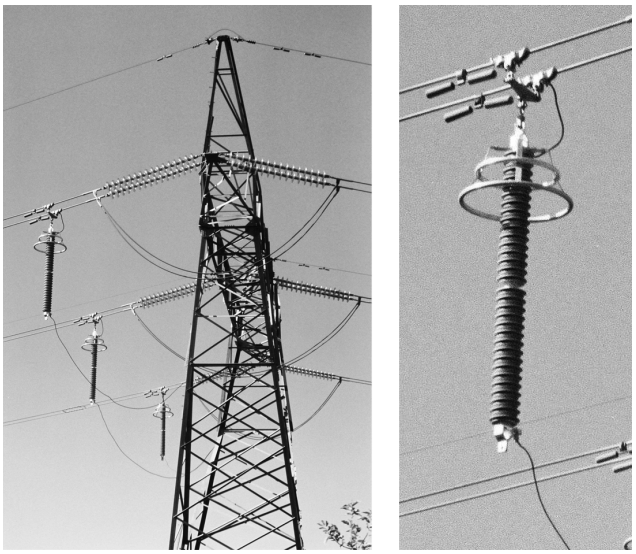


Figure A3.2-8 275-kV transmission-line surge arresters (Courtesy Eskom and ABB).

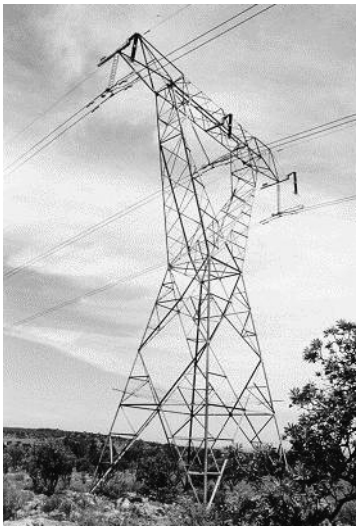


Figure 3.2-9 275-kV gapless arresters on an Eskom line (Courtesy Eskom and NGK).

Table A3.2-1 Common Applications of TLAs

Topic	Usage and Application Considerations
Handling	TLAs are typically more delicate than other equipment used on transmission lines and require special handling (storage, tools, torque requirements, etc.).
Installation	TLAs may be installed phase-to-ground, either in parallel with the line insulators or built into the insulators
Double-circuit lines	TLAs have been applied on single circuits of a double-circuit line in order to reduce double-circuit interruptions due to lightning.
Unshielded lines	TLAs have been used in areas of moderate ground flash densities on unshielded lines on the topmost phase, effectively transforming the phase into a shield wire to protect the other phases. This approach to lightning protection could be cost-effective in areas where the following conditions exist: • Difficult grounding, with resistivity in excess of 1000 Ω-m • Relatively low ground flash density • Relatively high incidence of icing or (ice + wind) loading • Areas of environmental sensitivity where line height is an issue
Vertical phase configurations	Since for vertical phase configurations the lowest phase would experience the lowest coupled voltage and the highest insulator voltage stress, for strokes on the shield wire, some apply TLAs on the bottom phases only. This would improve the performance against backflashovers of shielded vertical configurations. In such configurations, TLAs can effectively create another grounded conductor and hence improve the coupling to the remaining phases, which reduces the probability of a backflash on the phases without TLAs.
Poor grounding	TLAs may be installed on just the sections of line that have poor grounding due to soil conditions, or that have exceptional exposure to lightning strokes (e.g., river crossings, lakes). However, care is required in applying TLAs in such a fashion, or protecting adjacent segments with good ground impedance may be problematic. See discussion later.
Protective levels of TLAs vs. line CFO	The protective level of TLAs should be below the CFO of the line insulators. The selection of energy requirements depends on the application and whether the line is shielded or not. If a lightning stroke terminates on the overhead shield wire, most of the lightning current will discharge through the tower footing, with relatively little current flowing through the TLA. Hence, for a well-shielded line, the energy duty on the line arresters can be reduced compared to nonshielded lines. Even in the event of a shielding failure (i.e., some lightning strokes terminating directly on a phase conductor), for low-current magnitudes (5 to 20 kA), the TLA energy duty is still relatively low. Therefore line arresters may be applied to shielded lines to improve the backflashover performance with little concern for energy duty on the arresters. Protection with line arresters of unshielded lines often requires station class arrester types, as these lines have a higher probability of being subjected to direct strokes. TLAs in all phases on each tower eliminate the need for both shield wires as well as good footing resistance. In areas with moderate ground flash densities, one arrester in the top phase may be used instead of shield wires.
Protective level of TLA vs. substation arresters	The protective level of TLAs should be greater than the protective levels of the adjacent substation arresters to reduce the energy absorbed by the line arresters due to switching surges. Hence TLAs should have slightly higher MCOV than arresters applied in the substation.
Benefits to substation protection	Placing TLAs on the towers closest to a substation results in a reduction of steepness and amplitude of incoming surges to the substation. This dramatically improves the protection of the substation against backflashovers.
Reduced insulation levels	TLAs may be used to protect transmission line structures, or spans, with reduced insulation levels.
Open points	TLAs may be used on certain open points on the system exposed to voltage surge doubling.
Switching overvoltage control	For switching overvoltage control, line arresters are usually installed in all phases. Protection against switching typically requires one energy class lower for TLAs, than what is used for arresters installed at the substations. TLA can be used instead of closing resistors on circuit breakers. They can either replace, or supplement, controlled switching (see needs to be looked at carefully for compensated lines). For switching overvoltage control, TLAs are usually installed in all phases. The number of TLAs needed is dependent on the length of the line. For shorter lines, it may be sufficient to have TLAs at both line ends. For longer lines, studies need to be conducted to determine how many are needed. (Experience has shown that TLAs close to the middle or at one-third plus two-thirds of the line length have resulted in noticeable improvement over no TLAs.) The lower the protection level of the surge arrester, the lower are the overvoltages. However, the temporary overvoltage capability of the arrester is lower for a reduced protection level, and the energy to be absorbed is higher.
Reduction of insulation	TLAs can be used to intentionally reduce the insulation on certain structures, resulting in increased clearances to ground along the span. This is a recommended use.
Upgrading	Upgrading or compacting new lines may need TLAs in every tower for one or all phases, depending on the system requirements.

the tower ground resistance, with less sharing at lower resistance.

Application of TLAs on segments of the line with high grounding resistance: If there are differences in the ground resistance between different towers (for example, a struck tower having a TLA while the adjacent towers have a lower resistance and no TLA), it can be shown that the insulation stress will transfer to the adjacent tower that has no TLA. Hence it is recommended that, if TLAs are to be used only on a section of line with poor grounds, they should also be applied on at least the next one or two towers with good grounds. The above illustrates that lower ground resistance does not always improve the lightning performance of an overhead line with arresters.

Special Considerations Related to Standards and Specifications for TLAs

TLAs are not specifically addressed in IEEE Standard C62.11-1999 (IEEE 1999b), although the arresters used in these applications are part of the standard. Most of the test requirements that apply to line arresters are based on station-class requirements. When specifying line arresters, it should be noted that the following points are inherent to C62.11-1999.

1. Lightning energy-handling capability can be a major factor in selecting line arresters. The requirement of lightning-related energy is typically much more significant for lines than stations. Although present standards do contain some lightning-related tests, there is not presently an accepted test to quantify the lightning energy handling capability of surge arresters. The published energy-handling capability of arresters is typically based on switching-related tests.
2. Short-circuit tests permit polymer arresters to fall apart as long as the pieces fall within specific areas. The tests allow 2 minutes before the arrester must self-extinguish. These allowances in the present standards may not be acceptable for certain areas on a line right-of-way.

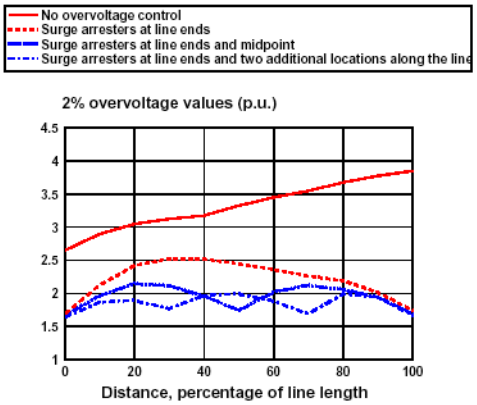


Figure A3.2-10 2% overvoltage values, line to ground, for 100-km line with different measures to control switching surge overvoltages (Stenström and Mobedjina 1998).

Analytical Requirements for TLA Applications

Most line arrester applications for lightning protection should be preceded by computer simulations to assess:

1. Which sections of the line should be protected by TLAs
2. Lines containing major differences in resistance and grounding methods
3. Only certain phases (typically top) being protected
4. Multiple circuits on the same tower

The following are some recommendations for performing a TLA application for lightning studies:

1. **Number of towers:** Start with at least 10 to 20 spans.
2. **Time Step Selection:**
   - For energy calculation, time steps can be as long as one-half span travel time (approximately 1 μ s for every 300 m), time steps of 0.25-0.5 μs have been used.
   - Shorter time steps must be used for the flashover calculation.
3. **Run Time:**
   - Typically several hundred μ s for arrester energy discharge calculations
   - 25-75 μ s for flashover calculations.
4. **Line model:** Start with a constant distributed parameter model. Add frequency dependence and corona to the final runs for more accurate answers.
5. **Current Levels:** Many currents must be run to determine a critical current level for both flashovers and arrester energy duty. These results may be used with stroke current probability distributions and ground flash density to obtain flashover and arrester failure rates.

Use of Line Arresters to Reduce Line Flashover Frequencies for Power Quality Considerations

Recent industry experience has shown that transmission-line surge arresters are reliable and effective as designed at voltage levels of 115 kV and 138 kV. Programs have been initiated to apply TLAs on 230-kV lines with both shielded and unshielded conditions. The effectiveness of arrester application is generally being monitored by comparing the number of "challenges" (nearby ground stroke terminations) before and after treatment. One interesting development at some utilities is the execution of performance improvement contracts with key customers, who fund the purchase and installation of transmission-line surge arresters in order to obtain premium power quality.

Arresters can be applied to unshielded lines as a substitute for overhead shield wires—advantages being that shield wire losses are eliminated, line compaction is improved, and the maximum expected turning moment of support structures (and consequently cost) is reduced. For this application, arresters must absorb energies from the complete spectrum of lightning flashes to the line, with a substantially higher risk of failure than the same arresters on lines with shield wires to attract and divert most of the stroke currents to ground.

Software for Selecting Arrester Locations

For cases where the span lengths and footing impedances are known, a number of modeling tools can be applied to analyze the effectiveness and reliability of transmission-line surge arrester applications. EPRI's TFlash, and the Electromagnetic Transients Program (EMTP) have been used by a number of researchers (Tarasiewicz et al. 2000; Lambert 1988; Zanetta 2002).

Summary

The modern surge arrester is a metal-oxide surge arrester (MOSA), which has largely replaced the older silicon-carbide arrester that was widely used. The arrester discharge voltage for a given surge-current magnitude is directly proportional to the height of the valve element stack, and is a function of the rate of rise of the current surge, with higher voltages occurring for faster rates of rise and vice-versa. Line arresters may be installed phase-to-ground, either in parallel with the line insulators or built into the insulators. While transmission-line arresters were initially envisioned for control of lightning overvoltages, they can (and have) also be used for the control of switching surge and temporary overvoltages. The energy requirements for TLA applications vary based on applications.

Recent industry experience has shown that transmission-line surge arresters are reliable and effective as designed. TLA applications are available for all HV and EHV systems up to and including 800 kV. Application of TLA opens up the possibilities for compacting lines and upgrading of existing lines.

TLAs offer a robust, efficient, and cost-effective alternative for minimizing/eliminating outages due to lightning surges and for limitation of switching surges along transmission lines.

APPENDIX 3.3 INSULATION COORDINATION METHODOLOGIES

Introduction

As previously described, line insulation coordination includes the selection of phase-to-ground and phase-to-phase clearances, tower strike distances, tower footing resistance, insulator lengths, and the leakage or creepage distance of insulators. Any overvoltage countermeasures, such as surge arresters and breaker-closing resisters, must also be selected if required. The lowest values of the withstand voltages of the insulation must meet desired line performance criteria when subjected to service conditions.

Two approaches to insulation coordination for transient overvoltages are in use today: a deterministic method and a probabilistic or statistical method. Many commonly-used procedures, however, are a mixture of both methods. Both are discussed extensively in the reference literature (EPRI 1982; IEC 1996; IEEE 1999a; Greenwood 1991). Obviously the universal availability of computers and software such as the applets in this Reference Book allows designers to use sophisticated probabilistic techniques as easily as the simpler deterministic methods, providing that appropriate stress and strength data are available. It is also recognized that many utilities simply continue to use old proven designs rather than risk potential savings against problems with new optimized designs, unfamiliarity of workers with new configurations for construction and maintenance, and requirements for new families of spare parts.

The principles described here are applicable to all three types of voltage stress and insulation strength—namely, lightning, switching surges, and power frequency voltage.

Deterministic Method

The deterministic method assumes that there is a known maximum overvoltage, V_{max}, which may stress the insulation, a known minimum insulation withstand voltage V_W, and that these occur simultaneously. Insulation is designed so that V_W is larger than V_{max} by a safety margin, as shown in Figure A3.3-1 (EPRI 1982). This safety factor covers only the uncertainties involved in the designer's evaluation of V_{max} and V_W. The safety factor should not be confused with

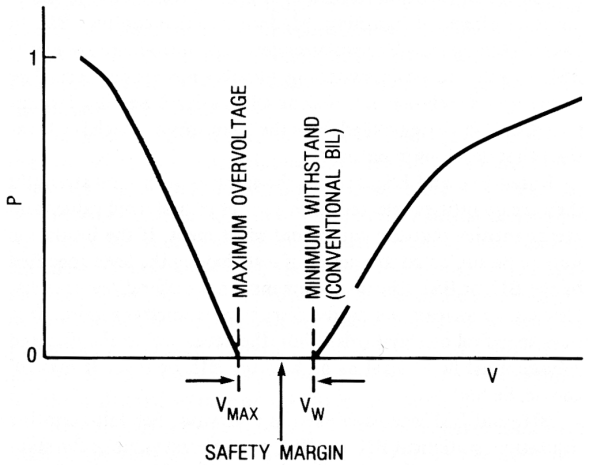


Figure A3.3-1 Illustration of deterministic method for insulation design (EPRI 1982).

the protective ratio, which is used in connection with internal insulation that is protected by an external surge arrester (Greenwood 1991).

Transmission lines designed in the past using the deterministic method characteristically have very conservative clearances and strike distances. Designs based on such an approach can be more expensive than those obtained from modern probabilistic methods. Today the deterministic method is usually applied when no statistical information on stress or strength is available, especially for coordination and design of non-self-restoring insulation.

Probabilistic (Statistical) Method

In actuality, both the stress (overvoltage) and the strength (insulation withstand) exhibit probabilistic behavior. The potential benefit of a probabilistic approach is that the combination of maximum overvoltage and minimum insulation strength rarely occurs. Therefore considerable economy may be achieved for self-restoring insulation by modeling the probabilistic nature of both the voltage stress and the insulation strength. This approach nearly always results in a substantial decrease in line insulation, tower dimensions, weight, width of right-of-way, and cost. That decreased cost must then be weighed against the increased risk of failure and the costs of such failures.

The probabilistic method is applied by modeling and combining the probability distributions of the overvoltages and the insulation strength. By repeating the calculations for different types of insulation and for different states of the network, the total outage rate of the system due to the insulation failures can be estimated. The application of probabilistic insulation coordination makes it possible to estimate the failure frequency directly as a function of the selected system design factors. In theory, optimization of the insulation could be possible, if outage costs could be related to the different types of faults. In practice, it is very difficult to evaluate the consequences of insulation faults in different operation states of the network and the uncertainty of the cost of the undelivered energy. Hence it is usually better to slightly overdimension the insulation system rather than optimize it. The design of the insulation system is then based on the comparison of the risks corresponding to the different alternative designs. Detailed computation is discussed below.

Virtually all probabilistic calculation methods embody a nonzero risk of failure. This results from the inability of statistical models to precisely represent insulation strength or insulation stresses. As an example, the typical statistical model for air gap behavior gives a flashover rate that is never zero, even for very small voltages. Designers recognize that in designing for nonzero levels of failure, limitations in modeling techniques result in conservatism in the designs. As will be described later, even designs with a relatively high 10% failure rate for switching surges have never in practice flashed over.

Statistical Properties of Withstand Voltage of System Components (EPRI 1982)

The withstand voltage of system components can be defined in statistical terms. Suppose that a number, *n,* of tests is performed with each of the voltages V_{T1}, V_{T2}, V_{T3} ...., V_{Tr}. The relative frequencies of failure, v_k/n, where v_k denotes the number of failures at the voltage V_{Tk} (k = 1,…, *r*), would then represent the estimates of probabilities of failure for the voltages V_{T1}, V_{T2},...., V_{Tk}. The graph expressing the dependence of the failure probability estimate, $p = v_k/n$ on V_{Tk}, would approach a curve continuously increasing from 0 to 1. At small voltages, there would be no failures, and at high voltages, all tests would lead to failure. This function, denoted $F(V_T)$, represents a probability that at a given instance the withstand voltage would be smaller than the applied voltage (i.e., the probability of disruptive discharge). This function is a cumulative distribution function,

$$F\left(V_T\right) = P\left\{V_W < V_T\right\} \qquad \text{A3.3-1}$$

and its derivative,

$$f\left(V_T\right) = \frac{d}{dV_T} F\left(V_T\right) \qquad \text{A3.3-2}$$

is the corresponding density function (see Figure A3.3-2).

For high-voltage gaps, this function is well approximated by the normal distribution (Gaussian) function:

$$F\left(V_T\right) = \frac{1}{\sigma\sqrt{s\pi}} \int_{-\infty}^{V_T} \exp - \frac{1}{2\sigma^2}\left(t-\mu\right)^2 dt = \Phi\left(\frac{V_T-\mu}{\sigma}\right) \qquad \text{A3.3-3}$$

where:

$$\Phi\left(u\right) = \frac{1}{\sqrt{2\pi}} \int_{-\infty}^{u} \exp\left(-\frac{z^2}{2}\right) dz \qquad \text{A3.3-4}$$

with:

$$z = \frac{V_T-\mu}{\sigma} \qquad \text{A3.3-5}$$

The function $\Phi(u)$ is given in tables. The constant μ is the mean value or median of the withstand voltage, and for lightning is called the critical flashover voltage (CFO). CFO is the crest value of the impulse that under specific conditions causes flashover of the insulation on 50% of the applications.

The voltage withstand strength is quite often expressed in terms of basic insulation levels, BIL and BSL. BIL, an abbreviation of basic insulation level, was originally related to the short-duration effects of lightning. Modern practice confines BIL to basic lightning impulse insulation level, and introduces the newer BSL to refer to basic switching impulse insulation level. Rated BIL and BSL are not the same as withstand strength; they are quantities that the equipment must meet, selected from a series of preferred values. If the insulation were to be subjected to a series of tests having the level specified by the BIL or BSL, the insulation must not suffer disruptive discharges, or at least not suffer disruptive discharges more often than specified by standards. Thus the actual value of withstand voltage must be at least as high as the BIL or BSL. It may, of course, be higher.

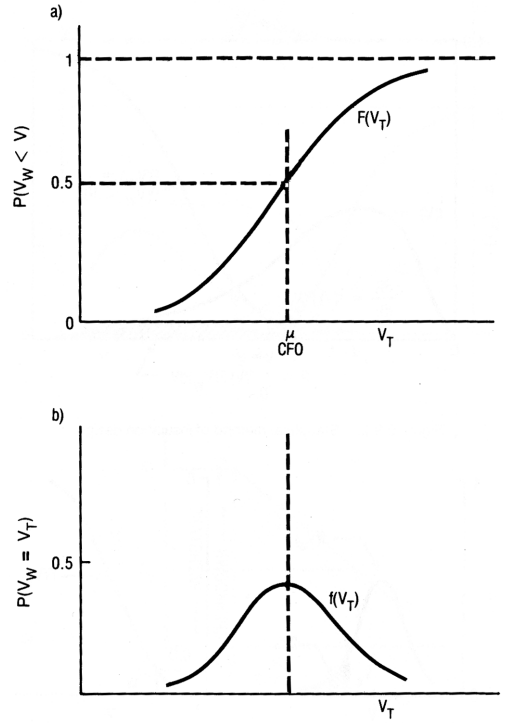


Figure A3.3-2 Probability functions: (a) cumulative distribution; and (b) density-derivative (EPRI 1982).

BIL and BSL are each used in two ways. For self-restoring insulation, statistical BIL (or BSL) is the crest value of the standard impulse for which the insulation exhibits 90% probability of withstand (or 10% probability of failure). On the other hand, conventional BIL (or BSL) used for non-self-restoring insulation is a value for which the insulation shall not exhibit disruptive discharge when subjected to a specific number of impulses. A summary of the recommended voltage-withstand characteristics is shown in Table A3.3-1. Table A3.3-2, from IEEE Std 1313-1993 (IEEE

Table A3.3-1 Withstand Voltage Characteristics

Type of Insulation	Withstand Voltage	
	Switching Impulse	Lightning Impulse
Non-Self-Restoring (Internal)	Conventional BSL	Conventional BSL
Self-Restoring (External)	CFO (50%) plus Statistical BSL (90%)	CFO plus Statistical BIL (50%)

Table A3.3-2 Preferred BILs and BSLs for V_m > 242 kV (IEEE 1999a)

Maximum System Voltage V_m (rms) (kV)	Base for per Unit Values $\sqrt{2}$ V_m $\sqrt{3}$ (crest) (kV)	BSL (per unit)	BSL (kV)*	BIL (kV)*
362	296	2.53 2.79 3.04 3.55	750 825 900 1050	825 900 1050 1175 1300
550	449	2.17 2.34 2.62 2.90 3.17	975 1050 1175 1300 1425	1175 1300 1425 1550 1675 1800
800	653	1.99 2.18 2.37 2.57	1300 1425 1500 1675	1675 1800 1925 2050 2175 2300
1200	980	†	†	

* Various values of BIL and BSL may be used in combination as appropriate to specific apparatus or system elements.

† These values are not presently specified.

1993), shows the preferred values of BIL and BSL for equipment. The recommended values apply both to statistical and conventional quantities. The BIL shall be chosen from the list in Table A3.3-2, and the associated BSL, as determined by the relationship, may differ from the values in the list.

Probability of Overvoltage Occurrence

The magnitudes of the overvoltages occurring in the system are also statistical in nature. This section clarifies some of the statistical concepts used in describing overvoltages. To illustrate the practical meaning, consider the example of overvoltages when energizing a line with a transformer from a given system (see Figure A3.3-3[a]). The three phases of the line are energized by a breaker, whose poles are not mechanically linked. When a command to close is given, generally by energizing the closing solenoids, the three poles begin to close independently. The timing of the closing impulse is usually random with respect to the timing of the supply-side power frequency voltage (see Figure A3.3-3[d]). The actual closing occurs after the solenoids are energized, and the actual closing times of the breaker poles—t_A, t_B, and t_C—display some statistical variations from operation to operation. Moreover, even the mean values of those times may be different, depending on the manufacture and adjustment of breakers in the field. It cannot be predicted exactly when the breaker poles will actually close and energize the circuit. There are other random variables—such as prestrike in the breaker, or functions of the circuit depending on the past history of the circuit (e.g., trapped flux in the transformer or charge on the line). All of these influence the overvoltages that are developed as the breaker closes.

Of interest are the observed overvoltages at the end of the line, V_A, V_B, and V_C. These voltages may be treated as an outcome of a statistical experiment, although the voltages in the three phases are not really independent variables. For simplicity, consider as an example voltages V_a of phase A as they would be measured in $n = 300$ tests. Instead of recording the voltages according to the sequence in which they were measured, they may be tabulated in order of their amplitudes. The table could be simplified by selecting some voltage interval and showing the number, v, of voltages that occurred in the interval $V < V_a < V + \Delta V$. This could be plotted in the form of a bar chart, such as in Figure A3.3-4, in which the vertical axis gives the number, v, of overvoltages in each voltage interval, ΔV, in relation to the total number of tests, n. It is noted that the ratio of v/n may be used as an estimate of the probability that the overvoltage will be in the given interval, ΔV, that is:

$$p\{V < V_a < V + DV\} = \frac{v}{n} \qquad \text{A3.3-6}$$

Of course, the higher the number of tests, n, the closer that estimate P would be to the true probability, which by definition is:

$$P\{V < V_a < V + DV\} = \lim_{n \to \infty} \frac{v}{n} \qquad \text{A3.3-7}$$

With n sufficiently high, ΔV approaches dV, and the histogram of Figure A3.3-4 approaches the continuous distribution function shown in Figure A3.3-5(a).

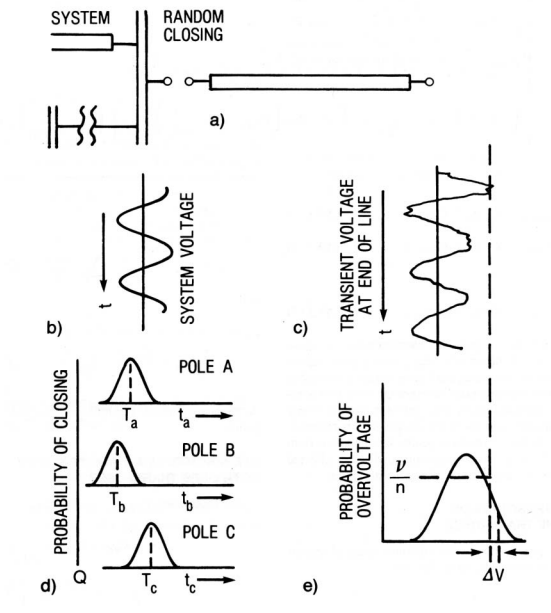


Figure A3.3-3 Statistical overvoltages: (a) circuit; (b) voltage on bus; (c) voltage at end of line; (d) probability of pole closing times; and (e) probability of indicated overvoltages (EPRI 1982).

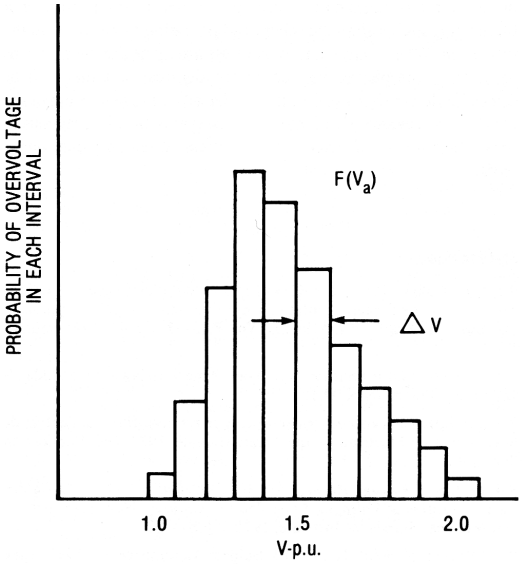


Figure A3.3-4 Histogram of overvoltage.

The cumulative distribution function is commonly defined by mathematical statistics as the function that gives the probability that the random variable V_a will be smaller than the value of interest, V. In this case, the cumulative distribution function (disregarding the polarity of the voltage) would be:

$$F(V_a) = P\{V_a < V\} = \sum_{v=0}^{n} \frac{v}{n} \quad \text{A3.3-8}$$

as shown in Figure A3.3-5(b), or:

$$F(V_a) = P\{V_a < V\}' = \int_0^v f(V_a)dV \quad \text{A3.3-9}$$

As far as insulation is concerned, it is really more appropriate to know the probability of a given voltage being exceeded. If the insulation were able to withstand exactly the specified or a lower voltage, that probability would also give the probability of failure. Such a probability function complementary to the cumulative distribution is:

$$P\{V_a > V\} = Q(V_a) - 1 - F(V_a) \quad \text{A3.3-10}$$

where:

$$Q(V_a) = V\int_V^{\infty} f(V_a)dV \quad \text{A3.3-11}$$

which is a monotonically decreasing function in the interval $Q(V_a)$ between 0 and 1.

A Monte Carlo procedure can be performed to obtain the probability distribution of switching overvoltages. From the repetitive simulation, a histogram of switching overvoltages and a cumulative probability curve are obtained. An example is shown in Figure A3.3-6. If the overvoltages were characterized by a purely Gaussian distribution, the plot would be a straight line, giving a definite, though perhaps small, probability of very large overvoltages, and giving a definite, though perhaps small, probability that some of the overvoltages would have amplitudes less than the crest value of the system voltage. Overvoltages are, by definition, greater than the supply voltage. Furthermore, there are fundamental limits to the maximum overvoltage that may be obtained, limits in addition to the fact that the extreme overvoltages may be limited by surge arrestors, corona, saturation, or other physical effects. Because the distribution may be only approximately Gaussian, and is in

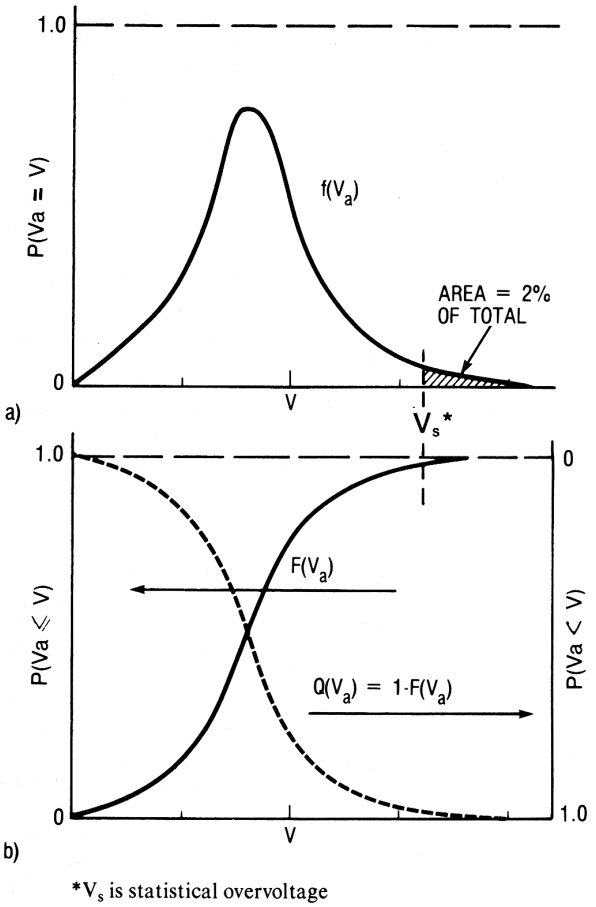


Figure A3.3-5 Probability of overvoltage: (a) overvoltage density $f(V_a)$; and (b) cumulative function $F(V_a)$.

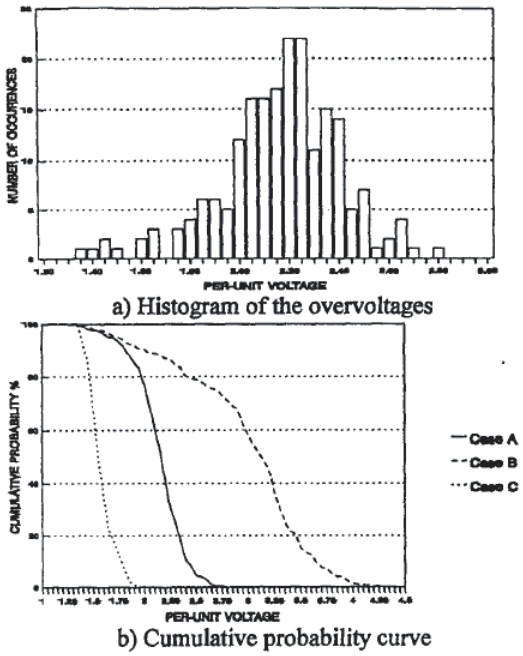


Figure A3.3-6 Cumulative probability of switching overvoltage (Martinez et al. 2000)

any event likely to be truncated at its upper and lower extremes, it is perhaps unwise to place much reliance on any calculated value of deviation as a measure to estimate the probability of occurrence of extreme overvoltages. If an analytic approximation to the measured distribution is needed, it is probably best to fit a straight line (or lines) to the curve. A straight-line approximation of the upper end of the distribution is generally possible, and it is usually only the upper end that is of importance.

The measured distribution, since it is from a limited number of tests, is only an approximation of the actual distribution. Truax et al. (Truax et al. 1978) give some quantitative data on how the number of experiments affects the maximum estimated overvoltages. In the case of TNA studies, it is quite common practice to base the output data on 300 switching operations.

The preceding explanations define only the basic terms. It should be noted that these terms may deserve further study, depending on how the data are used. For example, an explanation was given for voltages in one phase. Overvoltages in different phases could be treated separately (insulators in each phase are stressed only by the overvoltage in that phase) or in some relationship. One common practice is to rank the overvoltages without regard to the phase in which they occur. (If there is a flashover, it is not really of importance on which phase it occurs or whether it occurs simultaneously on more than one phase.) Figure A3.3-7 presents an example of how the final distribution may differ depending on the method of evaluation. The curves *A, B*, and *C*, give the distributions separately for 300 points measured in each specific phase *A, B*, and *C*, during 300 operations. Curve D represents the distribution of all 1900 measurements in all three phases during the 300 operations. Even though the overvoltages in the three phases are not really independent, it may be seen that the likelihood of closing angles, α, β, and γ, may be the same for any sequence of phases. This may be justified by considering not the distribution for one specifically adjusted breaker but the probability of the adjustments of any breaker in the field.

This statistical treatment is open to further refinement, depending on how the data are to be used. For example, most of the treatments have been single-phase analyses. Commonly, when a statistical analysis of overvoltages is made, the highest voltage on any of the three phases is selected. The statistical ranking of voltages from a number of tests is then made using only that highest voltage. This analysis implies that each of the phases is equally likely to flash over. Actually, for any particular operation of the breakers, the voltages on the three phases will be different, one of them being higher than the others and providing more stress on the insulation. When a large number of tests are made, the distributions for each of the phases may be nearly identical, but they will be somewhat lower than the distribution based on the maximum of the three phases as shown in Figure A3.3-7. It may be advantageous to make the analyses of strength versus stress on an individual-phase basis.

Combining Stress and Strength

The probabilistic method of insulation coordination is based on matching the probabilities of insulation stress and strength, as discussed above. The criterion is the acceptable risk of failure. The risk of failure may be calculated as shown in Figure A3.3-8. The probability of insulation breakdown is given by the function $F(V_W)$. The probability distribution or density of the overvoltage is given by the function of $f(V_a)$. The probability that the overvoltage V_1, will occur is $f(V_1)$. The probability that the insulation will fail at the voltage V_1 is $F(V_1)$. Hence the probability of both experiencing the overvoltage V_1 and not being able to withstand it indicates the probability of failure at that voltage as

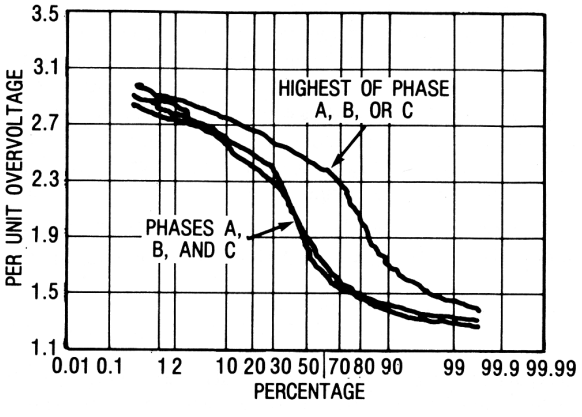


Figure A3.3-7 Distribution on a phase-by-phase basis (based on 300 breaker operations).

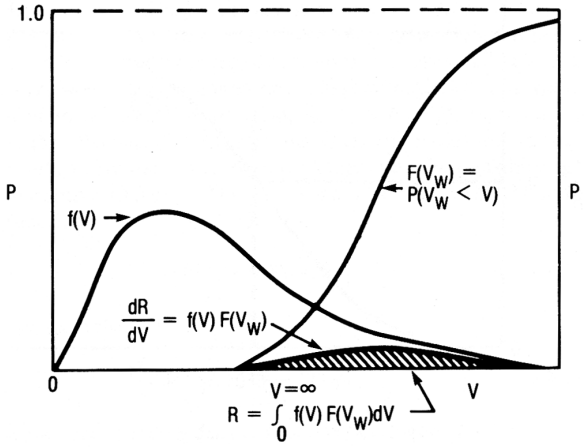


Figure A3.3-8 Statistical method of insulation coordination (EPRI 1982).

$f(V_1)$ x $F(V_1)$. The risk of failure R of the insulation, as shown by the shaded area in Figure A3.3-8, is the sum of all the preceding probabilities for all the possible voltages.

$$R = \int_0^\infty F(V) f(V) dV \qquad \text{A3.3-12}$$

The preceding explanation lays the groundwork for economic considerations, but it is rather elementary, principally because the functions that describe the probability of breakdown and the probability of overvoltage occurrence depend on many factors. There is no assurance that either function can be expressed in any analytical form. Computer techniques are needed to calculate the risk of failure and to optimize the line design.

If the actual distributions of overvoltage and withstand are not known, an approximation of the risk may be obtained by the simplified statistical method. This method is based on the premise that the actual shape of the low-voltage end of the overvoltage distribution is not too important, because those low overvoltages will not cause failure. Likewise, there is little need to keep accurate track of how likely it is that the insulation strength is greater than normal. Accordingly, the actual distributions are replaced by simple distributions, generally Gaussian, that may be characterized by the standard deviation σ and one measured point. The overvoltage distribution is characterized by the term "statistical overvoltage," V_S, this being the overvoltage at the 2% point. The distribution of withstand voltages is described by V_W, the statistical withstand voltage measured at the 90% withstand, or 10% breakdown, point. These points are illustrated in Figure A3.3-9. The ratio of the two values defines the quantity γ, the statistical safety factor, which is analogous to the conventional safety factor:

$$\gamma = \frac{V_W}{V_S} \qquad \text{A3.3-13}$$

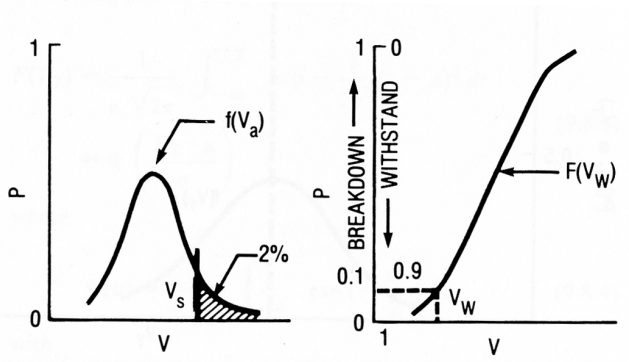


Figure A3.3-9 Reference probabilities: (a) probability of system overvoltage; and (b) probability of withstand voltage (EPRI 1982).

If V_S and V_W are known, and the rest of the distribution is assumed, it is possible to evaluate the risk and to plot a curve relating the statistical safety factor and the risk. The procedure is illustrated in Figure A3.3-10.

The actual numerical value of the risk depends on the shape assumed for the distributions. This shape may be described in terms of the standard deviations of the two curves. Although the standard deviation may not be known from test, it may sometimes be estimated from experience on similar tests. The curve relating statistical safety factor and risk, Figure A3.3-10(c), is valid only for the particular set of standard deviations assumed.

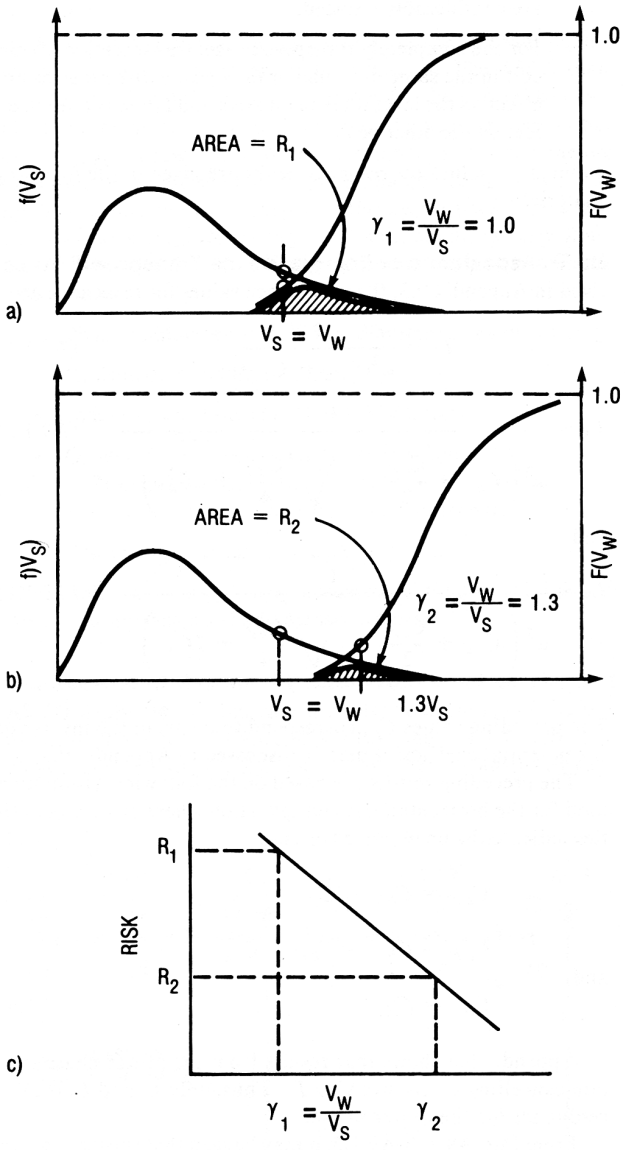


Figure A3.3-10 Simplified statistical method: (a) small statistical safety factor; (b) large statistical safety factor; and (c) risk versus safety factor (EPRI 1982).

Figure A3.3-11 shows one set of relationships between risk and statistical safety factor. The figure, for switching surges, assumes a standard deviation of 6% for the withstand voltage and various standard deviations for the stress. The effect of truncating the distributions of stress is also shown. Figure A3.3-12 shows a similar correlation for lightning surges.

It should be noted that the discussion above gives a general description of the line insulation coordination procedure. Detailed implementation should consider the characteristics of system overvoltages, system components, and environment factors, especially for operating voltages and temporary overvoltages, switching overvoltages, and lightning overvoltages. Comprehensive coverage of this can be found from references (IEC 1996; IEEE 1999a; IEEE 1997a; IEEE 1999a; Hileman 1999).

Summary

As previously described in the main body of this chapter, line insulation coordination includes the selection of phase-to-ground and phase-to-phase clearances, tower strike distances, tower footing resistance, insulator lengths, and the leakage or creepage distance of insulators. Two approaches to insulation coordination for overvoltages are in use today:

1. Deterministic method
2. Probabilistic (or statistical) method

The probabilistic method is applied by modeling and combining the probability distributions of the overvoltages and the insulation strength. The application of probabilistic insulation coordination makes it possible to estimate the failure frequency directly as a function of the selected system design factors.

Today, the universal availability of powerful computers and software (such as the applets in this Reference Book) allows designers to use sophisticated probabilistic techniques as easily as the simpler deterministic methods that were used in the past, providing that appropriate stress and strength data are available. Yet probabilistic techniques are not used across the board above 200 kV, due to the fact that many utilities continue to use old "proven designs," which are based on deterministic approaches because sufficient probability distributions are not known or are of dubious accuracy.

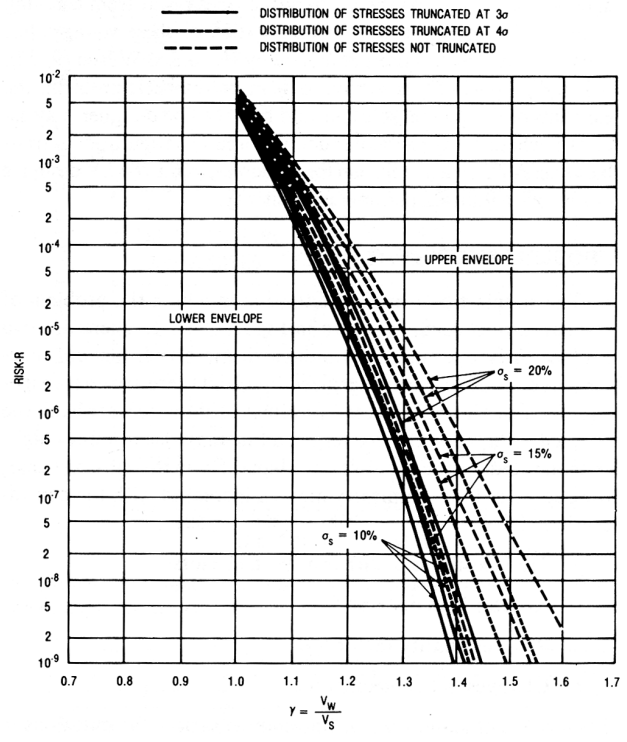


Figure A3.3-11 Correlations between risk of failure *R* and statistical safety factor γ for various switching surge distributions (IEEE 1976).

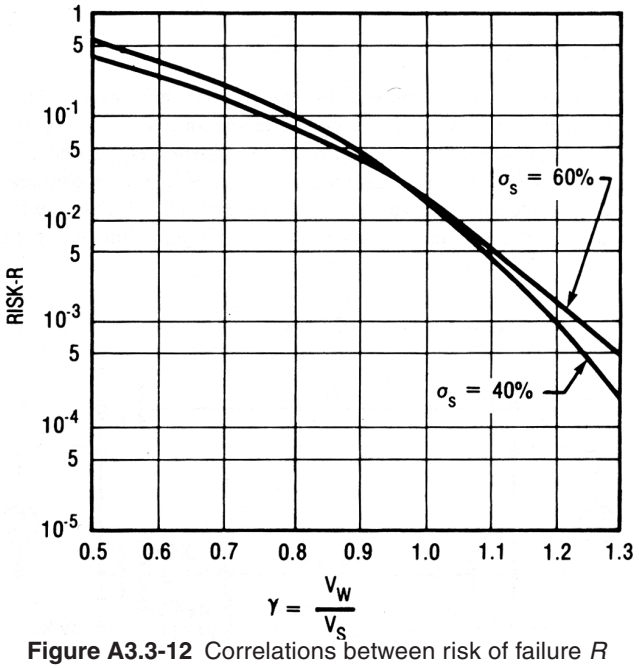


Figure A3.3-12 Correlations between risk of failure *R* and statistical safety factor γ for various lightning surge distributions (IEEE 1976).

APPENDIX 3.4 APPLICATION OF INSULATION COORDINATION ACCORDING TO IEC 71-2 INSULATION COORDINATION APPLICATION GUIDE

Introduction

This section is extracted from IEC 71-2 (Copyright © 1996, Geneva, Switzerland. www.iec.ch.), Insulation Coordination Application Guide, with minimum changes. It is intended to give the reader a roadmap to follow in the line insulation coordination procedures according to the IEC.

According to IEC 71-2, transmission-line insulation coordination follows to a great extent the same procedure used for other equipment, which is described more fully in IEC 71-1 (IEC 1993). Line insulation coordination is a simplified version (it stops at step 3 of 5 steps) of the general procedure (due to the self-restoring characteristics of line insulation). Hence the line insulation coordination follows the following steps.

Table A3.4-1 General Procedure for Insulation Coordination per IEC-71-1

General Procedure per IEC-71-1	Applicable Overhead Transmission Line
Step 1: Determination of the representative overvoltages (Urp)	**Yes**
Step 2: Determination of the coordination withstand voltages (Ucw)	Yes
Step 3: Determination of the required withstand voltages (Urw)	Yes
Step 4: Determination of the standard withstand voltages (Uw)	No
Step 5: Selection of standard insulation levels	No

IEC 71-2 provides the following guidelines for transmission-line insulation coordination:

- The operating voltage and the temporary overvoltages determine the required insulator string length and the shape of the insulator unit for the pollution site severity.
- In directly grounded neutral systems with ground fault factors of 1.3 and below, it is usually sufficient to design the insulators to withstand the highest phase-to-ground system voltage.
- For higher ground-fault factors, and especially in isolated or resonant grounded neutral systems, consideration of the temporary overvoltages may be necessary.
- Where consideration must be given to free-swinging insulators, the clearances should be determined under extreme swing conditions.
- An insulation failure due to ground-fault overvoltages causes a double phase-to-ground fault.
- Ground-fault overvoltages should be taken into account in systems with high ground-fault factors—i.e. for transmission lines in resonant grounded-neutral systems.
- As a guide, acceptable failure rates between 0.1 and 1.0 flashovers/year are typical.
- Special considerations are necessary for lines where energization and re-energization overvoltages are normally controlled to low amplitudes, since in this case the slow-front overvoltage generated by ground faults may be more severe.
- An insulation failure due to re-energization overvoltages causes an unsuccessful reclosure.
- As a guide, suitable acceptable failure rates for energization are on the order of 0.005–0.05 flashovers/year.
- Re-energization overvoltages require attention for transmission lines when fast three-phase reclosing is applied, because of trapped charges. Acceptable failure rates of 0.005–0.05 flashovers/year may be suitable.
- Re-energization overvoltages can be disregarded when single-phase reclosing is used on transmission lines.
- Slow-front overvoltages are among the factors determining the air clearances and, for some types of insulators, the insulator fittings. Usually their importance is restricted to transmission lines in the higher system voltage range of 123 kV and above. Where free-swinging insulators are applied, air clearances for slow-front overvoltages are generally determined assuming moderate (mean) swing conditions.

The IEC procedure is outlined in Figure A3.4-1. This is extracted from Figure 1 of IEC 71-1.

Insulation Coordination for Power-Frequency and Temporary Overvoltages

The coordination withstand voltage for the continuous (power-frequency) voltage is equal to the highest phase-to-phase system voltage, and this voltage divided by the square root of 3 for phase-to-earth insulations.

For coordination using the deterministic method, the short-duration withstand voltage is equal to the representative temporary overvoltage. When a statistical procedure is adopted, and the representative temporary overvoltage is given by an amplitude/duration distribution frequency characteristic, the insulation that meets the performance criterion is determined, and the amplitude of the coordination withstand voltage is equal to that corresponding to the duration of 1 min on the amplitude/duration withstand characteristic of the insulation.

When contamination is present, the response of external insulation to power-frequency voltages becomes important,

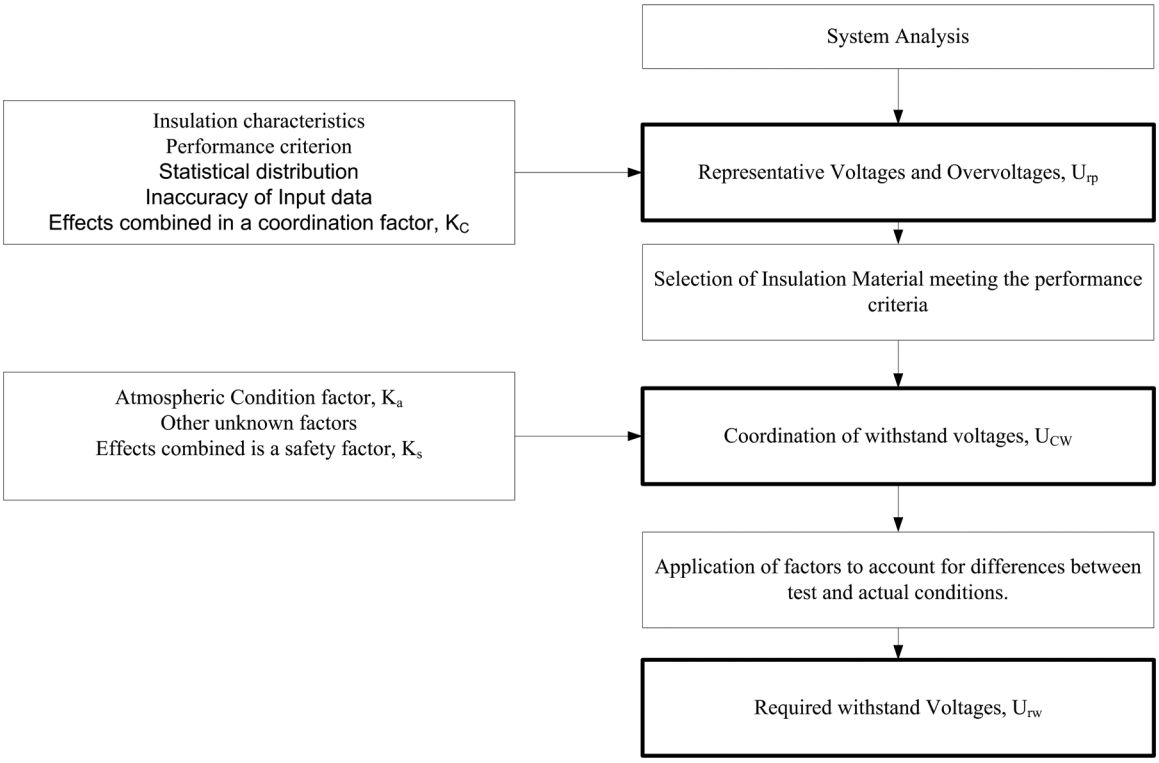


Figure A3.4-1 Insulation coordination procedure according to IEC 71-1. (Copyright © 1993, Geneva, Switzerland. www.iec.ch.)

and may dictate external insulation design. Flashover of insulation generally occurs when the surface is contaminated and becomes wet due to light rain, snow, dew, or fog without a significant washing effect.

Insulation Coordination for Slow-Front Overvoltages

Deterministic Method

The deterministic method involves determining the maximum voltage stressing the equipment and then choosing the minimum dielectric strength of this equipment with a margin that covers the uncertainties inherent in the determination of these values. The coordination withstand voltage is obtained by multiplying the assumed maximum value of the corresponding representative overvoltage by a safety factor called the deterministic coordination factor.

Statistical Method for Slow-Front Overvoltages

The statistical method for slow-front overvoltage is the same as discussed above. Slow-front overvoltages of interest for overhead lines are phase-ground fault overvoltages and energization and re-energization overvoltages.

Insulation Coordination for Fast-Front Overvoltages

Deterministic Method

For fast-front lightning overvoltages, a deterministic safety factor of 1 is applied to the assumed maximum value of the overvoltages. This is because, for lightning, the representative overvoltage includes probability effects. For fast-front switching overvoltages, the same relationships apply as for slow-front overvoltages.

Statistical Method

The statistical method recommended in this guide is based on the probability distribution of the representative lightning overvoltages. For internal insulation, the assumed withstand voltage has a withstand probability of 100%. The withstand probability at higher voltages is assumed to be zero. This means that the coordination withstand voltage is equal to the representative lightning overvoltage amplitude at a return rate equal to the adopted acceptable failure rate.

For external insulation, the conventional deviation of the discharge probability is usually small as compared to the dispersion of overvoltages. As a simplification, it can be neglected, and the same formula as for the internal insulation applied.

Insulation Coordination Example for a System with Nominal Voltage of 735 kV (Phase-Ground Only)

The general procedure is illustrated with an example, also extracted from IEC 71-2, for a system with a nominal voltage of 735 kV. In matching the voltage stresses with the electric strength, it is necessary to take into account the various types of voltage stresses and the corresponding response of the insulation. This involves making a distinc-

tion between self-restoring (external) insulation and non-self-restoring (internal) insulation. For non-self-restoring insulation, the stress-strength coordination is made using deterministic methodology, whereas for self-restoring insulation (e.g., transmission-line insulation), a statistical methodology can be used where this is convenient. For illustration purposes, the following example attempts to present all considerations about external insulation. The reader can refer to IEC 71-2 for details about internal insulation. The insulation performance of overhead lines has a large impact on the insulation performance of substations. The transmission-line outage rate due to lightning primarily determines the frequency of re-energization operations, and the lightning performance rate close to the substation determines the frequency of fast-front overvoltages impinging on the substation.

Furthermore, procedures of surge arrester selection and associated insulation coordination are described to protect the transmission systems. Insulation coordination of the transmission line is also discussed, and results from deterministic and statistic methods are compared.

For the purposes of illustrating the insulation coordination process, an example from the application guide is shown here. Assume the following basic data:

- Highest system voltage is: U_s = 765 kV.
- Pollution level is low to medium.
- Altitude is: H = 1000 m. (for all locations).

The pollution level is assumed sufficiently mild that the standard insulation levels (and clearances) can be determined by the voltage stresses (usually the slow-front overvoltages for systems with nominal voltage of 345 kV and above).

For overhead line insulation coordination, and where the design employs free-swinging insulators, the dielectric strength of air clearances should take into account conductor movement.

Step 1: Determination of the Representative Overvoltages—Values of Urp
The representative temporary and slow-front overvoltages are usually determined from system studies. For this example, results from such studies confirmed the following values:

- Temporary overvoltages: U_{rp} = 660 kV (r.m.s., phase-to-ground);
- Slow-front overvoltages: U_{e2} = 1200 kV (peak, phase-to-ground; phase-peak method).

Power-Frequency and Temporary Overvoltages
The high level of temporary overvoltage (1.5 p.u.) is associated with situations involving long lines radially fed after a major load rejection. For systems with nominal voltage of 345 kV and above, the two standard withstand voltages normally specified are the lightning and the switching impulse levels.

Slow-Front Overvoltages
The slow-front overvoltage is related to line reclosing, and is limited to about 2.0 p.u. by the use of closing resistors on line circuit breakers.

The surge arrester rating is also determined from these same system studies (normally from the temporary overvoltage characteristics: amplitude and duration) and, for the particular case of this example, the following protection levels were determined:

- Switching impulse protective level: U_{ps} = 1300 kV (peak value);
- Lightning impulse protective level: U_{pl} = 1500 kV (peak value).

Fast-Front Overvoltages
The simplified statistical method for fast-front overvoltages will be used, leading directly to the coordination withstand voltage.

In this step and those that follow, only the phase-to-ground insulation is considered. Phase-to-phase insulation coordination will be treated at the end of the example as a separate item.

Step 2: Determination of the Coordination Withstand Voltages–Values of Ucw
The coordination withstand voltage is obtained by applying a coordination factor (K_c) to the representative overvoltages, this factor being either K_{cd} for the deterministic method or K_{cs} for the statistical method.

Determination of the coordination withstand voltage for external insulation is carried out for slow-front overvoltages using the statistical method because of the nature of the insulation. A statistical method could also be applied to fast-front overvoltages, but this is generally not necessary for systems with nominal voltage of 345 kV and above.

Ucw for Temporary Overvoltages
For this class of overvoltages, the coordination withstand voltage is equal to the representative temporary overvoltage—in other words, the coordination factor K_c = 1. Therefore phase-to-ground U_{cw} = 660 kV.

Ucw for Slow-Front Overvoltages
The value of the statistical coordination factor K_{cs} comes from choosing a risk-of-failure of the insulation that has

been proven from experience to be acceptable. For a usually acceptable value of R in the range of 10^{-4}, the value of K_{cs} is 1.15. Hence the coordination withstand voltage is U_{cw} = 1200 kV x 1.15 = 1380 kV:

- Statistical overvoltage: U_{e2} = 1200 kV;
- Statistical coordination factor: K_{cs} = 1.15;
- Coordination withstand voltage: U_{cw} = 1380 kV.

Ucw for Fast-Front Overvoltages

The determination of the coordination withstand voltage for fast-front overvoltage is not necessary since the lightning impulse withstand voltage of the minimum clearances that result from the switching impulse withstand voltage will be far in excess of those that should be determined solely by the lightning impulse withstand voltage required for the non-self-restoring insulation.

Step 3: Determination of the Required Withstand Voltages – Values of Urw

The required withstand voltage is obtained by applying a safety factor K_s to the coordination withstand voltage. The values of K_s are given as:

- For external insulation: K_s = 1.05.

For external insulation, an atmospheric correction factor K_a is also applied.

For power-frequency voltage, determine the atmospheric correction factor assuming a short-duration power-frequency test on polluted insulators, for which m = 0.5 and assuming H = 1000 m, K_a = 1.063.

Hence U_{rw} = 660 x 1.063 x 1.05 = 737 kV:

- U_{cw} for temporary overvoltages: U_{cw} = 660 kV;
- Atmospheric correction factor: K_a = 1.063;
- Safety factor: K_s = 1.05;
- U_{rw} for temporary overvoltage: U_{rw} = 737 kV.

The atmospheric correction factor K_a for slow-front overvoltages is based on the assumed altitude. For H = 1000 m and m = 0.6, then $K_a = e_{0,07}$ = 1.07. Hence U_{rw} = 1380 kV x 1.07 x 1.05 = 1550 kV:

- U_{cw} for slow-front overvoltages: U_{cw} = 1380 kV;
- Atmospheric correction factor: K_a = 1.07;
- Safety factor: K_s = 1.05;
- U_{rw} for slow-front overvoltages: U_{rw} = 1550 kV.

Summary

This section described line insulation coordination procedures according to IEC 71-2, Insulation Coordination Application Guide. Since this section has been extracted from the IEC guidelines, the reader is urged to obtain the full standards from the IEC.

Presentation of the information in this appendix is intended to complement the information presented in the main body of this chapter. It provides some guidelines, as well as typical design figures or targets.

REFERENCES

Abi-Samra, N. C. 2000. "Transmission Line Insulation Coordination." IEEE Tutorial. Orange County, California.

Aleksandrov, G. N., V. Y. Kizvetter, V. M. Rudakova, and A. N. Tushnov. 1962. "The AC Flashover Voltages of Long Air Gaps and Strings of Insulators." *Elektrichestvo.* No. 5. pp. 27-32.

Ametani, A. 1973. "Modified Traveling-Wave—Techniques to Solve Electrical Transients on Lumped and Distributed Constant Circuits." *IEEE Proceedings.* 133. Vol. 120. No. 4. April. Pp. 497–503.

Anderson, R. B. and A. J. Eriksson. 1980. "Lightning Parameters for Engineering Application," *Electra.* 69. March. Pp. 65-102.

Arturi, C. M. 1991. "Transient Simulation and Analysis of a Three-phase Five-limb Step-up Transformer Following an Out-of-phase Synchronization." *IEEE Transactions on Power Delivery.* Vol. 6. No. 1. pp. 196-207. January.

Bewley, L. V. 1951. *Travelling Waves on Transmission Systems.* 2nd Edition. New York: J. Wiley and Sons.

Bickford, J. P. and A.G. Heaton. 1986. "Transient Overvoltages on Power Systems." *IEE Proceedings.* Vol. 133. Part C. pp. 201-225. May.

Boonyubol, C., C. Calabrese, and J. R. Tudor. 1970. "A Mathematical Analysis of Transmission-line Transients Related to Fault Surges." *IEEE Transactions on Power Apparatus and Systems.* Vol. PAS-89. No. 6. pp. 1207-1215. July/August.

Bui-Van, Q. and M. Rousseau. 2001. "Control of Overvoltages on Hydro-Quebec 735 kV Series-Compensated System During a Major Electro-mechanical Transient Disturbance." International Conference on Power Systems Transients (IPST)'01. Rio de Janeiro, Brazil. June.

CEA (Canadian Electricity Association). 1996. "CEA Purchasing Specification Line Post Composite Insulator for Overhead Distribution Lines." LWIWG-02 (96).

CIGRE. 1971. CIGRE Working Group 13-05. "The Calculation of Switching Surges, I: A Comparison of Transient Network Analyzer Results." *Electra.* No. 19. December. Pp.67–78.

CIGRE. 1972. CIGRE Working Group 05 1972. "The Calculation of Switching Surges. Part I." *Electra.* No. 19. pp. 67-78 and CIGRE Working Group 05 1974. "The Calculation of Switching Surges. Part II." *Electra.* No. 32. pp. 17-42.

CIGRE. 1973. CIGRE Working Group 33.03 1973-1. "Switching Impulse Test Procedure for Phase-to-Phase Air Insulation." *Electra.* No 30. pp. 55-69 and CIGRE Working Group 13.02 1973-2. "Switching Overvoltages in EHV and UHV Systems with Special Reference to Closing and Reclosing Transmission Lines." *Electra.* No. 30. pp. 70-122.

CIGRE. 1974. CIGRE Working Group 13-05. "The Calculation of Switching Surges II: Network Representation for Energization and Re-energization Studies on Lines Fed by an Inductive Source." *Electra.* No. 32. January. pp. 17–42.

CIGRE. 1979. CIGRE Working Group 13-05. "The Calculation of Switching Surges III: Transmission Line Representation for Energization and Re-energization Studies with Complex Feeding Networks." *Electra.* No. 62. January. pp. 45–48.

CIGRE. 1979. Study Committee 33. "Phase-to-Phase Insulation Coordination." *Electra.* No. 64. pp. 137-236.

CIGRE. 1990. CIGRE Working Group 02 (SC 33). "Guidelines for Representation of Network Elements when Calculating Transients."

CIGRE. 1991a. CIGRE Working Group 01 (Lightning) of Study Committee 33 (Overvoltages and Insulation Coordination). "Guide to Procedures for Estimating the Lightning Performance of Transmission Lines." Technical Bulletin 63. Paris: CIGRE. October.

CIGRE. 1991b. CIGRE Working Group 22.09 (Overall Design) of Study Committee 22. "Parametric Studies of Overhead Transmission Costs." *Electra.* No. 136. June. pp 31–67.

CIGRE. 1991c. CIGRE WG 22.09 (Overall Design) of Study Committee 22. "International Survey of Component Costs of Overhead Transmission Lines." Appendix to the document published in *Electra.* 136. *Electra.* No. 137. August. Pp. 61–79.

CIGRE. 1996. CIGRE Working Group 22.09 (Overall Design) of Study Committee 22. "Foundation Cost Study." *Electra.* No. 165. April. Pp. 37-51.

Clerici, A. 1972. "Analog and Digital Simulation for Transient Overvoltage Determination." *Electra.* No. 22. pp. 111-138.

Colclaser, Jr., R. G., C. L. Wagner, and D. E. Buettner. 1970. "Transient Overvoltages Caused by the Initiation and Clearance of Faults on a 1100-kV System." *IEEE Transactions on Power Apparatus and Systems.* Vol. PAS-89. No. 8. pp. 1744-1751. November/December.

Cortina, R., M. Sforzini, and A. Taschini. 1976. "Strength Characteristics of Air Gaps Subjected to Interphase Switching Surges." *IEEE Transactions on PA&S Mat.* Pp. 448-452.

Darveniza, M. 1980. *Electrical Properties of Wood and Line Design.* St. Lucia, Queensland, Australia. University of Queensland Press.

Diesendorf, W. 1974. *Insulation Coordination in High-Voltage Electric Power Systems.* London: Butterworth & Co.

Dommel, H. W. 1969. "Digital Computer Solution of Electromagnetic Transients in Single and Multiphase Networks." *IEEE Transactions on Power Apparatus and Systems.* Vol. PAS- 88. pp. 388–399. April.

Durie, R. C. and C. Pottle. 1993. "An Extensible Real-time Digital Transient Network Analyzer." *IEEE Transactions on Power Delivery.* Vol. 8. No.1. pp. 84–89. February.

EPRI. 1978. *Transmission Line Reference Book: 115-138 kV Compact Line Design.* Electric Power Research Institute, Palo Alto, California.

EPRI. 1982. *Transmission Line Reference Book, 345 kV and Above.* 2nd Edition.

EPRI. 1986. TLWorkstation™ Code: Version 1.0. Volume 6: TLOP Manual, EL 4540CCM, Research Project 2151-1. Palo Alto, CA: EPRI. July.

Gallet, L. R. et al. 1975. "General Expression for Positive Switching Impulse Strength Valid up to Extra Long Air Gaps." *IEEE Transactions on PA&S.* pp 1989-1993. November/December.

Grant, I. S. and A. R. Paulson. 1980. *Phase to Phase Switching Surge Design.* EPRI EL 1550. September.

Greenwood, A. 1991. *Electrical Transients in Power Systems.* 2nd Edition. New York: John Wiley & Sons, Inc.

Hileman, A. R. 1979. "Transmission Line Insulation Coordination." Twenty-eighth Bernard Price Memorial Lecture. South African IEEE. September. Pp. 3-15.

Hileman, A. R. 1980. "Transmission Line Insulation Coordination." Transaction of the SA Institute of Electrical Engineers. Vol. 71. Part 6. June.

Hileman, A. R. 1999. *Insulation Coordination for Power Systems.* New York: Marcel Dekker, Inc.

IEC. 1986. "Guide for the Selection of Insulators in Respect of Polluted Conditions." 60815.

IEC. 1989. "High Voltage Testing Techniques." Publication 60-1.

IEC. 1993. IEC Standard 71-1. Insulation Coordination, Part 1: Definitions, Principles, and Rules.

IEC. 1996. IEC Standard 71-2. Insulation Coordination, Part 2: Application Guide.

IEEE. 1970. IEEE Committee Report. "Switching Surges, Part III: Field and Analyzer Results for Transmission Lines. Past, Present, and Future Trends." *IEEE Transactions on Power Apparatus and Systems.* Vol. PAS-89. pp. 173–189. February.

IEEE. 1976. *Insulation Coordination, Part 2, Application Guide.* Genève, Switzerland: Bureau Central de la Commission Electrotechnique Internationale. IEEE Publication 71-2. 2nd Edition.

IEEE. 1985. Working Group on Lightning Performance of Transmission Lines. "A Simplified Method for Estimating the Lightning Performance of Transmission Lines." *IEEE Transactions on PA&S.* April. Pp. 919-932.

IEEE. 1993. IEEE Standard C37.015-1993. *IEEE Application Guide for Shunt Reactor Switching.*

IEEE. 1994. IEEE Standard C37.011-1994: IEEE Application Guide for Transient Recovery Voltage for AC High-Voltage Circuit Breakers Rated on a Symmetrical Current Basis.

IEEE. 1995. IEEE Standard 957-1995. *IEEE Guide for Cleaning Insulators.* (ISBN 1-55937-519-1).

IEEE. 1997a. IEEE Standard C62.22-1997. *IEEE Guide for the Application of Metal-Oxide Surge Arresters for Alternating-Current Systems*. New York.

IEEE. 1997b. IEEE Standard 1243-1997. *IEEE Guide for Improving the Lightning Performance of Transmission Lines.*

IEEE. 1999a. IEEE Standard 1313-2-1999. *IEEE Guide for the Application of Insulation Coordination.*

IEEE. 1999b. IEEE Standard C62.11-1999. *Standard for Metal-Oxide Surge Arresters for AC Power Circuits (> 1 kV).* March.

IEEE. 2001. Task Force. Chowdhuri, P. (ed.). "Bibliography of Research on Parameters of Lightning Strokes." Web page at www.ieee.org/pes-lightning.

Kawamura, T., M. Nagano, M. Ichihara, K. Ishikawa, S. Mizoguchi, T. Imakoma, and T. Shimomura. 1994. "Development of Metal-Oxide Transmission Line Surge Arrester and Its Effectiveness." CIGRE 1994 Session.

Kim, J-B., E-B. Shim, and J-W. Shim. 2000. "Switching Overvoltage Analysis and Air Clearance Design on the KEPCO 765 kV Double Circuit Transmission System." *IEEE Transactions on Power Delivery.* Vol.15. No.1. pp. 381–386. January.

Kimbark, E. W. and A. C. Legate. 1968. "Fault Surge Versus Switching Surge: A Study of Transient Overvoltages Caused by Line-to-Ground Faults." *IEEE Transactions on Power Apparatus and Systems.* Vol. PAS-87. No. 9. pp. 1762-1769. September.

Kishizima I., K. Matsumoto, and Y. Watanabe. 1984. "New Facilities for Phase-to-Phase Switching Impulse Tests and Some Test Results." *IEEE PAS-103.* pp. 1211-1216. June.

Lambert, S. R. 1988. "Effectiveness of Zinc Oxide Surge Arresters on Substation Equipment Probabilities of Flashover. *IEEE Transactions on Power Delivery.* Vol. 3. No. 4. October. Pp. 1928–1934.

Martinez, J. A., R. Natarajan, and E. Camm. 2000. "Comparison of Statistical Switching Results Using Gaussian, Uniform and Systematic Switching Approaches." IEEE Power Engineering Society Summer Meeting. Vol. 2. Pp. 884 –889.

Martinez-Velasco, J. A. 1998. "ATP Modelling of Power Transformers." European EMTP-ATP Users Group. *EEUG News.* Pp. 63–76. August-November.

Mathur, R. M. and X. Wang. 1989. "Real-time Digital Simulation of the Electromagnetic Transients of Power Transmission Lines." *IEEE Transactions on Power Delivery.* Vol. 4. No.2. pp. 1275–1280. April.

McElroy, A. J. and J. H. Charkow. 1967. "Probabilistic Aspects of Transmission System Switching Surge Reliability." *IEEE PAS-86.* pp. 1012-1024. August.

McLaren, P. G., R. Kuffel, R. Wierckx, J. Giesbrecht, and L. Arendt. 1991. "A Digital TNA for Testing Relays." *Proceedings of the 1991 IEEE PES Transmission and Distribution Conference.* Pp. 370–375. September.

Mork, B. A. 1998. "Five-legged Wound-core Transformer Model: Derivation, Parameters, Implementation, and Evaluation." Paper PE-414-PWRD-0-12-1997. Presented at the 1998 IEEE PES Winter Meeting. February 1-5. Tampa.

Naidu, M. S. and V. Kamaraju. 1995. *High Voltage Engineering.* McGraw-Hill. (Reproduced with permission of The McGraw-Hill Companies.)

NESC. 2002a. National Electrical Safety Code, IEEE/ANSI. 2002 Edition. Document C2-2002.

NESC. 2002b. National Electric Safety Code. References.

Petcharaks, N., C. Yu, and C. Panprommin. 1999. "A Study of Ferranti and Energization Overvoltages Case of 500 kV Line in Thailand." Eleventh International Symposium on High Voltage Engineering. Vol. 1. pp. 291-294.

Peyrot, A. H., E. M. Peyrot, and T. Carton. 1992. "Interaction and Interaction in Power Line Design." *IEEE Computer Applications in Power.* Vol. 5. No. 4. October. pp.19-23.

Pratico, E. R. and M. A. Eitzmann. 1994. "A Microcomputer-based Data Acquisition System for Transient Network Analyzer Operation." *IEEE Transactions on Power Systems.* Vol. 9. No. 2. Pp. 812–817. May.

Prikler, L. 1998. "Lightning Performance and Switching Overvoltage Studies of an Uprated Transmission Line." European EMTP-ATP Users Group. *EEUG News.* Pp. 109–117. August-November.

Ringler, K. G., P. Kirkby, C. C. Erven, M. V. Lat, T. A. Malkiewicz. 1997. "The Energy Absorption Capability and Time-to-Failure of Varistors Used in Station-Class Metal-Oxide Surge Arresters. *IEEE Transactions on Power Delivery.* Vol. 12. No. 1. January. Pp. 203–212.

Rizk, F. 1989. “A Model for Switching Impulse Leader Inception and Breakdown of Long Air Gaps.” *IEEE PWRD-4.* pp. 596-606. January.

Shih, C. H., R. M. Hayes, D. K. Nichols, R. E. Koch, J. A. Timoshenko, and J. G. Anderson. 1985. “Application of Special Arresters on 138-kV Lines of Appalachian Power Company.” *IEEE Transactions on Power Apparatus and Systems.* Vol. 104. No. 10. October. Pp. 2857-2863.

Stemler, G. E. 1976. “BPA's Field Test Evaluation of 500 kV PCBs Rated to Limit Switching Overvoltages to 1.5 per Unit.” *IEEE Transactions on PA&S.* Pp. 352–361.

Stenström, L. and M. Mobedjina. 1998. “Limitation of Switching Overvoltages by the Use of Transmission Line Arresters.” Paper presented at CIGRE SC-33 International Conference. Croatia.

Stuehm, D. L. 1993. “Final Report. Three Phase Transformer Core Modeling.” Bonneville Power Administration Award No. DE-BI79-92BP26700. February.

Tarasiewicz, E. J., F. Rimmer, and A. S. Morched. 2000. Transmission Line Arrester Energy, Cost, and Risk of Failure Analysis for Partially Shielded Transmission Lines. *IEEE Transactions on Power Delivery.* Vol. 15. No. 3. July. Pp. 919–924.

Thanassoulis, P., N. De Franco, A. Clerici, and M. Cazzani. 1975. “Overvoltages on a Series-compensated 750-kV System for the 10000 MW Itaipu Project.” *IEEE Transactions on Power Apparatus and Systems.* Vol. PAS-94. No. 2. pp. 622-631. March/April.

Thoren, H. B. and K. L. Carlsson. 1979. “A Digital Computer Program for the Calculation of Switching and Lightning Surges on Power Systems.” *IEEE Transactions on Power Apparatus and Systems.* Vol. PAS-89. January. pp. 212–218.

Truax, C. J., J. D. Brown, and W. Neugebauer. 1978. “TNA Study of Reclosing Transients on a 765-kV Shunt Compensated Transmission Line.” *IEEE Transactions on Power Apparatus and Systems.* Vol. PAS-97. Pp. 1447–1457. July/August.

Wagner, C. F. and A. R. Hileman. 1963. “The Effect of Predischarge Currents on Line Performance.” *IEEE Transactions on PA&S.* Vol. 82. pp. 117-131.

Yasuda, E. J. and F. B. Dewey. 1980. “BPA's New Generation of 500-kV Lines.” *IEEE Transactions on PA&S.* Pp. 616–624.

Zaffanella, L. E., G. Balderston, J. M. Schamberger, and G. W. Juette. 1972. “UHV AC Transmission Line Design Based on Project UHV Test Results.” CIGRE 1972. Report 31-12.

Zanetta, L. C., Jr. 2002. “Evaluation of Line Surge Arrester Failure Rate Using Multipulse Lightning Stresses.” IEEE Power Engineering Society Summer Meeting. Vol. 1. Pp. 21-25. July.

The authors thank the International Electrotechnical Commission (IEC) for permission to reproduce information from its International Standards IEC 60071-1 and IEC 60071-2. All such extracts are copyright of IEC, Geneva, Switzerland. All rights reserved. Further information on the IEC is available from www.iec.ch. IEC has no responsibility for the placement and context in which the extracts and contents are reproduced by EPRI, nor is IEC in any way responsible for the other content or accuracy therein.

BIBLIOGRAPHY

Bhargava, B., A. Khan, A. Imece, and J. DiPietro. 1992. "Effectiveness of Pre-Insertion Inductors for Mitigating Remote Overvoltages Due to Shunt Capacitor Energization." Paper 92 SM 495-2. Presented at IEEE PES Summer Meeting. July.

Colclaser, R. G., C. L. Wagner, and E. P. Donohue. 1969."Multistep Resistor Control of Switching Surges." *IEEE Transactions on Power Apparatus and Systems*. Vol. PAS-88. No. 7. July. pp. 1022–1028.

Holm, A., R. Alvinsson, U. Akesson, and O. Karlen. 1990. "Development of Controlled Switching of Reactors, Capacitors, Transformers, and Lines." CIGRE Paper No. 13-201.

Khodabakchian, B. et al. 1992. "TRV and the Non-zero Crossing Phenomena in Hydro-Québec's Projected 735 kV Series Compensated System." Proceedings from CIGRE. Paris.

Legate, A. C., J. H. Brunke, J. J. Ray, and E. J. Yasuda. 1988. "Elimination of Closing Resistors of EHV Circuit Breakers." *IEEE Transactions on Power Delivery.* Vol. 3. No. 1. pp. 223-231. January 1988.

Puente, H. R., M. L. Burgess, E. V. Larsen, and H. Elahi. 1989. "Energization of Large Shunt Reactors Near Static VAR Compensators and HVDC Converters." 88WM 092-9 T-PWRD. January. pp. 629-636.

Ribeiro, J. R. and M. E. McCallum. 1989. "An Application of Metal Oxide Surge Arresters in the Elimination of Need for Closing Resistors in EHV Breakers." *IEEE Transactions on Power Delivery.* Vol. 4. No. 1. pp. 282-291. January 1989.

CHAPTER 4

Insulation for Power Frequency Voltage

Andrew Phillips
Christiaan S. Engelbrecht

This chapter provides an overview of insulator technology and its relationship with the ac performance of the line. It includes information on insulator types and components, the contamination flashover mechanism, the long-term performance of insulators, laboratory test methods, the electrical performance of insulators and air gaps under power frequency voltage, performance in freezing conditions, insulation design, and the distribution of the electric field along insulators.



Dr. Andrew Phillips is a project manager, Transmission and Substations, Power Delivery and Markets Group at the Electric Power Research Institute (EPRI) in Charlotte, North Carolina. His responsibilities are mainly with the Overhead Transmission Program, with special areas of interest in polymer insulators, lightning and grounding, inspection and assessment of components, sensor developments, and daytime corona inspection. Dr. Phillips joined EPRI in January 1998.

Before joining the Institute, Dr. Phillips worked with J. A. Jones Power Delivery, where he was a project manager and lead researcher in the fields of insulation, aging, and lightning. Prior to that, Dr. Phillips worked at the University of the Witwatersrand, performing research for the South African electric power industry.

Dr. Phillips received his BSc, MSc, and PhD degrees in Electrical Engineering from the University of the Witwatersrand in Johannesburg, South Africa. Dr. Phillips holds one U.S. patent and is the author of over 60 journal and conference publications. He is a member of the IEEE, SAIEE, and CIGRE, and is a registered professional engineer.



Christiaan S. Engelbrecht is a Senior Consultant with KEMA based in Arnhem, The Netherlands. He has more than 15 years experience in the contamination design of insulators and insulation co-ordination studies, having also worked with ESKOM in South Africa and STRI in Sweden. He is convener of the newly formed CIGRE Working Group C4AG03-03, "Pollution and Environmental Influence on the Electrical Performance of Power Systems," and a member of IEC TC36 WG 11, which deals with the revision of IEC 60815, "Selection and Dimensioning of High-Voltage Insulators for Polluted Conditions." He has also been involved in insulation coordination audits of transmission and distribution systems and the study of corona losses due to hoarfrost.

4.1 INTRODUCTION

Traditionally the external insulation design of high-voltage transmission lines in the EHV and UHV range has been dominated by the requirements to withstand switching or lightning overvoltages. It was assumed that the insulation designs based on these requirements were also sufficient for power-frequency voltage because of the high relative strength of the air under ac even during rain. However, it has become apparent that the line performance might be severely affected if the insulation was not adequately dimensioned to withstand the effects of insulator contamination. This phenomenon has been studied extensively over the years and has resulted in a number of important review documents (Looms 1988; CIGRE 2000; IEEE Working Group on Insulator Contamination 1979; Lambeth 1971). Furthermore, standardized laboratory test methods for evaluating the contamination performance of ceramic and glass insulators have been developed (IEC 1991; IEEE 1978); guidelines for the selection of insulators with respect to contamination conditions have also been developed (IEC 1986).

Insulator technology has also seen many developments to improve its electrical and mechanical characteristics. Notable in this respect is the development of polymer insulators and the use of hydrophobic properties of insulating materials to improve the flashover performance of insulators under contamination conditions (Houlgate and Swift 1989). The introduction of this new technology has not been without problems, as the polymeric insulating materials are more sensitive to the effects of aging than the traditionally used ceramic and glass materials (CIGRE 1986; CIGRE 1990). Furthermore, it was also found that the guidelines and test methods developed for ceramic and glass insulators are not directly applicable to polymer insulators. Although much progress has been made in addressing these issues (Gorur et al. 1999), more work is needed to obtain general agreement on test procedures and rules for dimensioning.

This chapter provides an overview of the present understanding of the ac performance of transmission lines. This overview also covers insulator technology because of the intimate relationship between the selected insulator and the ac performance of the line.

Background information on insulator technology, typical applications, and important concepts are discussed in Section 4.2. This section starts with a concise description of the history of insulator development, highlighting important milestones. Insulator types and important terms, such as the “unified specific creepage distance” and “hydrophobicity” are defined and explained. The section closes with a description of typical insulator components and the materials and concepts used in manufacturing of insulators. The focus in this section is more on polymeric than glass and porcelain insulators.

Section 4.3 describes the contamination flashover mechanism for both hydrophilic and hydrophobic insulator types. It covers the buildup of contaminants on the insulators, as well as wetting processes and the development of discharges into flashover under critical levels of contamination. The effect of insulator profile and the material characteristics on the flashover process is highlighted.

The long-term performance, or aging characteristics, of various insulator technologies are discussed in Section 4.4, with many photographs illustrating examples from service and laboratory testing experience. The section closes with a summary of failure rates and dominant failure types as experienced by the users of polymer insulators.

Laboratory test methods for insulators are described in Section 4.5. The section starts with a description of the general requirements for laboratory testing, which is followed by summary descriptions of common methods used to verify the long-term performance of polymer insulators. This is followed by a discussion of presently used contamination flashover test methods and developments to establish a representative test method for polymer insulators.

In Section 4.6, a summary is presented of the electrical performance of air gaps and insulators under power frequency voltage. Information is presented on the effect of rain on clean hydrophilic and hydrophobic insulators, as well as the effect of rainfall rate and resistivity on the flashover strength. The latter part of the section concentrates on the contamination flashover strength of both hydrophilic and hydrophobic insulator types. Important influencing factors such as the contamination severity level, type of contamination, amount of nonsoluble components, and the linearity of flashover results are presented. Some information is also provided on the flashover performance of polymer insulators and the effect of hydrophobicity on the flashover voltage. The section closes with a short discussion of the contamination performance of resistive glaze insulators.

A summary of important aspects regarding the performance of insulators in freezing conditions can be found in Section 4.7. This section highlights the importance of considering the performance under ice conditions when dimensioning insulators. Test results from different laboratories are presented.

Insulation design and the factors that influence it are discussed in Section 4.8. The section starts with a broad discussion of insulation dimensioning concepts and how they are applied to problem of insulator contamination. Information

is provided on different methods for site severity estimation and developments in the IEC to standardize these. The choice of insulator technology is discussed in some detail, as well as important aspects that should be taken into account when utilizing polymer insulators. This section closes with detailed descriptions of both the deterministic and statistical methods for selecting the insulator dimensions to obtain a good contamination flashover performance.

The final section of this chapter, Section 4.9, is devoted to the distribution of the electric field along insulators and the design of grading rings. Polymer insulators, in particular, may suffer premature aging if the E-field grading is not considered carefully. This section highlights effects that an overly high E-field gradient may have on insulators, methods to control the gradient, and calculation methods. Some guidelines are provided on the selection of grading rings for insulators.

Three applets are associated with this chapter:

- Applet I-1: "Insulator Equivalent Salt Deposit Density (ESDD) and Parameter Evaluation." This applet calculates the leakage length, surface area, and form factor of an insulator, given its profile. Top and bottom surface parameters can be evaluated separately. The applet also guides the user to the measurements of ESDD and NSDD (Non-Soluble Deposit Density) and their calculation. The recommendations for measurements and calculations are made according to international practice using the methods described in this chapter.
- Applet I-2: "Electric Field Distribution for Polymer Insulators: Effect of Dimensions and Location of Corona Ring." This applet calculates the electric field in the space near the end fittings of a polymer insulator. This parameter is important when applying polymer insulators, as highlighted in Section 4.9. In fact, the electric field needs to be kept below certain limits in order to eliminate corona under dry conditions, reduce corona and arcing under wetting conditions (as these aging mechanisms reduce life expectancy), and prevent internal discharges due to defects or voids that may initiate a failure. The factor that dominates the application and design of corona rings is the electric field magnitude on the surface of the sheath close to the energized end region. If the electric field in this region exceeds a critical value, excessive corona activity can occur under wetting conditions, resulting in premature degradation of the rubber and reduction in life expectancy. The applet solves the field problem in 3-D. It accounts for a single conductor, which must be sufficiently long so that the end effects do not affect the region near the insulator. Both energized and grounded end fittings can be simulated, as well as the tower truss from which the insulator may be suspended. The corona ring is simulated by a toroid. This applet does not account for the dielectric properties of the rubber or rod, and is intended only as an educational tool for the user. The user may change the position and dimensions of a corona ring, and observe how the electric field distribution surrounding the polymer insulator end fitting is affected.
- Applet I-3: "Statistical Method for Dimensioning Insulators to Meet Contamination Flashover Requirements." This applet applies a statistical method to evaluate the risk of flashover of a specific insulator design at a site with a given contamination severity. As input data, the applet requires the statistical parameters that characterize the contamination severity of the site, the statistical and mathematical parameters that characterize the flashover performance of the insulator selected for the site, and the number of insulators. Based on the risk of flashover, calculated by the applet, the insulator creepage distance can be adjusted until the desired performance is achieved. The algorithms used by the applet are an implementation of statistical method discussed in Section 4.8.5. The input data used in the demonstration example of the applet is the same as was used to derive Figures 4.8-20, 4.8-21, 4.8-22, and 4.8-23.

4.2 INSULATOR TECHNOLOGY

4.2.1 Historical Perspective

The manufacture, design, and application of electrical insulators have posed a challenge to electrical engineers since the beginnings of power transmission. The first insulators were developed for telegraph lines, which were introduced around 1835 (Looms 1988). These were made mostly of annealed glass, or "dry-pressed" porcelain (Berry 1995). With the advent of power transmission in 1882, the telegraph insulators were initially scaled-up for use at higher voltages and mechanical loadings (see Figure 4.2-1). The higher demands associated with power transmission soon revealed serious shortcomings in both the materials and designs available at the time. For example, dry-press porcelain insulators suffered from punctures due



Figure 4.2-1 Examples of porcelain telegraph insulators.

to the porosity of the material. This gave impetus to the development of wet-process porcelain (1896), and soon thereafter the use of a vacuum extrusion process to eliminate air from the porcelain insulating body, thereby obtaining a vitreous porcelain that is essentially the same as used in modern applications (Berry 1995). Also glass has undergone considerable developments in the choice of ground materials and the introduction of toughening in the 1930s (Looms 1988; Pyrex 1933).

The first polymer insulator designs were developed during the 1960s, with the first test installations during the 1970s (Hall 1992). The advantages of polymer insulators included their light weight, resistance to vandalism, small profile, and in some cases improved contamination performance (Burnham and Waidelich 1997; CIGRE 1986, 1990; EPRI 2003b). As with ceramic and glass insulators, the initial designs were plagued by problems and suffered especially from material-aging effects. Through a continuous evolution of designs, polymer insulators have developed into a mature product that has since the 1980s become generally accepted and used in large numbers on transmission lines (EPRI 2003b).

Another challenge to be overcome in development of insulators has concerned the mechanical demands that insulators on transmission lines must withstand. Traditional insulating materials (i.e., porcelain and glass) are much stronger under compression than tension loads, whereas the insulators are generally placed under tension on transmission lines (Looms 1988). Designs, such as the disc (or cap and pin) type, had to be developed that place the dielectric under compression, although the insulator as a whole is under a tension load.

Pin insulators, which are direct descendants of the telegraph insulator, are still being produced today, but their use is limited to distribution lines. The first successful disc insulators were introduced in 1909 (porcelain) and 1930 (glass) (Looms 1988; Pyrex 1933). Pedestal post insulators, used mostly in substations, were introduced around 1910, and longrod insulators appeared in the 1920s (Looms 1988). Porcelain post insulators were only introduced in 1940 (Looms 1988). The first polymer insulators were of the longrod type, but since the early 1980s, they have also become available as post insulators.

Nearly all designs have certain vulnerabilities. The development of insulator designs and manufacturing technology has been a process of trial and error rather than an orderly progression. The designs and manufacturing methods used for porcelain and glass insulators stabilized in the 1950s and 1960s. Insulators from reputable manufacturers are widely used since they are reliable and offer a long service life.

Development of polymeric insulators has been ongoing—with big advances, in terms of their reliability, being made during the 1980s and 1990s. Presently most manufacturers have stable designs, which is underlined by the increasing use of polymer insulators worldwide. In 2002, a polling of 70 American utilities showed that 65 utilized polymer insulators, while figures obtained from four of the major manufacturers indicated that more than 4 million polymer transmission-class insulator units had been sold in the U.S. alone (EPRI 2003b).

This survey further indicated that the percentage of utilities applying polymer insulators reduces with increasing system voltage, as shown in Figure 4.2-2. The largest percentage of the polled utilities apply polymer insulators at the 115–138 kV level, and the second largest percentage at the 220-230 kV level (EPRI 2003b).

Based on data captured from five of the major polymer insulator manufacturers, the 2002 survey indicated that the total number of suspension and post units, including and above 69 kV, sold to the North American market was 3,938,000. The total number of service years indicated was 25,163,000 (the service years indicated is based on the date of sale, not the date of installation). The average age of the polymer insulators sold was 6.4 years. For individual manufacturers, the average values varied between 2.8 and 8.7 years. It should be noted that these are average values. Although all of the major manufacturers servicing the market in 2002 were represented, one design still installed in great quantities was excluded since it was no longer marketed at the time.

National (ANSI) and International (IEC) standards have followed the developments and usage trends of the different insulator technologies (ANSI 1996, 2002b, 2002c; IEC

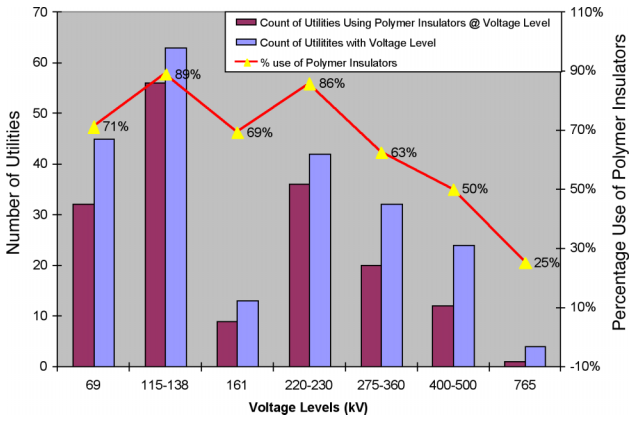


Figure 4.2-2 Number of utilities that apply polymer insulators at each voltage level, as well as the number of utilities that have transmission lines at each voltage level. The line indicates the results as a percentage.

1992, 2002a, 2002b, 2003). For glass and ceramic insulators, the standards have been available for many years, while the standards applicable to polymer insulators are still relatively new, or in many cases, are still under development.

4.2.2 General Insulator Terms and Classification

Insulators consist normally of an insulating body with one or more fixing devices. The insulating bodies have traditionally been made of porcelain or toughened glass, but with the development of polymer insulators, the insulating body may also comprise a fiber-reinforced plastic (FRP) rod that is covered by a rubber housing to provide the necessary leakage distance and to protect the rod from the environment.

The IEC names insulators according to the material from which the insulating body is manufactured. Specifications are produced for either glass and ceramic, or polymer insulators. Polymer insulators can again be subdivided into resin and composite insulator types. All transmission-line polymer insulators may be classified as composite by the IEC definition; however, a number of terms are used interchangeably in the industry when describing such insulators: composite, polymer, nonceramic insulators, or NCI. For the purposes of this Reference Book, the term "polymer insulator" will be used.

Resin insulators are not used at transmission voltage levels and are, hence, not further discussed in this chapter. For each of these general types of insulator, various designs exist, as illustrated in Figure 4.2-3.

It should be noted, however, that ANSI/IEEE standards use a slightly different naming convention. For example, what the IEC calls a "cap and pin" insulator is named "suspension disc" by ANSI. Figure 4.2-3, therefore, lists both IEC and ANSI terms, with the IEC term first. In this chapter, the naming convention of ANSI will be used.

General Classification

The standards recognize two classes of insulators according to the possibility of internal puncture (see Figure 4.2-4) (IEC 1993). For Class "A" insulators, the length of the shortest possible puncture is at least equal to half the external arcing distance. These insulators are regarded as puncture proof. Class "B" insulators, on the other hand, have a

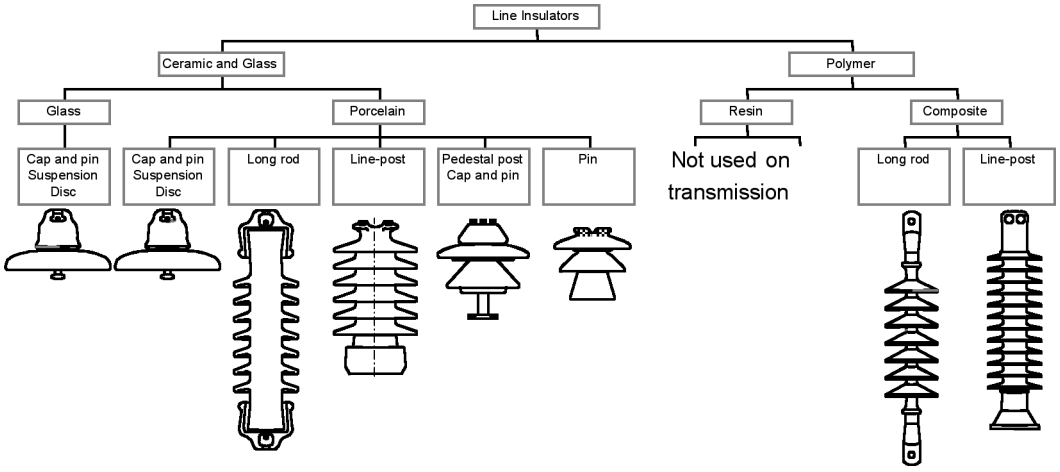


Figure 4.2-3 A general overview of insulator types used on transmission overhead lines.

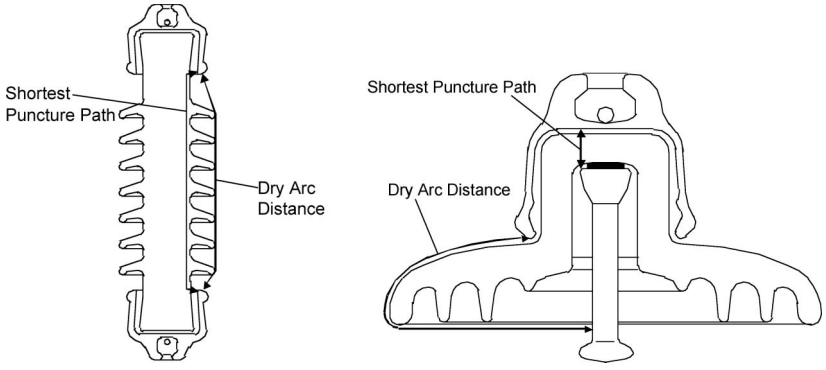


Figure 4.2-4 The general classification of insulators as Class A (*left*) or B (*right*).

shortest puncture path that is less than half the external arcing distance. These insulators are regarded as "puncturable."

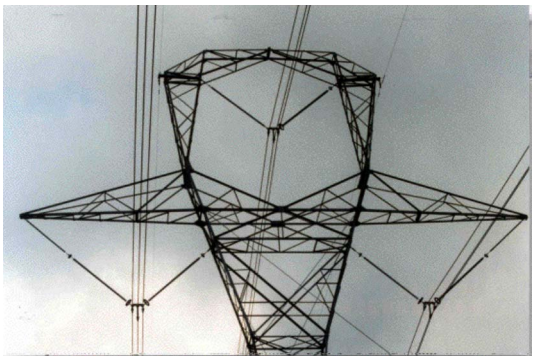
Typical Applications

Typical applications of transmission-line insulators are shown in Figure 4.2-5. Disc, longrod, and polymer longrod insulators are utilized in dead-end, I-string, and V-string assemblies. In these assemblies, the insulators are placed under tension loads to attach the conductor to the transmission-line structure. Longrod and disc insulators are generally not designed to withstand cantilever or compression loads.

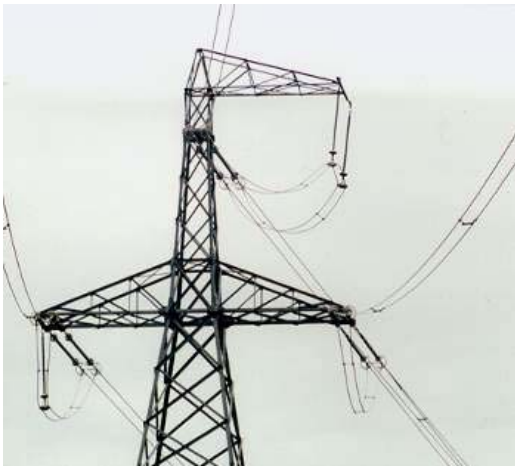
Post insulators, both polymer and porcelain, are attractive because they can be used in single-pole structures, reducing the structure footprint and in some cases, the required right-of-way. These units have to withstand cantilever, compression loads, and to a limited extent, even tension loads. The rod sizes are, therefore, larger than those of longrod insulators used at the same voltage level.



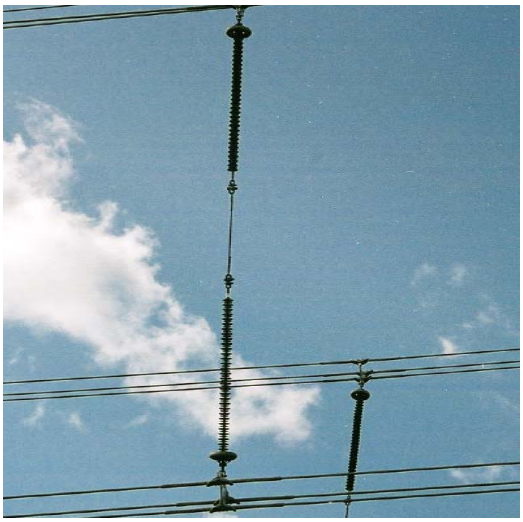
I-suspension



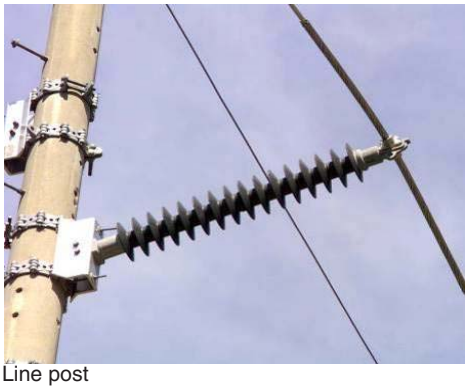
V-suspension



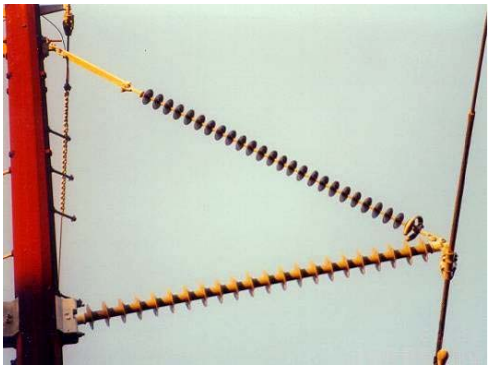
Strain or dead end



Phase spacer



Line post



Brace post or horizontal V

Figure 4.2-5 Examples of different insulator string configurations.

Post insulators can also be used in combination with longrod insulators to form a Horizontal V or braced post, as shown in Figure 4.2-5. This arrangement is used to obtain a more rigid mechanical structure to support the conductors.

Polymer or porcelain longrod insulators are also used in phase spacer applications. These applications need special consideration, since the insulators may by subject to compressive forces due to the conductor movement (Imakoma et al. 1994; Kito et al. 1975).

Parameters that Characterize Insulators

Various parameters have been defined that can be used to characterize insulator shape and dimensions. The most often used parameters are defined in this section.

- **Section length.** The section length (also known as connecting length) refers to the shortest distance between fixing points of the live and grounded (earthed) hardware, ignoring the presence of any stress control rings, but including intermediate metal parts along the length of the insulator (see Figure 4.2-6).
- **Dry arc distance.** The shortest distance in the air external to the *insulator* between those parts that normally have the operating voltage between them. The dry arc distance of various types of insulator configurations are illustrated in Figure 4.2-7.
- **Strike distance.** The strike distance is the shortest distance from the energized hardware to the grounded hardware or structure (see Figure 4.2-8). The strike distance may correspond to the dry arc distance.
- **Leakage (or creepage) distance.** The shortest distance over the insulator surface between the end fittings is the leakage or creepage distance. Since there is a linear relationship between the contamination flashover strength

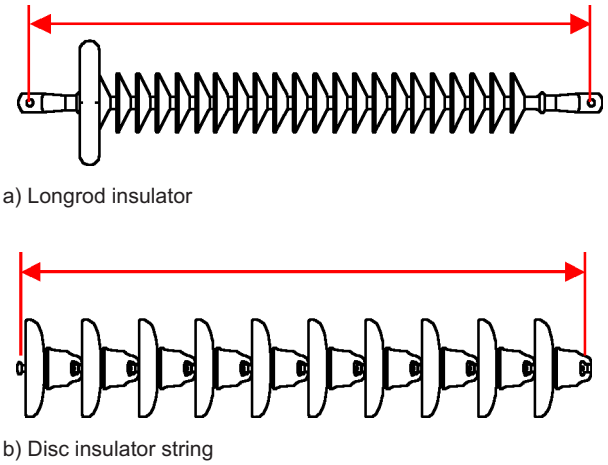


Figure 4.2-6 Definition of section length.

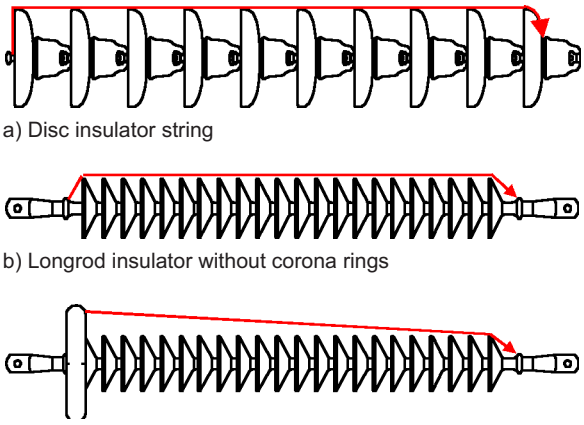


Figure 4.2-7 Definition of dry arc distance.

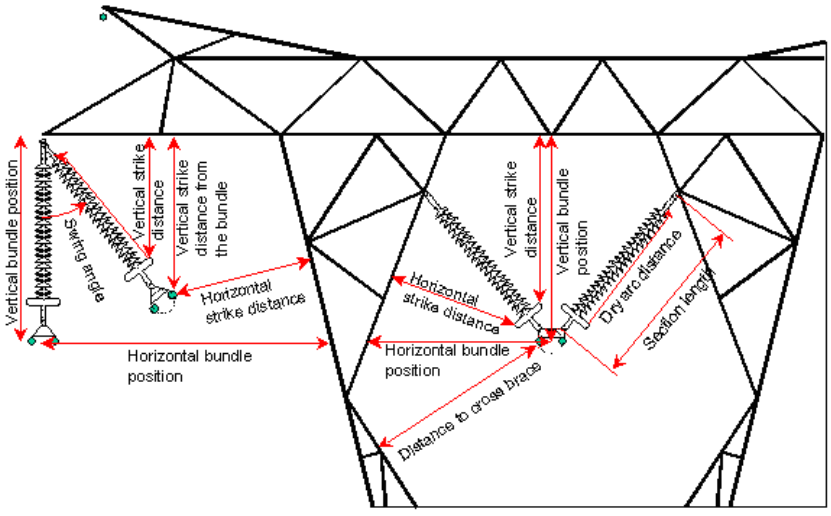


Figure 4.2-8 Definition of strike distance in comparison to dry arc distance and section length. I-string on the left and V-string on the right.

and leakage distance, the concept of specific leakage distance is commonly used. In the first edition of IEC publication 60815 (IEC 1986), the specific creepage distance was defined as the leakage distance divided by the phase-to-phase value of the maximum voltage for the equipment. This definition was based on the assumption that the insulation was installed between phase and ground, which is not always the case. To overcome this deficiency, IEC introduced the "*unified specific creepage distance*" concept, which is the leakage distance divided by the maximum operating voltage across the insulator. For the same pollution class, the *unified specific creepage distance* is √3 times the *specific creepage distance*. Both are usually expressed in mm/kV.

- **Protected leakage (or creepage) distance.** This parameter is the part of the leakage distance that is not easily accessible to natural cleaning. It is defined as the part of the creepage distance on the illuminated side of the insulator that would lie in shadow if light were projected on to the insulator at 90˚ (or 45˚ in special cases) to the longitudinal axis of the insulator (see Figure 4.2-9).
- **Form factor.** The form factor gives the relationship between the resistivity of a surface layer and the overall resistance of that same surface. This dimensionless ratio is calculated by the integral of the reciprocal value of the insulator circumference along the length of the leakage path (L) (see Figure 4.2-10).
- **Surface area.** When Equivalent Salt Deposit Density measurements are being performed, it is necessary to know the surface area of the insulator over which the measurement is performed. Evaluating the integral of the insulator circumference along the length of the leakage path (L) gives the surface area, as shown in Equation 4.2-1.

$$Area = \int_0^L 2\pi \cdot r(l) \cdot dl \qquad 4.2\text{-}1$$

Example: The insulator parameters can be obtained from the manufacturer or by using a scan of the insulator profile and a numerical evaluation of the surface integrals. Figure 4.2-11 and Table 4.2-1 show an example for a typical disc insulator used in multiple disc strings on many transmission lines. Applet I-1 provides a software implementation of the calculation of these insulator parameters based on coordinates that describe the insulating surface profile.

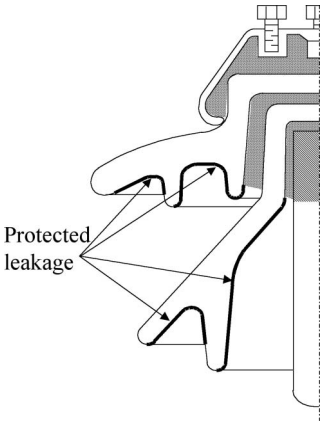
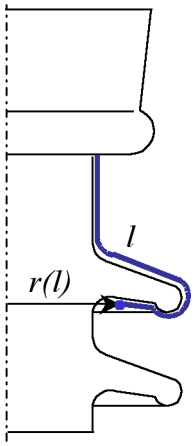
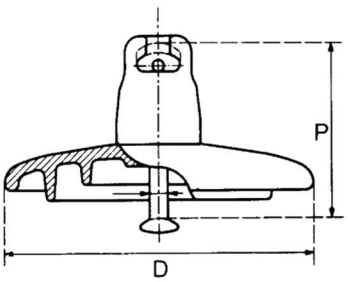


Figure 4.2-9 Protected leakage, or creepage, distance.



$$FF = \int_0^L \frac{dl}{2\pi \cdot r(l)}$$

Figure 4.2-10 Definition of form factor.



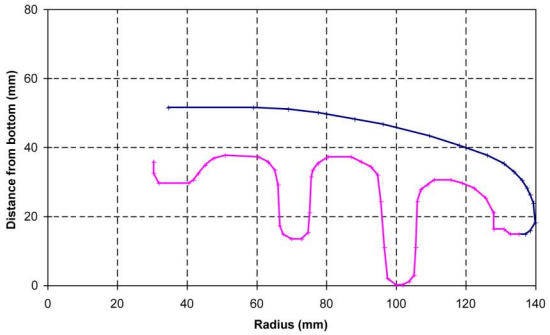


Figure 4.2-11 Insulator meaurements.

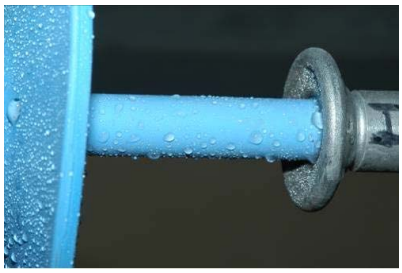
Table 4.2-1 Calculated Parameters for the Insulator Shown in Figure 4.2-11.

	Top	Bottom	Total
Section Length (mm)			146
Leakage distance (mm)	125.18	214.46	339.64
Surface area (cm^2)	746.95	1151.44	1898.39
Form Factor	0.24	0.46	0.70

For the example above, the 146-mm ($5^3/_4$ in.) spacing from cap to pin of the insulator, multiplied by the number of insulators in the string, gives a close estimate of the dry arc distance of the insulator. The sum of the top-surface and bottom-surface leakage distances (340 mm, [13.4 in.]), multiplied by the number of insulators, gives the overall leakage distance. If 25 of the insulators shown in Figure 4.2-11 are used, the dry arc distance will be about 3.65 m (143.75 in.), and the leakage distance will be 8.5 m (335 in.).

4.2.3 Hydrophobicity

One of the most important surface characteristics of an insulator is how it interacts with water on its surface. This is normally described in terms of its hydrophobicity. As illustrated in Figure 4.2-12, the surface condition may be anything between water-repellent (called *hydrophobic*) to easily wettable (called *hydrophilic*). This section provides a concise description of this phenomenon and some of the methods available to assess this characteristic on insulators. In 2003, the IEC published a guide that describes three methods for determining the wettability of insulators (IEC 2003).



a) A hydrophobic surface (i.e., high hydrophobicity).



b) A hydrophilic surface (i.e., low hydrophobicity)

Figure 4.2-12 Examples of a hydrophobic and a hydrophilic polymer surface.

Hydrophobic Surfaces

Hydrophobic surfaces have a low surface tension, which causes water to bead when coming into contact with it. In contamination conditions this provides an advantage because it inhibits the formation of a continuous water layer on such a surface. This reduces leakage currents and the likelihood for flashover.

Hydrophobic surfaces are normally associated with polymer insulators and more specifically with silicone rubber (SIR) insulators. Certain formulations containing low-molecular-weight silicone (LMWS) chains have the added advantage that through the migration of LMWS hydrophobicity may be transferred to the pollution layer, making it hydrophobic as well (Kindersberger and Kuhl 1989).

It should, however, be noted that there are conditions when these materials might temporarily or permanently lose their hydrophobicity. This occurs normally during either prolonged wetting events or under long-term discharge activity.

Hydrophilic Surfaces

A hydrophilic surface is characterized by a high surface tension that causes water to form a thin film on the surface. In polluted conditions the surface conductance of the insulator increases during wetting conditions, allowing increased leakage currents across the surface of the insulator. Under critical contamination and wetting conditions, the conductivity may become high enough to result in flashover (CIGRE 1979b).

Glass and porcelain insulators are the best examples of insulators that have a hydrophilic surface. Polymer insulators that are typically classified as hydrophilic are those with a housing of ethylene propylene rubbers (EPR). In some cases, however, silicone additives have been added to EPR material to give it hydrophobic properties for better performance in contaminated environments.

Categorization of Hydrophobicity

Because hydrophobic insulators may lose their hydrophobicity, it may be necessary to evaluate the condition of an insulator by categorizing its level of hydrophobicity. This may be done using a number of methods:

- Measuring the contact angle between the surface of the insulator and a water drop.
- Measuring the surface tension of the insulator housing.
- Comparing a section of wetted surface material against images of standard wetted surfaces.

Measurement of the Contact Angle

An indication of the surface wetting properties of a given material may be obtained by placing a water drop on a flat section of the material and measuring the static contact

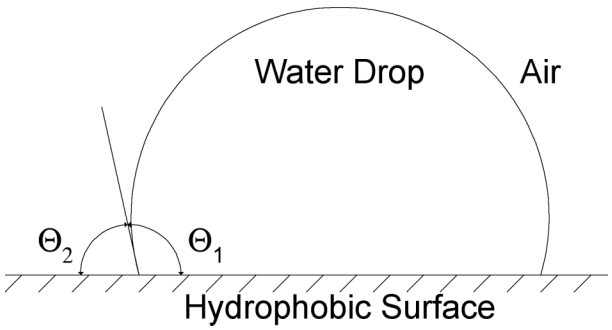


Figure 4.2-13 Definition of the static contact angle.

angle, Θ_1, as defined in Figure 4.2-13. (Although Θ_1 is usually defined as the contact angle, some publications refer to Θ_2 as the contact angle.).

The static contact angle is related to the surface tension—and therefore the degree of hydrophobicity—if the solid material is perfectly smooth and homogeneous. This relationship is given by the so-called Young's equation (Pigini and Tomba 1993). Larger angles (i.e., values of Θ_1) indicate a higher level of surface hydrophobicity, and vice versa.

Since the surfaces of polymer insulators are generally not homogeneous or smooth, the static contact angles do not conform scientifically with Young's equation, which limits the accuracy by which this method can be used to determine the wettability of the insulator surface (Pigini and Tomba 1993). However, this method is still considered as a practical alternative in determining the ability of the polymer to repel water.

Several permutations of the contact angle method have been devised to improve its accuracy and practical applicability. This was done, for example, by taking account of the effect of temperature and gravity. Some of the most commonly used alternatives are:

1. A small water drop on the material surface is viewed through a stereoscopic microscope. If the water drop is small (≈ 0.001 ml), the effect of gravitational forces can be neglected. By measuring the height of the drop and the radius at the base of the drop, as seen in Figure 4.2-14, the contact angle Θ_1 can be calculated by the formula shown in Equation 4.2-2 (Souheng 1982).

   $$\tan(\Theta_1/2) = h/r \qquad 4.2\text{-}2$$

   Where:
   Θ_1 = the contact angle.
   h = the drop height.
   r = the radius at the base of the drop.

   These measurements are usually performed at specific temperatures after the drop has been allowed to settle for a predetermined length of time.
2. Once again, a small water drop on the material surface is viewed through a stereoscopic microscope or a high-powered lens. An image is captured using either analog or digital methods (i.e., photograph or video digitizer). A line tangent to the water drop surface is projected, and the contact angle is measured as shown in Figure 4.2-14. If the image is digitized, automated software measurements are available to make this measurement (University of Oslo 1998).
3. A small water drop is placed on an inclined section of material, and the receding Θ_r and advancing Θ_a contact angles are measured as shown in Figure 4.2-15. The mean surface tension may then be calculated by subtracting Θ_r from Θ_a (Pigini and Tomba 1993).

Other methods not considered here include the use of a goniometer and extrapolation from digitized images to measure the contact angle.

Measurement of the Surface Tension

The IEC (IEC 2003) describes a method whereby the surface tension of an insulator is measured by spraying the surface with a range of organic liquid mixtures with predefined surface tension. An indication of the surface tension is obtained by measuring the time the sprayed-on liquid takes to break into distinct droplets. The surface tension of the insulator surface is lower than that of the liquid if the time to break up is less than 2 s. Different liquid mixtures are sprayed on until one is found with a breakup time that is closest to 2 s. The surface tension of this liquid can be considered to be indicative of that of the insulator.

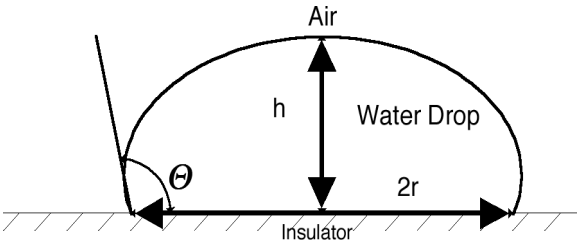


Figure 4.2-14 Measuring height and radius of a drop.

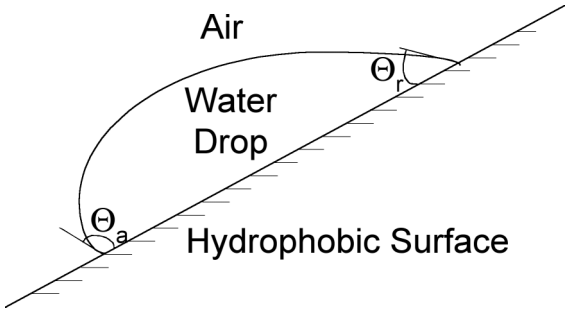


Figure 4.2-15 Contact angle on an inclined surface.

Classification Against Standard Samples

A simple and practical approach to classify the hydrophobicity of insulators has been developed (STRI 1992). This method is used extensively in the industry and has been adopted by the IEC (IEC 2003). With this method, a common spray bottle is used to spray the area of interest with a fine mist of uncontaminated water from a distance of between 10 and 25 cm for a duration of 20-30 s. Within 10 s after the completion of the spraying, the wetted surface is inspected and categorized according to standardized photographs and descriptions.

While the results are somewhat subjective, they are considered adequate in most situations. Seven hydrophobicity classes (HC) are defined, ranging from 1, which is completely hydrophobic, to 7, which is completely hydrophilic. These classes are described in Table 4.2-2, and the corresponding photos are presented in Figure 4.2-16 (STRI 1992).

4.2.4 Components of Ceramic and Glass Insulators

Suspension Disc

Glass and porcelain disc type insulators consist of a dielectric shell cemented between a cap and pin metal end fitting. The end fittings are normally a malleable or ductile cast iron cap and a forged steel pin, both hot dip galvanized. The shape of the cap-and-pin is designed so that the dielectric material is placed under compression under the normal loading condition. The dielectric material of modern insulators is either made of electrical porcelain or toughened glass. Porcelain shells have a glazed surface that provides a smooth surface and places the porcelain under compression to further enhance the mechanical strength of the porcelain. Glass shells are toughened by heating, followed by rapid cooling of the glass surface. This process produces a stress pattern that places the internal part of the shell under compression, thereby obtaining a dielectric element with a high mechanical strength. Both the porcelain and glass offer very high dielectric and mechanical strengths. Cement is used to fix the metal end fittings to the dielectric shell. Figure 4.2-17 shows the components of a disc insulator type (Gorur et al. 1999; Looms 1988).

Table 4.2-2 Relationship between the Hydrophobicity Class (HC) and Contact Angle (STRI 1992)

HC	Description
1	Only discrete droplets are formed. $\Theta_r > 80$ degrees for the majority of the droplets
2	Only discrete droplets are formed. $50 < \Theta_r < 80$ degrees for the majority of the droplets
3	Only discrete droplets are formed. $20 < \Theta_r < 50$ degrees for the majority of the droplets. Usually they are no longer circular.
4	Both discrete droplets and wetted traces form the water runnels are observed (i.e., $\Theta_r = 0$). Completely wetted areas < 2 cm^2, together they cover < 90% of the tested area.
5	Some completely wetted areas > 2 cm^2, which cover <90% of the tested area.
6	Wetted areas cover >90%, i.e., small unwetted areas (spots / traces) are still observed
7	Continuous water film over the whole tested area.

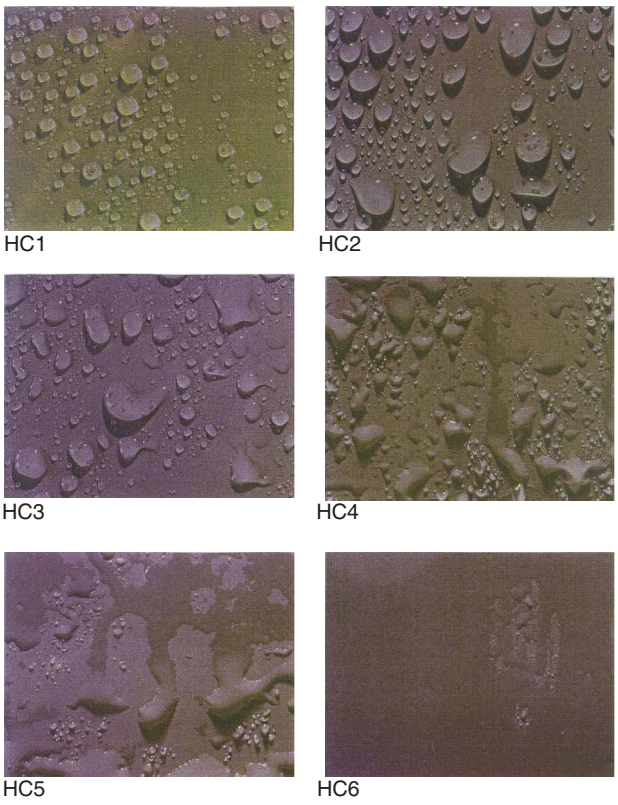


Figure 4.2-16 Standard pictures of the different STRI hydrophobicity classifications (STRI 1992). HC7, a completely wetted surface, is not shown.

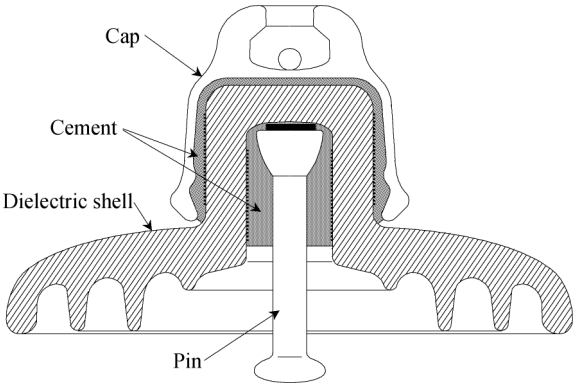


Figure 4.2-17 Components of a ceramic or glass disc insulator.

Longrod

Porcelain longrod insulators comprise a high-strength porcelain body, with metal end caps cemented to each end, as illustrated in Figure 4.2-18. As with disc insulators, the dielectric body of the longrod insulator is manufactured of glazed electrical porcelain. The end caps are fixed to the porcelain body with cement or with a lead-antimony alloy.

4.2.5 Components of Polymer Insulators

In its simplest form, a polymer insulator consists of a load-bearing core covered by a polymeric housing with sheds. Metal end fittings are provided at both ends of the core for connecting the insulator to the supporting tower, conductor, or other pieces of equipment. The main components of a polymer insulator are illustrated in Figure 4.2-19.

Core Rod

The internal insulating part of a polymer insulator is a fiberglass reinforced plastic (FRP) rod, which is designed to carry the mechanical loading of the insulator. It consists of axially aligned glass-fibers that are imbedded by a pultrusion process into a resin matrix to achieve maximum mechanical strength. The fibers are typically 5 to 25 μm in diameter and make up 75 – 80% of the total weight of the rod (EPRI 1998). E-Type glass fibers are often used, but corrosion-resistant fibers are also finding increasing use. "Corrosion resistant" refers to the ability of the glass fibers to resist stress corrosion cracking (brittle fracture), which is discussed later (Armentrout et al. 2003). This resistance is obtained by reducing the level of boron in the fibers. It should be noted that, although boron-free rods do reduce the possibility of failure by brittle fracture, they are still susceptible to the other failure modes, such as flashunder (see Section 4.4.3) and destruction of rod by discharge activity, discussed later in this chapter. A hydrolysis-resistant resin—epoxy, vinyl-ester, or polyester based—is used as the resin matrix. Figure 4.2-20 is a scanning electron microscope (SEM) image taken of a rod cross section, and shows the fibers and resin.

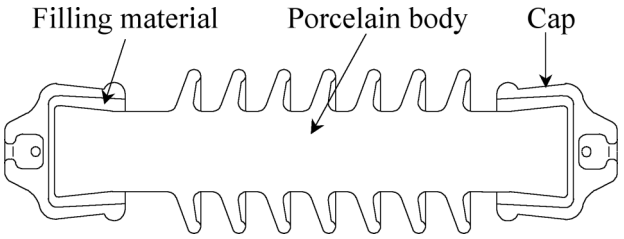


Figure 4.2-18 Components of a porcelain longrod insulator.

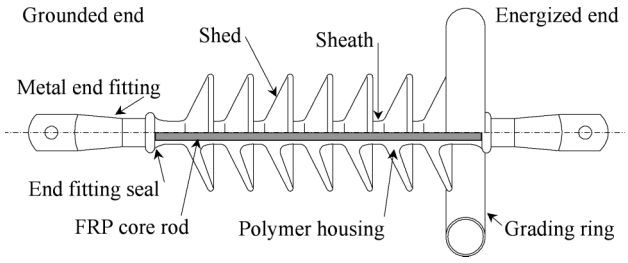


Figure 4.2-19 Basic components of a polymer insulator (note: U.S. naming convention).

The mechanical strength of a FRP rod is much higher under a tension load than it is under compression, torsion, or bending (cantilever) loads. This is evident in the much thicker rods that are required for polymer post insulators, which have to withstand compression and cantilever loads, compared with longrod units that are purely subjected to tension loads. Electrically, the rod is a good insulator as long as it is dry and uncontaminated.

Polymer Insulator Housing Material

The function of the polymer housing is to hermetically seal the rod from the environment, and to provide sufficient leakage distance to withstand both environmental and electrical stresses to which the insulator may be subjected. The housing typically comprises sheds and sheath (shank) sections. For transmission-line polymer insulators, the housing may be based on either an ethylene propylene rubber (EPR) or a silicone rubber (SIR). Distribution insulators may also utilize other materials such as cycloaliphatic epoxy or ethylene vinyl acetate.

Although housing materials are generally classified as EPR or SIR, the composition of these materials may vary considerably from one manufacturer to another. Some manufacturers even provide combinations of both. Furthermore, even the manufacturing process utilized affects the long-term performance of the rubber material. Therefore one has to be careful in making assumptions about the performance of a particular type of housing material based solely on the family of rubbers from which it comes.

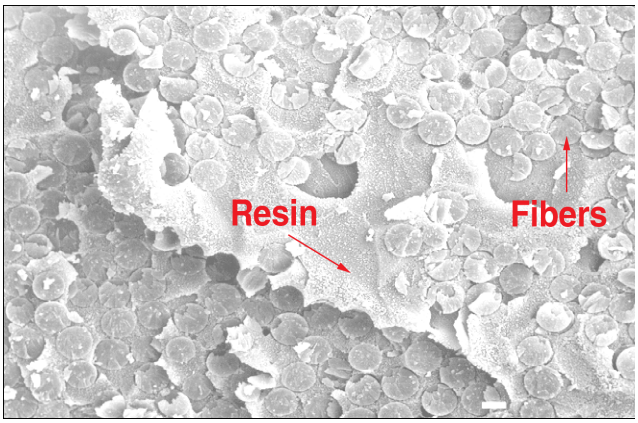


Figure 4.2-20 SEM image showing the resin fiber matrix.

In general, SIR-based materials provide a hydrophobic weathershed surface, and EPR-based materials provide a hydrophilic surface. (A more complete definition of hydrophobicity and its measurement is given in Section 4.2.3.) The implication of hydrophobic properties is discussed in more detail in the section below on silicone rubber.

It can be seen from the discussion that the choice of materials, especially for contaminated conditions, is not simple and may involve a certain degree of compromise. It is recommended, therefore, that data on previous experience with specific formulations in similar environments be obtained where possible (i.e., relevant service or outdoor test site experience).

Ethylene Propylene Rubber

There are several types of EP rubbers. The first generation of polymer insulator rubbers utilized ethylene and propylene monomers (EPM). Today most EP rubber insulators are made from three monomers: ethylene, propylene, and diene (EPDM). Some manufacturers also add small amounts of silicone polymer and indicate this by naming the material an "alloy" (Gorur et al. 1999).

Various additives are added to the polymer compositions to improve performance and satisfy manufacturing processes. For example:

- Inorganic powders such as Aluminumtrihydrate (ATH) are added to improve resistance to discharges, arcing, and tracking.
- UV stabilizing agents such as zinc oxide or titanium oxide are used.
- Cross-linking agents, such as dicumyl peroxide, may be used for vulcanizing.
- Chemicals are also added to obtain the required color.

The chemical structure of EP rubbers consists of a backbone of organic carbon molecules, and the side chain consists of hydrocarbon elements, as shown in Figure 4.2-21. The carbon content in EPDM is considerably higher than in silicone-based rubbers, and therefore, it is critical that it is prevented from degrading as the by-products are more likely to be carbon. Carbon can form a conductive path or track. To increase the tracking resistance, EPDM rubbers have large quantities of inorganic fillers—e.g., ATH (Gorur et al. 1999). One of the methods by which ATH increases tracking resistance is by forming moisture, which, in turn, cools the discharge activity (Meyer et al. 2004).

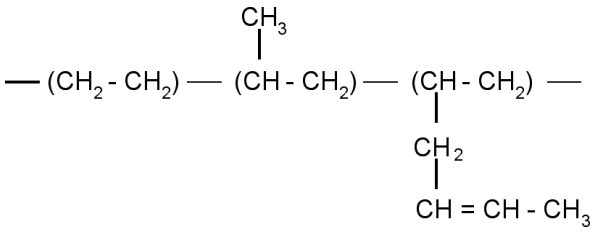


Figure 4.2-21 Chemical building block of an EPDM rubber.

EP-based rubbers have been shown to have good resistance to degradation due to surface discharges, and have performed well in many applications. Furthermore, EPDM usually have a higher tear resistance than silicone rubbers (Gorur et al. 1999). On the other hand, EPR surfaces wet out more easily, which permits a greater level of leakage current activity and a reduced flashover performance under contaminated conditions. Even so, leakage current and the associated discharge activity do not degrade EPR materials as significantly as silicone-based units. This is only a consideration when units are installed in environments where contamination is a concern. It should further be mentioned that EPR-based materials often show hydrophobic properties initially, but this may deteriorate significantly with exposure to the environment.

Silicone Rubber (SIR)

Three broad categories of silicone rubber used for insulation are:

- High Temperature Vulcanizing (HTV), also known as High Temperature Cured Rubber (HCR)
- Room Temperature Cured Vulcanizing (RTV)
- Liquid Silicone Rubber (LSR), also referred to as Liquid Injection Molding (LIM)

Most transmission-line applications today utilize HTV or LSR rubbers.

The chemical building block for silicone rubber is shown in Figure 4.2-22. It consists of an inorganic silicon-oxygen (Si-O) backbone and two organic side chains attached to the silicon atom. A methyl group (CH_3) is most often utilized for high-voltage applications, but other organic groups, such as phenyl or vinyl, may also be used.

Aluminumtrihydrate (ATH) or silica is added to improve resistance to discharges, arcing, and tracking. The proportion of filler compounds to silicone rubber and the form in

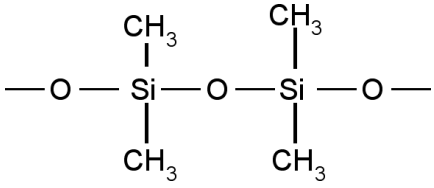


Figure 4.2-22 Chemical building block of silicone rubber (Gorur et al. 1999)

which they are added is an ongoing area of research (Meyer et al. 2004).

Silicone rubbers are characterized by having a low surface energy that results in highly hydrophobic surfaces. This property is considered important because it prevents the insulator surface from becoming completely wet, thereby suppressing leakage currents under contaminated conditions. Consequently, silicone rubber insulators generally offer a high contamination withstand and good aging properties, as long as they retain their hydrophobicity. Additionally, silicone rubbers have a unique property whereby lightweight silicone molecules continuously migrate to the rubber surface and can encapsulate contamination, resulting in a transfer of hydrophobicity. There are, however, conditions during which the silicone rubber may temporarily lose its hydrophobic properties. If the insulator is subjected to significant levels of discharge activity for long periods of time, the result may be a significant degradation of the rubber material and in extreme cases the exposure of the core rod (Phillips et al. 1999a, 1999b).

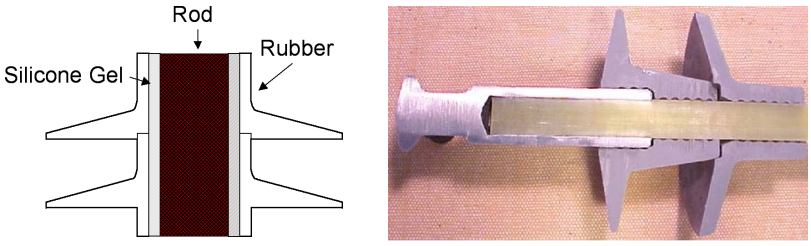
A unique feature of silicon rubber insulators is their ability to regenerate surface hydrophobicity once it has been lost. It is generally believed that after hydrophobicity is lost, if the factors causing this loss are removed, then the insulator will regain its surface hydrophobicity within 24 to 48 hours.

Housing Core Interface

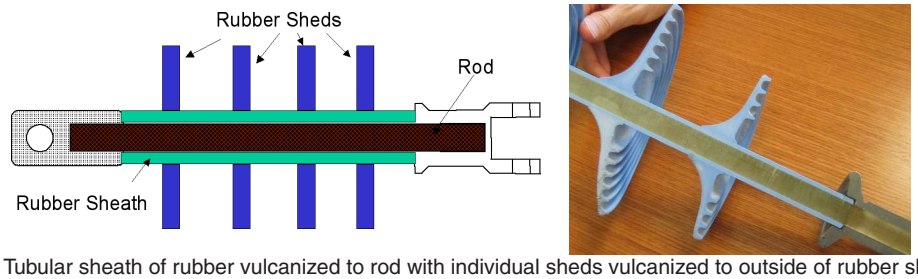
Some common methods for attaching the housing to the core rod are (EPRI 2002b):

- One-shot compression molding the rubber weathershed system onto the rod.
- High-temperature vulcanizing a tubular sheath of rubber to the rod to form the sheath. Individual sheds are then vulcanized to the outside of the sheath.
- One–shot, high–temperature, and pressure molding of the rubber weathershed system onto the rod.
- Sliding individual or multiple shed/sheath units over the rod with an active silicone gel interface between the rod and rubber.

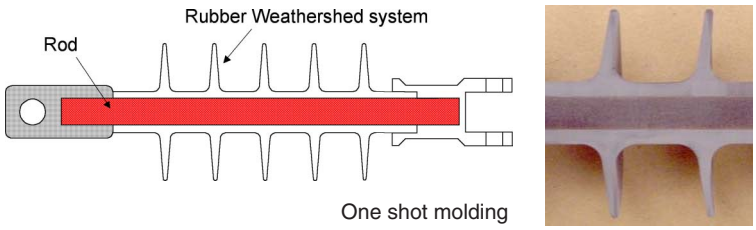
These methods are illustrated graphically and with photos in Figure 4.2-23.



Single or multiple shed units slipped over rod with a silicone gel interface



Tubular sheath of rubber vulcanized to rod with individual sheds vulcanized to outside of rubber sheath.



One shot molding

Figure 4.2-23 Different methods of constructing polymer insulators (note photographs of dissections of actual insulators) (EPRI 2002b).

Metal End Fittings

The metal end fittings serve two functions. The first function is that they provide the mechanism by which the fiberglass rod is attached to the structure and conductor hardware. The second function is to act as part of the ceiling system designed to prevent moisture ingress into the insulators' rod and rod-rubber interface. These components are made of hot-dipped, galvanized, forged steel or ductile iron. Transmission polymer insulator end fittings are not manufactured from aluminum since the melting point of aluminum is lower than the arc root temperature of a power arc (EPRI 1998).

A range of connection methods are available that can be fitted to longrod insulators. Some of the most often used include socket, ball, oval eye, and Y clevis. For post-type units, both rigid and bendable bases are used at the grounded end and are manufactured from ductile iron, rolled steel, or aluminum. The conductor is attached to the energized end of the post insulator, utilizing either a horizontal clamp top, as shown in Figure 4.2-24, or a drop tongue.

Today, metal end fittings are generally swaged or crimped onto the rod by a compression process, but in the past, other fixing methods, such as epoxy cones or metal wedge designs, have also been used. The crimped end fitting design is preferred because the stress concentrations inherent in the other designs can be avoided by grading the compressive forces during fitting attachment. Figure 4.2-25 shows typical cross-sections of swaged, epoxy, and cone end fittings (EPRI 2002b). Care needs to be taken to avoid over-compressing during manufacture, resulting in stress concentrations and possibly rod fracture. Care also needs to be taken to avoid under-compression, resulting in a mechanically weak insulator that may fail due to pull-out (Mobasher 2003).

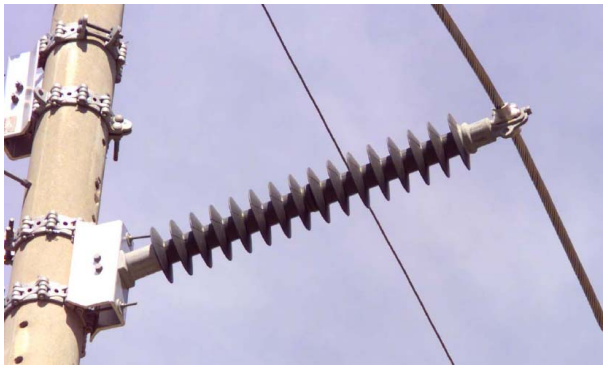
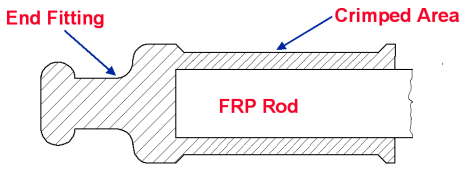
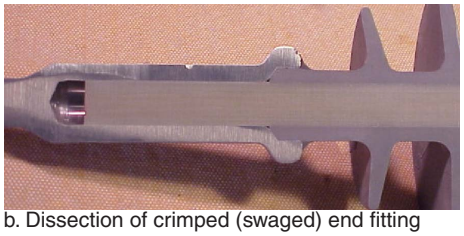


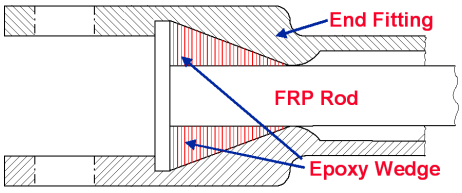
Figure 4.2-24 An example of a polymer post insulator with a horizontal clamp top and bendable base.



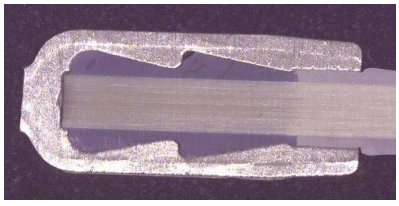
a. Schematic of crimped (swaged) end fitting



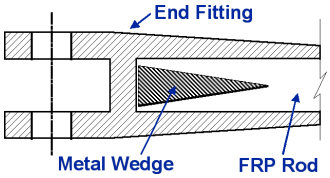
b. Dissection of crimped (swaged) end fitting



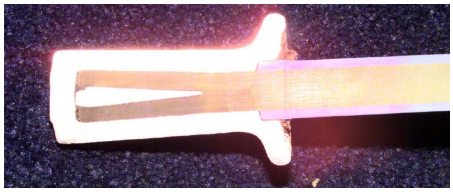
c. Schematic of epoxy wedge end fitting



d. Dissection of epoxy wedge end fitting



e. Schematic of metal wedge end fitting



f. Dissection of metal wedge end fitting

Figure 4.2-25 Dissection of different end fittings / rod attachment methods (note: most insulators in service are of crimped, or swaged, end fitting design) (EPRI 2002b).

End Fitting Seal

One of the most vulnerable regions of a polymer insulator is the interface between the end fitting, polymer housing, and the core rod, known as the end fitting seal. Its function is to prevent moisture or contamination from penetrating to the FRP rod, an event that is likely to precipitate a failure.

End fitting seals may be made in a number of ways, including (EPRI 2002b):

- Direct bonding of the rubber weathershed system to the metal end fitting.
- Single or double O-rings.
- A compression seal between the polymer housing and the metal end fitting.
- A metal connection piece between polymer housing and the metal end fitting.
- An external or internal sealant applied in the interfacial region. In some cases, a so-called metastable sealant is utilized, which is one that does not fully cure and remains "tacky." This allows for different coefficients of expansion between the materials used in the sealing interface.

Some designs incorporate more than one of the above sealing methods. Figure 4.2-26 shows examples of the different approaches.

E-field Grading Devices

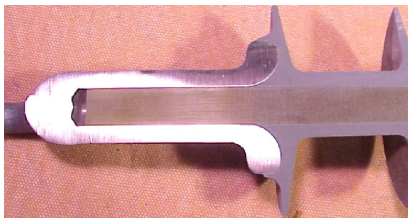
Research and service experience have shown that the electric field (E-field) within the rubber and rod material, as well as in the air close to the surface of a polymer insulator, needs to be controlled because it affects both the long- and short-term performance (Phillips et al. 1999a, 1999b; EPRI 2000a, 2002a, 2003a, 2004a). Reasons for this are discussed further in Section 4.4.3 on polymeric insulator aging and in the section on E-fields, Section 4.9.

The E-field needs to be controlled in the following regions (EPRI 1999):

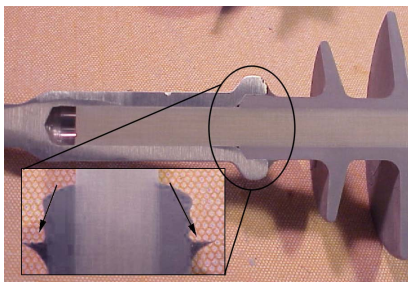
- Within the rubber and rod material
- On the surface of the metal end fittings, hardware, and corona rings
- On the surface of the polymer housing.

One or more of the following three methods may be used to achieve a proper E-field grading:

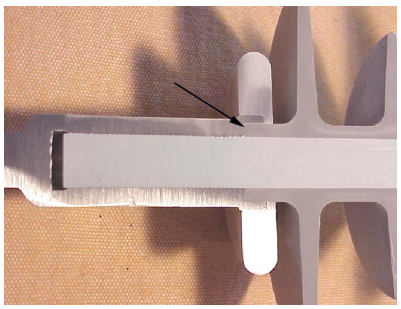
- The dimensioning and geometry design of the metal end fitting
- Attached E-field grading devices (often made of aluminum)
- Attachment of corona ring(s) at the high- and low-voltage ends (also called grading rings).



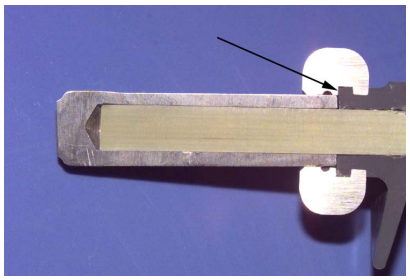
a) Direct Bonding of rubber onto metal end fitting



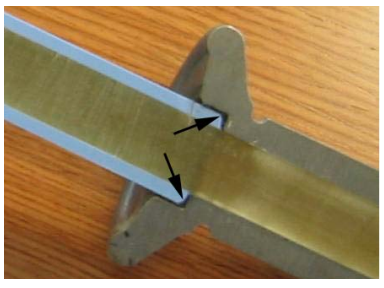
b) O-ring seal with outer sealant



c) Compression end fitting seal



d) Intermediate Al ring forms part of end fitting seal. Sealant, compression, and internal gel all form part of end fitting seal.



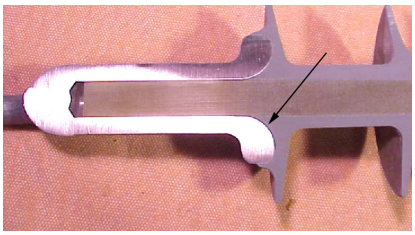
e) Metastable sealant

Figure 4.2-26 Examples of approaches to end fitting seals.

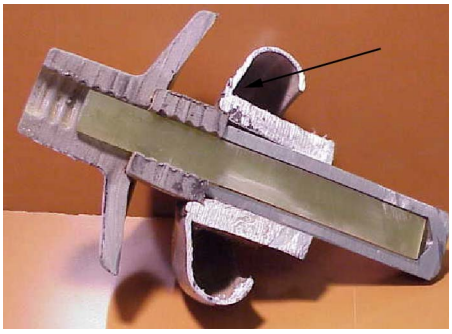
These methods are illustrated in Figure 4.2-27. Depending on the manufacturer and insulator application, one or all of the above may be utilized.

Corona rings need to be dimensioned by considering the system voltage, hardware geometry, structure dimensions, conductor bundle configuration, insulator parameters, and manufacturer recommendations. Depending on the system voltage level, corona rings may be necessary at the live end or/and at the grounded end of the insulator. Section 4.9 describes corona ring selection in more detail.

Other aspects that need to be considered when designing corona rings is their power arc withstand capability and attachment method.



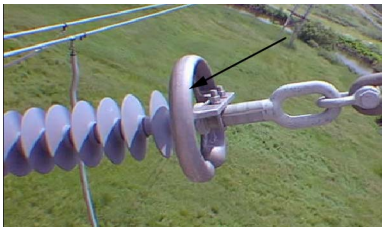
a) Dimensions and geometry of end fitting used to grade E-field. Note large and curved end fitting. (Manufacturer-specific)



b) E-field grading devices permanently attached to end fitting. Note large dimensions and curved edges. (Manufacturer-specific)



c) Corona (grading) ring attached at energized end of insulator. (Not all applications – installed in incorrect location with respect to end fitting for test purposes)



d) Corona (grading) ring attached at grounded end of insulator. (Not all applications)

Figure 4.2-27 Examples of E-field grading devices.

4.3 THE MECHANISM OF CONTAMINATION FLASHOVER

4.3.1 Introduction

Contamination-related outages came to the fore soon after the introduction of high-voltage transmission in the 1930s, which prompted the development of many of the presently used insulator monitoring-techniques, such as leakage current measurement. (Note: In other parts of the world, the term insulator "pollution" is also used. The words "pollution" and "contamination" will be used interchangeably in this text.) Since then, the study of transmission-line performance under contaminated conditions has become increasingly important. Both the IEEE and CIGRE have active and long-standing working groups dealing with this subject. The work of these groups culminated in a series of important review publications (Lambeth 1971; IEEE 1979; CIGRE 2000b). Also, during this time, polymer insulators were developed, which proved to be effective in reducing the number of contamination-related outages, especially if the insulator housing material was hydrophobic. Polymer insulators are, however, more prone to the effects of aging—an issue that will be dealt with in Section 4.4.

Power frequency flashovers on transmission systems are normally the result of airborne contamination that is deposited on the insulators. These contaminants may originate from natural sources such as the sea or desert, or they may be generated by industrial, agricultural, or construction activities. One of the most common contaminants is sea-salt (sodium chloride), which may cause severe problems on transmission-line insulators in coastal areas. Other types of salt, such as magnesium chloride, may cause problems in inland areas, where it is increasingly used on highways to combat ice during the winter season. In industrial or agricultural areas, a great variety of substances, such as gypsum, sulfuric acid, fly ash and cement, may be present as contamination on the insulators. Generally these deposits do not decrease the insulation strength when dry; they only become a threat under wet conditions, when the salts contained in the deposit dissolve to form a conductive layer on the insulator. Often, however, the contamination may already be in the dissolved state when deposited onto the

insulator, as may happen when the insulators are exposed to a saltwater fog. Under certain extreme cases—for example, close to certain types of mining activity—the deposits themselves could be conductive (e.g., metallic or carbon deposits); wetting is not required to reduce the strength of the insulator.

The formation of a conductive layer on an energized insulator leads to the flow of leakage current and the formation of dry bands in the areas with a high current density. When this happens, the voltage distribution along the insulator becomes highly nonuniform, with most of the voltage stress concentrated over the dry bands. This concentration of voltage stress may cause the dry bands to spark over. If this happens, a partial arc is established in series with the resistance of the conductive layer on the insulator. Depending on the layer conductivity, this partial arc may grow to span the whole insulator, leading to flashover.

In summary, there are three aspects that play an important part in the contamination flashover process (CIGRE 1979b):

1. Buildup of contaminants on the insulator surfaces
2. Wetting of the insulator
3. Discharge activity and its development into flashover.

Each of these aspects may comprise several subprocesses, as highlighted in Table 4.3-1. Although these are listed as individual items in the table, they actually combine into one seamless process. Some of the listed items may occur simultaneously, while others may happen at different times.

In practical situations, two types of contamination are generally identified: in this chapter, the terms "solid" and "liquid" contamination will be used. In the revised edition of the IEC 60815 (IEC Forthcoming b), these types are identified as Types A and B, respectively. These two types can be described as follows (CIGRE Forthcoming):

- **Solid contamination, or predeposited contamination.** Contaminants are deposited. Flashover may occur in a separate phase when the insulator is critically wetted by rain, fog, or condensation.
- **Liquid contamination, or instantaneous contamination.** Contaminants and wetting are deposited on the insulator surface simultaneously, which may result in flashover.

Of these two, solid contamination occurs more frequently, and it may originate from industry, agriculture, mining, bird feces, road-salt, or the sea. Examples of liquid contamination are conductive fog (or salt-fog) conditions or liquid salt spray directly from the sea.

The deposition and wetting conditions associated with solid and liquid contamination are distinctly different, as will be highlighted in the sections that follow.

4.3.2 Buildup of Contaminants on Insulator Surfaces

Types of Contaminant

Solid Contaminant

The deposited dry contaminants can be described in terms of two distinct components (CIGRE 2000b):

1. *Soluble contaminant* that, when in dissolved in water, will form a conductive solution. Examples include ionic salt such as sea-salt (NaCl), gypsum, and $CaSO_4$, or other constituents such as fly ash and cement.
2. *Nonsoluble contaminant*, which reduces the insulator's flashover voltage due to retention of water and the resulting influence on the formation of the conductive layer. Nonsoluble pollution may also be hydrophobic, such as oily or greasy substances that may enhance the insulator flashover characteristics.

Liquid Contaminant

The active component of liquid contamination is already in the dissolved state when it is deposited on the insulator surface. Typical examples are: saltwater spray close to the coast or gases in solution, such as SO_2, H_2S, or NH_3 close to chemical plants. Liquid contamination generally contains little or no nonsoluble contaminants.

Mechanism of Contaminant Deposit

There are several mechanisms by which solid or liquid contaminants can be deposited onto the insulators.

- **Aerodynamic action.** Contamination particles suspended in the air can be carried over great distances by wind (Fikke et al. 1993). When this contaminant-laden air encounters an insulator, the air is deflected around the insulator body. The particles suspended in the air are, however, not deflected to the same extent and are deposited on the insulator. Denser particles (e.g., sand) will be deposited on the windward side of the insulator since they are not sufficiently deflected by the airflow, as illustrated in Figure 4.3-1. Less dense particles will fol-

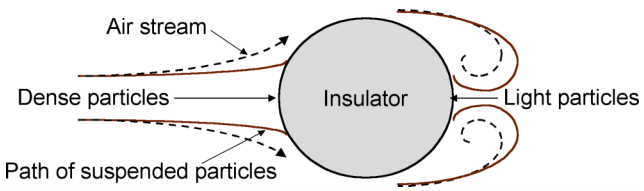
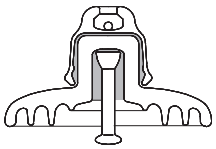
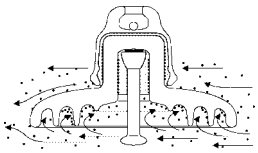
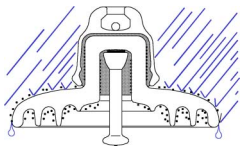
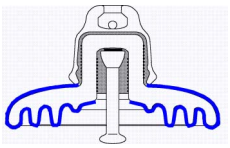
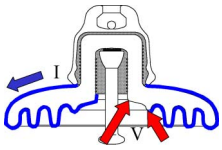
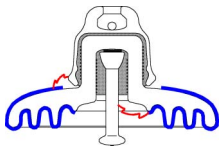
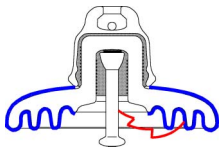
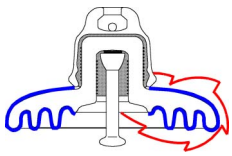


Figure 4.3-1 Pollution deposit by aerodynamic action (Looms 1988).

Table 4.3-1 Key Processes of the Contamination Flashover Process

	Description and Mechanisms	Influencing Factors	
	1.Clean Insulation surface	None	
Contaminant Build-up	2. Contamination Deposited a. Airborne particles b. Salt spray c. Under dry conditions, surface remains a good insulator	- Aerodynamic properties - Surface properties - Contamination type - Electric field (mainly dc)	
	3. Cleaning (removal of contamination) a. Rain b. Wind	- Insulator profile - String orientation - Precipitation type and intensity	
Wetting	4. Wetting of Contamination Layer a. Condensation b. Fog c. Rain d. Absorption e. Chemical Diffusion	- Contamination type (e.g., salt solubility) - Insulator profile - Surface properties - Wetting type	
Discharge Activity and Flashover	5. Formation of Dry Bands a. Leakage current flows on surface b. Increased heating in regions of high current density c. Dry bands form in regions of increased heating	Surface resistance • Humidity of air • Rate of rainfall • Level of contamination - Distribution of contamination - Insulator geometry	
	6. Dry Band Arcing a. Dry bands interrupt leakage current flow b. Full voltage across dry bands c. Air/surface cannot maintain potential difference d. Arcs form across dry bands e. Leakage currents surge when arcs form	- Surface properties - Degree of wetting - Level of contamination - Size of dry band	
	7. Growth/Quenching of Dry Band Arcs a. Dry band arcs sustained if surface resistance of entire string is low enough b. Increased heating at arc roots dries out contamination, increasing dry band size and hence arc length c. Surface resistance decreases with increases in arc lengths, resulting in increased leakage current magnitudes c. Arc grows and may self-extinguish as gap bridged becomes too large for arc to maintain itself. d. Arcs may be quenched by precipitation	-Surface Resistance • Rate of precipitation • Humidity • Amount and type of contamination • Surface properties - Insulator profile	
	8. Flashover a. If dry band arcs bridge a critical length of insulator, flashover occurs b. Multiple arcs may join (coalesce) c. Single arc may grow entire length	-Surface Resistance • Rate of precipitation • Humidity • Amount and type of contamination • Surface properties - Insulator profile	

low the airflow more closely and will only be deposited in areas where the airflow becomes turbulent (i.e., small curvature of the airflow), such as on the leeward side of the insulator or between the shed under-ribs (Looms 1988). Figure 4.3-2 shows the concentration of the contamination deposit in areas of turbulence, as indicated by the arrows. Aerodynamic action is, with a few exceptions, the dominant mechanism of contamination deposit (Taniguchi et al. 1979).

- **Precipitation by gravity.** Under low wind or still conditions, suspended particles in the air will precipitate and settle on horizontal surfaces under the influence of gravity. Precipitation by gravity may be the dominant mode of pollution deposition in areas close to a distinct contamination source, such as an industrial plant.
- **Heating effect of leakage current.** During conductive fog conditions, the heating effect of the current evaporates the water from the wet contaminant, leaving a salt residue behind. This residue is normally concentrated around the areas of the insulator with the highest current density. Heating by leakage current occurs on insulators installed close to the coast that are exposed to salt-fog.
- **Electric field.** Contamination may be deposited on the insulator surfaces due to the force exerted by the electric field on charged particles. This effect is, however, negligible under power-frequency energization, because of the alternating polarity of the field. It is more relevant for direct current energization, which falls outside the scope of this document.

Natural Cleaning of Surface Contaminant

Generally, two agents may remove contaminants from the insulator surface, thereby reducing the risk of flashover. These are:

1. **Precipitation.** High-intensity rain is very effective in removing contaminants from insulator surfaces. Exposed (i.e., top) surfaces that come in direct contact with the rain are most effectively cleaned. The more protected, or bottom, surfaces on the insulator may also undergo a significant amount of cleaning, but it is reduced as the amount of "protected" creepage increases (Kimoto et al. 1972).
2. **Wind.** In desert areas, strong winds may carry large sand particles that have a "sand blasting" effect, removing pollutants from the windward side of the insulator.

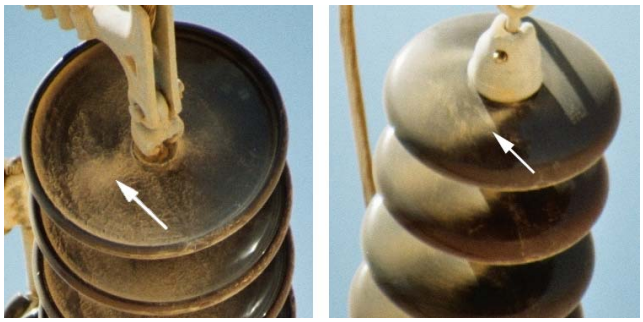


Figure 4.3-2 Photographs showing typical particle distribution on aerodynamically contaminated insulators. Note the concentration of the contaminants in areas of turbulence, as indicated by the arrows.

Accumulation of the Contaminants on the Insulator Surface

Solid Pollution

Contamination settles on the insulating surfaces in the form of dusty deposits. The contamination may be naturally removed from the insulators by the mechanisms indicated. The extent of this removal is related to the intensity and duration of the cleaning event. As a result, the level of contamination deposit varies over time, with the highest levels occurring at the start of cleaning events. Over time, equilibrium is reached when the rates of deposition and cleaning are in balance with random variations. Depending on the environment, it may take from weeks to years to reach this equilibrium (Looms 1988). In cold climates, where icing performance is a concern, the longest periods without rain tend to occur over the winter season. For example, climate norms for Minneapolis, Minnesota in the U.S. suggest that maximum temperature will be below freezing from December to March, a period of 120 days, well in excess of the days between rain events during the spring, summer, and fall.

Liquid Pollution

Wet pollution is characterized by the fast buildup of contaminants during events when the insulator is exposed to simultaneous pollution and wetting. In this case, the heating effect of the leakage current plays a major role in the deposition process, with the highest pollution deposit occurring in the areas with the highest current density on the insulator (IEEE 1979). The buildup of the deposit on the insulator may, in fact, be so fast that a clean insulator can build up sufficient contaminants to flash over during a single event. Thus natural cleaning has little influence on the flashover process in the case of liquid pollution.

Effect of Insulator Properties on the Accumulation of Contaminants

From the description above, it should be clear that the level and distribution of contamination are the result of a complex interaction between the insulator and the environment. This process is influenced by the profile of the insulator, its surface properties, and the orientation in which the insulator is installed. All these factors need to be taken account of when selecting insulators for a particular environment. Some guidelines are provided below:

Profile

- When insulators with convoluted profiles are exposed to wind-borne pollution, vortices are created by the underribs, which are conducive to the deposition of pollution, as illustrated in Figure 4.3-3 (Looms 1988). These regions are also sheltered, reducing natural cleaning and resulting in high contamination levels over time.
- Insulators shapes having large horizontal surfaces are at a disadvantage when contaminated by gravitational precipitation, as these surfaces present large areas on which the contaminants can settle.

Based on these principles, it can be concluded that: Open aerodynamic profiles tend to be beneficial in areas where there is a risk of a long-term buildup of airborne contaminants since these profiles collect generally less pollution and are accessible for natural or artificial cleaning. When there is a risk of a rapid buildup of contaminants, such as during storm conditions, profiles with a more convoluted design can be advantageous since large parts of the surface are "protected" from fast pollution accumulation. Likewise, profiles with large horizontal surfaces should be avoided when there is a significant gravitational precipitation.

Surface Properties

The insulator surface properties are also important in determining how much pollution attaches to the surface:

- Smooth surfaces accumulate less pollution than rough ones.
- Dry surfaces retain less pollution than damp ones.
- Studies have shown that silicone rubber insulators, due to the presence of the silicone oils, collect more contaminants than glass or ceramic surfaces (Naito et al. 1999); however, this is offset by the hydrophobicity encapsulation of the pollution layer (Kindersberger and Kuhl 1991). The surface hydrophobicity also influences the uniformity of the pollution deposit. The surface hydrophobicity causes the contaminated water drops to bead on the surface, leaving distinct spots of contamination behind when the water evaporates (Karady et al. 1995). On the other hand, solid pollution is not affected in the same way—due to absence of water—resulting in a more uniform deposit (Besztercey and Karady 2000; Engelbrecht et al. 2003).

Insulator String Orientation

Vertically orientated insulator strings (I-strings) collect more contamination than angled (V-strings) or horizontally (dead ends) installed units since there are large sheltered areas on the underside of the insulator where natural cleaning is less effective.

Horizontally orientated insulator strings pointing to, or from, a well-defined source may collect more contamination than strings pointing in other directions due to the larger windward and leeward regions where airborne deposition may occur (Houlgate et al. 1982).

4.3.3 Wetting Processes

Wetting Mechanisms

It is commonly recognized that flashovers caused by contamination generally occur during drizzle, fog, or high humidity conditions due to a reduction in the surface resistance. Four wetting processes are recognized (Karady 1975; Leclerc et al. 1982; Chrzan et al. 1989):

- **Collision of water droplets.** The insulator is wetted by the collision of free water droplets in the air (e.g., during rain, mist, or fog) with the insulator. The distribution of the wetting on the insulator is dependent on the insulator shape and the droplet size. Small droplets are more likely to wet the insulator underside since they are more influenced by air movement around the insulator.

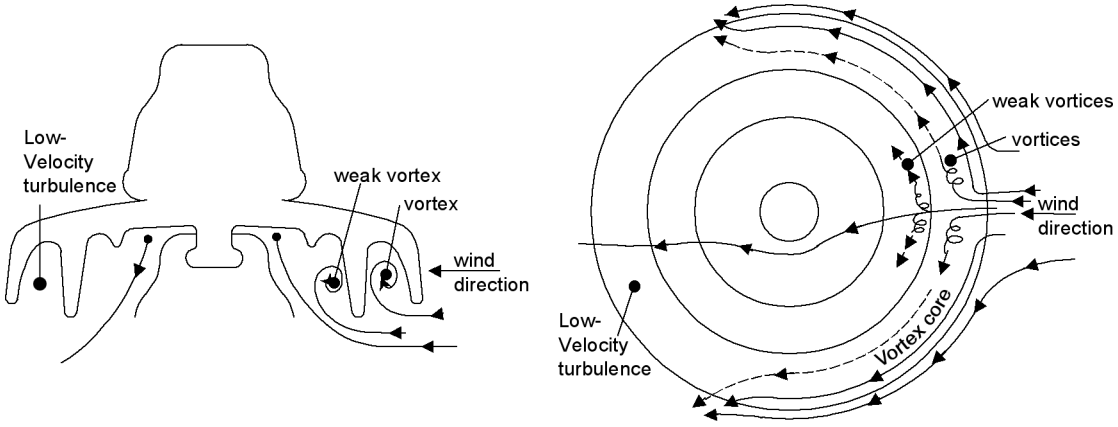


Figure 4.3-3 Airflow around a disc insulator (Looms 1988).

- **Hygroscopic behavior of surface deposits (absorption).** Surface contamination absorbs water molecules from the air by the process of deliquescence if it is salt, or absorption if it is a nonsoluble material. For typical contamination layers, this process occurs when the partial vapor pressure of the ambient is greater than the vapor pressure of the salt; for sodium chloride, this occurs approximately at a relative humidity of 75%. The type of salt and inert material present determines the distribution and amount of the wetting.
- **Condensation.** Condensation occurs when the insulator surfaces are colder than the ambient temperature and are below the dew point temperature. The temperature difference is due to thermal lag or radiation, and is therefore influenced by the thermal properties of the insulator. Polymer insulators, due to their low thermal conductivity and thermal mass, adjust quickly to the ambient temperature, resulting in small temperature differences, while a larger temperature difference would occur with glass and porcelain insulators during the same conditions. Hence polymer insulators have less condensation than glass or porcelain insulators (Engelbrecht et al. 2003).
- **Chemical diffusion.** The condensation rate is higher for solutions than for pure liquids due to the phenomenon of chemical diffusion. This is a contributing factor that results in a higher rate of condensation on moist contaminated surfaces than on clean surfaces.

These wetting processes combine during different ambient conditions to produce a characteristic wetting-pattern on the insulator surface. Some examples are:

- **Clear conditions.** Under clear air conditions, moisture can only be deposited on the insulator via condensation or moisture absorption. The whole insulator surface is likely to be wetted during these conditions. Typically this occurs during late night or early morning when the insulator may be cooler than the ambient air due to thermal radiation or thermal lag.
- **Fog or mist:** Fog occurs when the ambient air is cooled down sufficiently that condensation occurs in the air itself, resulting in suspended water droplets. The wetting of the insulator surface is mainly through collisions of fog droplets with the insulator surface, but condensation and absorption also make a significant contribution. The whole insulator surface is likely to be wetted during these conditions, unless there are deep shed under-ribs present that prevent effective droplet collision with the protected parts on the insulator.
- **Salt spray.** In areas close to the coast, wind can transport the salt-spray produced by the breaking waves. Wetting occurs due to the collision of the droplets with the insulator surface. The distribution of the wetting is mainly determined by the aerodynamic properties of the insulator and the size of the salt-water droplets. Logically, the exposed upper surfaces are wetted most effectively, but the insulator underside may also be wetted to some extent due to the turbulence created by the under-ribs, if present.
- **Rain.** Rain wets the insulator surface by the collision of the raindrops with the insulator surface. It is mostly the upper surfaces of the insulator that are wetted while the "protected creepage" remains relatively dry.

The rate by which the moisture impinges on a contaminated insulator may vary from light, during mist or fog, to heavy, during rain. It may further impinge on the insulator surface gently, as during a light drizzle, or violently as during a wind-driven downpour. As the rate of the wetting increases, so does its natural cleaning effect, as was discussed in the previous section. These are important factors that need to be considered when identifying when wetting conditions pose the greatest risk to the insulators.

Critical Wetting on Solid or Predeposited Contamination

In an area characterized by a predeposited contamination layer, the soluble electrolytes within the contamination coating gradually dissolve. A thin film of conducting liquid then forms on the insulator surface if it is hydrophilic, or droplets form if the surface is hydrophobic. As the wetting continues, a redistribution of the contamination may take place, and some of the contamination may even leach by run-off. Because of these processes taking place, the surface resistivity initially decreases due the salts that dissolve and increases after a while due to the leaching effect.

The minimum resistivity of the layer (i.e., highest conductivity) and the time at which it occurs are very dependent on solution characteristics of the predeposited contamination layer. Both the solubility and the speed by which it goes into solution play an important role (Williams et al. 1974; Ramos et al. 1993).

- The impact of the wetting rate on the flashover voltage is greater for low-solubility than for high-solubility salts. This was illustrated during laboratory tests that found a greater reduction in flashover voltage as a function of the steam input rate on insulators polluted with gypsum, as compared with insulators polluted with sea-salt (Campillo et al. 1995).
- The amount and type of nonsoluble contamination present also influence the wetting process. The nonsoluble contamination "binds" water to the insulator surface, which helps the formation of the low-resistance layer, resulting in a lowering of the flashover voltage.
- Different kinds of inert material influence the time it takes to reach the minimum resistivity and the value of

the minimum resistivity depending on its hygroscopic and hydrophobic properties (Matsuoka et al. 1996).

It can thus be seen that the surface conductivity of the insulator is the result of a complex process that depends not only on the amount of moisture and the chemical composition of the soluble and nonsoluble contaminants, but also on the material and shape of the insulator itself. On this basis, the critical wetting is defined as a wetting rate that is fast enough to wet the pollution sufficiently for the flashover process to take place and slow enough not to wash the pollutants from the insulator surface. In general, it can be stated that low wetting rates, such as during fog or mist, are critical for fast dissolving salts, and a heavy wetting rate is required to produce critical conditions for slow dissolving salts. For instance, in coastal areas where the main pollutant is sea-salt (NaCl), condensation or fog conditions generally provide sufficient wetting to dissolve the contamination layer, whereas in certain industrial areas, where gypsum is prevalent, a more severe wetting condition, such as rain, is needed to dissolve the contamination layer.

Wetting Aspects When Dealing with Liquid Contamination

Under conductive-fog conditions, the contaminants are deposited in the dissolved state. This is typical of sea storms when sea spray may be carried inland by wind, or close to industrial plants where the insulators may be exposed to a conductive rain or fog. The dissolving characteristics of the salts involved are in this case not important; what is important is the conductivity of the solution itself. A higher conductivity solution results in a greater risk of flashover. Leakage current flowing in the surface layer will cause a drying out in the areas of the insulator with the highest current density, and the initiation of dry-band activity (Lambeth et al. 1973). This electrical activity may also enhance the deposition of salt on the surface due to the heating effect of the current.

4.3.4 Discharge Activity and Development of Flashover

A critical part of the contamination flashover process is the formation of the conductive layer on the insulator's surface. The presence of such a layer invariably leads to a very nonuniform voltage distribution along the insulator and the inception of discharge activity. Depending on the conductivity of this layer, the wetting conditions, and the surface properties of the insulator, the discharge activity may develop into a flashover. The discharge development is basically the same for both solid and liquid pollution types, so no distinction will be made in the text that follows. However, the discharge development is markedly different on hydrophilic (e.g., ceramic and glass) and hydrophobic (e.g., silicone rubber) insulators. These two types of insulator will, therefore, be treated separately.

Hydrophilic Insulators

Contamination Flashover Process on Single-Unit Insulators

Development of electrical discharges on contaminated insulators will be discussed with reference to the simplified diagram presented in Figure 4.3-4.

The following description covers the flashover process from the formation of dry bands to the final arc in terms of the steps identified in Figure 4.3-4.

- **Condition A.** As wetting increases, the impedance of the insulator lowers and changes from mainly capacitive, at the start of the wetting, to mainly resistive. This is demonstrated by the change of surface impedance over time presented in Figure 4.3-5 (Kawai 1971; Standving 1934; John and Clark 1939), as measured during laboratory tests. The increase of the capacitance shown in the figure is a result of the increase in the conductive area on the insulator surface.
- **Condition B.** This drop in impedance leads to an increased level of leakage current across the insulator, which, in turn, leads to the formation of dry bands in the areas with the highest current density due to localized heating. On disc insulators, this is around the pin-and-cap area. The dry band blocks the flow of leakage current, which results in a concentration of the applied voltage over the dry bands. Figure 4.3-6 shows this voltage drop around the pin area of the disc insulator, as measured during laboratory tests. Corona and sparking activity ensues, which leads to a further drying out and an increase in the size of the dry band, until a stable con-

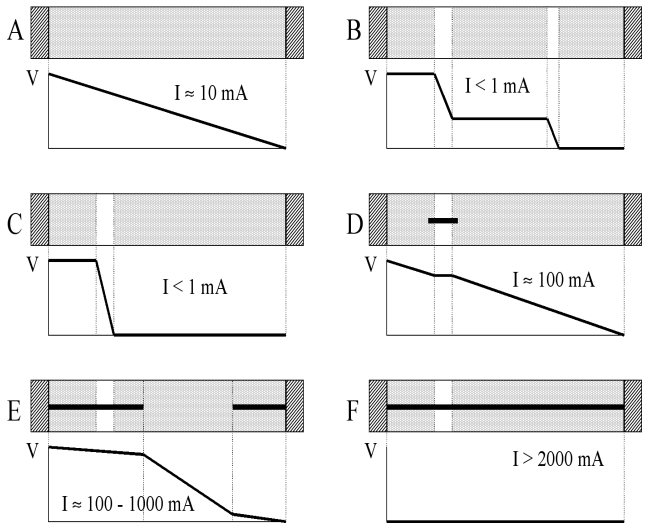


Figure 4.3-4 Typical steps and their associated voltage distribution, in the discharge development of contaminated insulators. (A - Wetting begins, B - Dry bands form, C - Consolidation of dry bands, D - Scintillation, E - Discharges extend, F - Flashover) (Lambeth 1971).

dition is reached where the dry band can withstand the applied voltage with occasional sparkovers (Lambeth 1971).

The degree to which dry bands form initially and the rate at which they reabsorb moisture depend on the intensity of the wetting process and the drying effect of the leakage current. In falling rain conditions, the wetting action may be so intense that dry band formation may not be possible until after the rain ceases.

- **Condition C.** When the dry band is established, the general level of leakage current over the insulator drops, which allows the wetting process to overcome the drying effect of the leakage current. On long-rod insulators, this may lead to the re-wetting of the smaller dry bands and the formation of only one dominant dry band, which is maintained by the heating effect of the discharge and corona activity (Chrzan 2003).
- **Condition D.** During the occasional sparkovers of the dry band, the voltage distribution over the insulator becomes more linear. This is supported by experimental findings, such as those presented in Figure 4.3-7, which shows the average measured voltage distributions along the insulator surface for different levels of leakage current. This linearization is more pronounced at higher levels of leakage current, and it is caused by the voltage drop associated with the current flow through the conductive surface layer (Lambeth 1971).
- **Condition E.** Exactly how the scintillation activity develops into flashover is not yet fully understood, as there are many factors that influence this process. Most theoretical studies have been based on a simplified model that assumes the contaminated insulator surface is already wetted and highly conductive (Rizk 1981; Hampton 1964; Nasser 1968; Woodson and McElroy; 1970). However, these models ignore the drying effect of the leakage current and partial arcs on the wet pollution layer, which in some cases can be so intense that it extinguishes the partial arc over the insulator, preventing flashover despite a high level of leakage current.

  However, on single-disc insulators, it is known that the arc develops from the high-voltage electrode, and that the complete flashover is the result of the growth of the partial discharges to span the whole insulator length.
- **Condition F.** At an advanced stage of discharge development, flashover is determined by the breakdown strength of the contamination layer, which holds most of the voltage (Lambeth 1971).

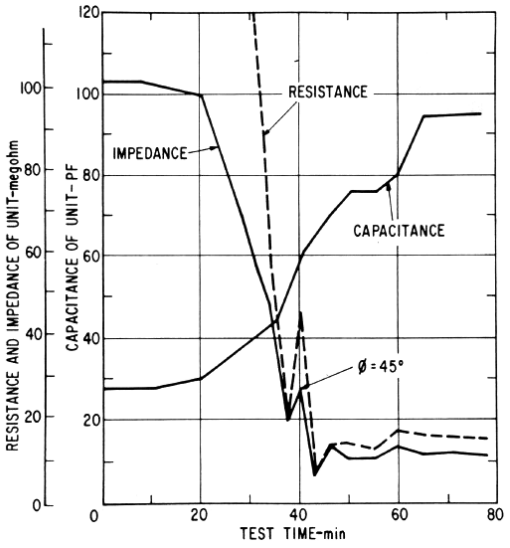


Figure 4.3-5 Example of dynamic surface impedance of standard insulators. (Salt-deposit density = 0.07 mg/cm^2; kaolin = 40 g/l.) Applied voltage per 5 $^3/_4$ in. (146 mm) disc = 6.3 kV.

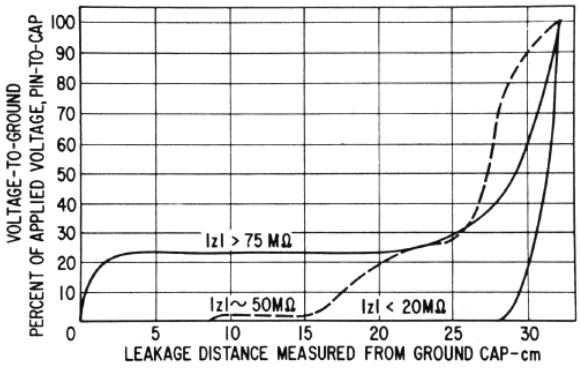


Figure 4.3-6 Voltage distribution measured from grounded cap before onset of scintillation for different values of surface impedance magnitude.

Flashover Mechanism of Long Insulator Strings under Light Wetting Conditions

During the contamination tests at Project UHV (EPRI 1982), which were performed under a relatively low degree

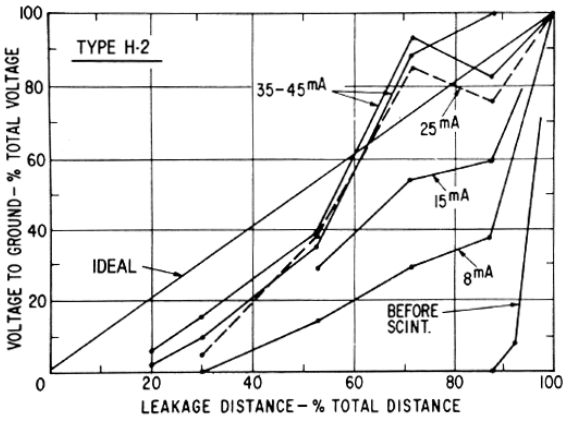


Figure 4.3-7 Typical measurement results of the dynamic voltage distribution on a disc type insulator under various levels of leakage current.

of wetting, it was found that a nonlinear voltage distribution on the insulator string might exist. This suggests that the contamination flashover of long insulator strings might be different from that of single insulator discs. From observations, the following phases in the flashover process were identified:

- Initially, the contaminated insulator surface is completely dry. Consequently, the voltage distribution on the string may be regarded as the same as that on a dry, clean insulator string (i.e., mainly capacitive). The equivalent circuit may be represented by a network of capacitances only, since the leakage resistance of the insulator surface may be ignored (see Figure 4.3-8). This distribution is usually nonuniform, with the highest voltage stress on the insulators closest to the high-voltage end.
- As the wetting progresses, the resistance of the insulator becomes more important. The value of this resistance is influenced by the drying effect created by leakage current and corona discharges, which are functions of the voltage across individual discs. Since the electric field distribution along the string is not uniform, the voltage across the units closest to the conductor is higher, and hence these units dry out first, forming a dry zone.

  The surface temperature of the discs in the dry zone is much higher than that of the insulators on the remaining section of the string. A wet zone is usually formed at the midsection of the string, where the voltage drop is the lowest. Thus the nonuniform voltage distribution can be held throughout the time of wetting. Surface leakage current in this period is about 100–600 mA (rms).
- As the dry zone dries out further and the wet zone becomes wetter, the voltage across the dry zones increases. Finally, the units on the bottom section can no longer withstand the voltage stress, and they flash over. This is observed when an arc bridges several units at the bottom of the string.
- The activity develops upward. The arcs bridging the bottom section result in an overvoltage over the rest of the string, producing heavier activity along the string. This activity appears as leakage current surges, usually having peak values ranging from 500 to 700 mA (rms).
- The leakage currents dry the insulator surfaces in the wet zone, linearizing the voltage distribution along the entire string and reducing the voltage drop across the initial dry zone, extinguishing the arc. However, this heavy activity does not make the insulator surfaces in the wet zone as dry as those of the dry zone of the string.
- After the activity has ceased, the insulator surfaces under low-voltage stress begin to absorb moisture, making the values of surface impedance lower. The units in the high field region do not absorb as much moisture due to their higher temperature. Therefore, the voltage distribution along the string again becomes nonuniform enough to produce another surge. This process is repeated either until a flashover develops or until the surge activity gradually disappears as the contaminants are leached from the insulator surface.

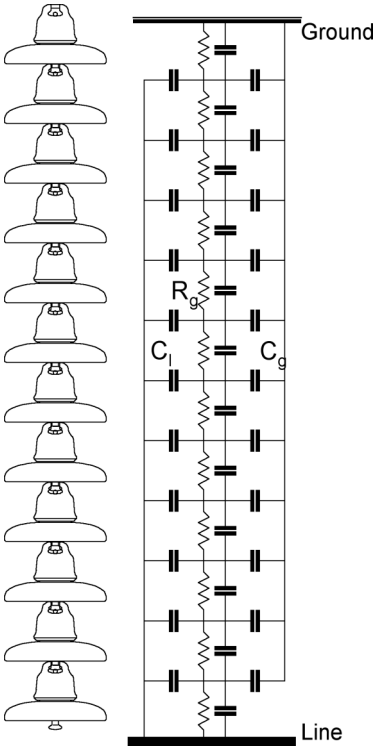


Figure 4.3-8 Equivalent circuit for voltage distribution along a contaminated insulator string.

Because it is a thermal process that causes the nonlinearity of the voltage distribution along the string (Boehne and Weiner 1966, 1967), it does not appear when the rate of surface wetting is fast enough to overwhelm the drying effect of the leakage current. Since the rate of wetting in natural conditions is often low, this nonlinear phenomenon has only been found for those tests in which the wetting condition was arranged to duplicate a natural wetting process. These nonlinear effects are reduced when the voltage distribution along the insulator string is made more uniform by the application of a grading/corona ring, an effect that has been illustrated in tests.

Influence of Pollution Level and Degree of Wetting on Flashover Development

Observations of artificially polluted insulators under natural wetting conditions have shown that the degree of discharge activity is a function of both the contamination severity and the degree of wetting (EPRI 2004f). These observations were performed during times when condensation and moisture absorption were the main wetting pro-

cesses. A schematic diagram, based on the observations, is presented in Figure 4.3-9, to illustrate this dependency. Images taken with a daylight ultraviolet camera during the different zones identified in Figure 4.3-9 are presented in Table 4.3-2.

The following distinct phases, or zones, were observed:

Zone I No discharges occur on dry insulators independent of the contamination level. Clean insulators also showed no discharges independent of the degree of wetting.

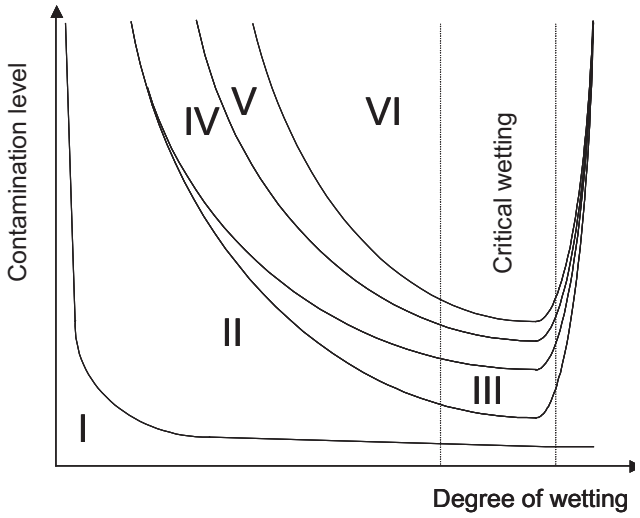


Figure 4.3-9 A schematic diagram of typical discharge activity on artificially polluted insulators, as observed during natural wetting conditions. Zone I: No activity, Zone II: Corona, Zone III: Scintillation, Zone IV: Quiet, Zone V: Intermittent sparking, Zone VI: Flashover. The different zones are described in more detail in the accompanying text.

Zone II In this zone, the insulator is partly wet, and corona discharges occur at the edges of the wet areas. These are generally concentrated in the high E-field stress areas of the insulator string.

Zone III A dry band is established, and sparking activity occurs—Condition B in Figure 4.3-4. This level of activity can be maintained for a relatively long time since the heating effect of leakage current is insufficient to increase the size of the dry band. Therefore this type of activity is mostly common on insulators with a critical to subcritical level of pollution.

Zone IV If the degree of wetting is balanced by the drying-out effect of the leakage current, a stable condition arises that is characterized by a low level of discharge activity—Condition C in Figure 4.3-4.

Zone V If the wetting rate is high enough to overcome the drying effect of the leakage current, occasional sparkovers of the dry band occur. This corresponds to Conditions D and E in Figure 4.3-4.

Natural cleaning and a quenching of the discharge activity take place if the degree of wetting is higher than the critical wetting rate.

Effect of the Insulator Properties

On convoluted insulator designs, scintillation discharges may take shortcuts between the shed protrusions, rendering a part of the leakage distance ineffective (Woodson and McElroy 1970; Baker and Kawai 1973). This is generally more apparent at lower contamination levels where the capacitive steering of the voltage across the insulator is still significant. A comparison of different insulator types

Table 4.3-2 Photos of the Typical Discharge Patterns That May Be Observed During the Zones Defined in Figure 4.3-9

Zone I: No activity	Zone II: Corona	Zone III: Scintillation	Zone IV: Quiet	Zone V: Intermittent sparking	Zone VI: Flashover
					

at low contamination severities shows that the flashover strength of insulators is not proportional to the leakage distance. At a higher degree of contamination, the conductivity of the surface layer is low enough so that the scintillation discharge follows the surface more closely, and the flashover strength is more proportional to the leakage distance.

On both single insulator discs and long insulator strings, the flashover process is driven by the nonuniform voltage distribution caused by thermal phenomena related to the leakage current. Recognizing this, some measures to improve the contamination performance may be proposed. For instance, employing insulators having high capacitance between cap-and-pin can reduce the nonuniformity of voltage distribution on long insulator strings, because the voltage distribution along the string would be greatly linearized. Also, a better contamination performance of single insulator units can be expected when the voltage concentration around the pin is greatly reduced (Akizuki et al. 2002).

Flashover Process on Hydrophobic Polymer Insulators

The flashover process on hydrophobic polymer insulators is markedly different from that of hydrophilic insulators such as porcelain and glass. Observations of the leakage current behavior of polymer insulators show a continuous low level of current that is interspersed with single high current spikes (Gorur et al. 1997). This is in contrast with the gradual buildup of current over ceramic and glass insulators and the densely spaced high current pulses. The main reason for the difference in behavior is the hydrophobicity that inhibits the formation of a continuous conducting layer of the polymeric insulator.

When a hydrophobic insulator is wetted—by condensation, fog, or rain—the water on the surface forms into droplets due to the hydrophobic properties. Through a process of diffusion, some of the salt on the insulator dissolves into the water, making the droplets conductive. The water from the drops also migrates into the dry pollution to form a damp layer with a high resistance. At this stage, a high resistive layer with conductive water drops scattered over it covers the insulator. The leakage current across the insulator reaches a stable, but low, value once equilibrium is reached between the evaporation caused by the heating effect and the reduction of the surface resistance by wetting (Karady 1999).

The scattered water drops on the insulator surface react to the presence of the oscillating electric field in two ways: first, the water drops elongate on the sheath sections and flatten under the oscillating force that the electric field exerts on the polar water molecules, and second, the electric field is enhanced at the edges in the wet areas as a result of the high permittivity of the water. If neighboring droplets are close enough, these may coalesce to form runnels, leading to a further strengthening of the electric field at the edges. The electric field may be increased sufficiently to cause corona discharges (Phillips et al. 1999b; Karady 1999). The discharge activity may reduce the surface hydrophobicity locally, which may help the formation of longer runnels.

On short insulators with a relatively uniform E-field distribution, the leakage current across the insulator may increase sufficiently over time to cause the formation of a dry band on the shank (or sheath) of the insulator, which is the area of the highest current density (Vosloo and Holzhausen 2003). As the hydrophobicity breaks down further in the high-stress zones, the dry-band activity extends to the sheds. The discharges extend as the water runnels extend further, resulting in sparking that bridges the wet areas. Depending on the conductivity of the water, the sparking may eventually extend to reach a flashover.

On long insulators (transmission voltages), the electric field along the insulator is very nonuniform, and the initial corona and sparking activity occurs in the area of the highest electric field close to the high voltage end. This causes the highly stressed section of the insulator to dry out more than the rest of the insulator, forming a high resistance area compared with the rest of the insulator (Gorur et al. 1997). This effectively blocks the leakage current from flowing. The highly nonuniform field concentrations at the ends of this high-resistance area may initiate a streamer breakdown process. If the streamer discharge spans the high resistance section, and the width of this region is large enough, a condition will arise whereby the wet section of the insulator is overstressed. The streamer can then quickly develop into a flashover. This flashover process is characterized by a general absence of leakage current, until the breakdown of the high resistance section, leading to single high current pulses or flashover.

4.4 LONG-TERM PERFORMANCE OF INSULATORS

4.4.1 Causes of Degradation and Damage

Degradation and damage to insulators can be divided into the following categories:

- **Manufacturing defects.** Manufacturing defects can be any flaw that results from an improper manufacturing and assembly process, or a lack of quality control (EPRI 2002a).
- **Damage from handling.** The insulator may be damaged during installation due to improper handling, such as improper storage, dropping, or using incorrect hoisting techniques. There is also the possibility that insulators

may be damaged during maintenance due to improper cleaning procedures (EPRI 2001a, c).

- **Service-induced damage or deterioration.** Service-induced damage may result if the insulator is not dimensioned correctly for the particular environment in question. This may result in damaging discharge activity or mechanical overload conditions. Degradation of correctly dimensioned insulators may also occur due to normal aging as a result of environmental and electrical stresses (EPRI 2004c).
- **Vandalism.** Vandalism is damage inflicted on the insulator by human activity other than that related to installation or maintenance. Gunshot damage or damage from projectiles are examples (Burnham and Waidelich 1997; EPRI 2004c).
- **Damage caused by animals.** Rodents and birds may damage polymer insulator housings through pecking or gnawing (EPRI 2004c).

In this section the discussion will focus exclusively on service-induced damage and deterioration since this should be taken account of when dimensioning the insulators.

4.4.2 Porcelain and Glass Insulators

Deterioration of Ceramic and Glass Insulators

High-quality porcelain and glass insulators can be kept in service for more than 30 years with little to no change in their electrical and mechanical properties. For example, there are records of porcelain insulators with more than 70 years of service life. Accelerated degradation does occur, but only when insulators are electrically or environmentally overstressed. A typical example is surface erosion of the glass or porcelain on insulators that are subjected frequently to elevated levels of leakage current (see Figure 4.4-1). These units may also exhibit corrosion of the pin and, in severe cases, the cap as well (Parraud and Dumora 2001).

Failure Modes of Glass Disc Insulators

Glass insulators may experience infant mortality to some degree—that is, it is not unusual to have a very small number of units shatter within a short time of installation.

Electrical Puncture

Glass insulators are highly resistant to electrical puncturing. However, in the event that they do puncture, the residual tensile stress in the glass, due to the toughening process, will cause the glass shell to shatter. Therefore, no hidden punctures can exist within a glass insulator (Looms 1988).

Punctures and subsequent shattering of the glass shell can be caused by:

- Concentrated electrical discharges under thick pollution layers may cause localized heating, leading to a thermal puncture.
- Thermal punctures due to heating caused by dielectric losses in the glass.
- Punctures or thermal shock due to lightning or high-energy power frequency power arc flashover.

Mechanical Failure

There are reasons other than electrical puncture that may also cause the glass shell to break. Internal mechanical stresses can build up in the glass shell and can lead to its eventual breaking. These stresses include:

- Erosion due to leakage currents, or in desert conditions due to "sand blasting," may lead to a disturbance of the internal mechanical forces, causing the glass shell to shatter.
- Vandalism is also a major contributor to insulator breakages. Gunshot and rocks thrown at insulator strings are common types of vandalism.
- Under dc energization, the migration of ions in sodium-rich glass cause the sodium to aggregate or deplete under the insulator cap. This may lead to a redistribution of mechanical forces inside the shell that can eventually shatter it (CIGRE 1994b).

Hardware corrosion (i.e., corrosion of the metal end fittings) may also lead to deterioration of the mechanical strength of the insulators.

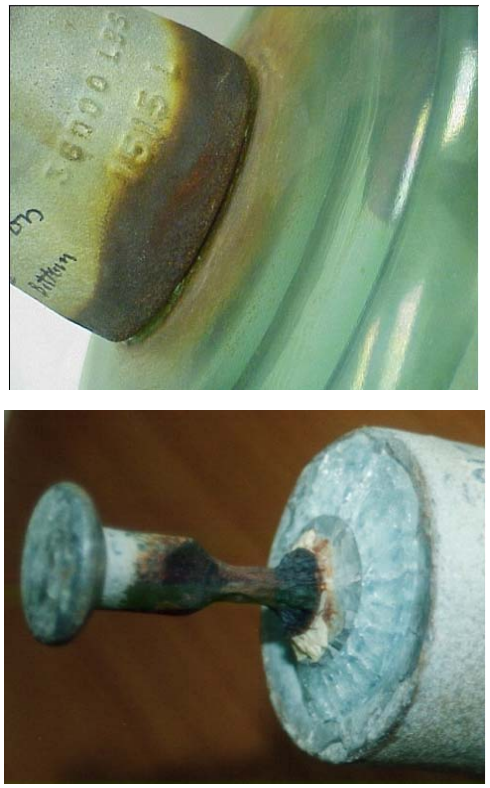


Figure 4.4-1 Examples of glass disc erosion and corrosion of the metal end fittings.

Failure Modes of Porcelain Disc Insulators

Electrical Puncture

An electrical failure on porcelain disc insulators normally manifests itself as a pinhole through the porcelain shell between the cap and pin (see Figure 4.4-2). The causes for puncture are varied, and some causes include (Looms 1988):

- Steep electrical impulse normally caused by lightning.
- Thermal runaway as a result of the heat generated by dielectric losses.
- Long-term high electric field stressing.

Mechanical Failure

A porcelain disc may be considered to have mechanically failed when it can no longer hold mechanical load or when there is significant damage to the porcelain shell. Examples of mechanical failures are as follows: (also see Figures 4.4-3 and 4.4-4):

- A radial crack of porcelain shell.
- A donut crack of porcelain shell
- A crack in the porcelain under the metal cap or in the porcelain head.
- Mechanical separation of the cap or pin hardware
- Mechanical failure of the porcelain shell



Figure 4.4-2 Examples of electrically induced failures.

These cracks may be formed due to one or a combination of the following:

- Stresses generated by ion movement within the porcelain under dc energization.
- Material erosion due to corona activity and/or high E-fields.
- Localized stresses induced by corrosion of metallic parts of the insulator.
- Mechanical stresses or forces created by the swelling of some of the components in the cement such as gypsum (Looms 1988; Gorur et al. 1999).
- Stresses created by unequal thermal expansion and contraction of the various insulator components (porcelain, metals, glazing, sand band, and bituminous material between the metal and cement, etc.).
- Mechanical overload conditions, such as those occurring during severe conductor icing conditions.
- Cracks and shell breakage caused by an impact and/or vandalism.
- Mechanical stresses in the disc that are induced by the electrical puncture of the porcelain.

Failure Modes of Porcelain Longrod Insulators

Electrical Puncture

Since porcelain longrod insulators fall under IEC Class A (see Figure 4.2-4), they are regarded as puncture proof.



Figure 4.4-3 Examples of mechanical failures.



Figure 4.4-4 Erosion of the cement around the pin caused by electrical discharges.

Mechanical Failure
Mechanical breakage on longrod insulators is normally associated with a failure of the end-caps or the cement or lead-antimony filling material that fixes the cap to the porcelain body. Breakages of the porcelain body may also occur when its dynamic or static mechanical strength has been exceeded.

4.4.3 Polymer Insulators

Degradation Mechanisms
Stresses that result in degradation of polymer insulators may be categorized into the following broad areas:

1. Environmental stresses
2. Mechanical stresses
3. Electrical stresses

Environmental stresses include temperature cycling, precipitation, solar radiation, and contamination, while *mechanical stresses* include static and dynamic loading (e.g., compression and tension loads, vibration, bending, twisting, and torque loads). If applied within the manufacturer-specified ranges, today's designs of polymer insulators are designed and tested to withstand these *individual* stresses without significant degradation. Hence environmental and mechanical stresses alone may be considered secondary as regards long-term degradation. However, some of the above stresses in combination with electrical stresses may result in significant degradation.

Electrical stresses may result in degradation of polymer insulators either alone or when combined with environmental stresses, such as precipitation and contamination (EPRI 1999; Maxwell et al. 2002; EPRI 1998; Maxwell and Hartings 2000). The electrical stresses considered are:

- Electric field distribution along the insulator
- Voltage applied across the insulator

These electrical stresses may result in discharge activity and leakage currents that, in turn, may degrade the rod, polymer weathershed material, interfaces, end-fittings, and end fitting seals. The ability of the insulator to withstand these stresses is a function of the insulator design, manufacturing process, and application. It should be noted that polymer insulator designs and manufacturing processes vary considerably from manufacturer to manufacturer and, hence, so does the ability to withstand these stresses.

Degrading discharge activity and leakage currents may be classified into distinct categories that are described in detail in the following sections:

- Discharges internal to the FRP rod and polymer weathershed material or, at the interface between the rod and housing
- Corona activity from metallic end-fittings or corona rings under dry conditions
- Discharges due to nonuniform wetting of the polymer rubber material
- Dry band arcing under contaminated conditions
- Damage due to external power arcs

The following sections provide an overview of each of these.

Discharges Internal to the Fiberglass Rod and Polymer Weathershed Material
If a critical E-field magnitude is exceeded, internal defects—such as voids, inclusions, or poor bonding between the rod and rubber sheath—may result in internal discharge activity (Cherney 1991). This internal discharge activity may have one or more of the following results:

- Destruction of the fiberglass rod resulting in a mechanical failure.
- Damage of rubber weathershed material, exposing the fiberglass rod to the environment and precipitating an electrical or mechanical failure. Possible failure modes are described in detail in a later section.
- Tracking along or through the fiberglass rod. This tracking may propagate axially along the length of an insulator, resulting in a larger conductive defect. If the conductive defect becomes a critical length, a flashunder electrical failure may occur. Figure 4.4-5 is an example of tracking along the interface between the fiberglass rod and rubber sheath.

Degradation due to internal discharges may be avoided by reducing the occurrence of internal defects in the manufacturing process and controlling the E-field internal to the insulator by the correct application of corona rings.

Internal discharge activity may also be initiated by moisture and/or contaminants that have penetrated the weather-

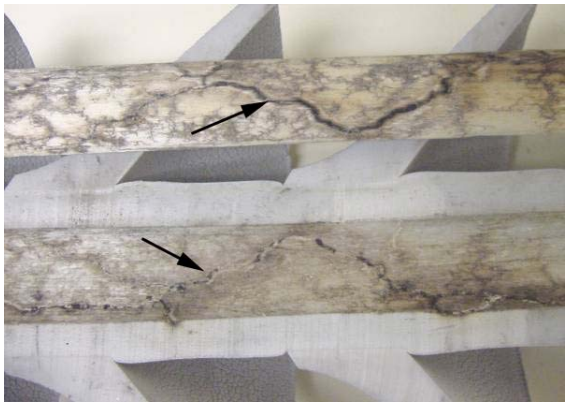


Figure 4.4-5 Tracking along the interface between the fiberglass rod and rubber sheath.

shed system. It is not feasible to control the internal E-field to prevent discharge activity caused by moisture present due to ingress.

Corona Activity from Metallic End-fittings or Corona Rings under Dry Conditions

High E-field magnitudes on the surface of, and surrounding, the metallic end fittings and corona rings can result in corona activity under dry conditions. These discharges result in radio interference and audible noise that, in turn, may result in complaints. If this discharge activity is in contact with the rubber weathershed system, or end fitting seal, degradation may occur. Figure 4.4-6 shows such activity and resulting degradation.

Sustained corona activity from galvanized end fittings has been shown to result in localized loss of galvanization from the steel end fitting and resulting localized corrosion.

Correct design and application of corona rings will ensure that the surface E-field magnitudes are below the threshold values required for dry corona activity. Tests are specified in most standards to ensure that corona activity under dry conditions does not occur (ANSI 2002a, 2002c; IEC 1992). It should be noted that these tests are usually only applicable to a single configuration type (usually an I-suspension string with minimal hardware), and testing may be necessary for other configurations.

Discharges due to Nonuniform Wetting of the Polymer Rubber Material

Discharge activity may occur on the surface of polymer insulators due to the presence of moisture. Moisture may be in the form of discrete droplets or water patches, depending on the surface properties of the rubber and the type of wetting. This type of discharge activity occurs due to the high dielectric constant of water and hence is not dependent on contamination being present—i.e., it occurs under low, or even clean, conditions (Phillips et al. 1999a, 1999b; Lopez et al. 2002; Lopez et al. 2001).

The discharge activity takes on different forms on hydrophobic and hydrophilic insulators.

Hydrophobic Insulators (e.g., Silicone Rubber)

Water drops and patches on the rubber surface enhance the electric field due to the high permittivity of water ($\varepsilon_r = 80$). If the electric field (E-field) is enhanced above a critical value, corona activity will result from the edge of the water. Figure 4.4-7 shows how a water drop enhances an electric field.

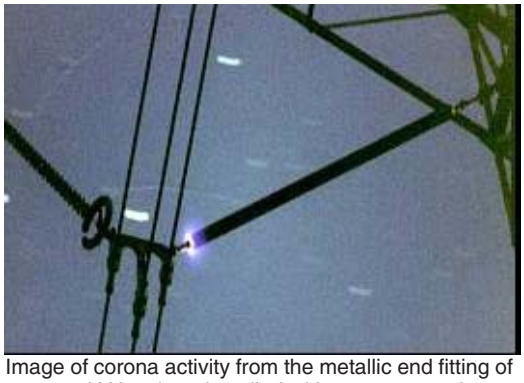
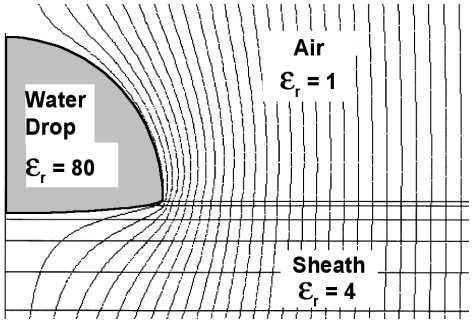


Image of corona activity from the metallic end fitting of a 500-kV insulator installed without a corona ring.

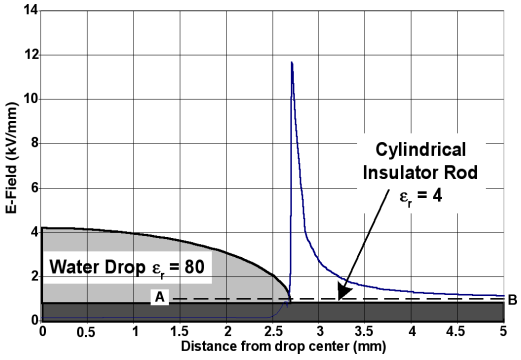


Erosions on the rubber weathershed material as a result of corona activity.

Figure 4.4-6 Corona activity from energized end fittings and the resulting damage.



(a) Equipotential lines surrounding a water drop on the surface of a polymer insulator in an electric field.



(b) Graph showing the increase in the E-field magnitude surrounding a water drop.

Figure 4.4-7 Results of finite elements modeling, showing enhancement of the E-field surrounding a water drop on the surface of a polymer insulator (Phillips et al. 1999a).

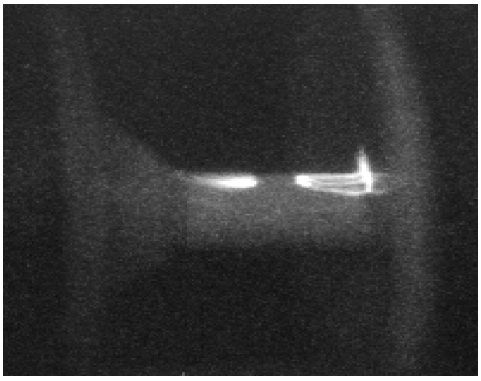
As can be seen from Figure 4.4-8, the E-field is significantly enhanced at the water/air/rubber interface. The enhanced E-field, in turn, results in corona discharge activity from the tip of the drop, as shown in the figure. This discharge, in turn, may degrade the polymer material.

The unperturbed, or dry, E-field magnitude necessary to result in corona activity from water drops is primarily a function of drop size and hydrophobicity. The larger the drop and lower the hydrophobicity, the lower the E-field magnitudes required. The E-field magnitudes for water drop corona on the sheath and shed are different due to the orientation of the E-field. Single drop experiments have shown that drops on the sheath have an onset field of greater than 4 kV/cm, depending on the hydrophobicity, while drops on the shed surfaces require an E-field of 8.5 kV/cm.

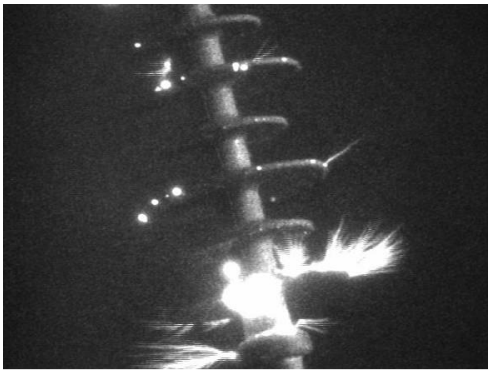
EPRI research has verified the occurrence of water drop corona and has shown that it may result in localized loss of hydrophobicity on silicone rubber insulators, as shown in Figure 4.4-9 (Phillips et al. 1999a, 1999b; EPRI 2000a, 2002a, 2003a, 2004a). This loss can be attributed to either the chemical by-products of the corona together with the moisture present or thermal increases due to the localized ionization (Goldman et al. 1989). Research indicates that the effect of the temperature increases due to corona is minimal, while the effects of chemical by-products, together with moisture, are more significant. It is unlikely, however, that water drop corona alone will result in significant degradation of the polymer weathershed system (Moreno and Gorur 2001, 2003).

Recent findings have indicated that water drop corona may just be the initial phase of the following, more severe, degradation mechanism that affects the long-term performance of the insulator:

1. Water drop corona in the high electric field regions results in localized loss of hydrophobicity. Regions affected have E-field magnitudes above the water drop corona onset threshold.
2. Under wetting conditions, patches of water form in the regions of lower hydrophobicity. These surface water patches are separated by dry regions or bands.
3. Localized arcs form, bridging the gaps between the water patches (EPRI 2003a).

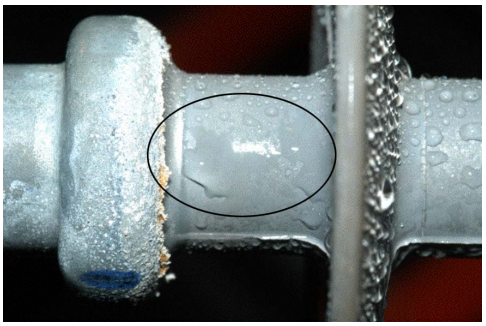


(a). Corona activity from a single water drop.

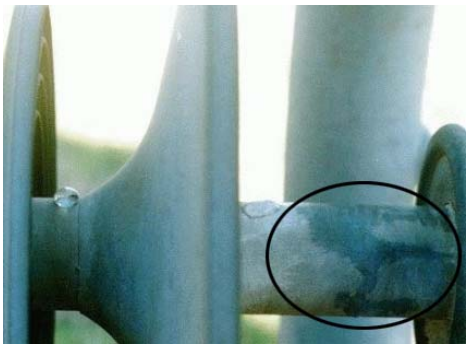


(b). Wetting corona activity at the live end of a polymer insulator.

Figure 4.4-8 Image intensifier image showing corona activity wetting activity (Phillips et al. 1999a).



Aging chamber



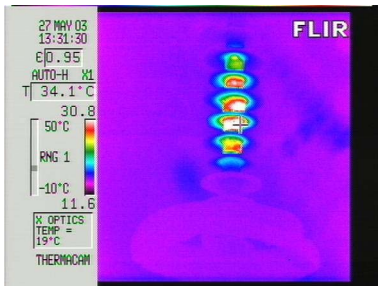
Insulator removed from service

Figure 4.4-9 Photos illustrating localized loss of hydrophobicity in the aging chamber and its effects on an insulator removed from service.

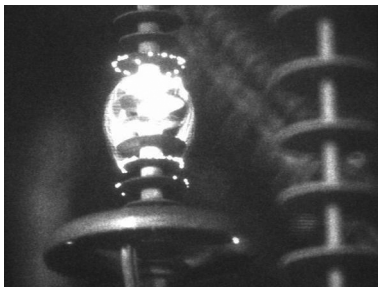
4. The energy and temperature of these localized arcs are significantly higher than that of water drop corona, stressing the rubber weathershed surface further (Gubanski 2003).
5. Over time, as the affected regions lose hydrophobicity, and completely wet out, the E-field in the adjacent regions is enhanced above the water drop corona onset threshold under wetting conditions.
6. The aging mechanism is then initiated in the previously unaffected regions. In this manner, the region affected is increased.

The activity described above is initially localized to the high electric field region of the insulator—i.e., the energized or grounded ends. The rest of the insulator remains hydrophobic and in good condition, hence there will be no significant increase in the leakage currents measured at the grounded end. Observations from the EPRI accelerated aging tests have indicated that, after 30 years of simulated aging, the loss of hydrophobicity can encompass as much as one-quarter of the insulator length (EPRI 2003a, 2004a).

Figure 4.4-10 shows an example of arcing activity observed in the high electric field region of a silicone rubber insulator.



Infrared image



Ultraviolet image

Figure 4.4-10 Localized arcing activity observed on a 230-kV silicone rubber insulator. The observed activity was correlated with localized loss of hydrophobicity in the high field region. Apart from the region showing activity, the rest of the insulator had a high level of hydrophobicity, and no leakage currents were measured at the grounded end.

Hydrophilic Insulators (e.g., EPDM)

During wetting conditions, the rubber surfaces of hydrophilic polymer insulators are covered with distinct droplets and patches of water. Dry regions separate these patches, and due to E-field enhancement, sparking may occur between patches. These discharges may degrade the rubber material. Figure 4.4-11 shows an example of this arcing activity.

Observations have shown that this activity may occur away from the high electric field region; however, casual observation in aging tests indicates that it is more prevalent in the high electric field regions.

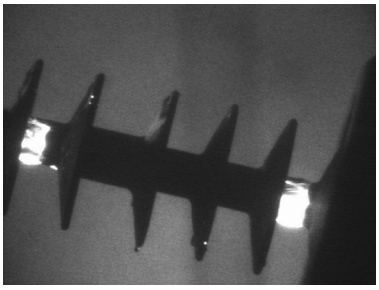
Dry Band Arcing under Contaminated Conditions

Contaminated insulators may have surface leakage currents and dry band arcing on the polymer weathershed system surfaces. For most types of contaminants, these phenomena occur only under wetting conditions due to the increased conductivity of the contamination layer.

As explained in Section 4.3.4, the dry band arcing on long polymer insulators is usually concentrated around the end fittings of the insulator, resulting in increased degradation in these areas. This discharge activity may result in degradation of the rubber housing as well as the end fitting seal. This degradation may include erosion, tracking, and localized loss of hydrophobicity. Loss of hydrophobicity is a



Infrared image



Ultraviolet image

Figure 4.4-11 Infrared and ultraviolet images of dry-band arcing activity on a polymer insulator (EPRI 2003a).

concern with silicone rubber insulators only. Severe examples of erosion and tracking are presented in Figure 4.4-12.

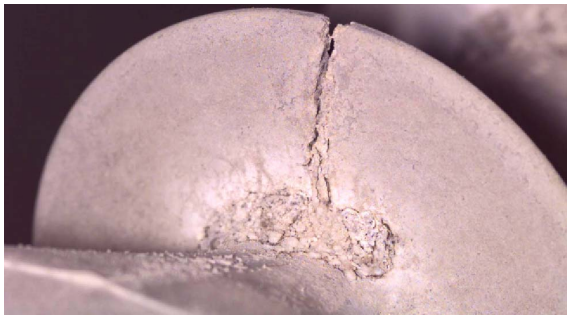
Damage due to External Power Arcs

Insulators may flash over due to lightning, switching, bird contact, or other activity, resulting in a power arc that terminates on the insulator or associated components. Termination points include end fittings, either energized or grounded, or the corona rings.

If the arc terminates on the end fittings, the intense arc root temperatures and energy dissipation may result in:

- Damage to end fitting seals.
- Loss of the galvanization.
- Localized heating that may damage the fiberglass rod or rubber weathershed system.
- Short-term loss in mechanical strength (Matsuoka 1998).

Damage to the end fitting seals is the largest concern. This concern is accentuated when aluminum components are integral to the seal mechanism since the melting temperature of aluminum is often lower than the arc root temperatures. Figure 4.8-9 shows an example of an end fitting seal damaged by power arcs.



Severe erosion along a mould line



Tracking on a polymer insulator

Figure 4.4-12 Examples of erosion *(top)* and tracking *(bottom)* along mould lines.

Testing has shown that a 60% reduction can occur in the ultimate strength of units during a power arc event (corresponding to 80% of specified mechanical load). A long-term loss of 10 to 20% in ultimate strength was recorded, but the units were still able to hold the specified mechanical load (Matsuoka et al. 1998).

Localized damage to galvanization will result in corrosion. In most cases, damage to the weathershed system is secondary.

Failure Modes

A failure may be defined when a polymer insulator is unable to fulfill either of its principal roles (EPRI 2003b, 2004c):

- Unable to insulate under power frequency conditions.
- Unable to hold everyday mechanical load.

The inability of an insulator to withstand transient overvoltages or temporary mechanical overloads within rating may also be considered a failure. However, in most cases, it is almost impossible to know the magnitude of these events for in-service units.

Mechanical failure modes include:

- Brittle fracture (stress corrosion cracking of fiberglass rod)
- Destruction of rod by discharge activity
- Mechanical failure due to end fitting pullout or mechanical failure of the rod

Electrical failure modes include:

- Flashunder (tracking along or through the fiberglass rod and the resulting flashover)
- Flashover due to contamination

The first four failure modes listed above relate to failure of the fiberglass rod, or the interface between the rod and rubber. Hence one of the most common reasons for failure is exposure of the fiberglass rod to the environment. This may occur through the functional failure of either the rubber weathershed system or the end fitting seal.

The following sections provide more detail on each of the failure modes.

Brittle Fracture (Stress Corrosion Cracking of Fiberglass Rod)

A brittle fracture is a mechanical failure of the fiberglass rod—i.e., a complete separation of fiberglass rod, as shown in Figure 4.4-13 (Burnham et al. 2002; CIGRE 1992b; Chandler et al. 1983; Chandler and Reynders 1984).

Features of a brittle fracture are:

- One or more smooth, clean planar surfaces, mainly perpendicular to the axis of the fiberglass rod giving the appearance of the rod being cut.
- Several planar fracture planes separated by axial delaminations.
- Residual mechanical fracture surfaces—i.e., broomstick.

Brittle fractures are caused by chemical attack of the FRP rod when nonsiliceous ions are leached from the fibers, and the surrounding thermoset resin matrix is hydrolyzed. This chemical attack, together with the mechanical load, results in transverse cracking. The cracking will progress until the remaining cross section of the rod can no longer support the applied load, and total separation occurs. Brittle fracture is more accurately defined as stress corrosion cracking. In many instances, failures may be misdiagnosed as being due to brittle fracture through simple visual examination. To properly identify a brittle fracture failure, it is helpful to utilize SEM and chemical analyses techniques.

Research indicates that brittle fracture occurs due to the presence of acids in proximity of the rod. There are a number of competing theories on how these acids are formed (Montesinos et al. 2003; Kumosa et al. 2004; de Tourreil et al. 2000).

Flashunder (Tracking Along or Through the Fiberglass Rod and the Resulting Flashover)

This is an electrical failure mode. This failure mode occurs when internal discharge activity results in carbonization within or on the surface of the fiberglass rod. Internal discharge activity may occur due to moisture ingress or internal defects—e.g., voids, poor bonding, or conductive defects. Internal tracking grows in or on the rod until a critical distance along the insulator is reached and the applied voltage can no longer be withstood and a flashunder occurs.

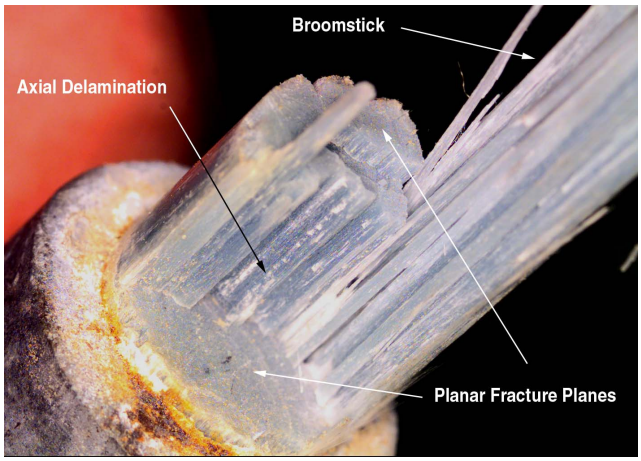


Figure 4.4-13 Brittle fracture. Note the several separate flat transverse fracture planes and the "broomstick."

Features of a flashunder include:

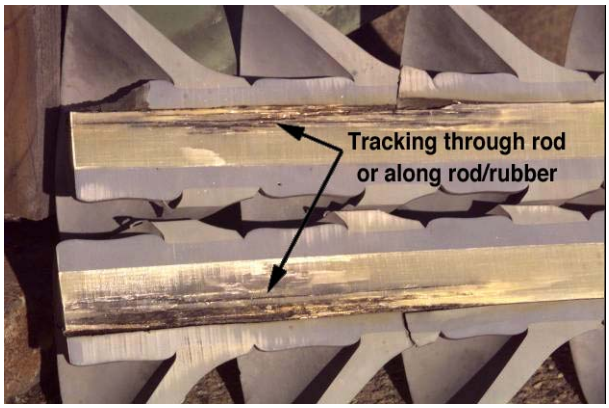
- Tracking through the rod or along the rod/rubber interface.
- Puncture holes and splits along the length of insulator due to internal discharge activity and a power arc during failure.

Figure 4.4-14 shows images of a flashunder and the associated features.

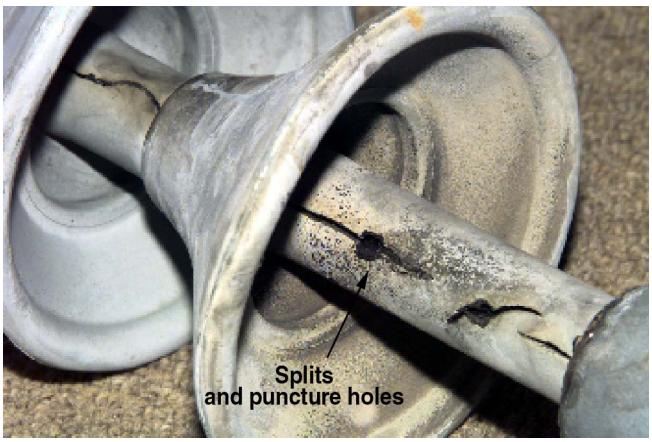
In a number of cases, after a flashunder occurred, and the line was re-energized, the insulator has been able to provide insulation adequate to prevent an immediate outage. This is due to the resulting power arc drying out the insulator and improving the insulation ability of the unit. However, with time or renewed wetting, the unit may precipitate further outages, leading to further damage that eventually results in complete electrical or mechanical failure.

Destruction of Rod by Discharge Activity

Destruction of the rod by discharge activity is a mechanical failure mode. Internal defects or moisture or contaminant ingress may result in internal discharge activity. If the rod



Two halves of a dissected polymer insulator that has failed due to a flashunder.



External photograph of the live end of an insulator that has failed due to a flashunder.

Figure 4.4-14 A flashunder and associated features.

becomes carbonized, a larger conductive defect is formed. These discharges degrade the rod until the unit is unable to hold the applied mechanical load and the rod separates. Figure 4.4-15 shows images of a rod damaged by discharge activity.

Mechanical Failure due to End Fitting Pullout or Mechanical Failure of the Rod

These are mechanical failure modes where either the insulator mechanically fails when the rod separates from the end fitting or the rod itself mechanically fails. These failures may occur due to mishandling, errors in the manufacturing process, and/or degradation—e.g., overheating of the fiberglass rod during manufacturing, or decomposition of the epoxy in an epoxy-cone-type end fitting, etc.

Figure 4.4-16 shows an example of a fiberglass rod that failed mechanically in-service. The reason for failure was traced back to a manufacturing defect.

Figure 4.4-17 shows an example of a unit that has failed due to the rod pulling out of the end fitting due to decomposition of the epoxy cone.



Dissected rod and end fitting of failed unit.



End fitting and rod of failed unit.

Figure 4.4-15 Unit that failed due to destruction of the rod by discharge activity.



Figure 4.4-16 Mechanically failed rod due to manufacturing defect.

Flashover due to Contamination

As explained in Section 4.3, the two main modes of insulator contamination flashover are solid and liquid contamination flashover. Flashovers occur mainly due to power frequency stress. Switching impulses may result in contamination-related flashovers, but this is rare. Contamination flashovers are not included in the EPRI failure database, as flashovers are mainly attributed to inadequate design, exceptionally harsh environments, or extraordinary contamination events.

Summary of Failures

In 1997, EPRI started a database recording failures of transmission polymer insulators in the field. Information and images, where possible, were obtained on each individual failure and stored in an electronic database, which may be queried at a later date. Information on failures as far back at the 1970s was obtained. The database continues to track failures on an ongoing basis, and the data presented in the following section was current as of September 2004 (EPRI 2003b).

Information is obtained from the relevant utility using a questionnaire containing a range of standard questions. Often the utility is unable to answer all of the questions in the questionnaire. This is often the case when utilities provide information on failures that did not occur recently.

For purposes of the database, a failure was defined as either of two conditions:

- Electrical: The insulator was unable to electrically insulate the energized conductor and hardware from the grounded structure. This may occur internally or externally along the surface of the polymer insulator.
- Mechanical: The insulator loses its ability to hold its everyday mechanical load and, consequently, the mechanical load that it is holding is released.



Dissected end fitting of failed unit.



Rod from failed unit.

Figure 4.4-17 Unit that has failed due to decomposition of the epoxy cone.

Precluded from this survey are three types of failures:

- Flashover due to external contamination—e.g., due to marine pollution.
- Failure due to extreme mishandling—e.g., the unit is broken during installation.
- Failure due to extreme mechanical loads—e.g., icing or hurricanes.

Although the database contains a comprehensive number of failures in North America, no attempt was made to collect information on a significant number of failures internationally due to the logistics involved. As of June 2003, EPRI has collected 189 failures from 53 different utilities. With four exceptions, all of the failures were collected from North American utilities. Of the 189 failures, 159 occurred in North America. Figure 4.4-18 shows the distribution of the failures between the different failure modes (EPRI 2003b).

A review of a recent paper, *IEEE Task Force Report: Brittle Fracture in Nonceramic Insulators* (Burnham et al. 2002), indicates that there are an additional 46 international brittle fracture failures that are not included in the EPRI failure database. The Task Force report only reported brittle fracture failures, and hence the total number of failures worldwide may be larger. The total number of recorded failures worldwide, therefore, exceeds 220.

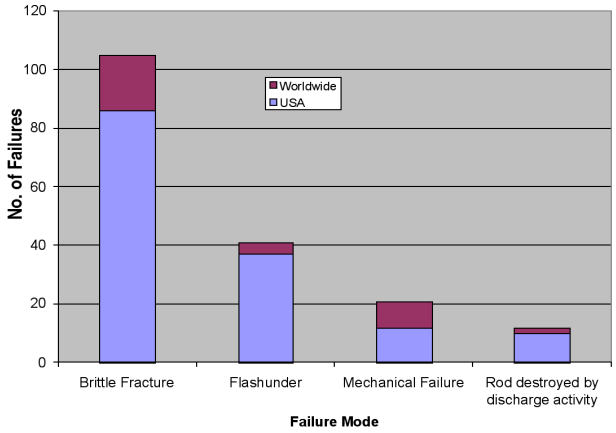


Figure 4.4-18 Failure mode distribution from EPRI failure database. Failures within and outside of the USA are indicated (EPRI 2003b).

It should further be noted that the failure database has by no means captured all of the failures that have occurred. In reality, it is the authors' opinion that a large percentage have not been captured in the EPRI failure database. EPRI is continuing to obtain failure information to increase the accuracy of the database and results.

Failure Rates

Of the 188 failures reported in North America, 89 related to the manufacturers that provided information to EPRI on the number of units sold. Based on this information, the average failure rate for all the manufacturers that provided sales information was 1 in every 45,000 units sold. Apart from one manufacturer for which there are no recorded failures, the individual manufacturer failure rates varied from 1 in every 65,000 to 1 in every 31,000 units sold (EPRI 2003b).

Utilizing the average failure rate data indicated above may be misleading, as 100 of the failures recorded in the database were from manufacturers that did not provide data or are no longer selling product and hence did not provide sales information.

Occurrence of Failures

An analysis of the data captured in the database has shown that 40% of failures occur within three years of installation (see Figure 4.4-19). This may be attributed to the weeding out of defective units or minor damage during installation. Although the number of units installed has increased over the years, the number of failures has not, indicating improved manufacturing techniques and materials have resolved early issues.

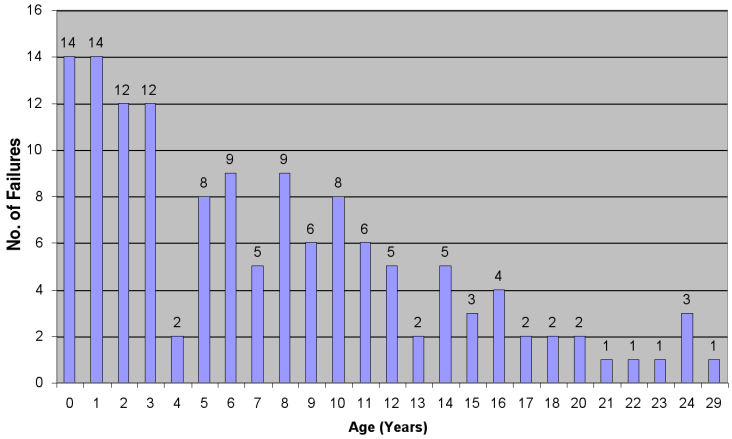


Figure 4.4-19 Age of failures (the age of failure for 57 failures could not be determined). Note: Installation year is used rather than year of manufacture, as the data is more readily available (EPRI 2003b).

4.5 LABORATORY TESTING

4.5.1 Introduction

Laboratory testing of insulators aims to verify by relatively short-term testing in a controlled environment, that the insulator is capable of withstanding the highest level of service voltage and the expected environmental stress without flashover or irreversible degradation (CIGRE 1999a). In this respect the validity of a laboratory test method can be measured in terms of the following concepts:

- **Representativity.** A test method must represent actual service conditions. Because it is impossible to simulate completely all of the many conditions in nature, only those conditions essential to determining insulator performance should be considered. A test method can be considered representative if the ranking order of different types of insulator produced by the test corresponds to that obtained in the service environment.
- **Repeatability.** If the test method gives consistent results from test to test performed in the same laboratory, then the test method can be considered repeatable. This requires that all test parameters be controlled as well as possible to eliminate excess dispersion in test results.
- **Practicality.** Insulator tests can be time consuming especially if the method is complicated. From the utility engineer's point of view, the insulator tests must be accomplished within a limited time and cost due to construction schedules and budgets. This obviously requires simplified test procedures.
- **Reproducibility.** If consistent results are obtained when different laboratories perform the test, then the test method can be considered reproducible. This aspect requires that all the test parameters are well defined and an unambiguous description of the method itself. Insulator manufacturers particularly emphasize the need for the development of reproducible test methods.

All laboratory test methods represent a compromise between the above requirements. Any particular method can, therefore, be criticized because of the necessary simplifications to achieve a practical method. On the other hand, research-oriented methods involve more complicated procedures, possibly with an increased dispersion in the results, and longer, time-consuming test durations. These problems are inevitable when trying to duplicate natural conditions.

There are two aspects that need to be considered when selecting tests to verify the performance of insulators. These are test methods that verify:

1. **Long-term performance of the insulator.** The exposure of the insulator to the environmental stresses may cause deterioration. This is mainly a concern for polymer insulators that may be influenced by electrical discharges and environmental factors.
2. **Electric flashover performance.** It is expected that the insulator, in the aged condition, will withstand the highest level of service voltage and the level of contamination to which it will be exposed with an acceptable Risk of flashover.

The first aspect is normally addressed by so-called "aging" tests, while the latter is verified by contamination tests.

4.5.2 Test Methods to Determine the Long-Term Performance of Insulators (Aging Tests)

Since the required life expectancy for polymer insulators is often 30 years or greater, a number of accelerated aging tests have been used worldwide to evaluate the long-term performance of polymer insulators. These tests are intended to simulate specific environments around which an aging cycle is developed. The design of the aging cycle is dependent on the primary aging mechanism under consideration. For example, if a highly contaminated environment is being considered, a higher number of pollution events may be included in the cycle. In the case of an aging test simulating a low-contamination environment, the number, or duration, of wetting events may be increased.

When considering the results of an existing test, or implementing a new aging test, care should be taken to consider the environment in which units will be installed and what the primary and secondary degradation modes are. The aging cycle should be designed to simulate the degradation phenomena that will occur in the field as accurately as possible. If a degradation mode is introduced that does not occur in the field, the test results may not be relevant.

Acceleration rates quoted for the individual tests are only approximate and are specific to the environment being simulated. Determining the acceleration rate requires a thorough understanding of the aging mechanisms, and in some cases, research performed at a later date may require the readjustment of initial acceleration rates. For example, at the time of development of the EPRI "Deserts with a Distinctly Cold Season" aging test, the assumption was made that the elevated temperature present in the desert was the primary aging process. Later research indicated, however, that wetting time was instead the primary aging factor; hence the initially calculated acceleration factor of between 12 and 20 was revised at the end of the test to a value between 7 and 14 (EPRI 2000a).

Also important when designing an aging cycle is to include rest periods where silicone rubber-based insulators are able to recover their hydrophobicity. These rest periods were not always included in the early versions of accelerated aging tests, leading to pessimistic and unrepresentative test results. The required conditions and duration of rest peri-

ods remain undefined and a topic of ongoing research via comparisons with service experience and natural testing sites where relevant and available.

It is, furthermore, essential to compare the results from accelerated aging tests against field-aged units to confirm that the aging mechanisms simulated in the tests are relevant to actual service conditions. In a number of cases, the accelerated aging results have compared favorably with both field-aged and outdoor test station units (EPRI 2000a, 2002a, 2003a, 2004a; Maxwell et al. 2002).

A number of accelerated aging tests have also been performed to assess the performance of one or possibly two components of an insulator but not the entire insulator (e.g., end fitting seal, mechanical performance, or rubber insulator housing). Examples include the incline plane test, the CEA tracking wheel test, EPRI's end fitting seal test, and EPRI's long-term dynamic and mechanical loading tests. These tests do not provide an indication of life expectancy; rather they provide a performance comparison between different designs, or highlight design weaknesses in the component being evaluated.

Some, but not all, of the accelerated aging tests are described in a document produced by a CIGRE Working Group (CIGRE 1999a). A summary of these tests, together with tests that have subsequently been implemented, is provided in this section.

IEC 601109 5000-h Test (CIGRE, Electricité de France Specification)

This 5000-h test, which was developed by Electricité de France (EDF) and subsequently adopted by the IEC, introduces multiple stresses in 24-h cycles while energized to the highest system voltage $V_m/\sqrt{3}$ kV (IEC 1992; Riquel 1993; CIGRE 1986). One cycle consists of different periods during which the insulator is exposed to demineralized rain, heating, humidification, fog generated from saltwater, and ultraviolet (UV) radiation, as shown in Figure 4.5-1. The representativity of the test was confirmed by comparing the damage sustained during the test with that occurring at an outdoor test station. Based on this comparison, an acceleration factor of 10 was determined for this test. Due to practical and cost limitations, the 5000-h test is normally performed in a small test chamber with a test voltage of between 14 and 20 kV. However, an aging chamber with a test voltage of $245/\sqrt{3}$ kV has been installed in France for full-scale testing at higher voltage levels.

ENEL 5000-h Test

This test is based on the same types of stresses as the IEC/CIGRE test, but it comprises a seven-day cycle (Fini et al.1993), of which details are presented in Figure 4.5-2. Other differences between the ENEL and IEC/CIGRE tests concern the salinity of the saltwater used for the pollution

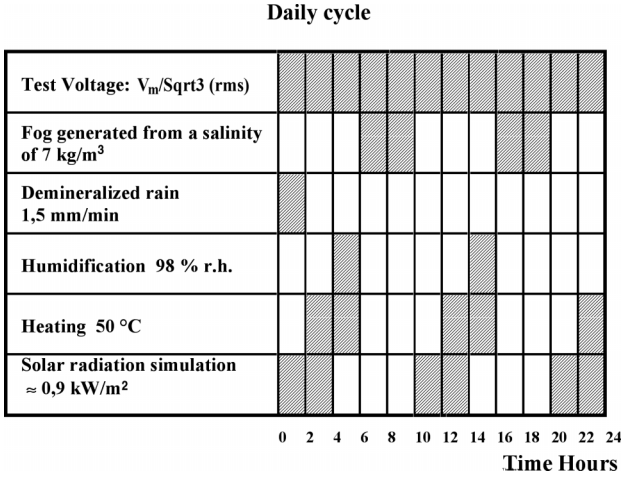


Figure 4.5-1 The aging cycle for the IEC/CIGRE 5000-h test.

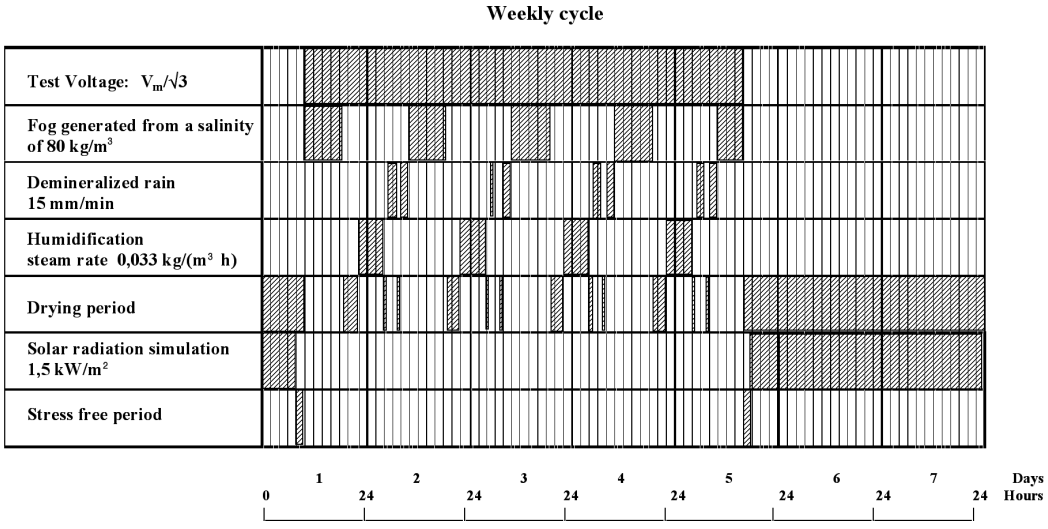


Figure 4.5-2 The aging cycle of the ENEL 5000-h test.

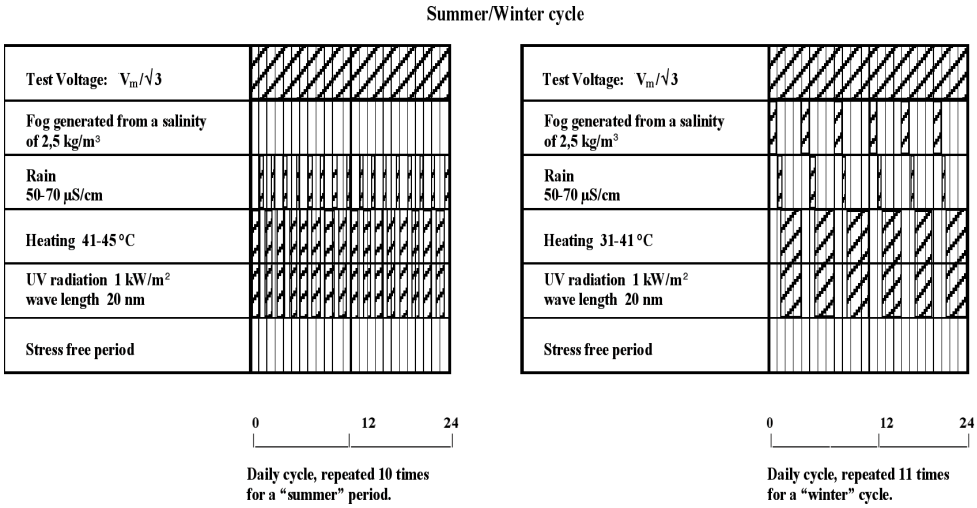


Figure 4.5-3 Aging cycle for the EPRI summer/winter cycle test.

period (i.e., ENEL uses 80 g/m^3 instead of 7 g/m^3) and the intensity of the solar radiation (i.e., ENEL uses 1.5 kW/m^2 instead of 0.9 kW/m^2). The test was devised for the selection of polymer insulators based on Italian conditions. It can be performed on full-scale insulators for system voltages of up to 540 kV.

EPRI Summer/Winter Cycle Test

This test was devised to simulate the weather conditions of the Florida seacoast area. There are two different 24-hour cycles, one for the summer and one for the winter. One year of service is represented by 10 summer cycles, which is followed by 11 winter cycles. The schematic of the cycles is shown in Figure 4.5-3. By this definition of the test cycles, the acceleration factor is about 17. The test has been performed on full-scale insulators at 138 and 15 kV (EPRI 1992; Schneider et al. 1992).

EPRI Test to Simulate "Deserts with a Distinctly Cold Season"

This test has been devised to simulate the weather conditions of the western part of the United States, where there is light rainfall, extensive UV duration, and elevated temperatures with relatively little contamination, which can be described as "deserts with a distinctly cold season." The aging cycle of this test is shown in Figure 4.5-4. One year of service is represented by 30 daily cycles. By this definition, the acceleration factor lies between 7 and 14. The test duration depends on the number of years that have to be simulated.

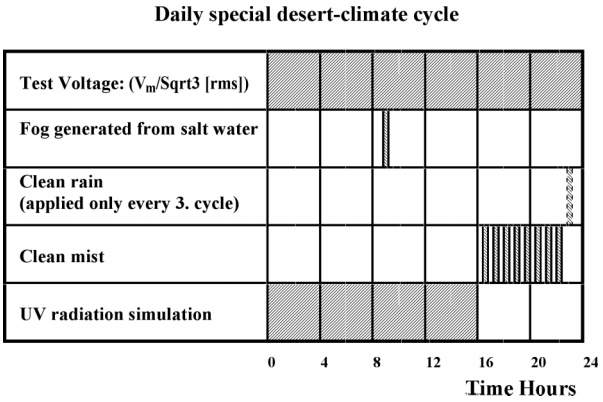


Figure 4.5-4 Aging cycle for EPRI Test to Simulate "Deserts with a Distinctly Cold Season."

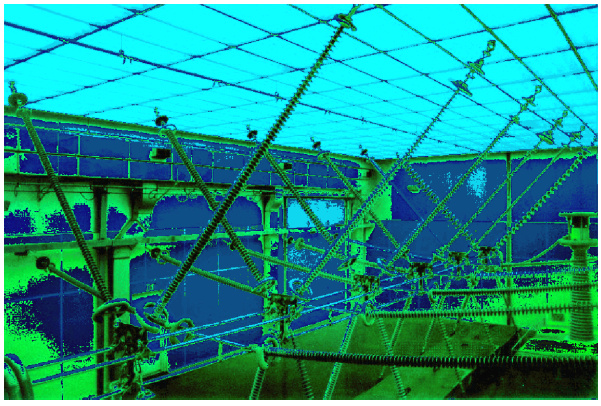


Figure 4.5-5 EPRI 500-kV accelerated aging test.

This test was performed on full-scale 500-kV insulators in both a horizontal and V-string setup. The V-suspension insulators were placed under a static mechanical load of 27 kN each. The horizontal insulators were not mechanically loaded. Figure 4.5-5 shows a general view of the 500-kV test set-up. The test was completed after six years on 22 insulators from five different manufacturers. The results of the test and comparison between the performance of different designs may be reviewed in the appropriate EPRI reports (EPRI 2000a; Schneider 1993).

EPRI Test to Simulate a "Warm Temperate" Climate

This full-scale multi-stress test was designed to simulate the climate of the southeastern United States, although the results may be translated to regions with similar climates. The aging cycle is presented in Figure 4.5-6, and the stresses applied to the insulator include voltage, UV, light fog, rainstorms, salt fog, mechanical loading, and temperature cycling. The level of contamination applied in this test is relatively low. One year of experience is simulated by 36 days of aging. Units are assessed biannually using a detailed visual inspection, as well as infrared and discharge inspection tools under energized conditions. The test is currently under way simulating a system voltage of 230 kV with 43 I-string, V-String, dead-end, post, and braced post units under test. This test also includes transmission-line surge arresters, fiberglass cross-arms, and fiber optic polymer insulators. Suspension units are mechanically loaded to their routine test load (RTL) and post units to their maximum design cantilever loads. The current test is expected to end in December 2004 after four years of aging. Figure 4.5-7 is an image of the 230-kV aging test chamber (EPRI 2002a, 2003a, 2004a).

FGH 5000-h Test

This test produces accelerated aging on polymer insulators under 100-kV dc test voltage at a specific leakage distance of 20 mm/kV_{DC}. A simple 14-day cycle is used, including a stress-free period of five days. The test duration is 5000 h (see Figure 4.5-8).

Inclined Plane Test

Flat rubber samples are placed at a predefined angle with two electrodes touching the surface at a predefined distance. A saline solution is then dripped onto the rubber surface between the electrodes, which results in leakage currents and arcing activity. The test is intended to evaluate the ability of the rubber formulation with withstand tracking and erosion (ASTM D2303).

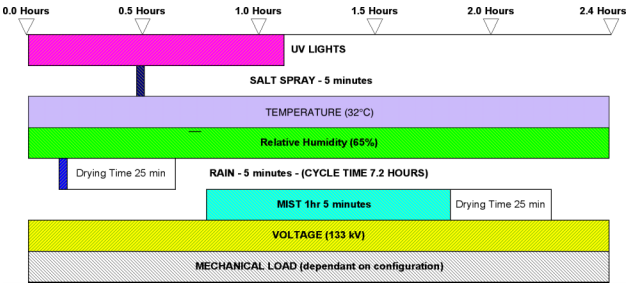


Figure 4.5-6 Aging cycle for EPRI test to simulate a warm temperate climate.



Figure 4.5-7 Some of the insulators installed in 230-kV accelerated aging chamber.

CEA Tracking Wheel Tests

There are two tracking wheel test methods commonly utilized as tests for polymer insulators. The tests are not accelerated aging tests with a fixed acceleration factor. The intent of the tests is more as a material and design screening test. During the tests the insulators are subjected to surface arcing generated through wetting with a saline solution and applied voltage. The properties of the insulator examined are material suitability, design (shed spacing and thickness, housing thickness), and the sealing system.

EPRI End Fitting Evaluation Tests

The end fitting regions of suspension polymer insulators are subjected to electrical and environmental stresses, while the entire insulator is subjected to both a static and vibration mechanical load. The test apparatus used to apply these stresses to the insulators is shown in Figure 4.5-9.

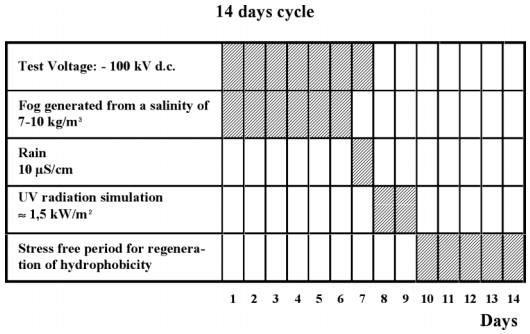


Figure 4.5-8 Aging cycle for FGH 500-h test.

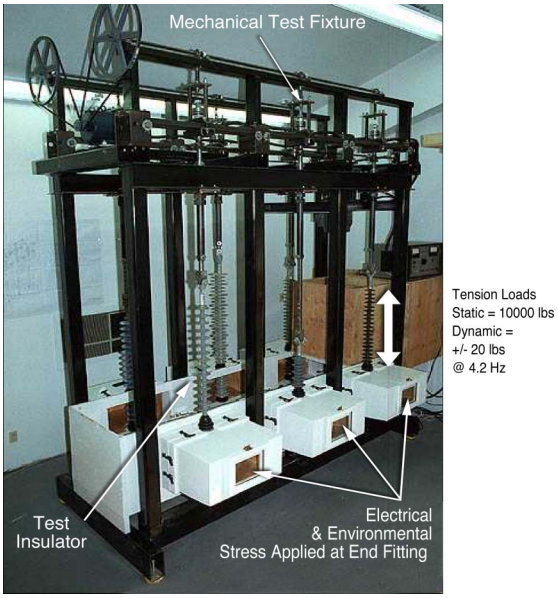


Figure 4.5-9 Overall view of test rig used for evaluating the end fitting seal and the mechanical performance of the insulator.

An electrical stress is applied to insulator end fitting regions using a remote electrode. The electrode geometry is designed to ensure that the peak magnitude of the E-field surrounding the end fitting is 0.7 kV/mm. Wetting is applied at regular intervals together with temperature cycling.

A static tension load is applied to each insulator with two leaf springs. Each insulator is loaded to 10,000 lb (4,535 Kg). In addition, large pulleys apply a 4.2-Hz dynamic tension load (an oscillating load of +/- 20 lb [9 Kg]).

After 365 days of testing, the failure load of the insulators is obtained and compared against reference units. Dye penetration, together with dissection, is used to evaluate the effectiveness of the end fitting seals (EPRI 2002b).

EPRI Mechanical Loading Tests

Suspension polymer insulators are subjected to the following simultaneous mechanical stresses using the apparatus shown in Figure 4.5-10:

- 50% of SML (specific mechanical load)
- 4.2-Hz dynamic tension load (an oscillating load of +/-20 lb [9Kg]).
- A twisting of $\pm 25^{o}$ is applied at 0.1 Hz

After 365 days of testing the units, the failure load of the insulators is obtained and compared against reference units (EPRI 2002b).

4.5.3 Contamination Flashover Tests

The aim of performing laboratory contamination flashover tests is to obtain a reliable and quick estimation of the contamination-withstand characteristics of insulators. This information can then be used to dimension insulators with respect to actual contamination conditions at their proposed installation site. It has been shown through results from natural test sites that the flashover voltages of insulators in service exhibit a larger standard deviation than those tested under artificial conditions. This can be ascribed to the greater nonuniformity of the pollution deposit and wide range in natural wetting intensity that occurs under natural conditions. A laboratory test, by contrast, aims to reduce the standard deviation of the flashover strength—without a change in its withstand value—by eliminating the factors that contribute to the large standard deviation observed in service. Laboratory contamination testing should still emulate the service environment of the insulator in a realistic manner to ensure that the withstand level obtained under artificial conditions corresponds to that under natural conditions.

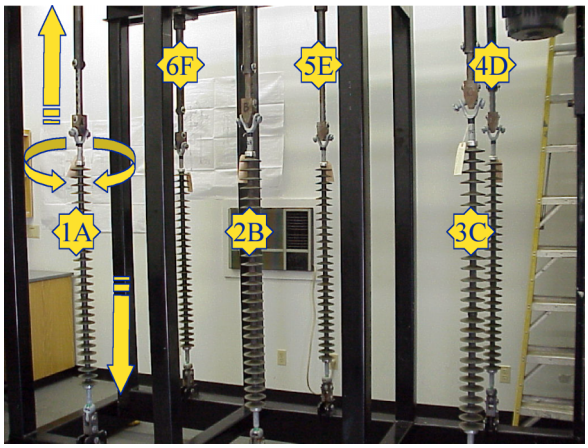


Figure 4.5-10 Test to evaluate mechanical performance (arrows indicate the static and dynamic loading applied).

The most often used laboratory contamination tests are those standardized by the IEC—namely, the Salt-Fog and the Solid-Layer methods (IEC 1991). These methods proved to be unsuitable for polymer insulators, since the hydrophobic nature of the insulator surface and its transfer to the contamination layer, as well as the dynamic nature of the surface conditions, adversely affect the uniformity of the pollution deposit and the repeatability of the test results (CIGRE 1999a; Gorur et al. 1989; Kindersberger and Kuhl 1993). This has prompted the development of alternative techniques for the artificial deposition of contaminants and new nonstandardized simulated environment tests such as the "Dust-Cycle" and the "Dry-Salt-Layer" methods (Marrone et al. 1987; Engelbrecht et al. 2003). However, to date, there is no formal agreement on a contamination test regimen for polymer insulators.

In the standards, the procedure for performing withstand tests is described. This type of testing aims to verify that the insulator can withstand (i.e., has a less than 10% probability for flashover) a specific voltage and contamination stress. The applied test voltage remains at a constant level for the duration of the withstand test. Although this test strategy has its advantages—that is, the insulator is subjected to a low number of flashovers and the test result is a clear pass / no pass verdict—little information is obtained about the flashover characteristics of the tested insulators. Variable voltage tests, or quick flashover tests, have, therefore, been devised to obtain statistical information (e.g., 50% flashover voltage and standard deviation) on the insulator flashover characteristics at a specific contamination severity level. During these tests the applied voltage is increased in a stepwise fashion until flashover occurs (Lambeth 1988). These voltage "ramps" are repeated throughout the test to obtain the required statistical information.

Conditioning

Conditioning is a precursory treatment of the insulator before the contamination test is performed to get the test insulator in a state that is representative of an aged insulator in service and to ensure consistent test results (CIGRE 1999a).

The conditioning on glass and ceramic insulators aims to clean the insulator from grease and dirt so that a completely hydrophilic insulating surface is obtained. For the Salt-Fog Test, this entails washing the insulator, as well as a series of eight conditioning flashovers across the insulator prior to testing. For the Solid Layer methods, the insulator surface can be made hydrophilic by repeated applications of the pollution layer after the insulator has been washed.

For polymer insulators, it is not so easy to define an appropriate method for conditioning, since the aged surface condition is not easily defined. Some polymer insulators, notably silicone rubber ones, may retain a high degree of hydrophobicity throughout their service life. There may be instances, however, when the hydrophobic properties of these insulators may temporarily be suppressed, after which they may recover fully. Other insulator types, such as EPDM insulators, lose their initial hydrophobic properties completely after some time in service. A third group of insulator types may retain some intermediate level of hydrophobicity. Also the level of surface roughness will be different for the various makes of insulator; some maintain the same level of surface roughness as new units, while others exhibit an increasing level of surface roughness with increasing service aging.

The choice of representative surface condition for polymer insulators is very important since it has been shown that the hydrophobic properties greatly affect recorded flashover voltages. An additional complication is that the hydrophobicity of the insulators may change during the testing procedure, due to the electric discharge activity that the insulator is subjected to during the test (Kindersberger and Kuhl 1993). This will lead to inconsistent results during repetitive testing.

Various treatments of the polymeric surface have been proposed. Nearly all of them are aimed at suppressing any hydrophobicity for the duration of the test. This approach has the advantage of ensuring consistent results and making the application of the pollution layer easier, but at the risk of obtaining pessimistic results in the case of insulators with good long-term hydrophobic properties. Some of these treatments put forward are:

- Application of inert materials, such as kaolin or tonoko, to mask the surface's hydrophobicity.
- Abrasive techniques such as scrubbing or sandblasting the insulator to roughen up the surface and to remove any hydrophobicity.
- Chemical treatments with wetting agents or detergents to remove the surface's hydrophobicity.
- Exposure to electrical discharge activity for prolonged times.
- Combinations of the above.

These methods can be criticized as unrealistic since they all aim to suppress the insulator's hydrophobicity completely, which may not be representative of actual service conditions. However, several laboratories seem to prefer the use of inert materials to temporarily mask the hydrophobic properties of the insulator, as this may actually occur in service (De La O et al. 1994; Matsuoka et al. 1996; Xidong et al. 1999; Gutman et al. 2001).

Contamination Test Methods

Before standardization there were a host of different contamination test methods in use. These were compared and reviewed by CIGRE (CIGRE 1979a), and a few were subsequently standardized (IEC 1991) for use on ceramic and glass insulators. Developments are now focused to obtain a suitable contamination test method for polymeric insulators (CIGRE 1999a). These developments are further highlighted at the end of this section.

The most often used contamination test methods can be grouped as follows:

1. Salt-Fog test
2. Solid Layer tests
3. Simulated environment tests

There are significant differences among these test methods since each simulates a different aspect that may occur in service. This has led to disagreement in test results: an insulator rated high by one test method may receive a lower rating with other test methods. It is, therefore, important to select the test method that will best represents the environment for which the insulators are intended.

The Salt-Fog Test

This method, first derived in 1960-1964 in Great Britain, was given its final form as the result of a collaboration between the Central Electricity Generating Board (CEGB) in Britain, EDF in France, and Ente Nazionale per L'Energia Elettrica (ENEL) in Italy (Lambeth et al. 1973). In this method, the insulator is energized at the service voltage, which is held constant through the test, and subjected to a salt fog. The salt-fog salinity, expressed in kilograms of salt per cubic meter of the solution, defines the severity of the contamination condition. The salinity values used are chosen from values increasing in a geometric progression, usually from 2.5 to 224 kg/m^3. The fog is produced by arrays of nozzles on opposite sides of the insulator, directing a fog of droplets at the insulator by means of compressed air. The highest salinity at which there is a withstand, in at least three out of four one-hour tests, is called the withstand salinity and is regarded as the criterion of performance (IEC 1991).

In a variation of the Salt-Fog test, named the quick flashover method, a variable voltage is applied to obtain statistical information on the flashover voltage at a given salinity

(Lambeth 1988). This method is regarded as more cost and time efficient than the standardized method. After an initial stabilization period, the voltage is raised in a step-wise fashion until flashover. The process is repeated with a starting voltage that is 90% of the previous flashover voltage. Each step comprises a rise in voltage of between 2.5 and 3.5% and a duration of 5 min. It has been shown that there is a good relationship between the withstand salinity and the average flashover voltage obtained from the quick flashover method.

The validity of the Salt-Fog test was evaluated by natural contamination tests. First, a set of various types of insulators was selected to serve as a test sample in different laboratories. The relative performance of the insulators was determined with natural contamination tests by recording surge leakage currents. Then, the same set of insulators was tested with the Salt-Fog method, and the order of merit was determined by withstand salinity. In the Salt-Fog test, there is a relationship between maximum leakage current and fog salinity; thus the comparison of insulator performance is made in terms of leakage current. Good correlation in order of merit between both tests was reported (Lambeth et al. 1973). For polymer insulators, however, it was found that the Salt-Fog test produced inconsistent results that did not correlate well with flashover results from natural testing stations (Houlgate and Swift 1989). This method is, therefore, not generally recommended for the contamination testing of polymer insulators.

Solid Layer Tests

The IEC describes two variants of the Solid-Layer test (IEC 1991):

- Wetting before and after energization
- Wetting after energization

In both methods the insulators are contaminated by spraying or flow-coating the contaminant mixture—comprising a mixture of saltwater and an inert material such as Kaolin, Tonoko, or Kieselguhr—onto the insulator surface. The applied layer of pollution is allowed to dry on the insulator before the actual test starts.

Wetting before and after energization (Wet Contaminant Test). In this test, the insulator is placed in its test position, and the fog generation is started. During this time, surface conductance measurements are performed at regular intervals, and the test voltage is applied when the measurements indicate that the surface conductance has reached its maximum value. The constant amplitude test voltage is applied instantaneously and only for a period of 10 min while the fog generation continues. This process is repeated a maximum of four times, and the insulator is only recontaminated if the conductance measurements have deteriorated by more than 10% from the target value. The insulator has passed the test if no more than one flashover has occurred during four tests. This test method simulates wet contaminant conditions such as cold switch-on. The test severity is normally expressed in terms of the layer conductance. Steam fog is the preferred wetting method for this type of test, but other types of fog may also be used.

Wetting after energization (Clean Fog Test). In this second variant the dry test object is placed in its test position and energized to the test voltage. The steam-fog generation is then started, and the test ends on flashover or if the insulator withstands the voltage and fog for 100 min. Again, this procedure is repeated a maximum of four times, and the insulator has passed the test if it has not flashed over more than once. The Clean-Fog test is regarded as an approximation of inland conditions where condensation is the main mechanism of wetting. Wetting of the insulators is established by a steam-fog of a specific fog density. The severity of this test is normally expressed in the Salt Deposit Density of the contamination on the insulator.

Both these methods are normally performed with constant applied voltage to determine whether an insulator will withstand the applied contamination and voltage stress. Variable voltage tests have also been used in conjunction with the latter method to obtain statistical information about the flashover voltage of an insulator at a specific contamination severity (Lambeth 1988). The application of variable voltage testing is, in this case, more complicated than with the Salt-Fog test, since the flashover voltage changes during the test. It decreases initially due to the wetting of the pollution layer and then increases because the contaminants are leached from the insulator surface.

Experience with the solid layer methods indicates that it cannot be used to test polymer insulators unless changes are made to the test. The main difficulty is to obtain a uniform contamination layer on the insulator. In service, the insulator surface is mostly exposed to dry or humid contamination particles that are not influenced by the insulator's surface hydrophobicity. This leads to a fairly uniform distribution of contamination on the insulator surface. When a contamination layer is artificially applied, as described above, the contamination does not stick to the hydrophobic surface, leading to an irregular distribution of the contamination (Matsuoka et al. 1996).

Various methods have been suggested; the most common variant is to mask insulator's hydrophobicity by the application to the insulator surface of a light dusting of dry Kaolin or Kieselguhr. The contamination solution can then be applied with the normal methods, as described in the standards (De La O et al. 1994; Xidong et al. 1999). It was found that Kieselguhr has an advantage over Kaolin as a masking agent since it resulted in a faster and more predictable hydrophobicity recovery rate (Gutman et al.

2001). This method has subsequently been adopted by a CIGRE Task Force (CIGRE Forthcoming). In order to compare the performance of insulators with different hydrophobicity characteristics, the Task Force suggests that a range of Solid Layer tests (wetting after energization variant) be performed at specified time intervals after the pollution application. In this way, the flashover performance under the best and worst hydrophobicity can be quantified, irrespective of the insulator type. In addition to using a masking agent, the Task Force also suggests that a wetting agent can be used to suppress the hydrophobicity (Swift et al. 2001). NGK has developed a similar method to contaminate polymer insulators. Dry Tonoko powder is applied to the wet insulator surface; after a drying and washing process, the insulator can be contaminated with a slurry of Tonoko and saltwater (Matsuoka et al. 1996).

As was mentioned in Section 4.3, polymer insulators have different wetting characteristics than glass and ceramic insulators due to their low thermal capacity. The insulator adjusts quickly to the ambient conditions, which poses a problem when using a steam-fog wetting that relies on condensation to wet the insulator. Experimental results have shown that a high fog density is an important parameter that has a strong influence on the flashover values obtained on silicone rubber insulators, as shown in Figure 4.5-11. On the strength of these results, it is suggested that polymer insulators be tested with a steam-fog density of 13-15 g/m^3 (Matsuoka et al. 1996).

Another method that has been devised to contaminate hydrophobic polymer insulators uses a so-called Dry-Mixing contamination method (Besztercey and Karady 2000). A special dry mixing nozzle has been developed to produce a mixture of solid contaminant particles and an atomized salt solution in a turbulent jet of air. This nozzle can be used to produce a predictable, uniform, dry contamination layer on hydrophobic or hydrophilic insulators. The coated insulators can subsequently be tested using the standard Clean-Fog method described above.

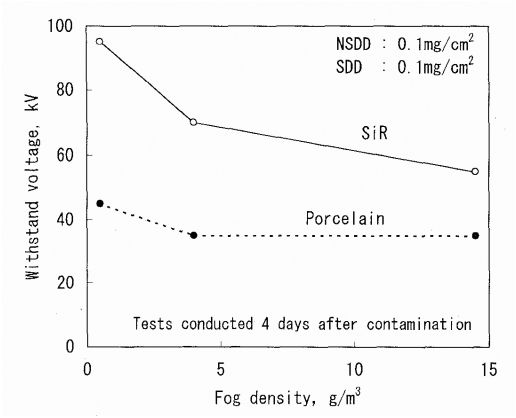


Figure 4.5-11 The relationship between fog density and the contamination withstand voltage of porcelain and silicone rubber insulators (Matusuoka et al. 1996).

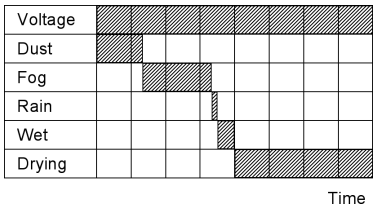
Simulated Environmental Flashover Tests

Simulated environment tests have been developed in order to improve on the aspects where the standardized laboratory tests were perceived to be weak. Two aspects were seen as important:

1. Testing of polymer insulators without the need for surface conditioning before the test
2. Evaluation of the insulator profile and its effect on the "pollution catch" of the insulator.

Two variants of simulated environment tests have so far been developed. These are the Dust-Cycle method (Eklund et al. 1994; Suzuki et al. 1999) and the Dry-Salt-Layer method (Engelbrecht et al. 2003). Both these methods expose the tested insulators to airborne contaminants.

In the case of the Dust-Cycle method, a "wind tunnel" is used to blow a mixture of salt and inert material toward the insulator under humid conditions. With this method, a predetermined stress cycle is repeatedly applied to accumulate contamination on the insulator until the insulator flashes over. This stress cycle simulates the pollution deposition by windborne contaminants, "natural" cleaning by rain, and a dry period where the polymer insulators get a chance to recover some of their hydrophobicity. The cycle is shown schematically in Figure 4.5-12, together with a view of a typical test chamber. It is also possible to adjust the cycle to fit specific types of environment. For example, a special



Stress cycle



General view of the test chamber

Figure 4.5-12 The Dust-Cycle method: the test cycle *(top)* and test chamber *(bottom).*

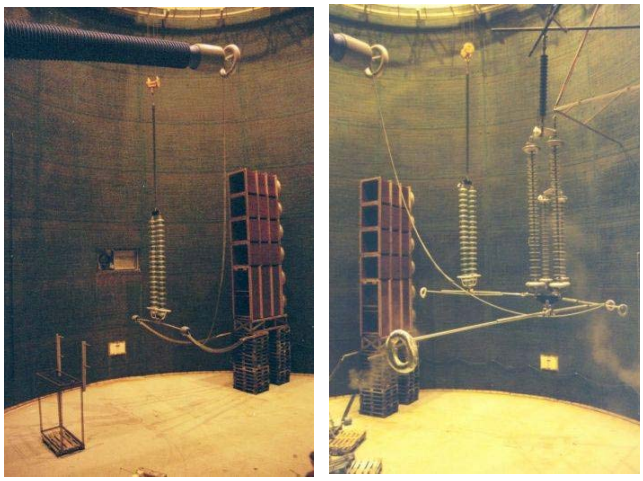
cycle, that included a period of wind cleaning, has been devised to simulate desert conditions (Engelbrecht et al. 2000). It was found that this type of testing produced the same flashover ranking of insulators as was found at field test stations (Znaidi 2001).

For the Dry-Salt-Layer method, a set of fans are used to circulate salt-laden air in the test laboratory and toward the test object under energized conditions, as shown in Figure 4.5-13. As with the Dust-Cycle method, this method also includes separate deposition and wetting phases. During the deposit phase, the insulators are exposed for a predetermined time to the salt-laden air to obtain a target Salt-Deposit Density while energized. After a short rest period, when the contamination layer is allowed to dry on the insulator, the wetting phase begins. A modified steam-fog wetting is utilized, where the steam is gently blown toward the test objects to obtain optimal wetting on polymer insulators. The wetting phase lasts 100 min or until the insulator flashes over. No conditioning of the insulators is necessary because they are exposed to dry, or nearly dry, contaminants so the hydrophobic properties do not influence the formation of a realistic pollution layer in a negative way.

Comparison of Flashover Test Methods

It is important to understand how contamination test methods differ from each other. Each test method presented above essentially simulates a different phenomenon. A factor that is important for one method may not be significant for other methods.

All the wet contaminant tests (e.g., Salt-Fog test) have been established on the assumption that the surface of the contaminated insulator is already wet when voltage is applied. A different approach is taken for the Clean-Fog test, in which a wetting condition, usually fog, is applied to the energized dry insulators. Different assumptions are also made regarding the manner in which the contaminant is deposited onto the insulator surface. For instance, the Dust-Cycle and Dry-Salt-Layer methods use an artificially generated wind to transport and deposit the contamination nonuniformly onto the insulator. This is in contrast to the Solid Layer methods, where the contaminants are applied uniformly to the insulator surface, or the Salt-Fog test, where a significant amount of contamination is accumulated on the insulator surface through the heating effect of the leakage current.



Deposit phase Wetting Phase

Figure 4.5-13 A view of the test set-up during the Dry-Salt-Layer method. Note the cabinet with fans on the right-hand side that blow the salt-laden air toward the test object, at center.

Aspects that should be considered when choosing a representative laboratory test method are:

- The way the insulator is conditioned to obtain a surface condition representative of an aged insulator.
- The type of contamination that the insulator is exposed to during the test: The contaminant can either be in liquid form, as in the Salt-Fog test, or as a dry contaminant layer, as in the Solid Layer tests.
- The way that the insulator is polluted: This can be either an artificially applied pollution layer, as in the Solid Layer tests, or some sort of environmental simulation that brings the pollution onto the insulator by a natural contamination process, such as during the Salt-Fog test.
- Voltage application: Contamination tests are either performed as constant voltage tests (i.e., withstand tests) or with a variable voltage (e.g., quick flashover method).

There is no direct relationship between the results of the Salt-Fog, Clean-Fog, and Wet-Contaminant methods, and one single method cannot simulate the breakdown phenomena created by the others. Thus, it is unreasonable to discuss the order of merit for several types of insulators by employing different test methods. For practical design, it is very important to choose the test method that will simulate the particular natural condition found in service. This means that nature is the ultimate standard to be used in contamination studies.

Clean-Fog tests are normally regarded as the most representative of contamination flashovers in the United States, which are commonly caused by contaminant deposition followed by a wet-weather condition. This test method closely simulates the slow wetting condition regarded as an essential component of almost any natural fog- or dew-initiated flashover. The high wetting rate present in Salt-Fog tests is more representative of coastal conductive fog conditions, and wet contaminant tests are more relevant to cold

switch-on conditions, which is when a completely wetted insulator string on a de-energized line is switched on.

4.6 ELECTRICAL PERFORMANCE OF INSULATORS AND AIR GAPS UNDER AC VOLTAGE

4.6.1 Introduction

An insulator needs to withstand all the electrical stresses that it is exposed to for the whole of its expected life. These stresses include transient overvoltages, such as switching and lightning, as well as more long-term voltage stresses, such as ac temporary overvoltage and the continuous ac supply voltage.

This section will concentrate on the insulation strength under ac voltages. Information can be obtained on the switching and lightning performance in Chapter 5 (Section 5.6.3) and Chapter 6 (Section 6.5), respectively.

4.6.2 Dry and Wet AC Flashover Strength of Air Gaps and Insulators

When insulators are dry, they have an ac flashover characteristic that is between that of a rod-rod and rod-plane gap, unless special field grading is employed, as shown in Figure 4.6-1 (Aleksandrov et al. 1962). This figure presents the flashover strength of a group of basic insulation configurations. The flashover stress of smaller gaps is presented in Figure 4.6-2 (IEEE 1974). Since the dry ac flashover strength of insulators is not a determinant in the insulation design, this data is used in the most cases to set the minimum clearances for power-frequency voltages in tower configurations during the initial design stages. For tower configurations for which the gap factor, "K", is known (see Chapter 5 [Section 5.2.4]), the ac 50% flashover strength can be estimated from (IEC 1996):

$$V_{a.c.50} = 750(1.35K - 0.35K^2)Ln(1 + 0.55L^{1.2}) \qquad 4.6\text{-}1$$

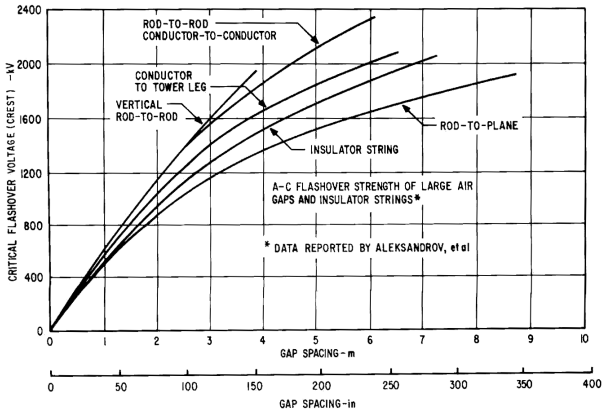


Figure 4.6-1 AC flashover strength of large air gaps *(*Aleksandrov et al. 1962*).*

This equation is valid for gap spacings greater than or equal to 2 m. A standard deviation of 2% may be assumed for the ac flashover strengths of air gaps. If the withstand voltage is assumed to be at the 3-σ level, its voltage would be 94% of the 50% flashover voltage (CFO).

Fires under transmission lines have proven to be a major cause of transmission-line outages. For example, in South Africa, 15.6% of transmission-line faults were classified as due to fires under the lines (Vosloo and Van Rooyen 2001). Investigations have shown that fires under lines cause a dramatic reduction in the withstand strength of the air between phases and between phase and ground (Fonseca et al. 1990; Sadurski and Reynders 1989; CIGRE 1992a; Swift and Naidoo 1993; Hoch and Sukhnandan 2003; Deno and Zaffanella 1987).

The heat in the flame associated with a fire reduces the air density according to the well-known expression:

$$\delta = p\frac{293}{273 + t} \qquad 4.6\text{-}2$$

Where:

δ = the air density relative to a pressure of 1.0 bar and a temperature of 20°C.

p = the pressure in bar.

t = the air temperature in °C.

Bearing in mind that temperatures as high as 900 °C are found in the flames of a large fire, the equation shows that the air density can be reduced to 25% of its value at 20 °C. Since breakdown strength is directly proportional to air density, the heat of the fire can reduce the strength of the air to 25% of its value at 20 °C (CIGRE 1992a). However, elevated temperature is not the only mechanism present in a fire that causes a reduction in the breakdown strength. Wilderness (bush) and agricultural-land fires produce conducting particles in the air gap, which increase the conductance of the gap. The carbonized particles in the gap

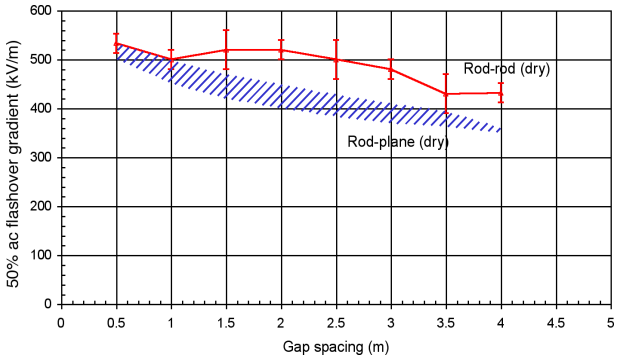


Figure 4.6-2 AC flashover gradient of small rod-rod and rod plane gaps under dry conditions. Note that the rod-plane data is represented by a band (IEEE 1974).

shorten the electrical length of the gap, and they are also sources of electrons, contributing in two ways to increasing the conductivity of the air (Hoch and Sukhnandan 2003). Long carbon particles, like those produced by sugarcane fires, lead to the greatest reduction in breakdown strength (Fonseca et al. 1990; Swift and Naidoo 1993). Measurements have shown that the resistivity of an air gap in a fire ranges between 5 MΩ-m and 25 MΩ-m (ESKOM 2003). As a consequence of the combined effect of these mechanisms, the withstand gradient, in the presence of a fire, can be reduced to as little as 10% of that without the fire. Flashovers are most common at mid-span, since that is where the clearance to ground is the least (ESKOM 2003; Fonseca et al. 1990; Deno and Zaffanella 1987).

Fires also lead to deposits on the surface of the line insulation. However, it has been found that the conductivity of the deposits is very small compared with other environmental deposits and does not make a significant contribution to insulator flashover (Fonseca et al. 1990).

When considering the impact of fires on line design, investigations have shown that it is necessary to achieve an average gradient between conductors and between conductors and ground of not more that 11 kV/m if fire flashovers are to be eliminated (Sadurski and Reynders 1989). Table 4.6-1 gives representative values for the average field associated with modern transmission lines (taken from data in ESKOM 2003).

Table 4.6-1 Average Gradient to Ground, at Mid-span, as a Function of Transmission-Line Voltage

Max System voltage, kV (rms)	145	245	300	420	800
Average gradient, kV (rms)/m	13	20	23	30	31

From the table, it is obvious that the gradients of transmission lines of 200 kV and above are too high to prevent flashover to ground in the event of a bush fire. The cost of increasing the clearances to values where the probability of flashover is negligible is so significant that it is not done. The strategy is to manage the right-of-way by regular clearing of the vegetation under the line and controlling the nature of farming activity in the right-of-way.

Bird excrement may also lead to flashover directly across the air gap by forming a continuous streamer of up to 2.5 m (for large birds). This may span enough of the air gap in the tower window to cause flashover under steady-state ac conditions. This proved to be the explanation of many "unknown" flashovers in the U.S. (Burnham 1995), Germany (Kaiser 1970) and South Africa (Vosloo and Van Rooyen 2001). The only solution is to install bird guards to prevent the birds from sitting above critical gaps in the tower—e.g., as shown in Figure 4.2-5 for the I-suspension string configuration (IEEE 2004a, 2004b). This aspect is further discussed in Chapter 12 (Section 12.16).

Rain may substantially reduce the ac strength of insulator strings, depending on the rate of rainfall, conductivity of the rainwater, and the insulator configuration considered. Typical flashover stress levels on glass and porcelain cap-and-pin insulators are between 250 and 300 kV per meter of section length during standard wet tests, with a low conductivity artificial rain (Sediver Catalog). Figure 4.6-3 shows the wet ac flashover strength of a selection of typical disc insulator strings. The main insulator parameters that influence the flashover voltage are the spacing of the individual discs and their diameter. The results in Figure 4.6-4 show the wet ac flashover voltage of a typical silicone rubber insulator. This curve has been based on catalog data (Lapp catalog). A comparison of these curves shows that there is not much difference between the wet flashover strength of ceramic and glass disc and hydrophobic composite insulators. Hydrophilic polymer insulators may have a wet ac flashover voltage that is 10–20% lower than that of the hydrophobic ones (Shaowu et al. 2000).

The rainfall rate mainly influences the flashover strength by the amount of water that cascades down from one unit to the next. The effect is greatest on vertically orientated

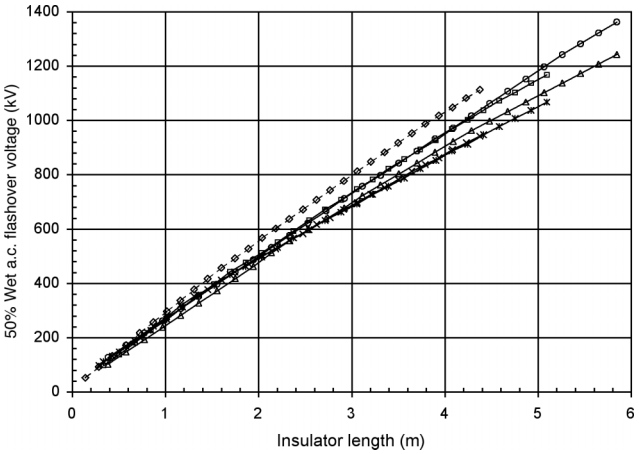


Figure 4.6-3 Wet ac flashover voltage of various shapes of cap-and-pin insulator strings (Sediver Catalog).

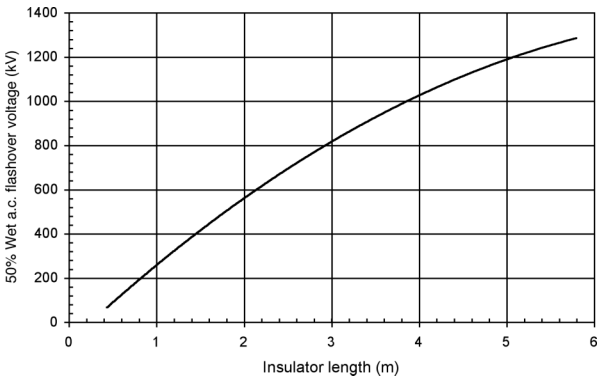


Figure 4.6-4 Wet ac flashover voltage of a silicone rubber insulator (Lapp Catalog).

strings (I-strings). For testing purposes, ANSI Standard C-29.1-1961 has specified a rain rate of 5 mm/min. This is equivalent to an extremely heavy rain, which rarely occurs in nature, and it causes a reduction in strength on long insulator strings of about 30% from the clean, dry critical flashover voltage (Locke Insulator Catalogue and Engineering Handbook; AIEE 1958; Standring et al. 1963). While this heavy rain rate was used historically, current wet tests on power apparatus are performed at a more realistic rain rate of 1 mm/min and a resistivity of 100 ohm-meters (IEEE 1995; IEC Forthcoming a). Figure 4.6-5 shows the correction factor curve used at Project UHV for rain rate. The critical flashover voltage for clean, dry conditions is defined as 1 p.u. To find the critical flashover voltage at any rain rate, one multiplies the reference value by the corresponding correction factor.

Critical ac flashover voltage also depends on water resistivity. The resistivity of rain is affected by pollution of the air, salt particles near seacoasts, and different kinds of contaminants near industrial areas. As rain begins, the rainwater resistivity is lowest, thereafter increasing with time. Figure 4.6-6 shows the correction factor curves used at Project UHV for rain resistivity on glass and ceramic insulators. The curve corrects the per-unit critical flashover voltage versus water resistivity for the case of a rain rate of 5 mm/min. As a reference value, Figure 4.6-6 uses a resistivity of 17.8 kΩ/cm. The slope of this curve is less for a lower rain rate.

Increasing levels of rainwater resistivity also adversely affect the ac flashover voltage of polymer insulators. Hydrophilic insulators are more affected than hydrophobic insulators, as shown in Figure 4.6-7. However, even hydrophobic insulators are strongly affected for rainwater conductivities above 10 mS/cm.

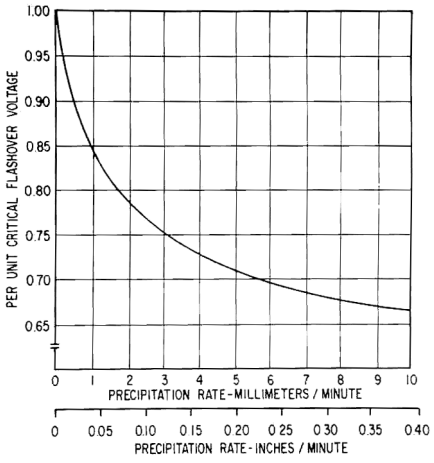


Figure 4.6-5 Correction factor for rate-of-rain on the a.c. flashover strength of I-strings (EPRI 1982).

4.6.3 Contamination Flashover Performance of Insulators

Over the years, many reports have been published on the performance of insulators under contaminated conditions. It is generally difficult to extrapolate results from one particular insulator to another, since small changes in the profile may lead to quite big differences in performance. On the other hand, most transmission lines are installed with very similar, or in many cases, the same type of insulator. In this section, some general conclusions are presented regarding transmission-line insulators, based on the assumption that most are installed with disc insulators or polymer longrod insulators. Some information is also provided regarding porcelain post insulators.

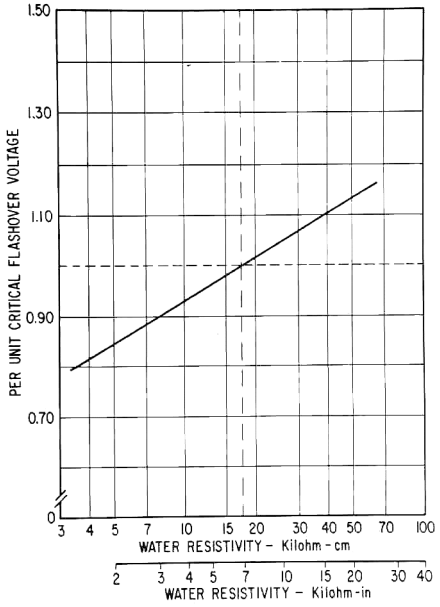


Figure 4.6-6 Correction factor for rainfall resistivity on the ac flashover strength of insulators (EPRI 1982).

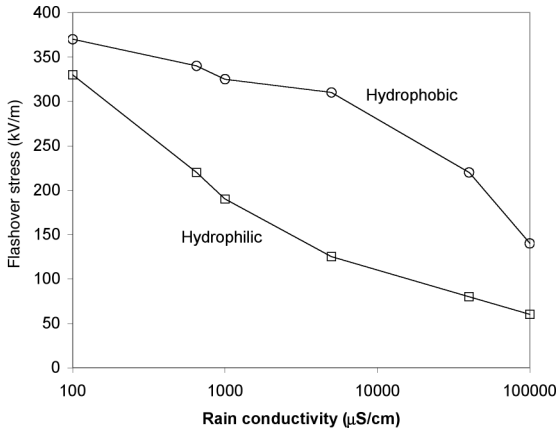


Figure 4.6-7 The relationship between ac wet flashover and rain conductivity for hydrophobic and hydrophilic polymer insulators (Shaowu et al. 2000).

Results are presented for both glass-and-porcelain insulators and polymer insulators separately since their characteristics differ considerably. It is, however, difficult to draw general conclusions for polymer insulators, since there is still no general agreement on a standardized method to determine the contamination performance of these insulators. Consequently, the results from different laboratories cannot be compared directly.

4.6.4 Glass and Porcelain Insulators

Flashover Voltage as a Function of Contamination Severity

Figure 4.6-8 shows withstand specific creepage distance as a function of contamination severity, based on a compilation of published results for standard-shape disc insulators (CIGRE 2000b). This relationship can be adequately described by:

$$\text{Flashover Gradient} = \frac{V}{L} = A \cdot \gamma^{-\alpha} \text{ or} \qquad 4.6\text{-}3$$

$$\text{Unified Specific Creepage Distance} = \frac{CD}{V} = B \cdot \gamma^{\alpha} \qquad 4.6\text{-}4$$

V = flashover voltage.
L = section length of the insulator.
CD = leakage distance of the insulator.
γ = contamination severity level.
A, B, and α are constants.

The value of α, which determines the "slope" of the curve, can be considered as a weighted average of the value for an electrolyte (α = 0.33) and that of air (α = 0). For line insulators, a value of α =0.2 can be considered typical (Looms 1988).

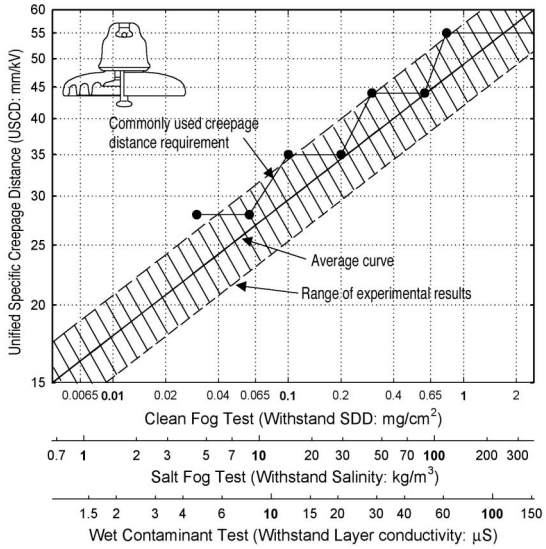


Figure 4.6-8 The withstand ac contamination performance of standard types of disc insulator based on the results from Salt-Fog and the Solid-Layer tests (CIGRE 2000b).

Table 4.6-2 presents the constants of the above equations associated with the curves in Figure 4.6-8. These values are based on the assumption that the flashover gradient is expressed in kV/m and the Unified Specific Creepage Distance (USCD) in mm/kV. (*Note: the unified creepage distance is the creepage, or leakage, distance of the insulator divided by the maximum operating voltage across the insulator, not the phase-to-phase system voltage as previously defined for the creepage distance, as used in the first version of IEC 60815.*) The values for *A* were derived from *B* by assuming a creepage distance to section length ratio of 2.21, which is typical for a standard-shape disc insulator.

Insulators with a long leakage distance, the so-called antifog insulators, have generally higher flashover strengths per unit length as compared with standard units, as shown in Figure 4.6-9. These results have shown:

- The performance of antifog insulators is not always proportional to leakage distance. The flashover values approach that of standard insulators at low contamination severity levels, while at high contamination levels, the performance becomes more proportional to the leakage distance.

Table 4.6-2 Experimental Parameters for the Withstand Curves Presented in Figure 4.6-8

Type of Laboratory Test (Severity Parameter)	Lower Limit			Average			Upper Limit		
	A	B	α	A	B	α	A	B	α
Salt – Fog (kg/m³)	115.7	19.1	0.22	134.8	16.4	0.22	156.7	14.1	0.22
Clean – Fog (mg/cm²)	38.8	56.9	0.22	45.1	49.0	0.22	52.6	42.0	0.22
Wet contaminant (μS)	126.3	17.5	0.28	148.3	14.9	0.28	175.4	12.6	0.28

- The spacing of the insulator discs is an important parameter at low pollution levels (i.e., SDD < 0.1). A greater spacing leads to a higher flashover voltage, even if the leakage distance is kept the same.
- Larger discs, with a diameter greater than 280 mm, have higher flashover strengths than regular disc insulators with a diameter of 254 mm.

Longrod and post insulators have approximately the same flashover performance as standard-shape insulators, as illustrated in Figure 4.6-10.

In Section 4.3.2, the importance of the nonsoluble components in the contamination layer was highlighted. Standardized solid layer tests utilize a nonsoluble deposit density (NSDD) of 0.1 mg per cm^2 of surface area of the insulator. In desert areas the NSDD may be much higher, which may severely affect the flashover voltage. As Figure 4.6-11 shows, longrod insulators are more affected by NSDD than disc insulators, and the reduction in flashover strength can be by as much as 40% in extreme cases (Matsuoka et al. 1996). These results show the importance of taking account of the nonsoluble deposit density when dimensioning insulators. It may even be prudent to confirm the insulator performance with testing at appropriate NSDD levels.

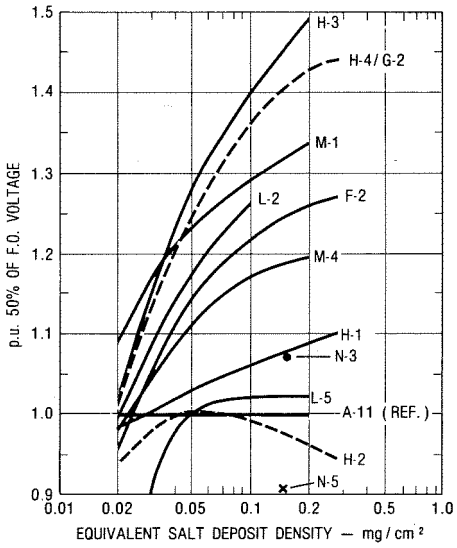


Figure 4.6-9 The flashover voltage of antifog insulators in relation to that of a standard-shape disc. (Labels on the graph refer to insulator types listed in Appendix 4.1) (EPRI 1982)

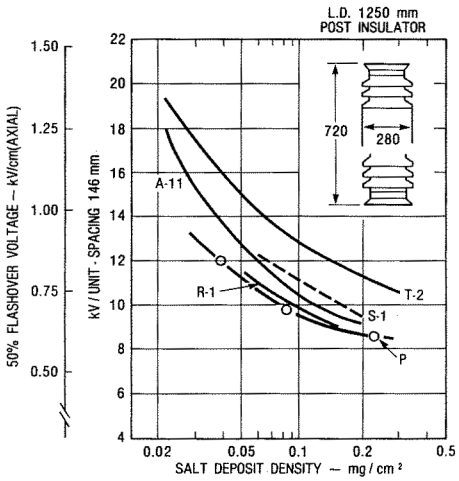


Figure 4.6-10 Performance of post insulators. (Standard disc A-11 is shown as a reference.) (EPRI 1982)

The type of soluble contaminants on the insulator may also affect the flashover under fog conditions (Ramos et al. 1993; Fujimura et al. 1979). Results from comparative Clean-Fog tests with different kinds of contamination salts are shown in Figure 4.6-12. These results show that low-solubility salts have a higher fog withstand voltage than high-solubility salts such as sodium-chloride.

Leakage Path Length

In most international standards the leakage path length is used as the main parameter for the dimensioning of

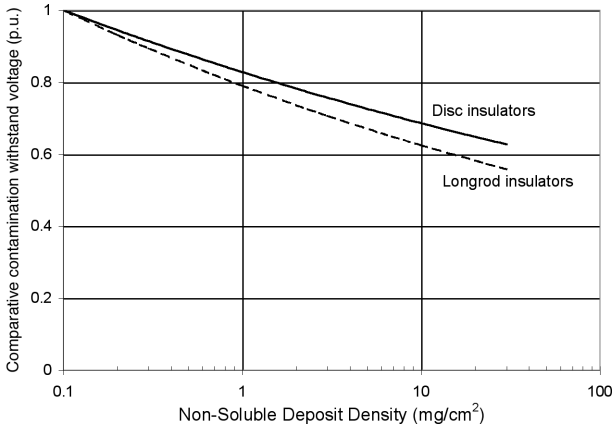


Figure 4.6-11 The influence of the amount of nonsoluble material on the contamination withstand voltage of disc and longrod insulators (CIGRE 2000b).

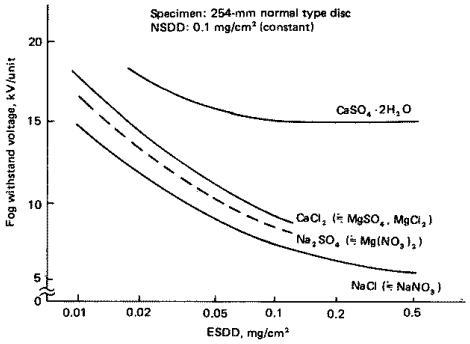


Figure 4.6-12 Influence of various salts in the contamination layer on the insulator fog withstand voltage (Fujimura et al. 1979).

insulators with respect to contamination. The guidelines commonly used are presented in Table 4.6-3. A comparison of this table with Figure 4.6-8 shows that the creepage distance guidelines agree well with the performance of standard-shape disc-type insulators. This agreement is probably due to the fact that the recommendations were based on the performance of standard-shape disc insulators in the first place.

The reasons for the differences in the classifications of the IEC and IEEE are not clear. It could be speculated that the differences may be due to differences in the NSDD levels of the typical environment on which each of these recommendations was based.

There is, however, a growing body of evidence to suggest that neither the leakage distance nor the section length can be used as a sole parameter for dimensioning (Swift 1996). This fact is also demonstrated in Figure 4.6-9, which shows that:

- At low pollution levels, the antifog and reference insulator have a similar flashover stress, despite the large differences in the leakage path length.
- At high pollution levels, the flashover voltage per unit length of the antifog units is much higher than that of the reference insulator.

Observations during low-pollution-level tests have shown that the growth of the dry-band arcing takes place through air, whereas at a high pollution severity, the breakdown takes place along the surface. The greater amount of inter-skirt breakdown at low pollution levels, therefore, reduces the leakage distance effectiveness of antifog insulators (Swift 1996). This is illustrated graphically in Figure 4.6-13.

There may also be other conditions when the leakage path may be rendered less effective. Field observations of longrod insulators with a close shed spacing have shown that the dry-band arcing often develops from the shed tips, as can be seen in Figure 4.6-14. This is in contrast to laboratory tests, with a higher degree of wetting, where the dry-band arcing follows the surface much closer.

In conclusion it can be said that the creepage distance concept seems to work well for those cases where the insulator profile has been selected to suit the environment. The concept breaks down, however, for inefficient profiles where nonlinear effects, such as inter-shed or inter-skirt breakdown, become important.

Natural Versus Artificial Contamination Tests

In Figure 4.6-15, the ac flashover voltage data obtained at three different natural test stations (situated in coastal areas) is compared against those of artificially polluted insulators under a Clean-Fog test (Naito et al. 1990). It shows that:

- The withstand voltage is about the same for the natural and artificial tests.
- The dispersion in the test results of natural tests is greater than that of artificial tests.

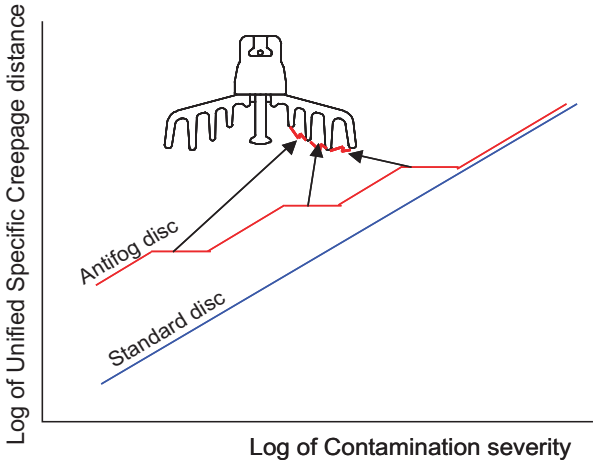


Figure 4.6-13 General effect of inter-skirt breakdown on the creepage distance requirement of antifog insulators.

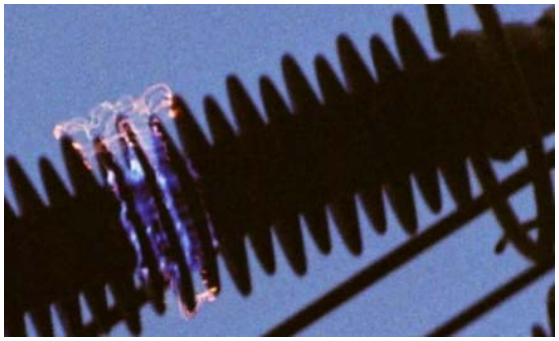


Figure 4.6-14 Discharge development on a porcelain longrod insulator under natural wetting conditions.

Table 4.6-3 Commonly Used Guidelines for the Selection of Creepage Distance Based on ESDD Measurements

Pollution Class	From IEC ESDD (mg/cm^2)	IEEE ESDD (mg/cm^2)	Unified Specific Creepage Distance (mm/kV_{p-g})
		< 0.03	21 (IEEE only)
1. Light	0.03 – 0.06	0.03 - 0.06	28
2. Medium	0.10 – 0.20	0.06 – 0.1	35
3. Heavy	0.30 – 0.60	>0.1	44
4. Very heavy	> 0.80		55

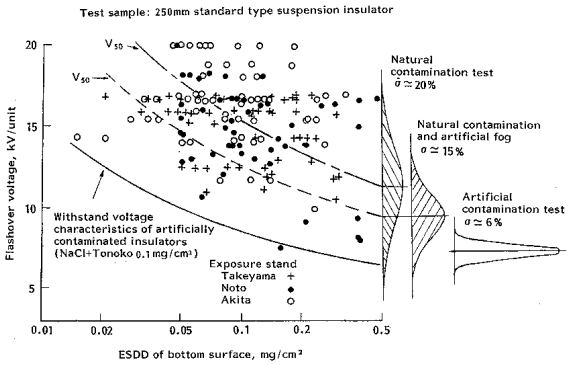


Figure 4.6-15 Results of ac natural contamination tests compared with Clean-Fog tests (Naito et al. 1990).

The larger dispersion of the natural test results is mainly due to variations in the wetting conditions, as well as the greater nonuniformity of the contamination deposit during the natural tests.

For inland areas, the agreement between artificial and natural contamination tests is not always as good. In most cases, this is due to the effects of higher levels of nonsoluble contaminants and the presence of low-solubility salts (Lin et al. 1992).

Linearity of Flashover Voltage as a Function of Insulator Length

In the preceding sections, the results were presented based on the assumption of a linear relationship between insulator length and flashover voltage. There seems to be general agreement, based on results from both natural and artificial contamination tests, that this is in fact correct (Fujimura et al. 1979; Houlgate et al. 1982; Looms 1988). There has been, however, some evidence from laboratory tests performed at Project UHV (EPRI 1982) to suggest a nonlinear relationship for insulator strings of over 3 m in length and low contamination levels (i.e., a Salt Deposit Density of below 0.02 mg/cm^2) (EPRI 1982). The results suggest further that this nonlinearity is accentuated by natural wetting conditions (i.e., noncritical wetting). Based on these tests, the concept of the long-string efficiency, λ, has been defined, which is expressed as:

$$\lambda = \frac{L_{EHV} \cdot V_{UHV}}{L_{UHV} \cdot V_{EHV}} \qquad 4.6\text{-}5$$

Where:

L_{UHV} = string length required at a UHV voltage level.
L_{EHV} = string length determined at a lower voltage level.
V_{UHV} = UHV voltage level.
V_{EHV} = lower voltage level.
λ = long-string efficiency.

The dependence of long-string efficiency on the line-to-earth voltage is shown in Figure 4.6-16, which applies to standard vertical insulator strings up to 11.5 m connection length (CIGRE 2000b). The equivalent salt deposit density (ESDD) is in the range of 0.01-0.04 mg/cm^2. For antifog insulators, the results for long-string efficiency are shown in Figure 4.6-17 for string connection lengths up to 8 m. In this case, the range of ESDD is 0.02–0.04 mg/cm^2 (CIGRE 2000b).

There is still no general agreement on how the long-string efficiency should be taken into account when dimensioning insulators, since this mainly occurs under light wetting and low contamination severities. This reduction in strength, which is only on the order of 5–10%, needs to be weighed against the greater uncertainty with which the site contamination severity is known.

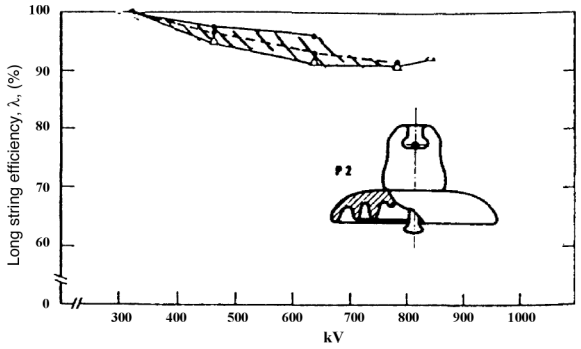


Figure 4.6-16 Long-string efficiency for ac energization as a function of line-to-earth voltage. Range of ESDD 0.01-0.04 mg/cm^2 (CIGRE 2000b). IEEE insulators (146 mm spacing, 254 mm diameter, and ratio leakage to spacing 2.1).

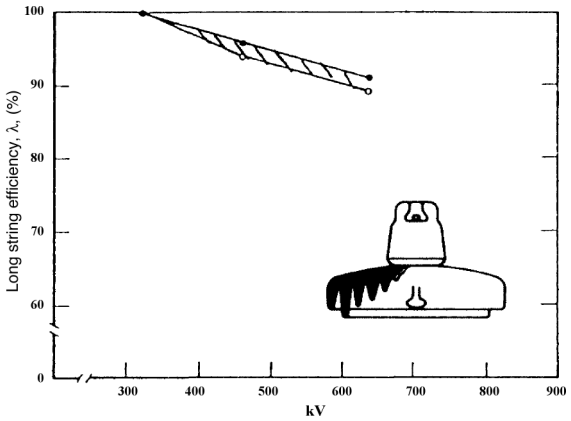


Figure 4.6-17 Long-string efficiency for ac energization as a function of line-to-earth voltage. Range of ESDD 0.02-0.04 mg/cm^2 (CIGRE 2000b). Antifog insulators (220 mm spacing, 420 mm diameter, and ratio leakage to spacing 3.3).

Effect of Insulator Orientation on Contamination Flashover Performance

It is generally agreed that inclined and horizontal line insulators have a better contamination performance than vertical insulators. The most important orientation effect is the accumulation of pollution, where inclined and horizontally installed insulators are more accessible for natural cleaning.

Also, during artificial testing, inclined and horizontally installed insulators may have significantly higher flashover voltages, as illustrated in Table 4.6-4, which presents the 50% flashover strength for the horizontal and V-string configurations as compared to equivalent flashover strength for I-strings. All tests were conducted on identical-length standard-shape insulators (Type A-11) at a Salt Deposit Density of 0.02 mg/cm^2 (average). Table 4.6-4 also gives a comparison of long-string efficiency (λ). From these results, it may be seen that the strength of horizontal configurations falls between the I- and V-configurations, and that they are somewhat more linear (higher λ). It would appear that these results, together with the available data on I- and V-strings, provide a sufficient guide for horizontal string usage.

The Flashover Performance of Closely Spaced Insulator Strings

Insulator assemblies consist sometimes of multiple insulator strings to fulfill mechanical or security requirements. Experimental results have shown that there is a reduction in flashover strength over and above that expected from statistical considerations. The following trends were observed (Sklenicka and Vokalek 1999; Petruch 1990):

- The flashover strength of closely spaced stings may be up to 30% lower than that of an identical single string. From purely statistical considerations, a reduction of only 7% is expected.
- The reduction in strength is caused by partial arcs bridging the gap between the parallel insulator strings.
- The proximity effect was independent of the laboratory test method used.
- Proximity effects have been observed on disc, longrod, and post insulator types.

Table 4.6-4 Comparison of 50% Flashover Strength and Long-String Efficiency for Different String Configurations (ESDD = 0.02 mg/cm^2)

Applied Voltage (kV l-g)	Relative Strength Using I-String as Reference		
	Horizontal	I-String (Ref)	V-String
370	1.22	1.0	1.60
740	1.29	1.0	1.63
	λ = 95%	λ = 90%	λ = 92%

- The proximity effect is independent of the orientation (i.e., vertical, inclined, or horizontal) of the parallel insulator set. Horizontal insulators are subjected to more frequent instances of natural cleaning, which may counter the proximity effect in practical situations.
- The reduction of strength increases with a decrease in the spacing between the parallel insulator sets.
- The reduction in strength was higher for longer insulator sets.

Based on the test results, an inter-string spacing of between 400 and 500 mm is recommended. Tapered insulator installations with a closer string spacing at the live end than at the grounded end may also offer a significant improvement in the flashover voltage of the double string.

4.6.5 Polymer Insulators

Overview of Contamination Flashover Performance

Hydrophobic polymer insulators generally have a superior contamination flashover performance when compared to that of glass and porcelain. Tests at Brighton insulator testing station showed that hydrophobic (i.e., silicone rubber) insulators exhibited a 60% higher flashover voltage than ceramic or glass insulators of the same axial length, and hydrophilic polymer insulators (i.e., EPDM) showed a 20% better flashover performance (Houlgate and Swift 1990). Most transmission-line owners who have changed the line insulation from glass or porcelain to polymer insulators have reported a major improvement in line contamination outage performance (Ravera et al. 1996; Fierro-Chavez and Ramirez-Vazquez 1999). The reasons for this are:

- **Surface hydrophobicity**. Good hydrophobicity is very efficient in preventing the formation of a uniform wet surface that is so fundamentally important to the contamination flashover process (Xidong et al. 1999). A part of the contamination deposit may also be "neutralized" by the hydrophobicity transfer phenomenon (Kindersberger and Kuhl 1989).
- **Thermal characteristics**. Polymer insulators adjust quickly to the ambient temperature. The wetting is, therefore, less efficient than on ceramic and glass insulators under critical wetting conditions.
- **The slender shape of the insulators**. For a given surface conductance, insulators with a slender shape will have a higher overall resistance than insulators with a larger diameter.
- **Longer leakage distances**. Polymer insulators are often installed with a longer leakage distance than ceramic and glass insulators (Maxwell and Hartings 2000). This is often done to avoid material deterioration due to leakage currents.

The above discussion does not account for differences between the contamination collection on polymer and ceramic or glass insulators (e.g., aerodynamic profile and surface roughness).

There are certain exceptions where the implementation of polymer insulators was not successful. In areas prone to bird streamer outages, an increased line outage rate was reported after the installation of polymer insulators. This was ascribed to presence of corona rings and the resulting shorter strike distance to the tower on replacement units (Burnham 1995). In extreme contamination conditions, polymer insulators may suffer from erosion and eventual electrical or mechanical failures due to the long-term exposure to damaging levels of leakage current (Fierro-Chavez and Ramirez-Vazquez, 1999).

Effect of Hydrophobic Properties on Insulator Flashover Performance

The level of surface hydrophobicity has a great influence on the surface conductivity of contaminated insulators during wetting conditions. Surface hydrophobicity measurements have shown that the surface layer becomes increasingly conductive for a level of hydrophobicity of above HC 4 (see Figure 4.2-16) (Eklund et al. 1995). This corresponds to the level of hydrophobicity when water runnels form on the surface. This behavior is reflected in the flashover gradient, as shown in Figure 4.6-18 (Xidong et al. 1999). (A runnel is defined as a narrow channel of water.)

Results from field inspections of hydrophobicity concluded that silicone rubber insulators showed good long-term hydrophobic properties (HC 1-4) in most environments, except close to the coast where hydrophobicity may regularly be suppressed. It was also noted that the loss of hydrophobicity is often very localized and concentrated around the end fittings, especially around the high-voltage end where the electric field is the highest (Xidong et al. 2001; Phillips et al. 1999a, 1999b). EPDM insulators do not have significant long-term hydrophobic properties (i.e., typically in the range of HC 5-7) (Maxwell and Hartings 2000; Montesinos et al. 2000).

Flashover Voltage as a Function of Contamination Severity

Laboratory tests on polymer insulators suggest that the performance of polymer insulators as a function of contamination severity can be expressed by the same power function as that used for ceramic and glass insulators. An example of typical results (NGK test method) is presented in Figure 4.6-19, which shows that silicone rubber insulators offer a significant improvement in insulator flashover stress as compared with standard disc insulators (Matsuoka et al. 1996). Tests indicated that this improvement may be between 20 and 70%, depending on the condition of the insulator's hydrophobicity when tested (Xidong et al. 1999).

The level of nonsoluble deposits in the contamination layer, as expressed by the NSDD, affects the flashover voltage of polymer insulators to the same extent as the ceramic longrod insulators (see Figure 4.6-11) (Matsuoka et al. 1996).

Laboratory test results suggest strongly that the contamination performance of hydrophobic polymer insulators should be evaluated under heavy wetting conditions (De la O and Gorur 1998; Matsuoka et al. 2002; Shaowu et al. 2000). Not only should the steam fog input rate used in Clean-Fog tests be much higher than specified in the standards, but also simulated rain tests on contaminated insulators are important to evaluate the shed profile and spacing in terms of water-cascading effects.

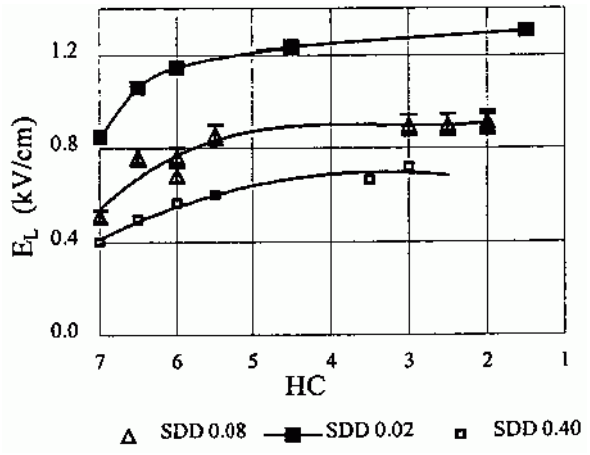


Figure 4.6-18 The flashover voltage over the leakage distance, as a function of the hydrophobicity class, as determined by modified Clean-Fog tests (Xidong et al. 1999).

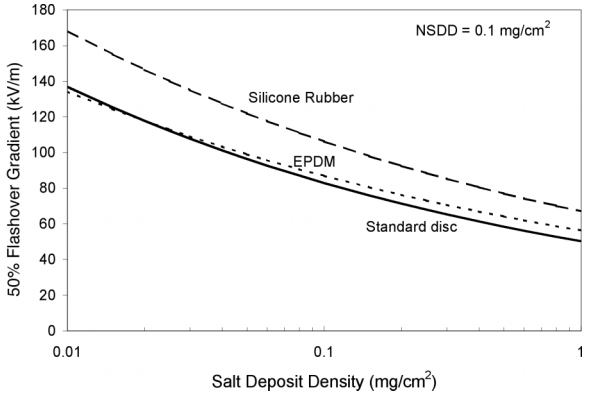


Figure 4.6-19 Comparison of the flashover stress of a hydrophobic silicone rubber insulator (Matsuoka et al. 1996) to that of a standard-shape disc insulator (derived from Figure 4.6-8 and based on a standard deviation of 8%).

4.6.6 Resistive Glaze Insulators

Insulators with semiconducting glaze have been available for some time. The use of these resistive coatings has been found effective both in suspension- and post-type insulators for EHV applications as a solution for insulation design in heavily contaminated areas. The presence of a resistive coating on the insulator surface results in two phenomena that lead to superior contamination performance. First, the continuous current flow of approximately 1 mA through the resistive layer provides enough heat on the surface of the insulators to keep them dry in dew or fog. Second, the resistive grading results in a significantly more uniform electrical stress along the insulator length. There have been some difficulties with the fabrication and field life of these insulators in the past. However, significant technological improvements have been made, and substantial service experience exists. Consequently, their use should be considered in the contamination design of UHV transmission lines.

Unfortunately, an operating stress of 10-12 kV/unit, suggested by several manufacturers for EHV applications, would impose a severe penalty on UHV line design. On an 1100-kV system, for example, 58 units would be required if the nominal rating were 11-kV/unit. The use of such long insulator strings raises performance- and cost-related questions. First, there is some concern as to the voltage distribution on these long strings, even if they are semiconducting. Second, the issue of thermal stability, with even a slightly nonuniform voltage distribution, should be considered. Finally, there is the economic consideration of the acceptability of a constant power loss due to resistive heating.

The voltage distribution on a long string of semiconducting glaze insulators will be more uniform than on a conventional string because of the resistance of each unit (Fukui et al. 1974). The thermal stability of a long string should also be better than that of a short string because changes in the impedance of one unit have a small effect on the total string impedance. Consequently, the total series current also does not change very much. Therefore, it is reasonable to expect that the test results obtained with short strings in fog tests at constant voltage will also apply to the long strings required for UHV because the primary mechanism involves the heating of the surfaces of each insulator.

To verify that the performance of semiconducting glaze insulators would exceed that of conventional insulators in the type of artificial contamination tests used at Project UHV, tests were conducted on suspension units with a predeposited contaminant and a clean fog. The insulators were the standard shape (146 mm by 254 mm) and were intended for energization at 11 kV per unit and a nominal resistive current of 1 mA. Short strings containing five units of these insulators were contaminated with a 40/100 mixture of Kaolin and NaCI (g/l) corresponding to a Salt Deposit Density of about 0.25 mg/cm^2, which represents a heavy level of contamination severity. The insulators were energized at a constant voltage of 11 kV/unit and exposed to the clean fog. The heat dissipation of 11 W/insulator kept the surfaces dry, and no flashovers occurred. Thus, it was verified that this type of insulator is effective for heavy contamination in areas where wetting usually occurs by fog.

The possibility of reducing string lengths with semiconducting glaze insulators was investigated with units designed for nominal 15-kV, 1-mA operation. Such insulators would be attractive for UHV line design. For example, on an 1100-kV system, 42 of these insulators would be required. This would mean a shorter overall string length than that possible with the number of conventional units (Massey 1972) necessary for even light contamination. (This assumes the semiconducting glaze units have the same spacing as the conventional ones.) Although the use of such semiconducting glaze units will aid in the power-frequency design of UHV lines, the resulting increased stress per unit in this case requires that attention be focused on the insulation strength during the energization of strings that are contaminated and wet, a condition known as cold switch-on. This situation occurs on lines that have been unenergized for a period of time long enough to render the heating, which results from the semiconducting glaze while the units are energized, ineffective in preventing the accumulation of moisture on the insulator surface.

Some data on the cold switch-on strength of semiconducting glaze insulators are available (Moran 1974). However, these data were obtained with relatively short strings, containing ten units (1.5 m) or less. The purpose of the tests reported here was to extend the data to strings that would be suitable for UHV transmission systems and to make a direct comparison with the cold switch-on strength of conventional insulators, which have a similar shape.

The cold switch-on test voltage was not applied to the insulator strings until they were thoroughly wet from the clean fog. To determine the time at which this condition was achieved, impedance measurements were made either on the strings to be tested or on an auxiliary monitor string that was prepared in an identical manner to the test strings. The impedance was found by applying a maximum voltage of 1 kV/unit to the insulators every five minutes for a duration that was only long enough to measure the current, generally 0.5 s or less. When the resistance reached its minimum value and was stabilized, the test series was begun.

In the test, two I-strings (one conventional and the other semiconducting glaze) were always tested in parallel by applying the full test voltage alternately to the conventional string for a maximum duration of 30 s and to the semicon-

ducting glaze units for 5 s, with another application of voltage on each string every 10 min. The 50% flashover voltage was determined by an up-and-down technique, in which the voltage for consecutive shots was raised or lowered by ~10% depending on whether a withstand, or a flashover, occurred. The total time of the test series was about 2-3 h. Consequently, the results of 10-15 voltage applications on each string were used to determine the 50% flashover voltage for a given string length and contaminant.

The preceding test procedure was devised after performing enough tests to verify that the short time durations, intervals, and total test time did not influence the performance. The data on cold switch-on strength are presented in Table 4.6-5 for the two types of insulators and two different contaminants. The results showing 50% flashover strength as a function of string length are given in Figure 4.6-20.

The issue of constant heat-energy dissipation and its economic penalty should be considered in any widespread application of the semiconducting glaze insulators. As an example, consider the possible use of these units for 1100-kV transmission. With 1 mA resistive current, each leg of a semiconducting glaze string would dissipate 581 W. Assuming a double V-string for each phase, the dissipation per tower would be 7.0 kW. With four towers per mile, the constant loss due to these insulators would be 28 kW per mile. For a typical 1100-kV design, the expected total average yearly I^2R and corona loss would amount to 110 kW/mile. This implies that the insulator losses are 30% of these other losses and are thus a factor that would contribute significantly to operating costs. These costs, however, must be balanced against the costs of over-insulation, greasing, or live-line washing, which might be required for conventional insulators. In cases of heavy contamination, the cost of power lost due to scintillation and dry band arcing of conventional insulators may also be worth considering.

Table 4.6-5 50% Cold Switch-on Flashover Voltage of Conventional and Semiconducting Glaze Insulators

Number of Units	Contaminant	50% Flashover Voltage (kV)	kV/unit
15	--	143 Conv.	9.5 Conv.
	--	173 S.C.	11.5 S.C.
31	--	285 Conv.	9.2 Conv.
	(40/20)	305 S.C.	9.8 S.C.
56	--	525 Conv.	9.4 Conv.
	--	525 S.C.	9.4 S.C.
64	--	575 Conv.	9.0 Conv.
	--	620 S.C.	9.7 S.C.
14	--	160 Conv.	11.4 Conv.
	--	155 S.C.	11.1 S.C.
25	--	275 Conv.	11.0 Conv.
	(40/40)	286 S.C.	11.4 S.C.
56	--	595 Conv.	10.6 Conv.
	--	615 S.C.	11.0 S.C.

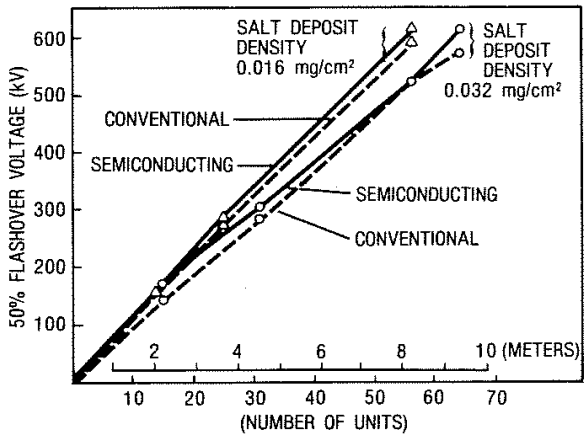


Figure 4.6-20 Cold switch-on flashover voltage as a function of string length (EPRI 1982).

4.7 PERFORMANCE OF INSULATORS IN FREEZING CONDITIONS

4.7.1 Introduction

Pollution accumulation, during or followed by ice or freezing fog accretion, has proved to create particularly severe conditions for insulators in power systems to withstand. In many areas, improvements in switching surge control led to the adoption of reduced insulation levels—for example, 1550-kV BIL for 500-kV systems, where many utilities had used 900-kV BIL for 230-kV systems. This insulation level has proved to be inadequate in cases where moderate pollution (often caused by road salting in the winter) can be exposed to freezing conditions that include fog or freezing rain.

In the years 1993-2001 (excluding 1997), the National Electric Reliability Council (www.nerc.com) reported 307 severe disturbance events. Of this total, six involved ice storms, and three of these were mainly mechanical problems, such as the collapse of 1300 hydro towers on January 4-9, 2003. Notable problems traced to the combined effects of pollution accumulation and winter precipitation are:

- **March 10, 1986**. Ontario Hydro nearly lost the operational use of its 500-kV network through a rare combination of contamination buildup (16 days without rain) and relatively mild winter icing conditions, leading to 57 flashovers on 500-kV lines and stations within a 2-h period. Nearby 230-kV and 115-kV lines were not affected.
- **December 14, 1994.** NERC Report on Western Systems Coordinating Council (WSCC) system disturbance affecting 1.7 million customers: "The three-terminal 345 kV (Idaho Power) Midpoint-Borah-Adelaide No.1 line protection scheme correctly detected a single line-to-ground fault when a contaminated insulator bell

flashed over to ground. These insulator strings are located in an agricultural area and are prone to collect dust and fertilizer contamination. The insulators had been washed the previous month."

- **December 20, 2000.** NERC Report on New Brunswick Power (NBP) Salt Contamination / Freezing Rain Related Loss of Transmission: NBP experienced a series of transmission system outages as a result of salt contamination on insulators combined with precipitation in the form of snow and freezing rain. The insulator contamination monitoring stations in the Saint John area recorded their highest level ever of contamination the day before the short circuits occurred. The contamination occurred following two days of strong southwesterly onshore winds (70 mph) off the Bay of Fundy, which deposited salt spray from high waves over a wide area in the south of the province. Light snow and freezing rain on the contaminated insulators caused five 345-kV flashovers and many lower-voltage flashovers in a 2-h period on December 20, 2000. As the precipitation turned to rain, the salt spray contamination on the insulators began to wash off, and the insulators regained their voltage withstand capability.

Most troubles have occurred on transmission lines and stations that are located near sources of salt, such as the ocean or urban expressways. With typical road salting levels of 16 tons per lane mile in the winter season for most provinces and states that perform winter maintenance, a location near an expressway is equivalent to a location 1 km from the seacoast.

A "Smart Washing" insulator monitoring and maintenance program using deionized water in freezing conditions has allowed one utility (IEEE 2000) to maintain adequate 500-kV network reliability without reinsulating a large number of stations and lines. With the relatively rare problem occurrence, this choice can be valid in many areas of limited exposure.

4.7.2 Clean- and Cold-Fog Test Results

Cold-Fog tests (Chisholm et al. 1996) on a variety of pre-contaminated insulators are summarized in Figure 4.7-1. Results are all expressed in terms of critical flashover strength (50%) for 30 min of exposure of line-to-ground voltage under cold fog conditions, including fog of moderate visibility (< 4 km) and temperatures rising from below to above 0°C. Results from conventional fog tests on strings of suspension insulators are plotted as circles to compare with the Cold-Fog test data.

According to IEC Standard 60815 (IEC 1986), and multiplying units of ESDD in mg/cm^2 by 1000, the four pollution levels shown in Table 4.7-1 are suggested for selection of insulator leakage distance.

Generally, the cold-fog requirements for leakage distance on transmission-line insulators are satisfied by IEC Standard 60815 recommendations, except for very heavy contamination levels above 300 µg/cm^2. The use of extended-leakage (fog-type) disc insulators is often needed to achieve the required specific leakage distance for EHV transmission lines. For example, with 500-kV system voltage and 25 disc insulators, the Level-III requirement of 11 m gives 440 mm per disc, while most standard-profile disks offer about 300 mm per disc. This leakage distance requirement for a single insulator string leaves no margin for system overvoltage or for exposure of several insulators in parallel.

4.7.3 Icing Test Results

Under conditions of moderate icing, it is common for icicles to form on insulator strings. These icicles tend to grow in length, bridging the air gaps between insulator caps or sheds and shorting out the leakage distance. Figure 4.7-2

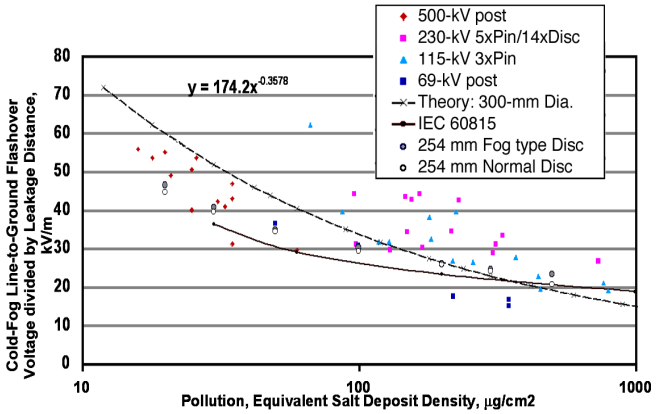


Figure 4.7-1 Cold-Fog and Clean-Fog flashover strength, kV of line-to-ground voltage per meter of leakage distance, decreases nonlinearly with increasing pollution level (Chisholm et al. 1996, Chisholm 1998).

Table 4.7-1 Specific Leakage Distance for Clean Fog and Cold Fog Conditions

Pollution Level	Unified Specific Leakage Distance for 20°C Fog	Unified Specific Leakage Distance for Cold Fog*
Level I (Light) – 2 to 30 µg/cm^2	28 mm per kV	19 mm per kV
Level II (Medium) – 30 to 60 µg/cm^2	35 mm per kV	24 mm per kV
Level III (Heavy) – 60 to 200 µg/cm^2	43 mm per kV	38 mm per kV
Level IV (Very Heavy) - > 200 µg/cm^2	54 mm per kV	68 mm per kV
* For transmission-line disc insulators.		

shows typical ice accretion levels on exposed 500-kV transmission disc insulators and on 230kV polymer insulators under conditions that led to line-voltage flashovers, at three orientations.

The electrical strength of the fully bridged insulator has been studied extensively, notably by Farzaneh et al. 1997; Farzaneh and Drapeau 1995; Farzaneh and Kiernicki 1997; Farzaneh et al. 2003; Farzaneh et al. 2004. Detailed modeling of the flashover process can be carried out using the Obenaus concept (Obenaus 1958), as adapted by Rizk (Rizk 1981) for ac flashover. On iced surfaces, the modeling uses different expressions for the voltage-current relation of the arc and the arc root voltage, compared to modeling of flashover on polluted surfaces (Farzaneh et al. 1997; Farzaneh et al. 2004). It is further complicated by several nonlinear factors, including the sensitivity of ice conductivity to temperature in the narrow range of –2 to 0°C and the nonlinear voltage distribution for EHV insulators, compared to HV systems.

One intermediate step in modeling the flashover process for engineering use was suggested in the CIGRE Task Force paper on Icing Test Methods (CIGRE 1999b). An "Icing Stress Product (ISP)," formed by the product of the ice conductivity and its weight per meter of dry arc distance, is proposed for evaluating performance. This product essentially defines the resistance of the deposit per unit length used in the Obenaus model.

$$ISP = \sigma \cdot \frac{\text{Deposit weight}}{\text{Dry arc distance}} \qquad 4.7\text{-}1$$

σ = the electrical conductivity of the ice deposit at 20°C in µS/cm.

Deposit weight = the weight of ice deposited on the whole insulator string in g.

Dry arc distance = the dry arc distance of the insulator string in cm.

The use of melted-water weight in the icing stress product automatically corrects for variations in ice or snow density. Figure 4.7-3 shows that the relations between electrical strength under melting conditions and icing stress product is well correlated over a wide range of conditions, including not just ice but also snow and cold-fog deposits.

The use of the icing stress product for evaluating dry-arc distance requirements is simple in experimental tests, using the recommended procedures as described in (Farzaneh et al. 2003; Farzaneh et al. 2004). This approach calls for the evaluation of insulator withstand performance using a fixed freezing-rain water conductivity of 100 µS/cm, corrected to 20°C. Ice accretion is measured, ideally both on the insulator surface and on a rotating reference cylinder of 25 to 29 mm diameter, similar to transmission-line conductors. The relationship between ice accretion thickness on the reference cylinder and ice weight on the insulator is

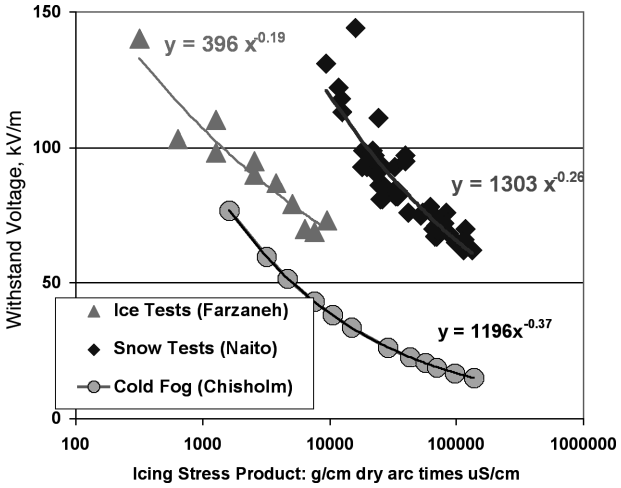


Figure 4.7-3 Relation between withstand voltage (line to ground) and icing stress product for ice, snow, and cold fog accretion.

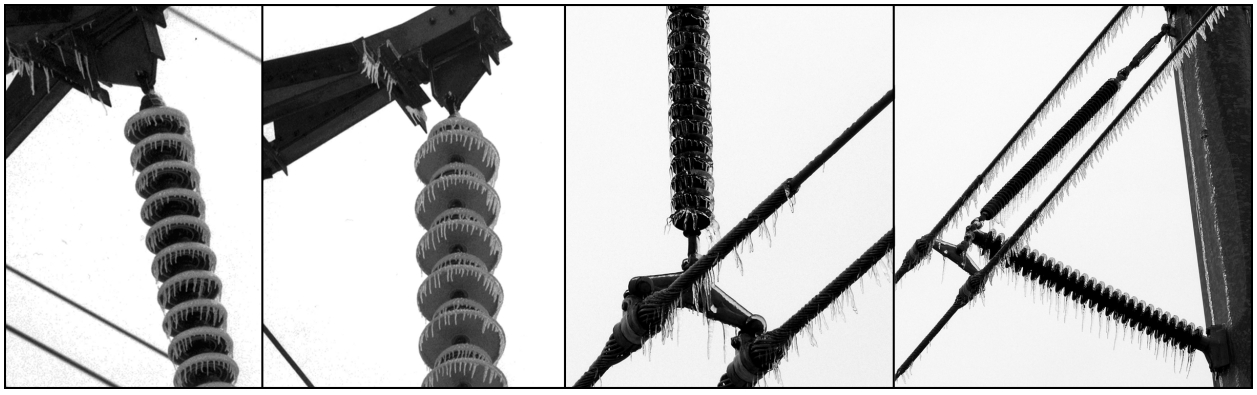


Figure 4.7-2 Examples of natural ice accretion on various types of transmission line insulator.

established by the insulator shape and size. Ice tends to accumulate only on one side of the insulator, and only the top surface of exposed disc insulators contributes any additional contamination to the native electrical conductivity of the freezing rainwater. Farzaneh and Kiernicki give the relation between ice accretion on a 25-mm reference cylinder and weight of wet-grown ice on IEEE standard disc insulators (Farzaneh and Kiernicki 1997):

$$Weight_{g/cm\,dry\,arc} = 3.2 \cdot Thickness_{mm} \qquad 4.7\text{-}2$$

Most tests suggest that the median electrical conductivity of snow, freezing rain, and rain samples at a particular site are roughly the same. There are large day-to-day variations in conductivity, often inversely correlated with daily precipitation amount, because the initial precipitation tends to capture most of the airborne pollution. At critical locations, site selection should probably rely on multiple measurements of snow conductivity to establish the probable values of freezing rain, which tends to have fewer opportunities for sampling without melting.

The process of freeze-thaw purification causes important gradients in the electrical conductivity of the ice deposit. Impurities from the ice itself and from surface pollution tend to migrate away from the ice caps and into the icicles, and also produce a radial gradient with highly conductive ice near the insulator surface.

The total icing stress product of an insulator string under natural conditions comprises the sum of two components:

1. A fixed contribution from the ice-coated area on the precontaminated top surface of the insulator
2. A variable contribution of the precipitation conductivity times the accumulation weight.

For example: The overall icing stress product of a disc insulator string can be evaluated as follows:

Insulator and ice characteristics:
Dry arc distance per insulator . . . . . 146 mm
Diameter of the insulator disc. . . . . 254 mm
Total top surface area . . . . . 647 cm² per disc
Surface area per insulator in contact with ice . . . . . .647 cm² / 4 = 162 cm²
Equivalent Salt Deposit Density . . . . . 100 µg/cm²
Salt from surface deposit in ice . . . . . 16,200 µg
Ice accumulation thickness on reference cylinder . . . . . 20 mm
Median freezing rain conductivity . . . . . .33 µS/cm

From Equation 4.7-2, the weight of wet grown ice per unit dry arc distance of the insulator can be estimated as 64 g/cm.

The contribution of the surface deposit can be calculated by evaluating the electrical conductivity of the melted ice deposit, corrected to 20°C:

$$\sigma = \left[\frac{ESDD \cdot Area}{0.42 \cdot Volume}\right]^{0.962} \qquad 4.7\text{-}3$$

ESDD is in µg/cm².
Area is in cm².
Volume is in ml.
Conductivity σ is in µS/cm at 20° C.

For each insulator, with a deposit weight of 64 g/cm, the ice weight per insulator is 64 g/cm × 14.6 cm = 934 g, corresponding to a water volume of 934 ml. Using Equation 4.7-3 and an ESDD of 100 µg/cm², the contribution of ESDD to the conductivity of the ice deposit is calculated as 35.8 µS/cm. The icing stress product of the predeposited contamination layer can then be evaluated from Equation 4.7-1 and is calculated as 2295 µS/cm x g/cm.

The surface deposit contributes a constant amount to the icing stress product, relatively independent of the amount of ice. For half the ice thickness, the concentration of the salt is doubled, giving no significant change in the series resistance of the ice deposit. For an ice deposit weight of 32 g/cm, the ice weight per insulator is 467 g, corresponding to a volume 467 ml. The electrical conductivity of the ice deposit at 20°C is 70 µS/cm, which translates as an icing stress product contribution of 2235 µS/cm x g/cm. Likewise, if the ice thickness is tripled to a deposit weight of 96 g/cm of dry arc distance (for the same insulator cross section), the ice volume per 146-mm insulator disc is 1402 ml, the conductivity is 24.3 µS/cm, and the icing stress product is nearly the same at 2329 µS/cm x g/cm.

The contribution from precipitation conductivity to icing stress product is evaluated directly from Equation 4.7-1. For an accumulation of 20 mm of ice, with a median freezing rain conductivity value of 33 µS/cm, the icing stress product on clean insulators would be 64 g/cm x 33 µS/cm, or 2112 µS/cm x g/cm.

The overall icing stress product of the precontaminated insulator exposed to the natural precipitation of 65 g/cm is the sum of the individual contributions, with (2295 + 2112), giving a total of 4407 µS/cm x g/cm.

Figure 4.7-4 gives an empirical expression for the electrical strength of the fully bridged iced insulator, in line-to-ground flashover voltage per meter of dry arc distance, as:

$$Ice\ Flashover_{kV_{l-g}/m\,dry\,arc} = 396 \cdot ISP^{-0.19}_{g/cm.\mu S/cm} \qquad 4.7\text{-}4$$

For the moderate accumulation on clean insulators, the ice flashover stress will be 92.5 kV/m, and a dry arc distance

of 3.28 m would be needed to withstand 500 kV ac system voltage using 5% above nominal or 303 $kV_{l\text{-}g}$. For the same accumulation on an insulator with ESDD of 100 μg/cm², the flashover stress is 80.4 kV/m, and a dry arc distance of 3.77 m (26 standard units) would be appropriate for a single insulator string.

4.7.4 Snow Test Results

Accumulation of snow on parallel strings of tangent (dead-end) insulator strings is a specific concern for EHV transmission lines. From Figure 4.7-3 it can be seen that snow becomes an electrical concern at an icing stress product of 30,000 g/cm x μS/cm for a typical voltage gradient of 100 kV/m. This value is valid for a dense snow accumulation (25% water equivalent density) of more than 50 cm on a pair of horizontal insulator strings spaced at 50 cm, with a typical snow conductivity of about 30 μS/cm. CIGRE (CIGRE 2000a) provides a detailed summary of test results for these special cases.

4.8 INSULATION DESIGN

4.8.1 Introduction

As with switching surge and lightning design of line insulation, the selection and dimensioning of insulators with respect to contamination and ice conditions involve the selection of the insulation strength relative to the stresses that it will experience during its service life to obtain a required performance. For both contamination and ice conditions, it is sufficient to assume that a voltage of constant magnitude will stress the insulator. In this case, it is the environment that presents itself as a statistical variable(s).

In many cases, the environmental stresses can be sufficiently characterized with a single stress parameter. The installation is then designed to withstand a single contingency—adverse weather stresses. Examples of this design philosophy for overhead lines include:

- The use of towers with adequate strength to withstand the static weight of accumulated ice.
- The use of overhead groundwires and grounding electrodes to protect against 95-99% of overvoltages resulting from direct lightning flashes.
- The use of insulators with adequate wet flashover performance under normal ac operating voltage for rain rates of 1-2 mm per min (both horizontal and vertical) with a rain resistivity of 100 Ω-m.

In other cases, a single-contingency approach is not sufficient since some composite adverse weather stresses are common enough that they should be included in transmission-line design analysis. Examples of two-contingency stresses include:

- The use of adequate parallel capacity (limited-time thermal rating) to carry summer peak load after loss of a double-circuit line from a severe lightning flash.
- The use of towers with adequate strength to withstand the static force of wind pressure on accumulated ice on conductors and overhead groundwires.
- The use of adequate clearance or galloping control devices (torsional dampers or inter-phase spacers) to limit the coupling of high-speed steady wind energy into lightly iced conductors.
- The use of adequate insulator dimensions to withstand the line voltage stress when insulator surfaces are coated (over a long time of exposure) with electrically conductive pollution, then wetted by fog.

Industry experience has shown that combinations of two or three moderate contingencies at the same time can be more damaging than single, extreme events. A good example is the series of three sequential ice storms that occurred from January 4 to 9, 1998, leading to 1300 toppled towers in Quebec, Ontario and the northeast U.S., and more than two million customers without power. No single storm was extreme, but the combined accumulation of ice onto previously iced conductors added more than 80 mm of radial ice and 1000 kg to each transmission span in some locations.

As a two-contingency design is significantly more complex to perform, assumptions are often made to simplify the problem to allow a single-contingency analysis. This will be explained by considering the design of insulation with respect to contamination.

When considering contamination on insulators, three statistical variables need to be considered:

1. Applied voltage
2. Level of contaminants and their distribution on the insulator surface
3. Degree of wetting

A worst-case design would dictate that insulation needs to be designed to withstand the:

1. Highest temporary overvoltage that may occur in the network
2. Highest level of contaminants that are distributed evenly over the insulator surface
3. Critical (or worst) wetting conditions that occur

By doing this, it is implicitly assumed that all three variables reach their maximum level at the same time. While often overly pessimistic, this assumption makes it very simple to specify a design requirement for the insulators.

A fully statistical design will consider the density functions of the applied voltage, the pollution level and its distribution, and the intensity of the wetting to obtain a distribution of the total stress on the insulator. This approach demands a lot of input information since sufficient data should be available to characterize the probability density function of each stress parameter.

A middle-of-the-road approach would be to simplify to a single-contingency stress by identifying which variables are correlated. One simplification is to assume that critical wetting occurs at the peak level of the pollution deposit. In many cases, this is a reasonable assumption, since after a critical wetting event, the contamination level is less due to the leaching of contaminants from the insulator surface. Another assumption that could be made is to say that there is no correlation between the level of temporary overvoltage (TOV) in the network and the occurrence of a critical wetting event when the insulator has its highest probability for flashover, which means that the design can be based on the maximum continuous operating voltage. By making these assumptions, the multiple contingency is reduced to a single-contingency problem that can be solved relatively easily.

Another aspect that should be considered when designing insulators is whether to design for an average or maximum failure rate. This is decided by the consequences of a failure. If the consequences of a failure are severe—for example, in the case of non-self-restoring insulation—then the statistical variables are quantified so that the maximum possible failure rate is evaluated. For self-restoring insulation, it is generally sufficient to consider average failure rates, since these types of faults are of transient nature, and a line can be auto-reclosed.

Contamination flashovers lie somewhere between the self-restoring and non-self-restoring cases, since it often proves difficult to restore the line in service after this type of outage. This manifests either as unsuccessful reclose operations or as subsequent flashovers shortly after a successful re-closing. However, after a relatively short period of time, the line can be successfully energized due to drying out of the contamination layer. In order to account for this when designing for contamination, conservative assumptions are made while evaluating average outage rates.

The basic steps necessary to select and dimension insulators are:

1. Characterize the environment in terms of both the type of contamination and its severity (Section 4.8.2).
2. Select the insulator characteristics that would be best suited to this environment—that is, the type of insulating material and the insulator profile (Section 4.8.3).
3. Determine the required insulator length or creepage (Section 4.8.4 and 4.8.5).

These steps will each be explained in the sections as indicated above.

4.8.2 Characterizing the Environment and its Severity

In designing transmission system insulation for contamination, it is essential to know the degree of contamination over the area where the power transmission system is to be constructed. Several methods to assess the site severity have been described in the literature (CIGRE 1979b; Lambeth et al. 1972). These methods range from very simple, such as directional dust deposit gauges, to complex, such as automated surface conductivity measurements (CIGRE 1994a). Also, not all methods are equally suited to assess the severity of a site, depending on the type of pollution present. Whereas the measurement of the Equivalent Salt Deposit Density is preferred at sites with solid, or predeposited, contamination, it may underestimate pollution levels at sites with liquid (or instantaneous) contamination. A first step in a site assessment should, therefore, be to determine the predominant type of contamination. Thereafter, the site assessment technique best suited to the particular circumstances can be selected. The most well-known site assessment techniques are listed in Figure 4.8-1 (CIGRE 2000b). These techniques can generally be classified as either a direct environmental measurement or a measurement of the insulator performance in the particular environment.

In the sections that follow, only a brief overview of the methods are given since they are well described in the standards and literature.

The results from the site severity measurements are used to classify the site according to a set of predetermined severity levels to allow the use of standardized insulation solutions. In Table 4.8-1, the five site severity categories used by the IEC are listed (IEC Forthcoming b), together with example descriptions of typical environments, based on the contamination accumulation characteristics of standard-shape insulators. It should be noted that these descriptions are illustrative only and not intended as a tool for site severity classification.

Environmental Severity Measurement

Environmental measurements aim to quantify the amount of contaminants at a particular site. The measurements can either be directly used to select the required insulator dimensions, based on service experience, or they can be used to specify a laboratory test. In both cases, a "calibration" curve is necessary that relates the site assessment measurement directly to either the insulator performance or the measure of severity used in the laboratory test method (Lannes and Schneider 1997).

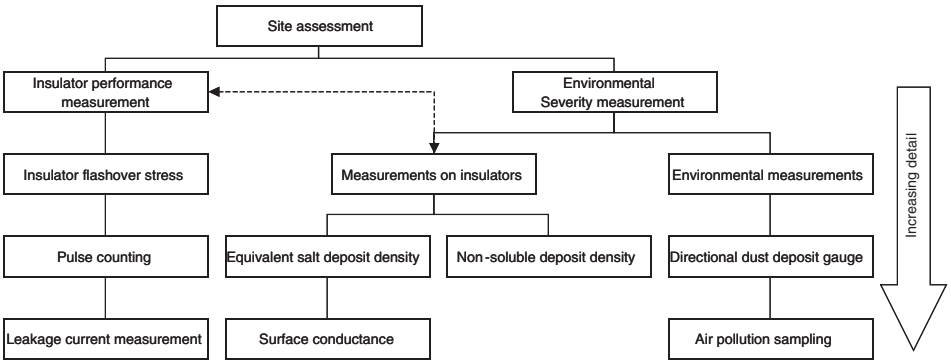


Figure 4.8-1 An overview of some site assessment techniques.

Table 4.8-1 Site Severity Classification and Sample Descriptions of Typical Environments (IEC Forthcoming b)

	Example Description of Typical Environment
Very Light	> 50 km from any sea, desert, or open dry land > 10 km from man-made pollution sources (e.g., industrial and agricultural activity such as crop spraying) or within a shorter distance, but: • the prevailing wind is not directly from these pollution sources • and/or subjected to regular monthly rain washing
Light	10-50 km from the sea, a desert, or open dry land 5-10 km from man-made pollution sources (e.g., industrial and agricultural activity such as crop spraying) or within a shorter distance, but: • the prevailing wind is not directly from these pollution sources • and/or subjected to regular monthly rain washing
Medium	3-10 km from the sea, a desert, or open dry land 1-5 km from man-made pollution sources (e.g., industrial and agricultural activity such as crop spraying) or within a shorter distance, but: • the prevailing wind is not directly from these pollution sources • and/or subjected to regular monthly rain washing or further away, but: • a dense fog (or drizzle) often occurs after a long dry pollution accumulation season (several weeks or months) • and/or heavy rains with a high conductivity occurs • and/or there is a high NSDD level, typically between 5 and 10 times the ESDD level
Heavy	Within 3 km of the sea, a desert, or open dry land Within 1 km of man-made pollution sources (e.g., industrial and agricultural activity such as crop spraying) or with a greater distance, but: • a dense fog (or drizzle) often occurs after a long dry pollution accumulation season (several weeks or months) • and/or there is a high NSDD level, typically between 5 and 10 times the ESDD
Very heavy	Within the same distance of pollution sources as specified for "Heavy" areas and: • directly subjected to sea-spray or dense saline fog • or directly subjected to contaminants with high conductivity, or cement type dust with high density, and with frequent wetting by fog or drizzle • Desert areas with fast accumulation of sand and salt, and regular condensation • Areas with extreme levels of NSDD, more than 10 times the level of ESDD

Furthermore, it is advisable to complement the measurements described below with a chemical analysis to identify the soluble deposits on insulator surfaces. This is especially useful in industrial areas where a great variety of chemicals may be deposited onto the insulators.

The environmental severity measurement methods can be described as follows:

ESDD and NSDD Measurement
(**E**quivalent **s**alt **d**eposit **d**ensity = ESDD, **N**on**s**oluble **d**eposit **d**ensity = NSDD)

The amount of soluble and nonsoluble contaminants on an insulator surface is determined by swabbing the insulator to obtain a solution of the contaminants, which is then analyzed to assess the contamination layer:

- **ESDD.** The amount of soluble contaminants is expressed as the equivalent deposit of sodium chloride on the total surface area of the insulator—in mg/cm^2—which has the same conductivity as that of the actual deposit dissolved in the same volume of water (Chisholm et al. 1994).

- **NSDD.** The amount of nonsoluble deposits is expressed as the weight of these deposits per unit square area of the insulating surface, also expressed in mg/cm^2.

These methods are being standardized by the IEC for the measurement of solid, or predeposited, contamination (IEC 60815 Forthcoming b). Applet A-1 can be used to calculate the ESDD and NSDD values from the measured conductivity of the contamination solution and weight of the nonsoluble residue.

The amount of contamination on the insulators is not constant. It accumulates on the insulators during periods without rain and is removed from the insulator during wet conditions. Thus it appears that the contamination on the insulator varies randomly over time, providing the equilibrium deposit has been reached. For the dimensioning process, it is necessary to know the statistical distribution of the maximum value of contamination stress on the insulator since:

- The peak value represents the weakest condition of the insulator.
- The peak occurs normally at the start of a natural cleaning event, which is also the time when the insulator has the greatest probability for flashover.

Usually the statistical distribution of the ESDD is characterized by its 2% value, which is the value that will be exceeded in 2% of the cases. It can be appreciated that a substantial number of measurements are required to get a good estimation of this value. As a result, it may be necessary to perform the ESDD measurements over an extended period of time. In some areas, notably those with extended dry periods, it may take several years to get a sufficient number of data points.

Another problem is that the peak values of the contamination severity occur at random. It is, therefore, difficult to time the ESDD measurements to obtain these peaks. From a practical point of view, the measurements are most often performed at a fixed time interval, resulting in a loss of accuracy in the evaluation of the maximum values, since the peak values are not necessarily measured. This error can be minimized by adjusting the sampling interval to be appropriate for the type of environment. Table 4.8-2 presents rough estimates for the different types of environment to help the user to choose an optimal measurement interval when this latter approach is followed (CIGRE Forthcoming b).

Standard insulator discs are used when attempting to quantify the severity of the environment for insulator selection purposes. When evaluating the accumulation characteristics of specific designs, the insulator under investigation is utilized. If the insulator is to be applied in a string, then the effect of the adjacent discs needs to be accounted for.

ESDD and NSDD measurements on a standard disc or longrod type insulator can be classified according to the diagrams in Figures 4.8-2 and 4.8-3, respectively (IEC Forthcoming b). This classification system takes account of the fact that the flashover performance deteriorates for increasing levels of nonsoluble deposits.

Table 4.8-2 Typical Measuring Intervals to Determine Maximum ESDD Values (CIGRE Forthcoming).

Type of Environment	ESDD Measurement Interval
Desert	From 12 to longer than 24 months
Coastal	1-6 months depending on duration of dry season or just after a rapid pollution event
Industrial	12-24 months
Agriculture	3-6 months
Inland (Low pollution)	3-6 months

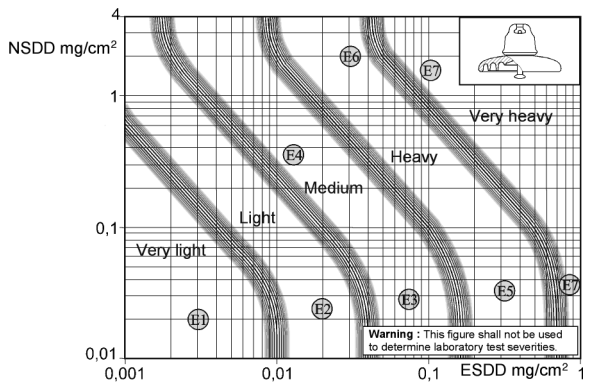


Figure 4.8-2 Solid type contamination: Relation between ESDD/NSDD and the site pollution severity for standard-shape disc-type insulator (IEC Forthcoming b).

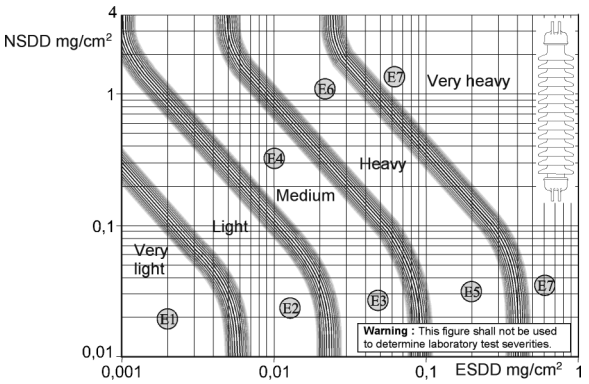


Figure 4.8-3 Solid type contamination: Relation between ESDD/NSDD and the site pollution severity for standard longrod type insulator (IEC Forthcoming b).

It should be noted that the ESDD does not always give a true value for the conductivity of the contaminant in actual service conditions. Two cases are worth mentioning:

- **Contamination with Different Types of Salts.** Insulators contaminated with different types of salts behave differently under natural wetting conditions, leading to different levels of flashover for identical ESDD values. This is primarily because of the difference in the hygroscopic characteristics of the deposited materials. For instance, gypsum has only 2% solubility, whereas sodium chloride has 40% solubility. Under natural wetting conditions, insulator surfaces contaminated with gypsum are not as conductive as those contaminated with sodium chloride because the amount of water on the surfaces is not sufficient to dissolve all of the gypsum. However, the gypsum is completely soluble if between 1000 and 2000 ml water is used to measure the ESDD (Lin et al. 1992; Ramos et al. 1993). This may result in an over-estimation of the contamination severity.
- **Encapsulation with Hydrophobic Silicone Oils.** Silicone rubber insulators may encapsulate pollutants on their surface with hydrophobic silicone oils. A portion of the contaminants are, therefore, not available to dissolve when the insulator is naturally wetted. When the ESDD measurement is performed, the hydrophobicity encapsulation is broken down, and all the salts are included in the measurement, leading to an over-estimation of the contamination severity on the insulator (Kindersberger and Kuhl 1991; Xidong et al. 1994; Engelbrecht et al. 2000).

Directional Dust Deposit Gauges

This is another method that is being standardized by the IEC. It can be used on sites independent of the contamination type—i.e., solid or liquid. With this method, a standardized gauge is used to collect windborne contaminants in a container over a monthly period (see Figure 4.8-4) (Lambeth et al. 1972). In this case, the contamination severity is expressed as the "Dust deposit gauge index – soluble," which is the average volume conductivity of the four containers, each dissolved in 500 ml water. Figure 4.8-5 shows the severity classification proposed by the IEC for this method (IEC Forthcoming b).

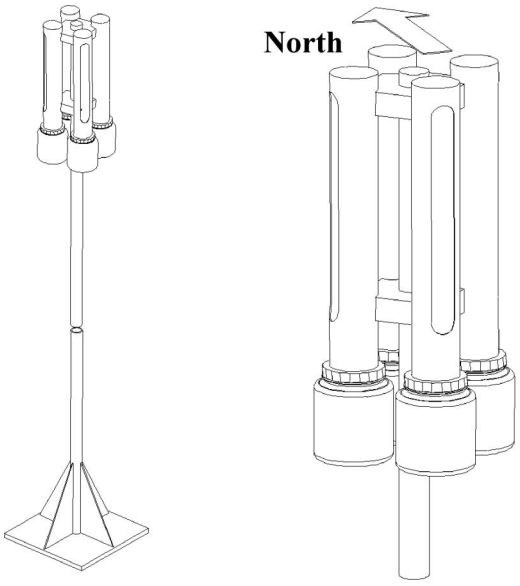


Figure 4.8-4 A directional dust deposit gauge.

It is recommended to "correct" the site severity classification for the presence of nonsoluble deposits, which is the average weight of the nonsoluble contaminants collected in the four containers, called the "Dust deposit gauge index – nonsoluble." Based on the average measured value over a year, a correction is made as follows (IEC Forthcoming b):

- No correction is made if the yearly average weight is below 0.5 g.
- The severity class is increased with one level if the average range value is between 0.5 and 1.0 g.
- The severity class is increased by two levels if the average value is higher than 1.0 g.

Air Pollution Sampling

A commercial standardized instrument is used to determine the amount and characteristics of the airborne pollution at a site, often called dustfall. A correlation needs to be established between the measurement performed and one of the standardized pollution severity measurements. For example, in Canada, it was found that the maximum buildup of ESDD over the winter months had a high correlation with "winter monthly dustfall," a standard environmental measure for local pollution (Chisholm et al. 1993):

$$ESDD_{Season\ peak} \approx 9 \times \left(\text{Dustfall}_{g/m^2/month}\right)^2 \qquad 4.8\text{-}1$$

Surface Conductance/Conductivity

The surface conductance, which is the ratio of the power frequency current flowing over a sample insulator to the applied voltage, is measured by "meggering" the insulator. The applied voltage should be high enough to obtain a good current reading, but not too high or of too long a duration, to avoid heating and discharge effects. Several automated instruments have been developed that measure

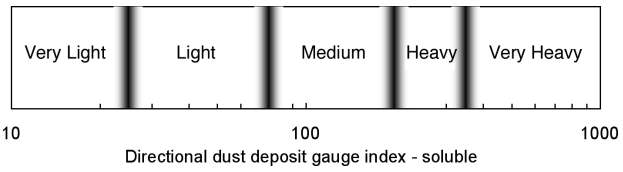


Figure 4.8-5 Relation between the average monthly directional dust deposit gauge index (soluble) and the site pollution severity (IEC Forthcoming b).

the surface conductance at preset intervals (CIGRE 1994a). The most sophisticated of these include built-in artificial wetting so that the surface conductance can be measured in dry weather conditions.

Surface conductance is not directly usable, since it is dependent on the dimensions of the insulator that is being measured. Therefore, it is common to calculate the surface conductivity from the surface conductance measurements with the help of the form factor, described in Section 4.2. The surface conductivity can also be measured directly with a hand-held probe, such as the one described in IEC 60507 (IEC 1991).

An approximate relationship between surface conductance and ESDD is:

$$ESDD_{mg/cm^2} \approx 0.01 \times \left(\text{Surface Conductivity}_{\mu S}\right) \quad 4.8\text{-}2$$

Surface conductance measurements are particularly suited for the measurement of the effective contamination severity on polymer insulators. These measurements can be made without disturbing the pollution layer—and destroying the encapsulation effect of silicone oils, if present. Several probes have been developed for this measurement (Kindersberger and Kuhl, 1991; Xidong et al. 1994). This conductance measurement can also be expressed in terms of the apparent salt deposit density (ASDD), which can be directly compared to ESDD measurements on the same insulator to obtain an indication of the extent of the encapsulation effect.

Insulator Performance Measurement

The performance of insulators can be measured as follows.

Insulator Flashover Stress

This is a very simple method to determine the minimum required length of insulators at a site. A sample insulator string is energized and a number of insulators are shorted out with explosive fuses, as shown in Figure 4.8-6. The fuses are selected so that the string length is successively increased with one, or more, discs if the leakage current reaches critical levels, or flashover occurs. This method is best applicable on disc-type insulator strings.

Pulse Counting

Pulse counting is one of the very first insulator monitoring methods that were developed. A counter is used to count the current pulses above a predetermined threshold. These counters can be made very simple and robust.

Leakage Current Measurement

The most sophisticated of the insulator performance measurements is the monitoring of leakage current over the insulator. This is readily enough done in a relatively controlled environment, such as an insulator testing station or a testing laboratory. A number of devices have been developed for on-line leakage current monitoring on line or substation insulators. These instruments are, however, rather expensive, which limits their widespread use.

Leakage current is used especially in areas with liquid contaminants. For such cases, the site severity is characterized by the equivalent Salt-Fog test severity that will result in the same level of peak current when performed on an identical insulator and voltage stress (see Figure 4.8-7) (Verma et al. 1978). In the revision of the IEC 60815, this is called the Site Equivalent Salinity (SES) (IEC Forthcoming b).

Contamination Maps

It would be desirable to arrive at a contamination map in which the degree of contamination condition is shown in the same manner as the isokeraunic levels for lightning

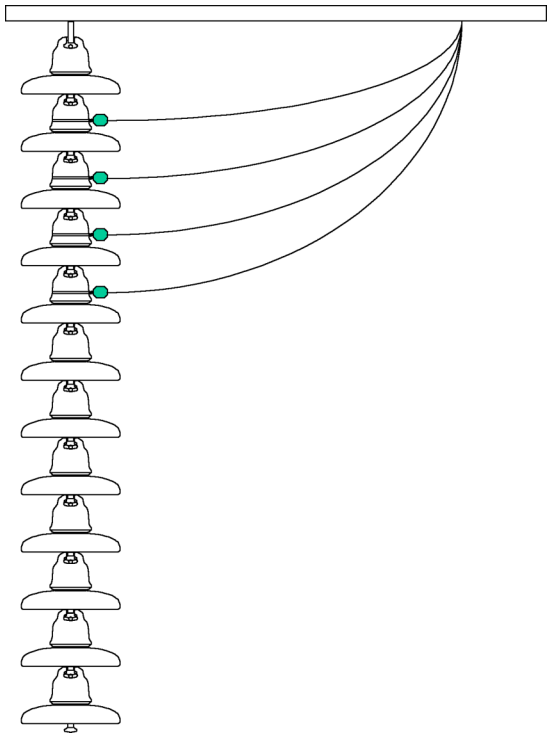


Figure 4.8-6 Application of explosive fuses to determine the minimum insulator flashover stress.

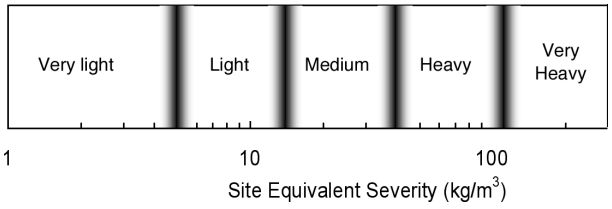


Figure 4.8-7 Relation between the site equivalent severity and the IEC pollution classification (IEC Forthcoming b).

(Kimoto et al. 1972). This will require an intensive investigation over large areas for several years, because the deposition of contaminants varies with weather conditions, such as wind and precipitation, and with specific locations. There is, of course, still much uncertainty surrounding the knowledge of weather conditions. In particular, it should be emphasized that many past contamination flashovers were caused by unusual weather conditions, such as an exceptional salt storm or a long dry period that allowed a heavy accumulation of pollutants (CRIEPI 1968; Sporn et al. 1964; Massey 1972). Also, industrial pollution levels change with the activity of industry in the vicinity of power systems. Application of air pollution controls should reduce artificial pollution in general.

It is recognized that the prediction of contamination conditions is an arduous and continuing task. In one country, the contamination map has been revised three times in 10 years (CRIEPI 1968). It is, therefore, advisable to use as far as possible automated, very simple site-assessment techniques, such as air pollution sampling. Figure 4.8-8 shows a typical example of how dustfall measurements have been used to obtain a pollution map of an area of heavy industry on the east shore of Lake Ontario. The HV transmission lines adjacent to this heavy industry will be exposed to relatively severe ESDD levels of up to 0.6 mg/cm^2.

4.8.3 Choice of Material

In the past, the choice of insulator material has often been based on historical experience and the confidence that has been gained in a specific product. As was highlighted in Section 4.4, all insulator technologies have their strengths and weaknesses. The choice of material is, therefore, a balancing act, where the advantages and disadvantages need to be weighed against each other in order to find the optimal solution. A broad overview of some of the advantages and disadvantages of using a particular technology are listed in Table 4.8-3.

In many companies, the decision to utilize glass or porcelain has been taken long ago and is generally based on many years of service experience. The electrical performance of these two materials is, for all practical purposes, the same, and the choice of material rests on previous good or bad experience. In comparison, polymer insulators have

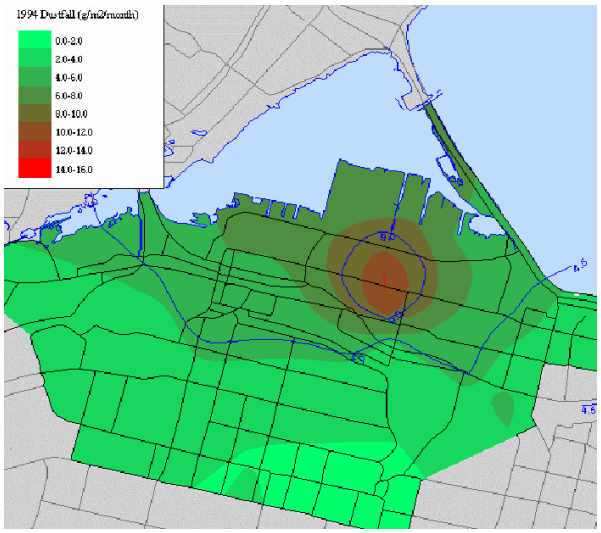


Figure 4.8-8 Typical variation in dustfall near urban industrial area of Hamilton, Ontario.

Table 4.8-3 Advantages and Disadvantages Associated with Different Insulator Technologies

Technology	Advantage	Disadvantage
Glass	– Give visual indication of internal defects – Good puncture resistance – Proven long-term reliability – Insulators from different manufacturers are interchangeable and generally have similar performance	– Prime targets for vandals because of shattering – Surface may be etched by long-term dry-band arcing resulting in shattering – May require long insulator strings in polluted conditions – Heavy – Lack of availability in certain regions
Porcelain	– Surface glazing resistant to etching from dry band activity – Do not shatter when shot by vandals – Proven long-term reliability – Insulators from different manufacturers are interchangeable and generally have similar performance	– May contain hidden internal defects – May require long insulator strings in polluted conditions – Heavy – Lack of availability and time to delivery in certain regions
Polymer	– Lighter weight (easier to handle and ship) – Lower cost – Better availability and shorter lead times – Enables single-pole structures (i.e., post application) – Better shock loading characteristics (post only). – Less susceptible to vandalism – Better contamination performance	– Unknown life expectancy – Limited service experience – Different designs, materials, and manufacturing processes between suppliers. – More susceptible to damage during handling. – May contain hidden defects – Concerns regarding live working – Difficult to identify high risk units prior to failure

been introduced relatively recently, and the designs of most manufacturers have evolved over time. Results from service inspections are also not always relevant due to the many revisions and refinements to the designs, and to the materials and manufacturing processes that have been made to improve the product and address degradation and failure modes. This is compounded by the facts that: (a) each manufacturer employs different materials, construction details, and manufacturing processes; and (b) many utilities are not certain of what vintage units they have in-service on a specific structure.

The aim of this section is, therefore, to focus more on the selection of polymer insulator materials than on glass or porcelain.

Insulator Selection Considerations

The following factors need to be considered when selecting the type of insulator to be utilized.

Cost and Availability

As manufacturing techniques improve, polymer insulators are becoming more cost competitive, and their inherently shorter lead times often make polymer insulators more attractive. Their light weight may also reduce shipping, handling, and most significantly, installation costs (EPRI 2003b; Burnham et al. 1994).

Standardization

Unlike porcelain and glass insulators, the basic dimensions and designs of polymer insulators are not well defined. Differences in materials and manufacturing techniques are significant, making the choice between different manufacturers' designs difficult. Utilities have to survey manufacturing techniques, materials, and designs to determine which is best for their environment and application. Often there are trade-offs to be made.

There are no standard connection lengths for polymer insulators. Concerns have arisen when replacing in-service units since connection length changes can have an effect on conductor tension and sag. Certain manufacturing processes allow the manufacture to almost any predefined length, while other processes are less flexible. Due to industry pressures, most manufacturers have addressed this issue by providing a comprehensive range of lengths.

There is no standardization of corona ring designs, attachment mechanisms, or effective performance criteria. The only performance criteria that has been put forward has been by EPRI and STRI, where the E-field is recommended to be below specific levels on the rubber housing and the end fitting seal (EPRI 1998; *Insulator News and Market Report* 2002).

Not only is it difficult for the utility engineer to evaluate differences in corona ring designs, but it may also result in confusion in the field. It is not uncommon to find corona rings from one manufacturer installed on another manufacturer's units. Since each manufacturer utilizes a unique attachment method specific to their end fitting design, a corona ring from another manufacturer may be installed in an incorrect location or backwards.

Power Arc Performance

The ability of polymer insulators to withstand power arcs terminating directly on the end fittings may be divided into three categories:

1. Short-term mechanical performance
2. Long-term mechanical performance
3. End fitting seal performance

Testing has indicated that there may be a short-term loss in mechanical strength during the power arc to approximately 60% of the ultimate strength of the insulator. For the design tested, this reduction corresponded to 80% of the specific mechanical load (SML) (Matsouka et al. 1998). Long-term reductions of 10 to 20% in ultimate mechanical strength have also been observed in testing. For the design tested, the long-term strength of units was above the SML. Since polymer insulators are applied at less than 50% of SML for extreme loading conditions, concerns are reduced (Matsouka et al. 1998)

Damage to the end fitting seal resulting in exposure of the fiberglass rod is a concern. Certain designs appear to be inherently more susceptible than others. The removal of galvanization and the resulting localized corrosion is of lesser concern. Figure 4.8-9 shows examples of units removed from service with damaged end fittings due to power arcs (EPRI 2004c). Standard tests exist to determine the ability of insulator strings to withstand power arcs. The tests specify how the power arc tests should be performed, together with visual and mechanical criteria by which the insulators are assessed after the test (IEC 1997 b).

The use of corona rings or arcing horns will reduce the effect of power arcs. Both the energized and grounded end fittings need to be addressed. Manufacturers should be consulted as to whether units that have experienced flashover should be removed from service.

Live Working

Concerns have been raised over working with polymer insulators under energized conditions. These concerns arise in two circumstances:

- **Installing new units.** Unlike manufacturers of porcelain/glass insulators, manufacturers of polymer insulators do not perform electrical routine tests on individual

polymer insulators, due to the high voltages required for such testing. In order to address this concern, some utilities test, tag, and package all new polymer insulators intended to be installed under energized conditions. Another approach is to utilize a high-voltage test set in the field to test the units. Utilizing the transmission line being worked on as a test source is another, although somewhat controversial, approach proposed (Harmon et al. 1996).

- **Working with or around in-service units.** Effective techniques to determine the condition of an in-service polymer insulator with respect to energized work remain illusive. Although concerns may arise for both the mechanical and electrical condition of in-service units, the mechanical concerns can be negated by installing strain sticks prior to applying mechanical load to the supported conductor. However, techniques are not available to assess whether a conductive (or semi-conductive) defect of sufficient size exists. Research projects are under way at EPRI and other institutions to address this issue (EPRI 2003d; EPRI 2004d).

Audible Noise, EMI, and RIV

Polymer insulators have been applied in some situations to address audible noise, EMI, and RIV complaints due to discharge activity. The unwanted discharge activity may have occurred due to contamination or poor connection between individual porcelain/glass bells on lightly loaded strings.



Figure 4.8-9 Examples of damage to end fittings due to power arcs.

High-Temperature Conductors

The maximum permissible conductor temperature has been generally limited by the maximum allowable conductor sag, which, in turn, is determined by conductor clearance regulations. Conductor sag is a function of the properties of the conductor, the current flowing through the conductor, mechanical load, ambient temperature, prevailing wind, and environmental conditions. In order to increase the power throughput, new conductors have been designed that have reduced sag at elevated temperatures. Some of these new conductors are able to operate at temperatures exceeding 200˚C (392˚F) without compromising clearance regulations.

With the advent of these new conductors, the factor limiting the temperature at which conductors may operate may shift from conductor sag to the maximum operating temperature of the attached line hardware and associated components. One of the components considered to be vulnerable to elevated temperatures is the polymer insulator due to the material used in its construction. Manufacturers of polymeric insulators generally specify a maximum ambient operating temperature of 50˚C (122˚F), and it is a concern that elevated conductor temperatures may lead to this value being exceeded.

A number of tests have been performed on polymer insulators connected to high-temperature conductors to determine the temperatures that the insulator end fittings will be subjected to. Figure 4.8-10 shows the results of some of these tests.

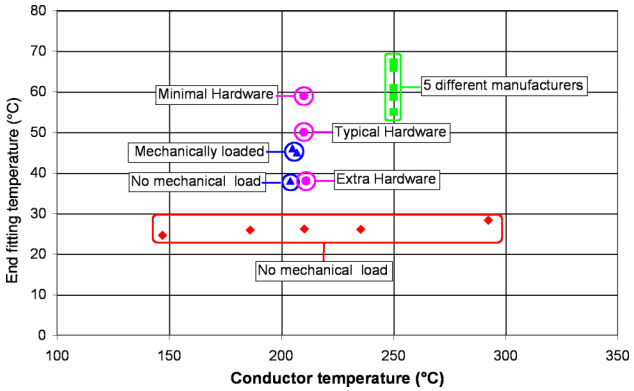


Figure 4.8-10 Summary of results obtained by different organizations with respect to the end fitting temperature of an insulator for different conductor temperatures. Ambient temperature in all cases was between 20 and 25ºC (EPRI 2000b, 2001b).

It was found that the polymer insulator end fitting temperature was a function of (EPRI 2001b):

- Conductor temperature
- Applied mechanical load. (Tests performed with no load provide lower end fitting temperatures due to the poor contact between the hardware. A relatively modest load of 235 kg (520 lb) ensures effective contact.)
- End fitting design of the polymer insulator.
- The type and length of hardware connecting the conductor and the polymer insulator.

It can be seen from Figure 4.8-10 that, in some cases, end fitting temperatures of almost 70°C were reached for conductor temperatures of 250°C when the ambient temperature was 25°C.

It has been indicated by a number of insulator manufacturers that these levels of end fitting temperature can be withstood. In a survey of manufacturers, the maximum recommended end fitting temperatures varied between 70° and 90°C, depending on manufacturer (EPRI 2001b).

Not evaluated or investigated in the testing was the impact of ambient conditions or solar radiation. The effect of these high temperatures on the long-term performance remains under investigation.

Ease of Inspection

Identifying high-risk polymer insulators prior to failure remains an issue. Conditions indicating an increased risk are relatively small, and inspection distances are large (EPRI 2003c; CIGRE 1996; Spangenberg and Riquel 1997). As the population of installed polymer insulators ages, utilities will be faced with an increased challenge. Detailed close-up visual inspection, at distances less than 0.5 to 1 m, remains the most effective method of inspection, but is impractical and not cost effective. It also requires considerable inspector expertise (EPRI 2004c).

Development of the EPRI daytime corona camera was intended to assist in this regard, but it has limited application since it does not address the main failure mode, brittle fracture (EPRI 2001d).

Developments currently under way to improve inspection methods, include:

- Inspection technique to evaluate the resonant characteristics of insulators (EPRI 2004b).
- "Self diagnosing" polymer insulator (EPRI 2003e).
- Design and vintage identification guides to assist in the identification of high-risk designs (EPRI 2004e).

These developments are currently under way and it is uncertain whether they will fully resolve the issue.

Wood Pole Fires

The use of polymer insulators has been effectively applied to reduce the occurrence of wood pole fires by reducing the leakage current. Silicone rubber units have been applied in most cases due to their hydrophobic properties and hence lower leakage currents.

Storing, Transporting and Installing

The root cause of numerous failures has been handling damage. The light weight and, apparent "toughness" of polymer insulators and the small size of the critical damage that they can incur appear to make polymer insulators more susceptible to handling damage. Education of warehouse and field personnel is essential to reduce the number of handling-related failures. Both utility and contractor personnel need to be addressed. A number of guides and an educational video are available to assist in this regard (EPRI 2001a, 2001c; CIGRE 2001).

Animal Damage

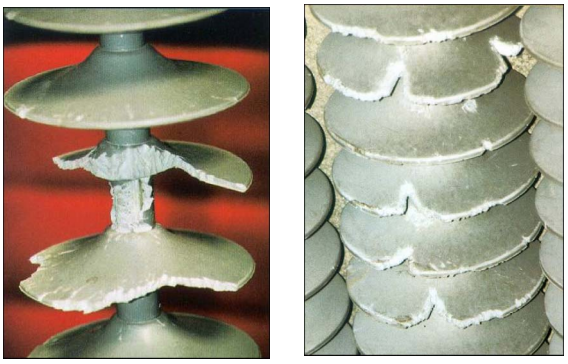
Polymer insulators at a number of utilities have experienced damage from rodents and birds, as shown in Figure 4.8-11.

Rodent damage has occurred to units while stored in warehouses or shipping yards. Effective packaging and storage procedures can be put in place to reduce concerns.

Utilities in Australia and the United States have experienced bird damage on installed units. Damage is more prevalent prior to energization; however, damage to energized units has also been reported. The cover-up of installed units prior to energization has been implemented to reduce damage.

Vandalism

Polymer insulators have been effectively applied in situations where vandalism is high. Unlike porcelain or glass units, polymer insulators provide little gratification when struck by a bullet and present a smaller profile to aim at (Burnham and Waidelich 1997).



Rodent Damage Bird Damage

Figure 4.8-11 Examples of rodent and bird damage to polymer insulators.

On the other hand, gunshot damage is difficult to identify on polymer insulators and can have a catastrophic result if the rod is exposed.

Resources

When determining which type of insulator, or what design of insulator to utilize, engineers can draw on a number of resources, including:

- Compliance with national and international standards
- Field experience
- Accelerated aging tests
- Stress testing
- Published application guides

International and National Standards

There is a wide range of international and national standards. In this document reference will be made to both IEC and ANSI standards. A list of the relevant IEC and ANSI/IEEE standards is provided in Tables 4.8-4 and 4.8-5.

Table 4.8-4 IEC Standards and Reports Covering AC Transmission Line Insulators

Code	Year	Title	Remarks
IEC 60383-1	1993	Insulators for overhead lines with a nominal voltage above 1000 V - Part 1: Ceramic or glass insulator units for a.c. systems - Definitions, test methods and acceptance criteria	
IEC 60383-2	1993	Insulators for overhead lines with a nominal voltage above 1000 V - Part 2: Insulator strings and insulator sets for a.c. systems - Definitions, test methods and acceptance criteria	
IEC 60305	1995	Insulators for overhead lines with a nominal voltage above 1000 V - Ceramic or glass insulator units for a.c. systems - Characteristics of insulator units of the cap and pin type	
IEC 60433	1998	Insulators for overhead lines with a nominal voltage above 1 000 V - Ceramic insulators for a.c. systems - Characteristics of insulator units of the long rod type	
IEC 60720	1981	Characteristics of line post insulators	
IEC 62217	New	Polymeric insulators for indoor and outdoor use with a nominal voltage greater than 1 000 V - General definitions, test methods and acceptance criteria	
IEC 61109	1992	Composite insulators for a.c. overhead lines with a nominal voltage greater than 1000 V - Definitions, test methods and acceptance criteria	Being Updated
IEC 61466-1	1997	Composite string insulator units for overhead lines with a nominal voltage greater than 1000 V - Part 1: Standard strength classes and end fittings	
IEC 61466-2	2002	Composite string insulator units for overhead lines with a nominal voltage greater than 1 000 V - Part 2: Dimensional and electrical characteristics	
IEC 61952	2002	Composite line post insulators for a.c. overhead lines with a nominal voltage greater than 1 000 V: definitions, test methods and acceptance criteria	Being Updated
IEC 60120	1984	Dimensions of ball and socket couplings of string insulator units	
IEC 60372	1984	Locking devices for ball and socket couplings of string insulator units - Dimensions and tests	
IEC 60471	1977	Dimensions of clevis and tongue couplings of string insulator units	
IEC/TR 60575	1977	Thermal-mechanical performance test and mechanical performance test on string insulator units	
IEC/TR 60797	1984	Insulators for overhead lines with a nominal voltage above 1000 V - Residual strength test for ceramic or glass string insulator units after mechanical damage of the dielectric	Being Updated
IEC/TS 61211	1994	Insulators of ceramic material or glass for overhead lines with a nominal voltage greater than 1000 V - Impulse puncture testing in air	Being Updated
IEC 60575 TR	New	Thermal-mechanical performance test and mechanical performance test on string insulator units - Development of the tests	
IEC/TS 61467	1997	Insulators for overhead lines with a nominal voltage above 1000 V - a.c. power arc tests on insulator sets	Being Updated
IEC 60437	1997	Radio interference test on high-voltage insulators	
IEC 60507	1991	Artificial pollution tests on high-voltage insulators to be used on a.c. systems	
	New	Minimum test requirements to cover brittle fracture of line composite insulators	Being Considered
IEC/TS 62073	2003	Guidance on the measurement of wettability of insulator surfaces	
IEC/TR 60815	1986	Guide for the selection of insulators in respect of polluted conditions	Being Updated
IEC 61467	1997	Insulators of ceramic material or glass for overhead lines with a nominal voltage greater than 1000 V – AC power arc tests on insulator sets	
CIGRÉ TB-158	2000	Polluted insulators: A review of current knowledge	
CIGRÉ	new	Guidelines for selection and dimensioning: Part 1: General principles and the a.c. case	Being Prepared

Table 4.8-5 ANSI standards and IEEE Guides Covering AC Transmission Line Insulators

Code	Year	Title	Remarks
ANSI C29.1	1988	Test methods for electrical power insulators	Revised 2002
ANSI C29.2	1986	Insulators – Wet process porcelain and toughened glass suspension type	Revised 1999
ANSI C29.4	1989	Wet Process porcelain insulators –strain type	Revised 2002
ANSI C29.7	1996	Porcelain Insulators high voltage line post type	Revised 2002
ANSI C29.11	1989	Tests to composite suspension insulation for overhead transmission lines	Revised 1996
ANSI C29.12	1997	For Insulators composite – suspension type	Revised 2002
ANSI C29.17	2002	For insulators – composite line post type	
IEEE Std 987	2001	IEEE Guide for Application of Composite Insulators	
IEEE Std 4	1995	IEEE Standard Techniques for High-Voltage Testing:	Amended 2001

The ANSI/IEEE standards listed in Table 4.8-5 refer to American Society for Testing and Materials (ASTM) that describe additional or complementary test methods to verify electrical, mechanical, physical, and chemical properties of the materials used in insulators. These test methods include:

Electrical Properties

- Dielectric strength (ASTM D 149)
- Dissipation factor (ASTM D 150)
- Arc resistance (ASTM D 495)
- Tracking and erosion resistance (ASTM D 2303)

Mechanical Properties

- Impact resistance (ASTM D 256)
- Tension (ASTM D 412)
- Compression (ASTM D 575)
- Fatigue (ASTM D 623)
- Tear (ASTM D 624)
- Shear (ASTM D 732)
- Flexural (ASTM D 790)
- Hardness (ASTM D 2240)
- Creep (ASTM D 2290)

Physical Properties

- Thermal expansion (ASTM D 696)
- Thermal resistance (ASTM D 756)

Chemical and Environmental Properties

- Fungi resistance (ASTM G 21)
- Chemical resistance (ASTM D 471)
- Ozone resistance (ASTM D 1149)
- Corona resistance (ASTM D 2275)

There are some differences in the terminology used in IEC and ANSI standards, as highlighted in Table 4.8-6.

Manufacturers' products are expected to comply with all requirements outlined in the applicable standards. It is often useful for decision makers to determine whether the product design complies with standards that may not be mandatory in their region.

Some of the "tracking and erosion tests" described in the standards are often called "aging tests" in the literature. It is important to note that these tests are not "accelerated aging tests" in the sense that these tests do not simulate exactly the real-life degradation conditions, nor do they accelerate them to give a life-equivalent test in a short time. Rather these tests use continuous, cyclic, or combined stresses to try to detect potential weaknesses that could compromise the insulators performance in-service. These tests can best be described as "screening tests" (IEC 1992; CIGRE 1999a; CEA 1996).

Field Experience

Even though an insulator may have passed all of the tests identified in the relevant international and national standards, further information is often required to obtain an

Table 4.8-6 Comparison of the Terminology used in IEC and ANSI

IEC	ANSI/IEEE	Definition
Design tests	Prototype tests	The purpose of these test are to verify the suitability of the design, materials and method of manufacture. Results are valid for the whole class of insulator. These tests do not provide an indication of life expectancy.
Type tests	Design tests	The purpose of these tests is to verify the main characteristics, which depend mainly on size and shape.
Sampling tests	Sample tests	These tests are for the purpose of verifying other characteristics, including those depending on the quality of manufacture and on materials used. They are made on insulator samples taken at random from production lots.
Routine tests	Routine tests	The aim of these tests is to eliminate insulators with manufacturing defects. They are made on every insulator of the production lot.

indication of the life expectancy for the environment and application in which the unit will be applied.

Field experience is one of the best methods to obtain life expectancy and performance information since the artificial stresses in aging/flashover tests are negated. This information is often not available since decades worth of experience is ideally necessary and the designs of units manufactured today are different from those manufactured 20 years ago.

When determining whether field experience information is relevant to a new installation, one must determine whether aging and flashover mechanisms are similar. Considerations include:

- Difference in environment between the field units being reviewed and the region in which the new units are to be applied. Care should be taken when basing the decision for units to be applied in a highly contaminated environment, on field units installed in a low contamination region and vice-versa.
- Differences in designs, manufacturing methods, and materials between the field units and the new units.
- Changes in the design of units presently manufactured and the field units.
- Differences in voltage level—to ensure that similar aging mechanisms occur (e.g., wet corona activity).
- Configuration and corona ring application, since the E-field distribution has a significant effect on the aging characteristics.
- Differences in mechanical loads—both everyday and under extreme loading conditions.

Not withstanding the above considerations, field experience remains the best resource on which to base a decision. Three areas from which this experience may be obtained include:

- Utility experience
- Test lines and structures
- Test stations

Utility experience on similar units installed in a similar environment for prolonged durations is required. Since modern-day polymer insulators only became available in the late 1970s, and since some of the designs changed significantly until the 1990s, this data is often not available. Approaches to reviewing field data should involve removal of units and include detailed visual inspection and dissection, and mechanical and electrical tests. Leakage current measurement, discharge observations, weather data, and material analysis have also been performed.

Care should be taken to ensure that field units reviewed are representative of the units being considered for application in terms of design, manufacturing, voltage level, and application. With a thorough understanding of the differences, these factors can often be accounted for in the decision-making process.

During the advent of polymer insulators, a number of utilities applied small numbers on test structures or installed test lines. The information from these installations has provided important guidance and verification. Since many of these test installations were initiated prior to mass production, units may have been hand crafted or not representative of the designs available today. Differences in environment, insulator design, voltage, and application should be noted when utilizing this information.

A number of outdoor test stations exist where large numbers of test units have been installed and monitored on a regular basis. In some cases, these test stations were also instrumented for leakage current measurement and weather parameters. Observations and analyses were performed using a range of techniques.

Test stations have been constructed in both high- and low-contamination locations (Houlgate and Swift 1990; Houlgate 1993; Vosloo and Holtzhausen 1996; Gutman et al. 1999; Maxwell et al. 2002), which have provided valuable information. In some cases, the test sites have been located in extremely highly contamination environments to accelerate degradation. Care needs to be taken when interpreting results to ensure that the aging and flashover mechanisms in these harsh environments are representative of the application in which new units will be installed.

Configurations in test stations should also be applied in a manner that the E-field distribution is similar to that in service. The voltage levels should also be representative. Test stations that provide an acceleration aging environment, due to exceptionally harsh environmental conditions not experienced on normal transmission lines, should be considered as an accelerated aging test rather than a field test when considering experience.

Multi-Stress Accelerated Aging Tests

Since the required life expectancy for polymer insulators is often 30 years or more, a number of accelerated aging tests have been used worldwide to evaluate the long-term performance of polymer insulators. The accelerated aging tests are intended to simulate specific environments, around which an aging cycle is developed. The design of the cycle to accelerate aging is dependent on the primary aging mechanism under consideration. For example, if a highly contaminated environment is being considered, the number of pollution events in a year may be increased. In

the case of an aging test simulating a low-contamination environment, the number, or duration, of wetting events may be increased

When considering the results of an existing test, or implementing a new aging test, care should be taken to consider the environment in which units will be installed, and to evaluate the primary and secondary degradation modes. The aging cycle should be designed to simulate the degradation phenomena that will occur in the field as accurately as possible. If a degradation mode is introduced that does not occur in the field, the results may not be relevant.

Acceleration rates quoted for the individual tests are only approximate and are specific to the environment being simulated. Determining the acceleration rate requires a thorough understanding of the aging mechanisms, and in some cases, research performed at a later date may require initial acceleration rates be adjusted. For example, at the time of development of the EPRI "Deserts with a Distinctly Cold Season" aging test, the assumption was made that elevated temperature was the primary aging process. Future research indicated that time of wetness was the primary aging factor; hence the initially calculated acceleration factor of between 12 and 20 was revised at the end of the test to between 7 and 14 (EPRI 2000a).

In designing an aging cycle, care has to be taken to allow rest periods where silicone rubber-based insulators are able to recover their hydrophobicity. The inclusion of these rest periods was not always accounted for in early accelerated aging tests. The required conditions and duration of rest periods remain undefined and an area of ongoing research.

Comparison of accelerated aging test results against field-aged units, to confirm that the aging mechanisms are relevant, is essential. In a number of cases, the accelerated aging results have compared favorably with field-aged and outdoor test station units (Maxwell et al. 2002; EPRI 2000a, 2004a).

A number of tests, to determine the long-term performance, have also been developed to assess the performance of one, or possibly two, components of an insulator, but not the entire insulator (e.g., end fitting seal or rubber). Examples include the incline plane test, EPRI's end fitting seal test, and EPRI's long-term dynamic and mechanical loading tests. These tests do not provide an indication of life expectancy; rather they provide a performance comparison between different designs or highlight design weaknesses in the component being evaluated. Summaries of these tests, together with recently implemented tests, are described in Section 4.5.1 (EPRI 2002b; CEA 1996; CIGRE 1999a)

4.8.4 Flashover Probability of Contaminated Insulators

The flashover probability of a contaminated insulator string during critical wetting conditions is a function of both the contamination severity and the applied voltage. An increase in either of these variables leads to a higher flashover probability, as illustrated in Figure 4.8-12.

Since variable voltage tests are easier to perform, it is usual to express the probability for flashover in terms of voltage at a constant pollution severity. In most cases, flashover probability as a function of applied voltage is approximated by a normal distribution function (Carrara and Hauschild 1990). However, a Weibull distribution function has also been used to take account of the truncation of the distribution function. That is, at a specific contamination severity, there is a voltage below which flashover is not possible (Ivanov and Solomonik 1995).

This distribution function is usually characterized by the critical or 50% flashover voltage (V_{50}) and the standard deviation (σ). It has been shown that laboratory tests have a normalized standard deviation (i.e., σ / V_{50}) of between 6 and 10%. For field tests, it is approximately 20%. This difference between laboratory and natural testing can be ascribed to the larger variation in wetting and contamination distribution on the insulator surface under service conditions.

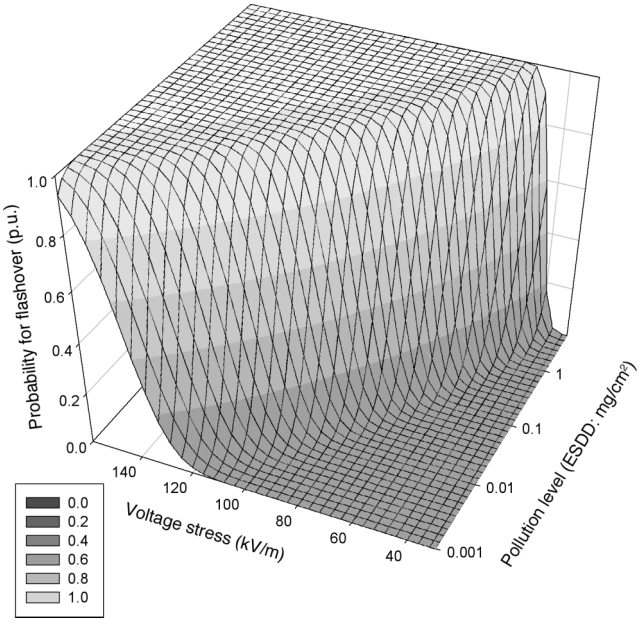


Figure 4.8-12 A three-dimensional representation of the probability for flashover during critical wetting as a function of the voltage stress across the insulator and the pollution severity level.

When considering the flashover probability of a transmission line, or station, it is also necessary to take account of the number of insulator strings that are exposed to the same environment. The Risk of flashover increases with more insulator strings exposed to the environment. The flashover probability of "n" insulator strings, "P_n", can be calculated from the flashover probability of one insulator string, "P_1" as follows:

$$P_n = 1 - (1 - P_1)^n \qquad 4.8\text{-}3$$

This relationship assumes that all the strings have the same single-string flashover probability and that they are statistically independent. It is, therefore, only possible to apply this relationship to a group of strings if they all are exposed to the same contamination severity, and all subjected to the same wetting conditions. The assumption of statistical independence implies that the flashover mechanism on one string does not affect the mechanism of others. Consequently, this relationship cannot be applied to closely spaced strings where the sub-strings are close enough to interact.

An experimental study was conducted for a setup of 14 parallel strings of eight-unit, Type A-11 insulators to prove the validity of this relationship. The results of these tests and two computed curves are plotted on normal distribution paper in Figure 4.8-13. Curves are shown for an assumed standard deviation, 10% and 8%, respectively of the V_{50}.

The relationship between flashover voltage and the number of strings in parallel is shown in Figure 4.8-14. In this figure the flashover voltage of all the strings in parallel is expressed in percentage of the V_{50} of a single string, while assuming a normal or Gaussian distribution function, with a normalized standard deviation of 10%.

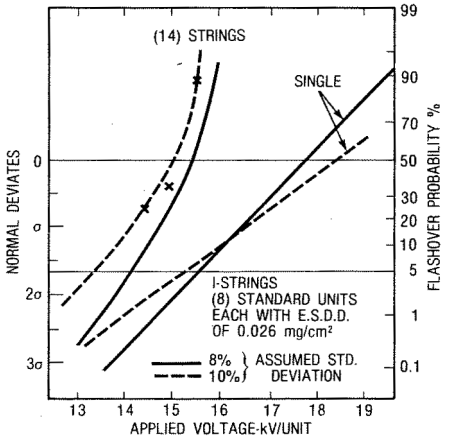


Figure 4.8-13 Test results of flashover probability of 14 I-strings.

For a single string, the withstand voltage (i.e., 10% flashover voltage, V_{10}) is 84% of $V_{50,}$ but this percentage deteriorates as the number of parallel strings increases. For example, a section of single-circuit, 10-mile-long, transmission line with four suspension towers per mile would contain 120 vertical strings. Under contaminated conditions, the withstand voltage of these 120 strings together would only be about 69% of the V_{50} of a single string.

The decrease of flashover voltage with the number of strings shows a trend of saturation for the case of more than 100 strings. For instance, the difference in withstand voltage between 100 and 500 strings is about 6.5%.

It is also necessary to take account of the effect of the parallel strings when performing laboratory tests on naturally contaminated insulators removed from a line that has experienced flashover. The naturally contaminated single string that has a V_{50} of 135% of the nominal line-to-ground voltage may be indication enough to verify that a contamination flashover has indeed taken place. This is because the V_{50} of 120 strings is 75% that of a single string, as shown in Figure 4.8-13. It was often found that units that experienced flashover have higher flashover voltages, from 110 to 150% of the nominal line-to-ground voltage, during laboratory testing.

These points emphasize that contamination flashovers on transmission lines, in areas of widespread contamination, occur at much lower voltages than the test voltages used in the laboratory (where the number of parallel strings is limited). This should be carefully reviewed during line design.

4.8.5 The Insulator Dimensioning Process

To dimension an insulator, the following aspects need to be considered:

- Basic Lightning Impulse Insulation Level (BIL) or Lightning Critical Impulse flashover

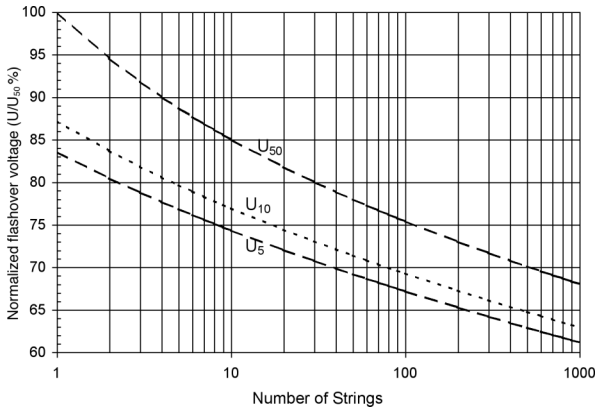


Figure 4.8-14 Relationship between flashover voltage of a single string and multiple strings, for 10% standard deviation.

- Basic Switching Impulse Insulation Level (BSL) or Switching Critical Impulse flashover
- Uncontaminated dry and wet power frequency flashover
- Contamination flashover
- Mechanical strength

In this section, the description of the dimensioning process will only cover the contamination requirements since the lightning and switching aspects are treated in Chapter 3, and the mechanical characteristics fall outside the scope of this book. The uncontaminated dry and wet power frequency flashover voltage is rarely a dimensioning criterion, so they will not be discussed further.

The aim of any dimensioning method is to select the properties of the insulator so that it has an acceptable flashover performance for its whole service life. This means that an insulator must be selected so that it can withstand the stresses placed on it without failing. It would be very easy if the insulator had a well-defined strength above which it will fail and below which it will withstand, and if the stresses to which it is subjected had a definitive maximum value that would never be exceeded. In reality, both the stress and the strength are probabilistic variables. That is, the stress placed on the insulator varies randomly over time, and for any particular level of stress there exists a probability that the insulation will flash over. As a result, there is always a chance that the stress may exceed the strength, leading to a flashover.

The risk of flashover can be determined with reference to Figure 4.8-15, as follows:

- The insulators are energized with an ac voltage with constant amplitude, corresponding to the maximum continuous operating voltage. In special cases, where the insulators are exposed to extended periods of temporary overvoltages, it could be necessary to base the design on a higher voltage level.

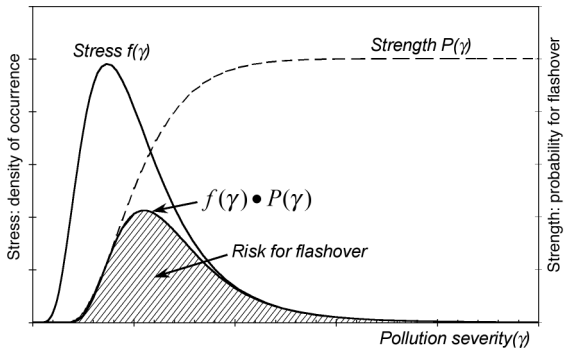


Figure 4.8-15 The stress-strength concept for the calculation of the risk of flashover with respect to polluted conditions.

- The variation of the pollution stress to which the insulator is exposed is represented by the probability density function "$f(\gamma)$", which is expressed in terms of the site severity "γ".
- A cumulative distribution function "$P(\gamma)$" describes the strength of the insulation—that is, the probability of flashover as a function of the same measure of site severity "γ" as was used to describe the pollution stress.
- The multiplication of the f and P functions gives the probability density of flashover of the insulator at the given site, and the area under this curve expresses the risk of flashover.

The risk of flashover can be minimized by "moving" the P curve to the right relative to the f curve—i.e., by selecting an insulator with a higher flashover strength, taking into account reasonable economics. In practice, it is not always possible to evaluate the risk of flashover in this way since these probabilistic functions are often time consuming or difficult to obtain. Generally the following methods are used, listed from simple to complex:

- Service experience
- Selection of creepage distance
- Deterministic method using laboratory tests
- Statistical method utilizing flashover performance data

Service Experience

In a great majority of cases, there are operating lines or substations in the area for which the insulation needs to be designed. If these installations have had an acceptable performance, the same insulation configuration can be used. Results from different voltage levels may even be extrapolated, based on the linearity principle discussed in Section 4.6.5. When introducing a new type of insulator, some network owners have opted for establishing test stations where the performance of insulators can be evaluated under natural conditions without risking system security. This provides a secure way to dimension insulators, but unless special testing is performed (e.g., using explosive fuses to determine the insulator flashover stress), this method does not offer much to optimize the insulation length. The IEC recommends that typically a period of 5-10 years of service, and 2 to 5 years in testing stations, may be needed to be able to adequately select insulators based on service experience (IEC Forthcoming b). These values are naturally dependent on the characteristics of the environment and the testing philosophy used.

Selection of Creepage Distance

Most national and international standards provide a simple table with four or five site severity categories and corresponding levels of minimum creepage distance. The site severity is determined through one of the methods described in Section 4.8.2 or by using a set of descriptions

Table 4.8-7 IEC and ANSI Guidelines for the Selection of Creepage Distance for Different Site Severity Classes

Pollution Class	Unified Specific Creepage Distance (mm/kV_{p-g})
1. Very light	22
1. Light	28
2. Medium	35
3. Heavy	44
4. Very heavy	55

of typical environments provided in the standard. The recommended creepage distance levels listed in the IEC and ANSI guidelines are provided in Table 4.8-7.

As discussed in Section 4.6.3, when using this method, many factors other than creepage distance that affect the insulator flashover strength need to be factored in. Documents providing leakage distance recommendations, therefore, contain a set of limits within which the creepage distance recommendations are valid. In some cases, correction factors are provided to adjust the recommended values for insulators outside these limits (Vladimirski et al. 2001). In other documents, such as the revision of the IEC 60815 Draft, factors are only provided to compensate for the effect of diameter, whereas profiles that fall outside the limits are disqualified (IEC Forthcoming b).

This method makes it possible to specify insulators, within a limited profile range, based on the collected long-term service and test experience of many countries without the need to perform additional laboratory or field-testing. All insulators within the profile limitations and with the minimum required creepage distance are approved for service.

Deterministic Method

The deterministic approach is used when there is insufficient statistical information available to warrant a full risk analysis. A minimum performance criterion is specified based on a worst-case analysis. Laboratory testing may be used to verify that a candidate insulator fulfills this criterion. With reference to Figure 4.8-16, this approach can be described as follows:

1. The maximum site contamination severity that the insulation will be exposed to is determined through site severity measurements or a subjective judgment based on the available site severity information.
2. The minimum contamination severity that the insulator must withstand is selected so that it exceeds the maximum site severity with a safety factor, which is chosen to cover the uncertainties in the designer's evaluation of the strength and stress parameters.
3. Candidate insulators may then be subjected to a withstand or flashover test to verify that their characteristics are above the minimum level determined in the previous step. The test method used is selected to be representative of the service environment.

Step 1: Determine the Maximum Site Severity

More often than not, an insufficient number of site severity measurements will be available. Depending on the number of measurement points available, the user may choose one of several strategies to estimate the maximum contamination severity:

- The user has many (i.e., more than 30) measurements available: The maximum site severity is then simply taken as the maximum value of the values available.
- The user has several measurement values available but not sufficient to feel confident that the maximum value can be taken as representative. This would be the case where the user has between 10 and 30 points available. In this case, it can be assumed that the measurements provide a good estimate of the average contamination severity of the site. The average value of the measurements, ($\gamma_{average}$), is then calculated, and the maximum site severity, (γ_{max}), can be estimated with:

$$\gamma_{\max} = \gamma_{average} \cdot e^{\left[2.06 \cdot \sigma - \frac{\sigma^2}{2}\right]} \qquad 4.8\text{-}4$$

  Where σ is the standard deviation of natural logarithm of the site severity measurements. Typical values of σ for ESDD measurements range between 0.4 and 0.9.
- The user has only single measurement values available. In this case, it would be best to assume that measured values correspond to the mode—i.e., the most likely level of pollution severity. In this case, the maximum

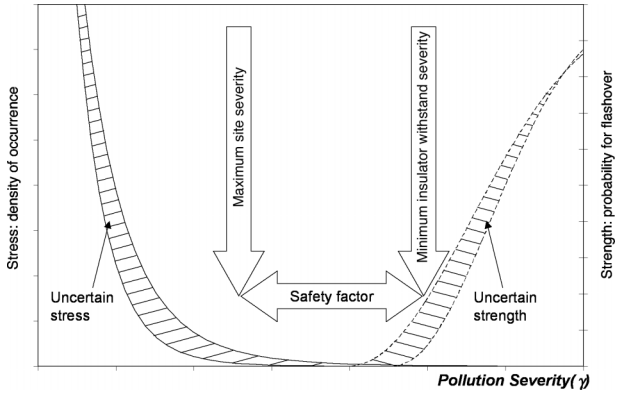


Figure 4.8-16 A graphical illustration of the deterministic approach.

site severity can be calculated from the most likely level of pollution severity, (γ_{mode}):

$$\gamma_{max} = \gamma_{mode} \cdot e^{\left[2.06 \cdot \sigma + \sigma^2\right]} \quad 4.8\text{-}5$$

Where the other parameters are as above.

Step 2: Determine the Minimum Contamination Withstand Severity

The minimum withstand is determined by multiplying the maximum site severity by a safety factor, which should be determined by taking the following factors into account:

- Number of insulators that will be exposed to the same environment (i.e., parallel insulators).
- Differences in pollution accumulation characteristics of the insulator used for the site pollution severity measurement and the candidate insulator. See Section 4.3.2.
- If contamination measurements were performed on unenergized units, it could be necessary to adjust the measured values if heating by leakage current contributes significantly to the contamination deposit.
- Difference in pollution type of the pollution deposit at site and in the test. It was shown in Section 4.6.5 that low-solubility salts have a higher flashover value than marine salt contamination under Clean-Fog tests. In some cases, it may be warranted to test at a lower severity level with the standard test to adjust for this.
- Differences in the uniformity of the pollution deposit at site and in the test and the wetting conditions in service and those during the test; the effects of these two factors have been shown in Section 4.6.5.
- Differences in the equipment assembly.
- Effect of aging on the pollution catch and wettability of the insulation during the expected lifetime.
- Number of critical wetting events per year.

Statistical flashover risk calculations have been performed to obtain a guideline for suitable safety factors that can be used in a deterministic design (Engelbrecht et al. 2005). The results are presented in Figure 4.8-17, which shows the safety factor as a function of the number of insulators exposed to the same environment (i.e., parallel insulators). These calculations were based on the following assumptions:

- The risk of flashover is once in 50 critical wetting events—i.e., 0.02.
- The contamination comprises mostly marine salt.
- The insulator flashover voltage determined during testing has a normalized standard deviation, C_{ins}, of between 6 and 10%.
- The statistical distribution of site severity can be described as lognormal, with a standard deviation of the logarithm of the severity between 0.4 and 0.9.
- The withstand characteristic of the insulator is described by the voltage or contamination severity, where the insulator has a 10% flashover probability.

For typical lines, as indicated by the shaded area in Figure 4.8-17, the safety factor lies between 1.3 and 1.8.

Step 3: Verify the Insulator Withstand Characteristic with Laboratory Tests

The performance of the insulator can be verified by laboratory tests. In the standards, withstand tests are described that consist of a maximum of four tests during which only one flashover is allowed. These tests aim to show that the insulator does not have a flashover probability of below 10% for the voltage and contamination severity at which the test was performed. There is an uncertainty in the test outcome, however—i.e., an insulator with a lower than 10% flashover probability may pass the test, because only a limited number of tests are performed.

It is possible to overcome this lack of discrimination by performing more than the prescribed four laboratory tests, but this can be costly. Another method is to perform the withstand test at a higher voltage or contamination severity to compensate for the limited number of tests performed.

For line insulators, it is more feasible, however, to base the verification tests on determining the 50% flashover voltage, V_{50}. This can be achieved by a relatively small number of tests if variable voltage application techniques are used (Lambeth 1988). These tests are performed at the minimum withstand severity, as determined by the deterministic method. The withstand voltage, V_{10}, for the tested can then be calculated by:

$$V_{10} = (1 - 1.28 \cdot c_{ins}) V_{50} \quad 4.8\text{-}6$$

where C_{ins} is the normalized standard deviation of the flashover voltage, which is typically on the order of 0.06 to 0.1 for laboratory tests.

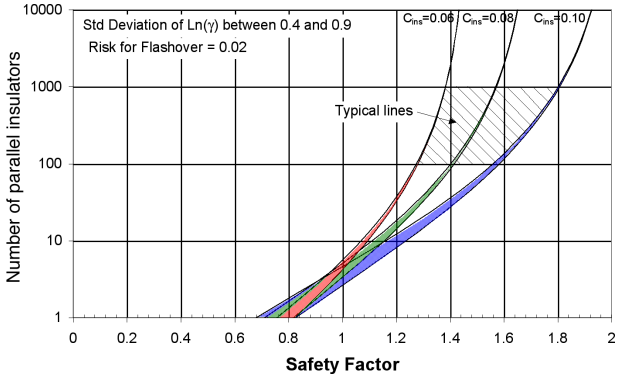


Figure 4.8-17 Typical range of a safety factor for transmission-line insulators (Engelbrecht et al. 2005).

The insulator is approved for service if the calculated withstand voltage level is above the maximum continuous operating voltage.

Statistical Method

A statistical method can be used to calculate the required insulator dimensions for a specific site based on a full risk of flashover assessment. When performing the statistical method, the following aspects should be taken into account:

- Number of insulators that will be exposed to the same environment (i.e., parallel insulators).
- Differences in pollution accumulation characteristics of the insulator used for the site pollution severity measurement and the candidate insulator. See Section 4.3.2.
- If contamination measurements were performed on unenergized units, it could be necessary to adjust the measured values if heating by leakage current contributes significantly to the contamination deposit.
- Difference in pollution type of the pollution deposit at the site and in the test. It was shown in Section 4.6.5 that low-solubility salts have a higher flashover value than marine salt contamination under Clean-Fog tests. In some cases, it may be warranted to test at a lower severity level with the standard test to adjust for this.
- Differences in the uniformity of the pollution deposit at the site and in the test, and the wetting conditions in service and those during the test; the effects of these two factors have been shown in Section 4.6.5.
- Differences in the equipment assembly.
- Effect of aging on the pollution catch and wettability of the insulation during the expected lifetime.
- Number of critical wetting events per year.

The statistical method methodology has the following steps:

1. Site contamination severity and wetting intensity
   - *Input:* A sufficient number of site severity measurements.
   - *Output:* A probability density function describing the site severity.
2. Insulator flashover characteristic
   - *Input:* Laboratory flashover test results at a range of contamination severity.
   - *Output:* A curve describing the flashover voltage as a function of the contamination severity.
3. Insulator flashover probability as a function of the pollution severity
   - *Input:* A curve describing the flashover voltage as a function of the contamination severity.
   - *Output:* The flashover probability as a function of the contamination severity for a specific insulator length.
4. The effect of parallel insulators
   - The probability function obtained in step 3 is adjusted for the number of parallel insulators.
5. Risk of flashover evaluation
   - *Input:* A probability density function describing the site severity.
     The flashover probability as a function of the contamination severity for a specific insulator length and number of parallel insulators.
   - *Output:* The risk of flashover.

Each will be discussed in some detail below with the help of a practical example. In this example, ESDD measurements are used, since it is the most representative of the American environment. It should be noted that this method is essentially the same for other site severity and laboratory testing techniques, such as the Site Equivalent Salinity and the Salt-Fog test.

Step 1: Site Contamination Severity and Wetting Intensity

With sufficient pollution-severity measurements available, a suitable distribution function can be fitted to obtain a statistical description of the pollution stress at the site. An example of ESDD measurements on a standard-shape glass disc insulator string over a period of 55 months is shown in Figure 4.8-18.

These values are sorted from low to high, and each point represents a *1/(number of data points)* drop in the cumulative probability. A suitable cumulative distribution function, such as the lognormal distribution function, can be fitted through these points by utilizing statistical techniques (e.g., the method of maximum likelihood) or by graphical means (i.e., a straight line fit on lognormal graph

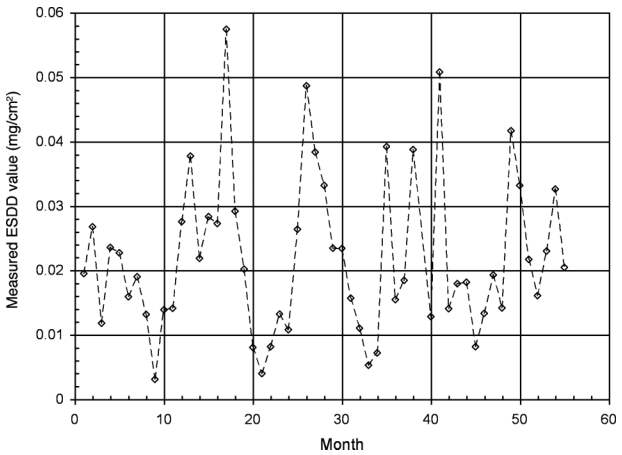


Figure 4.8-18 ESDD measurements at a coastal site.

paper) (Carrara and Hauschild 1990). The sorted site severity measurements and the fitted distribution function are shown in Figure 4.8-19.

The pollution severity of a site is usually characterized by the 2% severity, which is the severity having a 2% probability of being exceeded, and the standard deviation of the logarithm of the site severity measurements. In the example presented here, the 2% severity level is an ESDD level of 0.06 mg/cm^2 and the standard deviation of ln (ESDD) of 0.55.

It has been suggested that double-contingency analysis be performed (see Section 4.8.1) to take account of the independent variation of the contamination severity and the degree of wetting (Suzuki et al. 1999). This would require a two-dimensional risk-of-flashover assessment. However, this approach is rarely feasible, as the insulator strength is not evaluated under different wetting conditions (i.e., the standard laboratory tests only test insulators under critical wetting conditions). To enable a single-contingency analysis, it is conservatively assumed that all wetting events are critical.

Step 2: Insulator Flashover Characteristic

The insulator flashover probability needs to be described in terms of the contamination severity. In order to do this in a cost-effective way, laboratory tests (e.g., Clean-Fog —see description in Section 4.5.2) are performed to determine the 50% flashover voltage, (V_{50}), and standard deviation, (σ), at two or, preferably, more test severities. A power law function can then be fitted through the data points to obtain a mathematical description of the V_{50} as a function of the contamination severity, as discussed in Section 4.6.5. An example of such a relationship is shown in Figure 4.8-20. This example uses the average relationship for standard-shape insulators listed in Table 4.6.1 for the Clean Fog test.

This V_{50} curve can then be used to calculate a family of curves, each describing a different probability of flashover, as shown in Figure 4.8-20. This is relatively easily done by using the inverse probability function characteristics found in standard tables. For example, at a specific contamination severity and assuming a normal distribution function, the 10% flashover value, V_{10}, can be calculated from the 50% flashover voltage, V_{50}, and the normalised standard deviation, $c_{ins} = \sigma_{ins} / V_{50}$, from Equation 4.8-6.

Similar relations exist for the other flashover probabilities.

Step 3: Insulator Flashover Probability as a Function of the Pollution Severity

The curves in Figure 4.8-20 can then be used to derive a function describing the probability of flashover in terms of the contamination severity of a specific insulator. This process is illustrated in Figure 4.8-21 for an insulator with a unified specific creepage distance of 28 mm/kV. As illustrated in the figure, the probability of flashover for each contamination level is where the service stress line intersects with the probability curves. It can also be derived analytically if the insulator flashover voltage is described by a Weibull distribution function (Engelbrecht et al. 2004).

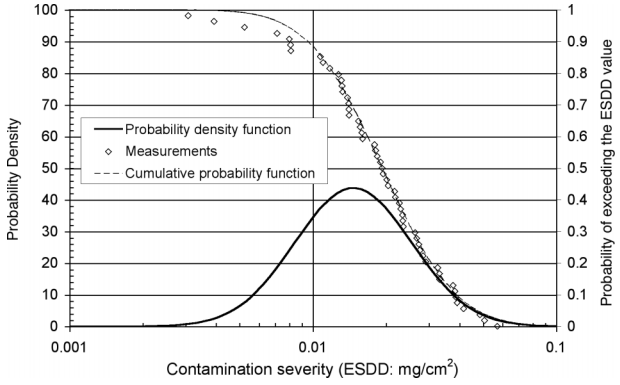


Figure 4.8-19 Typical results from pollution site severity measurements and the fitted lognormal distribution.

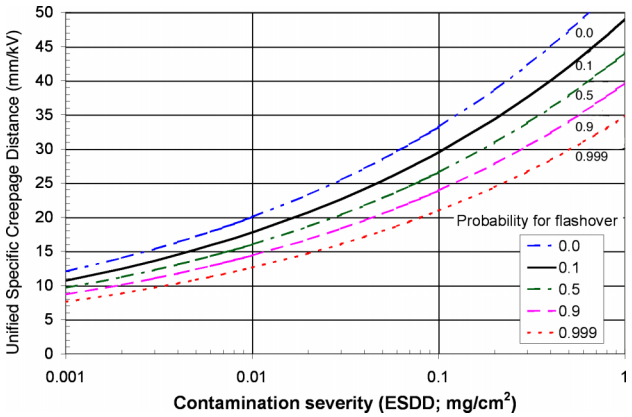


Figure 4.8-20 Insulator flashover characteristic as derived through laboratory tests. The standard deviation is assumed to be 8%. (The solid curve is the withstand characteristic (V_{10}) of the standard shape insulator presented in Figure 4-6.8.)

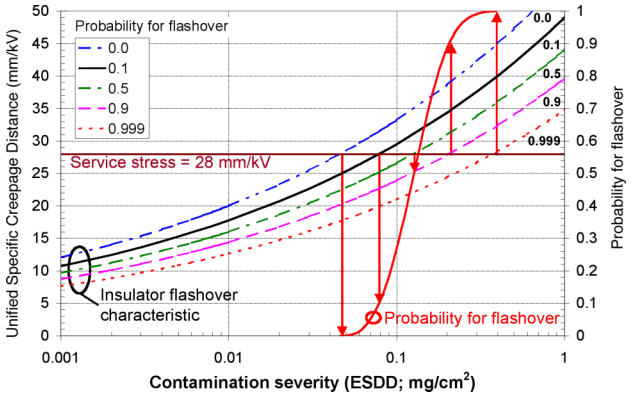


Figure 4.8-21 Derivation of the insulator flashover probability as a function of contamination severity.

Effect of Parallel Insulators

The next step is to take account of the number of insulators exposed to the same conditions. As mentioned previously this can be done with the relationship:

$$P_n = 1 - (1 - P_1)^n \qquad 4.8\text{-}7$$

Figure 4.8-22 shows the flashover characteristic of one insulator, from Figure 4.8-21, and that derived for 120 parallel insulators.

Evaluation of the Risk of Flashover

Enough information is now available to evaluate the risk of flashover for 120 insulators installed in the environment with a severity characteristic as derived in the first step. This is shown in Figure 4.8-23, where the contamination severity density function (from Figure 4.8-19) is multiplied with the insulator flashover probability curve (from Figure 4.8-22), and the area beneath this derived curve is the risk of flashover. This has numerically been calculated to be 0.028, or approximately one flashover in 36 critical wetting events.

With this calculation the fraction of critical events that will lead to flashover has been determined. This value can be expressed as the contamination flashover rate (CFOR) per year by taking account of the average number of wetting events (N_{events}) that take place each year:

$$CFOR = N_{events} \cdot \text{Risk per event} \qquad 4.8\text{-}8$$

For a site where there are 10 critical wetting events per year, the CFOR can be calculated as 0.28 flashovers per year, or on average one flashover each 3.6 years.

If this flashover rate is unacceptably high, an insulator with a higher unified specific creepage distance is selected and the risk of flashover is re-evaluated. This process is repeated until an insulator with an acceptable risk of flashover is found.

This calculation can then be repeated at different contamination severities to obtain a "design curve" for that particular insulator type. An example of such a curve is shown in Figure 4.8-24 in comparison with a typically used creepage distance requirement. The performance is expressed in risk of flashover per critical wetting event.

A software implementation of the statistical method has become available, and its results show good agreement with Russian dimensioning criteria (Gutman et al. 2004).

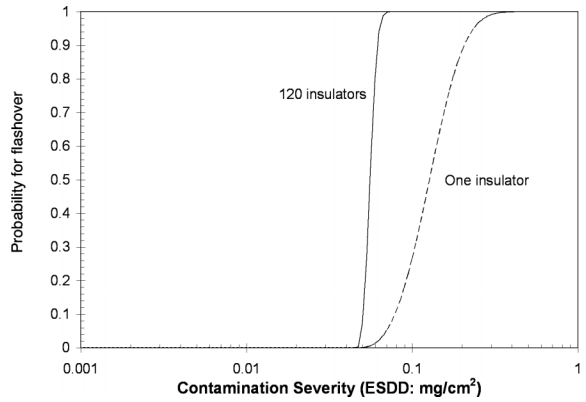


Figure 4.8-22 The derived probability for flashover characteristic for one and 120 insulators.

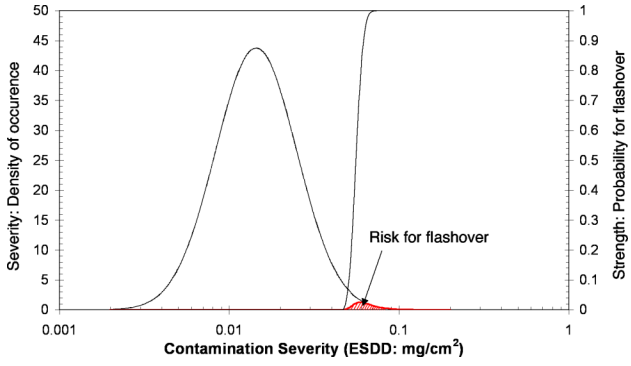


Figure 4.8-23 Calculating the risk of flashover from the site severity and the insulator flashover characteristic.

4.9 ELECTRIC FIELD ON INSULATORS AND GRADING RINGS

4.9.1 E-Field Distribution on Polymer Insulators

The E-field distribution on the surface of and within polymer insulators is a function of numerous parameters including voltage class, insulator design, tower configuration, phase spacing, etc. The following discussion will provide generalized information that relates to the E-field

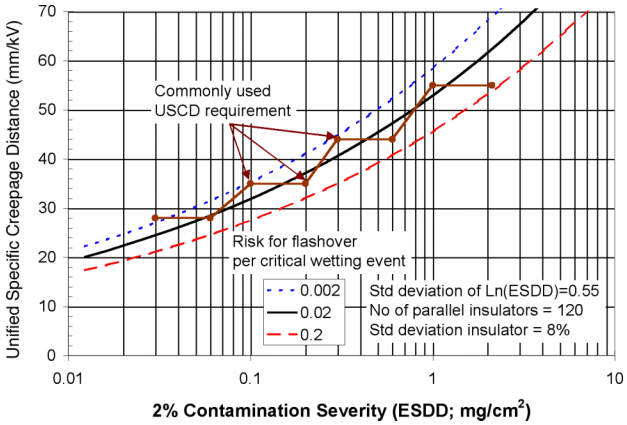


Figure 4.8-24 Design curve for a typical standard-shape disc insulator for three different levels of the risk of flashover.

distribution of most transmission-line applications. It should be kept in mind that there are applications, both on transmission lines and in substations, where the E-field distributions will differ from those presented in the following section.

In general, the E-field magnitudes are larger close to the energized and grounded ends of a polymer insulator. In some cases, the position of highest E-field occurs adjacent to the end fitting, while in other cases, it may occur a short distance away from the end fitting. The case where the position of highest E-field magnitude occurs adjacent to the end fitting is illustrated in Figure 4.9-1 that shows a shaded plot of the E-field magnitude distribution on the polymer weathershed surface of a 230-kV suspension polymer insulator as well as lines of equal potential.

As can be seen from Figure 4.9-1, the magnitude of the E-field close to the energized end is higher than that at the grounded end. It can also be seen from the equipotential lines surrounding the polymer insulator in Figure 4.9-1 that the direction of the E-field is mainly axial—i.e., in the same direction as the fiberglass rod (EPRI 1999; Zhao 2000; CIGRE 1992c).

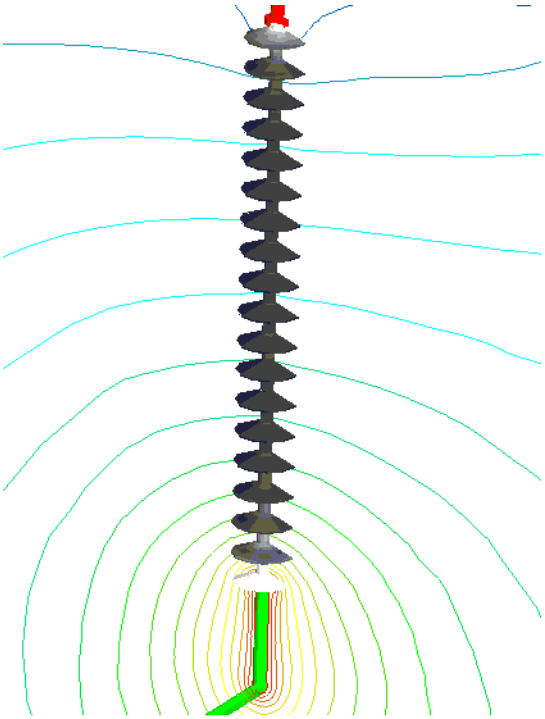


Figure 4.9-1 Shaded plot of the E-field distribution on the surface of a polymer insulator and the equipotential lines in the air surrounding the unit. The E-field magnitude is indicated in grayscale, with white being the highest and black the lowest.

Figure 4.9-2 is a plot of the normalized E-field magnitude within the fiberglass rod of a 115-kV I-sting measured along an axial line.

As can be seen from Figure 4.9-2, the E-field magnitude is high at the energized end and decreases exponentially. The field magnitude increases again at the grounded end, but the maximum value reached is lower than that at the energized end.

Although the distribution indicated in Figure 4.9-2 is common for many situations, there are applications where this may not be the case. Most significantly, for certain designs of overhead transmission-line polymer insulators, the corona ring results in the highest E-field magnitude occurring a short distance away from the end fitting rather than adjacent to the end fitting. An example of this is illustrated in Figure 4.9-3.

It can be seen in Figure 4.9-3 that the presence of the corona ring has shifted the position of highest E-field three sheds away from the energized end fitting. It should be noted that the application of a corona ring does not always result in the point of maximum E-field being shifted away from the area adjacent to the end fitting. Whether this will occur depends on the dimensions of the corona ring, its location, and the configuration geometry (EPRI 1999; Kondo 2002).

Factors That Influence the E-Field Distribution

Numerous factors influence the E-field distribution of polymer insulators. The most important factors include (EPRI 2003a):

1. Insulator geometry including weathershed system, fiberglass rod, and end fittings.

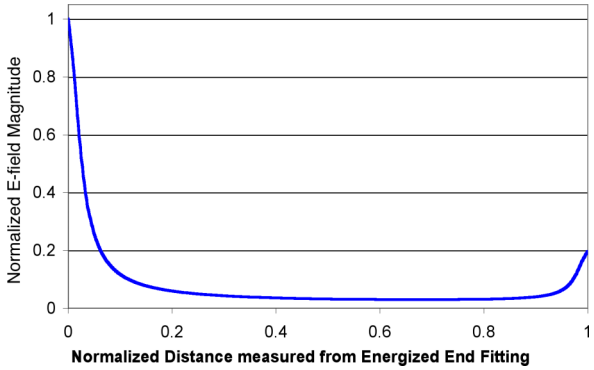


Figure 4.9-2 Example of the normalized E-field magnitude within the fiberglass rod of a suspension I-string 115-kV polymer insulator determined using three-dimensional finite elements modeling. The axial measurement line starts at the energized end fitting and ends at the grounded end fitting.

2. Electrical properties of polymer weathershed, fiberglass rod material, and any semiconductive grading that may be included.
3. The dimensions and position of the corona rings, as well as the attachment hardware.
4. The geometry of the attachment hardware, conductor bundles, grounded hardware, and line structure.
5. The orientation of the polymer insulator and its physical relationship to the attachment hardware, corona rings, conductor bundles, grounded hardware, and line structure.
6. Energized line voltage.
7. Presence of nearby phases.

Each of these parameters needs to be taken into account when determining the E-field distribution of a polymer insulator utilizing either modeling or measurement techniques. Depending on the case, these parameters may have a larger or reduced effect on the E-field distribution.

Due to the dependence of the E-field distribution on this range of parameters, identical polymer insulators applied in different situations may have different E-field distributions, and similarly, different polymer insulator designs applied in the same situation may have different E-field distributions.

Regions of Interest

There are three main regions of the polymer insulators where the distribution of the E-field distribution magnitude is of interest:

1. Within the fiberglass rod and polymer weathershed material.

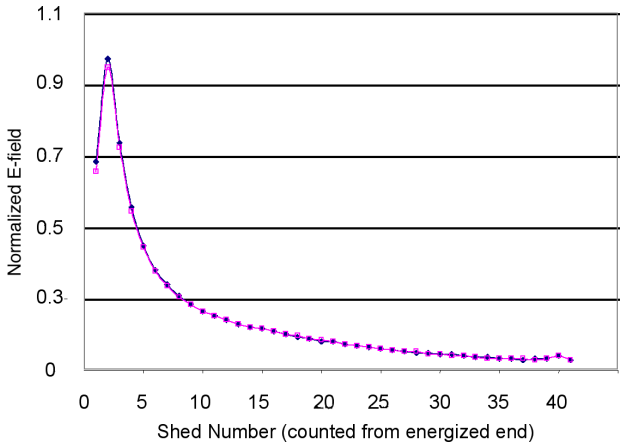


Figure 4.9-3 E-field profile measured along a suspension 500-kV V-sting polymer insulator using a field probe. The unit has a corona ring in place on both the live and grounded ends.

2. On the surface, and in the air surrounding, the polymer weathershed surface and surrounding the end-fitting seal.
3. On and in the air surrounding the metallic end fittings and attached corona rings.

If the E-field magnitude in any of these three regions exceeds critical values, unwanted or excessively large magnitudes of discharge activity may occur, affecting either the long- or short-term performance.

Discharge Activity

The presence, location, and magnitude of discharges are a function of both the E-field magnitude and direction. Four categories of discharges are of concern:

- **Discharges internal to the fiberglass rod and polymer weathershed material or at the interface between the rod and weathershed system.** If a critical E-field magnitude is exceeded, defects (such as voids or inclusions) may result in internal discharge activity. This internal discharge activity may result in destruction of the rod or weathershed material (Cherney 1991).
- **Corona discharges on the surface of, or in contact with, the polymer weathershed material and/or end-fitting seals.** Corona activity, either under dry or wetting conditions, has been shown to result in degradation or changes in the surface properties of the polymer weathershed material. Figure 4.9-4 is an example of such discharge activity (Phillips et al. 1999a, 1999b; Moreno and Gorur 2003; Lopez et al. 2001).

  Arcing activity that may occur in the high E-field region under wetting conditions will also result in degradation of the rubber material and/or end fitting seal. Arcing activity is generally more damaging than corona activity due to its high-energy nature. Arcing may occur between patches of water on the surface of the polymer insulator.

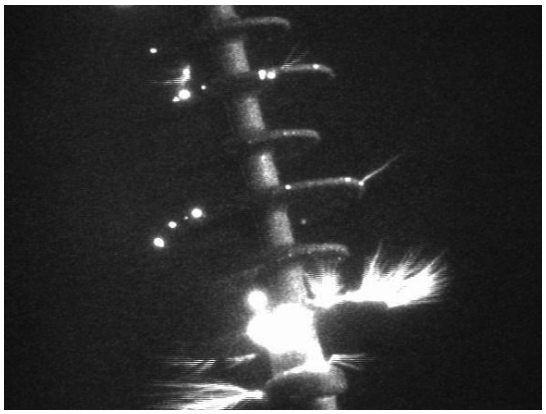


Figure 4.9-4 Example of discharge activity in contact with weathershed material.

This activity is more likely on surfaces that have lower values of hydrophobicity (EPRI 2003a).

Research has shown that corona activity, due to water drops or poorly graded metallic end fittings, may result in a hydrophobic surface losing some of its hydrophobicity. This loss of hydrophobicity allows patches of water to form that, in turn, result in arcing activity. The high energy of the arcing activity may result in more severe degradation of the rubber material.

- **Dry band arcing under contaminated conditions.** Under critical wetting conditions, contaminated insulators may have leakage currents and dry band arcing on the polymer weathershed surfaces. The occurrence and magnitude, and hence the destructive nature of the arcs, are influenced by the E-field magnitude.

  Electrostatic forces result in contamination and moisture being drawn in the direction of the high electric field, resulting in increased accumulation in the high E-field magnitude regions. This effect is considered secondary for polymer insulators applied on ac transmission lines.
- **Corona activity from metallic end fittings or corona rings.** High E-field magnitudes on the surface of the metallic end fittings and corona rings can result in corona activity under dry conditions. These discharges result in electromagnetic interference and/or audible noise that, in turn, may result in customer complaints. If this discharge activity is in contact with the rubber weathershed system or end fitting seal, degradation may occur. Figure 4.9-5 shows such activity (ANSI 2002c; EPRI 2001d).

Critical E-Field Values

In order to prevent or reduce the discharge activity, the maximum E-field magnitude in various regions should be kept below critical values. The following critical values have been mentioned in the literature. The values are for dry uncontaminated polymer insulators and are indicated in kV/cm (rms.):

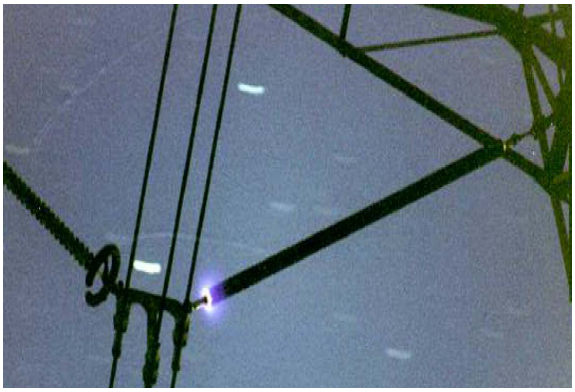


Figure 4.9-5 Image of corona activity from the metallic end fitting of a 500-kV insulator installed without a corona ring.

1. Internal to the fiberglass rod and rubber weathershed material: 30 kV/cm.
2. Surface E-field magnitudes on weathershed material: 4.5 kV/cm (rms) measured 0.5 mm above the surface of the sheath (EPRI 1998, 1999).
3. Surface E-field magnitudes on the metallic end-fittings and corona rings: These should be controlled such that the unit passes the radio corona / interference test indicated in ANSI and IEC standards (ANSI 2002c; IEC 2002a). A surface gradient of 21 kV/cm is often used as a reference value for hardware design (Kuffel and Zaengl 1984).

Correction factors need to be applied to the E-field magnitudes surrounding the metallic and corona rings to account for changes in relative air density if the unit is to be applied at altitudes above sea level (IEEE 1995).

No altitude corrections have been developed for the critical E-field magnitudes on weathershed magnitudes. Using standard altitude correction methods in this case is considered to be conservative, as the onset of corona from water drops is strongly dependent on the electrohydrodynamic forces. This has been shown for water drops attached to conductors (Phillips et al. 1996).

Factor 2 above, the E-field on the surface of the weathershed material, is usually the controlling value when considering corona ring and end-fitting design.

Control of E-Field Distribution

The E-field distribution may be controlled by:

1. **Polymer insulator end fitting design.** The design of the end fitting has an influence on the E-field distribution within the polymer insulator, on the surface of the weathershed material, and on the surface of the metallic end fittings. Large end fittings with rounded edges tend to reduce the maximum magnitude of the E-field in proximity of the end fittings. This grading of the E-field is integral in the design of the insulator. This obviously cannot be changed once a specific insulator design has been selected; however, it may need to be accounted for when selecting an appropriately dimensioned corona ring.
2. **Corona ring application and design.** The application of appropriately designed corona rings is also used to reduce the maximum E-field magnitudes and move the position of the maximum E-field away from the end-fitting (as the end-fitting seal is considered critical). The dimensions and location of the corona ring have a significant influence on the E-field distribution. Figure 4.9-10 shows an example of the E-field profile of a polymer insulator both with and without a corona ring installed. Corona ring design and application are discussed in more detail later in this section.

Corona rings are generally designed and tested for standard transmission-line applications. If polymer insulators are applied in nonstandard applications (e.g., in substations), the standard recommendations may not apply. Modeling and testing may be necessary (IEEE Forthcoming b). Figure 4.9-6 is an example of discharge activity from an insulator installed in a substation with a standard transmission-line corona ring that was inadequate for this application.

It is not uncommon for corona rings to be incorrectly installed in the field. Rings may be installed in the incorrect location with respect to the end fitting, not be sufficiently tightened, installed backwards (as shown in Figure 4.9-7), or not installed at all. In order to overcome these concerns, insulator manufacturers have designed attachment methods that minimize installation errors. An effective education and inspection program can limit errors.

3. **Application and Design of Extra Hardware.** The application of extra hardware—such as arcing horns, extra links, and additional field grading devices—influences the E-field distribution of the polymer insulator. For example, if an extra shackle or link is inserted between the polymer insulator and the conductor, it will increase the maximum E-field magnitude on the polymer insulator; similarly, if an arcing horn is applied, the maximum E-field may be reduced. Hardware that is in proximity to the polymer insulator has the largest effect on the E-field distribution. Hence, when an appropriate corona ring is being designed, selected, and evaluated for a specific application, the presence of hardware in proximity needs to be accounted for.

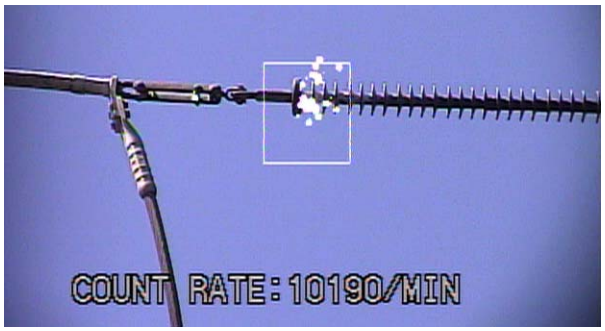


Figure 4.9-6 Corona activity from a 230-kV polymer insulator applied in a nonstandard application in a substation.

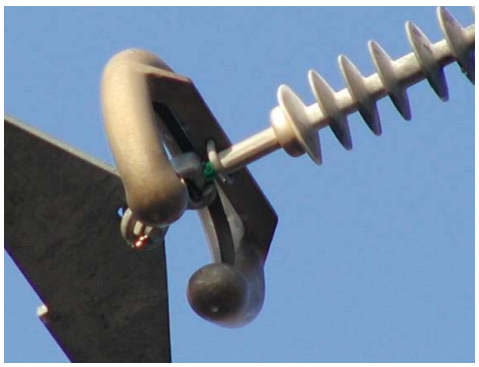


Figure 4.9-7 Corona ring installed backwards and in the incorrect location at 230 kV (EPRI 2004c).

Determination of E-Field Distribution on Polymer Insulators

The E-field distribution on polymer insulators may be determined by either modeling or measurement.

Modeling

Commercially available software packages employing one of the two mathematical methods for determining E-field distributions can be used: the finite element method (FEM) or the boundary elements method (BEM) (EPRI 1999). In order to obtain accurate results, the following needs to be accounted for in the model:

1. Three-dimensional nature of the problem.
2. Dimensions and material properties of the polymer insulator.
3. Dimensions and position of the corona ring.
4. Dimensions and material properties of the structure.
5. Conductor bundle.
6. Hardware that attaches the polymer insulator to the conductor and structure.
7. Nearby phases.
8. The presence of the earth (i.e., ground plane) and the height above.
9. Voltages (potential) of the components being modeled.

The degree to which all of the above are taken into account varies as a function of the region of interest and nature of the configuration. For example, if one was interested in the E-field distribution in the air surrounding the corona ring of a 500-kV insulator, it may not be necessary to take into account the separate properties of the fiberglass rod and rubber, while if one was interested in the E-field distribution inside the rod itself, one needs to take into account the different dielectric constants of the rod and rubber.

Whether each of the factors listed above should be accounted for, and to what degree, has been documented in reports and can be determined by sensitivity analyses (EPRI 1999). As computing power becomes more accessible and affordable, it will become increasingly feasible to include more detail in the modeling, resulting in improved accuracy.

Figures 4.9-1 and 4.9-2 are examples of outputs of such modeling, while Figure 4.9-8 is an example of the geometry of a 500-kV model to determine the E-field distribution on V-string insulators (EPRI 1999).

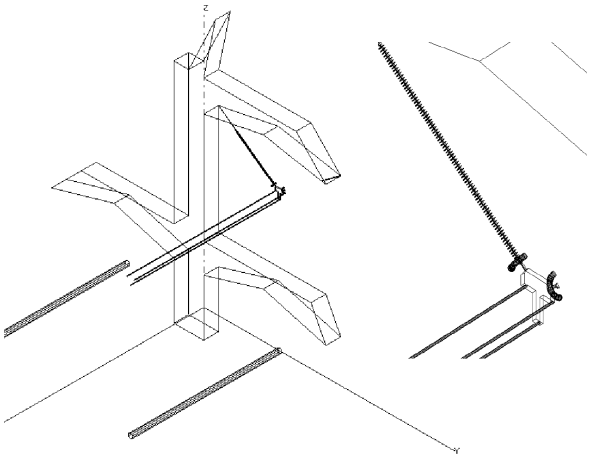


Figure 4.9-8 Example of a 500-kV three-phase geometry model. In this case, the presence of the nearby phases was accounted for by single conductors with the same equivalent radius as the bundle. It was only necessary to account for the presence of the dielectric material of the unit of interest.

Measurement

The E-field distribution may be measured using a range of techniques (Hartings 1994; Vaillancourt et al. 1997):

- By observing the deflection of phosphor bronze wire probe (Gosho 1969; Shen et al. 2004).
- Electro-optic space potential probes (Hartings 1994; Vaillancourt et al. 1997).

Measurement of E-field distribution has some limitations, including:

- Inability to measure in regions of interest—i.e., internal to the insulator or close to the rubber weathershed surface.
- Probe may distort the E-field being measured, reducing accuracy.
- Techniques are expensive and time consuming.

Representation of E-Field Magnitudes on Polymer Insulators

Since one is usually interested in the E-field close to the energized end fitting, the E-field is usually considered to be sinusoidal. Therefore, the rms E-field magnitude is usually considered (see Chapter 7 for more detail on E-field magnitudes). The E-field magnitudes may be represented in two forms: shaded plots or line plots. Figure 4.9-9 shows a shaded plot of the E-field magnitude surrounding the live end of a 500-kV polymer insulator (EPRI 1999).

As can be seen from Figure 4.9-9, the field magnitude is high surrounding the corona ring and live end fitting. The fields on the surface of the polymer insulator reduce as the distance from the end-fitting increases.

Line plots of the E-field magnitude are often plotted along the length of the insulator. Since one is often interested in the E-field in the air along the sheath of the unit, the measurement line often passes through the sheds of the unit. Figure 4.9-10 is an example of line plots for a polymer insulator both with and without a corona ring installed.

The sudden dips in the E-field magnitude in Figure 4.9-10 are when the measurement line passes through the rubber weathershed material, which has a permittivity higher than that of air, (ε_r approximately 4).

The influence of applying a corona ring is also evident in Figure 4.9-10. It can be seen that the peak E-field is

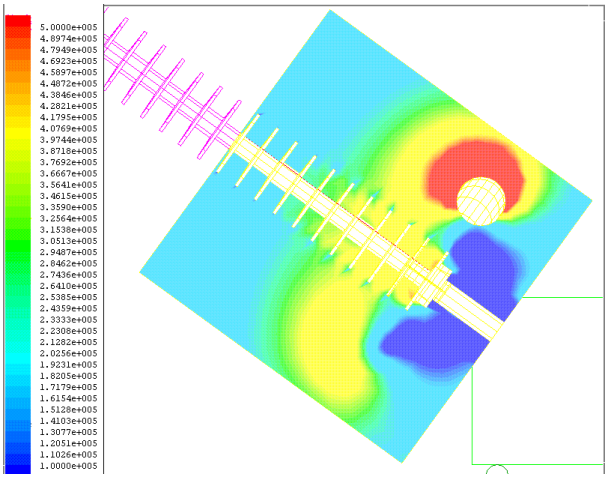


Figure 4.9-9 Example of shaded plot describing the E-field in the air surrounding the energized end fitting of a 500-kV polymer insulator.

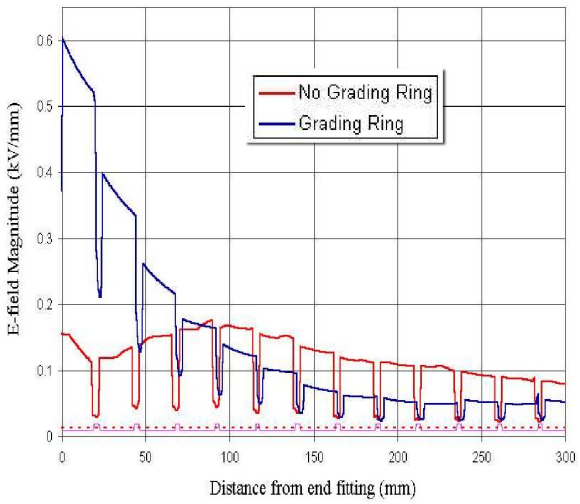


Figure 4.9-10 E-field magnitude in the air along the surface of a polymer insulator for 300 mm away from the live-end fitting. The E-field magnitude profile is shown both with and without a corona ring.

reduced in magnitude and shifted away from the end-fitting to between the third and fourth sheds.

E-Field Magnitudes on Polymer Insulators

The E-field magnitudes on polymer insulators may be divided into three areas of interest:

1. E-field magnitudes on the surface of, and surrounding, both the rubber weathershed material and the end fitting seal.
2. E-field magnitudes internal to the polymer insulator.
3. E-field magnitudes on the surface of the metallic end fittings and corona rings.

- **E-field magnitudes on the surface of, and surrounding, both the weathershed material and end fitting seal.** A considerable amount of modeling of configurations has been performed by numerous organizations. In some cases, different organizations have modeled the same configuration and compared results, illustrating that the results are repeatable. This has been done using both BEM and FEM modeling.

  Figure 4.9-11 plots the peak rms—E-field magnitudes as a function of system voltage for a range of configurations compiled by EPRI (EPRI 2002c). As can be seen, the suggested E-field magnitude level of 0.45kV/mm is exceeded in a number of cases, indicating inadequate corona ring designs. Utilities need to work together with insulator manufacturers to ensure that the E-field grading is acceptable to ensure life expectancy.

- **Internal E-field Magnitudes.** Figure 4.9-12 shows the maximum E-field magnitudes calculated internal to a

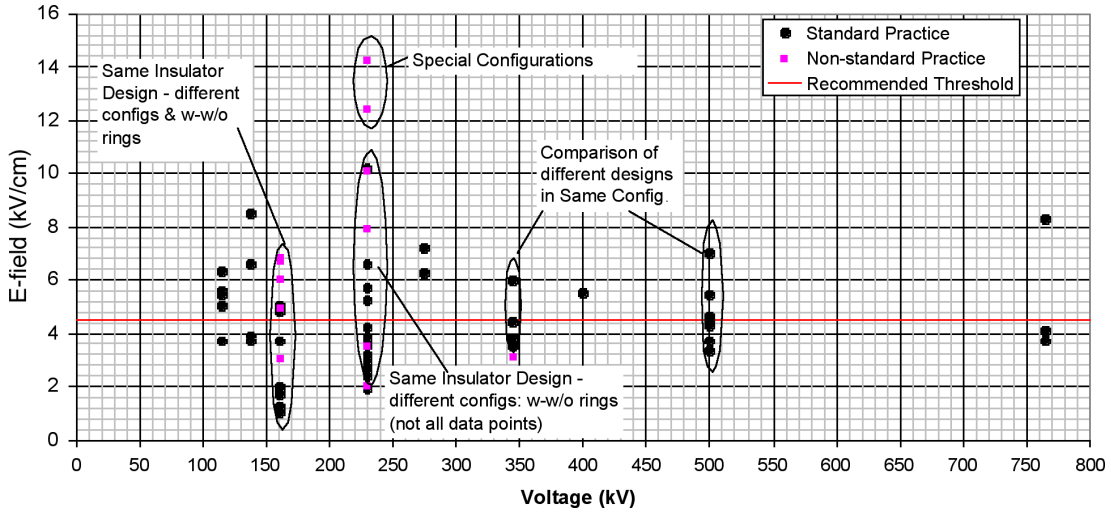


Figure 4.9-11 Maximum E-field magnitudes (rms) on the sheath sections of polymer insulators modeled as a function of system voltage. (All models account only for the presence of a single phase.) (EPRI 2002c).

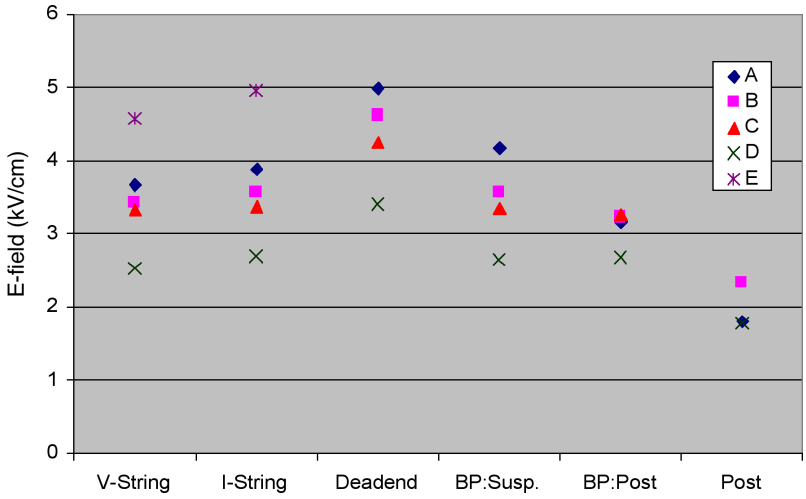


Figure 4.9-12 Maximum E-field magnitudes (rms) internal to a 230-kV polymer insulator applied in different configurations. For each configuration, the geometry is identical with only the manufacturer differing. (BP = braced post—all models account only for the presence of a single phase.)

230-kV polymer insulator in different configurations for five different manufacturers. As can be seen, the E-field magnitudes vary from 1.78 to 5 kV/cm, depending on the insulator/corona ring design and configuration. These levels are considerably lower than the critical 30 kV/cm mentioned previously.

- **E-field magnitudes on the surface of the metallic end-fittings and corona rings.** International and national standards and utility specifications require that insulators are corona free under dry conditions. This is verified by testing (IEC 1997 b; ANSI 2002a; IEEE Forthcoming b). The surface E-field magnitudes on the end fittings and the corona rings are, therefore, lower than the corona onset threshold. Figure 4-9.5 is an example of an insulator with dry corona activity from the end fitting due to elevated E-field magnitudes on the metallic surfaces (note: a corona ring was required for this application but was not installed).

Design and Selection of Corona Rings

Design of Corona Rings

In their simplest form, corona rings may be considered as toroids with three basic dimensions: overall diameter, *D3*, diameter of cross section, *D4*, and distance from end fitting, *L3*, shown in Figure 4.9-13.

Dimensions *D3*, *D4,* and *L3* may be optimized to ensure that the E-field distribution is within the required limits. Often there are limitations on the maximum and minimum dimensions. For example, the maximum value of *L3* may be defined due to strike distance requirements.

Applet I-2, Electric Field Distribution for Polymer Insulators (Effect of Dimensions and Location of Corona Ring) allows the user to investigate the effect of the corona ring, conductor, and end fitting dimensions on the E-field distribution. Although Applet I-2 takes into account the three-dimensional nature of the problem, it does not take into account the presence of the rubber or rod material. Hence Applet I-2 cannot be used to calculate the magnitude of the E-field accurately; however, the trend will be correct.

Often corona rings supplied by insulator manufacturers are not toroidal; rather, they have a horseshoe shape to allow for easy attachment after the insulators have been installed. Figure 4.9-14 shows some examples of corona rings provided by a number of manufacturers.

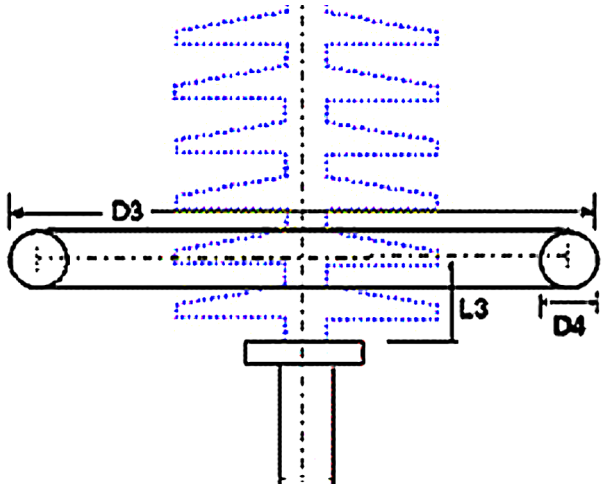


Figure 4.9-13 Definition of corona ring dimensions.



Figure 4.9-14 Examples of corona rings provided by different manufacturers for a range of applications. Both split ring and horseshoe types are shown. Note the different attachment mechanisms.

Corona rings are attached to the insulator end fittings using a variety of methods, depending on the insulator manufacturer. Some manufacturers have attempted to design attachment methods that prevent rings being incorrectly attached by field crews with varying success. Rings are not interchangeable between manufacturers due to difference attachment methods and end fitting designs.

Selection of Corona Rings

To address the aforementioned issues, corona rings are applied in many configurations. Although generic recommendations may be made, they often result in misapplication due to the variety of applications and the lack of definition of key parameters, such as ring size and location. It is preferable that the rings be selected based on E-field modeling, together with testing in accordance with electric field-based methods (IEEE Forthcoming b).

Recommendations in Table 4.9-1 are generic and do not take into account corona ring size or differences in configurations. The authors caution the reader in using the table for nonstandard applications.

As can be seen from Table 4.9-1, there is a degree of uncertainty in the recommendations for voltages between 100 and 161 kV—i.e., 115, 132, and 138 kV. The recommendations in Table 4.9-1 are an area of ongoing research, and the authors recommend that readers investigate the latest research results to determine the best application guidelines.

At voltages greater than 345 kV, separate E-field grading devices attached to the energized hardware may be used, together with the corona rings attached to the polymer insulator. The combination of the corona rings and grading devices controls the distribution of the E-field.

Due to the differences in geometry it may be possible to select different corona ring designs for suspension and dead-end applications on the same line. Most utilities select only one size to reduce confusion both during construction and maintenance.

It should also be noted that the dimensions and locations of corona rings from various manufacturers vary considerably, as do the E-field distributions as shown in Table 4.9-2

Table 4.9-1 Generic Recommendations for Corona Rings. (Note that ring dimensions and locations are not defined. Note that this table is under continual development as the industry's understanding of the issue increases.) (EPRI 1999,1998).

Insulator Type	System Voltage (kV)				
	V < 100 kV	100 kV < V < 161	161<= V < 230	230 <= V <= 345	345 < V
Suspension Units	-	Line-end maybe	Line-end	Line-end	Line-end Ground-end
Dead-End Units	-	Line-end maybe	Line-end	Line-end	Line-end Ground-end
Phase-to-Phase Spacers	-	Maybe both ends	Both ends	Both ends	Both ends
Braced Post	-	Maybe live end of suspension unit	Live end of suspension unit	Live end of suspension unit	
Line-Posts	-	-	Line-end maybe	Line-end	

Table 4.9-2 Comparison of Generic Recommendations Obtained for Four Different Insulator Designs (It should be noted that these are generic recommendations; manufacturers may adjust recommendations for different configurations or situations.)

	Manufacturer W		Manufacturer X		Manufacturer Y		Manufacturer Z	
	Energized end	Grounded end	Energized end	Grounded end	Energized end	Grounded end	Energized end	Grounded end
<138kV	None	None		None	None	None	None	None
161kV	None	None	6.4" or 7.8"	None	None	None	None	None
200-230kV	8"	None	6.4" or 7.8"	None	8"	None	11"	None
300-345kV	12"	None	7.8"	None	12"	None	11"	None
400kV	12"	8"	13.8"	None	12"	None (1)	15"	None (1)
500kV	15"	12"	17.7"	7.8"	17"	8"	15"	11"
756kV	15"	12"	(2)	(2)	17"	12"	16"	16"

Notes: 1. May be required in certain applications. 2. Special design required.

and Figure 4.9-11. Therefore it is impossible to determine the correct corona ring based on Table 4.9-1 alone since only whether one needs a ring is defined rather than the dimensions and location. Often E-field modeling is performed with the unit installed in the configuration of interest to confirm that the E-field magnitudes are kept below the limits specified in the sections above. Details on the correct E-field modeling methods to utilize are provided elsewhere (EPRI 1999, 1998).

A number of practical considerations need to be accounted for when designing/selecting a corona ring:

- A reasonable clearance is necessary between the corona ring and the weathershed system of the insulator being graded and nearby insulators.
  - –Concerns have been raised in braced post configurations, where the suspension unit corona ring touches the sheds of the post unit.
  - –Small gaps between the corona ring and the first shed have been shown to result in high levels of discharge activity.
- Interference between the corona ring and other hardware.
- Ease of installation and removal when insulator is installed.
- Should not prevent access to end hardware for live line work (e.g., access to cotter key).
- Have a simple locking/keying mechanism to ensure that it is installed in the correct location/position.
- The ring should be able to withstand the required level of vibration.
- Power arc termination on the ring should not expose the end fitting seal or weathershed system to undue stresses.
- The corona ring should be able to withstand specific levels of power arc current without sustaining considerable damage.
- The resulting reduction in the dry arc distance needs to be considered.
- Inclusion of corona rings in certain V-string (and possibly I-string) applications has increased the risk of bird streamer outages.

The selection or corona rings is often complicated when units from a range of manufacturers are installed on the same system. Since corona rings are manufacturer-specific, different corona ring designs need to be stocked for maintenance purposes, and maintenance staff need to be trained to select the correct ring for the insulator selected.

4.9.2 E-Field Distribution on Glass and Porcelain Insulator Strings

The E-field distribution on disc-type insulator stings is considerably different from polymer insulators due to the presence of the metallic cap and pins along the entire length of the unit. The self and mutual capacitance between the cap and pins have the effect of grading the field along the string length, resulting in maximum E-field magnitudes at the sting ends that are generally lower than that of a polymer insulator installed without a corona ring in the same application.

The E-field distribution on disc-type insulators may need to be considered for the following reasons:

- Corona activity under dry conditions may result in customer complaints due to audible noise or electromagnetic interference.
- Corona activity under dry conditions in the pin region may damage the grout, reducing the life expectancy. See Figure 4.9-15.
- Corona activity under dry conditions may result in damage to the glaze on porcelain units after extended exposure.
- Corona activity on the metallic surfaces under dry conditions may result in loss of galvanization, which, in turn, may result in localized corrosion after extended exposure.



Figure 4.9-15 *Top:* Images of corona activity on the first bell of a 765-kV insulator string with no grading devices installed. *Bottom:* Corona activity surrounding the pin of a porcelain insulator disc under dry conditions.

- Corona activity and/or high E-fields may damage the porcelain bulk material, resulting in donut-type failures, as previously discussed. See Figure 4.9-15 (Jagtiani and Booker 1995).
- Puncture due to lightning impulses. See Chapter 6 (Section 6.5.4).
- Corona-induced flashovers in clean environments (Landy and Reynders 2003).

Unlike polymer insulators, wet corona activity on porcelain and glass insulator stings is generally not a consideration due to the durability and aging characteristics of porcelain and glass.

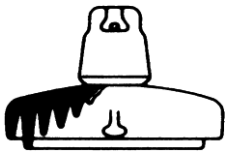
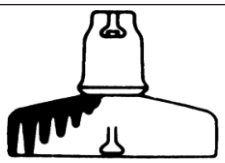
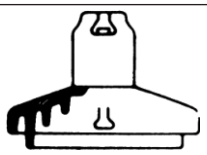
To address the above issues, corona rings and arcing horns may be applied. Another benefit of applying rings and horns is that they are often the preferential termination point for power arcs reducing the probability of damage to the insulator. Corona rings and arcing horns are usually applied to the line end hardware, not to the insulators themselves. The rings are designed to prevent corona from the hardware, as well as grade the E-field in, on, and around the insulators themselves.

Corona rings and E-field grading hardware are generally not utilized directly on insulator strings for applications at voltages lower than 345 kV. Field grading of 765-kV insulator strings has been shown to be important to prevent customer complaints and avoid reduction in life expectancy (see Chapter 15). Arcing horns have been applied at all voltage levels.

APPENDIX 4.1 INSULATOR TYPES REFERRED TO IN THIS CHAPTER

Table 4.1-1 Geometrical and Mechanical Characteristics of the Insulator Units Tested at Project UHV

Type	Spacing (SP)		Diameter		Leakage distance (LD)		Ratio	Mechanical strength	
	(mm)	(In.)	(mm)	(In.)	(mm)	(In.)	LD/SP	(Kg)	(Lb)
Standard-type									
A-11	146	5 3/4	254	10	305	12	2.08	7,500	15,000
Fog-type									
F-2	165	6 1/2	320	12 1/2	510	20	3.08	18,000	40,000
G-2	170	6 3/4	305	12	520	20 1/2	3.04	18,000	40,000
H-1	146	5 3/4	254	10	435	17	2.95	11,500	25,000
H-2	160	6 1/4	290	11 1/2	470	18 1/2	2.94	18,000	40,000
H-3	198	7 3/4	400	15 3/4	690	27	3,5	30,000	66,000
H-4	220	8 11/16	420	16 1/2	740	29	3.34	40,000	90,000
L-2	170	6 3/4	320	12 5/8	545	21 1/2	3.2	23,000	50,000
L-5	250	9 13/16	420	16 1/2	720	28 1/4	2.9	55,000	120,000
M-1	140	5 1/2	280	11	435	17	3.08	11,500	25,000
M-4	200	7 7/8	380	15	540	21 1/4	2.72	38,000	84,000
N-3	184	7 1/4	330	13	572	22 1/2	3.11	30,000	66,000
N-5	230	9 3/16	380	15	730	28 3/16	3.16	55,000	120,000

A-11	F-2	G-2	H1
			
H2	H3	H4	L2
			
L5	M1	M4, N3, N5	
			

REFERENCES

AIEE Committee Report. 1958. "The Influence of Water Resistivity and Precipitation Rate Upon 60-Cycle Wet Flashover Voltage." *AIEE Transactions Communication and Electronics.* Vol.77. Pt. I. pp. 350-358.

Akizuki, M., O. Fujii, S. Ito, T. Irie, and S. Nishimura. 2002. "A Study on Anti-contamination Design of Suspension Insulators—A Stress Grading Insulator." Power Engineering Society Summer Meeting. 2002 IEEE. Volume 1. 21-25 July. Pp. 300-307.

Aleksandrov, G. N., V.Y. Kizvetter, V. M. Rudakova, and A. N. Tushnov. 1962. "The AC Flashover Voltages of Long Air Gaps and Strings of Insulators." *Elektrichestvo.* No. 5. pp. 27-32.

ANSI. 1996. American National Standard for Composite Suspension Insulators for Overhead Transmission Lines - Tests: ANSI C29.11-1989 (R 1996). ANSI. New York, N.Y.

ANSI. 2002a. American National Standard for Electrical Power Insulators – Test Methods: ANSI C29.1-1988 (R2002). ANSI. New York, N.Y.

ANSI. 2002b. American National Standard for Insulators – Composite Line Post Type: ANSI C29.17-R2002. ANSI. New York, N.Y.

ANSI. 2002c. American National Standard for Insulators – Composites – Suspension Type: ANSI C29.12-1997 (R2002). ANSI. New York, N.Y.

Armentrout, D. L., M. Kumosa, and T. S. McQuarrie. 2003. "Boron-free Fibers for Prevention of Acid Induced Brittle Fracture of Composite Insulator GRP Rods." *IEEE Transactions on Power Delivery.* Volume 18. Issue 3. July. Pp. 684–693.

ASTM D2303. "Standard Test Method for Liquid-contaminant – Inclined-plane Tracking and Erosion of Insulating Materials."

Baker, A. C. and M. Kawai. 1973. "A Study on Dynamic Voltage Distribution on Contaminated Insulator Surface." *IEEE Transactions on Power Apparatus and Systems.* Vol. PAS-92. pp. 1517-1524. September/October.

Berry, B. 1995. "A Brief History of Porcelain Insulators." http://www.insulators.com/porcelain/history.htm.

Besztercey, G. and G. G. Karady. 2000. "An Artificial Contamination Method for Composite Insulators." *IEEE Transactions on Power Delivery.* Volume 15. Issue 2. April Pp. 732–737.

Boehne, E. W. and C. S. Weiner. 1966. "Contamination of EHV Insulation - An Analytical Study." IEEE Summer Power Meeting. Conference Paper 31 CP-66-48l. July.

Boehne, E. W. and C. S. Weiner. 1967. "Contamination of EHV Insulation—II: Power Losses and Their Distribution." IEEE Winter Power Meeting. Conference Paper 31 CP-67-l53. January/February.

Burnham, J. T. 1995. "Bird Streamer Flashovers on FPL Transmission Lines." *IEEE Transactions on Power Delivery.* Volume 10. Issue 2. April. Pp. 970–977.

Burnham, J. T., P. S. Givens, and T. M. Grisham. 1994. "High Strength Polymer Post Insulators Enable Economical Transmission Lines with Low Environmental Impact." Transmission and Distribution Conference. *Proceedings of the 1994 IEEE Power Engineering Society.* 10-15 April. Pp. 494–503.

Burnham, J. T. and R. J. Waidelich. 1997. "Gunshot Damage to Ceramic and Nonceramic Insulators." *IEEE Transactions on Power Delivery.* Volume 12. Issue 4. October. Pp. 1651–1656.

Burnham, J. T., T. Baker, A. Bernstorf, C. de Tourreil, J.-M George, R. Gorur, R. Hartings, B. Hill, A. Jagtiani, T. McQuarrie, D. Mitchell, D. Ruff, H. Schneider, D. Shaffner, J. Yu, and J. Varner. 2002. IEEE Task Force Report: Brittle Fracture in Non-ceramic Insulators." *IEEE Transactions on Power Delivery.* Volume 17. Issue 3. July. Pp. 848–856.

Campillo, M. T., J. I. Montesinos, and M. A. Ponce. 1995. "Conductivity and Flashover Voltage of Low Soluble Materials Deposited on High Voltage Insulators." 9th International Symposium on High Voltage Engineering (ISH). Graz, Austria. Paper 3217. August 28–September 1.

CAN/CSA (Canadian Standards Association). 1998. C411.4–98. Composite Suspension Insulators for Transmission Applications. (Reaffirmed 2003).

Carrara, G. and W. Hauschild. 1990. "Statistical Evaluation of Dielectric Test Results." *Electra.* Ref. No: 133.1.

CEA. 1996. CEA Purchase Specification: "Dead-end/Suspension Composite Insulator for Overhead Distribution Lines." CEA LWIWG-01. November.

Chandler, H., R. Jones, and J. Reynders. 1983. "Stress Corrosion Failure of Composite Long Rod Insulators." Paper No. 23.09. Presented at the Fourth International Symposium on High Voltage Engineering. Athens. September.

Chandler, H. and J. Reynders. 1984. "Electro-Chemical Damage to Composite Insulators." Paper No. 33-08. Presented at the International Conference on Large High Voltage Electric Systems (CIGRÉ). August.

Cherney, E. A. 1991. "Partial Discharge, Part V: PD in Polymer Type Line Insulators." *IEEE Electrical Insulation Magazine.* March/April. Vol. 7. No. 2.

Chisholm, W. A., P. G. Buchan, and T. Jarv. 1994. "Accurate Measurement of Low Insulator Contamination levels." *IEEE Transactions on Power Delivery.* Volume 9. Issue 3. July. pp. 1552–1557.

Chisholm, W. A., Y. T. Tam, R. C. Heics, and T. Jarv. 1993. "Insulator Contamination Levels in Southern Ontario." Ontario Hydro Technologies report A-G-93-14 P.

Chisholm, W. A., K. G. Ringler, C. C. Erven, M. A. Green, O. Melo, Y. Tam, O. Nigol, J. Kuffel, A. Boyer, I. K. Pavasars, F. X. Macedo, J. K. Sabiston, and R. B. Caputo. 1996. "The Cold-Fog Test [for outdoor insulators]." *IEEE Transactions on Power Delivery.* Volume 11. Issue 4. October. Pp. 1874–1880.

Chisholm, W. A. 1998. "Effects of Flue Gas Contamination on Ceramic Insulator Performance in Freezing Conditions." EPRI, Palo Alto, CA. Tennessee Valley Authority, Chattanooga, TN. TR-110296.

Chrzan, K., Z. Pohl, and T. Kowalak. 1989. "Hygroscopic Properties of Pollutants on HV Insulators." *IEEE Trans. on Electrical Insulation.* Vol. EI-24. No. 1. February. pp. 107-112.

Chrzan, K. L. 2003. "Concentrated Discharges and Dry Bands on Polluted Outdoor Insulators." 13th International Symposium on High Voltage Engineering (ISH). Delft, the Netherlands.

Chrzan, K. L., J. Vokalek, V. Sklenicka, W. Petrusch, and J. Kindersberger. 2003. "Pollution Flashover of Long Rod Insulators with Different Profiles." 13th International Symposium on High Voltage Engineering (ISH). Delft, the Netherlands.

CIGRE. 1979a. "A Critical Comparison of Artificial Pollution Test Methods for HV Insulators." Working Group 33.04. *Electra.* No. 64. pp. 117-136.

CIGRE. 1979b. "The Measurement of Site Pollution Severity and its Application to Insulator Dimensioning for AC Systems." Working Group 33.04. *Electra.* Ref. No. 64. pp. 101-116.

CIGRE. 1986. Field Experience and Laboratory Research on Composite Insulators for Overhead Lines. Paris. Report 15-12.

CIGRE. 1990. "Worldwide Service Experience with HV Composite Insulators." CIGRÉ Subworking Group 03.01 of Study Committee 22. *Electra.* No. 130. pp. 69-77.

CIGRE. 1992a. "Guidelines for the Evaluation of the Dielectric Strength of External Insulation." CIGRÈ Study Committee 33. Technical Brochure No. 72. CIGRE. Paris.

CIGRE. 1992b. "Guide for the Identification of Brittle Fracture of Composite Insulator FRP Rod." CIGRÉ Working Group 03 of Study Committee 22. *Electra.* No. 143. August. pp. 61-66.

CIGRE. 1992c. "Use of Stress Control Rings on Composite Insulators." CIGRE Working Group 03 of SC 22. *Electra.* No. 143. August. pp. 69-71.

CIGRE. 1994a. "Insulator Pollution Monitoring." Working Group 33.04. *Electra*. Ref. No. 152. pp. 79-89.

CIGRE. 1994b. "Failure of Cap-and-pin Insulators Subjected to HVDC." Task Force 33.04.02 of Study Committee 33. *Electra.* No. 153. April. pp. 22-31.

CIGRE. 1996. "Review of 'In-Service Diagnostic Testing' of Composite Insulators." *Electra.* No. 169. p. 105. December.

CIGRE. 1999a. *Natural and Artificial Ageing and Pollution Testing of Polymeric Insulators.* Report 142. Task Force 33.04.07. June.

CIGRE. 1999b. "Influence of Ice and Snow on the Flashover Performance of Outdoor Insulators. Part I: Effects of Ice." Working Group 33.04. *Electra*. Ref. No. 187.

CIGRE. 2000a. "Influence of Ice and Snow on the Flashover Performance of Outdoor Insulators. Part 2: Effects of Snow." Working Group 33.04. *Electra.* Ref. No. 188.

CIGRE. 2000b. "Polluted Insulators: A Review of Current Knowledge." Cigré Task Force 33.13.01. Brochure 158. June.

CIGRE. 2001. *Composite Insulator Handling Guide Working.* Report 184. Group 22.03. April.

CIGRE. Forthcoming. "Polluted Insulators: Guidelines for the Selection and Dimensioning Part 1: General Principles and the a.c. Case." CIGRÉ Task Force C4-13-01. Brochure to be published. 2005.

CRIEPI. 1968. "An Investigation of Salt-Contamination Problem on 500 kV Transmission System Insulation." Tokyo. Japan. CRIEPI 500-kV Special Committee Report. August.

De La O, A. and R. S. Gorur. 1998. "Flashover of Contaminated Nonceramic Outdoor Insulators in a Wet Atmosphere." *IEEE Transactions on Dielectrics and Electrical Insulation.* Volume 5. Issue 6. December. pp. 814-823.

De La O, A., R. S. Gorur, and J. Chang. 1994. "AC Clean Fog Tests on Nonceramic Insulating Materials and a Comparison with Porcelain." *IEEE Transactions on Power Delivery.* Volume 9. Issue 4. October. pp. 2000–2008.

Deno D. W. and L. E. Zaffanella. 1987. "Field Effects of Overhead Transmission Lines and Stations." *Transmission Line Reference Book: 345 kV and Above*. 2nd edition. 1987.

de Tourreil, C., L. Pargamin, G. Thevenet, and S. Prat. 2000. "Brittle Fracture of Composite Insulators: Why and How They Occur." Power Engineering Society Summer Meeting. IEEE. Volume 4. 16-20 July. Pp. 2569 – 2574.

Eklund, A., I. Gutman, and R. Hartings. 1994. "The Dust Cycle Method: A New Pollution Test Method for Ceramic and Non-ceramic Insulators." Proceedings of the International Conference on Power System Technology. October 18-21. Beijing, China. Vol. 2. pp. 1254-1257.

Eklund, A., I. Gutman, and R. Hartings. 1995. "Conditioning of Silicone Rubber Insulators: Loss and Recovery of Hydrophobicity." 9th International Symposium on High Voltage Engineering (ISH). Graz, Austria. August 28–September 1.

Engelbrecht, C. S., A. Eklund, R. Hartings, and R. Znaidi. 2000. "Field and Laboratory Testing for the Choice of Optimum Composite Insulator Design for a Marine-Desert Environment." CIGRE. Paris session. Paper 33-202.

Engelbrecht, C. S., R. Hartings, H. Tunell, B. Engström, H. Janssen, and R. Hennings. 2003. "Pollution Tests for Coastal Conditions on an 800 kV Composite Bushing." *IEEE Transactions on Power Delivery.* Volume 18. Issue 3. July. pp. 953–959.

Engelbrecht, C. S., R. Hartings, and J. Lundquist. 2004. "Statistical Dimensioning of Insulators with Respect to Polluted Conditions." *IEE Proc. Gener. Transm. Distrib.* Vol. 151. No. 3. May. pp. 321-326.

Engelbrecht, C. S., I. Gutman, and R. Hartings. 2005. "A Practical Implementation of Statistical Principles to Select Insulators with Respect to Polluted Conditions on Overhead a.c. Lines." Submitted to IEEE Power Tech. St. Petersburg, Russia.

EPRI. 1982. *Transmission Line Reference Book: 345 kV and Above*. Second Edition. Revised. EPRI. Palo Alto, CA.

EPRI. 1992. *Clean Fog Flashover Tests on 138-kV Nonceramic Line Post Insulators Before and After Artificial Aging.* Technical Report – 100886.

EPRI. 1998. *Application Guide for Transmission Line NCI.* TR 111-566.

EPRI. 1999. *Electric Field Modeling of NCI and Grading Ring Design and Application.* TR 113-977. EPRI. Palo Alto, CA. December.

EPRI. 2000a. *500 kV Aging Chamber – Testing and Final Results.* 1000719.

EPRI. 2000b. *Initial Investigation into the Effect of Elevated Conductor Temperature on the Operation of NCI.* 1000033. EPRI. Palo Alto, CA. April.

EPRI. 2001a. *Educational Video: Guide to Storing, Transporting and Installing Polymer Insulators.* 1006353. EPRI. Palo Alto, CA. August.

EPRI. 2001b. *Effect of Elevated Conductor Temperature Operation on Polymer Suspension Insulators and the Effect of Elevated Temperatures on the Mechanical Performance of Polymer Post Insulators.* EPRI. TC Report to funders only.

EPRI. 2001c. *Storing Transporting and Installing Polymer Insulators–A Practical Guide.* EPRI. TC Funder Report.

EPRI. 2001d. *Guide to Corona and Arcing Inspection of Transmission Lines.* 1001910. October.

EPRI. 2002a. *230 kV Accelerated Aging Chamber: Description of Test and Condition of NCI After One Year of Aging.* 01001745. Palo Alto, CA. November.

EPRI. 2002b. *Non-Ceramic Insulator End Fitting Analysis.* 1001744 EPRI. Palo Alto, CA. November.

EPRI. 2002c. *Results of Electrostatic Modelling of the Electric Field Magnitude on the Surface of Polymer Insulator Sheaths*. TC Funder report. EPRI. September.

EPRI. 2003a. *230 kV Accelerated Aging Chamber: Condition of NCI After 2 Years of Aging.* 1001746. EPRI. Palo Alto, CA.

EPRI. 2003b. *Polymer Insulator Survey 2002: Utility Field Experience and In-service Failures*. EPRI. Palo Alto, CA. 1007752. March.

EPRI. 2003c. *Promising Technologies for the Inspection of Polymer Insulators.* Technology Review and Evaluation. EPRI. Palo Alto, CA. 1002025. September.

EPRI. 2003d. *Development of Field Test Equipment for Live Working With Polymer (NCI) Insulators: Preliminary Study.* EPRI. Palo Alto, CA. 1002029.

EPRI. 2003e. *Develop New Polymer Insulator Design and Inspection Methods for Transmission Applications.* Palo Alto, CA.1009084.

EPRI. 2004a. *230 kV Accelerated Aging Chamber: Condition of NCI After 3 Years of Aging.* Palo Alto, CA. 1008737

EPRI. 2004b. *Damage Detection of Polymer Insulators Using Vibration Response: Evaluation of Remote Excitation Techniques.* Technical Update. EPRI. Palo Alto, CA. 1002026. July.

EPRI. 2004c. *Field Guide: Visual Inspection of NCI: Revision 1.* EPRI. Palo Alto, CA.1008739. May.

EPRI. 2004d. *Electrical Condition Assessment of Polymer Insulators for Live Working: Development of a Simple Portable Tester.* EPRI. Palo Alto, CA. 1002030.

EPRI. 2004e. Transmission and Substations 2005 Membership Offering: 2005. www.epri.com.

EPRI. 2004f. "Transmission Line and Substation Insulation—Assessing Contaminated Insulation Using Discharge Inspection: Not a Feasible Technique." NMAC Memo. EPRI. Palo Alto, CA. November. pp. 20-22. 10011355.

ESKOM. 2003. *Transmission Line Design Manual.* Eskom.

Farzaneh, M. and J. F. Drapeau. 1995. "AC Flashover Performance of Insulators Covered with Artificial Ice." *IEEE Trans. on Power Delivery.* Vol. 10. No. 2. pp. 1038-1051.

Farzaneh, M. and J. Kiernicki. 1997. "Flashover Performance of IEEE Standard Insulators under Ice Conditions." *IEEE Transactions on Power Delivery.* Volume 12. Issue 4. October. pp. 1602 –1613.

Farzaneh, M., J. Zhang, and X. Chen. 1997. "Modeling of the AC Arc Discharge on Ice Surfaces." *IEEE Transactions on Power Delivery.* Vol. 12. No. 1. January.

Farzaneh, M., T. Baker, A. Bernstorf, K. Brown, W. A. Chisholm, C. de Tourreil, J. F. Drapeau, S. Fikke, J. M. George, E. Gnandt, T. Grisham, I. Gutman, R. Hartings, R. Kremer, G. Powell, L. Rolfseng, T. Rozek, D. L. Ruff, D. Shaffner, V. Sklenicka, R. Sundararajan, and J. Yu. 2003. "Insulator Icing Test Methods and Procedures." A position paper prepared by the IEEE task force on insulator icing test methods. *IEEE Transactions on Power Delivery.* Volume 18. Issue 4. October. pp.1503–1515.

Farzaneh, M. (Chair) et al. 2004. "Selection of Station Insulators with Respect to Ice or Snow - Part I: Technical Context and Environmental Exposure and Part II: Methods of Selection and Options for Mitigation." A position paper prepared by IEEE Task Force on Icing Performance of Station Insulators. *IEEE Transactions on Power Delivery.* March. Acceptance ref. TPWRD-00110-2004.

Fierro-Chavez, J. L. and I. Ramirez-Vazquez. 1999. "Mexican Experience with the Use of Polymeric Silicone Rubber Insulators for Transmission Lines." 11th International Symposium on High-Voltage Engineering (ISH). London. Paper 4.96.S25.

Fikke S. M., J. E. Hanssen, and L. Rolfseng. 1993. "Long Range Transported Pollutants and Conductivity of Atmospheric Ice on Insulators." *IEEE Trans. on Power Delivery.* Vol. 8. No. 3. July.

Fini, G., G. Marrone, L. Sartore, and E. Sena, 1993, "Qualification Tests Performed on Composite Insulators for 132-150 kV Overhead Lines." Paper presented at the 12th International Conference on Electricity Distribution. Birmingham, England. May.

Fonseca, J. R., A. L. Tan, R. P. Silva, V. Monassi, L. A. R. Assuncao, W. S. Junqueira, and M. O. C. Melo. 1990. "Effects of Agricultural Fires on the Performance of Overhead Transmission Lines." *IEEE Transactions on Power Delivery.* Volume 5. Issue 2. April. pp. 687–694.

Fujimura, T., K. Naito, T. Irie, and Y. Suzuki. 1979. "Anticontamination Design of Insulators." Pacific Coast Electrical Association Meeting. March 15-16.

Fukui, H., K. Naito, T. Irie, and I. Kimoto. 1974. "A Practical Study on Application of Semiconducting Glaze Insulators to Transmission Lines." *IEEE Transactions on Power Apparatus and Systems.* Vol. PAS-93. pp. 1430-1443. September/October.

Goldman A., M. Goldman, R. Sigmond, and T. Sigmond. 1989. "Analysis of Air Corona Products by Means of Their Reactions in Water." Proceedings of 9th International Symposium on Plasma Chemistry. Pugnochiuso, Italy. pp. 1654-1658.

Gorur, R. S., S. Sundhara Rajan, and O. G. Amburgey. 1989. "Contamination Performance of Polymeric Insulating Materials Used for Outdoor Insulation Applications." *IEEE Trans. on Electrical Insulation.* Vol. 24. No. 4. August. pp. 713-716.

Gorur, R. S., A. De La O, H. El-Kishky, M. Chowdhary, H. Mukherjee, R. Sundaram, and J. T. Burnham. 1997. "Sudden Flashover of Nonceramic Insulators in Artificial Contamination Tests." *IEEE Transactions on Dielectrics and Electrical Insulation.* Volume 4. Issue 1. February. pp. 79–87.

Gorur R., E. Cherney, and J. Burnham. 1999. *Outdoor Insulators*. Ravi S. Grour Inc. Phoenix, AZ.

Gosho, Y. 1969. "Measurement of Potential Distribution between Electrodes by the Electrostatic Probe Method." 9th International Conference on Phenomena in Ionized Gases. Bucharest, Romania. September 1-6. p. 625.

Gubanski, S. M. et al., 2003. "Research Findings on the Ageing Factors of Silicone Rubber." *Proceedings: World Conference & Exhibition on Insulators, Arresters & Bushings*. Pp. 285-296. Marbella, Spain.

Gutman, I., R. Hartings, and W. L. Vosloo. 1999. "Field Testing of Composite Insulators at Natal Test Stations in South Africa." Eleventh International Symposium on High Voltage Engineering (Conf. Publ. No. 467). Volume 4. 23-27 August. pp. 50–53.

Gutman, I., R. Hartings, U. Åström, and D. Gustavsson. 2001. "Procedure to Obtain a Realistic Degree of Hydrophobicity on Artificially Polluted Silicone Rubber Insulators." 12th International Symposium on High Voltage Engineering (ISH). Bangalore, India. Paper 5-2.

Gutman, I., K. Halsan, D. Hübinette, E. Solomonik, and L. Vladimirsky. 2004. "New Developed Insulator Selection Tool (IST) Software: Results of Application Using Known Russian Service Experience." 12th Asian Conference on Electrical Discharge. 19-22 November. Shenzhen, China.

Hall. J. 1992. "History and Bibliography of Polymeric Insulators for Outdoor Applications." Paper 92 WM 265-9 PWRD. Presented at the IEEE 1992 Winter Meeting. New York, N.Y.

Hampton, B. F. 1964. "Flashover Mechanism of Polluted Insulation." IEE Proceedings. Vol. 111. p. 5. May.

Harmon, R., G. Karady, and O. Amburgey. 1996. "Electrical Test Methods for Non-Ceramic Insulators Used for Live Line Replacement." Paper No. 0-7803-3522-8/96. Prepared by the IEEE Task Force on Electrical Testing of Polymer Insulators for Hot Line Installation, Transmission and Distribution Committee.

Hartings, R. 1994. "Electric Fields Along a Post Insulator: AC Measurements and Calculations." *IEEE Transactions on Power Delivery.* Volume 9. Issue 2. April. pp. 912–918.

Hoch, D. A. and A. Sukhnandan. 2003. "Fire Induced Flashovers of Transmission Lines: Theoretical Models." IEEE Africon. George, South Africa.

Houlgate, R. 1993. "Natural Testing of Composite Insulators at Dungeness Insulator Testing Station." Non-ceramic Outdoor Insulation International Workshop. SEE. Paris, France. April.

Houlgate, R. G., P. J. Lambeth, and W. J. Roberts. 1982. "The Performance of Insulators at Extra and Ultra High Voltages in a Coastal Environment." CIGRE 29th Session. Paris. Paper no. 47-15.

Houlgate, R.G. and D. A. Swift. 1989. "Polymeric Insulators: A.C. Flashover Voltage under Artificial Salt-pollution of New and Naturally-aged Units Compared to Porcelain." 6th International Symposium on High Voltage Engineering (ISH). New Orleans, LA. August 28–September 1. Paper 47-30.

Houlgate, R. G. and D. A. Swift. 1990a. "Composite Rod Insulators for AC Power Lines: Electrical Performance of Various Designs in a Coastal Testing Station." *IEEE Trans. on Power Delivery.* Vol. 5. No. 4. October. pp. 1944-1955.

Houlgate, R. and D. Swift. 1990b. "Composite Rod Insulators for AC Power Lines: Electrical Performance of Various Designs at a Coastal Testing Station." Paper No. 90 WM 026-5 PWRD. Presented at IEEE/PES.

IEC. 1986. "Guide for the Selection of Insulators in Respect of Polluted Conditions." IEC/report 60815 - Ed. 1.0.

IEC. 1991. "Artificial Pollution Tests on High-voltage Insulators to be used on a.c. Systems." IEC 60507 - Ed. 2.0, 1991-04.

IEC. 1992. IEC International Standard 1109: 1992 – Composite Insulators for A.C. Overhead Lines with a Nominal Voltage Greater than 1,000 V – Definitions, Test Methods, and Acceptance Criteria. Geneva, Switzerland.

IEC. 1993. "Insulators for Overhead Lines with a Nominal Voltage above 1000 V - Part 1: Ceramic or Glass Insulator Units for a.c. Systems - Definitions, Test Methods and Acceptance Criteria." IEC 60383-1 - Ed. 4.0, 1993-04.

IEC. 1996. "Insulation Co-ordination – Part 2: Application Guide." IEC 60071-2, 1996-12.

IEC. 1997a. "Insulators for Overhead Lines with a Nominal Voltage above 1000 V – A.C. Power Arc Tests on Insulator Sets." IEC 61467, 1997-02.

IEC. 1997b. IEC 6124. Overhead Lines–Requirements and Tests for Fittings. Second Edition. 1997-09.

IEC. 2002a. IEC International Standard 61466-2. "Composite String Insulator Units for Overhead Lines with a Nominal Voltage Greater than 1 000 V – Part 2: Dimensional and Electrical Characteristics." First Edition.

IEC. 2002b. IEC International Standard 61952. "Composite Line Post Insulators for a.c. Overhead Lines with a Nominal Voltage Greater than 1,000 V: Definitions, Test Methods and Acceptance Criteria."

IEC. 2003. IEC International Standard 62073. "Guidance on the Measurement of Wettability of Insulator Surfaces."

IEC. Forthcoming a. Draft IEC 60060-1: High-Voltage Test Techniques—Part 1: General Definitions and Test Requirements. Clause 9.

IEC. Forthcoming b. Draft IEC 60815-1, TS: Selection and Dimensioning of High-voltage Insulators for Polluted Conditions - Part 1: Definitions, Information and General Principles.

IEEE. 1974. Working Group on Characteristics of Protective Gaps of the Surge Protective Devices Committee. "Sparkover Characteristics of High Voltage Protective Gaps." *IEEE Trans. on Power Apparatus and Systems.* Vol PAS-93. January/February. pp. 196-205.

IEEE. 1978. Standard Techniques for High-Voltage Testing. IEEE Standard 4-1978. pp. 27-29. IEEE Power Engineering Society.

IEEE. 1979. Working Group on Insulator Contamination, Lightning and Insulator Subcommittee. "Application of Insulators in a Contaminated Environment." *IEEE Transactions on Power Apparatus and Systems*. Vol. PAS-98. No. 5. September/October. pp. 1676-1695.

IEEE. 1995. IEEE Standard Techniques for High-Voltage Testing: IEEE Std 4-1995. (Amended 2001). October.

IEEE. 2000. Session 5 – Insulator Cleaning Methods. ESMO 2000 Proceedings. 8-12 October. Montreal.

IEEE. 2001. Guide for Application of Composite Insulators. IEEE Std 98 –2001.

IEEE. 2004a. Task Force on Reducing Bird Related Power Outages. Insulator Contamination Working Group of the Transmission and Distribution Committee. "Preventive Measures To Reduce Bird Related Power Outages: Part I – Electrocution and Collision." *IEEE Transactions on Power Delivery.* Volume 19. Issue 4. Pp. 1843-1847.

IEEE. 2004b. Task Force on Reducing Bird Related Power Outages, Insulator Contamination Working Group of the Transmission and Distribution Committee. "Preventive Measures To Reduce Bird Related Power Outages: Part II – Streamers and Contamination." IEEE Transactions on Power Delivery. Volume 19. Issue 4. October. pp. 1848-1853.

IEEE. Forthcoming a. Electric Field Distribution on ac Composite Transmission Line Insulators. IEEE Task Force Paper.

IEEE. Forthcoming b. Guide for Corona Testing of Insulators and Line Hardware.

Imakoma, T., Y. Suzuki, O. Fujii, and S. Kawamura. 1994. "Electrical and Mechanical Characteristics of Non-ceramic Phase-to-phase Spacers and Akimbo Insulator Assemblies." SEE Conference. Paris. June 7-8.

Insulator News and Market Report. 2002. "Verification of Grading Rings Takes on Growing Importance in Selection of Silicone Insulators." July-August. page 40.

Ivanov, V. V. and E. A. Solomonik. 1995. "Statistical Flashover Voltage Studies of Wet Polluted High Voltage Insulators." 9th International Symposium on High Voltage Engineering (ISH). Graz, Austria. Paper 3227. August 28–September 1.

Jagtiani, A. S. and J. R. Booker. 1995. "Aging of Porcelain Suspension Insulators under Mechanical and Electrical Stress on EHV AC Lines." ESMO-95 Proceedings. Seventh International Conference on Transmission and Distribution Construction and Live Line Maintenance. 29 October–3 November. Pp. 80–86.

John, W. and C. Clark. 1939. "Testing of Transmission-Line Insulators Under Deposit Conditions." *Journal IEE* (London). Vol. 85. pp. 590-624.

Kaiser, G. 1970 "The Mouse Buzzard as a Cause of Breakdown on 110 kV Single Pole High Tension Lines." ETZ-A. June.

Karady, G. G. 1975. "The Effect of Fog Parameters on the Testing of Artificially Contaminated Insulator in a Fog Chamber." *IEEE Trans. on Power Apparatus and Systems*. Vol. PAS-94. No. 2. March/April. pp. 378-387.

Karady, G. G. 1999. "Flashover Mechanism of Non-ceramic Insulators." *IEEE Transactions on Dielectrics and Electrical Insulation.* Volume 6. Issue 5. October. pp. 718–723.

Karady, G. G., M. Shah, and R. L. Brown. 1995. "Flashover Mechanism of Silicone Rubber Insulators Used for Outdoor Insulation-I." *IEEE Transactions on Power Delivery.* Volume 10. Issue 4. October. pp. 1965–1971.

Kawai, M. 1971. "A Study of the Performance of Contaminated Insulators under Various Test Conditions." *IEEE Transactions on Power Apparatus and Systems*. Vol. PAS-90. p. 2568. November/December.

Kimoto, I., K. Kito, and T. Takatori, 1972, "Antipollution Design Criteria for Line and Station Insulators. *IEEE Transactions on Power Apparatus and Systems.* Vol. PAS-91. pp. 311-316. January/February.

Kindersberger, J. and M. Kuhl. 1989. "Effect of Hydrophobicity on Insulator Performance." Paper No. 12.01. Presented at the Sixth International Symposium on High Voltage Engineering. New Orleans, LA. August.

Kindersberger, J., and M. Kuhl. 1991. "Surface Conductivity of Polluted Silicone Rubber Insulators." 7th International Symposium on High Voltage Engineering (ISH). Dresden, Germany. August 26-30. Paper 43.15.

Kindersberger, J. and M. Kuhl. 1993. "Performance of Silicone Rubber insulators under Wetted Conditions and Influence Thereof on Hydrophobic Properties." SEE workshop "Non-Ceramic Outdoor Insulation." Paris. April 16-17.

Kito, K., T. Imakoma, and K. Shinoda. 1975. "Phase to Phase Spacers for Transmission Lines." IEEE PES summer meeting. San Francisco. July 20-25. Paper A 75 498-6.

Kondo, K. 2002, "Corona Ring Position of Polymer Insulators and Electric Field Stress," CIGRE session 2002. Paris. Group 33. Answer to Questions 4.1.5 and 4.2.4

Kuffel, E. and W. Zaengl. 1984. *High Voltage Engineering.* Pergamon International Library of Science. Technology, Engineering and Social Studies. Oxford, England.

Kumosa, M., L. Kumosa, and D. Armentrout. 2004. "Can Water Cause Brittle Fracture Failures of Composite Non-ceramic Insulators in the Absence of Electric Fields?" *IEEE Transactions on Dielectrics and Electrical Insulation.* Volume 11. Issue 3. June. Pp. 523 – 533.

Lambeth, P. J. 1971. "Effect of Pollution on High-Voltage Outdoor Insulators." *Proc. IEE.* IEE Reviews. Vol. 118. No. 9R. September. pp. 1107-1130.

Lambeth, P. J. 1988. "Variable-Voltage Application for Insulator Pollution Tests." *IEEE Trans. on Power Delivery.* Vol. 3. No. 4. October.

Lambeth, P. J., H. Auxel, and M. P. Verma. 1972. "Methods of Measuring the Severity of Natural Pollution as It Affects HV Insulator Performance." *Electra.* No. 20. pp. 37-52.

Lambeth, P. J., J. S. T. Looms, M. Sforzini, R. Cortina, Y. Porcheron, and P. Claverie. 1973. "The Salt Fog Test and its Use in Insulator Selection for Polluted Localities." *IEEE Trans. on Power Apparatus and Systems.* Vol. PAS-92. No. 6. November/December. pp. 1876-1887.

Landy, R. C. and J. P. Reynders. 2003. "Corona Inception on Cap-and-pin Insulators in Clean Environments." 13th International Symposium on High Voltage Engineering (ISH). Delft, the Netherlands.

Lannes, W. and H. Schneider. 1997. "Pollution Severity Performance Chart: Key to Just-in-time Insulator Maintenance." *IEEE Transactions on Power Delivery.* Volume 12. Issue 4. October. pp. 1493–1500.

Lapp Rodurflex insulator catalogue.

Leclerc, M., R-P. Bouchard, Y. Gervais, and D. Mukhedkar. 1982. "Wetting Processes on a Contaminated Insulator Surface." *IEEE Trans. on Power Apparatus and Systems.* Vol. PAS-101. No. 5. May. pp. 1005-1011.

Lin, X., Z. Chen, X. Liu, K. Chu, K. Morita, R. Matsuoka, and S. Ito. 1992. "Natural Insulator Contamination Test Results on Various Shed Shapes in Heavy Industrial Contamination Areas." *IEEE Trans. on Electrical Insulation.* Vol. EI-27. No. 3. June. pp. 593-600.

Locke Insulator Catalogue and Engineering Handbook. No. 61. Section 2. p. 6. Baltimore: General Electric Company.

Looms, J. 1988. *Insulators for High Voltages*. IEE Power Engineering Series No. 7. Peter Peregrinus Ltd.

Lopez, I., S. H. Jayaram, and E. A. Cherney. 2001. "A Study of Partial Discharges from Water Droplets on a Silicone Rubber Insulating Surface." *IEEE Transactions on Dielectrics and Electrical Insulation.* Vol. 8. No. 2. April. p. 262.

Lopez, I. J. S, S. H. Jayaram, and E. A. Cherney. 2002. "A Method for Detecting the Transition from Corona from Water Droplets to Dry Band Arcing on Silicone Insulators." *IEEE Transactions on Dielectrics and Electrical Insulation.* Volume 9. Number 6. December.

Marrone, G., F. Marinoni, and F. Galluci. 1987. "Set Up of a Dust Chamber Providing Artificial Insulator Contamination Suitable to Reproduce Conditions Occurring in the Field." 5th International Symposium on High Voltage Engineering (ISH). Braunschweig, Germany. Paper 52.18. August 24-28.

Massey, J. R. 1972. "Control of Insulator Contamination in Substations." *Journal of the Franklin Institute.* Vol. 294. No. 6. December. pp. 375-383.

Matsuoka, R., H. Shinokubo, K. Kondo, Y. Mizuno, K. Naito, T. Fujimura, and T. Terada. 1996. "Assessment of Basic Contamination Withstand Voltage Characteristics of Polymer Insulators." *IEEE Transactions on Power Delivery.* Volume 11. Issue 4. October. pp. 1895 – 1900.

Matsuoka, R., K. Kondo, K. Naito, and M. Ishii. 1996. "Influence of Nonsoluble Contaminants on the Flashover Voltages of Artificially Contaminated Insulators." *IEEE Transactions on Power Delivery.* Volume 11. Issue 1. January. pp. 420–430.

Matsuoka, R., K. Tanaka, H. Shinokubo, J. T. Burnham. 1998. "Damage of Nonceramic Insulator End Fittings by Power Arc Currents." *Proceedings of 1998 IEEE 8th International Conference on Transmission & Distribution Construction, Operation & Live-Line Maintenance.* 26-30 April. pp. 278 – 284.

Matsuoka, R., K. Naito, T. Irie, and K. Kondo. 2002. "Evaluation Methods of Polymer Insulators under Contaminated Conditions." Transmission and Distribution Conference and Exhibition 2002. Asia Pacific. IEEE/PES. Volume 3. 6-10 October. pp. 2197-2202.

Maxwell, A. J. and R. Hartings. 2000. "Evaluation of Optimum Composite Insulator Design using Service Experience and Test Station Data from Various Pollution Environments." CIGRE session. Paper 33-203.

Maxwell, A.J., I. Gutman, C. S. Engelbrecht, S. M. Berlijn, R. Hartings, D. Loudon, R. Lilja, and A. Eriksson. 2002. "Selection of composite insulators for AC overhead lines: implications from in-service experience and test-station results" CIGRE session 2002, Paper 33-402

Meyer, L. H., E. A. Cherney, and S. H. Jayaram. 2004. "The Role of Inorganic Fillers in Silicone Rubber for Outdoor Insulation—Aluminum Tri-hydrate or Silica." *IEEE Electric Insulation Magazine.* Volume 20. Number 4. July/August.

Mobasher, B., D. Kingsbury, J. Montesinos, and R. S. Gorur. 2003. "Mechanical Aspects of Crimped Glass Reinforced Plastic (GRP) Rods." *IEEE Transactions on Power Delivery.* Volume 18. Issue 3. July. pp. 852–858.

Montesinos, J., R. S. Gorur, and J. Burnham. 2000. "Estimation of Flashover Probability of Aged Nonceramic Insulators in Service." *IEEE Transactions on Power Delivery.* Volume 15. Issue 2. April. pp. 820 – 826.

Montesinos, J., R. S. Gorur, B. Mobasher, and D. Kingsbury. 2003. "Mechanism of Brittle Fracture in Nonceramic Insulators." *IEEE Transactions on Dielectrics and Electrical Insulation.* Volume 9. Issue 2. April. pp. 236 – 243.

Moran, J. H. 1974. "The Effect of 'Cold Switch-on' on Semiconducting Glazed Insulators." IEEE PES Winter Meeting. Paper C74-071-7.

Moreno, V. M. and R. S. Gorur. 2001. "Effect of Long-term Corona on Non-ceramic Outdoor Insulator Housing Materials." *IEEE Transactions on Dielectrics and Electrical Insulation.* Volume 8. Issue 1. February. pp. 117 – 128.

Moreno, V. M. and R. S. Gorur. 2003. Impact of Corona on the Long-term Performance of Nonceramic Insulators." *IEEE Transactions on Dielectrics and Electrical Insulation*.Volume 10. Issue 1. February.

Naito, K., R. Matsuoka, and K. Sakanishi. 1990. "Investigation of the Insulation Performance of the Insulator Covered with Lichen." *IEEE Transactions on Power Delivery.* Vol. 5. No. 3. July.

Naito, K., R. Matsuoka, T. Irie, and K. Kondo. 1999. "Test Methods and Results for Recent Outdoor Insulation in Japan." *IEEE Transactions on Dielectrics and Electrical Insulation.* Volume 6. Issue 5. October. pp. 732 – 743.

Nasser, E. 1968. "Some Physical Properties of the Electrical Discharges on Contaminated Surface." *IEEE Transactions on Power Apparatus and Systems.* Vol. PAS-87. pp.957-963. April.

Obenaus, F. 1958. "Fremdschichtueberschlag und Kriechweglaenge, Deutche Elektrotechnik." Vol. 4. pp. 135-136.

Parraud, R. and D. Dumora. 2001. "Corrosion Mechanism of Insulators in Tropical Environment." Symposium CAIRNS. CIGRE 2001. Paper 300-04.

Petruch, W. 1990. "Insulation Performance of Longrod Double Chain Insulators in Artificial Pollution Tests." Isolierverhalten von doppelketten bei leitfähigen oberfächen-Ablagerungen, Technicher Bericht. 1-271 der FGH.

Phillips, A. J., I. R. Jandrell, and J. P. Reynders. 1996. Consideration of Corona Onset from a Water Drop as a Function of Air Pressure." *IEE Proceedings on Science, Measurement and Technology.* Volume 143. Issue 2. March. pp. 125 – 130.

Phillips A. J., D. J. Childs, and H. M. Schneider. 1999a. "Ageing of Non-Ceramic Insulators due to Corona from Water Drops." *IEEE Transactions on Power Delivery.* Vol. 14. pp. 1081-1086.

Phillips, A. J., D. J. Childs, and H. M. Schneider. 1999b. "Water-Drop Corona Effects on Full-Scale 500 kV Non-Ceramic Insulators." *IEEE Transactions on Power Delivery.* Vol. 14. pp. 258-263.

Pigini A. and A. Tomba. 1993. "Set Up of a Method to Evaluate the Surface Hydrophobicity of Insulators." Paper No. 41.03. Presented at the Eighth International Symposium on High Voltage Engineering. Yokohama, Japan. August.

Pyrex. ca 1933. "Pyrex suspension and strain insulators." http://www.peninsulators.org/Pyrex/index.html.

Ramos, G., M. T. Campillo, and K. Naito. 1993. "A Study on the Characteristics of Various Conductive Contaminants Accumulated on High Voltage Insulators." *IEEE Trans. on Power Delivery.* Vol. 8. No. 4. October.

Ravera, C., A. C. Britten, J. Olivier, and D. A. Swift. 1996. "Service Experience with Polymeric Insulators in Eskom, South Africa." Paper presented at IEE Conference on Transmission and HVDC. London. May.

Riquel, G. 1993. "Accelerated Ageing Test for Nonceramic Insulators: EdF's Experience." Workshop paper, presented at the Nonceramic Outdoor Insulation Workshop. Paris. April.

Rizk, F. A. M. 1981. "Mathematical Models for Pollution Flashover." *Electra.* Ref. No. 78. pp. 71-103.

Sadurski, K. J. and J. P. Reynders. 1989. "High Voltage ac Breakdown in the Presence of Fire." Sixth ISH. New Orleans. Paper 13.32.

Schneider, H., W. Guidi, J. Burnham, R. Gorur, and J. Hall. 1992. "Accelerated Aging and Flashover Tests on 138 kV Nonceramic Line Post Insulators." Paper No. 92 WM 264-2 PWRD. Presented at the IEEE/PES Winter Meeting. New York, N.Y. January.

Schneider, H., W. Guidi, J. Slocik, J. Burnham, J. Hall, R. Brown, D. Chaply, J. Ellsworth, R. Robarge, and L. Wakefield. 1993. "Accelerated Aging Facility for Full Scale 500 kV Nonceramic Insulators." Paper No. 47.07. Presented to the 8th International Symposium on High Voltage Engineering. Yokohama, Japan. August.

Sediver catalog. *Toughened Glass Disc Insulators for Overhead Lines.* TG 87.

Shah, M., G. G. Karady, and R. L. Brown. 1995. "Flashover Mechanism of Silicone Rubber Insulators Used for Outdoor Insulation-I." *IEEE Transactions on Power Delivery.* Volume 10. Issue 4. October. pp. 1972–1978.

Shaowu, W., L. Xidong, G. Zhicheng, and W. Xun. "Hydrophobicity Transfer Properties of Silicone Rubber Contaminated by Different Kinds of Pollutants." CEIDP. Victoria, Canada. pp. 373-376.

Shaowu, W., L. Xidong, and H. Lengceng. 2000. "Experimental Study on the Pollution Flashover Mechanism of Polymer Insulators." IEEE Power Engineering Society Winter 2000 Meeting. Volume 4. January 23-27. pp. 2830-2833.

Shen,Y, E. Cherney, Fellow, and S. Jayaram. 2004. "Electric Stress Grading of Composite Bushings Using High Dielectric Constant Silicone Compositions." Conference Record of the 2004 IEEE International Symposium on Electrical Insulation. Indianapolis, IN. September 19-22.

Sklenicka, V. and J. Vokalek, 1999, "Pollution Performance of Double Insulator Assemblies." 11th International Symposium on High-Voltage Engineering (ISH). London, UK. Paper 4.337.P2.

Souheng, W. 1982, *Polymer Interface and Adhesion.* Marcel Dekker.

Spangenberg, E. and G. Riquel. 1997. "In Service Diagnostic of Composite Insulators: EDF's Test Results." Presented at the 10th International Symposium on High Voltage Engineering. Montreal, Quebec, Canada. August.

Sporn, P., F. Cahen, and M. Magnien, 1964, "Progress Report of Study Committee 9 on Extra-High Voltage a.c. Transmission." Paris, France. CIGRE. Paper No. 420.

Standving, W. 1934. "Some Measurements on the Electrical Characteristics of Insulator Strings." *Journal lEE.* London. Vol. 75. pp. 111-118.

Standring, W. G., R. C. Hughes, and W. J. Roberts. 1963. "Factors Affecting the Results of 50 c/s West Flashover Tests." *IEE Proceedings.* Vol. 110. No. 6. pp. 1072-1076.

STRI. 1992. *Hydrophobicity Classification Guide.* STRI Guide 1. 92/1.

Suzuki, Y., S. Ito, M. Akizuki, and T. Irie. 1999. "Artificial Contamination Test Method on Accumulated Contamination Conditions." Eleventh International Symposium on High Voltage Engineering. Conf. Publ. No. 467. Volume 4. August 23-27. pp. 192–195.

Suzuki, Y., T. Fukuta, Y. Mizuno, and K. Naito. 1999. "Probabilistic Assessment of Flashover Performance of Transmission Lines in Contaminated Areas." *IEEE Transactions on Dielectrics and Electrical Insulation.* Volume 6. Issue 3. June. pp. 337-341.

Swift, D. A. 1996. "Pollution Flashover Performance of Ceramic High-Voltage Insulators: A Critique of Using Solely Specific Leakage Distance for Dimensioning Purposes." South African Universities Power Engineering Conference'96. Johannesburg. January 22-23. pp. 61-66.

Swift, D. A. and P. Naidoo. 1993. "Large Particle Initiated Breakdown of an Atmospheric Airgap, Relating to ac Power Line Faults Caused by Sugar Cane Fires." Eighth International Symposium on High Voltage Engineering. Yokohama, Japan.

Swift, D. A., C. A. Spellman, and A. Haddad. 2001. "Leakage Current on Silicone Rubber Insulators and RTV Coatings in Clean Fog: Hydrophobicity Transfer to Pollution." 12th International Symposium on High Voltage Engineering (ISH). Bangalore, India. Paper 5-7.

Taniguchi, Y., N. Arai, and Y. Imano. 1979. "Natural Contamination Test of Insulators at Noto Testing Station Near Japan Sea." *IEEE Trans. on Power Apparatus and Systems*. Vol. PAS-98. No. 1. January/February. pp. 239-245.

University of Oslo. 1998. *Drop: A Program System for Interfacial Tension Measurements by Image Analysis.* University of Oslo. Oslo, Norway.

Vaillancourt, G., S. Carignan, and C. Jean. 1997. "Experience with the Detection of Faulty Composite Insulators on High-Voltage Power Lines by the Electric Field Measurement Method." *IEEE Transactions on Power Delivery.* PE-23-PWRD-0-05-1997.

Verma, M. P., H. Niklasch, W. Heise, H. Lipken, G. F. Luxa, and H. Schreiber. 1978. "The Criterion for Pollution Flashover and Its Application to Insulation Dimensioning and Control." CIGRE 27th session. Paris. Paper no. 33-09.

Vladimirski, L. L., E. A. Solomonik, and E. N. Orlova. 2001. "Russian Guidelines for Selection of Outdoor Insulation." ICEE. Xián, China. July 22-26. Paper 0006.

Vosloo, W. L. and J. P. Holtzhausen. 1996. "The Design Principles of On-line Insulator Test Stations to be Used on Power Distribution and Transmission Networks." AFRICON. IEEE AFRICON 4th. Volume 1. September 24-27. pp. 241-246.

Vosloo, H. and C. Van Rooyen. 2001. "Guarding Against Bird Outages. Eskom's Transmission System Project Achieves Goal to Eliminate 'Bird Streamer Faults,'" *Transmission and Distribution World*. April. pp. 70-80.

Vosloo, W. L. and J. P. Holzhausen. 2003. "Observation of Discharge Development and Surface Changes to Evaluate the Performance of Different Outdoor Insulator Materials at a Severe Coastal Site." 13th International Symposium on High Voltage Engineering (ISH). Delft, the Netherlands.

Williams, L. J., J. H. Kim, Y. B. Kim, N. Arai, O. Shimoda, and K. C. Holte. 1974. "Contaminated Insulators - Chemical Dependence of Flashover Voltages and Salt Migration." *IEEE Trans. on Power Apparatus and Systems*. Vol. PAS-93. No. 5. September/October. pp.1572-1580.

Woodson, H. H. and A. J. McElroy. 1970. "Insulators with Contaminated Surfaces: Pt. II. Modeling of Discharge Mechanism." *IEEE Transactions on Power Apparatus and Systems.* Vol. PAS-89. pp. 1848-1858 November/December.

Xidong, L., C. Xupeng, T. Feng, and X. Jiaqi, 1994, "The Special Problem of Composite Insulators in Pollution Test." ICPST'94. Beijing, China. pp. 1263-1266.

Xidong, L., W. Shaowu, H. Lengceng, S. Qinghe, and C. Xueqi. 1999. "Artificial Pollution Test and Pollution Performance of Composite Insulators." 11th International Symposium on High-Voltage Engineering (ISH). London, UK. Paper 4.337.P2.

Xidong, L., W. Shaowu, G. Zhicheng, Y. Jun, and S. Qinghe. 2001. "Hydrophobicity Status of Silicone Rubber Insulators in the Field." 12th International Symposium on High Voltage Engineering (ISH). Bangalore, India.

Yasui, M., Y. Takahashi, A. Takenaka, K. Naito, Y. Hasegawa, and K. Kato. 1987. "RI, TVI and AN Characteristics of HVDC Insulator Assemblies under Contaminated Condition." Paper No. 87 SM 578-8. Presented at the IEEE/PES Summer Meeting. San Francisco, CA. July.

Zhao, T. and M. G. Comber. 2000. "Calculation of Electric Field and Potential Distribution along Nonceramic Insulators Considering the Effects of Conductors and Transmission Towers." *IEEE Transactions on Power Delivery.* Volume 15. Issue 1. January. pp. 313 – 318.

Znaidi, R. 2001. "Recherche de correlation entre la pollution artificielle et la pollution naturelle dans un milieu marin et desertique en Tunisie." Symposium CAIRNS. CIGRE. Paper 200-17.

CHAPTER 5

Switching Surge Performance

Luciano Zaffanella

This chapter discusses the strength of phase-to-ground and phase-to-phase transmission-line insulation when subject to switching surges. The chapter describes switching impulse test methods and provides flashover voltages versus distances for various types of insulation arrangements. The chapter also reviews the effects on switching impulse strength of several factors, including surge shape, atmospheric conditions, and gap geometry. Physical models are provided that describe the mechanism of switching surge flashover. The chapter also discusses the impact of switching surges during live line maintenance and the application of insulation strength data to transmission line design.



Dr. Luciano E. Zaffanella is one of the original authors of *EPRI Transmission Line Reference Book*. When the first and second editions were published he was directing General Electric's staff that was operating Project UHV on behalf of EPRI. Under his direction this project became a High Voltage Transmission Research Center, an internationally renowned facility for the study of overhead high voltage transmission lines with HVAC voltages up to 1500 kV three-phase, and HVDC voltages of + and – 1200 kV, including their switching surge performance. His research into the switching impulse strength of air insulation started before joining GE when he was managing the Research Section of CESI in Milan, Italy. He pioneered research into phase-to-phase switching impulse strength, behavior of gaps at low flashover probability, effect of air density on switching impulse strength, and switching impulse tests on outdoor full-scale transmission line tower insulation systems for Ultra High Voltages. His research on switching surge strength is documented in about 15 IEEE and CIGRE papers.

5.1 INTRODUCTION

External insulation of transmission systems must withstand, with a high degree of reliability, both transient and power frequency voltage stresses. Among the transient voltage stresses, particular attention must be given to those created by system operations—i.e., the voltage surges that may occur at line energization, or as a result of fault clearing or reclosure after clearing a fault. These voltage stresses are called *switching surges*. Chapter 3 discusses how these stresses are generated, how their magnitudes can be calculated, and how the surge amplitudes can be controlled. This chapter discusses the strength of transmission-line insulation elements when subjected to switching surges. The transmission-line insulation elements that are discussed consist of air gaps and insulators in various arrangements.

This chapter reports strength data obtained in high-voltage laboratories around the world using *switching impulses*—i.e., voltages that have the general shape of an impulse approximating the shape of actual switching surges. The switching impulses used to develop strength data for various insulation systems vary in shape. Particular attention is given to switching impulses with a shape that corresponds to the lowest possible flashover voltage for the same crest value. Studies of switching surge strength started in the 1960s simultaneously with the growth of EHV transmission, when it was found that switching impulses of the worst shape and polarity could cause flashovers of air gaps at unexpectedly low voltages. In addition, it was found that the relation between the length of air gaps and their switching surge strength is markedly nonlinear. Thus, switching surges become of increasing concern as the transmission voltage increases. It was this concern that caused a proliferation of research on the switching surge strength of air gaps and insulators during the 1970s and 1980s, when there were prospects for construction of UHV transmission in several countries.

The previous edition of this book, written at a time when there was a rapid increase in the use of higher voltage lines and there was a prospect of transmission lines with voltages above 1000 kV, emphasized the data on long air gaps. The current chapter presents data that cover the entire range of transmission voltages starting from 220/230 kV.

The design of several transmission-line elements is determined by the power frequency voltage and by lightning. Lightning may control the length of insulator strings, especially for lower voltage lines and in conditions of high ground resistance or high incidence of lightning. The power frequency voltage controls the design of insulator strings in contaminated conditions. The power frequency voltage controls also the air clearance between the conductors and the grounded objects when the conductor and insulator string swing in conditions of extreme winds. Conductor and insulator swings are of concern also for switching surges. However, the wind pressure used for switching surge design is generally assumed to be much lower than for the power frequency voltage because of the extremely low probability of coexistence of elevated winds and elevated switching surges.

Power frequency voltages influence the choice of the distances between phases because of the need to limit radio and audible noise. This is particularly true for voltages of 345 kV and above. Switching surge stresses between phases are seldom a limiting factor, except perhaps for compact lines at lower voltages, for which corona effects may not be significant. Power frequency voltages, rather than switching surges, often control the height of the conductors above ground because of the need to maintain adequate clearances in extreme conductor temperature conditions and also to limit the electric field induction in vehicles and the electric field at ground.

Although switching surges at the lower line voltages may not have as much an impact on line design as the case would be for UHV transmission, their consideration continues to be necessary. Once the insulation for power frequency and lightning is satisfied, the switching surge performance must be verified. In most cases, power frequency and lightning requirements control the insulation, and lines have a very low or no risk of failure due to switching surges. This is due in large part to the use of modern methods to limit switching surge amplitude, as discussed in Chapter 3.

The insulation utilized in transmission systems must be sufficient to ensure reliable operation of the line at all times. However, a line designed for no insulation failures may be extremely expensive, and the increased reliability may not be justifiable. The problem of designing insulation for switching surges is complicated because of the great variety of surges and meteorological conditions that the line may experience, and because of the statistical fluctuations of the insulation strength itself. Switching surges appear in all shapes and with different amplitudes. Each type of surge may occur during most meteorological conditions, all of which affect the flashover strength differently. The larger surges occur more rarely than the smaller ones, and the largest possible surge may have an extremely low probability of occurrence in actual service. The expense of providing insulation sufficient to withstand such a surge may be so great that it may be more practical to take the risk, clear the infrequent fault, and reclose. When reclosing breakers are utilized, flashover on transmission lines does not usually result in permanent failure or in unacceptable stability problems. The probability of successful reclosing

is quite high, thus encouraging efforts toward designing the lines to meet a given reliability criterion rather than attempting to ensure that no flashover will ever occur.

This chapter begins by briefly reviewing the principal variables in switching surge flashover. Sections 5.3 and 5.4 describe the switching impulse flashover process and test methods and equipment. In Sections 5.5 through 5.7, the discussion reviews the switching impulse strength of air gaps, line insulation, and station insulation. Techniques for characterizing phase-to-phase switching surge strength are covered in Section 5.8. Section 5.9 explains a calculation method for determining the flashover probability with voltage. The effects of various factors on switching impulse strength—including waveshape, air density and humidity, and rain and other wet- weather conditions—are described in Sections 5.10 through 5.12. Section 5.13 considers the risk of failure of phase-to-ground insulation.

The chapter concludes in Section 5.14 with a discussion of switching surge during live line maintenance. For most modern lines, the clearances between conductors and towers are designed to allow live-line maintenance operations on the line, such as replacing insulator strings. To ensure the safety of the personnel performing these operations, the gaps between conductive tools or personnel and conductors or energized hardware must not flashover even assuming the worst possible switching surge. In order to limit tower insulation requirements that this condition would impose, some utilities use portable gaps to control where a possible switching surge flashover occurs. This chapter also discusses other issues where switching surges impact live-line maintenance: the strength of air gaps with floating objects and the performance under switching surges of insulator strings with broken insulators, an issue of importance in order to assess when insulator strings must be changed.

Switching surge design methods may be very refined. It is possible to assess the relative frequency of occurrence of all the combinations of surges and meteorological events, combine stress with strength taking into account the probabilistic nature of the two and the entire set of insulation systems that are stressed, evaluate the risk of insulation failure, and evaluate how this risk would change as insulation type and dimensions are changed. These methods require special computer programs and a systematic evaluation of meteorological conditions and surge shapes and amplitudes. This chapter provides the strength data in the form of probability of flashover for different insulation types, surge amplitudes, shapes, and meteorological conditions. Insulation strength may be obtained from the many curves presented in this chapter or by applying an analytical model, which is described in Appendix 5.2.

In addition, the user may exercise the following applets:

- Applet S-1: "Switching Surge Flashover Model." The user who is interested in a particular insulation system may exercise Applet S-1 to calculate the critical 50% flashover voltage. This applet is based on an advanced model of the discharge process developed following great advances in the understanding of the mechanism of switching surge flashover. Despite the progress in analytical modeling, the use of data obtained from full-scale switching impulse tests is still preferable.
- Applet S-2: "Risk of Failure." This applet may be used to calculate the risk of failure for a transmission line subject to a set of switching surges. This applet accounts for the statistical distribution of surges, the statistical nature of switching surge strength, the statistics of weather conditions, and the number of insulating elements. With regard to the insulation strength, the standard error in the determination of the flashover voltage in tests among different laboratories is about 3%. This error, in combination with the standard deviation of the flashover voltage (see Section 5.9) and in combination with the accuracy expected from the determination of surge amplitudes in an actual system means that the risk of failure of phase-to-ground insulation of a line can be determined within about two orders of magnitude, for instance 1 in 10^4 instead of 1 in 10^6 surges. The use of absolute risk of failure values may seem questionable in view of such apparently poor accuracy. However, the use of a relative risk of failure is a useful tool to compare different designs. In most cases, even the most conservative switching surge risk of failure values may be significantly lower than those due to lightning and power frequency.
- Applet S-3: "Analysis of Results of Switching Surge Tests." This applet considers a switching impulse test consisting of a series of applied impulses with different crest voltages, each resulting either in a withstand or a flashover. The applet calculates the best estimates of the two parameters that define the switching impulse strength: 50% flashover voltage and standard deviation.

5.2 PRINCIPAL VARIABLES IN SWITCHING SURGE FLASHOVER

5.2.1 Switching Surges and Switching Impulses

Throughout this chapter, the terms "switching surge" and "switching impulse" are used. A *switching surge* is a transient overvoltage occurring on a power system as a result of a switching operation. A switching surge is a stress, specifically a voltage stress, applied to the power system insulation. A switching surge may result in a fault—i.e., the failure of an insulation element, such as a particular air gap. The failure consists of a flashover followed by a power

arc. The insulation failure of one element equates to the insulation failure of the entire line or system to which that element belongs; it will require a momentary or permanent de-energization of the line to clear the fault and restore the voltage. The generation, measurement, calculation, and control of switching surges are described in Chapter 3.

A *switching impulse* is a voltage transient produced in the laboratory for insulation testing. Amplitudes and shapes of switching surges differ from surge to surge. In contrast, switching impulses have shapes, often standardized, that try to reproduce the shape of the most frequently occurring or of the most severe switching surges. Laboratory tests are conducted by repeated application of switching impulses to a test object, normally an element of the external insulation of transmission lines or substations. External insulation consists of air gaps or insulators or their combination. External insulation is usually "self-restoring", meaning that it regains its strength after the application of a switching impulse, whether or not the impulse caused a flashover.

The strength of an insulation element is determined with switching impulse tests, consisting of a number of applications of impulses with varying amplitudes, each resulting in either a *withstand* or a *flashover*. Testing techniques are described in Section 5.4. A complete knowledge of stresses (switching surges), number and types of insulation elements, and their strength is needed to assess the risk of failure of an entire line. This issue is discussed in Section 5.13.

The switching impulse strength of elements of the external insulation of lines is a statistical quantity, because it fluctuates from one impulse to another even when all the test parameters are kept constant. In addition, the strength depends on:

- Polarity
- Waveshape
- Geometry of the insulation element under test
- Meteorological parameters: temperature, air pressure, humidity, rain, and other foul-weather conditions

5.2.2 Switching Impulse Polarity

The switching impulse strength is greatly affected by the polarity of the surge because of the asymmetry of the geometry of practical insulation elements. In most cases the grounded electrode is either the ground plane or a massive structure or the combination of the two. The dimensions of the energized electrode, however, are much smaller. Thus the electric field in the gap between the electrodes is very nonuniform with the higher field intensity at the energized electrode. The switching surge flashover is initiated by positive polarity streamers, which are predischarge phenomena occurring at the positive electrode. For most practical configurations the positive-polarity switching surge strength is lower than the negative-polarity switching surge strength. The more nonuniform the field, the more pronounced is the polarity effect. In power systems, positive- and negative-polarity surges occur statistically with the same frequency and amplitude. Phase-to-ground insulation of transmission lines and stations designed to withstand positive-polarity surges is minimally affected by negative-polarity surges. Therefore, it is common practice in the design of phase-to-ground insulation to disregard switching surges of negative polarity.

5.2.3 Switching Impulse Waveshape

The switching impulse strength of external insulation does not depend on the crest value of the applied voltage alone. Since the early stages of switching surge research, it was found that flashover could be obtained with lower crest voltages when the impulse has a shape similar to a switching surge, which reaches crest with a time much longer than for lightning impulses (a few microseconds) but much shorter than a power frequency waveform (4.2 ms for 60 Hz, 5 ms for 50 Hz). Indeed this worrisome peculiarity spurred the large amount of research conducted in high-voltage laboratories around the world, particularly in the period from 1960 to 1980.

Switching surges have a wide variety of waveshapes. Because the waveshape has a significant influence on the flashover strength, one of the first requirements of switching surge insulation research has been to adopt some sort of consistent waveshape for testing purposes. The waveshape most frequently used to emulate switching surges is a double exponential wave generated by a conventional impulse generator, such as the double exponential waveform shown in Figure 5.2-1. The wave has a "front" and a "tail," separated by the "crest." A double exponential waveform is characterized by two parameters: the time-to-crest, defined as the time interval between the beginning of the impulse and the instant when the voltage reaches its peak value (crest value), and the time-to-half value, defined as the time interval from the beginning of the impulse and the instant on the tail of the impulse when the voltage is one-half of the crest value. The time-to-crest, t_{cr}, of double exponential waveforms used during switching impulse tests usually ranges from 50 μs to 1000 μs. The time-to-half value usually ranges from 3 to 10 times the time-to-crest value. Flashovers may occur either on the front, at the crest, or on the tail of the waveform. For each gap, there is a critical time-to-crest for which the insulation strength reaches a minimum. It is interesting to note that flashovers generally occur on the tail for waveforms with time-to-crest shorter than critical, and on the front for waveforms longer than critical.

Long front waveforms, with times-to-crest greater than 1000 μs, are often more conveniently generated with a transformer, using different techniques of which the most common consists of discharging a capacitor into the low-voltage winding (Thione et al. 1975; Lloyd and Zaffanella 1981). Transformers can be cascaded for the purpose of generating switching impulses with higher crest values by discharging a capacitor in the low-voltage winding of each transformer in the cascade. Transformers are used to generate switching impulses because of the desire for a better emulation of the actual overvoltages occurring in high-voltage systems and also for performing switching impulse tests between phases, for which two generators are required. The resulting waveform, shown in Figure 5.2-1, is similar to the function *1-cos(ωt)*. Because flashovers, if any, occur on the front of the transformer-generated waveform, the shape of the waveform after crest is not important and, therefore, these waveforms are characterized by the time-to-crest only. A transformer-generated waveform stresses external insulation differently than a double exponential waveform of the same crest value and time-to-crest. The important parts of the flashover process, such as leader inception and propagation (see Section 5.3), take place at voltages between 60-75% and 100% of the crest value of impulses corresponding to a 50% probability of flashover. Thus the "active" portion of the waveform may be defined as that between the 70% point and the crest value of the impulse. The duration of the active portion is $t_{0.7} = T_{100} - T_{70}$. A double exponential waveform and a transformer-generated waveform having the same value of $t_{0.7}$ cause the same stress, even though their times-to-crest are quite different. Transformer-generated waveforms are characterized by $t_{cr,eq}$ (equivalent time-to-crest), which is the time-to-crest of a double exponential waveform with the same crest value and causing the same stress. For instance, a transformer-generated impulse with a time-to-crest of 1700 μs and a $t_{0.7}$ of 840 μs is equivalent to a double exponential waveform with a time-to-crest of 1220 μs and time-to-half value equal to 5 times the time-to-crest. Therefore, $t_{cr,eq}$ = 1220 μs. The ratio between t_{cr} and $t_{cr,eq}$ of a transformer-generated waveform depends somewhat on the time-to-half value; for a time-to-half value equal to 5 times the time-to-crest, the ratio is about 1.4 (Arada et al. 1973; EPRI 1982).

Switching impulse tests have also been performed with nonconventional impulse waveforms, such as waveforms with a double peak (Menemenlis et al. 1978b), waveforms with a double impulse (Les Renardieres Group 1978), and waveforms with a bump on the crest (Carrara et al. 1970; Lalot and Hutzler 1978), mainly for the purpose of understanding the flashover mechanism. The influence of a preceding voltage stress was also studied, using the ac power frequency voltage or a dc voltage before the impulse (Watanabe 1968; Knudsen and Iliceto 1970). These studies did not result in changes in the application of switching impulse data to line design. The voltage stress is defined by crest value and equivalent time-to-crest of the impulse. Several sets of data showing the dependence of switching impulse strength, expressed in terms of the 50% flashover voltage, V_{50}, (see Section 5.4), on time-to-crest, t_{cr}, have been generated by various researchers and are shown in Sections 5.5, 5.6, and 5.10. Qualitatively this dependence is shown in Figure 5.2-2.

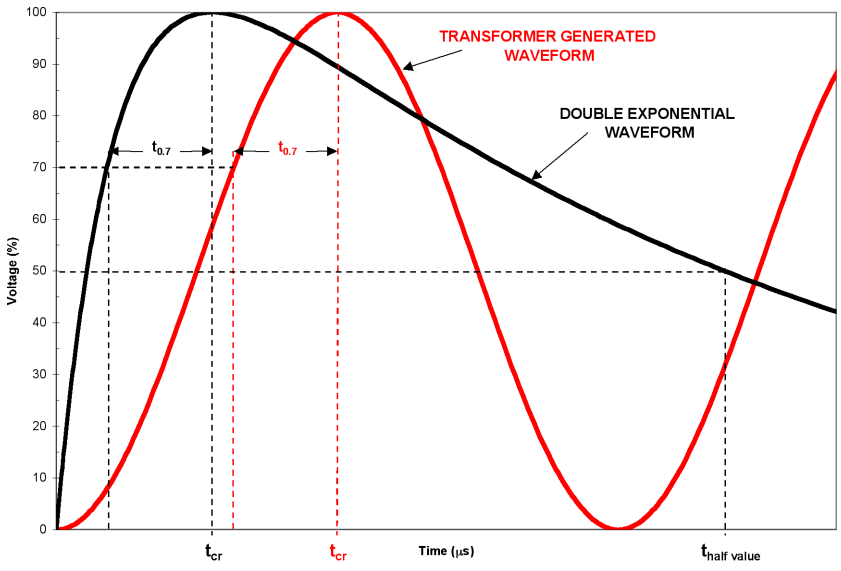


Figure 5.2-1 Typical switching impulse waveforms: double exponential and transformer-generated.

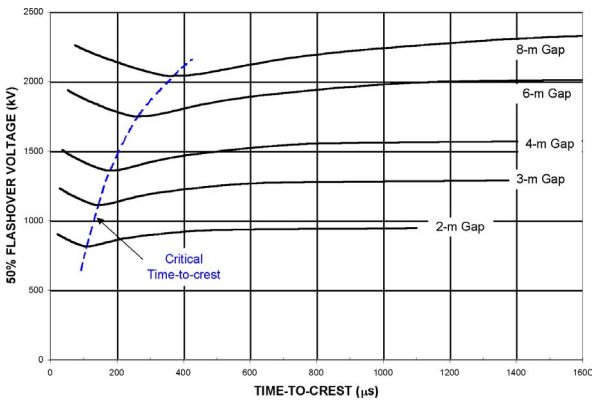


Figure 5.2-2 Examples of dependence of switching impulse strength on time-to-crest.

Switching surges encountered in power systems have times-to-crest ranging from 50 μs to 2000 μs or more (AIEE 1961; IEEE 1966; see also Chapter 3). As the crest values of the surges are reduced by means of advanced methods, such as circuit breakers with resistor insertion, the surges become longer, closely resembling a half-cycle of power frequency oscillation. Thus in those systems for which surge limitation is important, the great majority of the equivalent times-to-crest will be greater than 1000 μs.

5.2.4 Influence of Geometry on Switching Impulse Strength

The switching impulse strength of air gaps is not only a function of the gap length but also of the shape of the two electrodes between which a flashover may occur. For phase-to-ground insulation, the two electrodes are the line (or "energized") electrode and the grounded electrode. For phase-to-phase insulation, both electrodes are energized.

The shape of the electrodes influences the flashover process and the switching surge strength, especially for large gaps (i.e., gap length greater than 2 m). If the energized electrode has small dimensions, such as a rod or a small conductor, the presence of the ground plane or of large structures causes pronounced reductions in phase-to-ground flashover strength for positive polarity switching surges. The physical size of a tower can adversely influence the breakdown strength of the insulation, particularly if the tower approximates a ground plane. Small, lightweight towers have greater switching impulse strength than large massive ones with the same gap length. The walls of a laboratory may enhance the ground plane effect. Adequate laboratory clearances for reliable results must be considered (Carrara and Zaffanella 1968). When tower insulation is tested using a laboratory mockup, it is important to perform the tests outdoors using a full-scale model, which includes placing the conductors at the proper height above ground. Earlier tests of 345-kV and 500-kV tower insulation performed inside high-voltage laboratories showed a lower strength than when the same configurations were tested outdoors.

A large amount of research on the switching impulse strength of air gaps was performed on electrodes with simple geometry, some of which do not bear much resemblance to typical line or station configurations but were useful to develop today's knowledge of the flashover process. The technical literature reports results of tests on the following basic phase-to-ground electrode configurations:

- Rod-plane (see Section 5.5.1)
- Rod-rod, vertical arrangement (see Section 5.5.2)
- Rod-rod, horizontal arrangement (see Section 5.5.3)
- Sphere-plane (see Section 5.5.4)
- Conductor-plane (see Section 5.6.5)

Of particular interest is the rod-plane configuration, because it exhibits the lowest switching impulse strength, which occurs for positive polarity impulses of critical shape. It is about 400 kV/m for a 1-m gap, and it decreases with gap length to about 105 kV/m for a 30-m gap. At the other end of the spectrum, the strongest gap is the plane-to-plane, whose strength is about 3,000 kV/m independently of the shape of the impulse and gap length. The positive-polarity 50% flashover voltage of a rod-plane configuration is often taken as the reference value. The strength of any other configuration with the same gap spacing is defined by the "gap factor," which is the ratio between the positive polarity 50% flashover voltage of the configuration and the positive polarity 50% flashover voltage of a rod-plane configuration (Paris 1967). The gap factor of any configuration is always greater than or equal to one.

The technical literature reports results of tests on the following basic phase-to-phase electrode configurations:

- Rod-rod, horizontal arrangement (see Section 5.8)
- Conductor-conductor, horizontal arrangement, short section (see Section 5.8)

A large amount of test data is available also on more practical phase-to-ground line and station insulation, with or without the presence of insulators and with or without the presence of corona shields or similar hardware:

- Conductor-to-grounded object on the ground plane (see Section 5.6.5)
- Conductor with protrusion (broken spacer)-to-ground plane (see Section 5.6.5)
- Conductor-to-tower leg (see Section 5.6.4)

- Conductor-to-tower window (see Section 5.6.1)
- Conductor-to-tower, outside phase (see Section 5.6.2)
- Conductor-to-bus support structure (see Section 5.7.3)
- Horizontal insulator string, corona shield-to-support structure (see Section 5.7.2)

Finally, data on practical phase-to-phase line and station insulation configurations are also available:

- Conductor-to-conductor, long span (see Section 5.8)
- Corona shield-to-corona shield (see Section 5.8)

5.2.5 Meteorological Influence on Switching Impulse Strength

The most important weather parameters affecting the switching surge design of transmission lines are: air density, humidity, rain, and wind. Air density and humidity affect the switching impulse strength of air gaps.

Rain may affect the switching impulse strength of insulators, but it does not cause any appreciable change in the strength of air gaps. Heavy streams of water cascading over insulators greatly reduce the negative-polarity switching impulse strength, sometimes even reducing it below the positive-polarity strength. The conductivity of the water plays a significant role (Malaguti and Zaffanella 1968). The effect of rain is minimal for very long strings, such as those for 500-kV or 765-kV transmission or for V-strings (Kachler et al. 1971a).

When insulator strings are free to swing in the tower window or on an outside phase, a conservative design requires an increased horizontal gap distance to reflect that a switching surge may occur when the insulator string is swinging closer to a tower leg (see Section 5.13 and Appendix 5.1).

5.2.6 Statistical Fluctuations in Switching Impulse Strength

Nowhere in the insulation area is the statistical nature of the breakdown process in a gaseous dielectric more apparent than in switching impulse breakdown. After all determinable meteorological, geometrical, and electrical influences have been accounted for, a significant element of randomness persists.

The variation in strength of a single insulation element, when tested repeatedly under the same apparent conditions, is such that its flashover voltage may be expressed only in terms of probability. This is why the switching impulse strength is characterized by the 50% flashover voltage, V_{50}. This is the voltage at which 50% of the applied impulses result in a flashover and the other 50% result in a withstand. The flashover probability varies with voltage according to a distribution, which, for practical design purposes, can be assumed Gaussian. This was shown to be valid at least down to voltages equal to V_{50} — 4 times the standard deviation (see Section 5.9). On normal probability paper the flashover probability versus voltage is represented by a straight line. This distribution is defined by:

$$p(V) = \frac{1}{\sigma\sqrt{2\pi}} \cdot \int_{-\infty}^{V} e^{-\frac{1}{2}\left(\frac{x-V_{50}}{\sigma}\right)^2} dx \qquad 5.2\text{-}1$$

$p(V)$ is the flashover probability, V_{50} is the voltage corresponding to a 50% probability of flashover, and σ is the standard deviation.

A reliable value of the standard deviation is difficult to obtain with a single test with a limited number of repeated voltage applications. It is much better to use median values of the standard deviation derived from a large number of tests on similar insulation type and geometry. The value of the standard deviation depends on waveshape, polarity, geometry, and weather conditions. For gaps in which the energized electrode resembles a rod and for positive polarity waveshapes having critical time-to-crest, the median value of the standard deviation is between 4 and 5% of V_{50}. A conservative value equal to 5% is generally used. For gaps in which the energized electrode is a conductor or is close to a conductor, the median value of the standard deviation is less than or equal to 3% of V_{50}.

Even if V_{50} and σ are accurately determined, their values fluctuate for reasons that are often unknown. Comparisons of test results among different laboratories demonstrate that the results obtained by one laboratory deviate from those obtained by another, both working at their highest degree of accuracy. The differences in V_{50} are of a statistical nature. The magnitude of the standard deviation of all possible measurements of the V_{50} obtained in different laboratories is assumed to be about 3% (Brasca et al. 1967).

5.3 FLASHOVER MECHANISM

There are two reasons for the importance of switching surges in transmission-line design. First, the waveshape of the surges may fall in the region of times-to-crest, which, for positive polarity, are critical for the insulation strength of air gaps of typical overhead lines and stations—i.e., the strength is much lower than for lightning impulses and for power frequency voltages of the same amplitude. Second,

switching impulse strength increases less than proportionally with the gap length, whereas the increase in lightning impulse strength is linear with gap length.

To explain these phenomena, many studies of the physics of switching impulse flashover in air have been performed by researchers in high-voltage laboratories around the world (Ganger and Maier 1972; Les Renardieres Group 1972; Menemenlis and Isaksson 1974; Les Renardieres Group 1974; Baldo et al. 1975; Hutzler and Hutzler 1975, Menemenlis and Isaksson 1975; Suzuki 1975; Menemenlis and Harbec 1976; Les Renardieres Group 1977; Los and Schneider 1978; Menemenlis et al. 1978a; Alexandrov and Podporkyn 1979; Alexandrov et al. 1980; Alexandrov and Podporkyn 1982). As a result, much is known about the flashover mechanism, and several models based on physical considerations have been developed to determine the strength of air gaps (Lemke and Mosh 1973; Jones 1973; Carrara and Thione 1976; Kline 1977; Los 1978; Hutzler and Hutzler 1978; Rizk 1989a, 1989b, 1992, 1993, 1995, 1996; Podporkin 1995). What is summarily described in this chapter is the result of a considerable amount of work performed by many researchers over several years. The cited references provide a much more in-depth description to the interested reader.

The electric field in insulation configurations of overhead transmission lines and stations is highly divergent, and is much larger at the energized electrode than at the grounded electrode. When a positive-polarity switching impulse is applied, the positive electric field occurring at or near the energized electrode may cause the initiation of a process that may eventually lead to a flashover of the entire gap and that, under certain critical conditions, corresponds to the lowest possible flashover voltage. Most research has been focused on these critical conditions.

An example of flashover produced by applying a positive polarity switching impulse to a high-voltage conductor suspended by insulators in a tower window is shown in Figure 5.3-1.

The positive-polarity switching impulse flashover process can be broken down into different successive stages:

- In the first stage there is no discharge, while the voltage rises from zero to the corona inception voltage.
- At a certain voltage there is the first appearance of corona, called “first corona.” Corona appears as a bundle of filaments called “streamers” that start from the same point on the high-voltage electrode. Streamers emit mostly blue and ultraviolet light. Each streamer follows a different path from the previous one except for a short stem that is common to all (see Figure 5.3-2). Streamers propagate at a velocity of a few meters per microsecond and, for divergent field distributions, penetrate the gap up to distances from a few tens of centimeters to a few meters. The streamer length depends little on the gap spacing, but mainly on the degree of nonuniformity of the electric field in the gap and on the corona inception field, which may have wide statistical fluctuations from one impulse to the next. The electric field necessary for streamer initiation is predominantly a function of the shape of the high-voltage electrode, increasing with its radius of curvature. For smooth bundle conductors, a streamer inception field of about 36 kV/cm was measured (Los and Schneider 1978). The streamer inception field depends also significantly on the rate of rise of the voltage, being larger for a faster rising front. If the electrode is below a critical size, differences in streamer activity have no impact on the flashover voltage, which is dominated by the phenomena occurring during later stages of the flashover process. Corona emits light, which is detectable using photomultipliers, and causes a current pulse with short front times (tens of nanoseconds) and short tail times (hundreds of nanoseconds). First corona may be followed by a dark period during which there are no discharges because the space charge produced by the streamers reduces the electric field at the electrode below the value necessary to initiate more streamers. There is no ionization activity for a time dependent on the rate of rise of the voltage. Following the dark period, another burst of corona, or secondary corona, occurs. The propagation of the streamer depends on the degree of nonuniformity of the electric field in the gap. If the field is uniform, the streamers reach the ground electrode, secondary emission is produced there, and the discharge current is increased until a direct breakdown occurs.

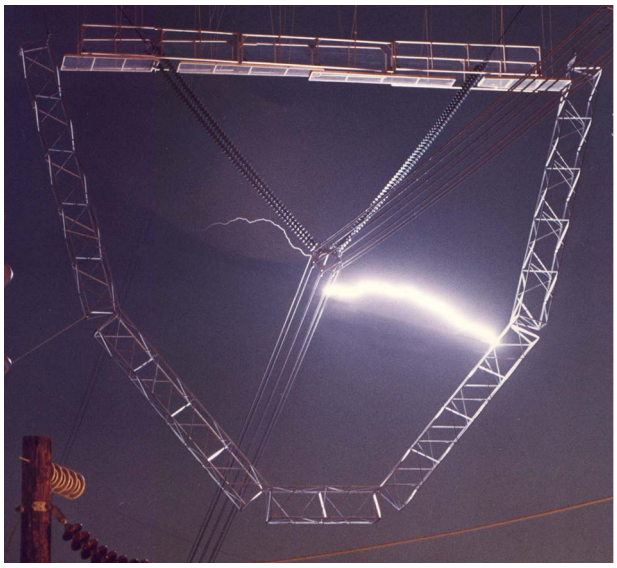


Figure 5.3-1 Switching impulse flashover of a tower window gap.

- The most important stage in the flashover process is the formation of a leader and the propagation of the leader into the gap. With or without a dark period, corona is followed by the initiation of a highly ionized channel called a "leader." The leader channel has a high conductivity and a radius of about 1 mm. The leader starts from the tip of the streamer stem (see Figure 5.3-2) and proceeds into the gap, often along a crooked path and in an irregular fashion characterized by sudden arrests of its propagation, pauses, restrikes, and restarts. At the tip of the leader the electric field is very intense and causes the formation of leader corona, composed of a bundle of luminous streamers. The luminosity of the leader is low, but its various phases can be detected using image converter cameras because of the luminosity of leader corona. Restrikes can be detected because of the illumination of the leader. The number of restrikes depends on the length of the gap. For a 5-m gap, there is at most one restrike; for a 10-m gap, there could be up to five restrikes. Under the critical conditions leading to the lowest switching impulse strength of the gap, the leader propagates in a fairly continuous and mostly straight fashion. The leader is the most important feature of the flashover process, and its properties have been extensively measured. It appears that the leader axial velocity (velocity of the leader tip projection on the axis of the gap) is about constant and equal to 1 ~ 2 cm/μs. As the leader progresses, a charge of 40 ~ 50 μC/m of axial leader length is injected into the gap. This charge resides near the leader channel and forms a space charge column with a radius of the order of 0.5 m. The electric field along the leader channel varies from a value of about 400 kV/m for a newly formed channel segment to an ultimate value of 50 kV/m with a time constant of about 50 μs. The potential at the tip of the leader remains about constant and equal to the leader inception voltage. The left side of Figure 5.3-1 shows the path of a leader that did not develop into a flashover. The brightness of this leader's channel is caused by the sudden transfer of the leader space charge to the high-voltage electrode when the voltage collapsed to zero. Without the voltage collapse, the leader would not have been visible.
- The final stage of the flashover process is the "final jump." When the leader bridges about two-thirds of the gap, its velocity suddenly and dramatically increases and, with a final jump, flashover of the gap occurs. The final jump occurs when streamers from the tip of the leader reach the grounded electrode (see Figure 5.3-2). The gap bridged by the streamers at that moment is called the "height of the final jump." Just before the final jump occurs, the mean electric field along the unbridged gap is 400–500 kV/m, while the electric field at the grounded electrode is lower and must reach a critical value to cause flashover.
- Usually no significant discharge activity appears at the negative electrode until the flashover process is nearly complete.

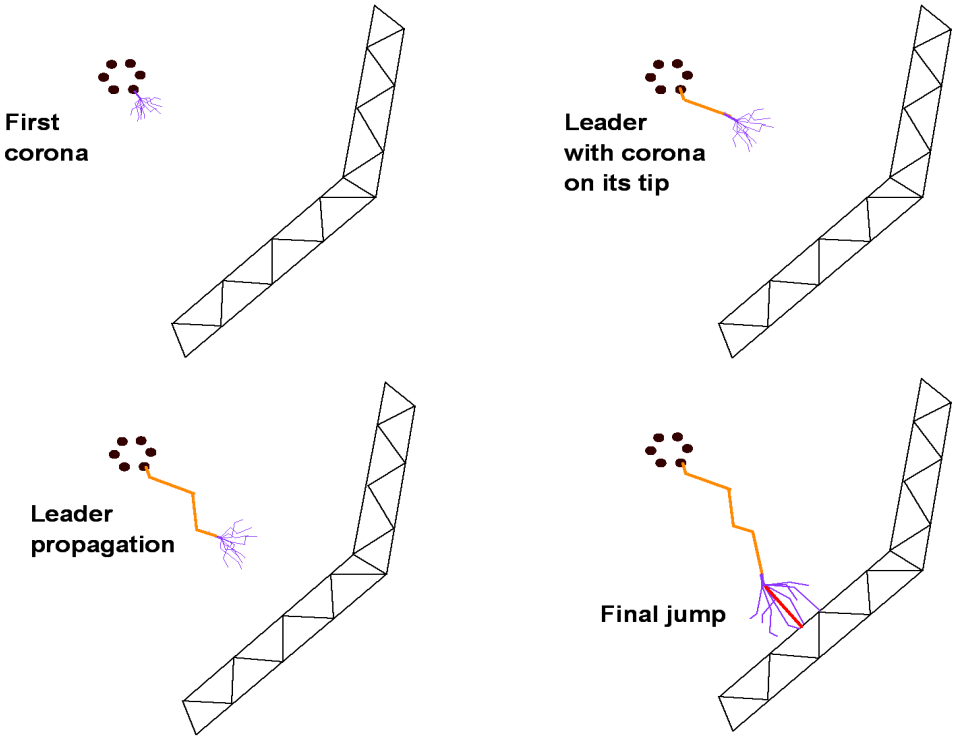


Figure 5.3-2 Stages of the positive switching impulse flashover process.

- Leader initiation and propagation depend on the geometry of the electrodes and on the shape and crest value of the applied voltage. There are critical waveforms for which these phenomena occur in such a way to cause flashover with the lowest possible value of crest voltage. These waves have been determined experimentally for a number of gaps. Models of the flashover process have focused on predicting the critical flashover voltage. Appendix 5.2 describes the most practical and promising model developed so far, based on the work of (Carrara and Thione 1976; Rizk 1989a, 1989b). The critical flashover voltage of any practical gap can be determined by exercising Applet S-1.

5.4 SWITCHING IMPULSE TESTING TECHNIQUES

5.4.1 Switching Impulse Generators, Test Circuits, Test Objects

Switching impulse tests are performed in high-voltage laboratories either indoors or outdoors. Outdoor tests are preferable whenever the dimensions of the test object are significant relative to the distances to the laboratory walls or test equipment. Tests performed indoors would result in lower flashover voltages, unless the dimensions of the test hall are much larger than the height of the energized electrode above ground (Carrara and Zaffanella 1968). Transmission-line tower design has been developed with full-scale models erected outdoors (Rohlfs et al. 1961; Kalb 1963; Johnson et al. 1963; Rawls et al. 1964; Atwood et al. 1965; Aubin et al. 1966; Guyker et al. 1966; Armstrong and Miller 1967; Saruyama et al. 1967; Hauspurg et al. 1969; Kachler et al. 1970; Dillard and Hileman 1970; Annerstrand et al. 1971; Pokorny and Flugum 1975; Young et al. 1980; Cortina et al. 1985; Yasui and Murooka 1988; Kim et al. 2000)

Switching impulse tests may be performed using either conventional impulse generators, such as that shown in Figure 5.4-1 or transformers, single or cascaded, such as those shown in Figure 5.4-2. Typical schematics of the test



Figure 5.4-1 Conventional impulse generator for generating double exponential waveforms at the EPRI Laboratory in Lenox, MA, USA.



Figure 5.4-2 Cascaded transformers for generating oscillatory waves at the EPRI Laboratory in Lenox, MA, USA.

circuits are shown in Figure 5.4-3 for the conventional impulse generator, and in Figure 5.4-4 for the transformer-generated impulses.

A switching impulse is generated by charging capacitors and then discharging them using various techniques. The impulse is applied to a test object, which may be a piece of equipment or an insulation element of overhead transmission lines or substations. For phase-to-ground switching impulse tests, the impulse is applied between the high-voltage electrode of the test object and ground, to which all the grounded parts of the test object are connected. The

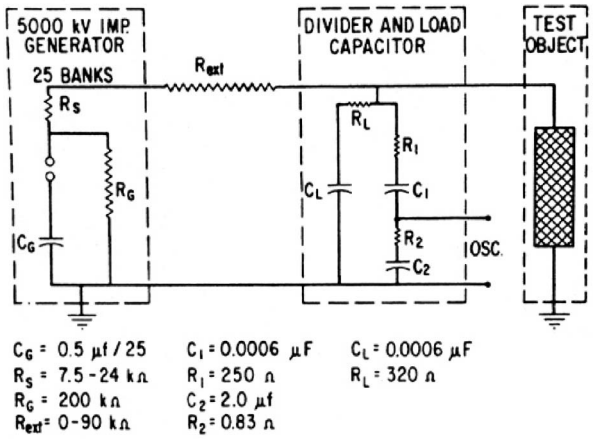


Figure 5.4-3 Schematic of a double exponential switching impulse testing circuit.

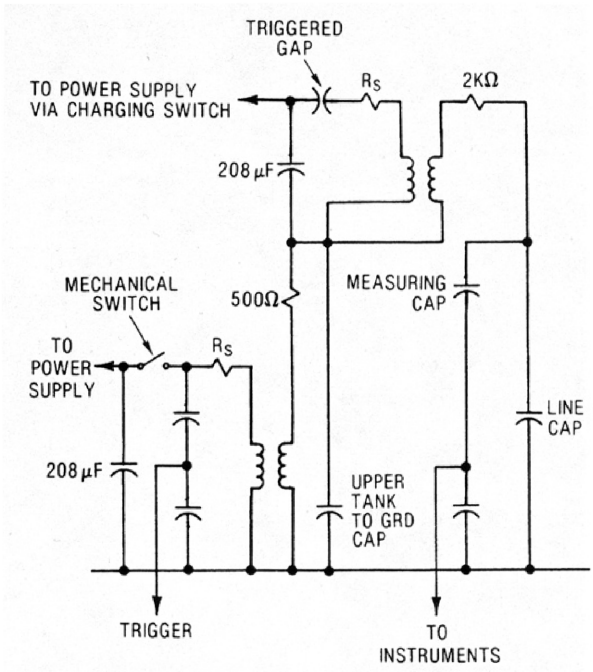


Figure 5.4-4 Schematic of a transformer-generated switching impulse testing circuit.

applied impulse is defined by its polarity (positive or negative applied between high-voltage electrode and ground), its crest voltage, and its waveform. The waveform is defined by the time-to-crest and the time-to-half value. Most important, for switching surge design of line insulation, is the time-to-crest—actually, the time-to-crest of the equivalent double-exponential waveform described in Section 5.2. The procedure and definitions relative to phase-to-phase tests are discussed in Section 5.8.

The result of the application of a switching impulse may be either a *withstand* or a *flashover*. The insulation elements of overhead lines and substations are self-restoring—i.e., their strength is not affected by a previous flashover. Therefore, a switching impulse test may consist of a series of switching impulse applications with the same or different crest voltages, some of them resulting in withstand and some in flashover. Normally, the time-to-crest is kept constant throughout the test, and the crest voltage is varied.

The crest voltage and sometimes the time-to-flashover are measured at each application. The voltage is measured using high-voltage capacitive dividers and analog or digital oscilloscopes. Calibration must be done by comparison with approved devices. Calibration can also be done using sphere gaps, which have a very well-defined strength (Gockenbach 1991). With switching impulses of positive polarity, flashovers frequently occur at random times before the crest. In presenting the results of flashover tests, the relationship of flashover probability to voltage is expressed in terms of the prospective crest value. The results of a test—i.e., the results of a series of voltage applications—are the 50% flashover voltage, V_{50}, and the standard deviation, σ. These two parameters define the strength of the test object for the time-to-crest and polarity of the applied switching impulse. The 50% flashover voltage is the prospective crest voltage of the impulse that has 50% chance of causing a flashover (and 50% chance of being withstood). The standard deviation is an important parameter that is used to define the strength at low flashover probabilities if the shape of the curve defining probability of flashover versus prospective crest voltage can be assumed Gaussian (see Section 5.9).

The test object is generally a mockup of an insulation system that may include conductors, insulator strings and associated hardware, and tower members. The final geometry must be replicated as close as possible, including the height of the conductors above ground. The walls of the laboratories must be as distant as possible in order not to affect the electric field near the high-voltage electrode and in the gap where flashover may take place. It is always preferable to perform tests on full-scale models of the line insulation systems erected outdoors. The conductor geometry

must also replicate the eventual geometry as closely as possible, although it is not necessary to use stranded conductors. The conductors must extend sufficiently on either side of the location where the flashover is expected to occur. The conductors must be terminated in a way to avoid flashovers to ground or other grounded objects from unintended locations. The high-voltage lead connecting the output of the impulse generator or the test transformers to the test objects must be placed away from the critical parts of the test object and from ground. If the test setup is not carefully designed, anomalous flashovers may occur during switching impulse tests with positive polarity (see Section 5.6.6).

All the parameters that affect the strength must be carefully defined and measured. These include: gap geometry and in particular the dimensions of the high-voltage electrodes and the gap length, temperature, air pressure, humidity, and precipitation. Often the results of a test are modified by applying weather correction factors in order to obtain the strength that would have been obtained under standard atmospheric conditions (see Section 5.11).

5.4.2 Test Methods

The two significant parameters that define the results of a switching impulse test are the 50% flashover voltage, V_{50}, and the standard deviation, σ. Various practical test methods to determine one or both of these parameters with the highest possible accuracy for a given number of voltage applications have been developed (Brasca et al. 1967; Brown 1969; Carrara and Dellera 1972; IEC 60-1 1989; IEEE Std 4 1995).

Ordinary Method (Multilevel Method)

The ordinary method, used in most past switching impulse tests, consists of applying a number of impulses (e.g., 20) with the same crest value at each of a number (e.g., 5) different voltage levels in a flashover probability range from below 20% to above 80%. The flashover fraction is determined at each level and is plotted versus the voltage level on normal probability paper. Assuming that the curve describing flashover probability versus voltage is a Gaussian (see Section 5.9), a straight line is fitted to the results. An example of this procedure is shown in Figure 5.4-5. The intersection with the 50% line gives V_{50} and the standard deviation, in per unit, is given by Equation 5.4-1.

$$\sigma = \frac{V_{50} - V_{15.9}}{V_{50}} \qquad 5.4\text{-}1$$

Up and Down Method

The most efficient method for the accurate determination of V_{50} is the "up and down method": the crest voltage of each impulse is adjusted depending on the result of the previously applied impulse—namely, the voltage level is increased or decreased by a fixed step, ΔV, depending on whether the previous result was a withstand or a flashover, respectively. The first useful application is defined as the one whose result is different from that of the successive application. The impulses that are applied before the first useful application are discarded. If there are N useful impulse applications, the 50% flashover voltage is calculated averaging the crest values of all the N impulses.

Extended Up and Down Method

If the curve describing flashover probability versus voltage is considered to be Gaussian (see Section 5.9), the most efficient method for the accurate determination of σ is the "extended up and down method." This consists of the regular up and down method used to determine V_{50}, plus a special up and down method devoted to the determination of V_x, where x is a low flashover probability. In the extended up and down method, N series of M impulses with the same crest value are applied. The crest voltage of a series depends on the results of the previous series: the voltage level is increased or decreased by a fixed step, ΔV, depending on whether all the M impulses of the previous series were withstood or if at least one impulse resulted in a flashover, respectively. The standard deviation is then calculated from V_{50} and V_x. For instance: with M = 10, x = 6.7%, and

$\sigma = \frac{V_{50} - V_{6.7}}{1.5}$; with $M = 20$, $x = 3.4\%$, and $\sigma = \frac{V_{50} - V_{3.4}}{1.83}$.

Analysis of Data Using the Principle of Maximum Likelihood

The determination of V_{50} and σ can be done independently of the test method using the principle of maximum likelihood (Brown 1969; IEEE Std 4 1995). The flashover probability function, $p = f(V)$, is assumed Gaussian. The probability that a flashover occurs at the i_{th} switching impulse application is $p_i = f(V_i, V_{50}, \sigma)$, where V_i is the crest voltage of the applied impulse. The probability that a withstand occurs is $q_i = 1 - f(V_i, V_{50}, \sigma)$. The likelihood function, L_i, is equal to p_i if the result is a flashover and is

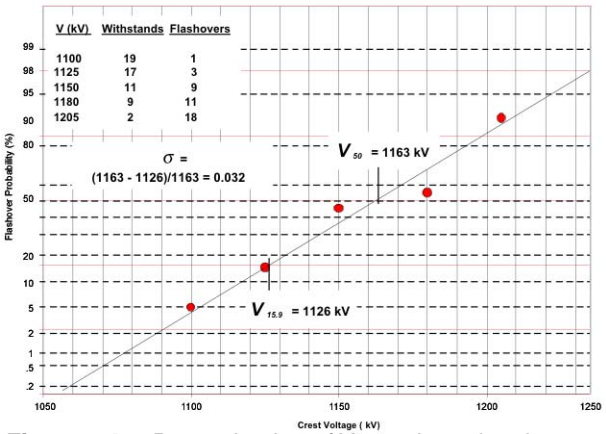


Figure 5.4-5 Determination of V_{50} and σ using the ordinary method.

equal to q_i if the result is a withstand. Given a series of N voltage applications, the likelihood of obtaining the actual results is the product of the individual likelihoods:

$$L = \prod_{i=1}^{N} L_i \qquad 5.4\text{-}2$$

The likelihood, L, is a function of the assumed values V_{50} and σ. The best estimates of the values of V_{50} and σ are those that maximize the likelihood: $L(V_{50}^*, \sigma^*) = L_{\max}$. The x% confidence interval of the estimates can be found by determining the range of values of V_{50} and σ for which the likelihood is greater than $2\frac{(100-x)}{100}L_{\max}$. For instance, the 95% confidence limits of the 50% flashover voltage are V_{50}^{lower} and V_{50}^{upper}, these limit values being such that $L(V_{50}, \sigma^*) > 0.1 \cdot L_{\max}$ for any V_{50} in the entire interval between the two limits.

Calculations of V_{50} and σ and of their confidence intervals can be done using Applet S-3, "Calculation of the 50% Flashover Voltage and Standard Deviation from a Set of Test Data". For example, the principle of maximum likelihood applied to the series of tests shown in the insert of Figure 5.4.5 gives the following results: V_{50} = 1163.4 kV (95% CI from 1151.1 to 1176.1 kV) and σ = 3.38% (95% CI from 2.42% to 5.23%). Comparison with the visual fitting of a straight line to the data points in the figure is quite favorable. The principle of maximum likelihood has the advantage of taking into account also the impulse applications at voltage levels where there were no flashovers or no withstands, whereas the visual straight-line fitting cannot utilize these data.

5.5 SWITCHING IMPULSE STRENGTH OF SIMPLE AIR GAPS

5.5.1 Rod-Plane

The switching impulse strength of air gaps depends on the geometry of the electrodes and on the polarity of the impulse. The strength of an air gap is characterized by the 50% flashover voltage, V_{50}, and by the standard deviation, σ. The lowest values of V_{50} occur for a positive polarity impulse applied to a rod protruding toward a plane. For this reason this configuration has been studied extensively for design purposes (Rohlfs et al. 1961; Udo 1965; Watanabe 1967; Paris 1967; Carrara and Zaffanella 1968; Paris and Cortina 1968; Kachler et al. 1970; Harada et al. 1970; Carrara et al. 1970; Harada et al. 1971; Barnes and Winters 1971; Carrara and Zaffanella 1972; Harada et al. 1973; Gallet et al. 1975; Suzuki and Miyake 1975; Lloyd and Zaffanella 1981; EPRI 1982; Cortina et al. 1985) and to gain an understanding of the physical mechanism of switching surge flashover (Les Renardieres Group 1972; Les Renardieres Group 1974; Baldo et al. 1975; Carrara and Thione 1976; Les Renardieres Group 1977; Rizk 1989a, 1989b, 1992). An exhaustive compilation of published data was prepared as a part of an EPRI project on live line work (Gela 1994).

The 50% flashover voltage of rod-plane gaps is a function of the time-to-crest of the impulse. For a given gap length and a given weather condition (relative air density and absolute humidity), there is a critical time-to-crest that corresponds to the lowest V_{50}. The corresponding voltage is $V_{50,crit}$. $V_{50,crit}$ is a nonlinear function of the gap length. An interpolation of available test data for rod-plane gap lengths between 1 and 23 m is expressed by the well-known "EdF equation" 5.5-1, introduced by researchers of the Electricité de France (EdF) (Gallet et al. 1975).

$$V_{50,crit,Rod-Plane} = \frac{3400}{1+\frac{8}{L}} \qquad 5.5\text{-}1$$

V_{50} is expressed in kV and the gap length, L, in m. The equation is valid for standard atmospheric conditions of relative air density, δ, and absolute humidity, h: δ = 1 and h = 11 g/m³.

Taking advantage of more available data, researchers at the Japanese laboratory CRIEPI improved the EdF formula, and developed Equation 5.5-2, which is valid for gap lengths between 1 and 25 m (Kishizima et al. 1984).

$$V_{50,crit,Rod-Plane} = 1080 \cdot \ln(0.46 \cdot L + 1) \qquad 5.5\text{-}2$$

A slightly different expression for the 50% flashover voltage of rod-plane gaps was developed on the basis of a model of continuous leader inception and breakdown of long gaps with critical times-to-crest (Rizk 1989). For gap lengths L > 4 m, the critical 50% flashover voltage of rod-plane gaps in standard atmospheric conditions is given by Equation 5.5-3.

$$V_{50,crit,Rod-Plane} = \frac{1830 + 59 \cdot L}{1+\frac{3.89}{L}} + 92 \qquad 5.5\text{-}3$$

The critical 50% flashover voltages of rod-plane obtained with Equations 5.5-1,5.5-2, and 5.5-3 are plotted versus gap spacing in Figure 5.5-1. A fundamental difference between the empirical EdF formula expressed by Equation 5.5-1 and the CRIEPI's and Rizk's Equations 5.5-2 and 5.5-3, is that the EdF formula predicts saturation of the crit-

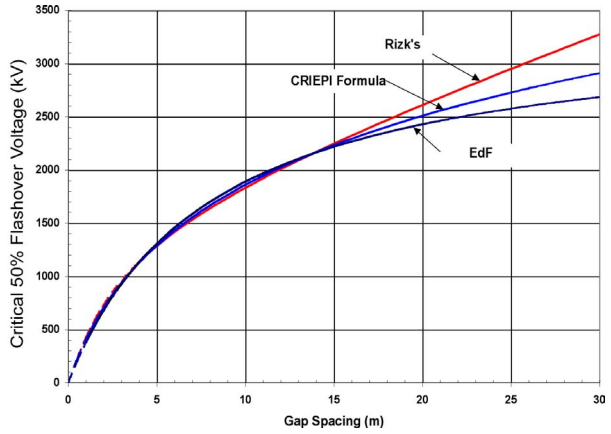


Figure 5.5-1 Critical 50% flashover voltage of rod-plane gaps versus gap length for standard atmospheric conditions.

ical 50% flashover voltage at 3400 kV. Rizk's model predicts saturation of the continuous leader inception voltage but not of the voltage drop along the leader, which will continue to increase with gap length. The differences between the critical 50% flashover voltages obtained with the three equations are small in the practical range of gap lengths but become significant for lengths greater than 17 m. The CRIEPI equation (5.5-2) has gained legitimacy from IEC, which is using it to define the gap factor of other gaps.

Rain does not affect the strength of rod-plane gaps. The effect of relative air density and absolute humidity are discussed in Section 5.11.

The critical time-to-crest is a function of gap length and humidity, as shown in Figure 5.5-2.

The standard deviation of rod-plane gaps depends on the time-to-crest. For critical times-to-crest, it is of the order of 4.5%.

5.5.2 Vertical Rod-Rod

Figure 5.5-3 shows the critical 50% flashover voltage versus gap length for different vertical rod-rod geometries characterized by different ratios between the height, H, of the grounded rod and the gap length, L. The lowest curve of Figure 5.5-3 is for rod-plane, which is a special case of rod-rod when the grounded rod height is zero. Figure 5.5-3 clearly shows the dramatic effect of geometry. As H/L is increased, the 50% flashover voltage of a given gap length increases. For positive polarity, the greatest strength is achieved by the ideal rod-rod gap, with the ground plane removed, corresponding to $H/L = \infty$. For this ideal rod-rod, the positive polarity and the negative polarity strengths coincide. This is the condition corresponding to the lowest negative polarity strength. The negative polarity strength

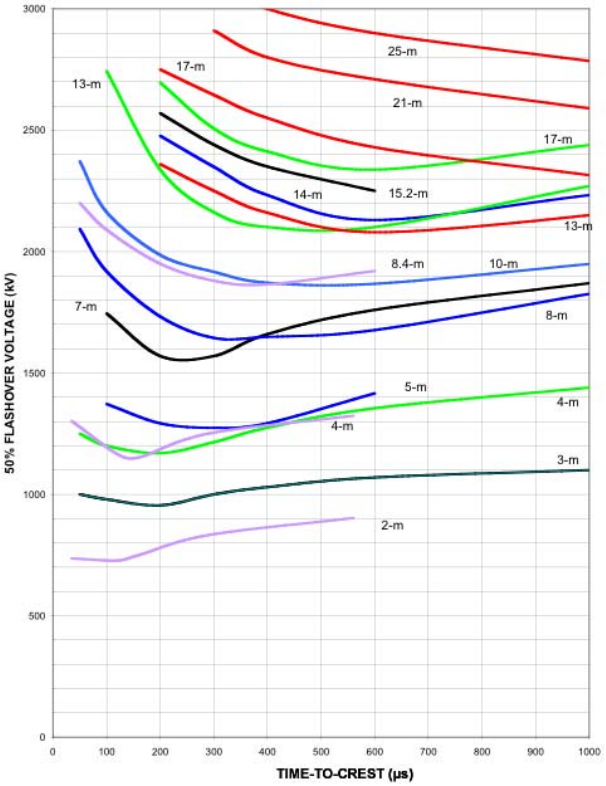


Figure 5.5-2 50% flashover voltage of rod-plane gaps versus time-to-crest. Data from CRIEPI (2, 4, and 8.4 m), Project EHV-UHV (3, 7, and 15.2 m), CESI-ENEL (4, 13, and 17 m), Renardieres (5, 8, 10, and 14 m), AEP/OB (13, 17, 21, and 25 m).

increases with decreasing H/L. The highest negative polarity strength is obtained for $H = 0$ (rod-plane).

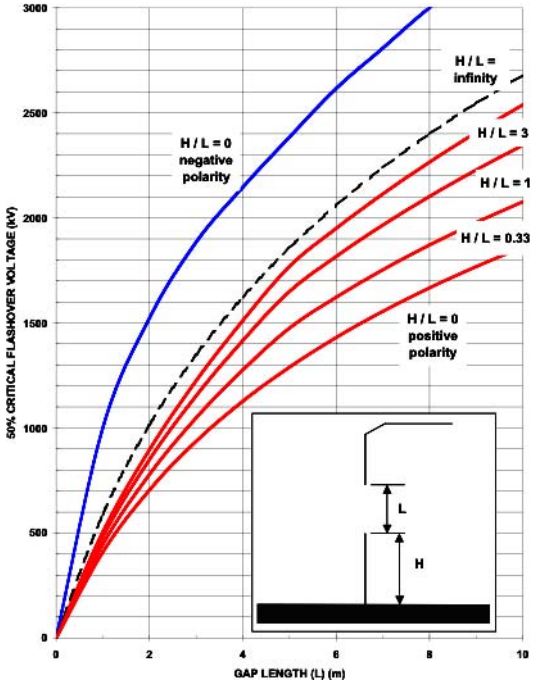


Figure 5.5-3 Critical 50% flashover voltage of vertical rod-rod gaps versus gap length.

This gap behavior demonstrates the critical importance of the positive polarity electrode and of the electric field near it. The presence of the ground plane, or of a massive structure at ground potential, enhances the electric field at the positive rod and decreases the switching impulse strength. When a negative polarity is applied to a rod-plane gap, the positive electrode is the ground plane, which has a much lower electric field. In most gap arrangements, the electric field at the energized electrode is greater than the electric field at the grounded electrode. In these cases the positive polarity switching surge strength is lower than the negative polarity strength. In some exceptional cases, however, the opposite may occur, such as, for instance, for the gap between a large bundle conductor and a tall pointed object at ground potential (conductor-rod).

The proximity effect of ground may be illustrated in another manner, as shown in Figure 5.5-4. The critical 50% flashover voltage of vertical rod-rod gaps is plotted versus the height, $H + L$, above ground of the upper rod. When the height of the rod above ground is small, less than about one-third of the total gap ($H/L \leq 0.5$), the rod has little effect on the positive polarity strength. In this case, flashovers, which start from the positive rod, may reach the ground plane, rather than the grounded rod.

5.5.3 Horizontal Rod-Rod

The critical 50% flashover voltage of horizontal rod-rod gaps is shown in Figure 5.5-5. The strength is practically independent of the height above ground, provided the height is greater than twice the gap length (Kachler et al. 1971).

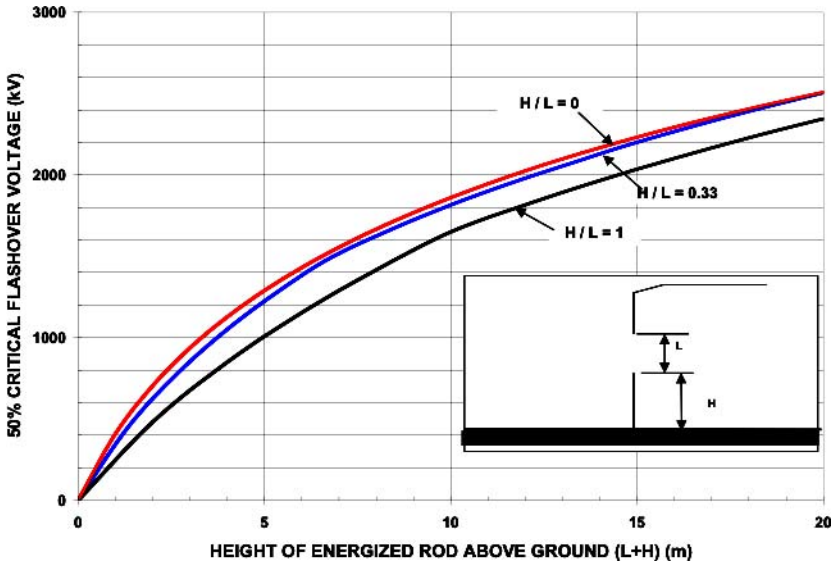


Figure 5.5-4 Critical 50% flashover voltage (positive polarity) of vertical rod-rod gaps versus height of the energized rod above ground.

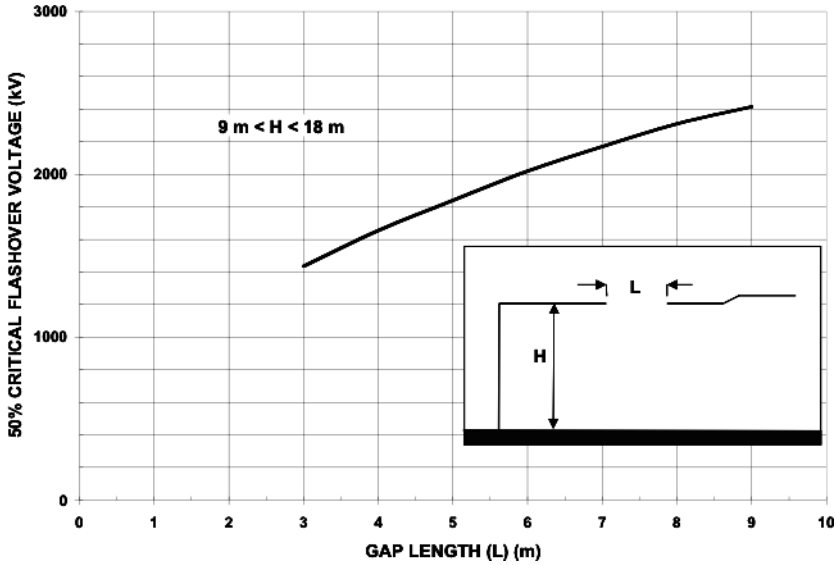


Figure 5.5-5 Critical 50% flashover voltage of horizontal rod-rod gaps versus gap length.

The horizontal rod-rod also shows a significant polarity effect, even for small gap lengths. For instance, for a height above ground of 9 m, the negative 50% flashover voltage of a 4.6 m gap was found to be 1.52 times greater than the positive, and that of a 0.9 m gap was found to be 1.28 times greater than the positive.

If the grounded electrode is a tower structure instead of a rod, the critical 50% flashover voltage may be significantly lower, by 20% or more, depending on the massiveness of the structure.

5.5.4 Sphere-Plane

The 50% flashover voltage for a 0.5-m diameter sphere-plane gap under dry conditions is shown in Figure 5.5-6 as a function of time-to-crest, for gap lengths from 1 to 5 m. For the 1-m gap, there is no dependence of the 50% flashover voltage on time-to-crest. As the gap length is increased, a more or less gradual transition occurs to U-curves. The 50% flashover voltage of sphere-plane gaps is greater or equal to that of rod-plane gaps, the difference between the two types of gap depending on the diameter of the sphere. For spheres of 0.5-m diameter, the sphere-to-plane 50% flashover voltage is twice that of the rod-plane for a 1-m gap, is about 10% greater for a 3-m gap, and is about the same for a 5-m gap.

The 50% flashover voltage for a 1-m diameter sphere-plane gap under dry conditions is shown in Figure 5.5-7 as a function of the time-to-crest. For this larger diameter sphere, the dependence of time-to-crest is not apparent up to 10-m gap lengths. The strength is always much greater than that of a rod-plane with the same gap spacing.

The critical 50% flashover voltages for rod-plane and different diameter sphere-plane gaps are compared in Figure 5.5-8. For each gap there is a critical sphere diameter, below which the sphere-plane gap has the same switching impulse strength as the rod-plane. This result has also been confirmed by physical considerations made during the study of the switching impulse flashover mechanism (Carrara and Thione 1976; Rizk 1989b). As the sphere diameter becomes larger than the critical, the U-curve that characterizes the dependence of the 50% flashover voltage on time-to-crest becomes flatter.

The data presented in Figures 5.5-6 to 5.5-8 refer to spheres with a smooth surface. Such spheres are only of theoretical interest. Practical spherical electrodes may be obtained as the envelope of many small diameter tubes. A sphere of this type with a diameter of 2.5 m has about the same strength as a smooth-surface sphere with half the diameter.

While the 50% flashover voltage of large electrodes is not much dependent on the time-to-crest when the electrodes are dry, it exhibits a significant U-curve when the electrodes are wet. For critical waveshape, rain reduces the switching impulse strength of large sphere-to-plane gaps to that of a rod-plane gap (Rizk 1976).

5.6 SWITCHING IMPULSE STRENGTH OF LINE INSULATION

5.6.1 Tower Window

The gap between conductor and tower is of great importance for tower design. The tower window, in which the tower structure completely surrounds the conductor, is generally the weakest and most important line insulation element.

Test Results

The critical 50% flashover voltage for tower window gaps is presented in Figure 5.6-1, which was derived from the work of many investigators (Rohlfs et al. 1963; Kalb 1963;

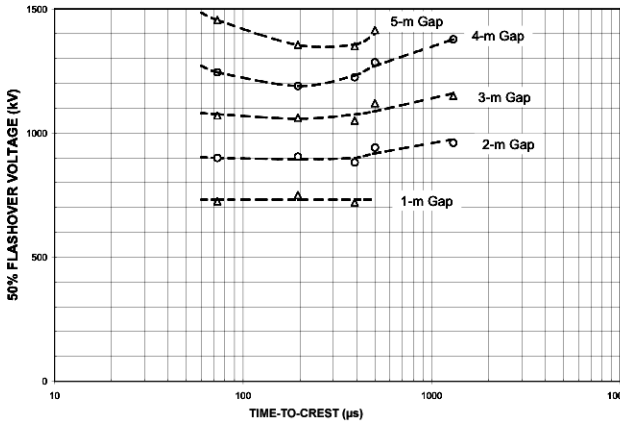


Figure 5.5-6 50% flashover voltage versus time-to-crest for 0.5-m diameter sphere-plane gaps in dry conditions.

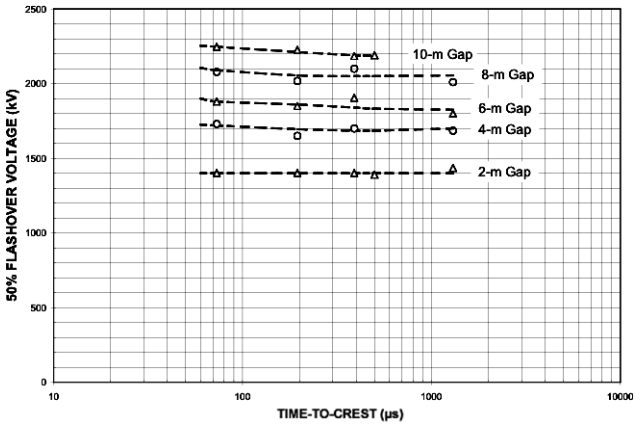


Figure 5.5-7 50% flashover voltage versus time-to-crest for 1-m diameter sphere-plane gaps in dry conditions.

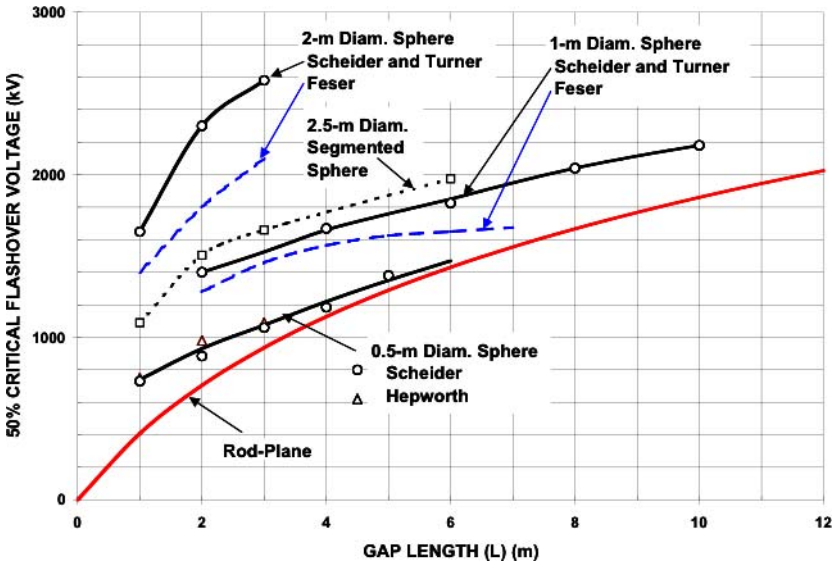


Figure 5.5-8 50% flashover voltage versus gap length for sphere-plane gaps for different sphere diameters. (Feser 1971; Hepworth et al. 1972; Schneider and Turner 1975).

Johnson et al. 1963; Rawls et al. 1964; Atwood et al. 1965; Aubin et al. 1966; Guyker et al. 1966; Armstrong and Miller 1967; Paris 1967; Saruyama et al. 1967; Hauspurg et al. 1969; Kachler et al. 1970; Dillard and Hileman 1970; Annerstrand et al. 1971; Kachler et al. 1971b; Carrara and Zaffanella 1972; Menemenlis and Harbec 1974; Pokorny and Flugum 1975; Young et al. 1980; Lloyd and Zaffanella 1981; Cortina et al. 1985; Yasui and Muruoke 1988; Kim et al. 2000).

Because test conditions (tower shape, tower width, height above ground, time-to-crest, and atmospheric conditions) were not identical, the results are quite scattered. The continuous curve of Figure 5.6-1 represents the best estimate of the results for a square window, tower width equal to 1.2 m, height of conductor above ground greater than twice the gap spacing, critical time-to-crest, relative air density = 1, and absolute humidity equal to 11 g/m^3. The test data were obtained with V-insulators with an insulator length as large as possible, so that the insulators would not affect the positive polarity switching impulse strength, in both dry and wet conditions. For comparison, Figure 5.6-1 reports the critical 50% flashover voltage curves of rod-plane (CRIEPI formula) and horizontal rod-rod gaps. The switching impulse strength of a tower window is intermediate to that of a rod-plane and a horizontal rod-rod with the same gap length.

The critical 50% flashover voltage of tower windows expressed by the continuous curve of Figure 5.6-1 may be expressed in terms of the critical 50% flashover voltage of rod-plane gaps through the gap factor, defined in Section 5.2.4. Tower windows gaps have a gap factor of approximately 1.2. The equation that fits the curve is:

$$V_{50,crit} = 1.2 \cdot \left[1080 \cdot \ln(0.46 \cdot L + 1)\right] \qquad 5.6\text{-}1$$

The height above ground of the conductor has little effect on the switching impulse strength of practical tower window gaps. In general, the critical 50% flashover voltage is minimally influenced by the conductor height above ground when the gap length is less than one-half the height.

Effect of Grading Rings

The gap spacing of a tower window gap is the minimum distance between the conductor and the tower. When there are grading rings, the continuous curve of Figure 5.6-1 still

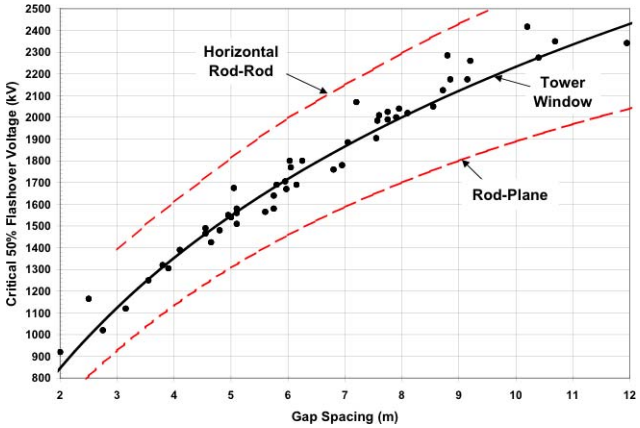


Figure 5.6-1 Critical 50% flashover voltage of tower windows. Continuous curve for square windows, tower width = 1.2 m, standard atmospheric conditions.

applies, provided that the gap length is taken as the minimum distance between the rings and the tower (Kachler et al. 1971b).

Effect of Length of V-Insulators

The effect of the length of the V-insulators, between the suspension hardware at the conductor and the hangers connected to the tower is shown in Figure 5.6-2 (Kachler et al. 1970). The data in this figure show that the critical 50% flashover voltage is reduced when the gap length across the insulators becomes less than the gap length conductor-to-tower. The insulator length is generally considerably greater than the gap length and, therefore, the presence of V-insulators does not affect the switching impulse strength.

Effect of Atmospheric Conditions

The effects of relative air density and absolute humidity are discussed in Section 5.11.

Rain does not affect the switching impulse strength of tower windows, except when the insulator length becomes comparable to, or less than, the gap length. In this case, rain and other wet weather conditions, such as fog, drizzle, wet snow, and high humidity, may, depending on the type of insulators, further reduce the switching impulse strength (see Section 5.12).

Effect of Time-to-Crest

The critical time-to-crest is a function of gap length and humidity, as for rod-plane gaps with the same gap length. The shape of the U-curve may be derived from the discussion in Section 5.10.

Standard Deviation

The standard deviation of the flashover probability function is discussed in Section 5.9.

Effect of Window Shape

The tower window shape may depart considerably from that of a square window, and its strength may be very difficult to predict. Some guidance may be obtained from test results on similar geometry or by exercising Rizk's flashover model (see Appendix 5.2 and Applet S-1). Whenever the geometry departs significantly from a simple known configuration, reliable strength data can be obtained only by performing switching impulse tests on full-scale models in an outdoor high-voltage laboratory.

The tower window results expressed by the continuous curve of Figure 5.6-1 and by Equation 5.6-1 apply to a square window, where the gaps to the top and bottom truss and to the tower legs have the same length. Tests on rectangular windows of various sizes and tower width equal to 1.2 m have shown that a variation, ΔX, in the distance to the top truss is equivalent to a variation equal to $0.6 \cdot \Delta X$ in the length of all the four gaps of a square window (Annerstrand et al. 1971). From this simple rule, it is possible to derive the correction factor to apply to the critical 50% flashover voltage of a square window in order to obtain that of a rectangular window. The correction factor is shown in Figure 5.6-3. For example, consider a rectangular window with a conductor-to-top truss gap length $X = 7$ m and conductor-to-tower leg gaps $Y = 8$ m. The 50% flashover voltage of this window is the same as that of a square window with a gap length equal to $8 - 0.6 \cdot (8 - 7) = 7.4$ m, which is equal to 1961 kV (from Equation 5.6-1). The same result is obtained from Figure 5.6-3. The correction factor for $X = 7$ m and $Y/X = 8/7 = 1.14$ is 1.03. This factor is to be applied to the critical 50% flashover voltage of a square window with a gap length $X = 7$ m, which is 1904 kV. Therefore, the critical 50% flashover voltage of the rectangular window is $1904 \cdot 1.03 = 1961$.

Effect of Conductor Size

Varying the size of the phase conductors, from single-conductor to 4-conductor bundles with a bundle diameter of 65 cm, does not significantly affect the flashover strength if the same gap length is maintained between the conductor and the tower. As the bundle diameter is increased further,

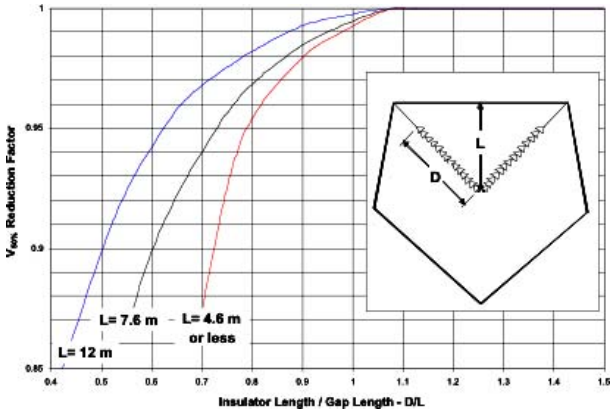


Figure 5.6-2 Effect of V-insulator length on the switching impulse strength of tower windows.

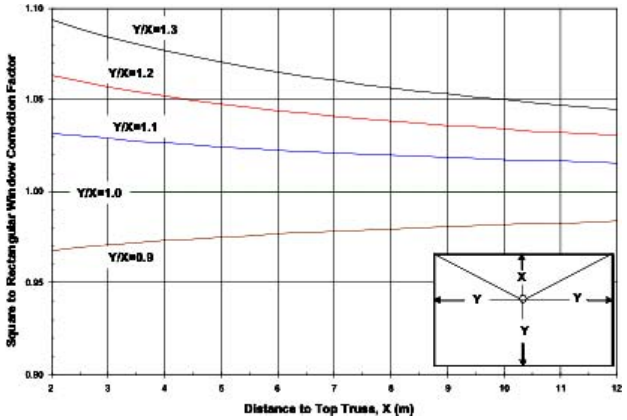


Figure 5.6-3 Voltage correction factor for rectangular window.

the strength may increase for the same gap length but remains practically constant or decreases for the same distance between the center of the bundle and the tower (Lloyd and Zaffanella 1981).

Effect of Entrance Angle

The entrance angle of the conductor to the tower face plays a role in determining the flashover path, but has only a slight effect on the critical 50% flashover voltage, as shown in the example of Figure 5.6-4 (Annerstrand et al. 1971). For instance, for an entrance angle of -7˚, the flashover voltage is only 1% lower than the maximum value, which occurs for an angle of +1.5˚. The data of Figure 5.6-4 were obtained for a tower window gap of 4.6 m; they can be tentatively applied to other gap lengths and also to outside phase gaps.

5.6.2 Outside Phase

The switching impulse strength of outside phase tower gaps with V-insulators is generally stronger than that of tower windows with the same gap length. The increase in strength depends on the geometry, particularly the dimensions of the tower arm and of the tower body and the horizontal distance to the tower body. If the outside phase conductor has the same distance to the tower arm and to the tower body, and if the tower arm and body have the same width of those of a square window, the outside phase strength is about 6% greater than that of the tower window for gap lengths less than 5 m. For gap lengths of 7 m or more, the outside phase strength is only slightly (2~3%) greater than that of the tower window.

As for the tower window, the outside phase is a complex geometry that is very difficult to predict. Some guidance may be obtained from test results on similar geometry or by exercising Rizk's flashover model (see Appendix 5.2 and Applet S-1). Whenever the geometry departs significantly from a simple known configuration, reliable strength data can be obtained only by performing switching impulse tests on full-scale models in an outdoor high-voltage laboratory.

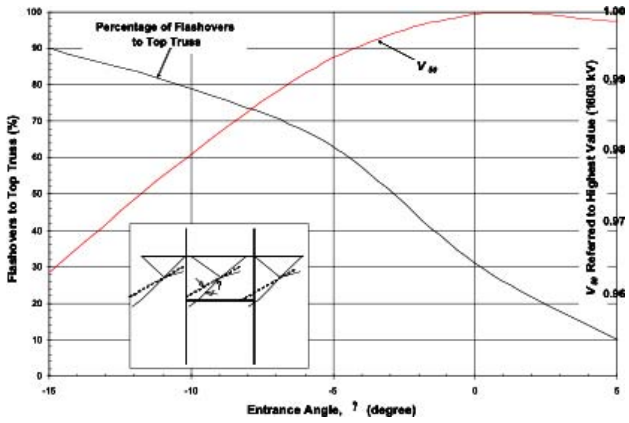


Figure 5.6-4 Percentage of flashovers to top truss and 50% flashover voltage versus entrance angle of the conductor at the tower. Data for 4.6-m tower window gap, 350-μs time-to-crest. The voltage is referred to the highest value (1603 kV).

5.6.3 Insulator Strings

Insulators affect the switching impulse strength of air gaps differently, depending on the type of gap. For positive polarity, the strength in fair weather is the same as the strength of the gap without insulators, provided the insulators are not placed directly along the possible flashover path. For instance, V-insulators in a tower window where flashovers occur from conductor to upper truss do not affect the tower window strength.

The positive dry switching impulse strength is reduced by up to 5% when the insulators are placed along the shortest gap distance, such as vertical insulators in a tower window or in an outside phase, or horizontal insulators in a dead-end structure.

Foul weather does not affect the positive polarity strength of gaps with insulators when the insulators are not placed directly along the possible flashover path. If the insulators are placed along the possible flashover path, the switching impulse strength may be significantly reduced in wet weather conditions (rain, fog, drizzle, and high humidity). The reduction depends on the type of insulators and on the degree of contamination. In clean areas, a 5% reduction over fair weather data should be considered. In areas with very light or light contamination, the suggested reduction is 10-20% (EPRI 1982). In these areas, however, the choice of the types of insulators may be determined by consideration of power frequency strength (see Chapter 4), and antifog or other special types of insulators may be considered. For these insulators, the reduction in positive-polarity strength caused by wet weather may be assumed equal to 5%, even for light degrees of contamination.

For negative polarity, the strength in fair weather is usually much higher than the positive-polarity strength. Some exceptions occur for insulators placed between a large energized electrode and a small, grounded element, such as the insulators shown on the right side of Figure 5.6-5. For these configurations, the negative polarity switching impulse strength may be equal or lower than the positive polarity strength. The negative polarity strength is generally significantly reduced by foul weather. Of concern are the situations where the negative polarity wet switching impulse strength becomes lower than the positive polarity strength. This is the case for the two arrangements on the right side of Figure 5.6-5. The data of Figure 5.6-5 are for clean insulators. For very light or light contamination, a

10-20% reduction is suggested. In these cases, and if the switching impulse strength becomes a limiting factor in line design, the use of antifog or other special types of insulators is recommended.

5.6.4 Conductor-to-Tower Leg

The 50% flashover voltage for the horizontal air gap between a conductor and a tower leg is shown in Figure 5.6-6 for a tower width of 1.2 m and a time-to-crest of 350 μs (Kachler et al. 1971a). Empirical rules were given to obtain the 50% flashover voltage for different values of the tower width (EPRI 1982). These rules, however, are quite cumbersome and unreliable. The conductor-to-tower leg strength may be very difficult to predict for complicated geometry. Some guidance may be obtained by exercising Rizk's flashover model (see Appendix 5.2 and Applet S-1). Whenever the geometry departs significantly from a simple known configuration, reliable strength data can be obtained only by performing switching impulse tests on full-scale models in an outdoor high-voltage laboratory.

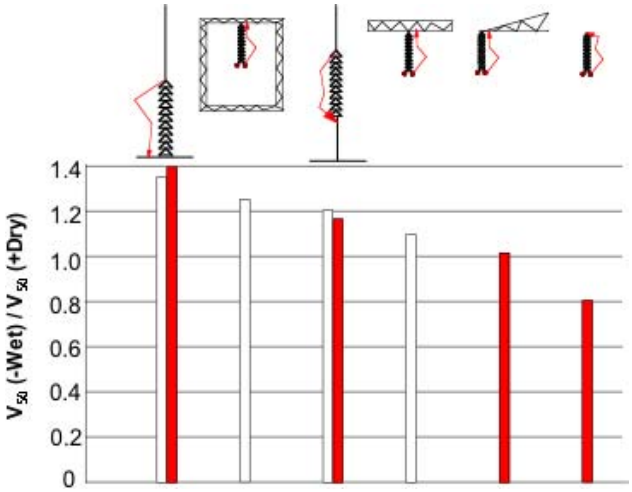


Figure 5.6-5 Ratio V_{50} (negative wet) to V_{50} (positive dry) for vertical insulator strings in different gaps.

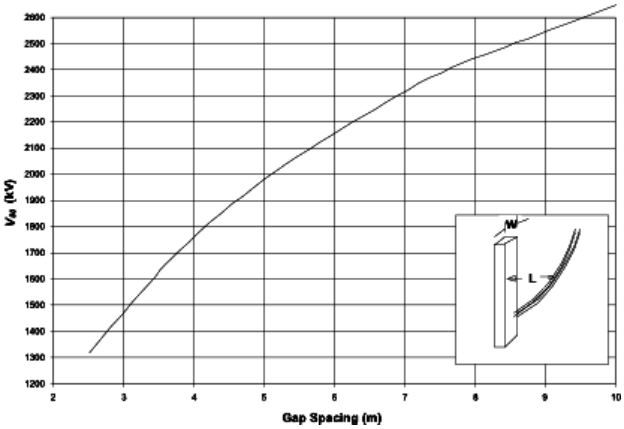


Figure 5.6-6 Switching impulse strength of conductor-to-tower gaps.

5.6.5 Conductor-to-Grounded Objects at Midspan

Minimum clearances of transmission-line conductors to ground are recommended by national standards, such as the National Electrical Safety Code in the U.S., which are based on, among other factors, the requirement that the gap between conductor and grounded objects should withstand switching surges with a high degree of reliability. Figure 5.6-7 shows the 50% flashover voltage of the gap between the conductor and the ground plane. These results were obtained with gap lengths up to 15 m and times-to-crest of 350 μs (Kachler et al. 1971a). Tests on an 11-m conductor to ground gap using one span of a test line and times-to-crest greater than 1000 μs have shown about the same results as the data obtained with 350 μs (Lloyd and Zaffanella 1981). The effect of time-to-crest on conductor-to-ground gaps, in fact, has been found much smaller than for rod-plane gaps (Gallet et al. 1976).

Figure 5.6-7 shows also the 50% flashover voltage of the gap between a conductor and a grounded structure (2.4-m wide and 15.3-m long) simulating a vehicle underneath the line (Lloyd and Zaffanella 1981).

A protrusion from the conductors, such as a broken spacer, reduces the flashover voltage only slightly, and the strength of the gap remains much higher than that of a rod-plane gap with the same length (Kachler et al. 1971a).

5.6.6 Anomalous Flashovers

During switching impulse tests with positive polarity, several investigators have noted anomalous flashovers, so called because they occurred over distances considerably longer than the gap under test. These flashovers are really not anomalous at all (Shindo and Suzuki 1995). They are caused by the breakdown characteristics of long gaps that resemble the rod-plane configuration. These flashovers occur more frequently when impulses with long times-to-

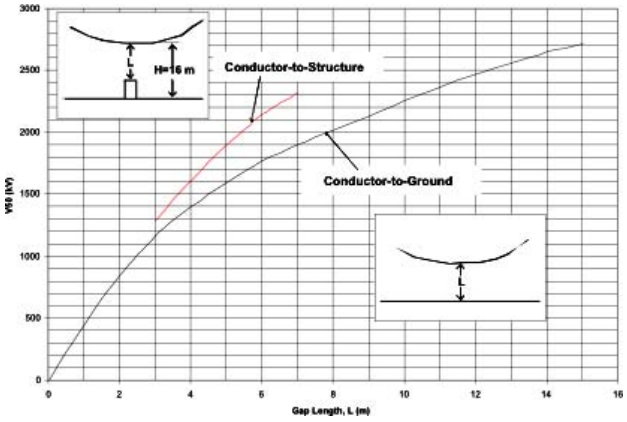


Figure 5.6-7 Switching impulse strength of conductor-to-ground and conductor-to-structure gaps.

crest are applied, because these correspond to the critical waveform for very long gaps (Lloyd and Zaffanella 1981). Because of the existence of this type of flashover, rod-plane data (Equation 5.5-1 plus some safety margin) should be used to determine the clearances between any energized part of a line (or a laboratory circuit) and grounded structures near locations where absolutely no flashover should occur.

5.7 SWITCHING IMPULSE STRENGTH OF STATION INSULATION

5.7.1 Introduction

Insulation elements of many different shapes may be encountered in a substation. Their treatment would exceed the scope of this book, which is about transmission lines. Some insulation elements such as horizontal insulator strings and station posts are encountered in a substation at the entrance of overhead lines and may be considered to also belong to the line. The switching impulse strength data for these elements are given in this section. Station posts have received the greatest attention (Killian and Moran 1964; Hertig and Kelly 1966; Moran and Alton 1968; Moran 1969; Hileman and Askins 1973; Boyd et al. 1974). For a discussion focused on station insulation, the reader may consult other work on the subject (Udo 1966; Menemenlis et al. 1981; Menemenlis et al. 1989).

5.7.2 Horizontal Insulator Strings

An important insulation element common in substations and also found at transmission strain towers is the horizontal gap containing insulator strings between the end of a conductor and the supporting tower face. Horizontal gaps in substations are generally weaker than those at transmission-line strain towers, because they may not have jumper loops, and they are generally closer to ground and to grounded structures.

The 50% flashover voltage of horizontal insulator strings is shown in Figure 5.7-1 (Boyd et al. 1974; Lloyd and Zaffanella 1981). The inset of this figure illustrates the gap geometry.

The results show the significant influence of the shield dimensions. Without a shield, the configuration approaches a rod-plane gap. The presence of large shields causes an increase in strength that is particularly large at shorter gaps. This is an effect similar to that of spheres (see Section 5.5). The effect of shields becomes smaller for larger gaps.

The 50% flashover voltage decreases as the dimensions of the grounded structure increase: the difference between a small truss (1.2 m) and a large truss (3.35 m) is of the order of 4%.

The insulators in the gap have a minor influence on the switching impulse strength, provided they cover more than two-thirds of the gap. Even with half of the gap short-circuited by a metallic connection, the 50% flashover voltage is reduced by only 10%.

5.7.3 Station Post Insulators

The positive polarity switching impulse strength of post insulators is shown in Figure 5.7-2, which summarizes results from several sources (Killian and Moran 1964; Hertig and Kelly 1966; Moran and Alton 1968; Moran 1969; Hileman and Askins 1973; Boyd et al. 1974). The data are for gap length (L) from 4.6 to 12.2 m.

The data shown in the figure are for a platform width of 1.21 m. Increasing the size, W, of the support structure to 3.7 m decreases the strength by 6% for a platform height, B, equal to the gap length, L. Decreasing W to essentially zero increases the strength by about 10% for B/L = 0.8 (Hileman and Askins 1973). Equation 5.7-1 is an empirical formula that provides correction factors (multipliers) to the V_{50} values of the curve for B/L = 1, which are valid for $0 \le W \le 3.7$ m (EPRI 1982).

$$Post\ \ Factor = 0.88 + 0.28 \cdot \frac{B}{L(W+1)} \qquad 5.7\text{-}1$$

For example, if B/L= 0.5, W = 1.22 m, and L = 7.5 m, the *Post Factor* from Equation 5.7-1 would be equal to 0.94. The V_{50} value from the curve for B/L = 1 in Figure 5.7-2 is 2275 kV. Therefore the corrected V_{50} is 2275 × 0.94 = 2139 kV.

The values reported in Figure 5.7-2 are for positive polarity switching impulses and fair-weather conditions. The values of V_{50} for positive polarity and wet weather are essentially

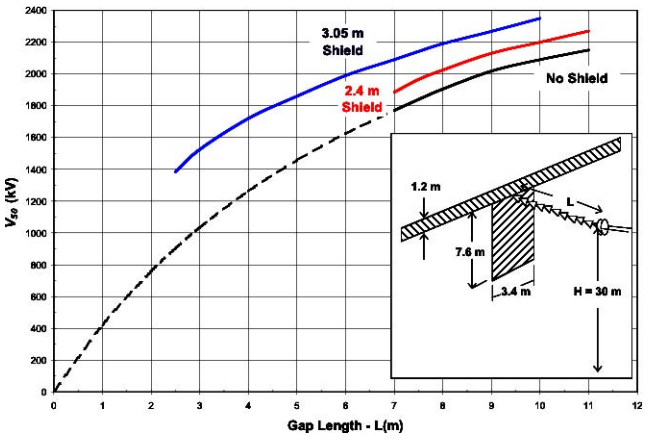


Figure 5.7-1 50% flashover voltage for horizontal insulator strings. Time-to-crest: 350 μs for no shield and 2.4-m shield, 1000 μs for 3.05-m shield.

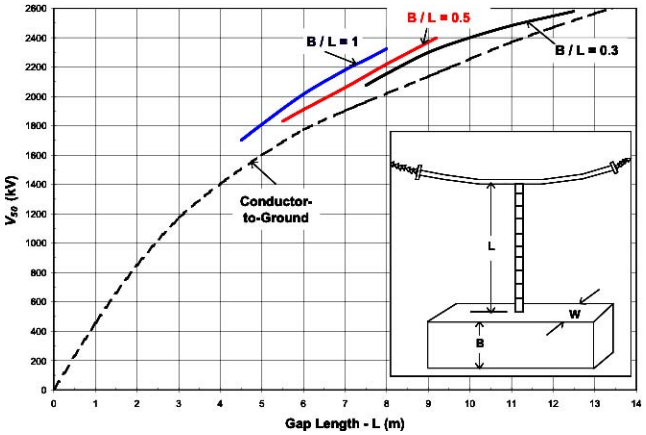


Figure 5.7-2 50% flashover voltage for post insulators for constant ratios between base height and gap length. Time-to-crest: 350 μs.

the same as those for fair weather (Boyd et al. 1974). For negative polarity, in both fair and wet weather, V_{50} is higher than for positive polarity.

5.8 PHASE-TO-PHASE SWITCHING SURGE STRENGTH

5.8.1 Introduction

A switching operation applies a stress not only to the insulation between each phase and ground or objects at ground potential, but also to the insulation between phases. The stress applied between two phases is more complex than that between one phase and ground because of the varying proportions of surges that may appear on the individual phases. For example, a positive-polarity switching surge of 2.0 per unit (i.e., twice the line-to-ground reference crest voltage) may appear on one phase simultaneously with a negative-polarity switching surge of 1.0 per unit on the adjacent phase. The phase-to-phase surge is referred to the same reference voltage as the phase-to-ground surges. The reference voltage is the peak power frequency phase-to-ground voltage immediately prior to a switching operation or to a switching cycle. In the previous example, if the two crests occur simultaneously, the amplitude of the surge between phases would be 3.0 per unit.

The strength of phase-to-phase insulation is a function not only of the surge between phases, but also of the relative proportion between the two phase-to-ground surges. In fact, the phase-to-phase insulation must be considered a system of two independently energized electrodes (the two phases) and objects at ground potential (including the ground). Actually a more accurate representation of a three-phase system should include also the third phase. For practical design purposes only two phase-to-phase insulation systems may be considered even when the system is actually three-phase. For example, the system of Figure 5.8-1 may be considered as the combination of three phase-to-ground insulations (A-G, B-G, and C-G) and two phase-to-phase insulations (A-B and B-C). The phase-to-phase insulation between electrodes A and C is not considered. It is generally assumed that the strength of the insulation between electrodes A and B does not depend on the voltage on electrode C. This is acceptable because the design of the insulation between A and B is based on the largest phase-to-phase surges occurring between A and B, V_{AB}. The voltage on C at the moment of the largest V_{AB} is generally sufficiently low to have no effect. However, this simplification is not possible for insulation systems such as that shown in Figure 5.8-2, which may be the case for some compact lines. Very little research of this case has been done.

An example of switching surges between phases is shown in Figure 5.8-3. The voltage between phases A and B, v_{AB}, is the difference between the voltage between phase A and ground, v_A, and the voltage between phase B and ground,

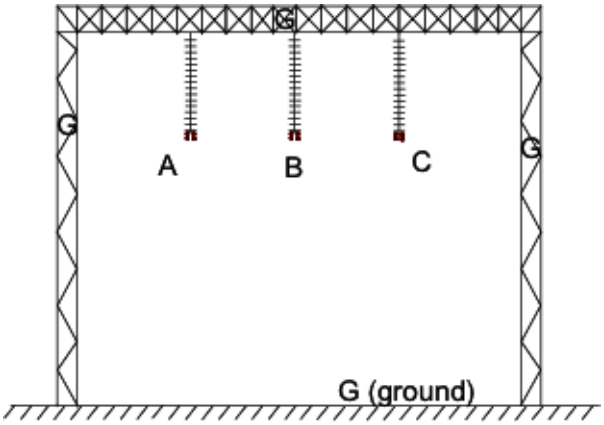


Figure 5.8-1 System of three phase-to-ground insulations (A-G, B-G, and C-G) and two phase-to-phase insulations (A-B and B-C).

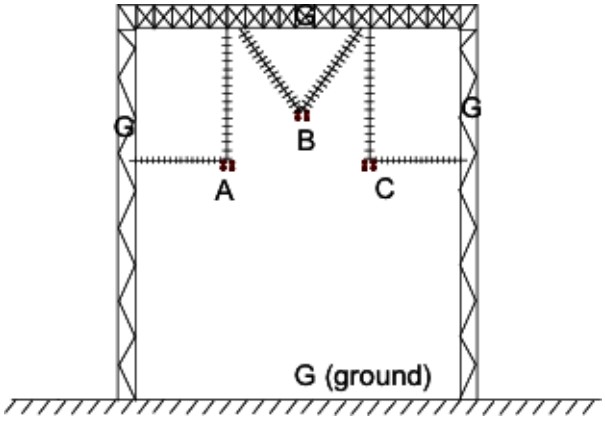


Figure 5.8-2 System of three phase-to-ground insulations (A-G, B-G, and C-G) and a complex phase-to-phase insulation system (A-B-C).

v_B. In Figure 5.8-3, at the instant of maximum phase-to-phase voltage, V_{AB}, the voltage of phase A is positive and that of phase B is negative. The parameters characterizing the phase-to-phase surge are: the crest voltages, V_A and V_B, of the phase-to-ground surges, the crest voltage, V_{AB}, of the phase-to-phase surge, the voltages to ground, V^+ and V^-, of the two phases at the instant of the maximum phase-to-phase voltage (V_{AB}), the voltage, v^-, on the negative phase at the instant of the maximum positive surge (V_A), the interval, ΔT, between the negative and the positive crests, and the equivalent times-to-crest of the surges, $t_{cr,eq.,A}$, $t_{cr,eq.,B}$, and $t_{cr,eq.,AB}$, which are characterized by the times above 70%, $t_{0.7,A}$, $t_{0.7,B}$, and $t_{0.7,AB}$ ($t_{0.7} = 0.69\ t_{cr,eq.}$, see Section 5.2).

Several experimental investigations were performed to determine the effect of each of the parameters described in Figure 5.8-3. The first phase-to-phase switching impulse tests were performed applying positive and negative polarity switching impulses having the same waveshape and simultaneous crests (i.e., $\Delta T = 0$) and varying the ratio between positive and negative crests, $\alpha = V^- / V_{AB}$ (Udo 1966a; Zaffanella et al. 1966). Two impulse generators were used for these tests. Previous testing of phase-to-phase insulation was performed with one phase energized and the other grounded ($\alpha = 0$) (Hertig and Kelly 1966).

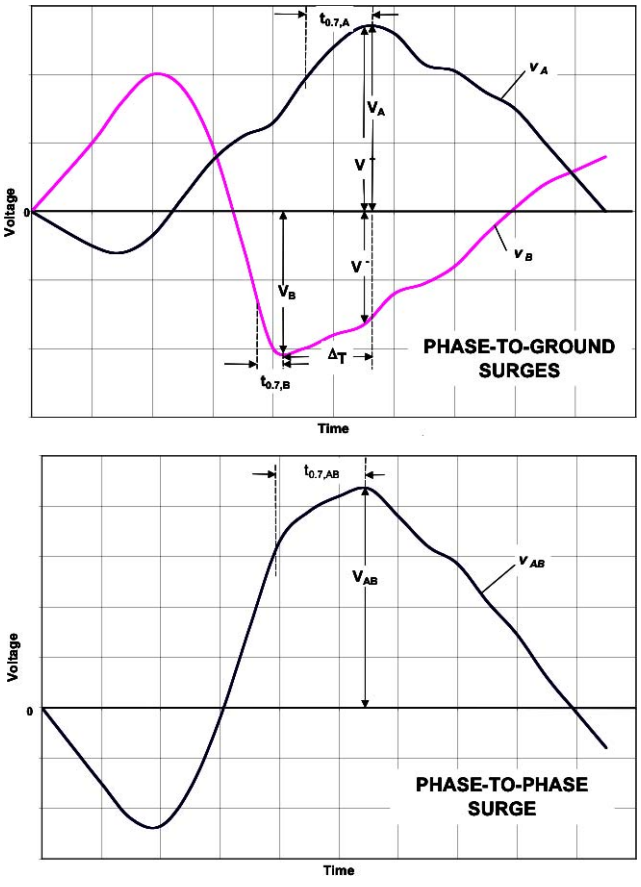


Figure 5.8-3 Example of a phase-to-phase surge.

The shape of the negative surge, which can be characterized by the time above 70%, $t_{0.7,B}$, was found to have little effect on the strength. For this reason, it is possible to test phase-to-phase insulation using an ordinary impulse generator for the positive electrode and a test transformer generating a power frequency voltage for the negative electrode (Dellera and Zaffanella, 1967), or using long-fronted transformer-generated impulses of negative polarity (Boyd et al. 1974; CIGRE 1973a).

The shape of the positive surge has a significant effect on phase-to-phase strength. Phase-to-phase tests have shown a dependence on the time-to-crest of the positive impulses characterized by u-curves that are similar to, but with a much less clearly defined minimum, those found for phase-to-ground insulation (CIGRE 1973a). Minimum phase-to-phase flashover voltages occur for times-to-crest of 50~60 μs for a 2-m rod-rod gap and 250~300 μs for a 10-m rod-rod gap. These times-to-crest are shorter than those for phase-to-ground insulation with the same gap length. Times-to-crest of 1000 μs or greater correspond to 10 to 15% greater strength. For conductor-to-conductor gaps, the effect of time-to-crest is even less pronounced.

The time interval, ΔT, between the negative and the positive surge crests has little effect on the phase-to-phase strength, if the stress is characterized by the maximum phase-to-phase voltage, V_{AB}, and by the positive and negative voltages, V^+ and V^-, of the two phases at the instant of the maximum phase-to-phase voltage (Boyd et al. 1974). On the other hand, if the stress is characterized by the sum, $V_A + V_B$, of the absolute values of the two crest values of the phase-to-ground surges, the influence of ΔT becomes significant. The minimum strength is reached for $\Delta T = 0$, in which case V_{AB} coincides with $V_A + V_B$ (CIGRE 1973a). The highest phase-to-phase voltage stresses recorded during system studies occur when the positive and negative peaks are synchronized (Cortina et al. 1970). The effect of ΔT, therefore, has mainly a theoretical value (Menemenlis et al. 1976; Koszaluk et al. 1981).

When switching surges between phases are being recorded using either a TNA or digital methods, only the highest peak value of a surge between phases is considered. Subsequent peaks occurring during the same switching event, even if they have about the same magnitude, do not constitute a greater stress and are not taken into account (CIGRE 1979b).

When both phase-to-ground surges are positive, or both are negative, the phase-to-phase voltages do not achieve sufficiently high values to be of concern.

The preceding observations justify the use of considerable simplifications in reproducing the switching surge stress between phases using switching impulses in the laboratory. The surge described in Figure 5.8-3 can be reproduced with the impulses shown in Figure 5.8-4. The strength is a function of the crest value of the phase-to-phase voltage $V_{p\text{-}p} = V^+ + V^-$, of the ratio $\alpha = V^-/ V_{p\text{-}p}$, and of the time-to-crest of the positive waveform. The results of laboratory tests on phase-to-phase insulation systems will be described in terms of these parameters.

5.8.2 Phase-to-Phase Strength for a Horizontal Rod-Rod

The horizontal rod-rod configuration is the geometry most tested to study the strength of phase-to-phase insulation (Udo 1966; Zaffanella et al. 1966; Dellera and Zaffanella 1967; Sforzini and Taschini 1970; CIGRE 1973a; Gallet et al. 1978). The rod-rod configuration has the advantage of being symmetric with respect to polarity; the results do not change by changing the positive with the negative electrode. A horizontal rod-rod is characterized by two geometrical parameters: the gap length and the height above ground. The data from the technical literature are summarized in Figures 5.8-5, 5.8-6, and 5.8-7.

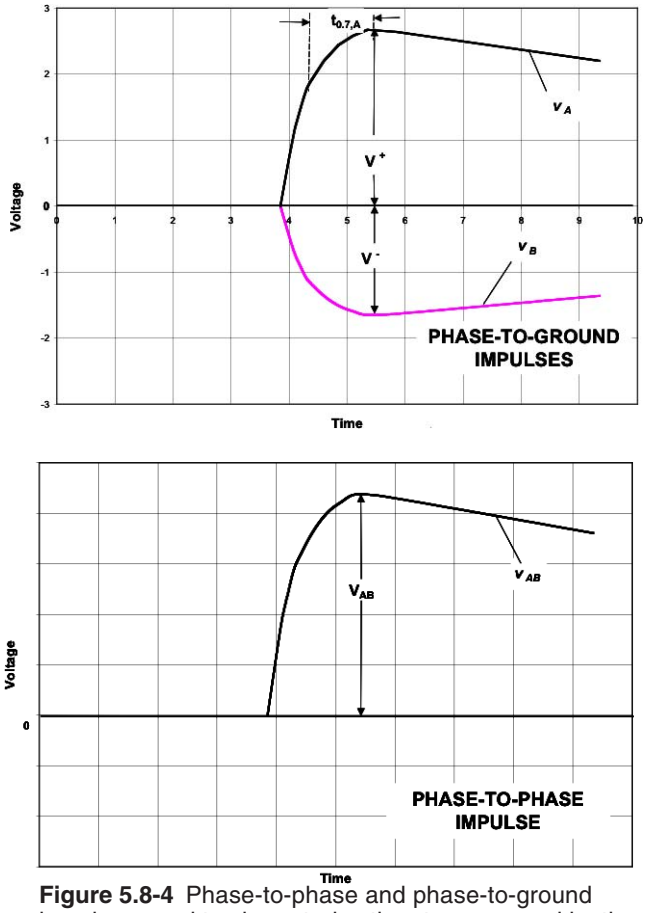


Figure 5.8-4 Phase-to-phase and phase-to-ground impulses used to characterize the stress caused by the switching surge described in Figure 5.8-3.

Figure 5.8-5 shows how the critical 50% flashover voltage varies with the parameter α. The lowest phase-to-phase flashover voltage is obtained when a positive voltage is applied to an electrode and the other is grounded. The highest flashover voltage is obtained when a negative voltage is applied to an electrode with the other grounded. The slope of the curves of Figure 5.8-5 depends on the height above ground. Ideally, for an infinitely large height, the strength of the gap is a function of the total voltage only and not of its components to ground, and the slope of the curves becomes zero.

Figure 5.8-6 shows the effect of the time-to-crest of the positive impulse.

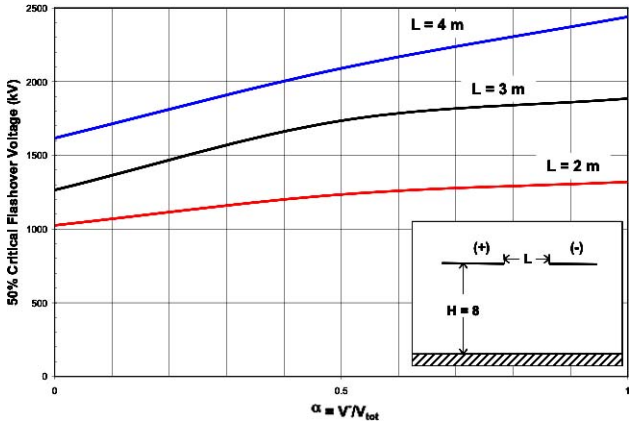


Figure 5.8-5 Phase-to-phase 50% critical flashover voltage for horizontal rod gaps. Effect of the ratio, α, between voltage applied to negative electrode and total phase-to-phase voltage.

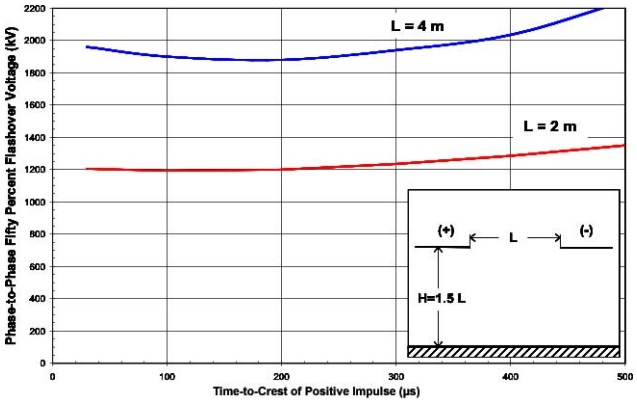


Figure 5.8-6 Effect of time-to-crest of positive impulse on phase-to-phase 50% flashover voltage. α = 0.5.

Figure 5.8-7 shows the effect of the height above ground. The curves of Figure 5.8-7 are for $\alpha = 0$ (positive polarity to a rod with the other grounded), $\alpha = 0.5$ (positive polarity to a rod and negative polarity of equal magnitude to the other), and $\alpha = 1$(negative polarity to a rod with the other grounded). The three curves will converge to the same value for an infinitely large height. For $\alpha = 0.5$, the phase-to-phase strength is only moderately affected by the height above ground.

5.8.3 Phase-to-Phase Strength of the Air Gap Between Conductors

The most important phase-to-phase insulation is the air gap between conductors. The issue is of particular importance for transmission lines because the strength decreases with increasing length of the conductors between which a surge is applied.

The technical literature reports results of tests on short sections of conductors, applicable to station insulation or to individual situations that may be encountered on a transmission line (Hertig and Kelly 1966; Cortina et al. 1970; Boyd et al. 1974; Gallet et al. 1978; CIGRE 1979b; EPRI 1982; Kishizima et al. 1984; Miyake et al. 1987). The data from the technical literature are summarized in Figures 5.8-8 and 5.8-9. The results are qualitatively similar to those obtained for horizontal rod-rod gaps.

The technical literature also reports results of tests on long sections of conductors, usually one or more spans of a test line (CIGRE 1979b; Paulson and Grant 1981; EPRI 1982; EPRI 1983; Vaisman et al. 1993). Equations 5.8-1 and 5.8-2 that give the phase-to-phase 50% flashover voltage were provided by (EPRI 1982) and (Vaisman et al. 1993), respectively. The curves corresponding to these equations are plotted in Figure 5.8-10.

$$\begin{aligned} V_{50} &= 1708 + 532\cdot(\alpha - 0.33) \\ &\quad +40.4\cdot(\alpha - 0.33)^2 \\ &\quad +269\cdot(L-4) - 9.81\cdot(L-4)^2 \\ &\quad +139\cdot(\alpha - 0.33)\cdot(L-4) \end{aligned} \qquad 5.8\text{-}1$$

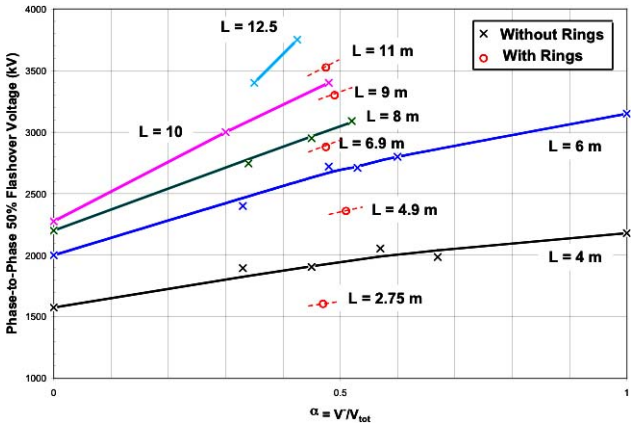


Figure 5.8-8 Phase-to-phase 50% flashover voltage conductor-to-conductor gaps. Conductor length is 12 m. Results for different gap lengths. Effect of the ratio, α, between voltage applied to negative electrode and total phase-to-phase voltage. Results for different phase-to-phase distances. Circles indicate results of tests with 2.1-m diameter toroids simulating corona rings protruding from the conductors.

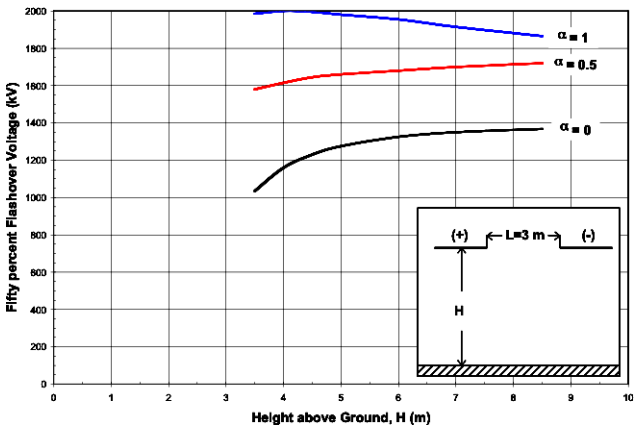


Figure 5.8-7 Effect of height above ground on phase-to-phase flashover voltage of horizontal rod-rod gap and for different values of the ratio, α, between voltage applied to negative electrode and total phase-to-phase voltage.

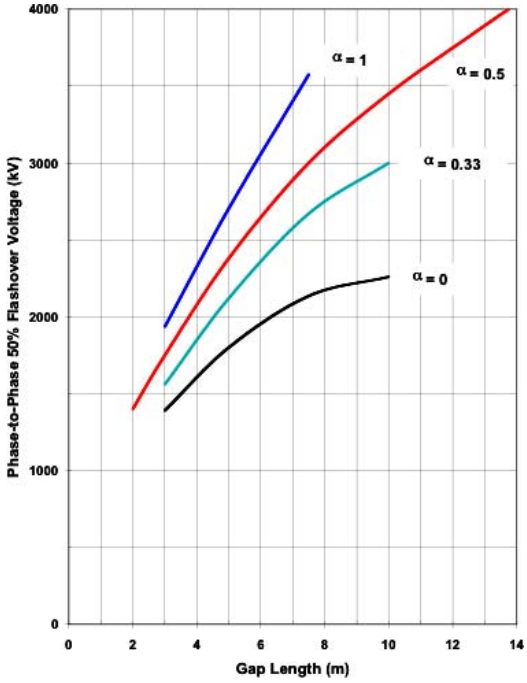


Figure 5.8-9 Phase-to-phase 50% flashover voltage of 12-m conductor sections for different phase-to-ground voltage combinations. Time-to-crest of positive impulse: 350 μs.

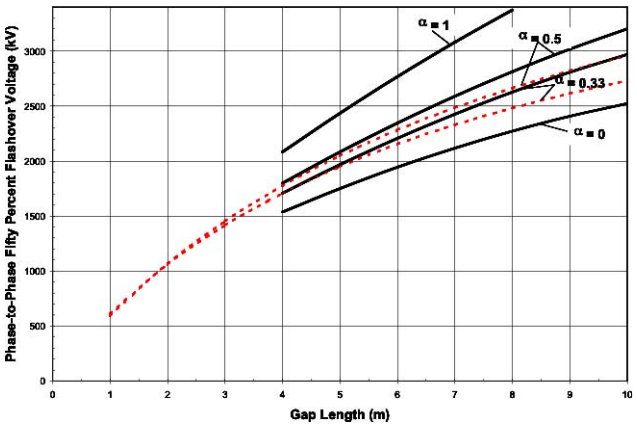


Figure 5.8-10 Conductor-to-conductor 50% flashover voltage versus gap length. Data for a 360-m span and average height above ground of 26 m. Solid curves: Equivalent time-to-crest = 1000 μs, 8-conductor bundles with subconductor diameter = 5.5 cm and bundle diameter = 1.22 m (EPRI 1982). Dashed curves: Time-to-crest = 250 μs, single and 4-conductor bundles with bundle diameter = 0.42 m (Vaisman et al. 1993).

V_{50} is in kV, L is the gap length in meters, and α is the ratio between the negative impulse crest and the phase-to-phase voltage. Data are for standard atmospheric conditions.

$$V_{50} = K_1 \cdot \left(2.17 \cdot (L/H)^{-0.15} \cdot (0.5-\alpha) + 3.24 \cdot \alpha\right) \cdot \frac{3400}{1+8/L} \qquad 5.8\text{-}2$$

V_{50} is in kV, L is the gap length in meters, α is the ratio between the negative impulse crest and the phase-to-phase voltage, H is the average height above ground, and K_1 is a correction factor for conductor length, given in Equation 5.8-3. Data are for standard atmospheric conditions.

$$K_1 = (1 - n \cdot \sigma) \quad ,$$
$$n = 0 \text{ for a conductor length, } S = 75 \text{ m}, \qquad 5.8\text{-}3$$
$$\text{otherwise } n = f(S/75)$$

σ = 0.04 for α = 0 and S= 0.033 for 0.33 ≤ α ≤ 0.5. The function $f(S/75)$ is calculated considering that a span, S, is equivalent to a number, $N_S = S/75$, of 75-m sections energized in parallel. A flashover probability of 50% for the span S corresponds to a flashover probability, p_{75}, of the 75-m section equal to $p_{75} = 1 - 0.5^{1/N_S}$. This probability corresponds to n standard deviations below the 50% value of the 75-m section. Assuming a Gaussian distribution of the flashover probability of a 75-m section, the value n can be derived from Table 5.13-1.

The curves from (EPRI 1982) and (Vaisman et al. 1993) have been plotted in Figure 5.8-10 for the same average height above ground (H = 26 m) and for the same span length (S = 360 m). The EPRI flashover data are higher because of the longer time-to-crest (1000 μs instead of 250 μs) and much larger conductors (8-conductor bundle instead of single or 4-conductor bundles).

Effect of Time-to-Crest

The critical time-to-crest for conductor-to-conductor configurations is proportional to the gap length and is approximately 25 μs per meter. For 0.33 ≤ α ≤ 0.5, the 50% flashover voltage for times-to-crest two times greater than critical is about 3.5% higher than the critical; for times-to-crest four times greater than critical, the increase is about 8%; and for times-to-crest 10 times greater than critical, the increase is about 10%.

Effect of Bundle Size

Very little (~ 1%) difference was found between a single conductor and a bundle of four conductors (Vaisman et al. 1993), as long as the gap length is intended as the minimum clearance between the phases and not as the distance between the two centers. The same conclusion was reached on the basis of theoretical considerations (Rizk 1996). It should be noted, however, that an increase in strength is reached when the conductor to which the positive impulse is applied is larger than a critical size, which is a function of the gap length (see Section 5.3 and Appendix 5.2).

The presence of an insulator string between phases does not appreciably alter the phase-to-phase switching impulse strength in fair weather, while a 5-10% reduction in wet weather should be expected.

5.8.4 Phase-to-Phase Strength of Other Insulation Geometries

The technical literature reports data on the switching impulse strength of several different types of geometrical configurations involving a phase-to-phase gap. These include data on vertical rod-rod (Udo 1966), conductor-to-conductor, stacked vertically (Kishizima et al. 1984), bus-to-orthogonal bus (Boyd et al. 1974, Menemenlis et al. 1981), ring-to-bus (Menemenlis et al. 1981), and ring-to-ring (Paris et al. 1973; CIGRE 1979).

5.8.5 Phase-to-Phase Insulation Stress

Most measurements of actual switching surge amplitudes and waveshapes have concentrated on phase-to-ground switching surges. Only a few data on phase-to-phase switching are available, as discussed in Chapter 3. The procedure outlined in Section 3.2.3 yields the 2% (S_2) and 50% (S_{50}) values of phase-to-phase surges and the standard deviation (σ_s) of the surge amplitude distribution that should be used for phase-to-phase gap length design.

5.8.6 Design of Phase-to-Phase Gap Length

Air distances to withstand phase-to-phase switching surges are designed by combining the strength data of Sections

5.8-2 to 5.8-4 with the stress data described in Section 3.2. The procedure is illustrated in the following example in which the minimum phase-to-phase distance of a 765-kV line is calculated. Assume the following conditions:

- Maximum system voltage: 800 kV.
- Stress distribution with 50% value, S = 2.47 p.u. and σ_S = 2.4 %.
- Strength: CFO data of Figure 5.8-10 for α = 0.5, continuous curve.
- Standard deviation of flashover voltage, σ_F = 3 %.
- Number of objects (spans) in parallel: 1000
- Desired probability of phase-to-phase flashover: less than one in a thousand switching operations.

The stress distribution is constructed using the maxima of the three phase-to-phase surges (A-B, B-C, and A-C). Assuming a configuration as the one shown in Figure 5.8-1, one-third of the switching operations produce maximum surges between nonadjacent phases (A-C) and are not of concern. Therefore, the flashover probability to consider is p = 1 / (1000 · 2/3) = 1/666.

The phase-to-phase flashover probability of the transmission line is a function of the strength/stress ratio defined in Section 5.13:

$$R = V_{50} / S_2 \qquad 5.8\text{-}4$$

S_2 is the statistical maximum switching surge. S_2 = 2.47 + 2 · (0.024 2.47) = 2.59.

The value of R may be determined from Figure 5.13-3. For N = 1000, σ_S = 2.4 %, and σ_F = 3 %, the value R = 1.13 is found. From Equation 5.8-4, V_{50} = 1.13 · 2.59 = 2.93 per unit. The maximum phase-to-ground voltage of an 800-kV line is $800\frac{\sqrt{2}}{\sqrt{3}}$ = 653 kV. Therefore, V_{50} = 2.93 · 653 = 1914 kV. From Figure 5.8-10 or Equation 5.8-1 for α = 0.5, the phase-to-phase distance, L = 4.4 m, is determined.

Minimum phase-to-phase distances between conductors of transmission lines were calculated using the data in Figures 3.2-5 and 3.2-6, N = 500 spans, Equation 5.8-1 for α = 0.5, and σ = 3 %. The results are shown in Table 5.8-1. The phase-to-phase distances are shown in Table 5.8-2. It is apparent that phase-to-phase distances of existing lines are very conservative. In general, corona phenomena are a more severe constraint on phase-to-phase design than switching surges.

Table 5.8-1 Expected Per-Unit Values of Statistical Maximum Phase-to-Phase Switching Surges and Required 50% Flashover Voltage

2% Phase-to-Ground Surge	2% Phase-to-Phase Surge	Standard Deviation, σ_S	σ = 3 %, N = 500, p = 1/10,000	
			R	V_{50}
(p.u.)	(p.u.)	(%)	(p.u.)	(p.u.)
1.5	2.43	10	1.255	3.05
1.75	2.77	13	1.290	3.57
2	3.1	16	1.315	4.08
2.25	3.42	19	1.340	4.58
2.5	3.75	21.5	1.36	5.10

Table 5.8-1 Minimum Distances between Conductors of Transmission Lines to Withstand Phase-to-Phase Switching Surges

Maximum System Voltage	Max (2% value) Phase-to-Ground Surge	Phase-to-Phase Distance
(kV)	(p.u.)	(m)
230	2.5	1.75
	2.25	1.54
	2.00	1.35
362	2.25	2.5
	2.00	2.1
	1.75	1.7
550	2.00	4.1
	1.75	3.3
800	2.00	7.3
	1.75	5.9
1200	2.00	16.0
	1.75	11.9
	1.5	8.9

5.9 VARIATION OF FLASHOVER PROBABILITY WITH VOLTAGE

The result of an application of a switching impulse to an external insulation system, such as the insulation between a conductor and a tower, is either a withstand or a flashover. The probability of obtaining a flashover increases with the crest voltage of the applied impulse. Laboratory tests are usually designed to derive with adequate accuracy the 50% flashover voltage, which is the crest voltage of the impulse corresponding to a probability of flashover equal to 50%. For application to line design, however, of great interest are the voltages corresponding to a very low flashover probability—i.e., a very high probability of withstand. Numerous investigations were made to determine the shape of the flashover probability distribution. Tests were performed at Project EHV (Edison Electric Institute 1968), at the CESI laboratory in Italy, and in Japan (Suzuki et al. 1969) on many identical test objects electrically connected so they would be identically stressed by an applied switching impulse. Many switching impulses of the same crest values were applied to such setups in order to determine

the voltages corresponding to extremely low probabilities of flashover. For instance, consider N equal test objects and apply M consecutive switching impulses having the same crest voltage V. If F flashovers (and M-F withstands) are obtained, the voltage V corresponds to a flashover probability equal to: $p = 1 - (1\text{-}F/M)^{1/N}$. For example, for 20 test objects and a series of 40 switching impulse applications, if only one flashover is obtained ($F = 1$), the best estimate of the flashover probability is $p = 0.00063$. By applying several series of impulses with different crest voltages, it is possible to assess the shape of the flashover probability distributions corresponding to relatively low flashover probabilities. The investigations have reached the conclusion that the flashover probability distribution in the low flashover probability region may be assumed Gaussian down to at least 4 standard deviations below the 50% flashover voltage. The assumption of a Gaussian distribution, in other words, cannot be refuted, although the actual shape of the distribution may never be known. Since the Gaussian distribution is relatively simple to express in mathematical terms, it has become normal practice to express the switching impulse strength of an object using two parameters, the 50% flashover voltage and the standard deviation, σ.

On a normal probability paper, a straight line, as shown in Figure 5.4-5, represents a Gaussian distribution. The flashover probability versus voltage can be calculated knowing the 50% flashover voltage and the standard deviation from Equations 5.13-2 to 5.13-4 and Table 5.13-1.

5.9.1 Withstand Voltage Level

With the assumption that the flashover probability distribution is Gaussian, there is no voltage level, however small, at which there is a sure withstand. This is not practical. Following the desire to define a withstand voltage level, V_{WS}, at which the probability of flashover is so low to be practically zero, the withstand voltage is defined as in Equation 5.9-1. At three standard deviations below the 50% flashover voltage, in fact, the flashover probability is less than 0.14%.

$$V_{WS} = (1 - 3\sigma) \cdot V_{50} \text{ (σ in per unit)} \qquad 5.9\text{-}1$$

5.10 EFFECT OF WAVESHAPE ON SWITCHING IMPULSE STRENGTH

The qualitative dependence of the 50% flashover voltage shown in Figure 5.2-2 cannot be easily generalized to all gap types. An attempt was made for line insulation as follows. The dependence of the switching impulse strength on the time-to-crest may be expressed by the function,

$$\frac{V_{50}}{V_{50,crit}} = f\left(\frac{T_f}{T_{f,crit}}\right)$$ where V_{50} is the 50% flashover voltage and T_f the time-to-crest of the actual wave and $V_{50,crit}$ and $T_{f,crit}$ are the corresponding values for the critical wave. A composite of data from different sources was used to derive the curve of Figure 5.10-1 (EPRI 1982; Yasui and Murooka 1988). The data for different gap factors, may be derived from those for rod-plane gaps (gap factor, $K = 1$), by considering that for the same gap length the critical time-to-crest and the increase in voltage caused by changing the time-to-crest are the same, independently of the gap factor. These considerations lead to Equation 5.10-1, which is valid for any gap factor, K.

$$\frac{V_{50}}{V_{50,crit}} = 1 + \frac{1}{K} \cdot \left[f_0\left(\frac{T_f}{T_{f,crit}}\right) - 1 \right] \qquad 5.10\text{-}1$$

f_0 applies to rod-plane ($K = 1$) and is given by the solid curve of Figure 5.10.-1.

The gap factor, K, is given by Equation 5.10-2

$$K = \frac{V_{50,crit}}{1080 \cdot \ln(0.46 \cdot L + 1)} \qquad 5.10\text{-}2$$

where L is the gap length in meters, and $V_{50,crit}$ is the critical 50% flashover voltage in kV.

The critical time-to-crest for double exponential impulses is given by Equation 5.10-3.

$$T_{f,crit} = A \cdot L + B \qquad 5.10\text{-}3$$

L is the gap length (in meters) and A and B are constants, $A = 35$ μs/m and $B = 40$ μs for $1 \le L \le 5$ m according to (Harada et al. 1973) or $A = 54$ μs/m and $B = -60$ μs for $5 \le L \le 15$ m according to (EPRI 1982). The critical time-to-crest increases significantly with increasing humidity. Equation 5.10-3 is approximately valid for standard absolute humidity (11 g/m^3).

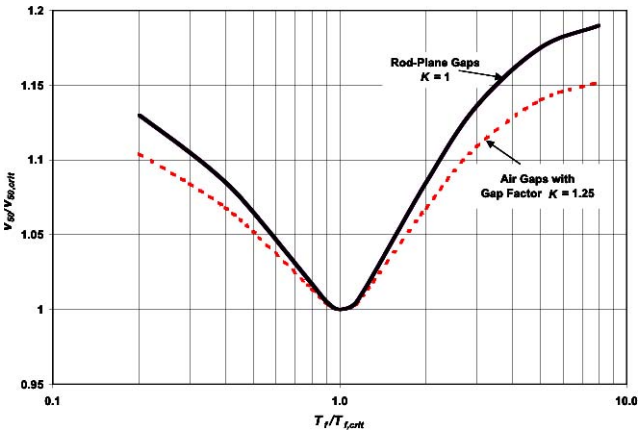


Figure 5.10-1 Influence of time-to-crest on switching impulse strength of air gaps.

5.11 EFFECT OF AIR DENSITY AND HUMIDITY ON SWITCHING IMPULSE STRENGTH: CORRECTION TO STANDARD CONDITIONS

5.11.1 Introduction

The strength of external insulation depends on the atmospheric conditions. Usually the strength increases when either the air density or the humidity increases. An exception may occur for high humidity conditions if the flashover develops close to insulator surfaces. This, however, rarely occurs for switching surges, especially those with positive polarity, which represent the most severe stress.

The effect of air density is particularly important for the design of transmission lines at high altitude, where the air density is low. In this respect, switching surges are particularly limiting because the switching impulse strength was found to decrease with altitude much more rapidly than the lightning impulse strength (Philips et al. 1967). This early finding stimulated much research based on switching impulse tests at laboratories located at different altitudes above sea level (Harada et al. 1970; Pigini et al. 1985; Ramirez et al. 1990) and based on studies of the flashover mechanism (Feser and Pigini 1987; Rizk 1992).

Although less important for switching surge design, the effect of humidity has also been the subject of experimental and theoretical studies (Kucera and Fiklik 1970; Kachler et al. 1971; Harada et al. 1971; Harada et al. 1973; Hahn et al. 1976; Busch 1978; CIGRE 1991).

5.11.2 Standard Air Density and Humidity Conditions

When high-voltage tests are performed on a specific insulation system that involves a possible flashover path in air, the air density and humidity at the time of the tests are recorded together with the test result. The result is corrected to standard atmospheric conditions—i.e., the operator calculates the value that would have been obtained for well-defined (standard) air density and humidity values. The calculations are made using correction factors derived from research or recommended by standardizing organizations (IEC 60-1 1989; IEEE Std 4 1995).

The standard atmospheric conditions are:

- Air density corresponding to a temperature, t_0, of 20°C and a pressure, b_0, of 760 mm Hg, corresponding to 101.3 kPa (1013 mbar)
- Absolute humidity, h_0, of 11 g/m^3

The air density is referred to the air density in standard conditions by using the relative air density, δ_r, which can be calculated for different temperatures, t, and pressures, b, using Equation 5.11-1.

$$\delta_r = \frac{b}{b_0} \cdot \frac{(273 + t_0)}{(273 + t)} \qquad 5.11\text{-}1$$

The absolute humidity, h, may not be directly known. Rather, the relative humidity, h_r (%), and the temperature, t, may be known. The absolute humidity may then be derived from the curves of Figure 5.11-1. When a high-voltage test is performed, the operator measures the air temperature and the temperature of a wet bulb thermometer and derives the absolute humidity using the curves of Figure 5.11-1.

5.11.3 Effect of Air Density

The effect of air density on the dielectric strength of air has long been known. It is based on Paschen law, which states that the breakdown voltage in a uniform electric field depends on the product of gas pressure and gap length. Figure 5.11-2 shows this effect for air (Loeb 1939). This figure applies to air gaps where the electric field is uniform and to very small distances. It is interesting to note that for points far to the right of the minimum, the steepness of the curve is one to one—i.e., the dc flashover strength becomes proportional to the product of gas pressure and gap length. For constant gap length, the strength is directly proportional to the air pressure, which, for constant temperature translates into a direct proportionality with δ_r. Indeed the effect of altitude on power frequency flashover strength of various types of insulators was taken into account by considering the flashover voltage proportional to the relative

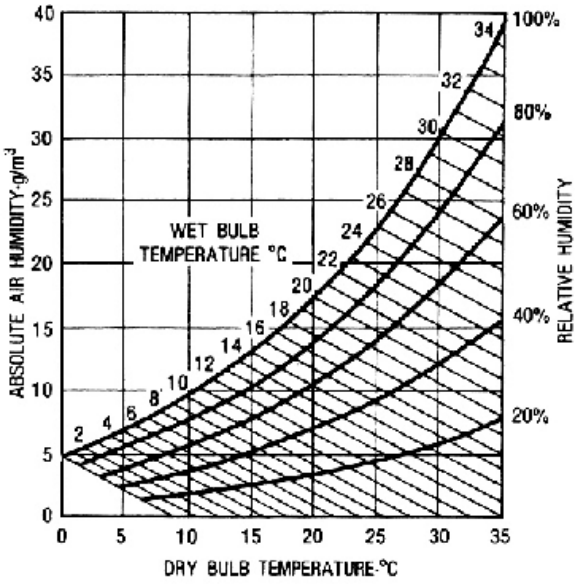


Figure 5.11-1 Absolute humidity of air as a function of relative humidity and temperature or of dry and wet bulb temperatures.

air density (Peek 1914). This behavior was confirmed for lightning impulses.

Nonlinear Air Density Effect on Switching Impulse Strength

The lightning impulse strength is proportional to the air density. A quite different behavior was found for switching impulses by different investigators who performed tests on identical gaps at two different altitudes, one close to sea level and the other at high altitude: at 3200 m at Leadville, Colorado, USA (Philips et al. 1967), at 1850 m on the top of Mount Nyugasa, Japan (Harada et al. 1970), at 1540 m at Apollo, South Africa and at 1800 m at Irapuato, Mexico (Pigini et al. 1985), and at 3000 m at Topilejo, Mexico (Ramirez et al. 1990).

Tests at different altitudes with switching impulses of positive polarity have shown that the flashover voltage is less than proportional to the air density. This effect is shown in Figure 5.11-3, which compares the curves of critical 50% flashover voltage versus gap spacing for rod-plane gaps at two different relative air densities: 1 and 0.8. For all types of air gaps, the effect of air density diminishes with increasing gap length and increasing proximity of the high-voltage electrode to ground. At the time when experimental results were available only for voltages up to about 1100 kV, it was thought possible to simplify the air density effect by applying a correction to the gap length rather than to the voltage. The effect of a reduced air density is assumed to be equivalent to a geometrical adjustment. Accordingly, two gaps with gap length in inverse proportion to the relative air density would have the same critical 50% flashover voltage (Zaffanella 1967). The dashed curve SC of Figure 5.11-3 shows that the gap length correction gives results in closer agreement to experimental result than a straight voltage correction (dashed curve VC). This gap length correction approach was recommended in the previous edition of this reference book (EPRI 1982).

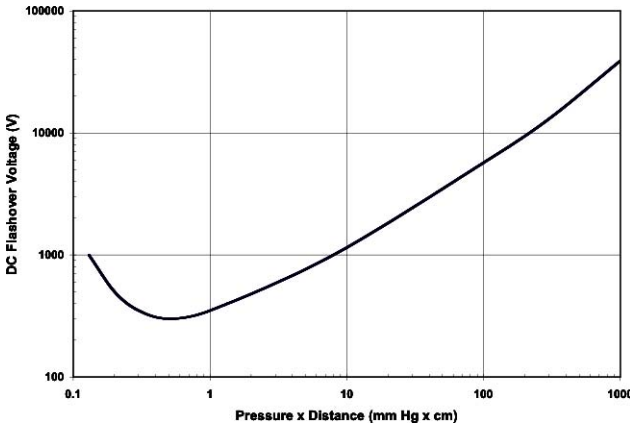


Figure 5.11-2 Dc flashover voltage as a function of pressure and spacing.

Air Density Correction Factor Recommended for High-Voltage Testing

The results of a gap length correction are not satisfactory for higher voltages, as shown by data obtained after 1967. Furthermore, a gap length correction is difficult to implement when an insulation system with given dimensions is tested. As a result, the latest IEEE standard for high-voltage testing recommends a complex procedure (IEEE Std 4 1995).

A measured 50% flashover voltage, V_{TEST}, may be converted to the value, V_{STD}, that would have been obtained under standard conditions ($\delta_r = 1$) by dividing by an air density correction factor k_δ.

$$V_{STD} = \frac{V_{TEST}}{k_\delta} = \frac{V_{TEST}}{\delta_r^n} \qquad 5.11\text{-}2$$

The exponent n is a function of the parameter G_0 given by Equation 5.11-3. The function relating n to G_0 is shown by Equation 5.11-4.

$$G_0 = \frac{V_{STD}}{500 \cdot L} \qquad 5.11\text{-}3$$

$$n = \frac{G_0(G_0 - 0.2)}{0.8} \text{ for } G_0 < 1 \qquad n = 1 \text{ for } G_0 \geq 1 \qquad 5.11\text{-}4$$

V_{STD} is in kV and must be estimated in order to calculate G_0, L is the gap length in meter.

Apart from being cumbersome, the air density correction method in the IEEE standards has serious limitations. For example, a 10-m rod-plane gap at a relative air density of 0.8 and an absolute humidity of 11 g/m^3 has a flashover voltage of 1720 kV. The parameter G_0 (from Equation

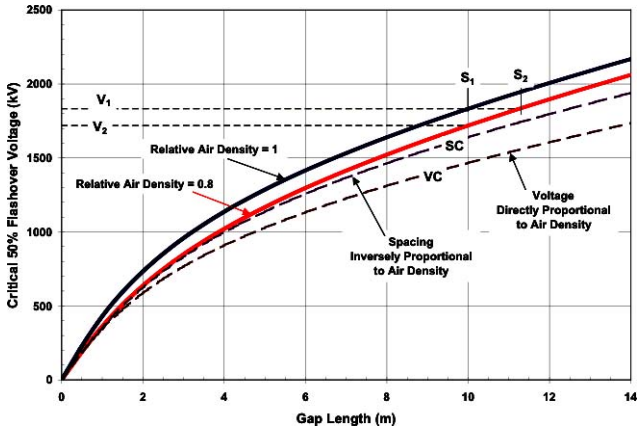


Figure 5.11-3 Critical 50% flashover voltage of rod-plane gaps. Top curve for $\delta_r = 1$. Bottom curve for $\delta_r = 0.8$.

5.11-3, using an estimated V_{STD} = 1830 kV) is equal to 0.37 and the exponent n (from Equation 5.11-4) is equal to 0.08. The correction factor is $k_1 = 0.8^{0.08} = 0.98$ and $V_{STD} = \frac{V_{TEST}}{k_1} = \frac{1720}{0.98} = 1750\,\text{kV}$. This result does not compare well with the value of flashover voltage expected for a 10-m rod plane gap at standard air density (1830 kV).

A closer value (1790 kV) is obtained applying the IEC correction factor, which is described by Equations 5.11-5 to 5.11-7.

$$G_0 = \frac{V_{STD}}{500 \cdot L \cdot [1 + (K-1)/3]} \quad 5.11\text{-}5$$

where K is the gap factor (see Table 5.13.-2) and V_{STD} must be estimated.

$$T = 1.4 \cdot \frac{1 - 0.8 \cdot G_0}{1 - 0.2 \cdot G_0} \cdot K^{1.6} \quad 5.11\text{-}6$$

$$k_\delta = \frac{0.8 \cdot [1 + T \cdot (1 - \delta_r)] \cdot (\delta_r - 0.2 \cdot G_0)}{1 - 0.2 \cdot G_0} + 0.2 \quad 5.11\text{-}7$$

Approach Based on Physical Model

An approach based on a physical model of the flashover mechanism was successfully developed and currently offers the best approach to the design of transmission lines at high altitude (Rizk 1992). The model accounts for the effect of air density on two key quantities that affect the flashover voltage: the continuous leader inception voltage and the leader length at the moment of the final jump. These parameters are described in Section 5.3 and Appendix 5.2. The effect of air density on the continuous leader inception voltage, V_{lc}, is described by Equation 5.11-8.

$$V_{lc} = \frac{V_{c\infty}}{1 + \frac{A}{\delta_r R}} \quad 5.11\text{-}8$$

$V_{c\infty}$, A, and R are parameters described in Appendix 5.2.

The leader length, l, at the moment of the final jump is:

$$l = d - \frac{V_{lc}}{\delta_r E_s} \quad 5.11\text{-}9$$

d is the gap length and E_s is the streamer gradient given by Equation 5.11-15 with h = 11 g/m^3.

The voltage drop, ΔV_l, along the leader is given by Equation 5.11-10:

$$\Delta V_l = 50 \cdot l + 37.5 \cdot \ln(8 - 7 \cdot e^{-1.33 \cdot l}) \quad 5.11\text{-}10$$

The 50% flashover voltage, V_{50}, is equal to:

$$V_{50} = \frac{V_{lc} + \Delta V_l}{1 - 3\sigma} \quad 5.11\text{-}11$$

σ is the standard deviation, which is taken as 0.05, although tests at high altitude show a tendency of the standard deviation to decrease with a decrease in air density (Philips et al. 1967; Pigini et al. 1985).

5.11.4 Effect of Humidity

The moisture content of the air has an influence on the breakdown strength of air gaps and insulators. The breakdown strength of air gaps increases with increasing humidity. This effect is caused by the tendency of water molecules to attract free electrons, thus causing an increase in the electric field necessary to cause ionization. The behavior of insulators with changing humidity is complicated by the condition of the insulator surfaces, whose conductivity depends on humidity. However, for positive polarity switching surges, which are the most limiting for insulation design, the possible flashover path develops mostly in air away from the insulator surface, and surface conductivity plays a negligible role.

The influence of humidity on positive polarity switching impulse breakdown is quite complicated. The previous edition of this reference book recommended a humidity correction factor equal to $\frac{1}{(H_0)}n$, where $1/H_0$ is the basic correction factor for short gaps, and the exponent n is equal to one for short gaps and decreases with increasing gap length. The exponent n was the same as that used for air density correction. Both H_0 and n were based on experimental data and depended on the waveform. The advancement in knowledge of the physical phenomena governing the switching impulse flashover mechanism (see Section 5.3), together with experimental data from different laboratories, has provided a more solid foundation to an improved correction procedure (CIGRE 1991).

Humidity Correction Factor Recommended for High-Voltage Testing

A measured flashover voltage may be corrected to the value that would have been obtained under standard conditions (h = 11 g/m^3) by dividing by the humidity correction factor k_h.

$$V_{STD} = \frac{V_{TEST}}{k_h} = \frac{V_{TEST}}{(K_0)^w} \quad 5.11\text{-}12$$

K_0, given by Equation 5.11-13, represents the basic correction factor applicable to short gaps. K_0 is the inverse of the factor H_0 previously employed. It must be noted that K_0 is

also a function of air density. It is expressed as a function of h/δ because an absolute humidity corresponds to a constant partial pressure of water vapor, which is independent of the changes in the partial pressure of air that occur when air density changes. This effect becomes important at high altitude

$$K_0 = 1 + 0.0095 \cdot (h / \delta_r - 11) \qquad 5.11\text{-}13$$

h is the absolute humidity expressed in g/m^3.

The exponent w is a function only of the parameter G_0 given by Equation 5.11-3, irrespective of electrode configuration and the type of stress (lightning or switching impulses). The function relating w to G_0 is shown by Equations 5.11-14.

$$\begin{aligned} &\text{For } G_0 < 1 && w = \frac{G_0 \cdot (G_0 - 0.2)}{0.8} \\ &\text{For } 1 < G_0 < 1.2 && w = 1 \\ &\text{For } 1.2 < G_0 < 2 && w = \frac{(2 - G_0)}{0.66\, G_0} \\ &\text{For } G_0 > 2 && w = 0 \end{aligned} \qquad 5.11\text{-}14$$

For $G_0 < 1$, the exponent w has the same value as the exponent n used for relative air density.

Effect of Humidity on the Physical Aspects of the Flashover Mechanism

The most significant humidity effect is the increase in streamer gradient with increasing humidity. This effect is expressed by Equation 5.11-15, which shows the effect of humidity on the breakdown of short gaps.

$$E_s = E_{s,0}(1 + 0.0095 \cdot (h / \delta_r - 11) \qquad 5.11\text{-}15$$

$E_{s,0}$ is the streamer gradient with standard humidity (h = 11 g/m^3) and relative air density (δ_r = 1). $E_{s,0}$ = 400 kV/m.

Contrary to the significant effect on streamer gradient, humidity has little effect on the gradient of the leader. The leader length becomes increasingly important as the gap length increases. This explains why humidity effects decrease with increasing gap length.

Humidity affects the net space charge injected by the first streamer corona. As humidity increases, the net space charge is reduced. This reduces the shielding effect of this space charge and facilitates the transition from streamers to leader. This phenomenon is dependent on the ratio h/δ_r. Humidity also affects the leader velocity, which increases with increasing humidity. The two effects of increasing humidity, more rapid leader formation and greater leader velocity, result in a reduction of the time from first corona to breakdown. Test results have shown that the critical

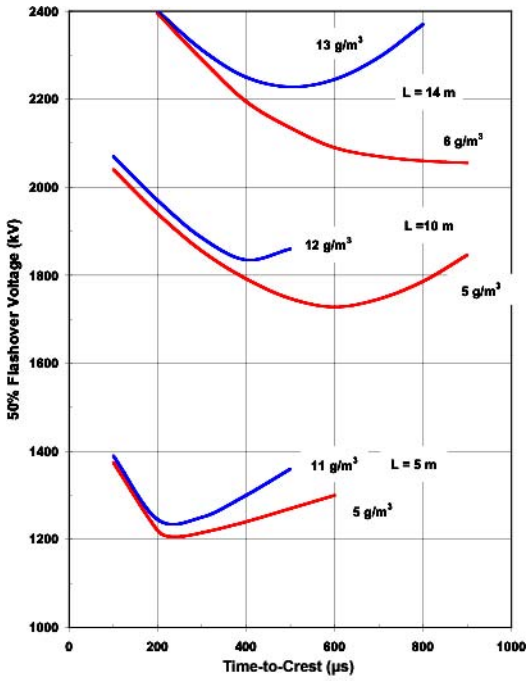


Figure 5.11-4 50% Flashover voltage of rod-plane gaps versus time-to-crest for different humidity.

time-to-crest decreases with increasing humidity (Kachler et al. 1971; Busch 1978; Aihara et al. 1983). This phenomenon is shown by the curves of Figure 5.11-4 (Busch 1978). The figure shows that different humidity effects can be found using different times-to-crest. Large humidity effects were found with waves having equivalent times-to-crest greater than 1000 µs (Lloyd and Zaffanella 1981; EPRI 1982).

5.12 EFFECT OF RAIN AND OTHER WET WEATHER CONDITIONS ON SWITCHING IMPULSE STRENGTH

5.12.1 Air Gaps and Clean Insulators

A significant amount of research has addressed the issue of how the switching impulse strength of transmission-line insulation systems is affected by rain and various types of wet-weather conditions (Udo 1966b; Armstrong and Miller 1967; Paris 1967; Malaguti and Zaffanella 1968; Paris and Cortina 1968; Hauspurg et al. 1969; Kachler et al. 1970; Kachler et al. 1971a; Kachler et al. 1971b; CIGRE 1979c; Riu et al. 1988).

Rain, drizzle, fog, snow, and any other type of precipitation do not affect the strength of air gaps. An exception occurs when the energized electrode is smooth and is larger than a critical size. The critical size is given by Equation 5.12-1 for spheres, and by Equation 5.12-2 for cylinders.

Critical radius of sphere for sphere-to-plane gaps:

$$R_c = 0.38(1 - e^{-L/L_0})(m) \quad 5.12\text{-}1$$

L is the gap length, $L_0 \approx 3.8$ m (EPRI 1982) or $L_0 \approx 5$ m (Carrara and Thione 1976)

Critical radius of cylinder for cylinder-to-plane gaps:

$$R_c = 0.0037 \cdot \ln(1 + L) \text{ (Rc and L in m)} \quad 5.12\text{-}2$$

When the energized electrode size is greater than the critical, rain, drizzle, snow, and other weather conditions that cause water drop or particle formation on the electrode surface, cause a reduction in switching impulse strength to values corresponding to electrode sizes below critical (Carrara and Thione 1976; Rizk 1978; Rizk 1989a). Efforts to improve switching surge performance by designing smooth electrodes are successful only in fair-weather conditions (Commellini 1971).

When insulators are present, the effect of wet weather depends on how much the flashover path develops along the insulator surface. For most transmission-line insulation systems, the positive polarity switching impulse strength is not affected by wet weather because flashover paths are in air away from insulators. Vertical insulator strings supporting a transmission-line conductor from a tower crossarm may be an exception, especially if the crossarm is slender. In these cases, the positive polarity flashover strength is quite high when the insulators are dry. The flashover develops close to the insulator string. When the insulators are wet, surface conductivity for some types of insulators in rain, drizzle, fog, wet snow, and even high humidity will increase significantly and will affect the flashover process. The positive polarity switching impulse strength may be reduced by a few percent, with a 5% reduction being a reasonably conservative value. The same behavior is shown by horizontal or V strings when the flashover path is along the insulators. As an approximate rule, the positive polarity strength is affected by wet weather when the gap factor of the insulator string gap is greater than 1.65. When the gap factor is 1.9, the reduction in switching impulse strength due to wetness of the insulators may reach 10%. For instance, assume that a 2-m-long insulator string is a part of an insulation system having a critical 50% flashover voltage of 1240 kV with flashovers along the insulator string. According to Equation 5.5-2, the critical 50% flashover voltage for a 2-m rod plane is 705 kV. The gap factor is 1240/705 = 1.76. The estimated reduction due to wet weather is 4.5%. The reduction depends on the type of insulators and on the insulator profile. The insulators that have a good performance in contaminated conditions under ac stress perform also better under switching surges. For instance, the switching impulse strength of insulation systems with nonceramic insulators is little affected by wet weather.

Switching impulse tests with artificial rain with the very high intensity (between 1 and 1.5 mm/min) prescribed by IEC (IEC 60-1 1989) have a poor reproducibility because of the difficulty in generating a consistent water spray and because of the random nature of the water cascading along the insulators (Riu et al. 1988).

The negative polarity strength of insulation systems with insulator strings is significantly affected by wet weather. This is consistent with the observation that negative polarity flashovers develop close to insulator surfaces. The reduction in negative polarity strength is of little concern regarding line performance, because negative polarity strength in dry conditions is generally much higher than the positive polarity strength. However, when the gap factor is high (1.8 ~ 1.9), the negative polarity wet strength may be as low as the positive polarity wet strength. It has also been observed that the reduction in negative polarity strength caused by insulator wetness increases as the time-to-crest increases. For long fronts (e.g., times-to-crest greater than 1000 μs), the negative polarity wet strength of insulator strings may be considered the same as the positive polarity wet strength.

Snow does not affect the insulation strength of insulation system, unless it succeeds in wetting the surfaces of the insulators along which flashovers may develop. This is not the case for dry snow or for wet snow and vertical or V-strings, but it may be the case for horizontal strings and wet snow. The design of insulator strings covered with ice or snow is based on power frequency voltage. Insulators designed to withstand the power frequency voltage when covered with ice or snow will also withstand switching impulses with crest values of at least 2.5 per unit (Yasui and Murooka 1988). This conclusion was reached on the basis of tests carried out in Japan (Watanabe 1978; Fujimura et al. 1979).

The standard deviation of the flashover voltage of air gaps and insulators is not affected by wet weather. The same value of 5% used for dry conditions may also be used for wet conditions.

5.12.2 Switching Impulse Strength of Contaminated Insulators

When insulators are contaminated and dry, the switching impulse strength is the same as for insulators clean and dry. When the insulator surface becomes conductive because of contamination and high humidity or fog, the switching impulse strength may be reduced (Okada and Koga 1970; Macchiaroli and Turner 1970; EPRI 1982). Insulators for

contaminated conditions are designed to withstand the power frequency voltage. If different contaminated insulators are ranked according to their behavior, the same ranking is obtained for switching surges and for power frequency (Macchiaroli and Turner 1970). Tests on strings with 10-25 standard insulator units and times-to-crest that were critical for the gaps in dry conditions have shown that the ratio of switching impulse to power frequency crest value for the same flashover probability is 1.9 to 2.5, depending on the severity of contamination and the type of insulation (Macchiaroli and Turner 1970). Tests with switching impulses having times-to-crest longer than 1000 μs applied to 4.4-m-long insulator strings have resulted in a ratio between switching impulse and power frequency crest for the same flashover probability equal to 1.7 for very light contamination and 1.2 for moderate degrees of contamination. Apparently the flashover process on contaminated insulators requires a much longer time than in air, and times to flashover are greater than 1000 μs. Therefore it would appear that serious insulation problems could occur if contaminated insulators, severe wetting conditions, and long- fronted switching surges were to occur simultaneously. The probability of simultaneous occurrence of these circumstances is very low, except perhaps for switching surges that may result from a line reclosure after a power frequency insulator flashover due to insulator contamination. In these circumstances, it may be difficult to re-energize the line. Therefore the design of insulators for contaminated conditions should be based on withstanding the power-frequency voltage (see Chapter 4).

5.13 RISK OF FAILURE OF PHASE-TO-GROUND INSULATION

5.13.1 Introduction

The behavior of transmission-line insulation when stressed by switching surges is dependent on a large number of parameters: crest value, polarity and shape of the surges, variation of the crest value of the surges along the line, number of insulation elements simultaneously stressed by the same surge, geometry of each insulation element, probability of flashover of each insulation element for each crest voltage and each waveshape, air density, humidity, rain, and wind.

The effect of these parameters and often the value of the parameters themselves are known with some degree of uncertainty. A design of transmission-line insulation based on the simultaneous occurrence of the worst estimated value of each parameter would be unnecessarily conservative. The use of statistical methods is necessary to deal with the complexity of the problem and optimize the design in an effective way (Anderson and Barthold 1964; McElroy and Charkow 1967; Barthold and Paris 1970; IEEE Std 4 1975; Kassakian and Otten 1975; Elovaara 1978; Brown 1978, Papadias 1979).

The behavior of transmission-line insulation can be defined by the *risk of failure*, which is the probability of an unwanted flashover of any insulation element of the transmission line when a switching operation that may create a voltage surge occurs.

This section discusses the determination of the risk of failure of phase-to-ground insulation. Phase-to-phase risk of failure is discussed in Section 3.2. In general, the risk of phase-to-phase failure is much lower than that of phase-to-ground.

5.13.2 Distribution of Switching Surges on Transmission Lines

Chapter 3 discusses methods to determine the distribution of switching surges on transmission lines. The amplitude and shape of a surge are determined by simulating several system conditions such as circuit breaker pole-closing characteristics, energizing versus reclosing, pre-insertion resistors, presence and behavior of surge arresters, line length, location along the line, and network configuration. By randomly varying each of the system conditions within their possible range, an infinite-sample distribution of switching surges is obtained. This distribution can be characterized by a function *F(V),* which expresses the probability that a switching surge crest voltage exceeds the value *V.*

Because of the physical nature of the system, or because of limitations caused by surge arresters, there will be a maximum switching surge level that cannot be exceeded, and the function *F(V)* will be truncated at its maximum value.

Switching Surge Amplitude and Waveshape Distribution

The switching surge amplitude distribution is characterized by the surge value, S_2, corresponding to 2% probability of occurrence, by the standard deviation, σ_s, and by the value of the probability of the truncation point (see Chapter 3). Chapter 3 discusses how the surge amplitude may vary along a transmission line and the variability of the surge waveshape, which has a significant effect on the stress applied to the line insulation (see Section 5.10).

5.13.3 Parameters Affecting Risk of Failure Caused by Switching Surges

The risk of failure of a transmission line is affected by the parameters of the surge distribution (S_2, σ_s, truncation point, variation of surge amplitude along the line, distribution of waveshapes) and by the strength characteristics of all line elements. Calculations can be performed with Applet S-2.

Vertical insulators are often free to swing because of wind. The gap between conductor and tower is reduced depend-

ing on wind speed and direction. The calculation of the swing angle is discussed in Appendix 5.1. The analysis of this situation involves also the assessment of the probability that any given swing angle will coincide with a switching surge. In general, this analysis shows that the worst stress is caused by the ever-present power frequency voltage, and that a design that avoids a flashover at power frequency in the highest expected wind conditions, would also be adequate for withstanding randomly occurring switching surges.

5.13.4 Simplified Design Procedure

A thorough design procedure requires the detailed knowledge of several parameters related to line insulation characteristics, switching surges, and weather conditions. This procedure is described in Applet S-2. A simplified procedure can be used if the following assumptions can be made:

- The switching surge amplitude distribution is considered Gaussian without a truncation point, and is defined by the statistical maximum surge (2% level), S_2, and by the standard deviation of the surge distribution, σ_s.
- The surge level is constant along the line.
- All surges are assumed to have the critical time-to-crest.
- All insulating elements have the same strength, defined by the value of V_{50}.
- The distribution of flashover probabilities is assumed Gaussian with a standard deviation, σ_F.
- There are N insulation elements per phase simultaneously subjected to a switching surge.

The probability of flashover of one insulation element subject to a surge of crest voltage, V, is expressed by Equation 5.13-1.

$$P(V) = \frac{1}{\sigma_F \sqrt{2\pi}} \int_{-\infty}^{V} e^{-\frac{1}{2}\left(\frac{x - V_{50}}{\sigma_F}\right)^2} dx \qquad 5.13\text{-}1$$

Introducing the parameter $z = \dfrac{x - V_{50}}{\sigma_F}$, Equation 5.13.1 may be written:

$$P(V) = \frac{1}{\sqrt{2\pi}} \int_{-\infty}^{Y} e^{-\frac{z^2}{2}} dz = f(Y) \qquad 5.13\text{-}2$$

$$Y = \frac{V - V_{50}}{\sigma_F} \qquad 5.13\text{-}3$$

Equation 5.13-2 expresses the flashover probability of an insulation element as a function of the number of standard deviations by which V_{50} differs from the surge crest, V. A tabulation of the probability $P(V)$ versus Y is shown in Table 5.13.1 for values of Y from 0 to –4.4. If Y is positive, the probability of flashover is greater than 0.5 and may be calculated as $1 - f(-Y)$ using the same table. For extremely low values of flashover probability ($Y < -4$), Equation 5.13-4 gives sufficiently accurate results.

$$P(V) \approx -\frac{e^{-Y^2/2}}{Y \cdot \sqrt{2\pi}} \qquad 5.13\text{-}4$$

For example, if the 50% flashover voltage of a gap is 1500 kV with a standard deviation of 5%, and a surge with a crest voltage equal to 1260 kV is applied, the flashover probability is calculated as follows: $Y = (1260 - 1500)/(0.05 \cdot 1500) = -3.2$ and, from Table 5.13-1, $P(V) = 6.87 \cdot 10^{-4}$.

The probability of flashover of one insulation element subjected to a switching surge of a given family depends on the probability of occurrence of a surge, expressed by the switching surge amplitude distribution density, $F(V)$, which expresses the probability, $F(V) \cdot dV$ that the crest value of a switching surge is between V and $V + dV$. $F(V)$ is assumed Gaussian, and is expressed by Equation 5.13-5:

$$F(V) = \frac{1}{\sigma_S \cdot \sqrt{2\pi}} \cdot e^{-\frac{1}{2}\left(\frac{V - S}{\sigma_S}\right)^2} \qquad 5.13\text{-}5$$

where $S = \dfrac{S_2}{1 + 2.05 \cdot \sigma_S}$

If a surge of the switching surge family characterized by $F(V)$ is applied to an insulation element characterized by V_{50} and σ_F, the probability of flashover can be calculated

Table 5.13-1 Flashover Probability P(V) versus the Variable Y = (V – V_{50}) / σ_F.

Y	P(V)	Y	P(V)	Y	P(V)
0	0.5	-1.5	0.0668	-3.0	0.00135
-0.1	0.460	-1.6	0.0548	-3.1	0.000968
-0.2	0.421	-1.7	0.0446	-3.2	0.000687
-0.3	0.382	-1.8	0.0359	-3.3	0.000483
-0.4	0.345	-1.9	0.0287	-3.4	0.000337
-0.5	0.309	-2.0	0.0228	-3.5	0.000233
-0.6	0.274	-2.1	0.0179	-3.6	0.000159
-0.7	0.242	-2.2	0.0139	-3.7	0.000108
-0.8	0.212	-2.3	0.0107	-3.8	0.000072
-0.9	0.184	-2.4	0.00820	-3.9	0.000048
-1.0	0.159	-2.5	0.00621	-4.0	0.000032
-1.1	0.136	-2.6	0.00446	-4.1	0.000021
-1.2	0.115	-2.7	0.00347	-4.2	0.000013
-1.3	0.0968	-2.8	0.00256	-4.3	0.000009
-1.4	0.0808	-2.9	0.00187	-4.4	0.000005

combining Equations 5.13-2 and 5.13-5, with the following result:

$$P = \frac{1}{\sqrt{2\pi}} \cdot \int_{-\infty}^{Y} e^{-\frac{z^2}{2}} dz = f(Y) \qquad 5.13\text{-}6$$

$$\text{where } Y = \frac{(S - V_{50})}{\sqrt{(\sigma_F \cdot V_{50})^2 + (\sigma_S \cdot S)^2}} \qquad 5.13\text{-}7$$

For example, assume S_2 = 1.8 p.u., σ_S = 10%, V_{50} = 2.2 p.u., and σ_F = 5%. It will be: S = 1.8 / (1+2.05 · 0.10) = 1.49 p.u. and $Y = \frac{(1.49 - 2.2)}{\sqrt{(0.05 \cdot 2.2)^2 + (0.10 \cdot 1.49)^2}} = -3.83$.

From Table 5.13-1, in correspondence to Y = -3.83, the flashover probability is $P(V) = 6.5 \cdot 10^{-5}$.

It must be noted that the surge distribution contains positive and negative surges in equal proportion, as is ordinarily the case for surge distributions derived with the TNA or with digital methods. The flashover probability derived with Equation 5.13-6 should be divided by 2, because it is assumed that negative polarity surges do not significantly stress the insulation.

The flashover probability of N identical insulation elements subjected to a switching surge of crest value, V, is given by Equation 5.13-8, which expresses the probability that at least one of the N elements will flash over.

$$P(N,V) = 1 - \left[1 - P(V)\right]^N \qquad 5.13\text{-}8$$

P*(V)* is given by Equation 5.13-1. *P(N, V)* is the stress distribution on N insulating elements. If *P(V)* is Gaussian, *P(N, V)* is not. An example of the stress distribution for a single insulation element and for a set of 100 elements is shown in Figure 5.13-1. Using the previous example with V = 1260 kV, V_{50} = 1500 kV, and σ_F = 75 kV, we obtain: $P(100, 1260\text{ kV}) = 1 - (1 - 6.5 \cdot 10^{-5})^{100} = 6.5 \cdot 10^{-3}$.

The probability of flashover of the set of 100 insulation elements becomes significant, even when the probability of flashover of a single element is negligible. Unfortunately, the accuracy with which *P(N, V)* is calculated is poor because *P(V)* is not well known at low flashover probabilities. Hence the value of σ_F and the assumption that *P(V)* is Gaussian become critical. Nevertheless, the Gaussian assumption still appears to be a good working assumption and conservative values of σ_F, 5% for a phase-to-ground insulation element and 3% for the phase-to-phase insulation of a transmission line span, are recommended.

The probability of flashover of a system of N identical insulation elements subjected to a switching surge of a given family is given by Equation 5.1-9.

$$P = \int_0^{\infty} F(V) \cdot \left\{1 - \left[1 - P(V)\right]^N\right\} \cdot dV \qquad 5.13\text{-}9$$

F(V) is given by Equation 5.13-5, and *P(V)* is given by Equation 5.13-1. When N = 1, Equation 5.13.9 becomes Equation 5.13-7.

The individual factors (stress density *F(V)* and strength of N insulation elements) appearing in the integrand of Equation 5.13-9 are plotted separately for a specific set of parameters in Figure 5.13-1. The product of the stress and strength curves, which is the integrand in the equation, is also plotted.

To facilitate the application of Equation 5.13.9, calculations were made for different combinations of the parameters N, σ_F, σ_S, and the strength to stress ratio, R defined by

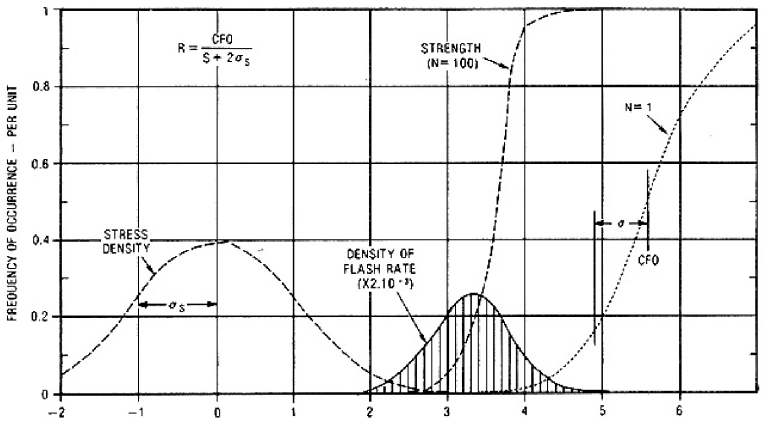


Figure 5.13-1 Stress density distribution and cumulative flashover probability (strength) distribution. Flashover rate per surge is given by the area under the flashover density distribution.

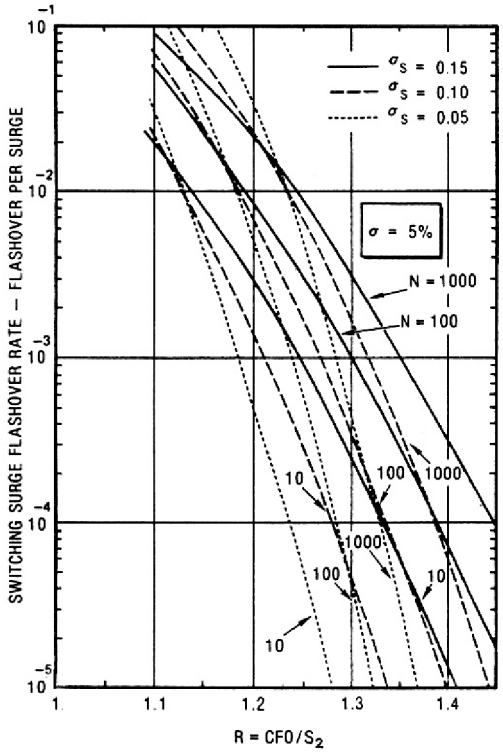


Figure 5.13-2 Flashover rate versus strength-to-stress ratio for different values of N and $\sigma_S \cdot \sigma_F$ = 5%.

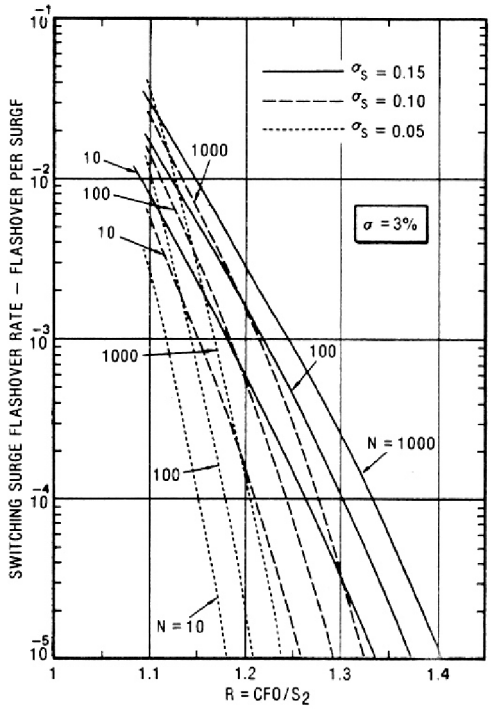


Figure 5.13-3 Flashover rate versus strength-to-stress ratio for different values of N and $\sigma_S \cdot \sigma_F$ = 3%.

Equation 5.13-10. The results are shown in Figures 5.13-2 and 5.13-3.

$$R = \frac{V_{50}}{S_2} \qquad 5.13\text{-}10$$

The use of R is justified by the common use of the statistical maximum surge to characterize the stress and by the convenient use of the 50% flashover voltage to characterize the insulation strength.

To illustrate the use of the curves of Figures 5.13-2 and 5.13-3, assume that a line with 1000 towers is subjected to switching surges having a statistical maximum S_2 of 1.75 per unit with a standard deviation σ_S of 10%. Further assume that the desired risk of failure rate is no more than one flashover every 10,000 switching operations. Ignoring the negative surges, the failure rate becomes $0.5 \cdot 10^{-4}$. Figure 5.13-2 for N = 1000, σ_F = 10%, and σ_S = 5% gives R = 1.385. Therefore, the design value of V_{50} corresponds to $1.75 \cdot 1.385 = 2.42$ per unit. For an 800-kV maximum system voltage, $V_{50} = 2.42 \cdot 800 \cdot \frac{\sqrt{2}}{\sqrt{3}} = 1580\ kV$. This is the minimum strength required by tower insulation in order to satisfy the desired failure rate requirement.

5.14 CONSIDERATION OF SWITCHING SURGES DURING LIVE-LINE MAINTENANCE

5.14.1 Introduction

The selection of tools, equipment, and work procedures for live-line maintenance are described in Chapter 13. In this section only the aspects of live-line maintenance that are affected by switching surges are discussed. Switching surges are indeed the major concern during live-line maintenance, since this is performed in fair weather when the possibility of lightning is remote, but the possibility of a switching operation exists.

Recommended minimum approach distances have been based on switching surge considerations (see Chapter 13). The insulation strength of individual live-line tools is normally estimated from the switching impulse strength of rod gaps with a safety margin. Live-line maintenance methods, however, may consist of complex tools, ladders, and lineman configurations where the critical gap distance cannot be easily defined. Furthermore, the presence of live-line tools may lower considerably the strength of an insulator string in some gap configurations. Therefore, switching surge tests are carried out for methods used on 220-kV lines and above (Reichman 1981; ESMOL 2002a).

In order to minimize the risk factor of a work method, the use of protective gaps has been promoted. These are special portable gaps that are installed on towers adjacent to that where live-line work must be carried out. These gaps are designed so that they will flashover whenever a surge of any shape exceeds a magnitude that may cause unacceptable risk at the work tower (Gela, Lux et al. 1996; ESMOL 2001).

Maintenance work can be performed with linemen at ground potential handling insulating tools or by placing linemen on the high-voltage conductor. During the transition between ground and line potential, a lineman is placed at a floating potential. This is the case of a lineman in a protective suit climbing an insulating ladder, or inside a work platform being raised to the conductor from ground, or a helicopter hovering near the conductor, or a robotic device being installed on the conductors. All these situations must be tested with switching impulses to determine the conditions leading to the lowest strength (ESMOL 2002a). Testing may be rationalized using analytical tools based on physical understanding of switching impulse flashover phenomena (Rizk 1995).

5.14.2 Minimum Number of Insulators to Withstand Switching Surges

The ability of a string of insulators to withstand a switching impulse depends on the number of defective units and their position in the string. A defective insulator is one that has lost some or all of its dielectric strength. Defective units may be shorted (all the dielectric strength is lost), broken (a portion of the porcelain or glass is missing), or punctured (with a visible hole). A healthy insulator is one that has retained all its dielectric strength.

The number and shape of the insulator units of a healthy string depend on line design criteria, such as limiting the line outage rate. Insulators either do not affect the strength of the gaps where they are placed (e.g., V-strings) or, if they do (e.g., vertical strings on an outside phase), the lowest strength occurs in wet weather. Therefore, the outage rate depends on the insulator design and on the contamination conditions of the area traversed by the line. No flashover due to healthy insulators is expected in dry conditions when live working is performed. In fact, the dry insulator performance is so much better than the wet performance that the insulator string can withstand the highest expected surge even when some insulator units are shorted.

Two methods are considered to determine the minimum number of healthy insulator units that can be accepted in a string during live line work (ESMOL 2002b). The first method is based on a formula that indicates the reduction in strength caused by defective units. The second method is a simplified approach based on an average withstand voltage of 55 kV for a single 146 mm × 254 mm (5 " × 10") insulator.

Method Based on the Reduction in Strength Due to Defective Units

The 50% flashover voltage, $V_{50,d}$, of an insulator string with N_d defective units is:

$$V_{50,d} = V_{50,0} \cdot (1 - 0.8 \frac{N_d}{N_0} \cdot k) \qquad 5.14\text{-}1$$

$V_{50,0}$ is the 50% flashover voltage with all healthy units,
N_0 is the total number of units in the string,
k is an empirical coefficient that characterizes the average dielectric strength of the defective units.

Broken glass insulators are considered shorted, therefore $k = 1$. Broken porcelain units may retain some strength; it is recommended to use $k = 0.75$, which is a conservative value.

Equation 5.14-1 assumes that the broken units are all in the worst location within the string—i.e., at the energized end of the string. The least reduction in strength occurs when the broken units are near the center of the string.

Simplified Method

The simplified method assumes that the healthy units have a withstand dielectric strength of 55 kV regardless of the insulator unit type. Tests have shown this to be a conservative value when an insulator string is subjected to switching impulses. The number of healthy units is derived by dividing the crest value (in kV) of the maximum expected surge by 55.

5.14.3 Performance of Portable Protective Gaps

Portable Protective Air Gaps (PPAG) are used as a live-line tool to control the maximum surge that can stress the insulation systems at the work site. The worker's minimum approach distance is a function of the flashover voltage of the PPAG. These devices and their use are described in Chapter 13.

PPAG are essentially rod-rod gaps that vary in length from about 0.5 to 1.04 m for applications in the range of voltages from 220 kV to 500 kV. These represent rather short gaps, where corona-starting voltage plays an important role in the flashover strength. The shape of the electrode must be carefully controlled to assure a consistent performance.

The performance of such gaps is greatly influenced by the proximity to either grounded parts or to the conductor. To assure a predictable behavior, the gap must be installed away from the conductor in a consistent way for which test data are available. In this case the lower strength is

obtained with positive polarity, which is desirable since that is the critical polarity for line insulation that is protected by the gap. The switching impulse strength depends very little on the waveshape.

5.14.4 Effect of Floating Objects

At any time a worker is in the air gap between conductor and grounded structures, he is considered a "floating object." The switching impulse flashover voltage of a gap with a floating object has been studied experimentally (Hutzler 1987) and theoretically (Rizk 1995). Because of the importance to worker safety, switching impulse tests using the exact dimensions and procedures of actual working methods should be performed. Rules governing the distance to be maintained by the worker in all the phases of the transitions between ground and conductor have been developed (ESMOL 2002a).

APPENDIX 5.1 COMPUTATION OF THE SWING ANGLE DISTRIBUTION

The calculation of the magnitude and frequency of the swing angle of free-swinging insulator strings requires information concerning wind statistics and the magnitude of the swing angle as a function of the wind velocity.

The method illustrated in this appendix was developed for switching surge performance calculations (EPRI 1982), not for mechanical design. The relation between swing angle and wind speed was derived from the results of the Hornisgrinde test project in Schwarzwald, Germany (Mors 1956a; Mors 1956b; Leibfried and Mors 1960). The wind speed distribution must be constructed on the basis of data available from stations such as those of the U.S. Weather Bureau.

Swing Angle as a Function of Wind Speed

The swing angle of free-swinging insulator strings is a function of the parameter:

$$K = \frac{D}{W} \cdot \frac{H}{V} \qquad \text{A5.1-1}$$

D is the diameter of the conductor (mm), W is the weight per unit of length of the conductor (kg/m), H is the horizontal span (m), and V is the vertical span (m).

The meaning of the parameters H and V is shown in Figure A5.1-1.

The swing angle versus the mean wind speed along the spans adjacent to the insulator strings is shown in Figure A5.1-2 for different values of the parameter K shown in Equation A5.1-1. All the curves are for single conductors. The wind is assumed normal to the line. Data for two- and four-conductor bundles show lower swing angles, especially at lower wind speed. It is conservative to use for bundles the same data as for single conductors. The curves are based on a span length of 300 m. Longer spans may have slightly lower swing angles, and shorter spans may have slightly higher swing angles. However, the difference is not significant for spans longer than 150 m. The data are based on the experience at a site with wind that is probably more uniform and has wider and longer lasting gusts than most other locations. For this reason, the data may be conservative.

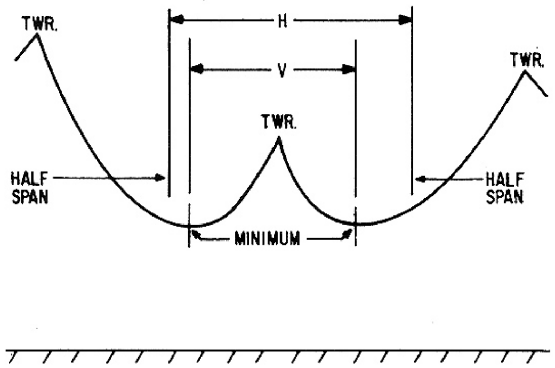


Figure A5.1-1 Illustration of the horizontal and vertical spans.

Wind Speed Statistics

Wind speed data from first-order U.S. Weather Bureau stations are housed at the National Climatic Data Center in Ashville, North Carolina. Hourly records of 2-minute-average wind speeds are available, as well as the daily peak 2-3 second gust (5-second gust for more recent records). The 2-minute hourly means may reasonably be used as hourly averages for statistical analyses. If this raw data is used for analysis, proper consideration must be made of the anemometer height and exposure, length of record, sampling error, averaging times, statistical analysis model, and height and exposure of the line under consideration.

For assessment of insulator swing angles, a recurrence interval wind speed (for example, 50-year recurrence means that the wind speed will occur every 50 years on average, or with a probability of 0.02 per year) should be used that is consistent with other design issues on the line. Recurrence interval gust wind speeds are available in ASCE 2003 (50-year nominal speeds are in maps, and tables can be used to convert to other recurrence intervals). The wind speed can be converted to a static load equivalent

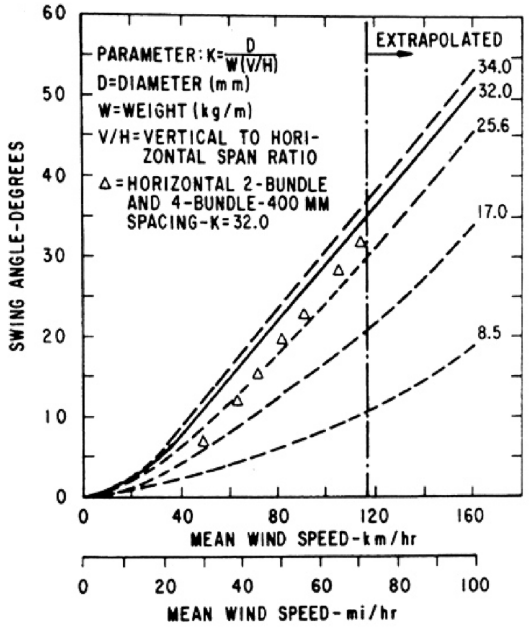


Figure A5.1-2 Swing angle as a function of mean wind speed. Curves are for single conductors. Data points for bundles of two and four conductors.

to an effective gust load for swing angle calculation using ASCE Manual of Practice (ASCE 1991). The 1991 version of this manual is based on older "fastest mile of wind" map that is obsolete. For use in this model, peak gust values from ASCE 7 can be converted to a "fastest mile" wind speed using Table A5.1-1.

Table A5.1-1 Conversion of Gust Wind Speed to Fastest Mile Wind Speed

Gust Speed (mph)	85	90	100	110	120	130	140	150	160
Fastest Mile Speed (mph)	70	75	80	90	100	110	120	130	140

APPENDIX 5.2 MODEL FOR THE CALCULATION OF SWITCHING IMPULSE STRENGTH OF AIR GAPS

Among the various models of the flashover process with positive switching impulses (see Section 5.3), the model proposed by Carrara and Thione (Carrara and Thione 1976) and later perfected by Rizk (Rizk 1989a, 1989b) appears to be the most practical and amenable to provide satisfactory results when applied to a variety of geometrical configurations. It should be emphasized that, while this model provides satisfactory results for most common situations, full-scale tests in outdoor high-voltage laboratories will provide more reliable results for an unusual situation or tower geometry and should be preferred.

The objective of the model is to calculate the critical 50% flashover voltage of air gaps with any given geometry. The model applies to positive polarity switching impulses with critical times-to-crest. It is based on the experimental observations regarding the various phases of the flashover process made by the Les Renardieres Group (Les Renardieres Group 1972, 1974, 1977, 1987).

The flashover process involves various phases: first corona, leader inception, leader propagation, and final jump (see Section 5.3). First corona is very difficult to assess; it is very dependent on the detailed shape of the high voltage electrode, and does not have a direct impact on the flashover voltage. For critical times-to-crest (corresponding to the lowest possible flashover voltage), the leader advances in the gap in a more or less straight fashion and in a continuous way (without sudden stops, dark periods, and re-illuminations) until, with a sudden final jump, the discharge reaches the grounded electrode. The initiation and propagation of the *continuous leader* are the two most important aspects of the model. Continuous leader inception appears to be dependent on the type of high-voltage electrode (for instance, conductor rather than rod), but less on the detailed shape of the electrode (conductor diameter or shape of rod tip). The model is based on the following assumptions:

1. The continuous leader starts when the streamer discharge activity at the high-voltage electrode has reached a critical stage, defined by the size and shape of the streamer space charge and by a critical electric field, E_c, at the tip of the streamers' stem, where the continuous leader initiates.
2. The stem of the streamers is assumed conductive, and its tip at the same voltage as the high-voltage electrode. The field, E_c, may be assessed assuming that the stem's tip is equivalent to a sphere with very small radius, r_{eq}, at the conductor voltage and located at a short distance from the electrode surface. The field, E_c, is then the sum of three components.

$$E_c = E_{lc} - E_a + E_b \qquad \text{A5.2-1}$$

E_{lc} is the field at the surface of the small sphere if there were no space charge; this field is proportional to the voltage and depends only on r_{eq}.

$$E_{lc} = \frac{V_{lc}}{4\pi\varepsilon r_{eq}} \qquad \text{A5.2-2}$$

E_a is the field at the surface of the small sphere caused by the space charge and by the image of the space charge in the high-voltage electrode. This field is of opposite direction to the electrostatic field, as the space charge tends to shield the streamer's stem. It is assumed that, at the critical stage, the value and location of the space charge are such that E_a is proportional to the voltage. This is a key assumption, based on experimental evidence.

$$E_a = \frac{V_a}{4\pi\varepsilon r_{eq}} = \frac{Q_0 / X}{4\pi\varepsilon r_{eq}} = \frac{c \cdot V_{lc} / X}{4\pi\varepsilon r_{eq}} \qquad \text{A5.2-3}$$

V_a is the space potential at the stem's tip caused by the space charge, Q_0, and by the image of Q_0 in the high-voltage electrode. The quantity X is a distance, function of the geometry of the high-voltage electrode, of the distribution of the space charge, and of the location of the small sphere. The parameter c, which has the dimension of capacitance, is the ratio between Q_0 and V_{lc} and will assume a certain value when the streamer discharge activity reaches the critical stage. It is not necessary to know the values of c and X, but only to realize that the electric field E_a depends only on the continuous leader inception voltage and on quantities related to the geometry of the high-voltage electrode and to the space charge at the critical stage.

E_b is the field at the surface of the small sphere caused by the image of the critical space charge in the grounded electrode. For calculating this field, the space charge may be assumed lumped at a point near the high-voltage conductor. It follows that, in addition to the small sphere

radius, E_b depends on the value of the critical space charge, and on the gap geometry.

$$E_b = \frac{V_b}{4\pi\varepsilon r_{eq}} = \frac{Q_0 / R}{4\pi\varepsilon r_{eq}} \qquad \text{A5.2-4}$$

V_b is the space potential at the stem's tip caused by the image of Q_0 in the grounded electrode. The quantity R is a distance, a function of the gap geometry. For instance, when the grounded electrode consists of the ground plane, $R = 2L$ (L is the gap length). R can be evaluated even for complex geometries of the grounded electrode, using the charge simulation method applied to 3-D configurations (Applet S-1).

3. The continuous leader inception voltage, V_{lc}, of a given air gap geometry with a given type of high-voltage electrode (conductor or rod), but a grounded electrode different from a plane is calculated by requiring that the critical electric field, E_c, at the tip of the streamers' stem is the same as that of an electrode (conductor or rod)-plane configuration with the same critical space charge: $E_c = E_{c,plane}$.

$$\begin{aligned} E_c &= E_{lc} - E_a + E_b \\ &= \frac{V_{lc}}{4\pi\varepsilon r_{eq}} - \frac{V_{lc}}{4\pi\varepsilon r_{eq}} \cdot \frac{c}{X} + \frac{Q_0}{4\pi\varepsilon r_{eq}} \cdot \frac{1}{R} \end{aligned}$$

$$\begin{aligned} E_{c,plane} &= E_{lc,plane} - E_{a,plane} + E_{b,plane} \\ &= \frac{V_{lc}}{4\pi\varepsilon r_{eq}} - \frac{V_{lc}}{4\pi\varepsilon r_{eq}} \cdot \frac{c}{X} + \frac{Q_0}{4\pi\varepsilon r_{eq}} \cdot \frac{1}{2L_{plane}} \end{aligned} \qquad \text{A5.2-5}$$

L_{plane} is the gap length of the electrode-plane configuration that produces the same continuous leader inception voltage and critical space charge. This occurs when

$$\frac{1}{R} = \frac{1}{2L_{plane}} \quad i.e. \quad L_{plane} = R/2 \qquad \text{A5.2-6}$$

Therefore, the continuous leader inception voltage of an air gap with any geometry of the grounded electrode is equal to the continuous leader inception voltage of the energized electrode-plane geometry with a gap length equal to $R/2$.

4. The continuous leader inception voltage for conductor-plane is given by Equation A5.2-7 and for rod-plane by Equation A5.2-8. The general forms of these equations were based on theoretical considerations, and the coefficients were derived from experimental data (Rizk 1989a, 1989b).

$$V_{lc} = \frac{2247}{1 + \dfrac{5.15 - 5.49 \cdot \ln(r)}{L \cdot \ln \dfrac{2L}{r}}} \text{ for conductor – plane} \qquad \text{A5.2-7}$$

$$V_{lc} = \frac{1556}{1 + \dfrac{3.89}{L}} \text{ for rod – plane} \qquad \text{A5.2-8}$$

V_{lc} is the continuous leader inception voltage in kV, L is the gap length in meters, r is the radius of the conductor in meters.

5. Equation A5.2-7 applies to cylinders with a radius smaller than a critical value, and Equation A5.2-8 applies to rods or spheres with a radius smaller than a critical value. For clean and dry electrodes with radius of curvature greater than a critical radius, the continuous leader inception voltage coincides with the first corona inception voltage. Critical radii for spheres and for cylinders are given by Equations A5.2-9 and A5.2-10, respectively. The first corona inception gradient is given by Figure A5.2-1 for cylinders and by Equation A5.2-11 for spheres.

$$R_c = 3.7 \cdot \ln(1 + L) \text{ for cylinders} \qquad \text{A5.2-9}$$

$$R_c \cdot \left(1 + \frac{0.224}{R_c^{0.37}}\right) = \frac{0.667}{1 + \dfrac{3.89}{L}} \text{ for spheres} \qquad \text{A5.2-10}$$

$$E_i = 2400\left(1 + 0.0113 / \sqrt{R} + 0.213 / \sqrt{R}\right) \text{ for spheres} \qquad \text{A5.2-11}$$

L, R_c, and R are in meters; E_i is in kV/cm

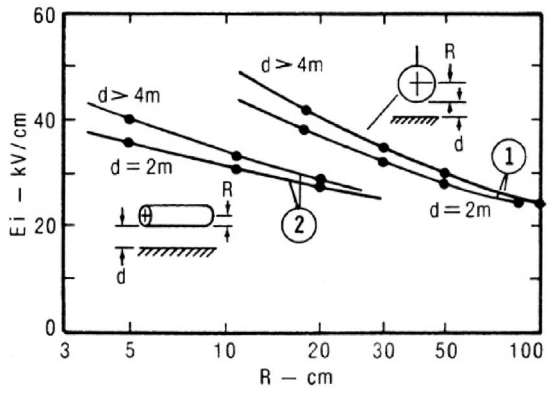


Figure A5.2-1 First corona inception gradient versus radius for cylinders.

6. The continuous leader propagates into the gap by maintaining a constant potential at its tip—i.e., the potential at the tip of the leader is always equal to the leader inception voltage, V_{lc}.
7. The continuous leader propagates toward the grounded electrode along the direction of highest electric field at a constant velocity v = 1.5 cm/μs.
8. The electric field along the continuous leader is E_i = 400 kV/m for a newly formed leader section. The electric field in a leader section decays to E_∞= 50 kV/m with a time constant θ = 50 μs (corresponding to $x_0 = v \cdot \theta$ = 75 cm of leader propagation).
9. The final jump occurs when the average electric field between the tip of the leader and the grounded electrode reaches a value, E_s = 400 kV/m when the grounded electrode is a plane or a structure and E_s = 500 kV/m when the grounded electrode is a rod.
10. The final jump occurs at great speed, and its duration may be considered zero.
11. The above criteria apply to the minimum flashover voltage, which is defined as $V_B = V_{50} / (1 + 3\sigma / 100)$. The standard deviation, σ, is taken as 3% when the high-voltage electrode is of conductor type and 5% when it is of rod type.

From items 6, 10, and 11, it is concluded that:

$$V_{50} = \frac{V_B}{1 + 3\sigma / 100} = \frac{V_{lc} + \Delta V}{1 + 3\sigma / 100} \qquad \text{A5.2-12}$$

ΔV is the voltage drop along the leader.

From items 6 and 9, the height, H, of the final jump is related to the leader inception voltage by:

$$H = \frac{V_{lc}}{E_s} \qquad \text{A5.2-13}$$

The length of the continuous leader at the instant of the final jump is:

$$L_{lc} = L - H = L - \frac{V_{lc}}{H} \qquad \text{A5.2-14}$$

Knowing the length of the continuous leader and considering items 7 and 8, Equation A5.2-15 is derived:

$$\Delta V = L_{lc} \cdot E_\infty + x_0 \cdot E_\infty \cdot \ln\left[\frac{E_i}{E_\infty} - \frac{E_i - E_\infty}{E_\infty} \cdot e^{-L_{lz} / x_0}\right] \qquad \text{A5.2-15}$$

The steps for the calculation of the 50% flashover voltage of an air gap subjected to a switching impulse of positive polarity and critical waveshape are shown in Figure A5.2-2. The calculation algorithms are implemented in Applet S-1.

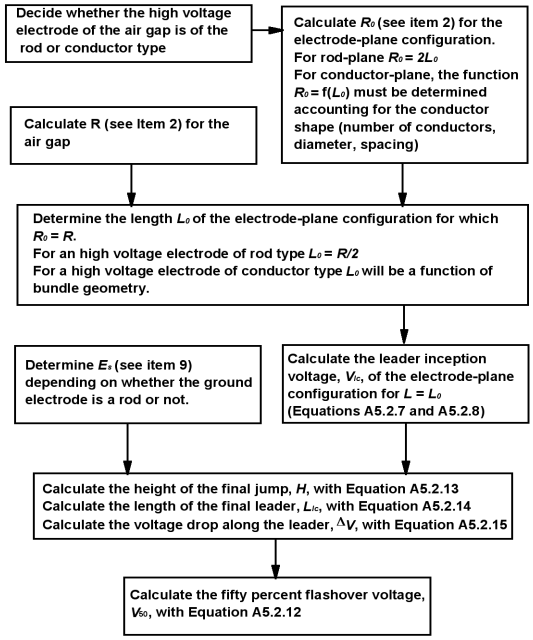


Figure A5.2-2 Steps for the calculation of the 50% flashover voltage of an air gap subjected to a switching impulse of positive polarity and critical waveshape.

REFERENCES

AIEE Committee Report. 1961. "Switching Surges: Part I, Phase-to-Ground Voltages." AIEE PAS-80. Pt. III. pp. 240-261. June.

Aihara, Y., Y.Watanabe, and I. Kishizima. 1983. "Analysis of New Phenomenon Regarding Effects of Humidity on Flashover Characteristics for Long Air Gaps." IEEE PAS-102. pp. 3778-3882.

Alexandrov, G. N. and G.V. Podporkyn. 1979. "Analysis of Experimental Data on the Electrical Strength of Long Air Gaps." IEEE PAS-98. pp. 597-605. March/April.

Alexandrov, G. N., G.V. Podporkyn, and H. Menemenlis.1980. "Further Improvement of the Critical Charge Method for the Theoretical Evaluation of the Breakdown Voltage of Conductor Bundle-to-Plane Air Gaps." IEEE PAS-99. pp. 687-694. March/April.

Alexandrov, G. N. and G.V. Podporkyn. 1982. "Control of the Electric Strength of Long Air Gaps." IEEE PAS-101. pp. 4395-4398. November.

Anderson, J.G. and L. O. Barthold. 1964. "METIFOR, A Statistical Method of Insulation Design of EHV Lines." IEEE PAS-83. pp. 271-280. March.

Annerstrand, S. A., J. J. LaForest, and L. E. Zaffanella. 1971. "Switching-Surge Design of Towers for UHV Transmission." IEEE PAS-90. pp. 1598-1603. July/August.

Armstrong, H. R. and C. J. Miller. 1967. "Insulation Characteristics of 345-kV Transmission Towers." IEEE PAS-85. pp. 666-677. June.

ASCE (American Society of Civil Engineers). 1991. *Guidelines for Electrical Transmission Line Loading.* ASCE Manuals and Report on Engineering Practice No. 74.

ASCE (American Society of Civil Engineers). 2003. *Minimum Design Loads for Buildings and Other Structures.* Chapter 6. (ASCE 7-02).

Atwood, A.W., A. R. Hileman, J. W. Skooglund, and J. F. Wittibschlager. 1965. "Switching Surge Tests on Simulated and Full-Scale EHV Tower-Insulation Systems." IEEE PAS-84. pp. 293-303. April.

Aubin, J., D. T. McGillis, and J. Parent. 1966. "Composite Insulation Strength of Hydro Quebec 735-kV Towers." IEEE PAS-85. pp. 633-645. June.

Baldo, G., I. Gallimberti, H. N. Garcia, B. Hutzler, J. Jouaire, and M. F. Simon. 1975. "Breakdown Phenomena of Long Gaps under Switching Impulse Conditions. Influence of Distance and Voltage Levels." IEEE PAS-94. pp. 1131-1140. July/August.

Barnes, H.C. and D. E. Winters. 1971. "UHV Transmission Design Requirements – Switching Surge Flashover Characteristics of Extra Long Air Gaps." IEEE PAS-90. pp. 1579-1589. July/August.

Barthold, L. O. and L. Paris. 1970. "The Probabilistic Approach to Insulation Coordination." *Electra*. 13. pp. 41-58. May.

Boyd, H. A., A. F. Rohlfs, and L. E. Zaffanella. 1974. "Phase-to-Ground and Phase-to-Phase Switching-Surge Flashover of External Insulation of UHV Stations." IEEE PAS-93. pp. 518-528. March/April.

Brasca, E., M. Tellarini, and L. Zaffanella. 1967. "The Confidence Limit of High Voltage Dielectric Test Results." IEEE PAS-86. pp. 968-975. August.

Brown, G. W. 1969. "Determination of Critical Flashover Voltage and Standard Deviation from Flashover Probability Data." IEEE PAS-88. pp. 189-193. March.

Brown, G. W. 1978. "Designing EHV Lines to a Given Outage Rate. Simplified Techniques." IEEE PAS-97. pp. 379-383. March/April.

Busch, W. 1978. "Air Humidity: an Important Factor for UHV Design." IEEE PAS-97. pp. 2086-2093. November/December.

Carrara, G. and L. E. Zaffanella. 1968. "UHV Laboratories: Switching Impulse Clearance Tests." IEEE Paper 68CP692-PWR. Summer Power Meeting. Chicago, IL. June 23-28.

Carrara, G., L. Dellera, and G. Sartorio. 1970. "Switching Surges with Very Long Fronts (above 1500 μs): Effect of Front Shape on Discharge Voltage." IEEE PAS-89. pp. 453-456. March.

Carrara, G. and L. Dellera. 1972. "Accuracy of an Extended Up-and-Down Method in Statistical Testing of Insulation." *Electra.* No. 23. July 1972.

Carrara, G. and L. E. Zaffanella. 1972. "UHV External Insulation. Challenging Aspects." *Electra.* No. 23. July 1972.

Carrara, G. and L. Thione. 1976. "Switching Surge Strength of Large Air Gaps: A Physical Approach." IEEE PAS-95. pp. 512-524. March/April.

CIGRE W.G. 05. 1972. "The Calculation of Switching Surges. Part I." *Electra.* No. 19. pp. 67-78.

CIGRE W.G. 33.03. 1973a. "Switching Impulse Test Procedure for Phase-to-Phase Air Insulation." *Electra*. No. 30. pp. 55-69.

CIGRE W.G. 13.02. 1973b. "Switching Overvoltages in EHV and UHV Systems with Special Reference to Closing and Reclosing Transmission Lines." Electra. No. 30. pp. 70-122.

CIGRE W.G. 05. 1974. "The Calculation of Switching Surges. Part II." *Electra.* No. 32. pp. 17-42.

CIGRE W.G. 05. 1979a. "The Calculation of Switching Surges. Part III." *Electra.* No. 62. pp. 46-78.

CIGRE SC 33. 1979b. "Phase-to-Phase Insulation Coordination." *Electra.* No. 64. pp. 137-236.

CIGRE TF 33.06-01. 1979c. "Switching-Impulse Performance of External Insulation in Natural Ambient Conditions. Results of an Interlaboratory Cooperative Experimental Research." *Electra.* No. 65. pp. 19-39.

CIGRE TF 33.07-03. 1991. "Humidity Influence on Non-Uniform Field Breakdown in Air." *Electra.* No. 134. pp. 63-89.

Clerici, A. 1972. "Analog and Digital Simulation for Transient Overvoltage Determination." *Electra.* No. 22. pp. 111-138.

Comellini, E. 1971. "Possible Improvements in EHV Overhead Line Insulation to Switching Surges." IEEE PAS-90. pp. 1574-1578. July/August.

Cortina, R., M. Sforzini, and A. Taschini. 1970. "Strength Characteristics of Air Gaps Subjected to Interphase Switching Surges." IEEE PAS-89. pp. 448-452. March.

Cortina, R., E. Garbagnati, A. Pigini, G. Sartorio, and L. Thione. 1985. "Switching Impulse Strength of Phase-to-Earth UHV External Insulation – Research at the 1000 kV Project." IEEE PAS-104. pp. 3161-3168. November.

Dellera, L. and L. E. Zaffanella. 1967. "Methods for Interphase Switching Impulse Tests on Air Insulation." CIGRE *Electra.* No. 3. p. 24.

Dillard, J. K. and A. R. Hileman. 1970. "UHV Transmission Towers Insulation Tests." IEEE PAS-89. pp. 1772-1884. November/December.

Edison Electric Institute. 1968. *EHV Transmission Line Reference Book.*

Elovaara, J. 1978. "Risk of Failure Determination of Overhead Line Phase-to-Earth Insulation Under Switching Surges." *CIGRE Electra.* No. 56. pp. 69-88.

EPRI. 1978. *Transmission Line Reference Book – 115-138 kV Compact Line Design*. Electric Power Research Institute. Palo Alto, California.

EPRI. 1982. *Transmission Line Reference Book – 345 kV and Above*. Second Edition. Electric Power Research Institute. Palo Alto, California.

EPRI. 1983. *Addendum to Transmission Line Reference Book: 115-138 kV Compact Line Design.* EL-3147. RP 1492. Electric Power Research Institute. Palo Alto, California. June.

ESMOL Subcommittee 15.07. 2001. "The Use of Portable Protective Air Gaps in Liveline Maintenance." IEEE PWRD-16. pp. 806-811. October.

ESMOL Subcommittee 15.07. 2002a. "Safety Considerations When Placing a Person with Tools in an Air Gap to Change Porcelain and Glass Insulators on Transmission Systems of 345 kV and above, Using Ladder and Aerial Lift Methods." IEEE PWRD-17. pp. 805-808. July.

ESMOL Subcommittee 15.07. 2002b. "Minimum Number of Good (Healthy) Porcelain or Glass Insulator Units in a String for Live Work." IEEE PWRD-17. pp. 809-814. July.

Feser, K. 1971. "Mechanisms to Explain the Switching Impulse Phenomena." *Schweizerische Technische Zeitschrift*. No. 16. November.

Feser, K. and A. Pigini. 1987. "Influence of Atmospheric Conditions on the Dielectric Strength of External Insulation." *Electra.* 112. pp. 83-95.

Fujimura, T., K. Naito, Y. Hasegawa, and T. Kawaguchi. 1979. "Performance of Insulators Covered with Snow and Ice." IEEE PAS-98. pp. 1621-1631.

Gallet, G., G. Leroy, R. Lacey, and I. Kromer. 1975. "General Expression for Positive Polarity Switching Impulse Strength Valid Up to Extra Long Air Gaps." IEEE PAS-94. pp. 1989-1993. November/December.

Gallet, G., M. Bettler, and G. Leroy. 1976. "Switching Impulse Results Obtained on the Outdoor Testing Area at Renardieres." IEEE PAS-95. pp. 580-585. March/April.

Gallet, G., B. Hutzler, and J-P. Riu. 1978. "Analysis of the Switching Impulse Strength of Phase-Phase Air Gaps." IEEE PAS-97. pp. 485-494. March/April.

Ganger, B.E. and E.G. Maier. 1972. "Studies of Spark Formation at High Switching Voltages of Positive Polarity." IEEE PAS-91. pp. 2427-2436. November/December.

Gela, G. 1994. "Air Gap Sparkover and Gap Factors – Analysis of Published Data." EPRI TR-104437. Project 3787. Final Report. December.

Gela, G., A. E. Lux, H. Kientz, D. A. Gillies, J. D. Mitchell, and P. F. Lyons. 1996. "Application of Portable Protective Gaps for Live Work on Compact 550 kV Transmission Lines." IEEE PWRD-11. pp. 1419-1429. July.

Gela, G., H. Kientz, H. J. Fox, J. D. Mitchell, and P. F. Lyons. 1996. "Defective Insulators in Live Working on a 550 kV Compact Steel Lattice Tower." IEEE PWRD-12. pp. 783-790. April.

Gockenbach, E. 1991. "Measurements of Standard Switching Impulse Voltages by Means of Sphere-Gaps (One Sphere Earthed)." *Electra.* 136. pp. 91-96. June.

Grant, I. S., A. S. Paulson, and M. A. Presser. 1981. "Phase-Phase Switching Surge Flashovers: Weather Correction Factors." IEEE PAS-100. pp. 1820-1828. April.

Guyker, W. C., A. R. Hileman, and J. F. Wittibschlager. 1966. "Full-Scale Tests for the Allegheny Power System 500-kV Tower-Insulation System." IEEE PAS-85. pp. 614-623. June.

Hahn, G., P. Zacke, A. Fischer, and H. Boecker. 1976. "Humidity Influence on Switching Impulse Breakdown of a 50-cm Rod Plane Gap." IEEE PAS-95. pp. 1145-1152. July/August.

Harada T., Y. Aoshima, Y. Ishida, Y. Ichihara, K. Anjo, and N. Nimura. 1970. "Influence of Air Density on Flashover Voltages of Air Gaps and Insulators." IEEE PAS-89. pp. 1192-1202. July/August.

Harada, T., Y. Y.Aihara, and Y. Aoshima. 1971. "Influence of Humidity on Lightning and Switching Impulse Flashover Voltages." IEEE PAS-90. pp. 1433-1442. July/August.

Harada, T., Y. Aihara, and Y. Aoshima. 1973. "Influence of Switching Impulse Wave Shape on Flashover Voltages of Air Gaps." IEEE PAS-92. pp. 1085-1093. May/June.

Hauspurg, A., V. Caleca, and R. H. Schlomann. 1969. "765-kV Transmission Line Insulation Testing Program." IEEE PAS-88. pp. 1355-1365. June.

Hepworth, J. K., R. C. Klewe, and S. A. Tozer. 1972. "Impulse Breakdown of Large Sphere-Plane Gaps." Proceedings IEEE. Vol. 119. No. 12. pp. 1751-1753. December.

Hertig, G. E. and W. B. Kelly. 1966. "Switching Surge Test Results EHV Substation Bus Configurations." IEEE PAS-85. pp. 846-858. August.

Hileman, A. R. and H. W. Askins. 1973. "Switching Impulse Characteristics of UHV Station Post Insulators." IEEE PAS-92. pp. 139-144. January/February.

Hutzler, B. and D. Hutzler. 1975. "Breakdown Phenomena of Long Gaps under Switching Impulse Conditions. Time to Breakdown Distribution and Breakdown Probability: Statistical Approach." IEEE PAS-94. pp. 894-898. May/June.

Hutzler, B. and D. Hutzler. 1978. "Leader Propagation Model for Predetermination of Switching Surge Flashover Voltage of Large Gaps." IEEE PAS-97. pp. 1087-1096. July/August.

Hutzler, B. 1987. "Switching Impulse Strength of Air Gaps Containing a Metallic Body at Floating Potential." 5th ISH (International Symposium on High Voltage). Brauschweig. Paper 11-11.

IEC Publication 71. 1972. "Insulation Coordination."

IEC Publication 60-1. 1989. "High Voltage Testing Techniques."

IEEE Committee Report. 1966. "Switching Surges: Pt. II, Selection of Typical Waves for Insulation Coordination." IEEE PAS-85. pp. 1091-1097. October.

IEEE Working Group. 1974. "Sparkover Characteristics of High Voltage Protective Gaps." IEEE PAS-93. pp. 196-205. January/February.

IEEE Working Group. L. E. Zaffanella et al. 1975. "Guide for Application of Insulators to Withstand Switching Surges." IEEE PAS-94. pp. 58-67. January/February.

IEEE Std. 4. 1995. "IEEE Standard Techniques for High Voltage Testing."

Johnson, W. R., E. G. Lambert, J. B. Tice, and F. J. Turner. 1963. "500-kV Line Design. II-Electrical Strength of Towers." IEEE PAS-82. pp. 581-587. August.

Jones, B. 1973. "Switching Surges and Air Insulation." *Phil. Trans. R. Soc. Lond. A.* Vol. 275. Pp. 165-180.

Kachler, A .J., J. J. LaForest, and L. E. Zaffanella. 1970. "Switching Surge Flashover of UHV Towers." IEEE PAS-89. pp. 1762-1771. November/December.

Kachler, A. J., J. J. LaForest, and L. E. Zaffanella. 1971a. "Switching Surge Flashover of UHV Transmission Line Insulation." IEEE PAS-90. pp. 1604-1611. July/August.

Kachler, A. J., J. J. LaForest, and L. E. Zaffanella. 1971b. "Switching Surge Results from Project UHV – Influence of Humidity and Grading Rings." IEEE PAS-90. pp. 2313-2320. September/October.

Kalb, J. W. 1963. "How the Switching Surge Family Affects Line Insulation." IEEE PAS-82. pp. 1024-1031. December.

Kassakian, J. G. and D. M. Otten 1975. "On the Suitability of a Gaussian Stress Distribution for a Statistical Approach to Line Insulation Design." IEEE PAS-94. pp. 1624-1628. September/October.

Killian, S. C. and J. H. Moran. 1964. "Characteristics of EHV Station Post Insulators." IEEE PAS-83. pp. 280-285. March.

Kim, J-B., E-B. Shim, and J-W. Shim. 2000. "Switching Overvoltage Analysis and Air Clearance Design on the KEPCO 765 kV Double Circuit Transmission System." IEEE PWRD-15. pp. 381-386. November/December.

Kishizima, I., K. Matsumoto, and Y. Watanabe. 1984. "New Facilities for Phase-to-Phase Switching Impulse Tests and Some Test Results." IEEE PAS-103. pp. 1211-1216. June.

Kline, L.E. 1977. "Corona Cloud Model Predictions of Switching Surge Flashover Voltages vs. Electrode Geometry." IEEE PAS-96. pp. 543-549. March/April.

Knudsen, N. and F. Iliceto. 1970. "Flashover Tests on Large Air Gaps with DC Voltage and with Switching Surges Superimposed on DC Voltage." IEEE PAS-89. pp. 781-788. May/June.

Kosztaluk, R., R. Lanoie, R. Malewski, C. Menemenlis, and D-H. Nguyen. 1981. "Effect of Time Shift between the Two Voltage Components on Phase-Phase Insulation Strength." IEEE PAS-100. pp. 3379-3386. July.

Kucera, J. and V. Fiklik. 1970. "Correction of Switching Impulse Flashover Voltages for Air Humidity." IEEE PAS-89. pp. 441-447. March.

Kucera, J., T. W. Liao, and A. F. Rohlfs. 1972. "Atmospheric Correction Factors for High Voltage Testing." *Electra.* No. 21. pp. 74-85.

Lalot, J. and B. Hutzler. 1978. "Influence of Non-Standard Switching Impulses on the Flashover Mechanism of an Air Gap." IEEE PAS-97. pp. 848-856. May/June.

Leibfried, W. and H. Mors. 1960. "The Mechanical Behavior of Bundled and Single Conductors – New Measurements at the Hornisgrinde Testing Station." CIGRE Report 209.

Lemke, E. and W. Mosh. 1973. "Long Air Gap Breakdown by Positive Switching Surges." *Elektrichestvo.* No. 12. pp. 30-33.

Les Renardieres Group. 1972. "Research on Long Air Gap Discharges." *Electra.* No. 23. pp. 10-53.

Les Renardieres Group. 1974. "Research on Long Air Gap Discharges." *Electra.* No. 35. pp. 26-49.

Les Renardieres Group. 1977. "Positive Discharges in Long Air Gaps at Les Renardieres." *Electra.* No. 53. pp. 31-153.

Les Renardieres Group. 1987. "Discharges in Long Air Gaps at Les Renardieres. Double Impulse Tests." *Electra.* No. 111. pp. 25-40.

Lloyd, K. J. and L. E. Zaffanella. 1981. "Switching Impulse Tests at Project UHV Using Long Wave Fronts." IEEE PAS-100. pp. 510-517. February.

Loeb, L. B. 1939. "Fundamental Processes of Electrical Discharges in Gases." New York. John Wiley and Sons.

Los, E. J. 1978. "A Model for the Study of Switching Surge Breakdown of Long Air Gaps." IEEE PAS-97. pp. 2382-2392. November/December.

Los, E .J. and H. M. Schneider. 1978. "Switching Surge Breakdown Development in Large Conductor-Tower Air Gaps." IEEE PAS-97. pp. 866-875. May/June.

Macchiaroli, B. and F. J. Turner 1970. "Switching Surge Performance of Contaminated Insulators." IEEE PAS-89. pp. 190-197. February.

Malaguti, C. and L. Zaffanella. 1968. "Switching Impulse Wet Tests." *Electra.* No. 5. pp. 40-61. June 1968.

McElroy, A. J. and J. H. Charkow. 1967. "Probabilistic Aspects of Transmission System Switching Surge Reliability." IEEE PAS-86. pp. 1012-1024. August.

Menemenlis, C. and G. Harbec. 1974. "Switching Impulse Breakdown of EHV Transmission Towers." IEEE PAS-93. pp. 255-263. January/February.

Menemenlis, C. and K. Isaksson. 1974. "The Front Shape of Switching Impulses and Its Effect on Breakdown Parameters." IEEE PAS-93. pp. 1380-1389. September/October.

Menemenlis, C. and K. Isaksson. 1975. "Influence of the Various Parts of Switching Impulse Front on Discharge Development." IEEE PAS-94. pp. 1725-1733. September/October.

Menemenlis, C., H. Anis, and G. Harbec. 1976. "Phase-to-Phase Insulation. Part I: Generalized Effects of Stress Parameters and Gap Geometry." IEEE PAS-95. pp. 643-650. March/April.

Menemenlis, C. and G. Harbec. 1976. "Particularities of Air Insulation Behavior." IEEE PAS-95. pp. 1814-1821. November/December.

Menemenlis, C., G. Harbec, and J. F. Grenon. 1978a. "Switching-Impulse Corona Inception and Breakdown of Large High-Voltage Electrodes in Air." IEEE PAS-97. pp. 2367-2374. November/December.

Menemenlis, C., G. Harbec, and J. F. Grenon 1978b. "Behavior of Air Insulating Gaps Stressed by Switching Overvoltages with a Double Peak." IEEE PAS-97. pp. 2375-2381. November/December.

Menemenlis, C., G. Harbec, A. Hould, B. R. Shperling, W. Pokorny, and S. Zelingher. 1981. "Air Insulation Design of UHV Stations Based on Switching Surges." IEEE PAS-100. pp. 891-898. February.

Menemenlis, C., G. Carrara, and P. J. Lambeth. 1989. "Application of Insulators to Withstand Switching Surges in Substations. Part I: Switching Impulse Insulation Strength." IEEE PWRD-4. pp. 545-557. January.

Miyake, K., Y. Watanabe, and E. Ohsaki. 1987. "Effects of Parameters on the Phase-to-Phase Flashover Characteristics of UHV Transmission Lines." IEEE PWRD-2. pp. 1285-1291. October.

Moran, J. H. and R. J. Alton. 1968. "Switching Surge Study of EHV Station Posts: I." IEEE PAS-87. pp. 1471-1480. June.

Moran, J. H. 1969. "Switching Surge Study of EHV Station Posts: II." IEEE PAS-88. pp. 238-244. March.

Mors, H. 1956a. "Wind Pressure on Overhead Transmission Line Conductors – Hornisgrinde Testing Station." CIGRE Report 220.

Mors, H. 1956b. "Wind Pressure on Stranded Conductors – Hornisgrinde Testing Station." CIGRE Report 220 BIS.

Okada, T. and S. Koga. 1970. "Switching Surge Flashover Characteristics of Long Disk Insulator Strings under Polluted Conditions." IEEE PAS-89. pp. 437-441. March.

Papadias, B. C. 1979. "The Accuracy of Statistical Methods in Evaluating the Insulation of EHV Systems." IEEE PAS-98. pp. 992-999. May/June.

Paris, L. 1967. "Influence of Air Gap Characteristics on Line-to-Ground Switching Surge Strength." IEEE PAS-86. pp. 936-947. August.

Paris, L. and R. Cortina. 1968. "Switching and Lightning Impulse Discharge Characteristics of Large Air Gaps and Long Insulator Strings." IEEE PAS-87. pp. 947-957. April.

Paris, L., A. Taschini, K. H. Schneider, and K. H. Weck. 1973. "Phase-to-Ground and Phase-to-Phase Air Clearances in Substations." *Electra.* No. 29. pp. 29-44.

Paulson, A. S. and I. S. Grant. 1981. "Phase-Phase Switching Surge Flashover: Design Data." IEEE PAS-100. pp. 3666-3672. July.

Peek, F. W. 1914. "The Effect of Altitude on Bushings, Leads and Insulators." AIEE-33. pp. 1721-1730.

Phillips, T. A., L. M. Robertson, A. F. Rohlfs, and R. L. Thompson. 1967. "Influence of Air Density on Electrical Strength of Transmission Line Insulation." IEEE PAS-86. pp. 948-961. August.

Pigini, A., G. Sartorio, M. Moreno, M. Ramirez, R. Cortina, E. Garbagnati, A.C. Britten, and K. J. Sadurski 1985. "Influence of Air Density on the Impulse Strength of External Insulation." IEEE PAS-104. pp. 2888-2900. October.

Podporkin, G.V. 1995. "Calculating the Switching Surge Critical Flashover Voltage of Phase-to-Ground and Phase-to-Phase Bundle Conductor Gaps." IEEE PWRD-10. pp. 365-373. January.

Pokorny, W.C. and R. W. Flugum. 1975. "UHV Tower Insulation Parameters Determined by Full-Scale Testing." IEEE PAS-94. pp. 518-526. March/April.

Ramirez, M., M. Moreno, A. Pigini, G. Rizzi, and E. Garbagnati. 1990. "Air Density Influence on the Strength of External Insulation under Positive Impulses: Experimental Investigation up to an Altitude of 3000 m a.s.l." IEEE PWRD-5. pp. 730-737. April.

Rawls, J. A., J. W. Kalb, and A. R. Hileman. 1964. "Full Scale Surge Testing of VEPCO 500-kV Line Insulation." IEEE PAS-83. pp. 245-250. March.

Reichman, J. 1981. "Safety Aspects of Live-Line Work Methods." IEEE PAS-100. pp. 3478-3485. July.

Riu, J. P., B. Hutzler, S. W. Rowe, J. Huc, and P. Maurin. 1988. "Wet Tests under A.C. Voltage and Switching Impulses – Procedure and Significant Parameters." IEEE PWRD-3. pp. 298-306, January.

Rizk, F. 1976. "Influence of Rain on Switching Impulse Sparkover Voltage of Large-Electrode Air Gaps." IEEE PAS-95. pp. 1394-1402. July/August.

Rizk, F. 1989a. "A Model for Switching Impulse Leader Inception and Breakdown of Long Air Gaps." IEEE PWRD-4. pp. 596-606. January.

Rizk, F. 1989b. "Switching Impulse Strength of Air Insulation: Leader Inception Criterion." IEEE PWRD-4. pp. 2187-2195. October.

Rizk, F. 1992. "Critical Switching Impulse Strength of Long Air Gaps: Modeling of Air Density Effects." IEEE PWRD-7. pp. 1507-1515. July.

Rizk, F. 1993. "Critical Switching Impulse Strength of Phase-to-Phase Air Insulation." IEEE PWRD-8. pp. 1492-1506. July.

Rizk, F. 1995. "Effect of Floating Conductive Objects on Critical Switching Impulse Breakdown of Air Insulation." IEEE PWRD-10. pp.1360-1370. July.

Rizk, F. 1996. "Critical Switching Impulse Breakdown of Long Bundle-Conductor Gaps." IEEE PWRD-11. pp. 373-383. January.

Rohlfs, A. F., H. E. Fiegel, and J. G. Anderson. 1961. "The Flashover Strength of Extra-High-Voltage Line and Station Insulation." IEEE PAS-80. pp. 463-470. August.

Rohlfs, A. F. and H. M. Schneider. 1983. "Switching Impulse Strength of Compacted Transmission Line Flat and Delta Configurations." IEEE PAS-102. pp. 822-831. April.

Saruyama, Y., M. Yasui, G. Ikeda, S. Nagasaki, and N. Mori. 1967. "500-kV Line Design: I-Insulation Characteristics of Towers." IEEE PAS-86. pp. 1083-1090. September.

Schneider, H. M. and F. J. Turner. 1975. "Switching-Surge Flashover Characteristics of Long Sphere-Plane Gaps for UHV Station Design." IEEE PAS-94. pp. 551-559. March/April.

Sforzini, M. and A. Taschini. 1970. "Strength Characteristics of Air Gaps Subjected to Interphase Switching Surges." IEEE PAS-89. pp. 448-452. March.

Shindo, T. and T. Suzuki. 1995. "A Method of Predicting Anomalous Flashovers." IEEE PWRD-10. pp. 1371-1377. July.

Suzuki, T. 1975. "Breakdown Process in Rod-to-Plane Gaps with Negative Switching Impulses." IEEE PAS-94. pp. 1381-1389. July/August.

Suzuki, T., I. Kishijima, Y. Ouch, and K. Anjio. 1969. "Parallel Multigap Flashover Probability." IEEE PAS-88. pp. 1814-1823. December.

Suzuki, T. and K. Miyake. 1975. "Breakdown Process in Long Air Gaps with Positive Switching Impulses." IEEE PAS-94. pp. 1021-1033. May/June.

Thione, L., J. Kucera, and K. H. Weck. 1975. "Switching Impulse Generation Techniques Using High Voltage Testing Transformers." *Electra.* No. 43. pp. 33-72. December 1975.

Truax, C. J., J. D. Brown, and W. Neugebauer. 1978. "TNA Study of Reclosing Transients on a 765 kV Shunt Compensated Transmission Line." IEEE PAS-97. pp. 1447-1457. July/August.

Udo, T. 1965. "Switching Surge and Impulse Sparkover Characteristics of Large Gap Spacings and Long Insulator Strings." IEEE PAS-84. pp. 304-309. April.

Udo, T. 1966a. "Minimum Phase-to-Phase Electrical Clearances for Substations Base on Switching Surges and Lightning Surges." IEEE PAS-85. pp. 838-845. August.

Udo, T. 1966b. "Switching Surge Sparkover Characteristics of Air Gaps and Insulator Strings Under Practical Conditions." IEEE PAS-85. pp. 859-864, August.

U.S. Weather Bureau. 1914. "Types of Storms in the United States and Their Average Movements." *Monthly Weather Review.* Supplement No. 1.

Vaisman, R., J. R. Fonseca, V. H. G. Andrade, et al. 1993. "Switching Impulse Strength of Compact Transmission Lines." IEEE PWRD-8. pp. 1570-1578. July.

Visher, S.S. 1966. "Climatic Atlas of the United States." Cambridge Howard University Press.

Watanabe, Y. 1967. "Switching Surge Flashover Characteristics of Extremely Long Air Gaps." IEEE PAS-86. pp. 933-936. August.

Watanabe, Y. 1968. "Influence of Preexisting DC Voltage on Switching Surge Flashover Characteristics." IEEE PAS-87. pp. 964-969. April.

Watanabe, Y. 1978. "Flashover Tests of Insulators Covered with Ice and Snow." IEEE PAS-97. pp. 1788-1794.

Yasui, M. and M. Murooka. 1988. "Practical Design of AC 1,000-kV Insulator Assemblies." IEEE PWRD-3. pp. 333-340. January.

Young, F. S., H. M. Schneider, Y. M. Gutman, and N. N. Tikhodeyev 1980. "USA-USSR Investigation of 1200-kV Tower Insulation." IEEE PAS-99. pp. 462-470. March/April.

Zaffanella, L. E. 1967. "Air Density Corrections." IEC Technical Committee 42. WG 2. Camogli, Italy. December 1967.

Zaffanella, L., G. Ceron, and M. Tellarini. 1966. "Design of Clearances between Phases in Air with Respect to Switching Surges." (in Italian, 67th Italian Electrical Association meeting, Alghero, Italy, October 1966). Results summarized in discussion by G. Carrara to (Udo 1966a) IEEE PAS-85. pp. 844-845.

Zaffanella, L. E., G. Balderston, J. M. Schamberger, and G. W. Juette. 1972. "UHV AC Transmission Line Design Based on Project UHV Test Results." CIGRE 1972. Report 31-12.

CHAPTER 6

Lightning and Grounding

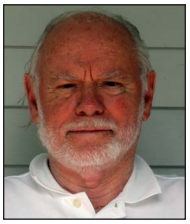
William A. Chisholm
John G. Anderson

This chapter describes the mechanisms of lightning flash, the effects of those mechanisms on transmission-line equipment, and the methods for mitigation of effects. Included are descriptions of measurement and detection systems, surge impedance effects, calculation methods for insulation strength and shielding failures, initiation of flashovers, and transmission-line grounding measurement techniques and tools.



Dr. William A. Chisholm is an internationally acknowledged expert in lightning protection, insulation, and thermal rating of power systems. He is a Senior Research Project Manager in the Transmission and Distribution Technologies group of Kinectrics, the former Research Division of Ontario Hydro, now a division of AEA Technologies PLC. In this capacity he has completed research contract and project work for more than 40 electric utilities, manufacturers and research organizations.

Dr. Chisholm was recognized as the editor of the "Best Standard" award in 1999 for the IEEE Standard 1243, *Guide to Improving the Lightning Performance of Overhead Transmission Lines.* He is a corresponding member of CIGRÉ Study Committee 33 working groups on lightning and insulator icing test methods. He is the chairman of the IEEE Power Engineering Society Lightning and Insulator Subcommittee and a member of the PES Editorial Board.



John G. Anderson is one of the original authors of the *EPRI Transmission Line Reference Book,* including the chapter on line lightning performance. He has had more than 50 years of high-voltage engineering experience, and is a Life Fellow of the IEEE and an elected member of the National Academy of Engineering. He is a former manager of the General Electric High Voltage Laboratory and served as a consulting engineer for General Electric and also as a senior consultant for Power Technologies, Inc. He was one of the original researchers at the Lenox, Massachusetts EPRI Project EHV and later Project UHV, and also carried out lightning research at the Empire State Building in New York City. He is the author/coauthor of more than 40 technical papers and coauthor of three books concerned with high-voltage transmission, lightning, and insulation performance.

6.1 INTRODUCTION

Lightning flashes occur many times over the design life of a transmission line. The initiation of a flashover across line insulation may occur in response to a severe flash. This flashover process involves poorly defined gas discharge physics, fast-changing electromagnetic fields relative to the structure size, time-dependent nonlinear effects of corona development, and time- and current-dependent impedance of the earth electrodes. The problem must be evaluated in the context of large uncertainties in the lightning parameters and smaller, but significant, uncertainties in the line description.

6.1.1 Historical Context

Depictions of lightning exist on Akkadian clay roll seals as far back as 2200 BC and in Leviticus (Golde 1977), and "thunder magic" was common in early cultures. However, it was not until the 18th century that the electrical nature of lightning was recognized by Franklin and others (Schonland 1964). The first physicist to be killed carrying out electrical experiments on lightning was G.W. Richmann in St. Petersburg, Russia. In 1752, he was duplicating Franklin's sentry-box experiment, a variation of Franklin's kite experiment, and was killed by a direct flash to his equipment.

The invention of the Boys camera (Boys 1926), in which photographic film was moved at high speed by an open lens at night, provided the first resolution of the initial downward leader velocity and the multiple return strokes that followed. This photographic technique has been used since that time to dissect all those characteristics of the lightning sequence that involve light, much of the early research being done by Schonland in South Africa (Schonland 1956), although now it is usually replaced by electronically-triggered streak or fast frame-rate pixel cameras.

In 1939 and later, direct stroke measurements were made at the Empire State Building, New York City, (McEachron 1939, Hagenguth and Anderson 1952) and by McCann (McCann 1944) in Pittsburgh. Such work was continued after World War II by many investigators, of which the researches by Berger at Mount San Salvatore in Switzerland from 1947 to 1975 were particularly outstanding (Berger et al. 1975). The widespread application of practical lightning location systems started in the late 1970s, with the theoretical and experimental work of Krider, Noggle, and Uman (Krider et al. 1976), combined with advancements in telecommunications to make real-time lightning detection economically feasible.

6.1.2 Lightning Protection of Transmission Lines

The use of overhead catenary wires for lightning protection started early in the electric power utility industry. Original design blueprints for the first power lines from Niagara Falls show intended mounting locations for overhead ground wires above each phase conductor, for a total of seven overhead groundwires per tower. The industry quickly established that a single wire, located several meters above the phases and acting as a horizontal lightning air terminal, gives nearly perfect protection at much lower cost. However, the true role of overhead groundwires in lightning protection was not fully described until the 1930s, after photographic methods led to a proper understanding of the lightning progression mechanism.

The 1930s were particularly fruitful in transmission-line lightning research, driven by a need to ameliorate plagues of serious lightning damage to transmission lines and station equipment occurring at that time. This period included some of the first direct measurements of lightning currents and resolutions of stroke current waveshapes, polarities, and magnitudes. This period also led to major advances in surge arrester design, insulator development, and the understanding of interactions between incoming transmission-line lightning transients and transformer windings.

In North America and many other parts of the world, lightning still remains the primary cause of transmission-line outages, momentary interruptions, and reliability and maintenance problems. On a multi-circuit line, simultaneous flashovers by lightning of two or more circuits can cause particularly severe disruptions to service, and 40-60% of flashovers on double-circuit towers can usually be expected to involve both circuits. A lightning strike can generate millions of volts across line insulators, sometimes leading to insulator tracking, punctures, and shed damage. Power frequency arcs triggered by lightning flashovers are then a major source of melting, burning, and pitting of wires, corona shields, and supporting hardware. High-voltage traveling waves injected onto phase conductors by tower flashovers or by shielding failures can travel for long distances to enter substations and present severe challenges to transformers, circuit breakers, and other components. The strong electromagnetic fields created by a flash to earth can induce enough voltage on a distribution or subtransmission line to flash over the line, even though the flash does not contact the line directly. Tower-mounted communications equipment and overhead shield wires with encased optical fibers are also vulnerable unless properly protected.

6.1.3 Simulation of Lightning on Transmission Lines

Lightning in all its complex physics is highly statistical in incidence, magnitudes, charge delivery, and all other electromagnetic effects that initiate line flashovers. In any given geographical area, meteorology dictates that the

number of hits to earth or to lines in the area can vary greatly around the observed averages—by 3:1 or more. Lines can be designed for a flashover return period of once in 20 years, and yet have a flashover the first year. Lines that require a very high reliability can be engineered and be largely successful, but may occasionally deliver a surprise from an unexpected and unusual lightning event. This chapter covers the principal statistics of this process in some detail.

Conversely, very often lightning has been designated as the culprit in a line tripout, when no lightning was actually involved. The recent growth of the North American Lightning Detection Network (NALDN) and similar networks around the world has made extensive data available on ground flash magnitudes, times, and locations. In principle, one can now determine whether a lightning flash at that location at the same time accompanied a line flashover, and—if so— the magnitude of the first stroke current in the flash. This technology provides estimates of stroke current parameters such as polarity, peak amplitude, and multiplicity. These estimates can often flag the root cause of the flashover, whether a shielding failure or a backflashover, so the proper remedial measures can be undertaken.

A wide range of software tools and design equations supplement the real-world laboratory of random stimulus (lightning strokes) and response (time-correlated records of transmission-line breaker operations). In this edition, the authors review some of the software simulation programs available to the reader to model lightning performance and discuss in some detail the advantages and limitations of each. A good simulation program has to handle the statistics of the process as well as the physics of breakdown and the response of the transmission system. Corrective actions for unsatisfactory performance can expend large quantities of money with little actual gain unless the user first determines the actual cause of the failures. Simulation programs can be very helpful in arriving at effective improvement strategies.

In the second edition of this Reference Book (EPRI 1982), a step-by-step, linearized numerical solution was developed to describe the problem in an approach that was developed for hand or programmable calculators. The industry (IEEE 1985, IEEE 1993, IEEE 1997b) found that this simplified method (based on a fixed 2-μs ramp wave, a deterministic volt-time description for insulator strength, simple models for corona effects, and relatively detailed traveling-wave analysis) gave results that were as satisfactory as any sophisticated prediction method. The "Red Book Method" was adapted into the IEEE FLASH program that forms part of IEEE Standard 1243 and formed an important basis for teaching the subject to a generation of graduate students and engineers.

Since the second edition, there has been considerable improvement in the ability to carry out numerical modeling on personal computers. An engineer or student would now use a simple spreadsheet or Internet applet rather than the eight-page schedule of calculations. Statistical and mathematical functions are available directly within these applications and do not require simple approximations. The computer even provides the new ability to visualize the downward and upward development of the leader, the traveling-wave response of the line, or the nonlinear effects of corona envelopes in the air and in the ground.

Hand in hand with this improved capability are improvements in our understanding of the individual components of the lightning problem. The overall level of risk in the second edition was based on the number of thunderstorm days per year, while this third edition makes use of observations from lightning location technologies. The statistics of stroke parameters based on measurements from around the world can be discussed quantitatively. The lightning attachment process no longer needs to rely fully on empirical description, as extrapolation of models for large-gap switching surge breakdown are found to give satisfactory predictions too. The physics of the lightning impulse flashover for typical 1-3 m insulation length has been studied, and improved numerical models have been proposed (CIGRE 1991). Details of tower and ground plane surge impedance have received scrutiny, and the entire subject of grounding has been simplified. Finally, and perhaps most importantly, utilities and researchers have tested the assertion in the second edition that "large negative first strokes cause the majority of transmission line outages" by comparing transmission-line flashover records with lightning location network records to form their own conclusions.

6.1.4 Capital Cost of Lightning Protection for Transmission Systems

The strength, weight, and cost of transmission towers are usually established by the transverse wind loading. The overturning moment on the transmission towers is the sum of traverse wind forces on each wire, multiplied by each wire height at the tower. The overhead groundwires are the tallest conductors, and in cold regions, they accumulate nearly the same ice thickness as phase conductors of larger diameter.

The tower weight needed to withstand traverse forces on conductors can be estimated simply from Equation 6.1-1:

$$W = K_m \sum ht \qquad 6.1\text{-}1$$

Where:

W = the tower weight (kg).
t = an individual traverse force (kg) located at attachment height h (m).
K_m = a coefficient of 0.014 kg/(m-kg) for double-circuit HV and EHV lattice towers.
K_m = a coefficient of 0.013 kg/(m-kg) for single-circuit horizontal EHV towers.
K_m = a coefficient of 0.021 kg/(m-kg) for single-circuit horizontal HV towers.

The coefficient relating tower weight and transverse forces varies depending on utility design practice and has trended downward over time. Good practice calculates the wind pressures on conductors and towers independently, and applies each force at the correct centroid, but for approximate purposes, the ratio of (Total) to (Conductor) overturning moment can be fixed at 1.9. Typical values of overturning moment for a double-circuit 345-kV line would be (t = 410 kg, h = 41 m) for two groundwires, and (t = 950 kg, h = 18 m, 25.5 m, and 33 m) for twelve conductors. The total tower moment from conductors would be 324 Mg-m, and the pressure of the wind on the tower adds 288 Mg-m. The total tower weight would be 8420 kg from Equation 6.1-1. If there were no overhead groundwires to support, the overturning moment would be only 549 Mg-m, and the tower weight would only be 7560 kg, a difference of 860 kg.

Table 6.1-1 shows the additional tower weights needed to support overhead groundwires for eight typical base-case conditions, as found in the appendix describing base cases. With four towers per km and a tower steel cost of $7/kg, the extra cost of supporting overhead groundwires above the 345-kV double-circuit base-case line is $2.4 M for a 100-km line.

6.1.5 Benchmark: Cost of Avoided Momentary Outages

The cost of supplying and supporting overhead groundwires (OHGW) is not the only cost of lightning protection using overhead groundwires. As transmission voltage increases, choices in the electrical layout have increasing influence in the extra costs of generation capacity and energy. Over the 50-year life of an overhead groundwire in areas of moderate lightning activity, there are three substantial costs: capital, peak loss, and energy loss. In an approximation with U.S. dollars in 2003, these costs are:

- **Capital Cost**—the capital cost of OHGW protection. This was established in Section 6.1.4 as $2.4 M per 100 km for the 345-kV double-circuit base-case line.
- **Peak Loss Cost**—the marginal cost of providing peak generation at peak load. As described in Section 7.9.2, and modeled using Applet EMF-8, currents of 92 A are induced in each of two overhead groundwires of the 345-kV double-circuit base case with "superbundle" or ABC/ABC phasing at a typical peak load of 1 A per kcmil of conductor cross-section. The loss at peak load of 2.6 MW per 100 km requires additional installed peak capacity at US_{2003}$ 2 M/MW, with a capital investment of $5.2 M per 100 km of OHGW.
- **Energy Loss Cost**—the present value of the continuous I^2R loss in the OHGW. Typical average loading would be one-third of peak; so continuous loss would be one-ninth of peak (290 kW per 100 km), and the cost of the energy loss at $0.05/kWh would be $120,000 per year per 100 km. This would have a present value of $3.2 M at 3% interest rate over 50 years.

The "superbundle" configuration was deliberately chosen to highlight the cost of energy losses in the overhead groundwires for EHV systems. Consider instead the situation where a low-reactance phasing, ABC/CBA, is used on the same 345-kV double-circuit line.

- Capital cost remains the same at $2.4 M extra per 100 km.
- Induced currents are reduced from 92 A to 11 A with the low-reactance phasing.
- Cost of additional generation capacity and energy are reduced by 98% and can now be neglected.

Table 6.1-1 shows that the control of overhead groundwire-induced currents, using favorable low-inductance phasing, optimal placement, or other methods in Applet EMF-8, becomes increasingly important as system voltage increases.

The load capability, and thus the number of customers affected by a transmission-line lightning outage, increases nearly as the square of line voltage. This results from the use of an increasing number of subconductors, providing greater ampacity. It is possible to compute the cost of an avoided momentary outage, using the difference in outage rate between a protected and an unprotected line. This calculation was carried out for an area of moderate ground flash density, N_g = 1.0 flash per km^2 per year. As an example, again using the 345-kV double-circuit line with 100 km length as a base case:

- The line would serve a summer peak of about 8500 MW, with each customer drawing 24 kW at a normal precontingency load of 3800 MW.
- A momentary outage on one circuit, successfully reclosed, would still introduce a voltage dip exceeding 50% for three cycles for 160,000 customers at the load end.
- Without lightning protection, there would be about 880 direct flashes to the unprotected upper phases over a 50-year exposure, and nearly all would cause phase-to-ground flashovers.

Table 6.1-1 Cost of Avoided Customer Momentary Outages using Overhead Groundwires in Area of Low Ground Flash Density (N_g = 1.0 (flashes/km²)/year)

System	Top Phase Height (m)	Extra Tower Weight (kg each)	Induced Current in OHGW[1] (A)	OHGW Loss /100 km at Peak Load	TOTAL[2] Capital in OHGW ($/ 100 km)	Cost Per Avoided Customer Momentary Outage[3]
230-kV Single Circuit	10.3	570	15.3	0.07 MW	$1.8 M	14¢
345-kV Single Circuit	12.5	710	33.7	0.3 MW	$3.1 M	9¢
500-kV Single Circuit	14.0	860	71.2	1.6 MW	$7.5 M	8¢
765-kV Single Circuit	18.5	1210	138.8	7.3 MW	$27 M	8¢
230-kV Double Circuit	15.3	620	26.7 SB 2.7 LowZ	0.2 MW 0.002 MW	$2.4 M $1.7 M	5¢ 4¢
345-kV Double Circuit	26.5	860	92.1 SB 11.2 LowZ	2.6 MW 0.04 MW	$10.8 M $2.5 M	8¢ 2¢
500-kV Double Circuit	31.0	940	140.8 SB 29.3 LowZ	7.5 MW 0.26 MW	$27 M $3.2 M	8¢ 1¢
765-kV Double Circuit	41.8	1300	262 SB 60.8 LowZ	26 MW 1.1 MW	$88 M $6.0 M	8¢ 1¢

SB = Superbundle phasing (ABC/ABC); LowZ = Low Reactance phasing (ABC/CBA).
1. Assuming 1 A per kcmil of conductor cross section at peak load for cost of capacity.
2. Cost of extra steel in towers, extra capacity at $2000/kW, and present value of energy at $0.05/kWh.
3. Assuming 24 kW per customer near summer peak load with dew point temperature > 25°C.

- With two overhead groundwires, there would be about 1000 direct flashes, and only 2% of these (17 over 50 years) are estimated to cause flashovers at a typical footing resistance.
- The overhead groundwires eliminated a total of (880-17) (160,000) customer momentary outages.
- With an overhead groundwire cost of $10.8 M using a high-loss superbundle configuration, the utility is spending about eight cents to prevent each momentary outage at a customer service entrance.
- The utility could provide the same protection at a cost of one cent per avoided customer momentary if it manages overhead groundwire circulating currents efficiently.

This investment level varies widely with customer and lightning ground flash density. The investment reaches nearly $1.00 per avoided momentary in some systems. The calculation can serve as a benchmark for regulation of other power quality investments, once suitable local values are substituted for the construction, generation, and energy costs; lightning flash density; transmission-line configurations; and number of customers affected by each momentary outage.

The cost of interruption to customers also varies widely, depending on the nature of the load. Table 6.1-2 summarizes costs of momentary outages, expressed as a sum of $US per kW (the momentary component) and $US per kWh (which can be neglected for momentary duration).

Table 6.1-2 Average Cost[1] of Single Interruption for Industrial Plants (IEEE 1997a, Table 2-5)

Industrial plants with <1 MW maximum demand	$15.61/kW + $27.57/kWh
All industrial plants	$6.43/kW + $9.11/kWh
Industrial plants with >1 MW maximum demand	$3.57/kW + $3.20/kWh

1. US$ 1997.

The cost of power interruption to commercial or office buildings is similar to the cost for small (<1 MW) industrial load (IEEE 1997a, Table 2-7). Clearly, from the industrial customer's point of view, utility investment in overhead groundwires and other lightning protection represents good value.

6.1.6 Organization and Contents of the Chapter

Section 6.2 describes the basic mechanisms of the lightning flash and results of recent analysis of these mechanisms. Section 6.3 reviews statistics and data on lightning flashes compiled through common measurement and detection systems. Section 6.4 discusses surge impedance and corona effects of lightning flash for a variety of conductors and tower shapes. Sections 6.5 and 6.6 provide calculation methods for insulation strength and shielding failure. Sections 6.7 through 6.9 explain the initiation mechanisms for backflashover, induced flashovers, and midspan flashovers. Section 6.10 describes tools and measurement methods for transmission line grounding. Appendix 6.1 discusses the disruptive effect algorithm to evaluate impulse failures of insulators. Appendix 6.2 gives some

additional details about the process of estimating lightning current from its distant radiated fields.

Several aspects of lightning can be calculated using simple software applications provided in the electronic version of this book. The user may exercise the following applets:

- L-1: "Transmission Line Lightning Performance." This applet calculates backflashover rate and shielding failure rate for each phase (number per km per year) given the input of line geometry at the tower, sag, phase voltages, insulator lightning impulse strength, span length, ground flash density, tower footing parameters, shield wire surge impedance, constants of the basic equations describing striking distance, and number of strikes to the line.
- L-2: "Stroke Attraction Model." This applet calculates the possible paths of lightning strokes as they descend from the cloud to hit the shield wires, the phase wires, or the ground.
- L-3: "Dynamic Tower Footing Resistance." This applet calculates the resistance of ground rods versus current and versus time, given the number and length of the rods, soil resistivity, soil dielectric strength, current peak value and waveshape.
- L-4: "Tower Lightning Flashover Tutorial." This applet calculates the currents and voltages that characterize the process of tower insulation flashover due to a lightning stroke that hits the tower. The applet is tutorial in nature, because it allows the user to verify in a friendly graphical way the effect of several physical parameters, such as stroke peak current, stroke waveshape, maximum stroke steepness, tower height, tower surge impedance, shield wire surge impedance, tower footing resistance characteristics, location of phase conductor in relation to the ground wire hit by lightning, height of the crossarm to which the insulators are attached, insulator string length, and span length. The applet shows how these parameters affect the current down the tower, the voltage between tower top and earth, the voltage between tower base and earth, the voltage across the phase insulator, and the disruptive effect on the insulators.
- L-5: "Tower Surge Impedance." This applet calculates the equivalent surge impedance of a tower to be used in simple models for lightning flashover calculations (Applet L-1 and Applet L-4) and shows how this surge impedance depends on the geometry of the tower. This applet calculates the response of a transmission tower when a unit current step is injected at the top of the tower and the response to a variety of current waveshapes. The applet shows the tower current, the tower top voltage, the tower base voltage, and the voltage at each crossarm versus time.
- L-6: "Step and Touch Potential." This applet calculates the potential of points on the ground with respect to earth, the step potential, and the maximum touch potential when lightning current flows from tower to earth. The potentials are calculated for the no-ionization case and are expressed as a percentage of the tower base-to-earth voltage. Potentials and step potentials are calculated at any desired point, or along a straight line, or in a rectangular area defined by the user. The applet can provide contour maps of potential and step potential.
- G-2: "World Map of Ground Flash Density and North American Map of Earth Resistivity." This applet provides some basic geophysical data that can be used to evaluate lightning protection in any region.

6.2 THE LIGHTNING FLASH

The following terms have been defined to encourage consistent description of lightning phenomena among engineers and researchers.

- ***Flash***—a term encompassing the entire electrical discharge from cloud to stricken object.
- ***Stroke***—the high-current components in a flash. A single flash contains a first stroke and may contain one or more subsequent strokes.
- ***Flashover***—an electrical discharge completed from an energized conductor to a grounded support. It may clear itself without tripping a circuit breaker.
- ***Backflashover***—an electrical discharge completed from a grounded support to an energized conductor. It may clear itself without tripping a circuit breaker.
- ***Tripout***—a flashover or backflashover of a line that does not clear itself. It must be cleared by momentary operation of a circuit breaker, removing ac power long enough for the flashover arc to extinguish.

6.2.1 Cloud Electrification

Figure 6.2-1 sketches one of the many possible configurations of a thunderhead. It functions much as a gigantic chimney, drawing moist heated air from the land and feeding the air high into the stratosphere, 15,000 m or more. The upward winds can reach speeds of 300 km per hour. The rising moisture, which first super-cools as it rises, finally turns to snow, hail, and ice in the upper regions. There can be severe turbulence in these clouds, which commercial aircraft must avoid. The turbulence—involving intermixing and friction of raindrops, snow, ice, and hail—causes a strong electrification to take place. Cooray (Cooray 2003b) summarizes cloud electrification models, and notes that negative charging occurs in the temperature range from -15 to -30°C (in the middle of the cloud), while positive charging occurs from 0 to -15°C (the bottom of the

cloud) and at temperatures below -30°C (the top of the cloud) (see Figure 6.2-1).

As Figure 6.2-1 shows, the lower regions of the cloud usually become strongly negatively charged, with small pockets of positive charge frequently interspersed. The upper regions of the cloud—at temperatures far below the freezing point of water—have widely distributed positive charges, and often these charges are embedded in an "anvil top" created by the rising air currents. The net negative charge at the base of the cloud induces a similar positive charge on the surface of the earth beneath, and voltages between the base of the cloud and the earth can increase to 100 million volts or more. This charge concentration increases the voltage between cloud and earth until the dielectric strength of the moist air between cloud and ground is overcome, and a spark—the lightning flash—occurs.

6.2.2 The Stroke Mechanism—Negative Downward Leaders

Lightning flashes may have to traverse several kilometers to complete a path to earth. The progression of the lightning channel toward the earth is sketched in Figure 6.2-2 for a typical negative downward leader. As shown in Figure 6.2-2, the leader usually starts from a negative charge pocket in the cloud as a "stepped leader," so called because the discharge proceeds as a series of steps toward the earth. Each step appears as a faint glow discharge whose core may be a few centimeters in diameter and approximately 50 m long, surrounded by a corona envelope a meter or more in diameter. The tip at the bottom end of the leader exhibits some enhanced illumination caused by strong corona activity, and typically appears on a streak camera photograph as a sequence on glowing spots proceeding toward the earth. Each step starts at the lower end of the previous step, zigzagging toward the earth, often accompanied by downward branching.

A time interval of about 50 μs occurs between successive steps, but this time between steps shortens as the leader nears the earth below. The average velocity is in the range of 3 x 10^5 m/s, one-thousandth the velocity of light. The entire stepped leader acts as a conductor carrying a strong distribution of negative charge in its corona sheath as it moves toward the striking point. As the leader progresses, it carries negative charge from the charge pocket from which it began, and this charge distributes along the leader channel in the manner shown in Figures 6.2-3 and 6.2-5.

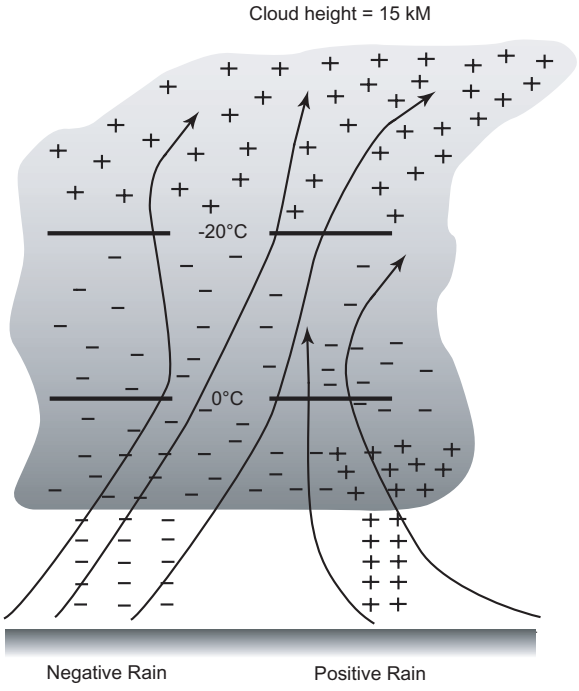


Figure 6.2-1 Electrification of a thunder cloud.

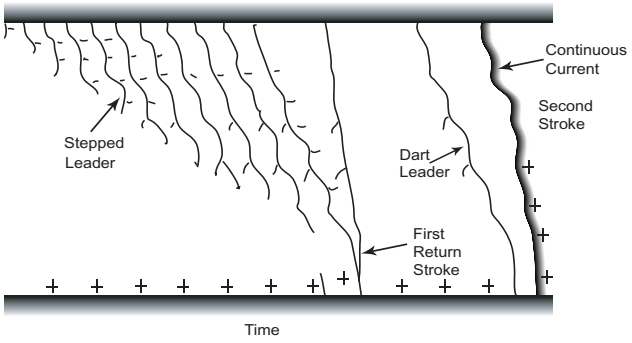


Figure 6.2-2 Progression of the downward leader and formation of the return stroke.

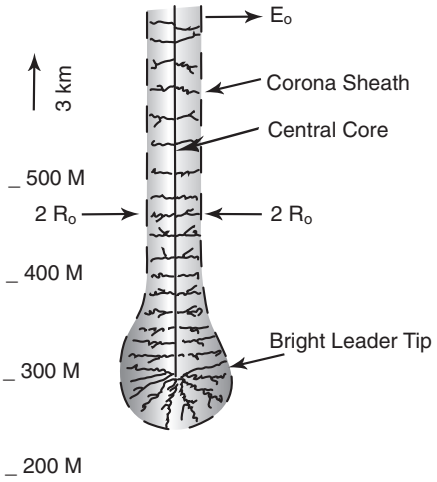


Figure 6.2-3 Storage of space charge in the corona envelope around the leader core (Hileman 1999).

In the stepping action, this charge is continually redistributing itself, feeding the leader tip as it moves and drawing more charge from the cloud charge pocket in what is essentially a progressive electrostatic process. As the leader tip approaches the earth, the leader charge creates a strong electric field at the earth's surface (or on a transmission-line conductor), and a leader is initiated from the earth and/or conductor, which moves upward to intercept the tip of the downward leader. When the two make contact, an electrical connection is created between cloud and earth.

This charge down near the lower end of the leader channel—not the charges in the cloud above—creates the very high and rapidly-changing currents injected into a transmission line. The charge distribution on the downward leader is not uniform. It is continually changing as the leader progresses, but the charge concentrates in the lower reaches of the channel, attracted by image charges in the earth below.

As the leader tip approaches within approximately 100 m of the earth (depending on the charge on the downward moving leader), the earth's electric field builds up to values greater than the dielectric strength of the air around pointed or protruding objects, and a positively charged upward leader rises from the ground or from a protruding object to meet the downward leader (Figure 6.2-2). When the two leaders merge, a current path now exists between cloud and ground. In classical terminology, the negative charges in the leader channel and its corona envelope now move down the completed channel toward the earth as the positive charges on the earth now move up the channel to meet them. The negative charge flowing down through an ammeter creates the same negative deflection as the positive charge flowing up through the other end of the same ammeter, so a powerful negative "return stroke" current moves skyward, eventually discharging most of the negative leader charge along the leader channel. The surge impedance of this return stroke channel is much higher than the impedance of any line conductor or transmission tower, so it can be considered to be a high-impedance current generator.

As shown in Figure 6.2-2, the first stroke can be followed by one or more subsequent strokes. A "dart leader" initiates each subsequent stroke. This dart leader progresses continuously down the ionized channel without stepping, and carries new charge extracted from other charge pockets in the cloud. As each dart leader reaches the ground terminal, it triggers another return stroke. These subsequent strokes tend to have lower magnitudes than the first stroke because the dart leader can move downward along the ionized path with less charge and less gradient at its tip. However, the higher conductivity tends to concentrate more charge per meter near its tip, and this creates a faster rate of rise of current, *dI/dt*. This high *dI/dt* can be an important contributor to the insulator flashover process for towers with high inductance, and is a dominant term in the electromagnetic pulse effects that affect nearby low-voltage or distribution systems. The mean number of strokes in a flash is three, but more than 20 strokes have been reported in unusual conditions.

Many return strokes are followed by continuing current flow of a few hundred amperes, representing a slow depletion of charge in the cloud. Because of its duration of many milliseconds, this low current can deliver more charge than that delivered by the return stroke, a characteristic similar to that of an arc welder. This charge transfer is primarily responsible for burning, melting, and other thermal effects associated with a lightning flash, including ignition of combustible material. Rakov and Uman (2003) estimate about 10% of the 1363 strokes in Florida and New Mexico had a continuing current of more than 40 ms.

6.2.3 The Stroke Mechanism—Upward Positive Leaders

When a tall object such as a river crossing tower, tall building, or mast is located on the earth under the same cloud electrification shown in Figure 6.2-1, a different triggering mechanism can occur. The electric field can build up around the top of grounded object so strongly that an upward leader is initiated from the object and moves toward a negative charge pocket at the base of the cloud, often accompanied by upward branching. This leader eventually completes the circuit, and negative current flows from the cloud to earth as a first stroke, and subsequent strokes can then follow. Analytical models from switching-surge flashover physics can be extrapolated (Rizk 1994) to give relatively simple estimates for the induced potential U_{ic} needed to initiate and propagate an upward positive leader from a vertical tower of height h (in m):

$$U_{ic} = \frac{1556\,kV}{1 + \frac{3.89}{h}} \qquad 6.2\text{-}1$$

One common lightning research strategy takes advantage of this upward initiation by firing small rockets toward a charged cloud with trailing wires attached to a grounded test object (Leteinturier 1990). An upward leader is emitted off the nose of the rocket as it approaches the cloud, completing the current path between the cloud and the ground, and a current flows down the wire. The wire vaporizes, but a complete ionized path then exists between the cloud and the test object for subsequent strokes to follow. This "triggered lightning" has been found to be very useful in simulating lightning hits to or near experimental objects such as

overhead wires, buried cables, arresters, or buildings (Barker et al. 1996; Schnetzer et al. 1995).

Structures having a height of 150 m or more (river crossings, tall masts, etc.) can initiate upward leaders directly without the necessity of an approaching downward leader. For this reason, they tend to collect a disproportionate share of lightning hits per year (Eriksson 1987; Gorin and Shkilev 1984). The 553-m CN Tower in Toronto, Ontario initiates an average of 70 upward flashes per year in an area of moderate ground flash density, some with upward leader development to charge centers more than 10 km away (Janischewskyj et al. 1997a).

6.2.4 The Stroke Mechanism—Positive Flashes

While the majority of lightning flashes deliver negative stroke currents, a small percentage are positive. Positive stroke currents tend to be of higher magnitudes and—although less frequent—can be more severe for surge arrester duty and metal erosion. Measurements from lightning location networks suggest a fairly wide variation of positive flash events over time and space, with a greater number of positive events in the winter, and areas in central North America and the Sea of Japan showing high positive-flash activity.

6.2.5 Charge and Voltage

Mazur and Ruhnke (Mazur and Ruhnke 2001) provide some recent experimental results for 24 low-current return strokes, measured from a lightning-location system. They measured time-correlated field changes associated with the return strokes at two locations. Figure 6.2-4 shows their estimates of leader potentials to earth as a function of leader charge.

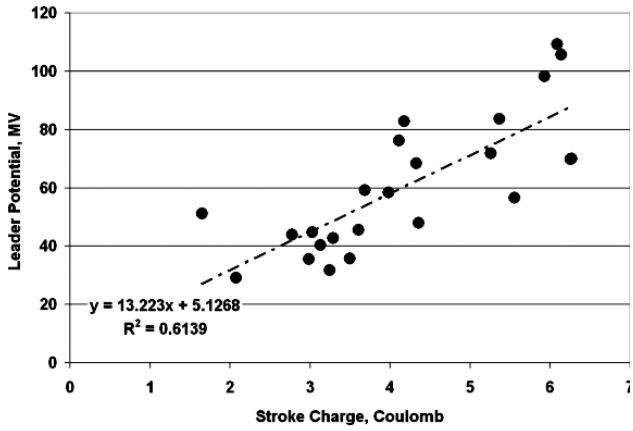


Figure 6.2-4 Experimental estimates of leader potential as a function of leader charge.

The leader potentials reached over 100 MV in two cases, with total charge approximating 6 C. Six coulombs released over a period of 100 ms corresponds to an average current of 60 A, but the same charge released in 100 μs corresponds to an average current of 60 kA.

6.2.6 Leader Diameter, Visibility, and Branching

Streak camera photographs of negative lightning usually show the stepping action as a series of bright dots along the channel, representing the strong ionization occurring at the leader tip at the end of each step. Between these tip discharges, little is to be seen, although ionization is occurring radially outward from the center of the channel as it moves. This radial ionization can extend from the core for a distance of a meter or more, as shown in Figure 6.2-4, and is responsible for the storage of the negative charge that is later swept up by the return stroke. If 31 kA is assumed for the median peak stroke current, and if this current is created by a linear charge moving at one-third the velocity of light, that charge equates to 3.1×10^{-4} C/m. Assuming the outer wall of this radial ionization expands until its gradient is less than a nonuniform field breakdown strength of air of approximately 20 kV/cm, application of Gauss' Law yields an ionization radius R_0 of 2.9 m in which charge is stored. Thus the downward leader can be regarded as a large cylindrical capacitor, which dumps its charge to earth via the return stroke.

In weak strokes, very little branching occurs, but if the downward leader channel contains excessive charge, the leader branches to maintain some kind of equilibrium at its walls. The branches proceed in the same direction at the main channel, usually downward because downward leaders initiate most flashes. If a flash is observed with upward branches, the assumption can usually be made that the flash was triggered by an upward leader emitted from a tall, earthed object. Two or more branches can sometimes reach the earth nearly simultaneously, creating multiple strikes to the earth or to a transmission line.

Both (Kitigawa et al. 1962) and (Rakov and Uman 1990b) report nearly 50% incidence of multiple earth terminations from the same downward leader. In some cases, distance between terminations can be more than 30 km, although most pairs are observed to hit the ground within 5 km of each other. This has led to discussion of whether it is more appropriate to evaluate lightning performance on the basis of ground stroke termination density, which could be as much as 1.7 times the traditional ground flash density. Another possibility is the use of the observed stroke flash density. At present, about 20% of flashes classed as first strokes by lightning location networks are probably the first of several subsequent strokes in events where the first stroke is difficult to observe remotely. Observation and

classification systems are being improved and validated using ground-truth (video) or high-performance Lightning Imaging Detection and Ranging (LIDAR) equipment. Accurate observation of multiple ground terminations and of subsequent stroke movements using lightning location systems may well prove to be of more value than the simple ground flash density values.

6.2.7 Structure and Progression of the Positive Upward Connecting Leader

The positive upward leader emitted from the earth or from a transmission line by induction from the downward leader negative charge (Figure 6.2-2) acts as the link to complete the lightning discharge circuit. The initiation characteristics and velocity of this upward leader play an important role in transmission-line shielding failures. The last step of the downward leader and its junction with the upward leader is frequently labeled the "final jump" or "striking distance," and several mathematical models of this striking distance have been proposed. Young, Clayton, Hileman, Brown, Armstrong and Whitehead proposed early models. The latter noted that this last step could appropriately be described by the switching surge behavior of large air gaps. Their application of the Paris-Cortina switching surge flashover data (CFO = 500 k_g $S^{0.6}$, kV, m) (Paris and Cortina 1968) led to the development of an early electrogeometric model for the shielding of transmission lines.

Later studies by (Dellera and Garbagnati 1990) and (Rizk 1989; Rizk 1994) have applied more comprehensive Leader Progression (LP) models of the switching-surge flashover process to the development of the upward and downward leader. The upward process in this case responds to the downward leader, initiating an upward streamer that, with increasing energy input, "thermalizes" into a leader, which then propagates upward. Rizk (Rizk 1994) defines the two conditions that must be satisfied—one for initiation of the positive upward "counter leader," and another for its stable propagation.

Electric Field Conditions

An upward leader from the earth initiates when the electric field at the earth's surface reaches some critical value. This field is from the combined effect of charges in the leader and in the cloud above it. For air at atmospheric pressure and 20°C, the balance between ionization and recombination occurs in uniform electric field strength of 2600 kV/m. The earth is invariably a nonuniform field electrode with projecting vegetation, rocks, or a variety of geologic features. Estimates of this critical gradient vary widely, depending on surface roughness, and the authors have used a median value of 500 kV/m for many common surfaces. Similarly, an upward leader from a transmission-line conductor initiates when the charge induced on the conductor by the approaching downward leader reaches some critical value, and 1500 kV/m on the wet conductor surface appears to be a workable value. Applet L-2 supplied in this chapter permits the user to experiment with different gradient values and actually observe the progression of the upward and downward leaders associated with one or two transmission lines on a right-of-way.

Structure of the Upward Leader

There are two distinct types of upward leaders: the upward leader initiated by the approach of a downward leader from the cloud, and an upward leader triggered from a tall structure in the absence of a downward leader. For a negatively charged cloud, both types carry positive charge and progress upwards as a continuous discharge without stepping and with an estimated velocity in the range of 0.6 to 1 m/μs, approximately twice the speed of the negative downward leader. The upward leader from a transmission line usually travels without branching since it is carrying a minimal charge, but the leader from a tall structure can display pronounced branching, which is one way of identifying by photography whether a flash to a tall structure was initiated by a downward leader from the cloud or by an upward leader from the structure.

Figure 6.2-5 shows the instantaneous magnitude of negative charge distributed on the leader channel as a downward negative leader approaches the earth. This charge distribution of the return stroke can be modeled with vari-

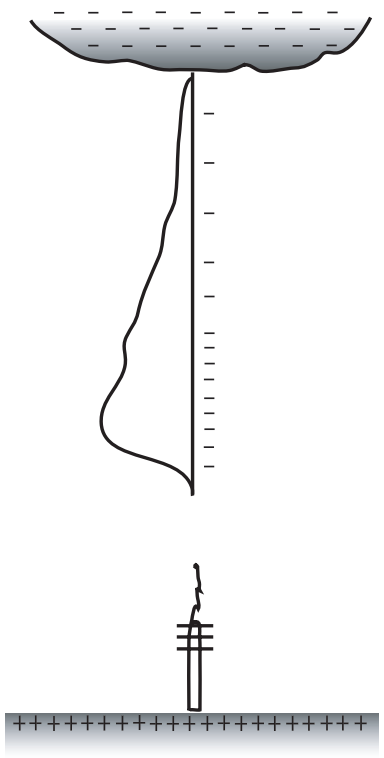


Figure 6.2-5 Distribution of charge on the downward leader.

ous return stroke models as a uniform distribution (Transmission Line, or TL model), a linear decay with height (Modified Transmission Line—Linear, or MTLL model), or an exponential decay with height (Modified Transmission Line—Exponential, or MTLE model) (Uman et al. 1975; Rakov and Dulzon 1991; Nucci et al. 1988 respectively). The peak charge can be 10^{-4} C/m or more. As the upward leader from the earth punches up through this channel charge on its way to the cloud above at approximately one-third the velocity of light (Figure 6.2-2), it can be thought of as an upward-moving grounded wire, collecting the channel charge as it moves. This collected charge moves down the return stroke channel at approximately the velocity of light, and the current waveshape measured at the ground end then replicates the charge distribution on the channel. The front time is greatly influenced by the way the stepping action distributes the charge on the lower end of the channel, as well as by the distribution of charge on the upward leader rising to meet it. This distribution makes the front of the first stroke concave, but subsequent strokes—being much faster—show much less concavity.

Junction with the Downward Leader

Figure 6.2-6, taken from (Anderson and Eriksson 1980), shows the observed "attractive radius" of a structure versus structure height. Attractive radius represents the radius measured outward from the top of a structure such that any downward leader tip within that radius initiates an ultimate strike to that structure. The attractive radius is closely related to "striking distance" in the electrogeometric model, which is the point of discrimination measured outward from the tip of the leader towards any nearby grounded object or line. Both models are partially correct: photographs show that the leaders develop from both ends simultaneously.

Attractive radius is seen to increase with height. Taking an extreme condition, if a wire is 1 cm above the ground, its attractive radius would approach 0, because the ground would reduce the gradient at the conductor surface to a very low value. Nevertheless, many proposed striking distance equations, including that recommended by the IEEE, include no direct conductor height correction. However, the IEEE recommends an indirect correction using a "Beta factor," which varies with line height, as will be discussed in Section 6.6.6.

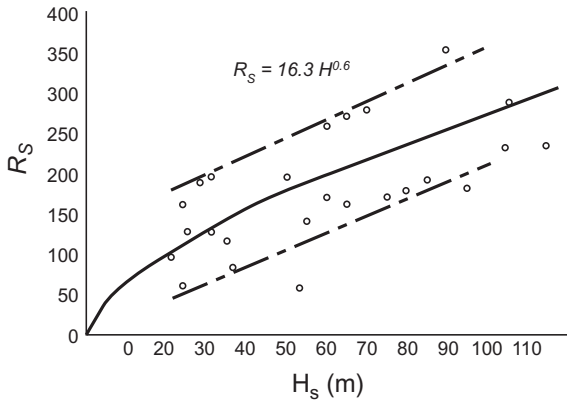


Figure 6.2-6 Observed variations of attractive radius with conductor height.

6.2.8 First Return Stroke Waveshapes

As discussed in Section 6.2.7, the return stroke current waveshape is initially determined by the distribution of charge on the downward leader channel at the moment of contact with the upward leader from a line conductor. The return stroke extracts the downward leader charge as it proceeds upward, and conducts this charge to earth in the form of a high transient current.

Velocity and Channel Charge Neutralization

The charged leader is neutralized by a zero-potential wave that sweeps upward, usually with a velocity that is considerably less than the speed of light. This return stroke velocity can be simulated in the laboratory by distributing multiple, short horizontal stubs at various angles along a vertical conductor, making a cylindrical brush. Each stub diverts and delays a fraction of the total current, and the average path length is increased. Corona streamers around the charged leader are ionized to a high level of conductivity and function nearly as metallic structures in this regard.

Channel Surge Impedance

It is generally assumed that the return stroke channel has a surge impedance much greater that the surge impedance of any transmission tower or line conductor (Wagner and Hileman 1960). Figure 6-2.7 shows observed values of return stroke surge impedance as a function of return stroke current (Mazur and Ruhnke 2001). While the data are widely scattered, in all cases, the impedance is 2000 Ω or higher, which supports the view that the return stroke

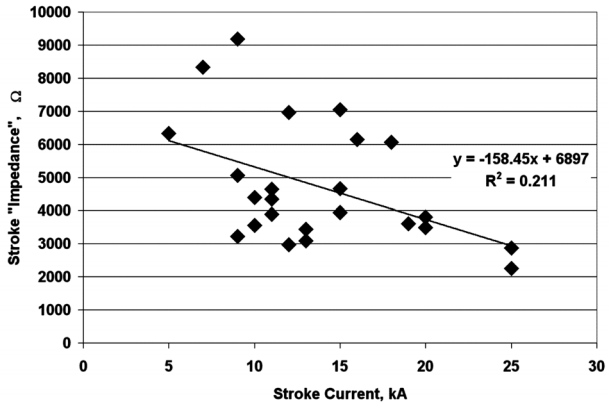


Figure 6.2-7 Return stroke "impedance" (potential / return stroke current) as function of return stroke current (Mazur and Ruhnke 2001).

can be regarded as a current source, not greatly influenced by the impedance of the object at the ground end. This means that the waveshapes and other parameters measured on tall, thin 60-m structures with 300 Ω surge impedance can be used with some confidence on transmission lines with parallel overhead groundwires that present a lower impedance.

Formation of the Surge Current Waveshape

Lightning currents and their corresponding overvoltages are unipolar impulses that may be represented by a waveform shown in Figure 6.2-8. The shape of the impulse consists of a fast-rising front, followed, after reaching a peak value, by a slowly decaying tail. It is usually characterized in terms of the peak value U_m, an equivalent front time t_f extrapolated from the 10 and 90% levels and the time of decay to half of peak voltage on the tail, t_h. The peak values of lightning overvoltage are usually much higher than the corona onset voltage U_0 of the conductor or conductor-bundle used on the transmission line. While the true waveshape has a concave front with relatively slow transition from 10 to 30%, the rise time of standard waves is in the range of 1-2 μs, and the time to half-value is in the range of 40-60 μs. Impulse voltages of this type are usually specified in terms of the peak voltage U_m and t_f/t_h values. The standard lightning impulse voltage, specified in IEEE Standard 4-2000 (IEEE 2000) as 1.2/50 μs, is closest to the lightning current waveshape. When the current is shunted by parallel connections to ground, the tail time reduces as a function of span length and resistance of those paths. Currents measured through nonlinear surge arresters also have longer front times of 4 to 8 μs when a 1.2/50 μs voltage is applied. This has led to the definition of 4/10 μs and 8/20 μs current waves for testing purposes, but these waveshapes do not correspond so well to the original source parameters and should not be used for calculating lightning performance.

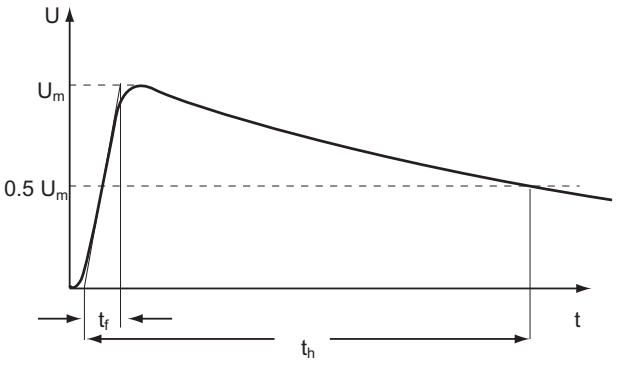


Figure 6.2-8 General voltage waveshape created on transmission lines by return strokes.

Double Exponential Waveshape

Many standards, including IEEE Standard 4, rely on a "double exponential" waveshape described by:

$$I = I_{pk} \cdot K(e^{-t/\tau_1} - e^{-t/\tau_2}) \qquad 6.2\text{-}2$$

For a 1.2 x 50 μs wave, $K = 1.037$, $\tau_1 = 68.5$ μs, $_2 = 0.404$ μs.

The "standard lightning impulse" has a virtual front time (defined as 1.67 times the 30-90% rise time) of 1.2 μs and a virtual time to half value of 50 μs. The current derivative is given analytically by:

$$\frac{dI}{dt} = I_{pk} \cdot K\left(\frac{e^{t/\tau_2}}{\tau_2} - \frac{e^{t/\tau_1}}{\tau_1}\right) \qquad 6.2\text{-}3$$

For the 1.2 x 50 μs wave, the maximum steepness of I_{pk} / 0.392 μs occurs at $t = 0$ (see Figure 6.2-9). The value for a median 31-kA flash would be 79 kA/μs, which is consider-

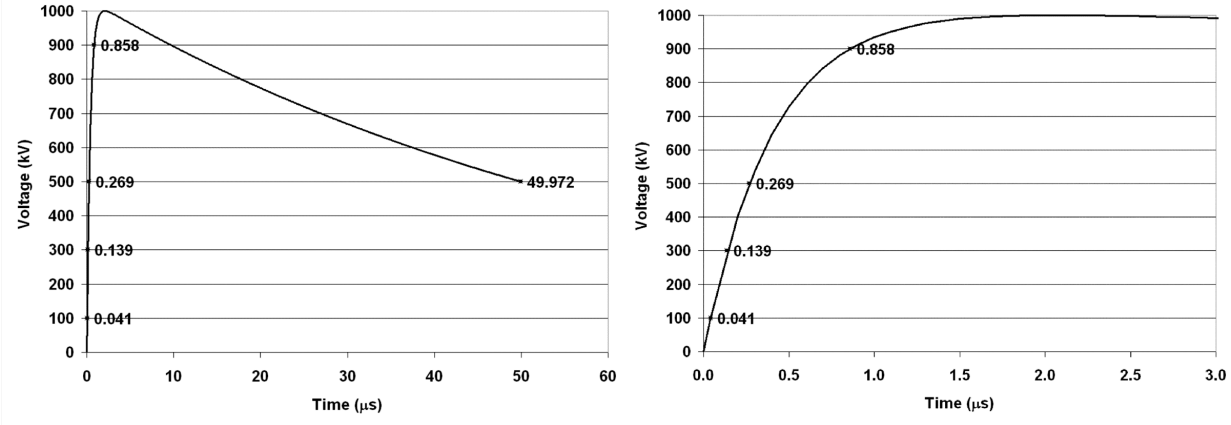


Figure 6.2-9 Front and tail profiles of a standard 1.2 x 50 μs double exponential voltage wave.

ably steeper than the correct 24 kA/μs value, but also occurs when the current is 0, rather than near its maximum. The double-exponential voltage wave is a poor approximation to the lighting stroke current in this regard and, like 4 x 10 μs and 8 x 20 μs current waves, should not be used to describe the input source current in lumped-circuit models.

Heidler Waveshape

Heidler et al. (Heidler et al. 1999) gives a functional form of current *I(t)* as:

$$\eta = e^{(-(\tau_1/\tau_2)(n\tau_2/\tau_1)^{(1/n)})} \quad 6.2\text{-}4$$

$$I(t) = \frac{I_{pk}}{\eta} \frac{\left(\frac{t}{\tau_1}\right)^n}{\left(\frac{t}{\tau_1}\right)^n + 1} e^{(-t/\tau_2)} \quad 6.2\text{-}5$$

Where:

I_{pk} = peak current.
τ_1 = rise time constant.
τ_2 = tail time constant.
n = concave factor (usually n = 5 since this factor mainly introduces delay rather than a change of shape).
η = the peak correction factor.

The Heidler function peak correction factor is valid for concave factors $n > 3$. In contrast, the expressions given in (Feizhou and Shanghe 2002) are valid for all values of n and have the advantage of smoother derivatives in work with Fourier transforms. Figures 6.2-10 and 6.2-11 show the current waveforms for typical waveform parameters.

For a 2 x 50 μs wave, η= 0.9566, τ_1 = 0.244 μs, and τ_2 = 67.5 μs. However, the lower part of the concavity contributes little to the development of severe insulator voltages, and—for this reason—a simple double-exponential current waveshape can be used to create nearly the same current characteristics in the vicinity of the crest of the wave (Figure 6.2-12).

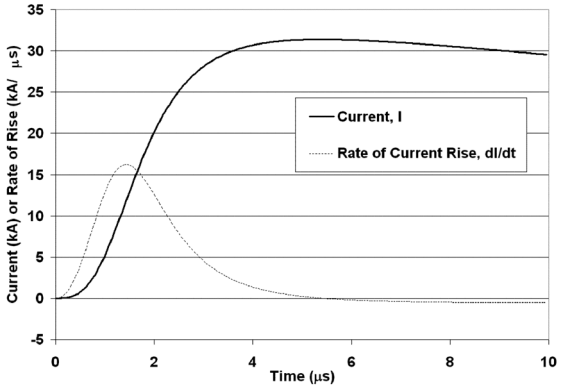


Figure 6.2-10 Heidler waveshape (Heidler et al. 1999).

In both cases, the peak value of *dI/dt* occurs 1.4 μs after the start of the wave, and is still not synchronized with the peak of wave. This feature persists even with high values of *n* and limits the use of either expression for computing the response of the transmission line. Measurements such as those in Figure 6.2-12 show that the peak *dI/dt* occurs at the same time as the current peak, meaning that resistive and inductive voltage rise should be simultaneous.

CIGRE Waveshape

A CIGRE working group has made an extensive analysis of measured stroke current waveshapes, taken mainly from the oscillograph records of Berger (CIGRE 1991). This group defined additional waveform parameters as shown in Figure 6.2-13.

The observed waveshapes (Figure 6.2-13) do not start at zero current, because a minimum current is always required to turn on the measuring equipment. The wavefronts are

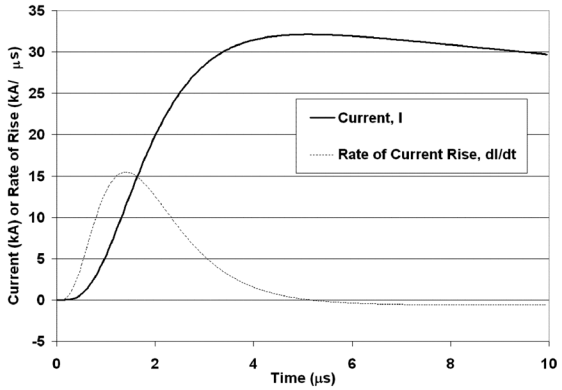


Figure 6.2-11 Feizhou waveshape (Feizhou and Shanghe 2002).

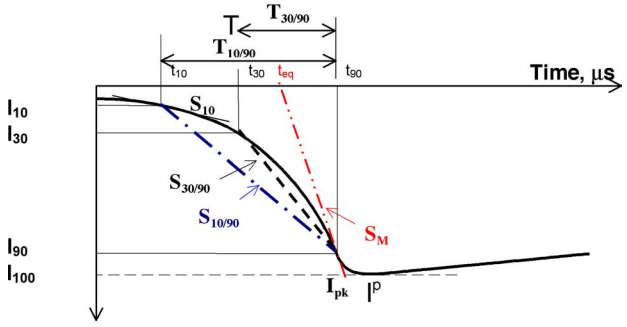


Figure 6.2-12 Crest and front time parameters for a CIGRE current wave.

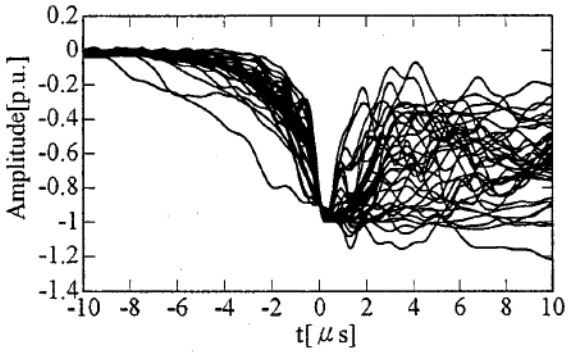


Figure 6.2-13 First stroke current waveshapes (Narita et al. 2000, pp. 429–435).

generally concave, and the steepest portions are near the current peak. The combination of crest current and maximum rate of rise determines the maximum tower top voltages that create insulator flashover. This means that a linear ramp to peak (front $S_{30\text{-}90,}$ or preferably S_M giving t_{eq} in Figure 6.2-12) is more appropriate than the double-exponential waveshape approximation of the stroke current conditions in flashover calculations near the crest of wave. CIGRE (CIGRE 1991) also recommend the following pair of equations for describing a typical first-stroke current if 31 kA with a steepness of 26 kA/μs, an equivalent front duration t_f of 3 μs and a time to half value t_h of 75 μs:

$$t < t_n: I = At + Bt^n$$
$$t > t_n: I = I_1 e^{-(t-t_n)/t_1} - I_2 e^{-(t-t_n)/t_2} \qquad 6.2\text{-}6$$

Where:
t_n = 4.67 us
n = 8.29
A = *3.24 kA/μs*
B = *3.65 x 10^{-5} kA/μs*
t_1 = *105μs*
t_2 = *0.12 μs*
I_1 = 31 kA
I_2 = 3.1 kA

6.2.9 First Negative Return Stroke Parameter Distributions

The Log-Normal Distribution

Figure 6.2-13 illustrates that the first stroke waveshapes vary greatly from flash to flash. This means that many observations must be analyzed to develop statistical descriptions, providing the mean, the dispersion, and the shape of the distribution. Most analysis leads to the use of a "log normal" distribution, with the logarithm of the parameter being normally distributed around a mean with a specified standard deviation.

$$p(x) = \frac{1}{\sqrt{2\pi}x\sigma_{\ln x}} \exp\left[-0.5\left(\frac{\ln x - \ln x_m}{\sigma_{\ln x}}\right)^2\right] \qquad 6.2\text{-}7$$

Where:
σ_{lnx} = the standard deviation of *ln x.*
x_m = the median value of *x.*

In many cases, classification of the statistical distribution using the (Pearson and Hartley 1972) criteria based on functions of skew and kurtosis do support the use of log-normal distributions.

First Negative Stroke: Peak Current Amplitude

A cumulative probability curve of peak amplitudes of first strokes is displayed in Figure 6.2-14. This distribution (Anderson and Eriksson 1980) can be approximated by a two-segment log-normal curve or a simple approximation, shown in the prominent dashed line, as suggested in previous editions of this Reference Book (EPRI 1982).

While Anderson and Eriksson note that each constituent distribution in Figure 6.2-14 had measurements greater than 3 kA, the deviation from a log-normal distribution in the low-current regime may be a result of experimental bias towards large flashes. Generally, oscilloscopes used for these measurements would have used a trigger level of between 3 and 10% of full scale, indicated by I_{trig} in their definition of impulse parameters. Since most experiments were set up to collect 200-kA peak currents, many flashes less than 10 kA may have been missed. With the improved dynamic range of digital instrumentation, more recent tower measurements would tend to have less of this bias.

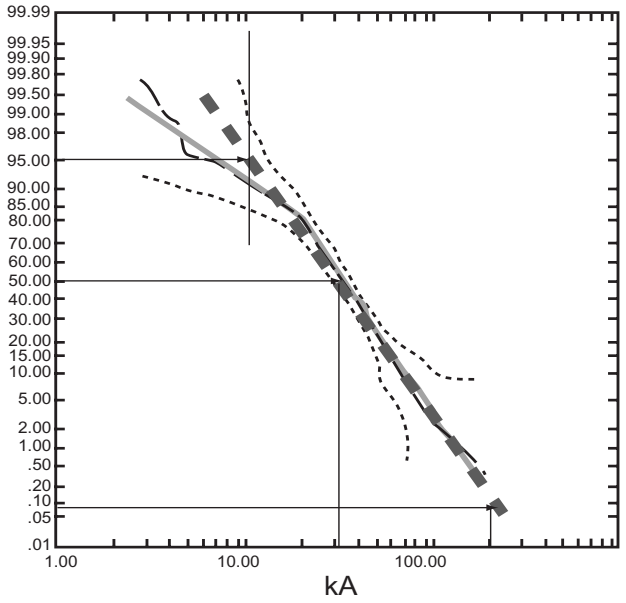


Figure 6.2-14 Cumulative distribution of first negative downward lightning flashes to objects < 60 m (Anderson and Eriksson 1980).

The dashed line in Figure 6.2-14 also shows the probability of a negative first stroke peak amplitude in excess of I_P, computed from Equation 6.2-8.

$$P = \frac{1}{1 + \left(\frac{I_P}{31}\right)^{2.6}} \qquad 6.2\text{-}8$$

This approximation differs from the log-normal distributions only at the extremes, where few data are available. In this regard, the reader should be aware that tall masts collect lightning in a significantly different way than horizontal transmission-line conductors or a flat earth, as will be discussed in Section 6.6. There may also be changes in stroke current characteristics with earth resistivity and latitudes. Rigor in mathematically-defining these statistical distributions may be academically satisfying, but our present knowledge is so limited that rigorous analytical methods contribute little to accuracy of final estimates of line lightning performance.

Lightning location systems provide measurements of peak-radiated field that are converted to stroke currents in kA using one of the transmission-line models. These measurements are precise, often reporting three significant figures, but are not accurate. Examples of anomalies that have been noted include:

- Correlation between sensor spacing and observed median amplitude (e.g., Orville and Huffines 2001), variables that should be independent
- A tendency to report a mixed distribution, with approximately 80-90% of first return strokes being correctly classified and 10-20% being incorrect reports of the first subsequent stroke amplitude. This can give a two-slope distribution that bends the opposite way to the kink in Figure 6.2-14 at 10 kA. This can also be deconvolved using the misclassification fraction if the two distributions have significantly different median currents.
- A wide range of attenuation rate with distance, depending on the local soil resistivity. The lowest attenuation is observed offshore, moderate attenuation is found in the USA NLDN (Cummins et al. 1998) and Florida (Idone 1993), and more than 50% attenuation over 400-km paths in Canada (Herodotou et al. 1990) and the Appalachian mountains (Orville and Huffines 2001).
- An ocean/land impedance discontinuity that gives 25 kA values over the ocean and 20 kA on the shore nearby, where electrogeometric models suggest the reverse should happen.
- No lake/land discontinuity in measured amplitudes over large bodies of water, such as the Great Lakes, with 80-130 Ω-m resistivity, similar to the surrounding land mass.
- Good agreement between lightning location system measurements and observations on 100-m instrumented towers (Diendorfer et al. 2002). Remote readings should be too high on tall towers, because the speed-of-light propagation velocity within the structure increases the radiated field efficiency compared to the return stroke to a shorter object.

Some impediments to the use of remote radiated field data for estimating peak stroke currents have already been addressed. For example, most of the "engineering models" of the return stroke discussed in Section 6.2.7—such as TL, MTLL, and MTLE— predict similar remote electromagnetic fields in practical networks. Studies of channel tortuosity (Levine and Meneghini 1978) show a strong effect later in the wave but little change to the peak-radiated field. Lightning has traditionally been used for geophysical prospecting, taking advantage of the strong current source to excite vertical and horizontal electric fields that give a "tilt angle" and an indication of the underlying strata. For calculations of induced overvoltage using (Agrawal et al. 1981), researchers now understand that this peak electromagnetic field itself, rather than the stroke current and return stroke velocity parameters, is the desired input parameter that illuminates distribution lines. The Sommerfeld-Norton model for sine-wave attenuation over lossy ground is described in Appendix 6.2. This model can be used to invert the observed variations in lightning peak amplitudes to characterize the soil resistivity with better detail than now available through Extra-Low Frequency (ELF) and AM broadcast attenuation maps, as shown in Section 6.10.

Present research suggests that, in spite of the anomalies listed above, there may be regional variations in stroke current amplitude of up to 50%, and that the median current may be somewhat lower than 31 kA. A focus on estimating the density of "damaging" lightning, such as the high density of positive-flash events over 85 kA in north-central U.S. and central Canada (Boccippio et al. 2001), as shown below in Figure 6.2-22, will continue to quantify the extent and significance of the observed variations in parameters.

First Negative Stroke: Rate of Current Rise

The probability of maximum *dI/dt* of a negative first stroke exceeding S_m in Figure 6.2-12, is given by:

$$P = \frac{1}{1 + \left(\frac{S_m}{24}\right)^{4}} \qquad 6.2\text{-}9$$

Where:

S_m is expressed in kA/μs.

First Negative Stroke: Charge

The probability of negative first stroke charge exceeding Q is given by:

$$P = \frac{1}{1+\left(\frac{Q}{5}\right)^2} \qquad 6.2\text{-}10$$

Where:

Q is expressed in coulomb (1 C = 1 A x 1 s).

Correlations Among First Negative Stroke Parameters

The joint probability density function between two parameters, both with log-normal distributions, is given by:

$$p(x,y) = \frac{\exp\left[\frac{-0.5}{1-\rho_c^2}\left(A_1 + A_2 - A_3\right)\right]}{2\pi \cdot x \cdot y \cdot \sigma_{\ln x}\sigma_{\ln y}\sqrt{1-\rho_c^2}} \qquad 6.2\text{-}11$$

Where:

ρ_c = the coefficient of correlation, and:

$$A_1 = \left(\frac{\ln x - \ln \bar{x}}{\sigma_{\ln x}}\right)^2$$

$$A_2 = \left(\frac{\ln y - \ln \bar{y}}{\sigma_{\ln y}}\right)^2 \qquad 6.2\text{-}12$$

$$A_3 = 2\rho_c\left(\frac{\ln x - \ln \bar{x}}{\sigma_{\ln x}}\right)\left(\frac{\ln y - \ln \bar{y}}{\sigma_{\ln y}}\right)$$

The conditional probability density function of the variable y, given $x = x_0$, is:

$$p(y \mid x = x_0) = \frac{p(x,y)}{p(x)} = \frac{\exp\left[-\frac{(\ln y - b)^2}{2\sigma^2}\right]}{\sqrt{2\pi}\, y\sigma} \qquad 6.2\text{-}13$$

$$b = \ln \bar{y} + \rho_c \frac{\sigma_{\ln y}}{\sigma_{\ln x}}\left(\ln x_0 - \ln \bar{x}\right)$$

$$\sigma = \sigma_{\ln y}\sqrt{1-\rho_c^2}$$

Narita et al. (Narita et al. 2000) give observations of 36 peak stroke currents on transmission towers, along with their maximum rate of rise, in Figure 6.2-15. A higher correlation coefficient of $\rho_c = 0.85$ for Equations 6.2-11 and 6.2-12 found between the two variables than for the CIGRE data. The Japanese UHV design point of 200 kA/μs in Figure 6.2-15 is seen to be roughly twice their highest observed values of 100 kA/μs.

In their correlation studies between electric field change and peak stroke current estimate (from lightning location systems), Mazur and Ruhnke (Mazur and Ruhnke 2001) develop a weaker experimental relationship between stroke current and leader charge, shown in Figure 6.2-16.

6.2.10 Positive Return Stroke Parameter Distributions

Since they are relatively infrequent, the parameters of first positive strokes have not been characterized as reliably as negative first strokes. The following approximations of positive return stroke parameter cumulative probabilities were derived from an accumulation of data from several sources (Anderson and Eriksson 1981; Rakov and Uman 2003). All currents are in kA, all charges are in coulomb (C).

Probability of positive peak stroke magnitude:

$$P = \frac{1}{1+\left(\frac{I}{34}\right)^{1.5}} \qquad 6.2\text{-}14$$

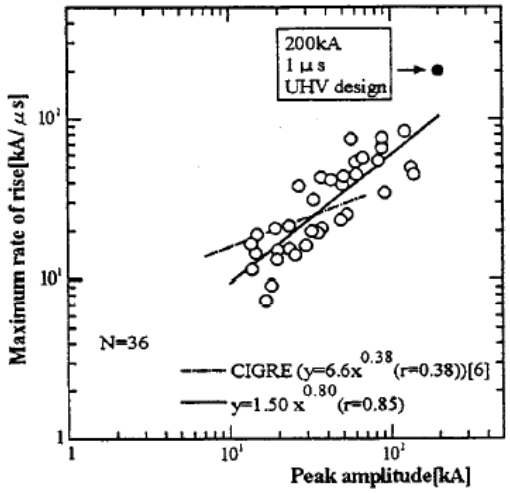


Figure 6.2-15 Observed relationship between peak amplitude and maximum rate of rise (Narita et al. 2000).

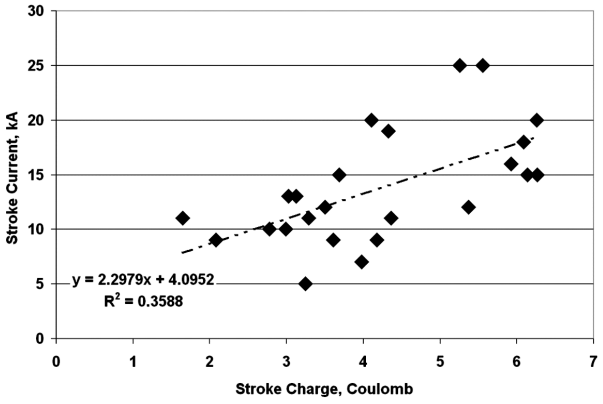


Figure 6.2-16 Return stroke current as a function of leader charge.

Probability of charge delivered by a positive first stroke:

$$P = \frac{1}{1 + \left(\frac{Q}{19}\right)^{1.34}} \quad 6.2\text{-}15$$

Where:
Q is expressed in coulomb.

Probability of total charge delivered by a positive flash:

$$P = \frac{1}{1 + \left(\frac{Q}{85}\right)^{2}} \quad 6.2\text{-}16$$

Where:
Q is expressed in coulomb.

6.2.11 Subsequent Stroke Parameters

After the passage of a return stroke, the lightning channel can re-illuminate quickly with a dart leader, resulting in a subsequent return stroke at or near the initial termination. In some measurements, 10% of the flashes have ten or more strokes per flash. The subsequent strokes tend to have lower values of charge and current, faster return stroke velocity, and less overall impact on transmission-line lightning performance. Special issues related to subsequent strokes include:

- Coordination of steep rates of voltage change (> 2500 kV/μs) with insulator puncture strength and endurance.
- Coordination of the steep rates of current rise (> 40 kA/μs) with nearby electronic equipment.
- Coordination of subsequent-stroke shielding failure flashover in cases of shielding failure where the first stroke is weak.
- Coordination of breaker reclosing times to prevent double trips and lockouts.
- Coordination of lightning surge arrester and accessory energy capability under multi-pulse excitation.

Many researchers have used artificial structures, either tall towers or rocket-triggered thin wires, to increase the probability of lightning flashes to their experimental setups. Research does support the hypothesis that, once the artificially-ionized channel from the upward leader has warmed to its task, the dart leaders and subsequent strokes along the same channel are similar to those found in nature. The median stroke current distributions, distant electromagnetic fields, and other features of natural subsequent strokes are similar to all records taken from artificially triggered lightning (Uman and Rakov 2002; Janischewskyj 1997a). However, differences in time to half value and rates of current rise have been found in some comparisons (Cooray 2003b).

As mentioned above, some of subsequent strokes are misclassified as small first strokes in lightning location systems, and some of the lower-amplitude events fall below the local detection threshold of the networks. However, multiple ground terminations are also counted as a first and a subsequent stroke, rather than two different first strokes. Both of these factors are being addressed in a process of continuous improvement for lightning location technologies.

Subsequent Stroke: Average Number

Uman (Uman 1987) suggests a mean of three subsequent strokes per flash, based on studies of Schonland in South Africa and Master in Florida. Anderson and Eriksson (Anderson and Eriksson 1981) recommend a global average ground-flash multiplicity of three, one first stroke and two subsequent strokes, for negative downward lightning. Observations from lightning location systems in the United States (Orville and Huffines 2001) show a mean negative multiplicity of 2.6 in Florida and most of the central U.S., falling to less than 2.0 in the west. Practically all positive flashes have a single stroke.

Subsequent Stroke: Interstroke Interval

The interstroke interval between subsequent strokes has been studied widely using video cameras (Anderson and Eriksson 1980) and, more recently, time-tagged observations of lightning location system data. The following expression is recommended for $t_{I\text{-}S}$, the interstroke time interval:

$$P = \frac{1}{1 + \left(\frac{t_{I-S}}{35\,ms}\right)^{1.7}} \quad 6.2\text{-}17$$

If regional variations in multiplicity occur, there could also be some regional variation of interstroke interval. Values for South Africa (Schonland 1956) and Thompson et al. (1984), areas of relatively high multiplicity, are 51 and 68 ms, respectively.

Subsequent Stroke: Overall Flash Duration

Figure 6.2-17 shows typical distributions of the duration of multiple-stroke flashes for three regions, along with a recommended relation as a solid line. The extreme values of this distribution are used for establishing protective settings for relays, especially for single-pole reclosing on unshielded lines, to ensure that the lightning event is over before the line is re-energized.

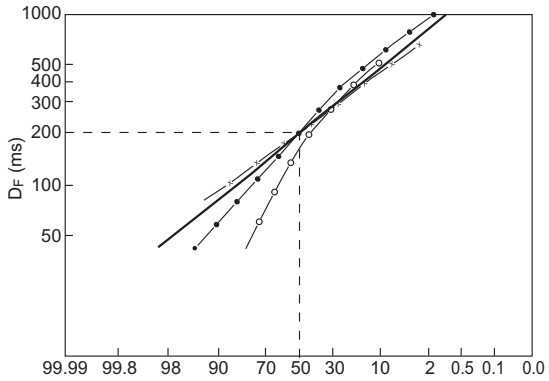


Figure 6.2-17 Percent of multiple-stroke flashes having duration exceeding vertical-axis value (Anderson and Eriksson 1980).

Subsequent Stroke: Peak Current Magnitude

Probability of negative subsequent stroke peak current > 0:

$$P = \frac{1}{1 + \left(\frac{I_P}{12}\right)^{2.7}} \qquad 6.2\text{-}18$$

Subsequent Stroke: Time to Crest

The definition of time to crest for subsequent strokes is compromised by the fact that many observations with wideband sensors show a 100-ns step from 50 to 90% of the wave.

Subsequent Stroke: Maximum dI/dt

The maximum rate of current rise of lightning determines the peak values of electromagnetically-induced voltage in closed or open loops in the vicinity of the tower (Hasse 2000). Also, the fast-rising voltages impressed across transmission-line insulators will eventually puncture cap-and-pin porcelain insulators electrically.

The maximum steepness of lightning occurs near the peak of wave. Anderson and Eriksson (Anderson and Eriksson 1980) used the maximum slope S_m to the current waveform to describe this feature. As shown in Figure 6.2-12 and 6.2-18, this portion of the wave has much greater steepness than the tangent at 10% and steepness associated with 10-90% and 30-90% points on the wave.

The dashed line in Figure 6.2-18 shows an approximate fit to the probability of maximum steepness S_{max} using:

$$P(S_{\max}) = \frac{1}{1 + \left(\frac{S_{\max}}{40\ kA/\mu s}\right)^{2.1}} \qquad 6.2\text{-}19$$

Measurements of radiated fields and return stroke currents from rocket-triggered lightning tend to have steeper distributions of maximum steepness. A mean value of 180 kA/μs for 100 measurements was reported by (Weidman and Krider 1980) based on a constant return stroke velocity assumption of $c/3$. Similar results have also been reported from rocket-triggered lightning experiments at Camp Blanding in Florida (Rakov and Uman 2003).

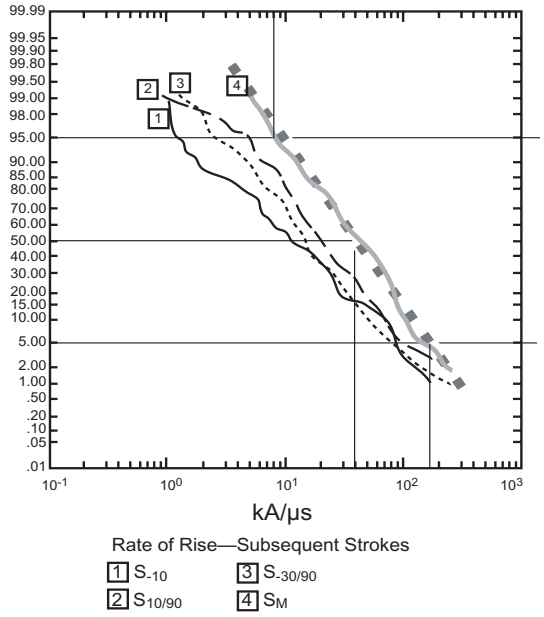


Figure 6.2-18 Probability of rate of rise of subsequent strokes.

Subsequent Stroke: Charge

The charge delivered by subsequent strokes has been shown to contribute to thermal stress on distribution surge arresters and disconnectors. The approximate model of a first stroke (median 5 C) and two subsequent strokes (each median 1 C), giving a total of 7 C, is reasonable. The probability of charge delivered by a negative subsequent stroke is estimated from:

$$P = \frac{1}{1 + \left(\frac{Q}{1}\right)^{2.2}} \qquad 6.2\text{-}20$$

Where:

Q is expressed in coulomb.

The overall probability of total charge delivered by a negative flash (including first and subsequent strokes) is given by:

$$P = \frac{1}{1 + \left(\frac{Q}{7}\right)^{1.7}} \qquad 6.2\text{-}21$$

Where:

Q is expressed in coulomb.

These values are also used for specifying adequate energy absorption capability when gapped or gapless Transmission Line Surge Arresters (TSLAs) are used on unshielded transmission lines.

6.2.12 Electromagnetic Fields from Return Strokes

LeJay (LeJay 1926) reported a relationship between the charge moment (product of charge and separation distance) of a vertical source *M* and the horizontal component of magnetic field B_h:

$$B_\phi = \frac{\mu_o}{4\pi c D^2}\left[c\frac{dM}{dt} + D\frac{d^2M}{dt^2}\right] \qquad 6.2\text{-}22$$

Where:

μ_o = the permittivity of free space, $4\pi\ 10^{-7}$ H/m.
D = the distance in m.
c = the speed of light, 3.10^8 m/s.
t = time in s.

Uman et al. (Uman et al. 1975) noted that, in effect, a current *i(t)* moving vertically upward with uniform velocity *v* produces a second derivative of charge moment that matches the current as follows:

$$\frac{d^2M}{dt^2} = 2\,vc\;i(t) \qquad 6.2\text{-}23$$

At distances greater than about 5 km from a lightning source, the induction term *dM/dt* can be ignored, meaning that the distant radiated field waveshape becomes a faithful copy of the return stroke current:

$$B_\phi\left(t+\frac{D}{c}\right) = \mu_o H_\phi\left(t+\frac{D}{c}\right) \approx \frac{\mu_o v}{2\pi c D} i(t) \qquad 6.2\text{-}24$$

For a peak stroke current of 30 kA, moving upwards at a velocity of $v = c/3$, the peak magnetic field at a distance D = 100 km is B = 20 nT. Since this is a radiated field, the impedance of free space relates the horizontal magnetic field to the vertical electric field as follows:

$$Z_o = \sqrt{\frac{\mu_o}{\varepsilon_0}} = 377\ \Omega \qquad 6.2\text{-}25$$

$$\begin{aligned} E_z\left(t+\frac{D}{c}\right) &= Z_o H_\phi \\ &= \frac{1}{c} B_\phi\left(t+\frac{D}{c}\right) \\ &= \frac{4\pi\cdot 10^{-7} v}{2\pi D} i(t) \\ &= 60\frac{v}{c}\frac{i(t)}{D} \end{aligned} \qquad 6.2\text{-}26$$

Here, E_z is expressed in V/m. For the 30-kA stroke at 100 km, E_z = 6 V/m.

This model ignores observations that neither the return stroke speed nor the source current (or its surrogate, the optical radiation strength) is constant as the wave travels up the transmission line. A wide range of modified models is discussed critically in Cooray (2003b). Many details in the use of the transmission-line model with distant radiated electric and magnetic fields to estimate lightning return stroke parameters, including location and peak current, remain to be resolved through cross-calibration and experimental validations, and this work is ongoing.

6.2.13 Upward Flashes from Tall Structures

Rizk (Rizk 1994) worked forward from the success of a switching-surge flashover model in describing the final jump to a downward leader. He described a second condition necessary for stable propagation of an upward leader. After analysis and interpretation, this model gives an estimate of the ground-level electric field E_Z that will cause an upward flash from a structure of height *h*:

$$E_Z = \frac{1600kV}{h} \qquad 6.2\text{-}27$$

Equation 6.2-26 suggests that upward leaders develop from a 100-m structure at a ground-level vertical electric field of about 16 kV/m. This electric field would be calculated from the charge structure in the cloud, prior to development of downward leaders. The upward leaders from tall structures have low currents during their development, but often bring dart leaders and subsequent return strokes to tall structures. Berger and other researchers have been careful to identify upward flashes and to segregate their parameters from downward flash results (Berger et al. 1975). Eriksson (Eriksson 1987) had previously related the observed incidence of upward flashes to structure height in the range of 80 to 550 m using

$$\%\ \text{Upward} = 52.8\ \ln(H_{\text{meters}}) - 230 \qquad 6.2\text{-}28$$

Measurements carried out on tall 553-m telecommunication towers (Rachidi et al. 2001) have established relatively low subsequent-stroke amplitudes, relative to shorter towers. Some of this bias is attributed to the ability to record an "initial uncontaminated" wave as it travels down the tower and, 3 μs later, to measure the imperfect reflection from ground. Figure 6.2-19 shows a typical fast-front record.

In the stroke current waveform, top right of Figure 6.2-19, the initial wave is an 8-kA step, and a reflection from ground of approximately 3 kA arrives at the measurement point 3μs later. The imperfect reflection coefficient, corresponding to a transient impedance of 55 Ω, is a result of the electromagnetic response of the ground plane, as described in Section 6.4. The electric and magnetic fields measured so close to the tower are influenced by several factors, such as reflections up and down the tower, as discussed in (Rachidi et al. 2001).

6.2.14 Experience on 60–140 m Towers

Narita (Narita et al. 2000) carried out 36 measurements of lightning stroke currents on transmission towers in the height range of 60 to 140 m. Table 6.2-1 (Narita et al. 2000) shows the peak current characteristics from this study, along with values from (Berger et al. 1975; CIGRE 1991) and (Eriksson 1987; Visacro et al. 2004) for first negative downward flashes.

Anderson and Eriksson (Anderson and Eriksson 1980) advanced a hypothesis that, for structures up to 60 m height, the stroke current distribution is independent of height. Figure 6.2-20 from (Narita et al. 2000) shows only a weak trend to higher currents with structure height of 60-140 m, supporting Anderson and Eriksson's idea.

6.2.15 Winter Lightning

Winter lightning, although infrequent, can be more severe, with a higher fraction of positive flashes having large peak currents, long wave fronts, and high delivered charge. Winter lightning appears to be more attracted to tall structures than summer lightning, and has been observed to strike two or more structures with the same flash (Miyake et al. 1990; Yokoyama et al. 1990). It often starts from tall structures, and the leader progresses upwards. Udo (Udo 2004) has

Table 6.2-1 Comparison of Peak Current Statistics

Reference	95% Value	50% Value	5% Value	σ of ln I	Sample Size
Berger 1975	14 kA	30 kA	80 kA		101
CIGRE 1991	6 kA	31 kA	90 kA	0.32	408
Narita 2002	11 kA	39 kA	135 kA	0.33	36
Eriksson 1987		36 kA		0.31	22
Visacro 2004	22 kA	40 kA	75 kA		79

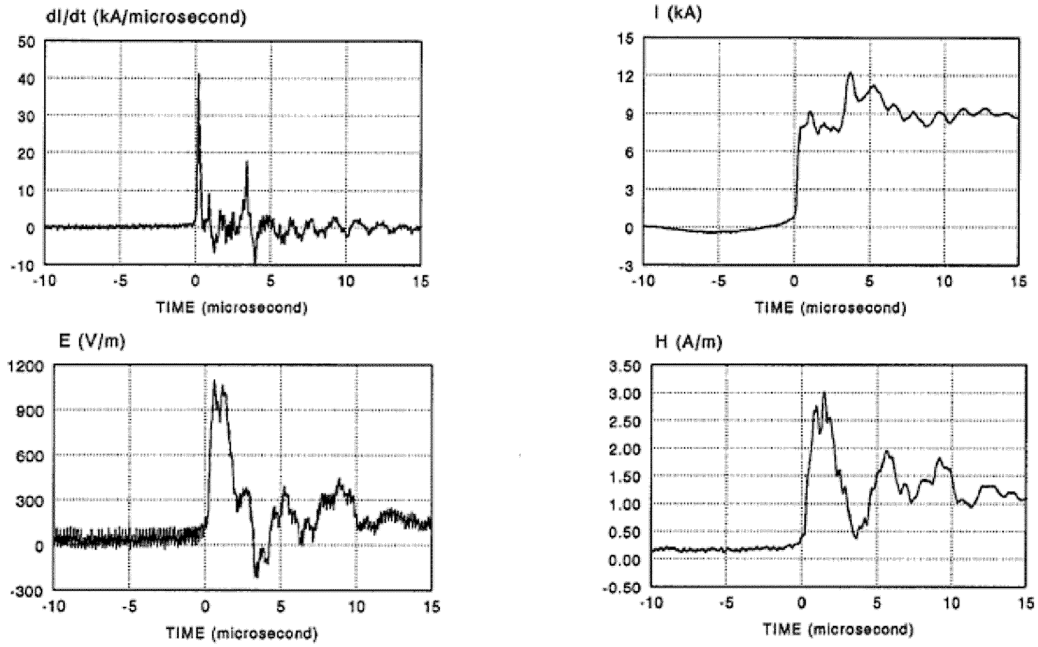


Figure 6.2-19 Typical current record at 553-m CN Tower (Rachidi et al. 2001) along with electric and magnetic fields at 2 km.

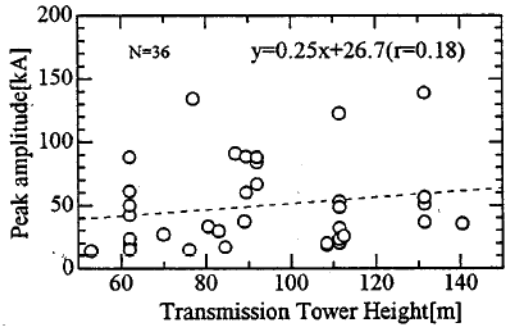


Figure 6.2-20 Observed relation between peak amplitude and tower height (Narita et al. 2000).

reported that the probability of a double-circuit flashover from a winter lightning flash is substantially higher than for summer lightning.

Evidence from a number of studies in Japan suggests that local conditions in the Sea of Japan lead to a strong local incidence of winter lightning. Physically, the dividing line of -15°C in the cloud, separating positive and negative charge centers, is closer to the ground. This factor, combined with stronger upper-level winds that tend to push the cloud top in front of the base, means that more positive lightning could develop to ground. Lightning location system data in continental U.S. also supports a summer/winter classification based on the ratio of positive-to-negative flashes, as shown in Figure 6.2-21.

6.2.16 Arc Damage from Flash Charge

As stated in Section 6.2.2, a low continuing current often flows between one or more of the high current peaks. This current can deliver substantially more charge than all the high current peaks combined, and is largely responsible for conductor ablation, burning, and general heat damage,

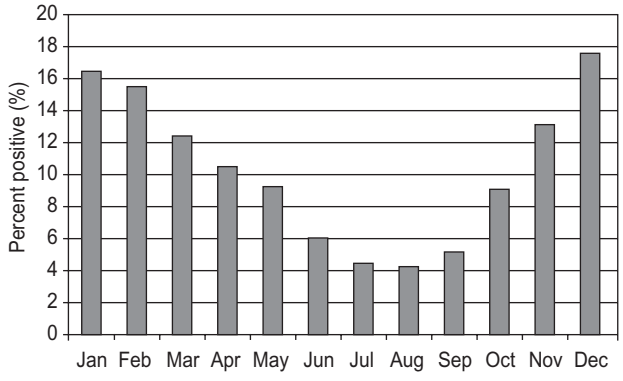


Figure 6.2-21 Mean percentage of positive cloud-to-ground lightning observed with U.S. National Lightning Detection Network (Orville and Huffines 2001).

exceeded only by arc damage from power frequency arcing in many cases. Probability approximation equations for the delivered total coulombs from a flash are given by Equations 6.2.15 and 6.2.20. Using these equations, there is a 10% probability that delivered negative charge from a flash would equal or exceed 25 C, and delivered charge from a positive flash would equal or exceed 255 C. This is equivalent to a dc arc welder applying a current of either 25 A or 255 A to a stricken object for a second.

Lightning plasma temperature is well above the melting point of metals used in transmission-line construction. In cases where continuous transfer of charge between return strokes occurs (mainly for negative flashes), or the charge of the first return stroke is large (mainly for positive flashes), there will be sufficient thermal energy to damage overhead groundwires. Lightning plasma will contribute thermal energy in three ways: radiation, arc root voltage, and chemical energy liberated by oxidation of the material. The radiation is strong, but has low energy density and can be ignored when studying damage to areas of 1 cm^2. The arc root voltage tends to be constant over a wide range of currents (Cobine 1958), so the energy contribution is simply related to the charge (the product of current and time for a rectangular pulse of current). Charge ablates (burns up) metal components in ways that are similar to industrial plasma cutting torches. The chemical energy from oxidation of the melted metal is typically as large or larger than the energy of the arc root, with aluminum providing higher energy compared to iron or zinc and being more susceptible to lightning arc damage. It should be recognized that the action integral i^2dt gives a poor estimate of heat damage in this case, because the arc terminates on either a cathode or anode spot, depending on polarity, instead of on a constant resistance.

Coulomb Probabilities

Arc root damage is an important concern in the successful application of optical fibers within overhead groundwires. IEEE Standard 1138 defines test methods and levels, depending on local flash density, the observed proportion of positive flashes, and the best data available for the parameters of impulse and flash charge. With a ground flash density N_g, and using the model of Eriksson (Eriksson 1987), each of two optical-fiber groundwires of height H would receive:

$$N_{flashes/100\,km/\,yr} = \frac{N_g}{10}\left(14\,H^{0.6}\right) \qquad 6.2\text{-}29$$

Where:

N_g = the ground flash density in flashes per km^2 per year.

H = the tower height in m.

10 provides unit conversion (attractive width in meters times 100 km length) to km^2.

For a two-year return period between damaging events on a 37-m-tall 100-km line with a ground flash density of 4 per km^2 per year, the design threat level would be 98 flashes. In an area with a 10% positive flash rate, this would give 10 positive (N^+) and 88 negative (N^-).

Design threat levels for negative flashes (N^- = 88) are computed as follows:

Negative first-stroke peak current is obtained by inverting Equation 6.2-8:

$$N^- \approx \left(\frac{I^-}{31kA}\right)^{2.6} \qquad 6.2\text{-}30$$

$$I^- \approx 31kA \cdot (N^-)^{1/2.6} = 31kA \cdot (N^-)^{0.38}$$

I^- =173 kA

Similarly, negative impulse charge is obtained by inverting Equation 6.2-9:

$$N^- \approx \left(\frac{Q^-}{7C}\right)^{1.7} \qquad 6.2\text{-}31$$

$$Q^- \approx 7C \cdot (N^-)^{1/1.7} = 7C \cdot (N^-)^{0.59}$$

Q^- = -97 C

The design threat levels for positive flashes (N^+=10) follow the same process, for example inverting Equation 6.2-15 to give a positive flash charge of:

$$N^+ \approx \left(\frac{Q^+}{85C}\right)^{2} \qquad 6.2\text{-}32$$

$$Q^+ \approx 85C \cdot (N^+)^{1/2} = 85C \cdot (N^+)^{0.5}$$

Q^+ = +266 C

It is worth noting that negative charge is about three times more damaging than positive charge per coulomb, a fact that is commonly used in electric arc welding and cutting. Typically, wire strand size of about 3 mm is needed to avoid breaking with this charge injection. Also, Boccippio et al. (Boccippio et al. 2001) present strong evidence of a regional variation in the occurrence of large positive flashes, as shown in Figure 6.2-22, and areas with many large positive flashes should use more robust Optical Fiber (OPGW) and overhead groundwires.

Test Methods

Optical-fiber overhead groundwires are tested by applying a dc current for a duration of 0.5 s. The magnitude of the current is adjusted to match the Q^- level: with the example above, a current of 194 A (negative polarity on rod, positive return on conductor) would give a charge of (194 A x 0.5 s) = 97 C. For OPGW, the performance of the optical fiber during the test and the possibility of moisture penetration are the most important pass/fail criteria. For conventional overhead groundwires, the loss of zinc galvanizing or aluminum cladding, and number of broken strands, remain as the conventional criteria.

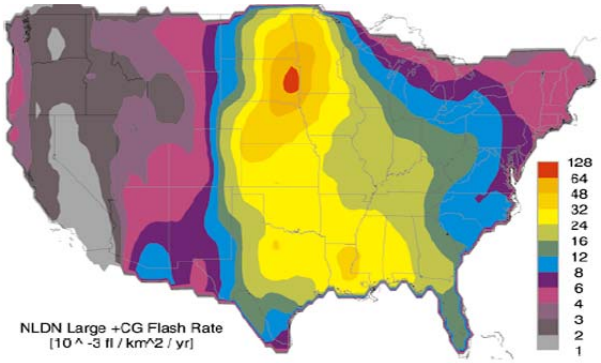


Figure 6.2-22 Occurrence of positive cloud-to-ground flashes with estimated peak currents exceeding 75 kA (Boccippio et al. 2001).

6.3 REGIONAL LIGHTNING FLASH STATISTICS AND DATA

The calculation of lightning flashover rate divides into two main areas, stimulus and response. The stimulus is described by the incidence of lightning, preferably grouped into specific ranges of stroke current amplitude. There are two important regimes of response:

1. The case where a low-amplitude flash excites an energized conductor and causes a flashover to ground. This is a *shielding failure*.
2. The case where a high-amplitude flash excites a grounded support, which responds imperfectly, causing a *backflashover* to one or more energized conductors.

Ishii (Ishii et al. 2002) used lightning location system (LLP) data to categorize lightning flashes that caused 187-kV transmission line outages. Their observations and calculations in Figure 6.3-1 suggest a roughly equal divi-

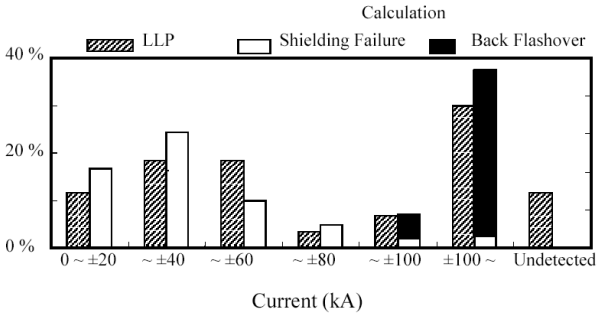


Figure 6.3-1 Lightning currents that caused 187-kV shielded transmission-line outages (Ishii et al 2002, corrected). Solid: Calculated. Hashed: Observed from Lightning Location System.

sion between shielding failures (0-60 kA) and backflashovers (>80 kA) as the root cause of tripouts.

The calculated occurrence of shielding failures at current levels greater than 40 kA is generally associated with nonvertical angles of stroke incidence. Ishii at al. also confirms in Figure 6.3-2 a hypothesis of the linear relationship between observed transmission line outage rates and observed ground flash density. The slope of this relation will be different for each voltage class of line, because higher-voltage lines have greater insulation strength.

6.3.1 Isokeraunic Maps, OTD Measurements, and Lightning Flash Counters

In the second edition of the EPRI Red Book, there was a heavy reliance on the use of the meteorological observations of "Thunderstorm Day" (*TD)* as defined by World Meteorological Association standards (see Figure 6.3-3).

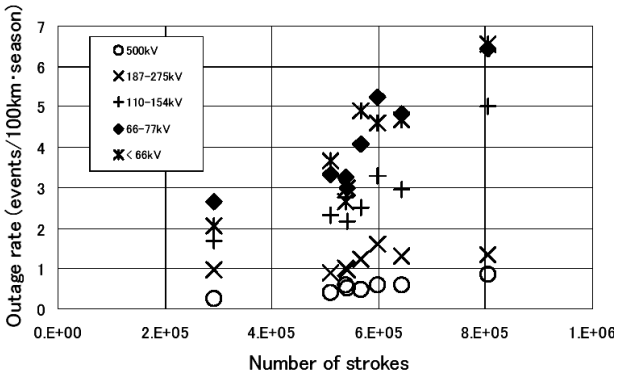


Figure 6.3-2 Transmission outage rate versus total number of lightning ground strokes in Japan (Ishii et al. 2002).

Various expressions were given to relate TD observations to the area density of ground flashes, *GFD,* usually expressed in flashes per square kilometer per year. Generally, ten years of observations are needed in areas of moderate thunderstorm activity (TD = 40 days/year) to obtain the 400 counts needed for a 5% relative standard deviation. Values obtained from areas with TD = 5 need 80 years of data to have the same certainty. This rule-of-400-counts applies to all GFD measurement methods.

Independent measurements of ground flash density have become increasingly sophisticated. In the 1970s, several long-term studies were initiated with the use of CIGRE 10-kHz lightning flash counters. In their 4-m vertical antenna configuration, these instruments advance a mechanical counter whenever a rapid, 26 V/m electrostatic field change occurs. Cross-calibration experiments and calculations support an average detection radius of 20 km, although the counters can respond to some strong flashes as far as 50 km away. An extensive program of measurements was carried out in South Africa, covering a broad range of flash density values over an 11-year period with the results in Figure 6.3-4.

The following expression was recommended for relating thunderstorm day levels in South Africa to ground flash density (CIGRE 1991):

$$GFD = 0.04TD^{1.25} \qquad 6.3\text{-}1$$

Figure 6.3-4 also introduces data from the Optical Transient Detector (OTD) experiment (Christian et al. 2003), which was established in 1995 to measure lightning flash characteristics using a satellite. The strong trend for higher ground flash density in the east of South Africa forms one

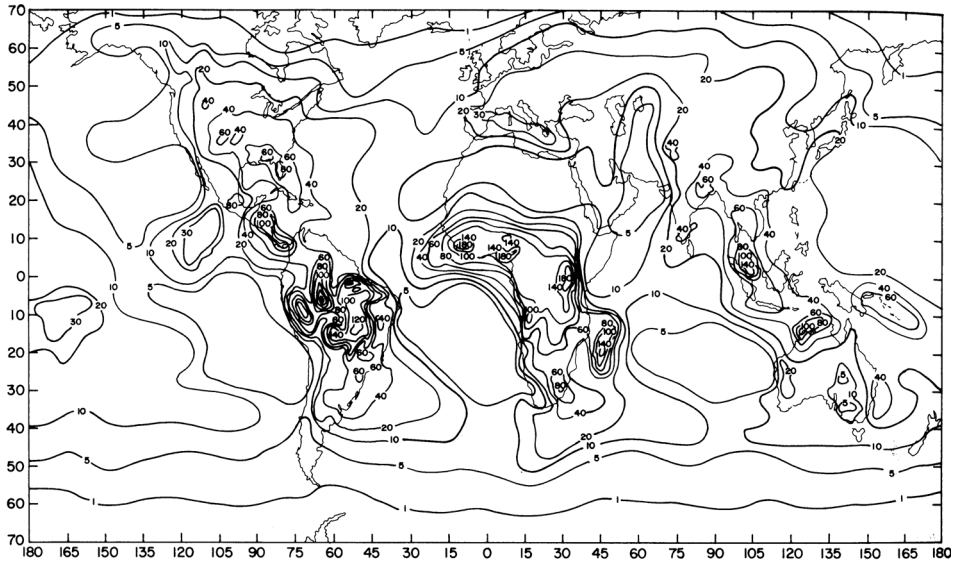


Figure 6.3-3 Global map of Thunderstorm Days per year (WMO 1953, www.wmo.int).

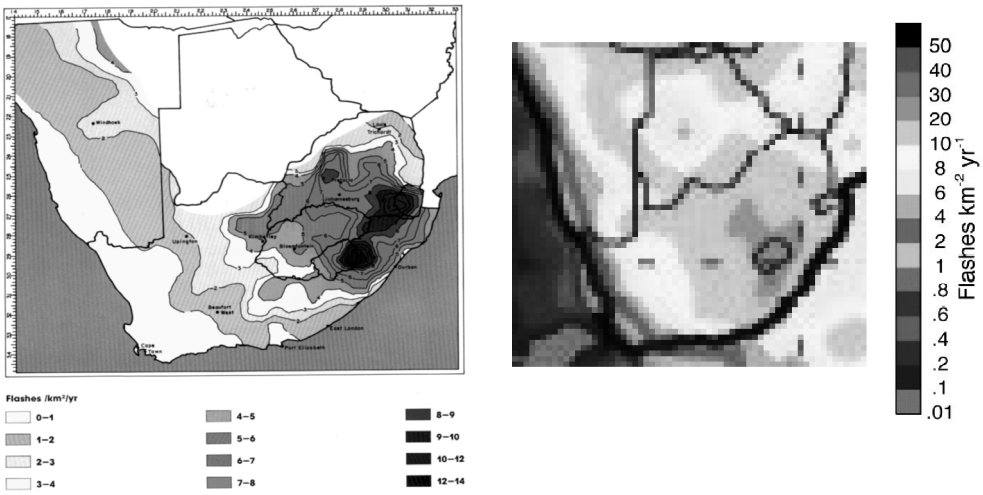


Figure 6.3-4 *Left:* Records of ground flash density from CIGRE 10-kHz lightning flash counters, 1975-1986; *Right:* Records of (CC+CG) flash density from optical transient detector (Christian et al. 2003).

of the best areas for intercomparison and calibration of the OTD data, which are less reliable because there are far fewer samples in each grid square. The OTD data are discussed below.

When applied to the continental U.S. map of *isokeraunic* lines of equal lightning density in Figure 6.3-5, the South African expression suggests peak ground flash density values of $0.04\ (130)^{1.25} = 17.5$ flashes per km^2 per year in central Florida, with values reaching 11 flashes per km^2 per year in areas of nine states that have TD levels greater than 90 days per year. The high local density of thunderstorm days in the central U.S. does not translate directly into an elevated level of ground flash density obtained from lightning location systems (MacGorman et al. 1984), leading to a hypothesis that thunderstorm-hour data would have a more linear relationship. Figure 6.3-6 shows the ground flash density estimates based on the recommended expression, $GFD = 0.054\ (TD)^{1.1}$, for the continental U.S.

Later studies by Chisholm, Janischewskyj, and Beattie (Chisholm and Janischewskyj 1992; Janischewskyj, Chisholm et al. 1997) showed, however, that the relationship between TH and ground flash density also has a regional dependence, comparing continental U.S. and Canada. There are more thunderstorm hours per year than thunderstorm days, so fewer years are needed to obtain the desired 400 observations, and this is perhaps the strongest advantage of TH measurements.

A more direct resource has become available to estimate lightning ground flash density in the absence of lightning location network or lightning flash counter data. Optical transient detectors, operated in low-earth orbit since 1995,

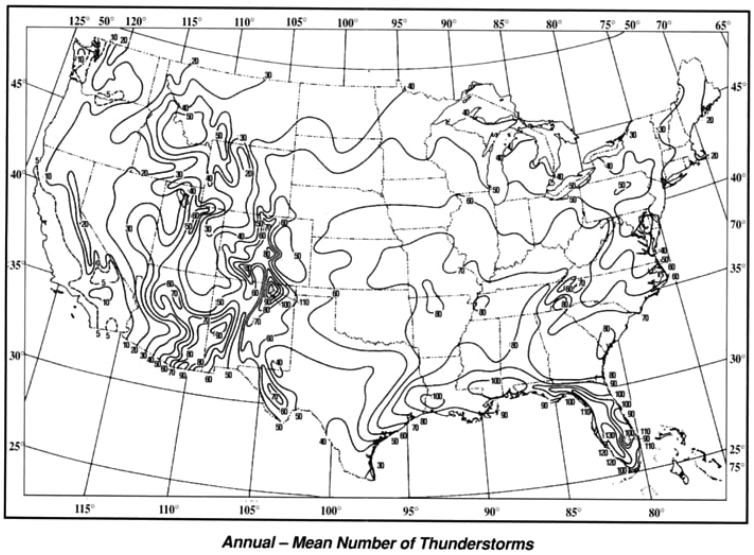


Figure 6.3-5 Isokeraunic map of the contiguous United States (MacGorman et al. 1984).



Figure 6.3-6 Estimate of ground flash density from Thunderstorm Hour (TH) values (MacGorman et al. 1984).

contribute another 10^6 flash observations per year, sampling most of the world's surface. These instruments provide an estimate of ground flash density in areas where lightning location systems have not been operated. Figure 6.3-7 shows the mission summary, which has been corrected for uneven sampling in each area and converted to a (Cloud-to-Cloud + Cloud-to-Ground) flash density.

Intercomparison of the OTD data and values from a second satellite, with a Lightning Imaging Sensor (LIS) with lightning location system data in the continental U.S. has validated an average value of (IC:CG) ratio $Z = 2.94$, with a standard deviation of 1.28 (Boccippio et al. 2001). However, by comparing Figure 6.3-7 with other measurements of ground flash density in Australia, Brazil, Canada, China, Colombia, Italy, Japan, and South Africa, the best estimates of ground flash density are obtained by dividing the (intracloud + ground flash) density values in Figure 6.3-7 by $(Z + 1) = 3.0$ rather than 3.94.

For ease of use, Applet G-2 provides the observed OTD count and the estimated ground flash density (using a factor of 3.0 OTD per ground flash) for any value of longitude and for latitudes from -60° to 60°. Figures 6.3-8 to 6.3-10 show the raw OTD data used in this applet, using expanded scales and the native 0.5x 0.5° resolution of the data. The strongest advantage of the OTD data over other observations is a lack of location bias, but the number of counts in each grid square is less than 50 in areas of low density. Additional studies, integrating more recent LIS data, may

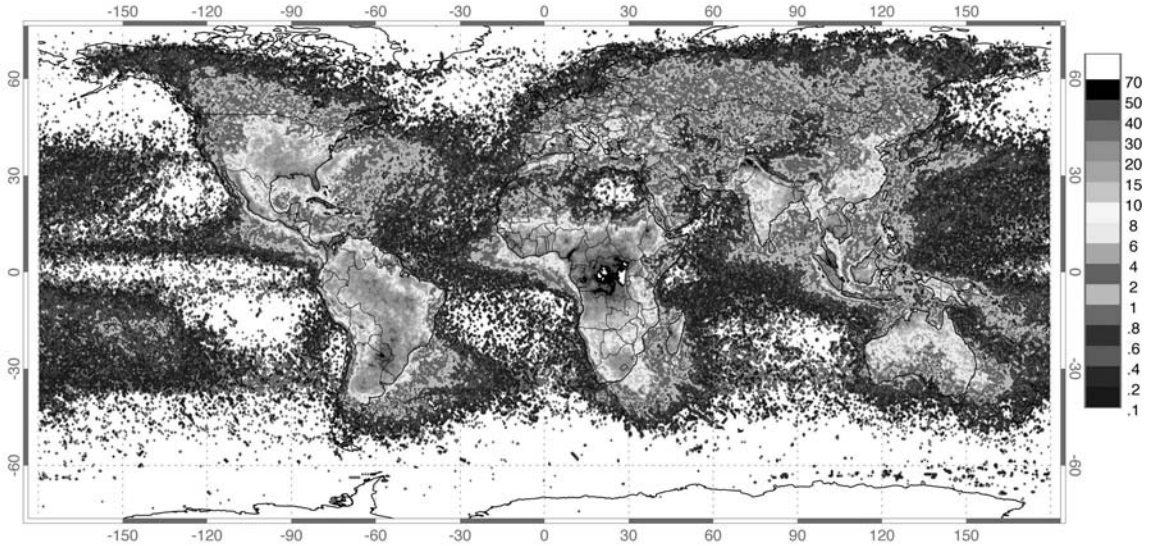


Figure 6.3-7 Global frequency and distribution of combined Inter-Cloud (IC) and Cloud-to-Ground (CG) lightning, as observed from space by the Optical Transient Detector and Lightning Imaging Sensor satellites (Christian 2002).

eventually improve the statistics and refine the value of Z in equatorial regions where existing observations can be unreliable and where the lightning flash density has its largest regional variations.

Wide-area lightning location systems, such as those using a combined time-of-arrival and direction finding approach (Cummins et al. 1998), offer important improvements in observations of ground flash density compared to any of the methods described above. The basic instrumentation, using magnetic loop antennas and regulated power supply, retains its calibration better than lightning flash counters, and its measurement range is 10 to 20 times larger. There has been a steady improvement in the detection efficiency and location accuracy of networks (Cummins et al. 1998) and better understanding of the need for sensors outside the area of interest. For example:

- Lightning observations up to 200 km south of the U.S.–Canada border improved when the North American Lighting Detection Network (NALDN) integrated a number of sensors in Canada (Orville 2002).
- Lightning observations in Brazil improved when a cooperative network of lightning location sensors was integrated from five independent systems (Cherchiglia et al. 2002).
- Observations along the U.S.–Mexico border retain a variety of measurement errors related to lack of sensors in Mexico.

6.3.2 General Observations

Latitude Effects

Several researchers have studied the possibility that there are differences between lightning in tropical areas and lightning in temperate climates. Most studies have traditionally been carried out in Australia, Europe, Japan, North America, and South Africa, where there have been more resources to apply and protect. This has led to problems, for example, in the basic estimate of ground flash density from thunderstorm-day level in areas where there are more than 150 TD per year, each tending to be of short duration. However, high levels of lightning, combined with difficult grounding conditions and increasing rate of development,

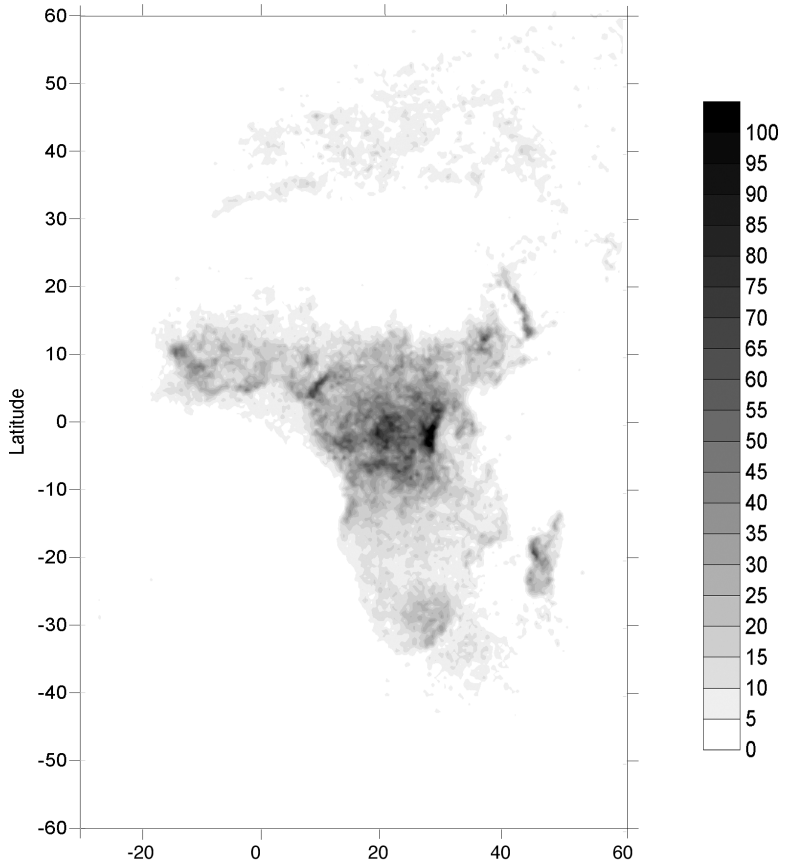


Figure 6.3-8 Combined LIS/OTD data for Africa and Europe. Units: (Cloud + Ground) flashes per km^2 per year.

have resulted in important contributions from Brazil, China, Colombia, and other regions.

Prentice and Mackerras (Prentice and Mackerras 1977) have studied the relationship of the IC:CG ratio Z as a function of latitude. This parameter changes significantly from storm to storm, but the researchers noted a tendency for Z to increase to $Z = 6$ at the equator, compared to $Z = 3$ in temperate regions from 30 to 60°. Their later work (Mackerras and Darveniza 1994) found Z largely independent of latitude. Boccippio (Boccippio et al. 2001) did not find any trend of Z variation with latitude either, but did note a strong increase in Z in the central U.S., possibly as a function of the fraction of positive-to-total flashes.

Measurements of peak stroke current distribution across the U.S. and Canada presently show a strong cross-border influence, with median lightning in Canada being less than 18 kA, a level observed only in limited areas of the U.S., where the earth resistivity is also high. At the fringe of the lightning location network used to gather the data in Figure 6.3-11, small-amplitude flashes are not detected, and the median value increases.

The median current level of 18 to 20 kA in much of continental U.S. is well below the 31-kA median reported by (Berger et al. 1975) and adapted into lightning calculations, including those presented here. It should be noted that the median from the lightning location system includes several competing biases, such as:

- A small fraction of misclassified subsequent strokes (12 kA median versus 31 kA); for example, a distribution with 20% subsequent strokes and 80% first strokes would have a median of about 27 kA.
- Correct identification of multiple ground terminations, each of which may have a reduced leader charge and peak amplitude compared to single-termination events collected at tall, instrumented towers.
- A single model for attenuation of normalized signal strength (Cummins et al. 1998) for the entire region,

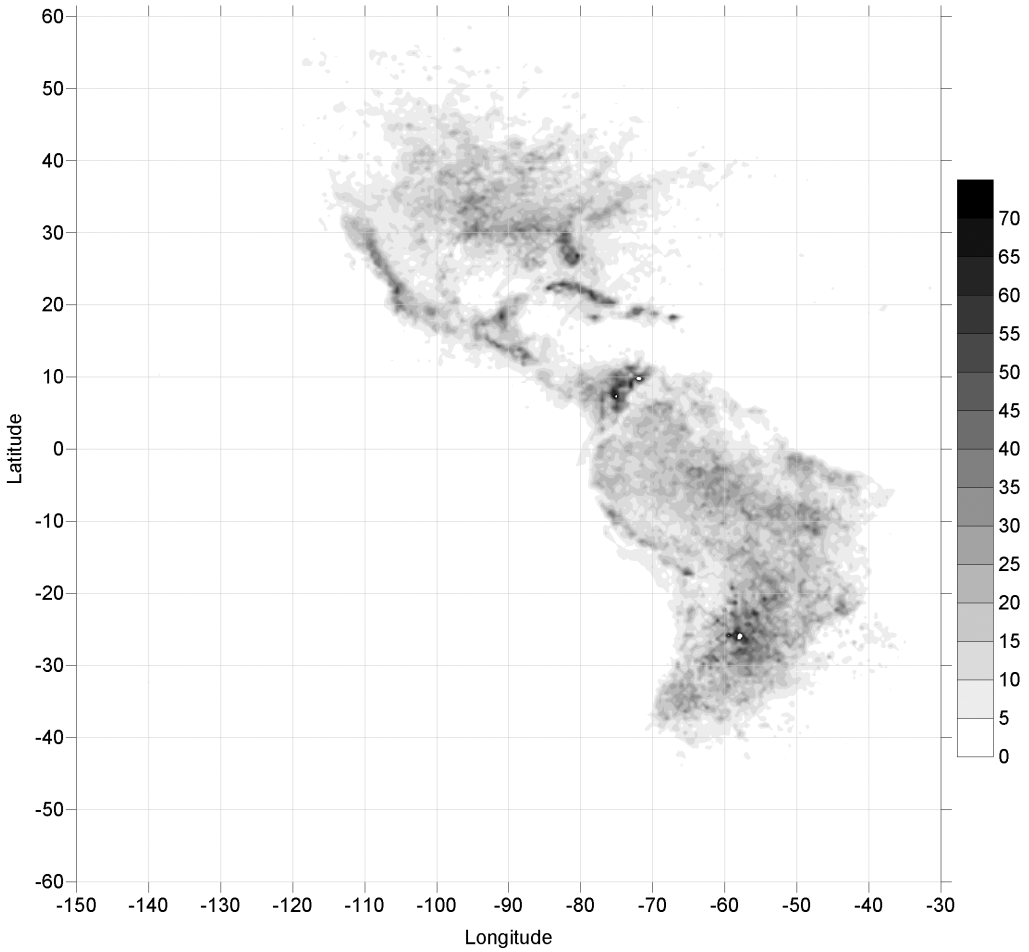


Figure 6.3-9 Combined LIS/OTD data for the Americas. Units: (Cloud + Ground) flashes per km^2 per year.

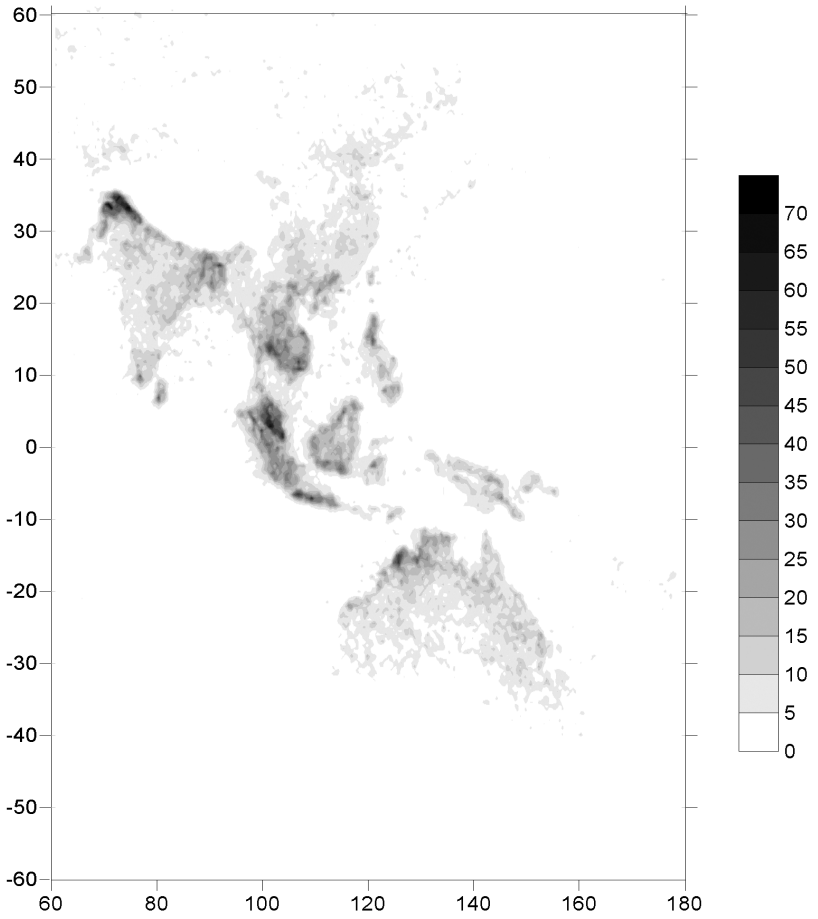


Figure 6.3-10 Combined LIS/OTD data for Asia. Units: (Cloud + Ground) flashes per km^2 per year.

which has a wide range of resistivity values given in Section 6.10 and Applet G-2.

- A wide range of baseline distances between sensors, as shown in Figure 6.3-14.

The saltwater-to-land transition has more of an effect than any variation with latitude in Figure 6.3-11. There is no such effect over large bodies of fresh water, which has a resistivity 400 times higher than saltwater. There are at least three hypotheses that can explain why observed lightning amplitudes are about 20% higher over the ocean:

- An abrupt reflection coefficient for ground-wave impedance occurs at the ocean-to-land interface, increasing the apparent source strength of electromagnetic waves arriving from the ocean side.
- The propagation of the electromagnetic wave from the return stroke is minimally attenuated over saltwater compared to its theoretical inverse-distance relation, but the peak signal strength attenuates by 10-30% over a typical 10-100 km land path.

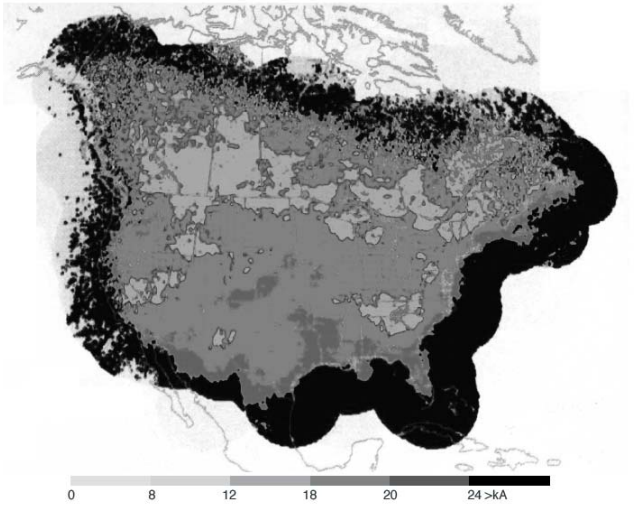


Figure 6.3-11 Observed median negative peak stroke current for North American Lightning Detection Network, 1998-2000 (Orville at al. 2002).

- The internal source impedance of the lightning flash, described as about 3000 Ω in Figure 6.2-7, encounters the minimum (35 Ω) surge impedance of a hemisphere electrode in the low 0.25 Ω-m resistivity of the ocean and a higher 600-Ω average impedance in a typical lightning termination on 100-1000 Ω-m soil.

The second and third hypotheses both argue for the use of the stroke current distribution observed over the ocean for well-grounded transmission-line structures. However, in view of these uncertainties, the important questions about the correct stroke current amplitude distribution, and its regional dependence, remain to be resolved by additional research and discussion. One possible treatment in the meantime would be to tabulate the incidence of stroke currents above a given backflashover critical current. Also, advanced studies of the leader charge and its relation to stroke current may refine the shielding failure model as well.

Time-of-Year, Time-of-Day Variation

Lighting shows a significant time-of-day variation, with low levels of activity from midnight to 10 a.m. local time, and high levels of activity peaking from 2 to 5 p.m., as shown in Figure 6.3-12. This is well understood by most electrical utility transmission line maintenance staff, and is reflected in a biased workday that starts early (6 to 7 a.m.) to minimize risk of interruption from lightning. In the northern hemisphere, Figure 6.3-13 shows a strong seasonal lightning variation with a peak in July and August.

6.3.3 The North American Lightning Detection Network

History of Commissioning

At the time of preparation of the second edition of the Red Book, the basis of modern lightning location technology had been described by Krider et al. (Krider et al. 1976) and tested for finding forest fires. EPRI and its members have promoted the technology for the NALDN through the 1980s, leading to successful commercialization in 1989. As a direct result of this work, there has been an increase in the number of observations of lightning:

- **1978:** approximately 10^6 observations per year in 1978, mainly registrations of lightning flash counters.
- **1989:** 12 x 10^6 measurements of gated wideband peak magnetic field and analog bearing per year in the continental U.S. alone (Orville and Huffines 2001).
- **1998:** 25 x 10^6 measurements of peak-radiated field and global positioning system (GPS) synchronized time per year in the continental U.S. (Orville and Huffines 2001).

Present Detection Technology—Magnetic Direction-Finding and Time-of-Arrival

In the mid-1990s, experience demonstrated that the combined use of magnetic direction finding (DF) and time-of-arrival (TOA) offers more robust estimates of lightning locations. The time-of-arrival technique proved to be less dependent on local site errors than direction finding, which is affected by reradiation from local conducting loops of various dimensions. The combined technology was optimized (Cummins et al. 1998), using GPS receivers to give accurate local time references.

Detection Efficiency and Location Accuracy

Since the peak-radiated field from lightning return strokes falls off more than inversely with distance, the sensitivity of a sensor network is established to some extent by the distance from the lightning to the nearest sensors. In the original (DF only) network, two time-synchronized sensors were needed to obtain a unique location. The addition of time-of-arrival capability increased the average number of sensors responding (ANSR) requirement to three or more if the DF data were not used in the computation. At least one IMPACT magnetic-field sensor reading is still needed in the NALDN to compute stroke amplitude. Figure 6.3-14 shows that baseline distance between magnetic-field amplitude

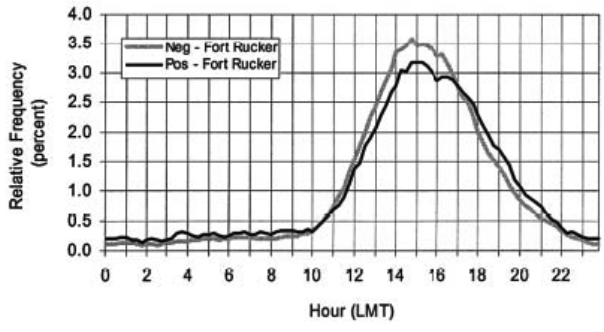


Figure 6.3-12 Observed summertime diurnal variation in lightning occurrence at Fort Rucker, Florida (Zajac and Rutledge 2001).

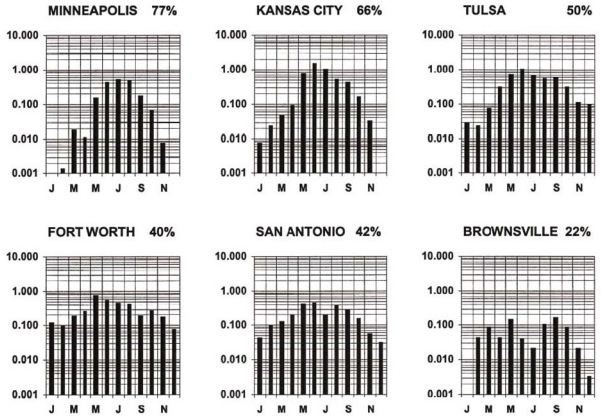


Figure 6.3-13 Lightning occurrence by month for six U.S. locations (Zajac and Rutledge 2001).

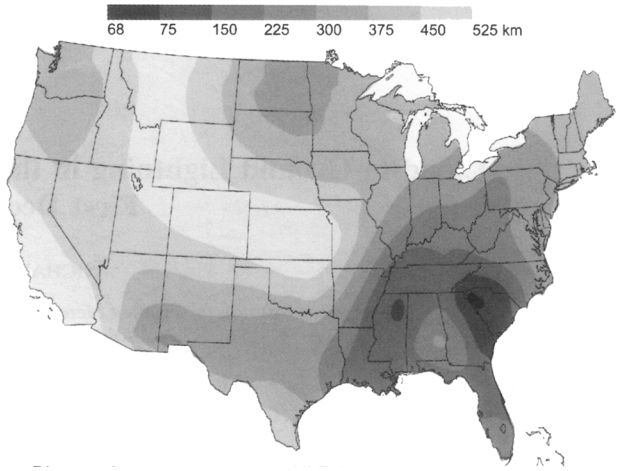


Figure 6.3-14 Distance between nearest pairs of IMPACT DF sensors in NALDN (Orville et al. 2002).

sensors in the U.S. NLDN network vary from 100 km in the Southeast and more than 400 km in the West.

Cummins (Cummins et al. 1998) has computed that the variation of baseline distance in Figure 6.3-14 does not affect the probability of detection and has focused network development on improving fringe coverage along the U.S.-Canada border by combined operation as a single NALDN. Experience with co-operative networks of lightning location sensors in Japan, Europe, Canada (Alberta/BC), and Brazil has demonstrated that accurate and uniform probability of detection within a region requires that sensors be placed on the border of, and preferably a distance of 200 km outside, the region. As an example, the increased ground flash density in U.S. states on the 49° latitude in Figure 6.3-16, compared to Figure 6.3-15, is most likely a function of the improved probability of detection when the two networks were integrated in 1998**.** Values within the center of an extensive network are relatively stable, while values at the edges of the network change considerably with improvements to network configuration.

Ground Flash Density Maps

Procedures to Perform an Adequate Study

When data are being binned, sampling error is defined as the square root of the number of counts. If the bin size is too small, it becomes impossible to say whether any particular count (say, a square km with 10 flashes per year) is significantly different from an adjacent area (say, with only 8 flashes per km^2 per year). For counting lightning events, it is recommended that a minimum of 400 counts should be aggregated. With typical ground flash density of less than 1 flash per km^2 per year in the western United States, year-by-year comparisons of 20 x 20 km grids would be valid, and the minimum grid size of 6 x 6 km would be acceptable in an 11-year study.

Insights from FALLS (Fault Analysis and Lightning Location System) Studies

It has always been an interesting challenge to establish the parameters of lightning flashes that actually cause transmission-line outages. In 1962, the Edison Electric Institute (EEI) initiated a ten-year study, called the "Pathfinder Project," to establish root causes. This research was carried out at a time when the U.S. utilities were spending several

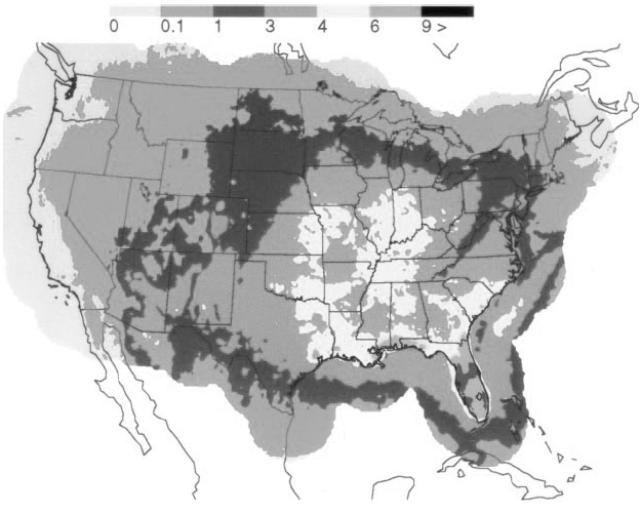


Figure 6.3-15 Mean annual negative lightning ground flash density, contouring 216 x 10^6 flashes from 1989 to 1998, without correction for detection efficiency (Orville et al. 2002).

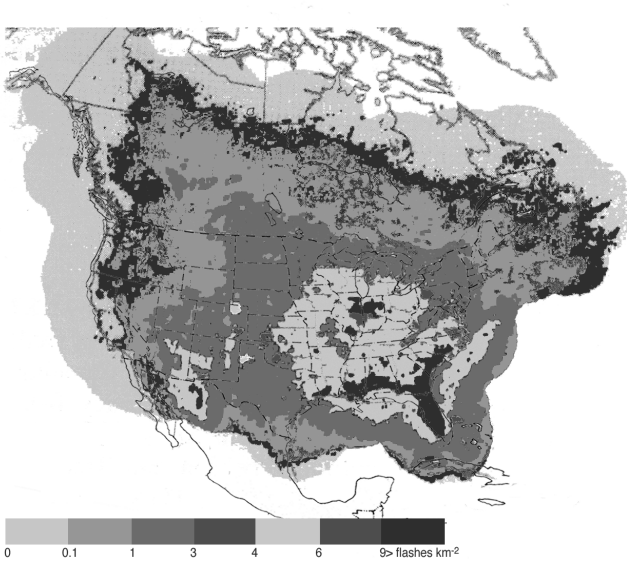


Figure 6.3-16 Mean annual lightning ground flash density, 1998-2002, after extension of network into Canada.

billion dollars per year on EHV infrastructure. Approximately 4600 instruments were installed on 400 miles (644 km) of transmission line, giving 138 operations on 89 separate strokes. Of these, 48 were identified as shielding failures, and 39 were backflashovers. Figure 6.3-17 provides a summary of operations for the project.

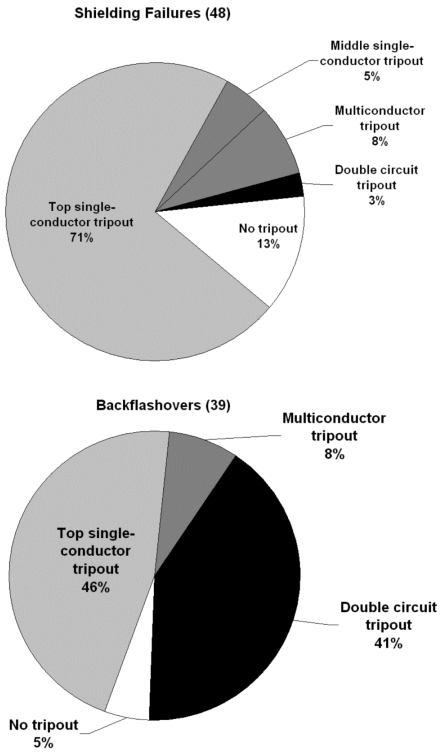


Figure 6.3-17 Summary of "Pathfinder" instrument operations for root cause analysis of lightning tripouts.

Whitehead (Whitehead 1971) found a 93% proportion of negative flashes in this study and developed a more conservative model of transmission-line shielding, taking advantage of the concurrent work on switching-impulse flashover by Paris and Cortina (Paris and Cortina 1968). Most utilities now overlay LLS data onto geographic information systems to establish specific outage causes on existing lines.

6.3.4 Inter-comparison of Lightning Detection Methods

Cross Calibrations

Chisholm and Janischewskyj (Chisholm and Janischewskyj 1992) carried out an inter-comparison of a DF80-02 lightning location network with 70-km baselines and registrations of CIGRE 10-kHz lightning flash counters (LFC). They found that, while the nominal detection radius of the LFC was 20 km, some flashes were detected as far as 45 km from the LFC. Tests with an all-sky camera located 50 km from the nearest DF 80-02 receiver showed an overall detection efficiency of 70% using this older technology.

Boccippio et al. (Boccippio et al. 2002) compared registrations of the lightning location network in the United States with observations of optical transients viewed from above. While low sampling density at any one location remains a problem, these researchers were able to establish a ratio of cloud flashes to ground flashes (Z) of 2.94.

Calibration using Features that Attract Lightning

While it would seem logical to look for a concentration of lightning flashes around tall structures, this has not always led to success. Measurements on a 100-m tower in Austria have been quite successful, leading to an estimate of 400-m location accuracy (Diendorfer et al. 2002). Correction of the signal strength for the additional radiation caused by the presence of the tower leads to a moderate discrepancy of 20% in the recorded amplitudes.

In contrast, the lightning location systems tend to reject electromagnetic signals from taller towers. As illustrated in Figure 6.2-19, there is a pronounced second peak, in the current measured on the 553-m CN Tower. The second peak is delayed by the two-way propagation time of current down and up the tower, and is significantly higher than the first peak. Signals like this fail a lightning location system waveform test meant to reject signals that have been distorted by excessive propagation distance (>600 km) through ionospheric reflection.

Local orographic features, such as oceans and mountain ridges, exert show a strong influence on ground flash density. The land-water contrast also leads to differences in estimated peak current over seawater and land, as shown previously in Figure 6.3-11. This difference does not, however, show up over the Great Lakes, which have a resistivity of 80 to 125 Ω-m, similar to the surrounding land, and thus may be an electromagnetic effect (such as a partial reflection of the incoming waves).

6.4 SURGE IMPEDANCE AND CORONA EFFECTS

Surge impedance concepts are used to provide a sufficiently accurate and detailed transfer function between the majority of input currents described in Section 6.3 and the dominant descriptions of insulation strength, based on voltage waveforms, in Section 6.5. For some aspects, such as slow input currents or late times to flashover, surge impedance effects are not important, but tower surge response and travel time have significant sensitivity in the predicted lightning performance of tall transmission lines.

Analysis of the response of transmission lines to lightning currents has been carried out with a variety of approaches. There is a broad range of excitation described in Section 6.2. Table 6.4-1 classifies these features in terms of time, frequency, and distance.

Table 6.4-1 Time-Domain and Frequency-Domain Features of Lightning Components

Parameter	Feature	Time-domain Description	Equivalent Bandwidth and λ/10 Wavelength
Subsequent Stroke	50-90% rise time	100 ns	1.7 MHz, 18 m
Subsequent Stroke	Peak	12.kA with 40 kA/μs	520 kHz, 58 m
First Stroke	30-90% rise time	2.3 μs	91 kHz, 330 m
First Stroke	Peak	31 kA with 24 kA/μs	124 kHz, 242 m
Continuing Current	Duration	100 ms	5 Hz, 6 x 10^6 m

The equivalent bandwidth is computed using one of two expressions:

$$f = \frac{0.35}{t_{10\%-90\%}} \qquad 6.4\text{-}1$$

$$f = \frac{dI/dt}{2\pi\hat{I}} \qquad 6.4\text{-}2$$

The λ/10 wavelength corresponds roughly to the size of structure for which traveling-wave or antenna-mode representation starts to become important.

The concave shape of the lightning stroke current ensures that the maximum steepness occurs at the same time as the peak of the current wave. This means that any insulator voltage rise from inductive effects ($L\ dI/dt$) will be added to the voltage rise from resistive components ($R\ I$) at the crest of wave. Fourier analysis of double-exponential and concave-front waves with the same peak magnitude does not highlight this important difference.

6.4.1 Surge Impedance of Single Wires and Bundles

Under Linear Conditions

A lightning stroke to a conductor produces a traveling wave of current I and voltage V, related by a surge impedance $Z = V/I$. This surge travels along the conductor at the speed of light unless there is a dielectric or a convoluted path. The surge impedance is purely resistive, so V and I have the same waveshape. Surge impedances of transmission lines and cables are functions of their distributed self-inductance L_{11} and self-capacitance C_{11} per unit length:

$$Z = \sqrt{\frac{L_{11}}{C_{11}}} \qquad 6.4\text{-}3$$

$$v = \frac{1}{\sqrt{L_{11}C_{11}}} \qquad 6.4\text{-}4$$

In cases where there is no dielectric between the conductor and ground, the speed of propagation v will equal the speed of light c, 3 x 10^8 m/s. In this case, it is easy to estimate the inductance L or capacitance C using the travel time τ of the line segment L_{seg} and its surge impedance Z. Equation 6.4-5 shows that this process, for speed-of-light propagation, simplifies to the well-known $\tau = ZC$ and $\tau = L/Z$ expressions for time constants in electric circuits.

$$\tau = \frac{L_{seg}}{c} \quad L = Z\tau \quad C = \frac{\tau}{Z} \qquad 6.4\text{-}5$$

From installing 75-Ω cable for television (CATV), many people are now familiar with the surge impedance of coaxial cables, defined for two concentric cylinders of inner radius r_1, outer radius r_2, and insulation dielectric constant ε_r as:

$$Z = \frac{60}{\sqrt{\varepsilon_r}} \ln\frac{r_2}{r_1} \qquad 6.4\text{-}6$$

The speed of propagation is reduced by the presence of dielectric material to:

$$v = \frac{c}{\sqrt{\varepsilon_r}} \qquad 6.4\text{-}7$$

Under lightning surge conditions, some of the air around the conductor ionizes and makes a temporary corona dielectric that functions in the same way as the plastic core of a coaxial cable, to reduce the surge impedance and slow down the velocity of propagation.

The surge impedance of a round wire of radius r at a height H over perfectly conducting ground plane can be calculated from expressions for the per-meter inductance and capacitance of the wire and its image at $2H$. The surge impedance is defined as the square root of the ratio of the self-inductance to the self-capacitance:

$$Z = \sqrt{\frac{L_{11}}{C_{11}}} = \sqrt{\frac{\frac{\mu_o}{2\pi}\ln\left(\frac{2H}{r}\right)}{\frac{2\pi\varepsilon_0}{\ln\left(\frac{2H}{r}\right)}}} = 60\ln\left(\frac{2H}{r}\right) \qquad 6.4\text{-}8$$

In the case of bundles of multiple conductors, an equivalent radius is obtained using the geometric mean of the wire self radius r_{11} and the distances r_{12}, r_{13} … r_{1n} to the other wires in the bundle:

$$R_{eq} = \sqrt[n]{r_{11} \cdot r_{12} \cdot r_{13} \cdots r_{1n}} \quad 6.4\text{-}9$$

In the case of a conductor in corona, the wire or bundle radius will increase as a function of voltage to model the additional capacitance, as described below in Equations 6.4-22 and 6.4-23.

The surge impedance relates the conductor potential that will be reached after injection of a unit step current. While it is defined for an infinite wire, the surge impedance values of relatively short wire segments are still useful for describing the electromagnetic response using electrical circuits. This will be discussed in further detail in Section 6.4.2.

If there is a step change in geometry that leads to a change in surge impedance, then the voltages and currents will change on both sides of the interface. It is useful to define a reflection coefficient for the interface from a surge incident from Z_1 to Z_2 as follows:

$$\rho_{12} = \frac{Z_2 - Z_1}{Z_2 + Z_1} \quad 6.4\text{-}10$$

The reflection coefficient from a surge moving from Z_2 towards the interface is ρ_{21}, which does not equal ρ_{12}. The voltage at both sides of the interface is constant after the surge arrives, and the sum of the currents moving towards and away from the interface must also be zero. This gives the following relationships:

	$t<t_o$	$t>t_o$
V_1	$I_o Z_1$	$(1+\rho_{12})\, I_o Z_1$
I_1	I_o	$\rho_{12}\, I_o$
V_2	0	$(1+\rho_{12})\, I_o Z_1$
I_2	0	$(1-\rho_{12})\, I_o$

6.4-11

The relationship that $V_2 = Z_2 I_2$ can be used to obtain an expression for Z_2 as a function of a known source impedance Z_1 and an observed reflection coefficient ρ_{12}:

$$Z_2 = \frac{1+\rho_{12}}{1-\rho_{12}} Z_1 \quad 6.4\text{-}12$$

This relationship is used for single or multiple reflections in a measurement technique called Time Domain Reflectometry, or *TDR*. TDR methods have been used to study the lightning surge response of transmission-line towers since the 1950s in full-scale and miniature model experiments.

As an example, a wire of 10-mm radius at a height of 30 m above ground is connected to a bundle of four wires, each with 10 mm radius but spaced in a square of 450 mm. The equivalent radius of the bundle is 0.189 m. The surge impedance of the single wire is Z_1 = 522 Ω. The surge impedance of the bundle is Z_2 = 346 Ω. The reflection coefficient at the interface is ρ_{12} = –0.203. A surge current of I_1 = 1 kA surge injected into the single wire over ground produces a surge voltage of 522 kV with the same waveshape. This surge propagates at the speed of light until it arrives at the interface. Then a surge current of I_2 = 1203 A continues in the bundle conductor away from the source, and a reflection of $-\rho_{12} I_1$ = 203 A starts to travel back towards the source, satisfying Kirchoff's law at the junction. The voltage wave propagating into the bundle conductor is 416 kV, computed either from $I_2 Z_2$ or from $(1 + \rho_{12}) V_1$. A negative voltage wave component with magnitude $\rho_{12} V_1$ = -106 kV reflects back towards the source (see Figure 6.4-1).

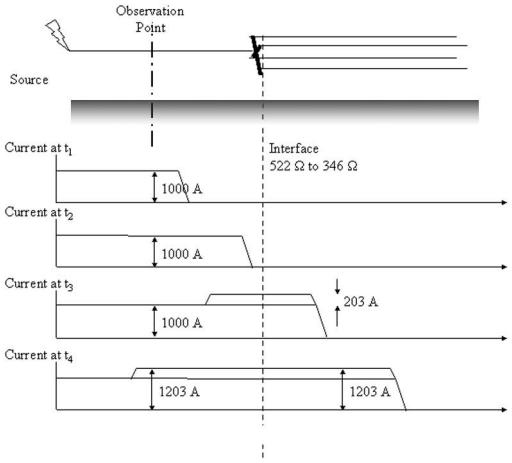


Figure 6.4-1a Time and space evolution of traveling current waves at interface.

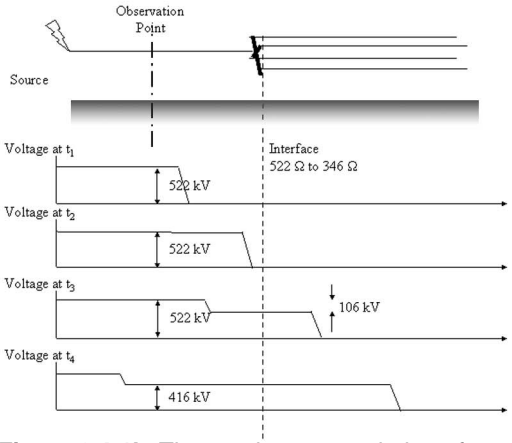


Figure 6.4-1b Time and space evolution of traveling voltage waves at interface.

The concept of getting more current into the bundle conductor than was originally injected into the single wire is sometimes difficult. However, when the single-wire section is considered as a voltage source with series impedance Z_1, it is more readily grasped that the open-circuit voltage is double the voltage into a matched load $Z_2 = Z_1$ (and the open-circuit current is zero). The short-circuit current is double the current into a matched load, and the short-circuit voltage is zero. The open-circuit, matched-load, and short-circuit cases correspond to $\rho_{12} = 1$, $\rho_{12} = 0$ and $\rho_{12} = -1$.

Conventional TEM Coupling Coefficients

When an undriven conductor is placed in parallel to a conductor that is excited by a surge source, the mutual capacitances and inductances combine to make a mutual surge impedance. This mutual surge impedance causes a faithful copy of the original wave, reduced in magnitude, to appear on the undriven conductor. The calculations of this Transverse ElectroMagtnetic (TEM) response are valid for all frequencies. At higher frequencies, corresponding to conductor height h of more than a tenth of a wavelength ($h > \lambda/10$, λ = 300 m or about 1 MHz for 30-m conductors) other modes of electromagnetic response also contribute, but the TEM mode remains a dominant term. For very fast rise times, there is a time delay in establishing coupling, which will be discussed in the next section.

Figure 6.4-2 shows the dimensions to be used in calculating the TEM coupling coefficients, based on the direct distance from driven to undriven conductor (D_{12}) and the distance from the undriven conductor to the image in a perfectly conducting earth of the driven conductor (D'_{12}).

$$Z_{11} = 60 \ln \frac{2H_1}{r_1} \quad Z_{22} = 60 \ln \frac{2H_2}{r_2} \qquad 6.4\text{-}13$$

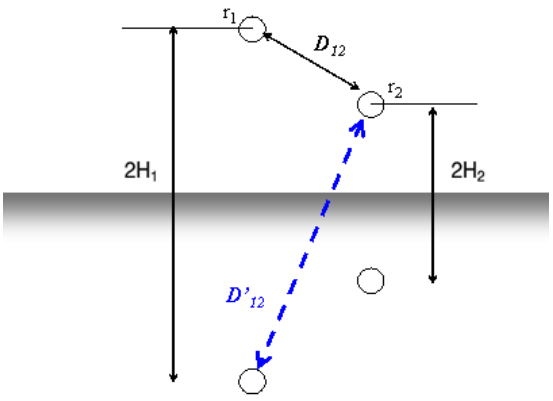


Figure 6.4-2 Dimensions for calculation of TEM coupling coefficient.

$$Z_{12} = Z_{21} = 60 \ln \frac{D'_{12}}{D_{12}} \qquad 6.4\text{-}14$$

$$v_1 = i_1 Z_{11} + i_2 Z_{12} \qquad 6.4\text{-}15$$

$$v_2 = i_1 Z_{21} + i_2 Z_{22} \qquad 6.4\text{-}16$$

With no current source on an undriven conductor, $i_2 = 0$ and the induced voltage v_2 simplifies to:

$$v_2 = \frac{Z_{21}}{Z_{11}} v_1 = c_n v_1 \qquad 6.4\text{-}17$$

The coupling coefficent c_n provides important mitigation of lightning. The line insulation is stressed by the difference in potential, $(v_1 - v_2)$. Any increase in the coupling factor reduces this potential difference (see Figure 6.4-3). On typical transmission lines, TEM coupling reduces insulator stress by 30 to 50% under backflashover conditions, and this can reduce transmission outage rates by a factor of three. Coupling can be deliberately enhanced by using more overhead groundwires, placed closer to (or under) the phases. This tends to increase losses from induced currents, and can cause other problems with clearances, electromagnetic compatibility (EMC), or mechanical loads.

Time Delay in Establishing Coupling

The TEM propagation assumes a uniform plane wave, and also assumes that the current in the undriven conductor is zero. Two exercises in nanosecond-model simulation of the TEM coupling can contribute insight into the value and limitations of this model. Nanosecond models use signal sources such as current step or impulse generators with >1ns rise time, along with wideband sampling oscilloscopes to allow efficient simulation of the complex electromagnetic waves using miniature wires and towers over conducting ground planes (Fisher et al. 1960).

If a wideband current transformer is placed around the driven conductor, a fast-rising step of current is measured as the wavefront passes. If a second CT is placed around the undriven conductor, an impulse, corresponding to the derivative of the first current, is measured. This impulse is also delayed in time, depending on how far along the measurement is taken from the excitation source. The source

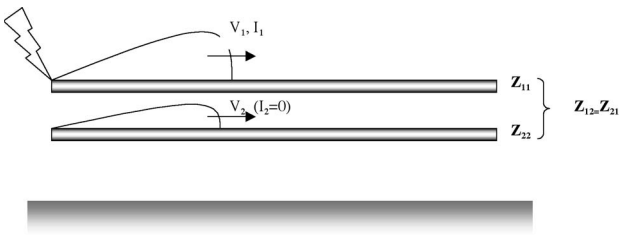


Figure 6.4-3 TEM coupling factor for two overhead lines.

excites a spherical wave that, in the limit of great distance, eventually flattens out into a plane. However, the lightning calculation is carried out near the source, and this time delay adds to insulator stress.

It is also useful to try out a technique for measuring voltage, using a probe technique originated by (Newi 1968) for fast high-voltage measurements. A high–impedance probe tip is connected to the driven or undriven conductor, and the probe sheath is maintained at a constant height over ground. Since the geometry is constant and the surge impedance can be relatively low compared to the probe, the relative error would be expected to be small. With a 5-kΩ probe impedance working into the usual 50-Ω coaxial cable of good high-frequency equipment, a 500-Ω surge impedance would introduce a 10% error at late time. However, a comparison of the current and voltage records quickly establishes that the voltage probe rise time is slowed to several times the wire height divided by the speed of light. This again is the time to establish the TEM coupling, and the degraded rise time is not real: the voltage and current should have the same waveshape. In general, the most useful voltage measurements in nanosecond model studies (or full-scale studies) are those taken across small distances (for example, from an undriven conductor to a nearby tower or across insulator strings) and measured locally or brought out to the oscilloscope on an optical fiber link. Measurements of currents are preferred because the results are unambiguous and less sensitive to probe routing.

Nanosecond modeling is an important complement to calculation of electromagnetic fields using advanced computer methods. One set of numerical results from (Baba and Ishii 2000) illustrates the concept of time variation of coupling coefficient using the NEC-2 computer software. Figure 6.4-4 shows this variation for a step function case without towers, and for more realistic cases where a 120-m tower and 2μs wavefront are introduced.

The delay in establishing TEM coupling is an important issue in the calculation of lightning outage rates for tall overhead lines, which remains to be integrated into future evaluation methods.

Impulse Corona Onset Voltage

At voltages below corona onset, the current resulting from a lightning impulse is purely capacitive. Above corona onset, however, the movement of corona-generated space charge near the conductor produces an additional current component. Impulse corona characteristics of transmission-line conductors are generally obtained as charge-voltage diagrams or *q-v* curves, with the simultaneous recording of the voltage *v(t)* and charge *q(t)* displayed along the x and y axes of the curve. The *q-v* curves on conductors may be obtained in laboratory (Davis and Cook 1960) or outdoor (Maruvada et al. 1977) cages and sometimes on a transmission line (Gary et al. 1989). A typical *q-v* curve is shown in Figure 6.4-5.

As the voltage increases from zero up to the corona onset voltage v_0, the current is purely capacitive (i.e., dielectric displacement current), and is given as

$$i(t) = C_0 \frac{dv}{dt} \qquad 6.4\text{-}18$$

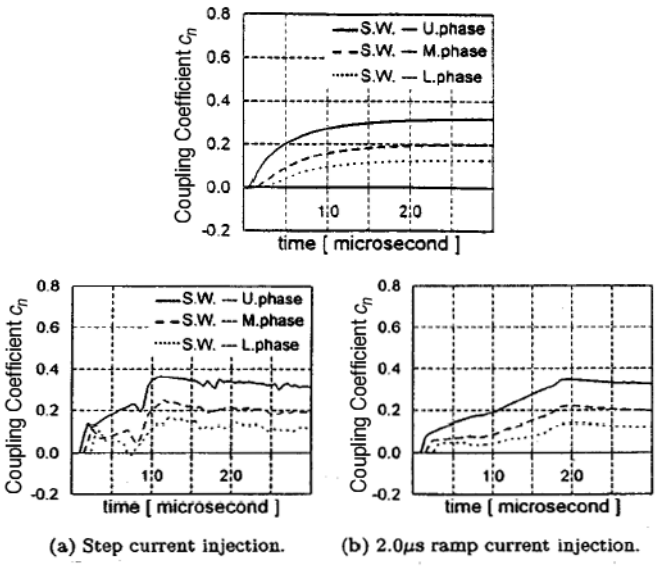


Figure 6.4-4 Time variation of shield-wire to phase-conductor coupling coefficient for step and 2-μs ramp injection (Baba and Ishii 2000).

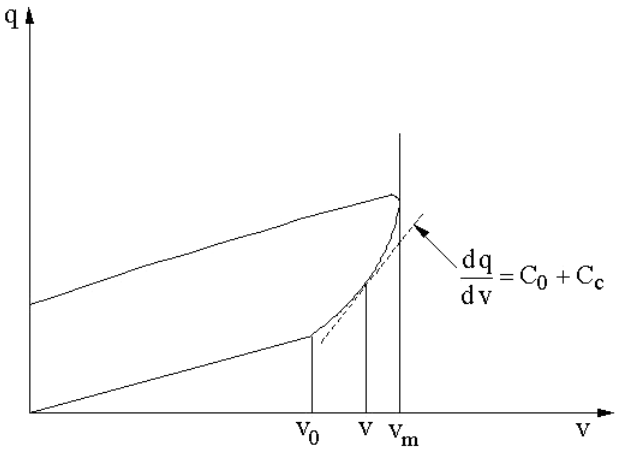


Figure 6.4-5 Charge-voltage curve for lightning impulse.

and the charge is given as

$$q(t) = \int i(t)\,dt = C_0\,v(t) \qquad 6.4\text{-}19$$

Where:

C_0 is the geometric capacitance of the conductor configuration.

Above the corona onset voltage v_0, however, the current consists, in addition to the capacitive component, a component due to the creation and movement of corona-generated space charge. The total current is then given as

$$i(t) = C_0 \frac{d\,v}{d\,t} + \frac{d\,q_c}{d\,t} \qquad 6.4\text{-}20$$

Where:

q_c is the charge produced by corona.

The second term in this equation may be expressed as

$$\frac{d\,q_c}{d\,t} = \frac{d\,q_c}{d\,v}\cdot\frac{d\,v}{d\,t} = C_c\cdot\frac{d\,v}{d\,t} \qquad 6.4\text{-}21$$

The term $\frac{dq_c}{dv}$ may be interpreted as an equivalent corona capacitance C_c, which is dynamic, nonlinear, and time-varying. Referring to the *q-v* curve between v_0 and the peak voltage v_m, the slope at any point corresponds to the total capacitance $C_t = C_0 + C_c$. After reaching the peak value v_m, the voltage decreases gradually to zero and the upper, more or less straight line, part of the *q-v* curve is obtained.

The shape of the *q-v* curve affects the attenuation characteristics of lightning impulses propagating on a transmission line. The principal parameters defining the *q-v* curve are: corona onset voltage v_0, corona capacitance C_c, and the energy absorbed due to corona, which is given by the area included in the *q-v* curve.

Experimental studies have shown (Davis and Cook 1960; Maruvada et al. 1977; Gary et al. 1983) that the corona onset gradient of a conductor, and hence the onset voltage, is higher for impulse voltages than that given by Peek's formula for power-frequency voltages. In fact, the onset gradient increases with the steepness of the impulse wavefront. For lightning impulses, the onset gradient may be 10-15% higher (Maruvada et al. 1977) than that given by Peek's formula in Equation 11.4-2. Although the corona capacitance varies nonlinearly with voltage above onset, a simplified linear representation is often used for the total capacitance C_t between v_0 and v_m, as shown in Figure 6.4-6. In the simplified representation, the return part of the *q-v* curve is represented by the geometric capacitance C_0. The ratio C_t/C_0 is found to vary between 1.5 and 5, depending on conductor configuration and the steepness of the impulse wavefront. The ratio is also found to increase with conductor size, but decrease with the number of conductors in the bundle (Maruvada et al. 1977). The energy absorbed by corona also depends on the impulse wavefront. For the same peak voltage, the energy absorbed is higher for steep-front lightning impulses than for slower-front impulses.

Modeling corona for studies on the attenuation of lightning impulses are carried out (Davis and Cook 1960) by taking into account the reduced speed of propagation due to the increased corona capacitance. More recently, Suliciu proposed (Suliciu and Suliciu 1981) a method of propagation analysis, which takes into account the overall *q-v* curve.

Reduction in Impedance Under Corona

The production of corona under lightning impulse conditions can be modeled as a dielectric loading near the driven conductor, leading to reduced surge impedance and a slower propagation time. In the second edition of the Red Book (EPRI 1982), the negative corona was modeled using an envelope approach, with a critical gradient E_o = 1500 kV/m in Equation 6.4-22. This expression converges quickly to the corona radius R_c for a conductor voltage V by starting with an initial value of R_c = 0.01 m.

$$R_C = \frac{V}{E_o \ln\left(\frac{2h}{R_C}\right)} \qquad 6.4\text{-}22$$

The corona envelope modifies the capacitance but not the inductance, so the self surge impedance of the conductor is given by:

$$Z_{Corona} = 60\sqrt{\ln\left(\frac{2h}{R_C}\right)\ln\left(\frac{2h}{r}\right)} \qquad 6.4\text{-}23$$

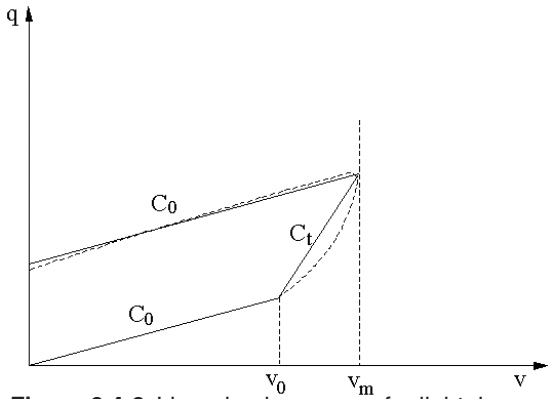


Figure 6.4-6 Linearized *q-v* curve for lightning impulse.

In Equation 6.4-23, r is the self radius r_{11} for single conductors and R_{eq} from Equation 6.9-4 for bundles.

Figure 6.4-7 shows the predictions of this model for a driven wire of 30 m height and 10 mm diameter, an undriven wire of 25 m height and 20 mm diameter, and a horizontal separation of 2 m, along with a calculation of surge impedance using (Gary 1989).

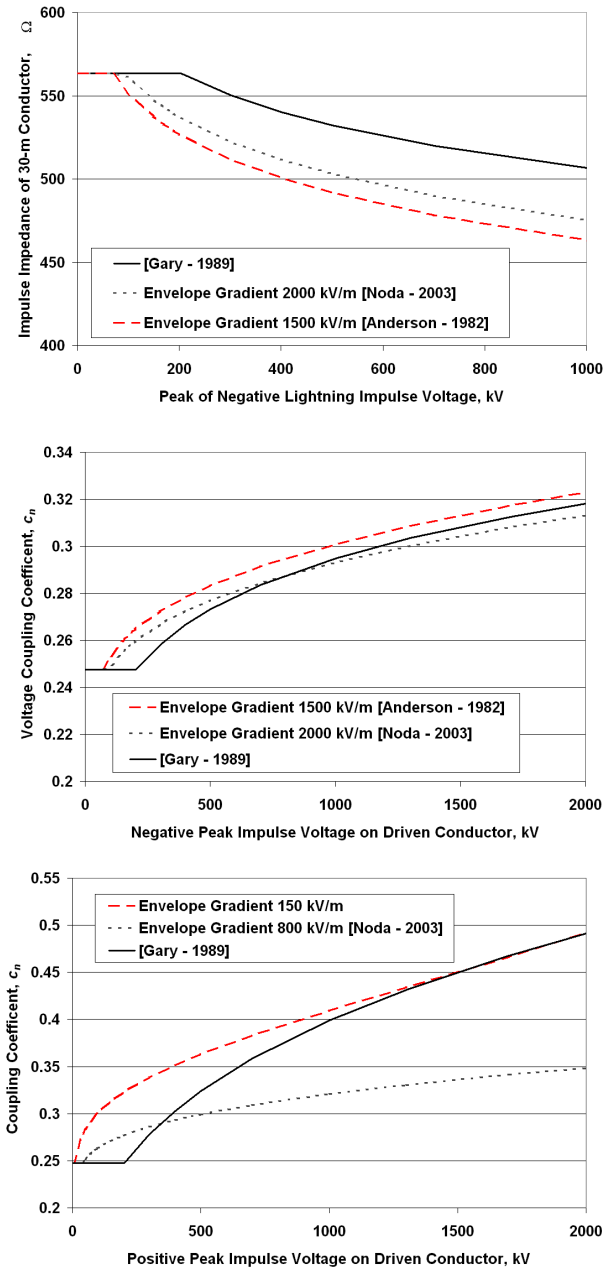


Figure 6.4-7 Changes in impedance (*top*), coupling under negative impulse corona (*middle*), and coupling under positive impulse corona (*bottom*).

The 1500-kV/m gradient model is found to be satisfactory, although a value of 2000 kV/m fits the Gary model slightly better. The 2000 kV/m surface state coefficient for negative corona was also recommended by Noda (Noda et al. 2003). For positive corona, the envelope gradient must be reduced to about 150 kV/m for good predictions of coupling coefficient above a conductor voltage of 1000 kV. This is much higher than the value of positive corona surface state gradient of 800 kV/m recommended by Noda, and will overstate the size of the zone in calculations of the corona radius, as discussed in the section on midspan flashovers. The strong increase in coupling coefficient for positive lightning is an important mitigation factor in calculations of positive-stroke backflashover rate.

6.4.2 Surge Impedance of Towers

The typical EHV transmission tower has a height that is relatively large compared to the rise time of some components of the lightning strokes. There are three options open to describe the role of the tower.

1. It can be considered as a series of one or more lumped circuit elements, usually inductances.
2. It can be modeled as a short transmission-line section with constant or variable surge impedance.
3. It can also be modeled as a series of electromagnetically coupled objects—for example, using moment methods to calculate self and mutual impedances as a function of frequency, and then convolved with input currents in the frequency domain, using inverse Fourier transforms to obtain a time-domain response.

It is possible to convert back and forth between inductance and surge impedance models using the tower travel time where this is well defined. However, measurements show that surges take a variety of path lengths down and back along tower crossarms, making estimation of travel time more difficult. This section describes the basic approaches to transmission tower modeling and recommends a simple surge impedance treatment, commensurate with the sensitivity of tower impedance and travel time in the calculation of backflashover rates.

Approximate Model—Self-Capacitance for Travel Time

The capacitance C_o of a finite cylinder of radius r of length L_{seg} at a height H over a conducting ground plane is given by (Markuviz 1986):

$$C_o = \frac{2\pi\varepsilon_o L_{seg}}{\cosh^{-1}\left(\frac{H}{r}\right)} \qquad 6.4\text{-}24$$

This expression retains its accuracy close to the ground for large objects like transmission towers, unlike the approximate expression $Z = 60\ ln\ (2H/r)$ used in Equation 6.4-8. The travel time τ of the cylinder, when excited from one end, is l/c, where c is the speed of light. The travel time and capacitance can be combined to give the surge impedance of the infinite element as follows:

$$Z_o = \frac{\tau}{C_o} = \frac{L_{seg}\ \cosh^{-1}\left(\frac{H}{r}\right)}{2\pi\,\varepsilon_0 L_{seg} c} = 60\ \cosh^{-1}\left(\frac{H}{r}\right) \quad 6.4\text{-}25$$

The effect of finite conductor length can be evaluated with a calculation of self-capacitance C_{11} using the surface area A, shape factor C_f, and geometric radius g:

$$C_{11} = \varepsilon_0 C_f \sqrt{4\pi A} \quad 6.4\text{-}26$$

$$g = \sqrt{2r^2 + (\frac{L_{seg}}{2})^2} \quad 6.4\text{-}27$$

$$A = 2\pi r L_{seg} + 2\pi r^2 \quad 6.4\text{-}28$$

$$C_f = \frac{3.54g}{\sqrt{A}\ln\left(\frac{23.7g^2}{A}\right)} \quad 6.4\text{-}29$$

$$C_{12} = 8\pi\varepsilon_0 H \quad 6.4\text{-}30$$

$$C_o = \frac{1}{2\left(\frac{1}{C_{11}} - \frac{1}{C_{12}}\right)} \quad 6.4\text{-}31$$

The shape factor C_f is a slowly-varying or "variational" parameter (Chow and Yovanovic 1982) that does not change much from unity for a fairly wide range of objects. The mutual capacitance term C_{12} between the tower element and its image can usually be neglected. This approach leads to estimates of stub impedance, as shown in Figure 6.4-8.

The circuit model, treating the finite wire as a capacitance, leads to a reasonable approximation of the sinusoidal input impedance in the frequency range from 10 kHz to 200 kHz for stub lengths of 10 to 100 m compared to the reference expression, $Z = Z_o \cot(\beta L_{seg})$ where $\beta = 2\pi f/c$. At higher frequencies, such as the curve shown for 1 MHz, traveling-wave effects start to affect the results. The deviation in behavior at 1 MHz starts to occur at $\lambda/10 = 30$ m.

The transmission tower can be treated in the same way to establish a surge response. The overall surface area of the tower is the sum of the face area of the tower (in the plane at right angles to the line direction) and the tower perimeter, multiplied by the thickness of the tower along the line direction. For any smooth body, such as a cone or cylinder, the estimate of tower surge impedance obtained using the known travel time (at speed of light propagation) and the calculated capacitance is in close agreement with theoretical estimates using expressions for conical or cylindrical towers, given next.

Tower as Single Inclined Overhead Line

The simplest approach to transmission tower surge impedance modeling may be developed from the following sequence of waveforms. In Figure 6.4-9, a step voltage with unit amplitude is launched into an overhead wire, having a constant surge impedance of $Z_o = 60\ ln\ (2H/r_o)$. At the junction, there is a step increase in radius, leading to a change in surge impedance $Z_1 = 60\ ln\ (2H/r_1)$. The figure shows a larger radius, so the impedance is lower. A voltage wave of 82% of the initial surge continues on in the section with larger radius, and a negative reflection of 18% arrives back at the source after a delay calculated from the conductor length and the speed of light.

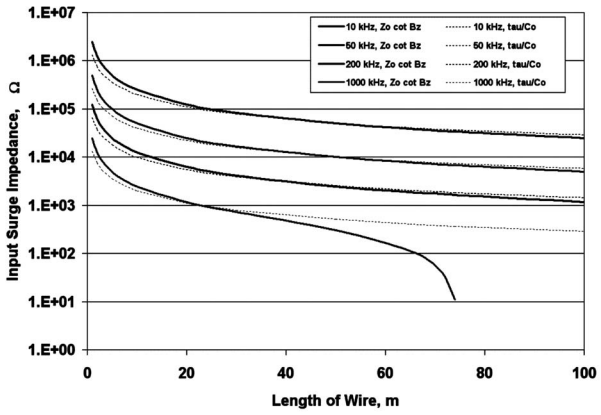


Figure 6.4-8 Input surge impedance of finite wire over ground using exact expression and capacitance approximation.

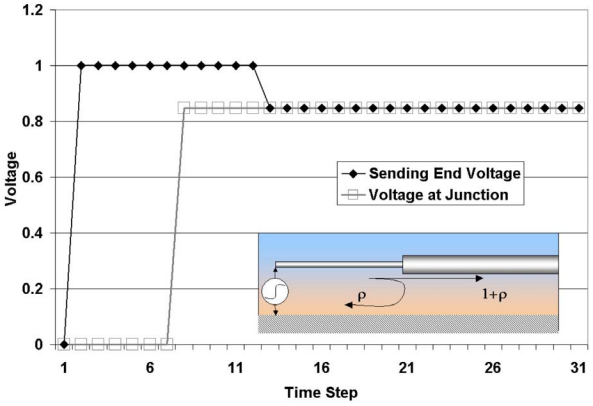


Figure 6.4-9 Sending-end and junction voltages for overhead wire with step change in radius.

If there are multiple changes in radius, these changes set up multiple reflections that can be computed with the use of a Bewley lattice diagram using a spreadsheet. Figure 6.4-10 shows the results from a geometry with constant wire height above ground but increasing radius.

The traveling wave response is no longer "crisp" and starts to approximate an exponential decay. The situation where the wire radius is held constant, but the height is reduced at each step until it reaches the ground, is shown in Figure 6.4-11. The transmission line here is terminated in a low impedance of 20 Ω. The voltage at the junction in Figure 6.4-11 shows a gradual reduction, eventually reaching a constant value given by the division of the open-circuit source voltage between the source impedance and the grounding resistance.

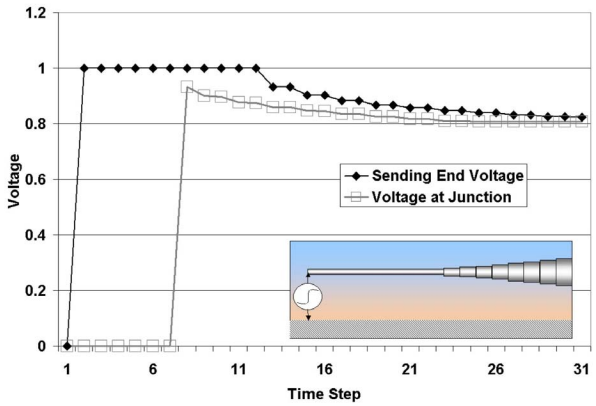


Figure 6.4-10 Sending-end and junction voltages for overhead wire with gradual change in radius.

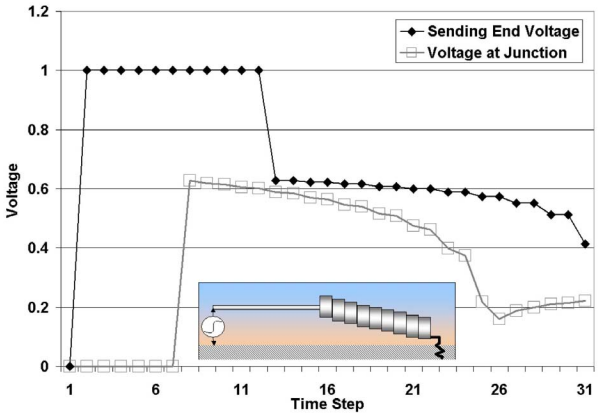


Figure 6.4-11 Sending-end and junction voltages for overhead wire with gradual change in height, terminated in 20 Ω.

The gradual modification of the horizontal line to a vertical tower is now apparent. With the knowledge that, electromagnetically, the orientation of each of the discs does not have a strong influence on its impedance, the voltage at the junction in Figure 6.4-11 is nearly the same as the voltage that appears on the top of a cylindrical tower of stacked elements with the same radius.

There remains one interesting surprise in this analysis. If the tower has a large radius at the top and a small radius at the base, then its impedance tends to be constant. Figure 6.4-12 shows that this establishes a constant junction (tower-top) voltage until a sharp reflection occurs from the 20-Ω termination at tower base. This behavior differs from the case where a vertical current is injected into a vertical cone: there, injection at the cone vertex gives a constant impedance (Markuviz 1986).

The response of a vertical tower to a surge in a horizontal wire is relevant for strokes to overhead groundwires near the tower. Since it is relatively simple to understand where the impedance values come from with this model, it is also the case covered in Applet L5 for showing why the tower travel time is so long compared to the tower height divided by the speed of light.

Tower as Solid Cone or Cylinder

The spherically symmetric TEM electromagnetic field formed between a pair of cones is well understood (Markuvitz 1968; Jordan and Balmain 1968; Kraus 1988) and useful in many antenna designs, such as the familiar bow-tie antenna for UHV television reception.

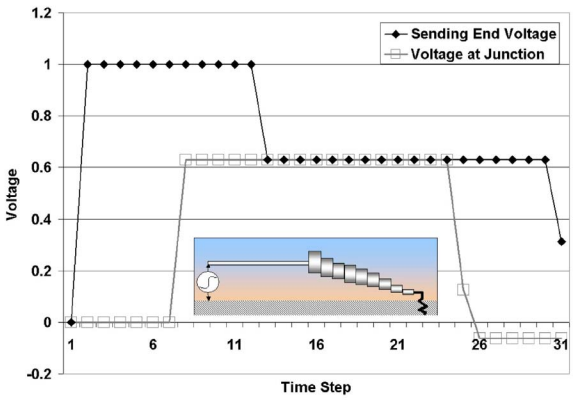


Figure 6.4-12 Sending-end and junction voltages for overhead wire with gradual reduction in both height and radius (inverted cone), terminated in 20 Ω.

The surge impedance is defined in general between two cones, each with half-angle θ_1 and θ_2, and the inner cone $\theta_1 < \theta_2$, as in Equation 6.4-32 and Figure 6.4-13.

$$Z = 60 \ln \frac{\cot\left(\frac{\theta_1}{2}\right)}{\cot\left(\frac{\theta_2}{2}\right)} \quad 6.4\text{-}32$$

The cone does not need to be perfect to have constant surge impedance. Triangular plates and wire-frame "bow-tie" approximations to a bicone can also be designed to present constant impedance over a wide range of frequencies. In the special case of the inner cone (tower) over a ground plane, θ_2 becomes 90°, the cotangent of 45° is unity and the tower impedance becomes as shown in Equation 6.4-33 and Figure 6.4-14.

$$Z = 60 \ln \cot\left(\frac{\theta_1}{2}\right) \quad 6.4\text{-}33$$

Equations 6.4-32 and 6.4-33 describe the impedance seen at a current injection point at the cone apex and remain valid for finite-length cones until two "tower travel times," given by the height of the cone divided by the speed of light.

In the case where the apex of the tower is excited by a vertical filament of current, Sargent and Darveniza (Sargent and Darveniza 1969) derived a constant surge impedance, shown in Equation 6.4-34 and Figure 6.4-15.

$$Z = 60 \ln \frac{\sqrt{2}}{\sin\theta} \quad 6.4\text{-}34$$

For slender towers with cone angles of less than 10°, the impedance to vertical injection at the apex is calculated to be 21 Ω higher than the impedance of the conical tower excited over a ground plane. This estimate has been verified by calculations of Baba (Baba and Ishii 1999), who found that the tower impedance for a vertical lead was 10% higher than for a horizontal lead.

When cylindrical towers are treated in the same way as the cones of Figure 6.4-13, a "bi-cylindrical" transmission line is nonuniform, with a capacitance per unit length and surge impedance that vary along the line. Jordan and Balmain (Jordan and Balmain 1968) note that, for thin antennas, each cylinder slice of thickness *dh* can be considered as an element of a biconical line with cone angle $\theta_1 = r/h$, with *r* being the cylinder radius and *h* being the distance from the excitation point to the element *dh*. The impedance of a bicylindrical transmission line is:

$$Z_o(h) = 120 \ln\left(\frac{2}{\theta_1}\right) = 120 \ln\left(\frac{2h}{r}\right) \quad 6.4\text{-}35$$

The impedance increases as the wave moves away from the injection point. An average impedance of the bicylinder antenna is given by integrating over the antenna height *H*:

$$Z_o(H) = \frac{1}{H}\int_0^H 120 \ln\left(\frac{2h}{r}\right) dr = 120\left[\ln\left(\frac{2H}{r}\right) - 1\right] \quad 6.4\text{-}36$$

Wagner and Hileman (Wagner and Hileman 1960) rederived the original approach of Jordan (Jordan 1934) to obtain the transient response of a vertical cylinder to an

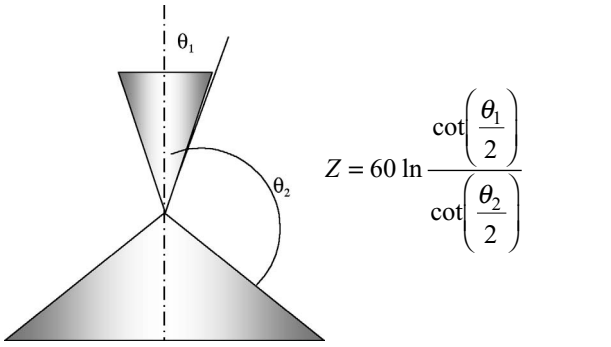


Figure 6.4-13 Surge impedance of two-cone antenna.

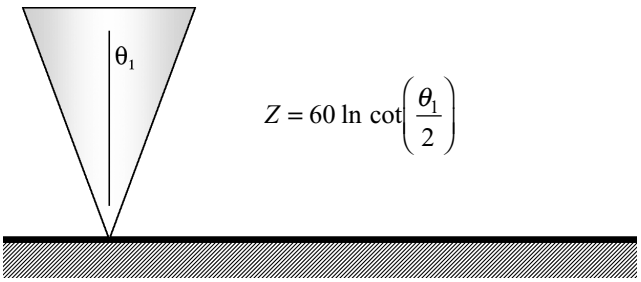


Figure 6.4-14 Surge impedance of vertical cone over ground plane.

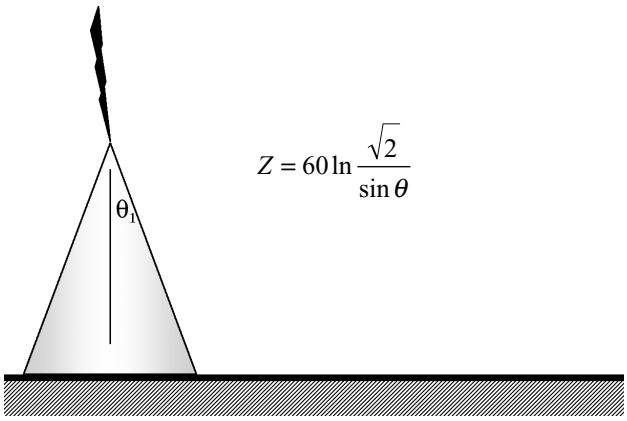


Figure 6.4-15 Surge impedance of cone with vertical current source at apex.

impressed lightning current using electromagnetic field theory. They express a transient tower surge impedance of a cylinder of radius *r* as shown in Equation 6.4-37 and Figure 6.4-16.

$$Z = 60 \ln \sqrt{2}\,\frac{ct}{r} \qquad 6.4\text{-}37$$

The highest value of tower-top potential is achieved at a time $t = 2h/c$. The transient impedance of the cylinder at this time differs from the impedance of a wire of the same radius over ground ($Z = 60 \ln (2h/r)$) by 21 Ω. Sargent and Darveniza (Sargent and Darveniza 1969) noted that the average surge impedance of the cylinder was 60 Ω less than the maximum value.

Chisholm (Chisholm et al. 1983) established that the response of transmission towers depends on the direction of current injection. In tests with time-domain reflectometry, inverted to obtain impedance as a function of distance down the tower, experiments showed that:

- The impedance of a cone over a ground plane is constant and is accurately estimated by Equation 6.4-33.
- The impedance of a cylinder over a ground plane starts out at a low value and increases, and is about 21 Ω lower than estimated by Equation 6.4-37.
- The impedance of a tower, excited by an incoming wave on a horizontal conductor, differs from the impedance when excited by a vertical current.
- For horizontal excitation, the cone with the apex at the ground has constant surge impedance while the cone with the apex at the wire has a highly variable surge impedance, as shown in Figure 6.4-17.

It is possible to estimate the surge impedance of individual sections of towers using the same expression for the surge impedance of that section over ground, for both horizontal and vertical portions of complex towers. The TEM impedance of *Z = 60ln (2H/r)* for thin wires was used in the previous section. For towers with a wide cross section at the base, the impedance based on the cone angle θ in Equation 6.4-32 is more physical. For horizontal excitation of a vertical cylinder of radius *r*, the transient impedance is calculated to be (Chisholm et al. 1985):

$$Z = 60 \ln \cot\frac{1}{2}\tan^{-1}\left(\frac{r}{H - ct}\right) \qquad 6.4\text{-}38$$

As in Wagner and Hileman, *t* is the time after a current step reaches tower top. The expression for the cone of base radius *r* with apex pointing up is:

$$Z = 60 \ln \cot\frac{1}{2}\tan^{-1}\left(\frac{rct}{H(H - ct)}\right) \qquad 6.4\text{-}39$$

Numerical integration of these transient impedances over the tower height gives average values that are 54 to 57 Ω less than the maximum values given at $t = 2h/c$, similar to the results of Sargent and Darveniza for vertical injection to a cylinder. For a wide range of tower shapes and with 5% accuracy, (Chisholm et al. 1985) recommended the following expression for the average impedance of a transmission tower, as shown in Figure 6.4-18.

$$Z_{avg} = 60 \ln \cot\frac{1}{2}\tan^{-1}\frac{r_1H_2 + r_2(H_1 + H_2) + r_3H_1}{\left(H_1 + H_2\right)^2} \qquad 6.4\text{-}40$$

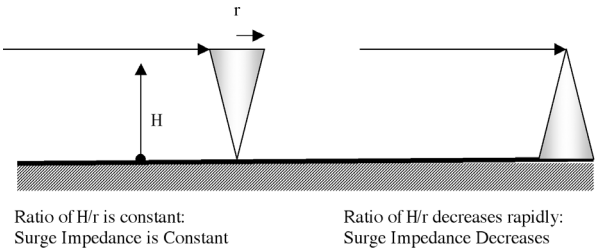


Figure 6.4-17 Surge impedance of cones for horizontal current injection.

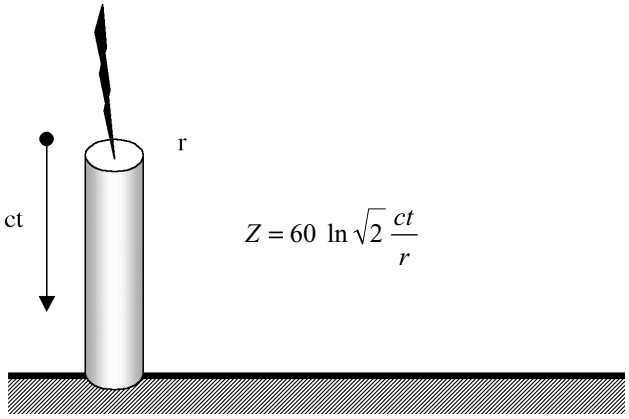


Figure 6.4-16 Surge impedance of cylindrical tower.

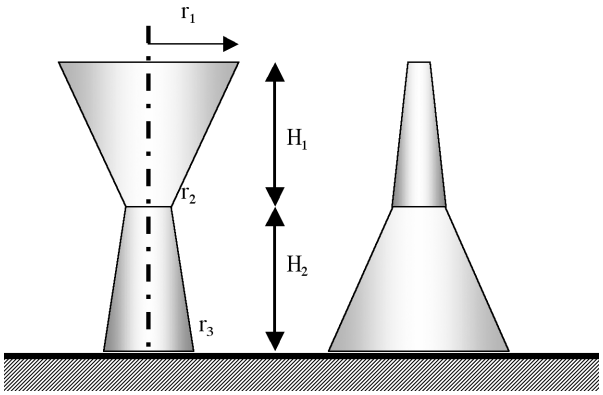


Figure 6.4-18 Surge impedance of two-section towers using conical model.

Towers with Crossarms

Many experimental results, obtained by measuring the time needed to observe a reflection (voltage reduction) from the tower base, suggest that the wave does not travel at the speed of light. Estimates of propagation speed by (Kawai 1964) ranged from 0.71 to 0.89 c, and measurements on scale models of typical towers also show effective propagation speed of 0.61 to 0.73 c. The extra travel time is a consequence of the convoluted and extended path length for the traveling waves.

Lattice mesh techniques are finite-difference (FD) methods for analyzing transients on traveling-wave systems. The "Telegrapher" equations of propagation on a lossless transmission line are solved in the time domain (TD) with a suitable FD scheme. Nonuniform transmission lines, such as slanted wires over ground or vertical cylinders, are treated with the use of reflection and refraction coefficients at each physical interface between sections. The use of an impulse for the source function allows direct calculation of transfer functions and efficient convolution at any point in the system.

Bewley (Bewley 1963) presented a lattice diagram method for analyzing traveling-wave systems in 1931. A typical lattice diagram is shown in Figure 6.4-19.

In Figure 6.4-19, time increases as the waves progress down the page. The total potential at any point in time and space can be calculated by superposition of all the reflected and refracted wave components that reach that point. At impedance discontinuities, the normal reflection and refraction coefficients (ρ and (1 + ρ) for voltage) are applied to the wave components.

Simple transmission-line systems can be analyzed efficiently with lattice diagrams because there are only a few interfaces. However, when the impedance of a system varies continuously or there are several interfaces, the multiple reflections in the diagram proliferate. At a certain point (typically more than three discontinuities), it is more efficient to formulate the problem in terms of general left-going and right-going waves above and below each interface. This is fully equivalent to a Lax-Wendroff central-difference operator for numerical solutions of the wave equations (Mitchell and Griffiths 1980):

$$U_x^{t+1} = 2\,(1-a)\,U_x^t + a\,U_{x-1}^t + a\,U_{x+1}^t - U_x^{t-1} \qquad 6.4\text{-}41$$

The subscript x refers to the discrete distance elements (the horizontal axis in Figure 6.4-18), and the superscript t refers to time steps, incrementing vertically from the top of the lattice diagram. The value a is used to speed up the calcula-

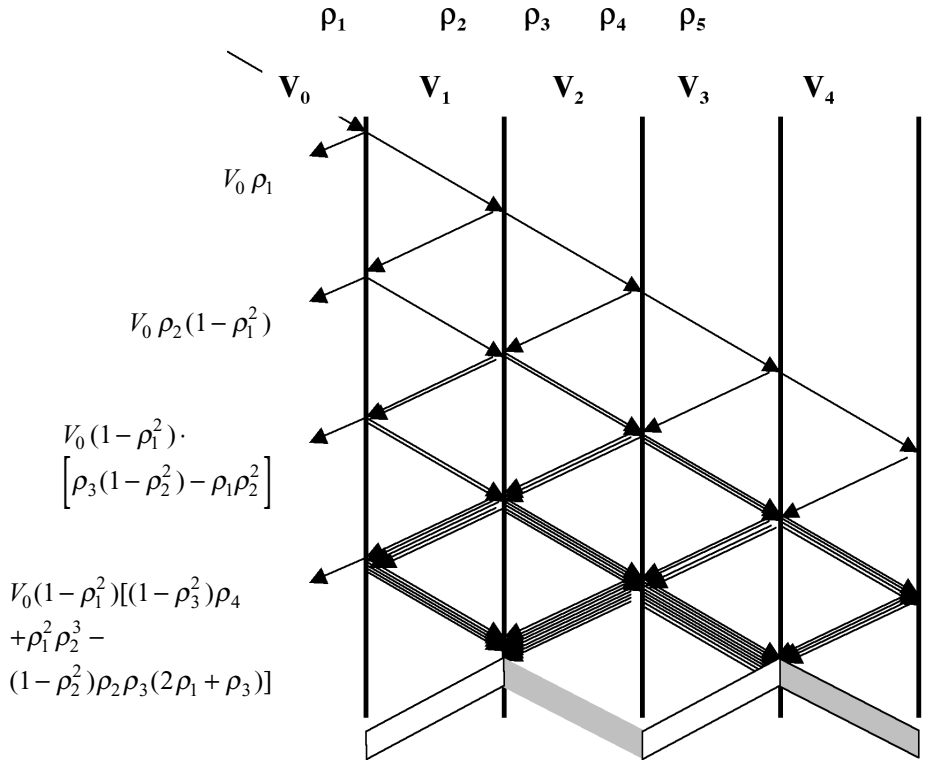


Figure 6.4-19 Lattice diagram for traveling waves with multiple reflections.

tions while maintaining the numerical stability of the calculation. The formulation in Equation 6.4-41 can be simplified by choosing a = 1, which simplifies programming and stability while increasing computation time. The boundary conditions for left-going and right-going waves are:

$$\begin{aligned} (right-going) \quad & U_x^{t+1} = \rho U_x^{t-1} + (1+\rho) U_{x-1}^t \\ (left-going) \quad & U_x^{t+1} = \rho U_x^{t-1} + (1+\rho) U_{x+1}^t \end{aligned} \qquad 6.4\text{-}42$$

Source terms in the form of derivatives of electric and magnetic field components from nearby lightning (or other electromagnetic illumination) can be included in the finite-difference scheme of Equation 6.4-42. Examples of formulations include (Taylor et al. 1965) for mixed fields, (Agrawal et al. 1980) for vertical and horizontal electric fields, and (Rachidi 1993) for vertical and horizontal magnetic fields.

When the transmission line is not uniform, every spatial location has nonzero reflection coefficients relative to its neighbors. Extension of the Lax-Wendroff equations for this case leads to an eight-point FD scheme. This is normally addressed by using different reflection coefficients for left-going (ρ_{12}) and right-going (ρ_{21}) waves with $\rho_{12} \neq \rho_{21}$, in fact $\rho_{12} = -\rho_{21}$. To show the equivalence of Bewley lattice calculations and the finite-difference methods for partial differential equations, it is more convenient to break the problem into left-going (*VL*) and right-going (*VR*) components, with the total voltage at any time and position given by the sum of these two components:

$$\rho_n = \frac{Z_{n+1} - Z_n}{Z_{n+1} + Z_n}$$

$$\begin{aligned} VR_n^{t+1} &= (1+\rho_n) VR_{n-1}^t - \rho_n VL_{n+1}^t \\ VL_n^{t+1} &= (1-\rho_n)\, VL_{n+1}^t + \rho_n VR_{n-1}^t \end{aligned} \qquad 6.4\text{-}43$$

$$U_n^{t+1} = VR_n^{t+1} + VL_n^{t+1}$$

As a double-check and to help visualize the various components, for the uniform-line case, the value of ρ will be 0, leading to:

$$\begin{aligned} U_n^{t+1} &= VR_{n-1}^t + VL_{n+1}^t \\ &= (U_{n-1}^t - VL_{n-1}^t) + (U_{n+1}^t - VR_{n+1}^t) \\ &= U_{n-1}^t + U_{n+1}^t - VL_n^{t-1} - VR_n^{t-1} \\ &= U_{n-1}^t + U_{n+1}^t - U_n^{t-1} \end{aligned} \qquad 6.4\text{-}44$$

This is the desired central-difference scheme of Equation 6.4-41, with *a = 0*.

The method can be extended to handle the case of a stub transmission line or parallel path. This is important for modeling the effects of tower crossarms and overhead groundwires. The reflection coefficients at a three-way interface with main path Z_1 to Z_2 and side path Z_3 will be ρ_1 from the incident wave in Z_1 to the parallel combination of $Z_2||Z_3$, ρ_2 from Z_2 to $Z_1||Z_3$ and ρ_3 from Z_2 to $Z_1||Z_3$.

$$\rho_1 = \frac{Z_2 Z_3 - Z_1(Z_2 + Z_3)}{Z_2 Z_3 + Z_1(Z_2 + Z_3)}$$

$$\rho_2 = \frac{Z_1 Z_3 - Z_2(Z_1 + Z_3)}{Z_1 Z_3 + Z_2(Z_1 + Z_3)} \qquad 6.4\text{-}45$$

$$\rho_3 = \frac{Z_1 Z_2 - Z_3(Z_1 + Z_2)}{Z_1 Z_2 + Z_3(Z_1 + Z_2)}$$

$$\begin{aligned} VR_{stub}^{t+1} &= \rho_3\, VL_{stub}^t + (1+\rho_1) VR_{n-1}^t + (1+\rho_2) VL_{n+1}^t \\ VR_n^{t+1} &= \rho_2\, VL_{n+1}^t + (1+\rho_1) VR_{n-1}^t + (1+\rho_3) VL_{stub}^t \\ VL_n^{t+1} &= \rho_1\, VR_{n-1}^t + (1+\rho_2) VL_{n+1}^t + (1+\rho_3) VL_{stub}^t \end{aligned} \qquad 6.4\text{-}46$$

Applet L-5, Tower Surge Impedance, implements the above method for lattice diagrams to illustrate some important points in tower surge response. The individual impedances of each section are estimated very simply with the expression $Z_n = 60\ ln(2h_n/r_n)$, where h_n is the average height of segment *n* above ground, and r_n is the radius of the circle that gives the same surface area as the segment. This expression is valid with some error (about 21 Ω) for both vertical and horizontal directions of propagation. For square segments of side length *C*, the perimeter is 4C, and the equivalent radius is $r_n = 2C/\pi$.

In Figure 6.4-20, a screen capture from Applet L-5, the surge current is injected into the apex of one of the overhead groundwire supports. At this point, the current splits into two components, one into the parallel impedance of the nearest overhead groundwire, and another into the support arm. At the center of the tower, the surge current splits again. A component travels back up the support arm to the opposite overhead groundwire, a portion is reflected back to the source, and the remainder travels vertically down the tower body. At each of the three crossarms, additional reflections and refractions occur. Voltages at the injection point and at the ends of each insulator crossarm are presented as a function of time. In addition, the time integral of the transfer impedance (in units of inductance) is also

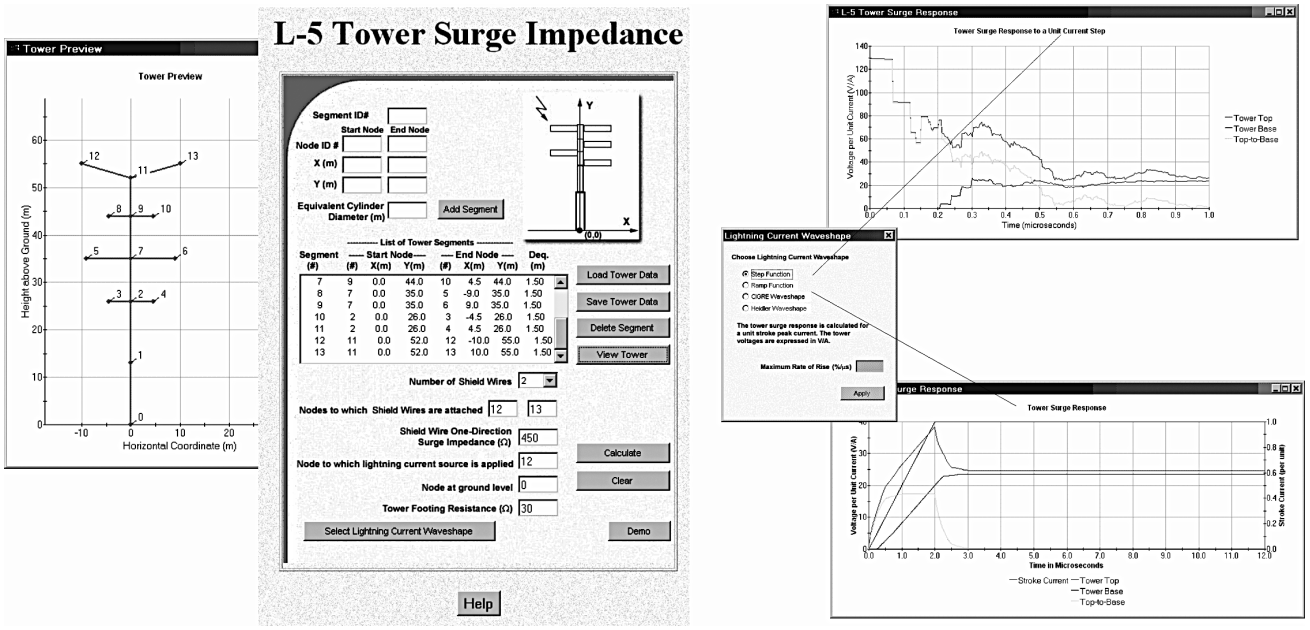


Figure 6.4-20 Traveling-wave model of transmission tower features.

calculated for comparison with estimates using simpler models. With the impulse injection source, it is possible to observe voltage doubling at the open-circuited ends of tower crossarms. This can be verified experimentally as well and contributes slightly to insulator stress. The dominant contribution, however, is the extended travel time associated with the additional propagation (at the speed of light) out and back along each stub element.

Towers with Multiple Parallel Paths to Ground

Some important tower types, including those with guy wires and H-frames, can be modeled as several inclined paths in parallel. While it is possible to compute and use the mutual coupling between these paths, this is not done in Applet L5, because this does not give better accuracy than a simple parallel combination of the individual impedance values. For a guyed-V tower of 60 m with 1-m diameter sections, a 206-Ω surge impedance is reduced to 170 Ω with two guy wires of radius 0.01 m. The L5 applet can be used to study this effect by adding guywire segments from the tower bridge (horizontal element above ground) down to near the ground plane, then adding another horizontal segment to terminate them to the central ground point at the apex of the tower.

Since guy wires carry considerable transient impulse current for short durations, they should not be electrically insulated or mounted in insulating anchors. Instead, the guy anchors should be used as launching points for radial crowfoot electrodes in areas of high soil resistivity, as described in Section 6.10.

Surge Impedance of Perfect Ground Plane

At the tower base, the surge impedance response of the tower continues. This surge response adds to the resistive rise from the tower footing resistance, as described in Section 6.8. Even with a perfectly conducting sheet of metal at the tower base, there is no "magic cancellation" that gives an immediate and perfect short circuit with reflection coefficient of $\rho = -1$. Instead, there is a distributed reduction in impedance that can be approximated in at least three ways.

The first model for ground plane surge response uses the expression for the surge impedance of a cone, excited at its apex. For a cone angle θ, this is given above in Equation 6.4-33 as:

$$Z_{cone} = 60 \ln\left(\cot\frac{\theta}{2}\right) \qquad 6.4\text{-}47$$

While the wave is propagating down the cone, the ratio of radius to distance from the apex remains constant, so the surge impedance is also constant. At the base, the radius of the perfectly conducting ground plane starts to increase, but the vertical distance remains constant, so that θ increases and Z starts to decrease.

- At two tower travel times ($\tau = H/c$), the wave will be a distance H away from the base, giving an angle θ of about 45° with a corresponding impedance of $Z = 53\Omega$.
- At 3τ, $\theta = \tan^{-1}(2H/H) = 63°$ and $Z = 29\ \Omega$.
- At 4τ, $\theta = \tan^{-1}(3H/H) = 72°$ and $Z = 20\ \Omega$.

Eventually, the cone angle will reach θ = 90°, and the "perfect" short circuit at low frequency will be established.

Experimentally, the reflection coefficients measured at the base of conical towers in a pair of parallel planes are imperfect, but not as high as suggested by the first ground-plane surge response model. A second model, based on the excitation impedance of a cylindrical waveguide, gives a simple expression for ground-plane surge response at the base of a tower of height H_{tower}:

$$Z_{ground} = \frac{60 H_{tower}}{ct} \qquad 6.4\text{-}48$$

This expression becomes valid for $ct > h$ and means that the initial (high-frequency, short-time) reflection coefficient at the base of a thin 300-Ω tower is approximately:

$$\rho_g = \frac{60\ \Omega - Z_{tower}}{60\ \Omega + Z_{tower}} \approx -0.7 \qquad 6.4\text{-}49$$

The imperfect ground reflection at the base of tall, thin, conical towers has been observed (Gorin et al. 1977; Janischewskyj 1997 and Willet et al. 1989) and verified experimentally (Bermudez et al. 2003) on full-scale measurements of lightning on tall towers. The effect can be analyzed comprehensively using advanced electromagnetic models such as NEC2 (Baba and Ishii 2001). Bermudez (Bermudez 2003) used measurements of lightning stroke currents at two heights on a tall tower to derive the reflection coefficient as a function of frequency, as shown in Figure 6.4-21.

With the experimental results in Figure 6.4-21, it is possible to propose a third, very simple model for the ground reflection at high frequency: the use of a constant value of $\rho = -0.7$ to terminate the transmission line model at the tower base. This model is appropriate for studying the effects of tower features, but is not relevant to calculation of outage rates because the low-frequency resistance is a function of the soil resistivity and the shape and size of the tower footing.

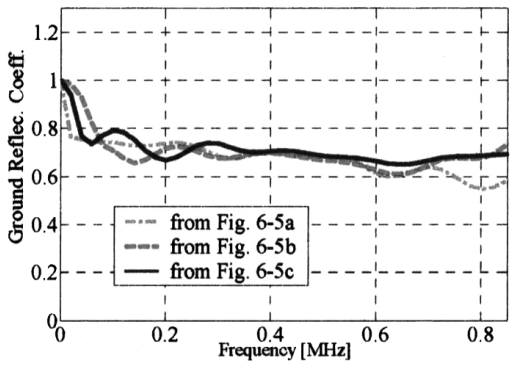


Figure 6.4-21 Observed ground reflection coefficient versus frequency for three pairs of tall-tower current measurements (*top and bottom*).

6.4.3 Calculation of Insulator Voltage and Lightning Performance

Figure 6.4-20 shows the schematic of Applet L-5, which is used to illustrate how the transmission tower affects the waveshape and magnitude of insulator voltage.

For simple cases, such as cylindrical or conical cross sections, Applet L-5 predicts transmission-line surge response that matches the corresponding equations from antenna literature. These cases should be explored first, using short crossarms to evaluate the influence of tower position on the insulator stress.

Crossarms provide a mixed effect in Applet L-5. They tend to lower the tower surge impedance and increase the tower travel time. Waveshapes on the bottom phases of the tower tend to have slower fronts, while the top phases can show significant oscillations that are predicted to increase the probability of flashover by accelerating the development of leaders across the insulation.

For short towers of less than 20 m, the tower surge response should not have much influence on the overall line performance, and the dominant result is that the insulator voltage is simply the input current, divided by the parallel impedance of the overhead groundwire network and the local footing resistance. This simple relationship exists until reflections return from adjacent towers, as shown in the Applet L-4. However, for taller towers of 50 m or more, the additional stresses associated with convoluted propagation paths and ground-plane surge impedance play an increasing role in the lightning performance.

6.5 INSULATION STRENGTH FOR LIGHTNING IMPULSES

Lightning performance is calculated by comparing the insulator stress with strength. The insulator stress is a function of:

- Input current parameter distributions, as described in Section 6.2.
- Lightning incidence statistics, as described in Section 6.3.
- The transfer function between the input current to the tower/overhead groundwire structure and the insulator voltage, as described in Sections 6.4 and 6.10, occasionally leading to backflashover, as computed in Section 6.7
- The transfer function between input current to the phase conductor and the insulator voltage, as described in Section 6.6, usually leading to shielding failure flashover

Section 6.2 has shown that there is no "one" lightning waveshape, and that a statistical approach is needed to define the stress correctly. The response of transmission-line insulation to lightning surge voltages was shown in Section 6.4 to be complex and dynamic. Steep-rising overvoltages with duration that is limited by the distance to adjacent structures can be far less prone to flashover than test results obtained with a standard 1.2 x 50 μs voltage wave. As a rough guide, the 50% increase in strength for short-time impulse strength (2 μs), compared to standard impulse flashover, can decrease transmission outage rates by a factor of three. Reliable calculation methods for transmission outage rates in Sections 6.6 and 6.7 all have models for the increase in impulse strength with decreasing time, however crude or empirical.

6.5.1 Volt-Time Curve Penetration Algorithm, Evaluated at Span Reflection Time

The second edition of the Red Book used a simple empirical description (Darveniza et al. 1975) of the flashover process. The dielectric strength of an insulator string as a function of time to flashover for a standard lightning impulse voltage wave is approximated as:

$$V_{50\%} = \left[400 + \frac{710}{t^{0.75}}\right][L] \qquad 6.5\text{-}1$$

Where:
$V_{50\%}$ = the median flashover voltage in kV.
t = the time to flashover in μs.
L = the length of the insulator string in meters.

This expression is valid for the case of a negative lightning to the overhead groundwires, making the conductor positive relative to the tower. For wet tower insulation in center or outside phases, Hileman (Hileman 1999) recommends a positive-polarity gradient for Critical Flashover (+ CFO) of 560 kV/m for positive polarity (corresponding to evaluation of Equation 6.5-1 at 7 μs) and 605 kV/m for negative polarity (- CFO). Hileman recommends the same gradients for both line and substation clearances and gives an alternate expression to Equation 6.5-1 for volt-time characteristic, illustrated in Figure 6.5-1. The difference between median and critical flashover levels is set by international standards and typically uses a relative standard deviation of 3% for lightning impulses. For this reason, the use of V_{50} is common in lightning calculations, including those in the applets.

The use of volt-time curves like those in Figure 6.5-1 is correct only while the applied waveform matches the standard 1.2/50 μs wave. If the applied voltage deviates from the standard wave, in particular by the arrival of canceling reflections from adjacent towers that reduce the voltage, then the model becomes less useful. The most appropriate applications of the volt-time curve are to model the flashover strength exactly at the span reflection time, as done in the IEEE FLASH program (IEEE 1997b), and to validate parameters of more sophisticated models, as shown in the next two sections.

6.5.2 The Disruptive Effect (DE) Algorithm, Typically for Faster-Front Flashover/Puncture

Below a critical flashover level V_o, shown in Figure 6.5-2, the applied voltage can be withstood for a relatively long time. This leads to models where all voltage above an ionization threshold contributes to the development of the flashover path. A general form used for many models of

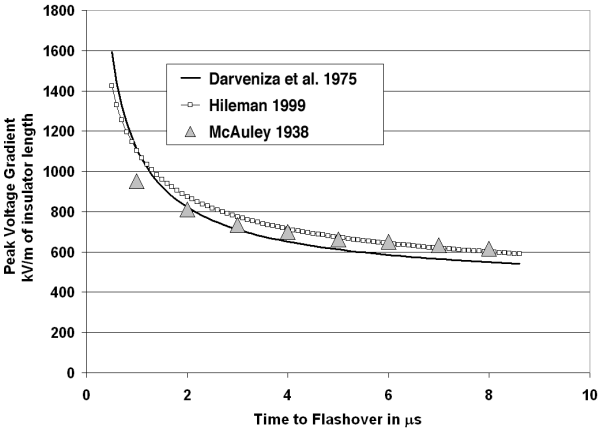


Figure 6.5-1 Volt-time characteristic of porcelain insulators under standard positive lightning impulse voltage (tower negative relative to conductor).

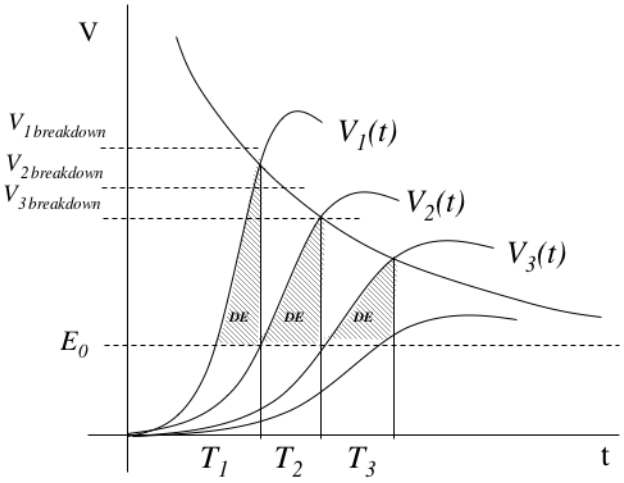


Figure 6.5-2 Disruptive effect for three nonstandard voltage waves.

insulation is the Disruptive Effect, given in Equation 6.5-2 and discussed in more detail in Appendix 6.1.

$$DE = \int_{t_o}^{T_d} (V(t) - E_0)^{\,n} dt \qquad 6.5\text{-}2$$

(Caldwell and Darveniza 1973) found that the DE method with $n = 1$ gave good results, with better than 10% agreement between measured and calculated values. An IEEE Task Force (IEEE 1996b) noted that the use of $n = 2.5$, DE of 10^{10}, and E_0 of 300 kV gave the best match to the volt-time characteristics of porcelain insulators in Equation 6.5-1, with a relative standard deviation of 6% for both front-of-wave and tail-of-wave flashover. Figure 6.5-3 shows, however, that good results (constant value of DE for a wide range of times to flashover) can be obtained with a wide range of exponents after the wave crest at 1.2 μs.

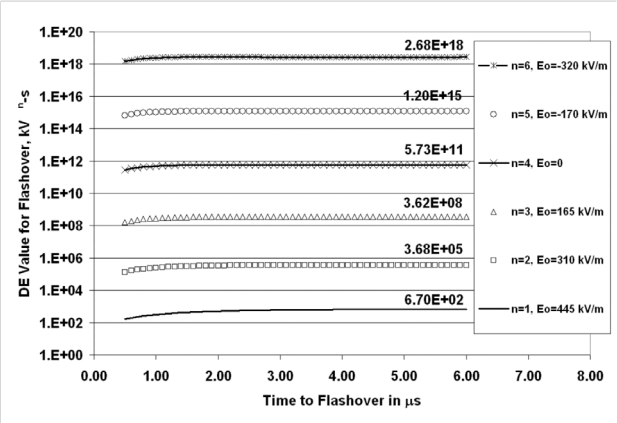


Figure 6.5-3 Disruptive effect at flashover of 1.2/50 μs standard lightning impulse wave for various exponents n and optimal value of E_o for fitting Equation 6.5-1.

6.5.3 The Leader Progression Model, Typically Evaluated for Several Span Reflection Times

The insulator voltage $v(t)$ is a source term for a differential equation that describes the growth of a leader across the gap. The growth rate and coupling terms are established from experimental results. By solving the differential equation, the leader progression models can lead to more realistic breakdown characteristics for nonstandard impressed waveforms, especially across air gaps. There are two times of interest in the high-voltage flashover process: t_s, the time to develop streamers across the gap from both electrodes, and t_l, the time for a leader to propagate across the gap.

The streamer propagation time is a function of the average voltage overstress in the gap, compared to its 50% flashover voltage V_{50}. (Pigini et al. 1989) gives the following estimate of streamer time for impulse voltages of either polarity:

$$t_s = \frac{1}{1.25\left(\dfrac{V}{V_{50}}\right) - 0.95} \quad \text{for } t_s \text{ in } \mu\text{s} \qquad 6.5\text{-}3$$

The streamer time t_s in Equation 6.5-3 is relatively constant at 0.5 to 2 μs. The difference between streamer time and total time to flashover in Equation 6.5.1 provides an estimate of the leader propagation velocity as a function of applied voltage as follows. The leader propagation time, using Equations 6.5-1 and 6.5-3, becomes, for a CFO of 560 kV/m:

$$t_l = \left(\frac{710}{E - 400}\right)^{1.333} - \left(\frac{448}{E - 426}\right) \qquad 6.5\text{-}3\text{A}$$

E is the peak breakdown voltage per meter of insulation, expressed in kV/m, and the leader time is given in μs. The leader propagation velocity dg/dt is simply the gap length divided by the leader propagation time. Figure 6.5-4 shows how this velocity is predicted to increase as a function of voltage stress for two insulator string lengths.

The results suggest that leaders need a minimum of 500 kV to develop, and also suggest that the average leader velocity is faster for longer gaps.

The expression proposed by (CIGRE 1991) for the leader progression process is:

$$\frac{dg}{dt} = kV(t)\left[\frac{V(t)}{l - g} - E_0\right] \qquad 6.5\text{-}4$$

Where:

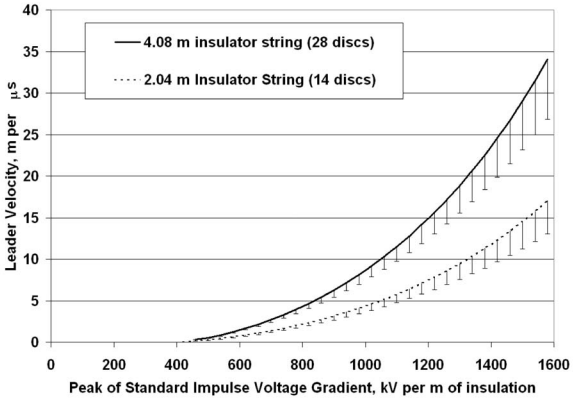


Figure 6.5-4 Estimate of leader velocity across porcelain insulator string, based on (flashover time) minus (streamer time) for E_o = 520 - 560 kV/m.

dg/dt = the leader velocity in m/s.
k = a constant given in Table 6.5-1.
$V(t)$ = the voltage across the gap in kV.
g = leader length in m.
l = the air gap length in m.
E_0 = the breakdown gradient as given in Table 6.5-1.

CIGRE recommends the matrix of values for E_0 and k shown in Table 6.5-1.

Table 6.5-1 Recommended Values for Leader Progression Model of Lightning Impulse Flashover

Configuration	Polarity	k $m^2/(kV^2\text{-}\mu s)$	E_0 KV/m
Air gaps, post insulators, long-rod polymer insulators	Positive	0.8×10^{-6}	600
	Negative	1×10^{-6}	670
Cap-and-pin porcelain and glass insulator strings	Positive	1.2×10^{-6}	520
	Negative	1.3×10^{-6}	600

A common simplification for implementation in the Electromagnetic Transient Program (EMTP) or other modelling programs is to assume a constant leader velocity, but Figure 6.5-4 suggests this may not be appropriate.

Figure 6.5-5 shows the CIGRE recommendations for leader propagation modelling along with the reference volt-time characteristic for standard lightning impulse voltage on a 1-m insulator string, described empirically by Equation 6.5-1. At the important times to flashover between 1.5 and 4 μs, the leader propagation estimate of strength for cap-and-pin insulators is 30% too high, and this would understate lightning outage rates by a factor of two. The Motoyama model (Motoyama 1996) is more satisfactory in the time of greatest interest, but drifts away from the reference for longer times to flashover, where the CIGRE model for cap-and-pin flashover begins to converge to observations.

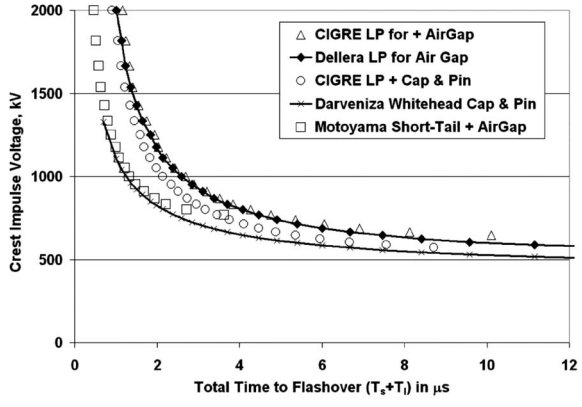


Figure 6.5-5 Comparison of predicted crest flashover voltage for leader progression (LP) models and observed volt-time characteristic of Equation 6.5-1.

6.5.4 Insulator Puncture Strength

Every lightning flash generates high transient stresses across the insulators. A typical subsequent stroke with rate of current rise 40 kA/μs, working into the minimum transient impedance of 60 Ω at tower base, generates a voltage wave with steepness of 2400 kV/μs. Shielding failures are particularly severe because the surge impedance of the stricken phase conductor would be three times greater. Some national insulator standards (CSA C411.1, ANSI C29.1) for cap-and-pin porcelain insulators call for twenty steep-front tests at the 2500 kV/μs level to establish adequate long-term performance. Morita (Morita et al. 1997) endorses this recommendation and provides experimental data on the puncture and flashover strength of individual insulators.

Insulator B in the left graph of Figure 6.5-6 has a longer leakage distance. Morita noted that, for time-to-flashover of less than 0.2μs, there was a stronger relationship between flashover voltage and insulator leakage distance, compared the usual relationship between standard lightning impulse strength and dry-arc distance for 1-10 μs times to flashover. In this case, the puncture strength of Insulator A is greater than the external flashover strength, so a single steep-front application is not likely to cause puncture. However, Figure 6.5-7 shows that repeated impulses with high steepness eventually cause wear-out failures. Impulses with higher peak magnitude, shown as $V_{0\text{-}4}$ in Figure 6.5-7, lead to a 2% failure rate for 20 impulses at 415 kV peak, but a 95% failure rate if the voltage is increased to 560 kV. This range of voltage stress per insulator disc is common on single-conductor high voltage lines when subsequent strokes follow the same path as a shielding failure. The puncture wear-out process occurs at lower stress levels on insulators with lower grades of porcelain, leading to insulator string end-of-life, when the number of sound insulators in a string falls below safe levels for live maintenance. The insulator puncture process can be summarized by noting that puncture will occur when voltage rise times become so extreme that the volt-time strength of the air along the surface of the insulator becomes higher than the volt-time strength of the insulator material. The latter has little volt-time turn-up at short times.

6.6 SHIELDING FAILURE CALCULATIONS

Overhead groundwires on a transmission line can be thought of as horizontal lightning air terminal. Their purpose is to intercept any lightning flash that would otherwise terminate on one of the phase conductors. Usually overhead groundwires are quite successful in intercepting

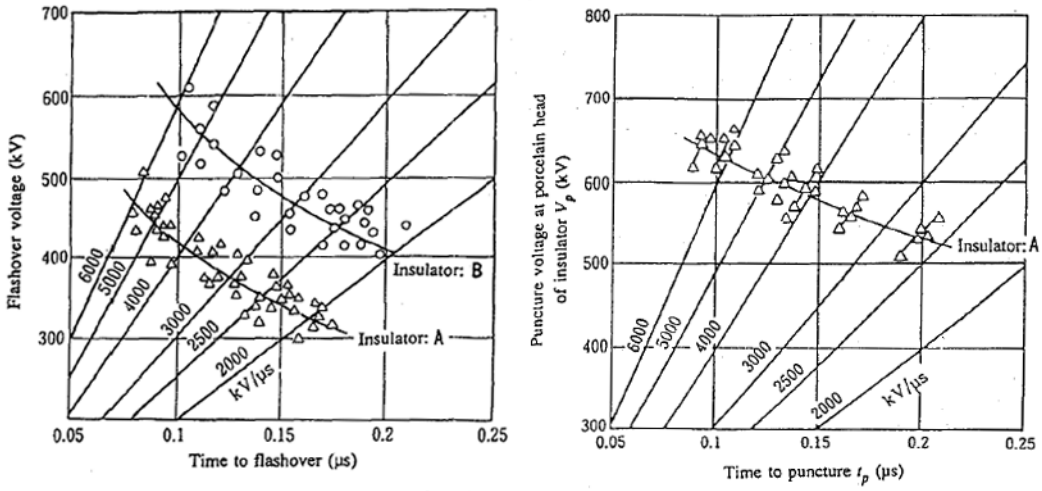


Figure 6.5-6 *Left:* Steep-impulse flashover characteristic of cap-and-pin porcelain disc insulators; *Right:* Steep-impulse puncture characteristic of cap-and-pin porcelain disc insulator (Morita 1997).

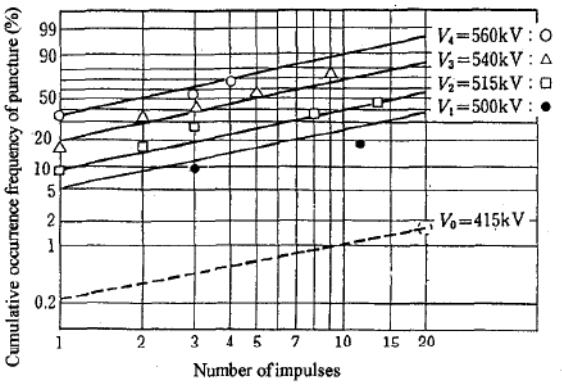


Figure 6.5-7 Number of impulses needed to cause electrical puncture on new cap-and-pin insulator at 5000 kV/μs steepness (Morita 1997).

lightning flashes, but sometimes a leader appears in such a location that it gets by the shield wire protection and strikes a phase conductor. This "shielding failure" can be a common cause of transmission-line lightning flashovers, and has been extensively studied for more than 50 years.

6.6.1 The Shielding Failure Process

The basic shielding failure process is sketched in Figure 6.6-1. A descending leader carrying a high negative charge is approaching the vicinity of a transmission line. As it moves earthward, it induces positive charges on the transmission-line conductors and on the earth below. The positive charges build up on the wires to magnitudes sufficient to trigger positive upward leaders from both the shield wires and the rightmost phase, and in some cases from the earth beneath the downward leader tip. At this moment, a race develops between the shield wire leader and the phase wire leader to resolve which will reach the tip of the downward leader first and complete the link. If the phase wire leader reaches the downward leader tip first, a shielding failure occurs, which may or may not cause a flashover, depending on the stroke current amplitude, the insulation strength, and the phase surge impedance. If the downward leader is sufficiently far away, the leaders from the wires are unable to

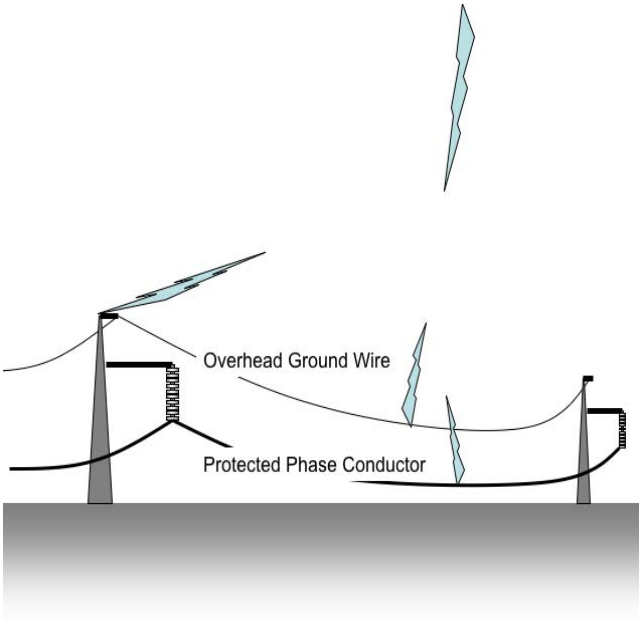


Figure 6.6-1 Upward leader competition for a line-shielding failure.

reach the downward leader and the latter terminates on the ground. Applet L-2 attached to this chapter provides a graphic simulation of this entire process, including a step-by-step downward leader progression (either for a straight leader channel, or a degree of randomization typical of what is seen in lightning photographs) and upward leaders from the conductors of either one or two transmission lines on either flat terrain or on a hillside.

In Figure 6.6-2, as a leader approaches a transmission line, each conductor emits an upward leader with striking distance R_s for the shield wire and R_p for the phase. If the downward leader tip penetrates Zone A, a strike to the shield wire occurs, or if it penetrates Zone B, a shielding failure occurs, or if Zone C, the flash is to ground. The striking distances R_s and R_p are determined by the charge on the downward leader, and hence on the first stroke current that the flash will deliver. Note in Figure 6.6-2, a distance to ground R_g is required in some algorithms to represent the striking distance to earth of the downward leader. Other algorithms simply consider a strike to ground to be a default condition if the downward leader is beyond the reach of R_s and R_p.

6.6.2 Uncovered Areas in the Shielding Failure Models

The classical "electrogeometric" analysis of shielding failure frequency considers that the flashover process originates at the tip of the downward leader, which develops downward until it achieves a point of discrimination among conductors and ground. The striking distance models from leader to conductor, and the attractive radius of later models, as shown in Figure 6.6-2, have much in common with regard to overall dimensions, increasing reach with current level and moderate sensitivity to height. The

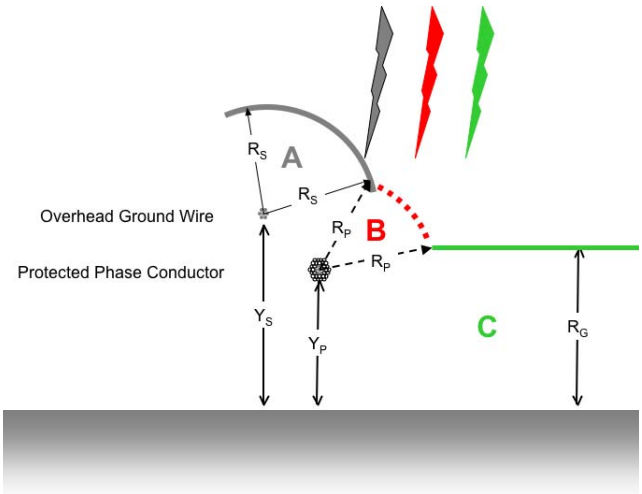


Figure 6.6-2 Shielding failure striking distances for a two-conductor line.

equations of striking distance as a function of stroke current and conductor height comprises the fundamental basis of the electrogeometric theory of shielding failures, and many variations of these equations have been proposed. It has also become common to compare striking distance and attractive radius equations directly, because they are both imperfect models of the same process, with leader development now observed to develop from both ends towards the middle.

6.6.3 Recommended Strike Distance Equations

A table of proposed strike distance equations was included in a previous edition. Recent ones include the following:

IEEE Standard 1243—1997

$$R_s = R_p = 10.0I^{0.65} \qquad 6.6\text{-}1$$

$$R_g = [3.6 + 1.7\ln(43 - y_c)]I^{0.65} \quad y_c < 40\ \text{m} \qquad 6.6\text{-}2$$

$$R_g = 5.5I^{0.65} \quad y_c >= 40\ \text{m} \qquad 6.6\text{-}3$$

Rizk—1990

$$R_s = 1.57I^{0.69}y_s^{0.45}; R_p = 1.57I^{0.69}y_p^{0.45} \qquad 6.6\text{-}4$$

Eriksson—1987

$$R_s = 0.67I^{0.74}y_T^{0.6}; R_p = 0.67I^{0.74}y_p^{0.6} \qquad 6.6\text{-}5$$

Where:

R_s = strike distance to shield wire, m.
R_p = strike distance to phase wire, m.
R_g = strike distance to ground from leader tip, m.
I = peak stroke current, kA.
y_c = average height of any conductor
y_p = average phase conductor height
y_s = average shield wire height
y_T = shield wire height at the tower

The average height of a conductor in a span is given by its height at the tower, minus two-thirds of the midspan sag.

At present, there is controversy over which of these strike distance equations correlates best with experience, but Rizk's equation (Equation 6.6-4) is recommended. In Applet L-1, all three can be used, and the highest number of shielding flashovers used as the most conservative value. Applets L-1 and L-2 permit the user to experiment with application of these equations. If the height exponent is selected to be zero in any of the above, Applet L-1 uses an approximation of Equations 6.6-2 and 6.6-3 for strikes to ground.

Usually lower current strokes under 20 kA are responsible for shielding failure flashovers, although leaders approaching a transmission line at an acute angle from the vertical

can cause high-current shielding failures. Historically, cosine or cosine-squared angle distribution has been used, but most present shielding failure theories usually assume only vertical leaders can develop. This simplifies the mathematics, but downward leaders are rarely straight and vertical.

6.6.4 Perfect Shielding

In the past, much has been made of the concept of "essentially perfect shielding," wherein the shield wires and outermost phases are so located with respect to each other that shielding failure flashovers can never occur. This is mathematically possible but of dubious reality. Figure 6.6-3 shows one conceptual perfect shielding model. For a downward leader carrying a current I, R_s represents the horizontal striking distance from the shield wire S to the downward leader, and R_p represents the striking distance from the outermost phase. Depending on which striking distance formula is used, R_s and R_p do not have to be of the same length. The heights Y_p of the phase and Y_s of the shield wire are usually set by clearance and code requirements, but the horizontal position of the shield wire with respect to the phase can be determined by tower design. In Figure 6.6-3, the phase conductor is given the relative x coordinate of zero, and it is desired to move the shield wire horizontally until perfect shielding is attained.

The current I_{crit} to use is the minimum stroke current required to initiate a flashover. It is given by:

$$I_{crit} = \frac{2 \cdot CFO}{Z_0} \qquad 6.6\text{-}6$$

Where:

I_{crit} = critical stroke current causing flashover, kA.
CFO = insulator critical flashover voltage for the stricken phase, kV.

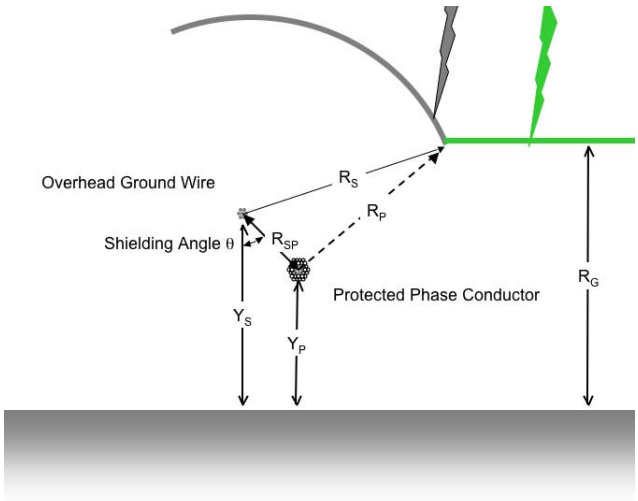


Figure 6.6-3 A conceptual zero shielding failure model.

Z_0 = phase surge impedance, ohms as modified by corona.

It is suggested that the Rizk equation (Equation 6.6-4) be used to calculate R_S and R_P using I_{crit}. Then, in Figure 6.6-3, the required horizontal distance X_{sp} between the shield wire and the outermost phase given by:

$$X_{sp} = R_s - \sqrt{R_p^2 - (Y_s - Y_p)^2} \qquad 6.6\text{-}7$$

and the required shield angle θ is:

$$\theta = \tan^{-1}\left(\frac{X_{sp}}{Y_s - Y_p}\right) \qquad 6.6\text{-}8$$

This ensures that $I < I_{crit}$, so that any remaining shielding failure is too weak to cause a flashover. Even if R_s and R_p are the same length, the shield wire is likely to absorb a preponderance of the flashes, since—being higher—the upward leader from the shield wire initiates sooner than the upward leader from the phase conductor.

One of the limiting problems in the use of "perfect" shielding angles is that, on average, two subsequent strokes tend to follow the same ionized path as the first stroke. Thus, while the first stroke may be less than I_{crit} in (Equation 6.6-6), one of the subsequent strokes may well have a current that is greater. The subsequent stroke current distribution seems to be independent of the first-stroke current, so the conditional probability that one of the subsequent peaks is greater than the first peak becomes large as the first-peak amplitude falls below 15 kA.

6.6.5 The Method of Maximum Heights

Analytical formulas for shielding failure flashover rates have been published by a number of authors and summarized in (CIGRE 1991), but when a multiplicity of wires, asymmetry of wire positions, and variations of striking distance with wire height are involved, an analytical approach becomes extremely complex, and step-by-step digital algorithms become much more tractable. One such algorithm is the "method of maximum heights," which is used in Applet L-1.

In Figure 6.6-4, a leader channel is positioned near an example set of two line conductors. This channel does not have to be vertical, but can be tilted in a Monte Carlo method to represent leaders approaching the line from a side. The striking distance from each conductor is calculated and connected to the channel, and flashover is assumed to occur to the conductor whose striking distance intercept reaches the highest position on the channel. The leader is assumed to occupy an area A_s, having a width of 1 m and a length consisting of the line length of 100 km.

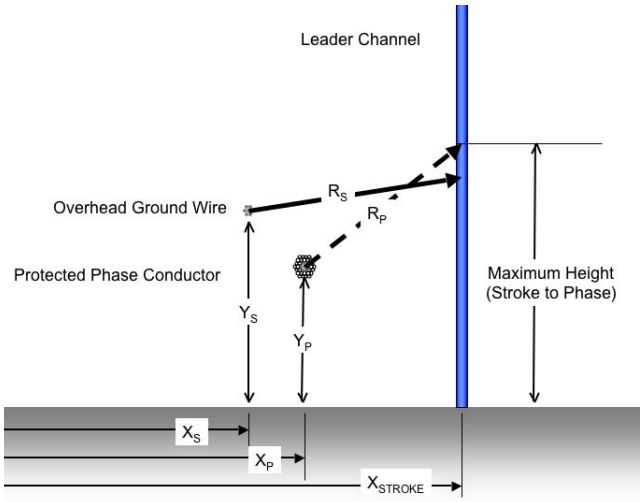


Figure 6.6-4 The method of maximum heights.

Then, if the ground flash density (GFD) is known, the total expected flashes N_t to area A_s per year can be determined. From the IEEE stroke current probability equation:

$$P = \frac{1}{1+\left(\frac{I}{31}\right)^{2.6}} \qquad 6.6\text{-}9$$

Where:

P = cumulative probability distribution of peak stroke currents.

I = peak stroke current, kA.

The question about the correct shape of the stroke current distribution in the shielding failure domain, from 3 to 20 kA, remains open. The data used to establish the two-slope distribution in (CIGRE 1991) mix measurements from systems with different trigger thresholds that were on the order of 5% of 200-300 kA full scale. All measurement systems probably captured 30-kA flashes, but fewer would have responded to 10-kA flashes, giving bias at the low end of the distribution. Data from lightning location systems are interesting strictly from the large number of observations, but also because cross-calibration with independent observations of low-amplitude events has been successful. The combination of time-synchronized tripout and non-tripout events from travelling wave fault recorders, along with lightning location records, remains a resource to be exploited to establish which stroke currents cause shielding failures (and which ones do not).

The probability of occurrence of any stroke of magnitude I ± 1 kA can be determined within the total population N_t. By scanning the complete range of stroke magnitudes from 2 kA to 160 kA in each area A_s, moving the leader area from the far right of the line to the far left in 1-m steps, and calculating the maximum heights to the leader channel of all the wire striking distances, one can count the number of flashes per 100 km per year to each wire. Several special strategies were adopted in Applet L-1 to speed the processing time.

6.6.6 Cascading Flashovers

In actual forensic examinations of lightning flashover damage in the field, insulator burns and/or structural damage usually leads one to conclude which support structure was associated with the lightning event. However, it is frequently the case that the structure with the observed damage is located one or more spans remote from the actual lightning strike location. A flashover at one tower can inject voltage on one or more phases, which travels to adjacent towers in both directions, causing them to flashover also, and the flashover closest to the generation holds in and turns off the others. These "cascading flashovers" can occur as far as three spans or more beyond the strike location.

6.6.7 Transmitted Stress to Terminals

A lightning event—either a shielding failure or a backflashover—can inject severe transient voltages on a phase that can travel for kilometers to enter a substation and—at the same time—create a severe power frequency fault that must be cleared. The power frequency fault can create severe mechanical stresses from magnetic forces, particularly in transformers. The high-voltage transient may arrive as an open breaker or disconnect switch tries to double, so even if it has been attenuated by corona and lossy ground effects, the increased voltage can still exceed the substation insulation level, leading to a failure of insulation coordination. The distance from the lightning backflashover to the open terminal at the station plays a fundamental role in the level of this transient overvoltage. It is important that, whenever possible, transmission lines within a kilometer or more of a substation or generating plant should be well shielded, grounded, and insulated to ensure that any transient voltages have to propagate over sufficient distance to minimize transferred stresses. Surge arresters, located near the open terminals or possibly on the transmission-line entrance, can play a role in limiting the overvoltage exposure economically.

6.6.8 Calculation Procedures

One of the most successful ways to estimate the lightning shielding failure flashover rate of a new transmission circuit is to perform a multiple linear regression of the observed performance for nearby lines against the most sensitive parameters. This is especially helpful when comparing lines with similar conductor geometry, tower style, and span length. Linear regression against remaining variables such as local ground flash density, shielding angle, height of adjacent vegetation, and right-of-way width can be as successful at predicting future performance as the most sophisticated treatment. In this context, equal weight

is given to describing simplified and complex models for the lightning performance of transmission lines.

6.6.9 Simplified Models

Rolling Sphere Methods

Many lightning protection standards now make use of a "rolling sphere" method (Lee 1978) adapted from transmission-line electrogeometric shielding calculations to identify protected and unprotected areas on buildings and lower structures. Lee's insight was that a sphere, with radius R_s associated with a critical current I_{crit}, rolled around a three-dimensional model of a set of ground-based shield wires, was an efficient way to evaluate shielding. This approach assumes that Whitehead's validation (Whitehead 1977) of the electrogeometric (EGM) from transmission-line data was sufficiently applicable to buildings.

According to the "Standard for the Installation of Lightning Protection Systems (NFPA 1997, Standard 780), 2000 Edition:

> "The zone of protection shall include the space not intruded by a rolling sphere having a radius of 150 ft (46 m). Where the sphere is tangent to earth and resting against a strike termination device, all space in the vertical plane between the two points of contact and under the sphere shall be considered to be in the zone of protection. A zone of protection shall also be formed where such a sphere is resting on two or more strike termination devices and shall include the space between those devices [see Figure 6.6-5]. All possible placements of the sphere shall be considered when determining the zone of protection using the rolling sphere model."
>
> "For structure heights exceeding 150 ft (46 m) above earth or above a lower strike termination device, the zone of protection shall be considered to be the space in the vertical plane between the points of contact and under the sphere where the sphere is resting against a vertical surface of the structure and the lower strike termination device or earth. The zone of protection shall be limited to the space above the horizontal plane of the lowest terminal unless it can be extended by further analysis, such as in rolling the sphere to be tangent to earth."

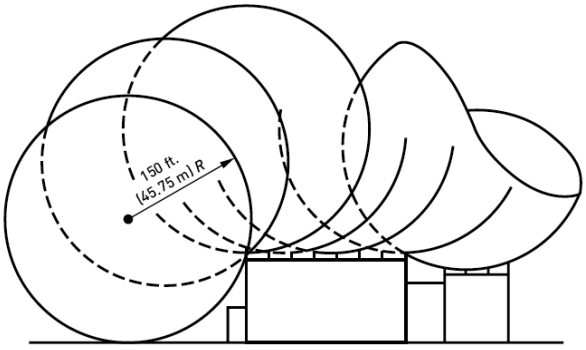


Figure 6.6-5 Rolling sphere method for analysis of shielding (NPFA 2004) (Reprinted with permission from NPFA 780-2004, *Installation of Lighting Protection Systems*, Copyright © 2004, National Fire Protection Association).

In international standards, R_s is defined directly to give an appropriate level of protection from shielding failures, with more critical installations calling for smaller radii (corresponding to less-probable weak first strokes). Typical values for the rolling sphere radius are found in Table 6.6-1.

Table 6.6-1 Recommended Values of Rolling Sphere Radius from International Standards

Standard	Rolling-Sphere Radius (m)	Equivalent Current (kA)
NFPA 780 / 2000	46 m	10.5 kA (94% protection)
NFPA 780 / 2000	30.5 m (flammable)	5.6 kA (99% protection)
BS 6651	60 m	15.7 kA (85% protection)
IEC TC81 Level I	20 m	2.9 kA (99% protection)
IEC TC81 Level II	30 m	5.4 kA (97% protection)
IEC TC 81 Level III	45 m	10.1 kA (91% protection)
IEC TC81 Level IV	60 m	15.7 kA (84% protection)
IEEE Std 998	$8\ I^{0.65}$	I = CFO/Bus Impedance

(Mousa and Srivastava 1989) recommends that a reduced striking distance expression and reduced median current of 25 kA be used for substation protection, and these have both been implemented in IEEE Standard 998 (IEEE 1996b).

The rolling sphere method can be applied in three dimensions to transmission lines near ground. This approach can be particularly helpful in areas where lines cross one another or enter a substation.

FLASH 1.8 Calculation of Shielding Failures

The IEEE Working Group on Estimating the Lightning Performance of Transmission Lines studied various methods for calculating the line flashover performance, including the methods of (Brown 1978; Darveniza 1979; EPRI 1982) and the method described in the second edition of this book. After comparing calculation results with observations on a calibration set of more than 20 transmission lines, the Working Group published a pair of papers recommending the following:

- Use of a height-dependent value for β, the factor that relates striking distances to ground and conductor, which varies with height. Originally, a value of $\beta = 22/H$ was selected to force the EGM to agree with the stroke incidence model, based on a shadow width of $(b + 4H^{1.09})$ for average overhead groundwire height H and separation b in meters. This factor was later revised in IEEE Standard 1243 (IEEE 1997b) to match the stroke incidence model of (Rizk 1990).

- Use of a striking distance of $R_s = 8\ I^{0.65}$ (IEEE 1985), intended to give a conservative shielding practice, but also leading to a gross overestimate of the shielding failure rate on 500-kV double-circuit lines with 6° shield angle. This expression was returned to its original value of SD = $10\ I^{0.65}$ in (IEEE 1993).

The Anderson method (EPRI 1982), as revised by the IEEE, was made available to the electrical industry in a variety of formats. With the difficulty of error-free completion of the schedule of calculations, even with scientific calculators, the program was converted to a series of computer languages, starting with FORTRAN, then Commodore BASIC, DOS (within a 64-k memory limit), C++, and most recently Excel. Versions of the DOS executable and BASIC versions are provided with IEEE Standard 1243. The Excel version, FLASH 1.8.1, is available on-line at www.ieee.org/pes-insulators.

The success of the FLASH program in predicting accurate transmission-line outage rates relates more to its use of accurate, but empirical models, than in its careful reproduction of the lightning interception process. For example, the effect of corona on the surge impedance of the stricken phase conductor is described using a gradient of 1500 kV/m at the edge of the envelope. This increases the capacitance (but not the inductance) of the phase and gives a realistic voltage dependence that matches experimental results by (Gary 1989). The FLASH program does not, however, consider subsequent-stroke shielding failure flashover effects, and this limitation can be addressed by assuming with little error that all shielding failures result in flashovers.

APPLET L-2

Applet L-2 attached to this chapter is designed as a tutorial for examination of the electrical and geometric parameters involved in the shielding failure process. It incorporates randomness in downward leader progression, influence of charges on the line conductors in attracting the tip of the downward leader and initiation of upward leaders from the line conductors, the contributions of line geometries and multiple circuits to the shielding failure process, effects of stroke current magnitudes, and general electrogeometric modeling. Four different mechanism options are provided to the user for simulation of the shielding failure process:

Option 1. Leader initiates from a conductor when induced charge on the conductor reaches some critical value.

Option 2. Leader initiates from a conductor when the average gradient between the tip of the conductor and the tip of the descending leader reaches some critical value.

Option 3. Upward leader length from a conductor is governed by the parameters in the general electrogeometric striking distance equation:

$$R_s = Ah^B I^C$$

Where:
R_S = striking distance, m.
A = striking distance parameter.
h = wire height, m.
B = a height exponent.
I = stroke peak current, kA.
C = a current magnitude exponent.

Option 4. Rizk attractive distance algorithm. Similar to Option 3 with specific values of the parameters;

$$D = 1.57h^{0.45} I^{0.69}$$

Where:
D = an attractive distance.

The user can modify any of the following default variables involved in the propagation process:

- Cloud-to-earth electric field at leader initiation: 15 kV/m.
- Distributed charge in lower regions of the leader channel: 15 μC/m.
- Critical gradient at wire corona wall: 30 kV/cm.
- Critical wire charge for upward leader initiation: 10 μC/m.
- Ratio of upward leader velocity to downward leader velocity: 2.0.
- Critical gradient at earth's surface for initiation of upward leader: 300 kV/m.
- Electrogeometric critical striking distance parameters.
- Critical gradient between leader tip and line conductors for final strike.

Figure 6.6-6 shows a graphic display of downward and upward leader progression created by the Applet L-2 for the base case of a shielded and unshielded transmission line running in parallel and for the choice of random leaders. A total of 100 flashes are shown, with 58 being inter-

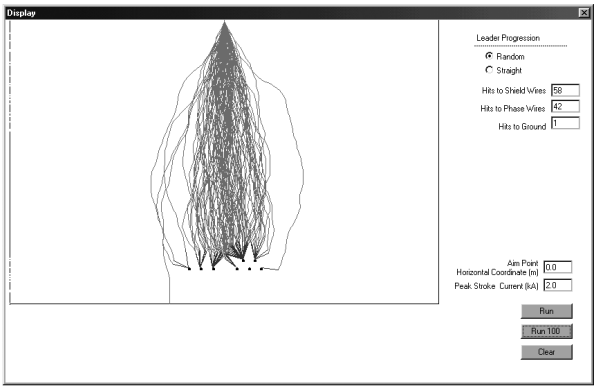


Figure 6.6-6 Graphic display of downward leaders by the Applet L-2.

cepted by the overhead groundwires, and 42 terminating on the phase conductors, mostly on the unshielded line but 3 on the shielded line.

A detailed description of the operation of the Applet L-2 is located in the Applet Help File.

6.7 INITIATION OF BACKFLASHOVERS

Backflashovers from negative first downward lightning strokes are the dominant root cause of transmission-line momentary outages.

6.7.1 The Backflashover Process

Backflashovers start with the normal interception of the lightning onto the overhead groundwires, as described in Section 6.6. For every intercepted lightning flash, the tower rises in potential relative to the phase conductors. Under these conditions, streamers can form from the tower to the phase conductors, ionize into leaders, and quickly bridge the tower-conductor gap. Phases with ac voltage in opposition to the stress tend to develop leaders most efficiently, and are most likely to initiate the backflashover from tower to phase. Once the leader has bridged the gap, the ac current can maintain this plasma channel continuously. The fault must be detected by protective relaying, so that automatic circuit breakers can remove the voltage for a sufficient time to allow the arc to cool and extinguish. The discussion here focuses on effectively grounded systems, but backflashovers may also occur on three-phase delta networks in other areas.

Contributions of Ground Resistance and Ground Plane Surge Impedance

Ground resistance is the most important variable in an insulator voltage equation. For typical transmission towers, the parallel resistance of four tower legs to remote earth is in the initial range of 60 Ω, rising or falling to a low-frequency value of 10-100 Ω within a few tower travel times. The initial surge response can be approximated as an inductance that varies with tower height, with 17 μH corresponding to a typical 30-m tower (Chisholm and Janischewskyj 1989). With a median peak current of 31 kA and a median rate of current rise of 25 kA/μs at peak from Section 6.2, the potential rise at the base of a tower is thus 700 to 3500 kV. Typical lightning impulse insulation strength for standard impulse waves is 540 kV per meter of distance, and a quick calculation shows that high-resistance grounds on 230-kV lines with 2 m of insulation are likely to have a high fraction of backflashovers in response to each lightning flash. As insulation level increases, this fraction decreases significantly, but even UHV lines at 735 kV and 765 kV are not immune to backflashovers.

Transmission towers are spotted with typical span lengths of 300 m. This means that, as the lightning surge current spreads out into the ladder network formed by footings and overhead groundwires, the impedance and resulting surge voltage drop continuously. Simplified methods of analysis achieve some success by performing an evaluation just before the first of these reflections from adjacent tower returns, making the local resistance at each tower a dominant input parameter.

Contributions of Tower Surge Impedance/Tower Inductance

The total voltage rise at the top of the transmission tower is the sum of two components:

- RI voltage rise from the footing resistance R and the peak current I.
- $L\ dI/dt$ voltage rise from the tower inductance L and the rate of current rise at the current peak.

The studies of lightning parameters show that the peak rate of rise occurs only slightly before the maximum of the current, so an arithmetic sum gives the peak voltage stress:

$$V_{tower-top} = R_{footing}\hat{I} + L_{tower}\frac{dI}{dt} \qquad 6.7\text{-}1$$

The correlation between I and dI/dt, for example as shown in Figure 6.2-14, is relatively high. This coupling of stress parameters can be exploited by using an analysis with an equivalent front time t_f, obtained by extrapolating back in time from the peak of wave to zero current at the maximum steepness.

Tower inductance can be calculated in a number of ways. As described in Section 6.4.2, some towers are relatively complex structures, with crossarms that provide multiple traveling wave path lengths. In most cases, it is efficient to calculate the capacitance C_t of the tower to free space using its surface area and shape factor, and the surge impedance of the body of the tower Z_t using a cylinder or cone expression from antenna theory. These two values are combined to give an average tower travel time ($\tau = Z_t C_t$) and the equivalent inductance ($L_{tower} = \tau Z_t = Z_t^2 C_t$). Anderson (EPRI 1986, Chapter 12) demonstrated that a realistic value of tower inductance will be higher than $L = \tau Z_t$ and is a function of tower footing resistance, but the classical value is generally used because the footing resistance itself is generally nonlinear with current.

Contributions of Shield Wire Coupling

The presence of overhead ground wires reduces the stress on insulation in two important ways. First, the parallel combination of all OHGW can give a surge impedance of about 120-140 Ω, which will appear in parallel with $R_{footing}$ to form a limiting case. For a ramp current with equivalent

front time t_f, the tower-top voltage with parallel OHGW impedance Z_{gw} becomes:

$$V_{tower-top} = \hat{I}\frac{\left(R_{footing} + \frac{L_{tower}}{t_f}\right)Z_{gw}}{R_{footing} + \frac{L_{tower}}{t_f} + Z_{gw}} \qquad 6.7\text{-}2$$

Second, and more sensitive in the calculation, is that the surge currents in the overhead groundwires produce voltages that are electromagnetically coupled to the phase conductors. This is normally modeled with an equivalent circuit of the mutual and self-impedance of the OHGW and phase conductor, leading to a coupling coefficient C_n as follows for the single OHGW case:

$$\begin{aligned} Z_{11} &= 60\ln\frac{2H_1}{r_1} \\ Z_{12} &= 60\ln\frac{D'_{12}}{d_{12}} \\ C_n &= \frac{Z_{12}}{Z_{11}} \end{aligned} \qquad 6.7\text{-}3$$

Here, D'_{12} is the distance from the phase conductor to the image of the OHGW in the earth, and d_{12} is the direct distance. For typical geometries, between 15 and 35% of the voltage appearing on tower top also appears with the same waveshape on the phase conductor, delayed in time but faithful to the original waveshape in most respects. Since the voltage on the insulator is the difference in potential between tower and phase conductor, the insulator voltage becomes, for insulators close to the top of the tower:

$$V_{insulator}(t) \approx V_{tower-top}(t) - C_n V_{tower-top}(t - \frac{2H}{c}) \qquad 6.7\text{-}4$$

The $2H/c$ term in Equation 6.7-4 is twice the travel time from the shield wire to its image in the earth, and represents the delay in creating the coupled voltage.

Contributions of Corona

High electric fields accelerate stray electrons, and these electrons can knock off other electrons from neutral air molecules, in a process called *ionization*. This process occurs at points of high stress under normal ac voltage, and is responsible for wet-weather corona loss, and electromagnetic and audible noise. Since the lightning surge voltages are so much higher than the normal ac voltage, it is correct to assume that impulse corona phenomena affect lightning backflashovers.

As an energy absorber, corona plays three roles in mitigating backflashover. These roles both enhance the contribution of overhead groundwire protection. First, the corona energy reduces the surge impedance of the overhead groundwire system. Second, there is an improvement in the efficiency of voltage coupling. Above the corona inception voltage, the value of C_n increases, and this reduces the stress across the insulation. The voltage-dependent corona model described in Section 6.4.1 is used to model these two aspects, using an envelope gradient of -2000 kV/m for negative flashes. Finally, the tower itself can be in corona during the flashover process (particularly for wood poles), tending to reduce the tower surge impedance and the apparent ground resistance.

Contributions of Power Frequency Voltages

The lightning impulse appears at a random time relative to the power frequency voltage. At any particular time, one or two of the phases have instantaneous ac potentials that add to the stress across the insulation. However, the phase voltages are also affected by tower position, mostly related to the lower values of coupling coefficient for phases that are farther from the overhead groundwires. Generally, the presence of ac voltage increases the chance of backflashover, and—importantly for high-voltage double-circuit lines—influences the order of phase conductor flashovers.

6.7.2 Dynamic Models for Electrical Insulation Strength

Section 6.5 described various models for the increase in electrical strength of air insulation as surge duration decreases. The empirical description of the insulator string flashover, using a volt-time curve, is useful when applied correctly to establish the magnitude of a voltage wave. A "correct" application is generally restricted to cases dominated by resistive response (for example, no strong tower or ground plane inductive peaks) and prior to the wave becoming "nonstandard," as canceling reflected waves arrive from adjacent towers after two span travel times.

When a detailed tower and ground plane surge response model is introduced, it shows that the insulator voltage can be significantly distorted from the traditional lightning impulse. Exercise of Applet L-4 in Section 6.5 demonstrates that the insulator voltage waveforms on the bottom phases can be quite different in nature from the top phases of the same tower. The Destructive Effect (DE) model from Section 6.5.2 is recommended to evaluate the flashover of insulators exposed to these nonstandard waves. Some mathematical aspects of the disruptive effect are discussed in Appendix 6.1.

6.7.3 Calculation Procedures

One of the most successful ways to estimate the lightning performance of a new transmission circuit is to perform a multiple linear regression of the observed performance for nearby lines against the most sensitive parameters. This is especially helpful when comparing lines with similar conductor geometry, tower style, and span length. Linear regression against remaining variables as insulation strength, footing resistance, local ground flash density, and TEM coupling coefficient can be as successful at predicting future performance as the most sophisticated treatment. In this context, equal weight is given to describing simplified and complex models for the lightning performance of transmission lines.

6.7.4 Digital Models for Backflashover

FLASH 1.8: Backflashover Aspects

The IEEE Working Group on Estimating the Lightning Performance of Transmission Lines studied various methods for calculating the line backflashover performance, including DCORTL (Sargent and Darveniza 1967), the methods of Brown (Brown 1978), and the method described in the second edition of the Red Book (EPRI 1982). After comparing calculation results with observations on a calibration set of more than 20 transmission lines, the Working Group published papers (IEEE 1985; IEEE 1993) recommending the following:

- Adoption of the Anderson simplified method (EPRI 1982), using evaluation of the volt-time curve at 2 μs (revised in 1993 to the span reflection time), and 6 μs along with traveling wave models of the tower, overhead groundwires that incorporate voltage-dependent coupling from corona effects.
- Elimination of the surge reduction factor in the Anderson method relating high-current footing resistance to measured low-current values. A constant factor of 0.6, applied to the calculation results to account for the reduced susceptibility of flashover for strokes to midspan compared to strokes to tower, should vary between 0.6 and 1.0 depending on footing resistance.

The Anderson method, as revised by the IEEE, was made available to the electrical industry in a variety of formats. With the difficulty of error-free completion of the schedule of calculations, even with scientific calculators, the program was converted to a series of computer languages, starting with FORTRAN, then Commodore BASIC, DOS (within a 64-k memory limit), C++, and most recently Excel. Versions of the DOS executable and BASIC versions are provided with IEEE Standard 1243 (IEEE 1997b). The Excel version, FLASH 1.8.1, is available online at www.ieee.org / pes-insulators.

The success of the FLASH program in predicting accurate transmission-line outage rates relates more to its use of accurate, but empirical, models than in its careful reproduction of every aspect of the complex lightning surge response. In particular, the use of the volt-time curve at 2-3 μs, just before the return of reflections from adjacent towers, is both technically correct and insensitive to error, compared to faster-front or slower-front times to flashover. The IEEE has been slow to adopt leader-progression models for flashover mainly because of the high sensitivity of the newer model to small errors in late-time voltage calculations, compared to the two-point evaluation recommended by Anderson at 2 μs and 6 μs.

DCORTL

Anderson and Thompson (Anderson and Thompson 1966) incorporated a digital weather model as the basis for calculating insulation performance of EHV transmission lines. This model built on Anderson's initial use of Monte Carlo methods strictly for lightning calculations. Sargent and Darveniza (Sargent and Darveniza 1967) refined and extended the use of Monte Carlo methods for dealing with the wide range of uncertainties in selecting parameters for analyzing double-circuit lightning performance of transmission lines. They sampled randomly from a range of parameter values, such as rise times from 2 to 6 μs and peak stroke current distribution of 13 kA median (5% level 60 kA, 1% 110 kA) from (AIEE 1950). The selected strokes were simulated in a traveling wave model, and calculations were repeated enough times to aggregate useful results. This work was supported by nanosecond models of the tower and phase conductor response, and was able to successfully predict the ratio of single-circuit to double-circuit outages on a number of 132-kV, 220-kV, and 230-kV lines in a wide range of grounding conditions and lightning exposure.

CIGRE Model

The CIGRE Technical Brochure 63 (CIGRE 1991) summarizes recommendations for calculating the lightning performance of transmission lines, and also facilitates modeling of the surges appearing at line terminals. A number of researchers have adapted parts or all of the CIGRE approach into calculation models, often using versions of the EMTP software package. Torres et al. (Torres et al. 2002) report the use of an implementation called DESCARGA, considering a concave front current, constant tower surge impedance, no corona effects, soil ionization, a leader progression model for insulation strength under nonstandard voltage impulse, and other important features in (CIGRE 1991). A comparison using data from four lines in Colombia was made among the IEEE FLASH program, DESCARGA, and the observed line performance. Both tools were found to be useful, but some adjustments, such as an appropriate relation between thunderstorm day and

ground flash density, were suggested for use in tropical regions.

Hileman DOS Programs

Hileman (Hileman 1999) accompanied his book *Insulation Coordination in Power Systems* with a diskette containing a group of MS DOS programs and help files for analysis of transmission-line and substation lightning performance. These include both CIGRE and IEEE programs for calculation of shielding failures and backflashovers, plus calculations of many of the parameters required in lightning analysis. Some of the initial versions of these programs were written for EPRI and are now updated.

EPRI TFLASH

In the years 1998-2003, EPRI developed a comprehensive transmission-line lightning simulation program TFLASH. This program evaluates all the aspects of lightning reliability of a large library of line geometries, insulator types, line arresters, conductor sizes, grounding arrangements, and transmission voltages. It is under continuous development, and is available to both EPRI and non-EPRI members through EPRI, 115 East New Lenox Road, Lenox, Massachusetts 01240, U.S. It accommodates multiple lines on the same right-of-way, distribution underbuild, branch circuits, and different exposures, and includes NLDN maps of regional ground flash densities over which a line can be located. It also permits economic evaluations of strategies for obtaining the best lightning performance of a line for a limited investment, or estimating how much investment would be necessary to attain a specified flashover rate of a proposed or existing line.

NEC2 and Other Electromagnetic Codes

The Numerical Electromagnetic Code (NEC) software program is a general-purpose routine that allows users to specify the endpoints of wire segments, and then to explore the response of this structure to electromagnetic fields at specified frequencies. The NEC code uses the method of moments (Harrington 1993). The original NEC2 was developed by Burke and Poggio (Burke and Poggio 1980) for the U.S. Navy. The code started as a "card image/batch run" operation initially designed for mainframe computers, similar to EMTP. It has been ported to many other machines with improved user interfaces as described at www.nec2.org. There are other public-domain electromagnetic codes, such as MININEC, that could also be used for this purpose. NEC2 uses the Sommerfield-Norton ground interaction for wire structures above lossy ground.

Baba and Ishii made excellent use of NEC2 in a series of analyses of transmission-line surge response to lightning (Baba and Ishii 1997, 1999, 2000, 2001), including a tutorial to describe the complete process of accurate frequency-domain modeling and conversion to time domain using Fourier transforms. The NEC2 code cannot be used to model nonlinear phenomena such as corona, ionization, or leader progression. This limitation can be addressed through the use of a "Thin Wire Time Domain" code, and research into this alternative for lightning electromagnetic effects has been initiated (Mozumi et al. 2003).

The electromagnetic models can give a detailed description of the potential difference across insulation without the approximations involved in adapting surge impedance models for this purpose. Properly-constructed computer models, validated in preferred research with experiments on full or reduced-scale models, have automatically dealt with causality and propagation effects that influence voltage coupling, and tower and ground plane surge response.

EMTP Codes

The Electromagnetic Transients Program (EMTP) was developed by Dommel (Dommel 1969) and was adopted at Bonneville Power Authority in the late 1960s. Some aspects of this development remain in the public domain through the Alternative Transients Program (ATP) program. The EMTP software proved to be a valuable tool for simulating power system transients in the frequency and time domain, using modules to describe system elements (lines, cables, transformers, lumped elements), their interconnections, and their interactions. Since that time, the following development dates are notable:

1982	The EMTP Development Coordination Group was founded.
1987	Version 1.0 released.
1989	Version 2.0 (DCG/EPRI EMTP) released.
1996	Version 3.0 (EMTP96) released.
2003	EMTP-RV released.

With improving computer processing power and memory, it is now practical to carry out simulations of lightning on multiple spans of transmission lines that include corona and frequency-dependent effects on wave propagation, (IEEE 1996), nonlinear tower and ground plane surge response, electromagnetic wave coupling (from an external source code such as LIOV), leader-progression models of insulator flashover, and accurate models for the response of line surge arresters.

One difficulty that still tends to limit the use of EMTP codes for lightning performance evaluation (Martinez and Castro-Aranda 2003) is the need to construct manual or supervisory routines (Zanetta 2003) to run multiple cases (for example, ramping up surge currents from 10 to 200 kA, and noting when flashover or arrester failure occurs) and to consolidate results. However, the new tools in later versions of EMTP for constructing the models, for visualizing the waveforms, and for saving results of case studies have facilitated many advanced research and analysis projects.

Web-based Resources

The recent development of online resources for retrieval of conference proceedings and journal articles offers a great wealth of new perspective to the lightning researcher. Recommended resources for further study include (but are not limited to):

- Search engines such as "Google" at www.google.com using keywords such as "lightning" and key phrases such as "transmission line" or "rolling sphere."
- Posted papers from conferences such as International Conference on Lightning Protection (ICLP).
- IEEE Xplore and Digital Library resources.
- *Electra* (four CD collection of papers from 1968 to 2002).
- Standards such as IEEE 1243, IEC 61024, and IEC 61312.
- EPRIweb resources, listing abstracts of important work.
- www.emtp.com.

6.7.5 Applet Descriptions

Two applets are provided with this book to help the user to integrate the technical descriptions in Sections 6.2 to 6.6.

Applet L-4

Applet L-4 attached to this chapter is a tutorial program to display the various voltage and current waveshapes created by a lightning flash to a tower top under different electrical and geometric conditions. Its operation is covered in more detail in the Applet Help File. The user selects a stroke waveshape—CIGRE first stroke, CIGRE subsequent stroke, Heidler waveshape stroke, or ramp function—and crest current. The general electrical parameters, including tower and shield wire characteristics, are keyed in as well as the low-frequency footing resistance. It assumes that the footing resistance dynamics can be described by the Korsuncev curve (Section 6.10.13), and—if ionization around the ground electrode is to be included—the Korsuncev *S* dimension must be specified. The applet then displays a table of values of some of the calculated variables as a function of time, followed by a graphic colored display of the voltage and current waveshapes created by the lightning strike and—if insulator performance is to be studied—a plot of the Disruptive Effect integration (Section 6.5.2) toward flashover is included. The applet is simplified and may not compare accurately with similar calculations made by EMTP or EPRI TFLASH, but should be sufficient for tutorial purposes.

Figure 6.7-1 shows, for a ramp function waveshape, the Disruptive Effect integrated waveshape calculated from the voltage across the insulator. When this waveshape reaches 100%, a flashover occurs.

Applet L-1

Applet L-1 attached to this chapter comprises a tutorial program to evaluate lightning performance of an idealized line for a variety of dimensional and grounding conditions. Procedures for using this applet are given in the Applet Help File. It is a traveling wave model for strikes to a tower top with two other equally spaced transmission towers on each side of it. CIGRE first-stroke current waveshapes are employed, but the user has the option of shifting the time to crest. Tower grounds can be ground rods, concrete foundations, or continuous or radial counterpoise. Radial counterpoise can consist of up to eight radials. Shielding failures

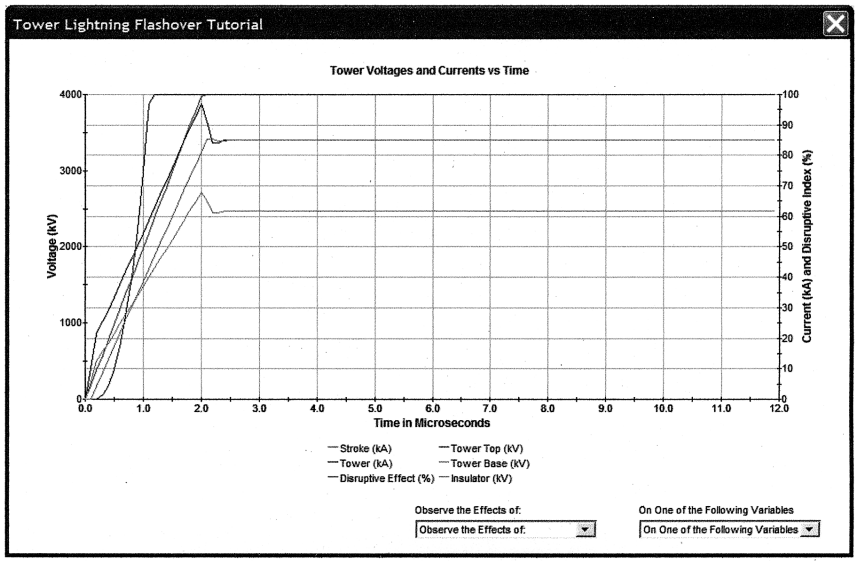


Figure 6.7-1 Example output waveforms of Applet L-4.

are calculated using the method of maximum heights (Section 6.6.5) and backflashovers as described in Section 6.7.1. Volt-time flashover of insulators is computed using the Disruptive Effect (DE) algorithm described in Section 6.5.2. When two or more insulators are equally stressed, the flashovers are shared equally between them. Simultaneous flashovers on more than one phase, as may often occur on a double-circuit line, are not reported. For any stroke, the calculation stops as soon as a flashover occurs, and the program then proceeds to the next stroke.

Ground rods can be in asymmetrical locations with respect to one another if desired, and their combined ground resistance is calculated as a dynamic value for every time step using the Liew-Darveniza algorithm (Liew and Darveniza 1974), with some conceptual modifications as described in Section 6.10.12.

Concrete foundations are assumed sufficiently large so that resistance reductions due to soil ionization can be neglected. If the total low-frequency ground resistance of the concrete foundations is unknown, the program provides an estimated value depending on the foundation surface area and soil resistivity, plus an adjustment for a fixed amount of metal reinforcing inside the concrete. The frequent practice of driving one or more ground rods adjacent to concrete foundations is not simulated, but should be recognized as providing additional reductions of Applet L-1 backflashover estimates.

For radial counterpoise, up to eight radial wires—all of the same length and diameter—can be utilized as the tower ground electrode. The low-frequency resistance of the counterpoise is calculated and displayed by Applet L-1 when earth resistivity is specified. The low-frequency counterpoise resistance is calculated using the Dwight equations (Dwight 1936) in Table 6.10-1. For any counterpoise subjected to a high-frequency transient, the initial impedance is the combined surge impedance of the counterpoise, but the counterpoise impedance rapidly decays down (or sometimes up) in approximately three round-trip travel times to the combined low-frequency resistance, or even lower when ionization is involved. For high currents, computer models show most earth ionization appears at the tower end of the counterpoise, because currents are depleted rapidly as they move along the wires. Applying travel times to the Applet L-1 counterpoise models is beyond the capability of the applet, and the approximate dynamic resistance is assumed similar to a set of horizontal ground rods modified by the presence of the earth's surface above them.

To more accurately represent surge impedance at high currents, corona envelopes are simulated on all shield wires and—for shielding failure analysis—on any phase conductor that is struck. The simulation follows Section 6.4.1 above.

Applet L-1 is intended as a tutorial model or rough estimation tool. It does not model:

- Multiphase flashovers
- Different tower footing resistances (all towers on either side of the struck tower must have the same footing resistance as the struck tower)
- Different tower exposures to lightning
- Arrester applications
- Subsequent stroke flashovers
- Distribution underbuild
- Counterpoise traveling wave effects
- Shielding failures on hillsides
- Corona attenuation of traveling waves

A much larger program, such as the EPRI TFLASH described in Section 6.7.4, would be necessary to make a thorough analysis of all the complexities inherent in the lightning flashover of all types of transmission lines.

6.8 INITIATION OF INDUCED FLASHOVERS

6.8.1 Induction from EM Fields of the Lightning Flash

The electromagnetic field coupling problem from a lightning flash near a conductor can be solved in three equivalent ways, using combinations of the electric and magnetic fields that illuminate the line. Near the lightning flash, these magnetic and electric source terms are not necessarily inter-related by the impedance of free space, 377 Ω. Rachidi (Rachidi 1993) showed the equivalence of these approaches, described generally in Appendix A2, and an excellent review of the entire induction process by Nucci and Rachidi is available in (Cooray 2003b, Chapter 8). These models predict that vertical lightning strokes terminating near, but not directly attaching to, overhead power lines and cables can still induce significant voltages and currents.

6.8.2 Simplified Model for Induced Overvoltages

Rusck (1958) described a simple model for the field-to-line coupling over perfectly conducting ground. For a linear leader charge q moving upward with velocity v:

$$I_o = vq_o \qquad 6.8\text{-}1$$

$$Z_o = \frac{1}{4\pi}\sqrt{\frac{\mu_o}{\varepsilon_o}} = 30\ \Omega \qquad 6.8\text{-}2$$

$$V_1(x,t) = Z_o I_o h \frac{v}{c} \frac{ct - x}{y^2 + (v/c)^2 (ct - x)^2} \left(1 + \frac{x + (v/c)^2 (ct - x)}{\sqrt{(vt)^2 + \left(1 - (v/c)^2\right)\left(x^2 + y^2\right)}} \right) \quad 6.8\text{-}3$$

$$V = V_1(x) + V_1(-x) \quad 6.8\text{-}4$$

Where:

q_o = the charge per unit length, C/m.
v = the return stroke velocity, m/s.
c = the speed of light, 3 x 10^8 m/s.
x = the coordinate along the horizontal conductor, with $x = 0$ at the point closest to the lightning.
y = the coordinate perpendicular to the horizontal conductor, with $y = 0$ at the lightning stroke.
h = the height of the horizontal conductor above perfect ground.

Figure 6.8-1 shows the induced voltages from a 10-kA flash at four locations along a 10-m-high conductor.

The highest voltage occurs at the conductor location nearest to the lightning stroke. The peak voltage for 10 kA is only 70 kV, well below the critical flashover level of high-voltage transmission lines. For this situation ($x = 0$), and with a typical return stroke velocity of $v = 0.3\ c$, Equation 6.8-3 simplifies to give a peak overvoltage estimate of:

$$V = 29 \frac{Ih}{y} \quad 6.8\text{-}5$$

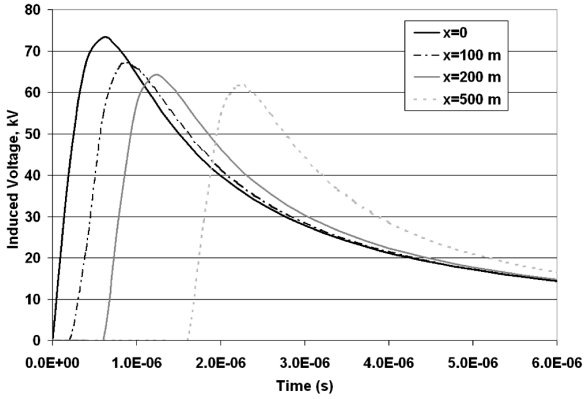


Figure 6.8-1 Induced voltage on horizontal conductor, h = 10 m above perfect ground, y = 50 m from I_o = 10-kA lighting stroke with $v = 0.3\ c$.

Field-measured induced voltages, such as the South African test line (Eriksson et al.1982) and an experimental line at Camp Blanding, Florida (Rubenstein –et al. 1989), the latter exposed to triggered lightning flashes, tend to verify Equation 6.8-5. The Rusck equation fails for small distances between the line and the flash or for the case of high earth resistivity.

6.8.3 Protection against Induced Flashovers

Generally, transmission lines have minimum insulation strength of at least 300 kV. This has led to a hypothesis (Gilman and Whitehead 1973) that induction cannot cause outages on transmission circuits. Any stroke with sufficient amplitude and close enough to cause an induced overvoltage flashover has a striking distance that is sufficiently high to terminate on the line.

There are cases where the induced overvoltage has a stronger engineering significance. First, a tall structure with large attractive radius can reduce the dimension y, which normally cannot be less than the striking distance of the lightning flash to the conductor. The return stroke velocity v will also equal the speed of light within the tall structure. These factors can combine to increase the overvoltage level.

In the case of tall transmission towers, the phase conductors are located below the tower top. The fraction of the lightning surge current in the tower can be within 3 m of the phases. Calculations (Baba and Ishii 2000) using an advanced electromagnetic program, NEC2, show that the resulting induced voltages have substantial peak amplitudes of up to 10% of the tower voltage, but tend to be bipolar. The bipolar-induced voltages with pulse widths corresponding to the tower travel time will not add to, or subtract from, the destructive index integral in any way that is substantiated by test results.

6.8.4 Importance for Subtransmission and Underbuilt Distribution

In some cases, joint-use imperatives force transmission-line towers to carry additional conductors for lower-voltage subtransmission, distribution, or communication systems. Since the transmission line receives many direct strokes over its life, the resulting exposure risk to attached equipment must be well managed. The transmission tower carries appreciable surge current, and this, combined with the physical proximity, can lead to severe induced overvoltage or side flashes. The term “backflow current” is generally applied to cases where lightning surges flow down a target (tower and overhead shield wire), through interconnected grounds, and back up into the susceptible system. The number of flashes to the overhead line often makes the use of line surge arresters effective on the lower-voltage system. The parallel impedance of the low-voltage network tends to reduce the surge impedance and improve the

coupling coefficient, either when it flashes over or when its surge arresters operate. However, the insulation strength on distribution lines can be much less than 300 kV, so significant (even high) induced overvoltage flashover rates can occur on such lines.

6.9 INITIATION OF MIDSPAN FLASHOVERS

Line flashovers caused by lightning strikes at or near midspan between two adjacent towers are infrequent for normal midspan clearances. Exceptions can occur if shield wire-to-phase spacings are small (as in distribution circuits), or if span distances are large (300 m or more). The high-voltage phenomena involved in these failures is well understood in principle, and has been confirmed by field tests (Wagner and Hileman 1964; Los 1980), but is highly nonlinear, and represents an interesting application of traveling wave theory.

6.9.1 The Failure Mechanism

In Figure 6.9-1, a high-magnitude stroke current is injected into a shield wire at midspan. The voltage at the strike point on the shield wire builds up according to the standard equation:

$$V_s = \frac{I_s Z_s}{2} \qquad 6.9\text{-}1$$

Where:

V_s = shield wire surge voltage to ground at the hit point, kV.

I_s = instantaneous stroke current, kA.

Z_s = shield wire surge impedance (modified by corona calculated from Equation 6.4-23), ohms.

6.9.2 Corona Coupling at Midspan

By the standard coupling equation, treating the self and mutual surge impedances as a coupled set of potential dividers with the phase current $I_p = 0$, the voltage V_p coupled onto the phase becomes:

$$V_p = \frac{Z_{sp} V_s}{Z_s} \qquad 6.9\text{-}2$$

Where:

Z_{sp} = mutual impedance between shield wire and phase conductor, ohms.

Equations for calculation of self and mutual surge impedances Z_s and Z_{sp} under corona conditions are given in Section 6.4.

Combining Equations 6.9-1 and 6.9-2, the voltage difference between phase and shield wire is

$$V_{sp} = V_s - V_p = \frac{I_s Z_s}{2}\left[1 - \frac{Z_{sp}}{Z_s}\right] \qquad 6.9\text{-}3$$

and the average gradient E_{sp} between shield wire and phase conductor is

$$E_{sp} = \frac{I_s Z_s}{2 S_{sp}}\left[1 - \frac{Z_{sp}}{Z_s}\right] \qquad 6.9\text{-}4$$

The ratio Z_{sp}/Z_s is called the "coupling factor." It normally has a value in the 0.2-0.3 range, increasing with voltage, as shown in Figure 6.4-7, and establishes the ratio of phase voltage to shield wire voltage for a hit to the shield wire.

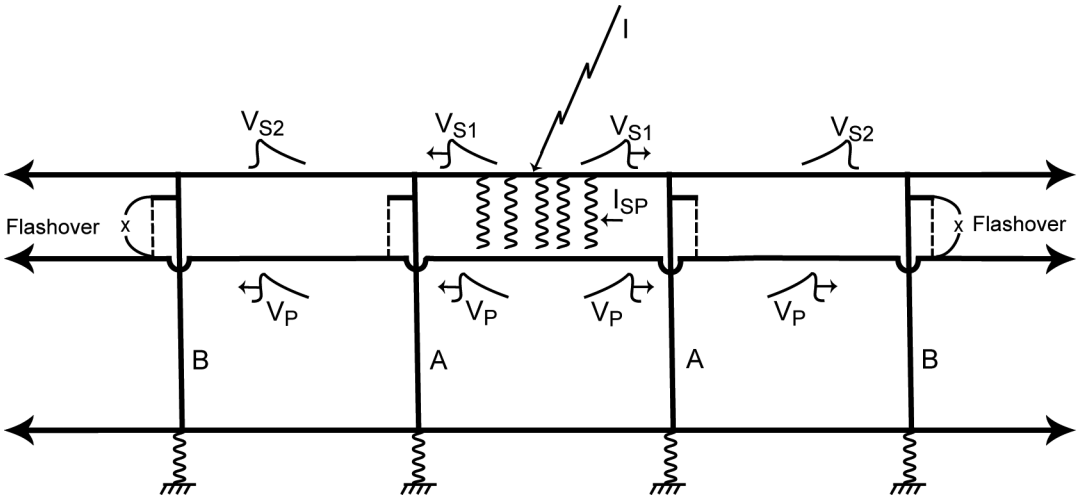


Figure 6.9-1 Lightning breakdown processes at midspan.

6.9.3 Current Injection into Phase Conductors

High-voltage tests (Wagner 1964; Wagner and Hileman 1964; Los 1980) have shown that the breakdown gradient E_{sp} between shield wire and phase occurs at approximately 610 kV/m for a standard 1.2 x 50 μs waveshape. This breakdown is observed to begin with strong predischarge currents flowing from the shield wire to the phase. This current flow into the phase can reach many hundreds of amperes before complete breakdown, increasing the phase voltage and maintaining the gradient between the two wires at its critical 610 kV/m value during the breakdown process. At a gradient of 610 kV/m between the two wires, the breakdown process is relatively slow, and can require many microseconds to complete. In the meantime, the stroke current injected into the shield wire (less the current flowing across the gap) splits and travels to the transmission structures at each end of the span (Figure 6.9-1). Here the currents reflect with reversed polarity off the structures (unless footing resistance is extremely high), and the reversed polarity currents return to the strike point where they combine, greatly reducing the shield wire voltage and stopping the breakdown before it can complete.

6.9.4 Tower Flashovers Caused by Midspan Strokes

Predischarge current injection into the phase conductor, as introduced above, can still cause flashovers at towers one or two spans away in some cases, even though the flashover process at midspan stalls before completion. As an example, in Figure 6.9-1, a 50-kA midspan stroke into a shield wire with a combined surge impedance (with corona) of 200 ohms would develop 10 MV on the shield wire at the strike point. If the spacing to the nearest phase is 7 m, then the voltage between the two wires at the critical gradient of 610 kV/m would be held to 4.3 MV during the breakdown process. This is equivalent to the total predischarge currents injecting a voltage onto the phase of 10 – 4.3 = 5.7 MV. This 5.7 MV transient, V_p, then travels in both directions along the phase conductor and appears an the line ends of the nearest insulators at towers *A* at the same time that shield wire voltages V_{s1} are arriving at the tower *A* tower tops (Figure 6.9-1). The difference created between the tower top voltage and the phase voltage may be insufficient to cause insulator flashovers at tower *A*, depending on footing resistance and difference between shield wire and phase voltages, but the phase voltage transients then continue to travel to the next set of towers where shield wire voltages V_{s2} are small and the difference between tower top and phase voltage is large, initiating phase flashovers at those locations.

The assumption is usually made that midspan flashovers do not make a significant contribution to the total backflash rate, but this assumption does not hold for some lines, particularly for lines with low basic insulation level (BIL), long spans, or tight clearances between shield wires and phases at midspan. Applet L-1 also does not determine if predischarge currents injected into phase conductors by a midspan hit are sufficient to cause flashovers at nearby towers. It operates on the assumption that approximately 60% of span hits are near enough to be considered as tower hits and that the other 40% are far enough out on the spans to not cause flashovers.

6.9.5 Cascading Flashovers at Adjacent Structures

Note also that if a midspan flashover does occur, the voltages arriving at insulators for towers *A* and *B* are usually sufficient to cause one or more insulator flashovers. The insulator flashover nearest to the generation source holds in, turning off or greatly limiting the voltage to the other flashovers. This can leave only failure evidence of burn marks on the insulator that held in, and no evidence whatsoever of the root cause at midspan.

6.9.6 Rules for Midspan Spacing

Generally, conductor clearances to other phase conductors, overhead shield wires, and grounded metallic objects should be specified to be sufficiently large that flashover at adjacent towers occur under lightning impulse conditions. Factors that influence the required spacing include:

- The conductor surge impedance, raising potential near the strike point relative to potential near the insulators.
- The number of nearby insulators in parallel with the gap; generally, only the two closest insulators should be considered.
- The presence of ac system voltage, unsynchronized with the lightning, and appearing essentially as a static bias voltage for the duration of the lightning surge.
- The wind speed, pressure on the conductor, and the horizontal displacement.
- The variability of wind gusts, which can get conductors swinging out-of-phase.
- The phasing of ac voltage on double-circuit lines, since reduced distance or contact between two conductors of the same phase and voltage are unlikely to cause outages.
- Special factors, such as the presence of ice and low torsional damping, which can cause a vertical “galloping” motion.

Electrical safety standards such as the NESC (IEEE/ANSI C2) generally use a linear relation between electrical guard distance and lightning impulse level (BIL) of 540 kV/m. Other details are discussed in Chapter 3.

6.9.7 Importance for Subtransmission and Underbuilt Distribution

If subtransmission or underbuilt distribution circuits are supported on transmission towers, very poor lightning performance on the former is a likely result. The insulation on these circuits is usually much weaker than the transmission circuit insulators, while the lightning transient voltages are usually as high or higher than those created across the transmission circuit insulators. In many cases, practically every lightning flash that hits the line (and being taller, more flashes are attracted to the line), as well as many flashes near the line, result in a subtransmission or distribution circuit flashover. Remedies can include liberal application of line arresters, installing the subtransmission or distribution circuits on separate poles, or using insulators with a BIL substantially above conventional practice.

6.10 TRANSMISSION-LINE GROUNDING

The grounding or earthing system is the total set of measures used to connect an electrically conductive part of the power system to earth. The grounding system is an essential part of both high- and low-voltage electric power networks, and has at least four important electrical roles:

1. To protect against lightning, eliminating hazards by:
   - Providing a mechanically and electrically robust path to ground
   - Limiting potential differences across electrical insulation on stricken towers
   - Reducing the number of flashovers that occur
2. For correct operation of the power system, minimizing energy by:
   - Providing unambiguous identification of faults, so that the correct protection systems operate.
   - Providing low zero-sequence impedance for return of unbalanced fraction of ac system currents
3. To ensure electrical safety, minimizing energy by:
   - Rapidly identifying system faults, leading to reduced fault duration
   - Limiting touch or step voltages to levels that restrict body currents to safe values
4. To contribute to electromagnetic compatibility, eliminating some hazards and reducing energy of others.

All these functions are provided by a single grounding system. Some elements of this system may have specific electrical purposes, but all elements are normally bonded or coupled together, forming one system to be designed or analyzed.

6.10.1 Mechanical Integrity

The main design challenges in transmission-line engineering are mechanical. The conductors must be sized to carry the load current, typically at a density of 1 A/kcmil (1000 circular mils or 0.001 sq. in.). National electrical safety standards define the necessary physical clearances to other electrical circuits and to ground for a variety of land uses. The towers are spotted at intervals of 200 to 400 m with sufficient strength to support the conductor weight, including possible ice loads, at attachment heights that will maintain adequate clearance at maximum conductor operating temperatures. The towers must also withstand some, but possibly not all, wind loads with well-controlled failure modes. Lines need sufficient margin for broken insulators or conductors over irregular terrain, with a wide range of soil load-bearing capabilities. There are, however, mechanical engineering solutions that have positive or negative impact on the effectiveness of overhead groundwires for grounding and lightning protection, such as:

- The spacing of the tower legs. Towers with a wide base, relative to the depth of the footings, perform better electrically because they have a larger contact patch to the earth. Steel pole towers tend to perform less effectively for the same reason.
- The use of guy wires. Towers with one or two central footings and four or more widely spaced guy wires have a large footprint and can perform well with adequate electrical grounding of each guy wire.

Designers often choose narrow-base towers for agricultural areas, then specify extensive buried ground conductors that are vulnerable to damage from agricultural machines. Steel poles, selected for appearance in areas of high public exposure, must also be specified with ground electrodes of sufficient size and shape to control risk of touch potentials.

6.10.2 Guy Anchors for Additional Strength

In areas where agriculture is less productive and the terrain is more rugged, tower designers tend to prefer the use of guyed V-type towers. These are economical, especially when helicopter installation is feasible. It is important to include analysis of the ground electrodes formed by the soil anchors for the guy wires. Also, the addition of four parallel guy wires to a conventional V-type lattice tower can reduce the tower surge impedance by a factor of two. The lower profile of guyed structures compared to free-standing towers also reduces lightning incidence, which is related to the attractive radius of overhead groundwire height, as described in Section 6.5.

6.10.3 Corrosion and End-of-Life Aspects

Buried wire electrodes, such as radial or continuous counterpoise, have a lifetime of 10 years or less in many applications. End of life can be accelerated when there is unrestricted public access to buried copper conductor, when there is acidic soil, or when there are appreciable steady-state neutral voltages.

6.10.4 Steady-State Tower Potentials

Currents induced in overhead groundwires can reach 30 A under normal load conditions. In lines where all spans are equal, the net current in each footing is zero. However, for lines with unequal span lengths, each tower has a different current that can reach a significant fraction of the total. Transmission tower ground electrodes provide steady-state dissipation of this current. The power dissipation can dry out the soil around concentrated electrodes such as rods, generally leading to higher local resistivity and contact resistance.

For an impressed current, the potential rise of a ground electrode relative to remote earth is obtained through the following analytical process:

- A distribution of the current is assumed, typically ignoring the resistance of the metallic parts of the buried electrode.
- The potential at distance *R* in the surrounding medium of resistivity ρ is calculated by superposition of potentials *dU* from the currents *dI* leaving each conductor element using $dU = \rho dI/(4\pi R)$.
- The potential is integrated (summing the contribution of each element of current *dI)* and evaluated at infinite distance (to obtain the rise in potential relative to remote earth) or at a close distance such as 1 m (to obtain touch or step potential exposures).

When an electrode consists of two or more components, the mutual resistance between the two elements is computed, often by using the average distance between the two. but sometimes using a double (Neumann) integral. The potential of an electrode buried in a half space is computed by considering a nearby image that makes a plane of symmetry at the surface of the earth.

Low-Frequency Ground Resistance Equations

Dwight (1936) and Sunde (1949) published expressions used to calculate the resistance to remote earth of electrodes for a number of practical shapes (see Tables 6.10-1 and 6.10-2).

Simple Model for all Smooth, Solid Electrode Shapes

While the tables of equations cover a wide range of situations, they do not provide particularly accurate estimates for fairly simple cases where vertical and horizontal electrodes are combined, such as two vertical rods connected together by a buried wire or a circular ring with a buried connection to a central tower. There is an approach that can treat an extremely wide range of electrode shapes with reasonable accuracy. This approach was developed from techniques for computation of electrode capacitance in free space with variational methods (Chow and Yovanovic 1982; Chisholm 2001). For a uniform half-space of resistivity ρ, the resistance of solid electrodes is accurately described by:

$$R_{geometric} \approx \frac{\rho}{2\pi g}\ln\left(\frac{11.8g^2}{A}\right) \qquad 6.10\text{-}1$$

Where:

$R_{geometric}$ = the electrode resistance to remote earth.
ρ = the resistivity in Ω-m.
g = the geometric sum of the length, width and depth of the electrode, $\sqrt{r_x^2 + r_y^2 + r_z^2}$
A = the surface area of the electrode.

The value 11.8 is theoretically $(2\pi e^{\sqrt{3}})/3$ or 11.838, but 12 is easier to remember.

The strength of the simple expression in Equation 6.10-1 is that it is adequately accuracy over an extremely wide range of electrode shapes. This means that geometric resistance for electrodes of any intermediate shapes (thick buried discs, fat cylinders, combinations of vertical rods and surface grids) can be estimated with similar accuracy using the same expression. Examples of the level of accuracy achieved, along with insight into the effect of electrode shape on resistance, follow by comparison to derived resistances of hemisphere, rod, disc, and arbitrary objects of revolution in the literature.

The *hemisphere* of radius *s* has a surface area of $A = 2\pi s^2$ and a value of $g = 1.732\ s$. For this important theoretical result, the geometric resistance from Equation 6.10-1 is:

$$R_{geometric} = \frac{\rho}{2\pi\sqrt{s^2+s^2+s^2}}\ln\left(\frac{11.8(\sqrt{s^2+s^2+s^2})^2}{2\pi\, s^2}\right)$$
$$= \frac{\rho}{2\sqrt{3}\pi s}\ln\left(\frac{11.8\cdot 3}{2\pi}\right) = \frac{\rho\cdot 1.73}{2\sqrt{3}\pi s} = \frac{\rho}{2\pi s} \qquad 6.10\text{-}2$$

This is in perfect agreement with the accurate value obtained by integrating the potential from the hemisphere surface to infinity.

Equation 6.10-1 gives a geometric resistance for a *rod* of length *s*, radius *r*, area $A = 2\pi rs + \pi r^2$ and $g \approx$ s for $s >> r$ of:

$$R_{geometric} = \frac{\rho}{2\pi s}\ln\left(\frac{11.8s^2}{2\pi rs}\right)$$
$$= \frac{\rho}{2\pi s}\left(\ln\left(\frac{11.8}{2\pi}\right) + \ln\left(\frac{s}{r}\right)\right)$$
$$= \frac{\rho}{2\pi s}\left(0.63 + \ln\left(\frac{s}{r}\right)\right)$$

Expressed in the same form as Equation 6.10-3, classical derivations of the resistance of a single rod of length s and radius r differ in the value of K_{rod}, as shown in Table 6.10-3.

$$R_{geometric} = \frac{\rho}{2\pi s}\left(K_{rod} + \ln\left(\frac{s}{r}\right)\right) \qquad 6.10\text{-}3$$

Generally, the value of $\ln(s/r)$ in Equation 6.10-3 will be about 6, leading to a ±9% change in $R_{geometric}$ from the variation in K_{rod} for different assumptions about the currents and fields around a vertical rod. Applet L-6 can be used to calculate the current and potential distribution along a vertical rod more accurately than any of the derivations in Tables 6.10-1, 2, or 3.

Table 6.10-1 Low-Frequency Ground Resistance of Electrodes (Dwight 1936)

Electrode	Dimensions	Equation
Single vertical rod	Length *L*, radius *a*	$R = \frac{\rho}{2\pi L}\left(\log_e \frac{4L}{a} - 1\right)$
Two vertical rods	Separation *s* with *s>L*	$R = \frac{\rho}{4\pi L}\left(\log_e \frac{4L}{a} - 1\right) + \frac{\rho}{4\pi s}\left(1 - \frac{L^2}{3s^2} + \frac{2}{5}\frac{L^4}{s^4} + \ldots\right)$
Two vertical rods	Separation *s* with *s<L*	$R = \frac{\rho}{4\pi L}\left(\log_e \frac{4L}{a} + \log_e \frac{4L}{s} - 2 + \frac{s}{2L} - \frac{s^2}{16L^2} + \frac{s^4}{512L^4} - \ldots\right)$
Buried horizontal wire	Length *2L*, depth *s/2*	$R = \frac{\rho}{4\pi L}\left(\log_e \frac{4L}{a} + \log_e \frac{4L}{s} - 2 + \frac{s}{2L} - \frac{s^2}{16L^2} + \frac{s^4}{512L^4} - \ldots\right)$
Right-angle turn of wire	Arm length *L*, depth *s/2*	$R = \frac{\rho}{4\pi L}\left(\log_e \frac{2L}{a} + \log_e \frac{2L}{s} - 0.2373 + 0.2146\frac{s}{L} + 0.1035\frac{s^2}{L^2} - 0.0424\frac{s^4}{L^4}\ldots\right)$
Three-point star	Arm length *L*, depth *s/2*	$R = \frac{\rho}{6\pi L}\left(\log_e \frac{2L}{a} + \log_e \frac{2L}{s} + 1.071 - 0.209\frac{s}{L} + 0.238\frac{s^2}{L^2} - 0.054\frac{s^4}{L^4}\ldots\right)$
Four-point star	Arm length *L*, depth *s/2*	$R = \frac{\rho}{8\pi L}\left(\log_e \frac{2L}{a} + \log_e \frac{2L}{s} + 2.912 - 1.071\frac{s}{L} + 0.645\frac{s^2}{L^2} - 0.145\frac{s^4}{L^4}\ldots\right)$
Six-point star	Arm length *L*, depth *s/2*	$R = \frac{\rho}{12\pi L}\left(\log_e \frac{2L}{a} + \log_e \frac{2L}{s} + 6.851 - 3.128\frac{s}{L} + 1.758\frac{s^2}{L^2} - 0.490\frac{s^4}{L^4}\ldots\right)$
Eight-point star	Arm length *L*, depth *s/2*	$R = \frac{\rho}{16\pi L}\left(\log_e \frac{2L}{a} + \log_e \frac{2L}{s} + 10.98 - 5.51\frac{s}{L} + 3.26\frac{s^2}{L^2} - 1.17\frac{s^4}{L^4}\ldots\right)$
Ring of wire	Diameters ring *D*, wire *d* depth *s/2*	$R = \frac{\rho}{2\pi^2 D}\left(\log_e \frac{8D}{d} + \log_e \frac{4D}{s}\right)$
Buried horizontal strip	Length *2L*, section *a* by *b*, (*a>8b),* depth *s/2*	$R = \frac{\rho}{4\pi L}\left(\log_e \frac{4L}{a} + \frac{a^2 - \pi ab}{2(a+b)^2} + \log_e \frac{4L}{s} - 1 + \frac{s}{2L} - \frac{s^2}{16L^2} + \frac{s^4}{512L^4} - \ldots\right)$
Buried horizontal round plate	Radius *a*, depth *s/2*	$R = \frac{\rho}{8a} + \frac{\rho}{4\pi s}\left(1 - \frac{7}{12}\frac{a^2}{s^2} + \frac{33}{40}\frac{a^4}{s^4} + \ldots\right)$
Buried vertical round plate	Radius *a*, depth *s/2*	$R = \frac{\rho}{8a} + \frac{\rho}{4\pi s}\left(1 - \frac{7}{24}\frac{a^2}{s^2} + \frac{99}{320}\frac{a^4}{s^4} + \ldots\right)$

Table 6.10-3 Value of K_{rod} for different assumptions about potential gradient around driven rod in half-plane of conducting soil

Researcher	Based On	K_{rod}
Liew and Darveniza 1974	Cylinder + Hemisphere Equation 6.10-11	0.003*
Dwight 1936	Table 6.10-1	0.38
Sunde 1949	Table 6.10-2 Average potential from constant current density	0.38
Chisholm 2001 using Oettle 1988	Equation 6.10-1	0.63
Rudenberg 1945, Sunde 1949	Ellipsoid of revolution Equation 6.10-5	0.69
Chisholm and Janischewskyj 1989	Deformed Hemisphere	1.00

*s = 3 m, r = 0.01 m

For a circular, solid *disc* of radius s, surface area $A = \pi s^2$ and $g = 1.414\,s$, Equation 6.10-1 gives:

$$R_{geometric} = \frac{\rho}{2\pi g}\ln\left(\frac{11.8\cdot 2s^2}{\pi s^2}\right) = \frac{\rho}{2\sqrt{2}\pi s}\ln(7.51) = \frac{0.226\rho}{s}$$

The "correct" theoretical derivation gives:

$$R_{geometric} = \frac{\rho}{4s} \qquad 6.10\text{-}4$$

Table 6.10-2 Footing Resistance Expressions from Sunde (1949)

Electrode	Dimensions	Equation
Single vertical rod	Length *L*, radius *a*	$R = \frac{\rho}{2\pi L}\left(\log_e\frac{4L}{a} - 1\right)$
Two vertical rods on circle of diameter *D*	Length *L*, radius *a*	$R = \frac{1}{2}\frac{\rho}{2\pi L}\left(\log_e\frac{4L}{a} - 1 + \frac{L}{D}\right)$
Three vertical rods on circle of diameter *D*	Length *L*, radius *a*	$R = \frac{1}{3}\frac{\rho}{2\pi L}\left(\log_e\frac{4L}{a} - 1 + \frac{2L}{D\sin\pi/3}\right)$
Four vertical rods on circle of diameter *D*	Length *L*, radius *a*	$R = \frac{1}{4}\frac{\rho}{2\pi L}\left(\log_e\frac{4L}{a} - 1 + \frac{2L}{D\sin\pi/4} + \frac{L}{D}\right)$
Six vertical rods on circle of diameter *D*	Length *L*, radius *a*	$R = \frac{1}{6}\frac{\rho}{2\pi L}\left(\log_e\frac{4L}{a} - 1 + \frac{2L}{D\sin\pi/6} + \frac{2L}{D\sin\pi/3} + \frac{L}{D}\right)$
n vertical rods on circle of diameter *D*	Length *L*, radius *a*	$R = \frac{1}{n}\frac{\rho}{2\pi L}\left(\log_e\frac{4L}{a} - 1 + \frac{2nL}{\pi D}\log_e\frac{2n}{\pi}\right)$
n rods in line, separation *s*	Length *L*, radius *a*	$R = \frac{1}{n}\left[\frac{\rho}{2\pi L}\left(\log_e\frac{4L}{a} - 1\right) + \frac{\rho}{\pi s}\left(\frac{1}{2} + \frac{1}{3} + \frac{1}{4} + \ldots + \frac{1}{n}\right)\right]$
Buried horizontal wire	Length *L*, radius *a*, depth *d*	$R = \frac{\rho}{\pi L}\left(\log_e\frac{2L}{\sqrt{2ad}} - 1\right)$
n buried horizontal radial wires	Length *L*, radius *a*	$R = \frac{\rho}{n\pi L}\left[\log_e\frac{2L}{a} - 1 + \sum_{m=1}^{n-1}\left(\log_e\frac{1+\sin(\pi m/n)}{\sin(\pi m/n)}\right)\right]$

The resistance of an *ellipsoid of revolution* with major semi-axis *s* and minor semi-axis *r* was derived by (Sunde 1949, Equation 3.12) as follows:

$$R_{geometric} = \frac{\rho}{4\pi s}\frac{\alpha+1}{\alpha-1}\ln(\alpha)$$
$$\alpha = \frac{\alpha_o}{2}\left[1+\sqrt{1-\frac{4}{\alpha_o^2}}\right] \qquad 6.10\text{-}5$$
$$\alpha_o = \left(\frac{2s}{r}\right)^2 - 2$$

For ellipsoids that are wider than they are long, α in Equation 6.10-5 becomes complex, and evaluation must use complex arithmetic. Figures 6.10-1 shows the overall effect of electrode shape. Figure 6.10-2 shows that the simple expression of Equation 6.10-1 is significantly closer to the Sunde derivation than either rod or disc expressions 6.10-3 or 6.10-4 for a wide range of electrode shapes that have roughly equal depth and radius.

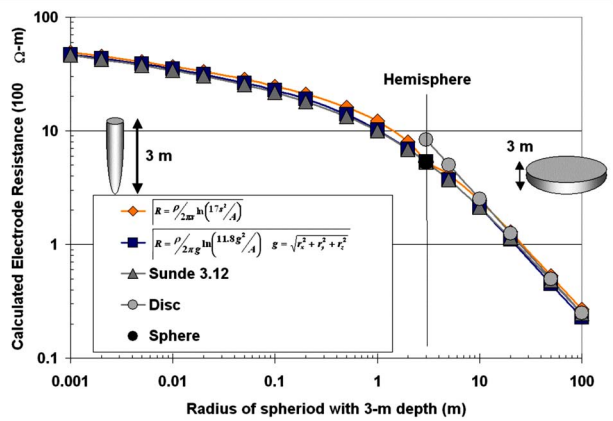


Figure 6.10-1 Comparison of expressions for resistance of rod, hemisphere, and disc electrodes.

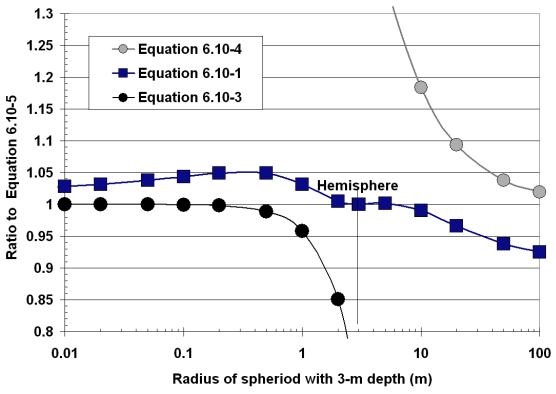


Figure 6.10-2 Ratio of expressions for geometric resistance to Sunde (Equation 6.10-5).

Correction from Solid to Wire-Frame Electrodes

The difference in resistance between solid electrodes and wire-frame approximations to the same shape is often small. This difference is called a "contact resistance." One estimate for contact resistance can be derived from the difference between the resistance of a circular ring of diameter *D,* wire diameter *d,* and burial depth *s/2*:

$$R = \frac{\rho}{2\pi^2 D}\left(\log_e\frac{8D}{d} + \log_e\frac{4D}{s}\right) \qquad 6.10\text{-}6$$

and the resistance of a circular plate of identical dimensions *D* and *s*:

$$R = \frac{\rho}{2D}\left(0.5 + \frac{D}{2\pi s}\right) \qquad 6.10\text{-}7$$

Figures 6.10-3 and 6.10-4 show the contact resistance for practical transmission tower ring and radial electrodes.

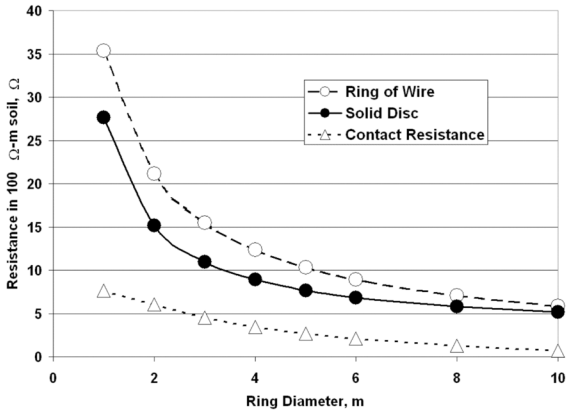


Figure 6.10-3 Contact resistance: Difference between ring and solid circular plate electrode resistances, buried at 1.5 m.

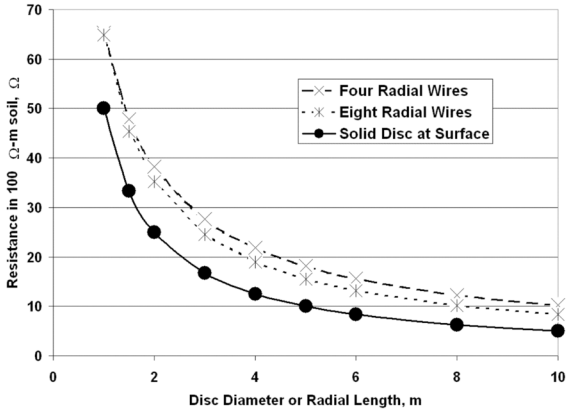


Figure 6.10-4 Contact resistance: Difference between radial wire and solid circular plate electrode resistance for shallow 0.5-m burial.

For buried grids of total length L, it is common to estimate the contact resistance using a simple expression:

$$R_{contact} \leq \frac{\rho}{L} \qquad 6.10\text{-}8$$

This upper bound is accurate for practical radial electrodes and too high for ring electrodes.

6.10.5 Earth Resistivity—Its Importance and Measurement

Soil resistivity has a direct influence on the potential rise from lightning flashes. Uncertainties in estimates of resistivity dominate our ability to compute transmission-line backflashover rates. Electrical resistivity ρ, with units of Ω-m, is a physical property of all materials that relates the electric field E (V/m) to the current density J (A/m^2) using $E = \rho J$.

The electrical resistivity of different materials at room temperature can vary by over 20 orders of magnitude. There are strong dependencies on temperature, moisture content, and frequency for many materials, including most soils and rock types. No single technique or instrument can measure resistivities over this wide range. This section focuses on techniques and instruments for practical measurement of soil resistivities and an assessment of the related experimental errors.

Since it is difficult to measure current density J in the soil, measurement techniques tend to use geometries that allow accurate calculation of current density as a function of source current I. This allows the use of an accurate four-terminal resistance meter, which accommodates a wide range of resistance in the excitation current source without affecting the high-impedance potential readings on inner terminals. A Wenner array, consisting of four, equally-spaced surface probes, is recommended for most work in uniform or layered soil. Figure 6.10-5 shows this configuration.

Equation 6.10-9 is used to convert the resistance measurements to resistivity at each probe spacing s, correcting for probe length l_w:

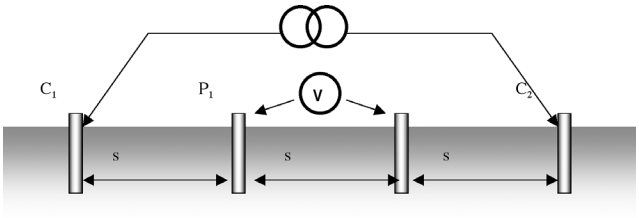


Figure 6.10-5 Wenner probe technique for measurement of resistivity.

$$\rho_a(s) = \frac{4\pi s \cdot R_{measured}}{1 + \frac{2s}{\sqrt{s^2 + 4l_w^2}} - \frac{s}{\sqrt{s^2 + l_w^2}}} \qquad 6.10\text{-}9$$

While it gives good accuracy, especially when used with a wide range of probe spacing 1 m < s < 200 m, the Wenner measurements are relatively slow to carry out and are more common in substation site selection and design. Transmission-line designers can review other sources of earth resistivity data in the design and site selection stage, and can also rely on airborne electromagnetic survey methods to establish design data for specific routes.

One important starting point for resistivity data is in the public domain. With every AM broadcast antenna, a "Proof of Performance" has been filed, consisting of measurements of radiated power as a function of distance from the antenna. This data can be used to estimate the earth resistivity over the path. If the earth resistivity is low, then the signal strength falls off uniformly with distance. For poorly conducting soil, the decay rate can increase to nearly 1/d^2. In the U.S., the Federal Communications Commission (FCC) has generated contour maps of conductivity σ (= 1/ρ) that give an approximation to the surface-layer resistivity and its variability. Applet G-2 can be used to explore the strong variation in resistivity across North America. The screen capture in Figure 6.10-6 shows resistivity of more than 1000 Ω-m in an area of Canadian Shield (granite). Resistivity of 100 Ω-m is reported for much of the central USA, with higher values in the Appalachian and Rocky mountain ranges.

6.10.6 Influence on Dielectric Strength of Soils

Certain soils contain more air pockets and are more prone to ionization effects as a consequence. This shows up as variations in the electric field gradient E_o, with values of 100-300 kV/m being low and 1000 kV/m being an upper limit. Oettle (Oettle 1988) studied the relationship of dielectric strength with resistivity, and reported a weak relationship that can be neglected. The median gradient of 300 kV/m was recommended by (Mousa 1994) after a literature review.

6.10.7 Vertical and Horizontal Layering

One method for estimating the effect of layering is to compare the very low frequency (VLF) (< 30 kHZ) and MF (1 MHz) conductivity maps for a region (see Figure 6.10-7). From the skin effect, the lower-frequency signals have deeper penetration, and the attenuation derived for those frequencies tend to represent a thicker layer than the 1-MHZ values.

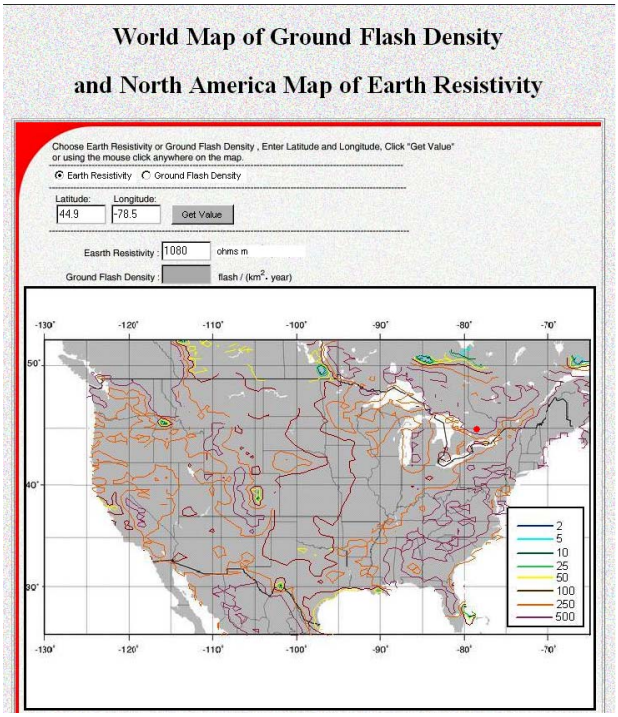


Figure 6.10-6 Screen capture from Applet G2. Estimates of resistivity based on the FCC records of AM broadcast can be obtained by clicking elsewhere on the map in Applet G2 or by entering the local latitude (a positive number) and longitude (a negative number) and clicking the "Get Value" button.

6.10.8 Measurement Techniques and Typical Results of Field Tests

The variation of surface layer depth and resistivity over horizontal distances of 300 m can be quite remarkable.

In cases where there is a pronounced change in soil resistivity with probe separation, the apparent resistivity $\rho_a(s)$ for the probe spacing s equal to the tower electrode diameter is a good approximation to the effective resistivity of the multi-layer earth. Alternately, the data can be interpolated with two-layer or multi-layer soil models, and the resulting values of upper-layer resistivity, depth, and lower-layer resistivity can be used along with an infinite series of reflection coefficients to compute an effective resistivity. Dawalibi (Dawalibi 1982, Chapter 4) provides guidance for this calculation process.

6.10.9 Capacitance, Electrolytic and Dielectric Effects

Bewley (Bewley 1963) observed a transient counterpoise capacitance of about 8 x 10^{-11} F/m. For a 50-m counterpoise, if soil conditions are such that the total leakage resistance is 20 ohms, this corresponds to a leakage resistance per meter of 1000 ohms. The RC time constant is 8 x 10^{-11} x 1000 = 8 x 10^{-8} s or 0.08 μs. This extremely small time constant indicates that resistance effects quickly swamp out capacitance effects during counterpoise current

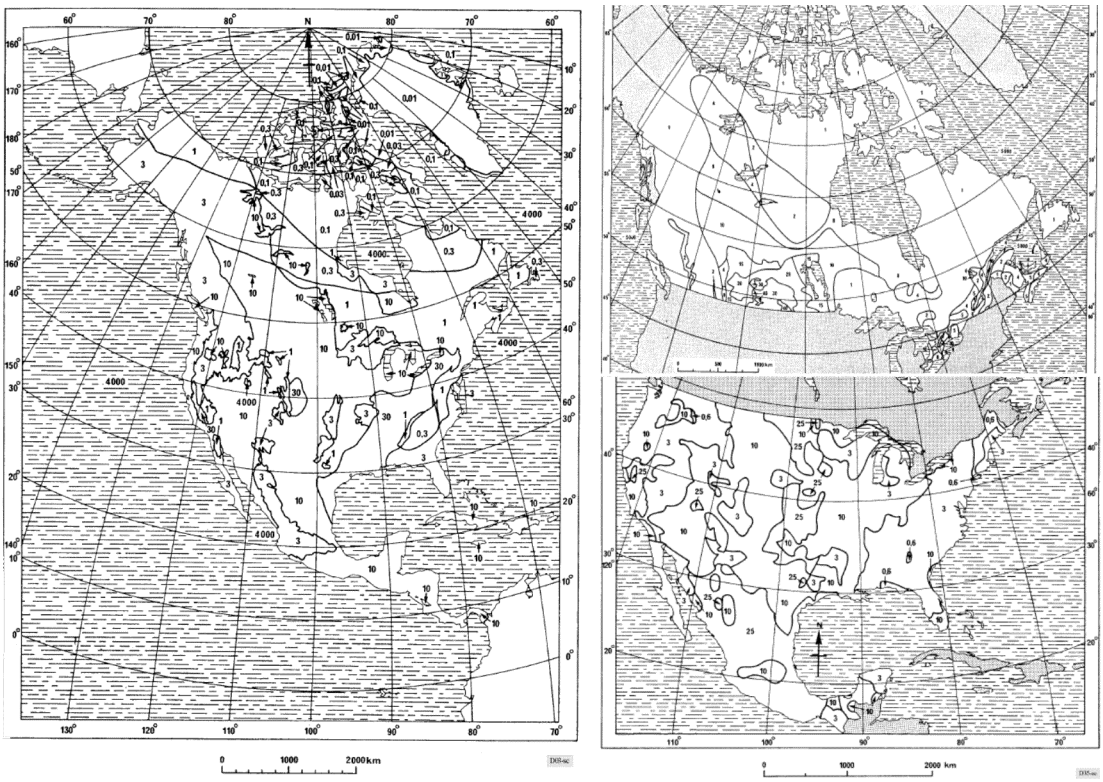


Figure 6.10-7 *Left*: ELF (deeper penetration) conductivity map. *Right*: MF (surface layer) conductivity maps for North America (CCIR 1982) (Reproduced with the kind permission of ITU).

propagation. A general measure of this is the "relaxation time" τ of the earth:

$$\tau = \varepsilon \times \rho \qquad 6.10\text{-}10$$

Where:

τ = earth relaxation time, s.
ε = earth permittivity, F/m.
ρ = earth resistivity, ohm-m.

A typical earth permittivity of 8 x 10^{-11} F/m and a resistivity of 300 ohm-meters yield a relaxation time of 2.4 x 10^{-8} s, or 0.024 μs. Hence resistance quickly dominates as a current wave propagates along the counterpoise.

6.10.10 Dynamics of Ground Resistance (Applets L-1 and L-3)

Applet L-1 (Transmission Line Lightning Performance) and Applet L-3 (Tower Dynamic Footing Resistance) are closely related. One of the mathematical difficulties that L-1 has to face is the nonlinearity of tower ground resistance at high stroke currents, brought about by the fact that earth is a poor dielectric. For large concrete foundations, surface areas are sufficient to maintain current densities at the surface of the concrete to values low enough to limit dielectric failures in the earth, but for ground rods and counterpoise wires, large currents have to flow from small surface areas, and the current density multiplied by the soil resistivity can create voltage gradients higher than the soil can endure. The resulting ionization appears as reduced resistivity of the soil (Oettle 1988). This effect can significantly reduce the voltage created at the base of a tower from what would be anticipated using the normal low-frequency resistance, and hence the lightning flashover rate.

6.10.11 Nonlinear Dynamics of Ground Rods

At high dielectric stresses, air spaces in many types of ground ionize and break down. This tends to increase the effective size of electrodes, in the same way that a corona envelope forms around overhead conductors. The limiting gradient in soils tends to be in the range of 100 to 1000 kV/m, compared to the recommended corona envelope in air of 1500 – 2000 kV/m used in Section 6.4.1. The increased radius of the corona envelope reduces the resistance of small or thin electrodes such as ground rods or counterpoise. The nature and the extent of this reduction in resistance are important research aspects into lightning response of small ground electrodes (EPRI 2002a; EPRI 2002b).

Figure 6.10-8 shows a typical test series, with increasing currents injected into a single ground rod. For 1-kA current, there is no effect, but as current increases to 7 kA, the impedance is halved late in the current wave.

For 1-kA current, there is no effect, but as current increases to 7 kA, the impedance is halved late in the current wave. The test levels of 7-34 kA are important, because there are typically two to four ground rods at each tower, each sharing a fraction of the impressed lightning current. Also, reflections from adjacent towers tend to shorten the tail of the impressed current, an effect that can be estimated using a ladder network of adjacent tower footing impedances connected by the overhead groundwire surge impedances.

An important nonlinear characteristic of multiple ground rods appears when they are all impulsed with the same voltage, as is usually the case. If the rods are asymmetrically located (for example, three rods in a row, so that the earth voltage coupling of the center rod to the other two is different from that of the outermost rods), the outer rods initially draw more current than the center rod. This, in turn, causes the outer rods to ionize sooner and their resistance drops more rapidly, causing them to draw still more current compared to the center rod. The situation is somewhat similar to an attempt to parallel several surge arresters when one has a different volt-ampere characteristic from another—the arrester with the lowest volt-ampere characteristic draws practically all the current.

6.10.12 The Liew-Darveniza Calculation of Rod Dynamic Resistances

In 1974, Liew and Darveniza (Liew and Darveniza 1974) published an important paper describing their development of theoretical models of the dynamic response of ground rods to high currents and comparisons with field tests.

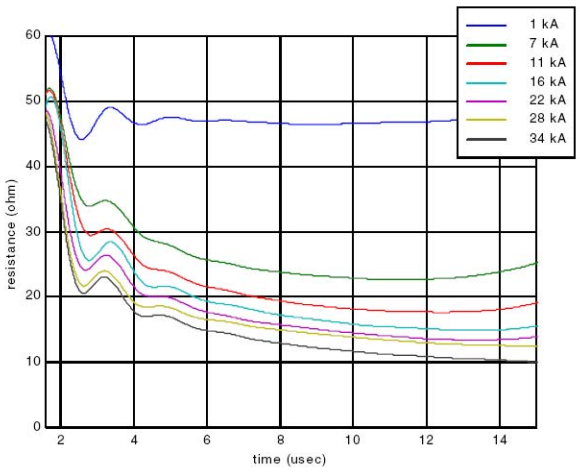


Figure 6.10-8 Resistance of 48-Ω driven rod for various impulse currents for 2.5 / 15 μs impulse current (typical of subsequent stroke).

Basically, they assumed each ground rod to be surrounded with a series of concentric shells (Figure 6.10-9).

Impulse current applied to the rod flows radially outward through each shell. Depending on the resistance of each shell and the current density, the soil in the shell starts ionizing and the shell resistance drops. Assuming uniform current flow out of the rod, the current density in each shell is easily calculated. If this current density is sufficient to create a shell gradient greater than E_0, where E_0 is the critical dielectric ionizing gradient of the soil, the shell resistance decays exponentially with time. When the surge current eventually decays, the gradient across one or more of the shells falls below E_0, and those shells start deionizing, their resistances increasing exponentially with time to their original low-current values.

Liew and Darveniza derived an equation for the sum of the nonionizing resistance of an infinite number of shells surrounding a single rod, and compared the result with the classical formula for the resistance of a single rod. The result was close to the theoretical value, demonstrating that the shell algorithm met the theoretical requirements. The resulting Liew-Darveniza equation for low-frequency resistance of a single rod is:

$$R = \frac{\rho}{2\pi L} \ln\left(\frac{r_0 + L}{r_0}\right) \qquad 6.10\text{-}11$$

Where:
R = rod low-frequency resistance, ohms.
ρ = earth resistivity, ohm-m.
L = rod length, m.
r_0 = rod radius, m.

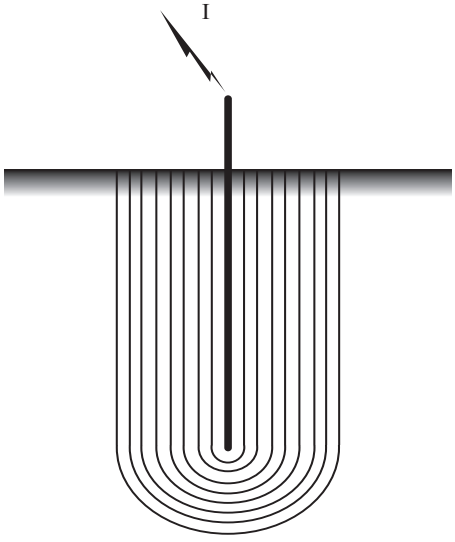


Figure 6.10-9 Liew-Darveniza ground rod surrounded by concentric shells of earth.

The relation between Equation 6.10-11 and other estimates of rod resistance was discussed previously in Table 6.10-3.

Shell ionization of any shell occurs when

$$J_C = \frac{E_0}{\rho_0} \qquad 6.10\text{-}12$$

Where:
J_C = critical current density, amperes/ m^2.
E_0 = earth critical ionizing gradient, volts/m.
ρ_0 = earth resistivity, ohm-m.

Ionization is marked by an exponential decay in resistivity:

$$\rho = \rho_0 \exp\frac{-t}{\tau_1} \qquad 6.10\text{-}13$$

Where:
ρ = shell resistivity during ionization, ohm-m.
ρ_0 = low current soil resistivity, ohm-m.
t = time in μs after start of ionization.
τ = a soil ionization time constant, μs (assumed 2.0 μs for many tests).

During the later deionization process of the shells, the deionization resistivity ρ of any shell increases exponentially, and Liew-Darveniza suggests the equation:

$$\rho = \rho_i + (\rho_0 - \rho_i)\left(1 - \exp\frac{-t}{\tau_2}\right)\left(1 - \frac{J}{J_C}\right)^2 \qquad 6.10\text{-}14$$

Where:
J = current density, ohm-m.
τ_2 = deionization time constant, μs.
ρ_i = value of resistivity when $J = J_C$ on current decay.
t = time measured from onset of deionization, μs.

Liew-Darveniza found reasonably good correlation between published ground rod volt-time data and their theoretical calculations using the concentric shells model, and the concentric shells model is used in all applets in this edition of the Red Book where analysis of ground rod response is required.

6.10.13 Use of the Korsuncev Criterial Curve

Korsuncev (Korsuncev 1958) carried out a dimensional analysis of the nonlinear behavior of ground electrodes of several different shapes, using what is known in North America as the Buckingham "Pi" method. Dimensionless ratios of relevant parameters in a complex problem are manipulated to give insight. Familiar dimension-less ratios used in thermodynamics are the Reynolds and Nusselt

numbers. Korsuncev recommended the following ratios Π_1 and Π_2:

$$\Pi_1 = \frac{s\,R}{\rho} \qquad \Pi_2 = \frac{\rho\,I}{E_o s^2} \qquad \text{6.10-15, a, b}$$

Where:

s = the characteristic distance from the center of the electrode to its outermost point.

ρ = the earth resistivity in the ionization zone near the electrode.

E_o = the critical breakdown gradient, typically 400 kV/m.

I = the instantaneous value of current, kA.

R = the footing resistance in Ω.

Chisholm and Janischewskyj (1989) consolidated observed relations between Π_1 and Π_2, as shown in Figure 6.10-10 for a variety of electrode shapes, ranging from hemisphere to thin rod. There are two separate regions of response. For low values of Π_2 at the left side of Figure 6.10-10, there is insufficient current to cause ionization, and the resulting resistance is independent of current. There is a unique value of Π_1 for each electrode shape, given closely by:

$$\Pi_1^o \approx \frac{1}{2\pi}\ln\left(\frac{2\pi\, e\, s^2}{A}\right) \approx \frac{1}{2\pi}\ln\left(\frac{2\pi e^{\sqrt{3}}\, g^2}{3A}\right) \qquad \text{6.10-16}$$

Π_1^o ranges from 0.159 for a hemisphere to about 1.26 for a 10-m long, 10-mm radius rod. The second expression is valid for smooth objects of revolution, using the dimension g as used by Oettle: $g = \sqrt{(r_x^2+r_y^2+r_z^2)}$.

The value of Π_1 to use in Equation 6.10-15a is the lesser of Π_1^o or an empirical expression relating Π_1 and Π_2 in the region of interest:

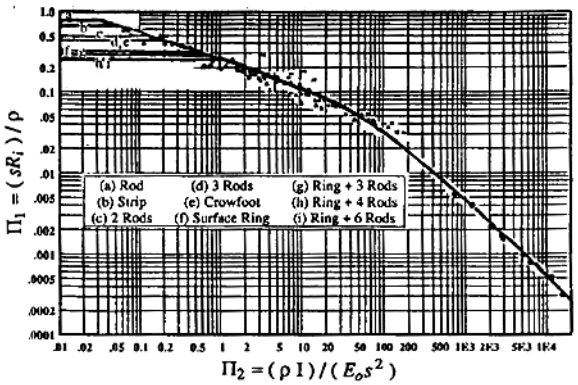


Figure 6.10-10 Observed relation between dimensionless parameters for ionized resistance of ground electrodes from Popolansky and Korsuncev.

$$\Pi_1 = \min\left(\Pi_1^o,\ 0.263 \cdot \Pi_2^{-0.308}\right) \qquad \text{6.10-17}$$

An EPRI study (EPRI 2002a) showed that the simple Korsuncev model provides good dynamic tracking of the voltage-current relationship for simple ground electrodes under lightning impulse conditions up to 40 kA. The shape of the ionized zone can be estimated from the resulting value of Π_1, knowing that the area A increases, but dimension s does not change if $\Pi_1 > 0.159$. For $\Pi_1 < 0.159$, the footing is fully ionized, the zone is hemispherical, and the zone radius can be calculated from the expression for the resistance of a hemisphere.

A step-by-step procedure using the Korsuncev relations to calculate dynamic resistance at high currents is as follows:

1. Calculate Π_2 for the required I current using Equation 6.10-15b.
2. Calculate Π_1 Equation 6.10-15a using g or s as appropriate.
3. Check that $\Pi_1 < \Pi_1^o$ from Equation 6.10-17 and then calculate the dynamic resistance using Equation 6.10-15.

6.10.14 Metal Tower and Reinforced Concrete Foundations

A basic calculation using the resistivity and relative permittivity of steel compared to copper shows that, at low currents, the surge impedance of a steel structure can be substantially higher than the impedance of an equivalent nonmagnetic structure.

$$L = \frac{1}{4\pi r}\sqrt{\frac{\mu_0}{\pi\sigma}}\,\frac{1}{\sqrt{f}} \qquad \text{6.10-18}$$

For copper:
Resistivity $\rho_{copper} = 1/\sigma_{copper} = 1.55 * 10^{-8}$ Ω-m.
Relative magnetic permeability = $\mu_r = 1$.

For reinforcing steel such as bare rebar:
Resistivity $\rho_{steel} = 1/\sigma_{steel} = 9*10^{-8}$ Ω-m at room temperature.
Relative magnetic permeability = μ_r = 100 to 1000 at low current.

$$\frac{L_{Steel}}{L_{Copper}} = \frac{\frac{1}{4\pi r}\sqrt{\frac{\mu_0\mu_{rs}}{\pi\sigma_s}}\,\frac{1}{\sqrt{f}}}{\frac{1}{4\pi r}\sqrt{\frac{\mu_0\mu_{rc}}{\pi\sigma_c}}\,\frac{1}{\sqrt{f}}} = \sqrt{\frac{\rho_{steel}\,\mu_{r\,steel}}{\rho_{copper}}} = 24-76 \qquad \text{6.10-19}$$

The capacitance per unit length of steel and copper wires would be equal, so the surge impedance of a pure steel wire would be five to nine times higher than the surge impedance

of a bare copper wire. However, several mitigating factors lead to lower inductance for steel wires:

- **Galvanizing.** Most steel wires are not exposed directly to the environment. The outer surfaces are galvanized with zinc or clad with aluminum or copper.
- **Saturation.** The current density is high in steel elements near the point of lightning attachment, and they tend to saturate. The current density at the surfaces is also elevated due to the skin effect, which tends to limit the cross-sectional area available to the lightning strike current by forcing the current to the perimeter of the member. This high current density saturates the steel near the surface of the conductor and significantly lowers the relative permeability. In the vicinity of the strike point, the relative permeability is much closer to that of free space (1.0) than it is to the maximum value of 1000 for unsaturated steel rebar at low currents. Since the permeability is much reduced, the inductive component is similarly reduced, reducing the surge impedance.
- **Corona**. As described in Section 6.4, the tower members are usually not sufficiently large to limit the electric field gradient to less than 1500 kV/m, so an impulse corona envelope forms, at least for small towers. This envelope increases the effective radius of the members and reduces their surge impedance.

For lightning strokes, the surge impedance of a structural rebar grid is found to be much lower than that of the conventional external copper or aluminum down-conductor system. In cases where the rebar is encased in concrete, the resulting electrode has a low inductance, and this makes the metal/concrete cross-section the preferred path for lightning surge currents.

In rocket-triggered natural lightning strike tests on instrumented reinforced concrete structures, (Schnetzer 1995) found that 75 to 90% of the strike current was carried by the steel rebar, and the remainder was carried by the external Lightning Protection System (LPS) down-conductors. This was true during the entire lightning waveform, even during the high *dI/dt* early-time phase, where the inductive component of the rebar would prevail. This clearly indicates that the surge impedance of the rebar grid is substantially lower than that of the LPS down-conductors during lightning strikes.

In an extreme example, the CN Tower is a 553-m reinforced-concrete structure with three 80-mm by 10-mm copper bars as an internal lightning protection system. Measurements by (McComb et al. 1980) with a current shunt in the lightning protection system and a Rogowski coil around the entire tower show that the copper carries less than 0.03% of the total current.

Generally, steel rebar in concrete foundations of transmission towers should be electrically continuous, and an external connection should be welded to the tower steel. The large surface area and relatively low resistivity of the concrete make the tower foundations preferred electrodes. Lightning will find its way into and out of the footings, with or without the bonds. A pre-engineered conductive path mitigates any concerns related to cracking or spalling.

The resistance of an individual concrete footing is formed by two terms: the contact resistance of the rebar length in the concrete, using a value of $\rho_{Concrete}$ = 70 to 250 Ωm in Equation 6.10-8, and the geometric resistance of the concrete electrode, given by Equation 6.10-1. Four concrete footings in parallel can be treated with the use of Applet L-6.

6.10.15 Radial and Continuous Counterpoise

An extensive compilation of low-frequency ground resistance formulas was published by Dwight (Dwight 1936) for rods, counterpoise, rings of wire, and buried strips and plates. His equations are reproduced in Table 6.10-1. Radial counterpoise, consisting of one or more horizontal buried wires, is similar in lightning response to one or more ground rods, the difference being that the proximity of the earth's surface to the horizontal wires increases the low frequency and dynamic resistance. For long wires (25 m or more), propagation times are also involved, so that—for very fast transients—the counterpoise impedance is initially governed by the combined surge impedances of all the wires (approximately 200 ohms per wire) and rings down or up exponentially to the final low-frequency resistance of all the wires in approximately three round-trip travel times. The addition of ionization brush discharges around the wires at high currents, particularly near the input end, further complicates the analysis.

Continuous counterpoise, wherein a buried conductor runs continuously from tower to tower, shows zero low-frequency footing resistance when conventional measurements are made. However, for high-frequency lightning transients, propagation times along the counterpoise render it ineffective for distances exceeding 60 to 90 m (Bewley 1963). Several radial wires of the same combined length have a much better transient response. The L-1 applet in this chapter assumes that a continuous counterpoise has the same high-frequency transient response as two radial wires, each with a length of 75 m.

6.10.16 Recommendations for Line Flashover Calculations

The strongest advantage of simple, empirical methods for calculating lightning flashover rate is that they can be applied efficiently to vectors of footing resistance data. For example, the FLASH program accepts a distribution of

footing resistance values as a histogram, and computes a composite flashover rate by summing the contributions of each element. It is now feasible to assemble the footing resistance or resistivity data in a spreadsheet, and to calculate the outage rate span by span. If additional line parameters, such as structure heights and conductor spacing, are also available electronically, these values can also be included.

User experience with the FLASH program, in the calibration process based mainly on outage data reported by Whitehead (Whitehead 1983), showed that aggregation of footing resistance into 10 or more subsets gave significant improvement in the predicted transmission outage rates.

6.10.17 Step, Touch and Transferred Potentials

Ground resistance calculations normally assume that the earth is an infinite, uniform half-plane with a given value of resistivity. With these assumptions, it is possible to derive exact equations for the ground resistance of some important electrode shapes. These exact theoretical equations are used in this section to illustrate the relationships among voltage, current, and potential distribution along the earth surface, using the variables shown in Figure 6.10-11.

With uniform resistivity ρ, there is spherical symmetry, and the current flows radially away, uniformly in every direction. The surface of the hemisphere, as well as any hemispherical cross-sections *dx* of the ground centered at the hemisphere, is an equipotential, and the current lines are perpendicular to these surfaces.

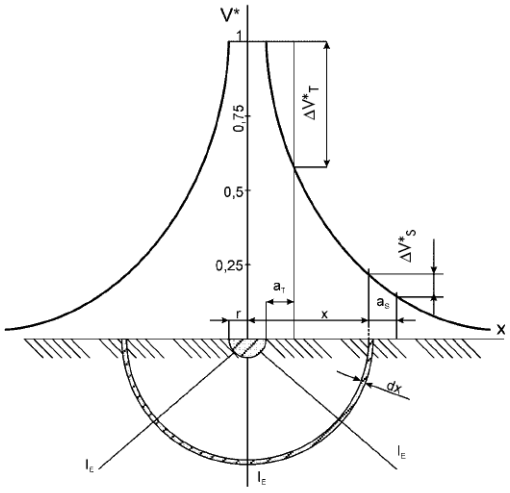
The current density is highest at the surface of the electrode (thinking of an uninflated balloon) and becomes thinner as the distance *x* increases (as the balloon inflates). The total current (weight of the balloon) remains constant at any inflation level, so the current density is given by the current divided by the surface area of the hemisphere, $A = 2\pi x^2$.

Under these conditions the resistance of the hemispherical element of thickness *dx* and the radius *x*:

$$dR = \frac{\rho}{2\pi \cdot x^2} dx \qquad 6.10\text{-}20$$

The electrode resistance is the integral of dR from the hemisphere surface to infinity:

$$R = \frac{\rho}{2\pi} \int_r^{\infty} \frac{dx}{x^2} = \frac{\rho}{2\pi r} \qquad 6.10\text{-}21$$



r = Electrode radius.
x = Distance from the center of the electrode.
a_T = Touch distance (normally 1 m).
a_S = Step distance (normally 1 m).
ΔV_T = Touch Voltage from the electrode itself to a position near the electrode.
ΔV_S = Step Voltage between two points, both remote from the electrode.

Figure 6.10-11 Potential profile of hemispherical electrode in uniform soil, showing parameters for calculating ground resistance, step and touch potentials.

The potential of any point located at distance *x* from the center of the hemisphere electrode, in which an earth current I_E flows, is given by:

$$V_X = \frac{\rho I_E}{2\pi x} \qquad 6.10\text{-}22$$

The shape of the potential profile for hemisphere electrodes gives a benchmark for comparing profiles of other electrode shapes. Ring or mesh electrodes have potential profiles that fall off less rapidly than $1/x$, while vertical driven rods have a greater change in surface potential with distance.

The potential difference between the electrode ($x = r$) and a point on the earth surface, one at distance $x = r + \Delta x$, is given by:

$$V_T = \frac{\rho I_E}{2\pi} \left(\frac{1}{r} - \frac{1}{r + \Delta x} \right) \qquad 6.10\text{-}23$$

In many electrical safety standards, such as IEEE Guide 80, Δx = 1 m, representing the reach of a 2-m (6 ft, 7-in.) person. A similar calculation can be carried out to determine the step potential V_S, existing between the feet of a person standing at a position x with foot separation Δx:

$$V_S = \frac{\rho I_E}{2\pi}\left(\frac{1}{x} - \frac{1}{x+\Delta x}\right) \qquad 6.10\text{-}24$$

where $x > r$.

Figure 6.10-12 shows a practical illustration of touch and step voltages. Persons at locations *A* and *B* are subject to the touch potentials V_T, while the person at C is subject to a step potential V_S.

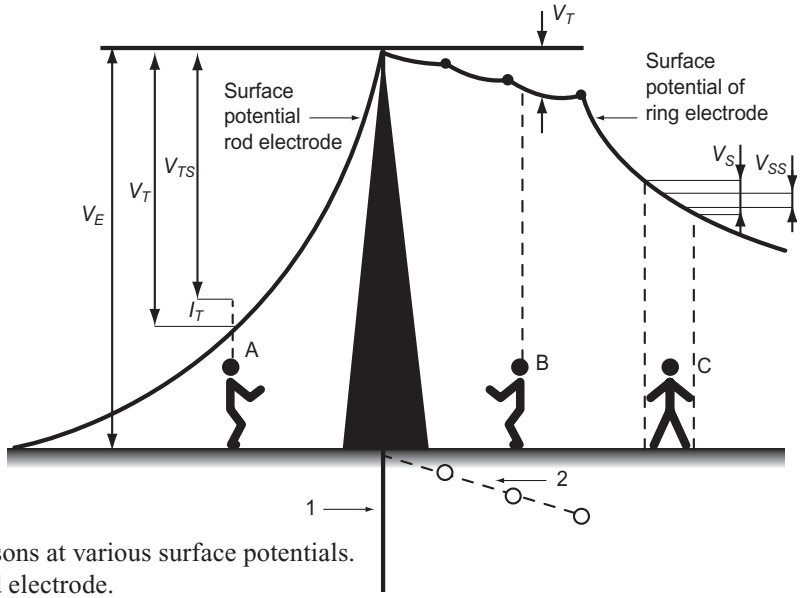
The left side of Figure 6.10-12 shows the situation for a rod electrode, while the right side shows the potential profile of a ring electrode. The rod electrode (1) may have a low resistance, but it also has the steepest (most unfavorable) potential distribution. The ring electrode (2) has a much flatter earth potential profile. The touch potential for person *A*, near the rod electrode, is considerably larger for person *B*, near the meshed electrode. Step potentials for person *C* are higher near the edge of the ring, but not as high as the step potential at an equal distance away from the rod.

The electrode resistance determines the value of potential rise, and its configuration establishes how the potential rise distributes along the earth surface. The configuration also influences the grounding resistance, as described by the geometric resistance and effective resistivity. Adequate design needs to consider both resistance and configuration, usually in an iterative process.

A ring electrode has some important benefits for many grounding conditions. The ring is has large dimension *g* and area *A*, giving a lower resistance, and the ring shape has a lower surge impedance than a long vertical rod or horizontal counterpoise. Also, within the ring is an area of approximate equipotential, but at the edges of the electrode there is a strong potential gradient. The touch potential is limited, because practical rings extend beyond several meters beyond any metal structure, but high step voltages can still occur.

Risk of exposure to step voltage is much preferred to touch voltage, because several of the following mitigation factors are present:

- Higher body path impedance (and the two feet appear in series rather than in parallel).



A,B,C = Persons at various surface potentials.
1 = Rod electrode.
2 = Mesh (grid or radial / ring) electrode.
V_E = Potential rise of composite electrode relative to remote ground.
V_T, V_{TS} = Touch voltage (open circuit) and shocking touch voltage (into body impedance).
V_S, V_{SS} = Step voltage (open circuit) and shocking step voltage (into body impedance).
I_T = Shocking touch current (V_{TS} / (impedance of body path + two feet in parallel).
I_S = Shocking step current (V_{SS}/(Impedance of body path + two feet in series).

Figure 6.10-12 Comparison of surface potential distribution for rod and mesh electrodes.

- Lower fraction of heart current for leg-to-leg electrocution compared to arm-to-legs contact.
- High resistivity of many common surface layers, including grass, asphalt, and gravel.

There are other disadvantages to ring electrodes: it is not practical to bury them deeply, so they are more susceptible to changes in soil moisture content and more easily damaged or vandalized. Improved stability of resistance can be achieved by including a number of long vertical rods in the mesh.

6.10.18 Coordination With Safe Body Withstand Levels

The risk of electrocution increases with duration of exposure, as shown for two standard models in Figure 6.10-3. At typical transmission-line clearing times of 3 ac cycles (50 ms), the graph shows that Biegelmeier (Biegelmeier and Lee 1980) recommends a safe limit of 500 mA for all short-duration surges. The level calculated from the Dalziel electrocution equation (Dalziel and Lee 1968) will be 116 mA divided by the square root of time in seconds, giving 519 mA.

A body impedance of 1000 Ω is used at 60 Hz to convert electrocution current into tolerable step and touch potentials. Additional factors, such as the foot-to-surface contact resistance, are also described in the IEEE Guide 80 (IEEE 2000a). A wide range of bioelectric impedance measurements shows that this impedance is also reasonable at 50 kHz for a wide range of body shapes, including children and the elderly.

For particularly fast exposure, such as the 100-µs "monophasic" (one-sided pulse) lightning surge current, Figure 6.10-14 shows a factor of 30 increase in ventricular fibrillation current relative to the 500-mA level of Biegelmeier, shown as level (2). An impulse current of 15 A from hand to foot would require an impulse potential of about 15 kV.

6.10.19 Calculation of Surface Potentials Using L-6 Applet

One excellent tool for evaluating the touch and step potentials around typical transmission tower electrodes is the L-6 applet. Using a sophisticated three-point moment method, this tool allows efficient modeling of foundation components as large or small cylinders, horizontal buried wires or rings. A screen capture for the demonstration electrode, a tower with ring and radial wires, is shown in Figure 6.4-15.

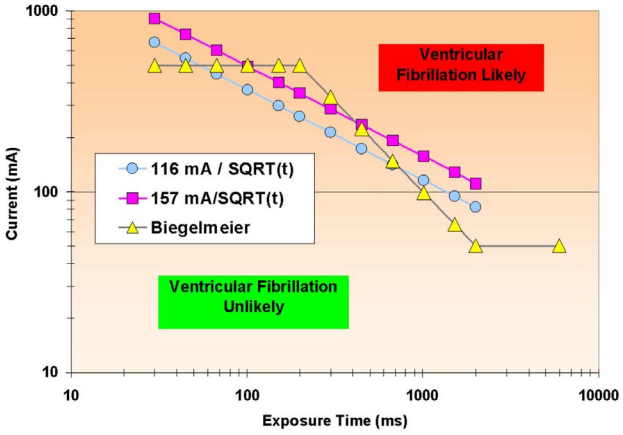


Figure 6.10-13 Comparison of IEC and IEEE Guide 80 Standards for electrocution current.

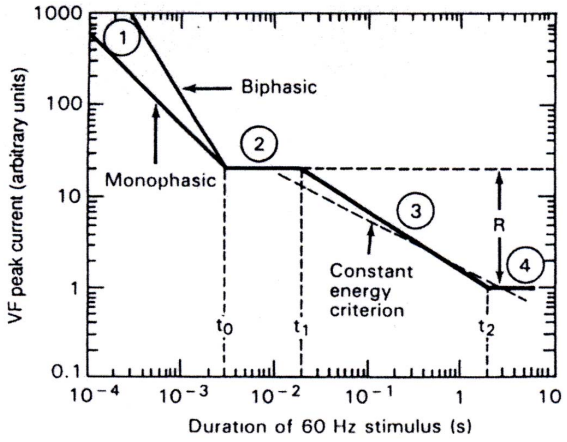


Figure 6.10-14 Ventricular fibrillation current versus duration of 60-Hz stimulus for wide range of exposure duration (Reilly 1998)

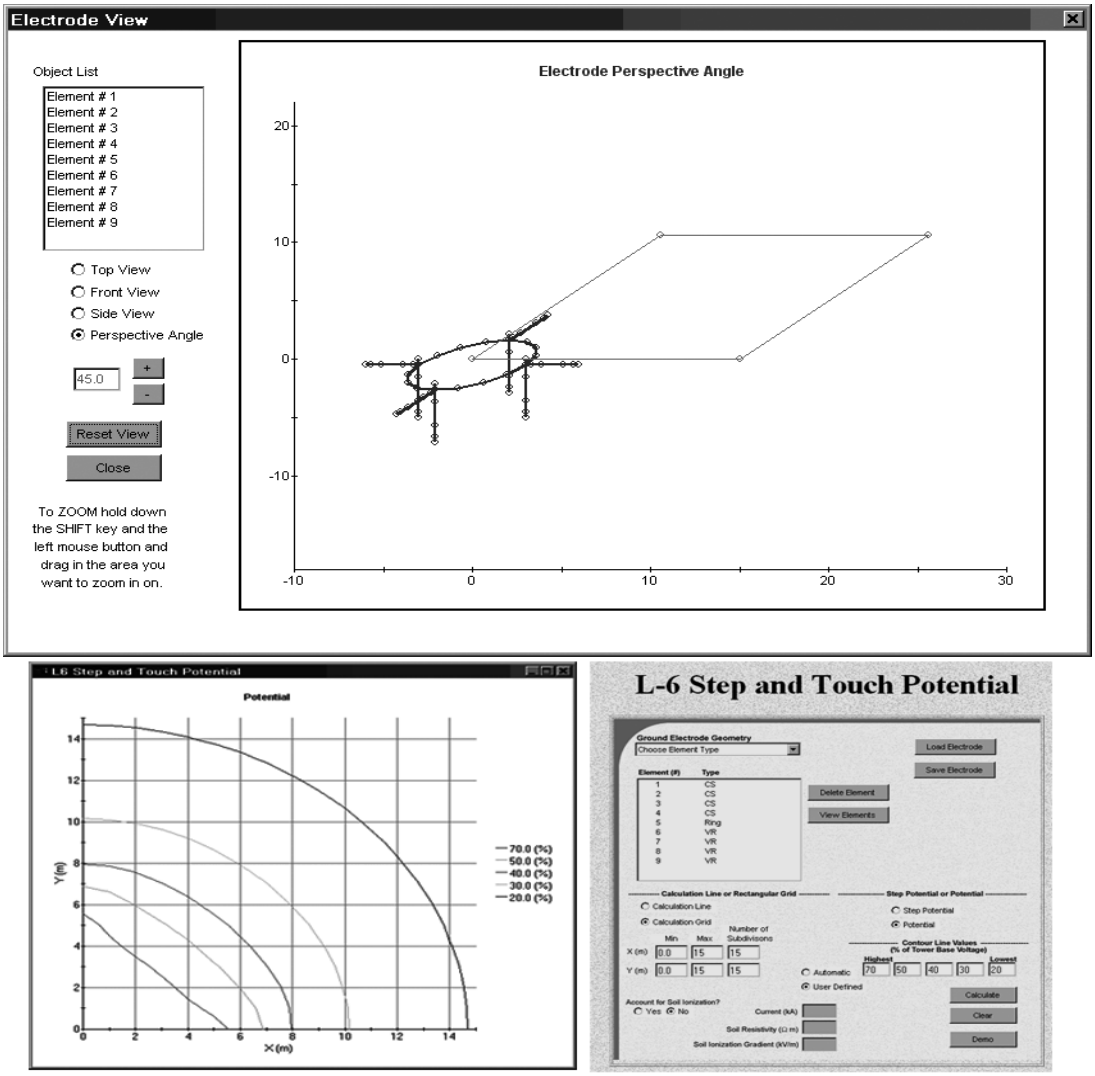


Figure 6.10-15 Screen Capture showing input geometry and calculation results for L-6 Applet.

APPENDIX 6.1 THEORY OF THE DISRUPTIVE EFFECT ALGORITHM

The disruptive effect algorithm was originally developed by Witzke and Bliss (1958) to evaluate impulse failures of transformers. In the quasi-uniform fields of power transformers, the formative time lag of a breakdown (the time required for a discharge to bridge a gap once it starts) is quite small compared to the statistical time lag which has to wait for the weak links (free electrons, ions, contaminating particles, etc.) to start the process, so the statistical time lag dominates the breakdown process and it becomes a matter of probability when the breakdown will begin. Once it begins, the formative time lag is practically instantaneous.

Disruptive Effect as a Probability Equation

In Figure A6.1-1, an impulse wave is simulated by a series of voltage impulses, each of a width t. Let the probability of withstand P_N of the gap for impulse *n* be approximated by:

$$P_N = \varepsilon^{-\alpha(V-V_0)\Delta t} \quad \text{A6.1-1}$$

Then the total probability of withstand of all the impulses is the product of all the individual probabilities and if this total probability is 0.5 for critical flashover, then:

$$0.5 = P_1.P_2.P_3 \ldots\ldots.P_N \quad \text{A6.1-2}$$

and substituting Equation A6.1-1 into Equation A6.1-2:

$$0.5 = \varepsilon^{-\varepsilon(V_1-V_0)\Delta t}.\varepsilon^{-\alpha(V_2-V_0)\Delta t}.....\varepsilon^{-\alpha(V_N-V_0)\Delta t} \quad \text{A6.1-3}$$

Taking the log of both sides of Equation A6.1-3:

$$-0.6931 = -\alpha\sum_{V_1}^{V_N}(V_K - V_0)\Delta t \quad \text{A6.1-4}$$

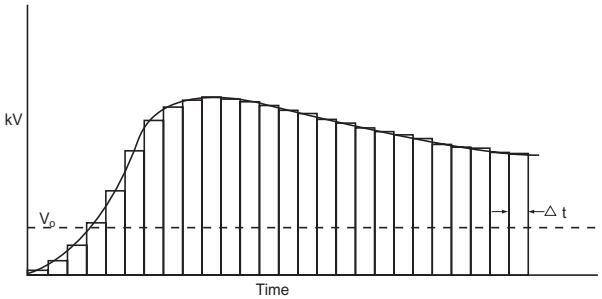


Figure A6.1-1 Voltage waveshape as contiguous impulses.

which in the limit becomes:

$$DE = \int_{V_1}(V(t) - V_0)dt \quad \text{A6.1-5}$$

Where:

$DE = 0.6931/\alpha$

Equation A6.1-5 is the "equal-area: criterion." A better fit to empirical data is often attained if $(V(t) - V_0)$ is raised to some exponent *n*.

Disruptive Effect as a Formative Time Lag Equation

The disruptive effect equation can also be viewed as a description of the flight of the breakdown streamer across a gap (a leader progression model). If the distance *x* that the streamer travels during a time *t* is given by:

$$\Delta x = \alpha(V(t) - V_0)^n \Delta t \quad \text{A6.1-6}$$

and then the gap is completely bridged when:

$$S = \sum_{t_0}^{t_S} \alpha(V(t) - V_0)^n \Delta t \quad \text{A6.1-7}$$

where *S* = gap length and t_S is the time to bridge the gap.

and once again in the limit:

$$DE = \int_{t_0}^{t_S}(V(t) - V_0)^n \Delta t \quad \text{A6.1-8}$$

where for this condition, $DE = S/\alpha$.

In Equation A6.1-8, α is a function of gap length, as is *DE*. *DE* does not vary so widely if gradient is used in the equations instead of voltage. The starting time t_0 in Equation A6.1-8 is the time at which the voltage just reaches the V_0 value. Values of *n* ranging from 1 to 4 have been proposed for the exponent.

Summary

The disruptive effect equation appears to simulate either a statistical time lag or a formative time lag (leader progression), and it seems reasonable to apply it for some combination of both. In practice it is easier to apply than a standard CIGRE leader progression model, and as long as the experimental parameters *n* and V_0 can be determined in advance, it should provide reasonably acceptable results for a variety of waveshapes.

APPENDIX 6.2 ELECTROMAGNETIC FIELDS FROM LIGHTNING

Source Strength

Electromagnetic radiation occurs whenever charge is accelerated. Current is the time derivative of charge flow, so a high rate of current rise *dI/dt* from lightning generates strong electromagnetic fields. An elegant model for this electromagnetic radiation (Uman et al. 1975) treats the lightning channel as a vertical transmission line of constant impedance in free space. Lightning is assumed to propagate upwards with a uniform return stroke velocity, often $v = c/3$, where c is the speed of light. With this model, the distant electric and magnetic fields, coupled by the 377-Ω impedance of free space, will be faithful copies of the return stroke current waveform, delayed in time and attenuating linearly with distance as follows:

$$H(D,t + D/c) = \frac{v}{2\pi cD} i(t) \qquad \text{A6.2-1}$$

Where:

$H(D,t+D/c)$ = the magnetic field (A/m).
$E(D,t+D/c)$ = 377 Ω x $H(D,t+D/c)$.
$i(t)$ = the lightning stroke current (A).
D = the distance from the flash to the receiver (m).
v = the return stroke velocity (m/s).
c = the velocity of light (3.0×10^8 m/s).
t = time (s).

At close range, Equation A6.2-1 has limitations, but still provides a good estimate of the peak incident energy for calculating induced overvoltages into horizontal conductors near ground. The average fields of 16 mA/m or 6 V/m at 100 km can be measured with good signal-to-noise ratio using wideband loop or plate antennas of dimension 0.1 to 1 m.

Measuring Lightning Locations

Wideband Gated Direction Finding (DF)

Several technologies have taken advantage of the strong source radiation for real-time detection of lightning ground flashes. The first gated, wideband receivers in commercial use (Krider et al. 1976) measured horizontal magnetic fields in north-south and east-west orientation, along with vertical electric field. Since the measured magnetic field is perpendicular to the direction from the source, its orientation can be used to determine a bearing towards the source. With two or more bearings, a source location can be placed on the surface of the earth. Peak magnetic field strengths were also reported. Networks with these LLP receivers were extended across the U.S. and operated until 1995, when a combined technology was implemented.

Site-to-site installation variations were significant limitations in the original networks. Nearby loop structures also introduced systematic site errors in bearing and amplitude. Continuous identification and elimination of these site errors led to satisfactory operation of extensive networks.

Wideband Time-of-Arrival Methods

The Global Positioning System (GPS) is a network of 24 Rockwell Navstar satellites. Each 900-kg satellite orbits the earth every 12 hours in a constellation that keeps every point on the planet in radio contact with at least four satellites. The first operational GPS satellite was launched in 1978, and the system reached full 24-satellite capability in 1993. Figure A6.2-1 shows the performance after "Selective Availability", a deliberate degradation of the signals, was discontinued.

The GPS achieves 5-m Standard Error Probable (SEP) or 3-m Circular Error Probable (CEP) through the use of time signals with 20-ns accuracy. Inexpensive GPS receivers can thus allow precise synchronization of waveform recorders for accurate location of remote electromagnetic transients, including power system faults and lightning strokes.

In a time-of-arrival (TOA) lightning location network, the time difference between two received signals establishes a hyperbola along which the lightning has occurred. With three received signals, it is usually possible to define a unique stroke location. An LPATS (Lightning Position And Tracking System) technology, using simple electric field antennas, operated with this approach until 1995. At that time, a combined technology, taking advantage of both DF and TOA data, was implemented (Cummins, Murphy et al. 1998).

Limitations of the TOA approach relate mainly to differences in the rate of signal attenuation at low and high frequencies, leading to an increase in signal rise time to peak with distance.

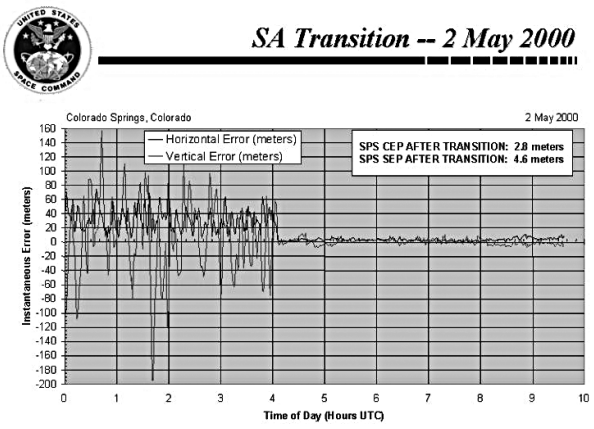


Figure A6.2-1 Reduction of GPS location error after removal of "Selective Availability" degradation on 2 May 2000.

Measuring Lightning Amplitudes

The principles for computing the effective radiated power from a vertical monopole antenna are well established (IEEE 1991). A measurement of signal power at a remote location can be inverted to give the source power. While the Sommerfeld-Norton approach is formulated for sinusoidal waves, it is relatively simple to implement the procedure using a Fourier transform of the lightning current impulse. This gives a lossy-earth correction that can be applied to the basic Equation A6.2-1 above.

Lightning is an impulse with a broad frequency spectrum, but peak features of interest have equivalent frequencies given by:

$$f_{equivalent} = \frac{dI/dt}{2\pi I} \qquad \text{A6.2-2}$$

For first strokes, 24 kA/μs and 31 kA give 120 kHz. For subsequent strokes, 40 kA/μs and 12 kA give 500 kHz. At frequencies below 5 MHz, the ground-wave propagation is most important. The following empirical process implements the ground-wave model in (IEEE 1991), supplemented by (Jordan and Balmain 1968) and (Volland 1968). The process is valid for distances:

- greater than five times the vertical height of the lightning channel
- less than 8000 km/(Hz)$^{1/3}$

Inputs:

ρ = soil resistivity (Ω-m)
ε_r = the relative permittivity of the earth
D = the path length (m)
f = the frequency (Hz)
λ = the free space wavelength = (3 x 10^8 m/s)/f (m)

$$x = \frac{1.8 \cdot 10^{10}}{\rho\, f}$$

$$b = \tan^{-1}\frac{\varepsilon_r + 1}{x} \text{ (Degrees)}$$

$$p = \frac{\pi D}{x\,\lambda}\cos(b)$$

$$A_0 = \frac{2 + 0.3p}{2 + p + 0.6p^2}$$

$$A_1 = 0.0143353\,b - 0.000143317\,b^2 + 5.94888 \cdot 10^{-7}\,b^3$$

$$n = 2.967 - 0.024719\ b + 0.00027614\ b^2 - 1.3469 \cdot 10^{-6}\,b^3$$

$$A_2 = \frac{37}{38 + \left|p - 2\right|^n}$$

$$\begin{cases} p < 1, & A_3 = p^{(0.252 - 0.00151b - 0.1 \cdot \log_{10} p)} \\ p \geq 1, & A_3 = 1 \end{cases}$$

$$A_{total} = A_0(1 - A_1 A_2 A_3)$$

$$F(p) = A_{total} \times \exp\left[j\pi \frac{(1.4 + p)\sqrt{p}}{2.5 + (1 + p)\sqrt{p}} \right]$$

The complex attenuation function *F(p)* is the difference in attenuation of the signal propagation over lossy ground, compared to that of a signal in free space. The function *F(p)* is multiplied by the Fourier transform of the lightning return stroke waveshape, and an inverse Fourier transform gives the distorted waveform. Table A6.2-1 shows the calculated loss of peak signal strength for a 1.2 x 50μs surge waveform.

Table A6.2-1 Signal Attenuation over 500-km Path for 1.2 μs x 50 μs Wave

ρ, Soil Resistivity	ε_r, Relative permittivity	Attenuation
0.2 Ω-m	81	0.999
100 Ω-m	81	0.990
100 Ω-m	10	0.992
1,000 Ω-m	5	0.912
1,000 Ω-m	10	0.911
1,000 Ω-m	20	0.909
10,000 -m	10	0.708

Generally, within the range of validity of the Sommerfeld-Norton approach and for most terrain, the attenuation of signal strength with distance introduces small 10% (or less) corrections into the field-source inversion process. At present, distance normalization to 100 km using an exponent of $D^{-1.12}$ rather than D^{-1} is used to provide attenuation correction for lightning location data in the continental U.S. and Canada (Cummins, Murphy et al. 1998).

Illumination of Nearby Power Lines

The strong electromagnetic field from lightning will induce voltages and currents in nearby horizontal conductors. The electromagnetic field coupling problem from a lightning flash near a conductor can be solved in three equivalent ways, using combinations of the electric and magnetic fields that illuminate the line. Near the lightning flash, these magnetic and electric source terms are not necessarily inter-related by the impedance of free space, 377 Ω. Rachidi (Rachidi 1993) showed the equivalence of these approaches, described generally in Table A6.2-2, and an excellent review of the entire induction process by Nucci and Rachidi is available in (Cooray 2003b, Chapter 8). These models predict that vertical lightning strokes terminating near, but not directly attaching to, overhead power lines and cables can still induce significant voltages and currents.

Table A6.2-2 Models for Traveling Waves on Horizontal Conductor under External Electromagnetic Field Illumination

Model	Basis	Wave Equation 1	Wave Equation 2
Taylor et al. 1965	Total Voltage V(x)	$\frac{dV(x)}{dx} + j\omega LI(x) = -j\omega \int_0^h B_y^i(x,z)dz$	$\frac{dI(x)}{dx} + j\omega CV(x) = -j\omega C \int_0^h E_z^i(x,z)dz$
Agrawal et al. 1980	Scattered Voltage $V_{Sxat}(x) = V(x) + \int_0^h E_z^i(x,z)dz$	$\frac{dV_{sxat}(x)}{dx} + j\omega LI(x) = E_x^i(x,h)$	$\frac{dI(x)}{dx} + j\omega CV_{scat}(x) = 0$
Rachidi 1993	Scattered Current $I_{Sxat}(x) = I(x) - \frac{1}{L}\int_0^h B_y^i(x,z)dz$	$\frac{dV(x)}{dx} + j\omega LI_{scat}(x) = 0$	$\frac{dI_{sxat}(x)}{dx} + j\omega CV(x) = \frac{1}{L}\int_0^h \frac{\partial B_x^i(x,z)}{\partial y}dz$
Rusck 1957	Total Voltage $V_1(x) + V_1(-x)$	See Equation 6.8-3	Assumes $E_x=0$ For perfect ground
Chowdhuri 1989	Total Voltage	$\frac{\partial^2 V(x)}{\partial x^2} - \frac{1}{c}\frac{\partial^2 V(x)}{\partial t^2} = -\frac{1}{c^2}\frac{\partial^2 V_i(x)}{\partial x^2} = F(x,t)$	Refer to Chowdhuri 1989 for V_i and $F(x,z)$

The model of (Agrawal et al. 1980) is formulated in terms of horizontal and vertical electric fields, coupled as source terms to a surge impedance description of a line over ground. The peak vertical electric fields can be obtained from distance-normalized signal strength. The peak horizontal electric field, which is small compared to the vertical field except over lossy ground, must be estimated using a wavetilt formula. This approach is most common in the electric power industry, particularly for evaluation of lightning performance of distribution lines. Generally, induced overvoltages from nearby lightning are roughly unipolar with narrow pulse width, corresponding to the stroke current rise time, and they do not often exceed 300 kV, except over poorly conducting earth (Borghetti et al. 2001). For special cases of tall objects near transmission lines, induced surges can be large, but they would also be bipolar with narrow pulse width corresponding to the height of the conductor above ground. The bipolar surges will not contribute much stress to insulator flashovers.

REFERENCES

Agrawal, A. K., H. J. Price, and S. H. Gurbaxani. 1980. "Transient Response of a Multiconductor Transmission Line Excited by a Nonuniform Electromagnetic Field." *IEEE Transactions on Electromagnetic Compatibility.* Vol. EMC-22. May. Pp. 119–129.

AIEE (American Institute of Electrical Engineering). 1950. "A Method of Estimating Lightning Performance of Transmission Lines." *AIEE Transactions on Power Apparatus and Systems.* Vol. 69. Part III. Pp. 1187-1196. AIEE Committee Report.

Anderson, J. G. 1961. "Monte Carlo Computer Calculation on Transmission Line Lightning Performance." *IEEE Transactions on Power Apparatus and Systems*. Vol. PAS-80. Pp. 414-419.

Anderson, J. G. and R. L. Thompson. 1966. "The Statistical Computation of Line Performance Using METIFOR." *IEEE Trans.* PAS-85. No. 6. Pp. 677-686. June.

Anderson, R. B. 1971. *A Comparison Between Some Lightning Parameters Measured in Switzerland with Those in South Africa.* Pretoria, South Africa: CSIR. Report ELEK 6.

Anderson, R. B. and A. J. Eriksson. 1979. *Lightning Parameters for Engineering Applications.* Pretoria, South Africa: CSIR. June. Report ELEK 170.

Anderson, R. B. and A. J. Eriksson. 1980. "Lightning Parameters for Engineering Application." *Electra.* No. 69. March. Pp. 65-102.

Armstrong, H. R. and E. R. Whitehead. 1968. "Field and Analytical Studies of Transmission Line Shielding." *IEEE Transactions on Power Apparatus and Systems*. Vol. PAS-87. Pp. 270-281.

Baba, Y. and M. Ishii. 1997. "Numerical Electromagnetic Field Analysis of Tower Surge Response." *IEEE Transactions on Power Delivery.* Vol. 12. No. 1. January. Pp. 483-488.

Baba, Y. and M. Ishii. 1999. "Numerical Electromagnetic Field Analysis on Measuring Methods of Tower Surge Impedance." *IEEE Transactions on Power Delivery.* Vol. 14. No. 2. April. Pp. 630–635.

Baba, Y. and M. Ishii. 2000. "Numerical Electromagnetic Field Analysis on Lightning Surge Response of Tower with Shield Wire." *IEEE Transactions on Power Delivery.* Vol. 15. No. 3. July.

Baba, Y. and M. Ishii. 2001. "Numerical Electromagnetic Field Analysis of Lightning Current in Tall Structures." *IEEE Transactions on Power Delivery.* Vol. 16. April. Pp. 324–328.

Baba, Y. and M. Ishii. 2003. "Characteristics of Electromagnetic Return-Stroke Models." *IEEE Transactions on Electromagnetic Compatibility.* Vol. 45. No. 1. Pp. 129-135. February.

Barker, P. P., T. A. Short, A. R. Eybert-Berard, and J. P. Berlandis. 1996. "Induced Voltage Measurements on an Experimental Distribution Line during Nearby Rocket Triggered Lightning Flashes." *IEEE Transactions on Power Delivery.* Vol. 11. No.2. Pp. 980-95. April.

Bellaschi, P. L., R. E. Armington, and A. E. Snowden. 1942. "Impulses and Sixty-Cycle Characteristics of Driven Grounds—I." *AIEE Transactions on Power Apparatus and Systems.* Vol. 61. Pp. 349-363.

Berger, K., R. B. Anderson, and H. Kroninger. 1975. "Parameters of Lightning Flashes." *Electra.* No. 41. July. Pp. 23-37.

Bermudez, J. L., M. Rubinstein, F. Rachidi, F. Heidler, and M. Paolone. 2003. "Determination of Reflection Coefficients at the Top and Bottom of Elevated Strike Objects Struck by Lightning. *Journal of Geophysical Research. Vol. 108*(D14). P. 4413.

Bewley, L. V. 1963. *Traveling Waves on Transmission Systems.* 2nd ed. New York: Dover Publications.

Biegelmeier, G. and W. R. Lee. 1980. "New Considerations on the Threshold of Venticular Fibrillation for AC Shocks at 50-60 Hz." *Proceedings of IEE.* Vol. 127. No.2. Pt. A. March.

Boccippio, D. J., K. L. Cummins, H. J. Christian, and S. J. Goodman. 2001. "Combined Satellite- and Surface-Based Estimation of the Intracloud–Cloud-to-Ground Lightning Ratio over the Continental United States." *Monthly Weather Review.* Vol. 129. January. Pp. 108-121.

Borghetti, A., C. A. Nucci, M. Paolone. 2001. "Lightning Performances of Distribution Lines: Sensitivity to Computational Methods and to Data." Power Engineering Society Winter Meeting. IEEE. Vol. 2. 28 Jan.-1 Feb. 2001. Pp. 796–798.

Boys, C. V. 1926. "Progressive Lightning." *Nature.* Vol. 118. Pp. 749-750.

Brown, G. W. 1978. "Lightning Performance. I—Shielding Failures Simplified." *IEEE Transactions on Power Apparatus and Systems.* Vol. PAS-97. Pp. 33-38.

Brown, G. W. 1978. "Lightning Performance. II—Updating Backflash Calculations." *IEEE Transactions on Power Apparatus and Systems.* Vol. PAS-97. Pp. 39-52.

Brown, G. W. and E. R. Whitehead. 1969. "Field and Analytical Studies of Transmission Line Shielding II."*IEEE Transactions on Power Apparatus and Systems.* Vol. PAS-88. No. 5. Pp. 617-626.

Burke, G. J. and A. J. Poggio. 1980. "*Numerical Electromagnetic Code (NEC)—Method of Moments*." Naval Ocean Systems Center. San Diego, CA. Tech. Doc. 116.

Caldwell, R. O. and M. Darveniza. 1973. "Experimental and Analytical Studies of the Effect of Non-Standard Waveshapes on the Impulse Strength of External Insulation." *IEEE Transactions on Power Apparatus and Systems.* Vol. PAS-92. Pp. 1420-1428.

CCIR 1982. (International Radio Consultative Committee, precursor to ITU-T). Recommendation 832: World Atlas of Ground Conductivities. 48 pp.

Cherchiglia, L. C. L., A. Cazetta, R. J. dos Reis, G. E. S. Amorin. 2002. "CEMIG Experience in Improving Transmission Line Lightning Performance Using a Lightning Location System," Proceedings of CIGRE 2002 Session. Paper 33-207.

Chisholm, W. A., Y. L. Chow, and K. D. Srivastava. 1983. "Lightning Surge Response of Transmission Towers." *IEEE Transactions on Power Apparatus and Systems.* Vol. 102. No. 9. Pp.3232-3242. September.

Chisholm, W. A., Y. L. Chow, and K. D. Srivastava. 1985. "Tower Travel Time." *IEEE Trans Transactions on Power Apparatus and Systems.* Vol. 104. No. 10. October. Pp. 2922-2928.

Chisholm, W. A. and W. Janischewskyj. 1989 "Lightning Surge Response of Ground Electrodes." *IEEE Transactions on Power Apparatus and Systems.* Vol. 4. No. 2. April. Pp. 1329-1337.

Chisholm, W.A. and W. Janischewskyj. 1992. "Lightning Ground Flash Density Measurements in Canada (March 1, 1984 to December 31, 1991)." Final Report for Canadian Electrical Association Contract 179 T 382.

Chisholm, W.A. 2001. "Transmission System Transients – Grounding." Section 10.7 of *The Electric Power Engineering Handbook* (ed. L. L. Grigsby). Boca Raton, FL: CRC Press.

Chow, Y. L. and M. M. Yovanovic. 1982. "The Shape Factor of the Capacitance of a Conductor." *Journal of Applied Physics.* Vol. 52. December.

Chowdhuri, P. 1989. "Analysis of Lightning-induced Voltages on Overhead Lines." Including six discussions. *IEEE Transactions on Power Delivery.* Vol. 4. No.1. Pp. 479-492.

Chowdhuri, P. (ed.). 2001. "Bibliography of Research on Parameters of Lightning Strokes." Web page at www.ieee.org/pes-lightning.

Christian, H. J., R. J. Blakeslee, D. J. Boccippio, W. L. Boeck, D. E. Buechler, K. T. Driscoll, S. J. Goodman, J. M. Hall, W. J. Koshak, D. M. Mach, and M. F. Stewart. 2003. "Global Frequency and Distribution of Lightning as Observed from Space by the Optical Transient Detector." *Journal of Geophysical Research.* Vol. 108. No. D1. p. 4005.

Cianos, N. and E. T. Pierce. 1972. *A Ground Lightning Environment for Engineering Usage.* Menlo Park, CA: Stanford Research Institute. August. SRI Project 1834. Technical Report No. 1.

CIGRE. 1991. Working Group 01 (Lightning) of Study Committee 33 (Overvoltages and Insulation Co-ordination). "Guide to Procedures for Estimating the Lightning Performance of Transmission Lines." Brochure #63. Paris: CIGRE. October.

Cobine, J. D. 1958. *Gaseous Conductors: Theory and Engineering Applications.* Dover Publications, New York.

Colebrook, F. M. 1940. "The Electric and Magnetic Fields of a Linear Radiator Carrying a Progressive Wave." *Journal I.E.E.* Pp. 169-178.

Cooray, V. 2003a. "On the Concepts Used in Return Stroke Models Applied in Engineering Practice." *IEEE Transactions on Electromagnetic Compatibility.* Vol. 45. No.1. February. Pp.101-108.

Cooray, V. 2003b. *The Lightning Flash, IEE Power & Energy Series 34*. (London: IEE).

Cummins, K. L., E. P. Krider, and M. D. Malone. 1998. "The U.S. National Lightning Detection Network™ and Applications of Cloud-to-Ground Lightning Data by Electric Power Utilities." *IEEE Transactions on Electromagnetic Compatibility.* Vol. 40. No. 4. November. Pp. 465-480.

Cummins, K. L., M. J. Murphy, E. A. Bardo, W. L. Hiscox, R. B. Pyle, and A. E. Pifer. 1998. "A Combined TOA/MDF Technology Upgrade of the US National Lightning Detection Network." *Journal of Geophysical Research*. Vol. 103. No. D8. April. Pp.9035-9044.

Dalziel, C. F. and W. R. Lee. 1968. "Reevaluation of Lethal Electric Currents." *IEEE Transactions.* Vol. IGA-4. No.5. September/October. Pp. 467-476.

Darveniza, M., F. Popolansky, and E. R. Whitehead. 1975. "Lightning Protection of UHV Transmission Lines." *Electra.* No. 41. July. Pp. 39-69.

Darveniza, M. et al. 1979. "Modelling for Lightning Performance Calculations." *IEEE Transactions on Power Apparatus and Systems.* Vol. PAS-98. Pp. 1900-1908.

Davis, R. and R. W. E. Cook. 1960. The Surge Corona Discharge. IEEE Proceedings. Part C. Monograph No. 4155.

Dawalibi, F. 1982. "Transmission Line Grounding (2 Vol)". Final Report EL-2699 for EPRI Research Project 1494-1. October.

Dellera, L. and E. Garbagnati. 1990. "Lightning Stroke Simulation by Means of the Leader Progression Model." *IEEE Transactions on Power Delivery.* Vol. 5. No. 4. Pp. 2009–2029.

Diendorfer, G., W. Hadrian, F. Hofbauer, M. Mair, and W. Schultz. 2002. "Evaluation of Lightning Location Data Employing Measurements of Direct Strikes to a Radio Tower." *CIGRE Session 2002 Proceedings.* Paris, France. Paper 33-206.

Dommel, H.W. 1969. "Digital Computer Solution of Electromagnetic Transients in Single and Multiphase Networks." *IEEE Transactions on Power Apparatus and Systems.* Vol. PAS-88. April. Pp. 388-399.

Dwight, H. B. 1936. "Calculation of Resistances to Ground." *Electrical Engineering.* Vol. 55. Pp. 1319-1328.

EPRI. 1975. *Transmission Line Reference Book—345 kV and Above.* Palo Alto, CA: Electric Power Research Institute.

EPRI. 1982. *Transmission Line Reference Book—345 kV and Above.* Second Edition. Palo Alto, CA: Electric Power Research Institute.

EPRI. 2002a. *High Current Impulse Testing of Full-Scale Ground Electrodes.* Report no. 1006866.

EPRI. 2002b. *Tower Grounding and Soil Ionization*. Report no. 1001908. Palo Alto, CA.

Eriksson, A. J. 1987. "The Incidence of Lightning Strikes to Power Lines." *IEEE Transactions on Power Delivery.* Vol. 2. No. 3. Pp. 859-870.

Eriksson, A. J., M. F. Stringfellow, and D. V. Meal. 1982. "Lightning-induced Overvoltages on Overhead Distributions Lines." *IEEE Transactions on Power Apparatus and Systems.* Vol.-PAS 101. No 4. Pp. 960-966.

Feizhou, Z. and L. Shanghe. 2002. "A New Function to Represent the Lightning Return-Stroke Current." *IEEE Trans EMC.* Vol. 44. No. 4. November. Pp. 595-596.

Fink, D. B. and H. W. Beaty. 1999. *Standard Handbook for Electrical Engineers.* 14th ed. New York: McGraw-Hill.

Finke, U. and O. Kreyer. 2002. "Detect and Locate Lightning Events from Geostationary Satellite Observations, Report Part I: Review of Existing Lightning Location Systems." Hannover: Institute für Meteorologie und Klimatologie EUM/CO/02/1016/SAT.

Fisher, F. A., J. G. Anderson, and J. H. Hagenguth. 1960. "Determination of Transmission Line Lightning Performance by Means of Geometrical Models." *IEEE Transactions on Power Apparatus and Systems.* Vol. PAS-78. Pp. 1725-1736.

Fisher, R. J., G. H. Schnetzer, R. Thottappillil, V. Rakov, M. A. Uman, and J. D. Goldberg. 1993. "Parameters of Triggered Lightning Flashes in Florida and Alabama." *Journal of Geophysical Research.* Vol. 98. No. 22. Pp 887-902.

Gary, C., D. Critescu, and G. Dragan. 1989. "Distortion and Attenuation of Travelling Waves Caused by Transient Corona." CIGRE Study Committee 33 Technical Brochure.

Ghannoum, E. and S. J. Yaacoub. 1989. "Optimization of Transmission Towers and Foundations Based on Their Minimum Cost." *IEEE Transactions on Power Delivery.* Vol. 4. No. 1. January. Pp. 614 –620.

Gilman, D.W., and Whitehead, E. R. 1973. "The Mechanism of Lightning Flashovers on High-Voltage and Extra-High-Voltage Transmission Lines." *Electra.* No. 27. Pp. 65-96.

Golde, R. H. 1977. *Lightning, Vol. 1: Physics of Lightning.* New York, NY: Academic Press.

Gorin, B. N. 1985. "Mathematical Modeling of the Lightning Return Stroke." *Elektrichestvo.* Vol. 4. Pp. 10-16.

Gorin, B. N., V. I. Levitov, and A.V. Shkilev. 1977. "Lightning Strikes to the Ostankino TV Tower." *Elektrichestvo.* Vol. 8. Pp. 19-23.

Gorin, B. N. and A. V. Shkilev. 1984. Measurements of Lightning Currents at the Ostankino Tower." *Elektrichestvo*. Vol. 8. Pp. 64-65.

Grigsby, L. 2000. *The Electric Power Engineering Handbook.* Boca Raton, FL: CRC Press. September.

Hagenguth, J. H. and J. G. Anderson. 1952. "Lightning to the Empire State Building— Part III." *AIEE Transactions.* Vol. 71. Part III. August. Pp. 641-649.

Harrington, R. F. 1968. (Reprinted 1993). *Field Computation by Moment Methods.* New York: Wiley/IEEE Press.

Hasse, P. 2000. *Overvoltage Protection of Low-Voltage Systems*. Revised edition. (London: IEE).

Heidler, F., J. M. Cvetic, and B.V. Stantic. 1999. "Calculation of Lightning Current Parameters." *IEEE Transactions on Power Delivery.* Vol. 14. April. Pp. 399-404.

Herodotou, N., W. A. Chisholm, and W. Janischewskyj. 1993. "Distribution of Lightning Peak Stroke Currents in Ontario Using an LLP System." *IEEE Transactions on Power Delivery.* Vol. 8. pp. 1331-1339.

Hileman, A. R. 1999. *Insulation Coordination for Power Systems*. New York: Marcel Decker.

Horváth, T. 1962. "The Probability Theory of Lightning Protection." *Elektrotechnika.* Vol. 55. Pp. 49-61.

Idone, V., A. B. Saljoughy, R. W. Henderson, P. K. Moore, and R. B. Pyle. 1993. "A Reexamination of the Peak Current Calibration of the National Lightning Detection Network". *Journal of Geophysical Research*. Vol. 98. Pp. 18323-18332.

IEEE. 1983. IEEE Standard 81. *Guide for Measuring Earth Resistivity, Ground Impedance, and Earth Surface Potentials of a Ground System.* New York, NY: IEEE.

IEEE. 1985. Working Group (J. G. Anderson, W. A. Chisholm, I. S. Grant, A. R. Hileman, W. Janischewskyj, G. E. Lee, V. G. Longo, D. Parrish, N. Roukos, E. Whitehead, and J. T. Whitehead). "A Simplified Method for Estimating Lightning Performance on Transmission Lines." *IEEE Trans. PAS.* Vol. 104. No. 4. April. Pp. 919-927.

IEEE. 1991. Standard 291. IEEE Standard on Field Strength of Sinusoidal Continuous Waves, 30 Hz to 30 GHz.

IEEE. 1993. Working Group (J. G. Anderson, W. A. Chisholm, I. S. Grant, A. R. Hileman, W. Janischewskyj, G. E. Lee, V. G. Longo, D. Parrish, N. Roukos, E. Whitehead, and J. T. Whitehead). "Estimating Lightning Performance of Transmission Lines II—Updates to Analytical Models." *IEEE Transactions on Power Delivery*, Vol. 8. No. 3. July. Pp. 1254–1267.

IEEE. 1996a. Fast Front Transients Task Force. "Modeling Guidelines for Fast Front Transients." *IEEE Transactions on Power Delivery.* Vol.11. No.1. Pp 493-506. January.

IEEE. 1996b. IEEE Standard 998. IEEE Substations Working Group. *IEEE Guide for Direct Lightning Stroke Shielding of Substations.* Piscataway, N. J.: IEEE.

IEEE. 1997a. IEEE Standard 493. *IEEE Recommended Practice for the Design of Reliable Industrial and Commercial Power Systems* (IEEE Gold Book). Piscataway, N.J.: IEEE. Table 2.5.

IEEE. 1997b. IEEE Standard 1243. IEEE Working Group on Estimating the Lightning Performance of Transmission Lines. *IEEE Design Guide for Improving the Lightning Performance of Transmission Lines.* Chisholm, W. A. (ed.). Piscataway, N.J.: IEEE.

IEEE 1997c. IEEE Standard 1410. IEEE Working Group on Estimating the Lightning Performance of Distribution Lines. *IEEE Design Guide for Improving the Lightning Performance of Electric Power Overhead Distribution Lines*. Short, T. A. (ed.). Piscataway, N.J.: IEEE

IEEE. 2000a. IEEE Standard 80. IEEE Working Group D7, Substation Grounding Safety. *Guide for Safety in AC Substations*. Keil, R. P. (ed.). Piscataway: IEEE

IEEE. 2000b. IEEE Standard 4. *IEEE Guide for High Voltage Testing.* Piscataway, N.J.: IEEE.

Inoue, A. 1978. "High Voltage Traveling Waves with Corona Discharge on Bundled Conductors." IEEE Paper A78–170-3.

Ishii, M. and Y. Baba. 2000. "Advanced Computational Methods in Lightning Performance. The Numerical Electromagnetics Code (NEC-2)." Power Engineering Society Winter Meeting. IEEE. Vol. 4. Pp. 2419-2424.

Ishii, M., T. Shindo, T. Aoyama, N. Honma, S. Okabe, and M. Shimizu. 2002. "Lightning Location Systems in Japan and Their Applications to Improvement of Lightning Performance of Transmission Lines." CIGRE Session 2002. Paper 33-201.

Janischewskyj, W., W. A. Chisholm, and J. Beattie. 1997a. "Lightning Ground Flash Density Measurements in Canada (January 1, 1990 To December 31, 1996)." Final Report for Canadian Electrical Association contract 179 T 382A.

Janischewskyj, W., A. M. Hussein, V. Shostak, I. Rusan, L-Z. Li, and J. S. Chang. 1997b. "Statistics of Lightning Strokes to the Toronto Canadian National Tower (1978-1995)." *IEEE Transactions on Power Delivery.* Vol. 12. No. 3. Pp. 1210-1221. July.

Jordan, C. A. 1934. "Lightning Computation for Transmission Lines with Groundwires". *General Electric Review.* Vol. 37.

Jordan, E. C. and K. G. Balmain. 1968. *Electromagnetic Waves and Radiating Systems.* 2nd ed. Englewood Cliffs, N. J.: Prentice-Hall.

Kawai, M. 1964. "Studies of the Surge Response on a Transmission Line Tower." *Transactions on Power Apparatus and Systems.* Vol. PAS-83. Part III. Pp. 30-34. January.

Kitigawa, N., M. Brook, and E. J. Wortman. 1962. "Continuing Currents in Cloud-to-Ground Lightning Discharges." *Journal of Geophysical Research*. Vol. 67. Pp 637-647.

Korsuncev, A. V. 1958. "Application on the Theory of Similarity to Calculation of Impulse Characteristics of Concentrated Electrodes." *Elektrichestvo*. No. 5. Pp.31-35.

Kraus, J. D. 1988. *Antennas.* 2nd Edition. New York: McGraw Hill.

Kraus, J. D. and D. A. Fleish. 1999. *Electromagnetics.* New York: WCB/McGraw-Hill.

Krider, E. P., R. C. Noggle, and M. A. Uman. 1976. "A Gated Wideband Magnetic Direction Finder for Lightning Return Strokes." *Journal of Applied Meteorology.* Vol. 15. No. 301.

Lee, R. H. 1978. "Protection Zone for Buildings against Lightning Strokes using Transmission Line Protection Practice." *IEEE Transactions on Industrial Applications.* Vol. 14. Pp. 465-470.

Leteinturier, C., C. Weidman, and J. Hamelin. 1990. "Current and Electric Field Derivatives in Triggered Lightning Return Strokes." *Journal of Geophysical Research*. Vol. 95. January. Pp. 811-828.

Levine, D. M. and R. Meneghini. 1978. "Simulation of Radiation from Lightning Return Strokes: The Effects of Tortuosity." *Radio Science*. Vol. 13. No. 5. Pp. 801-809.

Lewis, W. W. 1959. *Protection of Transmission Systems Against Lightning.* New York: John Wiley & Sons.

Liew, A. and M. Darveniza. 1974. "Dynamic Model of Impulse Characteristics of Concentrated Earths." *Proceedings IEE.* Vol. 121. No. 2. February. Pp. 123-135.

Los, E. J. 1980. "Transmission Line Lightning Design with Surge Suppressors at Towers." *IEEE Transactions on Power Apparatus and Systems.* Vol. PAS-99. No. 2. Pp. 720-728.

Love, R. R. 1973. "Improvements on Lightning Stroke Modelling and Applications to the Design of EHV and UHV Transmission Line." M. Sc. Thesis. University of Colorado.

Lundholm, R., R. B. Finn, and W. S. Price. 1957. "Calculation of Transmission Line Lightning Voltages by Field Concepts." *AIEE Transactions on Power Apparatus and Systems.* Vol. 76. Part III. Pp. 1271-1283.

MacGorman, D. R., M. W. Maier, and W. D. Rust. 1984. "Lightning Strike Density for the Contiguous United States from Thunderstorm Duration Records." Report to U.S. Nuclear Regulatory Commission. # NUREG/CR-3759

Mackerras, D., M. Darveniza, R. E. Orville, E. R. Williams, and S. J. Goodman. 1998. "Global Lightning: Total, Cloud and Ground Flash Estimates." *Journal of Geophysical Research.* No. 103. pp. 19791–19809.

Marcuvitz, N. 1986. *Waveguide Handbook (IEE Electromagnetic Waves Series, No. 21).* London: IEE

Martinez, J. and F. Castro-Aranda. 2003."Lightning Performance Analysis of Transmission Lines Using the EMTP." IEEE Power Engineering Society General Meeting. Vol. 1. Pp. 295-300. 13-17 July.

Maruvada, P. S., H. Menemenlis, and R. Malewski. 1977. "Corona Characteristics of Conductor Bundles Under Impulse Voltages." *IEEE Transactions on Power Apparatus and Systems.* Vol. PAS-96. No. 1. Pp. 102-115.

Mazur, V. and L. Ruhnke. 2001. "Evaluation of Lightning Protection System at the WSR-88D Radar Sites." *NOAA Final Report.* May.

McAuley, P. H. 1938. "Flashover Characteristics of Insulation." *Electric Journal*. July.

McCann, G. D. 1943. "The Effect of Corona on Coupling Factors Between Ground Wires and Phase Conductors." *AIEE Transactions on Power Apparatus and Systems.* Vol. 62. Pp. 818-826.

McCann, G. D. 1944. "The Measurement of Lightning Currents in Direct Strokes." *AIEE Transactions*. Vol. 63. Pp. 1157-1164.

McComb, T., E. A. Cherney, H. Linck, and W. Janischewskyj. 1980. "Preliminary Measurements of Lightning Flashes to the CN Tower in Toronto, Canada." *Canadian Electrical Engineering Journal.* Vol. 5. Pp. 3-9.

McEachron, K. B. 1939. "Lightning to the Empire State Building." *Journal of the Franklin Institute.* Vol. 227. Pp.149-217.

Mitchell, A. R. and D. F. Griffiths. 1980. *The Finite Difference Method in Partial Differential Equations.* Chichester: John Wiley & Sons.

Moini, R., B. Kordi, G. Z. Rafi, and V.A. Rakov. 2000. "A New Lightning Return Stroke Model Based on Antenna Theory." *Journal of Geophysical Research.* Vol. 105. No. 29. Pp. 693-702.

Morita, K., Y. Suzuki, and H. Nozaki. 1997. "Study on Electrical Strength of Suspension Insulators in Steep Impulse Voltage Range." *IEEE Trans. PWRD.* Vol.12. No.2. April.

Motoyama, H. 1996. "Experimental Study and Analysis of Breakdown Characteristics of Long Air Gaps with Short Tail Lightning Impulse." *IEEE Transactions on Power Delivery.* Vol. 11. No. 2. April. Pp 972 – 979.

Motoyama, H. and H. Matsubara. 2000. "Analytical and Experimental Study on Surge Response of Transmission Tower." *IEEE Transactions on Power Delivery.* Vol. 15. No. 2. April. Pp. 812–819.

Mousa, A. M. and K. D. Srivastava. 1989. "The Implications of the Electrogeometric Model regarding Effect of Height of Structure on the Median Amplitude of Collected Lightning Strokes."*IEEE Transactions on Power Delivery.* Vol. 4. No. 2. April. Pp. 1450-1460.

Mousa, A. M. 1994. "The Soil Ionization Gradient Associated with Discharge of High Currents into Concentrated Electrodes." *IEEE Transactions on Power Delivery.* Vol. 9. No. 2. July. Pp. 1669-1677.

Mozumi, T., Y. Baba, M. Ishii, N. Nagaoka, and A. Ametani. 2003. "Numerical Electromagnetic Field Analysis of Archorn Voltages during a Back-flashover on a 500-kV Twin-Circuit Line." *IEEE Transactions on Power Delivery***.** Vol. 18. No. 1. Pp.207-213. January.

Naccarato, K. P., O. Pinto Jr., and I. Pinto. 2003. "Influence of the Sensor Network on the Geographical Distribution of the Cloud-to-Ground Strokes Reported by a Lightning Location System." *Proceedings of VII SIPDA*. Curitiba, Brazil. Pp. 17-22.

Narita, T., T. Yamada, A. Mochizuki, E. Zaima, and M. Ishii. 2000. "Observation of Current Waveshapes of Lightning Strokes on Transmission Towers." *IEEE Transactions on Power Delivery.* Vol. 15. No. 1. January. Pp. 429–435.

Newi, G. 1968. "A High-Impedance Nanosecond Rise Time Probe for Measuring High-Voltage Impulses." *Transactions of IEEE (PAS)*. Vol. 87. No. 9. September.

NFPA. 2004. *Installation of Lightning Protection Systems.* NFPA 780-2004. National Fire Protection Association.

Noda, T, T. Ono, H. Matsubara, H. Motoyama, S. Sekioka, and A. Ametani. 2003. "Charge-Voltage Curves of Surge Corona on Transmission Lines: Two Measurement Methods." *IEEE Trans. PWRD.* Vol. 18. No. 1. January.

Norton, K. A. 1937. "The Propagation of Radio Waves over the Surface of the Earth and in the Upper Atmosphere." *Proceedings of the IRE.* Vol. 25. Pp. 1203-1236.

Norton, K. A. 1941. "The Calculation of Ground-Wave Field Intensity Over a Finitely Conducting Spherical Earth." *Proceedings of the IRE.* Vol. 29. No. 12. Pp. 623-639.

Nucci, C. A., C. Mazzetti, F. Rachidi, and M. Ianoz. 1988. "On Lightning Return Stroke Models for LEMP Calculations." *Proceedings of the 19th International Conference on Lightning Protection.* Graz, Austria. Pp. 463-469.

Nucci, C. A., G. Diendorfer, M. A. Uman, F. Rachidi, M. Ianoz, and C. Mazzetti. 1990. "Lightning Return Stroke Current Models with Specified Channel Base Current: A Review and Comparison." *Journal of Geophysical Research.* Vol. 95. No. 20. Pp. 395-408.

Nucci, C. A., F. Rachidi, M. Ianoz, and C. Mazzetti. 1993. "Lightning Induced Voltages on Overhead Lines." *IEEE Transactions on Electromagnetic Compatibility.* Vol. 35. No. 1. February. Pp. 75-86.

Nucci, C.A., 1995a. Cigré Working Group 33.01 (Lightning). "Lightning-Induced Voltages on Overhead Power Lines, Part I: Return-Stroke Current Models with Specified Channel-Base Current for the Evaluation of the Return-Stroke Electromagnetic Fields." *Electra*. No.161. August. Pp. 75–102.

Nucci, C.A. 1995b. Cigré Working Group 33.01 (Lightning). "Lightning-Induced Voltages on Overhead Power Lines, Part II: Coupling Models for the Evaluation of the Induced Voltages." *Electra.* No. 162. October. Pp.121–145.

Oettle, E. E. 1988. "A New General Estimating Curve for Predicting the Impulse Impedance of Concentrated Earth Electrodes." *IEEE Transactions on Power Delivery.* Vol. 3. No. 4. Pp. 2020-2029.

Orville, R. E. and G. R. Huffines. 2001. "Cloud-to-Ground Lightning in the United States: NLDN Results in the First Decade, 1989–98." *AMS Monthly Weather Review.* Vol. 129. May. Pp. 1179-1193.

Orville, R. E., G. R. Huffines, W. R. Burrows, R. L. Holle, and K. L. Cummins, 2002. "The North American Lightning Detection Network (NALDN) - First Results: 1998-2000." *Monthly Weather Review.* No. 130. Vol. 8. Pp. 2098-2109.

Paris, L. and R. Cortina. 1968. "Switching and Lightning Impulse Discharge Characteristics of Large Air Gaps and Long Insulator Strings." *IEEE Transactions on Power Apparatus and Systems.* Vol. PAS-87. Pp. 947-957.

Pearson, A. V. and H. O. Hartley. 1972. *Biometrica Tables for Statisticians.* Vol. 2. Cambridge, England: Cambridge University Press.

Pigini, A., et. al. 1985. "Influence of Air Density on the Impulse Strength of External Insulation." *IEEE Transactions on Power Apparatus and Systems.* Vol. 104. Pp. 2888–2900.

Pigini, A., G. Rizzi, E. Garbagnati, A. Porrino, G. Baldo, and G. Pesavento. 1989. "Performance of Large Air Gaps under Lightning Overvoltages: Experimental Study and Analysis of Accuracy of Predetermination Methods." *IEEE Transactions on Power Delivery.* Vol. 4. No. 2. April. Pp. 1379-1392.

Popolansky, F. 1970. *Measurement of Lightning Currents in Czechoslovakia and the Application of Obtained Parameters in the Prediction of Lightning Outages of EHV Transmission Lines.* Paris, France. CIGRE. Report 33-03. Vol. 2.

Popolansky, F. 1972. "Frequency Distribution of Amplitudes of Lightning Currents." *Electra.* No. 22. Pp. 139-147.

Prentice, S. A. 1977. "Frequency of Lightning Discharges." *Lightning.* Vol. 1. Edited by R. H. Golde. New York: Academic Press. Pp. 465-496.

Prentice, S. A. and D. Mackerras. 1977. "The Ratio of Cloud to Cloud-Ground Lightning Flashes in Thunderstorms." *Journal of Applied of Meteorology.* Vol.16. Pp. 545-549.

Rachidi, F. 1993. "Formulation of the Field-to-Transmission Line Coupling Equations in Terms of Magnetic Excitation Fields." *IEEE Transactions on Electromagnetic Compatibility.* Vol. EMC-35. No. 3. Pp. 404-407. August.

Rachidi, F., W. Janischewskyj, A. M. Hussein, C. A. Nucci, S. Guerrieri, B. Kordi, and J.-S. Chang. 2001. "Current and Electromagnetic Field Associated with Lightning—Return Strokes to Tall Towers." *IEEE Transactions on Electromagnetic Compatibility.* Vol. 43. No. 3. August.

Rakov, V. A. and A. A. Dulzon. 1987. "Calculated Electromagnetic Fields of Lightning Return Stroke." *Tekh. Elektrodinam*. Vol. 1. Pp. 87-89.

Rakov, V. A. and A. A. Dulzon. 1991. *9th International Symposium on EMC.* Zurich, Switzerland. 44H1. Vol. 229.

Rakov, V. A. and M. A. Uman 1990. "Some Properties of Negative Cloud-to-Ground Lightning Flashes versus Stroke Order." *Journal of Geophysical Research.* Vol. 95. Pp. 5447-5553.

Rakov, V. A. and M. A. Uman. 1998."Review and Evaluation of Lightning Return Stroke Models Including Some Aspects of Their Application." *IEEE Transactions on Electromagnetic Compatibility.* Vol. 40. Pp. 403-426. November.

Rakov, V. A. and M. A. Uman. 2003. *Lightning: Physics and Effects.* Cambridge, England: Cambridge University Press.

Reilly, J. P. 1998**.** *Applied Bioelectricity: From Electrical Stimulation to Electropathology.* New York: Springer Verlag.

Les Renardieres Group. 1977. "Positive Discharges in Long Air Gaps at Les Renardieres: 1975 Results and Conclusions." *Electra.* No. 53.

Les Renardieres Group. 1981. "Negative Discharges in Long Air Gaps at Les Renardieres: 1978 Results." *Electra.* No. 74. January.

Richmond, J. H. 1974. *Computer Program for Thin-Wire Structures in a Homogeneous Conducting Medium.* NASA Report CR-2399. National Technical Information Service. Springfield, VA.

Richmond, J. H. 1992. "Radiation and Scattering by Thin-Wire Structures in the Complex Frequency Domain." *Computational Electromagnetics.* Edited by E. K. Miller. New York: IEEE Press.

Rizk, F. A. M. 1989. "Switching Impulse Strength of Air Insulation: Leader Inception Criterion." *IEEE Transactions on Power Delivery.* Vol. 4. No. 4. Pp. 2187–2195.

Rizk, F. A. M. 1990. "Modeling of Transmission Line Exposure to Direct Lightning Strokes." *IEEE Transactions on Power Delivery.* Vol. 5. Pp. 1983-1997. October.

Rizk, F. A. M. 1994. "Modelling of Lightning Incidence to Tall Structures." Part I: Theory and Part II: Application. *IEEE Transactions on Power Delivery.* Vol. 9. No. 1. January. Pp. 162-193.

Rubenstein, M. A., T. Tzeng, M. A. Uman, P. J. Medelius, E. M. Thompson, and E. M. 1989. "An Experimental Test of a Theory of Lightning Induced Voltages on an Overhead Wire." *IEEE Transactions on Electromagnetic Compatibility.* Vol. 31. No. 4. November. Pp. 376-383.

Rudenberg, R. 1945. "Grounding Principles and Practice. I—Fundamental Considerations on Ground Currents." *Electrical Engineering.* Vol. 64. January. Pp. 1-13.

Rusck, S. 1958. "Induced Lightning Over-Voltage on Power Transmission Lines with Special Reference to the Overvoltage Protection of Low-Voltage Networks." *Transactions of the Royal Institute of Technology.* No.120.

Sargent, M. A. and M. Darveniza. 1967. "The Calculation of Double Circuit Outage Rates of Transmission Lines." *IEEE Trans.* PAS-86. No. 6. Pp. 665-678. June.

Sargent, M. A. and M. Darveniza. 1969. "Tower Surge Impedance." *IEEE Transactions on Power Apparatus and Systems.* Vol. PAS-88. Pp. 680-687. May.

Schelkunoff, S. A. and H. T. Friis. 1952. *Antennas Theory and Practice.* New York: John Wiley & Sons.

Schonland, B. F. J. 1956. *The Lightning Discharge.* Handbook of Physics. Vol. 22. Pp. 576-628.

Schlonland, B. F. J. 1964. *The Flight of Thunderbolts.* Oxford: Clarendon Press.

Schnetzer, G. H., J. Chael, R. Davis, R. J. Fisher, and P. J. Magnotti. 1994. "Triggered Lightning Test Program: Measured Responses of a Reinforced Concrete Building Under Direct Lightning Attachments." Technical Report SAND95-1551. Vols. 1 and 2. For U.S. DOE Contract AC04-94AL85000. Sandia National Laboratories. August. Available online at www.osti.gov.

Schnetzer, G. H., R. J. Fisher, and P. J. Magnotti. 1995. "Triggered Lightning Program: Temporary Lightning Protection Experiments, Direct Strike MILVAN and Concrete Building Test." Report 96-01, U. S. Army Armament Research, Development and Engineering Center, March.

Sommerfeld, A. 1909. "Propagation of Waves in Wireless Telegraphy." *Ann D. Phys.* Vol. 28. Pp. 665-736. March.

Sommerfeld, A. and F. Renner. 1942. Strahlungsenergie und Erdabsorption bei Dipolantennen. *Ann. Physik.* Vol. 41. Part 1.

Suliciu, M. M. and I. Suliciu. 1981. "A Rate Type Constitutive Equation for the Description of the Corona Effect." *IEEE Transactions on Power Apparatus and Systems.* Vol. PAS-100. No. 8. Pp. 3681-3685. August.

Sunde, E. O. 1949. *Earth Conductor Effects in Transmission Systems.* New York: Van Nostrand.

Szpor, S. et al. 1974. *Lightning Current Records on Industrial Chimneys in Poland.* Paris, France: CIGRE. Paper 33-10.

Taylor, C. D., R. S. Satterwhite, and W. Harrison, Jr. 1965. "The Response of a Terminated Two-Wire Transmission Line Excited by a Nonuniform Electromagnetic Field." *IEEE Transactions on Antennas and Propagation.* Vol. AP-13. No. 6. Pp. 987-989. November.

Thompson, E. M., M. A. Galib, M. A. Uman, W. H. Beasley, and M. J. Master. 1984. "Some Features of Stroke Occurrence in Florida Lightning Flashes." *Journal of Geophysical Research.* Vol. 89. Pp. 4910-4916.

Torres, H., M. Vargas, J. Herrera, E. Pérez, C. Younes, L. Gallego, and J. Montaña. 2002. "Comparative Study of Two Methodologies for Evaluating the Lightning Performance of Transmission Lines Applied in Tropical Zone." International Conference on Lightning Protection (ICLP). Krakow, Poland. September.

Udo, T. 2004. "Multiline Simultaneous Faults on Transmission Lines due to Winter Lightning." *IEEE Transactions on Power Delivery.* Vol. 19. No. 1. January. Pp. 248-254.

Uman, M.A. 1987. *The Lightning Flash*. San Diego: Academia Press.

Uman, M. A. and D. K. McLain. 1969. "Magnetic Field of Lightning Return Stroke." *Journal of Geophysical Research.* Vol. 74. Pp. 6899–6910.

Uman, M. A. et al. 1973. "Currents in Florida Lightning Return Strokes." *Journal of Geophysical Research.* Vol. 78. Pp. 3530-3537.

Uman, M. A., D. K. McLain, and E. P. Krider. 1975. "The Electromagnetic Radiation from a Finite Antenna." *American Journal of Physics.* Vol. 43. Pp. 33-38.

Uman, M. A. and E. P. Krider. 1989. "Natural and Artificially Initiated Lightning." *Science.* Vol. 246. October. Pp. 457-464.

Uman, M. A. and V. Rakov. 2002. "A Critical Review of Nonconventional Approaches to Lightning Protection." *American Meteorological Society.* Pp.1809-1820.

van Blaricum, M. and E. K. Miller. 1972. *TWTD–A Computer Program for Time-Domain Analysis for Thin-Wire Structures.* Lawrence Livermore National Laboratory. Report UCRL-51277.

Visacro, S., A. Soares Jr., M. A. O. Schroeder, L.C. L. Cherchiglia, and V. J. de Sousa. 2004. "Statistical Analysis of Lightning Current Parameters: Measurements at Morro do Cachimbo Station." *Journal of Geophysical Research.* Vol. 109. D01105.

Volland, H. 1968. *Propagation of Long Waves.* Germany: F. Veiweg & Son.

Wagner, C. F. 1964. "Application of Predischarge Currents of Parallel Electrode Gaps." *IEEE Transactions on Power Apparatus and Systems.* Vol. PAS-83. Pp. 931-944.

Wagner, C. F. and A. R. Hileman. 1960. "A New Approach to the Calculation of the Lightning Performance of Transmission Line. III—A Simplified Method: Stroke to Tower." *AIEE Transactions on Power Apparatus and Systems.* PAS-Vol. 79. Part III. Pp. 589-603. October.

Wagner, C. F. and A. R. Hileman. 1964. "Predischarge Current Characteristics of Parallel Electrodes." *IEEE Transactions on Power Apparatus and Systems.* Vol. PAS-66. Pp. 1236-1242.

Weck, K. H. and A. R. Hileman. 1978. *Application of Lightning Parameters—Lightning Current Shape and Amplitudes of Multiple Strokes.* CIGRE WG 33-01. Document 33-78.

Weidman, C. D. and E. P. Krider. 1978. "The Fine Structure of Lightning Return Stroke Wave Forms." *Journal of Geophysical Research.* Vol. 83. Pp. 6239-6247

Weidman, C. D. and E. P. Krider. 1980. "Submicrosecond Risetimes in Lightning Return-Stroke Fields." *Geophysical Research Letters*. Vol. 7. No. 11. Pp. 955-958. November. Correction: *Journal of Geophysical Research.* Vol. 87. p.7351.

Whitehead, E. R. 1971. *Final Report of Edison Electric Institute: Mechanism of Lightning Flashover Research Project.* EEI Project RP50. Publication 72-900. February.

Whitehead, E. R. 1977. "Protection of Transmission Lines." *Lightning.* Vol. 2. Edited by R. H. Golde. New York: Academic Press. Pp. 697-745.

Whitehead, J. T. 1983. "Lightning Performance of TVA's 161-kV and 500-kV Transmission Lines." *IEEE Trans. PAS.* Vol. 102. No. 3. March. Pp. 752-768.

Whitehead, J. T. and R. Driggans. 1983. "TVA's Experience with the SUNYA Lightning Detection Network". *IEEE Transactions on Power Delivery.* Vol. 5. No. 4. October. Pp. 2054-2062.

Willett, J. C., J. C. Bailey, V. P. Idone, A. Eybert-Berard, and L. Barret. 1989. "Submicrosecond Intercomparison of Radiation Fields and Currents in Triggered Lightning Return Strokes Based on the Transmission-Line Model." *Journal of Geophysical Research*. Vol. 94. No. D11. Pp. 13275-13286. September.

Witzke, R. L. and T. J. Bliss. 1950. "Coordination of Arrester Location with Transformer Insulation Level." *AIEE Transactions.* Vol. 69. Pp. 964-975.

WMO (World Meteorological Organization). 1953. "World Distribution of Thunderstorm Days." WMO No. 21, Part 2. Geneva, Switzerland. Also www.wmo.int

Yamada, T., A. Mochizuki, J. Sawada, E. Zaima, T. Kawamura, A. Ametani, M. Ishii, and S. Kato. 1995. "Experimental Evaluation of a UHV Tower Model for Lightning Surge Analysis." *IEEE Transactions on Power Delivery.* Vol. 10. No. 1. January. Pp. 393–402.

Yokoyama, S., K. Miyake, T. Suzuki, and S. Kanao. 1990. "Winter Lightning on Japan Sea Coast – Development of Measuring System on Progressing Feature of Lightning Discharge." *IEEE Transactions on Power Delivery.* Vol. 5. No. 3. July. Pp. 1418-1425.

Young, F. S., J. M. Clayton, and A. R. Hileman. 1963. "Shielding of Transmission Lines." *AIEE Transactions on Power Apparatus and Systems.* Special Supplement. Paper No. 63-640. Pp. 132-154.

Zajac, B. A. and S. A. Rutledge. 2001. "Cloud-to-Ground Lightning Activity in the Contiguous United States from 1995 to 1999." *AMS Monthly Weather Review.* Vol. 129. May. Pp. 999-1019.

Zanetta, Jr, L. C. 2003. "Evaluation of Line Surge Arrester Failure Rate for Multipulse Lightning Stresses." *IEEE Transactions on Power Delivery.* Vol. 18. No.3. Pp.796-801. July.

CHAPTER 7

Electric and Magnetic Fields

Luciano Zaffanella

This chapter presents engineering issues related to electric and magnetic fields produced by high-voltage transmission lines and to their effects. Methods of calculations and measurements are described. Evaluations of currents, voltages, and energies induced on objects and assessments of their effects are discussed. While the emphasis in previous editions was on electric field, magnetic field is also covered in detail in this edition. Methods of field reductions are illustrated and the analytical tools for their design are provided.



Dr. Luciano E. Zaffanella is one of the original authors of the *EPRI Transmission Line Reference Book*. When the first and second editions were published, he was directing General Electric's staff that was operating Project UHV on behalf of EPRI. Under his direction this project became a High Voltage Transmission Research Center, an internationally renowned facility for the study of overhead high voltage transmission lines with HVAC voltages up to 1500 kV three-phase, and HVDC voltages of + and – 1200 kV, including their environmental impact. He pioneered engineering studies of electric and magnetic fields, the development of low magnetic field lines, and methods of field reduction of existing lines. Prior to joining project UHV, he was the Head of the Research Section of the High Voltage Department of CESI, in Milan, Italy. He is currently Vice President of Research of Enertech, a company well known for its EMF expertise.

7.1 INTRODUCTION

Overhead transmission lines generate electric and magnetic fields at power frequency. These fields play an important role in transmission-line design and operation. This chapter presents practical methods for calculating and measuring electric and magnetic fields, discusses the effects of these fields, and presents the criteria by which the fields are to be evaluated.

The previous edition of this book, written at a time when there was a rapid increase in the use of higher voltage lines and there was a prospect of transmission lines with voltages above 1000 kV, emphasized electric fields. Electric fields are still to be considered in many aspects of line design and operation. They are important in terms of induction on vehicles and other conductive objects, shocks caused by spark discharges, interference with pacemakers, and pole fires. Some jurisdictions have electric field limits, so an electric field analysis is required to obtain permits for construction of new lines or upgrading of existing lines. This is true for all voltage levels considered in this book. At 230 kV, electric fields are of marginal interest, but must still be addressed in a permit application.

The emphasis today has shifted to magnetic fields. Magnetic field induction in parallel wires is one aspect. Interference with the proper operation of computer monitors is another. However, the major focus of attention is on the level of magnetic fields outside the right-of-way where long-term exposure of people to magnetic field and its possible health effects is of concern. Concern for health effects from exposure to power frequency electric and magnetic fields surfaced in the 1960s with the introduction of Extra High Voltage (EHV) transmission systems (Kowenhoven et al. 1967). These concerns were highlighted by a 1972 report of Russian workers becoming ill as they worked in high-voltage substations (Korobkova et al. 1972). Later in the decade, a report was published detailing an epidemiological study correlating a surrogate for 60-Hz magnetic fields with childhood leukemia (Wertheimer and Leeper 1979). This report triggered a massive research effort to find answers to the question: "Can power frequency magnetic fields of the type generated by transmission lines have an adverse effect on people's health?" Some jurisdictions have introduced magnetic field limits for transmission lines, so transmission-line magnetic fields must be analyzed in order to obtain permits for new lines or for uprating of existing lines. Magnetic field depends on the line current and remains a significant issue even when the voltage is 220 kV or lower.

The efforts to determine whether there are health effects associated with electric and magnetic fields have generated an abundant literature but are not discussed in this book, which is about engineering issues. At the time this reference book is being written, health effects due to long-term exposure to electric fields are generally considered irrelevant, but long-term exposure to magnetic fields is still a subject of investigations (NIEHS 1998; NRPB 2001).

As a result of the emphasis on magnetic fields, there have been significant advancements in the development of instrumentation for measuring these fields, advanced methods of calculations, and techniques for reducing magnetic fields. This chapter presents the different practical options that are available for reducing electric and magnetic fields. Because construction of new lines or modification to existing lines is subject to review in the regulatory process and to intense public scrutiny, the transmission-line design process often includes efforts to minimize electric and magnetic fields compatibly with safety and reliability.

Electric and magnetic fields and several related quantities can be calculated using simple software applications provided in the electronic version of this book. The user may exercise the following applets:

- EMF-1: "Field Ellipse." This applet calculates the maximum and minimum axes of the field ellipse given the orthogonal field components.
- EMF-2: "Transmission Line Electric Field (2-D)." This applet may be used to calculate the electric field and the space potential at any desired location near a transmission line and also to draw contour lines to separate regions with different electric fields or space potentials. This applet considers two-dimensional line geometry.
- EMF-3: "Single Conductor Equivalent to a Bundle." This applet may be used to calculate the diameter of the single conductor that has the same capacitance to ground as a bundle with a given geometry.
- EMF-4: "Transmission Line Electric Field (3-D)." This applet may be used for three-dimensional geometry. Applet EMF-4 also considers objects with various shapes at ground potential and may be used to assess the shielding effect of these objects.
- EMF-5: "Electric Field Shielding by Grid." This applet may be used to calculate the electric field reduction that is obtained with either vertical or horizontal grids of grounded wires.
- EMF-6: "Transmission Line Magnetic Field (2-D)." The user may exercise this applet to calculate the magnetic field at any desired location near a transmission line and also to draw contour lines to separate regions with different magnetic fields. This applet considers two-dimensional line geometry.
- EMF-7: "Transmission Line Magnetic Field (3-D)." This applet may be used for the calculation of magnetic

fields with three-dimensional geometry. In fact, the user may consider any combination of straight cylindrical segments, catenaries, busses, and coils.

- EMF-8: "Induction in Parallel Wires." This applet may be used to calculate the current induced in shield wires grounded at every tower, or the currents and voltages induced in shield wire sectionalized, transposed, and grounded at given intervals, or the voltage induced in long wires grounded at one end and isolated from ground at the other end.
- EMF-9: "Distant Field Equations for Parallel Lines." This applet may be used to find the equations giving the distant magnetic field from any set of infinitely long conductors with known current and position in space.
- EMF-10: "Electric Field Induction In Objects." This applet may be used to calculate the short-circuit current of objects to ground induced by the electric field produced by high-voltage conductors.
- EMF-11: "Magnetic Field Reduction Using Cancellation Loops." This applet may be used to design cancellation loops for the purpose of reducing magnetic field of transmission lines. The geometry of the line and of the loop are described in three dimensions. The results of the calculations include the current in the cancellation loop wires, and the magnetic field before and after the introduction of the loops.
- EMF-12: "Magnetic Field Reduction with Fourth Wire Scheme." This applet calculates the magnetic field reduction resulting from a special line design, called the "fourth wire scheme" (see Section 7.17.7).

7.2 BASIC ELECTRIC AND MAGNETIC FIELD PRINCIPLES

7.2.1 EMF: Electric and Magnetic Fields

Electric and magnetic fields (EMF) are generated by electrical charges and by their movement (electric currents).

The term *electromagnetic fields* refers to electric and magnetic fields that are coupled, as in high-frequency radiating fields. When the rate of change (frequency) of these fields is sufficiently low, as for power system fields, EMF can be separated into electric (related to voltages) and magnetic (related to currents) fields. In this case, the word EMF should be understood as meaning *Electric and Magnetic Fields*, as opposed to *Electromagnetic Fields*.

There is a spectrum of frequencies of electromagnetic fields. The product of frequency and wavelength of an electromagnetic wave equals the speed of propagation of the wave, which, in free space, is equal to the speed of light: $c \approx 3 \times 10^8$ m/s. The wavelength associated with 60 Hz is 5000 km and that associated with 50 Hz is 6000 km. By comparison, the wavelength of FM broadcast transmission at 100 MHz is 3 m. When the distance to the source is large compared to the wavelength, electric and magnetic fields are linked and considering them together is justified. In this case, the electric field, E (V/m), and the magnetic field strength, H (A/m), are related to each other through the intrinsic impedance, η, of the medium where the electromagnetic wave travels at a speed, v. This is called the "far field" or radiation field.

$$E = \eta H \quad \eta = \sqrt{\frac{\mu}{\varepsilon}} \quad v = \frac{1}{\sqrt{\mu\varepsilon}} \qquad 7.2\text{-}1$$

In free space, $\mu = 4\pi 10^{-7}$ H/m.
$\varepsilon \approx 8.85 \times 10^{-12}$ F/m.
$\eta \approx 377\ \Omega$.

However, when the distance from the source is small, such as in the case of electric and magnetic fields near power transmission lines, the fields are independent and should be considered separately as electric and magnetic fields, not as electromagnetic fields. These near fields form the "quasistatic" region, where the time variation of the fields is sufficiently slow that static formulas can be applied for many purposes. Effects related to coupled voltages and currents predominate in the quasistatic region. The radiation field is negligible in the quasistatic region.

The electromagnetic spectrum has been divided into several portions. Most of the electric and magnetic fields associated with the power system are within the "extremely low frequency" (ELF) band, which goes from 3 Hz to 3 kHz. This range encompasses both the fundamental frequency and its measurable harmonics.

Ionizing and Nonionizing Fields

This chapter discusses fields that are sufficiently low in magnitude and in frequency not to cause ionization. Power system electric and magnetic fields belong to the nonionizing portion of the electromagnetic spectrum. Fields are ionizing when they are capable of ejecting electrons from their orbits around a normal atom. Electromagnetic fields capable of producing ionization have frequencies that fall between 10^{16} and 10^{22} Hz. These include ultraviolet light, X rays, and gamma rays. Electromagnetic fields at frequencies below 10^{16} Hz are nonionizing, but may be capable of producing energy in the form of heat.

AC and DC Electric and Magnetic Fields

Power frequency ac electric and magnetic fields are also quite different both in nature and in their effects from dc electric and magnetic fields, like those occurring in natural ambient conditions or near HVDC power transmission lines. The main difference consists in the ability of ac fields to induce currents, the ac electric field through capacitive coupling and the ac magnetic field through inductive coupling. On the other hand, dc electric fields have other

effects, such as the ability to affect the trajectory of air ions and to affect the deposition of charged particles on surfaces, phenomena that have little significance for ac electric fields. The dc magnetic field of the earth has a nearly constant intensity and direction at any given location. Its intensity and direction are primarily a function of the latitude. Its intensity is generally much greater than the maximum instantaneous value of the ac magnetic field generated by transmission lines at points accessible by the general public, but the two fields cannot be compared on the basis of their magnitude alone because ac fields can induce currents in circuits and conductive bodies, whereas dc fields cannot (unless a conductive body is moving).

7.2.2 Phasors and Vectors

Electric and magnetic fields near transmission lines are described using phasors and vectors. A vector is characterized by a magnitude and an angle in space, whereas a phasor is a quantity with a sinusoidal time variation described by a magnitude and a phase angle. The three orthogonal components of a vector may be phasors with different magnitudes and phase angles. In this chapter, a vector is indicated with an arrow ($\vec{E}, \vec{B}$) and a phasor with a wave sign ($\tilde{E}, \tilde{B}$) or with a sinusoidal function of time.

7.2.3 Electric Field

Definition

The magnitude and direction of the force exerted on a stationary electrical charge define an *electric field*. The electric field is a vector. If a unit electric charge, one coulomb, is in a unit electric field, one volt per meter, it will be subjected to a unit force, one newton, in the direction of the field.

A more intuitive visualization of an electric field is obtained by considering two parallel conductive plates separated by an insulating medium, such as air. If a voltage is applied between the two plates, an electric field will be created between them, directed from one plate to the other. If the plates are sufficiently large with respect to their separation, *S*, the electric field is uniform and its magnitude is equal to $E = V/S$.

The unit of measurement of the electric field is the volt per meter (V/m).

The electric field is defined by its space components along three orthogonal axes. Each space component is a function of time.

$$\vec{e}(t) = e_x(t) \cdot \vec{u}_x + e_y(t) \cdot \vec{u}_y + e_z(t) \cdot \vec{u}_z \qquad 7.2\text{-}2$$

$\vec{u}_x$, $\vec{u}_y$, $\vec{u}_z$ are the unit vectors in the directions of the *x, y,* and *z* axes, respectively. $e_x(t)$, $e_y(t)$, and $e_z(t)$ are periodic functions of time, and each can be expressed as the sum of sinusoidal electric fields at the power frequency and its harmonics. Transmission-line electric fields have very little harmonic content because voltages are usually close to sinusoidal. For instance, the amplitude of the component along the *x* axis may be written:

$$e_x(t) = \sqrt{2} E_x \sin(\omega t + \alpha_x) \qquad 7.2\text{-}3$$

E_x is the rms (root-mean-square) value, $\sqrt{2}E_x$ is the maximum amplitude, and α_x is the phase angle of the electric field component along the *x* axis, and $\omega = 2\pi f$, with *f* being the frequency. Similar expressions can be written for the other two axes.

Electric Field Ellipse

In an electric field created by a three-phase system, the vector $\vec{e}$ changes in magnitude and direction with time. If the field is represented by an arrow anchored at a point, the tip of the arrow describes an ellipse, the "electric field ellipse."

The field ellipse (see Figure 7.2-1) can be characterized by its major and minor axes. When the axes are equal in magnitude, the ellipse becomes a circle, the field is constant in magnitude, but its direction varies with time. On the other hand, when the minor axis becomes very small with respect to the major axis, the ellipse becomes very narrow, until it eventually collapses into an oscillating vector. In this case, the field is represented by a vector with constant direction, but with a magnitude that varies with time.

When the field vector has a constant direction in space, the field is "linearly polarized." This occurs, for instance, on the surface of the transmission-line conductors, on the surface of conductive objects, and at or near a conductive ground.

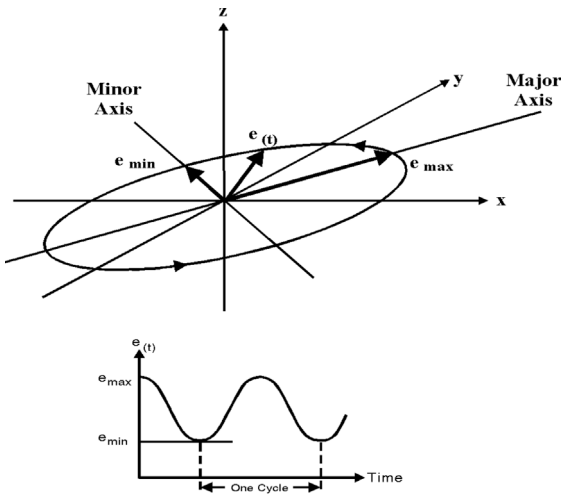


Figure 7.2-1 Electric field ellipse and variation of electric field with time.

If the field vector describes an ellipse, the field is "elliptically polarized." Away from the surface of conductive objects, a system of 50- or 60-Hz voltages not in phase with each other, such as three-phase transmission lines, will, in general, generate elliptically polarized fields. The degree of polarization is defined by the axial ratio. The axial ratio can range from zero to one. When the axial ratio is equal to zero, the field is linearly polarized. When the axial ratio is equal to one, the field is "circularly polarized."

$$\text{Degree of polarization} = \text{axial ratio} = e_{min}/e_{max} \qquad 7.2\text{-}4$$

RMS Value

The rms (root-mean-square) value of the electric field is used to characterize the intensity of the field, despite its possibly complicated variations in space and time. This is the quantity used to characterize the electric field, unless otherwise specified. In mathematical terms, the rms value can be derived from the function expressing the amplitude of the electric field vector versus time as follows:

$$E_{rms} = \sqrt{\frac{1}{T}\int \left[e(t)\right]^2 dt} \qquad 7.2\text{-}5$$

The variable t is the time; the integration must be performed for the duration of one period, T, of the time function (e.g., 1/60 s for a 60-Hz field). The rms value of the field has a simple relationship with the rms values of the three orthogonal space components:

$$E_{rms} = \sqrt{E_x^2 + E_y^2 + E_z^2} \qquad 7.2\text{-}6$$

The above equation is valid no matter what the periodic time functions are—i.e., it is valid also if the field contains harmonics of the power frequency. If the field is purely sinusoidal, the rms value is related to the minimum and maximum axes of the field ellipse by Equation 7.2-7.

$$E_{rms} = \sqrt{E_{\max}^2 + E_{\min}^2} \qquad 7.2\text{-}7$$

E_{max} and E_{min} are the rms values of the components of the electric field measured in the directions of the major and the minor axis of the field ellipse, respectively. The minimum and maximum axes of the field ellipse can be calculated from the three orthogonal components as shown in Appendix 7.1.

Spatial Characteristics of the Electric Field

The electric field is perpendicular to the surface of conductive bodies. In particular, it is perpendicular to the surface of the ground. When the ground is flat and without disturbing objects, the electric field caused by a distant source (high-voltage equipment, high-voltage conductors) is vertical and relatively uniform. In general, however, the electric field is rather nonuniform. This is especially true near conductive objects like the human body. The electric field is greatly perturbed by the presence of the body.

The effects of the electric field, such as induced currents and voltages on objects, are often expressed in terms of the *unperturbed field*, which is the field at the location of the object if the object were not there to perturb it. Because conductive objects perturb the field, special techniques are needed for electric field measurements (see Section 7.5).

Temporal Stability of Electric Fields

Electric field magnitudes have practically no variations in time. This reflects the fact that voltages are usually constant, even when the electrical loads are variable. Electric fields away from high-voltage conductors are affected very little by corona. The space charge generated by a conductor in foul weather, when the conductor is in corona, affects its equivalent capacitance, but the effect is small, particularly for a bundle of two or more subconductors.

Harmonic Content of Electric Fields

Power system voltages and electric fields have little harmonic content. Electric fields near transmission lines generally have a total harmonic distortion less than 1%. The largest harmonic is generally the 5th.

Electric Field Transients

Voltage surges in overhead transmission lines cause electric field transients characterized by a large rate of change of the electric field, *dE/dt*. Electric field transients occur also in nature, due to lightning.

Space Potential

An electric field region can be characterized not only by the electric field but also by the potential of each point, which is the voltage between the point and a reference, usually the electrical ground whose potential is taken equal to zero. The space potential is a phasor. Space potentials at the power frequency are characterized by an rms value and a phase angle. The following relation exists between electric field and space potential:

$$\vec{E} = -\nabla \tilde{V}_{sp} \qquad 7.2\text{-}8$$

The electric field is equal to the gradient of the space potential. For example, the component, $\tilde{E}_x$, of the vector electric field in the x direction is equal to the partial derivative of the space potential in that direction.

$$\tilde{E}_x\vec{u}_x = -\frac{d\tilde{V}_{sp}}{dx}\vec{u}_x$$
$$\tilde{E}_y\vec{u}_y = -\frac{d\tilde{V}_{sp}}{dy}\vec{u}_y \qquad 7.2\text{-}9$$
$$\tilde{E}_z\vec{u}_z = -\frac{d\tilde{V}_{sp}}{dz}\vec{u}_z$$

$\vec{u}_x$, $\vec{u}_y$, and $\vec{u}_z$ are the unit vectors in the directions of the *x, y,* and *z* axes, respectively. The voltage difference between two points is the difference in space potential between the two points and can be obtained by integrating the electric field along any line connecting the two points:

$$\tilde{V}_{AB} = \tilde{V}_{sp,A} - \tilde{V}_{sp,B} = \int_A^B -\vec{E}\cdot d\vec{l} \qquad 7.2\text{-}10$$

Coulomb's Law - Electric Flux Density - Surface Charge

Electric fields are caused by electric charges. *Coulomb's law* states that the electric field created by a charge, $\tilde{Q}$, at a distance, *R*, is given by:

$$\tilde{E} = \frac{\tilde{D}}{\varepsilon} = \frac{\tilde{Q}}{4\pi\varepsilon R^2} \qquad 7.2\text{-}11$$

$\tilde{D}$ is the magnitude of the electric flux density vector, $\vec{D}$. The total flux exiting a volume is equal to the sum of all the charges inside that volume (Gauss' law). The flux emanating from a point charge is uniformly distributed over the surface of a sphere centered on that charge, hence Equation 7.2-11. ε is the dielectric constant of the medium. For air, $\varepsilon = 8.854\cdot10^{-12}$ (F/m).

The electric flux through a surface is equal to the integral of the component of $\vec{D}$ normal to the surface. When the surface is that of a conductive object, the electric flux density vector is perpendicular to the surface and its magnitude, $\tilde{D}$, is equal to the charge density, $\tilde{q}$ (C/m²), which is equal to the ratio between the charge, $\tilde{Q}$, and the area, *A*, over which the charge is distributed. Thus, the electric field on the surface of conductive object is related to the surface charge density by Equation 7.2-12:

$$\tilde{q} = \tilde{Q}/A = \tilde{D} = \varepsilon\tilde{E} \qquad 7.2\text{-}12$$

Line Charge

The charge on a transmission-line conductor may often be considered uniformly distributed over the length of a line section. The geometry may be considered two-dimensional. The charge per unit of length is expressed using the unit of coulomb/meter. Although the charge is distributed on the surface of the conductor, for the purpose of calculating the electric field outside the conductor, the charge is often treated as a "line charge" located at the center, as if the conductor consisted of a line with zero dimensions. The electric flux emanating from a line charge is distributed over a cylindrical surface. The electric flux density and the electric field at a distance, *R*, from the line conductor are vectors directed away from the line charge and with magnitudes given by:

$$\tilde{E} = \frac{\tilde{D}}{\varepsilon} = \frac{\tilde{Q}}{2\pi\varepsilon R} \qquad 7.2\text{-}13$$

Potential Coefficients

The calculation of electric fields is relatively straightforward when the charge values and locations are known. Equation 7.2-11 is used for point charges and Equation 7.2-13 for line charges. In practice, however, the voltages rather than the charges are known. The voltage, $\tilde{V}_i$, on an object (*i*) is related to the charge, $\tilde{Q}_j$, on another object (*j*) through the potential coefficient, P_{ij}:

$$\tilde{V}_i = P_{ij}\tilde{Q}_j \qquad 7.2\text{-}14$$

Potential coefficients have different expressions, depending on the geometry of objects. The calculation of electric fields in two dimensions makes use of the potential coefficients between cylinders, as described in Section 7.3. For three-dimensional problems, complex expressions of potential coefficients are available for the case of sphere-to-sphere (EPRI 1999) and cylindrical segments-to-cylindrical segments (see Appendix 7.6), when spheres or cylindrical segments are used to simulate the geometry of objects.

Grounded and Floating Objects

Most objects near transmission lines may be considered conductive for the purpose of electric field calculations. Conductive objects include cars, trucks, the body of people and animals, live vegetation, moist surfaces, and the ground itself. Very dry wood, dry gravel, dry clothes and shoes, and rocky soil may be considered insulators. Conductive objects that rest on a conductive ground are "grounded"—i.e., at the potential of the ground, normally taken as the zero reference potential. Conductive objects that are well insulated from ground are considered "floating," because their potential floats between ground potential and the line potential. The total charge on a floating object is zero, although charges may be located on different parts of its surface. Many objects are neither grounded nor floating, because they are connected to ground through a resistance. This is, for example, the case of cars and trucks connected to the electrical ground through tires and dry pavement, of people connected to ground through partially conductive shoes, and of gutters connected to ground through not perfectly insulating wooden surfaces.

Electric Field for Simple Geometry

Electric field expressions are provided in Table 7.2-1 for pairs of electrodes with simple shapes. *V* is the voltage between electrodes. When the geometry is even slightly

more complex, such as for transmission line conductors parallel to each other above a flat ground, there are no simple closed-form solutions and more complex calculation methods, such as those described in Section 7.3 must be employed.

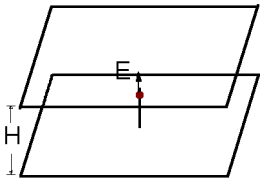
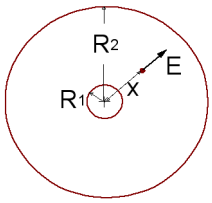
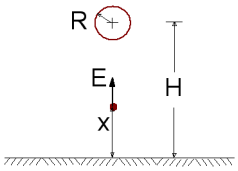
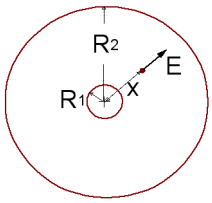
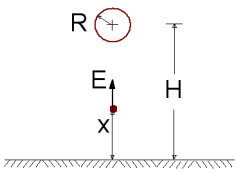
7.2.4 Magnetic Fields

Definition

The magnitude and direction of the force exerted on a moving electric charge define the magnetic field. If an electric charge is moving into a magnetic field, or if a field moves past the charge, the charge will be subjected to a force. If the unit electric charge—i.e., 1 C (one coulomb)—moves at a unit velocity—i.e., 1 m/s (one meter per second)— perpendicular to a magnetic field of a unit flux density— i.e., 1 T (one tesla)—it will be subjected to a unit force—i.e., 1 N (one newton)—in a direction orthogonal to both the direction of the motion and the direction of the magnetic field. The quantity described is the *magnetic flux density*, which is the magnetic flux in the unit area perpendicularly traversed by the flux.

The above definition, although correct, is not very intuitive. To gain better physical insight into the meaning of magnetic flux density, consider a single long wire carrying a current, I. The magnetic flux density in the surrounding air at a distance R from the wire is equal to $2 \cdot 10^{-7}\ I/R$ tesla. For

Table 7.2-1 Electric Field for Simple Geometry

Geometry		Capacitance	Charge on Electrode	Electric Field
Plate-to-plate		$C=\frac{\varepsilon}{H}$ (F/m²)	$Q=\frac{\varepsilon V}{H}$ (C/m²)	$E=\frac{V}{H}$ (V/m)
Concentric spheres		$C = 4\pi\varepsilon\frac{R_1R_2}{R_2-R_1}$ (F)	$Q = 4\pi\varepsilon V\frac{R_1R_2}{R_2-R_1}$ (C)	$E = V\frac{R_1R_2}{x^2(R_2-R_1)}$ (V/m)
Sphere above ground (for H>>R)		$C = 4\pi\varepsilon R$ (F)	$Q = 4\pi\varepsilon RV$ (C)	$E = V\frac{2R(H^2+x^2)}{(H^2-x^2)^2}$ (V/m)
Concentric cylinders		$C = \frac{2\pi\varepsilon}{\ln(R_2/R_1)}$ (F/m)	$Q = \frac{2\pi\varepsilon V}{\ln(R_2/R_1)}$ (C/m)	$E = \frac{V}{x\cdot\ln(R_2/R_1)}$ (V/m)
Cylinder above ground (for H>>R)		$C = \frac{2\pi\varepsilon}{\ln(2H/R)}$ (F/m)	$Q = \frac{2\pi\varepsilon V}{\ln(2H/R)}$ (C/m)	$E = \frac{2VH}{(H^2-x^2)\cdot\ln(2H/R)}$ (V/m)

instance, if the wire carries 1 ampere at the distance of 1 meter, the magnetic flux density is equal to $2 \cdot 10^{-7}$ tesla. The magnetic flux density is a vector that, in this example, is tangential to the circle with radius *R*. If the current is a phasor, the magnitude of the magnetic flux density is also a phasor.

Units of Measurement

Magnetic flux is measured in weber (Wb). The "magnetic flux density," often indicated by the letter B, is the magnetic flux per unit area. Magnetic flux density is measured in weber per square meter, or tesla. 1 T = 1 Wb/m^2.

$$\Phi = B \cdot A \qquad 7.2\text{-}15$$

The "magnetic field strength," indicated using the letter H, is measured in ampere per meter (A/m). $\vec{B}$ and $\vec{H}$ are related to each other through the permeability of the medium:

$$\vec{B} = \mu \vec{H} \qquad 7.2\text{-}16$$

The permeability, μ, is a characteristic that gives an indication of how a material affects the magnetic flux density that penetrates it. The permeability of vacuum, air, and biological matter is nearly the same: $\mu = \mu_0 = 4\pi\ 10^{-7} = 1.257 \cdot 10^{-6}$ henry/meter (H/m).

When engineers talk about a magnetic field, they refer to the rms value of the magnetic flux density, B. The international unit for magnetic flux density is the tesla (T). The unit commonly used in the United States is the CGS unit gauss (G). 1G = 0.0001T = 10^{-4}T. However, since most magnetic fields experienced by people are much lower than one tesla and one gauss, more commonly used units are the microtesla (μT), used in European publications, and the milligaus (mG), used in the U.S.: 1 mG = 0.001G = 10^{-7}T = 0.1 μ T

Like electric fields, magnetic fields can have constant direction (dc) or a direction that varies during the power frequency cycle (ac). The earth has a dc magnetic field ranging from about 280 to 660 mG (0.28 to 0.66 gauss), depending upon the location on the earth (the continental United States has a dc field of about 480 to 560 mG).

Magnetic Field Components, Magnetic Field Ellipse, RMS Value

The same concepts and definitions illustrated for the electric field are applicable to the magnetic field as well. The quantity used to characterize the magnetic field is the rms value, unless otherwise specified.

Harmonics of the Magnetic Field

The magnetic field of transmission lines has a low harmonic content, contrary to the field of most sources of magnetic field that can be encountered in common environments. Typical values inside and outside the right-of-way are shown in Table 7.2-2.

Table 7.2-2 Harmonic Content of Magnetic Fields from Transmission Lines (as a Percentage of the Fundamental)

Harmonic	2	3	4	5	7	9	11	13
Transmission Line (within ROW)	0.1	0.5-0.9	0.0	0.6-1.3	0.2	0.0-0.1	0.1	< 0.1
Transmission Line (outside ROW)	0.2-1.4	0.5-3	0.1-0.4	0.5-1.1	0.1-0.3	0.1-0.3	0.1-0.2	0.1

Temporal Stability of Magnetic Fields

The magnetic field from a power transmission line has the same variability as the transmission-line load current.

The Current Carrying Wire, Biot-Savart Law, Ampere's Law

The most familiar source of magnetic field is the current carrying wire, usually treated as a "line current"—i.e., the current travels along a line whose thickness can be ignored. A line current can, in general, follow any contour through space. A simple case of line current is the straight infinitely long line current. The magnetic field at a distance, *R*, from an infinitely long line current, *I*, forms circles around the wire, and its magnitude is given by:

$$B = \frac{\mu_0 I}{2\pi R} \qquad 7.2\text{-}17$$

The field direction is given by the right-hand rule (see Figure 7.2-2). The *right-hand rule* states that if the right thumb points along the wire in the direction of current flow, the fingers will encircle the wire in the direction of the magnetic field. The current, *I*, can be alternating, and Equation 7.2-17 indicates that the magnetic field produced by an ac current is in phase with the current.

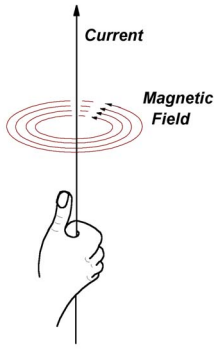


Figure 7.2-2 The right-hand rule.

For a line current following any contour through space, the magnetic field is given by the Biot-Savart law (see Section 7.4.4). Application of the Biot-Savart law leads to the development of equations for simple wire geometry as shown in Table 7.2-3.

Another fundamental law is Ampere's law, expressed by:

$$\int \vec{B} \cdot d\vec{l} = \mu_0 I_{enclosed} \qquad 7.2\text{-}18$$

Ampere's law states that the integral of the component of the magnetic field vector along any closed contour line equals μ_0 times the net current passing through the contour. As an example of its application, consider an infinitely long wire carrying a current *I*. The application of Ampere's law is illustrated in Figure 7.2-3, where an imaginary circular contour is drawn symmetrically around the current carrying wire. Note that at every point on the contour, the vector $d\vec{l}$ points along the contour. It is known from the right-hand rule that $\vec{B}$ also points along the contour. Therefore, at every point on the contour, $\vec{B}$ and $d\vec{l}$ are parallel. The integration of the scalar product around the contour gives: $B \cdot 2\pi R$. The total current enclosed by the contour of Figure 7.2-3 is the current in the wire, *I*. Therefore, Equation 7.2-18 becomes:

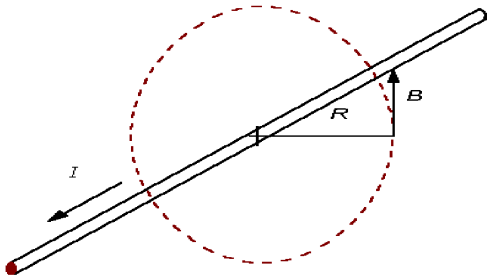


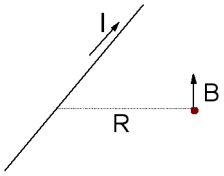
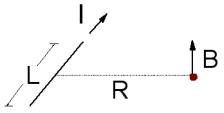
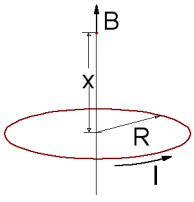
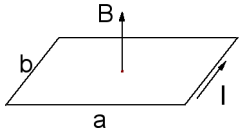
Figure 7.2-3 Magnetic field of an infinitely long current-carrying wire.

$$B = \mu_0 I / (2\pi R) \qquad 7.2\text{-}19$$

Faraday's Law of Induction, Induced Currents

Time-varying magnetic fields induce currents in conductive objects. These currents can flow in wires, or are induced as circulating currents in bulk matter. The latter are sometimes called "eddy currents." The physical law governing this phenomenon is called *Faraday's law.* This law states that there is an induced voltage around any closed path (loop) that equals the time rate of change of

Table 7.2-3 Magnetic Field for Simple Geometry

Geometry (Current in ampere, distances in meter)		Magnetic Field (tesla)	Magnetic Field (milligauss)
Infinitely long line		$B = \mu_0 \frac{I}{2\pi R}$	$B = \frac{2I}{R}$
Line segment (measurements in the axial plane)		$B = \frac{\mu_0 LI}{2\pi R\sqrt{L^2 + 4R^2}}$	$B = \frac{2LI}{R\sqrt{L^2 + 4R^2}}$
Circular Loop (measurements along loop axis)		$B = \frac{\mu_0 R^2 I}{2(R^2 + x^2)^{3/2}}$	$B = \frac{2\pi R^2 I}{(R^2 + x^2)^{3/2}}$
Rectangular Loop (measurements at the loop center)		$B = \frac{2\mu_0\sqrt{a^2 + b^2}}{\pi ab} I$	$B = \frac{8\sqrt{a^2 + b^2}}{ab} I$

magnetic flux through the loop (adjusted by a negative sign to give the correct direction). In mathematical form:

$$\tilde{V} = -\frac{d\tilde{\Phi}}{dt} \qquad 7.2\text{-}20$$

As an example of Faraday's law, consider a circular loop of wire one meter in radius (see Figure 7.2-4). The loop is placed in a region that has a uniform 60-Hz magnetic field with an rms value of 100 mG in the vertical direction, perpendicular to the plane of the loop. The field varies with time according to equation $\tilde{B} = \sqrt{2} \cdot 100 \cdot \sin(\omega t)$.

The flux through the loop is:

$$\tilde{\Phi} = \int \vec{B} \cdot d\vec{a} \qquad 7.2\text{-}21$$

The integration is over the area enclosed by the loop, and *da* is the elemental area vector.

Since the vectors $\vec{B}$ and $d\vec{a}$ are parallel everywhere over the area of integration, the scalar product in Equation 7.2-21 becomes simply the product of the magnitudes of $\vec{B}$ and $d\vec{a}$. Since the magnitude of $\vec{B}$ is constant,

$$\tilde{\Phi} = \pi \cdot \sqrt{2} \cdot 100 \cdot 10^{-7} \cdot \sin(\omega t) \text{ Wb}$$

The voltage induced in the loop is:

$$\tilde{V} = -d\tilde{\Phi} / dt = -\pi \cdot \sqrt{2} \cdot 10^{-5} \cdot \omega \cdot \cos(\omega t) \quad \text{V}$$

and in polar notation

$$= 0.012 \angle -90$$

where 0.012 is rms value.

In conclusion, the voltage induced in the loop by the magnetic field has an rms value equal to 0.012 V at a phase angle of 90° with respect to the field.

The loop will, in general, have an impedance formed by an inductance and a resistance as shown schematically in Figure 7.2-4. This impedance, along with the induced voltage, determines the current that flows in the loop.

Positive, Negative, and Zero Sequence Currents

The system of alternating currents of a three-phase transmission line can be considered as the geometric sum of a three symmetrical phasor system: positive, negative, and zero sequences, which are called *symmetrical components* (Grainger and Stevenson 1994). A positive sequence, the principal sequence for working current of power networks, is formed from three phasors of equal magnitude and with phase angles between the first phasor and the other two equal to 120° and 240°. A negative sequence is formed by three phasors equal in magnitude and with phase angles between the first phasor and the other two equal to -120° and -240°. Zero sequence current is formed from three phasors, equal in magnitude and in phase. Figure 7.2-5 presents an example of a phasor diagram of positive, negative, and zero sequence phase currents. Although the power system is designed for the positive sequence component, small negative and zero sequence components may exist.

Consideration of the symmetrical components is important for the assessment of methods of magnetic field reduction. Effectively reducing the magnetic field produced from transmission lines primarily requires dealing with the positive sequence currents. The negative sequence currents are of little importance because they are small. Furthermore, magnetic field reduction methods that apply to positive sequence currents apply to the negative sequence as well. The magnetic field produced by zero sequence currents, however, is not suppressed by the same measures effective for positive sequence currents. This concept is further discussed in Section 7.17, where different options for reducing transmission-line magnetic fields are examined.

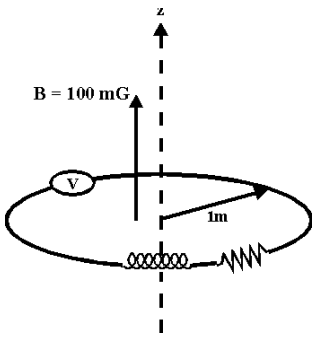


Figure 7.2-4 Voltage induced in a loop by an ac magnetic field.

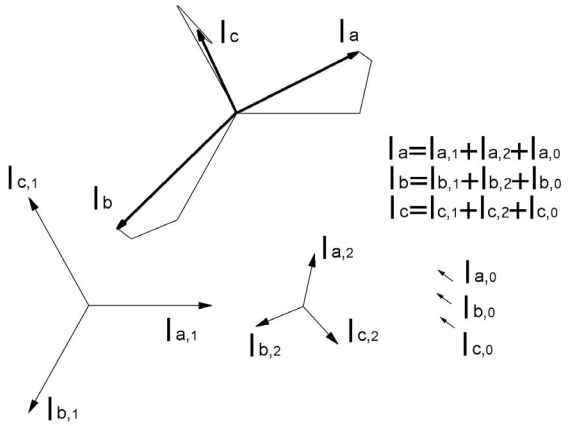


Figure 7.2-5 System of three nonsymmetric phase currents (I_a, I_b, I_c) presented as a sum of three symmetric components: (1) positive sequence, (2) negative sequence, and (0) zero sequence.

7.3 CALCULATION OF ELECTRIC FIELDS

7.3.1 General Method for Transmission Lines

The focus of this section is the electric field some distance from the conductors. In general, the methods described here do not apply to the electric field at the surface of the conductors, for which the reader is referred to Chapter 2. In most cases, the electric field generated by power transmission lines may be calculated with sufficient accuracy using a two-dimensional simplified analysis. The assumptions on which this analysis is based are the following:

- Electric fields in proximity to ac transmission lines are calculated assuming that there is no space charge, the charges being only on the surfaces of the conductors, on the ground, and on grounded objects. Corona, when present, creates a space charge near the conductor that affects the electric field but in an insignificant way, even in foul weather when corona is greater.
- Power line conductors may be simulated with a set of infinitely long cylindrical conductors, parallel to each other above a flat earth.
- The earth is assumed to be a perfect conductor because the time required for charges to redistribute on the earth surface under the action of a change in applied field (relaxation time, $\tau = \rho\varepsilon$) is extremely small (0.1 to 100 ns) compared to the period of the power frequency. The dielectric medium between conductors and earth is air, whose permittivity is practically independent of weather conditions and is equal to the permittivity of free space, $\varepsilon = 8.854 \cdot 10^{-12}$ F/m.
- Once the presence of the earth is accounted for using the images of the conductors, the time-varying electric field generated by a power transmission line may be treated as quasistatic—i.e., as essentially a static field because the wavelength is much larger than the dimensions under consideration.

The problem is two-dimensional and can be solved quite accurately using the charge simulation method. The electric field can be calculated using Applet EMF-2. The charges distributed on the surface of a conductor are simulated by a charge placed at the center of the conductor. The charges on the earth surface are simulated by image charges equal in magnitude but with opposite polarity to the charges on the conductors. These image charges are placed below the surface of the earth as if the earth were a perfect mirror reflecting the conductors. This system of charges creates electric fields in the space between conductors and earth that are equal to those created by the actual charges distributed on the surfaces of conductors and earth. The electric field at a point in space can be calculated from the charges. The charges are calculated knowing the voltage, V_k, applied to each conductor, k, and the geometry of the problem. It is required to solve the matrix equation:

$$[Q] = [P]^{-1}[V] \qquad 7.3\text{-}1$$

Where:

$[Q]$ is the array of the line charges (coulomb/meter).
$[V]$ is the array of the conductor voltages (volt).
$[P]$ is the array of the Maxwell potential coefficients (meter/farad).

Charges and voltages are alternating quantities at the power frequency and may be expressed by complex numbers, with a real and an imaginary part. For instance, the voltage of a conductor: $v(t)=\sqrt{2}V\cos(\omega t+\varphi)$ can be written as $\tilde{V}=\tilde{V}_r+j\tilde{V}_i$. V_r is the rms value of the real component (phase angle equal to zero) and V_i is the rms value of the imaginary component (phase angle equal to 90°):

$$v_r(t) = \sqrt{2}V\cos(\varphi)\cos(\omega t)$$
$$v_i(t) = \sqrt{2}V\sin(\varphi)\cos(\omega t + 90)$$

Equation 7.3-1 can be written for both real and imaginary quantities.

$$[Q_r] = [P]^{-1}[V_r] \quad \text{and} \quad [Q_i] = [P]^{-1}[V_i] \qquad 7.3\text{-}2$$

Conductors can be at any voltage including zero. Conductors with zero voltage include wires for lightning protection or wires intentionally used for electric field shielding.

The potential coefficients for a system of parallel conductors have simple expressions:

$$P_{kk} = \frac{1}{2\pi\varepsilon}\ln\left(\frac{4H_k}{d_k}\right) \qquad 7.3\text{-}3$$

$$P_{kl} = \frac{1}{2\pi\varepsilon}\ln\left(\frac{S'_{kl}}{S_{kl}}\right) \qquad 7.3\text{-}4$$

Where:

P_{kk} is the self potential coefficient of conductor k.
P_{kl} is the mutual potential coefficient between conductors k and l.
d_k is the diameter of conductor k.
H_k is the height above ground of conductor k.
S_{kl} is the distance between conductor k and conductor l.
S'_{kl} is the distance between conductor k and the image of conductor l (see Figure 7.3-1).
ε $= 8.854 \cdot 10^{-12}$ F/m.

The matrix of potential coefficients is symmetric: $P_{kl} = P_{lk}$.

In the case of a bundle of conductors, rather than considering each conductor separately, an equivalent single conductor may be considered. The equivalent conductor is a

conductor that would hold the same charge as the bundle when the same voltage is applied to it. The equivalent conductor can also be thought of as the conductor with the same capacitance to ground.

The diameter of a single conductor equivalent to a regular bundle—i.e., to a bundle of identical conductors disposed on the vertices of a regular polygon, is:

$$d_{eq} = d_b \cdot \sqrt[n]{\frac{nd}{d_b}}; \quad d_b = \frac{s}{\sin(\pi / n)} \qquad 7.3\text{-}5$$

Where:

d_b is the bundle diameter.
n is the number of subconductors in the bundle.
d is the diameter of the subconductors.
s is the spacing between subconductors.

The equivalent diameter of an asymmetric bundle—i.e., when the subconductors are not disposed on the vertices of a regular polygon, or of a bundle with subconductors with different diameters can be calculated using Applet EMF-3, "Single Conductor Equivalent to a Bundle."

Solution of Equations 7.3-2 yields the line charges on each conductor. Once the line charges are obtained, the desired electric fields and space potentials are calculated.

Each conductor's charge contributes to the electric field. The electric field is calculated by adding the contributions of all the charges. With reference to Figure 7.3-2, the electric field, $\vec{E}_k$, at point *M* caused by the line charge, $\tilde{Q}_k$, on conductor *k*, is the vectorial sum of the fields, $\vec{E}_{k1}$, due to $\tilde{Q}_k$, and $\vec{E}_{k2}$ due to the image, $-\tilde{Q}_k$, of $\tilde{Q}_k$ inside the earth.

The horizontal distance from conductor *k* and the height above ground of the measuring point, *M*, are indicated with X_M and H_M, respectively, while H_k indicates the height of the conductor. The magnitude of the horizontal and vertical components of the electric field caused by the charges on conductor *k*, $\tilde{E}_{kx}$ and $\tilde{E}_{ky}$, are given by Equations 7.3-6 and 7.3-7.

$$\tilde{E}_{kx} = \frac{\left(\tilde{Q}_{rk} + j\tilde{Q}_{ik}\right)}{2\pi\varepsilon} \cdot \left[\frac{X_M}{X_M^2 + (H_k - H_M)^2} - \frac{X_M}{X_M^2 + (H_k + H_M)^2}\right] \qquad 7.3\text{-}6$$

$$\tilde{E}_{ky} = \frac{\left(\tilde{Q}_{rk} + j\tilde{Q}_{ik}\right)}{2\pi\varepsilon} \cdot \left[\frac{H_M - H_k}{X_M^2 + (H_k - H_M)^2} - \frac{H_M + H_k}{X_M^2 + (H_k + H_M)^2}\right] \qquad 7.3\text{-}7$$

The vertical and horizontal components of the electric field vector are calculated by adding the contributions of all the conductors:

$$\tilde{E}_x = \sum_k \tilde{E}_{kx} = E_{rx} + jE_{ix} \qquad 7.3\text{-}8$$

$$\tilde{E}_y = \sum_k \tilde{E}_{ky} = E_{ry} + jE_{iy} \qquad 7.3\text{-}9$$

The rms value of the real and imaginary, horizontal and vertical components, E_{rx}, E_{ix}, E_{ry}, and E_{iy}, fully characterize the vector field. For instance, the rms value of the electric field is given by:

$$E_{rms} = \sqrt{E_{rx}^2 + E_{ix}^2 + E_{ry}^2 + E_{iy}^2} \qquad 7.3\text{-}10$$

The electric field vector describes an ellipse. The parameters of the field ellipse can be calculated as shown in Appendix 7.1 or using Applet EMF-1.

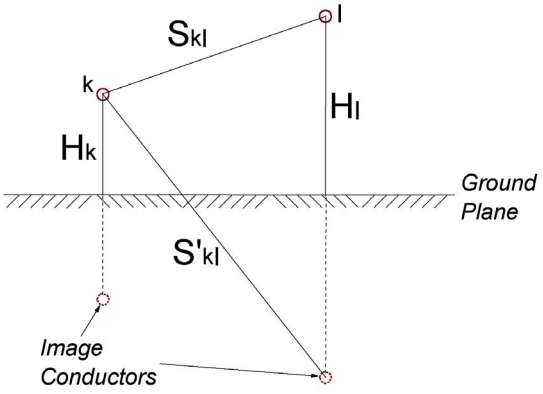


Figure 7.3-1 Conductors and their images.

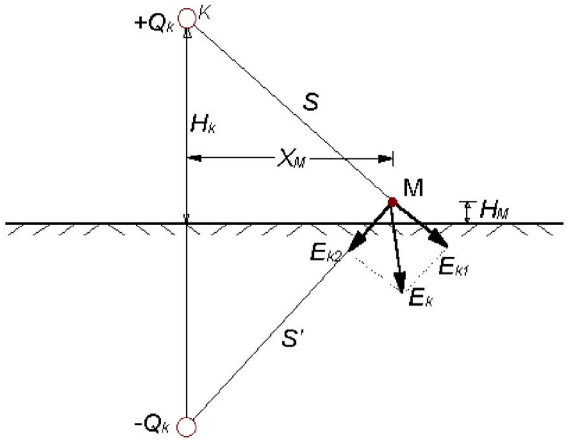


Figure 7.3-2 Calculation of the electric field from a line charge.

The space potential at the measuring point, *M*, may be evaluated by adding the contribution of each charge:

$$V_{sp} = \sum_k \frac{(Q_{rk} + jQ_{ik})}{2\pi\varepsilon} \cdot \ln\left(S_k / S'_k\right) \qquad 7.3\text{-}11$$

Where: S_k is the distance between conductor *k* and the measuring point.

S'_k is the distance between the image of conductor *k* and the measuring point.

Example

The following example guides the reader through the calculation of potential coefficients, charges on the conductors, electric field (real, imaginary, vertical, and horizontal components and resultant), and space potential (magnitude and phase angle). Consider a three-phase 525-kV line with the phases (*a*, *b*, *c*) in a flat configuration, 10 m between phases, 10.6 m height above ground, and bundles of three conductors, 3.3 cm in diameter, with 45 cm spacing. The electric field is calculated at a point 20 m from centerline and 2 m above ground.

Each phase is reduced to a single equivalent conductor, whose diameter is calculated with Equation 7.3-5:
d_b = 0.52 m, d_{eq} = 0.30 m.

The self-potential coefficients are calculated using Equation 7.3-3, using the conductor height of 10.6 m and the equivalent single conductor diameter of 0.30 m.

$P_{aa} = P_{bb} = P_{cc} = 8.91 \cdot 10^{10}$ m/F

The mutual potential coefficients are calculated using Equation 7.3-4.

$P_{ab} = P_{ba} = P_{bc} = P_{cb} = 1.53 \cdot 10^{10}$ m/F

$P_{ac} = P_{ca} = 6.77 \cdot 10^{9}$ m/F

The potential coefficients form a 3 by 3 square matrix, [P].

$$[P] = \begin{bmatrix} 8.91 & 1.53 & 0.68 \\ 1.53 & 8.91 & 1.53 \\ 0.68 & 1.53 & 8.91 \end{bmatrix} \cdot 10^{10} \quad \text{m/F}$$

Solution of Equations 7.3-2 requires the inversion of [P]. The elements of the matrix [C] = $[P]^{-1}$ are:

$C_{aa} = C_{cc} = 11.6 \cdot 10^{-12}$ F/m

$C_{bb} = 11.9 \cdot 10^{-12}$ F/m

$C_{ab} = C_{ba} = C_{bc} = C_{cb} = -1.90 \cdot 10^{-12}$ F/m

$C_{ac} = C_{ca} = -0.56 \cdot 10^{-12}$ F/m

$$[C] = [P]^{-1} = \begin{bmatrix} 11.6 & -1.90 & -0.56 \\ -1.90 & 11.9 & -1.90 \\ 0.56 & -1.90 & 11.6 \end{bmatrix} \cdot 10^{-12} \quad \text{F/m}$$

The real and imaginary components of the voltages to be used in Equations 7.3-2 are evaluated by assuming that the three-phase voltages are 120° apart and by referring the phase angles to that of the center-phase voltage. If the phase-to-phase voltage is 525 kV, the voltage to ground is 303.1 kV.

$V_{ra} = -0.5 \cdot 525 / \sqrt{3} = -151.6$ kV $\quad V_{ia} = 0.5 \cdot 525 = 262.5$ kV

$V_{rb} = 525 / \sqrt{3} = 303.1$ kV $\quad V_{ib} = 0$

$V_{rc} = -0.5 \cdot 525 / \sqrt{3} = -151.6$ kV $\quad V_{ic} = 0.5 \cdot 525 = -262.5$ kV

The charges can now be calculated with Equations 7.3-2:

$Q_{ra} = -2.25 \cdot 10^{-6}$ C/m $\quad Q_{ia} = 3.19 \cdot 10^{-6}$ C/m
$Q_{rb} = 4.18 \cdot 10^{-6}$ C/m $\quad Q_{ib} = 0$
$Q_{rc} = -2.25 \cdot 10^{-6}$ C/m $\quad Q_{ic} = -3.19 \cdot 10^{-6}$ C/m

The horizontal and vertical components of the field vector at a measuring point, *M*, can now be calculated with Equations 7.3-6 and 7.3-7 for each conductor and then added according to Equations 7.3-8 and 7.3-9. Point *M* is at a distance of 20 m from centerline and at a height of 2 m above ground. Equations 7.3-8 and 7.3-9 give:

$$\tilde{E}_x = (-100 + j\,141) + (481) + (-762 - j\,1080)$$
$$= -381 - j\,939 \quad \text{V/m}$$
$$\tilde{E}_y = (838 - j\,1189) + (-3055) + (3967 + j\,5627)$$
$$= 1750 + j\,4438 \quad \text{V/m}$$

The rms value of the electric field is given by Equation 7.3-10:

$$E_{rms} = \sqrt{381^2 + 939^2 + 1750^2 + 4438^2} = 4877 \quad \text{V/m}$$

The space potential at the measuring point, *M*, is calculated with Equation 7.3-11:

$$V_{sp} = \frac{1}{2\pi\varepsilon}\cdot(-2.25\cdot10^{-6} + j3.19\cdot10^{-6}) \cdot(-0.0417) + \frac{1}{2\pi\varepsilon}\cdot(-4.18\cdot10^{-6} + j0)\cdot(-0.081) + \frac{1}{2\pi\varepsilon}\cdot(-2.25\cdot10^{-6} - j3.19\cdot10^{-6})\cdot(-0.198) = (1687 - j\,2393) + (-6179) + (8026 + j\,1138) = 3535 + j\,8991 \quad \text{V}$$

The rms value of the space potential is

$$E_{rms} = \sqrt{3535^2 + 8991^2} = 9661 \quad \text{V}$$

The electric field and space potential can be calculated using Applet EMF-2, "Transmission Line Electric Field -2D."

7.3.2 Lateral Profile of Electric Field at Ground Level

Standards and guidelines prescribe measurements at 1-m height. However, there is very little difference between the electric field values calculated at 1 m and those calculated at ground level. The calculation of the electric field at ground level is a considerable simplification of the general method. The charges on the conductors and the image charges create field vectors with the same values but different orientation, with the resulting vector being vertical, as shown in Figure 7.3-3. The field caused by conductor *k* is given by Equation 7.3-7 with $H_M = 0$.

$$\tilde{E}_k = \frac{\left(Q_{rk} + jQ_{ik}\right)}{2\pi\varepsilon}\cdot\frac{2H_M}{X_M^2 + H_M^2} \qquad 7.3\text{-}12$$

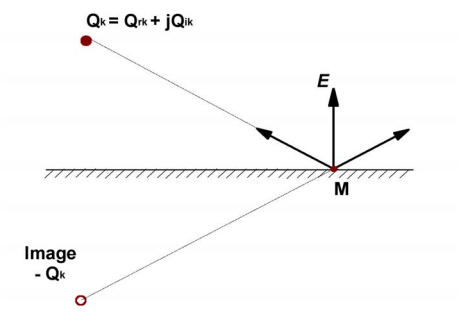


Figure 7.3-3 Electric field at ground caused by a line charge.

The field caused by the line is calculated by adding the contributions of all the conductors. The result is a phasor:

$$\tilde{E} = \sum_{k=1}^{n}\tilde{E}_k = E_r + jE_i \qquad 7.3\text{-}13$$

The magnitude of the field is:

$$E = \sqrt{E_r^2 + E_i^2} \qquad 7.3\text{-}14$$

The phase angle, θ, is:

$$\theta = \tan^{-1}(E_i / E_r) \qquad 7.3\text{-}15$$

The analysis of electric field effects on long objects that are not parallel to transmission lines requires the evaluation of both amplitude and phase angle of the electric field at different points.

If the calculation of the electric field at ground is repeated at different points in a cross-section of the transmission line, the *lateral profile* of the transmission line electric field is obtained. For an actual line with sag, the lateral profile is calculated at the section where the line has the lowest clearance to ground.

An example of lateral profile is shown in Figure 7.3-4. The maximum value of the electric field (the peak of the lateral profile) and the electric field at the edge of the right of way are particularly important for line design. The peak of the lateral profile generally occurs within the right-of-way, even though for flat configurations the lateral profile has two peaks occurring slightly outside the outer phases.



Figure 7.3-4 Example of lateral profile of electric field at ground. 525-kV line with flat configuration, 10-m phase spacing, 10.6-m height above ground, regular 3-conductor bundles, 3.3-cm diameter, 45-cm spacing.

7.3.3 Maximum Electric Field at Ground – Generalized Curves

Figures 7.3-5 to 7.3-9 show nomograms using nondimensional quantities. These curves are relatively simple to use and, even with easily accessible software, they may be preferable for a preliminary evaluation of the maximum electric field at ground for different single-circuit line types.

The use of Figure 7.3-5 is illustrated by the following example. Consider a single-circuit line with flat configuration, phase-to-phase voltage V = 525 kV, phase conductors consisting of regular three-conductor bundles with 3.3-cm diameter conductors and 45-cm spacing between conductors, phase spacing S = 10 m, and height above ground H = 10.6 m. The equivalent single-conductor diameter, calculated with Equation 7.3-5 is D = 0.3 m. In correspondence to H/D = 10.6/0.3 = 35.3 and S/H = 10/10.6 = 0.94, Figure 7.3-5 gives HE/V = 0.179. Therefore, the maximum field at ground is E = 0.179 × 525 / 10.6 = 8.8 kV/m, which is confirmed in Figure 7.3-4. Figures 7.3-5 – 7.3-9 do not consider the presence of overhead ground wires, which have a negligible effect on the field at ground level (see Section 7.3.4).

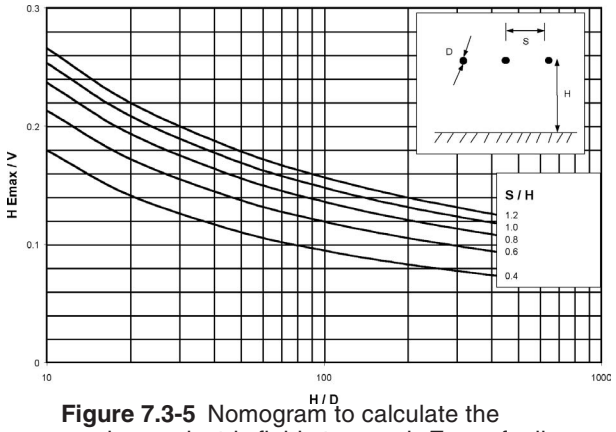


Figure 7.3-5 Nomogram to calculate the maximum electric field at ground, *Emax*, for lines of flat configuration.

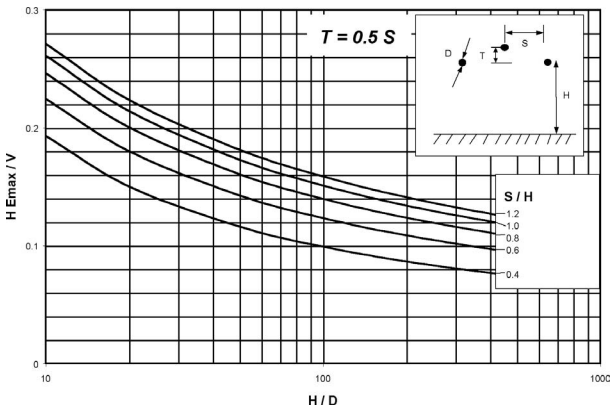


Figure 7.3-6 Nomogram to calculate the maximum electric field at ground, *Emax*, for lines of delta configuration (with T/S = 0.5).

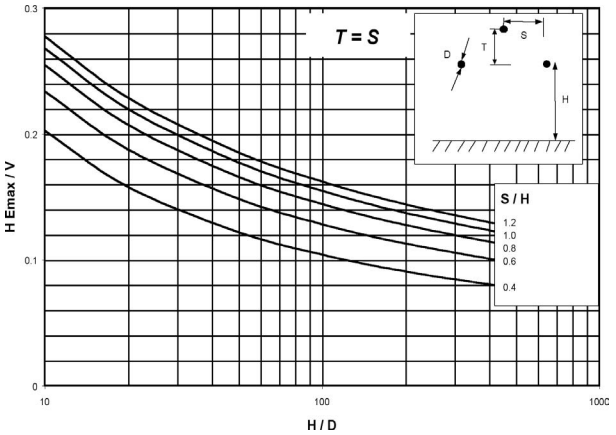


Figure 7.3-7 Nomogram to calculate the maximum electric field at ground, *Emax*, for lines of delta configuration (with T/S = 1).

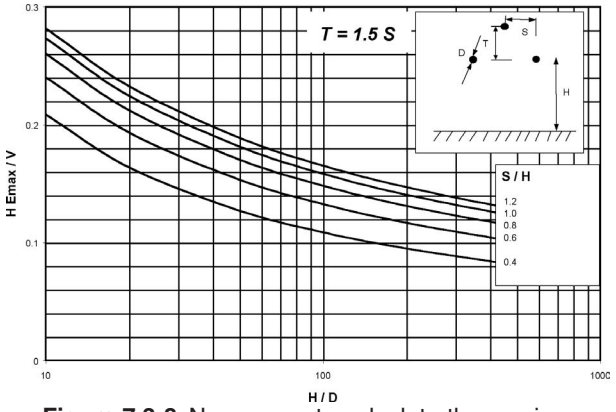


Figure 7.3-8 Nomogram to calculate the maximum electric field at ground, *Emax*, for lines of delta configuration (with T/S = 1.5).

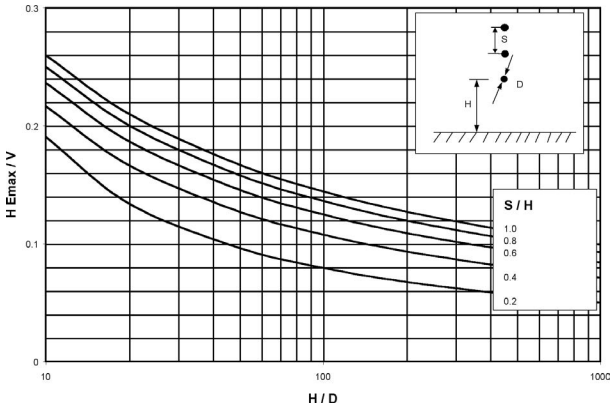


Figure 7.3-9 Nomogram to calculate the maximum electric field at ground, *Emax*, for lines of vertical configuration.

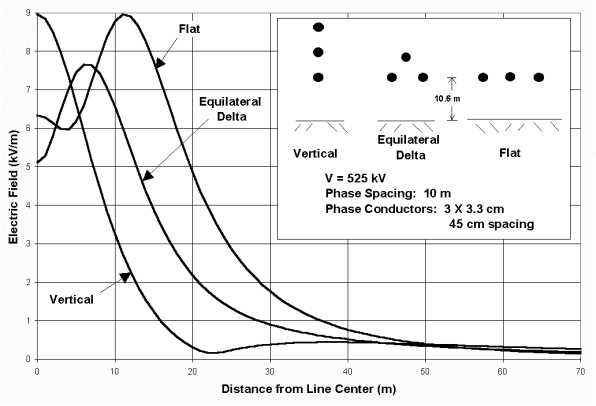


Figure 7.3-10 Effect of line configuration on the electric field at ground level.

7.3.4 Effect of Line Parameters

Effect of Line Configuration

Figure 7.3-10 shows the electric field profiles of three different single-circuit line configurations: flat, equilateral delta, and vertical. Voltage, phase spacing, conductor diameter, and clearance to ground are the same. The maximum electric field at ground is the lowest for the equilateral delta configuration. The electric field of the vertical line is the lowest at the edge of the right-of-way and beyond, while the field of the flat configuration is the highest.

Effect of Line Height

The line height is the parameter that has the greatest influence on the maximum field at ground. However, increasing the line height requires taller or more frequent towers. The effect of line height cannot be easily observed from the curves of Figures 7.3-5 – 7.3-9. The vertical axis variable implies an inverse proportionality between maximum field at ground, E_{max}, and height, H. However, H is contained also in the horizontal axis variable and in the parameter S/H. The relation between H and E may be expressed by the empirical equation:

$$\frac{E_1}{E_2} = \left(\frac{H_1}{H_2}\right)^m \qquad 7.3\text{-}16$$

E_1 and E_2 are the maximum fields for lines of minimum heights H_1 and H_2, respectively. The value of m depends on the line configuration. For single-circuit lines with a flat configuration $m \approx -1.4$ and for lines with an equilateral delta configuration $m \approx -1.6$. For instance, assume that the maximum field of a line with flat configuration is 8.8 kV/m for a 10.6 m height above ground. An increase of 1 m to a height of 11.6 m, will reduce the maximum field at ground to $8.8\ (11.6 / 10.6)^{-1.4} = 7.8$ kV/m.

The field at ground outside the transmission-line corridor is influenced by a change in line height in a completely different way. An example is shown in Figure 7.3-11. An increase in line height causes a decrease in the electric field up to a critical distance, L_c, but causes an increase in electric field at greater distances. Thus, increasing the line height is not desirable if the greatest concern is the electric field outside the transmission corridor. As a corollary of this discussion, the electric field outside the transmission corridor is generally greater toward the towers than at midspan.

The critical distance, L_c, at which a change in line height does not cause a change in electric field, is a function of the line parameters, particularly the line height. For lines of horizontal configuration, $L_c \approx (1.8 – 2.6)$ times the height H.

Effect of Sag

The effect of sag is normally neglected if the lateral profile is taken at the lowest point of the catenary. In this case, the difference in the calculation of the electric field near ground with and without accounting for the sag is less than 1% within the transmission corridor. This difference, expressed as a percentage of the field, increases with the distance from the line, but in absolute value is always negligible. For instance, for the 525-kV line of Figure 7.3-4, the field at 76 m from the line center at midspan calculated accounting for the sag is 128 V/m, while it is 116 V/m when the sag is not taken into account. This result was obtained using a 3-D electric field computer program (see Appendix 7.6) for an example in which the sag was 16.8 m and the span was 300 m. The effect of sag is negligible, not only at the point of minimum clearance, but also when the lateral profile is calculated with Equations 7.3-6 – 7.3-10 in the middle third of the catenary (middle third of the span when the two suspension points are at the same level), provided the height used in the calculations is the height of the conductors at the cross section where the profile is calculated. Closer to the suspension points, however, electric

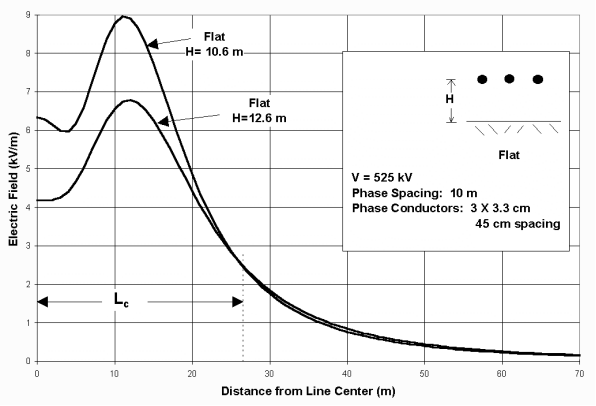


Figure 7.3-11 Effect of line height on the electric field at ground level.

field calculations made with 2-D algorithms may be significantly in error because of the cusp formed by the conductor at the suspension point and because the tower has a shielding effect. Both these factors may be taken into account using a 3-D electric field computer program.

Effect of Conductor Dimensions

The ground level electric field increases with conductor size. The effect of conductor size is practically independent of location. The field is approximately proportional to *log(P/D)* where *P* is the phase spacing and *D* the conductor diameter (equivalent diameter in the case of conductor bundles).

Effect of Phase Spacing

More compact lines produce lower electric fields at ground level. The electric field is approximately proportional to *log(P/D)* where *P* is the phase spacing and *D* the conductor diameter (equivalent diameter in the case of conductor bundles). Depending on the level of compaction, the line design may be controlled by support structure design, corona, radio and audible noise, insulation, maintenance, and other considerations.

Effect of Shield Wires

The overhead shield wires used for lightning protection and increasingly for communications do not have any appreciable effect on the ground-level electric field. Their presence causes a reduction of only 1 - 2% of the ground-level electric field.

Effect of Voltage

The electric field is proportional to the power line voltage. For the purpose of calculating electric fields, the voltages of a three-phase line may be considered perfectly symmetric (at 120° phase angle with each other).

Effect of Soil Conductivity

The conductivity of the soil is the least influential parameter. Even relatively dry soil has a conductivity much greater than that of air. Compared to air, the soil may be considered a perfect conductor. Extremely dry gravel or rock may lower the effective location of the ground plane representing the conductive earth only by a few tens of centimeters, which has a negligible effect on the electric field. If there is grass or other compact vegetation, the effective ground plane rises to be near the top of the vegetation.

Effect of Line Bends

Calculation of the electric field near line bends requires computational procedures for 3-D geometry (see Appendix 7.6 and Applet EMF-4). An example of electric field contour lines calculated for a 345-kV line making a 45° angle is shown in Figure 7.3-12. The field outside the right-of-way is increased inside the bend and decreased outside the bend.

Effect of Uneven Terrain

Calculation of the electric field above an uneven terrain requires advanced analytical techniques (Simpson and Brice 1987; Appendix 7.6). If the terrain is rolling, the electric field will be increased at the top of the roll and decreased at the bottom of the roll. The terrain factor, defined as the ratio between the electric field with the actual terrain and the electric field with a flat ground is shown in Figure 7.3-13. The terrain factor is a function of the terrain and not of the type of line. The maximum terrain factor, TF_{max}, at the top of the roll, and the minimum terrain factor, TF_{min}, at the bottom of the roll, can be estimated (for $B/A < 0.3$) as indicated in Equations 7.3-17 and 7.3-18.

$$TF_{max} = 1 + 1.6\ B/A \quad (7.3\text{-}17)$$

$$TF_{min} = 1 - 1.6\ B/A \quad (7.3\text{-}18)$$

First, calculations should be made for a flat terrain at the bottom of the rolls, and then the field at the top and at the bottom of the rolls should be calculated multiplying the flat-terrain electric field by the terrain factor.

Effect of Trees and Objects

The presence of conductive objects at ground potential has a significant effect on the electric field. In general, the effect consists in a field reduction. Shields consisting of grounded wires can be specifically designed for that purpose. Shielding caused by trees and other objects is discussed in Section 7.16.

7.3.5 Electric Field of Double-Circuit Lines

The relative phasing of the two circuits has a profound effect on the electric field at ground level. Figure 7.3-14 shows an example of the electric field lateral profile of a 525-kV double-circuit line with the conductors of each circuit configured vertically with different phase arrangements. Figure 7.3-15 shows an example of a 345-kV double-circuit line consisting of two delta circuits side by

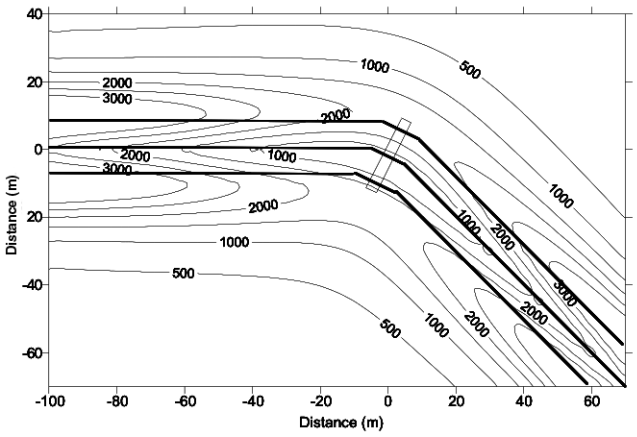


Figure 7.3-12 Electric field contour line near a line bend. Example of a 345-kV vertical line and a 45° angle.

side. If the phasing of one circuit is kept the same, there are six combinations of the phases of the other circuit, of which five result in different electric field profiles (arrangement ABC/CAB gives a profile symmetric to that of arrangement #4: ABC/BCA). Phase arrangement #1 in both cases is called "superbundle," because phase A and A^l, B and B^l, C and C^l in Figure 7.3-14 and phases A and A^l, B and B^l in Figure 7.3-15, may be considered as one large bundle of conductors at the same voltage. The superbundle arrangement corresponds to the highest electric fields (and also magnetic fields) at ground and to the lowest electric field at the conductors. Therefore, the superbundle corresponds to the lowest possible level of corona effects: corona loss, radio noise, and audible noise.

Phase arrangement # 5 corresponds to the lowest electric (and magnetic) fields at ground and to the highest electric field at the conductors and, therefore, produces the highest level of corona effects. This arrangement is called "low-reactance," because it also corresponds to the lowest reactance of the transmission line should this be composed of the two circuits tied together and carrying power in the same direction. Phase arrangement #6 consists of one circuit energized and the other grounded.

All the field values plotted in Figures 7.3-14 and 7.3-15 were calculated accounting for the presence of shield wires. Their influence on the electric field, however, was found negligible.

7.3.6 Electric Field in Substations

Electric field effects in substation are of the same type as those close to transmission lines. Induced currents and spark discharges depend on the particular situation and on the intensity of the electric field. The electric field at one meter above ground is a useful parameter to characterize the electric field environment of a substation as well.

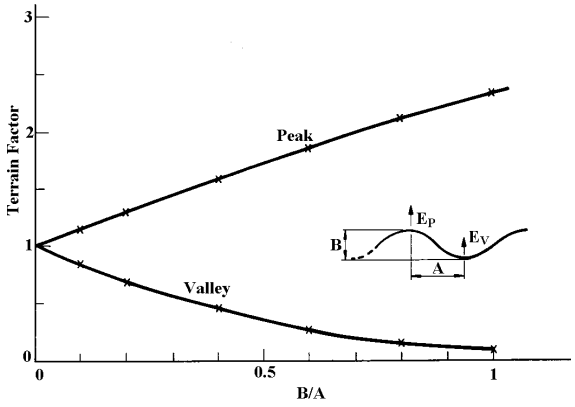


Figure 7.3-13 Terrain factor for rolling terrain.

In designing a new substation, the electric field of existing substations is a useful reference. The electric field at one meter above ground may be conveniently described by electric field contour lines traced on the plan view of the substation (EPRI 1982). Contour maps are a convenient way to show how the electric field at ground level is distributed within the substation area. For example, in a 500-kV substation, the maximum measured electric field at ground level was 8.5 kV/m. Typically, electric fields of about 2 kV/m were measured close to breakers and disconnects between phases, whereas values close to 6 kV/m were measured off the outside phases, where access roads or walk areas may be present.

Working areas usually have lower electric fields. For instance, if the breaker heads are de-energized for servicing, the fields around the heads will be lower unless they are close to an energized bus. The electric field near substation structures is very nonuniform. All the support structures are at ground potential and shield the region near ground.

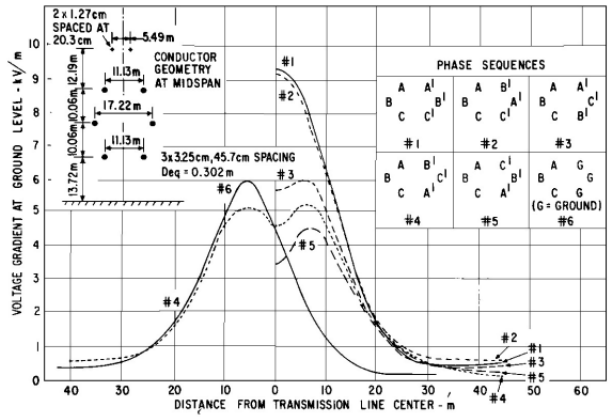


Figure 7.3-14 Electric field at ground level for a double-circuit 525-kV line consisting of two vertical circuits, different phase arrangements.

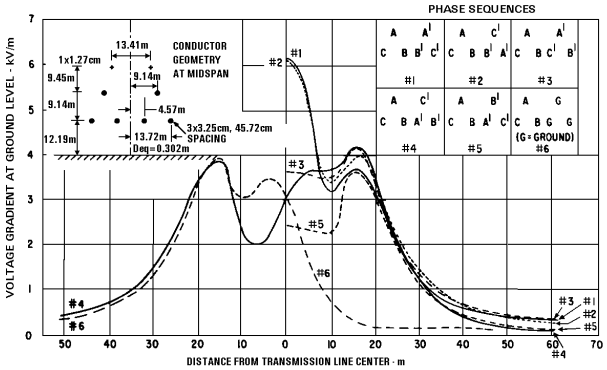


Figure 7.3-15 Electric field at ground level for a double-circuit 345-kV line consisting of two delta circuits, different phase arrangements.

The maximum values of the electric field at one meter above ground and typical geometrical characteristics of substation buses in North America are listed in Table 7.3-1. A limited amount of data on maximum electric field at ground measured in substations in different countries is available (Vinh and Yi 1982).

Table 7.3-1 Electric Field at One Meter Above Ground in Substations

Voltage	Max. Measured Electric Field	Typical Values Off Outer Phase[1]	Bus Height	Bus Phase Spacing	Base Height
(kV)	(kV/m)	(kV/m)	(m)	(m)	(m)
230		5.0	5.5	3.5	3.5
345	7.5	6.5	7	4.5	4.0
500	8.5	6.0	9	5.0	5.0
765	9.0	8.5	12	6.5	6.5

1. Representative maximum electric fields at ground level encountered along buses far from terminations and discontinuities.

The maximum electric field occurs at a distance of a few meters off the outer phases. The electric field may be reduced by designing substations with a large value of the bus height. Simpler procedures, however, may reduce the field even more. For instance, a grid of grounded wires strung off the outer phases at the height of the base will easily reduce the electric field by a factor of two or more, depending on the number and separation of the wires (see Section 7.16).

Air model facilities, using both power-frequency or high-frequency (24-kHz) voltages, have been used in the past to assess the electric field of substations (Sebo 1978; EPRI 1982). The use of calculation techniques for three-dimensional geometry, discussed in Appendix 7.6 and used in Applet EMF-4, makes the use of these models obsolete.

7.4 CALCULATION OF MAGNETIC FIELDS

7.4.1 General Method for Transmission Lines

In most cases, the magnetic field generated by transmission lines may be calculated with sufficient accuracy using a two-dimensional simplified analysis. Magnetic fields can be calculated using Applet EMF-6. The assumptions on which this analysis is based are the following:

- The conductors form infinitely long straight lines parallel to each other.
- The earth is a poor conductor for magnetic fields. The presence of the earth can be simulated by images of the conductors placed at a complex depth, which may be approximated by a real depth. The image depth is usually so large that, for calculations near transmission lines, the images may be neglected without loss of accuracy.
- Once the presence of the earth is accounted for using the images of the conductors, the time-varying magnetic field generated by a transmission line may be treated as quasistatic—i.e., as essentially a static field because the wavelength is much larger than the dimensions under consideration.

Consider the cross section of a conductor above the earth shown in Figure 7.4-1.

The figure shows the conductor and its image, placed at the image depth. For a detailed discussion of image depth, see Appendix 7.5. The image depth is approximately equal to 1.31 δ, where δ is the skin depth of the earth given by Equation 7.4-1.

$$\delta = \sqrt{\frac{\rho}{\pi f \mu}} \qquad 7.4\text{-}1$$

Where:

f is the frequency.
ρ is the resistivity of the soil.
μ is the permeability of the soil.

In most practical cases, the permeability of the soil is close to that of air ($\mu = 4\ \pi\ 10^{-7}$ H/m). For example, for a frequency of 60 Hz and a soil resistivity of 100 Ω m, the image depth is 850 m. This is such a large distance that, for many practical purposes, the contribution of the image conductor to the magnetic field may be neglected.

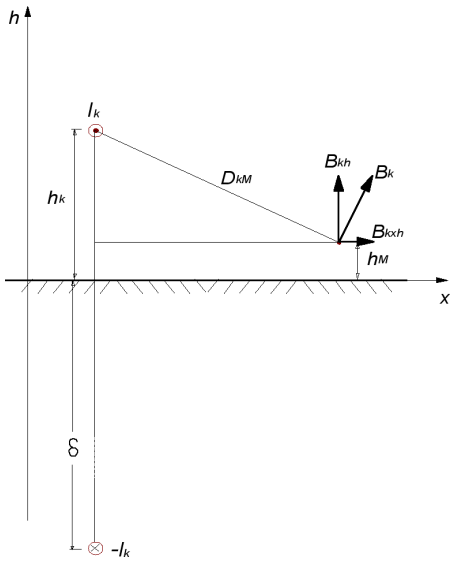


Figure 7.4-1 Magnetic field of an infinitely long conductor above the earth.

The calculation of the magnetic field is relatively straightforward if the amplitude and phase angle of the currents in all the conductors are known.

Consider a conductor, k, with the current I_k and phase angle ϕ_k. The current can be expressed as the sum of its real and imaginary components:

$$\tilde{I}_k = I_{kr} + jI_{ki} \quad 7.4\text{-}2$$

The magnetic field produced by this current has a real and an imaginary component. The real component of the magnetic field, B_{kr}, is caused by the real component of the current, I_{kr}, and is evaluated as indicated in Figure 7.4-1 and Equation 7.4-3. The field, B_{kr}, at a point M is represented by a vector that lies in the plane perpendicular to the conductor k and perpendicular to the line connecting M with the conductor k.

The magnitude of B_{kr} is given by Equation 7.4-3.

$$B_{kr} = 2 \cdot 10^{-7} I_{kr} / D_{kM} \quad 7.4\text{-}3$$

D_{kM} is the distance between conductor k and point M. The field is expressed in tesla, the current in ampere, and the distance in meter. If the field were expressed in mG, Equation 7.4-3 would become the simple expression 7.4-4.

$$\tilde{B}_{kr} = 2\tilde{I}_{kr} / D_{kM} \quad 7.4\text{-}4$$

Equation 7.4-4 neglects the contribution to the field by the image of conductor k in the ground. The image of a line current is not a mirror reflection (see Appendix 7.5). For practical purposes, the earth current can be lumped at an equivalent image location inside the earth as discussed above. The field contributed by the image of conductor k is calculated in the same fashion as for the conductor itself, except that the current in the image conductor should have the opposite direction. Even so, the image depth is usually so large that, for many practical purposes, the contribution of the image conductors to the magnetic field at a point near a transmission line can be neglected.

Using a system of orthogonal coordinates, x (lateral distance) and h (height above ground), as indicated in Figure 7.4-1, the magnitude of the magnetic field, B_{kr}, and of its horizontal and vertical components, B_{krx} and B_{krh}, are given by:

$$B_{kr} = \frac{2 \cdot 10^{-7} I_{kr}}{\sqrt{(x_M - x_k)^2 + (h_M - h_k)^2}} \quad 7.4\text{-}5$$

$$B_{krx} = \frac{2 \cdot 10^{-7} I_{kr}(x_M - x_k)}{(x_M - x_k)^2 + (h_M - h_k)^2} \quad 7.4\text{-}6$$

$$B_{krh} = \frac{2 \cdot 10^{-7} I_{kr}(h_M - h_k)}{(x_M - x_k)^2 + (h_M - h_k)^2} \quad 7.4\text{-}7$$

It should be noted that there is no field in the direction parallel to the conductor.

The same calculations are made to calculate the imaginary part of the magnetic field, B_{ki}, and its horizontal and vertical components, B_{kix} and B_{kih}. The imaginary component of the current, I_{ki}, should be used instead of the real component.

If a power line contains n conductors, with currents I_k and phase angles ϕ_k $(k = 1,n)$, the real and imaginary components of the horizontal and vertical magnetic field at point M are calculated separately for each conductor and then added. The resulting real and imaginary, horizontal and vertical magnetic fields at point M are:

$$B_{rx} = \sum_{k=1}^{n} B_{krx} \quad B_{rh} = \sum_{k=1}^{n} B_{krh} \quad B_{ix} = \sum_{k=1}^{n} B_{kix} \quad B_{ih} = \sum_{k=1}^{n} B_{kih} \quad 7.4\text{-}8$$

A magnetic field meter placed at point M with its probe oriented to measure the horizontal component will measure a magnetic field, B_x, given by:

$$B_x = \sqrt{B_{rx}^2 + B_{ix}^2} \quad 7.4\text{-}9$$

Similarly, the vertical component of the magnetic field is given by:

$$B_h = \sqrt{B_{rh}^2 + B_{ih}^2} \quad 7.4\text{-}10$$

The resultant magnetic field is:

$$B = \sqrt{B_x^2 + B_h^2} = \sqrt{B_{rx}^2 + B_{ix}^2 + B_{rh}^2 + B_{ih}^2} \quad 7.4\text{-}11$$

If the currents used are rms values, the resultant field also is an rms value.

The field components B_{rx}, B_{ix}, B_{rh}, and B_{ih} fully characterize the vector field $\vec{B}$. The parameters of the field ellipse can be calculated as shown in Appendix 7.1 or using Applet EMF-1.

The results for a particular application can be obtained by using Applet EMF-6, "Transmission Line Magnetic Field – 2D." The input data required by this applet are the lateral and vertical coordinates of each conductor, the current and phase angle of each conductor, and the lateral and vertical coordinates of the point at which the magnetic field is calculated.

7.4.2 Example Calculation

The magnetic field was calculated for the same example of 525-kV transmission line used for the electric field (see Figure 7.3-4). The line current in this example is 1000 A. The currents are assumed to be balanced and symmetric. The results are shown in Figure 7.4-2. In addition to the resultant magnetic field, both the maximum field component (in the direction of the major axis of the field ellipse) and the minimum field components (in the direction of the minor axis of the field ellipse) are shown. The figure uses a log scale for the magnetic field, because often the magnetic field is of interest at locations outside the right-of-way, where the field levels may be two orders of magnitude lower than the peak level measured inside the right-of-way. The following observations are noteworthy:

- The magnetic field decays with the distance from the line much less than the electric field. As a corollary of this conclusion, conductor height affects both electric and magnetic fields, but the effect is more pronounced for the electric field.
- The magnetic field varies approximately in inverse proportion with the square of the distance from the center of the conductor configuration. This is shown in Figure 7.4-2 by the dashed line: $B = 3.46IP/D^2$, where I is the current, P is the phase spacing, and D is the distance between measuring point and the center phase.
- Conductor diameter affects electric fields but not magnetic fields.
- The minor axis of the ellipse becomes negligible in relation to the major axis as the distance from the line increases. This indicates that the field ellipse collapses into an oscillating vector with constant direction in space. This is a characteristic of lines with flat configurations.
- The magnetic field is proportional to the line current. While the electric field, which is proportional to the line voltage, is relatively stable in time, the magnetic field has temporal variations depending on the fluctuations of the load. There may be a pronounced dependence on the hour of the day, the day of the week, and the season. For this reason, the current for which calculations are made should be well specified. The results may be better presented in a unit of mG/A, or may be given for the maximum expected load.
- Up to a few hundred meters from the line, the earth return currents have a negligible effect compared to the currents in the line conductors, as shown in Table 7.4-1.
- No effect of shield wires was assumed on the results shown in Figure 7.4-2. This is the case when shield wires are either not present or they are sectionalized and do not carry any current. If shield wires are present and grounded at each structure, they carry currents that may have a small but detectable effect on the magnetic field. Shield wire currents are calculated as shown in Section 7.9 or using Applet EMF-8. An example of the shield wire effect on magnetic field is shown in Table 7.4-2. The effect is different on the two sides of the line; the field is slightly increased on one side and slightly decreased on the other.

7.4.3 Calculation of Magnetic Field from Power Lines Using Simple Equations

The customary method of calculation of the magnetic field produced by a power line is to calculate the field caused by each phase separately and then add up the contributions of all the phases. For the purpose of designing low-field lines or reducing the field of existing lines, it is worthwhile to examine the structure of the magnetic field produced by simple arrangements of conductors.

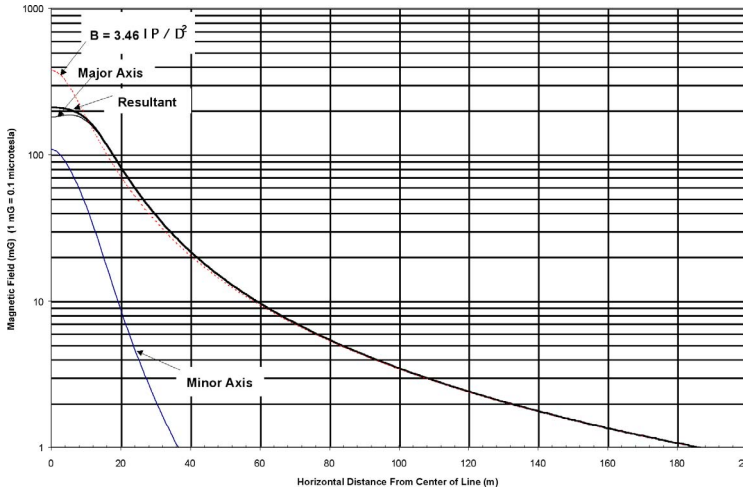


Figure 7.4-2 Magnetic field calculated at 1 m above ground for a three-phase line of flat configuration with 1000 A, phase spacing P = 10 m and height above ground of 10.6 m.

Table 7.4-1 Field Component Due to Earth Currents

Distance from Line Center (m)	Field Due to Conductor Currents (mG)	Field Due to Earth Currents (mG)
0	210	0.08
100	3.5	0.08
200	0.9	0.075
500	0.14	0.05
1000	0.035	0.024
2000	0.009	0.008
5000	0.0014	0.0014

Line: Flat configuration, P = 10 m, H = 10.6 m, I = 1000 A (balanced and symmetric), ground resistivity = 100 Ωm.

Table 7.4-2 Example of Effect of Shield Wires on Magnetic Field of a Three-Phase Line

Distance from Line Center (m)	Field Neglecting Shield Wire Currents (mG)	Field Accounting for Shield Wire Currents (mG)
-200	0.86	0.78
-100	3.47	3.31
0	210.5	210.4
100	3.47	3.65
200	0.86	0.96

Line: Flat configuration, P = 10 m, H = 10.6 m, I = 1000 A (balanced and symmetric); two shield wires at + and – 6.5 m from center, 15.6 m above ground, resistance = 6.7 Ω/mi, reactance = 1.8 Ω/mi @ 1 ft spacing; ground resistivity = 100 Ωm. Shield wires currents are 16.3 A @ 174° (from center phase current) and 15.4 A @ 27°.

The field of a power line can be analyzed efficiently by reducing the set of line currents that form a power line into basic line current elements: monopoles, dipoles, quadrupoles, and higher-order elements. These are described in Appendix 7.2. The equivalent monopole, dipole, and quadrupole of a given set of line currents can be found using Applet EMF-9. Using these elements, the "distant field" of a power line can be predicted accurately using simple equations. Distant field is defined as the field at distances from the center of the power line conductors that are large (e.g., greater than three times) compared to the largest distance between conductors of the power line. Simple equations for the "distant" field of lines with different configurations are shown in Table 7.4-3. The derivation of these equations is in Appendix 7.2.

7.4.4 Calculation of Magnetic Field from Sets of Conductors in Three Dimensions

When currents flow in conductors that can be approximated by straight lines infinitely long and parallel to each other, the magnetic field can be calculated with the method described in Section 7.4.1. Two-dimensional approximations, however, are not practical in many cases. Accurate results require calculations in three dimensions.

For current filaments, one-dimensional paths with zero cross section area, the Biot-Savart law, illustrated in Figure 7.4-3, offers the most convenient calculation tool. Each element, *dl*, of the path of the current *I*, generates a field at the measuring point *P* equal to:

$$d\vec{B} = \frac{\mu}{4\pi r^3} \cdot I \cdot d\vec{l} \times \vec{r} \qquad 7.4\text{-}12$$

$d\vec{l} \times \vec{r}$ is the cross product of the vector $d\vec{l}$ with the vector $\vec{r}$, which is a vector with amplitude $dl \cdot r \cdot \sin(\alpha)$ (α is the angle included by the two vectors) direction orthogonal to both $\vec{r}$ and $d\vec{l}$, and orientation according to the right-hand rule.

The magnetic field caused by a current flowing in a path from point A_1 to point A_2 is obtained by integrating Equation 7.4-12 from A_1 to A_2.

$$\vec{B} = \frac{\mu I}{4\pi} \int_{A_1}^{A_2} \frac{d\vec{l} \times \vec{r}}{r^3} \qquad 7.4\text{-}13$$

The units in 7.4-13 are meter, ampere, and tesla. The field can be expressed in mG by eliminating the term $\frac{\mu}{4\pi}$ (which is the same as multiplying by $\frac{4\pi}{\mu} = 10^7$).

Biot-Savart Law Applied to a Segment

1. If the measuring point is in the plane axis of the segment (Figure 7.4-4)

$$B = \frac{2LI}{R\sqrt{L^2 + 4R^2}} \qquad 7.4\text{-}14$$

(meter, ampere, milligauss)

2. If the segment is infinitely long (L = ∞):

$$B = 2I/R \qquad 7.4\text{-}15$$

(meter, ampere, milligauss)

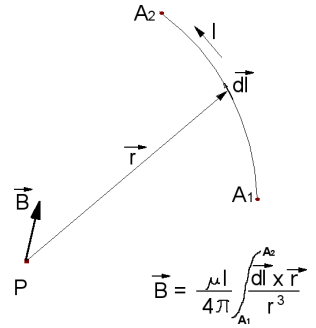
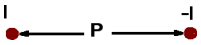
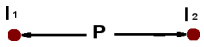
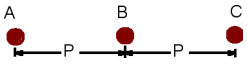
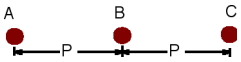
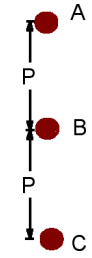
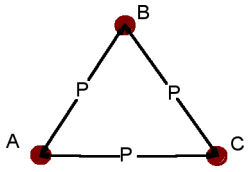
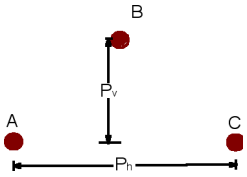
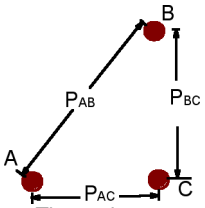
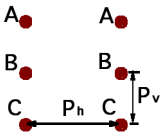
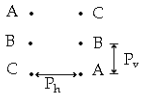
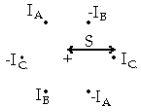
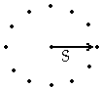
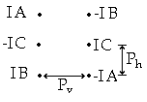


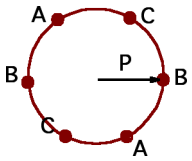
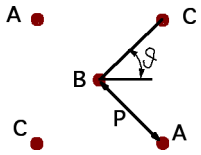
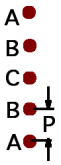
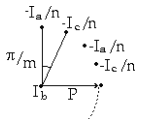
Figure 7.4-3 Illustration of Biot-Savart law.

Table 7.4-3 Distant Field Equations for Different Line Configurations

Configuration	Field[1] at Distance R	Configuration	Field[1] at Distance R
Single Wire	$B = 2I/R$	 Two wires, balanced	$B = 2PI/R^2$
 Two wires, unbalanced	$B_M = 2(I_1 + I_2)/R$ $B_D = P(I_2 - I_1)/R^2$	 Three-phase, flat, balanced	$B = 2\sqrt{3}PI/R^2$ linearly polarized
 I_o, I_1, I_2 Symmetrical components	$B_M = 6I_o/R$ $B_D = 2\sqrt{3}(\tilde{I}_1 - \tilde{I}_2)/R^2$ $B_Q = 2P^2(\tilde{I}_1 + \tilde{I}_2 - 2\tilde{I}_o)/R^3$	 Three-phase, vertical, balanced	$B = 2\sqrt{3}PI/R^2$ linearly polarized
 Three-phase, equilateral delta	$B = \sqrt{6}PI/R^2$ Circularly polarized $B_{MAX} = B_{MIN} = \sqrt{3}PI/R^2$	 Three-phase, non-equilateral delta	$B = \sqrt{3P_h^2 + 4P_v^2} \cdot I/R^2$ Elliptically polarized $B_{MAX} = \sqrt{3}P_h I/R^2$ $B_{MIN} = 2P_v I/R^2$
 Three-phase, general, balanced	$B = \sqrt{6}P_{eq} I/R^2$	 Double circuit, Currents: I_1, I_2 Same phasing	$B = 2\sqrt{3}P_v(I_1 + I_2)/R^2$
 Double circuit, Currents: I_1, I_2 Reverse phasing	$B_d = 2\sqrt{3}P_v(I_1 - I_2)/R^2$ $B_{q\max} = 2P_v^2(I_1 + I_2)/R^3$ $B_{q\min} = 2\sqrt{3}P_v P_h(I_1 + I_2)/R^3$ $B_q = 2P_v\sqrt{P_v^2 + 3P_h^2}(I_1 + I_2)/R^3$	 Six-phase, circular	$B_{\max} = B_{\min} = 6SI/R^2$ $B = 6\sqrt{2}SI/R^2$ Circularly polarized (I is the current in each phase)
 Twelve-phase circular	$B_{\max} = B_{\min} = 12SI/R^2$ $B = 12\sqrt{2}SI/R^2$ (I is the current in each phase)	 Six-phase vertical	$B_{\max} = 4P_h I/R^2$ $B_{\min} = 4\sqrt{3}P_v I/R^2$ $B = 4\sqrt{P_h^2 + 3P_v^2} \cdot I/R^2$ Elliptically polarized (I is the current in each phase)

1. B (mG) is the magnetic field, R (m) is the distance from the center of the set of wires, P (m) is the spacing between wires, and I is the current (A). B_M (mG) is the monopolar component, which varies in inverse proportion to distance, B_D (mG) is the dipolar component, which varies in inverse proportion to the square of the distance, and B_Q (mG) is the quadrupolar component, which varies in inverse proportion to third power of the distance. Bmax is the component along the major axis of the field ellipse and Bmin is the component along the minor axis of the field ellipse.

Table 7.4-3 Distant Field Equations for Different Line Configurations (Continued)

Configuration	Field[1] at Distance R	Configuration	Field[1] at Distance R
A • • C B • • B C • • A Three-phase, split phases, vertical.	$B_{max} = 2\sqrt{3}P_v P_h I/R^3$ $B_{min} = 2P_v^{\,2} I/R^3$ $B = 2P_v\sqrt{3P_h^{\,2} + P_v^{\,2}}\, I/R^3$ Elliptically polarized (I is the current per phase, twice the conductor current)	 Three-phase, split phases, circular.	$B_{max} = B_{min} = 3P^2\, I/R^3$ $B = 3\sqrt{2}P^2 I/R^3$ Circularly polarized (I is the current per phase, twice the conductor current)
 3-Phase, split phases, cruciform.	$B_{max} = 2\sqrt{3}P^2 \cdot \sin(2\vartheta) I/R^3$ $B_{min} = 2P^2 \cdot \cos(2\vartheta) I/R^3$ $B = 2P^2 \cdot (I/R^3) \cdot \sqrt{3\sin^2(2\vartheta) + \cos^2(2\vartheta)}$	 3-Phase, split phases, vertical.	$B = 2\sqrt{13}P^2\, I/R^3$ Linearly polarized (I is the current per phase, twice the conductor current)
A B C B A Three-phase, split phases, horizontal.	$B = 2\sqrt{13}P^2\, I/R^3$ Linearly polarized (I is the current per phase, twice the conductor current)		$B = \dfrac{2\sqrt{3n!}\,P^n \cdot I}{2^{\frac{n(n-1)}{2}} \cdot R^{n+1}}$ Linearly polarized

1. B (mG) is the magnetic field, R (m) is the distance from the center of the set of wires, P (m) is the spacing between wires, and I is the current (A). B_M (mG) is the monopolar component, which varies in inverse proportion to distance, B_D (mG) is the dipolar component, which varies in inverse proportion to the square of the distance, and B_Q (mG) is the quadrupolar component, which varies in inverse proportion to third power of the distance. Bmax is the component along the major axis of the field ellipse and Bmin is the component along the minor axis of the field ellipse.

3. In the general case: measuring point (x_p, y_p, z_p); segments from A_1 (x_1, y_1, z_1) to A_2 (x_2, y_2, z_2)

$$B = B_x\vec{u}_x + B_y\vec{u}_y + B_z\vec{u}_z \qquad 7.4\text{-}16$$

$\vec{u}_x, \vec{u}_y, \vec{u}_z$ are the unit vectors in the x, y, z directions

$$B_x = \frac{2I}{L} K\left[(z_p - z_1)(y_2 - y_1) - (y_p - y_1)(z_2 - z_1)\right] \qquad 7.4\text{-}17$$

$$B_y = \frac{2I}{L} K\left[(x_p - x_1)(z_2 - z_1) - (z_p - z_1)(x_2 - x_1)\right] \qquad 7.4\text{-}18$$

$$B_z = \frac{2I}{L} K\left[(y_p - y_1)(x_2 - x_1) - (x_p - x_1)(y_2 - y_1)\right] \qquad 7.4\text{-}19$$

$$K = \frac{1}{D^2 - D_0^2} \cdot \left[\frac{L + D_0}{\sqrt{L^2 + 2LD_0 + D^2}} - \frac{D_0}{D}\right] \qquad 7.4\text{-}20$$

L is the length of the segment
D is the distance between point P and point A_1
D_0 is the projection of the segment PA on the line A_1A_2.

$$D_0 = \frac{(x_1 - x_p)(x_2 - x_1) + (y_1 - y_p)(y_2 - y_1) + (z_1 - z_p)(z_2 - z_1)}{L}$$

The units in the above equations are m, A, and mG.

The field produced at a point P by a set of current-carrying segments is calculated by adding the contributions of all segments to the field components along each coordinate axis, calculated using Equations 7.4-17 to 7.4-21. These calculations can be performed for a variety of practical geometry by using Applet EMF-7.

Effect of Line Sag

The effect of line sag can be found using the 3-D method of magnetic field calculations (Applet EMF-7). This effect is appreciated by examining the magnetic field contour

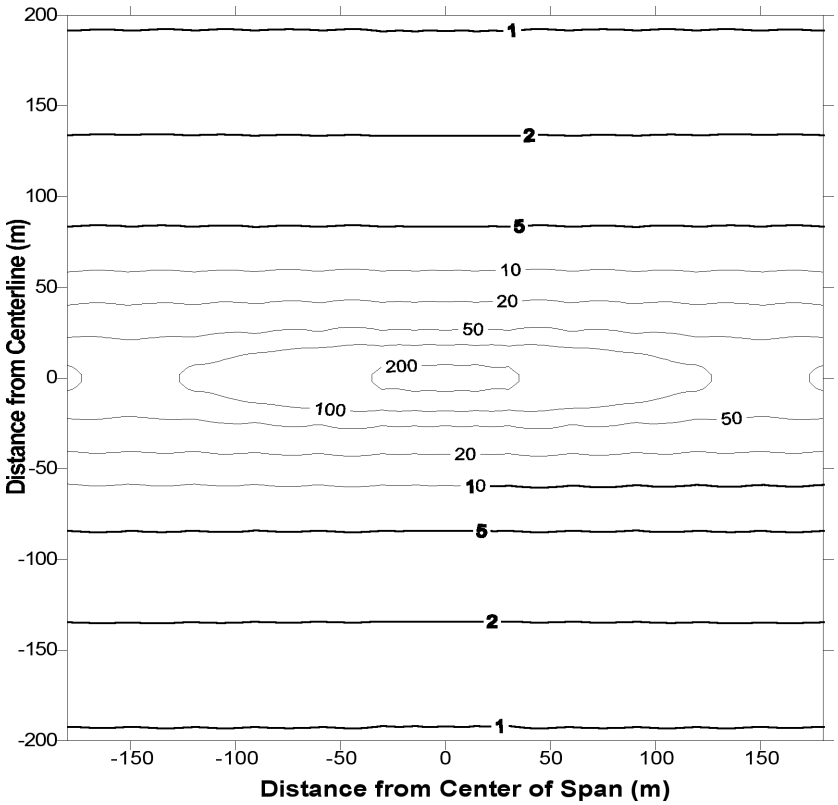


Figure 7.4-5 Example of magnetic field (mG) contour lines at 1 m above ground for one span (300 m) of a line with flat configuration, 10-m phase spacing, 10-m sag and 20 m at the tower attachment points. Line current is 1000 A.

lines calculated at 1 m above ground in an area encompassing one span. An example is shown in Figure 7.4-5.

If a lateral profile is taken at the lowest point of the catenary, the difference in the calculation of the magnetic field at ground level with and without accounting for the sag is negligible. For instance, for the line of Figure 7.4-5, the magnetic field at 1 m above ground under the center phase is 223 mG accounting for the sag and 227 mG if the line is assumed at constant height (same as the minimum height). At a distance of 100 m from centerline, the field at 1 m above ground is 3.55 mG accounting for the sag and 3.53 mG assuming a constant line height.

Magnetic Field in Substations

An application of the 3-D method of calculation is the calculation of magnetic field in substations. Substations for 230 kV and above are largely outdoor, open-air substations. Of interest is the magnetic field inside and outside the substation, particularly at the substation boundary.

The electrical equipment that must be considered for calculating the magnetic field are the overhead high-voltage lines entering or exiting the substation, the substation buses connecting these lines to the transformer bushings, and the underground cables that exit the substation. Each section of line, or bus, or cable must be simulated with a current-carrying segment. The magnetic field from transformers or other substation equipment is frequently negligible compared with the magnetic fields from lines, buses, and cables. It is frequently observed that the largest magnetic fields around the perimeter of a substation are those produced by lines entering or leaving the substation.

The magnetic field is calculated applying the Biot-Savart law (Equations 7.4-12 to 7.4-20). Magnetic field can also be calculated by exercising Applet EMF-7.

7.5 MEASUREMENT OF ELECTRIC FIELDS

7.5.1 Techniques for Measuring the Unperturbed Electric Field

There are different types of meters suitable for the measurement of electric fields from ac power lines. IEEE Standard 644: “Standard Procedures for Measurement of Power Frequency Electric and Magnetic Fields from AC Power Lines” recommends a free-body type meter (IEEE 1994a).

This meter measures the current between two halves of a conductive, isolated body (Deno 1976). The free-body meter is suitable for survey-type measurements because it is self-contained and portable, allows measurements above ground, and does not require a known ground reference.

Other types of electric field meters include ground-reference-type meters, which measure the current to ground of a probe, and electro-optic field meters that measure changes in the transmission of light through a fiber or crystal due to the influence of the electric field. Ground-reference-type meters should be used above grounded conducting surfaces and have found only limited applications. Several electro-optic methods can be used for measuring electric fields, but their application has been limited to laboratory situations.

An electric field meter consists of two parts, the probe and the detector. The probe is the field sensor that produces an electrical signal that is processed by the detector. For free-body meters, the detector is contained in the probe or is an integral part of it and is battery operated. The probe and detector measure the power-frequency-induced current generated by the charge oscillating between the conductive halves (electrodes) of the probe.

Figure 7.5-1 shows the two electrodes of a portable electric field meter. A box containing the detector circuit and the visual display is located between the electrodes. An insulating handle allows the user to hold the meter away from the body at a distance long enough not to affect the measurements (see Figure 7.5-2).

The free-body electric field meter measures the oscillating current flowing between the top electrode and the bottom electrode. This current provides the surface charge to the two electrodes that are at the same potential. A closed-form mathematical expression for the current induced by the electric field is possible when the meter is shaped like a sphere and the two electrodes are hemispheres oriented in the direction of the field to be measured (see Figure 7.5-3).

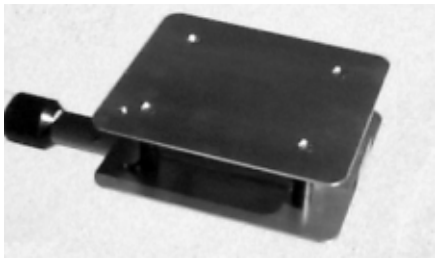


Figure 7.5-1 Free-body ac electric field meter.

Equation 7.5-1 gives the surface charge density, σ, on a conductive sphere in a uniform electric field.

$$\sigma = 3\varepsilon \cdot e \cdot \cos\theta \ \left(\mathrm{C/m^2}\right) \qquad 7.5\text{-}1$$

Where:

- ε is the dielectric constant of air, ($\varepsilon = 8.854 \cdot 10^{-12}$ F/m).
- e is the unperturbed electric field.
- θ is the angle between the direction of the field and the point on the sphere surface where the charge density is calculated.

Integrating the charge density over a hemisphere gives the instantaneous value of the total charge on the hemisphere:

$$q = \int_{\Phi=0}^{2\pi} \int_{\theta=0}^{\pi/2} 3\varepsilon\, e \cos\theta \cdot r \sin\theta \, d\Phi \cdot r \, d\theta \quad = 3\pi\varepsilon \cdot e \cdot r^2 \qquad 7.5\text{-}2$$

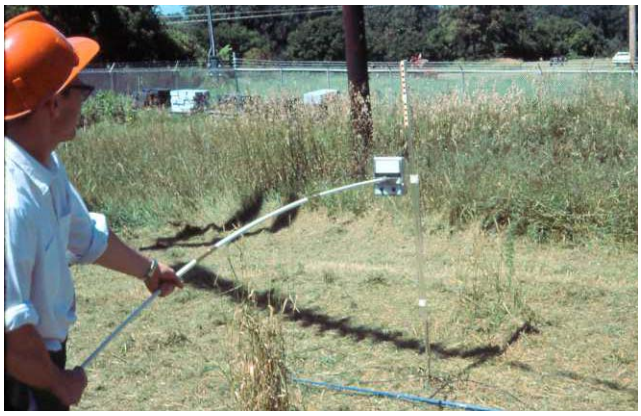


Figure 7.5-2 Measurement of the unperturbed electric field near ground.

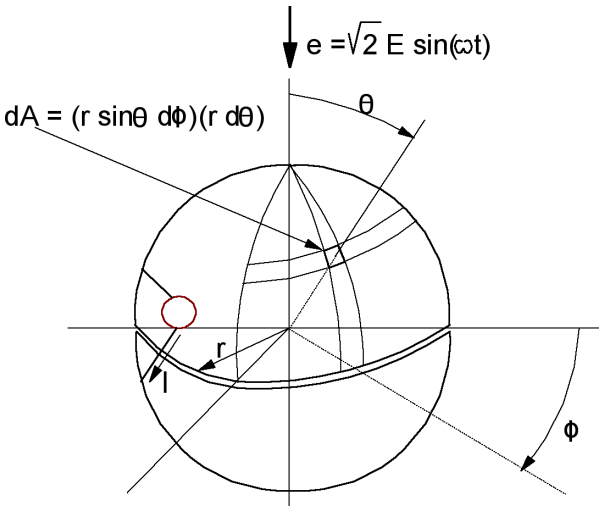


Figure 7.5-3 Current between two hemispheres induced by an electric field.

If the electric field is sinusoidal at a frequency *f*, it can be expressed by Equation 7.5-3, where *E* is the rms value of the field.

$$e = \sqrt{2}E\sin(\omega t)$$
$$\omega = 2\pi f \qquad 7.5\text{-}3$$

The current between the two hemispheres is:

$$i = dq/dt = 3\pi\omega\varepsilon r^2\sqrt{2}E\cos(\omega t) \qquad 7.5\text{-}4$$

The rms value, *I*, of the current is related to the rms value of the field, *E*, by:

$$I = 3\pi\omega\varepsilon r^2 E \qquad 7.5\text{-}5$$

For instance, if E = 1 kV/m and r = 0.1 m, at 60 Hz, the induced current is I = 0.315 μA.

For practical reasons the electrodes are not shaped like a sphere. Therefore, calibration of the meter in a known electric field is necessary. In all cases, however, there is a direct proportionality between induced current and unperturbed electric field. This allows setting the calibration constant independently of the field value.

$$E = \frac{kI}{f} \qquad 7.5\text{-}6$$

Free-body electric field meters are calibrated to read the rms value of the electric field component along the axis of the instrument. The axis of the instrument coincides with the axis of symmetry. If the electrodes are not symmetric, the meter axis must be specified. Equation 7.5-5 applies only to electric fields that are sinusoidal, such as those of most power lines, and at the frequency for which the meter has been calibrated. For these fields, any type of detector (rms, rectified average, etc.) is adequate for accurate measurements. If the electric field contains harmonics, however, the readings of the instrument depend on the type of detector. Some meters may be switched from one type of detector to another and provide a measure of the amount of electric field harmonics.

Equations 7.5-5 and 7.5-6 assume a uniform electric field. However, nonuniform fields also are measured with negligible errors.

The electrodes of the free-body meter cannot be placed in contact with the conductive surface of a body without severely perturbing the field. However, measuring the electric field close to the surface of grounded objects causes very little error. For instance, if the distance between the center of the instrument and the surface of a grounded object is greater than the largest dimension of the meter, the measurement error is less than 5%.

Since the meter measures only one component of the electric field, it is common practice to change the orientation of the meter axis by turning the handle or rotating it in the vertical plane until a maximum electric field value is read. This is the maximum field component, and it lies along the major axis of the field ellipse. In power line situations, measurements are often made near the ground (for instance, at a height of about 1 m). In these cases, the field meter may be held to measure the vertical component of the electric field. The vertical component practically coincides with the maximum field, while the horizontal component is negligible in comparison.

Measurement standards provide guidance for the measurement of power-frequency electric fields from ac power lines (IEEE 1994a). Calibration of the meter may be performed in a parallel plate system that generates a known electric field (Shih et al. 1977; Takuma et al. 1985). The recommended geometry consists of parallel plates 1.5 m x 1.5 m, with 0.75 m spacing between plates. The electric field strength at the center of this system is within 1% of the uniform field given by the voltage between plates divided by the plate spacing. This small error is predicated on the condition that the electric field meter has no diagonal dimension greater than 0.23 m. Once an electric field meter has been calibrated in a parallel plate system, its calibration can be more conveniently checked by injecting a known current between the electrodes.

Another calibration method is to measure the current flowing between a conductive plate of known area and a flat ground (EPRI 1982). Although this method is less accurate than the parallel plate method, it is convenient for transmission-line work because it employs the ac field generated by the line itself. The current induced in a 1×1-m plate by an electric field at a frequency, *f*, has a magnitude given by:

$$I = 2\pi f\varepsilon E \qquad 7.5\text{-}7$$

In a 60-Hz field of 1 kV/m, the current collected by the plate is 3.34 μ A; in a 50-Hz field, the current is 2.78 μ A. Conversely, if the measured induced current is *I* (ampere), the electric field is:

$$E = \frac{I}{2\pi f\varepsilon} = 3\cdot 10^8 I \ (\textit{for } 60\ \textit{Hz}),$$
$$= 3.6\cdot 10^8 \ (\textit{for } 50\ \textit{Hz}) \ \left(\mathrm{V/m}\right) \qquad 7.5\text{-}8$$

To obtain accurate results, an insulating sheet must be placed between the plate and the ground, and a guard ring must be placed around the plate and grounded through a

separate connection, other than that between plate and ground through the measuring ammeter (see Figure 7.5-4). For best accuracy, the plate should be a little less than 1 m^2. The air gap that separates the plate from the guard ring must have the edges perfectly aligned on a flat plane so that the dielectric flux is divided equally between plates and guard ring. The effective area of the plate is equal to the area of the center panel plus one half the area of the gap. The width of the guard ring should be at least five times the height of the plate above the virtual ground. The virtual ground may be a few centimeters below the surface of dry gravel, macadam, or the like. To minimize field distortion, the meter and the operator should be away from the plate and the operator must kneel.

The procedure recommended by the IEEE for measuring the lateral profile of the electric field of transmission lines consists of holding the meter at the height of 1 m above ground, at a distance of at least 2.5 m from the operator (see Figure 7.5-2) (IEEE 1994a). Usually, however, only small errors are encountered when the meter is kept at 1 m height even when the meter is kept at 1.5 m from the operator (DiPlacido et al. 1978). The measured field would be greater than the unperturbed field if the meter were kept at a height greater than 1 m, because the body of the operator would enhance the field at those heights. At heights lower than 1 m, the operator would partially shield the meter and the measured field would be lower than the unperturbed field.

The typical accuracy of practical outdoor electric field measurements is near 10%, but in controlled conditions it is easily better than 5%. The accuracy is limited by a number of factors that include:

- distortion of the field caused by the body of the person holding the meter,
- conductivity of the handle (measurements in the presence of moisture may give erroneous results),
- error in reading a display at a distance,
- error in calibrating the meter,
- difficulty in positioning the meter at the desired point and with its axis in the desired direction,
- an error dependent on the detector type, particularly if the field has a significant harmonic content.

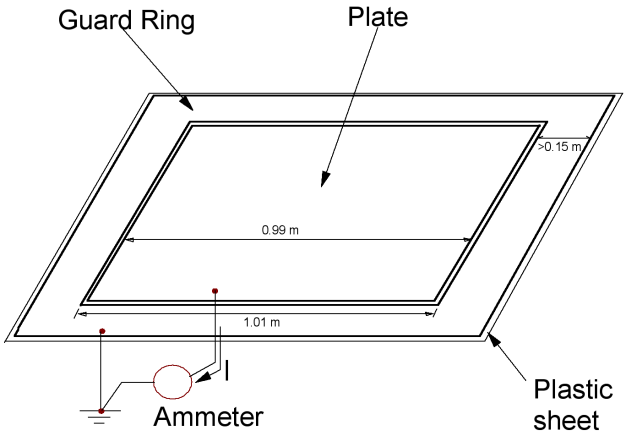


Figure 7.5-4 Conductive plate arrangement for field meter calibration near a power line.

When comparing measured and calculated values of the electric field, it must be noted that errors may occur both in the measurements and in the calculations. Calculation errors may occur because the geometry may not be well known or is not well simulated, the terrain may not be flat, and objects that cannot be well simulated in the calculations may perturb the field. If the terrain is not flat, the field close to ground will be enhanced by hills and reduced by valleys. If the ground is irregular or if there is tall grass, a virtual average ground that accounts for these irregularities should be assumed for the calculations and the measurements should be made away from any protuberance. The presence of bushes or trees will reduce the field at ground, often by a significant amount (see Section 7.16).

7.5.2 Measurement of the Electric Field on a Boundary Surface

The electric field, E, on a boundary surface may be determined by measuring the current, I, induced in a known area, S, and using Equation 7.5-9.

$$I = 2\pi f \varepsilon E S \qquad 7.5\text{-}9$$

An example of an application is the measurement of the electric field at ground by means of a flat plate, as shown in the previous section. The technique used for more complex surfaces is shown in Figure 7.5-5. In this example, the current is measured from a sensor consisting of a small square of copper foil surrounded by more copper foil that acts as a guard ring. A coaxial cable, with its shield connected to the



Figure 7.5-5 Measurement of electric field on a boundary surface.

guard ring and grounded, is used to connect the sensor to the ammeter.

7.5.3 Measurement of the Space Potential

The space potential is a very useful parameter to characterize the induction by electric fields in tall vertical objects in a transmission-line environment or in objects in a nonuniform electric field such as in a substation. In fact, the currents induced in objects in a nonuniform field are a function of the unperturbed space potential and not of the unperturbed electric field.

A technique suitable for the measurement of space potential is shown in Figure 7.5-6. The probe consists of a conductive object of small dimensions, placed at the measuring point and grounded through a shielded wire. An ammeter is placed in series with the wire between the probe and the ground. The shield of the wire is connected to the case of the meter and to ground. The current collected by the shield should flow to ground bypassing the meter. The measuring system is shown schematically in Figure 7.5-7.

The current induced in the probe is given by:

$$I_{probe} = k\,[(V_{sp} - V_{probe}) + L \cdot E] \qquad 7.5\text{-}10$$

Where:

- k is a coefficient of proportionality, which depends on the shape of the probe.
- V_{sp} is the space potential before insertion of the probe (unperturbed space potential). V_{probe} is the voltage of the probe.
- E is the unperturbed electric field at the probe location.
- L is a dimension function of the geometry of the probe.

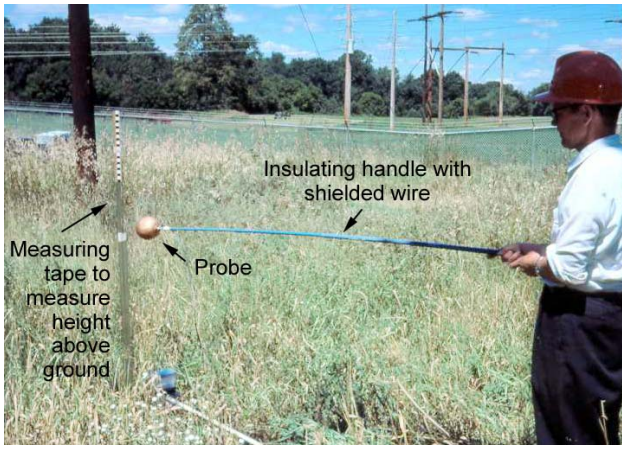


Figure 7.5-6 Measurements of the unperturbed space potential.

If the probe consists of a sphere of radius R, then $L = 3R$. For probes of small dimensions with respect to the distance to ground, the term $L \cdot E$ is very small in comparison to V_{sp} and can be neglected. If the probe is grounded, $V_{probe} = 0$, Equation 7.5-10 becomes:

$$I_{probe} \approx kV_{sp} \qquad 7.5\text{-}11$$

Equation 7.5-11 indicates that the current induced in the probe is directly proportional to the space potential. The probe calibration constant k is determined through a calibration procedure. The probe is placed in the center of the parallel plate setup used to calibrate the field meter (see Section 7.5.1), as shown in Figure 7.5-8. A known voltage, V (e.g., 100 V), is applied to the entire measuring system (probe, shielded cable, and ammeter all connected together), while the two plates are connected together and kept at ground potential. If the ammeter measures a current I, the probe calibration constant is I/V.

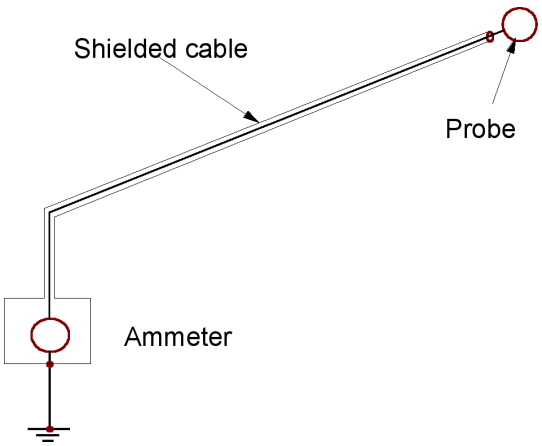


Figure 7.5-7 Schematic diagram of the space potential measuring system.

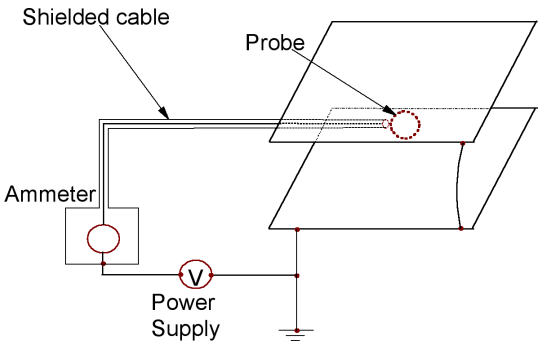


Figure 7.5-8 Schematic diagram of the calibration of a space potential probe.

7.6 MEASUREMENT OF MAGNETIC FIELDS

7.6.1 Magnetic Field Meters

A vast array of magnetic field meters is available. The IEEE has provided specifications to characterize instrumentation for measuring magnetic fields with sinusoidal frequency content in the range of 10 Hz to 3 kHz (IEEE 1994b).

Magnetic field meters consist of two parts: the sensor (or sensors) and the detector. The sensor can be made of wire coils from several inches to a fraction of an inch in diameter. For use near power lines, the coils must be electrically shielded in order to be immune from interference caused by the electric field. Small coils are sometimes wound around ferromagnetic cores. This arrangement has the same effect as increasing the area of the coil. The sensor coil is connected to a detector that measures the voltage across the coil. If the coil has N turns and an equivalent area A (see Figure 7.6-1), the voltage induced by a magnetic field is given by:

$$V = NA\frac{db_z}{dt} \qquad 7.6\text{-}1$$

Where:

b_z is the component of the magnetic field perpendicular to the area of the loop.

The measured quantity depends on the circuitry of the detector. In some cases, the voltage is integrated, and the rms value of the integrated quantity is measured. In this way, the rms value of the field is obtained. Some meters have a detector circuit that filters all frequencies but one—for instance, 60 Hz. Other meters operate in a wide frequency range. For example, some magnetic field meters measure the rms value of the magnetic field in the frequency range from 40 to 800 Hz. Filtering out the low frequencies is important if the meters are used for surveys requiring movements in the magnetic field of the earth. In fact, even though the magnetic field of the earth is constant (dc), movements may cause changes in the magnetic flux in the coil and therefore (see Equation 7.6-1) may induce a voltage. In this respect, body movements are relatively slow, and filtering out frequencies up to 10 Hz is usually sufficient to avoid interference even when measuring the lowest power-frequency fields.

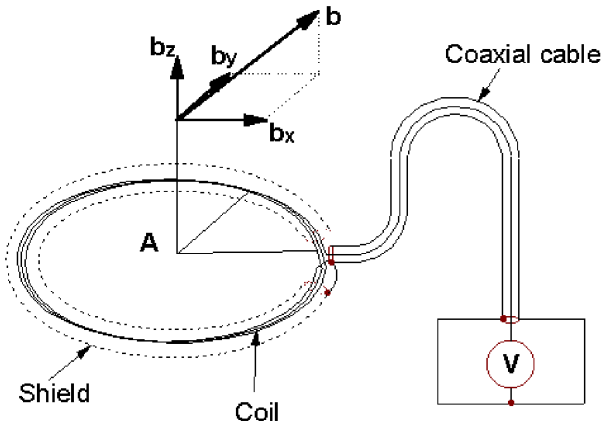


Figure 7.6-1 Magnetic field meter with sensor coil and voltmeter detector.

The recommended procedure for calibrating magnetic field meters is to introduce the meter (or the probe only, if separate from the meter) into a uniform magnetic field of known magnitude and direction (IEEE 1994a; Frix et al. 1994). Helmholtz coils are frequently employed for this task. A single square loop of many turns, N, of wires can also be used. In this case, the uniformity is reduced, but sufficient accuracy can still be obtained. The magnetic field in milligauss, B, in the center of the loop is perpendicular to the plane of the loop and is given by:

$$B = \frac{8\sqrt{2}NI}{L} \qquad 7.6\text{-}2$$

Where:

I is the current in a wire.

N is the number of turns.

L is the length of the side of the square loop.

Magnetic field meters with only one sensor coil are called single-axis meters. They measure the component of the field along the axis of the coil. For completeness, the field components along three orthogonal directions should be measured by orienting the sensor coil along these directions. If the measured field components, B_x, B_y, and B_z are rms values, the rms value of the resultant magnetic field, B, is given by:

$$B = \sqrt{B_x^2 + B_y^2 + B_z^2} \qquad 7.6\text{-}3$$

If the field is at the power frequency with no significant harmonics, the vector field rotates in space describing an ellipse. The component along the major axis of this ellipse, B_{max}, is measured by changing the orientation of the probe until the maximum reading is obtained.

Single-axis meters are useful for finding the location of field sources consisting of hidden conductors (e.g., underground water pipes) carrying a net current. In proximity of these sources, the maximum reading is obtained when the coil (see Figure 7.6-1) lies in the plane containing the field-producing conductor. The location of the wire may be estimated by making measurements at two different points.

Modern digital magnetic field meters have three sensor coils that measure simultaneously three orthogonal compo-

nents. The value of the three components is processed internally by the meter according to Equation 7.6-3. The meter directly provides the resultant field B. The rms resultant field read by a three-axis meter does not change with the orientation of the meter, because the value of B is independent of the choice of the three orthogonal axes. Magnetic field meters of this type usually do not provide information about the phase angle of the measured field. The value of B_{max} cannot be derived from three orthogonal component magnitude measurements.

Three-axis digital meters can be of two types: survey meters and digital recorders. Survey meters display the value of the field. As the field changes, the display is refreshed and the new value is displayed. The time between two successive measurements should be short (e.g., 0.5 s or less) to allow for rapid search of sources of field. Digital recorders not only display the value of the field but also store it in memory. The field may be measured at a fixed time interval and the values may be stored in memory. These meters have a provision for downloading the data into a PC at the end of the measurement period. Meters of this type may have additional features that allow measurements of the field versus time, field versus distance, and area mapping of the field. The last two features are made easy by the use of a calibrated wheel that sends to the meter information about the distance traveled.

7.6.2 Measurement of Magnetic Field from Power Lines

According to the IEEE, the magnetic field should be measured at a height of about 1 m above ground level (IEEE 1994-2). The value of the field is not very sensitive to variations of height. However, if another height is used, it should be explicitly indicated. If a single-axis meter is used, the probe should be oriented alternatively in three orthogonal directions in order to measure the vertical field (B_z), the horizontal field perpendicular to the power line (B_x), and the horizontal field parallel to the power line (B_y). The maximum value (magnitude of the field ellipse major axis) can also be measured if desired to obtain a measure of the field polarization. The component of the field parallel to the line, in the case of a long line without changes in direction, is negligible. Most conveniently, however, measurements are made with a three-axis digital recorder. B_x, B_y, and B_z are measured simultaneously and their resultant $B = \sqrt{B_x^2 + B_y^2 + B_z^2}$ is displayed. Orthogonal components and resultant are stored in memory.

The body of the operator does not affect the magnetic field. Therefore, the operator may stay close to the meter. Most objects are nonmagnetic and do not affect the measurements. Objects containing magnetic materials (e.g., cars and trucks) should be kept away (at least three times the largest dimension of the object).

The magnetic field of a power line is described by the magnetic field "lateral profile." This is a plot of the magnetic field versus distance in a direction perpendicular to the power line. A lateral profile can be obtained by carrying the meter. At known locations, the operator may stop and record the information. The lateral profile can be easily obtained using the special wheel mentioned earlier. The operator must walk slowly in the direction perpendicular to the line. It is a good practice to measure the height of the line at the location of the profile. Line height can change with current and weather conditions. These changes affect the field under the conductors and to a much lesser extent the field at the edge of the right-of-way and beyond.

The magnetic field depends on the current of the line, which may vary in time. Therefore, the date and time of the lateral profile must be recorded. If the line current at the time of the measurements is known, the lateral profile may be expressed in mG/A, and the magnetic field can be estimated for other current values, such as those corresponding to future loads.

A magnetic field recorder placed at a fixed location may be used to record temporal variations of magnetic field. Variations of magnetic field may be significant, although not as large as those caused by many other common field sources. Figure 7.6-2 shows two 24-hour plots of the magnetic field measured in two different residences—one in which the field was caused predominantly by a transmission line, and the other in which the field was caused by currents in the residence's grounding system, which is the most common source of residential magnetic field in North America (Zaffanella 1993). Both plots show a dependence of the field on the hour of the day. Short-term variability of the transmission-line field, however, is comparatively small. Daily and seasonal variations may be significant. Magnetic fields that are calculated on the basis of line current rating are worst-case scenarios because transmission lines are typically operated well below rating. Utilities and power pools variously define the rating of a transmission line: peak load, emergency load, design load, winter normal continuous capacity of the circuit, winter normal continuous capacity of the conductors, winter short-time emergency rating of the conductors, etc. The relation between actual magnetic field and calculated magnetic field at line rating is a function of the type of line. For instance, New York State utilities in 1990 estimated that the yearly average magnetic field at the edge of the right-of-way of their EHV transmission lines was only about 10% of the magnetic field calculated using winter short-time emergency rating. However,

the values calculated in these emergency conditions may be reached or approached for short periods of time.

Magnetic field measurements, in general, compare well with computer modeling calculations (Olsen et al. 1988). The uncertainty of magnetic field measurements results from the combination of calibration errors, temperature effects, and influence of extraneous fields. For carefully made measurements, the error should be well within ± 10%. The uncertainty of the results of calculations may be larger because of errors in measuring conductor heights, uncertainty in the values of the current at the time of the measurements, errors in the calculation of shield wire currents, and lack of knowledge about buried conductors that may carry induced currents. At large distances from the transmission line, magnetic field from earth currents may become important, and magnetic field from line current unbalance may dominate the measurements.

7.6.3 Waveform Capture Instrumentation

Instruments that capture and digitize the waveshape of the magnetic field are available. The field is measured along three orthogonal axes. The instantaneous values of the field components along each axis are sampled at a high rate in order to correctly measure harmonics of the field. For instance, a sampling rate greater than 2000 Hz is needed to measure harmonics up to 720 Hz (11th harmonic of 60 Hz). Some instruments also measure the dc field along three orthogonal axes. One cycle of the power frequency is sufficient to characterize the waveshape of transmission-line fields.

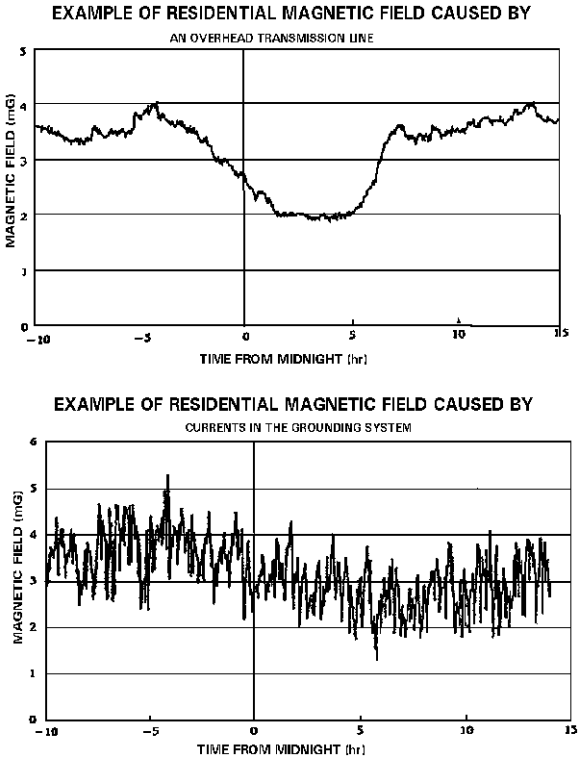


Figure 7.6-2 24-h magnetic field recordings. Top: field from a transmission line. Bottom: field from currents in a residential grounding system.

Waveshape capture instruments store the digitized waveshape in their internal memory. The data are downloaded to a PC and analyzed after the measurements. Some instruments display the waveshapes of the three orthogonal components. The parameters of the wave can be calculated after downloading the data into a PC or may be displayed directly by the instrument. These parameters include the coefficients of the Fourier series of each space component, the rms value of each frequency component, and the degree of polarization at the fundamental frequency and at each harmonic frequency.

The magnetic field of an ac transmission line is, in general, characterized by a relatively pure sinusoidal wave with little harmonic content. Within the right-of-way, the harmonic content is similar, but not equal, to the harmonic content of the line current. Typically, the third and fifth harmonics are of the order of 0-1% of the fundamental. Higher harmonics are, in general, less than 0.1%. The third harmonic field is monopolar. It decays at a slower rate than the field at the fundamental frequency and of the fifth harmonic, which are generally dipolar. Therefore, the magnetic field third harmonic percentage increases with the distance from the line.

Waveform capture instrumentation also provides the phase angle of each field component and, therefore, makes it possible to measure the polarization of the field.

7.7 COMPARISON BETWEEN HV TRANSMISSION-LINE AND COMMON ENVIRONMENT ELECTRIC AND MAGNETIC FIELDS

The power-frequency electric fields that exist near ground within the right-of-way of EHV transmission lines are practically the highest to which people may be exposed. The power-frequency magnetic fields are also significantly higher than ambient fields, but there are many other common environments with comparable or higher magnetic field values. Table 7.7-1 shows typical values of the electric and magnetic field for 230-kV and 500-kV transmission lines. Electric and magnetic fields that are encountered in other common environments are shown in Table 7.7-2.

Table 7.7-1 Typical Transmission Line Electric and Magnetic Field Levels

Line Voltage (kV)	Electric Field				Magnetic Field[1]			
	Max (kV/m)	Edge of Right-of-Way (kV/m)	At 30 m (kV/m)	At 60 m (kV/m)	Max (mG)	Edge of Right-of-Way (mG)	At 30 m (mG)	At 60 m (mG)
230	2	1.5	0.3	0.05	60	20	7	1.8
500	7	3	1	0.3	100	30	13	3.2
1. 1 mG = 0.1 μT								

Table 7.7-2 Electric and Magnetic Field Levels in Common Environments (Data from the U.S.)

Electric Field		Magnetic Field[1]	
Largest field at ground level near overhead distribution lines [2]	For 50% of the lines: > 8 V/m For 5% of lines: > 60 V/m	**Residential field at center of rooms [3]**	
Sofa/chair near lamp [4]	4 – 15 V/m	50% of houses, average for all rooms	0.6 mG
Under fluorescent light [4]	4 – 7 V/m	50% of houses, room with highest field	1.1 mG
Middle of rooms with lights and appliances [4]	0.5 – 8 V/m	5% of houses, average for all rooms	2.6 mG
Workshop with electric tools [4]	8 – 55 V/m	5% of houses, room with highest field	5.6 mG
Under electric blanket [4]	10 – 50 V/m [5]	1% of houses, average for all rooms	5.8 mG
Shopping mall [4]	4 – 7 V/m	1% of houses, room with highest field	12.2 mG
Classrooms w/o fluorescent lights [2]	< 0.5 V/m	Average field in 50% of classrooms [2]	0.4 mG
Classrooms with fluorescent lights [2]	2 – 15 V/m	Average field in 5% of classrooms [2]	1.3 mG
Magnetic Field near Appliances		Average for grocery stores [7]	1.9 mG
Electric range, 27 cm away [3]	2 – 28 mG [6]	5% of the area of grocery stores [7]	7.5 mG
Television, 27 cm away [3]	3 – 12 mG [6]	Average for hospitals [7]	1.3 mG
Air conditioner, window unit, 27 cm away [3]	0.5 – 9 mG [6]	5% of the area of hospitals [7]	3.7 mG
Microwave oven, 27 cm away [3]	17 – 67 mG [6]	Average for office buildings [7]	0.7 mG
Analog clock/radio, 27 cm away [3]	2.5 – 25 mG [6]	5% of the area of office buildings [7]	2.5 mG
Fluorescent light, 27 cm away [3]	1 – 23 mG[6]	Average for machine shops [7]	3.9 mG
Aquarium pumps, 27 cm away [3]	1.2 – 63 mG [6]	Time distribution for welders in machine shops [7]	50%: 5.2 mG 5%: 25 mG
Toaster oven, at 27 cm [3]	1 - 20 mG [6]		
Electric heater, at 27 cm [3]	1.6 - 41 mG [6]		
Dishwasher, at 27 cm [3]	5 - 15 mG [6]		
Can opener, at 27 cm [3]	12 - 325 mG		

1. 1 mG = 0.1 μT
2. From (Zaffanella 1999).
3. From (Zaffanella 1993).
4. From (Silva 1985).
5. The value depends on the electric field exposure equivalence criteria. Localized equivalent surface fields may be as high as a few hundred volts per meter.
6. Range of values applicable to 90% of the appliances.
7. From EMF RAPID Program of DOE, "Environmental Field Surveys," Engineering Project #3, April 1996. The values reported here are area measurements weighted by the number of people and the time spent.

7.8 ELECTRIC FIELD INDUCTION IN OBJECTS

7.8.1 Introduction

The electrical quantities that define the effects of transmission-line electric field on an object are:

- The current, I_{sc}, that would flow in a short circuit from the object to ground or to another grounded object.
- The voltage, V_{og}, induced between object and ground or another grounded object.
- The energy, J, that is discharged in a spark occurring when a contact is made between the object and ground or another grounded object. If the spark occurs at the peak of the voltage wave, J represents the maximum energy stored (excluding trapped charge effects).

The electrical parameters of the object are:

- The equivalent surface area, S, of the object. This quantity is defined as the area of a flat plate that would collect the same short-circuit current, I_{sc}, as that collected by the object. The plate is placed at ground level in a uniform field of the same value as the average unperturbed field to which the object is exposed (Deno 1975).
- The power-frequency impedance, Z_{og}, of the object to ground. This impedance is measured at the power frequency (50 or 60 Hz). For some objects, it can be represented with a Norton equivalent impedance consisting of a resistance in parallel with a capacitance. For certain other objects, such as vehicles on rubber tires, the impedance to ground consists of a complex network of resistances and capacitances (see Figure 7.8-1) that cannot be represented by a simple resistance in parallel with a capacitance.
- The spark-discharge capacitance, C_s. This is the capacitance of the object to ground that is discharged with a short time constant, not affected by the resistances to ground of the object, when the object contacts the ground (Maruvada and Hylten-Cavallius 1975). If the object is well insulated from ground, the impedance to ground is due only to this capacitance: $Z_{og} = 1/(2\pi f C_s)$.

The unperturbed average electric field, E, at the location of the object represents the source of induction. It allows the evaluation of the induction on an object without considering the actual geometry and electrical parameters of the conductors that generate the electric field. Without this simplification, the calculation would be very complicated. This simplification is justified because the presence of the object has a negligible effect on the electrical charges on the conductors that generate the electric field at the object. If the unperturbed field is nonuniform over the volume occupied by the object, the average unperturbed field should be considered. For tall objects, the average unperturbed field can be substituted by the space potential divided by the height of the object. For long objects, over whose length the electric field is not constant either in magnitude or in phase, an equivalent uniform electric field must be calculated (see Section 7.8.4). The current induced in an object in a uniform field can be calculated using scale models of the object (EPRI 1982) or analytical techniques (Tranen and Wilson 1971; Appendix 7.6).

Given the unperturbed average electric field, E, and the electrical parameters of the object, S, Z_{og}, and C_s, the induction quantities are calculated as follows:

$$\tilde{I}_{sc} = j2\pi f \varepsilon \tilde{E} S \qquad 7.8\text{-}1$$

The phase angle of the current is 90° greater than that of the field.

For 60 Hz, $I_{sc} = ES/(3 \cdot 10^8)$.
For 50 Hz, $I_{sc} = ES/(3.6 \cdot 10^8)$.

$$V_{og} = I_{sc} \cdot Z_{og} \qquad 7.8\text{-}2$$

$$J = \frac{1}{2} C_s \left(\sqrt{2} V_{og}\right)^2 = C_s \cdot V_{og}^2 \qquad 7.8\text{-}3$$

Where:

J is the energy that is discharged when the object-to-ground voltage is at its peak, which is $\sqrt{2}$ times greater than the rms value.

The capacitance C_s is used because other capacitances (e.g., the tire capacitance to ground C_g) would be discharged with a longer time constant (see Figure 7.8-1). Spark discharges take place with time constants of 1μs or less. The series resistance R_s is sufficiently large to make the spark-discharge contribution of C_g negligible. The impedances to ground in the equivalent circuit are subject to a large degree of uncertainty, and the open-circuit volt-

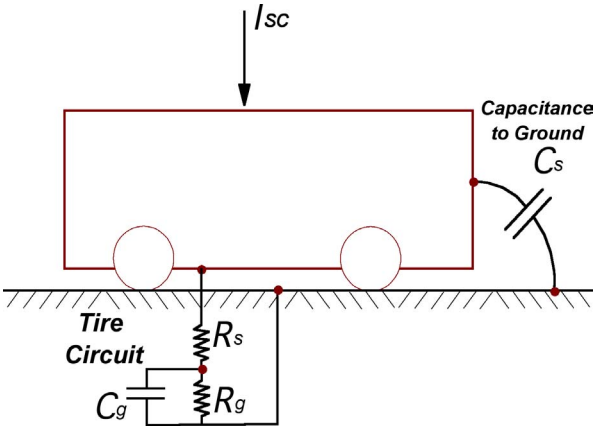


Figure 7.8-1 Equivalent circuit of a vehicle for power-frequency electric field induction.

age to ground is extremely variable (Reilly 1982). The most reliable measurement is that of the short-circuit current, which is the basic quantity that defines the electric field induction.

7.8.2 Electrical Parameters of Objects with Different Shapes

Sphere above Ground

A sphere of radius r at a height h above ground has an equivalent charge-collecting area given by Equation 7.8-4

$$S = \frac{4\pi h}{\frac{1}{r} - \frac{1}{2h}} \quad \text{for} \quad h >> r \quad \text{s} = 4\pi hr \qquad 7.8\text{-}4$$

When this equation is considered in combination with Equation 7.8-1 and with the concept that in a uniform electric field, the space potential at the sphere is $V_{sp} = Eh$, the result is:

$$I_{sc} = j\omega\varepsilon V_{sp} \frac{4\pi}{\frac{1}{r} - \frac{1}{2h}} \quad \text{for} \quad h >> r$$
$$I_{sc} = j\omega\varepsilon V_{sp} 4\pi r \qquad 7.8\text{-}5$$

Equation 7.8-5 is applicable also when the electric field is nonuniform.

The capacitance of a sphere is:

$$C_s = 4\pi\varepsilon r \qquad 7.8\text{-}6$$

Hemisphere on a Ground Plane

The equivalent charge-collecting area is:

$$S = 3\pi r^2 \qquad 7.8\text{-}7$$

This area is three times larger than the projected area. The shape factor, defined as the ratio between equivalent charge-collecting area and the projected area, is 3.

Half-Ellipsoid on a Ground Plane

The equivalent charge-collecting area of a hemisphere given in Equation 7.8-7 may be extended to a half-ellipsoid with semi-axes equal to a and b on the ground plane as follows:

$$S = 3\pi ab \qquad 7.8\text{-}8$$

Cylinder above Ground

The equivalent charge-collecting area of a long cylinder above ground must be referred to the unit of length, L, of the cylinder and is:

$$S/L = \frac{2\pi h}{\ln(2h/r)} \qquad 7.8\text{-}9$$

The short-circuit current, expressed as a function of the space potential, is:

$$I_{sc} = j\omega\varepsilon V_{sp} \frac{2\pi}{\ln(2h/r)} \qquad 7.8\text{-}10$$

If the cylinder is not very long in relation to its height above ground, the end effects will significantly affect the value of S. The end effects may be estimated equivalent to the addition of the equivalent charge-collecting area of a sphere with radius and height above ground equal to those of the cylinder.

$$S = \frac{2\pi h}{\ln(2h/r)} \cdot L + \frac{4\pi h}{\frac{1}{r} - \frac{1}{2h}} \qquad 7.8\text{-}11$$

Half-Cylinder on a Ground Plane

The equivalent charge-collecting area per unit of length, L, of a long half-cylinder on a ground plane is:

$$S = 4rL \qquad 7.8\text{-}12$$

This area is two times larger than the projected area. The shape factor, previously defined for a hemisphere, is 2.

If the half-cylinder is not very long in relation to its height above ground, the end effects will significantly affect the value of S. The end effects may be estimated equivalent to increasing the length of the cylinder by an amount equal to the radius of the cylinder.

$$S = 4r(L + r) \qquad 7.8\text{-}13$$

Vertical Cylinder

The equivalent charge-collecting area of a vertical cylinder (see Figure 7.8-2) is given by Equation 7.8-14 (Reilly 1978).

$$S = \frac{\pi L^2}{\ln\left[\frac{L}{r}\sqrt{\frac{4h + L}{4h + 3L}}\right]} \qquad 7.8\text{-}14$$

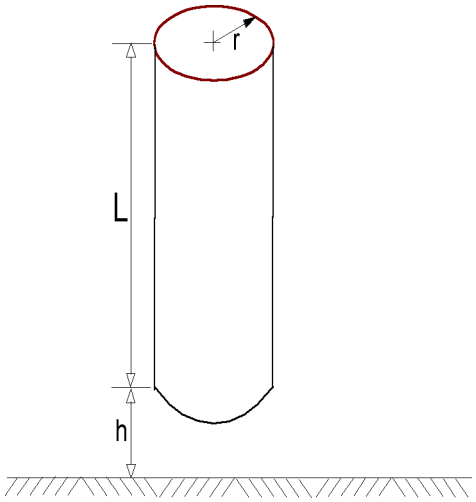


Figure 7.8-2 Vertical cylinder above ground.

Box

The equivalent charge-collecting area of a box may be obtained from the curves of Figure 7.8-3, which give the shape factor (*S/AB*) of a box with length *A*, width *B*, and height *H* of the top surface above the ground plane. The curves are given for the box placed on the ground plane (*C = 0*, see Figure 7.8-3). However, the curves may also be used with an error less than 10% for *0 < C < B/2*. These curves were obtained from experimental data using boxes formed with metallic wire mesh placed on a flat ground in a known electric field.

The use of Figure 7.8-3 is indicated in the following example. Assume that *A* = 1.22 m, *B* = 0.61 m, and *H* = 0.71 m. Then *A/B* = 2 and *H/B* = 1.16. The shape factor is obtained by interpolation of the data obtained in correspondence of *A/B* = 2 from the curves in Figure 7.8-3 for *H/B* = 1 and *H/B* = 2. A shape factor *S/AB* = 6.2 is obtained. Thus the equivalent charge-collecting area of the box is *S* = 4.62 m².

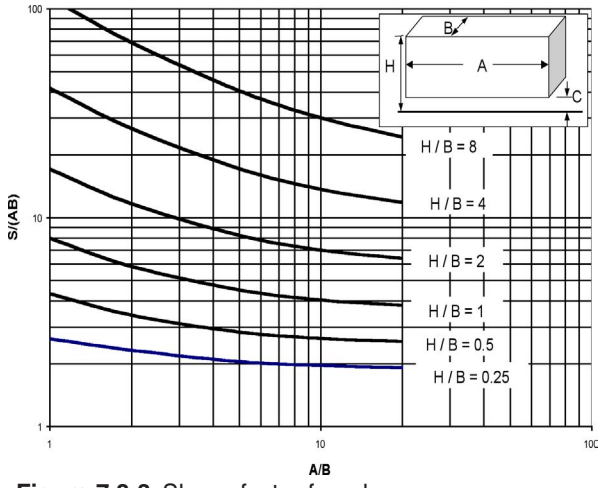


Figure 7.8-3 Shape factor for a box.

Horizontal Rectangular Plate

The equivalent charge-collecting area of a horizontal rectangular plate may be obtained from the curves of Figure 7.8-4, which give the shape factor (*S/AB*) of a plate with length *A*, width *B*, and height *H* of the plate above the ground plane. These curves also were obtained from experimental data.

The use of Figure 7.8-4 is indicated in the following example. Assume that *A* = 1.22 m, *B* = 0.61 m, and *H* = 0.71 m. These are the same parameters of the example for the box. The shape factor obtained from the data of Figure 7.8-4 is *S/AB* = 5. Thus the equivalent charge-collecting area of the plate is *S* = 3.72 m².

Objects with Any Shape Close to Ground—The 45° Shield Angle Approximation

When an object has a complex shape, its equivalent area may be estimated by projecting the top edges of the object on the ground using 45-degree cones. The total area of the projections obtained in this way is taken as the equivalent charge-collecting area. An example of an application of this method is shown in Figure 7.8-5. In this case. the equivalent charge-collecting area is: $S = AB + 2H(A+B) + \pi H^2 = 4.9$ m².

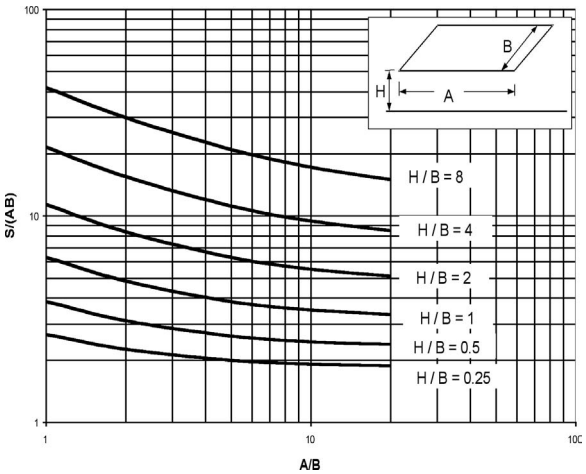


Figure 7.8-4 Shape factor for a horizontal plate.

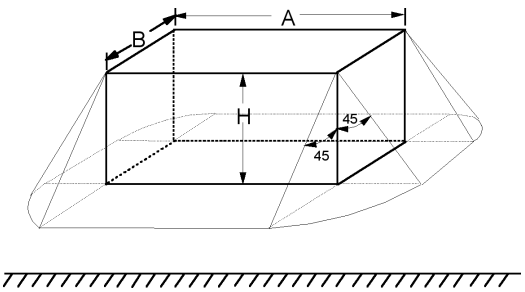


Figure 7.8-5 Equivalent area calculated using the 45° shield angle approximation.

Silos

The shape factor for a silo with diameter D and height H is given by the curves of Figure 7.8-6. The equivalent charge-collecting area, S, is obtained multiplying the silo area projected on the ground, $\frac{\pi D^2}{4}$, by the shape factor.

Houses

The shape factor for buildings with a rectangular cross plan (A x B) is given by the curves of Figures 7.8-7 to 7.8-9. The equivalent charge-collecting area, S, is obtained by multiplying the building area projected on the ground, $A \cdot B$, by the shape factor.

Antennas

The short-circuit current of antennas mounted on buildings in proximity of transmission lines may flow in the body of a person during installation or maintenance. The short-circuit

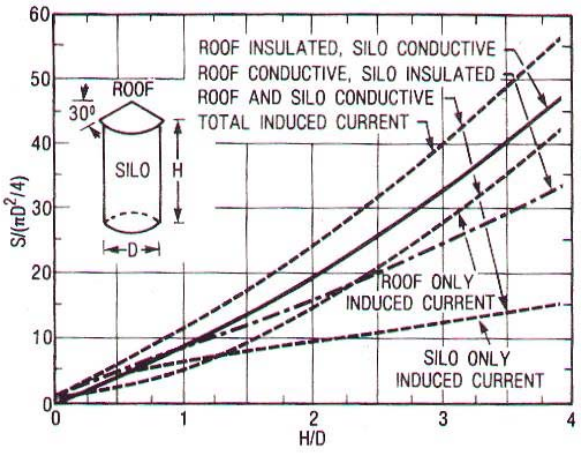


Figure 7.8-6 Shape factor for silos.

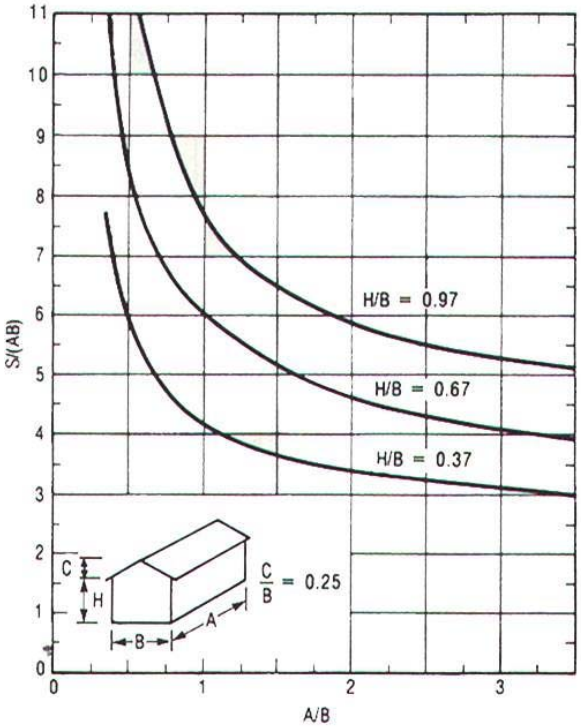


Figure 7.8-7 Shape factor for conductive gable roofs with insulating buildings.

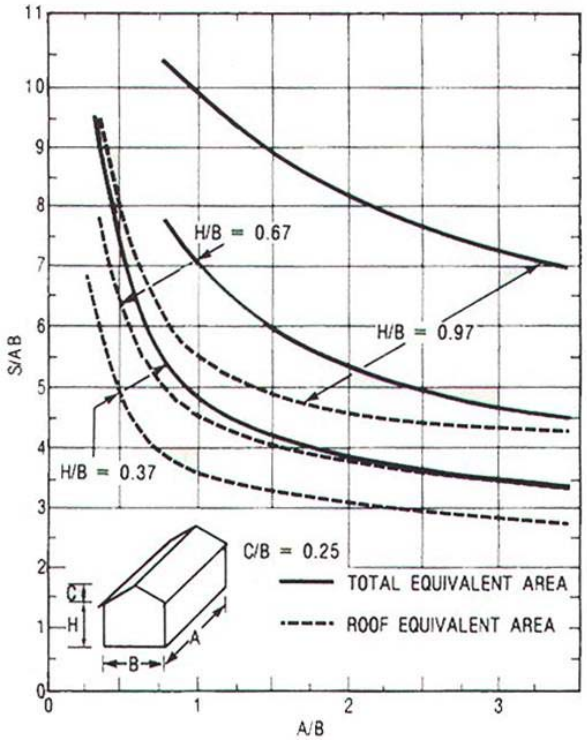


Figure 7.8-8 Shape factor for conductive buildings with conductive gable roofs.

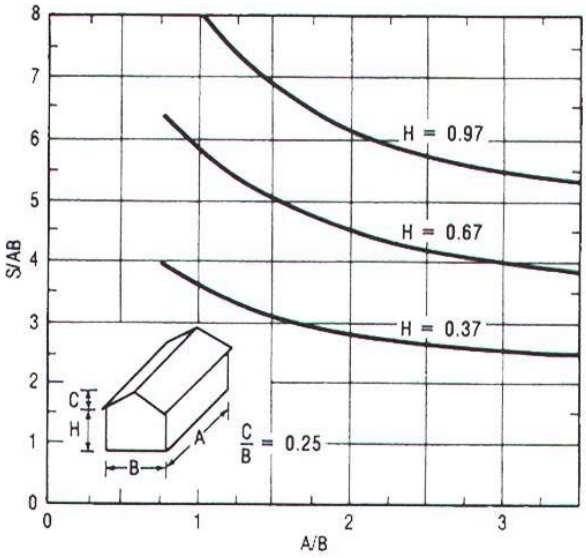
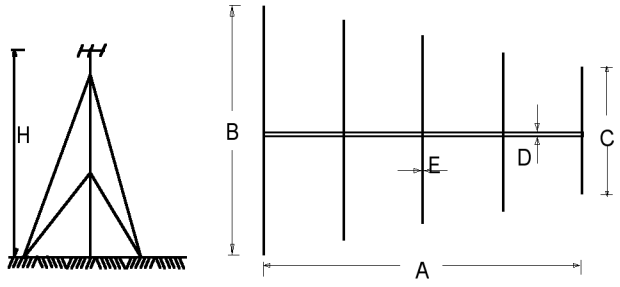


Figure 7.8-9 Shape factor for conductive buildings with insulating gable roofs.

current is given by Equation 7.8-1, in which E represents the average electric field over the antenna height perturbed by the presence of the building, and S is the equivalent charge-collecting area of the antenna. The field perturbation caused by the building, assumed conductive, is shown in the example of Figure 7.8-12. An accurate calculation of the perturbed field can be made using 3-D electric field computer programs. The equivalent charge-collecting areas of three different antennas (shown in Figure 7.8-10) are given by the curves of Figure 7.8-11. The spark-discharge capacitance, C_s, of an antenna depends on its dimensions. The value of C_s is indicated in Figure 7.8-10 for heights above ground of 10 m or greater. The capacitance increases when the height above ground is decreased and becomes 20–50% higher when the height is 1 m.



	A (m)	B (m)	C (m)	D (m)	E (mm)	No. of elements	Cs (pF)
TV ch. 6	1.75	1.83	1.58	0.019	9.55	5	48
TV all ch.	3.80	2.04	1.84	0.254	9.55	28	102
FM "S"	0.765	1.19	----	----	9.55	2	31

Figure 7.8-10 Dimensions of antennas whose equivalent charge-collecting area is given in Figure 7.8-11.

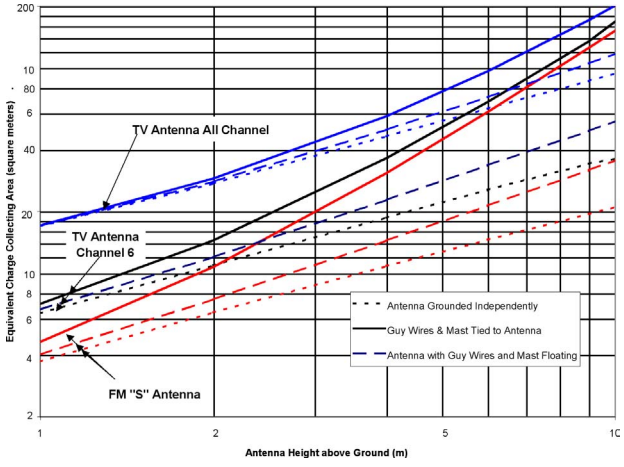


Figure 7.8-11 Equivalent charge-collecting area for three different antennas (see Dimensions in Figure 7.8-10).

Rain Gutters (Reilly and Cwiklewski 1981; EPRI 1982)
The current flowing in a conductive connection between a gutter and a building is given by Equation 7.8-1. The equivalent charge-collecting area is given by Equation 7.8-15.

$$S = \frac{2\pi h_{eq}}{\ln(2h_{eq}/r_{eq})} L \qquad 7.8\text{-}15$$

This is the same equation as Equation 7.8-9 for a cylinder above ground. However, an equivalent radius, r_{eq}, is used instead of r, and an equivalent height above ground, h_{eq}, instead of the real height above ground. The equivalent radius of a gutter is about equal to its largest dimension divided by two. The equivalent height is equal to the unperturbed space potential at the gutter with the building present, divided by unperturbed electric field at the gutter without the building. For one- or two-story buildings, the equivalent height of the gutter can be estimated as one fifth of the height of the gutter above ground.

The capacitance of the gutter to ground is given by:

$$C_s = \frac{2\pi\varepsilon}{\ln(2h_{eq}/r_{eq})} L \qquad 7.8\text{-}16$$

For a gutter well insulated from the roof, the impedance to ground coincides with its capacitive impedance.

$$Z_{og} = \frac{1}{j\omega C_s} \qquad 7.8\text{-}17$$

For example, assume h = 3 m, E = 2000 V/m at 60 Hz, a rain gutter length L = 20 m, and a rain gutter equivalent radius r = 0.65 m. Then h_{eq} = 0.6 m, S = 123 m² (The large charge-collecting area of the gutter results from its height above ground. See Figure 7.8-5.), Isc = 0.82 mA, C_s = 1810 pF, and, for a well-insulated gutter, Z_{og} = 1.47 MΩ and V_{og} = 1200 V.

Summary Tables
The equations and the methods for calculating the induction quantities (equivalent charge-collecting area, spark-discharge capacitance) of different objects are summarized in Table 7.8-1. These quantities can also be calculated for a variety of objects in practical transmission-line situations using Applet EMF-10. The equivalent charge-collecting area of an object is used to calculate the short-circuit current in a uniform electric field. If the electric field is nonuniform along the height of the object, the average electric field should be used, or the space potential at the top of the object divided by the object's height. If the electric field is nonuniform along the length of the object, the average electric field calculated as shown later in this section should be used.

Table 7.8-1 Equivalent Charge-Collecting Area and Spark-Discharge Capacitance of Objects in a Uniform Electric Field

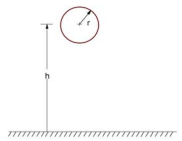
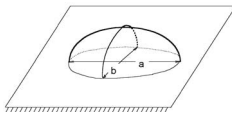
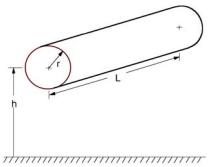
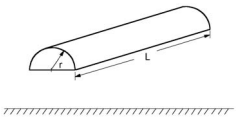
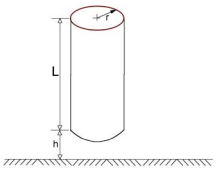
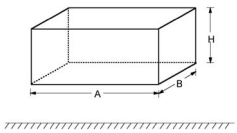
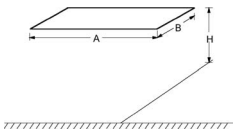
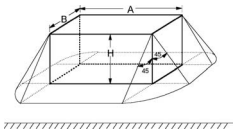
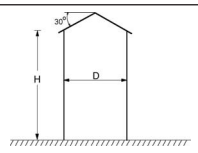
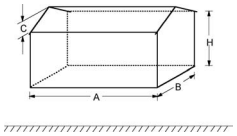
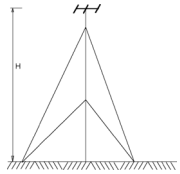
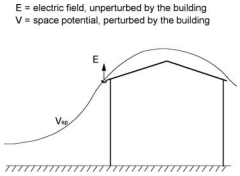
Object		Equivalent Charge-Collecting Area	Spark-Discharge Capacitance
Sphere above ground		$S = \dfrac{4\pi h}{\dfrac{1}{r} - \dfrac{1}{2h}}$ for $h >> r \quad S = 4\pi hr$	$C_s = 4\pi\varepsilon r$
Hemisphere on the ground		$S = 3\pi r^2$	
Half-ellipsoid on the ground		$S = 3\pi ab$	
Cylinder above ground		$S = \dfrac{2\pi h}{\ln(2h/r)} \cdot L + \dfrac{4\pi h}{\dfrac{1}{r} - \dfrac{1}{2h}}$	$C_s = \dfrac{2\pi\varepsilon}{\ln(2h/r)} L$
Half-cylinder on the ground		$S = 4r(L + r)$	
Vertical cylinder		$S = \dfrac{\pi L^2}{\ln\left[\dfrac{L}{r}\sqrt{\dfrac{4h+L}{4h+3L}}\right]}$	
Box		See Figure 7.8-3	
Flat plate		See Figure 7.8-4	
45° shield angle approximation		Top area with 45° cones projection on the ground	
Silos		See Figure 7.8-6	
Houses with gable roofs		Conductive roof, insulating house: see Figure 7.8-7 Conductive roof, conductive house: see Figure 7.8-8 Insulating roof, conductive house: see Figure 7.8-9	

Table 7.8-1 Equivalent Charge-Collecting Area and Spark-Discharge Capacitance of Objects in a Uniform Electric Field

Object		Equivalent Charge-Collecting Area	Spark-Discharge Capacitance
Antenna		See Figure 7.8-11	See Figure 7.8-10
Rain gutters		$h_{eq} = \frac{V_{sp}}{E}$ $S = \frac{2\pi h_{eq}}{\ln(2h_{eq}/r)} L$	$C_s = \frac{2\pi\varepsilon}{\ln(2h_{eq}/r)} L$

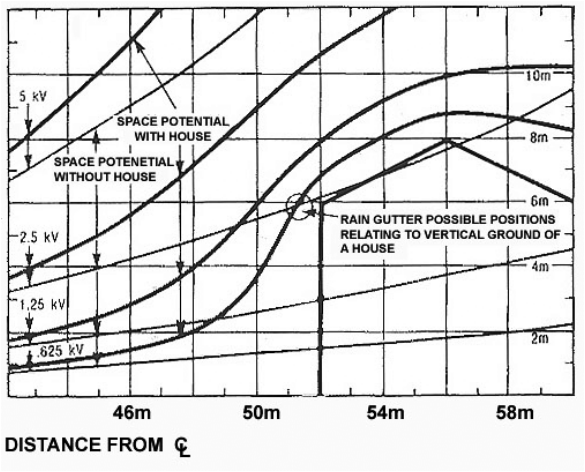


Figure 7.8-12 Example of space potential contour lines about a two-story house.

Table 7.8-2 shows experimental data for the ratio between short-circuit current and electric field and for the spark-discharge capacitance of different objects.

7.8.3 Accuracy Expected in Calculating Short-Circuit Currents

The accuracy of the results of calculations of short-circuit currents depends on the assumptions about their shape. Practical engineering problems do not involve perfect spheres or cylinders but objects of complicated shapes. Tables 7.8-1 and 7.8-2 contain data for many different objects. The accuracy of these data is of the order of ±5% for uniform electric fields. If approximations are used, accuracy depends on the subjective judgment in approximating the actual shape with one with known solution. Experienced engineers may achieve accuracy of the order of 10–20% even for complicated shapes. If better accuracy is desired, the user may exercise Applet EMF-10 "Equivalent Area of Objects in an Electric Field," based on the algorithms illustrated in Appendix 7.6.

Table 7.8-2 Induced Current Coefficient and Spark Discharge Capacitance of Different Objects

Object	Induced Current Coefficient I_{sc}/E (mA per kV/m)	Spark-Discharge Capacitance (pF)
Large tractor - trailer Total length 15.75 m Trailer: L=12.2 m, W=2.4 m, H=3.7 m	0.64	2000 ~ 3000
Tractor – Milk tanker Total length: L=13.8 m Tanker: L=10.3 m, W=2 m, H=2.6 m	0.40	
Large school bus L=10.4 m, H=2.8 m, W=2.44 m	0.39	1800
Small farm tractor L=3.7 m, W=1.95 m, H=1.5 m	0.06	
Combine L=9.15 m, W=2.3 m, H=3.5 m	0.38	
Wagon L=4.6 m, W=1.8 m, H=1.7 m	0.11	1000
Pickup truck L=5.2 m, W=2 m, H=1.7 m	0.10	
Car L=5.7 m, W=1.9 m, H=1.5 m	0.11	
Car L=4.6 m, W=1.78 m, H=1.37 m	0.088	800
Person: height = 1.75 m	0.016	100
Horse L=2 m, shoulder H=1.26 m, 385 kg	0.027	180
Cow L=2 m, shoulder H=1.17 m, 318 kg	0.024	200

Example: Electric Field Induction for an Automobile

Consider the automobile shown in Figure 7.8-13. The calculation of short-circuit current and open-circuit voltage may be made according to the following steps.

- The automobile may be approximated by a box with length A = 4.6 m and width B = 1.78 m.
- The height of the equivalent box is a weighted average of the heights of the different sections:
  $H = (0.86 \cdot 1.73 + 1.37 \cdot 1.83 + 0.94 \cdot 1.04)/4.6 = 1.08$ m

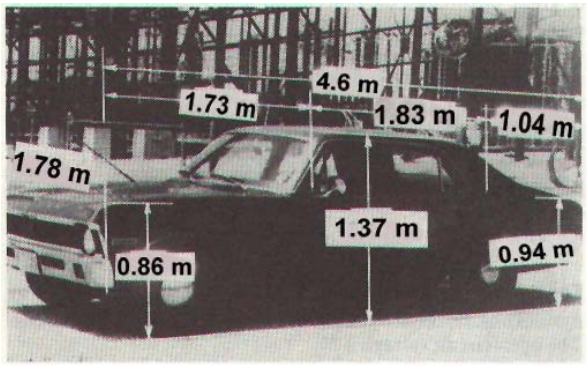


Figure 7.8-13 Automobile dimensions for short-circuit current evaluation.

- The shape factor, *S/(AB)*, is found from Figure 7.8-3, in correspondence to $A/B = 4.6/1.78 = 2.6$ and $H/B = 1.08 / 1.78 = 0.61$.
  $S/(A \cdot B) = 3.25$
- The equivalent charge-collecting area is:
  $S = 3.25\ A \cdot B = 26.5\ m^2$
- The short-circuit current is given by Equation 7.8-1. For an electric field of 1 V/m at the frequency of 60 Hz:
  $I_{sc} = 2\pi f \cdot 8.854 \cdot 10^{-12} \cdot 26.5 = 8.84 \cdot 10^{-8}$ A, i.e., $I_{sc} = 0.084$ mA/(kV/m)
- This result is close to that indicated in Table 7.8-2 for the same car.
- The capacitance to ground of an automobile depends on the type of pavement. The value of 800 pF listed in Table 7.8-2 is a typical value. If the tires and pavement provide a perfect insulation from the electrical ground, the impedance to ground is due only to the capacitance and is:
  $Z_{og} = 1/(2\pi f \cdot 800 \cdot 10^{-12}) = 3.32\ M\Omega$
- The open-circuit voltage is:
  $V_{og} = 3.32 \cdot 10^{6} \cdot 8.84 \cdot 10^{-8} = 0.29$ V/(V/m).

In an electric field of 9 kV/m, the short-circuit current for the automobile of this example would be $0.084 \cdot 9 = 0.76$ mA, and the open-circuit voltage would be $0.29 \cdot 9000 = 2610$ V.

The open-circuit voltage (2610 V) and the spark-discharge capacitance (800 pF) characterize the intensity of the discharge occurring when a person touches the automobile (see Section 7.10). For this example, Figure 7.10-7 indicates that the discharge will be above the annoyance level for most people.

7.8.4 Electric Field Induction in Long Objects in a Nonuniform Electric Field

There are two sources of errors in applying single-phase, uniform-field data to three-phase fields. First, the magnitude of the field and, second, the phase angle of the electric field may vary significantly over the dimensions of the object (Reilly 1979). Therefore, a different procedure should be used as illustrated by the following two examples.

Vehicle Perpendicular to the Transmission Line

Assume that a 10.4-m-long school bus is centered under the maximum electric field and is perpendicular to a three-phase line. The average electric field over the equivalent bus length should be considered, rather than the field at the peak of the lateral profile. The equivalent length is the actual bus length plus an extra length (~ 3.5 m) to account for end effects. The real and imaginary components of the uniform electric field that causes the same induction are the real and imaginary components of the field calculated over the equivalent length, L, of the bus, from x_1 to x_2:

$$\tilde{E}_{eq} = \frac{\int_{x_1}^{x_2} \tilde{E}(x) \cdot dx}{L} \qquad 7.8\text{-}18$$

Equation 7.8-18 applied to the data of Table 7.8-3 shows that the equivalent uniform electric field is 86% of the maximum field. Therefore, the induced short-circuit current for the bus perpendicular to the line is 86% of the current induced in a bus parallel to the line at the point of maximum field.

Table 7.8-3 Example Calculation of Equivalent Electric Field for a Vehicle Perpendicular to a Three-Phase Line

Distance from Centerline (m)	Electric Field Magnitude (kV/m)	Electric Field Phase Angle (degree)	Real Component (kV/m)	Imaginary Component (kV/m)
6 (end effect)	4.78	70.5	1.59	4.48
7 (end effect)	5.14	79.3	0.96	5.05
8	5.54	86.5	0.34	5.53
9	6.05	93.9	-0.41	6.04
10	6.36	98.1	-0.90	6.30
11	6.63	102.2	-1.40	6.48
12	6.71	104.5	-1.68	6.50
13	6.68	106.3	-1.87	6.41
14	6.55	107.6	-1.98	6.24
15	6.26	109.0	-2.04	5.92
16	5.97	110.0	-2.04	5.61
17	5.64	110.0	-1.93	5.30
18 (end effect)	5.29	111.0	-1.90	4.94
19 (end effect)	4.88	11.0	-1.75	4.56
Total			-15.02	79.36
Total (magnitude)			80.77	
Average Magnitude			80.77/14 = 5.8 kV/m	

For large vehicles, including tractor-trailers, the mitigation effect of the field nonuniformity and of the phase change are significant, and they should be included in the calculations because these vehicles are critical for the application of the National Electric Safety Code (NESC) 5-mA criteria.

Fence Near a Transmission Line

If a fence has different sections in different electric fields, or if it is not parallel to the line, computations should be made using an equivalent electric field calculated with Equation 7.8-18, or by adding the currents induced in different sections, as shown in this example. Consider a 120-m fence (60 m on each side of the centerline), 1-m above ground, with wire diameter of 0.64 cm. Assume that the fence is perpendicular to the double-circuit line of Figure 7.3-15, with phase sequence C, A, B, C′, B′, A′ (from left to right). The fence is sectioned into eight 15-m-long sections. The field magnitude and phase angle are calculated for each section, as shown in Table 7.8-4. The short-circuit currents of the different sections are added accounting for magnitude and phase angle. The total current is 0.268 mA. The capacitance to ground does not depend on the fence location and is C = 1070 pF. The open-circuit voltage for a well-insulated fence is 690 V.

Table 7.8-4 Induced Current in a Fence not Parallel to a Transmission Line

Fence Section	Average Electric Field (kV/m)	Average Phase Angle (degree)	Induced Short-Circuit Current (mA)
1	0.4	140	0.017
2	0.8	125	0.035
3	2.7	100	0.120
4	2.8	-20	0.124
5	3.7	-75	0.164
6	2.4	-20	0.107
7	0.5	0	0.022
8	0.15	30	0.007

7.8.5 Impedance of Vehicles to Ground

Short-circuit currents and spark-discharge voltages are a function of vehicle-to-ground and person-to-ground impedances. The largest currents and voltages occur when the vehicle is perfectly insulated from ground and the person well grounded. This is seldom the case.

Impedances depend on a number of variables. To overcome the difficulty of defining the effect of each variable, a series of statistical measurements were made for different types of vehicles, in different weather conditions, and for different types of ground surfaces (EPRI 1982). The experiments were conducted under a three-phase test line. Three different types of ground surfaces were prepared: dirt, macadam (the American term “black top” is used in the figures), and gravel. The test vehicles were a school bus (10.4 m long, 2.44 m wide, 2.8 m high), a farm tractor (3.76 m long, 1.95 m wide, 1.46 m high), and a small truck (4.6 m long, 1.9 m wide, 1.65 m high). The measurements were performed twice each month for an entire year. The dates were selected in advance to cover all types of weather without bias. The following quantities were measured:

- Unperturbed electric field, E_g, at the height of one meter above ground
- Vehicle short-circuit current, I_{sc}
- Vehicle open-circuit voltage
- Person-to-vehicle open-circuit voltage
- Person-to-vehicle short-circuit current
- Person-to-ground open-circuit voltage
- Person-to-ground short-circuit current

The results confirmed that the short-circuit current, I_{sc}, is proportional to the unperturbed electric field near ground, E_g. The measured values were:

- For the school bus: I_{sc} / E_g = 0.39 mA/(kV/m)
- For the farm tractor: I_{sc} / E_g = 0.06 mA/(kV/m)
- For the small truck: I_{sc} / E_g = 0.11 mA/(kV/m)

The data for the farm tractor showed some dispersion because of changes in the position of the driver.

The major statistical parameters of interest are the impedance vehicle-to-ground, the current person-to-vehicle, and the voltage person-to-vehicle. These parameters are shown in terms of probability of occurrence in Figures 7.8-14 to 7.8-22.

The impedance vehicle-to-ground was calculated as the ratio between the open-circuit voltage and the short-circuit current: $Z_g = V_{oc} / I_{sc}$.

The current person-to-vehicle was referred to the short-circuit current, I_{sc}. The median value of the person-to-vehicle current was between I_{sc} /100 and I_{sc} /25 for the school bus and less for the other two vehicles.

The induced voltage between a person and a vehicle is a useful parameter to assess the severity of spark discharges. For all the vehicles tested, the maximum induced voltage was $V_{pv} \approx 0.3\ E_g$, whereas the median values were between 0.008 E_g and 0.07 E_g. These voltages were lower than those between vehicle and ground, indicating that a person assumes a potential intermediate between that of the vehicle and ground. Although the worst-case condition was never experienced during the test program, it may conceivably occur under unusual circumstances. The U.S. National

Electric Safety Code prescribes that the induced current should be less than 5 mA in the worst case (NESC 1997). For the school bus tested, this translates into an electric field of 12.8 kV/m. In this field, the median values of the current bus-to-person would be between 0.02 and 0.05 mA, and the median values of the induced voltages would be between 100 and 900 V. Therefore, if a line is designed according to code, short-circuit currents vehicle-to-person would generally not be perceptible (see Section 7.10), Spark discharges, however, may exceed perception level and occasionally annoyance levels (see Section 7.10). In none of the conditions experienced during the test program would the spark discharge voltage have been sufficient to cause gasoline ignition during refueling operations (see Section 7.14).

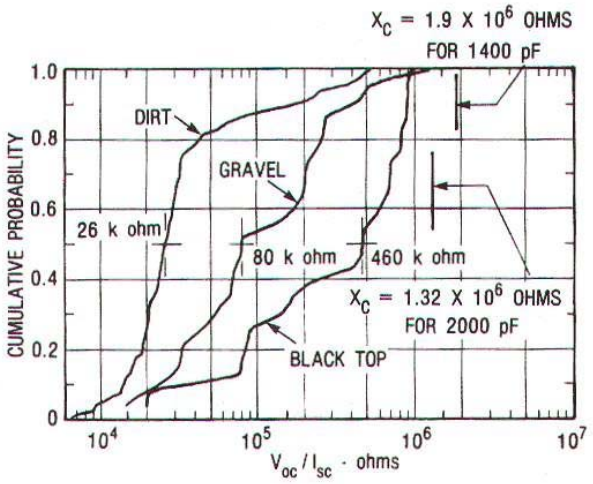


Figure 7.8-14 Probability that a given value of vehicle-to-ground impedance, $Z_g = V_{oc} / I_{sc}$, will not be exceeded. Data for a school bus.

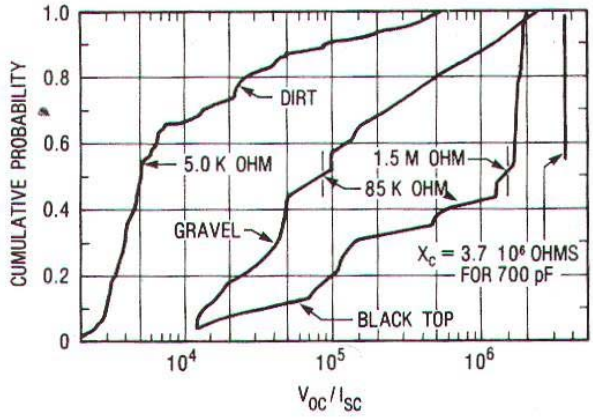


Figure 7.8-15 Probability that a given value of vehicle-to-ground impedance, $Z_g = V_{oc} / I_{sc}$, will not be exceeded. Data for a farm tractor bus.

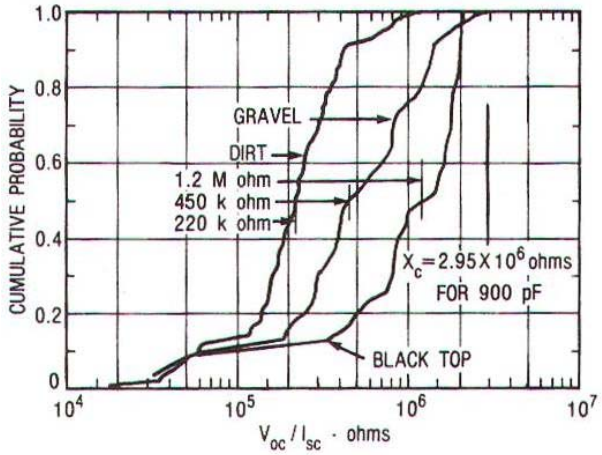


Figure 7.8-16 Probability that a given value of vehicle-to-ground impedance, $Zg = V_{oc} / I_{sc}$, will not be exceeded. Data for a small truck.

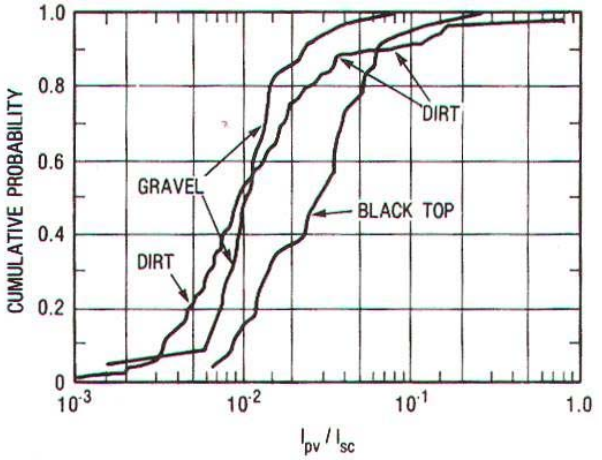


Figure 7.8-17 Probability that a given value of vehicle-to-person current, I_{pv} / I_{sc}, will not be exceeded. Data for a school bus.

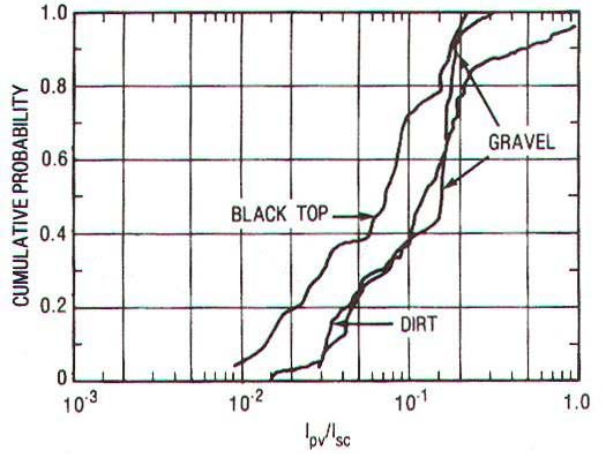


Figure 7.8-18 Probability that a given value of vehicle-to-person current, I_{pv} / I_{sc}, will not be exceeded. Data for a farm tractor.

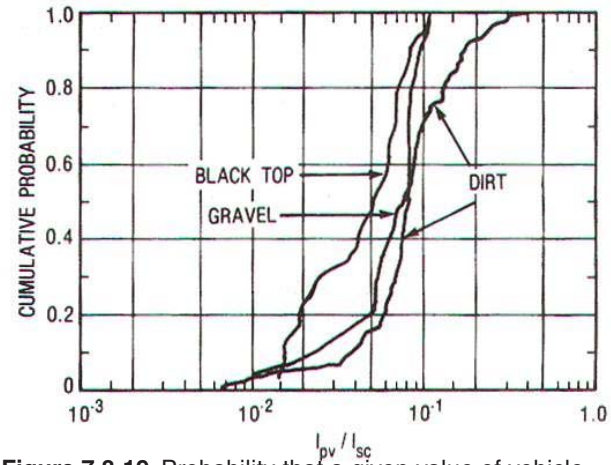


Figure 7.8-19 Probability that a given value of vehicle-to-person current, I_{pv} / I_{sc}, will not be exceeded. Data for a small truck.

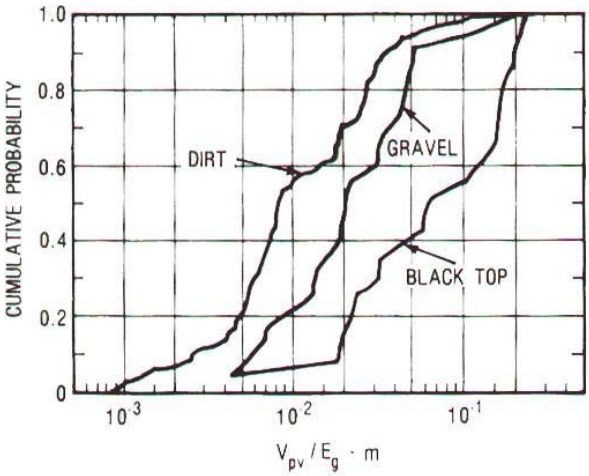


Figure 7.8-20 Probability that a given value of vehicle-to-person voltage, V_{pv} / E_g, will not be exceeded. Data for a school bus.

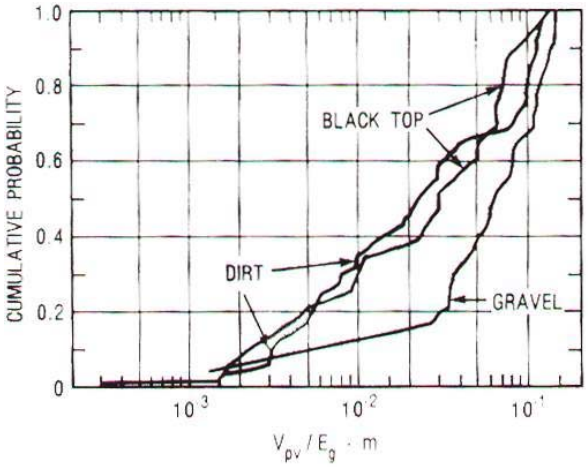


Figure 7.8-21 Probability that a given value of vehicle-to-person voltage, V_{pv} / E_g, will not be exceeded. Data for a farm tractor.

7.9 MAGNETIC FIELD INDUCTION IN OBJECTS

7.9.1 Short-Circuit Currents and Open-Circuit Voltages of Sets of Conductors Parallel to Transmission Lines

A power transmission line may induce significant voltages in conductive objects that have a considerable length parallel to the line, such as fences, pipes, rails, and wires. If these conductors are a part of a loop or a network, currents may flow in these objects or in the connections between these objects and people, giving rise to important safety issues. Induced currents and voltages in parallel wires are important considerations for the safety of personnel who work on de-energized lines parallel to energized lines. The inductive coordination problem has been studied since the start of the power industry and a rich literature on the subject is available, covering subjects such as pipes (Dabkowski and Taflove 1979; Taflove and Dabkowski 1979a; Taflove and Dabkowski 1979b; Taflove et al. 1979; Jaffa and Stewart 1981; EPRI 1985; Frazier et al. 1986), railroads (EPRI 1985; Frazier et al. 1986), fences (Jaffa 1981), and the general issues of inductive coordination (Dabkowski 1981; Olsen and Jaffa 1984).

Magnetic induction is responsible for currents in shield wires used for lightning protection when these wires are bonded to more than one transmission structure. When the shield wires are sectionalized, grounded only at one structure, and insulated at other structures in order to reduce losses, the magnetic induction generates a voltage between

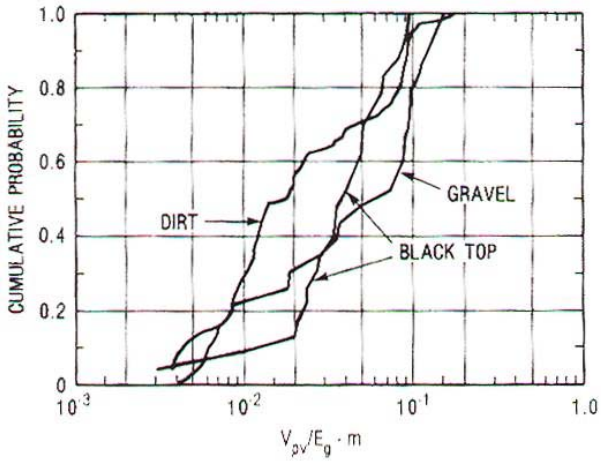


Figure 7.8-22 Probability that a given value of vehicle-to-person voltage, V_{pv} / E_g, will not be exceeded. Data for a small truck.

shield wires and these structures. Magnetic induction generates currents and voltages in conductor networks located near the transmission lines: distribution line neutrals and their ground connections, water pipe systems, and building steel columns and beams. In some cases, the induction in these networks reduces the magnetic field at locations where a reduced magnetic field is desired. Indeed, a special passive conductor network can be designed for that purpose (see Section 7.17).

The voltage, $V_{a,b}$, induced in a loop formed by two conductors, *a* and *b*, parallel to a transmission line and connected to each other at the ends of a long section of length *L*, is given by:

$$\tilde{V}_{a,b} = L \cdot \sum_i \frac{j\omega\mu \tilde{I}_i}{2\pi} \ln \frac{D_{ib}}{D_{ia}} \qquad 7.9\text{-}1$$

The distances D_{ia} and D_{ib} are from conductor *i* of the transmission line. The summation is extended to all the conductors. In most practical situations, the earth return currents may be neglected.

The voltage $V_{a,b}$ may be regarded as the difference of two voltages assigned to each individual conductor. For instance, the voltage assigned to conductor *a* is:

$$\tilde{V}_a = L \cdot \sum_i \frac{j\omega\mu \tilde{I}_i}{2\pi} \left(\ln \frac{2L}{D_{ia}} - 1 \right) \qquad 7.9\text{-}2$$

It can be verified that:

$$\tilde{V}_{a,b} = \tilde{V}_a - \tilde{V}_b \qquad 7.9\text{-}3$$

Equation 7.9-2 may be written:

$$\tilde{V}_a = \sum_i Z_{ia} \tilde{I}_i \qquad 7.9\text{-}4$$

Z_{ia} is the mutual impedance between conductor *a* and conductor *i*.

$$Z_{ia} = L \cdot \frac{j\omega\mu}{2\pi} \left(\ln \frac{2L}{D_{ia}} - 1 \right) \qquad 7.9\text{-}5$$

If there are two or more conductors parallel to the transmission line, voltages and currents are related through matrix Equation 7.9-6.

$$[V] = [Z][I] \qquad 7.9\text{-}6$$

The matrices contain variables that refer to all conductors, those of the transmission line and those where voltages are induced by the transmission lines. [*V*] is the array of voltages per unit of length of the conductors (the longitudinal electromotive force (LEF), also called the longitudinal electric field), [*I*] is the array of conductor currents, and [*Z*] is an impedance matrix containing self and mutual impedances. All variables are complex numbers. The mutual impedance between two conductors is given by Equation 7.9-5. The self-impedance of a conductor, for instance conductor *a*, is given by:

$$Z_a = L\left[R_a + \frac{j\omega\mu}{2\pi} \left(\ln \frac{2L}{GMR} - 1 \right) \right] \qquad 7.9\text{-}7$$

Where:

R_a is the resistance (ac resistance at the power frequency of 50 or 60 Hz).

GMR is the Geometric Mean Radius.

For a conductor of radius *r* and with uniform current distribution:

$$GMR = 0.779\, r \qquad 7.9\text{-}8$$

For transmission-line conductors, the value of *GMR* (in meters) may be derived from tables giving the conductor self-reactance, X_a, in ohm per mile for 1-ft spacing at the frequency $f = 60$ *Hz*, using Equation 7.9-9:

$$GMR = 0.305 \cdot e^{-(2\pi X_a/(1610 j 2\pi 60\mu)} \qquad 7.9\text{-}9$$

If the reactance were given in ohm per kilometer for 1-m spacing at the frequency of 50 Hz, Equation (8.9-10) should be used:

$$GMR = e^{-(2\pi X_a/(1000 j 2\pi 50\mu)} \qquad 7.9\text{-}10$$

It is useful to partition matrix Equation 7.9-6 as shown in Equation 7.9-11.

$$\left[\begin{array}{c|c} Z_{tt} & Z_{tp} \\ \hline Z_{pt} & Z_{pp} \end{array} \right] \left[\begin{array}{c} I_t \\ \hline I_p \end{array} \right] = \left[\begin{array}{c} V_t \\ \hline V_p \end{array} \right] \qquad 7.9\text{-}11$$

Where:

t indicates the transmission-line conductors,

p denotes the conductors parallel to the transmission line where induction takes place.

Assume, for instance, that the parallel conductors are connected to each other at their ends. In this case, all the voltages induced on the parallel conductors are equal, and the sum of the parallel conductor currents is zero. The currents and the voltage drop along the parallel conductors can be calculated solving the system (7.9.12) consisting of *2p+1* equations with *2p+1* unknowns (V_p, V, I_p).

$$\begin{aligned} &[V_p] = V[1] \quad \text{All the voltages are equal to V} \\ &\sum_p I_p = 0 \quad \text{Kirchoff law} \\ &[Z_{pt}][I_t] + [Z_{pp}][I_p] = [V_p] \quad \text{Derived from (7.9 - 11)} \end{aligned} \qquad 7.9\text{-}12$$

Assume, instead, that the parallel conductors are not connected to each other or to the ground (except at one point). In this case, the currents are all zero. The induced voltages can be calculated, from Equation 7.9-13, which is derived from 7.9-11.

$$[V_p] = [Z_{pt}][I_t] \qquad 7.9\text{-}13$$

Calculations of induced voltages and currents for simple geometry can be made using Applet EMF-8.

Effect of Conductive Ground

If the ground were perfectly conductive, then the image of each conductor should be considered—i.e., a conductor carrying an opposite current and placed below the ground in a mirror location. Since the earth is not perfectly conductive, the earth currents move deeper into the earth and a phase delay occurs. In most practical cases and for the power frequency, the earth may be considered nonconductive in comparison to the line conductors, and the earth return current, if any, may be placed at an infinitely large distance from the conductors. The detailed analysis of how to account for earth return current is shown in Appendix 7.5. The main results of the analysis are reported here. The depth of the return current is given by Equation 7.9-14:

$$return\ depth = 1.31\delta = 1.31\sqrt{\frac{\rho}{\pi f \mu}} \qquad 7.9\text{-}14$$

Where:
ρ is the soil resistivity.
μ is the soil permeability.
f is the frequency.
δ is the skin depth.

In most cases the permeability of the soil is the same as that of air. Assuming a soil resistivity of 100 Ωm, the earth return depth at 60 Hz is approximately 850 m. Therefore, in most practical cases, the earth return currents may be neglected. This is especially true for transmission-line currents that are balanced, because all the conductor return currents are placed at nearly the same location inside the earth. If there is an unbalance, the return current may affect the induction of parallel conductors that are at distances from the power lines comparable to the return depth. Accounting for earth return current, the mutual impedance per unit of length between two conductors *a* and *i*, at a distance d_{ia} from each other, is given by Equation 7.9-15.

$$Z_{ia} = \frac{\omega\mu}{8} + \frac{j\omega\mu}{2\pi} \ln \frac{1.31\sqrt{\frac{\rho}{\pi f \mu}}}{D_{ia}} \qquad 7.9\text{-}15$$

7.9.2 Shield Wire Currents

The phase currents induce shield wire currents. The shield wire currents are calculated assuming that no current flows from the shield wires to ground through the towers. This assumption is valid only for the middle span of a long line with uniform earth resistivity and tower-to-earth impedance. Transposition of the line, discontinuity of the ground wires, and line terminations also invalidate this assumption.

Shield wire currents are calculated solving the matrix Equations (7.9-16).

$$\begin{bmatrix} Z_{aa} & Z_{ab} \\ Z_{ba} & Z_{bb} \end{bmatrix} \cdot \begin{bmatrix} I_a \\ I_b \end{bmatrix} = \begin{bmatrix} V_a \\ V_b \end{bmatrix} \qquad 7.9\text{-}16$$

Where:
I_a is the array of line currents.
I_b is the array of shield wire currents.
V_a and V_b represent line and shield wire voltages, respectively.
Z_{aa}, Z_{ab}, Z_{ba}, and Z_{bb} are impedance matrices.

The shield wire currents are calculated by requiring that the shield wire longitudinal voltages (*V/m*) be zero. This means no voltage drop from one tower to the next because both towers are at earth potential, since no current flows from shield wire to ground along the towers. If $V_b = 0$, the system (7.9.16) can be solved for the shield wire currents, I_b.

$$[I_b] = -[Z_{bb}]^{-1} \cdot [Z_{ba}] \cdot [I_a] \qquad 7.9\text{-}17$$

Shield wire currents should be treated as line currents in the calculation of magnetic field induction on wires parallel to the transmission line. The presence of shield wires slightly reduces the magnetic field and the magnetic field induction in objects.

Shield wire currents can be calculated using Applet EMF-8.

7.10 RESPONSE OF PEOPLE TO TRANSMISSION-LINE FIELDS

This section is useful for analysis, design, and mitigation of situations of short-term exposure to electric fields that may result in complaints. It reports the values of currents and spark-discharge energies that cause different levels of sensations. Also reported are the levels of electric field that cause various degrees of sensations caused by hair stimulation. This section also reports some data on electric currents inside the human body but does not discuss their biological importance.

7.10.1 Induced Currents and Their Distribution

Power-frequency currents are induced in the body of people who are in an electric field produced by high-voltage transmission lines. Knowledge of these currents and of how they are distributed inside the body is useful to relate results of biological studies conducted in the laboratory to the electric field produced by transmission lines. Simplistic models are able to estimate the current distribution in the human body with very little accuracy (Spiegel 1977). Determining the distribution of the currents in the internal organs requires the knowledge of the relative resistance of the various tissues of the body (Dawson et al. 1998). In contrast, it is relatively easy to determine experimentally the amount of currents that enters the various surfaces of the body and the total current that flows in a cross section of the body. These experiments were conducted with a special manikin used as the power-frequency electric equivalent of a human body (Deno 1977b; EPRI 1982). The manikin was made of insulating material, and its surface was covered with copper foil. The foil covering a section of the body was separated from the foils of adjacent sections by small gaps bridged by wire connections. This arrangement allowed measuring the current flowing between sections. Measurements were made for various body postures, for body either grounded or insulated from ground, and for uniform and nonuniform electric fields. When the body was at ground potential, the total current to ground was measured in a low-impedance connection to ground.

Total Body Current Induced in a Person Erect and Grounded

The short-circuit current, I_{sc}, for a person in the erect position over a flat ground and away from other objects is given by:

$$I_{sc} \approx 9 \cdot 10^{-11} f \cdot h^2 \cdot E \qquad 7.10\text{-}1$$

The current is proportional to the power frequency, f, the unperturbed uniform electric field, E, and the square of the height of the person h. For instance, a person 1.75 m tall standing erect and grounded in a 1-kV/m 60-Hz electric field would have a short-circuit current equal to about 0.017 mA. The equivalent charge-collecting area of a person is obtained combining Equations 7.8-1 and 7.10-1:

$$S \approx 1.62 \cdot h^2 \qquad 7.10\text{-}2$$

A person 1.75 m tall has an equivalent charge-collecting area equal to about 5 m^2. If the person is grounded through the feet, the current I_{sc} is flowing through the feet. Grounding may occur when a person is barefoot, has conductive or wet shoes, or is in tall grass that makes contact with the legs.

Current Induced in a Person Insulated from Ground

If the person is insulated from ground, as occurs when the person is standing or walking with insulated shoes on dry ground, the body acquires a voltage to ground, V_{og}, which is a function of the capacitance, C, of the person to ground.

$$V_{og} = \frac{I_{sc}}{2\pi f C} \qquad 7.10\text{-}3$$

The short-circuit current flows through the capacitance C. Part of this capacitance is between feet and ground. The current flowing through the feet to ground is:

$$I_{sc} \approx 9 \cdot 10^{-11} f \cdot h^2 \cdot E \cdot \left(1 - 2.9 \cdot 10^{-11} \frac{h}{C}\right) \qquad 7.10\text{-}4$$

The value of the capacitance between a person and ground is a function of the height of the top of the sole of the shoes above a conductive ground, as shown in Figure 7.10-1. For a 1.75-m tall person and a typical capacitance value of 150 pF, the current flowing through the feet, calculated with Equation 7.10-4 is 0.011 mA, or about two-thirds of the current that flows through the feet when the person is grounded through the feet.

Current Induced in a Person for Different Body Postures

Person erect, grounded, hands by sides, and with feet at a height, L, above ground:

$$I_{sc} \approx 9 \cdot 10^{-11} f \cdot h^2 \cdot E \cdot (1 + 2L/h) \cdot (1 - 0.2L/h) \quad \text{for } L < h$$
$$I_{sc} \approx 9 \cdot 10^{-11} f \cdot h^2 \cdot E \cdot (1 + 2L/h) \cdot 0.8 \quad \text{for } L > h \qquad 7.10\text{-}5$$

Person erect, grounded, with one outstretched hand, and with feet at a height, L, above ground:

$$I_{sc} \approx 1.07 \cdot \left(9 \cdot 10^{-11} f \cdot h^2 \cdot E \cdot (1 + 2L/h) \cdot (1 - 0.2L/h) \right) \quad \text{for } L < h$$
$$I_{sc} \approx 1.07 \cdot \left(9 \cdot 10^{-11} f \cdot h^2 \cdot E \cdot (1 + 2L/h) \cdot 0.8 \right) \text{for } L < h \qquad 7.10\text{-}6$$

Person erect, grounded, on the ground with one hand overhead:

$$I_{sc} \approx 1.12 \cdot \left(9 \cdot 10^{-11} f \cdot h^2 \cdot E \right) \qquad 7.10\text{-}7$$

Current Induced in a Person Who Is Not Erect or Is in a Nonuniform Electric Field

The space potential approach is particularly useful when the electric field is not uniform or the person is not erect. Nonuniform fields occur close to nonflat boundaries, such as near vehicles, substation equipment, towers, trees, and bushes. The most practical approach for determining the current induced in the body of the person is to determine the unperturbed space potential, V_{sp}, at the location of the chest of the person and calculate an equivalent electric field, E_{eq}, which is equal to the unperturbed uniform electric field that would induce the same current in the body of the person standing erect in a uniform field.

$$E_{eq} = V_{sp} / h_c \qquad 7.10\text{-}8$$

Where:

h_c s the height of the chest above ground when the person is erect.

The induced current may be calculated using Equation 7.10-1, but with E_{eq} instead of E.

For example, consider a person standing near a grounded fence that perturbs the field in such a way that, at the position of the chest, the electric field is 12 kV/m and the space potential is 10.4 kV/m. If the height of the chest above ground is 1.3 m, the equivalent electric field is 8 kV/m. The current flowing into a contact with ground is 0.13 mA. Using the actual electric field of 12 kV/m would have yielded results 50% higher. A grounded fence does indeed shield a person, even though the local electric field may be enhanced.

7.10.2 Field Enhancement on the Surface of the Body

The electric field on the surface of the body, E_s, does not coincide with the unperturbed field, E, because the field is changed by the presence of the body:

$$E_s = kE \qquad 7.10\text{-}9$$

Where:

k is the field enhancement.

The field enhancement may be calculated for simple geometry. For a complicated geometry, it may be more accurate to measure the surface field using the technique illustrated in Figure 7.5-5. Results of measurements are shown in Table 7.10-1 (EPRI 1982).

Surface irregularities such as body hair and clothing produce an ill-defined surface field.

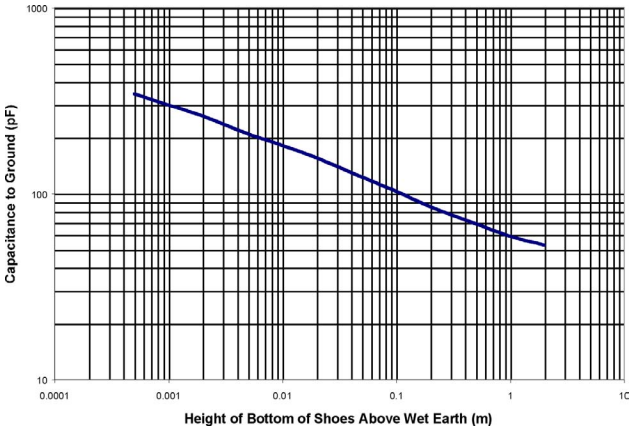


Figure 7.10-1 Person-to-ground capacitance measured with dry thin-soled shoes.

Table 7.10-1 Field Enhancement on the Surface of the Body (Person Grounded)

Position	Subject	Field Enhancement
Forehead	Manikin (h = 1.84 m) Person (h = 1.75 m)	23.3 20.0
Top of head	Manikin Person	16.6 18.3
Back of head	Manikin Person	18.3 15.2
Arm by side	Person	7.7
Arm outstretched	Person	9.3

Field enhancement is a function of the body posture and of the nonuniformity of the field. The surface field depends to a larger degree on the unperturbed space potential than on the unperturbed local electric field.

The current density on the surface of the upper portion of the body is the best parameter to characterize electrical quantities such as the total induced current, the electric field on the skin or hair, and the open-circuit voltage to ground. For this reason, personal electric field exposure monitors are based on the principle of measuring the induced current in a portion of the upper body surface. Such monitors are worn on arms, shoulders, and safety hats. The most accurate electric field exposure monitors are based on measuring the current induced in a conductive vest worn over insulating clothing and connected to an electrode in contact with the body.

7.10.3 Currents Induced by Spark Discharges

During a vehicle refueling operation, if there is a critical mixture of fuel and air in the gap and in the surrounding volume and if the spark discharge voltage is sufficiently high, fuel may ignite, although the probability that it happens is so low that in practice ignition will never occur (see Section 7.14).

A spark discharge is self-extinguishing, but may be repetitive because the voltage between the two bodies may be restored under the action of the ac electric field. After the contact between the two bodies is made, the discharges will cease, but a steady-state current at the power frequency will flow. The combination of transient and steady-state currents may be below the level of perception or may cause various sensations from perception without annoyance to a severe startle that may cause uncontrolled reactions.

The effects of spark discharges in an ac electric field depend on the peak value of the transient currents, their waveshape, and their repetition rate. These parameters, in turn, are a function of the type of contact and of the resistance of the discharge circuit. For the same type of contact and the same value of resistance, the transient currents depend on the voltage existing across the contact just before the spark and on the capacitance discharged by the spark. The value of the instantaneous voltage at the moment of the spark is difficult to determine. Therefore, it is preferable to define as the spark-discharge voltage the rms value of the voltage between the objects across which the discharge occurs.

The equivalent circuit for a spark discharge between a charged person and a grounded object is shown in Figure 7.10-2. This circuit shows lumped parameters to simulate the nonlinear distributed parameters of actual situations.

The spark-discharge voltage is:

$$V_{oc} = V\frac{C_2}{C_1 + C_2} \qquad 7.10\text{-}10$$

Where:

C_2 is the person-to-line capacitance and is negligible in comparison to C_1, which is the person-to-ground capacitance.

The capacitance of the person being discharged is:

$$C = C_1 + C_2 \approx C_1 \qquad 7.10\text{-}11$$

The person-to-ground capacitance is a function of the height of the bottom of the shoes above a conductive earth, as shown in Figure 7.10-1. Practical values of C are between 120 and 200 pF.

The terms R_B and R_S in Figure 7.10-2 represent the body-discharge resistance and the discharge resistance through the skin at the point of spark, respectively. The body resistance is the resistance from the charged surfaces of the body to the point of the spark. It is concentrated in the area of the body close to the spark. When the contact is made with a firmly held metal object, the total resistance is equal to the body resistance and has a minimum value of 250-400 Ω. When the spark occurs at a point on the skin, the spark-discharge resistance through the skin, R_S, becomes predominant. This resistance is nonlinear with voltage and is time varying. The equivalent initial resistance assumes values between 2,000 and 40,000 Ω.

The person-to-ground voltage, V_{oc}, is a function of the electric field, of the person's position, and of the impedance to ground. Measurements have shown that, for a person standing on insulating ground, or on an insulating platform, or in a switchyard with crushed stones, $V_{oc}/E = 0.18 – 0.42$ m, with an average value of 0.275 m (EPRI 1982). In the case of perfect insulation, the voltage to ground is

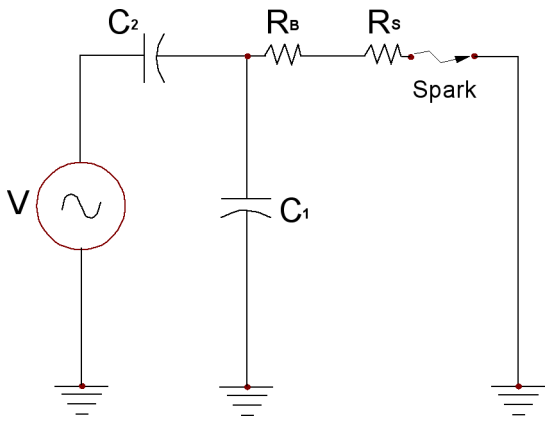


Figure 7.10-2 Equivalent circuit for a person-to-ground spark discharge.

$V_{oc} = I_{sc}/(\omega C)$, where C is derived from Figure 7.10-1 and I_{sc} is calculated according to Equation 7.10-4. For a person wearing shoes and walking on conductive ground (wet ground or grass), $V_{oc}/E = 0 – 0.3$ m, depending on the insulation of the shoes.

For a person standing on macadam, or "black top," beside a vehicle (thus partially shielded by it):

	Median Value	Maximum Value
School Bus	$V_{oc}/E = 0.06$ m	0.16 m
Farm Tractor, or Small Truck	$V_{oc}/E = 0.13$ m	0.22 m

The equivalent circuit for a spark discharge between a charged object and a person is shown in Figure 7.10-3. The resistance R_C in this circuit represents the contact resistance at the point where the person is grounded, such as a hand contact with a conductive object or a contact through conductive shoes on conductive ground.

The transient currents caused by spark discharges have a shape described in Figure 7.10-4, which shows a sequence of current pulses followed by a steady state current after the contact is fully established. Figure 7.10-5 shows an example of waveshape for one current pulse. The waveshape is not a simple exponential, such as that occurring in a linear R-C circuit, because the contact resistance varies in time. Two equivalent resistances are defined in the example of Figure 7.10-5: the initial resistance equal to the voltage before the contact divided by the initial current, and the resistance during the main part of the discharge, calculated through the average time constant.

The transient current propagation through the body is dominated by resistances and not by inductances. In fact, the skin depth for the propagation of these transient currents is

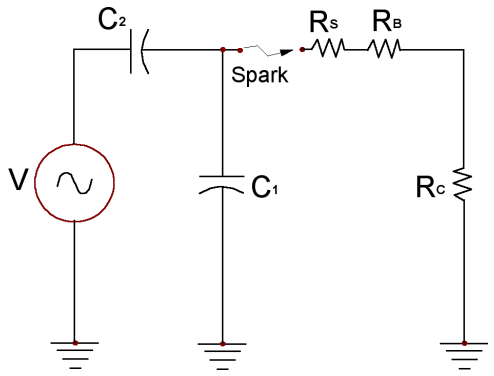


Figure 7.10-3 Equivalent circuit for a spark-discharge object-to-person.

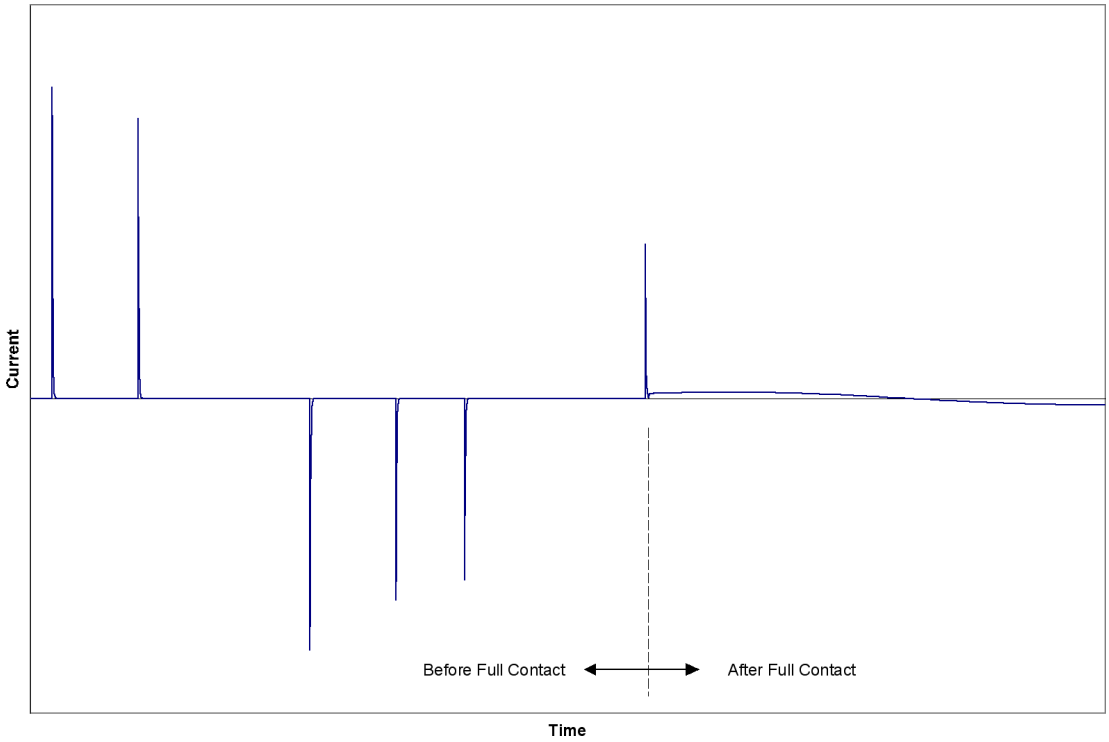


Figure 7.10-4 Sequence of current pulses in a spark discharge and current after contact.

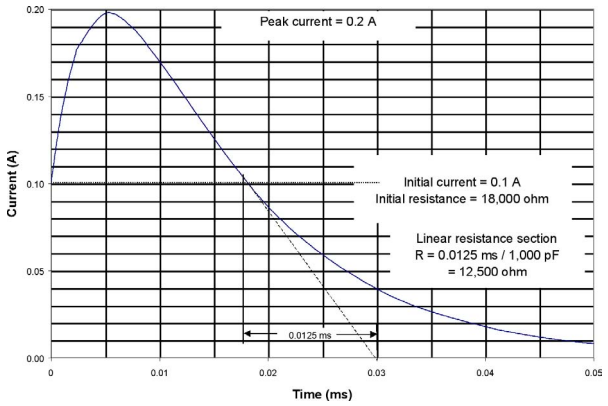


Figure 7.10-5 Waveshape of a current pulse in a spark discharge at a wet index finger. Peak voltage of 1800 V, capacitance = 1,000 pF.

sufficiently large for the hand and arm current distribution to be independent of inductances, even for the shortest time constants. The spark resistance is concentrated at the point of spark. Consequently, the current wave through the body has the same shape. The distribution of the transient currents inside the body depends on the point of contact and on the relative resistance of the different organs.

Comparison with Carpet-Induced Spark Discharges

Spark discharges occurring in proximity to high-voltage transmission lines are similar to those occasionally experienced by people walking on carpets in very dry rooms and touching a metallic object. People walking on carpets in very dry rooms may charge themselves with negative dc voltages with values depending on the insulating characteristics of the shoes and carpet and the type and degree of shuffling the shoes over the carpet. Voltages around 4 kV are a common occurrence, and voltages up to 8 kV may be generated indoors in dry winter climates. The capacitance of a person on a carpet is about 200 pF.

Comparison with the spark-discharge parameters in the case of person-to-ground spark discharges induced by high-voltage transmission line electric field shows that crest voltages and capacitance values are of the same order. In fact, for V_{oc}/E = 0.275 m, a crest voltage of 4 kV may be reached in an electric field of 10 kV/m. A notable difference, however, is the spark repetition that occurs in an alternating electric field when the contact is slow or brushing.

7.10.4 Transient Currents Induced by Switching Surges

Usually switching surges have peak voltages less than twice the peak value of the phase-to-ground voltage and times-to-crest exceeding 100 μs. If a person is in contact with an insulated object near the line at the time of the surge, a transient current will flow through the person's body.

The transient current caused by a switching surge is a single pulse. The crest value of this pulse is much lower than the crest value of a spark discharge. Assume a single-phase source, with a power frequency voltage, V, causing a short-circuit current, I_{sc}, in a conductive object. The source-to-object capacitance is $C_1 = I_{sc}/(2\pi fV)$. If the source voltage is an exponential transient with peak value $V_c = k\sqrt{2}V$ and time constant τ, a person touching the object would be subject to a transient current with the same time constant and crest value, I_c, equal to:

$$I_c = V_c \frac{C_1}{(RC_1 + \tau)} \approx V_c \frac{C_1}{\tau} = I_{sc} \frac{k\sqrt{2}}{2\pi f\tau} \qquad 7.10\text{-}12$$

If k = 1.8, τ = 400 μs, and f = 60 Hz, the crest voltage of the transient current is 17 times greater than the rms value of the short-circuit current. For I_{sc} = 2 mA, I_c = 34 mA. This value is much lower than the crest value of spark-discharge currents that may be of the order of hundreds of milliampere.

There has been no report of people sensing the electrical effect of switching surges. Switching surge exposure is infrequent compared to exposure to spark discharges, which, furthermore, have much higher peak currents and may occur repeatedly while making or breaking a contact.

7.10.5 People Response to Short-Term Exposure to Electric Field

Short-term exposure to electric field produced by ac transmission lines, substations, and overhead high-voltage apparatus may be classified according to the type of effect causing a sensation in people.

- Spark discharges, which cause transient currents in the body of a person when the electrical breakdown of an air gap occurs between the person's body and a conductive object, or ground
- Electric fields on the surface of the body, which exert forces on hair with consequent hair stimulation
- Steady-state ac currents, which enter a person contacting an object

The effects were listed in order of practical frequency of occurrence above perception levels. Spark discharges, causing a startled reaction or aversion to ac field exposure, are of major importance in establishing threshold of annoyance or uncomfortable sensations. The effects of electric field on hair are of minor importance and are present only in very high electric fields. Responses to steady-state currents are used to establish safety limits with respect to the possible largest charged object that a person might contact in conditions of good insulation of the object and good grounding of the person. Such situations are infrequent and

in almost all cases are preceded by spark discharges of considerable values.

The intensity of stimulation is classified according to the type of human response. Four categories of stimuli may be identified (EPRI 1982):

- Primary shock
- Secondary shock
- Perception
- Below perception

Primary shocks may produce direct physiological harm, such as heart fibrillation, respiratory tetanus, and inability to voluntarily control muscles.

Secondary shocks cannot produce such harm but are annoying and may produce involuntary muscle reactions. Secondary shocks are of subjective interpretation and may be defined in various ways: annoyance, startle, and aversion. Annoyance occurs when a person would consider the sensation to be mildly irritant if it occurred repeatedly. A startle would occur unexpectedly and would be likely to produce an unintentional muscular effect that may be hazardous under a defined set of circumstances. Aversion occurs when the person is motivated to avoid situations that would lead to a similar experience.

Perception occurs without shock when a person consciously detects the presence of a stimulus. The sensation is gentle and not necessarily unpleasant.

The following levels separate the preceding four categories:

- Minimum primary shock level
- Minimum secondary shock level
- Threshold of perception

Each of these levels is definable only in conjunction with a probability of occurrence in a well-defined set of circumstances. This probability is expressed as the percentage of people who have reactions above a particular level.

Response to Spark Discharges

Spark discharges induced by transmission-line electric fields do not have enough energy to cause primary shocks. They may, however, cause perceptible and annoying sensations to a person touching an insulated object or to an insulated person touching a grounded object. Sensitivity to spark discharges depends on the point of contact. The most sensitive points of contacts are the back of fingers or hands and the ankles. The electric field must be increased by a factor of about 1.5 to reach the same sensitivity with the tips of fingers, and by another factor of about 1.5 for contact with the palm (EPRI 1982). There is little difference in the response to spark discharges between men and women, with the exception of sparks to the tips of index fingers, in which case, women's perception is generally greater, probably due to more sensitive skin corresponding to a lower resistance (EPRI 1982). Temperature and humidity have a significant effect on the sensitivity to spark discharges. Weather conditions may cause variations in perception and annoyance levels by a factor of 2 or greater (EPRI 1982). The skin is most insensitive in dry and cold weather, which causes high values of skin resistance.

Discharges between a Person and Ground or between a Person and an Umbrella

Figure 7.10-6 shows the percentage of people who may experience sensations above the threshold of perception and above the minimum annoyance level for different spark-discharge situations (IEEE 1978; EPRI 1982). Different curves correspond to different situations.

Group 4 curves correspond to spark discharges between the thumb and the metallic shaft of an umbrella. The umbrella is held at the insulating handle, and the thumb is moved slowly until it touches the metallic shaft, and then it is removed. Different curves were obtained for rainy and fair-weather days. During rainy days, the umbrella's material becomes wet, and the equivalent surface area of the umbrella increases. Also during rainy days, finger sensitivity is higher because of higher humidity. In this situation the discharge capacitance is that of the umbrella (about 60 pF when dry and about 70 pF when wet).

Group 5 curves correspond to spark discharges between a small, grounded wire, simulating a blade of grass and the ankle. The person is erect and slowly touches the wire with the ankle and then moves the ankle away from the wire.

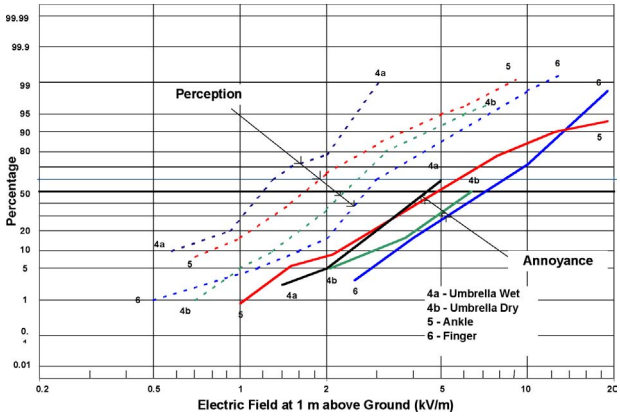


Figure 7.10-6 Percentage of people experiencing perceptible or annoying spark discharges in different situations in different electric fields. Data for 136 adults (EPRI 1982).

The discharge capacitance is that of a person to ground (see Figure 7.10-1).

Group 6 curves correspond to spark discharges between the tip of the index finger and a grounded object. The approach is made slowly, and then the contact is broken by withdrawing the finger. The discharge capacitance is that of a person to ground (see Figure 7.10-1). Considering a median value of 170 pF and a median value of the person-to-ground open circuit voltage equal to 0.275 kV / (kV/m), curves 6 of Figure 7.10-6 indicate the following median values for perception and annoyance thresholds:

- Perception threshold
  E = 2.7 kV/m V_{oc} = 740 V C = 170 pF
- Annoyance threshold
  E = 7 kV/m V_{oc} = 1900 V C = 170 pF

Straight lines reasonably match the data in Figure 7.10-6 when the field is plotted using a log scale and the probabilities of perception and annoyance are plotted using a normal probability scale. The data indicate a wide variability in human response. The ratio between fields corresponding to 84% and 16% probability is between 2.5 and 4.3. The curves for annoyance have about the same slope as the curves for perception. The ratio between annoyance and perception fields ranges between 2.6 and 3.8. At fields corresponding to 50% probability of perception, the probability of annoyance is 2~3%— i.e., when 50% of the people do not perceive any sensation there are a few people who judge the sensation annoying.

The data presented in Figure 7.10-6 correspond to repeated contacts. If the contact is casual, the voltage at the moment of the spark is likely to be less than the crest voltage of the open-circuit voltage. In fact, it is possible to make contact at $V = 0$ if the speed of approach is sufficiently high (greater than 15 cm/s). With repeated contacts, the chance that the voltage at the moment of the spark equals the crest voltage is high. In addition, with a slow approach and rapid withdrawal after the spark, the instantaneous spark voltage may be up to twice the crest of the open-circuit voltage.

Discharges between a Person and an Insulated Object

The severity of spark discharges between a person and an insulated object depends on the following parameters:

- V_{oc}: the open-circuit voltage of the object to ground
- C_s: the capacitance of the object to ground
- I_{sc}: the short-circuit current when the object is connected to ground through a low impedance.

If a person at ground potential touches an insulated object, the capacitance C_s will be discharged through the contact. The discharge may be flowing directly through the skin or, if the instantaneous voltage between person and object at the moment of the spark is sufficiently high, through a spark. If the contact is not made firmly, there could be a series of sparks. The current in the contact may be described as in Figure 7.10-4. After the contact is established, a current at the power frequency will flow. If the object is insulated and the person is electrically grounded, this current will approach the value of the short-circuit current, I_{sc}. The person can be considered effectively grounded not only when touching a grounded metallic object, but also when standing barefoot or wearing wet or conductive shoes on grassy or wet ground.

A person contacting a metallic object in an electric field may sense the capacitive discharge occurring when a contact is made or broken, or the short-circuit current occurring after a contact is made, or both.

Data regarding the values of V_{oc}, C_s, and I_{sc} that correspond to the threshold of perception and annoyance are few and based on people's subjective interpretation (especially in what constitutes annoyance). A summary of the data (EPRI 1982; IEEE 1978, Reilly 1992) that are relevant to spark discharges between a person and an insulated conductive object near a high-voltage transmission line is shown in Figure 7.10-7. The data from the Red Book (EPRI 1982) are for a well-insulated object. The perception threshold data from Reilly are given for different values of the parameter k, which is given by Equation 7.10-13.

$$k = \frac{V_{oc}}{V_{highest}} \qquad 7.10\text{-}13$$

$V_{highest}$ is the largest possible object-to-ground voltage. $V_{highest}$ occurs for a perfectly insulated object ($R = \infty$), when all the current I_{sc} flows in the capacitance C_s.

$$V_{highest} = \frac{I_{sc}}{\omega C_s} \qquad 7.10\text{-}14$$

When the leakage resistance becomes of the same order or smaller than the capacitive impedance, $1/C_s$, the voltage is less than the highest possible by the factor k.

If the leakage resistance is known, the value of k may be derived from Equation 7.10-15.

$$k = \frac{R}{\sqrt{R^2 + (1/\omega C_s)^2}} \qquad 7.10\text{-}15$$

The response of a person to the electrical stimulus occurring when touching an object varies with the value of k. For the same values of C_s and V_{oc}, a low value of k means a higher value of I_{sc}. Therefore, while the discharges occurring when

the contact is made or broken produce the same sensations, there is a stronger sensation during the contact.

The following example illustrates the concepts presented in this section. Assume an object, for instance a gutter system, with C_s = 400 pF and I_{sc} = 0.2 mA. The capacitive impedance of the gutter to ground is $1/\omega C$ = 6.6 MΩ. If the leakage resistance of the gutter is much greater than this value, the voltage between the gutter system and ground, given by Equation 7.10-14, is $V_{highest}$ = 1320 V. According to Figure 7.10-7, in correspondence to C_s = 400 pF, V_{oc} = 1320 V, and k = 1, the situation may produce sensations well above perception and corresponding to the annoyance levels for 50% of the people. Assume now that the gutter system has a leakage resistance to ground of 2 MΩ. According to Equation 7.10-15, k = 0.29; according to Equation 7.10-13, V_{oc} = 385 V. According to Figure 7.10-7, in correspondence to C_s = 400 pF, V_{oc} = 385 V, and k = 0.25, the situation may produce sensations just about at the level of perception for 50% of the people.

Effect of Frequency

The frequency of the electric field has an effect on sensation because it causes a different spark repetition rate during the approach, and it affects the short circuit current after the contact is established. Test data obtained with dc voltages are not applicable to the ac case and could be quite misleading, resulting in much higher open-circuit voltages. Results of tests (EPRI 1982) performed with electric fields at different frequencies are shown in Figure 7.10-8. The data indicate that people are more sensitive to spark discharges in electric fields with higher frequency. However, the difference between the effects of 50 Hz and of 60 Hz electric fields is very small and insignificant when compared with the large dispersion of human response data.

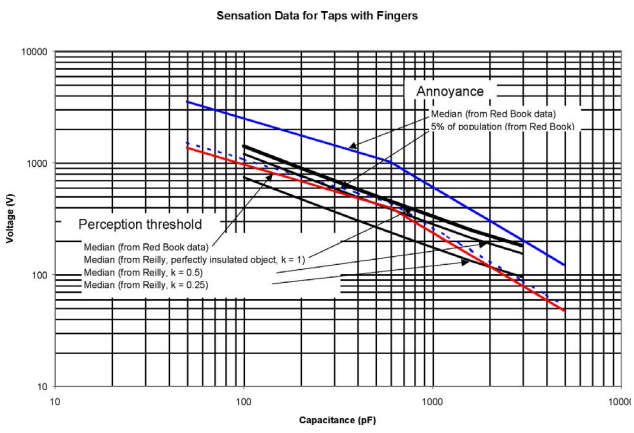


Figure 7.10-7 Perception and annoyance data for taps with fingers. Median values correspond to 50% of people.

Response to Steady-State Currents

Of practical interest for transmission-line design and operation applications are the ac currents flowing into the body of a person from hand to hand or from hand to feet when touching a large object, which collects current induced by the ac electric field. Only a few data are available for this case. Most data refer to laboratory tests in which people held the electrodes firmly in their hands.

Experimental results are shown in Figure 7.10-9 for perception of direct current and in Figure 7.10-10 for perception of alternating current (Dalziel 1954, 1972). The data follow a normal distribution with a large dispersion (the 99% values are four times larger than the 1% values). Average values for men equal 5.2 mA for dc current and 1.1 mA for currents alternating at 60 Hz. The first sensation for direct current is that of heat, whereas the first sensation for alternating current is a stinging sensation. Insufficient data are available for women, although the comparison of average values indicates a 2:3 ratio in the threshold of perception levels (Thompson 1933).

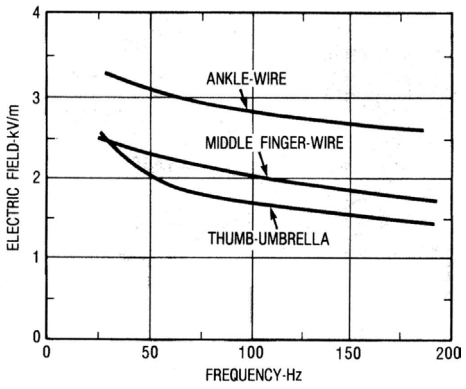


Figure 7.10-8 Median values of threshold of perception of spark discharges as a function of the frequency of the electric field.

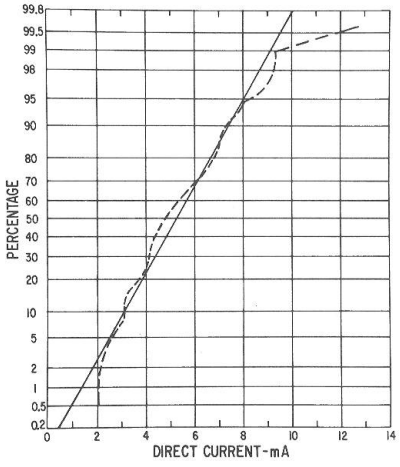


Figure 7.10-9 Distribution of minimum direct currents perceptible by men. Data for 115 men.

As the intensity of the current increases, control of the muscles in which the current flows becomes increasingly difficult. Above a certain value of current, it is not possible to release the grip on an object. The current for which this situation first occurs is called the "let-go current." Figure 7.10-11 shows the distribution of let-go values of direct currents. Figure 7.10-12 shows the distribution of let-go values of currents alternating at 60 Hz (Dalziel and Massoglia 1956; Dalziel 1972). The minimum let-go 60-Hz current values, arbitrarily defined as those corresponding to a probability of 0.5%, are 9 mA for men and 6 mA for women. A more conservative value of 5 mA might be applied for children. The National Electric Safety Code has specified that transmission-line clearances shall be consistent with a maximum induced current of 5 mA, to be calculated for the largest expected sag and for the largest vehicle anticipated under or near the transmission line (Banks and Vinh 1984; NESC 1997).

The effect of frequency on let-go current is shown in Figure 7.10-13 (Dalziel et al. 1943). There is practically no difference between 50 Hz and 60 Hz.

Increasing the value of the current above let-go may produce ventricular fibrillation (Dalziel 1960). Fibrillating current values are available for some animals. The fibrillating current is proportional to the body weight as shown in Figure 7.10-14. In addition to body weight and current

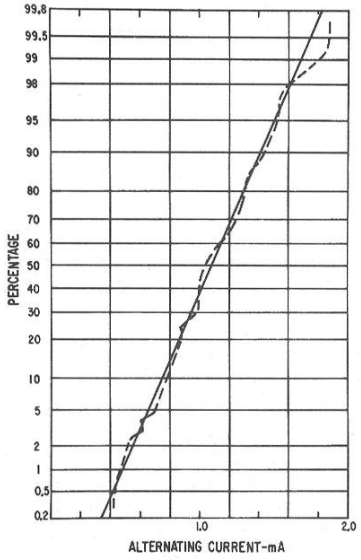


Figure 7.10-10 Distribution of minimum 60-Hz currents perceptible by men. Data for 167 men.

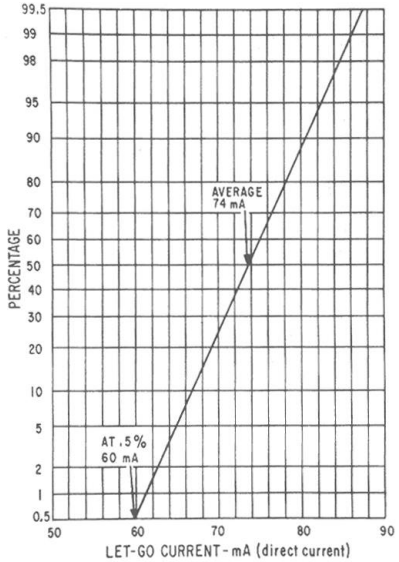


Figure 7.10-11 Distribution of let-go direct current values for men. Data for 28 men.

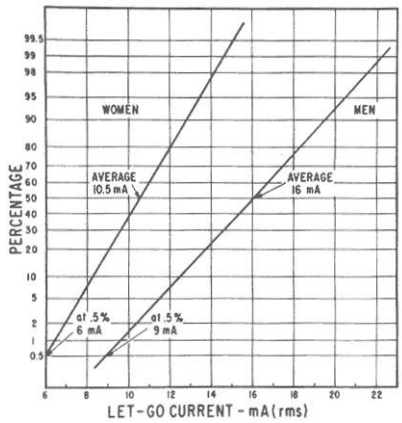


Figure 7.10-12 Distribution of let-go 60-Hz currents value. Data for 28 women and 134 men.

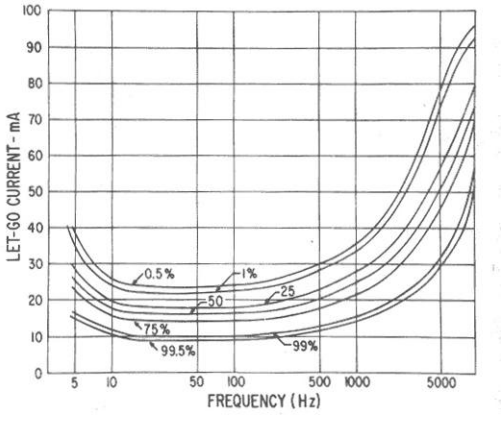


Figure 7.10-13 Effect of frequency on let-go current for men. The curves refer to different percentages of the population.

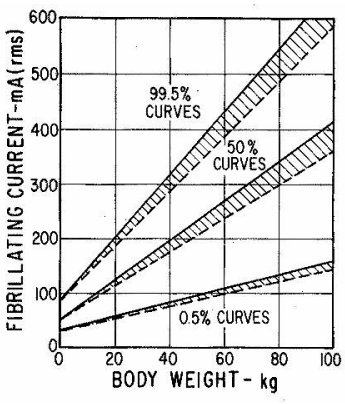


Figure 7.10-14 Fibrillating current versus body weight for six species of animals (calves, dogs, sheep, cats, rabbit, and guinea pigs). Continuous curves: All animals considered. Dashed curves: Guinea pig omitted.

magnitude, fibrillation is a function of the shock duration, according to the classic electrocution Equation 7.10-16 (Dalziel 1968, 1972; Dalziel and Lee 1969).

$$I = \frac{k}{\sqrt{t}} \quad (I \text{ in mA and } t \text{ in seconds}) \qquad 7.10\text{-}16$$

Dalziel gives a value of k = 116 for "normal adult worker" (Dalziel 1972), while in previous work had indicated a range of 116 to 185 (Dalziel and Lee 1969).

A summary of the response of adult men to steady-state ac electric currents is shown in Figure 7.10-15 (EPRI 1982).

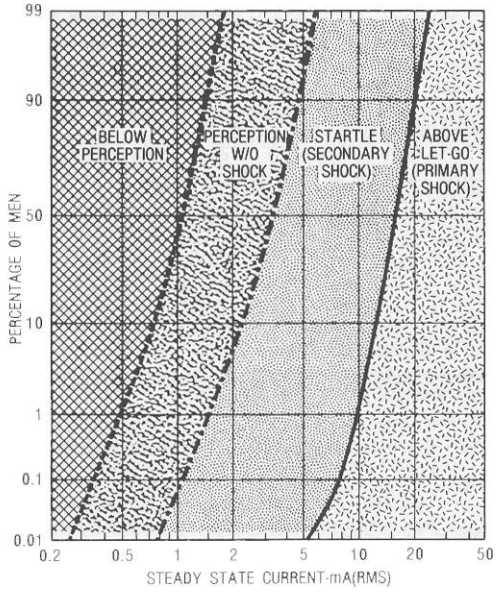


Figure 7.10-15 Statistical distribution of responses of adult men to steady-state ac currents through a gripped contact.

The few data available for women indicate levels approximately two-thirds those for men. Data for children are not existent.

Response to Hair Stimulation

In high electric fields, sensation is also caused by stimulation of hair nerves. Such stimulation occurs when skin with hair is exposed directly to the electric field or when currents pass from clothes to body through hair. Figure 7.10-16 presents the percentage of people who experience sensations above the threshold of perception and above the minimum annoyance level.

The curves marked with 1 correspond to stimulation of the hair of the hand when a person extends the arm over the head searching for the position where the sensation is strongest. Curves 2 correspond to stimulation of the hair of the head (forehead, eyebrows, sideburns), with the arms on the side of the body. Curves 3 correspond to a tingling sensation in parts of the body covered with clothes (elbow, shoulder, sides). Straight lines match reasonably well the data when the field is plotted in a log scale and the probability in a normal probability scale. The dispersion is much larger than for spark discharges (see Figure 7.10-6). There is a 7~9 ratio between 84% and 16% probability levels. The ratio between annoyance and perception fields is 6 ~10. The median values of the threshold of perception levels are:

Hand hair: 7 kV/m
Head hair: 23 kV/m
Between body and clothes: 20 kV/m

Median annoyance levels are much higher and are never reached in practical conditions.

Women, probably because of less hair, appear to be much less sensitive than men to this type of electric field effect. For a group of 8 women, the 50% value of perception for hand hair was 17.5 kV/m, as opposed to 6.7 kV/m for a group of 60 men tested the same day (EPRI 1982). Low

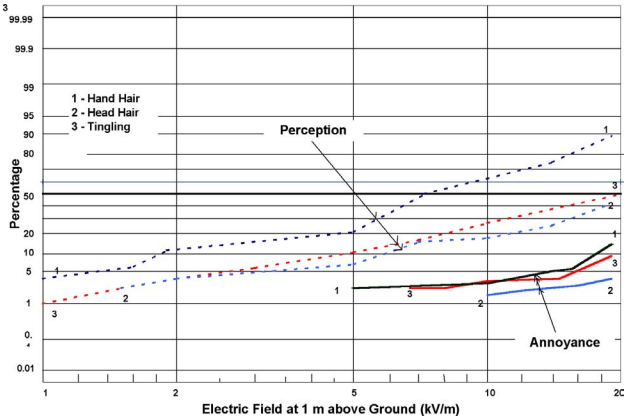


Figure 7.10-16 Hair stimulation and tingling (136 persons).

humidity and low temperature lower sensitivity, although the effect of individual parameters is not clear.

The frequency of the electric field affects the sensation, as shown by the curves of Figure 7.10-17. Greater sensitivity occurs at lower frequencies. The difference between 50 Hz and 60 Hz is small and insignificant when compared with the large dispersion of these data.

The basic mechanism of hair stimulation is not fully understood. It is assumed that hair collects charges that give origin to a force acting on the hair, thus causing vibration. Hair vibration has been observed at the power frequency and at twice the power frequency. These observations produce different interpretations of the nature and polarity of the charges on the hair. Conductive hair, such as wet hair, has a charge of the same polarity as that on the skin. Thus, the mechanical force on the hair has a frequency double that of the power frequency. However, if hair is insulating, a net charge of fixed polarity could remain on the hair, thus justifying a force at the power frequency.

7.11 BIOLOGICAL EFFECTS OF ELECTRIC FIELDS

Electric fields from electrical facilities have been studied for a variety of reasons and for many purposes. Much of the investigation of electric field from transmission lines and stations has included health concerns, particularly since the advent of EHV transmission in the 1960s and the subsequent great expansion of EHV systems. This Reference Book does not discuss the research performed on health effects of the electric field. The body of literature on possible biological and health effects of electric fields on people, animals, and plants has been reviewed and commented upon by many organizations (Bridges 1978; AMA 1994; NIEHS 1998; NRPB 2001).

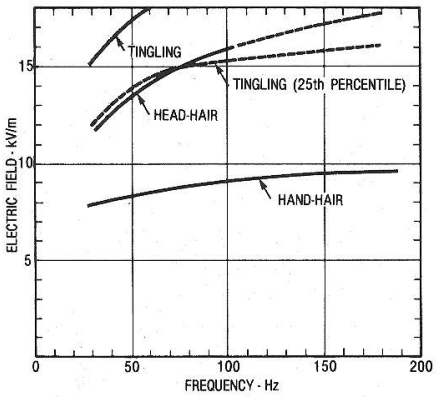


Figure 7.10-17 Median value of the threshold of perception of hair stimulation versus the frequency of the electric field.

To date, no health effect of ac electric fields of the type and value as those existing in transmission-line and station environments has been conclusively found nor accepted by the scientific community. Although health complaints by substation workers in the former Soviet Union were reported (Korobkova et al. 1972), medical examinations of transmission-line workers in the U.S. (Kouwenhoven et al. 1967), in Sweden (Knave 1980), and in Canada (Roberge 1976) failed to find health problems attributable to the electric field.

Even after considerable research, it is not possible to draw definitive conclusions. It is often necessary, nevertheless, for system planners, line designers, and state and federal regulatory agencies to take decisions on the values of electric field for which electrical facilities can be designed and operated. No rules for electric field intensity inside and outside the transmission corridor have been widely accepted. International Commission on Non-Ionizing Radiation Protection (ICNIRP) guideline document regards a current density of 100 mA/m^2 as the threshold for changes in the nervous system and recommends not exceeding one-tenth of this value—i.e., 10 mA/m^2 (ICNIRP 1998). For a person, 10 mA/m^2 may be reached in an unperturbed electric field of 25 kV/m. Recommendations and guidelines for electric field are presented in Appendix 7.3. Most of these rules are not based on accepted scientific findings. Some rules have been established with the purpose of allowing construction of new facilities while offering a guarantee that these new facilities would not exceed field values normally found in facilities that already exist in the same region.

7.12 CURRENTS INDUCED IN THE HUMAN BODY BY TRANSMISSION LINE MAGNETIC FIELDS AND A COMPARISON WITH THOSE INDUCED BY ELECTRIC FIELDS

The currents induced inside the body of a person exposed to ac electric and magnetic fields depend on the electrical characteristics of the different organs, tissues, and membranes of the body. A detailed electrical representation of the body has been developed and used to calculate current distributions in various parts of the body caused by electric (see Section 7.10.1 and Dawson et al. 1998) and magnetic fields (Stuchly and Zhao 1996). A discussion about this rigorous treatment and the presentation of the results of calculations is beyond the scope of this Reference Book. However, a simplified model is presented that provides an approximate comparison between electric-field and magnetic-field induced currents resulting from exposure to transmission-line fields.

The magnetic-field induced currents in the human body may be calculated by approximating the body cross section with a circle of radius *r*. Consider the rms value, *B*, of the component of the magnetic field normal to this cross section. The current density, *j*, at a distance *x* from the center of the cross section is calculated with Equation 7.12-1.

$$j = v / (2\pi x \rho) \qquad 7.12\text{-}1$$

Where:

ρ is body resistivity.

v is the voltage induced in a circular area of radius x.

The induced voltage is given by:

$$\begin{aligned} v &= -\frac{d\Phi}{dt} \\ &= -\frac{d}{dt}\left(\pi x^2 \sqrt{2} B \sin(2\pi f t)\right) \\ &= 2\pi f \sqrt{2} \cos(2\pi f t) \cdot \pi x^2 \end{aligned} \qquad 7.12\text{-}2$$

In the steady state:

$$V = -j 2\pi f \sqrt{2} B \cdot \pi x^2$$

The rms value of the current density is:

$$J = \frac{V}{2\pi x \rho} = \frac{\pi f B x}{\rho} \qquad 7.12\text{-}3$$

The highest current density occurs on the periphery of the cross section ($x = r$).

The comparison between currents induced by a 1000 V/m electric field in a person erect and grounded and the currents induced in a 100 mG (10 μT) vertical magnetic field is shown in Table 7.12-1. These field values were chosen because they are representative of electric and magnetic field in outdoor situations near the right-of-way. The highest electric-field induced current is in the ankle. Magnetic-field induced currents are lower. The highest magnetic-field induced current is in the chest. Even at that location, the magnetic-field induced currents are significantly lower than the current induced by the electric field.

Electric-field induced currents may be significantly greater when a person touches a conductive object. In this situation, part or all of the object's short-circuit current will flow to ground through the body of the person. In this respect, it should be mentioned that electric-field induced currents resulting from touching a conductive body in an electric field are the same as touching an appliance or any other object that may have a small amount of conductive current leakage. Electric field induction often causes transient spark-discharge currents, with peak values that may be 1000 times greater than the steady-state current peak. The current density at the point of entrance in the body may be 10^6 times greater. No similar phenomena are caused by magnetic-field induction.

Table 7.12-1 Comparison of Currents Induced in the Body of a Person by Electric and Magnetic Fields Typical of Situations near the Right-of-Way

Electric Field	Person 1.75 m high, standing in a 1000 V/m (See Section 7.10)		
Position	**Current**	**Circumference**	**Current Density**
Neck	48 μA	38 cm	0.42 mA/m²
Waist	126 μA	91 cm	0.19 mA/m²
Ankle	164 μA	23 cm	4.0 mA/m²
Magnetic Field	**Person standing in a 100 mG (10 μT) vertical magnetic field. Body resistivity ρ = 10 Ωm**		
Position		**Radius**	**Current Density**
Chest		17 cm	0.032 mA/m²
Head		9 cm	0.017 mA/m²

7.13 BIOLOGICAL EFFECTS OF MAGNETIC FIELDS

Magnetic fields from electrical facilities have been studied for a variety of reasons and for many purposes. This chapter discusses the currents and voltages that are induced in long conductors parallel to transmission lines and that may generate safety issues for fences, pipelines, de-energized parallel lines, and shield wires. Appendix 7.4 discusses the possible monitor jitter caused by power line magnetic fields. This chapter covers engineering issues that may also be applicable for the consideration of possible health effects of long-term exposure to power-frequency magnetic fields such as calculations, measurements, design rules, and methods for field reductions.

Much of the investigation of magnetic fields from transmission lines and stations has included health concerns, particularly since the publication of the results of epidemiological studies starting in 1979 and continuing in different countries for the following 20 years (Wertheimer and Leeper 1979; Tomenius 1986; Savitz et al. 1988; London et al. 1991; Feychting and Ahlbom 1993; Verkasalo et al. 1993; Olsen et al. 1993; Linet et al. 1997; Tynes and Haldorsen 1997; Michaelis et al. 1998; McBride et al. 1999; UK Childhood Cancer Study Investigators 1999; Ahlbom et al. 2000; Greenland et al. 2000). This Reference Book does not discuss the research performed on health effects of the magnetic field. The body of literature on possible biological and health effects of magnetic fields on people, animals, and plants has been reviewed and commented

upon by many organizations (AMA 1994; NIESH 1998; NRPB 2001).

In their information booklet on EMF, the National Institute of Environmental Health Sciences and the National Institute of Health report the following conclusion (NIEHS-NIH 2002): "Electricity is a beneficial part of our daily lives, but whenever electricity is generated, transmitted, or used, electric and magnetic fields are created. Over the past 25 years, research has addressed the question of whether exposure to power frequency EMF might adversely affect human health. For most health outcomes, there is no evidence that EMF exposures have adverse effects. There is some evidence from epidemiological studies that exposure to power-frequency magnetic field is associated with an increased risk of childhood leukemia. This association is difficult to interpret in the absence of reproducible laboratory evidence or a scientific explanation that links magnetic fields with childhood leukemia. EMF exposures are complex and come from multiple sources in the home and workplace in addition to power lines. Although scientists are debating whether EMF is a hazard to health, the NIEHS recommends continuing education on ways of reducing exposure."

Several countries and state regulatory agencies have developed recommendations and guidelines for magnetic fields. No U.S. federal recommendations for occupational or residential exposure to 60-Hz magnetic fields currently exist. Various recommendations and guidelines are presented in Appendix 7.3.

Magnetic field levels are frequently an issue when a line is sited, when developments are planned near transmission lines and substations, and when health effects are attributed to the proximity of electrical facilities. Because of the importance of this issue, considerable effort has been spent in researching practical cost-effective ways to reduce magnetic fields (see Section 7.17).

7.14 FUEL IGNITION

This section discusses electric-field induced fuel ignition during refueling and fuel ignition induced by corona at the conductor surface. There is no apparent real problem in these situations, yet the power industry's deep concern for public safety has led to research whose results are presented here. There has been no report of accidental ignition of fuel caused by spark discharges induced by transmission-line electric fields. Corona discharges do not have sufficient energy to create fuel ignition except in special cases.

7.14.1 Fuel Ignition Caused by Spark Discharges

Lewis and von Elbe determined the minimum discharge energy required in ideal conditions for ignition of flammable mixtures of hydrocarbon vapor and air (Lewis and von Elbe 1951). Their work covered different fuels and different types of discharges. An excellent summary of the subject was prepared by McKinney (McKinney 1962).

The minimum energy required to cause ignition of a specific mixture varies with the test setup. For example, a minimum ignition energy spark requires such high voltage that corona at the electrodes may partially discharge the circuit before the spark occurs. The energy dissipated in the spark goes in different proportions to heat the mixture and the electrodes. The dissipation of energy in heating the electrodes causes the quenching of the flame, and plays a dominant role in the process of ignition causing significant differences between different electrode arrangements. For example, electrodes with round edges and minimum corona will be massive thermal sinks that tend to quench an ignited flame. Most of the investigations reported in the literature were aimed at finding the arrangements corresponding to the minimum discharge energy, whereas EPRI research focused on the discharge energy required for fuel ignition in realistic conditions associated with refueling near a high-voltage transmission line (EPRI 1982).

Three methods of causing ignition were considered by McKinney:

- Ignition by discharge of capacitive circuits between fixed or closing electrodes
- Ignition by interruption of inductive circuits between opening contacts
- Ignition by hot wires

In proximity to overhead ac transmission lines, the main concern is with capacitive discharges from large objects caused by electric field induction.

The discharges induced by the power-frequency electric field may be repetitive, and, owing to the effect of trapped charges, more voltage (and energy) may be available after the first spark if the electrodes are moved apart (withdrawing electrodes). Sequences of sparks to ground from an insulated object modify the object potential, as shown in Figure 7.14-1. When the spark gap is kept constant and the voltage is raised, the voltage at the moment of the spark is equal to or less than the peak voltage existing without a spark. The same situation occurs if the voltage is kept constant and the gap distance is decreased by closing the electrodes. However, if the gap distance is increased by withdrawing one of the electrodes from the other, the spark voltage may reach values higher than the open-circuit voltage with no spark, as shown in Figure 7.14-2. The maximum spark voltage could conceivably be twice the open-circuit voltage. This phenomenon is influenced by the leakage resistance to ground and by corona appearing on the

electrodes (in the case of small objects when higher voltages are required). The voltage-doubling effect may be reached with high parallel leakage resistance for objects of large capacitance to ground.

The energy required for ignition is a function of the fuel-to-air ratio of the mixture. In most cases, the minimum ignition energy corresponds to the stoichiometric mixture. For a single capacitive discharge, the minimum ignition energy of hydrogen is about 0.02 mJ. The minimum ignition energy for the majority of hydrocarbons that make up the most commonly used fuels is much higher, being equal to about 0.25 mJ.

The dielectric loss of the capacitor used in the discharge circuit, the ignition quenching characteristics of the electrodes, and the electrode wetting by the fuel are important parameters (EPRI 1982). For these reasons, fuel ignition tests are difficult to reproduce. Tests simulating realistic situations were performed using electrodes shaped like gasoline cans and open containers filled with gasoline connected to objects having different capacitances to ground

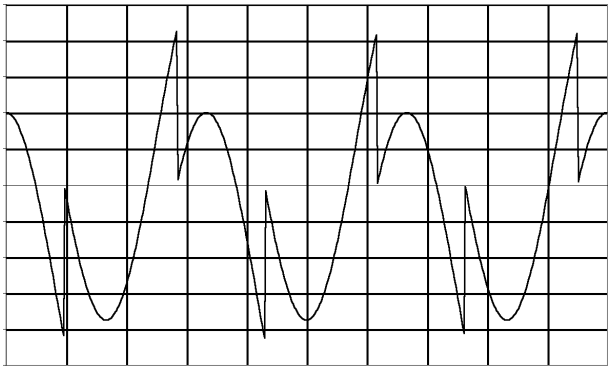


Figure 7.14-1 One spark per cycle. Large object.

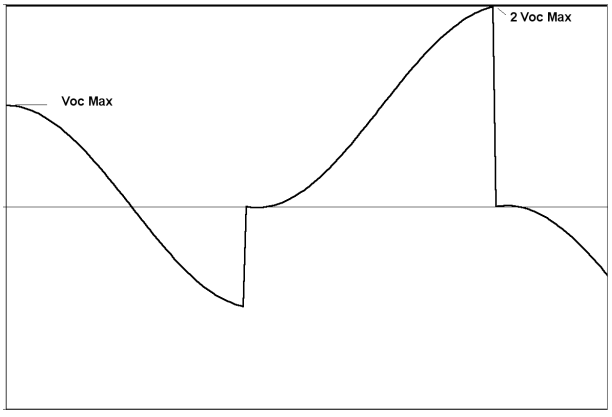


Figure 7.14-2 Voltage-doubling effect.

in an electric field produced by a 60-Hz high-voltage test line (EPRI 1982). The results were plotted as shown in Figure 7.14-3. A straight line was drawn through the points representing the minimum ignition voltage obtained. The equation for minimum ignition voltage is:

$$V_{oc} = 4.6 \cdot C^{-0.3} \quad (V_{oc} \text{ in volt rms and } C \text{ in farad}) \qquad 7.14\text{-}1$$

The actual ignition voltages obtained during several experiments ranged from 1 to 2 times the minimum values. Sparks originating from a sharp point, such as a pin, lowered the minimum ignition voltage obtained with a spout by a factor of 1.5.

The curve in Figure 7.14-3 that gives the minimum ignition voltage is not a constant energy curve; therefore, it is not possible to refer to the energy as the only parameter that characterizes the potential for ignition. The minimum ignition energy is 2.1 mJ with a 100 pF capacitor and 13 mJ with 10,000 pF. For a large vehicle with a typical capacitance value of 1,500 pF, the minimum ignition voltage is 2,000 V rms, and the energy stored at the peak of the voltage is 6 mJ.

In order to characterize the potential for ignition, it is necessary to provide both the value of the rms voltage existing prior to the discharge and the value of the capacitance. The actual voltage at the instant of ignition may be greater than the crest value of the open-circuit voltage prior to the discharge owing to the voltage-doubling effect previously illustrated. In fact, the minimum ignition voltages were obtained by withdrawing the spout from the gasoline container.

Figure 7.14-3 also contains a curve from McKinney (McKinney 1962) obtained by rearranging the Lewis and

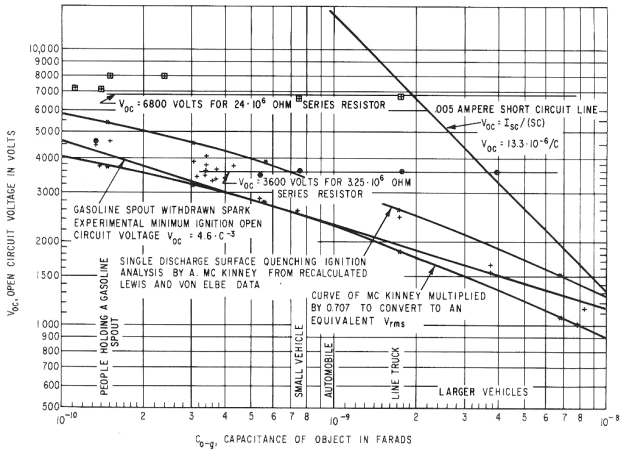


Figure 7.14-3 Minimum open-circuit voltage for ignition of gasoline caused by spark discharges between a can spout and a vehicle tank.

von Elbe data on ignition of mixtures of natural gas and air with single capacitor discharges with plain electrodes (Lewis and von Elbe 1951). Translating McKinney's curve to ac rms voltages produces a relatively close agreement with Equation 7.14-1. It is, therefore, suggested that this equation be used for situations that might occur near overhead ac transmission lines. Also in Figure 7.14-1, the curve of V_{oc} and C corresponding to a short-circuit current of 5 mA is drawn. According to the U.S. National Electric Safety Code, 5 mA is the maximum short-circuit current allowed from a vehicle located under a transmission line. It can be seen that spark discharges that have the potential of igniting gasoline correspond to situations in which the short-circuit current is much less than 5 mA. However, spark discharges at the level of potential gasoline ignition cause a painful sensation, a strong warning sign that fueling operations in such conditions may result in fuel ignition.

It must be noted that in realistic conditions, even when the open-circuit voltage and the capacitance values are above the minimum required, gasoline ignition is very improbable because several conditions must occur simultaneously in order to obtain ignition:

- The vehicle must have high impedance to ground, such as well-insulated tires on a very dry pavement.
- The gasoline must be fresh and easily ignitable.
- Warm dry sunny day. When the temperature is less than 10 ºC, the minimum ignition voltage may be as much as twice the minimum given by Equation 7.14-1.
- The gasoline container must be grounded—for instance, through the body of a person standing on wet ground or vegetation.
- The spark must occur in an area where the fuel and air are close to the stoichiometric proportion.
- There must be a sequence of sparks with the gasoline-pouring spout being slowly withdrawn from the tank.
- The operator ignores spark discharges above the perception level that are likely to occur in a situation where there is a potential for gasoline ignition. In a practical scenario, a person will experience perceptible and annoying spark discharges and is likely to consider them as a warning against proceeding with fueling operations without suitable precautions.

Section 7.8 describes the statistical nature of the voltage that exists between a person and a vehicle. This voltage is always lower than that needed for fuel ignitions. It can be concluded that the probability of an ignition occurring is so low that in practice it will never occur. The fact that no fuel ignition due to sparks caused by transmission-line electric field has been reported substantiates this conclusion (Deno and Silva 1985). Furthermore, the potential consequence of fuel ignition is not catastrophic. Analysis indicates that an ignition would cause only a "puff" at the filler neck, similar to the effect produced by lighting a gasoline stove (EPRI 1982). In fact, the gasoline partial pressure inside the tank at a temperature greater than –18 ºC results in a fuel-air mixture too rich to support combustion. For extremely low temperatures, at which combustion becomes possible, the spark energy required for ignition is much greater.

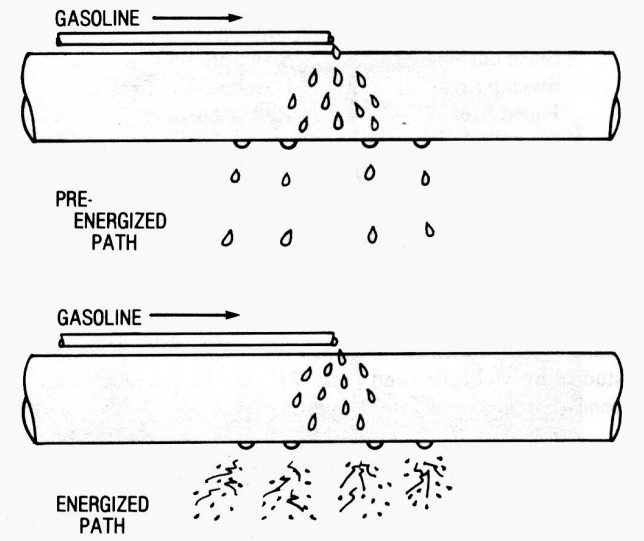


Figure 7.14-4 Effect of electric field on dripping of fuel droplets from a conductor.

7.14.2 Corona-Induced Fuel Ignition

In some situations, such as with gas line blow off on a shared right-of-way, combustible hydrocarbon gases may approach transmission-line conductors where there is corona. Ignition by hydrocarbon vapors by transmission-line corona was investigated by EPRI (EPRI 1982).

The high electric field at and near the surface of a conductor in corona greatly affects the shape of the droplets of fuel and the dripping from the conductor surface, as shown in Figure 7.14-4. In the presence of a high electric field, the dripping fuel is pulled off the dripping path.

Ignition occurs only in calm wind conditions (wind velocity less than 5 km/hr). Humidity and temperature have little effect on ignition. The surface electric field necessary for ignition is dependent on the conductor diameter: 15.3 kV/cm for a 5.5-cm diameter conductor, 17.4 kV/cm for a 3.3-cm diameter conductor, and more than 30 kV/cm for a 1.6-cm diameter conductor.

7.15 EFFECTS OF HIGH-INTENSITY ELECTRIC FIELDS

High-intensity electric fields may cause burning of transmission-line wood poles with grounded hardware and also of poles without any hardware, burning of dead trees or dead tree branches, damage to tree tips, corona from grounded objects, and damaging currents on the surface of fiber optic cables strung near the high-voltage conductors (Karady and Devarajan 2001). The phenomena discussed in this section occur only at high-intensity electric fields, such as those that exist near the conductor support structures of EHV transmission lines. Some of the effects were a common experience in proximity of UHV test lines (EPRI 1982), but are rarely experienced at EHV voltages. The phenomena described in this section are of little or no concern at 220/230 kV or lower voltage levels.

7.15.1 Wood Pole Burning

The grounding and bonding of the hardware of wood structures have been used to prevent the insulator leakage current from flowing on the wood surface. However, the current induced by the electric field on wood surfaces when they are wet or moist flows to the nearest hardware. If the current density at the hardware is high enough, the wood surface near the hardware may form a dry band, the voltage builds up across the dry band, arcing starts, and the wood gets slowly carbonized and eventually burns. A photograph of the initial burning of a wood pole near hardware is shown in Figure 7.15-1.

Wood poles are used for lines with voltages up to 345 kV. They are seldom used for 500-kV lines. Most wood structure burning reports are for 345-kV lines (Lusk 1975; Lusk and Mak 1976).

The phenomenon of wood pole burning near hardware is affected by many parameters, such as the conductivity of the wood surface, the dryness of the wood below the surface, the shape of the hardware, and the highest space potential to which the surface of the pole is exposed. Experience has suggested that a condition for the occurrence of wood burning near hardware is that the surface of the pole at some point exceeds a space potential of 100 kV (EPRI 1982). The space potential is that which exists without the object present—i.e., the unperturbed space potential. Burning occurred at the first moisture after a long period of dry weather or in the winter in cold and dry weather but with snow covering the surface of the pole (EPRI 1982).

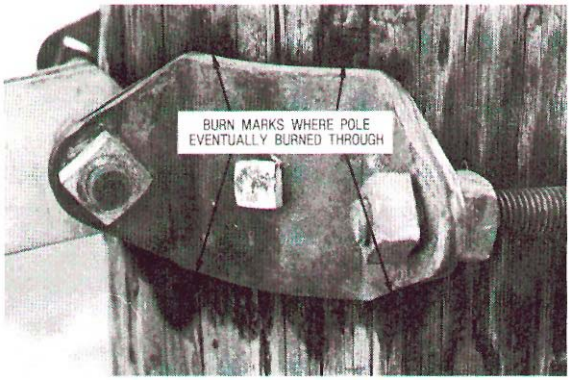


Figure 7.15-1 Initial burning around a collar holding guy wires of a wood pole installed in a high electric field region.

Pole fires may also occur on poles without hardware. These poles may be installed near transmission lines for various reasons—for instance, for the purpose of supporting instrumentation of some kind. The current flowing on a moist surface may encounter discontinuities, and may form dry bands and arcing along the pole. This phenomenon is similar to that occurring on contaminated insulators in humid weather and to that causing damage to fiber optic cables strung near the conductors of high-voltage lines (Karady and Devarajan 2001). Experience has suggested that, for poles without hardware, just as for those with hardware, a condition for the occurrence of wood burning is that the surface of the pole at some point exceeds an unperturbed (without the pole) space potential of 100 kV (EPRI 1982). This rule of thumb may be applied in the analysis of wood pole-burning situations.

The possibility of wood pole burning may be analyzed by calculating the space potential at various points along the pole and determining whether any of these exceeds the 100 kV limit. Space potential contour lines can be obtained using Applet EMF-2 (2-D geometry) or Applet EMF-4 (3-D geometry). Figure 7.15-2 shows the space potential contour lines around a 550-kV transmission line. Any dead tree or wood pole that protrudes inside the 100-kV contour line may be subject to burning caused by the transmission-line electric field.

7.15.2 Dead Tree Burning

Unlike live trees, dead trees have a very high resistance in dry weather because they have no sap. In dry weather, therefore, dead trees cause very little perturbation of the electric field produced by a transmission line. In wet weather or when the surface is covered with melting frost or snow, however, the surfaces of the branches form conductive sheaths that collect electrical charges and discharge them to the ground. There will be no current inside the tree but only on the surface. The phenomenon is the same as previously illustrated for wood poles. Figure 7.15-3 shows branches of a dead tree broken because of burning. Details of a stump show clear signs of burning.

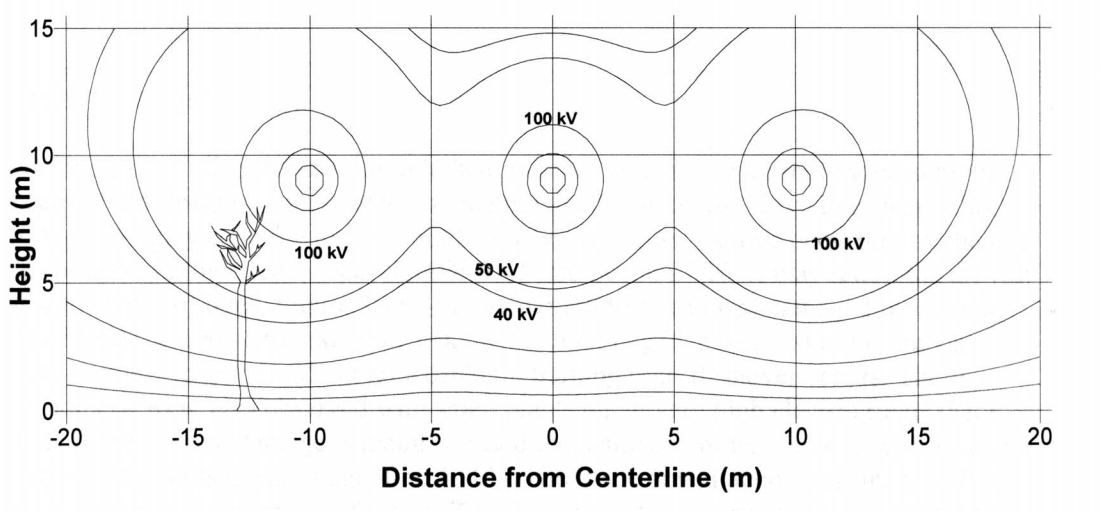


Figure 7.15-2 Space potential lines for a 525-kV transmission line (bundles of 3 x 3.3 cm, 46-cm spacing, 10-m phase spacing, 9-m height at midspan).

The 100-kV space potential rule also applies to dead trees. Experience indicates that burning occurs only at space potentials greater than 100 kV (EPRI 1982). Figure 7.15-2 shows space potential contour lines for a 500-kV line. The portion of dead trees that intrude inside the space delimited by the 100-kV contour line may experience burning.

7.15.3 Tree Tip Damage

Live trees are well grounded through their conductive sap. The current induced by the electric field flows to ground without creating much power loss. Live trees near a high-voltage line may continue to grow until a flashover occurs. Corona occurring on the tree tips because of the intense local electric field (see Section 7.15.4) may retard the growth of some types of trees. Figure 7.15-5 shows a birch tree with tips damaged by corona. Other types of trees—for example, oaks with round-edged leaves and blunt branch buds—appear to grow without noticeable tip burning until flashover occurs. These phenomena were also observed with small plants but at very high electric fields (McKee et al. 1978) Corona damage is mainly caused by positive corona, whose inception occurs at space potentials greater than 30 to 40 kV. The space potential contour lines, such as those shown in the example of Figure 7.15-2 are useful to determine the potential impact of this phenomenon.



Figure 7.15-3 Dead tree in a high electric field region. Branches that have burnt through and a stump detail.

7.15.4 Corona on Grounded Objects

A common experience near single UHV test lines, especially if single-phase, was the observation at night of corona on wood poles, bushes, and trees in the immediate proximity of the line (EPRI 1982). If a sharp metallic object, such as a key, is held high toward the line, audible and visual corona may be experienced. These phenomena may be experienced near some EHV transmission lines. An example is shown in Figure 7.15-4, which shows corona from needles of a tall pine tree near a 500 kV line.

Corona occurs on grounded objects when the electric field at their surface exceeds the breakdown electric field of air



Figure 7.15-4 Corona from needles in the top part of a tall pine tree near a 500 kV transmission line, photographed with a DayCor camera. Courtesy of the Bonneville Power Administration.

(~30 kV/cm). Such high levels may be reached when the height of the object is large and the tip of the object is sharp. At sharp points, corona appears first during the negative polarity half-cycle (negative corona). Corona onset is a function of the shape of the tip of the object and of the space potential. At larger space potential, corona also appears on the positive half-cycle (positive corona). While negative corona onset is critically dependent on the shape of the tip of the object, positive corona onset depends little on the shape. The space potential at positive corona varies from 30 kV for small objects to 40 kV for objects resembling plates 2.5 cm thick and 25 cm in diameter (EPRI 1982).

Negative corona produces very little visible light and audible noise. Positive corona, on the other hand, is clearly visible at night and audible if the ambient is quiet. The audible noise of a corona source is detected by the human ear but not by an instrument above ambient levels of 40 – 45 dBA. Each positive corona point generates radio noise currents between 1.5 and 5 mA. Negative corona radio noise is about 15 dB lower. Radio noise currents of such magnitude would be of concern if the line radiated them. In all cases, however, the radio noise current circulates in a very small circuit from the corona point to ground and is not propagated by the line. The radio noise decays very fast with distance from the source, and falls below ambient at a distance twice the height of the object.

Ozone is generated in measurable, but very minute, quantities only by positive corona. To detect ozone, the ozone sensor must be placed closer than a few centimeters from the source. Ozone is generally not detectable away from the transmission line. Since, in practical conditions, positive corona onset is not reached on the tips of most crops, no crop damage by corona is expected. Positive corona may occur on the tips of the branches of tall trees near 500-kV or higher voltage lines, depending on the type of tree, and damage can be observed (see Figure 7.15-5).



Figure 7.15-5 Black birch with electric-field-damaged branches photographed from the ground.

7.16 METHODS FOR REDUCING TRANSMISSION-LINE ELECTRIC FIELDS

7.16.1 Introduction—Passive and Active Shielding

A method often used to minimize the effects of the electric field is to shield the area of interest from the high-voltage conductors by placing conductive objects above or around that area. Shielding reduces the electric field and consequently its effects. Because most field effects occur close to ground, and are a function of the magnitude of the unperturbed electric field, the reduction of the field at 1 m above ground is the primary objective of the shielding methods discussed in this section. It should be pointed out, however, that there are other methods to reduce electric field effects such as the grounding of structures, the use of conductive straps on vehicles, and the use of conductive suits to reduce currents induced on line workers.

Different shielding methods represent alternative means of reaching specific objectives. The choice of the method depends on subjective considerations that are often a function of local conditions and on the selection of the admissible field in the area to be shielded.

Methods of shielding may be classified as "passive," if shielding is provided by grounded conductive objects, or as "active," if shielding is provided by conductors energized at appropriate voltages and phases. Each shielding method changes the value of the electric-field intensity and of the space potential from the value without the shield. A useful parameter to categorize the degree of shielding is the shielding factor, *S*, defined in Equation 7.16-1 as:

$$E_s = E_u \cdot S \qquad 7.16\text{-}1$$

Where:

E_s is the electric field at ground with the shield present.

E_u is the unperturbed electric field without shield.

Also, a shielding efficiency, *SE*, may be defined, as shown in Equation 7.16-2.

$$SE = 1 - S = \frac{E_u - E_s}{E_u} \qquad 7.16\text{-}2$$

Also used is the "field reduction factor," *F*, which is the inverse of the shielding factor, as shown by Equation 7.16-3:

$$F = 1/S = E_u / E_s \qquad 7.16\text{-}3$$

The concepts of shielding factor, shielding efficiency, and field reduction factor may be applied to objects in nonuniform fields or to objects not close to ground. In these cases,

however, it is preferable to use the space potential of a point, as shown by Equation 7.16-4 for the shielding factor, *S*.

$$V_{sp,s} = V_{sp,u} \cdot S \qquad 7.16\text{-}4$$

Where:

$V_{sp,s}$ is the space potential with the shield present.

$V_{sp,u}$ is the unperturbed space potential without the shield.

7.16.2 Shielding by a Horizontal Grid of Grounded Wires

A horizontal grid of wires at ground potential placed at height, *H*, above ground provides an effective shield of the electric field caused by transmission lines either above the grid or at a distance from the grid, as shown in Figure 7.16-1 (Deno 1977a).

Infinite Grid

The width of the grid, *W*, is shown in Figure 7.16-1. If the grid can be considered infinitely large ($W = \infty$), and the unperturbed field is uniform over the extent of the field, the average field under the grid can be calculated in a straightforward manner.

The shielding efficiency of an infinite grid, SE_∞ (defined by Equation 7.16-2 is given by Equation 7.16-5).

$$SE_\infty = \frac{2\pi\, H/S}{\ln\frac{2H}{R} + \ln\left[\frac{e^{2\pi H/S} - e^{-2\pi H/S}}{4\pi H/S}\right]} \qquad 7.16\text{-}5$$

Where:

H is the height of the grid also ground.

S is the spacing between wires (assumed uniform).

R is the radius of the wires.

For instance, a grid of 0.0048-m wires, spaced 3.43 m apart, and at a height above ground of 6.85 m provides a shielding efficiency of 0.73 (73%). The field under the grid is reduced to 27% of its unperturbed value (shielding factor = 0.27).

Even if the unperturbed field is not uniform over the grid, Equation 7.16-5 can still be used to calculate the shielding efficiency, which is independent of the unperturbed field.

Finite Grid

The shielding efficiency is the product of two factors: the shielding efficiency of an infinite grid, SE_∞, and the edge factor, which is a function of the ratio between the distance, *x*, from the edge of the grid and the height, *H*, of the grid.

$$SE(x) = SE_\infty \cdot f(x/H) \qquad 7.16\text{-}6$$

The values of the function *f(x/H)* are given in Figure 7.16-2.

The edge effect is negligible below the grid at distances greater than *2 H* (*H* is the height of the grid's wires) from the closest grid's edge. At the edge of the grid, the edge factor is about 0.73. The edge factor applies only to the closer of the two grid terminations.

This method of calculating the shielding efficiency of a horizontal grid is sufficiently accurate for closely spaced wires.

When the ratio of grid-wire spacing, *S*, to grid height, *H*, exceeds 1.8, the shielding efficiency varies significantly from point to point even under the grid. For widely spaced wires, the shielding efficiency at any point may be calculated by adding the shielding efficiency of each wire, using wires that are no further than *3H* from the calculation point. For this purpose, the shielding efficiency of each wire is individually calculated by multiplying SE_∞, calculated for $S/H = 1.8$, by the edge factor for a single wire (dashed curve in Figure 7.16-2). For instance, assume that $S = 2H$, $R = 0.0002\ H$, and that the calculations are performed directly under a grid wire. The shielding efficiency

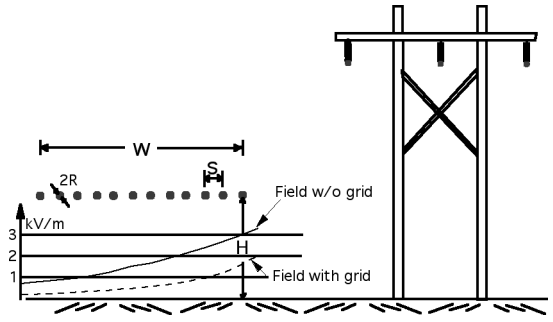


Figure 7.16-1 Horizontal grid of grounded wires as an electric field shield.

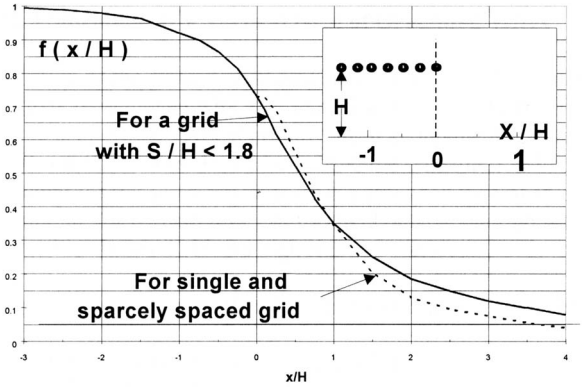


Figure 7.16-2 Edge factor for a horizontal grid of shield wires.

is contributed by three wires, one directly above, and two at a distance *2H*. The shielding efficiency due to the grid is $SE = SE_\infty \cdot (f(0) + 2 \cdot f(2))$ For this example: $SE_\infty = 0.33$, f(0) = 0.73, f(2) = 0.12, and, *SE* = 0.32.

If the calculation point were at the midpoint of two grid wires, $SE = SE_\infty \cdot (2f(1) + 2f(3)) = 0.28$. Note that the shielding efficiency for an infinite grid calculated with Equation 7.16-5 would have resulted in *SE* = 0.30.

An accurate solution of transmission-line electric field shielding by a horizontal grid of wires parallel to the transmission-line wires can be obtained by accounting for all shield wires and transmission-line wires and using the algorithms described in Section 7.3. The electric field in the presence of a grid of shield wires can be calculated using Applet EMF-5.

7.16.3 Shielding By a Vertical Grid of Grounded Wires

Reduction of the ground-level electric field off the edge of a transmission-line right-of-way may be achieved with a vertical, fencelike set of parallel wires. Wood poles may be used to support the vertical grid in a most economical manner. The position of these "electrostatic" fences should be outside the transmission-line outer phases at a distance sufficient for flashover clearance. This grounded type of shielding is particularly appropriate for reducing the electric field outside the right-of-way in areas of low admissible electric field and high right-of-way cost.

The geometry of a vertical grid is shown in Figure 7.16-3. The design parameters are:

H_{max} = height above ground of the top wire
H_{min} = height above ground of the bottom wire
n = number of wires
d = diameter of wires
S_i = spacing between the wire i and the wire $i+1$

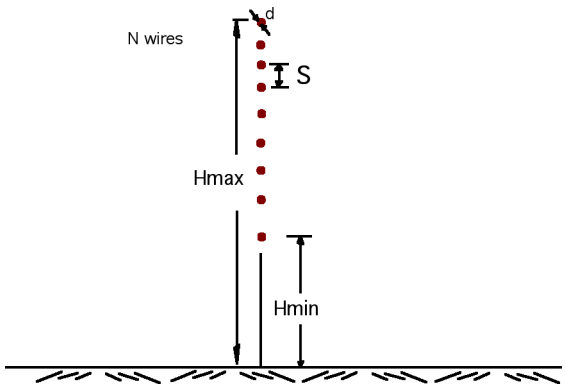


Figure 7.16-3 Geometry of a vertical grid.

$R = \frac{S_{n-1}}{S_1}$, with the condition that $\frac{S_{i+1}}{S_i} = \frac{S_i}{S_{i-1}}$, i.e., consecutive spacings are in the same geometric ratio. When $R = 1$, the wires are equally spaced.

The bottom wire of the grid should be at a height sufficient to allow the movement of vehicles. The distance between shield and phase conductors should be greater than the minimum clearances prescribed by the National Electrical Safety Code. This should not constitute a limitation to the use of this type of shield, because the grid may be positioned effectively away from the wires. The other parameters should be chosen to achieve the desired reduction of the electric field outside the right-of-way.

Both E_u and E_s vary with the distance from the vertical grid, and the shielding efficiency is a function of that distance. The functions $E_u(x)$ and $E_s(x)$ depend in a complicated way on the characteristics of the line (flat, delta, vertical, double circuit). This renders a generalized characterization of the shielding efficiency as a function of the distance, *x*, from the grid, *SE(x)*, impossible.

A modified concept of shielding efficiency, the "shielding function," *f*, is of more practical application.

$$f = \frac{\tilde{E}_u - \tilde{E}_s}{\tilde{E}'_u} = \frac{-\tilde{E}_G}{\tilde{E}'_u} \qquad 7.16\text{-}7$$

Where:
$\tilde{E}_u$ and $\tilde{E}_s$ are calculated at the point where the shielding is calculated.
E_G is the magnitude of the field induced by the grid charges.
$\tilde{E}'_u$ is the unperturbed field at the grid location.

$$\tilde{E}_s = \tilde{E}_u + \tilde{E}_G = \tilde{E}_u - f \cdot \tilde{E}'_u \qquad 7.16\text{-}8$$

The shielding factor is:

$$\tilde{SF} = \frac{\tilde{E}_s}{\tilde{E}_u} = 1 - f \cdot \frac{\tilde{E}'_u}{\tilde{E}_u} \qquad 7.16\text{-}9$$

For a practical range of parameters of the grid, the shielding function at a distance *x* from the grid, *f(x)*, is independent of line characteristics and is a function only of the characteristics of the grid. The field E_G has the same phase as the field $\tilde{E}'_u$. Therefore, the grid-shielding function, *f(x)*, is a scalar. For example, assume that the unperturbed field at the grid is E'_u = 4 kV/m and, 20 m away, E_u = 2 kV/m (with the same phase angle of E'_u). The shielding efficiency *SE* is 50%, so that E_s = 1 kV/m (with the same phase angle of E'_u). The grid shielding function is $f = \frac{2-1}{4} = \frac{1}{4} = 0.25 \cdot$

When the unperturbed field has a phase angle that varies as a function of the distance from the grid, this angle should be included in the calculations. It has the effect of reducing the shielding efficiency. For instance, assume that the grid (with $f = 0.25$ as in the previous example) is used when $E'_u = 4$ kV/m and $E_u = 2$ kV/m (with a phase angle of 30° relative to $\tilde{E}'_u$). Equation 7.16-6 gives $E_s = 1.24$ kV/m, instead of 1 kV/m obtained when the unperturbed field at the calculation point ($\tilde{E}_u$) and the unperturbed field at the grid location ($\tilde{E}'_u$) have the same phase angle.

The grid-shielding function, *f(x)*, coincides with the shielding efficiency of a grid in a uniform electric field. It is given in Figures 7.16-4 and 7.16-5 as a function of the distance from the grid for different number of wires. Figure 7.16-4 is for a maximum grid height of 18 m. Figure 7.16-5 is for a maximum grid height of 12 m. The minimum grid height was kept constant at 6 m, a height that would not prevent the movement of most vehicles. Increasing the height of the bottom wire (while keeping the number of wires constant) reduces the shielding close to the grid, but has little effect on the shielding at distances from the grid greater than 2/3 H_{max}. The diameter of the wires has a small effect on shielding. The design curves presented are for a wire diameter of 0.95 cm (3/8 in.). The wires were considered uniformly spaced (spacing ratio $R = 1$). A spacing ratio $R = 3$ achieves a slightly better shielding. Placing the top wires of the grid closer to each other also reduces the electric field on the grid wire surface and the possibility of corona on the top wire.

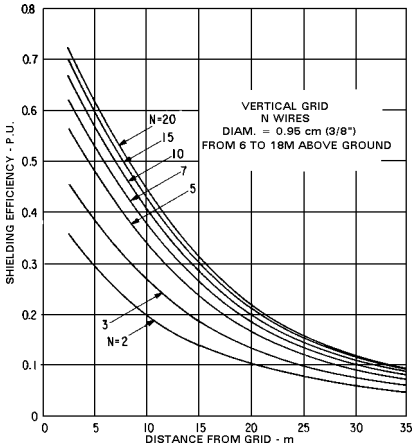


Figure 7.16-4 Shielding function (shielding efficiency in a uniform electric field) of a vertical grid. Wires uniformly spaced between 6 and 18 m above ground.

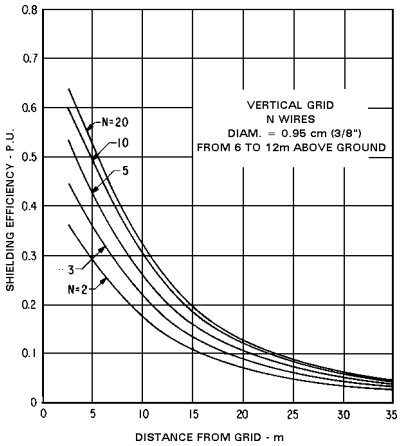


Figure 7.16-5 Shielding function (shielding efficiency in a uniform electric field) of a vertical grid. Wires uniformly spaced between 6 and 12 m above ground.

An accurate solution of transmission-line electric field shielding by a vertical grid of wires parallel to the transmission line can be obtained by accounting for all shield wires and transmission-line wires and using the calculation method illustrated in Section 7.3. The electric field in the presence of a grid of shield wires can be calculated using Applet EMF-5.

7.16.4 Shield Wire Mesh

It is expedient to use meshes of grounded wires rather than parallel wires to shield working areas or walkways. The shielding efficiency of meshes can be calculated using a 3-D electric field calculation program. An approximate solution can be obtained by translating the mesh into a set of parallel wires, for which electric field may be more easily calculated, using the methods of Section 7.16.2 for horizontal grids and Section 7.16.3 for vertical grids.

Assume that the mesh consists of two sets of wires: a set of wires with radius r_1 and spacing S_1 between wires and another set, perpendicular to the first, with wire radius r_2 and wire spacing S_2. An equivalent grid of parallel wires is obtained by removing one of the two wire sets—for instance, the second set—and increasing the radius of the wires of the first set from its value r_1 to a value r_{eq} given by Equation 7.16-10.

$$r_{eq} = \left(r_1 \cdot r_2 \cdot S_1^3 \Big/ \left(32 \cdot S_2\right)\right)^{1/4} \qquad 7.16\text{-}10$$

This equation is valid for $S_1/5 < S_2 < 5\ S_1$.

For example, if $r_1 = r_2$, $S_1 = 80\ r$, and $S_2 = 40\ r_1$, then $r_{eq} = 4.5\ r_1$. The effect of the mesh is equivalent to increasing the wire diameter of the first grid by a factor of 4.5.

7.16.5 Shielding by Objects

Calculations of electric field in the presence of conductive objects can be performed using 3-D electric field programs capable of simulating the geometry accurately. When the geometry is simple, accurate results may be obtained using

Applet EMF-4. The shielding factor of an object is a function not only of the shape of the object but also of the position of the object relative to the transmission line (Deno et al. 1987).

$$\tilde{SF} = 1 - f(x) \cdot \frac{\tilde{E}'_u}{\tilde{E}_u(x)} \qquad 7.16\text{-}11$$

Where:

$\tilde{SF}$ is the shielding factor—i.e., the ratio between the field with the object and the field without the object.

Note that $\tilde{SF}$ is a phasor—i.e., the field is not only modified in magnitude but also shifted in phase. Actually, $\tilde{SF}$ is a complicated operator that transforms an elliptically polarized vector in another elliptically polarized vector. However, for applications close to ground, where the electric field is practically a vertical vector, the shielding function, $f(x)$, may be considered a scalar, function only of the geometry of the object and of the location x relative to the object, and Equation 7.6-11 provides usefully accurate answers. $\tilde{E}'_u$ is the unperturbed field at the object location, and $\tilde{E}_u(x)$ is the unperturbed field, without the object, at the calculation location x.

Equation 7.16-11 is valid if the field does not vary significantly with height above ground. If the field is not uniform with height, Equation 7.16-11 is applied by substituting $\tilde{E}'_u$ with $\tilde{V}_{sp}/h$, where $\tilde{V}_{sp}$ is the unperturbed space potential at the top of the object (at a height, h, above ground).

The shielding function, $f(x)$, can be expressed in closed form for simple geometry (Deno et al. 1987).

Sphere above Ground

(radius r, height h)

$$f(x) = 2h^2 r \Big/ \left(h^2 + x^2\right)^{3/2} \qquad 7.16\text{-}12$$

Where:

x is the horizontal distance from the sphere.

Single Tree

A single tree may be equated to a sphere above ground with diameter W and height above ground h as indicated in Figure 7.16-6.

Cylinder above Ground

(radius r, height h)

$$f(x) = \frac{2h^2}{\ln\left(\frac{2h}{r}\right) \cdot \left(h^2 + x^2\right)} \qquad 7.16\text{-}13$$

Where:

x is the horizontal lateral distance from the cylinder.

Row of Trees

A row of trees can be equated to a cylinder above ground, as indicated in Figure 7.16-6

Vertical Cylinder

(height h, radius r)

$$f(x) = e^{-\frac{(x-r)/h}{(x_0-r)/h}} \qquad 7.16\text{-}14$$

$$\left(x_o - r\right)\Big/h = \left(1 - e^{-r/(1.4H)}\right)^{1/3} \qquad 7.16\text{-}15$$

Box

(W x L x H)

$$f(x) = e^{-\alpha\left(x - r_o\right)/h} \qquad 7.16\text{-}16$$

Where:

r_o is the distance from the box center to the box perimeter (see Figure 7.16-7).

$$\alpha = \left(1 - e^{-\sqrt{L^2 + W^2}/(2.8H)}\right)^{1/3} \qquad 7.16\text{-}17$$

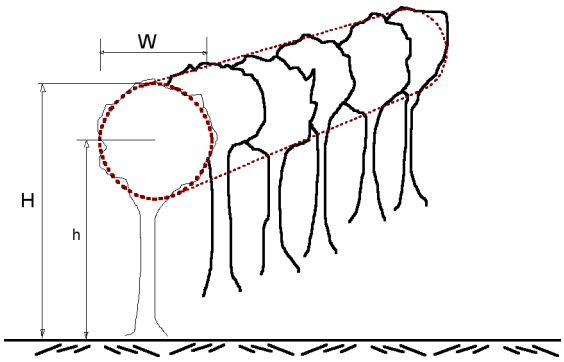


Figure 7.16-6 Representation of a row of trees with an equivalent cylinder.

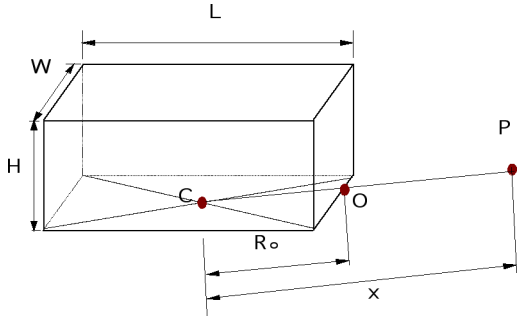


Figure 7.16-7 Parameters of a box for shielding evaluation.

Equation 7.16-16 applies when $H \leq 4W$ and $L \leq 4W$.

Complex Objects

For objects of complex shape, the shielding function may be determined by:

- Full-scale measurements near actual transmission lines
- Calculation using, for instance, the method presented in Appendix 7.6. Calculations should be performed using a uniform unperturbed field such as the field produced by a conductor located at a long distance from the object.

Multiple Shielding

The shielding calculations developed for individual objects assume that there is no other object affecting the field at the calculation point. When this is not the case, the mutual shielding among objects may have a significant effect.

The overall shielding may be calculated by using the approximate Equation 7.16-18.

$$\tilde{S}F = \tilde{E}_S / \tilde{E}_U = \prod_i (1 - f_i \tilde{E}_{oi} / \tilde{E}_U) \qquad 7.16\text{-}18$$

Where:

$\tilde{E}_s$ is the field at the measuring location in the presence of all shielding objects.

$\tilde{E}_u$ is the unperturbed field at the measuring location without the shielding objects.

f_i is the shielding function for object i calculated for the measuring location.

$\tilde{E}_{oi}$ is the unperturbed field (without object i present) at the location of object i.

7.16.6 Effect of Underbuilt Lines on Electric Field (Active Shielding)

While passive shielding of an electric field is provided by conductors at ground potential, active shielding is provided using energized conductors. However, it is not practical to energize conductors solely for the purpose of reducing electric field. Active shielding may be achieved by placing lower voltage lines at appropriate locations and phase arrangements.

Lower voltage lines built beneath EHV lines can provide a large reduction of the electric field at ground level. Position, bundle diameter, voltage, and phase angle of each phase conductor must be properly selected. Calculations of electric field and space potentials can be made using the methods illustrated in Section 7.3 or using Applet EMF-2. Calculation programs for three dimensions (see Appendix 7.6 or use Applet EMF-4) are needed if the underbuilt line has a different span and sag than the EHV line to be shielded.

An example of a 500-kV transmission line with two underbuilt 161-kV lines is shown in Figure 7.16-8. The line configuration is indicated in Figure 7.16-9. The calculated electric field at 1-m height above ground is shown in Figure 7.16-10. The calculations were performed for three conditions: no underbuilt lines, underbuilt line present and energized, and underbuilt lines present and grounded.

There are several practical considerations to take into account for the design, construction, and operation of

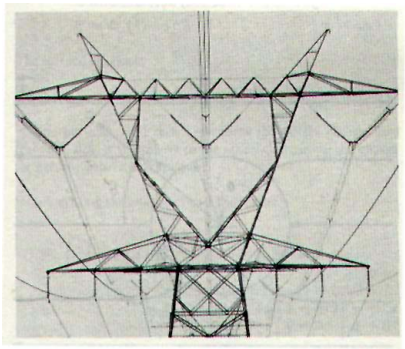


Figure 7.16-8 Tower with a 500-kV line and two underbuilt 161-kV lines (TVA).

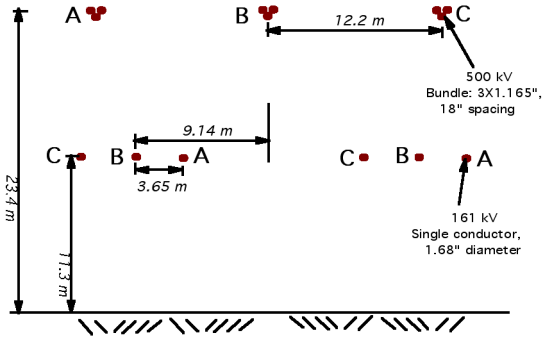


Figure 7.16-9 Geometry of a 500-kV line with two underbuilt 161 kV lines.

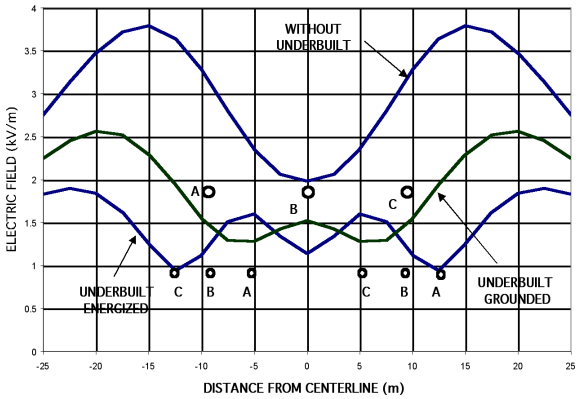


Figure 7.16-10 Electric field profiles for 500-kV line with underbuilt 161-kV line.

underbuilt lines. Underbuilt lines may be built in order to conserve right-of-way and not for the specific purpose of reducing electric field. In general, underbuilt line sections are relatively short, and coupling between EHV line and underbuilt is not significant. The EHV tower heights should be increased to obtain adequate clearances between conductors of different lines. Tower strength must be increased to support the underbuilt lines. Work on the underbuilt or on the EHV line, while the other line is energized, should be considered live work. Finally, currents induced by the higher voltage line during ground faults may affect the lower voltage underbuilt power system relaying. In order to keep underbuilt relaying sensitive, negative sequence relaying logic may be appropriate.

7.17 METHODS FOR REDUCING TRANSMISSION-LINE MAGNETIC FIELDS

7.17.1 Line Design for Low Magnetic Field

Magnetic field of transmission lines is a factor in line design. Several jurisdictions require that magnetic field levels outside the right-of-way do not exceed prescribed values (see Appendix 7.3). Public sensitivity to health issues may require designing for even lower magnetic field levels, particularly in areas with high population density or where particular activities take place.

The information in this chapter is useful for the design of new lines with fields lower than those of lines of traditional design and for reducing magnetic field levels of existing lines.

How much reduction of the magnetic field of overhead transmission lines can be achieved? The answer to this question depends on the level of effort that is justifiable to achieve the field reduction goal. While it is technically possible to reduce electric field to extremely low values using grounded grids of densely spaced wires (see Section 7.16), similar large reduction in magnetic field are often not practical. It is technically possible using traditional technology to significantly reduce the magnetic field for overhead 115-kV lines. With pipe-type cables, it is possible, although quite expensive, to practically eliminate the magnetic field of transmission lines with voltages from 69 kV up to 345 kV. Solid dielectric cables, which are being used for voltages up to 230 kV, offer an opportunity for significant field reductions except in the area above or very near the cables. Significant reductions are also possible for overhead lines, including those with voltage greater than 345 kV, using special techniques, such as the application of cancellation loops, which will be discussed in this section. The effort required to accomplish magnetic field reductions may or may not be justified. Several options may be available, and their field reduction effectiveness should be weighed against their cost and performance. This process is a part of what has been called "magnetic field management," which is defined as the prudent use of resources to effectively reduce exposure of people to power system magnetic field levels while maintaining power system reliability, safety, and effectiveness (EPRI 1999).

A particular technique that can be used to achieve significant magnetic field reductions is the use of a split-phase arrangement for either short sections or the entire length of a line. Split-phase arrangements are discussed in this section. However, split-phase arrangements are very expensive to construct for voltages of 345 kV or greater. For these voltages, the phases cannot be split without practically doubling the cross section of each phase. This is because the number of subconductors and the conductor diameter of each sub-phase are in large part governed by corona performance. The result is that split-phase sections of single-circuit transmission lines with voltages of 345 kV or greater approach the complexity and cost of double-circuit lines.

7.17.2 Optimization of Line Parameters

Modifying the parameters on which the field levels depend can reduce transmission-line magnetic fields. Changes in line parameters may affect electric field differently than magnetic field and may have another different effect on quantities such as radio noise, audible noise, resistive loss, corona loss, insulation performance, etc. Some changes in line design may affect the magnetic field under or close to the line, where the field is largest, differently than farther away from the conductors. Magnetic field, therefore, should be considered in the context of the overall line design.

The magnetic field depends on the following parameters: line currents, line configurations, height above ground, phase spacing, shield wires, and relative phasing of multiple circuits on the same right-of-way. Given these parameters, the magnetic field of a power line is calculated using the algorithms described in Section 7.4.

Line Currents

The magnetic field is proportional to the currents in the phase conductors, provided they vary in the same proportion and their phase angle remains constant. Unlike voltage, the current of a power line may vary significantly. Some transmission lines are steadily loaded; their magnetic field varies little with time. Some other lines have variable loads, showing pronounced seasonal, weekly, and daily variations. Even the most variable transmission-line loads, however, are not as variable as the loads of many other sources, such as electrical appliances, house wiring, and most distribution lines.

For assessing exposure to transmission-line magnetic field, the statistics of the line current over a long period of time is needed. A sample taken every hour during several days distributed over the period of time provides sufficient information to determine average current, load profiles, and 50%, 5%, and 1% exceedance levels. These parameters are affected by events such as outages and load capacity changes.

Line ratings are insufficient for the characterization of actual magnetic fields. In fact, average line currents and even the 1% exceedance levels are significantly lower than line ratings.

Phase Angles

For the purpose of calculating magnetic fields, the currents of most transmission lines may be considered symmetric (at 120º phase angle with each other). Transmission lines are also generally balanced, i.e., the phasor sum of the three phase currents is zero. However, certain system characteristics may give rise to an unbalance, which, however small, may have a measurable effect on the magnetic field outside the right-of-way. This may be of some significance should extreme magnetic field reductions be required at large distances from a transmission line. In fact, the unbalanced current constitutes a monopole (see Section 7.4), whose field decays in inverse proportion to the distance, while the balanced components of the line currents form a dipole, whose field decays in inverse proportion to the square of the distance. Thus, at some distances, the monopolar field generated by the unbalanced current becomes greater than the dipolar field, which exists with balanced currents.

Line Configuration

The line configuration affects both the magnitude and the polarization of the magnetic field. Simple expressions are presented in Section 7.4 for each line configuration. Expressions for flat, delta, and vertical configurations are shown in Table 7.4-3 and Figure 7.17-1. For instance, the magnetic field produced by a single-circuit line with flat configuration outside the right-of-way is linearly polarized, has an angle with the vertical equal to twice the line azimuth, and a magnitude, *B*, given to a good approximation by:

$$B = 2\sqrt{3}P\,I/R^2 \text{ (mG)} \qquad 7.17\text{-}1$$

Where:

P is the phase spacing (meter).
I is the line current (ampere).
R is the distance between measuring point and center of line.

For the same current and phase spacing, the equilateral delta configuration produces the lowest field (lower than the field of flat and vertical lines by a factor equal to $\sqrt{2}$).

Phase Spacing

The magnetic field outside the right-of-way is nearly directly proportional to phase spacing.

Line Height and Lateral Distance

The magnetic field decreases with the distance, *D*, to the center of the line phase configuration. If *L* is the lateral distance and *H* the height of the center of the phase configuration above ground:

$$D = \sqrt{H^2 + L^2} \qquad 7.17\text{-}2$$

Therefore, an increase in line height, *H*, will decrease the field at points near ground level, although not to the same extent as an increase in line height decreases electric field. For three-phase single-circuit lines, the field decreases with the square of the distance *D*. For double-circuit lines, the field may have two components—a dipolar component that decreases with the square of the distance *D,* and a quadrupolar component that decreases with the third power of the distance *D*.

For a double-circuit line with the same currents, reverse phasing, and symmetrical geometry, and for split-phase lines with symmetrical geometry, the dipolar component is zero, and the field decreases proportionally to the third power of the distance *D*.

Shield Wires

Currents may flow on overhead shield wires used for protecting transmission lines from lightning. These currents can be calculated using the method outlined in Section 7.9. Currents in shield wires have a small effect on the magnetic field close to the line, but may have a measurable effect on the distant field. Because of the presence of shield wire currents, the lateral profile of the magnetic field is asymmetric even for symmetrical line configurations.

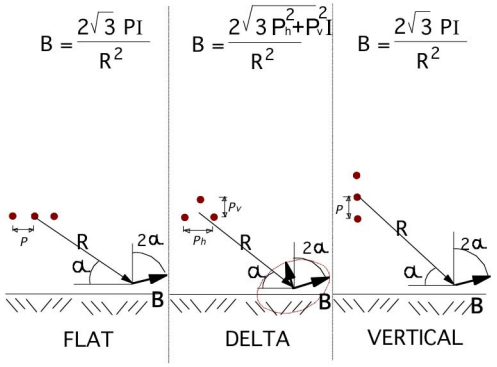


Figure 7.17-1 Effect of line configuration on magnetic field of single-circuit lines.

Phasing of Double-Circuit Lines

The magnetic field of double-circuit lines can be calculated using the algorithms described in Section 7.4. Similar to what occurs for the electric field, the relative phasing of the two circuits profoundly affects the magnetic field. For calculating the electric field, the voltages of the two circuits could be considered practically equal in magnitude and phase angle. For calculating the magnetic field, however, the currents in the two circuits may be considered equal only when the two circuits are tied together at the same sending and receiving substations. The phasing indication (A, B, C) is normally reserved for the voltages. It can be adopted also for the currents only if the power flow of the two circuits is in the same direction. There are cases when the two circuits have opposite power flow, such as when one circuit originates and the other ends at the same substation bus. In this case, if the phases of the currents of the first circuit are indicated by A, B, and C, then the phases of the currents of the second circuit must be indicated using the symbols -A, -B, -C. In fact, the phases of the currents of the second circuit are opposite (180º difference) from those of the first circuit.

Figure 7.17-2 shows the magnetic field lateral profile for the same double-circuit 525-kV line of Figure 7.3-14, assuming a current of 1000 A for both circuits (configurations #1 to #5) or in one circuit only (configuration #6).

Figure 7.17-3 shows the magnetic field lateral profile for the 345-kV double-circuit line of Figure 7.3-15, assuming the same current of 1000 A from both circuits.

If the currents in the two circuits were not equal, the magnetic field would be different, especially for the low reactance configuration, even if the average current stays the same. However, the different phase arrangements would have the same relative behavior indicated in Figures 7.17-2 and 7.17-3.

The same observations made for electric fields apply to magnetic fields. The superbundle arrangement (#1) corresponds to the highest magnetic field and the low-reactance arrangement (#5) to the lowest.

In the distant field, at distances from line center greater than 60 m for Figure 7.17-2 and greater than 80 m for Figure 7.17-3, the magnetic field can be calculated using the approximate expressions shown in Table 7.17-1. These expressions apply only if the two circuits have exactly the same current. The effect of inequality between the currents in the two circuits on the low-reactance arrangement magnetic field is shown in Figure 7.17-4.

The low reactance arrangement (arrangement #5) has generally the lowest field. For the double-circuit line of Figure 7.17-2, the field becomes even lower relative to that of the other arrangements as the distance, *R*, from the line center increases. This phenomenon occurs because the field of this configuration is quadrupolar and decreases with the third power rather than with the second power of the distance, as is the case for the other phasing arrangements. It should be noted that arrangement # 5 of Figure 7.17-3 does not generate a quadrupolar field (see Table 7.17-1). The low reactance arrangement does not necessarily generate a field that decreases with the third power of the distance.

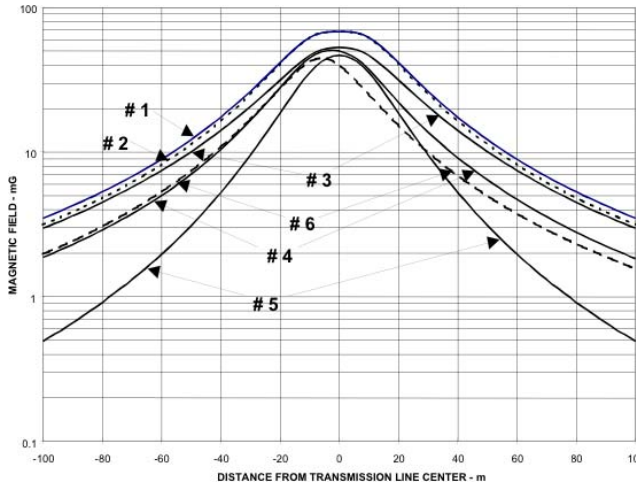


Figure 7.17-2 Magnetic field at ground level for a double-circuit 525-kV line consisting of two vertical circuits. Different phase arrangements. Same geometry and phasing as Figure 7.3-14.

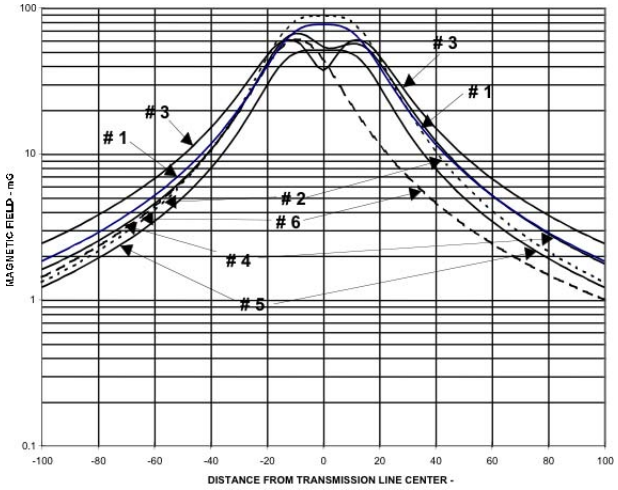


Figure 7.17-3 Magnetic field at ground level for a double-circuit 345-kV line consisting of two delta circuits. Different phase arrangements. Same geometry and phasing as Figure 7.3-15.

The low field that can be achieved by the optimum phasing of the two circuits is rapidly increased when one of the two carries less current than the other. The largest field values are reached when one of the circuits is de-energized and the other still carries the full load.

When the two circuits of a double-circuit line originate and end on the same substation bus, phase arrangement #5 in both Figure 7.17-2 and Figure 7.17-3 provides the lowest magnetic fields. If the currents were equal (an unlikely occurrence in practical situations), the field would be expressed by the last row of equations in Table 7.17-1. For the case of Figure 7.17-2, the field would vary in inverse proportion to the third power of the distance.

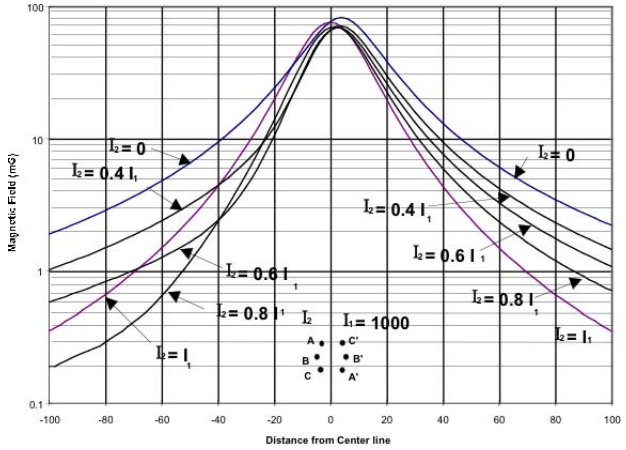


Figure 7.17-4 Effect of inequality of current in two circuits of a low-reactance double-circuit 345-kV line. (Horizontal phase spacing: 7.32 m and 9.15m, vertical phase spacing: 6.10 m, minimum height above ground: 12.19 m.)

7.17.3 Line Compaction

Advantages and Disadvantages of Line Compaction

Compacting a transmission line means reducing the overall dimensions of its support structure, including distances between phases, phase-to-shield wire distances, and height above ground. The advantage of compaction is a lower visibility of the line and possibly a lower cost. An additional advantage consists of lower magnetic (and electric) fields, particularly if compaction is limited to reducing the distances between conductors without reducing line height. In fact, magnetic fields are approximately directly proportional to the phase spacing.

Arranging the phases in a delta configuration as close as possible to equilateral is the first step of line compaction for the purpose of reducing the magnetic fields near ground level. For the same minimum distance between phases, the equilateral triangle configuration gives the lowest magnetic field. The distant magnetic field of this configuration is lower than that of a flat configuration by a factor equal to $\sqrt{2}$. It should be noted that the magnetic field of an equilateral delta line is circularly polarized, while that of a flat configuration is linearly polarized. If the comparison is made on the basis of the magnitude of the maximum field component, the equilateral delta produces a magnetic field, which is one-half that of a flat configuration.

Table 7.17-1 Distant Field of Double-Circuit Lines with Different Phase Arrangements (Same current, *I*, in the Two Circuits)

Phase Arrang.	Figure 7.3-14 and Figure 7.17-2	Figure 7.3-15 and Figure 7.17-3
#1	$4\cdot\sqrt{3}P_v\, I/R^2$	$4\cdot P_v\, I/R^2$
#2	$2\sqrt{9P_v^{\,2}+3\Delta P^2}\cdot I/R^2$	$2\sqrt{P_v^{\,2}+\frac{3}{4}P_h^{\,2}-3P_h\Delta P+3\Delta P^2}\cdot I/R^2$
#3	$2\sqrt{9P_v^{\,2}+3\Delta P^2}\cdot I/R^2$	$2\sqrt{3P_h^{\,2}+4P_v^{\,2}}\cdot I/R^2$
#4	$2\sqrt{3}\sqrt{P_v^{\,2}+\Delta P^2}\cdot I/R^2$	$2\sqrt{P_v^{\,2}+\frac{9}{4}P_h^{\,2}}\cdot I/R^2$
#5	$4\sqrt{3P_v^{\,2}P_h^2+P_v^4+\Delta P^2\left(P_h+\Delta P\right)^2-2\Delta P\cdot P_v^2\left(P_h+\Delta P\right)}\cdot I/R^3$	$2\sqrt{P_v^{\,2}+\frac{3}{4}P_h^{\,2}}\cdot I/R^2$
#1, but with A'=-A, B'=-B, C'=-C	$2\sqrt{3}P_h\cdot P_v\cdot I/R^3$	$2(P_h+\Delta P)\sqrt{4P_v^2+3P_h^2}\cdot I/R^3$

P_v is the vertical phase spacing between bottom conductors and intermediate conductors for Figure 7.3-14 and top conductors for Figure 7.3-15. P_h is the horizontal phase spacing between the bottom conductors of the two circuits for Figure 7.3-14 and of the same circuit for Figure 7.3-15. ΔP is the horizontal offset of the intermediate conductors over top and bottom conductors for Figure 7.3-14 and the horizontal distance between the two closest phases of 7 of the two circuits for Figure 7.3-15.

In regard to magnetic field, compaction affects the dipolar component, but does not affect the monopolar component, the magnetic field produced by the zero sequence current component, I_o, of the line. The distant field, B_o, produced by the zero sequence component is equal to $6I_o/R$ (R is the distance from the center of the phases in meters, I_0 is in ampere, and B_o in milliGauss). In the case of an equilateral delta configuration, this field becomes equal to that produced by the positive sequence, I_1, at a distance, R_x, from the center of the phases equal to:

$$R_x = \frac{P}{\sqrt{6}} \cdot \frac{I_1}{I_o} \qquad 7.17\text{-}3$$

For instance, if the zero sequence is 3% of the positive sequence, and P = 7 m, R_x = 95 m. At distances greater than 95 m, the zero sequence field dominates. Reducing the phase spacing will reduce the positive sequence field at these distances, but will be practically ineffective in reducing the overall field.

Depending on the level of compaction, line design may be controlled by considerations of practical support structure design and aspects of line performance other than electric and magnetic fields near ground. There are obvious limits to line compaction, dictated by insulation and corona noise requirements. From the lowest transmission voltages up to 230 kV, insulation requirements are likely to be a limiting factor. At these voltages, significant degrees of compaction over traditional designs may be achieved at relatively low incremental cost. At voltages of 345 kV and above, corona noise is the major obstacle to phase compaction. Cost of compaction may escalate rapidly as larger conductors or more conductors in a bundle are required to keep corona noise within acceptable limits.

Factors limiting phase-to-phase distances are:

- dielectric strength of air gaps between phases
- mechanical movements of the conductors and wires produced by wind and ice
- electric field on the conductor surface determining corona loss, audible noise, and radio interference
- requirements of live-line maintenance

Dielectric strength determines the smallest possible distance (i.e., maximum possible degree of compaction). Such distances represent the maximum possible compaction effect on magnetic field if other restrictions are overcome. The approximate values of the minimum phase-to-phase distances that can withstand the electrical stresses are shown in Table 7.17-2.

Table 7.17-2 Minimum Requirements for Phase-to-Phase Distances

Rated Voltage of Transmission Line	Minimum Air Gap Permissible Phase-to-Phase	
(kV)	(ft)	(m)
230	6	1.84
345	9	2.74
500	13	3.96

Practical limitations to reducing the spacing between phases to the distances of Table 7.17-1 are caused by phase-to-ground clearance requirements at the structures and flashovers along the span due to wires swinging toward each other.

Flashovers due to the mechanical movements of conductors under wind and ice loading are prevented by adopting large distances between phases, determined after many years of service experience. Flashover can also be overcome by applying phase-to-phase insulating spacers that fix the distance between conductors at one or more points between the structures.

The electric field on a conductor surface will not create practical limitations to compaction of most 220/230-kV lines, but may be a problem for 345-kV lines, and will certainly be a problem for lines with voltages of 500 kV and above. Specially designed conductor bundles could be used in these cases, and optimization of their positioning may allow further compaction.

General Compaction

Distances between conductors can be reduced at the tower and, consequently, all along the span. Conductors are parallel along the span. General compaction requires towers with smaller clearances between energized and grounded parts, making live-line maintenance more difficult but allowing the maximum effect from compaction. Restraint of conductor motion at towers during wind and ice events, possibly by use of post insulators, is required for the greatest compaction.

The magnetic field of a single-circuit transmission line is reduced by an amount approximately equal to the phase spacing reduction factor. The magnetic field reduction, for low-reactance double-circuit lines, is approximately equal to the product of the horizontal and vertical phase spacing reduction factors. The field reduction factor for superbundle double-circuit lines is approximately equal to the geometric mean of the horizontal and vertical phase spacing reduction factors.

In-Span Compaction

Compaction for the purpose of magnetic field reduction can be achieved by reducing the distances between conduc-

tors in the span while leaving the line geometry unchanged at the tower. The advantages of this method over general compaction are:

- clearances for the purpose of maintenance work on insulators and hardware at the tower are not affected,
- compaction of existing lines may be possible simply by adding in-span spacers.

On the other hand, the field reduction effectiveness of the option is less than that of general compaction. Additionally, the in-span spacers may constitute weak points where insulation failure may occur. Some of the in-span compaction options are illustrated in Figures 7.17-5 and 7.17-6. The magnetic field reduction effectiveness of these options is presented in Table 7.17-3.

In-span compaction can be obtained in three ways:

- Bringing conductors closer using insulating spacers at locations in the span (see Figure 7.17-5).
- Bringing conductors closer at midspan due to their transposition on the towers (see Figure 7.17-6, for example). No spacers may be needed in this case, unless dictated by mechanical problems, such as galloping or ice shedding.
- Sagging upper conductors closer to lower conductors by using different tensions.

Table 7.17-3 Magnetic Field Reduction with In-Span Compaction

Line Description	Phase-to-phase Distance Reduction Factor	Field Reduction Factor (average at 30 to 200 m)
Compaction Using In-span Spacers		
500 kV Flat, 1 spacer/span	2.2	~1.4
500 kV Flat, 2 spacers/span	2.2	~1.7
500 kV Delta, 1 spacer/span	2.2	~1.5
500 kV Delta, 2 spacers/span	2.2	~1.7
230 kV Horizontal Delta compacted in-span using 2 spacers	4.0 (both horizontal and vertical)	3.2
230 kV Double Circuit Vert., low reactance, 2 spacers	4.0	Up to 11 near line
Compaction using Conductor Transposition		
500 kV Delta 1 rotation/3 spans	2.0	~1.5
500 kV Delta Cruciform 1 rotation/4 spans	1.4	~2.0

Compaction Using Covered Conductors

The distance between phases can be reduced beyond the values suggested in Table 7.17-2 by employing conductors with an insulating cover. The concept is similar to a tree-wire used for distribution lines. The insulation cover is not required to withstand the full voltage except for brief periods of time during accidental contacts with grounded objects or between the phases.

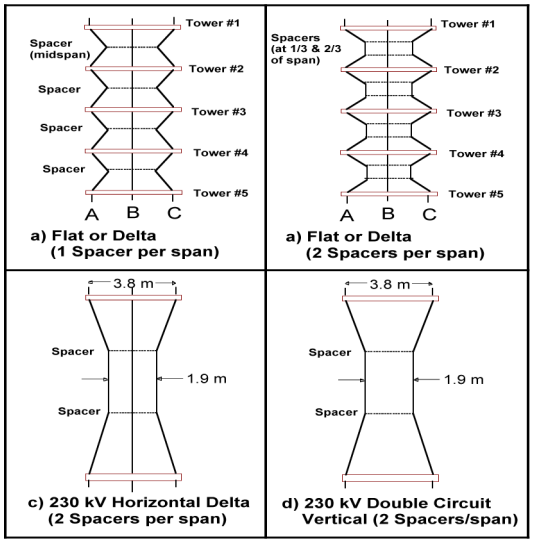


Figure 7.17-5 230-kV in-span compaction option.

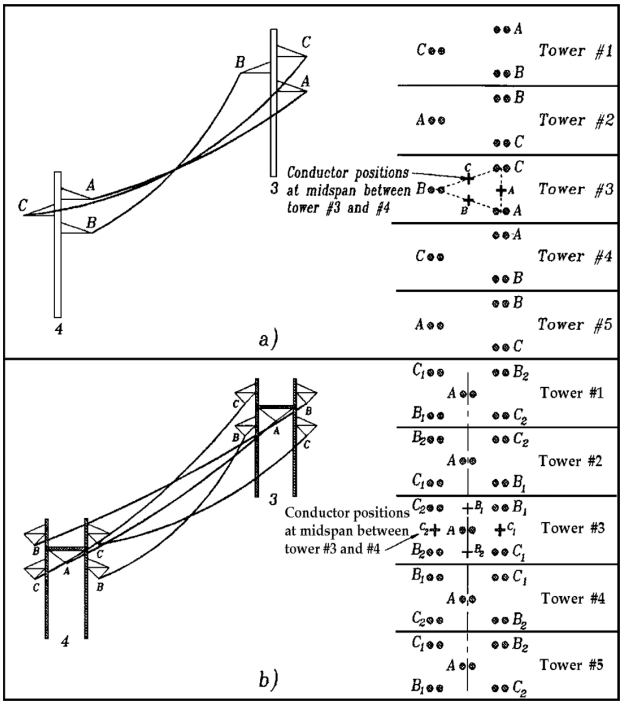


Figure 7.17-6 500-kV in-span compaction option.

The technology of insulated conductors is available for distribution voltages, but has not been applied to transmission voltages, except on an experimental basis up to 230 kV.

7.17.4 Split-Phase Lines

A split-phase line is a line that has one or more phases split into two or more subphases placed in different positions. Split-phase lines were introduced specifically for the reduction of magnetic field, although they are also effective in reducing the electric field. Section 7.4 shows how the magnetic field can be regarded as the resultant of field components of different order (monopole, dipole, quadrupole, and higher-order components). To reduce the magnetic field, particularly the distant field, it is advantageous to reduce or eliminate the lower-order components (monopolar or dipolar), which have a slower decay with distance.

The monopolar component is reduced to zero when the sum of all the currents ("net current") is zero. For a three-phase transmission line, this occurs when the zero sequence current is zero, or, if the line has ground wires, when the zero sequence current is carried exclusively by the ground wires.

The reduction of the dipolar component requires a system with more than three wires. For instance, a double-circuit line of the low-reactance type carrying equal current in the two circuits produces a much lower distant field than a single-circuit three-phase line. In fact, such a double-circuit line can be shown to correspond to a quadrupole. The field decays in inverse proportion to the third power of the distance from the center of the line conductors. This concept can be extended to split-phase lines for which the field is also quadrupolar (or of higher order) and varies in inverse proportion to the third (or higher) power of the distance from the center of the line.

A split-phase line is still a three-phase line. However, one or more of the phases is split into two or more subphases (see Figure 7.17-7). If the position of these subphases is chosen properly, significant magnetic field reductions can be achieved.

For magnetic field calculation purposes, the like-phased conductors appear as a single conductor at the midpoint of all of the like-phases. Observe the phasing of the conductors in Figure 7.17-7. The conductor positions are chosen such that the midpoints of each pair of like-phased conductors coincide. The transmission line appears, from a distance, as three conductors at the same location, as if it were a three-phase cable. The resulting magnetic field is very small.

The magnetic field lateral profiles of several split-phase arrangements are compared to that of a traditional vertical design in Figure 7.17-8, which corresponds to a 230-kV line carrying 240 MW. The field produced by the split-phase designs is considerably lower than that produced by the traditional design, and the field reduction becomes increasingly greater as the distance from the line increases.

An even greater distant field reduction can be obtained by splitting phases in more than two subphases. For instance, if phase A is placed in the center of the configuration and phases B and C are split in three subphases each, placed at alternative vertices of an hexagon surrounding phase A, the distant field is:

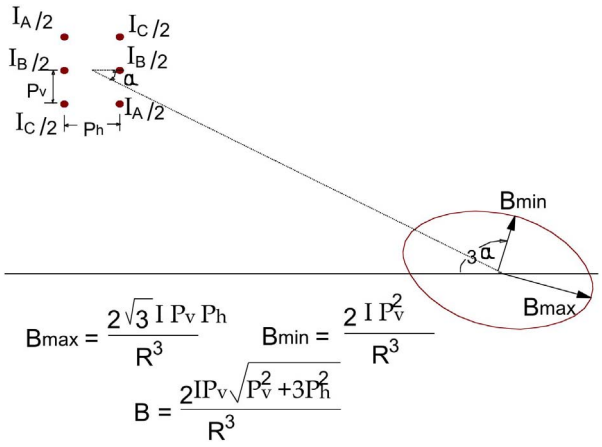


Figure 7.17-7 Split-phase transmission line example.

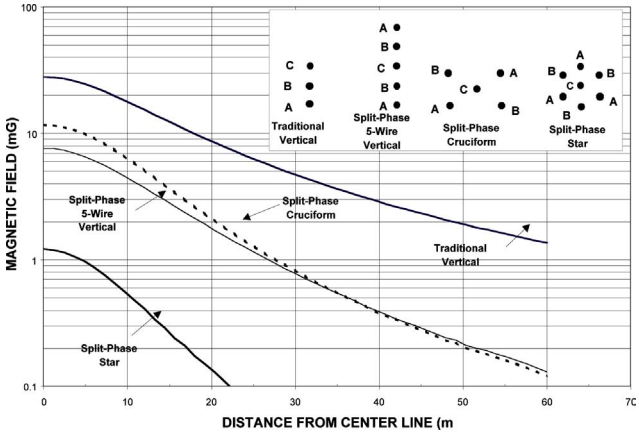


Figure 7.17-8 Lateral profiles of split-phase arrangements compared with traditional design – 230 kV line carrying 240 MW.

$$B = 1.5\frac{IP^3}{R^4} \qquad 7.17\text{-}4$$

Where:

P is the phase-to-phase distance.

In this case, the field decays with the fourth power of the distance. The distant field reduction is dramatic. For instance, at $R = 5P$ (R = 30 m for P = 6 m), the field would be about 2.5% of that produced by an equilateral delta three-phase line, and at $R = 10P$ (R = 60 m), the field would be less than 1% of that of a traditional three-phase line.

A special symmetry is required for maximum magnetic field reduction from split-phase lines. If such symmetry does not exist, then the field will have two components, one (B_d) that varies in inverse proportion to the second power of distance and the other (B_q) that varies in inverse proportion with the third power of the distance. An example is the two-over-four-phase configuration shown in Figure 7.17-9.

Assume $P_{h3} = \frac{P_{h1} + P_{h2}}{2}$, then the dipolar field, B_d, and the quadrupolar fields, B_q, are:

$$B_d = \frac{2IP_V}{R^2} \qquad 7.17\text{-}5$$

$$B_q = \frac{I}{2R^3}\left(P_{h1} - P_{h2}\right)\left(13P_{h1}^2 + 22P_{h1}P_{h2} + 13P_{h2}^2\right)^{1/2} \qquad 7.17\text{-}6$$

Split-phase lines result also in reduced electric field, although the reduction is not as much as that of the magnetic field. An additional potential benefit is the significant reduction of the line surge impedance, although the self- and mutual-line impedances may become sufficiently unbalanced to require phase transposition.

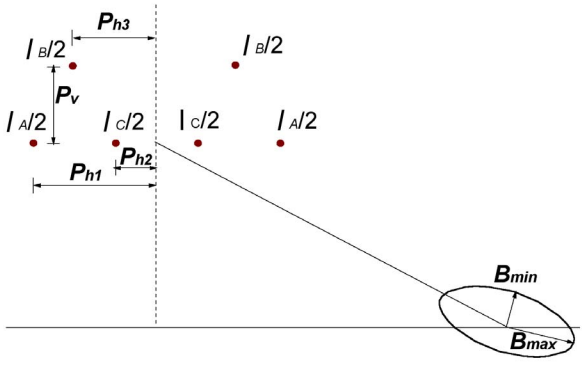


Figure 7.17-9 Conductor configuration for a split-phase two-over-four arrangement.

Split-phase designs may produce significantly higher levels of audible and radio noise than traditional lines because the conductor surface gradient may be significantly increased, unless the total cross-sectional area is increased beyond what is economically desirable. For line voltages less than 230 kV, splitting the phases while keeping the total conductor cross-sectional area constant may still result in acceptable noise levels. In fact, the design of the conductors for these lines is generally not limited by audible and radio noise design considerations. At 230 kV, phase splitting while maintaining the some total conductor cross-sectional area may result in designs that are marginal from the point of view of radio and audible noise. Additional conductor cross-sectional area may be needed for split-phase lines at 345 kV and even more at 500 kV. Each subphase of a 500-kV split-phase line may require bundles of two or three conductors of the same dimensions as that of a phase of a traditional three-phase 500-kV line. Thus, the required total cross-sectional area may be twice that of a traditional line. Therefore, the cost of this option will be substantially higher than that of a traditional line.

Applying the split-phase concept to existing construction is difficult because of the constraints imposed by the conductor support structures on the line geometry, such as tower modifications to allow the change from single circuit to double circuit. Examples of adding two or three conductors to existing lines of traditional design are shown in Figure 7.17-10. Adding two conductors allows only two of the phases to be split. Even though the geometry is such that a pure quadrupole cannot be created, the dipolar component of the magnetic field can be reduced to a minimum by designing the additional conductors with such impedance to create an equal current split. The field reduction in the distant field would still be substantial for balanced line currents. The costs of these options would be significant, but it should be weighed against potentially significant costs of alternative solutions should magnetic field reduction be necessary.

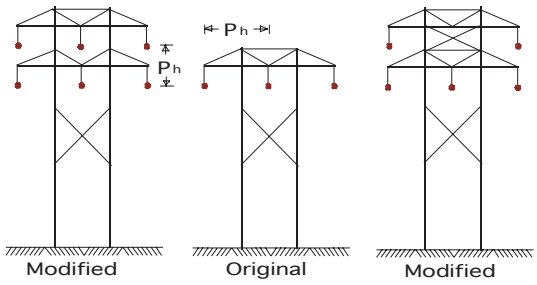


Figure 7.17-10 Split-phase modification to a three-phase line.

It is important to note that the split-phase option may be applied as a local solution involving a limited number of spans. This issue may be relevant should certain areas traversed by the line be particularly sensitive to magnetic field exposure.

The distant field for the configurations described in Figure 7.17-10 is given by:

Original configuration:

$$B = 2 \cdot \sqrt{3} \frac{PI}{R^2} \qquad 7.17\text{-}7$$

Where:

R is the distance from the center of the conductors to the measuring point.

Modified configuration (left side):

$$B = 4 \frac{P^2 I}{R^3} \qquad 7.17\text{-}8$$

Modified configuration (right side):

$$B = 1.2 \frac{PI}{R^2} \qquad 7.17\text{-}9$$

Comparison of Different Split-Phase Designs

For comparison purposes, calculations of magnetic fields were performed for 230-kV lines assuming that the phase currents are 1000 A each. Since magnetic field levels are linear with current levels, the shape of the magnetic field profile for a given line will not change with the line load, but will only shift up or down. The phase-to-phase and phase-to-tower clearances are 2.75 m and 1.6 m, respectively. The horizontal separation between adjacent phases is set to 3.8 m. For the purpose of comparison, the ground clearance of the middle phases is set equal to 13.8 m for all configurations. The geometry of four different split-phase configurations is shown in Figure 7.17-11. This figure shows the midspan geometry and is not intended to imply any particular tower design. Figure 7.17-12 shows the calculated magnetic field profiles.

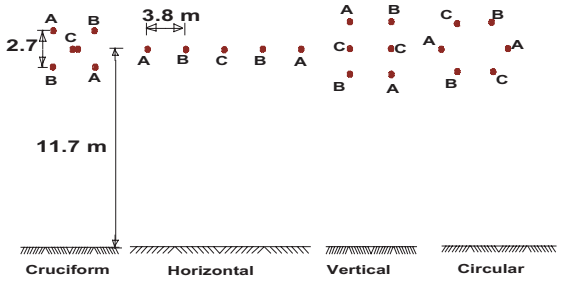


Figure 7.17-11 Split-phase line configurations.

For the cruciform and the horizontal configurations, phase C conductor must carry the entire phase C current. The other two phases are split into two subphases, each with half the cross-sectional area of phase C conductor. Phase C could be bundled by using two conductors if there were an incentive to do so, such as requirements for transpositions.

7.17.5 Passive Shielding of Transmission Line Magnetic Field Using Cancellation Loops

Introduction

Reducing magnetic field exposure, without significant modifications to the transmission line or disruption of the activities of the exposed people, is an attractive magnetic field management option. A technique that has these requisites is the application of "passive cancellation loops," so named because the currents circulating in these loops are induced by the transmission-line magnetic field without the need of separate sources and create a magnetic field that partially cancels the previously existing field.

Cancellation loops may provide one of the most practical options for reducing transmission-line fields. Cancellation loops can be applied to new or existing lines, to an entire line, or to a short section. Several utility applications have been designed. Although commercial installations are limited, analytical techniques, experimental verifications, and pilot projects are sufficiently advanced for including this technology in this Reference Book (Walling et al. 1993; Jonsson et al. 1994; Spherling et al. 1996; Zaffanella 1995).

Several challenges remain that prevent cancellation loops from becoming widely accepted. Although their cost is small compared to the cost of the transmission lines, cancellation loops are expensive to install, even when applied to only a few spans. The cost of losses is not negligible either. Also, cancellation loops can cause operational constraints on the utility. Finally, the additional poles and conductors required by the cancellation loops may be

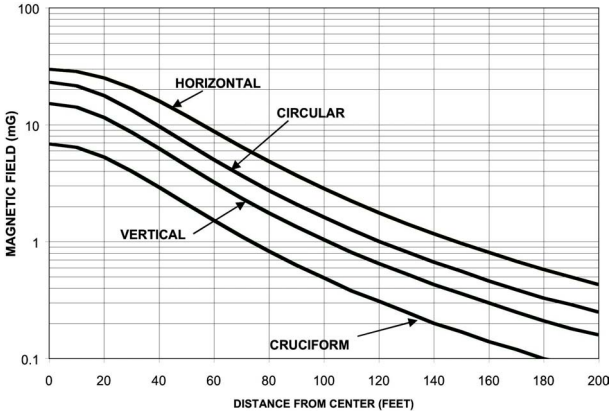


Figure 7.17-12 Low field line magnetic field profiles.

aesthetically unpleasant. Nevertheless, cancellation loops remain one of the more attractive options for reducing the magnetic field of existing transmission lines. They may be the only option to achieve significant field reduction for transmission lines with voltages of 345 kV or above.

The Concept of Cancellation Loops

Cancellation loops reduce magnetic fields by producing fields with the same direction in space but with phase opposite to that of the fields produced by the phase conductors. Cancellation loops can be placed around a work area to reduce the field produced by external sources ("subject shielding"), or they can be placed around a source to reduce the field of the source ("source shielding"). They can be passive, when the loop currents are induced by the magnetic field of the source, or active, when the loop current is generated by an independent power supply.

Passive loops are more attractive than active loops because independent power supplies and controls of the loop current are not needed. The general principle of passive loop operation is quite simple, and is described in the example of Figure 7.17-13. A passive concentric circular loop is placed close to the source, in this case a circular loop. A portion of the magnetic field flux generated by the source current, *I*, will be linked with the passive loop. The extent of the flux linkage is expressed by the mutual inductance, *M*, between the two loops. The voltage induced in the passive loop by the current in the source loop is given by:

$$Vs = -j\omega MI \qquad (\omega = 2\pi f;\ f \text{ is the power frequency}) \qquad 7.17\text{-}10$$

This voltage will cause a circulating current in the passive loop, given by:

$$I_s = V_s / \left(R_s + j\,\omega L_s\right) \qquad 7.17\text{-}11$$

Where:

R_S is the resistance and L_S is the inductance of the passive loop.

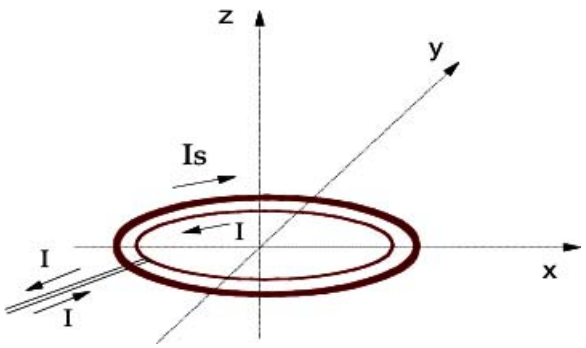


Figure 7.17-13 Circular passive loop concentric to a source current loop.

It is assumed that the effect of the induced current in the passive loop will not appreciably modify the impedance, and thus the current, of the source circuit. This is true for transmission-line applications involving short sections.

Combining Equations (7.17-10) and (7.17-11) yields:

$$I_s = \left(j\omega MI\right) / \left(R_s + j\omega L_s\right) \qquad 7.17\text{-}12$$

This equation indicates that the passive loop current, I_s, is equal and opposite to the source current, *I*, when the loop resistance is zero, and the mutual inductance is equal to the self-inductance of the loop. Therefore, when there is a good coupling between source conductors and cancellation loop and when the cancellation loop resistance is small, the loop current will tend to produce an equal but opposite effect to that of the source current.

When the source is a transmission line, the passive cancellation loops consist of conductors installed parallel to the line conductors for the desired line section length and connected at the ends of the line section to form loops. The magnetic field produced by the currents in the transmission-line conductors induces currents in the cancellation loops. If the geometry and the electrical characteristics of the loops are properly chosen, the additional currents generate a magnetic field that, at some desired locations, will be opposite to that produced by the line and therefore will reduce the line field. The challenge for the designer is to select an option that is effective in reducing the field at desired locations and is acceptable from the viewpoint of safety, reliability, aesthetics, and cost. It should be noted that, while magnetic fields are decreased at certain locations, there could be a field increase at other locations. The parameters of the cancellation loop design depend to a very large extent on the transmission-line configuration, the area to be shielded, and the desired field reduction factor.

For best results, a capacitor should be placed in series with the loop conductor. The value of this capacitor is of critical importance for adjusting the loop current magnitude and phase angle to their optimum values. Calculations of magnetic field with and without the application of a cancellation loop can be performed using Applet EMF-11.

Example of Field Reduction for a Flat Configuration Line

Figure 7.17-14 shows an example of the loop geometry for a transmission line with horizontal phase configuration, and Figure 7.17-15 shows the magnetic field reduction effectiveness.

The impedance of the loop affects the loop current. For practical conductors, the largest component of this impedance is the reactance. Reducing the conductor reactance,

therefore, will increase the loop current and its field cancellation effect. One method to reduce the loop reactance, without increasing the total conductor weight, is to use bundles of smaller size conductors rather than a single large conductor. As indicated in Figure 7.17-16, this is equivalent to increasing the conductor geometric mean radius, which reduces the reactance, increases the loop current, and achieves greater magnetic field reduction.

Another method to reduce the loop reactance without bundling the conductors is to place a capacitor in series with the loop. The capacitance must be adjusted for optimum results. The effect of series capacitance is shown in Figure 7.17-17. In this example, a 480-m long loop may require a capacitor bank of approximately 7.4 mF, rated for 480 V (to withstand also possible overvoltages). Distribution-type capacitors would be required when loop length exceeds several miles. Nonstandard capacitors may be required for short loops.

The loop conductor resistance is a critical parameter. Greater field reduction requires lower resistance.

The loop current can be 30-80% of the phase current.

The loop conductors should be grounded at least at one point. Multiple grounds may deteriorate the field reduction performance of the loop, although not significantly if the loop length is only a few spans.

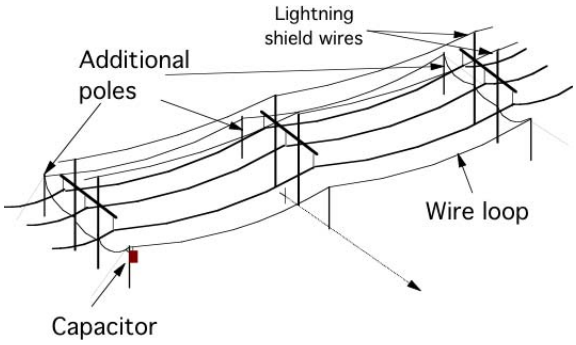


Figure 7.17-14 Horizontal cancellation loop for reducing the magnetic field of a transmission line with flat configuration.

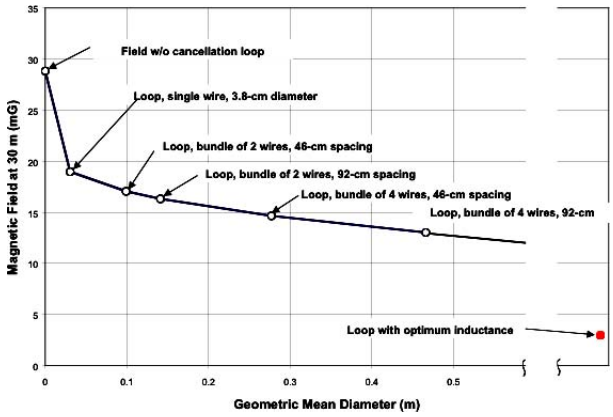


Figure 7.17-16 Effect of loop reactance on magnetic field (345-kV line with 1000 A, flat configuration, phase spacing 8 m, loop wires 11 m from center line and 1 m below the phase wires, loop wire resistance $3.85 \cdot 10^{-5}$ Ω/m).

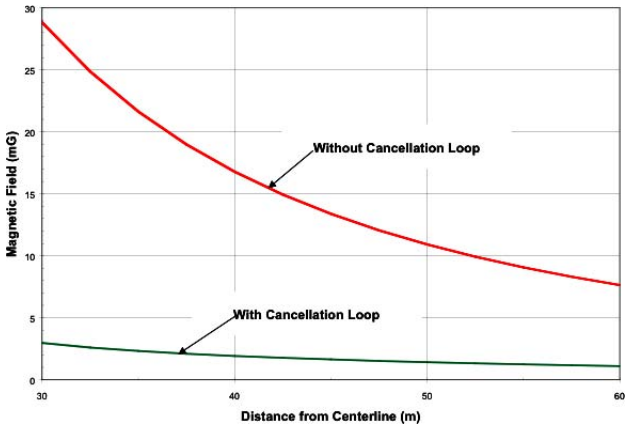


Figure 7.17-15 Magnetic field calculated with and without a wire loop with optimum conductor placement and capacitive compensation (345-kV line with 1000 A, 60 Hz, flat configuration, phase spacing 8 m, loop wires 11 m from center line and 1 m below the phase wires, loop wire resistance $3.85 \cdot 10^{-5}$ Ω/m).

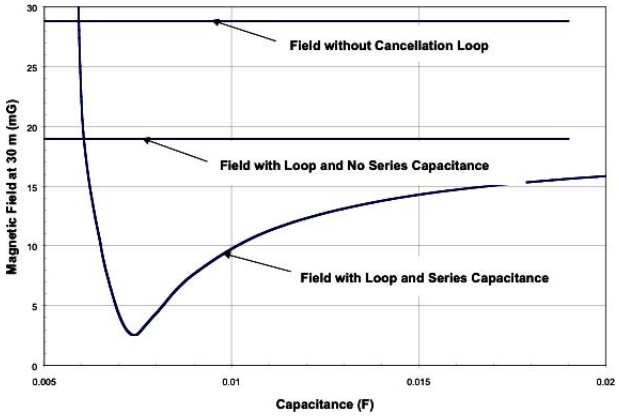


Figure 7.17-17 Effect of capacitance in series with a cancellation loop (345-kV line with 1000 A, flat configuration, phase spacing 8 m, loop wires 11 m from center line and 1 m below the phase wires, loop with single 3.8-cm diameter wire with resistance $3.85 \cdot 10^{-5}$ Ω/m, loop along two spans with total length of 480 m).

The geometry of the loop must be tailored to the geometry of the line. A vertical phase configuration requires a vertical cancellation loop.

A few examples of passive cancellation loops are presented in this section. Several variables affect the choice of the optimum design parameters and the performance of cancellation loops. The design parameters that most affect the design of cancellation loops are:

- Transmission-Line Configuration: flat, delta, vertical, and double circuit.
- Cancellation Loop Wire Set Type: for instance, 2-wire set, 3-wire set, and two 2-wire sets.
- Optimization of Shielding in a Given Area: distant, near on both sides, and near on one side only.
- Transmission-Line Geometrical Variables: horizontal and vertical phase spacing.
- Cancellation Loop Conductor Geometrical Variables: variables that describe the location of the conductors of the cancellation loops.
- Cancellation Loop Conductor Electrical Parameters: *GMD* (geometric mean diameter), *R* (resistance), *C* (series capacitance), and I_s (cancellation loop conductor current).

Wire Set Types

The optimum geometry of a set of cancellation loop wires depends on the transmission line configuration. Figures 7.17-18 through 7.17-21 show schematically some of the possible arrangements of cancellation loops. The connection arrangements for a 2-wire cancellation loop are shown in Figure 7.17-14. Figures 7.17-22, and 7.17-23 illustrate the connection arrangements for a 3-wire cancellation loop,

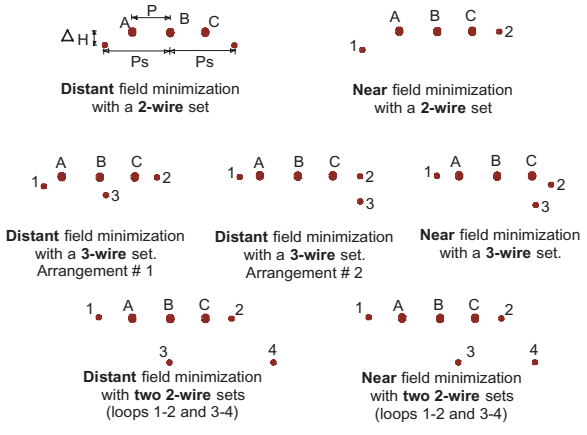


Figure 7.17-18 Cancellation loop arrangements for shielding 3-phase transmission lines with flat configuration.

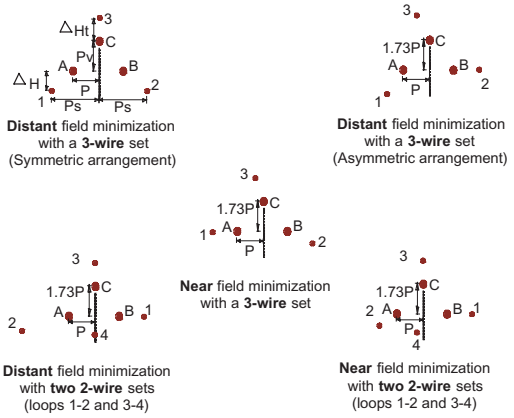


Figure 7.17-19 Cancellation loop arrangements for shielding 3-phase transmission lines with delta configuration.

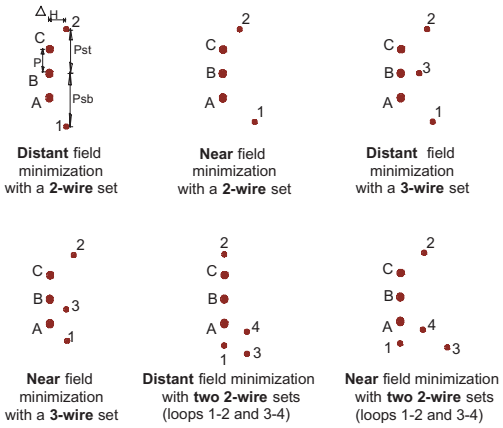


Figure 7.17-20 Cancellation loop arrangements for shielding 3-phase transmission lines with vertical configuration.

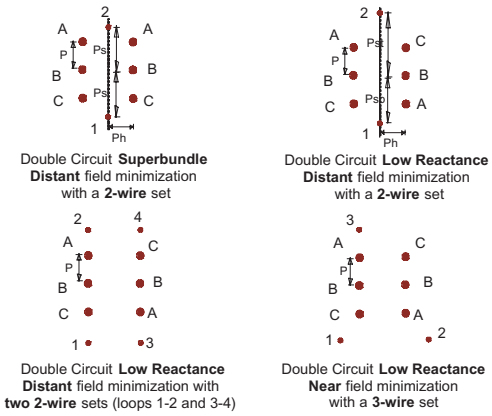


Figure 7.17-21 Cancellation loop arrangements for shielding double-circuit transmission lines.

and two 2-wire cancellation loop sets, respectively. Generally, two 2-wire cancellation loops provide better shielding than a 3-wire cancellation loop, and this, in turn, provides better shielding than a single 2-wire cancellation loop.

Optimization of Shielding in a Given Area

The choice of the geometry and of the design parameters of a cancellation loop system depends on the selection of the area to be shielded. It makes a significant difference whether the magnetic field is to be reduced at a single point only or whether the field is to be reduced over a large area. Furthermore, if the field must be reduced over a large area, it may make a significant difference whether the field parameter to be minimized is the maximum or the average field in that area.

The geometry of the cancellation loop and the value of the capacitor to be placed in series with the loop may be chosen to minimize the distant field—i.e., the field at distances much greater than the distance between phases. The shielding factors at points within or near the right-of-way may be higher (less shielding) or lower (more shielding) than that which could have been obtained if the geometry and capacitor were selected to minimize the field inside the right-of-way. To illustrate this concept, consider the line geometry shown in Figure 7.17-24. The magnetic field lateral profile was calculated for different conditions as shown in Figure 7.17-25.

Curve B of Figure 7.17-25 gives the magnetic field profile when the capacitor in series with the loop is chosen to minimize the field at long distances from the line. A series capacitor of 5.9 mF is required for a 480-m loop length. At a distance of 330 m from centerline, the field is reduced by a factor of 3. At these distances, however, the field is

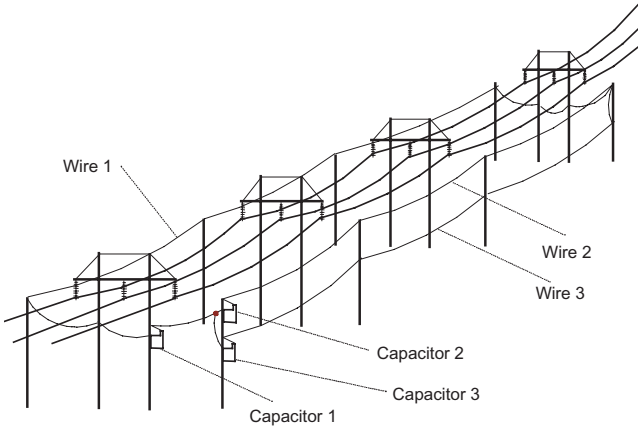


Figure 7.17-22 Example of connection arrangement for a 3-wire cancellation loop.

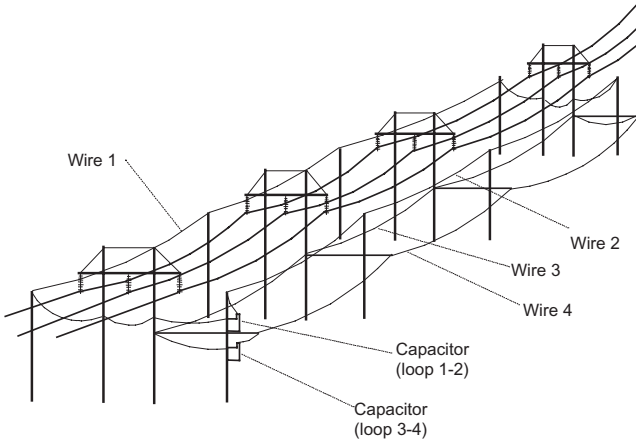


Figure 7.17-23 Example of connection arrangement for two independent 2-wire loop sets.

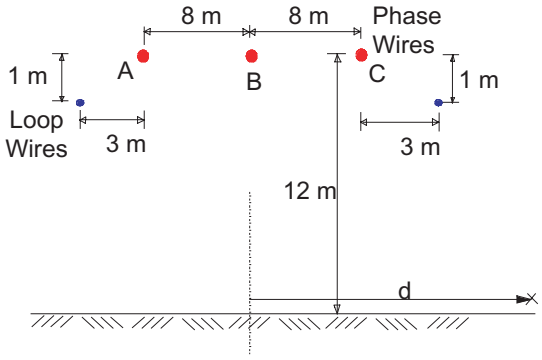


Figure 7.17-24 Example of passive cancellation loop applied to a transmission line with flat configuration (345-kV line with 1000 A, phase spacing 8 m, loop wires 11 m from center line and 1 m below the phase wires, loop with single 3.8-cm diameter wire with resistance $3.85 \cdot 10^{-5}$ Ω/m, loop along two spans with total length of 480 m).

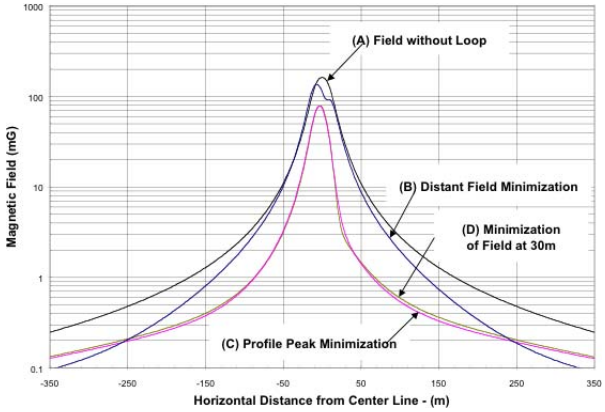


Figure 7.17-25 Magnetic field lateral profiles at 1-m above ground for different conditions: No cancellation loop (Curve A), minimum distant field (Curve B), minimum lateral profile peak field (Curve C), minimum field at 30 m from centerline (Curve D).

already very low (0.3 mG or less). Of much greater interest is reducing the field near the right-of-way. Curve C shows the field profile when the series capacitor is chosen to minimize the peak of the magnetic field profile—i.e., the largest value that the magnetic field can reach at the height of 1 m above ground. With a capacitor of 7.2 mF, the peak of the profile is reduced from 162 to 80 mG. In some cases, the field reduction is required on one side of the line, starting from a given distance. Curve D shows the field profile when the field is minimized on one side of the line at 30 m from centerline. The series capacitance required is 7.4 mF. At 30 m, the field is reduced to 2.5 mG (see curve D) from 29 mG without loop (see curve A). If a capacitance of 7.2 mF were used, as required by profile peak minimization (curve C), the field at 30 m would have been 3 mG. If the optimization were made for large distances (curve B), the field at 30 m would be 25 mG.

Note that curves C and D are not symmetrical. Field reduction is easier on the side of the phase wire with current lagging the current of the center phase. It should be noted that curves C and D practically coincide.

Better shielding may be provided when the cancellation loop wires can be placed asymmetrically with respect to the power line. This is true for both distant-field and near-field minimization. Calculations of magnetic field with and without the application of a cancellation loop can be performed using Applet EMF-11.

Electrical Parameters of Cancellation Loop Wires

The shielding factor is a function of the electrical parameters (resistance and inductance) of the cancellation loop wires. The inductance is controlled by wire length and geometry and geometric mean diameter (GMD*)*. It is practically impossible to provide design curves for every type of line geometry and loop arrangement types. An example of design curves is shown in Figure 7.17-26. These curves apply to a horizontal line configuration and a horizontal 2-wire cancellation loop placed symmetrically around the line. The loop wires have the same height above ground as the phase conductors ($\Delta H = 0$); the distance between loop wires and centerline is 1.5 times the phase spacing ($P_s/P = 1.5$). To provide design curves of general applications, *GMD* is given as a function of phase spacing, *P*, and design curves are given for different values of the parameter *GMD/P*. The shielding factor is a function of the ratio, *R/f*, where *R* is the resistance per unit of length and *f* is the frequency. For instance, a reduction of the frequency from 60 to 50 Hz would require a 17% reduction of *R* to obtain the same shielding.

The series capacitance for greatest shielding is given in the design curves of Figure 7.17-27. The optimum value of capacitance is a function of the length of the cancellation loop. Therefore, the curves in Figure 7.17-27 provide the value of the product of optimum capacitance times the loop length.

The loop wire current is proportional to the power line current. Therefore, the curves shown in Figure 7.17-28 provide the ratio I_s/I, where I_s is the loop wire current and I is the power line current.

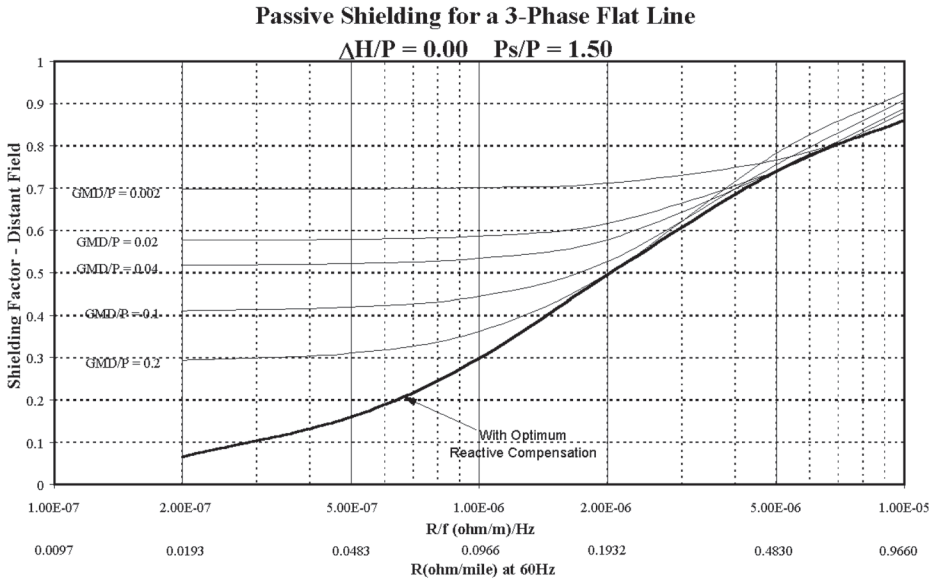


Figure 7.17-26 Design curves for distance field of three-phase lines with horizontal configuration and a two-wire cancellation loop. Shielding factor versus loop wire resistance.

The following example shows how the design curves of Figures 7.17-26 to 7.17-28 are used. Assume that the power line has a phase spacing of 6.1 m, a flat configuration, and the cancellation loop is applied to a 550-m section of the line and is formed by two wires located at the same height as the phase conductors and 3.05 m outside the outside phase conductors. Assume that the loop wire is a 1590 kcmil ACSR "Lapwing" conductor. Assume 1000 A phase current.

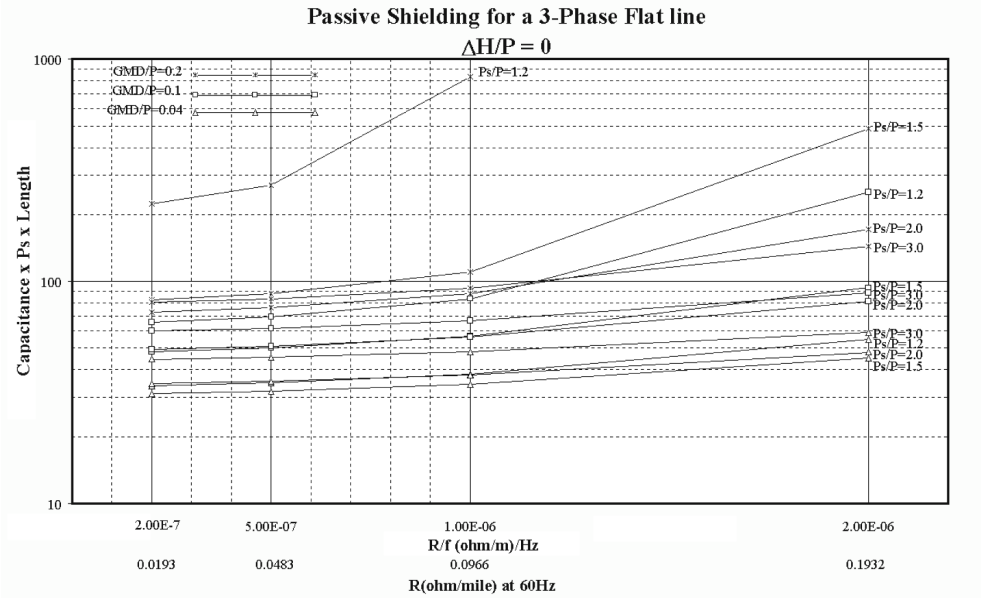


Figure 7.17-27 Design curves to obtain optimum series capacitor for a two-wire cancellation loop applied to a three-phase line with horizontal configuration.

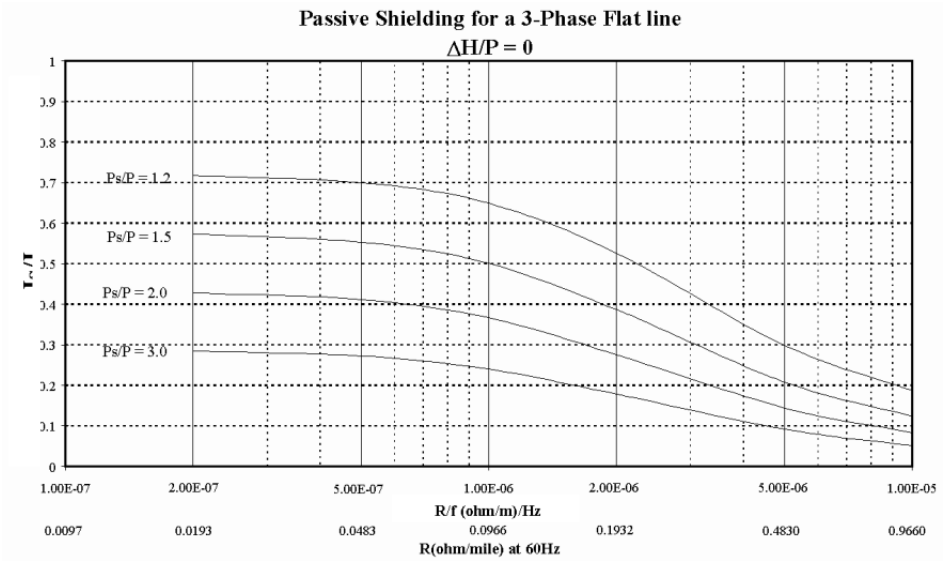


Figure 7.17-28 Design curves (I_s/I versus R) to determine loop wire current with optimum series capacitor for a two-wire cancellation loop applied to a three-phase line with horizontal configuration.

From conductor tables, the resistance and the GMD of the loop wire are found: R = 0.0622ohm/mile @ 60 Hz and 25°C; GMD = 2(0.0497) = 0.0994 feet = 3.03 cm. The parameters needed for the use of the design curves are: $\Delta H/P$ = 0; P_s/P = 1.5; GMD/P = 0.005; R/f = 6.44 · 10^{-7} (Ω/m)/Hz.

From Figure 7.17-26, the shielding factor corresponding to the values of GMD/P and R/f of this example is about 0.5. This is the shielding factor without any series capacitor. If the optimum capacitance is used, the shielding factor is about 0.2. This value is read on the curve for "optimum reactive compensation" in correspondence to R/f = 6.44 · 10^{-7} (Ω/m)/Hz.

The optimum value of capacitance is found with the help of Figure 7.17-27. A value of $C_{opt} \cdot P_s \cdot Length = 35(F \cdot m^2)$ is found in correspondence of P_s/P = 1.5; GMD/P = 0.005; R/f = 6.44 · 10^{-7} (Ω/m)/Hz. Therefore, $C_{opt} = 35/(9.15 \cdot 550) = 6 \cdot 10^{-3} F$.

The loop current is found with the help of Figure 7.17-28. A value of I_s/I = 0.54 is found in correspondence of P_s/P = 1.5 and R/f =6.44 · 10^{-7} (Ω/m)/Hz. The loop current varies in proportion to the line current. The loop current corresponding to a line current of 1000 A is 540 A.

The voltage across the capacitor is given by: $V = I_S/(2\pi fC)$ = 205 V. This is the maximum operating voltage. This voltage corresponds to the minimum capacitor voltage rating. The actual capacitor voltage rating depends on the magnitude of possible overvoltages and any capacitor protection that may be implemented.

Effect of Loop Wire Resistance

The shielding of a passive loop is, in general, more effective if the loop resistance is smaller. The value of the optimum capacitance practically does not change as the resistance is changed. The lateral profile of the magnetic field as a function of the wire resistance of a 2-wire loop is shown in Figure 7.17-29, which refers to the geometry described in Figure 7.17-24.

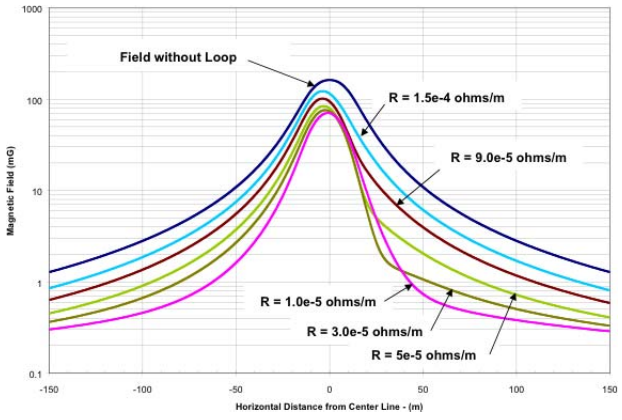


Figure 7.17-29 Effect of loop conductor resistance.

Examples of Field Reduction with Different Passive Loop Arrangements

Examples of magnetic field reduction are shown in Figures 7.17-31 to 7.17-33. The results can be obtained with Applet EMF-11. These examples illustrate the effect of the type of loop wire arrangement (2-wire, 3-wire, and two 2-wire loops). The examples refer to a 345-kV line with the flat configuration geometry shown in Figure 7.17-30.

Engineering Considerations for Passive Loops

*Cost. A*spects other than field reduction effectiveness, such as cancellation loop costs, effects on system performance, reliability, safety, and maintenance must be evaluated. It is important to assess the cost of a cancellation loop and to compare it with the cost of implementing other magnetic field management options. It is also important to compare

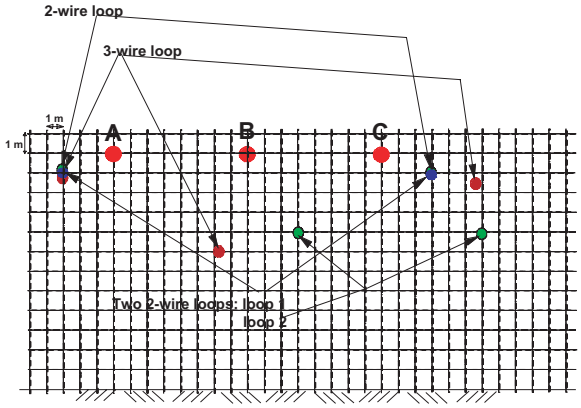


Figure 7.17-30 Geometry of the line and cancellation loop for the examples of Figures 7.17-31 to 7.17-33.

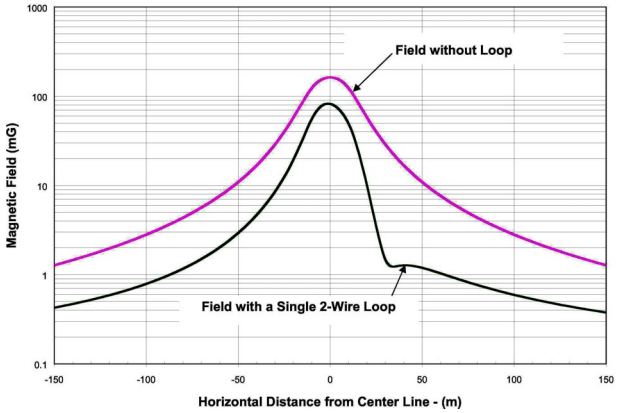


Figure 7.17-31
Minimization of near field with a 2-wire cancellation loop (345-kV line with 1000 A, phase spacing 8 m, loop wires 11 m from centerline and 1 m below the phase wires, loop with single 3.8-cm diameter wire with resistance 3.85·10^{-5} Ω/m, loop along two spans with total length of 480 m, series capacitance 7.4

the cost of different cancellation loop options to select the most cost-effective design.

Actual loop implementation costs will vary widely between individual utilities due to local conditions and utility practices. The following list provides the basic cost elements that must be considered for the implementation of passive cancellation loops:

- Cancellation loop engineering costs
- Loop conductor (material costs)
- Loop conductor hardware

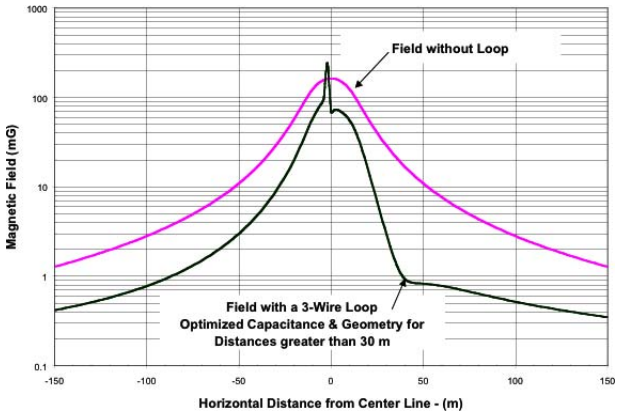


Figure 7.17-32 Minimization of near field with a 3-wire cancellation loop (345-kV line with 1000 A, phase spacing 8 m, loop wires 11 m from centerline and 1 m below the phase wires, each loop wire is a single 3.8-cm diameter wire with resistance $3.85 \cdot 10^{-5}$ Ω/m, loop along two spans with total length of 480 m, series capacitances in series with the wires, from left to right: 9 mF, 1 mF, 32 mF).

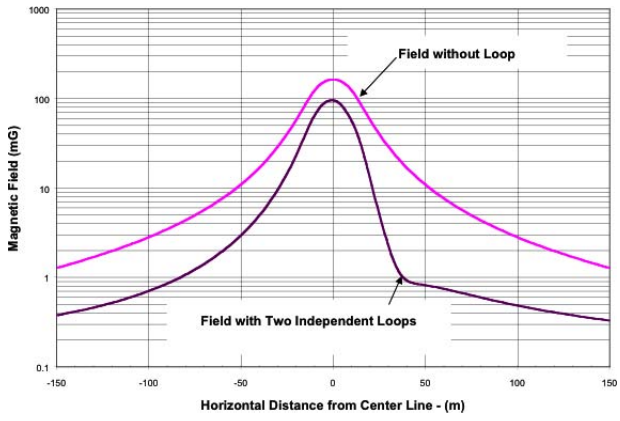


Figure 7.17-33 Minimization of near field with two 2-wire cancellation loops (345-kV line with 1000 A, phase spacing 8 m, loop wires 11 m from centerline and 1 m below the phase wires, each loop wire is a single 3.8-cm diameter wire with resistance $3.85 \cdot 10^{-5}$ Ω/m, loop along two spans with total length of 480 m, series capacitances in series with the loops, first loop: 7.4 mF, second loop: 4 mF).

- Additional poles (if needed)
- Structure modifications (if needed)
- Dead-end structures and hardware at loop ends
- Capacitors
- Insulators
- Capacitor enclosure and mounting platform
- Capacitor protective equipment
- Loop construction costs
- Cost of possible line de-energization during construction (lost revenue)
- Cost of losses
- Cost of inspection and maintenance

The cost of losses, inspection, and maintenance are annual costs. They can be translated into present worth and added to the initial costs of engineering, materials, and construction. The evaluation of the present worth requires specifying a rate of return and a total number of years.

Grounding of Cancellation Loop Wires

A voltage may exist between a point of the cancellation loop wires and ground. This voltage may result from electric and/or magnetic induction.

A large electric-field induced voltage may exist only if the loop is not connected to ground. A magnetically induced voltage between a loop point and ground would always be present when the source wires are carrying current. If the cancellation loop is ungrounded, the electric-field induced voltage depends on the geometry of the loop and of the line. The current that flows to ground through an object contacting the loop wires is a function of the loop length. The cancellation loops should be grounded at least at one point. If the cancellation loop is grounded at one point, the loop-to-ground voltage at the ground connection is equal to the electric-field induced short-circuit current multiplied by the resistance to ground. In general, the loop-to-ground voltage will be relatively low. For instance, if the short-circuit current of the cancellation loop to ground is 0.5 A and the ground resistance is 10 ohm, the voltage to ground is 5 V. Higher currents and voltages, however, may result if the cancellation loop is more than a few spans.

When the cancellation loop is grounded at only one point, there will be no magnetically induced current in the ground connection. The magnetically induced loop-to-ground voltage is zero at the point of grounding and increases as one moves away from that point. The maximum loop-to-ground voltage occurs at the opposite end of the loop from the grounding point if there is no series capacitor, or it will occur at the capacitor if a capacitor is present.

If the cancellation loop is grounded at more than one point, there will be a magnetically induced current in all the ground connections with a consequent modification of the loop wire current and of the magnetic field reduction effectiveness of the cancellation loop. In general, however, the magnetic field reduction effectiveness is only slightly reduced by the presence of multiple grounds. Multiple grounds, however, do little to increase safety because they are not very effective in reducing the loop-to-ground voltages, which depend little on the value of ground resistances in the range from 5 to 400 ohm.

Safety and Maintenance

A "passive" cancellation loop is designed to operate without the need of a feedback system. The current in the cancellation loop is induced by the line itself and varies proportionally to the line current, maintaining a constant shielding factor (for transmission lines). The cancellation loop must be grounded at least at one point. With the exception of very short loops for which the voltage of the loop to ground is very small, the cancellation loop must be treated as an energized conductor. Nevertheless, for most applications, there is no need to insulate the cancellation loop conductors from the supporting structures, if they are wood or concrete poles. If the cancellation loop conductors are supported by metallic structures, such as transmission towers, they must be insulated from the structure.

The voltage of the loop conductor to ground is dependent on the position along the cancellation loop. The largest voltage is across the capacitor terminals. The capacitor must not be made accessible to the public. Safe work practices require the capacitor to be switched out of service, shorted across the terminals, and grounded on both ends before being maintained. This can be done by means of a low contact resistance switch that is capable of interrupting large currents. The switch should be protected from corrosion and tampering. The open-circuit voltage across the switch depends on the length of the shielded section, on the line current, and on the cancellation loop design. For cancellation loops applied to a few spans, the open-circuit voltage across the switch is generally less than 25 V under normal load conditions.

The procedure for a periodic check of the shielding factor must be established. It is expected that inspection and maintenance requirements would be minimal.

Lightning Shield Wires

Overhead ground wires are used for lightning protection of transmission lines. These wires are generally grounded at every structure. Occasionally they are sectionalized, with each ground wire section grounded at only one tower and insulated from the other towers. If the overhead ground wires are grounded at every tower, current will be induced in the wires due to the same principle that induces current in cancellation loops. The method of calculating shield wire current is described in Section 7.9. Overhead ground wire currents are relatively small, because the wires are made of steel and have low conductivity. The effect of shield wire currents on transmission-line magnetic field is measurable but small. Issues related to shield wires and cancellation loops are:

- Is there an effect of lightning shield wires on the cancellation loops?
- Can one take advantage of lightning shield wires to form cancellation loops?

Effect of Lightning Shield Wires on the Design of Cancellation Loops: The presence of lightning shield wires has an effect on the design of cancellation loops. If the cancellation loop design is optimized without accounting for the presence of lightning shield wires, the actual presence of these wires will change the shielding factor, typically making it less effective. Therefore, it is preferable to optimize the loop wire design accounting for the presence of the lightning shield wires. Unfortunately, the current in a span of lightning shield wires depends on the values of tower impedances, which may vary from tower to tower, and on the distance of the span from a substation. Furthermore, lightning shield wire currents add a monopolar component to the transmission-line field, which cannot be eliminated in the distant field using cancellation loops. Since the shield wire currents are not known with great accuracy, they cannot be readily considered in the loop design. In view of the above considerations, it is preferable to sectionalize the overhead ground wire for the length of line where the cancellation loop is applied. In this way, there would be no current in the lightning shield wires and no interference with the performance of the cancellation loop. However, sectionalizing the shield wire affects the zero sequence impedance of the transmission line and may have an impact on the line's relay protection.

Use of Lightning Shield Wires in Cancellation Loops: In general, lightning shield wires are not effective when included in cancellation loops. For example, a portion of a cancellation loop for a vertical line configuration could be made of the lightning shield wire, located above the phase conductors, with an additional wire installed below the phase conductors. The analysis of such a design shows that this cancellation loop has little shielding effect. The reason is the elevated value of the lightning shield wire resistance. Even ground wires made of copperweld or alumoweld, which have lower resistance then steel conductors, have too high a resistance to be used as cancellation loop wires. Effective cancellation loops require wire resistances of the order of 0.05 mΩ/m or less. Such resistances cannot be obtained with the wires commonly used for lightning

protection. It would be possible to replace the steel wires with more conductive wires and achieve effective shielding. In this case, however, there is a concern about lightning strikes to the cancellation loop and their effect on the series capacitor reliability and safety.

End and Sag Effects

Cancellation loops can be applied to reduce the field in short sections of transmission lines. If the loop is designed to minimize the field in the middle of the section, the field will be significantly larger near the ends of the section. Calculations of end effects must be made using a three-dimensional computational procedure.

As a rule of thumb, to ensure a uniform field reduction for a desired length, the cancellation loop must extend beyond each end of the section by an amount equal to about 2-3 times the distance between measuring point and loop wires.

The sag of the phase conductors and the loop wires affects the shielding factor. It is preferable to match the loop wire sag to the phase conductor sag as much as possible.

7.17.6 Example of Cancellation Loops Applied to a 345-kV Corridor

Introduction

In 1995, the New York Power Authority (NYPA) initiated an R&D project to demonstrate the cancellation loop concept (Spherling et al. 1996). The project consisted of the design, installation, and evaluation of a passive shielding system for a large transmission corridor carrying two separate 345-kV lines. The shield was applied to a short section of line consisting of two spans located in upstate New York near the city of Utica. Several cancellation loop types were studied, and their designs optimized to reduce the magnetic field at the edge of the right-of-way and beyond. A system consisting of two 2-wire loops was chosen. The project successfully demonstrated that two 2-wire loops were capable of reducing the magnetic field outside the right-of-way by a factor of about ten. The long-term performance of the cancellation loop was very satisfactory. The conclusions reached as a result of this project are useful for the design of future similar systems.

The area where the magnetic field was to be reduced was in a wooded area along two spans of the NYPA Cross-State Corridor, which contains two 345-kV lines, each with flat configuration. Figure 7.17-34 shows the dimensions of the average cross section of the corridor. The right-of-way width is 91.4 m. The circuits are located symmetrically on the corridor, with a 45.7-m separation between centers. The phase spacing on both circuits is 10.5 m, and the phasing is A-B-C from south to north on both circuits.

The cancellation loop system was designed to provide maximum shielding when the magnetic field from the lines is near its maximum. This corresponds to a load of 1200 A per phase (maximum loading is 1700 A), and to a sag of 12 m. With this sag and a tower attachment height of 21.3 m, the ground clearance at midspan is 9.3 m.

The Optimized Cancellation Loop System Design

The basic steps taken in developing an optimized system are outlined below:

- Constraints on the shield design were identified. Most important was to identify the regions in space in which loop wires may, and may not, reside. Because shield conductors are essentially at ground potential, there are minimum distances from the 345-kV conductors that must be maintained. Wind and heavy ice loading must be taken into account. The loop wires must remain at least 1.8 m from the line conductors in all wind and ice conditions. In addition, the loop wires must maintain a ground clearance of 4.9 m and cannot go beyond the edge of the right-of-way. Poles and guy wires must remain inside the corridor. The permissible locations of the loop wires at midspan in relation to a phase conductor are indicated in Figure 7.17-35.
- Different cancellation loop configurations (a 2-wire loop, a 3-wire loop, and two 2-wire loops) were analyzed. The first analysis was made in 2-D, assuming all the wires of the line and of the cancellation loops parallel to each other. Then the best configuration was analyzed and optimized in 3-D accounting for the sags. For each type, the optimum wire location and the optimum value of capacitance to be placed in series with the wires were determined. The 2-wire loop consisted of one large

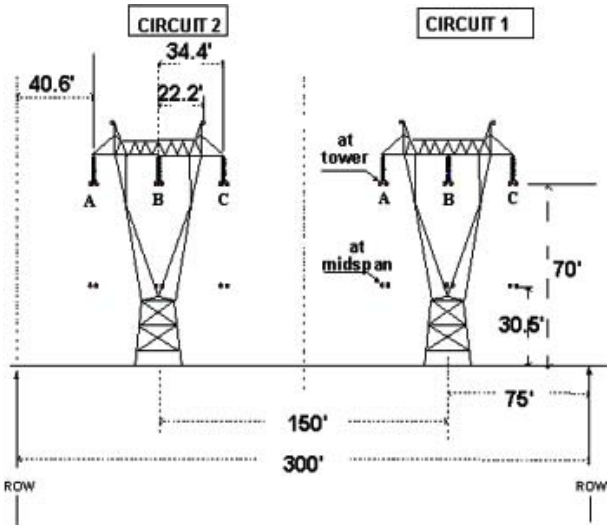


Figure 7.17-34 Cross Section of the 345-kV corridor at the site to be shielded.

loop encircling the two lines, with a series capacitor. The 3-wire loop consisted of three long conductors connected at their far ends, each conductor with its own series capacitor. Two 2-wire loops consisted of two independent (but magnetically coupled) loops, one around each line, each loop with its own series capacitor. Various conductor sizes were also considered. In addition, a wide range of locations of the loop wires were considered, such as on new wood poles, attached to the existing towers, and underground.

- The optimum configuration within the constraints described above was determined. The optimum was defined in terms of maximum reduction of the average magnetic field from the edge of the right-of-way up to 15 m beyond the right-of-way on each side of the corridor. A two 2-wire loop configuration was chosen. The two loops would be comprised of 1431 kcmil ACSR conductors, with a diameter of 3.6 cm and a resistance of 4.2510^{-5} Ω/m at 25 ºC, supported on wooden poles. Each loop has its own series capacitor. The optimized design is shown in Figures 7.17-36 and 7.17-37. The two legs of the south loop are labeled S1 and S2, and those of the north loop are labeled N1 and N2. The calculated optimum distances of N1 and S2 from centerlines were sufficiently close that it was possible to design one supporting pole for both conductors without much altering the optimum design. The calculated optimum capacitance values, the induced loop open-circuit voltages, and the induced currents in the loops are indicated in Table 7.17-4. The magnetic field profiles at midspan and at the tower with and without shielding loops calculated with 3-D software are shown in Figure 7.17-38. The 3-D calculations at midspan give results close to those obtained with the 2-D model. Profile calculations at the tower are

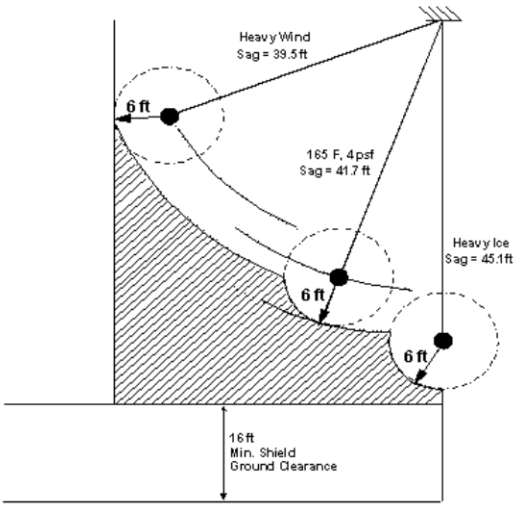


Figure 7.17-35 Determination of permissible locations for shield wires.

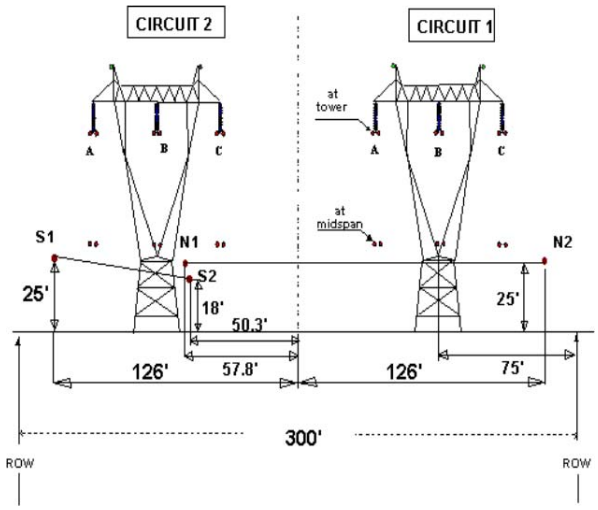


Figure 7.17-36 Corridor cross section in 2-D with the cancellation loop system in place.

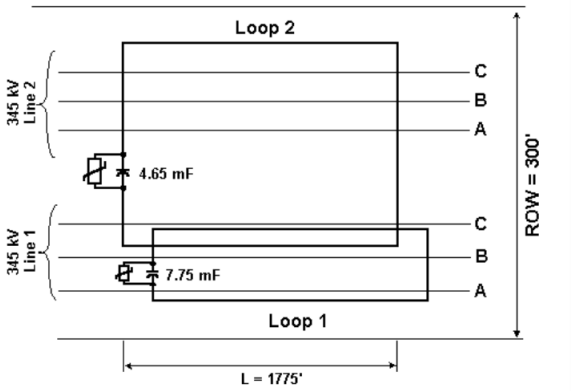


Figure 7.17-37 Plan view of cancellation loop system layout.

Table 7.17-4 Calculated Optimum Parameters of the Two Independent Loops

Parameter	2-D Model		3-D Model	
	S Loop	N Loop	S Loop	N Loop
Optimum series capacitance	8.31 mF	5.34 mF	7.75 mF	4.65 mF
Capacitor Voltage @ 1200 A/phase	175 V	229 V	177 V	311 V
Cancellation loop current @ 1200 A/phase	519 A	522 A	518 A	545 A
Phase angle of the loop current (degree)	165	146	166	149

accurate only with the 3-D model. At the tower, the magnetic field values with the cancellation loop system present are lower than at midspan, both within and outside the right-of-way.

A sensitivity analysis was performed on the various parameters of the optimized shield design. In an actual implementation of cancellation loops, there are unavoidable deviations from the idealized design. It is important to study these deviations in order to observe the sensitivity of field reduction to variations in the individual parameters. From this, it could be determined which parameters have critical tolerances, and which do not. The parameters analyzed were series capacitors, transmission-line sags, and transmission-line currents. The effect of one line being out of service was also analyzed. It was found that the overall shielding efficiency was not significantly affected by capacitance deviations up to 12% from the optimum values. However, tuning the capacitance in place was recommended to optimize the performance. If the sag of the line conductors changes relative to the sag of the cancellation loop wires because of temperature and loads, there is some, but not significant, loss of shielding efficiency. A significant amount of shielding is lost when one line is out of service. However, the field remains below the levels when both lines are energized and the cancellation loops are present. The data indicate that a significant amount of field reduction is lost when there is a significant level of net current. Transmission lines, however, are generally very well balanced.

- The final details of the design were established.

Capacitor Selection

The capacitor ratings determined from the 3-D model were 7.75 mF, 480 V for the south loop and 4.65 mF, 480 V for the north loop. The types of capacitors recommended for this application were power factor correction capacitors. Each of the two capacitors used consisted of a housing with a number of internal smaller capacitor cans wired in parallel. Some of these cans are of higher capacitance than others. It was necessary to have a number of smaller capacitance cans in order to fine-tune the capacitors in-place. Also, 10% more capacitance than indicated above was purchased in the event a higher capacitance was found to be required. The sensitivity analysis demonstrated that the shielding effectiveness of the loops is insensitive to capacitance deviations up to about 12%. Therefore, it was recommended that each of the two capacitors contain individual cans of 0.1 mF up to about 10% of its total capacitance, and another set of cans of 0.2 mF up to another 20% of its total capacitance. The remaining capacitance consists of a combination of larger cans. Table 7.17-5 summarizes the recommendations.

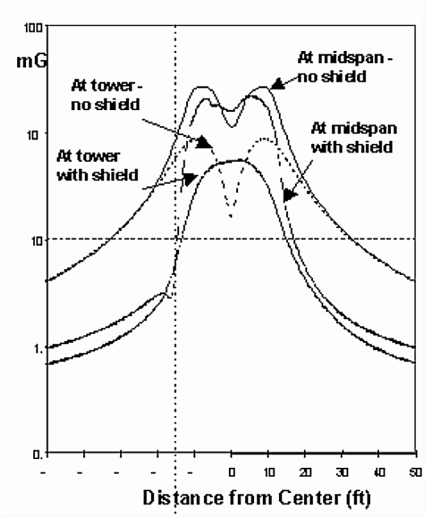


Figure 7.17-38 Magnetic field profiles at midspan and at the tower with and without cancellation loops.

Power factor correction capacitors are capable of enduring significant levels of overvoltages (up to as much as 100% overvoltage) for brief periods of time. However, overvoltages can degrade and destroy capacitors. Two types of protection were recommended: surge arresters and fuses. Surge arresters will protect the capacitors from sudden overvoltages caused by line faults, lightning, etc. Fuses were also recommended because the capacitor manufacturer normally supplies them. The capacitor housings come with fuse holders, and they supply an extra layer of protection. The capacitors were fused according to their 480-V ratings.

The capacitors and arresters were mounted on a suitable platform with suitable housing. Personnel had access to the capacitors for tuning. The arresters were mounted in parallel to the capacitors, and the capacitors were grounded on one side. A switch was provided to short the capacitors during tuning. A schematic of the assembly is shown in Figure 7.17-39.

It was important not to inadvertently introduce any extraneous resistances into the cancellation loops, such as at connections. Care was used to make resistance-free connections. This included cleaning the areas of contact prior

Table 7.17-5 Capacitor Recommendations

	Specified Value	With 10% margin	No. of 0.1 mF Tuning Cans	No. of 0.2 mF Tuning Cans
South Loop	7.75 mF	8.52 mF	9	10
North Loop	4.65 mF	5.12 mF	5	6

to making connections to remove oxidation and other contaminants. An oxide inhibitor was applied to contact points, and all connections were made appropriately secure.

Grounding and Safety

It is critical that each shielding loop be grounded at least at one point immediately adjacent to one side of each capacitor. Experimental studies and analysis indicated that there is no significant loss in shielding efficiency if there are multiple grounded points on each loop, such as at each pole. However, the exact effect of multiple grounds on such full-scale loops is not well known. Because the loops are grounded at a minimum of one point, they are at low potentials relative to the transmission line. However, there are induced voltages along the loops that can be on the order of a few hundred volts (especially across the capacitors). Therefore, they need to be treated similar to the distribution-line conductors.

Installation of the Shielding System

The shielding system was constructed as close to specifications as practical. The sensitivity analysis demonstrated that small deviations from the optimum geometry would not significantly affect the shielding performance. The loop conductors were strung from crossarms mounted on wood poles, and were attached with small insulators. The conductors near the outer edges of the corridor (conductors S1 and N2 of Figure 7.17-36) were supported on their own poles, and the two conductors running along the inside of the corridor (N1 and S2) were supported on common poles. The series capacitors and arresters were mounted on a platform located near one end of the shielding loops. The platform was a metal grate mounted 4.5 m above ground on wood poles.

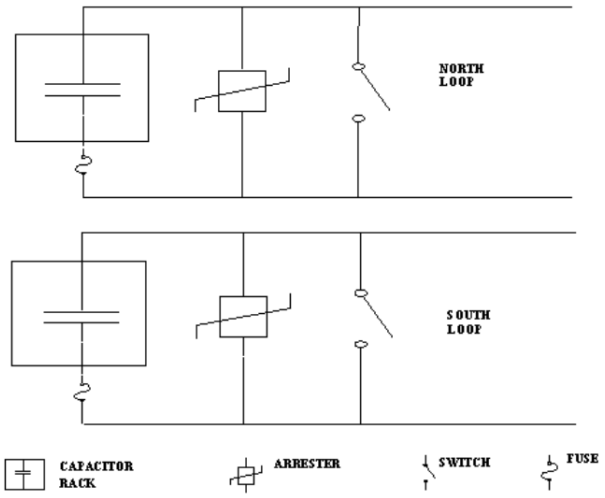


Figure 7.17-39 Electrical schematic of the capacitor assemblies.

Figure 7.17-40 shows a view of the shielding system. Figure 7.17-41 shows the details of the loop wire N1 and S2 attachments to the pole.

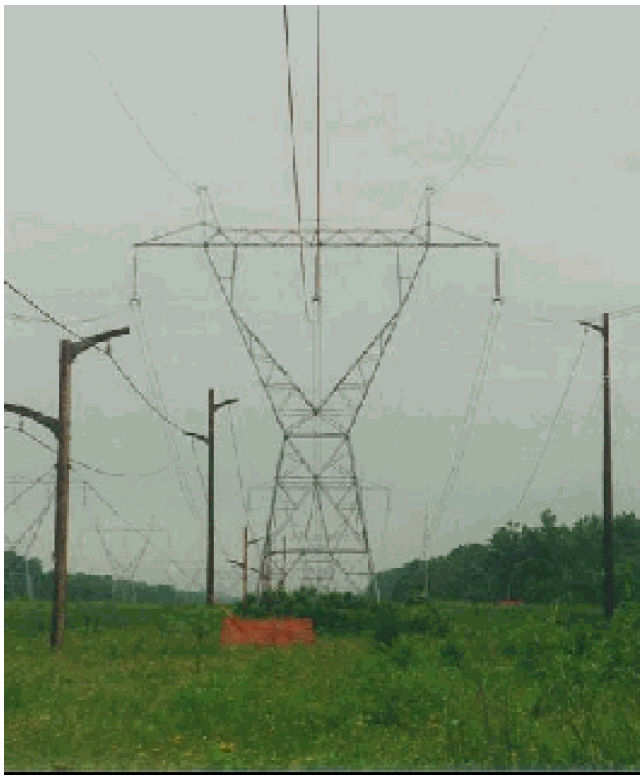


Figure 7.17-40 View of the shielding system looking east. A tall wood pole on the south side of the corridor supports conductor S1, and shorter poles support conductors S2 and N1.



Figure 7.17-41 Details of loop wires N1 and S2 attachment to wood pole.

Actual Performance of the Shielding System

Figure 7.17-42 shows the measured values of the magnetic field profile for the case in which the south loop had a series capacitance of 7.815 mF and the north loop had a series capacitance of 4.522 mF. These were the capacitance values that provided the best overall shielding at the site, and were the values adopted for the long term. Calculations and measurements match reasonably well. However, the actual (measured) shielding was somewhat better than predicted on the south side of the corridor, and was slightly worse on the north side.

Measured and calculated currents induced in the cancellation loops are shown in Table 7.17-6. The measured and calculated induced currents in the south loop compared favorably. However, the measured induced currents in the north loop were significantly lower than predicted. This, however, did not significantly affect the overall performance of the cancellation loop system.

Table 7.17-6 Comparison between Measured and Calculated Currents in the Shielding Loops

South Loop		North Loop	
Measured (A)	**Calculated (A)**	**Measured (A)**	**Calculated (A)**
335	364	341	419

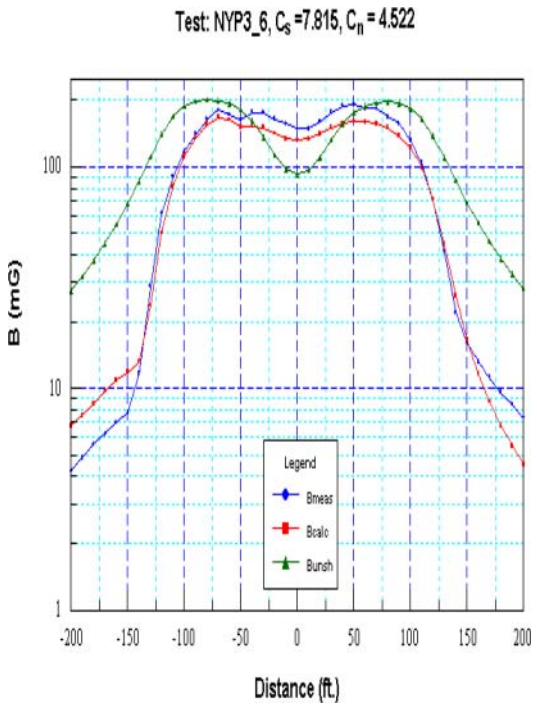


Figure 7.17-42 Comparison between measured and calculated magnetic field lateral profiles.

Following the construction and the evaluation of the cancellation loop system, the system was left unattended. For the first year of its operation, magnetic field recorders were placed outside the right-of-way 3 m from the edge of right-of-way on both sides of the corridor at shielded midspan locations and at unshielded midspan locations. These instruments recorded the rms magnetic field every 10 minutes. The site was visited approximately once each month, and the recorders were downloaded and reset. The data collected over the year indicated that the magnetic fields at these locations were reduced, on average, by about 88% on the south side of the corridor, and by about 87% on the north side. The field reduction did not change with time.

7.17.7 Fourth-Wire Scheme

A significant field reduction can be obtained with a relatively simple arrangement consisting of splitting one of the phases in two and placing this fourth wire in a strategic location (Pettersson 1996). An example of the fourth-wire scheme is shown in Figure 7.17-43.

The current in phase A is split into two wires. The impedance of the two wires and the mutual inductances with the other two phases determine the current split. This scheme can reduce magnetic field by a factor of 2 or more by proper selection of the size and characteristics of the fourth wire. The scheme can be applied to an existing line and to a few spans only, when the field reduction is only locally required.

The magnetic field can be calculated using Applet EMF-12, "Magnetic Field Reduction with Fourth Wire Scheme."

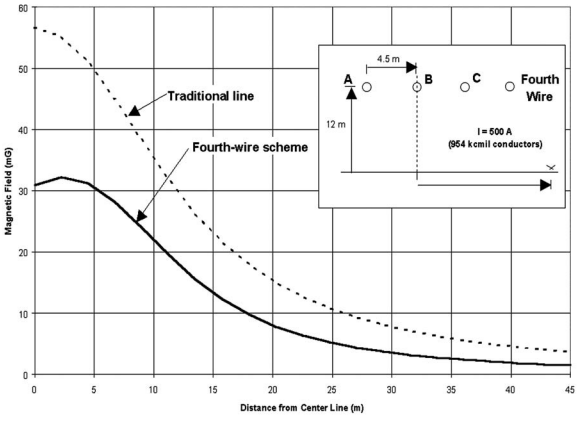


Figure 7.17-43 Example of fourth-wire scheme for magnetic field reduction.

APPENDIX 7.1 CALCULATION OF FIELD ELLIPSE PARAMETERS

The concepts illustrated here apply to both the electric and the magnetic field. The concept of a field ellipse is particularly important for magnetic fields. The electric field ellipse is rarely of importance, because electric fields are measured near ground or near conductive surfaces, where they tend to be perpendicular to the surface and where, therefore, the ellipse collapses into an oscillating vector.

The equations in this appendix are written for the electric field. The same equations may be used for the magnetic field by substituting the symbol *E* with the symbol *B*.

If all the components of the field at a point, P, are sinusoidal functions of time at a frequency *f*, the field can be described by a vector, $\vec{e}$, anchored at P, with a length proportional to the instantaneous value, *e*, and with its tip describing an ellipse at the frequency *f*.

A major and a minor axis characterize the field ellipse. The maximum instantaneous field occurs when the field vector is aligned along the major axis and its value is represented by one-half of the length of the major axis: the semi-major axis. Similarly, the semi-minor axis represents the minimum instantaneous field.

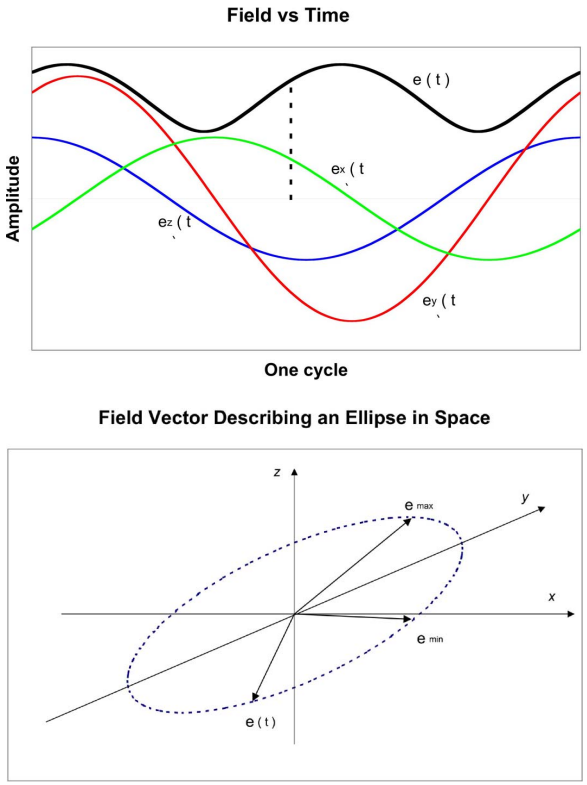


Figure A7.1-1 Field ellipse and variation of field with time.

When the major and minor axes are equal in magnitude, the ellipse becomes a circle; in this case, the field is constant in magnitude, but its direction varies with time in a plane with constant angular velocity. In this case, we say that the field is circularly polarized. On the other hand, when the minor axis becomes very small with respect to the major axis, the ellipse becomes very narrow, until it eventually collapses into an oscillating vector. In this case, the field is linearly polarized and is represented by a vector that has a constant direction in space, but a magnitude that varies in a sinusoidal fashion with time. This occurs, for instance, for the electric field when all the voltages are in phase, and for the magnetic field when all the currents are in phase. Also, the electric field on the surface of conductive objects is always linearly polarized, with a direction perpendicular to the surface. In situations involving three-phase systems, the fields are in general elliptically polarized.

The degree of polarization is defined by the axial ratio—i.e., the ratio between the minor and the major axes of the field ellipse.

$$Polarization = axial\ ratio = e_{min} / e_{max} \qquad \text{A7.1-1}$$

Polarization ranges from zero (linear polarization) to one (circular polarization). The component of the field in the direction of the major axis of the ellipse is the "maximum field" that can be measured with a single axis probe. The rms value of the maximum field is $E_{max} = e_{max}/\sqrt{2}$. Similarly $E_{min} = e_{min}/\sqrt{2}$. The parameters of the field ellipse (E_{max}, E_{min}, polarization) can be calculated if the rms values of real and imaginary parts in all three orthogonal directions (ER_x, EJ_x, ER_y, EJ_y, ER_z, EJ_z), or the rms amplitude and phase angles of the three orthogonal components of the field (E_x, ϕ_x, E_y, ϕ_y, E_z, ϕ_z) are known.

Real and imaginary components are related to amplitude and phase angles by Equations A7.1-2.

$$\begin{aligned} ER_x &= E_x \cdot \sin\phi_x \\ EJ_x &= E_x \cdot \cos\phi_x \\ ER_y &= E_y \cdot \sin\phi_y \\ EJ_y &= E_y \cdot \cos\phi_y \\ ER_z &= E_z \cdot \sin\phi_z \\ EJ_z &= E_z \cdot \cos\phi_z \end{aligned} \qquad \text{A7.1-2}$$

The instantaneous value of the field is expressed by Equation A7.1-3.

$$\begin{aligned}\vec{e}(t) &= \sqrt{2}E_x \cdot \sin(\omega t + \phi_x) \cdot \vec{u}_x \\ &+ \sqrt{2}E_y \cdot \sin(\omega t + \phi_y) \cdot \vec{u}_y \\ &+ \sqrt{2}E_z \cdot \sin(\omega t + \phi_z) \cdot \vec{u}_z\end{aligned} \quad \text{A7.1-3}$$

$\omega = 2\pi f$ (f is the frequency)

$\vec{u}_x, \vec{u}_y, \vec{u}_z$ are unit vectors in the direction of the *x, y*, and *z* axes, respectively.

The maximum and minimum axes of the field ellipse correspond to the value of *t* for which the field expressed by Equation A7.1-3 is maximum or minimum. This occurs for:

$$\omega t = \frac{1}{2}\tan^{-1}\left(-\frac{E_x^2 \cdot \sin(2\phi_x) + E_y^2 \cdot \sin(2\phi_y) + E_z^2 \cdot \sin(2\phi_z)}{E_x^2 \cdot \cos(2\phi_x) + E_y^2 \cdot \cos(2\phi_y) + E_z^2 \cdot \cos(2\phi_z)}\right) \quad \text{A7.1-4}$$

Equation A7.1-4 gives two solutions ωt_1, and $\omega t_2 = \omega t_1 + \pi/2$. Substituting ωt in Equation A7.1-3 with ωt_1 and ωt_2 gives the instantaneous values of the maximum and minimum fields. The rms values of the field in the direction of the major and minor axes of the ellipse are:

$$\begin{aligned}E_{\max} = \{ &\left[E_x \cdot \sin(\omega t_1 + \phi_x)\right]^2 \\ &+ \left[E_y \cdot \sin(\omega t_1 + \phi_y)\right]^2 \\ &+ \left[E_z \cdot \sin(\omega t_1 + \phi_z)\right]^2 \}^{1/2}\end{aligned} \quad \text{A7.1-5}$$

$$\begin{aligned}E_{\min} = \{ &\left[E_x \cdot \sin(\omega t_2 + \phi_x)\right]^2 \\ &+ \left[E_y \cdot \sin(\omega t_2 + \phi_y)\right]^2 \\ &+ \left[E_z \cdot \sin(\omega t_2 + \phi_z)\right]^2 \}^{1/2}\end{aligned} \quad \text{A7.1-6}$$

It is interesting and important to note that the rms value of the field expressed by Equation A7.1-3 is given by:

$$E_{r.m.s.} = \sqrt{E_{\max}^2 + E_{\min}^2} = \sqrt{E_x^2 + E_y^2 + E_z^2} = \sqrt{ER_x^2 + EJ_x^2 + ER_y^2 + EJ_y^2 + ER_z^2 + EJ_z^2} \quad \text{A7.1-7}$$

For two-dimensional situations, Equations A7.1-4, A7.1-5, and A7.1-6 apply with one of the field components, for instance E_y, equal to zero.

Major and minor axes of the field ellipse can be calculated with Applet EMF-1.

Example Calculation:

Assume that the magnetic field real and imaginary components at a point are:

BR_x = 10 mG	BR_z = -2 mG	BR_y = 0
BJ_x = 18.03 mG	BJ_z = 15 mG	BJ_y = 0

The real and imaginary components are first converted into field magnitude and phase angle for each axis:

Field Amplitude	Phase Angle
B_x = 10.2 mG	ϕ_x = -11.3 degrees
B_z = 18.03 mG	ϕ_z = 56.3 degrees

Equation A7.1-4 becomes

$$\omega t = \frac{1}{2}\tan^{-1}(8.98)$$

ωt_1 = 41.8 degrees, ωt_2 = 131.8 degrees

Equations A7.1-5 and A7.1-6 give:

$B_{\max} = 18.6\,\text{mG}$ and $B_{\min} = 9.1\,\text{mG}$

The axial ratio (polarization) is 9.1 / 18.6 = 0.49.

APPENDIX 7.2 USE OF TWO-DIMENSIONAL DIPOLES AND QUADRUPOLES FOR CALCULATING TRANSMISSION-LINE MAGNETIC FIELDS

The magnetic field produced by a power line can be analyzed efficiently by reducing the set of line currents that form a power line into basic line current elements: monopole, dipoles, quadrupoles, and higher-order elements (Kaune and Zaffanella 1992; Petterson 1992; Zaffanella 1999b).

Monopole

A current-carrying, infinitely long, straight conductor (line current), is defined as a *monopole*. The structure of the field produced by a monopole is quite simple, as shown in Figure A7.2-1. The field has the following features:

1. The magnetic field vector, $\vec{B}$, at a measuring point, T, is orthogonal to the conductor and to the vector $\vec{R}$. The direction of the field can be determined using the right-hand rule. If the right thumb points along the direction of the current, the fingers encircle the conductor in the direction of the magnetic field. In Figure A7.2-1, the conductor carrying the current is shown with a dot in its center to signify that the direction of the current is through the page toward the reader. This dot represents the tip of the arrow indicating the direction. A × sign inside the conductor would signify a direction away from the reader.
2. As $\vec{R}$ is rotated by an angle α, the field vector $\vec{B}$ also rotates by α.
3. The field magnitude is independent of α.
4. The field magnitude is inversely proportional to the distance *R*. If the field is expressed in milligauss, the current in ampere, and the distance in meter, the field is given simply by:

$$B = 2I/R \qquad \text{A7.2-1}$$

If *B* is desired in microtesla, the result of Equation A7.2-1 should be divided by 10.

5. The field is in phase with the monopole current and is linearly polarized.

Dipole

A pair of equal, but opposite, line currents is defined as a *dipole*. The structure of the field, $\vec{B}$, produced by a dipole is shown in Figure A7.2-2. The field has the following features:

1. When the measuring point, T, is in the plane of the two line currents, $\vec{B}$ is orthogonal to the conductors and to the vector distance, $\vec{R}$.
2. As $\vec{R}$ is rotated by an angle α, $\vec{B}$ rotates by 2α and ceases to be perpendicular to $\vec{R}$.
3. The field magnitude is independent of α.
4. The field magnitude is inversely proportional to the square of the distance *R*. The field is given by:

$$B = \frac{2IP}{R^2} = \frac{2D}{R^2} \qquad \text{A7.2-2}$$

The units in Equation A7.2-2 are milligauss, ampere, and meter. If *B* is desired in microtesla, the result of Equation A7.2-2 should be divided by 10.

The field depends on the product of *I* and *P*. Doubling the current while halving the spacing between conductors does not change the field. For this reason, the product *IP* can be substituted by the quantity $\vec{D}$ (dipole), which can be thought of as a vector with magnitude *IP*, centered between the two conductors, and with a direction from the × sign to the dot.

5. The field is in phase with the dipole current (current in the conductor with the dot) and is linearly polarized.

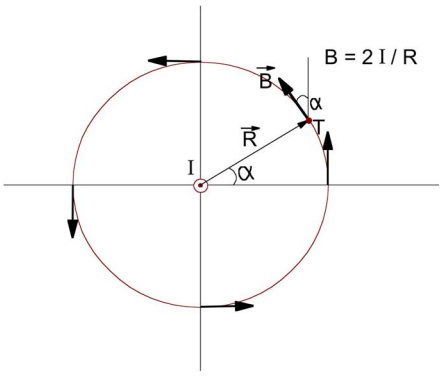


Figure A7.2-1 Magnetic field of a monopole.

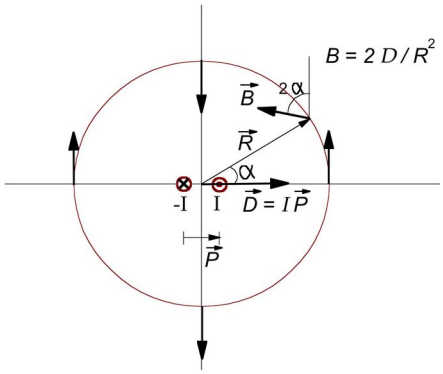


Figure A7.2-2 Magnetic field of a dipole.

Quadrupole

A pair of equal, but opposite, dipoles is defined as a *quadrupole*. The structure of the field produced by a quadrupole is shown in Figure A7.2-3. The field has the following features:

1. When the vector $\vec{R}$ has the same direction of the dipole $\vec{D}$, the field is perpendicular to the vector $\vec{P}_{12}$ connecting the two dipoles.
2. As $\vec{R}$ is rotated by α, $\vec{B}$ rotates by 3α.
3. The field magnitude is independent of α.
4. The field magnitude is inversely proportional to the cube of the distance *R*:

$$B = \frac{4 \cdot P_{12} \cdot D}{R^3} = 4\frac{Q}{R^3} \qquad \text{A7.2-3}$$

   The units in Equation A7.2-3 are milligauss, ampere, and meter. If *B* is desired in microtesla, the result of Equation A7.2-3 should be divided by 10.
5. The field is in phase with the dipole current (current of the conductor with the dot of the first dipole) and is linearly polarized.

The quadrupole can be characterized by a vector $\vec{Q}$, with magnitude equal to $P_{12} \cdot D$ and direction from the center to the point at which the field, $\vec{B}$, is perpendicular to the vector $\vec{R}$. The direction of $\vec{Q}$ is obtained by rotating $\vec{D}$, by δ/2, where δ is the angle between $\vec{P}_{12}$ and $\vec{D}_1$.

Higher-Order Elements

Elements can be constructed beyond the quadrupole, by considering a pair of equal, but opposite, quadrupoles, and then a pair of newly constructed elements, and so on. The monopole can be considered a first-order element, the dipole a second-order element, and the quadrupole a third-order element.

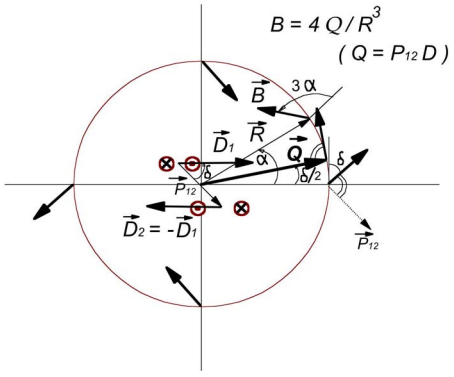


Figure A7.2-3 Magnetic field of a quadrupole.

Rules for Combining Monopoles, Dipoles, and Quadrupoles

The field created by two different basic elements—for instance, two dipoles—can be added using conventional vectorial rules. It is also desirable to represent basic elements by vectors that can be combined, so that the resulting vector represents the basic element that can be used to calculate the field. However, the combination of vectors representing basic elements of different orders—for instance, a dipole and a quadrupole—does not have any meaning. Basic elements of the same order can be combined if the elements are concentric and if special procedures are followed.

- Monopoles are represented by a scalar, not by a vector. Monopoles can be combined simply by adding the values of the currents. The result is a monopole with a value equal to the sum of all the individual currents.
- Dipoles can be represented by a vector (see Figure A7.2-2). The rule for combining two dipoles is quite simple. The combination of two dipoles is represented by a vector equal to the vectorial sum of the vectors representing the individual dipoles. When combining several dipoles with different phase angles, the real and imaginary components should be treated separately. The result is a real dipole vector and an imaginary dipole vector. They can be combined as shown in Appendix 7.1 to obtain a "dipole ellipse." The magnetic field generated by such a dipole has a degree of polarization (ratio between minor and major axes of the field ellipse) equal to that of the dipole ellipse.
- Quadrupoles can be combined as follows:

1. Each quadrupole is represented by a vector (see Figure A7.2-3).
2. Each vector is rotated by an angle equal to *-3β*, where *β* is the angle of the vector with an arbitrary reference axis (for instance, the horizontal axis). As a result of this operation, the "normalized" vector is obtained.
3. The normalized vectors are added using traditional rules for vectors. The result of this operation is the "normalized vector sum" representing the combination of the quadrupoles.
4. The vector representing the combination of quadrupoles is obtained by rotating the normalized vector sum by an angle equal to $\frac{3}{2}(2\pi - \delta)$, where δ is the angle of the normalized vector sum with the reference axis.

Derivation of Monopoles, Dipoles, and Quadrupoles From Sets Of Line Currents

Monopoles, dipoles, and multipoles can be readily derived from a set of line currents. Calculations can be performed using Applet EMF-9. Assume that there are n line currents, and the k^{th} line current has a magnitude *I(k)*, and a phase

angle $\phi(k)$, a lateral distance $x(k)$, and a height above ground $h(k)$. The calculation procedure (see the example of Figure A7.2-4) is the following:

1. Choose an arbitrary point as the center of the line current set. The choice of the center will not affect the monopole value, will not affect the dipole value if the monopole is zero, and will not affect the quadrupole value if both monopole and dipole are zero.
2. The monopole is calculated by adding all the currents:

$$\tilde{I}_m = \sum_{k=1}^{n} \tilde{I}_k \qquad \text{A7.2-4}$$

3. If the monopole $\tilde{I}_m$ and the opposite of each current: $-\tilde{I}_1, -\tilde{I}_2, \ldots, -\tilde{I}_n$ are placed at the center, the system is not changed because the sum of the currents placed at the center is zero. This operation, however, creates a monopole $\tilde{I}_m$ and n nonconcentric dipoles: $\vec{D}_1 = \tilde{I}_1 \cdot P_{10}$, $\vec{D}_2 = \tilde{I}_2 \cdot P_{20}$, …, $\vec{D}_n = \tilde{I}_n \cdot P_{n0}$. Each of these dipoles has real and imaginary, vertical and horizontal components.
4. If the dipole sum $\vec{D} = \sum_{k=1}^{n} \vec{D}_k$ is placed at the center, together with the dipoles $-\vec{D}_1, -\vec{D}_2, \ldots, -\vec{D}_n$, the system is not changed because the sum of the dipoles placed at the center is zero. However, a dipole $\vec{D}$ and n nonconcentric quadrupoles: $\vec{Q}_1 = P_{10} \cdot \vec{D}_1 / 2$, $\vec{Q}_2 = P_{20} \cdot \vec{D}_2 / 2$, ……, $\vec{Q}_n = P_{n0} \cdot \vec{D}_n / 2$ are created. Note that the sum of the dipoles is a vectorial sum. Each vector is also a phasor. The resultant dipole $\vec{D}$ will have real and imaginary, vertical and horizontal components from which the dipole ellipse can be calculated.

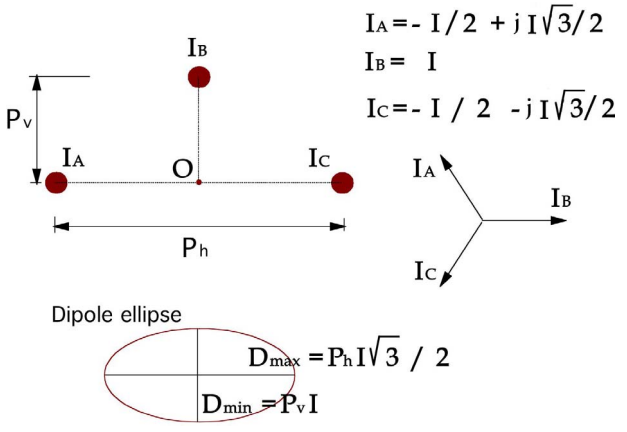


Figure A7.2-4 Example of dipole and quadrupole calculation.

5. Place all the quadrupoles in the center together with their opposites $-\vec{Q}_1, -\vec{Q}_2, \ldots, -\vec{Q}_n$. This operation creates a quadrupole and n nonconcentric fourth-order multipoles. The quadrupole is calculated by adding the n individual quadrupoles according to the multipole addition rules previously illustrated—that is, (1) each quadrupole vector is first rotated by -3β, where β is the angle with the horizontal axis, then (2) the vertical and horizontal components and the quadrupole ellipse are calculated.
6. The operation is repeated up to the desired order of multipole.

For the example of Figure A7.2-4, the previous steps result in the following:

1. The center O is chosen midway between phases A and C.
2. The monopole $I_m = 0$. This is the case for all power lines with balanced currents, such as transmission lines with no zero sequence current and distribution lines in which all the phase unbalance returns into the neutral and none of it flows into the ground.
3. Each conductor forms dipoles as follows:

$$D_{A,horizontal,real} = -\frac{P_h}{2} \cdot \frac{-I}{2} \quad D_{A,vertical,real} = 0$$

$$D_{A,horiz,imaginary} = -\frac{P_h}{2} \cdot \frac{\sqrt{3}}{2} I \quad D_{A,vert,imag} = 0$$

$$D_{B,horizontal,real} = 0 \quad D_{B,vertical,real} = P_v \cdot I$$

$$D_{B,horiz,imag} = 0 \quad D_{B,vert,imag} = 0$$

$$D_{C,horizontal,real} = \frac{P_h}{2} \cdot \frac{-I}{2} \quad D_{C,vertical,real} = 0$$

$$D_{C,\mathbf{horiz},imag} = \frac{P_h}{2} \cdot \frac{-\sqrt{3}}{2} I \quad D_{C,vertical,imaginary} = 0$$

The dipole formed by the line is obtained by adding the dipoles of the three phases:

$$D_{horiz,real} = 0 \quad D_{vert,real} = P_v \cdot I$$

$$D_{horiz,imag} = -\frac{\sqrt{3}}{2} P_h \cdot I \quad D_{vert,imag} = 0$$

The resultant dipole is:

$$D = \sqrt{D_{horiz,real}^2 + D_{vert,real}^2 + D_{horiz,imag}^2 + D_{vert,imag}^2}$$

$$D = \frac{I}{2}\sqrt{4P_v^2 + 3P_h^2}$$

The magnitude of the dipolar field, B_D, at a distance R, is given by Equation A7.2-2, and is:

$$B_D = \frac{2D}{R^2} = \frac{I}{R^2}\sqrt{4P_v^2 + 3P_h^2} \qquad \text{A7.2-5}$$

The real vector is vertical and the imaginary vector is horizontal. Since real and imaginary vectors are perpendicular to each other, they coincide with major and minor axes of the ellipse:

$$D_{MAX} = \frac{\sqrt{3}}{2} P_h \cdot I \quad D_{MIN} = P_v I$$

4. The conductors form the following quadrupoles:

$$Q_{A,real} = (-P_h / 2)(-P_h / 4)(-I / 2) = -\frac{1}{16} P_h^2 I$$

$$Q_{A,imag} = (-P_h / 2)(-P_h / 4)(I\sqrt{3} / 2) = \frac{\sqrt{3}}{16} P_h^2 I$$

The direction of $\vec{Q}_A$ is horizontal. The normalized vector $\vec{Q}_{A,O}$ coincides with $\vec{Q}_A$.

$$Q_{B,real} = P_v(P_v / 2)I = \frac{1}{2} P_v^2 I \quad Q_{B,imag} = 0$$

The vector $\vec{Q}_B$ is vertical, downward. The normalized vector $\vec{Q}_{B,O}$, is equal to $\vec{Q}_B$ but rotated by 270°, thus ending up being in the opposite direction of the horizontal axis.

$$Q_{C,real} = \frac{P_h}{2} \cdot \frac{P_h}{4} \cdot \frac{-I}{2} = -\frac{1}{16} P_h^2 I$$

$$Q_{C,imag} = \frac{P_h}{2} \cdot \frac{P_h}{4} \cdot \frac{-\sqrt{3}}{2} I = -\frac{\sqrt{3}}{16} P_h^2 I$$

The vector $\vec{Q}_C$ is horizontal. The normalized vector $\vec{Q}_{C,O}$ coincides with $\vec{Q}_C$.

Adding the three normalized quadrupole vectors $\vec{Q}_{A,O}$, $\vec{Q}_{B,O}$, and $\vec{Q}_{C,O}$ yields:

$$Q_{horiz,real} = -\frac{4P_v^2 + P_h^2}{8} I \quad Q_{horiz,imag} = 0$$

$$Q_{vert,real} = 0 \quad Q_{vert,imag} = 0$$

$$Q_{MAX} = \frac{\left(4P_v^2 + P_h^2\right)}{8} I \quad Q_{MIN} = 0$$

$$\text{and} \quad Q = \frac{\left(4P_v^2 + P_h^2\right)}{8} I$$

The magnitude of the quadrupolar field, B_Q, at a distance R, is given by Equation A7.2-3, and is:

$$B_Q = \frac{4Q}{R^3} = \frac{I}{2R^3} \cdot (4P_v^2 + P_h^2) \qquad 7.2\text{-}6$$

At practical distances, the field of the quadrupole, given by Equation A7.2-6, is negligible when compared to that of the dipole, given by Equation A7.2-5. In fact, assuming $P_v = P_h / 2$, the dipole field is greater than the quadrupole field at any distance $R > P_h / 2$.

APPENDIX 7.3 STANDARDS AND GUIDELINES

Introduction

Electric and magnetic field exposure guidelines have been established in some countries and by some international organizations. In 2002, however, there was no U.S. federal government health standard or guideline related to power-frequency electric and magnetic fields. Two organizations have developed health guidelines for occupational and public exposure to electric and magnetic fields: the International Commission on Non-Ionizing Radiation Protection (ICNIRP 1998) and the American Conference of Governmental Industrial Hygienists (ACGIH 1998).

Some U.S. states have electric or magnetic field limits for certain voltage classifications of transmission lines within the right-of-way or at the edge of the right-of-way. These standards were established to limit electrical effects rather than from a health risk perspective. Standards or guidelines for exposure to electric and magnetic fields exist in some foreign countries. Some countries have simply adopted or modified international organizational guidelines, while some guidelines seem to have been developed for a particular occupation (such as welders). Many other states and countries have considered setting magnetic field standards. Sweden has established standards related to computers and computer monitors.

State Standards and Recommendations Related to Transmission Lines

There are at least six states in the U.S. that have adopted engineering-based guidelines or standards for transmission-line electric fields; two of these states also have standards for magnetic fields. The purpose of most of these standards is to make the field levels from new power lines similar to the field levels from existing lines or to minimize the potential for spark discharge from large vehicles in the electric fields of 345- to 765-kV transmission lines. Table A7.3-1 presents a summary of these standards (NIEHS and DOE 1995).

In 1989, the California State Department of Education released a school site selection and approval guide (CSDE 1989) that contains recommendations related to electric and magnetic fields. The School Facilities Planning Division has established the following limits for locating school sites near certain high-voltage power transmission-line easements:

- 100 feet from edge of easement for 100- to 110-kV power line
- 150 feet from edge of easement for 220- to 230-kV power line
- 250 feet from edge of easement for 345-kV power line

These limits are based on an electric field strength graph developed by EPRI (EPRI 1987). The guide also recommends that the local electric utility be contacted to determine if any additional power lines or upgrades to existing power lines are planned.

The IEEE developed a standard for measuring power-frequency electric and magnetic fields near power lines. This standard, initially developed in 1979, has been periodically revised and updated through March 1997 (IEEE 1997). The purpose of this standard is to establish uniform procedures for the measurement of power-frequency electric and magnetic fields from overhead power lines. The standard also describes procedures for the calibration of instrumentation used to conduct these measurements. In addition to the transmission-line electric and magnetic field standard, the IEEE has also developed a guide for the measurement of quasi-static magnetic and electric fields (describing various types of survey characteristics, goals, and measurement methods) (IEEE 1997).

Health Guidelines for Electric and Magnetic Fields

Two organizations have developed health guidelines for occupational and public exposure to electric and magnetic fields: the International Commission on Non-Ionizing Radiation Protection (ICNIRP 1998) and the American Conference of Governmental Industrial Hygienists (ACGIH 1998). Tables A7.3-2 and A7.3-3 present a summary of the electric and magnetic field levels of these guidelines respectively.

The ICNIRP established these guidelines to provide protection against known adverse health effects. While the ICNIRP reviewed all of the scientific literature, the adverse effects on humans that were fully verified by a stringent evaluation were short-term, immediate health consequences (such as nerve and muscle stimulation, shocks and burns, etc.) (ICNIRP 1998).

The ACGIH established threshold limit values to which it is believed that nearly all workers may be exposed repeatedly without adverse health effects, based upon an assessment of available data from laboratory research and human exposure studies. The threshold limit values were developed as a guideline to assist in the control of health and safety hazards (ACGIH 1998).

Both the ICNIRP and ACGIH guidelines are based on established adverse health effects (such as burns, shocks, nerve stimulation, etc.). Electric and magnetic field levels as specified in these guidelines, and which would cause

these types of effects, are much higher than typical levels found in residential and most occupational environments.

Table A7.3-1 State Regulations that Limit Field Strengths on Transmission-Line Rights-of-Way

State	Electric Field Limit		Magnetic Field Limit	
	Within the Right-of-Way	Edge of Right-of-Way	Within the Right-of-Way	Edge of Right-of-Way
Florida	8 kV/m for 69- to 230-kV lines 10 kV/m for 500-kV lines	3 kV/m for 69- to 230-kV lines 2 kV/m for 500-kV lines	-------	150 mG for 69- to 230-kV lines (max load) 200 mG for 500-kV lines (max load) 250 mG for double-circuit 500-kV lines (max load)
Minnesota	8 kV/m	-------	-------	-------
Montana	7 kV/m maximum for highway crossings	1 kV/m	-------	-------
New Jersey	-------	3 kV/m	-------	-------
New York	11.8 kV/m 11 kV/m for private road crossings 7 kV/m for highway crossings	1.6 kV/m	-------	200 mG (winter normal conductor rating)
North Dakota	9kV/m	-------	-------	-------
Oregon	9 kV/m	-------	-------	-------

Table A7.3-2 Summary of ICNIRP 50/60 Hz Exposure Guidelines

International Commission on Non-Ionizing Radiation Protection Guidelines		
Exposure (60 Hz)	**Electric Field**	**Magnetic Field**
Occupational: Reference Levels for Time-Varying Fields Current Density for Head and Body	8.333 kV/m (8,333 V/m) 10 mA/m^2 (25 kV/m)	4.167 G (4,167 mG) 10 mA/m^2 (5 G)
General Public: Reference Levels for Time-Varying Fields Current Density for Head and Body	4.167 kV/m (4,167 V/m) 2 mA/m^2 (5 kV/m)	0.833 G (833 mG) 2 mA/m^2 (1 G)

Table A7.3-3 Summary of ACGIH 60 Hz Exposure Guidelines

ACGIH Occupational Threshold Limit Values for Sub-Radio Frequency Fields	
Electric Field	**Magnetic Field**
Occupational exposures should not exceed: 25 kV/m (from 0 Hz to 100 Hz) Prudence dictates the use of protective devices (e.g., suits, gloves, insulation) in fields above 15 kV/m. For workers with cardiac pacemakers, maintain exposure at or below 1 kV/m.	Occupational exposures should not exceed: 60 Hz: 10 G (10,000 mG) 50 Hz: 12 G (12,000 mG) For workers with cardiac pacemakers, the field should not exceed 1 G (1,000 mG).

International Standards

Electric and magnetic field exposure guidelines have been established in some countries and by some international organizations. These standards vary in regulatory power, from guidelines and recommendations to proposed or existing standards to established regulations and orders. Tables A7.3-4 and A7.3-5 present a summary of international electric and magnetic field standards (Maddock 1998).

Table A7.3-4 Summary of International Electric Field Standards – kV/m

	Public	Occupational	Status	Basis
Country:				
Australia [1]	As IRPA	As IRPA	G	C
Austria [2]	5, 10[a]	10 to 30[b]	PS	C
Czechoslovakia [3]		15	S	P, H
Germany – BFE [4]			O, R	C
Exposure area 1[c]		21.32, 30, 30[c]		
Exposure area 2[e]		6.67	O, R	C
Italy [5]	5[f], 10[g,h]		O	H
Poland [6, 7]	1[i], 10	15, 20[k]	O	P, H
Switzerland [8, 9]	5	12.3	G, O[r]	C
UK – NRPB [10]	12	12	G, R	C
USA – (ACGIH 1998)		25	G	C
USSR [11]		5 to 25[m]	O	P, H
Organization:				
CENELEC [12]	10	10 to 30[b]	PS, R	C, P
CEU [13]		6.1, 12.3, 19.6[n]	PD	C
IRPA [14]	5[p], 10[a]	10 to 30[b]	G	C
ICNIRP (ICNIRP 1998)	5	25	G	C, P

Table A7.3-5 Summary of International Magnetic Field Standards – Gauss (rms)

	Public	Occupational	Status	Basis
Country:				
Australia [1]	As IRPA	As IRPA	G	C
Austria [2]	1, 10[a]	5, 50[bm, d]	PS	C
Germany – BFE [4]				
Exposure area 1[c]		13.6, 25.5, 42.4[c, d]	O, R	C
Exposure area 2[e]		4.24	O, R	C
Italy [5]	1[gm], 10[h, jm]		O	H
Poland [15]		5[pm], 50[s, d]	O	C
Switzerland [8, 9]	1	4	G, O[r]	C
UK – NRPB [10]	16	16	G, R	C
USA – (ACGIH 1988)		10	G	C
USSR [16]		18 to 75[km]		W
Organization:				
CENELEC [12]	6.4, 100[c]	16[d]	PS, R	C
CEU [13]		2, 4, 6.4[mm]	PD	C
IRPA [14]	1[nm], 10[a]	5[pm], 50[bm, d]	G	C
ICNIRP (ICNIRP 1998)	1	5	G	C

All at 50 Hz except IRPA (50/60 Hz) and ACGIH (60 Hz). Where levels for 16 2/3 Hz are specified, they are three times those at 50 Hz.

C: Limitation of induced current density.

G: Guideline or recommendation.

H: Health – concern for possible effects.

O: Order, rule, regulation or decree, often with legal force.

P: Perception of spark discharges or tingling sensations.

PD: Proposed Directive regarding the exposure of workers to physical agents (annex IV).

PS: Pre-Standard.

R: Reference or investigation levels – may sometimes be exceeded.

S: Standard, sometimes with legal force.

W: These values seem to have been developed primarily for electric-arc welding.

a: For up to a few hours per day and can be exceeded for a few minutes (up to 20 kV/m for 5 minutes and up to 20 G for 5 minutes in Austria) per day provided precautions are taken to prevent indirect coupling effects (additional body currents in Austria).

b: Depending on the duration (t, hours per work day) of exposure, $t < 80/E$ for E between 10 and 30 kV/m, although the exact interpretation of this formula differs between the three standards that use it.

bm: Maximum exposure duration is 2 hours per work day.

c: 'Exposure area 1' (controlled areas or short-time exposure) – 8, 2 and 1 hours/day respectively.

d: Higher values are given for limbs.

e: 'Exposure area 2' (longer-time exposure or areas where fields are not normally expected).

f: In areas or environments in which it may reasonably be expected that members of the public will spend a significant part of the day.

g: In cases in which exposure may reasonably be assumed to be limited to a few hours per day.

gm: In areas or environments in which it may reasonably be expected that members of the public will spend a significant part of the day.

h: Minimum distances of buildings to overhead power lines are also specified.

j: 1 kV/m applies where there are homes, hospitals, schools and the like.

jm: Minimum distances of buildings to overhead power lines are also specified.

k: 2 hours maximum.

km: Depending on duration of exposure from 8 to 1 hours per work day.

m: Depending on the duration (t, hours per work day) of exposure, $t = 50/E - 2$ for E between 5 and 20 kV/m; between 20 and 25 kV/m, only 10 minutes exposure is permitted.

mm: Various actions would have to be carried out or requirements met before exceeding each of these levels.

n: Various actions would have to be carried out or requirements met before exceeding each of these levels.

nm: For up to 24 hours per day—this restriction applies to open spaces in which members of the general public might reasonably be expected to spend a substantial part of the day, such as recreational areas, meeting grounds, and the like.

p: For up to 24 hours per day—this restriction applies to open spaces in which members of the general public might reasonably be expected to spend a substantial part of the day, such as recreational areas, meeting grounds, and the like.

pm: For whole working day.

r: Public—Federal recommendation (legally binding ordinance being considered); occupational – legally binding protection of workers.

s: Depending on duration (t, hours per work day) of exposure according to D = H2 t, where H is the field strength in kA/m and D = 1.28 (kA/m)2 h (this gives 8 hours at 5 G and 5 minutes at 50 G).

1. "Interim Guidelines on Limits of Exposure to 50/60 Hz Electric and Magnetic Fields (1989)," National Health and Medical Research Council, Canberra, 1989.
2. "Low-Frequency Electric and Magnetic Fields – Permissible Limits of Exposure for the Protection of Persons in the Frequency range 0 Hz to 30 kHz," Austrian Standard S1119, 1994 (in German).
3. "Protection Against the Influence of Electrical Fields in the Closeness of Electrical Transmission Systems for 750 kV and Above," CSN 33 2040, Prague, 1979 (in Czech).
4. "Regulations for Safety and Health Protection in the Workplace for Exposure to Electric, Magnetic, or Electromagnetic Fields," Berufsgenossenschaft der Feinmechanik und Electrotechnik, June 1995 (in German).
5. "Maximum Limits of Exposure to Electric and Magnetic Fields Generated at the Rated Power Frequency (50 Hz) in Indoor and Outdoor Environments," Decree of the Prime Minister, Gazzetta Ufficiale della Repubblica Italiana, N.104, 1992 (in Italian).
6. "Order of the Council of Ministers dates 5 November 1980 in the Matter of Detailed Principles of Protection Against Non-Ionizing Electromagnetic Radiation Harmful to People and the Environment," Law Gazette, no. 25, item 101, pp. 277-278, 17 November 1980 (in Polish).
7. "Effects of Electromagnetic Fields Caused by EHV Overhead Power Lines," *J. Arciszewski and A. Pilatowicz*, CIGRÉ SC36, Warsaw, 1989.
8. "Biological Effects of Electromagnetic Fields, Part 2, Frequency Range 10 Hz to 100 kHz," Report of a Working Group, Environment Text Series No. 214, Swiss Federal Office for Environment, Forests and Countryside (BUWAL), Berne, 1993 (in German).
9. "Limit Values in the Workplace," Schweizerische Unfallversicherungsanstalt (SUVA), Luzern, 1994 (in German).
10. "Board Statement on Restrictions on Human Exposure to Static and Time Varying Electromagnetic Fields and Radiation," Documents of the NRPB, 4, 1-69, 1993.
11. "Electric Fields of Industrial Frequency," USSR Official State Standard, GOST 12.1.002-84, Moscow, 1984 (in Russian).
12. "Human Exposure to Electromagnetic Fields – Low Frequency (0 Hz to 10 kHz)," European Prestandard ENV 50166-1, CENELEC, Brussels, 1995.
13. "Proposal for a Council Directive on the Minimum Health and Safety Requirements Regarding the Exposure of Workers to the Risks Arising from Physical Agents," OJ No. C 230, 3-29, 19.8.94.
14. "Interim Guidelines on Limits of Exposure to 50/60 Hz Electric and Magnetic Fields," International Non-Ionizing Radiation Committee of the International Radiation Protection Association, *Health Physics*, 58, 113-122, 1990.
15. Order of the Ministry of Health, 23 December 1994 (in Polish).
16. "Environmental Health Criteria 69: Magnetic Fields," World Health Organization, Geneva, 1987.

APPENDIX 7.4 MONITOR JITTER CAUSED BY TRANSMISSION-LINE MAGNETIC FIELDS

Magnetic fields at power frequency (50 or 60 Hz) may interfere with the image displayed by computer monitors that utilize a cathode ray tube (CRT). The interference manifests itself as rapidly moving or wiggling characters or images on the display—called "jitter." The level of interference depends not only on the value of the magnetic field but also on the monitor design. Monitor design has changed over time. Some changes, such as the use of longer electron beam paths and lower electron gun acceleration voltages for larger screens, have resulted in monitors that are less immune than older and smaller monitors (Baishiki et al. 1990). Manufacturers of computer monitors have done little to decrease the immunity to external magnetic fields, even fields that are present in common environments. In fact, the most typical situations where complaints about monitor jitter are made do not involve high-voltage transmission lines, but rather proximity to an electrical panel, appliance, or building wires. On the other hand, the steady growth in usage of flat-panel liquid crystal displays (LCD), which are not affected by external magnetic fields, may some day render this issue irrelevant.

Cathode Ray Tubes for Computer Monitors

Cathode ray tubes (see Figure A7.4-1) utilize an electron gun at one end of the tube that sends a beam of electrons to the other end of the tube, consisting of a screen covered by a phosphorous layer. The phosphorous layer emits light when the beam hits the screen. The electron beam is accelerated inside the gun and exits the gun in the axial direction with a velocity dependent on the characteristics of the gun. The electrons maintain their axial velocity inside the vacuum tube, but are accelerated horizontally and vertically by the magnetic field generated by the deflection coils. The beam then proceeds in a straight line until it reaches the phosphorous screen. The deflection coils are controlled in such a way that the electron beams constantly scan the phosphorous screen creating the image on the monitor. The electron beam starts from the upper left-hand edge of the screen, moves horizontally across the screen to the end of the line, and moves back to the beginning of the next line, and so on until the entire screen is traced. The number of times that this process is performed in a second is called the "refresh rate" or "vertical scan rate." Typically, refresh rates for standard monitors range from about 50 to 120 Hz. To the human eye, however, the image on the screen appears steady. Jitter occurs whenever the external power frequency magnetic field is of sufficient strength to change the deflection of the electron beam in an appreciable way. The deflection caused by the power-frequency magnetic field varies in intensity during the cycle, and it is superimposed on the deflection caused by the deflection coils. The result is an apparent movement of the image at a frequency equal to the difference between the refresh rate and the power frequency.

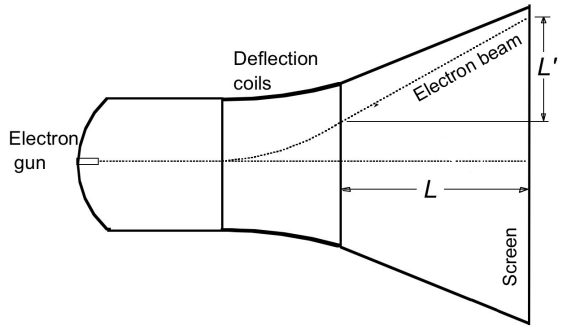


Figure A7.4-1 Cathode ray tube for computer monitor.

Jitter Characteristics

A jitter is characterized by its magnitude, frequency, and mode.

The *magnitude* of the jitter is defined as the maximum displacement (mm) of one character on the screen. The displacement occurs because, under the action of a magnetic field, an electron is accelerated by a force proportional to the magnetic field and to the component of the velocity of the electron orthogonal to the magnetic field. The force is orthogonal both to the field and to the electron velocity. For instance, consider the electrode beam hitting the center of the screen. An external magnetic field horizontal and parallel to the screen will accelerate the electrons in a vertical direction (perpendicular both to the velocity of the electrons and to the magnetic field). The acceleration, a, is proportional to the electron axial velocity, W, and to the magnetic field, b:

$$a = kbW \qquad \text{A7.4-1}$$

This acceleration will create a vertical deflection, d, during the time of flight, T, of the electrons from the area of the deflection coils (which is shielded from the action of an external field) to the screen.

$$T = L / W \qquad \text{A7.4-2}$$

The time T is very short in comparison to the period of the power frequency. Therefore, the field b may be considered constant during the travel time of the electrons.

$$d = \frac{1}{2} a T^2 = \frac{kbL^2}{2W} \qquad \text{A7.4-3}$$

If the frequency of the magnetic field is different from the frequency of vertical scanning, the deflection will be different for each scanning period. The deflection will change at a frequency equal to the difference between magnetic field frequency and scanning frequency. The maximum dis-

placement of a character on the screen (jitter, *J*) is proportional to the peak-to-peak value of the magnetic field.

$$J = \frac{\sqrt{2}kBL^2}{W} \qquad \text{A7.4-4}$$

Where:
B is the rms value of the magnetic field.

When the magnetic field is horizontal and parallel to the screen, the jitter will be approximately the same throughout the screen.

A vertical magnetic field will accelerate the electrons in a horizontal direction. The jitter is still given by Equation A7.4-4, but will occur in a different mode, as described below.

A magnetic field perpendicular to the screen will not deflect the beam that hits the center of the screen, but it will deflect the beam that reaches other points. For a corner of the screen, where the jitter is the largest, the velocity of the beam has a component parallel to the screen given by:

$$W' = L' / T = W\frac{L'}{L} \approx W\frac{G}{2L} \qquad \text{7.4-5}$$

L' is the length traveled by the beam outside the deflection coil in the direction parallel to the screen. This dimension is approximately one-half of the diagonal of the screen, *G*. The jitter is still given by Equation A7.4-4, where *W'* is substituted for *W* and *L'* = *G*/2 is substituted for *L*.

$$J \approx \frac{\sqrt{2}kBGL}{2W} \qquad \text{7.4-6}$$

The maximum jitter for this situation is less than the maximum jitter when the field is parallel to the screen in proportion to the ratio between half the screen diagonal and the length of the tube from the deflection coils to the screen.

In summary, when the magnetic field is parallel to the screen, the jitter sensitivity (mm/mG) is proportional to the square of the length, *L*, of the tube. When the magnetic field is perpendicular to the screen, the jitter is zero in the center and maximum in the corners of the screen where it is proportional to the product of the length of the tube and the half diagonal (*G*/2) and is therefore considerably lower than when the field is parallel to the screen.

Smaller (14- or 15-inch) monitors have jitter sensitivity equal to 0.008 - 0.011 mm/mG for a magnetic field parallel to the screen and 0.004 – 0.008 mm/mG for a magnetic field perpendicular to the screen. The sensitivity increases with monitor size: 17-inch monitors have jitter sensitivity equal to 0.014 - 0.017 mm/mG for a magnetic field parallel to the screen and 0.006 – 0.011 mm/mG for a magnetic field perpendicular to the screen. Large (21-inch) monitors have jitter sensitivity of about 0.019 mm/mG for a magnetic field parallel to the screen and about 0.013 mm/mG for a magnetic field perpendicular to the screen.

The *frequency* of the jitter is equal to the difference between the power frequency and the refresh rate. The same jitter is perceived differently depending on the frequency. When the refresh rate is equal to the power frequency the jitter frequency is zero. In this case, the image is distorted, but it does not move and the distortion is perceived only when it becomes very large. As the jitter frequency increases, the jitter is perceived more easily. The minimum jitter is perceived at a frequency of 4-15 Hz. As the frequency is further increased, jitter perception becomes more difficult. Above 30 Hz, the jitter becomes a blur and can be perceived only by increasing its level.

Jitter may occur in different *modes* depending on the direction of the power frequency field relative to the cathode ray tube. Figure A7.4-2 presents a sample of the magnetic field interference displayed on the monitor when the external magnetic field is perpendicular to the path of the electron beam (parallel to the screen) and is aligned horizontally. In this orientation, the image displacement will result in the vertical squeezing and enlarging of the characters. Figure



Figure A7.4-2 Jitter caused by a power-frequency magnetic field horizontal and parallel to the screen.

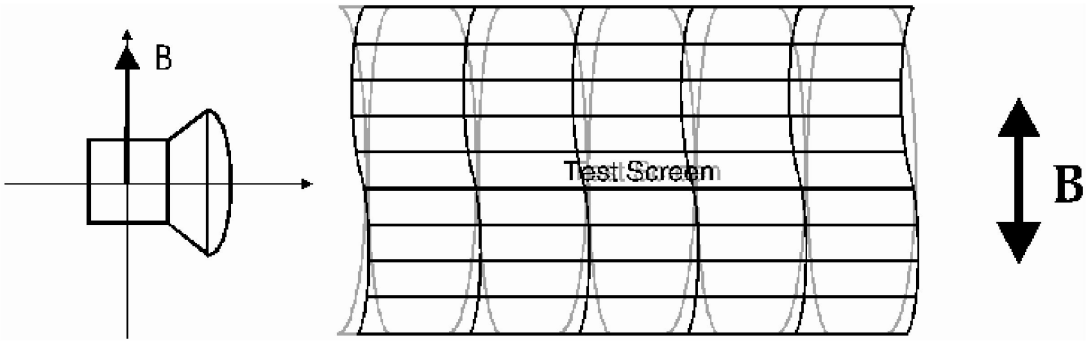


Figure A7.4-3 Jitter caused by a power-frequency magnetic field vertical and parallel to the screen.

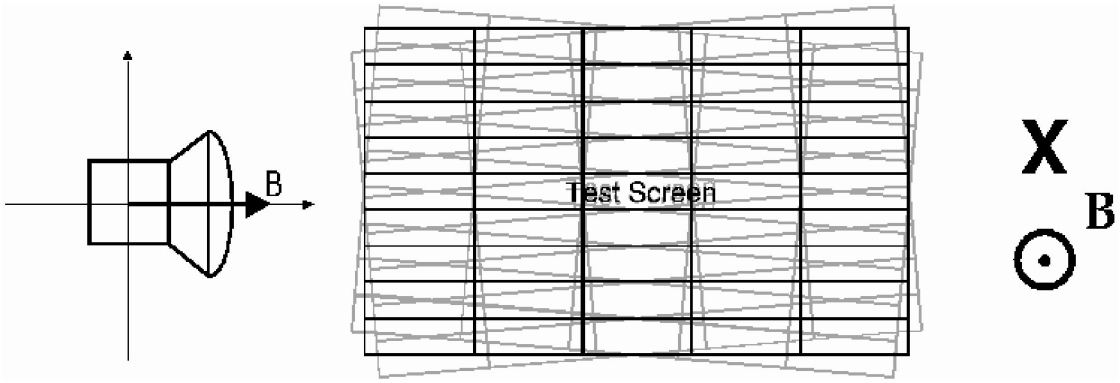


Figure A7.4-4 Jitter caused by a power-frequency magnetic field perpendicular to the screen.

A7.4-3 presents a sample of the magnetic field interference displayed on the monitor whenever the external magnetic field is perpendicular to the path of the electron beam (parallel to the screen) and is aligned vertically. In this orientation, the image displacement will result in a horizontal oscillating motion. Figure A7.4-4 presents a sample of the magnetic field interference displayed on the monitor whenever the external magnetic field is aligned in the direction of the path of the electron beam (perpendicular to the screen). In this orientation, the image will be displaced both horizontally and vertically, and the image will shift in a rotational pattern.

The human sensitivity to jitter is greatest when the magnetic field is vertical and the image has a horizontal oscillating motion (Figure A7.4-3). In this mode, the threshold of observed jitter for a large group of people had a mean value of 0.127 mm, with a standard deviation of 13% when the jitter frequency was 4 Hz, and a mean value of 0.142 mm with a standard deviation of 11% when the jitter frequency was 12 Hz (Banfai et al. 2000). When the magnetic field is horizontal and parallel to the screen (Figure A7.4-2), the vertical squeezing and enlarging of the characters are perceived less readily, and the minimum observed jitter is somewhat larger (20 – 50% larger) (Baishiki and Deno 1987). When the magnetic field is perpendicular to the screen (Figure A7.4-4), the minimum detected jitter is considerably larger.

Other orientations will create a combination of different image displacements, depending upon the angle of orientation between the monitor and the external magnetic field. When the magnetic field is elliptically polarized, as is often the case for transmission lines, more than one mode of jitter will be present.

In summary, the most easily detectable jitter occurs when the field is vertical. The jitter sensitivity (mm/mG), the minimum observable jitter (mm), and the corresponding minimum field (mG) are presented in Table A7.4-1.

Color Monitors

A color monitor has three electron guns, and the three beams converge into three adjacent dots, having the phosphor corresponding to the three basic colors: red, green, and blue. A color picture is made by varying the intensity of each beam and achieving the proper mixture of the basic colors. The color purity of an image is obtained when the proper phosphors are excited. This occurs only when the alignment is properly adjusted and the necessary magnetic field free region is maintained inside the CRT. A power-frequency magnetic field may cause the loss of color purity, which can be seen as mottled or incorrect colors, and color

Table A7.4-1 Minimum Magnetic Field for Perceptible Jitter

Monitor Size	Jitter Sensitivity	Minimum Observable Jitter		Minimum Field for Perceptible Jitter	
		Jitter Frequency = 4 Hz			
		Mean Value	5% of People	Mean Value	5% of People
(inch)	(mm/mG)	(mm)	(mm)	(mG)	(mG)
14–15	0.008 – 0.011	0.127	0.10	11.5 - 16	9 – 12.5
17	0.014 – 0.017	0.127	0.10	7.5 - 9	6 - 7
21	0.019	0.127	0.10	7	5
		Jitter Frequency = 12 Hz			
14–15	0.008 – 0.011	0.142	0.12	13 - 18	11 – 15
17	0.014 – 0.017	0.142	0.12	8.5 - 10	7 – 8.5
21	0.019	0.142	0.12	7.5	6

fringes at edges of characters or graphics. These phenomena are difficult to detect at the magnetic field levels corresponding to the threshold of jitter.

Mitigation Options

A number of options can be employed to reduce or eliminate computer monitor jitter:

- Adjust the monitor refresh rate to be as close to the power frequency as possible. However, the tendency today is to increase the refresh rate well above the power frequency in order to reduce flicker, which is a temporal variation in character or background luminance independent of power frequency magnetic field. When jitter is more objectionable than flicker, making the refresh rate equal to the power frequency may be an acceptable solution.
- Increase the refresh rate so that the jitter frequency becomes greater than 30 Hz. At this frequency the jitter is not perceptible. The image, however, becomes blurred and may create eye fatigue for long-term usage of the monitor. Also the necessary change in refresh rate is not always possible and depends on the graphic card and monitor.
- Adjust the orientation of the monitor to minimize effects. This is possible if the interfering field is horizontal and the monitor can be turned until the field becomes perpendicular to the screen. This is equivalent to a field reduction by a factor of 1.5 – 2.
- Install a magnetic field shield around the monitor. Shields made of high-permeability materials may achieve significant field reduction and are commercially available.
- Use active shielding (Mellik and Garry 1996). This is accomplished with external coils that generate a magnetic field that cancels all or part of the interfering field.
- Replace the CRT monitor with an LCD monitor.

APPENDIX 7.5 MAGNETIC INDUCTION WITH RESISTIVE GROUND RETURN

The material in this appendix is the same contributed by Dr. Don Deno in the last edition of this book (EPRI 1982). The material is not easily found in other publications.

The techniques to calculate the self- and mutual-impedance between two parallel wires above a resistive ground were developed by Carson (Carson 1926). The impedances have the following expressions:

$$Z_{ii} = R_i + j\frac{\omega\mu}{2\pi}\left(\ln\frac{r_{ii}^{'}}{r_{ii}} - j2(P+jQ)\right) \quad \text{A7.5-1}$$

$$Z_{ij} = j\frac{\omega\mu}{2\pi}\left(\ln\frac{r_{ij}^{'}}{r_{ij}} - j2(P+jQ)\right) \quad \text{A7.5-2}$$

Where:

Z_{ii} is the self-impedance of wire *i*.
Z_{ij} is the mutual-impedance between wire *i* and wire *j*.
r_{ii} is the geometric mean radius of wire *i*.
r'_{ii} is the distance between wire *i* and its image.
r_{ij} is the distance between wire *i* and wire *j*.
r'_{ij} is the distance between wire *i* and the image of wire *j*.
P and *Q* are the Carson series.

Despite being based on restrictive assumptions and being often of difficult application, Carson's equations have survived the test of time and have been widely used. A simpler equation for Z_{ij} can be derived from a series expansion by appropriately choosing the truncation point to obtain acceptable engineering accuracy. Careful choice of the truncation point is also important to achieve self-consistent results of the associated magnetic field expressions. All of the Z_{ij} equations, including Carson's, are derived from the quasi-static field theory yielding solutions valid for low frequencies. However, for high frequencies, their accuracy is questionable. The simplified equation is:

$$Z_{ij} = j\frac{\omega\mu}{2\pi}\left[\ln\frac{r_{ij}^{'}}{r_{ij}} - \frac{1}{12}\left(\frac{2}{\gamma r_{ij}^{'}}\right)^4\right] \quad \text{7.5-3}$$

The image depth is modified by adding the term 2/γ, so that:

$r_{ij}^{'} = \sqrt{(x_i - x_j)^2 + (y_i + y_j + 2/\gamma)^2}$ where x_i and x_j are the horizontal coordinates and y_i and y_j are the vertical coordinates of conductors *i* and *j*, respectively.

$$\gamma = \left[j\omega\mu(\sigma + j\omega\varepsilon)\right]^{1/2} \quad \text{7.5-4}$$

σ = the earth conductivity.
ε = the earth permittivity.

And, since

$$\sigma >> \omega\varepsilon \qquad \gamma = \left[j\omega\mu\sigma)\right]^{1/2} = \frac{1}{\delta}(2j)^{1/2} \quad \text{A7.5-5}$$

In the above equation, δ is the skin depth of the earth:

$$\delta = \sqrt{\frac{2}{\sigma\omega\mu}} \quad \text{A7.5-6}$$

When the heights of the wires above earth are much smaller than the skin depth,

$$r_{ij}^{'} \approx \frac{2}{\gamma} = (1-j)\delta \quad \text{A7.5-7}$$

Substitution of Equations A7.5-6 and A7.5-7 into Equation A7.5-3 yields:

$$Z_{ij} = j\frac{\omega\mu}{2\pi}\left[\ln\frac{(1-j)\delta}{r_{ij}} - \frac{1}{12}\right] = \frac{\omega\mu}{8} + j\frac{\omega\mu}{2\pi}\ln\frac{1.31\delta}{r_{ij}} \quad \text{A7.5-8}$$

This simplified equation was reported in the first edition of this book. Equation A7.5.8 may also be written in the form:

$$Z_{ij} = \frac{\omega\mu}{8} + j\frac{\omega\mu}{2\pi}\cdot\frac{1}{2}\left[2\ln\frac{0.79\delta}{r_{ij}} + 1\right] \quad \text{A7.5-9}$$

Equation A7.5-9 was reported when studying voltages induced on buried pipelines (Taflove and Dabkowski 1979a and 1979b).

Derivation of the Conductor's Complex Image

For the purpose of calculating the magnetic field, it is useful to separate the contribution of the conductor and of its image in the earth. The image of the conductor, however, is a difficult concept when dealing with a resistive earth. The derivation of a somewhat intuitive conductor image is illustrated in the following.

The magnetic field $\vec{H}$ may be calculated through consideration of Equations A7.5-10 to A7.5-12.

$$E = Z_{ij} I_i \quad \text{A7.5-10}$$

The electric field is directed parallel to the line.

$$curl\ \vec{E} = -\frac{\partial\vec{B}}{\partial t} = -\mu\frac{\partial\vec{H}}{\partial t} = -j\omega\mu\vec{H} \quad \text{A7.5-11}$$

$$curl\ \vec{E} = \frac{\partial E_z}{\partial y}\vec{u}_x - \frac{\partial E_z}{\partial x}\vec{u}_y \quad \text{A7.5-12}$$

Where $\vec{u}_x$ and $\vec{u}_y$ are the unit vectors along the axes *x* and *y* (see Figure A7.5-1), and E_z is the (only) component of the field, *E*, parallel to the line. Hence,

$$\vec{H} = \frac{1}{-j\omega\mu}\left(\frac{\partial E_z}{\partial y}\vec{u}_x - \frac{\partial E_z}{\partial x}\vec{u}_y\right) \quad \text{A7.5-13}$$

A combination of Equation A7.5-10 and A7.5-3 gives the expression for E_z to enter into Equation A7.5-13. The induced voltage relative to the earth is:

$$E_z = j\frac{\omega\mu}{2\pi} I_i \left[\ln\frac{r'_{ij}}{r_{ij}} - \frac{1}{12}\left(\frac{2}{\gamma r'_{ij}}\right)^4 \right] \qquad \text{A7.5-14}$$

The derivatives $\partial E_z/\partial x$ and $\partial E_z/\partial y$ may be simplified, noting that

$$\frac{\partial}{\partial x_j}\ln\frac{r'_{ij}}{r_{ij}} = -\frac{x_i - x_j}{r'^2_{ij}} + \frac{x_i - x_j}{r^2_{ij}} \qquad \text{A7.5-15}$$

$$\frac{\partial}{\partial y_j}\ln\frac{r'_{ij}}{r_{ij}} = \frac{y_i + y_j + \frac{2}{\gamma}}{r'^2_{ij}} + \frac{y_i - y_j}{r^2_{ij}} \qquad \text{A7.5-16}$$

The contribution of the term $\ln\frac{r'_{ij}}{r_{ij}}$ to $\vec{H}$ calculated with Equation A7.5-13 then becomes

$$\frac{I_i}{2\pi r_{ij}}\left[-\frac{y_i - y_j}{r_{ij}}\vec{u}_x + \frac{x_i - x_j}{r_{ij}}\vec{u}_y\right] - \frac{I_i}{2\pi r'_{ij}}\left[\frac{y_i + y_j + \frac{2}{\gamma}}{r'_{ij}}\vec{u}_x + \frac{x_i - x_j}{r'_{ij}}\vec{u}_y\right] \qquad \text{A7.5-17}$$

This expression may be simplified by identifying the unit vector associated with the distance between observation at conductor *j* and line *i*:

$$\vec{\Phi}_{ij} = -\frac{y_i - y_j}{r_{ij}}\vec{u}_x + \frac{x_i - x_j}{r_{ij}}\vec{u}_y \qquad \text{A7.5-18}$$

and the unit vector associated with the distance between the complex image of conductor *j* and line *i*:

$$\vec{\Phi}'_{ij} = \frac{y_i + y_j + \frac{2}{\gamma}}{r'_{ij}}\vec{u}_x + \frac{x_i - x_j}{r'_{ij}}\vec{u}_y \qquad \text{A7.5-19}$$

The corrective term in Equation A7.5-14 is taken into account, noting that

$$\frac{\partial}{\partial x_j} r'^{-4}_{ij} = -4r'^{-5}_{ij}\frac{\partial}{\partial x_j} r'_{ij} = \frac{4(x_i - x_j)}{r'^6_{ij}} \qquad \text{A7.5-20}$$

and similarly

$$\frac{\partial}{\partial y_j} r'^{-4}_{ij} = -\frac{4\left(y_i + y_j + \frac{2}{\gamma}\right)}{r^i_{ij}{}^6} \qquad \text{A7.5-21}$$

The corrective term contribution to $\vec{H}$ becomes

$$\frac{I}{2\pi r'_{ij}}\cdot\frac{1}{3}\left(\frac{2}{\gamma r'_{ij}}\right)^4 \vec{\Phi}'_{ij} \qquad \text{A7.5-22}$$

Combining Equations A7.5-17 and A7.5-22, a simple expression for the field at conductor *j* due to the current of conductor *i* is obtained:

$$\vec{H}_{ij} = \frac{I_i}{2\pi r_{ij}}\vec{\Phi}_{ij} - \frac{I}{2\pi r'_{ij}}\left[1 - \frac{1}{3}\left(\frac{2}{\gamma r'_{ij}}\right)^4\right]\vec{\Phi}'_{ij} \qquad \text{A7.5-23}$$

Equation A7.5-23 is of intuitive appeal because it separates the conductor from its complex image and identifies a relatively simple correction term. A geometric description of the complex image is shown in Figure A7.5-1.

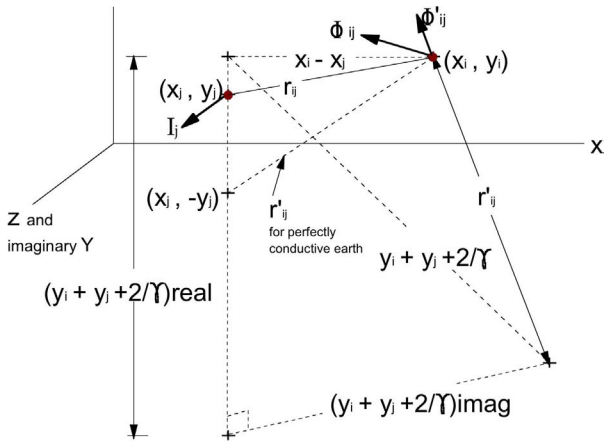


Figure A7.5-1 Coordinate system for complex distance mutual-impedance with earth return.

APPENDIX 7.6 ELECTRIC FIELD CALCULATIONS FOR THREE-DIMENSIONAL GEOMETRY

The application of two-dimensional methods for the calculation of the electric fields (see Section 7.3) is made possible by simplifying assumptions: parallel, infinitely long conductors, over a perfectly flat earth. In many cases, these assumptions lead to acceptable accuracy. Practical situations, however, can be properly described only in three dimensions. Even a relatively simple feature, such as the line sag, requires a three-dimensional approach for the calculation of the electric field away from midspan. A three-dimensional approach is absolutely essential when dealing with complex arrangements of conductors, such as in a substation, or to account for the presence of conductive objects.

Charge Simulation Method Using Cylindrical Segments

The charge simulation method using cylindrical segments is particularly suited to the calculation of the electric field and the space potential for three-dimensional geometry when objects can be reasonably well simulated with sets of cylindrical segments (Augugliaro et al. 1979; Liu and Zaffanella 1996). Examples include: substation bus arrangements, power lines with sag, power lines with angles, line transposition spans, lines crossing each other, and situations in which the presence of poles and lattice towers must be considered. Calculations can be made also for objects with non-cylindrical geometry (e.g., vehicles, houses) provided these objects can be reasonably well simulated with a set of cylindrical segments. Calculations using the algorithms presented in this appendix can be made with Applet EMF-4, "Transmission Line Electric Field – 3D."

The electrical charges on each cylindrical segment are simulated by a line charge with a density (coulomb/meter) linearly varying from one end of the segment to the other, as shown in Equation A7.6-1 and Figure A7.6-1.

$$q(x) = Q + DQ \cdot \frac{x - a - L/2}{L} \qquad \text{A7.6-1}$$

The potential at a point P in space (see Figure A7.6-2) due to the charge distributed on the segment BE is given by Equation A7.6-2.

$$4\pi\varepsilon V_P = \int_a^{a+L} \frac{q(x)}{r} dx = Q \cdot \ln \frac{\delta_1 + \delta_2 + L}{\delta_1 + \delta_2 - L} + DQ \cdot \left[\frac{\delta_1 - \delta_2}{L} - \frac{\delta_1^2 - \delta_2^2}{2L^2} \cdot \ln \frac{\delta_1 + \delta_2 + L}{\delta_1 + \delta_2 - L} \right] \qquad \text{A7.6-2}$$

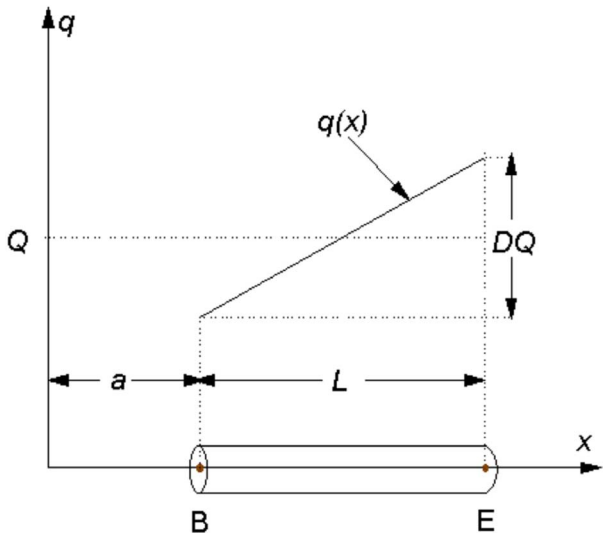


Figure A7.6-1 Charge density linearly distributed on a cylindrical segment.

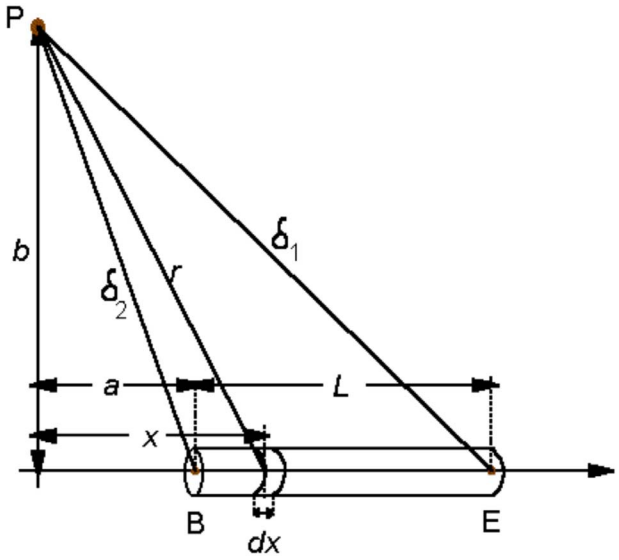


Figure A7.6-2 Geometry of a charged segment for electric field calculation at point P.

If the segment BE is above a ground plane (see Figure A7.6-3), its image also contributes to the potential of P, given by Equation A7.6-3.

The parameters A and B represent the potential coefficients relating the charge density quantities Q and DQ to the potential at point P. Given N segments with known voltages, the problem consists of finding Q and DQ. A system of 2N equations must be written.

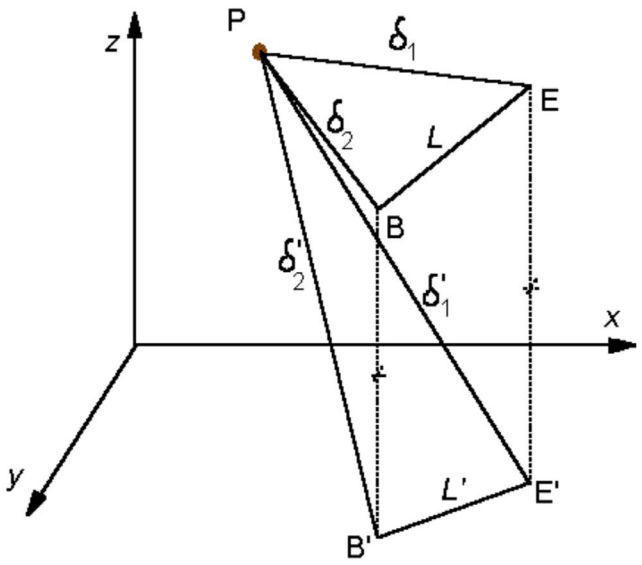


Figure A7.6-3 Charged segment, BE, and its image (B'E') below the ground plane.

Consider the geometry of Figure A7.6-4. The coordinates of its beginning and end points, B and E, its radius, R, and its voltage, V, characterize each segment. The problem consists of determining the charge density parameters (Q and DQ) that would cause the given voltages on the surfaces of the segments. Since the charge density distributions have been characterized only by two parameters, only two potential points are needed to provide a sufficient number of equations. Accurate results are obtained if the potential points, F (first) and S (second), are placed at the 1/3 and 2/3 points of each segment. The potentials are calculated as the average potential on the circumference of the conductor at F and S. The average potential on the surface of one segment caused by charges on other segments is practically the same as that of the center.

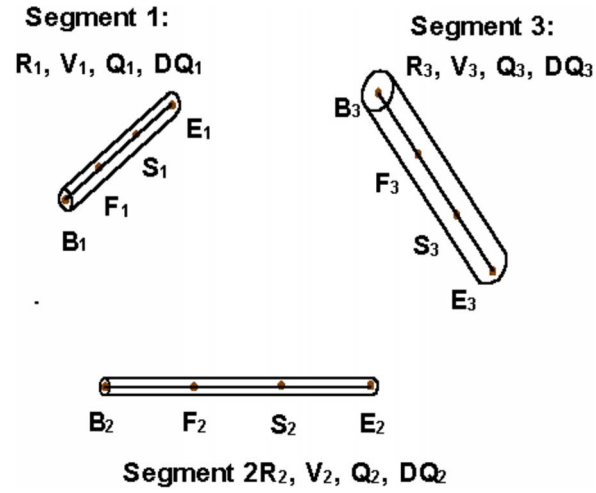


Figure A7.6-4 Voltages, charge densities, and potential points in a system of three charged cylindrical segments.

For instance, the mutual coefficients between charge density Q_2 on segment 2 and the first potential point of segment 1 is found by calculating the potential at point F_1, caused by the charge Q_2:

$$4\pi\varepsilon V_1 = Q_2 \cdot AF_{12} \qquad \text{A7.6-4}$$

Where:

AF_{12} is the coefficient of Equation A7.6-3 calculated between point F_1 and segment 2.

Self-potential coefficients are the ratios between charge density parameters and the potentials at the first and second potential points of the same segment. The potentials are calculated on the circumference. For instance, the potential at point F_1 on segment 1 caused by charge distribution Q_1 on segment 1 is derived from:

$$4\pi\varepsilon V_1 = Q_1 \cdot AF_{11} \qquad \text{A7.6-5}$$

AF_{11} is the coefficient A of Equation A7.6-3.

The parameters δ_1 and δ_2 are the distances between the circumference at F_1 and the beginning and end points of segment 1, as shown in Equations A7.6-6 and A7.6-7.

$$\delta_1 = \sqrt{(L/3)^2 + R^2} \qquad \text{A7.6-6}$$

$$\delta_2 = \sqrt{(2L/3)^2 + R^2} \qquad \text{A7.6-7}$$

Similar expressions hold for the potential coefficient B of Equation A7.6-3.

$$4\pi\varepsilon V_P = Q \cdot \ln\frac{\delta_1+\delta_2+L}{\delta_1+\delta_2-L} \cdot \ln\frac{\delta_1'+\delta_2'-L}{\delta_1'+\delta_2'+L} + DQ \cdot$$

$$\left[\frac{\delta_1-\delta_2}{L} - \frac{\delta_1'-\delta_2'}{L} + \frac{\delta_1'^2-\delta_2'^2}{2L^2} \cdot \ln\frac{\delta_1'+\delta_2'+L}{\delta_1'+\delta_2'-L} - \frac{\delta_1^2-\delta_2^2}{2L^2} \cdot \ln\frac{\delta_1+\delta_2+L}{\delta_1+\delta_2-L}\right] \qquad \text{A7.6-3}$$

$$= Q \cdot A + DQ \cdot B$$

The potential equations written at all points F and S appear as system (A7.6-8), which is written in matrix notation.

$$\begin{aligned} 4\pi\varepsilon\left[V\right] &= \left[AF\right]\cdot\left[Q\right]+\left[BF\right]\cdot\left[DQ\right] \\ 4\pi\varepsilon\left[V\right] &= \left[AS\right]\cdot\left[Q\right]+\left[BS\right]\cdot\left[DQ\right] \end{aligned} \qquad \text{A7.6-8}$$

The solutions of system (A7.6.8) are shown in Equations A7.6-9 and A7.6-10:

$$\begin{aligned} \frac{1}{4\pi\varepsilon}\left[DQ\right] = &\left[\left[BS\right]-\left[AS\right]\left[AF\right]^{-1}\cdot\left[BF\right]\right]^{-1} \\ &\cdot\left[\left[1\right]-\left[AS\right]\left[AF\right]^{-1}\right]\cdot\left[V\right] \end{aligned} \qquad \text{A7.6-9}$$

$$\frac{1}{4\pi\varepsilon}\left[Q\right] = \left[AF\right]^{-1}\cdot\left[V\right]-\left[AF\right]^{-1}\cdot\left[BF\right]\cdot\left[DQ\right]\cdot\frac{1}{4\pi\varepsilon} \qquad \text{A7.6-10}$$

Once all the charges are known, potential and electric field can be evaluated at any point. The potential is calculated using Equation A7.6-3. The electric field components are calculated along two directions, one (E') orthogonal and one (E") parallel to the charged segment (see Figure A7.6-5).

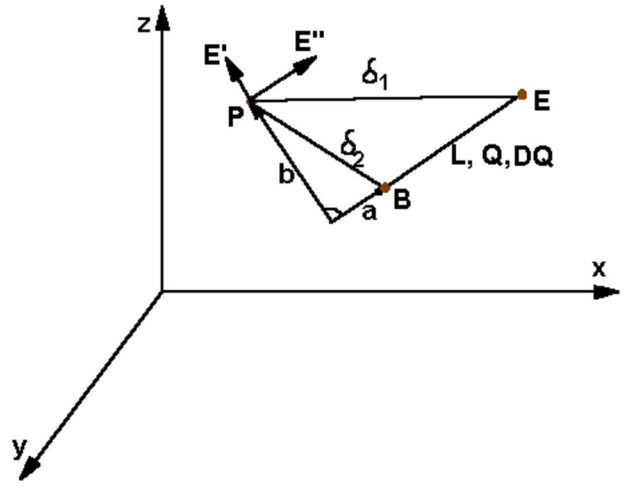


Figure A7.6-5 Electric field and its components at point P due to the charge density distributions Q and DQ on segment BE.

For a segment characterized by a length L and charge density quantities Q and DQ, the values of E' and E'' are given by Equations A7.6-11 and A7.6-12, respectively.

$$\begin{aligned} 4\pi\varepsilon E' = &\left[Q - DQ\frac{\delta_1^2-\delta_2^2}{2L^2}\right]\cdot 2L\cdot b \\ &\cdot\frac{\delta_1+\delta_2}{\delta_1\cdot\delta_2\cdot(\delta_1+\delta_2-L)\cdot(\delta_1+\delta_2+L)} \\ &-\frac{DQ}{L}\left[\frac{b}{\delta_1}-\frac{b}{\delta_2}\right] \end{aligned} \qquad \text{A7.6-11}$$

$$\begin{aligned} 4\pi\varepsilon E'' = &\left[Q - DQ\frac{\delta_1^2-\delta_2^2}{2L^2}\right]\cdot\left[\frac{1}{\delta_1}-\frac{1}{\delta_2}\right] \\ &-\frac{DQ}{L}\cdot\ln\frac{\delta_1+\delta_2+L}{\delta_1+\delta_2-L} \\ &-DQ\frac{(\delta_1+\delta_2)\cdot\left[(\delta_1-\delta_2)^2-L^2\right]}{2\cdot\delta_1\cdot\delta_2\cdot L^2} \end{aligned} \qquad \text{A7.6-12}$$

The components of E' and E'' along the x-axis are evaluated using Equations A7.6-13 and A7.6-14.

$$E'_x = E'\frac{X_B+\frac{a}{L}(X_E-X_B)-X_P}{b} \qquad \text{A7.6-13}$$

$$E''_x = E''\frac{X_E-X_B}{L} \qquad \text{A7.6-14}$$

The field component along the x-axis, caused by the segment is $E_{x,s} = E'_x + E''_x$. Similar expressions apply for the field components, E_y and E_z, along the y and z-axes.

The same operation must be performed to find the field components, $E_{x,image}$, $E_{y,image}$, $E_{z,image}$, caused by the mirror image of the segment below ground, with charge quantities $-Q$ and $-DQ$. Finally, the contributions of all the segments must be added:

$$E_x = \sum_{i=1}^{N}(E_{x,s}+E_{x,image}) \qquad \text{A7.6-15}$$

The space potential at point P caused by the charges on the segment shown in Figure A7.6-5 is given by:

$$\begin{aligned} V_s = &Q\cdot\ln\frac{\delta_1+\delta_2+L}{\delta_1+\delta_2-L} \\ &+DQ\cdot\left[\frac{\delta_1+\delta_2}{L}-\frac{\delta_1^2+\delta_2^2}{2L^2}\cdot\ln\frac{\delta_1+\delta_2+L}{\delta_1+\delta_2-L}\right] \end{aligned} \qquad \text{A7.6-16}$$

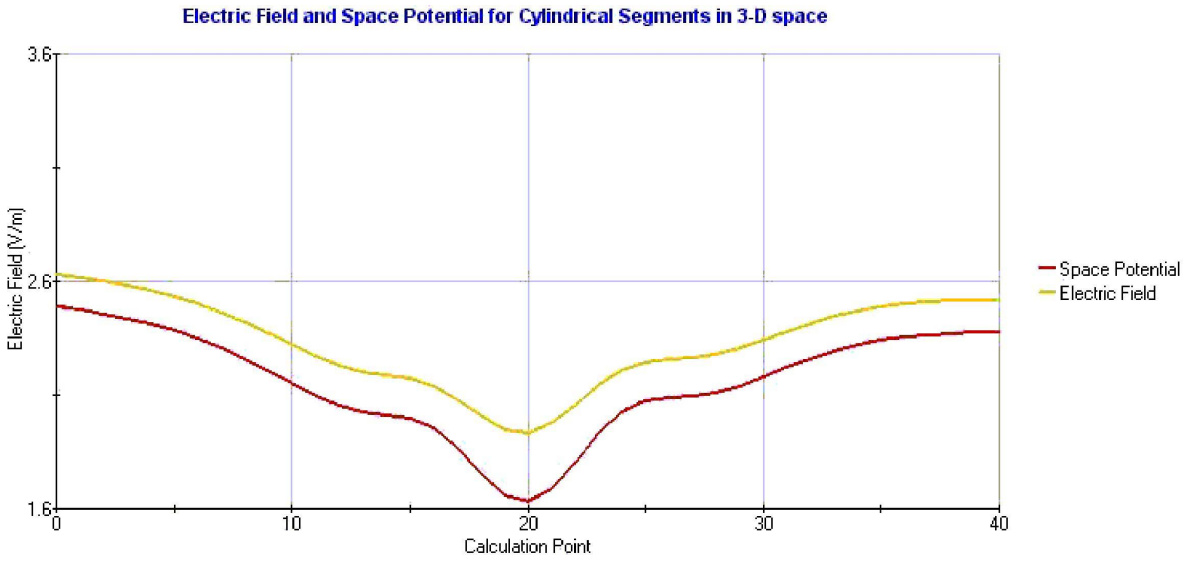


Figure A7.6-7 Electric field and space potential for example of Figure A7.6-6 calculated with Applet EMF-4.

The same operation must be performed to find the space potential, V_{image}, at P, caused by the image of the segment, with charge quantities $-Q$ and $-DQ$. Finally, the contributions of all segments must be added:

$$V = \sum_{i=1}^{N} (V_s + V_{image}) \qquad \text{A7.6-17}$$

If the voltages have different phase angles, such as for a three-phase line, calculations must be performed twice, once for the real parts and once for the imaginary parts. The potential at a point is a phasor defined by a real and an imaginary component or a magnitude and a phase angle:

$$V_P = V_{P,real} + jV_{P,imaginary} = V_P \cdot \cos(\omega t + \alpha) \qquad \text{A7.6-18}$$

The electric field is characterized by the major and minor axes of the field ellipse, the calculation of which is discussed in Appendix A7.1 (see also Applet EMF-1). Calculation of electric fields using the method described in this section can be made using Applet EMF-4, "Transmission Line Electric Field – 3D." The following is an example of electric field calculation using the method described in this appendix. The geometry is illustrated in Figure A7.6-6. A 115-kV line crosses a 500-kV line at a right angle. Each catenary between the towers of Figure A7.6-6 is simulated with seven segments. Past the points of attachment, a long segment parallel to ground simulates each conductor. Because the crossing does not occur close to a tower, the presence of the tower is neglected. In total, the geometry consists of 54 cylindrical segments. Using Applet EMF-4 requires inputting for each catenary the conductor diameter, the magnitude and phase angle of the voltage to ground, the x, y, and z coordinates of the attachment points at the towers, and the sag at midspan. The input data for all other conductor segments are the same as for a catenary, except that the sag is zero. In addition, the points where the field is calculated must be specified. In this example, the field is calculated on the line from point F (-20,0,1) to point L (20,0,1).

The results are shown in Figure A7.6-7. Solution of this problem using the finite element method would have been extremely laborious and practically impossible.

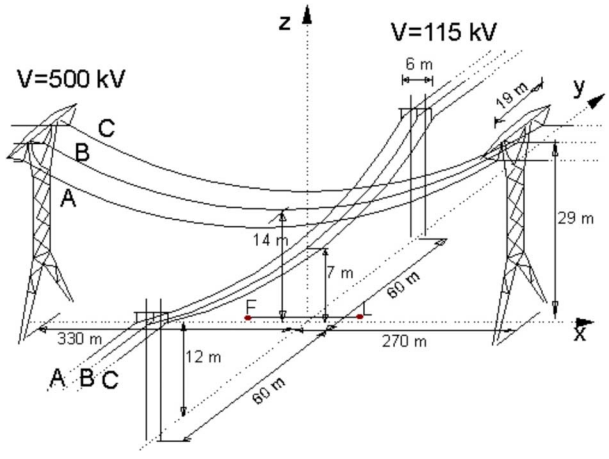


Figure A7.6-6 Geometry requiring electric field calculations with charge simulation method using cylindrical segments (Applet EMF-4).

REFERENCES

ACGIH. 1998. "Threshold Limit Values for Chemical Substances and Physical Agents," American Conference of Governmental Industrial Hygienists (ACGIH), Cincinnati, ISBN 1-88-2417-23-2.

Ahlbom, A., N. Day, M. Feychting, E. Roman, J. Skinner, J. Dockerrty, M. Linet, M. McBride, J. Michaelis, J.H. Olsen, T. Tynes, and P.K. Verkasalo. 2000. "A Pooled Analysis of Magnetic Field and Childhood Leukemia." *British Journal of Cancer.* 83: 692-698.

AMA. 1994. American Medical Association; Council of Scientific Affairs. "Effects of Electric and Magnetic Fields." Chicago: AMA. December.

Augugliaro, A. 1979. "A Computer Aided Analysis of Electric Fields of Overhead Conductors." 3rd International Symposium on High Voltage Engineering. Milan. August.

Baishiki, R.S. and D.W. Deno. 1987. "Interference from 60 Hz Electric and Magnetic Fields on Personal Computers." *IEEE PWRD-2*. pp. 558-563. April.

Baishiki, R.S., G.B. Johnson, G.B. Rauch, and L.E. Zaffanella. 1990. "Studies of Power System Magnetic Fields: Characterization of Sources in Residential Environments, Measurements of Exposure, Influence on Computer Screens." CIGRÉ.

Banfai, B., G.G. Karady, C.J. Kim, and K.B. Maracas. 2000. "Magnetic Field Effects on CRT Computer Monitors." *IEEE PWRD-15*. pp. 307-312. January.

Banks, R.S. and T. Vinh. 1984. "An Assessment of the 5 mA 60 Hz Contact Current Safety Level." *IEEE PAS-103*. pp. 3608-3614. December.

Bridges, J.E. 1978. "Environmental Considerations Concerning the Biological Effects of Power Frequency (50 or 60 Hz) Electric Fields." *IEEE PAS-97*. pp. 19-27. January/February.

Carson, J.R. 1926. "Wave Propagation in Overhead Wires with Ground Return." *Bell Syst. Tech. Jour.* Vol. 5. pp. 539-554.

CSDE. 1989. "School Site Selection and Approval Guide." California State Department of Education. Sacramento, CA.

Dabkowski, J. 1981. "The Calculation of Magnetic Coupling from Overhead Transmission Lines." *IEEE PAS-100*. pp. 3850-3860. August.

Dabkowski, J. and A. Taflove. 1979. "Prediction Method for Buried Pipeline Voltages Due to 60 Hz AC Inductive Coupling. Part II: Field Test Verification." *IEEE PAS-98*. pp. 788-794. May/June.

Dalziel, C.F. 1954. "Threshold of Perception Currents." *Electrical Engineering*. Vol. 73. pp. 625-630.

Dalziel, C.F. 1960. "Threshold 60-Cycle Fibrillating Currents." *AIEE Trans*. Vol.79. Part III. pp. 667-673. October.

Dalziel, C.F. 1968. "Re-evaluation of Lethal Electric Currents." *IEEE Transactions on Industry and General Applications*. No 4. pp. 467-476. October.

Dalziel, C.F. 1972. "Electric Shock Hazard." *IEEE Spectrum*. pp. 41-50. May.

Dalziel, C.F., E. Ogden, and C.E. Abbott. 1943. "Effect of Frequency on Let-Go Currents." *AIEE Transactions-62*. pp. 745-750. December.

Dalziel, C.F. and F.P. Massoglia. 1956. "Let-Go Currents and Voltages." *AIEE Transactions Part II Application and Industry-75*. pp. 49-55. May.

Dalziel, C.F. and W.R. Lee. 1969. "Lethal Electric Currents." *IEEE Spectrum*. pp. 44-50. February.

Dawson, T.W., K. Caputa, and M.A. Stuchly. 1998. "High-Resolution Organ Dosimetry for Human Exposure to Low-Frequency Electric Fields." *IEEE PWRD-13.* pp. 366-373. April.

Deno, D.W. 1975. "Electrostatic Effect Induction Formulae." *IEEE PAS-94*. pp. 1524-1536. September/October.

Deno, D.W. 1976. "Transmission Line Fields." *IEEE PAS-95*. pp. 1600-1611. September/October.

Deno, D.W. 1977a. "UHV Transmission Line Electric Field Reduction with a Set of Horizontal Wires." *IEEE PAS-96*. pp. 1507-1516. September/October.

Deno, D.W. 1977b. "Currents Induced in the Human Body by High Voltage Transmission Line Electric Field – Measurements and Calculation of Distribution and Dose." *IEEE PAS-96*. pp. 1517-1527. September/October.

Deno, D. W. and J. M Silva. 1985. "Probability and Consequence of Gasoline Ignition Under HVAC Transmission Lines." *IEEE Transactions on Power Apparatus and Systems.* Vol. PAS-104. No. 11. November. pp. 3181-3188.

Deno, D.W., L.E. Zaffanella, and M. Silva. 1987. "Transmission Line Electric Field – Shielding by Objects." *IEEE PWRD-2.* pp. 269-280. January.

DiPlacido, J., C.H. Shih, and B.J. Ware. 1978. "Analysis of the Proximity Effects in Electric Field Measurements." *IEEE PAS-97*. pp. 2167-2177. November/December.

Dockerty J.D., J.M. Elwood, D.C. Skegg, and G.P. Herbison. 1998. "Electromagnetic Field Exposures and Childhood Cancer in New Zealand." *Cancer Causes and Control.* 9:299-309.

EPRI. 1982. *Transmission Line Reference Book – 345 kV and Above*. Second Edition. Electric Power Research Institute. Palo Alto, California.

EPRI. 1985. "Utility Corridor Design: Transmission Lines, Railroads, and Pipelines. Engineering Analysis and Site Study." EPRI EL-4147. Project 1902-2. Electric Power Research Institute. Palo Alto, California.

EPRI. 1987. "Background on Electromagnetic Fields and Human Health." Electric Power Research Institute. February.

EPRI. 1999. *Electric and Magnetic Field Management Reference Book*. First Edition. EPRI. Palo Alto, California. TR-114200.

Feychting, M. and A. Ahlbom. 1993. "Magnetic Field and Cancer in Children Residing Near Swedish High-Voltage Power Lines." *American Journal of Epidemiology.* 138: 467-481.

Frazier, M., H. Robertson, J. Dunlap, P. Thomas, and T. Morgan. 1986. "Transmission Line, Railroad and Pipeline Common Corridor Study." *IEEE PWRD-1*. pp. 294-300. July.

Frix, W.M., G.G. Karady, and B.A. Venetz. 1994. "Comparison of Calibration Systems for Magnetic Field Measurement Equipment." *IEEE PWRD-9*. pp. 100-109.

Granger, J.J. and W.D. Stevenson. 1994. *Power System Analysis*. McGraw-Hill.

Greenland, S., A.R. Sheppard, W.T. Kaune, C. Poole, and M.A. Kelsh. 2000. "A Pooled Analysis of Magnetic Fields, Wire Codes and Childhood Leukemia. EMF Study Group." *Epidemiology.* 11: 624-634.

ICNIRP. 1998. "Guidelines for Limiting Exposure to Time-Varying Electric, Magnetic, and Electromagnetic Fields (Up to 300 GHz)." International Commission on Non-Ionizing Radiation Protection (ICNIRP). *Health Physics*. 74: 494-522.

IEEE Working Group. 1978. "Electric and Magnetic Field Coupling from High Voltage AC Power Transmission Lines – Classification of Short-Term Effects on People." *IEEE PAS-97*. pp. 2243-2252. November/December.

IEEE. 1994a. "Standard Procedures for Measurements of Power Frequency Electric and Magnetic Fields from AC Power Lines." ANSI/IEEE Std. 644-1994. New York, NY.

IEEE. 1994b. "Recommended Practices for Instrumentation: Specifications for Magnetic Flux Density and Electric Field Strength Meters. 10 Hz to 3 kHz." IEEE Std. 1308-1994.

IEEE. 1997. "IEEE Guide for the Measurement of Quasi-Static Magnetic and Electric Fields." IEEE Standard 1460-1996. IEEE Standards Coordinating Committee on Non-Ionizing Radiation (SCC28). March.

Jaffa, K.C. 1981. "Magnetic Field Induction from Overhead Transmission and Distribution Power Lines on Parallel Fences." *IEEE PAS-100*. pp. 1624-1636, April.

Jaffa, K.C. and J.B. Stewart. 1981. "Magnetic Field Induction from Overhead Transmission and Distribution Power Lines on Buried Irrigation Pipelines." *IEEE PAS-100*. pp. 990-1000, March.

Jonsson, U., A. Larsson, and J-O. Sjodin. 1994. "Optimized Reduction of the Magnetic Field Near Swedish 400 kV Lines by Advanced Control of Shield Wire Currents. Test Results and Economic Evaluation." *IEEE PWRD-9*. pp. 961-969, April.

Karady, G.G. and S. Devarajan. 2001. "Algorithm to Predict Dry-Band Arcing in Fiber-Optic Cables." *IEEE PWRD-16*. pp. 286-291, April.

Kaune, W.T. and L.E. Zaffanella. 1992. "Analysis of Magnetic Fields Produced far from Electric Power Lines." *IEEE PWRD-7*. pp. 2082-2091, October.

Knave, B. 1980. "Long-Term Exposure to Electric Fields. A Cross-Sectional Epidemiological Investigation of Occupationally Exposed Workers in High Voltage Substations." *Electra*. No 65. June.

Korobkova, V.P., Y.A. Morozov, M.D. Stolarov, and Y.A. Yakub.1972. "Influence of the Electric Field in 500 and 750 kV Switchyards on Maintenance Staff and Means for Its Protection." Proceedings of the International Conference on Large High-Voltage Electric Systems, August. 28-September. 6. CIGRÉ. Paris.

Kouwenhoven, W.B., O.R. Langworthy, M.L. Singewald, and G.G. Knickerbocker. 1967. "Medical Evaluation of Men Working in AC Electric Fields." *IEEE PAS-86*. pp. 506-511. April.

Lewis, B. and G. von Elbe. 1951. "Combustion, Flames, and Explosions of Gases." New York: Academic Press, Inc.

Linet, M.S., E.E. Hatch, R.A. Kleinerman, L.L. Robison, W.T. Kaune, D.R. Friedman, R.K. Severson, C.M. Haines, C.T. Hartsock, S. Niwa, S. Wacholder, and R.E. Tarone. 1997. "Residential Exposure to Magnetic Fields and Acute Lymphoblastic Leukemia in Children." *New England Journal of Medicine.* 337:1-7.

Liu, Y. and L.E. Zaffanella. 1996. "Calculation of Electric Field and Audible Noise from Transmission Lines with Non-Parallel Conductors." *IEEE PWRD-11*. pp. 1492-1497, July.

London, S.J., D.C. Thomas, J.D. Bohman, E. Sobel, T.C. Cheng, and J.M. Peters. 1991. "Exposure to Residential Electric and Magnetic Fields and Risk of Childhood Leukemia." *American Journal of Epidemiology.* 134: 923-937.

Lusk, G.E. 1975. "Reducing Fires on EHV Wood Poles." *Electrical World.* September 15.

Lusk, G.E. and S.T. Mak. 1976. "EHV Wood Pole Fires: Their Cause and Potential Cures." *IEEE PAS-95*. pp. 621-629. March/April.

Maddock, B.J. 1998. "A Summary of Standards for Human Exposure to Electric and Magnetic Fields at Power Frequencies." Joint Working Group 36.01/06. *Electra*. No. 179: 51–65. August.

Maruvada, P.S. and N. Hylten-Cavallius. 1975. "Capacitance Calculations for Some Basic High Voltage Electrode Configurations." *IEEE PAS-94*. pp. 1708-1713. September/October.

McBride, M.L., R.P. Gallagher, G. Theriault, B.G. Armstrong, S. Tamaro, J.J. Spinelli, J.E. Deadman, B. Fincham, D. Robson, and W. Choi. 1999. "Power-Frequency Electric and Magnetic Fields and Risk of Childhood Leukemia in Canada." *American Journal of Epidemiology.* 149: 831-842.

McKee, G.W., D.P. Knievel, D.T. Poznaniak, and J.W. Bankowske. 1978. "Effect of 60-Hz High Intensity Electric Fields on Living Plants." *IEEE PAS-97*. pp. 1177-1181, July/August.

McKinney, A.H. 1962. "Electrical Ignition of Combustible Atmospheres." *ISA Transactions*. Vol.1. No. 1. pp. 45-64. January.

Mellik, Garry. 1996. "Magnetic Field Mitigation to Reduce VDU Interference." Electricity Supply Association of Australia Limited. July.

Michaelis, J., J. Shuz, R. Meinert, E. Zemann, J.P. Grigat, P. Kaatsch, U. Kaletsch, A. Meisner, K. Brinkmann, W. Kalkner, and H. Karner. 1998. "Combined Risk Estimates for Two German Population-Based Case-Control Studies of Residential Magnetic Field and Childhood Leukemia." *Epidemiology.* 9: 92-94.

NESC. 1997. National Electric Safety Code. ANSI C2-1997.

NIEHS and DOE. 1995. "Questions and Answers About Electric and Magnetic Fields Associated with the Use of Electric Power." National Institute of Environmental Health Studies (NIEHS) and U.S. Department of Energy (DOE). DOE/EE-0040. U.S. Government Printing Office. Washington, DC. January.

NIEHS. 1998. C.J. Portier and M.S. Wolfe. "Assessment of Health Effects from Exposure to Power-Line Frequency Electric and Magnetic Fields." Working Group Report No. 98-3981. Research Triangle Park: National Institute of Environmental Health Sciences.

NIEHS-NIH. 2002. "Questions and Answers: Electric and Magnetic Fields Associated with the Use of Electric Power." NIEHS. T: 919-541-3419; F: 919-541-3687; cdm@niehs.nih.gov.

NRPB. 2001. National Radiological Protection Board. "ELF Electromagnetic Fields and the Risk of Cancer." Vol. 12:1. Chilton, Didcot, Oxon. UK OX11 ORQ.

Olsen, J.H., A. Nielsen, and G. Schulgen 1993. "Residences Near High Voltage Facilities and Risk of Cancer in Children." *British Medical Journal*. 307: 891-895.

Olsen, R.G., D.W. Deno, and R.S. Baishiki. 1988. "Magnetic Fields from Electric Power Lines. Theory and Comparison to Measurements." *IEEE PWRD-3*. pp. 2127-2136.

Olsen R.G. and K.C. Jaffa. 1984. "Electromagnetic Coupling from Power Lines and Magnetic Field Safety Analysis." *IEEE PAS-103*. pp. 3595-3607, December.

Pettersson, P. 1992. "Simple Method for Characterization of Magnetic Fields from Balanced Three-Phase Systems." CIGRÉ. 36-103. 1992 Session. August-September.

Pettersson, P.1996. "Principles in Transmission Line Magnetic Field Reduction." *IEEE PWRD-11*. pp. 1587-1593. July.

Reilly, J.P. 1978. "Electric Field Induction on Sailboats and Vertical Poles." *IEEE PAS-97*. pp. 1373-1383. July/August.

Reilly, J.P. 1979. "Electric Field Induction on Long Object – A Methodology for Transmission Line Impact Studies." *IEEE PAS-98*. pp. 1841-1852. November/December.

Reilly, J.P. 1982. "Characteristics of Spark Discharges from Vehicles Energized by AC Electric Fields." *IEEE PAS-101*. pp. 3178-3186. September.

Reilly, J.P. 1992. "*Electrical Stimulation and Electropathology.*" Cambridge University Press.

Reilly, J.P. and M. Cwiklewski. 1981. "Rain Gutter Near High-Voltage Power Lines: A Study of Electric Field Induction." *IEEE PAS-100*. pp. 2068-2081. April.

Roberge, F. 1976. "State of Health of Maintenance Electricians Engaged in the Maintenance of Hydro Quebec 735 kV Stations." Hydro Quebec Report. May.

Savitz, D.A., H. Wachtel, F.A. Barnes, E.M. John, and J.G. Tvrdik. 1988. "Case-Control Study of Childhood Cancer and Exposure to 60-Hz Magnetic Fields." *American Journal of Epidemiology.* 128: 21-38.

Sebo, S.A. 1978. "Model Study of Electric Field Effects on Substations." EPRI Project RP 753. Final Report EL-632.

Shih, C.H., J. DiPlacido, and B.J. Ware. 1977. "Analysis of Parallel Plate Simulation of the Transmission Line Electric Field as Related to Biological Effect Laboratory Studies." *IEEE PAS-96.* pp. 962-968. May/June.

Silva, J.M., 1985. "AC Field Exposure Study: Human Exposure to 60-Hz Electric Fields." EPRI Report. EA-3993. April.

Simpson, T.L. and C.W. Brice. 1987. "Moment Method Analysis of the Electric Field under EHV Transmission Lines." *IEEE PWRD-2*. pp. 1264-1270, October.

Spherling B., L. Menemenlis-Hopkins, B. Fardanesh, B. Clairmont, and D. Childs. 1996. "Reduction of Magnetic Fields from Transmission Lines Using Passive Loops." CIGRÉ 36-103.

Spiegel, R.J. 1977. "Magnetic Coupling to a Prolate Spheroid Model of Man." *IEEE PAS-96*. pp. 208-212. January/February.

Stuchly, M.A. and S. Zhao. 1996. "Magnetic Field Induced Currents in the Human Body in Proximity to Power Lines." *IEEE PWRD-11*. pp. 102-109. January.

Taflove, A. and J. Dabkowski. 1979a. "Prediction Method for Buried Pipeline Voltages Due to 60 Hz AC Inductive Coupling. Part I: Analysis." *IEEE PAS-98*. pp. 780-787. May/June.

Taflove, A. and J. Dabkowski. 1979b. "Mitigation of Buried Pipeline Voltages Due to 60 Hz AC Inductive Coupling. Part II: Pipeline Grounding Methods." *IEEE PAS-98*. pp. 1814-1823. September/October.

Taflove, A., M. Genge, and J. Dabkowski. 1979. "Mitigation of Buried Pipeline Voltages Due to 60 Hz AC Inductive Coupling. Part I: Design of Joint Rights-Of-Way." *IEEE PAS-98*. pp. 1806-1813. September/October.

Takuma, T., T. Kawamoto, and Y. Sunaga. 1985. "Analysis of Calibration Arrangements for AC Field Strength Maters." *IEEE PAS-104*. pp. 489-496. February.

Thompson, G. 1933. "Shock Threshold Fixes Appliance Insulation Resistance." *Electrical World.* 101: 793-795, June.

Tomenius, L. 1896. "50-Hz Electromagnetic Environment and the Incidence of Childhood Tumors in Stockholm County." *Bioelectromagnetics.* 7: 191-207.

Tranen, J.D. and G.L. Wilson. 1971. "Electrostatically Induced Voltages and Currents on Conducting Objects under EHV Transmission Lines." *IEEE PAS-90.* pp. 768-775. March/April.

Tynes, T. and T. Haldorsen 1997. "Electromagnetic Field and Cancer in Children Residing Near Norwegian High-Voltage Power Lines." *American Journal of Epidemiology.* 145: 219-226.

UK Childhood Cancer Study Investigators. 1999. "Exposure to Power Frequency Magnetic Fields and the Risk of Childhood Cancer: A Case/Control Study." *Lancet.* 354: 1925-1931.

Verkasalo, P.K., E. Pukkala, M.Y. Hongisto, J.E. Valjus, P.J. Jarvinen, K.V. Heikkila, and M. Koskenvuo. 1993. "Risk of Cancer in Finnish Children Living Close to Power Lines." *British Medical Journal.* 307: 895-899.

Vinh T., C.W. Yi, and C.H. Shih. 1982. "Measurements and Analysis of Electric Fields in HV and EHV Stations." *IEEE PAS-101*. pp. 4122-4130. October.

Walling, R.A., J.J. Paserba, and C.W. Burns. 1993. "Series-Capacitor Compensated Shield Scheme for Enhanced Mitigation of Transmission Line Magnetic Fields." *IEEE PWRD-8.* pp. 461-469. January.

Wertheimer, N. and E. Leeper. 1979. "Electrical Wiring Configurations and Childhood Cancer." *American Journal of Epidemiology.* 119: 273-84.

Zaffanella, L.E. 1993. "Survey of Residential Magnetic Field Sources." EPRI. TR-102759-V1 and -V2. September.

Zaffanella, L.E. 1995. "Magnetic Field Management for Overhead Transmission Lines: Field Reduction Using Cancellation Loops." EPRI. TR-105571. December.

Zaffanella, L.E. 1999a. "Electric and Magnetic Field Exposure Assessment of Powerline and non-Powerline Sources for Public School Environments." Report to California Department of Public Health. EMF Program. Oakland, CA. April.

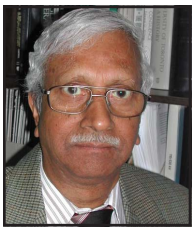
Zaffanella, L.E. 1999b. "Electric and Magnetic Field Reference Book – Section 4.6." EPRI. Palo Alto, CA: 1999. TR-114200.

CHAPTER 8

Corona and Gap Discharge Phenomena

P. Sarma Maruvada

This chapter describes the basic physical processes involved in corona and gap discharges and their electrical characteristics. The chapter presents the criteria for the onset of corona on conductors, and discusses the general concepts of the different corona effects that play a role in transmission-line design.



Dr. P. Sarma Maruvada has been involved in theoretical and experimental research studies of the corona performance of high-voltage ac and dc transmission lines for more than thirty-five years. He made important contributions to the calculation of conductor surface electric fields, analysis of corona onset phenomena, space charge fields and corona losses of dc transmission lines, analysis and measurement of radio noise and audible noise, and to the development of design criteria for radio noise and audible noise of ac and dc transmission lines as well as for electric fields and ion currents in the vicinity of dc lines. He contributed to experimental studies of corona on conductors subject to lightning, switching and temporary overvoltages, and to the modeling and analysis of corona attenuation of overvoltages on transmission lines.

Dr. Maruvada's research and analysis of corona is presented in his landmark book *Corona Performance of High-Voltage Transmission Lines*. He served on the Executive Committee of the IEEE/PES Transmission and Distribution Conference and Exposition and as Chairman of CIGRÉ Study Committee 36 on Power System Electromagnetic Compatibility. He is an Honorary Member of CIGRÉ, has been elected Fellow of IEEE, and received the IEEE Herman Halperin Electric Transmission and Distribution Award.

8.1 INTRODUCTION

Corona discharges occur on transmission-line conductors when the electric field intensity at the conductor surface is above a certain critical value. High levels of electric field give rise to a chain of ionization events in the surrounding air that culminates in the formation of corona discharges. A number of effects, such as power loss, electromagnetic interference, audible noise, gaseous effluents, and light are produced due to corona on conductors. Some of these corona effects have important implications for the electrical design of transmission lines, particularly in the choice of conductor size.

In order to evaluate the corona performance of a transmission line, as defined by the magnitudes and variations of the various corona effects, it is necessary to understand the basic discharge phenomena involved. Without going into too much detail, the physical mechanisms of corona discharges and of the resulting effects are discussed in this chapter. Engineering aspects of the corona effects, necessary for evaluating the corona performance of a transmission line, are discussed in Chapters 9 through 11.

The chapter begins with a review of the physics of ionization processes and electrical breakdown in air and a description of the different modes of corona discharges occurring on transmission-line conductors. A brief discussion of gap discharges on transmission and distribution lines is also included. The chapter continues with a description of the criteria for the onset of corona on conductors and a discussion of the influence of atmospheric and weather conditions on corona onset gradient, as well as on the different corona effects. Following that is an explanation of the generation quantities of the main corona effects, which are necessary for predicting the corona performance of a transmission line from test results on short lengths of conductors. Finally, the chapter concludes with the role of corona in attenuating the different types of power system overvoltages. Corona attenuation of overvoltages has an influence on the insulation performance of transmission lines, presented in Chapters 3 through 6.

An applet is included in this chapter to enable the user to calculate the corona onset gradient of any conductor and the corona onset voltage of any given transmission line configuration.

8.2 MECHANISM OF CORONA DISCHARGES

Corona discharges occurring on conductors and hardware give rise to several effects that play an important role in the electrical design of high-voltage transmission lines. The principal corona effects that describe the corona performance and, therefore, influence the design of transmission lines are corona (power) loss (CL), electromagnetic interference (EMI) in general and radio interference (RI) in particular, and audible noise (AN). In order to evaluate the corona performance of transmission lines, it is necessary first to understand the basic physics of corona discharges and also the physical mechanisms underlying the various corona effects.

8.2.1 Basic Discharge Physics

Atmospheric Air

The most widely used insulating medium for electrically isolating the conductors of overhead power transmission lines is atmospheric air. Although insulator strings provide the necessary structural support for the conductors, ambient air provides the bulk of insulation between the high-voltage conductors and the grounded parts of the tower structure as well as the ground plane. A good understanding of the insulation properties of air is, therefore, essential in evaluating the corona and insulation performance of overhead lines.

Atmospheric air is composed mainly of a number of gaseous components and water vapor (Humphreys 1964), the volume percentage of the latter depending mainly on ambient temperature, with the highest values occurring near the equator. The volume percentage of the gaseous components of dry air does not vary significantly, however, from one region of the earth to the other. The principal gaseous constituents of dry air are: nitrogen (78.1%), oxygen (21%), argon (0.9 %), and traces of carbon dioxide, neon, helium, krypton, etc.

Natural Sources of Ionization

Atmospheric air is almost a perfect insulating material under normal conditions. Some naturally occurring phenomena give rise, however, to conducting particles such as electrons and ions and make air an imperfect insulator. For example, gamma rays produced by radioactive processes in the soil have sufficient energy to ionize electrically neutral gas molecules, giving rise to free electrons and positive ions. Cosmic radiation, originating outside earth's atmosphere, also acts as a source of ionization at earth's surface. Naturally occurring ultraviolet light may also cause photoionization in air, but because of its much lower energy, makes only a minor contribution to ionization in air. The free electrons created by natural ionization processes attach quickly (in less than a microsecond) to oxygen molecules in air, forming negative ions. Thus, atmospheric air contains mainly positive and negative ions. As a consequence of all the natural ionization processes, atmospheric air at sea level contains approximately 1000 positive ions and approximately an equal number of negative ions per cubic centimeter. Although remaining almost electrically neutral due to the presence of equal numbers of positive and negative ions, their presence makes air slightly conducting and,

therefore, susceptible to the occurrence of electrical discharge phenomena such as corona and breakdown.

Ionization Processes

A brief review of basic ionization processes in gases (Cobine 1958) is essential for an understanding of the physics of corona and breakdown. The classical Bohr's model of atom, rather than the more accurate quantum theory, is most often invoked to understand the various ionization processes. In this model, an atom consists of a nucleus composed of neutrons and protons, surrounded by electrons in orbital motion. The number of orbital electrons for any element is equal to the number of protons in the nucleus, making the atom electrically neutral. In Bohr's model, the electrons occupy different orbits, or in quantum-mechanical terms, different shells, each characterized by a permissible energy state. The electron orbit closest to the nucleus has the lowest energy, while that farthest away has the highest energy. Any energy imparted to the atom, such as by mechanical impact or by electromagnetic radiation, affects mostly the electron in the outermost orbit. The ionization behavior of molecules, which are made up of two or more atoms, is quite similar to that of the constituent atoms.

Excitation and Ionization

If sufficient energy is imparted to an atom, the electron in the outermost orbit may be made to jump to the next higher permissible energy orbit, and the atom is said to be *excited*. An excited atom quickly (in less than about 10^{-8} seconds) relaxes to its original energy state, releasing the excess energy in the form of a photon. The frequency of the photon released in this process depends on the difference between the energy levels through which the electron jumps.

If an even larger amount of energy is imparted, the electron can be made to jump so far away from its orbit that it will not be able to return to its original state or even to the atom. The atom is then said to be *ionized*. The process of ionization, therefore, gives rise to a positive ion, i.e., the atom deprived of an electron, and a free electron. For discharges of interest in transmission-line engineering, the energy required to cause excitation and ionization of atoms and molecules is provided either by electrons accelerated to high energies in an electric field or by photons with sufficient energy hf_p, where f_p is the frequency of the photon radiation and h is Planck's constant. The processes of excitation and ionization may be illustrated by the following symbolic equations:

By Electron Impact

$$A + e \rightarrow A^* + e \text{ (excitation)} \qquad 8.2\text{-}1$$

$$A + e \rightarrow A^+ + e + e \text{ (ionization)} \qquad 8.2\text{-}2$$

By Photon

$$A + hf_p \leftrightarrow A^* \text{ (photo-excitation or photon emission)} \qquad 8.2\text{-}3$$

$$A + hf_p \rightarrow A^* + e \text{ (photo-ionization)} \qquad 8.2\text{-}4$$

Equations 8.2-1 and 8.2-2 indicate that an electron e colliding with the atom A with sufficient energy gives rise to an excited atom A^* or a positive ion A^+ and another free electron. Equation 8.2-3 indicates the process of photo-excitation as well as the reverse process of photon emission from an excited atom, while Equation 8.2-4 indicates the process of photo-ionization.

Electron Attachment and Detachment

In some gases, known as *electronegative* gases, like oxygen, chlorine, etc., the outermost shell is not completely filled in the neutral state, leaving one or two positions readily available to receive free electrons. As a result, although the gas atoms are electrically neutral, they have a definite capability, or *affinity*, to capture free electrons to form stable negative ions. The formation of negative ions by electron attachment may be illustrated by the following symbolic equation,

$$A + e \rightarrow A^- \text{ (attachment)} \qquad 8.2\text{-}5$$

In a reverse process, called electron detachment, a negative ion may shed its electron to revert to its neutral state. A certain amount of energy, known as *electron affinity*, is required to cause electron detachment. In atmospheric air, oxygen is an electronegative gas and, therefore, permits the formation of negative ions. Water vapor is also electronegative and, when present in ambient air, leads to the formation of negative ions.

Recombination

The coexistence of positively and negatively charged particles in a gas leads to the process of recombination, in which charge neutralization takes place. The process may be represented symbolically by the equation,

$$A^+ + B^- \rightarrow AB + hf_p \text{ (recombination)} \qquad 8.2\text{-}6$$

In this process, A^+ is the positive ion and B^- may be an electron or a negative ion. The process shown above, in which photon emission takes place, and which occurs only with electrons, is known as *radiative recombination*, and may be considered in some respects as the reverse of photo-ionization.

Ionization, Attachment and Recombination Coefficients

The ionization processes described above play important roles in the various phases of the development of gas discharges including breakdown and corona. One of the fundamental processes involved in the initiation and development of discharges is ionization of atoms and molecules by high-

energy electrons. In the absence of any applied electric field, the electron moves randomly, colliding with gas molecules. In the presence of an applied electric field, however, the electron acquires energy from the electric field and a velocity in the direction of the field. Townsend (Townsend 1915) defined the *ionization coefficient* α, known also as Townsend's first ionization coefficient, as the number of electron-ion pairs produced in the gas by a single electron, in moving through a unit distance in the direction of movement of the electron. If *n(x)* electrons advance a distance *dx* in a gas in the field direction, the number of additional electrons produced by ionization is

$$dn = n(x)\,\alpha\,dx \qquad 8.2\text{-}7$$

If the initial number of electrons is n_0 at x = 0, then integrating Equation 8.2-7,

$$\ln\frac{n}{n_0} = \int_0^x \alpha\,dx$$

In general, the coefficient α varies as a function of the electric field. In a uniform electric field, α is constant and

$$n = n_0 e^{\alpha x} \qquad 8.2\text{-}8$$

In a nonuniform field, α varies with the electric field and, therefore, with *x* and

$$n = n_0 e^{\int_0^x \alpha\,dx} \qquad 8.2\text{-}9$$

Analogous to the ionization coefficient, the *attachment coefficient* η is defined as the probability that a free electron will attach itself to a neutral atom to form a negative ion when moving a unit distance through the gas in the direction of the applied electric field. Proceeding as described above, the number of electrons remaining as a consequence of electron attachment is

$$n = n_0 e^{-\eta x} \text{ in uniform fields} \qquad 8.2\text{-}10$$

$$\text{and, } n = n_0 e^{\int_0^x -\eta\,dx} \text{ in nonuniform fields} \qquad 8.2\text{-}11$$

If ionization and attachment are present simultaneously, as in the case of electronegative gases, the number of electrons at a distance *x* is obtained as

$$n = n_0 e^{(\alpha-\eta)x} \text{ in uniform fields} \qquad 8.2\text{-}12$$

$$\text{and, } n = n_0 e^{\int_0^x (\alpha-\eta)\,dx} \text{ in nonuniform fields} \qquad 8.2\text{-}13$$

In the presence of attachment $(\alpha - \eta)$ may be considered as the effective ionization coefficient. In other words, the effective boundary of ionization can be considered as when $\alpha = \eta$, since the probability of ionization is then equal to the probability of attachment. Finally, the recombination coefficient R_i is defined as the number of recombining events per unit time and per unit density of positive and negative ions. The rate of decrease of positive and negative ions is then given by

$$\frac{dn_+}{dt} = \frac{dn_-}{dt} = -R_i\,n_+\,n_- \qquad 8.2\text{-}14$$

where n_+ and n_- are concentrations of positive and negative ions at the location of interest in the gas. All the three parameters α, η and R_i described above have been found to be functions of *E/p*, where *E* is the electric field intensity and *p* is the gas pressure.

Secondary Ionization

Free electrons produced by natural ionization processes, such as by gamma rays and cosmic radiation, initiate electrical discharges in air. In the presence of a sufficiently high electric field, these electrons are accelerated and reach energies high enough to ionize the air molecules. This is the primary mechanism of ionization responsible for the development of discharges. Other processes, generally known as *secondary ionization*, are essential, however, for producing sustained discharges.

For corona discharges in air, secondary ionization can take place either on a conducting surface or in ambient air. On conducting surfaces, secondary ionization may be caused by several mechanisms, but the most likely one for discharges at atmospheric pressure is by positive ion impact. Photons, either produced by an external light source or released by excited atoms or molecules in the gas, may also impinge on the conducting surface and cause secondary ionization and release of secondary electrons. The main source of secondary ionization in air, however, is photons released by excited atoms or molecules generated in the discharge itself.

Drift and Diffusion of Charged Particles

In a gas discharge, the concentration of charged particles, either electrons or ions, is generally very low compared with that of the neutral gas molecules. Thus, the gas molecules may be assumed to act as fixed scattering centers and remain almost unaffected by collisions with the charged particles. The bulk movement of charged particles in a gas consists of two components:

1. *diffusion* due to the existence of a density gradient and
2. *drift* due to the force exerted on the charged particles by the applied electric field.

The drift velocity $\vec{v}$ of a charged particle in a gas is generally proportional to the applied electric field $\vec{E}$,

$$\vec{v} = \mu\vec{E} \qquad 8.2\text{-}15$$

where μ is known as the *mobility* of the charged particle. The mobility of ions is nearly constant over wide ranges of *E/p* values, but that of electrons varies as a function of *E/p*, where *E* is the magnitude of electric field and *p* is gas pressure.The diffusion coefficient *D* of charged particles is almost negligible compared to the mobility at normal ambient temperatures.

8.2.2 Discharges in Uniform Fields

Before proceeding with a discussion of the physics of corona discharges on conductors, it is useful to understand how a discharge develops in a uniform field air gap at atmospheric pressure. Consider an electrode system specially designed to produce a uniform electric field in the air gap when a high direct voltage *V* is applied between them. If the air gap distance between the electrodes is *d*, the applied electric field is $E = V/d$.

Electron Avalanche

Free electrons may be produced near the cathode surface either by natural ionization processes or by artificial ultraviolet illumination. The free electrons are accelerated by the electric field in the gap, from the cathode towards the anode. The electrons collide with the neutral oxygen and nitrogen molecules, and almost all the energy acquired by them in the electric field is imparted to the gas molecules. At sufficiently high electric field, the gas molecules are ionized, and new electron-positive-ion pairs are created. The newly created electrons also gain energy from the electric field and proceed to ionize other gas molecules, leading to a process called *field-intensified ionization*. This process is illustrated in Figure 8.2-1. The initial electron collides with a neutral molecule, as shown in (a), giving rise to a positive ion and two free electrons, which collide with two neutral molecules, as shown in (b). This gives rise to two more positive ions and four free electrons colliding with four neutral molecules, as shown in (c), and so on. Most of the electrons created in this process attach to neutral oxygen molecules to form negative ions. The exponential growth of ionization from a single electron near the cathode and moving towards the anode is called an *electron avalanche*, as shown in Figure 8.2-2. Since electrons move about 100 times faster than the ions, they move to the head of the avalanche, leaving behind the slow-moving ions.

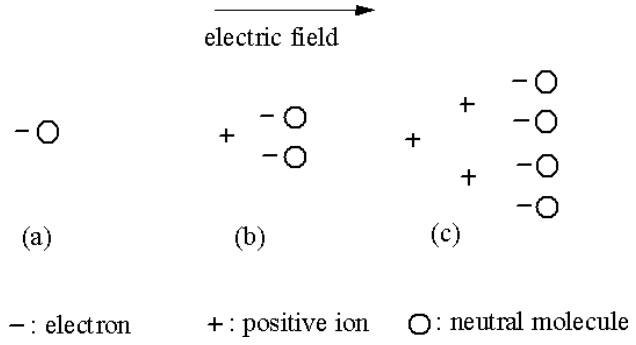


Figure 8.2-1 Field-intensified ionization.

Figure 8.2-3 shows a uniform field gap with positive voltage applied to the anode and the cathode grounded through an ammeter, sufficiently sensitive to measure the small currents produced by the discharge process in the gap. An electron avalanche created by a free initial electron at the cathode is also shown in the figure.

A spherical head and a conical volume trailing behind characterize the electron avalanche. Most of the electrons are located on the surface of the spherical volume facing the anode, while the positive ions are distributed throughout the spherical and the conical volumes of the avalanche. Some of the collisions between the electrons and the molecules produce excited rather than ionized molecules, followed by photon emission. These photons also play an important role in the discharge development. Most of the electrons created in the discharge attach themselves eventually to the molecules of the electronegative components (mainly oxygen) of the gas, forming negative ions. While the electrons move very rapidly towards the anode, the positive and negative ions move rather slowly towards the cathode and anode, respectively.

Voltage-Current Characteristic and Breakdown

As the voltage across the electrodes is increased gradually, the typical voltage-current characteristic shown in Figure

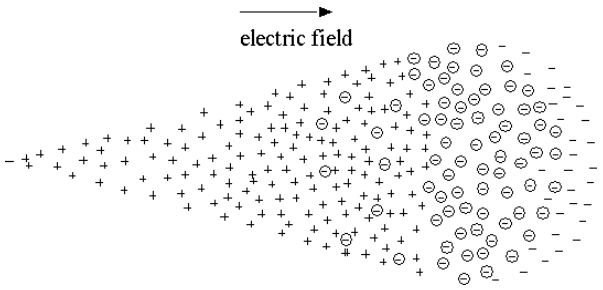


Figure 8.2-2 Electron avalanche.

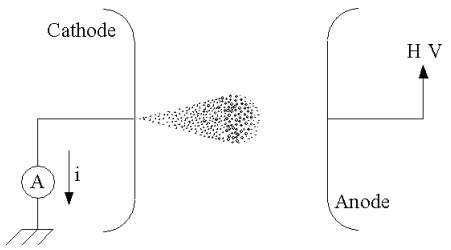


Figure 8.2-3 Discharge in a uniform-field gap.

8.2-4 is obtained. The current increases almost linearly with voltage at the beginning and then saturates gradually as the voltage approaches V_0. As the voltage is increased above zero, any free electrons that are continually created in the gas by natural processes being swept into the anode produce the current. The linear part of the characteristic corresponds to a rate of creation of electrons higher than that of removal, while saturation occurs when all the free electrons are drawn into the anode. At voltages above V_1, the electric field in the gap is sufficiently large to give rise to excitation and ionization by electron collision and to field-intensified ionization, and the formation of electron avalanches. The exponential nature of this process produces a current characteristic of the form, $i = i_0 e^{\alpha d}$, where i_0 is the saturation current at V_0. The value of the ionization coefficient α increases with the magnitude of the electric field. Above a certain voltage V_2, the current starts to increase more rapidly than the exponential relationship shown above, leading ultimately to breakdown at the voltage V_b.

This rapid increase in current is caused by secondary ionization at the cathode surface, mainly due to the impact of positive ions in the primary avalanche, which creates new electrons capable of producing new electron avalanches. The creation of secondary electrons at the cathode surface makes the discharge process self-sustaining—i.e., not dependent on the source of the initiatory electrons—and leads ultimately to electrical breakdown of the gap. Only the external circuit impedance limits the current at this stage. In order to understand the transition of the discharge process to electrical breakdown, it is useful to look at a simplified mathematical model of the discharge.

Assuming that n_c is the total number of electrons emanating from the cathode, of which n_0 is the number of free electrons initially created near the cathode, then the number of electrons emitted by secondary ionization process is

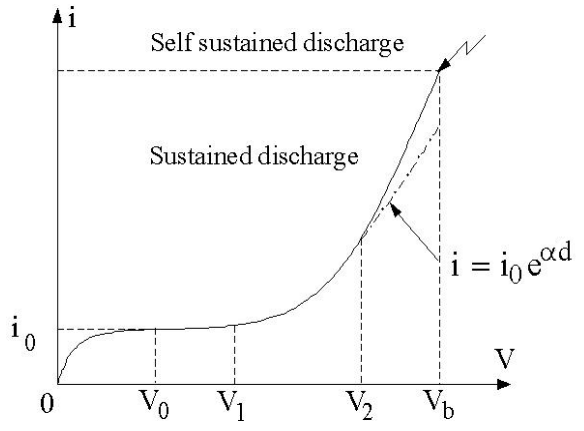


Figure 8.2-4 Voltage-current characteristic (Maruvada 2000). (Reproduced with permission of Research Studies Press.)

$(n_c - n_0)$. Neglecting creation of negative ions for the moment, the total number of electrons n_t created in the avalanche, by the time it reaches the anode, is

$$n_t = n_c e^{\alpha d}$$

The number of positive ions returning to the cathode and capable of producing secondary electrons on impact is also n_t. If γ denotes the efficiency of the secondary ionization by positive ion impact, also known as *secondary ionization coefficient*, the number of secondary electrons is

$$\left(n_c - n_0\right) = \gamma n_t = \gamma n_c e^{\alpha d}$$

$$\text{or, } n_c = \frac{n_0}{1 - \gamma e^{\alpha d}} \qquad 8.2\text{-}16$$

Equation 8.2-16 provides the criterion, known as the Townsend criterion, for breakdown. It is seen from Equation 8.2-16 that the total number of electrons n_c emanating from the cathode tends to infinity if

$$\gamma e^{\alpha d} = 1 \qquad 8.2\text{-}17$$

The voltage V_b at which the Townsend criterion (8.2-17) is reached is the breakdown voltage.

From a physical point of view, the discharge occurring at voltages below V_b is known as a *sustained discharge*, since it ceases to exist if the source of primary electrons is removed. The discharge becomes *self-sustaining*, however, at the breakdown voltage V_b, since the total number of secondary electrons n_c tends to infinity according to Equation 8.2-16—i.e., the discharge will continue to develop even if the source of initiatory electrons is removed.

In gases such as air, containing electronegative gas components such as oxygen, some of the electrons attach themselves to neutral molecules to become negative ions and, consequently, the effective ionization coefficient becomes $(\alpha - \eta)$ and the breakdown criterion is modified to,

$$\gamma e^{(\alpha - \eta) d} = 1 \qquad 8.2\text{-}18$$

8.2.3 Discharges in Nonuniform Fields

In most practical situations related to transmission lines, the electrode geometries of interest, such as a cylindrical conductor above a ground plane, are characterized by highly nonuniform electric field distributions. The highest electric field occurs at the surface of the electrode with the smallest radius of curvature, the cylindrical conductor in this case, and decreases rapidly at first and then more gradually across the gap, with the lowest electric field at the ground plane. As the voltage across the gap is increased, ionization and the discharge process are initiated at the surface of the

highly stressed cylindrical conductor. At a certain distance from the conductor surface, however, the electric field becomes so low that ionization by electron impact of gas molecules cannot take place. Thus, unlike in a uniform field gap, the discharge process is confined to a small volume in the vicinity of the highly stressed electrode.

The discharge process in a nonuniform field gap proceeds through the same stages as in a uniform field gap—namely, cumulative ionization, electron avalanches, secondary ionization, and eventually to breakdown. However, the self-sustained discharge is limited to only a part of the gap and is known as "partial breakdown," or more commonly as *corona* discharge. Similar discharges occurring inside high-voltage electrical apparatus are known as *partial discharges*. Depending on the degree of nonuniformity of the gap, the voltage at which breakdown of the entire gap takes place is much higher than that at which corona occurs.

Since the ionization coefficient α at any point in the gap varies as a function of the electric field and, therefore of its position, the criterion 8.2-17 should be modified for the onset of corona discharge as

$$\gamma\, e^{\int_0^d \alpha\, d\,x} = 1 \qquad 8.2\text{-}19$$

The integral in 8.2-19 is carried out from the surface of the highly stressed electrode ($x = 0$) to distance d, at which ionization stops. Again, if electron attachment takes place, creating negative ions, Equation 8.2-19 should be modified to,

$$\gamma\, e^{\int_0^d \left(\alpha-\eta\right) dx} = 1 \qquad 8.2\text{-}20$$

Equation 8.2-20 may be rewritten as

$$\int_0^d \left(\alpha-\eta\right) dx = \ln\left(\frac{1}{\gamma}\right) \qquad 8.2\text{-}21$$

The criterion 8.2-21 has been used in different forms to calculate the corona onset gradients of nonuniform field electrode systems. In practice, however, the complexities of the actual discharge process and the unavailability of good experimental data on some of the ionization parameters involved make it rather difficult to calculate the voltage corresponding to corona onset. For air at atmospheric pressure, good data is available for the parameters α and η, but it is quite difficult to determine the parameter γ.

In nonuniform fields, electron avalanches are initiated at either the cathode or the anode, whichever is the highly stressed electrode. When the cathode is the highly stressed electrode, the avalanche is initiated at the cathode, similar to the case of the uniform field gap described above, but it develops in the direction of decreasing electric field intensity. In the case of a highly stressed anode, however, the avalanche is initiated not at the electrode surface, but at a certain distance away from the surface where the electric field intensity is sufficiently high that a free electron is more likely to ionize than be attached to a neutral molecule. The electron avalanche near the anode develops, unlike near the cathode, in the direction of increasing electric field intensity.

In both uniform and nonuniform field discharges, the cumulative effect of a rapid succession of electron avalanches gives rise to the accumulation of space charges and the enhancement of electric field in the region away from the electrode surface. As a result of the field enhancement, a transition takes place from avalanche to streamer discharges. Conditions that favor rapid clearing of space charges in the case of nonuniform field discharges give rise to unstable filamentary discharges known as *streamers*. Under certain conditions, however, equilibrium may be reached between the ionization processes and the clearing of space charges, resulting in a stable discharge known as *glow.*

8.2.4 Modes of Corona Discharge

The physical manifestations of corona discharge may vary widely depending mainly on the following aspects:

1. electrode geometry;
2. magnitude and distribution of electric field near the highly stressed electrode; and
3. composition of the gaseous medium between the electrodes.

From the point of view of high-voltage transmission lines, an understanding of corona discharges occurring on cylindrical conductors placed above a ground plane are of particular interest. Although practical transmission-line conductors are of stranded construction and their surfaces are often characterized by defects and unwanted deposits of foreign material, it is useful first to consider corona discharges on ideally smooth cylindrical conductors. Also, since corona on conductors at alternating voltages are composed essentially of discharges occurring during the positive and negative half cycles, it is necessary to understand the types of corona discharge at positive and negative direct voltages.

Adapting from the excellent treatment of the subject in published literature (Trinh and Jordan 1968, 1970; Trinh 1995), a description is given in the following pages of the different modes of corona discharge occurring on conductors at negative and positive dc as well as at ac. In order to

improve the quality of the discharge photographs in these studies, a protrusion of conical or spherical shape was fixed on the conductor to stabilize the discharge site as well as in the development of the different corona modes. Since oxygen, one of the main components of air, is an electronegative gas, negative ions are much more stable negative charge carriers than electrons. The faster moving electrons are the principal source of ionization and excitation of molecules in a corona discharge, while the comparatively slower moving ions of both polarities, created by successive electron avalanches, tend to accumulate in the gap and form quasi-stationary space charge clouds. These space charge clouds modify the electric field distribution, giving rise to significant changes in the spatial and temporal development of the discharge process and eventually to different corona modes.

Negative DC Corona Modes

A cylindrical conductor to plane air gap is shown in Figure 8.2-5, with high direct voltage of negative polarity applied to the conductor and the plane maintained at ground potential. A nonuniform field distribution is produced in the gap, reaching the highest value at the conductor surface and decreasing gradually towards the plane. As the applied voltage is increased, the electric field near the conductor becomes high enough to start the discharge process. Free electrons, created by natural processes at the conductor surface, initiate electron avalanches, which progress in the decreasing electric field region away from the conductor.

The progress of the electron avalanche stops at a certain boundary *B*, as shown in the Figure 8.2-5, where the effective ionization coefficient (α - η) becomes zero. Before reaching this boundary, some of the electrons created by the field-intensified ionization process attach themselves to oxygen molecules to form negative ions, while the remaining electrons continue to produce field-intensified ionization. Beyond the boundary *B*, however, all the free electrons form negative ions by attachment and no more field-intensified ionization takes place. The impact of the returning positive ions, as well as of the photons created in the avalanche, on the conductor surface produces the secondary electrons necessary for a self-sustained discharge or the onset of corona.

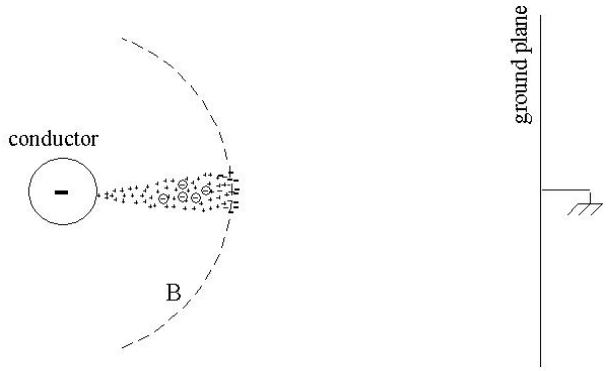


Figure 8.2-5 Negative dc corona.

At the completion of the development of the initial electron avalanche, two ion space charge clouds are formed, the positive moving towards the conductor and the negative towards the ground plane, as shown in Figure 8.2-6. The field distribution near the conductor is modified due to the presence of these space charge clouds as shown in Figure 8.2-7. The original and space-charge-modified field distributions are represented by curves 1 and 2, respectively. As indicated by curve 1, the conductor surface electric field at the initiation of the electron avalanche is E_{c1}, while E_i is the electric field at which effective ionization stops at a distance r_{i1} from the conductor. The effect of space charges is to increase the electric field near the conductor to E_{c2} and

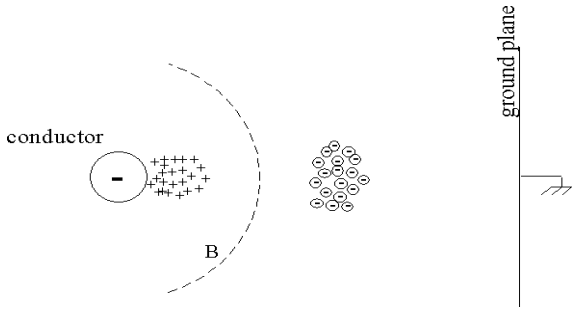


Figure 8.2-6 Development of negative dc corona.

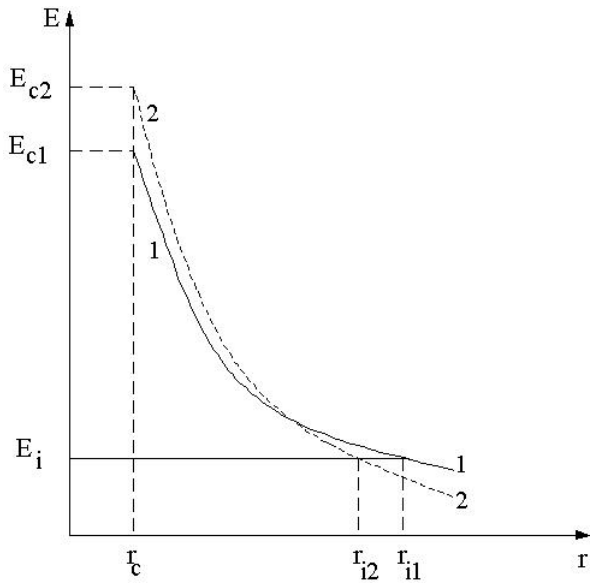


Figure 8.2-7 Field distribution near the conductor: 1 – Original field distribution; 2 – Space-charge modified field distribution.

decrease it correspondingly away from the conductor. This modified field distribution, shown by curve 2, results in the subsequent electron avalanche to develop in a region of slightly higher field intensity, but extending over a shorter distance r_{i2}.

The extent to which the field is modified by the space charge clouds has a direct influence on the discharge development and gives rise to three different modes of negative corona, each with distinct electrical, physical, and visual manifestations. These modes, in the order of increasing field intensity at the conductor surface, are:

- Trichel Streamer
- Negative Glow
- Negative Streamer

Trichel streamer corona occurs at a conductor surface electric field slightly above the onset value. The positive space charge created by the initial streamer, consisting essentially of a succession of electron avalanches of decreasing magnitude, is absorbed and neutralized by the conductor, leaving only a negative space charge at a distance away from the conductor. This tends to decrease the conductor surface electric field below E_{c1} and suppresses the discharge. Following a short interval of time, in which the negative space charge is cleared from the immediate vicinity of the conductor, the electric field at the conductor surface reverts to E_{c1} and the process of streamer formation is repeated.

The duration of the growth and suppression of the streamer is of the order of a hundred nanoseconds, while the time interval between two successive streamers may vary from a few microseconds to a few milliseconds. The discharge current resulting from this process, attributable mainly to the movement of electrons in the electric field, consists of a train of pulses of small amplitude and short duration. The pulse frequency may vary from one to several tens of kHz.

Figure 8.2-8 shows the visual manifestation of a typical Trichel streamer, while Figure 8.2-9 indicates the resulting current pulse waveform. As the conductor voltage is increased, the Trichel pulse frequency increases until it reaches a critical value. Above this voltage, the Trichel streamers effectively merge and a new mode of corona called *negative glow* appears, characterized by a change in the visual appearance of the discharge. The bright spherical discharge, followed by a conical positive column, as shown in Figure 8.2-10, is the typical visual manifestation of the negative glow mode of corona. This mode is also characterized electrically by a steady corona current.



Figure 8.2-8 Trichel streamer.

The glow mode of corona continues over a certain range of voltage, above which a transition takes place to *negative streamer* corona. The extended streamer channel characterizing this mode of corona is shown in Figure 8.2-11. The discharge current in this case consists of pulses superposed on a dc component, the presence of which signifies that, unlike the case of Trichel streamer corona, the discharge process never completely stops. Further increases in the applied voltage eventually lead to complete breakdown of the conductor-plane gap.

Positive DC Corona Modes

In the conductor-plane air gap considered, if direct voltage of positive polarity is applied to the conductor, as shown in

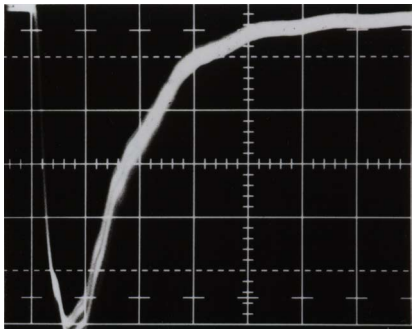


Figure 8.2-9 Trichel current pulse.



Figure 8.2-10 Negative glow.

Figure 8.2-12, the resulting discharge phenomena are known as positive corona. The electron avalanche in this case is initiated by free electrons created by natural processes, not at the conductor surface, but in air at a boundary surface *B*, where the effective ionization coefficient $(\alpha - \eta)$ is greater than zero. The avalanche develops towards the conductor in the continuously increasing electric field. The highest field-intensified ionization activity occurs near the conductor surface, with the spherical volume close to the conductor and the conical volume directed away from the conductor.



Figure 8.2-11 Negative streamer.

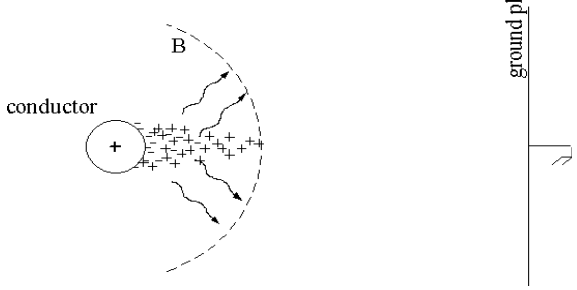


Figure 8.2-12 Positive dc corona.

The secondary electrons necessary for producing a self-sustained discharge of positive corona are generated exclusively by photo-ionization in the gas. As in the case of negative corona, electrons attach to neutral oxygen molecules to form negative ions, and ions of both polarities form relatively immobile space charge clouds compared to the fast moving electrons. Most of the negative ions are created away from the immediate vicinity of the conductor, since electrons are more likely to be neutralized on contact close to the conductor than form negative ions. Similar to the case of negative corona, the positive and negative space charge clouds affect the field distribution near the conductor and influence the discharge development. This interaction gives rise to the following positive corona modes, in the order of increasing conductor surface electric field:

- Burst Corona
- Onset Streamer
- Positive Glow
- Breakdown Streamer

Burst corona occurs just at the onset of positive corona and is caused by electrons that lose their energy due to ionization activities just before they are absorbed in the conductor. The positive ions created in the immediate vicinity of the conductor build up cumulatively to form a positive space charge and suppress the discharge. The spread of electrons then moves to another part of the conductor. Each time ionization spreads around the conductor surface and is suppressed subsequently by space charge, a small positive corona current pulse is produced. Figure 8.2-13 shows the visual manifestation and discharge current characteristic of burst corona.

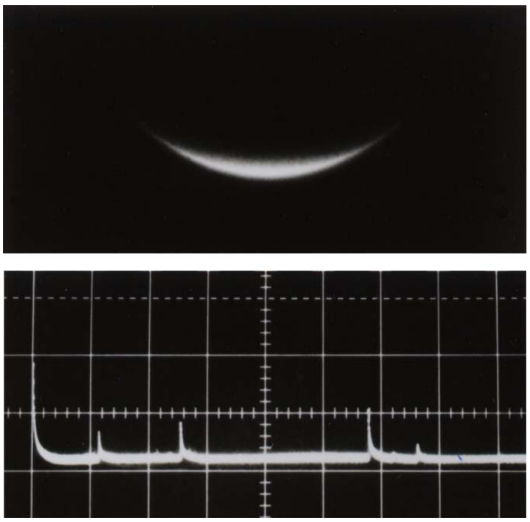


Figure 8.2-13 Positive burst corona and current pulse.

Unlike burst corona, which is caused by the spread of ionization on the conductor surface, *onset streamer*, sometimes also known as "plume," results from the radial development of the discharge. Due to the higher electric field in this case, the positive ion space charge near the conductor enhances the electric field away from the conductor sufficiently to cause subsequent electron avalanches and lead to the development of a streamer channel in the radial direction. The positive ion space charge created by successive avalanches away from the conductor reduces the electric field near the conductor surface and eventually suppresses the streamer. The discharge activity stops during an interval of time necessary to clear the space charge and resumes as soon as the original field distribution is restored. Thus, the positive onset streamer mode of corona is pulsative in nature, producing corona current pulses with larger amplitudes and lower repetition rates than those of negative Trichel streamers. On practical transmission-line conductors, positive onset streamers are the main source of RI and AN. The visual appearance and the resulting current pulse waveform of onset streamers are shown in Figure 8.2-14.

Under some special conditions of electric field distribution near the highly stressed positive conductor, the discharge may progress from burst corona mode to a stable glow corona mode of nonpulsative discharge rather than to the onset streamer mode. The *positive glow* corona mode occurs as the result of a particular combination of rate of creation and removal of positive ions near the conductor. The field distribution should be such that the positive ion space charge is removed rapidly from the anode, while at the same time the field intensity is not sufficient to allow radial development of the discharge and streamer formation. Figure 8.2-15 shows the visual manifestation of positive glow corona. It should be emphasized that positive glow corona is difficult to obtain even in the laboratory and may occur on transmission-line conductors only under very special conditions. Finally, as the voltage applied to the conductor is further increased, streamers similar to onset streamers but of much more vigorous nature are produced that eventually lead to a complete breakdown of the conductor-plane gap.

AC Corona Modes

When an alternating voltage is applied to a conductor-plane gap, the electric field in the gap and, therefore, in the vicinity of the conductor surface, varies continuously in magnitude as well as polarity or direction. As the voltage goes above the corona onset value in each of the positive and negative half cycles, different modes of corona occur at the conductor surface. The discharge process under ac differs from that under dc mainly due to the presence of a residual space charge, having the same polarity as that of the previous half cycle, before the onset of corona in the current half cycle. In spite of this difference, however, the modes of corona occurring in each half cycle are very similar to those under direct voltages of the same polarity.

The development of different modes of corona in the negative and positive half cycles, as a function of the applied voltage, may be identified in Figure 8.2-16. For this case studied in a laboratory setup (Trinh and Jordan 1968), onset streamers are suppressed in favor of glow corona in the positive half cycle. On stranded conductors of large diameter generally used on transmission lines, however, onset streamers are the most commonly observed corona mode in the positive half cycle. Under ac, corona first appears in the negative half cycle in the form of Trichel streamers. The corona modes observed in the negative half cycle, as the voltage is increased, are Trichel streamers and glow. In the positive half cycle, breakdown streamers fol-

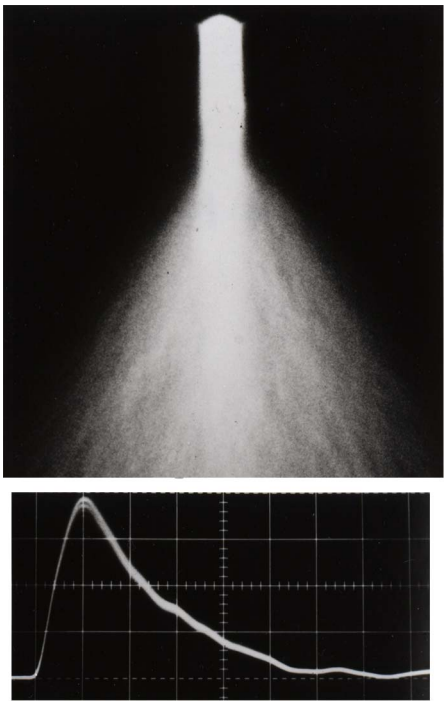


Figure 8.2-14 Positive onset streamer.

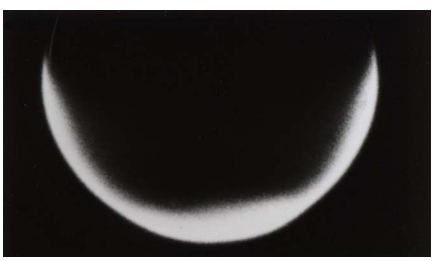


Figure 8.2-15 Positive glow.

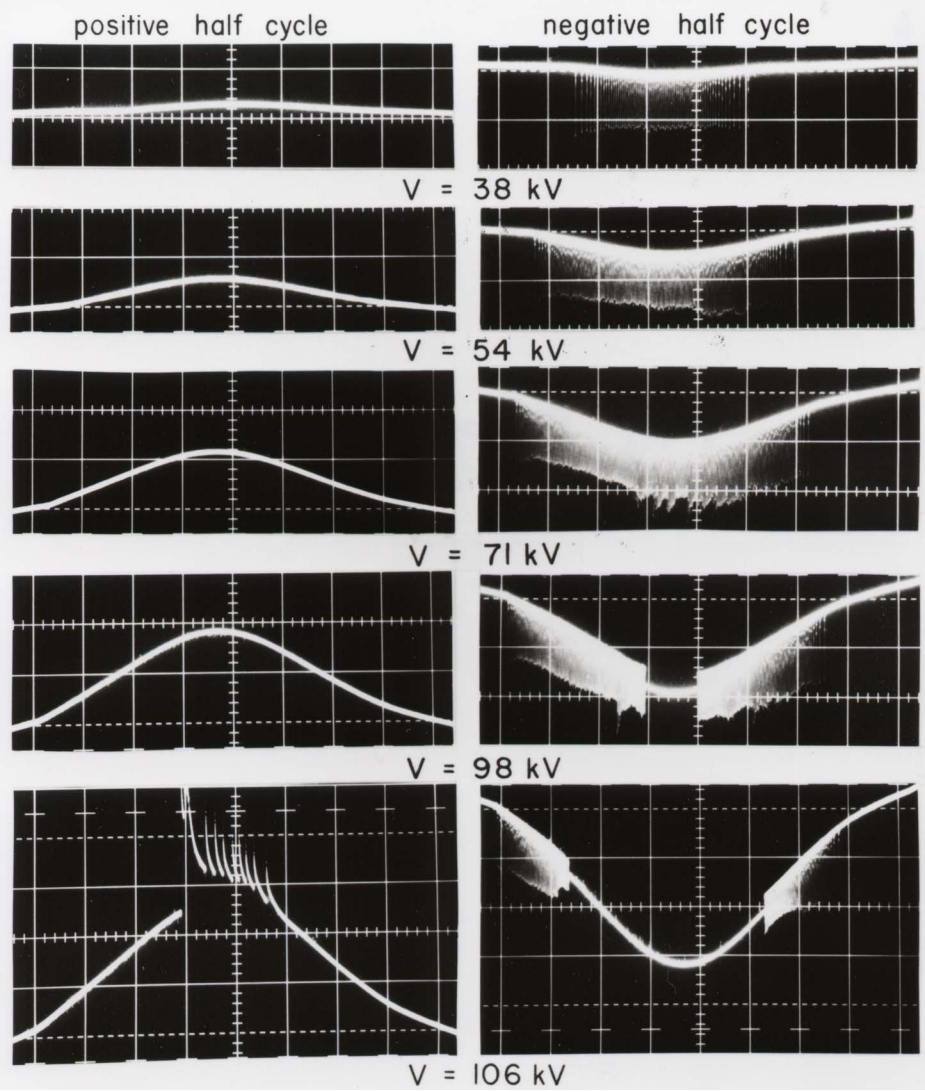


Figure 8.2-16 AC corona modes.

low glow corona. Although corona first appears in the negative half cycle, breakdown of the gap always occurs in the positive half cycle and, consequently, negative streamers do not appear.

Experimental studies (Uhlig 1956) have shown that on very thin and clean wires, only glow corona mode, called *ultra corona*, occurs. Studies were also carried out (Héroux et al. 1982) on stranded conductors wrapped with very thin smooth wires in order to promote ultra corona, eliminate positive onset streamers and, therefore, reduce RI and AN problems on ac transmission lines. This technique, although reducing RI and AN, has been found to increase CL significantly.

On insulators, both ceramic and nonceramic, corona discharges may occur near hardware or insulator protrusions, where the electric field distribution is sufficiently high to produce sustained discharges. Both positive and negative corona may occur near hardware protrusions, while only positive corona occurs near insulating surfaces.

8.3 GAP DISCHARGES

While partial breakdown near the highly stressed electrode of a nonuniform field air gap is generally known as corona, complete breakdown of air insulation between two electrodes separated by a short gap is known as a *gap discharge*. Although most gap discharges on power lines occur between two metallic electrodes, they may also occur between a metallic electrode and the surface of an insulator. The gap spacing in these discharges is usually of the order of a few millimeters.

Parts of metallic hardware used in the construction of power lines, which are normally in electrical contact with each other, may become separated during the operation of the line and give rise to a short air gap. One of the separated hardware parts may then become electrically isolated, leading to a voltage buildup across the gap and eventually to breakdown. On high-voltage transmission lines, for example, an air gap may form between the cap and pin of a mechanically lightly loaded suspension insulator string. On lower voltage distribution lines, a metallic staple holding the ground wire to a wood pole may become loose, giving rise to a short air gap. An example of the conductor-insulator gap is that which may exist between the tie wire and a pin insulator on a distribution line.

The physical mechanism of gap discharges occurring on power lines may be illustrated using the equivalent circuit shown in Figure 8.3-1. The voltage applied to the power line conductor is represented by the voltage source *V.* The impedance between the conductor and the floating electrode of the gap is represented by Z_1, while Z_2 represents the impedance between the floating electrode and ground. In most cases, the impedances Z_1 and Z_2 are purely capacitive. In special cases, such as a wood pole line in a humid environment, one or both of these impedances may be predominantly resistive.

Due to voltage division along the divider formed by Z_1 and Z_2, a voltage V_g appears across the gap. If the voltage V_g is sufficiently high, complete electrical breakdown takes place across the air gap, which in turn causes short-circuit and reduces the voltage across the gap to nearly zero. The discharge is then extinguished and the air gap reverts to an insulating state. This cycle of complete breakdown and full insulation recovery continues as long as the power line is energized.

Extensive laboratory studies (Janischewskyj and Arainy 1983; Arai et al. 1985) have been carried out to understand the physical mechanisms involved in gap discharges and to determine the magnitude, shape and repetition rate of the discharge current waveform produced. The basic mechanisms of gap discharge are similar to those described earlier in this chapter for uniform field gaps. The initiation, progression, and culmination of the breakdown process depend on the actual gap geometry.

Typical current waveform produced by a gap discharge is shown in Figure 8.3-2. The amplitude of currents produced by gap discharges depend on the gap spacing and the coupling impedances Z_1 and Z_2 and are generally orders of magnitude higher than those produced by any modes of corona discharge described in Section 8.2.4.

Studies have shown (Arai et al. 1985) that the magnitudes of coupling impedances have a large influence on the pulse repetition rate, but not on the current waveshape. The main consequence of gap discharges is the generation of electromagnetic interference (EMI) and will be discussed in more detail in Section 8.5.

Gap discharges occur almost exclusively on distribution lines and rarely on the higher voltage transmission lines. This is mainly due to differences in hardware assemblies and construction practices used for these lines. Since gap discharges occur as a consequence of unwanted changes taking place in the hardware assemblies, they are more amenable to corrective maintenance practices rather than to changes at the design stages. This is in stark contrast to corona on transmission-line conductors, which is taken into account at the design stage in order to limit the resulting corona effects to acceptable values during the normal operation of the line.

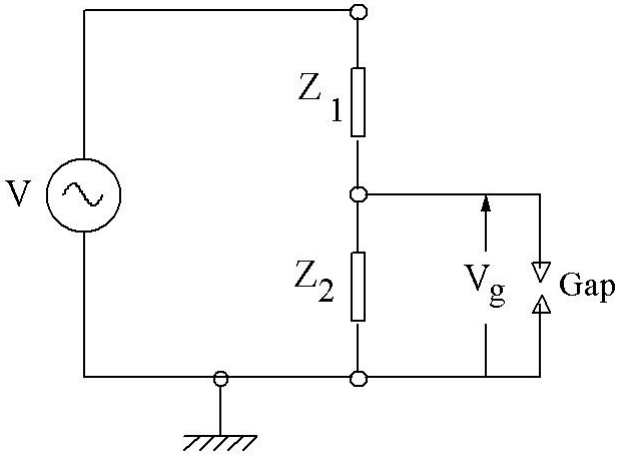


Figure 8.3-1 Equivalent circuit for gap discharge.

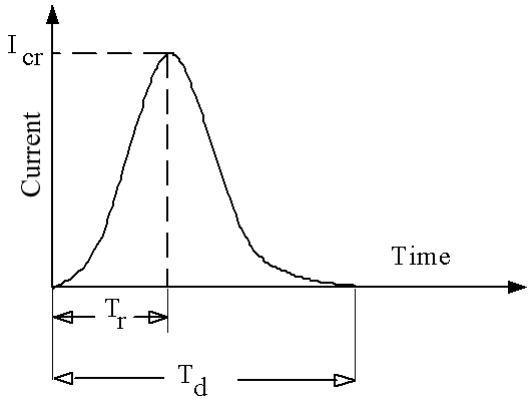


Figure 8.3-2 Gap discharge current pulse.

8.4 CORONA ONSET ON CONDUCTORS AND HARDWARE

8.4.1 Conductors

High-voltage power transmission lines are generally designed to reduce, and in some cases, limit the undesirable effects produced by corona on the conductors. Ideally, it would be preferable to operate a transmission line at a voltage below that necessary to cause corona to occur on the conductors. It would be uneconomical, however, to design a line so that the conductors are corona-free under all operating conditions. Although not playing a direct role in the corona design of transmission lines, it is useful to determine the threshold voltage for the onset of corona on the conductors for any given line configuration.

Corona Onset Gradient

As discussed in Section 8.2.3, corona onset on a conductor is defined as the occurrence of a self-sustained discharge, and it is theoretically possible to determine the conductor surface gradient at which onset of corona occurs, known as the *corona onset gradient*, using Equation 8.2-20. From a practical point of view, however, it is very difficult to determine the corona onset gradient purely from theoretical considerations. A number of experimental studies have, therefore, been carried out, using a concentric cylindrical setup, to determine the corona onset gradient of smooth cylindrical conductors. One of the most commonly used methods is an empirical formula developed (Peek 1929) using data of laboratory measurements at alternating voltages on smooth cylindrical conductors, and is given as

$$E_c = m E_0 \delta \left[1 + \frac{C_1}{\sqrt{\delta r_c}} \right] \qquad 8.4\text{-}1$$

Where:

E_c is the corona onset gradient in kV/cm.

E_0 is an empirical constant.
Peek found E_0 = 29.8 kV/cm (peak value) or 21.1 kV/cm (rms value).

C_1 is an empirical constant that Peek found to be 0.301 cm $^{-1/2}$.

m is the conductor irregularity factor that takes the surface condition of the conductor into account. (See subsection below.)

δ is the relative air density defined in Equation 8.4-2 below.

The corona onset gradient was found to be a function of the *relative air density* δ, given as

$$\delta = \frac{273 + t_0}{273 + t} \cdot \frac{p}{p_0} \qquad 8.4\text{-}2$$

Where:

t is the temperature (° C).

p is the pressure (mm) of ambient air.

t_0 is the reference temperature, usually 25° C.

p_0 is the reference pressure usually 760 mm or 1.013 bar.

For transmission lines traversing mountainous regions, determination of corona onset gradient as well as the overall corona performance requires knowledge of δ as a function of the altitude above sea level. Equation 8.4-2 shows that δ varies inversely as the absolute temperature and directly as the pressure. Variation of the ambient temperature with altitude is a complex function of several parameters and is generally difficult to evaluate. Available data indicate (Humphreys 1964, p. 43) that the average temperature of the surface decreases approximately at the rate of 1°C per each 180 m, 200 m, and 250 m increase of height on mountains, hills and, plateaus, respectively. An average decrease of 1°C per each 200 m may, therefore, be used to determine δ as a function of altitude.

It is comparatively easier to determine the variation of pressure with altitude. Based on a large number of measurements taken in summer and winter, the variation of pressure with altitude has been presented (Humphreys 1964, p. 80) in tabular form for altitudes up to 40 km. An abridged version of this data, giving the average atmospheric pressure for the summer and winter seasons, normalized to 760 mm at sea level, as a function of altitude up to 10 km, is shown in Table 8.4-1.

Table 8.4-1 Variation of Atmospheric Pressure with Altitude

Altitude, km above sea level	Average atmospheric pressure, mm
0.0	760.00
0.5	714.84
1.0	673.07
1.5	633.18
2.0	595.03
2.5	559.02
3.0	524.87
4.0	461.78
5.0	405.06
6.0	354.10
7.0	308.40
8.0	267.43
9.0	230.99
10.0	198.71

The data presented above may also be represented by an empirical formula,

$$p/p_0 = 1 - A/k \qquad 8.4\text{-}3$$

Where:
A is the altitude in km.
k is an empirical constant.

For altitudes of practical interest, up to 5 km, a value of k = 10 gives the best fit with data (Mercure 1989).

It can be seen from the data presented above that the variation of δ with altitude is largely due to the variation in atmospheric pressure. If temperature and pressure data are available from existing meteorological stations along the transmission line route, they can be used directly to determine the value of δ. In the absence of such data, however, the atmospheric pressure may be obtained either from the table or formula given above and a default value for temperature of 25°C may be used to determine the value of δ.

A factor m, known as the *conductor surface irregularity factor*, is introduced in the formula to take into account the fact that practical conductor surfaces are generally not perfectly smooth.

For a given transmission-line configuration, the voltage necessary to make the conductor surface electric field equal to the corona onset gradient is known as the *corona onset voltage*.

Factors Influencing Corona Onset

The most important factor influencing the corona onset gradient is the conductor radius. Peek's formula shows that, all other parameters remaining the same, the corona onset gradient of a conductor varies as an inverse function of its radius. The simple case of a transmission line with a single conductor per phase is used to illustrate how conductor size affects corona onset characteristics. For a given line voltage and configuration, the conductor surface electric field E_s varies inversely as the conductor radius r_c, as shown in Figure 8.4-1. At the same time, the corona onset gradient E_c of the conductor varies, according to Equation 8.4-1, as a slower inverse function of r_c, also shown in the figure. For values of conductor radius $r_c < r_{c1}$, $E_s > E_c$ and corona discharges occur on the conductor. In order to prevent the occurrence of corona, therefore, it is necessary to choose a conductor with a radius greater than r_{c1}.

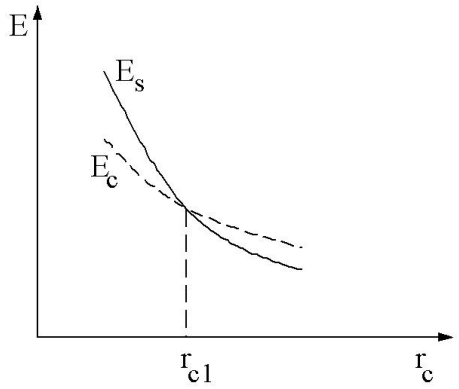


Figure 8.4-1 Conductor size and onset of corona.

Peek's formula was derived based exclusively on experimental data on smooth conductors of small diameter. Extrapolation of this formula to practical conductors of larger diameter has been shown to predict higher corona onset gradients than those measured. In spite of this discrepancy, Peek's formula continues to be used for practical transmission-line conductors, partly because the onset gradient itself plays only a minor role in line design and partly due to the fact that the factor m introduced in the formula masks to some extent the influence of conductor radius.

The influence of conductor surface irregularity factor m on the corona onset gradient is somewhat similar to that of conductor size. For ideally smooth cylindrical conductors, such as those used in early experimental studies, the value of m is equal to 1. However, the surface of a practical transmission line conductor is far from ideal, mainly due to stranding and presence of defects such as nicks, scratches, etc. All such irregularities tend to enhance the electric field in the immediate vicinity of the conductor surface and, consequently, reduce the onset gradient calculated using the nominal conductor radius. This reduction in onset gradient can be taken into account by choosing a value of m less than 1. Thus, the factor m takes into account the uncertainties arising out of practical conductor surface conditions and may be defined as the ratio between the measured onset gradient and that calculated for an ideal smooth cylindrical conductor of the same radius. Experimental studies show that the value of m varies between 0.75 and 0.85 for clean stranded conductors, depending on the radii of the outer strand and of the overall conductor. Presence of nicks, scratches, etc., may reduce the value of m to between 0.6 and 0.8. Any deposits on the conductor surface such as insects, vegetable matter, water drops, snow, ice, etc., may further reduce the value of m in the range of 0.3 to 0.6. Extreme conditions such as insects and vegetable matter deposited on a greasy conductor in a tropical forest, or cumulative deposition of soil and moisture resulting in thick uneven layers of soil on the conductor in a dry offshore region, may reduce m to values as low as 0.2. Such extreme conditions, which result in very high corona losses, have been reported in some regions of the world (Mombello and Maruvada 2001).

The factors considered above, relating mainly to the size and surface conditions of the conductor, affect the electric field distribution near the conductor surface and, as a result, influence the corona onset gradient. Other factors

characterizing the ambient air affect the ionization processes leading to corona discharges and may, therefore, also affect the corona onset gradient. Relative air density δ influences corona onset in a complicated manner, as shown in Equation 8.4-1. Due to the presence of δ in the second term in parenthesis, corona onset gradient varies somewhat less than proportionally with δ. For example, an analysis of laboratory test results lead to the conclusion (Peterson 1933) that the onset gradient varies proportionally with $\delta^{2/3}$. Since relative air density decreases with altitude above sea level, special attention has been paid to the insulation and corona design of transmission lines operating in high-altitude regions (Phillips et al. 1967). Based on results of the Leadville high-altitude tests (Robertson and Dillard 1961), corona onset gradient was found to vary proportionally with $\delta^{1/2}$.

Although humidity in ambient air affects some of the ionization parameters such as electron attachment, there is no clear evidence that relative humidity, in the absence of any condensation on the conductor surface, has any measurable influence on corona onset gradient. All the factors influencing the onset of corona on a conductor also influence the different corona effects that characterize the corona performance of a transmission line. However, while the corona onset gradient or onset voltage serves only as a rough guideline, actual design of a transmission line is based on the magnitudes and statistical distributions of corona effects.

8.4.2 Hardware

In the overall corona design of transmission lines, it is necessary to ensure that different types of hardware, such as toroidal electrodes used with insulator assemblies, spacer dampers required on bundled conductors etc., are corona-free at the operating voltage of the line. For hardware composed of geometrically well-defined electrodes such as toroids, spheres, ellipsoids etc., the surface electric field may be calculated either analytically or numerically using appropriate field calculation software. Design of these types of hardware for corona-free operation can be achieved using analytical methods if their corona onset characteristics are also known. However, if it is not possible to calculate the surface electric field either analytically or numerically, corona testing of hardware, as described in Appendix 8.1, would be required in order to select corona-free hardware.

Knowledge of corona onset characteristics of different types of electrodes is, therefore, an essential part of any analytical design of transmission-line hardware. However, very few studies have been reported on this subject in the technical literature, and no empirical formulas, similar to that of Peek for cylindrical conductors, have been proposed. Based on theoretical considerations of the corona onset criterion for general electrode shapes and some unpublished experimental data on corona onset gradients, guidelines are proposed below for the corona design of electrodes and hardware used on high-voltage transmission lines.

Equation 8.2-21 provides the general criterion for the onset of corona on conductors or hardware of any given geometrical shape. Knowledge of the electric-field distribution in the immediate vicinity of the surface permits evaluation of the ionization integral on the left-hand side of this equation and determination of the corona onset gradient. In the case of a smooth cylindrical conductor, for example, the electric field decreases inversely as the radial distance away from the conductor surface. Taking this field distribution into account, the ionization integral may be evaluated to derive the corona onset criterion, which actually turns out to be very similar to Peek's formula (Cobine 1958, pp. 256-258). For stranded cylindrical conductors, such as those used on transmission lines, the electric-field distribution in the vicinity of a strand can be calculated analytically and the corona onset gradient evaluated (Yamazaki and Olsen 2004) using Equation 8.2-21.

For a general electrode configuration, the electric field distribution in the vicinity of the conductor surface needs to be determined either analytically or numerically and substituted in Equation 8.2-21 to derive the corona onset gradient. A simpler approach may be used, however, for regular surfaces using a principle in electric field theory (Pedersen 1989), which states that the variation of electric field as a function of radial distance from the surface of the electrode depends on the mean curvature H at a given point P on the electrode surface,

$$H = \frac{1}{2}\left[\frac{1}{r_1} + \frac{1}{r_2}\right] \qquad 8.4\text{-}4$$

where r_1 and r_2 are the radii of curvature of the curves through the point P of the normal sections of two mutually perpendicular planes. In practice, r_1 and r_2 correspond to the two principal radii of curvature, or the maximum and minimum values of all possible sets of r_1 and r_2.

An investigation of electrodes for which the electric-field distribution near the surface is calculated using the principle described above and substituted in Equation 8.2-21 has shown (Pedersen 1989) that the corona onset gradient remains the same for different electrode shapes that have

the same mean curvature or, in more practical terms, the same equivalent radius r_{eq} defined as

$$r_{eq} = 2\frac{r_1 r_2}{r_1 + r_2} \quad 8.4\text{-}5$$

It may be noted that electrodes generally fall somewhere between the two extreme cases: a sphere for which r_{eq} is equal to its radius and a cylinder for which r_{eq} is equal to twice its radius.

Experimental studies have shown that the influence of any surface pollution in reducing the corona onset gradient is more pronounced for the larger hardware electrodes than for conductors used on transmission lines. Smooth and polished electrodes have the highest corona onset gradients. Under natural pollution conditions, corona onset starts at low surface gradients and shows improvement with successive voltage applications as the pollution is either removed or burnt off. This phenomenon may lead to a relatively large dispersion in the measured corona onset gradients of electrodes.

Some experimental data on the corona onset gradients of different types of electrodes are available in laboratory reports, but not in published literature. Figure 8.4-2 shows the measured corona onset gradient as a function of r_{eq} for toroidal, spherical and spheroidal electrodes (Maruvada 1973). For purposes of comparison, corona onset gradients of smooth cylindrical conductors, given by Peek's formula, are also shown in this figure. As shown in the figure, the solid straight line drawn below all the data points provides a basis for the design of electrodes to ensure corona-free operation. The relationship between the design gradient E_d on the electrode surface and the equivalent radius r_{eq} of the electrode may be obtained from this line and expressed by the empirical equation:

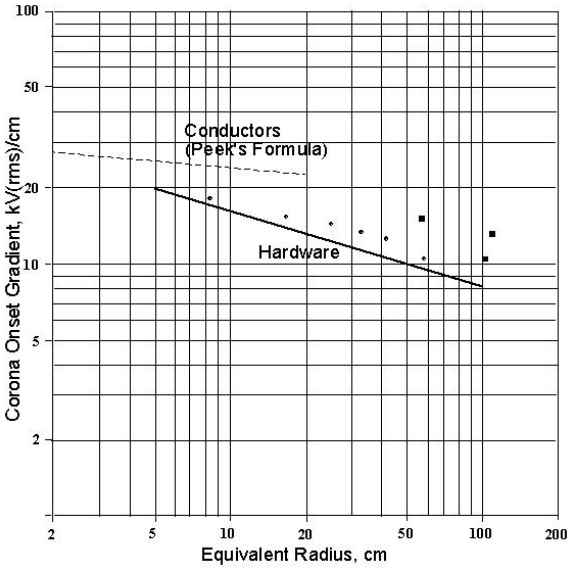


Figure 8.4-2 Corona onset gradient of hardware electrodes (● Toroids; ■ Spheres and Spheroids).

$$E_d = 32.4\left(r_{eq}\right)^{-0.3} \quad 8.4\text{-}6$$

In the absence of more extensive and reliable experimental data, Equation 8.4-6 provides a reasonable basis for the corona design of hardware electrodes. However, if a more conservative design is required (i.e., corona-free operation under some degree of pollution), the empirical equation may be modified as:

$$E_d = 32.4m\left(r_{eq}\right)^{-0.3} \quad 8.4\text{-}7$$

where m is the surface roughness factor, usually of the order of 0.9 or less depending on the expected degree of pollution.

8.5 CORONA EFFECTS

All the diverse ionization processes involved in producing corona discharges in the highly stressed regions near the conductors of transmission lines, as well as the creation and movement of charged particles in the electric field, require an expenditure of energy. This energy is supplied by the high-voltage power source connected to the transmission line, which generates the high electric field near the conductors necessary to sustain corona discharges. Most of the energy is converted to thermal energy for heating the air in the immediate vicinity of the conductors. A small proportion of the energy is converted to electromagnetic radiation including light emission, to acoustic energy, and to electrochemical energy required to produce gaseous effluents ozone and nitric oxides.

8.5.1 Corona Loss

The power loss, defined by the rate at which energy is drawn by corona from the high-voltage power source, is known as *corona loss*. Since the electromagnetic, acoustic, and electrochemical components are only a small part of the overall energy, corona loss is effectively caused by the movement of positive and negative ions in the electric field. The lifetime of electrons created in the discharge, before they attach to neutral molecules and become negative ions, is very short, and consequently, their movement in the electric field gives rise only to short-duration current pulses, which do not contribute significantly to corona loss.

On an ac transmission line, the sinusoidal voltage applied to the conductors causes a capacitive current to be drawn from the power source. Before the onset of corona, the

power source is called upon to supply mainly the capacitive current. The capacitive current flowing in the conductor gives rise to a small amount of I^2R power loss. At voltages above corona onset, however, the oscillatory movement of the ionic space charge in the alternating electric field near the conductor gives rise to an additional alternating current component. Unlike the capacitive current, the current produced by the movement of ions is mostly in phase with the voltage and, therefore, gives rise to power loss, known as corona loss. The corona current also contributes to a small component in phase with the capacitive current, thus causing an apparent increase in the capacitance of the conductor configuration. Analytical treatment of corona loss on ac transmission lines is very complex and requires the solution of time-varying space charge fields. Information required for design purposes is obtained mainly through experimental studies.

8.5.2 Electromagnetic Interference

Corona on transmission-line conductors is generally confined to a number of point sources randomly distributed along the length of each conductor. The linear density of corona sources depends very much on the ambient weather and environmental conditions, with the lowest density occurring in fair weather and the highest in foul weather such as rain. At the conductor surface gradients that transmission lines are generally designed for, the corona modes occurring are usually Trichel streamers during the negative half cycle and the onset streamers during the positive half cycle. Both these modes of corona give rise to current pulses with fast rise time and short duration, as shown in Figure 8.5-1, quite similar to those shown in Figure 8.3-2 for gap discharges.

However, the parameters defining the three pulse shapes—namely, the amplitude, rise time, and duration—are quite different, as shown in Table 8.5-1 (Maruvada 2000). It is seen that gap discharge pulses have the highest amplitudes, fastest rise times, and shortest duration. The amplitudes of positive corona pulses are about an order of magnitude higher than those of negative corona, while the latter have faster rise times and shorter duration.

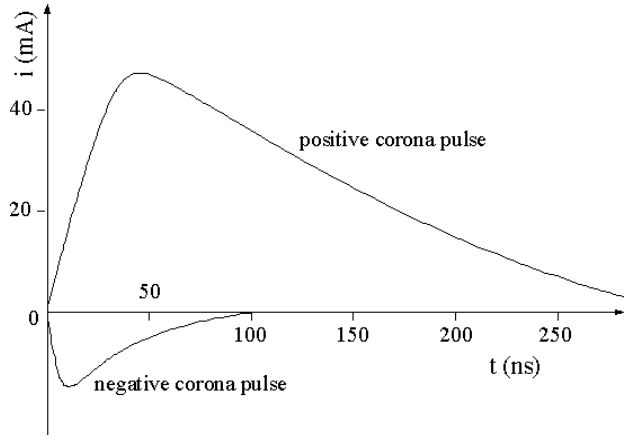


Figure 8.5-1 Corona discharge current pulses.

Table 8.5-1 Characteristics of Corona and Gap Discharge Current Pulses (Maruvada 2000) (Reproduced with permission of Research Studies Press.)

Type of Pulse	Amplitude (mA)	Rise-time (ns)	Duration (ns)	Repetition Rate (pulses/s)
Positive Corona	10 – 50	50	250	$10^3 – 5.10^3$
Negative Corona	1 – 10	10	100	$10^4 - 10^5$
Gap Discharge	500 - 2000	1	5	$10^2 – 5.10^3$

Transient current pulses such as those produced by corona and gap discharges generate EMI over a broad range of frequencies. The characteristics of EMI depend directly on the frequency spectral characteristics of current pulses, which are functions of the parameters defining the pulses as well as on the pulse repetition characteristics. The amplitude of the frequency spectrum of a pulse is proportional to the product of the pulse amplitude and duration (charge content), while the bandwidth is an inverse function of the pulse rise time. The relative frequency spectra of corona and gap discharges are shown in Figure 8.5-2. Positive corona and gap discharge pulses have the highest amplitude of frequency spectrum, and gap discharges also have the widest frequency bandwidth, extending into the GHz range. The frequency spectrum of positive corona pulses begins to fall off rapidly at frequencies between 1 and 2 MHz, while that of negative corona pulses may

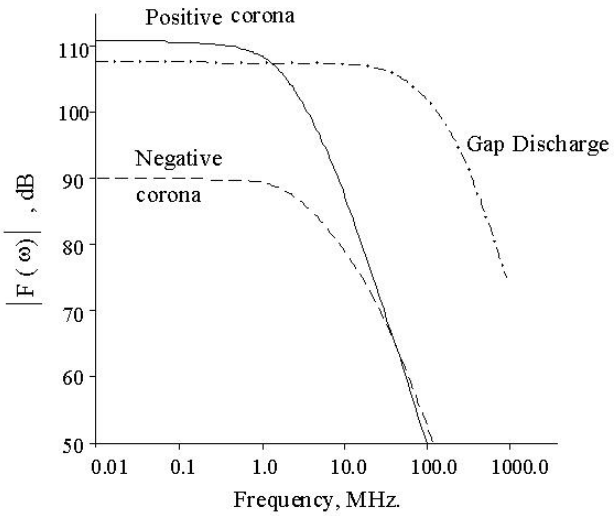


Figure 8.5-2 Frequency spectra of corona and gap discharge current pulses (Maruvada 2000). (Reproduced with permission of Research Studies Press.)

extend up to about 100 MHz. Gap discharges produce EMI covering both radio and television frequency bands and extending up to 1 GHz.

Because of the high impedance to ground, corona as well as gap discharges may be considered as current sources, injecting current pulses into the conductors of transmission and distribution lines. On transmission lines, each corona source injects a random train of current pulses into the conductor on which it is located. Sources on any conductor also induce currents of much lower amplitude in the other conductors of the line. The current pulse injected at any point divides into two pulses, each with half the amplitude of the original pulse, traveling in opposite directions along the conductor. The pulses are subject to attenuation and distortion as they travel, until the amplitude becomes insignificant. Depending on the impedance characteristics of the transmission line, the influence of a corona source extends only up to a finite distance on both sides. Thus, the resultant current flowing at any point along the line is composed of randomly spaced pulses of varying amplitudes arriving from the randomly distributed sources and traveling in both directions. Analysis of corona-generated EMI on transmission lines is quite complex and is generally carried out in the frequency domain, using classical electromagnetic theory of propagation. Since the EMI generated by gap discharges, occurring mainly on distribution lines, extends to frequencies in the GHz range, analytical treatment becomes even more complex.

8.5.3 Audible Noise

The principal modes of corona on transmission lines—namely, negative Trichel streamers and positive onset streamers—consist essentially of repetitive transient discharges in which rapid ionization takes place during a short interval of time on the order of a few hundred nanoseconds. During the development of streamers, the gas within the streamer channel is heated to very high temperatures, while its physical volume cannot expand sufficiently. As a result, the local pressure inside the streamer channel is increased in accordance with physical laws governing gases. The local increase in the gas pressure corresponds, by definition, to the generation of an acoustic pressure wave propagating outwardly from the discharge site.

The typical shape of a single acoustic pulse generated by a pulsative corona discharge (Héroux and Trinh 1976) is shown in Figure 8.5-3. The acoustic pulses due to both positive and negative corona have similar shapes, but the amplitudes at positive polarity are an order of magnitude higher than those at negative polarity, similar to current pulse amplitudes. As in the case of EMI, therefore, positive corona is the main source of AN on transmission lines. The frequency spectrum of the corona-generated acoustic pulse extends wider than the normal audible range of humans—i.e., above 15 kHz.

The random trains of acoustic pulses produced by different sources distributed along the conductor travel different distances in air to arrive at a point in space near ground level where a human observer may be located. Because of their random distribution in space and time, acoustic waves arrive at the point of observation with random phase relationships. Analytical treatment of AN from transmission lines is, therefore, carried out in terms of acoustic power, which does not require any phase information. Contributions from all phases of the line are added to determine the acoustic power perceived at the point of observation.

In addition to the random component described above, AN from ac transmission lines also includes one or more pure tones, which are produced by the oscillatory movement of ionic space charges created in the vicinity of the conductor in both half cycles of the alternating voltage. As they oscillate in the alternating electric field near the conductor, the ions transfer their kinetic energy through elastic collisions to the air molecules and give rise to an acoustic pure tone called *hum* at a frequency twice that of the power frequency (i.e., 120 Hz for a 60-Hz system). Higher harmonics may also be present in hum, but usually of much lower magnitudes. Because of the similarities in the physical mechanisms involved, hum noise is well correlated with corona loss.

8.5.4 Ozone and NO_X

Complex electrochemical reactions take place within the discharge processes of positive and negative corona, resulting in the generation of ozone, O_3, and various oxides of nitrogen, collectively known as NO_x. Dissociation of oxygen molecules in air due to the ionization processes

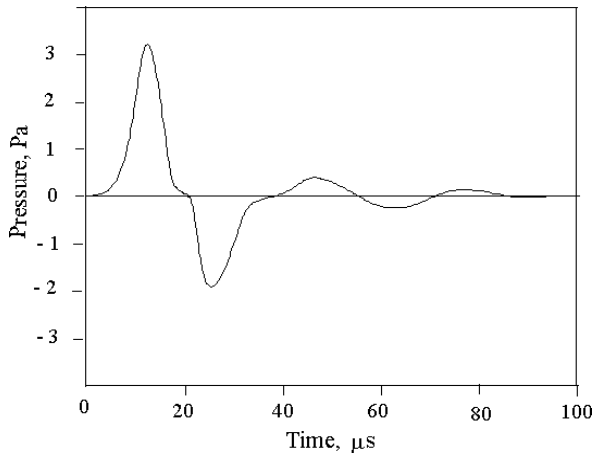


Figure 8.5-3 Corona-generated acoustic pulse.

creates atomic oxygen, which in subsequent reactions gives rise to ozone and nitric oxides. A detailed discussion of ozone generation due to corona on transmission lines is given in Chapter 11.

8.5.5 Light Emission

The processes leading to corona discharges in air give rise to excitation as well as ionization of molecules. As explained in Section 8.2.1, the excited molecules, in which the outermost orbital electrons are bumped to a higher energy state, emit photons when they revert to their original energy state. Other molecules in air absorb some of the photons, but some of them manage to escape and contribute to the visual manifestation of corona discharges. Visual observations show that the light is of pale bluish color. Studies of the emission spectra of corona discharges (Grum and Costa 1976) indicate that most of the light is emitted from excited nitrogen molecules. Figure 8.5-4 shows the typical spectrum of light emitted by corona discharges in air. The spectrum of visible solar radiation is also shown in the figure. It is seen that corona produces mainly low-intensity ultraviolet radiation at the edge of the solar light spectrum.

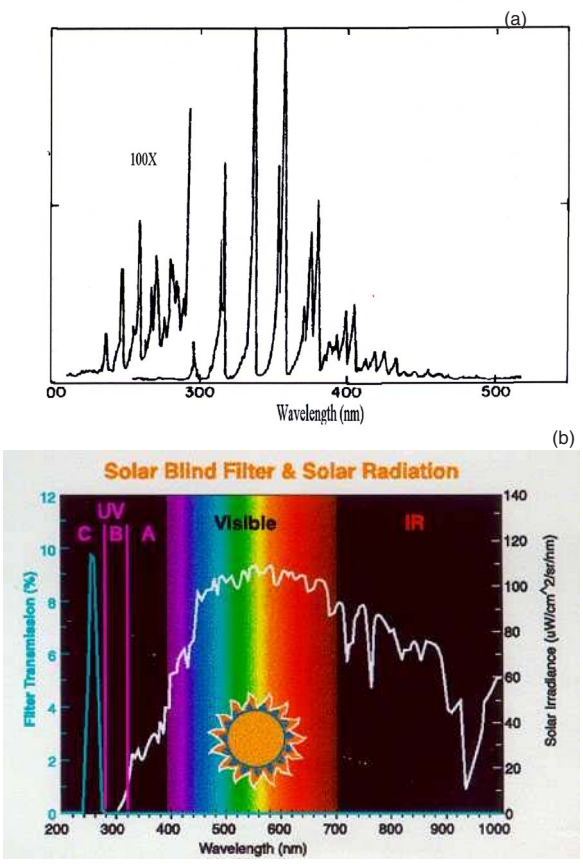


Figure 8.5-4 (a) Corona light spectrum; (b) visible solar light spectrum.

8.5.6 Electrical Wind and Corona-Induced Vibrations

In addition to the widely observed effects described above, corona discharges also produce less well-known effects such as electrical wind and corona-induced vibrations. In cases of both positive and negative corona, ions of the same polarity are created and repelled from the highly stressed conductor. The momentum gained by the ions in the electric field is transferred to the neutral gas molecules, which create a pressure difference in the gas and a flow of gas in motion away from the conductor. This phenomenon is generally known as *electrical wind* (Loeb 1965). Electrical wind is, therefore, a steady-state version of acoustic pulse generation described in Section 8.5.3.

The presence of water drops on conductors during rainy weather may sometimes cause the conductors to vibrate at very low frequency (1-5 Hz) (Newell et al. 1968), giving rise to *corona-induced vibrations*. Water drops on conductors are elongated in the presence of high levels of conductor surface electric field, causing them to eject water droplets. The repulsive electrostatic forces between the ejected drop and the suspended drop, along with the reactive force produced by corona-generated electrical wind as well as by water ejection, exert an upward force on the conductor. Meanwhile, the suspended drop is replenished and is again elongated in the electric field (Adachi and Phan 1981). Corona-induced vibration is excited, first, by electrostatic forces, mainly the Coulombic repulsive forces and reactive force caused by ionic wind. The amplitude of the vibration is then amplified by the mechanical reactive force in the ejection of drops or droplets from the suspended drops.

8.5.7 Other Effects

In addition to the various effects described above that have been subject to experimental and analytical investigations, there has been some speculation in environmental public hearings and even in scientific literature that corona on transmission-line conductors may give rise to other effects that lead to adverse environmental impact. It is useful to consider the plausibility of some of the more notorious of these effects.

Since corona discharges are known to produce electromagnetic radiation, as described in Sections 8.5.2 and 8.5.5, questions have been raised on the possibility of microwave radiation and X rays being produced by corona on transmission-line conductors. Corona-generated EMI at frequencies up to 1 GHz have been measured (Pakala and Chartier 1971) from power lines operating at voltages up to 800 kV. EMI measurements have also been made more recently (Chartier et al. 1986) at 900 MHz on 230-kV and 500-kV double-circuit lines in rainy weather. These studies indicate that measurable EMI may be produced by trans-

mission lines even at frequencies above 1 GHz, but the levels fall off inversely proportional to the frequency. Consequently, any EMI produced by transmission lines in the low microwave frequencies could be detected only in rainy weather, and the levels are so low as not to pose any health risks.

It was also speculated that electrons created by corona on conductors may interact with ambient water molecules to produce microwave radiation in the X and K bands (9 – 25 GHz). A laboratory study (DeVore and Ungvichian 1975) has shown, however, that no measurable radiation was produced at these frequencies. Similarly, the possibility of X ray production due to corona on transmission-line conductors was raised at some environmental hearings, but consideration of the physics involved shows that it is not plausible. Ionization processes in air at atmospheric pressure produce photons at energies corresponding to visible and ultraviolet light as shown in Figure 8.5-4. Since photons of X rays have energies that are two to three orders of magnitude higher than those of ultraviolet radiation, it is physically not possible for corona and gap discharges to produce X rays. In a recent study (Silva et al. 2004), all potential mechanisms for the production of X-rays by transmission line corona were analyzed and evaluated from basic physical principles, and it was concluded that none could produce any detectable amounts of X-rays.

It has been suggested in a recent paper (Fews et al. 1999) that corona ions emitted by high-voltage ac transmission lines will produce charged pollutant aerosols, which in turn may have adverse health implications for any exposed human population. An analysis of the oscillating space charge environment of corona shows, however, that any contribution to charged atmospheric aerosols by high-voltage ac transmission lines is negligible. Support for this conclusion has also been provided (Houlgate 1986) by measurements made on a 400-kV transmission line.

Apart from conductors and hardware, corona may occur on the surfaces of insulation, such as nonceramic insulators and fiber optic cables, causing erosion and eventually leading to insulation failure. Finally corona may also occur on the sharp tips of leaves, vegetation, and other objects located in close proximity of transmission-line conductors, as described in Section 7.15 of Chapter 7.

8.6 FACTORS INFLUENCING CORONA PERFORMANCE

Although onset of corona on the conductors of a transmission line is an important indicator, corona performance of the line is generally described in terms of the three main parameters: CL, RI, and AN. All the factors influencing corona onset described in Section 8.4.2 also affect the corona performance in a similar manner. Generally, if the corona onset voltage of the line is lowered by any of the factors, there will be a corresponding increase in corona loss, radio interference, and audible noise of the line. Laboratory studies have shown good correlation between RI and AN and also between corona loss and the hum component of AN.

8.6.1 Fair Weather Corona Sources

Fair weather may be defined as the absence of any precipitation or of any condensation on the conductors. A number of studies carried out on operating transmission lines (Newell et al. 1967, 1968; Laforest 1968) have shown that the principal sources of corona in fair weather are not defects on conductors such as nicks and scratches, but airborne organic and inorganic substances such as insects, vegetable matter, dust, etc. Any conductor defects produced during manufacture and installation are found to give rise mostly to glow corona and to be smoothed out gradually after about a year following installation. Data collected on operating lines by Project UHV have shown that the number of fair weather sources does not depend very much on the line voltage or the conductor surface gradient, but varies significantly with the seasons of the year. Few sources are present in the winter and the largest number are found in late summer. Depending on the geographical location of the line and ambient weather conditions, the number of fair weather corona sources may vary from 1 to 400/km.

8.6.2 Conductor Surface Conditions

The corona performance of a transmission line under conditions of water deposition, either by condensation (fog) or by precipitation (rain), depends very much on the properties of the conductor surface. The polished metallic surface of a newly installed conductor interacts chemically with the components of ambient air, including moisture and pollution, leading to corrosion or oxidation and formation of a layer of metallic compounds on the surface. Sometimes, particularly on HVDC transmission lines, corona discharges themselves cause changes in the surface conditions. The process, which progresses gradually and changes the chemical nature and physical properties of the conductor surface, is generally called *aging*. The rate at which the actual process of aging takes place depends on the nature of the newly installed conductor and the prevailing environmental conditions.

On stranded aluminum conductors used on high-voltage transmission lines, aging produces gray- or black-colored surface layer. The gray coloring arises mainly due to preferential corrosion in silicon-rich areas. Black-colored coating that is noticeable after several years of operation is formed by aggressive corrosion, which takes place in the presence of water and industrial or organic deposits.

The behavior of water deposited on a transmission-line conductor depends very much on the properties of the surface layer. On reaching the conductor surface, water forms into drops, the shape of which depends on the surface tensions

of water, solid (conductor surface) and water-solid interface (Wernick and Pinner 1972). Surfaces that allow the formation of stable individual water droplets are known as *hydrophobic*, while those on which water spreads and wets the whole surface are known as *hydrophilic*.

New conductor surfaces are usually hydrophobic. A thin layer of grease present on new conductors makes the surface even more hydrophobic. The layers of aluminum compounds formed by the process of aging change the conductor surface and make it hydrophilic. Studies have shown (Héroux et al. 1982; Tong et al. 1975; Héroux 1981) that corona performance of hydrophilic conductors under conditions of rain and fog is generally much better than that of hydrophobic conductors. The reasons for this difference in corona performance are described in the next section.

Because of the improved corona performance of conductors with a hydrophilic surface, attempts have been made (Héroux et al. 1982) to artificially make the surface of a new conductor hydrophilic, a process sometimes known as artificial aging. Two such methods are worth mentioning: 1) sandblasting and 2) wrapping the conductor with cotton or stainless steel fiber. Sandblasting increases the roughness of the conductor surface, which increases its wettability or makes it hydrophilic. Tests have confirmed that sandblasting leads to a significant improvement in the overall corona performance, very similar to natural conductor aging. Wrapping a conductor with cotton tape increases its wettability due to the capillary action of cotton fibers and thus makes the conductor surface more hydrophilic. Wet cotton fibers as well as thin metallic wires wrapped around a conductor promote the formation of glow (ultra-corona) rather than streamer discharges. This tends to decrease RI and AN generated, but increases CL.

8.6.3 Influence of Water on Conductors

Water may be deposited on transmission-line conductors either by condensation during dense fog with high humidity content or by precipitation such as drizzle or rain. Water drops form on the conductor surface, and their subsequent behavior depends very much on the physical properties of the surface. If the surface is hydrophobic, individual water drops form all around the conductor surface. Continuous supply of water from ambient weather makes the water drops coalesce and ultimately fall off due to gravitational forces. If the conductor is hydrophilic, water deposited on the surface flattens out to form a thin film. Water also accumulates in the inter-strand volumes by capillary action. As water accumulates, drops form at the bottom of the conductor and are ultimately ejected by forces of gravity.

The presence of an electric field around the conductor of an energized transmission line exerts additional electromechanical forces on any water drops formed on the surface (English 1948). The combined effect of the electromechanical and gravitational forces tends to flatten any drops on top of the conductor and elongate those located on the bottom side. Since any water drop, flattened or elongated, increases the conductor surface irregularity and reduces the value of m, the corona onset voltage of the line is decreased. This leads to an increase in the CL, RI, and AN levels of the line.

Since water drops may form all around the surface of a hydrophobic conductor, compared to only at the bottom of a hydrophilic conductor, the number of corona sources on the former are likely to be more than those on the latter. This relationship may partly explain the higher values of CL, RI, and AN on new conductors that tend to be hydrophobic, as compared to aged conductors, which are generally hydrophilic. Laboratory studies (Hoburg and Melcher 1975) have shown that there may be another reason for reduced levels of corona effects, particularly RI and AN, from hydrophilic conductors. Results from these studies indicate that, depending on the electric field and water flow rate, electrohydrodynamic forces make the water drops at the bottom of the conductor elongate in the vertical direction, exhibiting fine long tips that eventually break off, ejecting small water drops. This behavior, termed by the authors of the study as "Mode III" behavior, results in a reduction of the amplitudes of the electric as well as acoustic pulses generated and to a reduction of the RI and AN levels.

Particles such as raindrops, snowflakes, dust etc., passing nearby a conductor but not coming in direct contact with it may lead to corona and electrical breakdown of the particle-conductor air gap. The particles' approach causes a local field distortion and may initiate the discharge process. Water drops in particular become elongated, causing further field distortion. The field enhancement thus produced may lead to corona discharge on the moving particle or even to complete breakdown and a gap discharge. Experimental studies have shown (Hatanaka 1981) that gap discharges occurring due to raindrops passing near conductors give rise to television interference.

8.6.4 Influence of Weather Conditions

Weather conditions comprise a broad range of factors including ambient temperature, pressure, and humidity; wind velocity and direction; as well as the occurrence of precipitation such as rain, snow, etc. The atmospheric pressure at any particular location generally does not vary over a wide range, while the temperature may vary significantly from summer to winter conditions. Relative air density, which is a function of both temperature and pressure as shown in Equation 8.4-2, is thus higher in winter than in summer. Seasonal variations in the corona performance of a transmission line may to some extent be explained by variations in ambient temperature, with the corona onset voltage being the highest in winter and lowest in summer.

The influence of relative humidity on corona performance is not well understood. At sufficiently high velocities, wind may be able to move the charged particles away from the discharge region near the conductor. However, there is not enough data to permit conclusions to be drawn on the quantitative influence of wind.

The influence of fog, drizzle, and rain, which deposit water on conductor surfaces, on the corona performance is discussed in the preceding section. Other forms of precipitation, such as snow, ice, hoarfrost, etc., also have a significant influence on corona onset and corona performance. Dry snow occurring at low ambient temperatures forms a surface deposit on the conductor, reducing the value of *m* and increasing CL, RI, and AN. Close to 0° C, however, the precipitation is in the form of wet snow, which sticks to the conductor surface and may cause water drops to form. The corona performance in this case would be similar to that in rain.

Under certain conditions, precipitation in the form of freezing rain may occur, leading to ice accretion on the conductor and formation of icicles, and a consequent reduction in the value of *m*. Although ice-tip corona may not be as severe as that from water drops, it may still cause high levels of CL, RI and AN. Hoarfrost is a different form of precipitation, which occurs when water vapor freezes directly on the conductor at subzero surface temperatures (Lahti et al. 1997). Depending on ambient weather conditions, two types of hoarfrost have been observed (Tikhodeev 2000): crystalline hoarfrost and granular hoarfrost with ice. Experimental studies have shown that crystalline hoarfrost does not usually form on heated conductors and that, when it does, the quantity is smaller than on a cold conductor. Some of the highest levels of corona loss have been reported in hoarfrost. Under conditions of crystalline hoarfrost, corona losses as high as four times those under heavy rain have been observed.

8.6.5 Influence of Conductor Heating

Although not a part of weather conditions, conductor heating caused by the flow of load current affects the atmospheric conditions in the immediate vicinity of the conductor and, therefore, influences the corona performance of the transmission line. Load current flowing through the conductor resistance gives rise to power loss and generates heat, thus raising the conductor temperature above the ambient value. The heat generated also raises the temperature of a thin layer of air surrounding the conductor, the same layer in which corona discharges are likely to occur. This increase in temperature causes the relative air density δ in this layer to decrease, which in turn reduces the corona onset gradient of the conductor. The heat transfer from the conductor and the temperature distribution within the layer of air depend to a large extent on ambient wind conditions and to some extent also on the local air currents created by the rapid movement of ions in the discharge process.

The process by which conductor heating affects the corona performance of a transmission line is quite complex. In addition to reducing the corona onset gradient as described above, conductor heating may also inhibit the formation of water drops under conditions of high humidity, fog, drizzle, etc. While the levels of corona effects tend to be increased due to a decrease in corona onset gradient, inhibition of water drops results in a reduction of these effects. Studies on practical transmission lines (Chartier 1993) show a net reduction in corona effects due to conductor heating.

The highest temperatures attained by conductors presently used on transmission lines are on the order of 100° C. New technologies are making it possible, however, to operate the conductors at temperatures as high as 240° C. At such temperatures, the conductor surface deposits under all types of precipitation will be markedly different. Corona performance of transmission lines using the new type of conductors will, therefore, be significantly different from that of lines presently in operation. Experimental studies, combined with a theoretical analysis of the discharge processes taking place in the corona layer, can provide data necessary to evaluate the corona performance of transmission lines using high-temperature conductors.

8.6.6 Statistical Consideration of Corona Performance

Corona performance of transmission lines, generally defined in terms of CL, RI, and AN, is strongly influenced by weather conditions. Minor variations are caused by seasonal changes in ambient temperature, but different types of precipitation cause major variations, the highest levels usually occurring in heavy rain. The levels of CL, RI, and AN may vary by more than two orders of magnitude over the duration of a year. Any quantitative description of corona performance should, therefore, include a description of the prevailing weather conditions. In some cases, such as evaluating corona losses, possible variation of weather conditions along the length of the line should also be taken into account. Since variations in weather conditions are notoriously unpredictable, their influence on corona performance can be described only in probabilistic terms. Each of the corona effects is represented by a random variable, and the performance during a certain period of time (day, month, or year) is represented statistically as a cumulative distribution, sometimes simply known as *statistical distribution*.

While describing corona effects in statistical terms, it is often useful to present data for specific weather categories, such as fair weather, foul weather, rainy weather, etc.

Definitions of weather categories used in the analysis of corona performance are given in an IEEE Standard (IEEE

Standard 1990). The category *all-weather* is also used to describe the statistical distribution of data collected under all possible weather conditions.

Typical statistical distribution of a corona effect (CL, RI, or AN), plotted on a probability paper, is shown in Figure 8.6-1 for fair and foul weather categories. The all-weather distribution is also shown as the sum of the two individual distributions. Certain quantities derived from the statistical distribution, known as *exceedance levels*, are generally used to represent the overall distribution. Referring to Figure 8.6-1, the exceedance level L_x is the level on the abscissa that is exceeded $X\%$ of the time. In this representation, L_{50} is the median value. Values L_{95} and L_5 are often used to represent the minimum and maximum values, respectively, of the distribution.

8.7 GENERATION QUANTITIES OF CORONA EFFECTS

The complexity of corona discharge processes and the large number of factors influencing corona effects make it impractical to evaluate the corona performance of transmission lines based only on theoretical considerations. Since the first instance when corona was discovered to be a limiting factor in the design and operation of transmission lines, experimental studies were necessary to understand the physics of corona discharges as well as to obtain data for design purposes. The principal test methods used for determining the corona performance characteristics of conductors are indoor laboratory cages, outdoor test cages, and full-scale single-phase or three-phase test lines.

The main purpose of the tests is to obtain data that can be used to predict the corona performance of new line designs. Measurements on operating lines are often used to assess the validity of any prediction methods developed. Studies have shown that results of corona effect measurements in the different test configurations cannot be used directly to predict the performance of practical line configurations. Concepts of generation quantities of CL, RI, and AN have, therefore, been developed mainly for the purpose of converting measured data in test facilities into prediction methods for transmission lines. The basic principle of generation quantities is that they depend only on the physical processes occurring in the immediate vicinity of the conductor and not on the overall test or line configuration.

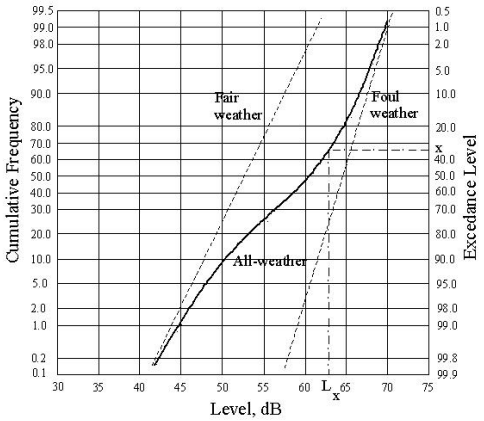


Figure 8.6-1 Statistical distribution of corona effects.

8.7.1 General Principles of Corona Testing

Before discussing the concept of generation quantities, it is useful to review the different test methods used for corona performance evaluation of conductors. The purpose of tests is usually to measure one or more of the following parameters: corona onset gradient, CL, RI, and AN.

Laboratory studies on conductors are generally carried out in a *cage* configuration, in which the test conductor is placed concentrically inside a metallic cylinder, usually made of some form of a wire-mesh and called the cage, of a much larger diameter than the conductor. High conductor surface electric fields are produced by applying sufficient voltage between the conductor and the outer cage, which is connected to ground, sometimes through small measuring impedance. The main advantage of the cylindrical cage configuration is that the conductor surface gradient E_c can be calculated easily as

$$E_c = \frac{V_t}{r_c \ln\left(\frac{r_g}{r_c}\right)} \qquad 8.7\text{-}1$$

Where:

r_c is the conductor radius.
r_g is the inner radius of the cage.
V_t is the test voltage.

Different values E_c are obtained, therefore, by varying the test voltage V_t.

Early test cage setups were small and were used mainly to determine corona onset gradient of smooth conductors of relatively small diameter. They were also used to study the physical characteristics of corona discharges, including the electrical and acoustical characteristics of corona pulses, at direct and alternating voltages. Studies on larger-diameter stranded conductors, of the type used on transmission lines, require larger cages and higher voltages. With sufficiently large cages, some studies of corona loss and ozone generation could also be carried out. It is not possible, however, to obtain useful RI and AN data from laboratory cage tests.

For tests on conductors and conductor bundles normally used on transmission lines, cages with large diameter (a few meters) are required. Also, to be able to make any meaningful measurements of CL, RI, and AN, the cage should also be sufficiently long (a few tens of meters). Because of the larger dimensions of the test setup, such

cages can be built mainly outdoors. Due to the larger dimensions required, outdoor cages are often built with a square rather than a circular cross section (Trinh and Maruvada 1977; Comber and Zaffanella 1974; Gary and Moreau 1976). Although they are usually equipped with some kind of sprinkler systems for studies of corona performance under artificial rain conditions, outdoor cages can also be used (Gary and Moreau 1976) for studies under natural weather conditions.

Although outdoor cages are inexpensive to build and easy to operate, they are suitable for studies only under heavy rain conditions and not for obtaining statistical data under all weather conditions. For obtaining long-term data under different weather conditions, short sections of full-scale transmission lines, called test lines, are used. Either single-phase or three-phase test lines may be used for ac corona studies. Since three-phase test lines accurately reproduce the electric field conditions of normal transmission lines, most corona studies at high voltages were carried out using such installations (Nigol and Cassan 1961; Shankle et al. 1965; Perry et al. 1979). However, they are more expensive to build, and it is more difficult to analyze radio noise measurements on short three-phase lines. Single-phase test lines are comparatively less expensive, and it is easier to predict the corona performance of transmission lines of different configurations based on measurements from single-phase test lines.

Outdoor test cages and test lines provide the information necessary for selecting conductors or conductor bundles used on transmission lines. It is also important, however, to select hardware used on transmission lines as well as on equipment so that corona discharges do not occur under normal operating conditions. Corona testing of both line and equipment hardware and methods generally used for corona detection indoors and outdoors are described below.

Corona Testing of Hardware

The basic electrical requirement for selecting hardware, used for supporting conductors as well as for connecting equipment to transmission lines, is that corona discharges do not occur at normal operating voltage. Corona testing of hardware is generally carried out in the laboratory on a single-phase test configuration, which is preferred mainly to avoid the inconvenience and cost of performing three-phase tests. It is necessary, however, to select the single-phase test voltage that produces the same electric field conditions on the hardware as under normal three-phase operation. This can be done in principle using three-dimensional field calculations. A completely experimental technique for producing the necessary field conditions on the hardware is based on the use of a sphere calibrator (Nigol 1979). Guidelines for corona testing of hardware are described in Appendix 8.1.

Corona Detection

It is often necessary to detect the onset of corona accurately in the laboratory and also the presence of corona or gap discharges on transmission and distribution equipment in operation. In both cases, one of the different manifestations of the discharges may be used for detection. Devices have been developed based on detection of either electromagnetic energy in the radio and television frequency bands or of acoustic energy emitted by corona. It is difficult using such techniques, however, to determine the location of the discharge accurately.

It is possible to locate the source of discharge more accurately by detecting the light energy emitted. As mentioned in Section 8.5.5, most of the light emitted by corona and gap discharges is in the ultraviolet (UV) region, just bordering the high-frequency end of visible light spectrum. Detection of UV radiation emitted by discharges with the naked eye is possible only in a darkened laboratory or against a dark background at night outdoors. Light amplification devices may be used in the laboratory or for night vision outdoors to enhance the sensitivity of corona detection. Some advanced UV detection devices have been developed recently, using either a gated imaging technique (Vosloo et al. 1997) or a dual spectrum system (EPRI 2002), which combines solar-blind UV detection with a visible light camera to image the discharge source, for daytime detection of corona on transmission and distribution systems. The dual-spectrum camera system seems to be the most sensitive method currently available for daytime corona detection.

8.7.2 Generated Corona Loss

The concept of generated corona loss requires the identification of a corona loss parameter that is independent of the conductor configuration and can be used to predict the CL of any line configuration based on data obtained in a test installation. For a clear understanding of the concept, consider the concentric cylindrical configuration shown in Figure 8.7-1, with a conductor of radius r_c placed inside a larger cylinder of radius r_g.

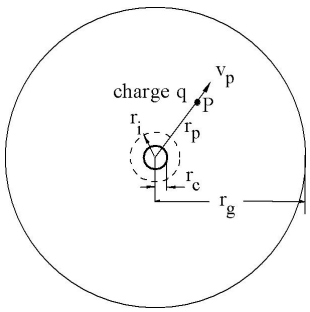


Figure 8.7-1 Generated corona loss in a cylindrical configuration.

The ionization zone in which corona discharges occur is shown as a thin layer around the conductor with a radius r_i. Ions created by corona discharge move out of this zone and are subject to an oscillatory movement in the alternating electric field. The maximum radius r_m, attained by the ions before they are forced to return to the conductor, is generally much less than r_g for practical cage installations.

The oscillatory movement of each ion in the alternating electric field induces a current, which is drawn from the power source connected to the conductor and thus gives rise to power loss. The cumulative effect of all the ions created by corona and moving in the electric field corresponds to the total corona current and to the corona loss of the conductor. The conductor surface electric field E_c, corresponding to the voltage V_1 on the conductor at any given time t, is

$$E_c = \frac{V_1}{r_c \ln\left(\frac{r_g}{r_c}\right)} \qquad 8.7\text{-}2$$

The electric field E_p at a point P, at a radial distance r_p is

$$E_p = \frac{V_1}{r_p \ln\left(\frac{r_g}{r_c}\right)} = \frac{E_c\, r_c}{r_p} \qquad 8.7\text{-}3$$

For an ion with a charge q located at P, the velocity v_p is in the radial direction, similar to the electric field, and is given as

$$v_p = \mu\, E_p = \mu \frac{E_c\, r_c}{r_p} \qquad 8.7\text{-}4$$

The movement of the ion, caused by the force exerted on it by the electric field, induces a current in the conductor. The amplitude of the current at the instant t may be obtained using Shockley-Ramo theorem (Appendix 8.2) as

$$i_c(t) = q \cdot \frac{1}{r_p \ln\left(\frac{r_g}{r_c}\right)} \cdot v_p = q \cdot \frac{1}{r_p \ln\left(\frac{r_g}{r_c}\right)} \cdot \mu \frac{E_c\, r_c}{r_p}$$

The instantaneous power loss $p(t)$ is then obtained as

$$p(t) = U_1\, i_c(t) = U_1 \cdot q \cdot \frac{1}{r_p \ln\left(\frac{r_g}{r_c}\right)} \cdot \mu \cdot \frac{E_c\, r_c}{r_p}$$

which simplifies, using Equation 8.7-1, to

$$p(t) = q\,\mu \cdot \left(\frac{E_c\, r_c}{r_p}\right)^2 \qquad 8.7\text{-}5$$

Equation 8.7-5 shows clearly that the instantaneous power loss $p(t)$ is a function only of the ionic charge q and the electric field conditions existing in the immediate vicinity of the conductor surface and is independent of the voltage applied to the conductor and the parameters defining the conductor configuration. If the same conductor is placed at a certain height H above a ground plane rather than in a cylindrical cage as considered above, the voltage that has to be applied to conductor in order to obtain the same gradient E_c will be different. However, if a derivation is made, following the same steps as described above, the instantaneous power loss will be given exactly by Equation 8.7-5. This conclusion can be extended to corona loss, which is obtained by summing the contributions due to all charged particles created by corona and integrated over a complete cycle of the alternating voltage. It should be emphasized that the conclusion is valid in the case of all practical conductor configurations, provided the corona-generated space charge is confined to a region close to the conductor surface.

The *generated corona loss* may, therefore, be defined as the loss per unit length of the conductor, and it is a function only of the conductor radius and the electric field distribution near its surface and not on the overall conductor configuration. Thus, for the same conductor surface gradient, the generated CL is the same whether the conductor is in a cage or on a single- or three-phase transmission-line configuration.

8.7.3 Radio Noise Excitation Function

The level of radio noise produced by a transmission line depends on the characteristics of the current pulses generated by corona activity near the conductor as well as on the propagation of these pulses along the line. Characterizing the generation activity by a quantity that depends only on the electric field and space charge distribution near the conductor, and not on the actual conductor or line configuration, greatly simplifies the RN propagation analysis. Adams (Adams 1956) was the first to provide the concept of such a quantity. Gary (Gary 1972) subsequently refined Adams's proposal and introduced the concept of RN *excitation function*, which can be measured experimentally in a cage or test line facility and then used in a propagation analysis to determine the RI characteristics of any given line configuration. The concept of excitation function for single- or multiple- conductor systems is explained below.

Considering a single-conductor configuration, cage or line, the movement of a charge q (mainly electrons in the case of current pulses) created by corona induces a current i in the

conductor, which can be calculated using Shockley-Ramo theorem (Appendix 8.2) as

$$i = q \cdot \frac{C}{2\pi\varepsilon_0} \cdot \left(\frac{1}{r_p}\right) \cdot v_p \qquad 8.7\text{-}6$$

where C is the capacitance per unit length of the conductor in the configuration being considered, r_p is the radial distance of the point where charge q is located and v_p is the radial velocity with which the charge moves. Equation 8.7-6 may be rearranged as

$$i = \frac{C}{2\pi\varepsilon_0} \cdot \left(\frac{q}{r_p} \cdot v_p\right) = \frac{C}{2\pi\varepsilon_0} \cdot \Gamma \qquad 8.7\text{-}7$$

The term Γ in this equation is a function only of corona activity near the conductor. The current induced in the conductor depends, therefore, on two independent factors:

1. the capacitance, which is a function of the geometrical parameters of the configuration; and
2. the density and the velocity of movement of space charges, which depend on the electric field distribution and corona activity near the conductor.

The term Γ in Equation 8.7-7 is defined as the RN *excitation function*.

In the context of RN generation, i represents random current pulse trains induced in the conductor. In frequency domain, it represents the current measured at a certain frequency by a radio noise meter with a specified bandwidth. For purposes of propagation analysis, the rms value of the current, expressed in terms of power spectral density, measured by the RN meter is considered. Since RN excitation function Γ as defined above is independent of the conductor geometry, it can be measured in a simple geometry, such as a cylindrical cage or a single-phase test line, and used in the propagation analysis of any transmission-line configuration.

On a multiconductor line, corona activity near one conductor may induce RN currents in all the other conductors. Considering the n-conductor line configuration shown in Figure 8.7-2, corona activity near conductor k induces currents in the conductor k itself as well as in all the other conductors of the line. The current induced in conductor k may be obtained, using the Shockley-Ramo theorem (Appendix 8.2), by setting $V_k = 1.0$ and $V_j = 0$ for $j \neq k$, and calculating the charge densities induced on the conductors as

$$\begin{bmatrix} q_1 \\ q_2 \\ \vdots \\ q_k \\ \vdots \\ q_n \end{bmatrix} = [C] \begin{bmatrix} 0 \\ 0 \\ \vdots \\ 1.0 \\ \vdots \\ 0 \end{bmatrix} \qquad 8.7\text{-}8$$

where $[C]$ is the square capacitance matrix of the line. It follows from Equation 8.7-8 that

$$q_j = C_{jk}, \quad j = 1, 2, \ldots n \qquad 8.7\text{-}9$$

Where:

C_{jk} is the mutual capacitance between conductors j and k.

The electric field near the surface of conductor k at a radial distance r_p where the charge created by corona, q_c, is located, is given as

$$E(r_p) \approx \frac{q_k}{2\pi\varepsilon_0} \cdot \left(\frac{1}{r_p}\right) = \frac{C_{kk}}{2\pi\varepsilon_0} \cdot \left(\frac{1}{r_p}\right) \qquad 8.7\text{-}10$$

In calculating the field $E(r_p)$ as shown above, the influence of charges on all conductors other than k are neglected, since r is generally much smaller than the inter-conductor distances. The current induced in conductor k due to the movement of q_c with a radial velocity v_p is

$$\begin{aligned} i_k &= E(r_p) \cdot q_c \cdot v_p \\ &= \frac{C_{kk}}{2\pi\varepsilon_0} \cdot \left(\frac{q_c}{r_p}\right) \cdot v_p \end{aligned} \qquad 8.7\text{-}11$$

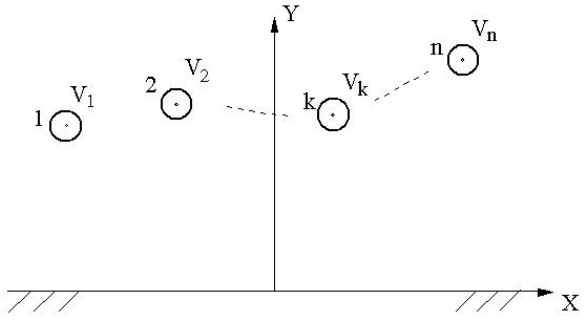


Figure 8.7-2 Multiconductor transmission line.

The term $\left(\frac{q_c}{r_p}\cdot v_p\right)$, which depends only on the electric field and space charge conditions near the conductor k, may, therefore, be defined as the excitation function Γ_k. Therefore,

$$i_k = \frac{C_{kk}}{2\pi\varepsilon_0}\cdot\Gamma_k \qquad 8.7\text{-}12$$

The current in conductor j due to corona near conductor k may be obtained with similar reasoning as

$$i_j = \frac{C_{kj}}{2\pi\varepsilon_0}\cdot\Gamma_k \qquad 8.7\text{-}13$$

Equations 8.7-12 and 8.7-13 may be generalized, and since $[C]^T = [C]$ for a transmission line, to obtain

$$[i] = \frac{1}{2\pi\varepsilon_0}[C][\Gamma] \qquad 8.7\text{-}14$$

Where:

$[i]$ is the column matrix of currents induced in the conductors.

$[\Gamma]$ is the column matrix of generated RN excitation functions.

$[C]$ is the capacitance matrix of the line.

Data on RN excitation function obtained from corona test facilities may be used along with Equation 8.7-14 to carry out RN propagation analysis for any transmission-line configuration.

8.7.4 Generated Acoustic Power Density

Similar to the cases of CL and RN considered above, the concept of a generation quantity provides a bridge between AN data obtained in test installations and predicting the AN performance of any transmission-line configuration. A conductor with uniformly distributed corona sources is a linear source of acoustic power generation. However, an elemental length dx of a conductor may be considered as a point source. If the *generated acoustic power density* due to corona on the conductor is A W/m, the point source will have a power of Adx watts. Spherical sound waves emanate from the point source, so that the acoustic power dJ_p received at a point of observation P is given as

$$dJ_p = \frac{A\,dx}{4\pi r_p^2} \qquad 8.7\text{-}15$$

Where:

r_p is the radial distance from the source to the point P.

If ℓ_T is the length of conductor in the test installation, then the total acoustic power J_p measured at P using appropriate instrumentation is obtained as

$$J_p = A\cdot\int_{\ell_T}\frac{1}{4\pi r_p^2}\,dx \qquad 8.7\text{-}16$$

Since the conductor surface gradient is assumed to remain the same along the length of the test conductor, the generated acoustic power density A is constant, while the distance r_p is a function of x. Thus, Equation 8.7-16 provides the basis for determining the generation quantity A, which depends only on the electric field and space charge distribution near the conductor, from measurements made in test installations. The quantity A can be used subsequently in a propagation analysis to predict the AN performance of different transmission line configurations.

8.8 CORONA ATTENUATION OF POWER SYSTEM OVERVOLTAGES

Most of the corona effects described in the preceding sections may be considered as problems affecting transmission-line design, which should be limited to acceptable levels in order to meet the economic and environmental design criteria. However, corona on conductors can also play a positive role by improving the insulation performance of transmission lines. In particular, the energy dissipated by corona tends to reduce the magnitudes and severity of any overvoltages to which the line insulation may be subject, thus reducing the probability of insulation failure.

Overhead transmission-line insulation consists mainly of the different air gaps between the energized conductors themselves and between the conductors and ground, as well as of the insulating supports (ceramic and nonceramic insulators) required to keep the conductors in place. The insulation is called upon to withstand the stresses produced not only by the normal system operating voltage, but also by the overvoltages that may be imposed on the conductors. The principal categories of overvoltages that might occur on transmission lines are lightning, switching, and temporary overvoltages (IEC Standard 1993).

Design of transmission lines from the point of view of corona performance is carried out for operation at the nominal system voltage. The steady-state voltage used for insulation design, however, is the maximum system voltage that occurs under normal operating conditions at any time and at any point on the system. An *overvoltage* is any transient voltage with a peak value higher that of the maximum system voltage. An important distinction is generally made between overvoltages of short duration (lightning and switching) and those of relatively long duration (temporary).

Lightning discharges occurring in the vicinity of high-voltage transmission lines (*see* Chapter 6) cause transient overvoltages of very short duration to appear on the conductors. The overvoltages may be caused by the lightning stroke directly hitting the phase conductor or ground wire or indirectly the ground in proximity to the line. Currents of enormous magnitude (several tens of kA) are injected by the direct impact of lightning on conductors and ground wires, producing overvoltages as they pass through the complex impedance network to ground. Lightning strokes to ground occurring close to a line produce overvoltages on conductors by electromagnetic induction. Lightning overvoltages are usually unipolar impulses with a rise time on the order of a few microseconds and duration on the order of 100 μs, which propagate along the conductors in both directions away from the point of incidence.

Switching overvoltages occur due to switching operations such as line energization or reclosing (*see* Chapter 5), fault occurrence, and clearing and switching of capacitive and inductive currents. Although switching overvoltages may have different oscillatory, aperiodic and repetitive waveforms, for the purpose of insulation design, they are generally represented by unipolar impulses with a rise time on the order of a few hundred microseconds and duration on the order of a few milliseconds. They also propagate along the conductors, away from the point of occurrence.

Temporary overvoltages, sometimes also called dynamic overvoltages, are oscillatory voltages of relatively long duration and arise from ground faults (*see* Chapter 4), sudden load changes, resonance, and ferroresonance. The frequency of oscillation is very close to the power frequency, and the overvoltage may persist until removed by some sort of switching operation. Temporary overvoltages also propagate along the transmission line. While the amplitude of lightning overvoltages depends on external factors such as the amplitude of lightning stroke current, that of switching and temporary overvoltages depends mainly on the system voltage and other system parameters.

As they propagate along the line, all overvoltages are subject to attenuation and distortion, the extent of which depends on the impedance characteristics of the line and waveshape of the overvoltage itself. The main sources of attenuation are resistive losses in the conductors and ground, losses caused by the occurrence of corona on conductors, and any insulation leakage losses. From the point of view of insulation design, it is important to determine in a realistic manner the overvoltage levels to which transmission systems are exposed. These levels should, therefore, be determined taking into account the specific influence of corona on conductors in attenuating different overvoltages, which may be defined as corona attenuation. The following subsections describe the physical aspects of corona under different types of overvoltages described above, the influence of corona-generated space charge on conductor capacitance and energy dissipation, and possible corona models that may be used in electromagnetic transients programs to evaluate corona attenuation of overvoltages.

8.8.1 Lightning Overvoltages

As mentioned above, lightning overvoltages are unipolar impulses that may be represented by a waveform shown in Figure 8.8-1. The shape of the impulse consists of a fast-rising front, followed, after reaching a peak value, by a slowly decaying tail. It is usually characterized in terms of the peak value V_m, front time t_f and time to decay to half of peak voltage on the tail, t_h. The peak values of lightning overvoltages are usually much higher than the corona onset voltage V_0 of the conductor or conductor-bundle used on the transmission line. The rise time is in the range of 1-2 μs, and the time to half value is in the range of 40-60 μs. Impulse voltages of this type are usually specified in terms of the peak voltage V_m and t_f/t_h values. Standard lightning impulses are usually specified as 1/50 μs.

At voltages below corona onset, the current resulting from a lightning impulse is purely capacitive. Above corona onset, however, the movement of corona-generated space charge near the conductor produces an additional current component. Impulse corona characteristics of transmission-line conductors are generally obtained as charge-voltage diagrams or *q-v* curves, with the simultaneous recording of the voltage *v(t)* and charge *q(t)* displayed along the x and y axes of the curve. The *q-v* curves on conductors may be obtained in laboratory (Davis and Cook 1960) or outdoor (Maruvada et al. 1977) cages and sometimes on a transmission line (Gary et al. 1983). A typical *q-v* curve is shown in Figure 8.8-2.

As the voltage increases from zero up to the corona onset voltage v_0, the current is purely capacitive (i.e., dielectric displacement current), and is given as

$$i(t) = C_0 \frac{dv}{dt} \qquad 8.8\text{-}1$$

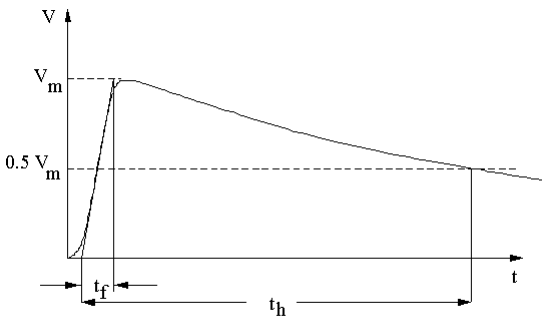


Figure 8.8-1 Lightning impulse waveform.

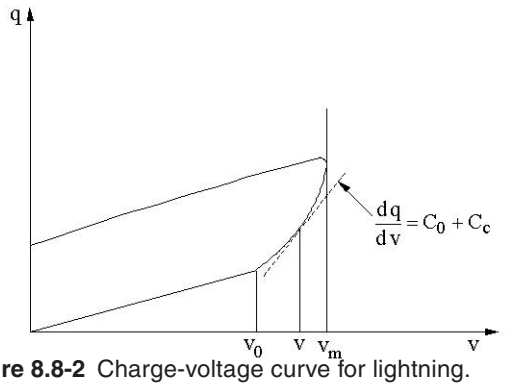


Figure 8.8-2 Charge-voltage curve for lightning.

and the charge is given as

$$q(t) = \int i(t)\,dt = C_0\,v(t) \qquad 8.8\text{-}2$$

Where:

C_0 is the geometric capacitance of the conductor configuration.

Above the corona onset voltage v_0, however, the current consists, in addition to the capacitive component, a component due to the creation and movement of corona-generated space charge. The total current is then given as

$$i(t) = C_0 \frac{dv}{dt} + \frac{dq_c}{dt} \qquad 8.8\text{-}3$$

Where:

q_c is the charge produced by corona.

The second term in this equation may be expressed as

$$\frac{dq_c}{dt} = \frac{dq_c}{dv}\cdot\frac{dv}{dt} = C_c\cdot\frac{dv}{dt} \qquad 8.8\text{-}4$$

The term $\frac{dq_c}{dv}$ may be interpreted as an equivalent corona capacitance C_c, which is dynamic, nonlinear and time-varying. Referring to the *q-v* curve between v_0 and the peak voltage v_m, the slope at any point corresponds to the total capacitance $C_t = C_0 + C_c$. After reaching the peak value v_m, the voltage decreases gradually to zero and the upper, more or less straight line, part of the *q-v* curve is obtained.

The shape of the *q-v* curve affects the attenuation characteristics of lightning impulses propagating on a transmission line. The principal parameters defining the *q-v* curve are: corona onset voltage v_0, corona capacitance C_c and the energy absorbed due to corona, which is given by the area included in the *q-v* curve.

Experimental studies have shown (Davis and Cook 1960; Maruvada et al. 1977; Gary et al. 1983) that the corona onset gradient of a conductor, and hence the onset voltage, is higher for impulse voltages than that given by Peek's formula for power-frequency voltages. In fact, the onset gradient increases with the steepness of the impulse wavefront. For lightning impulses, the onset gradient may be 10-15% higher (Maruvada et al. 1977) than that given by Peek's formula. Although the corona capacitance varies nonlinearly with voltage above onset, a simplified linear representation is often used for the total capacitance C_t between v_0 and v_m as shown in Figure 8.8-3. In the simplified representation, the return part of the *q-v* curve is represented by the geometric capacitance C_0. The ratio C_t/C_0 is found to vary between 1.5 and 5, depending on conductor configuration and the steepness of the impulse wavefront. The ratio is also found to increase with conductor size, but decrease with the number of conductors in the bundle (Maruvada et al. 1977). The energy absorbed by corona also depends on the impulse wavefront. For the same peak voltage, the energy absorbed is higher for steep-front lightning impulses than for slower-front impulses.

Modeling corona for studies on the attenuation of lightning impulses are carried out (Davis and Cook 1960) by taking into account the reduced speed of propagation due to the increased corona capacitance. More recently, Suliciu proposed (Suliciu and Suliciu 1981) a method of propagation analysis, which takes into account the overall *q-v* curve.

8.8.2 Switching Overvoltages

Switching surges play a greater role in the insulation design of higher voltage transmission lines (≥ 400 kV). However, because of the differences in waveform, corona attenuation of switching surges is lower than that for lightning impulses. Although a realistic evaluation of the magnitude, including the influence of corona attenuation is desirable, recent developments in switching technology may have reduced the importance of switching overvoltages in the overall insulation design of transmission lines.

For standardized unipolar switching impulses, the corona characteristics may also be represented by *q-v* curves as shown in Figure 8.8-4. Because of a slower-rising wave-

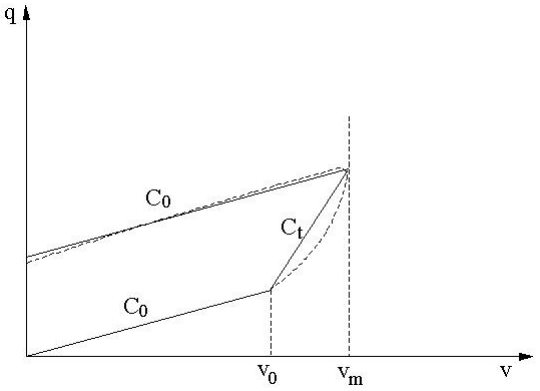


Figure 8.8-3 Linearized *q-v* curve for lightning impulse.

front, the corona onset gradient under switching impulses is nearly the same as that given by Peek's formula. Above corona onset, the slope of the *q-v* curve increases slowly until the peak voltage is reached and then reverts slowly to the slope corresponding to the geometric capacitance of the conductor on the tail of the impulse. The ratio of C_t/Co varies in the range of 1.5 to 2.5 for different conductor configurations and the energy absorbed by corona is lower than in the case of lightning impulses. Based on results of experimental studies, an empirical formula has been developed (Maruvada et al. 1977) for the energy *W* as

$$W = k_1\left(\frac{v_m}{v_0} - 1\right)^{k_2} \qquad 8.8\text{-}5$$

Where:

v_m is the peak value of the impulse voltage.

v_0 is the corona onset voltage.

Empirical constants k_1 and k_2 are determined by the least-square approximation of experimental data. Values of k_1 and k_2 determined for single and bundled conductors tested using different switching impulse waveforms are summarized in Table 8.8-1.

Equivalent circuit models of switching impulse corona have been proposed (Maruvada et al. 1977; Kudyan and Shih 1981) for use in analog and digital studies of corona attenuation. A typical analog corona model (Maruvada et al. 1977) is shown in Figure 8.8-5. Under the application of a switching impulse voltage *v(t)*, the circuit presents the geometric capacitance C_0 for voltages less than v_0. Above the voltage v_0, two additional components are brought into the circuit: the corona capacitance C_c and the conductance G_c, representing the energy loss due to corona. After the impulse peak voltage v_m is reached, for voltages $v_0<v(t)<v_m$, G_c alone remains in the circuit in parallel with C_0. The parameter G_c is chosen to obtain the energy dissipated equal to the experimental value.

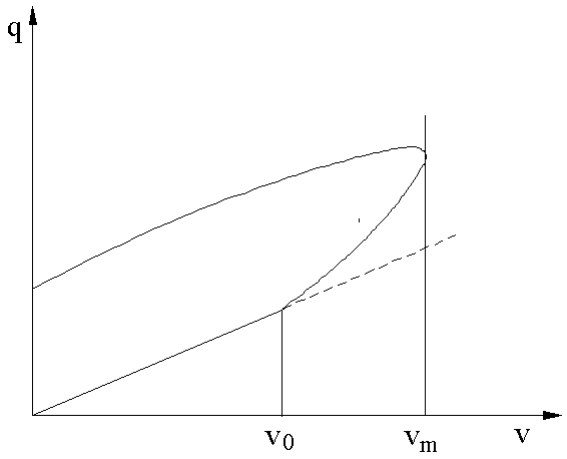


Figure 8.8-4 *q-v* curve for switching impulse.

Equivalent circuit parameters calculated for different conductor bundles and for the longest of the switching impulse waveforms used (~ 260/2500 μs) are shown in Table 8.8-2.

The measured and simulated *q-v* curves for a four-conductor bundle (Maruvada et al. 1977) are shown in Figure 8.8-6.

Table 8.8-1 Empirical Constants Determined for Different Conductor Bundles and Switching Impulse Waveforms (Maruvada 1977)

Conductor Bundle (number x diameter)	Switching Impulse (positive polarity)	k_1	k_2
1 x 1.2”	260/2700 μs 75/2500 μs	76.2 75.2	1.55 1.41
1 x 1.823”	250/2600 μs 75/2500 μs	87.9 82.9	1.06 1.22
4 x 1.2”	260/2300 μs 75/2300 μs	570.9 353.9	1.17 0.91
6 x 1.823”	260/2500 μs 75/2300 μs	1962.5 823.2	1.61 0.75

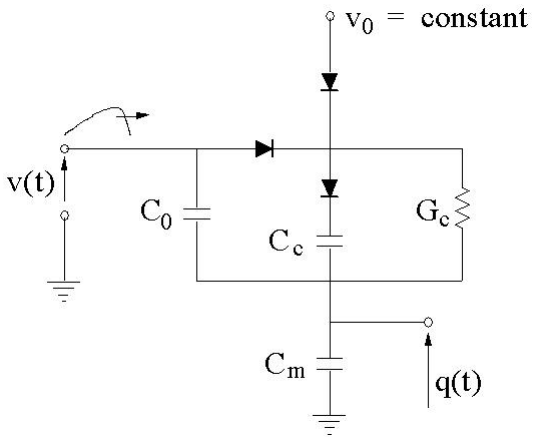


Figure 8.8-5 Analog corona model for switching impulses.

Table 8.8-2 Equivalent Circuit Parameters for Switching Impulse Corona (Maruvada 1977)

Conductor Bundle (number x diameter)	C_0 (nF)	C_c (nF)	G_c (μS)
1 x 1.2”	0.65	0.50	0.10
1 x 1.823”	0.70	0.63	0.11
4 x 1.2”	1.20	0.70	0.20
6 x 1.823”	1.60	0.90	0.25

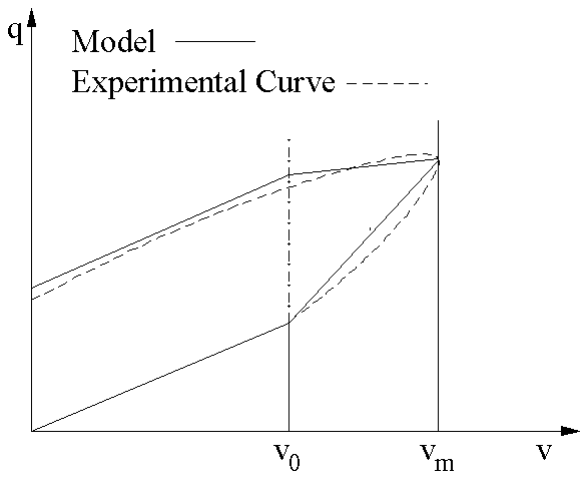


Figure 8.8-6 Measured and simulated *q-v* curves for switching impulses.

8.8.3 Temporary Overvoltages

Corona attenuation of temporary overvoltages becomes important only in special cases, such as in evaluating the overvoltages caused by the energization on no load or load shedding of very long lines (several hundreds of km or more). Since the frequency of oscillation of temporary overvoltages is close to power frequency, corona characteristics obtained on conductor configurations under the application of power frequency voltages may be used for evaluating corona attenuation of temporary overvoltages.

The increase in capacitance due to corona in this case is quite small and, therefore, need not be taken into account for attenuation calculations. Knowledge of corona losses is essential, however, for determining the attenuation of temporary overvoltages. Although a large number of studies, both theoretical and experimental, have been carried out over the years, most of the data and empirical formulas for practical conductor configurations were obtained for voltages only 20-30% above corona onset, since the normal operating voltage of transmission lines is close to the corona onset voltage. In order to determine corona attenuation of temporary overvoltages, however, corona loss data at almost twice the normal operating voltage are required.

In some studies of corona attenuation of temporary overvoltages (Iliceto et al. 1984; Iliceto and Cinieri 1988), empirical formulas obtained from tests on smooth conductors in the laboratory and large-scale extrapolation of existing data were used to model corona. In one study (Maruvada et al. 1989), experimental corona loss data were obtained for two- and four-conductor bundle configurations at voltages up to twice the normal operating voltages of any transmission lines using these bundles. Corona losses were measured under fair weather as well as heavy rain conditions. The results showed that the losses increased very rapidly at higher voltages. For both bundles, the fair weather corona losses were negligible compared to those under rain at the normal operating voltages. They increase very rapidly with voltage, and the fair weather losses become very nearly equal to those under rain at twice the normal operating voltage. This observation is very important since corona loss data under fair weather conditions were practically nonexistent. An empirical formula, obtained based on the results of this study, is given as

$$P = K_p n f r^2 \left(E - E_0\right)^2 \qquad 8.8\text{-}6$$

Where:

P is corona loss in W/m.
n is the number of subconductors in the bundle.
f is the power frequency in Hz.
r is the conductor radius in cm.
E is the peak value of the operating conductor surface gradient in kV/cm.
E_0 is the peak value of corona onset gradient of the conductor in kV/cm.
K_p is an empirical constant.

The applicability of the empirical formula shown above is limited to the range of parameters for which the data is obtained (Maruvada et al. 1989). Under heavy rain, the value of K_p is found to be independent of n and equal to 0.0008. In fair weather, however, the following values are obtained: $K_p = 0.0022$ for $n = 4$ and $K_p = 0.0014$ for $n = 2$. More experimental studies for a wider range of n and r are required to derive formulas of wider applicability.

Two corona models are developed for attenuation studies using the results obtained in this study. The first is a nonlinear resistance model, in which piecewise linear sections represent the nonlinear voltage-current characteristic of corona. The slope of each of these sections is simulated by a resistance element, valid at voltages corresponding to the extremities of the section. The second corona model is based on the general Suliciu model (Suliciu and Suliciu 1981), originally developed for unipolar impulses. It is extended to oscillatory voltages of double polarity such as temporary overvoltages. Studies using the improved corona models mentioned above have clearly established the important role played by corona in attenuating temporary overvoltages. Results obtained for typical cases of line energization on no load and of load shedding show (Maruvada et al. 1989) that corona limits temporary overvoltages to the same extent or even better than arresters.

APPENDIX 8.1 GUIDELINES FOR CORONA TESTING OF HARDWARE

Introduction

The choice of hardware used on transmission lines and in substations is based to a large extent on corona tests carried out in a high-voltage laboratory. A uniform test procedure is, therefore, a prerequisite to ensure that the hardware is either free of visible corona or does not add appreciable radio interference (RI) to that already being generated by the transmission line or substation conductors. This appendix describes guidelines regarding test arrangements and procedures for carrying out the two types of corona tests—the first test to determine the corona onset or extinction voltage of the test object and the second test to determine the radio influence voltage (RIV) produced.

The first test uses techniques for determining the onset or extinction of positive corona (Nigol 1979, IEC 1997), while the second prescribes methods for the measurement of RIV (ANSI 1996, NEMA 1992, IEC/CISPR 1999, IEC/CISPR 1986). Questions regarding the specification of corona onset or extinction voltages or of permissible RIV limits are not addressed in these guidelines since they are usually set by regulation or by agreement between the utility and hardware manufacturer.

Two basic test methods are available to determine the corona onset or extinction voltages as well as to measure RIV:

1. Calculation, or the Voltage method in which three-dimensional field calculations are made for the laboratory test configuration and the test voltage determined to obtain the same conductor surface gradient as in the case of the actual transmission line or substation configuration;
2. Calibration, or the Voltage Gradient method in which the test voltage is determined to obtain the required conductor surface gradient using a particular device and calibration procedure.

Test Arrangements

The test arrangement essentially comprises a length of single or bundled conductor with the hardware attached as in normal use. The conductor or subconductor used in the test configuration should be either a stranded conductor or a smooth metallic tube with the same diameter (± 5%) as on the transmission line or in the substation.

The test conductor should be positioned parallel to a conducting reference ground plane represented by a suitable ceiling, wall, floor or a structure specifically built for the purpose. The reference ground plane should be at least 30% longer than the test conductor and at least twice as wide as the specified clearance between the conductor and reference ground plane. Further, the conductor and suggested ground plane structure should be so positioned that the conductor is centered with respect to the ground plane. The connection to the test supply should be made from one end of the test conductor and the connection should be positioned so as not to affect the gradient on the test object. No other grounded object should be closer to any point on the test conductor than 1.4 times the distance between the conductor and the reference ground.

In the test on any hardware item, regardless of type, freedom from positive corona at the end of the test conductor and at the connection to the high-voltage test transformer should be ensured by using appropriate toroidal or spherical shield electrodes. All corona shields and auxiliary hardware used for the purpose should be of such size that the surface voltage gradient at the midpoint of the test conductor is unaffected.

For the different test arrangements and voltages generally used, recommended clearances and dimensions are given in the IEC Standard 61284 (IEC 1997).

Suspension Assemblies

The test conductor should be mounted horizontally. At the midpoint, support should be provided by the suspension clamp test specimen in combination with suspension-type insulators. Insulating rods or ropes or nonceramic insulators may be used to provide tension or support for the ends.

The minimum conductor length on either side of the suspension point should be 5 m for single conductors and ten times the diameter of the shield electrode for bundled conductors (IEC 1997). The clearance between the test conductor and the reference ground plane should be provided so that uniform electric fields are attained in the vicinity of the test specimen.

Tension Assemblies

The test setup should be assembled as in service and should include the dead-end tension clamp, complete with jumper terminals and conductors. The test conductor, or bundle, should be mounted either vertically or horizontally. Regardless of what other means for support or for tensioning are used, such as rods or rope, the conductor should be secured at one end by the dead-end assembly test specimen in combination with the appropriate suspension type insulator units. The other end of the conductor should be connected to the test transformer. The minimum length of conductor should be 5 m for single conductors and ten times the diameter of the shield electrode for bundled conductors (IEC 1997).

Other Hardware

Other hardware such as spacers, vibration dampers, compression sleeves, etc. should be set up as in service. The conductor or bundle should be supported, or tensioned, either horizontally or vertically, by any of the means described above. The conductor free length and the minimum clearance to the reference ground plane should be as specified above.

Station Rigid Bus Hardware

Rigid bus should be represented by smooth tubing of appropriate diameter. The test bus should be supported by standard station bus insulator units in one or more stacks. The conductor should be connected at one end to the test transformer. The conductor free length and the minimum clearance to the reference ground plane should be as specified above.

Test Procedures

Determination of Test Voltage

The test voltage is determined to obtain the same electric field distribution around the hardware installed in the single-phase laboratory setup as exists on the operating transmission line or substation. This is achieved by obtaining the same conductor surface gradient in the test as well as the actual line or substation configuration. Although clearances between conductor(s) and the reference ground of the test setup need not be specified, they should be chosen such that relatively uniform conductor surface gradients are obtained in the vicinity of the test hardware. Since the electric field for a given configuration is directly proportional to the applied voltage, only a single reference point relating the voltage and electric field is required. Two approaches may be used to determine the linear relationship between the voltage and electric field and subsequently the test voltage.

Calculation Method

It is well known that the nominal electric field at the surface of conductor(s) of three-phase transmission lines can be calculated accurately using two-dimensional electric field algorithms (see Chapter 2, Section 2.2, Applet CC-1). For single-phase laboratory test configurations, however, three-dimensional field calculation programs (see Chapter 7, Appendix 7.6, Applet EMF-4) may be necessary to obtain accurate results of conductor surface gradient. For simple test configurations, two-dimensional field calculations may be sufficient.

Calibration Method

A device to determine the correct voltage needed to expose insulator and hardware assemblies being tested in single-phase arrangements in high-voltage laboratories to the same electric fields that they will be exposed to on the operating line was developed several years ago by Ontario Hydro (Nigol 1979). The device, known as a sphere calibrator, consists of a steel ball bearing of specified diameter, complete with a clip by which the sphere can be held onto the surface of the test conductor. The calibration method is based on the principle that the positive corona onset on a small sphere placed on the surface of a cylindrical conductor takes place at the same value of conductor surface gradient, irrespective of the actual conductor configuration. Spheres with diameters in the range of 2 to 5 mm are used as calibrators on conductors of 20 to 60 mm diameter, with larger diameter spheres used on larger conductors. Figure A8.1-1 shows the sphere calibrator with its attachment wire and how it is attached to a stranded conductor.

For a given conductor or subconductor, the nominal conductor surface gradient at which positive corona onset occurs on the sphere may be predetermined by placing the conductor with the sphere mounted on it in either a concentric cylinder of known diameter or at a known height above a ground plane. The conductor surface gradient E_C corresponding to positive corona onset on the sphere is then given as

$$E_C = V \Big/ r \ln\left(R/r\right) \qquad \text{A8.1-1}$$

for the concentric cylindrical geometry,

Where
V is the voltage applied to the conductor.
R is the radius of the test concentric cylinder.
r is the radius of conductor.

and

$$E_C = V \Big/ r \ln\left(2h/r\right) \qquad \text{A8.1-2}$$

for the conductor ground plane geometry,

Where
h is the height of conductor above the ground plane.

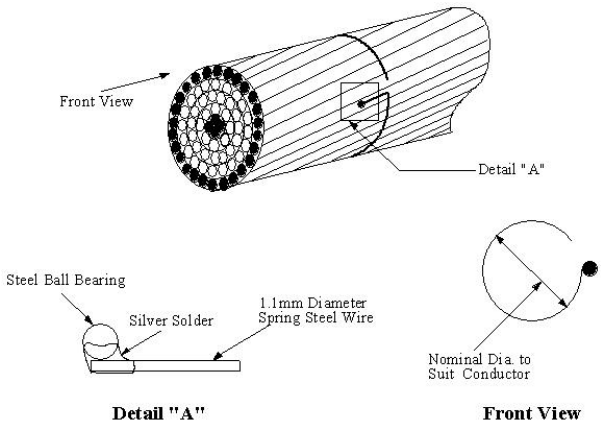


Figure A8.1-1 Attachment of a sphere calibrator to a conductor.

Before the test voltage can be determined, the conductor surface gradient E_S, which gives the standard of acceptance, must be specified. The standard of acceptance is that there be either no visible corona or the measured RIV not exceed the specified limit at the specified E_S. To determine the test voltage, a calibrated sphere is located on the conductor. For a single conductor, the sphere should be positioned toward the closest ground plane, while for a bundled conductor, it should be located at the point of maximum conductor surface gradient. For stranded conductors, it should also be located on the tip of an outer strand. For tests on hardware assemblies other than compression connectors, the sphere should be placed at the midpoint of the test conductor free length. When a compression connector is being tested, the sphere should be 280 ± 20 mm from one end of the connector.

Before the calibration sphere is located on the test conductor, it should be wiped clean with a lint-free cloth. Voltage should then be applied to the conductor. This voltage should be steadily increased to the minimum value at which positive corona occurs on the calibration sphere, and the corresponding voltage noted. This positive corona onset voltage is used to determine the test voltage, which can be calculated using

$$V_T = \frac{E_S}{E_C} V_C \qquad \text{A8.1-3}$$

Where

V_T is the calculated test voltage.
V_C is the voltage applied at positive corona onset on the sphere.
E_C is obtained from Equation A8.1-1 or A8.1-2.
E_S is the specified conductor surface gradient.

It is important to note that V_C may vary as much as ± 5% since the corona onset gradient for the bus or conductor mounted calibration sphere is only a mean value. When using the calibration sphere, it is important to ensure that positive corona is not confused with negative corona. The two are easily distinguishable, especially for the calibration spheres. As the voltage is raised, the negative corona occurs first, but it usually cannot be heard (might put out a slight hiss) and generates very little RIV. It is also very difficult to observe visually unless a light amplification device is used. On the other hand, positive corona onset is abrupt, is easily heard, and is easily seen in a darkened laboratory. Also, the RIV increases dramatically. The negative corona emits a soft blue light at the surface of the calibration sphere. Once the whiter light from the positive corona streamers 25 mm or more in length appears, the negative corona can no longer be seen. A recent round robin investigation in different high-voltage laboratories around the world (Kuffel et al. 2001) has confirmed that the voltage gradient rather than the voltage method is more appropriate for corona testing of hardware.

Adjustment for Altitude (Relative Air Density)

The relative air density, δ, or the altitude above sea level that a particular transmission line will be exposed to cannot be simulated in high-voltage laboratories. But, since it is well known that corona onset is a function of both voltage and relative air density, the voltage can be adjusted to account for the difference in δ between the test laboratory and the proposed line location. Most HV laboratories are located at altitudes less than 300 m above sea level, which means altitude needs to be considered when one of these laboratories is used to test hardware that will be used at much higher altitudes. Since the corona onset voltage for the same test setup decreases as δ decreases or as altitude increases (see Section 8.4.2), the hardware in the low-elevation laboratories should be tested at a higher voltage to account for the increased altitude.

To compensate for the difference in altitude between the testing laboratory and the location at which the hardware will be used, it is necessary to apply a correction factor to determine the appropriate test voltage. Research carried out by Peek (Peek 1929), Peterson (Peterson 1933) and at Leadville (Robertson and Dillard 1961) indicate that corona onset gradient varies proportional to δ, $\delta^{2/3}$ and $\delta^{1/2}$, respectively. Subsequent studies on corona effects from transmission lines indicate, however, that the data are more consistent with corona onset gradient being proportional to $\delta^{2/3}$ as suggested by Peterson. For this reason, the following formula is recommended for calculating the test voltage:

$$V = V_0 \left(\delta_0 / \delta\right)^{2/3} \qquad \text{A8.1-4}$$

Where

V is the required test voltage.
V_0 is the specified voltage for acceptance.
δ is the relative air density for the altitude at which the hardware will be used.
δ_0 is the relative air density for the altitude of the testing laboratory.

If a more conservative estimate of the test voltage is required, however, Peek's formula, in which the corona onset gradient is proportional to δ, may be used to correct for the altitude.

Test Circuit and Instrumentation

Two test procedures can be performed. The first is a measurement of the RIV, and the second is a visible corona test.

RIV Measurement

The RIV measurements should be performed according to ANSI Standard C63.2-1992 and NEMA Standard 107-1992 or CISPR Publication 16 (1999) and CISPR Publication 18-2 (1986). After the apparatus to be tested has been

mounted in the test assembly, a voltage should be applied that is 1.2 times greater than the acceptance test voltage for a period of at least 5 minutes. The voltage should then be reduced to 0.3 times the acceptance test voltage, and then increased again to 1.2 times the acceptance test voltage for a period of another 5 minutes. Then the voltage should be decreased in steps of 25 kV and the RIV should be recorded. The apparatus being tested passes this test if the RIV is less than the specified RIV.

Visible Corona Test

The visible corona test should be performed in a fully darkened laboratory using an image intensifier with a light amplification greater than 40,000. The following procedure should be used:

1. Increase the applied voltage slowly until positive corona is observed on the apparatus being tested. This is the corona onset voltage.
2. Increase the voltage by 10% and maintain for 1 minute.
3. Lower the voltage slowly and note at which voltage extinction of positive corona occurs.
4. Repeat steps 1 through 3 three times.

Photographic records of the corona can be made by mounting either a still or a video camera to the light image intensifier. The apparatus being tested passes this test if the positive corona onset and extinction voltage is greater than the specified corona onset and extinction.

Data Presentation

The test procedure and the data should be described fully and presented in a complete and consistent form. The following information should be provided:

1. Description of apparatus being tested
2. Details of test setup
3. Air temperature, barometric pressure and relative humidity during testing.
4. Description of instrumentation used during testing
5. Corona onset and extinction voltages
6. RIV data plotted versus voltage
7. Any photographs taken during testing

APPENDIX 8.2 CURRENTS INDUCED BY MOVING CHARGED PARTICLES

Charged particles such as electrons and ions created by the ionization processes taking place in a corona discharge are subject to forces in the prevailing electric field. The motion of any charged particle depends on the amount of charge on the particle and the magnitude and direction of the electric field. In a multielectrode system such as a transmission line, the moving charged particles induce currents in all the electrodes. The currents induced in conductors due to corona discharges are the result of contributions from all the charged particles created in the discharge. Since corona effects on transmission lines depend directly on the transient and steady-state corona currents in the conductors, it is useful to be able to calculate these currents.

The instantaneous value of the current induced in any electrode of a multielectrode system due to a moving charged particle was derived independently by Shockley (Shockley 1938) and Ramo (Ramo 1939). Derived originally to facilitate the analysis of multigrid vacuum tubes, the result of this derivation is commonly known as Shockley-Ramo theorem. Considering a system of n electrodes, all of them at ground potential, as shown in Figure A 8.2-1, the Shockley-Ramo theorem states that the instantaneous value of the current i_k induced in conductor k by a particle with a charge q located at any point P and moving with a velocity $\vec{v}_p$ is given as

$$i_k = q\,\vec{e}_{pk} \cdot \vec{v}_p \qquad \text{A8.2-1}$$

Where: $\overrightarrow{e_{pk}}$ is the unit electric field vector at the point P due to a potential of one volt applied to the kth electrode and zero potential to all other electrodes.

The velocity vector $\vec{v}_p$ has a magnitude that is a function of the magnitude of the actual electric field E_p, produced at P due to the potentials applied to all the electrodes and any space charges in the interelectrode space, and has the same direction as E_p. For ions, the velocity is given as $v_p = \mu E_p$, where μ is the ion mobility. The instantaneous value of the corona current in conductor k may then be calculated if the spatial distributions of the charged particles, as well as of the electric field distributions as defined above, are known. The total instantaneous corona current is the sum of the contributions due to the movement of all charged particles in the discharge.

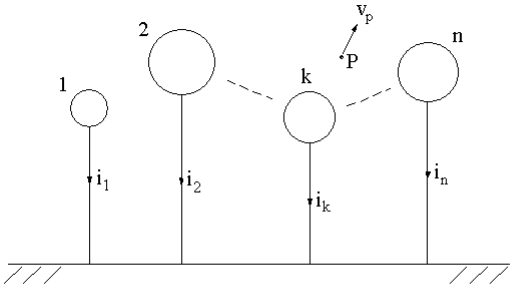


Figure A8.2-1 Currents induced by a moving charged particle.

If the electrodes in Figure A8.2-1 are all infinitely long cylindrical conductors, and if the point P is located very close to the conductor k (corona layer), the unit electric field at P may be calculated considering only the linear charge λ_k (Coulombs/meter) on the conductor k as

$$\vec{e}_{pk} = \frac{\lambda_k}{2\pi\varepsilon_0}\left(\frac{1}{r_p}\right)\cdot\vec{u}_r \qquad \text{A8.2-2}$$

Where:

r_p is the radial distance of P from the center of conductor k.

$\vec{u}_r$ is the unit vector in the radial direction.

However, since the potentials applied to the conductors are $V_k = 1.0$ and $V_j = 0$, for $j = 1,2\ldots n$, $j \neq k$, the charge $\lambda_k = C_{kk}$, where C_{kk} is the self capacitance per unit length of conductor k. Thus,

$$\vec{e}_{pk} = \frac{C_{kk}}{2\pi\varepsilon_0}\frac{1}{r_p}\cdot\vec{u}_r \qquad \text{A8.2-3}$$

Since it is reasonable to assume that very near the conductor k, $\vec{v}_p$ has only a radial component, and the current i_k induced is obtained as

$$i_k = q\,\frac{C_{kk}}{2\pi\varepsilon_0}\left(\frac{1}{r_p}\right)v_p \qquad \text{A8.2-4}$$

For a single-conductor system, such as a conductor in a cage or a conductor above ground, Equation A8.2-4 reduces to

$$i_k = q\,\frac{C}{2\pi\varepsilon_0}\left(\frac{1}{r_p}\right)v_p \qquad \text{A8.2-5}$$

Where:

C is the capacitance per unit length of the conductor in the configuration considered.

REFERENCES

Adachi, T. and L.C. Phan. 1981. "A Laboratory Study of Corona-Induced Vibration of High-Voltage Smooth Aluminum DC Conductors in a Mass-Spring Configuration," *Journal of Electrostatics*. 9. pp. 273-288.

Adams, G.E. 1956. "The Calculation of Radio Interference Level of Transmission Lines Caused by Corona Discharges," *AIEE Trans*. Part III. pp. 411-419. June.

ANSI C63.2-1995. "American National Standard Specification for Electromagnetic Noise and Field Strength Instrumentation, 10 Hz to 1 GHz."

Arai, K., W. Janischewskyj, and N. Miguchi. 1985. "Microgap Phenomena and Television Interference." *IEEE Transactions on Power Apparatus and Systems*. Vol. PAS-104. No. 1. pp. 221-232. January.

Chartier, V.L. 1993. "Effect of Load Current on Conductor Corona," CIGRÉ SC 36 Committee Report.

Chartier, V.L., R. Sheridan, J.N. DiPlacido, and M.O. Loftness. 1986. "Electromagnetic Interference Measurements at 900 MHz on 230 kV and 500 kV Transmission Lines." *IEEE Transactions.* Vol. PWRD-1. pp. 140-149. April.

Cobine, J.D. 1958. *Gaseous Conductors*, Dover Publications, Inc.

Comber, M.G. and L.E. Zaffanella. 1974. "The Use of Single Phase Overhead Test Lines and Test Cages to Evaluate the Corona Effects of EHV and UHV Transmission Lines." *IEEE Transactions on Power Apparatus and Systems*. Vol. PAS-93. pp. 81-91. January/February.

Davis, R. and R.W.E. Cook. 1960. "The Surge Corona Discharge." *IEEE Proceedings* Part C. Monograph No. 415 S.

DeVore, R. and V. Ungvichian. 1975. "Corona Radiation at X and K-Bands." IEEE/PES Paper C 75 121-9.

Draft IEEE Standard, 1997. *IEEE Guide for Conducting Corona Tests on Hardware for Overhead Transmission Lines and Substations*.

English, W.N. 1948. "Corona from a Water Drop." *Phys. Rev.* Vol. 74. pp. 179-189.

EPRI. 2002. *Guide to Corona and Arcing Inspection of Substations*. Report 1001792.

Fews, A.P., D.L. Henshaw, R.J. Wilding, and P.A. Keitch. 1999. "Corona Ions from Power Lines and Increased Exposure to Pollutant Aerosols." *Int. J. Radiat. Biol.* Vol. 75. no. 12. pp. 1523-1531.

Gary, C.H. 1972. "The Theory of Excitation Function: A Demonstration of its Physical Meaning." *IEEE Transactions on Power Apparatus and Systems*. Vol. PAS-91. pp. 305-310. January/February.

Gary, C.H. and M.R. Moreau. 1976. *L'effet Couronne en Tension Alternative.* Eyrolles, Paris. Chapter 4. pp. 45-51.

Gary, C.H., A. Timotin, and D. Cristescu. 1983. "Prediction of Surge Propagation Influenced by Corona and Skin Effect." IEEE Proceedings. Vol. 130. Pt. A. No. 5. pp. 264-272. July.

Grum, F. and L.F. Costa. 1976. "Spectral Emission of Corona Discharges." *Applied Optics.* Vol. 15. No. 1. pp. 76-79. January.

Hatanaka, G.K. 1981. "Field Measurement of VHF Noise from an Operating 500 kV Power Line." *IEEE Transactions on Power Apparatus and Systems*. Vol. PAS-100. No. 2. pp. 863-872.

Héroux, P. 1981. *Reduction of Audible Noise of High-Voltage Transmission Lines*. Canadian Electrical Association. Report No. 77-28. July.

Héroux, P. and N.G. Trinh. 1976. "A Study of Electrical and Acoustical Characteristics of Pulsative Corona." IEEE Paper no. A 76 122-2. IEEE/PES Winter Meeting. New York. 25-30 January.

Héroux, P., P. S. Maruvada, and N.G. Trinh. 1982. "High Voltage Transmission Lines: Reduction of Corona Under Foul Weather." *IEEE Transactions on Power Apparatus and Systems*. Vol. PAS-101. No. 9. pp. 3009-3017. September.

Hoburg, J.F. and J.R. Melcher. 1975. "Current-Driven, Corona-Terminated Water Jets as Sources of Charged Droplets and Audible Noise." *IEEE Transactions on Power Apparatus and Systems*. Vol. PAS-94. No.1. pp. 128-136.

Houlgate, R.G. 1986. "Atmospheric Ions Beneath High-Voltage Transmission Lines." Discussion Meeting on Atmospheric Ions and Industrial Activity, IEE London.

Humphreys, W.J. 1964. *Physics of the Air*. Dover Publications, Inc.

IEC 71-1. 1993. *Insulation Coordination, Part 1: Definitions, Principles and Rules.* Seventh Edition. International Electrotechnical Commission. Geneva, Switzerland.

IEC Standard 61284 – 1997. "Overhead Lines – Requirements and Tests for Fittings."

IEC/CISPR Publication 16, Part 1 1999. "C.I.S.P.R. Specifications for Radio Interference Measuring Apparatus and Measurement Methods."

IEC/CISPR Publication 18-2 1986 "Radio Interference Characteristics of Overhead Power Lines and High-Voltage Equipment; Part 2: Methods of Measurement and Procedure for Determining Limits."

IEEE Standard No. 539.1990. *IEEE Standard Definitions of Terms Related to Corona and Field Effects of Overhead Power Lines***.**

Iliceto, F., E. Cinieri, and A. Di Vita. 1984. "Overvoltages due to Open-Phase Occurrence in Reactor Compensated EHV Lines." *IEEE Transactions on Power Apparatus and Systems*. Vol. PAS-103. No. 3. pp. 474-482. March.

Iliceto, F. and E. Cinieri. 1988. "Analysis of Half-Wave Length Transmission Lines with Simulation of Corona Losses." *IEEE Transactions on Power Delivery.* Vol. 3. No. 4. pp. 2081-2091. October.

Janischewskyj, W. and A. Arainy. 1983. "Microgap Discharges as Sources of Television Interference." IEEE International Electrical and Electronics Conference. Toronto, Canada. pp. 638-641. September.

Kudyan, H. and C.H. Shih. 1981. "A Nonlinear Circuit Model for Transmission Lines in Corona." *IEEE Transactions on Power Apparatus and Systems* Vol. PAS-100. No. 3. pp. 1420-1430. March.

Kuffel, J., Z. Li, V. L. Chartier, S. Grzybowski, J. Vandermaar, and B. Gunasekaran. 2001. "Round Robin Investigation of a Corona Test Procedure Based on Gradient Calibrating Spheres." International Symposium on High Voltage Engineering (ISH). Bangalore, India. 20-24 August.

Laforest, J.J. 1968. "Seasonal Variation of Fair Weather Radio Noise." *IEEE Transactions on Power Apparatus and Systems*. Vol. PAS-87. pp. 928-931. April.

Lahti, K., M. Lahtinen, K. Nousiainen. 1997. "Transmission Line Corona Losses Under Hoar Frost Conditions," *IEEE Transactions on Power Delivery.* Vol. 12. pp. 928-933. April.

Loeb, L.B. 1965. *Electrical Coronas: Their Basic Physical Mechanisms*. The University of California Press. Berkeley and Los Angeles. pp. 402-406.

Maruvada, P.S. 2000. *Corona Performance of High-Voltage Transmission Lines*. Research Studies Press Ltd. Baldock, Hertfordshire, England. pp. 113-118.

Maruvada, P.S. and N.G. Trinh. 1973. "A Preliminary Report on Tests Conducted at IREQ on Large High Voltage Electrodes." IREQ Report No. 73-912-01. Presented to CIGRÉ WG 33.03. Measuring Technique.

Maruvada, P.S., H. Menemenlis, and R. Malewski. 1977. "Corona Characteristics of Conductor Bundles Under Impulse Voltages." *IEEE Transactions on Power Apparatus and Systems*. Vol. PAS-96. No. 1. pp. 102-115.

Maruvada, P.S., D.H. Nguyen, and H. Hamadani-Zadeh. 1989. "Studies on Attenuation of Dynamic Overvoltages." *IEEE Transactions on Power Delivery.* Vol. 4. No. 2. pp. 1441-1449. April.

Mercure, H.P. 1989. "Insulator Pollution Performance at High Altitudes: Major Trends." *IEEE Transactions on Power Delivery.* Vol. 4. No. 2. pp. 1461- 1468. April.

Mombello, E. and P.S. Maruvada. 2001. "Measurement and Analysis of Corona Losses Generated by Heavily Contaminated Conductors." International Symposium on High-Voltage Engineering (ISH). Bangalore, India. 20-24 August.

NEMA Standard Publication No. 107–1992. "Methods of Measurement of Radio Influence Voltage (RIV) of High-Voltage Apparatus."

Newell, H.H., T.W. Liao, and F.W. Warburton. 1967. "Corona and RI Caused by Particles on or near EHV Conductors: I - Fair Weather." *IEEE Transactions on Power Apparatus and Systems*. Vol. PAS-86. pp. 1375-1383. November.

Newell, H.H., T.W. Liao, and F.W. Warburton. 1968. "Corona and RI Caused by Particles on or near EHV Conductors: II - Foul Weather." *IEEE Transactions on Power Apparatus and Systems*. Vol. PAS-87. pp. 919-927. April.

Nigol, O. 1979. "Development and Testing of Corona-Free High Voltage Line and Station Hardware." International Symposium on High Voltage Engineering (ISH). Milan, Italy. August 28-31.

Nigol, O. and J.G. Cassan. 1961. "Corona Loss Research at Ontario Hydro Coldwater Project." *AIEE Transactions, Power Apparatus and Systems*. Vol. 80. Pt. III. pp. 388-396. August.

Pakala, W.E. and V.L Chartier. 1971. "Radio Noise Measurements on Overhead Power Lines from 2.4 to 800 kV." *IEEE Transactions on Power Apparatus and Systems.* Vol. PAS-90. Pp. 1155-1165. May/June.

Pedersen, A. 1989. "On the Electrical Breakdown of Gaseous Dielectrics: An Engineering Approach." *IEEE Transactions on Electrical Insulation.* Vol. 24. No. 5. pp. 721-739. October.

Peek, F.W. 1929. *Dielectric Phenomena in High-Voltage Engineering*. McGraw-Hill.

Perry, D.E., V.L. Chartier, and G.L. Reiner. 1979. "Bonneville Power Administration's 1100 kV Transmission Development – Corona and Electric Field Studies." *IEEE Transactions on Power Apparatus and Systems*. Vol. PAS-98. pp. 1728-1738. September/October.

Peterson, W.S. 1933. (Discussion) in: Carrol, J.S. and B. Cozzens. "Corona Loss Measurements for the Design of Transmission Lines to Operate at Voltages Between 200 kV and 300 kV." *AIEE Transactions*. Vol. 52. pp. 55-63.

Phillips, T.A., A.F. Rohlfs, L.M. Robertson, and R.L. Thomson. 1967. "The Influence of Air Density on the Electrical Strength of Transmission Line Insulation." *IEEE Transactions on Power Apparatus and Systems*. Vol. PAS-86. pp. 948-961. August.

Ramo, S. 1939. "Currents Induced by Electron Motion." *Proceedings of the I.R.E.* pp. 584-585. September.

Robertson, L.M. and J.K. Dillard. 1961. "Leadville High-Altitude EHV Test Project, Part I – Report on 4 years of Testing." *AIEE Trans*. Vol. 8. pp. 715-725. December.

Shankle, D.F., S.B. Griscom, E.R. Taylor, and R.H. Schloman. 1965. "The Apple Grove 750 kV Project – Equipment Design and Instrumentation." *IEEE Transactions on Power Apparatus and Systems*. Vol. PAS-84. pp. 541-550. July.

Shockley, W. 1938. "Currents to Conductors Induced by a Moving Point Charge." *J. Appl. Phys*. Vol. 9. pp. 635-636. October.

Silva, J. M., H. H. Fleishmann, and C. H. Shih. 2004. "Transmission Line Corona and X-Rays." *IEEE Transactions on Power Delivery.* Vol. 19. No. 3. pp. 1472-1482. July.

Suliciu, M.M. and I. Suliciu. 1981. "A Rate Type Constitutive Equation for the Description of the Corona Effect." *IEEE Transactions on Power Apparatus and Systems*. Vol. PAS-100. No. 8. pp. 3681-3685. August.

Tikhodeev, N.N. 2000. "Mitigation of Corona Losses on EHV Overhead Lines Through Voltage Control." *Proceedings of St. Petersburg IEEE Chapter.* pp. 3-13.

Tong, D.W., G.L. Wilson, and I. Johansen. 1975. "Effects of Surface Wettability on Audible Noise and Capillary Absorption as a Noise Reduction Scheme." IEEE Paper A 75 566-0.

Townsend, J.S. 1915. *Electricity in Gases*. Oxford University Press.

Trinh, N.G. 1995. "Partial Discharges XIX: Discharges in Air – Part I: Physical Mechanisms." *IEEE Electrical Insulation Magazine*. Vol. 11. pp. 23-29. March/April.

Trinh, N.G. and J.B. Jordan. 1968. "Modes of Corona Discharges in Air." *IEEE Transactions on Power Apparatus and Systems*. Vol. PAS-87. pp. 1207-1215. May.

Trinh, N.G. and J.B. Jordan. 1970. "Trichel Streamers and Their Transition to Pulseless Glow Discharge." *J. Appl. Phys*. Vol. 41. pp. 3991-3999. September.

Trinh, N.G. and P.S. Maruvada. 1977. "A Method of Predicting the Corona Performance of Conductor Bundles Based on Cage Test Results." *IEEE Transactions on Power Apparatus and Systems*. Vol. PAS- 96. pp. 312-325. January/February.

Uhlig, C.A.E. 1956. "The Ultra Corona Discharge, a New Discharge Phenomenon Occurring on Thin Wires." *Proc. High Voltage Symposium*. National Research Council of Canada. pp. 15-1 –15-13.

Vosloo, W.L., G.R. Stolper, and P. Baker. 1997. "Daylight Corona Discharge Observation and Recording System." *Proceedings.* International Symposium on High Voltage Engineering. Montreal. pp. 161-164. August.

Wernick, S. and R. Pinner. 1972. *The Surface Treatment and Finishing of Aluminum and its Alloys*. Draper.

Yamazaki, K. and R. G. Olsen. 2004. "Application of a Corona Onset Criterion to Calculation of Corona Onset Voltage of Stranded Conductors." *IEEE Transactions on Electrical Insulation.* Vol. 11. No. 4. pp. 674-680. August.

CHAPTER 9

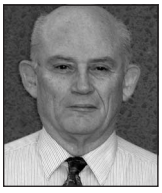
Electromagnetic Interference

Robert Olsen
Vernon Chartier

This chapter describes the nature of electromagnetic interference produced by corona and gap discharges on high-voltage transmission lines. The chapter outlines in detail the procedures for calculating the EMI due to corona from 100 kHz to 1 GHz produced by any practical line configuration. Also covered in the chapter are methods for measurements, criteria for assessing EMI tolerability, and compliance with industry guidelines and limits. In addition, the discussion includes two types of passive interference.



Dr. Robert G. Olsen earned a Ph.D. in electromagnetic theory from the University of Colorado in 1974, and—aside from temporary positions at GTE Labs, ABB Corporate Research, and EPRI—has been a member of the electrical engineering faculty at Washington State University since then. The bulk of his research work has been in the area of power system electromagnetic compatibility (EMC). One portion of his research was the development of a comprehensive theory for predicting corona-generated electromagnetic interference from power lines. He has also worked on problems with the compatibility of fiber optics and the high-voltage environment, shielding of extremely low-frequency electromagnetic fields, wideband power line communications, and the electromagnetic environment of power lines. Dr. Olsen is a Fellow of the IEEE, and has served as chair of the IEEE Power Engineering Society Corona Effects and AC Fields Working Groups, and as United States National Committee representative to CIGRÉ Study Committee 36 (Electromagnetic Compatibility).



Vernon L. Chartier has conducted pioneering research on all the corona effects associated with high-voltage ac and dc transmission lines. While he was at the Westinghouse Electric Corporation from 1963 to 1975, he conducted corona and 60-Hz electric field research at the Apple Grove 750-kV Project, which was a joint project of American Electric Power and Westinghouse. During that period, he also conducted research and consulted on projects for the electric utility industry. In 1975, he joined the Bonneville Power Administration (BPA), where he was associated with the Lyons 1200-kV Project and managed several high-voltage research projects for BPA to gain a better understanding of the electrical environment of high-voltage ac and dc lines. After retiring from BPA in 1995, he has been a power system EMC consultant. Chartier has managed several long-term EMI measurement programs on ac lines operating at 230, 500, 765, and 1200 kV. His research on EMI has been documented in more than 30 technical papers, which include the comprehensive measurement program conducted from 1965 to 1968 for the United States Air Force on lines operating from 2.4 to 800 kV. He has played a leading role in the corona and fields work of IEEE, CIGRÉ, and CISPR. For his contributions he was elected a Fellow of the IEEE in 1980, and received the IEEE Herman Halperin Transmission and Distribution Award in 1995.

9.1 INTRODUCTION

In previous editions of the *Transmission Line Reference Book* (EPRI, 1982), the primary emphasis of the chapter on "radio noise" was interference to the frequency band occupied by what the Federal Communications Commission (FCC) calls the Standard Broadcast Band. This range, which is better known as the AM Broadcast Band, covers the frequency range of 535 - 1605 kHz. By definition, the term "radio" covers the entire radio frequency spectrum, which is roughly 10 kHz to 100 GHz. However, in the electric utility industry, the term "radio noise" has meant radio interference (RI) to the AM Broadcast Band. Interference to the Television Broadcast Band has been called television interference (TVI), which was also covered in the last edition of the "Red Book." Over the past 20 years, as more and more communication devices have been developed, it has become necessary to develop the ability to determine if interference from overhead power lines is compatible with these devices. Within the electromagnetic compatibility (EMC) community, the term *electromagnetic interference* (*EMI*) has become the preferred term over the term radio noise. For this reason, the title of this chapter has been changed from the previous edition, and the text now devotes a greater emphasis to discussion of the electromagnetic compatibility between overhead power lines and a wide range of communication systems.

Electromagnetic interference (EMI) from overhead power lines can be classified as follows:

- Corona from
  —Conductors
  —Insulator assemblies and hardware
- Gap discharges (sparks) due to
  —Loose hardware
  —Floating hardware
  —Dissimilar dielectrics
  —Insulator dry-band arcing
- Passive interference, including
  —Reradiation of broadcast signals
  —Ghosting
  —Blocking

Corona and gap discharges can also be found in substations, and substation structures can also cause passive interference. Sources of EMI associated primarily with substation equipment are:

- Partial discharges in transformers and other high-voltage equipment
- Periodic Switching from FACTS (STATCOM, UPFC) type equipment
- Occasional switching from
  —Utility switching
  —Customer switching
- Harmonics

The occasional switching conducted by the utility or its customers is usually not a source of harmful interference to communications systems of nearby residences or other facilities. Most utilities make a major effort to control this type of EMI, since it is a source of interference to their own communication systems.

The EMI caused by periodic switching associated with thyristors in FACTS-type equipment has not been very well documented, mainly because of the newness of the technology and the lack of measurements. However, it is well known that the EMI from thyristors is usually much less than the EMI from mercury arc valves that were employed in the first high-voltage direct current (HVDC) systems.

Harmonics that cause interference in the telephone voice band (300 to 3600 Hz) can be created either by the utility system or by a customer system.This phenomenon has been studied for more than 60 years, and solutions to make the two systems electromagnetically compatible have been well documented.

The source of interference that causes more than 90% of the EMI complaints received by utilities are gap discharges, which are also called gaps or sparks and sometimes microsparks. Gap discharges are complete electrical discharges across two electrodes of two dissimilar dielectrics. The main source of gap discharges is loose hardware, and they can be found on lines of every voltage classification. They tend to be found the most often on wood pole structures where hardware has a greater probability of becoming loose as the wood poles and wood crossarms dry out. Lattice steel structures, concrete poles, and tubular steel poles are much better structures from an EMI standpoint than wood because the hardware on the structure usually stays very tight, and the weight of the long spans tends to keep hardware well bonded.

The source of interference from overhead lines where the most research over the past 60 years has been conducted is corona—especially as the industry was considering moving to higher and higher voltages in the 1940s through the 1970s. Corona can be a source of severe EMI in the AM Broadcast Band, particularly during foul weather when the corona can be as much as 10 times greater than in dry weather. However, over the past 20 or so years, electric utilities have received very few EMI complaints in this frequency band that were due to corona. This trend is primarily because of the popularity of the FM Broadcast Band, which is not affected by power line EMI and the fact that the AM Broadcast Band tends to have a lot of static due to atmospheric EMI, especially where the signal strengths are not very strong. Corona is also a significant source of conducted interference in the power line carrier band. This subject is beyond the scope of this book, but interested

readers should know that there is an IEEE standard (IEEE 1980) that can be used to estimate the corona being generated on the conductors.

Overhead structures and buildings can cause passive interference. In the AM Broadcast Band, metal transmission line structures can reradiate broadcast signals that can change the propagation pattern of the radio station that has the license from FCC. This is especially true for directional antennas. The license given to the radio station not only specifies the transmitting power of the antenna, but also specifies the propagation pattern that the station must maintain. If the pattern is changed or distorted, the utility could be responsible for fixing the problem.

The other type of passive interference of great concern to customers living near metal transmission and substation structures is ghosting and blocking of TV signals.

Outside the electric utility industry, there is the mistaken impression that EMI increases with line voltage. This is not true, as will be explained throughout the chapter. Gap discharges are the main source of EMI complaints, and they are pretty much independent of the voltage of the line. In fact, distribution lines are a much larger source of gap discharges than transmission lines. Gap discharges can be controlled through proper line design and maintenance; therefore, techniques used by the industry to minimize gap discharges will be discussed as well as techniques to locate such sources. Industry practices to control corona from conductors and hardware are also discussed as well as industry practices for controlling passive interference.

From the standpoint of overhead lines, the two most important EMI sources are corona and gaps. Section 9.2 describes the characteristics of these two sources. Section 9.3 discusses industry guidelines and limits. Included in this section are noise tolerability criteria, the importance of different weather conditions, and the effect of line and conductor geometry on EMI performance. Section 9.4 presents a discussion of how to measure EMI based on industry standards. Sections 9.5 and 9.6 describe models for predicting EMI levels from conductor corona below and above 30 MHz. Section 9.7 covers two types of passive interference.

EMI can be calculated using the following simple software applications provided in the electronic version of this book. The first three methods can be used to calculate the conductor corona EMI versus distance from a transmission line of given characteristics in different weather conditions. Since all three methods have a strong empirical component, they will not necessarily give the same EMI level as explained below:

- Applet RN-1: “Electromagnetic Interference up to 30 MHz.” This applet may be used to calculate the conductor corona EMI as measured by a CISPR standard quasi-peak receiver with a 9-kHz bandwidth connected to either a rod or a loop antenna. It uses the wideband analytical method (WBNOISE) developed by Olsen and his coworkers and described later in this chapter. It is valid for field points at any distance (and any direction including vertical) from the transmission line. An L_{50} rain excitation function was created by calibrating it to the best long-term EMI data from operating lines found in the literature. An L_{50} fair weather excitation function is calculated by subtracting 21.6 dB from the L_{50} rain excitation function.
- Applet RN-2: “EMI Calculations Using Empirical Method.” This applet calculates the EMI from 100 kHz to 1000 MHz for different detectors and different bandwidths. It has two empirical methods developed by Chartier when he was at the Bonneville Power Administration, and is in a computer program called “Corona and Field Effects.” The data used to develop the empirical method for calculations up to 30 MHz came from a large number of long-term measurements at a single frequency and short-term lateral profile and frequency spectrum measurements. The L_{50} levels during fair weather were the primary data used to develop this method, since most regulations are based on fair weather. To calculate the L_{50} rain EMI, 25 dB is added to the L_{50} fair weather level. To calculate the L_{50} EMI level during foul weather (conductors are wet), 17 dB is added to the L_{50} fair weather level. Above 30 MHz, long-term foul-weather data collected primarily at 75 MHz and the results of lateral profile and frequency spectrum measurements were used to develop an empirical method over the range of 30 MHz to 1000 MHz. In general, this applet up to 30 MHz will give results that are within a few dB of RN-1.
- Applet RN-3: “Radio Noise Base Case Curves.” This applet uses the approach described in the second edition of this Reference Book. Since it is based on generation functions measured on conductors in a test cage under very heavy artificial rain rather than generation functions that were developed from mean values from long-term measurements on operating lines, there can be significant differences for some cases between RN-3 and the first two methods. The excitation functions in this applet were determined from measurements at a single frequency over a wide range of conductors at Project UHV under both heavy rain and under what Project UHV called “wet conductor” conditions. The L_{50} fair-weather generation function is determined by subtracting 17 dB from the wet-conductor generation function.
- Applet RN-4: “EMI Base Case Curves and Effect of Line Parameters.” This applet is based on Applet RN-3

and may be used to calculate the EMI measured at a reference location and the effect of individual line parameters—such as conductor diameter, number of conductors, phase spacing, and height above ground—for a large number of base case line voltages and configurations.

9.2 CHARACTERISTICS OF TRANSMISSION-LINE EMI

As previously mentioned, gap discharges are the cause of more than 90% of the interference complaints received by utilities (IEEE 1976). This is because the EMI magnitude of a single spark can be relatively large and usually extends over a much wider frequency range than corona. The extensive EMI measurements that were conducted for the United States Air Force (USAF) between 1965 and 1968 on 20 overhead power lines from 2 to 800 kV illustrate the difference between corona and gap discharge EMI (Pakala and Chartier 1971). Figure 9.2-1 (IEC/CISPR 1982) shows a comparison of the EMI frequency spectra from corona and a single gap discharge over the frequency range of 100 kHz to 1000 MHz. This figure was developed from the measurements conducted for the USAF (Pakala and Chartier 1971). Figure 9.2-1 shows quite clearly why gaps are the primary source of interference in the TV Broadcast Band. It also illustrates why fair weather corona, no matter how intense, does not cause television interference (TVI). Foul weather corona has been a source of TVI from a few noisy transmission lines in rural areas where TV signals tend to be weak (Loftness et al. 1981). However, TVI during foul weather has been a minor problem for lines designed to industry guidelines.

9.2.1 EMI Due to Conductor Corona

The EMI due to conductor corona from an ac transmission line will be highest during heavy rain, when the conductors are saturated with water drops acting as corona sources; lower in fair weather, when the number of corona sources, typically insects and particles of vegetation, are relatively few; and lowest after a rainstorm has washed foreign particles off the conductors and the conductors have dried.

The EMI level of a line due to conductor corona is often expressed as a single number referring to a particular set of measuring conditions: (1) the climatic conditions, (2) the measuring location, (3) the characteristics of the detector of the measuring instrument, and (4) the measuring frequency. For example, the EMI level may be that corresponding to the conditions of fair weather, a location 15 m (50 ft) laterally from an outside phase, a quasi-peak detector (see discussion on measurements in Section 9.4), and a measuring frequency of 0.5 MHz. However, this single measure is of limited use in assessing the impact of the line noise on interference to most communication systems. For such an assessment, a more detailed description is required that makes use of three principal characterizations: (1) frequency spectrum, (2) lateral profile, and (3) statistical distribution.

Frequency Spectrum

A frequency spectrum displays the variation of noise level as a function of measuring frequency. The shape of the spectrum depends on the shape of the originating corona-current pulses and the extent to which these pulses are attenuated as they travel along the line. In turn, the current-pulse shape varies with the mode of corona (see Chapter 8). In addition, the form of the frequency spectrum depends on the distance of the measuring location from the line. Thus, there does not exist a unique frequency spectrum for all lines, but for practical line designs, a certain amount of generalization may be applied. Typical frequency spectra, derived from measurements of corona-produced EMI for different measuring locations (Pakala and Chartier 1971) are shown in Figure 9.2-2.

Lateral Profile

A lateral profile describes how the noise level falls off with increasing distance from the line. Beneath the line and within 15 m (50 ft) from the outermost phase of the line,

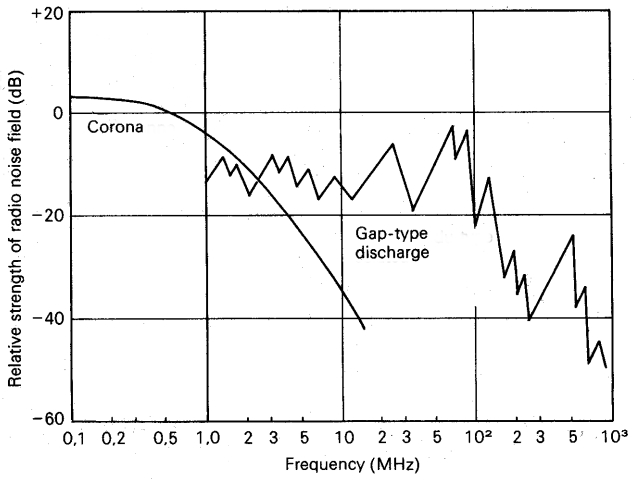


Figure 9.2-1 Example of the relative strength of corona and gap-type discharges as a function of frequency in fair weather (IEC/CISPR 1982).

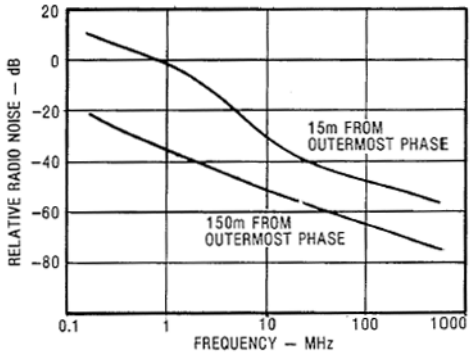


Figure 9.2-2 Typical frequency spectra of corona-produced EMI.

the actual line geometry plays an important part in determining the shape of the lateral profile. The profile of a single-circuit horizontal configuration, for example, would differ in shape from that of a vertical configuration. At moderate distances, the overall height of the line closest to the point of measurement influences the rate at which the noise level falls off with distance, the attenuation being greater for lower line heights. At far distances, the shape of the lateral profile is practically independent of the line geometry. What constitutes moderate and far distances depends on the frequency of measurement. The rate of the lateral attenuation of EMI from a source is a complex function of frequency and distance (Pakala and Chartier 1971). In the very low frequency (VLF) (3–30 kHz) and low frequency (LF) (30–300 kHz) bands, antennas used to make measurements will be in the near field or in an induction field, and the rate of attenuation of the EMI is $1/R^2$, where R is the radial distance from the conductor to the antenna. In the mid frequency (MF) (300–3000 kHz) band, as the antenna is moved away from the line, the field changes from an induction field to a surface wave field at a radial distance of about $\lambda/2\pi$ from the conductor, where λ is the wavelength in meters. The attenuation rate for the surface wave field begins at 1/R, but will eventually attenuate more rapidly depending on the ground conductivity. From 3 MHz to about 30 MHz, the field is a combination of a surface wave and a radiated field. Above 300 MHz, the field is a direct wave, but at distances far from the conductors, it can be a combination of a direct wave and a ground-reflected wave.

Typical profiles also derived from measurements for different frequencies (Pakala and Chartier, 1971) are shown in Figure 9.2-3.

Statistical Distributions

EMI levels due to conductor corona vary with time, primarily owing to variations in the weather conditions. From conditions of heavy rain to fair weather, levels may change by as much as 25-30 dB. Even within a particular weather-condition category (fair weather, for example), variations of as much as 10-15 dB may occur simply because the number of corona sources changes with time. It is possible to describe noise variations in statistical terms only, for example, by cumulative frequency (of occurrence) distribution curves (see Section 8.6.6). These curves show the percentage of time that the noise level is below a certain value. The total time represented may comprise all weather conditions or particular categories, such as rain, snow, or fair weather. For example, one may speak of the 95% rain level of radio noise, meaning that the noise is less than this level during 95% of the total period of rain.

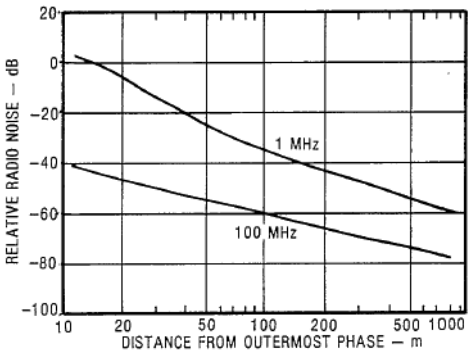


Figure 9.2-3 Typical lateral profiles of EMI.

All-weather statistical distribution curves generally exhibit an inverted S-shape, the points of inflexion being a function of the percentage of occurrence of the various conditions. The inverted-S shape is the sum of two statistical distributions—one during fair weather and one during foul weather, which includes anytime the conductors are wet. This all-weather cumulative distribution can also be described as being made up of three Gaussian (normal) distributions—one for fair weather, one for measurable foul weather, and one for the transition period between fair and measurable foul weather, as indicated in Figure 9.2-4. The transition distribution consists of light rain, light snow, fog, dew, hoarfrost, etc. However, some of the data in the transition distribution could consist of high EMI levels during fair weather and even EMI levels occurring from wet conductor corona sources several kilometers down the line.

It has become standard practice among acousticians to express audible noise in terms of exceedance levels, denoted L_x, signifying a level that is exceed x% of the time. Thus, the 95% rain level referred to earlier would be expressed as the L_5 rain level. In an attempt to achieve consistency in the reporting of transmission-line EMI and audible noise data, exceedance levels are used in the remainder of this chapter and in Chapter 10 on audible noise.

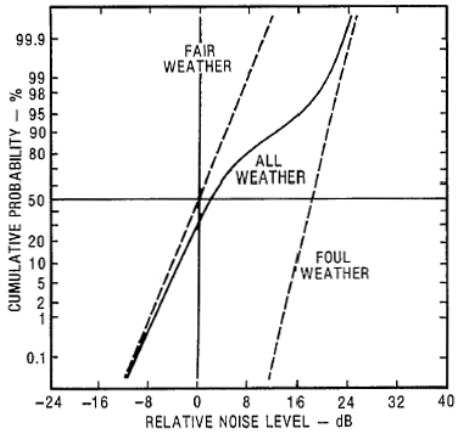


Figure 9.2-4 Typical all-weather cumulative frequency distribution of conductor corona EMI, and approximation by Gaussian distributions.

Acousticians also prefer to plot the audible noise in dBA on the ordinate of probability plots and the exceedance level on the abscissa since they are primarily interested in determining the noise level for a particular exceedance level. Examples of such plots can be found in Chapter 10. Figure 9.2-5 is an example of a probability plot, where the abscissa is plotted in exceedance percentages. The data for Figure 9.2-5 came from long-term measurements conducted on two parallel 500-kV lines near Scio, Oregon by the Bonneville Power Administration. The audible noise distribution for these parallel lines is shown in Figure 10.6-1. Similar plots can be found for audible noise, RI, and TVI (Chartier et al. 1987) for a double-circuit 500-kV line in Montana.

Line Geometry

In assessing the options available for reducing or limiting the overall level of EMI produced by line conductor corona, the designer will obviously pay particular attention to the line geometry. In general terms, any change in line geometry that results in a reduction of the conductor surface gradient on the surface of the conductors will reduce EMI levels.

Parameters that have the most significant effect on EMI levels are the number of conductors in a phase bundle and the diameter of the conductors. An increase in either will result in a reduction of EMI. For a fixed amount of total conductor material (measured in terms of weight per unit length), a large number of small-diameter conductors result in a lower EMI level than a smaller number of larger-diameter conductors. Thus, for example, a phase bundle of 3 x 33-mm (1.3-in.) conductors, which might be used for 500-kV lines, will produce less noise than a bundle of 2 x 41-mm (1.6-in.) conductors, the two bundles having approximately the same amount of material (approximately 6 kg/m [4 lb/ft] for ACSR conductors). The spacing of the conductors within a bundle has a more complex effect on noise levels. Any set of conductors has an optimum spacing, above or below which the conductor surface gradient and hence the noise level increases. However, except for very small spacings, the variation from the optimum is slight.

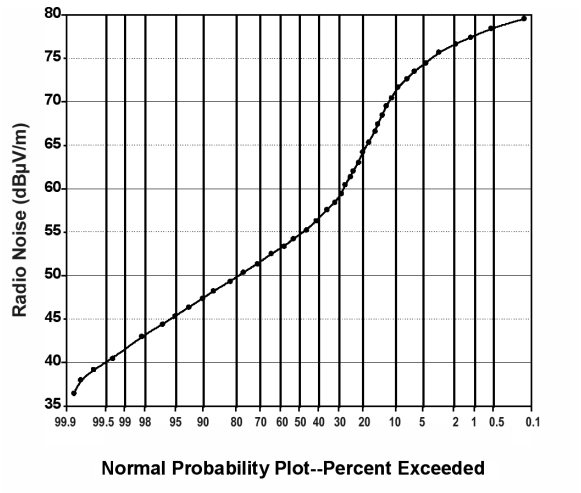


Figure 9.2-5 All-weather RI distribution at 834 kHz obtained at 15 m from outside phase of Marion-Lane and Marion-Alvey 500-kV lines near Scio, Oregon.

Increasing the phase spacing of single-circuit lines lowers the conductor surface gradient, and thus, the EMI produced. However, in terms of dB-per-dollar, this method is generally not an economic proposition unless the spacing needs to be increased for other reasons. For double-circuit lines, the net result depends to some extent on the relative phasings of the two circuits. "Low reactance" phasing, which is often used to reduce 60-Hz magnetic fields, generally results in higher EMI levels than "super-bundle" phasing. Increasing the line height has only a small effect on the conductor gradient, but may have a somewhat more significant effect on the lateral profile of the radio noise. Under and close to the line, the noise levels will be reduced, but the rate at which the EMI attenuates away from the line is also reduced. Consequently, at distances beyond the edge of the right-of-way, EMI levels may even be increased beyond their original levels.

The quantitative effects of variation of each of the parameters previously discussed are incorporated in the methods for calculating EMI due to conductor corona. It should be recognized that variation of line parameters affects several other aspects of the electrical performance of the line and that no one effect should be studied exclusively of all others.

Conductor Surface Conditions

Although hardly under the control of the designer, the conductor surface condition plays an important part in determining the EMI levels in both fair and foul weather. The lowest EMI levels result from clean, dry conductors. As previously mentioned, the accumulation of insects and particles of vegetation will increase fair-weather EMI levels. Similarly, the EMI performance will be impaired if the conductor surface is nicked or scratched, since the irregularities act as corona sources. If the damage occurs during the line-stringing process, one should expect EMI levels during the first several months of energization to be significantly higher than would be predicted from methods described later in Section 9.5.

As the conductors age through exposure to the weather and corona, these sources tend to smooth out, until they become insignificant. An example of this phenomenon is illustrated by measurements conducted on a 345-kV line in central Iowa in the 1960s. The stringing of the conductors had been completed several months before it was energized. On the day the line was energized, RI measurements were conducted. The RI decreased about 6 dB in the first

20 minutes as electrostatic forces blew off loose aerosols that had collected on the conductors during the time it was unenergized. Over another 6 months, the RI decreased another 6 dB, probably as aluminum burrs and insects and dirt that were stuck to the conductors were burned off by the corona.

The highest EMI levels under dry weather conditions occur near some industrial plants. For example, a 400-kV line within 6 km of an oil refinery was found to have a greasy surface. Another example is a 345-kV line near a factory that produced plasterboard. The conductors and the towers were covered with plaster dust that significantly increased the corona activity.

In foul weather, when the conductors are saturated with water drops, the effect of all the fair-weather sources is generally negligible. However, the surface condition of the new conductor in foul weather is important from another point of view. New conductors generally have a somewhat greasy surface that causes water to form in small droplets all around the surface. Consequently, on bundled conductors, water drops (corona sources) are present in the region of maximum gradient on all conductors. In foul weather, conductors that have been energized and exposed to the weather elements for some time (on the order of a few months) exhibit a different property that causes water drops to form only on drip lines on the bottom of the conductors (see also Section 8.6.2). In this case, fewer conductors in the bundle have water drops at the point of maximum gradient, and noise levels tend to be lower. This effect is particularly noticeable under light-rain conditions and at moderate surface gradients, and is less pronounced at high gradients or in heavy rain.

Effect of Weather Conditions and Load Current

The influence of weather conditions and conductor heating on general corona performance is discussed in Section 8.6 Because of the relative importance of minimizing audible noise from overhead lines, a detailed discussion of the effect of weather conditions and load current on audible noise is discussed in Section 10.3.1. Since the effect of weather and load current on audible noise is not exactly the same for RI, some of the differences will be discussed. After the cessation of rain, moderate-to-heavy load current can dry off a conductor very rapidly, thereby lowering the audible noise to ambient levels in as little as 5 minutes. This attenuation may or may not happen with radio noise. Audible noise is a local phenomenon, whereas RI is not. RI levels can still be quite high on a span where measurements are being made, even though it may have stopped raining on that span. RI currents attenuate very slowly up and down the line; therefore, the RI can still be high on a single span because of rain occurring somewhere else on the line. Also, load current does not necessarily dry out support hardware like corona rings; as a result, even if the rain has ceased on most of the line, the corona sources might still be relatively strong on the hardware. TVI is more of a local phenomenon; therefore, TVI levels might decrease more rapidly than RI levels once the rain has stopped, but not as quickly as audible noise because of corona sources from the insulators and the hardware.

Load current has the greatest effect on corona during fog because of the resistive heating effect. However, the resistive heating effect does not keep moisture from building up on insulators and hardware. As a result, RI and TVI levels could still be relatively high, but there have not been enough measurements to determine the magnitude of the RI or TVI levels during fog on lines that are moderately to heavily loaded.

Hoarfrost, like fog, is also formed by condensation but at temperatures below 0°C. Corona off the sharp, icy points is more of a glow corona, which usually has a lower RI level than during rain. Experience has shown that once the load current becomes high enough to melt the hoarfrost, the RI will increase.

Load current can have an effect on fair weather RI because increasing the conductor temperature lowers the relative air density (RAD) at the conductor surface. This effect decreases the corona onset gradient. Figure 9.2-6 shows time plots of magnetic field, A-weighted AN, >6.5 kHz AN, radio noise, solar radiation, and ambient temperature from a corridor of the Bonneville Power Administration (BPA) where one of the 500-kV lines was a very noisy line that used a single 6.35-cm conductor on each phase. It is easily seen in Figure 9.2-6 that the RI is tracking the magnetic field, which, of course, is a measure of load current. It is also tracking the measurement of solar radiation and ambient temperature, which helps heat the conductors.

Effect of Air Density

Air density affects the generation of corona sources. At higher altitudes above sea level, corona inception occurs at lower conductor surface gradients. Based on measurements conducted at the Leadville Project (Robertson 1961) in the 1950s, Pakala and Chartier (IEEE, 1973b) developed the following term to correct RI calculated at sea level to another altitude.

$$\text{dB, adder} = 40\,(1 - \delta r) \qquad 9.2\text{-}1$$

$$\delta_r = 0.392\,\frac{b}{273 + T} \qquad 9.2\text{-}2$$

Where:

δ_r is the relative air density (referred to standard atmospheric conditions: 760 mmHg and 25 ºC).

b is the absolute barometric pressure (mmHg).

T is the temperature (ºC).

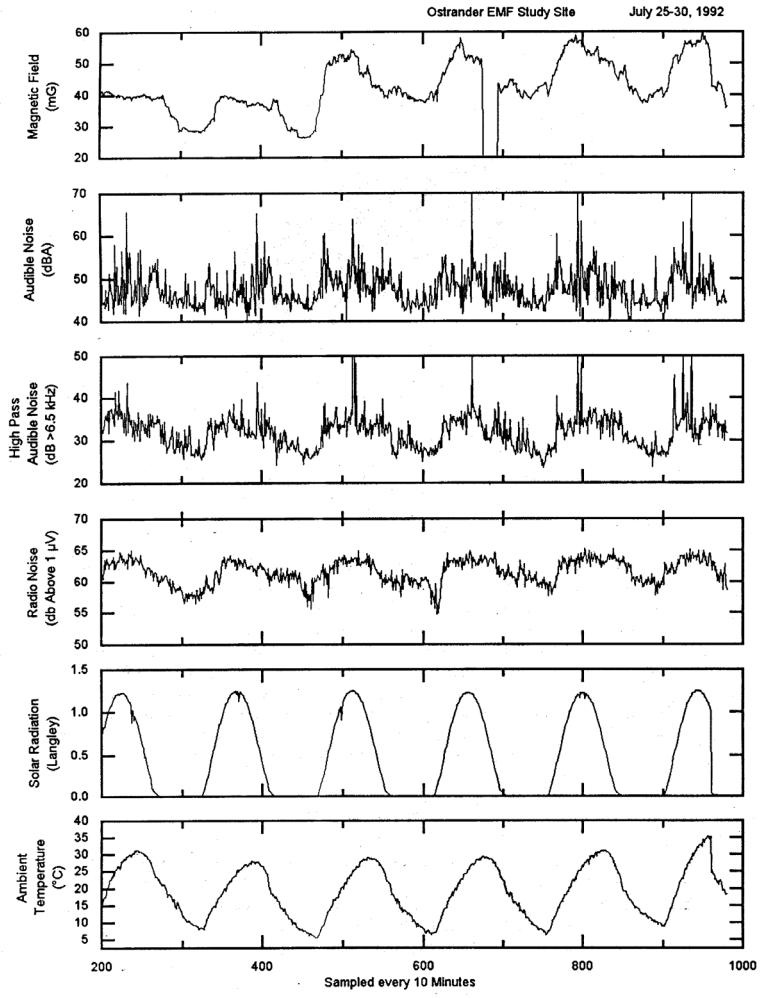


Figure 9.2-6 Magnetic field (top plot), A-weighted AN (2nd plot), >6.5 kHz AN (3rd plot), RI (4th plot), solar radiation (5th plot), and ambient temperature (bottom plot) vs. time (Chartier 1994).

A correction based on elevation above sea level that is much easier to apply can be found in the Italian RI formula (Paris and Sforzini 1968). This term was also developed from the RI data collected at the Leadville Project, and shows that the RI increases with altitude above sea level by $A/300$, where A is the elevation in meters.

The Westinghouse and Italian terms give practically the same results as can be seen in Figure 9.2-7, but the correction for elevation is much easier to apply than the one for relative air density. The temperature and pressure used to calculate the upper abscissa, δ_r in Figure 9.2-7 came from the International Standard Atmospheric Table, which can be found in many reference books.

9.2.2 EMI due to Hardware Corona

EMI from transmission-line hardware is usually not a large source of EMI, but it can be if the hardware is not designed properly. Like corona from conductors, corona from hardware will be higher during rain than fair weather. Because of the much larger number of corona sources from the conductors during foul weather, the hardware corona is usually a very small contributor to the overall EMI level from the line. Corona rings are commonly used to prevent the

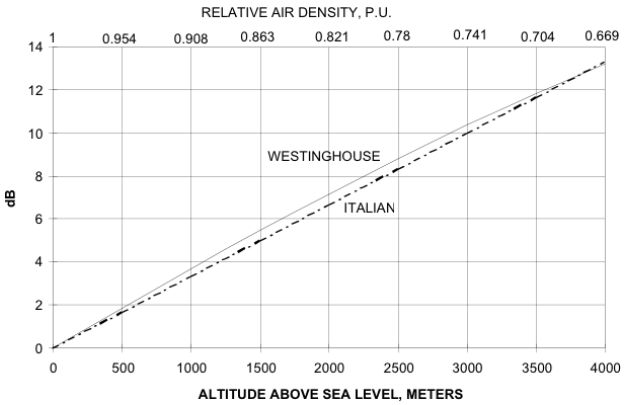


Figure 9.2-7 Westinghouse and Italian terms for altitude effect on RI.

clamping hardware at the line end of insulator strings from going into severe corona. However, the corona rings must be designed properly or they may be a severe EMI source in dry weather. Similar to the conductors, corona rings with larger diameters have a lower electric field at the surface of the ring for the same voltage. Experience at Project UHV has shown, however, that corona rings made up of a composite of several rings that are small in diameter are not only better from a corona performance standpoint, but are easier to manufacture than a single ring (EPRI 1982).

In the particular case of polymer insulators, corona rings are used to suppress the aggressive chemical by-products (nitric acid in particular) formed by any corona discharges at the fitting at the live end of the insulator. Measurements of radio influence voltage (RIV) on polymer and ceramic insulators by Eskom in South Africa has shown that the RIV from polymer insulators is generally lower.

Prediction techniques do not exist for determining the EMI from hardware corona. However, if one is concerned about the overall contribution of hardware EMI in the AM Broadcast Band, analytical techniques are available (IEC/CISPR 1982). This approach, however, requires the corona current to be measured from the hardware assembly in a high-voltage laboratory (IEC/CISPR 1986; IEEE/PES 1997).

A phenomenon called *dry-band arcing* along contaminated insulator stings can create some of the highest EMI levels. When the insulator is dry and contaminated, dry-band arcing does not occur. The worst dry-band arcing is caused by fog and early morning dew where the contaminate is wetted but not wetted enough to wash off the contaminate. Depending on the level of contamination and the voltage, the EMI can become very large and has been the source of severe TVI. Unfortunately, this statement is based primarily on anecdotal evidence rather than actual measurements. This EMI source can be eliminated either by replacing or washing the insulator strings. Dry-band arcing seems to be a problem mainly with ceramic and glass insulators and much less of a problem with polymer insulators.

9.2.3 Gap Discharge EMI

Sparks or gap-type discharges are the primary source of EMI from overhead power lines. They are called gap-type discharges because they are caused by the electrical breakdown of air across a small gap. The gap where the spark is created can be 2.54 mm or less. Avalanche ionization initiates the development of an arc across the gap. Once the gap is formed, the potential difference across the gap drops to a low level, whereby the arc is extinguished. The whole process can be repeated once the parts become recharged. The repetition rate of this sequence of events depends on the charging and discharging time constants of the circuit, the magnitude of the surrounding electric field, and the length of the gap. Individual sparks can occur at many hundreds to a few thousand times per second. However, the repetition rate is usually one order of magnitude lower than the repetition rates for corona. Gap discharges have steep rise times, which means even a single gap discharge can cover a very wide frequency range (see Section 8.5.2).

Propagation along the line is important for gap discharges. The EMI currents produced by a gap discharge will propagate some tens of kilometers at frequencies in the AM Broadcast Band. In the TV Band, the propagation is very short. This phenomenon is taken advantage of in locating gap discharges that cause EMI (Pakala 1964; Loftness 2002; Roets and Britten 1992).

Gap discharges are the main source of EMI from wood-pole distribution lines caused primarily by unbonded conducting parts such as loose hardware. Gap-type discharges are not often found on steel-structured lines, but are often found on wood-pole transmission lines. Hardware on steel-structured lines tends to remain tight throughout the life of the line, whereas hardware on wood-structured transmission lines can become loose in a manner similar to loose hardware on distribution lines. Figure 9.2-8 is a frequency spectrum measured on a wood-pole 345-kV line where the gap discharge was caused by a steady spark between the vertical ground wire running down one of the poles of the H-framed structure and a floating cross-brace. Obviously, the cross-brace had become loose over time. The most common source of gap discharges on steel-structured lines is poor metal-to-metal contact between the units in an insulator string. This poor contact often occurs at what are called “slack spans”—spans where there is not enough weight to keep the units in solid metal-to-metal contact with each other. To solve this problem, some utilities

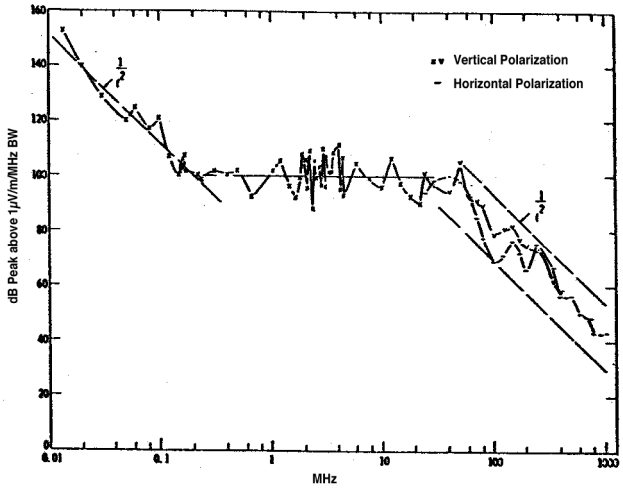


Figure 9.2-8 Frequency spectrum of a natural gap on the wood tower of a 345-kV horizontal configuration line. Measurements made 200 ft from outside phase at the tower(Pakala and Chartier 1971).

replace the ceramic insulator string with a polymer insulator, or they hang weights on the end of the insulator string. It has also been found that voids in the porcelain of porcelain insulator strings can produce gap discharges. Such voids can be found in broken insulator strings. This illustrates that gap discharges are caused not only by metal-to-metal sparks, but also by porcelain-to-porcelain and even metal-to-porcelain sparks.

Unlike the steady gap discharge that was measured on the 345-kV wood-pole line shown in Figure 9.2-8, most gap discharges are very erratic. Some gap discharges may continue for many hours or even days, then suddenly stop. A short time later they may start up again, but sometimes it may be days or months before they start up. Gap discharges are often called "fair-weather" sources because they are usually shorted out during rain or under moist conditions. However, internal gap discharges—such as a gap discharge inside of a lightning arrester—are not shorted out during wet weather.

9.3 DESIGN CONSIDERATIONS AND EMI GUIDELINES AND LIMITS

EMI due to gap discharges can be controlled in the design process by ensuring that hardware is properly bonded together. Then, if hardware becomes loose over time, it can be located and corrected. EMI due to corona from the conductors and hardware cannot be totally eliminated in either the design process or after the line is energized; therefore, it is important that both the conductors and the line hardware are properly selected. The determination of the absolute EMI level of a transmission line due to corona depends on many factors, one of them being the prevailing weather conditions. Thus the whole problem of EMI determination and annoyance evaluation must be approached from a statistical viewpoint.

Over the past 40 years, the electric utility industry has developed design guides and limits for the evaluation of the corona performance of overhead lines (IEEE 1971). The IEEE has developed a comprehensive guide that shows all the technical considerations that need to be considered in assessing the RI and TVI impact of transmission lines (IEEE 1980). Internationally, IEC/CISPR has developed what they call a "Code of Practice for Minimizing the Generation of Radio Noise" from overhead power lines (IEC/CISPR 1986b), and CIGRÉ has published two guides that are widely used (CIGRÉ 1974; CIGRÉ 1996). As far as actual EMI limits for overhead power lines are concerned, none exists in the U.S., but they do exist in Canada and other countries. Because of the variability of EMI from overhead lines, a number of factors must be considered: (1) line-design options for reducing the overall level of the noise, (2) the subjective evaluation of the interfering effect of the noise, (3) the population density of the areas through which the line passes, and (4) the availability and quality of existing radio communication service. These aspects are discussed in the following sections.

9.3.1 EMI Tolerability Criteria

In practice it is unrealistic to say that a particular EMI level produced by a transmission line will or will not cause unacceptable interference because the strength of the received signal, the sensitivity of the receiver, the orientation of the receiving antenna, and the ambient EMI play important roles in determining whether the EMI from the transmission line will cause degradation to communication system. In the AM Broadcast Band, the EMI from a line may produce unacceptable levels of RI in rural areas where both the ambient RI and the signal strengths from distant cities may be low; however, the EMI may be considered quiet in an urban area where there are a much larger number of strong signals, but possibly higher ambient RI levels. Rather than use absolute EMI levels as a criterion for rating interference levels, it is more logical to use a relative measure such as signal-to-noise ratio. This parameter has been used in several studies to assess the effect of transmission-line noise on AM radio-broadcast and television-broadcast reception. Discussion here is confined to RI and TVI, but the general approach is useful in rating the interference of line noise to the operation of any communication device.

Signal-to-Noise Ratio

The term *signal-to-noise ratio (SNR)* is almost self-explanatory. Properly, it is defined as the ratio of average signal power in a given bandwidth to average noise power in the same bandwidth. However, for use in RI and TVI assessments, an alternative definition may be employed: the ratio of signal strength, measured by a particular instrument (antenna and meter), to the strength of the RI or TVI at the same location. This definition generally must be further qualified with respect to the detector used for measuring signal and noise. In this section, unless otherwise specified, it is understood that signal levels are as measured with the average, or field intensity (FI), detector, and the noise is as measured with the quasi-peak (QP) detector. If a signal were being received with a strength of 5 mV/m in the presence of noise measured at a strength of 500 μV/m, the SNR would be as follows:

$$\text{SNR} = \frac{5 \times 10^{-3}\ \text{V/m}}{500 \times 10^{-6}\ \text{V/m}} = 10 \qquad 9.3\text{-}1$$

Often the SNR is expressed in terms of decibels (dB). For the preceding example, the expression would be as follows:

$$\text{SNR} = 20 \log_{10}(10) = 20\ \text{dB} \qquad 9.3\text{-}2$$

Signal and noise strengths are commonly expressed in terms of decibels referred to as 1μV/m (dBμV/m), in which

case the SNR is obtained by subtracting the RI level from the signal level, as illustrated by the following:

$$\text{Signal} = 5\ \text{mV/m} = 20 \log (5 \times 10^3) / 1 = 74\ \text{dB}\mu\text{V/m}$$
$$\text{RI} = 500\ \mu\text{V} = 20 \log_{10} (500) / 1 = 54\ \text{dB}\mu\text{V/m}$$
Then the SNR (as before) is obtained,
$$\text{SNR} = \text{Signal} - \text{RI} = 20\ \text{dB} \qquad 9.3\text{-}3$$

RI Tolerability Criteria

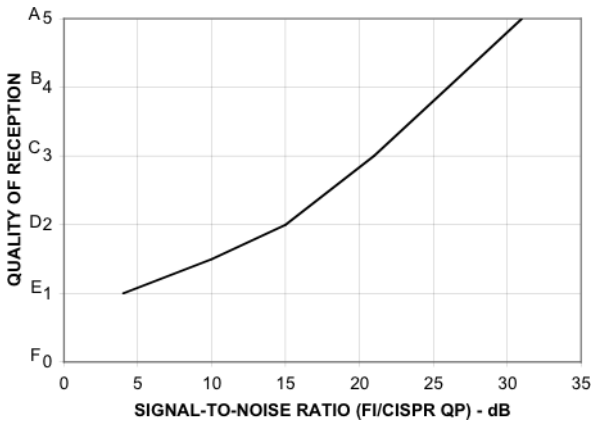
The rating of the quality of radio reception is a subjective matter. Two listeners may rate the same reception quite differently, even though the SNR is the same in both instances. Several investigators have considered these problems and have, from listening tests, statistically evaluated the effect of SNR on reception quality. Such tests were performed as early as 1940 in an attempt to evaluate the effectiveness of radio-noise meters as devices whose objective was to give readings proportional to annoyance for all types of radio noise (Burrill 1942). Later investigations concentrated on radio noise emanating from transmission lines and used meters with quasi-peak detector time constants conforming to present-day standards (Nigol 1964; Lippert et al. 1951; Taylor and Bonska 1962). All investigators reported a certain correlation between SNRs, measured with a quasi-peak detecting instrument, and the quality of reception.

Based on the published listening tests that used transmission-line noise, an IEEE committee presented a curve of quality-of-reception versus quasi-peak SNR that is believed to give "a reasonably good evaluation of the effect of transmission-line radio noise on the quality of AM broadcast radio reception" (IEEE 1965). This curve is shown in Figure 9.3-1. The abscissa is scaled in decibels adjusted to SNRs of average signal to CISPR QP noise. The SNR scale of the equivalent figure in the IEEE Committee Report (IEEE 1965) reflects quasi-peak signal to quasi-peak noise with a meter based on the old ANSI QP detector. Typically the average value of an amplitude-modulated signal is 3 dB below its QP value, and the CISPR QP is about 2 dB below the old ANSI QP detector for corona noise. These factors were used in translating Figure 9.3-1 from the equivalent figure in the IEEE report. If the limit of tolerability is assessed as the point at which reception quality becomes less than satisfactory, then the quasi-peak radio-interference level of a transmission line should be 22 dB or more below the average strength of the desired signal.

A complete summary of all of the SNRs that have been obtained based on listening tests for corona noise from high-voltage ac lines can be found in an IEC/CISPR document (IEC/CISPR 1986a).

This criterion, in itself, is rarely the complete answer to the tolerability question. In any given location, the received-signal strength (in the absence of the line noise) may vary over a wide range, depending on the period of the day, with the distinct possibility that certain signals are received at such a low strength that it would be unreasonable to enforce a line design that would not result in unacceptable reception of these signals. The tolerability problem then becomes one of what percentage of radio-signal receptions, originally considered acceptable, are rendered unacceptable by introduction of the line noise. It has been a common practice of many utilities, therefore, to measure the AM broadcast-signal strengths along the edges of a proposed right-of-way prior to the design of the line to determine the impact any particular design might have on AM broadcast signals. Generally, the only AM signals considered in such a study are those from broadcasting stations for which the measuring location falls within the stations "primary coverage area." The FCC defines three coverage or service areas (FCC 1968)

1. Primary service area the area in which the ground wave is not subject to objectionable interference or objectionable fading



A 5 - ENTIRELY SATISFACTORY

B 4 – VERY GOOD, BACKGROUND UNOBSTRUSIVE

C 3 – FAIRLY SATISFACTORY, BACKGROUND PLAINLY EVIDENT

D 2 – BACKGROUND VERY EVIDENT, BUT SPEECH EASILY UNDERSTOOD

E 1 – SPEECH UNDERSTANDABLE WITH SEVERE CONCENTRATION

Figure 9.3-1 AM radio reception quality vs. signal-to-noise ratio.

2. Secondary service area the area served by the skywave and not subject to objectionable interference or variations in intensity
3. Intermittent service area the area receiving service from the ground wave but beyond the primary service area and subject to some interference and fading

TVI Tolerability Criteria

Almost from the introduction of television, TVI has been of concern to investigators. The problem was identified as early as 1941 by C. M. Burrill (Burrill 1941), who, in discussing developments in the field of radio-noise measuring instruments, concluded that "visual interference is a subject by itself, as yet practically unexplored, which must be left for treatment elsewhere." Rapid advancement in television technology delayed the need for such research until the last decade. Television interference from transmission lines has in the past generally been confined to gap discharges due to loose hardware. In such cases, the offending source or sources may be located, the situation remedied, and the customer satisfied (Loftness 1992). However, with increasing transmission-system voltage, the possibility of TVI caused by conductor corona during foul weather became a problem, especially in rural areas where TV signals can be relatively weak (Clark and Loftness 1970). The problem is not localized, but distributed, and is not easily or inexpensively remedied once a line has been built and is in operation. Because of the many options available to improve the strength of TV signals at any particular location, this TVI phenomenon has not been researched as thoroughly as the RI problem.

Several years ago, the utility industry, in attempting to formulate guidelines for assessing the impact of TVI, had to face the question of what type of detector to use to measure the noise. In contrast to the case of RI, no meter had been developed for the specific purpose of correlating subjective ratings of the interference to television reception. Nevertheless, several investigators attempted to relate viewer tolerance with SNR by using conventional radio-noise meters. For impulsive-type noise, Eteson (Eteson 1967) and Cortina et al. (Cortina et al. 1968) found that good correlation of viewer annoyance with SNRs could be obtained by using the average detector. However, Juette (Juette 1972) found that the peak detector resulted in good correlation for gap-type noise, whereas Sawada et al. (Sawada et al. 1974) used a quasi-peak detector for the evaluation of noise emanating from insulator strings. In investigations of TVI due to conductor corona when the conductors were wet, the peak detector (Juette 1972) and the average detector (Clark and Loftness 1970) have been used. These many different findings illustrate the problems involved in quantitatively assessing the annoyance value of TVI.

The most extensive investigation was sponsored by EPRI (Janischewskyj et al. 1983). It involved the evaluation by more than 500 people of the interfering effect of transmission-line TVI due to gap discharges and rainy weather corona and superimposed on television signals. Two base signal levels were chosen: 70 dB above 1 μV/m, corresponding to an excellent picture quality if no noise were present, and 50 dB above 1 μV/m, corresponding to an adequate picture quality. The two levels may be related approximately to the Grade A and Grade B signal levels, respectively, defined by the FCC for the low VHF range (channels 2-6) (FCC 1968). Master videotapes of color television program material were contaminated by superimposing different levels of transmission-line noise. The resulting picture material (master with superimposed noise) was re-recorded to obtain a contaminated master tape containing material for two signal levels, 70 dB and 50 dB, and SNRs from 50 dB down to 10 dB. Three noise sources were used: foul-weather corona noise, small gap discharge noise, and large gap discharge noise. An edited, test videotape was created from 132 randomly mixed 10-second clips of the contaminated master tape and played to more than 500 human subjects in Canada and the United States. Each subject was asked to rate each clip according to a six-point rating scale, ranging from (1) noise imperceptible to (6) noise so objectionable that picture is unusable. Results of the study are summarized in Figures 9.3-2 to 9.3-4. Each point corresponds to the mean rating of all test subjects for each SNR.

SNRs in Figures 9.3-2 to 9.3-4 correspond to average signal levels and quasi-peak noise levels, both measured with a Stoddart NM30A radio-noise meter having a 6-dB bandwidth of 150 kHz. If noise data measured with an instrument having a different bandwidth are available, then a bandwidth correction factor must be applied to the data before computing the SNR to use with these figures. From

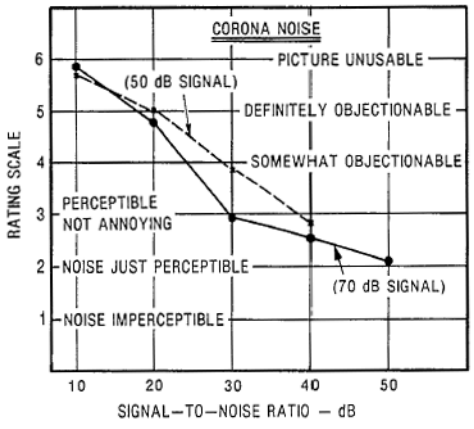


Figure 9.3-2 Television noise rating vs. signal-to-noise ratio for corona noise.

measurements made with different instruments in connection with the preceding TVI study (Janischewskyj et al. 1983) and from other test measurements (IEEE 1977), (Hatanaka 1981), the following bandwidth correction factors are suggested for converting quasi-peak data from a 6-dB bandwidth of BW (in kHz) to the 150-kHz bandwidth of the NM30A meter:

for corona noise
$$\Delta = 12 \log10 (150/BW) \text{ dB} \quad 9.3\text{-}4$$

for gap discharge noise
$$\Delta = 17 \log10 (150/BW) \text{ dB} \quad 9.3\text{-}5$$

From the results presented in Figure 9.3-2, it would appear that an SNR of at least 30-40 dB is required if corona noise is not to cause objectionable interference. Higher SNRs are required for gap discharge noise (Figures 9.3-3 and 9.3-4). However, gap discharge noise is usually associated with broken insulators or other defective or loose-fitting hardware and is not generally used as a design criterion.

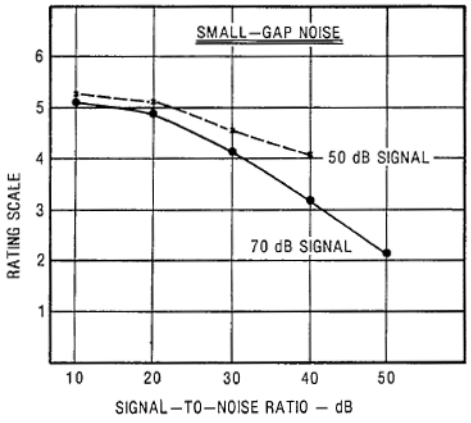


Figure 9.3-3 Television noise rating vs. SNR for small gap discharge noise. (Rating scale same as in Figure 9.3-2.)

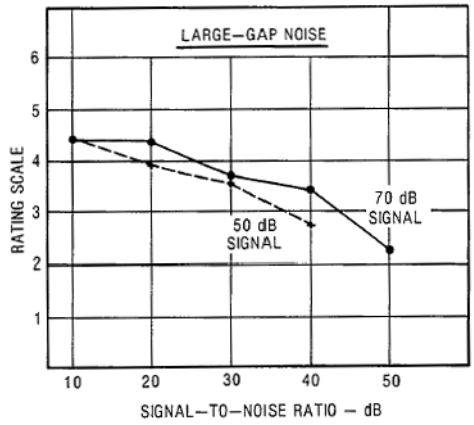


Figure 9.3-4 Television noise rating vs. SNR for large gap discharge noise. (Rating scale same as in Figure 9.3-2.)

The study described previously used color program material. The effect of interference on black-and-white television reception compared to color has been investigated (Fredenall 1953). The results indicate that color reception is only slightly more susceptible to random noise (such as corona), whereas there is virtually no difference for impulse noise (such as gap discharge noise).

As with RI, a criterion based on SNR alone is rarely the complete answer to the tolerability criterion. The FCC regulations specify that the minimum field intensity that must be provided over the entire principal community to be served is 74 dB above 1 μV/m for channels 2-6, 77 dB for channels 7-13, and 80 dB for channels 14-83. However, it is recognized that in many areas (presumably outside the principal community), usable signals are received with strengths considerably lower than these levels. In fact, in the same FCC regulations, reference is made to Grade A and Grade B service contours of signal strength lower than those previously mentioned (see Table 9.3-1). These contours are used for station authorization purposes to estimate the median signal strength at 50% of the receiving locations. The exact definition or significance of these contour grades is not clear from the regulations; however, an interpretation is offered in the following example. If the Grade A contour encloses 10,000 receiving locations, then 5000 of these would receive a signal strength greater than 68 dB above 1 μV/m for channels 2-6 (see Table 9.3-1) for more than 50% of the time. The remaining 5000 would receive lower signals most of the time. Recognizing that people in their service area are using signals at very low levels, the Bonneville Power Administration has gone further in defining Grades C and D (Clark and Loftness 1970). (See Table 9.3-2). It would be economically prohibitive to design a high-voltage transmission line that at all times and under all conditions would not result in objectionable interference in areas covered by Grade C and Grade D service. Generally, however, such situations are relatively few and may be treated on an individual basis. Mitigation techniques such as repositioning the antenna at a greater distance from the line or, for more widespread problems, the installation of a local cable television or satellite system may be considered (Loftness et al. 1981).

Table 9.3-1 FCC Television Service Grades

Television Channel	Signal Level (dB above 1μV/m)	
	Grade A	Grade B
2–6	68	47
7–13	71	56
14–83	74	64

Table 9.3-2 Television Service Grades Defined by Bonneville Power Administration

Television Channel	Signal Level (dB above 1μV/m)	
	Grade C[1] (fringe)	Grade D[2] (far fringe)
2–6	34–46	20–33
7–13	42–55	33–41

1. Usable with high-gain antenna and low ambient noise.
2. Very poor picture (but people are found to be watching TV in this area). Below minimum of this range, the signal is unusable.

For the design of a new transmission line, a philosophy may be established to take into account population densities, received-signal strengths, percentage of time that corona noise will exist (foul weather), and absolute noise levels. Guidelines similar to those proposed for RI could also be used for the television interference problem (IEEE 1980).

Digital TV and Radio

All of the previous discussion on tolerability criteria may soon become obsolete as the radio and TV broadcasting industry converts to digital systems. Direct Broadcast Satellite (DBS) television has been available for a number of years. DBS radio is already operating in Africa, the Middle East, and in the United States. Since DBS TV and radio operate at frequencies above 1 GHz, EMI due to corona or sparks is not expected to interfere with these systems.

There is a worldwide push to convert all analog TV broadcasting to digital. A pure DTV system is one where the local TV station transmits pure digital television signals along with the reception and display of those signals on a digital TV set. The digital signals might be broadcast over the air or transmitted by cable or by a satellite system to the home. In the home the signal is fed into a decoder and uses it, in digital form, to directly drive the TV set. The class of DTV that is now available is called high-definition television (HDTV). HDTV is high-resolution digital television combined with Dolby Digital surround sound. There are HDTV stations "on the air" in many large cities. In the United States the FCC has mandated that all existing TV broadcast stations be capable of broadcasting HDTV by 2006. Since HDTV will be broadcast over the air using the existing licensed frequencies, there is a need to determine the susceptibility of these digital signals to power line EMI.

There is also a global trend toward adoption of digital technology in radio broadcasting. FM sound broadcasting is moving toward digital broadcasting, but, as is well known, coverage in the 88-108 MHz (VHF) band is limited. Because of the superior coverage of long, medium, and short wave, there is a push to implement digital technology in the AM bands. The IEC has given the DRM (Digital Radio Mondiale) on-air system its endorsement with the adoption of the DRM standard IEC 62272-1 Ed. 1: Digital Radio Mondiale (DRM) – Part 1: System Specification. As most EMI engineers know, analog AM radio is extremely susceptible to atmospheric EMI. If DRM systems can be built to be immune to atmospheric EMI, it is highly likely they will also be immune to power line EMI.

Tolerability criteria for digital radio and TV will not necessarily have grades of reception. It is more likely that there would be a threshold where the program being received by the radio or TV could no longer be heard or seen below a particular signal-to-noise ratio.

Tolerability Criteria for Other Communications Systems

There are innumerable types of communication systems. Such systems include radio telescopes, aircraft instrument landing systems, telecommunications data transmission, public safety (fire, police, ambulance) communications, amateur and citizens-band radio, pagers, wireless telephones, etc. Some of these systems are analog, and others are digital. The QP measure of RI that can be estimated for any frequency through procedures described in this chapter may not be applicable to many of these communication systems. The susceptibility of all the various communications systems to transmission-line EMI is not known and usually has to be assessed on a case-by-case method. However, for many communications services, it appears that a noise power or an rms measurement of the noise is needed to assess the interfering impact of the noise. Very few rms measurements have been made on actual lines, especially with the newest EMI instrumentation.

Rms noise measurements were made during the last three configurations tested at Project UHV (bundles of 16 x 3.31 cm tested at 1450 kV, 8 x 5.59 cm tested at 1300 kV, and 6 x 5.59 cm tested at 1100 kV). Measurements were made at 0.47 MHz, just below the AM Broadcast Band, and were compared to QP measurements made concurrently at the same frequency and off the same antenna. Average foul-weather differences between QP and rms were found to be 14 dB, 10 dB, and 11 dB, respectively, for the three Project UHV configurations. On the basis of these data, and in the absence of additional information, one could estimate the rms level of transmission-line RI, in a 5-kHz bandwidth, by subtracting 12 dB from the QP level.

Chartier has conducted many measurements using a variety of EMI meters that did not have all of the detectors that are in the modern EMI instruments. Based on analysis of all this data, he recommends that, between 150 kHz and 30 MHz, the rms level can be determined by subtracting 8 dB from the QP (CISPR) measurement of the EMI (Chartier 1988). Rms measurements on 230- and 500-kV lines during rain at 75 and 900 MHz showed smaller differences (Chartier et al. 1986); however, those rms measurements

were made with an add-on box that was difficult to calibrate. The mean difference between QP and rms measurements on both the 500-kV line and 230-kV line at 900 MHz in a 1.0 MHz bandwidth was 5.2 dB. The difference was 4.1 dB in a 0.1 MHz bandwidth. The mean difference at 75 MHz with a 0.1 MHz bandwidth was 5.0 dB. These differences seem too small based on the differences seen between QP and FI measurements at 50, 75, and 160 MHz during an extensive IEEE measurement program (IEEE 1977). For both wet and dry corona, the mean difference between QP (CISPR) and FI was about 14 dB, which was similar to the difference seen between the measurements conducted at 0.5 and 1.0 MHz. Therefore, until more complete measurements have been conducted using the newer, more stable EMI meters, the rms level of corona EMI during both fair and rainy weather should be determined by subtracting 8 dB from the QP calculation of EMI from 150 kHz to 1000 MHz.

Since EMI in rms units varies with the square root of the bandwidth, in another bandwidth, BW (kHz), the EMI noise would be

$$EMI = EMI_0 + 10 \log (BW/BW_0)$$

From 150 kHz to 30 MHz, the rms level calculated by subtracting 8 dB from the QP (CISPR) calculation, using the prediction techniques in this chapter, is based on a bandwidth of 9 kHz. From 30 MHz to 1000 MHz, the reference bandwidth is 120 kHz if the TVI is calculated using the TVI prediction techniques described later in this chapter.

An assessment of whether the calculated noise level would cause unacceptable interference to a particular communication system would need additional information such as sensitivity of the communication system and acceptable SNRs if they are known. Obviously, these ratios will be different for different types of communication systems, and each system would have to be examined on a case-by-case basis.

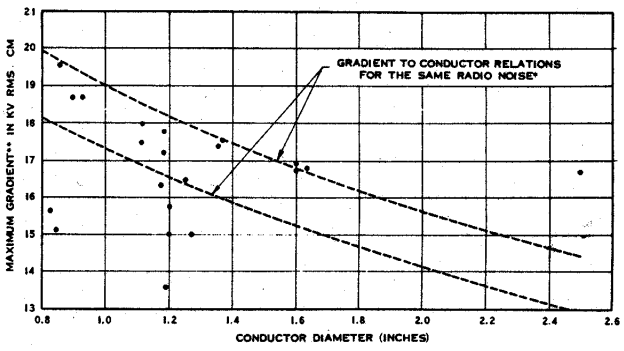
9.3.2 Design Guidelines and Limits

There are no EMI limits for overhead power lines in the U.S. Overhead power lines are covered by the FCC incidental radiation device rule, which can be found in Part 15 of the FCC Rules and Regulations (FCC 2001). By FCC definition, an incidental radiator is "a device that generates radio frequency energy during the course of its operation although the device is not intentionally designed to generate or emit radio frequency energy." According to the FCC, "an incidental radiation device shall be operated so that the radio frequency energy that is emitted does not cause harmful interference." The FCC also defines harmful interference as "any emission, radiation or induction which endangers the functioning of radio navigation service or of other safety services or seriously degrades, obstructs or repeatedly interrupts a radio communications service operating in accordance with this chapter." Basically this rule says if an incidental radiation device is causing harmful interference, the device must be turned off. Since this isn't possible with overhead power lines, the FCC allows utilities to find other solutions to eliminating harmful interference. In the case of gap discharges the solution is to find the gap(s) and eliminate them (Loftness 1996). In the case of corona, which for the most part is designed into lines and substations, utilities have used other solutions such as relocating antennas, connecting customers to cables, paying for the purchase of satellite antennas, etc. (Loftness et al. 1981).

IEEE Radio Noise Design Guide

The IEEE published two design curves in 1971 (IEEE Line Design Working Group 1971). Those curves showed the range of operating conductor surface gradients and conductor sizes for single or bundle conductors that would give comparable radio noise levels due to conductor corona. These curves are independent of the number of conductors in the bundle based on research conducted in the AM Broadcast Band over the years. The working group that produced those curves (reproduced as Figure 9.3-5) came to the conclusion that lines that were designed based on the upper curve would produce a fair weather radio noise level of approximately 40 dBμV/m (100 μV/m) at 1 MHz at 100 ft lateral distance from the outside conductor of a overhead line.

Figure 9.3-5 illustrates the importance of the conductor surface gradient and the conductor diameter on the



* Fair weather level below 100 μV/m (optional QP) at 100 ft lateral distance from outside conductor.

** Maximum gradient around the periphery of a subconductor on any phase.

• Lines in operation in 1971.

Figure 9.3-5 Range of operating gradient and conductor size for single or bundle conductors for comparable noise levels (IEEE Working Group on Line Design 1971).

generation of the conductor corona that produces the RI. But the curves in Figure 9.3-5 are for lines operating at sea level. Since many lines operate at high elevations, the family of curves in Figure 9.3-6 were created, and they show not only the range of operating gradients and conductor sizes that give comparable RI levels at sea level, but also at elevations from 0 to 6000 meters above sea level. These curves were created by multiplying the upper curve of Figure 9.3-5 by $\delta^{2/3}$, where δ is the relative air density. The equation for the calculation of relative air density can be found in Chapter 8.

RI Limits

Canadian utilities working with the Department of Communications (DOC) in Canada developed RFI limits (Canadian Standards Association) for overhead power lines that are based on work conducted at Hydro-Quebec (Maruvada and Trinh 1975). These limits are reproduced in Table 9.3-3. It should be noted, however, that the Canadian Limits are independent of the source of the RFI. In other words, they are applicable for both corona and gap discharges. Canada, however, is no different than the U. S. in terms of the primary source of RFI. Gap discharges are responsible for more than 90% of the RFI complaints, and the Department of Communications working with the Canadian utilities spends a lot of time and effort locating and correcting RFI sources due to gap discharges.

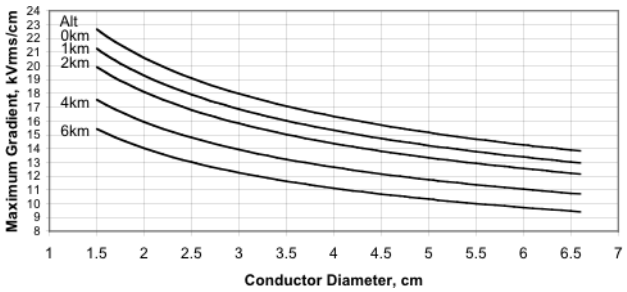


Figure 9.3-6 Range of operating gradients, conductor diameters, and altitudes above sea level for comparable RI levels.

Table 9.3-3 Canadian Standards Association Maximum Fair Weather Limits for Interference Fields - 0.15 - 30 MHz

Nominal Phase-to-Phase Voltage (kV)	Interference Field Strength (dBμ/m)
below 70	43
70-200	49
200-300	53
300-400	56
400-600	60
600-800	63

It needs to be noted that these limits are based upon: (1) a frequency of 0.5 MHz, (2) the IEC/CISPR-type meter, (3) the maximum RI level that occurs during fair weather, and (4) a distance of 15 m from the outside phase. As mentioned earlier, the IEC/CISPR-type meter measures corona about 2 dB less than the older ANSI type meters. Also, the maximum RI level during fair weather is about 6 dB larger than the mean radio noise level during fair weather.

From an international perspective, IEC/CISPR has attempted at times to create RI limits for overhead power lines. These attempts have not been successful because many nations feel that RI from overhead power lines is a national, not an international, concern. However, IEC/CISPR in 1986 did produce what they call a "code of practice for minimizing the generation of radio noise" (IEC/CISPR 1986b). Some countries have RI limits, but it is not clear how current these limits are. The IEEE Power Engineering Society in a 1980 paper (IEEE 1980) showed that regulations existed in Czechoslovakia, the USSR, Switzerland, and Poland. Since the USSR and Czechoslovakia no longer exist, it is not clear that these limits still exist or have been replaced. The Swiss standard, issued in 1966, covers a vast range of electrical equipment and installations, among which are included high-voltage power systems. The standard states that the RI level, measured at a frequency of 0.5 MHz and at a distance of 20 m from the outside phase during dry weather and 10ºC, should not exceed 34 dB for lines operating at less than 100 kV and 46 dB for lines operating at more than 100 kV. The Polish standard, issued in 1969, also covers a wide range of equipment. For transmission lines, the interference field strength, measured during normal operation at a lateral distance of 20 m from the outermost conductor, should not exceed 750 μV/m (57.5 dB), for air humidity not exceeding 80%, for the temperature not less than +5ºC and for the frequency of 500 kHz ±10 kHz.

Finally the IEEE in 1980 (IEEE 1980) produced an excellent review of all the technical considerations needed to develop limits for overhead power lines and stations. Much of the material in this paper in setting limits in the AM Broadcast Band came from the work of Maruvada and Trinh (Maruvada and Trinh 1975) and also from previous efforts of the IEEE Radio Noise Subcommittee. The material related to the television bands came from Clark and Loftness (Clark and Loftness 1970), the IEEE and other sources.

9.4 MEASUREMENT OF EMI

Ideally, to measure the true level of interference to a particular communication device, the EMI instrumentation should have the same response characteristics as the communication device, with only the final output stage

modified to measure the EMI in quantitative terms. However, since a wide variety of communication devices operate throughout the radio-frequency band, such an ideal cannot be practically realized for the general investigation of transmission-line EMI. On the other hand, it is very desirable that different investigators of transmission-line EMI use similar instrumentation and measuring techniques. This consistency provides a straightforward means of comparing data collected by different investigators and providing data that will be useful to the transmission-line designer. Consequently, a certain amount of standardization has been undertaken, in both the areas of instrumentation and of measuring procedures (ANSI/IEEE 1986; ANSI 1996; IEC/CISPR 1999).

The theory and principal characteristics of radio-noise meters covered by standards have been discussed in considerable detail in the literature (Aggers et al. 1940; Burrill 1941; Frick 1945; Burgess 1948; Frick 1954; Showers and Eckersley 1954). In addition, reports on the comparative performance of different instruments in measuring transmission-line EMI are available (IEEE 1968; IEEE 1977). Thus, only the most important features of radio-noise instrumentation are discussed in this section. Similarly, the measuring procedures are well documented elsewhere (ANSI/IEEE 1986), and specific requirements are dealt with only briefly here. However, even when prescribed measuring procedures are carefully followed, erroneous or misleading measurements can still occur unless precautionary steps are taken. The text on measuring procedures describes several steps that can be taken to ensure good data collection.

9.4.1 EMI Instrumentation

An EMI meter is a frequency-selective voltmeter. The basic EMI meter is a superheterodyne receiver specially designed to accurately measure signal or noise amplitude. (Another instrument that is also used to measure EMI is the spectrum analyzer. See Section 9.4.4.) The block diagram in Figure 9.4-1 illustrates the signal-processing chain in the basic EMI meter. For the example illustrated, widely separated pulses (1) enter the meter via the RF (radio frequency) input. Each pulse may be considered as a generator of a spectrum of frequency components. The RF amplifier amplifies a relatively narrow portion of this spectrum, determined by the bandwidth of the amplifier. The output of the amplifier is a train of modulated oscillatory pulses (2), the oscillation frequency being the tuning frequency of the meter. The envelope of the pulses have a peak amplitude, A, which is proportional to the bandwidth of the amplifier, and a width, *W*, which is inversely proportional to the bandwidth. (*W* is defined as the width of a rectangle having the same area and height as the pulse envelope.)

In the mixer, the pulse oscillation frequency is converted to an intermediate frequency (IF). The pulses then pass through the IF amplifier, whose output is again a train of oscillatory pulses. At this stage, the width and peak amplitude of the pulses are determined by the narrowest bandwidth of the IF circuit.

The pulses then enter the detector, which rectifies the pulses (3) and filters out the high-frequency components leaving the monopolar envelopes of the pulses (4), which are applied to the weighting circuits. These circuits, often considered part of the detector, determine whether the voltmeter reads the peak, rms or the average of the envelope, or some intermediate quasi-peak (QP) value (5). Some instruments provide an automatic gain control to reduce the gain of the IF amplifier for large signals (noise levels) so that the deflection of the voltmeter is proportional to the logarithm of the input signal amplitude. The voltmeter is calibrated to indicate the rms value, in microvolts (μV) or decibels above 1 μV (dBμV), of a sinusoidal input signal whose frequency is equal to the tuning frequency of the meter. For example, suppose a certain noise input results in a meter deflection when the meter is tuned to 1 MHz. If a 1-MHz sinusoidal voltage adjusted to yield the same meter deflection replaces the noise α, then the original noise level would be defined to be the rms value of the sinusoidal voltage, and the meter scale would be marked accordingly.

9.4.2 Weighting Circuits

Weighting circuits are often considered part of the detector and are identified by terminology such as *average detector, rms detector, peak detector, and quasi-peak detector.* These

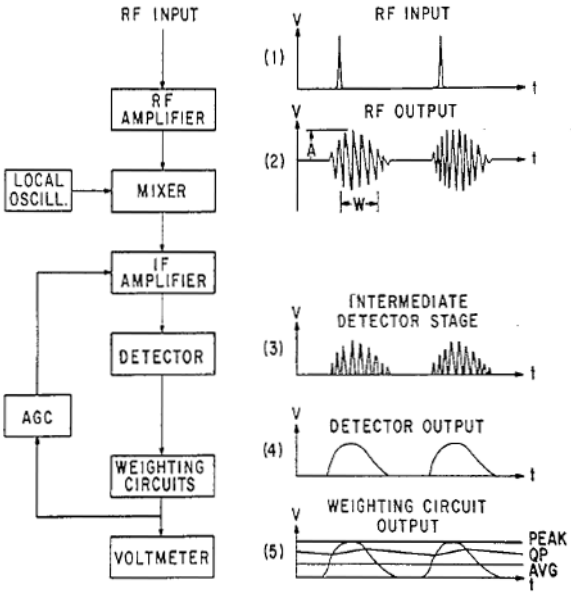


Figure 9.4-1 Signal processing of an EMI meter.

detectors have been standardized, and can be found in the previously mentioned standards. A schematic representation of the average, peak, and quasi-peak detectors are shown in Figure 9.4-2.

Average

If a uniform train of pulses, V, is applied to the input of the average weighting circuit, the output, V_1, will vary about the time-average value of the pulses, the amplitude of the variation being practically determined by the time constant R_1C_1. If this time constant is sufficiently large, the output voltage will be essentially constant (for a uniform pulse train input) and will not be affected by very short-duration pulses superimposed on the input. The average weighting circuit, which thus measures the longtime average of the input signal, is particularly suitable for measuring the field strength of radio-frequency carriers since its indication will not depend on the carrier modulation whose longtime average is zero. For this reason, the average detector is also known as the field intensity (FI) or carrier detector.

Root-Mean-Square (rms)

The rms detector measures the energy of the input signal. Since the response of an rms meter is proportional to the square root of the bandwidth for any type of broadband interference, rms measurements can be easily corrected to any other bandwidth. The rms measurement of EMI is preferred for analysis of interference to many communication receivers.

Peak

Two types of peak detectors are discussed in the standards: Direct Peak or Slideback Peak. Until recently, the Slideback Peak detector was exclusively used whereby the meter reads a dc voltage, V_1. The difference between this voltage and input voltage, V, is rectified and applied to the input of an audio-amplifier, the output of which is zero when V_1 is adjusted to the peak of the input, V. The Direct Peak detector is the preferred detector and is similar in concept to the QP detector. According to the standards, "the direct-peak detector circuit shall have a charging circuit with a time constant in seconds that is much shorter than the reciprocal of the widest bandwidth in hertz. The discharge time constant (that is, peak hold) shall be a minimum of five times the time constant of the output indicating device." The peak detector is particularly applicable to measurements of repetitive, impulse-type noises.

Quasi-peak

The QP detector is the standard detector for measuring EMI from overhead lines in the AM and TV Broadcast Bands. It was originally designed to relate the meter indication for a particular noise to the annoyance effect that the noise would have when interfering with AM radio broadcast reception. The response of the circuit is determined by the charge and discharge time constants, RC and R_1C_1 respectively. If R_1 is infinite, then C can discharge only through its own leakage resistance, and the output would effectively be the peak of the input pulse train. This principle is essentially the basis of the direct peak detector,

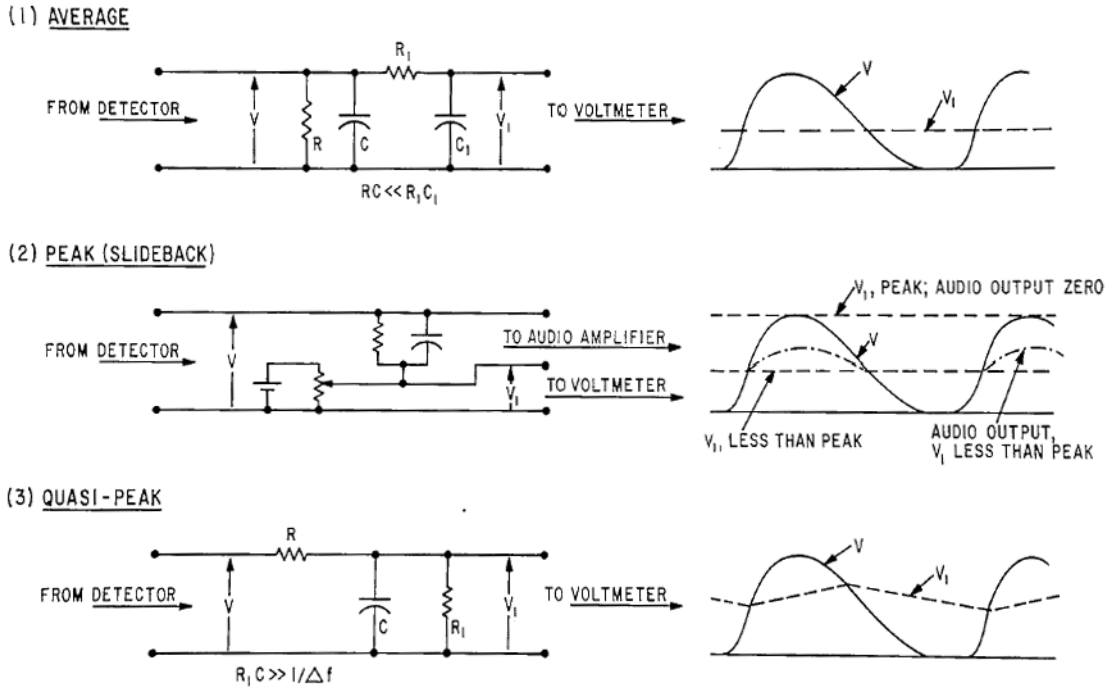


Figure 9.4-2 Detector weighting circuits.

mentioned earlier, where in practice R_1 is some finite value such that R_1C is on the order of several seconds. The annoyance value of any noise, however, depends not only on the peak value, but also on the repetition rate of noise pulses. This relationship was first found to be true for audible noise by Steudel (Steudel 1933) and reported by Davis (Davis 1938) who, in discussing sound level meters suitable for measuring repetitive-type noise, stated that the meter "must have an appropriate leak, for the loudness of a slow series of repetitions is less than that of a rapid series." This concept of a leaking peak meter was carried over into the design of radio-noise meters, the end product being the QP detector circuit. Present-day standards (ANSI 1996; IEC/CISPR 1999) call for QP time constants as indicated in Table 9.4-1.

The optional discharge time constant in the frequency range of 150 kHz to 30 MHz is a time constant associated with much earlier versions of ANSI C63.2. Several years ago ANSI adopted the time constants associated with the CISPR 16 standard (IEC/CISPR 1999). However, ANSI C63.2 allows the use of meters with the 600-ms discharge time constant in the frequency range of 150 kHz to 30 MHz for the special case of "interference or radio-influence (RIV) associated with electrical power apparatus." The older instruments that have this discharge time constant have a 6-dB bandwidth of about 4.5 kHz, whereas the CISPR requirements have a 1-ms charge, a 160-ms discharge, and a 6-dB bandwidth of 9 kHz (IEC/CISPR 1999). For most types of electrical discharges instruments that conform to the old ANSI C63.2 standard and the CISPR 16 standard, the meters will read essentially the same. However, special comparison tests conducted by the IEEE Radio Noise Subcommittee have shown that for corona and gap noise from overhead power lines, meters conforming to the old ANSI C63.2 standard read from 1 to 2 dB higher than meters conforming to the IEC/CISPR 16 standard. The recommendation for corona noise is to subtract 2 dB from measurements conducted with the instruments that conform to the old ANSI C63.2 standard to obtain a measurement that conforms to instruments designed to the IEC/CISPR standard (IEEE 1977).

Investigators of transmission-line EMI have historically concentrated on the QP measurement because the potential interference to AM radio-broadcast reception from corona-produced EMI was the main concern of the utility industry. Now there are a host of telecommunication receivers. It is known that the QP detector does not necessarily provide EMI data suitable for evaluating interference to all of the various receivers. For example, many communication devices such as radio telescopes and wireless telephone are better evaluated using the rms measure of EMI.

Other measures of noise besides those previously mentioned have been suggested, and in some instances have been used for transmission-line radio noise. One such measure is the amplitude probability distribution (APD) (Lauber 1976). APD provides an indication of the probability with which the amplitude of the envelope of the IF output exceeds a given value. From such data, any noise parameter that is a function of the instantaneous amplitude (such as rms or average) may be calculated. However, equipment for APD measurements is quite specialized, can be found in only a limited number of laboratories, and has not found wide application in the measurement of transmission-line noise.

9.4.3 Meter Response – Bandwidth and Pulse Repetition Rate

A single pulse may be considered a generator of a continuous spectrum of frequencies. The RF amplifier of the radio-noise meter has a relatively small bandwidth Δf centered about its turning frequency f_o. Consequently, it amplifies only a small portion of the pulse frequency spectrum—namely, that portion between $(f_o\text{-}\Delta f/2)$ and $(f_o+\Delta f/2)$. For the simplest case of a rectangular pulse, amplitude A and duration δ, it can be shown that the output of an ideal bandpass filter of bandwidth Δf and tuned to f_o is as follows:

$$U = A\delta \bullet 2\Delta f \frac{\sin \Delta f t}{\Delta f} \sin 2\pi f_0 t \qquad 9.4\text{-}1$$

$$\delta << 1/f_0 \qquad 9.4\text{-}2$$

Equation 9.4-1 describes a modulated high-frequency oscillation, as shown in Figure 9.4-3. The output of the

Table 9.4-1 Standard Bandwidths and Circuit Time Constants for QP Detector

Frequency Range	Bandwidth at 6 dB	Charge Time Constant[1] (ms)	Discharge Time Constant[1] (ms)	Optional Discharge Time Constant[1] (ms)
10 Hz-20 kHz	Full Range (Wideband)	1	160	-
10 – 150 kHz	200 Hz	45	500	-
150 kHz-30 MHz	9 kHz	1	160	600
30 MHz-1 GHz	120 kHz	1	550	-
Above 1 GHz	N/A	N/A	N/A	N/A

1. A tolerance of ±20% about these nominal values is suggested.

filter is essentially a series of pulses, the largest of which has a peak amplitude $2A\delta\Delta f$ and a duration of $2/\Delta f$. Subsequent pulses have amplitudes that are attenuated at the rate of $2/(2n - 1)\pi$, where n is the number of the pulse, and can usually be neglected. Thus, for a single pulse input, the output of the RF amplifier of the radio-noise meter will effectively be a pulse whose amplitude is proportional to the amplifier bandwidth and whose duration is inversely proportional to the bandwidth. If the single pulse input is replaced by a series of pulses sufficiently separated in time, the amplifier output will be a series of non-overlapping pulses; that is, the response of the amplifier to one pulse will have died away before the arrival of the next pulse. In this case the magnitudes of the output pulses are not dependent on the repetition rate. In practice, two pulses can be considered non-overlapping if the interval between them is greater than $1/\Delta f$, the reciprocal of the amplifier bandwidth. Usually the RF and IF amplifiers are considered *en bloc*: Δf represents the smallest bandwidth in the amplifier chain and is the characteristic meter bandwidth. Consider now how the overall meter response is affected by the pulse repetition rate. Figure 9.4-4 illustrates the effects for two different pulse rates, neither of which results in overlapping pulses at the amplifier output (detector input). The peak response is unaffected by the repetition rate. In fact, the pulses may occur quite randomly, provided they are separated by at least $1/\Delta f$, without affecting the peak reading. Quasi-peak, average, and rms readings all increase with increasing repetition rate, as indicated in Figure 9.4-4. If the pulses occur randomly, with no two pulses closer to each other than $1/\Delta f$, then the quasi-peak, average, and rms responses will be as if the pulses were regularly separated by a time period equal to the mean interval of the randomly occurring pulses. The ratio of quasi-peak to peak readings is known as the quasi-peak factor and is shown in Figure 9.4-5 for both ANSI and CISPR radio-interference meters. It may be noted that this factor approaches unity as the pulse repetition rate approaches the bandwidth of the meter. If the repetition rate increases further, the amplifier output will be dependent on the phase relationship between the high-frequency components of the pulses. As illustrated in Figure 9.4-6, a reinforcing or canceling effect will occur, which in the extremes could cause a double amplitude or a zero amplitude output. For randomly occurring pulses, this phase relationship is randomly distributed. When two pulses are superimposed within the meter bandwidth, the amplitude of the resulting detector pulse is the rms value of the envelopes (Maruvada et al. 1974). Hence all readings will increase at a rate approximately proportional to the square root of the mean repetition rate.

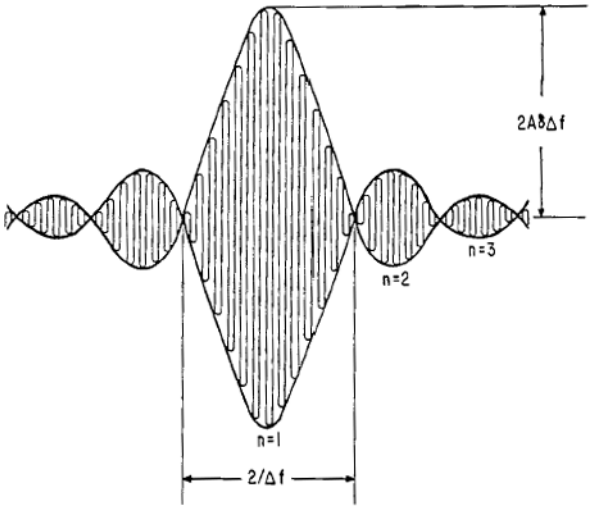


Figure 9.4-3 Output of an ideal band-pass filter for a rectangular pulse input.

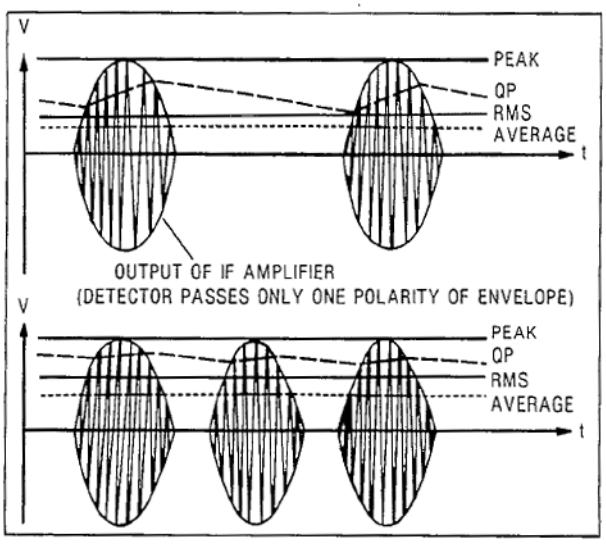


Figure 9.4-4 Meter response for different pulse repetition rates.

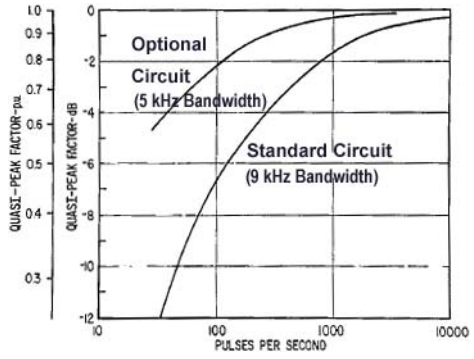


Figure 9.4-5 Comparison of quasi-peak factors for the optional and standard time constants in ANSI C63.2.

Now consider the effect of different bandwidths. As shown in Equation 9.4-1 and Figure 9.4-3, the peak reading will increase linearly with meter bandwidth for sufficiently separated pulses. The average reading is effectively determined by the area under the envelope of the pulse at the detector output. It can readily be shown that this area, and thus the average reading, is independent of the bandwidth, again for sufficiently separated pulses. The rms reading will increase with the square root of the bandwidth, whereas the quasi-peak reading will increase somewhat less than linearly with the bandwidth by an amount that is dependent on the repetition rate. The effect of bandwidth is illustrated in Figure 9.4-7, in which all responses are shown relative to a 5-kHz bandwidth. If the pulse repetition rate is greater than the meter bandwidth, the overlapping of pulses will result in responses that increase approximately with the square root of bandwidth for all detectors.

The preceding discussion has been confined to regular pulses occurring at a more or less regular rate, which may or may not result in overlapping pulses within the meter. The regular and overlapping pulses may be broadly classified as impulse noise and random noise, respectively—the term *random* referring to the random phase relationship of the high-frequency components of overlapping pulses. A single-source, gap-type noise, such as a sparking insulator, would generally fall into the impulse-noise category.

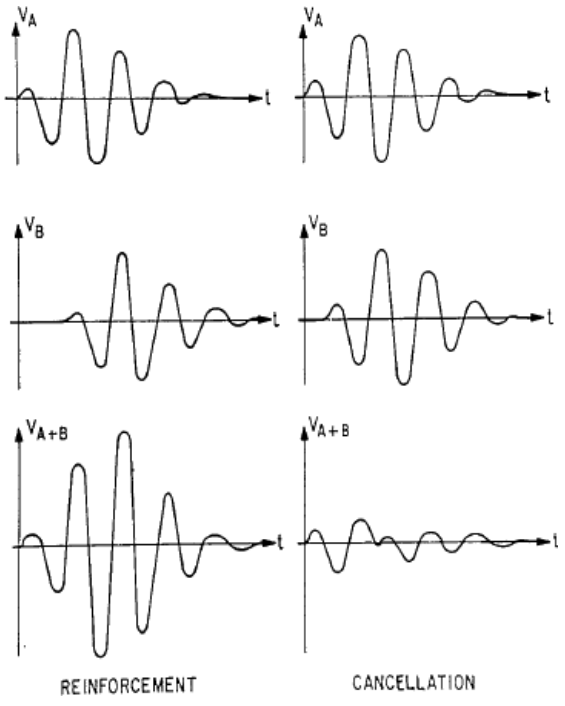


Figure 9.4-6 Reinforcing and canceling effects of overlapping pulses.

Corona noise does not fall completely into either category because, in general, corona noise consists of isolated packets of random-amplitude, high-repetition-rate pulses—individual packets being separated in time by one-half period of the power-frequency voltage cycle, as illustrated by Figure 9.4-8. If corona on the conductors is well established and reasonably uniform, the meter's response will be very close to its response to random noise, with little difference between peak and quasi-peak readings. If corona is well established, but one or two predominant sources are producing distinct intermittent pulses, the peak detector will respond as if to impulse noise, although the quasi-peak response may remain unaffected. For dry-weather corona, where noise pulses are usually well separated, both peak and quasi-peak detectors will generally respond as if to impulse noise.

The effect of bandwidth on the QP detector is somewhat moot because IEC/CISPR 16 and ANSI C63 define single

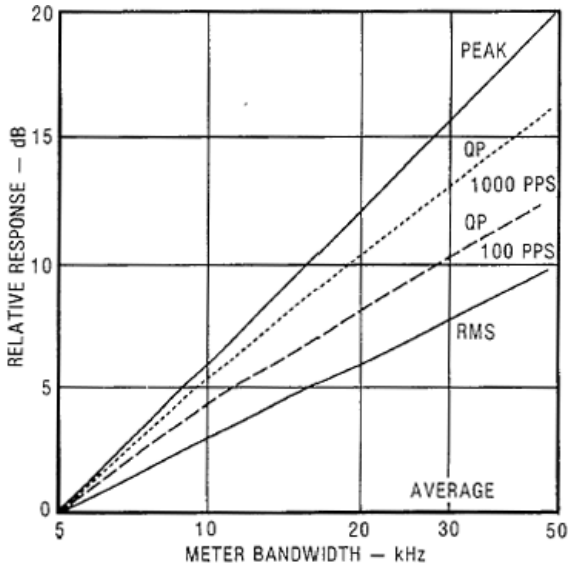


Figure 9.4-7 Meter response for different bandwidths relative to the response for a 5-kHz bandwidth.

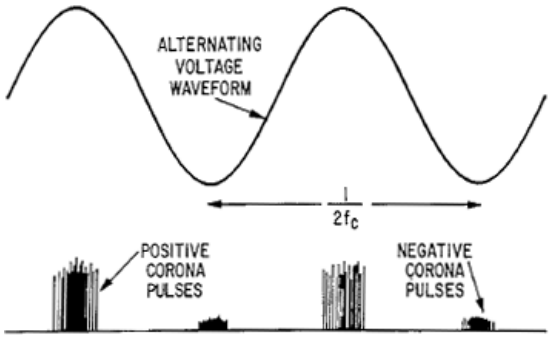


Figure 9.4-8 Corona noise packets for power frequency fc.

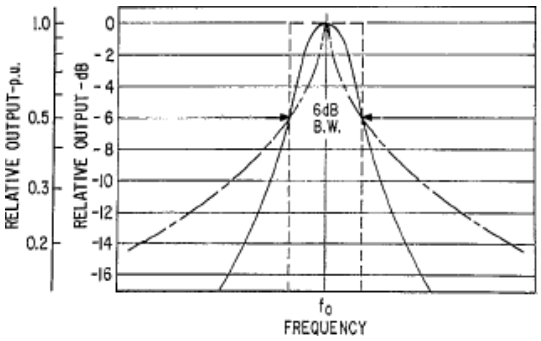


Figure 9.4-9 Different band-pass characteristics for the same 6-dB bandwidth.

6-dB bandwidths for the QP detector for the frequency ranges shown in Table 9.4-1. Some EMI instruments have more than one IF bandwidth built into them, which allows QP measurements to be made in other bandwidths. However, in some of those meters, the QP readings at other than the standard bandwidth made no sense whatsoever; e.g., the QP measurement at some frequencies in one meter decreased drastically when a larger bandwidth was switched in. Obviously the instrument was not designed to make QP measurements at the nonstandard bandwidths. This fact indicates the importance of using meters that conform exactly to standards when QP measurements are required.

9.4.4 Actual Band-Pass Characteristics

In the preceding discussion of meter responses, the amplifier band-pass characteristics were considered ideal in that complete rejection occurred for frequencies below $(f_o - \Delta f/2)$ and above $(f_o + \Delta f/2)$, where f_o is the tuning frequency and Δf is the amplifier bandwidth. In practice, however, this is not the case. The degree to which the actual band-pass characteristic approaches the ideal depends on the amplifier filter circuit design. Often the 6-dB bandwidth of an amplifier is specified. This quantity is measured as the difference between the two frequencies at which the output drops to one-half of its maximum value when the input is sinusoidal. However, this definition does not completely define the band-pass characteristic of the amplifier, as can be seen from Figure 9.4-9. The figure shows three band-pass characteristics that have the same 6-dB bandwidth but that are otherwise quite different. The band-pass characteristics of radio-noise meters are further defined by the effective impulse bandwidth and the effective random-noise bandwidth. The effective impulse bandwidth is defined as the reciprocal of the width in seconds of a rectangle having the same area and maximum amplitude as the impulse-response envelope. The effective random-noise bandwidth is defined as the width in hertz of a rectangle of the same area and maximum amplitude as the square of the amplifier-frequency response to a sinusoidal input.

What have been described so far are the basics of the superheterodyne-type EMI receivers. Another instrument that has been widely used to measure EMI is the spectrum analyzer. A *spectrum analyzer* is a heterodyne receiver in which the local oscillator (LO) is swept across a certain frequency band. The input signal is fed into a mixer where it mixes with the local oscillator signal. If any of the mixed signals falls within the passband of the intermediate frequency (IF) filter, it is further processed, detected by the detector circuit, digitized, and used as the vertical deflection on a display. A ramp generator provides the tuning voltage for the LO as well as the horizontal deflection for the display. The horizontal axis of the display is calibrated in frequency. The vertical axis is calibrated in amplitude, which can either be a linear scale calibrated in volts or a logarithmic scale calibrated in dB.

Modern spectrum analyzers have a "Max Hold" trace, where the highest signal encountered at any given frequency point during multiple sweeps can be displayed. This is particularly advantageous when the EMI is very erratic—e.g., natural gap discharges.

One of the disadvantages of using spectrum analyzers over a wide frequency range is the possibility of system overload due to out-of-band signals. This is particularly important in outdoor measurements when low-level EMI from transmission lines is being measured in the presence of very strong broadcast signals. That is the reason a preselector is used in conjunction with the spectrum analyzer.

Some of the modern EMI receivers can display the output of more than one detector. This is particularly advantageous when frequency spectra are being measured in an outdoor environment. For example, if both the QP and average measurements are measured simultaneously, the EMI from the line can be separated from broadcast signals since the QP and average levels for broadcast signals are approximately the same.

One of the disadvantages of conducting frequency sweeps of QP with the automated EMI meters or spectrum analyzers is that in order to capture low-repetition-rate impulse EMI, the minimum scan rate for the 9-kHz bandwidth needs to be 200 sec/MHz. This scan rate requires a scanning time of about 95 minutes to sweep from 150 kHz to 30 MHz. Anyone who has conducted EMI measurements on overhead power lines knows that either corona or gap-discharge EMI can change quite rapidly over relatively short time periods. Since corona has a fairly high repetition rate, the sweep rate for corona can probably be done at a faster rate than the ones recommended in the standards.

9.4.5 Antenna Systems

As mentioned previously, radio-noise meters are very sensitive radio-frequency voltmeters, capable of measuring down to fractions of a μV. To measure radio-frequency noise fields, the meters must be used in conjunction with an antenna that is placed in the field to be measured. The antenna output voltage is proportional to the field strength, the relationship between these two quantities being the antenna factor. Typically there is a considerable impedance mismatch between the antenna and the radio-noise meter, and a coupling network between the two devices is generally required to provide either maximum system response at the frequency of measurement or a good flat response over a broader range of frequencies. The antenna coupler is usually supplied by the antenna manufacturer. Curves of antenna factor, which include the effect of the antenna coupler, are also provided by the manufacturer. When the antenna is used according to the manufacturer's instructions, the radio-noise field, *E,* is given by the following:

$$E = V + AF = dB \text{ above } 1\ \mu\text{V / m} \qquad 9.4\text{-}3$$

where V is the radio-noise meter reading in dB above 1 μV, and AF is the antenna factor in dB 1/m.

Several different types of antennas are available, and the selection of a particular antenna is often dictated by the type of noise to be measured and the frequency of measurement. At frequencies up to 30 MHz, vertical rod and loop antennas are commonly used. A rod antenna is sensitive to the electric component, *E,* of the electromagnetic field (and thus for ground-level measurements is used in a vertical position), whereas the loop antenna is sensitive to the magnetic component, *H,* of the field. At distances greater than about 15% of a wavelength from the transmission line (approximately 48 m for a frequency of 1 MHz), conditions exist in which the electric and magnetic components of the field are directly related through the following expressions (Olsen and Rouseff 1985):

$$E \cong H \cdot Z \qquad 9.4\text{-}4$$

where Z is the impedance of free space

$$Z = \sqrt{\mu_0 / \varepsilon_0} = 377\ \Omega \qquad 9.4\text{-}5$$

in which μ_o and ε_o are the permeability and permittivity of air, respectively. Antenna factors provided for loop antennas take this relationship into account, and thus the field determined by adding the antenna factor to the meter reading is, in fact, the electric component of the field even though a loop antenna is used. For transmission-line noise measurements, a loop antenna is generally preferred because of its directional characteristics and the fact that it is the FCC standard antenna for measuring the field strength of AM broadcast signals. It can often be oriented for maximum response to line noise (with its plane parallel to the line and perpendicular to the ground) while excluding, to some extent, unwanted noise or signals from other sources. A rod antenna is responsive to noise and signals from all directions, and is highly dependent on its reference to ground.

For frequencies above 30 MHz, it becomes increasingly difficult to match the impedance of rod and loop antennas to the standard 50-Ω input impedance of the radio-noise meter (over a broad range of frequencies). For frequencies in the range 30-200 MHz, a dipole antenna is often used. The dipole antenna, with its two arms of continuously adjustable length, may be tunable. Often only one value of antenna factor is given for the complete frequency range. This value corresponds to the 1/2-wavelength resonant length (tip to tip) of the antenna. Thus the antenna must be readjusted for each different frequency. An alternative to the tuned dipole is the broadband dipole antenna. It has one basic length to which one or two extender elements may be added to provide two or three different lengths, each covering a certain range of frequencies for which a curve of antenna factors is provided. Care must be used in using antenna factor at these frequencies because antenna factor assumes that the field is a wave arriving in the direction of the antenna's maximum response. Since the noise signal, especially from transmission lines, arrives from a variety of directions, the antenna factors are not always useful (Paul 1992). Obviously the maximum response is obtained only at one particular frequency for each of the different lengths, but for measurements requiring frequency sweeps, an antenna such as the broadband dipole is preferable over the tunable variety. For those occasions when even the use of the different elements of a broadband dipole antenna is inconvenient, a bi-conical antenna may be used. This antenna typically has an optimum response around 70-80 MHz, but it is supplied with curves of antenna factors over the range 20-200 MHz.

At frequencies above 200 MHz, calibrated dipole antennas are available; however, more exotic antennas such as log-spiral, log-periodic, or bi-triangle are usually used. For most transmission-line work, however, the level of corona-produced noise at such frequencies is so low that measurements are very difficult unless one uses high-gain antennas and low-noise preamplifiers. Consequently such measurements are made only to evaluate possible interference to special communication facilities.

When only detection of noise is required without a quantitative measure, other special antenna systems may be of greater use. Yagi antennas, and others offering high sensitivity and good directionality at particular frequencies, are often used in these cases. (Some investigators have used such antennas for quantitative noise measures.) Generally

antenna factors are not available for these antennas, and thus the factors have to be determined experimentally.

The antennas described so far are the basic antennas that have been available for a number of years. Antennas for EMI measurements above 30 MHz have become much more sophisticated. The features of the bi-conical and log-periodic antennas have been combined so that EMI measurements can be made from as low as 25 MHz to as high as 7.0 GHz in a single antenna. These antennas have names such as Biconilog, Bilogical, Combilog, and Ultralog. They operate over a very wide frequency range, but the ranges vary depending on the manufacturer.

9.4.6 Measurement of Transmission-line EMI

In measuring transmission-line EMI, one must first determine the purpose of the measurement. If the purpose is to determine the performance of an existing line or to determine compliance with guidelines or limits, then ANSI/IEEE Standard 430 definitely applies. If the purpose is to measure the EMI to determine compatibility between a communication site and a proposed transmission-line, then there are other considerations. In either case, particular attention must be given to the selection of the measuring location, the calibration of the measuring instruments, the background noise level (to ensure that atmospherics, other spurious signals, and/or broadcast signals are not contaminating the measurements), and to a number of other factors. In the EMC case, a number of questions must be asked before the measurement program is conducted. The ANSI/IEEE Standard covers the most important aspects of transmission-line EMI measurement from 15 kHz to 1 GHz, and it is recommended reading for those who intend to carry out their own field measurements. It is worthwhile here, however, to discuss a few general items that are not covered in the standard but that should be considered in establishing a measuring program.

AM Broadcast Band

Since there are existing guidelines and limits for RI from overhead lines in the AM Broadcast Band, measurements are sometimes required to determine compliance with those guidelines or limits. One of the most important measurement requirements in this frequency band is the use of the loop antenna. There are two reasons the loop antenna is the preferred antenna for conducting either short-term or long-term measurements of RI in the AM band. First, it is the antenna recommended by the FCC for measuring broadcast signals in the AM band; therefore, it only makes sense that it should be also be used to measure the RI. Second, the rod antenna is not recommended because it is easily perturbed by the presence of conducting or partially conducting objects such as vehicles, trees, fences, and people. Also the determination of the antenna factor for the rod antenna is based on the rod being situated above a very large conducting ground plane, which cannot be ensured in practice. The ground plane supplied with most rod antennas is a very small ground plane, which may be adequate when situated on most loamy soil, but has been found to be inadequate when situated on dry, sandy soil. The loop antenna does not rely on a ground plane; therefore, it can be operated above ground, which is desirable for conducting long-term measurements where heavy snowfall may occur. Also, being able to raise the antenna above ground offers protection from vandalism.

Another problem with rod antennas is that the tip can go into corona in high electric fields. Therefore, checks should be made to ensure that the rod antenna is corona free. Loop antennas, because of their shape, are less likely to go into corona, although the likelihood increases as the antenna's height above ground is increased. Corona on an antenna will generally result in very high and steady readings on the EMI meter. An abrupt drop in the reading as a person approaches the antenna or as the antenna is moved farther away is a good indication of an antenna-corona problem.

In some areas of the world it is very difficult to measure the RI in the long-wave, and medium-wave bands because of atmospheric EMI caused by near and even distant lightning disturbances. This is especially true in areas such as Florida and Mexico that have high isokeraunic (IKL) levels and less true in areas like the Pacific Northwest of the U.S. where the IKL is very low. Atmospheric EMI from distant lightning storms can travel for many kilometers at frequencies below 1 MHz. For example, atmospheric disturbances in the Caribbean can interfere with AM Broadcast signals in many of the states in the U.S. during the summer months when lightning storms are the most prevalent. The needle on an analog meter takes large jumps due to such EMI, and in many cases, it never settles down so a measurement of the transmission-line RI can be taken. One of the difficulties in using the modern computer-controlled EMI meters or spectrum analyzers is that they do not discriminate between EMI due to atmospherics and EMI due to the transmission line. That is why it is important to conduct measurements not only at the standard distance of 15 m from the line recommended in ANSI/IEEE 430, but also at distances farther from the line to ensure that only the EMI due to the line is being measured.

When conducting manual measurements, the use of headphones or a small loudspeaker (plugged into the EMI meter's audio output) can help in determining when readings are due to broadcast signals. If such equipment is not available, the meter readings themselves may provide a good indication of the presence of signals. In the absence of signals, there should be little variation in the meter readings for small changes in tuning frequency (this applies to

measurements up to 30 MHz only). If line noise only is being measured, the difference between QP and FI readings should be substantial (in the order of 14 dB or more). If FI and QP readings are approximately the same, or if small variations in tuning frequency cause significant fluctuations in meter readings, the presence of signals is indicated. One of the advantages of the modern EMI receivers is that QP and FI levels can be swept simultaneously, which makes it easier to separate carrier signals from transmission-line EMI.

TV Broadcast Band

In the TV broadcast range, signal frequencies are well established and can be easily avoided. In the FM broadcast range (88-108 MHz), it may be more difficult to find a clean area. It is perhaps best to avoid the FM region if possible. (It may be noted that FM transmissions are inherently immune to pulsative-type noises.) A frequency between 73 and 76 MHz is a good choice for monitoring TVI since this is in the low VHF range, between TV channels 4 and 5, and within a frequency range reserved for radio astronomy and aeronautical navigation. Consequently this frequency is generally free of signals of significant magnitude.

At 75 MHz, the wavelength is only 4 m. Small variations in the location of an antenna may result in significant changes in indicated EMI levels. Measurements could be made for several antenna locations in proximity to the nominal position to check for maximum values. A better approach would be to fix the antenna location and make noise measurements at several frequencies close to the nominal frequency to check for maximum values.

The 50/60-Hz electric field can have a significant effect on antennas used to measure TVI since the antenna has to be raised at least 3 m above the ground (ANSI/IEEE 1986). The tips of dipole antennas can easily go into corona. This effect has been solved in the past by replacing the small spheres on the ends of the standard dipole antennas with larger spheres. Most TVI measurements are now measured with bi-conical or log-periodic antennas. The elements of bi-conical antennas usually do not go into corona, but gap discharges can occur in the antenna's balun when placed in a high 50/60-Hz electric field. Such discharges have damaged the input electronics of some EMI meters. Log-periodic antennas are similar to commercial TV antennas; therefore, they have pointed tips. If these antennas are used to measure TVI, one must be alert to those tips going into corona.

A comparison of peak and quasi-peak readings can sometimes help in determining if the noise being measured is corona noise or gap discharges. With corona noise, peak readings will be only slightly higher than quasi-peak (up to about 5 dB typically). With gap discharge noise, large differences (up to 15 dB or more) are typical. With the aid of headphones, a trained ear can readily detect the difference between corona noise (more a random, white noise) and gap discharge noise (more or less a fixed, repetition-rate, pulsative noise).

Other Communication Bands

Sometimes measurements in frequency bands other than the radio or TV bands are required to determine if an existing or proposed transmission line will be compatible with a particular communication system. Before the measurements are conducted, a number of questions need to be asked such as: (1) at frequencies below 30 MHz, is the communication system antenna detecting the electric or magnetic field, (2) at frequencies above 30 MHz, what is the antenna polarization, (3) what are acceptable signal-to-noise ratios if known, (4) what is the overall sensitivity of the communication system, (5) what detector should be used to make the measurements, and (6) what is the bandwidth of the receiver. Once these questions are answered, the measurement program can be designed. An example of such a measurement program at 900 MHz can be seen in (Chartier et al. 1986). This was a case where there was concern that an existing 345-kV corridor might cause EMI to a very sensitive phased-arrayed radar system operating at about 900 MHz. The preferred site for the radar system was about 2000 m from the transmission-line corridor that had more than one 345-kV line. After several discussions between the manufacturer of the phase-arrayed radar system and the utility, a measurement program was designed. A highly sensitive measurement system was put together to measure the noise energy of the corona noise during wet weather.

9.4.7 Pre-construction, Pre-energization and Post-energization Measurements

Before a new line is built, many utilities measure the ambient EMI along the proposed corridor(s). These are called *pre-construction measurements*. After a line is built, but before it is energized, a few utilities have conducted what have been called *pre-energization surveys*. After the line is energized, *post-energization measurements* are also conducted. Over the years these three types of measurements have become less important, as is discussed in this section.

Pre-construction Measurements

When 550- and 800-kV lines were first being considered in the 1960s, the effect of RI on radio reception to nearby residences was the main corona phenomena issue from a design standpoint. The pre-construction surveys were considered very important because they determined the quality of AM radio signals along proposed rights-of-way. From this information, conductors were selected to minimize fair-weather RI as much as economically possible, and in

some cases lines were slightly relocated to avoid coming close to residences where radio signals were not very strong.

After the radio signals were measured, thorough analysis techniques of the AM Broadcast signals (TVI was not a concern in those days) were developed. Two approaches that have been used are described in two references (Guyker et al. 1966; Maruvada and Trinh 1975) and summarized in (IEEE 1980).

Pre-energization Measurements

In the 1960s and 1970s, some utilities would repeat the pre-construction measurements after the line was built but before it was energized. This was done for several reasons. First, they wanted to know if the construction of the line affected the magnitude of the broadcast signals. Some investigators claimed the physical presence of the line reduced the level of the AM Broadcast signal, whereas other investigators claimed the signals were increased. This question has never been fully resolved, but it is known that the presence of the line will have a greater effect on a signal measured with a rod antenna than with a loop antenna. Second, some utilities wanted to know if the ambient levels that were measured before the line was built have changed. This finding is very difficult to prove one way or another because of the randomness of EMI. Also some noise sources such as gap discharges from nearby distribution lines that may have been present before construction may have disappeared after construction. It has been observed that at AM Broadcast frequencies, currents from a gap discharge traveling along a distribution line can couple into a nearby transmission line whether the line is parallel to the distribution line or whether it crosses the distribution line.

It is well known that the physical presence of overhead lines can affect TV signals. The largest effect is ghosting due to reflected signals off the steel structures, but signal reduction can also take place if the metal transmission tower is between the transmitting and receiving antennas. Measurements of this effect are usually not conducted for obvious reasons. In the TV broadcast band, signals can vary significantly over time and just by moving the antenna a few meters.

Post-energization Measurements

Measurements after a line is energized are made to determine if the line is performing as predicted. Two types of measurements can be made: short term and long term. ANSI/IEEE Standard 430 should be referred to before conducting either short- or long-term measurements. The Canadian Standards Association (CSA) in their voluntary standard for interference from high-voltage ac power systems has a measurement procedure similar to ANSI/IEEE 430. It is not clear at this time if utilities are required to measure the RI from new lines after they have been energized, and if so, when the measurements are to be performed. It is well known that conductors undergo both long-term and short-term aging. As was previously mentioned, the RI can decrease by 6 dB or more over a period of less than $^1/_2$ hour when a line is first energized. A decrease of another 6 dB or more may occur over the next 6 to 8 months as aluminum burrs and aerosols stuck on the conductor are burned off by the corona. Since the RI levels predicted for a line are based primarily on well-aged conductors, relatively high RI levels would be expected if the measurements were conducted shortly after the line was energized.

Since the corona process is erratic, the best method for validating the EMI performance of an overhead line is to conduct long-term measurements. RI from overhead lines can vary as much as 30-40 dB over a period of a year and even between some dry conductor conditions and heavy rain conditions. The calculated values are usually a mean or median value for either fair weather or for measurable rain; therefore, statistical analysis of long-term measurements is the only valid method to verify that the line is performing as predicted. Again ANSI/IEEE Standard 430 should be consulted before embarking on a long-term measurement program.

A good summary of the measurement of EMI and other corona phenomena from overhead power lines can be found in (Chartier 1991).

Argument for Not Conducting Preconstruction, Pre-energization, and Post-energization Measurements

The Bonneville Power Administration for the most part has stopped making these measurements. BPA's general philosophy is that if their lines create interference to radio or TV, they will do whatever is necessary to correct the interference—including complaints about TV signal reduction and ghosting. This philosophy falls in line with the FCC Incidental Radiation Device Rule. Interference caused by sparks are located and eliminated. For interference due to corona, BPA has provided new antennas, relocated antennas, built mini-cable TV systems, provided connections to cable systems, provided satellite dishes, etc. to resolve interference caused by their lines. Because of this policy and because BPA designs their lines to meet an audible noise limit of 50 dBA at the edge of the right-of-way, BPA feels that their lines are quite adequate from an EMI standpoint, and all of the above measurements are not needed. If a valid complaint comes in, then steps are taken to either eliminate the interference or to improve the signal-to-noise ratio at the residence of the complainant.

9.5 CALCULATION OF EMI FROM CONDUCTOR CORONA BELOW 30 MHZ

Ever since it was recognized that radio noise from transmission-line corona posed a potential threat to the unimpaired reception of AM broadcast signals, proposals have been developed for calculating EMI levels (IEEE 1973b; IEEE 1971). The basic idea behind all these proposals can be understood by referring to the series of events shown in Figure 9.5-1. In (a), the gradient of the power frequency electric potential at the surface of transmission-line phase conductors (i.e., the surface electric field) is shown. It is large enough to cause ionization of the air (i.e., corona) near the conductors, as shown in (b). This corona consists of electric charges that are moved rapidly in both directions by the 50/60-Hz electric field. These charges can be modeled as an electric dipole with a time-varying (impulsive) current as shown in (c) (Schennum and Olsen 1994). Because the current is impulsive, its frequency spectrum extends over a wide range of frequencies. In (d) the process by which the dipole capacitively couples electric currents into the conductors is shown. Finally, as shown in (e), these currents (i.e., the propagating radio frequency currents) create electromagnetic interference fields in the vicinity of the transmission line over a wide range of frequencies. Note that, although the corona discharges also directly generate EMI, their contribution is much less than that of the induced currents (Olsen 1983).

The 50/60-Hz conductor surface electric field (i.e., surface potential gradient) can be determined from knowledge of the voltages and locations of the phase and shield conductors as well as the size, number, and geometrical arrangement of subconductors (IEEE 1979) that constitute each phase conductor in Chapter 2. The corona "amplitude" is a function of the surface gradient, the size, number, and arrangement of subconductors, weather, and altitude. Additional parameters needed to describe the amplitude of the current induced on the conductors are the electrical permittivity and conductivity of the earth. Finally the EMI fields depend on the measurement frequency and the location of the point at which the field is calculated. This section describes two general classifications of calculation techniques (analytical and empirical) used to calculate EMI from transmission lines in the low-, medium- and high-frequency range (i.e., approximately 100 kHz to 30 MHz). Generally, empirical methods are based more on extrapolations of EMI measurements near common transmission lines, while analytical methods are based more on the fundamental principles of physics. It should be emphasized, however, that no method is entirely "empirical" or "analytical." The former, for example, use analytical expressions to calculate the surface gradient and the effect of distance away from the line. The latter use empirical data from test corona cages to describe the corona amplitude on the line as a function of surface gradient, bundle geometry, weather conditions, and altitude that is used to determine the level of corona current. Despite this fact, the distinction between empirical and analytical methods will be retained.

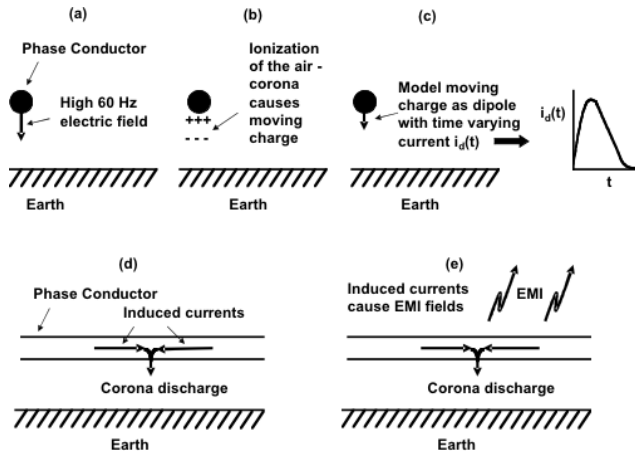


Figure 9.5-1 The process by which EMI is generated.

In this reference book, both empirical and analytical methods will be described. In each case, EMI data measured over long periods of time were used to calibrate the models used to predict corona noise. Both methods have been validated over the 500 kHz to 30 MHz frequency range and for field points at an arbitrary distance from the power line. While they are probably also useful from frequencies from 100 kHz to 500 kHz, they should not be used above 30 MHz for reasons discussed in Section 9.6. For continuity with previous editions of this book, the relationship between these methods and the more restrictive modal propagation methods presented in previous editions that are valid for frequencies less than 2 MHz and distances less than 50-100 m will be discussed in some detail.

9.5.1 Philosophy of Modeling

It is important to realize that any model is limited in its applicability. One of the reasons for this is that the physical model used to predict EMI is only an approximation of an actual transmission line. This fact can be easily observed by reference to Figure 9.4-2, which shows a simple physical model used to predict the EMI from a single-conductor transmission line. It is clear that the earth has been assumed to be flat and homogeneous, (i.e., hilly terrain is ignored), that the conductors are assumed to be infinite and horizontal (i.e., the site is "very far" from a substation, where "very far" is usually on the order of 5 km at 1 MHz, and conductor sag has been ignored), that the corona activity has been assumed to be nearly uniformly distributed along the conductors (i.e., gap and insulator noise are ignored), that the corona amplitude (which can be determined only by experiment in a statistical sense) is

known, and that the effect of towers has been ignored (i.e., enhancement or shielding of the power frequency field near a tower is ignored). Because of these approximations to the actual transmission line, the EMI prediction theory will not be completely correct even if the mathematical methods used to calculate the EMI fields for the model are exact. This is not, however, necessarily a cause for great concern. In fact, it has been found that the physical approximations (when properly used and interpreted) do not lead to predicted EMI levels that deviate significantly from measured values of EMI. Nevertheless, the fact that approximations are made does emphasize the need to validate and/or calibrate any model by comparison to measured data.

One characteristic of the EMI problem is that the corona pulses, and hence the EMI measurements, are not deterministic; neither the exact location nor the current pulse shape of any corona source is known. In fact, any two pulses can be treated as uncorrelated, and hence powers rather than fields add. Further, the exact number of corona pulses is unknown. As a result, it is not possible to precisely predict the level of the interference fields. Instead the corona sources must be treated as a stochastic or random process, and the EMI can only be predicted as the expected value of a function of a random variable. This problem can be observed while taking data since the measured value of EMI will generally not be stable.

In addition to the problem posed by the random distributions of corona position and amplitude, there is another reason why the EMI fields are not deterministic. This is the fact that the number and amplitude of corona pulses change with different weather conditions. Hence the EMI will vary, and long-term measurements of EMI will generally exhibit characteristics of the distribution shown in Figure 9.5-3. More specifically, EMI tends to be significantly larger (i.e., approximately 18 - 25 dB) in foul weather than in fair weather. This is because raindrops collect on phase conductors and cause local enhancement of the 50/60-Hz electric field that causes additional corona.

The most reasonable way to ensure the accuracy of an EMI prediction program is to calibrate it using long-term measured data. More specifically, some average value for the EMI (e.g., L_{50} [median] level during measurable rain or L_{50} [median] fair-weather data as determined from a distribution such as shown in Figure 9.5-3) should be used to calibrate the method. In doing this, it is important to state the specific definition of the conditions satisfied by the data used for calibration (e.g., median EMI level during measurable rain). This information will make it possible for the user to specify an experiment that, in principle, would give the same results as predicted by the program. Finally the calibration process will result in an estimate of the accuracy to which the predicted EMI will match measured data.

In addition to physical approximations made to the model, there are usually mathematical approximations that further

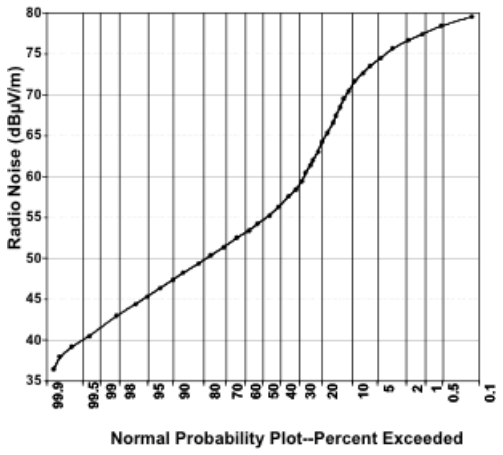


Figure 9.5-3 Typical long-term distribution of EMI measurements.

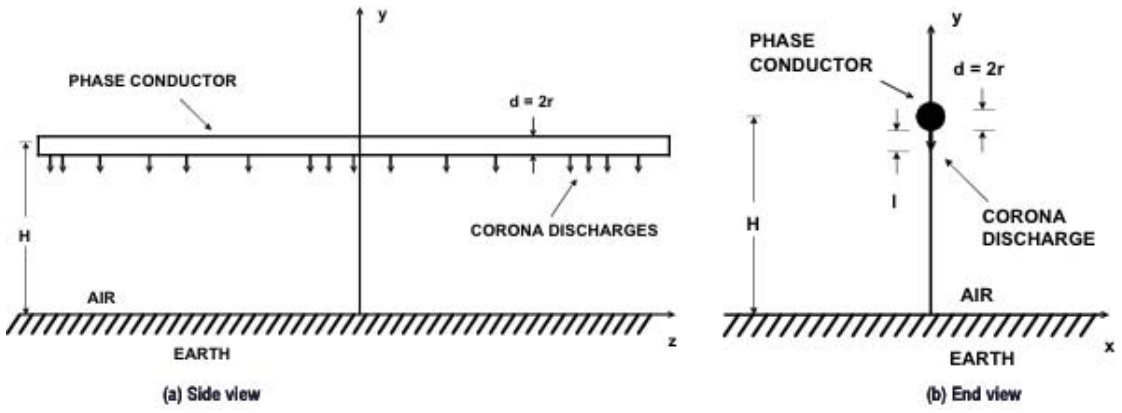


Figure 9.5-2 A simple model for EMI from a single-conductor transmission line.

restrict the validity of the model. For example, in most traditional analytical models (e.g., the model described in the second edition of this book), induced currents on the conductors are assumed to be the quasi-TEM modes of a multiconductor transmission line. This assumption is acceptable as long as the frequency is low enough that the spacing between conductors is a small fraction of a wavelength—i.e., the frequency in megahertz is less than approximately 30 divided by the conductor spacing in meters (Olsen 1988; Olsen and Rouseff 1985; Olsen et al. 1992). Further, the EMI fields are usually calculated using a quasi-static method that is relatively simple but that limits the calculation to field points less than approximately 50/(frequency in megahertz) meters away from the line. Finally most methods use expressions for the EMI field that limit field points to within 2 – 3 m from the earth's surface. For typical transmission lines, methods that use the approximations mentioned above are restricted to frequencies less than approximately 2 MHz and field points near the earth's surface and within 50-100 m from the line.

The wideband analytic method (i.e., WBNOISE) described in this section does not incorporate any of the approximations listed in the last paragraph (Olsen and Wu 1991; Schennum and Olsen 1995). In that sense it is more general than others that have been developed. Nevertheless, because the physical approximations described earlier have been made, its accuracy is open to question. For this reason, long-term measurements of EMI from operating transmission lines have been used to calibrate the method. Comparisons of the calibration data to EMI predictions have been used to delineate the expected accuracy of the method (e.g., the L_{50} or mean level during measurable rain predictions are expected to be within ± 2 or 3 dB of the measured results).

Finally it should be emphatically stated that a model is expected to produce the results of an experiment that could have been done but need not be done because the model exists. It should be completely clear to the user what the parameters of this experiment are and what differences should be expected between the model's prediction and the experiments.

9.5.2 Analytical Methods

Introduction

This section describes analytical methods for predicting EMI from power lines. Although results are given that are applicable for any frequency in the MF or HF range, emphasis is placed on approximate low frequency methods when applicable in order that the development not be obscured by an excessive amount of mathematics. A derivation of the more exact theory is presented completely in the appendices and is referred to extensively within this section.

The first subject to be described is that of defining the "generation function" (Γ) that relates the wideband induced currents on transmission-line conductors to the corona source. This definition will be made in the context of a single-conductor power line such as shown in Figure 9.5-2 because it is simpler and because the generation function is essentially related only to local conditions near the conductor and, thus, can also be used on multiconductor transmission lines. The generation function is often measured (usually at 0.5 or 1.0 MHz with a quasi-peak receiver) in a device called a corona cage, which is essentially a very large diameter coaxial cable with its inner conductor in corona, as described in Section 8.7.1. The second subject is that of calculating the EMI fields for the single-conductor problem. This calculation is made by relating the induced current on the transmission-line conductors to the electric and magnetic fields they generate. Following this is a description of analytical methods for calculating EMI from two- and three-conductor transmission lines and finally the extension to multiple-circuit transmission lines. This discussion refers to the traditional theory that uses multimode expansions as well as the more general wideband theory that does not utilize modal expansion.

Temporal and Spatial Frequency Domains

It has been found helpful to use temporal and spatial Fourier transforms to determine the currents induced on phase conductors by corona. The former is quite familiar to electrical engineers and can be described by the transform pair

$$P(\omega) = \int_{-\infty}^{\infty} p(t) e^{-j\omega t} dt \qquad \text{9.5-1a}$$

$$p(t) = \frac{1}{2\pi} \int_{-\infty}^{\infty} P(\omega) e^{j\omega t} d\omega. \qquad \text{9.5-1b}$$

Here a function of time $p(t)$ is transformed into the temporal frequency domain to obtain the temporal frequency spectrum $P(\omega)$ using the first equation. ω is the radian frequency, where $\omega = 2f$ and f is the frequency in hertz. This spectrum can be thought of as the amplitude of a continuous set of exponential functions that is equivalent to $p(t)$. Less familiar to electrical engineers is the fact that the same operation can be carried out in a Cartesian spatial coordinate. If the geometry of the problem (not including sources) does not vary with that coordinate, then it will be possible to easily apply boundary conditions in the transform domain. This is advantageous since differential equations in the spatial domain become algebraic equations in the transformed domain. In our case, this can be done in the spatial dimension along the length of the power line since the power line is considered to be infinite. In the case

for which this coordinate is z, the transform pair can be written

$$Q(\gamma) = \int_{-\infty}^{\infty} q(z) e^{+j\gamma z} dz \qquad 9.5\text{-}2a$$

$$q(z) = \frac{1}{2\pi} \int_{-\infty}^{\infty} Q(\gamma) e^{-j\gamma z} d\gamma \qquad 9.5\text{-}2b$$

Since the concept of a spatial transform may be new to power engineers, a few words of interpretation may be useful. $Q(\gamma)$, the transformed $q(z)$, may be considered as the continuous amplitude of exponentially varying functions of the form $\exp(-j\gamma z)$. Thus, just as time-varying signals are expanded into components of the form $\exp(j\omega t)$, spatially varying functions are expanded into functions of the form $\exp(-j\gamma z)$. The advantage of doing this is that a derivative with respect to the spatial coordinate is replaced by $-j\gamma$ in the same way that derivatives with respect to time are replaced with $j\omega$ (for the Fourier transform) or s for the Laplace transform. By analogy to the temporal frequency domain, $Q(\gamma)$ can be thought of as the spatial frequency spectrum of $q(z)$ and the spatial frequency γ plays the role of the temporal frequency ω in the temporal transform. Later it will be shown that γ can become complex (i.e., $\gamma = \beta - j\alpha$) for lower frequency fields. In this case, α represents the attenuation of propagating currents along the power line.

The problems in this section are solved by first transforming expressions for the electric and magnetic fields into the temporal and spatial frequency domains. After finding the solution in these domains, it is necessary to transform back into the spatial domain using (9.5-2b). It is not necessary, however, to transform back into the time domain, since the receivers used to measure EMI measure the energy within a narrow range of frequencies.

Theory of the RI Generation Function

For the purposes of calculating transmission-line EMI, the corona process is quantitatively expressed in terms of the EMI generation function, Γ, a concept used to relate the corona ionization near the conductor to the amplitude of the interference current induced in the conductor, which was introduced in Section 8.7.3. The generation function is nearly independent of the ground geometry and depends only on electric-field conditions and conductor geometry in the immediate vicinity of the conductor under test. Thus generation functions determined from single-phase tests may be used as the starting point for calculating three-phase transmission-line EMI.

Here the physical basis for the generation function is described. Following this, specific generation functions developed from measurements at a number of laboratories are described.

The principle of current induction and its relationship to the generation function is first demonstrated with the simple case of a single transmission-line conductor above ground. Consider such as conductor of radius "r" located a distance "H" above an earth with permittivity ε_g, conductivity σ_g (= $1/\rho_g$ where ρ_g is the earth resistivity), and permeability μ_0 as shown in Figure 9.5-2. The corona source is modeled by an infinite number of electric dipoles with impulsive currents $i_{dn}(t)$ and length ℓ randomly distributed just below the conductor and along its length. These corona sources induce currents on the conductor that will, in turn, produce electromagnetic interference fields.

Since the current density for a vertical electric dipole in free space at (x,y,z) = (0,0,0) is

$$j_y(x,y,z,t) = i_{dn}(t)\ell\delta(x)\delta(y)\delta(z) \quad A/m^2, \qquad 9.5\text{-}3$$

where $\delta(p)$ is the Dirac delta function of argument p, the current density of a distribution of corona discharges (oriented in the –y direction) is (Olsen 1983)

$$j_y(x,y,z,t) = -\sum_{n=-\infty}^{\infty} i_{dn}(t)\ell\delta(z-z_n)\delta(x)\,\delta\,[y-(H-r-\ell/2)] \quad A/m^2 \qquad 9.5\text{-}4$$

where the nth corona source is located at $(x,y,z) = (0,H\text{-}r\text{-}\ell/2,z_n)$. Note that each discharge may have its own current $i_{dn}(t)$ amps.

This source function will be transformed into the frequency domain using the Fourier transform defined in Equation 9.5-1a. The result is

$$J_y(x,y,z,\omega) = -\sum_{n=-\infty}^{\infty} I_{dn}(\omega)\ell\delta(z-z_n)\delta(x)\,\delta[y-(H-r-\ell/2)] \quad A/m^2 \qquad 9.5\text{-}5$$

To determine the generation function, it is first necessary to find the current induced on the conductor. The steps for doing this are described in detail in Appendix 9.1. Here the steps are outlined and the final result given.

1. An expression is found for the temporal and spatial transform of the axially (i.e., z) directed electric field at the conductor surface due to the corona discharge currents given in Equation 9.5-5.
2. An expression is found for the temporal and spatial transform of the axially (i.e., z) directed electric field at the conductor surface due to the (yet unknown) induced current on the conductor.

3. The axial electric fields of the corona and conductor currents are added and set equal to the surface impedance of the conductor multiplied by the unknown current.
4. This equation is then solved for the temporal and spatial transform of the unknown induced current.
5. The frequency spectrum of current as a function of the z coordinate is found by performing the inverse spatial Fourier transform (i.e., Equation 9.5-2b).

Again the details of this derivation are found in Appendix 9.1. The result (Equation A9.1-14) is an expression for the frequency spectrum of the induced current that is valid throughout the MF and HF frequency ranges. It is

$$I_w(z,\omega) = \frac{1}{2\pi}\int_{-\infty}^{\infty} I_w(\gamma,\omega)e^{j\gamma z}d\gamma \qquad 9.5\text{-}6a$$

where

$$I_w(\gamma,\omega) = \sum_{n=-\infty}^{\infty} I_{wn}(\gamma,\omega) \qquad 9.5\text{-}6b$$

and

$$I_{wn}(\gamma,\omega) = \frac{-\gamma}{\left(Z_{11}(\gamma,\omega) + Z_{si} - \gamma^2 A_{11}(\gamma,\omega)\right)} \frac{1}{\pi\omega\varepsilon_0} I_{dn}(\omega)e^{+j\gamma z_n} \qquad 9.5\text{-}6c$$

where $I_{wn}(\gamma,\omega)$ is the temporal and spatial Fourier transform of the current induced on a single-phase conductor above earth by a single corona discharge at $(x,y,z) = (0,H\text{-}r\text{-}\ell/2,z_n)$, and $Z_{11}(\gamma,\omega)$, Z_{si} and $A_{11}(\gamma,\omega)$ are defined in Appendix 9.1 in Equation A9.1-12 and A9.1-13.

It turns out that finding an analytic expression for $I_{wn}(z,\omega)$ by taking the inverse Fourier transform is very difficult because $Z_{11}(\gamma,\omega)$ and $A_{11}(\gamma,\omega)$ are complicated functions of γ. By contrast, the low-frequency approximation for $I_{wn}(\gamma,\omega)$ has a simple dependence upon γ that facilitates a simple evaluation of the inverse transform (Equation 9.5-6a) for $I_{wn}(z,\omega)$ in terms of the transmission line propagation mode for a wire over the earth.

In order that the mathematics not obscure the physics here, the low-frequency approximation for $I_{wn}(z,\omega)$ is given. More specifically, for conductors that are less than approximately $\lambda/10$ from the earth, where λ is the wavelength equal to $300/f$(MHz) for the interference frequency of interest, $Z_{11}(\gamma,\omega)$ and $A_{11}(\gamma,\omega)$ are no longer functions of γ, and the evaluation of the inverse Fourier transform becomes straightforward. More specifically from Equation A9.1-16, (Olsen 1983)

$$I_w^{lf}(\gamma,\omega) = \sum_{n=-\infty}^{\infty} I_{wn}^{lf}(\gamma,\omega) \qquad 9.5\text{-}7a$$

$$I_{wn}^{lf}(\gamma,\omega) = \frac{-j2\gamma}{\ln(2H/r)\left(\gamma^2 - \gamma_p^2\right)} I_{dn}(\omega)e^{+j\gamma z_n} \qquad 9.5\text{-}7b$$

$\gamma_p = \beta_p - j\alpha_p$ is the propagation constant for a transmission-line mode that travels on the conductor/earth transmission line. The value for this propagation constant can be obtained as

$$\gamma_p = \sqrt{Z_{11}(\omega)Y_{11}(\omega)}, \quad \alpha_P > 0 \qquad 9.5\text{-}8$$

where the series impedance per unit length is

$$Z_{11}(\omega) = \frac{j\omega\mu_0}{2\pi}\left\{\ln(2H/r) - J_c(0, H-r, 0, H, \omega)\right\}. \qquad 9.5\text{-}9$$

$$J_c(x,y,x',y',\omega) = \frac{2}{k_g^2}\int_0^{\infty}(u-\lambda)e^{-\lambda(y+y')}\cos(\lambda(x-x'))d\lambda \qquad 9.5\text{-}10$$

is Carson's integral, where $u = (\lambda^2\text{-}k_g^2)^{1/2}$, $\mathrm{Re}(u) > 0$ and $k_g = (\omega\mu_0\sigma_g)^{1/2}e^{-j\pi/4}$ $\mathrm{Re}(k_g) > 0$ (Carson 1926). The shunt admittance per unit length is

$$Y_{11}(\omega) = \frac{1}{A_{11}(\omega)} = \frac{j2\pi\omega\varepsilon_0}{\ln(2H/r)}. \qquad 9.5\text{-}11$$

Because γ appears in the denominator of Equation 9.5.7b as the very simple form $(\gamma^2 - \gamma_p^2)$, the inverse transform of Equation 9.5-7b can be found in closed form using the theory of residues as discussed in Appendix 9.2. Thus the induced conductor current in the frequency domain can be written as (Olsen 1983)

$$I_w^{lf}(z,\omega) = \sum_{n=-\infty}^{\infty} I_{wn}^{lf}(z,\omega) \qquad 9.5\text{-}12a$$

$$I_{wn}^{lf}(z,\omega) = \frac{-1}{\ln(2H/r)}\frac{(z-z_n)}{|z-z_n|} I_{dn}(\omega)e^{-j\gamma_p|z-z_n|} \qquad 9.5\text{-}12b$$

The current consists of traveling waves that propagate in opposite directions away from each point z_n at which they are injected by a corona source as shown in Figure 9.5-1d. Note that even though the number of sources is infinite, the induced current is not. This is because the current decays exponentially between source and measurement point since $\alpha_p = \mathrm{Re}(j\gamma_p) \neq 0$, and distant sources (i.e., those more than

about 5 – 10 km away for frequencies between 500 kHz and 1 MHz) contribute little to the total current at the measurement point (Olsen 1983). Equation 9.4.12 is the form of the induced current used in the second edition of this book. This form is restricted to frequencies below approximately 2 MHz.

The Role of Statistics

Of course, it is still not possible to determine the exact induced current since the corona discharge locations and currents are unspecified. Here some reasonable assumptions about the corona current will be made that lead to a more compact expression for the current in terms of statistical averages.

The conductor is divided into equal-length cells of length Δz as shown in Figure 9.5-4a. Within each of these cells, a corona discharge is located at a value $z_n = n\Delta z + \delta z_n$, where n is the number of the cell and δz_n is a random variable uniformly distributed between 0 and Δz. Thus each cell has one discharge randomly distributed within it. Further, each corona pulse shape is assumed to be the same except for a random starting time τ_n centered around the time at which the surface 50/60-Hz electric field is maximum. The latter is justified since measurements show that corona pulses occur randomly within a small interval of time near the phase voltage peak as shown in Figure 9.5-4b. It will later be assumed that τ_n is a Gaussian distributed random variable centered at the peak of the 60-Hz voltage and with a standard deviation much smaller than the period of a 60-Hz sine wave.

Mathematically, the corona pulses can be written as

$$i_{dn}(t) = I_d(t - \tau_n) \qquad 9.5\text{-}13$$

where it is assumed here that each pulse is the same except for some random starting time τ_n that is distributed near the peaks in the 60-Hz voltage as described above. A solution for which the amplitude of the current can also vary from pulse to pulse can be found in (Olsen and Wu 1989). In the frequency domain the corona current can be written

$$I_{dn}(\omega) = I_d(\omega)e^{-j\omega\tau_n} \qquad 9.5\text{-}14$$

Because of the random locations, and start times, the source current is still not completely specified, and thus, the induced current is also not completely known. However, with a reasonable assumption about the distribution of start times (i.e., that they are randomly distributed around the 60-Hz voltage peak), it is possible to find an expression for the expected value of the spectral density of the current that is defined as

$$< S_i(\omega) > = < I_w(z,\omega) I_w^*(z,\omega) > = \frac{\left|I_d(\omega)\right|^2}{\ln^2(2H/r)} \bullet$$
$$\sum_{n=-\infty}^{\infty}\sum_{m=-\infty}^{\infty} e^{-j\gamma_p\left|z-n\Delta z\right|} e^{+j\gamma_p^*\left|z-m\Delta z\right|} \frac{(z-z_n)}{\left|z-z_n\right|}\frac{(z-z_m)}{\left|z-z_m\right|}$$
$$< e^{-j\gamma_p(\delta_n-\delta_m)} >_\delta < e^{-j\omega(\tau_n-\tau_m)} >_\tau \qquad 9.5\text{-}15$$

where (δ_n, δ_m) and (τ_n, τ_m) are pairs of independent random variables that represent the locations within each cell and starting times of the nth and mth corona pulses, respectively. It has been assumed that the random variables in location and starting time are independent. The symbol < > represents the expected value (i.e., an average over the probability distribution of a random variable) of the function inside it. The subscript $\tau(\delta)$ means an average over the probability distribution of τ_n (δ_n). Here only the expected value of the starting time function will be considered for reasons that will be discussed shortly.

It is shown in Appendix 9.2 that $<exp(-j\omega(\tau_n-\tau_m)>$ = 1, if $m = n$ and 0, if $m \neq n$, provided that the measurement frequency is well above 1 kHz (Olsen 1983). Since this is true, the remaining expected values need be evaluated only for the case $m = n$. Since $<exp(-j\gamma_p(\delta_n-\delta_m)>$ = 1 for $m = n$, the double summation in Equation 9.5-15 reduces to a single summation given below.

$$< S_i(\omega) > = < I_w(z,\omega) I_w^*(z,\omega) >$$
$$= \frac{\left|I_d(\omega)\right|^2}{\ln^2(2H/r)} \sum_{n=-\infty}^{\infty} e^{-2\alpha_p\left|z-n\Delta z\right|} \cong \frac{\left|I_d(\omega)\right|^2}{\ln^2(2H/r)(\alpha_p\Delta z)}. \qquad 9.5\text{-}16$$

In the final expression it is assumed that $z = \Delta z/2$ and the corona sources are close together with respect to the attenuation length of the transmission line mode (i.e., $\alpha_p\Delta z << 1$). Finally the expected magnitude of the induced current can

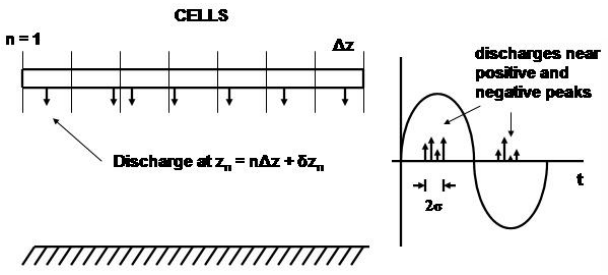


Figure 9.5-4 Corona discharges in space and time. σ is a measure of the temporal spread of the pulses.

be written as the square root of Equation 9.5-16. It is (Olsen 1983)

$$\left|I_w(\omega)\right| \cong \frac{\left|I_d(\omega)\right|}{\ln(2H/r)(\alpha_p \Delta z)^{1/2}} = \frac{C}{4\pi\varepsilon_0\sqrt{\alpha_p}}\Gamma(\omega) \qquad 9.5\text{-}17a$$

Where:

$$\Gamma(\omega) = \frac{2\left|I_d(\omega)\right|}{\sqrt{\Delta z}} \qquad 9.5\text{-}17b$$

is the EMI generation function and $C = 2\pi\varepsilon_0/\ln(2H/r)$ is the capacitance per unit length between the conductor and the earth. $\Gamma(\omega)$ represents twice the corona current induced on the conductor per square root length. The reason why the square root appears is that the corona sources are incoherent, and hence, the power emitted by each adds. Thus the total power emitted is proportional to the cell length Δz, and since power is proportional to current squared, the effective induced "current" per unit length is proportional to the square root of Δz.

$\Gamma(\omega)$ must be determined experimentally. This experiment is generally performed using corona test facilities, mainly test cages such as described in Section 8.7.1. Since $\Gamma(\omega)$ must be measured, "analytic" methods that use it are not fully analytic. Note also that since the currents generated by corona sources are wideband, the measured value of $\Gamma(\omega)$ depends on the receiver's bandwidth and detector type. It will be assumed here that the receiver used to measure $\Gamma(\omega)$ is a CISPR standard receiver with a 9-kHz bandwidth and a quasi-peak detector that is specified in the standard. It is important to note that the generation function is a function of frequency and that, since noise is wideband, the amount of noise measured is dependent on the instrumentation used for the measurement. The frequency dependence of $\Gamma(\omega)$ will be discussed in more detail later.

Experimentally Determined EMI Generation Functions

Several generation functions have been developed over the years, including those developed at Electricité de France, Project HVTRC, IREQ, Bonneville Power Administration, CIGRÉ, ENEL, and Eskom. Several of these functions are described here. In each case a large number of different conductor geometries were tested, and the EMI data collected were used in the development of a general formula for the generation function of any conductor configuration. It is assumed that the generation functions presented here were measured using standard CISPR receiver at a measurement frequency of 500 kHz. Any generation function measured using a different receiver or at a different frequency has been modified to reflect this. An extensive comparison of these generation functions has been published by Olsen et al. (1992). These will not be repeated here.

The Electricité de France (EdF) Generation Function (Moreau and Gary 1972)

This generation function is defined by its authors as a "natural heavy rain" generation function, where this condition is defined as the average EMI generation for all natural rain rates exceeding 1 mm per hour. It is

$$\Gamma_e = G'(E_{\max}, r) + A(n)r - B(n) \quad dB/1\mu a/\sqrt{m} \qquad 9.5\text{-}18$$

where $A(n)$ and $B(n)$ are given in Table 9.5-1 and G' is given in Figure 9.5-5. E_{max} is the "average maximum bundle gradient" on the surface of a subconductor of the conductor bundle shown in Figure 9.5-6, where r is the radius of the subconductor, S is the subconductor spacing, and n is the number of subconductors. E_{max} is defined in Chapter 2.

Table 9.5-1 Constants for the EdF Generation Function

Number of Subconductors (n)	1	2	3	4	5	6
$A(n)$ $=(11.5+\log_{10}(n^2))$ dB/cm	11.5	12.1	12.5	12.7	13.0	13.3
$B(n)$ - dB	0	5	7	8	9	9.5

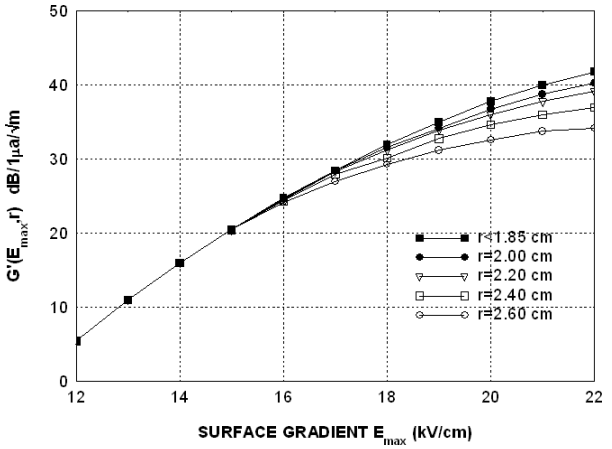


Figure 9.5-5 Portion (G') of the EdF generation function under heavy rain (dB/1μa/√m).

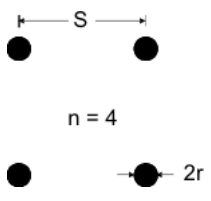


Figure 9.5-6 Bundle geometry.

The average maximum bundle gradient E_{max} (measured in kV/cm) used in Equation 9.4-18 is that discussed in Chapter 8. It should be noted that E_{max} is calculated assuming the presence of both phase conductors and shield wires above ground.

Project HVTRC Generation Functions (EPRI 1982)
Two generation functions were developed at Project HVTRC: one (Γ_{hr}) for artificial "heavy rain" defined at rain rates of 8 – 12 mm/hour, and the other (Γ_{hw}) defined as that obtained when the artificial heavy rain is turned off, but the conductors are still wet. This is now referred to as the "L_{50} rain" generation function. The two functions are defined as

$$\Gamma_{hr} = 81.1 - 580/E_{max} + 38\ log_{10}(2r/3.8)\ \text{dB/1}\mu\text{a}/\sqrt{\text{m}} \quad 9.5\text{-}19$$

and

$$\Gamma_{hw} = 89.3 - 580/E_{max} + 38\ log_{10}(2r/3.8) - 14.2E_c/E_{max}\ \text{dB/1}\mu\text{a}/\sqrt{\text{m}} \quad 9.5\text{-}20$$

Where:

$24.4/(2r)^{0.24}$ *for* $n \le 4$

$Ec =$

$24.4/(2r)^{0.24} - 0.5(n-4)$ *for* $4 \le n \le 8$

IREQ Generation Function (Trinh and Maruvada 1977)
The IREQ generation function is described as appropriate for "heavy rain" conditions. This generation function is

$$\Gamma_i = -90.25 + 92.42\ log_{10}(E_{max}) + 43.02\ log_{10}(2r) - B(n,S)\ \text{dB/1}\mu\text{a}/\sqrt{\text{m}} \quad 9.5\text{-}21a$$

Where:

$B(1,S) = 0$, $B(2,S) = 3.7$ *dB* and $B(n,S) = 6$ *dB for* $n \ge 3$. 9.5-21b

BPA "Generation Function" (Chartier 1988)
The BPA formula is not a true generation function in the sense that it was developed using measurements in a corona cage. Rather, it has been deduced from the BPA formula for calculating EMI. Because of this, it has an unknown constant (Γ_{bo}) that will be determined later when the generation functions are calibrated by comparison to long-term EMI data. It is included here since it contains the same functional dependencies (i.e., E_{max}, and r) as generations functions reported earlier.

The BPA foul weather "generation function" is

$$\Gamma_b = \Gamma_{bo} + 120\ log_{10}(E_{max}/15) + 40\ log_{10}(2r/4)\ \text{dB/1}\mu\text{a}/\sqrt{\text{m}} \quad 9.5\text{-}22$$

CIGRÉ Generation Function (CIGRÉ 1974)
Again the CIGRÉ method has been derived in the same way as the BPA method and thus has an unknown constant Γ_{co}.

The CIGRÉ foul weather "generation function" is

$$\Gamma_c = \Gamma_{co} + 3.5E_{max} + 12r\ \text{dB/1}\mu\text{a}/\sqrt{\text{m}} \quad 9.5\text{-}23$$

Note that the generation functions are all different due to differences in experimental conditions, but mostly because they were developed for different weather conditions. This issue will be addressed again when the prediction method is calibrated using long-term EMI data from operating lines.

Dependence of Γ on Weather Conditions, Frequency and Altitude
Later in this section each generation function will be modified by an additive constant in order to calibrate it using long-term EMI data from operating lines. At the same time the effect of weather conditions (i.e., rain vs. fair), measurement frequency, and altitude on the generation function will be discussed.

EMI from a Single-Conductor Transmission Line Above Ground
Once the induced current on the conductor is known, it is possible to calculate the electric and magnetic fields surrounding the wire. In Appendix 9.4, expressions for the electric and magnetic fields that are valid for an arbitrary distance and direction from the conductor are presented. From these expressions, the simpler low frequency approximations that have been commonly used in the power line EMI literature are derived.

The current induced on an infinitely long conductor above earth by a single corona source, such as that shown in Figure 9.5-2, is given in Equation 9.5-6c and is repeated here as

$$I_{wn}(\gamma,\omega) = \frac{-\gamma}{\left(Z_{11}(\gamma,\omega) + Z_{si} - \gamma^2 A_{11}(\gamma,\omega)\right)} \frac{1}{\pi\omega\varepsilon_0} I_{dn}(\omega) e^{+j\gamma z_n} \quad 9.5\text{-}24$$

Once the induced current is known, it is possible to calculate the electric and magnetic fields associated with this current. Note that since the fields generated by the corona discharges themselves are relatively small, they are ignored. The most commonly measured electric (vertical) and magnetic (horizontal) fields from a z-directed line current $I_{wn}(\gamma,\omega)$ at $(x,y) = (X,H)$ are shown in Equations 9.5-25a through 9.5-26b (Olsen and Wu 1991)

Here $D = ((x-X)^2 + (y-H)^2)^{1/2}$ and $D' = ((x-X)^2 + (y+H)^2)^{1/2}$ are the lateral distance between the observation point at (x,y) and the conductor and its image, respectively. The integrals in Equations 9.5-25b and 9.5-26b are Sommerfeld integrals that are valid at arbitrary frequencies, conductor spacings, and distances from the transmission line. The definitions of the remaining parameters in these equations can be found in Appendix 9.1, and wideband approximations for F_{ey}, F_{hx} and the axial electric field E_{zw} that do not require the numerical evaluation of infinite integrals can be found in Appendix 9.4. Note that although corona

$$E^{n}_{yw}(x,y,X,H,\gamma,\omega) = I_{wn}(\gamma,\omega)F_{ey}(x,y,X,H,\gamma,\omega)$$

Where: 9.5-25a

$$F_{ey}(x,y,X,H,\gamma,\omega) = \frac{-j\gamma}{4\omega\varepsilon_0}\left\{\zeta_0\left[\frac{(y-H)}{D}H_1^{(2)}(\zeta_0 D) - \frac{(y+H)}{D'}H_1^{(2)}(\zeta_0 D')\right]\right.$$

$$\left. - \frac{j2k_0^2}{\pi}\int_{-\infty}^{\infty}\left[\frac{1}{u_0+u_g} - \frac{\lambda^2+\gamma^2}{\left(k_0^2 u_g + k_g^2 u_0\right)}\right]\frac{e^{-u_0(y+H)}e^{-\lambda(x-X)}}{u_0}d\lambda\right\} \quad 9.5\text{-}25b$$

and $\zeta_0 = \left(k_0^2 - \gamma^2\right)^{1/2}$, $\mathrm{Im}(\zeta_0) < 0$.

$$H^{n}_{xw}(x,y,X,H,\gamma,\omega) = I_{wn}(\gamma,\omega)F_{hx}(x,y,X,H,\gamma,\omega) \quad 9.5\text{-}26a$$

Where:

$$F_{hx}(x,y,X,H,\gamma,\omega) = -\frac{j}{4}\left\{\zeta_0\left[\frac{(y-H)}{D}H_1^{(2)}(\zeta_0 D) - \frac{(y+H)}{D'}H_1^{(2)}(\zeta_0 D')\right]\right.$$

$$\left. + \frac{j2}{\pi}\int_{-\infty}^{\infty}\left[\frac{\lambda^2-k_0^2}{u_0+u_g} + \frac{k_0^2\gamma^2}{\left(k_0^2 u_g + k_g^2 u_0\right)}\right]\frac{e^{-u_0(y+H)}e^{-\lambda(x-X)}}{u_0}d\lambda\right\} \quad 9.5\text{-}26b$$

sources also create an electromagnetic field, the field of the induced wire current is dominant. This is because the "length" of the current induced on a conductor is much longer than the length of a corona source, and the radiated fields from electrically short antennas are proportional to both the current and the length.

To calculate the EMI at general frequencies, the effect of all corona sources must be added. This calculation can be done formally as follows.

First, the parts of $I_{wn}(\gamma,\omega)$ that are peculiar to the nth corona source are separated out. Here, as earlier, it has been assumed that all corona source currents are the same except for a random starting time. Thus

$$I_{dn}(\omega) = I_d(\omega)e^{j\omega\tau_n} \quad 9.5\text{-}27$$

and

$$I_{wn}(\gamma,\omega) = I'_w(\gamma,\omega)e^{j\omega\tau_n}e^{j\gamma\left(n\Delta z+\delta_n\right)} \quad 9.5\text{-}28a$$

$I_w'(\gamma,\omega)$ then can be written as

$$I'_w(\gamma,\omega) = \frac{-\gamma}{\left(Z_{11}(\gamma,\omega) + Z_{si} - \gamma^2 A_{11}(\gamma,\omega)\right)}\frac{1}{\pi\omega\varepsilon_0}I_{dn}(\omega) \quad 9.5\text{-}28b$$

Then the spectral density of the vertical electric field generated by $I_{wn}(\gamma,\omega)$ can be found as shown in Equation 9.5-29.

$$\left\langle S_E(x,y,X,H,\omega)\right\rangle = \left\langle E_{yw}(x,y,X,H,\gamma,\omega)E^*_{yw}(x,y,X,H,\gamma,\omega)\right\rangle =$$

$$\frac{1}{(2\pi)^2}\int_{-\infty}^{\infty}\int_{-\infty}^{\infty} I'_{wn}(\gamma,\omega)I'^*_{wn}(\gamma,\omega)F_{ey}(x,y,X,H,\gamma,\omega)F^*_{ey}(x,y,X,H,\gamma,\omega) \quad 9.5\text{-}29$$

$$\sum_{n=-\infty}^{\infty}\sum_{m=-\infty}^{\infty}\left\langle e^{j\omega(\tau_n-\tau_m)}\right\rangle_\tau\left\langle e^{-j(\gamma\delta-\gamma'\delta_m)}\right\rangle_\delta e^{+j\gamma(z-n\Delta z)}e^{+j\gamma'(z-m\Delta z)}d\gamma d\gamma'$$

Now as before,

$$\left\langle e^{j\omega(\tau_n-\tau_m)}\right\rangle_\tau = \begin{cases}1, & m=n\\ 0, & m\neq n\end{cases} \qquad 9.5\text{-}30$$

because the sources can be considered to be incoherent. Thus the double sum reduces to the single sum

$$e^{j(\gamma-\gamma')z}\sum_{n=-\infty}^{\infty} e^{j(\gamma-\gamma')n\Delta z} = e^{j(\gamma-\gamma')z}\,\frac{2\pi}{\Delta z}\,\delta(\gamma-\gamma') \qquad 9.5\text{-}31$$

where the last identity can be found in (Olsen and Wu 1991), and $\delta(p)$ is the Dirac delta function of argument p. Thus,

$$\left\langle S_E(x,y,X,H,\omega)\right\rangle = \frac{\left|\Gamma(\omega)\right|^2}{(2\pi)^3(\omega\varepsilon_0)^2} \int_{-\infty}^{\infty} \frac{\left|F_{ey}(x,y,X,H,\gamma,\omega)\right|^2\gamma^2}{\left|Z_{11}(\gamma,\omega)+Z_{si}-\gamma^2A_{11}(\gamma,\omega)\right|^2}d\gamma \qquad 9.5\text{-}32$$

where the "effective vertical electric field" can be written as

$$E_{eff}(x,y,X,H,\omega) = \left(S_E(x,y,X,H,\omega)\right)^{1/2} \qquad 9.5\text{-}33$$

The result given as Equations 9.5-32 and 9.5-33 is valid over the entire medium- and high-frequency ranges (i.e., 500 kHz – 30 MHz) and can probably be extended to lower frequencies. F_{ey} as given by Equation 9.5-24b can be approximated by an expression that is not as difficult to evaluate but is valid throughout the entire frequency range of interest. This expansion can be found in Appendix 9.4 along with wideband approximations for the denominator of the integrand of Equation 9.5-32. It should also be noted that when Equation 9.5-32 is evaluated, the integrand should not be expanded into modes because the mode structure of the denominator is complicated and involves both discrete modes such as the transmission-line mode mentioned earlier as well as modes that are characterized as "radiation" modes that are related to branch cuts in the complex plane (Wait 1972; Chang and Olsen 1975; Kuester et al. 1978). This issue is discussed further in Appendix 9.2. Thus Equation 9.5-32 is evaluated by integrating over the real axis of the γplane with the recognition that the infinite integral can be truncated to a finite integral since the integrand decays as γapproaches +/- ∞.

Finally it should be pointed out that a similar expression can be developed for the horizontal magnetic field H_x. In this case Equation 9.5-26 should be used instead of Equation 9.5-25. The result is

$$\left\langle S_H(x,y,X,H,\omega)\right\rangle = \frac{\left|\Gamma(\omega)\right|^2}{(2\pi)^3(\omega\varepsilon_0)^2} \int_{-\infty}^{\infty} \frac{\left|F_{hx}(x,y,X,H,\gamma,\omega)\right|^2\gamma^2}{\left|Z_{11}(\gamma,\omega)+Z_{si}-\gamma^2A_{11}(\gamma,\omega)\right|^2}d\gamma \qquad 9.5\text{-}34$$

and

$$H_{eff}(x,y,X,H,\omega) = \left(S_H(x,y,X,H,\omega)\right)^{1/2} \qquad 9.5\text{-}35$$

It is appropriate at this point to consider how the results for E_{eff} and H_{eff} compare to those given in the second edition of this book (EPRI 1982). To do this, $I_{wn}(\gamma,\omega)$ is replaced by its low frequency equivalent as given in Equation 9.5-7b. In addition, F_{ey} is replaced with an approximate form that is valid when the field point is less than approximately 100/(frequency in MHz) away from the conductor. This approximation is

$$F_{ey}^{lf}(x,y,X,H,\gamma,\omega) \approx \frac{+\gamma}{2\pi\omega\varepsilon_0}\left[\frac{(y-H)}{D^2}-\frac{(y+H)}{D'^2}\right] \qquad 9.5\text{-}36$$

For the low-frequency approximation to the current given in Equation 9.5-7b, the vertical electric field of a single corona source at $(0,H\text{-}r\text{-}\ell/2,z_n)$ is

$$E_{ywn}^{lf}(x,y,X,H,\gamma,\omega) \cong \frac{-jI_{dn}(\omega)}{\pi\omega\varepsilon_0\ln(2H/r)}\left[\frac{(y-H)}{D^2}-\frac{(y+H)}{D'^2}\right] \int_{-\infty}^{\infty}\frac{\gamma^2}{(\gamma^2-\gamma_p^2)}e^{-j\gamma(z-z_n)}d\gamma \qquad 9.5\text{-}37$$

Due to the simplicity of the integrand's denominator, this integral can evaluated in closed form using the theory of residues (see Appendix 9.2). The result is

$$E_{ywn}^{lf}(x,y,X,H,z,\omega) = \frac{-\gamma_P I_{dn}(\omega)}{2\pi\omega\varepsilon_0\ln(2H/r)}\left[\frac{(y-H)}{D^2}-\frac{(y+H)}{D'^2}\right]e^{-j\gamma_p|z-z_n|} \qquad 9.5\text{-}38$$

where γ_p is the transmission-line propagation constant that is given by Equation 9.5-8. The spectral density of the electric field from all sources can be written as the expected value of the electric field multiplied by its complex conjugate. The result is

$$\begin{aligned}&\left\langle S_E^{lf}(x,y,X,H,z,\omega)\right\rangle \\ &=\left\langle E_{yw}(x,y,X,H,z,\omega)E_{yw}^{*}(x,y,X,H,z,\omega)\right\rangle \\ &= \left\{\frac{\left|I_d(\omega)\right|\left|\gamma_p\right|}{2\pi\omega\varepsilon_0\ln(2H/r)}\left[\frac{(y-H)}{D^2}-\frac{(y+H)}{D'^2}\right]\right\}^2 \\ &\sum_{n=-\infty}^{\infty}\sum_{m=-\infty}^{\infty}\left\langle e^{j\omega(\tau_n-\tau_m)}\right\rangle_{\tau}\left\langle e^{-j\gamma_p(\delta_n-\delta_n)}\right\rangle_{\delta} e^{-j\gamma_p|z-n\Delta z|}e^{+j\gamma_p^{*}|z-m\Delta z|}\end{aligned} \quad 9.5\text{-}39$$

As illustrated earlier, the double summation can be reduced to a single summation by using Equation 9.5-30. The result is

$$\begin{aligned}&\left\langle S_E^{lf}(x,y,X,H,z,\omega)\right\rangle \\ &= \left\{\frac{\left|I_d(\omega)\right|\left|\gamma_p\right|}{2\pi\omega\varepsilon_0\ln(2H/r)}\left[\frac{(y-H)}{D^2}-\frac{(y+H)}{D'^2}\right]\right\}^2 \\ &\sum_{n=-\infty}^{\infty} e^{-2\alpha_p|z-n\Delta z|}\end{aligned} \quad 9.5\text{-}40$$

where the infinite series can be summed in closed form in the same way as the one in Equation 9.5-16. If it is assumed that $z = \Delta z/2$ and $\alpha_p\Delta z << 1$ then, using the definition of generation function in Equation 9.5-17b

$$\begin{aligned}&\left\langle S_E^{lf}(x,y,X,H,\omega)\right\rangle \\ &=\frac{1}{\alpha_p}\left\{\frac{\Gamma(\omega)\left|\gamma_p\right|}{4\pi\omega\varepsilon_0\ln(2H/r)}\left[\frac{(y-H)}{D}-\frac{(y+H)}{D'^2}\right]\right\}^2\end{aligned} \quad 9.5\text{-}41$$

where $\Gamma(\omega)$ is defined in Equation 9.5-17b and D and D' are defined in the discussion accompanying Equation 9.5-26b. It should be noted that, while this expression was computed at $z = \Delta z/2$, it is valid at any z.

The "effective" vertical electric field is defined as the square root of this spectral density. It is

$$E_{eff}^{lf}(x,y,X,H,\omega)=\left(S_E^{lf}(x,y,X,H,\omega)\right)^{1/2} \quad 9.5\text{-}42$$

For $x = 0$ and $\gamma_P \approx k_0$ (true in most cases), this is the same result as found in the second edition of this book. Clearly it is valid only at frequencies less than approximately 2 MHz and distances from the line less than approximately 50 m.

A similar expression can be written for the effective magnetic field except that F^{lf}_{ey} must be replaced with

$$\begin{aligned}&F_{hx}^{lf}(x,y,X,H,\gamma,\omega) \\ &=\frac{1}{2\pi}\left[\frac{(y-H)}{D^2}-\frac{(y+H+\alpha_g)}{(y+H+\alpha_g)^2+(x-X)^2}\right]\end{aligned} \quad 9.5\text{-}43$$

where $\alpha_g=\sqrt{2}\delta_g\exp(-j\pi/4)$ and $\delta_g=\sqrt{2/(\sigma_g\mu_0\omega)}$ is the skin depth of the earth. The second term of Equation 9.5-43 has been identified as a "complex image" of the current source above ground. Either this term or an approximation to it can be found in some of the radio-noise literature (Wait and Spies 1969; Olsen and Pankaskie 1983). It is often ignored at 60 Hz because $\delta \approx 650$ m for a typical earth conductivity (σ_g) of 0.01 S/m. However, at 1 MHz, for the same conductivity, $\delta_g \approx 5$ m, and this term cannot be ignored. It is interesting to note the ratio $E_y/H_x = F_{ey}/F_{hx} \approx 120\ \pi$ ohms, the impedance of free space, if δ_g can be ignored. This is true even at points that are not in the "far field" of the conductor. The reason for this is that the mode that propagates on the conductor is nearly transverse electromagnetic (TEM) and TEM modes have the property that E/H = 120π ohms (Olsen and Rouseff 1985).

The resulting value for the low-frequency spectral density of the horizontal magnetic field is

$$\begin{aligned}&\left\langle S_H^{lf}(x,y,X,H,\omega)\right\rangle = \\ &\frac{1}{\alpha_p}\left\{\frac{\Gamma(\omega)}{4\pi\ln(2H/r)}\left[\frac{(y-H)}{D^2}-\frac{(y+H+\alpha_g)}{(y+H+\alpha_g)^2+(x-X)^2}\right]\right\}^2\end{aligned} \quad 9.5\text{-}44$$

and the effective low-frequency magnetic field equal to

$$H_{eff}^{lf}(x,y,X,H,\omega)=\left\langle S_H^{lf}(x,y,X,H,\omega)\right\rangle^{1/2} \quad 9.5\text{-}45$$

EMI from a Two-Conductor Transmission Line Above Ground

The problem of interest here is the symmetric two-conductor transmission line with conductors at *(x,y) = (+/-X/2,Hd)*, shown in Figure 9.5-7.

It is shown in Appendix 9.1 that the current induced on this pair of conductors by the *n*th corona source on conductor "*p*" is

$$I_1(\gamma,\omega) = -\frac{1}{2}\left(\frac{I_{dn}^{p}(\omega)\gamma e^{+j\gamma z_n}}{\pi\omega\varepsilon_0}\right)$$
$$\left\{\frac{Y_{11}(\gamma,\omega)+Y_{12}(\gamma,\omega)}{\gamma^2-G_1^2(\gamma,\omega)}+(-1)^{p-1}\frac{Y_{11}(\gamma,\omega)-Y_{12}(\gamma,\omega)}{\gamma^2-G_2^2(\gamma,\omega)}\right\} \quad 9.5\text{-}46$$

$$I_2(\gamma,\omega) = -\frac{1}{2}\left(\frac{I_{dn}^{p}(\omega)\gamma e^{+j\gamma z_n}}{\pi\omega\varepsilon_0}\right)$$
$$\left\{\frac{Y_{11}(\gamma,\omega)+Y_{12}(\gamma,\omega)}{\gamma^2-G_1^2(\gamma,\omega)}-(-1)^{p-1}\frac{Y_{11}(\gamma,\omega)-Y_{12}(\gamma,\omega)}{\gamma^2-G_2^2(\gamma,\omega)}\right\}$$

where $p = 1$ or 2 and the parameters Y_{11}, Y_{12}, G_1, and G_2 are defined in Appendix 9.1. This expression has been obtained by decomposing the current into its common (i.e., $I_1 = I_2$) and differential (i.e., $I_1 = -I_2$) components and finding the propagation constants for each of these separately. It is reasonable to do this in this case because the decomposition is found to be independent of the spatial transform variable, γ. In more general cases (i.e. any line with three or more conductors), this approach will not be as useful. Despite this simplification, Equation 9.5-46 is still rather complex and cannot be easily evaluated. For example, the denominators of the terms within the brackets do not have a simple pair of values at which they equal 0 (i.e., simple poles) as does the denominator of Equation 9.5-37. This is because G_1 and G_2 are complicated functions of γ. As a result, the inverse spatial transform of Equation 9.5-46 cannot be easily evaluated except in the low-frequency case. This result is consistent with the observation noted earlier when commenting on Equation 9.5-32 for the single-wire case. It will be shown shortly, however, that if the low-frequency approximation is made, then the evaluation of the inverse spatial transform will be relatively simple. It is also useful to note here that a corona source on one conductor will induce a current on the second by induction from the current induced on the first.

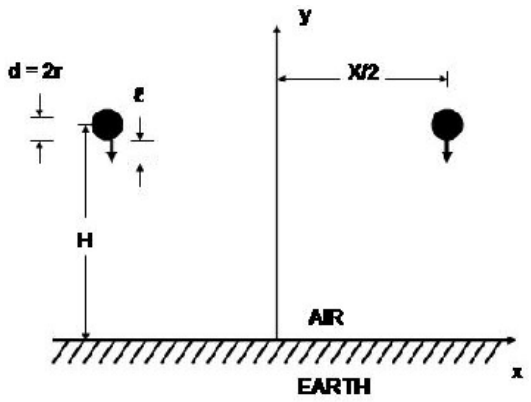


Figure 9.5-7 A symmetric two-conductor transmission line above earth with corona sources.

The vertical electric and horizontal magnetic fields can be found by multiplying each current by F_{ey} in Equation 9.5-25b and F_{hx} in Equation 9.5-26b, respectively for their appropriate values of x (i.e., $x \rightarrow x/2$ and $-x/2$ for conductors at $x/2$ and $-x/2$ respectively). However, as in the single-wire case, these fields are not yet fully specified because of the randomness of the corona source currents. In order to find measurable quantities, expressions for the spectral density of each field will be written in the same manner as earlier.

In the case for general frequencies, the following steps will be followed since inverse transformation to the space (i.e., z) domain is difficult due to the complicated spectrum. The steps will be outlined for the vertical electric field, but the steps for the horizontal magnetic field are identical. These steps are nearly identical to those explicitly written down for the single-wire case.

1. An expression for the vertical electric field in the temporal and spatial frequency domains of all corona sources is written by adding Equation 9.5-44 for each corona source on each conductor.
2. This expression for the vertical electric field is transformed to the spatial domain by using the inverse transform given in Equation 9.5-2b.
3. The spectral density of the vertical electric field (i.e., the magnitude squared of the field) is found by multiplying the field by its complex conjugate. In doing this, the integration variables for the field and its conjugate are γ and γ', respectively.
4. The expected value of the spectral density is computed by averaging over the random starting times and locations of the corona sources.
5. The result in Equation 9.5-30 is applied to each pair of corona sources, including pairs that involve one source on one wire and one on the other. Only the average over a source with itself is nonzero. This reduces the doubly infinite sum to a single infinite sum.
6. The identity, Equation 9.5-31, is used to express the remaining infinite sum in closed form as a Dirac delta function.
7. The γ' integration can be performed easily due to the factor $\delta(\gamma-\gamma')$ in the integrand.

After following this sequence of steps, the expression for the expected value of the spectral density of the vertical electric field can be written as shown in Equations 9.5-47 and 9.5-48.

In Equation 9.5-47, $F_{ey}(x,y,x',y',\gamma,\omega)$ is defined in Equation 9.5.25b and $Y_{ij}(\gamma,\omega)$ and $G_i(\gamma,\omega)$ can be found in

Appendix 9.1 as Equations A9.1-23 and A9.1-29, respectively. Wideband approximations for each of these can be found in Appendix 9.4. $\Gamma_1(\omega)$ and $\Gamma_2(\omega)$ are the generation functions for conductors 1 and 2, respectively.

A similar expression can be found for the expected value of the spectral density of the horizontal magnetic field $\langle S_H(x,y,\omega)\rangle$ and its corresponding "effective magnetic field" $H_{eff}(x,y,\omega)$ by substituting F_{hx} from Equation 9.4-26b for F_{ey} of Equation 9.2-25b and evaluating in the same way as for the single-conductor case.

Without going into the details of the derivation, low-frequency approximations for Equations 9.5-47 and 9.5-48 can be found in Equations 9.5-49 and 9.5-50, respectively.

$$\left\langle S_E\left(x,y,\omega\right)\right\rangle = \frac{1}{\left(2\right)^2}\frac{1}{\left(2\pi\omega\varepsilon_0\right)^2}\bullet$$
$$\left\{\Gamma_1\left(\omega\right)\int_{-\infty}^{\infty}\left|\left(\frac{Y_{11}\left(\gamma,\omega\right)+Y_{12}\left(\gamma,\omega\right)}{\gamma_1^2-G_1^2\left(\gamma,\omega\right)}+\frac{Y_{11}\left(\gamma,\omega\right)-Y_{12}\left(\gamma,\omega\right)}{\gamma_1^2-G_2^2\left(\gamma,\omega\right)}\right)F_{ey}\left(x,y,-X/2,H,\gamma,\omega\right)\right.$$
$$\left.\left(\frac{Y_{11}\left(\gamma,\omega\right)+Y_{12}\left(\gamma,\omega\right)}{\gamma_1^2-G_1^2\left(\gamma,\omega\right)}-\frac{Y_{11}\left(\gamma,\omega\right)-Y_{12}\left(\gamma,\omega\right)}{\gamma_1^2-G_2^2\left(\gamma,\omega\right)}\right)F_{ey}\left(x,y,X/2,H,\gamma,\omega\right)\right|^2 d\gamma \qquad 9.5\text{-}47$$
$$+\Gamma_2\left(\omega\right)\int_{-\infty}^{\infty}\left|\left(\frac{Y_{11}\left(\gamma,\omega\right)+Y_{12}\left(\gamma,\omega\right)}{\gamma_1^2-G_1^2\left(\gamma,\omega\right)}-\frac{Y_{11}\left(\gamma,\omega\right)-Y_{12}\left(\gamma,\omega\right)}{\gamma_1^2-G_2^2\left(\gamma,\omega\right)}\right)F_{ey}\left(x,y,-X/2,H,\gamma,\omega\right)\right.$$
$$\left.\left(\frac{Y_{11}\left(\gamma,\omega\right)+Y_{12}\left(\gamma,\omega\right)}{\gamma_1^2-G_1^2\left(\gamma,\omega\right)}+\frac{Y_{11}\left(\gamma,\omega\right)-Y_{12}\left(\gamma,\omega\right)}{\gamma_1^2-G_2^2\left(\gamma,\omega\right)}\right)F_{ey}\left(x,y,X/2,H,\gamma,\omega\right)\right|^2 d\gamma\Big\}$$

$$E_{eff}\left(x,y,\omega\right)=\left\langle S_E\left(x,y,\omega\right)\right\rangle^{1/2} \qquad 9.5\text{-}48$$

$$\left\langle S_E{}^{lf}\left(x,y,\omega\right)\right\rangle = \frac{1}{\left(8\pi\omega\varepsilon_0\right)^2}$$
$$\frac{\left|F_{ey1}^{lf}\right|^2}{\left|\gamma_1\right|^2}\left\{\left(\Gamma_1^2+\Gamma_2^2\right)\left(\frac{\left|Y_{11}+Y_{12}\right|^2\left|\gamma_1\right|^2}{\alpha_1}+\frac{\left|Y_{11}-Y_{12}\right|^2\left|\gamma_2\right|^2}{\alpha_2}\right)\right.$$
$$\left.+4\left(\Gamma_1^2-\Gamma_2^2\right)\mathrm{Re}\left(\frac{\left(Y_{11}+Y_{12}\right)\left(Y_{11}-Y_{12}\right)^*\gamma_1\gamma_2{}^*}{\left(\alpha_1+\alpha_2\right)+j\left(\beta_1-\beta_2\right)}\right)\right\}$$
$$+2\,\mathrm{Re}\left\{\frac{F_{ey1}^{lf}F_{ey2}^{lf}}{\gamma_1\gamma_2}\left(\Gamma_1^2+\Gamma_2^2\right)\left(\frac{\left|Y_{11}+Y_{12}\right|^2\left|\gamma_1\right|^2}{\alpha_1}-\frac{\left|Y_{11}-Y_{12}\right|^2\left|\gamma_2\right|^2}{\alpha_2}\right)\right\} \qquad 9.5\text{-}49$$
$$\frac{\left|F_{ey2}^{lf}\right|^2}{\left|\gamma_2\right|^2}\left\{\left(\Gamma_1^2+\Gamma_2^2\right)\left(\frac{\left|Y_{11}+Y_{12}\right|^2\left|\gamma_1\right|^2}{\alpha_1}+\frac{\left|Y_{11}-Y_{12}\right|^2\left|\gamma_2\right|^2}{\alpha_2}\right)\right.$$
$$\left.-4\left(\Gamma_1^2-\Gamma_2^2\right)\mathrm{Re}\left(\frac{\left(Y_{11}+Y_{12}\right)\left(Y_{11}-Y_{12}\right)^*}{\left(\alpha_1+\alpha_2\right)+j\left(\beta_1-\beta_2\right)}\right)\right\}$$

$$E_{eff}=\left\langle S_E^{lf}\left(x,y,\omega\right)\right\rangle^{1/2} \qquad 9.5\text{-}50$$

The spectrum and effective value of the magnetic field can be found by substituting F_{hx}^{lf} in Equation 9.5-43 for F_{ey}^{lf}.

EMI from a Three-Conductor Transmission Line Above Ground

The problem of interest here is to calculate the EMI from a three-conductor transmission above earth. Here the geometry shown in Figure 9.5-8 will be considered. This geometry might represent a horizontally configured line if $H_1 = H_2 = H_3$, a delta configured line if $H_1 = H_3$, or a vertically configured line if $X = 0$.

The starting point for this problem is the current induced on each of the three transmission-line conductors by a single corona source on pth conductor. This current can be found by solving the matrix equation that can be found as Equation A9.1-35 in Appendix 9.1, where all but one of the sources on the pth conductor is suppressed. The resulting equation is shown in Equation 9.5-51.

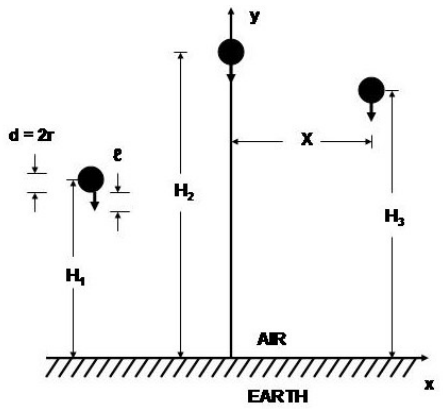


Figure 9.5-8 A three-conductor transmission line above earth with corona sources.

Here the terms $\exp(+j\omega\tau_{np})$ and $\exp(+j\gamma\delta_{np})$ represent the random starting time and location of the nth corona source within the nth cell $(n\Delta z)$ on the pth conductor. In these expressions, the explicit functional dependence of Z_{ij}, Z_{si}, and A_{ij} on geometry and transform variables is not given in order to conserve space.

As mentioned in Appendix 9.1, it is not useful to expand the currents in the eigenvectors of the matrix $[Z][Y]$ for the general frequency case since the eigenvectors are complicated functions of γ. Later, however, this can be (and generally is) done for the low-frequency case.

An expression for the vertical electric field of the induced currents of this single source can be found by multiplying each current by F_{ey} with its source location at the appropriate conductor. The currents shown in Equation 9.5-52 can be found by solving Equation 9.5-51. The result is shown in Equation 9.5-53 (Olsen and Wu 1991).

An expression for the vertical electric field of all corona sources on conductor p in the temporal and spatial domains can now be written by adding Equation 9.4-52 for each corona source on the pth conductor and transforming it to the spatial domain by using the inverse transform given in Equation 9.4-2b. The result is shown in Equation 9.5-54.

The spectral density of the vertical electric field (i.e., the magnitude squared of the field) is found by multiplying the field by its complex conjugate. In this calculation, the integration variable for the field and its conjugate are g and g', respectively. Following this, the expected value is calcu-

$$\begin{bmatrix} Z_{11}+Z_{si}-\gamma^2 A_{11} & Z_{12}-\gamma^2 A_{12} & Z_{13}-\gamma^2 A_{13} \\ Z_{21}-\gamma^2 A_{21} & Z_{22}+Z_{si}-\gamma^2 A_{22} & Z_{23}-\gamma^2 A_{23} \\ Z_{31}-\gamma^2 A_{31} & Z_{32}-\gamma^2 A_{32} & Z_{33}+Z_{si}-\gamma^2 A_{33} \end{bmatrix} \begin{bmatrix} I_{w1} \\ I_{w2} \\ I_{w3} \end{bmatrix} = \begin{bmatrix} \delta_{1p} \\ \delta_{2p} \\ \delta_{3p} \end{bmatrix} \left(\frac{-\gamma}{2\pi^2 \omega \varepsilon_0} \right) I_d^p(\omega) e^{j\omega\tau_{n_p}} e^{j\gamma\delta_{n_p}} e^{j\gamma n_p \Delta z} \qquad 9.5\text{-}51$$

where δ_{ij} is the Kronecker delta function that is equal to 1, when $i = j$, and 0 otherwise.

$$E_y^{pn_p}(x,y) = \begin{bmatrix} F_{ey}(x,y,-X/2,H_1) & F_{ey}(x,y,0,H_2) & F_{ey}(x,y,X/2,H_3) \end{bmatrix} \begin{bmatrix} I_{w1} \\ I_{w2} \\ I_{w3} \end{bmatrix} \qquad 9.5\text{-}52$$

$$\begin{bmatrix} I_w \end{bmatrix} = \begin{bmatrix} Z-\gamma^2 A \end{bmatrix}^{-1} \begin{bmatrix} \delta_{1p} \\ \delta_{2p} \\ \delta_{3p} \end{bmatrix} \left(\frac{-\gamma}{2\pi^2 \omega \varepsilon_0} \right) I_d^p(\omega) e^{j\omega\tau_{n_p}} e^{j\delta_{n_p}} e^{j\gamma n_p \Delta z} \qquad 9.5\text{-}53$$

$$E_{yw}^{p}(x,y,z,\omega) = \frac{-1}{4\pi^3\omega\varepsilon_0}\cdot$$
$$\int_{-\infty}^{\infty}\gamma\left[F_{ey}(\gamma,\omega)\right]\left[Z(\gamma,\omega)-\gamma^2 A(\gamma,\omega)\right]^{-1}\begin{bmatrix}\delta_{1p}\\ \delta_{2p}\\ \delta_{3p}\end{bmatrix} I_d^p(\omega)\sum_{n_p=-\infty}^{\infty} e^{j\omega\tau_{n_p}}\, e^{j\gamma\delta_{n_p}}\, e^{-j(z-n_p\Delta z)}\,d\gamma \qquad 9.5\text{-}54$$

$$\left\langle S_E^p(x,y,z,\omega)\right\rangle = \left(\frac{1}{4\pi^3\omega\varepsilon_0}\right)^2\int_{-\infty}^{\infty}\int_{-\infty}^{\infty}\left(\gamma\left[F_{ey}(\gamma,\omega)\right]\left[Z(\gamma,\omega)-\gamma^2 A(\gamma,\omega)\right]^{-1}\begin{bmatrix}\delta_{1p}\\ \delta_{2p}\\ \delta_{3p}\end{bmatrix} I_d^p(\omega)\right)$$
$$\left(\gamma'\left[F_{ey}(\gamma',\omega)\right]\left[Z(\gamma',\omega)-\gamma'^2 A(\gamma',\omega)\right]^{-1}\begin{bmatrix}\delta_{1p}\\ \delta_{2p}\\ \delta_{3p}\end{bmatrix} I_d^p(\omega)\right)^{*} \qquad 9.5\text{-}55$$
$$\sum_{n_p=-\infty}^{\infty}\sum_{m_p=-\infty}^{\infty}\left\langle e^{j\omega(\tau_{n_p}-\tau_{m_p})}\right\rangle\left\langle e^{j(\gamma\delta_{n_p}-\gamma'\delta_{m_p})}\right\rangle e^{-j\gamma(z-n_p\Delta z)}\, e^{+j\gamma'(z-m_p\Delta z)}\,d\gamma d\gamma'$$

lated by averaging over both the random starting time and the random source location. The result is shown in Equation 9.5-55.

The result in Equation 9.5-30 is applied to each pair of corona sources. Only the statistical average over a source with itself is nonzero. This reduces the doubly infinite sum to a single infinite sum. In addition, the identity, Equation 9.5-31, is used to express the remaining infinite sum in closed form as a Dirac delta function. Finally, the γ' integration can be performed easily due to the factor $\delta(\gamma-\gamma')$. With this operation, the result becomes independent of z. The result is (Olsen and Wu 1991)

$$\left\langle S_E^p(x,y,\omega)\right\rangle = 2\pi\left(\frac{1}{4\pi^3\omega\varepsilon_0}\right)^2\Gamma_p^2(\omega)$$
$$\int_{-\infty}^{\infty}\left|\gamma\left[F_{ey}(\gamma,\omega)\right]\left[Z(\gamma,\omega)-\gamma^2 A(\gamma,\omega)\right]^{-1}\begin{bmatrix}\delta_{1p}\\ \delta_{2p}\\ \delta_{3p}\end{bmatrix}\right|^2 d\gamma \qquad 9.5\text{-}56$$

Where:

$$\Gamma_p(\omega) = I_d{}^p(\omega)/(\Delta z)^{1/2} \qquad 9.5\text{-}57$$

is the generation function. The total EMI from all conductors can be calculated as (Olsen and Wu 1991)

$$\left\langle S_E(x,y,\omega)\right\rangle = \left\langle S_E^1(x,y,\omega)\right\rangle + \left\langle S_E^2(x,y,\omega)\right\rangle + \left\langle S_E^3(x,y,\omega)\right\rangle \qquad 9.5\text{-}58$$

since the statistical average over any source on one conductor with one on another is zero. The specific equations used to calculate the different parts of Equation 9.5-56 will be indicated later in this section when the program WBNOISE is described.

As earlier, the "effective electric field" can then be written

$$E_{eff} = \left\langle S_E(x,y,\omega)\right\rangle^{1/2} \qquad 9.5\text{-}59$$

A similar expression for the effective magnetic field can be written if F_{ey} in Equation 9.5-56 is replaced by F_{hx} found as Equation 9.5-26b.

Traditionally Equations 9.5-56 – 9.5-58 have been written in terms of the natural modes of the transmission-line conductors above the earth, as was done in the previous discussions of the one- and two-conductor transmission lines. This is not done here for several reasons. First, as mentioned above, the decomposition in terms of modes can only be done when either there is special symmetry (e.g., the two-conductor symmetric transmission line) or when the frequency is less than approximately 2 MHz. While a

certain amount of insight may result from the expansion into modes, this insight can be camouflaged by the complexity of the modal expansion. The details of this expansion can be found in the second edition of this book (EPRI 1982), but will not be repeated here due to space limitations.

EMI from a Multiple-Circuit Transmission Line Above Ground

EMI from multiple-circuit transmission lines can be found in a way completely analogous to that used for the three-conductor case. The only change is that the matrices in Equation 9.5-56 have dimension equal to the number of phase conductors rather than just three. As a result, Equation 9.5-58 will be written as

$$\left\langle S_E\left(x,y,\omega\right)\right\rangle = \sum_{p=1}^{N_p}\left\langle S_E^p\left(x,y,\omega\right)\right\rangle \qquad 9.5\text{-}60$$

where N_p is the total number of phase conductors.

Frequency and Altitude Corrections

Prior to using the generation functions described earlier in the section in the program WBNOISE to compare calculations with measurements, corrections were included for both altitude and frequency. The altitude correction was simply

$$\Gamma(A) = A/300 \text{ dB} \qquad 9.5\text{-}61$$

where "A" is the altitude of the experiment in meters above sea level (Burns et al. 1985; Chartier et al. 1987). The frequency correction term added to each generation function is shown in Figure 9.5-9. This dependence is different from that known for the frequency spectrum of the field since the source spectrum is changed by the process of current induction and field propagation. It was found by adjusting the source spectrum so that the fields calculated by the program WBNOISE had the known frequency variation. The field spectrum used for this calculation was the CISPR standard frequency dependence up to 20 MHz and a $1/f$ dependence between 20 and 30 MHz (IEC/CISPR 1982; Chartier 1988). More specifically, the WBNOISE source function was adjusted to provide a best fit with the BPA Corona and Field Effects (CFE) program from 0 – 100 m from a power line at a number of frequencies (Schennum and Olsen 1995). Each generation function was then corrected by adding the term

$$\Gamma(A, f) = A/300 + \Gamma_f(f) \text{ dB} \qquad 9.5\text{-}62$$

Calibration of the Wideband EMI Prediction Method Using Long-Term Data

A number of long-term experiments of EMI have been made at various locations in Europe and North America (Olsen et al. 1992). A list of these experiments, along with the relevant properties of the transmission lines, is shown in Tables 9.5-2 and 9.5-3.

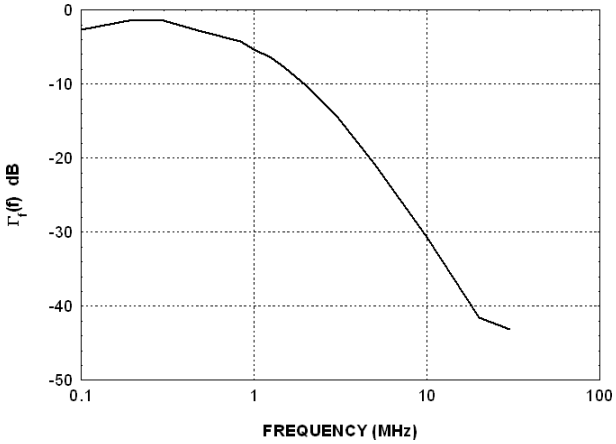


Figure 9.5-9 Frequency spectrum of the generation function.

Table 9.5-2 Properties of Transmission Lines Used for Long-Term Measurements (I). References (a – j) identified in Table 9.5-5

Line #	Ref.	line-line Voltage	Cnd. Dia.	# Sub.	Sub. Sp.	Horizontal location of phases			Average height of Phases		
			d	n	S	A	B	C	A	B	C
		(kV)	(mm)		(cm)	(m)	(m)	(m)	(m)	(m)	(m)
1	a	530	40.7	3	45.7	-4.6	-7.6	-4.6	16	25.5	35
		530	40.7	3	45.7	4.6	7.6	4.6	35	25.5	16
2	b,c	400	50	1	0	-9.6	0	9.6	14	14	14
3	d	400	31.7	2	45	-12	0	12	14	14	14
4	e	735	35.1	4	45.7	-15.2	0	15.2	17.1	17.1	17.1
5	f	387	21.7	4	40	11.3	14.8	7.8	35.7	25.2	25.2
		230	21.7	2	40	-11.3	-14.8	-7.8	35.7	25.2	25.2
6	g	760	29.6	4	45.7	-13.7	0	13.7	19.8	19.8	19.8
7	h	525	40.7	2	45.7	-6.1	0	6.1	16	24.5	16
		525	40.7	2	45.7	39.6	45.7	51.8	16	24.5	16
8	i	540	63.5	1	0	-10.4	0	10.4	16	16	16
		540	40.7	2	45.7	-49.3	-38.1	-26.9	16	16	16
9	j	735	30.5	4	45.7	-13.7	0	13.7	27.4	27.4	27.4

Table 9.5-3 Properties of Transmission Lines Used for Long-Term Measurements (II). References (a – j) identified in Table 9.5-5

Line #	Ref.	Altitude A	Earth Resistivity $\rho_g = 1/\sigma_g$	# Shield wires	Shield wire diameter	Horizontal spacing of shield wires	Height of shields
		(m)	(Ω-m)		(mm)	(m)	(m)
1	a	1935	250	2	12.7	3.7	40
		1935					
2	b,c	350	250	2	12.5	12	21
3	d	50	250	2	10.8	22	24
4	e	60	250	2	11.1	21.6	30
5	f	200	300	1	21.7	0	56.5
		200					
6	g	250	125	2	14.6	21.4	30.5
7	h	150	250	0			
		150		0			
8	i	100	250	0			
		100		0			
9	j	50	250	2	12.2	18	32.6

Table 9.5-4 Measurement Characteristics and Results for Long-Term Experiments

Line #	Conductor Gradient (calculation)			Ant.	Ant. ht.	Freq.	Horiz. Meas. dist. from reference	Detector	Avg. meas.rain	Avg. Fair
	kVrms/cm				(m)	(MHz)	(m)		dB/(μV/m) CISPR	
	A	B	C							
1	14.97	14.25	15.06	loop	2	0.5	22.6	ANSI	74	48
	14.98	14.13	14.88							
2	15.07	15.93	15.07	loop	3	0.5	24.6	CISPR	73	52
3	15.42	16.21	15.42	loop	2	0.5	27.0	CISPR	66	39
4	16.19	17.29	16.19	loop	2	1.0	0.0	ANSI	73	46
5	13.36	15.16	14.92	loop	1.7	0.5	14.8	CISPR	58	43
	11.69	13.85	12.52							
6	19.50	20.95	19.5	loop	5	1.025	28.7	ANSI	70.5	50
7	17.42	16.95	17.7	loop	2	0.5	66.8	ANSI	74	50
	17.74	16.95	17.37							
8	17.24	17.45	16.13	loop	3	0.5	56.1	ANSI	68	46
	16.70	18.14	17.62							
9	18.37	19.80	18.37	loop	1	1.0	28.7	ANSI	68	55

In Table 9.5-4, calculations of the conductor gradient for each of these lines, along with the details of the measurement system and results of the measurements, are shown. Note that measurements made using ANSI receivers were converted to CISPR by subtracting 2 dB.

The average fair-weather noise and average noise under measurable rain conditions shown in Table 9.5-4 were determined from the long-term statistical EMI distribution in the following way. Consider, for example, the distribution shown in Figure 9.5-3. The average EMI under measurable rain conditions was the average of the upper portion of the curve. In this case the average would be taken over the data from approximately the 7% point to the 0.1% of the curve. The result (at 3.5%) is approximately 75 dB μV/m. The average fair-weather EMI is the average of the lower portion of the curve from 99.9% to approximately 46%. The result (at 73%) is approximately 52 dB μV/m.

The references given in Tables 9.5-2 and 9.5-3 can be identified by reference to the key given in Table 9.5-5.

The data given in Table 9.5-4 were used to calibrate the wideband EMI prediction program (WBNOISE) in the following way.

1. Each of the generation functions given earlier in this section was augmented by an additive constant.
2. Each augmented generation function was incorporated into the program WBNOISE and used to calculate the EMI (average measurable rain conditions and fair weather) for each of the nine experiments reported in Table 9.5-4.

Table 9.5-5 Key for References in Table 9.5-3

Reference #	Section Reference
a	(Chartier et al. 1987)
b	(Cortina et al. 1970)
c	(IEEE 1973)
d	(Flink and Svensson 1975)
e	(Lacroix and Charbonneau 1968)
f	(Bartenstein and Schafer 1962)
g	(Kolcio et al. 1979)
h	(Chartier et al. 1979)
i	(Chartier 1989)
j	(Trinh et al. 1982)

3. The additive constant for each generation function was chosen so that the rms difference between the predictions and the actual measurements

$$\left[\frac{1}{N}\sum_{n=1}^{N}\left(X_p(n)-X_m(n)\right)^2\right]^{1/2} \qquad 9.5\text{-}63$$

was minimized where N is the number of experiments (9 in this case), and $X_p(n)$ and $X_m(n)$ are the predicted and measured results, respectively. This optimization was done separately for fair-weather and measurable rain conditions.

4. The augmented generations function that resulted in the least rms error between measurements and predictions was the one chosen for the final version of the program.
5. The generation function found to give the best error when averaged over both fair-and foul-weather conditions was the HVTRC heavy rain generation function in Equation 9.5.19. The value of the additive constant used to optimize the generation function was –2.0 dB. With this constant, the rms error for measurable rain conditions weather was 2.2 dB. Average fair-weather noise was predicted by subtracting 21.6 dB from the average measurable rain noise. The rms error for this calculation was 5.1 dB, consistent with the fact that fair-weather noise is much more variable.

The results of the comparison between measured results and the optimized calculation for average measurable rain conditions and average fair weather are shown in Figure 9.5-10 (Schennum and Olsen 1995). It is clear that the results of measurable rain measurements are much easier to predict than the results of fair-weather experiments.

The Computer Program WBNOISE

The computer program WBNOISE is designed to predict the EMI (i.e., effective vertical electric and horizontal magnetic fields) during fair-weather and measurable rain conditions at any point near one or more high-voltage transmission lines. The approximate frequency range of the predictions is from 500 kHz to 30 MHz (Schennum and Olsen 1995), but it probably can be extended to frequencies as low as 100 kHz.

In principle, the number of phase conductors and shield wires is not limited. However, any particular version of the program will have limits for the number of each. It should first be noted that the shield wires are used only for the calculation of the 50/60-Hz electric field at the surface of each phase conductor (i.e., the surface gradient E_{max}). E_{max} is the "average maximum bundle gradient" for a bundled conductor and is calculated using the methods described in (IEEE 1979) or Chapter 2. It is one of the inputs that determines the value of the corona generation function. The remainder of the EMI calculation involves only the phase conductors. For these calculations, a bundled phase conductor is replaced by an equivalent single conductor with the geometric radius of the bundled conductor.

The core generation function used by WBNOISE is the "heavy rain" generation function given by Equation 9.5-19. It has been modified by adding the altitude and frequency spectrum corrections given in Equations 9.5-61 and 9.5-62 and Figure 9.5-9. In addition, it has been modified by subtracting 2 dB, as required by the calibration process that is described in Figure 9.5-10. When so modified, this generation function is used to calculate the average EMI during measurable rain conditions.

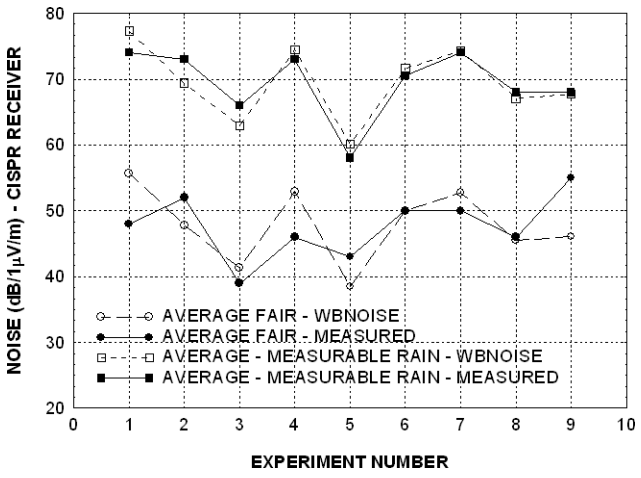


Figure 9.5-10 Comparison between measured fair weather and measurable rain noise and calculations using the WBNOISE with the optimized HVRAIN generation function. The HVRAIN generation function has been optimized by subtracting 2 dB. The average fair-weather noise has been obtained by subtracting 21.6 dB from the average foul-weather calculation. This value was chosen to minimize the difference between fair-weather calculations and measurements over the entire set of experiments.

The specific method used to calculate the vertical electric field EMI (e.g., that measured using a vertical rod antenna) is given in Equations 9.5-56 – 9.5-59 suitably generalized to N_p phase conductors. Numerical integration is used to evaluate Equation 9.5-56, and the specific forms used for F_{ey}, A, and Z are given in Appendix 9.4. For the calculation of horizontal magnetic field EMI (e.g., that measured using a loop antenna with its normal vector horizontal and normal to the transmission line), F_{ey} (Equation 9.5-56) is replaced by F_{hx}, which is given in detail in Appendix 9.4.

The calculations of EMI in measurable rain conditions are expected to have an rms error of ±- 2.2 dB. The average fair-weather EMI is calculated to be 21.6 dB smaller than the average measurable rain EMI and is expected to have an rms error of ±- 5.1 dB. It should be noted that the data used to calibrate WBNOISE were from transmission lines of between approximately 400 and 750 kV; the rms error for lines outside of this range may be larger. The 230-kV transmission line from experiment number 5 was not included in this range since it was paired with a 387-kV line that produced most of the EMI.

In principle, the EMI calculated by WBNOISE will predict the results of a long-term experiment using a CISPR quasi-peak receiver. More specifically, the "average measurable rain" output is the average EMI during rain conditions, and the "average fair weather" output is the average EMI during fair weather conditions over a period of at least one year. For both of these calculations, the transition data between fair weather and rain were not used.

9.5.3 Empirical Methods

There are several empirical formulas in the technical literature, and most of them have been summarized in (IEEE 1979). As with the traditional analytical method, most empirical methods are limited by use of the quasi-static field approximation. That, of course, means they cannot be used above 2 MHz and at distances of greater than 50/f meters, where f is the frequency in MHz. There is one empirical formula that has been found to be valid up to 30 MHz and at distances far from the line. This formula was developed at the Bonneville Power Administration (Chartier 1988). It is

$$EMI = 46 + 120\log_{10}\left(\frac{E_{\max}}{17.56}\right) + 40\log_{10}\left(\frac{2r}{3.51}\right) \quad dB(1\mu V/m) \tag{9.5-64}$$

where E_{max} is the average maximum bundle gradient in kV/cm rms, and r is the conductor radius in cm. This formula gives a prediction for the noise measured from any one phase conductor using a CISPR standard quasi-peak receiver tuned to 1 MHz and a horizontal loop antenna at 1 m above ground and 15 m from the phase conductor during average fair-weather conditions. For average EMI during measurable rain, it is suggested that 25 dB be added to Equation 9.5-64. For average EMI during foul weather, which is a wet conductor condition due to rain, fog, mist, snow, sleet, etc., it is suggested that 17 dB be added to Equation 9.5-64.

Other terms may be added to Equation 9.5-64 to take into account values of measuring frequency, altitude above sea level, and lateral distances that differ from the reference values. The term added to correct for a measuring frequency f (in MHz) different from 1 MHz is

$$RI_f = 10\cdot\left[1-\left(\log\left(10\cdot f\right)\right)^2\right] \quad dB \tag{9.5-65}$$

The reference altitude for Equation 9.5-64 is sea level. The additive correction used for any altitude A in km above sea level is

$$RI_q = A/0.3 \; dB \tag{9.5-66}$$

The additive term used to correct for distances different from 15 m from the conductor is

$$RI_D = -C_1 + C_2 \quad dB \tag{9.5-67}$$

where C_1 is a constant for the reference line and C_2 is a constant for the new line for which EMI is being calculated. The values of C_1 and C_2 can be determined from

$$C_i = 10\log\left(DW^2 + ESU^2 + EIND^2\right), \quad i = 1,2 \quad dB \tag{9.5-68}$$

where DW is the direct wave component, ESU is the surface wave component, and EIND is the induction field component. These three components are calculated as follows

$$DW = \frac{H}{k_0 D}, \quad for\ D \le \frac{12\ H\ h_a}{\lambda} \tag{9.5-69}$$

$$= \frac{H}{k_0 D}\cdot\frac{12\ H\ h_a}{\lambda D}, \quad for\ D > \frac{12\ H\ h_a}{\lambda}$$

$$ESU = \frac{g\left(\Delta\right)H}{k_0 D} \tag{9.5-70}$$

$$EIND = \frac{H}{\left(k_0 D\right)^2} \tag{9.5-71}$$

where, H is the height of the conductor in meters, h_a is the height of the antenna in meters, D is the radial distance

between the conductor and the antenna in meters, f is the frequency in MHz, λ is the wavelength in meters and

$$k_0 = \frac{2\pi}{\lambda}$$

$$g(\Delta) = \frac{2 + 0.3\Delta}{2 + \Delta + 0.6\Delta^2}$$

$$and \quad \Delta = \frac{52.5D}{\sigma_g \lambda^2}$$

σ_g being the ground conductivity in milli-siemens per meter (mS/m). The reference parameters for calculating C_1 are

$$D_1 = 21.04 \qquad DW_1 = \frac{31.1}{f}$$

$$EIND_1 = \frac{70.55}{f^2} \qquad \Delta_1 = \frac{276.16}{\lambda^2}$$

$$f(\Delta_1) = \frac{2 + 0.3\,\Delta_1}{2 + \Delta_1 + 0.6\,\Delta_1^2} \qquad ESU_1 = \frac{31.1\, g(\Delta_1)}{f}$$

9.5-72

where the reference value for σ_g = 4 mS/m.

The RI level for each phase is calculated using this formula. The final RI level is the highest value at the distance at which the calculation is being made. In other words there is no addition of the RI levels calculated from each phase. The total RI could also be determined using the method described in IEC/CISPR 18-3 (IEC/CISPR 1986b). The maximum difference between the two approaches is 3 dB.

It has been shown that the BPA formula is in agreement with the WBNOISE predictions if another 3.4 dB is added to the formula. With this addition, the rms difference between the two formulas is less than approximately 4 dB in measurable rain for frequencies between 500 kHz and 20 MHz and distances from the line of up to 100 m.

9.6 CALCULATION OF EMI FROM CONDUCTOR CORONA ABOVE 30 MHZ

9.6.1 Introduction

In foul weather and below 30 MHz, corona noise from conductors is usually the dominant source of EMI from high-voltage transmission lines. In fair weather and above 30 MHz, gaps (if they exist) are usually the dominant source of EMI for both high-voltage transmission and lower-voltage distribution lines. There are several reasons for this. First, the frequency spectrum of a gap source decays less rapidly at higher frequencies than that of a corona source. Thus, the energy emitted by a gap source is generally larger than that of a corona source above 30 MHz. Second, gap sources can be shorted by water during foul weather. When this occurs, they are no longer sources of EMI, and the emissions from conductor corona sources may dominate. Further, conductor corona is increased in foul weather due to the fact that raindrops form on the conductor surface. These drops enhance the 50/60-Hz field there and hence create additional sources of corona. Thus, despite the smaller energy radiated in the VHF and UHF range, conductor corona noise can be the dominant source of EMI in foul weather. This behavior is more pronounced for higher-voltage transmission lines because the amount of corona activity generally decreases as the line voltage decreases; but there are exceptions since corona activity is related to the electric field at the surface of the conductor. However, at voltages less than 200 kV, corona is usually too small to be a source of EMI above 30 MHz.

In this section, methods for predicting EMI from conductor corona will be discussed. The one method (i.e., the Bonneville Power Administration Corona and Field Effects Program) that is useful for EMI predictions between 30 and 1000 MHz is reproduced here. It should be noted that this model does not predict gap EMI. In fact, to the authors' knowledge, no model for predicting gap EMI exists. Part of the reason for this is the extreme variability of gap EMI and the fact that it is usually treated as a maintenance issue. Gaps are repaired when they occur. In contrast, EMI due to conductor corona is reasonably predictable and cannot be repaired after construction of the line. Therefore it is a design issue.

In principle, the method introduced in Section 9.5 could be used to calculate the effective vertical electric and/or horizontal magnetic fields from conductor corona at frequencies in excess of 30 MHz. The fundamental reason that this will not be done here is that it is not appropriate to simply calculate the electric and/or magnetic field at one point in space as done in Section 9.5. While this method can be used to calculate the effective fields at nearby points, it does not allow calculation of the phase difference at different points for the fields of a single source. This information is needed to calculate the output voltage of any antenna that is not much smaller than a wavelength in size. Below 30 MHz, rod and loop antennas typically used for EMI measurements are electrically small (i.e., their dimensions are much smaller than a wavelength). As a result, their output voltage is proportional to the value of the electric or magnetic field at the center of the antenna, and phase is not important. Above 30 MHz, however, the antennas typically used to measure EMI are comparable in size to a wavelength. As a result, their output voltage is determined by the electric or magnetic field distribution (especially the phase) over the entire antenna. Since these fields can vary

considerably over the antenna, it is no longer possible to characterize the EMI by a single field value. It is much more appropriate to include the receiving antenna in the model and to calculate the antenna output voltage.

Only one such analytic model has been reported that does this (Olsen and Stimson 1988). Unfortunately, because so little data exists for conductor corona EMI at these frequencies, this model is not well enough calibrated to release for public use. Nevertheless, the model will be described here because: (1) it leads to some insight about the nature of VHF and UHF EMI from conductor corona, and (2) some practical guidance about how to minimize the effect of this EMI can be developed.

9.6.2 Analytical Methods

Consider again corona sources on power line conductors, as shown in Figure 9.6-1. If the *n*th corona source on the *p*th conductor is located at z = z_{np}, the methods introduced in Section 9.5 can be used to determine the current that the corona source induces on the *n*th conductor. After appropriate high-frequency approximations are made, the temporal and spatial transform of this current can be found as

$$I_{wn}(\gamma,\omega) = \frac{4\gamma}{2j\zeta^2 \ln\left(\zeta a_n\right) - 4\omega\varepsilon_0\pi Z_{si}} e^{+j\gamma z_{np}} \qquad 9.6\text{-}1$$

Where:
$\zeta = (k_0^2 - \gamma^2)^{1/2}$, Im ($\zeta$) > 0, and $k_0 = \omega(\mu_0\varepsilon_0)^{1/2}$ is the propagation constant of free space where μ_0 and ε_0 are the permeability and permittivity of free space, respectively, and a_n and Z_{si} are, respectively, the radius and impedance per unit length of the *n*th conductor. It has been assumed here that the coupling between the conductors can be ignored. This assumption is reasonably valid at these higher frequencies. Note here that Equation 9.6-1 is a single-frequency component of the total impulsive current from the corona source. The impulsive current can be written in the time domain by evaluating the inverse temporal Fourier transform of Equation 9.6-1.

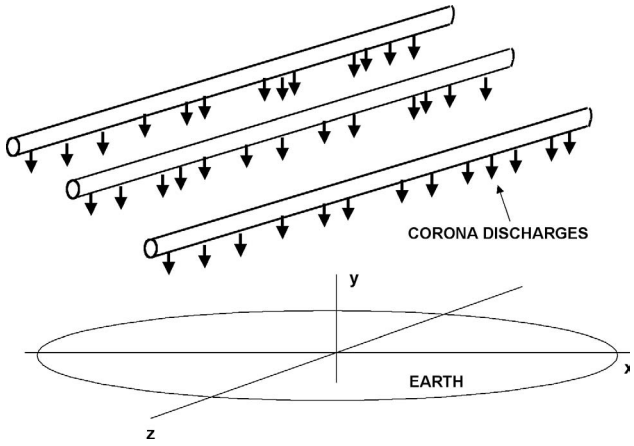


Figure 9.6-1 Corona discharges on power line conductors.

As mentioned in Section 9.5, it is difficult to evaluate the inverse spatial Fourier transform of Equation 9.6-1 because the denominator does not have the form ($\gamma^2 - \gamma_p^2$) that leads to simple residue integration. Nevertheless, it is possible to show that the induced current as a function of z can be reasonably well approximated as

$$I_{wn}(z,\omega) = Ae^{-\left(\alpha + jk_0\right)\left|z - z_{np}\right|} \qquad 9.6\text{-}2$$

where α is an attenuation constant that is due to resistive and radiation losses as the currents propagate. It can be inferred from this result that the induced current consists of a pair of traveling waves that propagate on the conductor in opposite directions away from the corona source and decay in a roughly exponential manner as shown in Figure 9.6-2.

Since the frequency is above 30 MHz, the wavelength is less than 10 m. As a result, the points at which the EMI are measured are usually at least one wavelength from the conductor and hence in the range for which the "radiation" terms dominate.

Since the current induced on the conductor by a single corona source is a pair of traveling waves, the electromagnetic fields generated by it behave like those of a "traveling wave antenna." More specifically, the fields more than a few wavelengths from the antenna have the following characteristics. First, they do not radiate directly down the wire. Second, and more surprising, they do not radiate perpendicular to the line. This occurs because the electromagnetic fields from the two traveling wave currents cancel in this direction. This behavior is summarized by the "radiation pattern" of the induced current as illustrated in Figure 9.6-3. For any given angle away from the source, the radiated field is proportional to the distance between the center point and the curve. Thus, for the example shown, the radiated field is maximum at about 45º from the conductor and zero normal to it.

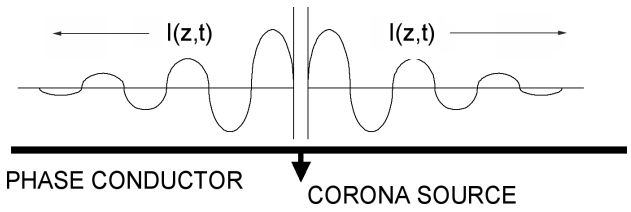


Figure 9.6-2 Traveling wave currents induced on a phase conductor by a corona source.

Again the reason why this interpretation can be made at VHF and UHF, but not in the MF and HF range, is that the concept of radiation pattern is only valid in the far field of the source. In the MF and HF range, the source/field point distances are usually only a small fraction of a wavelength.

Consider now the effect of having several (five in this case) corona sources on the phase conductor, as shown in Figure 9.6-4. The total EMI field is the superposition of the EMI from each source. Note again that since the starting time for each impulsive source current is "random," the pulses are "incoherent," and the total radiated power density in any direction is the sum of the power densities radiated by each source.

Some of the characteristics of conductor corona EMI at these frequencies can be illustrated by considering the output of an antenna typically used to measure EMI at these frequencies. An example of such an antenna is a directional antenna that is shown at the bottom of Figure 9.6-5. This antenna is characterized by its radiation pattern that can be described as follows. The signal at the terminals of the receiving antenna is proportional to the amplitude of the incoming signal and to the amplitude of its radiation pattern in the direction of the incoming signal. This amplitude is inversely proportional to the distance between the center of the antenna and the radiation pattern boundary in the direction at which the radiation arrives. Thus, in Figure 9.6-5, the maximum signal is induced by a signal (if any) arriving from the top of the figure.

In Figure 9.6-5, the directional antenna is oriented directly at the phase conductor. By this is meant that the maximum of its radiation pattern is "pointed" at corona source #3 on the phase conductor.

The total signal at the terminals of the directional antenna shown in this figure can be determined in the following way. First, consider source #3 at the center. Since this source radiates nothing in the direction of the antenna, it causes no signal at the receiver's terminals, even though the antenna's radiation pattern is maximum for signals arriving in this direction. Next, consider sources #2 and 4. Because of the source's radiation pattern, only a very small signal is radiated from these sources in the direction of the receiving antenna. Thus, even though the radiation pattern of the directional antenna is nearly maximum in this direction, only a very small signal is caused at these terminals by corona sources #2 and 4. For sources #1 and 5, the situation is a little different. The corona sources radiate a significant amount of energy toward the receiving antenna. However, since the receiving antenna is further away from the source, the amplitude of the signal arriving at the receiver is attenuated. Further, the amplitude of the antenna's radiation pattern for signals arriving from this direction is smaller. The result is only a small signal induced in the receiving antenna. The sum of all signals introduced to the terminals of the directional antenna is nonzero but relatively modest.

Next, consider the case for which the directional antenna is rotated away from the center of the phase conductor, as shown in Figure 9.6-6. The total signal at the terminals of the receiving antenna can be determined in the following way. First, consider source #1. This source radiates a significantly strong signal toward the receiving antenna. However, because of the orientation of the antenna's radiation

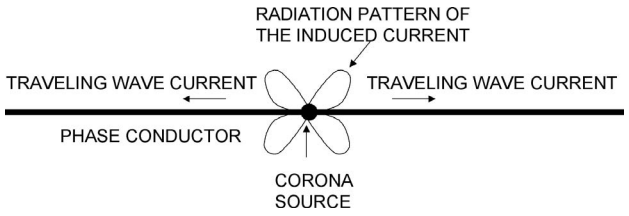


Figure 9.6-3 Radiation pattern of the traveling wave currents induced on the conductor.

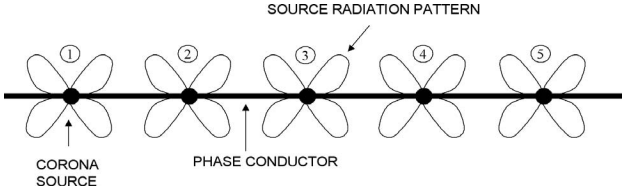


Figure 9.6-4 Radiation from five corona sources on a phase conductor.

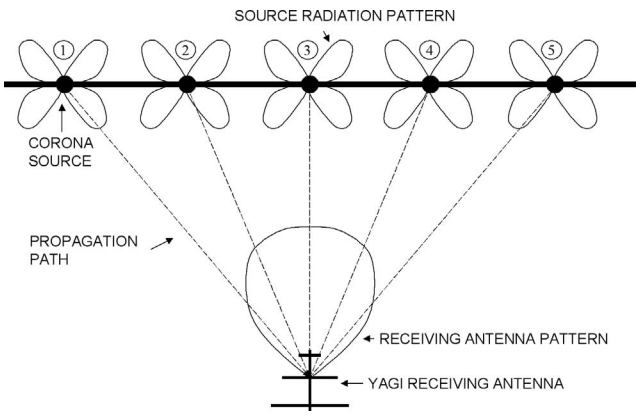


Figure 9.6-5 Yagi antenna oriented normal to a power line conductor receiving EMI from several corona sources on the conductor.

pattern, the signal at its terminals is essentially zero. For source #2, both the signal radiated toward the receiving antenna and the response of the antenna are small. This combination results in only a very small signal at the yagi's terminals. Source #3 does not radiate in the direction of the receiver. Source #4 does radiate some energy toward the receiving antenna, but because the amplitude of the radiation pattern of the directional antenna is large in this direction, there is a moderate signal induced at the antenna terminals. Source #5 is the most interesting source. Here the source radiates its maximum toward the receiving antenna, and the receiving antenna has its maximum response. Thus, even though source #5 and the receiving antenna are not close, the EMI picked up by antenna is relatively large.

The final result is that the EMI is minimized when the directional antenna is oriented directly at the phase conductor! As the antenna is rotated away from this position, the noise increases.

The ideas developed in the discussion of Figures 9.6-5 and 9.6-6 are further illustrated in Figure 9.6-7. Here the results of an experiment are plotted. In this case EMI from a 1200-kV test line at 75 MHz was measured with a commercial high gain directional antenna and a CISPR quasi-peak receiver (Perry et al. 1979). The EMI was plotted as a function of the receiving antenna orientation with respect to the transmission line; zero degrees corresponds to the case for which the axis of the antenna is pointing directly at the line. Also plotted is a computer simulation using the method described above (Olsen and Stimson 1988). It is clear that the ideas presented above are validated by experiment.

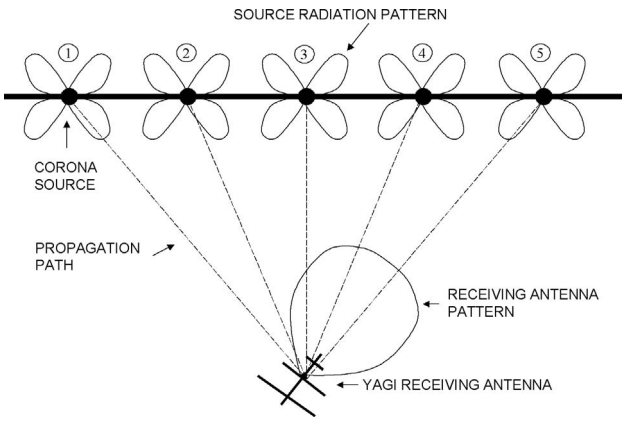


Figure 9.6-6 Directional antenna oriented 45° with respect to a power line conductor receiving EMI from several corona sources on the conductor.

It can be concluded that the EMI received from conductor corona can be minimized by orienting a directional antenna directly at the transmission line. This conclusion at first appears to be counterintuitive but has been validated by both theory and experiment.

A final conclusion that can be made about the characteristics of the EMI is that the radiation will be nearly horizontally polarized. This occurs because the currents that generate the EMI are almost horizontal, and it is well known that horizontal currents produce horizontally polarized waves. Thus the use of a vertically polarized receiving antenna will minimize the conductor corona EMI at the receiver terminals. Of course, this statement may not apply if the conductors have a significant amount of sag.

9.6.3 Empirical Methods

Above 30 MHz, EMI due to fair weather is generally so small that it does not cause interference even to the most sensitive communication systems. The only exception to this statement might be radio telescopes, which are extremely sensitive systems. Because of the proliferation of communication systems that now operate above 30 MHz, it is important that the industry have the ability to estimate EMI from conductor corona during foul weather, at any frequency, for any detector, and at any distance from the line.

The previous edition of the reference book (EPRI 1982) did not have a complete method for predicting EMI from conductor corona above 30 MHz. However, it did have a method for calculating TVI; but that method was only valid for the low VHF band (54 – 88 MHz), since it only included a single attenuation rate of 6 dB per doubling of

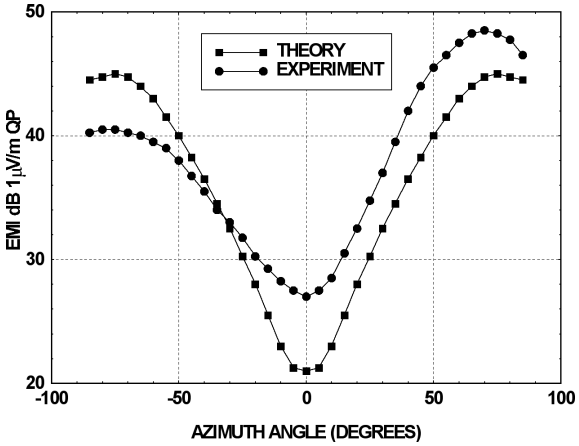


Figure 9.6-7 Theoretical and measured EMI at 75 MHz from a 1200-kV transmission delta line as a function of receiving antenna orientation. Zero degrees corresponds to antenna pointing directly at the transmission line.

distance. At the higher VHF and UHF frequencies, the attenuation rate changes from 6 dB per doubling of distance to 12 dB per doubling of distance (Pakala and Chartier 1971). A complete method for calculating EMI above 30 MHz not only models the attenuation rate correctly, but also includes the effect of conductor surface gradient, conductor diameter, frequency, and altitude, and also has correction terms for bandwidth and the detector. Such a procedure for calculating the L_{50} EMI level per phase above 30 MHz during measurable rain conditions can be expressed as:

$$EMI/phase = E_0 + E_g + E_d + E_f + E_A + E_{det} + E_{bw} + E_D \quad 9.6\text{-}3$$

where E_0 is a reference value and the rest of the terms are adjustment factors for the effects of conductor surface gradient (E_{max}), subconductor diameter (d), frequency (f), altitude (A), detector (det), bandwidth (bw), and radial distance from the conductor (D).

Equation 9.6-3 can be broken up into two parts—that is, a field value at 15 m laterally from the nearest conductor, and a field factor. The first six terms on the right-hand side of E_0 are corrections to the reference field value at 15 m for the transmission line and receiver for which calculations are being made. E_d is the distance term, and it is generally (but not always) very complex, since it is a function of not only distance from the conductor, but also of frequency, ground conductivity, and the heights of the antenna and the conductor. Also, in calculating E_d, a plane earth is assumed, because calculations for uneven terrain are very complex.

The most complete empirical method for predicting EMI above 30 MHz is the method developed by the Bonneville Power Administration (Chartier 1983). The BPA method was first developed to predict TVI from overhead lines during rain, but the method has been expanded so that EMI above 30 MHz can be calculated at any frequency, at any distance from the line, at any antenna height, for any bandwidth, and for any detector.

Before discussing the BPA prediction method, it is appropriate to introduce the characteristics of the experiment used to develop the empirical formula. TVI above 30 MHz from overhead power lines has been measured primarily with horizontally polarized, directional, or bidirectional antennas. The measured noise voltage at the antenna terminals is converted to an equivalent incident electric field by using the "antenna factor" of the receiving antenna. Details of this conversion can be found in the ANSI/IEEE standard 430 (ANSI/IEEE 1986). The measurements have been primarily made at midspan at the IEEE standard distance of 15 m from the outside phase with the antenna placed at a height of 3 m above the ground (ANSI/IEEE 1986). Measurements have also been made at distances up to 60 m from the outside phase (Pakala and Chartier 1971). Most of the measurements have been made using the quasi-peak detector. During rainy weather, the antenna is oriented to give the maximum reading on the meter that is connected to the antenna. When the antenna is located at the 15 m lateral distance, the maximum level usually occurs with the antenna pointing up and down the line if the antenna is bidirectional and either up or down the line if the antenna is unidirectional. This behavior is consistent with the discussion found in Section 9.6.2.

The BPA method for calculating the TVI/phase due to conductor corona for a CISPR quasi-peak receiver is expressed as:

$$TVI/phase = 10 + 120\log\left(\frac{E_{\max}}{16.3}\right) + 40\log\left(\frac{d}{3.04}\right) + TVI_f + TVI_D(L) + TVI_A \quad dB\mu V/m \quad 9.6\text{-}4$$

Where:

E_{max} is the conductor surface gradient in kV/cm
d is the subconductor diameter in cm
L is the distance between antenna and phase in m
A is the altitude in km

$$TVI_f = 20\log\left(\frac{75}{f}\right)$$

$$TVI_D(L) = 20\log\left(\frac{L_0}{L}\right), \text{ for } L \text{ and } L_0 \le L_c$$

$$= 20\log\left(\frac{L_0}{L_c}\right) + 40\log\left(\frac{L_c}{L}\right), \text{ for } L \ge L_c \text{ and } L_0 \le L_c$$

$$= 20\log\left(\frac{L_c}{L}\right) + 40\log\left(\frac{L_0}{L_c}\right), \text{ for } L \le L_c \text{ and } L_0 \ge L_c$$

$$= 40\log\left(\frac{L_0}{L}\right), \text{ for } L \text{ and } L_0 \ge L_c$$

L_0 = 61 m, reference radial distance between phase and antenna

$$L_c = \frac{12\, h_a\, H}{\lambda}$$

$$TVI_A = \frac{A}{0.3}(dB), \text{ altitude correction}$$

h_a is the antenna height in m, H is the conductor height in m, λ is the wavelength in m, and f is the frequency in MHz. For TVI, the detector is a CISPR QP detector where the bandwidth is 120 kHz. The TVI values calculated for each phase are not added. Rather, the phase that gives the highest level is considered to be the level for the line. The maximum error by not adding the fields from each phase is

3 dB. Measurements conducted by BPA (Perry et al. 1979; Chartier et al.1986; Chartier et al.1987) have verified that the above calculation procedure is valid from 30 to 1000 MHz and is probably valid at frequencies above 1000 MHz.

Now, if EMI calculations for other bandwidths or other detectors are needed, the following procedure should be used (Chartier 1988). First, the QP calculation should be corrected to another detector using the corrections shown Table 9.6-1.

Table 9.6-1 Corrections from QP to Other Detectors

Detector	Correction
Peak	+5 dB
RMS	-10 dB
Average	-14 dB

The corrections for the detectors in Table 9.6-1 were determined using older EMI instrumentation and need to be verified with the newer, more stable instruments.

Once the detector correction has been made, then the correction for bandwidth is made. For the peak detector, measurements have indicated that EMI due to rainy weather conductor corona is directly proportional to the bandwidth, or

$$\Delta E_{pk} = 20 \log_{10} (BW/BW_0) \quad 9.6\text{-}5$$

For the rms and average detectors, the EMI is proportional to the square root of the bandwidth or

$$\Delta E_{rms} = 10\log_{10} (BW/BW_0) \quad 9.6\text{-}6$$
$$\Delta E_{avg} = 10\log_{10} (BW/BW_0) \quad 9.6\text{-}7$$

Quasi-peak should never be corrected for bandwidth since CISPR specifies single bandwidths for specific frequency ranges for this detector.

9.6.4 Calculation of TVI – Low VHF Band

In the previous edition of the reference book (EPRI 1982), two procedures for calculating TVI were discussed. The EPRI method relied on RI calculations at 1 MHz, which were extrapolated to VHF frequencies and then corrected for bandwidth and distance from the line. The BPA method discussed in (Perry et al. 1979) and (EPRI 1982) was a simple comparative formula that assumed a single attenuation rate. However, as was discussed in Section 9.6.3, the attenuation rate changes from $1/D$ to $1/D^2$, and the point at which the change takes place is a function of frequency (Pakala and Chartier 1971).

A few investigators have conducted TVI measurements during foul-weather conditions. The lines for which measurements have been conducted are shown in Table 9.6-2, and the measurement parameters and the data are shown in Table 9.6-3. Also shown in Table 9.6-3 is a comparison of the levels predicted by the BPA EMI formula and the measurements. The BPA formula obviously underestimates the TVI levels that were measured on the test lines at Project UHV. However, the estimates are not that bad for the BPA lines and the Ontario Hydro 500-kV line. The TVI prediction method developed at Project UHV, which is shown in the second edition of the reference book (EPRI 1982), shows better agreement with the TVI measurements made on the three Project UHV test lines, but it overestimates the TVI levels for most of the BPA lines. The prediction of TVI is not expected to be as accurate as the prediction of AN and RI because of the lack of research. For example, it is not clear that the corona from the water drops is the primary source of the TVI. It may also be due to microsparking between the conductor and the water drops as they leave the conductor and microsparking between the charged water drops in space as postulated by (Janischewskyj and Arainy 1979). Also, it has been observed by many investigators that the corona activity from the insulator assemblies and the associated hardware can sometimes be quite high. It has been observed (Pakala and Chartier 1971) that if measurements above 30 MHz are conducted opposite the support structures, the antenna will almost always point directly at the structure, which would not be the case if the corona on the conductors was the sole source of the TVI according to the theory described in Section 9.6.2.

9.7 PASSIVE INTERFERENCE

Another type of EMI that the electric utility industry has dealt with over the years is *passive interference.* In this type of EMI, the electric power system is not an independent source of electromagnetic fields as it is with corona- or gap-generated noise. Rather, metallic objects that are part of the transmission system distort electromagnetic fields from other sources. For example, transmission-line structures and ground wires can reradiate radio signals being transmitted by nearby AM Broadcast Band antennas and hence distort the fields radiated by the antennas. In the TV Broadcast Band, interactions with the transmission-line system can cause reradiation that may result in ghosting and/or blockage. These effects can also be seen in communication channels other than AM radio and TV, but it is the AM and TV Broadcast Bands where the problem has been the most prevalent.

9.7.1 AM Broadcast Reradiation

When radio waves are transmitted, they encounter many man-made structures that contain metal. The wave induces an electric current in the metal, which can, in turn, radiate a radio wave at the same frequency as the original transmitted wave. In some cases, parts of the transmission-line structure may be nonlinear (e.g., junctions between bolts and tower members). If this is the case, signals at harmonic frequencies may be generated (Elsner 1982). This wave is

Table 9.6-2 Parameters of Line Configurations Used for Comparison of Calculated and Measured TVI

	Line	No. of Cond.	Cond. Diam.	Line Voltage	Horizontal Arrangement of Phases			Minimum Conductor Heights			Conductor Gradient	
											Outside Phase	Center Phase
					A	B	C	A	B	C		
			cm	kV	m	m	m	m	m	m	kV/cm	kV/cm
1	Project UHV 6 (EPRI 1982)	6	5.59	1100	19.8	0.0	19.8	22.9	22.9	22.9		
2	Project UHV 8 (EPRI 1982)	8	5.59	1300	-19.8	0.0	19.8	21.3	21.3	21.3	11.8	12.9
3	Project UHV 8 (EPRI 1982)	8	3.31	1050	-19.8	0.0	19.8	22.9	22.9	22.9	14.3	15.3
4	Ontario Hydro (Hatanaka 1981)	4	2.15	490	-12.8	0.0	12.8	18.0	18.0	18.0		
5	BPA Lyons 8 (Perry 1979)	8	4.07	1200	-11.0	0.0	11.0	24.4	42.7	24.4	14.48	14.50
6	BPA Lexington-Ross (Chartier 1981)	1	2.81	240	-8.2	0.0	8.2	12.2	12.2	12.2	14.94	15.75
7	BPA Marion-Alvey-Lane (Perry 1979)	2	4.07	540	-6.1	0.0	6.1	12.2	20.7	12.2	See Note #1	
8	BPA McNary-Ross (Chartier 1981)	1	4.07	343	-9.8	0.0	9.8	16.5	16.5	16.5	15.4	16.2
9	BPA Ostrander-Pearl) (Chartier 1981)	1	6.35	540	-10.4	0.0	10.4	18.3	18.3	18.3	16.4	17.4
10	BPA Oregon City-Keeler (Chartier 1981)	3	3.31	535	-10.2	0.0	10.2	15.2	15.2	15.2	16.97	18.25
11	BPA dble ckt (Montana) (Chartier 1987)	3	4.07	530	-4.6	-7.6	-4.6	12.8	22.3	31.8	See Note #2	
12	BPA dble ckt (Oregon) (Chartier 1987)	2	4.07	542	-4.6	-7.6	-4.6	12.8	22.3	31.8	See Note #3	

1. Two identical single circuit lines. Distance between centerlines is 45.7 m. Gradients: A1 = C2 = 18.13 kV/cm; B1 = B2 = 17.34 kV/cm; C1 = A2 = 18.38 kV/cm
2. Double circuit low reactance line, altitude of 1935 m: A1 = C2 = 14.70 kV/cm; B1 = B2 = 14.10 kV/cm; C1 = A2 = 15.0 kV/cm
3. Double circuit low reactance line, A1 = C2 = 14.70 kV/cm; C1 = B2 = 15.5 kV/cm; B1 = C2 = 15.2 kV/cm

Table 9.6-3 Comparison of Calculated and Measured TVI for Configurations Given in Table 9.6-2

Config.	TVI Measuring Location - L (m)	Antenna Type	TVI Antenna Height (m)	TVI Measuring Frequency (MHz)	Calculated TVI - QP (dBμV/m)	Measured TVI - QP (dBμV/m)	Difference Calc-Meas (dB)
1	43	Bi-conical	3	75	8.7	17.4	-8.7
2	43	Bi-conical	3	75	7.8	20.8	-13.0
3	43	Bi-conical	3	75	7.7	25.1	-17.4
4	40	Bi-conical	9.2	70	13.6	21.0	-2.5
5	16/25	Winegard	3	75	16.4/11.6	14.0	2.4/-2.4
6	15	Bi-conical	3	75	15.0	21.1	-4.0
7	15	Dipole	3	75	31.4	27.0	+3.4
8	15	Bi-conical	3	75	21.0	23.1	0.0
9	15	Bi-conical	3	75	32.2	34.0	-1.8
10	15	Bi-conical	3	75	21.1	24.0	-2.9
11	15	Dipole	3	75	26.0	21.5	+4.5
12	15	Dipole	3	75	19.5	16.0	+3.5

called *reradiation*. It is a form of passive interference if it distorts the effective far field radiation pattern (i.e., the amplitude of the signal as a function of direction) being transmitted by the radio station (Madge and Jones 1986).

AM Broadcasters are licensed to broadcast their signals at certain power levels and certain directional patterns. The pattern may be either omnidirectional or directional. In the U.S., the directional pattern for any given broadcaster is approved by the Federal Communications Commission and must be maintained by the broadcaster. Failure to do so may result in loss of the license. Practically all of the interference problems encountered by radio stations involve AM transmission with directional orientation. Many different kinds of antenna arrays are used depending upon the desired pattern. Figure 9.7-1 adopted from (Huyck 1985) shows a typical directional pattern produced by an antenna and the same signal pattern distorted by a nearby transmission line.

Vertical structures are the most effective at reradiation when they are close to a quarter wavelength ($\lambda/4$) tall (IEEE 1996). Quarter wavelengths in the AM Broadcast Band of 535 to 1705 kHz result in $\lambda/4$ heights of 44 to 140 m, which are typical heights for transmission structures. For power lines, reradiation may be caused either by interaction with isolated towers or with loops formed by two or more grounded towers connected with overhead ground wire. The reradiation is directly proportional to the AM radio frequency currents in these towers and overhead ground wires. These currents are dependent on the wavelength, tower design, and tower spans.

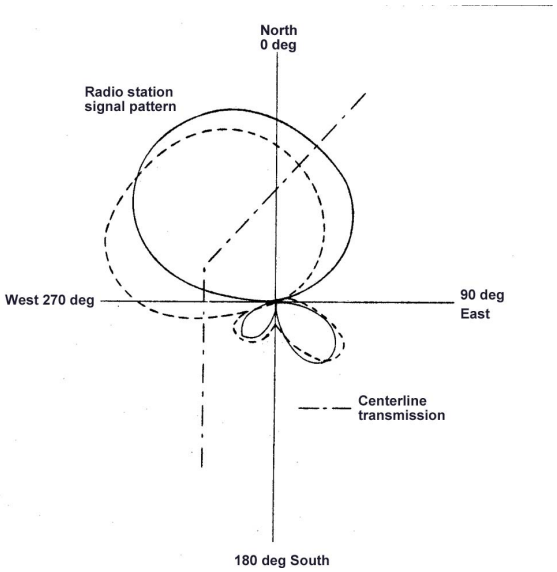


Figure 9.7-1 Radio station signal pattern (solid line) and signal pattern distorted by nearby transmission line (dotted line) (Huyck 1985).

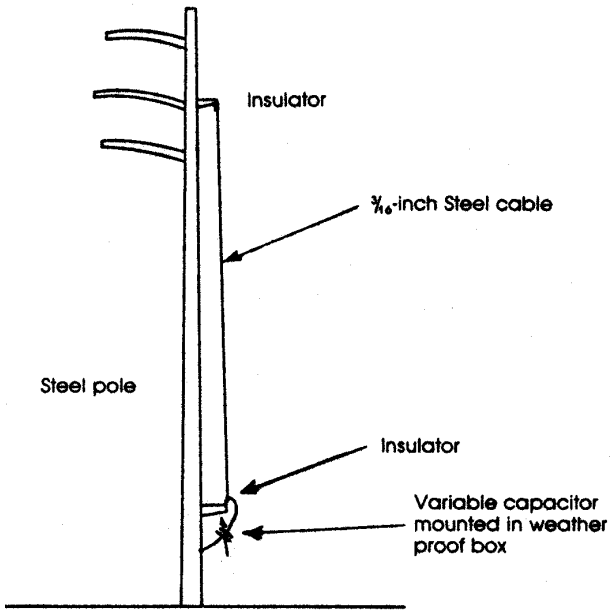


Figure 9.7-2 Schematic showing installation of detuning wire on a steel pole (Huyck 1985).

Fortunately the IEEE has addressed this problem and produced a standard that shows the techniques that have been developed over the years for predicting, measuring, analyzing, and remedying reradiation (IEEE 1996). The reader is referred to this standard for an in-depth understanding of reradiation of AM signals by transmission structures.

One of the solutions to this problem is to install a single detuning wire. The detuning wire does not eliminate radio-frequency currents in the structure. What it does is to provide a path for an equal current that is out of phase with the induced current. Figure 9.7-2 taken from (Huyck 1985) shows a typical installation of a detuning wire on a steel pole. A tuning capacitor is installed in series with the wire. The capacitor is adjusted to resonate with the frequency of the AM signal.

Sometimes reradiation is caused by the ground wire running down a wooden pole. One solution that has been used for this problem is to install a spark gap in the wire (Huyck 1985). For lattice structures, detuning wires are often used, but another solution is to isolate the tower from ground by installing insulating material under the legs of the lattice structure (Huyck 1985). If this is done, then a spark gap must be installed to provide for lightning protection.

Huyck (1985) also provides some general guidelines for utilities to consider to avoid this problem when siting a line:

1. transmission lines should be at least 1 mile from a directional antenna,
2. transmission lines should be at least 2 miles from stations with more than four towers or with power of 25-50 kW, and
3. transmission lines should always pass behind the station's pattern—that is, through the area of minimum radiation.

9.7.2 TV Broadcast Reradiation

The ghosts seen on TV sets are caused by reflected signals arriving out of time phase with the direct signal being transmitted by the broadcaster. Ghost signals are very prevalent in mountainous areas. Tall metallic structures, such as buildings and transmission structures, can also be a source of severe ghosting. Ghosting has always been a large problem in downtown areas of large cities that have many tall buildings. However, this problem can generally be solved by connecting television sets to cable TV or installing satellite dishes.

The physical presence of a steel transmission-line tower can also partially block a TV signal, which means the signal does not arrive at full strength.

The only known analytical studies of these effects have been undertaken in Japan, where apparently large concentrations of television-watching households are close to high-voltage transmission lines (Toyoda and Hashimoto 1979; Takeshita et al. 1979). In Japan and throughout the world, these effects do not significantly factor into the design of a transmission line, but may arise in the form of complaints after line construction. Such complaints are usually mitigated on a case-by-case basis (Loftness 1996). The easiest solution to ghosting and blocking is to connect the customer's TV set to an existing cable system or to a satellite dish antenna. If these solutions are not possible, the customer's antenna can be relocated or replaced with a highly directional antenna system that has a very high front-to-back ratio and also a good front-to-side ratio. Such an antenna system reinforces the main desired signal and reduces the weaker reflected signals arriving from various angles (Loftness 1992).

APPENDIX 9.1 CALCULATION OF CORONA-INDUCED CURRENT ON PHASE CONDUCTORS

Introduction

The problem that will be solved in this appendix is illustrated in Figure A9.1-1. A high-voltage transmission line consists of N_P infinitely long phase conductors (or phase bundles) and N_S infinitely long grounded shield wires. It is assumed that there is a distribution of corona discharges modeled as electric dipoles just below each phase conductor. The shield wires, however, are assumed not to have any corona. In fact, the only function of the shield wires in this solution is to affect the 60-Hz electric fields and hence the corona "amplitude." Any effect they have on propagation will be ignored. This will include the contribution of the ground wires to the series impedance terms Z and the parallel admittance terms Y and hence to the propagation of EMI currents. The ultimate object of this appendix is to identify expressions for the electric current induced on the transmission-line conductors. These results will be used in Section 9.5 to calculate the electric and magnetic fields near the transmission line.

The problem is to find the electric current induced on the phase conductors by the corona. To do this, it is necessary to write expressions for:

1. the electromagnetic fields of N_P linear distributions of vertical corona sources, and
2. the electromagnetic fields of the (yet to be determined) induced electric currents on the N_P phase conductors.

The geometry for these two problems for a single-phase conductor is shown in Figure A9.1-2.

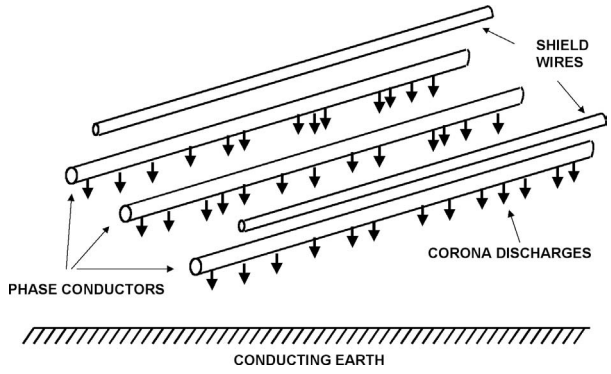


Figure A9.1-1 Geometry of the problem to be solved.

In Figure A9.1-2a, a set of corona discharges above earth is shown. The total field of all corona discharges along the phase conductor is found by adding up the fields due to sources at z_n along the line $(x,y) = (X, H\text{-}a\text{-}\ell/2)$, where the associated phase conductor is located at (X,H). The associated phase conductor is shown in Figure A9.1-2b. An end view of each of these problems is shown in Figures A9.1-2c and A9.1-2d, respectively.

The Temporal and Spatial Frequency Domains

It has been found useful to solve this problem using temporal and spatial Fourier transforms. The former is quite familiar to electrical engineers and can be described by the transform pair

$$P(\omega) = \int_{-\infty}^{\infty} p(t) e^{-j\omega t} dt \qquad \text{A9.1-1A}$$

$$p(t) = \frac{1}{2\pi} \int_{-\infty}^{\infty} P(\omega) e^{j\omega t} d\omega \qquad \text{A9.1-1B}$$

Here a function of time $p(t)$ is transformed into the temporal frequency domain to obtain the temporal frequency spectrum $P(\omega)$ using the first equation where ω is the radian frequency $= 2\pi f$ and f is the frequency in Hertz. This spectrum can be thought of as the amplitude of a continuous set of exponential functions that is equivalent to $p(t)$. Less familiar to electrical engineers is the fact that the same operation can be carried out in a spatial coordinate if the geometry of the problem (not including sources) does not vary with that coordinate. In our case, this will be true in the spatial dimension along the length of the power line since the power line is considered to be infinite. In the case

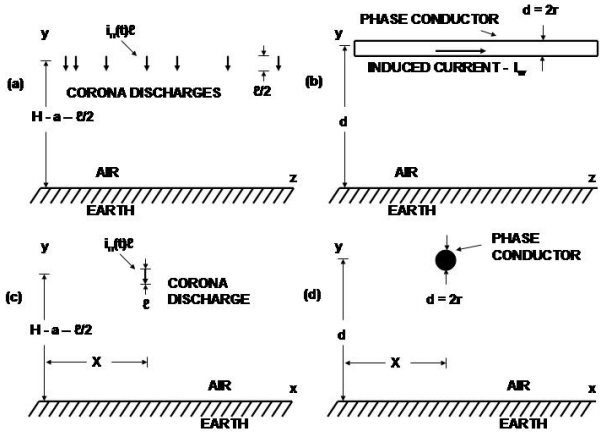


Figure A9.1-2 Components of the problem for a single-phase conductor.

for which z is this coordinate, the transform pair can be written

$$Q(\gamma) = \int_{-\infty}^{\infty} q(z) e^{+j\gamma z} dz \qquad \text{A9.1-2A}$$

$$q(z) = \frac{1}{2\pi} \int_{-\infty}^{\infty} Q(\gamma) e^{-j\gamma z} d\gamma \qquad \text{A9.1-2B}$$

Since the concept of a spatial transform may be new to power engineers, a few words of interpretation may be useful. $Q(\gamma)$, the transformed $q(z)$, may be considered as the continuous amplitude of exponentially varying functions of the form $exp(-j\gamma z)$. Thus, just as timevarying signals are expanded into components of the form $exp(j\omega t)$, spatially-varying functions are expanded into functions of the form $exp(-j\gamma z)$. The advantage of doing this is that a derivative with respect to the spatial coordinate is replaced by $-j\gamma$ in the same way that derivatives with respect to time are replaced with $j\omega$ (for the Fourier transform) or with s (for the Laplace transform). By analogy to the temporal frequency domain, $Q(\gamma)$ can be thought of as spatial frequency spectrum of $q(z)$ and the spatial frequency γ plays the role of the temporal frequency ω in the temporal transform.

Expressions Needed for Determining the Induced Current

The z-directed electric field due to the array of vertical dipoles of length ℓ (oriented in the –y direction) carrying current $i_d(t)$ and located at $(x,y,z) = (X, H\text{-}a\text{-}\ell/2, z_n)$, as shown in Figure A9.1-2a can be shown to be (Olsen and Aburwein 1980) (Olsen 1988)

$$E_{zd}(x,y,X,H-a-\ell/2,z,t) = \frac{1}{2\pi}\int_{-\infty}^{\infty} E_{zd}(x,y,X,H-a-\ell/2,z,\omega)e^{+j\omega t}d\omega \qquad \text{A9.1-3A}$$

where

$$E_{zd}(x,y,X,H-a-\ell/2,z,\omega) = \frac{1}{2\pi}\int_{-\infty}^{\infty} E_{zd}(x,y,X,H-a-\ell/2,\gamma,\omega)e^{-j\gamma z}d\gamma \qquad \text{A9.1-3B}$$

and

$$E_{zd}(x,y,X,H-a-\ell/2,\gamma,\omega) = \frac{j_0\ell\gamma}{4\omega\varepsilon_0}\sum_{n=-\infty}^{\infty} I_{dn}(\omega)e^{+j\gamma z_n}\left[\varsigma_0\frac{\left(y-H+a+\ell/2\right)}{D_d}H_1^{(2)}(\zeta_0 D_d)\right] \qquad \text{A9.1-3C}$$

where Equations A9.1-3b and A9.1-3c are the temporal and temporal/spatial Fourier transforms of the dipoles' electric field.

Note that in this expression the effect of the earth has been ignored since the sources are very close to the conductor. An expression for this field that contains all of the earth interaction terms can be found in (Olsen and Aburwein 1988). Since the dipole fields will be evaluated here only at the conductor, the "earth" terms have been shown to be negligible. The variables in Equation A9.1-3 are:

$I_{dn}(\omega)$ is the temporal Fourier transform of the nth corona current.

$k_0 = (\mu_0\varepsilon_0)^{1/2}$ is the free space propagation constant, where μ_0 is the permeability of free space and ε_0 is the permittivity of free space

$\varsigma_0 = (k_0^2 - \gamma^2)^{1/2}$, $Im(\zeta_0) < 0$

$H_1^{(2)}(x)$ is the Hankel function of second kind and order 1.

$D_d = ((x\text{-}X)^2 + (y\text{-}H+a+\ell/2)^2)^{1/2}$ is the lateral distance from the dipole to the observation point at (x,y).

It can generally be assumed that $D_d << \lambda$ for all frequencies of interest here, where $\lambda = 300/(\text{frequency in MHz})$ m. Thus the small argument approximation for the Hankel function

$$H_1^{(2)}(\zeta_0 D_d) \cong \frac{2j}{\pi\zeta_0 D_d} \qquad \text{A9.1-4}$$

can be used and

$$E_{zd}(x,y,X,H-a-\ell/2,\gamma,\omega) \cong \frac{-\ell\gamma}{2\pi\omega\varepsilon_0}\frac{\left(y-H+a+\ell/2\right)}{D_d^2}\sum_{n=-\infty}^{\infty} I_{dn}(\omega)\gamma e^{+j\gamma z} \qquad \text{A9.1-5}$$

Similarly, the z-directed electric field of a z-directed wire current $I(z,t)$ at $(x,y) = (X,H)$ is (Wait 1972; Chang and Olsen 1975; Olsen and Rouseff 1985; Olsen and Wu 1989)

$$E_{zw}(x,y,X,H,z,t) = \frac{1}{2\pi}\int_{-\infty}^{\infty} E_{zw}(x,y,X,H,z,\omega)e^{+j\omega t}dt \qquad \text{A9.1-6A}$$

where

$$E_{zw}(x,y,X,H,z,\omega) = \frac{1}{2\pi}\int_{-\infty}^{\infty} E_{zw}(x,y,X,H,\gamma,\omega)e^{-j\gamma z}d\gamma \qquad \text{A9.1-6B}$$

and

$$E_{zw}(x,y,X,H,\gamma,\omega) = F_{ez}(x,y,X,H,\gamma,\omega)I_w(\gamma,\omega) \quad \text{A9.1-6C}$$

where

$$F_{ez}(x,y,X,H,\gamma,\omega) = \frac{-1}{4\omega\varepsilon_0}\cdot \left[\begin{array}{l}\zeta_0^2(H_0^{(2)}(\zeta_0 D) - H_0^{(2)}(\zeta_0 D')) \\ +k_0^2(P(x,y,X,H,\gamma,\omega) - Q(x,y,X,H,\gamma,\omega))\end{array}\right]$$

Here Equations A9.1-6b and A9.1-6c represent the temporal and temporal/spatial Fourier transforms of the wire's electric field.

In Equation A9.1-6c

$$P(x,y,X,H,\gamma,\omega) = +\frac{j2}{\pi}\int_{-\infty}^{\infty}\left(\frac{1}{u_0+u_g}\right)e^{-u_0(y+H)}e^{-j\lambda(x-X)}d\lambda \quad \text{A9.1-6D}$$

$$Q(x,y,X,H,\gamma,\omega) = +\frac{j2}{\pi}\int_{-\infty}^{\infty}\left(\frac{\gamma^2}{k_0^2u_g+k_g^2u_0}\right)e^{-u_0(y+H)}e^{-j\lambda(x-X)}d\lambda \quad \text{A9.1-6E}$$

where $P(x,y,X,H,\lambda,\omega)$ and $Q(x,y,X,H,\lambda,\omega)$ are two-dimensional Sommerfeld integrals that account exactly for the earth interaction, and $I_w(\gamma,\omega)$ is the temporal and spatial Fourier Transform of the induced wire current $I_w(z,t)$. The previously undefined variables are:

$\eta_0 = (\mu_0\varepsilon_0)^{1/2}$ is the impedance of free space.

$k_g = \omega(\mu_0\varepsilon_g - j\mu_0\sigma_g/)^{1/2}$, $Re(k_g) > 0$ is the propagation constant of the earth where σ_g is the earth conductivity and ε_g is the earth dielectric constant = $\varepsilon_0\varepsilon_{rg}$.

$H_0^{(2)}(x)$ is the Hankel function of second kind and order 0.

$u_0 = (\lambda^2 + \gamma^2 - k_0^2)^{1/2}$, $Re(u_0) > 0$.

$u_g = (\lambda^2 + \gamma^2 - k_g^2)^{1/2}$, $Re(u_g) > 0$.

$D = ((x-X)^2 + (y-H)^2)^{1/2}$ and $D' = ((x-X)^2 + (y+H)^2)^{1/2}$ are the lateral distance between the observation point at (x,y) and the conductor and its image respectively.

In Appendix 9.4, an approximation to E_{zw} is given that is valid over the entire frequency range of interest in this section (i.e., 300 kHz – 30 MHz). This expression does not involve an infinite integral that must be evaluated numerically and hence is used in the computer program WBNOISE used in this section to implement the formulas for induced conductor current introduced here.

Equation A9.1-6c can be rewritten in a form that will lead naturally to the standard formulas traditionally used at lower frequencies for propagation on power lines.

$$E_{zw}(x,y,X,H,\gamma,\omega) = -\left\{Z(x,y,X,H,\gamma,\omega) - \gamma^2 A(x,y,X,H,\gamma,\omega)\right\}I_w(\gamma,\omega) \quad \text{A9.1-7A}$$

$$Z(x,y,X,H,\gamma,\omega) = \frac{\omega\mu_0}{4}\left(H_0^{(2)}(\zeta_0 D) - H_0^{(2)}(\zeta_0 D') + P(x,y,X,H,\gamma,\omega) - Q(x,y,X,H,\gamma,\omega)\right) \quad \text{A9.1-7B}$$

$$A(x,y,h,d,\gamma,\omega) = \frac{-1}{4\omega\varepsilon_0}\left(H_0^{(2)}(\zeta_0 D) - H_0^{(2)}(\zeta_0 D')\right) \quad \text{A9.1-7C}$$

Now it can be shown that for frequencies such that all relevant distances (i.e., r, *H, D,D', D_d and D_d'*) are small compared to a wavelength (for power lines, this is up to several MHz), the terms listed above can be simplified to expressions familiar to power engineers (i.e., Carson's equations). More specifically (Carson 1926; Olsen 1988)

$$H_0^{(2)}(\zeta_0 D) \cong \frac{-j2}{\pi}\ln(\zeta_0 D), \quad H_0^{(2)}(\zeta_0 D') \cong \frac{-j2}{\pi}\ln(\zeta_0 D') \quad \text{A9.1-8}$$

$$Z(x,y,X,H,\gamma,\omega) \cong Z(x,y,X,H,\omega) = \frac{j\omega\mu_0}{2\pi}\left\{\ln(D'/D) - J_c(x,y,X,H,\omega)\right\} \quad \text{A9.1-9A}$$

Where J_c is Carson's integral and is written as

$$J_c(x,y,x',y',\omega) = \frac{2}{\hat{k}_g^2}\int_0^{\infty}(u-\lambda)e^{-\lambda(y+y')}\cos(\lambda(x-x'))d\lambda \quad \text{A9.1-9B}$$

$$u = \left(\lambda^2 - \hat{k}_g^2\right)^{1/2}, \ \mathrm{Re}(u) > 0, \quad k_g \cong \hat{k}_g = \left(\omega\mu_0\sigma\right)^{1/2}e^{-j\pi/4}, \ \mathrm{Re}\left(\hat{k}_g\right) > 0, \ \frac{\sigma}{\omega\varepsilon_g} >> 1$$

Finally,

$$A(x,y,X,H,\gamma,\omega) \cong A(x,y,X,H,\omega) = \frac{1}{Y(x,y,X,H,\omega)} = \frac{-j}{2\pi\omega\varepsilon_0}\ln(D'/D) \quad \text{A9.1-10}$$

where $A(x,y,X,H,\omega)$ is the Maxwell potential coefficient for a single conductor above the earth. Note that both $Z(x,y,X,H,\omega)$ and $A(x,y,X,H,\omega)$ are independent of γ.

Setting Up an Equation for the Induced Current

To find the unknown current induced on one or more parallel conductors by the corona discharges, an electromagnetic boundary value problem is solved (Pogorzelski and Chang 1977; Olsen and Aburwein 1980). This is done by setting the total tangential electric field on the conductor surface to an appropriate value. By first assuming that each conductor is "thin" compared to wavelength and other dimensions, this may be done by setting the total axial (i.e., z directed) electric field (i.e., sum of the field from the corona sources and that due to the unknown current induced on each conductor) at only one point on the circumference of each conductor to the "surface impedance" (Z_{si}) of that conductor multiplied by the current. This surface impedance is the ratio of the *z* component of the electric field (i.e., voltage per unit length) to the current (i.e., $2\pi r$ times the azimuthal magnetic field at the surface of the conductor). For good conductors, this impedance has been found to be related only to the properties of the conductor. The resulting equation is

$$E_{zd}\left(X, H-r, X, H-r-\ell/2\right)+E_{zw}\left(X, H-r, X, H\right) = Z_{si} I_w\left(\gamma,\omega\right) \qquad \text{A9.1-11}$$

The Single-Wire Problem

As a first example of how this works, consider a *z*-directed wire above the earth at a location *(x',y') = (0,H)*. Using Equation A9.1-11 and expressions for the appropriate fields in Equations A9.1-5 and A9.1-7 presented above to match the boundary condition at *(x,y) = (0, H-r)*

$$\frac{-\gamma}{\pi\omega\varepsilon_0}\sum_{n=-\infty}^{\infty} I_{dn}\left(\omega\right)e^{-j\gamma z_n} - \left[Z_{11}\left(\gamma,\omega\right)-\gamma^2 A_{11}\left(\gamma,\omega\right)\right] I_w\left(\gamma,\omega\right) = Z_{si} I_w\left(\gamma,\omega\right) \qquad \text{A9.1-12A}$$

where

$$Z_{11}\left(\gamma,\omega\right) = Z(0, H-r, 0, H, \gamma, \omega) \qquad \text{A9.1-12B}$$

$$A_{11}\left(\gamma,\omega\right) = A(0, H-r, 0, H, \gamma, \omega) \qquad \text{A9.1-12C}$$

In this expression the subscript notation 11 indicates that the field of conductor #1 is evaluated at the surface of conductor #1. The form of this notation will also be used later when the number of conductors is increased.

Finally, in Equation A9.1-12a

$$Z_{si}(\omega) = \eta_w / 2\pi r \text{ where } \eta_w = (j\omega\mu_0/\sigma_w)^{1/2},\ Re(\eta_w) > 0 \qquad \text{A9.1-13}$$

is the surface impedance of the conductor and σ_w is the wire conductivity.

Equation A9.1-12 can now be solved algebraically for the induced current $I_w(\lambda,\omega)$. The result is (Olsen and Wu 1989):

$$I_w(\gamma,\omega) = \frac{-\gamma}{\left(Z_{11}(\gamma,\omega)+Z_{si}-\gamma^2 A_{11}(\gamma,\omega)\right)}\frac{1}{\pi\omega\varepsilon_0}\sum_{n=-\infty}^{\infty} I_{dn}(\omega)e^{+j\gamma z_n} \qquad \text{A9.1-14}$$

Once the temporal and spatial Fourier transform of the induced current is known, the current as a function of *z* can be found by evaluating the inverse Fourier transform as

$$I_w(z,\omega) = \frac{1}{2\pi}\int_{-\infty}^{\infty} I_w\left(\gamma,\omega\right)e^{j\gamma z}\,d\gamma \qquad \text{A9.1-15}$$

In principle, this integral can be solved, but because Z_{11} and A_{11} are complicated functions of γ, the integral must be evaluated numerically. There are other alternatives; for example, a spectral decomposition could be used, but these also are quite complicated and will not be pursued here (Kuester et al. 1978). Perhaps most relevant is that it is not (in general) possible to represent the current in the form *exp(-jγ_P|z|)* as it is for the low-frequency case to be discussed next.

Using the low-frequency approximation given in Equations A9.1-8 – A9.1-9, Equation A9.1-14 becomes (Olsen 1983)

$$I_w^{lf}(\gamma,\omega) = \frac{-j2\gamma}{\ln(2H/r)\left(\gamma^2-\gamma_p^2\right)}\sum_{n=-\infty}^{\infty} I_{dn}(\omega)e^{+j\gamma z_n} \qquad \text{A9.1-16A}$$

where

$$\gamma_p = \left[-Y_s\left(Z_{si}+Z_{ss}+Z_g\right)\right]^{1/2},\ \ \mathrm{Im}(\gamma_P) < 0. \qquad \text{A9.1-16B}$$

Here

$$Y_s = \frac{j2\pi\omega\varepsilon_0}{\ln\left(2H/r\right)} \qquad \text{A9.1-16C}$$

is the inverse of the Maxwell potential coefficient *A* and is the shunt admittance per unit length of a conducting earth,

$$Z_{ss} = \frac{j\omega\mu_0}{2\pi}\ln\left(2H/r\right) \qquad \text{A9.1-16D}$$

is the series impedance per unit length of a conductor over perfectly conducting earth, and

$$Z_g = \frac{-j\omega\mu_0}{2\pi} J_c(0, H-r, 0, H, \gamma, \omega) \qquad \text{A9.1-16E}$$

is the series impedance per unit length due to the finite conductivity of the earth.

What is significant about this result is that both $Z = Z_{si} + Z_{ss} + Z_g$ and $Y_s = 1/A$ are independent of γ. As a result:

1. it is relatively simple to determine the exact value for the inverse Fourier Transform of Equation A9.1-16a using residue theory as described in Appendix 9.3, and
2. the current as a function of z has an especially simple form.

The inverse Fourier transform for the current is:

$$I_w(z,\omega) = \frac{-2\pi}{\ln(2H/r)} \sum_{n=-\infty}^{\infty} \frac{(z-z_n)}{|z-z_n|} I_{dn}(\omega) e^{-j\gamma_P |z-z_n|} \qquad \text{A9.1-17}$$

The Two-Wire Problem

It is possible to set up a similar solution for the problem of N parallel conductors driven by an array of corona sources (Wait 1977). However, in the interest of developing insight, the first multiwire example will be that for two wires located a distance X apart at the same height H above an earth, as shown in Figure A9.1-3. Generalizing Equation A9.1-12,

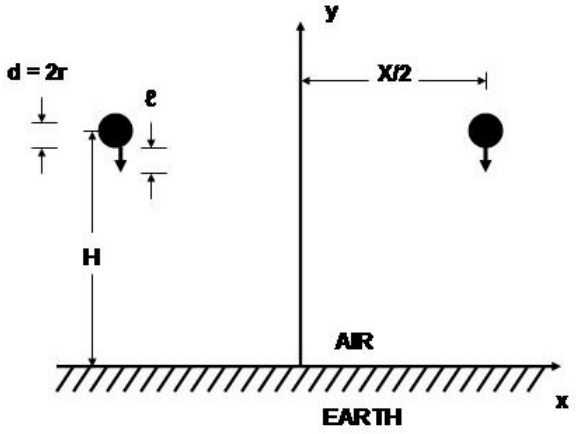


Figure A9.1-3 Geometry for the symmetric two-conductor problem.

$$\left(Z_{11}(\gamma,\omega) + Z_{si} - \gamma^2 A_{11}(\gamma,\omega)\right) I_{w1}(\gamma,\omega) + \left(Z_{12}(\gamma,\omega) - \gamma^2 A_{12}(\gamma,\omega)\right) \cdot I_{w2}(\gamma,\omega) = E_{zd1}(\gamma,\omega) \qquad \text{A9.1-18A}$$

$$\left(Z_{21}(\gamma,\omega) - \gamma^2 A_{21}(\gamma,\omega)\right) I_{w1}(\gamma,\omega) + \left(Z_{22}(\gamma,\omega) + Z_{si} - \gamma^2 A_{22}(\gamma,\omega)\right) \cdot I_{w2}(\gamma,\omega) = E_{zd2}(\gamma,\omega) \qquad \text{A9.1-18B}$$

where

$$Z_{11}(\gamma,\omega) = Z(-X/2, H-r, -X/2, H, \gamma, \omega) \qquad \text{A9.1-18C}$$

$$Z_{12}(\gamma,\omega) = Z(-X/2, H-r, +X/2, H, \gamma, \omega) \qquad \text{A9.1-18D}$$

$$A_{11}(\gamma,\omega) = A(-X/2, H-r, -X/2, H, \gamma, \omega) \qquad \text{A9.1-18E}$$

$$A_{12}(\gamma,\omega) = A(-X/2, H-r, +X/2, H, \gamma, \omega) \qquad \text{A9.1-18F}$$

and

$$E_{zd1}(\gamma,\omega) = \gamma f_{zd1}(\omega) = \gamma\left(\frac{-1}{\pi\omega\varepsilon_0} \sum_{n_1=-\infty}^{\infty} I_{dn_1}(\omega) e^{+j\gamma z_{n_1}}\right), \qquad \text{A9.1-19A}$$

$$E_{zd2}(\gamma,\omega) = \gamma f_{zd2}(\omega) = \gamma\left(\frac{-1}{\pi\omega\varepsilon_0} \sum_{n_2=-\infty}^{\infty} I_{dn_2}(\omega) e^{+j\gamma z_{n_2}}\right) \qquad \text{A9.1-19B}$$

$Z_{11}(\gamma,\omega)$ and $Z_{12}(\gamma,\omega)$ are, respectively, the generalized self and mutual impedances of the two conductors above earth, while $A_{11}(\gamma,\omega)$ and $A_{12}(\gamma,\omega)$ *are,* respectively, the generalized self and mutual Maxwell potential coefficients of the two conductors above earth. Note that in this case, $Z_{11}(\gamma,\omega) = Z_{22}(\gamma,\omega)$ and $A_{11}(\gamma,\omega) = A_{22}(\gamma,\omega)$ due to the symmetry of the problem and that $Z_{12}(\gamma,\omega) = Z_{21}(\gamma,\omega)$ and $A_{12}(\gamma,\omega) = A_{21}(\gamma,\omega)$ by reciprocity.

The equations can be written in more compact matrix form as:

$$\left\{[Z] - \gamma^2[A]\right\}[I_w] = \gamma[f_{zd}(\omega)] \qquad \text{A9.1-20A}$$

Where [Z] and [A] are the 2 x 2 matrices

$$\begin{bmatrix} Z_{11}(\gamma,\omega) & Z_{12}(\gamma,\omega) \\ Z_{21}(\gamma,\omega) & Z_{22}(\gamma,\omega) \end{bmatrix} \quad \text{and} \quad \begin{bmatrix} A_{11}(\gamma,\omega) & A_{12}(\gamma,\omega) \\ A_{21}(\gamma,\omega) & A_{22}(\gamma,\omega) \end{bmatrix} \qquad \text{A9.1-20B}$$

respectively, while $[I_w]$ and $[f_{zd}]$ are 2 x 1 matrices

$$\begin{bmatrix} I_{w1}(\gamma,\omega) \\ I_{w2}(\gamma,\omega) \end{bmatrix} \quad \textit{and} \quad \begin{bmatrix} f_{zd1}(\omega) \\ f_{zd2}(\omega) \end{bmatrix} \qquad \text{A9.1-20C}$$

The components of the matrix f_{zd} are defined in Equation A9.1-19.

This equation can be formally solved for the wire currents by premultiplying by the matrix

$$\left\{\left[Z\right]-\gamma^2\left[A\right]\right\}^{-1} \quad \text{A9.1-21}$$

To get

$$\left[I_w\right]=\left\{\left[Z\right]-\gamma^2\left[A\right]\right\}^{-1}\gamma\left[f_{zd}\right] \quad \text{A9.1-22}$$

In general this is the way that the currents on multiconductor systems should be found. However, as will be illustrated in this section, there are cases for which an alternative method of solution lends additional insight and should be pursued. The general two-wire case is one of these.

The alternative method is to first premultiply Equation A9.1-22 by

$$[Y] = -[A]^{-1}, \quad \text{A9.1-23}$$

the generalized admittance matrix that is the inverse of the generalized Maxwell potential coefficient matrix [*A*]. Doing this results in

$$\left\{-\left[Y\right]\left[Z\right]+\gamma^2\right\}\left[I_w\right]=\left[Y\right]\gamma\left[f_{zd}\right] \quad \text{A9.1-24}$$

In the special case for two symmetric conductors, the matrix [*Y*][*Z*] is symmetric and has equal diagonal elements. Because of this, its eigenvectors are particularly simple (i.e., they are constant and independent of γ), and an eigenvector expansion of the current I_w leads to additional insight. This simple property of the eigenvectors, however, will not be true for more general multiconductor cases, and hence some of the material below is not applicable to those cases. Nevertheless, it will be pursued for the two-conductor case because its simplicity will not obscure the physics of the problem. Because [*Y*][*Z*] is symmetric and has equal diagonal elements, it has the very simple set of orthonormal eigenvectors

$$\left[\eta\right]=\frac{1}{\sqrt{2}}\begin{bmatrix}1 & 1\\ 1 & -1\end{bmatrix} \quad \text{A9.1-25}$$

It is known that the column matrix of unknown currents can be expanded as a sum of the eigenvectors. If this is done, then

$$\left[I_w\right]=\left[\eta\right]\left[\Lambda_w\right] \quad \text{A9.1-26}$$

where $[\Lambda_w]$ is a matrix of mode amplitudes.

This expansion can be physically interpreted as follows. The first of the eigenvectors ([1 1]√2) is often called the "common" mode, and is the mode for which the currents on the two conductors are equal with a return current through the earth. The second ([1 -1]√2) is often called the "differential" mode and is the mode for which the currents on the two conductors are equal in magnitude but opposite in sign. In this case, there is no return current in the earth.

If Equation A9.1-26 is substituted into Equation A9.1-24 and is premultiplied by $[\eta]^{-1}$, then

$$\left[-\left[\eta\right]^{-1}\left[Y\right]\left[Z\right]\left[\eta\right]+\left[\eta\right]^{-1}\gamma^2\left[\eta\right]\right]\left[\Lambda\right]=\left[\eta\right]^{-1}\left[Y\right]\gamma\left[f_{zd}\right] \quad \text{A9.1-27}$$

which reduces to

$$\left[\left[G_p^2\right]-\left[\gamma^2\right]\right]\left[\Lambda\right]=-\left[\eta\right]^{-1}\left[Y\right]\gamma\left[f_{zd}\right] \quad \text{A9.1-28}$$

In this form the matrix equation is separated into two scalar equations for the mode amplitudes because $[G_p^2(\gamma,\omega)]$ is a diagonal matrix of the eigenvalues of [*Y*][*Z*] where

$$G_1^2\left(\gamma,\omega\right)=\left(Z_{11}\left(\gamma,\omega\right)+Z_{12}\left(\gamma,\omega\right)\right)\left(Y_{11}\left(\gamma,\omega\right)+Y_{12}\left(\gamma,\omega\right)\right) \quad \text{A9.1-29A}$$

$$G_2^2\left(\gamma,\omega\right)=\left(Z_{11}\left(\gamma,\omega\right)-Z_{12}\left(\gamma,\omega\right)\right)\left(Y_{11}\left(\gamma,\omega\right)-Y_{12}\left(\gamma,\omega\right)\right) \quad \text{A9.1-29B}$$

so that

$$\begin{bmatrix}\Lambda_1\\ \Lambda_2\end{bmatrix}=\frac{1}{\sqrt{2}}\begin{bmatrix}\dfrac{\gamma}{\gamma^2-G_1^2\left(\gamma,\omega\right)}\left(f_{zd1}\left(\omega\right)+f_{zd2}\left(\omega\right)\right)\left(Y_{11}\left(\gamma,\omega\right)+Y_{12}\left(\gamma,\omega\right)\right)\\ \dfrac{\gamma 1}{\gamma^2-G_2^2\left(\gamma,\omega\right)}\left(f_{zd1}\left(\omega\right)-f_{zd2}\left(\omega\right)\right)\left(Y_{11}\left(\gamma,\omega\right)-Y_{12}\left(\gamma,\omega\right)\right)\end{bmatrix} \quad \text{A9.1-30}$$

Finally, the individual wire currents can be written as shown in Equation A9.1-31

$$\begin{bmatrix} I_1(\gamma,\omega) \\ I_2(\gamma,\omega) \end{bmatrix} = \frac{1}{2} \begin{bmatrix} \dfrac{\gamma}{\gamma^2 - G_1^2(\gamma,\omega)} \Big(f_{zd1}(\omega) + f_{zd2}(\omega)\Big)\Big(Y_{11}(\gamma,\omega) + Y_{12}(\gamma,\omega)\Big) \\ \quad + \dfrac{\gamma}{\gamma^2 - G_2^2(\gamma,\omega)} \Big(f_{zd1}(\omega) - f_{zd2}(\omega)\Big)\Big(Y_{11}(\gamma,\omega) - Y_{12}(\gamma,\omega)\Big) \\ \dfrac{\gamma}{\gamma^2 - G_1^2(\gamma,\omega)} \Big(f_{zd1}(\omega) + f_{zd2}(\omega)\Big)\Big(Y_{11}(\gamma,\omega) + Y_{12}(\gamma,\omega)\Big) \\ \quad - \dfrac{\gamma}{\gamma^2 - G_2^2(\gamma,\omega)} \Big(f_{zd1}(\omega) - f_{zd2}(\omega)\Big)\Big(Y_{11}(\gamma,\omega) - Y_{12}(\gamma,\omega)\Big) \end{bmatrix} \quad \text{A9.1-31}$$

At this point it is generally desired to identify the currents as a function of z by taking the inverse spatial Fourier Transform using

$$I_i(z,\omega) = \frac{1}{2\pi} \int_{-\infty}^{\infty} I_i(\gamma,\omega) e^{j\gamma z} d\gamma \quad \text{A9.1-32}$$

Unfortunately, this integral cannot be evaluated as simply using residue theory as could Equation A9.1-16. The reason is that $Z_{ij}(\gamma,\omega)$ and $Y_{ij}(\gamma,\omega)$, and hence $G_i^2(\gamma,\omega)$, are transcendental functions of γ, and hence the singularities in the γ plane are much more complex than the simple poles found when evaluating Equation A9.1-16. As a result, the current will not have the simple form $exp(-j\gamma_i z)$, and some of the insight is lost. Although the integration in the complex plane can be done (Chang and Olsen 1975), it is difficult, and one may rather choose to evaluate the induced currents by numerically integrating Equation A9.1-32. If, however, the frequency is low enough that significant distances are much smaller than a wavelength, the impedances and admittances can be approximated by Carson's equations as before. For this problem

$$Z_{11}^{lf}(\omega) \cong \frac{\omega\mu_0}{2\pi}\Big\{\ln(2H/r) - J_c(-X/2, H-r, -X/2, H, \omega)\Big\} \quad \text{A9.1-33A}$$

$$Z_{12}^{lf}(\omega) \cong \frac{\omega\mu_0}{2\pi}\left\{\ln\left(\sqrt{(2H)^2 + X^2}\,/\,X\right) - J_c(-X/2, H-r, +X/2, H, \omega)\right\} \quad \text{A9.1-33B}$$

$$A_{11}^{lf}(\omega) \cong \frac{-j}{2\pi\omega\varepsilon_0}\ln(2H/r) \quad \text{A9.1-33C}$$

$$A_{12}^{lf}(\omega) \cong \frac{-j}{2\pi\omega\varepsilon_0}\ln\left(\sqrt{(2H)^2 + X^2}\,/\,X\right) \quad \text{A9.1-33D}$$

The most significant thing to note about this result is that the impedances and admittances are independent of γ. As a result, $G_1(\gamma,\omega) = \gamma_1(\omega)$ and $G_2(\gamma,\omega) = \gamma_2(\omega)$ are not functions of γ, and the singularities of the denominator of Equation A9.1-31 are simple poles in the complex γplane. Given this, simple residue integration (see Appendix 9.3) can be used, and the currents take on the form shown in Equation A9.1-34.

In Equation A9.1-34, the terms multiplied by $Y_{11}(\omega) + Y_{12}(w)$ represent the "common" mode component of the current that propagates with propagation constant γ_1. Similarly, the terms multiplied by $Y_{11}(\omega) - Y_{12}(\omega)$ represent the "differential" mode component of the current that propagates with propagation constant γ_2. Because the return current for the common mode flows in the lossy earth, while the differential mode return current does not, it is generally true that the attenuation constant $\alpha_1 = Re(\gamma_1)$ is much larger than the attenuation constant $\alpha_2 = Re(\gamma_2)$.

The Three-Wire Problem

It is important to also consider the three-wire problem since most transmission lines are "three-phase" lines that have "three" phase conductors for a single circuit or six-phase conductors for a double-circuit line. The formulation of the problem is straightforward, given what has been presented above. Here the simple geometry shown in Figure

$$\begin{bmatrix} I_1(z,\omega) \\ I_2(z,\omega) \end{bmatrix} = \frac{j}{4\omega\varepsilon_0} \begin{bmatrix} \left(Y_{11}(\omega)+Y_{12}(\omega)\right)\left[\sum_{n_1=-\infty}^{\infty} \frac{(z-z_{n_1})}{|z-z_{n_1}|} I_{dn_1}(\omega) e^{-j\gamma_1|z-z_{n1}|} + \sum_{n_2=-\infty}^{\infty} \frac{(z-z_{n_2})}{|z-z_{n_2}|} I_{dn_2}(\omega) e^{-j\gamma_1|z-z_{n2}|}\right] \\ +\left(Y_{11}(\omega)-Y_{12}(\omega)\right)\left[\sum_{n_1=-\infty}^{\infty} \frac{(z-z_{n_1})}{|z-z_{n_1}|} I_{dn_1}(\omega) e^{-j\gamma_2|z-z_{n1}|} - \sum_{n_2=-\infty}^{\infty} \frac{(z-z_{n_2})}{|z-z_{n_2}|} I_{dn_2}(\omega) e^{-j\gamma_2|z-z_{n2}|}\right] \\ \left(Y_{11}(\omega)+Y_{12}(\omega)\right)\left[\sum_{n_1=-\infty}^{\infty} \frac{(z-z_{n_1})}{|z-z_{n_1}|} I_{dn_1}(\omega) e^{-j\gamma_1|z-z_{n1}|} + \sum_{n_2=-\infty}^{\infty} \frac{(z-z_{n_2})}{|z-z_{n_2}|} I_{dn_2}(\omega) e^{-j\gamma_1|z-z_{n2}|}\right] \\ -\left(Y_{11}(\omega)-Y_{12}(\omega)\right)\left[\sum_{n_1=-\infty}^{\infty} \frac{(z-z_{n_1})}{|z-z_{n_1}|} I_{dn_1}(\omega) e^{-j\gamma_2|z-z_{n1}|} - \sum_{n_2=-\infty}^{\infty} \frac{(z-z_{n_2})}{|z-z_{n_2}|} I_{dn_2}(\omega) e^{-j\gamma_2|z-z_{n2}|}\right] \end{bmatrix} \quad \text{A9.1-34}$$

A9.1-4 will be considered. This geometry might represent a horizontally configured line (if $H_1 = H_2 = H_3$), a delta configured line if $H_1 = H_3$, or a vertically configured line if $X = 0$.

Setting up the equations for the current induced on these conductors by the corona sources can be done in the same way as for the two-conductor line in the last section. The only difference will be that the three-phase line has less symmetry that can be exploited in finding a solution to the equations.

Using the same method as for the two-conductor line, the following matrix equation can be set up for the induced currents. Here the explicit dependence of the variables Z_{ij},

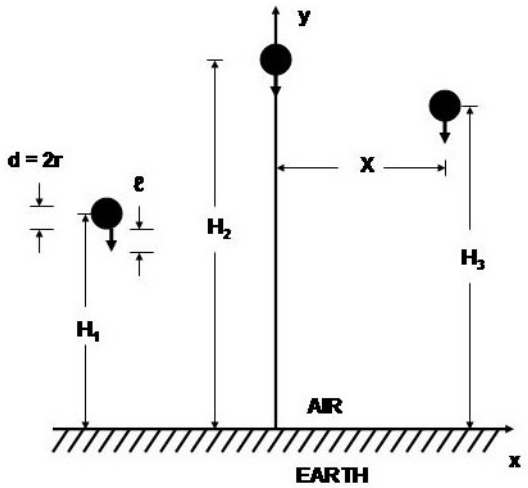


Figure A9.1-4 A three-conductor line with distributions of corona sources.

A_{ij}, I_{wi}, and E_{zdi} on γ and ω has been dropped for economy of notation (Olsen and Wu 1991).

$$\begin{bmatrix} Z_{11}-\gamma^2 A_{11} & Z_{12}-\gamma^2 A_{12} & Z_{13}-\gamma^2 A_{13} \\ Z_{21}-\gamma^2 A_{21} & Z_{22}-\gamma^2 A_{22} & Z_{23}-\gamma^2 A_{23} \\ Z_{31}-\gamma^2 A_{31} & Z_{32}-\gamma^2 A_{32} & Z_{33}-\gamma^2 A_{33} \end{bmatrix} \begin{bmatrix} I_{w1} \\ I_{w2} \\ I_{w3} \end{bmatrix} = \begin{bmatrix} E_{zd1} \\ E_{zd2} \\ E_{zd3} \end{bmatrix} \quad \text{A9.1-35A}$$

where

$$Z_{ij} = Z\left(X_i, H_i, X_j, H_j, \gamma, \omega\right) \quad \text{A9.1-35B}$$

$$A_{ij} = A\left(X_i, H_i, X_j, H_j, \gamma, \omega\right) \quad \text{A9.1-35C}$$

are defined further in Equations A9.1-7b and A9.1-7c and $X_1 = -X/2$, $X_2 = 0$, $X_3 = H/2$.

In Equation A9.1-35, the following definitions are used.

$$D = D_{ij} = \left[\left(X_i - X_j\right)^2 + \left(H_i - H_j\right)^2\right]^{1/2} \quad \text{A9.1-36A}$$

$$D' = D'_{ij} = \left[\left(D_i - D_j\right)^2 + \left(H_i + H_j\right)^2\right]^{1/2} \quad \text{A9.1-36B}$$

$$P\left(x, y, X, H, \gamma, \omega\right) = P_{ij}$$
$$= +\frac{j2}{\pi}\int_{-\infty}^{\infty}\left(\frac{1}{u_0 + u_g}\right)e^{-u_0\left(H_i + H_j\right)}e^{-j\lambda\left(X_i - X_j\right)}d\lambda \quad \text{A9.1-36C}$$

$$Q\left(x, y, X, H, \gamma, \omega\right) = Q_{ij}$$
$$= +\frac{j2}{\pi}\int_{-\infty}^{\infty}\left(\frac{1}{k_0^2 u_g + k_g^2 u_0}\right)e^{-u_0\left(H_i + H_j\right)}e^{-j\lambda\left(X_i - X_j\right)}d\lambda \quad \text{A9.1-36D}$$

$$E_{zdi} = \mathcal{V}_{zd1} = \gamma\left(\frac{-1}{\pi\omega\varepsilon_0}\sum_{n_i=-\infty}^{\infty} I_{dn_i}\left(\omega\right)e^{+j\gamma z_{n_i}}\right) \quad \text{A9.1-36E}$$

It is tempting to premultiply Equation A9.1-35a by $[Y] = [A]^{-1}$ as in the two-conductor case. If this is done, Equation A9.1-35a becomes

$$\left\{-\left[Y\right]\left[Z\right] + \gamma^2\right\}\left[I_w\right] = \left[Y\right]\left[E_{zd}\right] \quad \text{A9.1-37}$$

An evaluation of the parameters Z_{ij} and A_{ij} shows that $Z_{ij} = Z_{ji}$ and $Y_{ij} = Y_{ji}$ by reciprocity, and that $Z_{12} = Z_{32}$, $Y_{12} = Y_{32}$, $Z_{11} = Z_{33}$ and $Y_{11} = Y_{33}$ by symmetry. Despite these symmetries in $[Y]$ and $[Z]$, the matrix $[Y][Z]$ is not symmetric, as it was for the symmetric two-conductor case. As a result, the eigenvectors of $[Y][Z]$ are dependent upon γ. Given this, the equation for the mode amplitudes analogous to Equation A9.1-30 becomes

$$\begin{bmatrix} \Lambda_1 \\ \Lambda_2 \\ \Lambda_3 \end{bmatrix} = -\begin{bmatrix} \gamma / \left(G_1^2(\gamma,\omega)\right) & 0 & 0 \\ 0 & \gamma / \left(G_{21}^2(\gamma,\omega)\right) & 0 \\ 0 & 0 & \gamma / \left(G_3^2(\gamma,\omega)\right) \end{bmatrix} \bullet$$
$$\begin{bmatrix} \eta_{11}(\gamma) & \eta_{12}(\gamma) & \eta_{13}(\gamma) \\ \eta_{21}(\gamma) & \eta_{22}(\gamma) & \eta_{231}(\gamma) \\ \eta_{31}(\gamma) & \eta_{32}(\gamma) & \eta_{33}(\gamma) \end{bmatrix} \begin{bmatrix} Y_{11} & Y_{12} & Y_{13} \\ Y_{21} & Y_{22} & Y_{23} \\ Y_{31} & Y_{32} & Y_{33} \end{bmatrix} \begin{bmatrix} f_{zd1} \\ f_{zd2} \\ f_{zd3} \end{bmatrix} \quad \text{A9.1-38}$$

where the explicit dependence the terms of [η] on γ has been indicated. The fact that this is true makes the computation of [Λ] much more complicated, since when performing the inverse Fourier transform to calculate the currents in the space domain, the eigenvectors must be calculated for every value of γ. Further, the insight that comes from having simple "common" and "differential" modes in the symmetric two-wire case disappears. Given these difficulties, any advantage of expanding the currents in the eigenvectors of the $[Y][Z]$ matrix disappears. As a result, the final expression for the current will be found simply by multiplying Equation A9.1-35a by the inverse of the $[Z\text{-}\gamma^2 A]$ matrix. The result is

$$\left[I_w\right] = \left\{\left[Z\right] - \gamma^2\left[A\right]\right\}^{-1}\left[E_{zd}\right] \quad \text{A9.1-39}$$

which is in the same form as the result for the two-conductor case in Equation A9.1-22.

As earlier, if low-frequency approximations are made, then it becomes reasonable to use modal expansion to calculate the currents. This is the approach that has been used as the basis for classical radio noise programs (Adams and Barthold 1960; Barthold 1964; Hedman 1965; EPRI 1982; Olsen 1988).

APPENDIX 9.2 STATISTICAL AVERAGES

This expected value can be written as (Papoulis 1965)

$$< e^{j\omega(\tau_n - \tau_m)} > = \int_{-\infty}^{\infty}\int_{-\infty}^{\infty} p(\tau_n, \tau_m) e^{-j\omega(\tau_n - \tau_m)} d\tau_n d\tau_m \qquad \text{A9.2-1}$$

where $p(\tau_n, \tau_m)$ is the joint probability density function of the pair of random variables. If the reasonable assumption is made that these two variables are independent, then

$$p(\tau_n, \tau_m) = p(\tau_n)\, p(\tau_m) \quad m \neq n \qquad \text{A9.2-2}$$

The probability density function assumed for the purpose of evaluating the expected value is

$$p(v) = \frac{1}{\sqrt{2\pi}\sigma} e^{-v^2/2\sigma^2} \qquad -\infty < v < \infty \qquad \text{A9.2-3}$$

This is a Gaussian, where if $\tau < 0.25$ msec, most of the corona will occur near the peak in the 50/60-Hz voltage cycle (here assumed to occur at $t = 0.0$ sec). If Equation A9.2-1 is evaluated,

$$< e^{-j\omega(\tau_n - \tau_m)} > = e^{-\omega^2\sigma^2} \cong 0 \quad m \neq n \qquad \text{A9.2-4}$$

if $\omega >> 1/\sigma = 4\text{x}10^3$ rad/sec (i.e., $f >> 636$ Hz). This is certainly justified at the frequencies of interest to us, and thus it can be assumed that the individual corona sources are effectively incoherent (i.e., powers add). Since $\langle e^{-j\omega(\tau_n - \tau_m)} \rangle = 1$ for m = n.

APPENDIX 9.3 EVALUATION OF INVERSE SPATIAL TRANSFORMS

An integral that is commonly found after making low-frequency approximations is given in Equation A9.3-1

$$I(z) = A\int_{-\infty}^{\infty} \frac{\gamma e^{-j\gamma(z - z_n)}}{\left(\gamma^2 - \gamma_P^2\right)} d\gamma \quad = \quad A\int_{-\infty}^{\infty} \frac{\gamma e^{-j\gamma(z - z_n)}}{(\gamma - \gamma_P)(\gamma + \gamma_P)} d\gamma \qquad \text{A9.3-1}$$

where the denominator has been factored to explicitly show the two poles at +/- γ_P and $\gamma_P = \beta_P - j\alpha_P$ and $\alpha_P > 0$. This integral can be evaluated in closed form using residue integration. This can be done in the following way (Churchill et al. 1976).

Consider the complex plane γ shown in Figure A9.3-1. The real part of γ is plotted on the horizontal axis, while the imaginary part is plotted on the vertical axis. Shown on this plane are the two poles at +/- γ_P that are marked by *x*'s, as well as the contour of integration from $-\infty$ to ∞ that is marked as $C_{0l} + C_{0r}$.

It can be shown that the integral of an analytic function on a closed contour, i.e., one that begins and ends at the same point—in the complex plane is zero. Since the integrand of Equation A9.3-1 is analytic except at the poles indicated above, this property can be used to find a value for Equation A9.3-1. Consider a closed contour in the complex plane that consists of the segments $C = C_{0l} + C_- + C_P + C_+ + C_{0r} + C_\infty$, where all but $C_{0l} + C_{0r}$ are shown as dashed lines in Figure A9.3-1. This contour was chosen since the pole at γ_P has been excluded from the region inside the closed contour, and therefore the integrand of Equation

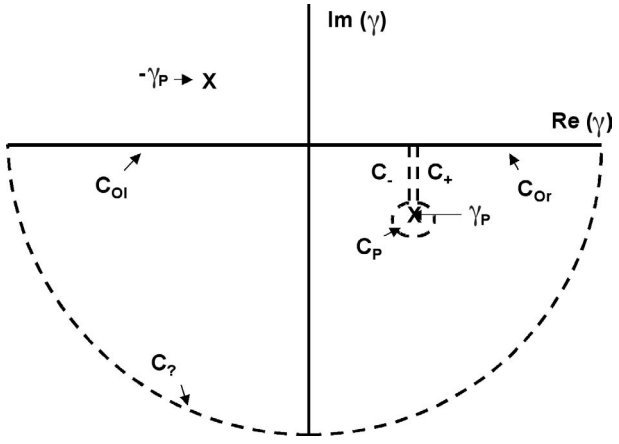


Figure A9.3-1 The complex γ plane for evaluating Equation A9.3-1.

9.3-1 is analytic there, and the integral around the contour is zero. Thus,

$$\int_C \frac{\gamma e^{-j\gamma\left(z-z_n\right)}}{\left(\gamma-\gamma_P\right)\left(\gamma+\gamma_P\right)}d\gamma = 0 \qquad \text{A9.3-2}$$

Since $\alpha_P > 0$, it can easily be shown that the integrand is zero along C_∞ as long as $z > z_n$. Therefore the portion of integral (Equation A5.3-2) along C_∞ is also zero. Next, since integrals along C_- and C_+ integrate the same integrand but in opposite directions, the portions of Equation A9.3-2 along these two contours cancel. The only remaining contours are $C_0 = C_{0l} + C_{0r}$, the original contour and C_P and

$$\begin{aligned} & A\int_{C_{0l}+C_{0r}} \frac{\gamma e^{-j\gamma\left(z-z_n\right)}}{\left(\gamma-\gamma_P\right)\left(\gamma+\gamma_P\right)}d\gamma \\ & = A\int_{-\infty}^{\infty} \frac{\gamma e^{-j\gamma\left(z-z_n\right)}}{\left(\gamma-\gamma_P\right)\left(\gamma+\gamma_P\right)}d\gamma = I\left(z\right) \\ & = -A\int_{C_P} \frac{\gamma e^{-j\gamma\left(z-z_n\right)}}{\left(\gamma-\gamma_P\right)\left(\gamma+\gamma_P\right)}d\gamma \end{aligned} \qquad \text{A9.3-3}$$

The last integral in Equation A9.3-3 can be evaluated explicitly by using the transformation $\gamma = \gamma_P + s$, where $s = re^{j\theta}$, $r <<< \gamma_P$ and then using polar coordinates to integrate counter clockwise around the circle from $\theta = -3\pi/2$ to $\pi/2$. The differential length along this circular contour is $d\gamma = ds = jre^{j\theta}d\theta$. If $\gamma$is set equal to γ_P in the portion of the integrand that does not include the pole, the integral can be written and evaluated as follows.

$$\begin{aligned} I\left(z\right) &= \frac{-A\gamma_P e^{-j\gamma_P\left(z-z_n\right)}}{2\gamma_P}\int_{-3\pi/2}^{\pi/2} \frac{jre^{j\theta}}{re^{j\theta}}d\theta \\ &= -j\pi A e^{-j\gamma_P\left(z-z_n\right)}, \quad z > z_n \end{aligned} \qquad \text{A9.3-4}$$

The method by which this result was obtained is called *residue integration* and has been done assuming that the only characteristic of the integrand that makes it nonanalytic is the pole at γ_P. This result can be generalized to the case for arbitrary values of z by repeating the integration for $z < z_n$. When this is done, the integration contour used will be in the upper half plane since, for $z < z_n$, the integral along the upper C_∞ contour will be zero. The result for $I(z)$ will be of the opposite sign to that above. This makes sense since the current injected into the conductor is in opposite directions on different sides of the corona discharge, as shown in Figure 9.5-1d. In addition, the term $exp(-j\gamma_P(z-z_n))$ will become $exp(+j\gamma_P(z-z_n))$ because the current is propagating in the opposite direction. The final result for the current can then be written

$$I\left(z\right) = -j\pi A\frac{\left(z-z_n\right)}{\left|z-z_n\right|}e^{-j\gamma_P\left|z-z_n\right|} \qquad \text{A9.3-5}$$

The question that will be investigated now is whether a similar integration can be carried out if the low-frequency approximation for the current cannot be made. In this case the integral of interest has the form

$$I\left(z\right) = B\int_{-\infty}^{\infty} \frac{\gamma e^{-j\gamma\left(z-z_n\right)}}{\left(Z_{11}(\gamma,\omega)-\gamma^2 A_{11}\left(\gamma,\omega\right)\right)}d\gamma \qquad \text{A9.3-6}$$

Unfortunately, the behavior of the integrand of Equation A9.3-6 is much more complex than that of (D1). More specifically, it can be shown that the identification of an integration contour such that the integrand will be analytic inside it requires that at least two poles be isolated and more importantly that at least two points and branch cuts be identified (Chang and Olsen 1975; Kuester et al. 1978). These poles, γ_{P1} and γ_{P2}, branch points and branch cuts are identified in Figure A9.3-2.

Given this result, it is not possible to evaluate Equation A9.3-6 without retaining at least two infinite integrals on contours that surround the branch cuts. While there are times that it makes sense to evaluate Equation A9.3-6 in this way, it does not here, and the integral along the original contour is retained.

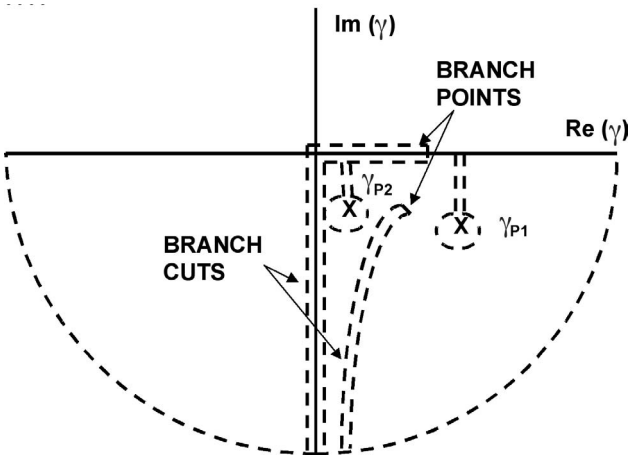


Figure A9.3-2 The complex γplane for evaluating Equation A9.3-6.

APPENDIX 9.4 APPROXIMATIONS FOR F_{EY}, F_{HX}, AND F_{EZ}

Calculation of the vertical electric field, F_{ey} (Wu et al. 1990)

$$\left(\frac{j4\omega\varepsilon_0}{\gamma}\right)F_{ey}\left(x,y,X,H,\gamma,\omega\right)=\zeta_0\left[\frac{\left(y-H\right)}{D}H_1^{(2)}\left(\zeta_0 D\right)-\frac{\left(y+H\right)}{D'}H_1^{(2)}\left(\zeta_0 D'\right)\right]$$
$$-\frac{j2k_0^2}{\pi\left(k_g^4-k_0^4\right)}\left\{j\pi k_0^2\frac{\partial}{\partial y}H_0^{(2)}\left(\zeta_0 D'\right)-\frac{k_0^2k_g^4}{k_0^2+k_g^2}I_{p1}\left(x,y+H\right)\right.$$
$$-jk_g^2\zeta_g I_{p2}\left(x,y+H\right)+\frac{jk_g^2}{2\zeta_g}\left[\lambda_p^2\left(1+\frac{\lambda_p^2}{4\zeta_g^2}\right)I_{p2}\left(x,y+H\right)\right.$$
$$\left.\left.-j\pi\left(1+\frac{\lambda_p^2}{2\zeta_g^2}+\frac{k_t^2}{4\zeta_g^2}\right)\frac{\partial^2}{\partial y^2}H_0^{(2)}\left(\zeta_0 D'\right)-\frac{j\pi}{4\zeta_g^2}\frac{\partial^4}{\partial y^4}H_0^{(2)}\left(\zeta_0 D'\right)\right]\right\} \quad \text{A9.4-1}$$

where

$$I_{p1}\left(X',Y'\right)=0.5\left[G_{XY}(\zeta_0,k_t)+G_{XY}(\zeta_0,-k_t)\right] \quad \text{A9.4-2}$$
$$I_{p2}\left(X',Y'\right)=-j\pi H_0^{(2)}\left(\zeta_0 R'\right)-j0.5k_t\left[G_{XY}(\zeta_0,k_t)-G_{XY}(\zeta_0,-k_t)\right]$$
$$\zeta_0=\left(k_0^2-\gamma^2\right)^{1/2},\quad \mathrm{Im}\left(\zeta_0\right)<0$$
$$\zeta_g=\left(k_g^2-\gamma^2\right)^{1/2},\quad \mathrm{Im}\left(\zeta_g\right)<0$$
$$\lambda_p=\left[\frac{k_0^2k_g^2}{k_0^2+k_g^2}-\gamma^2\right],\quad \mathrm{Im}\left(\lambda_p\right)<0 \quad \text{A9.4-3}$$
$$k_t=\left(\zeta_0^2-\lambda_p^2\right)^{1/2}\quad \mathrm{Im}\left(k_t\right)<0$$
$$R'=\left(X'^2+Y'^2\right)^{1/2}$$

D and D*'* are defined in Section 9.5 below Equation 9.5-26,

$$G_{XY}\left(\zeta_0,k\right)=\frac{e^{+jkY}}{\lambda_p}\left\{2B_0\cos\left(\lambda_p X'\right)-2\left(\pi/2-\theta\right)\sin\left(\lambda_p X'\right)\right.$$
$$\left(+j\pi/2\right)\left[\left(-kX'+\lambda_p Y'\right)e^{j\lambda_p X}He_0^{(2)}\left(\alpha_1,\zeta_0 R'\right)\right. \quad \text{A9.4-4}$$
$$\left.\left.\left(+kX'+\lambda_p Y'\right)e^{-j\lambda_p X}He_0^{(2)}\left(\alpha_2,\zeta_0 R'\right)\right]\right\}$$

where

$$\alpha_1 = j\left(-kY' - \lambda_p X'\right)$$
$$\alpha_2 = j\left(-kY' + \lambda_p X'\right)$$
$$B_0 = -\ln\left[\left(k + j\lambda_p\right)/\zeta_0\right] \quad k = k_t$$
$$B_0 = -j\pi + \ln\left[\left(k + j\lambda_p\right)/\zeta_0\right] \quad k = -k_t$$
$$\theta = \arctan(Y'/X'), \quad \alpha_1 = j\left(kY' - \lambda_p X'\right), \quad \alpha_2 = j\left(kY' + \lambda_p X'\right)$$
$$He_0^{(2)}(\alpha,\beta) = \frac{2j}{\pi} J_0\left[\beta EV_2(\alpha)\right] + H_0^{(2)}\left[\beta EV_1(\alpha)\right]$$

where

$$J_0\left[\beta EV_2(\alpha)\right] = \sum_{n=0}^{\infty} a_n EV_2^{2n}(\alpha)$$
$$H_0^{(2)}\left[\beta EV_1(\alpha)\right] = \left[1 - \frac{2j}{\pi}\left(\ln(\beta/2) + C_0\right)\right]\sum_{n=0}^{\infty} a_n EV_1^{2n}(\alpha) + \frac{2j}{\pi}\sum_{n=1}^{\infty} b_n EV_1^{2n}(\alpha)$$
$$a_n = \frac{(-1)^n}{(n!)^2}\left(\frac{\beta}{2}\right)^{2n}, \quad b_n = a_n \sum_{k=1}^{n}\frac{1}{k}$$
$$EV_1^{2n}(\alpha) = \sum_{m=0}^{\infty}\frac{\alpha^m}{m!(2n+1+m)}$$
$$EV_2^{2n}(\alpha) = \sum_{m=0}^{\infty}\frac{\alpha^m}{m!(2n+1+m)^2}$$

Numerical difficulties arise in calculations of G_{XY} for large values of $\zeta_0 R$ and $\zeta_p R$.
Asymptotic expansions for these cases used to circumvent this problem can be found in (Olsen and Wu 1989).

For the horizontal magnetic field, F_{hx} (Olsen and Wu 1991)

$$\begin{aligned}(4j)F_{hx}(x,y,X,H,\gamma,\omega) &= \zeta_0\left[\frac{y-H}{D}H_1^{(2)}(\zeta_0 D) - \frac{y+H}{D'}H_1^{(2)}(\zeta_0 D')\right] \\ &+ \frac{2j}{\pi\left(k_g^2 - k_0^2\right)}\left[j\pi\frac{\partial^3}{\partial y^3}H_0^{(2)}(\zeta_0 D') - \pi\zeta_g\frac{\partial^2}{\partial y^2}H_0^{(2)}(\zeta_0 D')\right. \\ &+ \frac{\pi}{2\zeta_g}\left(\zeta_0^2\frac{\partial^2}{\partial y^2}H_0^{(2)}(\zeta_0 D') + \frac{\partial^4}{\partial y^4}H_0^{(2)}(\zeta_0 D')\right) \\ &+ \gamma^2\left(\frac{k_0^2 k_t^2 + k_0^2\left(\zeta_g^2 - \lambda_p^2\right)}{\left(k_0^2 + k_g^2\right)}I_{p1}(x, y+H)\right. \\ &- j\pi\frac{\partial}{\partial y}H_0^{(2)}(\zeta_0 D') + j\zeta_g I_{p2}(x, y+H) - \frac{j}{2\zeta_g}\left[\lambda_p^2\left(1 + \frac{\lambda_p^2}{4\zeta_g^2}\right)I_{p2}(x, y+H)\right. \\ &\left.\left.\left.- j\pi\left(1 + \frac{\lambda_p^2}{2\zeta_g^2} + \frac{k_t^2}{4\zeta_g^2}\right)\frac{\partial^2}{\partial y^2}H_0^{(2)}(\zeta_0 D') - \frac{j\pi}{4\zeta_g^2}\frac{\partial^4}{\partial y^4}H_0^{(2)}(\zeta_0 D')\right]\right)\right]\end{aligned} \qquad \text{A9.4-5}$$

where I_{p1} and I_{p2} are defined above.

For the axial electric field, F_{ez} (Wu et al.1990)

$$F_{ez}\left(x,y,X,H,\gamma,\omega\right)=-\left[Z\left(x,y,X,H,\gamma,\omega\right)-\gamma^2 A\left(x,y,X,H,\gamma,\omega\right)\right]$$

where

$$A\left(x,y,X,H,\gamma,\omega\right)=\frac{-1}{4\omega\varepsilon_0}\left(H_0^{(2)}\left(\zeta_0 D\right)-H_0^{(2)}\left(\zeta_0 D'\right)\right)$$

$$Z\left(x,y,X,H,\gamma,\omega\right)=\frac{\omega\mu_0}{4}\left(H_0^{(2)}\left(\zeta_0 D\right)-H_0^{(2)}\left(\zeta_0 D'\right)\right)+\frac{jk_0^2}{\pi}M_z\left(x,y,X,H,\gamma,\omega\right)$$

where for $|\zeta_g(y+H)| < 2.5$

$$M_z\left(x,y,X,H,\gamma,\omega\right)\cong\frac{1}{k_g^2-k_0^2}\left\{-j\pi\frac{\partial^2}{\partial y^2}H_0^{(2)}\left(\varsigma_0 D'\right)-\frac{j\pi\varsigma_g}{2}\left[H_1\left(j\varsigma_g Z\right)-\frac{Y_1\left(j\varsigma_g Z\right)}{Z}+\left(H_1\left(j\varsigma_g Z^*\right)-\frac{Y_1\left(j\varsigma_g Z^*\right)}{Z^*}\right)\right]\right\}$$

where $H_1(x)$ is the Struve function of order 1, and argument x, $Y_1(x)$ is the Bessel function of second kind, order 1 and argument x and $Z' = Y' + jX'$ and $X' = x - X$, $Y' = y + H$.

For $|\zeta_g(y+H)| > 2.5$

$$\begin{aligned}M_z(x,y,X,H,\gamma,\omega)\cong\frac{\pi}{k_g^2-k_0^2}\Bigg\{&-j\frac{\partial^2}{\partial y^2}H_0^2\left(\varsigma_0 D'\right)+\left[\varsigma_g\left(1-\frac{\varsigma_0^2}{2\varsigma_g^2}-\frac{\varsigma_0^4}{8\varsigma_g^4}\right)\right.\\&\left.+\frac{k_0^2\gamma^2}{2\varsigma_g\left(k_g^2+k_0^2\right)}\left(1+\frac{\lambda_p^2}{2\varsigma_g^2}+\frac{k_t^2}{4\varsigma_g^2}\right)\right]\frac{\partial}{\partial y}H_0^2\left(\varsigma_0 D'\right)\\&-\frac{1}{2\varsigma_g}\left(1+\frac{\varsigma_0^2}{2\varsigma_g^2}-\frac{k_0^2\gamma^2}{4\varsigma_g^2\left(k_g^2+k_0^2\right)}\right)\frac{\partial^3}{\partial y^3}H_0^2\left(\varsigma_0 D'\right)\\&-\frac{1}{8\varsigma_g^3}\frac{\partial^5}{\partial y^5}H_0^2\left(\varsigma_0 D'\right)-\frac{\gamma^2}{\pi\left(k_g^2+k_0^2\right)}\left[k_g^2 I_{p2}\left(x-X,y+H\right)\right.\\&\left.-jk_0^2\varsigma_g\left(1-\frac{\lambda_p^2}{2\varsigma_g^2}-\frac{\lambda_p^4}{8\varsigma_g^2}\right)I_{p1}\left(x-X,y+H\right)\right]\Bigg\}\end{aligned}$$

APPENDIX 9.5 GROUND CONDUCTIVITY

Figure A9.5-1 is an earth conductivity map of the United States, which may be used to estimate ground resistivity in any particular area. The indicated conductivity (mS/m) may be converted to resistivity (Ω · m) by taking the reciprocal of the indicated numbers and multiplying by 1000—i.e., 2 mS/m = 500Ω · m. Additional ground conductivity plots can be found in Chapter 6, Figures 6.10-14 through 6.10-18. More extensive plots can be found in the World Atlas of Ground Conductivities that is available for free download at http://www.itu.int/itudoc/itu-r/publica/op/091-1.html.

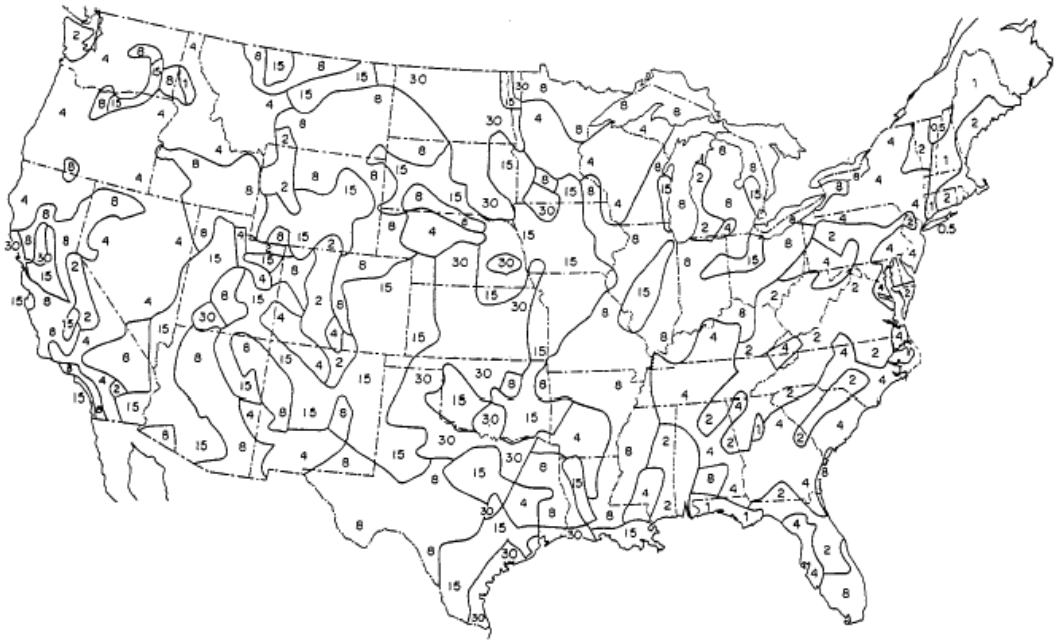


Figure A9.5-1 Estimated effective ground conductivity in the United States. The numbers are in mS/m. The conductivity of sea water (not shown) is assumed to be 5000 mS/m. This chart is from the book, *Reference Data for Radio Engineers, Sixth Edition*, courtesy Howard W. Sams and Co., Inc., subsidiary of International Telephone and Telegraph Corporation.

REFERENCES

Adams, G.E. and L.O. Barthold. 1960. "The Calculation of Attenuation Constants for Radio Noise Analysis of Overhead Lines." *AIEE Transactions on Power Apparatus and Systems.* Vol. 79. Pt. III. pp. 975-981. December.

Aggers, C.V., D.E. Foster, and C.S. Young. 1940. "Instruments and Methods of Measuring Radio Noise." *AIEE PAS-59*. pp. 178-192.

ANSI/IEEE Standard 430-1986 (R1991). IEEE Standard Procedures for the Measurement of Radio Noise from Overhead Power Lines.

ANSI Standard C63.2-1996. American National Standard for Electromagnetic Noise and Field Strength Instrumentation. 10 kHz to 40 GHz-Specifications.

Bartenstein R., E. Schafer. 1962. "Continuous Measurements of the High Frequency Interference Level of H. V. Transmission Lines and their Statistic Evaluations." *CIGRÉ paper #409*.

Barthold, L.O. 1964. "Radio Frequency Propagation on Polyphase Lines." *IEEE Transactions on Power Apparatus and Systems.* Vol. PAS-83. pp. 665-670. July.

Burgess, R.F. 1948. "The Response of a Linear Diode Voltmeter to Single and Recurrent RF Impulses of Various Shapes." *IRE-95. Pt. III*. pp. 106-110. March.

Burns, A.L., M.W. Tuominen, V.L. Chartier, and L.Y. Lee. 1985. "The Effect of Altitude on Conductor Selection for High Voltage AC Transmission Lines." *Proceedings of the 1985 American Power Conference-47*. pp. 665-674.

Burrill, C.M. 1941. "Progress in the Development of Instruments for Measuring Radio Noise." *IRE-29*. pp. 433-42. August.

Burrill, C.M. 1942. "An Evaluation of Radio-Noise Meter Performance in Terms of Listening Experience." *IRE-30*. pp. 473-478. October.

Canadian Standards Association, Standard, CAN3-C108.3.1.M84. "Limits and Measurement Methods of Electromagnetic Noise from AC Power Systems, 0.15-30 MHz." Canadian Standards Association. 178 Rexdale Boulevard, Rexdale, Ontario, Canada M9W 1R3.

Carson, J.R.1926. "Wave Propagation in Overhead Wires with a Ground Return." *Bell Sys. Tech. J-5* 5. pp. 539-554. October.

Chang, D.C. and R.G. Olsen. 1975. "Excitation of an Infinite Horizontal Wire Above a Dissipative Earth." *Radio Science-10*. pp. 823-831. August-September.

Chartier, V.L. 1983. "Empirical Expressions for Calculating High Voltage Transmission Corona Phenomena." *Proceedings of the First Annual Seminar Technical Career Program for Professional Engineers*. Portland, Oregon. pp. 75-82. April.

Chartier, V.L. 1988. "Comprehensive Empirical Formulas for Predicting EMI from Overhead Power Line Corona." *Proceedings of the 1988 U.S.-Japan Seminar on Electromagnetic Interferences in Highly Advanced Social Systems (Modeling, Characterization, Evaluation and Protection)*. Honolulu, Hawaii. pp. 5-1 to 5-11, August.

Chartier, V.L. 1989. "Results or Long-Term Audible Noise Measurements Made Before and After Reconductoring of the Spans from Tower 6/4 to 7/4 of Ostrander-Pearl 500 kV Transmission Line." BPA Division of Laboratories Report No. ELE-89-34. March.

Chartier, V.L. 1991. "Measurement of Corona Effects." Paper presented at the Panel Session on Corona Effects at the 1991 IEEE T&D Conference and Exposition. Dallas, TX. September 23-27.

Chartier, V.L. 1994. "Effect of Load Current on Conductor Corona from High Voltage AC and DC Overhead Transmission Lines." *Proceedings of the 1994 Japan-U.S. Science Seminar on Electromagnetic Field Effects Caused by High Voltage Systems (Modeling, Characterization, Measurements, Mitigation).* Sapporo, Japan. pp. 47-56. June 28 - July 1.

Chartier, V.L., A.L. Gabriel, J.D. Simpson, and R.D. Stearns. 1979. "EMI Performance of Bonneville Power Administrations Prototype 1200 kV Transmission Line." *3rd Symposium on Electromagnetic Compatibility.* Rotterdam. pp. 475-480. May .

Charter, V.L. and R.D. Stearns. 1981. Discussion of Hatanaka G.K. "Field Measurements of VHF Noise from an Operating 500 kV Power Line." *IEEE PAS-100*. pp. 863-872. February.

Chartier, V.L., R. Sheridan, J.N. DiPlacido, and M.O. Loftness. 1986. "Electromagnetic Interference Measurements at 900 MHz on 230-kV and 500-kV Transmission Lines." *IEEE PWRD-1*. pp. 140-149. April.

Chartier, V.L., L.Y. Lee, L.D. Dickson, and K.E. Martin. 1987. "Effect of High Altitude on High Voltage AC Transmission Line Corona Phenomena." *IEEE PWRD-2*. pp. 225-236. January.

Churchill, R.V., J. Brown, and R.F. Verhey. 1976. *Complex Variables and Applications.* McGraw-Hill. New York.

CIGRÉ Committee Report. 1974. "Interference Produced by Corona Effect of Electric Systems." International Conference on Large High Voltage Electric Systems. 112. bd Haussmann. Paris. 1974.

CIGRÉ Committee Report 1996. "Addendum to CIGRÉ Document No. 20 (1974) Interferences Produced by Corona Effect of Electric Systems (Description of Phenomena and Practical Guide for Calculation)." 21 rue d'Artois – F-75008. Paris. December.

Clark, C.F. and M.O. Loftness. 1970. "Some Observations of Foul Weather Television Interference." *IEEE PAS–90*. pp. 1157-1168. July/August.

Cortina, R., F. Demichelis, W. Serravalli, and M. Sforzini. 1968. "I Disturbi Alle Communicazioni Radio e Televisive Prodotti Dalle Linee Aeree a Media Tensione." Rendiconti Della LXIX Riunione Annuale AEI.

Cortina, R., W. Serravalli, and M. Sforzini. 1970. "Radio Interference Long-Term Recording on an Operating 420-kV Line." *IEEE PAS-89*. pp. 881-892. May/June.

Davis, A.H. 1938. ""An Objective Noise-Meter for the Measurement of Moderate, Loud, Steady and Impulsive Noises." *IEE-83*. pp. 249- 260. August.

Elsner, R.F. 1982. "'Rusty Bolt' Demonstrator." *IEEE EMC-24. pp. 420-421.* November.

EPRI. 1982. "Transmission Line Reference Book – 345 kV and Above/Second Edition." Electric Power Research Institute. Palo Alto, California.

Eteson, D.C. 1967. "The Subjective Effects of Power System Sparks on Television Picture Quality." IEEE Summer Power Meeting. Portland, Oregon. Conference Paper 31 CP 67-432. July.

FCC Rules. Part 15.5 and 15.13. 10-1-2001 Edition.

Federal Communications Commission. 1968. *Federal Communications Commission Rules and Regulations.* Vol. III. March.

Flink, B. and L. Svensson. 1975. "Report by the Swedish National Committee on Recordings of Radio Interference from a 400 kV Power Line." International Electrotechnical Commission CISPR/C. UDC 621.391.8. April.

Fredenall, G.L. 1953. "A Comparison of Monochrome and Color Television with Reference to Susceptibility to Various Types of Interference." *RCA Review-14*. pp. 341-358. September.

Frick, C.W. 1945. "A Study of Wave Shapes for Radio-Noise Meter Calibrations." *AIEE PAS-64*. pp. 890-901.

Frick, C.W. 1954. "The Quasi-Peak Voltmeter." *AIEE PAS-73. Pt. 1*. pp. 417-425.

Guyker, W.C., J.E. O'Neil, and A.R. Hileman. 1966. "Right-of-Way and Conductor Selection for the Allegheny Power System 500-kV Transmission System." *IEEE PAS-85*. pp. 624-632. June.

Hatanaka, G.K. 1981. "Field Measurements of VHF Noise from an Operating 500 kV Power Line." *IEEE PAS-100*. pp. 863-872. February.

Hedman, D.E. 1965. "Propagation on Overhead Transmission Lines: II – Earth Conduction Effects and Practical Results." *IEEE Transactions on Power Apparatus and Systems.* Vol. PAS-84. pp. 205-210. March.

Huyck, M.F. 1985. "Designing Lines to Avoid Radio-Interference." *Transmission and Distribution*. September.

IEC/CISPR. 1982. "Radio Interference Characteristics of Overhead Power Lines and High-Voltage Equipment, Part 1: Description of Phenomena." Publication 18-1. Bureau Central de la Commission Electrotechnique Internationale. 3, rue de Varembe, Geneve, Suisse.

IEC/CISPR. 1986a. Publication 18-2. "Radio Interference Characteristics of Overhead Power Lines and High-Voltage Equipment; Part 2: Methods of Measurement and Procedure for Determining Limits."

IEC/CISPR. 1986b. Publication 18-3. "Radio Interference Characteristics of Overhead Power Lines and High-Voltage Equipment; Part 3: Code of Practice for Minimizing Generation of Radio Noise."

IEC/CISPR Publication 16 (Part 1-1999). C.I.S.P.R. Specifications for Radio Interference Measuring Apparatus and Measurement Methods.

IEEE Committee Report. 1965. "Transmission System Radio Influence." *IEEE PAS-84*. pp. 714-724. August.

IEEE Committee Report. 1968. "Correlation of Various RI Meters and Reading Comparison of RI Meter Operators on a 735-kV Line." *IEEE PAS-87*. pp. 1249-1259. May.

IEEE Line Design Working Group of the Radio Noise Subcommittee. 1971. "Radio Noise Design Guide for High-Voltage Transmission Lines." *IEEE PAS-90.* pp. 833-842. March/April.

IEEE Committee Report. 1973a. "CIGRÉ/IEEE Survey on Extra High Voltage Transmission Line Radio Noise." *IEEE* PAS-92. pp. 1019-1028. May/June.

IEEE Committee Report. 1973b. "Comparison of Radio Noise Prediction Methods with CIGRÉ/IEEE Survey Results." *IEEE PAS-92*. pp. 1029-1042. May/June.

IEEE. 1976. "The Location, Correction and Prevention of RI and TVI Sources from Overhead Power Lines." Tutorial Course Text 76 CH1163-5-PWR. Piscataway, New Jersey.

IEEE Committee Report. 1977. "A Field Comparison of RI and TVI Instrumentation." *IEEE PAS-96*. pp. 863-87. May/June.

IEEE Committee Report. 1979. "A Survey of Methods for Calculating Transmission Line Conductor Surface Voltage Gradients." *IEEE PAS-98*. pp. 1996-2014. November/December.

IEEE Committee Report. 1980. "Review of Technical Considerations on Limits to Interference from Power Lines and Stations." *IEEE PAS-99*. pp. 365-388. January/ February.

IEEE Standard 1260-1996. "IEEE Guide on the Prediction, Measurement, and Analysis of AM Broadcast Re-Radiation by Power Lines."

IEEE Standard 643-1980 (R1992). "IEEE Guide for Power-Line Carrier Applications."

IEEE/PES Corona Testing Task Force 1997. "IEEE Guide for Conducting Corona Tests on Hardware for Overhead Transmission Lines and Substations." (This document is a working document that has only been circulated within the task force.)

Janischewskyj, W. and A.A. Arainy. 1979. "Corona Characteristics of Simulated Rain." Paper A79 496-1. IEEE/PES Summer Meeting. Vancouver, BC. July 15-20.

Janischewskyj, W., E.B. Harvey, and M.G. Comber. 1983. "Power Line Interference and Assessment of Television Picture Quality." *IEEE PAS-102*. pp. 1039-1049. May.

Juette, G.W. 1972. "Evaluation of Television Interference From High-Voltage Transmission Lines." *IEEE PAS-91*. pp. 865-873. June.

Kolcio, N., J. Di Placido, R.J. Haas, and D.K. Nichols. 1979. "Long Term Audible Noise and Radio Noise Performance of American Electric Power's Operating 765 kV Lines." *IEEE PAS-98*. pp. l853-1859. November/December.

Kuester, E.F., D.C. Chang, and R.G. Olsen.1978. "Modal Theory of Long Horizontal Wire Structures Above the Earth, 1, Excitation." *Radio Science-13*. pp. 605-613. July-August.

Lacroix, R. and H. Charbonneau. 1968. "Radio Interference from the First 735-kV Line of Hydro-Quebec." *IEEE PAS-87*. pp. 932-939. April.

Lauber, W.R. 1976. "Amplitude Probability Distribution Measurements at the Apple Grove 775-kV Project." *IEEE PAS-95*. pp. 1254-1266. July/August.

Lippert, G.D., W.E. Pakala, S.C. Bartlett, and S.D. Fahrnkopf . 1951. "Radio Influence Tests in Field and Laboratory 500-kV Test Project of the American Gas and Electric Company." *AIEE PAS-70*. Pt. I. pp. 251-269.

Loftness, M.O. 1992. "Power Line Interference – A Practical Handbook." National Rural Electric Cooperative Association. 1800 Massachusetts Avenue, N.W. Washington, D.C. 20036.

Loftness, M.O. 1996. "AC Power Interference Manual." Percival Publishing. P.O. Box 4122. Tumwater, WA 98501.

Loftness, M.O. 2002. "AC Power Interference Handbook." Percival Publishing. P.O. Box 4172. Tumwater, WA 98501

Loftness, M.O., V.L. Chartier, and G.L. Reiner. 1981. "EMI Correction Techniques for Transmission Line Corona." *Proceedings of the 1981 IEEE International Symposium on Electromagnetic Compatibility.* 81CH1675-8. Boulder, Colorado. pp. 351-358.

Madge, R.C. and D.E. Jones. 1986. "Effects of Power Lines on AM Radio Broadcast Radiation Patterns." *IEEE PWRD-1*. pp. 163-168. April.

Maruvada, P.S., N. Hyltén-Cavallius, and N.T. Chinh. 1974. "Radio Noise Meter Response to Random Pulses by Computer Simulation." *IEEE PAS-93*. pp. 905-915. May/June.

Maruvada, P.S. and N.G. Trinh. 1975. "A Basis for Setting Limits to Radio Interference from High Voltage Transmission Lines." *IEEE PAS-94*. pp. 1714-1724. September/October.

Moreau, M.R. and C.H. Gary. 1972. "Predetermination of the Radio-Interference Level of High Voltage Transmission Lines, I - Predetermination of the Excitation Function." *IEEE PAS-91*. pp. 284-293. January/February.

Nigol, O. 1964. "Analysis of Radio Noise from Higher-Voltage Lines. I-Meter Response to Corona Pulses." *IEEE PAS- 83*. pp. 524-553. May.

Olsen, R.G. 1983. "Radio Noise Fields Generated by Corona Streamers on a Power Line." *Radio Science*. Vol. 18. No. 3. pp. 399–408. May-June.

Olsen, R.G. 1988. "Radio Noise Due to Corona on the Multiconductor Power Line Above a Dissipative Earth." *IEEE* PWRD-3. pp. 272-287. January.

Olsen, R.G. and A. Aburwein. 1980. "Current Induced on a Pair of Wires Above Earth by a Vertical Electric Dipole for Grazing Angles of Incidence." *Radio Science.* Vol. 15. No. 4. pp. 733–742. July-August.

Olsen, R.G. and T.A. Pankaskie. 1983. "On the Exact, Carson and Image Theories for Wires at or Above the Earth's Interface." *IEEE PAS-102*. pp. 769-774. March.

Olsen, R.G. and D. Rouseff. 1985. "On the Wave Impedance for Power Lines." *IEEE PAS-104*. pp. 711–717. March.

Olsen, R.G. and D. Rouseff. 1985. "Radio Noise Fields Generated by Corona Streamers on a Power Line Above Dissipative Earth," *Radio Science-20*. pp. 601-610. May-June.

Olsen, R.G. and B. Stimson. 1988. "Predicting VHF/UHF Electromagnetic Noise from Corona on Power Line Conductors." *IEEE EMC-30*. pp. 13–22. February.

Olsen, R.G. and M. Wu. 1989. "A Wideband Model for Electromagnetic Interference from Corona on Electric Power Lines." *Radio Science.* Vol. 24. No. 3. pp. 340–350. May-June.

Olsen, R.G. and M. Wu. 1991."A Wideband Model for Electromagnetic Interference from Corona on Multiconductor Power Lines." *Radio Science-26*. pp. 73-88. January-February.

Olsen, R.G., S.D. Schennum, and V.L. Chartier. 1992. "Comparison of Several Methods for Calculating Power Line Electromagnetic Interference Levels and Calibration with Long-Term Data." *IEEE PWRD-7*. pp. 903–913. April. (In Table VI replace (13) and (11) with (11) and (8), respectively.)

Pakala, W.E. 1964. "A Practical Handbook for Location and Prevention of Radio Interference from Overhead Power Lines." Westinghouse Electric Corp. Research Report. 64-9E4-565-RI.

Pakala, W.E. and V.L. Chartier. 1971. "Radio Noise Measurements on Overhead Power Lines from 2.4 to 800 kV." *IEEE PAS-90*. pp. 1155-1165. May/June.

Papoulis, A. 1965. *Probability, Random Variables and Stochastic Processes.* McGraw-Hill. New York.

Paris, L. and M. Sforzini. 1968. "RI Problems in HV-Line Design." *IEEE PAS-87*. pp. 940-946. April.

Paul, C.R. 1982. "Introduction to Electromagnetic Compatibility." Wiley. New York. pp. 202-205. April.

Perry, D.E., V.L. Chartier, and G.L. Reiner. 1979. "Bonneville Power Administration's 1100 kV Transmission Development - Corona and Electric Field Studies." *IEEE PAS-98*. pp. 1728-1738. September/October.

Pogorzelski, R.J. and D. C. Chang. 1977. "On the Validity of the Wire Approximation in Analysis of Wave Propagation Along a Wire Over a Ground." *Radio Science.* Vol. 12, No. 5, pp. 699-707. September/October.

Robertson, L.M., W.E. Pakala, and E.R. Taylor, Jr. 1961. "Leadville High-Altitude Extra-High-Voltage Test Project, Part III - Radio Influence Investigations." *AIEE PAS-80*. pp. 732-743. December.

Roets, H.A. and A.C. Britten, 1992. "Guidelines for the Identification, Location, and Correction of Radio and Television Interference from High Voltage Lines." National Energy Council. Pretoria. 1992.

Sawada, Y., M. Fukushima, M. Yasui, I. Kimoto, and N. Naito. 1974. "A Laboratory Study on RI, TVI and AN of Insulator Strings Under Contaminated Conditions." *IEEE PAS-93*. pp. 712-719. March/April.

Schennum, S.D. and R.G. Olsen. 1994. "A Multipole Model for Coupling Between Electrical Discharges and Wires." *Proceedings of the 1994 Japan-U.S. Science Seminar on Electromagnetic Field Effects Caused by High Voltage Systems (Modeling, Characterization, Measurements, Mitigation).* Sapporo, Japan. pp. 57-65. June 28 - July 1, 1994.

Schennum, S.D. and R.G. Olsen. 1995. "A Method for Calculating Wideband Electromagnetic Interference from Power Line Corona." IEEE *PWRD-10*. pp. 1535-1540. July.

Showers, R.M. and A. Eckersley.1954. "Research Investigations of Interference Measuring Instruments." *Proceedings of the First Conference on Radio Interference Reduction.* Chicago. pp. 70-85.

Steudel, U. 1933. "Hochfrequentztechnik and Elektroakustik." Vol. 41, p. 1.

Takeshita, K., S. Takeshita, and H. Hachimoto. 1979. "Scattering Characteristics of VHF Television Broadcasting Waves by Steel Towers of Overhead Power Transmission Lines." *IEEE EMC-21*. pp. 33-40. February.

Taylor, F.L. and J.F. Bonska. 1962. "An Investigation of Radio Influence Voltages on Transmission and Distribution Lines on the Same Right-of-Way." *AIEE PAS-81*. pp. 1062-1066. February.

Toyoda, S. and H. Hashimoto. 1979. "Scattering Characteristics of VHF Television Broadcasting Waves by Steel Towers of Overhead Power Transmission Lines." *IEEE EMC-21*. pp. 62-65. February.

Trebby, F.J. 1959a. "Development of a Square-law Radio-Noise Meter-I." *AIEE PAS-78. Pt. III-A.* pp. 522-528. August.

Trebby, F.J. 1959b. "Development of a Square-law Radio-Noise Meter-II," *AIEE PAS-78. Pt. III-B.* pp. 1186-1191. December.

Trinh, N.G. and P.S. Maruvada. 1977. "A Method of Predicting the Corona Performance of Conductor Bundles Based on Cage Test Results." *IEEE* PAS-96. pp. 312-325. January/February.

Trinh, N.G., P.S. Maruvada, J. Flamand, and J.R. Volotaire. 1982. "A Study of the Corona Performance of Hydro Quebec's 735-kV Lines." *IEEE PAS-101*. pp. 681-690. March.

Wait, J.R. 1972. "Theory of Wave Propagation along a Thin Wire Parallel to an Interface." *Radio Science-7*. pp. 675-679. June.

Wait, J.R. 1977. "Excitation of an Ensemble of J Parallel Cables by an External Dipole Over an M Layered Ground." *Arch. Elektrotech. Ubertrag.* 31. pp. 489-493. December.

Wait, J.R. and K.P. Spies. 1969. "On the Image Representation of the Quasi-Static Fields of a Line Current Source Above Ground." *Canadian Journal of Physics-47*. pp. 2731-2733. December.

Wu, M., R. G. Olsen, and S. W. Plate. 1990. "Wideband Approximate Solutions for the Sommerfeld Integrals Arising in the Wire Over Earth Problem." *Journal of Electromagnetic Waves and Applications.* Vol. 4. No. 6. pp. 479-504.

CHAPTER 10

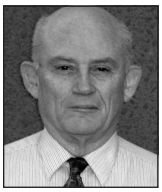
Audible Noise

Tony Britten
Vernon Chartier
Luciano Zaffanella

This chapter describes the nature of the acoustic noise produced by corona on high-voltage transmission lines. The chapter offers detailed procedures for calculating the noise produced by any practical line configuration. It also includes methods for measurements and criteria for assessing annoyance or compliance with noise regulation.



Tony (AC) Britten has worked many years as Technical Specialist in Eskom, the South African power utility. He has done research and development in the disciplines of electromagnetic compatibility in power systems, external insulation, insulation coordination and corona effects on transmission lines. He was responsible (in the mid-1980s) for the selection of the field effect and conductor corona parameters of Eskom's first high-altitude 800-kV transmission lines. Since then, he has led various theoretical and experimental studies of the corona properties (especially audible noise) of high altitude, compacted 400-kV lines, and is presently doing research into HVDC corona phenomena. He has written several conference papers on power line corona. He is a registered Professional Engineer in South Africa, and is a Fellow of the South African Institute of Electrical Engineers.



Vernon L. Chartier is a leading expert on corona effects of high-voltage transmission lines. He performed pioneering work on radio and audible noise while he was with the Westinghouse Electric Corporation. This included corona research for the Apple Grove 750-kV Project in the 1960s. In 1975, he joined Bonneville Power Administration, where he was associated with the Lyons 1200-kV Project and managed several high-voltage research projects. Since 1995, he is a Power System EMC consultant. He has conducted long-term audible noise measurements on lines at 230-, 500-, 765-, and 1200-kV. His research on audible noise has been documented in about 20 technical papers. He had a leading role in IEEE, CIGRÉ, and CISPR work on corona. For his work, he has been elected a Fellow of IEEE and received the Herman Halperin T&D Award.



Dr. Luciano E. Zaffanella is one of the original authors of *EPRI Transmission Line Reference Book*. When the previous editions were published, he was directing General Electric's staff that was operating Project UHV on behalf of EPRI. Under his direction this project became an internationally renowned facility for the study of overhead high-voltage transmission lines with HVAC voltages up to 1500 kV three-phase, and HVDC voltages of + and - 1200 kV, including audible noise. He pioneered the application of cage tests to determine the audible noise generation of conductors and the use of asymmetric bundles to reduce audible noise in wet weather. He is the author of 5 technical papers on the subject of audible noise. He is currently Vice President of Research at Enertech. He is a Fellow of the IEEE.

10.1 INTRODUCTION

Audible noise continues to be of concern in today's society. Normally, transmission systems contribute very little compared with the everyday occurrences of other more common environmental noises such as vehicular, aircraft, and industrial noises. Transformer noise is a source of occasional complaints and is a significant consideration in modern transformer and urban substation design. With increasing transmission-system voltages (from 230 kV up to the highest voltages), audible noise produced by corona on transmission-line conductors has emerged as a design constraint. At lower operating voltages, little attention was paid to this problem because the noise levels were low enough to be of no concern.

Since the publication of the first and second editions of the Red Book (1975 and 1982 respectively, and a revision in 1987), it has indeed been shown that audible noise is a significant, and sometimes overriding, design factor. This trend has been seen not only in North America, but also in other parts of the world. The driving factors in countries such as Venezuela, South Korea, Brazil, and South Africa, for example, have been 765-kV lines and new 400- and 500-kV designs with tighter phase spacing. In the South African case, new 400- and 765-kV lines have been built at altitudes of up to 1600 m above sea level, a factor that significantly increases corona and corona-produced audible noise.

Audible noise from transmission lines occurs primarily in foul weather. Water drops impinging or collecting on the conductors produce a large number of corona discharges, each of them creating a burst of noise. In dry conditions, the conductors usually, but not always, operate below the corona-inception level, and very few corona sources are present. In the case of compact lines operating at high altitudes in particular, noise levels in dry conditions can be significant. In such situations, the dry-noise limits may become an important design issue.

This chapter describes the nature of the noise and the instrumentation for its measurement. Procedures for evaluating the audible noise of any practical transmission-line configuration are given in detail with methodologies and equations that allow rigorous, direct evaluation. The criteria for annoyance evaluation and assessment of design limits are discussed. The chapter concludes by presenting different methods for the reduction of audible noise.

Audible noise can be calculated using software applications (applets) provided in the electronic version of this book. The user may exercise the following applets:

- AN-1: “Audible Noise of Transmission Lines (2-D).” This applet calculates the sound-pressure level versus the distance from a transmission line of given characteristics in different weather conditions. This applet considers two-dimensional line geometry.
- AN-2: “Audible Noise of Transmission Lines (3-D).” This applet may be used for three-dimensional geometry, such as a transposition span or lines crossing at an angle. It calculates the audible noise at any desired location given the dimensions and the voltages of all the conductors.
- AN-3: “Bundle Geometry for Minimum Audible Noise.” This applet may be used to determine the optimum location of individual conductors within multiconductor bundles corresponding to the lowest audible noise level in wet weather.
- AN-4: “Audible Noise, Hum.” This applet may be used to calculate the hum profile, i.e. the sound pressure level of a pure tone at twice the power frequency versus the distance from a line.
- AN-5: “Audible Noise—Base Case Curves and Effect of Line Parameters.” This applet calculates the audible noise at a reference location and the effect of individual line parameters, such as conductor diameter, number of conductors, phase spacing, and height above ground for a large number of base case line voltages and configurations.
- AN-6: “Audible Noise vs. Rain Rate.” This applet provides data on how line noise and rain noise vary with rain intensity.

10.2 CHARACTERISTICS OF TRANSMISSION-LINE NOISE

Audible noise generated by corona on power transmission lines has two major components: the “broadband noise” and the “hum.”

The broadband noise has a significant high-frequency content that distinguishes it from most common environmental noises. It is generated primarily by positive-polarity streamers (see Chapter 8) forming at the surface of the conductors. Each streamer generates a local sudden change in air pressure, which causes an impulsive pressure wave to propagate in the surrounding air. The pressure waves of different streamers occur at different instants in time and, therefore, each frequency component of the broadband noise spectrum is the result of many pressure wave components having a random phase relationship with each other. The combination of many uncorrelated pressure waves and their high-frequency content results in the cracking, frying, or hissing characteristics of transmission-line noise. The frequency spectrum of an impulsive wave is flat up to a drop-off frequency. The flat part of the broadband noise spectrum extends well beyond the sonic (audible) range—

that is, beyond about 15 kHz to several tens of kilohertz (Sforzini et al. 1975). In practice, the drop-off frequency of the noise spectrum depends on the frequency response of the microphone used for the measurements and on the air absorption of sound energy, which increases with frequency (see Figure 10.4-4). A microphone orthogonal to the direction of the sound wave cannot respond to frequencies with wavelengths smaller than the microphone diameter. For example, the frequency response of a 2.54-cm diameter microphone orthogonal to the direction of the sound wave starts dropping off at about 6.5 kHz.

The hum is a pure tone that is superimposed over the broadband noise. The hum has a frequency equal to twice the power frequency (namely, 100 Hz for a 50-Hz system and 120 Hz for a 60-Hz system). It is the result of a pressure wave caused by the movement of air ions alternatively attracted to and repelled from the conductors. The positive-polarity corona discharges, initiated when the electric field at the surface of the conductor reaches some critical positive value, create electrons that are attracted to the conductor and positive ions that are pushed away from the conductors by the electric field. When the electric field changes sign, the positive ions return to the conductor. Similarly, negative-polarity corona discharges, initiated at some critical negative electric field value, create electrons that attach to air molecules to form negative ions that are pushed away from the conductor. When the electric field changes sign, the negative ions return to the conductor. Ion movement causes alternative changes in air density and air pressure twice each power frequency cycle. A sound pressure wave with frequency twice the power frequency is established. The pressure variations are not purely sinusoidal and may occur differently during the positive and negative cycles. Therefore, a power frequency component and harmonics of the hum may also be present, even though their amplitude is much smaller than the hum. Among the harmonics, the second (200 / 240 Hz) is often measurable above the broadband noise.

Not all ac corona modes (see Chapter 8) create broadband noise and hum in the same proportions. The broadband noise is created primarily by positive-polarity streamers, whereas glow corona may produce intense ionization and consequently a strong hum. In different weather conditions the relative magnitude of broadband noise and hum may be different. For example, during rain the broadband component generally dominates, whereas under icing conditions the hum dominates. Figure 10.2-1 shows a typical measured frequency spectrum of a 60-Hz transmission-line audible noise emission in rain. The figure shows the 120-Hz hum and a less significant 240-Hz tone. The bandwidth of the measuring instruments affects the readings of the broadband spectrum (pressure level proportional to the square root of the bandwidth) but does not affect the pure tones. The noise levels at frequencies below 100 Hz are greatly affected by ambient noise. The broadband noise extends in frequency above 10 kHz. The rolloff of the broadband noise above 10 kHz results from the frequency response of the measuring microphone and from the increasing effect of air absorption of sound energy with frequency.

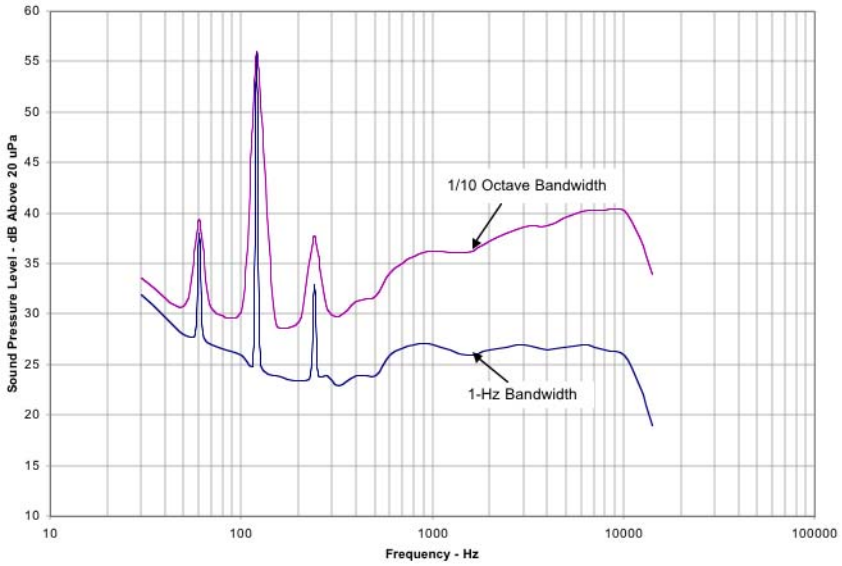


Figure 10.2-1 Typical frequency spectrum of ac transmission-line audible noise in rain.

In the absence of attenuation due to air absorption of sound energy, the sound-pressure levels of both broadband noise and hum vary in inverse proportion to the square root of the distance away from the line. This means that the audible noise decreases by 3 decibels for each doubling of distance away from the line. Air absorption and attenuation by trees or structures increase with frequency and, therefore, affect much more significantly the broadband noise than the hum. Reflection of noise by the ground has a negligible effect on the broadband noise and can be disregarded, while it has a profound effect on the hum.

An important difference between broadband noise and hum is due to the difference in the phase correlation between pressure waves from different sources. The pressure waves generated by different sources of broadband noise, either on the same or on a different phase, may be considered uncorrelated. Their pressure levels combine in a random way. To calculate the combined effect the energies of the waves are added (see Section 10.4). An example of lateral profile of the broadband noise soundpressure level is shown in Figure 10.2-2. By contrast, the pressure waves that form the hum have a definitive temporal relation with each other. For a three-phase line, the pressure wave generated by each phase has a fixed phase angle with the charge on the conductor, which is practically in phase with the voltage. Thus, the difference in phase angles of the pressure waves generated by different phases is 120º. The pressure waves arriving at a measuring point from different phases add up as phasors. Their phase depends on the phase angle of the generated wave and on the time of travel from the phase to the measuring point. To this, the waves reflected from the ground are added, each with its own phase. The result is a pressure level extremely dependent on the location of the measuring point, including its height above ground. At some point the different pressure waves may all be in phase and cause a large increase in pressure level, while at some other point, they may tend to cancel each other. The lateral profile of the hum, an example of which is shown in Figure 10.2-3, reflects these wide variations.

During rain and in other wet-weather conditions when there are water drops hanging at the bottom of the conductors and the wind is calm, corona may cause the conductors to vibrate at very low frequency (Newell et al. 1968). These corona-induced vibrations are caused by the intermittent space charge produced by corona at the water drops hanging at the bottom of the conductors and by the fact that corona is modulated by the deformation of the water drops during the oscillation cycle itself. This phenomenon is self-excited and results in the conductor vibrating at any of its natural frequencies with increasing amplitude until the deformation of the water drops causes corona out of synchronism with the motion (Farzaneh and Phan 1984; Farzaneh and Teisseyre 1988; Farzaneh 1992). Corona-induced vibrations do not cause conductor fatigue because the frequency is relatively low (1–5 Hz) and the peak-to-peak amplitude is relatively small (2–10 cm). They cause, however, a modulation of the audible noise, which makes the noise more detectable and distinguishable from the rain noise.

10.3 AUDIBLE NOISE AS A DESIGN FACTOR

There are no specific regulations that limit the level of audible noise that a transmission line may produce. There are many state and local ordinances that by the nature of their generality may implicitly include transmission lines (Bragdon 1980). It has been argued that, since transmission-line noise differs sufficiently in characteristics from other man-made noise sources, hardly any of the existing ordinances properly reflect the true impact. Because of the unique nature of transmission line audible noise, in the 1980s a

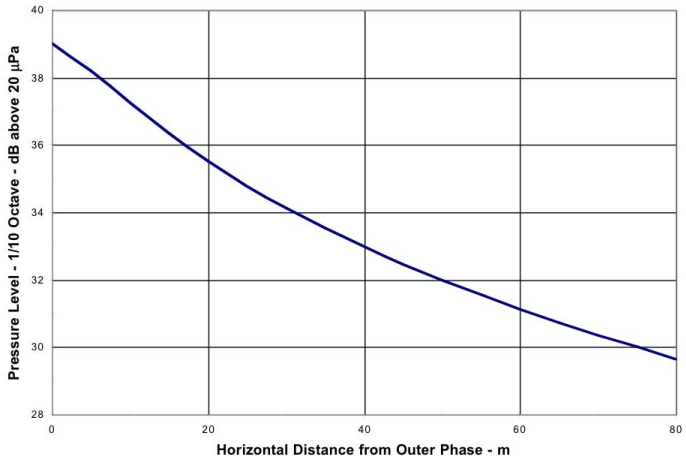


Figure 10.2-2 Example of a lateral profile of the 1000-Hz component of the broadband audible noise of a three-phase transmission line. Line voltage 525-kV; 2 x 4.07-cm conductor bundles, flat configuration with 10.4-m spacing between phases, 12.2-m height above ground, measurements at 1.5 m above ground.

number of psychoacoustic studies were performed to assess the impact of transmission-line noise on humans (Wells 1974; Molino et al. 1979). These studies produced interesting results, but no regulatory body has used them to develop noise limits specifically for transmission lines for obvious reasons. Every man-made noise source has some unique characteristics, no regulatory body wants to create separate limits for transmission lines, or they might be required to create separate limits for many sources.

10.3.1 Effect of Weather Conditions and Load Current

Generally, transmission-line audible noise is a concern only in foul weather; especially in moderate, relatively clean environments. For lines that are designed for acceptable levels of radio noise, the fair-weather audible noise is usually very low and can't be heard on most lines except for an occasional burst of corona. It is known, however, that in dry climates where the conductors operate at relatively high conductor surface gradients, where they are exposed to particles such as dust, insects, etc., and where they experience very few rain storms to wash off the particles, the fair weather audible noise can be sufficiently high to be detected by the human ear. The highest audible noise levels occur, however, in conditions of foul weather because of the potential for a large concentration of corona sources, such as water drops or snowflakes that collect on the conductor surface.

It is well known that load current affects foul weather corona from transmission lines (Gross et al. 1951; LaForest et al. 1963; Anderson et al. 1966; Chartier et al. 1970). The resistive heating effect of load current discourages the formation of condensation on the conductors in the early morning hours and during fog. Depending upon its magnitude, it can discourage the formation of hoarfrost on the conductors and even melt hoarfrost if it has already formed; and it can melt snow that lands on the surface of the conductors. It can also increase the rate at which conductors dry after rain.

Observations on a 500-kV line of the Bonneville Power Administration have shown that load current also affects fair-weather corona phenomena (Chartier 1994). It is well known that the conductor surface gradient at which corona onset occurs decreases as the relative air density (RAD) decreases. Since RAD is inversely proportional to temperature, increased load current increases the conductor temperature and decreases the RAD at the conductor surface. Reduced RAD at the conductor surface decreases the corona onset gradient. Because transmission lines operate at relatively fixed voltages, the noise increases with increased conductor temperature. This phenomenon can be enhanced in the summertime when the air temperature can also be very high. It is discussed further for each of the following weather conditions.

Rain

Perhaps the most important weather condition, from a design point of view, is rain because of all foul-weather conditions this is the one most often encountered. Noise levels in rain may vary over a wide range. In the initial stages of a rain, when the conductors are not thoroughly wet, there may be considerable fluctuation in the noise level as the rain varies. When the conductors are thoroughly wet and dripping, the noise fluctuations will be less significant because, even as the rain intensity lessens, the conductors will still be saturated with water drops that act as corona sources. The variability of the noise levels during

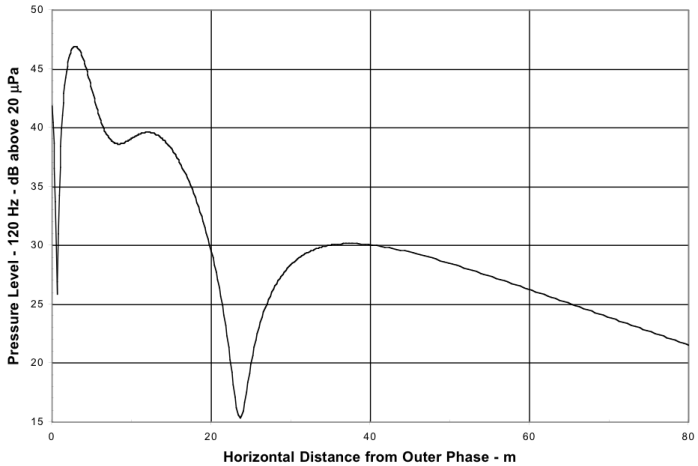


Figure 10.2-3 Example of a lateral profile of the hum of a three-phase transmission line operating at 60 Hz. Flat configuration with 10.4-m spacing between phases, 12.2-m height above ground, measurements at 1.5 m above ground.

rain depends greatly on the condition of the conductor surface and on the conductor surface gradient at which the conductors are operating. At high operating gradients, the noise level is less sensitive to rain rate than at low gradients. Consequently, the dispersion of noise levels is less for the higher gradients. An example of the variation of audible noise during rain for a three-phase test line is shown in Figure 10.3-1 (EPRI 1982).

Load current has little effect on the audible noise during measurable rains. Therefore, if the audible noise limit is based upon the L_{50} level during measurable rain, load current does not have to be considered. Load current is important after the cessation of rain. In Figure 10.3-1, it can be seen that the rain stopped at about 1400 hours, but the noise did not reach ambient levels until about 1530 hours. The drying time, therefore, was about 1-1/2 hours. For 500-kV lines that carry load, the drying time can be as short as 5 minutes. Rapid drying of the conductors affects the shape of the audible noise probability distribution. As will be seen later, some noise regulations are based upon equivalent sound levels, which is an energy average A-weighted noise level over a specific time period. If the specific time covers all weather conditions, then the load current will have an impact on the calculation of the equivalent sound level.

Fog

When lines carry little or no load current, the audible noise during fog can reach high levels, depending upon the intensity of the fog. At the Apple Grove 750-kV Project, which was very close to the Ohio River, audible noise during very heavy, intense fogs even reached the levels experienced during measurable rain (Kolcio et al. 1974; Kolcio et al. 1977). An example of noise buildup during a lengthy period of fog for a three-phase test line without load current is shown in Figure 10.3-2 (EPRI 1982).

The resistive heating effect of load current discourages the formation of moisture on the conductors due to condensation. When a line carries a significant load current, water drops will not form on the surface of the conductors, thereby causing the noise to be barely audible. Conversely, high noise levels would be encountered if condensation would take place

Snow

Noise level in snow is primarily dependent on the nature of the snow and may vary over a wide range. At air temperatures close to 0º C, there may be a fine distinction between snow, sleet, and rain. Moderate-to-heavy wet snow results in noise levels essentially the same as those obtained during rain. At temperatures below 0º C, the snow, depending upon how dry it is, can result in much lower noise levels, especially on lightly loaded lines. For test lines without load current, heavy snowfalls at very low temperatures produce very little increase in noise level (EPRI 1982).

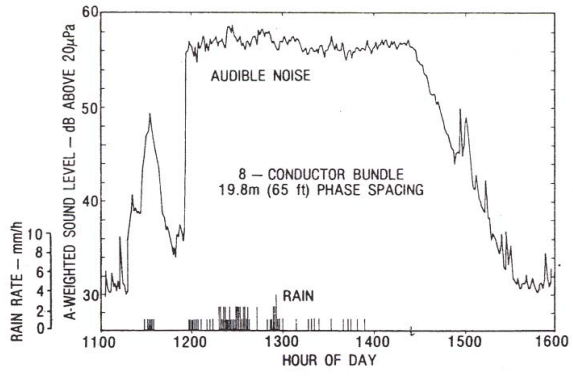


Figure 10.3-1 Variation of audible noise before, during, and after a rain period. Eight-conductor bundles with 3.31-cm diameter conductors; center phase gradient = 15.3 kV/cm; outer phase gradient = 14.2 kV/cm; test line without load current.

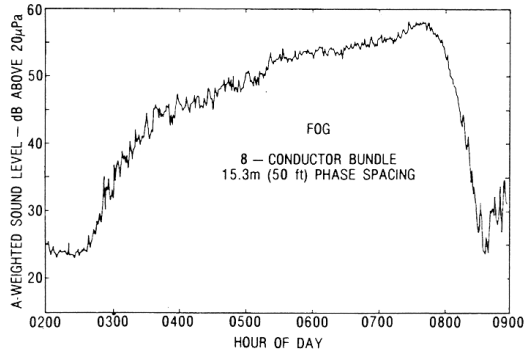


Figure 10.3-2 Variation of audible noise during a period of fog. Eight-conductor bundles with 3.31-cm diameter conductors; center phase gradient = 16.3 kV/cm; outer-phase gradient = 15.6 kV/cm; test line without load current.

An example of the variation of noise for a three-phase configuration during a period of snow is shown in Figure 10.3-3 (EPRI 1982).

If snow lands on conductors that are very warm, it can melt, turn to water, and drip off of the conductors. Therefore, even during relatively dry snows, the noise can reach the same levels as during rain if the load current is high enough.

Hoarfrost

Experience has shown that when hoarfrost builds up on test lines with no current or on lightly loaded operating lines, the corona losses can be very large. Hoarfrost consists of many sharp, icy points. Corona from these sharp points produces glow discharges or what some researchers call ultra-corona. Such corona produces very high corona losses. At the Apple Grove Project (Kolcio et al. 1974), there were many occasions when the conductors and the towers were covered with heavy hoarfrost in the early morning hours during the winter months. During periods when the simulated load current circuits were disconnected, the noise coming from the conductors was a pure, very large 120-Hz hum, similar to the audible noise produced by a transformer. This was due to glow corona from the sharp ice tips. On a 60-Hz line, the glow corona oscillates at 120 Hz, thereby creating a very strong 120-Hz hum. On a 50-Hz line, the hum frequency would be 100 Hz. Hoarfrost, like fog, is formed by condensation, but at temperatures below 0º C. As during fog, the heat produced by moderate-to-heavy load currents can discourage the formation of hoarfrost. Hoarfrost formed during light load conditions can quickly turn to water once the load current is increased.

Fair Weather

As stated earlier, in dry environments where an occasional rain is not sufficient to wash the conductors, the fair-weather noise can reach measurable levels, even for lines operating at normal conductor surface gradients. Fair-weather audible noise may become a source of complaints for lines whose conductors operate at very high conductor surface gradients for the size of their conductors. One of the Apple Grove test lines had bundles of four 2.54-cm conductors, and the conductor surface gradient on the center phase was 24.4 kV/cm. This center phase was in heavy corona even during dry weather. At 16.8 m from the outer phase, this line had a mean fair-weather noise level of about 55 dBA (Kolcio et al. 1974). Another abnormal line was the first 500-kV line built by the Bonneville Power Administration and for which a single 6.35-mm conductor was used. The mean audible-noise level during measurable rain from this line at 20 m from the outside phase is about 62 dBA. During the cold winter months in Oregon, the fair-weather audible noise from this line is below 40 dBA; but during the hot summer months the fair-weather level can be above 50 dBA.

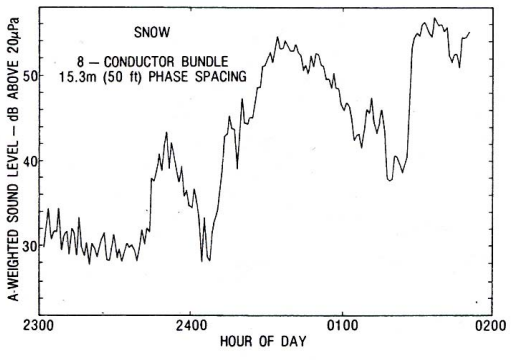


Figure 10.3-3 Variation of audible noise during a period of snow. Same conductors and gradients as Figure 10.3-2. Test line without load current.

Fair-weather audible noise can be very erratic; therefore, it is not easy to predict. Long-term audible noise measurements conducted in clean environments has shown that the L_{50} audible noise level during fair weather is about 25 dBA less than the L_{50} audible noise during measurable rain. This difference will be smaller in dirtier, drier environments. This difference will also be smaller for lines operating at higher conductor surface gradients. Because of the lack of long-term audible noise measurements in dusty and dry environments or in situations conducive to measurable levels of fair weather noise (extremely low ambient levels, high surface gradient, high altitude and dusty environment), it is very difficult to predict fair-weather audible noise.

As mentioned earlier, the heating effect of load current can affect fair-weather corona phenomena by increasing the conductor temperature at the surface of the conductor where the corona forms. Increased conductor temperature lowers the air density at the conductor surface, thereby decreasing the corona onset gradient. Figure 10.3-4 shows time plots of magnetic field, A-weighted sound-pressure level, and sound-pressure level above 6.5 kHz from a corridor where one of the 500-kV lines used the single 6.35-cm conductor. It is easily seen in Figure 10.3-4 that the audible noise is tracking the magnetic field, which, of course, is a measure of load current.

To fully evaluate the audible noise performance of a given line, one should consider all foul-weather conditions and might have to consider even fair-weather conditions depending upon the particular noise code a line has to comply with. This requires detailed information on the noise variability for the given line in all foul- and fair-weather conditions. Often, such information is not available unless long-term measurements have been conducted on lines operating in an environment similar to the one where the proposed line will be built.

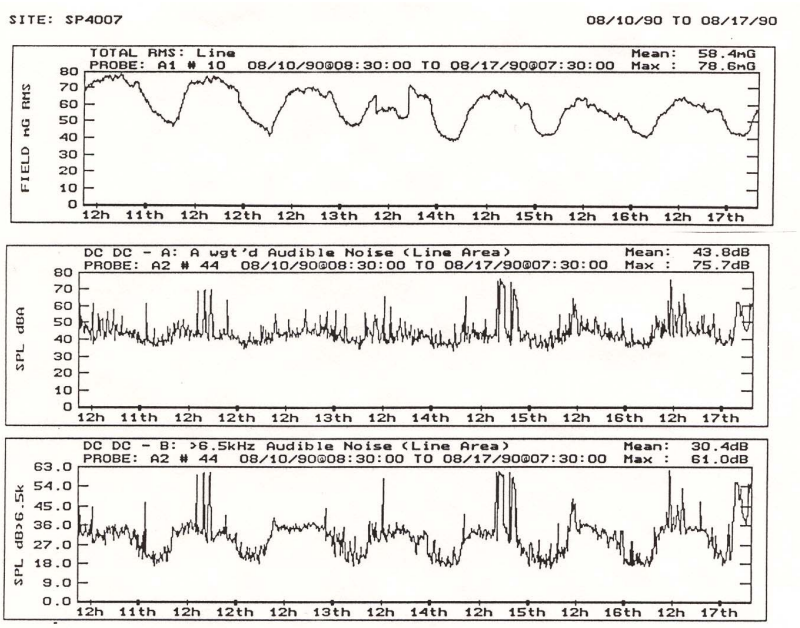


Figure 10.3-4 Magnetic field, A-weighted sound-pressure level, and sound-pressure level above 6.5 kHz versus time. Measured on a transmission corridor where one of the lines was a 500-kV line with a single 6.35-cm conductor.

10.3.2 Effect of Line Geometry and Conductor Surface Conditions

The dispersion of audible-noise levels produced by a transmission line during rain depends both on the operating conductor surface gradient and on the conductor surface conditions. Lower overall levels and greater overall dispersion of noise are obtained as the conductor surface gradient is reduced. The line parameters that have the greatest effect on the conductor surface gradient are the number and diameter of conductors in a phase bundle. The discussion on the effect of variation in these and other line parameters on the radio-noise performance (see Chapter 9) also applies to audible noise.

Conductor Surface Electric Field (Conductor Surface Gradient)

The most important parameter affecting audible noise and other corona phenomena is the electric field at the surface of the conductor. It is important that this be accurately calculated. The conductor diameter, number of conductors, the height of the conductors above ground, and the distance between the phases affect the conductor surface gradient. The height above ground is not constant along a span. For the purpose of audible-noise calculations, it is customary to consider an average height equal to the minimum height plus one third of the sag. This approximation gives the most accurate results. From audible-noise measurements in test cages and test lines, several empirical relations have been developed, showing the relationship between audible noise and conductor surface electric field (EPRI 1982; Chartier and Stearns 1981; IEEE 1982).

Conductor Diameter

The diameter of the conductor(s) is also an important factor, and again there are several empirical terms that have been developed showing the relationship between audible noise and conductor diameter (EPRI 1982; Chartier and Stearns 1981; IEEE 1982). Audible noise (and all the other corona phenomena) decreases as the conductor diameter is increased, if the line voltage remains constant. However, if the conductor diameter is increased while the conductor surface gradient remains constant, the audible noise increases. This is because the decay of the electric field from the conductor surface is slower for larger conductors. Larger conductors have longer corona streamers, which produce higher audible noise levels.

Number of Conductors

Audible noise, unlike radio noise, increases as the number of conductors in the bundle increases. Again, several empirical relations have been developed showing the relationship between audible noise and the number of conductors when all of the other parameters are kept constant (EPRI 1982; Chartier and Stearns 1981; IEEE, 1982).

Generally, one thinks of a bundle of conductors as being regular—i.e., the individual conductors in the bundle are regularly spaced along an imaginary circle, whose diameter is the bundle diameter. Often, for two, three-, and four-

conductor bundles, the spacing between adjacent conductors is used to describe the size of the bundle; however, for larger conductor bundles, the diameter is more often referred to. Most of the available audible-noise data were obtained with regular bundles. The design rules in Section 10.4 place considerable emphasis on the effect of variation of the basic geometrical parameters of regular bundles. However, some reduction in audible noise can be achieved through optimization of conductor placement within a bundle—i.e., through the use of asymmetric bundles. Methods to determine optimum bundle geometries and expected reduction in noise with respect to regular bundles are given in Section 10.7.

Conductor Surface Conditions

Since audible noise is essentially a foul-weather phenomenon, conductor-surface conditions are important only inasmuch as they affect water drop formation. This subject was discussed in Chapter 8 (Corona Phenomena). Two extremes of surface condition may be identified: (1) hydrophobic, in which water tends to bead in many small droplets all over the conductor surface (with the exception of nonspecular conductors, brand new conductors, fresh off the reel, exhibit this type of surface condition); (2) hydrophilic, in which the conductor appears almost to absorb water until a point of saturation is reached when large drops begin to appear only at the bottom of the conductor (a well-aged conductor, one that has been exposed to the elements for a long period of time exhibits this type of surface condition). Conductors exhibiting a hydrophilic condition have better audible-noise performance than those exhibiting a hydrophobic surface condition (EPRI 1982). The improvement is especially notable at low surface gradients and in light rain or fog, but it diminishes with increasing gradient or increasing rain rate. During the time between stringing and first energization of a transmission line, the surface oil on conductors that is responsible for beading of the water drops breaks down. Beading can disappear from nonenergized conductors as rapidly as 4-7 months in the environment of northern Indiana (Booker 1986). However, colder weather appears to inhibit this aging process by as much as 5 months. Depending upon when new lines are energized, the surface condition would be somewhere between hydrophobic and hydrophilic. Parameters involved in the aging process include the time of exposure to the elements and the general atmospheric conditions and cleanliness of the air. These can vary so much from case to case that it is difficult to quantify the effect in terms of an expected audible-noise reduction. The effect of surface aging on audible noise is greater at lower gradients. For a three-phase test line with an eight-conductor bundle, a noise reduction of about 2 dB was noted after 5 months of exposure, 4 dB after 10 months, and 8 dB after approximately 3 years (Comber and Nigbor 1979).

10.3.3 Audible Noise from Insulators and Fittings

If line hardware, fittings, and insulators are not designed properly, they can produce audible noise of a level that some people might find objectionable. Insulators by themselves, generally, produce very little audible noise unless they become contaminated, and a phenomenon called "dry-band arcing" occurs under certain environmental conditions. When the insulators are dry and contaminated, dry-band arcing is not a problem. The conditions that cause the worst dry-band arcing are fog, mist, and dew, which wet the insulators but not enough to wash the contaminant off their surface. Depending upon the level of contamination and the voltage, the audible noise can become quite loud. The problem can be corrected either by replacing or washing the insulators. Audible noise seems to occur more frequently with porcelain and glass insulators than with polymer insulators.

Line hardware and fittings are a different problem. Like for the conductors, if the electric fields over the surface of fittings exceed a critical gradient, then corona will occur. During rain, fittings will have corona streamers where water drops are collecting. However, the audible noise created by these corona streamers is not a problem because the noise is usually masked by the noise created by the much larger number of corona sources that occur up and down the conductors.

Audible noise created by corona sources on fittings during fair weather has an erratic behavior. The noise is usually not loud enough to violate local noise regulations, but the industry has received complaints from individuals living close to structures that have had relatively loud, erratic corona sources on fittings.

Audible noise from fair-weather corona from fittings becomes a more significant problem as the industry moves towards upgrading existing lines and building lines with tighter phase spacing. An example of excessive corona on fittings from a 115-kV substation that was upgraded to 230 kV can be seen in Figure 10.3-5 (EPRI 1992). Similar corona sources occurred at fittings along the line, which prompted some complaints by residents who were used to living next to a quiet 115-kV line. The corona performance of this substation and associated 230-kV line was improved by employing special hardware for corona suppression (e.g., corona rings).

Another example of excessive corona from fittings under dry conditions was reported by (Chartier et al. 1995). In this case, polymer post insulators were designed to support conductors to be used on a compact horizontal line configuration. The conductors were clamped directly to the insulator without corona rings. Once the line was energized, the insulator assembly was found to produce objectionable noise levels. Nighttime viewing determined that the objectionable corona was coming from the clamps.

It is important that fittings designed for lines are tested in the laboratory before being used on new lines. A common practice is to test fittings in HV laboratories by energizing a single-phase mockup of the conductor insulator assembly at a voltage around 10% above the operating line-to-ground voltage. If the assembly is corona free, then it passes the test. However, this test ignores the fact that corona onset is a function of surface gradient rather than voltage. It also does not take altitude into consideration. A more correct way of testing hardware for overhead lines and substations is described in Appendix 8.2. This technique was used to test the hardware assembly for another compact 230-kV line using a compact horizontal line configuration structure in the State of Washington. When a corona ring and a special washer were added to the line post insulator, the assembly in the laboratory mockup was rendered corona free. This behavior has been confirmed by the operating experience since the line was energized in the early 1990s.

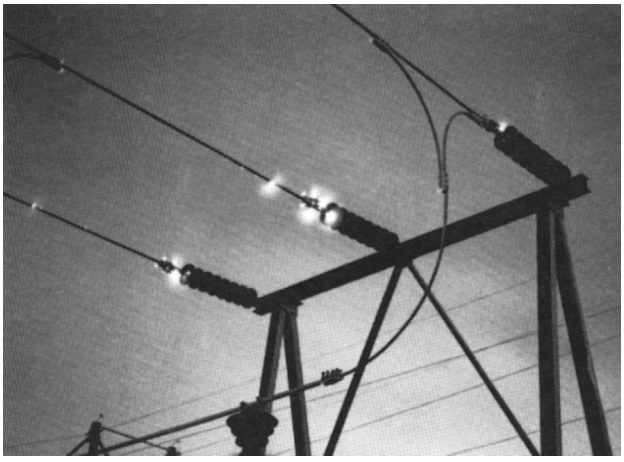


Figure 10.3-5 Nighttime photo illustrating corona on clamps on end of dead-end insulator string. Right-hand conductor has reduced corona because of a better clamp arrangement than the other two phases (EPRI 1992).

10.4 CALCULATION OF TRANSMISSION-LINE AUDIBLE NOISE

10.4.1 Introduction

Transmission-line audible noise first became a problem in the U.S. in the late 1960s and early 1970s when 500- and 765-kV lines were introduced (Perry 1972; Kolcio et al. 1974). Because of the complaints associated with these lines, corona-generated audible noise became an important transmission-line consideration. As a result, the industry launched a major effort to measure and develop a better understanding of corona-generated audible noise, especially in the 1970s when research began on transmission voltages above 1000 kV. In other countries, such as Brazil and South Africa, audible noise became a design issue in the 1980s when 765-kV and compact 400-kV lines were first built. From a design standpoint the accurate prediction of audible-noise levels is most important. The calculation of audible-noise levels is much simpler than the calculation of radio-noise levels because audible noise is concerned only with the generation and propagation of sound-pressure waves. Unlike radio noise, propagation of sound along the conductor does not occur, and is not an issue. The generation of audible noise is determined empirically, usually as a function of conductor characteristics such as the surface gradient, diameter, and number of conductors in the phase bundle. The propagation of the sound may be evaluated using the laws of acoustics.

Audible-noise calculation methods may be divided into two general types: (1) methods that are specific to a particular type of line design (e.g., a single-circuit, horizontal configuration), and in some instances specific to a voltage class (e.g., 550 kV); and (2) methods that are general and may be applied to any particular design. The first methods are described in (IEEE 1982). Because of the flexibility and accuracy of the second methods, the first methods are not widely used and will not be discussed further in this chapter.

Methods of the second type calculate the noise level produced by each phase of the line at the point of measurement and then sum the contributions of each phase to determine the overall noise level. Generally, a formula similar to Equation 10.4-1 is used to calculate the noise of each phase.

$$P = P_0 + k_1 \cdot f_1(E_{\max}) + k_2 \cdot f_2(n) + k_3 \cdot f_3(d) + k_4 \cdot f_4(D) \quad \text{10.4-1}$$

Where:

P is the predicted noise level.
P_0 is a reference noise level.
E_{max} is the conductor surface gradient.
n is the number of subconductors in each phase bundle.

d is the subconductor diameter.
D is the distance from the conductor to the measuring point.
$k_1 - k_4$ are constant coefficients.

Data used in the formulation may come from tests on three-phase lines using mathematical or experimental techniques to separate the noise of individual phases, or the data may come from special tests on single-phase conductor geometries in test cages or on test lines. Once the noise for each phase is obtained, the total line noise is found from

$$P_{tot} = 10 \log \sum_{i=1}^{N_p} 10^{P_i/10} \qquad 10.4\text{-}2$$

N_p is the number of phases and P_i is the noise level (expressed in N/m^2) produced by phase i.

Methods of this type are more generally useful than those of the first type because less restriction is imposed on the line configuration. Lines may be single-circuit, double-circuit, horizontal, vertical, triangular, or they may have a higher phase order and could even have different conductor geometries on different phases. Ac transmission-line noise is mostly of concern in foul weather, primarily rain. In fair weather, the audible-noise level is often much lower than in rain, and few transmission lines have experienced fair-weather complaints. All presently available calculation methods predict A-weighted sound pressure levels primarily for conditions of rain. However, some methods give an estimate of the fair-weather level.

For the purpose of calculation, audible noise in rain has to be defined. The most commonly used calculation methods (Chartier and Stearns 1981; EPRI 1982) refer to the median value, which is the L_{50} exceedance level, during periods of measurable rain. In addition to the L_{50} rain value, some methods calculate audible noise during periods of heavy rain. Heavy rain is variously defined as the maximum levels that would be encountered during rain or the L_5 exceedance level during periods of measurable rain. The heavy rain concept came about when test cages were first being used. The artificial rain spray systems used to wet conductors produce very heavy rain intensities that are rare in nature. A research facility that has used cages extensively defines heavy rain as any rain intensity above 1 mm/h (Coquard and Gary 1972; Clade et al. 1976), which is closer to the mean rain intensity in many moderate climates. At the EPRI Project UHV site, where many audible-noise data were obtained, the L_{50} natural rain intensity corresponded to about 0.75 mm/h and the L_5 natural rain intensity to about 6.5 mm/h (EPRI 1982). At this site many tests were performed with a test line under natural rain conditions and using cages with both natural and artificial rain. A special procedure was adopted for the cage tests with artificial rain resulting in "heavy rain" and "wet conductor" noise levels (see the glossary of terms). The heavy rain level was equated to the L_5 level in natural rain, and the wet conductor noise level was equated to the L_{50} noise level in natural rain and also to the highest level of noise that could be reached during fog.

10.4.2 Generation and Propagation of Audible Noise

The audible-noise performance of a transmission line is determined primarily by the noise generation, the propagation of the noise away from the line not being affected by the particular line configuration. The noise generation is composed of two components: broadband noise and a 100- or 120-Hz hum component for 50- and 60-Hz lines, respectively. Each corona burst initiates a broadband sound-pressure wave. The movement of ions generated by corona, alternately attracted and repelled by the 50/60-Hz line voltages, produces the 100/120-Hz hum. The laws of acoustics govern the propagation of corona-generated noise from conductors into the surrounding space. There are two cases to consider: the propagation of the broadband (random) component of the noise and the propagation of the pure-tone (hum) component of the noise.

The Audible-Noise Generation Function

For the purpose of calculating transmission-line audible noise, the corona process is quantitatively expressed in terms of the audible-noise generation function, A, a concept introduced in Chapter 8. Since audible noise has a broadband component and a 100/120-Hz hum component, a generation function for each component is required. During the years in which Project UHV was essentially a single-phase transmission research facility, a very large number of different conductor geometries were tested, both on the overhead test line and in the test cages (EPRI 1982). Audible-noise data collected during these tests were used in the development of two general formulas that could be used to calculate the generation function of the broad-band and hum components for any conductor configuration. The generation quantity is independent of the ground geometry and depends only on the electric field conditions in the immediate vicinity of the conductor under test. If the electric field conditions around a conductor on a three-phase line are reproduced around a similar conductor under test in a single-phase test cage or on a test line, then the corona generation per unit length is also reproduced. Thus, generation functions determined from single-phase tests may be used as the starting point for calculating three-phase transmission-line audible noise.

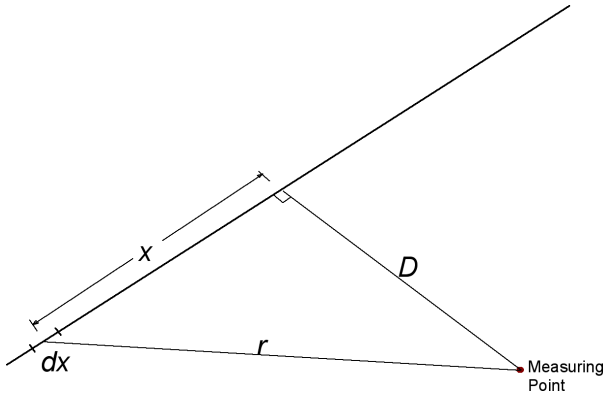


Figure 10.4-1 Geometry for a single conductor far from ground.

Single-Conductor, Broadband Components

To apply the laws of acoustics to transmission lines, certain assumptions must be made concerning the nature of the noise source. Consider an ideal case of a single conductor far removed from ground. Assume that corona is uniformly distributed along the length of the conductor, so that the noise power generated per unit length, A, is constant. Also assume that the microphone with which the measurements are made is ideal, responding equally to sound-pressure waves irrespectively of the angle of incidence. Further, assume that no energy is lost by the waves as they travel through the air.

For this case, each elemental length dx (Figure 10.4-1) generates a noise power equal to $A \cdot dx$. This elemental length approximates a point source of noise from which the sound propagates in the form of a spherical wave. At a distance, r, from the source, the sound energy is uniformly distributed over the imaginary sphere of radius r with an acoustic power density equal to

$$dJ = \frac{A \cdot dx}{4\pi r^2} \qquad 10.4\text{-}3$$

The sound pressure, dP, resulting from the noise generation of the element, dx, is related to the acoustic power density by

$$dP = \sqrt{\delta v \cdot dJ} = \sqrt{\frac{\delta v A}{4\pi r^2}\,dx} \qquad 10.4\text{-}4$$

δ is the air density and v is the velocity of propagation.

Due to the uncorrelated nature of the corona sources, the pressure waves from each individual element of conductor arrive at the point of observation with a random phase relationship. The sound pressure due to corona from the entire line length is therefore determined from the quadratic summation of the sound pressures from the individual elements according to Equation 10.4-5.

$$P = \sqrt{\sum_i dP_i^2} \qquad 10.4\text{-}5$$

Changing the summation into an integral form results in

$$P = \sqrt{\int_l \frac{\delta v A}{4\pi r}\,dx} \qquad 10.4\text{-}6$$

l indicates an integration over the length of the line.

From Figure 10.4.1

$$r^2 = D^2 + x^2 \qquad 10.4\text{-}7$$

D is the radial distance from the line to the point of observation.

If the point of observation is midway along a line segment of length l, then

$$P = \sqrt{\int_{-l/2}^{l/2} \frac{\delta v A}{4\pi(D^2 + x^2)}\,dx} \qquad 10.4\text{-}8$$

from which

$$P = \sqrt{\frac{\delta v A}{2\pi D}\tan^{-1}\left(\frac{l}{2D}\right)} \qquad 10.4\text{-}9$$

For the practical case, when $l >> 2D$, Equation 10.4-9 reduces to

$$P = \sqrt{\frac{\delta v A}{4D}} \qquad 10.4\text{-}10$$

Equation 10.4-10 indicates that the sound pressure varies inversely with the square root of the distance from the line—i.e., the sound pressure decreases by 3 dB for every doubling of distance.

It is common practice to express the sound pressure, P, in terms of dB. To do this, a reference sound pressure must be chosen. If P_0 is the reference pressure, then Equation 10.4-10, in terms of dB, becomes:

$$P(dB) = 10\log A + 10\log\frac{\delta v}{4} - 10\log D - 20\log P_0 \qquad 10.4\text{-}11$$

The sound-pressure level of 20 μPa, which is approximately the threshold of hearing, has been adopted as the

reference level. In Equation 10.4-11, P_0 is 20 μPa, A is given in units of W/m, R in m, and for normal atmospheric

$$\delta = 1.29 \text{ kg/m}^3 \quad 10.4\text{-}12$$

$$c = 331 \text{ m/s} \quad 10.4\text{-}13$$

Equation 10.4-11 then becomes:

$$P(dB\ ref\ 20\,\mu Pa) = 10\log A + 10\log(106.8) - 10\log D - 20\log(20\cdot 10^{-6}) \quad 10.4\text{-}14$$

$$P(dB\ ref\ 20\,\mu Pa) = 114.3 + 10\log A - 10\log R \quad 10.4\text{-}15$$

In the following, it will be understood that when P is expressed in dB, it is referenced to 20 μPa.

Determination of Generated Acoustic Power from Cage and Single-Phase Line Tests

The generated acoustic power is independent of the location of the conductor with respect of other energized conductors and ground, as long as the conductor geometry, surface gradient, surface conditions, and corona sources are the same (Comber and Zaffanella 1974). The microphone is placed in the middle of the conductor section being tested either in a cage or on a single-phase line. Equation 10.4-9 is used to derive the generated acoustic power from the measured pressure level. In this equation, D is the distance between conductor and microphone, and l is the length of the conductor under test. Since the microphone is placed relatively close to the conductor, there is no need to consider any attenuation caused by the air absorption of sound energy, which is discussed later in this section.

Single-Conductor, Pure Tones

The 100/120-Hz pure-tone component of the noise produced by corona results from the motion of the positive and negative ions of the corona space charge, as they are alternately attracted to, and repelled from, the conductor under the influence of the alternating field in the immediate vicinity of the conductor. If corona is uniformly distributed along the conductor (as assumed), the resulting pressure wave propagates in a cylindrical fashion because all points along the conductor experience the same variation of field—i.e., the motion of the space charge is in phase along the conductor length. If A_h represents the pure-tone generated power per unit length of conductor, the sound energy at a distance, D, from the conductor is uniformly distributed over the imaginary cylinder of radius D, with an acoustic power density given by Equation 10.4-16.

$$J = \frac{A_h \cdot dx}{2\pi D \cdot dx} = \frac{A_h}{2\pi D} \quad 10.4\text{-}16$$

Using the relationship expressed in Equation 10.4-4, the pure-tone sound pressure is obtained:

$$P_h = \sqrt{\frac{\delta v A_h}{2\pi D}} \quad 10.4\text{-}17$$

As for the broadband noise, the pressure is inversely proportional to the square root of distance—i.e., the pressure decreases by 3 dB for each doubling of distance laterally away from the line.

Presence of Ground

The ground acts as a reflective surface that provides an indirect path of travel for pressure waves from the line source to the point of measurement (see Figure 10.4-2).

The ground is fairly absorbent at high frequencies, and the net effect of reflections on A-weighted measurements is practically negligible. For low frequencies (e.g., the 100/120-Hz component of the line noise), the ground is a good reflector.

The reflected wave arrives at the microphone with a pressure given by:

$$P\text{ref} = K \cdot P(S) \quad 10.4\text{-}18$$

K is the ground reflection coefficient (at 100/120 Hz this is practically unity) and $P(S)$ is the sound pressure found from Equation 10.4-17 by substituting the indirect travel distance S for the direct distance D.

For an n-conductor system above ground, there would be $2n$ sound waves arriving at the point of measurement, n direct and n reflected waves. The total pressure is the phasor sum of all the individual wave pressures. Since the pure-tone pressure waves are phase-related, there is an opportunity for phase addition or phase cancellation of waves. This pro-

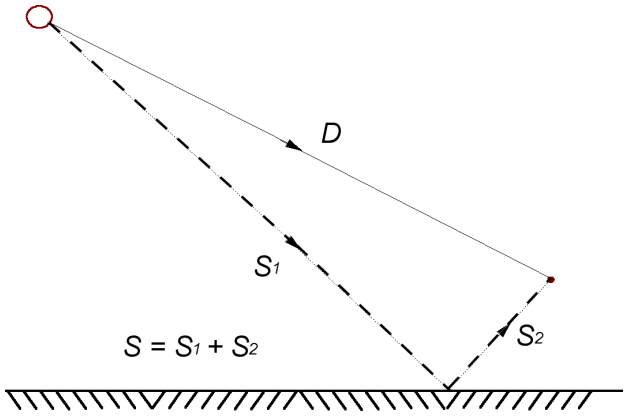


Figure 10.4-2 Direct and indirect (ground-reflected) paths from line source to microphone.

duces a very complicated profile of pure-tone sound-pressure measurements as indicated in Figure 10.4-3.

Air Absorption of Sound Energy

In a nondissipative medium, sound-pressure levels attenuate with distance away from a source by divergence only—i.e., the power generated by the source is spread over an ever-increasing area, as in the case of cylindrical divergence of the noise away from a line source. In reality, some energy is lost by molecular absorption as the sound waves travel through the air, resulting in additional attenuation. The absorption is thus a complex function of frequency, temperature, and relative humidity, as indicated in Figure 10.4-4 (S.A.E. 1964). Because of the number of variables involved, absorption cannot easily be incorporated into the calculation of transmission-line noise.

Typically, for distance up to about 100 m from the line, the absorption may result in a reduction of 1-2 dB of the A-weighted level. According to the EPRI method (see Section 10.4-3), the effect of absorption may be reasonably approximated by:

$$\text{Absorption} = -0.02\,D \text{ dB} \qquad 10.4\text{-}19$$

D is the distance from the line to the measuring point. This may be included in Equation 10.4-15 to give:

$$P = A + 114.3 - 10\log D - 0.02D \qquad 10.4\text{-}20a$$

Both P and A are expressed in dB.

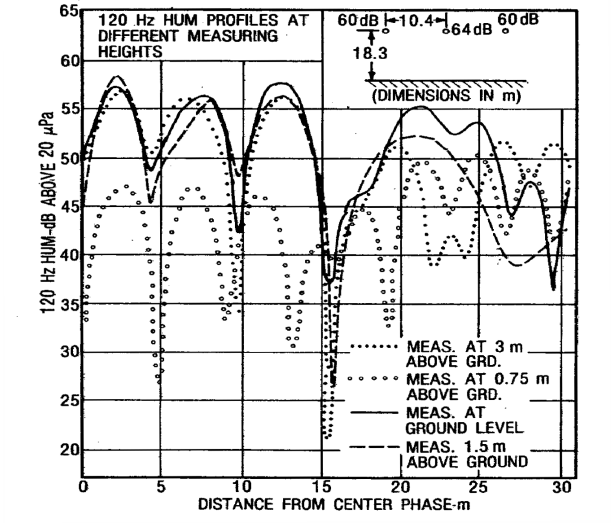


Figure 10.4-3 Example of 120-Hz pure-tone profiles for different heights of microphone above ground. Generation in dB above 1 μW/m.

According to the BPA method (see Section 10.4-3), the combined effect of divergence from a line source and absorption of sound energy by the air is estimated to cause an audible noise variation with distance proportional to $(1/D)^{0.57}$. Equation 10.4-20a becomes Equation 10.4-20b.

$$P = A + 114.3 - 11.4\log D \qquad 10.4\text{-}20b$$

Note that Equations 10.4-20a and 10.4.20b give the same result at a distance of about 150 m.

Figure 10.4-4 shows that air absorption is greater at higher frequencies. At frequencies below 500 Hz, it has a negligible effect. For the 100/120-Hz hum component, no attenuation should be considered.

Addition of Noise from Difference Phases

Each phase may be considered as a separate line source. The sound pressure of the multi-phase system may be found by summing the contributions from the individual phases (for bundled phase conductors, the entire bundle may be considered as a single line source).

For the broadband component of noise, a quadratic summation (square root of the sum of squares) is used because of the uncorrelated nature of the sources. The total pressure, P_{tot} (dB), resulting from the combination of the audible noise of the N_p phases may be calculated by

$$P_{tot} = 20\log\left[\sum_{i=1}^{N_p}\left(10^{P_i/20}\right)^2\right]^{1/2} \qquad 10.4\text{-}21$$

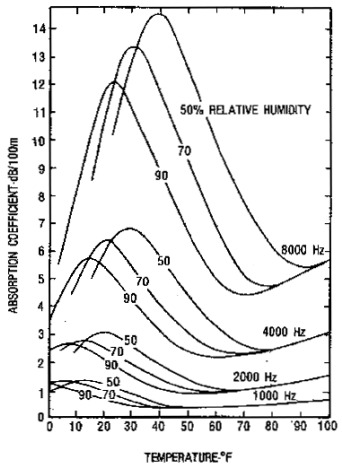


Figure 10.4-4 Effect of temperature, relative humidity, and frequency on air absorption of sound-pressure waves.

or, simplifying:

$$P_{tot} = 10 \log \sum_{i=1}^{N_p} 10^{P_i} / 10 \qquad 10.4\text{-}22$$

P_i is the audible noise produced by phase i in dB given by Equation 10.4-20a or 10.4-20b.

According to the EPRI method:

$$P_i = A_i + 114.3 - 10 \log D_i - 0.02 D_i \qquad 10.4\text{-}23a$$

According to the BPA method:

$$P = A_i + 114.3 - 11.4 \log D \qquad 10.4\text{-}23b$$

A_i is the generated acoustic power (dB above 1 W/m) of the i^{th} phase and D is the distance (m) from the i^{th} phase to the calculation point. Using Equations 10.4-22 and 10.4-23, the sound pressure from any single, double, or multiple-circuit line arrangement can be calculated.

For the pure-tone components, such as the hum at twice the power frequency, the phase of the individual pressure waves must be taken into account. The pure-tone sound pressure for phase i will be a sinusoidal function expressed as:

$$\tilde{P}_i = \sqrt{2} \sqrt{\frac{\delta v A_{hi}}{2\pi D_i}} \cos(\omega t - \Phi_i - 2\pi D_i / \lambda) \qquad 10.4\text{-}24$$

where A_{hi} is the rms, pure-tone, generated acoustic power due to corona on phase i, ϕ is the phase angle of the charge (practically coinciding with the phase angle of the voltage) of phase i, D_i is the distance from the phase to the measurement location, λ is the wavelength of the pure-tone pressure wave (3.42 m for 100 Hz, 2.85 m for 120 Hz, in air and for normal atmospheric conditions), δ is the air density, and v is the velocity of sound ($\sqrt{\delta v}$ = 20.5 for normal atmospheric conditions). In addition to the pure-tone direct wave, there may be an indirect or reflected wave. The pure-tone reflected wave will also be sinusoidal and may be expressed as:

$$\tilde{P}_{r,i} = K \cdot \sqrt{2} \sqrt{\frac{\delta v A_{hi}}{2\pi S_i}} \cos(\omega t - \Phi_i - 2\pi S_i / \lambda) \qquad 10.4\text{-}25$$

K is the reflection coefficient (usually 1 for a 100/120-Hz hum), S_i is the distance traveled by the reflected wave from point of generation to point of measurement (see Figure 10.4-2), and all other terms are the same as in Equation 10.4-24.

The total pressure from a line with N_p conductors may then be calculated by adding the direct and reflected phasors, or:

$$\tilde{P}_{total} = \sum_{i=1}^{N_p} (\tilde{P}_i + \tilde{P}_{r,i}) \qquad 10.4\text{-}26$$

Other Considerations

The preceding calculation methods apply only to the calculation of audible noise in the unobstructed space near a transmission line. Reflections from objects close to the point of measurement may have a significant effect. The attenuation of sound as it passes through structures may also have an important effect. If the sound has a broad frequency spectrum, the attenuation of different frequencies may not be the same, and hence the spectrum of the sound may change (EPRI 1982).

10.4.3 Calculation of A-Weighted Audible Noise-Levels in Rain

The two most widely used methods for the calculation of the A-weighted audible-noise levels during rain are the "EPRI method" developed at Project UHV (EPRI 1982) and the "BPA method" developed by the Bonneville Power Administration (Chartier and Stearns 1981). The detailed algorithms for these two methods are given in the following. These algorithms are incorporated in Applet AN-1, which the user may exercise to calculate the audible noise (dBA) produced by transmission lines of any voltage and geometry. The audible noise measured at a reference location and the effect of individual line parameters, such as conductor diameter, number of conductors, phase spacing, and height above ground may be calculated for a large number of line voltages and configurations using Applet AN-5.

EPRI Method

The method calculates a heavy rain value and an L_{50} level during measurable rain. The empirical equations to make these calculations are based on research and tests on a large variety of bundle configurations strung in special test cages (Juette and Zaffanella 1972; Comber and Zaffanella 1974) and on full-scale single-phase (Anderson and Zaffanella 1972) and three-phase test lines of various configurations (Comber and Nigbor 1976; Zaffanella et al. 1978). The EPRI method gives the audible noise for the condition of "heavy rain" and "wet conductor". During cage tests the heavy-rain audible noise was obtained with an artificial rain spray system that delivered uniform rain with diameter of water drops characteristics of natural rain (MacCarthy and Doyle 1969). On the basis of comparisons with tests in natural rain, the heavy-rain noise determined with cage

tests was equated to the L_5 level in natural rain—i.e., with the audible noise level exceeded for 5% of the time during which a measurable amount of rain was detected. This corresponded to rain intensity for the site equal to about 6.5 mm/h. During cage tests the wet-conductor audible noise was defined as the audible noise measured one minute after the rain spray system was turned off, when there were no more drops impinging on the conductors but water drops were hanging from the conductors. On the basis of comparisons with tests in natural rain, the wet-conductor audible noise determined with cage tests was equated to the L_{50} level in natural rain—i.e., with the audible noise level exceeded for 50% of the time when a measurable amount of rain was detected. The "wet conductor" term has caused some confusion in the industry. Some line designers in environmental impact statements have called the wet-conductor calculation an A-weighted audible noise level after the cessation of rain, when instead it is an L_{50} level during measurable rain. To prevent further confusion, in this edition of the reference book, the "wet-conductor audible noise" is called the "L_{50} audible noise level during periods of measurable rain" or simply the L_{50} rain audible noise.

To calculate the corona-generated audible noise in the vicinity of a power transmission line during heavy rain conditions, the following equations are used. The generated acoustic power, A, produced by a phase consisting of a bundle of n subconductors is given by:

For $n < 3$

$$A = 20\log n + 44\log d - 665/E_{\max} + K_n - 39.1 \qquad 10.4\text{-}27$$

For $n \geq 3$

$$A = 20\log n + 44\log d - 665/E_{\max} + (22.9(n-1)d/d_{eq}) - 46.4 \qquad 10.4\text{-}28$$

The sound-pressure level, P, due to each phase, is obtained combining the above equations with Equation 10.4.20:

For $n < 3$

$$P = 20\log n + 44\log d - 665/E_{\max} + K_n + 75.2 - 10\log D - 0.02D \qquad 10.4\text{-}29$$

For $n \geq 3$

$$P = 20\log n + 44\log d - 665/E_{\max} + (22.9(n-1)d/B) + 67.9 - 10\log D - 0.02D \qquad 10.4\text{-}30$$

Where:

P is the audible noise in dBA above 20 μPa.
A is the generated acoustic power in dBA above 1 W/m.
n is the number of subconductors in the bundle.
d is the subconductor diameter in cm.
E_{max} is the maximum surface gradient in kV/cm, calculated for an average height above ground equal to the minimum height plus 1/3 of the sag.
d_{eq} is the bundle diameter in cm.
D is the distance from the phase to the measuring point in m.
K_n is equal to 7.5 dB for $n = 1$ and 2.6 dB for $n = 2$.

Equations 10.4-27 to 10.4-30 were developed for conductor diameters in the range between 2 and 8 cm, which cover the practical range of transmission-line conductors. Audible-noise data for diameters up to 31 cm were developed for application to substation buses (EPRI 1982).

The sound-pressure level is calculated separately for each phase. The total sound-pressure level for all the N_p phases is then calculated using Equation 10.4-31.

$$P_{tot} = 10\log\sum_{i=1}^{N_p} 10^{P_i/10} \qquad 10.4\text{-}31$$

The L_{50} level during measurable rain is calculated by adding a correction factor to the heavy-rain level. To calculate the correction factor, the "6-dB gradient," E_c, must be calculated. The 6-dB gradient is the gradient at which the L_{50} level during measurable rain will be 6 dB below the heavy-rain level. The value of E_c depends to some extent on the number of subconductors and is given by Equations 10.4-32 and 10.4-33.

For $n \leq 8$ $E_c = 24.4/d^{0.24}$ 10.4-32

For $n > 8$ $E_c = 24.4/d^{0.24} - 0.25(n-8)$ 10.4-33

Where:

E_c = 6-dB gradient, kV/cm.
n = number of subconductors.
d = subconductor diameter, cm.

The correction to apply to the heavy generated acoustic power in order to obtain the L_{50} level during measurable rain, ΔA, is:

For $n < 3$ $\Delta A = 8.2 - \dfrac{14.2E_c}{E_{\max}}$ 10.4-34

For $n \geq 3$

$$\Delta A = 10.4 - \frac{14.2E_c}{E_{\max}} + [8(n-1)d/d_{eq}] \qquad 10.4\text{-}35$$

To calculate the L_{50} level during measurable rain:

1. Calculate the heavy-rain (L_5 rain) sound-pressure level for each phase according to Equation 10.4-29 or 10.4-30.
2. Calculate the 6-dB gradient, E_c, using Equation 10.4-32 or 10.4-33.

3. Calculate the L_{50} correction for each phase using Equation 10.4-34 or 10.4-35.
4. Add the L_{50} correction to the L_5 sound pressure level calculated in step 1 for each phase.
5. Sum the sound-pressure levels calculated in step 4 using Equation 10.4-31.

BPA Method

The BPA method was developed mainly from long-term statistical data collected on full-scale operating and test lines that for the most part had conductors that were well aged. The BPA method calculates the L_{50} level during measurable rain conditions. Long-term audible-noise and rain measurements show that the L_{50} A-weighted audible noise level occurs at an L_{50} rain intensity level of about 1 mm/h.

The BPA method does not have a separate equation for calculating heavy-rain audible noise. As was mentioned earlier, heavy rain is not easily defined. The heavy artificial rains used in test cages at various research centers are not the same; the rain intensities produced by these artificial rain spray are not common in nature; and there are no noise regulations based upon heavy rain. If a heavy-rain value is required, the BPA method recommends that 3.5 dB be added to the L_{50} rain calculation. The BPA method assumes that the slopes of the A-weighted audible-noise statistical distributions for measurable rains are about the same when plotted on a probability paper for all lines in all climates. This assumption has been pretty much verified by measurements on three-phase lines in both wet and dry climates; at different altitudes; and over a wide range of conductor surface gradients. Figure 10.4-5 shows all-weather A-weighted audible-noise probability distributions for two lines that were about 6 miles from each other in western Oregon. The upper portions of the curves (values exceeded for more than about 10% of the time are close to straight lines and represent the measurable rain distributions; and as can be seen, they have exactly the same slopes, even though the conductor surface gradients are quite a bit different. The maximum conductor surface gradient for the 7 x 4.1 cm conductors on the 1200-kV test line operating at 1160 kV was 15.9 kV/cm, whereas the maximum conductor surface gradient for the two parallel 500-kV lines operating at 540 kV was 18.4 kV/cm.

The L_{50} measurable rain A-weighted generated acoustic power, A, of each phase is given by:

For $n < 3$ $A = 55\log d + 120\log E_{\max} + Alt./300 - 229.7$ 10.4-36

For $n \geq 3$

$$A = 26.4\log n + 55\log d + 120\log E_{\max} + Alt./300 - 242.7$$ 10.4-37

The sound-pressure level, P, is obtained combining the above equations with Equation 10.4-20a:

For $n < 3$

$$P = 55\log d + 120\log E_{\max} + Alt./300 - 115.4 - 11.4\log D$$ 10.4-38

For $n \geq 3$

$$P = 26.4\log n + 55\log d + 120\log E_{\max} + Alt./300 - 128.4 - 11.4\log D$$ 10.4-39

Where:

- P is the audible noise in dBA above 20 μPa.
- A is the generated acoustic power in dBA above 1 W/m.
- n is the number of subconductors in the bundle.
- d is the subconductor diameter in cm.
- E_{max} is the maximum gradient in kV/cm, calculated for an average height above ground equal to the minimum height plus $^1/_3$ of the sag.
- $Alt.$ is the altitude above sea level in m.
- D is the distance from the phase to the measuring point in m.

The total sound-pressure level, expressed in dBA, produced by a line with N_p phases is given by Equation 10.4-31.

10.4.4 Audible Noise in Fair Weather

A transmission line designed to have an acceptable audible-noise level in rain will usually not generate appreciable audible noise in fair weather. In fair weather, corona noise of most lines, even when detectable by the human ear, cannot be measured above ambient noise unless the ambient is extremely quiet. Fair-weather audible noise has large daily and seasonal variations. The number of audible fair-weather sources in corona for high-voltage transmission lines in the United States was found to vary from none to forty per 100 m of three-phase line (EPRI 1982). The lowest number corresponds to winter months and the highest to the month of August. Audible corona sources also depend on the climate, especially on the amount of rainfall, being washed out by a thunderstorm and accumulating during a long period without rain. For this reason, fair-weather noise data are almost nonexistent and, if they exist, they are anecdotal. When a value for audible noise in fair weather is to be provided for lines operating at normal conductor surface gradients, a customary approach is to subtract a fixed amount of dB from the L_{50} rain noise—e.g., 25 dB (Chartier and Stearns 1981). This correction, even though it may not be accurate in all cases, may be safely applied if the conductor surface gradient is below 15 kV/cm and the altitude above sea level is below 1000 m.

While fair-weather audible noise is of little significance in most cases, its level increases rapidly with the surface gra-

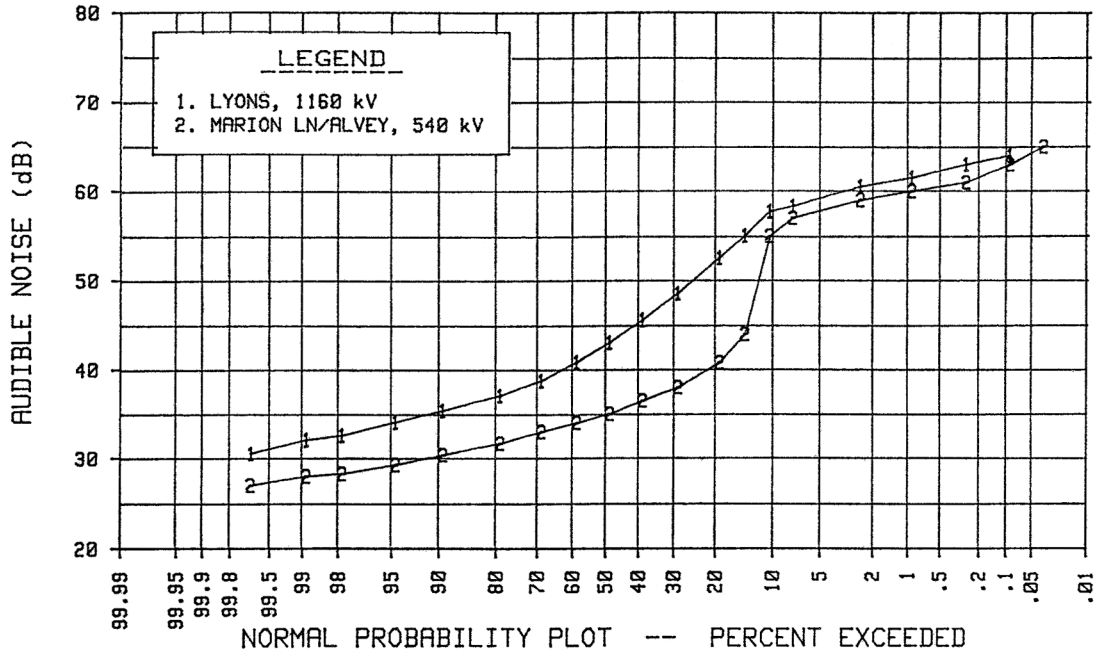


Figure 10.4-5 A-weighted all-weather night-time audible-noise distributions comparing the unloaded Lyons 3-phase, 7 x 4.1 cm configuration with two loaded BPA 500-kV lines located near Lyons, Oregon. Measurements made at 15 m (Stearns 1980).

dient to the point that, at very elevated gradients it may reach and even surpass the noise level in rain (see Figure 10.4-12). The difference between rain and fair-weather noise is not a constant but decreases with increasing conductor surface gradient. Fair-weather noise on a line can suddenly increase due to the presence of dust particles, insects, and other aerosols. For example, when fair-weather noise data was being logged over a 24-h period on a 500-kV line in southern California in February, the noise suddenly increased from about 32 dBA to as high as 48 dBA during evening hours at the measurement distance of 15 m from the outer phase. Levels above 40 dBA lasted for about 90 minutes and never occurred again during the 24-h measurement period. Corona plumes could be seen up and down the conductors with the naked eye. It is not clear what caused the sudden increase in fair-weather noise, but the most likely cause was either insects or dust particles suddenly appearing on the conductors in this dry area of California. The L_{50} dry weather level during this 24-h period was 32 dBA.

As was mentioned earlier, fair-weather audible noise tends to be lower during the winter months and higher during the summer months. Not only does the number of sources increase during the summer months, but also the noise may increase due to the increased conductor temperatures as shown in Figure 10.3-4. The data shown in Figure 10.3-4 were collected on a BPA corridor that had a combination of 500-kV and 230-kV lines. In fair weather during hot summer days and especially during daytime hours, loud bursts of corona could be heard from the 500-kV line with a single 6.35-cm conductor, whereas very little noise could be heard from the 500-kV line with bundles of three 3.3-cm conductors. The mean fair-weather audible noise produced by the line with the single 6.35-cm conductor during hot summer days was estimated to be about 50 dBA at 15 m from the outside phase. Observations on this line during the winter months and long-term measurements on other BPA lines using the single 6.35-cm conductor have shown that even on this noisy line the difference between L_{50} rain and L_{50} (year-round) fair-weather levels can be as high as 25 dBA.

A few examples of lines for which fair-weather audible-noise data are available are shown in Table 10.4-1. It needs to be mentioned that the center phase of the Apple Grove C-line was audibly very noisy, independent of the time of the year. The spread in the A-weighted fair-weather audible noise from this line over a year was only 5 dB (Kolcio et al. 1974), whereas the spread on the BPA 500-kV line with the single conductor has been estimated to be around 14 dB. The fair-weather values in Table 10.4-1 for the BPA Marion-Alvey-Lane 500-kV line and the BPA double circuit line at 1935 m in Montana are the L_{50} values from the lower normal distributions in Figures 10.4-5 and 10.6-3. The Montana line, where it goes over the Continental Divide is in a very clean environment. The Marion-Alvey-Lane lines are in a relatively clean rural environment. More accurate estimates of fair-weather audible noise levels of a

given line design would require long-term measurements on a similar line in a similar environment.

It is possible to estimate the fair-weather audible noise by using data derived from test lines and test cages on a variety of conductors performed at the EPRI laboratory (EPRI 1982) and from cage tests at high altitude performed by Eskom (South Africa). The data are presented in Figure 10.4-6 as the fair-weather noise relative to the L_5 rain noise versus the maximum conductor surface gradient. At a sufficiently high gradient, which depends on the conductor diameter, the fair-weather noise tends to be equal to the rain noise. In order to report the high-altitude data on the same graph as the data obtained at the EPRI laboratory, the difference between fair-weather and L_5 rain noise is reported versus the equivalent sea-level surface gradient, obtained by dividing the actual gradient by the relative air density. Figure 10.4-6 shows a large possible range of values, which reflects the variability and the ill-defined nature of fair-weather corona sources. Data obtained in one climate may not be reproduced in another climate.

The data of Figure 10.4-6 are incorporated in Applet AN-1, which the user may exercise to calculate the possible range of fair-weather audible noise (dBA) produced by transmission lines of any voltage and geometry.

10.4.5 Influence of Tower, Sag, and Ground Wires

In general, audible noise is calculated considering the line as a two-dimensional geometry. Calculations of audible noise for three-dimensional geometry can be made using the same equations for generated acoustic power, for instance, Equations 4.10-27 and 4.10-28. The generated acoustic power, however, must be calculated for short conductor segments along which the surface gradient may be considered constant. Thus, it is necessary to divide the conductors in a large number of segments, to calculate the surface gradient for each segment, and then calculate the generated acoustic power and the pressure level. These algorithms are incorporated in Applet AN-2, which may be used for three-dimensional geometry, such as a transposition span or lines crossing at an angle. This applet may also be used to calculate the effect of sag and the presence of the towers.

Usually, the effect of both sag and towers are ignored. These elements affect the conductor gradient as shown in Figure 10.4-7. The figure shows the separate and combined effects of the presence of the tower and of the height of the conductor above ground on the conductor gradient. It can be seen that the conductor gradient changes very little. In addition, the sag influences the noise at ground level along the transmission line from midspan to tower, especially within, or close to, the right-of-way because of the different distances of conductor to ground. This is shown in Fig-

Table 10.4-1 Fair Weather Data from 3-Phase Lines

Line	No. of Cond.	Cond. Diam. (cm)	Line Volt (kV)	Conductor Gradient		Estimated Fair-Weather Range (dBA)	L_{50} Rain (dB)	L_5 Rain (dB)
				Outside Phase (kV/cm)	Center Phase (kV/cm)			
Apple Grove C (Kolcio et al. 1974)	4	2.54	775	22.8	24.4	53 - 57	62	64
Eskom High-Altitude=1500 m	2	3.55	420	15.3	15.8	41 - 46	56.5	
BPA Marion-Alvey-Lane (Chartier and Stearns 1981)	2	4.07	540	See Note # 1		28 - 40	60.5	64
BPA dble ckt Altitude=1935 m (Chartier et al. 1987)	3	4.07	530	See Note # 2		20 - 43	55.5	60
BPA Ostrander 1 (Perry 1972; Chartier 1989; Chartier 1994)	3	6.35	525	15.8	16.8	36 - 50	61.4	64

Note 1.Gradients: A1=C2=18.3 kV/cm; B1=B2=17.34 kV/cm; C1=A2=18.38 kV/cm.

Note 2.Gradients: A1=C2=14.70 kV/cm; B1=B2 14.10 kV/cm; C1=A2=15.0 kV/cm.

Apple Grove C-line: fair-weather range shows L_5 and L_{95} levels from Figure 8 (Kolcio et al. 1974).

Eskom High Altitude: fair-weather range determined from measurements conducted over a 4-h measurement period from 00H00 to 04H00.

BPA-Marion-Alvey-Lane and BPA double circuit: nighttime fair-weather ranges determined from probability distributions; see Figures 10.4-5 and 10.6-2.

BPA Ostander: fair-weather ranges determined from two different long-term measurement periods.

ure 10.4-8 for lateral distances, *L*, from the line center of 0, 30, and 90 m.

The ground wires do not appreciably contribute to the total audible noise of the transmission line. Because of their small size, the ground wires do not significantly increase the surface gradient of the phase conductors. The ground wires generally have a low operational surface gradient and therefore do not produce visual corona, audible noise, and radio noise. Furthermore, from a corona consideration, the ground wire will not degrade PVC-insulated lash-type fiber optic cable that may be later strapped to the ground wire. This applies to voltages up to 500 kV; at 765 kV and higher, long-term degradation may occur.

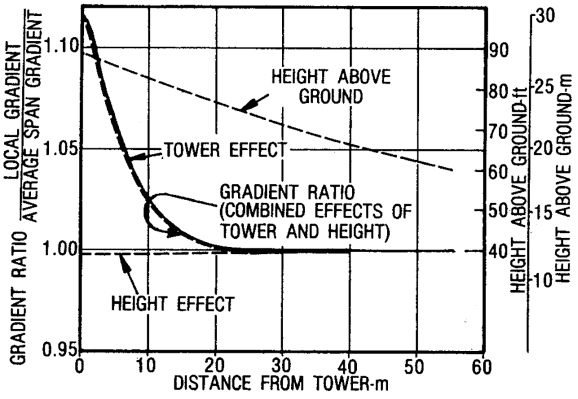


Figure 10.4-7 Influence of the tower and of the height above ground on the gradient for the center phase of a 500-kV transmission line.

10.4.6 Effect of Rain Rate

The audible noise generated by a transmission line varies as a function of the rain rate. The highest levels of noise are associated with the highest rain rates. Hence, if two transmission lines, identical in all respects, were located in dif-

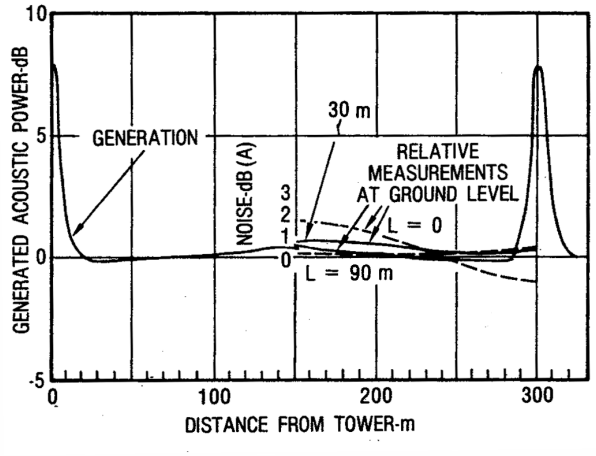


Figure 10.4-8 Noise generation along the span of a 500-kV transmission line. Audible noise at ground level referred to the noise of the ideal line with constant height and without towers.

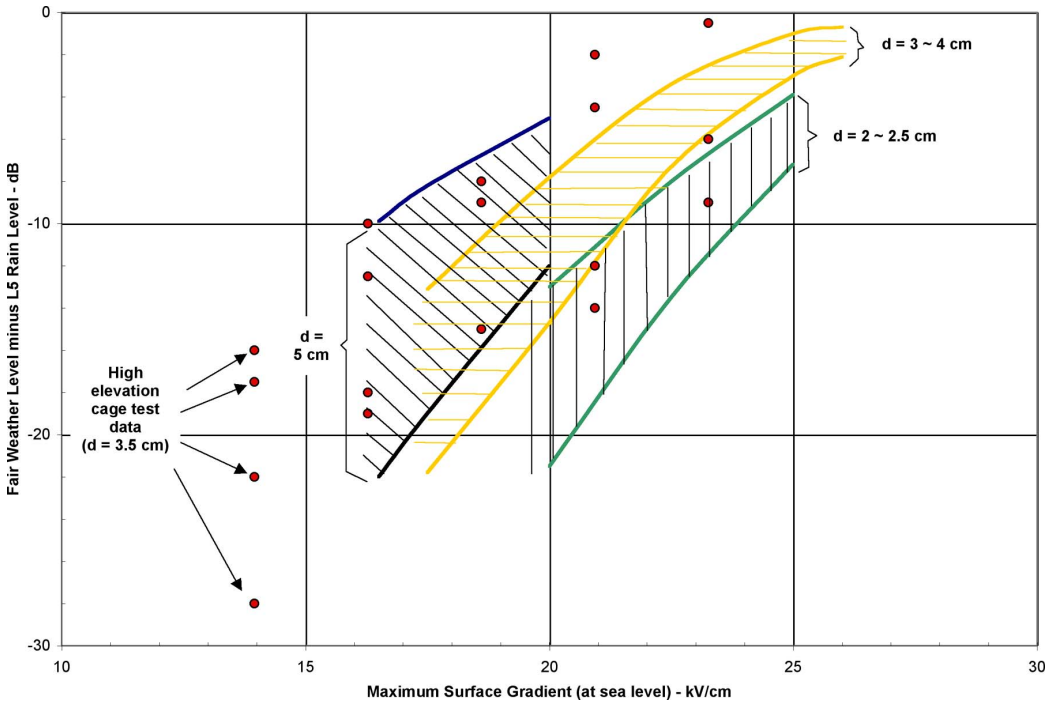


Figure 10.4-6 Fair-weather audible noise dBA referred to the L_5 rain noise value.

ferent regions of the country that had substantial differences in their rain rate distributions, then the audible-noise levels recorded would reflect those differences in rate.

The long-term rain rate, obtained over several years at the EPRI site in western Massachusetts where many audible noise data were obtained, is given in Figure 10.4-9. The L_{50} rain rate is 0.75 mm/h. The reference book audible-noise calculation made according to the EPRI method represents levels that would occur in a region having a similar long-term rain rate distribution. If calculated levels are required for a particular region whose long-term rain rate distribution deviates significantly from those shown by Figure 10.4-9, then a correction to the calculated levels should be applied.

The A-weighted audible noise varies in linear proportion to the logarithm of the rain rate (Lundquist 1990). The equations relating the generated acoustic power versus rain rate are of the type:

$$A = A_0 + k_r \log(RR) \qquad 10.4\text{-}40$$

Where:

A is the generated acoustic power expressed in dBA.
k_r is a coefficient (dB per decade).
RR is the rain rate (mm/h).
A_0 is the generated acoustic power, expressed in dBA, for a rain rate of 1 mm/h.

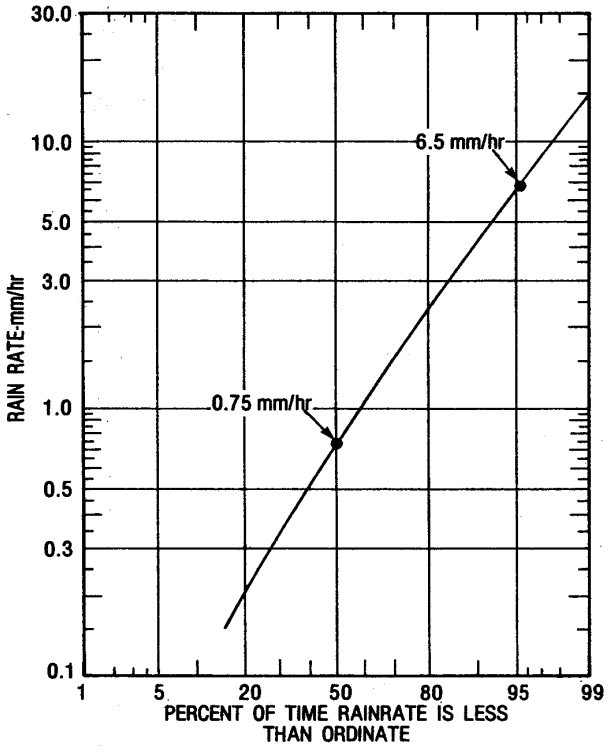


Figure 10.4-9 Long-term rain rate distribution at the EPRI site in western Massachusetts.

The coefficient k_r can be calculated using the EPRI method by noting that the difference between L_5 and L_{50} levels in rain is given by Equation 10.4-34 or 10.4-35 and that the long-term rain distribution at the location of the EPRI Laboratory had a 5% rain rate equal to 6.5 mm/h and a 50% rain rate equal to 0.75 mm/h (see Figure 10.4-9). Thus,

$$k_r = \frac{L_5 - L_{50}}{\log(6.5 / 0.75)} = 1.07 \cdot \Delta A \qquad 10.4\text{-}41$$

If the audible-noise levels are calculated for a line in a region whose long-term rain distribution deviates from that of Figure (10.4-9), then the L_5 and L_{50} levels in rain are calculated as follows:

1. The difference, ΔA, between L_5 and L_{50} measurable rain are calculated for each phase according to Equation 10.4-34 or 10.4-35. This is the difference between the noise levels corresponding to rain rates of 6.5 mm/h and 0.75 mm/h, which are the 5% and 50% rain rates in the climate where the EPRI method was developed.
2. The coefficient, k_r, is calculated with Equation 10.4-41.
3. The 5% and 50% rain rate levels (RR_5 and RR_{50}) are obtained from the rain records of the region.
4. The sound-pressure level L_{50}, is calculated for each phase using the EPRI method.
5. The L_5 and L_{50} levels are calculated for each phase as follows:

For the L_{50} level: $$P = L_{50} + k_r \cdot \log\left(\frac{RR_{50}}{0.75}\right) \qquad 10.4\text{-}42$$

For the L_5 level: $$P = L_{50} + k_r \cdot \log\left(\frac{RR_5}{0.75}\right) \qquad 10.4\text{-}43$$

The user may calculate the audible noise versus rain intensity using Applet AN-6, which incorporates the algorithms of this section.

10.4.7 Effect of Conductor Aging

The effect of conductor aging on corona phenomena is discussed in Chapter 8 (Corona Phenomena). Its specific effects on audible-noise generation are discussed here.

Rain

Most new conductors have an oily surface that is part of the manufacturing process. The exception is non-specular conductors whose surfaces are blasted with fiberglass beads. This manufacturing process was developed primarily to eliminate the shiny surface on conductors, but it also eliminates most of the oil that creates a hydrophobic surface. When water is sprayed on a hydrophobic conductor, small beads of water are formed all over its surface. As the conductor is exposed to the elements, the oil breaks down and the water flows to the bottom of the conductor where it

forms a drip line. The rate at which it breaks down depends upon the time of the year. This oily surface can disappear as quickly as 4-7 months in an environment that is hot and humid in the summertime and cold and windy in the wintertime (Booker 1986). He also indicated that cold weather could inhibit this aging process by as much as 5 months.

Audible-noise measurements at the EPRI laboratory and other research facilities have shown that new conductors can be as much as 8 dBA noisier than aged conductors (EPRI 1982). Figure 10.4-10 shows the effect of aging on the audible-noise performance of an eight-conductor bundle installed on a three-phase test line.

The beading process not only increases the A-weighted audible noise, but also significantly increases the 100/120-Hz hum. When the BPA 500-kV line that had a single 6.35-cm conductor for each phase was first energized, the 120-Hz hum was quite large (Perry 1972). Over time this 120-Hz hum decreased significantly, as can be seen in Figure 10.4-11. The small water beads on a new conductor produce a lot more corona sources than what is formed on the drip line at the bottom of an aged conductor. It is speculated that the glow corona off of these small beads produces an intense space charge and, therefore, a significant 100/120-Hz hum. When the space charge that causes the hum is very intense, it inhibits the formation of positive-polarity streamers that are responsible for the broadband noise. This effect is shown in Figure 10.4-11 by the increase in the noise components above 500 Hz as the conductor ages and the hum decreases in intensity. A similar effect occurs under icing conditions, when the hum and the corona loss are significantly above values obtained in

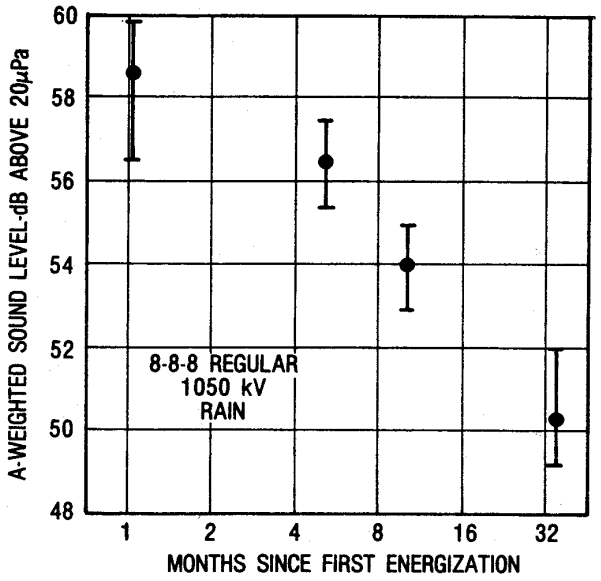


Figure 10.4-10 Effect of aging on the audible-noise performance of eight-conductor bundles.

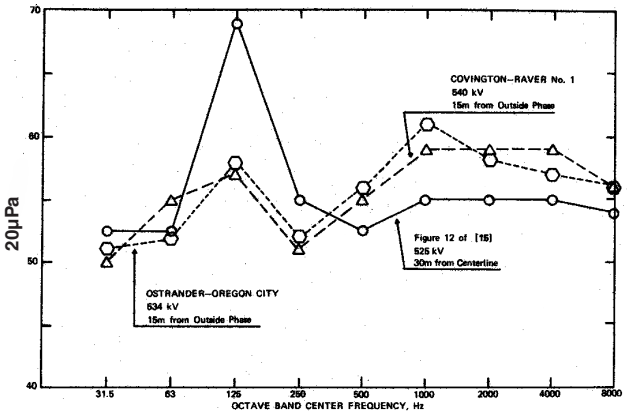


Figure 10.4-11 Octave band frequency spectra, single 6.35-cm conductor on BPA 500–kV lines.

rain, while the broadband noise is greatly reduced over the value in rain.

Another factor needs to be mentioned. When new conductors have been tested in cages or in HV laboratories, a rain spray system is normally used to wet the conductors. Researchers in conducting measurements of audible noise using these artificial rain systems have sometimes observed an increase in the audible-noise level when the rain spray is turned off. This phenomenon has not been observed on operating lines. At the EPRI laboratory this phenomenon was observed at very high surface gradients, and it was explained by the noise-reducing effect of the space charge, which is generated in large amounts at high gradients and at high rain rates. Tests on degreased conductors in the BPA HV laboratory have shown that the audible noise does not change when the spray system was turned off, whereas tests on new conductors have shown that the audible noise increases when the spray system was turned off. The explanation for this phenomenon appears to be that while the new conductors are being sprayed on, the downward force of the spray prevents some beading, especially at the top of the conductor. Once the spray is turned off, the beading reforms and the audible noise increases.

There is some indication that the expected audible-noise reduction due to conductor-surface aging diminishes as the operating conductor surface gradient is increased, but good quantitative information is not available. A qualitative illustration of the performance of new and aged conductors at different surface gradients and in different weather conditions is given in Figure 10.4-12.

Dry Conductors

When conductors are strung on new lines, they normally are not energized for several months. During this time, depending on the environment, they tend to collect dust, insects, etc. New conductors can also have a few aluminum

burrs all along the length of the conductors, which occurred during the manufacturing process. Because of these burrs and because of the particles that collect on the conductor during the months when the line was not energized, corona activity can be quite high when lines are first energized. Measurements conducted many years ago on a 345-kV line in central Iowa showed that the radio noise decreased about 6 dB in the first 20 minutes after the line was first energized. This data was taken before audible noise was an issue, but a similar decrease in audible noise would be expected. It is suspected that electrostatics forces blew off a lot of the loose aerosols. Over another 6 months the radio noise decreased another 6 dB. Here it was suspected that the reduction was the slow elimination by corona of the aluminum burrs and the insects and dirt that were stuck to the conductor.

10.4.8 Effect of Altitude above Sea Level

Air density affects both the generation and propagation of audible noise from transmission-line conductors. The greatest effect is on the generation, because air density affects both the inception and the development of positive-polarity streamers. At higher altitudes, streamer inception occurs at lower conductor surface gradients. Using a simplistic model, streamer inception and development can be considered the same as those occurring at standard air density but at conductor surface gradients multiplied by $1/\delta$, where δ is the relative air density referred to standard atmospheric conditions: 760 mmHg and 25 ºC. For instance, a conductor surface gradient of 15 kV/cm at an altitude of 1500 m, where the relative air density is 0.863, is equivalent to a conductor surface gradient of 17.4 kV/cm. For a 4.07-cm diameter conductor, the EPRI method calculates an increase in L_{50} rain noise of 8.3 dB, and the BPA method calculates an increase in L_{50} rain noise of 7.8 dB. The noise caused by each streamer is a pressure wave generated by the collapse of the pressure at the source. Therefore, the sudden variation in noise pressure is proportional to the air density. This effect translates into a decrease in noise. For instance, for a relative air density of 0.863 (1500-m altitude), the decrease in noise is 1.3 dB. The propagation of sound also is affected because it depends on the air density, as shown in Equation 10.4-11. At high altitudes this effect may be included by calculating the 10 log (δc/4) term in Equation 10.4-11 for both the standard air density and the actual air density. The effect of altitude on noise propagation results in a corrective term equal to 10 log δ, to be added to Equation 10.4-11. This corrective term is small (0.6 dB for an altitude of 1500 m), and it represents a decrease in noise with altitude. The combination of the generation and propagation effects illustrated by the above simplistic model results in an increase in noise of 5.9–6.4 dB for an altitude of 1500 m. Experimental results, however, indicate a smaller increase equal to 5 dB.

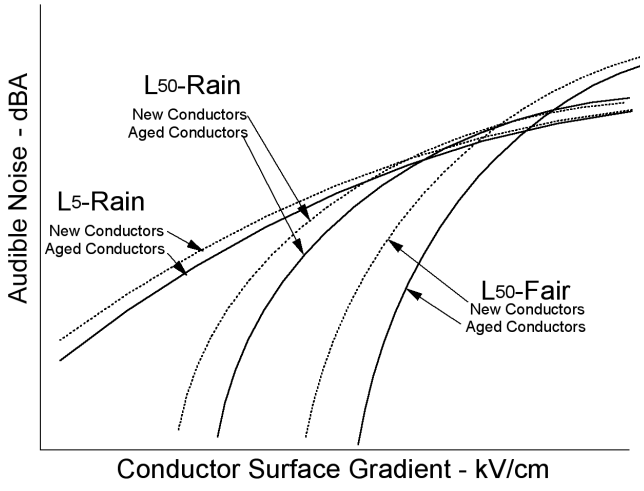


Figure 10.4-12 Qualitative curves for audible noise versus surface gradient for new and aged conductors in different weather conditions.

Audible-noise measurements conducted by BPA (Chartier, et al. 1987) have shown that the audible noise increases with altitude above sea level by an amount in dB equal to about *Alt.*/300 where *Alt.* is the elevation in meters. This term had previously been used in an Italian radio-noise formula (Paris and Sforzini 1968; IEEE 1973) and, based upon the audible-noise measurements conducted on the BPA 500-kV double-circuit line at 1935 m above sea level, appears to be valid for audible noise as well.

10.4.9 Effect of Bundle Orientation

In order to reduce subconductor oscillations, line designers sometimes prefer to use a vertical, rather than a horizontal, configuration for the two-conductor bundle and a diamond configuration, rather than a square configuration, for the four-conductor bundle. Cage tests performed at the EPRI laboratory determined that the bundle orientation does not have an appreciable effect on audible-noise generation for bundles with three or more conductors (EPRI 1982). For vertical two-conductor bundles, however, 1.5 dB should be added to calculations of L_{50} audible noise in rain since the prediction equations were developed for horizontal configurations (EPRI 1982). Because BPA was considering using four-conductor bundles for the first time on 500-kV lines at higher elevations, designers wanted to know whether the diamond configuration would be noisier than the square configuration. To answer this question, BPA conducted radio- and audible-noise tests on several different types of new and aged (degreased) conductors in their high-voltage laboratory under artificial rain conditions (Chartier et al. 1994). Two-conductor bundles were tested in a vertical and

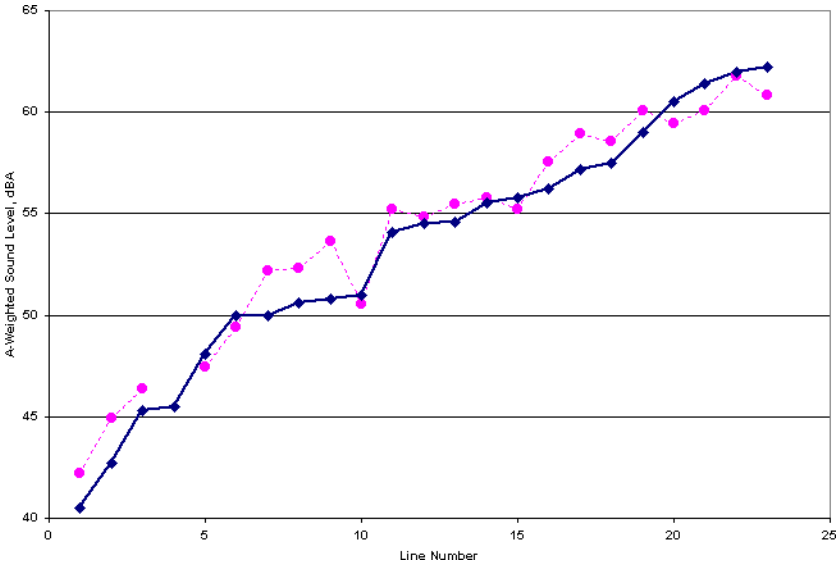


Figure 10.4-13 Comparison between L_{50} rain values calculated with the EPRI method and measured values (from Table 10.4-1).

horizontal configuration; three-conductor bundles in a vee and an inverted vee configuration; and four-conductor bundles were tested in a square and diamond configuration. No consistent difference in the audible- or radio-noise performance under artificial rain conditions could be found between each of the two configurations that were tested in a two-, three-, or four-conductor bundle.

10.4.10 Comparison of Audible-Noise Calculation Methods with Measured Data (Rain)

Several long-term audible-noise data from three-phase transmission lines are available. These data are reported in the technical literature and come from test and operating lines throughout the world. The data reported can be found in (Chartier and Stearns 1981; Yang et al. 2000), and are presented in Table 10.4-2. Figure 10.4-13 shows a comparison of the calculated and measured L_{50} measurable rain levels using the EPRI method and Figure 10.4-14 shows a similar comparison using the BPA method. Good agreement can found using both methods.

10.4.11 Generation and Calculation of Hum

The audible noise produced by transmission-line corona includes pure tones, the most significant of which occurs at twice the power frequency: 100 Hz for 50-Hz systems and 120-Hz for 60-Hz systems. This noise is referred to as the "hum."

In general the hum is not as objectionable as the high-frequency random noise. The A-weighted sound pressure level commonly used to quantify transmission-line audible noise is little affected by hum levels. However, there have been reports of occasional complaints about the hum, specifically, in contrast to the broadband component, from 500-kV lines in Japan (Tanabe 1991a, 1991b). The hum is particularly noticeable in heavy rain, ice, wet snow, or similar conditions that are also associated with a large amount of corona loss. In fact, the physical phenomenon that is responsible for corona loss—i.e., the alternating movement of air ions toward and away from the conductor surface twice during the power frequency cycle—is also responsible for the alternating change in air pressure. Laboratory tests have found a near-perfect correlation between corona loss and hum during rain with a 14-dB variation in hum level for a 10-fold increase in corona loss for different bundle configurations tested (EPRI 1982).

The hum is only slightly attenuated by air, trees, and walls. Therefore, at larger distances from the line or inside houses, the hum may become more noticeable in relation to the high-frequency random noise.

There are few experimental data on the level of hum (EPRI 1982; Tanabe 1991a). The generation of hum under conditions of heavy rain is expressed by the empirical Equation 10.4-44 derived from single-phase line and cage tests (EPRI 1982).

$$A_h = 58.1 - 41/d - 505.5/E_{\max} + k_1 - k_2/(n + k_3) \qquad 10.4\text{-}44$$

Where:

A_h is the hum-generated acoustic power in heavy rain, dB above 1 μW/m.

E_{max} is the maximum conductor surface gradient, kV/cm.

d is the conductor diameter, cm.

n is the number of conductors in the bundle.

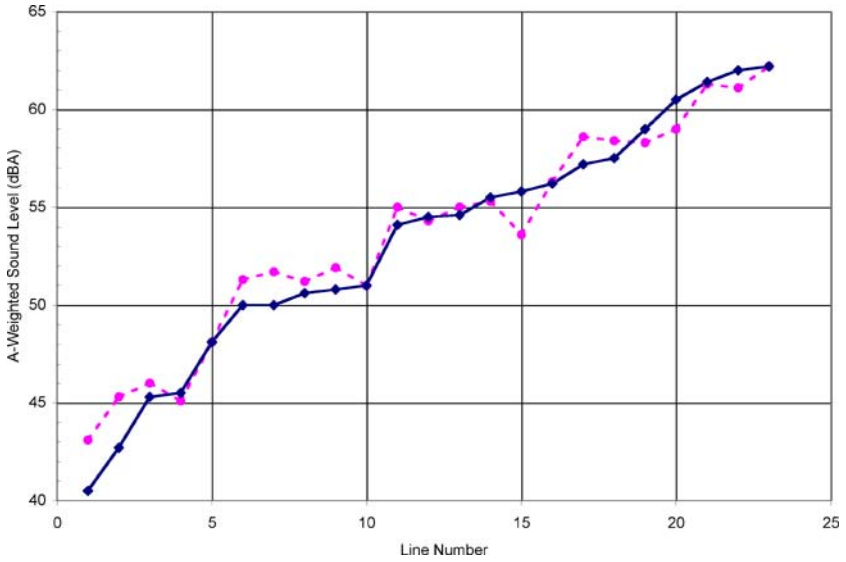


Figure 10.4-14 Comparison between L_{50} rain values calculated with the BPA method and measured values (from Table 10.4-1).

k_1, k_2, and k_3
are constants dependent on conductor diameter as follows:
For d = 2.3 cm k_1 = 47.4 k_2 =1000 k_3 =15
For d = 4.63 cm k_1 = 24.1 k_2 =390 k_3 =10
For other diameters, linear interpolation or extrapolation is suggested.

The hum is very sensitive to rain intensity, much more than the broadband noise (Tanabe 1991a). Equation 10.4-44 applies to a heavy rain level of about 6.5 mm/h. For a rough estimate of the hum level at the rain intensity of 0.75 mm/h (L_{50} level at the EPRI Laboratory in Lenox, MA) the difference between L_5 and L_{50} levels found with Equations 10.4-34 and 10.4-35 should be increased by 3 dB.

The hum-generated acoustic power expressed in W/m is obtained using Equation 10.4-45.

$$A\,(W/m) = 10^{A_h/10} \cdot 10^{-6} \qquad 10.4\text{-}45$$

The hum level at a measuring point is the result of the addition of pressure waves coming from each phase of the line, both directly or after a reflection at ground, as shown in Figure 10.4-15.

The sound pressures of direct and reflected waves are given (in units of Pascal) by Equations 10.4-24 and 10.4-25, respectively. The reflection coefficient K in Equation 10.4-25 is approximately equal to 1 for most practical terrains. The total pressure is calculated by adding the pressures from all direct and reflected waves, as indicated by Equation 10.4-26. Finally the hum dB-level is obtained from the pressure level, P, expressed in Pa, using Equation 10.4-46.

$$P\,(dB\,above\,20\,\mu Pa) = 10\log\left(\frac{P}{20\cdot 10^{-6}}\right) \qquad 10.4\text{-}46$$

The lateral profile of the hum level can be calculated using Equations 10.4-44, 10.4-45, 10.4-24, 10.4-25, 10.4-26, and 10.4-46. These algorithms were incorporated in Applet AN-4. With applet AN-4, the user may calculate the hum profile for any line voltage and geometry.

The hum pressure level fluctuates widely as the height above ground and the distance from the line are changed. At some location the pressure waves add to each other,

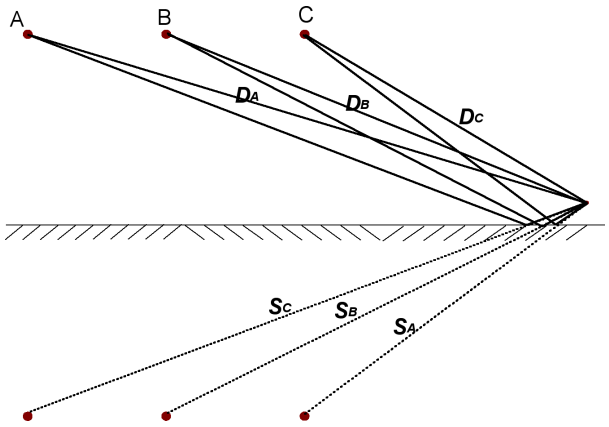


Figure 10.4-15 Direct and reflected pressure wave paths from a three-phase line.

Table 10.4-2 A-Weighted Audible Noise Data from Three-Phase Lines[1]

	Line	No. of Cond.	Cond. Diam. (cm)	Line Volt. (kV)	Horizontal Arrangement of Phases 1 (m)	2 (m)	3 (m)	Minimum Conductor Heights 1 (m)	2 (m)	3 (m)	Conductor Gradient (kV/cm) Outside Phase	Center Phase	L_{50} Rain (dBA)
1	BPA Lexington-Ross (Chartier and Stearns 1981)	1	2.81	240	-8.2	0.0	8.2	12.2	12.2	12.2	14.94	15.75	40.5[2]
2	Sweden 400 kV (Larsson 1988)	2	3.17	420	-11.0	0.0	11.0	12.0	12.0	12.0	15.60	16.58	42.7
3	BPA Ostrander 3 (Perry 1972)	3	3.31	525	-10.4	0.0	10.4	12.2	12.2	12.2	15.69	16.86	45.3[3]
4	Puget Power, Sedro-Woolley (Chartier et al. 1995)	1	3.30	235	-1.92	1.92	1.92	15.2	16.8	13.7	See Note #4		45.5
5	KEPCO dble ckt (Lee 1997)	6	3.04	765	-11.4	-11.84	-12.3	24.3	40.3	56.3	See Note #5		48.1
6	BPA Oregon City-Keeler (Chartier and Stearns 1981)	3	3.09	535	-10.2	0.0	10.2	15.2	15.2	15.2	16.97	18.25	50.0
7	Project UHV 8 (EPRI 1982)	8	3.31	1050	-19.8	0.0	19.8	18.6	18.6	18.6	14.46	15.42	50.0
8	Hydro-Quebec 1 (Trinh 1982)	4	3.50	735	-15.3	0.0	15.3	19.8	19.8	19.8	16.06	17.30	50.6
9	Project UHV 16 (EPRI 1982)	16	3.31	1450	-19.8	0.0	19.8	18.3	18.3	18.3	12.41	13.34	50.8
10	BPA McNary Ross (Chartier and Stearns 1981)	1	4.07	356	-9.8	0.0	9.8	16.5	16.5	16.5	15.74	16.66	51.0
11	BPA Lyons 8 (Chartier and Stearns 1981)	8	4.07	1200	-11.0	0.0	11.0	24.4	42.7	24.4	14.48	14.50	54.1
12	BPA Ost.-2	2	4.07	525	-10.4	0.0	10.4	12.2	12.2	12.2	16.79	17.91	54.5[3]
13	Hydro-Quebec 2 (Trinh 1982)	4	3.05	735	-13.7	0.0	13.7	19.8	19.8	19.8	18.29	19.82	54.6
14	BPA dble ckt (Montana) (Chartier et al. 1987)	3	4.07	530	-4.6	-7.6	-4.6	12.8	22.3	31.8	See Note # 6		55.5
15	Project UHV 12 (EPRI 1982)	12	3.31	1300	-19.8	0.0	19.8	16.9	16.9	16.9	13.66	14.59	55.8
16	Apple Grove A (Kolcio et al. 1974)	4	3.51	775	-13.7	0.0	13.7	13.7	13.7	13.7	17.56	18.77	56.2
17	Apple Grove B (Kolcio et al. 1974)	4	3.04	775	-13.7	0.0	13.7	15.2	15.2	15.2	19.58	21.03	57.2
18	AEP (Popeck and Knapp 1981)	4	2.96	760	-13.7	0.0	13.7	15.2	15.2	15.2	19.77	21.13	57.5
19	BPA Lyons 7 (Stearns 1980)	7	4.07	1200	-11.0	0.0	11.0	24.4	42.7	24.4	15.87	15.90	59.0

1. All measurements are 15 m from an outside phase unless noted otherwise. The altitude of the lines is assumed to be sea level unless otherwise noted.
2. Measurements were made directly under the outer phase.
3. Measurements were made 20.1 m from an outside phase.
4. There is an underbuilt distribution line on this structure (Chartier et al. 1995).
5. Double-circuit low-reactance line: A1= C2 = 14.70 kV/cm; B1 = B2 = 14.73 kV/cm; C1 = A2 = 14.99
6. Double-circuit low-reactance line, altitude of 1935 m: A1 = C2 = 14.70 kV/cm; B1 = B2 = 14.10 kV/cm; C1 = A2 = 15.0 kV/cm.
7. Two identical single-circuit lines. Distance between centerlines is 45.7 m. Gradients: A1 = C2 = 18.13 kV/cm; B1 = B2 = 17.34 kV/cm; C1 = A2 = 18.38 kV/cm.

Table 10.4-2 A-Weighted Audible Noise Data from Three-Phase Lines[1] (Continued)

	Line	No. of Cond.	Cond. Diam. (cm)	Line Volt. (kV)	Horizontal Arrangement of Phases 1 (m)	2 (m)	3 (m)	Minimum Conductor Heights 1 (m)	2 (m)	3 (m)	Conductor Gradient (kV/cm) Outside Phase	Center Phase	L_{50} Rain (dBA)
20	BPA Marion-Alvey-Lane (Chartier and Stearns 1981)	2	4.07	540	-6.1	0.0	6.1	12.2	20.7	12.2	Note #7		60.5
21	BPA Ostrander 1 (Perry 1972)	1	6.35	525	-10.4	0.0	10.4	18.3	18.3	18.3	15.82	16.84	61.4[3]
22	USSR 1150 kV (Azernikova and Emelyanov 1985)	8	2.72	1180	-24.5	0.0	24.5	18.0	18.0	18.0	19.41	21.90	62.0
23	Apple Grove C (Kolcio et al. 1974)	4	2.54	775	-13.7	0.0	13.7	14.3	14.3	14.3	22.81	24.41	62.2

1. All measurements are 15 m from an outside phase unless noted otherwise. The altitude of the lines is assumed to be sea level unless otherwise noted.
2. Measurements were made directly under the outer phase.
3. Measurements were made 20.1 m from an outside phase.
4. There is an underbuilt distribution line on this structure (Chartier et al. 1995).
5. Double-circuit low-reactance line: A1= C2 = 14.70 kV/cm; B1 = B2 = 14.73 kV/cm; C1 = A2 = 14.99
6. Double-circuit low-reactance line, altitude of 1935 m: A1 = C2 = 14.70 kV/cm; B1 = B2 = 14.10 kV/cm; C1 = A2 = 15.0 kV/cm.
7. Two identical single-circuit lines. Distance between centerlines is 45.7 m. Gradients: A1 = C2 = 18.13 kV/cm; B1 = B2 = 17.34 kV/cm; C1 = A2 = 18.38 kV/cm.

while at some other locations they tend to cancel each other. An example is shown in Figure 10.4-3.

To assess the hum level for the purpose of line design, it has been proposed to use the rms value of the sound-pressure level in the space of interest (based on considerations of mean power value), rather than the highest value at the worst location. If the hum is evaluated on this basis, a hum value less than 50 dB is recommended to avoid complaints (Tanabe 1991a).

10.5 MEASUREMENT OF AUDIBLE NOISE

The terminology used most frequently when referring to audible noise generated by transmission lines will be presented as defined in the IEEE Standard for the measurement of audible noise from overhead transmission lines (ANSI 1992). Explanation of the various terms can also be found in the Glossary incorporated in this book.

10.5.1 Sound Pressure, Sound-Pressure Level, the Decibel

The sound pressure of the wave may be characterized by the magnitude or size of a sound wave. For steady sounds in air, such as transmission-line noise, this characteristic is usually observed in terms of the root-mean-square amplitude of the small variations in atmospheric pressure that accompany the passage of the sound wave. It is usually expressed in terms of micropascal, abbreviated μPa (1 μPa = $1\mu N/m^2 = 10^{-5}\mu bar$).

The range of pressure variations that the human ear can detect is extremely wide. The levels of some common noise sources are shown in Table 10.5-1. As this table shows, human ears can experience sounds of vastly differ-

Table 10.5-1 Common Noise Levels

Sound Pressure in Pascal	Sound Level in dBA	Environmental Conditions
200	140	Threshold of pain
	130	Pneumatic chipper
20	120	Loud automobile horn (at 1 m)
	110	
2	100	Inside (New York) subway train
	90	Inside motor bus
0.2	80	Average traffic on street corner
	70	Conversational speech
0.02	60	Typical business office
	50	Living room suburban area
0.002	40	Library
	30	Bedroom at night
0.0002	20	Broadcasting studio
	10	Threshold of hearing
0.00002	0	

ent pressure levels. A very loud sound may have as much as 1,000,000 times the rms sound pressure of a very quiet sound. For reporting convenience, a compressed scale has been devised on the basis of the logarithm of the sound pressure: this is the sound-pressure level, and it is expressed mathematically in decibel (dB) as

$$\text{Sound - pressure level} = 20 \log_{10}\left(\frac{\textit{sound pressure}}{\textit{reference pressure}}\right) \text{dB} \qquad 10.5\text{-}1$$

It is a good practice to state the reference pressure when sound-pressure levels are reported. For example, a particular noise may have a sound-pressure level of 50 dB above 20 μPa. Unless otherwise explicitly stated, it is understood that the sound pressure is the root-mean-square sound pressure and that the reference pressure is 20 μPa.

10.5.2 Weighted Sound Level

The human ear is more sensitive to the midrange of frequencies, where most speech information is carried. This characteristic may be accounted for in sound measurements by adjusting the spectrum of the measured sound-pressure level for the sensitivity of human hearing. In standardized sound-measuring instruments, this is implemented with selectable A-, B-, and C-weighting networks (ANSI 1983). The terms "weighting" or "weighted" are used because some frequencies are given more or less importance, or weight, than other frequencies. By far the most commonly used noise-rating scale is the A-weighted sound level, expressed in dBA. A-weighting is commonly used for transmission-line sounds, although experiments have indicated that subjective reaction to corona noise might correlate better with the B-weighted (Wells 1974) or with the D-weighted (Molino et al. 1977) measures of the noise. A-, B-, C-, and D-weighting characteristics are shown in Figure 10.5-1, along with the characteristics of the average human ear. The A-weighted measure of noise is the one most often used. The A-weighted level is much less affected than the B-, C-, and D-weighted levels by the variations in the 100/120-Hz component of transmission-line audible noise.

10.5.3 Statistical Descriptors

Many sounds have pressure levels that are not constant in time and cannot, without qualification, be adequately characterized by a single value of sound-pressure level. One method for dealing with fluctuating or intermittent sounds is to examine the sound level statistically as a function of time. Statistical descriptors are often applied to A-weighted sound levels and are called exceedance levels or L- levels. For example, the L_5 level is the A-weighted sound level exceeded for 5% of the time over a specified time period. For the other 95% of the time, the sound level

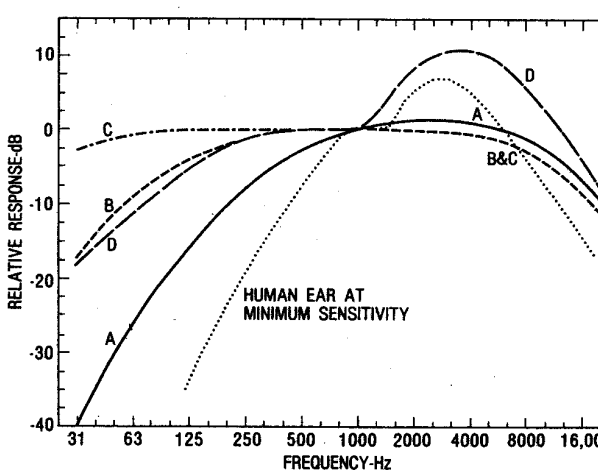


Figure 10.5-1 Attenuation of different weighting networks used in sound-level measurements.

is less than the L_5. Similarly, the L_{50} level is the sound level exceeded 50% of the time.

10.5.4 L_{eq}, L_{dn} and CNEL

The simplest and most popular method for rating intermittent or fluctuating noise intrusions is to rely upon some measure of the average sound magnitude over time. The most common such average is the equivalent sound level, L_{eq}. The equivalent sound level is the energy average of the level (usually A-weighted) of a varying sound over a specified period of time. The term "equivalent" signifies that a steady sound having the same level as the L_{eq} would have the same sound energy as the fluctuating sound. The term "energy" is used because the sound amplitude is averaged on an rms-pressure-squared basis, and pressure squared is proportional to energy. For example, two sounds, one of which contains 24 times as much energy as the other, but lasts for 1-hour instead of 24 hours, would have the same equivalent sound level. The L_{eq} rating does not account for the fact that noise intrusions will be more annoying at night. The L_{dn} (day/night) rating, calculated similarly to the L_{eq} rating, accounts for this fact by adding a 10-dB penalty to all sounds occurring between 10 p.m. and 7 a.m. The Community Noise Equivalent Level (CNEL) includes a 5-dB penalty on noise during the 7:00 p.m. to 10:00 p.m. time period and a 10-dB penalty on noise during the 10:00 p.m. to 7:00 a.m. time period.

10.5.5 Instrumentation

The instrumentation required to make audible-noise measurements is composed of three basic components: a transducer (microphone) to convert acoustical pressure into electrical signals, a processing device to weight and/or filter the electrical information, and an output device to determine the levels of the acoustical signals. The equipment available to perform these measurements varies sig-

nificantly in sophistication and price from simple, handheld instruments to more complex, computer-controlled systems. Transmission-line noise measurements are unique in that, generally, they require the measurement of low-noise levels, they are concerned with a noise having high-frequency content, and for the most part they must be performed outdoors in foul weather. These requirements affect the measurement system with regard to sensitivity, frequency response, and ability to operate in wet conditions. The characteristics of sound-level meters are described in several standards (IEC 2000, 2001). The sound-level meter measures the overall sound pressure level. To provide a better measure of the effect a given sound will have on people, most sound-level meters provide the A-weighting network. More sophisticated meters will usually provide the A-, B-, and C-networks along with a flat or unattenuated noise scale. A few meters provide also the D-network.

When more detail than can be provided by a simple measure of the noise (e.g., A-weighted) is desired, a complete determination of the frequency spectrum should be made using frequency analyzers. For field measurements, an octave-band filter set is often used. For better definition, narrow-band frequency analyzers with one-third or one-tenth octave filters are also used. One octave is defined as a bandwidth for which the ratio between upper and lower frequency of the band is 2. For the one-third and one-tenth octave bands, the ratios are $2^{1/3}$ and $2^{1/10}$, respectively. As the bandwidth is increased, the pressure level measured for random noise (having a flat spectrum within the band) is proportional to the square root of the bandwidth, whereas for pure tones (e.g., the 120- Hz hum), the measurement is independent of the bandwidth.

The microphone is an important part of the noise-measuring system. There are several types and sizes of microphones available. Each has its own characteristics, and thus its own advantages and disadvantages. If the characteristics of a given microphone and the basic characteristics of the noise being measured are understood, the limitations of a particular microphone may then be determined. As long as these limitations are recognized and adjustments for them are made, the particular type of microphone used is not of major importance. IEEE Standard 656 provides a comprehensive discussion on characteristics and use of different types of microphones (ANSI 1992). For measurement of audible noise during rain, some means of microphone protection will be required for all but the very shortest-duration measurements. Microphone manufacturers have products designed specifically for measurements during rain. These products must be checked to verify that they are suitable for the transmission-line environment and for the measurement of corona noise.

10.5.6 Measurements

The techniques of transmission-line audible-noise measurements should be made according to IEEE Standard 656-1992 (ANSI 1992). However, since the last revision of this standard, the instruments for conducting audible-noise measurements have evolved from primarily analog sound-level meters to integrating sound-level meters. Most of the electric utility industry's experience has been with the older instruments. The newer, more sophisticated instruments allow the user to log data at very fast rates over any time period desired. The outdoor microphone systems are smaller and much easier to use. These instruments can store large amounts of data depending upon the internal memory. Software makes it relatively easy to process the data. The basic procedures in 656 are still valid. This section provides a summary of some of the important features in 656 for conducting short-term manual measurements and long-term automated measurements.

The Sound Level Meter (SLM) should be an ANSI/IEC Type 1 integrating SLM with a 1/2-in. (1.27-cm) free-field microphone. The preferred free-field microphone should have a sensitivity of at least –27 dB (referred to 20 μPa), and the frequency response should be from about 2.6 Hz to 20 kHz. The overall sensitivity of the SLM and the microphone should be less than 20 dBA. Most of the integrating SLMs have very large dynamic ranges up to 110 dB, which makes them suitable for outdoor measurements. Most of them also have large memory (up to 30 Mbytes) allowing data to be logged at very high rates over fairly long time periods. And, all of them have software built into the instrument so that the user-selected L_n values and the $L_{eq's}$ are automatically calculated. With the RS-232, interface data can be easily downloaded into portable computers.

Short-Term Manual Surveys

Anyone who has made outdoor audible-noise measurements with an analog meter has experienced the needle on the meter bouncing back and forth. This is due to the meter responding to many noise sources besides the transmission-line noise. For most lines, fair-weather measurements can only be conducted in remote areas where the background levels are very low. That can also be true for conducting foul-weather measurements on lines where the anticipated audible-noise level is less than 50 dBA. Even then, background noise can distort the measurements. With the advent of handheld data-logging integrating sound-level meters (SLM), many data points can be collected over a short time period. Most of these meters have user-selectable L_n values. Therefore, if the L_{50} level is desired for a certain weather condition over a certain time period, one of the L_n values that can be calculated from the logged database is $L_{50,}$ which is much better than trying to eyeball the L_{50} value from a fluctuating needle on an analog meter. Some of these integrating meters allow for the concurrent measure-

ment of the octave bands and the discrete or statistical measurements. That feature allows for the simultaneous measurement of A-weighted noise and 8-kHz or 16-kHz octave band levels. It has been shown for corona noise there is a direct correlation between measures of A-weighted, 8 kHz and 16 kHz noise (EPRI 1982; Lundquist 1990). Noise measured with the higher octave bands is less contaminated by ambient noise and can be used effectively to obtain dBA data as described in Appendix 10.1.

When conducting short-term measurements, it is important that the noise being received by the SLM be monitored with headphones so that unwanted background noise can be observed and eliminated. If the noise data are being logged, the observer can stop the logging until the intruding noise goes away. For most short-term measurements, the polyurethane wind screens provided by the manufacturer also are good rain covers.

Long-term Automatic Measurements

Long-term measurements are made to characterize the audible-noise statistics of the transmission-line noise over a long time period at a particular location under a variety of conditions and for checking regulatory compliance. IEEE Standard 656 recommends that these measurements be made with the microphone 1.5 m above ground and 15 m measured horizontally from an outside phase conductor of an ac transmission line. However, for regulatory compliance, the measurements might have to be made at the edge of the right-of-way. If a free-field microphone is used, it must be oriented so that the axis of the microphone diaphragm is pointed at the center phase of the transmission line. The center phase is usually the phase with the highest conductor surface gradient (e.g., the highest noise level).

For long-term outdoor measurements, an outdoor microphone must be used. When transmission-line noise first became a problem in the late 1960s, outdoor microphones did not exist (Kolcio et al. 1974; Perry 1972). At the EPRI laboratory, researchers used air-condenser microphones that were back-vented through a desiccative cartridge (EPRI 1982). This arrangement provided durability in conditions of high humidity. Microphones specifically designed for outdoors became available in the late 1970s. One version that was expensive and bulky, but highly reliable, was first applied at the Lyons 1100-kV Project (Perry et al. 1979).

The same integrating SLMs can be used in conjunction with the outdoor microphones for long-term measurements. If measurements are required at several locations, more sophisticated instruments that can accept several microphone inputs are required. Fully packaged outdoor systems that can be monitored remotely are available from various manufacturers.

Long-term measurements are also sometimes carried out for the purposes of research and performance verification. Monitoring sites may have to be at remote locations, so that the intrusive influences of high ambient background noise may be minimized or avoided. These measurements should preferably comply with IEEE 656. At sites where grid power is not available, it is important to ensure that a reliable power supply is engineered. Solar power augmented by batteries is usually viable. The measurement equipment must of course be securely housed, thereby ensuring protection against vandalism and the weather.

10.6 ASSESSING THE IMPACT OF TRANSMISSION-LINE AUDIBLE NOISE—AUDIBLE-NOISE REGULATIONS

With one or two exceptions, existing noise ordinances were not developed with transmission-line noise in mind. The purpose of this section is to provide information on how some utilities have targeted noise levels to be used for line design and how some noise ordinances have been interpreted for transmission-line noise.

Community noise regulations specify levels based upon A-weighting expressed as dBA. Other weighting networks have been examined for transmission-line noise, but the advantage of using these other measures from a regulatory standpoint is marginal. Some noise ordinances also specify octave band levels.

10.6.1 Noise Evaluation Studies

Transmission-line audible noise first became a problem in the U.S. in the late 1960s and early 1970s when 500- and 765-kV lines were first introduced. The conductor chosen for the first 500-kV line of the Bonneville Power Administration (BPA) was a single-conductor, 6.35-cm diameter, expanded ACSR. Although it was anticipated that the radio noise for this line would be somewhat above that of previous lines, this conductor selection allowed the mechanical analysis and design to be consistent with the practice and experience of the past. Energization of BPA's first 500-kV line during the rainy season on the west side of the Cascade Mountains was swiftly followed by numerous complaints about audible noise.

As time went on, BPA changed from using a single 6.35-cm conductor per phase to using two 4.07-cm conductors per phase and eventually to using three 3.31-cm conductors per phase. The audible noise performance of these three designs is well documented (Perry 1972). Based upon the complaint experience of BPA, Perry drew the guidelines shown in Figure 10.6-1 (Perry 1972). Since that time, several studies have been undertaken, but Perry's guidelines are still widely referenced. Based upon this

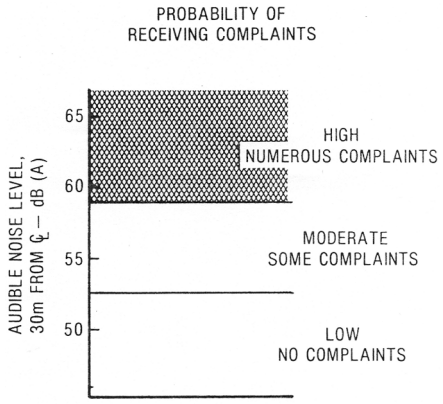


Figure 10.6-1 Audible-noise complaint guidelines (Perry 1972).

complaint experience, BPA adopted an initial design limit of 53 dBA at the edge of the right-of-way, which is an L_{50} level during measurable rain. Long-term measurements of audible noise and rain intensity on lines in Oregon on the west side of the Cascade Mountains have shown that the median rain rate that corresponds to the L_{50} audible noise level during measurable rain is about 1 mm/h.

There have been other studies to assess the impact of audible noise on people living near transmission lines (Wells 1974; Molino et al. 1979; Pearson et al. 1979). In one of these studies, an acoustic-menu technique was used to determine subjects' preferences for different types of noise, including transmission-line noise and other more commonly encountered environmental noises (Molino et al. 1979). The conclusion was that the A-weighted network underestimates the aversiveness of corona noise, relative to other environmental sound by about 3 dB.

Transmission-line audible noise has been an issue in many public hearings on line certification applications. The most notable cases were, perhaps, the New York State Public Service Commission Cases 26529 and 26559—"Common Record Hearing on Health and Safety of Extra-High Voltage Transmission Lines." It was concluded by the commission that an L_{50} rain level of 52 dBA at the edge of the right-of-way is a reasonable standard (State of New York 1978). It was recognized, however, that a sound of this level might produce sleep interference beyond the right-of-way in a limited number of cases. This was based on the general conclusion from the hearing testimony that 35 dBA is a proper maximum level for bedrooms, but that under average rainy conditions the noise from the line could result in levels of approximately 36.5 dBA in a bedroom with partly open windows. This assumes 15.5-dBA attenuation through the partly open window and a noise level immediately outside the window of 52 dBA. The attenuation figure was derived from tests performed on several houses in the vicinity of the proposed line. In a subsequent agreement between the Public Service Commission and one of the utilities involved in the hearing, it was accepted that the utility would implement mitigation measures if, after receiving a noise complaint, it was demonstrated through a prescribed measurement procedure that the long-term median foul-weather sound level due to the transmission line would be 35 dBA or greater in the complainant's regular sleeping room.

The State of Montana, based on land-use issues related to proposed 500-kV lines, adopted limits specifically for transmission lines. The State of Montana requires that noise from transmission lines not exceed 50 dBA L_{dn} at the edge of the right-of-way in residential and subdivided areas (Montana Major Facility Siting Act 1984). This is 5 dB less than the level specified in the EPA noise guideline that is discussed later. The State of Montana, based upon the Molino study, felt that transmission-line noise should have a more stringent limit.

10.6.2 Noise Ordinances—United States

With the exception of the State of Montana (Montana Major Facility Siting Act 1984), no existing noise ordinances in the U.S. specifically refer to transmission lines as noise sources. However, many ordinances by virtue of their general nature may implicitly include transmission lines. Some regulations may overstate the impact of line noise because the noise occurs primarily during foul weather. Most regulations are based on other more commonly encountered noise sources such as vehicular traffic, aircraft, and industrial and general community noises. However, by working with the regulatory agencies, utilities have been able to interpret these audible-noise regulations for transmission-line noise.

A number of regulatory bodies have developed regulations based upon the Environmental Protection Agency's so-called "levels document" (U.S. EPA 1974), general noise-level limits that are identified as "requisite to protect public health and welfare with an adequate margin of safety." It is specifically noted that the levels are not to be construed as standards since they do not take into account cost or feasibility. Table 10.6-1 summarizes the levels recommended to avoid outdoor and indoor activity interference and annoyance.

In Table 10.6-1, $L_{eq(24)}$ represents the sound-pressure level calculated on the basis of the sound energy averaged over a 24-h period, whereas L_{dn} represents the L_{eq} with a 10-dB nighttime adder—i.e., during nighttime hours, 10 p.m. to 7 a.m., a 10-dB penalty is assessed to reflect a greater potential for annoyance of a given sound during nighttime hours. Thus, an L_{dn} of 55 dB is more restrictive than an $L_{eq(24)}$ of 55 dB. For a noise that occurs on an essentially regular, daily basis, it is clear how these suggested levels

Table 10.6-1 Summary of EPA Noise Guidelines

Effect	Level	Area
Outdoor activity interference and annoyance	$L_{dn} \leq 55$ dBA	Residential areas and farms and other areas where people spend widely varying amounts of time and other places where quiet is a basis for use
	$L_{eq(24)} \leq 55$ dBA	Areas where people spend limited amounts of time, such as school yards and playgrounds
Indoor activity interference and annoyance	$L_{dn} \leq 45$ dBA	Residential areas
	$L_{eq(24)} \leq 45$ dBA	Other areas where human activities take place, such as schools

might be interpreted. In the case of transmission-line noise, which occurs primarily during foul weather, which is fairly infrequent in most parts of the world, the interpretation is not clear. One approach, which has been used, suggests that the L_{dn} should be computed on an annual basis, taking into account those periods of fair weather in which most lines do not make noise (Keast 1980). However, as was mentioned earlier, some lines can be noticeably noisy at times during fair weather; therefore, the approach is still valid if the L_{dn} is calculated for all-weather.

In a 110-page book, Bragdon presents the most comprehensive list of existing municipal noise control legislation within the United States (Bragdon 1980). The book tabulates existing noise ordinances alphabetically by state and municipality. Ten noise ordinance provisions are categorized in this book including nuisance, zoning, vehicles, recreation vehicles, railroad, aircraft, construction, building code, animals, and entertainment. At the time of publication, no noise ordinance provision existed specifically for transmission-line noise. The book is somewhat dated, but still provides a useful guidance about noise ordinances in the United States.

A few states have adopted land-use noise regulations that specify allowable noise levels within certain areas depending on whether their primary use is residential, commercial, or industrial. Table 10.6-2 summarizes some typical state ordinances. One must be alert to the fact that many counties and other municipalities within the 50 states have adopted their own ordinances. Many noise ordinances can be found on the Internet. For example, if a search for California noise ordinances is conducted, one can see that hundreds of counties and communities in California have adopted noise ordinances. Fortunately, it looks like most of those ordinances are based upon some variation of the EPA "levels document."

Table 10.6-2 Examples of State Noise Regulations Based on Land-Use Levels

State	Maximum Noise Allowed Within Residential Area		Comments
	Day	Night	
Colorado	55 dBA	50 dBA	
Illinois	55 dBA	45 dBA	Class A (residential areas) noise source
	55 dBA	45 dBA	Class B (commercial areas) noise source
	61 dBA	51 dBA	Class C (industrial areas) noise source
New Jersey	65 dBA	50 dBA	Octave band levels also specified
Montana	Ldn – 50 dBA		Can be waived by affected landowner
Oregon	L_{50} – 55 dBA	L_{50} – 50 dBA	In any one hour
	L_{10} – 60 dBA	L_{10} – 55 dBA	In any one hour
	L_1 – 75 dBA	L_1 – 60 dBA	In any one hour

The Noise Control Act of 1972 gave the states in the United States the responsibility for noise control. Executive Order No. 12088 requires that all federal agencies comply with these state and local noise control regulations. Since the Bonneville Power Administration (BPA) is an agency of the Department of Energy of the U.S. federal government, they were required to meet state and local noise control regulations.

Washington and Oregon are two states in BPA's service territory that have audible-noise limits based essentially on the L_{50} level during any one-hour period. Since most areas of Washington and Oregon have rain periods that last one hour or longer, the L_{50} level during measurable rain would have to be equal to or less than the appropriate limit. Both of these noise codes allow the audible noise to exceed these L_{50} levels for a very short period.

Many ordinances use some variation of the EPA L_{dn} criteria. The State of Montana has a limit of 50 dBA L_{dn}. Two measurement scales commonly used in the State of California are the Community Noise Equivalent Level (CNEL) and the day-night level (L_{dn}). In order to account for increased human sensitivity at night, the CNEL level includes a 5-dB penalty on noise during the 7:00 p.m. to 10:00 p.m. time period and a 10-dB penalty on noise during the 10:00 p.m. to 7:00 a.m. time period. The L_{dn} level includes only the 10 dB weighting for late-night noise. These values are nearly identical for all but unusual noise sources.

10.6.3 Case Study: Example of Limits Based on Any One Hour

Since interpretation of the Washington Noise Code has been well documented (Chartier et al. 1995), it will be used as the example for determining limits based upon any one hour.

The Department of Ecology in the State of Washington developed "Maximum Environmental Noise Levels" (WAC 1975). Soon after these maximum noise levels were adopted, BPA held discussions with personnel from the Department of Ecology to determine how to apply these noise limits to transmission lines.

This Washington Administrative Code (WAC) divides land into three classes according to typical land uses and their need for protection from noise sources:

(a) Residential areas - Class A EDNA

(b) Commercial areas - Class B EDNA

(c) Industrial areas - Class C EDNA

The EDNA (Environmental Designation for Noise Abatement) establishes permissible noise levels.

According to the WAC, "no person shall cause or permit noise to intrude into the property of another person, which noise exceeds the maximum permissible noise levels set forth in this section."

(a) "The noise limitations established are as set forth in the Table 10.6-3 after any applicable adjustments provided for herein are applied."

(b) "Between the hours of 10:00 p.m. and 7:00 a.m. the noise limitations in Table 10.6-3 shall be reduced by 10 dBA for receiving property within Class A EDNA."

(c) "At any hour of the day or night the applicable noise limitations in (a) and (b)" above may be exceeded for any receiving property by no more than:

(i) "5 dBA for a total of 15 minutes in any one-hour period; or"

(ii) "10 dBA for a total of 5 minutes in any one-hour period; or"

(iii) "15 dBA for a total of 1.5 minutes in any one-hour period."

The Department of Ecology, based on discussions with BPA engineers, classified transmission corridors as being a Class C noise source. Since transmission lines operate during both daytime and nighttime hours, they are required to meet the 50-dBA nighttime limit for EDNA Class A receiving properties. Since rain can occur in any hour of the day and can last for more than an hour, then the L_{50} audible noise level during measurable or fairly stable rains has to be assumed.

Because of the long rainy periods in the U.S. Pacific Northwest, some utilities have chosen to design their lines to meet Class A EDNA noise requirements (Chartier et al. 1995). The nighttime requirement for a Class A noise source propagating into a Class A receiving property is 45 dBA.

10.6.4 Case Study: Example of Limits Based on Some Variation of the EPA "Levels Document"

The State of Montana has a limit of 50 dBA L_{dn} that is specifically for transmission-line noise. San Diego County in California has daytime and nighttime sound level limits based upon land use as shown in Table 10.6-4.

The San Diego County regulations go on to say, "if the measured ambient level exceeds the applicable limit noted above, the allowable one-hour average sound level shall be the ambient noise level. The ambient noise level shall be measured when the alleged noise violation source is not

Table 10.6-3 Washington State Noise Limits for Different Environmental Designations for Noise Abatement (EDNAs)

EDNA of Noise Source	EDNA of Receiving Property		
	Class A	Class B	Class C
Class A	55 dBA	57 dBA	60 dBA
Class B	57 dBA	60 dBA	65 dBA
Class C	60 dBA	65 dBA	70 dBA

Table 10.6-4 San Diego County Sound Level Limits Day/Night dBA Average per Hour (L_{eq})

Land Use	Daytime	Nighttime
	dBA Average per hour (L_{eq})	
Low-Density Residential	50	45
High-Density Residential	55	50
Commercial	60	55
Industrial	70-75	70-75

operating. Fixed-location public utility distribution or transmission facilities located on or adjusted to a property line shall be subject to the noise level limits of this section, measured at or beyond six feet from the boundary of the easement upon which the equipment is located."

Since the San Diego County sound level limits are based upon one hour, the L_{50} level during rain might apply. Even in dry climates, rain can sometimes last for one hour or more. It appears that these limits apply to transmission line noise; but it isn't clear exactly how they should be interpreted in light of the fact that measurable rain only occurs about 3% of the time in San Diego County.

Calculation of L_{eq} and L_{dn} from Probability Distributions

Keast recommended that the L_{dn} should be computed on an annual basis, taking into account those periods of fair weather in which most lines do not make noise (Keast 1980). That proposal was made when it was assumed that transmission lines made very little noise during fair weather. As was discussed earlier, this assumption is not necessarily true. In order to calculate an annual $L_{dn,}$ all-weather statistics of audible noise for at least a year are needed. Fortunately, BPA has been able to conduct long-term audible noise measurements over periods of at least one-year or more in areas where the ambient noise was quite low.

It is important to note that normal transmission lines in moderate, relatively clean climates produce very little audible noise during fair weather. One can walk under most transmission lines, and the audible noise during dry weather is barely noticeable. In very quiet rural areas, especially during nighttime hours, BPA has been able to measure fair-weather audible noise from their normal 500-kV lines. These long-term measurements have shown that the difference between the L_{50} audible noise during stable rain and the L_{50} audible noise during fair weather is 25 dBA or more. Figure 10.6-2 shows two all-weather nighttime probability distributions. One distribution was collected next to a corridor that contains two single-circuit 500-kV operating lines. The other one was collected next to an 1200-kV test line that BPA operated about 10 km from the operating 500-kV lines.

Figure 10.6-3 shows similar all-weather distributions collected on a BPA double-circuit 500-kV operating line in Montana (Chartier et al. 1987). The difference between the 500-kV audible-noise distributions in Figures 10.6-2 and 10.6-3 are that the data collected on the 500-kV line near Scio, Oregon is based on nighttime data, whereas the noise data collected on the 500-kV line in Montana is both daytime and nighttime data. During the daytime, noise from activity at nearby farms and light traffic on a nearby dirt road made it difficult to collect meaningful daytime data in fair weather from the line in Oregon. The line in Montana, however, was near the Continental Divide of the Rocky Mountains several miles from any human activity. The ambient noise was very low even during daytime hours, and especially in the winter months.

Each one of the A-weighted distributions for the 500-kV lines in Figures 10.6-2 and 10.6-3 has three normal distributions. The lower normal distribution is the fair-weather distribution. The upper normal distribution is the stable rain distribution. Between these two distributions is a "transition" distribution. The weather that makes up the transition distribution is light rain, fog, mist, light snow, etc. Figure 10.6-2 shows that the transition distribution for the audible noise from the parallel 500-kV lines near Scio, Oregon was very steep, whereas the transition distributions for the double-circuit 500-kV line in Montana and for the 1200-kV test line near Lyons, Oregon were much more

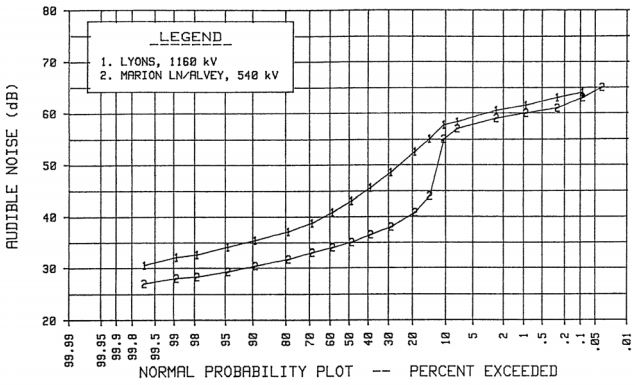


Figure 10.6-2 Comparison of A-weighted all-weather nighttime audible-noise distributions from the Lyons 1200-kV test line and parallel operating BPA 500-kV lines located near Scio, Oregon. Measurements were made at 15 m from the outermost phases. The conductor configurations were 7 x 4.1 cm for the 1200-kV test line and 2 x 4.1 cm for the 500-kV lines (Stearns 1980).

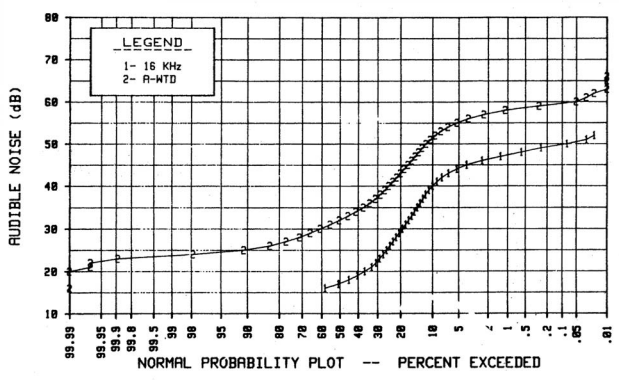


Figure 10.6-3 All-weather audible noise distributions for BPA double-circuit 500-kV line at 1935 m above sea level; A-weighted and 16 kHz. Sample size: 166,992. (Chartier et al. 1987)

gradual. The steep transition is due to the fact that the two parallel operating 500-kV lines in Oregon were carrying medium to heavy loads. It has been shown that medium to heavy loads heat up conductors enough to discourage condensation during early morning dew conditions and during fog (Chartier 1994). The load current also causes conductors to dry off a lot faster after the cessation of rain. The test line had no load current, which is why the transition distribution is quite gradual. The audible noise measured from the line in Montana was a combination of snow and rain over the one-year testing period. When snow lands and sticks on a conductor, it creates audible noise. If the conductor is warm because of the load current, the snow might melt and turn to water, which will run to the bottom of the conductor. Corona will occur where water drops form. The transition distribution for the Montana line consisted primarily of audible noise during light snow.

Once the all-weather distribution has been developed, statistical levels such as L_{eq} and L_{dn} can be calculated. The technique for doing this from probability distributions has been described in (Keast 1980). A process analogous to graphical integration is used to determine the L_{eq} for the all-weather distribution, i.e.:

$$L_{eq} = 10 \log_{10}\left[\frac{1}{100}\sum_{0}^{n}\left((P_c - P_{c-1})\cdot 10^{\frac{L_c}{10}}\right)\right] \qquad 10.6\text{-}1$$

P_c and P_{c-1} are selected adjacent steps along the abscissa, and L_c is the highest noise level in each step.

Table 10.6-5 shows the steps and the values that were used to calculate the L_{eq} for the A-weighted distribution in Figure 10.6-3.

The calculated all-weather L_{eq} for the double-circuit 500-kV line in Montana at 15 m from the outermost phase is 47.8 dBA.

The L_{dn} can be calculated from the following formula (Keast 1980), assuming that the daytime and nighttime L_{eq}'s are the same and that the number of hours that make up daytime and nighttime are 15 and 9 hours, respectively.

$$L_{dn} = 10 \log_{10} \{(1/24)\,[15 \text{ antilog } (L_d/10) + 9 \text{ antilog } (L_n + 10)/10]\} \qquad 10.6\text{-}2$$

L_d is the daytime L_{eq} and L_n is the nighttime L_{eq}; both equal to 47.8 dBA

The calculated L_{dn} for the 500-kV line at 26 m from centerline is 54.2 dBA.

Determination of the All-Weather Distribution

An all-weather distribution can be developed for any line knowing: (1) the L_{50} audible noise during rain; (2) the percent of time measurable foul weather occurs; and (3) the L_{50} audible noise level during fair weather. The L_{50} audible noise during foul weather can be calculated using either the EPRI or BPA L_{50} measurable rain formulas. The percentage of time that measurable foul weather occurs in the U.S. can be determined from weather data maintained by the National Climatic Data Center (NCDC) of the National Oceanic and Atmospheric Administration (NOAA). BPA has determined that the break point between the upper normal distribution and the transition distribution is very close to the percentage of time that measurable foul weather occurs. Therefore, the measurable rain foul-weather distribution can be drawn on a probability plot since two points are known. The slope of the straight line should be the same as one of the slopes for the measurable foul-weather distributions in Figures 10.6-2 or 10.6-3. The rest of the all-weather distribution can be traced using one of the distributions in Figures 10.6-2 or 10.6-3. To be conservative, the all-weather distribution with a gradual transition distribution should be used unless it is known that the proposed line will be moderately to heavily loaded most of the time. Then the all-weather distribution with the steeper transition slope could be used.

Table 10.6-5 Steps Used in Calculation of L_{eq} for A-Weighted Distribution in Figure 10.6-3.

P_c	P_{c-1}	L_c
0.01	0.05	62.0
0.05	0.1	60.0
0.1	0.2	59.5
0.2	0.5	59.0
0.5	1.0	58.5
1.0	2.0	58.0
2.0	3.0	57.2
3.0	4.0	56.5
4.0	5.0	55.5
5.0	10.0	55.0
10.0	20.0	51.5
20.0	30.0	44.0
30.0	40.0	37.0
40.0	50.0	35.0
50.0	60.0	32.0
60.0	70.0	30.0
70.0	80.0	29.0
80.0	90.0	26.0
90.0	95.0	25.0
95.0	98.0	24.5
98.0	99.0	24.2
99.0	99.5	24.0
99.5	99.8	23.8

The all-weather distributions in Figures 10.6-2 and 10.6-3 were obtained in clean environments. The differences between the L_{50} measurable rain and the L_{50} fair-weather levels for the operating lines in Figures 10.6-2 and 10.6-3 are 25 dBA or more. If the proposed line is to be located in an industrial environment or a dry, dusty environment, then the difference between the measurable rain and the fair-weather distributions should be made smaller. But the question is how much smaller should it be made? The problem is that there is essentially no long-term statistical audible-noise data from lines in dirtier environments. Without such data, the fair-weather distribution would have to be estimated. Once the predicted distribution is drawn, then L_{eq} and L_{dn} can be calculated as was described earlier.

10.6.5 Case Study: Example of Limits Based on South African Noise Code

There is no specific legislated limit applicable to noise generated by transmission lines in South Africa. Informal design limits have been adopted within the South Africa Electric Utility, Eskom, and have been based on what is achievable, affordable and compatible with the high-altitude environment in which most of the 400-kV lines operate. Some engineering background to the limits is given below.

In the case of Eskom's high-altitude 765-kV lines (1500 m above sea level), the limit adopted has been L_{50} rain = 53 dBA at the maximum line voltage at the edge of the ROW. This was based on the limit derived from the 1978 hearings into permissible noise from the New York State Power Board's (then) proposed 735-kV line. As Eskom's cage tests at the time showed that the L_{50} fair-weather level would be some 20 dB below the target for rain, it was concluded that the fair-weather levels from the line would not be intrusive. Spot noise readings in the field have subsequently shown this to be the case.

The building of a number of 400-kV lines with tight phase spacing, thereby creating relatively high conductor surface gradients—particularly with lines built in high-altitude areas in recent years—has necessitated the possible adoption of fair-weather noise limits. This is besides the 53 dBA L_{50} rain limit adopted at the edge of the ROW. Typical long-term fair-weather levels from a rural 400-kV line with well-aged conductors have been found to be of the order 12 to 15 dB below the L_{50} rain level in a temperate climate. The foregoing differences were also found to agree quite well with those predicted from tests in a high-altitude cage. The difference (12 to 15 dB) found between the L_{50} rain and L_{50} fair-weather levels of compact 400-kV lines at high altitude in South Africa is significantly smaller than the value of 25 dB found for BPA's 500-kV lines of normal design.

The question of fair-weather noise limits has resulted in investigations into the local legislative requirements.

Audible-noise limits can be inferred from criteria in existing legislation. The Environment Conservation Act of 1989 defines two conditions relevant to noise from power lines:

- Disturbing Noise
- Nuisance Noise

"Disturbing noise" is defined as the noise level that exceeds the so-called zone sound level, or if no zone sound level has been designated, a noise level that exceeds the ambient sound level at the same measuring point by 7 dBA or more. The method of measurement is described in the Act, and may require the average sound level to be determined over a period of 7 days.

The level for a "nuisance noise" is much more subjective. It does not require rigorous measurement—it may not even be measurable—and could arise from the complaint of a highly sensitive person. Local legal opinion is of the view that Eskom could be vulnerable to such a complaint if the relevant local authority has not specified zone sound levels.

Zone sound levels (rating levels) in dBA recommended for outdoors are given in Table 10.6-6.

Table 10.6-6 Sound Levels Recommended for Outdoors

Type of District	Daytime	Evenings, Weekends	Nighttime
Rural	45 dBA	40 dBA	35 dBA
Suburban	50 dBA	45 dBA	40 dBA
Urban	55 dBA	50 dBA	45 dBA
Industrial	70 dBA	65 dBA	60 dBA

The essential dilemma for Eskom is that for certain compact 400-kV designs, the mean fair-weather level at the edge of the ROW can exceed the 35-dBA sound zone level by more than 7 dB; this has caused a number of complaints from the public. In other cases, especially in deep rural areas, the 42-dBA guideline level (35 dBA + 7 dBA) for nighttime may be met, but because the mean background (ambient) noise level is often less than 35 dBA, the difference may exceed 7 dB. Besides this, and also any rational limit that may be met, the "noise nuisance" criterion could still be invoked.

The above issues have not yet been satisfactorily resolved. However, one approach will be to require audible noise to be measured as part of an Environmental Impact Assessment, both before and after a line is built. This will allow the designer to set a realistic noise limit or target, and also for the impact of the noise to be objectively assessed.

10.7 AUDIBLE-NOISE REDUCTION TECHNIQUES

10.7.1 Introduction

There is an incentive to reduce the audible noise produced by corona on transmission lines when audible noise represents a design constraint, or as a result of complaints about noise from specific line sections. Reducing noise from an operational line is a problem some utilities may face from time to time. Such problems are usually urgent, and also embarrassing to the utility.

Using traditional technology, audible noise is reduced by increasing the conductor diameter and, more effectively, by using a bundle of a greater number of conductors. For the same total cross-section, lower levels of audible noise are obtained with a greater number of conductors of smaller diameter. For instance, a bundle of four 3.2-cm diameter conductors for 500 kV produces less noise than a bundle of three 3.7-cm diameter conductors, which produces less noise than a bundle of two 4.5-cm conductors, which produces less noise than a single 6.35-cm conductor. In all four cases, the conductor cross-section is the same. Unfortunately, increasing the number of conductors increases wind and tower loads, and therefore the cost of conductor support structures.

Several techniques for audible-noise reduction have been explored (EPRI 1982). Most require new nontraditional technology, and some have significant drawbacks. The most practical method to achieve a significant reduction of audible noise when bundles of three or more conductors are used is to adjust the relative position of the conductors in the bundle to achieve an optimum performance. Bundle geometry optimization is discussed in detail in Section 10.7.2. Other techniques have mostly a theoretical interest and are only briefly discussed.

As a result of complaints, audible-noise reduction techniques may be required, but they need to be applied only to a short section of transmission line. The effective noise reduction depends on the ratio between the length, X, of the section treated and the distance, D, between line and point of measurement. The effective noise reduction, ΔP (dB), when the noise generation of the treated section is reduced by ΔA (dB), is given by:

$$\Delta P = 10 \cdot \log\left(1 - (1 - 10^{-\Delta A/10}) \cdot \tan^{-1}(X / (2D)) \cdot 2 / \pi\right) \quad 10.7\text{-}1$$

Assume, for example, that a noise reduction technique reduces the noise generation by 10 dB and is applied to a 400-m span of a transmission line. At a distance of 80 m from the center of the line, in correspondence to the center of the span, the noise is reduced by 5 dB. This value is derived from Equation 10.7-1, with ΔA = 10 dB and $X/(2D)$ = 400/(2 x 80).

An example of a technique successfully applied as a local fix consists of the application of large diameter conductive tubing around the conductors (Nourse 1978; Stearns 1979).

10.7.2 Bundle Geometry Optimization

The audible noise produced by a bundle of conductors depends on diameter and relative position of each conductor within the bundle. Generally transmission lines use regular bundles—i.e., the conductors have all the same diameter and are placed on the vertices of a regular polygon. The audible-noise calculation procedure, described in Section 10.4, applies to regular bundles. Of particular interest is the noise in the weather conditions (such as light rain, fog, and wet snow) most conducive to complaints because of relatively elevated line noise and relatively low ambient noise. The measure of audible-noise performance in these conditions may be identified with the L_{50} level in rain (median noise level during periods of measurable rain) discussed in Section 10.4, and which is called here for simplicity the "wet-weather" noise.

The wet-weather noise can be reduced by proper adjustment of the geometry of the bundle (Comber and Zaffanella 1973). The optimum bundle geometry is the one corresponding to the minimum wet-weather noise. This section describes how the bundle geometry can be optimized. Once the optimum bundle is determined, the fair-weather audible noise and the performance under wind, ice, and electrical load conditions should be checked to verify that an improvement in wet-weather audible noise performance is not achieved at the expense of an unacceptable worsening of other performance parameters.

The equations of Section 10.4 considered a regular bundle as a unit. To optimize the geometry of a bundle, however, each individual conductor of the bundle must be considered separately. The noise produced by each conductor must be calculated as a function of the conductor characteristics that determine the intensity of the noise produced by corona. The source of wet-weather audible noise is the crackling sound caused by positive-polarity corona streamer starting at water drops. The intensity of these streamers is a function of the following:

1. The shape of water drops, the distribution of drops on the surface, and the frequency of drop formation, all of which depend on surface conditions, rain intensity, and other weather conditions.
2. The electric field in the space where the streamers propagate. This means not only the electric field at the surface of the conductor but also the electric field up to

some distance from the surface (e.g., up to at least two diameters from the center of the conductor).

If two conductors are identical in terms of the two sets of parameters listed above, they will produce the same audible noise because everything associated with the water drops is identical. An example is the following: consider the bottom-left conductor of the four-conductor bundle and the left conductor of the two-conductor bundle shown in Figure 10.7-1. Both these conductors have the same diameter and the same ratio between maximum surface gradient and average gradient. The equipotential lines are practically the same in the region near the surface of the conductors, as indicated in the enlargement of the two conductors shown in Figure 10.7-2. The figures also show a water drop located at the bottom of the conductor. In both cases the water drop would be in the same electric field environment: it would be deformed by the field in identical way, corona from the water drop would be triggered and would propagate in the same way, and the audible noise would be the same.

The wet-weather-generated acoustic power of a conductor may be expressed as a function of four parameters: the conductor diameter, d; the maximum surface gradient, E_{max}; the average surface gradient, E_{av} (or the ratio between the maximum and the average surface gradients: $k = E_{max}/E_{av}$); and the point of maximum gradient on the

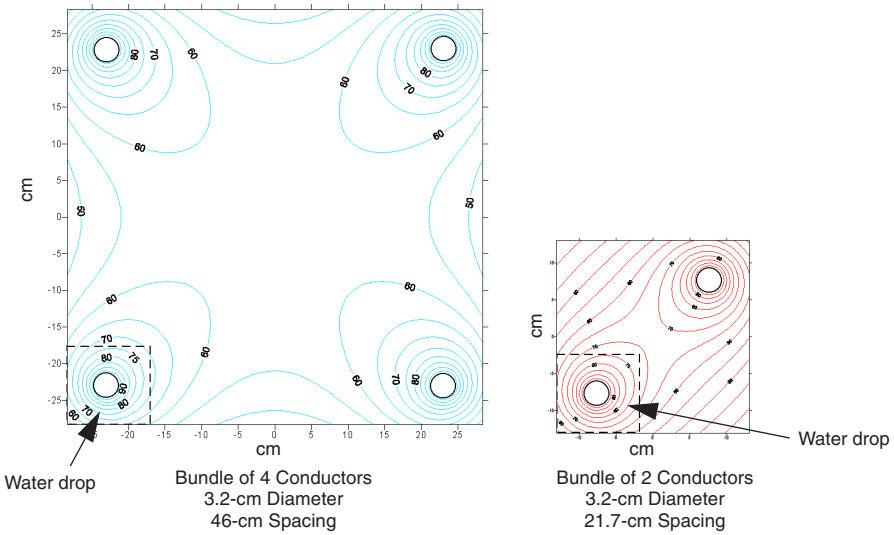


Figure 10.7-1 Equipotential lines (conductor surface = 100) for a bundle of four and a bundle of two conductors with the same average and maximum surface gradients.

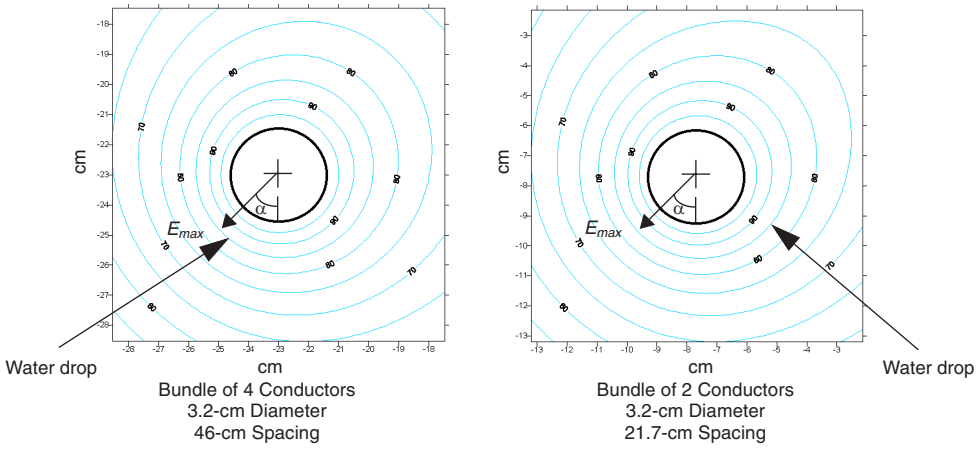


Figure 10.7-2 Enlarged portions of Figure 10.7-1. Equipotential lines near the surface of a conductor of a four-conductor bundle and of a conductor of a two-conductor bundle with the same average and maximum surface gradients and location of water drops.

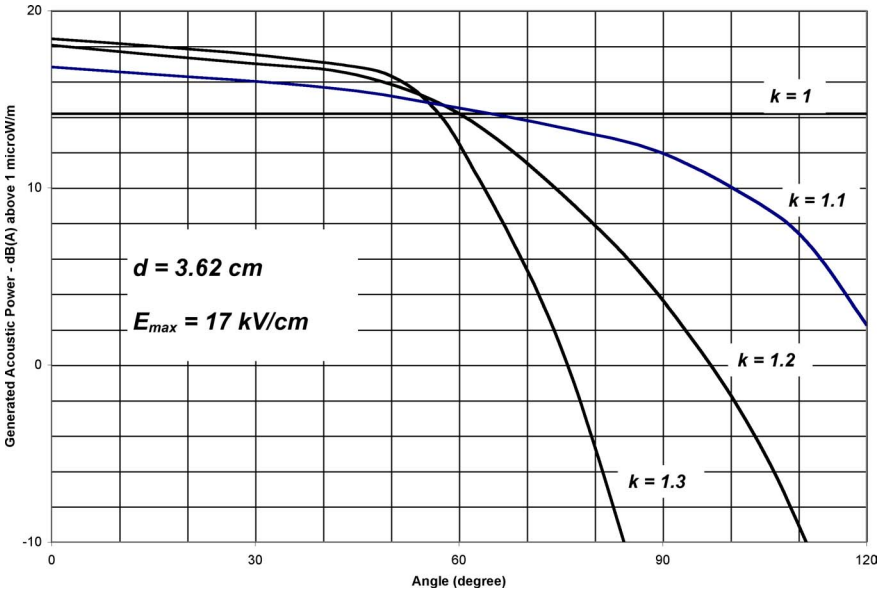


Figure 10.7-3 Example of wet-weather audible-noise-generated acoustic power versus the angle, α, that defines the angular position of the point of maximum gradient relative to water drops. Curves for a fixed conductor diameter and a fixed maximum surface gradient and different values of the ratio, *k*, between maximum and average surface gradients.

conductor surface in relation to the location of the water drops, defined by the angle, α, (see Figure 10.7-2).

$$A = f(d, E_{\max}, k, \alpha) \qquad 10.7\text{-}2$$

A complete set of audible-noise generation data was obtained for different values of d, E_{max}, k, and α (Comber and Cortina, 1976). A special test setup allowed the researchers to isolate the noise produced by an individual conductor and to vary the four parameters independently of each other. An example of the results obtained is shown in Figure 10.7-3. This figure shows that the largest noise is produced when the water drops are at the point of maximum gradient ($\alpha = 0$), in which case the noise is greater for the largest values of k. For a regular bundle and the same bundle diameter, a bundle with more conductors has a greater value of k, which is given by Equation 10.7-3.

$$k = 1 + (n-1)d / d_b \qquad 10.7\text{-}3$$

where n is the number of conductors, d is the diameter of the conductors, and d_b is the diameter of the regular bundle. Therefore, the bottom conductor(s) of a bundle with a greater number of conductors produce a greater level of audible noise for the same maximum surface gradient.

The data developed to express the noise of individual conductors apply to aged conductors—i.e., conductors whose surface has a hydrophilic property similar to the surface of conductors that have been exposed to the elements for a considerable period of time. In calm wind conditions, water accumulates in drops on the bottom of such conductors rather than beads all around the surface, as is the case for new conductors. Therefore, for aged surfaces and calm wind conditions, the angle α characterizes the position of the water drops with respect to the point of maximum gradient.

The individual conductors of a regular bundle do not produce the same audible noise in wet weather. For instance, assume that the bundle of four conductors shown in Figure 10.7-1 operates at a maximum surface gradient of 19 kV/cm. The individual conductor data show that each of the bottom two conductors generates 18.3 dB above 1 μW/m while each of the top two conductors generates 4.5 dB above 1 μW/m (i.e., about 14 dB less) (Comber and Cortina 1976).

The individual conductor noise data have been used to optimize the bundle geometry (Comber and Cortina 1976). The optimum geometry of a bundle can be found by exercising Applet AN-3, "Bundle Geometry for Minimum Audible Noise". In principle, it is possible to reduce wet-weather audible noise by optimizing the relative values of the diameter of the conductors in the same bundle. However, it is not practical to use conductors of different diameter because they would have different temperature, sag, creep, and stringing characteristics. Much more attractive is the optimization of the relative position of each conductor within a bundle. Since the bottom conductors of a regular bundle generate more noise, the noise is decreased by

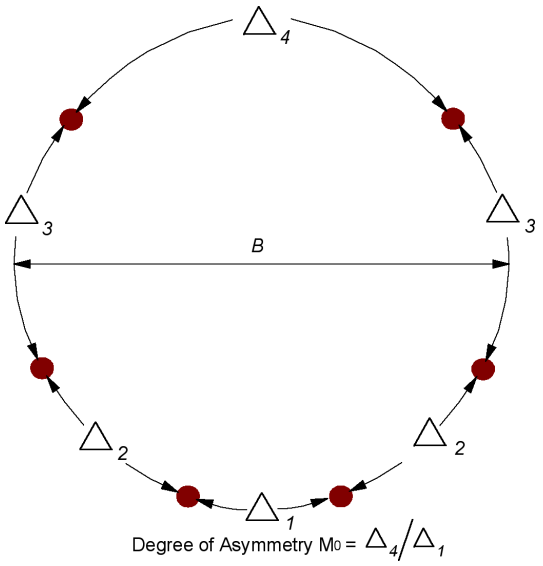


Figure 10.7-4 Asymmetric arrangement of a six-conductor bundle.

placing more conductors on the bottom than on the top part of the bundle, thus reducing the maximum surface gradient of the bottom conductors. This is shown in the asymmetric bundle of Figure 10.7-4. The circular spacing between adjacent conductor is the shortest for the bottom two (Δ_1) and the longest for the upper two (Δ_4), all the spacing being in a geometric progression ($\Delta_2/\Delta_1 = \Delta_3/\Delta_2 = \Delta_4/\Delta_3$). The degree of asymmetry is defined as the ratio $M = \Delta_4/\Delta_1$. The audible noise of the top conductors of the bundle is increased, but overall the bundle will be less noisy. There is an optimum degree of asymmetry, M_0, corresponding to the lowest noise generated by the bundle.

Cage tests were performed on a six-conductor bundle (conductor diameter equal to 4.63 cm and bundle diameter equal to 1.42 m) for the center phase of a 1050-kV line (EPRI 1982). The regular bundle operates at a maximum surface gradient of 16.0 kV/cm. The tests were performed for different degrees of asymmetry. The results, shown in Figure 10.7-5, confirmed the predictions based on individual conductor audible noise data. The optimum degree of asymmetry was found to be $M_0 \approx 3$. The optimum bundle produced about 6 dB less noise than the regular bundle. However, tests on a three-phase test line with the same bundle have shown only a 3-dB reduction in the L_{50} audible noise in rain, while an 8-dB reduction was observed in fog.

Similar results were obtained for an asymmetric 4 x 3.62-cm conductor bundle for 800-kV transmission (Baker et al. 1975). For this bundle, a reduction of about 4 dB in the L_{50} rain level was obtained, while no reduction in the L_5 rain level was obtained.

The noise performance of an asymmetric bundle in an actual three-phase installation in natural rain conditions is degraded by several facts, particularly by the fact that water drops do not form exactly at the bottom of the conductors because of imperfect surface conditions and wind, and because conductor twist and differential sags make the bundle geometry different from the desired optimum.

Another important factor is the noise caused by water drops impinging on the upper conductors of the bundle during rain. The impingement noise depends on the rain intensity and, for regular bundles and most rain conditions, is negligible with respect to the noise due to water drops formed on the conductor surface. The impingement noise is greater for asymmetric bundles because of the increase in surface gradient for the upper conductors. The impingement noise is absent in fog conditions and is negligible in light rain. It is in these conditions that the reduction in audible noise caused by bundle asymmetry can be significant.

The achievable noise reduction is larger at lower surface gradients and for bundles with a greater number of conductors. For these reasons, asymmetric bundles are attractive for transmission voltages of 800 kV and higher.

Asymmetric bundles designed for minimum wet-weather audible noise generation do not have a uniform load current distribution among the conductors, even though they have the same diameter. In fact, the current subdivision among the conductors of a bundle is controlled by the mutual inductances in addition to the self-inductances and resistances. Individual conductor currents may differ by 5 ~ 10% from the average conductor current. This causes an additional resistive loss of the order of 1 ~ 3%. However, the additional resistive loss may be more than compensated by the reduction in corona loss, which for optimum asymmetric bundles can be significantly lower than that of regular bundles.

10.7.3 Other Techniques of Audible Noise Reduction

Several techniques for audible noise reduction have been explored (EPRI 1982). Most require new nontraditional technology, and some have significant drawbacks. They are briefly described below.

Use of Small Protrusions that Generate Ultra Corona

Small wires or thin protrusions generate intense corona without the positive-polarity streamers that are the main cause of transmission-line audible noise. This kind of corona is usually referred to as “ultra corona.” The large amount of generated space charge reduces the gradient at the conductor surface and prevents the formation of positive-polarity streamers from the water drops that are close to the protrusions. This method has serious disadvan-

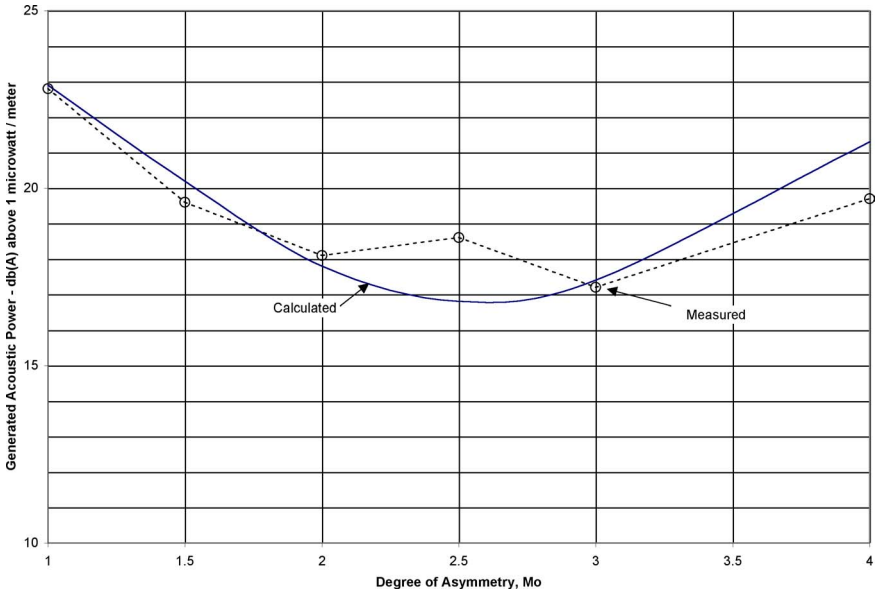


Figure 10.7-5 Test results and calculated performance of a six-conductor bundle with 4.63-cm conductor diameter and 1.42-m bundle diameter.

tages that limit its use only to local fixes in some circumstances. In fact, although a reduction of 10 to 20 dBA in noise may be achieved, the hum at twice the power frequency is drastically increased in value and occurs at all times independently of the weather conditions. This hum may become a new source of complaints. Furthermore, ultra corona causes a large increase in corona loss and, consequently, a severe economic penalty, especially if long sections of the transmission line are treated. Finally, in one application on a 765-kV line, it was found that ultra corona from thin wire loops clipped to the conductors caused unacceptable television interference. It is not clear, however, whether the television interference was caused by the ultra corona or by spark discharges due to inadequate contact between the small wires and the conductor.

Conductors Covered with a Thick Layer of Insulation

A layer of insulation on the conductor surface causes water drops to form in regions of lower gradients and introduces impedance between water drops and conductor. In order to cause a significant decrease in noise the insulation thickness must be significant. Insulated conductor technology is well known at distribution voltages (tree wires). At 138 kV and 230 kV, this technology has other potential advantages because it allows reducing the distance between phases, which is desirable in an urban setting where compaction and magnetic field reduction are needed. At these voltages, however, audible noise is not a design constraint. At higher voltages, where audible noise reduction is desirable, this technology is not available.

Conductors Covered with Insulating Tube or Wire Mesh

Placing an insulating tube or cylindrical wire mesh over a conductor has an effect similar to that of thick insulation. It has the advantage of simplicity and, if the tube or the wire mesh is not concentric but hangs on the conductor, the water drops will form further away from the conductor. The space between the tube or the wire mesh and conductor may be filled with air or another insulating material. It may also be possible to leave the upper portion of the conductor exposed. This would not be effective in heavy rain, but it would reduce the noise in other wet-weather conditions. This technique is effective in reducing audible noise. However, the use of tubes limits conductor heat dissipation and will increase wind loading. The wind loading will be much smaller if a cylindrical wire mesh instead of a tube is placed around the conductor, and the mesh does not limit heat dissipation.

The Bonneville Power Administration placed a 4.0-in. (10.16-cm) tube over some spans of two of their 500-kV lines that were originally built with a 2.5-in. (6.35-cm) conductor. During steady rain conditions the A-weighted audible noise from the spans with the tubes was about 8 dB less than from the nearby span without the tubes (Stearns 1979).

Application of a Negative DC Bias to Reduce the Positive Surface Gradient Peak

Since the main contributors to audible noise are the streamers that occur during the positive polarity cycle, reducing the positive peak while maintaining the same peak-to-peak amplitude of the surface gradient reduces the

audible noise. A practical application of this technique occurs when a HVDC line is adjacent to a HVAC line. When the positive pole of the HVDC line is the closest to the HVAC line, a negative charge is induced in the conductors of the HVAC line. The positive-polarity peak gradient is decreased and the negative polarity peak gradient is increased. This causes a decrease in audible noise (Chartier et al. 1981; Clairmont et al. 1989).

APPENDIX 10.1 ADJUSTMENT OF MEASURED AUDIBLE-NOISE LEVELS TO ACCOUNT FOR AMBIENT NOISE INTRUSIONS

When the ambient noise is of the same order as, or only a few dB below the transmission-line noise, measured A-weighted noise levels cannot reliably be attributed to corona from the line.

The most commonly encountered ambient noises, such as those from wind, vehicles, and aircraft, have the major portion of their energy concentrated in the lower frequency region of the noise spectrum (frequency less than 500 Hz), whereas the most significant components of corona noise are above 500 Hz. These contrasting characteristics of ambient and corona noises may be used to detect when the noise measurement is affected by ambient noise intrusions. They may also be used, with one reasonable assumption relating to the frequency spectrum of corona noise, to provide a means of correcting the measured sound-pressure levels. The assumption is that the shape of the frequency spectrum of corona noise, measured without the presence of significant ambient noise, remains the same even though the intensity of the noise may vary. This was shown to be true during audible-noise tests (Comber et al. 1978; Nourse 1978) and was used extensively by BPA in their long-term audible-noise measurement programs (Chartier et al. 1987). With this assumption, the A-weighted level of the noise would vary dB-for-dB in equal fashion for each of the octave-band levels above 500 Hz.

With a 1-in. (2.54-cm) microphone, the frequency response rolloff occurs above 12 kHz. With a 1/2-in. (1.27-cm) microphone, the frequency response rolloff occurs above 20 kHz. At these frequencies, the corona-spectrum is still quite flat, whereas typical ambient noises have little energy compared to lower frequencies. The measurements of the 8-kHz or of the 16-kHz octave band levels are thus considered to be best indicators of the true line noise. Figure A10.1-1 shows a plot of 8-kHz octave band measurements against corresponding dBA measurements during several days of testing of a three-phase line configuration. Included are data for different voltage levels, totaling approximately 5000 points. It may be seen that a large mass of points form a good dB-for-dB correlation. However, many points have a higher dBA level than expected from the main trend, and many points corresponding to the lower noise levels break out of the trend. These effects are caused by the intrusion of ambient noises that have little effect on the 8-kHz level, but significantly increase the A-weighted level.

Figure A10.1-2 shows a reduction of these data points. For each 8-kHz dB window, the 50% dBA level is plotted against the 8-kHz level. A line with slope 1 dBA/1 dB(8 kHz) may be drawn from the bulk of the points as shown. Assuming that the 8-kHz level is due entirely to line noise, the true A-weighted line noise, corrected for ambient noise, may be determined from the 8-kHz measurements. For this particular example, the adjusted dBA level is found by adding 7 dB to the measured 8-kHz level. Note that the relationship between dBA and dB(8 kHz) depends on microphone type, microphone location, and, to some extent, also line geometry. This relationship must be computed for each situation. For example, the relationship between the A-weighted and 16-kHz noise levels produced by a double-circuit line in Montana was found to be about 11 dB for a 1.27-cm microphone.

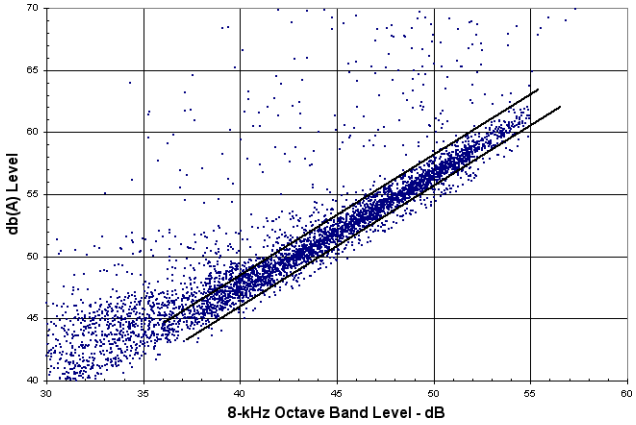


Figure A10.1-1 Measured A-weighted noise level plotted against 8-kHz octave band level.

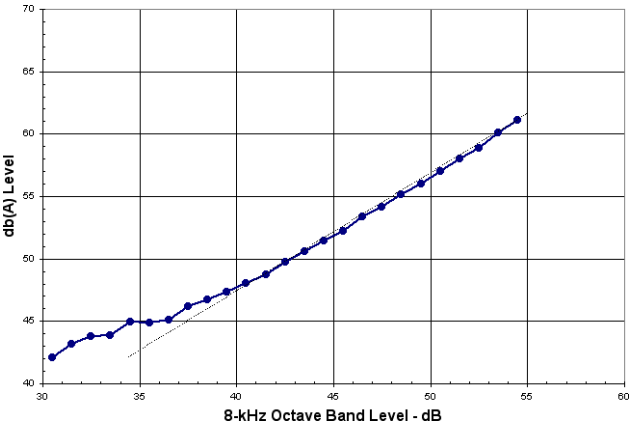


Figure A10.1-2 Median A-weighted noise level for each 1 dB interval of 8-kHz octave band level (data from Figure 10.A1-1).

APPENDIX 10.2 AMBIENT NOISE DURING RAIN

Knowing the ambient levels during rainstorms becomes important when some noise codes (e.g. San Diego County, see Section 10.6) allow higher noise levels if the ambient level exceeds the applicable limit.

The background noise caused by rainfall depends on the location and the rain intensity. High noise levels may be achieved by rain falling on some types of roofs (metal or plastic). Some rainfalls are accompanied by wind, which also adds to the noise.

A typical frequency spectrum of rain noise is compared to a typical frequency spectrum of transmission-line noise in Figure A10.2-1. The figure shows that the ambient noise caused by rainfall decreases rapidly with frequency, whereas the transmission-line noise is quite different. Because of this difference in frequency spectra, the transmission-line noise may be distinguished from ambient rain noise of the same dBA level.

L. N. Miller developed an empirical procedure for predicting rainfall sound on the basis of rainfall rate, surface types, and wind speed (Keast 1980). Miller's results are shown in Figure A10.2-2. The conditions determining the curves R-1 through R-5 in Figure A10.2-2 are given in Table A10.2-1. The curve number to be selected is the one that best represents the type of ground, ground cover, and leaf conditions. Assuming a heavy rainfall (2.5 mm/h) and no wind, Figure A10.2-2 shows that the rainfall sound level can vary from 41 to 54 dBA, depending upon the type of surface on which the rain impacts. Therefore, the field experience of many observers that corona noise from ac lines during "heavy rain" is masked by the noise of the rain itself isn't necessarily true. The highest level is for large-leafed foliage, and the lowest for porous ground, sand, or snow. Rainfall on ordinary residential roofs is very quiet, while water dripping from eaves and wind-driven rain against windowpanes are much noisier (Keast 1980).

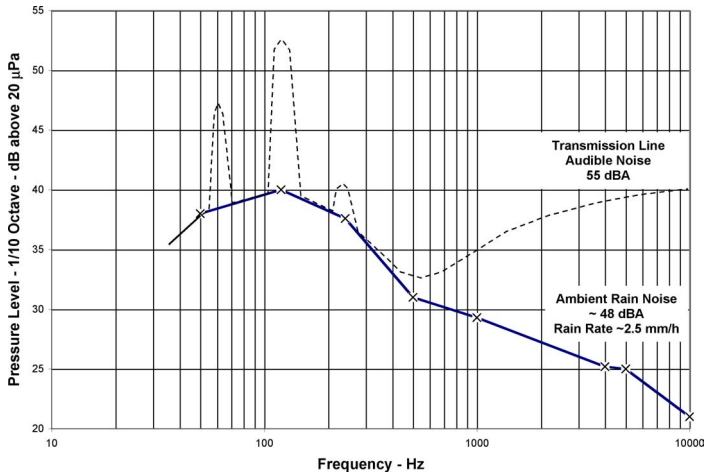


Figure A10.2-1 Audible-noise frequency spectrum (1/10 octave) of ambient noise caused by rainfall and corona noise of a transmission line.

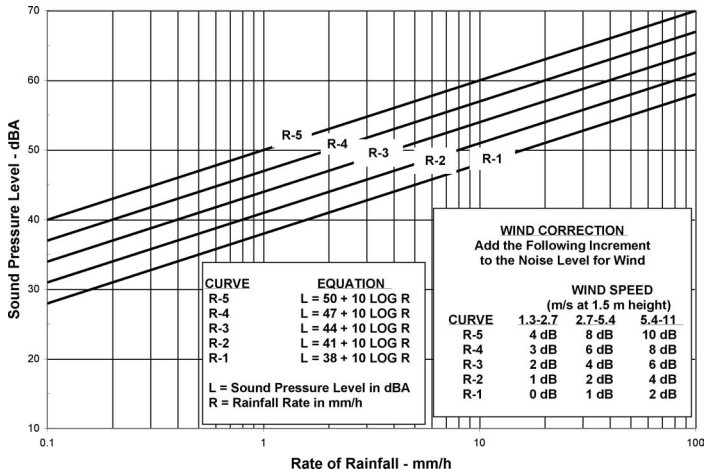


Figure A10.2-2 Family of curves for estimating sound levels due to rainfall (Keast 1980). Determine the appropriate curve number from ground and vegetation conditions given in Table A10.2-1.

Table A10.2-1 Curve Number to Be Used in Figure A10.2-2 for Estimating A-Weighted Sound Levels Due to Rainfall (Keast 1980)

Curve Number	Condition of Ground and Vegetation
R-1	Essentially bare, porous ground (i.e., plowed field or snow-covered ground); no standing puddles of water. Relatively small-leafed ground cover vegetation, such as grass lawn, meadow, hay field shortly after mowing, field of small-leafed plant.
R-2	Nonporous hard bare ground or paving. Falling rain drops splash on thin layer or puddles of collected water. In or beside wooded areas of deciduous trees without leaves or with small leaves. In or besides wooded areas of trees with needles, not leaves. Thin-leafed ground cover or crop, such as hay, clover, or grain.
R-3	A few small, fully leafed deciduous trees at 15–30 m. A few large, fully leafed trees at 30–90 m.
R-4	Large area of fully leafed trees or large-leafed crops or vegetation, such as corn, starting at 15–30 m distance.
R-5	Large area of fully leafed trees or large-leafed crops or vegetation entirely surrounding area of interest.

REFERENCES

Anderson, J.G., M. Baretsky, and D.D. MacCarthy. 1966. "Corona-Loss Characteristics of EHV Transmission Lines Based on Project EHV Research." *IEEE PAS-85*. pp. 1196-1212. December.

Anderson, J.G. and L.E. Zaffanella.1972. "Project UHV Test Line Research on the Corona Performance of a Bundle Conductor at 1000 kV." *IEEE PAS-91.* pp. 223-232, January/February.

ANSI/IEEE Standard 656-1992. IEEE Standard for the Measurement of Audible Noise from Overhead Transmission Lines.

ANSI. American National Standard Specification for Sound Level Meters. ANSI/S1.4-1983 (reaffirmed 2001).

Azernikova, T.I. and N.P. Emelyanov. 1985. "The Problem of Acoustical Noise in the Development of 1150 kV Transmission Lines." Izvestiya Akademii Nauk SSSR. *Energetika I. Transport*. Vol. 26, no. 3.

Baker, A.C., M.G. Comber, and K.E. Ottosen.1975. "Investigation of the Corona Performance of Conductor Bundles for 800-kV Transmission." *IEEE PAS-94*. pp. 1117-1130. July/August.

Booker, J.R. 1986. "Natural Aging of Non-Energized Aluminum Conductors." *IEEE PWRD-1*. pp. 269-274. October.

Bragdon, C.R. 1980. *Municipal Noise Legislation*. Atlanta, Georgia: The Fairmont Press, Inc.

Britten, A.C., E.G. Clarke, and H.E. Konkel.1987. "Radio Interference, Corona Losses, Audible Noise and Power Frequency Electric Fields as Factors in the Design of Eskom's 765 kV Lines." CIGRÉ Regional Conference. Johannesburg. October.

Britten, A.C., D.H. Cretchley, K.J. Sadurski,B. Druif, and H.A. Roets.1991. "The Compaction of Conductor-to-Tower Clearances on Eskom's 765 kV Transmission Lines." CIGRÉ Symposium. Leningrad. June.

Chartier, V.L. 1989. "Results of Long-Term Audible Noise Measurements Made Before and After Reconductoring of the Spans From Tower 6/4 to 7/4 of Ostrander-Pearl 500-kV Transmission Line." U.S. Department of Energy–Bonneville Power Administration, Division of Laboratories Report No. ELE-89-34. March 22.

Chartier, V.L. 1994. "Effect of Load Current on Conductor Corona from High Voltage AC and DC Overhead Transmission Lines," Paper presented at The Seminar on Electromagnetic Field Effects Caused by High Voltage Systems (Modeling, Characterization, Measurements, Mitigation). Japan-U.S. Cooperative Science Program of the National Science Foundation and the Japan Society for the Promotion of Science Program. Hokkaido University. Sapporo, Japan. June 28–July 1.

Chartier, V.L., D.F. Shankle, and N. Kolcio. 1970. "The Apple Grove 750-kV Project: Statistical Analysis of Radio Influence and Corona-Loss Performance of Conductors at 775 kV." *IEEE PAS-89*. pp. 867-881. May/June.

Chartier, V.L. and R.D. Stearns.1981. "Formulas for Predicting Audible Noise From Overhead High Voltage AC and DC Lines." *IEEE PAS-100*. pp. 121-129. January.

Chartier, V.L., S.H. Sarkinen, R.D. Stearns, and A.L. Burns. 1981. "Investigation of Corona and Field Effects of AC/DC Hybrid Transmission Lines." *IEEE PAS-100*. pp. 72-80. January.

Chartier, V.L., L.Y. Lee, L.D. Dickson, and K.E. Martin. 1987. "Effect of High Altitude on High Voltage AC Transmission Line Corona Phenomena." *IEEE PWRD-2*. pp. 225-236. January.

Chartier, V.L., D.E. Blair, R.D. Stearns, and D.J. Lamb. 1994. "Effect of Bundle Orientation on Transmission Line Audible and Radio Noise." *IEEE PWDR-9*. pp. 1538-1544. July.

Chartier, V.L., D.E. Blair, M.D. Easley, and R.T. Raczkowski. 1995. "Corona Performance of a Compact 230-kV Line." *IEEE PWDR-10*. pp. 410-420. January.

Clade, J., C. Gary, and M. Moreau.1976. "Results of Studies on Corona Effects Undertaken at the Experimental Station at Renardieres." CIGRÉ Paper 31-08.

Clairmont, B.A., G.B. Johnson, L.E. Zaffanella, and S.V.L. Zelingher.1989. "The Effect of HVDC – HVAC Separation in a Hybrid Corridor." *IEEE PD-4 No. 2.* pp. 1338-1350. April.

Comber, M.G. and L.E. Zaffanella.1973. "Audible Noise Reduction by Bundle Geometry Optimization." *IEEE PAS-92*. pp. 1782-1791. September/October.

Comber, M.G. and L.E. Zaffanella. 1974. "The Use of Single-Phase Overhead Test Lines and Test Cages to Evaluate the Corona Effects of EHV and UHV Transmission Lines." *IEEE PAS-93.* pp. 81-90. January/February.

Comber, M.G. and R. Cortina. 1976. "Audible Noise Generation of Individual Subconductors of Transmission Line Conductor Bundles." *IEEE PAS-95*. pp. 528-535. March/April.

Comber, M.G. and R.J. Nigbor. 1976. "Audible Noise Performance of the First Three-Phase Ultra-High Voltage Transmission Test Line At EPRI's Project UHV." *IEEE PAS-95*. pp. 1105-1114. July/August.

Comber, M.G., L.E. Zaffanella, and F.S. Young. 1978. "Three-Phase UHV Transmission Line Research at EPRI's Project UHV." CIGRÉ 31-10.

Comber, M.G. and R.J. Nigbor. 1979. "Audible Noise Performance of Regular and Asymmetric Bundles and Effect of Conductor Aging on Project UHV's Three-Phase Test Line." *IEEE PAS-98*. pp. 561-572. March/April.

Coquard, A. and C. Gary.1972. "Audible Noise Produced by Electrical Power Transmission Lines at Very High Voltage." CIGRÉ Paper 36-03.

EPRI. 1982. "Transmission Line Reference Book – 345 kV and Above/Second Edition." Electric Power Research Institute, Palo Alto, California.

EPRI. 1992. "Substation Voltage Upgrading – Volume 2: Substation Insulation Tests and Design for Fast Front Lightning Impulses." Prepared by GE Industrial and Power Systems. Schenectady, New York. EPRI EL-6474. Volume 2. Project 2794-1. Final Report. April.

Farzaneh, M. and L.C. Phan.1984. "Vibration of High Voltage Conductors Induced by Corona from Water Drops or Hanging Metal Points." *IEEE PAS-100.* pp. 2746-2752. September.

Farzaneh, M. and Y. Teisseyre. 1988. "Mechanical Vibrations of High Voltage Conductors Induced by Corona: Roles of the Space Charge and Ionic Wind." *IEEE PWRD-3.* pp. 1122-1130. July.

Farzaneh, M. 1992. "Effects of the Intensity of Precipitation and Transverse Wind on the Corona Induced Vibrations of High Voltage Conductors." *IEEE PWRD-7.* pp. 674-680. April.

Gross, I.W., C.F. Wagner, O. Naef, and R.L. Tremaine. 1951. "Corona Investigation on Extra-High Voltage Lines—500-kV Project of the American Gas & Electric Company." *AIEE Transactions*. Vol. 70, pt. I. pp. 75-94.

IEC 60804. 2000. Integrating-averaging sound level meters. October.

IEC 60651. 2001. Sound Level Meters. October.

IEEE Committee Report. 1973. "Comparison of Radio Noise Prediction Methods with CIGRÉ/IEEE Survey Results." *IEEE PAS-92.* pp. 1029-1042. May/June.

IEEE Corona and Field Effects Subcommittee Report. 1982. "Calculating Audible Noise Produced by HV Lines; Comparison of Calculation Methods." *IEEE PAS-101*. pp. 4090-4099. October.

Juette, G.W. and L.E. Zaffanella. 1972. "Radio Noise, Audible Noise, and Corona Loss of EHV and UHV Transmission Lines Under Rain: Predetermination Based on Cage Tests." *IEEE PAS-91*. pp. 211-222. January/February.

Keast, D.N. 1980. "Assessing the Impact of Audible Noise from AC Transmission Lines: A Proposed Method." *IEEE PAS-99*. pp. 1021-1031. May/June.

Kolcio, N., B.J. Ware, R.L. Zagier, V.L. Chartier, and F.M. Dietrich. 1974. "The Apple Grove 750 kV Project: Statistical Analysis of Audible Noise Performance of Conductors at 775 kV." *IEEE PAS-93*. pp. 831-840. May/June.

Kolcio, N., J. DiPlacido, and F.M. Dietrich.1977. "Apple Grove 750 kV Project –Two Year Statistical Analysis of Audible Noise from Conductors at 775 kV and Ambient Noise Data." *IEEE PAS-96*. pp. 560-570. March/April.

LaForest, J.J., C.B. Lindh, D.D. MacCarthy, F. Olsen, and M.W. Schultz.1963. "Radio Noise and Corona Loss Results from Project EHV." *AIEE Transactions*. Vol. 82. pp. 735-750. October.

Larsson, C., B. Hallberg, and S. Israellsson. 1988. "Long Term Audible Noise and Radio Interference Performance from an Operating 400-kV Transmission Line." *IEEE PWRD-3*. pp. 1842-1846. October.

Lee, D.I., J.B. Kim, K.H. Yang et al.1997. "Audible Noise Performance of 6-Rail Conductors on a 765-kV Double Circuit Test Line." *IEEE PWRD-12*. pp. 1343-1351. July.

Lundquist, J. 1990. "Results from AC Transmission Line Audible Noise Studies at the Anneberg EHV Test Station." *IEEE PWRD-5.* pp. 317-323. January.

MacCarthy, D.D. and J.R. Doyle. 1969. "New Method for Simulating Rainfall in High-Voltage Testing." *IEEE PAS-88*. pp. 126-133. February.

Molino, J.A. 1977. "Initial Psychoacoustics Experiments on the Human Response to Transmission Line Audible Noise." U.S. Department of Energy, Contract EA-77-A-06110-A0-17-1, Report DOE/ET/6010-1.,

Molino, J.A., G.A. Zerdy, N.D. Lerner, D.L. Harwood, and S.G. Tremaine.1979. "Use of the 'Acoustic Menu' in Assessing Human Response to Audible (Corona) Noise from Electric Transmission Lines." *J. Acoust. Soc. America*. Vol. 66, No, 5. pp. 1435-1445. November.

Montana Major Facility Siting Act. 1984. "Linear Facilities, Minimum Impact Standard." Rule ARM 36.7 3507. Montana Board of Natural Resources and Conservation. December 10.

Newell, H.H., T.W. Liao, and F.W. Warburton.1968. "Corona and RI Caused by Particles on or near EHV Conductors: II – Foul Weather." *IEEE PAS-87.* pp. 911-927. April.

Nourse, G.R. 1978. "Development and Trial Installation of an Aluminum Tubing Audible Noise suppressor for 765 kV Lines." *IEEE PAS-97*. p. 1009. July/August.

Paris, L. and M. Sforzini. 1968. "RI Problems in HV-Line Design." *IEEE PAS-87.* pp. 940-946. April.

Pearson, K.S., R.L. Bennett, and S.A. Fidell. 1979. "Initial Study on the Effects of Transformer and Transmission Line Noise on People." EPRI Final Report EA-1240, Project 852, December.

Perry, D.E. 1972. "An Analysis of Transmission Line Audible Noise Levels Based upon Field and Three-Phase Test Line Measurements." *IEEE PAS-91*. pp. 857-865. May/June.

Perry, D.E., V.L. Chartier, and G.L. Reiner. 1979. "Bonneville Power Administration's 1100 kV Transmission Development - Corona and Electric Field Studies." *IEEE PAS-98*. pp. 1728-1738. September/October.

Popeck, R.A. and R.F. Knapp.1981. "Measurements and Analysis of Audible Noise from Operating 765-kV Transmission Lines." *IEEE PAS-100*. Pp. 2138-2148. April.

S.A.E. 1964. "Standard Values of Atmospheric Absorption as a Function of Temperature and Humidity for Use in Evaluating Aircraft Flyover Noise." New York, NY: Society of Automotive Engineers. Report ARP 866. August.

Sforzini, M., R. Cortina, G. Sacerdote, and R. Piazza. 1975. "Acoustic Noise Caused by AC Corona on Conductors: Results of an Experimental Investigation in the Anechoic Chamber." *IEEE PAS-94*. pp. 591-601. March/April.

State of New York Public Service Commission. 1978. "Opinion and Order Determining Health and Safety Issues, Imposing Operating Conditions, and Authorizing, in Case 26529. Operation Pursuant to Those Conditions." Opinion No. 78-13. June 19.

Stearns, R.D. 1979. "Audible Noise (AN), and Radio Interference (RI) Performance of the AN Boot Located on the Oregon City-Ostrander 500-kV Line near the E. R. Hursh Residence." U.S. Department of Energy—Bonneville Power Administration Laboratory. Report No. ERJ-79-128. December 31.

Stearns, R.D. 1980. "Corona and Electric Field Performance of the Lyons Test Line Utilizing the Symmetric 7 x 41 mm Configuration." U.S. Department of Energy—Bonneville Power Administration 1200 kV Project Report. Report No. EL-80-7. September 11.

Tanabe, K. 1991a. "Hum Noise Performance of 6, 8, 10 Conductor Bundles for 1000 kV Transmission Lines at the Akagi Test Site: A Comparative Study with Cage Data." *IEEE PWRD-6.* pp. 1799-1804. October.

Tanabe, K. 1991b. "Second Harmonics of Audible Noise from AC Transmission Lines – Random Walk Model on Space Distribution." *IEEE PWRD-6*. pp. 216-222. January.

Trinh, N.G., P.S. Maruvada, J. Flamand, and J.R. Valotaire.1982. "A Study of the Corona Performance of Hydro-Quebec's 735-kV Lines." *IEEE PAS-101*. pp. 681-690. March.

U.S. Environmental Protection Agency. 1974. "Information on Levels of Environmental Noise Requisite to Protect Health and Welfare with an Adequate Margin of Safety. Document 5519-74-004. U.S. Government Printing Office. 546-318/366 1-3.

WAC. 1975. Chapter 173-60. Washington Administrative Code (WAC). "Maximum Noise Levels." Adopted April 22, 1975. Amended August 1, 1975. Department of Ecology. Noise Section. Olympia, Washington.

Wells, R.J. 1974. “Subjective Analysis of the Noise from High Voltage Transmission Lines.” Proceedings of a Workshop on Power Line Noise as Related to Psychoacoustics. IEEE Publication 74CH0967-0-PWR.

Yang, K. H, D. I. Lee, G. H. Hwang, J. H. Park, and V. L. Chartier. 2000. “New Formulas for Predicting Audible Noise from Overhead HVAC Lines using Evolutionary Computations.” IEEE PWRD-4. Pp. 1243-1251. October.

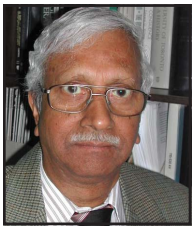
Zaffanella, L.E., M.G. Comber, H.M. Schneider, and R.J. Nigbor. 1978. “Three-Phase UHV AC Transmission Research.” EPRI Report EL-823. July.

CHAPTER 11

Corona Loss and Ozone

P. Sarma Maruvada

This chapter describes the mechanism of generation and techniques for measurement of corona losses on transmission lines. The chapter outlines methods for calculation of corona losses in different weather conditions, as well as calculation of mean annual and maximum corona losses. In addition, the discussion includes evaluation of corona-generated ozone from transmission lines.



Dr. P. Sarma Maruvada has been involved in theoretical and experimental research studies of the corona performance of high-voltage ac and dc transmission lines for more than thirty-five years. He made important contributions to the calculation of conductor surface electric fields, analysis of corona onset phenomena, space charge fields and corona losses of dc transmission lines, analysis and measurement of radio noise and audible noise, and to the development of design criteria for radio noise and audible noise of ac and dc transmission lines as well as for electric fields and ion currents in the vicinity of dc lines. He contributed to experimental studies of corona on conductors subject to lightning, switching and temporary overvoltages, and to the modeling and analysis of corona attenuation of overvoltages on transmission lines.

Dr. Maruvada's research and analysis of corona is presented in his landmark book *Corona Performance of High-Voltage Transmission Lines*. He served on the Executive Committee of the IEEE/PES Transmission and Distribution Conference and Exposition and as Chairman of CIGRÉ Study Committee 36 on Power System Electromagnetic Compatibility. He is an Honorary Member of CIGRÉ, has been elected Fellow of IEEE, and received the IEEE Herman Halperin Electric Transmission and Distribution Award.

11.1 INTRODUCTION

Chapter 8 describes the physical nature of corona discharges and the conditions under which they occur on transmission-line conductors, as well as the various corona effects that may be produced. One of the consequences of corona on conductors is power loss, known as corona loss, which needs to be supplied by the power source connected to the transmission line. Annual corona energy loss, which depends on the magnitude and variation of corona loss during different weather conditions occurring in a year, has an impact on the economic choice of conductors. The economic impact depends to a large extent on the prevailing cost of energy. However, for higher voltage transmission lines that use bundled conductors, EMI and AN play a more important role in the choice of conductors than corona loss. With the current trend towards deregulation, there is an increasing need to allocate the various costs to appropriate parties and, consequently, the ability to evaluate the cost of losses, including corona loss, becomes important.

Part of the corona loss is converted to electrochemical energy, leading to the generation of gaseous effluents, such as ozone and the various oxides of nitrogen, collectively known as NO_X. The possible environmental impact of these effluents was first raised in the late 1960s, when 750-kV lines were introduced in the United States (Frydman et al. 1973). This chapter discusses the factors influencing, and general characteristics of, generation of corona loss and gaseous effluents from high-voltage ac transmission lines. Although corona-generated ozone may not presently be an important design consideration for transmission lines, it usually has to be addressed in Environmental Impact Statements.

Excessive corona loss was historically the first corona phenomenon observed on high-voltage transmission lines that played an important role in the choice of conductor size. Fair weather corona loss was the main design criterion for transmission lines at voltages in the range of 220-330 kV (Wagner et al. 1948; Peterson et al. 1950). At higher transmission voltages, conductor size had to be increased to obtain lower conductor surface electric field and, consequently, reduced corona loss. The resulting conductor cross section was generally much higher than that required to carry the current. In order to meet the conflicting requirements of large-diameter conductors for lower corona loss and smaller conductor cross section needed for carrying the current, hollow or expanded type conductors were introduced. With the introduction of transmission voltages close to 400 kV, however, conductor bundles consisting of smaller-diameter stranded subconductors replaced the hollow or expanded conductors. Depending on the line voltage and the altitude at which it is located, bundles of 2, 3, 4, 6 and even 8 subconductors have been used. At the same time, the economic importance of very high corona losses under foul weather conditions—such as rain, snow and hoarfrost—also became evident. At the end of 1950s, the importance of corona losses from lines considered for operation at high altitudes were being studied (Robertson et al. 1957).

Starting with the basic physical concepts of corona discharges described in Chapter 8, Section 11.2 explains the mechanism of generation of corona losses at alternating voltages. The section also describes the role of generation and movement of charged particles in the alternating electric field at the conductor surface in producing the corona loss current. Following an explanation of the need for experimental data, Section 11.3 outlines the methods generally used for measuring ac corona loss and the specific methods of measurement applicable to different test techniques—namely, indoor and outdoor test cages, outdoor test lines, and operating transmission lines. A brief outline is also given in this section of the experimental studies carried out in different countries in order to obtain experimental data on the influence of the relevant parameters on corona loss.

Section 11.4 describes the characteristics of corona losses occurring in fair weather conditions and presents some of the empirical formulas developed for predicting fair weather corona losses. The section also describes special cases in which high levels of fair weather corona loss occurred and some empirical methods developed for calculating these losses. Section 11.5 discusses the influence of different foul weather conditions—namely, fog, mist, rain, snow, and hoarfrost—on corona losses from transmission lines and the empirical methods derived for predicting these losses. Section 11.6 presents the effect of altitude on corona losses. Section 11.7 discusses the importance of annual corona energy losses and maximum corona loss of a transmission line and the methodologies for calculating them. Finally, Section 11.8 explains the mechanism of generation of ozone and NO_X due to corona on transmission-line conductors. The section also describes experimental studies carried out to determine the rates of ozone generation and presents the dispersion model used for evaluating ground-level ozone concentrations in the vicinity of high-voltage transmission lines. Existing environmental regulations are used to assess the possible contribution of transmission lines to ambient ozone levels. Several applets are included in this chapter for the calculation of corona losses under different weather conditions and ozone levels for different transmission-line configurations:

The following applets are included in this chapter to enable the user to calculate the corona losses and ozone levels for typical transmission-line configurations.

- CL-1: "Corona Loss." This applet may be used for calculation of fair- and foul-weather corona losses, and for calculation of mean annual and maximum corona losses.
- CL-2: "Corona Loss Heavy Rain Base Case Curves." Users may exercise this applet to calculate corona losses in heavy rain.
- CL-3: "Ozone Concentration." This applet may be used to calculate corona-generated ozone levels near high-voltage transmission lines.

11.2 PHYSICAL MECHANISM OF CORONA LOSS

As explained in Section 8.5.1, corona loss is caused by the movement of positive and negative ions produced by corona discharges around the conductors of a transmission line. The mechanism of corona loss on ac transmission lines is explained considering a simple configuration consisting of a single conductor placed concentrically inside a cylindrical cage. In order to simulate the effect of large conductor-to-ground-plane clearances of transmission lines, the radius of the cage is assumed to be much larger than the maximum radius attained by the oscillating space charge around the conductor. A high-voltage ac power source is assumed to be connected between the conductor and the cage.

The alternating voltage applied between the conductor and the cage gives rise to a highly nonuniform electric field distribution, with the highest field occurring at the conductor surface. At voltages below the corona onset voltage for this configuration, a predominantly capacitive current, 90^{o} out of phase with the voltage, is drawn from the power source, and there is a small but almost negligible I^2R power loss due to the capacitive current flowing in the conductor resistance. At voltages above corona onset in the positive and negative half cycles, however, corona discharges occur on the conductor. Oscillatory movement of positive- and negative-charged particles created by corona discharges in the alternating electric field gives rise to an additional component of current, superimposed on the capacitive current. This additional current component, also drawn from the power source, is in phase with the voltage and, therefore, gives rise to power loss.

The mechanism of generation of corona loss is better understood by following the events during one complete cycle of the alternating voltage (Cobine 1958). The voltage, as well as the capacitive and corona current waveforms, are shown in Figure 11.2-1. The sequence of generation, movement, recombination, and neutralization of the ions during one voltage cycle is shown in Figure 11.2-2.

Starting at the point a, when the voltage swings from the negative to the positive half cycle, going through zero, a band of residual negative ions created by corona in the negative half-cycle is located at some distance away from the conductor, as shown in Figure 11.2-2(a). The presence of a ring of negative charge around the conductor creates a small electric field, even at zero conductor voltage, exerting a force on the ions and making them move towards the conductor. As the voltage increases from point a to b, the magnitude of the electric field increases steadily, and the ring of negative ions moves with increasing speed towards the conductor. The conductor surface electric field equals the positive corona onset voltage at point b, and corona discharges begin to occur. The electrons and negative ions created in the discharge move rapidly towards the conductor and are neutralized on contact. The positive ions created in the discharge move outwards, mixing with the incoming band of negative ions. The mixing of ions of opposite polarity results in some amount of recombination and neutralization of the ions. However, the majority of the negative ions continues moving towards the conductor and is neutralized on contact with the conductor surface. The space charges at the onset of positive corona are shown in Figure 11.2-2(b).

Positive corona discharges continue to occur and intensify as the voltage reaches the peak value and then starts decreasing. At a certain point c, on the decreasing part of the voltage cycle, the electric field at the conductor surface is reduced to a value that is insufficient to sustain the discharge, leading to corona extinction. Generation of ions stops, therefore, at point c, but the positive ions already created continue to move away from the conductor, as shown in Figure 11.2-2(c). As the voltage continues to decrease and reach zero at point d, no corona discharges are occurring, but the ring of residual positive ions con-

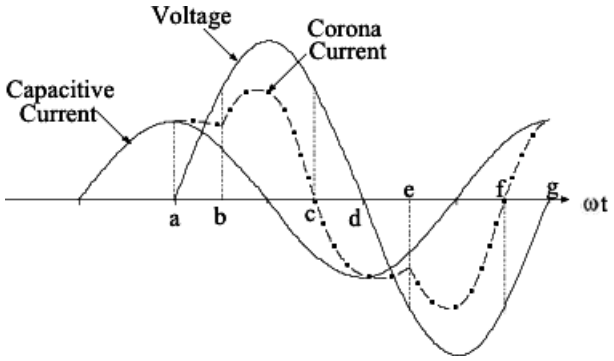


Figure 11.2-1 Capacitive and corona current components.

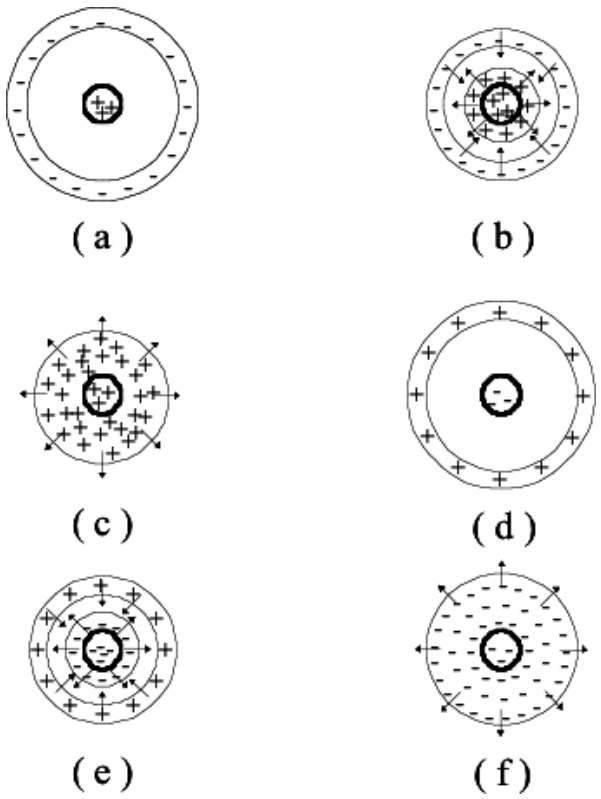


Figure 11.2-2 Generation and movement of space charges in ac corona.

tinue moving outward and attain the maximum radius at the point d, as shown in Figure 11.2-2(d).

At the beginning of the negative voltage half-cycle, the space charge situation is similar to that at point a, excepting for the change in polarity. Subsequent activities of positive ion movement, onset and extinction of negative corona discharges, ion recombination and neutralization at the conductor surface are also similar to those that took place in the positive half-cycle and are shown in Figures 11.2-2(e) and (f).

The corona current, produced due to the creation and movement of ions in the corona discharge, is shown superimposed on the capacitive current component in Figure 11.2-1. The negative corona onset gradient of conductors is generally lower than that at positive polarity. The practical implication of this difference is to impart a degree of asymmetry to the corona current waveform. The fundamental sinusoidal component of corona current is essentially in phase with the voltage waveform and gives rise to corona power loss. There may be a small out-of-phase corona current component that contributes to a small increase in the capacitance. Any increase in capacitance due to corona occurs only at voltages well above corona onset. Corona current also contains a number of even and odd harmonic components, but none of them give rise to any power loss since the voltage waveform is essentially sinusoidal and, therefore, has only the fundamental component.

11.3 MEASUREMENT OF CORONA LOSS

Knowledge of the corona loss characteristics of different conductors and conductor bundles, under all possible weather conditions, is necessary to make an informed economic choice of conductors for a new transmission line. The highly complex nature of corona discharges makes it very difficult (Maruvada 2000), however, to obtain the necessary information using only theoretical considerations. Experimental data is essential for the development of prediction methods for the corona performance of high-voltage transmission lines. Accurate measurements of corona effects are important, therefore, in order to obtain good experimental data.

As explained in the preceding section, measurement of corona loss requires the accurate detection of a very small corona current component in the presence of a large capacitive current component. This detection necessitates accurate power measurement at very low power factors, sometimes as low as 0.01. Low-power-factor wattmeters were used in many of the early corona investigations (Peterson et al. 1950; Tremaine and Lippert 1947; Naef et al. 1951; Nigol and Cassan 1961; Robertson et al. 1961; Shankle et al. 1965). The accuracy of corona loss measurements using wattmeters is limited, however, by the precision of the meters as well as that of any instrument transformers used for the purpose. Such limitations in accuracy made it difficult in many cases to measure fair weather corona losses at normal operating conductor surface gradients.

High-voltage bridge methods, originally developed for determining the dissipation factor of dielectric materials, are found to be well suited for measuring corona loss at very low power factor. The most commonly used method for this purpose is the Schering bridge, or some variation of it. Figure 11.3-1 shows the basic Schering bridge circuit, which consists of two high-voltage arms and two low-voltage arms. Measurement is accomplished by manipulating the low-voltage arms to balance the bridge. The conductor for which corona losses are to be measured forms one of the high-voltage arms of the bridge, the other being a standard high-voltage lossless capacitor C_S. The conductor with corona is represented by the parallel circuit with capacitance C_C and resistance R_C. The purpose of the measurement is to determine the parameters C_C and R_C, and subsequently the corona loss.

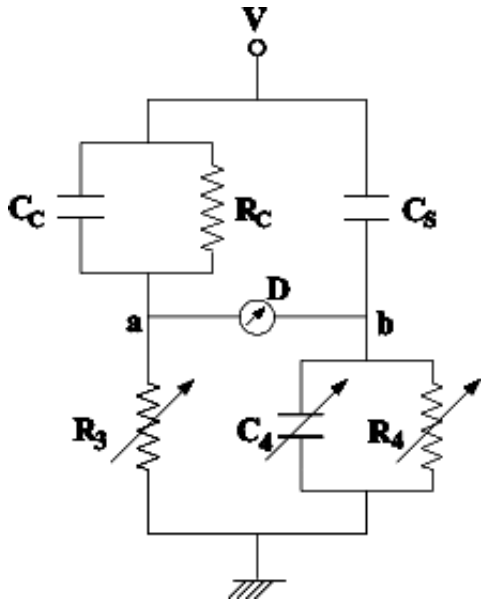


Figure 11.3-1 Schering bridge for corona loss measurement.

The low-voltage section of the bridge comprises one arm, consisting of a variable resistance R_3, and the other a parallel circuit made up of variable resistance and capacitance R_4 and C_4, respectively. A detector D, essentially a very sensitive ammeter, is connected between the junction points a and b, between the high- and low-voltage arms. The balancing procedure consists of manipulating the variable components C_3, R_3, and R_4 in order to obtain a zero or null reading of the detector. With a high-voltage V applied to the conductor and the bridge, the capacitance and dissipation factor of the conductor in corona are obtained in terms of the parameters R_3, C_4, and R_4 required to balance the bridge and the standard capacitance C_S, as follows:

$$C_C = C_S \cdot \frac{R_4}{R_3} \quad \text{11.3-1}$$

$$D = \tan\delta = \omega C_4 R_4 \quad \text{11.3-2}$$

Where:

C_C is the conductor capacitance.

D is the dissipation factor.

δ is the loss angle (90^o-δ is the power factor angle).

ω is the angular frequency of voltage and current.

The corona loss is then obtained as

$$P = V^2 \omega C_C \tan\delta \quad \text{11.3-3}$$

The Schering bridge method can be used to measure corona losses of conductors and conductor bundles accurately at different voltages and under fair as well as foul weather conditions.

Other bridge methods, such as a high-voltage capacitance bridge based on the current comparator principle (Petersons 1964), have also been used for corona loss measurement. The self-balancing feature of the bridge, achieved using a negative feedback loop, is very useful in making continuous long-term measurement of corona loss (Morris and Petersons 1962). Also, high-precision wattmeters (Mazetta 1971; Tomota et al. 1968) replaced conventional low-power-factor wattmeters for corona loss measurement.

Different techniques were used to measure corona losses in different test installations such as test cages, test lines, and operating lines. Since the Schering bridge requires access to both terminals of a test object, it is well suited for measuring corona loss in test cages (Mombello and Maruvada 2001). Of course, all the methods mentioned above can be used in test cages.

In long-term studies using three-phase test lines, corona loss was measured either with wattmeters (Wagner et al. 1948; Nigol and Cassan 1961; Robertson et al. 1961; Shankle et al. 1965) or by using modified bridge methods (Foley and Olsen 1960; Gary and Moreau 1976, pp. 45-51; Keitley et al. 1966). In a Swedish study using a single-phase test line (Knudsen 1964), the capacitive coupling between the test conductor and a parallel, insulated unused conductor was used as the test object in a Schering bridge configuration for corona loss measurement. The author designated the second conductor used in this method as an antenna.

The question is often raised about the possibility of corona loss measurement on operating high-voltage transmission lines. The main problem faced in this case is the detection of the rather small amount of corona loss in the presence of the large quantity of power transmitted over the line. It is possible, in principle, to determine corona loss as the difference between the sending end power and the sum of the receiving end power, I^2R losses in the conductors and any insulator leakage losses. However, the accuracy of measuring the difference between two large quantities is inherently low. In spite of this difficulty, this type of measurement was used in a Finnish study (Larsson and Ponni 1964) to evaluate corona losses in hoarfrost on operating 400-kV transmission lines. By making energy measurements at both ends of the line with precision kWh-meters and simultaneously measuring voltage and current on the line, the I^2R and insulator leakage losses were calculated to determine corona loss. This method can probably be used to measure the high levels of corona loss that occur during heavy rain, heavy snow, and hoarfrost conditions—especially if the entire length of the line is experiencing one of these conditions. If not, then it is difficult to compare the measurements with predictions since

the latter are usually based on so many watts per unit length of the line.

Another method using small lengths of multiple antennas placed below the line conductors (Kravchenko et al. 1962 and 1964) was successfully used for measuring corona losses under different weather conditions on operating 400- to 500-kV transmission lines. Measurements using this method were made over long periods of time, on the order of a year, to successfully obtain corona loss data. In addition to measurement accuracy considerations, it is difficult to interpret results of measurements on operating lines since weather conditions are not likely to be uniform along the entire length of the line.

Probably the best technique for measuring corona losses on an operating line is under no-load conditions—especially during foul weather when the losses are high. Such measurements are not easy to carry out for one obvious reason: the difficulty in getting a line outage when a particular weather condition is impacting the entire length of the line. Such measurements were inadvertently made on an operating 345-kV line in New Mexico in 1984 during a period when the entire region was experiencing a combination of rain or wet snow. The line happened to be de-energized at one end, and the substation operator noticed that the power flowing at the energized end was 20 MW, which was attributed to corona losses and insulator leakage losses. The mean altitude of this line was estimated to be about 1830 m. More recently, corona losses were measured on two open-circuited 400-kV lines (Loxton and Britten 2002), in both dry and rainy weather conditions at an altitude of 1500 m. The total power loss on the unloaded transmission lines was measured using conventional instrument transformers and commercial precision wattmeters. Accurate measurement using this method requires knowledge of the response characteristics of the current transformers (CT) and the capacitive voltage transformers (CVT) used to measure the current and voltage signals, respectively. The no-load I^2R losses on the conductors were estimated and found to be less than 2.5% of the measured corona loss. Comparison with accurate cage measurements has shown good agreement for dry corona losses. Under rain, however, losses measured on the line were lower than those in the cage. The observed difference was attributed to the dispersed rain along the line.

11.4 CORONA LOSS IN FAIR WEATHER

In the early development of high-voltage transmission lines, fair weather corona loss was considered as the main design criterion in choosing the conductor. The conductor diameter was selected on the basis of not exceeding a certain level of fair weather corona loss. Experimental studies of corona onset and corona loss were carried out in test cages, as well as on short test lines, and empirical formulas were derived using the data. For example, Peek's formula for the corona onset gradient of a conductor has been discussed in Section 8.4. One of the first empirical formulas for corona loss of clean and dry conductors was also obtained by Peek (Peek 1929) and is given as

$$P = \frac{241\times10^{-5}}{\delta}\left(f+25\right)\sqrt{\frac{r_c}{D}}\left[\ln\left(\frac{D}{r_c}\right)\right]^2 r_c^2\left(E-E_c\right)^2 \qquad 11.4\text{-}1$$

Where:

P is corona loss in kW/km of conductor.

r_c is conductor radius and D the average phase spacing, both in cm.

f is power frequency, δ is relative air density.

E is the conductor surface gradient and E_c the corona onset gradient of the conductor, both in kV_{rms}/cm.

The corona onset gradient E_c is given (Equation 8.4-1) by

$$E_c = 21.1\,m\,\delta\left[1+\frac{0.301}{\sqrt{\delta\,r_c}}\right] \qquad 11.4\text{-}2$$

where m is the conductor surface irregularity factor that takes into account the uncertainties arising out of practical conductor surface conditions. It may be defined as the ratio between the measured onset gradient and that calculated for an ideal smooth cylindrical conductor of the same radius (see Section 8.4.2). For clean stranded conductors, m varies between 0.75 and 0.85, depending on the radii of the outer strand and of the overall conductor. Presence of nicks, scratches, etc., may reduce the value of m to between 0.6 and 0.8. Any deposits on the conductor surface—such as insects, vegetable matter, water drops, snow, ice, etc.—may further reduce the value of m in the range of 0.3 to 0.6. Extreme conditions—such as insects and vegetable matter deposited on a greasy conductor in a tropical forest, or cumulative deposition of soil and moisture resulting in thick uneven layers of soil on the conductor in a dry offshore region—may reduce m to values as low as 0.2.

Comparison with experimental data has shown that Peek's formula does not apply at voltages close to corona onset at which practical transmission lines normally operate. The formula has also been found to give too high losses for small conductors and too low losses for large conductors. Combining theoretical considerations and experimental

correction factors, Peterson (Peterson 1933) developed an empirical formula for corona loss as

$$P = \frac{2.09\times10^{-5}}{\left[\log\left(\frac{D_{eq}}{r_c}\right)\right]^2}\cdot f V^2 F\left(\frac{E}{E_c}\right) \qquad 11.4\text{-}3$$

Where:

V is the line voltage in kV_{rms}.

D_{eq} is the geometric mean distance between the phase conductors.

E is the conductor surface gradient and E_c the corona onset gradient, both in kV_{rms}/cm.

$F(E/E_c)$ is an empirical constant given in graphical form for two ranges of E/E_c, from 0.6 to 2.4 and from 1 to 18.

The formula is claimed to give accurate results for E/E_c in the vicinity of 1.3. Experimental studies have shown (Wagner et al. 1948) that measured corona loss data agreed well with Peterson's formula. Peek's formula predicted much higher losses than those measured. Figure 11.4-1 shows the empirical constant F as a function of E/E_c.

The main disadvantage of Peterson's formula is that it applies only to single-conductor transmission lines and not to lines with bundled conductors. The formula cannot, therefore, be used to predict fair weather corona loss for any lines above 230 kV that may use bundled conductors. For lines with single conductors, however, Peterson's formula may still be useful if an estimate of fair weather corona loss is required.

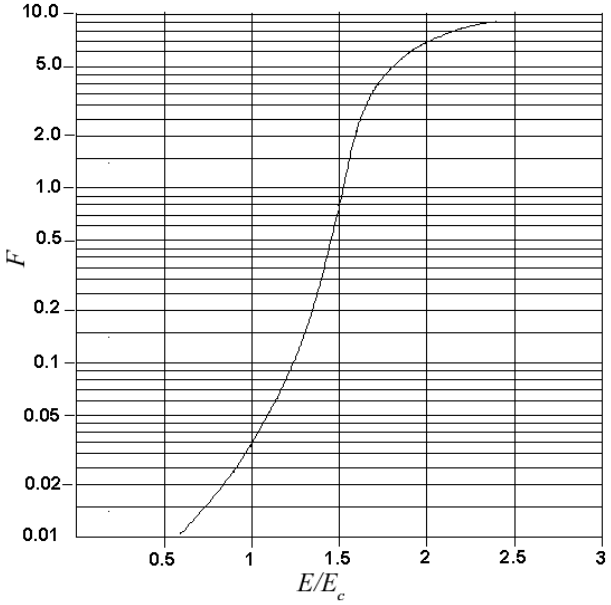


Figure 11.4-1 Empirical constant F in Peterson's formula.

Based on theoretical considerations of space charge in the case of localized corona on conductors and experimental data obtained in outdoor test cages, Electricité de France (EDF) developed (Gary and Moreau 1976, pp. 379-381) an empirical formula for evaluating fair weather corona losses on single, as well as bundled, conductors. Fair weather corona losses are given as

$$P = P_0\, r^{1.8}\left(n+6\right)^2\cdot10^{7\left(E^*-0.7\right)} \qquad 11.4\text{-}4$$

Where:

P is fair weather corona loss, W/m.

P_0 = 1.5×10^{-2} for new and contaminated conductors.
= 1.5×10^{-3} for aged and clean conductors.

E^* = E_{max}/E_c, E_{max} being the maximum conductor surface or bundle gradient, and E_c the critical corona onset gradient (given by Equation 11.4-2 with $\delta = 1$ and $m = 1$), both in kV_{rms}/cm.

r is the conductor radius, cm.

n is the number of conductors in the bundle.

Equation 11.4-4 may be used to estimate the maximum and minimum values of fair weather corona losses for transmission lines using either single or bundled conductors. For a majority of transmission lines above 230 kV, fair weather corona losses are insignificant in comparison with foul weather losses. However, fair weather losses occur for a large percentage of time in a year and may affect the total annual corona energy losses.

Since relatively smooth and clean conductors were used in early studies, corona occurrence was fairly uniform along and around the conductors. However, the use of stranded conductors, either in single or bundled configuration, makes corona to appear at discrete sources rather than uniformly on the conductor surface. As explained in Section 8.6.1, the number of fair weather corona sources on conductors varies from about 1 to 400 per kilometer, depending on the line location and ambient weather conditions. Such low linear density of corona sources makes it very difficult to measure corona losses on short lengths of conductors generally used in test installations, particularly in cages. Another factor that may adversely affect the accuracy of measurement of fair weather corona losses is insulator leakage losses. Measurements carried out at Project UHV (EPRI 1982) have shown that fair weather insulator leakage losses for 345- to 735-kV transmission lines with ceramic insulator strings are in the range of 1-2 kW/km. The leakage losses of polymeric insulators are probably an order of magnitude lower than those of ceramic insulators. Not much comparative data have been published, however, on the leakage losses of polymeric insulators. In most of

the experimental investigations of corona losses, however, the magnitude of insulator leakage losses was evaluated and was found to be negligible compared to corona losses, even in fair weather.

Although fair weather corona loss may not be important for transmission lines under normal operating conditions and with conductor surface gradients close to corona onset values, there are special cases in which it may become very important. For example, there is anecdotal evidence for the occurrence of very high levels of fair weather corona loss on transmission lines operating in the voltage range of 120 to 345 kV. One spectacular example describes the case of a newly commissioned line traversing a dense tropical forest region in an African country, where very little power was available at the receiving end, although the generators were operating at their full capacity at the sending end. An investigation by specialists from France apparently revealed that the new conductors installed on the line were covered with grease, which led to the deposition of insect and vegetal matter all along the length of the line and occurrence of very high levels of corona loss in fair weather. Most of the power input to the line seems to have been dissipated as corona loss before reaching the receiving end.

In the example given above and other similar cases, the conductor surface roughness increases to a degree even higher than under rain or snow. Such conditions greatly reduce the corona onset gradient of the conductors and give rise to very high levels of corona losses even under normal fair weather conditions and impose important economic penalties on the operation of transmission lines. A recent case of excessive fair weather corona loss involved a 230-kV transmission line in the coastal region of Peru (Mombello and Maruvada 2001). In this region, characterized by scarce rains, winds from the sea carry soil particles, sand, and organic material and deposit them on the conductor surface during the day. Because of high levels of humidity, dew, and possibly fog in the night, the contamination sticks to the conductor surface, causing thick and uneven layers of contamination and sometimes even the growth of small plants. The conductor surface irregularity factor m may be reduced to values in the range of 0.2 to 0.5.

Very few studies have been carried out, however, on the corona loss characteristics of heavily contaminated conductors. Some useful data have been provided by a recent laboratory study using artificially contaminated conductors (Mombello and Maruvada 2001). Using corona loss data on single ACSR conductors with diameters in the range of 2.59 cm to 4.60 cm and two conductor bundles of 2.19 and 2.59 cm diameter and values of m in the range of 0.2 to 0.8, the following empirical formulas were obtained:

For single conductors,

$$P = -59.8 + 42.5\log\left(E_m\right) + 19.7\log\left(d\right) - 21.9\log\left(m\right) \quad \text{11.4-5}$$

For two conductor bundles,

$$P = -71.7 + 46.7\log\left(E_m\right) + 23.0\log\left(d\right) - 33.2\log\left(m\right) \quad \text{11.4-6}$$

Where:

P is corona loss in dB above 1 W/m.
E_m is the maximum conductor surface gradient in kV_{rms}/cm.
d is the conductor diameter in cm.
m is the conductor surface irregularity factor.

These empirical formulas are useful at low values of m. They should be used, however, mainly in the range of values of parameters for which the empirical formulas were derived.

Another special case in which fair weather corona losses assume great importance is when transmission lines are subject to temporary overvoltages. As described in Section 8.8, temporary overvoltages are essentially at power frequency and, for some lines, may attain magnitudes as high as twice the nominal system voltage. At such voltages, fair weather corona losses increase very rapidly, equaling and even exceeding those under heavy rain. A more detailed discussion of fair, as well as heavy rain, corona losses at high power frequency overvoltages is given in Section 8.8.3. Fair weather corona losses should also be taken into account in designing lines at very high altitudes—e.g., above 1500 m.

There is good experimental evidence that moderate to heavy load currents affect foul weather corona losses (see Section 11.5-3). Chartier (Chartier 1993) has shown, based on measurements conducted near a noisy 500-kV line in Oregon, that fair weather radio and audible noise measurements tracked with the measurement of magnetic field, which, of course, is a measure of load current. What his data were really suggesting is that fair weather corona phenomena are functions of the relative air density, which is inversely proportional to conductor temperature. The temperature of the conductor itself is a function of the load current, air temperature, wind speed, and solar radiation. Since radio and audible noise are produced by conductor corona, his data suggest that load current would also affect fair weather corona losses. However, the industry does not have either the experimental data nor the analytical tools to make reasonable estimates of the effect of conductor heating on corona losses.

11.5 CORONA LOSS IN FOUL WEATHER

A general discussion of the influence of ambient weather conditions on the corona performance of transmission lines is given in Section 8.6.4. The main factor other than precipitation that influences corona loss is relative air density δ (see Sections 8.4.1 and 8.4.2). At high altitudes above sea level, for example, the value of δ decreases, giving rise to lower corona onset gradient and higher corona losses. Laboratory (Beattie 1969) as well as test line (Knudsen 1964) studies have shown that ambient relative humidity has no measurable influence on corona loss. Fog, which occurs at high levels of relative humidity, may lead to the formation of water droplets on the conductor surface and give rise to an increase in corona loss.

Precipitation in the form of drizzle, rain, snow, ice, and hoarfrost deposited on a conductor surface tends to decrease the conductor surface irregularity factor *m* and thus increase corona losses. Of these, rain and hoarfrost produce the highest levels of corona loss on transmission lines. Most of the experimental studies have, therefore, concentrated on obtaining corona loss data under varying conditions of rain and hoarfrost.

With the introduction of transmission voltages in the range of 400-500 kV, many experimental studies were carried out in different countries to determine foul weather corona losses. The emphasis in most studies was placed on obtaining corona loss data required for making an economic choice of conductors for a particular transmission line being planned. Only in a few of these studies were the experimental data also used to derive empirical formulas that may be useful in the design of other transmission lines in the future. For example, in the Ontario Hydro study (Nigol and Cassan 1961), an empirical formula was derived, based on experimental data as well as theoretical considerations of corona, to calculate the corona losses in different weather conditions.

11.5.1 Corona Losses in Rain

Corona losses were measured at Project EHV (Anderson et al. 1966) under different weather conditions for several conductor bundles and transmission-line configurations between 400 and 700 kV. The experimental data were used to obtain the following empirical formula for corona losses in rain:

$$\sum P = P_{FW} + \left[\frac{V}{\sqrt{3}} J r^2 \ln\left(1 + K \cdot RR\right)\right] \sum_{1}^{n} \left(E^m\right) \qquad 11.5\text{-}1$$

Where:

$\sum P$ is total three-phase corona loss, kW/km.

P_{FW} is total three-phase fair weather corona loss, kW/km.

V is phase-to-phase voltage, kV.

J is a loss current constant.

r is conductor radius, cm.

n is the total number of conductors (3 × number of conductors in the bundle).

E is the gradient at the bottom of each conductor, kV_{peak}/cm.

m is an exponent ≈ 5.

K is a wetting coefficient, equal to 10.

RR is the rain rate, mm/h.

Taking into consideration that corona sources are distributed around each subconductor, the magnitude of the current constant J was obtained, using data from Project EHV as well as from Swedish (Knudsen 1964) and German (Bartenstein and Rachel 1958) studies, as

$J = 7.04 \times 10^{-10}$ at 400-kV configurations

$J = 5.35 \times 10^{-10}$ at 500-and 700-kV configurations

At the time Equation 11.5-1 was proposed, it was realized that the relationship between corona loss and rain rate needed further study, and that the equation would not be valid for parameters outside the range used to derive it.

The possibility of using transmission voltages of 750 kV and higher led to a number of experimental studies using test lines and outdoor test cages to evaluate the corona performance characteristics of different conductor bundles. On test lines, the corona performance of each conductor bundle was studied over a long period of time, ranging from a few months to a year, under all naturally occurring weather conditions. It is difficult and quite expensive, however, to obtain sufficient data from test lines to derive empirical formulas for any of the corona effects, such as corona loss, as a function of the conductor parameters (number and diameter of conductors in the bundle and conductor surface gradient) as well as the principal weather variables such as rain rate. Test cages equipped with the means for producing artificial rain have been used, therefore, to test a large number of conductor bundles rapidly and inexpensively under artificial heavy rain conditions to derive empirical formulas. In some cases, data from test lines as well as test cages were used to develop the empirical formulas. Empirical methods derived for evaluating corona losses in rain based on three of these studies (Cladé and Gary 1970; Trinh and Maruvada 1977; EPRI 1982) are described below.

The concept of generated corona loss, described in Section 8.7.2, has been used in some form in deriving these empirical methods. By definition, generated corona loss depends only on the electric field distribution in the vicinity of the conductor surface, not on the actual configuration in which the conductor is placed, provided the

corona-generated space charge is sufficiently far away from the grounded cage or the ground plane. The concept of generated corona loss is derived in Section 8.7.2 considering only a single conductor. The question remains, therefore, whether the concept also applies to bundled conductors, since the space charge movement takes place over a much larger radius than in the case of a single conductor. The possibility that the corona loss of a conductor bundle depends not only on the conductor surface electric field but also on the capacitance of the configuration in which the bundle is placed casts some doubt on the validity of the concept of generated corona loss. A detailed investigation (Cladé and Gary 1970), using a computational model for calculating corona losses from single, as well as bundled, conductors placed in test cages or on test lines, has shown that differences in conductor capacitance may cause up to 30% variation in the calculated generated corona loss. However, considering the rather large inherent variability of corona losses, the influence of capacitance on the generated corona loss is not of any practical significance.

The IREQ empirical method (Trinh and Maruvada 1977) is based on cage tests on a large number of conductor bundles, with the number of subconductors varying from 1 to 16 and the subconductor diameter varying from 2.35 to 7.72 cm, under artificial heavy rain conditions. Somewhat similar to the Project EHV method described above, the distribution of water drops around the surface of a single conductor or the surfaces of all the subconductors in the bundle is taken into account in deriving the empirical formulas for corona loss. In the case of bundled conductors, the method takes into account the nonuniform field distribution around the surfaces of the individual subconductors.

The empirical formula obtained from experimental data for the generated corona loss P_s under heavy rain (> 10 mm/h) of a single conductor, is given as

$$P_s = K_1 E^{5.8} d^{2.46} \qquad 11.5\text{-}2$$

Where:

P_s is corona loss, W/m.
E is the conductor surface gradient, kV_{rms}/cm.
d is the conductor diameter, cm.
K_1 is an empirical constant = 2.75×10^{-8}.

For a conductor bundle used on a given transmission-line configuration, the electric field distribution around each subconductor of the bundle is calculated and corona loss of the conductor bundle is obtained using Equation 11.5-2 as

$$P_b = \frac{C_b}{C_s}\left[\sum_{1}^{n}\frac{1}{2\pi}\int_{\alpha}^{\beta} P_s\left(E,d\right)d\phi\right] \qquad 11.5\text{-}3$$

Where:

C_b is the capacitance of the conductor bundle in the phase being considered.
C_s is the capacitance of a single conductor of diameter d in a cage with an equivalent diameter of 5.35 m (the IREQ cage).
n is the number of subconductors in the bundle.
α, β are angles defining the portion of the conductor surface where water drops collect.

Since the electric field on the subconductor surface is a function of the angle ϕ, the corona loss $P_s(E,d)$ is also a function of ϕ. The angles α and β are chosen to reflect complete wetting of the conductor surface for new conductors and only partial wetting at the bottom of the conductors for aged conductors. For new conductors, $\alpha = 0$ and $\beta = 2\pi$, while for aged conductors, $(\beta - \alpha)$ is on the order of π or less.

Combining a computational model of the generation and movement of space charges according to the mechanism of corona loss described in Section 11.2 with extensive measurements in outdoor test cages, an empirical method was developed by EDF (Cladé and Gary 1970) to calculate corona losses of conductor bundles in rain. The influence of the rate of rainfall is taken into account by determining an empirical relationship between rain rate and the conductor surface irregularity factor m. The corona losses are determined using a chart of reduced or normalized losses as a function of relative conductor surface gradient for different values of m as shown in Figure 11.5-1. Corona losses are expressed as

$$P = K P_n \qquad 11.5\text{-}4$$

where P is corona loss and P_n the normalized corona loss, both in W/m, and K is the reduction coefficient, given as

$$K = \frac{f}{50}\cdot\left(nr\beta\right)^2\cdot\frac{\log\frac{r_{cyl}}{r_e}\times\log\frac{r_s}{r_e}}{\log\frac{r_{cyl}}{r_s}} \qquad 11.5\text{-}5$$

Where:

n is the number of subconductors in the bundle.
r is the radius of subconductors, cm.
r_e is the equivalent radius of the bundle, cm, given by $r_e = r_b\left[n\,r/r_b\right]^{1/n}$, r_b being the bundle radius, cm.
r_{cyl} is the radius of equivalent zero potential cylinder, cm.
f is the frequency of applied voltage $\beta = 1 + \frac{0.3}{\sqrt{r}}$
r_s is the average radius of space charge, cm; $r_s = 18\sqrt{r}$ for single conductors and $r_s = 18\sqrt{nr+4}$ for bundles.

The chart of normalized losses shown in Figure 11.5-1 was obtained from corona loss measurements in outdoor cages. The measured data was converted to P_n using the known bundle parameters and the reduction coefficient K for the test cages.

To determine the corona losses for each phase of a transmission line, the corresponding reduction coefficient K is calculated. The value of r_{cyl} is calculated to obtain the same capacitance of the bundle in the equivalent cylinder as for the particular phase of the line, i.e., $r_{cyl} = r_e\, e^{2\pi\varepsilon_0/C_p}$, C_p being the capacitance of the bundle for the given phase.

The chart in Figure 11.5-1 shows P_n as a function of relative gradient E/E_c with m as a parameter, where E is the average conductor surface or bundle gradient and E_c the corona onset gradient (given by Equation 8.4-1 for ac with m and δ set equal to 1), both in kV_{rms}/cm. The conductor surface irregularity factor m as a function of rain rate is given in Figure 11.5-2.

An empirical method has been developed at Project UHV (EPRI 1982), based essentially on corona loss measurements under artificial heavy rain conditions in outdoor test cages on a large number of conductor bundles and covering a wide range of subconductor diameters (1.1–5 cm) and number of subconductors (1–16). The method is based on the theoretical model of corona losses developed by EDF (Cladé and Gary 1970).

The corona loss P of a conductor bundle in any configuration is expressed as

$$P = K P_e \qquad 11.5\text{-}6$$

where P_e is the effective corona loss of the bundle and the factor K is defined as

$$K = \frac{ln\left(r_{cyl}/r_e\right)}{ln\left(r_{cyl}/r_s\right)} \qquad 11.5\text{-}7$$

Where:

r_e is the equivalent radius of the bundle (same as in Equation 11.5-5).

r_s is the average distance between the space charge and center of the bundle during the cycle.

r_{cyl} is the radius of the equivalent zero potential cylinder for the configuration.

The value r_s is obtained as follows:

$$r_s = \sqrt{\frac{16200}{f}\cdot n\, r + \left(r_b\right)^2} \qquad 11.5\text{-}8$$

Where:

f is the power frequency, Hz.

r_b is the bundle radius in cm.

r is the subconductor radius in cm.

n is the number of subconductors.

Figure 11.5-3 shows the effective corona loss P_e for six-conductor bundles, obtained by converting measured corona loss data in a test cage and using the appropriate value of K. For a different number of subconductors, the basic curves must be corrected by multiplying their values by a factor K_{CL}, an empirical corona loss correction factor shown in Figure 11.5-4. Systematic experimental data were obtained for bundles with subconductors having 2.33-cm and 4.63-cm diameters, plus a few data for 3.3-cm conductors. For other diameters, an interpolation through the curves of Figure 11.5-4 is suggested.

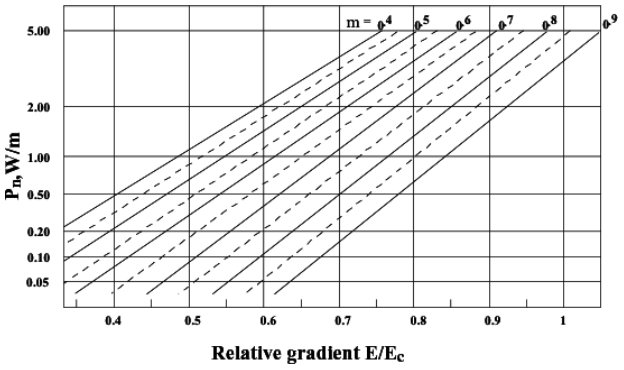


Figure 11.5-1 Normalized corona loss (Cladé and Gary 1970).

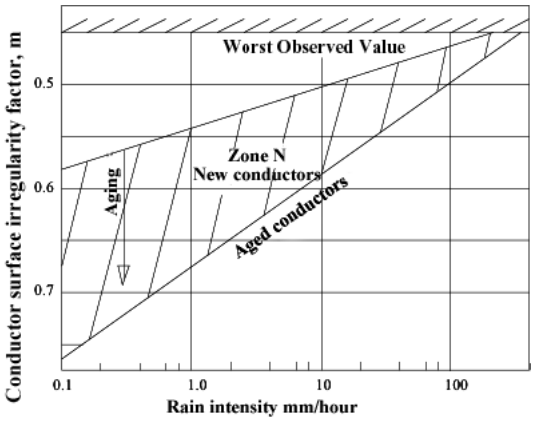


Figure 11.5-2 Conductor surface irregularity factor for different rain rates (Cladé and Gary 1970).

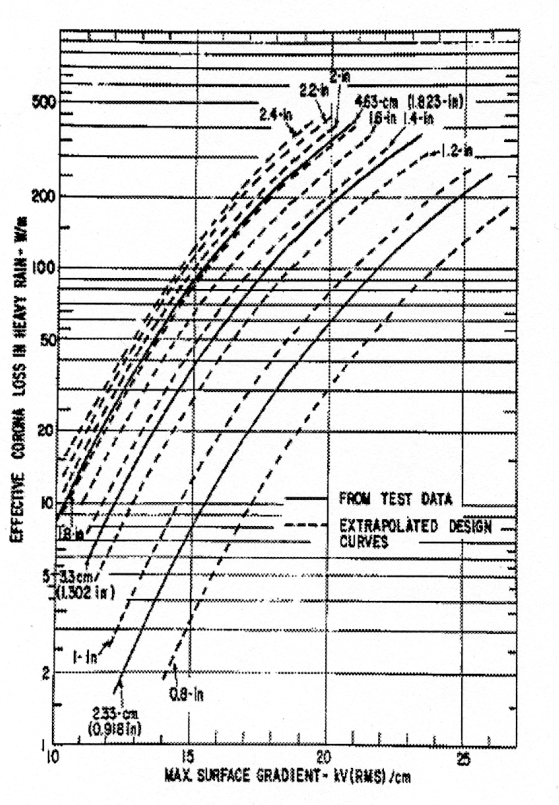


Figure 11.5-3 Effective corona loss for six-conductor bundles with subconductors of different diameters.

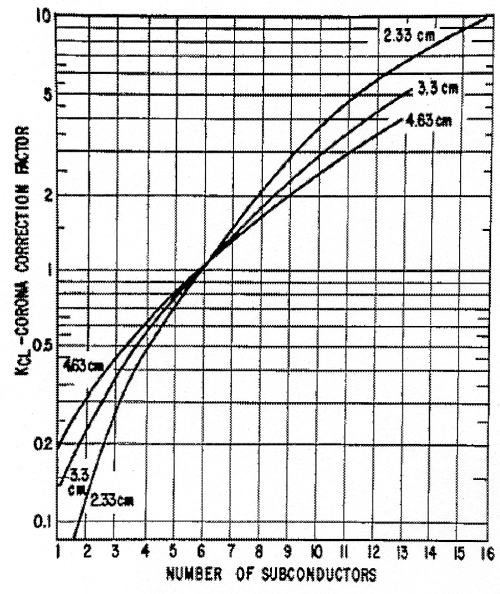


Figure 11.5-4 Correction factor to apply to the loss curves of Figure 11.5-3 to obtain the loss for different numbers of subconductors.

The corona losses of each phase of a transmission line are obtained by determining the effective corona loss P_e using the data presented in Figures 11.5-3 and 11.5-4 and calculating the value of K for that phase.

Of the three empirical methods presented above, the IREQ method may be used to determine corona loss under heavy rain for bundles with six subconductors or less, while for more than six subconductors, the Project UHV method may be more appropriate. The EDF method may be used to obtain corona losses at different rain rates and for bundles with up to four subconductors.

The highest levels of corona loss occur for most transmission lines under heavy rain conditions. Many studies have also shown, however, that the losses vary significantly with the rate of rainfall. In some of these studies (Nigol and Cassan 1961; Knudsen 1964; Anderson et al. 1966; Sugimoto 1968; Cladé and Gary 1970), rain rate was introduced as a parameter in the empirical methods developed. In most cases, corona losses were found to increase rapidly at low rain rates, but to saturate at high rain rates. The relationship between corona loss and rain rate is represented in some methods (Nigol and Cassan 1961; Knudsen 1964; Cladé and Gary 1970) by two linear approximations, with the higher slope at low rain rates. One of the principal difficulties encountered in many of these studies is accurately measuring the low rates of rainfall that occur normally. An accurate method of measuring low rates of rainfall has been developed (Kirkham 1980), but was used only in one study of corona loss (Kirkham 1981) at voltages corresponding to the UHV range (above 1000 kV).

Using the experimental data from the full-scale test lines at Tidd (Wagner et al. 1948), Leadville (Robertson et al. 1961), Apple Grove (Chartier et al. 1970), and Lyons (Chartier 1983), a simple but fairly accurate empirical formula was developed at Bonneville Power Administration (BPA) (Chartier 1983). The influence of rain rate and altitude above sea level are both included in this method. The influence of rain rate came from measurements by Kirkham (Kirkham 1981) and is represented by a two-slope piecewise linear approximation. The corona loss P, expressed in dB above 1 W/m, is given as

$$P(dB) = 14.2 + 65 \log\left(\frac{E_m}{18.8}\right) + 40 \log\left(\frac{d}{3.51}\right) + K_1 \cdot \log\left(\frac{n}{4}\right) + K_2 + \frac{A}{300} \quad 11.5\text{-}9$$

Where:

n is number of subconductors.

d is diameter of subconductor, cm.

E_m is the average maximum bundle gradient.

K_1 = 13 for n ≤ 4
= 19 for n > 4

K_2 is a term that adjusts corona loss for rain rate *RR*, and is given as

$$K_2 = 10 \cdot \log\left(\frac{RR}{1.676}\right), \text{ for } RR \le 3.6 \text{ mm/h}$$

$$= 3.3 + 3.5 \cdot \log\left(\frac{RR}{3.6}\right), \text{for } RR > 3.6 \text{ mm/h}$$

A is altitude, m.

To calculate corona loss in W/m, the antilog of *P(dB)* must be performed, or $P = 10^{P(dB)/10}$. The total loss for a line in W/m is the summation of the loss from all the conductor bundles. To calculate the mean fair weather corona loss, BPA recommends that 17 dB be subtracted from the mean loss calculated during rain. The difference of 17 dB was determined by comparing the mean corona loss measured from carefully controlled measurements during fair weather at the Apple Grove 750 kV Project with mean values obtained during rain (Chartier et al. 1970).

In the empirical methods described above, the power frequency *f* appears explicitly only in Equations 11.5-5 and 11.5-8. All the other formulas apply for *f* = 60, and results for other frequencies should be obtained taking into account that corona losses are proportional to frequency. The effect of altitude on corona losses is discussed in Section 11.7.

Precipitation in the form of drizzle may be considered equivalent to light rain in calculating corona loss. The BPA method may be used for a wide range of conductor bundle parameters, rain rates, and altitudes. Application of the methods of calculation of corona losses in fair weather and in rain to practical transmission lines is explained in Applet CL-1. Applet-CL-2 provides calculation of corona losses in heavy rain for base case transmission line configurations using the Project UHV method.

Accuracy of the results obtained using empirical formulas for corona effects is generally evaluated by comparing them with good measured data obtained on operating high-voltage transmission lines. Unlike RI and AN, however, sufficient measured data are not available for corona losses from operating lines and, therefore, it is not possible to make a realistic evaluation of the accuracy of corona loss empirical formulas.

11.5.2 Corona Losses in Snow, Ice, and Hoarfrost

At temperatures below the freezing point of water, precipitation may be in the form of snow, ice, or hoarfrost. Of these, snow is the most common form of precipitation occurring in most regions. In the northern regions of Russia, Finland, and Canada, hoarfrost is also a common occurrence.

Dry snow occurs at low ambient temperatures, well below the freezing point, while at temperatures close to the freezing point, precipitation is usually in the form of wet snow. Dry snow deposited on a conductor reduces the conductor surface irregularity factor *m* and, therefore, gives rise to high levels of corona loss. Wet snow deposited on a conductor melts and forms water drops just like rain. Corona losses under wet snow may equal, and sometimes even exceed, those under heavy rain.

Presently available data do not permit an accurate empirical relationship to be established between corona loss and rate of snowfall. In the empirical formula developed by Ontario Hydro (Nigol and Cassan 1961), for example, the rate of snowfall was taken into account by converting it to its equivalent water content (1 cm of snowfall is roughly equivalent to 1 mm of rainfall). Test data at Project EHV (Anderson et al. 1966) suggest the following equivalent rain rates for calculating corona loss:

Heavy snow: 2.5 mm/h of rain

Medium snow: 0.6 mm/h of rain

Light snow: 0.1 mm/h of rain

In addition, the data also suggest a loss multiplier of 2 for wet snow compared to dry snow.

The conditions leading to the formation of ice and hoarfrost on transmission-line conductors are quite different than those for dry or wet snow. Super-cooled water droplets, carried by freezing drizzle or rain, coming in contact with a conductor surface give rise to the formation of ice. As the water spreads around the conductor surface, an almost uniform layer of ice is formed. Such a uniform layer of ice on the conductor may not give rise to a significant increase in corona losses. However, if icicles protruding from the conductor surface are formed, high levels of corona loss may occur due to the development of ice-tip corona.

Hoarfrost is a different kind of ice accretion, which occurs when water vapor in atmospheric air freezes on contact with the conductor, forming crystalline or granular hoarfrost (Lahti et al. 1997; Tikhodeev 2000). If the temperature of conductors is below that of ambient air, crystals of ice start covering the conductor, resulting in crystalline hoarfrost. In the presence of fog at freezing temperatures and high wind velocities, however, granular hoarfrost is formed on the conductors. Because of the very high dielectric constant of ice (almost 100 time that of air),

the electric field at the tips of hoarfrost needles may reach very high levels. Observations at the Apple Grove 750-kV Project during early morning hours, when hoarfrost covered the conductors, trees etc., have shown that corona coming from the tips of the hoarfrost needles was glow corona, or what is also called "ultra corona," since the observed audible noise was a pure 120-Hz hum similar to that produced by transformers. Laboratory observations in North America have shown that ultra corona produces a pure 120-Hz hum; and it is well known that ultra corona produces very high corona loss levels. It appears, therefore, that the highest levels of corona loss occur when conductors are covered with crystalline hoarfrost. Studies conducted by the power company Imatran Voima Oy (IVO) in Finland (Laasonen and Lahtien 1996) have shown that the type, as well as the thickness, of hoarfrost has an impact on corona losses. However, IVO has also observed that high losses can occur even when the hoarfrost is nearly invisible. Experimental studies have shown (Tikhodeev 2000) that corona losses in hoarfrost may be as high as four times those in heavy rain.

11.5.3 Influence of Conductor Heating

On operating transmission lines, the flow of load current increases the conductor temperature above that of ambient air. The actual increase in the temperature depends on the magnitude of the load current, the electrical characteristics of the conductor, and the ambient weather conditions. The influence of conductor heating on the corona discharge process and, consequently, on corona loss is quite complex (Maruvada 2000) and is not well understood.

Some studies have been carried out on practical transmission lines (Larsson and Ponni 1964; Chartier 1993; Tikhodeev 2000) and in the laboratory (Morgan and Morrow 1977; Lahti et al. 1997) to determine the influence of conductor heating on corona loss. Under conditions of high humidity, fog, and mist, conductor heating may inhibit the formation of water drops and thus lower corona losses. For conductors normally used on transmission lines, however, corona losses in moderate to heavy rain may not be affected significantly by conductor heating. Dry snow and ice may be converted to water due to conductor heating, resulting in an increase in corona loss.

Studies have shown (Tikhodeev 2000) that the formation of crystalline hoarfrost is inhibited on a heated conductor. Hoarfrost accretion is reduced as the current in the conductor increases. For load currents on the order of 300 A and higher in a conductor of 3.29 cm diameter, the formation of hoarfrost was almost completely inhibited in laboratory studies (Lahti et al. 1997).

With the use of the new high-temperature conductors on transmission lines, corona loss as well as other corona effects should be drastically reduced in foul weather conditions when these conductors are carrying significant load current.

11.6 EFFECT OF ALTITUDE ON CORONA LOSS

As discussed in Section 8.4.1, relative air density δ has an important influence on the corona onset gradient of conductors. The value of δ is close to 1.0 at sea level and decreases with altitude mainly due to a decrease in atmospheric pressure as a function of the altitude, given by Equation 8.4-3. For a given transmission-line configuration and conductor surface gradient, the levels of EMI, AN, and corona loss increase with altitude because of the reduced corona onset gradient and a general increase in the ionization activity in the air surrounding the conductors. The effect of altitude on EMI and AN are discussed in Chapters 9 and 10, respectively.

Early studies of the effect of δ on corona loss (Peek 1929; Peterson 1933) were carried out in laboratory cages on smooth conductors and over a narrow range of values of δ centered on 1.0. The only study on the effect of altitude on corona loss for practical conductor configurations was conducted at the Leadville High Altitude Project (Robertson et al. 1961). Corona loss measurements made on the Leadville test line, located at an altitude of about 3200 m, were compared with those made at nearly sea level (195 m) on the Tidd test line (Wagner et al. 1948). The emphasis at both test projects was on fair weather corona loss.

Contrary to the results of Peek (Peek 1929), which showed that corona onset gradient varied directly proportional to δ, or those of Peterson (Peterson 1933), which showed proportionality with $\delta^{2/3}$, analysis of the Leadville fair weather corona loss data indicated that corona onset gradient varied as $\delta^{1/2}$.

Careful measurements of EMI and AN were made at an altitude of 1935 m on a 500-kV double-circuit transmission line (Chartier et al. 1987) and compared with data obtained on a similar line at an altitude of 277 m. Comparative analysis of the data led BPA to suggest that, as in the case of EMI and AN, corona losses increase with altitude above sea level by an amount in dB equal to $A/300$, where A is the altitude in meters. The rationale for using this term is explained in Section 10.4.8.

The term $A/300$ used in the BPA formulas for all the corona effects is consistent with the proportionality of corona onset with $\delta^{2/3}$ observed by Peterson. The reason why the Leadville corona loss data show a $\delta^{1/2}$ relationship rather than $\delta^{2/3}$ is not entirely clear. It may partly be due to the fact that the analysis was based only on fair weather corona loss data. In addition, the environment at Leadville was very clean, and the conductors did not show any signs of

aging, generally characterized by blackening of the conductor surface and reduction of corona losses over a period of time. The reduction of fair weather losses was seen at Tidd, but not at Leadville, as shown in Figure 11.6-1.

The effect of altitude is inherently taken into account in the empirical methods of Peek (Equation 11.4-1) and Peterson (Equation 11.4-2) through the presence of δ in corona onset gradient or voltage. In the EDF method (Equations 11.5-4 and 11.5-5), it is suggested (Gary and Moreau 1976, pp. 409-411) that the effect of altitude may be taken into account by expressing β in Equation 11.5-5 as a function of δ,

$$\beta = \delta\left(1+0.3/\sqrt{\delta r}\right) \qquad 11.6\text{-}1$$

It is recommended, however, that all empirical methods, for fair as well as foul weather corona loss, be used with δ = 1 and then adding the term A/300 in dB to correct for altitude above sea level, until further research is conducted.

11.7 EVALUATION OF CORONA LOSS

As discussed in preceding sections of this chapter, corona losses of a transmission line vary over a very wide range of values depending on the prevailing weather conditions. The highest values of corona loss can be 100 times or more than the lowest values. For a given transmission line, a practical description of corona losses over a period of time can be given only in statistical terms such as cumulative distribution.

Corona losses have two types of economic impact:

1. the annual cost of energy losses; and
2. the cost incurred due to the simultaneous occurrence of maximum corona loss and maximum demand.

The first type of impact refers to the annual operating cost of supplying the corona loss energy, while the second type of impact refers to the cost of any additional generating capacity required to take into account the possibility that maximum corona loss is coincident with the maximum load conditions of the transmission line.

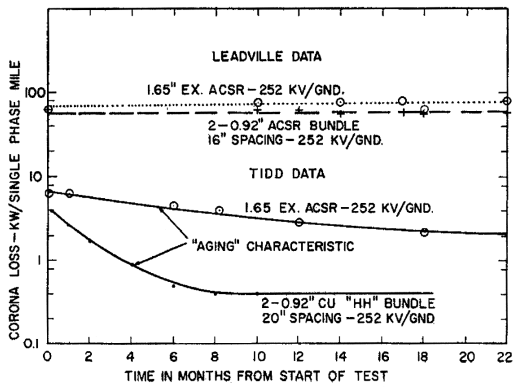


Figure 11.6-1 Corona loss variation with time at Tidd and Leadville (Robertson and Dillard 1961).

Unfortunately, neither of the two parameters of interest is directly available from test results obtained in cages or short test lines. High-voltage transmission lines generally cover long distances and may traverse regions with different weather patterns. Determination of annual corona energy losses or of maximum corona loss require, therefore, the use of statistical models that take into account the temporal variation of corona loss due to weather conditions as well as spatial variations along the length of the transmission line. Using U.S. Weather Bureau data for 10 to 15 years, Project EHV developed a statistical model (Edison Electric Institute 1968) for evaluating the frequency of corona loss occurrence for different locations and different transmission-line designs. For example, Figure 11.7-1 gives precipitation frequency areas, in terms of contours of mean annual number of days with 0.25 mm (0.1 inch) or more of rain, of the continental United States.

Any statistical model considered should enable the calculation, for a given transmission line, of the mean annual corona loss P_{ma} and the maximum corona loss P_{max}. The mean annual corona loss P_{ma} may be defined as

$$P_{ma} = \frac{1}{T_a}\sum_{i=1}^{n} P_i T_i \qquad 11.7\text{-}1$$

Where:

i = 1,2,....n are the n distinct weather categories occurring in a year.
T_i is the duration in hours of each weather category.
P_i is the average corona loss in the corresponding weather category.
T_a is the number of hours in a year, i.e., 8760.

The time durations T_i may also be expressed as fractions or percentages of T_a.

In order to use the simple statistical model given by Equation 11.7-1, two sets of information are required:

1. the generated corona loss for the conductor bundle being considered and for the different weather categories, as a function of the conductor surface gradient; and
2. statistical model of the weather categories for the region in which the transmission line is located.

The accuracy of the results obtained using this model depends on the available data of statistical weather model for the region and of corona loss data corresponding to the different weather categories in the model. Continued efforts to measure corona losses on operating transmission lines in different regions at different altitudes and under different weather conditions would, therefore, be very useful in providing such data.

For example, consider a region characterized by three weather categories: fair weather, rain, and snow. The weather model should then provide data on the durations of T_i for each of these categories and either the mean or the distribution of rainfall and snowfall rates. Empirical formulas described in the preceding sections may be used to determine the corresponding values of P_i. Snowfall rates are converted to equivalent rainfall rates before using the formulas.

Some transmission lines may traverse different regions characterized by different weather models. Calculations should be made in such cases taking into account the lengths of the line located in each region. If a line of length l traverses m regions, with lengths $l_j, j = 1,2,\ldots m$ of the line in each region, the mean annual corona losses are obtained as

$$P_{ma} = \frac{1}{l\,T_a}\sum_{i=1}^{n}\sum_{j=1}^{m} l_j\left(P_{ij}\;T_{ij}\right) \qquad 11.7\text{-}2$$

A similar model can also be applied to the case of a line traversing different altitudes above sea level, such as a line starting at a lower altitude and climbing into a higher elevation. A typical example of such a line is a BPA 500-kV line that begins at sea level near Portland and crosses the Cascade Mountains, where it goes from an altitude of zero to about 2000 m above sea level. Similar lines are in operation in other parts of the world, such as South America, South Africa, etc. The model described by Equation 11.7-2) can be used in such cases by dividing the line of length l into sections l_j, each defined by a mean altitude. An increment of about 300 m may be used for this stepwise representation of the line. Any variations in the weather conditions prevailing along each segment of the line may also be taken into account in calculating P_{ma}. The application of these models to practical cases of transmission lines is explained in Applet CL-1.

Determination of the maximum corona loss P_{max} of a transmission line, for the purpose of evaluating the maximum demand requirements, is more difficult because of the statistical variations of weather conditions at any given time along the length of the line. As a result of this statistical variation, the maximum corona loss in kW/km of a long transmission line is always less than that measured for the same conductor bundle in a cage or a test short line. In the Project EHV model, the maximum corona loss of a line is calculated by assuming that the spatial variation of corona loss along the length of the line may be replaced by the temporal variation of the highest corona losses—for example, with the prevailing rain rates. Such an approach may also be used in the case of a line traversing regions characterized by different weather models. Approaches for calculation of P_{ma} and P_{max} are illustrated by examples in Applet CL-1.

11.8 INFLUENCE OF CORONA LOSSES ON LINE DESIGN

Corona losses do not generally play an important role in the overall design of transmission lines. Under special conditions, however, they may influence the economic choice

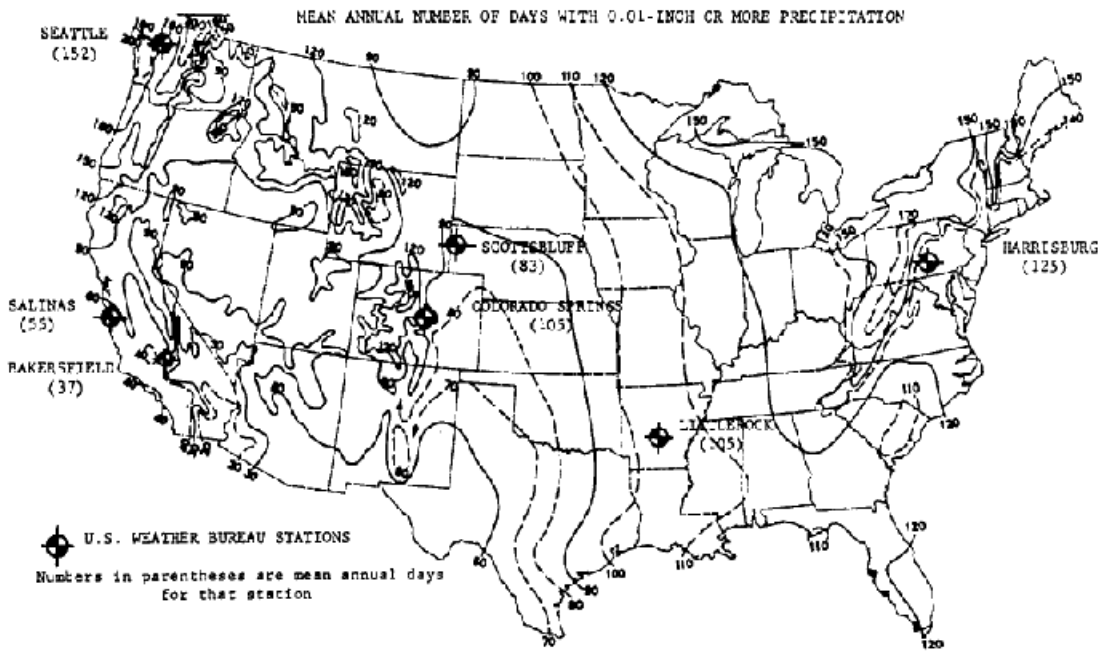


Figure 11.7-1 Precipitation frequency areas of the continental United States (Courtesy U.S. Government-Environmental Sciences Services Administration).

of conductors. The cost of transmission-line conductors, usually expressed in terms of an annualized cost, is made up of the annualized cost of capital investment and the annual cost of energy losses incurred during the operation of the line. The capital cost is almost directly proportional to the conductor cross section, or to d^2, where d is the conductor diameter, and is annualized over a specified duration of life of the conductor. In the absence of corona on conductors, the energy losses consist mainly of the resistive or I^2R losses, where I is the load current flowing through the line and R is resistance of the conductor. Insulator leakage losses are generally negligible compared to the resistive losses. Since the load current varies almost continuously with time, I represents the average current that produces the same energy losses over a year as the actual load current. However, for the sake of simplicity, the maximum load current of the line is often used for I in calculating the annual resistive energy losses. Since the conductor resistance R is almost inversely proportional to d^2, the annualized cost of energy losses is proportional to I^2/d^2.

For a given transmission voltage and load current, the economic choice of conductors involves minimizing the total annualized cost of conductors. Since the capital cost increases while the cost of resistive energy losses decreases with d, there is an optimum value of d for which the total cost attains a minimum. This is illustrated in Figure 11.8-1, in which curve 1 shows the variation of the total cost as a function conductor diameter d. The minimum total cost is obtained for an optimum conductor diameter d_1. For conductor sizes either lower or higher than d_1, the total cost will be higher. In practice, however, the increase in total cost for a conductor size slightly different from d_1 is generally quite small and depends on the magnitude of the load current and the relative importance of energy and capital costs. The increase in total cost may become important for lower load currents and/or higher energy costs.

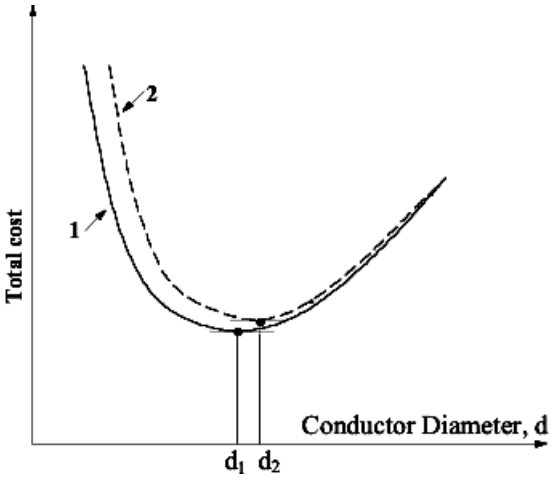


Figure 11.8-1 Economic choice of conductors.

In the presence of corona on conductors, the mean annual corona losses should be added to the resistive losses to determine the annualized cost of energy losses. As in the case of resistive losses, corona losses decrease as d increases, since the conductor surface gradient varies inversely with d for a given line voltage. This relationship is illustrated by curve 2 of Figure 11.8-1, which differs from curve 1 at lower values of d and merges asymptotically with curve 1 as d increases. The minimum total cost of curve 2 occurs at a slightly larger diameter d_2. The difference between d_2 and d_1 depends to a large extent on the relative importance of corona losses and resistive losses.

At higher transmission voltages, constraints imposed by EMI and AN may require a conductor size even larger than d_2, in which case the use of bundled rather than single conductors should be considered. If bundled conductors are used, curves similar to those in Figure 11.8-1 should be obtained for different numbers of conductors in the bundle and an optimum number and size of conductors determined in order to minimize the total cost and at the same time meet the requirements of EMI and AN.

With the increasing cost of energy, studies carried out in several countries have shown that it is important to take into account the cost of corona losses in the economic choice of conductors, particularly for lightly loaded or compact transmission lines in the range of 230 – 400 kV, lines traversing regions of high altitude or of extreme pollution, and also for normally loaded lines at voltages above 750 kV (Burns et al.1985).

The mean annual corona losses of high-voltage transmission lines are usually an order of magnitude lower than the resistive losses. However, the maximum corona losses can be of the same order of magnitude as the resistive losses. Some typical magnitudes of normal loads and resistive and corona losses of different transmission lines are shown in Table 11.8-1 (EPRI 1982).

Table 11.8-1 Comparison of Corona and Resistive Losses

Line Voltage kV	Conductor Bundle[1] n x d	Load MVA	I^2R Loss kW/km	Corona Loss (kW/km)	
				Average	Maximum
362	2 x 3.16	400	41	2	26
550	3 x 3.3	900	52	4	78
800	4 x 3.3	2000	93	8	208
1200	8 x 4.4	5000	73	9	221
1500	12 x 4.4	9000	103	10	230

1. n: number of subconductors; d: subconductor diameter, cm.

11.9 OZONE AND NO_X

Oxidants such as ozone and the various oxides of nitrogen collectively known as NO_X contribute to atmospheric air pollution. Studies have shown that ozone comprises more than 90% of all the photochemical oxidants responsible for air pollution. The formation of ozone at ground level is mainly due to the action of ultraviolet radiation on the gaseous emissions of combustion processes. For example, photochemical reactions taking place in automobile exhaust gases is known to generate ozone and contribute to increased pollution in urban areas. The rapid growth of high-voltage transmission in the early 1970s raised some concerns of the possibility of ozone generation by corona discharges on transmission-line conductors and its impact on ambient air quality. Ozone and NO_X were included, therefore, as part of an environmental impact consideration of transmission lines. Careful studies in the laboratory and measurements near transmission lines have clearly shown, however, that transmission lines do not make any significant contribution to ambient atmospheric ozone levels. Although corona-generated ozone may not presently be an important design consideration for transmission lines, it usually has to be addressed in Environmental Impact Statements.

11.9.1 Mechanism of Generation

The mechanism of generation of ozone and NO_X in corona discharges is very complex and not fully understood. According to present state of knowledge (Lunt 1959), the mechanism follows the steps described below. The first step is most likely the dissociation of oxygen molecules due to the absorption of UV radiation produced in the corona discharge or by electron impact,

$$O_2 + hf\ (\text{UV radiation}) \rightarrow 2\,O \qquad 11.9\text{-}1$$

$$O_2 + e \rightarrow 2\,O + e \qquad 11.9\text{-}2$$

In the second step, ozone is formed as a result of three-body collisions with another molecule M, as

$$O + O_2 + M \rightarrow O_3 + M \qquad 11.9\text{-}3$$

Different oxides of nitrogen such as NO, NO_2, NO_3, N_2O_5, N_2O, collectively known as NO_X, are also formed due to a series of reactions involving atomic and molecular oxygen. The oxidants O_3 and NO are not stable, however, and may recombine to form more stable O_2 and NO_2 molecules according to the reaction

$$O_3 + NO \rightarrow O_2 + NO_2 \qquad 11.9\text{-}4$$

At normal values of ambient temperature and humidity, ozone reverts back to molecular oxygen in about 20 to 30 minutes.

11.9.2 Rates of Generation

Part of the corona loss energy, mainly that required to produce atomic oxygen, is used to generate ozone through the mechanisms described above. One of the important parameters required to estimate the contribution of a transmission line to ambient ozone levels is the rate of ozone generation due to corona on the conductors. Theoretical estimates based mainly on electrochemical considerations indicate that energy on the order of 1.4 kWh is required to generate about 1 kg of ozone in air (Scherer et al. 1973). Practical efficiencies of ozone generation are much lower, however, being one or two orders of magnitude lower than the theoretical value given above. Commercial ozonizers with air attain a maximum efficiency of 90g/kWh (Cramariuc et al. 1999). Laboratory studies (Sebo et al. 1976) on transmission-line conductors have shown that the generation efficiency may be as low as 0.5g/kWh under dry conditions and up to 4.5g/kWh in rain. Several factors influence the rate of generation of ozone, the most important being conductor surface gradient, mode of corona discharge and the ambient weather conditions—i.e., temperature, humidity, precipitation, and wind. The presence of water and humidity, although increasing the efficiency of ozone generation, makes ozone decay faster than in dry weather.

Studies were also made (Sebo et al. 1976) on the rate of generation of NO_X, and the measured levels were found to be an order of magnitude lower than that for ozone. Since ambient ozone and NO_X levels are generally of the same order of magnitude, any contribution of transmission lines to ambient NO_X should be negligible.

11.9.3 Ozone Dispersion from Transmission Lines

In order to determine the contribution of transmission lines to ambient ozone levels, it is necessary to estimate the dispersion and dilution of corona-generated ozone near the conductors as a result of the weather-related activities in the atmosphere and the geometry of the terrain. The most important factors influencing the dispersion are the wind speed and direction, the turbulence in the air, and the configuration of the transmission line.

The diffusion of gaseous effluents in the atmosphere has been studied extensively in the past, and mathematical models based on Gaussian distribution have been developed (Roberts 1923; Smith 1968; Turner 1970) to analyze dispersion away from point and line sources of the effluent. These models have been adapted (Scherer et al. 1973; Roach et al. 1974; Roach et al. 1978) to the transmission-line ozone problem by considering each phase conductor (or conductor bundle) as a uniform linear source of ozone.

Considering a three-phase horizontal transmission-line configuration—with the coordinate system such that the line is located along the Y-axis, and the Z-axis is along the vertical direction above the ground plane—the center phase in the (X,Z) plane will be located at (0,H), while the outer phases are at (-D,H) and (D,H), where D is the phase spacing and H the average height above ground of the line. To account for the reflection of ozone at the ground surface (i.e., ignoring any destruction process at the surface), virtual line sources are located at the image positions below the ground surface. Expressions were derived (Roach et al. 1974) for dispersion of ozone for winds perpendicular and parallel to the line.

For winds blowing perpendicular to the line, the downwind concentration in the X-direction is estimated from (SI Units)

$$C(X,Z) \cong \sum_{i=1}^{3} \frac{\bar{S}_i}{U\,\sigma_z\sqrt{2\pi}} \left\{ \exp\left[-\frac{(Z-H)^2}{2\sigma_z^2} \right] + \exp\left[-\frac{(Z+H)^2}{2\sigma_z^2} \right] \right\} \qquad 11.9\text{-}5$$

Where:

$\bar{S}_i$ is the source strength of the ith line.
U is wind speed.
H is the average line height above ground.
σ_z is the spreading coefficient in the Z-direction.

For winds parallel to the transmission line, ozone concentrations are estimated for a line of finite length L_0. The line is arbitrarily located parallel to the X-axis for this calculation so that the downstream direction in this case is also along the X-axis. Each phase conductor bundle is divided into n equally spaced point sources of ozone. The strength of each point source on a given bundle is $\bar{S}_i L_0/n$, where $\bar{S}_i$ is the known source strength of the ith bundle. Summing the contributions from the n sources on each phase and their corresponding image, as well as for all three phases, the total ozone concentration at any point (X,Y,Z) is given (in SI units) by the equation shown below, in which $D_i = 0$ for the center phase and $D_i = \pm D$, for the outer phases D being the phase spacing

$$C(X,Y,Z) \cong \sum_{i=1}^{3} \frac{\bar{S}_i L_0}{\pi U n} \sum_{k=1}^{n} \frac{1}{\sigma_y \sigma_z} \exp\left[-\frac{(Y-D_i)^2}{2\sigma_y^2} \right] \cdot \left\{ \exp\left[-\frac{(Z-H)^2}{2\sigma_z^2} \right] + \exp\left[-\frac{(Z+H)^2}{2\sigma_z^2} \right] \right\} \qquad 11.9\text{-}6$$

For calculation of downwind concentrations using Equation 11.9-5 and 11.9-6, the spreading coefficients σ_z and σ_y are given by empirical relations (Smith 1968). For stable wind, the spreading coefficients can be approximated by

$$\sigma_z = 0.06\left(X - X_i\right)^{0.71}\ ;\ \sigma_y = 5\sigma_z \qquad 11.9\text{-}7$$

where X_i is the X coordinate of the ith line or point source. For unstable wind conditions, the spreading coefficients are approximated by

$$\sigma_z = 0.0315\left[\left(\frac{23}{U} \right) + 4.75\left(\frac{100}{H} \right)^{0.25} \right] \left(X - X_i\right)^{0.86}\ ;\ \sigma_y = 1.43\,\sigma_z \qquad 11.9\text{-}8$$

Highest ground-level ozone concentrations are obtained under conditions of rain, unstable wind parallel to the line, and at low wind speeds. Calculation of ground-level ozone concentrations near transmission lines will be explained considering some practical examples in Applet CL-3.

11.9.4 Ozone Levels Near Transmission Lines

In addition to laboratory investigations mentioned above on the ozone generation characteristics of transmission-line conductors, a number of studies were also carried out to determine the contribution of transmission lines to the ambient ozone levels. Ozone levels in ambient air are measured using chemiluminescent ozone detectors (Roach et al. 1978), which are based on the principle that when ozone is mixed with nitrogen monoxide (NO), the ensuing chemical reaction results in light emission that can be measured. Air samples containing ozone are drawn through nonreactive plastic or teflon pipe using a fan at the end of the pipe and are passed through the ozone detector at a known flow rate. The mouth of the intake pipe is placed at the desired height above ground and lateral distance from the transmission line. The first of these investigations was carried out along the American Electric Power (AEP) 765-kV transmission system (Frydman et al. 1973), in which short-term measurements of ozone were taken at 20 different locations along the line. No ground-level ozone contribution attributable to the transmission line was detected during the tests. Subsequently, a measurement program extending several months before and after the energization of a 765-kV line was carried out at one site (Frydman and Shih 1974) near the line. Detailed analysis of the data confirmed that the line did not contribute to ambient ozone level.

In order to maximize the probability of detecting ozone from a full-scale line, long-term measurements were conducted on the C-Line at the Apple Grove 750-kV Test Project (Roach et al. 1978). The Apple Grove C-Line was a

test line operating at 775-kV using a 2.54-cm conductor in a four-conductor bundle. This subconductor in a bundle of four was too small to ever be considered for an operating line because it created a very high conductor surface electric field of the center phase bundle of 24.41 kV/cm. Ozone sensors were placed at 0.6 m and 9.1 m above ground at a distance of 30 m from the center phase of the horizontally configured line. The results of the study showed that

1. ozone could be detected during foul weather at the 9.1 m sensor location;
2. it could not be detected at ground level under any weather conditions;
3. it could not be detected at the 9.1 m sensor location during dry weather conditions; and
4. the prediction model developed from laboratory tests (Roach et al. 1974) agreed quite well with the measurements.

The results of this study were used in the extensive hearings conducted in the State of New York. These hearings were the New York State Public Service Commission Cases 26529 and 26559 - "Common Record Hearing on Health and Safety of Extra-High Voltage Transmission Lines." The conclusion of those hearings was that ozone was not an issue in the design or siting of 765-kV transmission lines.

Measurements carried out in the vicinity of one of Hydro-Quebec's 735-kV lines (Varfalvy et al. 1985) showed that any ozone from the line could not be distinguished from the normal fluctuations of ambient ozone levels.

11.9.5 Standards for Ambient Ozone Levels

Air quality standards for photochemical oxidants, which comprise mostly ozone, are based on their possible impact on human health. In North America, the environmental regulations prescribe a level of 120 ppb (parts per billion) (EPA 1990) as a maximum one-hour mean concentration, not to be exceeded more than once a year. It is clear from the discussion presented in this section that corona-generated ozone from transmission lines is normally well below the prescribed standard. For all practical purposes, therefore, ozone has no impact on the design of high-voltage transmission lines.

REFERENCES

Anderson, J.G, M. Baretsky, Jr., and D.D. MacCarthy. 1966. "Corona Loss Characterization of EHV Transmission Lines Based on Project EHV Research." *IEEE Transactions on Power Apparatus and Systems*. Vol. PAS-85. No. 12. pp. 1196-1212. December.

Bartenstein, R. and E.A. Rachel. 1958. *The 400 kV Rhineau Research Establishment. Vol. II – Corona Measurements*. Heidelberg, Germany.

Beattie, J. 1969. *An Experimental Study of the Effects of Atmospheric Environment on High-Voltage Corona*. M. A. Sc Thesis. University of Toronto. Toronto, Canada.

Burns, A.L., M.W. Tuominen, V.L. Chartier, and L.Y. Lee. 1985. "The Effect of Altitude on Conductor Selection for High Voltage AC Transmission Lines." American Power Conference. Chicago, Illinois. April 24.

Chartier, V.L. 1983. "Empirical Expressions for Calculating High Voltage Transmission Line Corona Phenomena." First Annual Seminar Technical Program for Professional Engineers. Bonneville Power Administration (BPA).

Chartier, V.L. 1993. "Effect of Load Current on Conductor Corona." CIGRÉ SC 36 Committee Report.

Chartier, V.L., D.F. Shankle, and N. Kolcio. 1970. "The Apple Grove 750 kV Project: Statistical Analysis of Radio Influence and Corona-Loss Performance of Conductors at 775 kV." *IEEE Transactions on Power Apparatus and Systems.* Vol. PAS-89. pp. 867-881. May/June.

Chartier V.L., L.Y. Lee, L.D. Dickson, and K.E. Martin. 1987. "Effect of High Altitude on High Voltage AC Transmission Line Corona Phenomena." IEEE Transactions on Power Delivery. Vol. PWRD-2. No. 1. pp. 225-237. January.

Cladé, J.J and C.H. Gary. 1970. "Predetermination of Corona Losses Under Rain: Influence of Rain Intensity and Utilization of a Universal Chart." *IEEE Transactions on Power Apparatus and Systems*. Vol. PAS-89. No. 6. pp. 1179-1185. July/August.

Cobine, J.D. 1958. *Gaseous Conductors*. Dover Publications, Inc.

Cramariuc, R. I., V. Velisar, V. Milevschi, V. Munteanu, V. Ghiuta, and F.T. Tanasescu. 1999. "New Considerations of Ozone Generation and the Influence of NOX in Ozone Production and Water Treatment." Applications in Environment Protection. 9-12 November 1998. Bucharest Romania. Kluwer Academic Publisher. pp. 313-340.

Edison Electric Institute. 1968. "EHV Transmission Line Reference Book." New York.

EPA. 1990. *National Ambient Air Quality Standards.*

EPRI. 1982. *Transmission Line Reference Book – 345 kV and Above/Second Edition*. Electric Power Research Institute. Palo Alto, California.

Foley, A.H., and F. Olsen. 1960. "Project EHV – Preliminary Corona Investigations: The Effect of Harmonics on Corona Losses." *AIEE Transactions Power Apparatus and Systems*. Vol. 79. pp. 310-316. June.

Frydman, M., A. Levy, and S.E. Miller. 1973. "Oxidant Measurements in the Vicinity of Energized 765 kV Lines." *IEEE Transactions on Power Apparatus and Systems*. Vol. PAS-92. pp. 1141-1148. May/June.

Frydman, M. and C.H. Shih. 1974. "Effects of the Environment on Oxidants Production in AC Corona." *IEEE Transactions on Power Apparatus and Systems*. Vol. PAS-93. pp. 436-443. January/February.

Gary, C.H. and M.R. Moreau. 1976. *L'effet Couronne en Tension Alternative*. Eyrolles, Paris.

Keitley, R., D.F. Oakshott, and G.C. Stringfellow. 1966. "Corona Power Loss and Radio Interference Measurements at 400 kV and 750 kV on the Leatherhead Experimental Line." CIGRÉ Report 419.

Kirkham, H. 1980. "Instantaneous Rainfall Rate: Its Measurement and Its Influence on High-Voltage Transmission Lines." *Journal of Applied Meteorology.* Vol. 19. pp. 35-40.

Kirkham, H. 1981. "The Influence of Rain Rate on Transmission Line Corona Performance." *IEEE Transactions on Power Apparatus and Systems*. Vol. PAS-100. No. 1. pp. 420-430. January.

Knudsen, N. 1964. "Corona Loss and Radio Interference Measurements on High-Voltage A.C. Test Lines in Sweden." CIGRÉ Report 411.

Kravchenko, V.D., V.I. Levitov, and V.I. Popkov. 1962. "Measuring of Corona Losses on Operating 400-500 kV Lines." CIGRÉ Report 407.

Kravchenko, V.D., V.I. Levitov, and V.I. Popkov. 1964. "Corona Power and Energy Losses on the Conductors of Loaded 500 kV Lines." *Electrichestvo*. No. 5. pp. 7-12.

Laasonen, M. and M. Lahtien. 1996. "Corona Research Helps Curb Losses." *Energy Innovation 1996 – IVO Group's Research and Development Report*. pp. 45-46.

Lahti, K., M. Lahtinen, and K. Nousiainen. 1997. "Transmission Line Corona Losses Under Hoar Frost Conditions." *IEEE Transactions on Power Delivery*. Vol. 12. pp. 928-933. April.

Larsson, N. and K. Ponni. 1964. "Measurements of Corona Losses due to Hoarfrost and Winter Precipitation on 400 kV Operating Lines in Finland with Special Reference to Estimation of Hoarfrost Corona Losses Based on Meteorological Data." CIGRÉ report 409.

Loxton, A.E. and A.C. Britten, 2002. "The Measurement and Assessment of Corona Losses on 400 kV Transmission Lines." 6th Africon Conference in Africa. George, South Africa. pp. 613-616.

Lunt, R.W. 1959. "The Mechanism of Ozone Formation in Electrical Discharges." in *Ozone Chemistry and Technology*. American Chemical Society. Washington D.C. pp. 286-304.

Maruvada, P.S. 2000. *Corona Performance of High-Voltage Transmission Lines*. Research Studies Press Ltd. Baldock, Hertfordshire, England. pp. 113-118.

Mazetta, L.A. 1971. "A High Performance Phase-Sensitive Detector." *IEEE Transactions on Instrumentation and Measurement*. Vol. IM-20. No. 4. pp. 296-301. November.

Mombello, E. and P.S. Maruvada, 2001. "Measurement and Analysis of Corona Losses Generated by Heavily Contaminated Conductors." International Symposium on High-Voltage Engineering (ISH). Bangalore, India. 20-24 August.

Morgan, V.T. and R. Morrow, 1977. "The Effect of Electrical Corona on the Natural Convective Heat Transfer from a Circular Cylinder in Air." Second Australian Conference on Heat and Mass Transfer. University of Sydney. pp. 79-83. February.

Morris, R.M. and O. Petersons. 1962. "Measurement of Corona Losses at Alternating Voltages." *Bull. Radio and Elect.* Engg. Div. National Research Council of Canada. Ottawa. Vol. 12. pp. 20-23.

Naef, O., R.L. Tremaine, and A.R. Jones. 1951. "Techniques of Corona Loss Measurement and Analysis – 500-kV Test Project of the American Gas and Electric Company." *AIEE Transactions on Power Apparatus and Systems*, pp. 496-506.

Nigol, O. and J.G. Cassan, 1961. "Corona Loss Research at Ontario Hydro Coldwater Project." *AIEE Transactions on Power Apparatus and Systems*. Vol. 80. Pt. III. pp. 388-396. August.

Peek, F.W. 1929. *Dielectric Phenomena in High-Voltage Engineering*. McGraw-Hill.

Peterson, W.S. 1933. (Discussion) in: Carrol, J.S. and B. Cozzens. "Corona Loss Measurements for the Design of Transmission Lines to Operate at Voltages Between 200 kV and 300 kV." *AIEE Transactions*. Vol. 52. pp. 55-63.

Peterson, W.S., B. Cozzens, and J.S. Carrol. 1950. "Field Measurement of Corona Loss above 230 kV." CIGRÉ Report 401.

Petersons, O. 1964. "A Self-Balancing High-Voltage Capacitance Bridge." *IEEE Transactions on Instrumentation and Measurement*. Vol. IM-13. pp. 216-224. December.

Roach, J.F., V.L. Chartier, and F.M. Dietrich. 1974. "Experimental Oxidant Production Rates for EHV Transmission Lines and Theoretical Estimates of Ozone Concentrations Near Operating Lines." *IEEE Transactions on Power Apparatus and Systems*. Vol. PAS-93. pp. 647-657. March/April.

Roach, J.F., F.M. Dietrich, V.L. Chartier, and H.J. Nowak. 1978. "Ozone Measurements on the C-Line at the Apple Grove 750 kV Project and Theoretical Estimates of Ozone Concentrations Near 765 kV Lines of Normal Design." *IEEE Transactions on Power Apparatus and Systems*. Vol. PAS-97. No. 4. pp. 1392-1401. July/August.

Roberts, O.F.T. 1923. "The Theoretical Scattering of Smoke in a Turbulent Atmosphere." *Proceedings of the Royal Society of London*. A. Vol. 104. pp. 640-654.

Robertson, L.M., C.F. Wagner, and T.J. Bliss. 1957. "Colorado High-Altitude Corona Tests, Parts I – III." *AIEE Transactions on Power Apparatus and Systems*. Vol. 76. pp. 356-376. June.

Robertson, L.M., D.F. Shankle, J.C. Smith, and J.E. O'Neil. 1961. "Leadville High-Altitude Extra-High-Voltage Test Project: Part II-Corona Loss Investigations." *AIEE Transactions on Power Apparatus and Systems*. pp. 725-732. December.

Robertson, M. and J. K. Dillard 1961. "Leadville High-Altitude EHV Test Project Part I – Report of 4 Years of Testing." *AIEE Transactions on Power Apparatus and Systems*. pp. 715-725. December.

Scherer, H.N., Jr., B.J. Ware, and C.H. Shih. 1973. "Gaseous Effluents due to EHV Transmission Line Corona." *IEEE Transactions on Power Apparatus and Systems*. Vol. PAS-92. pp. 1043-1049. May/June.

Sebo, S.A., J.T. Heibel, M. Frydman, and C.H. Shih. 1976. "Examination of Ozone Emanating from EHV Transmission Line Corona Discharges." *IEEE Transactions*. Vol. PAS-95. pp. 693-703. March/April.

Shankle, D.F., S.B. Griscom, E.R. Taylor, and R.H. Schloman. 1965. "The Apple Grove 750 kV Project – Equipment Design and Instrumentation." *IEEE Transactions on Power Apparatus and Systems*. Vol. PAS-84. pp. 541-550. July.

Smith, M., Editor. 1968. *Recommended Guide for Prediction of the Dispersion of Airborne Effluents*. ASME Committee on Air Pollution Controls.

Sugimoto, T. 1968. "Corona Loss of Three-Conductor Bundle." *Electrical Engineering in Japan*. Vol. 88. No. 9. pp. 23-31.

Tikhodeev, N.N. 2000. "Mitigation of Corona Losses on EHV Overhead Lines Through Voltage Control." *Proceedings of St. Petersburg IEEE Chapter*. pp. 3-13.

Tomota, M., T. Sugiyama, and K. Yamaguchi. 1968. "An Electronic Multiplier for Accurate Power Measurements." *IEEE Transactions on Instrumentation and Measurement*. Vol. IM-17. No. 4. pp. 245-251. December.

Tremaine, R.L. and G.D. Lippert. 1947. "Instrumentation and Measurement – Tidd 500-kV Test Lines." *AIEE Transactions on Power Apparatus and Systems*. pp. 1624-1631.

Trinh, N.G. and P.S. Maruvada. 1977. "A Method of Predicting the Corona Performance of Conductor Bundles Based on Cage Test Results." *IEEE Transactions on Power Apparatus and Systems*. Vol. PAS- 96. pp. 312-325. January/February.

Turner, D.B. 1970. *Workbook of Atmospheric Dispersion Estimates*. Environmental Protection Agency. Research Triangle Park. North Carolina.

Varfalvy, L., R.D. Dallaire, P. Sarma Maruvada, and N. Rivest. 1985. "Measurement and Statistical Analysis of Ozone from HVDC and HVAC Transmission Lines." *IEEE Transactions on Power Apparatus and Systems*. Vol. PAS-104. pp. 2789-2797. October.

Wagner, C.F., A. Wagner, E.L. Peterson, and I.W. Gross. 1948. "Corona Considerations on High-Voltage Lines and Design Features of Tidd 500 kV Lines." *AIEE Transactions on Power Apparatus and Systems*. pp. 8-15.

CHAPTER 12

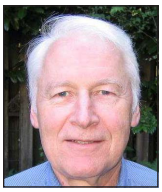
Shared Use of the Right-of-Way

Robert Olsen
T. Dan Bracken

This chapter reviews issues associated with shared uses of transmission-line corridors. Included is a discussion of the basic elements of electromagnetic compatibility and descriptions of 15 planned and incidental uses of the right-of-way—among them, railroads, pipelines, power line carrier communications systems, radio navigation systems, and agricultural operations.



Dr. Robert G. Olsen earned a Ph.D. in electromagnetic theory from the University of Colorado in 1974, and—aside from temporary positions at GTE Labs, ABB Corporate Research, and EPRI—has been a member of the electrical engineering faculty at Washington State University since then. The bulk of his research work has been in the area of power system electromagnetic compatibility (EMC). One portion of his research was the development of a comprehensive theory for predicting corona-generated electromagnetic interference from power lines. He has also worked on problems with the compatibility of fiber optics and the high-voltage environment, shielding of extremely low-frequency electromagnetic fields, wideband power line communications, and the electromagnetic environment of power lines. Dr. Olsen is a Fellow of the IEEE, and has served as chair of the IEEE Power Engineering Society Corona Effects and AC Fields Working Groups, and as United States National Committee representative to CIGRÉ Study Committee 36 (Electromagnetic Compatibility).



Dr. T. Dan Bracken received a Ph.D. in low-temperature physics from Stanford University in 1971. After teaching physics for three years at Reed College, he worked as a physicist for the Bonneville Power Administration (BPA) for seven years. At BPA he conducted research projects on field and corona effects from both ac and dc transmission lines and provided support for environmental studies. In 1981, he founded T. Dan Bracken, Inc. a scientific consulting firm that offers scientific and technical expertise in areas of electric and magnetic field measurements, exposure assessment, instrumentation, environmental effects of transmission lines, and project management. Initially, Dr. Bracken's research involved measurement and characterization of fields from ac and dc transmission lines. Most recently, the emphasis has been on occupational exposure assessment and compliance issues related to guidelines. Dr. Bracken is a Fellow of the IEEE, and has served as chair of working groups in the IEEE Power Engineering Society Corona and Field Effects Committee. He is also a member of the Bioelectromagnetics Society and an affiliate member of the American Conference of Governmental Industrial Hygienists (ACGIH).

The following individuals also made contributions to this chapter:

- Paul Wong, (PW International, Inc.)
  Sections 12.7 (ILS) and Section 12.8 (cordless and cell phones)
- Richard Harness (EDM International, Inc.)
  Section 12.16 (avian interaction)

12.1 INTRODUCTION

12.1.1 Background

The potential for man-made electromagnetic interference between separate systems has existed since the construction of the first electric power system in the late 1800s. These systems were sources of electromagnetic fields that could interfere with electrical receptors such as telegraph and telephone systems. In fact, it is likely that interference between ac power systems and telephone systems was the first reported electromagnetic compatibility (EMC) problem. In this context, *EMC* is defined broadly as the ability of devices, systems, or facilities to function as intended in an electromagnetic environment that might include the one generated by itself. In this chapter, the source of the electromagnetic environment is a high-voltage transmission line, and the devices, systems, or facilities include anything with a function that can be compromised by exposure to these electromagnetic fields.

In the early decades of the 1900s, the voltage levels at which transmission lines operated were increased, and additional EMC issues were encountered. More specifically, corona (as discussed in Chapters 8, 9, and 10 of this book) caused electromagnetic interference (sometimes called radio noise, electrical noise, or radio frequency interference) to radio and television receivers. As more systems and devices or facilities were either constructed or used on or near the transmission line right-of-way, even more EMC issues surfaced.

The entire set of EMC issues due to interactions between electric power lines and other devices, systems, and facilities that share its corridor is the main subject of this chapter. Devices, systems, and facilities with which transmission lines can cause EMC problems, and that will be discussed in this chapter, include railroads, pipelines, transmission-line communications, optical fiber communications, communication system antennas, aircraft warning systems, telephone systems, distribution lines, agricultural operations, radio navigation receivers, communication receivers, and large portable equipment. Parking lots, homes, and other structures, schoolyards, playgrounds, and recreational areas are also considered because they are inhabited by humans who may be influenced by the transmission-line electromagnetic fields. Finally, there are a few interactions that are not specifically electromagnetic in nature, but are considered here for completeness. These include structural issues such as tower foundation integrity and legal issues such as the protection of bird nests.

The consequences of electromagnetic interactions that will be examined here include:

- Malfunction or degraded performance of systems that rely on electromagnetic communication.
- Premature aging or failure of systems due to electromagnetic interactions.
- Potential for catastrophic failure or hazardous conditions due to transients.
- Safety of human workers while power lines are energized.
- Safety and comfort of the public near transmission lines.
- Legal limits on electromagnetic emissions or harmful interference to licensed communication systems.

It should also be noted that some of these EMC issues that are related to either 50/60-Hz or corona-generated electromagnetic fields have been discussed earlier in this book. In several sections of this chapter, the reader will be referred to the appropriate sections of the book for further reading. For example, there will be no discussion of possible long-term biological effects of 50/60-Hz electric or magnetic fields on people. For information on this subject, the reader is referred to Sections 7.11 and 7.13.

Finally, it will not be possible to exhaustively discuss each of these phenomena in this chapter. For this reason, the reader is provided an extensive list of references for further reading if more information is required.

12.1.2 EMC Regulations, Standards and Guidelines

As the number of EMC problems has increased, the interest in developing regulations, standards, and guides as tools to manage these problems has grown. The purpose of these tools is to protect devices and people from the unintended behavior of a device caused by interference. At appropriate points within this chapter, relevant regulations, standards and guides will be referenced. These documents will be helpful to the engineer who is considering proposals for location of other systems and facilities on a transmission-line right-of-way.

12.1.3 Elements of EMC

The EMC problem involves all aspects of the *generation, coupling,* and *reception* of electromagnetic energy. As illustrated in Figure 12.1-1, these three components are the basis of engineering work focused on solving EMC problems.

The source (also called a generator or emitter) produces electromagnetic energy that travels along one or more

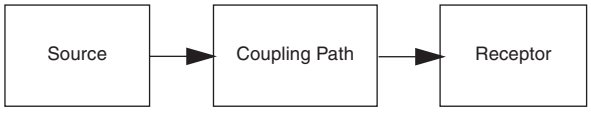


Figure 12.1-1 Components of the EMC process.

coupling paths to the receptor elements. In this case, the source is the power line. Unwanted electromagnetic energy from the power line could couple to the receptor via (for example) induction to nearby cables, its internal or external antenna, fields that interact directly with unshielded circuits, or the power supply cable attached to the receptor. Receptors can be radio or TV receivers, appliances, navigation equipment, electronic circuits, animals, birds, humans or just about anything that uses or can detect electromagnetic energy. Each of these three components of the EMI problem is discussed in more detail below.

12.1.4 Electric Power Transmission-Line Sources

Since the principal subject of this chapter is the interaction of power lines with other systems, the electromagnetic environment generated by these lines will be summarized here. This environment consists of the power-frequency (i.e., 50/60-Hz) and related harmonic electric and magnetic fields originating from power system operation. The environment also includes radio frequency (RF) carrier signals on the phase conductors, higher-frequency electromagnetic fields generated by corona discharges from power lines and equipment, arcing from small gaps in system hardware or tracking on the surface of contaminated insulators, and high-frequency fields from power electronic switching devices connected to transmission lines. A short description of each source follows.

Power-Frequency Voltages and Currents

These are voltages and currents at a frequency of either 50 or 60 Hz that are designed to carry power. The electric and magnetic fields associated with these generally have the largest amplitude of all those described here, and are discussed extensively in Chapter 7 of this book. Power-frequency electric and magnetic fields can be put in the context of background levels both in the home and away from the power system (Silva et al. 1989; Fraser-Smith and Bower 1992).

Harmonic-Frequency Voltages and Currents

Harmonic frequencies are integer multiples of the power frequency. Voltages and currents at these frequencies are caused by nonlinear devices on the power system, such as power transformers, and more importantly by nonlinear loads such as switching power supplies, variable-speed motor drives, and energy-efficient lighting connected to the power system. The first 10 harmonics are usually the ones of interest. On transmission lines, the amplitudes of fields associated with these harmonic voltages and currents are generally smaller than 5% of the 50/60-Hz fields, and in most cases even smaller. Fields at harmonic frequencies on distribution lines may be substantially larger than those on transmission lines. Again, measurements of background fields at these frequencies are available (Randa et al. 1995).

Transient Voltages and Currents

Voltages and currents of short duration (i.e., transient currents) occur on transmission lines from time to time. These can be caused by switching operations, unintended faults, and lightning. While they are generally of short duration, they may have very important effects because they can have large amplitudes compared to the normal voltages and currents on the transmission line, and (because they are generally unbalanced) can result in large voltages and currents in the earth. These earth voltages and currents can cause problems with a number of systems or facilities located near the transmission line.

Power Line Carrier Voltages and Currents

These are caused by low-frequency communication systems (i.e., power line carrier [PLC]) operated by a utility. Typical systems have "carrier" frequencies ranging from 40 to 490 kHz. Most PLC systems use some form of discrete frequency shifting to transmit digital information and operate at low power levels (typically 1-10 W). Typical bandwidths (i.e., the range of frequencies over which the receiver responds, usually within 3 dB of the peak response) for these systems are less than 3.4 kHz, although in some older systems, bandwidths of up to 10 kHz have been used.

More recently, broadband communication systems that use the power line as a transmission medium have been proposed. Although their use is not widespread at this time and has been restricted to lower-voltage distribution lines, they may be more common in the future if certain technical issues can be resolved.

Corona Noise

Generally, corona noise is important only on transmission lines with voltages of 345 kV and above. For these lines, the 50/60 Hz conductor surface electric fields are usually large enough to cause corona (i.e., ionization of the air). It should be noted, however, that some lower-voltage transmission lines of "compact" or "low magnetic field" design may also have large enough conductor surface electric fields to cause noticeable corona. The corona caused by these large electric fields at the conductor surface induces impulsive currents on the transmission line. These induced currents, in turn, cause wideband electromagnetic "noise" fields, which fill the entire frequency spectrum from below 100 kHz to almost 1000 MHz, although they are usually too small to be measured above 10–20 MHz. Weather has a large influence on corona noise. In fact, the noise is 15-30 dB higher during precipitation. A more extensive discussion of corona-generated noise can be found in Chapter 9. It should also be noted that corona generates audible noise. Although not an electromagnetic phenomena, it is generally considered when evaluating the environmental

impact of transmission lines. More information about this topic can be found in Chapter 10.

Spark or Gap Discharges

Spark discharges generally occur between different unconnected hardware components that are physically close but at different voltages due to high-impedance capacitive coupling. If the voltage difference becomes high enough, a tiny electric spark occurs across the gap between components. Due to the nature of this discharge, the electromagnetic noise fields from these sparks tend to dominate those from corona at frequencies above 10-20 MHz and can extend beyond 1000 MHz. Again, weather has a large influence on gap discharges. In fact, they generally occur only during dry weather; wet conditions tend to equalize voltages between different parts of the hardware and hence suppress gap discharges. In dry weather, when corona noise is reduced, fields from gap discharges can often dominate corona-generated fields even below 10 MHz. A different type of spark occurs on the surface of contaminated insulators that have become wet due to condensation or fog. These tiny arcs are part of a process, called *tracking* (or insulator scintillation), in which wet and dry bands form on the contaminated insulator surface and create differences in potential that allow arcing across the dry bands. This phenomenon is reduced or disappears when the entire insulator becomes dry or is cleaned by heavy rain or by mechanical means. The magnitude of the noise field due to scintillation is generally less that that of the gap discharge mechanism previously described. A more extensive discussion of spark discharges can be found in Chapters 8 and 9.

Power Electronic Devices

Wideband noise currents are induced on power line due to switching of HVDC converters or other nonlinear power electronics devices such as Flexible AC Transmission System (FACTS) devices or static VAR compensators (EPRI 2003a). It has been shown that noise near transmission lines that has been injected by a FACTS device can exceed that from foul weather corona noise by up to approximately 20 dB at frequencies up to approximately 1 MHz.

Miscellaneous Other Sources

Other sources of electric and magnetic fields are important for some EMC issues and thus should be recognized for completeness. These include: electromagnetic fields from cellular base stations located on transmission-line towers, electromagnetic fields from the utility microwave communications system, and electromagnetic fields from personal communication transceivers used by utility workers.

Relative Amplitude of Fields from the Different Sources

It is useful to summarize this section by indicating in Figure 12.1-2 the range of frequencies and relative amplitudes of fields for some of the different sources mentioned above. Note the "noise" amplitudes in Figure 12.1-2 are the magnetic-field equivalents (i.e., electric field divided by the impedance of free space = 120π Ω) of the electric field as measured with a CISPR standard quasi-peak receiver as described in Chapter 9. Also one should not infer from this figure that the noise from spark discharges is always less than corona noise for frequencies less than 20 MHz. Both sources depend on weather conditions, and thus, for example, in dry conditions, spark discharge noise will usually dominate corona noise at frequencies less than 20 MHz. Transients are not included; their amplitudes are highly variable but can easily exceed those indicated on the chart for short periods of time. Finally, noise from FACTS or similar power electronic switching devices is not shown on Figure 12.1-2 because: (1) these devices are not widespread at the time of this writing, and (2) it may be controlled by filtering. Nevertheless it should be recognized that at locations near ac/dc converter stations or FACTS devices, these high-speed electronic switching devices may be the dominant electromagnetic field source up to frequencies near 1 MHz.

12.1.5 Coupling Paths

Electromagnetic energy of the source may be coupled to a receptor by one of the following mechanisms: conducted (an electric current through a wire or resistive material such as the earth), coupled or induced (capacitively by an electric field or inductively by a magnetic field), or radiated (a propagating electromagnetic wave). There may be multiple coupling paths or a complex combination of path mechanisms, in which case it may be difficult to mitigate

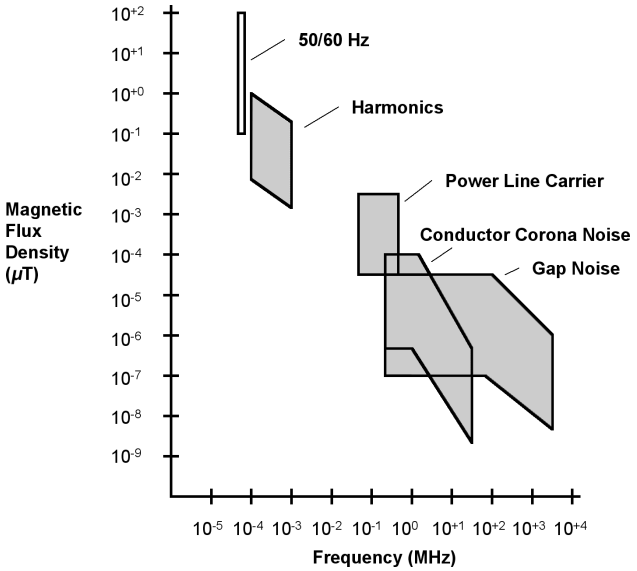


Figure 12.1-2 Relative amplitudes in microtesla (μT) and frequency ranges in megahertz (MHz) for different transmission-line electromagnetic fields. Corona and gap noise is expressed as the equivalent magnetic field for the noise measured in a CISPR standard quasi-peak receiver.

interference because reducing or eliminating one path may enhance another. Figure 12.1-3 illustrates these coupling mechanisms.

12.1.6 Receptors

Interference with the operation of an electronic "receptor" occurs when an electromagnetic noise field to which it is exposed causes improper operation of the device. For many electronic devices, it is only necessary to establish the external electric and magnetic field levels at the device location and to compare these to threshold field levels (i.e., susceptibility levels) below which the device operates as intended. Note that a margin of safety may be added when setting maximum exposure limits for equipment. To evaluate the effect of noise on communication and navigation receivers, however, it is necessary to compare the amplitude of the desired "signal" to that of the "noise." The ratio of these two is usually identified as the signal-to-noise ratio (SNR), but can alternatively be referred to as the signal-to-interference ratio (SIR). To decide whether the SNR is acceptable, it is necessary to know the minimum SNR for unimpaired operation of the receiver. A more extensive discussion of SNR can be found in Chapter 9. Examples of devices or systems that are receptors and that may be found near a power line right-of-way are computer monitors using cathode ray tubes; pacemakers and other medical devices; electron microscopes; medical diagnostic and treatment equipment; aircraft communications and navigation systems; military and government communications; AM, FM, and TV broadcasting; amateur radio; air traffic control equipment; railroad signaling equipment; farm irrigation control systems; global positioning system receivers; and utility control/ protection systems.

Another issue that will be discussed in this chapter is that of premature aging and/or failure of power system and/or shared system components due to electromagnetic interactions. These might include premature aging of dielectric materials such as all-dielectric self-supporting (ADSS) optical fiber cable due to corona and dry-band arcing or failure of components due to switching surges, faults, or lightning. Here the "receptor" is that portion of the system that degrades prematurely.

Personal safety issues will also be discussed where appropriate. In this case, a human is the "receptor." These discussions will include the safety of power system workers, workers employed by services that share the right-of-way, and the general public.

12.1.7 Organization and Contents of the Chapter

Systems that share a transmission-line corridor can be divided into: (1) those that are planned to share the corridor with the power line, and (2) those whose use on the corridor is incidental. The systems below will be categorized in that way. *Planned* uses that will be discussed in Sections 12.2 through 12.9 are:

- 12.2 Interference with the operation of railroads
- 12.3 Interference with the operation of pipelines

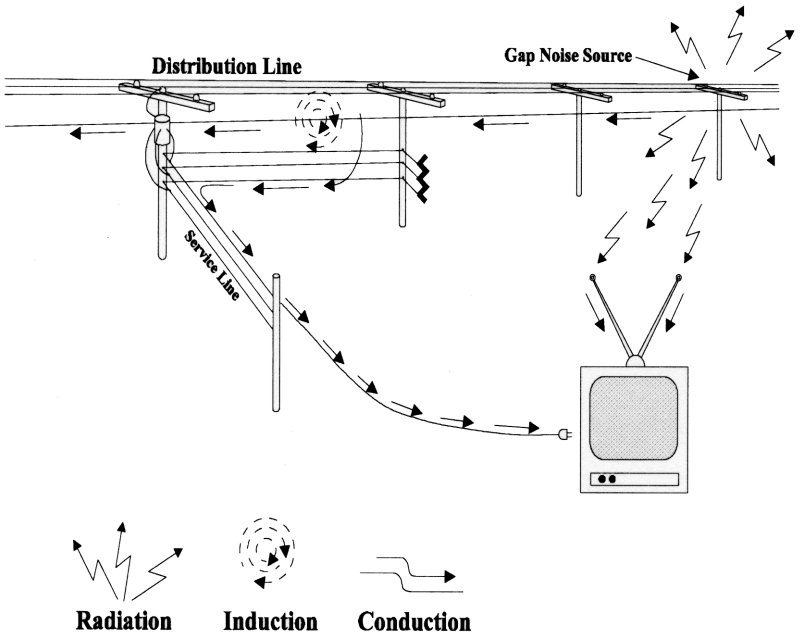


Figure 12.1-3 Example coupling paths between power system EMC source and a receptor.

- 12.4 Interference with the operation of power line communication systems
- 12.5 Interference with the operation of optical fiber communications
- 12.6 Consequences of installing communication system antennas on transmission line towers
- 12.7 Interference with the operation of systems for warning aircraft
- 12.8 Interference with the operation of telephone systems
- 12.9 Consequences of installing distribution lines under transmission lines

Incidental uses that will be discussed in Sections 12.10 through 12.16 are:

- 12.10 Interference with the operation of radio navigation systems
- 12.11 Interference with the operation of communication receivers
- 12.12 Impacts on agricultural operations near transmission lines
- 12.13 Use of vehicles and large equipment near transmission lines
- 12.14 Impacts on buildings near transmission lines
- 12.15 Impacts on public use of rights-of-way
- 12.16 Avian interactions with transmission lines

12.2 INTERFERENCE WITH THE OPERATION OF RAILROADS

12.2.1 Background

Shared corridors for railroads and power lines such as the one shown in Figure 12.2-1 are often an economic necessity. However, over the years, these joint-use corridors have led to a small but consistent number of EMC issues. In this context, EMC relates to the ability of one system (e.g., railroad signals) to operate in the presence of effects caused by a nearby system (e.g., electric power lines).

Any conductor carrying an alternating current creates time-varying electric and magnetic fields in its vicinity and distributions of current within conducting regions such as the nearby earth. These "induced" fields and currents cause separate alternating currents and voltages on any system of conductors (e.g., railroad tracks and associated electrical equipment) that are placed near the power line. In turn, these voltages and currents may interfere with the proper and safe operation of the nearby system. These effects become greatest with ac power lines and railroads that are parallel and in close proximity to each other over a long distance. Unfortunately, this is exactly the situation when ac power lines are located along a railroad right-of-way, as illustrated in Figure 12.2-1.

Effects considered here include compromised equipment operation, equipment damage, and personnel safety (i.e., direct electrical effects on a person touching the equipment). Of particular interest here is the fact that modern electrical communications technologies are not necessarily as robust as the simple electromechanical systems of the past.

It will be assumed here that the primary interference is between the electric power system and railroad equipment. This is certainly true for "diesel" locomotives (in reality "diesel electric" since the diesel turns an electric generator that provides power to motors that drive the wheels) that do not cause large currents in the rails. In some parts of North America and in most of Europe, however, electric traction is used. In these cases, electricity from another source, usually delivered through an overhead catenary wire or an electrified third rail, is used to drive the electric motors to turn the wheels. Because electric traction requires the railroads to have their own electric power distribution systems, railroads using electric traction can be sources of ac power interference. Problems specific to railroads using electric traction are covered in many IEC and European standards, but will not be discussed further here (CENELEC 1999; IEC 2003a-f).

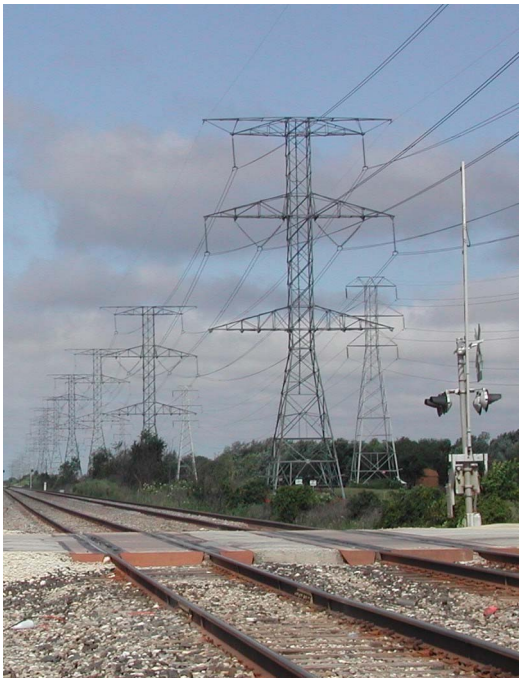


Figure 12.2-1 Joint railroad transmission-line corridor.

Programs to address ac interference challenges have been undertaken in the past. Most of these programs concentrated on the issues of ac induction (JCIIRC 1918; Leisenring 1926; AAR/EEI 1936; AAR/EEI 1977). The last of these references is known as *Principles and Practices for Inductive Coordination of Electric Supply and Railroad Communication/Signal Systems*. While it is not a standard, this document, commonly called the "Bluebook," is the closest thing in North America to an industry accepted guide.

EPRI and the American Association of Railroads (AAR) conducted several research projects on railroad/electric power inductive coordination in the 1980s (EPRI 1983b; EPRI 1985). These projects included development of CORRIDOR software to predict magnetic and electric coupling into railroads and pipelines. Included in this work was the creation of the Track Circuit Simulator to permit testing of any interference condition on actual equipment installed on simulated track. The EPRI work, as with most of the prior work, was concentrated on electric and magnetic field coupling. However, many of the problems that railroads have with newer signaling equipment technologies are caused by distributions of current injected into the earth. The most comprehensive discussion of this subject can be found in a recent EPRI publication entitled *Power System and Railroad Electromagnetic Compatibility Handbook* (EPRI 2004).

12.2.2 Introduction to Coupling Mechanisms between Power Lines and Railroads

It is well known that one electromagnetic system (e.g., a power line) can couple energy into another electromagnetic system such as a railroad signaling circuit. While, in general, this interaction is complex, it is possible to understand the most important mechanisms by considering electric-field, magnetic-field, and conductive induction separately, if all relevant dimensions of the systems are small compared to a wavelength in the air and the earth. This is, in part, because electric- and magnetic-field coupling can be superimposed under these conditions and, in part, because one of the three mechanisms usually dominates the others. For simplicity here, only coupling to the electrical circuits that involve the railroad tracks will be considered. Descriptions of coupling to other circuits, such as parallel communications networks, can be found in the publications mentioned above.

12.2.3 Electric-Field (Capacitive) Induction

Required Conditions

Electric-field induction is of concern whenever there are long and/or large objects near the power line that are not well grounded. Two cases for which electric-field coupling can be the dominant coupling mechanism are between power lines and insulated pole-top communication wires, and between power lines and long trains parked in parallel to power lines. In the former case, the impedance between the pole-top circuits and ground is large, which results in higher voltage on the wires. In the latter case, the induced voltage may be higher because the large surface area of the train results in a large power line/train capacitance. This type of induction occurs during both normal operating and fault conditions. The voltages, however, may be different under the two conditions.

Predictive Methods

Capacitive induction can be understood by referring to the circuit diagram in Figure 12.2-2. Note here that (for

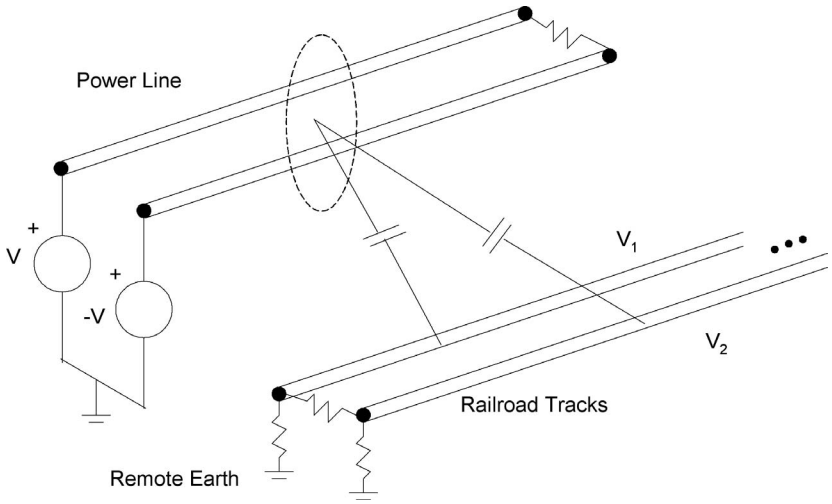


Figure 12.2-2 Electric-field (capacitive) coupling mechanism. Voltages V_1 and V_2 are the capacitively coupled voltages (with respect to remote earth) on each of the two tracks.

simplicity) the power line is a simple two-conductor line. In the absence of the railroad, no current will be injected into the earth by the power line in this simple system since it is "balanced." However, unequal coupling from the two conductors to the tracks causes a slight unbalance. The result is a current driven by the power line voltage through the capacitance between the power line and the railroad tracks and then to the earth through the impedances that connect the tracks to the earth. Because the capacitance between power line and tracks is so small, this current is usually limited to milliampere levels. Usually this level is either too small to interfere with the operation of railroad systems or is dominated by currents induced by other mechanisms and can be neglected. Further, the voltages induced on the tracks are usually small because the impedance between the tracks and ground is generally much smaller than the capacitive impedance between the power line and the tracks. More detailed discussions of electric-field coupling can be found in Sections 7.8 and 12.3.2.

Mitigation

Mitigation of capacitively induced voltages is usually achieved by either increasing the distance between the transmission line and the system on which the voltages are induced or (when possible) by installing additional grounds. The method used to evaluate potential hazards to personnel is essentially equivalent to the one described in Section 12.3.2 for capacitively induced voltages on pipelines. The reader is referred to that section for more detail on this subject.

12.2.4 Magnetic-Field (Inductive) Induction

Required Conditions

Magnetic-field induction is of concern whenever railroad tracks are parallel to transmission lines for long distances. It is often the dominant induction mechanism when the impedance between the tracks and ground is relatively small (i.e., the tracks are reasonably well grounded), so that effect of electric-field induction is reduced. Again, inductive coupling may be of concern during normal power system operation. During faults, however, the current may increase dramatically and hence dramatically increase the coupled currents and voltages.

Predictive Methods

Inductive coupling can be understood by referring to the circuit diagram in Figure 12.2-3. The mechanism by which coupling occurs is indicated by the magnetic field lines that pass through both the power line and the track circuit. Note that the "track circuit" here refers to loops that consist of current paths from: (1) one rail to the other and back again (i.e., the "differential" or "rail-to-rail" mode), and (2) the set of rails to ground and through the earth to the other end of the rails (the "common" or "rail-to-ground" mode).

Because the magnetic fields are generated by current, it is the power lines' current that drives this coupling mechanism. The equivalent sources (i.e., voltage sources in series with impedances connected to the railroad tracks that replace the power line) that drive the railroad circuit can be shown to have both a low open-circuit voltage and low impedance. For typical values of these parameters, the current induced into the railroad circuit may be on the order of amperes. Hence magnetic induction is usually the dominant coupling mechanism during normal power line operation, and can be responsible for malfunction of signals, equipment damage, and personnel safety. It should be noted that EMC problems related to inductive coupling may be driven by harmonic currents on the power system as well as the 50/60-Hz currents. Part of the reason for this

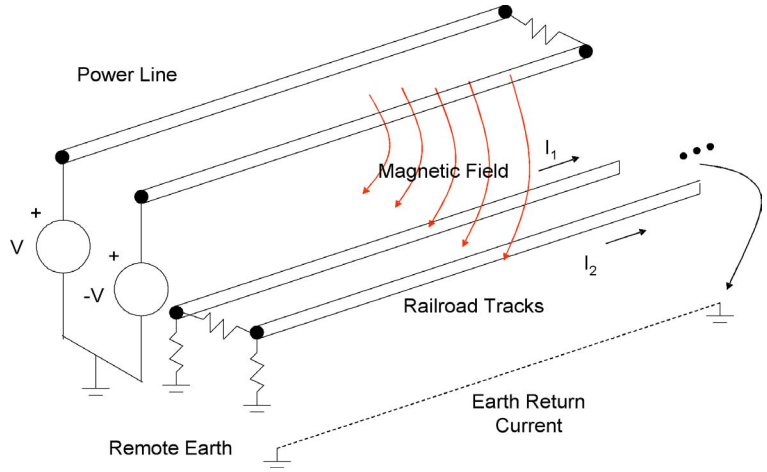


Figure 12.2-3 Magnetic field (inductive) coupling mechanism. Currents I_1 and I_2 are the inductively coupled currents on each of the two tracks.

is that inductive coupling increases in proportion to frequency. A more detailed discussion of magnetic field coupling can be found in Section 7.9 of this book.

Mitigation

As with electric-field induction, increasing the distance between the track and power lines will reduce magnetic-field induction. Other techniques used to reduce magnetic-field induction include minimizing the magnetic field at the rails by either reducing the spacing between phase conductors or phasing multiple circuit lines for minimum magnetic field levels. In some cases it may be possible to reduce the length of parallel exposure between the transmission line and the track. If the problem is related to fault currents, installing fault-current-limiting devices may help. Many other techniques for mitigating problems due to magnetic induction can be found in EPRI (2004).

12.2.5 Conductive (Resistive) Induction

Required Conditions

Whenever magnetic induction is suspected to be a problem, conductive induction should be considered as well. This is especially true under fault conditions since the currents will generally be unbalanced, and hence the probability of large earth currents is increased.

Predictive Methods

Conductive coupling can be understood by referring to the circuit diagram in Figure 12.2-4. In this figure, the power line is represented by a single conductor because the emphasis is on the current injected into the earth by the power line. Under ground-fault (i.e., the power line is shorted to ground) conditions, the power line is effectively grounded at various points along its length, and a significant amount of current flows into the earth. In the figure, the resistors between the power line, remote earth (the "ground" symbol in the circuit), and the railroad tracks represent the resistances through earth for each of these. Coupling from the power line to the railroad system occurs through the currents injected into the earth. The currents are then distributed throughout the railroad system because of its relatively low impedance back to the power-line source. The currents, in turn, cause voltages across the impedances through which they flow. If these voltages are comparable to, or greater than, the railroad equipment immunity level, improper equipment operation is possible.

It should be noted that conductive coupling is dependent on soil resistivity, which in turn, is dependent on the moisture content of the soil. Consequently, one indication of the presence of conductive coupling is a dependence of any problem on the moisture content of the soil.

Finally, while distribution systems are not the subject of this book, it should be noted that their multiple-grounded neutral system is often responsible for injection of significant current under normal (often unbalanced) operation.

Mitigation

For conducted induction, methods used to reduce electric or magnetic fields are generally not useful. Most mitigation methods that are effective require some modification of the railroad plant. For more specific information on recommended methods for reducing susceptibility due to conducted induction, the reader is referred to EPRI (2004).

12.2.6 Common and Differential Modes

Often it is helpful to identify the voltage between the rails and the average voltage of the rails with respect to remote earth. Similarly it is helpful to identify the portion of the current on each rail that returns to the source via the other rail and the portion that returns to the source via the earth. This can easily be done by defining two modes: the "common mode" and the "differential mode."

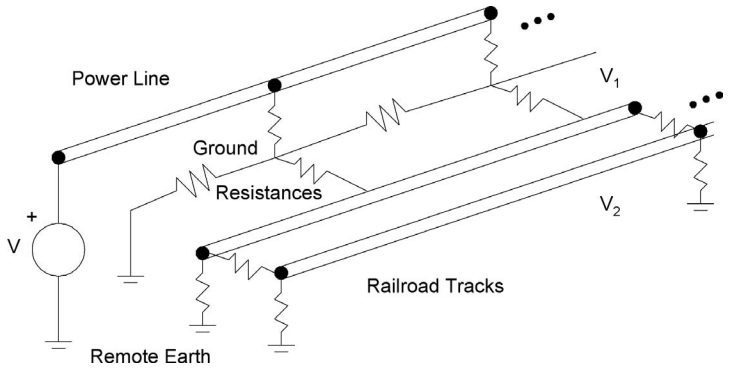


Figure 12.2-4 Conductive (resistive) coupling mechanism. Voltages V_1 and V_2 are the conductively coupled voltages on each of the two tracks.

The common-mode voltage (V_c) and current (I_c) are defined respectively as

$$V_c = \frac{V_1 + V_2}{2} \quad , \quad I_c = \frac{I_1 + I_2}{2}. \qquad 12.2\text{-}1$$

These represent the average voltage (with respect to remote earth) and current on the two rails. The former is relevant to issues relating to worker safety and equipment damage since voltages with respect to earth are the ones to which workers standing on the ground and equipment are exposed. The general rule is that these should not exceed 50 V rms rail to ground.

The differential-mode voltage (V_d) and current (I_d) are defined respectively as

$$V_d = \frac{V_1 - V_2}{2} \quad , \quad I_d = \frac{I_1 - I_2}{2}. \qquad 12.2\text{-}2$$

These voltages are generally the more significant sources of interference to railroad signals. They are of concern for abnormal operation of railroad systems if greater than equipment immunity. The American Railway Engineering and Maintenance of Way Association (AREMA) manual recommends 5 V or 10 V of ac rms immunity, depending on type of equipment. Grade-crossing equipment is particularly susceptible.

12.2.7 Coupling between Common and Differential Modes

Whenever there is an unbalance in the system (e.g., different resistances between each rail and the earth) common-mode currents can be converted into differential-mode currents. This is important because often the dominant currents induced magnetically are the common-mode currents that are induced in the rails and that return through the earth. While these currents (and associated voltages) do not interfere with most signaling systems, the differential-mode currents caused by system unbalances do.

12.2.8 Overview of Railroad Signaling

The most common types of railroad-signaling equipment usually fall into one (or more) of the following categories of systems designed to:

- Detect the presence of a train within an area defined by a track circuit "transmitter" and a track circuit "receiver."
- Communicate information (such as a train's location) along a railroad line (e.g., coded track circuits, wire-line circuits, radio communications).
- Measure a train's position or motion with respect to a fixed point (e.g., motion sensors, crossing predictors).
- Detect specific hazards to railroad operations (e.g., slide fences, dragging equipment detectors, etc.).
- Provide safety-critical information to trains or motorists (e.g., wayside signals, cab signals, crossing flashers, crossing gates, bells).
- Physically reconfigure the railroad tracks to construct a particular route of travel for a train (e.g., switch machines, switch heaters, switch locks, etc.).

Although most types of equipment listed above can suffer from interference due to nearby ac power transmission and distribution systems, the first indication of an ac interference problem will usually come from the motion sensors and crossing predictors used to control the warning devices at grade crossings. Since they are often the most sensitive detectors of unwanted ac electrical energy on railroad tracks, particular attention should be paid to these systems.

12.2.9 Abnormal Operation of Railroad Equipment

Railroad equipment is designed to fail in such a way that safety is maintained. So, if the track signals detect a problem, they slow or stop the trains. If the highway-crossing gate system detects an inappropriate input, it lowers the gates. The idea is that it is better to stop people and freight than to risk a collision. These "safe" failures are sometimes called "right-side" failures. The opposite would be "wrong-side" failures. These are simply unacceptable.

As mentioned earlier, the most common abnormal operations resulting from ac interference are false activation of highway-grade-crossing train detection equipment (the gates are down with no train). Another common problem is dropout of the locomotive cab signaling system that displays wayside signals inside the cab. Because these cab systems utilize inductive coupling from the track, operate at audio frequencies near power frequencies, and use very low power levels, they are more susceptible to ac interference than other systems.

12.2.10 Damage to Railroad Equipment

When damage is caused by transmission-line operation, it is usually due to surges from faults or switching operations. Steady-state ac interference does not often cause damage because railroad signal equipment is designed to withstand ac voltage levels well above those considered hazardous to personnel (50 V rms steady-state). Since steady-state interference levels are usually maintained below this level for safety, steady-state interference rarely causes damage.

Track surge protective devices (SPDs or arresters) used on railroad equipment are designed to withstand lightning. SPDs used on track circuits are designed to fail open (not

shorted). They fail when the energy flowing through them exceeds their i^2t capacity (i = current in amperes, t = time in seconds). While the current through an arrester will be an order of magnitude higher for lightning than for a power line fault, the duration of the current can be three to five orders of magnitude greater for the power line fault. Thus, the energy coupled by a power line fault can be much greater than from a lightning strike. The result is that the arrester is often destroyed, leaving the rest of the undamaged equipment vulnerable to lightning.

12.2.11 Personnel Safety Considerations (Steady-State Operation)

Ac interference sometimes can be large enough to have an effect on a person on the ground touching the railroad system. If the voltage levels are high enough, a shock hazard might exist. Where voltage is induced in railroad facilities by electric-field induction, the steady-state short-circuit current to ground should not exceed 5 mA ac rms. More specific information on this topic can be found in Section 12.3.6. A minimum criterion for steady-state voltage induced on railroad facilities by magnetic field induction would be to limit the voltage to a maximum of 50 V ac rms point-to-point (within reach) under worst case conditions.

Although it is highly unlikely that a spark could cause ignition (Deno and Silva 1985), care should also be taken when fueling machinery with gasoline under high-voltage lines. As a general rule, if fuel is to be transferred under high-voltage power lines, the fuel container should be electrically bonded to the equipment being fueled prior to and during fueling. Any fumes should be allowed to dissipate before removing the bond. Additional information on this subject can be found in Section 7.14.

Another aspect of personnel safety is exposure to electric and magnetic fields. More information on this subject can be found in Chapter 7.

12.2.12 Personnel Safety Considerations (Fault Conditions)

Computer modeling can be used to predict fault-current induction into railroad systems. For these calculations, the worst-case fault should be modeled. To this end, various fault locations should be used to identify the maximum exposure voltage, and more specifically, the closest phase conductor to the track under elevated temperature final sag conditions should be faulted if this conductor also carries the largest possible fault current.

Experience shows that the voltage induced in communication/signal circuits from power line faults may be tolerated if the rms value of the induced voltage does not exceed: 430 V rms for typical power line equipment and maintenance or 650 V rms for high reliability power lines with high-speed relaying and fault clearing (AAR/EEI 1977). In any case, it is reasonable to evaluate the situations using either the IEC (1987) or IEEE (2000) method (or both) to ensure adequate safety and to ensure mitigation is not unnecessarily expensive. More detail on how this should be done can be found in Section 12.3.6.

12.2.13 "Rules of Thumb" of Railroad Signals and AC Interference

In summary, evaluation of ac interference with railroad systems can be summarized by several basic tenets: (EPRI 2004)

- 90% of problems are related to induction on the track.
- Motion sensors and crossing predictors are the most sensitive devices connected to the track, and will usually be the first indicators or victims of ac interference.
- Railroad signal circuits respond to the voltage between the two rails (differential mode).
- Anything that unbalances the electrical characteristics of one rail with respect to the other can act as a catalyst in turning induced common-mode voltage into differential or "rail-to-rail" voltage.
- Many cases thought to be related to "induction" turn out to be related to "conduction."
- Just because there is some ac interference on the track, does not mean that this is the cause of the problem.
- Many railroad signal circuits are frequency-selective, but enough of even a non-adjacent frequency can cause operational problems.
- Transmission lines may look big, but ordinary distribution lines are often the source of ac interference.

Changes to power line alignment that tend to decrease ac interference levels include:

- Increasing the horizontal or vertical distance between the track and power lines.
- Phasing multiple circuits for minimum magnetic field levels at rails.
- Decreasing the length of the parallel exposure.
- Decreasing the spacing between phase wires.
- Adding a second circuit to a single-circuit corridor, and optimizing the phase arrangement for minimum magnetic field levels from both circuits.

Changes to equipment that tend to decrease ac interference levels include:

- Decreasing the current-carrying capacity of the lines (derating).

- Installing fault-current-limiting devices.

More detail about mitigation options can be found in the *Power System and Railroad Electromagnetic Compatibility Handbook* (EPRI 2004).

12.3 INTERFERENCE WITH THE OPERATION OF PIPELINES

12.3.1 Background

Like the railroads discussed in the previous section, oil, gas, and other pipelines are long parallel transportation systems that commonly share a corridor with electric transmission lines. The long conductive pipelines are subject to the same types of electromagnetic interference (EMI) from power lines as railroad tracks. EMI-induced currents and voltages on pipelines can degrade the pipeline coating and the pipe itself, disrupt the cathodic protection and other pipeline operating systems, and generate shock hazards for pipeline workers and the public. There is also a risk of gas ignition due to induced currents and voltages.

Concerns related to EMI impacts on pipelines have increased over the last decades. Competition for land and constraints on land use have encouraged the joint use of corridors by pipelines and electric transmission lines. In addition, improved pipeline coatings have reduced the number of defects (holidays) in the coatings where leakage to ground can occur (Bonds 1999; Shwehdi and Johar 2003). The lack of holidays increases the resistance of pipelines to ground and results in higher induced voltages.

Pipelines are subject to three types of coupling to the power line electric and magnetic fields: electric-field or capacitive coupling, magnetic-field or inductive coupling, and ohmic or conductive coupling through the earth. These three mechanisms are discussed in Sections 12.2.3, 12.2.4, and 12.2.5, respectively. Capacitive coupling to pipelines is only of concern when the pipe is above ground and ungrounded. It can be analyzed with straightforward methods commonly used for coupling to objects under transmission lines, as described in Section 7.8. Burial of pipelines complicates the nature of inductive coupling relative to that for a conductor in air. A pipeline buried in soil must be considered as a conductor in a lossy medium, where leakage of the induced currents to earth occurs continuously along the length of the pipeline. This presents a more difficult analysis problem than induction between power lines and railroad tracks, as was discussed in Section 12.2, since buried pipelines may be much lossier than railroad tracks. Burial of pipelines also introduces the possibility of conductive coupling through the earth during fault conditions, as was also discussed for railroad tracks.

Early prediction methods for induced currents on buried pipelines often relied on induction calculations for conductors in air. This approach overestimated induced voltages by up to a factor of 10 when compared with measured values (Taflove and Dabkowski, 1979). A more sophisticated and accurate prediction method for EMI from power lines to pipelines was developed during a comprehensive study of overhead ac transmission lines and pipelines sponsored jointly by the Electric Power Research Institute and the American Gas Association (EPRI/AGA) in the 1970s (EPRI 1978a; EPRI 1978b; Taflove and Dabkowski 1979; Dabkowski and Taflove 1979a; Taflove et al. 1979; Dabkowski and Taflove 1979b). The method developed in this study considers the pipeline as a lossy electrical transmission line in a conducting earth. An equivalent circuit for the pipeline is derived given the electrical characteristics and physical locations of the transmission line(s), pipeline(s), and the earth. The method predicts induced currents and voltages on pipelines in transmission corridors during steady-state conditions. This methodology produced results that compared favorably with measurements (Dabkowski and Taflove 1979a). This project also developed computational methods for predicting induced voltages and currents and mitigation strategies for reducing induced voltages on pipelines (Taflove et al. 1979; Dabkowski and Taflove 1979b; CEA 1979).

Two subsequent joint EPRI/AGA project in the 1980s also developed computation methods for interference from power lines to gas pipelines (EPRI 1983a; EPRI 1987; Dawalibi and Southey 1989; Dawalibi and Southey 1990). Besides addressing steady-state conditions, these subsequent projects emphasized inductive and conductive coupling during fault conditions.

12.3.2 Electric-Field Induction

Required Conditions

Electric-field induction is of concern whenever long sections of pipe are located above the ground without adequate grounding. This condition is of special concern for above-ground pipe storage that can occur during construction. In this case, electric fields from the overhead conductors can result in potentially hazardous voltages or currents on the pipe. Once a contiguous portion of the pipe is buried, an effective ground for mitigating electric-field coupling is established through the resistive pipe coating. However, such a ground may not reduce the potential for magnetic-field-induced voltages.

Predictive Methods

The nature of electric fields under transmission lines and the electric-field coupling to objects under transmission lines were discussed in Section 7.8, and a graphic that illustrates electric-field coupling is given in Figure 12.2-2.

The open-circuit voltage, V_{oc}, and induced short-circuit current, I_{sc}, to a pipe of length L, radius r, and height h above the ground in a uniform vertical electric field E is given by (EPRI 1982, p. 349; EPRI 1978a, p. 4-6):

$$V_{oc} \approx Eh \qquad 12.3\text{-}1$$

and

$$I_{sc} = j\omega EhL(2\pi\varepsilon_0 / (\ln(2h/r)) \qquad 12.3\text{-}2$$

If the pipe is located parallel to the line, the electric field varies somewhat as the conductor height changes along the line. In this case, the average field along the pipe length represents the equivalent uniform vertical field. However, if the pipe is perpendicular to, or at an angle to, the transmission line, then the magnitude and phase of the field have to be taken into account to develop an equivalent vertical field for the purpose of estimating induced voltage and short-circuit current (Reilly 1979).

From Equation 12.3-2, it is apparent that the magnitude of the potential current shock from the ungrounded pipe is directly dependent on the length of the pipe and on the electric field, and also dependent on the height and radius of the pipe.

Mitigation

Mitigation to avoid discharges and steady-state currents to workers from electric-field-induced voltages on above-ground pipelines can be accomplished by moving the pipe away from the power line or by installing a separate grounding system for the pipe when it is near the transmission line. The use of independent grounds is also used to mitigate for nuisance shocks from conducting objects found on or near rights-of-way, such as fences, large metal buildings, and large vehicles.

Grounding systems should be placed away from towers to mitigate the possibility of a transferred potential (conductive coupling) to the pipe during a fault at the tower. To achieve this, the recommended location for grounds is midway between towers and as far from the transmission line as possible (EPRI 1978a, p. 8-2). Redundant grounds at each location minimize problems due to failed grounds.

The short-circuit current to earth from the pipe, I_{sc}, follows parallel current paths through the worker with impedance of Z_w and through the grounding system with impedance to remote earth of Z_g. The impedance of the grounding system to remote earth that is required to limit the current to the worker, $I_{w,}$ to a given value can be determined from (Dabkowski and Taflove 1978a, p. 8-6).

$$Z_g = Z_w[I_w / (I_{sc} - I_w)] \qquad 12.3\text{-}3$$

If the limit on current through the worker is taken as the 3 mA limit for grasped contacts in IEEE Standard C95.6-2002 (IEEE 2002a, p. 15), then the maximum ground system impedance is given by

$$Z_g \leq 4500 / I_{sc} \qquad 12.3\text{-}4$$

where I_{sc} is in mA, I_{sc} is assumed to be much greater than I_w, and the worker impedance is taken as 1500 Ω, the wet skin impedance (EPRI 1978a, p. 8-6). The maximum short-circuit current for a pipe, I_{sc}, can be calculated from Equation 12.3-2.

For long pipes, single-point grounds to eliminate hazards from electric-field-induced voltage may exacerbate problems associated with magnetic-field-induced voltages on the pipe. With a single-point ground, magnetic-field induction may generate a voltage on the pipe between the ground and the worker. The worker standing on remote earth may then experience a shock when touching the pipe. This can be alleviated somewhat by the introduction of multiple grounds along the above-ground pipe with low-impedance grounds at each end to reduce magnetic-field-induced voltages. All grounds should be far removed from towers where the possibility of conductive coupling during faults exists.

Hazards to personnel from all types of coupled voltages and currents can be mitigated by the use of ground mats in work areas. These are conducting wire grids that are bonded to the pipe and extending away from the work area. The ground mat provides an equipotential area that is essentially at the same voltage as the pipe. This precaution eliminates the possibility of the worker being at remote earth potential when he/she touches the pipe. Safety procedures with respect to the installation and use of ground mats are described in the NACE Standard Recommended Practice for Mitigation of Alternating Current and Lightning Effects on Metallic Structures and Corrosion Control Systems (NACE 2000).

12.3.3 Magnetic-Field Induction

Required Conditions

Magnetic-field induction occurs on above-ground and buried pipeline segments that are adjacent to overhead transmission lines. A graphic that illustrates this process is given in Figure 12.2-3. The magnitude of the induced voltage will depend on the length of the segment and the grounding characteristics. The previously mentioned EPRI/AGA studies provided a comprehensive examination of prediction, mitigation, and design methodologies for induced voltages on gas transmission pipelines, The first study emphasized steady-state conditions (EPRI 1978a; EPRI 1978b). Subsequent studies investigated induction

and conduction to pipelines during both steady-state and fault conditions (EPRI 1983a; Dawalibi and Southey 1989; Dawalibi and Southey 1990).

The principal concerns related to steady-state magnetic-field-coupled voltages on pipelines are physical damage to coating and hazards to personnel or the public who might contact the pipeline. Other concerns are interference with the operation of electronic equipment ancillary to pipeline operation such as cathodic protection, communications, and monitoring systems, and corrosion of the pipeline. The larger voltages and currents conducted to the pipeline during fault conditions raise the additional concern of damage to the pipeline itself.

Concern for induced voltages on pipelines is not limited to those parallel to transmission lines. Jaffa and Stewart (1981) report that objectionable voltage levels can be induced on long buried irrigation pipelines by parallel distribution lines.

For buried pipelines, the largest induced voltages occur where there is a physical change or discontinuity in the pipeline. The physical change results in a change in the impedance or the driving electric field along the pipeline. Such locations include a bend in the pipe, a cathodic protection system, an insulated joint, or where the transmission line veers away from the pipeline.

Predictive Methods

The original EPRI/AGA study of induction on buried pipelines developed computational methods for determining induced steady-state voltages on pipelines in shared corridors with ac transmission lines (Taflove and Dabkowski 1979; Dabkowski and Taflove 1979a). In this approach, the pipeline is treated as a lossy electrical transmission line with impedance per unit length of Z and admittance per unit length of Y. The line is described by a characteristic impedance $Z_o = (Z/Y)^{1/2}$ and propagation constant $\gamma = (ZY)^{1/2}$. The lossy transmission line is subject to a distributed voltage source along its length, corresponding to the longitudinal electric field of the transmission line that is parallel to the pipeline. The longitudinal field is a function of the currents and geometries of the parallel power lines and other conductors in the corridor.

The differential equations describing this electrical model of a pipeline are identical to the classical transmission-line equations, plus a term for the distributed source (Taflove and Dabkowski 1979). Solution of these equations leads to an expression for the voltage as a function of distance along the pipeline. Another important result is that the voltage at a termination of the pipeline can be modeled as a Thevinen equivalent circuit.

The Thevinen equivalent voltage for the pipeline is dependent on the longitudinal electric field, the pipeline length, characteristic impedance and propagation constant, and the impedance at the other termination. The Thevinen source impedance is dependent on the pipeline length, characteristic impedance and propagation constant, and the impedance at the other termination. Sections of the pipeline with constant or variable longitudinal electric field can be modeled as Thevinen equivalent circuits.

With the Thevinen equivalent approach, methodologies were developed for electrically short ($L < 0.1/|\gamma|$) and electrically long ($L > 2$ Real(γ)) pipelines, for parallel and nonparallel pipelines, and for long pipelines terminating outside the corridor. Nonparallel pipelines and those terminating outside the corridor are characterized by a nonconstant driving electric field.

The common Thevinen equivalent circuit approach allows analysis of pipelines comprised of segments with different source terms. This capability is essential to analyze realistic scenarios where changes in the source term are introduced by, among others, pipe joints, grounds, cathodic protection systems, and transmission-line transpositions, as well as discontinuities in separation distance, pipeline coatings, and earth conductivity. The Thevinen voltages at the junctions between segments with dissimilar sources can be combined to estimate the induced voltages for the entire pipeline.

The prediction method for steady-state induced voltages requires computation of the longitudinal electric field, pipeline characteristics, and Thevinen circuits. These are determined by the physical and electrical characteristics of the transmission line, pipeline, other conductors, and earth. A series of calculations were developed to provide: the unknown currents in earth return circuits; the mutual impedances between adjacent, parallel earth return conductors; the pipeline propagation constant and characteristic impedance; and the Thevinen source voltage and source impedance.

These calculations were originally implemented in programs for a vintage handheld programmable calculator (TI-59) (EPRI 1978b; EPRI 1985). The programs are included in the reports and could be implemented on a modern PC or other platform.

Comparisons of the predicted induced voltages on pipelines in existing shared corridors agreed with measured values within about 10% (Dabkowski and Taflove 1979a). Both the predictions and the measurements exhibited local peaks in the induced voltage at electrical discontinuities in the pipelines.

As an example, the geometry and predicted and measured induced voltages for a pipeline parallel to a transmission line in the Mojave Desert are shown in Figures 12.3-1 and 12.3-2. The discontinuities are described in Table 12.3-1.

Additional computational methods to accurately simulate complex realistic right-of-way problems were developed in the second EPRI/AGA study (EPRI 1987; Dawalibi and Southey 1989; Dawalibi and Southey 1990). Electric- and magnetic–field induction and conductive coupling for steady-state and fault conditions are examined with an emphasis on the latter condition. The computer program that combines these methods predicts inductive and conductive coupling between power lines and arbitrarily positioned above-ground and buried pipelines. Both long and short conductor segments can be included, with the short segments often representing the grounding configuration of the towers or the pipeline. The grounding configuration is important for analyzing inductive and conductive coupling during fault conditions. The calculations also allow for inclusion of underground bare conductors, which can have different propagation characteristics than better insulated coated conductors.

For this approach to inductive coupling, short and long conductors are treated separately, at least initially. Ultimately, the different conductors are combined into a circuit model based on their voltage, ground impedance, and self and mutual impedances. Impedance to earth for grounding networks (short conductors) is determined with a field theory approach (Dawalibi and Southey 1989). The

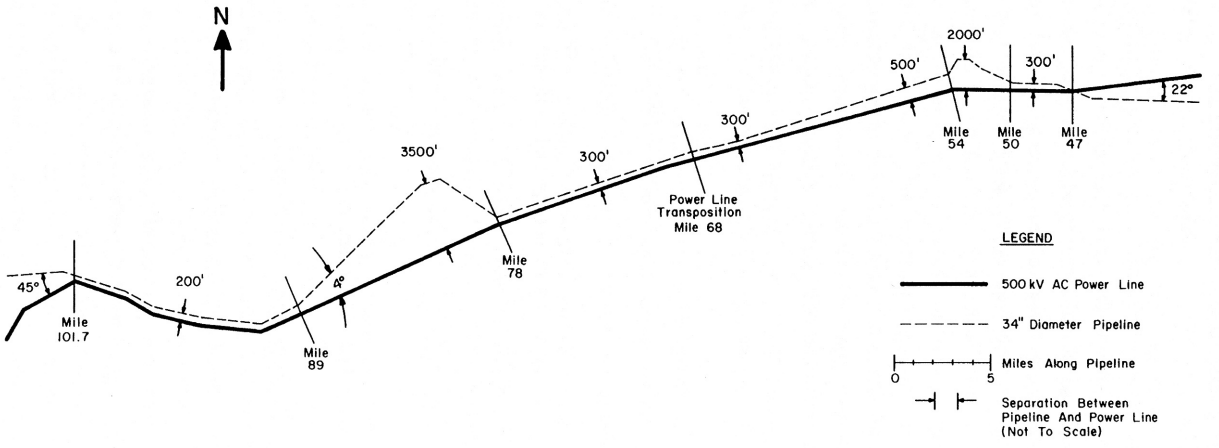


Figure 12.3-1 Mojave Desert pipeline-power line geometry. (EPRI 1978b)

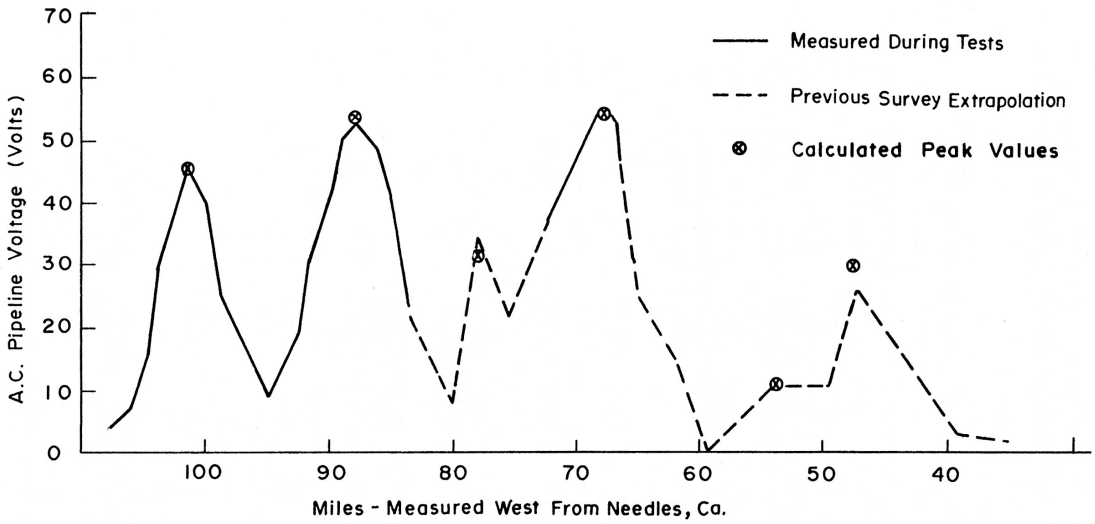


Figure 12.3-2 Mojave Desert pipeline voltage profile. (EPRI 1978b)

Table 12.3-1 Induced Voltage Peaks at Discontinuities along the Mojave Desert Pipeline (Dabkowski and Taflove 1979a)

Mile-post	Discontinuity	Predicted Voltage (V)	Measured Voltage (V)
101.7	Pipeline approaches power line	46.3	46
89	Change in separation from power line	54.0	53
78	Change in separation from power line	31.1	34
68	Power line phase transposition	54.8	51
54	Change in separation from power line	11.4	11
47	Pipeline departs power line	31.2	25

impedance-to–earth, per unit length of long buried conductors, is obtained from a similar approach. The self and mutual impedances for long conductors are obtained from expressions for conductors in air or equations for lossy underground conductors that have been developed over many years and are often used in analysis of transmission lines (Dawalibi and Southey, 1989, pp. 1842-1843).

The circuit model includes the voltages and impedances for all phase wires, overhead ground wires, pipelines, mitigation wires buried near pipelines, and tower grounds. The ground impedances for towers and other structures are also incorporated. Solution of the circuit model by the double-sided elimination method yields the magnetically induced voltages and currents in the pipeline and any mitigation wires (Dawalibi and Southey, 1989, p. 1845).

To incorporate conductive coupling into the model, computations are made of voltages and currents on the long conductors, due to known currents injected into the earth by the grounding systems. The results of computations for conductive effects are combined with those for inductive effects to produce the final prediction of pipeline voltages and currents due to steady-state or fault conditions on a nearby transmission line.

Predictions for coupled voltages and currents by the program were in agreement with measurements in previous tests under both steady-state and fault conditions. The program was also used to investigate the influence of various parameters on inductive and conductive coupling (Dawalibi and Southey 1990).

Mitigation

The parametric analysis of Dawalibi and Southey (1990) considered inductive and conductive coupling separately and suggested approaches to mitigation. For inductive coupling, separation between power line and pipeline is obviously an important factor: increased separation decreases coupling strength. The length of the pipeline is also important until the length exceeds the characteristic length of the pipeline (the inverse of the propagation constant), at which point, the induced voltage remains constant. This observation would suggest segmenting the pipeline into shorter sections with insulating junctions. However, the junctions can introduce higher cathodic protection costs and result in large voltage differences across the junctions during faults.

Grounding of the pipeline reduces the induced voltage and can be an effective mitigation tool at electrical discontinuities in the pipeline where peak-induced voltages occur. Mitigation wires that are parallel to, and near, the pipeline but are not bonded to the pipeline reduce the induced voltage on the pipeline. In this case, several smaller conductors are more effective than one large conductor.

NACE Standard RP0177-2000 describes design considerations for numerous protective devices to mitigate the effects of all types of ac coupling to metallic structures including pipelines (NACE 2000, pp. 4-10). Protection should be considered for locations that are restricted to workers and to those that are accessible to the general public. The protective devices include:

- *Electrical shields.* Mitigation wires or shields can be installed in the earth between the ac power systems and the pipeline. They can be a long, buried bare conductor or a group of electrodes surrounding a pipeline. Shields are intended to reduce the pipeline to earth potential and thus reduce the possibility of damage to the coating or to the pipe.
- *Grounding mats.* Grounding mats bonded to a structure may be placed at locations where persons may be in contact with hazardous step-and-touch potentials. For pipelines, these locations include areas near valves, metallic vents, cathodic protection test stations, and other components of a pipeline that protrude above ground, where contact can be made by a worker or the public. Ground mats should be large enough to ensure reduction of the step-and-touch potentials to acceptable levels for contact with the structure.
- *Isolating joints.* These joints divide the pipeline into shorter electrical segments or isolate a section in proximity to a power system from the remainder of the pipeline. Devices such as lightning arresters, polarization cells, or electrolytic grounding cells should be installed across the joints to protect them from breakdown under high-voltage conditions. These same devices can be installed between affected structures and grounds to reduce induced voltages during normal operation and surge conditions and to reduce the possibility of structure puncture.

- *Anodes and grounding cells.* Distributed anodes and/or electrolytic grounding cells used to prevent corrosion can be incorporated as part of a grounding system.

The NACE Standard recommends that during construction temporary electrical grounds be placed at intervals not to exceed 300 m (1000 ft) on long conducting structures such as pipelines (NACE 2000, p. 12). Bonding of temporary or permanent grounds to the existing structures of a power system is strongly discouraged because of the increased hazards during fault conditions.

12.3.4 Conductive Coupling

Required Conditions

During faults to ground, the earth is a conductive path for fault current to remote earth. A graphic that illustrates this phenomenon is given in Figure 12.2-4. This current results in a localized potential rise relative to remote earth at the faulted structure. The current and potential rise can couple into an adjacent pipeline and cause physical damage to the pipeline and create voltages hazardous to personnel. Although pipes are generally coated, the fault-generated potential difference between the soil and the metal pipe can puncture the coating and even damage the pipe itself. The ground potential rise near a faulted tower can increase the step-and-touch potentials near the structure as well as near a pipeline. Any associated voltage rise on a pipeline can be transferred to locations remote from the fault, and represent a hazard on pipeline components that are accessible to persons in contact with the earth.

An unbalanced distribution system with a grounded neutral can also be a source of earth currents. However, the magnitude of these currents is generally orders of magnitude smaller and does not give rise to the large potential differences between pipe and soil or to hazardous step-and-touch potentials. However, ground faults or lightning strikes to a distribution system can result in the same hazards experienced under fault conditions near a transmission line.

Predictive Methods

Conductive coupling requires that current be injected into the earth near a pipeline or other buried structure. The current is injected through the tower footings and any counterpoise that is present. The grounding systems for towers and pipelines are generally comprised of short conductors for which the assumptions used in computing impedances of long conductors are not valid. As noted earlier in this section, Dawalibi and Southey (1989) describe a hybrid method for determining potentials and currents in the earth and on pipelines for a system with both short and long conductors present.

First, the circuit model is solved for the inductively coupled currents and voltages. Then the known fault currents injected into the earth through the grounding systems are incorporated. With field theory and the known injected currents, the user can then determine the potentials near the ground systems and the potentials and currents in the long conductors. The potentials and currents in the long conductors computed in this manner are the result of conductive coupling. The conductive and inductive coupling results are then added together (with care taken to correctly combine currents with different phases) to produce the total interference level.

Mitigation

For conductive coupling, separation between the tower ground and the pipeline is obviously an important factor in reducing coupled voltages during faults. The parametric analysis of Dawalibi and Southey (1990) examined other factors that can affect conductive coupling. The tower ground impedance affects coupled voltages: lower tower impedance results in lower potential rise near the tower during faults and thus lower soil potentials near the pipeline. The tower impedance depends directly on the soil resistivity and the size and extent of the structure ground. Long mitigation wires situated between the pipeline and the tower perturb the potential distribution during a fault and reduce conductive coupling effects.

12.3.5 Damage to Pipelines

Induced voltages on pipelines are generally less than 50 V under steady-state conditions and less than 500 V during fault conditions (EPRI 1978a, p. 7-26). Consequently, most damage to pipelines from induction phenomena occurs during faults.

However, the relatively low voltages induced under steady-state conditions can damage the pipeline through various mechanisms (EPRI 1978a, p. 7-26). They can reduce the lifetime of cathodic protection rectifiers. They can cause current flow through unintended conducting bridges across insulating joints. This current flow can eventually heat up and damage the joint. Induced ac currents can interfere with data signals when the pipe is part of the communication system for the facility.

Under high-current conditions, due to either a power line fault to ground or a lightning strike to the power system, the fault current into the ground can cause a rise in soil-to-pipe potential. If this potential difference is of sufficient magnitude, it may break down the protective coating around the pipeline or, in extreme cases (5000 V), puncture a hole in the pipe itself. In this latter instance, there is a risk of ignition of leaking gas. A rise in the voltage on a pipeline can also damage isolating fittings between pipeline sections, bonding connections, lightning arresters, and

cathodic protection systems. Large fault currents can also cause glow or arc discharges at coating punctures or in the earth. The discharges can have sufficient energy to damage coaxial cables or ignite gas vapors (EPRI 1978a, p. 7-28).

The communications networks associated with pipelines generally employ newer wireless and fiber optic technologies that are immune to EMI from transmission-line sources (Association of Oil Pipe Lines 2004). Telephone land lines are also used but do not necessarily follow the pipeline and any parallel transmission lines. Thus, induced voltages and currents on pipelines could damage individual communications components located on the pipeline but not interfere with communications per se.

Corrosion of steel due to 60-Hz currents to buried structures is estimated to be about 0.01 to 0.1% of that for a dc current of comparable magnitude (EPRI 1978a, p. 7-8). Cathodic protection systems tend to mitigate the effects of ac corrosion. Consequently ac corrosion is generally not a problem with pipelines buried near transmission systems.

However, coupled currents and voltage can affect cathodic protection system components, such as rectifiers. In areas with known potential for interference or with observed rectifier failures, testing of cathodic protection systems should take place more frequently with safety precautions implemented to protect workers (NACE 2000, pp. 15-16).

12.3.6 Personnel Safety

Steady State

Personnel working on pipelines can be exposed to hazardous ac voltages due to coupling from adjacent power systems. The NACE Standard *Recommended Practice for Mitigation of Alternating Current and Lightning Effects on Metallic Structures and Corrosion Control Systems* cites 15 V (rms) as a level of anticipated shock hazard. This value is selected to limit currents to 10 mA through an assumed hand-to-hand or hand-to-foot resistance of 1500 Ω for an adult male (NACE 2000, pp. i and 11).

The IEEE standard for exposure to electromagnetic fields, 0–3 kHz, sets a lower limit of 3 mA for the maximum permissible exposure (MPE) for a grasp contact in controlled (occupational) environments (IEEE 2002a, p. 15). The IEEE MPE for a touch contact is 1.5 mA in controlled environments and 0.5 mA for the general public. The lower limits for the IEEE standard reflect the choice of "discomfort" as the criterion for the limit. The NACE standard is based on the maximum safe let-go current for adult males.

When the voltage level on a pipeline (or other structure) exceeds the hazardous level, NACE (2000) calls for reduction of the voltage to safe levels or implementation of other measures to prevent shocks to pipeline workers or the general public. These measures include temporary grounding of pipelines during construction, installing ground mats at work locations, and restricting public access to possible contact points.

Fault Conditions

The following discussion of hazardous voltage levels during faults is drawn from the *IEEE Guide for Safety in AC Substation Grounding* (IEEE 2000). Although this guide applies to substation grounding, it can also be used to analyze hazardous conditions near pipelines.

The response of individuals to short-duration current shocks is dependent on the magnitude and duration of the shock current passing through the body. To estimate tolerable voltage levels for short-duration, rarely-occurring shock scenarios, the IEEE guide uses, as an allowable current level, the current at which 99.5 % of persons do not experience ventricular fibrillation. Empirical findings indicate that this current level is dependent on duration of the shock and body weight, as follows:

$$I_B = k / \sqrt{t_s} \qquad 12.3\text{-}5$$

Where:

I_B is the current through the body in amperes.
k is a constant dependent on body weight (k = 0.116 for 50 kg, and k = 0.157 for 70 kg).
t_s is the shock duration in seconds.

The tolerable voltage is determined by the allowable current and the combined resistance of the body and the foot contacts. The tolerable voltage for step potentials is given by:

$$V_{step} = I_B (R_B + 2R_f) \qquad 12.3\text{-}6$$

Where:

V_{step} is the voltage between the feet at a 1-m separation.
R_B is the body resistance.
R_f is the contact resistance of one foot.

The tolerable voltage for touch potentials, V_{touch}, is:

$$V_{touch} = I_B (R_B + R_f / 2). \qquad 12.3\text{-}7$$

The IEEE guide (2000) assumes a body resistance of 1000 Ω and a foot resistance standing on homogeneous soil of:

$$R_f = \rho / 4b \qquad 12.3\text{-}8$$

Where:

ρ is the soil resistivity.
b is the radius of a metal disk equivalent to the foot contact, assumed to be 0.08 m.

If there is a layer of more insulating material spread over the soil, such as gravel in a substation, then the foot resistance is given by:

$$R_f = \rho_s C_s / 4b \qquad 12.3\text{-}9$$

Where:

ρ_s is the resistivity of the surface layer.

C_s is the surface layer derating factor that accounts for the finite thickness of the top layer.

The derating factor can be computed from models, determined from graphs, or determined from an empirical formula (IEEE 2000, pp. 22-23). For a homogeneous, single-layer earth, $C_s = 1$ and $\rho_s = \rho$.

Combining Equations 12.3-5, 12.3-6, and 12.3-9, and using a 1000 Ω body resistance, yield the following limit for maximum allowable step potential:

$$V_{step} = \left(1000 + 6\rho_s C_s\right) k / \sqrt{t_s} \qquad 12.3\text{-}10$$

Similarly, for the maximum allowable touch potentials, combining Equations 12.3-5, 12.3-7, and 12.3-9 yields:

$$V_{touch} = \left(1000 + 1.5\rho_s C_s\right) k / \sqrt{t_s} \qquad 12.3\text{-}11$$

Actual step or touch potentials should be less than these values to ensure safety of personnel during fault currents.

12.4 INTERFERENCE WITH THE OPERATION OF POWER LINE COMMUNICATION SYSTEMS

12.4.1 Power Line Carrier

For many years, power line carrier (PLC) systems have used power lines as a communications medium at frequencies between 40 and 490 kHz. Most of these systems have been used for utility applications such as relaying, automatic meter reading, load control, and distribution automation (ANSI/IEEE 1980; Tengdin 1987; Diamanti 1996; 1999; Hagamann 1989). The systems are economical (especially in mountainous areas where microwave systems are not easy to construct and operate successfully) and reliable, and can be used over long distances. Generally, however, they operate only at very slow speeds.

The primary compatibility concern about PLC systems is that they must satisfy limits on the amplitude of electromagnetic fields associated with them. In the United States, these regulations are written in Part 15 of the Federal Communications Commission regulations (FCC 1998). More specifically, according to Sections 15.109 and 15.209 of these regulations, the measured electric field strength using a CISPR quasi-peak receiver (ANSI 2000) at 300 m from the power line must not exceed 2400/f(kHz) μV/m, where f(kHz) is the operating frequency of the PLC system in kHz. Calculations of the electromagnetic fields associated with PLC can be easily made (Madge and Hatanaka 1992; Sarto 1998).

Over the years, PLC systems have caused interference to the operation of LORAN-C navigation systems that operate at 100 kHz (Arnstein 1986; Last and Bian 1993). This issue has declined in importance recently as the use of LORAN-C has decreased. Another concern has been raised is the potential for interference with receivers using the Nationwide Differential Global Positioning System (NDGPS) network. But this potential has been shown to be small and can be resolved easily by frequency separation if it becomes a problem (Silva and Whitney 2002).

Because PLC systems are often used for communicating information to relays, it is essential that they operate properly at all times. One issue is that the normal background noise from transmission-line corona and switching devices (e.g., FACTS facilities) should not degrade the PLC performance. Although corona has not been reported to cause problems, anecdotal information and measurements suggest that wideband noise from FACTS facilities may interfere with PLC communication (EPRI 2003a). During the occurrence of a fault, there may be additional noise generated by the impulsive voltages and currents associated with the fault. Generally the power of the PLC transmitter is set so that communication is maintained during these faults.

12.4.2 High-Speed Communications

More recently, PLC systems (e.g., in-home networks) have been developed that can operate at relatively high speed. For example, low-cost, short-range systems designed around the wireless RF standard 802.11b (i.e., “homeplug” devices), with 12 Mbps (megabits per second) data rates have been offered recently by several suppliers of networking products (O’Neal 1986; Radford 1996). These systems, however, are found only on secondary distribution systems and are limited in their range to distances comparable to the size of a small neighborhood.

In the last few years, the possibility of using power lines for high-speed Internet access has been seriously discussed (EPRI 2001; Brown 1996; Sanderson 2000a; Sanderson 2000b; Hansen, 2001). Such systems must utilize a broad range of frequencies (i.e., a broad bandwidth), and will be designated here as “broadband power line” (BPL) communication systems. Utilities have expressed interest because they can receive revenue from the sale of services and also have a system that can be used for their own communication needs. BPL systems are an attractive alternative to their wired competition (e.g., digital subscriber lines

[DSL] and cable modem) because: (1) little new infrastructure is needed—the wires go nearly everywhere; (2) utilities own the wires and thus control the communication medium; and (3) the regulatory and licensing strictures on PLC are relatively minimal, providing it does not cause interference.

To date, BPL systems have only been used on low- and medium-voltage power lines. Nevertheless, they are discussed in this book because they can, in principle, be used on higher-voltage transmission lines (e.g., in rural areas).

To realize these systems, it will be necessary to operate them over a long distance (i.e., multiple kilometers), and at high speed (i.e., 10s of megabits per second). Because of this high data rate, the bandwidth required for these systems extends to 10s of megahertz. Such systems have been developed only within the last few years. To be successful, these PLC products must: (1) operate as designed and meet the needs of the intended application; (2) be built, sold, and installed at a price that makes it commercially successful; and (3) satisfy all government regulations on EMC with licensed systems that use the same spectrum.

It is important to note that power lines were not designed to be operated at frequencies in the 10s of megahertz range. As a result, they do not necessarily have the desired characteristics at these frequencies. More specifically, unshielded and unbalanced low-and medium-voltage distribution lines are not primarily designed for communication purposes like DSL. Examples of problems with the power system architecture are: capacitors used for power factor correction, transitions from overhead to underground powerlines, multiple taps, and multiple grounds and transformers (EPRI 2001; Tesche et al. 2003; Tesche 1993). Each of these has a purpose and works well at 50/60 Hz, but causes deterioration in system performance (i.e., results in higher attenuation and/or additional radiation due to unbalanced currents) at 10s of megahertz. In addition, time-dependent loads, as well as EMI filters that block high-frequency signals, present difficulties for evenly distributing radio frequency (RF) energy on secondary distribution systems and within buildings.

Because of this, the most serious technical challenges to BPL systems have been found to be

- attenuation due to junctions such as taps, connected elements such as transformers, and the lack of matched transmitter/receiver impedances; and
- legal limits on electromagnetic emissions from these unlicensed systems.

Together, the first challenge listed above, which causes the attenuation rate for high-frequency signals to be quite high (Tesche et al. 2003), and the second challenge, which limits the input power, result in possibly unacceptable limits on the range of the system.

Recent experience with BPL systems installed on overhead distribution lines with relatively few (i.e., fewer than roughly one per 100 m) devices such as transformers, capacitors, taps, and underground risers suggests typical attenuation rates on the order of 3 dB/100 m. For the same lines, the maximum distance between repeaters is approximately 600 m for a communication rate of at least 10 Mbps. Note that the communication rate available to any one user may be smaller than this since the transmission system is shared by all of its users. Overhead distribution lines with a larger density of attached devices may exhibit similar attenuation rates and maximum distances between repeaters, but there can be no guarantee of this. Underground distribution lines typically exhibit attenuation rates that are three times as high as those for overhead lines. However, this is often compensated for by the substantially lower noise levels on most underground lines, since they do not tend to pick up radio broadcasts.

Experiments on sub-transmission lines (i.e., 69 kV) have shown that repeaters may be spaced as far as 1200 m or more apart for a communication rate of 10 Mbps. It can be inferred from this result that attenuation rates on higher-voltage lines may be even lower. The reason for this is likely related to the smaller number of attachments, and more uniform dimensions, of higher-voltage lines.

It should be emphasized here that one of the more difficult issues for BPL systems to deal with is the noise that is induced on the system from a variety of unconnected RF sources such as commercial radio stations. This occurs because the overhead power lines act as good receiving antennas for these signals. Such noise can be mitigated by the use of systems that adaptively select spectrum that maximizes the data rate for given interference conditions.

Of greatest concern here is the potential for meeting the legal limits on electromagnetic emissions. These vary from country to country and are much more liberal in the United States than other countries (EPRI 2001; Olsen 2002a). In the United States, the FCC is responsible for governing the emission of electromagnetic fields. According to FCC Part 15 regulations, the measured electric-field strength from a BPL system operating in the range 1.705–30 MHz must not exceed 30 μV/m. The measurements are made using a CISPR quasi-peak receiver (ANSI/IEEE 2001) at 30 m from the power line (EPRI 2001). In addition, since BPL systems are unlicensed, they must not cause harmful interference to authorized users of the spectrum. It is this part of the regulation that may be the most

difficult to satisfy since there are numerous users of the spectrum (e.g., amateur radio operators and government users) who are concerned about interference.

In Section 15.3m of the FCC regulations, harmful interference is defined as "any emission, radiation, or induction that endangers the functioning of a radio navigation service or other safety services or seriously degrades, obstructs or repeatedly interrupts a radiocommunications service in accordance with this chapter." The FCC requires that such devices employ good engineering practices to minimize the risk of harmful interference. If harmful interference does occur, the operator of the incidental radiator must take all necessary steps to correct the interference. In the case of power lines, the operator is not responsible for radio frequency noise generated by devices connected to the electric power system (e.g., motors, welding machines, manufacturing plants, etc).

In the early part of 2004, the FCC issued a notice of proposed rulemaking in which they identified BPL as a new technology that could "play an important role in providing additional competition in the offering of broadband services to the American home and consumers, and in bringing Internet and high speed broadband access to rural and underserved areas (FCC 2004)." In this document, the FCC proposed new rules to mitigate harmful interference and new rules to clarify how measurements to determine compliance with Part 15 regulations should be conducted. It remains to be seen how these new regulations will affect the BPL industry.

12.5 INTERFERENCE WITH THE OPERATION OF OPTICAL FIBER COMMUNICATIONS

12.5.1 Introduction

In recent years it has become common for utilities to locate optical-fiber communication systems on their transmission-line towers. The need for internal utility communications (to replace inadequate microwave links) and, for some utilities, the desire for revenue from leased fibers have driven this activity. Of the variety of cable options available (EPRI 1997; Austin et al. 1984), three are most common: the first is optical ground wires (OPGW) in which the fibers are installed at the center of shield wires normally used for lightning protection. The second (WRAP) is an all-dielectric cable that is wrapped around phase conductors on lower-voltage lines or shield wires on higher-voltage lines. The third is all-dielectric self-supporting (ADSS) cable, which is usually attached on a tower below the phase conductors.

This section first compares the advantages and disadvantages of each type. In doing so, several of the criteria that involve electromagnetic compatibility with the power line are noted with a "*". These topics are discussed in more detail later in the section.

12.5.2 Comparison of OPGW, ADSS, and WRAP

OPGW Advantages

- For new installations with ground wires, OPGW requires only that a different type of ground wire be specified.
- For new installations with ground wires, the additional cost of OPGW is minimal.
- OPGW is less susceptible to vandalism than ADSS.
- Operating experience with OPGW has been good (EPRI 2000).

OPGW Disadvantages

- OPGW is difficult, if not impossible, to install while the transmission line is energized.
- It is usually necessary to request extended outages to install or repair OPGW.
- There have been a number of lightning-related failures *.
- It may not be possible to retrofit OPGW on existing towers without ground wires due to loading limits.
- Ground potential rise is a concern for telecommunications terminal equipment*.
- OPGW is more expensive than ADSS for retrofit installations.
- In some cases, OPGW must be removed near substations due to fault current considerations*.
- OPGW in high lightning areas should be inspected periodically for strand breakage.
- For transmission lines that use segmented shield wires, special optical isolators will be needed at towers where shield wire segments are isolated.

WRAP Advantages

- Material cost of WRAP is smaller than ADSS or OPGW.
- WRAP is relatively easy to install and repair on energized circuits, although permission to work on the fiber while the line is energized is not always easily obtained or available.
- It is not necessary to request extended outages to install or repair WRAP, unless installed on energized conductors.

WRAP Disadvantages

- WRAP is more vulnerable to bird damage and vandalism than OPGW.

- WRAP cables can only be installed on conductors that have surface gradients less than approximately 10 kV/cm. On high-voltage transmission lines, this limits their installation to the shield wires since most high-voltage phase conductors have surface gradients that exceed 10 kV/cm.
- Care must be taken not to damage WRAP sheath during installation or re-sagging of conductors.
- Some utilities have experienced problems with loosening of WRAP cable over time.

ADSS Advantages

- Material cost of ADSS for retrofits or new designs without ground wires is smaller than OPGW.
- Fault and lightning protection is not an issue since ADSS is usually located below phase conductors.
- ADSS is much easier to install and repair on energized circuits.
- In some locations, ADSS will not require an extended outage to install or repair.
- It is not necessary to request extended outages to install or repair ADSS.
- Recent operating experience with properly designed ADSS installations has generally been very good (EPRI 2000).

ADSS Disadvantages

- ADSS is susceptible to excessive stretching due to icing (EPRI 1999a).
- ADSS is more vulnerable to vandalism (e.g., gunshots) than OPGW.
- Some ADSS cables have failed in the high-electric-field environment of transmission lines *.
- Although operating experience has been good, it is not clear whether or not the expected life of ADSS will be as long as OPGW (EPRI 1999b) *.
- It is not clear to utilities if the ADSS should be considered a dielectric or a conductor for deciding which work practices are appropriate *.
- ADSS cannot be used on spans longer than approximately 1000 m due to limited strength.
- Care must be taken not to damage ADSS sheath during installation.

12.5.3 Experience with WRAP

Operating experience with WRAP installations has generally been mixed. Experience in Europe has generally been reported to be positive. However, in North America, problems that include fiber pinching during re-sagging and loosening of WRAP cable from the conductor around which it is wrapped have caused interest in WRAP to decline. For this reason, the emphasis here will be placed on the OPGW and ADSS options.

12.5.4 OPGW EMC Issues

Considerations for Fault Currents

As for any other ground wire, it is important to evaluate the importance of fault currents. However, the OPGW case is different because the limiting factor is the protection of the temperature-sensitive fibers in the center of the cable. Normally, manufacturers supply OPGW with a specification on the maximum value of i^2t (where i is the rms fault current on the ground wire and t is the time until relay operation) that the cable can withstand without damage to the fibers. The user should determine that this value is not exceeded for any fault on the system. In some cases, it may be necessary to limit installation of OPGW at some distance from a substation since the value of i^2t at points closer to the substation may exceed the manufacturer's limit.

Lightning

Even if the OPGW is sized correctly for the expected fault current, lightning protection may still be an issue. This is a critical issue because it is known that lightning can have a serious effect on OPGW, as shown in Figure 12.5-1, and utilities often must guarantee the availability of communication circuits.

The procedure for ensuring that OPGW will withstand lightning strikes in any given area of the world is not completely understood. Given this, it is appropriate to summarize what is known about lightning failures from research, a detailed analysis of several operating failures, and interviews with utilities and companies that repair failures.

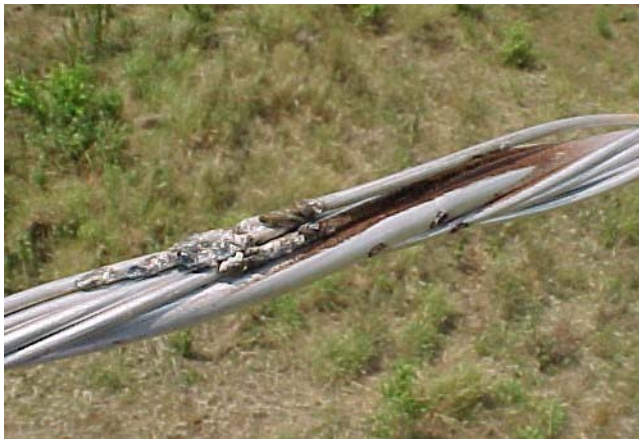


Figure 12.5-1 Observed lightning damage to OPGW in Brazil. Note that several strands have been damaged, leading to reduced strength, and the central aluminum buffer tube has been punctured. (Photo credit: Silverio Visacro.)

The procedure for selecting an OPGW that will withstand lightning strikes in any given area of the world has some uncertainties. The greatest of these are the local ground flash density N_g, the local fraction of negative-to-positive flashes (for example, shown in Figure 6.2-20) and the statistical distributions of the total charge, as described by (Berger et al. 1975; Eriksson 1987) and in Section 6.2 by Equations 6.2-15 and 6.2-20. In cases where little is known, Applet G2 provides an estimate of ground flash density based on observations of overall lightning transient density, and the ratio of 5% positive to 95% negative flashes can also be assumed. This information may be used as discussed in Section 6.2.16 to predict the probability of damage to OPGW.

- OPGW damage and/or failure rates range from 0.02 to 0.08 cases/100 km/year (Yokoya et al. 1994; Zischank and Wiesinger 1997).
- Distribution conductor damage rates tend to match OPGW damage rates, once corrected for the number of flashes to the line using Equation 6.2-27.
- Low-amplitude (≅ 400 A), long-duration (≅ 500 ms) continuing currents rather than short impulsive currents cause damage to ground wires. The larger the transferred charge (typically on the order of 100 coulombs or greater), the more destructive the stroke (Bonicel et al. 1995; Nourai 1992; Carter et al. 1984).

Figure 12.5-2 illustrates that the short impulsive component of a lightning current (i.e., the IEC Standard 60794 Component "A" impulse) does not transfer enough energy to the OPGW to generate serious damage to the cable strands. In contrast, the lower-amplitude, long-duration current pulses characteristic of lightning "continuing currents" (i.e., the IEC Standard 60794 Component "C") can cause considerable damage, as illustrated in Figure 12.5-3 for negative polarity current and in Figure 12.5-4 for a positive polarity current.

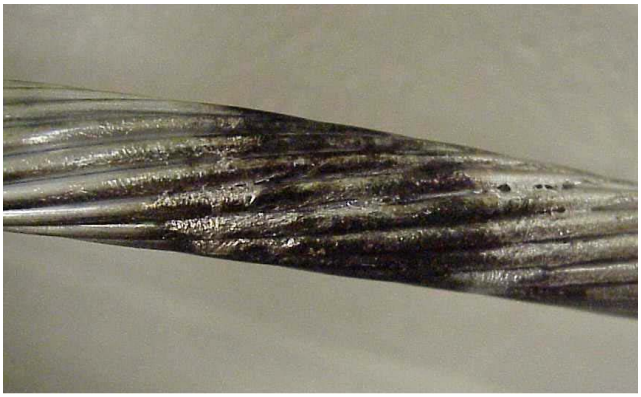


Figure 12.5-2 Effect of 160-kA 30/150 μs IEC Standard 60794 Component "A" impulse on OPGW. $I^2t = 2 \times 10^6$ A^2s. (Photo credit: Jody Levine, Kinectrics.)

Perhaps the best guidance that can be developed is from the ground wire or distribution conductor damage rates at locations near the new installation. Generally, if there is a history of conductor damage or the local overhead ground wire life is less than 30 years, extraordinary measures such as large (>3 mm) strands and large overall OPGW diameter may be warranted. In extraordinary cases, one might consider "lightning-resistant OPGW" (Yokoya et al. 1994; Kuboto 1983). However, the most effective scheme is the use of lightweight OPGW in a protected, underbuilt location beneath the phase conductors. In this location, the OPGW cable will also improve the transmission-line backflashover rate by increasing the common-mode electromagnetic coupling of lightning surges to the phase conductors, reducing the insulator voltage by as much as 25%. OPGW position in underbuilt locations relative to phase conductors can be controlled using lightweight,



Figure 12.5-3 Effect of negative IEC Standard 60794 Component "C" (500 ms x 400 A = 200 coulomb). (Photo credit: Jody Levine, Kinectrics.)



Figure 12.5-4 Effect of positive IEC Standard 60794 Component "C" (670 ms x 418 A = 280 coulomb). (Photo credit: Jody Levine, Kinectrics.)

nonceramic insulator spacers similar to interphase spacers used for conductor galloping control.

Safety of Working on OPGW on Energized Circuits

It is not unusual for utilities to conduct splicing operations on OPGW while the transmission line on which it is installed is energized. Given the possibility of faults occurring on the transmission line during this maintenance, there is concern about worker exposure to transferred potentials caused by ground potential rise during the flow of fault current to earth. This problem has been studied by Olsen and Meliopoulis (2002b). Their general conclusion was that grounding mats were needed to provide a safe working environment for this activity.

12.5.5 ADSS EMC Issues

Background

There have been a number of catastrophic failures of ADSS cable around the world, some within a year of installation (EPRI 1996; EPRI 2000; Keller et al. 1997). One example of a failed cable is shown in Figure 12.5-5. A few failures have occurred in environments previously thought to be benign (Kaidanov et al. 2000). As a result, some people have suggested a severely restricted lifespan for ADSS cables on high-voltage transmission lines (Carter 1998). Despite this pessimistic prediction, ADSS cables installed in North America have been in use near 345-kV transmission lines for more than 15 years and on 500-kV lines for more than 8 years without incident. It appears that these disparate reports can be reconciled by recognizing that significant advances have been made in the development of ADSS cables with tracking-resistant jackets (Wheeler et al. 1998) and in the procedures used to design ADSS installations. Thus more recent experience with properly designed ADSS cable installations has been significantly better than earlier experience.



Figure 12.5-5 An ADSS cable that has failed due to dry-band arcing. Note the heavy contamination on the cable and attachment hardware. (Photo credit: Wayne Kincheloe.)

At least two reasons for ADSS cable failures are related to the fact that the cable is suspended in a strong electric field. First, metallic hardware is used to attach the cable to a tower that is at ground potential. Electric fields are increased around the grounded hardware, and corona and/or microsparks may occur near hardware tips that are close to the cable sheath. These corona and/or microsparks have been shown to affect the long-term integrity of the cable sheath (Karady et al. 1999). Second, the midspan electrical potential of the cable is approximately that of the space potential at the cable position. At the tower, however, the cable is held at ground potential. Over time, all cables become contaminated and hydrophilic. When these cables are wet from rain or dew, the pollution layer on the cable sheath becomes conducting, and small electric currents can flow. As the cable dries, "dry bands" can form on the pollution that has a voltage across it approximately equal to the midspan space potential. If the pollution resistance is low enough, dry-band arcing can lead to cable sheath damage that may affect the cable sheath's long-term integrity (Carter et al. 1997; Wheeler et al. 1988; Carter and Waldron 1992).

Corona Damage

Three-dimensional electric-field modeling has been used successfully to understand the conditions under which corona can occur and to develop techniques to suppress it (Tuominen 1996). Based on this research, commercial devices such as the one shown in Figure 12.5-6 are now available to suppress corona by essentially shielding critical areas (such as tips armor rods). In most cases it is not necessary to use the full three-dimensional electric-field modeling when designing a new ADSS system. Rather, the two-dimensional space potential, calculated using the cross sec-

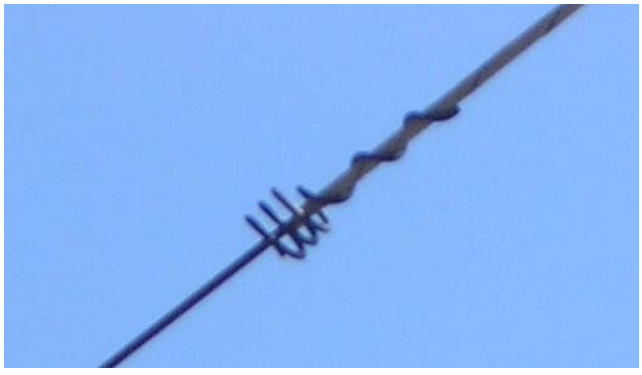


Figure 12.5-6 A "Corona Coil"® for suppressing corona on ADSS mounting hardware. (Photo credit: R. G. Olsen.)

tion of the transmission line at the tower location, can be used to indicate the need for corona-suppressing hardware.

Dry-Band Arcing Damage

Electrical design parameters that are useful for predicting dry-band arcing on ADSS cable in a high-voltage environment have been identified. These include contamination level and hydrophobicity of the ADSS cable, space potential, dry-band voltage, current available to an arc, and arc models (Tuominen and Olsen 2000). Of these, current available to the arc, available dry-band voltage, and contamination/hydrophobicity level appear to be the most useful predictors of performance. In fact, preliminary tests indicate that for a 26-kV dry-band voltage, available arc currents of 1.5 and 5 mA are sufficient to cause damage to nontracking-resistant and tracking-resistant ADSS cable sheaths, respectively (Carter and Waldron 1992; Johnson and Lo 1999; EPRI 1999b). Under normal conditions, these levels cannot be reached unless the resistance per unit length of the cable sheath under wet conditions (a measure of the contamination level) is less than approximately 10^6 Ω/m (i.e., moderate contamination).

Two computer models (shown to be equivalent) have been developed that can be used to predict values of current available to a dry-band arc and available dry-band voltage (EPRI 2000; Olsen 1998; Olsen 1999a; Tuominen and Olsen 2000). As mentioned above, these values are critically dependent upon the (generally unknown) level of contamination. For unknown contamination levels (the normal case), a typical contamination level, such as 10^6 Ω/m, or a range of contamination levels, such as 10^5 Ω/m to 10^7 Ω/m, can be used in the computer models mentioned above to evaluate the possibility of dry-band arcing. More specifically, there will not generally be a problem with dry-band arcing if the current available to a dry-band arc is less than 1 mA and tracking-resistant cable is used.

Simpler Method for Designing ADSS Installations

For those who do not have access to either contamination measurements or computer programs to predict the probability of dry-band arcs, a less precise but generally adequate method can be used (Tuominen and Olsen 2000). A description of this method follows.

ADSS cables are normally placed 3-6 m below phase wires. The determination of the specific location, however, is a much more complicated issue. This is especially true for transmission lines with voltages above 138 kV. As mentioned earlier, one measure of the induced currents and voltages on the cable is the space potential at midspan. It should be noted, however, that it is the electric field, not the space potential, that is the driving force behind both dry-band arcing and corona activity. Nevertheless, space potential is often used as a surrogate because it is the integral of the electric field from the tower to midspan.

For calculation of the space potential, towers are neglected, and it is normally assumed that the transmission line is two dimensional. Here this potential will be designated $V_{SP}(2D)$. Software such as Applet EMF-2, which is described in Chapter 7, can be used for this calculation.

Generally, ADSS cable placements have been successful in environments for which the space potential is less than approximately 12 kV. Above 12 kV (which is more common on transmission lines of 138 kV and above), manufacturers' recommendations differ. At least one is willing to install cables with tracking-resistant sheaths in space potentials of up to 25 kV. For space potentials in this range, dry-band arcing can occur if the contamination is sufficient and a more careful analysis is suggested. With such an analysis, ADSS cable has been successfully installed and operated on transmission lines with voltages of up to 500 kV. While above 25-kV space potential, the use of ADSS cable is not generally recommended, at least one utility has installed ADSS near 45 kV by employing extensive 3D electric-field analysis to design electric-field-reducing hardware.

Longevity of ADSS Cable

Since their introduction, questions about the longevity of ADSS cables have been studied (Alcoa 1995). As mentioned earlier, some have predicted dramatically reduced lifetimes for ADSS cable on high-voltage lines (Carter 1998). Nevertheless, as mentioned above, ADSS cables have been operated successfully in high-voltage environments for more than 15 years. Because the question of how long ADSS cable will last is important to utilities, EPRI conducted accelerated aging tests at its Lenox, MA laboratory using a test that simulates field conditions (EPRI 2000). Their conclusion was that tracking-resistant ADSS cables installed in severe climatic conditions have expected lives greater than 17 years when used in a space potential equal to 25 kV.

Safety of Working on ADSS Cable on Energized Circuits

In a recent survey of utilities, it was found that approximately half consider ADSS to be an insulator for the purpose of assigning work rules, and the other half consider it to be a conductor. In order to resolve this issue, a method has been developed for calculating the contact current through a grounded worker touching the ADSS cable while the power line is energized (Olsen 1999b). The model is valid for cable resistances between 10^5 and 10^7 Ω/m (typical of wet/polluted cables). Very close to the tower, the contact current is $V_{SP}(2D)/Z_0$, and a crude upper limit is $2V_{SP}(2D)/Z_0$. Here $V_{SP}(2D)$ is the two-dimensional space potential near the tower (typically 10s of kilovolts),

and Z_0 is the characteristic impedance of the ADSS cable above ground (typically 5–50 MΩ for wet/contaminated cables). More explicit results indicate that for cable resistances less than 10^6 Ω/m, workers within 25 m of structures could be exposed to contact currents in excess of the IEEE standard for contact currents in controlled (occupational) environments: maximum permissible exposure not to exceed 3.0 mA for grasp contacts and 1.5 mA for touch contacts (IEEE 2002a).

Since the above analysis is based on theory, some field tests were done at the Bonneville Power Administration to further study the question of worker safety (Edwards and Olsen 2002). In the limited set of conditions examined in this work, the short-circuit current through a worker touching ungrounded hardware while it was drying after rain could exceed the maximum permissible exposure defined in the IEEE standard (IEEE 2002a). Clearly, more study of worker safety is needed for ungrounded workers on wood poles in contact with grounded and ungrounded hardware in a variety of weather conditions.

Recommended Maintenance

As mentioned earlier, the variable that is both critical and least well known is the contamination level on the ADSS sheath. If there is concern about dry-band arcing, it is recommended that periodic checks of the contamination level be done using the method outlined in Edwards et al. (2003). Such tests at the Bonneville Power Administration have indicated that contamination levels in their territory are not as severe as might have been thought (Edwards et al. 2003). The lowest level measured was $10^{7.7}$ Ω ohm/m at Bandon, Oregon, one mile from the Pacific Ocean, on ADSS exposed to the local climate for about six years (Tuominen 2004).

Alternative Mitigation Techniques

Other mitigation devices have been proposed and tested (Carter 1993). These include insulating the ADSS cable from the tower and the use of a semiconducting rod in parallel with the ADSS cable. The latter technique is the most promising and has been used in the United Kingdom.

12.6 CONSEQUENCES OF INSTALLING COMMUNICATION SYSTEM ANTENNAS ON TRANSMISSION-LINE TOWERS

12.6.1 Introduction

In recent years, communications antennas have been installed on high-voltage transmission-line towers, such as those shown in Figure 12.6-1. Because of this, several issues have been raised. The first is whether the transmission line or its supporting towers has any influence on the performance of the antenna. The second is whether there are any special problems related to the low-voltage source used to supply power to the communications equipment. Finally, transmission-line workers (and the public) are exposed not only to the expected 50/60-Hz electric and magnetic fields, but also to radio frequency (RF) electromagnetic fields from the antennas. As a result, concern about how to properly evaluate worker (and public) safety in the combination of extremely-low-frequency (ELF) and RF electromagnetic fields has been raised.

12.6.2 Influence of the Power Line on the Antenna

Questions have been raised about whether transmission-line towers might influence the radiation pattern of the antennas and/or whether high-power-frequency electric fields might cause corona at the tips of communication antennas. Neither has been reported to be a major problem. The main beams of directional antennas (e.g., panel antennas), such as typically used for cellular telephone installations, are normally directed away from the tower and hence



Figure 12.6-1 A typical installation of communication antennas on a transmission-line tower.

are only minimally influenced by the tower. Nondirectional antennas mounted on the tower may experience modified patterns in the direction through the tower, but this appears to be a problem that the antenna's operator can accept. Finally, while corona could possibly occur on the sharp tips of RF antennas, no reports of either corona-related material degradation or electromagnetic interference with reception have been given.

12.6.3 Issues Relating to Grounding and Low-Voltage Feeds

When a communications antenna is installed on a high-voltage transmission-line tower, a cable (usually coaxial) is mounted on the tower to carry the RF signals from the communications hut on the ground to the antenna. The "grounding" of this cable is of concern to electric utilities since fault currents can have a significant effect on the potential of different parts of the "ground" with respect to "remote earth." Since grounding practices appear to vary among utilities, a typical practice will be outlined here. First, in this typical practice, the cable shield is bonded to the tower as close to the antenna location as possible using a commercially available grounding kit. In addition, the cable shield is connected to ground at the point near the earth just before it enters the communications hut. Here, it is connected to a small ground plate that is, in turn, connected to a large-diameter wire (typically 00 or 0000 wire) that surrounds the hut and is buried approximately 0.6 m (2 ft) in the ground. This wire is usually connected to between two and four ground rods that are typically 2.4 m (8 ft) in length and driven into the earth. The wire then runs underground from the hut to the transmission tower and is typically bonded to each of the four tower legs.

Because the wire is usually made of copper, and towers are usually made of galvanized steel, there is concern about galvanic action at the junction between these two metals. For this reason, an anticorrosion cell may be required.

Another issue that should be considered is the fact that power is provided to the communications hut from the low-voltage electric distribution system. If the transmission and distribution system grounds are connected together, ground potential rise (possibly thousands of volts), due to fault currents on the transmission line, may be carried to the distribution system via its "ground" and, hence, adversely affect any device connected to the distribution system. Although designs for isolation transformers to eliminate this problem have been developed by the Bonneville Power Administration, none are known to be commercially available at this time. Thus, in most systems known to the authors at this time, the transmission and distribution grounds are simply connected. The safety issue raised as a result of this connection needs to be investigated.

Finally, because of concerns about the effect of ground potential rise on their equipment, telephone companies generally do not install copper telephone wires within the "zone of influence" of a transmission-line tower. The "zone of influence" is defined by them as any point within approximately 150 m (500 ft) of a transmission-line tower. The communications operator is then responsible for installing the last section of the communications line with nonmetallic (usually fiber optic) medium.

12.6.4 Exposure to RF Electromagnetic Fields

Utility employees who must work close to RF antennas will be exposed to RF electromagnetic fields that may exceed government standards for human exposure to these fields (FCC 1997; IEEE 1999; ICNIRP 1998). Since there are now numerous antennas located on electric power transmission-line towers, acceptable RF exposure limits and work practices must be developed for utility employees working near these antennas (EPRI 2002). One of the tools used to evaluate the environment is an instrument called an RF survey meter, which is used to measure RF field levels. An example of one of these meters is shown in Figure 12.6-2.

It has been noted, however, that erroneous meter indications of the RF electromagnetic field strength occur when RF survey meters are exposed to strong ELF (e.g., 50/60-Hz) electric fields near power transmission lines (Aslan 1985; Mantiply 1988; Mantiply 1995). This phenomenon usually results in significantly higher indications of RF electric field strength than those which actually exist.



Figure 12.6-2 A typical RF survey meter. In this photograph, the probe (upper left) is connected to a preamplifier (center) and then to a readout unit in the operator's hand. The probe elements are contained within a "radome" structure to protect them from physical damage.

More specifically, they may indicate that RF fields exceed RF safety standards when, in fact, they do not.

To consider this issue more carefully, a study of the EMC of RF survey meters and 50/60 Hz electromagnetic fields was carried out by EPRI (EPRI 2003b; Olsen and Yamazaki 2004). This work showed that special care must be used in making RF electromagnetic field measurements whenever strong ELF fields are present. More specifically, broadband instruments commonly used to assess RF fields for safety purposes can be substantially interfered with when used in the presence of 50/60-Hz electric fields typical of those found in the electric power industry. While it can take considerable effort to conclusively identify whether an instrument is malfunctioning when used in strong 50/60-Hz fields, the following practical observations can be made by the user to gauge the likelihood of such problems.

1. If measurements are being made in a known, high-level 50/60-Hz field environment, the observer should be alert to the possibility of artifactual readings and focus more than casual attention on whether the indications on the instrument seem to make sense. In this regard, strong electric fields are potentially more suspect than strong magnetic fields.
2. The meter readout should be observed as the probe shaft is oriented from horizontal to vertical and back to horizontal while keeping the probe sensor itself at approximately the same location. If the meter reading increases significantly in one orientation or the other, this is an indication that low-frequency interference may be present. The orientation of the probe shaft for the greatest reading will suggest the polarization of the interfering low-frequency field. At ground level under power lines and away from structures, poles, and other objects, the principal electric-field component is usually vertical. Hence, most 50/60-Hz interference is observed when the probe shaft is vertical such that the electric field is aligned with the direction of the shaft.
3. If the RF meter reading appears to continue to increase in value as the probe is elevated above ground, without decreasing at some height, it can be inferred that low-frequency fields may be interfering with proper measurement of the intended RF field.
4. If 50/60-Hz electric field interference is suspected, the most accurate measurement will be accomplished by isolating the probe, meter, and cable from the observer by mounting it on a nonconductive stand. Figure 12.6-3 illustrates this technique for an older-style probe and meter. The cable should be formed into a small-diameter coil and taped to the side of the meter, while the probe should be positioned at the same height as the meter on the stand. In this fashion, the instrumentation components (i.e., probe, cable, and meter readout) are placed as close as possible to the same low-frequency space potential, which will result in the least amount of pickup. If the meter reading increases noticeably when touching the meter, while it is supported on the nonconductive stand, then this is a definite indication that the probe is responding to low-frequency artifact. Under this condition, RF field readings obtained when directly holding the meter should be considered suspect.

Another type of meter that may be used is an RF exposure monitor. These are compact RF field sensors carried by workers that are designed to warn them if they enter RF electromagnetic fields close to, or in excess of, RF safety standards. Concern has been expressed about whether these sensors are also susceptible to 50/60-Hz electric or magnetic fields. Two studies of these meters indicate that meters designed to be "ELF immune" by coating the inside of their cases with a conducting material work well in electric fields even up to 120 kV/m (Johnson 1999; EPRI 2004). This level of field is higher than that experienced by workers passing by phase conductors as they climb 500-kV transmission-line towers.



Figure 12.6-3 Older-style probe, meter, and cable placed on nonconductive support for measurement of medium-frequency RF fields near AM radio station. Placement of the entire measurement system at essentially the same space potential helps reduce the magnitude of low-frequency interference due to induction of common-mode currents on cabling.

12.7 INTERFERENCE WITH THE OPERATION OF SYSTEMS FOR WARNING AIRCRAFT

12.7.1 Introduction

The Federal Aviation Administration (FAA) establishes requirements for marking and/or lighting transmission-line towers and other tall structures that could potentially interfere with aircraft safety. Marking and/or lighting are required for any temporary or permanent object that is taller than 200 ft (61 m) above ground level or that exceeds the obstruction standard contained in Federal Aviation Regulations (FAR) (FAR 1971). The regulations establish buffer zones around airports where height restrictions are in effect. The FAA requires notification by the constructor of tall objects within these zones and provides recommendations for marking and/or lighting the obstructions.

FAA safety standards can be met by moving or lowering the obstruction or by marking and/or lighting the towers and/or conductors. Common methods of meeting FAA requirements are warning lights on towers, brightly colored marker balls on conductors, and painted towers. Both warning lights and marker balls are susceptible to damage from transmission-line fields. A new technology under test is an active system that detects the presence of an aircraft and turns on lights and initiates a radio warning if necessary (Lowe 2004).

12.7.2 Warning Lights

Warning lights on towers often require low-voltage electric power from a local utility. Supplying this power to warning lights is similar to the problem of supplying power to a communications system and antenna mounted on a tower, as discussed in Section 12.6.3. Direct connection of the tower to the low-voltage distribution system neutral introduces the possibility of conductively coupled voltage rise on the neutral conductor during a fault at the tower. Even the low-voltage distribution-phase conductors could be affected if the voltage rise is sufficient to break down their insulation. The increased voltage can damage equipment and cause hazardous conditions for personnel.

In areas where multiple towers require lighting and power supplies are limited, one utility uses the overhead ground wire as a conductor to supply power to adjacent towers (Tuominen 2004). In this way, only one connection to the distribution system is required. The overhead ground wire is energized (between 7.2 and 25 kV, depending on location) and feeds power to lights on an adjacent tower, usually on the other side of a river crossing. To prevent hazardous conditions from occurring on the operational voltage (nominally 120/240 VAC) circuit during maintenance, the system is continuously connected to ground through auxiliary loading resistors. This reduces induced voltages arising from capacitive coupling to the overhead ground wire to safe levels, when distribution supply breakers are open.

At least one other utility uses voltage that is capacitively coupled to a shield wire to light warning lights. This method eliminates questions of ground rise on the distribution system. Further, capacitively coupled voltage drops during a fault (except for voltage rise on unfaulted phases), as opposed to the sharp rise in inductively coupled voltage during a fault.

New warning systems may incorporate technologies that allow data acquisition and wireless transmission of the functional status of airway lighting (PSE&G 2004; Lowe 2004). However, as long as these systems rely on local low-voltage distribution systems for power, they will be susceptible to transferred potentials during fault conditions. The battery-powered warning lights that are sometimes used in remote areas are not susceptible to transferred potentials.

12.7.3 Airway Marking Balls

Highly visible marker balls may be required by the FAA at locations where conductors represent an obstacle in flight paths, such as at river and canyon crossings. The construction of the balls can make them prone to damage from corona (Tuominen 2004). The large, hollow plastic balls are coated inside with a thin metallic layer. In high-voltage gradients near the conductor, corona can occur at edges or imperfections of this coating. The heating due to the corona can cause burning of the plastic and a subsequent fall from the conductor.

Typically, corona damage occurs only at voltages of 500 kV or higher: it is generally not a problem on lower-voltage lines, where gradients near the conductors are lower. However, there was an instance of a marker ball on an overhead ground wire being damaged by corona. In this case, the two upper conductor bundles of a double-circuit 500-kV line had similar phasing, producing a high surface gradient on the overhead ground wire (Tuominen 2004). Methods under consideration for mitigating corona damage to marker balls are the use of grading rings in the attachment hardware and the use of all-aluminum balls.

12.8 INTERFERENCE WITH THE OPERATION OF TELEPHONE SYSTEMS

12.8.1 Telephone Lines

Over the years, there have been many cases of interference between electric power lines and telephone lines that parallel the power lines. These problems led to an IEEE standard that can be used both to design compatible systems and assist in the diagnosis of these “inductive

coordination" problems (IEEE 1992). Although many of the problems have involved distribution lines because there are so many more of these, there have also been issues with transmission lines. For this reason, these problems will be reviewed briefly here. Further, with the improvement in communication technology over the years (e.g., microwave systems and fiber optics), the number of inductive coordination problems has decreased. Nevertheless, inductive coordination remains an issue and does arise from time to time (Jewell et al. 2000).

The mechanisms by which coupling between these systems occurs are essentially identical to those discussed for railroads in Section 12.2.1. But, because communications lines are physically different from railroad tracks, some of the details are different. The most important difference is that communications lines are often closely spaced wires that are twisted together. Because of this, there is very little direct induction of a differential-mode current between the two wires (i.e., the mode for which the entire current on one of the wires returns on the other). Rather, essentially all of the induction on the communication wire is common mode for which the return current is through the earth. Interference, however, usually occurs because some of the common-mode current is converted into differential-mode current via unbalances in the system, as described in Section 12.2.7.

The Canadian Electrical Association published a comprehensive guide for power and telecommunications engineers to help prevent and solve electrical interference problems between power and telecommunications systems (CEA 1989). It describes the interaction between power and telecommunications systems at fundamental and harmonic frequencies under both normal and fault conditions. For each system, the guide covers the applicable calculations, measurements, and mitigation methods. The guide further discusses the administration of electrical coordination work and suggests a cooperative agreement with provisions for sharing costs.

12.8.2 Cordless Phones

A cordless phone operates like a radio receiver and a mini radio station in one unit. Radio signals are transmitted and received between the base unit and the handset. Both the base unit and the handset can be the transmitter and receiver at any one time. Cordless phones first appeared around 1980 with an operating frequency in the 27 MHz range. Later in the mid 1980s, the 43-50 MHz band was used to improve the sound quality but was still unsatisfactory due to its very limited range between the base station and the handset. These two types of cordless phones are no longer sold in stores, and very few units are probably still being used.

Today, cordless phones sold in stores operate in the 900-MHz and 2.4–GHz (gigahertz) range, with some newer units in the 5.8-GHz range. The useful range is about 0.5 km between the base unit and the handset, with some units reaching as high as 3 km. Modern cordless phones use digital spread spectrum (DSS) technology, which improves sound quality, provides security against eavesdropping and immunity against interference, and increases the usable range of the telephone when compared to older analog technology.

Like any electronic equipment, cordless phones contain electronic components that may be sensitive to radio interference. If the telephone does not have built-in interference protection, its performance may be affected by nearby radio communications or electrical noise. Telephones with more features contain more electronic components and need greater interference protection. A better quality telephone or one that uses a higher frequency is less likely to have interference problems.

Considering the high frequency of operation (900 MHz, 2.4 and 5.8 GHz) and the use of digital technology, it is highly unlikely that transmission-line radio frequency (RF) noise will interfere with the operation of cordless phones in the vicinity of transmission lines. In the unlikely event that an interference complaint occurs, an economical solution to resolve the complaint is to replace the older cordless phone with a newer and better quality unit.

12.8.3 Cell Phones

A cell phone is a mobile phone that sends and receives radio signals to and from low-power transmitters and receivers located within defined service areas called *cells*. Each cell ranges from a few to tens of kilometers. Each cell site is connected to one or more cellular switching exchanges. As the phone moves out of the service range of one cell and enters the adjacent cell, the signal carrying the conversation is transferred to the transmitter and receiver in the adjacent cell and the connection is switched to the new cell site by the switching exchange. Communication between cell sites and the public switched telephone network can be by optic fibers, microwave radio links, or copper wires connected with telephone exchanges.

The older cell phones use analog technology, whereas the newer units use digital technology, which is suitable for both voice and data communications. The digital technology allows a greater number of users within the available bandwidth and is more immune to interference. Different digital technologies in use include time division multiple access (TDMA), code division multiple access (CDMA), and Global System for Mobile communication (GSM). In North America, the older analog units operate only in the

800-MHz (800- to 900-MHz) band, while the newer digital units operate in both the 800-MHz and 2-GHz bands. Phones operating in the 2-GHz band are sometimes called PCS (Personal Communications Services) phones.

For cell phone systems in the 800-MHz band, the reliable service area of a cell is defined as having a signal strength of 35 dBμV/m at the cell perimeter (Industry Canada 2003). This standard is technology neutral, and supports analog cell systems and digital systems based on different technology platforms (e.g., TDMA, CDMA, GSM) as well as digital packet data (CDPD). For the purpose of protecting stations operating in adjacent service areas from co-channel interference, a base station is not allowed to generate a field strength exceeding 35 dB μV/m outside the operator's service area unless agreed by the affected operator. The 35-dB μV/m field level may be used as a rough guide for cell phone signal level in this frequency band. The channel bandwidth is 30 kHz.

For land mobile and fixed radio services in the 800-MHz band, the geographic separation between co-channel systems (Industry Canada 1999) is calculated based on a nonoverlap of the 40-dB μV/m service contour (i.e., usually calculated based on a probability of service of 50% of the time for 90% of the locations at edge of contour) of the existing station and the 22-dB μV/m interference contour (i.e., calculated using the probability that the signal level used is below the threshold 90% of the time for 90% of the locations) of the proposed station. The difference between the service and interference contours is 18 dB (40-22 dB μV/m), which may be used as a rough guideline for the required signal-to-noise ratio for satisfactory reception of mobile phone signal.

For the purpose of protecting stations operating in adjacent service area from co-channel interference for PCS phone systems in the 2-GHz range, a base station is not allowed to generate a field strength exceeding 47 dB μV/m outside the operator's service area unless agreed by the affected operator. The 47-dB μV/m field level may be used as a rough guide for cell phone signal level in this frequency band.

Many cell antennas are currently operating on top of transmission-line structures. The proper functioning of these cell antennas over the years gives a very good indication that perceptible interference from transmission lines with cell phones is a highly unlikely event. Because of the high operating frequency (above 800 MHz), the use of digital technology in the newer phones, and years of successful operation of cell antennas on transmission-line towers, it is highly unlikely that transmission-line radio noise will interfere with cell phone systems.

It should be noted that specific concerns about the consequences of locating cell phone system base stations on transmission-line towers are considered in Section 12.6. The interested reader is referred there for further information.

12.9 CONSEQUENCES OF INSTALLING DISTRIBUTION LINES UNDER TRANSMISSION LINES

Often, utilities find it advantageous to install overhead distribution lines on the same structures used to support a transmission line. Since there are potential negative consequences to this practice, some utilities have chosen either not to permit this "underbuilding" or to restrict it to lower-voltage transmission lines such as lines of 115 kV and below. Nevertheless, the practice continues even on transmission lines with voltages above 115 kV, because it is often convenient and utilities perceive that the negative consequences are manageable.

The most important issue in designing these underbuilt distribution lines is maintaining adequate clearance. The clearance between transmission and distribution conductors must be large enough to prevent failure during steady-state and fault conditions, and care must be taken to ensure that it is maintained under all possible combinations of transmission-and distribution-line sag (including icing). In addition, the clearance must allow for adequate working space for both transmission- and distribution-line workers. These maintenance access and clearance issues are addressed by the National Electric Safety Code (IEEE 2002b). In fact, many utilities (especially those in low-lightning areas) consider this reference to be their only guide when designing underbuilt distribution lines. While consequences other than those considered by the National Electric Safety Code may arise, they are believed to be manageable.

One set of potential negative consequences is related to electromagnetic coupling (as described in Sections 12.2.3, 12.2.4, and 12.2.5) that can occur and have a noticeable effect on system performance. This coupling is stronger for lines that are closer, have larger voltage differences (capacitive or electric-field coupling), larger currents (inductive or magnetic-field coupling) and/or longer parallel exposures. If the coupling is strong enough, there may be operational consequences, such as difficulty in maintaining voltage level on the distribution line or flashover of distribution-line insulators by induced voltages during transmission-line faults. Maintenance issues such as induced voltages and currents on the de-energized distribution line when the transmission line remains energized are also important. Another issue related to conductive coupling between the lines is the consequences of bonding the distribution neutral (if any) to transmission-line overhead

ground wires (if any). This connection may result in excessive voltage between the distribution phase conductors and the neutral (and possible failure) during transmission-line faults and the associated ground potential rise.

Other miscellaneous potential consequences include damage to the distribution circuit from transmission-line conductors that fall and come into contact with the distribution line, pole fires related to distribution-line hardware that may occur in some regions and that could cause the transmission line to flashover, and the possible need for separate poles for distribution-line transformers in order to reduce the chance of an accident during maintenance.

The number of lightning hits to an underbuilt distribution line is reduced due to electrostatic shielding by the transmission line. Nevertheless, the system may need to be modified to reduce the probability that strikes to the transmission line will flash over to the distribution line. This is often done by increasing the Basic Insulation Level (BIL) of the distribution line by using fiberglass crossarms or by using more transmission-line lightning arresters than would normally be used.

Finally, one positive result of using underbuilt distribution is that (because they are at a much lower voltage) the distribution conductors tend to shield the transmission line's electric field and hence reduce its amplitude at ground level. The theory behind this effect is essentially identical to that for shielding by a horizontal grid of grounded wires or underbuilt transmission lines, as discussed in Section 7.16.

12.10 INTERFERENCE WITH THE OPERATION OF RADIO NAVIGATION SYSTEMS

12.10.1 LORAN-C

Long-range navigation systems such as LORAN-C operate in the very-low-frequency (VLF) range near 100 kHz. One of the factors that limits the absolute positional accuracy of the LORAN-C system (i.e., approximately 0.25 nautical miles) is signal-to-noise degradation due to atmospheric noise generated by lightning (U.S. Coast Guard 2002). Since the system was primarily designed to be used for the navigation of ships in U.S. coastal waters, man-made noise sources do not usually add to this atmospheric noise. However, when LORAN-C is used on rivers or channels crossed by high-voltage power lines or on land near high-voltage power lines, radio noise due to corona can degrade its performance.

LORAN-C is also subject to errors caused by electromagnetic scattering of its ground waves by nearby large objects, such as bridges, power lines, and other large structures (e.g., petroleum refineries, steel mills) (U.S. Coast Guard 2002). The distance from the structure where LORAN-C position information becomes unusable varies among structures. In Coast Guard track line surveys, it was noted that some power lines caused noticeable errors, when as much as 500 m distant from the receiver, and distance errors up to 200 m, when directly under the power line (U.S. Coast Guard 1982; Olsen and Aburwein 1982).

Over the years, PLC systems operating near 100 kHz have also caused interference to the operation of LORAN-C navigation systems (Arnstein 1986; Last and Bian 1993). This problem can be mitigated by an appropriate choice of PLC operating frequency.

While all of these problems remain, LORAN-C systems have been generally supplanted by the global positioning system (GPS) and the future of LORAN-C is in doubt. Since GPS operates in the microwave frequency range, it is much less vulnerable to interference from power transmission lines. As a result, there will be no further discussion here of low-frequency navigation systems.

12.10.2 Instrument Landing Systems (ILS)

The Instrument Landing System (ILS) is a radio navigation system that provides a pilot with accurate guidance for the final approach in landing. It consists of three subsystems: localizer (LOC), glide slope (GS) or glide path, and marker (MKR) beacon. Each system is composed of: transmitters, transmitter antennas, receiver antennas, receivers, and indicators. The approach path is given by the intersection of the localizer beam (for horizontal guidance) and the glide slope beam (for vertical guidance). These beams activate a course deviation indicator in the aircraft that contains a horizontal needle sensitive to deviations from the glide slope and a vertical needle sensitive to deviations from the localizer. By keeping both needles centered, the pilot can guide the aircraft down to the centerline of the runway. False guidance can result from distortion of the radio beam by nearby buildings or mountains. Newer systems using microwave beams overcome most of these limitations. For example, the microwave landing system (MLS) uses frequencies in the 5.030 and 5.150 GHz range.

The localizer operates in a frequency band from 108 to 118 MHz. Within this band, there are 200 channels, each occupying 50 kHz. The carrier is modulated with audio tones of 90, 150, and 1020 Hz. The first two tones are for horizontal guidance, and the difference in tone characteristics results in a deviation on the course deviation indicator. The third tone is for identifying the facility. The minimum ICAO (International Civil Aviation Organization) performance standard requires a signal level of -77 dBm/m^2.

The glide slope or glide path operates in a frequency band from 329 to 335 MHz. Within this band, there are 40 channels, each occupying 150 kHz. Like the localizer, the carrier is modulated with 90 and 150 Hz tones, which are used for vertical guidance. The minimum ICAO performance standard requires a signal level of -65 dBm/m^2.

Marker beacons are installed at several locations along the approach path to inform the pilot of the plane's location along the approach path. These beacons operate near 75 MHz (74.8 to 75.2 MHz). Depending on the location of the marker beacon, the carrier is modulated with a 400-, 1300, or 3000-Hz tone. The minimum ICAO performance standard requires a signal level of -52 dBm/m^2.

According to a 1985 report, there are two major interference mechanisms affecting ILS receivers: automatic gain-control (AGC) capture and tone-filter capture (CEA 1985). AGC capture occurs when an extraneous signal is detected and causes the AGC to reduce gains in the first mixer and IF (intermediate frequency) stages, and the output level of the desired signal (or tones) is therefore reduced. Tone-filter capture occurs when the envelope of an undesired signal contains spectral components at or near the tone-filter frequencies. The report concluded that the flag deviation currents in the GS and LOC receivers degraded as a function of the average power of the interfering noise, and that both indicators were easier to measure than the AGC voltage. The sharpness of the tone filters in the ILS receivers varies among manufacturers, and receivers with "sloppy" filters degrade much more rapidly than those with sharp ones.

In the Canadian Electrical Association (CEA) project cited above, limited measurements of ILS receiver performance were made in the field near a 500-kV power line and within the perimeter of a distribution substation of a major power company. The antenna used for capturing noise was a pole–mounted, half-wave dipole tuned to 110 MHz, and located ~30 ft from the outside phase of a 500-kV line. The actual noise level, however, was not reported. Additional measurements were made in the laboratory using recorded power-line noise and independent, controllable noise sources. All measurements confirmed the theoretical premises that ILS receiver degradation occurs as a function of the average power level of power-line noise, and that the LOC receiver is the most susceptible element of the three ILS receivers (LOC, GS, and MKR).

The conservative EMI zoning criteria for electrical power systems established by Transport Canada require power lines with voltages greater than 100 kV be located no closer than 1.8 km from the runway centerline and no closer than 3.2 km from the ends of the runway; and AC electrical substations with voltages greater than 100 kV be located no closer than 3.2 km from the runway centerline and no closer than 16 km from the ends of the runway (Transport Canada 2004). Only Stage 1 of a three-stage project was completed by CEA and Transport Canada in 1985. Stage 2 (actual airborne radio noise measurements) and Stage 3 (more realistic EMI zoning criteria for airports under all weather conditions) were never carried out. Consequently, the Canadian utilities must continue to use the conservative EMI zoning criteria for airports, which results in added costs for routing and locating electric power facilities near airports.

There are no recorded incidences of ILS interference from power systems. This is probably because most, if not all, of the utilities are using unrealistically large separation distance between airports and electric power facilities, as dictated by their respective EMI zoning criteria near airports. Given this operating experience, it is highly unlikely that ILS interference from power systems will occur in the future as long as the same separation distances are maintained.

Although there is no recorded airborne radio noise data from power systems, it is possible to do a crude prediction on the likelihood of ILS interference with power systems by making the assumption that airborne radio noise from power systems are similar in characteristics to those measured near ground level, except possibly for a slower attenuation rate with distance from the power system. Using this assumption and the above technical information on ILS, one can estimate the likelihood of ILS interference from a transmission line by using a "postulated" 13-dB signal to noise degradation threshold, with noise measured in a bandwidth of 100 kHz, as given in the 1985 CEA report.

12.10.3 Global Positioning System (GPS)

GPS is a satellite-based radio navigation system that has many civilian applications for the position, velocity, and time information it can provide (Parkinson and Spilker 1996). At present, 28 GPS satellites are in place (Enge and Misra 1999). Each satellite, at an altitude of about 20,200 km, is moving at about 4 km/s and completes an orbit of the earth in approximately 12 hours. Precise determination of the transit time for a radio wave to travel from a GPS satellite with a known position in space to the user's receiver on earth is the basis for all GPS applications. For 3-D navigation, the GPS receiver requires range information from at least four satellites; the fourth satellite is needed to adjust for receiver clock errors. The position is given as latitude, longitude, and elevation, usually with respect to a reference ellipsoid model of the earth, such as the World Geodetic System (Kremer et al. 1990; Pietraszewski 1990).

Each GPS satellite broadcasts very weak, uniquely identifiable signals, using spread spectrum technology (Parkinson and Spilker 1996). Each satellite transmits its carrier signals on two different radio frequencies in the L-Band of the frequency spectrum: Link 1 (L1) at 1,575.42 MHz, and Link 2 (L2) at 1,227.60 MHz; each has a bandwidth of 20.46 MHz (Parkinson and Spilker 1996).

One issue that is sometimes raised is the potential for degraded performance of GPS receivers when they are used near electric power facilities. Of specific interest is the reception of GPS satellite-based microwave signals under or near power line conductors. At the surface of the earth, the satellite microwave signals are weak, and any reduction of signal intensity due to scattering by conductors or noise due to corona and/or gap discharges could degrade receiver performance or cause loss of signal lock.

The potential effects of EMI from transmission-line corona and/or signal scattering from overhead conductors have been evaluated analytically by Silva and Olsen (2002). More specifically, their analysis shows that scattering is unlikely to lead to significantly reduced signal strength, and that corona and gap noise are small enough at 1200–1500 MHz to be neglected. These conclusions have been supported by a small number of practical measurements made under transmission lines with GPS receivers. It is thus unlikely that power line conductors will interfere with use of the GPS satellite signals.

12.10.4 Differential Global Positioning System (DGPS)

There are a number of error sources for GPS receiver operation, including: satellite clock and orbit errors, ionosphere and troposphere delay, multipath, receiver noise, and errors due to satellite constellation geometry. There are also a number of applications (such as harbor navigation, positive train control, and precision agriculture) that require accuracies of 5-10 m or better (Enge and Misra 1999). Since the accuracy of the GPS system is not sufficient for these applications, the system is being improved with augmentations such as differential GPS (NDGPS). With NDGPS, corrections are provided to users to improve accuracy by compensating for some of the errors inherent in autonomous GPS use. More specifically, with DGPS, two GPS receivers are used: a reference unit and a mobile or rover unit. The reference receiver is placed at a stationary location with a position previously determined to a high degree of accuracy by surveying. This reference receiver determines its position using GPS signals, and a computer derives the position error and calculates differential corrections that can be applied by the rover to yield a more accurate position. Users with mobile GPS receivers that are equipped to receive and process these corrections in real time can realize significant improvements in accuracy improvements—in some cases, to the 1-3 m range or better (Parkinson and Spilker 1996; Enge and Misra 1999).

The DGPS correction messages can be made available by various methods. In one method (the Wide Area Augmentation System or WAAS), correction signals are broadcast from separate WAAS system geostationary satellites at the same L1 frequency (1575.42 MHz) as GPS. Because the L1 frequency is used (see Section 12.2.3), there is not expected to be any interference between high-voltage transmission lines and WAAS-enabled GPS receivers. Another system (the Nationwide Differential GPS System or NDGPS) can be expected to have interference from high voltage transmission lines under some conditions. This system consists of a network of broadcast stations operated in the 283.5-325 kHz band by the United States and many other governments. The reason why this may be interference is that EMI fields from corona on transmission lines during rain can be quite strong in this frequency range. In fact, anecdotal reports by agricultural users of coastal NDGPS stations indicate that power line electromagnetic noise can be a problem for NDGPS receivers if it exceeds the background atmospheric noise. Some GPS receiver manuals also mention the potential for noise/interference problems near to electric power lines.

The NDGPS messages are modulated onto the low-medium frequency carrier wave by minimum shift keying (MSK) with transmission rates that are presently 100 and 200 bits per second (USDOT 1998). The 99% power containment bandwidth of the MSK modulated signal is equal to 1.17 times the transmission rate (USDOT 1998). This means the NDGPS broadcast information is contained in a relatively small bandwidth (i.e., 117 or 234 Hz).

The specified minimum field strength for coverage of the NDGPS broadcast signal is usually 75 μV/m or 37.5 dBμV/m. Many NDGPS sites with a 200 bit per second transmission rate have a specified minimum field strength of 100 μV/m (or 40 dBV/m).

As an example, consider a calculation of the minimum signal-to-noise ratio (see Chapter 9) needed for a NDGPS receiver to properly operate in corona noise. It will be assumed here that that the NDGPS receiver has a bandwidth of 234 Hz. It will be further assumed that the electromagnetic noise is 58 dBμV/m as measured in a CISPR receiver (i.e., a 9-kHz bandwidth). This figure is typical of the interference measured near a 387-kV transmission line in average measurable rain, as quoted in Table 9.5-4. This noise can be converted to rms noise (see Section 9.3.1) by subtracting 8 dB and to the bandwidth of the NDGPS receiver by adding 10 $\log_{10}(234/9000)$ = -15.8 dB. The resulting noise level is 34.2 dB μV/m. If the signal strength is 100 μV/m or 40 dBμV/m, the receiver must operate

properly with a signal-to-noise ratio of 5.8 dB. If a receiver has a minimum signal-to-noise ratio for proper operation less than this, it will not work properly. Given typical minimum signal-to-noise ratios for digital receivers, it would be no surprise that this noise level could cause the receiver to malfunction. It should be noted here that the calculation reported above assumed a minimum signal strength for the NDGPS signal. In most cases, the signal strength will be significantly above this level.

It has been shown (Silva 2002) that NDGPS receivers, operated close to 345- to 765-kV transmission lines in corona, could experience a decreased SNR that may degrade receiver performance.

The practical consequences of poor NDGPS signal reception are illustrated by the results of measurements taken using an NDGPS-equipped vehicle driven slowly across a multiple transmission-line easement (double-circuit 120- and 345-kV transmission lines). The high-end GPS receiver carried by the vehicle was augmented with NDGPS and used a roof-mounted, shielded H-field antenna for both GPS and NDGPS signal detection. As the vehicle was driven, its position, as reported by the NDGPS system, was logged at 1-s intervals. The data were taken on two different days while driving along the same route under the transmission lines (at midspan) in fair weather and in light steady rain when corona would be more prevalent. The data collection route across the easement started about 100 m south of the 120-kV line and proceeded laterally on a straight line to traverse the easement by crossing first under the 120-kV line and then, in succession, under each of the two double-circuit 345-kV transmission lines. The results are shown in Figures 12.10-1 and 12.10-2 for fair weather and rain, respectively.

The plot of positions approximates a straight line in Figure 12.10-1 during fair weather as expected since the vehicle traverse was not exactly a straight line and the position accuracy was within 1 m or less. As Figure 12.10-2 indicates, the SNR was reduced by the corona noise until it went below the minimum required to maintain lock on the NDGPS beacon. At this point, the NDGPS receiver experienced a loss of the NDGPS differential correction messages and suddenly reverted to the standard positioning service with the associated lack of accuracy. Without NDGPS, the reported position suddenly jumped to a different position with significant error. As the measurement vehicle continued to traverse the easement, NDGPS operation was intermittently resumed, albeit with some aging of corrections (i.e., extrapolations using older corrections), which is representative of marginal or suboptimum receiver performance. Near the edge of the easement, NDGPS corrections were again received on a timely basis, and the final few positions shown in Figure 12.10-2 were close to the correct values.

Note that in this particular experiment, the signal from the closest NDGPS transmitter was significantly reduced by re-radiation from the power line ground wire and tower combination because the angle of arrival of the NDGPS signal was almost parallel to the transmission line. The next closest NDGPS transmitter (used by the receiver when the first was unavailable) was significantly further away, hence its signal was very small. This combination of conditions was unusual.

It should also be noted that the measurements reported in Figures 12.10-1 and 12.10-2 were taken before the "selective availability" option was removed by the U.S. government. This option intentionally reduced the position accuracy for the nonaugmented GPS system. After this option was removed, data taken when the NDGPS corrections were unavailable would not have errors as large as those shown in Figure 12.10-2.

These measurements demonstrate that, even with a very high quality digital GPS/NDGPS receiver and antenna, corona noise can degrade NDGPS receiver performance in the region near transmission lines. There was no apparent effect on the GPS satellite's microwave signal reception

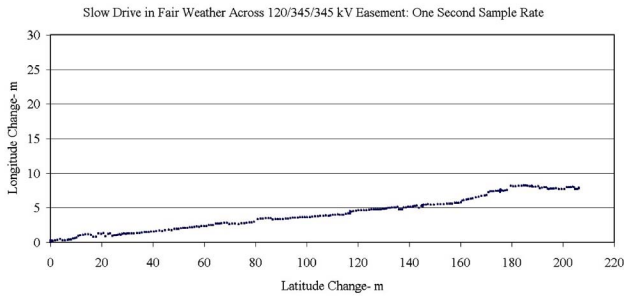


Figure 12.10-1 Plot of positions logged using digital GPS unit (augmented with NDGPS), taken while driving across 120/345/345-kV easement during fair weather.

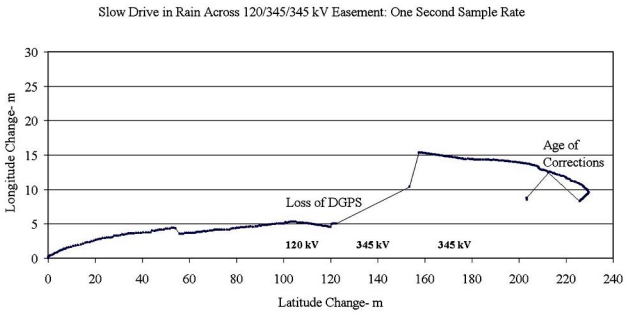


Figure 12.10-2 Plot of positions logged using Digital GPS unit (augmented with NDGPS), taken while driving across 120/345/345-kV easement during rainy weather.

quality. However, the NDGPS low-medium frequency signals could not be used at some locations close to the 345 kV lines, even with the closest NDGPS broadcast beacon only about 20 miles away.

Gap discharge sources on power lines can also generate radio frequency noise in the NDGPS band, as previously described. These potential RF noise sources are most commonly associated with ubiquitous distribution lines but can be found on transmission lines as well. It has been shown by Silva (2002) that gap discharge RF noise can significantly raise the noise floor in the NDGPS band. It is thus possible under certain conditions that NDGPS receiver performance may be degraded to suboptimal levels by gap discharge noise sources. Of course this will depend on many factors, such as NDGPS receiver and antenna design, signal strength, noise level, distance from source, and weather (gap sources are often quiet during wet weather). No further discussion of this will be given here since most gap sources are associated with distribution lines, which is not the major subject of this book.

12.11 INTERFERENCE WITH THE OPERATION OF COMMUNICATION RECEIVERS

It is well known that transmission lines can interfere with AM/FM/TV receivers, amateur radio receivers, aircraft communication receivers, and specialized devices such as radio astronomy antennas. At frequencies below approximately 10 MHz, corona noise may dominate during foul weather. Above 10 MHz, however, gap discharges will be the primary source of interference. Since these topics have been covered in detail in Chapter 9, the reader is referred there for further information.

12.12 IMPACTS ON AGRICULTURAL OPERATIONS NEAR TRANSMISSION LINES

12.12.1 Introduction

Issues that relate to agricultural operations near power lines include: (1) possible biological effects on plants, wildlife, and domestic animals; (2) the use of motorized equipment; (3) the possibility of shocks from metallic objects such as vehicles, fences, and support structures for crops; (4) the safety of using spray irrigation systems; and (5) interference with the operation of magnetically guided cornering arms associated with center-pivot irrigation systems.

Aside from the material covered in Section 12.16 on designing transmission lines to minimize avian interactions, the first issue is really outside the scope of this document. However, because the literature is not very well known, it is useful to refer to a relatively recent review of the literature (Lee et al. 1996). In this review, the authors concluded that plants growing near transmission lines generally experienced no adverse effects of power frequency electric and magnetic fields. One effect that was observed was damage due to corona on the sharp tips of leaves and branches (see Section 7.15.3). Honeybee hives were adversely affected by electric-field-induced shocks and current, but these effects can easily be mitigated by shielding. Finally, relatively few effects on wildlife and domestic animals have been reported.

The use of motorized equipment under transmission lines raises two questions. The first is the clearance required between them and the power line. This subject is discussed later in Section 12.13. The second is the possibility that a person who touches the equipment will experience either a transient or steady-state shock due to electric field effects. This subject is discussed in detail in Chapter 7, in Sections 7.8 and 7.10, and in Section 12.13.

Utilities that have a considerable amount of irrigated land within their service areas have conducted research on, and developed policies for, the installation and operation of irrigation systems near their transmission lines (BPA 1978; Starr et al. 1969; Ewy et al. 1981). In addition, the IEEE Corona and Field Effects (CFE) Subcommittee held discussions on this topic. While the results of these discussions were not published, they represent the thinking of a group of IEEE members on this subject. The following is a summary of the findings of the above-mentioned research and the IEEE discussions.

First, it was recommended that the minimum distances shown in Table 12.12-1 should be maintained between irrigation pipes and equipment and energized conductors. Since the height of conductors can change with the electrical load on the line, it is important to know the minimum height of the line before applying the distances in Table 12.12-1. Further, according to Bonneville Power Administration (BPA) policy, “all metal pipe lines, electrical power cables and communication cables should be kept 16 meters (53 feet) from any part of a BPA structure including any grounding system and perpendicular to the transmission line centerline” (BPA 1978). Finally, any underground water supply piping, electric power cables, and communi-

Table 12.12-1 Minimum Separation Distances between Irrigation Equipment and Transmission Lines. (Note that these distances should never be measured with devices such as tape measures, poles, etc.)

Voltage (kV)	Minimum Distance
765	7.30 m (24 ft)
500	5.79 m (19 ft)
345	4.88 m (16 ft)
230	4.26 m (12 ft)

cation cables crossing the right-of-way should do so at an angle of not less than 60° to the centerline of the transmission line and buried, if possible, a minimum of 2 ft underground.

It was also recommended that, to avoid nuisance shocks, the unloading of irrigation pipe sections from a vehicle should be done at least 15.24 m (50 ft) horizontally from the nearest conductor. Caution should also be used when touching irrigation equipment used near power lines. To avoid nuisance shocks, it is essential that the equipment be grounded. However, when long pipes (such as with center-pivot systems) are used, magnetic fields from power lines can induce voltages at the ungrounded end (if the irrigation system is parallel to the power line). Thus these ends should not be touched, and for maintenance, the long pipe should be oriented perpendicular to the transmission line to minimize magnetic-field induction.

12.12.2 Operation of Irrigation Equipment

Whenever possible, it is recommended that irrigation systems be operated so that there is no direct contact between the stream of water and the power line. A continuous stream of water should never be directed at energized conductors. However, when irrigation nozzles cause the water to break up into a spray, the probability of line-to-nozzle flashover is greatly reduced (Starr et al. 1969; Ewy et al. 1981). Thus, it is important that the irrigation system be designed to produce a spray rather than a continuous stream. Generally, any obstruction or discontinuity in the pipes, hoses, and nozzle (such as a ring insert) will cause breakup of the water stream.

The work of Starr et al. (1969) and Ewy et al. (1981) on determining minimum conductor-to-nozzle distances for safe operation of the irrigation system when the stream is in contact with an energized conductor can be summarized in the following way. Since it is nearly impossible to model the impedance of the spray, these results are based on measurements of leakage current flowing from the transmission line through the water spray (via conductance through droplets and capacitance between them) and to ground via the irrigation system. When a person touches the irrigation hardware, a portion of this current flows through him/her to ground. The process by which this occurs is illustrated in Figure 12.12-1. The fundamental criterion on which the recommendations are based is that this current through the person should not exceed 5 mA. Some example results are given in Table 12.12-2. For these calculations, it has been assumed that the person's body resistance is 1500 Ω, the irrigation system ground resistance is 10 Ω, the water conductivity is 1200 μS/cm, and the water pressure is 80 psi.

12.12.3 Interference with Cornering Guidance Systems

For many years, center-pivot irrigation systems have been used to provide automated uniform irrigation of agricultural fields. These systems consist of a long pipe mounted on motor-driven wheels (Figure 12.12-2). The system is driven in a circle around a field as shown in Figure 12.12-3. Water is connected to the pivot point at the center and sprayed on the field as the system rotates around the field. Since some of these systems are located near high-voltage transmission lines, questions have been raised about the potential for flashover initiation, the potential for shock hazards for personnel touching the system, and proper techniques for handling irrigation pipe. Responses to these questions have been summarized above.

One drawback of center-pivot irrigation systems is that most plots of land are square or rectangular in shape, while the footprint of the land irrigated by the system described above is circular. Thus, land in the corners of the field is not well irrigated. To resolve this problem, manufacturers

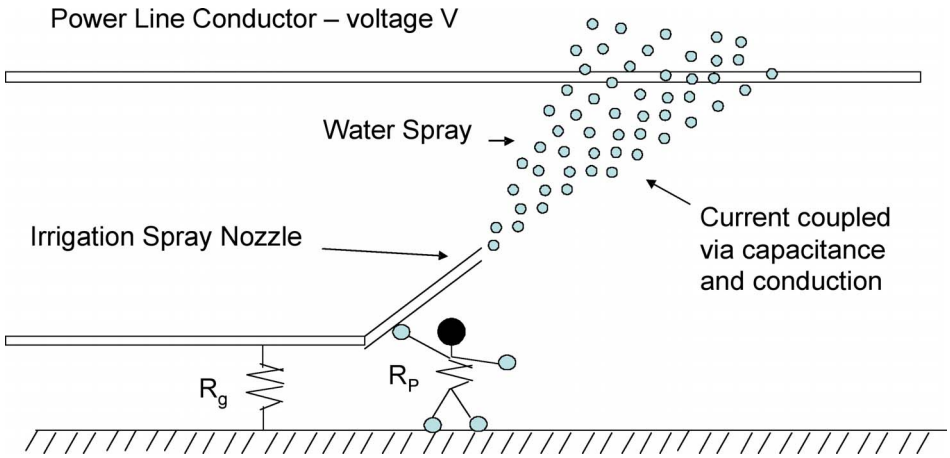


Figure 12.12-1 Illustration of current flow through spray, irrigation ground and person to ground.

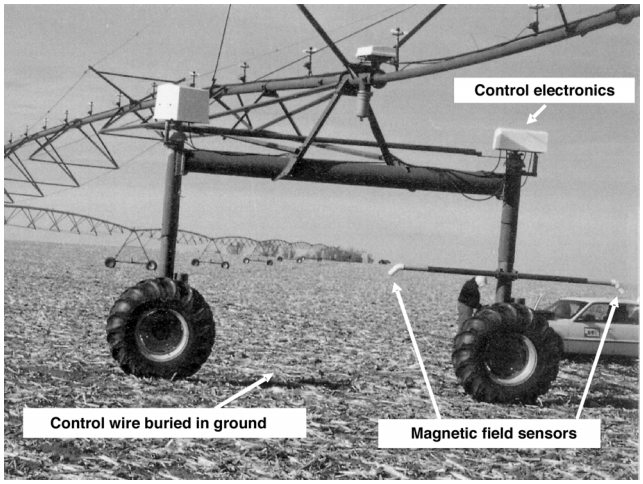


Figure 12.12-2 A center-pivot irrigation system. This particular one is a cornering unit with a section of pipe near the end that can rotate separately to fill in the corners of the field as shown in Figure 12.12-3.

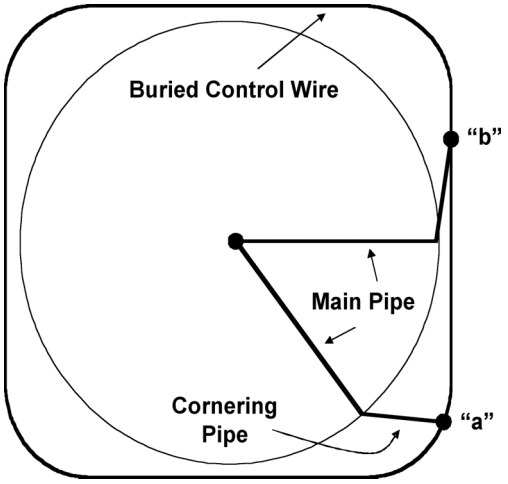


Figure 12.12-3 Diagram of a corner irrigation system from above.

developed "cornering" systems that consist of an additional length of pipe at the end of the system that can be swiveled with respect to the main pipe. This type of system is pictured in Figure 12.12-2 and diagrammed in Figure 12.12-3. The swiveling pipe tends to align with the main section of pipe when in a corner of the field and thus extends the length of the system into the corner (condition "a" in Figure 12.12-3). The swiveling pipe is perpendicular to the main section of the pipe when the system passes to the short edge of the field (condition "b" in Figure 12.12-3).

The orientation of the swiveled corner pipe is controlled by a magnetic-field guidance system. The guidance system employs a buried wire that carries a 1000-Hz current. More details of such systems can be found in (Olsen and Heins 1998). Although the system is designed to follow the 1000-Hz magnetic field, a strong 60-Hz field can interfere with the system. Thus, the operation of these systems near power lines can, in principle, be compromised.

Tests with one system indicated that a 50 μT magnetic field at 60 Hz was required to interfere with the operation of the guidance system (Olsen and Heins 1998). Of course, other manufacturers' systems may be designed with different filtering systems and hence may have different thresholds.

12.13 USE OF VEHICLES AND LARGE EQUIPMENT NEAR TRANSMISSION LINES

12.13.1 Introduction

Use of vehicles and large equipment on transmission-line rights-of-way gives rise to two safety concerns: inadvertent electrical contact with energized conductors, and capacitive coupling of currents and voltages to these large objects. Electrical contact with transmission-line conductors can produce fatal shocks for persons on or near a vehicle. Induced currents and voltages on large vehicles represent a potential source of nuisance or hazardous shocks when contacting the vehicles (Section 7.8). Under extremely rare circumstances, spark discharges associated

Table 12.12-2 Conductor-to-Nozzle Distance for Water Spray

	Conductor-to-Nozzle Distance[1] m (ft)				
Nozzle Diameter mm (in.)	115 kV	230 kV	345 Kv	500 kV	765 kV
19.5 (0.75)	3.66 (12.0)[3]	3.66 (12.0)[3]	4.7 (15.4)	6.4 (21.0)	7.8 (25.6)
22.9 (0.9)	3.66 (12.0)[3]	5.2 (17.1)	6.9 (22.6)	9.2 (30.2)	10.7 (35.1)
27.9 (1.1)	4.2 (13.8)	7.3 (23.9)	9.2 (30.2)	11.2 (36.8)	12.6 (41.3)
35.6 (1.4)	5.69 (18.7)	10.7 (35.1)	13.8 (45.3)	17.3 (56.8)	19.7 (64.6)
40.6 (1.6)	6.19 (20.3)	13.4 (44.0)	17.3 (56.8)	21.0 (56.8)	22.9 (75.1)
49.0 (1.93)[2]	6.19 (20.3)	13.4 (44.0)	16.7 (54.8)	19.9 (65.4)	22.1 (72.5)

1. For water spray, the water stream is broken up so there is no solid and continuous stream.
2. Ring insert.
3. Limited by regulations (OSHA).

with induced voltages can also cause fuel ignition (Section 7.14.1) (Deno and Silva 1985).

Electrical safety codes are intended to minimize the occurrence of situations that give rise to electrical contact and induction hazards. In addition, strict adherence to safe working practices near transmission lines is also required to ensure hazardous situations do not arise. Safe practices include limiting the height of vehicles, equipment, and accessories, such as antennas, masts, or booms, to maintain safe electrical clearances when passing under conductors. Reduced ground clearances should be anticipated in areas with heavy snow accumulation.

In the United States, the National Electrical Safety Code (NESC 2001) specifies the minimum clearance required for conductors over various areas such as roads and highways, railroads, bodies of water, and areas accessible to pedestrians only. These clearances are intended to provide safe electrical clearances for typical equipment, vehicles, and sailboats passing under the lines.

12.13.2 Induced Currents from Vehicles

For lines with voltage greater than 98 kV ac to ground, the NESC limits the induced short-circuit current to the largest vehicle anticipated under the transmission line. The maximum allowed short-circuit current is 5 milliamperes (mA). For a person to actually experience the maximum short-circuit current requires a very-well-insulated large vehicle and a well-grounded person. Occurrence of these two conditions is highly unlikely. In addition to the induced current, very perceivable and probably annoying spark discharges generally serve as a warning of the presence of annoying contact currents (Section 7.10.5).

The 5 mA criterion approximates the let-go current threshold for 99.5% of children; in other words, only 0.5% of children would be unable to release a gripped contact at this current level (Reilly 1992, p. 435). The Underwriters Laboratories uses a limit of 0.5 mA for continuous currents from hand-held appliances. This is the level at which most people can perceive a continuous current through their hands. Although a startle reaction with unintended movement is possible at the 0.5 mA level, it is not likely (Reilly 1992, p. 434).

An estimate of the short-circuit current from a vehicle requires both the electric field in the area of the vehicle and the size of the vehicle, as discussed in Section 7.8. The specified condition for computing the maximum induced current to a vehicle is with the line operating at maximum voltage and conductors at final unloaded sag at 50°C.

The largest anticipated vehicle at road crossings can be determined from the appropriate governing body for the area. In the United States, the federal and/or state governments set limits for the dimensions of trucks. The federal limit for vehicle length on the national highway network is a facilitating law that specifies the minimum lengths that states must allow on national highways: at least 48 ft (14.6 m) for semitrailers in a semitrailer configuration; and at least 28 ft (8.5 m) for trailers in a twin-trailer combination. (USDOT 2000, Vol. I, pp. II-11, II-16, II-17; Vol. II, p. III-11). Thus, limits on the total length of vehicles are generally set by the states, with many states allowing semitrailers longer than the federally stipulated minimum length of 48 ft (14.6 m).

The federal limit on truck width is 102 in. (2.6 m). Height limits on trucks in the United States are determined by the states, with western states limiting truck height to 14 ft (4.2 m) and eastern states (except Maine) limiting height to 13.5 ft (4.1 m). States may also allow oversize vehicles with special permits. Thus, information on the largest anticipated vehicle for highway and road crossings is best obtained from the government agency having jurisdiction.

At road crossings, the largest vehicles are generally oriented perpendicular to the line. In this case, both the magnitude and phase of the electric field may vary over the length of the vehicle. The induced current to the vehicle reflects an average of the field over the entire vehicle, including the effects of varying phase. Examples of computations of the average field over long objects are given in Section 7.8.4 and in Reilly (1979).

Large farm equipment, such as combines, also may need to be evaluated with respect to the 5 mA criterion. In agricultural areas, the minimum conductor clearance can be reduced from that at road crossings, resulting in higher electric fields with correspondingly higher induced currents. For large vehicles of odd shapes, their equivalent charge-collecting area may be estimated using the formulae for standard shapes in uniform fields, given in Table 7.8-1, or the 45° shield area approximation shown in Figure 7.8-5.

Estimates of the short-circuit current from a vehicle assume that the entire induced current to the vehicle passes through a person to ground. This is equivalent to no leakage current through the vehicle tires and zero impedance for the current path through the person. This is a worst-case estimate of the current that could pass through a person touching an ungrounded vehicle. In realistic situations, there is finite resistance to earth through the vehicle tires that offers an alternative current path.

Farm vehicles operating on soil are likely to have low resistance to ground. Dragging a chain from the vehicle is a commonly recommended method of reducing nuisance

shocks for such vehicles under transmission lines. However, the effectiveness of such a method has not been substantiated.

The impedance of the person to ground may be substantial due to contact resistance between the shoes and ground or the resistance of the shoes themselves (Section 7.8.5). The impedance of a thin, highly resistive layer on the surface of the earth can also limit current flow during contact (Section 12.2).

As discussed in Section 7.8.5, both of these practical conditions (vehicles not well insulated and person not well grounded) will tend to reduce the current through a person touching a vehicle in an electric field to values well below the worst-case short-circuit current. Short-circuit current measurements on various realistic surfaces are reported in Section 7.8.5. The results indicate that, for realistic conditions, the actual currents from vehicles to persons would generally not be perceptible even when the worst-case short-circuit current approaches the 5 mA criterion.

12.13.3 Spark Discharges (Induced Voltages) from Vehicles

As an insulated person contacts a grounded vehicle or as a grounded person touches an insulated vehicle in a 60-Hz electric field, a series of spark discharges may occur across the air gap between finger or hand and the vehicle (Section 7.10.3). After contact is established, a steady-state current flows. The intensity of the spark discharge depends on the field level, the voltage difference between person and vehicle, the level of insulation of person and vehicle, and the size of the electrically ungrounded vehicle. Perceivable spark discharges occur for contacts with other objects under transmission lines, such as fences or blades of grass. However, contacts with passenger, commercial, and farm vehicles probably represent the most common source of concern and complaints about nuisance shocks.

Reaction to spark discharges can range from imperceptible, to perceptible, to annoying, and to a startle with inadvertent movements (Section 7.10.5). Individuals vary widely in their response to spark discharges. The level of response is dependent on the voltage between the person and object, the capacitance of the charged object, and the leakage resistance of the charged object (Reilly 1992, p. 347). For example, the voltage threshold for perception of repetitive 60-Hz discharges (from a constant capacitance) decreases as the leakage resistance decreases.

An example of the evaluation of the response to spark discharges from a charged gutter is provided in Section 7.10.5. The approach used for the gutter can easily be applied to vehicles. As with induced currents, the actual value for the induced voltage on an object is usually much reduced from the worst-case situation with the object perfectly insulated from ground. This leads to a reduction in the level of response to potential spark discharges from that under worst-case conditions. Figures 7.8-20 to 7.8-22 provide statistical distributions for person-to-vehicle voltages under practical conditions.

12.13.4 Fuel Ignition

It is extremely unlikely that conditions for fuel ignition by a spark discharge from an insulated vehicle to ground will occur in an electric field under a transmission line, and no such event has been reported (Section 7.14) (Deno and Silva 1985). Nevertheless there are ideal conditions under which such an event could occur. In addition, the possibility of fires during refueling is not limited to those ignited by spark discharges. Therefore utilities often recommend against refueling under transmission lines for both public safety and line reliability reasons.

12.13.5 Parking Lots

The use of rights-of-way for vehicle and equipment parking lots is generally controlled by the transmission-line operator as the owner in fee or through easement language. A parking lot under a 345-kV line is shown in Figure 12.13-1. Concerns related to this use are physical damage to transmission-line structures, exceedance of the 5 mA criterion for large vehicles, frequent opportunities for person-vehicle contact in high electric fields that produce nuisance shocks, and vehicle fires arising from fuel ignition or mechanical problems, such as broken fuel lines, faulty catalytic converters, electrical failures, and overheating. By creating a public space and increasing human activity under energized lines, parking lots can also increase the opportunities for unsafe activities that are hazardous whenever they occur near transmission lines. Some of these would include unauthorized tower climbing, transport of excessively tall objects under lines, or kite flying. Corona-generated audible noise during foul weather

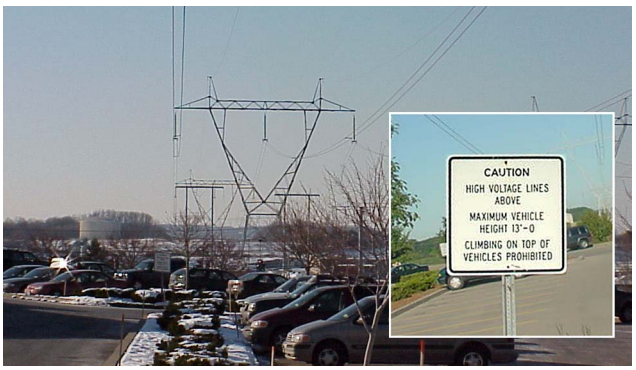


Figure 12.13-1 Parking lot directly under 345-kV line with an example of a warning sign (inset).

from lines directly overhead can also be a source of public complaints and/or unease when using parking lots.

Physical access to towers can be limited by no-vehicle zones around towers and anti-climbing barriers. Warning signs can also be used to advise the public of unsafe activities (see Figure 12.13-1, inset).

Induction effects related to electric fields can be controlled by exclusion of vehicles above a certain size from areas of peak field intensity or by reducing the fields in the parking lot area. One approach is to apply the NESC clearance for road crossings that is based on the 5 mA short-circuit current criterion to parking lots. However, the increased public use of a parking area beyond that at road crossings may result in an increased number of nuisance-shock complaints. To reduce the number of complaints requires measures that reduce the electric field in parking lots below levels required by the NESC 5 mA criterion.

Electric fields can be reduced by increasing the conductor clearance or by employing the shielding methods described in Section 7.16. For example, a horizontal grid of grounded wires can be employed in the area of minimum clearance to reduce ground level fields (Section 7.16.2). In instances where field reduction is required in a limited area, it may be possible to use grounded light poles or other conducting architectural objects to achieve the required field reduction (Section 7.16.5). Lower voltage lines suspended under transmission lines can also provide shielding of the electric field (Section 7.16.6). All shielding options should meet code requirements for electrical clearance and, if grounded, employ redundant grounds to minimize the possibility of a shock hazard caused by a damaged ground.

Trees and other vegetation also provide shielding. However, their susceptibility to damage and the need to maintain electrical clearances may preclude their use as permanent shields.

As discussed in Section 12.16.2, the surfaces of parking lots will help reduce the impact of induced currents and voltages. With the vehicle and person standing on the same surface, it is difficult to achieve the worst-case condition with the entire short-circuit current from a vehicle passing through a person.

The Bonneville Power Administration (BPA) policy on parking lots provides an example of criteria that are more stringent than the 5 mA criterion for short-circuit current (Lee et al. 1996, p. 5-5). Instead of let-go current, the BPA criteria for electric fields are based on limiting the probability of perception or annoyance from field effects. This results in a 3.5 kV/m limit for shopping center parking lots, with the stipulation that parking for large trucks is not allowed. This field produces a short-circuit current in sedans and pickup trucks of less than 1 mA in the worst-case situation. Under realistic conditions, the current level is well below 1 mA and is generally not perceptible. In commercial and industrial parking lots, the field limit is reduced to 2.5 kV/m with the intent of limiting the short-circuit current to 2 mA for large trucks. Shopping center and commercial parking lots are not permitted where fields exceed 3.5 and 2.5 kV/m, respectively.

Limiting the electric field and/or vehicle size in parking lots reduces the already low probability for fuel ignition by spark discharges during refueling (Deno and Silva 1985). Nevertheless the potential public health and transmission-line reliability impacts of a fire under a line lead to the recommendation of no refueling in parking lots. Posting signs advising of the restriction on refueling vehicles can serve as a warning to the public.

12.14 IMPACTS ON BUILDINGS NEAR TRANSMISSION LINES

In the United States, the expansion of urban and suburban areas into previously rural areas has increased the pressure to place houses and other buildings near new and existing transmission lines. Whether structures are allowed on the right-of-way or not is determined by the operator for lands owned in fee and otherwise by language in the easement agreement. Generally, buildings are not allowed under transmission lines in the United States. In other countries, buildings may be permitted on rights-of-way. The presence of buildings raises issues related to the reliability of the transmission line and the safety and annoyance of occupants.

Combustible materials, including structures, are generally prohibited from transmission-line rights-of-way to minimize the chance of fire. Flames or smoke can cause a flashover to ground. The presence of buildings also increases the level of human activity under and near transmission line, with opportunities for hazardous or unsafe activities. Of special concern is the possibility of a person or persons upending a long object and reaching unintentionally near the conductors (to within the flashover distance of the conductors). Construction of buildings on a right-of-way can also encroach on required safe electrical clearances and increase the required height of the conductors above ground.

Many of the safety and annoyance issues for occupants of structures near transmission lines have been discussed in previous sections: electric and magnetic field induction effects in Chapter 7; interference with computer monitors in Appendix 7.4; EMI, including radio and television interference, in Chapter 9; and audible noise in Chapter 10.

Induced current and voltage shocks from building components are possible even in the reduced electric field beyond the edge of the right-of-way. Such shocks can lead to inadvertent startle responses that could be hazardous. For example, a startle response while on a ladder cleaning gutters or installing an antenna could increase the risk of falling. Grounding of conducting building components, such as gutters, metal roofs, and metal siding, may be necessary to eliminate these objects as potential sources of shocks. However, this grounding does not remove the startle response initiated by the induced voltage shocks received by an insulated person touching a grounded building component. Electrically bonding the person to the grounded building component is the only way to eliminate such a hazard. Depending on the size of the component, grounding may be required off the right-of-way. Metal window frames or other conducting objects that penetrate the walls of a structure can be a source of shocks inside a structure as well as outside. Formulae for the charge collecting areas and spark-discharge capacitance of various structural components and shapes are described in Table 7.8-1 and Section 7.8.2.

The electric field on the roofs of buildings adjacent to transmission-line rights-of-way will be increased from the field at ground level. Consequently, construction and maintenance activities on the roof may require special precautions to avoid nuisance shocks. For example, grounding sheet metal ducting and other large metal objects may be required during installation.

Conducting metal objects are generally well separated from transmission-line structures. However, as houses and other buildings are placed along the edges of rights-of-way, separation requirements may be violated. When a fault to ground occurs at a tower with a nearby, long conducting object, a hazardous voltage may be transferred to distant points, as described for pipelines in Section 12.3. Similarly, hazardous conditions may arise when a grounded fence passes near a faulted tower and is also near or attached to a building. In such cases, the increased voltage at the transmission tower (or a portion of this voltage) may be transferred to the distribution line and internal building wiring designed for lower voltages. The result can be damaged equipment or fire as the insulation level of the lower voltage wires is exceeded, or possibly a severe shock if someone is in contact with the affected wiring.

Above-ground and in-ground swimming pools are not tall structures. However, their presence on rights-of-way can pose similar problems to those already discussed for other activities: the danger of upending a long pool cleaning tool into overhead lines and nuisance shocks from persons to ground and between persons near the pool. In addition, in the unlikely event of a nearby fault, swimming pools may concentrate fault currents and cause injury or death in a pool, just as faulty pool wiring can. For these reasons, some utilities discourage pools on rights-of-way.

12.15 IMPACTS ON PUBLIC USE OF RIGHTS-OF-WAY

12.15.1 Introduction

As open space declines in populated areas, pressure increases for the public use of transmission-line rights-of-way for parks, playing fields, playgrounds, pedestrian and equestrian trails, and other recreational activities. Whether the right-of-way is owned outright or acquired through an easement determines the extent to which these activities on the right-of-way can be controlled by the transmission-line operator. For example, the language of an easement may only allow control over activities that could affect operation and maintenance of the line, such as the presence of fires and structures in campgrounds, but not trails or playing fields.

As with other uses and activities on and near a transmission-line right-of-way, public safety remains the principal concern of the operator and the user. Thus operators prohibit or discourage unsafe activities that might compromise the required electrical clearances built into the design of a line. Some of these activities include flying kites and model airplanes, tipping up long objects such as irrigation pipes, and sailing boats with tall masts. In addition, preventing tower climbing and limiting access to the areas around towers is also a priority in areas where the public might congregate. Many of these issues were discussed in Sections 12.13 and 12.14 with respect to vehicles and buildings.

Avoidance of the areas at the base of towers is advisable in the unlikely event of a fault to ground. As discussed in Section 12.2, a fault to ground can cause touch potentials and step potentials. These voltage differences between the tower and ground or along the ground can cause serious or fatal shocks to persons in contact with the tower or standing on the ground near the faulted tower. Persons using the right-of-way are advised to get away from towers and the conductors during lightning in the area.

The other concerns besides electrical safety when the public uses open spaces on rights-of-way are the possibility of nuisance shocks and possible annoyance from corona-generated audible noise especially during foul weather (Chapter 10).

12.15.2 Exposure Guidelines for the General Public

The transient nature of public right-of-way use precludes extended exposures at the field levels found near transmission lines. However, the short-term exposures on rights-of-way do occur at field levels higher than those found in common residential or occupational settings. The possibility of health-related effects associated with extended exposure to low-level electric and magnetic fields or with short-term exposures to elevated levels remains a controversial issue after many years of investigation (Section 7.13). To date, limits for electric and magnetic field exposures have been established based on short-term stimulation of the nervous system (ICNIRP 1998; IEEE 2002). The IEEE Standard (2002) contains an extensive discussion of the physiological, statistical, and methodological base or electric-field limits based on responses to spark discharges and magnetic-field limits based on nerve stimulation. Standard-setting bodies generally have not found a basis for setting exposure limits in the results of research on long-term health effects.

Exposure guidelines for the general public for electric and magnetic fields are given in Appendix 7.3. The limits promulgated by the International Commission on Non-Ionizing Radiation Protection (ICNIRP 1998) and those from the IEEE Standard for Safety Levels with Respect to Human Exposure to Electromagnetic Fields, 0-3 kHz (2002) are shown in Table 12.15-1. In the United States, several states have established regulations of their own for electric and magnetic fields on and at the edge of rights-of-way (Table A7.3-1). Several of these limits are based on the fields from existing lines in the state rather than on effects. Other countries and international organizations tend to follow the ICNIRP guidelines but also have promulgated standards of their own (Tables A3.7-4 and A3.7-5).

The limits imposed on electric fields are generally intended to limit short-term nuisance effects such as spark discharges, field perception, and steady-state ac currents (Section 7.10.5). Spark discharges are the most frequently perceived effects and are most likely to produce an annoying response. In Japan, electric fields under transmission lines are limited to 3 kV/m to limit perception of spark discharges or tingling sensations (Maddock 1992).

Table 12.15-1 Exposure Guidelines for the General Public to 50/60-Hz Electric and Magnetic Field

Organization	Electric Field, kV/m[1]	Magnetic Field, G[1]
ICNIRP (1998)	5/4.167	1.0/0.833
IEEE (2002)	5[2]	9.04

1. ICNIRP limits are for 50/60 Hz; IEEE limits are for 50 and 60 Hz.
2. Limit is 10 kV/m within power line rights-of-way.

The limits in Table 12.15-1 are applicable to persons walking on transmission-line rights-of-way. The electric-field limits will not be exceeded on rights-of-way for transmission lines up to 230 kV. For line designs at voltages of 345-kV and above, there are areas of the right-of-way where the field could exceed the ICNIRP limits of 5 and 4.167 kV/m for 50 and 60 Hz, respectively. Whether the limit is exceeded depends on the design minimum line-to-ground clearance. The area in the right-of-way where the limit is exceeded will be much less for a 345-kV line than for a 500- or 765-kV line.

The IEEE 10-kV/m limit for public exposure on rights-of-way will not be exceeded under 345-kV lines and is unlikely to be exceeded under 500-kV lines. However, portions of a 765-kV line right-of-way under and directly beyond the outside conductors near the point of minimum clearance (typically near midspan) could have fields in excess of the 10-kV/m limit, depending on the design minimum line-to-ground clearance.

The exposure guideline levels for 50/60-Hz magnetic fields in Table 12.15-1 are very unlikely to be exceeded on transmission-line rights-of-way for lines at any voltage.

12.15.3 Nuisance Shocks

The response of persons to spark discharges and hair stimulation under a high-voltage line were investigated at the EPRI Project UHV site in Lenox, MA (EPRI 1982). Data collected for 136 people insulated from ground indicate the levels of response to spark discharge as a function of unperturbed electric field at ground level (Figure 7.10-6). The median electric field for perception of a spark discharge from a wire to ankle (simulating a blade of grass) was about 1.7 kV/m; from a hand-held wet umbrella to thumb was about 1.2 kV/m; and from a ground rod to a fingertip was 2.7 kV/m. The electric-field levels for annoyance under these same conditions were considerably higher. The median electric field for annoyance from a wire discharge to the ankle was about 5 kV/m; from an umbrella to thumb was 4.5 kV/m; and from a rod to finger was 7 kV/m.

The annoyance levels indicate that, under worst-case situations with perfect insulation, annoying spark discharges can occur under transmission lines. However, as is the case with vehicles discussed in Section 12.13, several factors reduce the probability of worst-case conditions arising under operating transmission lines. These factors could include leakage across the footwear that reduces the insulation level of the person, the presence of shrubs and other vegetation that reduces the ground-level electric field, and human activities taking place at locations other than where the peak field occurs on the right-of-way.

Hair stimulation by electric fields occurs in very high fields (Section 7.10.5). The median field for perception of hair stimulation on an up-stretched arm among 136 persons was 7 kV/m (Figure 7.10-16). The median annoyance level for this same group was well above 20 kV/m. Annoyance from hair stimulation is not of concern for public exposures under transmission lines.

Steady-state currents above the perception level generally arise from contact with large conducting objects such as vehicles and ungrounded metal buildings (Sections 7.10.5, 12.13, 12.14). An insulated person will have a short-circuit current to ground. However, the current-collecting area of a person is small enough so that the magnitude of the current induced on the ground under a transmission line will generally be below perception levels and well below annoyance levels.

Thus, annoying spark-discharge shocks are the effect of most concern for the public using open spaces on rights-of-way.

12.15.4 Open-Space Uses of the Right-of-Way

Access to rights-of-way has prompted public and commercial uses of the open space under transmission-line conductors. Such uses as parks, trails, and nurseries increase the number of people in proximity to transmission facilities. In allowing or promoting these uses, the benefits are weighed against the safety and reliability issues described previously in this chapter and the uncertainty about a possible association of long-term health effects with electric and magnetic field exposure. The latter concern has led some utilities and regulators to discourage public use of rights-of-way as a precautionary measure. For new transmission lines, users may object to the intrusion of an energy facility into an otherwise natural setting.

Schools

The location of schools near transmission lines has been an issue of particular concern to many areas. For example, the California State Department of Education defined limit distances from transmission-line easements as follows (Section A7.3; Lee 1996, p. 5-9):

- 100 ft for 50- to 133-kV lines
- 150 ft for 220- to 230-kV lines
- 350 ft for 500- to 550-kV lines

These distances would result in electric fields well below the levels where spark discharges would occur and are based on a conservative approach to electric and magnetic field exposures.

Buildings, including schools, are generally not allowed on rights-of-way. However, in the event that school grounds are located on rights-of-way, play structures, permanent objects, and fences should be grounded, and access to areas around towers should be restricted.

Building a new transmission line near a school facility, or a new school near a transmission line, will likely face increased public opposition and should be avoided if alternate routing or an alternate location can be found.

Parks and Recreation Areas

Heavily used parks may require restriction of access to tower areas and other actions, such as posting warning signs regarding electrical hazards to discourage unsafe activities. In parks with athletic playing fields, picnic grounds, or other gathering places on the right-of-way, grounding of metal structures such as goals are recommended. Depending on the electric field strength, ground conditions, and type of shoes, users may experience perceivable spark discharges between one another or from body to ground.

Recreation areas in more natural settings may have vegetation that provides shielding of the electric field and a reduced potential for spark discharges. Trails can be routed to bypass the highest field areas and towers.

Fisherman using rivers, streams, and lakes crossed by transmission lines should be aware of the presence of conductors and avoid casting into the conductors. Care should be taken even though conductor heights above rivers, streams, and lakes are often increased either to provide clearance for boats or by topography.

During periods of heavy snow, cross-country skiers, snowshoers, and snowmobilers should be aware of the possibility of reduced clearances and cross under lines at points nearer to towers instead of near the point of minimum line height, typically near midspan.

Trails

Linear parks such as pedestrian, bicycle, and equestrian trails are compatible with transmission-line rights-of-way as long as safety precautions are followed. Depending on the electric-field strength, ground conditions, and type of shoes, users may experience perceivable spark discharges between one another or from body to ground. Persons on horseback will experience an enhanced electric field at the surface of the body (Section 7.10.2) and be more likely to perceive hair stimulation than when standing on the ground.

Commercial Activities

Nurseries, garden centers, and other outdoor commercial activities can take place on rights-of-way provided the safety precautions described above for other uses are followed. Of special concern are the absence of any trees or

other tall objects (greater than 14 ft) and the moving of tall objects under the conductors. Security fencing must be properly grounded and located at a suitable safe distance from any towers. The use of vehicles in such operations was discussed in Section 12.13. It is advisable to provide safety training to all employees regarding working under transmission lines. Depending on the electric field strength, ground conditions, and type of shoes, customers and employees may experience perceivable spark discharges between one another or from body to ground.

12.16 AVIAN INTERACTIONS WITH TRANSMISSION LINES

12.16.1 Introduction

Issues that relate to avian interactions with transmission lines include: (1) bird contacts resulting in bird deaths and outages, (2) bird collisions, (3) nesting, (4) bird feces insulator pollution, and (5) bird feces streamer outages.

12.16.2 Bird Electrocutions

Transmission facilities typically have sufficient clearances to avoid phase-to-ground and phase-to-phase bird contacts. However, electrocutions have been recorded on both tubular steel (Figure 12.16-1) and lattice structures (Figure 12.16-2). Bird electrocutions typically only occur at the lowest transmission voltages. The Raptor Research Foundation recommends a minimum of 152 cm spacing between phases and phase to ground to minimize eagle electrocutions. Utilities should review design tolerances to ensure that there are adequate clearances for birds and animals that traditionally use utility structures. Incorporating proper clearance before construction is preferable to costly retrofits. This process will also avoid costly outages and a potentially negative impact on consumer relations.

In addition to causing outages, bird electrocutions can result in fines. In the United States, the Migratory Bird Treaty Act (MBTA) protects all migratory birds. Under the MBTA, bird electrocutions can result in a $15,000 (USD) fine per electrocution. Under the Bald and Golden Eagle Protection Act (BGEPA), eagle electrocutions can result in a $200,000 (USD) fine. Utilities electrocuting birds will, at a minimum, be required by law to reconstruct or modify lethal poles in a manner that eliminates the electrocution hazard.

12.16.3 Bird Collisions

The potential risk of birds colliding with transmission lines depends on factors such as habitat types, line orientation to migratory flyways and foraging flight patterns, number of migratory and resident bird species, species' composition



Figure 12.16-1 Electrocuted red-tailed hawk under a steel structure. (Photo credit: EDM International, Inc.)

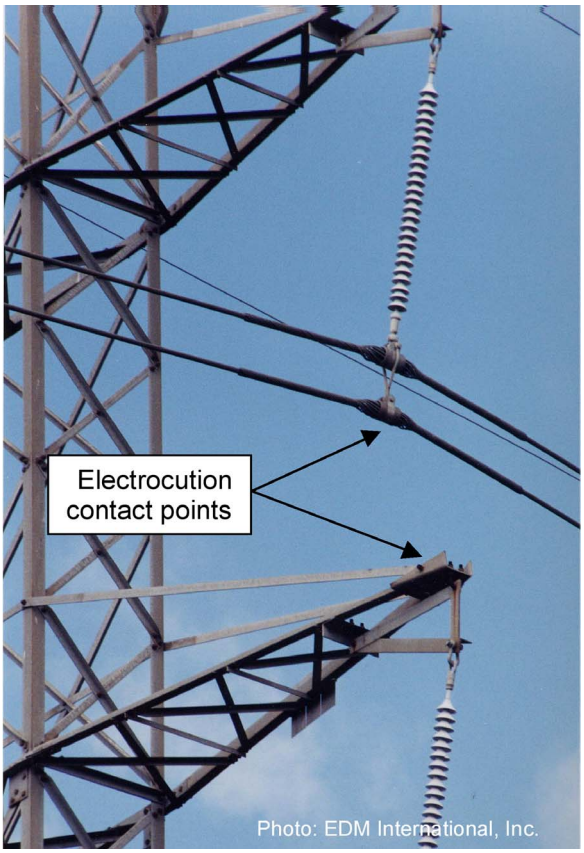


Figure 12.16-2 Lattice structure involved in vulture electrocutions. (Photo credit: EDM International, Inc.)

and area familiarity, types of human-related disturbance, and line design. Birds approaching at or below line height are most vulnerable to colliding with the conductors or static wires. Many species will alter their flight path to cross above larger primary conductors only to encounter the smaller overhead static wire.

Species with high wing loading and low aspect are at a higher risk of collision with power lines. Birds at greatest risk are species like rails and coots with short wings and heavy bodies. Some large, heavy-bodied birds such as herons, cranes, swans, and pelicans are sometimes collision casualties because of their large wingspans and lack of agility. Flying in flocks also restricts maneuverability and increases collision risk. The timing and duration of inclement weather and low-light conditions also may affect bird collision rates. Although bird collisions rarely result in outages, they can result in legal penalties, particularly when critically endangered species are involved.

A variety of markers are available to make power lines more visible. These devices consist of either rotating disks and plates (active devices) (Figure 12.16-3) or coils designed to simply increase the line profile (passive devices). The optimal diverter placement is to stagger the devices midway between each other on alternating lines to reduce the number of markers required. A significant portion of the cost associated with installing any marker is achieving the proper device placement. When stringing the conductors, it is important to mark where the diverter is to be placed rather than to perform measurements when the wires are in the air. This is more critical when installing markers with a helicopter or tall crane from a barge than when using a pull cart.

12.16.4 Nesting Issues—Structural

Nesting can become a structural issue in the case of very large birds or birds that build very large communal nests. For example, golden eagles build their nests in open habitats, preferring mountains and hills. As a result, these birds may build nests on transmission towers, and a typical nest is about 1 m in diameter. Once a nest is established, eagles often use the same nest year after year, adding new material. Nesting material typically consists of thick tree branches, twigs, and conifer needles. Over the years, some nests become enormous (Figure 12.16-4)—as much as 2 m in diameter, weighing more than 900 kg. In some cases, the added weight can become a structural concern.



Figure 12.16-3 Active type bird collision devices. (Photo credit: EDM International, Inc.)

Large nests can also be a barrier and hamper maintenance line crews. Birds defending their nests may pose an additional risk to linemen attempting to climb and work on structures. Depending on the type of nest and time of year, a permit may be necessary to remove or alter any nest (see Section 12.16.6). Utility employees should be aware that many diseases can be transmitted by contact with nests, and crews should wear gloves or use an inverted plastic bag to handle nest material. Breathing filters are also recommended because moving nests often disperses dried bird feces into the air.

12.16.5 Nesting Issues—Electrical

Birds typically construct nests using tree branches, twigs, and leaves. However, some larger birds, such as hawks, ravens, and golden eagles, incorporate pieces of bailing wire and barbed wire. Sometimes these conductive wires protrude from the nests, creating maintenance and safety issues (Figure 12.16-5). Even without conductive materials, these structures can be problematic if a nest falls or a strong wind blows the nest down. A collapsing wet nest can allow phase-to-ground faults.

If nests are removed, the established pair usually rebuilds at or near the site within a few weeks if it is near the breeding season. Permits may be required to relocate nests (see Section 12.16.6). Constructing alternative platforms in less critical portions of the structure is a good solution to avoid persistent nesting problems. Biologists should be consulted when installing alternative platforms to make sure the location, elevation, aspect, size, and shape are desirable for a particular bird species.



Figure 12.16-4 Golden eagle nest on a steel lattice transmission structure. (Photo credit: EDM International, Inc.)

12.16.6 Nesting Issues—Legal

Some birds nesting on power lines have special legal protection. In the United States, all active migratory bird nests are protected. Additional protection is afforded to eagles and threatened/endangered species. Under these laws, it is necessary to obtain federal permits to remove active nests from transmission structures. In the case of eagles and threatened/endangered species, a utility may not even disturb a nest without the necessary permit. These laws have utility operation and maintenance implications. For example, there may be transmission maintenance restrictions during the nesting season in order to avoid disturbance to eagle nests. It is important for a utility to contact the appropriate agency prior to removing any active nests or performing any activity near eagles or threatened/endangered species. There may also be additional state and local ordinances that pertain.

12.16.7 Nesting Issues—Liability

The monk parakeet is a South American species that has established feral populations in the United States after accidental and deliberate releases. These birds are a medium-sized with a long pointed tail and are distinguished by their bright-green color and gray throat, forehead, cheeks, and breast. The monk parakeet is unique because it is the only parrot that builds stick nests. These large, bulky, dome-shaped nests are made of woven twigs with numerous compartments. In southern Texas and Florida, these birds have readily adapted to using transmission towers (Figure 12.16-6).

In Texas, one utility caught a person illegally climbing one of their lattice transmission power structures in an attempt to retrieve young birds from a nest. This person wanted the birds to raise and sell. Handfed babies can be sold for $50 to $200. Although the utility was not having operational problems due to these nests, they elected to investigate methods to deter future nesting because of the potential liability associated with people climbing towers to capture birds. This utility also reviewed their warning signage and eliminated climbing rungs on nesting structures.



Figure 12.16-5 Osprey nest constructed with bailing twine on a steel lattice transmission structure. (Photo credit: Norbert Kilroe, Trans Alta Corp.)

12.16.8 Bird Pollution

An electrical fault can be caused by bird pollution when pollutant buildup takes place on the insulator disks. A coating of bird droppings undermines the insulating qualities of the insulator, ultimately resulting in a phase-ground flashover across the insulator string under wet conditions. Both large and small birds can cause such outages. Transmission structures can be fitted with shields (Figure 12.16-7) and insulated barriers (Figure 12.16-8) to reduce fecal contamination.

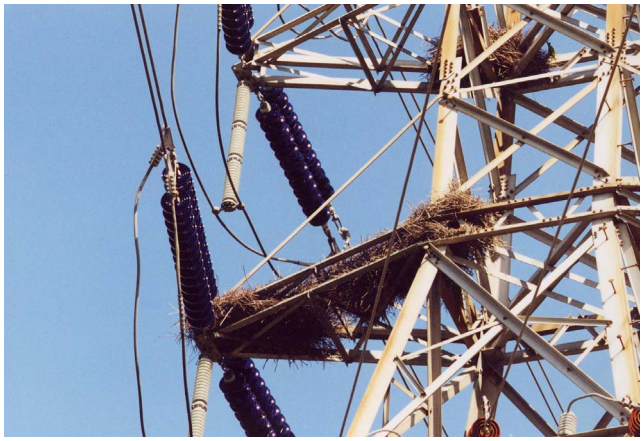


Figure 12.16-6 Monk parakeet nest on a steel lattice transmission structure. (Photo credit: EDM International, Inc.)



Figure 12.16-7 Lattice structure with six fecal contamination shields. (Photo credit: EDM International, Inc.)



Figure 12.16-8 Fecal contamination insulated barrier. (Photo credit: EDM International, Inc.)

12.16.9 Bird Streamers

A bird streamer is a long stream of excrement released by large birds, either perched or in flight near a transmission-line tower. A streamer bridging the entire distance, or sufficient part thereof, between a ground and the nearest live hardware point, acts as a fuse and an electrical fault is established. The fault initiates on the live hardware and propagates vertically toward the tower. The fault appears to flash across the air gap and does not follow an insulator creepage path as observed on pollution outages. Physiologically, only larger birds can cause such outages. Streamer outages are usually a localized problem, and transmission structures can be fitted with perching deterrents to prevent streamers. Perching deterrents include the use of high-density polyethylene (HDPE) cones and spikes (Figure 12.16-9). The goal of the deterrents is to move the bird more than 1 m away from a perch site over a conductor.

12.16.10 Other Bird Issues

Some birds are curious about their surroundings, sometimes creating unique problems for the transmission provider. In South Africa, communication cables have been lashed to overhead static wires only to have curious vultures chew off the lashing with their beaks. This has resulted in communication cables falling down into energized wires.

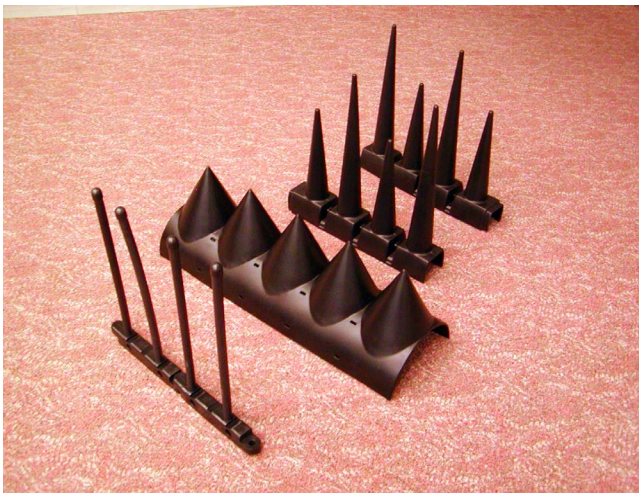


Figure 12.16-9 HDPE cones and spike-type perching deterrents. (Photo credit: EDM International, Inc.)

In Australia, the rose-breasted cockatoo (referred to as the Galah) is known for its curiosity and ability to chew. In one incident, a new transmission line constructed with nonceramic insulators had 200 units chewed before the line was energized. The rose-breasted cockatoos perched on corona rings and took bite-sized pieces out of the insulator sheds. Most of the insulators were replaced prior to line energization.

Vulture digestive acid is so strong it easily digests putrid substances. Their digestive systems have the unique ability to kill any almost virus and bacteria present in their food, and their resulting droppings are also acidic. These droppings and can damage metal surfaces and communication cables mounted on metal structures. In addition to simply fouling structures, the accumulation of bird feces can pose a human health issue. Feral pigeons and European starlings are suspected in the transmission of 29 different diseases to humans. For these reasons, transmission structures should be constructed in such a way as to minimize avian perching in critical areas, if possible.

Holes in tubular steel structures can attract cavity nesting birds. The accumulation of feces, prey items, and decaying nesting material can corrode the inside of tubular structures. For these reasons, holes should be plugged to prevent both bird and insect nesting. Holes in tubular steel can also create sound on windy days, which may irritate local landowners.

REFERENCES

AAR/EEI. 1936. "The Inductive Coordination of Electrical Supply and Communication Systems." *Report of the Joint General Committee of the AAR and EEI on Inductive Coordination.* October.

AAR/EEI. 1977. "Principles and Practices for Inductive Coordination of Electric Supply and Railroad Communication/Signal Systems." *Report of the Joint Committee of the AAR and EEI on Inductive Coordination.* September.

Alcoa Fujikura Ltd. 1995. "All-Dielectric Self-Supporting (ADSS) Fiber Optic Cable Reliability Study 1986-1994." *Alcoa Fujikura Ltd. Report.* June 23.

ANSI/IEEE Standard 643-1980. "ANSI/IEEE Guide for Power-Line Carrier Applications."

ANSI/IEEE Standard C63.4-2001. "American National Standard for Methods of Measurement of Radio-Noise Emission from Low-Voltage Electrical and Electronic Equipment in the Range of 9 kHz to 40 GHZ."

Arnstein, P. H. 1986. "LORAN-C and PLC: Partners or Adversaries." *Proceedings of the 15th Annual Technical Symposium, the Wild Goose Association.* pp. 21-28. October.

Aslan, E. 1985. "Non-Ionizing Radiation—Measurement Methods and Artifacts." *Proceedings of 39th Annual Broadcast Engineering Conference.* National Association of Broadcasters. Las Vegas, NV. pp. 645-655.

Association of Oil Pipe Lines. 2004. "Pipeline Control Systems."

Austin, K. A. et al. 1984. "Optical Communications Using Overhead Power Transmission Lines." *CIGRE Paper No. 35-04.*

Berger, K., R. B. Anderson, and H. Kroninger. 1975. "Parameters of Lightning Flashes." *Electra.* No. 41. July. pp. 23-37.

Bonds, R.W. 1999. "The Effect of Overhead AC Power Lines Paralleling Ductile Iron Pipelines." Ductile Iron Pipe Research Association. Birmingham, Alabama.

Bonicel, J, O. Tatat, U. Jansen, and G. Couvrie, 1995. "Lightning Strike Resistance of OPGW." *1995 International Wire and Cable Symposium Proceedings.* pp. 800-806.

BPA. 1978. "Guidelines for the Installation and Operation of Irrigation Systems near High Voltage Transmission Lines." Bonneville Power Administration. Portland, OR.

Brown, P. A. 1996. "Multi-Media Communications Over the Electricity Network." British Association Annual Festival. University of Birmingham. September 9-15.

Caola, R. J., D. W. Deno, and V. S. W. Dymek. 1983. "Measurements of Electric and Magnetic Fields in and Around Homes near a 500 kV Transmission Line." *IEEE Transactions on Power Apparatus and Systems.* Vol. PAS-102. pp. 3338-3347. October.

Carter, C. N. et al. 1984. "Lightning Simulation Tests on Power Transmission Conductors Carrying Embedded Optical Communication Cable." International Conference on Lightning and Power Systems. pp. 207-209.

Carter, C. N. and M. A. Waldron. 1992. "Mathematical model of Dry-Band Arcing on Self-Supporting, All-Dielectric, Optical Cables Strung on Overhead Power Lines." *IEE Proceedings-C.* Vol. 139. pp. 185-196. May.

Carter, C. N. 1993. "Arc Control Devices for Use on All-Dielectric Self-Supporting Optical Cables." *IEE Proc.-A.* Vol. 140. pp. 357-361. September.

Carter, C. N. 1998. "Presentation to the Optical Fiber Task Force" 1998 IEEE PES Winter Meeting, Tampa, FL.

CEA. 1979. *Study of Problems Associated with Pipelines Occupying Joint-Use Corridors with AC Transmission Lines.* Canadian Electricity Association (Former name: Canadian Electrical Association) Technical Report 75 T 02.

CEA. 1985. *Measurement System for Evaluating Power-Line Interference to Instrument landing Systems.* IITRI (Illinois Institute of Technology Research Institute) and Ontario Hydro for the Canadian Electrical Association (CEA) and Transport Canada. CEA Report 100 T 219/219A, March.

CEA. 1987. *Effect of Powerline Faults on Pipelines in a Common Corridor.* Canadian Electricity Association (Former name: Canadian Electrical Association) Technical Report 239 T 532.

CEA. 1989. *Electrical Coordination Guide.* Canadian Electricity Association (former name Canadian Electrical Association), Technical Report, May.

CEA. 1994. *Powerline Ground Fault Effects on Pipelines.* Canadian Electricity Association (Former name: Canadian Electrical Association). Technical Report 239 T 817.

CENELEC. 1999. *Railway Applications – Electromagnetic Compatibility – Part I – General*. The European Committee for Electrotechnical Standardization. Technical Report ENV50121-1.

Dabkowski, J. and A. Taflove. 1979a. "Prediction Method For Buried Pipeline Voltages Due to 60 Hz AC Inductive Coupling. Part II: Field Test Verification." *IEEE Transactions on Power Apparatus and Systems.* Vol. PAS-98. pp.788-794. May/June.

Dabkowski, J. and A. Taflove. 1979b. "Mitigation of Buried Pipeline Voltages Due to 60 Hz AC Inductive Coupling. Part II: Pipeline Grounding Methods." *IEEE Transactions on Power Apparatus and Systems*. Vol. PAS-98. pp.1814-1823. September/October.

Dawalibi, F. P. and R. D. Southey. 1989. "Analysis of Electrical Interference from Power Lines to Gas Pipelines. Part I: Computation Methods." *IEEE Transactions on Power Delivery.* Vol. PWRD-4, pp. 1840-1846. July.

Dawalibi, F. P. and R. D. Southey. 1990. "Analysis of Electrical Interference from Power Lines to Gas Pipelines. Part II: Parametric Analysis." *IEEE Transactions on Power Delivery.* Vol. PWRD-5. pp. 415-421. January.

Deno, D. W. and J. M Silva. 1985. "Probability and Consequence of Gasoline Ignition Under HVAC Transmission Lines." *IEEE Transactions on Power Apparatus and Systems.* Vol. PAS-104. No. 11. November. pp. 3181-3188.

Diamanti, P. 1996. "Power-line Carrier: Still the Lowest-Cost Medium for Communications." *Electrical World.* Vol. 20. pp. 30-35. August.

Edwards, K. S. and R. G. Olsen. 2002. "Safety Aspects of ADSS Cable Installations on High Voltage Transmission Lines." North American Power Symposium. Tempe, AZ. October.

Edwards, K. S., P. D. Pedrow, and R. G. Olsen. 2003. "Portable ADSS Surface Contamination Meter Calibrated in a High Voltage Environment." *IEEE Transactions on Power Delivery.* Vol. PWRD-18. pp. 888-894. July.

Enge, P. and P. Misra. 1999. "Scanning the Special Issue/Technology on Global Positioning System." *Proceedings of the IEEE*. Vol. 87. No. 1. January.

EPRI. 1978a. *Mutual Design Considerations for Overhead AC Transmission Lines and Gas Transmission Pipelines. Vol. 1: Engineering Analysis.* Report EL-904. September.

EPRI. 1978b. *Mutual Design Considerations for Overhead AC Transmission Lines and Gas Transmission Pipelines. Vol. 2: Prediction And Mitigation Procedures.* Report EL-904. September.

EPRI. 1982. *Transmission Line Reference Book: 345 kV and Above*. Second Edition.

EPRI. 1983a. *Power Line-Induced AC Potential on Natural Gas Pipelines for Complex Rights-of-Way Configurations, Volume 1: Engineering Analysis.* Report EL-3106-V1. May.

EPRI. 1983b. *Mutual Design of Overhead Transmission Lines and Railroad Communication and Signal Systems, Volume 1: Engineering Analysis and Volume 2: Appendixes.* Report EL-3301. October.

EPRI. 1985. *Utility Corridor Design: Transmission Lines, Railroads, and Pipelines. Volume 1:Engineering Analysis and Site Study and Volume 2: User's Manual for Computer Program CORRIDOR*. Report EL-4147. July.

EPRI. 1987. *Power Line Fault Current Coupling to Nearby Gas Pipelines*. Report EL-5472/PR176-510. November.

EPRI. 1996. "Workshop on Fiber Optic Cables Within High Voltage Transmission Corridors." Tempe, AZ. December 9-10.

EPRI. 1997. *Fiber Optic Cables in Overhead Transmission Corridors: A State-of-the-Art Review.* EPRI report TR-108959. November.

EPRI. 1999a. *Fiber Optic Cables in High Voltage Environments: ADSS Icing Test Report.* EPRI Report (Energy Utilization and Delivery Center. Lenox, MA), April 8.

EPRI. 1999b. *Accelerated Aging Tests of ADSS Fiber Optic Cables.* EPRI Report (Energy Utilization and Delivery Center. Lenox, MA). August.

EPRI. 2000. *Fiber Optic Cables in High Voltage Environments.* EPRI Report 1000444. December.

EPRI. 2001. *The Possible Use of the Electric Power Transmission/Distribution System as a Waveguide for Wideband Communication Systems*. Technical Report 1001891. November.

EPRI. 2002. *Radio Frequency Safety for the Electric Power Industry.* Technical Report 1005419. March.

EPRI. 2003a. *Electromagnetic Interference Emission Measurements Near FACTS Devices.* EPRI Technical Report 1007753. March.

EPRI. 2003b. *Evaluation of Radio Frequency Measurement Instruments in Strong Extremely Low Frequency Fields and High Voltage Protective Hoods in Strong Radio Frequency Fields.* Product Number 1008156. October.

EPRI. 2004. *Power System and Railroad Electromagnetic Compatibility Handbook*. Technical Report 1009492.

Eriksson, A. J. 1987. "The Incidence of Lightning Strikes to Power Lines," *IEEE Transactions on Power Delivery.* Vol. PWRD-2. pp. 859-870. July.

Ewy, K. A., D. R. Kallensen, L. E. Stetson, and R. E. Hanson. 1981. "Investigation of Power Line and Irrigation System Compatibility." *IEEE Transactions on Power Apparatus and Systems.* Vol. PAS-100. pp. 3535-3544. July.

FAR. 1971. Federal Aviation Regulations, Part 77, Subpart C, Section 77.23. (Federal Register 5970, April 1).

FCC. 1997. "Evaluating Compliance with FCC Guidelines for Human Exposure to Radiofrequency Electromagnetic Fields." *OET Bulletin 65. Edition 97-01*. Federal Communications Commission. Office of Engineering and Technology. Washington, DC. August.

FCC. 1998. "Code of Federal Regulations; Title 47 (Telecommunication), Chapter I, Part 15 (Radio Frequency Devices)." Federal Communications Commission, Washington, DC.

FCC. 2004. "Carrier Current Systems, including Broadband over Power Line Systems, Notice of Proposed Rulemaking." Federal Communications Commission. Washington, DC. February 23.

Fraser-Smith, A. C. and M. M. Bower. 1992. "The Natural Background Levels of 50/60 Hz Radio Noise." *IEEE Transactions on Electromagnetic Compatibility.* Vol. EMC-34. August.

Gohari, J. 1999. "Power Line Carrier." *The Standard Handbook for Electrical Engineers.* 14th Edition.

Hagmann, W. 1989. "Spread Spectrum Communications System for Load Management and Distribution Automation." *IEEE Transactions on Power Delivery.* Vol. PWRD-4. pp 75-81. January.

Hansen, D. 2001. "Megabits per Second on 50 Hz Power Lines?" *IEEE EMC Society Newsletter*. Winter.

ICNIRP. 1998. "Guidelines for Limiting Exposure to Time-Varying Electric, Magnetic, and Electromagnetic Fields (up to 300 GHz)." Prepared by the International Commission on Non-Ionizing Radiation Protection. *Health Physics*. Vol.74. pp. 494-522. April.

IEC Standard 479-2. 1987. "Effect of Currents Passing Through the Human Body."

IEC Standard 62236-1. 2003a. "Railway Applications, Electromagnetic Compatibility—Part 1: General." April.

IEC Standard 62236-2. 2003b. "Railway Applications, Electromagnetic Compatibility—Part 2: Emission of the Whole Railway System to the Outside World." April.

IEC Standard 62236-3-1. 2003c. "Railway Applications, Electromagnetic Compatibility—Part 3-1: Rolling Stock—Train and Complete Vehicle." April.

IEC 62236-3-2. 2003d. "Railway Applications, Electromagnetic Compatibility—Part 3-2: Rolling Stock–Apparatus." April.

IEC Standard 62236-4. 2003e. "Railway Applications, Electromagnetic Compatibility—Part 4: Emission and Immunity of the Signaling and Telecommunications Apparatus." April.

IEC Standard 62236-4. 2003f. "Railway Applications, Electromagnetic Compatibility— Part 5: Emission and Immunity of Fixed Power Supply Installations and Apparatus." April.

IEEE Standard 776. 1992. "IEEE Recommended Practice for Inductive Coordination of Electric Supply and Communication Lines."

IEEE Standard C95.1. 1999. "IEEE Standard for Safety Levels with Respect to Human Exposure to Radio Frequency Electromagnetic Fields, 3 kHz to 300 GHz."

IEEE Standard 80. 2000. "IEEE Guide for Safety in AC Substation Grounding."

IEEE Standard C95.6. 2002a. "IEEE Standard For Safety Levels with Respect to Human Exposure to Electromagnetic Fields, 0 to 3 kHz."

IEEE Standard C2. 2002b. "National Electric Safety Code."

Industry Canada. 1999. "Technical Requirements for Land Mobile and Fixed Radio Services Operating in the Bands 806-821/851-866 MHz and 821-824/866-869 MHz." *Spectrum Management and Telecommunications Standard Radio System Plan SRSP-502*. Issue 4. October.

Industry Canada. 2003. "Technical Requirements for Cellular Radiotelephone Systems Operating in the Bands 824-849 MHz and 869-894 MHz." *Spectrum Management and Telecommunications Standard Radio System Plan SRSP-503*. Issue 6. June.

Jaffa, K.C. and J. B. Stewart. 1981. "Magnetic Field Induction from Overhead Transmission and Distribution Power Lines on Buried Irrigation Pipelines." *IEEE Transactions on Power Apparatus and Systems*, Vol. PAS-100. pp. 990-1000. March.

JCIIRC. 1918. "Final Report of the Joint Committee on Inductive Interference to the Railroad Commission of the State of California." California State Printing Office. Sacramento.

Jewell, W., W. L. Miller, and T. Casey. 2000. "Filtering Dispersed Harmonic Sources on Distribution." *IEEE Transactions on Power Delivery.* Vol. PWRD-15. pp. 1045-1051. July.

Johnson, M. D. 1999. *Evaluation of Radio Frequency (RF) Exposure Monitors for Workers*. Bonneville Power Administration Engineering and Technical Services Report TNL (M) – 99-25. April 14.

Johnson, M. D. and J. O. Lo. 1999. *ADSS Jacket Arc Resistant Material Tests.* Bonneville Power Administration. U.S. Dept. of Energy. Laboratory Services Report TNF(M)-98-24a. January 21.

Kaidanov, F., R. Munteanu, and G. Sheinfain. 2000. "Damages and Destruction of Fiber Optic Cables on 161 kV Overhead Transmission Lines." IEEE *Electrical Insulation Magazine*. Vol. 16. pp. 16-23. July/August.

Karady, G. G., M. Torgerson, D. Torgerson, J. Wild, and M.W. Tuominen. 1999. "Evaluation of Corona-Caused Aging of ADSS Fiber-Optic Cables." Paper #TR08-080. 1999 IEEE Transmission and Distribution Meeting.

Kremer, G. T. et al. 1990. "The Effect of Selective Availability on Differential GPS Corrections." *Navigation*. Vol. 37. No. 1. Spring.

Kuboto. S. et al. 1983. "Field Trial of Composite Fiber Optic Overhead Groundwire." 1983 International Wire and Cable Symposium.

Last, D. and Y. Bian. 1993. "Carrier Wave Interference and Loran-C Receiver Performance." *Radar and Signal Processing. IEE Proceedings F.* Vol. 140. pp. 273–283. October.

Lee, J. M., K. S. Pierce, C. A. Spiering, R. D. Stearns, and G. VanGinhoven. 1996. *Electrical and Biological Effects of Transmission Lines: A Review.* Bonneville Power Administration. Portland, OR. December.

Leisenring, J. 1922. "Inductive Interference, Illinois Traction System." Joint Convention of the Illinois Gas Association, the Illinois State Electric Association, and the Illinois Electric Railways Association. Chicago. March.

Lowe, P. 2004. "Device Automatically Warns Pilots of Wires and Obstacles" *Aviation International News*. February.

Maddock, B. J. 1992. "Guidelines and Standards for Exposure to Electric and Magnetic Fields at Power Frequencies." (Panel 2-05. CIGRE meeting. August 30-September 5, 1992.) CIGRE. Paris.

Madge, R. C. and G. K. Hatanaka. 1992. "Power Line Carrier Emissions from Transmission Lines." *IEEE Transactions on Power Delivery.* Vol. PWRD-7. No. 4. October.

Mantiply, E. D. 1988. "Characteristics of Broadband Radiofrequency Field Strength Meters." *Proceedings of IEEE Engineering in Medicine and Biology Society 10th Annual International Conference*. pp. 889-891.

Mantiply, E. D. 1995. "Radiofrequency Radiation Meter Calibration, Methods, and Observations," *Proceedings of RF Radiation and Ultrawide Band Measurements Symposium*. U.S. Air Force Armstrong Laboratory. Brooks Air Force Base, TX. February.

NACE Standard RP0177. 2000. "Standard Recommended Practice: Mitigation of Alternating Current and Lightning Effects on Metallic Structures and Corrosion Control Systems." NACE International. Houston.

Nourai, A. 1992. *Simulated Lightning Tests on Optical Groundwires.* American Electric Power Service Corp. Reports 92-01, 92-02. February 24.

Olsen, R. G. and A. Aburwein. 1982. "LORAN-C Positioning Errors Caused by Scattering from Wires Above the Earth." *IEEE Transactions on Electromagnetic Compatibility.* Vol. EMC-24. pp. 381–388. November.

Olsen, R. G. 1998. "An Improved Model for Studying Dry Band Arcing on All- Dielectric Self-Supporting Fiber Optic Cable Located Near High Voltage Power Lines." EMC 98' ROMA. October.

Olsen, R. G. and G. L. Heins. 1998. "A Study of the Electromagnetic Compatibility of High Voltage Transmission Lines and the Guidance of Center Pivot Irrigation Units with Cornering Systems." *IEEE Transactions on Power Delivery.* Vol. PWRD-13. pp. 1230-1237. October.

Olsen, R. G. 1999a. "Laboratory Simulation of Dry Band Arcing on All-Dielectric Self-Supporting Fiber Optic Cable Near High Voltage Power Lines." *Proceedings of the 1999 IEEE EMC Society Symposium*. Seattle, WA.

Olsen, R. G. 1999b. "An Improved Model for the Electromagnetic Compatibility of All Dielectric Self Supporting Fiber Optic Cable and High Voltage Power Lines." *IEEE Transactions on Electromagnetic Compatibility.* Vol. 41. pp. 180 – 192. August.

Olsen, R. G. 2002. "Technical Considerations for Wideband Power Line Communication – A Summary." *2002 IEEE Power Engineering Society Summer Meeting*. Chicago, IL.

Olsen, R.G. and A. P. Sakis Meliopoulos. 2002. Personnel Grounding and Safety Issues / Solutions Related to Servicing Telecommunications Equipment Connected to Fiber Optic Cables in Optical Ground Wire (OPGW). NSF Power Systems Engineering Research Center (PSerc) Report. December.

Olsen R. G. and K. Yamazaki. 2004. "The Interaction Between ELF Electric Fields and RF Survey Meters: Theory and Experiment." *IEEE Transactions on Electromagnetic Compatibility.*

O'Neal, J. B. 1986. "The Residential Power Circuit as a Communications Medium." *IEEE Transactions on Consumer Electronics*. Vol. 32. pp. 567-577. August.

OSHA. 1910. Subpart S Electrical; 1926 Subpart K Electrical.

Parkinson B.W. and J. J. Spilker, ed. 1996. "Global Positioning System: Theory and Applications, Volumes I and II." *Progress in Astronautics and Aeronautics*. Vols. 163 and 164. AIAA.

Pietraszewski, D. 1990. "U.S. Coast Guard Differential GPS Navigation Field Test Findings." *Navigation.* Vol. 37. No. 1. Spring.

PSE&G. 2004. "Remote Monitoring of Aircraft Warning Lights on Transmission Structures." EPRI Overhead Transmission Conference. Monterey, CA.

Radford, D. 1996. "Spread-Spectrum Data Leap Through AC Power Wiring," *IEEE Spectrum*. pp. 48-53. November.

Randa, J., D. Gilliland, W. Gjertson, W. Lauber, and M. McInerney. 1995. "Catalogue of Electromagnetic Environment Measurements, 30-300 Hz." *IEEE Transactions on Electromagnetic Compatibility.* Vol. EMC-37.

Reilly, J. P., Principal Author. 1978. "Electric and Magnetic Field Coupling from High Voltage AC Power Transmission Lines - Classification of Short-Term Effects on People." *IEEE Transactions on Power Apparatus and Systems*. Vol. PAS-97. pp. 2243-2252. November/December.

Reilly, J. P. 1979. "Electric Field Induction on Long Objects—A Methodology for Transmission Line Impact Studies." *IEEE Transactions on Power Apparatus and Systems*. Vol. PAS-98. pp. 1841-1852. November/December.

Reilly, J. P. ed. 1992. *Electrical Stimulation and Electropathology.* Cambridge University Press New York, NY.

Sanderson, L.W. 2000a. "Broadband Communications over a Rural Power Distribution Circuit." *Proceedings of IEEE SoutheastCon2000*. pp. 497-504. Nashville, TN. April.

Sanderson, L. W. 2000b. "Broadband Communications over Distribution Circuits for Rural Communities (The PowerComm System)." *UTC Telecom2000.* Phoenix, AZ. June.

Sarto, M. S. 1998. "Electromagnetic Interference from Carrier Channels on Finite-Length Power Lines above a Lossy Ground in a Wide Frequency Range." *IEEE Transactions on Power Delivery.* Vol. PWRD-13. pp. 336-343. April.

Shwehdi, M. H. and U.M. Johar. 2003. "Transmission Line EMF Interference with Buried Pipeline: Essentials and Cautions." *Proceedings of the International Conference on Non-Ionizing Radiation at UNITEN (ICNIR 2003): Electromagnetic Fields and Our Health*. King Fahd University, Dhahran, Saudi Arabia. October 20-22, 2003.

Silva, J. M. 2002. "Evaluation of the Potential for Power Line Noise to Degrade Real Time Differential GPS Messages Broadcast at 283.5-325 kHz." *IEEE Transactions on Power Delivery.* Vol. PWRD-17. pp. 326–333. April.

Silva, J. M., N. P. Hummon, D. Rutter, and C. Hooper. 1989. "Power Frequency Fields in the Home." *IEEE Transactions on Power Delivery.* Vol. PWRD-4. pp. 465 – 478. January.

Silva, J. M. and R. G. Olsen. 2002. "Use of Global Positioning System (GPS) Receivers Under Power Line Conductors." IEEE *Transactions on Power Delivery.* Vol. PWRD-17. pp. 938-944. October.

Silva, J. M. and B. Whitney. 2002. "Evaluation of the Potential for Power Line Carrier (PLC) to Interfere with Use of the Nationwide Differential GPS Network." *IEEE Transactions on Power Delivery.* Vol. 17. pp. 349-352. April.

Starr, E. C., J. J. Managan, W. L. Boling, A.L. Kinyon, and F. Chambers. 1969. "Electrical Conducting and Flashover Characteristics of Large Irrigation Sprinkler Water Streams Near High Voltage Transmission Lines." *IEEE Transactions on Power Apparatus and Systems.* Vol. PAS-88. pp. 141-146. February.

Taflove, A. and J. Dabkowski. 1979. "Prediction Method for Buried Pipeline Voltages Due to 60 Hz AC Inductive Coupling. Part I: Analysis." *IEEE Transactions on Power Apparatus and Systems.* Vol. PAS-98. pp. 780-787. May/June.

Taflove, A., M. Genge, and J. Dabkowski. 1979. "Mitigation of Buried Pipeline Voltages Due to 60 Hz AC Inductive Coupling. Part I: Design of Joint Rights-of-Way." *IEEE Transactions on Power Apparatus and Systems*. Vol. PAS-98. pp. 1806-1813. September/October.

Tengdin, J. T. 1987. "Distribution Line Carrier Communications–An Historical Perspective." *IEEE Transactions on Power Delivery.* Vol. PWRD-2. pp. 321-329. April.

Tesche, F. M. 1993. "Investigation of Measured S- Parameters of an Allis-Chambers 1.2 kV – 120/240V Power Transformer." A report to Lawrence Livermore National Laboratory. May.

Tesche, F. M., B. A. Renz, R. M. Hayes, and R.G. Olsen. 2003. "Development and Use of a Multiconductor Line Model for PLC Assessments." *Proceedings of the 15th International Zurich Symposium on EMC.* February.

Transport Canada. 2004. *Land Use in the Vicinity of Airports, Part II – Protection of Telecommunications and Electronic Systems*. Report TP 1247E.

Tuominen, M. W. 1996. *ADSS Hardware Corona Prediction for Selected Towers Using EF3D.* U.S. Department of Energy Bonneville Power Administration. Portland, OR. Report No. TELE-96-3. January.

Tuominen, M. 2004. Bonneville Power Administration. Private Communication, August 4, 2004.

Tuominen, M. W. and R.G. Olsen. 2000. "Electrical Design of All-Dielectric Self-Supporting Optical Fiber Cable." *IEEE Transactions on Power Delivery.* Vol. PWRD-15. pp. 940-947. July.

U. S. Coast Guard. 1982. "Radionavigation Bulletin." No. 11. Navigation Center. 7323 Telegraph Road. Alexandria, VA.

U. S. Coast Guard. 2002. *LORAN-C User's Handbook, COMDTPUB P16562.6*. Stock number 050-012-00331-9. Superintendent of Documents. Order Section. U.S. Government Printing Office. Washington, DC. 20402.

USDOT. 1998. *Programmatic Environmental Assessment: Nationwide Differential Global Positioning System.* U.S. Department of Transportation. December.

USDOT. 2000. *Comprehensive Truck Size and Weight Study. Volume I. Summary Report.* Publication Number: FHWA-PL-00-029 (Volume I) HPTS/August.

Wheeler, J. C. G., M. L. Lissenburg, J. D. S. Hinchcliffe, and M.E. Slevin. 1988. "The Development of a Track Resistant Sheathing Material for Aerial Optical Fibre Cables." 5th International Conference on Dielectric Materials and Applications. Canterbury, U.K. pp. 73-76.

Yokoya, M, Y. Katsuragi, Y. Goda, Y. Nagata, and Y. Asano. 1994. "Development of Lightning-Resistant Overhead Ground Wire." *IEEE Transactions on Power Delivery.* Vol. 9. pp. 1517-1523. July.

Zischank, W. and J. Wiesinger, 1997. "Damages to Optical Ground Wires Caused by Lightning." *Proceedings of the 10th International Symposium on High Voltage Engineering*. Montreal, Quebec, Canada.

CHAPTER 13

Considerations for Inspection and Maintainability

Andy Stewart
George Gela

This chapter provides guidance on designing transmission lines for inspection and maintainability. It includes practical information, learned from experience, on design principles that will facilitate inspection, condition assessment, and maintenance activities. The chapter also provides information on line design features that will better enable maintenance and testing on equipment that is energized—live working.



Andrew Stewart is the president of EDM International, Inc. (EDM), located in Fort Collins, Colorado. He joined EDM as a senior research engineer in 1983, and his career activities encompass technical and managerial roles related to research, development, consulting and training associated with inspection and test methods, analysis procedures, maintenance plans, performance metrics, and new technologies for the management of transmission and distribution assets, and the thermal rating of overhead transmission lines. Mr. Stewart received a BS in civil engineering from the University of Rhode Island in 1981 and an MS in civil engineering from Colorado State University in 1984. He is a U.S. patent holder and the author of numerous publications. Mr. Stewart is also a director of Intec Services, Inc., a leading provider of inspection and maintenance services for T&D facilities, and Barlow Projects, Inc., a developer of renewable energy projects. He is a member of the ASCE, IEEE, and the West-Central Wind Research Consortium (W2RC). He is a member of the Executive Board of the W2RC, and serves as the Chairman of the IEEE Task Force on the Management of Existing Overhead Lines.



Dr. George Gela is the EPRI Project Manager, Transmission and Substations, in Lenox, Massachusetts. In this capacity, he is responsible for projects involving high-voltage testing, live working, compact and upgraded transmission lines, and maintenance of lines. Previously Dr. Gela conducted high-voltage research and taught graduate and undergraduate courses at The Ohio State University. Dr. Gela earned a Ph.D. in electrical engineering from the University of Toronto in 1980. He is the international chairman of IEC TC78 "Live Working," and past chair of the IEEE Corona and Field Effects Subcommittee. He has authored/co-authored more than 15 technical peer-reviewed papers.

Contributors to Sections 13.2.3, 13.2.4, and 13.3 include the following teams and individuals:

Insulators

- Team Leader
  —Andrew Phillips, EPRI, USA
- Contributors
  —Gail Carney, Central Hudson Gas and Electric, USA
  —Fabio Bologna, Eskom, South Africa
  —George Watt, Hydro One, Canada

Conductors, Overhead Ground Wires, and Splices

- Team Leader
  —John K. Chan, EPRI, USA
- Contributors
  —Lance Powell, Anchorage Municipal Light & Power, USA
  —George Watt, Hydro One, Canada

Grounding

- Team Leader
  —Kurt Bell, POWER Engineers, Inc., USA
- Contributors
  —Robert Kluge, American Transmission Company, USA
  —John Peckinpaugh, Tennessee Valley Authority, USA

Structures

- Team Leader
  —Cal Stripling, CenterPoint Energy, Inc., USA
- Contributors
  —Terry S. Eagar, Salt River Project, USA
  —Alan Holloman, Georgia Power Company, USA

Hardware

- Bill Hewitt, San Diego Gas & Electric, USA

Rights-of-Way

- Bill Hewitt, San Diego Gas & Electric, USA

Design Examples

- J. A. Tony Gillespie, Powerlink Queensland, Australia

13.1 INTRODUCTION

The electric power industry is a comparatively new industry, and the capability to transmit high-voltage electricity is even newer. It was circa 1930 before transmission voltages broke the 200-kV threshold, the mid-1950s for 345 kV, and it was not until the mid-1960s that both 500-kV and 765-kV lines were constructed. Therefore, many of the existing transmission lines operating at voltages of 200 kV and above were designed without a wealth of hindsight and foregoing experience related to durability and maintainability. For this reason, the lines were often over-designed in an attempt to ensure satisfactory long-term performance, even though essential data on possible failure modes and rates were not available. In many ways, today's designers are among the first generation that has the advantage of learning from reasonably long-term observations and experience. Chapter 13 was born out of this recognition.

Chapter 13 is a somewhat unique addition to this latest edition of the Reference Book. Whereas the majority of the chapters provide guidance on methods for calculating or estimating, and accounting for and understanding the behavior of electricity for the purpose of designing safe, cost-effective, and reliable overhead transmission lines, Chapter 13 is structured to provide very practical information learned from experience to promote consideration of maintainability during the design process. "Maintainability," as used herein, is intended to encompass consideration of principles during the design process that promote long-term reliable performance, facilitate inspection and condition assessment, and minimize the need for maintenance, while also facilitating the ability to efficiently perform unavoidable maintenance activities. Underlying this approach is the desire to encourage designers to engage maintenance personnel in the design process.

This chapter is divided into two primary sections:

- "Designing for Maintainability" (Section 13.2) provides background information and guidance on designing transmission lines for:

  —Inspection,

  —Condition assessment,

  —Maintenance, and

  —Durability and longevity.

  This section represents a compilation of information provided by experienced personnel from transmission operations and engineering departments from utilities across the world.
- "Optimizing the Design for Effective Live Working" (Section 13.3) provides information to encourage engineers to incorporate features in line design that will make lines more friendly for maintenance, construction, or testing on equipment and circuits that are energized, may become energized, or are close to energized facilities— i.e., live working.

Increasing opposition to the siting and construction of new overhead transmission lines, competition, and regulatory constraints combine to exert an unprecedented pressure to maximize the utilization and life of overhead infrastructure. Facilities are being operated in ways and long beyond what designers may have originally anticipated, demands for reliability are becoming more stringent, and in many areas it is increasingly difficult to schedule outages to enable maintenance to be performed. These constraints need to be considered in designing new facilities. The authors of and contributors to Chapter 13 hope that the information provided will encourage designers to incorporate desirable features and characteristics and avoid undesirable features and characteristics in the design of new lines in order to enhance maintainability.

One applet is associated with this chapter:

- M-1: "Minimum Approach Distance (MAD)." The applet calculates the MAD values using either the IEEE method or the IEC method.

13.2 DESIGNING FOR INSPECTION AND MAINTAINABILITY

13.2.1 Introduction

Maintainability of overhead transmission lines is too often overlooked during the design process. This is counterintuitive given the fact that designers may have responsibility for a transmission line for only a year or two while maintenance personnel will have it for the line's lifetime. Further, designing for maintainability may be more important than first cost in the case of any facility with a high capital cost, that is required to have a long service life, and whose systems, subsystems, and components are subject to deterioration. However, shortsighted tactical thinking, rather than strategic thinking, may cause this factor to be overlooked. Successful designs optimize costs, life, and performance (thereby minimizing maintenance and maximizing availability and power quality).

For transmission infrastructure, *maintainability is a designed-in feature that intrinsically minimizes the need for inspection, condition assessment and maintenance, and the man-hours and other resources required to easily and safely preserve a line in or restore it to a required operational state.* This relatively brief addition to the latest edition of the Reference Book is dedicated to conveying to future generations of designers some basic principles regarding designing for maintainability. It is based on lessons learned over the last nearly 80 years with transmission

lines operating at 200 kV and above, and on the knowledge and expertise of experienced transmission-line engineering and maintenance personnel from around the world.

Capturing institutional memory, especially the successes or mistakes of the past, is particularly important during this period of unprecedented change in business practices and the roles of personnel within the electric utility industry. Whereas in the past it was reasonable to expect that one organization would have primary oversight for an overhead line from cradle to grave, that is no longer the case. Today, it is not an unreasonable scenario to have an overhead transmission line designed by one group, maintained by a second, operated by a third, and owned by a fourth. Further, it is not unreasonable to expect that there will be a shift in stakeholders and their roles during the life of a line. Disassociation of the design process from consideration of maintainability can lead to designs that, while having low first costs, are difficult and expensive to maintain.

The objectives for this section are twofold:

- Foster consideration of features during transmission-line design that minimize the need for and cost of inspection, condition assessment and maintenance, and enhance the ability to inspect and maintain the line.
- Promote communication among design and maintenance personnel regarding the design of every new transmission line.

Inherent in the objective of minimizing the need for inspection, condition assessment, and maintenance activities is designing for durability and longevity.

This section is intended to stimulate a mindset that maintainability is a vital consideration if one's goal is to develop designs characterized by life-cycle cost-effectiveness; it is not intended to provide exhaustive coverage of maintainability considerations. To meet the aforementioned objectives, the following information is provided.

- *Background.* General interest information is provided on asset management; inspection, condition assessment, and maintenance including designing to facilitate these processes; and basic maintainability considerations.
- *Designing for Durability and Longevity.* This subsection identifies primary modes of degradation, and approaches to mitigate the impacts of these factors during design to help ensure durability and longevity of performance for several categories of transmission-line components.

This section focuses solely on the topic of designing for maintainability. Constructability is another key issue that should be accounted for during the design process; however, it is beyond the scope of this section.

It is important to note that live working is a component of many utilities' work practices; hence it is an important consideration when seeking to design for maintainability. For this reason, a new section (Section 13.3) devoted to the topic of optimizing transmission-line designs for live working is included in this edition of the Reference Book.

13.2.2 Background

This subsection presents information on the following four topics that are foundational to understanding the importance of maintainability:

- Asset management
- Inspection, condition assessment, and maintenance
- Basic maintainability concepts
- Route characteristics and other information to aid in designing for maintainability

First, a discussion of asset management is presented because it provides a context for the roles of inspection, condition assessment, and maintenance within electric utilities. This is followed by a discussion of basic maintainability concepts that provide guidance on how to think about maintainability, and finally, insights are provided on the types of information that can be useful when seeking to design for maintainability.

Asset Management

Asset management, enterprise asset management, and strategic asset management are somewhat synonymous terms that describe a business framework for all the activities of an electric utility including designing for maintainability, and inspection, condition assessment and maintenance functions. ***Asset management is a systematic process of cost-effectively planning, developing, acquiring, designing, constructing, utilizing, operating, maintaining, upgrading, and disposing of power generation and delivery assets so as to meet a required level of service for current and potential future customers*** (EPRI 2004b). It represents an organized approach to the allocation and use of resources that requires balancing risks, costs, and performance to achieve optimized returns while satisfying customer expectations. Implicit in this definition is the need to consider maintainability.

The business framework incorporates an organizational structure that includes three primary functional roles based on core competencies:

- **Asset Owner**: establishes performance constraints (e.g., capital and operations and maintenance budgets, etc.) and performance goals for the organization (e.g., customer satisfaction, earnings per share, etc.).
- **Asset Manager**: establishes policies in the context of its regulatory regime, strategies to accomplish performance

goals within performance constraints, procedures for planning, performance indicators, and management of contracts with service providers.

- **Asset Service Provider**: schedules resources and delivers the services needed. Service providers may be in-house or contractors.

Information and Communication are Vital to Designing for Maintainability

Asset management is driven by information and enabled by good communication. Effective communication is needed both horizontally and vertically among stakeholders. Horizontal communication is required across functional silos within an organization (e.g., finance, operations, safety, design, etc.) to promote a clear understanding of direction and objectives. Two-way vertical communication is required (i.e., from the asset owner to the asset manager and asset service provider, and from the asset service provider to the asset manager to the asset owner). Asset management is intended to enable personnel to focus on doing what they are specifically trained for and best equipped to do. Communication must extend beyond the walls of the organization because outsourcing is almost always a component of this approach to doing business. For example, today consultants are often used for the design of major new transmission lines. Consultants must be apprised of specific maintainability concerns of their customers; otherwise, their tendency will be to focus almost exclusively on developing designs that meet their client's transmission needs on an initial least-cost basis.

Effective asset management requires that maintainability be a consideration in transmission-line design and demands that maintenance personnel be engaged throughout the design process. The knowledge base of operating experience regarding what works and what does not work should be leveraged. The design phase of a transmission-line's life cycle represents an opportunity to minimize maintenance from the outset. Further, the inadvertent introduction of maintenance constraints into the design can be avoided.

Inspection, Condition Assessment, and Maintenance Information is Mission-Critical to Improving the Maintainability of New Line Designs

It is critical that adequate inspection, condition assessment, and maintenance information flow among the various stakeholders. Information on the conditions of overhead facilities collected by the asset service providers represents a powerful resource that needs to be conveyed to asset managers for use in planning, prioritizing, and justifying inspection, condition assessment, and maintenance activities, and enhancing the maintainability of future line designs. Further, as condition data are gathered and stored for the longer term, they can provide the basis for examining trends and determining rates of degradation of components, such as insulators and structure coatings, which, in turn, can provide the basis for enhancing the durability and longevity of future designs and determining the type and timing of needed inspection and maintenance activities. Ideally transmission-line designers have access to information that facilitates the development of designs that recognize the objectives for each new line, the unique attributes of proposed line routes, and the performance characteristics of the components and design features planned for utilization in the design of a new line.

Asset Management Requires Strategic Thinking about Maintainability

Asset management takes a holistic view of the assets of an organization. Asset management's view of the world is that assets are not discrete, independent items or systems, but rather they are interrelated and have a life cycle, and must be considered as such if an optimum allocation and utilization of resources are to be achieved. This involves a balancing of the overarching drivers that are in tension—i.e., maximizing profits (corporate and shareholder interests) and reliability, power quality, low-cost power (customer interests) in a way that is sustainable. Sustainability implies the need for strategic thinking that takes a long view of business operations. That is not to say that there is an absence of short-term goals, objectives, and plans, but rather that short-term/tactical planning will not be accomplished in a void, without consideration of the future implications of choices made today. From the perspective of transmission-line design, a focus on short-term profits alone can lead to higher future costs. Sustainability is a key consideration when it comes to designing for maintainability. This is because transmission-line designs that minimize the need for inspections and maintenance may not have the lowest first costs. However, their net-present-value life-cycle costs—which account for first costs coupled with those for inspection, condition assessment, and maintenance—should be favorable.

Line Inspection, Condition Assessment, and Maintenance

Inspection, condition assessment, and maintenance functions are vital to utility operations, and they are intimately related to the issue of maintainability. Several issues concerning these functions that are also salient to the topic of maintainability are addressed below.

In the absence of effective inspection, condition assessment, and maintenance activities, safety, availability, service life, and financial resources are exposed to undue risk. Further, if effective, continuous feedback mechanisms are provided, the knowledge gained from these functions will enable problematic conditions, line configurations, and components to be identified, thereby enabling improvements in the maintainability of future line designs.

Rationale for Inspection, Condition Assessment, and Maintenance Functions

The drivers and reasons for inspection, condition assessment, and maintenance should be considered when seeking to design for maintainability. Safety and performance are the two primary drivers, as illustrated in Figure 13.2-1.

In addition to these drivers, there are several reasons for the inspection, condition assessment, and maintenance functions including:

- Ensuring the inherent safety and availability of a specific line configuration are achieved,
- Restoring safety and availability following degradation,
- Enhancing existing facilities and the designs of new facilities,
- Forecasting and planning maintenance,
- Extending facility life, and
- Achieving safety, availability, and service life objectives at an optimal cost.

Approaches to Program Design

A variety of valid maintenance approaches are utilized to achieve the performance objectives for overhead transmission lines. Maintenance programs have been developed through experience, trial-and-error, knowledge of system conditions, and understanding of business processes within each organization. Cost-effective programs account for the diverse environmental and climatic conditions, terrain, equipment, and operating practices that may be associated with individual lines. Likewise, maintainable designs account for these many variables.

A cost-effective maintenance program generally encompasses corrective and preventative maintenance activities. Maintainable designs should minimize the need for both of these categories of activities.

- *Corrective Maintenance*: Unanticipated repair, rehabilitation, or replacement activities to correct failures or conditions characterized by deterioration beyond acceptable thresholds. Inspections to support corrective maintenance (pre- and post-failure event) are performed to ascertain the extent of deterioration that must be corrected or to determine what activities are needed to restore service and/or availability following a failure.
- *Preventative Maintenance*: Preplanned inspection and maintenance performed on schedules defined to preclude failure or avert deterioration beyond some predefined acceptable threshold (i.e., to maintain functional capabilities). The schedules may be based on combinations of fixed intervals, previously observed conditions, and estimated rates of change/deterioration.

The "preventative maintenance" category can be divided into two broad subcategories (Smith 1993):

- Scheduled Maintenance
- Condition-Based Maintenance

Scheduled maintenance can be time-based or use-based. For overhead transmission lines, time-based criteria are more commonly considered than use-based; use-based approaches are generally applied for equipment with moving parts. Condition-based maintenance can be scheduled based on experience, knowledge of component life/failure rates, results of visual inspections, results of periodically

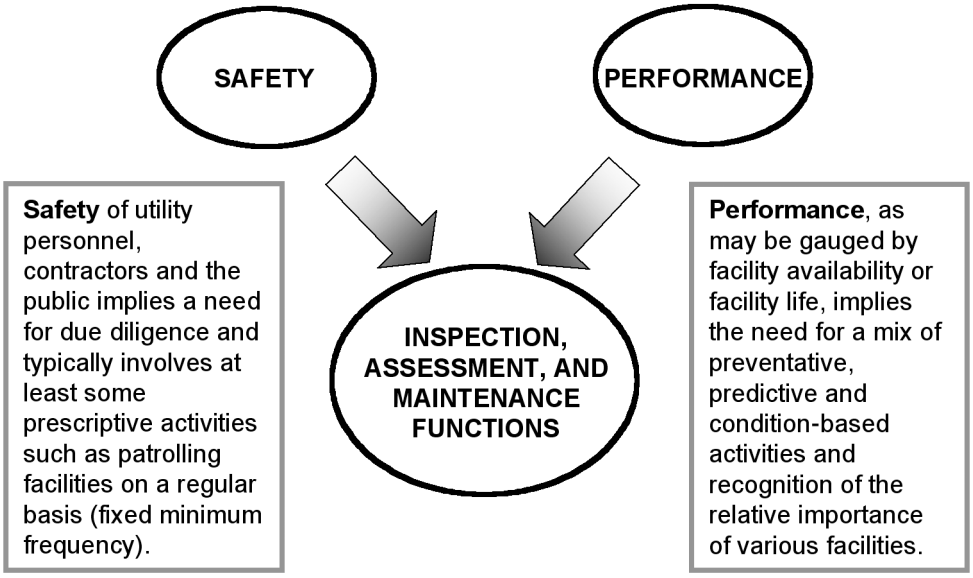


Figure 13.2-1 Primary drivers for inspection, condition assessment, and maintenance.

performed measurements (e.g., nondestructive tests that trigger the need for some sort of maintenance action), and/or on-line remote monitoring of conditions (although automated monitoring and diagnostics are seldom used for overhead transmission). The structure of a utility's maintenance program, and the predictability and detectability of component degradation and failure, will be accounted for during the design of new facilities if maintainability is to be optimized.

When developing or refining an inspection, condition assessment, and maintenance program, and/or designing for maintainability, utilities should consider the fact that the consequences of all failures and deterioration are not equal. Information on the consequences of various failures, the mechanisms that precipitate them, the ability to detect evidence of the failures or deterioration that is a precursor to the failures, etc. is a powerful resource when seeking to optimize maintenance practices and should impact the selection of components during the design of new lines. Optimizing line designs for maintainability and maintenance programs requires substantial information and a significant investment of time and resources. Historic data on conditions, deterioration rates, failures, component mortality, etc. are vital to determining best practices. Unfortunately, in many cases, available data are sparse at best. This shortcoming emphasizes the need for utilities to make a long-term commitment to the collection and management of relevant data.

In spite of some of the shortcomings in currently available data, there are tools/processes/principles that can help utilities to design cost-effective maintenance programs. Some of the same concepts can be used to optimize the maintainability of new line designs. Reliability-centered maintenance (RCM) is one such approach, and while RCM may have more to offer in maintenance arenas contending with moving parts, there are gems of truth that can be extracted from RCM for application to overhead transmission lines. RCM emphasizes maintaining performance, not simply conditions. For this reason, RCM directs users to implement failure modes and effects analyses to consider how components fail, why they fail, the causes of failure, and the consequences of failure. For a failure determined to have significant consequences, RCM seeks to define what can be done to prevent it and what can be done to detect evidence of the failure, or deterioration progressing towards a failure. Similarly, when new facilities are being designed, consideration of the consequences of failures can aid in prioritizing where investment should be focused to optimize maintainability.

Rating Component and Facility Condition

Transmission-line components whose condition/capacity/remaining life can be quantified using test devices or measurement techniques are the exception. By far, the majority of recommendations for maintenance or replacement of components in overhead transmission lines are based on visual inspections. As a result, determining how much deterioration can occur before a maintenance action is warranted presents a difficult challenge. Cost-effective decision-making is further complicated by the fact that the results of visual inspections—other than those represented by the ends of the condition continuum (i.e., new and failed, respectively)—are predominantly qualitative and subjective. In spite of these shortcomings, a properly designed condition-rating system can be a powerful resource for tracking changes in conditions and planning and forecasting inspection and maintenance needs, as well as providing valuable information to enable enhancement of the maintainability of future line designs.

The subjectivity associated with condition assessments based on visual inspections points to the need and opportunity for a new generation of "smart" components that are self-diagnosing or capable of being tested in a way that minimizes subjectivity.

Prioritization of Inspection, Condition Assessment, and Maintenance Activities

Prioritization represents an opportunity to utilize available resources more effectively. When planned actions are being prioritized, it is important to acknowledge that safety should supersede all other considerations. Therefore, if a practice jeopardizes safety (e.g., neglecting due diligence activities), or a situation/condition is detected that indicates that there is a palpable safety risk, then any prioritization scheme should call for corrective actions to become top priorities.

When safety is not compromised, then performance should become the primary driver for the allocation of resources. While line and component condition are important, performance should take precedent for purposes of setting priorities—except perhaps when conditions have deteriorated to the point that they are deemed to be an imminent threat to performance, or if unattended, may significantly impact facility life. A balanced approach to prioritization of inspection, assessment, and maintenance must account for a variety of factors. A partial list of factors is presented below. Consideration of some of these same factors can help designers to identify opportunities for investment to optimize new line designs for maintainability. Investment should be focused where it will pay the greatest dividends.

- Public and worker safety
- Line priority within the electrical system
- Redundancy of electrical supply/line configuration (e.g., radial versus loop)
- Load served

- Political issues
- Performance history
- Outage causes, frequencies, and durations
- Potential for forced outages
- Impact of forced outages on customers
- Criticality of component to performance or safety
- Potential for catastrophic failure and/or damage to other facilities
- Known problematic components and design flaws
- Materials used
- Local structural loading conditions and anomalies
- Local deterioration or environmental hazard
- Desired service life
- Planned modifications including upgrades or decommissioning
- Budgetary and manpower constraints

Periodicity/Frequency of Activities and the Impact of the Environment

A variety of factors, not the least of which is the perceived maintainability of a particular facility, should to be considered when determining the types and frequencies of inspections to be performed and requisite maintenance activities in response to findings. Likewise, choices made during design influence maintainability, and will impact the types and frequencies of inspection and maintenance activities that will be required.

Each utility must decide what factors it will consider, and the relative importance of the factors, when setting the appropriate frequency for the various types of visual inspections (e.g., aerial patrols, foot/driving patrols, climbing/bucket truck inspections) and diagnostic evaluations (e.g., splice temperature or resistance measurements, coating thickness measurements, etc.) that will be performed for each of its lines. However, when it comes to performance-driven activities, few, if any, factors influence the design of inspection programs more than the effects of the environment. Thus, when the required frequency of inspection for a given line is being determined, it is important to consider how certain environmental conditions can affect the service life/durability of components.

Tracking the change in state or condition of line components relative to environmental and special operating conditions (e.g., operating conductors at high temperatures resulting from high electrical loads) can prove useful in refining the required timing (seasonally) and frequency of patrols, enhancing predictive maintenance practices, and enhancing future line designs.

Performance Monitoring and Continuous Improvement

Customer availability/reliability indices have long been tracked as measures of electrical system performance. Only relatively recently, however, have more than a few utilities begun investigating or implementing performance metrics to gauge the effectiveness of inspection and maintenance functions. Well-designed performance monitoring tools can identify facilities needing attention, provide insight into opportunities for improving inspection and maintenance practices and future designs, and provide justification for level of investment in inspection and maintenance of existing facilities as well as components to be used in new lines. Use of a performance monitoring system is indicative of a utility that is committed to continuously improving its inspection and maintenance program. If a utility desires to also use the performance monitoring system to help identify opportunities for improvements in maintainability, then they must also commit to keeping good inventory, inspection, and maintenance records and tracking information such as degradation rates, the frequency of component failures, time between failures, and associated line operating and route conditions.

Maintainability Concepts

Transmissions lines are exposed to unforgiving conditions, including a wide variety of long-term environmental, mechanical, and electrical stresses that cause deterioration/degradation of conditions, performance, and integrity. Many lines are being operated in ways not intended and long beyond what designers may have originally anticipated. Demands for availability and reliability are becoming more stringent, and in many areas, it is increasingly difficult to schedule outages to enable maintenance to be performed. Increasing opposition to the siting and construction of new overhead transmission lines, competition, and regulatory constraints combine to exert an unprecedented pressure to maximize the utilization and life of overhead infrastructure. If the past is indicative of what the future holds, then these issues highlight the need to optimize the design of new transmission facilities for maintainability.

Experiences within the electric utility industry and other infrastructure-intensive industries have revealed important principles and considerations that can be used as a checklist to foster maintainability during design. A list of common considerations to facilitate inspection, condition assessment, and maintenance is presented below.

General Considerations

- **Opportunity during Design.** Capitalize on the opportunity to account for maintainability during design because excellence in inspection, condition assessment, and maintenance practices cannot make up for a poor design.
- **Simple Designs.** Seek to develop simple designs, as they are generally more maintainable.
- **Specific Characteristics.** Identify and consider the specific characteristics of the potential line configuration alternatives and line route.
- **Proven Track Record.** Use components, materials, and configurations with a proven track record or sufficient testing to ensure confidence in their performance when subjected to the deterioration mechanisms associated with a particular design alternative and line route, and for the target life of the line.
- **Specifications.** Develop proper component specifications, and remember that most national/international industry consensus standards and specifications provide minimum requirements that may not be sufficient for the line in question.
- **Failure Rate.** Determine an acceptable failure rate and design to exceed the minimum acceptable performance level.
- **Fail to Safe Modes.** Design line subsystems (e.g., structures) and components to fail to a safe mode.
- **Failure Containment.** Incorporate failure containment features to limit the possibility of major cascades.
- **Standardization.** Standardize in the use of components, and minimize the number and sizes of unique parts.
- **Unnecessary Connections.** Eliminate any unnecessary connections, as each point where two or more components are joined becomes a potential maintenance point.
- **Moisture.** Eliminate features/details where moisture can collect or be trapped.
- **Bird Nesting.** Eliminate features/details favorable for bird nesting and perching, especially over insulators/phases.
- **Labeling.** Require labeling that positively identifies components and their ratings.
- **Numbering.** Require use of easily visible structure numbering.
- **Quality Assurance.** Stress the importance of quality assurance and control activities during construction to ensure that construction matches design and to catch and correct mistakes.
- **Raking.** Maintain records of structures/poles that were raked during installation so that a "leaning" pole will not later be misidentified as having a problem.
- **Records.** Keep good records on all components installed, including manufacturer and year of manufacture.

Inspectability and Condition Assessment Considerations

- **Complex Configurations.** Avoid use of complex configurations.
- **Types/Frequencies of Activities.** Consider types and frequencies of anticipated inspection and maintenance activities.
- **Testing Components.** Use self-diagnosing and easily tested components to facilitate condition assessment and quickly isolate problems.
- **Initial Measurements.** Capture initial measurements of those components for which quantitative tests are available (e.g., initial measurement of splice resistance).
- **Lines-of-Sight.** Provide unobstructed lines-of-sight, both from ground and airborne perspectives, for all components that will be visually inspected.
- **Indicators.** Incorporate indicators/telltales of deterioration and failures of all major components and subsystems.

- **Visual Inspection.** Provide step bolts and/or ladders oriented so as to facilitate visual inspection of components in the upper portions of structures (e.g., insulators, conductors, and overhead ground wires and their attachment hardware).
- **Splice Location.** Specify locations of splices to be installed near mid-span, in easily accessible areas, and staggered so that they are not vertically aligned in order to facilitate inspection and testing.
- **IR Inspections.** Paint splices with infrared (IR) paint to facilitate IR inspections.
- **Vertical Bolts.** Install vertically oriented bolts (e.g., flange bolts) with heads in the downward position so that if there is a bolt failure, the bolt will fall out and the failure will be evident. This will also help prevent moisture from collecting around the threads in the annular space in a connection.
- **Visible Connections.** Make every connection point where two or more components come together visible and easily accessible.
- **Difficult-to-Inspect Components.** Give special attention to the design/selection of components whose condition will be difficult to inspect/assess.

Maintenance Considerations

- **Complex Configurations.** Avoid complex configurations.
- **Accessibility.** Consider ROW/route accessibility (e.g., availability of roads) for equipment and vehicles to be used to support maintenance activities.
- **Live Working.** Consider requirements of anticipated maintenance work methods, such as use of live working (hotstick or barehand methods) versus de-energized work techniques. (Refer to Section 13.3 for more detailed information on designing to facilitate live working [LW].)
- **Fastening/Unfastening.** Use connections that facilitate fastening and unfastening for those components likely to need replacement. This is particularly important for those components that may be maintained using LW techniques.
- **Hot-Line Hardware.** Use hot-line hardware (if live working is to be performed) to facilitate live working on attachments to conductors.
- **Broken Bells.** Establish the number of broken bells on glass and porcelain insulators used in different applications and configurations that will limit live working.
- **Polymer Insulators.** Review with maintenance department whether live working polymer insulators is an issue.
- **Corona Rings.** Review with maintenance department whether the corona rings and their attachment mechanism design will limit any work procedures.
- **Polymer Insulator Washing.** If applying polymer insulators in a contaminated environment, review with manufacturer whether washing is possible and what techniques are acceptable.
- **Insulator Strings.** If environmental conditions are such that replacement of a broken insulator bell with a new clean bell may lead to flashover, then plan to replace the entire string rather than individual broken units.
- **Attachment Points.** Provide attachment points for equipment used during maintenance work including live working (e.g., jack and hoist lift points, guides, etc.) with sufficient capacity to facilitate anticipated component repairs and replacements.
- **Component Replacement.** For those components likely to require replacement during the life of the line, limit the number of task steps required to perform a replacement, limit the number of fasteners utilized, and incorporate features to prevent components from slipping or falling as they are being unfastened for replacement.
- **Attachment Hardware.** Design attachment hardware (e.g., brackets, holes, fasteners, etc.) to accommodate functionally similar parts produced by different suppliers.

- **Mistake-Proof Components.** Use mistake-proof components that can only be installed correctly during construction and when replacements are performed.
- **Accessible Components.** Make components that are likely to require replacement readily accessible/reachable via the various means that may be used to deliver a lineman to the component--for example, climbing or bucket truck.
- **Vibration.** Use fasteners that resist loosening due to vibration.
- **Special Tools.** Minimize or eliminate the need for special tools/equipment.
- **Inventory of Components.** Maintain an inventory of components adequate for anticipated maintenance needs.

Economic and Risk Considerations

- **Strategic Value.** Consider strategic value of line configuration and component alternatives, not just first costs.
- **Intrinsic Value.** Consider the intrinsic value of the facility and its value to the system from the perspective of reliability, load served, and revenue generation when determining what investment can be justified in terms of facilitating inspection and maintenance and promoting durability and longevity.
- **Radial Lines/Redundancy of Supply.** Consider whether the line is radial or there is redundancy of supply.
- **Probability of Failure.** Identify components and subsystems subject to deterioration and projected to have a greater probability of repair, refurbishment, replacement, and failure; and consider risk and failure effects when weighing where to make investment.
- **Future Costs.** Perform net present value or similar economic analyses that consider future costs when weighing choices among line configurations and component options.

Route Characteristics and Other Information to Frame a Cost-Effective, Site-Specific Design for Maintainability

This section provides guidance on the types of site- and situation-specific background information that should be sought to enable a transmission-line design to be optimized for maintainability. Questions are provided for each of the following topics:

- General line and operations information
- Route characteristics and considerations
- Line configurations, components, and materials

The answers to these questions may help to guide design choices and identify opportunities for investment to enhance maintainability based on site-specific considerations. The questions are intended as examples to prompt designers to consider issues that may help them to design for maintainability.

General Line and Operations Information

- **Operating Voltage.** What is the operating voltage? Is it a nonstandard voltage for the utility that will require special training and tools?
- **Consequences of Failure.** What are the consequences of failures and forced outages?
- **Radial Line.** Is it a radial line?
- **Nearby Lines.** Are other lines located in the same corridor?
- **Third-Party Attachments.** Will the line support underbuilds or other third-party attachments (e.g., communications equipment such as antennae, fiber optics, etc.)?
- **Service Life.** What is the projected service life for the line?

- **Upgrades.** Are upgrades anticipated?
- **Uprating.** Is future uprating or high-temperature operation anticipated?
- **Maintenance Vehicles.** What types of vehicles will be used to access the line for maintenance?
- **Climbing vs. Bucket Trucks.** Will maintenance be performed by climbing or via bucket trucks?
- **Live Working.** Will the line be maintained using live working techniques?
- **Inspection.** How frequently will the line be inspected and by what methods?
- **Maintenance Approach.** What is the anticipated approach to inspection and maintenance-prescriptive, preventative (e.g., reliability-centered or condition-based), etc.?

Route Characteristics and Considerations

- **Comparable Performance.** How have other similar lines in the area performed?
- **Wind.** What are the wind characteristics along the route?
- **Climatic/Terrain Anomalies.** Are there climatic or terrain anomalies in the area that could lead to special problems (e.g., vibration, galloping, overloads, etc.)?
- **Precipitation.** What is the annual precipitation?
- **Humidity.** What is the average relative humidity?
- **Ice Accretion.** Is the area prone to ice accretion?
- **Heavy Icing.** Is heavy icing likely?
- **Snowfall.** Is the area prone to significant accumulation of snowfall?
- **Keraunic Level.** What is the keraunic level?
- **Soil/Foundation Types.** What soil/foundation types (e.g., gravel, sand, clay, rock) will be encountered along the route?
- **Stability of Soil/Foundations.** Are the soil/foundation conditions stable?
- **Below-Ground Corrosion.** Are the route conditions such that below-ground corrosion is likely?
- **Soil Chemistry.** What is the soil chemistry and pH?
- **Dissimilar Materials.** Will dissimilar materials be in ground contact?
- **Buried Facilities.** Are other buried facilities (e.g., pipelines) located nearby?
- **Ground Resistance.** What are the ground resistance characteristics?
- **Water Table.** Where is the water table and is it stable?
- **Water Crossings.** Will the line cross a body of water?
- **Standing Water.** Will there by standing water along the line?
- **Irrigated Land.** Does the route traverse irrigated land?
- **Flowing Water.** Is there flowing water along the route and will foundation scour be an issue?
- **Ice Flows.** Are ice flows likely to cause problems?
- **Freeze-Thaw Cycles.** Are the effects of freeze-thaw cycles likely to be a problem?
- **Contamination.** Are portions of the line likely to be contaminated by salt spray, fertilizers, pesticides, or airborne industrial pollutants?
- **Insulator Washing.** Is the need for insulator washing anticipated?
- **Wildlife Habitat.** Does the route traverse any sensitive wildlife habitat?
- **Protected Species.** Are there any protected or endangered species along the route?
- **Woodpecker Habitat.** Is the route characterized by woodpecker habitat?
- **Bird Nesting.** Is bird nesting or perching likely to be a problem?

- **Wetlands.** Does the route traverse wetlands?
- **Archaeological Sites.** Does the route cross known archaeological sites?
- **Vegetation.** What are the characteristics of the ROW vegetation?
- **ROW Uses.** What are the characteristics of the ROW use and adjacent areas (e.g., is there any vehicle traffic nearby that could result in impacts, are farm implements likely to be used near the structures, etc.)?
- **Future ROW Uses.** What future uses of the ROW are anticipated?
- **Vandalism.** Is vandalism likely? If so, what type?
- **Easement Issues.** Are there landowner and easement issues that will limit certain types of maintenance activities?
- **ROW Accessibility.** How accessible is the ROW? Are there problematic areas along the route?
- **Vehicles on ROW.** What types of vehicles will be able to traverse the ROW?
- **Line Accessibility.** How will the line be accessed for inspection and maintenance?

Line Configurations, Components, and Materials

- **Preferred Line Alternatives.** What are the preferred line design alternatives (e.g., structure types, components, etc.) and their characteristics?
- **Relevant Experience.** What are the utility's and industry's experiences with similar configurations and components?
  - —Are there known problems? If so, how will they be mitigated?
  - —Has reliability been acceptable?
  - —What is the projected service life?
  - —Has experience with inspection and maintenance been acceptable?
- **Live Working.** Are the preferred design alternatives maintainable using live working techniques?
- **Replacement Components.** Are replacement components readily available (e.g., in inventory)?
- **Remedial Actions.** Will remedial actions (such as painting, application of wood preservatives, replacement of sacrificial anodes) be required on a regular basis?
- **New Products.** Will any new products be incorporated in the design?
  - —If operating experience is less than the target service life, how will risk be mitigated?
  - —What has been the experience of other users?
  - —Has there been adequate testing?
  - —Are they inspectable (visually, NDE [Nondestructive Evaluation])?
  - —Are there hidden failure modes that could lead to a catastrophic failure without being preceded by detectable evidence of degradation?
  - —Are they maintainable?

13.2.3 Designing for Durability and Longevity

The following section provides guidance on designing for durability and longevity. Tabulated information is provided on prevalent modes of degradation associated with each of the following major categories of transmission-line components ("Component Categories"), along with guidance on approaches that can be taken during design to mitigate the impacts of the degradation.

- Insulators
- Conductors, Overhead Ground Wires, and Splices
- Grounding
- Structures
- Miscellaneous Hardware (marking devices, signs, steps, bird guards and diverters)
- Rights-of-Way

To facilitate logical grouping and presentation of the information, the table header provides the following labels:

1. *Component Category*: Identifies which of the broad groups of components listed above is being addressed.
2. *Component Type*: Identifies the specific type of component (e.g., polymer insulators) being addressed within a major "Component Category" (e.g., insulators). In some cases, due to commonality of attributes and performance characteristics, it may be appropriate to group various types of components together, in which case, a designation such as "All" is used for the Component Type.
3. *Modes of Degradation*: Identifies the list of broad categories of degradation modes that may be applicable to the Component Category and Component Type to be addressed. The following codes are used to designate broad categories of modes of degradation and organize information in a consistent format throughout the table:

   B = Biological

   C = Chemical

   E = Electrical

   M = Mechanical

   T = Thermal
4. *Cause*: Identifies the specific action or force of component degradation (e.g., vibration) to be addressed in the body of the table.
5. *Mode*: This letter code is provided as an organizational reference tool to associate the Cause being addressed with an individual Mode of Degradation. Multiple Causes may be described for an individual Mode.
6. *Mitigation Opportunities During Design*: The body of the table provides information on approaches that can be taken to enhance the durability and longevity of components subject to the specific "Cause" of degradation referenced.

INSULATORS

Insulators

Glass

Component Category:	Insulator
Component Type:	Glass Insulator
Modes of Degradation:	C, E, M, T

Cause:	Cement Expansion/Shrinkage	Mode:	C	Mitigation Opportunities During Design:
• Cement can react chemically with the metal components of the insulator and promote swelling or shrinkage, thereby degrading the insulator (e.g., expansion can create an excessive hoop stress that can lead to radial and circumferential cracks of the insulator shell.)				• Specify aluminous cement. • Ensure strict material control. • Specify cement sample testing to verify that the sample expansion does not produce excessive localized mechanical hoop stresses that could damage the glass shell. • Use a reputable manufacturer.

Cause:	Contamination	Mode:	E	Mitigation Opportunities During Design:
• Contamination of insulator surfaces can degrade the insulating properties leading to flashover. • Excessive leakage current activity can cause glass shell to shatter.				• Limit contamination-related problems by using the most appropriate profile, creepage length, etc. for the given environmental conditions. —Refer to appropriate design guides. • Atypical applications may require additional investigation.

Cause:	Corona	Mode:	E	Mitigation Opportunities During Design:
• Corona can cause the following: —Customer complaints due to audible noise and radio interference. —Degradation of the cement at the pin/glass interface.				• Specify the correct corona or grading ring.

Cause:	Leakage Current	Mode:	E	Mitigation Opportunities During Design:
• Excessive or sustained leakage currents can result in: —Deterioration of the galvanized coating on pin, thereby enabling corrosion. —Arcing may corrode pin, causing a mechanical failure.				• Select correct insulator parameters for environment and application. • Use corrosion retardation ring on pin.

Cause:	Lightning, Switching, and Power Arcing	Mode:	E	Mitigation Opportunities During Design:
• Steep front lightning or switching impulses may cause: —Shattering of glass shell. —Damage to cap and/or pin. —Removal of galvanization, enabling the formation of rust. • Melting of glass shell can occur, degrading the insulating capabilities under contamination conditions.				• Use corona rings or arcing horns to prevent termination on end fittings. • Apply line surge arrestors. • Use a reputable manufacturer.

Cause:	Mishandling	Mode:	M	Mitigation Opportunities During Design:
• Damage due to improper packaging, handling, and shipping procedures.				• Specify preassembly of strings in factory. • Specify packing in a palletized container. • Educate personnel on proper procedures. —Warehouse, transportation, and construction • Inspect units prior to installation.

Cause:	Vandalism	Mode:	M	Mitigation Opportunities During Design:
• Glass insulators are susceptible to vandalism, primarily from gunshot or other projectiles (e.g., a stone). —Damage can range from chipping to complete shattering of the skirt and can contribute to failure of the electrical performance of the insulator. Note: The string will remain intact mechanically even though the glass is shattered.				• Replace glass insulator string with a polymer insulator in high incident areas.

Cause:	Thermal Expansion	Mode:	T	Mitigation Opportunities During Design:
• Both glass and metal components expand and contract at different rates, and extreme changes can cause the glass shell to shatter.				• Ensure insulator can withstand cyclic thermal-mechanical loads. • Use a reputable manufacturer.

Insulators

Polymer Insulator (NCI)

Component Category:	Insulator		
Component Type:	Polymer Insulator (NCI)		
Modes of Degradation:	B, C, E, M		
Cause: Bird and Rodent Damage	Mode: B	Mitigation Opportunities During Design:	
• Rodents may eat rubber while units are in storage. • Birds may eat units while in storage or after installation. —Damage is more prevalent prior to units being energized.		• Rodent damage: —Specify durable packing of polymer insulators to prevent access by rodents during shipping and storage. —Ensure rodent-free storage areas. • Bird damage: —Store units in secure packaging prior to installation to prevent damage. —Cover up installed units prior to energizing to minimize attack.	
Cause: Mold, Fungus and Bacteria	Mode: B	Mitigation Opportunities During Design:	
• Mold, fungus, and bacteria grow on insulator surfaces. —Concerns mainly due to units losing hydrophobicity (silicone rubber units). —Has not been linked to any loss in performance.		• Casual observation indicates that certain activity is more prevalent on certain rubber types (EPRI 2004b).	
Cause: Chemical Attack	Mode: C	Mitigation Opportunities During Design:	
• Chemical pollutants from industrial plants or other sources attack polymer material.		• Check with manufacturer to ensure compatibility of rubber with specific environmental conditions of line site.	
Cause: Weathering	Mode: C	Mitigation Opportunities During Design:	
• Ultraviolet radiation, temperature fluctuations, and various forms of precipitation may slowly degrade polymer materials and end-fitting seals.		• Use a reputable manufacturer. • Today's polymer insulator designs are such that the materials are more resistant to such damage than earlier materials, allowing for extended life.	
Cause: Contamination	Mode: E	Mitigation Opportunities During Design:	
• Contamination builds up on weathershed surfaces. —Many types of contamination have insulating properties when dry but conduct when wet (especially in marine environments and environments subject to road salt). —Leakage currents flow along insulator surfaces under wetting conditions. —Dry bands form due to localized heating or nonuniform wetting. —Arcs bridge dry bands (i.e., dry band arcing). —Arcing may result in damage to rubber material and/or end-fitting seals (e.g., erosion, tracking, cracking, etc.).		• Select correct insulator parameters for environment and application (EPRI 1998a). (Also see Chapter 4 in this Reference Book.) • If in an environment where it is anticipated that washing will be needed, check with manufacturer to ensure insulator can be washed and determine recommended washing cycle. Select an insulator with minimum washing requirements.	
Cause: Corona	Mode: E	Mitigation Opportunities During Design:	
• Corona activity under dry conditions from metal end-fittings will degrade rubber weathershed and/or end-fitting seal. —May occur at either energized or grounded ends. —Activity erodes rubber and/or seal. —After prolonged corona, fiberglass rod may be exposed. —Degradation from wetting discharge activity will also be high. • Corona activity under wet conditions causes degradation. —Water drops and patches enhance electric field, resulting in discharge activity (corona and localized arcing). —Discharge activity degrades rubber material and end-fitting seals due to: • Kinetic forces • UV • Temperature • Chemical activity —Wetting discharge activity is: • More prevalent in high electric field regions (i.e., close to end fittings). • Less likely on units with high levels of hydrophobicity. • A long-term aging mechanism.		• Correct selection of corona rings: (EPRI 1998a; EPRI 1999) (also see Chapter 4 in this Reference Book) —Refer to appropriate guides. • Atypical applications require further investigation. —Perform E-field distribution modeling and analysis to ensure that the magnitudes are within recommended levels (see Chapter 4). • Correct application of corona rings: —Educate field personnel as to correct application of corona rings. —Ensure that manufacturer supplies corona rings and installation instructions in the same crate. —"Keyed" corona ring designs that limit mistakes by field personnel are preferable.	

Insulators

Polymer Insulator (NCI) (Continued)

Cause:	Flashover	Mode:	E	Mitigation Opportunities During Design:
• Power arc terminating on either energized or grounded end fitting(s) can: —Damage end-fitting seal. —Melt end fitting or seal (more prevalent with aluminum seals, end fittings). —Remove galvanization resulting in rust. —Note: The effects of localized heating on rod and long-term mechanical strength are unknown. • Power arc terminating on corona ring(s) can: —Damage corona ring, which will no longer grade electrical field effectively. —Damage corona ring, leading to customer noise complaints. • Arcs may or may not terminate on the insulator; regardless, however, hot gases from arcs may damage rubber weathershed system or end-fitting seals.				• Use of corona rings or arcing horns prevents arc termination on end fittings (EPRI 1998a; EPRI 2004a). • Choose polymer insulator without aluminum end fittings or seals (EPRI 1998a; EPRI 2004a).
Cause:	Mishandling	Mode:	M	Mitigation Opportunities During Design:
• Damage can be caused by improper packaging, handling, and shipping procedures. —Damage due to impact: • Tears or cuts in rubber material. • Rod-rubber bond destroyed. • End-fitting seals damaged. • Galvanization removed. —Damage due to bending or twisting: • Rod interfaces between fibers and resin matrix may be damaged. • Damage is often not externally apparent. • Note: Damage grows as units age – minor damage may grow over years until failure.				• Educate personnel on proper procedures (EPRI 2001). —Warehouse, transportation, and construction. • Specify durable packing of insulators: —Withstand transportation and handling. —Prevent rodent and bird damage. • Inspect units prior to and after installation. —Close-up inspection needed.
Cause:	Vandalism	Mode:	M	Mitigation Opportunities During Design:
• Polymer insulators are susceptible to vandalism primarily from gunshot. —Rubber weathershed system and corona rings are most susceptible to direct damage. —If rod is exposed, risk of failure is high.				• Polymer insulators are often applied in gunshot areas since: —Damage is less obvious than brittle materials, reducing enjoyment. —Units have smaller profiles and are harder to shoot. —Note that this does not mean that the units are “shot proof.” Exposed rod increases risk of failure.

Insulators

Porcelain Insulator

Component Category:	Insulator		
Component Type:	Porcelain Insulator		
Modes of Degradation:	C, E, M		
Cause: Cement Expansion/Shrinkage		Mode: C	Mitigation Opportunities During Design:
• Cement expansion due to chemical reaction in the cement creates an excessive hoop stress inside the porcelain head that can lead to radial and circumferential cracks of the insulator shell. • Shrinkage can lead to pin pull out or cap separation from the shell.			• Specify portland-type cement. • Specify cement sample testing to verify that the sample expansion does not produce excessive localized mechanical hoop stresses that could damage the porcelain shell. • Improve material quality control and assembly process requirements.
Cause: Corrosion		Mode: C	Mitigation Opportunities During Design:
• Most metals are susceptible to corrosion due to interaction with oxygen, water, acids, bases, salts, oils, and other solid and liquid chemicals, etc. to form surface oxides or other complex corrosion products. Corrosion can accelerate when rubbing of components, corona activity, or arcing compromises protective coatings such as zinc galvanizing. Atmospheric corrosion is the primary type of corrosion that degrades metal fittings of insulators: —The rate of corrosion measures metal wastage and is influenced by factors including relative humidity, temperature, concentration of sulphate and chloride pollution, etc. —The severity of corrosion depends on environmental conditions, such as proximity to power plants, chemical plants, and other industrial facilities, marine environments, and areas where there is heavy use of fertilizers and pesticides.			• Increase zinc coating thickness in aggressive environments. • Specify corrosion resistant material (e.g., stainless steel). • Apply metal collar or shield over the exposed region of the pin. • Install corona ring to suppress corona discharge. • Install anti-interference cotter key to suppress corona discharge. • Install proper-sized weight to increase tension of jumper loop support string.
Cause: Faults, Lightning, or Excess Surface Dry-band Arcing		Mode: E	Mitigation Opportunities During Design:
• Pitting and melting of glaze surface is a form of degradation that occurs in the case of discharge activities. • Corona discharge can induce pitting and corrosion.			• Specify proper-sized protective gaps/arcing horn. • Specify corona ring to suppress excessive corona discharge.
Cause: Flashover		Mode: E	Mitigation Opportunities During Design:
• Exposure of an insulator to ice, freezing rain, fog, and contamination from a polluted environment under certain weather conditions can contribute to insulator flashover. —Melting ice and snow combined with contamination can provide low-resistance paths for currents to flow. —Ice and snow can bridge sheds. —Adverse conditions are generally localized and sustained for a relatively short period (in hours).			• Consider economic and performance tradeoffs between increasing insulation and power washing to clean off the contaminants or reduce the contamination to a safe level. • Monitor the buildup of contamination level and use the ESDD methodology to develop information to assist with proper insulator selection and/or determining washing cycles. • Use V-string configuration to reduce frequency of washing. • Use resistive-glaze insulators. • Use rubber-coated insulators. • Use alternating diameter units or V-string to prevent ice bridging between units.
Cause: High Electric Fields		Mode: E	Mitigation Opportunities During Design:
• Strong electric fields from extra-high-voltage operation (e.g, 700 kV and above) causes continuous high electric stress at areas between the cap and pin, and could degrade the electrical properties of the insulator over time. —High-intensity localized fields may cause puncture of porcelain shell and slow erosion of pin cement.			• Install corona ring to suppress excessive corona discharge near the line-end units.

Insulators

Porcelain Insulator (Continued)

Cause:	Lightning, Switching, and Power Arcing	Mode:	E	Mitigation Opportunities During Design:
• Lightning, switching, and power arc faults degrade insulators. —Exposure to repeated steep front lightning or switching impulses will result in full or partial punctures of insulators. —Fault currents or lightning will result in annealing of metal fittings and cause loss of strength. —Melting of metal fittings may occur. —Rapid heating followed by rapid cooling of the metal may reduce its ability to withstand bending and dynamic forces. —Erosion of galvanization of metal fittings may occur.				• Specify proper-sized protective gaps/arcing horns. • Install corona ring to suppress excessive corona discharge near the line-end units. • Install metal-oxide arrester.
Cause:	Mishandling	Mode:	M	Mitigation Opportunities During Design:
• Damage due to improper packaging, handling, and shipping procedures.				• Specify preassembly of strings in factory. • Specify packing in a palletized container. • Educate personnel on proper procedures. —Warehouse, transportation and construction. • Inspect units prior to installation.
Cause:	Overloading	Mode:	M	Mitigation Opportunities During Design:
• Mechanical overloading is generally the result of excessive wind and/or ice loading. —The most common result of mechanical overload is separation of metal end-fittings from the insulator body. —Temporary overloading beyond the recommended rating normally does not cause complete separation of the insulator unit; however, it could result in reduction of rated mechanical failure load due to a time-load effect. —Insulators exposed to heavy or temporary overloads would typically have higher standard deviations of M&E strength than new insulators that are normally in the range of 5 to 10%.				• Install double or multi-string assembly. • Reduce the allowable design loads to a lower percentage of M&E ratings of insulators for various loading conditions (e.g., heavy ice, combined wind and ice, and everyday loads). • Use a probability approach to determine the mechanical stress and insulator strength requirements.
Cause:	Vandalism	Mode:	M	Mitigation Opportunities During Design:
• Porcelain insulators are susceptible to vandalism primarily from gunshot. —Damage can range from chipping to complete shattering of the skirt and can contribute to insulator failure.				• Replace porcelain with polymer units in high incident areas. • Change glaze color from dark brown to light gray or blue to reduce the sharpness of the target image.
Cause:	Vibration and Galloping	Mode:	M	Mitigation Opportunities During Design:
• Wind-induced conductor motion is one of the most common causes of shell and metal end-fittings degradation. Damage to zinc coating of metal fittings can lead to corrosion. —Aeolian vibration results in metal fatigue and eventual breakage of insulator end-fittings. —Galloping results in very high dynamic loading of the conductor and can lead to breakage of porcelain shell, metal fittings, and/or uncoupling of insulator units.				• Maintain conductor tension within its design limits. • Use vibration dampers and spacer dampers. • Use self-damping conductors. • Use anti-galloping devices. • Use stainless steel cotter key. • For line post insulator configurations. —Use polymer units. —Improve conductor attachment end-fitting design to allow more free movement.

CONDUCTORS, OVERHEAD GROUND WIRES, AND SPLICES

Conductors

All

Component Category:	Conductor
Component Type:	All
Modes of Degradation:	C, E, M

Cause:	Corrosion	Mode:	C	Mitigation Opportunities During Design:
• Most metals corrode in the presence of water, acids, bases, salts, oils, and other solid and liquid chemicals, as well as various gases including acid vapors, ammonia, and sulfur-containing gases. The rate of corrosion is dependent on a variety of factors, including the properties of the metal and the presence of water, oxygen, and various contaminates. Atmospheric and galvanic corrosion are two primary types of corrosion that degrade conductors. —Atmospheric corrosion occurs due to contact with substances such as oxygen, carbon dioxide, water vapor, and sulfur and chlorine compounds present in the atmosphere. Atmospheric corrosion is primarily a concern with the galvanized steel core of conductors. —Galvanic corrosion occurs when two dissimilar metals are brought together in the presence of moisture and electric potential. In the case of ACSR conductors, the zinc galvanizing is a sacrificial anode, and the aluminum is the cathode. However, if the zinc coating is compromised and the aluminum comes in contact with the steel, the aluminum becomes the sacrificial anode and begins to corrode at a higher rate. —The severity of corrosion problems depends on environmental conditions, and therefore, the proximity of a line to sources of contaminants should be considered. Sources might include power plants, chemical plants, and other industrial facilities, marine environments, and areas where there is heavy use of fertilizers and pesticides.				• A few mitigation measures can be adopted during design. Some of these options are: —Specify a thicker-than-standard galvanization for the steel wire. —Use Alumoweld and/or Copperweld-type core conductors. —Use a composite core conductor.

Cause:	Excessive Current	Mode:	E	Mitigation Opportunities During Design:
• Exposure of conventional conductors (ACSR, AAAC, AAC, ACAR) to temperatures of 90°C or greater due to continuous high-temperature operations, temporary fault, or lightning currents will result in annealing of aluminum, loss of conductor strength, elevated creep, and increased sag. —The resulting loss of strength depends on the cumulative duration at various temperatures above 90°C and the type of aluminum used. The effect of strength reduction will depend on the composition of the conductor (i.e., aluminum to steel ratio). —Because the durations of fault and lightning currents are short and the size of conductor is large, the impact on phase conductor is generally small. —Pitting and melting of the conductor surface could, however, occur in the case of power arc faults or lightning strokes. —Burndown could occur due to overheating from excessive current and significant reduction of tensile strength.				• The occurrence and effects of high-temperature operations on conductors can be mitigated in several ways: —The conductor can be selected to ensure sufficient cross-sectional area of aluminum to limit anticipated operating temperatures to less than 90°C. Marginal gain in area can be achieved by selecting a conductor with trapezoidal strands rather than round strands but with the same conductor diameter. —Conductors that are specially designed for high-temperature operation can also be utilized. There are a few High-Temperature Low-Sag conductors that are commercially available such as the aluminum conductor steel-supported (ACSS), the Invar conductor, and the Gap conductor. In addition, several promising new conductors, which use composite material in place of a steel core in order to provide reduced sags under high temperatures are currently being evaluated. —Lightning strokes on the conductor can be reduced substantially if overhead ground wires are installed to shield lightning from the phase conductors.

Cause:	Overloading	Mode:	M	Mitigation Opportunities During Design:
• Mechanical overloading is generally the result of excessive wind and/or ice loading, or due to impact load from interference of foreign objects such as planes, sail boats, and fallen trees. —The most common result of mechanical overloading is excessive sag. In the worst case, it could cause adjacent structures to fall. —Unless the conductor is overloaded to the point of breaking individual strands, overloading does not normally result in a measurable reduction in ultimate mechanical strength. It will, however, cause permanent elongation to the conductor.				• The effect of mechanical loads can be mitigated in the following ways: —Local weather data along with the appropriate safety and design code criteria should be used to determine proper loading for the conductor. —The permanent set created by heavy ice and wind loading should be factored into the design when the ground clearance of the conductor is determined. —The practice of cutting danger trees that might fall onto the conductor should be followed. —Warning signs and devices should be posted across flight paths, waterways, etc.

Conductors

All (Continued)

Cause:	Vandalism	Mode:	M	Mitigation Opportunities During Design:
• Gunshot is the primary type of vandalism to which conductors are susceptible. —Damage can range from nicking to severing strands and can contribute to long-term degradation.				• Different attempts have been made to discourage gunshots. Some of these are: —Provide an alternative target nearby. —Provide warning on the consequence of a fallen power line. —Distribute public awareness communications.
Cause:	Vibration	Mode:	M	Mitigation Opportunities During Design:
• Wind-induced conductor motion or vibration is the most common cause of conductor degradation. Wind-induced conductor motion includes aeolian vibration, galloping, and wake-induced oscillation. —Aeolian vibration, a high-frequency low-amplitude motion, results in fatigue and eventual breakage of strands at points of support or restraint, such as suspension points, spacer attachments, compression splices, and dead ends. —Galloping, a low-frequency high-amplitude motion, results in very high dynamic loading of the conductor and can lead to conductor damage and/or failure as well as damage to other components such as the insulator string. Broken strands may occur near suspension points or other attachments. The mid-span surface could be scarred with pitting and burn marks due to flashovers between adjacent phase conductors. —Wake-induced oscillation, a low-frequency motion caused by the shielding effect on the leeward subconductor in a conductor bundle, can lead to sufficient amplitude to cause adjacent conductors in a bundle to clash, resulting in wear at contact points and at attachments. • Vibration can cause wear of connected components.				• There are various ways to mitigate vibrations. —Maintaining a low-conductor tension at cold temperatures when the conductor is prone to vibration can control aeolian vibration. A proper conductor tension should be selected based on consideration of the terrain and local weather data. Dampers and cushioned suspension or support hardware are often installed to control aeolian vibration. Armor rods can also be used. —There is no simple means to control galloping. Galloping control devices such as interphase spacers, air-flow spoilers, and detuning pendulums have been used with partial success. The effectiveness of a galloping control device is dependent on its ability to provide damping at low frequencies. To avoid clashing or flashover of conductors during galloping, sufficient phase separation must be allowed in the design. —One of the mitigation options to alleviate wake-induced oscillations is to stagger the subspan distances. • Comprehensive information on conductor vibrations can be found in the EPRI *Transmission Line Reference Book: Wind-Induced Conductor Motion* (EPRI 1979). • Vibration/motion-induced wear of connected components can be minimized by avoiding use of relatively soft metals in connections.

Overhead Ground Wire

All

Component Category:	Overhead Ground Wire		
Component Type:	All		
Modes of Degradation:	C, E, M		
Cause: Corrosion	Mode: C	Mitigation Opportunities During Design:	
• For steel ground wires, atmospheric corrosion is a concern in industrial and polluted areas as well as near the coast. Corrosion occurs due to contact with substances such as oxygen, carbon dioxide, water vapor, and sulfur and chlorine compounds present in the atmosphere.		• A few mitigation measures can be adopted during design. Some of these options are: —Specify a thicker-than-standard galvanization for the steel wire. —Specify the use of a steel alloy. —Specify the use of Alumoweld or Copperweld-type overhead ground wires that have a higher resistance to corrosion.	
Cause: Excessive Current	Mode: E	Mitigation Opportunities During Design:	
• The overhead ground wire comprised typically of steel wire strands does not normally carry any current. Its main function is to protect the phase conductors from lightning that could cause a line outage. As a result, the overhead ground wire is often struck by lightning. Repeated strikes by lightning strokes can cause damages to the ground wires. —Melting of steel overhead ground wires may occur. —Rapid cooling following rapid heating from a lightning stroke may cause embrittlement of the steel, resulting in reduction of its ability to withstand bending and dynamic forces.		• Ground wire damage caused by lightning can be mitigated by: —Specifying a size of steel ground wire that is larger than that which would normally be required. Oversizing provides some buffer material that can be sacrificed in the event of a lightning strike without reducing the strength to an unacceptable level. It can also accept higher currents by providing a higher melting temperature. —Using Alumoweld or Copperweld in place of steel; both products offer higher conductivity than steel and better performance when subjected to lightning strokes.	
Cause: Overloading	Mode: M	Mitigation Opportunities During Design:	
• Mechanical overloading is generally the result of excessive wind and/or ice loading. Heavy ice loading affects the overhead ground wire more than the phase conductor due to its smaller size. —The most common result of mechanical overloading is excessive sag. —Excessive ice load can break overhead ground wires.		• The effect of mechanical loads on an overhead ground wire can be mitigated in the following ways: —Local weather data, along with the appropriate safety and design code criteria, should be used to determine proper loading for the overhead ground wire. —Excessive sag caused by temporary ice load should be considered in the selection of separation between an overhead ground wire and the phase conductors. —Overhead ground wires using high-strength steel can be selected for heavy ice areas.	
Cause: Vandalism	Mode: M	Mitigation Opportunities During Design:	
• Gunshot could be a source of vandalism to which the overhead ground wire is subjected. —Damage can range from nicking to severing strands, and can contribute to long-term degradation.		• The overhead ground wire, being smaller in size and higher from the ground, is less of a target than the phase conductor. Measures taken for the phase conductor can be applied to the ground wire as well. —Provide an alternative target nearby. —Provide warning on the consequence of a fallen power line. —Distribute public awareness communications.	
Cause: Vibration	Mode: M	Mitigation Opportunities During Design:	
• Fatigue from aeolian vibrations is the most common cause of overhead ground wire failures. It occurs at the suspension point. • Vibration can cause wear of connected components.		• Maintaining a low overhead ground wire tension at cold temperatures when it is prone to vibration can control aeolian vibration. A proper tension should be selected based on consideration of the terrain and local weather data. • Dampers and cushioned suspension or support hardware can also be installed to control aeolian vibration of overhead ground wires. • Armor rods can also be used. • Vibration/motion-induced wear of connected components can be minimized by avoiding use of relatively soft metals in connections.	

Splice
All

Component Category:	Splice			
Component Type:	All			
Modes of Degradation:	M			
Cause:	Insufficient Strength	Mode:	M	Mitigation Opportunities During Design:
• Splices form an integral part of the conductor system and are exposed to the same degradations as the conductor since similar materials are used. Although the ultimate mode of failure of a splice is most often mechanical, the degradation that precipitated the failure could be electrical due to high currents, thermal due to higher-than-normal splice temperature caused by high resistance of the splice resulting from improper installation, mechanical due to vibrations and overloading, and corrosion from dissimilar material used or ingress of water and contaminants into the splice. Degradation of a splice most often results from: —Improper selection of the type of splice for the application. —Improper installation.				• To avoid premature failure of a splice, and to help ensure that it will not fail before the conductor it connects, the following steps can be taken: —Select the proper splice for the application. If continuous high-operating temperature is expected, use a splice that is designed for high temperature with sufficient volume of material to avoid overheating, annealing, and thermal fatigue. Avoid using single-stage splices. —Select the implosive splice if good compression is a concern. —Follow diligently the procedure dictated by the manufacturer; ensure that the grease, die, and press as specified by the manufacturer are used. —Educate and train staff to ensure proper installation methods are followed to avoid water ingress and thereby minimize the likelihood of corrosion.

GROUNDING

Grounding

Caissons and Guy Anchors

Component Category:	Grounding		
Component Type:	Caissons and Guy Anchors		
Modes of Degradation:	C,E,M,T		
Cause: Corrosion	Mode: C	Mitigation Opportunities During Design:	
• A high salt content environment can cause corrosion to concrete-encased reinforcing steel.		• Reinforcing steel is encased in concrete to prevent corrosion. An additional precaution is to be aware of locations (such as along roadways) where high salt concentration might be present.	
Cause: Lightning, Switching Surges, and Power Arcing	Mode: E, T	Mitigation Opportunities During Design:	
• High current transients, such as lightning surges, can cause severe damage to concrete footings or anchors.		• Suggestions to avoid damage are as follows: —Use the reinforcing steel in a caisson foundation as a grounding component according to NESC (NESC 2002b). —Install a ground rod alongside the caisson foundation as protection against damage to the concrete.	
Cause: Mechanical Damage	Mode: M	Mitigation Opportunities During Design:	
• Ground connections to foundations or anchors can sustain mechanical damage due to causes such as impact from vehicles.		• Ground leads must be positioned or guarded per NESC (NESC 2002a) to limit the likelihood of mechanical damage.	

Grounding

Chemical Ground Rods

Component Category:	Grounding		
Component Type:	Chemical Ground Rods		
Modes of Degradation:	C		
Cause: Hazardous Materials	Mode: C	Mitigation Opportunities During Design:	
• The handling and replacement of hazardous chemicals are of concern with chemical ground rods.		• Chemical ground rods are available that are formed by adding nonhazardous minerals to the surrounding soil over an extended period of time.	

Grounding

Counterpoise—Copper, Galvanized Steel, and Zinc

Component Category:	Grounding		
Component Type:	Counterpoise—Copper, Galvanized Steel, and Zinc		
Modes of Degradation:	C, E, M		
Cause: Corrosion	Mode: C	Mitigation Opportunities During Design:	
• Galvanized steel and zinc conductors can corrode over time due to galvanic corrosion. • Counterpoise conductors may corrode over time due to microbic-induced corrosion in certain soil conditions. Presence of sulfur odor in soil may indicate presence of microbes. • Counterpoise conductors may corrode over time due to dc earth currents. • Some typical sources are as follows: —Pipelines with dc-impressed current or sacrificial cathodic protection systems. —Dc transmission lines. —Dc-powered railroads.		• In areas of known corrosive soil conditions, choose copper as counterpoise material. • There is no practical mitigation measure available for microbic-induced corrosion. • A measurement of the ground resistance at the time of installation should be made and documented as the basis for future measurements to verify counterpoise integrity. • Typical dc earth current mitigation measures are as follows: —Avoid placing counterpoise in proximity to facilities having impressed-current cathodic protection. —The amount of separation depends on the level of dc current imposed on the foreign facility. —Segmenting the overhead ground wire grounds. —Use of an independent cathodic protection system.	
Cause: Excessive Current	Mode: E	Mitigation Opportunities During Design:	
• Exposure of counterpoise conductors to elevated temperatures due to high fault currents or lightning can result in fusing or melting. • Connection hardware and conductors can melt due to high temperatures at high-resistance connections.		• The size of standard conductors can be selected so as to ensure a cross-sectional area of the conductor sufficient to limit anticipated temperatures for an expected transient duration to nondamaging levels. • Specify adequate size connectors and cleaning of contact surfaces to ensure low-resistance connections.	

Grounding

Counterpoise—Copper, Galvanized Steel, and Zinc (Continued)

Cause:	Mechanical Damage	Mode:	M	Mitigation Opportunities During Design:
• Exposure of counterpoise conductors to the following external mechanical forces can cause damage to strands or completely sever the counterpoise. —Excavation activities by property owners and contractors can uncover and damage counterpoise. —Erosion of soil can cause inadequate surface coverage, making counterpoise vulnerable to damage. —Excessive settling due to inadequate backfill and compaction can make counterpoise vulnerable to damage.				• The possibility of mechanical damage can be reduced by addressing the following site conditions: —Specify adequate depth of counterpoise installation. In cultivated areas where plowing is performed, additional depth is required. —Specify alternative grounding method (ground rods, etc.) in areas of high construction activity. —Specify counterpoise be installed on side of structure away from likely excavation activity. —Specify Best Method Practices to prevent erosion. —Specify installation by vibratory plow where possible to reduce the settling and erosion.
Cause:	Vandalism	Mode:	M	Mitigation Opportunities During Design:
• Theft of counterpoise for salvage value.				• Use Copperweld, galvanized steel, and zinc because they have a low salvage value relative to copper. • Make connection to structure below grade to decrease visibility of counterpoise.

Grounding

Direct Buried Tubular Poles

Component Category:		Grounding		
Component Type:		Direct Buried Tubular Poles		
Modes of Degradation:		C		
Cause:	Corrosion	Mode:	C	Mitigation Opportunities During Design:
• Many utilities directly bury metal structures or components. These structures are generally bonded to the overhead ground wires and may be used as grounding components. The metal structure can be subject to corrosion because buried steel (galvanized) structures are anodic relative to copper grounds if both metals are buried together in earth and bonded together.				• Typical methods to mitigate galvanic corrosion of the buried structure are as follows: —Coat the buried steel with a dielectric coating. (Some utilities only coat a portion of galvanized poles, leaving the base uncoated for grounding.) —Some coating types are: • Coal tar • Polyethylene —Encase the buried steel in concrete. —Use galvanized ground rods. —Electrically isolate the buried structure(s). • Install an insulator in the guy lead. • Segment the overhead ground wire.

Grounding
Driven Ground Rods and Pole Butt Wraps

Component Category:	Grounding
Component Type:	Driven Ground Rods and Pole Butt Wraps
Modes of Degradation:	C, M

Cause: Corrosion	Mode: C	Mitigation Opportunities During Design:
• Galvanic corrosion occurs when dissimilar metals are electrically connected and in a common earth electrolyte. —Examples of differing metals that may be used for ground rods include: • Copper • Stainless steel • Galvanized steel • Zinc • Variations in the electrical and chemical characteristics of the soil affect the rate of corrosion. The typical soil parameters that vary in a regional area (horizontal or vertical soil structure layers) are as follows: —Soil resistivity —Chemical consistency and pH • Alkaline or acidic soils are more corrosive, especially if the soil is low resistance (typically less than 50 ohm-meters).		• Noble metals such as copper have less affinity to oxidation and are generally preferred. • Dissimilar metals should be avoided. • If circumstances require ground rods of dissimilar metals, electrically isolate the metals. —Since distribution systems generally have a multi-grounded neutral, where distribution is attached to the transmission poles, it may not be acceptable to isolate the grounds. —On extra-high-voltage lines (345 kV and above), insulated shield wire sections have been used to reduce inductive power losses. Similar designs could be utilized to isolate ground rods of dissimilar metals. • Naturally occurring variations in the electrical and chemical characteristics of the soil cannot be avoided. Certain soil characteristics can be measured and the information used to enhance the design. —Soil resistivity can be measured. —The galvanic activity level of soil can be profiled. A copper – copper sulfate reference half-cell is generally used for the measurement.
Cause: Construction Damage	**Mode: M**	**Mitigation Opportunities During Design:**
• The impact of driving ground rods with threaded couplings can damage the electrical connections, reducing the effectiveness of the lower sections.		• Where installation is difficult (hard soils), or where multiple rod sections are required to obtain the desired ground resistance, use compression couplings that have been shown to be more resistant to damage during installation. • Resistance measurements after installation will readily identify whether electrical connections have been damaged.

Grounding
Grillages

Component Category:	Grounding
Component Type:	Grillages
Modes of Degradation:	C, M

Cause: Corrosion	Mode: C	Mitigation Opportunities During Design:
• Galvanized steel grillages will corrode over time due to galvanic corrosion. • Galvanized steel grillages may corrode over time due to microbic-induced corrosion in certain soil conditions. Presence of sulfur odor in soil may indicate presence of microbes. Designer is not likely to have information about presence of microbes. • Galvanized steel grillages may corrode over time due to dc earth currents. • Some typical sources are as follows: —Pipelines with dc-impressed current cathodic protection systems. —Dc transmission lines. —Dc-powered railroads.		• Specify adequate level of galvanizing. • Locate structures so grillages do not set in areas of fluctuating water levels. • In highly corrosive soils, install structures on concrete footings. • There are no known practical mitigation measures available for microbic-induced corrosion other than avoid metal in ground at these locations. • Typical dc earth current mitigation measures are as follows: —Avoid placing structures in proximity to facilities having impressed-current cathodic protection. —The amount of separation depends on the level of dc current imposed on the foreign facility. —Segmenting the overhead ground wires. —Use of independent cathodic protection system.

Grounding
Grillages (Continued)

Cause:	Mechanical Damage	Mode:	M	Mitigation Opportunities During Design:
• In many locations where the soil resistivity is relatively low, steel grillages with grounding enhancements (ground rods, counterpoise, etc.) are adequate for grounding purposes. • Mechanical damage to grillages can occur due to external mechanical forces as follows: —Excavation activities by property owners, developers, contractors, etc. can uncover and damage grillages. —Erosion of soil can cause inadequate surface coverage, making grillages vulnerable to damage. —Excessive settling of earth cover due to improper backfill and compaction can make grillages vulnerable to damage.				• The possibility of mechanical damage can be reduced by addressing the following site conditions and solutions: —For a structure that must be located close to a road, install barriers between road and structure. —For a structure that must be located close to an area of high construction activity, install barriers around structure. —Specify Best Method Practices to prevent erosion. —Specify tamping of earth backfill during installation.

Grounding
Ground Leads—Aluminum

Component Category:	Grounding
Component Type:	Ground Leads—Aluminum
Modes of Degradation:	E, M

Cause:	Lightning, Faults	Mode:	E	Mitigation Opportunities During Design:
• Aluminum has a lower melting point than copper; and, under fault or lightning currents, aluminum wire might melt and separate.				• Aluminum should be avoided for ground leads.
Cause:	**Mechanical Damage**	**Mode:**	**M**	**Mitigation Opportunities During Design:**
• Aluminum is easily cut or mechanically severed.				• Aluminum should be avoided for ground leads.

Grounding
Ground Leads—Copper (Soft and Hard), Copperweld

Component Category:	Grounding
Component Type:	Ground Leads - Copper (Soft and Hard), Copperweld
Modes of Degradation:	M

Cause:	Mechanical Damage	Mode:	M	Mitigation Opportunities During Design:
• Mechanical damage can occur due to: —Farm equipment near cultivated fields. —Vehicle bumpers in parking lots or along street and roadways.				• NESC (NESC 2002a) requires: —Leads of single-grounded systems must be covered. —Other ground leads shall be: • Substantially attached closely to the surface of the pole and located on a side having least exposure to mechanical damage, or covered. • Methods to protect ground leads are as follows: —Wood poles: • A shallow kerf sawed into the wood pole (height of eight (8) feet above ground) provides a secure, recessed location for the ground wire. This is one of the best protection methods against damage but is seldom utilized (the cost is high). • Wood molding (eight (8) feet long) is commonly used. These typically provide better protection than the plastic alternatives. —Steel poles: • Locate the ground wire attachment close to the ground line so the lead is as short as possible. • Provide two attachment points on opposite sides of the pole so the one having less exposure can be utilized. —Caisson foundations: • Secure the ground wire to the concrete with hammer-driven wire clips. • Cast the ground wire into the concrete. • Form a groove into the foundation for the ground wire.

Grounding
Ground Leads—Copper (Soft and Hard), Copperweld (Continued)

Cause:	Vandalism	Mode:	M	Mitigation Opportunities During Design:
• Theft of ground wire has been reported. • Typical locations of ground wire removal are: —For wood poles, the bottom eight (8) feet of ground wire from the structure. —For steel poles, the ground lead from a steel pole to the ground rod.				• Deterrents to theft include: —Use Copperweld wire that has no salvage value. —Use hard-drawn copper that is more difficult to cut. —Install molding or covering. —On wood poles, use more frequent staples. —For steel poles with caisson foundations, the ground lead can be secured to (or cast within) the concrete.

Grounding
Ground Wells

Component Category:	Grounding
Component Type:	Ground Wells
Modes of Degradation:	C

Cause:	Corrosion	Mode:	C	Mitigation Opportunities During Design:
• Galvanic corrosion can occur if there are dissimilar metals between the ground well and conductor installed in the well. —Examples of differing metals that may be used in ground wells include: • Copper • Stainless steel • Galvanized steel • Zinc				• Dissimilar metals should be avoided. • When installing conductive backfill in ground well, position the grounding conductor to avoid direct contact with ground well.

Grounding
Nails and Staples

Component Category:	Grounding
Component Type:	Nails and Staples
Modes of Degradation:	E

Cause:	Electric Fields/Leakage Current	Mode:	E	Mitigation Opportunities During Design:
• Nails and staples on ground leads can cause wood pole fires. As the ground wire passes through the electric field near the energized conductors, a voltage is induced in the ground wire. If the path of the wood pole is moist, current will also pass through the wood pole. Theoretically, the current dries and heats the wood at the tip of the staple where the current is concentrated. As the wood dries, it becomes a good insulator of heat so that the heat rises to the point of ignition. —Most occurrences have been reported at voltages of 138 kV and above, although pole fires could also occur at lower voltages if the conductor-to-ground wire spacing were close enough to generate a high electrical field. • Similar occurrences have occurred due to leakage current through the wood between the pole ground and pole hardware. See grounding of hardware for further details.				• Recommended design solutions to eliminate pole fires occurring at nails or staples and other hardware are as follows: —Install the nails and staples at close spacing near the energized conductor region. Because the weak electric current is dissipated at more locations, sufficient heat to ignite the wood would not be generated at any one nail or staple (Lusk and Mak 1975). —Use plastic wire holders (inserts) for the staples. —Use plastic (or nylon) nails or staples. • Choose a plastic nail or staple that will not work loose. Some have a wedge shape and do not stay in the pole. • Avoid installing ground wires such that they are driven (kinked) into the wood pole. —Specify adequate distance between the pole ground and other pole hardware. —Bond the pole hardware to the pole ground.

Grounding

Overhead Ground Wires

Component Category:	Grounding			
Component Type:	Overhead Ground Wires			
Modes of Degradation:	C, E, M			
Cause:	Corrosion	Mode:	C	Mitigation Opportunities During Design:
• Hardware corrosion can cause high-resistance connections, contributing to excessive heating at hardware connections.				• Use bonding lead as path between overhead ground wire and structure to reduce current flow through the hardware.
Cause:	Excessive Current	Mode:	E	Mitigation Opportunities During Design:
• Induced currents can cause excessive heating and failure at hardware connections.				• The possibility of excessive heating can be mitigated as follows: —Do not rely on mechanical contact between hardware components as a current path. Use a bonding lead as path between overhead ground wire and structure. —Isolate sections of overhead ground wire to reduce current flow.
Cause:	Vibration	Mode:	M	Mitigation Opportunities During Design:
• Excessive vibration can cause wear on various overhead ground wire hardware components and associated hangers on structure. • Gaps between hardware components during a vibration cycle contribute to arcing between components, causing additional deterioration and radio interference.				• Install dampers as required to reduce vibration. • Use bonding lead as path between the overhead ground wire and structure. —Select a fatigue-resistant wire for the bond, such as soft-drawn stranded copper, not hard-drawn solid wire.

Grounding

Passive Conductors (Pipelines, Railroads, Communication Cables, etc.)

Component Category:	Grounding
Component Type:	Passive Conductors (Pipelines, Railroads, Communication Cables, etc.)
Modes of Degradation:	C, E

Cause:	Corrosion	Mode:	C	Mitigation Opportunities During Design:
• Stray ac and dc earth currents can cause corrosion. —Whenever the transmission grounding system is a continuous path for ac and dc earth currents, the current from a foreign passive conductor source can cause corrosion. —Some typical foreign passive conductor sources are as follows: • Pipelines with dc-impressed current cathodic protection systems. • Dc transmission lines. • Dc-powered railroads. —The detrimental effects will be more severe for a series of ground rods installed along a pipeline or between the rectifier and a pipeline.				• Ac and dc earth currents can be detrimental to all types of buried metal structures, including transmission structure grounding systems such as copper ground rods. Some recommendations to prevent corrosion and other electrical effects are as follows: —Avoid placing horizontal conductors (such as counterpoise) or vertical rods in close proximity to structures having impressed-current cathodic protection. • The amount of separation depends on the level of ac and dc current imposed on the foreign structure. • Where a power line crosses perpendicular to a pipeline, consider omitting the horizontal conductor or ground rod(s) at the structure closest to the pipeline. (If it is a metallic structure, this may be trivial because the structure could become part of the dc circuit.) —Where corridor-sharing with a pipeline, railroad, communication cable, etc. is necessary, protection of the electrical grounds from corrosion may be advised. The following are possible solutions: • Segment the overhead ground wire grounds. • Use resistance bonds to receive a portion of the passive conductor's protective current. • Use independent cathodic protection. —At connections between passive conductors such as pipelines and electric transmission systems at generation stations and pumping stations, the following is recommended: • Isolate the station grounds or consider isolating the transmission grounds remote from the station. For example, insulate the overhead ground wire at a distance from the station where the fault currents have diminished. This pertains to the prevention of safety concerns.
Cause:	Lightning	Mode:	E	Mitigation Opportunities During Design:
• Overhead ground wires are designed to attract lightning and protect the transmission phase conductors. Lightning strikes are likely to dissipate energy to earth, particularly through the grounding system and ground rods. Insulated coverings of any nearby metallic conductors could be damaged.				• Locate transmission grounding system conductors at a minimum of thirty (30) feet from underground power and communication cables. Conversely, underground power and communication cables should be located at a minimum of thirty (30) feet from transmission ground rods. (It is important to note that a site-specific separation distance should be properly determined from an analytical study.)

Grounding

Personnel Protection at Switch Structures (Buried Mats or Grates at Ground Surface)

Component Category:	Grounding
Component Type:	Personnel Protection at Switch Structures (Buried Mats or Grates at Ground Surface)
Modes of Degradation:	C, E, M

Cause:	Corrosion	Mode:	C	Mitigation Opportunities During Design:
• Above-ground galvanized steel grates may corrode over time due to dc current flow. • Some typical sources are as follows: —Dc-impressed current or sacrificial cathodic protection systems. —Dc transmission lines. —Dc-powered railroads.				• Specify adequate level of galvanizing. • Use a suitable anode to the steel grate that would be sacrificial to the steel and protect the grate.
Cause:	Electrical Shock Hazard	Mode:	E	Mitigation Opportunities During Design:
• Improper grounding of the transmission switch at ground level could result in an electrical shock hazard during a possible line-to-ground electrical fault.				• Persons operating line switches should be insulated or isolated from ground potential according to the NESC (NESC 2002c). • A proper grounding system should provide protection to a person operating the switch from possible touch-and-step voltages in the case of a line-to-ground electrical fault. The grounding system should have the following characteristics: —The ground conductor leads to the above-ground grate or buried ground mats should be sized based on maximum fault current anticipated into the grounding system (IEEE 2003b). —The ground mats or above ground grates should be designed for mesh spacings to provide touch and step voltage safety according to (IEEE 2000).
Cause:	Mechanical Damage	Mode:	M	Mitigation Opportunities During Design:
• Exposure of above-ground grates or buried ground mats to excavation activities by property owners and contractors can damage the switch grounding system.				• The possibility of mechanical damage can be reduced by addressing the following site conditions: —Specify adequate depth of buried ground mat installation. In cultivated areas where plowing is performed, additional depth is required. —Provide markers or install a fence around the above-ground grate.

STRUCTURES (INCLUDING FOUNDATIONS)

Structures (including foundations)

Concrete Structures

Component Category:	Structures (including foundations)			
Component Type:	Concrete Structures			
Modes of Degradation:	C, E, M			
Cause:	Chemical Attack	Mode:	C	Mitigation Opportunities During Design:
• Chemical attack can be due to: —Acid attack. Portland cement is not very resistant to attack by acids, although weak acids can be tolerated. The products of combustion of many fuels contain sulfurous gases that combine with moisture to form sulfuric acid. Other possible sources for acid formation are sewage, some peat soils, and some mountain water streams. Disintegration of the concrete paste between the fine and course aggregate results. —Alkali-carbonate and alkali-silica reaction. Certain aggregates of carbonate rock have been reactive in concrete. Also some aggregates containing silica that is soluble in highly alkaline solutions may react to form expansive products that will disrupt the concrete. Pattern cracking of the concrete results. —Sulfate attack. Naturally occurring sulfates of sodium, potassium, calcium, or magnesium are sometimes found in soil or in solution in water. Map and pattern cracking results from this form of chemical attack.				• Some aspects of chemical attacks can be mitigated: —Alkali-carbonate and alkali-silica reaction may be minimized by using nonreactive aggregate in the concrete mix or by adding certain additive mixes to the concrete mix. —Using sulfate-resistance cement in the concrete mix may minimize sulfate attack.
Cause:	Lightning	Mode:	E	Mitigation Opportunities During Design:
• Pole punctures due to induced voltage from lightning strikes can occur when an external ground is used.				• When an external ground is used on a concrete pole, it should be bonded to the internal metal components, both at the top and bottom of the pole, to prevent large voltage differences between the internal metal components and to reduce the surge impedance of the pole.
Cause:	Overloading	Mode:	M	Mitigation Opportunities During Design:
• Cracks and/or spalling may develop from: —Thermal strain from fire —Overload or added load conditions —Collisions				• If the structure has been competently designed using the appropriate governing code as a minimum and taking into account known, unusual loading conditions, little else can be done to prevent overloading the structure from occurrences such as fires or unforeseen excessive or added loads. Locating structures as far as possible from vehicle pathways can minimize vehicle collisions.

Structures (including foundations)
Steel or Aluminum Structures

Component Category:	Structures (including foundations)
Component Type:	Steel or Aluminum Structures
Modes of Degradation:	C, M

Cause: Corrosion	Mode: C	Mitigation Opportunities During Design:
• Most metals corrode in the presence of water, acids, bases, salts, oils, and other solid and liquid chemicals, as well as various gases including acid vapors, ammonia, and sulfur-containing gases. The rate of corrosion is dependent on a variety of factors, including the properties of the metal and the presence of water, oxygen, and various contaminates. The severity of corrosion problems depends on environmental conditions and therefore the proximity of a steel or aluminum structure to sources of air contaminants such as power plants, chemical plants, and other industrial facilities, or water or soil contaminants such as marine environments, and areas where there is heavy use of fertilizers. Atmospheric, water and soil corrosion, localized corrosion cells, and galvanic corrosion are the four primary types of corrosion that can degrade steel or aluminum structures: —Atmospheric corrosion occurs due to contact with substances such as oxygen, carbon dioxide, water vapor, and sulfur and chlorine compounds present in the atmosphere. —Water and soil corrosion occurs due to contact with water or soils, both of which contain soluble minerals. This is a particular concern for directly embedded steel structures. —Localized corrosion cells are due to the induced currents from the transmission line itself flowing through a structure, especially where there are railroads and pipelines, and can cause below-ground steel to degrade at a much faster-than-normal rate. —Galvanic corrosion results from the use of dissimilar metals in a structure.		• Structures should not be designed with uncoated steel or aluminum in direct contact with earth. Specifications should provide requirements for handling and backfilling during construction to ensure that coatings remain intact. • Supplemental coatings (i.e., in addition to the primary coating) should be applied to the portion of the structure that will be in ground contact. The top edge of the supplemental coating should be feathered so that no ledge is created that can collect moisture. • Weldments and connections should be detailed so that they do not collect/trap water. • Vent and drainage details and access holes in pole structures should be detailed so that they do not collect/trap water or attract nesting of birds or other animals. • Atmospheric corrosion is generally not a concern with uncoated aluminum structures, except for particularly corrosive industrial or marine environments. The use of aluminum below ground should be avoided. • The rate of degradation of steel above and below ground due to the four types of corrosion can be reduced by using one or more of the following methods, as appropriate: —Galvanizing —Coating with organic or inorganic compounds —Thermal spraying —Fabrication using weathering steels —Increasing material thickness to allow for a specific rate of corrosion —Cathodic protection —Avoiding the use of dissimilar metals in a structure

Cause: Overloading	Mode: M	Mitigation Opportunities During Design:
• Buckles and kinks in plates and/or members and sheared or deformed bolts may develop from: —Thermal strain from fire —Overload or added load conditions —Collisions		• If the structure has been competently designed using the appropriate governing code as a minimum, and taking into account known, unusual loading conditions, little else can be done to prevent overloading the structure from occurrences such as fires, collisions, or unforeseen excessive or added loads. Locating structures as far as possible from vehicle pathways can minimize vehicle collisions.

Cause: Stress Concentrations	Mode: M	Mitigation Opportunities During Design:
• Stress concentration due to poorly designed structure details may cause metal cracking. • Stress concentration caused by metal fatigue resulting from vibration or other repetitive loadings may also cause cracking. • Improper torque applied to bolts and fasteners can cause stress concentrations and lead to metal fatigue.		• The occurrence of stress concentration cracking may be mitigated by paying attention to structure details and eliminating the following: —Re-entrant corners and any details with narrow notches at points of high stress (e.g., holes to facilitate galvanizing, vent and drainage details, access holes for conduits) —Large and abrupt changes in plate widths and/or thicknesses —Concentrations of heavy welds • Designs that eliminate repetitive loading or that reduce repetitive stress levels to a very low value may eliminate metal fatigue cracking. • Design configurations should be reviewed to ensure that they will not excite vibration due to vortex shedding. • Use of dampers on conductors and overhead ground wires will reduce the possibility of fatigue failures in arms and insulator brackets. • Proper torques should be specified for all bolts and connectors based on manufacturers' recommendations to minimize problems due to fatigue of bolts, improper load sharing and stress concentrations, over-tightening of connections designed to be free to rotate, and loosening of connections due to vibration.

Structures (including foundations)
Wood Structures

Component Category:	Structures (including foundations)
Component Type:	Wood Structures
Modes of Degradation:	B, E, M, T

Cause: Decay and Insects	Mode: B	Mitigation Opportunities During Design:
• Two of the primary causes of biological deterioration include decay and insects: —External decay. This form of fungal deterioration occurs on the outer surface of wood poles when there is untreated wood, when the treatment was not applied correctly during manufacturing, or when the treatment effectiveness is diminished due to factors such as leaching. If left untreated, external decay can rapidly diminish the strength of the pole. External decay can be stopped by removing the decayed wood and applying an approved remedial preservative treatment. —Internal decay. This type of decay occurs in the untreated interior of wood poles when it is exposed to decay fungi, moisture, and oxygen usually through drying checks. As with external decay, internal decay will diminish the strength of a wood pole. Internal decay can be stopped by application of fumigant or water-diffusible remedial treatments. —Pole top decay. While most decay is confined to the near groundline zone of poles, pole tops can decay, especially in regions with relatively high annual precipitation, when drying checks expose untreated wood to water and decay fungi or when treatment effectiveness is diminished due to weathering and leaching of preservatives. —Insect damage. Wood poles are susceptible to damage by termites, carpenter ants, and several other types of insects. In general, insects do not like preservative-treated wood; however, they will attack the untreated interior of poles by gaining access to the untreated wood through drying checks. Once initiated, insect damage can be significantly more difficult to arrest than decay. A knowledgeable pesticide applicator should be consulted if this type of damage is observed.		• Only use wood poles that are treated to industry standards, or more stringent standards if the line site represents a particularly aggressive environment, and inspected at the wood pole plant during the white wood stage and after treatment by a qualified independent inspector to ensure the specified preservative penetration and retention. Special care should be taken to make sure that wood poles are dried to the required moisture content prior to treatment so they will accept the preservatives. • In aggressive environments, special manufacturing requirements such as radial drilling or through boring can be specified to ensure penetration of preservatives near the groundline, at the pole top, or in both locations. • Pole top caps and devices that limit the opening of pole top drying checks can be specified for environments subject to pole top decay.

Cause: Woodpecker Holes	Mode: B	Mitigation Opportunities During Design:
• Woodpeckers cause significant damage to wood poles by creating surface holes and larger nest cavities. In addition to their direct effect on structure strength, cavities, if left unattended, will hold water that in turn will promote decay of untreated heart wood.		• Wood poles that are to be installed in areas that are known to have woodpecker activity should be covered with a barrier such as hardware cloth (screen mesh) to prevent as much damage as possible.

Structures (including foundations)
Wood Structures (Continued)

Cause:	Electric Fields/Leakage Current	Mode:	E	Mitigation Opportunities During Design:
• Nails and staples on ground leads can cause wood pole fires. As the ground wire passes through the electric field near the energized conductors, a voltage is induced in the ground wire. If the path of the wood pole is moist, current will also pass through the wood pole. Theoretically, the current dries and heats the wood at the tip of the staple where the current is concentrated. As the wood dries, it becomes a good insulator of heat so that the heat rises to the point of ignition. —Most occurrences have been reported at voltages of 138 kV and above, although pole fires could also occur at lower voltages if the conductor-to-ground-wire spacing were close enough to generate a high electrical field. • Similar occurrences have occurred due to leakage current through the wood between the pole ground and pole hardware. See grounding of hardware for further details.				• Recommended design solutions to eliminate pole fires occurring at nails or staples and other hardware are as follows: —Install the nails and staples at close spacing near the energized conductor region. Because the weak electric current is dissipated at more locations, sufficient heat to ignite the wood would not be generated at any one nail or staple (Lusk and Mak 1975). —Use plastic wire holders (inserts) for the staples. —Use plastic (or nylon) nails or staples. • Choose a plastic nail or staple that will not work loose. Some have a wedge shape and do not stay in the pole. • Avoid installing ground wires such that they are driven (kinked) into the wood pole. —Specify adequate distance between the pole ground and other pole hardware. —Bond the pole hardware to the pole ground.
Cause:	Mechanical Damage	Mode:	M	Mitigation Opportunities During Design:
• Mechanical damage can be caused by: —Vehicle striking a pole on a city street —Equipment working on the right-of-way (e.g., agricultural equipment, or right-of-way clearing equipment) —Vandalism				• To help prevent vehicle damage, set wood poles as far from the roadway as possible • Set limitations for the right-of-way crews (i.e., predetermined distances for them to stay away from the poles). • Educate landowners on the dangers of working too close to the poles.
Cause:	Fire Damage	Mode:	T	Mitigation Opportunities During Design:
• Many areas that have wood poles installed are susceptible to range and forest fires. Fires can damage most wood poles if the fire is slow moving and the fuel source on the right-of-way is sufficient. It is not uncommon for wood poles to burn completely off at the ground.				• When wood poles are to be installed in areas where fires are anticipated (e.g., controlled burns, brush fires, etc.), the poles should have some sort of protection applied near the groundline (i.e., protective fire-resistant coating, sheet metal wrap), and the area around each structure should be cleared to minimize the available fuel at the base of each pole.

MISCELLANEOUS HARDWARE

Miscellaneous Hardware

Anti-Climbing Barriers

Component Category:	Miscellaneous Hardware
Component Type:	Anti-Climbing Barriers
Modes of Degradation:	M

Cause:	Anti-Climb Barrier	Mode:	M	Mitigation Opportunities During Design:
• To prevent unauthorized personal from climbing the structures.				• Install barbed wire barrier around the structure about 8 to 10 ft off the ground.

Miscellaneous Hardware

Aerial Marker Balls

Component Category:	Miscellaneous Hardware
Component Type:	Aerial Marker Balls
Modes of Degradation:	E, M, T

Cause:	Corona	Mode:	E	Mitigation Opportunities During Design:
• Corona can develop on aerial marker balls on conductors and cause the following: —Customer complaints due to audible noise and radio interference. —Degradation of the marker ball particularly close to the conductor and where the halves of the ball are joined. Burning of aerial marker balls due to corona is known to occur.				• Specify a properly designed and tested product.
Cause:	**High Temperature**	**Mode:**	**M,T**	**Mitigation Opportunities During Design:**
• Fires on ROWs can generate sufficient heat to deform marker balls. The deformation can lead to vibration problems and wear and fatigue of the conductor or overhead ground wire. The deformation can also promote galloping.				• In areas where aerial marker balls are to be installed, vegetation management specifications should ensure effective vegetation/fuel load management under the spans of concern. • Specify heavy-duty hardware for the attachment of the aerial marker balls to the conductor or overhead ground wire to minimize the impacts of wear.
Cause:	**Overloading**	**Mode:**	**M**	**Mitigation Opportunities During Design:**
• Mechanical overloading of conductors, overhead ground wires, and structures can result from use of improperly designed marker balls: —Improperly sized/fitted marker balls can entrap water, thereby adding significant weight. —Improperly sized/fitted marker balls can attract nesting birds (e.g., via oversized openings around the conductor), and the accumulation of nesting materials and other debris can add significant weight.				• Specify a properly designed and fitted product. • Account for any anticipated additional weight associated with the aerial marker balls during the design of the conductor, overhead ground wire, and associated hardware.

Miscellaneous Hardware
Aerial Signal Lights

Component Category:	Miscellaneous Hardware			
Component Type:	Aerial Signal Lights			
Modes of Degradation:	E			
Cause:	Electric Field/Leakage Current, and Lightning, Switching Surges, and Power Arcing	Mode:	E	Mitigation Opportunities During Design:
• Aerial signal lights can be damaged by electric fields/leakage current as well as lightning, switching surges, and power arcing.				• Design the installation of aerial lights and wiring (for non self-contained units) to be isolated as far as practical from energized components. • Specify surge protection devices be incorporated in the aerial lighting circuits. • Specify use of transmission-line lightning arrestors and proper grounding.

Miscellaneous Hardware
Bird Guards – Anti-collision Marking Devices

Component Category:	Miscellaneous Hardware			
Component Type:	Bird Guards – Anti-collision Marking Devices			
Modes of Degradation:	C, E, M			
Cause:	Ultraviolet Degradation	Mode:	C	Mitigation Opportunities During Design:
• Ultraviolet rays may cause bird flappers and diverters to prematurely become brittle and deteriorate.				• Use devices with UV inhibitors.
Cause:	Corona	Mode:	E	Mitigation Opportunities During Design:
• Corona can develop on markers on energized conductors and cause the following: —Customer complaints due to audible noise and radio interference. —Accelerated aging of the marking device.				• Select anti-collision devices appropriate for use on energized lines.
Cause:	Overloading	Mode:	M	Mitigation Opportunities During Design:
• Ice and snow loads may build up on and damage marking devices.				• Select devices suitable for the appropriate ice and snow loading conditions.
Cause:	Vibration	Mode:	M	Mitigation Opportunities During Design:
• Active flapper type devices may fail due to wear and/or cause damage to conductors and overhead ground wires in areas with frequent occurrences of relatively high winds. • Flapper-type devices may also slide on wires with significant vibration.				• Select devices suitable for the appropriate wind and wire vibration conditions.

Miscellaneous Hardware
Bird Guards – Anti-perching

Component Category:	Miscellaneous Hardware			
Component Type:	Bird Guards – Anti-perching			
Modes of Degradation:	B, C			
Cause:	Corrosion	Mode:	B,C	Mitigation Opportunities During Design:
• Caustic bird feces can build up on anti-perching device hardware, resulting in corroded fasteners.				• Use heavy-duty fasteners or UV-rated nonmetallic straps.
Cause:	Ultraviolet Degradation	Mode:	C	Mitigation Opportunities During Design:
• Ultraviolet rays can cause devices to prematurely become brittle and deteriorate.				• Use materials with UV inhibitors.

Miscellaneous Hardware
Bird Guards—Fecal Shields

Component Category:	Miscellaneous Hardware			
Component Type:	Bird Guards – Fecal Shields			
Modes of Degradation:	B, C, M			
Cause:	Corrosion	Mode:	B,C	Mitigation Opportunities During Design:
• Caustic bird feces may build up on fecal shield hardware, resulting in corroded fasteners.				• Use heavy-duty fasteners or UV rated nonmetallic straps.
Cause:	Ultraviolet Degradation	Mode:	C	Mitigation Opportunities During Design:
• Ultraviolet rays may cause devices to prematurely become brittle and deteriorate.				• Use materials with UV inhibitors.
Cause:	Overloading	Mode:	M	Mitigation Opportunities During Design:
• Ice and snow loads may build up on large barrier shields and damage the shield and the structure.				• Design the barriers and structures with the appropriate ice, wind, and snow loading conditions.

Miscellaneous Hardware
Bird Guards—Hardware Cloth

Component Category:	Miscellaneous Hardware			
Component Type:	Bird Guards – Hardware Cloth			
Modes of Degradation:	B, C			
Cause:	Woodpecker Damage	Mode:	B	Mitigation Opportunities During Design:
• Woodpeckers may peck through some types of pole wraps.				• Use the appropriate gauge material (e.g., larger gauge for larger woodpeckers), and wrap all poles tightly.
Cause:	Corrosion	Mode:	C	Mitigation Opportunities During Design:
• Metallic wraps may rust and prematurely fail.				• Use galvanized metallic hardware cloth.
Cause:	Ultraviolet Degradation	Mode:	C	Mitigation Opportunities During Design:
• Ultraviolet rays may cause nonmetallic hardware cloth to prematurely become brittle and deteriorate.				• Use wraps with UV inhibitors.

Miscellaneous Hardware
Bird Guards—Nesting Platforms

Component Category:	Miscellaneous Hardware			
Component Type:	Bird Guards – Nesting Platforms			
Modes of Degradation:	B, C, M			
Cause:	Corrosion	Mode:	B,C	Mitigation Opportunities During Design:
• Caustic bird feces may build up on nesting device platform hardware, resulting in corroded fasteners.				• Use heavy-duty fasteners or UV rated nonmetallic straps.
Cause:	Overloading	Mode:	M	Mitigation Opportunities During Design:
• Ice and snow loads may build up on nesting platforms, and damage the platforms and the structure.				• Design the platforms and structures with the appropriate ice, wind, and snow loading conditions.

Miscellaneous Hardware
Climbing Steps

Component Category:	Miscellaneous Hardware			
Component Type:	Climbing Steps			
Modes of Degradation:	M			
Cause:	Climbing Steps	Mode:	M	Mitigation Opportunities During Design:
• To prevent unauthorized personal from climbing the structures.				• Remove all steps that are 10 to 15 ft above the ground. • Remove all step brackets that could be used to climb the pole.

Miscellaneous Hardware
Signs (Aerial and Near Ground)

Component Category:	Miscellaneous Hardware			
Component Type:	Signs (Aerial and Near Ground)			
Modes of Degradation:	C, M			
Cause:	Corrosion/Ultraviolet Degradation	Mode:	C	Mitigation Opportunities During Design:
• Signs can be damaged and their visibility/readability diminished by corrosion (atmospheric and galvanic) and ultraviolet degradation. Degradation of structure numbers can hinder inspection and maintenance activities, and degradation of warning signs can lead to increased risks for utility personnel and the public.				• Specify materials and coatings that resist corrosion and incorporate UV inhibitors. • Specify use of large numbers and letters to enhance long-term readability. —Install large numbers to facilitate ground and aerial inspections and maintenance. • Install even numbers on south or east face of structures. • Install odd numbers on north or west face of structures. —Install large “Xs” at the top of structures two to three spans before a wire crossing to alert aerial patrol pilots of crossings.
Cause:	Vandalism	Mode:	M	Mitigation Opportunities During Design:
• Signs on the lower portions of structures are subject to theft.				• Specify installation heights that are above normal reach. • Specify use of attachment hardware that is difficult to remove with standard tools.

RIGHTS-OF-WAY

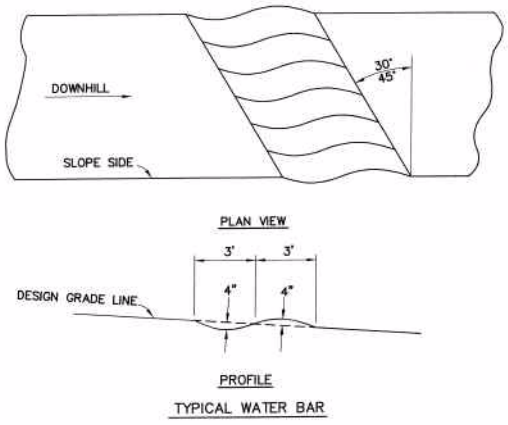
Rights-of-Way

Access Roads (Native Soil)

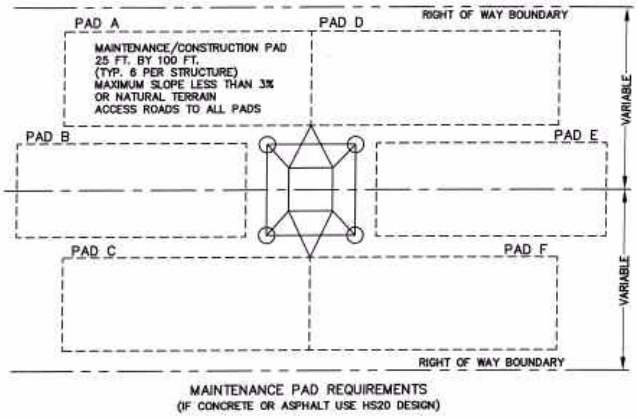
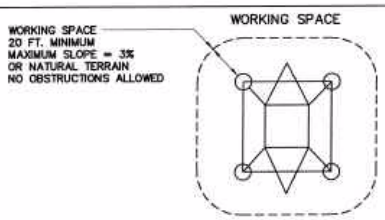
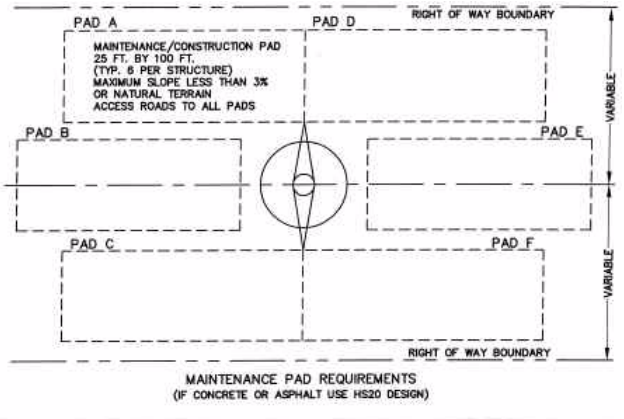
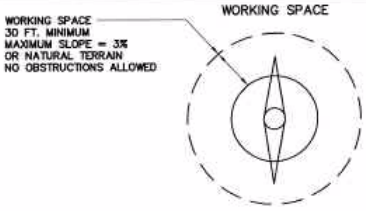
Component Category:	Rights-of-Way			
Component Type:	Access Roads (Native Soil)			
Modes of Degradation:	B, M			
Cause:	Rain Runoff	Mode:	M	Mitigation Opportunities During Design:

- Improper grading of the cross slope of access roads may allow pooling of water, which could lead to erosion.
- If the drainage system was improperly designed, the access road could erode.
- If water bars are not placed at set interfolds, the velocity of runoff may increase to the point where the runoff will erode the access road.

- When the proper cross slope is applied during design and construction, the expense to maintain and re-establish access roads in case of erosion will be minimized. Guidance on reasonable cross slopes based on centerline grades is provided below:
  - —Grade of centerline 0–4%; cross slope 2%
  - —Grade of centerline 5–7%; cross slope 3%
  - —Grade of centerline 8–10%; cross slope 4%
  - —Grade of centerline 11–12%; cross slope 5%
  - —Grade of centerline 13–15%; cross slope 6%
  - —Grade of centerline 16–17%; cross slope 7%
  - —Grade of centerline 18–20%; cross slope 8%
- Drainage system should be designed to handle the anticipated amount of runoff. When the access road meets a publicly maintained road, drainage (e.g., culverts) should be designed to meet the requirements of the municipality or agency having jurisdiction over the publicly maintained roads and including current storm water management requirements.
- Water bars should be open on the lower end to allow drainage, and should be placed at an approximate angle of 30 to 45°. The spacing of the water bars is dependent on the road grade. Guidance on typical spacing is provided below.
  - —Average road grade 0–5%; maximum spacing (water bars not required)
  - —Average road grade 5%; maximum spacing 125 ft
  - —Average road grade 10%; maximum spacing 80 ft
  - —Average road grade 15%; maximum spacing 60 ft
  - —Average road grade 20%; maximum spacing 50 ft

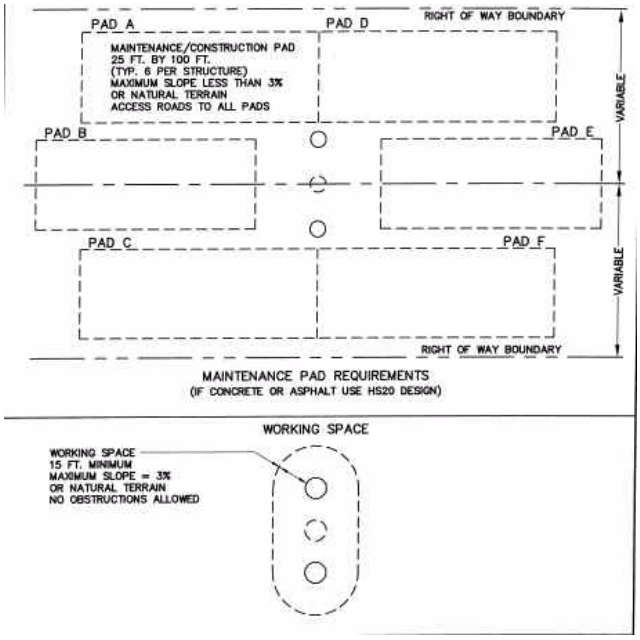


Rights-of-Way
Maintenance Pads

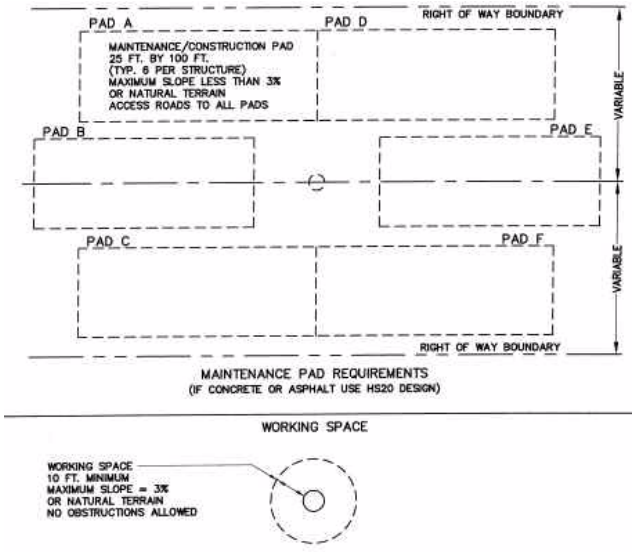
Component Category:				Rights-of-Way
Component Type:				Maintenance Pads
Modes of Degradation:				B, M
Cause:	Poor Maintenance	Mode:	B,M	Mitigation Opportunities During Design:
• If maintenance pads are not provided or they are not properly maintained (grading, mowing, brush cut, etc.), then emergency repairs or maintenance many be hindered. —Working area should be clear of all vegetation.				• Maintenance or construction pads for vehicles can be provided at six (6) positions per structure. Examples of typical maintenance pads for lines 230 kV and below (latticed tower, single steel pole, multiple wood pole, and single wood pole structures) and 500 kV and above (latticed tower and single steel pole structures). —230 kV and Below – Latticed Towers  MAINTENANCE PAD REQUIREMENTS (IF CONCRETE OR ASPHALT USE HS20 DESIGN)  —230 kV and Below – Steel Poles  MAINTENANCE PAD REQUIREMENTS (IF CONCRETE OR ASPHALT USE HS20 DESIGN) 

Rights-of-Way
Maintenance Pads (Continued)

—230 kV and Below – Multiple Wood Poles

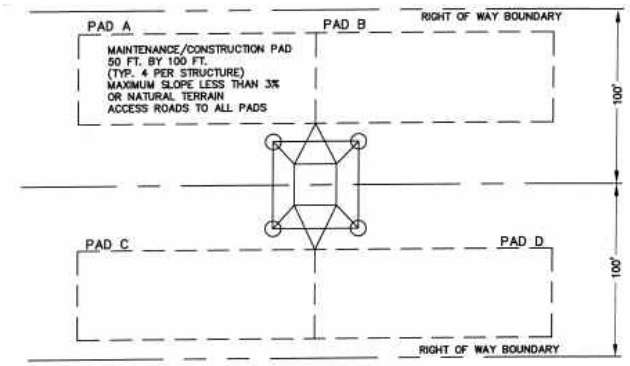


—230 kV and Below – Single Wood Poles

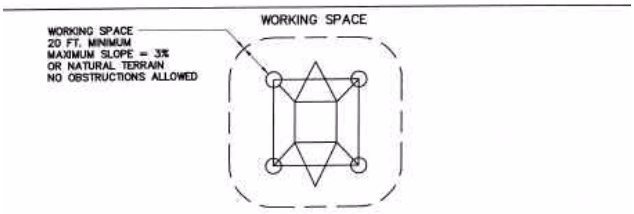


Rights-of-Way
Maintenance Pads (Continued)

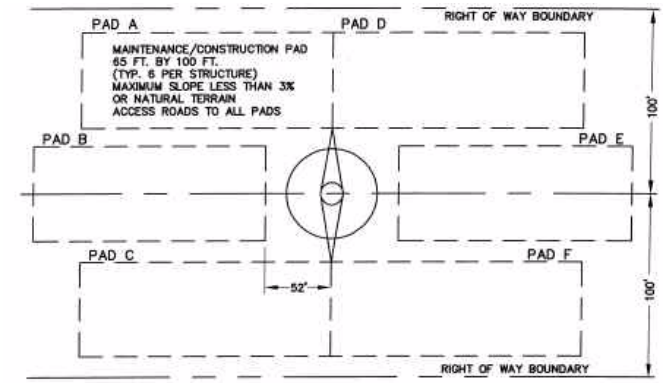
—500 kV and Above – Latticed Towers



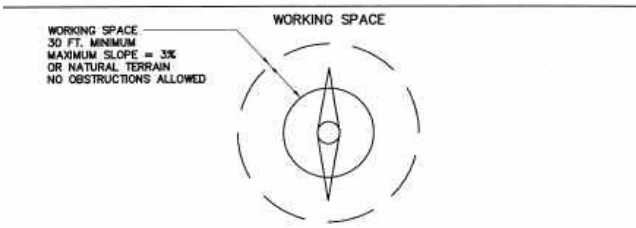
MAINTENANCE PAD REQUIREMENTS
(IF CONCRETE OR ASPHALT USE HS20 DESIGN)



—500 kV and Above – Steel Poles



MAINTENANCE PAD REQUIREMENTS
(IF CONCRETE OR ASPHALT USE HS20 DESIGN)



Rights-of-Way
Right-of-Way Width

Component Category:		Rights-of-Way		
Component Type:		Right-of-Way Width		
Modes of Degradation:		B		
Cause:	Vegetation	Mode:	B	Mitigation Opportunities During Design:
• Improper clearing and trimming of the vegetation inside and along the right-of-way may lead to failures, fires, and outages.				• Specifying proper horizontal clearances from vegetation to conductors will minimize the possibility of vegetation falling into conductors. (Obtain proper approval to trim any trees that are outside of the right-of-way that could fall on the conductors.) Examples of typical minimum right-of-way widths are provided below. —230 kV and below (steel structures) – 120 ft —345 kV and below (steel structures) – 160 ft —500 kV and below (steel structures) – 200 ft • Specifying proper vertical clearances from vegetation to conductors will minimize the possibility of vegetation contact with conductors. Guidance on minimum clearances is provided below. —200-300 kV – minimum radial clearances of 10 ft from any conductor (at maximum operating temperature) —300 kV and above – minimum radial clearances of 15 ft from any conductor (at maximum operating temperature)

Rights-of-Way
Vertical Clearance (Phase to Ground)

Component Category:		Right-of-Way		
Component Type:		Vertical Clearance (Phase to Ground)		
Modes of Degradation:		E, M		
Cause:	Insufficient Clearance	Mode:	E,M	Mitigation Opportunities During Design:
• Insufficient vertical clearances represent a significant safety hazard. They can result from a variety of factors, including construction errors such as poor conductor sagging techniques, and from changes in the elevation of the ground profile within the right-of-way resulting from depositing of material from excavations, and overlayments of existing streets.				• Specifying that a clearance buffer be added to minimum required design clearances at maximum operating temperature/sag will help minimize future problems. (A buffer of 2 ft is a commonly used value.) Minimum allowable clearances should meet local jurisdictional requirements and be appropriate for the anticipated use of the right-of-way. Examples of minimum design clearances (without buffer) for a variety of situations are provided below. • Areas accessible to pedestrians only (without buffer): —230 kV 18 ft, 6 in. to 25 ft, 0 in. —345 kV 21 ft, 0 in. to 26 ft, 2 in. —500 kV 24 ft, 0 in. to 30 ft, 0 in. • Along thoroughfares or when crossing areas capable of being traversed by vehicles or agricultural equipment (without buffer): —230 kV 22 ft, 6 in. to 30 ft, 0 in. —345 kV 25 ft, 0 in. to 31 ft, 2 in. —500 kV 28 ft, 0 in. to 35 ft, 0 in. • Crossings above tracks of railroads (without buffer): —230 kV 30 ft, 6 in. to 34 ft, 0 in. —345 kV 33 ft, 0 in. to 34 ft, 0 in. —500 kV 34 ft, 0 in. to 36 ft, 0 in. • Bodies of water not suitable for sailing or where use of sailboats is prohibited (without buffer): —230 kV 21 ft, 0 in. to 25 ft, 0 in. —345 kV 23 ft, 6 in. to 26 ft, 2 in. —500 kV 26 ft, 6 in. to 30 ft, 0 in. • Bodies of water accessible to sailboats and having surface areas greater than 200 acres and less than 2000 acres (without buffer): —230 kV 38 ft, 6 in. to 41 ft, 0 in. —345 kV 41 ft, 0 in. to 42 ft, 2 in. —500 kV 44 ft, 0 in. to 46 ft, 0 in.

13.2.4 Design Examples

The following examples illustrate how maintainability can be accounted for during the design process for new lines.

CASE STUDY #1

Line Design of 345-kV Double-Circuit Transmission Line to Connect a Power Station

Scope

A new 345-kV double-circuit line is required to connect a new 800-MW coal-fired power station to the network.

- Line length is 200 km and runs within 5 to 30 km of the coastline through rural areas.
- Regular rainfall occurs throughout the year.
- High lightning activity.
- Line life required is 50 years.

Structures

Self-supporting, steel-latticed towers are considered the lowest-cost option. Lower-cost guyed structures are not viable due to agricultural activity. Galvanizing is required to achieve the design life. In one section that traversed a particularly corrosive environment near the coast, a supplemental coating of paint was applied to selected structures to extend the life of galvanizing.

As a baseline, the structural strength must meet the minimum governing code requirements for wind- and ice-induced loads. In addition, the structural capability of the line must match the security requirements. Structural failure will result in significant outage time and power station income losses, so the line must have high security and commensurate high strength. Therefore, additional longitudinal capability is designed into the crossarms and body of suspension towers to provide for cascade containment. Anticipated construction and maintenance procedures, and the associated loads and points of application of those loads, were considered and accounted for during design.

Structure geometry is a conventional double-circuit configuration, but with increased vertical phase to phase and top phase to overhead ground wire clearance to allow helicopter in span maintenance. Refer to a photo of the suspension tower in Figure 13.2-2.

The line has diagonal phasing to minimize fields on the ground and series voltage drop for high loads.

Additional attachment points are provided for maintenance, adjacent to conductor strain and suspension insulator attachment points. The tower also incorporates lugs designated for square rigging to raise and lower conductors for maintenance.

The ends of suspension crossarms have a fitting to accept a live-working lifting yoke for insulator replacement.

Large strain towers have grid mesh platforms installed on the bottom of the crossarms to provide walkways for linemen.

For structural integrity, bolts are installed with punched threads or spring washers to limit loss of bolts due to vibration. Conductor and overhead ground wire attachment plates and plates to attach crossarms and ground wire peaks have double nuts installed for extra security.

Foundations

Foundations are mostly drilled piers. In one section near the coast, where the ground is soft, driven pile foundations are used. All below-ground steel is electrically connected by welding, and is also connected to an exposed cathodic protection test tag at the top of the pile cap. This tag allows testing with a half-cell to detect possible below-ground corrosion activity. If corrosion activity is detected, then sacrificial anodes or impressed current can be connected to this test tag. Care is taken during construction of the foundation to avoid direct metallic contact between tower stub angles and foundation reinforcing steel. This ensures that connection of cathodic protection systems will protect only the below-ground steel, and will not drain away from the structure via low-impedance overhead ground wires.

Right-of-Way

The right-of-way is 60 m wide, based on conductor blow-out and electromagnetic field calculations. Large trees are cleared mechanically, and undergrowth is chemically treated initially and also 12 months later. This approach to vegetation management has a high initial cost, but results in lower overall clearing costs on a net-present-value basis over the life of the line.

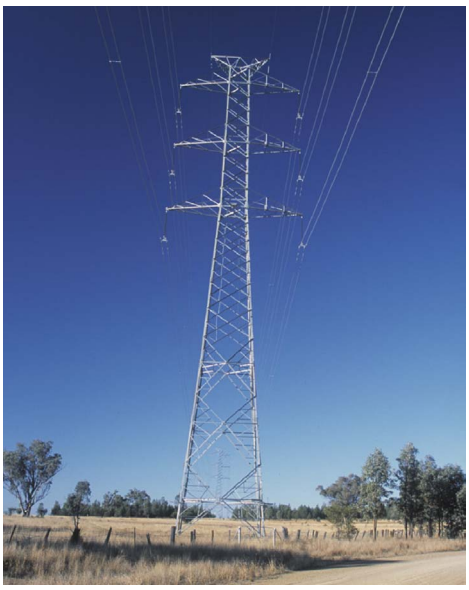


Figure 13.2-2 Suspension tower.

Conductor

The power transfer requirements for this line are high, and losses are an issue. For this reason, twin AAAC conductor is selected. This conductor has lower losses than ACSR and enables design of a lower-capital-cost line than was achievable with ACSR. Use of AAAC adds a little cost to the suspension structures because they must be taller than if ACSR were used; however, the costs of strain towers are reduced because less tension is applied by AAAC than ACSR. (Consideration must be given to an appropriate conductor operating temperature during normal and emergency operation when connecting to generating units. Generator lines are typically run at high continuous loads. To avoid annealing, AAAC should not be run continuously at more than 75º C, and not more than 90º C for short-term emergency conditions. This limit is not normally a constraint, because a larger conductor area than the minimum required for thermal rating is usually selected to minimize losses for power station lines. In some cases, it may be necessary to select another conductor alternative such as ACSR over AAAC as ACSR can be run at a higher continuous temperature.)

Transposition

Due to the length of the line, and structure geometry, transposition is required to control unbalance. This is achieved by splitting the double-circuit construction onto two modified single-circuit suspension towers to allow the rotation of phases.

A line of this length and loading may require two complete phase rotations to achieve the required unbalance criteria. For a very heavily loaded line, transpositions may be required as close as every 30 km.

Overhead Ground Wires

One 14-mm ACSR ground wire and one 14-mm OPGW (optical fiber in ground wire) are installed to provide shielding from lightning.

The ground wire and OPGW must be galvanically isolated from the power station. This is to prevent galvanic corrosion of the steel pipes and galvanized steel earthmat at the power station if they were electrically connected to the copper earthmat of the transmission substation at the other end of the line. For the overhead ground wire, one insulator unit is installed in the hardware assembly to achieve the required isolation. In the case of OPGW, the presence of downleads makes total isolation difficult. One way to achieve isolation with OPGW is to make the last span connection to the power station using an underground OPGW cable with a plastic, rodent-proof sheath.

Ground wires and OPGW should have a minimum individual strand size of no less than 3 mm to avoid breakage from direct lightning strikes. Twin ground wires should be electrically matched as close as possible so that fault currents are shared evenly between the two wires, and no one ground wire is electrically overloaded due to disparity in resistance or fault rating.

Hardware

The terrain is flat to undulating, with little natural shielding of the line, and conductor tension is high, so aeolian vibration needs to be controlled to prevent fatigue failure of conductor and ground wire strands. Stockbridge-type dampers are applied to the conductor, ground wire, and OPGW. Line guards are applied over the OPGW under the vibration damper. To make maintenance easier, line guards and the same size damper as on the OPGW are installed on the ACSR ground wire. For suspension attachment, armor grip suspension units are installed on the ground wire, OPGW, and conductor.

Compression fittings are used for dead ends and for splicing of the conductor. Wedge strain fittings are used on the ground wire and OPGW. Compression splices are installed on the ground wire.

Spacers are neoprene lined to prevent damage to the conductor.

OPGW is spliced with extra cable length looped up into the tower. This extra length allows splicing at ground level in an air-conditioned vehicle, and sufficient extra length is provided to enable splicing to be redone twice.

Corona rings are installed around the hardware of twin strain insulators to reduce audible noise, and radio and television interference in areas close to residents.

Hardware bolts and split pins are orientated in the same direction on all structures along the line to make inspection easier.

Insulation

Polymer insulators are selected over glass or porcelain options based on a net present value over the life of the line. Even though the polymer insulator's life is projected to be shorter than that of the glass and porcelain insulators, and therefore must be changed once more than the other options over the life of the line, they are still economically justifiable because of their significantly lower cost. Polymer insulators are also preferred for the coastal environment, as glass and porcelain suspension insulators suffer from pin corrosion. Polymer insulators have an order of magnitude less leakage current that reduces pin corrosion rates.

The location and severity of pollution sources associated with the power station should also be taken into account

when specifying the contamination performance of polymer insulators. Polymer insulators exhibit superior performance in areas of high pollution compared with glass and porcelain insulators, and are a good choice for line segments close to power stations that often have mining operations, coal stockpiles, spoil heaps, and convective cooling towers as contamination sources.

Corona rings are fitted to the live end to reduce the electric field on the sheath and seal to prolong insulator life. An arc distance equivalent to 20 units is selected. A minimum of 18 units is required for switching surge, but an extra two units are installed to achieve a low backflashover rate and, particularly, reduce the double-circuit, lightning outage rate.

Grounding

In areas frequented by people (e.g., at the power station), buried grading rings are installed around the tower. Additional grounding is installed to ensure good lightning performance. The target impedance is less than 5 ohms within 2.5 km of the switchyards at each end of the line, and 10 ohms for the middle of the line. Copper is used for grounding to ensure adequate life in soil contact.

Condition Monitoring

A number of weather stations are installed along the route to provide data to calculate real-time, conductor thermal rating and to estimate the probability of bush fires under the line. The weather stations also incorporate lightning location detection capabilities to assist with locating lightning flashovers and to indicate when storms are near the line.

An insulation leakage current monitor is installed on a tower at the power station to monitor accumulation of contamination. The monitor measures leakage current of six insulator strings.

Maintenance

Line outages are not desirable because they constrain the power station output. Some structures do not have all-weather ground access. The line is designed for live working of insulators, spacers, and dampers. Because there are concerns regarding sudden failures of polymer insulators due to brittle fracture, extra care is taken to ensure their integrity before performing energized maintenance. Before proceeding with live working activities, a thermographic inspection is performed, and insulators are checked with a corona camera, and finally, the integrity of the sheath and seals of each insulator is visually inspected to detect whether the fiberglass rod has been exposed. The results of these inspections are used to determine whether live working can be safely performed.

Suspension insulators are changed using hot sticks off the structure, and in some cases, helicopters are used to fly the insulators in and out. Strain insulators can be changed live, either with hot sticks or using barehand techniques. Barehand techniques are faster, but require ground access for an insulated elevated platform vehicle or crane to suspend a man box. Climbing is required on the structure to attach the live-working lifting yoke to the crossarms and to undo the dead end when changing insulators. Climbing is by step bolts on diagonal tower legs. For the case where a strain tower has a very large deviation angle and there is insufficient clearance to climb the tower live, the step bolts are removed on the inside of the angle and a warning sign is installed. Each step bolt has a loop to attach to, at all times, while climbing. Step bolt strength is designed to be adequate for fall arrest. Conductor vibration dampers are changed live off the structure with hot sticks. Ground wire dampers and spacers are inspected and changed live from helicopters.

CASE STUDY #2

Line Design of 220-kV Single-Circuit Transmission Line for a New Mine

Scope

A new 220-kV single-circuit line is required to supply a new iron ore mine.

- Line length is 150 km, and the line is in a dusty, low-rainfall, inland environment with a low incidence of lightning.
- Line runs along a road easement in flat-to-low undulating terrain.
- Some areas have cultivation.
- Close to the mine, the line is subject to iron ore dust.
- Mine and line life is 15 to 20 years.
- Mine load is 20 MVA.

Structures

Poles are considered the most suitable structures for the narrow space between the road and the property boundary. Wood, concrete, and steel are considered for the structures. Wood is subject to woodpecker attack and therefore incurs high maintenance costs. Concrete is heavy and expensive to transport. Corrosion rates are very low in the dry environment, and line life required is only 20 years. Consequently, self-weathering steel poles are selected. Galvanizing is not required to achieve the design life.

The structural strength must meet the minimum governing code requirements for wind- and ice-induced loads. In addition, the structural capability of the line must match the security requirements. Cascade containment philosophy is based on the pole, crossarms, and insulators deflecting under extreme longitudinal loads to reduce wire tensions. Therefore, additional longitudinal capacity is designed into these components. Anticipated construction

and maintenance procedures, and the associated loads and points of application of those loads, were considered and accounted for during design.

Steel crossarms with "I" strings are selected, rather than line post insulators, to enable a more structurally efficient and cost-effective line configuration with relatively long spans. The design incorporates a compact geometry, with conductors in a delta configuration and sufficient clearances to allow live working methods to be used for insulator replacements. The critical clearance for live insulator change is the clearance from the lowest crossarm to the phase above. The delta conductor configuration minimizes fields on the ground and unbalance, thereby eliminating the need to transpose the line. Strain, angle structures are guyed with the conductors stacked vertically.

The poles are directly embedded into bored holes and backfilled with a sand cement mix. The steel pole is both the downlead for the ground wire and the grounding electrode.

Conductor
The power transfer is low, at 20 MVA, so line losses are not a major issue. An AACSR conductor is selected. A galvanized steel core will be adequate for the low-corrosivity environment and the short life required. This conductor can be installed at high tension with low sag due to the combination of aluminum alloy and galvanized steel strands that allows long spans of approximately 400 m. Conductor size is selected based on the minimum diameter to prevent corona.

Overhead Ground Wire
One SC/GZ overhead ground wire is installed to provide shielding from lightning. Although lightning activity is low, this measure is taken because mine production would have to cease for lightning trips of the line due to the fact that the conveyor belts must be unloaded before equipment can be restarted. This downtime would result in considerable loss of production.

Fault levels at the substation are also low, which allows the use of single, high-resistance SC/GZ steel ground wire.

Hardware
The terrain is flat, with no natural shielding of the line, and conductor tension is high so aeolian vibration needs to be controlled to prevent fatigue failure of conductor and ground wire strands. Spiral vibration dampers are applied to the ground wire for their efficiency on wires smaller than 12.5 mm. Stockbridge-type dampers are applied to the conductor, as it is larger than 12.5 mm. For suspension attachment, line guards are applied over the conductor, and then trunnion clamps are installed.

Helical fittings are used for dead ends and for splicing the ground wire and small conductor. Helical fittings are lower cost than wedge or compression connectors, and will provide good service for the small conductor running at a low temperature due to the small mine load.

Hardware bolts and split pins are oriented in the same direction on all structures along the line to make inspection easier.

Insulation
Polymer insulation is selected over glass or porcelain options because of its superior performance in contamination conditions of cultivation dust and iron ore dust with little natural washing. Corona rings are fitted to the live end of the polymer insulators to reduce the electric field on the sheath and seal. An arc distance equivalent to 12 normal units is all that is required based on switching surge. Lightning activity is low.

Maintenance
Line outages are not desirable because there is only one line supplying the mine. There is all-weather, ground access to the base of all poles along the line. Insulated, elevated platform vehicles can be used to change insulators and vibration dampers live. Because there are concerns regarding sudden failures of polymer insulators due to brittle fracture, extra care is taken to ensure their integrity before performing energized maintenance. Before proceeding with live working activities, a thermographic inspection is performed and insulators are checked with a corona camera, and finally, the integrity of the sheath and seals of each insulator is visually inspected to detect whether the fiberglass rod has been exposed. The results of these inspections are used to determine whether live working can be safely performed. Climbing is required on the structure to attach the live-working lifting yoke to the crossarms and to undo the dead end when changing insulators. Climbing is by a central climbing style with step bolts on either side. Strength is adequate for fall arrest, and the design facilitates attachment at all times while climbing.

13.3 OPTIMIZING THE DESIGN FOR EFFECTIVE LIVE WORKING

13.3.1 Introduction

Live work (LW) is the performance of maintenance, construction, or testing on equipment and circuits that are energized or that may become energized.

Live work (work on energized circuits) is the preferred method of maintenance where system integrity, system reliability, and operating revenues are at a premium and removal of the circuit from service is not acceptable (Lombardet and Kiener 1995, Tomaseski 1998, Zarco Periñán

and Moreno Amescua 2002, Portillo Belinchón and Pérez Herranz 2002, Kovacs 2004). Live work may also be beneficial in construction and storm damage repair. Furthermore, LW is necessary and unavoidable in some cases, such as stringing over or under energized circuits or adjacent to parallel energized circuits. Another example is radial lines to small municipalities that must remain energized, even during maintenance, to avoid disruption of service to essential facilities such as hospitals, law enforcement offices, fire departments, and intrusion alarms. While there are many reasons for using LW methods, it does not always represent the most efficient or cost-effective solution for all situations. A proper perspective on LW is to view it as another tool at a utility's disposal for performing certain tasks.

Live work should not be performed, and should be discontinued if started, if there is any indication of lightning or other inclement weather conditions in the surrounding area (some utilities use five miles as a guide). Other inclement weather conditions may include high relative humidity, high wind speed, presence of fires (grass, forest), presence of debris in the air, etc.

As such, LW helps utilities avoid loss of revenue while maintaining transmission grid reliability and stability. However, if workers are to perform such work on energized lines and equipment, they must have knowledge of LW rules and regulations to ensure their safety and the safety of others. In addition, to perform LW safely, workers must maintain phase-to-phase and phase-to-ground minimum approach distances between energized parts and grounded objects for the specific voltage being worked. Insulating tools are used to bridge the air gap between energized parts and ground, and between parts energized at different voltages. Also, work on de-energized facilities often requires similar qualifications, since de-energized facilities that are close to energized parts can acquire significant voltages through electric and magnetic induction. For this reason, de-energized work is also included in the broad area of "live work."

It is not the purpose of this section to discuss details of LW methods, procedures, and tools. This is subject to two published EPRI guides on LW (EPRI 2002b, EPRI 2002c). Only a very brief overview of LW, including de-energized work, is presented on the following pages.

Rather, the purpose of this section is to:

- Alert designers to the needs of linemen performing LW (including de-energized work).
- Identify areas where relatively minor and inexpensive modifications to the design and/or construction can be implemented to render the line more "live-working friendly"— i.e., to remove impediments to safe, efficient, and cost-effective LW.
- Identify areas that could have a major effect on design, construction, and cost of a line if an "LW-friendly" approach is considered.
- Provide several examples and "lessons learned".
- Provide a "check list" for the designer to use to verify that the line can be maintained using LW methods.

This section also discusses aspects of design and construction that are important to LW. This will allow designers to develop an appreciation of the needs of linemen and how these needs can be incorporated into the design. Based on this foundation, the section discusses low-cost design modifications that can have a significant effect on the ease with which LW can be undertaken safely, efficiently, and cost-effectively. An informative subsection dealing with practical examples and lessons learned illustrates both the options available to the designer and the possible consequences of not considering LW at the design stage (Ackermann and Morton 1990, Forgie et al. 1990, Marshall and Visser 1998, Gela 1998).

The material covered in this section focuses on overhead transmission lines 230 kV and above, although many concepts are applicable down to 69 kV as well. The section is written with two audiences in mind: the line designer, and the line maintenance staff.

13.3.2 Brief Overview of Live Working (LW)

This subsection contains a brief description of LW methods that are applicable, but not limited, to lines 230 kV and above, namely:

- The temporarily de-energized method
- The insulating tool method ("hotstick method")
- The barehand method

In addition, the "gloving method" is used at distribution voltage levels. It is not discussed here in detail since this method is not used on lines operating at 230 kV and above. The four basic methods of live work are described as follows (see Figure 13.3-1):

1. **De-energized work.** Once the circuit has been disconnected from all known sources of electrical supply, the circuit is still considered energized until all system, equipment, and personal protective grounds have been installed at the worksite(s) using insulating tool(s).
2. **Gloving.** Distribution circuits are worked energized by using insulating gloves, blankets, line hoses, and other cover-up equipment. Work can be performed from grounded structures or from insulated aerial devices or platforms.

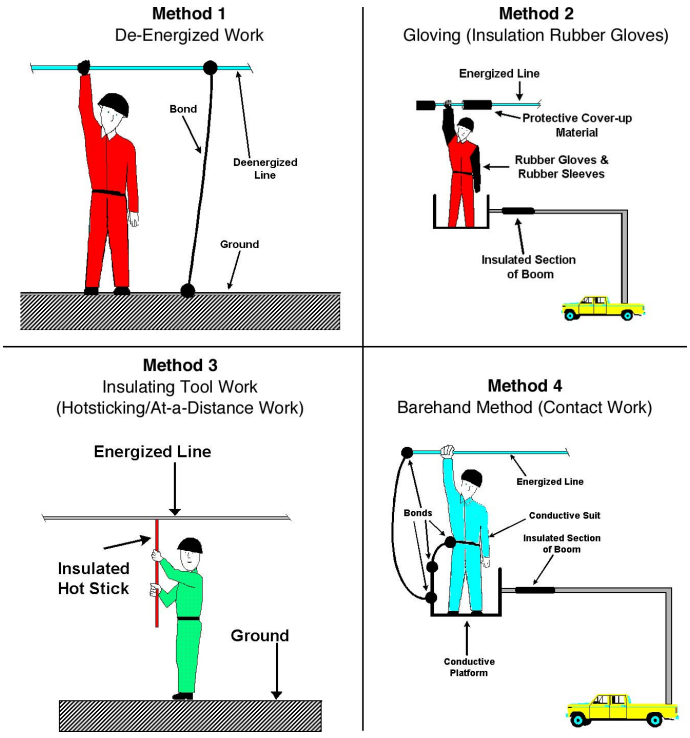


Figure 13.3-1 Sketches of the four types of Live Work.

3. **Insulating tool work** (also known as hotsticking and at-a-distance work). Work is done with insulating tools, non-conductive rope, and aerial devices. The worker is essentially at ground potential and is separated from the energized circuit by insulating tools. Insulating tool work may be done from an insulated or an uninsulated aerial device as long as the appropriate minimum approach distances are observed.
4. **Barehand method** (also known as contact work). The worker is in direct contact with energized parts and is separated from ground by air and a combination of insulating tools. Barehand work can be performed from insulating ladders or aerial devices.

Historical Overview

Live work is sometimes considered a recent development in the electrical power industry. However, forerunners of modern insulating tools made their appearance as far back as 1913. These initial tools were homemade, crude, and bulky; still, they launched the development of the efficient and refined tools that are used by utilities today.

In 1916, a tool known as an "electrical hook" was introduced in Atlanta, Georgia. This was essentially a spring-type clamp mounted on an insulating wooden stick that was used to tap energized circuits. Its use identified the need for LW tools for other applications, and tools were soon developed for applying parallel-groove clamps, handling conductors, pulling insulator cotter pins, and manipulating tie wires. Soon to come were a hacksaw, an LW come-a-long, and saddles that could be attached to structures (usually wood poles) for supporting other tools.

LW tools were first accepted for work on lines up to 34 kV; however, many linemen were hesitant to perform LW at this voltage. Because of this reluctance, many companies initially restricted LW to 22 kV or less. Linemen began to acquire confidence in performing LW when they realized that the tools always kept them at a safe distance from energized parts. Restrictions were gradually relaxed, and by 1930 several utilities permitted LW operations on 66-kV lines. The permitted voltage limit soon rose to 110 kV, and in the late 1930s, the astonishing news was circulated that a 220-kV line on the west coast had been successfully worked energized ("hot"). Another milestone was passed in March 1948, when linemen changed suspension insulators on a 287-kV Hoover Dam-Los Angeles transmission line with LW tools specifically designed for the job.

LW tools with fiberglass sticks were introduced in 1959. The fiberglass sticks consisted of layers of resin-coated glass fibers wound around and laid lengthwise over a plastic foam core. They were formed into a single unit by curing in an oven maintained at a constant temperature. It was the introduction of these fiberglass sticks, which were highly resistant to moisture absorption and damage that

allowed electric utilities to develop the LW maintenance practices that they currently employ on 345-kV, 500-kV, and 765-kV transmission lines.

The terms "liveline work" and "liveline tools" were natural selections for use in connection with work on energized facilities because, for a long time, transmission lines were the only application for LW. However, because today's market puts a premium on transmission grid reliability and stability as well as revenues, more and more maintenance is being performed on energized substation circuits. As such, the term "liveline" is evolving into the more general term "live work" because it is more descriptive of today's work practices. The term "live work" is consistent with international standards such as those developed by the International Electrotechnical Commission (IEC). Furthermore, since the term "hotstick" has been used as a trade name, it is now being replaced by the term "insulating tool" in national standards.

Minimum Approach Distance (MAD)

Workers performing LW must maintain the appropriate distance from energized and grounded parts. The term "distance" is typically used in standards to represent electrical distances between energized parts and grounded objects for maintenance and construction (i.e., minimum approach distance, MAD). Standards use the term "clearance" to represent the electrical clearances necessary for the design of structures and the operation of the system. Therefore, the MADs used in this section are for construction near and maintenance of energized facilities.

There are currently two widely accepted methods of determining (calculating) MADs for qualified electrical workers:

- The IEEE method, described in detail in (IEEE Std 516)
- The IEC method, described in detail in (IEC Publication 61472)

Both methods yield approximately the same MAD values. Both the IEEE and the IEC publications are reviewed periodically and amended as needed.

The MADs for qualified electrical workers (linemen) consist of two components:

- Basic electrical air distance based on the withstand/sparkover of the air gap and the anticipated overvoltage (SI and TOV) value
- An ergonomic (inadvertent movement) distance adder

Note: Qualified electrical workers are those who have been trained, have shown proficiency, and have a certificate of qualification for the specific (insulating tool, barehand, etc.) work in their permanent employee records file.

Applet M-1 can be used to calculate the MAD values using either the IEEE method or the IEC method. Calculations use the most recent editions of the relevant standards (IEEE Std 516— 2003 edition and IEC 61472–2004-07 edition). To perform calculations with the M-1 applet, the user is first requested to select the desired method of calculation (IEEE or IEC), and then is asked to provide the various data required to perform the computations according to Equations 13.3-1 or 13.3-2 through 13.3-6, respectively. The computational methods and the respective equations are described in detail below. The output of the applet is the MAD.

The IEEE Method (IEEE Std 516)

The IEEE method is the one used by the NESC C2 (ANSI C2 NESC), and OSHA 1910.269 Subpart R (OSHA 29CFR 1910.269) and 1926.950 Subpart V (OSHA 29CFR 1926.950). The IEEE method is conservative. OSHA uses the NESC tables.

Air gap sparkover data used to calculate the MAD for voltages up to 72.5 kV are presented in IEEE Std 4-1995. Air gap sparkover data used to calculate the MAD for voltages 72.6 kV and above are presented in IEEE Std 516-2003. The tables for the OSHA/NESC numbers for 72.5 kV and below are the numbers calculated from IEEE Std 4-1995 plus a 2-ft ergonomic (inadvertent movement) component. For voltages above 72.6 kV, the tables for the OSHA/NESC numbers are taken from IEEE Std 516–2003 plus a 1-ft ergonomic component. Therefore, there is an apparent discontinuity in the value at 72.5 kV; however, this is not an issue of practical importance. The IEEE method does not explicitly consider the effects of defective insulators or electrically floating conducting objects (floating electrodes). The effect of altitude is treated as a separate multiplying factor.

The electrical component of the MAD is calculated by the IEEE method using Equation 13.3-1:

$$D = (C_1 \times C_2 + a) \times T \times kV_{LG} \qquad 13.3\text{-}1$$

where:

D = insulation distance, ft.

C_1 = 0.01, or 1% of the line-to-ground system voltage.

C_2 = 1.0 for cases without tools in the air gap.

a = saturation factor for crest

$V_{crest} = \sqrt{2} \times T \times kV_{LG}$ voltages of 630 kV and above.

T = maximum anticipated per-unit switching impulse overvoltage, truncation value.

kV_{LG} = rms system phase-to-ground voltage—actual.

It is important to note that the per-unit values (the values of T in Equation 13.3-1) have been revised and changed

significantly in 2003. The new values are listed in IEEE Std 516-2003 as:

- 3.5 per-unit for voltages 72.6 to 362 kV,
- 3.0 per unit for voltages 500 to 550 kV,
- 2.5 per unit for voltages 700 to 800 kV.

IEEE Std 516-1995 and previous editions of Std 516 used lower per-unit values (3.0 per unit for voltages of 362 kV and below, 2.4 per unit for 500 to 550 kV, and 2.0 per unit for 700 to 800 kV). The reason for the change is that new 121- to 362-kV single-break-per-pole switching devices may produce per-unit values that are significantly higher than those used previously for cases of three-phase reclosing into trapped charges. Further engineering studies may be required to determine the expected per-unit values to allow calculation of new MAD values for systems and equipment that may have greater overvoltages than those listed above.

Consequently, there is a disparity in the tabulated MAD values between IEEE Std 516-2003 and the OSHA (OSHA 29CFR 1910.269, OSHA 29CFR 1926.950) and NESC (ANSI C2) documents, and this disparity will be eliminated in due course of revisions to the documents.

Table 13.3-1 gives the MAD values for qualified electrical workers listed in IEEE Std 516-2003 (Table 18, without tools but including the ergonomic or inadvertent movement factor). The per-unit values used in calculating the distances in Table 13.3-1 will not be exceeded if the automatic breaker reclosing devices are rendered inoperative (blocked reclosing). Table 13.3-1 reflects the MAD for workers and utilities that do not have knowledge of the overvoltages on their system or specific facilities. Interpolation of MAD for voltages not listed in Table 13.3-1 **is not permitted.** MAD for those voltages must be calculated in accordance with IEEE Std 516 plus the appropriate ergonomic adder.

The reader is encouraged to consult References (IEEE Std 516, ANSI C2 NESC, OSHA 29CFR 1910.269, OSHA 29CFR 1926.950) for additional details, explanations, and restrictions on the use of the values in Table 13.3-1. Table 13.3-2 contains the altitude correction factors used in the IEEE method.

The IEC Method

The IEC method is summarized in IEC Publication 61472 and is discussed in several recently published papers (Gela et al. 2000, Gela and Charest 1998, Gela and Kientz 2000, De Dona 2004). It is based on the CRIEPI formula for air gap sparkover (Kishizima et al. 1984). The IEC method is not in table form. It requires the MAD value to be calculated for each circumstance. The IEC method has the advantage of including in the calculations for effects of defective insulator units, electrically floating objects, and several other details that are not a part of the IEEE method. Whereas the IEEE method has a fixed ergonomic component, the IEC method allows the utility to determine this value. However, the IEC method is complicated to use and requires more information for computing the MAD values (see Equations 13.3-2 through 13.3-6):

$$D_V = 2.17\ (e^{V_{90}/(1080K_t)} - 1) \qquad 13.3\text{-}2$$

where:

$$V_{90} = K_s \times V_2 \qquad 13.3\text{-}3$$

$$V_2 = (\sqrt{2}\ /\ \sqrt{3}) \times V_s \times v_2 \qquad 13.3\text{-}4$$

V_s = the maximum nominal system voltage.

v_2 = the 2% per unit overvoltage. Note: v_2 is related to T in the IEEE method by:

$$v_2 = (T + 0.25) / 1.25 \qquad 13.3\text{-}5$$

K_s = statistical safety factor with the suggested value of 1.1

$$K_t = k_s \times k_g \times k_a \times k_f \times k_i \qquad 13.3\text{-}6$$

Table 13.3-1 MAD Values Calculated by the IEEE Method (Based on IEEE Std 516-2003)

Voltage in kV Phase-to-Phase	Distance to Employee			
	Phase-to-Ground		Phase-to-Phase	
	(ft)	(m)	(ft)	(m)
72.6–121	3.45	1.05	4.56	1.39
138–145	3.94	1.20	5.27	1.61
161–169	4.42	1.35	5.96	1.82
230–242	6.14	1.87	8.46	2.58
345–362	10.44	3.18	14.69	4.48
500–550	15.68	4.78	23.61	7.20
765–800	21.44	6.54	34.53	10.52

Table 13.3-2 IEEE Altitude Correction Factors

Altitude		Correction Factor
(m)	(ft)	
900	3000	1.00
1200	4000	1.02
1500	5000	1.05
1800	6000	1.08
2100	7000	1.11
2400	8000	1.14
2700	9000	1.17
3000	10 000	1.20
3600	12 000	1.25
4200	14 000	1.30
4800	16 000	1.35
5400	18 000	1.39
6000	20 000	1.44

k_s = conventional deviation factor with the value ks = 0.936 for the typical suggested normalized conventional deviation of 5%.

k_g = gap factor; suggested conservative value of 1.2, unless a more precise value can be chosen.

k_a = atmospheric factor, to allow for a range of elevations within a service area (see IEC Publication 61472).

k_f = factor to allow for the effects (in addition to their reduction of the air gap length) of electrically floating objects in the worksite gap (see IEC Publication 61472).

k_i = factor to be applied to determine the required minimum length of a defective insulator string near which live work is to be done (see IEC Publication 61472).

The reader is encouraged to consult IEC Publication 61472 for further details.

Control of Worksite Overvoltages

For barehanding LW activities, OSHA 1910.269 (q) (3) (I) (OSHA 29CFR 1910.269) requires that, if possible, the automatic reclosing feature be made inoperative ("blocking reclosure") on the circuit-interrupting devices that are used to protect the circuit on which work is to be performed. There is no such requirement for insulating tool work (hot-stick work); however, it is a good practice that has been adopted by many utilities to block reclosure of circuit breakers.

Blocking reclosures provides two primary advantages from the LW viewpoint:

- As switching overvoltage studies show, the highest overvoltages (pu values) occur, not as the result of the opening action of a circuit breaker, but as the result of reclosing the breaker immediately after opening, since the trapped charge (remaining voltage) on the line has not had sufficient time to bleed off. Hence, the resulting *re-closing* overvoltage can be significantly higher than the initial opening overvoltage. In fact, the 3 pu value mentioned above as a basis for the MAD values, is derived from reclosing (rather than one-time opening) overvoltages.
- In case of an unintentional electrical breakdown at the worksite, the resulting phase-to-ground fault is usually a low-impedance type and will be cleared by the breaker very quickly. This not only prevents repeated exposure to possibly lethal current if the breaker reclosed, but it also minimizes the initial exposure and possible harm to the worker.

Furthermore, blocking a circuit breaker reclosure requires a certain amount of internal coordination and paperwork, which help make a larger number of employees within several departments aware that LW is being performed. This further reduces the possibility of errors and hazardous situations.

From the MAD viewpoint, a significant advantage of blocking reclosures is that the possible magnitude of overvoltage at the worksite is contained and significantly reduced. This, in turn, allows recalculation of the value of D (in the IEEE method) or D_U (in the IEC method), resulting in a smaller D (in the IEEE method) or D_U (in the IEC method) value and therefore a smaller recalculated value of MAD. As the actual physical clearances on the structure are unchanged, a smaller recalculated MAD value provides an increased margin of safety during LW.

It should be noted that additional measures are also available to reduce worksite overvoltages even further, such as the use of Portable Protective Air Gaps (PPAG) (EPRI 1994, Gela et al. 1996, Gela and Ferraro 2002, Niamsorn et al. 2004), which have recently been developed for system voltages between 115 kV and 500 kV. The use of PPAG can limit worksite overvoltage to 1.7 pu or even lower, which in turn allows further recalculation of D (in the IEEE method) or D_U (in the IEC method), and of the MAD. Of course, if the available clearances are greater than the MAD, then those clearances should be utilized fully to reduce the risk to the worker.

Robotics

Robotic equipment and devices for LW range from sophisticated all-purpose remotely operated robots and computer-vision-guided aircraft, through specialized robotic arms, to rather simple mechanized conductor support equipment mounted on aerial devices (Figure 13.3-2) and automatically timed insulator cleaning nozzles (Udod et al. 1998, Campoy et al. 2000, Montambault 2002, Iwashita 2004). Remotely operated robots can have one or two insulated mechanical hands that are operated through hydraulics by a remote operator. There are basically two types of remotely operated robotic equipment, those with chassis-mounted cabs and those with boom-mounted cabs. A chassis-mounted cab uses video cameras to manipulate the robotic arms. A boom-mounted cab is placed at the end of an insulating boom and provides the operator direct line-of-sight control of the robotic arms. EPRI built a robotic unit dubbed "TOMCAT" (see Figure 13.3-3). Although EPRI has not pursued further robotic live work (the TOMCAT robot has been decommissioned), other countries such as Japan, France, and Spain continue active robotic maintenance programs (see Figure 13.3-4). Robotics is most effective in areas such as cities with high pedestrian activity and in substations, since little ground-level space is required compared to the size of staging areas required for human operation.

13.3.3 Design and Construction Aspects Important to LW

This subsection focuses on design and construction topics that are important to LW. Various types of structures, insulator assemblies, conductor hardware, and other installations (such as OPGW, ADSS) are discussed.



Figure 13.3-2 Specialized robotic conductor support arm.

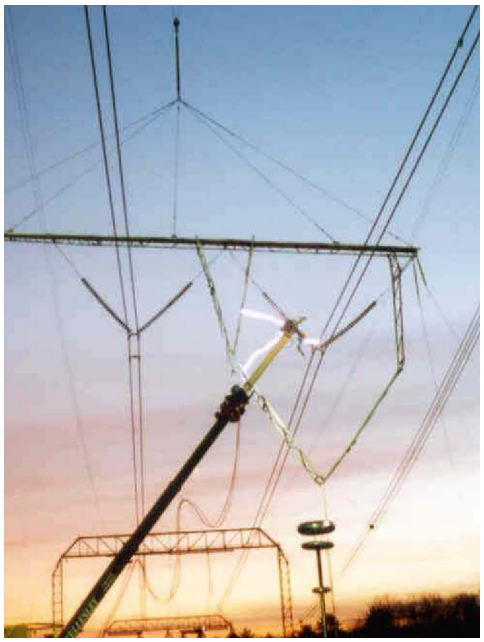


Figure 13.3-3 TOMCAT undergoing switching impulse tests at the EPRI Center in Lenox, MA.

Steel and Aluminum Lattice Structures

Lattice structures are relatively easy to climb and to attach tools such as strain and support sticks. From the LW viewpoint, it is important to ensure that structure members have sufficient strength (both initial, and aged after years of service) to allow climbing and to support tools.

On multi-circuit structures, sufficient climbing space must be available. The possibility of blocking breaker reclosure on both lines may also need to be available. Short-circuit current levels need to be known for both lines. For de-energized work on one or both lines, attachment points for temporary grounding cables must be available and an equipotential zone established for the de-energized circuit(s).

Structures with underbuilt lower-voltage lines require special consideration. When work is performed on the upper higher-voltage line(s), whether energized or de-energized, sufficient climbing space past the underbuilt lower-voltage line(s) must be available, or the lower-voltage line(s) must be de-energized and grounded. For work on the underbuilt lower-voltage line(s) while the upper higher voltage line(s) remain(s) energized, induction into the lower-voltage line(s) resulting from steady-state and switching operations, faults, and lightning strikes on the upper higher-voltage line(s) must be considered, or the higher-voltage line(s) must be de-energized but not necessarily grounded.

Steel, Concrete, and Wood Single-Pole Structures

Transmission single-pole structures are generally more difficult to climb and require one of the following:

- Step bolts that are appropriately spaced and located around the pole circumference
- Attached ladders for climbing
- The use of aerial devices

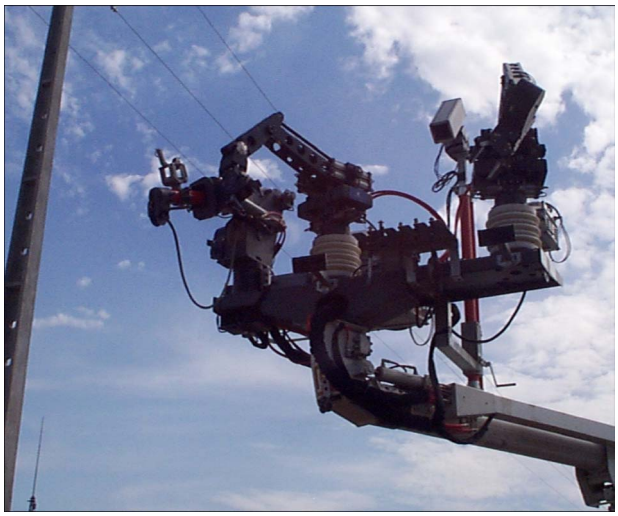


Figure 13.3-4 Example of a Spanish robot for live work.

Similar considerations as for lattice structures apply to multi-circuit poles. Step bolts and ladders generally start about 8 to 10 feet (2.4 to 3 m) above ground level to prevent climbing access to the public. Wood poles may or may not be equipped with step bolts.

Wood and concrete poles often have copperweld grounding wires as part of the lightning protection system. These ground wires are designed for system protection and are not sufficient to carry short-circuit currents; hence, they are not suitable attachment points for temporary grounds for de-energized work.

Also, workers have expressed concerns about climbing laminated poles using pole climbers, since the gaffs tend to slide off or sink into the laminate more easily that in the case of wood poles.

There are a variety of composite structures (i.e., wood H-frame using a prefab metal crossarm with attached overhead ground wire supports—so-called "goat head") that are composed of a variety of materials. These must be addressed separately as to appropriate work method.

Structures Made of Nonconductive Materials

Structures made of nonconductive synthetic materials, or containing nonconductive synthetic structural components, are not in common use yet; however, there are several trial installations. One advantage of such structures is the possibility of using structural components as part of the insulation system, thus reducing the length and weight of insulators. From the LW viewpoint, however, this approach can pose significant problems for workers climbing or performing insulating tool work from the structure. Namely, the presence of a worker's body, particularly when wearing a conductive suit, can short out a portion of the insulation system, and thereby possibly expose the worker to increased electrical risk. For LW purposes, all components should be considered to be conductive unless specific work procedures have been developed.

In addition, issues related to installation and interconnection of temporary grounds (including multi-circuit structures) are similar to, or even more severe than, those for wood and concrete poles.

Tangent, Angle, and Deadend Structures

Tangent (suspension) structures are designed primarily for nontension mechanical loads such as the vertical weight of conductors, overhead ground wires, and ice, as well as horizontal wind loads. They generally account for the majority of structures in a transmission line. A single climbing and maintenance procedure is required for these structures.

Angle structures (small, medium, and large angle) can vary significantly in construction and present different challenges to LW. The inside, center, and outside conductor(s) often have crossarms of different lengths and may use different insulator attachment hardware. Work procedures and specific tools must be considered for each phase.

Deadend structures, besides supporting vertical and horizontal loads, are designed to carry the tension loads of the conductors. They are normally designed such that if the tension on one side or the structure is lost, the structure will absorb the loss, including shock load, without failure. On long lines in severe storm areas, tangent deadend structures are often installed at specified intervals to prevent cascading or catastrophic failure of the system. Strain tools on deadend structures must accommodate both the tension and the angle of the conductor(s). Deadend structures have a "jumper" to electrically connect the conductors on either side of the structure. Like the angle structure, crossarm lengths and insulator attachment hardware can vary between phases, depending on the angle between the line directions on either side of the structure. The jumpers can use from none to two supporting insulator strings depending on the angle and the specific phase. Different work procedures and specific tools may need to be used for various angle structures and, possibly, for each phase on the angle structure. Tools supporting the tension loads and their structure attachment points must be given careful consideration.

Testing of Insulators Prior to Commencement of LW

Porcelain and Glass Insulators

Prior to beginning LW, the maximum allowable number of defective insulator units, or minimum number of good units, must be determined. This number (maximum number of defective units, or minimum number of good units) must be established by each utility.

Some utilities allow visual determination of defective suspension insulators, while many require electrical testing of each unit. Angle, tension, and inclined span insulators should always have electrical testing performed on each unit. All new units should be tested before installation. The cost of testing before installation is insignificant compared to the cost of a return visit to replace a defective unit that was not detected prior to installation.

Polymer Insulators

At this time, there are no low-cost techniques and instruments for rapid and reliable routine testing of polymer insulators at the worksite prior to maintenance. Consequently, some utilities do not perform LW on some lines that use polymer insulators, do not use polymer insulators altogether on certain lines that need to be maintained live, or have instituted programs to replace installed polymer insulator with porcelain or glass strings to allow LW.

Suspension and Deadend Insulator Assemblies

Suspension (tangent) insulators (porcelain, glass and polymer) are designed primarily for nontension loads, such as the vertical weight of conductors and ice, as well as horizontal wind loads. They generally account for the majority of insulators in a transmission line. A single work procedure is required for these insulators.

Deadend insulators are designed to carry the full tension load of the conductor(s) (with an NESC overload capacity factor [OCF]) as well as the vertical weight of conductors and ice and horizontal wind loads. Removal of deadend insulator porcelain and glass strings requires the use of a cradle. The common practice is to use the cradle to lower the insulator to the ground for repair. At 230 kV, it is sometimes possible to slide the insulators and the cradle toward the structure and replace individual units without lowering the cradle to the ground. Polymer deadend insulators are typically installed and removed without the use of a cradle, unless there is a possibility of bending or twisting of the long units (that are used at higher voltages) during installation or removal. Deadend jumper support insulators are handled much the same as suspension insulators.

Angle insulator strings carry a vertical, horizontal, and tension (specific to the angle) load. If strainsticks are used, care must be taken to duplicate, as closely as possible in the field, the conductor-to-structure attachment angle to maintain the required clearances. Misaligned strainsticks can make disconnection (reconnection) of the insulator string(s) from the conductor (or structure) difficult, and installation of the insulator string can become extremely difficult. Cradles may be used to remove and lower angle porcelain and glass strings to the ground. Polymer insulators are typically handled without a cradle, unless there is a possibility of bending or twisting of the long units (that are used at higher voltages) during installation or removal.

Insulator I- and V- Insulator Configurations

Suspension I-insulators (porcelain and glass strings, and polymer units) are vertical insulators that are free to sway in the wind. Their design accounts for the sway and any changes it makes in the electrical sparkover distance between the insulator attachment hardware, conductor, and the structure. Because LW is not performed during high winds, I-insulator swaying, and the problems associated with maintaining the required MAD values, is usually not an issue. During either energized or de-energized work on I-insulators, the vertical load on the strainsticks is concentrated near the insulator attachment point, providing adequate support for tools and equipment. I-insulators do not require the use of a cradle to lower them to the ground, but guide ropes (tag lines) may be needed, especially on structures with a vertical conductor phase configuration.

V-insulators are normally used on the center phase of a single-circuit structure and to eliminate side-swing on double-circuit structures. V-insulators may be used on the outside phases (to prevent side-swing) of single-circuit structures where right-of-way width is a concern (usually at higher transmission voltages). However, longer arms and additional structure material are required. Ceramic V-insulator strings require the use of a cradle to lower the string to the ground. Long polymer insulators (i.e., 345 kV and above) may require a cradle to prevent excessive bending. Workers must take care when attaching strainsticks to lattice steel bridges and crossarms. Attachment points where two or more lattice members meet on each of two bolted planes are preferred to prevent the bending of single members. Bridge loading points are usually not a concern in heavy loading areas because work is not done with ice and heavy wind on the conductor.

When planning LW on V-insulators, one must make sure that the required MAD is available, since the physical clearances required for V-insulators are less that those required for I-insulators. This is even more important for upgraded and compact lines.

V-insulators are also used when upgrading to a higher voltage. Elimination of I-insulator side-swing by the use of a V-insulator will often provide adequate operating clearance for the higher voltage.

Single- and Multiple-Insulator Assemblies

Multiple insulator assemblies (porcelain or glass, and polymer) are usually used only on bundled conductors or on critical spans such as interstate and railroad crossings. Usually, only one string of a multiple deadend assembly is replaced at a time or, if multiple replacements are required, they are replaced one at a time. When only one string is replaced at a time, the strain sticks only need to support the tension of the entire bundle divided by the number of insulator strings. For example, using a porcelain or glass double deadend insulator string on a two-conductor bundle with a total of 20,000 lb (9100 kg) tension, the strain sticks need only be rated for 10,000 lb (4550 kg) tension when replacing the insulator strings one at a time.

Because of the different way of specifying the mechanical strength for a polymer insulator than for ceramic or glass insulators, designers often use a single polymer insulator on a deadend, whereas a double string would have been used in the same situation if the strings consisted of ceramic or glass insulators. Hence, when removing the single polymer insulator, the strain sticks must support the entire tension of the deadend. This requires strainsticks of greater strength, diameter, weight, and cost. The maintenance department must have such strain sticks and must be aware that special high-strength sticks have to be used to remove the polymer unit. If high-strength sticks are not

available, the utility design department should be informed of this issue early in the design stage of the line. A simple solution to overcome this difficulty is to use two polymer insulators. This approach will double the cost of deadend polymer insulators, however, the cost of strain sticks and other tools is reduced and the work procedure places the worker at lower risk. Another important benefit of using double deadend polymer insulators is that this will double the strength of the assembly, and also in case of damage to one unit, the line will be placed in lesser risk of failure. The damaged unit could be replaced on a longer maintenance schedule rather than more urgently.

Ceramic, Glass, and Polymer Insulators Replacement

Ceramic and glass insulator strings should not be replaced with polymer insulators without checking the overall length (including attachment hardware), the electrical rating (including the Critical FlashOver Voltage, or CFO rating) and the mechanical-electrical (M&E) rating with the utility design department. The porcelain insulator string length for a given CFO is usually different from that of a polymer insulator. Hence, choosing the replacement insulator based only on CFO may result in different insulator lengths. Also, the M&E rating of ceramic insulators must be coordinated with the Specified Mechanical Load (SML) rating of the polymer insulator according to each manufacturer's specifications.

Insulator Hardware Type

It is essential that designers coordinate the design of insulator hardware with maintenance personnel, especially the craft that will be performing the LW. Including special provisions for LW, such as a yoke or tool attachment flange on the hardware, reduces the cost for developing special tools for LW, reduces work time, and decreases worker risk. For example, in the instance of multiple insulator strings, "single-pole strain carrier yokes" minimize tool requirements and worker stress.

Insulator Contamination and Cleaning Issues

Contaminated insulator units or strings may flash over during wet conditions. This situation can be detected by locating areas where several structures exhibit tracking on the insulator units or strings. Industrial areas and seaside locations are most likely to experience high pollution and contamination problems. Washing or cleaning (using various methods, such as CO_2 pellets, crushed vegetable matter, etc.) of contaminated insulator strings is recommended until it is no longer effective and replacement becomes necessary. Also, contamination-related flashovers tend to occur during fog, in morning dew, or very early in the day when the sun starts to warm up the units and moisture tends to condense on contaminated surfaces. Some utilities avoid these conditions by not performing live work until later in the day.

Also, cleaning of polymer insulators must be performed very carefully to avoid damage to the sheds and, more importantly, to the sheath (Burnham et al. 1995). Many utilities avoid cleaning of polymer insulators for this reason.

Coating of insulators to prevent contamination-related flashovers helps avoid outages, but has little effect on LW procedures. However, when insulators need to be re-coated (usually every few years), removal of the aged coating and application of new coating are typically performed with the line de-energized.

Conductor and Insulator Hardware

Tools dedicated to specific voltages and structure design are recommended for use in the insulating tool and barehand live work methods. The engineering department should be instructed to furnish permanent insulator LW ("hot fittings") hardware for insulator attachments to ease LW procedures and to accommodate standard insulating tool attachments. Special LW hardware provisions need only be furnished at insulator string connections that have been coordinated between engineering design and maintenance. This may be required on the cold-end, hot-end, or both.

Practice has shown that universal insulating tools may be too long and, as such, interfere with, restrict, or prevent effective LW. This is especially true when replacing ceramic insulator strings with polymer insulators and when performing live work on compact structures (EPRI 1998, EPRI 1997a).

Fog bells, (i.e., long-skirted) porcelain insulator units, may prohibit the use of standard cotter pin removal tools.

Overhead Ground Wires (Shield Wire, Static Wire), OPGW, ADSS

Overhead Ground Wires

The primary function of overhead ground wires (OGW) is to direct the energy of a lightning stroke to earth. The amount of energy that flows to earth at each ground point diminishes as the distance from the location of the stroke increases. A reduced overvoltage (i.e., lower than the original lightning strike) will be induced on the phase conductor(s) being worked.

During fault conditions, over 85% of the fault current will flow from the structure grounding system to the OGW. Portions of the current will drain at each consecutive structure; however, most of the current will return to the substation(s), and will, in turn, trip the protection relays.

The overhead ground wires are not designed and used specifically with LW, or for that matter, de-energized work in mind. Overhead ground wires, structure grounds, and footing resistance are designed for system and equipment

protection—*not for worker protection.* Therefore, the role of overhead ground wires in setting up of safe LW worksites (equipotential zones, for example) needs to be carefully considered.

OPGW and ADSS

Installation of fiber optic cables on transmission-line structures is a relatively new development and offers many advantages and challenges (Garcia et al. 2002, Fernández 2002). The most common types of fiber optic cables are:

- Optical Ground Wire (OPGW)
- All Dielectric Self-Supporting (ADSS) cable.

OPGW is installed in place of conventional OGWs. ADSS can be installed anywhere on the structure, but, to minimize mechanical loading, it is usually installed below the energized phases.

Servicing OPGW with the line energized is, for the most part, similar to servicing conventional OGWs. The main differences are:

- The skills needed to service both the OGW and the optical fibers
- The grounding of fiber optic equipment during work
- The establishment of an equipotential zone for workers.

Servicing ADSS raises similar points, and also raises the question whether the ADSS should be considered an insulator or a conductor. Full-scale and long-term tests indicate that the ADSS behaves as an insulator when new (i.e., during initial stringing, for example), but that it may accumulate contamination and experience surface or internal leakage currents after a period of exposure to the elements that results in degradation or damage to the cable jacket. Available standards and regulations (IEEE Std 516, ANSI C2 NESC, OSHA 29CFR 1910.269, OSHA 29CFR 1926.950) do not provide clear guidance at this time. However, the issue is under consideration. It should also be noted that the NESC (ANSI C2 NESC) and OSHA (OSHA 29CFR 1910.269) cite minimum safety (low-risk) rules. They **do not** establish work procedures. Work procedures and compliance with the rules are the responsibility of the utility.

As with any conductive object, induction (both from the energized circuit being worked and parallel energized circuits) during installation and maintenance of ADSS and OPGW *must* be included in the hazard analysis and as part of the work practice. In general, induction is dependent on the following considerations:

- Magnitude of the current on the parallel circuit(s)
- Proximity to the energized circuit(s)
- The line length that the circuits are parallel. Note: *The parallel section(s) may not be visible from the worksite.*

Surge (Lightning) Arresters

Surge arresters have traditionally been installed in substations. Recently, many utilities have installed arresters on transmission lines, in strategic locations, to improve lightning performance of lines. The arrester is connected between the energized conductor and the structure ground. New EPRI research (EPRI 2002c, EPRI 1997b) has shown that further improvements in line performance can be achieved by employing line arresters with automatic disconnects that effectively remove the arrester from service and break the connection to the arrester in case of arrester failure. The disconnecting device usually contains an explosive cartridge, such as a.22 caliber power tool load. In the case of arrester failure, the cartridge explodes and the arrester lead breaks away to prevent a phase-to-ground fault and the resulting power outage.

Two general arrangements are used:

- The disconnecting device is at the energized end of the arrester
- The disconnecting device is at the grounded end of the arrester.

In the first arrangement, the arrester is disconnected from the energized conductor when the disconnecting device operates. The arrester then swings away from the energized conductor and remains grounded, but is still free to swing. In the second arrangement, the arrester is disconnected from structure ground when the device operates. The arrester swings away from the structure ground and remains energized and free to swing.

In both cases, caution must be exercised and detailed LW procedures must be developed for LW on transmission lines that contain line arresters with explosive disconnects. Further research is needed to identify and resolve the pertinent LW issues that arise in such situations. LW procedures must be developed for both working in the vicinity of functioning arresters and for replacement of arresters that have been activated and require maintenance or replacement. Work procedures and tools related to the MAD for the specific voltage must be addressed.

Step, Touch, Transfer, and Induced Voltage Issues

Step, touch, and transfer voltages can occur on the ground at the worksite as result of an accidental short-circuit on the structure where LW is performed. Most of the fault current will return to the substation through the phase and shield wires (if present), and only a portion will travel to ground through the structure. However, even relatively small fault currents (relative to the total available short-circuit current) can produce hazardous step, touch, and transfer voltages at

the worksite (Dines and Melzer 1990, San Román Salcines 2000, McLean 2000, Lessard and Rajotte 2000, Gela 2002, Pierce 2002, Mougenet 2002). There is little that can be done at the design stage to minimize such hazards, except for the rather expensive option of installing extensive ground mats similar to those use in substations. Therefore, the onus falls on LW crews to be properly trained to minimize hazards by establishing equipotential zones.

De-energized lines that are in the vicinity of other energized lines may acquire significant induced voltage. Consequently, as in the case of work on OPGW and ADSS discussed earlier, induction must be included in the hazard analysis and as part of the work practice. In general, induction is dependent on the following considerations:

- Magnitude of the current on the parallel circuit(s)
- Proximity to the energized circuit(s)
- The line length that the circuits are parallel. Note: The parallel section(s) may not be visible from the worksite.

Worksite Access Issues

Access to structures is a major deterrent to LW at many utilities. In inaccessible mountainous, river bed, residential, industrial, or agricultural areas, aerial devices cannot be used due to lack of access roads and flat areas near structures. Helicopter use can often be hindered by fog, rain, and high winds. Therefore, climbing is often the only alternative, keeping in mind that the climbing option may not be viable due to the condition of structures discussed earlier, and due to prevailing environmental conditions at the time of work.

Climbing Issues and Worker Attachment Methods

There has been an effort by general industry and attachment manufacturers to require 100% attachment at all times while performing LW, and also while climbing. At present, the worker is permitted to free-climb to the worksite. Once at the worksite, or at rest, the worker must be attached. Workers must be attached while transitioning to and from a vertical or horizontal ladder. Climbing equipment and procedures are covered in IEEE Std 1307. Attachment and rescue (self and assisted) should be an integral part of every work procedure (Martin 1993, De Dona et al. 2002, Ross 2000, Thorne 2000, Thorne 2003, Martin 2004).

Climatic Conditions

Climatic conditions are important considerations that cannot be overlooked when assessing the practicability of LW. LW is normally not performed in inclement weather conditions, such as:

- High humidity (at several utilities, LW is typically not performed when humidity exceeds 85%)
- Rain or drizzle, fog
- Strong winds (while there are no specific or general limits, many utilities stop work when the crew finds it difficult to control long insulating tools)
- Thunder is heard, or lightning is seen within about 5 miles

Vegetation and Bird Control, Structure Painting

Vegetation control is essential to system stability and reliability. Right-of-way access must be maintained and kept clear of vegetation to prevent line maintenance delays. Management (trimming) of vegetation that can make contact with energized conductors in high wind or ice loading conditions is normally part of the utility's ongoing scheduled maintenance program; however, hazard trees, those along the edge of the right-of-way that could fall into the line, are often ignored. Vegetation near and under circuits that are heavily loaded tends to go into corona and may eventually ignite. Bird droppings may cause serious insulator contamination that may lead to flashovers and consequent outages (Wells 1998, Portillo Belinchón 2000).

Structure painting, whether performed by the utility or a contractor, must be closely controlled. Paint must not be allowed to be spilled, splashed, or drip onto insulators, such as shown in Figure 13.3-5. Compliance with worker climbing and attachment regulations is difficult to adhere to. The utility must plan these activities carefully and establish a training plan.

Conductor and overhead ground wires are often required to be marked for public safety in some manner. Aerial markers (balls) can be installed by aerial device, cable cart, traveling ladder, or helicopter. Installing these devices on energized lines is regularly done with established work procedures. Activities, such as painting large diameter and bundled conductors over interstate highways, is not in the realm of normal activities.These conductors are often painted black



Figure 13.3-5 Example of insulators inadvertently splashed with conductive graphite-based paint during structure painting.

with the intention of preventing sunlight reflection and glare. It is essential that the utility develop a program and train workers for these unusual and rare activities.

Special Considerations, Including Environmental and Worksite Conditions, PCS Antennae, Work Conditions, Preparatory Training, Worker Buy-in

Environmental issues may restrict the ability to perform LW by such considerations as:

- Limiting access to the worksite for workers, heavy equipment, helicopters
- Limiting the available worksite area, especially in public places such as road and parking lots
- Specific locations of structures, such as mountainous areas, river channels, highway crossings

Use of transmission structures as supports for radio frequency (RF) antennae and personal communications system (PCS) equipment is a new development (see Figure 13.3-6). Antennae are usually installed above energized phase conductors. Installation of, and maintenance work on, such equipment raises several new challenges, including:

- Need for new skills to handle and service the equipment
- Grounding of the equipment during work
- Protection of workers from exposure to high-frequency fields.

The high-frequency energy field of the antenna can cause concern to a climber (Carman and Woodhouse 2000, Van Waes et al. 2000, Kolcio et al. 2003, Poulin 2003). PCS operators are very reluctant to "power down" their equipment. Climbing near their equipment should not be attempted without contacting the utility management and obtaining appropriate approvals.

The IEEE/ESMOL Subcommittee is now in the process of considering these issues and preparing an IEEE standard. Manufacturers of conductive clothing are investigating the effectiveness of conventional conductive apparel to shield high-frequency fields. Test data indicate that commercially available conductive clothing with a face screen affords shielding, provided that electrical continuity of the entire apparel (including the face screen) is maintained.

Worksite conditions that may be affect LW include:

- Induction for nearby energized lines—this can result in significant steady-state and temporary overvoltages on the line on which LW is performed.
- Ambient temperature—LW is normally not performed on very cold days (to avoid frostbite) and on very hot days (to avoid excessive physical strain to workers, fainting, etc.).
- Conductor temperature—with the increasing interest in the use of conductors that are rated to operate at very high temperatures (200°C or more), the conductors and hardware may prove to be too hot for barehand work without special precautions.
- Worksites in multi-use corridors, such as along highways, railroads, pipelines, etc. may require special pre-



(a) Antennae installed on top of structure



(b) Antennae installed amid phases

Figure 13.3-6 Examples of shared use of transmission structures —PSC antennae.

cautions and procedures, hearing protection, and additional training of crews in avoidance of distractions.

- Shared use of structures (i.e., installations that include fiber optic cables or PCS antennae) as discussed above.
- Concerns about electric and magnetic field exposure (Pretorius 1993a, Pretorius 1993b, Udod et al. 1995, Engelmann and Kindersberger 2000, ESMOL Task Force 2000, Fernández et al. 2000, Moreno Barraza et al. 2000, Vincent et al. 2002).

Training of crews to perform new tasks is essential (Ascenção Gaspar and Trullench Marzo 2000, McLean 2002, EPRI 2002a, EPRI 2002b). It is also a very good investment in developing successful LW programs to involve the maintenance department and crews that will perform LW very early in the design process. This helps secure workers' buy-in into new work and tasks, facilitates a healthy debate of issues that helps avoid subsequent difficulties, and helps all stakeholders develop cost-effective LW programs.

Compact Lines

Compact lines are lines that have smaller phase-to-structure and/or phase-to-phase electrical distances than conventional lines (Ordon and Lindsey 1995). A line can generally become compact in one of three ways:

- An existing line is rebuilt with smaller electrical design and operating clearances,
- An existing line is upgraded in voltage (the operating voltage is higher than the original), but the finished line has smaller electrical design and operating clearances than a conventional line at the higher voltage
- A line is built initially with smaller electrical design and operating clearances

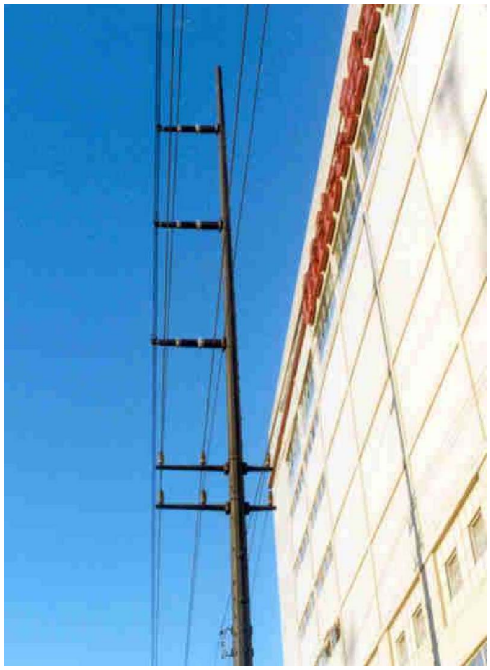
The above line designs are used more and more often due to difficulties faced by utilities in obtaining permits for new rights-of-way and construction of new lines, expense of purchasing new rights of way, restrictions on structure height and concerns about effects of electric and magnetic fields, and new commercial buildings that abut line the right-of-way.

Two examples of compact lines are:

- A 230-kV line with a vertical phase configuration and an original phase-to-phase distance of 16 ft (4.88 m) that was compacted to a phase-to-phase distance of 6 ft (1.83 m) (see Figure 13.3-7).
- A double-circuit 230-kV line that was upgraded to a single-circuit 550-kV line with the relevant shortest distances of 11 ft, 4 in. (3.45 m), which is about 20% smaller than a conventional 500-kV line (see Figure 13.3-8).

Line compaction can create three general problems for LW:

- The phase-to-structure and/or phase-to-phase distances may be insufficient to provide the MAD (minimum approach distance) for the line voltage without careful control of worksite overvoltages.

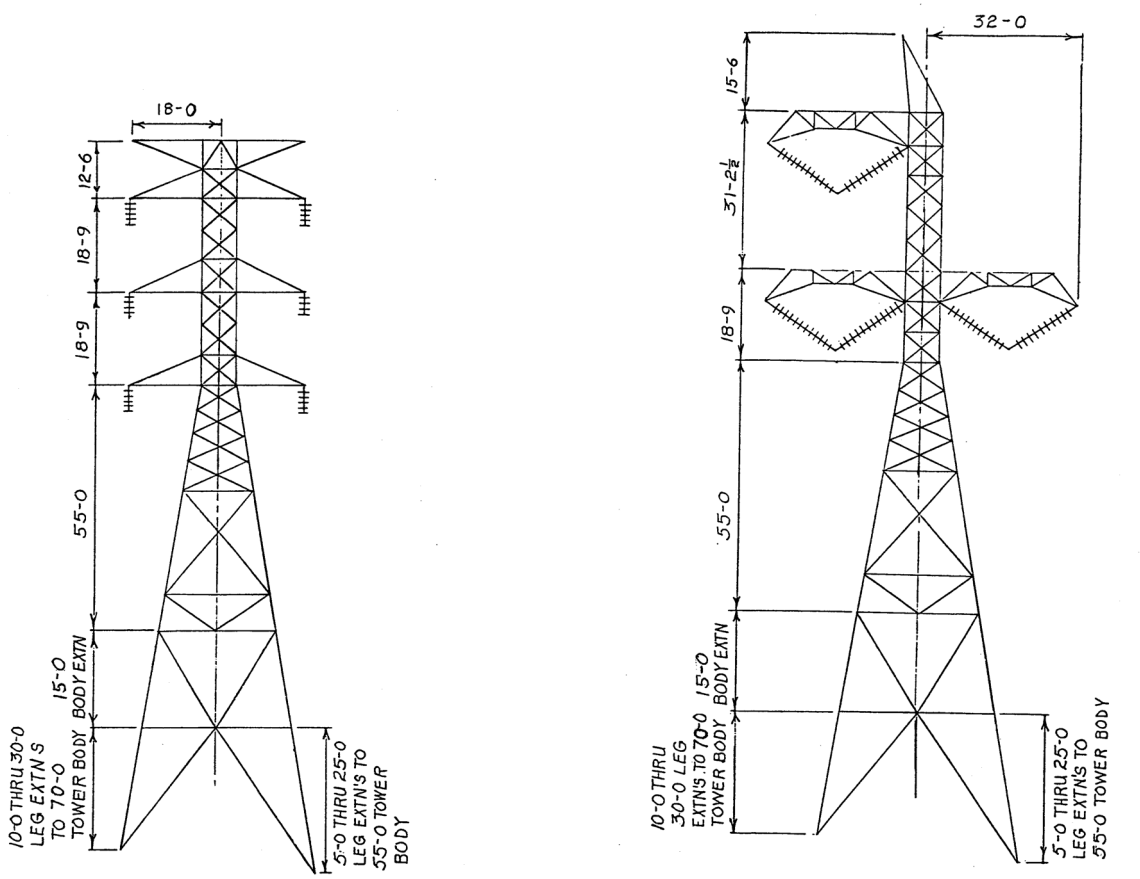


(a) Original 230-kV line, 4.9 m (16 ft) phase spacing.



(b) Compacted 230-kV line, 1.9 m (6 ft) phase spacing.

Figure 13.3-7 Example of a compacted 230-kV line.



(a) Original 230-kV double-circuit tower.

(b) Upgraded compact 550-kV tower, about 20% compaction.

Figure 13.3-8 Example of 230-kV line upgraded to 550 kV.

- Conventional LW tools may be too long for the available distances (EPRI 1998b, EPRI 1997a).
- Certain work methods, such as barehanding, may not be possible at all, or may only be possible with the use of additional innovative worksite overvoltage control measures.

As an example of this potential problem, Table 13.3-3 summarizes the required MAD values (based on 3 pu transient overvoltage factor) and the lengths of recommended tools (Hubble T95) for three system voltage levels (115/138 kV, 230 kV, and 345 kV). The connection lengths of the ceramic strings and polymer insulators are also included. The MAD values and the tool lengths are often taken from (Hubble T95), which is the common reference available to work crews. Although deviations from these recommendations are possible, if properly justified in engineering terms, it must be recognized that the work crews need to be fully aware of the changes, must understand them, must "buy into them," and must be convinced that tools other than those recommended in (Hubble T95), or equivalent

Table 13.3-3 MAD Values, Recommended Tool Lengths and Connection Lengths

System Voltage (kV_{ph-ph})	MAD (ft/m)	Strainstick Length (ft/m)	Cradle Stick Length (ft/m)	Connection Length Ceramic String (ft/m)	Connection Length NCI (ft/m)
345 (V, 20 units)	8.5/2.59	13.2/4.02	11.3/3.45	9.58/2.92	8.04/2.45
345 (V, 16 units)	8.5/2.59	13.2/4.02	9/2.74	7.98/2.43	8.04/2.45
230 (I, 13 units)	5.25/1.59	9.9/3.02	--	6.23/1.9	6.48/1.97
115/138 (I, 9 units)	3.6/1.09	8.7/2.64	--	4.31/1.31	4.58/1.4

sources available to them, are in fact appropriate and meet or exceed the required maintenance criteria.

Analysis of Table 13.3-3 clearly leads to the following observations:

- The required MAD values are smaller than the ceramic string connection lengths, except for the case of 16 units on the 345-kV system. This is due to line compaction (no links). Hence, overvoltage control needs to be employed when working on 16-unit ceramic strings.
- The required MAD values are smaller than the polymer insulator connection lengths for the 230- and 115/138-kV cases, but they are not smaller for the 345-kV cases. This is due to line compaction (no links). Hence, overvoltage control needs to be employed when installing polymer insulators on the 345-kV system.
- The lengths of the recommended adjustable strainstick are greater in all cases than the insulator connection lengths. This has been found to be a problem in the case of the 345-kV V-sting, and sticks that are shorter than recommended have to be used. This is due to line compaction (no links). For the I-string, no problems were found since the yoke plate was placed on top of the crossarm. However, there may be situations where sticks shorter than recommended may need to be used. If shorter sticks must be used, overvoltage control needs to be employed.
- The lengths of the recommended cradle sticks are greater than the insulator connection lengths for the 345-kV system, V-string configuration (cradles are not needed for I-strings). This is due to line compaction (no links), and results in mechanical interference shown in Figure 13.3-9. If shorter cradle sticks must be used, overvoltage control needs to be employed.



Figure 13.3-9 Close-up photograph showing that the recommended 11-ft, 4-in (3.45 m) cradle sticks for use on 345 kV system are too long.

13.3.4 Low-Cost-Impact Design Modifications That Help Facilitate LW

Overall structure design should recognize the need of performing LW and should accommodate, as much as possible, provisions that would help facilitate LW and render the work least strenuous and costly. When designing structures, it is possible to include design features and modifications that have a very low impact on line cost but are very useful from the viewpoint of executing LW tasks. Conversely, the cost of not including such simple and low-impact design modifications can result in a higher cost of performing LW, can hinder efficient execution of LW tasks, and in some cases can prevent LW altogether. Some general low-impact design modifications are described below. Examples of problems resulting from not including LW needs at design stage are presented in Section 13.3.6.

Tool attachment points are essential to efficient to LW. The designer should be able to incorporate tool attachment points (such as additional holes) into the hardware and structure members at little or no increased cost. For instance, work in the lattice window of the center phase with conductor(s) supported by V-insulators requires installation of tools that provide a near vertical lift to release the vertical load on the insulator attachment hardware. Tools should be attached at the intersection of two or more lattice members. Some structures have relatively long-angle iron members on each side of the crossarm with no connecting and reinforcing cross-members in the center portion of the crossarm. These long members must support the weight of workers as well as the redistributed weight of the conductor(s). Structures designed for heavy ice and wind loads may be able to easily support these no-design loads; however, structures designed for light loading may find angle iron members subjected to severe bending.

Tool attachment locations are also critical on angle structures. The tools must be attached such that as the tension is taken off of the conductor, the angle of the tool relative to the conductor and the structure does not change. Otherwise, tools placed at a wrong angle are not able to support the conductor tension. This results in severe hardship for workers and may reduce work efficiency. Furthermore, on the outside angle, the phase insulator assembly hardware attachment is at the termination of the crossarm. Therefore, there is no convenient place to attach tools, unless special provisions are made at the crossarm termination itself. Including tool attachment points at appropriate locations during the design stage can be done relatively easily if the designer is aware of the issue. Proper design will undoubtedly save on future maintenance costs and reduce risk of injury to the worker. Conversely, lack of appropriate attachment points may prevent LW altogether.

Similarly, attachment provisions for insulating ladders (both vertical and horizontal), and anchorages for hoisting equipment should be an integral part of each structure design, and can be provided relatively easily at the design stage.

Worker access to elevated work positions may be accomplished by the installation of step bolts or attached ladders. These should begin at about 8 to 10 ft (2.4 to 3 m) above the ground level to eliminate easy access by the public. More serious problems set in at crossarm level. Access to the worksite on a lattice structures is not a significant issue because of the available number of structure cross-members on which workers can step, walk, and attach restraint and rescue devices (provided these members are properly rated for mechanical loads). On steel and concrete poles, permanent working rings around the structure (at conductor height) should be provided for the worker's feet and another set of smaller rings, eyelets, or loops for worker climbing and rescue equipment attachment. Access to the insulator hardware attachments on tubular steel crossarms can been achieved by the use of catwalks with handrails or steel bar loops for hand and knee positioning.

Also, provisions for worker self and assisted rescue must be included in new designs.

Insulators and attachment hardware, especially at the energized end, should be selected to allow good visibility of the work area and easy removal/reinsertion of the cotter key. Fog-type units tend to obstruct access and visibility to the cotter key and should not be used as the first unit at the energized end of a string.

13.3.5 High-Cost-Impact Design Modifications That Help Facilitate LW

Design of structures on which LW will be performed must have appropriate distances (MAD) for the line voltage and the selected LW method. For instance, access by insulated ladder may require a greater working envelope (i.e., larger distances) than access by an aerial device positioned on the outside of the structure perimeter. Also, vertical configurations and multi-circuit structures will require greater working distances on the upper phases.

Providing sufficient distances may require structures to be larger than initially planned, which could result significant increase in the material and construction costs. This is an example of a high-cost-impact design modification that may not always be justified in economic terms and, therefore, is not used very often. On the other hand, the cost of an outage to perform needed work de-energized may outweigh the initial cost increase, or even the cost of subsequent modification of an existing line, and the designer may find good justification for increasing structure size to accommodate LW. In fact, some utilities have designed and erected structures with helicopter landing platforms on top of the structure for the specific reason of accommodating LW and aerial inspection, even at the much increased construction and material cost. Also, some utilities have constructed lines with significantly increased phase-to-phase distances for the specific reason of accommodating helicopter-based LW between phases.

Many utilities also have recently returned to the practice of using the traditional ceramic insulators instead of single polymer units, particularly in deadend assemblies on bundle conductors, because of the inability to test reliably the installed polymer units prior to LW. Also, some utilities double up polymer deadend insulators to allow the use of traditional LW tools (strainsticks) that do not have sufficient mechanical strength to support full bundle tension.

While such examples are rather rare at this time, they point to the advantages of employing innovative approaches to optimize not only the line design/construction process, but also the line maintenance process.

Of course, alternate solutions are often possible that do not necessarily require larger and/or more costly structures. For example, control of worksite overvoltage may be used in some situations to offset the need for larger distances, and future development of special tools may alleviate other difficulties. Therefore, the designer needs to be aware of available alternatives and approaches to arrive at the best overall line design.

13.3.6 Examples and Lessons Learned

This subsection includes actual examples of practical problems and effective solutions based on accumulated experience, discussions with utilities, and feedback from electrical contractors performing construction and LW tasks for utilities.

Insulator Types

Several utilities have found it difficult to use LW on clevis-type insulators. Namely, workers using the insulating tool method from a structure may find it quite difficult to remove cotter keys and the curved bolt (with or without the nut) to detach the insulator string, and even more difficult to re-insert the curved bolt and the cotter key upon re-assembly, especially at the energized end of the string that is remote from a worker working from the structure and using long insulating tools. While these difficulties are certainly real and can cause work delays or even interruption, for the most part they can be resolved and overcome. Several utilities have managed to eliminate such problems through careful field study of the problem, practice, additional specialized training for crews, and the development of spe-

cialized tools that are particularly suited for the job. Some utilities have undertaken wholesale replacement of clevis-type insulator with ball-and-socket type to facilitate LW.

Armor Rod

Workers often encounter difficulties working with preformed armor rods on deadend insulators. When workers are using the insulating tool method from a structure, it is physically difficult and demanding to install/remove preformed rods. It is also difficult to visually observe the progress of the work. One solution involves replacing preformed rods with compression fittings that are easier to work. While this is easy to implement on new construction, systemwide replacement of all already installed performed rods with compression-type deadends would be a very costly exercise, and it would require extended de-energization of lines. If armor rods are removed entirely, the addition of vibration dampers should be considered.

Structural Adequacy

Some utilities have installed aluminum structures in mountainous regions where access by heavy construction equipment such as cranes is difficult. Construction of the aluminum structures was done with helicopter, but early versions of cargo helicopters had a limited load capability and could not carry heavy steel components. Helicopters are also restricted to certain elevations. Hence, lightweight aluminum was the material of choice at the time. Unfortunately, aluminum structures are often not designed to carry the additional mechanical loading introduced during LW by several linemen and conductor support tools such as strain and support sticks. In fact many aluminum structures require guying to help withstand longitudinal loads. This severely restricts the ability to climb the structures and perform LW. Also, aluminum structures are subject to severe corrosion; bolts corrode, seize and disintegrate; and angle structural members corrode to the point of perforation. This not only dictates the need for mechanical maintenance and repair of the structures, but also hinders climbing and LW in general until the degraded structures have been repaired.

Also, in humid environments, accumulation of algae and moss on structures, both metal and wood, makes the structures slippery and renders climbing very treacherous. These difficulties exist both in LW and de-energized work.

Access

Access to structures is a major deterrent to LW for many utilities. In inaccessible mountainous areas, insulating boom aerial devices cannot be used due to lack of access roads and flat areas near structures. Use of helicopters can often be hindered by fog, rain, and high winds, and they are also restricted to certain elevations. Therefore, climbing is often the only alternative, keeping in mind that the climbing option may be not viable due to the condition of structures discussed earlier, and due to prevailing environmental conditions at the time of work. In addition, on certain environmentally sensitive or protected areas such nature sanctuaries, access can only be accomplished by horse or mule.

Climatic Conditions

Climatic conditions are important considerations that cannot be overlooked when assessing the practicability of LW. LW is normally not performed in inclement weather conditions, such as:

- High humidity (at several utilities, LW is typically not performed when humidity exceeds 85%)
- Rain or drizzle
- Strong winds (while there are no specific or general limits, many utilities stop work when the crew finds it difficult to control long insulating tools). It should also be noted that the wind speed increases with elevation above grade.
- Fog
- Thunder is heard, or lightning is seen within about 5 miles

Worker Preparation, Training, and Buy-in

Training of crews to perform new tasks is essential (this is required, for example, by OSHA 1910.269 (a)(2) and (q)(3), [OSHA 29CFR 1910.269]). It is also a very good investment in developing successful LW programs to involve the maintenance department and crews that will perform LW very early in the design process. This helps secure workers' buy-in into new work and tasks, facilitates a healthy debate of issues that helps avoid subsequent difficulties, and helps all stakeholders develop cost-effective low-risk LW programs (Verdecchio et al. 2004).

Implementation of a New LW Program

An example of successful implementation of a new LW program is a utility in the Northeast United States that decided to increase the gloving capability from 12.5 kV to 34.5 kV. The decision was based on economic and technical evaluation of the company's needs. When the decision was finalized, the craft personnel were informed of three points:

- The decision is firm, and LW will be extended to 34.5 kV because it makes good sense to the well-being of the utility.
- Craft personnel will be invited to fully participate in the implementation of LW at 34.5 kV.
- After LW at 34.5 kV has been implemented, the previously used insulating tool (hotstick) method of LW will remain an option to be utilized as needed.

Representatives from the craft personnel were selected as members of a special committee to work with management, engineering, safety and other departments on the

task of bringing the plan to fruition. This secured the all-important buy-in of the craft personnel.

Volunteers for the new LW program were selected based on best skills, attitude, ingenuity, and overall superior performance. No additional compensation was proposed; rather the prestige of being a part of the new team appeared to suffice. Following numerous meetings of the committee, adjustments to the original plan were made, adequate training was provided, and the goal of gloving 34.5 kV systems was achieved successfully. Of course, the insulating tool methods were retained as an alternative to be used when so selected by a particular crew.

On the other hand, a Midwest (U.S.) utility also decided to develop gloving procedures for a higher voltage than previously worked in-house, but unfortunately took the approach of imposing the decision on the craft personnel. As a result, workers' buy-in was not secured, resentment and distrust set in, and the new LW program started out on a very rocky road. The program was eventually implemented, but not until considerable effort was expended to repair strained relations.

Unique Structure Configuration
A utility designed unique and visually attractive structures with a star insulator configuration for a 400-kV line (see Figure 13.3-10). Unfortunately, little discussion was held at the design stage with the maintenance department, and no training was provided to work on the structure. LW crews expressed concern about the undefined voltage on the hardware of the star point of the insulator configuration ("floating point"). Furthermore, no immediate agreement was reached on the question of whether the connection of the insulators within the star configuration—i.e., between each phase and the star point—should be treated as phase-to-phase or phase-to-ground connection. Consequently, LW could not be performed on the line until these issues were resolved and thorough training was completed (Ackermann and Morton 1990).

Induction of Overvoltages from Parallel Circuits into De-energized Lines
Recent trends of upgrading and uprating transmission lines and corridors create very serious problems for maintenance and construction near energized circuits. The problems occur on both parallel circuits and double-circuit structures. When the de-energized circuit being worked parallels a single or, more seriously, multiple energized circuits, each energized circuit induces continuous switching impulses and temporary overvoltages onto the parallel circuit(s). Induction depends on three factors:

- The current magnitude and flow in the parallel "source" circuit(s)
- The proximity of the parallel "source" circuit(s) to the "receiving" circuit
- The length that the "source" and "receiving" circuits are parallel to each other

To compound the problem, the parallel portions of the "source" (energized) and the "receiving" (de-energized) circuits are often well removed and out-of-sight of the work location. The following are documented examples of potentially hazardous induction from one parallel circuit to another.

Induced Voltage Lower than System Voltage on Which Work is Performed
Voltage induced onto a de-energized 345-kV transmission line paralleling an energized 500-kV line for approximately 120 miles was measured at 15 kV phase-to-ground. An arc occurs when an attempt is made to install protective



Figure 13.3-10 Example of a star insulator configuration.

grounds. The hazards resulting from such an arc are unacceptable. Also, if the protective grounds are installed, it is extremely difficult, if not impossible, to remove them without introducing an arc hazard. Consequently, as an example, to replace damaged insulators under these conditions would require de-energizing the line and using protective grounds with built-in interrupters, or de-energizing the line and using live work practices rated for 345 kV. In the latter case, it may be more efficient to work the line energized using the appropriate live working procedures; however, a greater number of defective insulator units may be allowed with the de-energized method—provided that the induction voltage has been physically measured or determined by an engineering analysis.

Induced Voltage Higher than System Voltage on Which Work Is Performed

Voltage induced onto a de-energized 69-kV transmission line in a corridor with two 500-kV lines and a double-circuit 69-kV line was measured higher than the operating voltage of the 69-kV line. Switching impulses and temporary overvoltages on the parallel lines would result in overvoltages on the de-energized 69-kV line that are significantly above those expected on 69-kV systems. Consequently, live work procedures in such corridors must take appropriate precautions and make adjustments in the work procedure and the minimum approach distance for the actual overvoltages that are likely to occur at the worksite.

Insulator Replacement—Suspension Insulators

A utility constructed a 500-kV line with V-insulator suspension strings consisting of fog-type units. Due to the large profile of the fog-type units, cotter keys on the first units from the energized end are not visible from the structure and are not accessible using the insulating tool method. Consequently, the utility decided to replace the first unit from the energized end in each suspension string with a regular-type (disc) unit to facilitate LW with the insulating tool method.

Insulator Replacement—Deadend Insulators

A utility discovered that it is not possible to replace live double deadends on 345-kV steel pole structures (see Figure 13.3-11). This operation was attempted on at least two structures. The task was found impossible to perform and work was interrupted. The problem occurs when an attempt is made to remove one of the two strings with 22 insulator units of the double deadend assembly using special single-pole strain carrier yokes that are placed on the triangular cold-end insulator yoke plate, and on the rectangular hot-end insulator yoke plate. (Figure 13.3-12 shows the cold-end strain carrier yoke installed on the triangular insulator yoke plate. A similar strain yoke is installed on the hot-end rectangular insulator yoke.

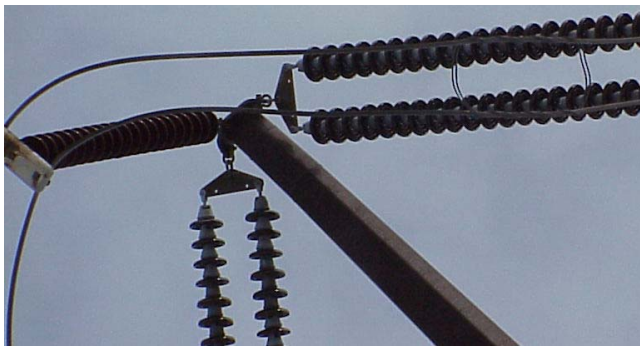


Figure 13.3-11 Photograph, from below, of a double deadend porcelain string (reproduced with permission of Northeast Utilities).





Figure 13.3-12 Two views of the cold-end strain carrier yoke installed on the triangular cold-end insulator yoke plate. A similar strain carrier yoke would be installed on the rectangular energized-end insulator yoke place (reproduced with permission of Northeast Utilities).

Figure 13.3-12 shows that the strain yoke has a round cutout that envelops and rests on the insulator ball shackle. When both strain carrier yokes are installed, an adjustable strain stick is installed to connect these yokes. The strain stick is tightened to relieve tension in the insulator string. The round cutouts rest on the shackles and thereby apply the compressive force to the string.

However, by doing so, the strain carrier yokes bind the shackles in place and prevent them from moving (rotating) with the insulator string.

As the result, when the string is compressed, the cold-end and hot-end insulator yokes are twisted out of parallel. The end shackles are twisted out of alignment, and it becomes impossible to uncouple the insulators. The end shackles cannot be moved or rotated to allow detaching the string, since they are held in fixed position by the pressure of the strain carrier yokes and the compressive force on the string that is to be removed. The play (flexibility) in the string consisting of individual bells is insufficient to allow removal of the entire string.

This situation is even worse in the case of polymer insulators that consist of one long unit. When the compressive force is applied, the unit tends to bow, and removal of its ends from the shackles becomes impossible.

Consequently, crews find it impossible to remove the insulator string. The crews noticed that forcing the string sideways resulted in bowing of the trunion, and work was stopped immediately. It was possible, however, to remove 20 units of the 22-unit string, leaving the cold-end and the hot-end units in place. These units could then be removed separately as subsequent isolated tasks.

Several solutions to this problem are available, including:

- The permanent yoke plates can be redesigned to provide an alternate support and pivot points for the strain carrier yokes that are installed to allow removal of the string.
- Alternate strainstick attachment holes could be provided.
- Additional shackles could be provided to increase the flexibility of the string and to allow removal of the units.
- The utility can contend with the two-step procedure where the 20 internal units are removed first, and then the remaining two end units are removed separately.

However, recognition of the situation prior to commencement of LW would eliminate the need for repeated trials and reduce physical strain on the workers.

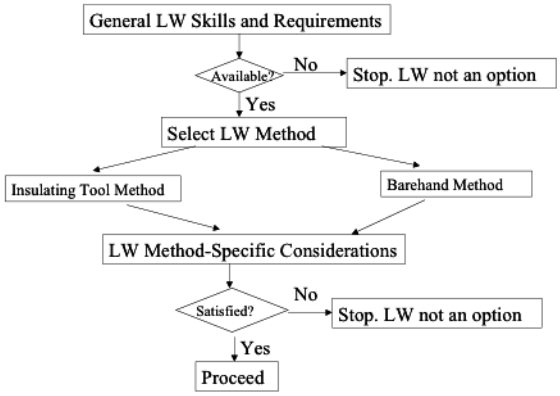


Figure 13.3-13 Decision flowchart to assess line maintainability using LW methods.

13.3.7 Determining Whether a Line is Maintainable Using LW Methods

The key to ensuring that a line is maintainable using LW methods lies in close cooperation among at least four groups: the line design department, the maintenance department with LW experience, the system operations department, and the safety department. Insulator type, material, and hardware have a direct bearing on the ease with which LW can be performed. These selections must also be coordinated with the choice of LW methods and tools to be used. Often the need to purchase new or different tools will affect design but may bring long-term cost advantages when maintenance expense and the cost of revenue loss due to outages are considered.

The information contained in this subsection cannot be exhaustive and comprehensive at this stage since many issues have not been fully studied and resolved. The flowchart shown in Figure 13.3-13 can be used to assess the compatibility of a line with LW requirements. The list is not yet complete, and the items are not necessarily listed in order of importance.

General LW Skills and Requirements

Below is a list of essential skills and requirements. They may be supplemented by additional skills and requirements in specific situations.

- Adequate LW training and certification
- Written work procedures in compliance with federal, state, local, and utility requirements, such as the NESC, OSHA, and local authority
- Adequate rescue equipment, first-aid facilities, and advanced medical help/facilities
- Attachment points and anchorage tools for body restraint, and for self- and assisted-rescue devices

- Positive communication system between elevated workers and ground personnel
- Positive communication system (a backup system is also recommended) between the worksite and operations (dispatcher, system controller, etc.)

LW Method-Specific Considerations

- Determination of the minimum approach distance for each type of work and each task, and, if necessary, for each structure and insulator type
- Determination of the need for use of conductive clothing (this is a requirement for workers positioned at the energized conductor while performing barehand work)
- Confirmation of adequate structure capacity for climbing, installation of tools, and rescue equipment
- Decision to use aerial devices or insulated ladders
- Selection of sufficient and appropriate tools for each LW method, type of structure, insulator, string, and insulator hardware
- Assessment of insulator string hardware: are LW fittings available, or are special yokes and tools required?
- Determination of the minimum number of healthy (or maximum number of defective) insulator units allowed for each type of work and each task. Additional insulation is required for altitudes above 900 m (3000 ft)
- Assessment of replacement materials: is the replacement item electrically and mechanically equivalent to, or greater than, that of the item being replaced?
- Possibility of using overvoltage control methods such as blocked reclosing, pre-insertion resistors, PPAG, etc.
- Possibility recalculating the MAD based on overvoltage control method(s) selected
- Possibility of establishing equipotential zones or erecting barrier for ground crew in case of a flashover or sparkover, especially on structures where PPAGs are installed

REFERENCES

AASHTO (American Association of State Highway and Transportation Officials). 1987. *Manual for Bridge Maintenance*.

AASHTO (American Association of State Highway and Transportation Officials). 2002. *Standard Specifications for Highway Bridges*. 17th Edition.

Ackermann, R.H. and R. J. Morton. 1990. "In-House Development and Application of Live-Line Techniques by ESKOM." *ESMO 1990 Proceedings.* pp. 15-18.

ACI (American Concrete Institute). 2002. *Manual of Concrete Practice*.

ANSI C2, NESC. 2002. "National Electrical Safety Code C2." 2002 Edition.

Ascenção Gaspar, J.A. and V. Trullench Marzo. 2000. "The Live Work Activity in the Context of an Strategic Alliance Between EDP and IBERDROLA." *ICOLIM 2000 Proceedings.* pp. 85-91.

Burnham, J.T., J. Frank, and M.R. Eby. 1995. "High-Pressure Washing Tests on Polymer Insulators." *ESMO 1995 Proceedings.* pp. 101-106.

Campoy, P., A. Barrientos, P.J. Garcia, J. del Cerro, I. Aguirre, R.G. Fernández, and J.M. Muñoz. 2000. "An Autonomous Helicopter Guided by Computer Vision for Visual Inspection of Overhead Power Cable." *ICOLIM 2000 Proceedings.* pp. 755-763.

Carman, W.D and D.J. Woodhouse. 2000. "Probabilistic Assessment of Risk Associated with Mobile Telephone Antennas on HV Towers." *ESMO 2000 Proceedings.* pp. 154-158.

De Dona, G., M. de Nigris, and C. Valaguessa. 2002. "Insulating Ropes for Live Lines Works. Laboratory Tests for Assessing Their Condition and for Determining the Selection Criteria as a Function of the Application." *ICOLIM 2002 Proceedings.* pp. 151-156.

De Dona, G. and C. Valagussa. 2004. "Live Working: A Method of Calculation of Minimum Approach Distances. Comparison between the New and Old Edition of IEC 61472 Standard." *ICOLIM 2004 Proceedings.* pp. 445-450.

Denis, R.J. and R.W. Melzer. 1990. "Development of a Portable Ground Interrupter at Bonneville Power Administration." *ESMO 1990 Proceedings.* pp. 32-34.

Dubail, R. 2002. "TST et isolateurs composites (Testing of Composite Insulators)." *ICOLIM 2002 Proceedings.* pp. 121-124.

Engelmann, E. and J. Kindersberger. 2000. "Magnetic Field Stress During Live Working in High Voltage Transmission Lines." *ICOLIM 2000 Proceedings.* pp. 187-195.

EPRI. 1979. *Transmission Line Reference Book: Wind-Induced Conductor Motion*. EL-100-V4.

EPRI. 1994. *Electrical Performance of a Portable Protective Gap (PPG) in a Compact 550-kV Tower.* TR-103860.

EPRI. 1995a. *Assessment and Inspection Methods (AIM) Field Experiment. Volume 1: Results of Transmission Line Inspection Experiment*. TR-104449.

EPRI. 1995b. *Assessment and Inspection Methods (AIM) Field Experiment. Volume 2: Inspection Limitations, Enhancements, Technology Gaps and Recommendations*. TR-104449.

EPRI. 1997a. *Energized Work on Idaho Power Company's Existing 345 kV Structures.* TR-108968.

EPRI. 1997b. *Guide for the Application of Transmission Line Surge Arresters 42-230 kV.* 108913.

EPRI. 1997c. *Inspection and Detection Techniques: Defects in Porcelain Insulator Strings.* TR-109451-V2.

EPRI. 1998a. *Application Guide for Transmission Line Non-Ceramic Insulators.* TR-111566.

EPRI. 1998b. *Evaluation of the Performance of Non-Ceramic Insulators for Live Working Applications: Replacing Ceramic Insulators with NCI.*

EPRI. 1999. *Electric Field Modeling of NCI and Grading Ring Design and Application*. TR-113977.

EPRI. 2000a. *Assessment and Inspection Methods (AIM) Methodology. Inspection Methodologies for Overhead Transmission Lines.* TR-108212-CD.

EPRI. 2000b. *Electrical and Mechanical Performance of Ceramic Insulators.* 1000505.

EPRI. 2001. *Storing, Transporting and Installing Polymer Insulators*. 1006353. Training Video.

EPRI. 2002a. *Inspection, Assessment and End-of-Service Life Guidelines for Porcelain Cap and Pin Insulators*. 1001911.

EPRI. 2002b. *Live Working Application Guide.* 1001917.

EPRI. 2002c. *Live Working Field Guide.* 1006898.

EPRI 2002d. *Transmission Line Lightning Performance Prediction Software (TFlash) Version 4.0.22.* 1001738

EPRI. 2003a. *Managing Transmission Line Steel Structures, Version 1*. 1002005.

EPRI. 2003b. *Overhead Transmission Inspection and Assessment Guidelines—2003.* 1001760.

EPRI. 2004a. *Field Guide—Visual Inspection of NCI, Revision 1*. 1008739.

EPRI. 2004b. *Overhead Transmission Inspection and Assessment Guidelines—2004*. 1002007.

Eskom. 2004. *The Fundamentals and Practice of Overhead Line Maintenance*. Eskom Power Series Book. Vol. 2.

ESMOL Task Force. 2000. "Service Aged Conductive Clothing Measurements – Revision of IEEE Std. 1067-1996." *ESMO 2000 Proceedings.* pp. 182-185.

Fernández, L.J., J.M. Muñoz, and A. Andrés. 2000. "Electric Field Measurement on Composite Insulators Using Live Working Techniques." *ICOLIM 2000 Proceedings.* pp. 169-178.

Fernández, L.J., R.G. Fernández, M.A.F. Fernández, and C.R. Visser. 2002. "Working Method for Live Line Optic Fibre Stringing." *ICOLIM 2002 Proceedings.* pp. 145-149.

Forgie, G.C., L.H.E. Freeman, and B.A. Williams. 1990. "The Introduction of Bare Hand Live Line Techniques for Reinsulating of the New Zealand HVDC Inter Island Link." *ESMO 1990 Proceedings.* pp. 145-148.

Garcia, D.E., C. Kuchciak, R. Neveleff, and B. Alessi. 2002. "O.P.G.W. Type Fibre Cable Optic Stringing with Live Line." *ICOLIM 2002 Proceedings.* pp. 133-138.

Gela, G. 2002. "Step, Touch, and Transfer Voltages: A New Nemesis?" ICOLIM 2002 Proceedings. pp. 111-114.

Gela, G., A. Lux, H. Kientz, D.A. Gillies, J.D. Mitchell, and P.F. Lyons. 1996. "Application of Portable Protective Gaps for Live Work on Compact 550 kV Transmission Lines." *IEEE Transactions on Power Delivery.* Vol. 11, No. 3. July. pp. 1419-1429.

Gela, G. and M. Charest. 1998. "IEC Method of Calculation of Minimum Approach Distances for Live Working." IEEE Transactions paper presented at ICOLIM 1998, Lisboa, Spain. October.

Gela, G., H.J. Fox, and R. Ferraro. 1998. "Live Working on Vintage 138 kV Steel Lattice Structures." *ESMO 1998 Proceedings*. pp. 27-32.

Gela, G. and H. Kientz, 2000. "Further Comparison of the IEC and IEEE Methods of Calculation of Minimum Approach Distance." Paper presented at ICOLIM 2000. Madrid, Spain. May.

Gela, G., P.W. Hotte, and M. Charest. 2000. "IEC Method of Calculation of Minimum Approach Distances for Live Working." *IEEE Transactions on Power Delivery.* Vol. 15, No. 2. April. pp. 635-640.

Gela, G., R. Ferraro, and T. Verdecchio. 2002. "Portable Protective Air Gaps." *ICOLIM 2002 Proceedings*. Berlin, Germany. pp. 103-107.

Gorur, R.S., E.A. Cherney, and J.T. Burnham. 1999. *Outdoor Insulators*. Ravi S. Gorur, Inc.

Hubble Chance Company. *Tool Catalog*. T95.

IEC. 2004. Publication 61472. *Live Working—Minimum Approach Distances for A. C. Systems in the Voltage Range 72,5 kV to 800 kV – A Method of Calculation*, Second edition. 2004-07.

IEEE. 1995. Standard No. 4. "IEEE Standard Techniques for High-Voltage Testing."

IEEE. 1996. Standard No. 1307. "IEEE Trial Use Guide for Fall Protection for the Utility Industry."

IEEE. 2000. Standard 80. "Guide for Safety in AC Substation Grounding."

IEEE. 2003a. Standard No. 516. "IEEE Guide for Maintenance Methods on Energized Power Lines."

IEEE. 2003b. Standard 1048. "Guide for Protective Grounding of Power Lines."

Iwashita, T., S. Noda, K. Kawamura, and M. Nakashima. 2004. "A Study on the Development of and Operator-Assisted Distribution Work Robot." *ICOLIM 2004 Proceedings.* pp. 13-19.

Kishizima, I., K. Matsumoto, and Y. Watanabe. 1984. "New Facilities for Phase-to-Phase Switching Impulse Tests and Some Test Results." *IEEE Transactions on Power Apparatus and Systems.* Vol. PAS-103. No. 6. June. pp. 1211-1216.

Kleinhans, K. 2000. *The Effect of Inserting a Spark Gap in Series with a Polluted Insulator String.* Eskom internal report. TSI/EL/00/009.

Kolcio, N., K.J. Brown, J.J. Jalics, R.E. Johnson, and J. Amato. 2003. "RF Protection of Personnel Working in the Vicinity of Wireless Communications Antennas Attached to Electric Power Line Structures." *ESMO 2003 Proceedings.* pp. 118-127.

Kovacs, G. 2004. "Impact of the LW Activities on the Service Quality Indices." *ICOLIM 2004 Proceedings.* pp. 359-365.

Lessard, G. and Y. Rajotte. 2000. "Safety Issues Related to the Connection of MV and HV Grounding Systems Outside Substations." *ESMO 2000 Proceedings.* pp. 159-162.

Lombardet, D. and A. Kiener. 1995. "Valuation of Non Guaranteed Energy for the Electricité de France Transmission Network." *ESMO 1995 Proceedings.* pp. 47-54.

Lusk, G. E. and S.T. Mak. 1975. "EHV Wood Pole Fires: Their Cause and Potential Cures." IEEE, F 75 512-4.

Marshall, C.E. and H. H. Visser. 1998. "Live Work in ESKOM Transmission." *ESMO 1998 Proceedings.* pp. 11-18.

Martin, J.P. 1993. "Selection and Use of Fall Protection and Rescue Equipment for Work on Towers." *ESMO 1993 Proceedings.* pp. 117-126.

Martin, J.P. 2004. "Fall Protection and Rescue—Transmission." *ICOLIM 2004 Proceedings.* pp. 153-206.

Martin, R. 1989. "Insulation Design: Toughened Glass Strings with Contamination." Congreso de Generation Transmision de Energia Electrica. Venezuela. November.

McLean, J.A. 2000. "Experiences and Concerns about Live Maintenance by a Regulator for Health and Safety." *ICOLIM 2000 Proceedings.* pp. 203-206.

McLean, J. 2002. "Development of Criteria for Assessing the Competence of Workers." *ICOLIM 2002 Proceedings.* pp. 51-58.

Montambault, S. 2002. "HQ LineROVer: A Remotely Operated Vehicle for Live-Line Work on Overhead Transmission Lines." *ICOLIM 2002 Proceedings.* pp. 77-81.

Moreno Barraza, M., K. Naito, and Y. Mizuno. 2000. "Report of Joint Research on Power Frequency Electric and Magnetic Fields Measurements in Mexico." *ICOLIM 2000 Proceedings.* pp. 705-717.

Mougenet, J.–F. 2002. "From Risk analysis to Live Working Techniques." *ICOLIM 2002 Proceedings*. pp. 189–193

Naval Facilities Engineering Command. 1992. "Inspection, Maintenance, and Procurement Procedures for Wood Poles." NAVFAC MO-312.3.

NESC. 2002a. (National Electrical Safety Code). Rule 093.D. "Grounding Conductor and Means of Connection."

NESC. 2002b. (National Electrical Safety Code). Rule 094.A.3. "Grounding Electrodes."

NESC. 2002c. (National Electrical Safety Code). Rule 443.A.1.b. "Work on Energized Lines and Equipment."

Niamsorn, V., K. Petchsanthad, and G. Gela. 2004. "Live-Line Maintenance for EGAT's 500 kV Compact Line: Application of Portable Protective Air Gaps (PPAG)." *ICOLIM 2004 Proceedings.* pp. 213-219.

Ordon, T.J.F. and K.E. Lindsey. 1995. "Considerations in the Design of Three Phase Compact Transmission Lines." *ESMO 1995 Proceedings.* pp. 108-114.

OSHA Federal Register 29CFR. Part 1910.269. Electric Power Generation, Transmission, and Distribution.

OSHA Federal Register 29CFR. 1926.950 Subpart V. Power Transmission and Distribution.

Pierce, A. D. 2002. "Management of Live Working."

Portillo Belinchón, M., J.R. Solés, and J.J.G. Camino. 2000. "Contribution of Live Working Techniques to the Improvement of Environmental Conditions. Protection of Bird Wildlife." *ICOLIM 2000 Proceedings*. pp. 671-676.

Portillo Belinchón, M. and A. Pérez Herranz. 2002. "The Role of Live Working Procedures in the Improvement of Power Transmission System Availability in Spain." *ICOLIM 2002 Proceedings*. pp. 169-174.

Poulin, J. 2003. "Safety Aspects Relates to the Installation of Mobile Telephone Antennas on HV Towers." *ESMO 2000 Proceedings*. pp. 163-164.

Pretorius, P.H. 1993a. "Assessing the Significance of Annual Magnetic Field Dosages Received by Live Line Maintenance Personnel." *ESMO 1993 Proceedings.* pp. 97-104.

Pretorius, P.H. 1993b. "Assessment of the Historical Magnetic Field Dosages Received by ESKOM's Live Line Maintenance Personnel." *ESMO 1993 Proceedings*. pp. 105-116.

Ross, N. 2000. "Rescue Practice Without the Risk." *ESMO 2000 Proceedings*. pp. 218-224.

San Román Salcines, L.F. 2000. A Project for Eliminating Accidents and Preventing Incidents in High Voltage Live Working Activities." *ICOLIM 2000 Proceedings*. pp. 25-36.

Sediver Glass Insulator. 1997. Catalog.

Smith, A.M. 1993. *Reliability-Centered Maintenance*. McGraw-Hill.

Thorne R. 2000. "Life Safety Rope Strategies for Transmission Structures." *ESMO 2000 Proceedings.* pp. 211-217.

Thorne, R.B. 2003. "Rope Access for Transmission Line Maintenance and Construction (TLM&C) Trends in Safety Managing Power Delivery Systems." *ESMO 2003 Proceedings.* pp. 138-148.

Thrash, R., G. Hudson, D. Cooper, and G. Sanders, Editors. 1994. *Overhead Conductor Manual.* First Edition. Southwire Company.

Tomaseski, J.R. 1998. "Deregulation of the Electric Power Industry." *ESMO 1998 Proceedings*. pp. 79-88.

Udod, E., V. Molchanov, V. Taloverya, N. Ivanov, V. Dyakov, A. Rubanenko, and G. Gela. 1998. "Automated Apparatus for Live Work on Overhead Transmission Lines." *ESMO 1998 Proceedings*. pp. 19-26.

Udod, E.I., V.L. Taloverya, and L.P. Nijnik. 1995. "Shielding of Worker's from Electric and Magnetic Fields During Live Line Work in Ukraine." *ESMO 1995 Proceedings.* pp. 163-170.

Van Waes, J.B.M., M.J.M. van Riet, A.P.J. van Deursen, and F. Provost. 2000. "Safety Aspects of GSM Systems on High Voltage Towers." *ESMO 2000 Proceedings.* pp. 165-168.

Verdecchio, T., J. Tomasesk, G. Gela, K. Buchholz, I. Buonincontri, J. Christensen, D. Dodds, E. Hunt, C. Kelly, N. Kolcio, and S. Thiese. 2004. "Development of an Industry Guide for Live Work on AC Transmission Lines." ICOLIM 2004 Proceedings. p. 291.

Vincent, C., M. Bourdages, D.H. Nguyen, R. Boissonneault, S. Lapierre, and M. Hamel. 2002. "Properties of Conductive Material (Fabric) under AC and DC Conditions." *ICOLIM 2002 Proceedings*. pp. 157-162.

Wells, R.H. 1998. "Effectively Managing Tree Growth and Pruning Cycles with Tree-Growth Regulators." *ESMO 1998 Proceedings*. pp. 210-216.

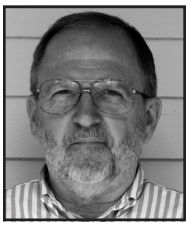
Zarco Periñán, P. and M. Moreno Amescua. 2002. "Comparative Study of the Costs of Live Working Activities." *ICOLIM 2002 Proceedings*. pp. 165-168.

CHAPTER 14

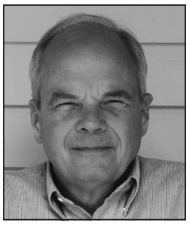
Voltage Upgrading of Existing Transmission Lines

Dale A. Douglass
James Stewart

This chapter concerns the process of increasing the operating voltage of an existing transmission line—voltage upgrading. It outlines in detail the successive stages of analysis and evaluation that may be required prior to the upgrading—including a system-level study of power flow need and voltage strategy, mechanical and electrical feasibility assessments, an evaluation of present line condition, and a detailed engineering design. The chapter also includes four brief examples of utility voltage upgrades.



Dr. Dale A. Douglass is a Principal Engineer of Power Delivery Consultants, Inc. based in Niskayuna, New York. He has more than 30 years of experience in transmission line engineering and conductor design, having worked with Power Technologies, Inc., Kaiser Aluminum, and Bell Laboratories. He is presently the Vice Chairman of IEEE's Towers, Poles, and Conductors Subcommittee and the convener of CIGRE Working Group B2-12 on Electrical Aspects of Transmission Lines. He has been involved in studies of overhead line sag-tension, high temperature operation, and both current and voltage upgrading of existing lines. In 1996, he was elected a Fellow of the Institute of Electrical and Electronic Engineers for "contributions to understanding the characteristics and applications of overhead power transmission conductors."



Dr. James Stewart is an independent consultant based in Scotia, New York. He has over 30 years of experience in power systems and transmission lines, having worked for Niagara Mohawk Power Corporation and Power Technologies, Inc. He has been involved in experimental and analytical research of compact overhead transmission lines, and is a co-author of the EPRI *Transmission Line Reference Book: 115-138 kV Compact Line Design* and subsequent EPRI reports on line compaction and DOE reports on high phase order power transmission. This compact line research was subsequently applied to voltage upgrading of existing transmission lines. Dr. Stewart participated in several of these upgrading studies. He was elected as a Fellow of the Institute of Electrical and Electronics Engineers in 1987 for "advances in transmission line theory and its reduction to practice through prototype demonstration." He is presently Chairman of the Transmission and Distribution Committee of the IEEE Power Engineering Society.

14.1 INTRODUCTION

This chapter concerns the process of increasing the operating voltage of an existing transmission line ("voltage upgrading"). Voltage upgrading ranges from the occasional case where it is possible to increase operating voltage with no modifications to the line itself, to cases where voltage increase is possible without replacement or major modification of existing structures, to virtual reconstruction of the line. Virtual reconstruction is the case where, for example, the tower below the waist and foundations are retained and the entire tower superstructure is redesigned and constructed with new insulation and conductors.

This chapter presents a summary of the items that need to be considered in any voltage upgrading study. It begins in Section 14.2 with a description of the factors that make up a system-level study of power flow need and voltage strategy—including consideration of reactance limits, voltage drop, and thermal uprating. Prior to any detailed engineering analysis, a feasibility study is conducted. Sections 14.3 and 14.4 describe the requirements for assessments of electrical and mechanical feasibility. For those lines that appear capable of operation at the proposed higher voltage level, but that require certain physical modifications or acceptance of reduced electrical performance criteria, a detailed evaluation of line condition and re-design may be required. Section 14.5 outlines items of concern in an evaluation of present line condition. Section 14.6 describes the later stage of voltage upgrading—a detailed engineering design. The chapter concludes in Section 14.7 with brief profiles of four examples of actual voltage upgrades.

It should be noted, however, that the emphasis in this chapter is on those situations where voltage upgrading is contemplated without virtually reconstructing the line. If the tops of the structures are removed and replaced with entirely new material, the design process is essentially that of a new line, albeit possibly a compacted line. (See Figure 13.3-8 and Example 4 in Section 14.7.) When the existing line components are retained to the maximum extent feasible, the design process contains more of the nature of re-engineering and reverse-engineering an existing facility. Aspects such as consideration of design criteria and margins come more heavily into play than they do with new designs. For the detailed technical aspects, references are made as necessary to the detailed technology developed in other chapters of this Reference Book.

Methods for increasing the maximum allowable line current ("thermal uprating") are described briefly and compared to voltage upgrading methods. Thermal uprating of existing transmission lines is discussed in considerable detail in other EPRI publications (EPRI 2003) and in the technical literature.

Each voltage upgrading situation is unique, requiring its own individual engineering study in part because of the wide variety of existing line designs and possibilities for modification. Differences in existing line design and condition, as well as differences in system needs, give each study its own special characteristics. Solutions vary depending on local conditions. This chapter lays out a framework for conducting a voltage upgrading study based on the technical data provided in the remainder of the book. Not every upgrading study will require every element presented herein. Nor will every study necessarily follow exactly the same sequence. However, adherence to sound engineering principles will go a long way toward an ultimately successful outcome.

Until the 1980s, transmission research was directed to the development of increasing transmission voltages. As presented in the earlier chapters of this Reference Book, much of this research focused on electrical insulation and corona and field effects issues. As a consequence of the increased technical understanding provided by the results of this research, the amount of extra margin designed into the lines diminished with increasing line voltage. Figure 14.1-1 (EPRI 1983) illustrates the trend by plotting the ratio of phase spacing to required power frequency flashover spacing as a function of transmission-line voltage class for typical historically conventionally designed lines. At 115 kV, the ratio exceeded 10 to 1. By the time 765 kV came along, the ratio was down to approximately 6 to 1.

Note that Figure 14.1-1 is intended only to illustrate the general trend with respect to voltage classes. Within each voltage class, there has been significant variation in phase spacing in traditional designs as a result of such factors as design span length, structure type (wood vs. steel), conductor sag, and switching surge overvoltage levels. However,

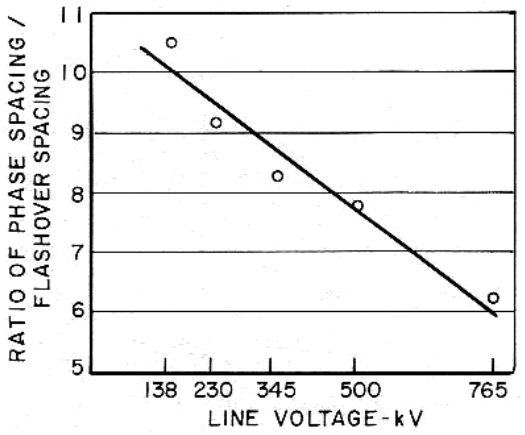


Figure 14.1-1 Phase spacing ratio vs. line voltage (EPRI 1983).

the general trend is valid, indicating greater possible margin for voltage upgrades for the lower voltage class lines.

Analysis of Figure 14.1-1 suggests the following possibilities:

1. It may be possible to design lower voltage transmission lines with tighter spacings than had been done previously. This was the origin of the concept of "compact high voltage transmission lines," as developed in the EPRI *Transmission Line Reference Book 115-138 kV Compact Line Design* (EPRI 1983).
2. There may be sufficient margin in existing lines, especially at lower voltages such as 115-138 kV, for increasing the line operating voltage (voltage upgrading) with relatively minimal modifications to the line. Higher voltage lines (e.g., 345 or 500 kV) may have less margin for exploitation at higher voltages.

By exploiting these design margins, one may be able to increase the power transfer capability of existing lines by increasing line current and/or line voltage, thus avoiding or delaying construction of new lines. Line modifications that yield increased current flow limits are referred to in this chapter as *thermal uprating,* and modifications that allow operation at a higher voltage are denoted as *voltage upgrading*.

The motivation to increase voltage on a transmission line should be driven by system considerations. Increasing the capacity of a particular transmission line may or may not yield a sufficient increase in overall power transfer capability. It is necessary to analyze the power flow problems to see if a voltage upgrade would provide an appropriate answer. Power flow limitations may be a result of thermal limitations of the line conductors or substation apparatus, or may be due to other factors such as voltage drop or stability problems. If voltage or stability concerns dominate, increasing the current-handling capability of a line is probably not the answer. A voltage increase may provide the needed improvement. The presence of higher voltages in nearby substations and higher voltage levels system wide are factors in making the decision to upgrade a specific transmission line. Overall system topology plays a part (i.e., whether the resulting flow patterns are worth the effort). The nature of the system problem driving the proposed upgrading (e.g., whether the increased power flow is required for contingency or continuous operation) also has an influence on the decision. Predictions of future load growth can affect the planned development of the system and future voltage classes.

Voltage upgrading studies emphasize three broad areas: insulation coordination; compact line design; and corona and field effects. Improved knowledge in each of these three areas has allowed engineers to re-evaluate existing line designs to better determine the existing design margins that can be utilized to operate at higher voltage.

A possibly crucial step in voltage upgrading is careful consideration of relevant criteria used for new line designs—criteria that might be relaxed, if necessary, to make a voltage upgrade possible. For example, a slightly higher switching surge probability of flashover (PFO) than would be applied to a new line, reduced insulator leakage distance, or higher conductor surface electric field may give adequate performance in the specific application under consideration. In contrast to new line design, in voltage upgrading, the operating history of the existing line is known. Laboratory contamination tests on insulators removed from the line might be used to justify a shorter insulator string at the increased voltage than would be used on a new line.

Once the rationale for voltage upgrading has been established, several factors must be addressed. These factors should be handled at two levels: a preliminary feasibility analysis and a detailed study. The preliminary study is valuable to scope the detailed study and to develop a degree of confidence in the project's ultimate success. Before a voltage upgrade is undertaken, the insulating, conducting, and structural components must be known, the design assumptions understood (especially the design margins), and the physical condition of the line established. Included in voltage upgrading studies are:

1. Analysis of the original design of the line, including design assumptions and criteria.
2. Electrical analysis of the line at existing and proposed voltages.
3. Examination of the physical condition of the line.
4. Evaluation of structure mechanical loading if conductor changes are required.

Assessment of economic trade-offs is also an essential part of the study, especially if conversion to more than one standard voltage is feasible. Consideration of criteria must be viewed in the overall context of the economic balance between risks, costs and benefits for new line construction versus the risks, and costs and benefits related to and obtained by upgrading the voltage of the existing transmission line. There is an element of the business rationale and business goals of the company in the overall voltage upgrading process. The following discussion focuses on the technical aspects of selection of design criteria, recognizing that the overall system factors of risks and benefits can play a significant role in the final choice of the project.

As a consequence of performing the detailed engineering study, some lines have required different levels of modification for upgrading:

1. Some lines have been successfully increased to the next voltage level without any modification.
2. Some lines have required additional insulation, perhaps adding a small number of units to insulator strings or changing to a different kind of insulator.
3. Some lines have been upgraded by addition of a second conductor per phase to make two conductor bundles. This usually requires appropriate reinforcement of support structures.
4. Occasionally double-circuit lines have been converted to single-circuit lines at a higher voltage by using the six-phase conductors as two three-conductor bundles for the new circuit.
5. Some lines have been found where the existing designs are sufficiently marginal that voltage upgrading is not a reasonable option.
6. Alternatives to voltage upgrading may also exist in a particular application, such as conversion to HVDC, addition of FACTS controllers, use of series or shunt compensation, or possibly conversion to six-phase lines. These options are more related to system studies than to voltage upgrading of a specific line as discussed in this chapter. While not strictly a critical part of a voltage upgrading effort, these studies might be performed to justify the upgrading.

The present chapter serves as a guide for the use of the technical information presented in this Reference Book for the electrical portion of a transmission-line voltage upgrading study. Chapter 3 of this book is an overview of insulation design of new lines and can profitably be consulted in conjunction with this chapter on voltage upgrading of existing lines. The fundamental difference between insulation design of a new transmission line and a voltage upgrading study is that the new design starts with a clean sheet of paper while an upgrading study starts with the existing line. The difference is partially philosophical in that a new line can be designed to whatever criteria the designer specifies. An upgrading is re-engineering an existing line and may involve different basic criteria from those used for a new line. While not without some risk, it is often found possible to operate closer to fundamental physical limits with an upgrading than would normally be tolerated on a new line. The amount of risk may be bounded or lessened because of the extensive operating experience with the existing line and the possibility of using the existing line in some sense as a test laboratory for the upgraded voltage.

Other EPRI references should be consulted in conjunction with this volume with regard to voltage upgrading, including the *Increased Power Flow Guidebook* (EPRI 2003), *Transmission Line Reference Book: 115-138 kV Compact Line Design* (EPRI 1983), and *Transmission Line Reference Book: Wind-Induced Conductor Motion* (EPRI 1979). The compact line and wind-induced motion books present considerations related to conductor motion as a result of wind, ice, and magnetic forces resulting from passage of through fault currents. These mechanical motions may become limiting factors in some cases as the clearances required to prevent flashover increase with increasing line voltage.

14.2 SYSTEM LEVEL STUDY OF POWER FLOW NEED AND VOLTAGE STRATEGY

The degree to which the maximum power flow can be increased for an existing overhead line is dependent on its length, the original design margins, environmental concerns, and many other issues. Because power flow on the transmission system is a function of the overall system topology (transmission lines, transformers, generation, series and shunt compensation, and load), system considerations can also limit the maximum power flow on a specific transmission line. Transmission-line ratings are frequently developed on a system basis rather than on an individual line basis. The overall limit may be between operating areas irrespective of ownership or individual lines, and may change during a day based on system condition. System limits can result from factors such as voltage drop, possibility of voltage collapse, and system stability, both steady state and transient.

When a transmission-line voltage upgrade project is being considered, the specific requirements may initially be very well defined, or may be only known in a general sort of way. To make intelligent choices, the following types of questions must be addressed:

1. What presently limits the flow on the line? Is it thermal rating, voltage drop, system stability, or some other concern?
2. What flows are anticipated in the future?
3. How much confidence can be placed in the load projections?
4. Are the anticipated flows baseload, peaking, or emergencies?
5. What other higher voltage levels exist in the area to which the line might be converted?

Because the motivation for voltage upgrading of a transmission line is the need to relieve system constraints, it is necessary to perform system studies to completely understand the issues and possible avenues of relief. It is necessary to clearly define the problem that is proposed to be addressed by upgrading the voltage of an existing transmission line. For example, the problem to be solved may be the ability to handle "normal" loading—that is, loading with all transmission facilities in service under system peak conditions. Another possibility is that the problem

may occur under short- or long-term emergency conditions, perhaps when a line or other facility is out of service for some reason or other. The best solution to the problem may be different depending on whether the condition of concern is under normal or emergency loading conditions.

In selecting the choice of a solution to a system problem, it is necessary to understand the fundamental factors limiting power flow on a transmission line. These factors include transmission-line conductor thermal ratings, voltage control, or transient or dynamic stability concerns. While thermal limitations can be addressed through line uprating, perhaps by reconductoring, voltage and stability issues are better handled through voltage upgrading. Thus, a thorough understanding of the nature of the problem is important to developing the solution, whether it should be uprating or upgrading of the existing line(s) or construction of new line(s). An additional factor to be considered is projected load growth rate. When either line uprating or voltage upgrading of the line voltage may solve the immediate problem, the choice between them may hinge on future load growth. Slow load growth might favor uprating current, while larger growth might favor upgrading voltage. Of course, voltage upgrading always yields a large increase in the MVA thermal rating of the existing line, but it may also result in an increase in the maximum allowable line current if reconductoring or adding an additional conductor per phase is necessary for acceptable corona performance at the higher operating voltage.

System studies include load flow and stability analyses to assess the effect of the voltage upgrade on system real and reactive power flow distribution, voltage profiles, and stability margins. Normal and contingency conditions must be modeled, especially if the limiting condition is contingency loading. System fault studies may also be required to assess the impact on substation and circuit breaker fault duties.

A fundamental consideration in system studies is the present topology of the system, especially with respect to location of facilities at different voltage levels. Voltage levels in use both in the local area of the line under consideration and in the overall system should be considered. Choice of voltage is tied with projected development of the system as a whole, and how the upgraded line fits in with planned future development. While it is not impossible to add a new voltage to an existing system, it is preferable to use an existing voltage if possible. Use of a new, or even a nonstandard voltage, should not be ruled out at the start, as that may prove to be the technically and economically advantageous solution. An autotransformer at each end of the line and switched with the line could conceivably allow the line to operate at the maximum possible voltage for the maximum possible loading capability, even if it is not standard. When this is considered, a load flow analysis is required to ensure that the reactance of the autotransformers does not reduce the loading on the upgraded line below that expected.

14.2.1 Reactance Limits, Stability, and Surge Impedance Loading

The division of power flow among the different transmission lines in a power system is primarily a function of the relative per unit line series inductive reactances. See Section 2.3 for a discussion of the equivalent circuit model of an individual transmission line. For a set of transmission lines in parallel, the total operating power limit is generally less than the sum of the thermal limits of the lines because the relative power flows relate to reactances rather than thermal capacity. While series reactance plays a major role, shunt admittance and their combination, surge impedance, are also relevant to system transfer limits. System planners have long recognized this relationship, particularly where there are prospects of changing the line impedance, either by adding equipment (e.g., series capacitors), or by modifying the line itself (e.g., reconductoring, voltage upgrading, etc.).

Transmission-line series inductive reactance is determined by conductor size, phase spacing, number of conductors, relative phasing (double-circuit lines) and line configuration. (See the discussion of transmission-line reactance in Section 2.3.) In transmission lines, the series reactance is significantly larger than the series resistance. *Therefore simple reconductoring of a transmission line (which has a minimal effect on series reactance) results in only minor changes in system power flows.*

Per unit reactance is a function of the square of the line voltage. Doubling the line voltage reduces the per unit reactance to one-quarter of what it was previously. This reduction in per unit reactance stiffens the system, alleviating voltage and stability problems. Per unit reactance reduction is one of the factors driving the use of increased transmission voltages.

A basic understanding of power flow and the role played by the line reactance is given by Equation 14.2-1. Equation 14.2-1 gives power flow on a transmission line, neglecting line resistance, and is derived from a simple circuit consisting of sending and receiving end voltage sources connected by a series reactance.

$$P = \frac{V_1 \bullet V_2 \bullet \sin(\delta)}{X} \qquad 14.2\text{-}1$$

Where:

P = Real power transfer on the transmission line in megawatts.

V_1 = Magnitude of sending end bus voltage in kilovolts.

V_2 = Magnitude of receiving end bus voltage in kilovolts.
X = Line series inductive reactance between V_1 and V_2 in ohms.
δ = Phase angle difference between V_1 and V_2 in degrees.

Alternatively, P, V_1, V_2, X, and δ can be expressed in per unit on a consistent set of bases. Either way, increasing the voltage causes an increase in power flow for the same phase angle difference between the ends of the line.

Increasing voltage magnitude for the same phase angle difference between ends increases the power flow. By increasing the voltages V_1 and V_2 together, the power transmitted increases by the square of the voltage for the same phase angle. This is a powerful motivation for use of higher transmission voltages and voltage upgrading. Power flow increases for the same end voltage magnitudes are accommodated by an increase in the phase angle difference between the voltages at the two line ends, possibly reducing the stability margin of the system.

The first observation from Equation 14.2-1 is that it imposes a fundamental limit on the amount of power that can be carried by a transmission line corresponding to a phase difference between line ends of 90º. Further increases in angle result in decreases in power flow. This is an unstable situation that can be realized in practice in two ways. If the steady-state power flow were to slowly increase to the point that the angle reached 90º, an attempt to further increase power flow would actually decrease the power flow. An increase in the power angle δ, when δ is in the range from 90 to 180º, results in a decrease in sin (δ) and a consequent decrease in power flow. The condition of trying to increase the flow on the line actually results in a decreased flow and system instability. *Thus any transmission line has a maximum power flow capability irrespective of the thermal rating of the line.*

Secondly, a system disturbance (for example, tripping of a line) causes a redistribution of power flow among the remaining lines, and consequent changes in the bus voltage angles. It is insufficient that the new angle differences on all the lines are less than 90º, because the angle differences must remain lower than 90º during all the transient system swinging from the time of the disturbance until the system settles in its new operating state. If a line were to experience its angle difference momentarily passing 90º, it would try to accommodate the power requirement by opening up the angle beyond 90º, decreasing the power flow. This is an unstable situation, and would cause the line to pass through the electrical point where its relay protection would sense a fault (even though none exists on the line), and result in a line trip and probable system separation. This is a brief statement of the transient stability problem.

Surge impedance loading (SIL, defined in Equation 14.2-2) provides a useful rule-of-thumb measure of transmission-line loading limitations as a result of the effects of reactance, including voltage drop and stability.

$$SIL = \frac{V^2}{Z_S} \qquad 14.2\text{-}2$$

Where V is the line voltage and Z_S is the surge impedance of the transmission line given by:

$$Z_S = \sqrt{\frac{L}{C}} \qquad 14.2\text{-}3$$

Surge impedance Z_S is a resistance in ohms. L and C in Equation 14.2-3 are positive sequence inductance and capacitance in henries per mile and farads per mile, respectively. Surge impedance loading is that loading on a three-phase power transmission line that it would have if it were loaded by a Y-connected set of resistances of Z_S ohms per phase. This is the same physical condition as a radio frequency transmission line impedance matched to its termination (72 ohm coaxial cable terminated in 72 ohms in television cable). In electromagnetic theory it corresponds to a pure TEM wave. The reactive power (vars) generated in the line capacitance is exactly canceled by the vars absorbed in the line inductance in a power transmission line at surge impedance loading (neglecting line resistance and real power losses). Surge impedance loading thus is a loading value based on physical principles related to the line design itself.

Surge impedance loading is a handy tool for estimating the relative loading capabilities of lines of different voltages, constructions, and lengths from a system standpoint (St. Clair 1953). SIL is oversimplified for use in specifying actual line ratings on an operating system. However, it is a useful guide both for assessing actual loading limits and for understanding the different factors that limit line loading. Figure 14.2-1 gives a curve of line loadability in per unit of SIL as a function of line length for heavy loading conditions (Federal Power Commission 1964). Slightly different versions of Figure 14.2-1 have been published, but they are all very similar (Gutman 1988). The fundamental observation from Figure 14.2-1 is that transmission-line loadability decreases as length of the line increases. Three different regions come into play in derivation of Figure 14.2-1. Short lines tend to be thermally limited, irrespective of system conditions. As line length increases, voltage drop considerations frequently come into play. At longer line lengths, stability factors may dominate. Short lines are

often loaded at 2 or 2.5 times SIL and thus need reactive power (var) support to maintain the voltage. Long lines may be limited to 1.0 times SIL or less.

An important observation from Equation 14.2-2 is that surge impedance loading is a function of the square of line voltage. This has been a driving force for increased transmission voltages over the years, especially for longer lines. For short, thermally limited lines, doubling the line voltage doubles the thermal capacity of the line, a considerable improvement that may forestall construction of an additional line. Doubling the line voltage for longer lines may increase the power-handling capacity of the line by the ratio of the line voltages squared. However, it is necessary to change the substation facilities at all taps along the upgraded line, which may be economically preferable to construction of an additional line or lines to gain the needed added capacity.

14.2.2 Voltage Drop

Voltage control on the power system is of major concern as system loadings increase. The longer the line, generally the lower the power flow required to reach a voltage drop limit. Increasing the voltage of a transmission line reduces the percent voltage drop along the line and increases the power flow for the same line current. Increasing the line voltage thus both increases the loadability of the line and improves voltage control. This effect is most obvious for a radial system. For a tightly interconnected mesh system, voltage control issues may be system related, and require modifications to more than a single transmission line. Methods to improve voltage control in addition to upgrading voltage of existing transmission lines take a variety of forms:

1. In some cases, bundled conductors have been used for short, lower voltage lines to reduce series reactance where the use of bundled conductors is required neither for thermal or corona reasons.
2. Supply of vars at various points on the system can be used to control voltage. The supply can be fixed, switched, or adjustable. In former years, synchronous condensers were used to supply vars in a continuously adjustable basis. Capacitor banks are commonly used, and may be switched on or off depending on the local voltage. Static var compensators (SVCs) are also used to control voltage on the bulk power system.
3. Shunt reactors may be used for long EHV lines where the var supply from the line capacitance is greater than the system can absorb.

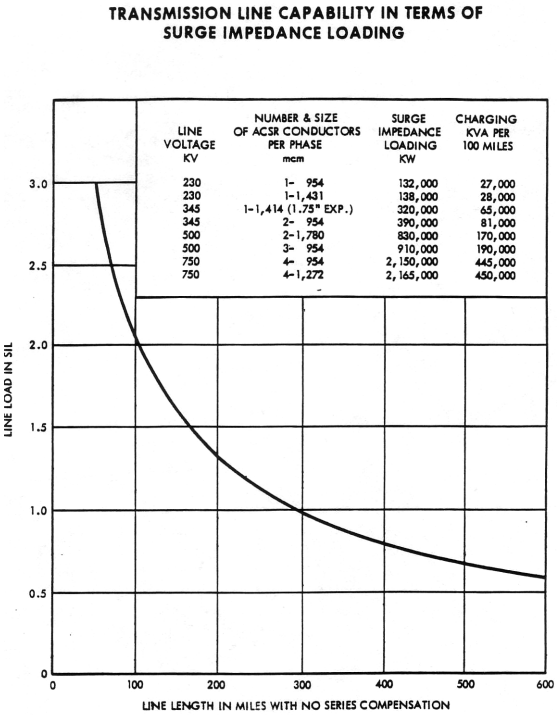


Figure 14.2-1 Line loadability in terms of surge impedance loading.

Because voltage drop is primarily a function of line reactance rather than resistance, simple reconductoring does very little to decrease the voltage drop per unit length. Reconductoring an existing 230-kV line by replacing the original 636 kcmil Hawk ACSR with a 954 kcmil Rail ACSR only increases the power flow corresponding to the voltage drop limit by 5%. Adding a second conductor per phase, to form two-conductor bundles, results in a more significant reduction in series reactance, and a greater improvement in voltage drop power limit.

While excessive voltage drop has long been known as a limitation on power transmission, attention has also been focused on voltage collapse (Koessler and Feltes 1993), which is a system instability that can occur under heavy loading conditions. Voltage collapse can occur for several reasons on a heavily loaded system where there is insufficient var support. Voltage collapse has occurred under peak load conditions. It has also occurred when var demands are unusually great or var supply is compromised. An example of the combination of increased var demands and loss of var support is seen in the geomagnetic storm of March 13, 1989, with its resulting voltage collapse and blackout. While the March 1989 storm increased attention to system problems that result from solar activity (Boteler 1994), it also highlighted possible problems of voltage collapse in general. Utilities in areas subject to geomagnetic disturbances monitor solar activity (Lesher et al. 1994) and can re-dispatch generation to reduce loading on affected facilities during times of high geomagnetic activity to deal with the var requirements.

This discussion of voltage control illustrates the variety of potential solutions to a specific system problem. Series and shunt reactive compensation can increase loadability of existing lines and improve var flow and voltage control. Other approaches include:

- Conversion of a line to dc to eliminate the effect of line reactance limitations, especially for long lines.
- Use of flexible ac transmission system (FACTS) devices to control flows and force them along desired paths.

More drastic approaches are sometimes considered, such as increased load shedding to alleviate contingency conditions and allow heavier normal line loading. Consideration of all these approaches is part of the system analysis that may be undertaken. They also form part of the economic analysis and justification behind line voltage upgrading.

14.2.3 Thermal Uprating

In certain cases, particularly with relatively short lines, the post-contingency overloads identified through power system analysis may be resolved by increasing the thermal capacity of an existing line by as little as 5%. A number of relatively inexpensive methods are available to allow such modest increases in capacity as described in the *Increased Power Flow Guidebook* (EPRI 2003) and in many other technical publications.

In comparison to the process of voltage upgrading, increasing the thermal capacity of an existing transmission line generally requires less capital investment, less outage time for construction, and limited replacement of substation equipment. In addition, the wide range of thermal uprating methods leads to a correspondingly wide range of changes in capacity and capital investment. Of course, increasing the thermal capacity of an existing line will do nothing to relieve power flow constraints, which involve either excessive electrical phase shift or voltage magnitude drop.

To illustrate the differences between thermal and voltage upgrading, consider the range of possible thermal uprating options for the 115-kV conventional single-circuit, wood pole H-Frame line shown in Figure 14.2-2. In this example, assume that the phase conductor is 26/7 795 kcmil (400 mm^2) "Drake" ACSR, that the present maximum allowable conductor temperature is 75°C, and that the line reaches the clearance limit at a conductor temperature of 100°C. Under conventional line rating assumptions of 35°C air temperature, full sun, and a 2 ft/s (0.61 m/s) crosswind, the thermal rating is 800 amperes/159 MVA. Span length is 600 ft (180 m).

- **Option 1.** Increase the maximum operating temperature of the Drake ACSR to 90°C. The line clearance limits are still met, the annealing of the aluminum strands will be negligible, and the thermal rating of the line will increase to 950 A/ 189 MVA. The cost of this action is limited to the engineering review, and there is no need for a service outage.
- **Option 2.** Install tension or sag monitors and begin rating the line dynamically. On a cool windy day when the air temperature is 20°C, the wind speed is 4 ft/s, and there is no sun, the rating will be 1200 A/239 MVA. On a hot windless day, the rating may be even lower than 800 A/ 159 MVA. The line rating will vary in a fashion that is partially predictable and partially random. The cost of the monitoring and calculating system is on the order of 10% of the cost of a new line, and no service outage is required.
- **Option 3.** Increase the maximum operating temperature of the line to 125°C by raising the crossarm attachment height and, where necessary, by installing so-called "floating dead-ends" to reduce the vertical dimension of the insulator assembly. The rating of the line is then 1220 A/243 MVA. The cost of these modifications is in the range of 20% of the cost of a new line, and only limited service outages are needed.
- **Option 4.** Replace the Drake ACSR conductor with a high-temperature low-sag conductor such as ACSS or ACSS/TW. ACSS conductors can be operated at temperatures as high as 200°C continuous if line clearance allows. In this line, with 600 ft (180 m) spans, without any structure or insulator modifications, a Drake ACSS or Suwannee ACSS/TW, both having the same diameter as Drake ACSR, might reach the clearance limiting sag at a conductor temperature of approximately 175°C. At 175°C, the line rating increases to 1485 A/296 MVA and

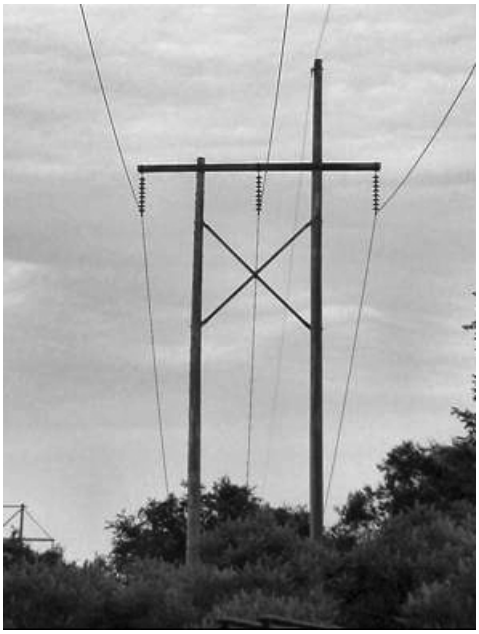


Figure 14.2-2 115-kV single-circuit wood pole candidate for thermal uprating.

1630 amps/325 MVA, respectively. Because of the greater cross-sectional area of aluminum, Suwannee ACSS/TW conductor yields the higher rating because of its 20% lower resistance. The cost of reconductoring the line may be as much as 50% of the cost of a new line, and service outages may be extended.

These options are compared in Table 14.2-1, where the voltage upgrade option is also listed.

Comments concerning these various methods of increasing the power flow limit on the example 115-kV line:

- None of the thermal uprating methods cause an increase in electrical losses unless the normal load on the line increases. Reconductoring with ACSS/TW and voltage upgrading from 115 to 230 kV actually reduces electrical losses if the normal electrical load remains the same (Suwannee ACSS/TW has about 20% less resistance than Drake ACSR), and operation of the line at twice the original voltage yields half the current flow and a 75% reduction in losses.
- The cost and service outage associated with voltage upgrading have much to do with the associated substation equipment. If the line is short, and a new substation bus at 230 kV must be built, the cost of the substation modifications could be several times the cost of the line modifications. The substation costs associated with large increases in line thermal capacity must also be considered important.
- Reconductoring the line, either with ACSS or with a larger standard conductor as part of a voltage upgrade, is likely to yield reduced maintenance costs and improved physical reliability. It is highly unlikely that increasing the maximum allowable temperature of a 50-year-old line from 75 to 125°C will result in a line that is as reliable as one that has been reconductored with a new conductor of any sort.

Table 14.2-1 Comparison of Thermal Uprating Options for 115-kV Example

Line Uprating Method	Cost Range (% of new line)	Duration of Outage Required	Power Flow Capacity – MVA (% increase)
Original			159
Higher Conductor Temp	0	None	189 (25%)
Dynamic Rating	10	Less than a day	159-239 (0-50%)
Raise Structures	20	Days or weeks	239 (50%)
Reconductor with ACSS	30–50	Weeks or months	296 (85%)
Reconductor with ACSS/TW	30–50	Weeks or months	325 (100%)
Voltage upgrade to 230 kV	20–80	None to Months	318 (100%)

14.3 ASSESSING ELECTRICAL FEASIBILITY

An engineering investigation to upgrade the voltage for an existing transmission line is generally conducted in two steps: a feasibility study and a subsequent detailed analysis. It is the purpose of the feasibility analysis to determine, in a general way, if upgrading might be possible. If voltage upgrading is feasible, it is then possible to proceed to a more detailed analysis in order to develop the upgraded line's design parameters. Because each voltage upgrading is unique, not all feasibility studies include the same elements or be conducted to the same degree of detail.

This section describes the many aspects of a voltage upgrade feasibility analysis. As an example, the section will consider the feasibility analysis that led to the successful upgrading, from 115 to 230 kV, of the double-circuit, steel lattice structure transmission line, of the type shown in Figure 14.3-1. The details of this voltage upgrade are described in Example 1 in Section 14.7. This example is chosen because double-circuit steel lattice structures are in common use around the world, so this case is an example of a voltage upgrading that might be attempted in many locations. Also, voltages in the 110/138 kV range are in common use around the world, and upgrading to voltages in the range of 220/275 kV would be of interest in many transmission systems. The voltage upgrade feasibility analysis described in this section might apply to any existing line where the major line components are in reasonably good physical condition.



Figure 14.3-1 115-kV double-circuit line.

14.3.1 Data Gathering

The first step in the feasibility analysis is to carefully gather data on the existing line. The amount of original line design information available may vary with each individual line, depending on its age and history of ownership. The line may have been designed to standard system specifications, in which case standard system designs can be initially assumed and later verified in the physical inspection described in Section 14.5. Required data includes:

- Plan/profile drawings
- Electrical and mechanical design criteria
- Structure drawings including dimensions
- Conductor type and size
- Shield wire type and size
- Insulator type and number
- Insulator bonding
- Hardware types
- Structure grounding configuration
- Footing resistance
- Operating history of the line (outage rate, repairs made, design changes introduced)
- Maintenance and live working considerations
- Most recent condition survey including clearance measurements

14.3.2 Review of Line Design

Two factors to keep in mind, during both the feasibility and any following detailed engineering studies, are the re-evaluation of the original design in the light of any improved technical data and calculation methods, and the appropriateness of the design criteria in light of the intended use of the upgraded line (e.g., high daily power flows or rare high post-contingency loading). This is a very important step for all aspects of voltage upgrading. Given the operating experience obtained with the existing line, it is sometimes possible to operate with less margin than would be customary in designing a new line. On the other hand, identification of problems with the existing line, perhaps previously unknown or ignored, may become important in setting design requirements for a successful upgrading.

A reasonable effort may be required in order to gather the necessary data on the original design assumptions, the outage rate of the existing line, the general condition of the line, and the geometric dimensions and wind conditions necessary for such an assessment (see Note 1). Some aspects may be obvious. For example, the structure dimensions, conductor type and size, and the insulator type and length can usually be readily obtained.

Note 1
115 to 230-kV Upgrade Example
Review of Line Design

Original Line Design Parameters

- Double-circuit steel lattice.
- Single 2167 kcmil Kiwi ACSR per phase.
- Nine standard porcelain suspension insulators per string.
- Limited vertical distance between conductor attachment points and structural members.

The purpose of the review of the line design is to provide the information for insulation and corona/field effects feasibility analysis and to identify other matters that may require attention in a detailed analysis. For example, conductor motion upon release of accreted ice is not a concern if the conductors are in a horizontal configuration, but this may become an issue for closely spaced conductors in a vertical configuration. Likewise, it is possible to add units to insulator strings, but clearances to ground and wind swing clearances to the structure may require careful attention. Detailed mechanical considerations, such as structure loading if conductor changes are necessary, will follow later if required.

14.3.3 Electrical Clearances and Right-of-Way

Factors to consider regarding electrical clearances and right-of-way are:

- Review of plan/profile drawings
- Conductor midspan ground clearance
- Right-of-way width
- Special local situations
- Comparison with electrical code clearances
- Electrical clearance to earth and objects
- Blowout clearance to edge-of-ROW

Design ground clearance levels, code clearance requirements, and clearance to objects at the edge of the right-of-way must be carefully defined (see Note 2). During this part of the study, special local situations and areas of special concern are identified. Areas of special concern may be environmentally sensitive areas, areas of possible increased contamination (e.g., salt contamination at crossings of interstate highways or industrial areas), or water crossings. Location and identification of spot contamination sources are important because additional insulation may be required in locations of higher-than-normal contamination.

Note 2
115 to 230-kV Upgrade Example
Electrical Clearances and Right-of-Way

Line Profile Observations

- 150-ft ROW adequate.
- Clearance at max temp adequate for 230 kV in all spans.
- Conductor motions due to galloping and ice shedding are not an issue at this location.

Conductor blowout clearances to the edge of the right-of-way under maximum wind swing conditions are essential to maintain code clearances and safety. Analysis of the plan/profile drawings will help identify any areas where conductor blowout may be a concern. Additional clearance will be required because of the increased air gap spacing needed for insulation withstand at the higher voltage.

Review of the plan/profile drawings also will identify issues along the edge of the right-of-way. The existing right-of-way width may need to be increased in a voltage upgrade of an existing line. This may require acquisition or leasing of additional land or an environmental assessment for the voltage upgrade. It may be necessary to widen the right-of-way to accommodate increased horizontal phase spacing or to meet "edge of right-of-way" electric field environmental regulations at the higher voltage. Increasing line voltage increases ground-level electric field, and such measures may need to be taken to ensure compliance. Edge of right-of-way radio and audible noise levels may also be considerations.

A comparison of the present code requirements to the ones that existed at the time the line was constructed is carried out to determine whether the present code allows the same clearances as presently exist on the line. As discussed later, it is also necessary to verify that the line meets the present code's mechanical loading requirements, which may be different from those in effect when the line was designed.

Maintenance of the National Electrical Safety Code (NESC) electrical clearances is essential for any transmission line. Code clearance for conductors above ground is a function of transmission-line phase-to-ground voltage. However, options exist that may allow the existing line to operate at a higher voltage with the present clearance. Many transmission lines constructed in former years were designed with generous ground clearances that would allow operation at a higher voltage without changing the present conductor sags or attachment heights. Also, occasionally, a line designed under provisions of one edition of the NESC will be found to have sufficient clearance to operate at a higher voltage under provisions of a more recent code. Ground clearance requirements have changed for individual voltage classes, in some cases allowing less clearance for the same voltage. The alternate clearance calculation provision in recent code editions allows reduced clearance for cases where switching surge levels are known or controlled. If switching surge levels are known, whichever distance is smaller can be used for compliance (the distance computed from the linear calculation or the switching surge calculation). As a result, lines designed under the former code with a simple voltage distance adder may comply with the present code at a higher voltage if switching surge levels are appropriate. In other situations it might be necessary to devise methods of increasing ground clearance during the detailed studies phase, such as re-sagging the conductors or raising the structure height.

A further note with regard to codes is that early editions of the NESC specified requirements for spacing between conductors within a single circuit. However, once it was recognized that spacing of conductors within a circuit was not the safety issue in the same manner as clearances to objects outside the circuit, these provisions were removed. This question of clearances between conductors within a circuit was an issue when compact high-voltage transmission lines were first contemplated.

14.3.4 Review of Electrical Design Criteria

Factors to consider with respect to electrical design criteria are:

- Preliminary definition of electrical design criteria
- Insulation probability of flashover
- Insulation leakage distance requirements
- Corona and field effects limits

A thorough understanding of criteria that had been used for the original design of the line is important, as is careful consideration of appropriate criteria to be applied to the upgrading (see Note 3). Such criteria include (but are not limited to) insulator leakage distance, desired probability of flashover under switching surge conditions, wind speeds for insulator swing calculations, allowable lightning tripout rates, radio noise limits, and ground-level electric and magnetic field limits.

For the feasibility analysis, it is sufficient to develop criteria only to the degree necessary to evaluate insulation and corona/field effects to see what the prospects are for a successful upgrading. Careful attention to applicable criteria must be given during the detailed design process. In some cases consideration will have to be given to modification of the criteria for a successful upgrading. For example, reconsideration of insulator leakage distance and switching surge

Note 3
115 to 230-kV Upgrade Example
Review of Electrical Design Criteria

- Probability of flashover for switching surge energization (PFO) might be 0.001 for new line.
- Insulator leakage distance 1.2 in. (3 cm) per kV phase to ground voltage.
- Radio noise at 230 kV comparable to new lines.
- Audible noise at 230 kV comparable to new lines.
- Items requiring detailed analysis: none.

probability of flashover criteria may be necessary to develop a workable design.

14.3.5 Insulation and Conductor to Structure Clearances

Factors to consider with respect to insulation requirements are:

- Insulation analysis
- Phase-to-ground spacing
- Insulator swing clearance
- Leakage distance/contamination requirements
- Switching surge flashovers (based on typical data)
- Lightning flashover rate

Careful evaluation of line insulation is essential for a voltage upgrading study (see Note 4). The preliminary evaluation of line insulation includes requirements for power frequency voltage, switching surge overvoltages, and lightning. One of the aspects of a voltage upgrading analysis is the need to make maximum possible use of the line insulation—in other words, to stress it to the maximum degree deemed possible. Thus, existing insulators must be carefully identified. Insulator type (post or suspension, porcelain, glass, or polymer) and number of units per string should be noted and dimensions determined. If leakage distance and CFO values are not in the design information, they can be determined from catalog information.

Air gap clearances between the phase conductors and the structures are important for insulation withstand for power frequency voltage, switching surges, and lightning. Design air gap clearances must be evaluated, both for normal (no wind) and maximum wind conditions. Because power frequency voltage is always present, adequate air gap clearance for power frequency voltage withstand must be maintained under maximum insulator wind swing. Assumed or typical values of insulator swing may be used in the feasibility analysis, but it may be necessary to do a careful weather study during the subsequent detailed design analysis. In some cases, it may be possible to determine the clearances assumed in the original design. Because of the statistical nature of switching surge overvoltages, less than maximum insulator wind swing is often assumed for a switching surge study.

Note 4
115 to 230-kV Upgrade Example
Insulation and Conductor to
Structure Clearances

Inspection Analysis

- Distance from phase conductor attachment point to tower arm below important for switching surge flashover to the next lower grounded steel member.
- Trade-off with insulator leakage distance.
- Reconsideration of normal design criteria.
- Lightning performance is presently adequate.

Key issues requiring detailed analysis.

- 230-kV insulator length vs. switching surge flashovers.
- Insulator leakage distance required for contamination in the area of the line.

The existing structure type establishes the geometrical framework of the line and defines some of the concerns that will require careful consideration during the detailed design phase. With double-circuit steel lattice structures, there is a distance limitation between the phase conductor attachment point at the bottom of the insulator "I" string and the next lower structure arm. Any attempt to increase the insulator length may reduce this distance and adversely affect switching surge performance. With single-pole structures and post insulators, longer post lengths can be substituted to increase the voltage withstand at a higher voltage, but the longer posts may not have sufficient mechanical strength to handle ice conductor loads.

Phase-to-grounded structure member clearance under normal and maximum wind swing conditions must be checked against power frequency air gap spacing requirements at the proposed higher voltage. Consideration may be given to bracing insulators to restrain wind swing if necessary. Present insulator leakage distance should be compared with a cursory review of contamination conditions to estimate an appropriate leakage distance per kilovolt for the upgraded line. Consideration should be given to the possibility of changing the type of insulators as well as simply

adding additional units to the present strings. Note that adding insulation may affect clearances to earth as well as grounded structure members.

Switching surges often play a significant role in a voltage upgrading because of the restricted available space. Control of switching surge overvoltages may be important at voltages as low as 115 kV. Occasionally addition of insulators to improve power frequency performance impinges on the air gap from a switching surge perspective so a tradeoff must be considered. For a feasibility analysis, it is sufficient to determine if spacing and clearances are generally adequate if proper control measures are applied. At this point, for an initial feasibility analysis, typical switching surge distribution may be assumed with assumed weather conditions rather than performing a detailed switching surge study.

Lightning analysis may be on a comparative basis to assess the effect of changes in the line on lightning performance. Voltage upgrading generally has only a minor impact on lightning performance of an overhead transmission line.

14.3.6 Corona and Field Effects

Factors to consider for the corona and field effects analysis are:

- Conductor and hardware corona
- AN, RN, TVI
- Possible need for hardware replacement
- Possible conductor options
  - — Bundling new and old conductors
  - — Reconductoring
  - — Retensioning existing conductor
- Electric and magnetic fields

Conductor type and size are significant for corona and noise calculations. Determining whether the original line phase conductor is of sufficient effective diameter to be used at the proposed higher voltage is a critical part of the electrical feasibility study for voltage upgrading. If the existing conductor will provide acceptable corona performance at the higher voltage, the structure mechanical loads will be unchanged. If the existing conductor must be replaced with a larger conductor or bundled with another similar conductor in order to meet corona performance limits, then the mechanical assessment becomes more challenging since the existing structure loads will be much higher. The existing structures may have to be reinforced or replaced.

Note 5
115 to 230-kV Upgrade Example
Corona and Field Effects

Summary comments. Given the relatively large conductor, corona is unlikely to be a problem at 230 kV.

Corona and Field Levels

- Calculation of radio noise for this line operated at 230 kV shows similar noise levels to existing conventionally designed 230 kV lines. The corona and field effects evaluation is carried out for completeness, but in this particular case, the dominant concerns are electrical insulation rather than environmental effects.

Conductor corona is often the limiting factor in how high the voltage can be increased on an overhead transmission line (see Note 5). Because conductor surface electric field at the higher voltage often approaches levels usually seen on EHV lines, factors such as audible noise and corona on insulators and hardware must be considered. The preliminary feasibility analysis must consider conductor corona performance (radio noise, television noise, audible noise, corona loss) of the line at the existing operating voltage and at possible higher voltages. Appropriate criteria must be developed to assess the corona performance, and to arrive at a maximum possible operating voltage for the existing conductor from a corona standpoint. Conductor surface electric field should be assessed at this time, and a preliminary recommendation made as to the adequacy of the present line hardware for operation at the higher voltage. Replacement of standard hardware with corona-free hardware may be necessary for operation at the higher field levels.

A wide range of possibilities exists for adequacy of the conductor to successfully operate at the higher voltage. A line designed with ample conductor size may successfully operate at a higher voltage with no adverse corona or noise impact. Smaller conductor may require more careful attention to noise to determine if it can be successfully used, while still smaller conductor may need more significant attention. Reconductoring or adding an additional conductor per phase are options to be given preliminary consideration.

Energized line hardware is subject to corona concerns, especially as the line voltage is increased. Armor rods may go into corona at the ends of the rods and be a source of radio and television noise. The type of conductor clamps is significant for corona, as discussed in the detailed analysis in Section 14.6. Corona testing of hardware may be important, and replacement of conventional clamps with corona-

free clamps is likely necessary. Very old lines may have ferrous clamps that are limited by magnetic field heating of the clamp in the amount of current that can pass through the clamp on the conductor. Replacement of the clamps with nonferrous clamps may be a relatively inexpensive way to thermally uprate the line at the same time as the voltage upgrade is in process. In addition to corona concerns, vibration dampers impinge on spacing and may have an effect on switching surge withstand strength of the line. Replacement of vibration dampers may be necessary if the line is re-tensioned to limit conductor vibration damage.

Evaluation of ground-level electric and magnetic field profiles is appropriate during the feasibility analysis to identify any concerns that may arise during the permitting process for the upgrade. This is especially significant in those jurisdictions that have specified maximum electric and magnetic field levels.

Analysis of corona and field effects is dependent on conductor clearances. Ground-level electric field is especially sensitive to conductor height above ground. If conductor retensioning is needed to meet code clearance requirements, the new clearance should be used for the corona and field effects feasibility analysis.

14.3.7 Grounding and Bonding

Grounding is not a primary concern in voltage upgrading, but increasing the line voltage may increase fault current levels. Other than this, there is no reason that existing shield wires cannot be re-used at the higher voltage.

In general, grounding considerations greatly determine the lightning performance of the line. The physical layout of shield wires with respect to the phase conductors relates to shielding failure lightning performance. Structure grounding configuration and footing resistance relate to backflashover lightning performance. Shield wire type and size and shield wire tension limits are factors in the mechanical loading of structures and foundations.

Utility practice varies with regard to bonding of insulator attachments on wood structures. Sometimes the attachments are bonded to the down leads, and sometimes the attachments are unbonded, leaving the wood in series with the insulators for added lightning impulse strength. Unbonded insulators are mostly found at lower voltages, such as 115 kV and occasionally 230 kV. The additional impulse strength of the wood must be balanced against the possibility of pole fires resulting from leakage currents in the wood.

14.3.8 Other Issues

Other issues include:

- Regulatory issues
- Line operation and maintenance

Any regulatory issues should be identified during the feasibility analysis, especially the degree of permitting required for the upgrading (see Note 6). This varies widely in different jurisdictions, and any regulatory issues should be identified at the outset. For example, some jurisdictions have specified editions of the NESC in their laws, and this can affect compliance requirements.

Note 6
115 to 230-kV Upgrade Example
Other Issues

- No additional problems were identified.

Key Issues in Detailed Review:

- However, as regulatory requirements become more stringent, additional issues may be expected to emerge.

It is helpful at an early stage in a voltage-upgrading project to enlist the input of the maintenance personnel. Higher voltages require greater clearances for live working, and the upgrading may change work practices, or even make live working impossible. Situations occur where live line maintenance is still possible, if proper attention is paid to maintenance practices during the design process.

Following the first feasibility evaluation of corona performance and insulation, conceptual line modifications can be developed to allow operation at a higher voltage. These modifications may include re-conductoring, adding a second subconductor per phase, lengthening insulator strings, replacement of insulators with a different type for increased leakage distance or contamination performance, bracing insulators to prevent swinging in the wind, or some combination of modifications. In the event re-conductoring or adding a second subconductor per phase is indicated, a preliminary structural analysis must be conducted to assess any structural modifications that may be necessary. As a conclusion to the voltage upgrading analysis, thermal and surge impedance loading for the new voltage may be calculated and compared to the existing line.

14.4 ASSESSING MECHANICAL FEASIBILITY

The electrical feasibility study, described in Section 14.3, may indicate that the original line design parameters (conductor diameter, ground clearance, phase spacing, insulator leakage length, right-of-way width, live line working dimensions, etc.) are adequate for operation of the line at the proposed higher voltage level. In that case, there is no need to perform a mechanical feasibility study, other than to verify that the line is in reasonably good physical condition.

The electrical feasibility study may also indicate that, short of completely rebuilding the line and purchasing additional right-of-way, there is no possibility of increasing the voltage of the existing line with acceptable insulation and environmental performance. Again, in this case, there is little need for a mechanical assessment.

Most commonly, the electrical feasibility study may show that the operating voltage of the existing line can be increased to the next higher system level if certain physical changes are made to the line. For example, the electrical feasibility study may identify issues related to conductor corona that could be resolved by replacing the original phase conductors with larger conductors, by adding an additional conductor per phase, or by retensioning the existing conductors to reduce sag and increase ground clearance. Or, if the electrical feasibility analysis shows the necessity of increasing structure dimensions to accommodate greater phase spacing, longer insulator string lengths, or larger air gap clearances, the mechanical feasibility study would emphasize whether the existing structures can withstand increased tension loads or the use of post-type insulators.

Typical of many voltage-upgrading projects, the goal of the mechanical feasibility study is to identify the types of physical modifications that are necessary to meet the changed electrical requirements and estimate how practical such changes might be. For example, if the voltage upgrade requires an increase in the mid-span ground clearance, the mechanical feasibility study might consider whether this is best accomplished by retensioning the existing conductor, raising the conductor attachment points on the structures, or reconductoring with a low-sag replacement conductor.

Existing line design parameters that might be studied include the structure type (e.g., the crossarm of a wood pole H-frame structure is relatively easy to raise), the number of tension structures per mile (e.g., with many tension structures, the cost of structure modification to handle retensioning may be prohibitive), the original tension limits used in sag-tension calculations (e.g., with a relatively high maximum ice and wind load tension, it may be possible to reconductor without needing to reinforce the angle and dead-end structures), and the maximum insulator loading.

To keep things simple, no detailed evaluation of cost or structure design changes should be included in this feasibility study. The question is: “Is it possible or practical?” It is not: “How much will the line modifications cost?” or “Which alternative is best?”

The example in the preceding discussion of an electrical feasibility analysis is not very interesting from a mechanical viewpoint since the engineers were lucky enough to be performing a voltage upgrade on an existing 115-kV line with a very large 72/7, 2167 kcmil ACSR Kiwi conductor that had sufficient ground clearance to allow operation at 230 kV without physical structure modifications to reduce sag.

Voltage upgrading a single-circuit 115-kV line, with wood pole H-frame structures, in a flat phase configuration (such as was used for the thermal uprating example in Section 14.2) may be considerably more challenging mechanically. Such lines are in wide use at 69 to 345 kV with conductors that are usually much smaller than Kiwi.

The mechanical feasibility procedure described in this section is generally applicable, but the voltage upgrading of a 115-kV wood pole H-frame line to 230 kV (see Figure 14.4-1) will be reviewed as an example.

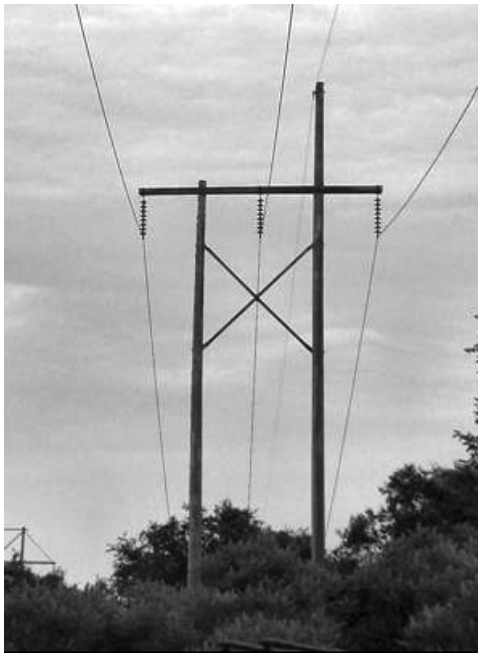


Figure 14.4-1 115-kV wood pole H-frame line.

14.4.1 Mechanical Data Gathering

As in the electrical feasibility analysis, the first step in the mechanical feasibility analysis is the location and collection of relevant operational data and original design data. If not available from plan profile drawings and detailed structure design drawings, some design information can be obtained simply by making field measurements. For example, the spans, pole spacing, and everyday "final" sag can be measured directly. The line may have been designed to standard utility specifications, in which case standard design parameters can be assumed in the feasibility analysis and later verified in the detailed physical inspection described in Section 14.5.

14.4.2 Review of Original Structure Loads

Structures and foundations are designed to withstand various loads produced by both phase conductors and shield wires under high winds, large ice loads, combined ice and wind loads, and broken conductor loads. In most lines, the majority of structures are tangent suspension towers, whose design is determined primarily by transverse wind and vertical ice loads. These transverse loads on tangent suspension structures are primarily determined by the diameter of phase conductors and shield wires, as shown in Equation 14.4-1 for vertical ice load (W_{ICE}), Equation 14.4-2 for combined ice and wind loads $W_{W\&I}$, and Equation 14.4-3 for high-speed horizontal wind load (W_{WIND}) per unit length of conductor, where the radial ice thickness on the conductor is t, the wind pressure for combined wind and ice load is P_{W1}, and the high-speed wind pressure is P_{W2}:

$$W_{ICE} = 1.244t(D_c + t) \quad \text{14.4-1}$$

$$W_{W\&I} = P_{w1}\frac{(D_c + 2t)}{12} \quad \text{14.4-2}$$

$$W_{WIND} = P_{w2}\frac{(D_c + 2t)}{12} \quad \text{14.4-3}$$

Suspension structure loads are less sensitive to the maximum conductor and shield wire tensions that determine the primary loads on the more expensive, but far less common, angle and dead-end structures. Given a strong ACSR conductor and a less strong all aluminum conductor of the same diameter, the magnitude of the design loads is similar on suspension structures, but much higher for the ACSR on angle and dead-end structures where transverse wind and ice loads are secondary to the design.

In a voltage upgrade, where the original conductor must be replaced with a larger diameter conductor, the loading on both suspension tangent and tension strain structures is increased. If the diameter increase is more than 10 to 20%, it is probable that many suspension and strain structures will require reinforcement or replacement.

If the diameter of the existing conductors is adequate at the higher voltage, but an increase in ground clearance is necessary, retensioning the existing conductors may leave the suspension structure loads largely unaffected, but require reinforcement or replacement of angle and dead-end structures. Retensioning the original conductor also increases aeolian vibration problems and reduces the conductor's safety factor under maximum ice and wind load.

As an alternative, when ground clearance must be increased in order to allow a voltage upgrade, selectively raising the conductor support points is attractive since it does nothing to increase loading on strain structures and only marginally increases the ground line moment on those suspension structures whose support points are raised. For many very practical reasons, the safety margins are often generous for mechanical conductor loadings on structures and for electrical clearances in spans along the original line. That is, the loading of many suspension structures may be only 60 to 80% of the maximum design load capability. Also, the minimum electrical clearance in most spans may be many feet greater than the minimum required. This occurs partly as a result of limitations on structure placement (e.g., structures cannot be placed in or too close to roads, buildings, and waterways), limited increments in available heights (e.g., leg extensions and pole lengths are available with 5-ft increments), and the engineering conservatism inherent in traditional line design processes. In any event, in many older existing lines, most structures are loaded to less than their maximum load capacity, and most spans have excess electrical clearance. As an example, Figure 14.4-2 shows the excess electrical clearance distribution for a wood pole H-frame line in the western U.S.

Clearly, in such a line, the mechanical challenges associated with a voltage upgrade may be modest.

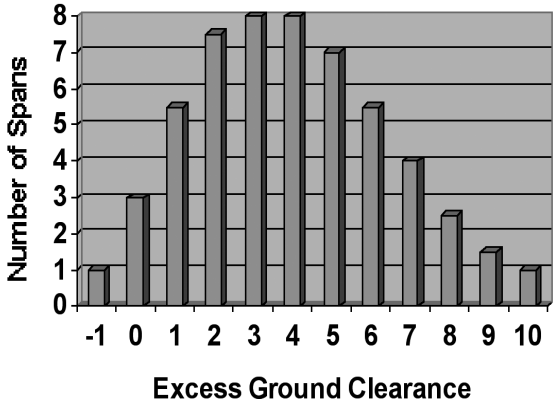


Figure 14.4-2 Typical excess clearance distribution for an existing transmission line.

As a very rough guide, in performing a mechanical feasibility analysis of a proposed voltage upgrade, one may conclude that modest increases in conductor diameter, in maximum conductor tension, and in maximum conductor sag can often be accommodated with a minimum of structural modification. That is, if the electrical feasibility review indicates that the original conductor needs to be replaced or re-tensioned, increases in maximum structure loads (transverse, vertical, or longitudinal) in the range of 5 to 10% can often be accommodated without extensive reconstruction. Similarly, modest increases in electrical clearance (e.g., 1 to 3 ft) required by the higher line voltage may often be met by the existing line with selective structure modifications to raise attachment points.

14.4.3 Sag-tension Calculations

In a new line, the initial sag of phase conductors and shield wires is chosen in order to limit wind-induced motions (e.g., ice galloping, aeolian vibration, and wind blowout at mid-span), to avoid over-tensioning angle and dead-end strain structures during heavy ice and high wind loading events, and to maintain adequate electrical clearance to ground and other lines under high electrical loading and high ice/wind loading events, throughout the life of the line.

The supporting structures of a new line are "spotted" along the right-of-way, such that minimum electrical clearances to ground and other conductors are met and the maximum structure design loads are not exceeded under all loading conditions. The maximum sag and maximum conductor tension from sag-tension calculations are a critical part of this process.

For example, consider Table 14.4-1. The bolded, italicized, and underlined values are:

- Initial installed sag (29.04 ft) at 60°F.
- Corresponding initial tension (4725 lbs) also expressed as a percentage of the breaking strength of the conductor (15%).
- "Final" sag (38.23 ft and 36.35 ft) at the maximum conductor temperature (257°F) and at the maximum ice load condition.
- The initial maximum tension for ice and wind.
- The unloaded tension at 60°F expressed as % of RTS.

Table 14.4-1 Sag-Tension Calculation Table

ALUMINUM COMPANY OF AMERICA SAG AND TENSION DATA

Sag-Tension Calculations

Conductor DRAKE 795.0 Kcmil 26/ 7 Stranding ACSR

Area= .7264 Sq. in Dia= 1.108 in Wt= 1.094 lb/f RTS= 31500 lb
Data from Chart No. 1-537
English Units
Using Exact Catenary Equations

Span= 1000.0 feet NESC Heavy Load Zone
Creep is NOT a Factor Rolled Rod

Design Points					Final			Initial		
Temp	Ice	Wind	K	Weight	Sag	Tension	RTS	Sag	Tension	RTS
°	in	psf	lb/f	lb/f	ft	lb	%	ft	lb	%
0.	.50	4.00	.30	2.509	31.47	10002.	31.8	31.47	***10002.***	31.8
32.	.50	.00	.00	2.094	32.76	8023.	25.5	31.44	8358.	26.5
32.	1.00	.00	.00	3.715	***36.35***	12845.	40.8	36.35	12845.	40.8
-20.	.00	.00	.00	1.094	25.90	5295.	***16.8***	24.66	5558.	***17.6***
0.	.00	.00	.00	1.094	27.15	5053.	16.0	25.78	5319.	16.9
30.	.00	.00	.00	1.094	28.96	4738.	15.0	27.43	5001.	15.9
60.	.00	.00	.00	1.094	30.71	4470.	14.2	29.04	4725.	15.0*
120.	.00	.00	.00	1.094	34.02	4039.	12.8	32.14	4272.	13.6
167.	.00	.00	.00	1.094	35.78	3844.	12.2	34.46	3987.	12.7
212.	.00	.00	.00	1.094	37.00	3716.	11.8	36.59	3757.	11.9
257.	.00	.00	.00	1.094	***38.23***	3598.	11.4	38.23	3598.	11.4

* Design Condition

Maximum tension under ice and wind

%RBS tension for aeolian vibration

Maximum sag for clearance calculations

In evaluating the mechanical feasibility of retensioning the existing conductor or replacing the existing conductor with a new conductor, the critical sag-tension parameters, as shown in Table 14.4-1, are:

- The maximum conductor tension under high wind, heavy ice, or combined ice and wind load, which is key to determining whether the existing structures can be used or reinforced rather than replaced.
- The conductor tension (expressed as a % of the Rated Breaking Strength or as tension divided by mass per unit length) for the "coldest month" of the year. This parameter determines the level of aeolian vibration, the need for dampers, and the likelihood of fatigue damage in the modified line.
- The final sags of the conductor at the upgraded line's maximum allowable conductor temperature and at maximum ice and wind load.

If the electrical feasibility study indicates that the ground clearance of the line must be increased, the original conductors could be re-tensioned or replaced. If re-tensioned, the conductor vibration activity would increase, the maximum tension on the existing structures would increase, and there would be some additional creep elongation. Vertical ice loads and transverse wind loads would be unchanged. If a sag-tension calculation for the re-tensioned line is performed, the increase in maximum tension and in vibration activity can be assessed. If either is excessive, the retensioning option can be dismissed.

If a new conductor is to be bundled with the original, the maximum structure loads would double. For many structures, this would require replacement of most structures—though, as shown in Example 3 in Section 4.7, this is sometimes possible.

If the existing conductor is replaced with a new conductor, then to avoid replacing the existing structures, the maximum tension, maximum sag, and aeolian vibration levels need to be similar to those of the original conductor.

Consider the mechanical feasibility of replacing the Drake ACSR with a special high-temperature, low-sag conductor, such as ACSS ("Aluminum Conductor Steel Supported" ASTM B-856). This conductor can be operated at temperatures as high as 200°C, has higher self-damping and lower thermal elongation than ACSR, and has a lower stiffness. Consider the sag-tension data in Table 14.4-2.

Table 14.4-2 Sag-tension for Drake ACSS

ALUMINUM COMPANY OF AMERICA SAG AND TENSION DATA

Sag-Tension Calculations

Conductor DRAKE/ACSS 795 Kcmil 26/ 7 Stranding ACSS

Area= .7264 Sq. in Dia= 1.108 in Wt= 1.093 lb/f RTS= 28000 lb

Data from Chart No. 3-945

English Units

Using Exact Catenary Equations

Span= 1000.0 feet NESC Heavy Load Zone

Creep is NOT a Factor

Design Points					Final			Initial		
Temp	Ice	Wind	K	Weight	Sag	Tension	RTS	Sag	Tension	RTS
°	in	psf	lb/f	lb/f	ft	lb	%	ft	lb	%
0.	.50	4.00	.30	2.508	31.47	10000.	35.7	31.47	10000.	35.7*
32.	.50	.00	.00	2.093	32.09	8186.	29.2	30.13	8714.	31.1
32.	1.00	.00	.00	3.714	37.59	12423.	44.4	37.59	12423.	44.4
-20.	.00	.00	.00	1.093	26.12	5245.	18.7	21.75	6292.	22.5
0.	.00	.00	.00	1.093	27.38	5005.	17.9	22.55	6071.	21.7
30.	.00	.00	.00	1.093	29.21	4693.	16.8	23.82	5749.	20.5
60.	.00	.00	.00	1.093	30.12	4553.	16.3	25.16	5443.	19.4
120.	.00	.00	.00	1.093	31.90	4301.	15.4	28.01	4893.	17.5
167.	.00	.00	.00	1.093	33.27	4125.	14.7	30.32	4522.	16.2
212.	.00	.00	.00	1.093	34.56	3972.	14.2	32.55	4215.	15.1
257.	.00	.00	.00	1.093	35.83	3832.	13.7	34.76	3949.	14.1

* Design Condition

Notice that the final high-temperature sags shown in Table 14.4-2 are less than with the original Drake ACSR, and that the maximum tensions under ice load are essentially the same. However, with this simple calculation, one can that the sag under heavy ice loading is almost 2 ft greater than the sag at 257°F. If clearances are to be met for this heavy ice condition, then the ACSS replacement conductor offers no advantage in voltage upgrading. It can also be seen that for a less severe ice loading assumption, appropriate to a medium or light loading area, ACSS might allow the necessary increase in clearance to go to the next voltage level without rebuilding the line structures.

14.4.4 Hardware/Connectors

Examples of hardware and connectors to be considered are:

- Full-tension connectors
- Armor rods
- Suspension clamps
- Vibration dampers

In most voltage upgrades, the capital investment and the circuit outage time required are both significant, but the cost and time required to replace hardware and connectors are not a major factor. Line connectors and hardware will be replaced as part of any reconductoring. When new conductors are bundled with old conductors, the hardware would need to be replaced, but original connectors may be left in place if in good condition. Any existing vibration dampers should also be replaced and, if the original conductor is re-tensioned to provide additional ground clearance, the entire vibration damping control system should be reviewed and upgraded.

14.4.5 Insulator Strength

Mechanical considerations for insulators include:

- Insulator type and number
- Insulator mechanical strength

If existing insulators are in good functional condition and are adequate for use at the higher voltage, the need for their replacement may hinge on their mechanical strength, especially if the line is to be reconductored with a larger conductor. Retensioning of existing conductor places added tension stress on insulators on dead-end and heavy angle structures. The ability of the insulators to handle the increased load must be evaluated.

14.4.6 Structure Phase Geometry

The basic structure type establishes the geometrical framework of the line. Part of the mechanical feasibility review should concern the trade-offs between increased insulator length and electrical clearances to ground. Single-pole structures with post insulators have room to lengthen the posts, but the ability to lengthen the posts may be limited by pole or insulator mechanical strength. (Lines have been modified by adding intermediate structures to halve the span length, but in some cases this can make the line look like a fence.) Material choice includes pole class for wood pole lines, and type of steel and size of members for steel lattice structures. Structural strength information is essential if it is found necessary to reconductor, re-tension, or add an additional conductor per phase. There may be sufficient design margin in the existing structures to handle the additional loading. It may be necessary to reinforce the dead-end and heavy angle structures. Or, reinforcement of all structures, including tangent structures, may be required.

14.4.7 Shield Wires

Shield wires can be a significant part of the structure loading tree. Tension, vertical, and transverse loads from shield wires occur at or near the top of the structure. Large ground line or overturning moments result from modest loads at the top of the structure.

If the original shield wires are in good condition, they may be re-used in the voltage upgrade. If the shield wires are in poor condition, or if the asset owner wants to consider the use of OPGW shield wire(s), the original structure load calculations have to be reviewed. It is unlikely that the voltage upgrade will require greater phase to shield wire spacing or that the arc currents seen by the shield wires will be higher.

If the original conductor is re-tensioned, the mid-span clearance of the loaded shield and phase conductors needs to be checked since it is likely to be reduced while the voltage is increased.

14.4.8 Right-of-Way

Right-of-way concerns are:

- Accessibility
- Width
- Possible increased width

Right-of-way accessibility relates to the ease of making modifications to the line. Existing and possible increased width relates to the possibility of making modifications that would increase the physical dimensions of the line. The very fact of the existence of a right-of-way should be verified. Some older transmission lines were constructed with structure easements rather than a right-of-way easement. In such cases, it may be necessary to formulate an agreed-upon deemed right-of-way width for environmental effects compliance issues.

Study of the plan/profile drawings of the line is essential to determine design ground clearance levels and to locate any areas of special concern, such as environmentally sensitive areas where construction would be especially difficult or water crossings. Ground clearance levels may be of major significance for a relatively small portion of the total number of conductor spans. In that case, fewer structures would need modification to increase clearances for the new voltage than would be required for a line on flat ground where the clearance is similar for most or all of the spans. It is essential to view the line in the evaluation of present condition in Section 14.5 to note any changes in land use that have occurred since the line was originally designed. Incursions on the right-of-way may have been made, or modifications made to the line not shown on the drawings.

14.4.9 Wind and Ice-Induced Conductor Motions

Conductor "blowout" clearances to the edge of the right-of-way, under maximum wind swing conditions, must be maintained for safety. Analysis of the plan/profile drawings may help identify long spans where conductor blowout is a concern. Additional clearance to the edge of the right-of-way will be required at any increased line voltage.

Ice galloping calculations should be reviewed during the mechanical feasibility calculations. Clearances between energized conductors, and between these conductors and ground wires during ice galloping, may need to be increased if the line voltage is to be increased. Ice galloping motions can be reduced by reducing the sag of line conductors (by retensioning, for example), by the addition of ice galloping control devices, or by re-conductoring with special anti-galloping conductors such as T2.

14.5 EVALUATION OF PRESENT LINE CONDITION

The feasibility studies described in Sections 14.3 and 14.4 provide an initial evaluation of whether the operating voltage of an existing line can be successfully raised to the next higher standard system voltage level. With certain lines, such as Example 1 in Section 4.7, the voltage may be raised with adequate electrical performance and with little need for physical modifications. Other lines may clearly be incapable of operation at higher voltage levels without being extensively rebuilt. Identification of lines that fall into one of these two categories without extensive analysis is the purpose of the electrical and mechanical feasibility analyses.

For those lines that appear capable of operation at the proposed higher voltage level, but that require certain physical modifications or acceptance of reduced electrical performance criteria, a detailed evaluation of line condition and re-design may be required. The actual condition of the existing line can only be determined from a detailed physical inspection. This section outlines the steps necessary to perform a detailed line evaluation, prior to a detailed voltage upgrade design.

The condition of the existing structures may range from being in original "as-built" condition to showing significant amounts of rust and degradation. Figure 14.5-1 shows apparent corrosion in an existing steel pole, and Figure 14.5-2 shows significant woodpecker damage to the wood poles on a 115-kV line. Both conditions warrant further investigation. A line in poor condition may be a candidate for major overhaul instead of a simple upgrading. A physical review of the original line is essential in determining whether there are incursions onto the right-of-way or other changes that adversely affect clearances to ground or to objects at the edge of the right-of-way.

It is important to make a careful review of historical electrical and mechanical failure rates of the line, especially failures that have never been satisfactorily explained. Increasing line voltage increases the electrical stress on



Figure 14.5-1 Apparent corrosion in an existing steel pole.

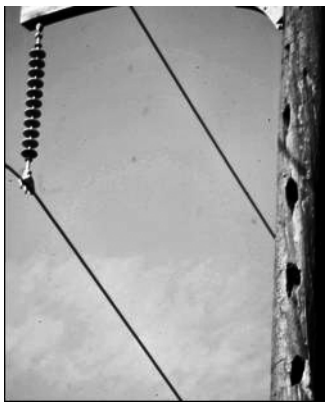


Figure 14.5-2 Woodpecker damage to a wood pole.

line components, and may make previously insignificant problems into major problems that could seriously compromise the line's operating performance.

14.5.1 Physical Examination

The physical inspection of the line may be performed in several ways:

- Driving inspection
  —Comparison to plan/profile drawings
  —Verify structures, etc.
- Helicopter inspection
- Satellite images

A physical inspection of the line route is necessary to compare presently existing conditions with those reported on the plan/profile drawings. Incursions on the right-of-way (Figure 14.5-3) must be identified, as well as any locations where clearances have been impaired. For example, piles of dirt may have been moved under a transmission line near midspan, creating a potentially dangerous condition, as shown in Figure 14.5-3. Swimming pools or other structures may have been built on the right-of-way. Large buildings may have been constructed immediately adjacent to the right-of-way, necessitating a careful consideration of conductor blowout.

A driving tour of the line will also verify that the structures, insulators, etc. are the type expected, based on the review of the line drawings. Obvious changes should be noted. A portion of the line may have been reconductored and resagged at one time. Theft of copper conductor may have resulted in replacement with ACSR, or reconstruction after storm damage may have been done with a different conductor. Some structures may have been added, modified, or replaced with a different type. An example of this may be where an interstate highway or flood dike was constructed after the transmission line was long in service, and it became necessary to modify the line for adequate clearances.



Figure 14.5-3 Right-of-way incursion with piles of construction materials.

In addition to the driving tour, other sources of field information should be identified and utilized to help ascertain the present condition of the line, such as:

- Video inspection records
- Detailed helicopter inspections and satellite images
- Maintenance records (as opposed to outage records)

Careful understanding of the present condition of the line and its environment is essential to preventing unpleasant surprises at a later stage of the project.

The condition of the insulators should be noted. The presence of broken insulators may indicate long deferred maintenance or may indicate areas of high vandalism. A transmission structure located near a sandpit used for target practice is especially vulnerable to gunshot insulator damage. The major items of concern are:

- Broken bells
- Contamination

Areas of high or potentially high insulator contamination should be identified. These may be locations near major highways where salt contamination could be an issue, seacoast locations, or near industrial plants. If a specific area appears to present a considerable degree of contamination, it should be noted for possible removal of an insulator string for subsequent testing at a high-voltage laboratory. Conversely, if the entire area appears to be one of low contamination, one may allow a reduction in the amount of insulator leakage distance that can be tolerated in the upgraded line.

While it is difficult to assess conductor condition in detail from an inspection from the ground, it is possible to determine some aspects of its condition. The main concerns with regard to conductor are:

- Sags
- Corrosion
- Broken strands
- Excessive number of splices

Sag should be compared with the plan/profile drawings. It may be found necessary to use surveying instruments to verify conductor sag, or simpler measurements may be adequate to obtain confidence in the drawings. Sag may be greater or less than expected. Excessive sag may point to

conductor weakened as a consequence of annealing from overheating.

The appearance of the conductor may give a clue as to the possibility of any corrosion damage. Whether the conductor is bright and shiny or discolored is an indication of its condition.

The existence of broken strands is an indication of vibration fatigue as shown in Figure 14.5-4. Such breaks typically occur near the mouth of suspension clamps and may be difficult to see without a "hand" inspection. Such fine damage is difficult to see from the ground or a helicopter. Missing or broken vibration dampers are a tip-off to excessive conductor vibration. Missing damper weights indicate excessive movement of the weights due to excessive vibration. The presence of broken or missing dampers should be a warning to check the conductor for broken strands.

Birdcaging might indicate improper installation. An excessive number of repair splices is an indication of frequent conductor failures and should lead to an investigation as to the cause.

The type and condition of hardware can be determined from a visual inspection. The major concerns with regard to hardware are:

- Wear
- Corrosion
- Conventional or "corona-free" design
- Broken dampers

Excessive wear in original yoke plates, suspension clamp bolts, etc. can be spotted fairly easily and worn hardware replaced. Identification of hardware such as bolted conductor clamps, armor grip suspension, and conventional or corona-free designs are especially important to an evaluation of possible hardware corona problems during voltage upgrading.

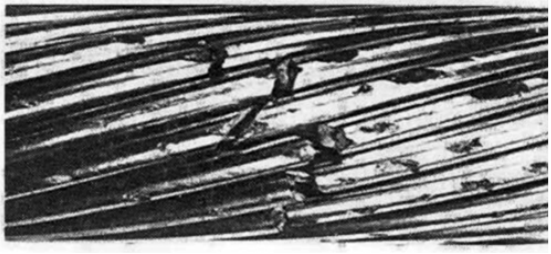


Figure 14.5-4 Broken conductor strands due to vibration-induced fatigue.

Inspection of structures and foundations can be complex and time consuming, especially if voltage upgrading involves a possible increase in original conductor loads. The main items to be included in any inspection would include:

- Overall condition
- Corrosion
- Overstressed components
- Fatigue
- Burning
- Clearances

The inspection of conductors and foundations is related to their type. The general overall condition of wood pole structures is related to presence of rot or cracking in the wood. Rust on steel structures is a clue to check for structural integrity. Unusual circumstances may be noted. For example, the natural buildup of the earth in wet locations may have raised the ground level so it is touching structure members, and corrosion has weakened them. Occasionally structural modifications will be noted, such as occasional replacement of a steel crossarm with a wooden crossarm, or vice versa.

The presence of overstressed components such as bent members on steel lattice structures is a warning that the structures are loaded, at least at certain times, to near their structural limits.

Broken structure members may be evidence of vibration-induced fatigue, and may be related to conductor strand damage, hardware wear, or broken or missing vibration dampers.

Occasionally burning may be noted on wood structures. If near the top of the structure, it may indicate lightning damage. Lower on the structure it may indicate incipient pole fires due to leakage currents in the wood, especially for unbonded insulators or unbonded pole line hardware close to the phase conductors. Un-bonded pole line hardware may be present on X-braces, for example.

Attention should be given to any indications of unusually small clearances, especially at angle structures where the insulator strings normally hang at an angle. Occasional conditions have been observed where, for one reason or another, the insulator rest position is at a greater-than-desired angle, resulting in smaller-than-anticipated clearance to the structure. Such a situation may be a cause of previously unexplained outages.

Clearly, in those cases where substation modifications are required to support the voltage upgrading of an existing line, the substation evaluation and modification can be complex. In the most basic sense, the following substation properties need to be noted:

- Equipment availability
- Space availability
- Voltage levels existing

Upgrading voltage of a transmission line requires connecting it to higher voltage buses in the terminating substations. The presence of the new voltage levels, layout of the substations, and availability of additional space relate to the ease with which the upgrading can be accomplished.

14.5.2 Historical Damage Report Examination

One of the advantages of voltage upgrading an existing line is that the designer has access to many years of field data reports. At a minimum, the following outage frequency reports need to be reviewed:

- Lightning
- Contamination
- Unexplained

Careful examination of the operating history of the line is essential to spot any incipient problems that might be magnified by the voltage upgrade. Outage rates and reported causes of the outages must be explained. Particular attention must be paid to unexplained outages, because these may be due to factors that may become significant with the upgrade. An example may be an angle structure where clearance from the conductor to the structure has been degraded by the insulator string hanging at a greater-than-expected angle. Another cause of unexplained outages is bird-related outages, especially bird-related insulator contamination.

Structure and foundation failures are especially serious and deserve considerable attention. Failures ascribed to deterioration may be an indication of problems to come with remaining structures. Field reports of structure and foundation failures should include failures:

- Due to deterioration
- Due to excessive ice and wind
- Unexplained

Failures due to ice and wind may represent a one-time event, but are still significant regarding design loading conditions if the company is contemplating increasing the structure loading as a result of conductor changes. Modifications to remaining structures as a result of failures affect the original design and should be addressed.

A thorough conductor inspection should be performed even if the original conductor is to be replaced as part of the voltage upgrading. The following field data can help in assessing the condition of the existing conductor and in refining design assumptions for conductors in the upgraded line:

- Connector failures
- Strand and hardware fatigue and wear due to aeolian vibration
- Excessive temperature

Conductor and shield wire failures may result from improper installation but rarely as a result of environmental damage. The fittings may have been improperly crimped, or the installer may have failed to insert the protective grease, resulting in corrosion damage. A record of splice or connector failures is especially significant if conductor retensioning is contemplated to increase ground clearance.

Conductor vibration may manifest itself as conductor failure or as vibration damage to, and possible failure of, conductor support hardware. If fatigue damage is evident on the existing line, any reconductoring effort should provide for improved mechanical damping. Retensioning of the existing conductors, as part of a voltage upgrade, can only make aeolian vibration problems worse. If uncertainty persists as to vibration levels in the existing line, vibration recorders could be placed in critical span locations during cold weather to assess the problem.

Transmission lines are normally operated at a relatively small fraction of their thermal capacity, and the resulting conductor temperature is rarely more than 5 or 10º above air temperature. In certain lines, however, extended periods of high current loading can occur and may result in annealing of the copper or aluminum strands. The only certain method of assessing the possibility of annealing is the testing of conductor samples. The loss of conductor strength from annealing can yield conductor or connector failure during periods of extreme ice loading.

Evidence of public complaints regarding corona-induced noise can provide some indication of problems that might appear after a proposed voltage upgrade. Public complaints normally focus on:

- TV/radio interference
- Audible noise

When an overhead transmission line has been properly designed for conductor corona, probably 95% of all radio noise complaints and 100% of all television interference complaints will be a result of sparking somewhere on the line. Sparking sources range from staples poorly contacting down leads on wood pole lines, corroded joints between insulators in slack strings of suspension insulators, and foreign objects hanging on the phase conductors. These sources can be located and corrected during normal maintenance operations. Increasing line voltage will increase the electrical stress everywhere on the line, including leakage currents in wooden members and potential sparking in defective insulators. Radio and television interference complaints must be taken seriously because they may point to problems that will become significantly worse at the higher operating voltage. A review of interference complaints and how they were resolved may prevent complications later when the voltage is raised, even though analysis of conductor corona indicates successful operation.

Audible noise is rare for lines at the voltages that will normally be considered for upgrading. As a consequence, it is necessary to take any audible noise complaints that have been received seriously, and to follow through with an understanding about how the problem was resolved. It may be that there is an area that is especially sensitive to noise (or an especially easily annoyed neighbor). On the other hand, there could be an issue that should be addressed before increasing the operating voltage.

14.6 DETAILED ENGINEERING DESIGN FOR VOLTAGE UPGRADING

The preliminary electrical and mechanical feasibility analyses indicate what upgrading options are feasible for the line in question, and the amount of power transfer increase possible by making the proposed changes. Before proceeding any farther, it may be necessary to perform a more detailed engineering analysis relating to some of the aspects of the proposed upgrading. The scope of the more detailed studies varies widely from one project to another. If significant structure modifications are necessary to accommodate increases in conductor spacing or use of heavier conductor, it will be necessary to analyze the structures in detail. If the insulation is to be stressed beyond conventional design practice for new lines, it will be necessary to perform a complete insulation analysis, possibly including computation of switching surge distributions and analysis of local weather data to develop the relative dielectric strength of the insulation. Laboratory tests may be required for those projects where it is desired to extend the design to near practical limits. In extreme cases, it may be appropriate to recommend construction of a few spans of experimental line to gain experience with the uprated design before committing to the complete upgrade installation. Because a voltage upgrading study partially involves re-engineering an existing line, it has the advantage that a wealth of operating experience is available with the line.

The detailed engineering design for upgrading voltage of an existing transmission line is an application of the technical data presented in the previous chapters of this book. This section is a guide to the use of the detailed information presented elsewhere in the book for an upgrading study, and as such does not reproduce that information here. Table 14.6-1 gives an overview of the different aspects of a voltage upgrading study as they relate to the different chapters in this book. As the various portions of the upgrading study are encountered, reference can be made to these earlier chapters for the detailed data and procedures needed for each kind of analysis. More specific references to previous chapters are made in connection with the text of this section.

Table 14.6-1 References to Earlier Chapters for a Voltage Upgrading Study

Topic	Chapter Number and Title
Conductor data used for corona calculations and mechanical analysis (e.g., structure loading)	2. Electrical Characteristics of Conductor Configurations and Circuits. See Appendix 2.1, “Electrical and Mechanical Characteristics of Conductors.”
Power frequency insulation, contamination performance, leakage distance, and insulator types and applicability	4. Insulation for Power Frequency Voltage
Switching surge insulation design	5. Switching Surge Performance
Lightning performance calculations, backflashovers and shielding failures; ways to improve tripout rate	6. Lightning and Grounding
Corona noise (radio and television interference) criteria, calculation methods, and evaluation procedure.	9. Electromagnetic Interference Chapter 9 presents the calculation and evaluation techniques for conductor corona interference. Section 8.3, “Gap Discharges,” relates to the practical matter that most interference complaints result from gap sources.
Audible noise criteria, calculation methods, and evaluation procedure.	10. Audible Noise
Ground-level electric and magnetic fields criteria, calculation methods, and evaluation procedure.	7. Electric and Magnetic Fields
Maintenance, live working, and Minimum Approach Distance.	13. Considerations for Inspection and Maintainability

The following items should be considered for a detailed voltage upgrading analysis, keeping in mind that careful study of all the technical areas may not be necessary. Each area should at least be considered to the extent necessary to verify that it is not a problem for the particular application under consideration. The sequence of topics presented below is not necessarily the sequence that these items would be addressed in an actual upgrading analysis. Some of the areas can profitably be investigated in parallel with one another. Because of the interaction between the different factors, it may become necessary to revisit one of the areas after changes are made to the design as a result of consideration of another area. Voltage upgrading studies take on the nature of an optimization analysis, where a number of variables are varied at one time in order to arrive at an optimal design.

Because a voltage upgrading involves stretching things nearer ultimate physical limits, it is important not to overlook any items that might impact the success of the project. For example, altitude and weather conditions affect not only the insulation strength of the air, but also the corona performance of the line. A design that works successfully at sea level may not give adequate performance at high altitudes. Because electrical stress is related to electric field, not necessarily voltage, it is important not to assume that traditional components and procedures used at one voltage level will work successfully on a lower voltage line upgraded to that same voltage level.

14.6.1 Detailed Review of Criteria Applied to Upgrading

The following are examples of criteria that may require detailed review:

- Insulation probability of flashover
- Insulation leakage distance requirements
- Corona and field effects limits

Different design criteria may be applied to a voltage upgrading study, as opposed to a new line design, for several reasons. It may be necessary to operate the upgraded line with reduced insulation margin than would be customarily applied to a new line in order to achieve the desired voltage without structure modifications. The reduced margin may be less insulator length (shorter insulators or less leakage distance per kV) or smaller-than-customary air gap clearances between phases or between conductors and the structures. Criteria for a new line design include values for probability of flashover for energizing switching surge distributions (PFO), or specified insulator leakage distance per kV phase to ground voltage. These criteria may be impossible to meet without increasing structure dimensions. However, upon proper analysis, it may be found that the line could meet altered (i.e., relaxed) criteria and still provide adequate performance. Allowing a slightly higher PFO, together with control of switching surge overvoltages, may make the difference that allows a successful upgrading. Alternatively, if structure modifications are required, reassessment of insulation criteria may have a significant impact on the ultimate design chosen.

The fact that experience exists for the presently operating line—experience that is not available for a new line—lends support to the upgrading analysis. For example, the operating record of the present line—together with analysis of the existing degree of insulator contamination and laboratory tests, if necessary—may warrant a relaxation of the insulator leakage distance deemed necessary at the higher voltage. Another possibility is that evaluation of the radio noise from the existing line compared to predictions, together with identification of the nearest residences, might lead to the conclusion that a certain increase in noise would be acceptable.

Re-evaluation of mechanical structure-loading criteria may also be necessary in light of needed structure modifications and the operating and weather experience of the line. Code changes may also impact structure-loading criteria.

The bottom line is that evaluation and possible reconsideration of all design criteria are important parts of the voltage upgrade analysis.

14.6.2 Power Frequency Insulation

Power frequency insulation studies include:

- Extreme wind study to investigate structure clearances
- Insulator leakage distance (fog chamber tests)
- Replacement of insulators (high leakage or hydrophobic)
- Insulating struts to prevent insulator movement during foul weather

Increasing phase to ground voltage increases the minimum allowable air gap spacing between conductors and grounded structural members to avoid flashovers resulting from the stress of the higher power frequency voltage. Suspension insulator I-strings swing in the wind, and clearances to the structural members are reduced under windy conditions. Power frequency voltage is continually present, requiring adequate clearances to be maintained under the most extreme wind conditions. Thus, a weather analysis and wind motion study may be necessary to investigate the minimum structure clearances that occur under extreme wind conditions for lines with I-strings. Insulator swing is not a consideration for post insulators or V-strings, and can be alleviated for I-string suspension insulators by bracing the insulator strings to prevent movement in wind. One of the design considerations for compact overhead transmission lines is to restrain conductor movement at the structures. Restraint of conductor motion at the structures

generally requires post insulators or insulating struts to prevent insulator movement during foul weather. This general principle may be useful for consideration of voltage upgrades, where restraint of insulator motion may be necessary to maintain adequate air gap clearance.

References to Other Sections for Power Frequency Insulation

Power frequency insulation design for new lines . . . . . Section 3.4.1

Insulator wind swing angle . . . . . Section 4.7.2
. . . . . Appendix 5.1

Power frequency air gap flashover . . . . . Section 4.7

Power frequency insulator dimensioning . . Section 4.5

Insulator contamination . . . . . Section 4.5.2

Polymer insulators . . . . . Section 4.5.2

Testing of insulators . . . . . Section 4.5.2

Resistive glaze insulators . . . . . Section 4.6

Another power frequency insulation consideration is insulator length required for adequate performance under contamination conditions prevailing at the line location. Increasing phase to ground voltage generally requires increased insulator leakage distance, and most likely, increased insulator string length to maintain the same leakage distance per kV. However, there may be insufficient space to lengthen the insulators to provide the same insulator leakage distance per kV at the new voltage, as there was at the previous operating voltage, and still maintain sufficient air gap clearances. Lengthening post insulators sufficiently to maintain the same leakage distance per kV may be inappropriate because of the reduced mechanical strength of the longer posts, unless a stronger class of posts is specified. It may turn out that longer posts may not be strong enough for the conductor mechanical loading conditions for the existing span lengths.

An advantage of voltage upgrading of an existing line is the availability of knowledge of contamination conditions of the existing line. Study of the performance of the existing line may lead to the conclusion that a reduced leakage distance per kV is acceptable for the upgrading. If there is a question about the contamination performance of the insulators at the higher voltage, it is possible to perform laboratory fog chamber contamination tests on insulators carefully removed from the existing line. The insulators must be handled and shipped in such a way so as not to disturb any surface contamination that may be present. These tests may provide valuable insight into existing conditions and the amount of leakage distance that is required for increased voltage. Insulator laboratory tests are not always required, but sometimes provide the degree of confidence needed to move ahead with the project. A possible alternative is to take samples of the contamination and to determine an equivalent salt deposit density for use in laboratory fog chamber tests.

If power frequency insulation contamination performance is a problem, consideration should be given to alternative approaches, such as:

- Fog or high-leakage-type insulators, where additional leakage distance is provided for the same axial string length.
- Semiconductive glaze insulators, where the porcelain glaze is deliberately made semiconducting to even out the voltage distribution along the insulator string and reduce the effects of dry bands.
- Nonceramic insulators whose qualities may reduce the amount of leakage distance required.

It is very important to carefully review operating experience with the line, including any instances of insulator contamination or other failures. Reliability of the line in its present form is an important clue to the way that the upgraded line will operate. Raising line voltage will increase the electrical stress on the line, and any incipient flashover problems will be magnified at the higher voltage. Therefore, it is necessary to resolve any previously unexplained flashovers in order to be sure that nothing is present that may cause inadequate performance at the new voltage. An example of this kind of outage is bird-related outages that may be tolerable at the former voltage but intolerable at the new voltage.

14.6.3 Switching Surge

Detailed switching surge studies include:

- Mitigation methods
- Surge arresters
- Increased air gap
- Lab tests to verify performance of the modified line

Switching surge studies have historically been considered for the higher transmission voltages, and are not customarily conducted on lower voltage lines. However, for voltage upgrading, where it is important to make maximum use of the available space, switching surges may become a limiting factor at lower voltages such as 230 kV or even 115 kV. A switching surge analysis may also be necessary to determine code clearance requirements. A successful upgrading may hinge on mitigation methods, such as limiting the surge overvoltage distribution by closing resistors or surge arresters.

A detailed switching surge study may be necessary when air gaps are tight. This detailed study starts with calcula-

tion of appropriate surge overvoltage distributions. A weather analysis provides an appropriate wind swing angle to use for suspension insulators. A weather analysis also provides a distribution of relative insulation strength of the air. Combining the weather information with insulating characteristics of the air gaps gives overall probability distributions for insulation strength. Statistical techniques then are used to provide the probability of flashover (PFO) for the expected line configuration.

It may be necessary to develop a compromise between power frequency and switching surge insulation requirements. For example, increasing insulator string length increases leakage distance, but may impinge on air gap clearances for switching surge strength. Even lacking this trade-off, the desired PFO might not be attained. Re-evaluation of the PFO criteria may be important at this point. The PFO may not meet the normal criteria for new line designs, but it may be judged adequate for the special conditions of a voltage upgrading.

References to Other Sections for Switching Surge

Switching surge insulation design for new lines . . . . . Section 3.4.2
Switching surge overvoltages
Mitigation methods

Switching surge insulation risk of failure . . . . . Section 5.13

Switching surge laboratory tests . . . . . Section 5.4

Simplified switching surge design procedure . . . . . Section 5.13.4

If an acceptable PFO cannot be achieved, mitigation measures are available. Circuit breaker preinsertion resistors, synchronous closing of circuit breaker poles, or surge arresters can be used to reduce the switching surge overvoltage distribution. For the same insulation strength, reducing the surge overvoltages improves PFO. Mitigation methods have the further advantage of controlling switching surge levels in the event that they can be used to reduce NESC clearance to ground requirements. On long lines, it may be necessary to apply surge arresters at the middle of the line in addition to arresters located at the ends of the line in order to control the overvoltages over the full length of the line. Modifications to the structure are less desirable than controlling the overvoltages, but they may be required to increase the air gap spacing. Laboratory tests may be necessary in critical cases to verify performance of the upgraded line.

In summary, a number of transmission lines have been successfully upgraded to a higher voltage by paying careful attention to control of switching surge overvoltages.

14.6.4 Corona and Field Effects

Corona and field effects studies include:

- Electric and magnetic fields
- Corona
  —Corona testing of insulators and hardware
  —Corona-free hardware
  —Possible need for hardware replacement
- AN, RN, TVI
- Possible conductor options
  —Bundling new and old conductors
  —Reconductoring
  —Retensioning existing conductors

Conductor, hardware, and insulator corona is one of the fundamental limiting factors for how high the voltage can be raised on an existing transmission line. The conductor surface electric field on an upgraded 115- or 230-kV line may equal that of an EHV line, so procedures and precautions normally reserved for the higher transmission voltages may be important for upgraded lines at lower voltages as well. Even audible noise, commonly ignored at 115 or 230 kV, may be important and should not be neglected in an upgrading study.

Corona and field effects would have been already evaluated to some extent during the feasibility study. However, a more careful analysis may be required during the detailed design phase. If it appears that conductor changes will be required because of corona at the higher voltage, it may be necessary to perform the corona studies with a higher degree of care than would be done for a feasibility analysis. It may be necessary to consider the effects of weather, even

References to Other Sections for Corona and Field Effects

Corona testing of hardware . . . . . Appendix 8.1

Audible noise as a design factor . . . . . Section 10.3

Audible noise reduction techniques . . . . . Section 10.7

Electromagnetic interference . . . . . Section 9.2
Corona, hardware, sparking

Radio and television noise design considerations and guidelines . . . . . Section 9.3

Conductor types . . . . . Section 2.2

Electric field induction on objects . . . . . Section 7.8

Magnetic field induction in objects . . . . . Section 7.9

corona loss in some situations. The need for a more careful analysis may be especially true with regard to corona on conductor support hardware and insulators.

Different types of conductor support hardware have traditionally been applied at 115 and 230 kV, compared to 345 kV and above. Bolted conductor clamps with the U-bolt threads protruding below the clamp and the nuts on the underside of the clamp are common at 115 and 230 kV, where the electric field on the clamp surface tends to be low. "Corona-free" hardware inverts the U-bolts so the threads and nuts are inside the clamp. While this hardware is harder to install and change because of the location of the nuts, the shape of the clamps grades the electric field and reduces the amount of corona on the clamps. Corona-free hardware is generally used at 345 kV and above. For compact transmission lines and voltage-upgrading applications, the electric field on lower voltage line conductors, insulators and hardware may equal that of EHV lines. Corona-free hardware may be necessary to prevent radio and television interference, and corona rings may be necessary to protect the skirts of polymer insulators. Corona testing of insulators and hardware may be necessary to verify operation at the higher electric field stress with the increased voltage. Corona testing of hardware and insulators needs to be specified at the anticipated electric field levels on the affected parts, not merely set up for the operating voltage. Traditional tests based on voltage have sometimes failed to identify components that would go into corona at the higher voltage. Replacement of conductor support hardware with corona-free hardware may be necessary for adequate noise performance.

Replacement of phase conductors may also be considered to obtain adequate corona performance of the conductors at the increased voltage. Options for improving the conductor corona performance include reconductoring with a larger diameter conductor or adding an additional conductor per phase to make a larger bundle. Conductor replacement and addition have consequences for the structures and insulators, and mechanical considerations are an important part of this analysis. Retensioning of the existing conductor may be an option to increase ground clearance to meet code requirements or to reduce ground-level electric fields.

Items may have been identified with respect to the "review of the condition of the existing line" that may have an effect on the ground-level electric and magnetic field requirements of the line. Land use alongside the right-of-way may have changed, and electric and magnetic field induction to objects near the line may become an issue. Permitting requirements may dictate more detailed electric and magnetic field studies to demonstrate compliance with local regulations.

14.6.5 Lightning

References to Other Sections for Lightning

Lightning design for new lines . . . . . Section 3.4.3
Insulation strength for lightning impulses . . . . . Section 6.5
Shielding failures . . . . . Section 6.6
Backflashovers . . . . . Section 6.7
Grounding. . . . . Section 6.10
Line arresters . . . . . Section 6.11

Lightning performance of an overhead transmission line is frequently little changed by upgrading the line voltage. For the backflashover analysis for half of the power frequency voltage sine wave cycle, the phase voltage adds to the lightning impulse voltage. For the other half of the power frequency voltage sine wave cycle, the phase voltage subtracts from the lightning impulse voltage. Half of the time, the power frequency voltage adds to the lightning voltage, increasing the stress on the insulation. The other half of the time, the power frequency voltage subtracts from the lightning voltage, decreasing the stress on the insulation. If there are minimal modifications to the line, the net effect is for the impact of the increased line voltage to essentially cancel out over a period of time, leaving a similar lightning backflashover tripout rate. With minimal line modifications, the shielding failure rate is little changed. Thus the overall tripout rate is similar before and after the upgrading. If the insulator CFO must be increased during the upgrading for other reasons, the result may be improved lightning performance.

An appropriate way to do a voltage upgrading lightning performance analysis is to calculate the tripout rate for the existing line and again for the line after the proposed modifications have been made. Compare the calculated tripout rate for the existing line with the known operating record of the line. This comparison calibrates the calculation with recorded data. The difference in calculated tripout rates before and after the upgrading, together with the operating record of the existing line, allows the lightning analysis to predict a change in performance from historical values. This prediction gives a clearer indication than a purely analytical prediction based on assumed data. If historic lightning performance has not been satisfactory, or if it is desired to improve the lightning performance of the upgraded design,

measures such as improving the footing resistance can be developed at this time. Consideration should also be given to how line surge arresters could now be used to mitigate any lightning problems associated with the upgraded line.

14.6.6 Structural Analysis and Reinforcement

Detailed structural analysis and reinforcement may become necessary, especially if increased clearances, reconductoring, or adding an additional conductor per phase are options. Structural analysis may not be necessary if changes to the line design are minimal. On the other hand, some voltage upgrades are practically reconstruction of the line, with major modifications to the structures, requiring thorough re-engineering of structures and foundations.

14.6.7 Detailed Economic Review

Economic analysis plays an essential role in the decision whether or not to upgrade a transmission line, as noted in Section 14.1. While cost and economic analysis considerations are outside the scope of this technical reference book, it is necessary to at least note that a detailed economic review is necessary at some stage in the decision-making process. The scope of the detailed economic review depends to a certain degree on the extent of the modifications anticipated for the transmission line. If several technically acceptable alternatives are identified during the detailed technical analysis that fit the system requirements, a detailed economic analysis will be required in order to make the proper selection from among the alternatives.

14.6.8 Maintenance and Minimum Approach Distance Requirements

Maintenance and clearance requirements are an important component of a voltage upgrading project. For this reason, it is helpful to bring maintenance people into the upgrading study at an early point. In some cases, slight modifications to the design may allow live line maintenance procedures that otherwise would be impossible. Assuming the existing line is not to be virtually reconstructed, presumably maintenance practices are already in place for the line. If live line working is presently practiced on the existing line, it will be necessary to evaluate how an increase in line voltage will impact the existing procedures, and what resulting design changes may be necessary to continue the practice of live line working.

Increasing the voltage of a transmission line necessarily increases the minimum approach distance (MAD) that is required for live line working (Section 13.3). For example, increasing the line voltage from 115 kV to 230 kV increases the MAD for a person (phase-to-ground voltage) from 1.05 to 1.87 m, according to the IEEE method (Table 13.3-1). It will probably also be necessary to consider the control of worksite overvoltages and the use of personal protective grounding or personal protective air gaps (Section 13.3.2).

References to Other Sections for Maintenance Considerations

Live line maintenance . . . . . Section 13.3
Minimum approach distance. . . . . Section 13.3.2
Inspection and maintenance . . . . . Section 13.3.1
Modifications for live working . . . . . Section 13.3.4

When contemplating modifications to an existing transmission line to make operation at a higher voltage technically feasible, it is appropriate to review the changes to determine if there are any low-cost modifications that could be employed to help facilitate live line working (Section 13.3.4). For example, if it is necessary to replace hardware, incorporation of tool attachment points (such as additional holes) may improve the maintainability of the line.

14.6.9 Conductor Motion

Conductor motion may require analysis to ensure adequate air gap clearances. Types of conductor motion that may be considered are:

- Differential blowout of conductors
- Ice dropping following an ice storm
- Ice galloping

In some cases involving very close conductor spacings, it may be necessary to look at conductor motions under adverse weather conditions. These motions may include differential blowout of conductors as a result of different conductor tensions and wind gust conditions. Reduction of phase-to-phase conductor spacing as a result of differential conductor motion is rarely of concern, but might be important for small conductors strung to low tensions. Shedding of ice from conductors following an ice storm (ice dropping) results in large vertical conductor motion (ice jump) and may cause flashover under extreme conditions. Ice galloping is a more common concern in open locations. Compact high-voltage transmission line research, in addition to addressing insulation coordination questions, has resulted in improved understanding of conductor spacing requirements for mechanical motions due to wind, ice, and fault currents. While it is not always necessary to consider mechanical motions in voltage upgrading, it is essential to be aware of their significance. Sometimes simple mechanical modifications, such as bracing insulators from swinging, can provide ample clearances to allow a voltage upgrading to proceed.

14.6.10 Laboratory Tests of Prototype Upgraded Structure

Laboratory tests of one or more prototype uprated structures may be necessary, especially if clearances or insulator lengths are especially tight. Contamination tests and switching surge flashover tests may be done in properly equipped high-voltage laboratories. However, in some cases, it may be desirable to construct a full-scale version of the upgraded line for testing. Such a prototype might be a few spans of line connected to a substation bus at the actual location of the proposed upgrading and left energized for a period of time to verify performance. Maintenance procedures can be demonstrated on the prototype line for application later.

14.7 EXAMPLES OF VOLTAGE UPGRADES

Four examples are included in this section to illustrate some actual voltage upgrades that have been successfully performed by various utilities. These examples were selected to illustrate the range of possible upgrading situations, from the most minimal modifications of the line to virtual reconstruction of the line. The types of studies performed are listed to show the different types of analysis that were required. The examples are deliberately sketchy, because each upgrading situation is unique and requires a set of studies specifically tailored to the application at hand. For other examples, see references (Broschat and Clayton 1981; Koller, 1986; Wale 1981). For an example of an upgrading that included construction of a prototype line section, see (Broschat and Clayton 1981). Example 1 contains some laboratory testing.

14.7.1 Example 1: 115 to 230 kV Voltage Upgrading

This is the ideal voltage upgrade, requiring a minimum of physical modifications in order to operate successfully at the higher voltage (see Figure 14.7-1).

Location
Maryland, U.S.

Initial and Final Voltages
Initial voltage:115 kV.

Final voltage:230 kV.

Structure Type and Modifications

- Double-circuit steel lattice structure.
- No modifications were necessary to the structure because the existing conductor and insulation were able to operate at the higher voltage with acceptable clearances and corona performance.

Studies Performed
Switching Surge

Note: One result of this study was preinsertion resistors were used in circuit breakers to limit surge overvoltage to 2.2 per unit. This allowed adequate PFO with the existing insulators.

- A transient network analyzer (TNA) study was performed to determine the switching surge overvoltage distribution.
- A weather analysis was performed to determine the angle to use for insulator wind swing.
- The switching surge withstand of the insulator strings and tower gaps were analyzed.
- As part of the insulation withstand strength study, a weather analysis was performed to determine the appropriate value to use for the relative insulation strength of air at the line location.

The conclusion of the switching surge analysis was that optimum switching surge performance occurred with the existing nine insulators per string. Shortening the strings led to increased breakdown across the insulator strings. Lengthening the strings led to increased breakdown across the air gaps. Limiting the surge overvoltage with resistor preinsertion allowed the line to be energized at 230 kV with acceptable PFO.

Lightning

- The probability of shielding failures was calculated by two different methods.
- The tripout rate due to backflashovers was calculated by two different methods.

Both shielding failure and backflash calculations were primitive by the standards of this Reference Book. They

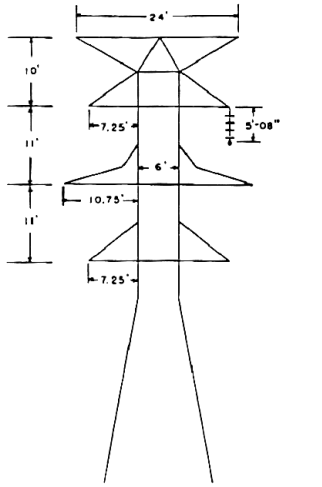


Figure 14.7-1 Suspension steel tower, energized at 230 kV.

indicated acceptable performance, which has been borne out by subsequent operating experience with the line.

60-Hz Voltage

- Insulator contamination was investigated for this line location.

Nine insulators per string is very short for 230-kV lines, with leakage distance of 1.88 cm/kV (0.74 in./kV). Contamination was determined to be very light at the line location, and the decision was made to use nine insulators per string. While performance has been satisfactory, part of the design was the decision that if a problem developed, either insulator cleaning would be enacted, or the insulators would be replaced with high-leakage-type units.

Radio Noise

Note: This line was originally constructed with a large Kiwi ACSR conductor.

- Measurements were made of radio noise at the existing 115-kV level.
- Laboratory tests were made of radio interference (RI) performance of the existing insulator strings at 230 kV.
- Comparison of predicted RI of the uprated line with "conventional" 230-kV lines indicated that radio noise performance would be satisfactory.

Special Problems or Trade-offs

- Increasing the insulator string length to increase leakage distance increases the switching surge probability of flashover because of the reduced air gap spacing to the nearest steel structure member

Criteria Relaxed (if any)

- Insulator leakage distance was 1.88 cm/kV (0.74 in./kV), less than would be used for a new line.

Laboratory or Test Line Studies

- Radio noise measurements were made of the existing 115-kV line.
- Laboratory tests were made of RI performance of the existing insulator strings when operated at 230 kV.

Special Considerations

- Switching surge overvoltage was controlled with circuit breaker resistors.

Reference (if public)

Nabet, G. 1975. "Reduced Insulation for Overhead 230 kV Transmission Line." Southeastern Electric Exchange Transmission Section. Bal Harbour, Florida. April 18 (Nabet 1975).

14.7.2 Example 2: 230 to 345 kV Voltage Upgrading

Location

Upper Midwest, U.S.

Initial and Final Voltages

Initial voltage:230 kV.

Final voltage:345 kV.

Structure Type and Modifications

Single-circuit lattice H-frame structure.

Analysis of the following structure modifications was performed:

- Structure rebracing was necessary to accommodate a second conductor per phase, to make two-conductor bundles as a result of the corona analysis.
- Structure height was increased to accommodate required ground clearance.

Studies Performed

Note: Sensitivity studies were performed to assess the effect of small changes in parameters in order to arrive at an optimum balanced solution.

Switching Surge

Note: One result of this study was that preinsertion resistors were used in the circuit breakers to limit surge overvoltages.

- A digital switching surge study was performed to determine switching surge overvoltage distributions for the following three cases:
  —Energizing.
  —Reclosing into trapped charge (high-speed reclosing following a fault).
  —Effect of application of preinsertion resistors in the circuit breakers.
- The overvoltage withstand of the tower air gaps was determined from published laboratory test data.
- A weather analysis was performed to determine a statistical distribution of the relative insulation strength of air at the line location.
- A weather analysis was performed to determine a statistical distribution of wind speed. Together with wind and weight span data, an appropriate insulator wind swing angle distribution was determined.

Lightning

- A shielding failure analysis was performed to determine an appropriate shield angle. Shield angle of the existing line was judged excessive.
- A backflashover analysis was performed to verify adequate performance.

- Midspan shield wire to phase conductor flashovers were considered, but determined to result in an insignificant number of tripouts.
- A calculation was performed to investigate lightning penetration to the center phase if the shield wires were moved farther apart.

60-Hz Voltage

- The effects of insulator contamination at the line location were investigated to determine the minimum number of insulators per string for adequate performance.
- The weather analysis described above for switching surges was used to determine insulator swing under extreme winds for maintenance of adequate power frequency voltage clearance.

Environmental

- The primary electrical environmental consideration was radio noise. Radio station signal strengths were estimated based on available data. The result of the radio noise analysis was that acceptable noise performance required addition of a second conductor per phase to make two-conductor phase bundles.
- Audible noise was calculated and determined not to be a problem.
- Television interference from conductor corona was estimated and determined to be at most a very minor problem.
- Gaseous oxidants produced by conductor corona were considered and predicted to be undetectable.
- Electric field induction to vehicles near the line was calculated for induced current, spark discharges, and consideration of the possibility of accidental fuel ignition. Recommendations were prepared for right-of-way use and grounding of nearby structures.
- Magnetic field induction to parallel facilities was calculated and determined not to be a major concern.

Code Clearances

- NESC clearances were investigated and determined to be adequate for the upgrade with control of switching surge overvoltages.

Special Problems or Trade-offs

- Switching surge performance was sensitive to tower dimensions and insulator string length.
- Contamination proved to be more of a problem than anticipated after the upgrading was completed.
- The original design had an unusually high shielding failure rate.

Criteria Relaxed (if any)
None.

Laboratory or Test Line Studies
None.

Special Considerations

- Switching surge overvoltage control was required and accomplished with circuit breaker resistor preinsertion.

14.7.3 Example 3: 300 to 420 kV Voltage Upgrading

Location
Norway.

Initial and Final Voltages
Initial: 300 kV.

Final: 420 kV.

Structure Type and Modification – Case 1
Portal steel lattice tower (Figure 14.7-2). Single circuit.

- Removed both shield wires.

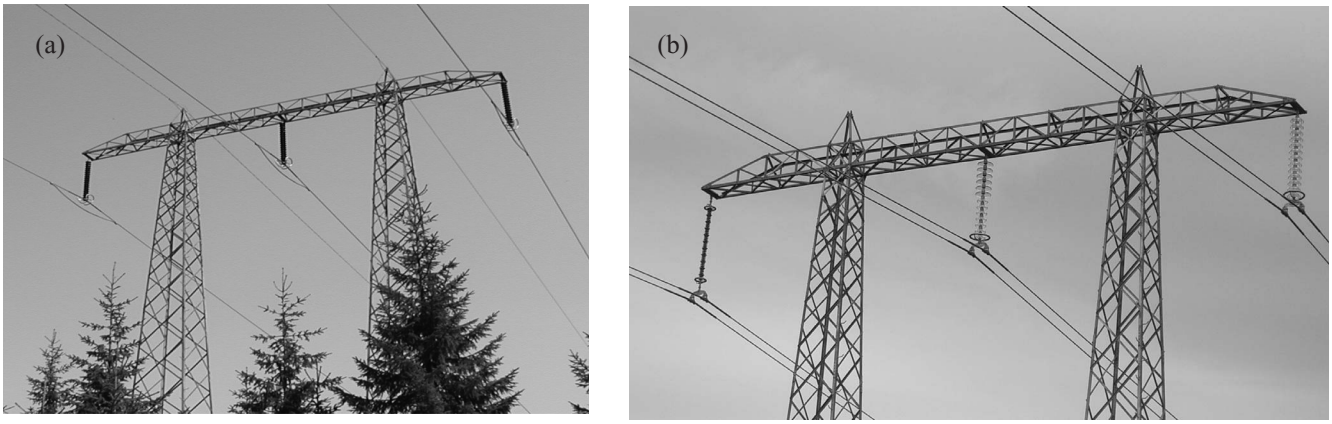


Figure 14.7-2 (a) 300-kV line Flesaker-Sylling before voltage upgrade, with single conductor and shield wire. (b) 300-kV line Flesaker-Sylling after voltage upgrade, with twin bundle conductor and without shield wire.

- Tower earthing (in each tower) connected to parallel line with shield wire.
- Single conductor (Plover) replaced with twin bundle (Grackle).
- Replaced old glass insulators (standard type) with glass fog type and composite (same length as earlier).
- Increased insulator strings in tension tower with four glass units.
- I-strings were in some towers replaced with L-strings in outer phases to limit problem with air clearances during insulator swing out.
- Installed line surge arresters in all phases at both section ends.
- Reinforcement of some towers.
- Two new tension towers.

Studies Performed – Case 1

Laboratory Studies

- A three-year research program was conducted, covering electrical testing of various profiles and lengths of both glass and composite insulators. The pollution tests were performed in full laboratory (DSL test, Ice test). New tests methods were developed, particularly with regard to insulators with ice.

Paper and Computer Studies

- A study of different requirements to air clearance in the Nordic countries.
- A computer program was developed to calculate and compare the line performance before and after upgrading with regard to over voltages (lightning and switching) and environmental impact (pollution, keraunic level, earthing condition) for various glass and composite insulator types, both profile and length.

Field Studies

- Line surge arresters were three years earlier installed in several towers in another line with poor earthing. Mostly testing the mechanical performance of the line arresters and earthing connections of the arrester.
- Installation of new type L-strings were tested in another line.

Monitoring

- The line has a monitoring station equipped with two video cameras, and a complete meteorological station. The collected data is presented in live format on a web page on the Internet. Analyzed data is also presented on the same web page. The station will give information on icing on conductor and insulators and insulator swing out. The monitoring will last for four more years.

Environmental

- Studies of magnetic field and audible noise changes.

Criteria Relaxed

- Reduced ice load with 20% and wind load with 16%.
- Reduced air requirements can be accepted with use of line surge arresters.
- Accepts increased number of failures due to lightning.

References

Laboratory studies published in International Conference on Large High Voltage Electric Systems (Conference Internationale des Grands Reseaux Electriques) (CIGRE), International Workshop on Atmospheric Icing of Structures (IWAIS), and International Symposium on High Voltage Engineering (ISH), etc.

Structure Type and Modification – Case 2

Portal steel lattice tower (Figure 14.7-3). Single circuit, twin bundle.

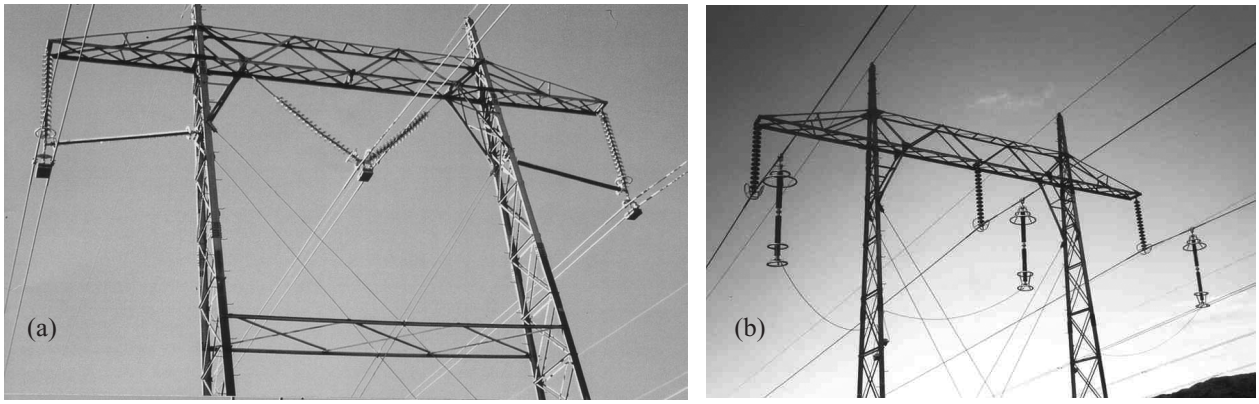


Figure 14.7-3 (a) Voltage upgraded where I-string has been replaced with L-string in outer phases and V-string in mid phase. (b) Line surge arresters installed on all phases to reduce the switching overvoltage of the line.

- Increased I-string glass insulator with 3-4 units.
- Increased insulator strings in tension towers with four glass units.
- I-strings were in some towers replaced with L-strings in both outer phases to limit problem with air clearances during insulator swing out.
- Some reinforcement of the tower cross arm.
- Installed line surge arresters in all phases at both ends and in the middle of the 75-km long line.
- Installed composite insulators to guide the conductor loops through tension towers with short air clearances.
- Installed new vibration dampers.

Criteria Relaxed

- Reduced ice load with 20% and wind load with 16%.

Studies Performed – Case 2
Same as mentioned under Case 1, except for monitoring.

Environmental

- A residential area has in the recent years been constructed very close to the transmission line. Since the voltage upgrade will result in higher levels of audible noise, protests from the neighbors are expected, and therefore a new route will be built for a 3-km-long section.

14.7.4 Example 4: 230 to 500 kV Voltage Upgrading

This is an example of virtual reconstruction of a transmission line. A double-circuit line was removed from the top of the structures and replaced with a single-circuit 500-kV line. Because of structure limitations, the 500-kV was a compact design and required all the engineering studies for a new compact transmission line. This conversion is also discussed in Section 13.3.

Location
California-Oregon, U. S.

Initial and Final Voltages
Initial voltage: 230 kV

Final voltage: 500 kV

Structure Type and Modifications

- Double-circuit steel lattice structure.
- Reconstructed into a single-circuit steel lattice structure (Figure 14.7-4).

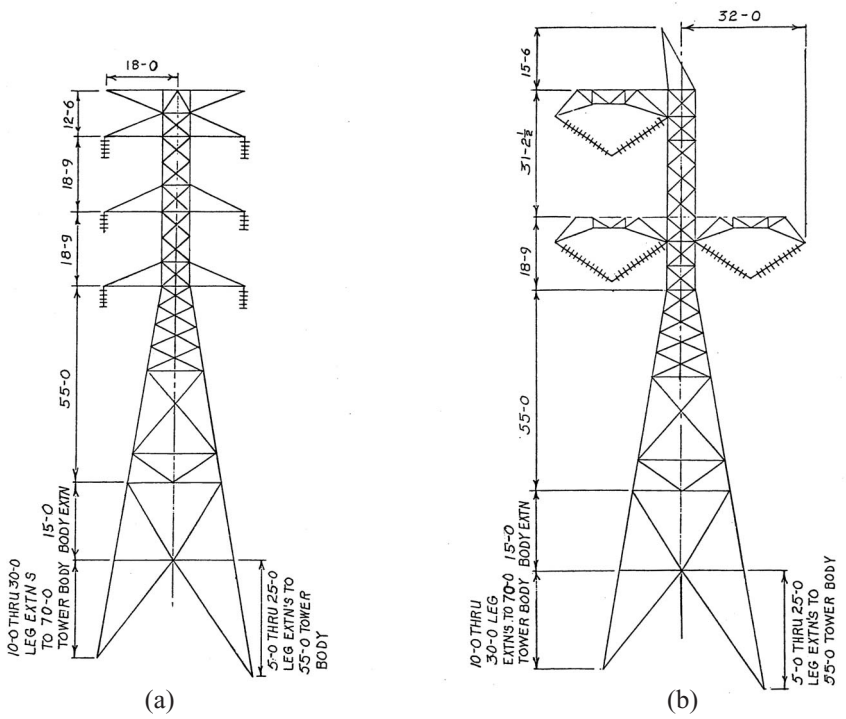


Figure 14.7-4 (a) Original 230-kV double-circuit line. (b) Upgraded 500-kV single-circuit line.

Studies Performed

- All studies that are normal for a new 500-kV line were performed.
- Special consideration was given to operational and maintenance issues.

Special Problems or Trade-offs

- Replacing the conductor required new crossarms, strengthening the towers, and increasing the tower height for tangent structures. Dead-end and heavy angle towers were replaced or heavily modified.
- Transient Overvoltage (TOV) control measures were required to reduce the minimum approach distance (MAD) for live line working. Research was conducted on determination of MAD and the minimum number of undamaged insulators for both the Known TOV Method and the Controlled TOV Method. Extensive study was made of personal protective gaps. See Section 13.3.

Special Considerations

- One shield wire was removed so the upgraded line had one shield wire instead of the two that previously existed on the 230-kV line.
- Evaluation of the number of undamaged insulators was performed as part of the live working study.

Reference (if public)

Gela, G., H. Kientz, D. A. Gillies, and P. F. Lyons, "Operational and Maintenance Issues of Lines Following Upgrading of the Operating Voltage." Presented at the 1996 EPRI "The Future of Power Delivery" Conference in Washington, D.C. (Gela et al. 1996).

REFERENCES

Boteler, D. H. 1994. "Geomagnetically Induced Currents: Present Knowledge and Future Research." *IEEE Transactions on Power Delivery*. Volume 9. Number 1. pp. 50-58. January.

Broschat, M. and R. Clayton. 1981. "Compaction Techniques Applied to Subtransmission Line Uprating 41.6 kV to 115 kV." *IEEE Transactions on Power Apparatus and Systems*. Vol. PAS-100. No. 4. pp. 1959-1965. April.

EPRI. 1979. *Transmission Line Reference Book: Wind-Induced Conductor Motion.* EL-100-V4.

EPRI. 1983. *Transmission Line Reference Book: 115/138 kV Compact Line Design*. EL-100-V3.

EPRI. 2003. *Increased Power Flow Guidebook: Overhead Transmission Lines*.1001817.

Federal Power Commission. 1964. *National Power Survey* Part II—Advisory Reports. U. S. Government Printing Office. Washington, D.C. October.

Gela, G., H. Kientz, D. A. Gillies, and P. F. Lyons.1996. "Operational and Maintenance Issues of Lines Following Upgrading of the Operating Voltage." Presented at the 1996 EPRI "The Future of Power Delivery" Conference in Washington, D.C.

Gutman, R. 1988. "Application of Line Loadability Concepts to Operating Studies." *IEEE Transactions on Power Systems*. Volume 3. Number 4. pp. 1426-1433. November.

Koessler, R. J. and J. W. Feltes. 1993. "Voltage Collapse Investigations with Time-Domain Simulation." IEEE/NTUA Joint International Power Conference "Athens Power Tech" Proceedings. Athens, Greece. September 5-8.

Koller, J. P. 1986. "Uprate 34-kV Line to 138-kV Emergency Tie." *Transmission and Distribution*. 1986; EPRI First Use Bulletin. "Adapting Compact Transmission Techniques." December.

Lesher, R. L., J. W. Porter, and R. T. Byerly. 1994. "Sunburst—A Network of GIC Monitoring Systems." *IEEE Transactions on Power Delivery*. Volume 9. Number 1. pp. 128-137. January.

Nabet, G. 1975. "Reduced Insulation for Overhead 230 kV Transmission Line." Southeastern Electric Exchange Transmission Section. Bal Harbour, Florida. April 18.

St. Clair, H. P. 1953. "Practical Concepts in Capability and Performance of Transmission Lines." *AIEE Transactions on Power Apparatus and Systems*. Volume 72. Part III. pp. 1152-1157. December.

Wale, C. T. 1981. "Compact Line Design-115 kV Project." NELPA 58th Annual Joint Spring Conference. April 28.

CHAPTER 15

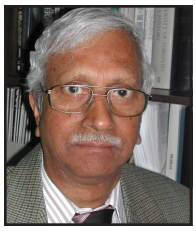
Transmission Lines Above 700 kV

Vernon Chartier
P. Sarma Maruvada

This chapter describes the transmission lines that have been built throughout the world to operate above 700 kV. The chapter provides information on the system planning, the electrical design, the mechanical and tower design, and the operation and maintenance experience of lines built in the U.S., Canada, South Africa, Brazil, Venezuela, Russia, Korea, India and Japan. Also briefly discussed is the research conducted around the world to develop systems to operate above 700 kV including the research conducted by EPRI at their high-voltage research facility in Lenox, Massachusetts, which has been documented in previous editions of this book.



Vernon L. Chartier has conducted pioneering research on the corona and field effects of several lines operating above 700 kV, which made him uniquely qualified along with Dr. Maruvada to write this chapter. From 1964 to 1975, he managed the Apple Grove 750-kV Project located along the Ohio River in West Virginia for the Westinghouse Electric Corporation. This facility was a joint project of the American Electric Power Service Corporation (AEP) and Westinghouse, which led to the extensive 765-kV network built by AEP, starting in the late 1960s. In 1968, while at Westinghouse, he conducted extensive EMI measurements for the United States Air Force from 30 Hz to 10,000 MHz on one of the Hydro-Quebec 735-kV lines. Starting in 1974, he was a consultant and expert witness for three electric utilities in New York State on proposed 765-kV lines that resulted in what is commonly known at the "Common Record Hearings on Health and Safety of Extra-High Voltage Transmission Lines." In 1975, he joined the Division of Laboratories of the Bonneville Power Administration (BPA), where he played a major role in BPA's research on a prototype 1200-kV line built near Lyons, Oregon. While at BPA, he also managed several high-voltage research projects to gain a better understanding of the electric environment on both high-voltage ac and dc lines. Three of the more significant projects were: (1) EMI and AN measurements on a double-circuit 500-kV line at an altitude of 1935 m above sea level near Basin, Montana; (2) EMI, AN, and ion-enhanced electric field measurements on the upgraded ±500-kV HVDC line near Grizzly Mountain in Oregon; and (3) EMI and AN measurements on a compact 230-kV line of Puget Sound Power and Light near Sedro-Wooley, Washington. He has also assisted the Korea Electric Power Research Institute (KEPRI) in the siting and associated research conducted at the Gochang 765-kV Full-Scale Double Circuit Test Line located on the western coast of Gochang-Gun, Jeon-buk Province in South Korea. His research has been documented in more than 50 technical papers. From 1995 to the present, he has been an independent consultant on Power System Electromagnetic Compatibility (EMC). He has played a leading role in the corona and fields work of IEEE, CIGRE, and CISPR. For his contributions he was elected a Fellow of IEEE in 1980; received the IEEE Herman Halperin Transmission and Distribution Award in 1995, and the IEEE Third Millennium Medal in 2000; and was inducted into the National Academy of Engineers in 2004.



Dr. P. Sarma Maruvada has been involved in theoretical and experimental research studies of the corona performance of high-voltage ac and dc transmission lines for more than 35 years. He has made important contributions to the calculation of conductor surface electric fields; analysis of corona onset phenomena, space charge fields, and corona losses of dc transmission lines; analysis and measurement of radio noise and audible noise; and development of design criteria for radio noise and audible noise of ac and dc transmission lines as well as for electric fields and ion currents in the vicinity of dc lines. He contributed to the research and development of the 1200-kV ac transmission option that was considered by Hydro-Québec in 1974 for the James Bay Project. He also assisted in the development of research facilities at the Central Power Research Institute (CPRI), Hyderabad, India, for carrying out the electrical studies at transmission voltages up to 1200 kV ac and ± 1000 kV dc.

Dr. Maruvada's research and analysis of corona are presented in his landmark book *Corona Performance of High-Voltage Transmission Lines*. He served on the Executive Committee of the IEEE/PES Transmission and Distribution Conference and Exposition and as Chairman of CIGRE Study Committee 36 on Power System Electromagnetic Compatibility. He is an Honorary Member of CIGRE, has been elected Fellow of IEEE and received the IEEE Herman Halperin Electric Transmission and Distribution Award.

Contributors to Chapter 15 include the following individuals:

Section 15.4, Hydro-Quebec 735-kV Lines in Canada

- J. P. Gingras, A. Dutil, H. Létourneau, L. Allard, J. M Gagnon, J. C. Carrière, D. Bouchard, M. Hamel, L. Vo Van, M. Lavoie, D. Goulet, and Y. Deshaies, TransÉnergie/Hydro-Québec.

Section 15.5, American Electric Power (AEP) Service Corporation 765-kV System in the U.S.

- Eric Engdahl and Ed Schnell, AEP, USA.

Section 15.6, Russian 750-kV and 1150-KV Lines

- Viktor Rashkes.

Section 15.7, EDELCA 765-kV Lines in Venezuela

- Jose Antonio Delgado Garcia, Javier Tarazona Gomez, Jose Antonio Pardinas, Carlos Garcia Cuestas, and Joaquin Oliveira Da Silva.

Section 15.8, FURNAS 750-kV Lines in Brazil

- Paulo Cesar Vaz Esmeraldo, FURNAS, Brazil.

Section 15.9, New York Power Authority (NYPA) 765-KV System in the U.S.

- Ben Shperling and Peter S. Muench, NYPA, USA.

Section 15.10, Eskom 765-kV Lines in South Africa

- Tony Britten, Fabio Bologna, Dave Cretchley, Dzevad Muftic, Logan Pillay, and Riaz Vajeth, Eskom, South Africa.

Section 15.11, POWERGRID 765-kV Lines in India

- R. P. Singh, R. N. Nayak, M. Krishnakumar, and Rajiv Gandhi, POWERGRID, India.

Section 15.12, Korea Electric Power Corporation (KEPCO) 765-kV System in South Korea

- Dong Il-Lee, KEPCO (KEPRI) and Chang-Hyo Oh, KEPCO, South Korea.

15.1 INTRODUCTION

Once high-voltage ac power transmission became feasible in the early twentieth century, there arose a continuing trend toward the use of increasingly higher voltages for transmitting large blocks of power efficiently over long distances. Higher-voltage transmission lines were also essential for the development of large interconnected power networks, one of the most important engineering achievements of the twentieth century. Transmission voltages progressed from the 30-40 kV range at the beginning to 132-150 kV by the year 1920, to 220 kV in 1923, and 287 kV by about 1934—all in the United States. The next important step was taken almost 20 years later with the introduction of 380-400 kV transmission in Sweden in 1954. The growth continued with the introduction of transmission voltages of 500 kV in the early 1960s and 700-800 kV in the mid-1960s. The first 735-kV transmission lines were built by Hydro-Québec in 1965. Although efforts continued to establish the technical feasibility of power transmission in the range of 1000-1500 kV, practical implementation of transmission systems at these voltages was not feasible because of a steady decline in load growth following the energy crisis that began in 1973. Transmission lines in the range of 1000-1200 kV were built in Russia (the former USSR) and Japan, but the Russian line, after a few years of operation at the design voltage of 1150 kV, has been operated at the lower level of 500 kV, while the Japanese 1000-kV line has been operated since it was built also at 500 kV. Thus, the highest operating transmission voltage in different countries around the world continues to be in the range of 700-800 kV.

Since the mid-1960s, transmission lines in the range of 700-800 kV were designed, built, and operated in several countries. Some of these lines have been in operation for 20-40 years, while others have been built more recently and in operation for only a few years. There are indications that more transmission lines will be constructed in the 700-800 kV range in many countries, and consequently, there is a need for information on the experience so far on the design, construction, operation, and maintenance aspects of lines at voltages above 700 kV. The main objective of this chapter, therefore, is to provide a summary of the relevant experience of utilities in different countries that have transmission lines above 700 kV.

A preliminary survey identified nine cases of transmission lines in the 700-800 kV range—in Canada, United States, Brazil, Venezuela, Russia, South Africa, South Korea, and India, and two lines in the 1000-1200 kV range in Russia and Japan. A survey of technical literature revealed many publications on the planning and design aspects of the first generation of 700-800 kV transmission lines, but relatively few papers on the operation and maintenance aspects. Few publications were found for the second generation of 700-800 kV lines as well as for the 1000-1200 kV lines. As a result, a survey-type questionnaire (Appendix 15.1) was prepared in order to obtain comprehensive information on all aspects of the identified transmission lines. EPRI solicited the participation of the concerned utilities in the survey, and distributed the questionnaire to those who agreed to participate. A workshop was held in 2004 to discuss the questionnaire with experts from the participating utilities. The information collected through a literature survey, responses to the questionnaire, as well as discussions at the workshop were all used in preparing this chapter.

Even though many of the utilities that built lines at voltages greater than 700 kV had their own research programs, they also relied heavily on the research of others, especially the research conducted at the EPRI facility at Lenox, Massachusetts, which has been documented in three previously published reference books. This facility has been in operation since 1959 under many names: Project EHV, Project UHV, and the High Voltage Transmission Research Center. It has conducted pioneering research in all of the electrical phenomena associated with overhead high-voltage transmission lines, and has provided basic information not only for the design of lines above 700 kV, but also for the construction of research facilities such as test lines, test cages, contamination chambers, impulse generators, etc. This updated reference book, which incorporates the results of worldwide research, should be even more heavily relied upon in the future.

The chapter begins with a brief review of the research and development efforts that were undertaken for the purpose of obtaining the data required for the design and construction of 700-800 kV and 1000-1200 kV transmission lines, followed by the main body of the chapter consisting of detailed case studies of nine 700-800 kV and two 1000-1200 kV lines. Each case study includes information on system planning, electrical design, mechanical and tower design, and operation and maintenance aspects. Finally, a summary is provided, mainly in the form of tables, at the end of the chapter. A comprehensive list of references, a bibliography, and an appendix describing the survey questionnaire complete the chapter.

15.2 RESEARCH TO DEVELOP TRANSMISSION SYSTEMS ABOVE 700 KV

15.2.1 Introduction

From 1934 to 1952, the United States had the only transmission systems in the world operating at voltages higher than 220 kV, which were the 287-kV lines from Hoover Dam in Nevada to Los Angeles in California. These lines,

which used copper conductors, were later upgraded to 500 kV. For various reasons, no other systems were built in the United States or other countries to operate at higher voltages. However, shortly after World War II, the utility industry determined that there would be a need for higher-voltage transmission lines because of the great expansion in the use of electricity. This determination resulted in the construction of high-voltage test lines throughout the world, such as the Tidd 500-kV test project of American Gas & Electric and the Westinghouse Electric Corporation Company (Sporn and Monteith 1947). Other projects that were built to study higher voltages were the Chevilly 500-kV Experimental Station of Electricité de France (Cahen and Pelissier 1952); the Coldwater 600-kV test project of Ontario Hydro (Cassan and McMurtrie 1960); the Mannheim-Rheinau 400-kV Research Station in Germany (Bartenstein 1956); the 600-kV Shiobara Laboratory in Japan (Sawada 1965); and the 400-kV Leatherhead test line in England (Banks et al. 1968). Another important project of that era was the Leadville High-Altitude Extra-High-Voltage Test Project of the Public Service Company of Colorado and the Westinghouse Electric Corporation (Robertson and Dillard 1961). All these projects had three-phase test lines, with the exception of the Leatherhead and Leadville test lines, which had single-phase lines. These research projects provided the primary research that led to the construction of 345-kV, 400-kV, and 500-kV systems throughout the world. However, it should be noted that projects like Project EHV and Apple Grove, which were built to study voltages up to 775 kV, provided additional research for the 500-kV voltage class. These latter two projects are discussed in the next section.

15.2.2 Research to Develop 800-kV Systems

In 1958, the General Electric Company determined that even higher voltages would be needed, which led to the construction of Project EHV in 1959 (Abetti 1960). This project provided research on corona and insulation for switching surge and power frequency voltages over the voltage range of 380-750 kV. It was located in the towns of Lenox and Lee, Berkshire County, Massachusetts. The location was chosen because it was only a few miles from the Pittsfield Transformer Plant of General Electric and from the General Electric High-Voltage Laboratory. The original Project EHV test line ran along the Housatonic River for a length of 4.3 miles (6.9 km) at elevations between 950 and 1080 ft (290 and 329 m) above sea level. The test line started operating as an open-ended line in 1960 at voltage levels between 460 and 500 kV. In 1961, terminal equipment was installed at the open end of the line, which completed the loop with a local 115-kV line. Project EHV was initially designed for two rated voltages, 460 and 650 kV. Insulation levels for the project were determined by conducting many impulse, switching surge, and 60-Hz tests on insulator strings, stacks of pedestal insulators, bushings, and various types of apparatus, under both wet and dry conditions.

Project EHV was operated under General Electric sponsorship from 1958 to 1964. The original project consisted of two EHV substations, a data acquisition and headquarters building, a 3000-kV outdoor impulse generator, and the test line. In 1964, General Electric proposed to the Edison Electric Institute that a two-year effort be undertaken to: (1) generalize the findings of the initial experience at the project, (2) bring to bear from this generalization all the analytical and computer models developed in parallel with the early project experience, and (3) continue experiments and tests at the project to fill in some important gaps in understanding that appeared necessary for effective generalized solutions (EEI 1968). This effort resulted in an EHV line design reference book (EEI 1968).

In 1960, the American Electric Power Service Corporation (AEP) entered into an agreement with the Westinghouse Electric Corporation to build a test project that could operate over the range of 500-775 kV. This project, which consisted of three test lines, was energized in 1961, and was called the Apple Grove 750-kV Project (Shankle et al. 1965). The original project was instrumented to measure corona loss on all nine phases, with the conductors carrying simulated load current. It had three types of radio noise meters located at the electrical center of each test line.

Apple Grove originally was designed to operate for about five years. During that period the primary research was conducted on conductors operating at 775 kV, but one of the three test lines was reconductored, and the project was operated at 515 kV for one year starting in November 1962 (Taylor et al. 1965). During this same one-year period, switching surge tests were conducted on this 525-kV test line by reducing the phase-to-ground clearances artificially on one of the 775-kV suspension towers (Barnes et al. 1965). The results from this research were used in the design of the Virginia Electric & Power 500-kV line, which was the first line at this voltage level.

In 1969, which was about one year after AEP energized their first 765-kV line, the Apple Grove project was instrumented to measure audible noise. In 1974, ozone and television interference instrumentation were added. Extensive measurements of electric fields and induced currents and voltages into objects were conducted in the late 1960s and early 1970s.

Test projects to study voltages above 500 kV were built in other countries, such as the Experimental Station at Les Renardieres in France (Magnien et al. 1966) and the

700-kV single-phase test line that was built next to the Leatherhead High Voltage Laboratory in England (Banks et al. 1968). Test lines that operated in this voltage range were also built and operated in the USSR (Burgsdorf et al. 1960). In 1993, the Korea Electric Power Institute built the first double-circuit 765-kV test line near the Yellow Sea in South Korea (Dong-IL Lee et al. 1997). This project, which was called the "Gochang 765-kV Full Scale Test Line," was instrumented to measure all the phenomena associated with conductor corona.

As part of the Les Renardieres Research Project, a test cage to study corona phenomena was built. Such cages were found to be invaluable and were built in conjunction with some of the UHV research projects, which are discussed in Section 15.2.3.

The majority of these test line projects were built to conduct research on conductor corona and ground-level electric fields. As was mentioned earlier, Project EHV had the capability of conducting lightning impulse and switching surge tests on tower configurations. In the development of 500-kV and 735/765-kV systems in the 1960s, utilities in North American conducted tests to determine the insulation needed for switching-surge overvoltages at Project EHV and/or at the high-voltage laboratories owned by manufacturers of high-voltage equipment. Most major manufacturers of high-voltage equipment—such as General Electric, Westinghouse, ASEA, Hitachi, etc.—had such high-voltage laboratories.

In 1979, Eskom entered into a collaborative program with both the Italian utility Ente Nazionale per L'Energia Elettrica (Enel) and the test lab Centro Elettrotecnico Sperimentale Italiano (CESI) of Italy. A high-altitude cage was built to study the effects of altitude on conductor corona phenomena, and in 1981/1982 two high-altitude 3300-kV UHV test laboratories (NETFA and CSIR) were built to study dielectric strengths of tower window shapes for 765-kV lines (Britten et al. 1987; Le Roux et al. 1987). Live-line working practices and insulation strengths were also studied. The laboratories were used, in addition, for the study of atmospheric correction factors for lightning and switching impulse breakdown, and also for the gap factors of various tower window shapes. The NETFA and CSIR labs were used mainly for switching and lightning impulse studies. Neither lab was equipped with a test line, and no laboratory studies of insulator pollution were conducted. However, some pollution severity measurements were done on a number of 88-kV test stations in the Johannesburg, KwaZulu Natal, and Cape areas. The equipment for these tests was acquired from Enel, and the work to some extent was guided by specialists in Enel and CESI. The 765-kV research at both laboratories was directed by Eskom specialists, but with guidance from Enel and CESI. The same applied to the research into conductor corona done at the Eskom Corona Cage.

Another major facility built in 1982 by Eskom was the vibration test line at Kroonstad. The main purpose of the test line at that time was to study the performance of spacer dampers on six-conductor bundles. It is still being used for research into conductor vibration on 275- and 400-kV lines.

Eskom never seriously considered the need for ac systems of 1000 kV and above. However, at the high operating altitudes of their present 765-kV system, the system is roughly equivalent to 1000 kV from a dielectric and corona point of view.

The research from these projects around the world resulted in the construction of thousands of miles of 735/765-kV lines in Québec, Canada and in the states served by AEP in the United States. The New York Power Authority (NYPA) and Commonwealth Associates built other lines operating at 765 kV in the U.S. In other countries, 765-kV lines were built in Brazil, Venezuela, South Africa, and South Korea. In the USSR, the lines that were built in this voltage range were classified as 787-kV lines.

15.2.3 Research to Develop Transmission Systems Above 1000 kV

Rapid load growth in the 1960s and the perceived prospects for continued load growth in the ensuing decades were the driving forces for research and development of ac power transmission lines at voltages above 1000 kV. Even as the first transmission lines at 500 and 750 kV were being built and operated in the 1960s, there was a heightened interest in developing the next higher transmission voltages in the so-called ultra-high-voltage (UHV) range of 1000 to 1500 kV (Anderson and Barthold 1968, Catenacci et al. 1968). In order to gather the vast amount of technical information necessary to design transmission lines above 1000 kV, research and test facilities were built in several countries in the 1970s. Information on the progress of research work carried out in six countries—Brazil, Canada, Italy, Japan, U.S., and USSR was presented in two excellent CIGRE Working Group (WG) reports (WG 31.04 1983; WG 38.04 1987).

The impetus for research on transmission lines above 1000 kV in Brazil was provided by the need for transmitting a block of power on the order of 20,000 MW from the Amazon Basin to the load centers at distances ranging from 1500 to 2300 km (De Franco and Morissy 1980). Research and test facilities required for carrying out studies at system voltages up to 1500 kV were built at the research institute Centro de Pesquisas de Energia Elétrica (CEPEL) in Adrianopolis, Brazil. In addition to a large

indoor high-voltage laboratory for tests on equipment, the facilities at CEPEL include an outdoor area where full-scale or mockup transmission towers can be tested for air insulation clearances and an outdoor experimental line and test cages for corona studies.

In Canada, the need for transmission systems above 1000 kV was foreseen in the provinces of British Columbia and Québec to bring large blocks of power from remote hydroelectric projects to the load centers. The main research and test facilities for studies at system voltages above 1000 kV were located at the Institut de Recherche d'Hydro-Québec (IREQ), Hydro-Québec's research institute. The test facilities at IREQ (Hylten-Cavallius and Train 1974) comprised a large indoor high-voltage laboratory, with capabilities for air insulation studies on tower window mockups for system voltages up to 1500 kV, a large pollution chamber for studies on insulators, and an outdoor experimental line and test cages for corona studies. A test line was also built at Magdalen Islands to study vibration performance of conductor bundles and development of spacer dampers.

Phase-to-ground and phase-to-phase air insulation tests on line and substation configurations at IREQ provided a large amount of data necessary for determining air gap clearances for transmission lines and substations at system voltages of 1200 and 1500 kV. Corona studies were carried out in the test cages on six and eight conductor bundles, and the 6 x 46.53 mm conductor bundle was selected for 1200-kV lines (Trinh et al. 1974).

In Italy, opportunities were foreseen to install large power generation facilities at a few sites relatively far from the load centers (Cladé et al. 1978). It became apparent that, in order to take advantage of this opportunity, a new transmission voltage around 1000 kV would be required to overlay the existing 420-kV network. Studies for system voltages above 1000 kV were carried out in Italy at several research and test facilities. At the Suvereto 1000-kV Project, a 1-km-long test line was used for air insulation and corona studies. In addition, an outdoor test cage was also used for corona studies. A test line at Pradarena Pass was used for ice and wind loading studies in winter and vibration, subspan galloping, and spacer performance studies in summer. Further studies on air insulation and performance of polluted insulators were carried out at the CESI laboratories in Milan.

Extensive research studies carried at the different facilities in Italy generated a large amount of data for determining phase-to-ground and phase-to-phase air clearances, selecting ceramic and nonceramic insulator strings, and selecting conductor bundles for a 1050-kV prototype transmission line. The test data were also used in the development of vibration dampers, spacers, and nonconventional tower structures and foundations for 1050-kV transmission lines.

In Japan, the need for overcoming stability problems of the existing 500-kV network and obviating the problems of excessive short-circuit currents led to the consideration of transmission above 1000 kV to overlay the existing network. As a consequence, research and test facilities were built (Udo et al. 1980), comprising mainly a large fog chamber designed for testing polluted insulators at line-to-ground voltages up to 900 kV, a double-circuit experimental line, and a test cage for corona studies. In addition, a test line of the Tokyo Electric Power Company (TEPCO) was used for wind and ice studies on conductor bundles and the NGK high-voltage test facilities were used for corona and pollution studies. A significant amount of information was obtained on the withstand voltages of contaminated and snow-covered insulator strings.

In the United States, transmission voltages above 1000 kV were seriously considered by two utilities: AEP and Bonneville Power Administration (BPA). In both cases, the purpose of the new transmission systems was to transmit large amounts of power, improve system stability, and reduce environmental impact. Three separate research and test facilities were built to evaluate the technical feasibility of transmission lines above 1000 kV:

1. The AEP/ASEA test facility, located near South Bend, Indiana, had the capability of testing single-phase conductor bundles at voltages corresponding to transmission-system voltages up to, and even beyond, 1500 kV (Nagel and Vassell 1974; Pokorny and Flugum 1975). A single-phase experimental line and two test cages were used to evaluate the corona performance of large conductor bundles.
2. At BPA, a full-scale three–phase, 1200-kV prototype test line (Annestrand and Parks 1977) near Lyons, Oregon, was used to evaluate the long-term corona performance of an eight-conductor bundle. In addition, the facility at Carey High Voltage Laboratory was used for studies on air insulation, while conductor vibration and galloping studies were carried out at the Moro mechanical test line.
3. The GE/EPRI Project UHV comprised a three-phase experimental line, a test cage, and a pollution chamber. The facility had the capability of testing the corona performance of conductor bundles, withstand strength of air gaps, and the pollution performance of line and station insulators. A detailed description of the test facilities is given in the second edition of the Red Book (EPRI 1982).

Data on the corona performance of several bundles, with up to 18 subconductors, were obtained at the AEP/ASEA test facility (Scherer et al. 1980). The results obtained at BPA included switching surge withstand strength of air gaps, pollution performance characteristics of ceramic and nonceramic insulator strings, and corona performance (Perry et al. 1979) of a seven- and an eight-conductor bundle. Eleven different conductor bundles, with subconductor diameters varying from 3.3 to 5.6 cm and the number of subconductors from 6 to 16, were tested at the GE/EPRI Project UHV at system voltages from 950 to 1450 kV to obtain a vast amount of data on the corona performance (EPRI 1982).

In the USSR, the need to strengthen the electrical links between integrated power systems, as well as the need for transmitting large quantities of power over long distances, spurred the research activities at transmission voltages in the range of 1150 to 1500 kV. A 1200-kV experimental line was constructed at the Bely Rast substation (Beliakov et al. 1976). Test data were obtained on the corona performance of conductor bundles and the strength of air insulation.

Although a large amount of research and test data was obtained from the different facilities around the world, the need to establish the technical feasibility of power transmission at voltages above 1000 kV, combined with economic and other considerations, persuaded the utilities concerned either to postpone indefinitely or abandon the plans for the construction of the transmission systems. A double-circuit 1000-kV transmission line was built in Japan, but has been operated only at 500 kV. The world's first 1200-kV transmission system (Burgsdorf et al. 1976) was built and operated for several years in the USSR. However, this system has been operated over the last few years at 500 kV.

15.3 CASE STUDIES OF TRANSMISSION LINES ABOVE 700 KV

The introduction of 735/765-kV systems began in the 1960s. There are three main reasons why such high-voltage systems were needed. The first reason was to transmit energy over long distances from remote generating sources to load centers. There are several examples that can be cited such as the Swedish 400-kV system, the Hydro-Quebec 735-kV system, and the 500-, 750- and 1150-kV systems in Russia.

Another important role of extra-high-voltage systems was to interconnect systems that had been previously isolated for the purpose of achieving economies in the use of generation sources. Examples can be found in Europe and on the Pacific Coast in the United States.

A third use of higher-voltage lines was to provide an overlay on an existing well-developed lower-voltage system. The purpose of such an overlay was to enable the bulk power transfer between generating plants and load centers, which permitted the integrated operation of the overall system in an economical and reliable manner. Such a system results in a complex network that is strongly interconnected with neighboring systems. Examples of such systems can be found all over the world, with the AEP 765-kV system as a prime example in the United States.

A number of transmission systems were designed, constructed, and operated at the 750-kV level in many countries around the world. At the 1000–1200-kV level, transmission lines were designed and built in Russia and Japan. The 1150-kV lines in Russia were operated at the nominal voltage for a few years and are presently being operated at 500 kV. The 1000-kV lines in Japan have been operated only at 500 kV since their construction, but are planned to be operated at their nominal voltage sometime in the future. Case studies of the following transmission lines at the 750-kV level as well as at the 1000-kV level are presented in the following sections:

15.4 Hydro-Québec 735-kV lines in Canada

15.5 American Electric Power Service Corporation (AEP) 765-kV lines in the U.S.

15.6 Russian 750-kV and 1150-kV lines

15.7 Electrificación del Caroni (EDELCA) 765-kV lines in Venezuela

15.8 Furnas Centrais Elétricas (FURNAS) 750-kV lines in Brazil

15.9 New York Power Authority (NYPA) 765-kV lines in the U.S.

15.10 Eskom 765-kV lines in South Africa

15.11 Power Grid Corporation of India Limited (POWERGRID) 765-kV lines in India

15.12 Korean Electric Power Corporation (KEPCO) 765-kV lines in South Korea

15.13 Tokyo Electric Power Company (TEPCO) 1000-kV lines in Japan

15.4 HYDRO-QUÉBEC 735-KV LINES IN CANADA

The first transmission lines above 700 kV in the world were designed, built, and commissioned by Hydro-Québec, the electric power utility in the province of Québec, Canada, in the fall of 1965. With the major hydroelectric potential located in the north and the load centers in the south, the need existed for transmitting large blocks of power over distances from 500 to 1000 km. When the first major hydroelectric power project was developed in the early 1960s on the Manicouagan and Outardes Rivers, with a combined output of 5300 MW, the power had to be transmitted over a distance of about 600 km to Montréal. Three transmission alternatives—at 315 kV, 525 kV, and 735 kV—were considered in a technical and economic evaluation. The alternative of 315 kV, Hydro-Québec's highest transmission voltage at the time, was abandoned immediately because of the large number of circuits required. Studies indicated that three lines of either 525 kV or 735 kV would be adequate, although the 525-kV circuits would require 50% series compensation. The costs of the two alternatives were approximately the same, but the 735-kV transmission without series compensation appeared more attractive since it was more flexible, could more easily lend itself to future expansion, and was a more reasonable overlay voltage to the existing 315 kV.

The 735-kV transmission was subsequently extended to connect with the Churchill Falls hydroelectric project in Labrador, with an output of about 5200 MW. This extension of the 735-kV transmission network comprised three lines between Churchill Falls and Manicouagan, an addition of two lines between Manicouagan and Québec city, and one line between Québec City and Montréal, in addition to the three lines already existing in the Manicouagan-Québec City-Montréal corridor. The integration of the Churchill Falls complex was completed in 1974.

To meet the growing energy demands of the province, Hydro-Québec decided in 1971 to develop the James Bay complex, generate about 16,000 MW, and transmit the power to the load centers about 1000 km to the south. Three alternatives—735 kV, 1100 kV ac, and ±600 kV dc—were evaluated for transmitting the power, but the decision was made to continue with the 735-kV lines for technical and economic reasons.

The Hydro-Québec transmission system at present comprises 76 single-circuit 735-kV line sections, for a total length of 11,280 km.

15.4.1 System Planning

System studies required to design the first 735-kV lines of Hydro-Québec were carried out on the Transient Network Analyzer facilities of General Electric, Schenectady, New York. The results showed that the maximum switching overvoltage would be 2.1 p.u., and the maximum dynamic (temporary) overvoltage would be 1.5 p.u. Subsequently, tests were carried out at the Project EHV in Pittsfield, Massachusetts, to determine the composite tower insulation—composite of the window size and the number of insulators in the window. The initial tests were carried out on a mock-up tower, and the results were later confirmed by tests on a full-scale 735-kV tower. Corona losses, calculated using the data obtained at Ontario Hydro's Coldwater test line, were considered in selecting the conductor bundle. The RI level of the selected bundle was checked using a Japanese empirical formula. Additional studies were carried out using the network analyzer and high-voltage test facilities at IREQ, the Research Institute of Hydro-Québec, for the design and optimization of subsequent generations of 735-kV transmission lines.

The new generations of Hydro-Québec's 735-kV lines were designed to withstand switching surge overvoltages of 1.8 p.u., achieved using circuit breakers with closing resistors. Based on the acceptable performance over ten years of operation of the first 735-kV lines, the tower insulation was designed to limit the risk of failure during line energization to less than 10^{-5} per tower and per event. The flashover risk was calculated from the distribution of the amplitudes of switching surges and the probability distribution of insulation flashover.

The James Bay 735-kV transmission system was planned originally according to the following criterion: Under full-transfer conditions, the system must be capable of withstanding a permanent single line-to-ground fault, normally cleared.

The Hydro-Québec 735-kV transmission system is a radial network made up of two 1000-km branches—one from the James Bay complex and the other from the Churchill Falls and Manic-Outardes complexes—connecting the generating stations in the north to the load centers of Québec City and Montréal in the south. A severe fault on such a system could result during the early stage of development in an out-of-phase condition between distant generating centers and, subsequently, in the separation of the two major transmission branches caused by simultaneous tripping of all lines when virtual faults (or near zero voltages) appear. Following a system separation, severe temporary overvoltages due to the Ferranti effect could appear on long unloaded lines that are still connected to the generators. A protection system, consisting of switched metal-oxide arresters and an unloaded line switching scheme, has been implemented.

A vast program of series compensation (about 11,000 MVAR) was launched in 1989 in order to increase the robustness of the system and to comply with more stringent design and operating criteria, particularly with the Northeast Power Coordinating Council (NPCC) criteria. Thirty-two sections of 735-kV lines have been equipped with series compensation. A defense plan, based on special protection system, was also put in place to increase the system security in case of severe extreme contingencies.

During normal system operation, shunt reactor switching, synchronous condensers, and Static Var Compensators (SVC) are used for overvoltage control. After contingencies, these devices are switched on predetermined voltage settings and time delays. In the early stages of developing the 735-kV system, bolted shunt reactors were used. Then circuit breakers were installed to switch off the reactors in case of high power flow on the lines. Synchronous condensers and SVCs were used to control the operating voltage and to provide voltage control after contingencies. In addition, precise detection of local voltage was used for automatic switching of shunt reactors to complement the action of the synchronous condenser and SVC for overvoltage and undervoltage situations.

Electromechanical distance protection—including fault-detection relays for phase-to-phase and phase-to-ground faults with a minimum of two zones, with under-reach permissive transfer trip and incorporating nonswitched measuring elements—was used up to 1990. On sections of the 735-kV lines on which series compensation was added, differential protection replaced distance protection. Single-pole reclosing was not used on 735-kV lines; however, reclosing has been permitted on some lines following a three-phase opening on a single-line-to-ground fault after a typical 1-s delay for uncompensated lines and 5-s delay for lines equipped with series compensation.

Microwave systems were used to provide the functions of communication and protection for the 735-kV lines. In recent years, however, Optical Ground Wire (OPGW) with 16 to 40 optical fibers have been increasingly used for purposes of both telecommunication and protection, with the microwave system used only as backup.

For more than 20 years, the selection of transmission-line routes at Hydro-Québec has been based on guidelines developed on the basis of the "Environmental Assessment Method for Transmission Lines and Substations." The main characteristic of the methodology is that an environmental perspective has been inserted into different planning, design, construction, and operation stages of the projects. The integration of this environmental perspective into the process has consisted of six operations: (1) technical understanding of the project; (2) knowledge of the environment; (3) project evaluation; (4) communication with different stakeholders; (5) selection of project and overall environmental assessment; and (6) environmental monitoring and follow-up.

The major difficulty encountered in siting the lines has been to take into account simultaneously the real human and natural environmental impacts of the project and the socio-political forces expressed by local groups with specific needs, which may not always be in harmony with environmental goals. Most of the high-voltage transmission projects, including 735 kV, have encountered opposition from specific groups of local communities. The opposition has come mainly from agricultural associations as well as from people living in the region who have concerns about nature, landscape, or the quality-of-life and who are intent on protecting their natural quality-of-life and the tourist potential of the region.

All the 735-kV lines in Québec are located in areas where the altitude above sea level does not exceed 1000 m. The lines cross farmland in the southern part of the network, while in the northern regions they traverse wooded areas. A small proportion of the lines cross hilly areas.

The isokeraunic level is about 20 in the St. Lawrence River Valley in the south and gradually decreases to about 5 in the northern James Bay area. A lightning location system (LLS), known as ORAGELECT, has been installed covering the entire transmission system of Hydro-Québec. The system is used primarily to help operating personnel during a thunderstorm by providing advance information about a possible line outage. It also helps maintenance personnel to locate a tower hit by a lightning strike that produced an outage, reducing the time required to inspect insulator strings for possible damage.

Two ground wires, each of 12.7 mm in the south and 11.1 mm in the north, were used on the 735-kV lines, with a shielding angle of less than 20°, which provides full protection against direct lightning strokes according to simulation studies. The size of the ground wires was determined, first, to provide sufficient mechanical strength considering severe ice and wind loadings and, second, to avoid excessive overheating during single line-to-ground faults. On some heavily loaded 735-kV lines, one ground wire has been insulated, sectionalized every 5 to 10 km, and grounded at only one point in each section to reduce losses.

In the St. Lawrence River Valley, the lines cross farmland where the ground resistivity is very low, with tower footing resistances as low as 1 Ω. In the northern regions, the soil resistivity may reach values as high as 10,000 Ω-m, and

the counterpoise is required to keep the ground resistance to a reasonably low value. On all 735-kV lines, a continuous counterpoise was used, except at river and road crossings, where ground rods were installed and connected to tower foundations, to obtain tower footing resistance less than 25 Ω.

In the region traversed by transmission lines in Québec, the temperature varies between slightly more than 30°C in summer to as low as -50°C in winter. Rain is frequent in spring, summer, and fall. During winter, snow occurs most of the time, but severe freezing rain may occur from time to time. Freezing rain and ice accretion are major considerations in line design, with some parts of the network getting 50 mm of freezing rain over a few days. Hydro-Québec uses a network of nearly 60 passive ice meters, which are essentially 25-mm-diameter steel tubes set horizontally 2 m above ground. Ice accretion data are collected twice a day and are then subject to statistical analysis to determine return periods of different ice accretion levels. Data are also being obtained through real-time monitoring, using ice rate meters mounted close to lines and ice-measuring stations located directly on the insulator string or overhead ground wires. The data obtained from these stations are used to develop improved design criteria, together with better operation and maintenance practices.

15.4.2 Electrical Design

The air gap clearances at the insulator strings of Hydro-Québec's 735-kV lines varied between 4.8 and 5.2 m, depending on the type of insulators used and the towers on which they were installed. The clearances between the phase conductors and any part of the tower were also variable. For V insulator strings, the distance varied between 4.1 and 4.6 m, while for suspension strings at rest the clearance varied between 4.3 and 6.0 m. For a suspension string displaced by strong wind, which might occur during one hour in a year, the clearance was reduced to between 3.1 and 4.5 m. The smallest air gap clearance occurred on guyed V towers on which, in a balanced position, it was as low as 2.8 m between the conductor and guy wires. The phase-to-phase clearance for the first generation of suspension towers was 15.3 m, and was reduced for subsequent generations of towers to 13.7 and 12.0 m. For Chainette towers, the phase-to-phase clearance was 12.7 m. The minimum conductor-to-ground clearances were 17.4 m above roads, highways, and railroads; 15.3 m in accessible regions; and 12.2 m in inaccessible zones.

Contamination was considered in selecting insulator strings, but it was not a serious concern since pollution levels were very low almost everywhere in the network (< 0.3 g/m^2). Leakage distance provided by the insulator strings was about 14 mm/ kV (phase to phase). Porcelain insulators were used exclusively on the first 735-kV lines of Hydro-Québec, but glass insulators have also been used later on. Some polymer insulators were installed mainly to test their field performance. Porcelain insulators continue to be used because of their excellent field performance. Glass insulators have also shown good field performance and are now being commonly used. However, polymer insulators have shown dielectric and mechanical weakness at their earlier stage, and it is also difficult to assess their dielectric integrity. The number of insulators in the string varied from 25 to 35 units depending on their spacing, mechanical strength, and coupling type. Electromechanical strengths of 110, 160, 220, and 300 kN were selected for use on the 735-kV lines.

Conductor bundles were selected mainly on the basis of corona performance. Both resistive and corona losses were considered in the economic choice of conductor cross section. Four conductor bundles with a subconductor spacing of 45 cm were used on all the 735-kV lines of Hydro-Québec. Bersimis conductors with a diameter of 35.1 mm were used on the first generation of lines, while the Carillon conductors with a diameter of 30.5 mm were used on the second-generation lines. For the James Bay transmission lines, Bersfort conductors with a diameter of 35.6 mm were used in the southern zone, while the Bersimis conductors continued to be used in the northern zone.

The RI level was limited for the first-generation lines to 67 dB at 1 MHz, ANSI meter, during foul weather at 30 m from the outside phase. The criterion was modified later on, to be in conformity with Canadian Standards, to the maximum fair weather level of 63 dB at 0.5 MHz, CISPR meter, at 15 m from the outside phase. The design criterion for audible noise was 60 dBA during foul weather at the edge of the ROW. The width of ROW for Hydro Québec's 735-kV lines has been fixed at 91.5 m.

Long-term measurements of RI at 1 MHz, ANSI meter, and AN in dBA, both made at 15 m from the outside phase, have shown the following results: mean fair weather RI and AN levels were 49.9 dB and 46.1 dBA, respectively, for the first-generation lines and 58.6 dB and 47.5 dBA, respectively, for the second-generation lines; mean foul weather RI and AN levels were 61.1 dB and 50.6 dBA, respectively, for the first-generation lines and 67.0 dB and 54.65 dBA, respectively, for the second-generation lines. Hydro-Québec audible noise design criterion is now fixed at 55 dBA at the edge of the right-of-way, under wet conductor.

The lines were designed to limit the electric field to 10 kV/m at midspan and for maximum conductor sag. Subsequently, the criteria of 2 kV/m at the edge of ROW and a

maximum value of 6.5 kV/m on roads were adopted in order to limit the induced currents in vehicles to a safe level. Consequently, the minimum clearance of conductors above ground is now 14.1 m in general and 17.5 m above road, and the ROW width is 80 m. No international standards exist for the magnetic fields from transmission lines.

15.4.3 Mechanical and Tower Design

The 735-kV transmission lines in Québec cover a fairly extensive territory exposed to great climatic variations with extreme conditions of wind, temperature, precipitation, and lightning. Because the lines are constantly exposed to wind conditions generating aeolian vibrations, spacer dampers are used on all lines with bundled conductors. In the early stages of development of 735-kV lines, commercially available spacer dampers were used, which resulted in an unsatisfactory operational experience. Hydro-Québec has, therefore, developed and commercialized its own design of spacer dampers, holding the cables by means of preformed rods as well as solid clamps, applicable to different number of subconductors in the bundle.

During winter in Québec, precipitation occurs mainly in the form of snow and freezing rain, often accompanied by strong winds. It is necessary, therefore, to design transmission lines for appropriate ice and wind loadings. The first generation of 735-kV lines was designed according to Canadian standards for a radial ice thickness of 12.7 mm, along with 385 Pa of wind pressure, using a deterministic approach with safety factors. However, after incidents of damage to the 735-kV lines due to ice storms in 1969 and 1973, Hydro-Québec revised the design criteria and sought to improve its understanding of meteorological phenomena that present danger to transmission lines. Following these extensive studies, new design criteria, using a probabilistic approach, were developed for ice and wind loadings: generally, in the southern zone, 45 mm of radial ice thickness or a combination of 20 mm of ice thickness and 300 Pa of wind pressure; in the northern zone, 32 mm of ice thickness or a combination of 10 mm of ice thickness and 230 Pa of wind pressure.

The most severe ice storm in the recorded history of Québec occurred in January 1998, covering the southwestern region of the province, causing an accumulation of more than 100 mm of ice in five days on the ground and loads exceeding the design criteria of transmission lines. A number of transmission lines at all voltages collapsed due to ice accumulation, resulting in extensive damage to the transmission system. Studies undertaken following this incident may lead to a revision of the design criteria.

Over the past 40 years, Hydro Québec has made continuous improvements in developing several tower designs, based on new design philosophy and criteria, to achieve the optimum balance between adaptability to the type of terrain and minimum cost. Four specific types of towers were used extensively on the 735-kV lines: (1) self-supporting steel lattice tower (1965); (2) narrow-base guyed lattice tower (1974); (3) steel guyed V tower (1976); and (4) Chainette tower (1980). The weights of these four generations of towers were 65 tons/km, 42 tons/km, 31 tons/km, and 19 tons/km, respectively. The weight of the Chainette tower is only 30% of the first-generation lattice towers but require extensive ground space. Tubular towers were also used on some sections of 735-kV lines, mainly for esthetic and economic reasons. A typical first-generation tower is shown in Figure 15.4-1, while Figures 15.4-2 and 15.4-3 show a Chainette suspension tower and a tubular self-supporting tower, respectively. Figure 15.4-4 shows a reinforced lattice steel tower for use in regions with a high risk of ice storms.

Mainly grillage-type foundations were used for the self-supporting suspension as well as for angle towers. For large angle towers, concrete foundations on piles were used because of the larger load components involved. Tubular structures were built on caisson-type foundations, which consist of a large-diameter tube of heavy-gauge steel filled with concrete. The main difficulty encountered with certain types of grillage footings has been frost heave. This situation has been corrected by increasing the depth of the foundation.



Figure 15.4-1 First-generation Hydro-Québec self-supporting 735-kV tower.



Figure 15.4-2 Hydro-Québec/TransÉnergie Chainette suspension tower.



Figure 15.4-3 Hydro-Québec/TransÉnergie tubular self-supporting tower.

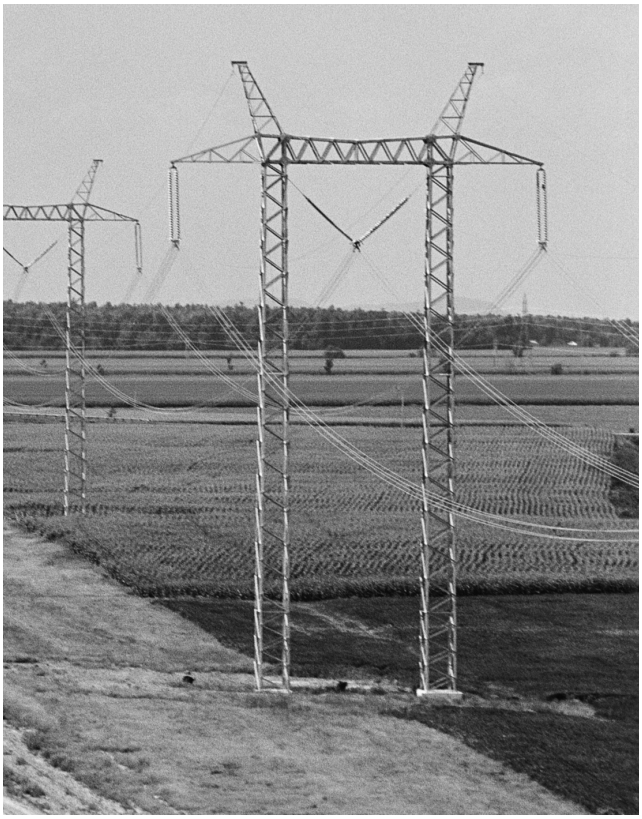


Figure 15.4-4 Hydro-Québec/TransÉnergie reinforced lattice steel tower.

Hydro-Québec has followed the classic techniques of erecting the towers with a gin pole. But this technique has been phased out by resorting mainly to high-capacity lift cranes. In the recent past, 99% of all construction has been carried out with lift cranes. The Chainette tower could be easily erected by means of conventional methods or by helicopter. The line conductors were installed using conventional pullers.

Hydro-Québec has developed an emergency plan for any event likely to happen on the power grid. Emergency centers are put in place, and include specialists from the utility. Three warehouses are equipped with material for immediate construction of 10 km of lines of different voltages. A particular feature of the Chainette tower is the possibility of quick repair in case of failure. In fact, the replacement of a Chainette tower takes about one-tenth the time required for a self-supporting tower. This feature makes the Chainette tower ideally suited for emergency replacement.

15.4.4 Operation and Maintenance

The maintenance frequencies adopted for inspection of Hydro-Québec 735-kV transmission lines are as follows:

- Line in rural and forest zone: helicopter patrol once a year and foot patrol once every two years.
- Line in urban zone: foot patrol twice a year.
- Earlier spacer dampers replaced by those of Hydro-Québec because of improved design and less damage to conductors.
- Replacement of some of the old insulators by the new porcelain and glass insulators because the old insulators suffered reduced mechanical resistance and a high rate of perforation.

The outage experience of the 735-kV transmission lines may be summarized as follows:

- Lightning is responsible for about one outage per 1000 km of line per year, based on 40 years of operating experience and more than 10,000 km of lines;
- On a few occasions, switching surges resulted in a fault, which was generally attributed to broken units in an insulator string.
- No outages could be attributed to polluted insulators.
- Some outages have been caused by forest fires and freezing rain that short-circuited insulators.

The cause of the most disruptive outage due to the ice storm of 1998 has been identified as combined ice and wind load in excess of design criteria. The changes in frost and ice accretion levels in southern regions of Québec, particularly on hill slopes, have been taken into account in line design. A few outages of the 735-kV transmission system occurred due to equipment failures, including shunt reactors, arresters, circuit breakers, and instrument transformers. However, no statistical data are available on these failures.

No complaints have been received about the audible noise from operating 735-kV lines. However, concerns about audible noise have been expressed at public hearings on the construction of new 735-kV lines. Electric and magnetic fields and possible health effects have been issues of public concern for more than 30 years when obtaining the construction permits for new 735-kV lines. These concerns are usually expressed at public hearings. Specialists at Hydro-Québec have developed several public information brochures on EMF and health, and the public has also been guided through a special interpretation center created by Hydro-Québec, called Electrium.

Since the introduction of the 735-kV transmission system, Hydro-Québec has practiced live line maintenance using insulated sticks as well as barehand techniques. In the early stages of operating the 735-kV lines, commercial equipment was used exclusively for live line work. Over the last 20 years, however, special equipment, such as a mobile insulated ladder all-terrain vehicle and a remote insulated jib, as well as working procedures, have been developed jointly with IREQ. Remotely Operated Vehicles (ROV), also known as Line ROVers, were developed recently for overhead ground wire de-icing. This equipment has since been used at Hydro-Québec for maintenance applications such as visual and infrared inspection, evaluation of the condition of compression splices (based on resistance measurements), replacement of conductors and ground wires (live), and cleaning and deicing of conductors, etc.

The 735-kV lines of Hydro-Québec are designed to carry 2000 MW. In winter, when the peak load is reached, some of the lines are loaded to their design value. It also occurs from time to time in summer, when some lines are out of service for maintenance purposes and the production is concentrated in a particular generating station to control the water level in reservoirs. Since series compensation has been added on many lines, during contingencies, the load on these lines may exceed 3000 MW for less than half an hour. Although not part of the initial design, the thermal margin associated with the conductor bundle allows this mode of operation.

15.5 AMERICAN ELECTRIC POWER SERVICE CORPORATION (AEP) 765-KV SYSTEM IN THE U.S.

To meet load growth in the AEP service area in the 1960s and 1970s, major generating plants with units as large as 1100 and 1300 MW were being added. Multiple units were added at some generating plants located in proximity to one another, which resulted in concentrations of generating capacity as large as 4000 to 5000 MW. To move such large amounts of generation required a higher voltage, and AEP chose 765 kV as an overlay of their existing 345- and 138-kV systems for two reasons: (1) it was the highest voltage technologically proven at the time, and (2) because of the five-fold increase in circuit capability, it effectively provided over 345 kV (Barnes and Nagel 1969). From AEP's viewpoint, this was a continuation of the company's basic philosophy that a strong transmission network, adequate at all times to meet the most severe outage conditions, was indispensable to the successful operation of a fully integrated power system. At that time, the use of electric power was doubling about every ten years, and the cost per kilowatt transmitted using 765 kV, rather than 345 kV, was about half. The economic advantage of 765 kV versus 345 kV arises because of the 5-to-1 transmission capability.

For many years, AEP has been a pioneer in the development of higher-voltage transmission. Many years of study, beginning with the Tidd 500-kV Project in 1946 and the Apple Grove Project in 1961, provided the technical information that determined the feasibility of operating voltages in the 500- to 800-kV range. AEP also had years of experience operating an extensive 345-kV system that had many of the challenges associated with extra-high-voltage systems, such as corona, resistance-capacitance, switching surge overvoltages, arc deionization, capacitive compensation, insulation coordination, lightning arrester performance, influence on relaying of transient currents and voltages, high-breaker duties, stability of large motors and generators, conductor and tower stresses, and many others. In essence, the 345-kV system was a laboratory that provided firsthand experience into the understanding of the multitude of technical issues associated with EHV transmission.

When AEP introduced the first 765-kV system in the United States, the main technical issues that needed to be addressed at that time were radio noise, corona losses, switching surge, and lightning performance. Since the lines were built in fairly pristine environments, contamination was not much of a concern. The energization of the first line brought forth some complaints about foul-weather audible noise, which resulted in audible noise research at the Apple Grove Project (Kolcio et al. 1974).

15.5.1 System Planning

AEP conducted comprehensive system planning studies for the first 765-kV lines, as is well documented in an IEEE paper (Vassell and Maliszewski 1969). This paper compares equipment costs and discusses the basic system performance characteristics of 765 kV versus 345 kV. One of the main differences between 345 and 765 kV is the large quantity of excess line charging that needs to be absorbed by the system from a lightly loaded 765-kV system compared to a correspondingly loaded 345-kV system. To control this large quantity of line charging, shunt-reactive compensation was built into the 765-kV system. AEP anticipated that 70–80% of the 765-kV line charging needed to be compensated by shunt reactors during the first few years of operation because the lines would be lightly loaded. In addition to installing 765-kV shunt reactors throughout the system, AEP has also installed 345-kV series reactors at one of their 765/345-kV stations so as to limit short-circuit fault currents.

One of the system planning studies that was required in the design of the 765-kV system was the determination of expected overvoltages, which can exceed 3 p.u. To determine these overvoltages, AEP engineers used the General Electric transient network analyzer (TNA), the Westinghouse Electric ANACOM, and the Allis-Chalmers electronic differential analyzer (EDA), supplemented by hand calculations and digital computer studies. These studies basically showed that the overvoltages could be controlled to 2.0 p.u. if preinsertion resistors were used (Hauspurg et al. 1969). AEP is currently using surge arresters located along the line's length to control overvoltages in lieu of breaker closing resistors.

AEP retained an outside consultant to conduct a meteorological study of the area transversed by the 765-kV lines. This study was undertaken in the 1960s and followed the conventions of that time; that is, wind was measured as the fastest mile, not the current 3-s gust, etc. No special techniques were used to measure ice accretion. The study was used to confirm/refine the ice and wind loadings that were used to design much of AEP's 345-kV and all the 765-kV transmission lines. The determined ice and wind loads, the combinations of these loads, and individual material overload factors (steel, conductor, insulators, etc.) became the ultimate loads applied to the 765-kV towers/conductors.

By 2004, AEP had built about 3400 km of 765-kV transmission, and another 145 km was under construction.

Since AEP was the first utility to build 765-kV lines in the U.S., they conducted a number of field studies to determine the line routing and the electrical and mechanical parame-

ters of the lines. They relied heavily on the research results that came out of the Apple Grove 750-kV Project and Project EHV, but they also conducted many other studies that will be described in this section.

As was mentioned earlier, when AEP was designing the initial 765-kV system, the main technical issues, from an electrical standpoint, were radio noise and corona loss due to conductor corona and switching surge and lightning performance. But, after the first line was energized, audible noise (AN) became an issue, as did induced voltages and currents into objects and people due to the 60-Hz electric field. This experience instigated research on both these phenomena at Apple Grove, Project UHV, and other research facilities around the world.

AEP chose not to transpose their 765-kV lines. The utility felt that transposing the lines would result in an added cost of building nonstandard towers to complete the transposition, introduce phasing complexities, and/or interfere with the placement of future stations along these initially long lines.

AEP uses power line carrier (PLC) quite extensively. The utility feels that it provides the most secure long-distance relaying channel if properly coupled and trapped. AEP uses Mode 1 coupling at all 765-kV substations. PLC is used for protection of the transmission lines, circuit breakers, and power transformers. The PLCs operate in the frequency range of 30–250 kHz, depending on line length. A 100-W carrier system has been found to give adequate signal-to-noise ratios, even for the Rail conductor, which is the smallest conductor used on the 765-kV system.

AEP has not used ADlash or ADSS types of fiber-optic cables on their system. They have used a tightly buffered OPGW design on some of their 765-kV lines. This OPGW consists of a 24-fiber design, with 12 fibers within a plastic tube and the plastic tubes inside a continuous aluminum tube. At the time this chapter was written, AEP had 26 km of OPGW installed with good experience.

15.5.2 Electrical Design

The phase conductors selected for the first 1500–1600 km of line were 4-Rail conductors. This conductor was slighter smaller than the conductor on the Apple Grove B-Line, which used 4-Cardinal conductors. It had been determined that the Cardinal conductor was adequate for 765-kV operation. The conductor selected for the next approximately 1800 km of line was a 4-Dipper conductor. Using this conductor reduced the audible and radio noise approximately 3 dB. Some lines using the 4-Rail conductors were built between 1000 and 1200 m above sea level in the Appalachian Mountains. At these altitudes, the AN was about 3 dB higher than the lines that were built closer to sea level. This higher AN produced some complaints from people who lived close to the lines. Because of these complaints, the conductors selected for the next line, which will be 145 km in length and will also be built at the higher elevations, are Tern conductors in a bundle of six subconductors. The Tern conductor has a diameter of 2.7 cm. The characteristics of the three conductors used by AEP at 765 kV are shown in Table 15.5-1, along with the nominal phase spacing and the minimum conductor heights. The minimum conductor heights are the minimum ground clearance. The minimum crossing clearance over other lines is 7.92 m. Minimum clearances of 13.7 m and 15.2 m were established over roads and railroads, respectively. It should be noted that some of the earlier AEP light tangent towers have phase spacing as small as 12.5 m and as large as 16.8 m. Also, all lines built after 1977 were designed to minimum ground clearances of 13.7 m at 120°F (49°C) across cultivated lands.

The overhead ground wires used on all of the AEP lines are seven No. 8 Alumoweld wires that have a diameter of 0.98 cm. The nominal attachment height is between 42.7 and 45.7 m, with a shield angle of 23°. AEP has sectionalized some of their overhead ground wires in an "open-loop" technique to reduce ground losses (Keri et al. 1984). The ground wires are insulated from the towers at every other tower by two insulators placed in-series with the ground wire at the tower (dead-ending the ground wire on each side of the tower). The insulators are installed with grounded arcing horns that facilitate flashover when the ground wire is struck by lightning. The ground wire is grounded at the tower in between the insulated towers.

Impulse and 60-Hz tests were conducted to determine the number of insulator units, air gap clearances, and tower

Table 15.5-1 Line Parameters for AEP 765-kV Lines

Conductor Type	No. of Cond.	Cond. Diam. (cm)	Sub. Cond. Spacing (cm)	Bundle Diam. (cm)	Stranding	Phase Spacing (m)	Min. Conductor Heights (m)
Rail (ACSR)	4	2.96	45.7	64.7	45/7	13.7	12.2
Dipper (ACSR)	4	3.52	45.7	64.7	45/7	13.7	12.2/13.7[1]
Tern (ACSR)	6	2.70	38.1	76.2	45/7	13.7	13.7

1. The 13.7-m minimum height was adopted after the 1977 NESC.

configuration (Hauspurg et al. 1969). From these tests, it was found that standard porcelain disc insulators, rather than a special design, would satisfy the electrical requirements. For tangent structures, two different suspension-insulator assemblies were used in either a single- or a double-V. Some single-V assemblies used 25,000-lb units and others used 36,000-lb units. This was also true for the double-V assemblies. The number of insulators used on the outside phase and center phases are 30 and 32 insulators, respectively. For dead-end structures, quad bundles are used. The number of insulators in the quad bundle is 32 insulators if the quad consists of 50K units and 34 if 36K units are used.

Since the AEP 765-kV lines were built in relatively pristine areas, insulator contamination was not an issue in the selection of the insulators.

Both the single- and double-V assemblies were designed with provision for hot-line maintenance. This was done by placing centering notches at the top of the yoke plates for both the single- and double-V insulator assemblies.

The vertical strike distances were 4.57 and 5.49 m for the outside and center phases, respectively. The comparable horizontal air gaps were 4.27 and 4.87 m.

At the time this chapter was being written, AEP was in the process of building their first 765-kV line that uses a six-conductor bundle. This line experienced significant siting problems, and it took more than 10 years from application to approval. One concern was AN, since the line would traverse a mountainous area of Virginia at altitudes between 1000 and 1200 m. The original 765-kV design built at these altitudes had some AN complaints. Since there was a need for another 765-kV line in the same state at these altitudes, AEP instigated a research project to look at other options, such as five or six conductors in a bundle. As part of this research effort, AEP reconductored four spans of an operating 765-kV line with 6-Tern conductors. The long-term measurements showed that the AN would be about 4 dBA lower than the original design. Calculations showed that the radio noise would be reduced as much 8.5 dB.

As was mentioned earlier, AEP has used standard porcelain insulators on all their 765-kV lines. However, for this new line, nonceramic insulators (NCI) insulators will be used on the majority of the structures; the remaining structures will use standard porcelain discs. The hot and ground ends of the polymer insulators will be protected from excessive corona by the installation of grading rings.

15.5.3 Mechanical and Tower Design

AEP not only conducted detailed studies to determine the line insulation and the conductor configuration, they also looked at a number of different tower types (Samuelson et al. 1969). The structures selected for suspension are the self-supporting and the guyed-V structure shown in Figures 15.5-1 and 15.5-2. In general, the guyed-V structures were used in the mountainous areas, and the self-supporting towers were used in the relatively flat areas. The guyed-V structures were constructed with helicopters, and the self-supporting structures were constructed using cranes.

AEP's standard practice is to conduct mechanical design load tests on all new 765-kV tower designs. This practice was continued for AEP's latest 765-kV line. Mechanical and electrical tests, as appropriate, were conducted to select the anchors, guys, insulator assemblies, conductor



Figure 15.5-1 AEP 765-kV self-supporting suspension tower with four-conductor bundle.



Figure 15.5-2 AEP 765-kV guyed-V suspension tower with four-conductor bundle.

fittings, and the spacers. A spring-type spacer was selected for the first AEP lines to limit subconductor contact.

Initially, AEP used Stockbridge dampers to control aeolian vibration, but later lines resorted to the use of spacer dampers to maintain the bundle shape and control vibration.

In spans that have only spacer dampers, the spacers are spaced asymmetrically. For example, the first spacer is placed 61 m from the tower, then 68.6 m to the next spacer, then 61 m to the next one, then 53.3 m to the next one, etc. AEP feels the vibration protection is improved with this asymmetrical spacing. For the new line being built, AEP will use a new spacer damper. An indicative example is shown in Figure 15.5-3.

AEP also tested several foundation types. For the self-supporting towers, they tested steel grillages, reinforced concrete auger caissons, and steel H pilings. All three are used, depending upon the type of soil.

15.5.4 Operation and Maintenance

At the January 1972 Winter Power Meeting of the IEEE Power Engineering Society in New York City, AEP presented a series of five papers on their initial experience with the first 30 months of operation of the 765-kV system (Scherer et al. 1972; Vassell et al. 1972; Scherer et al. 1972; Haas et al. 1972; Garrity et al. 1972). The first link of the 765-kV system had been energized on May 2, 1969, and by the time those papers were presented, AEP had 1078 km of 765-kV lines, with the associated terminal and transformation equipment in operation.

As part of their line inspection process, AEP has historically performed a minimum of one or two aerial surveys a year, a ground-based inspection every six to seven years, and a tower-climbing inspection every 12 years. These inspection intervals are constantly reviewed and modified as physical conditions warrant. From these inspections, the utility has found very few problems and none that required a redesign of the lines. AEP has experienced mechanical failure of the original spring-type spacers. The failed spring spacers were replaced with the new spacer dampers, and the original Stockbridge dampers have been retained. Replacing the spring spacers was difficult and costly due to scheduling outages, placing of carts on the conductors, or the use of large bucket trucks/cranes. Today, replacement of the spring spacers is completed by the use of helicopters working on energized conductors. This practice has resulted in some spans having a combination of spring spacers, Stockbridge dampers, and spacer dampers. The combination of spacer types and vibration protection has worked well, and has minimized spacer maintenance cost to the early lines built with the original spring spacer design.

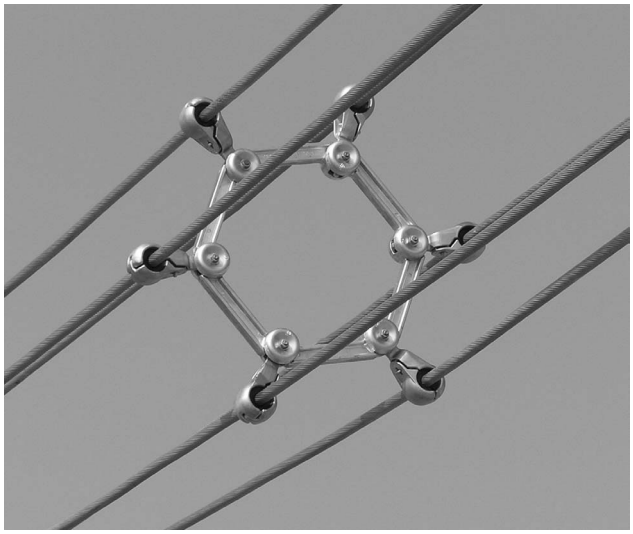


Figure 15.5-3 Six-conductor-bundle spacer damper.

In maintaining energized lines, AEP has used hot sticks, bucket trucks, and helicopters. AEP was a pioneer in the development and use of the barehand technique for maintaining overhead lines. Today, helicopters are used to replace spacers and sleeves. Except in the case of live-line maintenance with helicopters, AEP, in spite of being a pioneer in developing the barehand approach to performing maintenance, now does maintenance on their 765-kV system by obtaining outages. In fact, at the time of the writing of this chapter, AEP had not conducted any live-line maintenance over the last 15 years. AEP still maintains the proper training and equipment to perform live-line maintenance at 765 kV, but in recent years, the redundancy of AEP's 765-kV system has made it possible to schedule circuit outages without undue difficulty. AEP is prepared to return to live-line 765-kV maintenance for those components that cannot be maintained from a helicopter as system operating conditions make it difficult to obtain outages. Until that time, AEP is taking advantage of the lower maintenance cost associated with de-energized maintenance.

AEP did not grade the insulators on the original suspension towers, but that will be done on the suspension towers for the new line being built with a six-conductor bundle using nonceramic insulators. Some porcelain insulators on lines with four-conductor bundles have experienced what the utility refers to as a "donut effect." AEP's field personnel call these insulators "Donut Insulators," to describe punctured porcelain disc insulators, where the puncture initiates a circumferential crack in the porcelain body around the metal cap. The porcelain shell lets go from the remaining intact insulator cap and pin; the resulting porcelain shell,

without the center portion of the insulator, looks like a donut. To solve this problem, AEP prefers to reinsulate rather than install corona rings. The "donut effect" is not well understood, but AEP strongly suspects that it is a function of the high electrical stress across the bottom one to three disc insulators in the V-string and the physical makeup of the insulator. While all of the 765-kV disc insulators experience the same electrical stress at their relative position in the V-string, AEP has only experienced 15 "donut" insulators out of a population of roughly 1.4 million disc units. They have not seen this effect on any of their 345-kV or 500-kV lines. If AEP were to build a new 765-kV line with porcelain insulators, they would add grading rings to lower the electrical stresses. The electrical stress on the porcelain disc insulators used on AEP's new 765-kV line will be graded by the hardware grading ring installed on the six subconductor yoke plate.

AEP's lines are in an area of the U.S. that experiences tornadoes. They have experienced 765-kV tower failures from both tornadoes and icing. AEP has been operating their 765-kV systems for 35 years. During that time, they have lost about 5 towers to tornadoes and about 80 towers due to icing over a 32-km stretch. The tornadoes twisted the towers at their waist so that, from the waist up, the towers fell to the ground. The ice failure was a classic vertical overload failure. Once the first tower failed, the vertical span on the next tower was increased and it failed. The towers looked like someone had pushed them down from the top. The failure cascaded until it came to a tower with a greater vertical design capacity than the towers that had failed. The tower that stopped the cascading was a dead-end tower, mainly because all of AEP's dead-end towers are designed for a longer weight span than the corresponding tangent towers. AEP designs for 3.2 cm of ice, but the ice on the subconductors for this case was between 6.4 and 7.6 cm.

When it comes to lightning, AEP has had less than 1 outage per 100 miles (161 km)/yr. The original estimate was that line outages due to lightning would not exceed 1.0 per 100 miles (161 km) per year, which was the performance of comparable single-circuit 345-kV lines on the AEP system in isokeraunic levels between 40 and 50. AEP has not had any failures due to contamination or switching surges. However, they have had outages due to structure failures, as described in the previous paragraph.

In general, AEP's 765-kV lines have performed satisfactorily with respect to corona- produced effects such as RI, AN, and TVI. When the first line section was energized, there was an initial wave of AN complaints during foul-weather conditions. Subsequent analysis determined that the majority of these complaints occurred during an initial series of switching-surge tests conducted on an unloaded line at 800 kV. The complaints mainly came during heavy fog conditions from homes near a line that crossed the Ohio River. Subsequent lines were energized and tested with more care, and complaints diminished. This experience, however, instigated a major research effort at the Apple Grove 750-kV Project to gain a better understanding of foul-weather AN.

Over the 35 years that the AEP 765-kV system has been in operation, there have been scattered AN complaints. Lines built at higher elevations in the Appalachian Mountains in Virginia had the most AN complaints. To find solutions to the AN problems, AEP spent quite a bit of effort researching various techniques for reducing AN on spans near homes of complainants. The utility investigated the possibility of taking loops made of very small-diameter copper wires and clipping them to the subconductors to produce ultra-corona. This approach reduced the broadband AN, but increased the 120-Hz hum, the corona losses, and the TVI. The utility studied the effect of placing the four-conductor bundle in an asymmetrical arrangement. This method was found to reduce the AN during light rain and fog. The utility also tried placing a conductive tube over the subconductors. Placing a 7.6-cm aluminum tube over each subconductor reduced the AN as much as 10 dBA during light rain and fog conditions (Nourse 1969). A semiconductive neoprene rubber spacer was used to center the tubes and electrically bond the tubes to the subconductors. The last two techniques were actually used on some spans.

AEP has also experienced a few RI complaints in low-signal-strength areas, which were easily resolved. TVI complaints during foul-weather conditions in rural areas where the signals are not very strong were resolved by relocating antennas, connecting customers to cable systems, etc.

The possible generation of ozone and other gaseous products was raised by a number of property owners in the course of obtaining some of the original easements. AEP, along with others, thoroughly analyzed this problem through laboratory tests and measurements on operating lines and measurements on the test lines at the Apple Grove 750-kV Project and at Project UHV. All these measurements programs have determined that the amount of ozone and other gaseous effluents is too small to be a problem.

People living near the AEP 765-kV system have experienced some spark discharges when they touched fences, rain gutters, and other metallic objects. But these problems, for the most part, were easily resolved through proper bonding and grounding of the objects.

AEP maintains emergency material (towers, conductor, insulators, hardware, etc.) to replace 3 to 8 km of line in case any lines need to be quickly restored due to natural or manmade disasters. The system design permits extended outages of a single 765-kV circuit. Thus the restoration philosophy is not to make emergency repairs but to restore the damaged portion of line to its original condition. AEP did experience one ice-related failure that exceeded its emergency materials inventory. The circuit was out of service until new materials could be ordered, fabricated, and installed.

AEP has had some outages due to equipment failures. Examples are transformers, shunt reactors, CCVTs, etc.

15.6 RUSSIAN 750-KV AND 1150-KV LINES

The vast territory covered by the former USSR and even the present-day Russia (since 1991), combined with dispersed locations of energy resources and population centers, shaped the evolution of high-voltage power transmission systems in these countries. As a result, the distances over which electric energy had to be transported were generally larger than those in countries like the U.S., requiring the use of higher voltages. The electric power grid in Russia stretches from west to east for about 7000 km. The need to transmit large blocks of power from remotely located, huge power plants to the load centers, as well as the requirements of developing the power grid as a whole, played important roles in the choice of transmission voltages in Russia. Also, unlike the approach commonly used in many free-market countries, the choice of transmission voltages in Russia was made practically neglecting land costs, and the costs of labor and materials were taken into account quite differently than in western countries. One consequence of these differences, for example, was the selection, for the same transmission voltage, of a larger number of conductors of smaller diameter in the bundle.

Historically, two systems of gradually increasing nominal transmission voltages developed: 35 – 110 – 220 – 500 kV in the main territory and 35 – 150 – 330 kV in the western part of the country. Initially, the voltage 400 kV was superimposed over the 35 – 110 – 220 kV system, but subsequently all the 400-kV lines, except a few interconnecting with European countries, were up-rated to 500 kV. The selection of 750-kV and 1150-kV transmission systems was a natural extension, slightly more than doubling the existing 330-kV and 500-kV systems, respectively.

The first test/commercial 87-km-long, 750-kV transmission line was put into operation between Konakovo and Bely Rast in 1967. The substations at its ends served as full-size test sites for newly developed 750-kV equipment. The program of field tests here lasted for several years and was then followed by a nationwide program of field and commissioning tests on all the existing 750-kV transmission lines. The 750-kV transmission lines (nominal voltage: 750 kV; maximum permissible rated voltage: 787 kV) were built and commissioned in association with the construction of 3.6-6.4 GW steam and nuclear power plants (the largest hydro power plant was also 6.4 GW) and introduction of a new backbone to the existing grid for the purpose of enhancing its reliability, maneuverability, and economic performance. The total length of 750-kV lines in the former USSR approached 8000 km, of which about 3000 km now operate in Russia.

As the first step in introducing the new voltage class 1150 kV, the 750-kV substation at Bely Rast was complemented in 1973 with a 1150-kV switchyard and test line. Here full-scale tests were conducted by researchers representing both the manufacturers and the electric utility. It was used also to train utility staff. Later a second switchyard used only by the manufacturers was erected in Toljatti City. The first 1150-kV transmission lines (nominal voltage: 1150 kV; maximum permissible rated voltage: 1200 kV) were designed primarily to deliver power from clusters of thermal power plants in Kazakhstan and Siberia to the integrated power grid of the former USSR and provide backbone in regions where 500 kV had been the highest transmission voltage. From the total projected length of 1150-kV transmission lines of about 10,000 km, only 2350 km were constructed at the time of the dissolution of the USSR (950 km in Russia itself), and only 900 km operated at 1150 kV for several years. The first 1150-kV Ekibastuz-Kokchetav transmission line, 500 km long, was put into operation in 1985. The 390-km-long Kokchetav-Kustanai extension of the line was commissioned in 1988. Commissioning of both lines was immediately followed by full-scale tests, similar to those on 750-kV lines. Other sections of the line, although designed and built for 1150 kV, were operated at 500 kV. Since about 1995, all 1150-kV lines operate at 500 kV.

In the 1980s, a pilot program with appropriate tests was conducted to determine the maximum possible rated voltage for ac transmission lines. A large insulation test facility was built near Moscow for the VEI Electrical Research Institute, and the existing outdoor installations in Leningrad were upgraded for these tests. Taking into account the fast, nonlinear increase of required air gaps with voltage, 1800 kV ac, with switching surge limitation to 1.45 p.u., was chosen as the next voltage class. The program carried out the design of the line—with phase bundles of 11 subconductors, ACSR-240 mm^2—manufacturing of prototype equipment, and tests of the line. Then, with the collapse of the USSR and the lowering of demand for electric energy, this program was abandoned—at least for now.

15.6.1 System Planning

Standards were developed in Russia, through studies carried out jointly with equipment manufacturers, for permissible temporary overvoltages. The standards cover temporary overvoltage durations from 8 h to 0.1 s, with the permissible magnitudes varying from 1.025 p.u. for duration of 8 h to 1.35 – 2.4 p.u. for duration of 0.1 s, depending on the type of equipment and rated voltage. The 750-kV and 1150-kV transmission lines were designed to withstand switching overvoltages of 2.1 p.u. and 1.8 p.u., respectively. For the future generation of 750-kV and 1150-kV lines using metal oxide surge arresters, however, the withstand levels for switching overvoltages were reduced to 1.8 p.u. and 1.6 p.u., respectively.

The following overvoltage control measures were used on both the 750-kV and 1150-kV lines:

- Switchable shunt reactors installed at both ends of the line, their circuit-breakers being equipped with spark gaps for instant reactor connection, through spark and following arc, to the line at fault line trippings.
- Metal oxide arresters installed at shunt reactors and capable of withstanding switching surges and some temporary overvoltages.
- Programmed or/and automatically controlled planned operations and fault trippings.
- Pre-insertion resistors in line circuit-breakers (1150 kV only).

The main protection for the 750-kV and 1150-kV lines was based on the comparison of electrical parameters on line ends, using the combined power-line carrier current directional and phase comparison relay schemes. Multi-step reserve relay protection devices were also used on the lines. Although phase conductors were used for transmitting carrier current signals on lower voltage lines, insulated ACSR shield wires were used for this purpose on the 750-kV and 1150-kV lines. Two single-conductor ground wires, each insulated by two suspension insulators, were used to transmit the carrier current signals on 750-kV lines, while two two-conductor bundles, each insulated by four suspension insulators, were used on the 1150-kV lines. To reduce the induced power frequency voltages, the ground wires were transposed every 10–40 km, preferably at dead-end towers. The ground wires were grounded via high-frequency choke coils at intervals of up to 110 km, where the amplification of the communication signals was required.

The observation of local meteorological stations served as the main source of weather information for line design. In order to obtain information on ice accretion, a cylindrical conductor of 1 cm diameter was used. Wind measurements were made at 15 m above ground, and ice measurements were obtained at 10 m above ground. Special correction coefficients were found and standardized for taking into account the rise in wind velocity and ice wall thickness with the increase in the height of the conductor position and for reduction in wall thickness with the increase in the conductor diameter. The second important source of information about catastrophic wind and ice conditions was the operating experience of existing transmission lines in the same area.

15.6.2 Electrical Design

Extensive tests to determine the dielectric strength of air gaps and the application of probabilistic approaches were the basis for determining the various air gap clearances of 750-kV and 1150-kV transmission lines. Table 15.6-1 shows the minimum air gap clearances required on the 750-kV and 1150-kV lines. The actual values of the height above ground of conductors at midspan were higher than those in the table in order to meet the criteria for ground-level electric fields. Similarly, the phase-to-phase clearances were also larger than those shown in the table to meet other design considerations.

Toughened glass cap-and-pin insulators were used on the 750-kV and 1150-kV lines. The 750-kV transmission lines go mainly through areas of very light contamination, while the 1150-kV lines go through relatively clean areas. Insulators with a leakage distance of 1.5 cm/kV were used for both lines. Insulators with an electromechanical strength of

Table 15.6-1 Minimum Air Gap Clearances for 750-kV and 1150-kV Transmission Lines

Type of Gap	Voltage Applied	Gap Clearance for 750-kV Line, m	Gap Clearance for 1150-kV Line, m
Conductor to tower leg or cross arm	OV	1.5 - 1.6	2.6
Conductor to tower leg	SI(1)	4.1 – 4.5	6.5
Conductor to tower leg	SI(2)	2.7 – 2.8	5.2 – 5.3
Conductor to cross arm	SI(1)	4.7 – 5.0	6.5 – 6.9
Conductor to guy wire	SI(1)	3.9	
Conductor to ground at mid-span	SI(1)	6.2 – 7.5	9.3 – 10.5
Conductor to conductor of 330-kV or 500-kV crossing line	SI(1)	4.2 or 4.6 respectively	
Phase to phase	SI(1)	4.5	11.3

OV: Operating Voltage

SI(1): Switching Impulse limited to 2.1 p.u. for 750-kV and 1.8 p.u. for 1150-kV lines

SI(2): Switching Impulse limited to 1.8 p.u. for 750-kV and 1.6 p.u. for 1150-kV lines

120 and 160 kN were used in double suspension strings on 750-kV lines. The I V I configuration was used in the majority of cases. To avoid the need for grading rings or horns, a specially designed suspension clamp (in which the first insulator of the string went inside the fitting) was developed for the 750-kV lines. On the 1150-kV lines, the I V I configuration was used on the three phases with double insulator strings of 210 to 400 kN or single strings of 300 to 400 kN installed. No grading rings were used on these lines as well, but the local bundle spacing was increased from 40 to 57 cm to let the vertical insulator strings go through the bundle. A similar solution could not be applied for the V strings. Instead of lowering the first insulator into the fitting, the insulators closest to the phase bundle in each string were replaced with ones having larger capacitance. The types and characteristics of insulator strings used on 750-kV and 1150-kV lines are summarized in Table 15.6-2.

The regions traversed by the 750-kV and 1150-kV lines were characterized by a moderate lightning activity (20 to 50 h of thunderstorms a year) and relatively low values of earth resistivity, ranging between 200 and 400 Ω-m. The grounding resistance of towers could, therefore, be kept below 15 Ω.

Both resistive and corona losses were taken into account in the economic choice of the conductor cross section. Corona performance considerations, mainly RI and AN, were the basis for the selection of the number and diameter of conductors in the bundle. Typical conductor bundle configurations used on 750-kV and 1150-kV lines are shown in Table 15.6-3. The phase spacing for 750-kV lines varied from 17.5 to 19.5 m and for 1150-kV lines from 21.5 to 25 m. A horizontal conductor configuration was generally used, but the center phase was slightly raised for some lines to reduce ground-level EMF.

Limits to radio noise from transmission lines were set by Russian standards, according to which the permissible noise level at 100 m from the outside phase, not to be exceeded during 80% of a year, at different frequencies were as follows: 48 dB at 0.15 MHz; 43 dB at 0.5 MHz; 38 dB at 1 MHz; 21 dB at 10 MHz; 30 dB at 30-1000 MHz. According to health standards in housing areas in Russia, environmental audible noise is limited to 55 dBA in daytime and 45 dBA at nighttime. According to these standards, the AN level of 750-kV lines at 40 m from the outside phase was limited to 38 dBA in dry weather and 45 dBA for wet conditions. For the 1150-kV lines, the AN standards apply at a minimum distance of 300 m from the outside phase. Measurements of AN made at this distance have shown levels of 32 dBA in dry weather, 39 dBA from wet conductors, and 52 dBA from conductors and gaps in fittings in dry weather. AN from corona was acceptable both in dry and wet conditions, but additional noise from gap discharges during dry weather made the total AN exceed the norm for nighttime.

Table 15.6-2 Toughened Glass Cap-and-Pin Insulators and Insulator Suspension Strings in Russian 750- and 1150-kV Lines

Type	Electro-mechanical strength, kN	Dimensions, mm			Number of Insulators in Suspension String[1]		Remarks
		Height	Diameter	Leakage Distance	750 kV	1150 kV	
PS-120A	120	146	260	340	-/43-44	73/77	
PS-160B	160	170	280	368	-/41	63/67	
PS-210B	210	170	320	385	35	57/60	
PSK-210A	210	155	410	410	29	47/50	conical
PS-300B	300	195	320	420	31	56/59	
PSK-300K	300	175	450	457	27	45/47	conical
PS-400A	400	200	390	467	29	49/51	

1. Numerator: number of insulators in single string.
Denominator: number of insulators in double string.

Table 15.6-3 Conductor Bundles Used on 750-kV and 1150-kV Lines

Transmission Voltage, kV	Transmitted Power, GW	Type of ACSR Conductor and Cross Section, Aluminum/Steel, mm²	Number and Diameter of Conductors in the Bundle	Subconductor Spacing, cm
750	1	AS-240/56	5 x 2.24 cm	30
	1.5 – 1.9	AS-400/93	4 x 2.91 cm	60
	2.0 – 2.5	AS-500/64	4 x 3.06 cm	60
1150 kV	4.0 – 5.0	AS-330/43	8 x 2.75 cm	40
	5.5 – 6.0	AS-400/51	8 x 2.75 cm	40

Corona losses depend very much on the prevailing weather conditions. Table 15.6-4 shows the yearly distribution of weather conditions in some of the regions traversed by 750-kV and 1150-kV lines. Estimates of average corona losses under different weather conditions for these lines are shown in Table 15.6-5. The operating voltage of these lines was sometimes lowered in order to reduce corona losses during periods of heavy rain or severe hoarfrost.

The electric field directly under the midspan of 750-kV and 1150-kV lines was limited to 20 kV/m in difficult-to-reach areas where agricultural machines were not used, to 15 kV/m in unpopulated areas used for agriculture, and to 5 kV/m in populated areas. In addition, for utility personnel working on transmission lines and in substations, the daily exposures to electric fields were limited to: 5 kV/m – no limitation; 10 kV/m – 180 min; 15 kV/m – 90 min; 20 kV/m – 20 min; and 25 kV/m – 5 min. A summary of the maximum ground-level electric fields, as well as the minimum conductor heights, is shown in Table 15.6-6.

15.6.3 Mechanical and Tower Design

Design criteria for wind and ice loads in Russia were developed on the basis of long-term meteorological data. Wind velocities varied (in seven grades) between 30 and 45 m/s, while wind pressure varied between 550 and 1250 Pa. Thickness of ice accretion varied (in five grades) between 0.5 cm and more than 2.2 cm. For the 750-kV and 1150-kV lines, the following design wind and ice loadings were chosen:

- 750 kV – wind pressure of 540 to 640 Pa and ice thickness of 1.5 to 2.0 cm.
- 1150 kV – wind pressure of 700 to 800 Pa and ice thickness of 1.0 to 1.5 cm.

Combinations of weather conditions, representing the worst-case scenarios, were also used in line design. For the combined action of wind and ice, for example, full ice thickness was combined with 25% of the maximum wind pressure.

A number of different types of spacers—including bi-conductor and star-shaped for 3, 4, 5, and 8 subconductors—and spacer dampers were developed in Russia for use on all classes of transmission lines. On the 750-kV lines, bi-conductor spacers in groups, with distance between groups of 60–80 m were used. No dampers were deemed necessary. Star-shaped spacers were used for the eight-conductor bundles of the 1150-kV lines, at variable spacings up to 60 m. Subspan lengths were reduced to 40 m, using groups of bi-conductor spacers where it was necessary to suppress subspan oscillations. Spacers used for bundles with three to eight conductors are shown in Figure 15.6-1.

Self–supporting, as well as guyed lattice steel structures, were used for the 750-kV and 1150-kV lines. Typical tower configurations are shown in Figures 15.6-2 and 15.6-3. Full-scale mechanical testing of tower prototypes and foundations formed the basis of tower designs. Figure 15.6-4 shows a photograph of a 1150-kV tower.

Standardized designs were developed for the reinforced concrete foundations of both self-supporting and guyed towers. Line construction technologies for the 750-kV and 1150-kV lines did not differ from those already used for lower voltage lines, but larger dimensions and higher weights of the elements required more powerful machinery and more accuracy in erecting towers and stringing the conductors.

Table 15.6-4 Yearly Distribution of Different Kinds of Weather (in % of year)

Location	Ukraine, 787-kV Lines	Kazakhstan, Siberia, 1200-kV Lines
Dry weather	85.3	63.9
Increased humidity	-	25.1
Dry snow	4.7	3.4
Fog	0.5 (wet snow)	0.69
Rain	5.1	5.8
Frost	3.4	1

Table 15.6-5 Estimates of Average Corona Power Losses, kW/km, for Russian 750- and 1150-kV Lines When Operating at Nominal Voltage (Tamazov 2004)

Rated Line Voltage and Phase Bundle	750 kV 4xAS-400/93	1150 kV 8xAS-330/43
Dry (fair) weather	6.47	9.0
Increased humidity (over 90%)	21.4	33
Dry snow	29.4	44
Fog	37.3	62
Rain	66.5	102
Frost	118	184

Table 15.6-6 Maximum Electric Field and Minimum Conductor Height above Ground at Midspan

Location	E_{max}, kV/m	Height, m	
		750 kV	1150 kV
Unpopulated, inaccessible area (mountains, steep slopes, etc.)	-	6.5	8.5
Difficult-to-reach area with no appearance of agricultural machines	20	10	15
Unpopulated area used for agriculture	15	12	17.5
Populated area	5	23	-
Highways, roads	-	16	23
Railroads	-	20	28

15.6.4 Operation and Maintenance

Fifteen years of operating experience of the first two 1150-kV lines with a total length of about 1000 km, reported in (Krylov 2004), at different operating voltages (part of the time at 1150 kV; part of the time at 500 kV), provide an important insight into the mechanical behavior of an overhead line with a very large number of subconductors in the phase (eight) and very long (11 m) insulator strings. The line crosses an area with periods of wind velocities at least 10-100 times higher than those typical for the European part of the former USSR where a majority of EHV lines exist. Observed wind velocities here reached 40 m/s. The following mechanical failures were observed on the line:

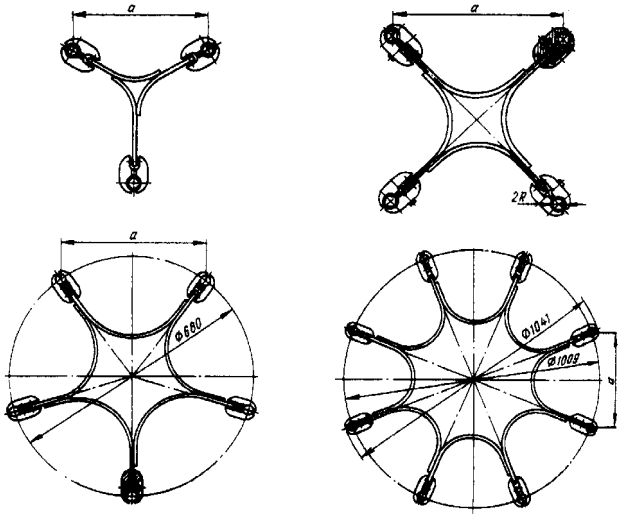


Figure 15.6-1 Spacers for bundles of three to eight conductors.

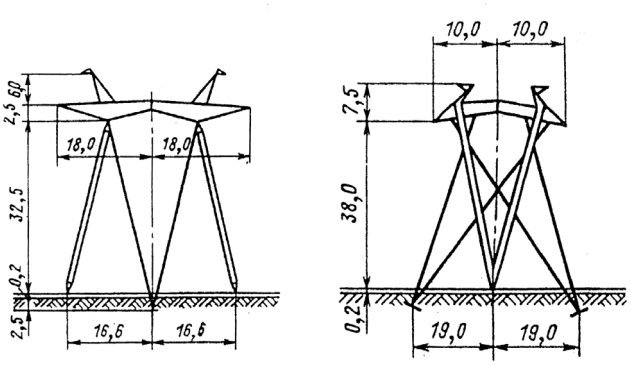


Figure 15.6-2 Typical 750-kV guyed V towers.

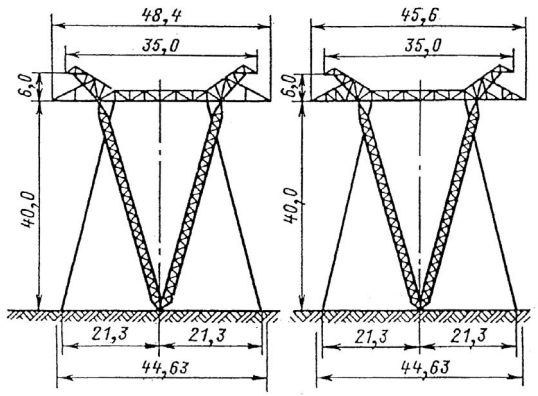


Figure 15.6-3 Typical 1150-kV guyed V towers.

- Breakage of insulators occurred in the supporting double V strings used on the line. Damages were concentrated near the middle of the circuits and at distances of one-quarter and three-quarters of their length. These damages were caused by low-frequency (1-2 Hz) string oscillations under the wind impact, and probably by moderate conductor galloping of approximately the same frequency. The wind velocity required for the insulator circuit to oscillate resonantly was estimated as 5 m/s. In these oscillations, the string length corresponds to a half wavelength (first harmonic) and/or full wavelength (second harmonic) of free mechanical oscillations of the string. When a small difference in self-frequencies of parallel strings brings them into opposite phases of their oscillations, the mechanical collision breaks the insulators. To overcome this problem, two specially developed spacers were installed between the parallel strings at distances of one-third and two-thirds of the string, which eliminated any further damage to the insulators.
- Disconnections of suspension insulator strings were caused by collision of parallel strings, as described above, as well as by conductor galloping discussed below. In some cases, the disconnections were caused by defective suspension hardware.
- Conductor galloping with double amplitude of at least 3-10 m at wind speeds of 6-11 m/s and ice wall thickness of at least 15 mm led to the fall of a support tower and part of the conductors and numerous damages to conductors and line accessories including clamps,

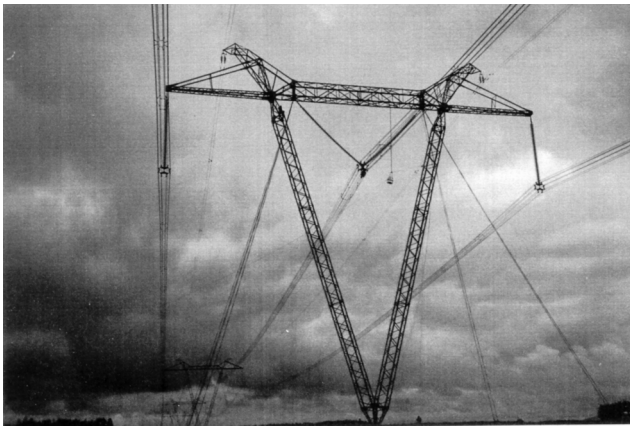


Figure 15.6-4 1150-kV tower.

shielding rings, and suspension hardware. Some accessories revealed evident signs of fatigue wear under cycles of changing and reversing loads. Galloping and ice thickness above 10 mm were not expected on this line, so it was necessary to introduce measures to strengthen the towers and to prevent galloping.

- High winds, with the direction perpendicular to the line route, and the velocity exceeding the design norm, led to damage and even destruction of numerous towers of the line. At the height of 7 m, the recorded wind velocity was 35 m/s, and it increased with height, whereas the design velocity was 30 m/s. It is evident that norms have to be reconsidered and must be based on values from longer periods than used initially.
- Damages occurred to suspension hardware related to dry friction wear under repetitive applications of changing mechanical loads. The accessories were redesigned, with an increase in contact area and with the introduction of rubber compensating elements, where needed.

An interesting environmental case was discovered following complaints about a rise in RI levels. As it happened, birds had begun to nest inside bundled phases of the line just near tension strings (Figure 15.6-5). Hay and pieces of aluminum wires found near the line were used as material of nests. The line is going through steppes—arid, treeless land. Acoustic noise, mechanical vibration, and strong gradients of electric field near conductors did not prevent the nesting.

The outage rate of transmission lines generally decreased as the line voltage increased. The average outage rate for 750-kV lines was 0.22 per 100 km/year. Although the amount of data may be insufficient, the average outage rate of 1150-kV lines was found to be on the order of 0.12 per 100 km/year. The outages on 750-kV lines were attributed to different causes as follows: 13.7% due to defects in construction or maintenance; 3.8% due to ice, wet snow, and conductor galloping; 20% due to lightning; 10.6% due to polluted insulators; 20.6% due to wind; 13.8% due to faulty maneuvers near the lines, fires, hunters shooting, etc.; and 17.5% due to unknown causes. For 750-kV lines, 98% of short circuits were single-line-to-ground, while for 1150-kV lines, practically 100% were single-line-to-ground. In 52%, single-pole high-speed reclosures were successful. Some outages were also caused by failures of substation equipment, mainly transformers and shunt reactors. If the outage was due to damaged line elements, the average restoration time for a 750-kV line was 5.8 h, and 10.5 h for a 1150-kV line. The number of 750- and 1150-kV transformer outages per year per phase was 0.107 and 0.13, respectively; and for shunt reactors 0.068 and 0.25. Average restoration time for 750-kV transformers was 112 h, and 198 h for 750-kV shunt reactors. Roughly, outages of substation equipment led to the same number of line outages as failures of the line itself. All types of relay protection devices used on these transmission lines operated properly in 99.55% cases, and automatic control devices in 99.73% cases.

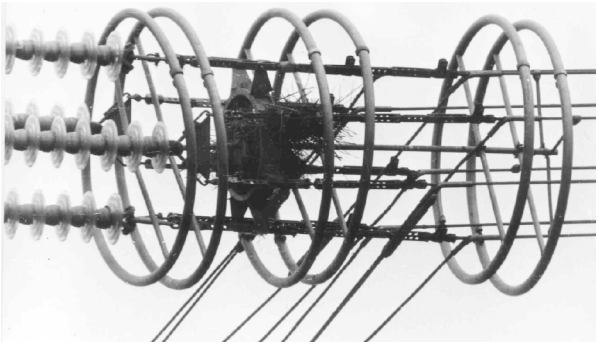


Figure 15.6-5 Bird nest on fittings of 1200-kV tension insulator strings.

Several line maintenance procedures were developed in the former USSR for transmission lines at or above 500 kV, but the one developed and widely used on the 750-kV line in Ukraine was found to be the most flexible and universal: an operator cradle is raised on an insulating rope by a winch to the repair area. Suspended in the cradle, the operator made the necessary repairs on the insulator string without disconnecting or lowering the string.

Standard maintenance practices were developed for the power grid in Russia, and regional maintenance divisions, equipped with the necessary material and human resources, were located at the 750-kV and 1150-kV substations. Also local unmanned shops with more frequently needed materials and tools were located along the line near communication amplification stations—i.e., at intervals up to 150 km.

15.7 EDELCA 765-KV LINES IN VENEZUELA

Large hydroelectric power plants with a generating capacity of 17,000 MW are situated on the Caroni River (Guri and Macagua in service and Caruachi and Tocoma now under construction) in the southern region of Venezuela, while the main load centers are located in the north and central regions near Caracas, the capital city. In terms of installed generating capacity, CVG EDELCA is the largest utility in Venezuela, and it has the responsibility for developing the generating stations on the Caroni River and the associated high-voltage transmission system. With the development of the Guri hydroelectric power station, the need arose for transmitting about 8000 MW of power over a distance of 600 to 800 km. The existing transmission network consisted of 230 kV and 400 kV lines. Studies were carried out to study the economic feasibility of three transmission alternatives:

1. Extend the existing 400-kV lines.

2. Build new 765-kV lines.
3. Build new ±600-kV dc transmission system.

Following these studies, the 765-kV ac transmission system was selected because it was the best economic choice, in particular with respect to the dc alternative. The number of 400-kV circuits required was too large, and involved too many rights-of-way—six to eight, rather than three or four, for the 765-kV circuits. The 765-kV system was also found to contribute to greater reliability.

The system was constructed in two stages. In the first stage, between 1980 and 1985, two 765-kV lines, with a total length of 1237 km, and five 765-kV substations, were constructed. After extensive field tests, they were put in commercial operation in February 1986. The second stage was constructed from 1987 to 1990, and it was put in commercial operation in 1991. The system added a third line and the interconnection between the receiving-end substations, with a total of 835 km, and two new 765-kV substations.

15.7.1 System Planning

Design of the 765-kV transmission system of EDELCA was based on the requirement of transient system stability and voltage stability for a permanent single line-to-ground fault, with a clearing time of 4.5 cycles on any line section and other secondary criteria. The basic design philosophy was to ensure reliability, control overvoltages, and limit the impact of corona and electric field effects near the lines, as well as to facilitate the use of locally manufactured materials such as the self-supporting tower structures and ACAR conductors.

Measures such as preinsertion resistors in line circuit breakers, shunt reactors at the receiving end of the lines, and switching of the reactors and lines when necessary were used to control overvoltages. The power frequency overvoltages were limited to 1.5 p.u., and the switching overvoltages to 1.75 p.u. Zinc oxide lightning arresters are used at the line terminals and near transformers and reactors. However, they were not primarily designed to control overvoltages in the lines, but to protect the open circuit breakers in case of multiple lightning strokes.

Series compensation was not used for the first three lines, but provisions were made for future installation. Instead, two static compensators with thyristor-controlled reactors and thyristor-switched capacitors, rated +300/-280 MVAr, were installed. Line protection relays consisted of duplicate static directional comparison type, using power-line carrier for transfer trip. Single- and three-phase reclosing was allowed. A scheme with a neutral reactor in the shunt reactors was conceived to facilitate single-phase reclosing, but the scheme has not been implemented because of operational considerations. Blocking relays were also installed to avoid units from operating in case of system oscillations, and a tripping scheme was incorporated for loss of synchronism. In addition, overvoltage protection was used for each line, with a traveling-wave type of relay used on the third line.

The line routes were determined considering different alternatives based on technical, economic, and security studies. The following considerations also played important roles in the choice of the line routes: topography, rights-of-way, line angles, deforestation, access, foundations, vibrations, corrosion, corona effects such as RI and AN, future installations, etc. For reasons of security, electrical and wind storms, floods, contamination, flight accidents, fires, and access to maintenance were all taken into account. It was decided to locate each of the two initial lines, which run parallel over 60% of the route, on different rights-of-way separated by at least 1 km. The right-of-way was 120 m for the first two lines and 90 m for the third line.

Some difficulties were encountered in siting the lines, such as the presence of other transmission lines and passage through national parks. The problem of crossing the very wide Orinoco River was solved by using an island, so that spans of 1150 m and 850 m were created on each side of the island. Some opposition was encountered from landowners for siting the line in a sector about 30 km long, and consequently, the line construction was delayed by about 18 months.

The EDELCA 765-kV transmission lines were transposed at 1/6, 1/3, 1/3, and 1/6 of line length. The main reasons for transposition were to have a balanced system, to improve the line protection, and to simplify the single-pole reclosing scheme. Only power-line carrier was used to transmit line-protection communication and transfer trip signals. Interference due to corona and switching were not taken into account, and two-phase coupling with frequencies in the range of 50 to 500 kHz and a bandwidth of 4 kHz was used for each channel. Although OPGW was used on 230-kV and 400-kV lines after the 765-kV lines were in operation, they were not adopted for the 765-kV lines. Weather data required for both the electrical and mechanical design of the lines were obtained from stations located along the line route, and no special techniques were used.

15.7.2 Electrical Design

The electrical design of the first two 765-kV lines was based mainly on the *EPRI Transmission Line Reference Book: 345 kV and Above*, first edition, and the third line was based on the second edition.

For most of the length, the lines pass through plains and relatively uninhabited terrain, with altitudes below 300 m. In the northern region, the lines pass through hills and

mountainous areas with altitudes near 1000 m. However, the altitude was not an important parameter in the line design, except for changing the ground wire protection angle from 20° on flat terrain to 0° in mountainous areas.

The mean ambient temperature along the line route was 26°C, with a minimum of 10°C and a maximum of 40°C. The relative humidity varied between 65% and 85%, but reached almost 100% during nights. No ice or tornadoes occur in the region, but it is subject to earthquakes. A seismic evaluation was, therefore, made of the transmission towers and foundations for a maximum acceleration of 0.5 G. The lines were designed for a maximum ground resistance of 50 Ω, although the actual values turned out to be much lower, being less than 20 Ω almost along the entire length of the line.

Self-supporting towers were used on all three lines. The conductor-to-tower structure clearances were determined to withstand the expected maximum switching overvoltages. In the tower window, where the conductors were supported by V string insulators, the conductor-to-tower clearances were 5.5 m for the first two lines and 5.07 m for the third line. For the outer phases of all three lines, where the conductors were supported by a single insulator string, the conductor-to-tower clearance was 4.0 m for an average wind speed of 62 km/h. Taking into account the probabilistic distributions of switching overvoltages and wind speeds, the conductor-to-tower clearance for the maximum wind speed of 125 km/h was determined to be 1.5 m. For the first two lines, the minimum conductor-to-ground clearance was 14.7 m, and the phase-to-phase clearance was 15.0 m, while for the third line, the corresponding clearances were 13.7 m and 13.2 m, respectively.

Strings of porcelain, as well as glass cap-and-pin insulators, with a zinc sleeve for protection against corrosion, were used on all the lines. The I V I configuration was used with 37 insulators in each string. Performance under pollution conditions was the main consideration for the selection of the type of insulators. In low contamination areas with ESDD of 0.05 mg/cm^2, 37 insulators of 170 x 280 mm with a leakage distance of 370 mm were used, while in high contamination areas, insulators of 170 x 320 mm with a leakage distance of 540 mm were used. The electromechanical strength of the insulators were 160 kN and 210 kN, respectively.

On tension towers, double strings of 45 and 35 insulators of 195 x 320 mm with a minimum leakage distance of 370 mm and electromechanical strength of 300 kN were used in high and low contamination areas, respectively. All insulator strings were required to have no visible corona at 500 kV phase to ground, an RIV level of less than 1300 μV, and to withstand a power-arc current of 32 kA.

Selection of conductor bundles was made using the program LOP-T, in which resistive losses, but not corona losses, were considered for the economic choice of the total conductor cross section. Following technical and economic evaluation, a four-conductor bundle, with a subconductor diameter of 3.332 cm, and subconductor spacing of 45 cm, was selected. ACAR conductors were selected since they could be manufactured in Venezuela and EDELCA had good operating experience with these conductors. The lines were designed to meet the criteria of RI level at 0.5 MHz of 50 dB, and AN level of 55 dBA at the edge of the right-of-way. Since there were no regulations in Venezuela, these criteria were adapted from the experience in other countries.

Electric fields were limited to 10 kV/m below the line and 2 kV/m at the edge of the right-of-way, which was 60 m from the center of the line for the first two lines and 45 m for the third line. No magnetic field criteria were used for the design of these lines.

With an isokeraunic level of 50 to 80 thunderstorm days per year along the line route, two ground wires, each with a protection angle of 20° on flat terrain and 0° in mountainous areas, were used. Alumoweld conductors with a diameter of 0.978 cm were selected for ground wires on the basis that they withstand a maximum short-circuit current of 28 kA with a duration of 15 cycles, for a phase-to-ground fault at the Guri substation. With protection angles of 20° or less and ground resistance values less than 50 Ω, the lightning flashover rate was expected to be less than 1 per 100 km per year.

From ground resistance measurements, the region traversed by the lines may be divided into two zones—the first from Guri to about the midpoint with high earth resistivity of 2000 Ω-m, and the second from the midpoint to the receiving-end substations with low resistivity of 50 Ω-m. In the low resistivity zone, four radial counterpoises, each 10-m-long copperweld wires of 5.19 mm diameter, were used, while a double continuous counterpoise was used in the high resistivity zone.

15.7.3 Mechanical and Tower Design

Based on field tests on aeolian vibrations and subconductor oscillations, and laboratory tests to verify the effectiveness of damping, spacer dampers were developed and installed at intervals of approximately 50 m on the lines in order to control wind-induced conductor vibrations. Spacer dampers from three different manufacturers were used on the

conductor bundles. Stockbridge dampers were used on ground wires.

The maximum 5-s duration wind speed of 125 km/h at 10 m height and a 200-year return period were used as the wind-loading criterion for line design. Self-supporting towers with a horizontal conductor configuration were used on all three lines. Studies were made of guyed V towers, and although they had a small cost advantage over self-supporting towers, the use of self-supporting towers was preferred because of EDELCA's good experience with them on lower voltage lines. Several designs were developed for towers at line angles in the ranges of 0°-5°, 30°-60°, dead-end towers and transposition towers. The mean tower height was 33 m. On the Orinoco River crossings, towers of 115 m high, and AACSR conductors with 54 wires of aluminum alloy and 37 alumoweld wires and quadruple insulator strings were used. There is also a special tower type designed to bring ten 765-kV circuits through a highly constricted corridor from the Guri plant to the switching station, which is a double-circuit flat configuration tower with one circuit above the second, and nearly 70 m high. Figure 15.7-1 shows a sketch of a typical transmission suspension tower used for EDELCA 765-kV transmission lines. Figure 15.7-2 shows the double-circuit 765-kV towers used by EDELCA.



Figure 15.7-2 EDELCA's double-circuit 765 kV transmission towers.

Several types of foundations were used, but the most common was the spread footing with concrete pad and concrete pyramid and chimney, mainly because it is versatile and does not need any special equipment for laying it in different types of soil. Concrete drilled foundations were used

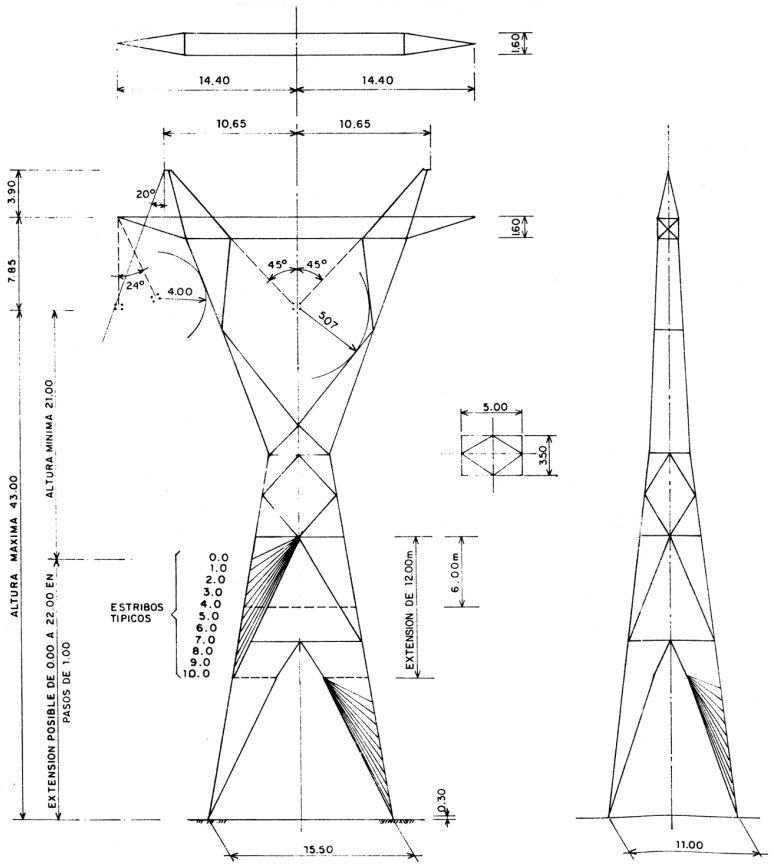


Figure 15.7-1 EDELCA's 765 kV suspension tower.

for ground anchors. In some types of soil, pile foundations with raking piles were used instead of spread footing because, although they require special equipment, they were more economical.

Conventional construction techniques were used for all lines. The towers were assembled on site using cranes, and the conductors were tensioned using 16-ton, simultaneous four-conductor stringing equipment.

15.7.4 Operation and Maintenance

The operational experience over about twelve years (1991-2003) of the EDELCA 765-kV lines has shown that there have been 0.956 forced outages per 100 km of line per year. Of these, 40% (0.383 faults/100 km) were caused by fires, 16.1% (0.155 faults/ 100 km) by lightning, 5.8% (0.055 faults/ 100 km) by contamination, 8.1% (0.077 faults/ 100 km) by vegetation, 22.3% (0.213 forced outages/ 100 km) by faults in equipment, 1.9% (0.018 faults/ 100 km) by humans and 5.8% (0.055 faults/ 100 km) due to other causes. This outage experience did not lead to any redesigns of the lines. Also, no complaints were received from the public on RI, TVI, AN, or EMF.

The lines are inspected by ground once a year and by air using helicopters four times a year. Infrared thermo-vision is sometimes used during line inspection. There have not been any particular failures of line components such as hardware or insulators and, consequently, no replacements were required. Only some spacer dampers had to be replaced because of missing conductor clamps. The lines are maintained by conventional methods, mainly barehand with the lines out of service.

In general the operating loads on the lines have been below the original design loads, normally below 80%.

15.8 FURNAS 750-KV LINES IN BRAZIL

The Itaipu hydroelectric power project, located on the Parana River and developed by the binational company Itaipu Binacional on the basis of a joint agreement between Brazil and Paraguay, is one of the largest in the world, with a generating capacity of 12,600 MW. The agreement established that each of the two countries would have the right to 50% of the power generated and also the right of each to purchase from the other the power it could not utilize. Because of the comparatively low load growth in Paraguay, it was decided that the transmission system to Brazil should be capable of transmitting all the power generated at Itaipu.

15.8.1 System Planning

In the initial transmission system feasibility studies (Peixoto 1980), several alternatives and configurations of transmission were examined, including 500 kV, 750 kV, and 1100 kV ac, as well as ±600 kV dc. It was concluded from these studies that the indicated transmission voltage for the Itaipu system was 750 kV with series compensation. Following the feasibility studies, detailed studies were carried out to define the configuration of the 750-kV transmission system. Based on the system studies and detailed economic analysis, a transmission system with five 750-kV series compensated ac lines was selected. It was assumed at this stage that all the power generated at Itaipu would be available to Brazil at 60 Hz. Subsequently, it became evident that Paraguay would maintain its system at 50 Hz and, therefore, the Itaipu generation was divided equally between machines generating power at 50 Hz and 60 Hz. Due to this special feature of generation at two frequencies, system studies indicated that a hybrid ac/dc system was best suited for transmitting the power from Itaipu to the remote load centers in Brazil.

From the studies made for the complete 750-kV ac system, some important data were already obtained on the maximum power that could be lost without jeopardizing the reliability of the interconnected system and on the location of the switching substations. Studies were then performed to choose the most appropriate ac voltage of the hybrid ac/dc system. Load flow, stability, and economic studies were carried out for the following voltage combinations:

1. Five 500-kV ac lines and two ±600-kV dc lines
2. Three 750-kV ac lines and two ±600-kV dc lines

The final choice between these two was based on economic considerations. The second alternative, with three 750-kV ac and two ±600-kV dc lines, was selected. Each of the 750-kV lines was about 900 km long, with two intermediate substations. Criteria for the design of both the ac and dc components of the hybrid transmission system were developed based on a number of analog and digital simulation studies.

The basic design criteria for the steady-state and dynamic operating conditions of the Itaipu transmission system were developed (Peixoto 1980) by considering the 50-Hz and 60-Hz generating stations, as well as both the ac and dc transmission systems, as one entity such that the total transmission capacity is defined with any one element (transformer, line section, valve group but not dc pole or smoothing reactor) out of service. The hybrid nature of the transmission system required, therefore, a more complex series of load flow, stability, and overvoltage studies than those for a simple ac system. For design purposes, a maximum dynamic overvoltage for substation equipment was 1.4 p.u., while for circuit breaker locations that may open a line after load rejection, it was limited to 1.5 p.u. Following load rejection, the maximum temporary overvoltage at the

open end of transmission lines with lightning arrester was limited to 1.6 p.u. The maximum transient voltage, which occurs on clearing of a three-phase-to-ground bus fault at the sending end, was found to be 2.0 p.u.

Besides line and busbar shunt reactors, transfer trip was also considered to control power frequency overvoltages. Shunt reactors connected at the ends of the lines control the power frequency overvoltages during light load conditions. To increase the power transfer capability, series capacitors were installed in all the lines. Since there are three parallel lines along the whole length, stability studies demonstrated that single-pole reclosing was not necessary. Traveling wave and digital protection for the lines included directional comparison unblock and direct unblock transfer trip schemes.

Geographical maps of the region were carefully studied to determine the shortest line route, while at the same time avoiding urban areas, airports, and areas designated for rainforest and wildlife preservation. Some difficulties were encountered in siting the lines, particularly in regions of rough terrain and proximity to urban areas. Opposition to line routing came mainly in areas designated for areas of permanent vegetation preservation and wildlife preservation.

Each section of the transmission line between two substations was transposed at intervals of 1/6, 1/3, 1/3, and 1/6 of its length. Because of the long distances covered by these lines, transposition was necessary in order to avoid unbalances in each of the parallel circuits. The best transposition scheme was selected on the basis of studies carried out of resonance by induction, electromagnetic fields, induced voltages in ground wires, etc.

Power line carrier with three-phase coupling was used for purposes of both telecommunications and protection on the first 750-kV circuit between Sao Paulo and Parana. Later on, FURNAS changed the coupling and telecommunication configuration scheme for the first two circuits into a scheme with just the primary teleprotection path in the PLC with phase-to-phase coupling, and the alternate teleprotection path and voice communication over a microwave analog system. Presently, all three transmission circuits use this scheme with one teleprotection path using PLC and the other protection and communication provided by microwave. The frequencies used for PLC ranged from 64 to 160 kHz. Some corona problems were encountered with the PLC equipment used on the first two circuits. All other services along the transmission corridor from Sao Paulo right up to the Itaipu dam—such as voice for dispatch and administrative purposes, telemetering, load dispatch etc.—use a 960-channel, 6-GHz microwave analog system. Recently, FURNAS installed a 24-fiber OPGW system on the third 750-kV circuit, which is expected to replace the PLC system eventually. The performance of the OPGW with the external layer of alumoweld or galvanized steel has been satisfactory, but the OPGW with aluminum alloy covering suffered damage due to lightning, mainly to the external layer and not to the fibers.

15.8.2 Electrical Design

System operating voltages, switching overvoltages, and lightning overvoltages were considered in determining the conductor-to-tower structure clearances of the transmission lines. The air gap clearances were determined for two types of transmission towers, self-supporting and guyed, that were used for these lines. Altitude above sea level was not an important factor in the design of the lines, since the average and maximum values of the altitude along the line route were 800 m and 1200 m, respectively. For self-supporting towers, a clearance of 7.0 m was selected for the external phase to structure and 5.0 m for the central phase to structure. For guyed towers, the external and center phase to structure clearances were 6.5 m and 5.0 m, respectively.

System operating voltages and lightning overvoltages were taken into account in determining the number and type of insulator strings used on the lines. The region traversed by these lines is characterized by low levels of contamination (0.016 to 0.02 mg of $NaCl/cm^2$). Taking these low contamination levels into account, the choice of insulators was as follows: For the first circuit, 35 glass suspension-type ball-and-socket insulators, in accordance with IEC 120, 146 x 254 mm with rated electromechanical strength of 120 kN. For the second and third circuits, 30 glass insulators, 170 x 280 mm with a rated electromechanical strength of 160 kN.

Economic and corona performance criteria were considered in the selection of conductor bundles for the Itaipu transmission lines. Cost of resistive losses was the basis for determining, in the traditional manner, the economically optimum cross section of the conductor bundles. The contribution of the mean annual corona losses, calculated assuming rainy weather for 15% of the time and on 20% of the total length of the line, was considered only in a qualitative manner. Conductor bundles with three and four subconductors, spaced 40 cm to 50 cm apart, were considered. However, three conductor bundles were rejected because the subconductor diameter required to obtain acceptable levels of RI and AN was too big. The criterion for RI was 42 dB at 1 MHz and at the edge of the right-of-way, not to be exceeded 50% of the time in a year. This criterion ensures a 24-dB signal-to-noise ratio for a minimum radio signal level of 66 dB during 50% of the time. The criterion for AN was that it should not exceed 58 dBA at the edge of the right-of-way under light rain (less than 0.148 mm/h), or four hours of fog or 15 minutes after rain. The width of right-of-

way was 94.5 m for a single transmission line and 175 m where two lines run parallel in the same right-of-way.

A general criterion used for determining the minimum conductor-to-ground clearance was to limit the current induced in a person touching the largest road vehicle, located directly under the line to 5 mA. Criteria were also in place to limit the maximum electric field to 15 kV/m in rural zones, 10 kV/m near roads, and 5 kV/m in zones where people may gather (city streets, squares, etc.). No criteria were specified for magnetic field levels under the lines.

Lightning protection of the lines was based on an assumed isokeraunic level (IKL) of 100 thunderstorm days per year. Because of the high IKL, two ground wires were used all along the transmission lines, and the size of the ground wires was selected on the basis of expected short-circuit current levels and also on telecommunication requirements. The ground wires on the first circuit were Minorca single–layer, extra-high-strength (EHS) ACSR conductor with a diameter of 1.219 cm, while on the second and third circuits, both Minorca and Dotterel, also a single-layer EHS ACSR conductor with a diameter of 1.542 cm, were used. To ensure acceptable lightning performance, an average value of 15 Ω ground resistance was achieved through the use of four radial counterpoises, 15 to 60 m long, for each tower. The ground wires were sectionalized in order to reduce losses. Sections of ground wires were insulated, with grounding only at one point per section.

15.8.3 Mechanical and Tower Design

With the use of four-conductor bundles, it was necessary to consider aeolian vibrations and develop appropriate control measures. On Itaipu transmission lines, spacer dampers were used on the conductor bundles, and Stockbridge dampers for the overhead ground wires.

For the design of tower structures, a survey was carried out to establish the design wind velocities using available data from the meteorological stations in the states of Parana and Sao Paulo, in a strip 300 km wide along the proposed route of the transmission lines. Based on a statistical study of the wind data, a design wind velocity of 150 km/h was adopted, corresponding to an integration period of 30 s, at a height of 30 m, and for a 50-year return period.

As mentioned earlier, two types of towers were used for the Itaipu transmission lines: self-supporting (36%) and guyed (64%), according to the ground profile, mechanical stresses, etc. The first two circuits had grillage foundations, but concrete foundations were used for the third circuit because of the appearance of corrosion problems on the grillage foundations.

In cases of emergency, FURNAS has developed a global plan to ensure a quick restoration of service. The plan consists of a strategy for coordinating different units of the company so that personnel and material are provided in a quick and efficient manner. Complete emergency kits consisting of the special equipment and tools are made available in emergencies. Spare parts and towers of all types are kept in a stockroom in Campinas located along the line route.

15.8.4 Operation and Maintenance

The operational experience of the Itaipu transmission lines over the past 20 years has shown that an average of 0.26 outages/100 km were experienced per year due to lightning. No outages were attributable to switching overvoltages. Although the lines were subject to some industrial pollution and sea side salt, no outages occurred due to pollution flashover of the insulators. Some outages were experienced as a result of falling towers due to strong winds, explosion, and collisions with a farm tractor or truck.

Since 1982, nine incidents have been caused by high wind velocities, resulting in 39 damaged structures, of which 26 occurred in the last three incidents. In all cases, investigations were made jointly with the tower manufacturers, and it was concluded that the tower structures were struck by strong winds of short duration, restricted to a small area, and in two cases there was strong evidence that the structure was struck by tornados.

The outage experiences of the FURNAS 750-kV transmission lines over the past 20 years are summarized in Table 15.8-1.

One major outage was attributed to a failure in the driving mechanism of a 800-kV SF_6 circuit breaker.

Since most outages were caused by lightning, a lightning location system known as RINDAT (Integrated National Network for Detection of Atmospheric Discharges), has been employed. It covers with very good reliability the entire FURNAS system, including the 750-kV system. The RINDAT system has been used for viewing the displacement of thunderstorms in real time and for helping in the operation and maintenance of the transmission system, as well as for obtaining statistical data on lightning strike or flash density and other parameters of interest for transmission-line design.

Following the outage experience described above, design criteria for the tower structures were developed for wind speeds of 150 km/h and 170 km/h. Some towers were mechanically reinforced as a result of the structural failures of the towers. A photo of the reinforced self-supporting 750-kV tower is shown in Figure 15.8-1.

Table 15.8-1 Outage Experience of FURNAS 750-kV Transmission Lines

Year		85	86	87	88	89	90	91	92	93	94
Lightning	Outages	2	0	1	4	1	8	3	3	2	5
	Length (km)	568	891	891	891	1783	1783	1783	1783	1783	1783
	Outages / 100 km	0,35	0,00	0,11	0,45	0,06	0,45	0,17	0,17	0,11	0,28
Fire Under the Line	Outages	1	0	0	0	0	1	0	0	6	1
	Length (km)	568	891	891	891	1783	1783	1783	1783	1783	1783
	Outages / 100 km	0,18	0,00	0,00	0,00	0,00	0,06	0,00	0,00	0,34	0,06
Fall of Towers due to Wind		2							-	-	3

Year		95	96	97	98	99	2000	2001	2002	2003	Average
Lightning	Outages	4	4	6	8	6	3	7	10	11	
	Length (km)	1783	1783	1783	1783	2114	2386	2698	2698	2698	
	Outages / 100 km	0,22	0,22	0,34	0,45	0,28	0,13	0,26	0,37	0,41	0,26
Fire Under the Line	Outages	1	0	0	0	0	4	0	2	0	
	Length (km)	1783	1783	1783	1783	2114	2386	2698	2698	2698	
	Outages / 100 km	0,06	0,00	0,00	0,00	0,00	0,17	0,00	0,07	0,00	0,06
Fall of Towers due to Wind		-	-	2	2	-	-	-	-	-	

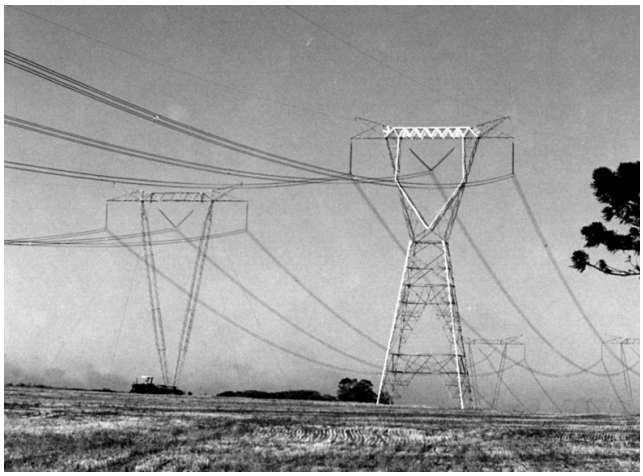


Figure 15.8-1 Reinforced self-supporting 750-kV tower.

Few complaints were experienced about audible noise or radio and television interference. More complaints were received, however, about electric shocks, probably caused by electric field induction effects and grounding problems. As a result of these complaints, electric and magnetic field measurements were made, and the grounding systems improved to solve the problems. Public information brochures on electric and magnetic fields were developed and distributed, particularly to people living close to the lines. Some doubts and questions persist, however, on the influence of EMF on health.

Before the transmission lines were commissioned, detailed land inspections were carried out. These involved climbing all the towers, giving special attention to the spacer dampers, were carried out. The relay settings were determined by conducting short-circuit studies and model tests in a real-time network simulator. Panel/control circuits were thoroughly checked before commissioning.

Two kinds of inspection are carried out every year on the Itaipu lines. The first, called land inspection, is made by car or motorcycle. In this, the inspectors climb one of every five towers, while the remaining four are inspected using binoculars. The second kind of inspection is made by air using helicopters. Some of the most common failures detected are related to vegetation that grows too close to the conductors, illegal use of transmission corridors, broken and polluted insulators, loose spacer dampers, and damaged conductors. It is planned to change some insulator strings and ground wires since they were damaged by corrosion in polluted areas.

Sticks, barehand, and helicopter methods are all used to maintain the lines, but the most commonly used is the barehand method. Due to the great importance of these lines to the Brazilian transmission system, almost all of the maintenance work is done live line.

The operating loads on the FURNAS transmission lines are around 70% of the design and limit loads.

15.9 NEW YORK POWER AUTHORITY (NYPA) 765-KV SYSTEM IN THE U.S.

In 1973, the Power Authority of the State of New York (PASNY) applied for a certificate of environmental compatibility and public need, under Article VII of the Public Service Law of the State of New York, for a proposed 765-kV transmission line from the Canadian border, near Massena, New York, to Marcy, New York, a distance of about 155 miles. PASNY today is called New York Power Authority (NYPA). Early in 1974, Rochester Gas & Electric Corporation and Niagara Mohawk Power Corporation applied for a certificate for a 765-kV line from the Pannell Road Substation in Monroe County, New York, a distance of about 66 miles. The main reason for the 765-kV line from Massena to Marcy was the need to provide additional transfer capability from the St. Lawrence Hydro Plant down to the south. In addition, NYPA system planners wanted the ability to make a future connection to the Hydro-Québec system for buying energy during summer months and selling energy during wintertime. This resulted in the construction of a 765-kV line from Massena to Chateauguay, Canada. Today NYPA shares ownership of this line with Hydro-Québec—NYPA owns 21 miles of the total 55 miles of this line. At the time of the line's construction, the projected load growth in New York State was about 7% per year, and there were plans to build multiple nuclear power plants on Lake Ontario. With this in mind, NYPA, Niagara Mohawk, and New York State Electric and Gas built some additional transmission lines: Marcy-New Scotland-Alps, Marcy-Volney, and BG-Leeds using 765-kV towers. However, these lines today are being operated at 345 kV.

The Massena-to-Marcy 765-kV line is 134 miles long, and much of it parallels two 230-kV lines. The Massena-Marcy and the Massena-Chateauguay lines are another example of lines that were built to transmit energy over a long distance from remote generating sources to load centers. Some of those generating sources belong to the Hydro-Québec system.

Opposition to these 765-kV lines resulted in what were called the "Common Record Hearings on Health and Safety of Extra-High Voltage Transmission Lines." Those hearings produced 14,000 pages of testimony by 31 expert witnesses and close to 150 exhibits. The issues that were addressed were: ozone production; effect on cardiac pacemakers; induced electric shock; audible noise; and biological effects. The hearings were conducted in two phases. Phase I was devoted to examining the operating characteristics of the transmission lines, while Phase II was intended to consider the health and safety implications of the information in Phase I. The conclusions and recommendations of the administrative law judges were basically that the right-of-way width be approximately 350 ft, instead of the 250 ft proposed by the applicants, and that information concerning the possible effects of the lines on users of cardiac pacemakers be distributed to cardiologists in the state. The judges also recommended the use of the right-of-way for recreational purposes be discouraged and that complaints concerning shock and audible noise be reported to and monitored by the judges. They also found no need for any other proposed protective measures and no need to take any action regarding the lines being operated at voltages lower than 765 kV. As a result of the Common Record Hearings, NYPA purchased another 50 ft on each side of the line, except for where the line paralleled an existing 230-kV line. Even though the utility purchased this additional right-of-way, they do not have to maintain it. NYPA, however, does not allow any houses to be built on this additional easement.

15.9.1 System Planning

System planning studies in the conventional sense were not performed before NYPA made the decision to build their 765-kV network in the State of New York. These lines were driven by the need to receive power from Hydro-Québec and for NYPA to have the capability of sending power to Hydro-Québec. No TNA studies were performed before the lines were designed and built. TNA studies were conducted, however, after the lines were energized, to confirm certain solutions to particular problems. Also, NYPA, unlike Hydro-Québec and AEP, did not conduct impulse or 60-Hz tests to determine the number of insulator units, air-gap clearances, and tower configuration. However, they did conduct corona tests on the hardware selected for the lines.

NYPA operates only two 765-kV lines: Massena-Chateauguay (55 miles), which was energized on August 29, 1978, and Massena-Marcy (134 miles), which was energized on December 22, 1978. As mentioned earlier, the Massena-Chateauguay line is operated mutually between NYPA and Hydro-Québec. Neither line is transposed.

Since the Massena-Marcy line, for the most part, parallels an existing 230-kV line, extensive line-routing studies were not conducted.

To control power frequency overvoltages, two shunt reactors were installed on the Massena-Marcy line and one on the Massena-Chateauguay line. All reactors are connected to the lines through circuit breakers. Shunt capacitors are only used on the 345-kV system.

When NYPA made the decision to build the Massena-Marcy 765-kV line from the Canadian border to the Utica, New York area, they had the benefit of the research conducted at the Apple Grove 750-kV Project, Project EHV,

Project UHV, and the operating experience of the Hydro-Québec 735-kV lines and the AEP 765-kV lines. The first AEP lines had a few AN, RI, and TVI complaints and some complaints regarding spark discharges in the electric fields near the lines. The first Hydro-Québec 735-kV line, which was a more conservative design, did not have these problems. As will be seen later, the NYPA 765-kV line design was similar to the first Hydro-Québec line.

15.9.2 Electrical Design

The conductor bundle used on the NYPA 765-kV line consisted of 4-1351.5 kcm 45/7 ACSR (Dipper) conductors. The diameter of each conductor was 3.52 cm, with a subconductor spacing of 45.7 cm. Like the first Hydro-Québec line, the phase spacing was 15.24 m. The average heights of the conductors were 26.2 m. The minimum ground clearance at midspan was 15 m, compared to 12.2 m for the first AEP designs. NYPA initially selected a 250-ft right-of-way-width for this line; but the common record hearings mandated a 350-ft right-of-way. The first Hydro-Québec 735-kV line was built on a 250-ft right-of-way, and the first AEP 765-kV line was built on a 200-ft right-of-way.

The overhead ground wires were 7#8 Alumoweld, spaced 20.7 m apart, with a shield angle of 20°. The overhead ground wires were not sectionalized, nor were they insulated. Also, NYPA has not installed fiber optic cables on these lines.

The L_{50} audible noise during rain at the edge of a 350 ft right-of-way width was determined from the long-term measurements conducted on the A-Line at the Apple Grove 750-kV Project. The ability to accurately predict L_{50} AN during rain was not well developed at the time that these lines were being designed. But, since the conductors on the Apple Grove A-line had essentially the same diameter as that proposed by NYPA, only slight adjustments had to be made for the differences between the Apple Grove design and the NYPA design to obtain an accurate prediction of the L_{50} audible noise during rain. The L_{50} AN level predicted during rain at 125 ft from centerline was 53.2 dBA. At the edge of a 350-ft right-of-way, the AN would decrease to about 51.7 dBA.

The 60-Hz electric field at the edge of the 350-ft right-of-way is about 1.6 kV/m. The administrative law judges mandated the 350-ft right-of-way width on the basis that they wanted the electric field at the edge of the 765-kV right-of-way to be essentially the same as what existed in the State of New York at the edge of the rights-of-way of existing 345-kV lines. The widths of the rights-of-way of most of the 345-kV lines in New York State are about 150 ft.

NYPA used standard porcelain insulators on the 765-kV line. The M&E ratings for the suspension structures were 30,000-lb units. The suspension and angle structures were V-stings, two strings on each side, and 35 units per string. The M&E ratings for the dead-end and angle structures were 40,000 lb. The dead-end structures consisted of four strings for each phase. The creepage distance for the 30K units was 12-in. per kV, whereas for the 40K units, it was 12.5-in.

15.9.3 Mechanical and Tower Design

The NYPA 765-kV line was built with self-supporting structures using weathering steel. A suspension tower can be seen in Figure 15.9-1.

The original spacers on the lines were bare groove, with a rigid top and springs on the bottom and sides. NYPA has not found any conductor damage from the use of these spacers, but they have found that the springs deform over time and crush very quickly with ice loading. The utility is replacing them on a priority basis with shear nut, spacer dampers. The shear nut units have been found to be a lot easier to install by helicopter than the crimp type because the crimping tool is difficult to use. After the first spacer is installed at a specific span-related distance from the center of the V-string, the rest are mounted 200 ft apart.

15.9.4 Operation and Maintenance

To inspect the 765-kV line, NYPA uses helicopters to conduct two aerial patrols each year. A ground patrol is also conducted annually on all lines from 115 to 765 kV. A detailed comprehensive aerial inspection is also performed



Figure 15.9-1 NYPA 765-kV suspension tower.

every five years on all of these lines. A NYPA lineman and a contract helicopter conduct the aerial patrols. NYPA linemen patrol the lines on foot with the use of four-wheel drive trucks and all-terrain vehicles. From these inspections, they have found the following damage and failures: (1) insulator separation, (2) shackle failure, (3) lattice tower collapse during an ice storm, (4) wood H-frame structure failures, (5) pole fires, (6) shield wire failure, and (7) conductor failures due to vibration, gun shot, and ice loading. However, on the 765-kV lines, they have found only one serious failure and that was a splice.

In maintaining energized lines, NYPA uses hot sticks and helicopters. If hot-line maintenance needs to be done, NYPA prefers the use of helicopters. However, their first preference is to conduct maintenance during the planned two- or three-day outages that are scheduled each year.

From a lightning standpoint, the NYPA design has experienced about one outage per 100 miles per year, which was their design criteria. The lines have had no outages due to switching surges or contamination. The NYPA 765-kV lines are in a fairly pristine environment, which has not changed over the years.

The NYPA 765-kV lines were designed to withstand 2.54 cm of ice and 2.03 cm of ice in the substations. In 1998, the lines experienced 5 cm of ice on the line, but it only affected the shield wires. This ice storm broke the overhead groundwire in numerous locations. The wire, which is a 7#8 Alumoweld, has an ultimate strength of about 15,400 lb. Since some of the spans on the 765-kV lines exceed 1400 ft, it does not take much ice to exceed the strength of the wire. The wire broke in four places; only one was at the AGS units, and the other three were tensile failures. At these three locations, it is suspected that the wires were weakened due to vibration effects accumulated over 20 years of service. At the time, two stretches of the line, totaling about 50 miles, had a radial equivalent of 4.5 cm of ice.

The other 765-kV failure was a shackle rated at 80 K positioned in the outside string of the outside phase of an SA1 tower. That threw the four-conductor bundle into the tower. NYPA had to splice in about 300 ft of wire per subconductor, and they had to rebuild part of the tower. Metallurgical tests showed galvanizing in a flaw in the pin, indicating that the flaw pre-existed the hot dip galvanizing. Thus, the ice increased the load; it did not exceed what the shackle should have held. Shortly thereafter, NYPA replaced all the shackles on all the SA1 towers because they were from the same batch. NYPA has had some outages due to equipment failure such as transformers, shunt reactors, etc.

The utility has had a few AN, RI, TVI, EF, and MF complaints, but these complaints have all been resolved satisfactorily. Mitigation measures have included improving the grounding system and installing better antenna systems. One concern is that homes are being built closer and closer to the lines.

In conducting commissioning procedures and tests, NYPA relied upon their own workforce. Before energizing the line, they did line inspection, phasing checks, verification of relay operation, etc.

The operating loads on the 765-kV lines at times have been comparable with the original estimation or lower.

NYPA used power line carrier (PLC) for communication. Two spread spectrum (SS) frequency bands were used on the Massena-Chateauguay line: 474 ± 4 kHz for the transmitter and 184 ± 4 kHz for the receiver and 436 ± 4 kHz for the transmitter and 166 ± 4 kHz for the receiver. One SS frequency band and one microwave channel were used on the Massena-Marcy line. The frequency band was 344 ± 4 kHz for the transmitter and 356 ± 4 kHz for the receiver. NYPA has not used any types of fiber optic cables or optical ground wires for communication.

After the 1998 ice storm, NYPA developed a Transmission Emergency Response Plan. For 345-kV lines and below, the plan specifies wood until permanent towers can be replaced. In the case of 765-kV lines, the utility has the capability of restoring up to one mile of line using Lindsey towers.

NYPA presently has a lightning detection system, correlated with GPS coordinates of their transmission structures, that gives them the ability to locate lightning-caused faults within a one-mile radius.

NYPA collects weather data from local weather forecasts, weather websites, and the Federal Aviation Administration (FAA) offices. They have not developed any special techniques for measuring ice accretion.

The other 765-kV lines that are operating at 345 kV in New York State have towers that use weathering steel similar to the NYPA 765-kV lines. However, the dead-ends have box assemblies on the ends of the arms to give linemen a better perch for hot stick maintenance. The jumpers are supported by strut instead of suspension insulators. Like NYPA, the National Grid has a 345-kV line originally built to be operated at 765 kV. That line has a three-conductor bundle and was constructed using green steel poles, which is quite a bit different from any of the other 765-kV structures discussed in Chapter 15.

15.10 ESKOM 765-KV LINES IN SOUTH AFRICA

Eskom supplies about 95% of the electrical energy used in South Africa. All of the company's major baseload power stations are located near the inland coalfields. Much of the load is also concentrated in the inland area relatively close to the coalfields, but there are significant loads in the coastal centers, some of which are 1500 km from the inland stations. Before 765 kV, these distant load centers were supplied by a three-line 400-kV system.

Eskom has standardized on using six 600-MW generators at each of their coal-fired stations, which means that up to 3600 MW has to be transmitted out of each station. The distances involved in connecting the Matimba Power Station to the system, or in connecting their Tutuka Station to KwaZulu Natal, or to the first distribution station of the Cape system, vary from 330 to 500 km, an average about 400 km. Since the loads in the links to the Cape and Natal were expected to exceed 2300 MW in the early 1990s, the use of 765 kV for these links was felt to be fully justified. For the Matimba link, the case for 765 kV was marginal, as the load would barely exceed 2300 MW when all six sets were operating at full output, and the 400-kV lines connected to this station would take up to 900 MW of the station output. From 1975 to 1980, the average load growth in South Africa averaged 8.2%, but from 1980 to 1985, it dropped to 3.7%. As a result, Eskom decided to use 400 kV, instead of 765, to connect Matimba to the system and for the next line to Natal. However, they have used 765 kV to overlay their 1500-km transmission system to the Western Cape. At this time they have about 1200 km of 765-kV line in service.

H. B. Norman in a 1976 paper (Norman 1976) showed that 765-kV transmission was economic in South Africa for loads exceeding approximately 2300 MW and distances over 200 km. This is especially true since, in general, 765-kV lines cost less than twice the cost of 400-kV lines, but they can carry four times the load of 400-kV lines. The planning studies that were used to choose the voltage needed and the number of lines assumed a 7.5% load growth and the transfer of large amounts of power over a distance of 1500 km.

At the time 765 kV was being considered in South Africa, only two utilities were operating lines above 700 kV: Hydro-Québec in Canada and American Electric Power Service Corporation in the United States. Norman in the same 1976 paper mentioned these two systems and that they had had some problems in the technical areas of switching surges, audible noise, ground gradients, etc., which had led to extensive investigations in those countries. However, because of the unique problems, such as high altitude, that would be encountered in introducing 765-kV transmission in South Africa, Eskom in 1979 entered into a collaborative agreement with CESI, the Italian research organization, to study electromagnetic and insulation problems associated with reduced air density at high altitude.

As of the writing of this book, Eskom has two lines operating at 765 kV and a third line built for 765 kV, but operating at 400 kV. The first two lines are called Alpha-Beta-1 and Alpha-Beta-2. They are both 436.4 km in length and were built in 1987. The third line is called Beta-Hydra-2. It is 280 km long and was built in 1990, and is scheduled to be energized at 765 kV in 2004.

15.10.1 System Planning

Eskom conducted the usual system planning studies based on an assumed load growth of 7.5%. Studies showed that 765 kV would be needed to transfer large quantities of power from the coal-fired generating stations. In addition, Eskom had a vision for a strongly interconnected and firm transmission network that would connect these load centers to the generation. As a result of these studies, Eskom has built the following 765-kV lines:

- Line 1 – Alpha-Beta 1 – 436.4 km (Built in 1985)
- Line 2 – Alpha-Beta 2 – 434.4 km (Built in 1985)
- Line 3 – Beta-Hydra 2 – 280 km (Built in 1990)
- Line 4 – Beta-Hydra 2-Turn-In – 5 km (Built in 2003)

Since the 765-kV lines would be built at altitudes as high as 1500 m above sea level, Eskom needed to determine the electrical design with these higher altitudes in mind. With the assistance of CESI and Enel in Italy, Eskom built a corona test cage at Megawatt Park, Johannesburg at an altitude of 1584 m to study AN, RI, and CL due to conductor corona.

The results of a TNA study for the 765-kV system indicated that the CFO voltage of the towers in the first leg of the transmission system should be 1350 kV, which translated into conductor-window clearances of approximately 5 to 5.5 m at an altitude of 1500 m. In order to verify the validity of the initial design estimates to local conditions, an extensive series of tower window breakdown studies were conducted at the NETFA facility from June 1981 to June 1983. An extended test series was also conducted in March/April 1982 at the CSIR facility. The NEFTA tests also included assessments of live-line working clearances and safety.

To optimize the air-gap clearance, Eskom built two 765-kV structures (guyed and self-supporting) at the NETFA laboratory at Apollo for intensive testing at a high-altitude location. On the center phase of the self-supporting tower,

two different conductor-earth clearances (5.5 and 5.1 m) were tested, so as to allow the relevant gap factors to be optimized. These gap factors were found to depend slightly on the relative air density. No cognizance of fire flashovers was taken in choosing the phase-to-phase and phase-to-ground clearances. Clearances for withstanding fire were determined to be prohibitively large and expensive. Avoidance of fire, as far as possible, is Eskom's practice.

Eskom's system studies determined that surge arresters would be required at both ends of the substation, and closing resistors would be required on line breakers. The studies also showed that switchable shunt reactors would be needed at both ends of the line. Eskom also uses switchable busbar reactors on their 765-kV lines. No series compensation is used.

The Alpha and Beta substations, which are GIS protected by Eskom's Phase II standard protection schemes, are designed to the performance levels required for a 6000-MW interconnection, as described in (Coney 1982). This allows for single-pole reclosing, as well as three-phase reclosing. Although single-pole reclosing was designed for, it is not used.

To determine the routes for the 765-kV lines, Eskom conducted environmental impact studies along with extensive field investigations. The lines were built over a prevailing open country environment, and the company's main concern was in the utilization of guyed structures. The company encountered some opposition to the lines from farmers, and some concern was expressed over EMF and TVI. Eskom sought to overcome opposition by promoting the economic benefits of the project and building a mockup. The company also designed a pamphlet on the project and distributed it to the public.

The presence of two equi-spaced line transpositions on the 765-kV lines necessitated careful design of the power line carrier system. In particular, low-carrier frequencies (in the 50-70 kHz range) were used. Compatibility between the line configuration and feasible operation of the power line carrier system were very important design considerations. In fact, the delta configuration was rejected because of the likelihood of mode cancellation at power line carrier frequencies.

15.10.2 Electrical Design

As mentioned earlier, Eskom conducted impulse tests on a full-scale tower to determine the insulation requirements. Those tests indicated that a 5.5-m air gap was probably adequate, and the 765-kV towers were designed around this figure. However, when allowances were made for variations in the hardware dimensions and insulator tolerance, the actual air gap clearance in the suspension tower windows became approximately 5.9 m. Once full-scale structures became available, a self-supporting and a guyed suspension tower were retested at the high-voltage test facility at Apollo to determine the actual performance of the structures. These tests showed that the flashover performance was higher than necessary. A new-guyed structure was designed with a reduced clearance of 5.2 m. The original phase spacing was reduced by almost 2 m to 13.5 m.

The lightning density in the areas where the 765-kV lines were built was 6 to 9 flashes/sq km/annum, which translated into about 3.1 strikes/km/yr. The estimated annual outage rate based on these numbers was 0.25 outages/100 km/year. The ground resistivity is from 500 to 1500 ohm-meters, but mostly around 500. For analysis purposes, Eskom adopted a tower-footing resistance of 50 ohms, compared to a measured value of 5-20 ohms.

A study of the loads on the system indicated that 300 kN insulators in a V formation on the suspension towers and triple parallel strings of 300 kN insulators on the strain assembly were required. The insulators selected were glass cap-and-pin, which were designed specifically for the 765-kV lines. Eskom has had very good experience with glass insulators, and the insulators could at the time be manufactured in South Africa. They are no longer manufactured in South Africa. The final cap-and-pin insulator that was selected has the following properties:

Minimum failing load:	300 kN
Connecting length:	195 mm
Creepage length:	440 mm
Shed diameter:	320 mm
Pin diameter:	28 mm

The pin diameter of these insulators is one size larger than what is specified by IEC. According to (Cretchley et al. 1987), this allows less sophisticated materials and metallurgical treatment to be used in the cap and pin.

Each sting of insulators on the Alpha-Beta lines consists of 33 discs giving an overall insulator length of 6435 mm and a specific creepage of 18.2 mm/kV. However, a new suspension tower designed for future lines will have 30 discs per string.

As can be imagined, the V suspension assemblies and the triple insulator string strain assemblies required the development of new 300-kN hardware. Also, since the strain assembly terminated on a single tower attachment, a 900-kN shackle was required.

The conductor selected was 54/7/3.18 "Zebra" ACSR. The diameter of the subconductor is 2.862 cm. The conductors are arranged in a level, regular hexagon formation. The

optimum bundle diameter for corona performance was approximately 56 cm, but this was increased to 64 cm for fear of subspan oscillation.

The electromagnetic performance of this bundle was predicted to be as follows:

Conductor surface gradient:
16.1 kV/cm (center phase); 15.8 kV/cm (outer phase)

Audible noise (L_{50} rain):
53.3 dBA, edge of the right-of-way (80 m right-of-way)

Radio noise (L_{50} rain):
72 dBμV/m at 0.5 MHz, edge of right-of-way

Corona loss (L_{50} rain):
<10 kW/km/phase

Corona loss (L_5 rain, heavy rain):
55.6 kW/km/phase

The line was designed so that the maximum electric field at 1.8 m above ground would not exceed 10 kV/m. This resulted in a minimum ground clearance of 15 m at 70°C and assuming a 10-year creep on the conductors. Clearance over structures, poles, etc. is 10 m, and clearance to other power lines or telephone lines is 7.5 m.

Two continuous 19/2.65 mm 1100 Mpa galvanized steel earth conductors are used. The shield angle to the outer phases is 15° and 60° to the center conductor.

Many utilities do not use corona grading rings on four-conductor bundles, but corona rings are necessary for suspension structures that have six-conductor bundles. Eskom, however, has used corona rings on four-conductor bundles on suspension structures at 400 kV. This has been done for two reasons: namely, to meet their radio interference voltage (RIV) limit, and in the case of polymeric insulators, to suppress deleterious corona discharges at the polymer sheath-metal interfaces. Eskom designed the corona rings for all of the structures on the 765-kV lines. Figure 15.10-1 shows the corona ring used in the center phase of one of the suspension structures. The RIV tests associated with the photo are conducted at an altitude of 1500 m above sea level. Besides the RIV limit, the RIV test also uses the absence of visible corona on the end fittings as a criterion for acceptable corona performance. Eskom uses only glass and polymeric insulators at transmission voltages. Apart from one case in which porcelain long-rod insulators have been installed, porcelain insulators are not used. This is due to the susceptibility of porcelain cap-and-pin insulators to puncturing.

15.10.3 Mechanical and Tower Design

The towers were designed to encounter loads under the worst possible climatic conditions and the worst combination of broken phase and earth conductors under "every day" climatic conditions. The towers were designed for 32 m/s wind on the conductors and 45 m/s wind (1.4 gust factor) on the tower. The details can be found in (Cretchley et al. 1987).

The flat terrain of the Alpha-Beta lines allowed extensive use of guyed structures. Self-supporting suspension towers were used only at positions where the installation of guyed structures was impractical due to side slopes or physical constraints. Of the 1900 structures erected on the first two Alpha-Beta lines, guyed suspension towers make up 95%, self-supporting suspensions 1%, and strain towers 4%.

Eskom's practice of using twin spacers on the horizontal pairs of multiple conductors could not be used on the 765-kV six-conductor bundle because the bundle shape has to be maintained from a corona phenomena standpoint. Therefore, Eskom spent a considerable period of time developing a suitable spacer for the 765-kV lines. They even built a test facility near Kroonstad in terrain that is open and flat to evaluate spacer dampers. This terrain gives rise to laminar flow winds that aggravate aeolian and wake-induced conductor vibration, which makes the tests fairly severe. The facility consisted of four spans of six "Zebra" ACSR with lengths of 400, 350, 350, and 400 m, respectively. A total of eight types of spacer dampers were found to be acceptable, and three different makes were installed on the first line. In his 1987 paper, Cretchley said that the first spacers had been installed for three years with no



Figure 15.10-1 Corona grading rings on 765-kV suspension assembly used to limit the RIV to 65 dBμV/300 ohms at 0.5 MHz. This limit applies irrespective of the altitude. (Photo courtesy Eskom.)

problems (Cretchley 1987). At the 2004 workshop, Eskom representatives stated that no problems have been encountered with the spacer damper. The maximum spacing between spacer dampers on the first line was 65 m. This was reduced to 55 m on the second line.



Figure 15.10-2 Eskom guyed-V structure. (Photo courtesy Eskom.)

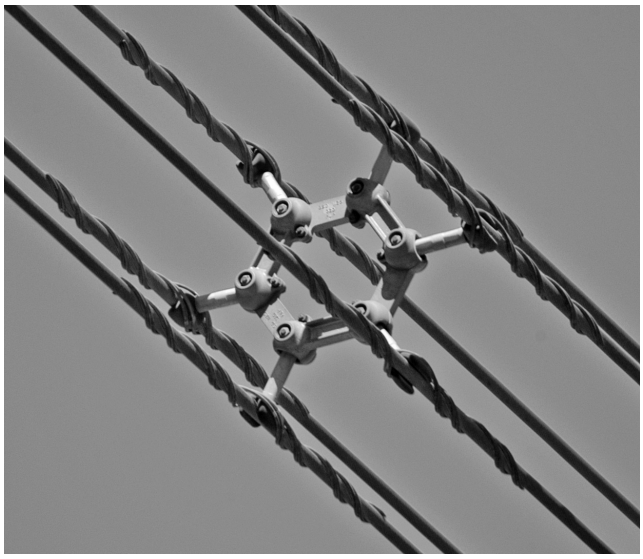


Figure 15.10-3 Space damper for six-conductor bundle. (Photo courtesy Eskom.)

The first 765-kV lines cross the central and northeastern Free State. The route follows rolling terrain. Elevation varies between 1350 m and 1750 m above sea level, with little change in climatic conditions. The expected temperature extremes for a 50-year return period vary from -10°C to 40°C, with the average daily temperature above 15°C. Snow and icing are quite rare occurrences. Rainfall varies from about 800 mm per year for the northern part of line down to about 400 mm for the southern end. Dust storms and bush fires generally occur during the dry winter periods.

Since some 765-kV lines will eventually traverse the Beaufort West area of South Africa, the 50-year return wind speeds for this area were used to design the 765-kV lines. Available data predicted a maximum hourly wind speed of 32 m/s, with 3-s gusts reaching 45 m/s.

Full-scale testing of the selected guyed-V suspension tower was conducted at the SAE testing station in Lecco, Italy during the Christmas period of 1983. All the other towers were tested at Eskom's Tower Test Station at Rosherville, which is 15 km east of Johannesburg. As a result of these tests, an alternative design was developed for the guyed-V suspension tower for the second Alpha-Beta line. The details are described in (Cretchley et al. 1987); the changes resulted in a reduction in mass of approximately 1600 mg.

The foundations used for the self-supporting towers were of the conventional types—i.e., pad and chimney—with alternatives such as 400-mm piles for normal soils, 100-mm piles for rock, and special types for waterlogged and sandy conditions.

Because Eskom was using guyed structures, the company had to carefully design the guy anchors. The guy anchors had to withstand a maximum design load of approximately 70 metric tons in the direction of the guy (56° to the horizontal). Two types of guy anchors were designed for the majority of the soils that were likely to be encountered on the lines:

1. An 800-mm diameter pile, which was suitable for soils ranging from certain types of clay to decomposed rocks.
2. A 100-mm pile solution with six piles connected to the guy through a pile cap. Two different types of this anchor were developed: one with vertical piles, and the other with the piles inclined at the same slope as the guy.

"Dead-man" anchors were also designed as an alternative to the above basic types for conditions unsuitable for drilling, and for sandy and waterlogged conditions.

All types of guy anchors were fully tested in the field. The 800-mm piles proved to be particularly successful.

To construct the towers, Eskom used cranes and temporary crossarms for the guyed-V structures. To string the line, 2 x 3 conductors were pulled simultaneously with two winches and two brakes.

15.10.4 Operation and Maintenance

To inspect the 765-kV lines, Eskom does a ground patrol every six months and an aerial patrol every three years. These inspections have discovered failed spacer dampers, some conductor damage due to line vibration, and a few broken insulators. All composite rubber-elastomer spacer dampers replaced the failed units. Six different makes of spacer dampers have been used on the 765-kV lines with a staggering scheme. An example of the staggering scheme is shown in Table 15.10-1.

Eskom has had some outages on the 765-kV system for which the exact cause could not be established. It is speculated that such faults were caused by bird streamers and/or light pollution, light wetting flashover phenomena. These outages are still under investigation, however, and no final conclusions at this time have been reached. Eskom has had some outages due to fires and one outage due to sabotage (a bomb in the late 1980s). The utility has had 18 reactor failures, which, of course, affected the network. No failures have been due to switching surges. In recent years, three fire-induced flashovers have occurred on the 765-kV lines. In two of the three cases, one occurred near the midspan position, and the other at a position where the conductor height is 27 m. The average electric field gradient at the midspan position is 461/15 = 30.6 kV/m. This exceeds the assumed fire flashover withstand gradient of 20 to 25 kV/m, so flashover is to be expected. Because of the lower gradient at the second position (namely, 17 kV/m), flashover should not be expected, but one did occur and the result was quite surprising. What this experience shows is that the 765-kV lines are inherently susceptible to fire flashover. Furthermore, the second flashover suggests that the withstand gradient is below 17 kV/m.

As regards birds, Eskom has not installed bird guards on the 765-kV towers. Bird guards are plastic rods mounted vertically on crossarms and the middle section of the tower to prevent birds from perching and excreting directly down to the suspension insulators and phase conductors. The 5.5 m air gap on the 765-kV lines is large enough to prevent bird streamers from causing flashovers. The 3.3 m gaps on the 400–kV lines, however, are vulnerable to bird streamer flashovers.

The outages that have occurred have been primarily due to lightning, but the outage rate has been in line with predictions.

In general, the performance of the power line carrier system on the 765-kV lines has been excellent. No corona noise problems have occurred, nor have the transpositions caused any signal propagation problems.

ADLash optical fiber has recently been installed on the 765-kV shield wires. It is too early to determine whether the corona discharges predicted from simulation and cage tests will cause any long-term damage to the cable sheath.

The design specifications for the guyed-V tower in the 1980s created some changes in the tower specification. Also, guy anchor failures due to corrosion created some changes.

Eskom has not received any AN, RI, or TVI complaints from anyone living near their 765-kV lines. Nor have they received any electric shock complaints due to the 50-Hz electric field. And, they have received no complaints about electric and magnetic fields, especially from farmers who may be concerned about possible effects on their livestock.

Eskom has developed all three of the commonly used methods to maintain the lines: sticks, barehand, and helicopters. They have used all three depending on specific task and conditions. Eskom does not use protective gaps in their live-line working operation. However, in general, most of their maintenance work is conducted with the 765-kV line de-energized, due to cost effectiveness and the possibility of getting outages. Eskom makes use of the guidelines in IEC 61472 in calculating the minimum safe approach distances to be used. The corrections for a nominal altitude of 1500 m are based on local research. The

Table 15.10-1 Example of Staggering Scheme for Spacer Dampers

Span Length	Subspan Length (m)												
	Spacer No.												
(m)	1	2	3	4	5	6	7	8	9	10	11	12	13
300	28	51	46	53	44	49	29						
400	29	44	54	46	53	44	55	46	29				
500	29	51	45	55	48	42	52	45	54	49	30		
600	30	47	54	44	50	42	49	55	44	53	47	55	30

minimum safe approach distance (for phase-to-ground) in the case of 765 kV is 5.5 m. This includes the ergonomic distance of 0.5 m.

In commissioning lines, the company does not do anything special. Standard commissioning procedures and various energization tests are conducted.

The loadings of the lines have been about 50% of the design load due to load growth smaller than anticipated.

The so-called Hydra Turn-In 765-kV line is a 2.5 km extension to the existing Beta -Hydra line 765 kV, which has been operating at 400 kV since its construction in the late 1980s. The entire line, which was completed in 2004, is scheduled to be energized at 765 kV in December 2004. The Hydra Turn-In line uses composite insulators, which represents Eskom's first use of polymeric insulators on 765-kV lines. The specific creepage in this case is 25 mm/kV, and the dry arcing distance is 5.5 m. The rated mechanical strengths are 300 and 400 kN for the suspension and strain assemblies, respectively. To facilitate handling on site, all insulators consisted of two units in series. Figure 15.10-4 shows a terminal tower at the start of the Tee-off section. Note that in Figure 15.10-4, the jumpers have been omitted to keep the Tee-off de-energized. Note also that the Tee-off was constructed without an underpass arrangement, which was enabled by a 3D analysis to ensure that clearances would not be infringed. It should also be noted that the grading rings on the earth end of the polymeric insulators are yet to be installed.

Until recently, Eskom has not needed to apply Emergency Restoration Procedures to the 765-kV lines. This is because of the few noncritical mechanical failures occurring since their commissioning in 1986. However, a comprehensive program is now being developed for the transmission grid as a whole, including the 765-kV lines. The procedures will be based on a hierarchy of the criticality of the lines—i.e., rapid, emergency repair of the most important lines, slower methods for the less important lines, etc. Various technical methods are now being evaluated. Technical teams to perform the repair tasks are also being formed.



Figure 15.10-4 Terminal tower in Eskom's Hydra Turn-In 765-kV line. (Photo courtesy Eskom.)

In general, Eskom feels the 765-kV lines have been well designed and that their performance is quite satisfactory. Plans are already under way to extend the 765-kV network by several hundred kilometers to the Western Cape area of South Africa.

15.11 765-KV TRANSMISSION LINES IN INDIA

In India, the central and state governments have joint responsibility and jurisdiction for the development of the power sector. The generation, transmission, and distribution sectors are, therefore, developed through various central and state sector utilities. For administrative and operational reasons, the power systems spread throughout the 32 state territories are grouped into five regional grids: northern, eastern, western, southern, and northeastern regions.

The natural energy resources in the country are unevenly distributed—with coal reserves concentrated in the eastern region, and hydro potential located mainly in the northeastern and northern regions. Large pithead thermal generating stations have been established near coal reserves, and hydro power generating potential is also gradually being exploited. The load centers, however, are situated across various regions, and there are constraints on rights-of-way. Therefore, it has become necessary to establish flexible and high-capacity systems for transmitting large blocks of power between regions.

Power Grid Corporation of India Limited (POWERGRID) is the central transmission utility having the responsibility for establishing and operating regional and national power grids to facilitate transfer of power within and across the regions with reliability, security, and economy based on sound commercial principles. POWERGRID has established high-capacity, high-voltage ac and dc transmission lines, as well as HVDC back-to-back links, leading to formation of a national grid.

The choice of a 765-kV ac transmission system by POWERGRID was to provide an overlay on the vast 400-kV system already in operation to facilitate transfer of large blocks of power over long distances and to conserve rights-of-way. Construction of the first two 765-kV single-circuit lines, with a total length of 563 km, was completed in 2001, but the lines are being initially operated at 400 kV,

and will be operated at the rated voltage depending on the growth of power generation in the region by 2010-11. The construction of two more 765-kV lines is nearing completion. Future plans include construction of a ring of 765-kV transmission lines interconnecting eastern, western, and northern regional grids by the year 2010.

15.11.1 System Planning

The first 765-kV transmission lines in India comprised two single-circuit lines between Kishenpur in the State of Jammu and Kashmir and Moga in the State of Punjab. The transmission voltage of 765 kV was chosen on the basis of technical and economic considerations after evaluating various alternatives: six double-circuit 400-kV lines, two single-circuit 765-kV lines, or one HVDC bipole.

The design of 765-kV lines was made on the basis of national codes and standards, international practices, and consultants' recommendations. The basic reliability criterion for the transmission system design was that the power angle does not exceed 30˚ with one line out of service. Also, a reliability level corresponding to 150-year-return-period loads was considered in the design of transmission towers and other components.

Since the lines are initially operated at 400 kV, no special measures were incorporated to control overvoltages. When the lines are eventually operated at 765 kV, measures such as preinsertion resistors in circuit breakers, controlled switching, surge arrestors, shunt reactors, etc., will be incorporated for overvoltage control. Similarly, series compensation may be considered, depending on future load growth.

The nominal transmission voltage was 765 kV, with the maximum system voltage of 800 kV. The lines were designed to withstand power frequency overvoltage of 830 kV, switching overvoltage of 1550 kV, and lightning overvoltage of 2400 kV.

Power line carrier (PLC) was used for protection signaling. For the transmission lines presently under construction and eventually operated at 765 kV, carrier–aided-distance-type relays will be used as Main-I and Main-II protections. Conducted interference due to corona has been taken into account in designing the PLC system. OPGW is being used as one of the two ground wires on one of the lines, mainly for the purposes of communications and load dispatch.

The lines traverse through agricultural plains as well as hilly areas, with the altitude above sea level varying between 200 and 1000 m. The altitude was not taken into account in the electrical design of the lines. The lines experience mainly tropical weather conditions, with the possibility of occasional heavy wind conditions and wind storms. The isokeraunic levels in the regions traversed by the line vary between 50 and 60, and the ground resistivity between 100 and 600 Ω-m. Two ground wires were used to provide a shielding angle of 15˚. Pipe-type earthing or counterpoise-type earthing (comprising four counterpoise wires, each 25 m long) were used for each tower in order to bring the tower footing resistance to about 10 Ω.

Preliminary surveys were carried out to identify and select the line routes. Detailed surveys were also carried out during execution stage. Although some difficulties were encountered in siting the lines in populated areas, hilly terrain, etc., no active opposition was encountered in these regions.

The transmission lines were transposed at one-third of their length to reduce the effect of unbalance in line configuration.

15.11.2 Electrical Design

Based on studies carried out on lightning, switching, and power frequency voltage withstand requirements, the following conductor-to-tower air-gap clearances were selected: 5.1–5.6 m under stationary conditions, 4.4 m for 25˚ swing of insulator string, and 1.3 m for 55˚ swing of insulator string. The minimum conductor-to-ground clearance was kept at 15 m.

Both porcelain and toughened glass cap-and-pin disc insulators, with electromechanical ratings of 120 kN and 210 kN were used. Since the transmission lines pass through areas of light pollution, performance under polluted conditions was not a major consideration in selecting the insulators. The insulator strings comprised 35 units of 280 x 170 mm discs, each with a leakage distance of 370 mm (in the case of 210 kN) and 40 units of 255/280 x 145 mm discs, each with a leakage distance of 320 mm (in the case of 120 kN).

Conductor bundles were selected on the basis of technical and economic considerations. Economic conductor cross section was selected, taking only resistive losses into account, while the choice of the number and diameter of conductors in the bundle was based on the corona performance characteristics, mainly RI and AN, of the line. The bundle consisted of four Bersimis conductors of 35.05 mm diameter with a subconductor spacing of 457 mm. Taking into account the existing international practices, as well as the operating experience of the 400 kV lines in the country, the 765-kV lines were designed to meet the following criteria: RI at the edge of the right-of-way, and at 1 MHz should not exceed 50 dB for 80% of the time during a year; AN at the edge of right-of-way limited to 55-58 dBA under wet conductor conditions.

The electric field at 1.8 m above ground was limited to 10 kV/m within the right-of-way and to 2 kV/m at the edge of right-of-way. The magnetic field under the line was limited to 1 mT. The width of the right-of-way for the first 765-kV lines in India was 85 m, but for the new generation of lines, it has been reduced to 64 m. Two ground wires, each with a diameter of 10.98 mm, were used for lightning protection. In one of the lines, one of the ground wires is a 24-fiber OPGW. In addition to providing the required protection angle, the ground wires were also designed to carry fault currents.

15.11.3 Mechanical and Tower Design

Spacer dampers were used on the four conductor bundles, while rigid spacers were used for jumpers. Clamping systems in both cases were metal-to-metal. Vibration dampers were also installed on the ground wires. For transmission lines built so far in India, snow/ice loading was not a design criterion, but for some of the lines planned in the northern regions, it is being considered. Wind speeds corresponding to a 150-year return period and narrow front wind loading equivalent to 250 km/h were also considered for line design. Some failures of towers occurred during the construction stage due to heavy wind conditions. However, no failures occurred after the lines were commissioned.

Single-circuit horizontal conductor configuration was used for the first group of 765-kV lines in India. The towers were mainly self-supporting, fully galvanized steel lattice structures. For approximately 64% of the locations of the two lines, 0˚ (type A), 5˚ (type B), and 15˚ (type C) suspension towers were used, while for the remaining locations, 30˚ (type D) and 60˚ (type E) tension/dead-end towers were used. The future 765-kV lines will have a delta phase configuration, as shown in Figure 15.11-1.

15.11.4 Operation and Maintenance

Because the transmission lines designed for 765 kV have been operated only at 400 kV since their construction, not much operational experience can be reported. Ground inspection of the lines is carried out by linemen, either monthly or biannually, depending on the type of terrain. Thermo-vision inspection is carried out annually on the conductors; detection of punctured insulators and signature printouts using offline fault locators are also conducted annually. The line maintenance is presently carried out through manual patrolling and use of conventional methods, but provisions are being made for live-line maintenance in the future.

Quick restoration of damaged transmission lines, due to either natural or man-made disasters, using Emergency Restoration System (ERS) and helicopters, has been carried out on lower voltage lines. The use of ERS is also foreseen to be extended to 765-kV lines.

The ERS is designed and fabricated with a modular concept, which can be easily transported and erected at site. The major components of the ERS are:

- Modular structures to constitute different configurations of guyed towers suited to various failure scenarios and site conditions
- Insulated cross-arms
- Guy wires
- Temporary foundation and guy anchor arrangements
- Erection tools like winches, gin-poles, etc.

Presently under development at POWERGRID is an in-house design of an ERS that is applicable to transmission lines of 132–800 kV ac and ± 500 kV dc, with either single conductors or multiconductor bundles.

POWERGRID has implemented a program of wildlife and environmental protection. Under this program, care is taken during transmission-line route selection to avoid wildlife sanctuaries, national parks, and forest lands with rare flora and fauna. Where routing through forest lands is unavoidable, route length in the forest is kept to a minimum, and wherever required, towers with extensions of

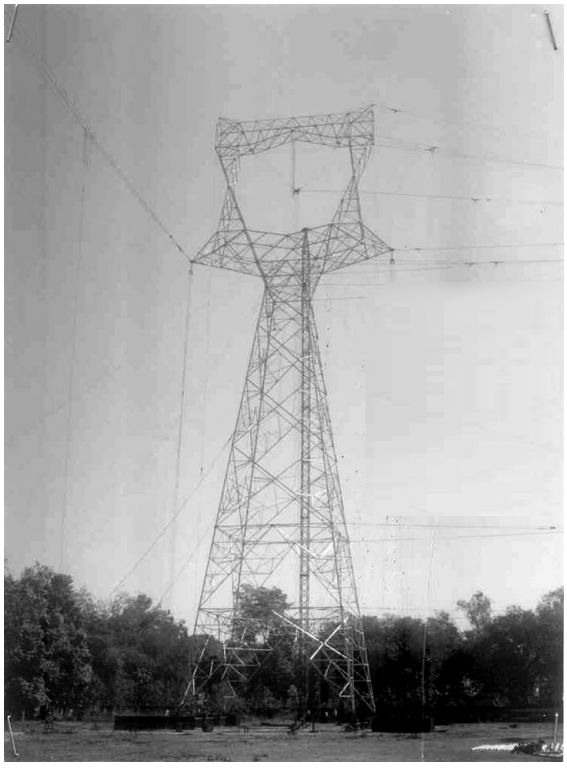


Figure 15.11-1 765-kV delta tower configuration.

18/25 m are used to minimize tree cutting. Similarly, where the line is passing through areas near wildlife sanctuaries, and movement of elephants is expected within the right-of-way, tower heights are increased by 6 to 9 m so that even elephants with raised trunks would have adequate safety clearances from the live conductors. As an initiative in environmental conservation and to optimize land use, towers have been designed with delta configurations that require a reduced right-of-way of 64 m, and prototypes have been tested for use in ongoing and future projects.

Further, for lines passing through hills and mountain slopes, towers with a narrow base and unequal leg extensions are used to facilitate locating them with fewer disturbances to natural slopes. In addition, foundations with unequal chimneys and pedestals are also used to reduce disturbance to natural slopes.

15.12 KOREA ELECTRIC POWER CORPORATION (KEPCO) 765-KV SYSTEM IN SOUTH KOREA

The Korea Electric Power Corporation (KEPCO) determined in the 1980s that 765-kV transmission was going to be needed in South Korea because of rapid economic growth.

When these studies were being performed, the load growth in South Korea was between 8 and 10% per year. KEPCO already had a 345-kV backbone system. Being a small country, 765-kV was not needed to transmit large blocks of power over extremely long distances from remote power stations, but their situation was similar to that of AEP. The rapid growth required more and larger generating stations, and the 345-kV system was no longer adequate for transmitting such large blocks of power throughout South Korea. As of the writing of this section, KEPCO had three double-circuit 765-kV lines in operation: (1) Dangjin Thermal Plant to Sinseosan substation (40 km); (2) Sinseosan to Sinanseong substation (138 km); and SinTaebaek substation to SinGapyeong substation (155 km). Because of the difficulties in obtaining land for the lines and the requirement of the public for environmental friendliness, all of the 765-kV substations of KEPCO are outdoors and full-GIS systems.

15.12.1 System Planning

Table 15.12-1 shows the results of a study conducted by KEPCO to determine the lines needed to transmit various loads. This study, like most studies of this nature, clearly shows the economic advantage in using 765–kV, rather than 345 kV, to transmit larger loads.

KEPCO was the first utility in the world to construct double-circuit 765-kV lines. Since there was no experience with double-circuit 765-kV systems anywhere else, KEPCO, through the Korea Electric Power Research Institute (KEPRI), built the "Gochang 765-kV Full-Scale Test Line," which is located on the western coast of Gochang-Gun, Jeon-buk Province. Before this test line was constructed, various kinds of conductors were tested in a corona cage at the Korea Electric Research Institute (KERI). Also, the basic technology of insulation design for 765-kV transmission lines and substations was developed during this initial period.

To determine overvoltages that would be expected on the 765-kV system, KEPCO conducted TNA studies at KEPRI. The system studies indicated that, to control overvoltages, surge arresters and shunt reactors would be needed in the substation, and closing resistors would be required in the breakers. Series compensation is not used anywhere on the 765-kV system.

Because of the increasing awareness of people to their environment, securing land for the 765-kV line was somewhat difficult. Concern over EMF was one of the biggest issues raised by opponents of the line to block its siting. A geographic information system (GIS) was introduced to select the optimal route considering all of the environmental factors.

Even though transposition was studied using ElectroMagnetic Transients Program (EMTP), the result of this study showed that transposition was not necessary for the double-circuit line since a low-reactance phase arrangement was being used. Therefore, KEPCO did not transpose any of these lines. Optical ground wires (OPGW) were used for communications rather than PLC.

15.12.2 Electrical Design

The conductor for the 765-kV line was selected after comprehensive studies of RI, AN, transmission capacity, maintenance of above-ground conductor heights, etc. The stronger ACSR 480 mm^2 Cardinal conductor in a bundle of six was selected over the ACSR 480 mm^2 Rail conductor, which has been generally used for the 345-kV transmission lines. In the Dangjin Thermal power plant, the ACSR/AW conductor was used to prevent deterioration from corrosion. The properties of these conductors are shown in Table

Table 15.12-1 Transmission Capacity of Overhead Lines

Division		154 kV	345 kV	765 kV	
Circuit		Double Circuit	Double Circuit	Double Circuit	Single Circuit
Transmission Capacity		480 MW	1800 MW	8400 MW	4200 MW
In Terms of Capacity	Number of Lines	18	5	1	2
	Site Area	2304 m^2	960 m^2	512 m^2	760 m^2

15.12-2. For this double-circuit line, the conductors were arranged in a low-reactance configuration.

The minimum, maximum, and mean altitudes that the 765-kV lines traverse are 50 m, 1000 m, and 300 m, respectively.

The main electrical environmental design criteria of the 765-kV line were that the audible noise should be ≤50 dBA (L_{50} rain), radio interference should have a SNR ≥26 dB (L_{50} fair), and the electric field should be ≤3.5 kV/m. Even though the audible noise criterion in the residential areas is 50 dBA, in the mountainous areas where there are no residences KEPCO adopted 60 dBA by using the 1-dBA/300 m altitude correction factor.

The audible noise level of 50 dBA at the edge of the 37-m right-of-way width was determined from environmental regulations of the Korean government and the long-term AN measurements conducted by KEPRI on the test line at Gochang.

These tests indicated that the AN (L_{50} during rain) would be below 50 dBA. From an RI standpoint, the goal was to protect all radio signals whose strengths were 71 dB or larger with a 26-dB signal-to-noise ratio during mean fair-weather conditions.

For the 765-kV lines, KEPCO has used both regular ground wires and optical ground wires. For lightning protection, the shield angle was -8˚, which placed the overhead ground wires 1 m outside of the outermost conductors. The properties of the overhead ground wires are shown in Table 15.12-3. The ground wires were neither sectionalized nor insulated.

Table 15.12-4 shows the results of studies KEPCO conducted to determine the location of the overhead ground wires for lightning protection and the resulting strike distances for both the suspension towers and the tension towers. The assumptions used in this study were 0.35 lightning flashes/100 km/year at an Iso-Keraunic Level (IKL) of 20 and a tower ground resistance of 15 ohms.

For the suspension structure, KEPCO increased the "standard insulation" distances to 5600 mm at altitudes greater than 1000 m. For the tension structures, this distance was not increased.

The IKL assumed by KEPCO in designing the 765-kV system was 20; however, they are now accumulating lightning data using the Lightning Positioning and Tracking System (LPATS). The information obtained by this system will be used in the future rather than IKL.

The number of insulators required for the double-circuit line was not fixed. It depended upon the height of the line above sea level and whether the area through which the line was passing was clean or not. Table 15.12-5 shows the required number of insulators. In the design of the insulation for

Table 15.12-2 Conductors Used on 765-kV Lines

Kinds of Conductor	Stranded Wire (Cable) Composition	Calculated Sectional (mm^2)	Tensile Strength (kg)	Outer Diameter (mm)	Weight (kg/km)	Coefficient Of Elasticity	Coefficient of Linear Expansion (106/°C)
ACSR 480 mm^2 (Cardinal)	Al 54/3.38 Aw 7/3.38	Al 484.53 Aw 62.81	15,300	30.42	1,836	7,987	19.53
ACSR/AW 480 mm^2 (Cardinal)	Al 54/3.38 Aw 7/3.38	Al 484.53 Aw 62.81	15,300	30.42	1,760	7,565	20.5

Table 15.12-3 Overhead Ground Wires Used on 765-kV System

Kinds of Wires	Stranded Cable Composition	Calculated Cable Composition (mm^2)	Tensile Strength (kg)	Outer Diameter (mm)	Weight (kg/km)	Coefficient of Elasticity	Coefficient of Linear Expansion	Application Area
AW 200 (Conductivity 40%)	AW 19/3.7	204.3	12,870	18.5	961	11,100	15.5	Clean area
AW 200 (Conductivity 30%)	AW 19/3.7	204.3	16,547	18.5	1162	13,500	13.8	Snow or heavy snow area
OPGW 200 (Conductivity 40%)	AW 12/3.8 AW 10/2.81	198.1	12,480	19.0	1006	11,100	15.5	Clean area
OPGW 200 (Conductivity 30%)	AW 12/3.8 AW 10/2.81	198.1	16,046	19.0	1201	13,500	13.8	Snow or heavy snow area

lightning protection, the design criterion of lightning flashes number was smaller than 0.35 flashes/100 km/year at an IKL of 20, which determined the arcing horn interval.

The minimum height of the conductors at midspan of the 765-kV lines was calculated based upon electric field strength at ground level, height of trees under transmission line, types of electrical devices under the line, and separation needed when crossing other types of structure. These minimum ground heights are shown in Table 15.12-6. For regions frequented by people, KEPCO designed the lines to limit the maximum electric field to 3.5 kV/m. In the mountainous areas, the minimum clearance was selected so that the ground-level electric field would not exceed 7.0 kV/m.

Table 15.12-4 Lightning Overvoltage Insulation Design for KEPCO 765-kV Transmission Line

Item		Lightning Endurance Design	
Thunderstorm for a year		20	
Arm length of ground wire		1 m longer than arm of the most outer phase conductor or shielding-angle reference –8 (or over)	
Tower ground resistance		15 ohms	
Flashover route		Suspension device	Tension device
		Insulator string Horn	Jumper Horn
Horn distance		4800 mm	4600 mm
Standard Insulation distance	Applied method	1.115 Z + 21 [Z : Horn distance (mm)]	
	Isolation distance	Suspension tower	Tension tower
		5380 mm	5150 mm

Table 15.12-5 Required Number of Insulators for 765-kV Lines[1]

Height Above Sea Level	Location Class of Pollution		Clean Area		Contaminated Area[2]				
			Clean I	Clean II	A[3]		B[4]	C	D
	ESDD[5] (mg/)		~0.01	~0.03	~0.063		~0.125	~0.25	~0.5
	Kinds of Insulators		General Insulators			Anti-fog Insulators			
1000m and less	Suspension	300 kN	30	37	44	34	39	45	50
		400 kN	29	36	41	33	38	45	50
		V-String 210 kN	38	43	50	39	45	51	58
	Tension	400 kN	28	36	41	33	38 (48)	45	50
More than 1000m	Suspension	300 kN	31	37	44	34	39	45	50
		400 kN	39	36	41	33	38	45	50
		V-String 210 kN	38	43	50	39	45	51	58
	Tension	400 kN	28	36	41	33	38 (48)	45	50

1. Note: The dimension of insulators follows IC-305 (1978).
2. Division of contaminated area follows the ESDD measurements of 765-kV routes by Electric Power Research Institute (1994.6~1995.12).
3. Contaminated area A: General insulators are used.
4. Contaminated area B: For suspension device, anti-fog insulators are applied. For tension device, general insulators.
5. ESDD (mg/cm^2) is at underside outer attachment of standard suspension insulators.

Table 15.12-6 Ground Clearances for 765-kV Lines

Division	Facility Standard (m)	Added Value (m)	Designed Value	Remarks
Flat ground area	13.68		28	Region frequented by people
Mountainous area	12.68		19	Region seldom visited by people and with no trees
Railway (including electric railway)	14.18		28	
Road	13.68		28	Express highway, national road and other
Other trees	10.88	16.2	27	
Larches	10.88	21.2	32	Collective afforestation area
Rigida pine trees, Big cone pines	10.88	21.2	32	Collective afforestation area
Farmland	13.68		28	
Scheduled residential area (3 stories)	10.88		28	
Other structures crossing separating	10.88	4	15	Overhead electric wires, Overhead low-voltage line

15.12.3 Mechanical and Tower Design

The main members of the towers use steel tubular pipes, whereas the arm members use angle steel. Figure 15.12-1 is a drawing of a suspension tower, and two photographs of KEPCO 765-kV towers can be seen in Figure 15-12-2. KEPCO prefers double circuit to single circuit because more bulk power can be transmitted over a given corridor, and the width of the right-of-way can be smaller. Because the towers are close to 100 m in height, the use of tubular steel is preferred over angle steel, because of the extra strength needed during strong winds. KEPCO also believes the steel tubular structure is simpler, more environmentally friendly, and easier to assemble. To build the towers, KEPCO used a "tower crane," which is similar to the cranes used in the construction of high-rise buildings.

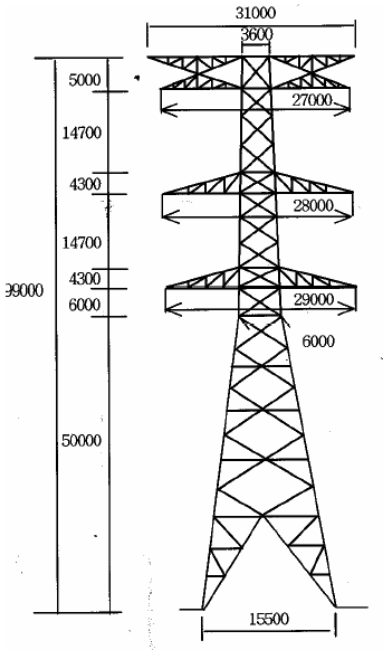


Figure 15.12-1 KEPCO 765-kV suspension tower.

Because the foundation load would be between 400 and 700 tons, and a lot of the construction would take place in mountainous terrain, KEPCO used a pier-type foundation. The depth of these pier foundations varied between 15 and 25 m depending upon the soil.

Because of the large heights of these double-circuit towers, a track is mounted on each tower that can accommodate a gas-powered car that is used as an elevator. The purpose is to improve safety and prevent worker fatigue, which is quite likely on such tall towers. Also, tools and other small material can be transported up the tower much more

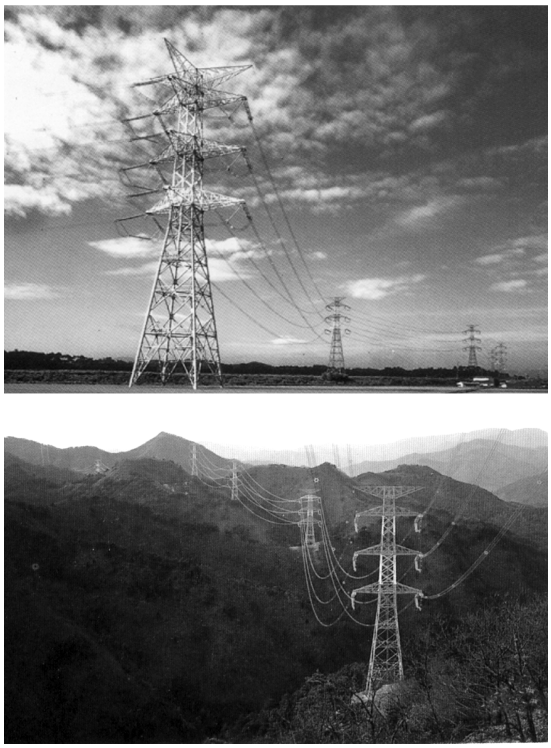


Figure 15.12-2 KEPCO 765-kV line.

quickly. Figure 15.12-3 shows an elevator attached to the rail on one of the 765-kV structures and a closeup of the elevator.

Many of the 765-kV lines were constructed in mountainous areas and on slopes. To minimize the destruction of the environment in these mountainous regions and to improve work efficiency, KEPCO built what they called "work stages," which could be dismantled once a tower was built. Figure 15.12-4 shows an example of a work stage.

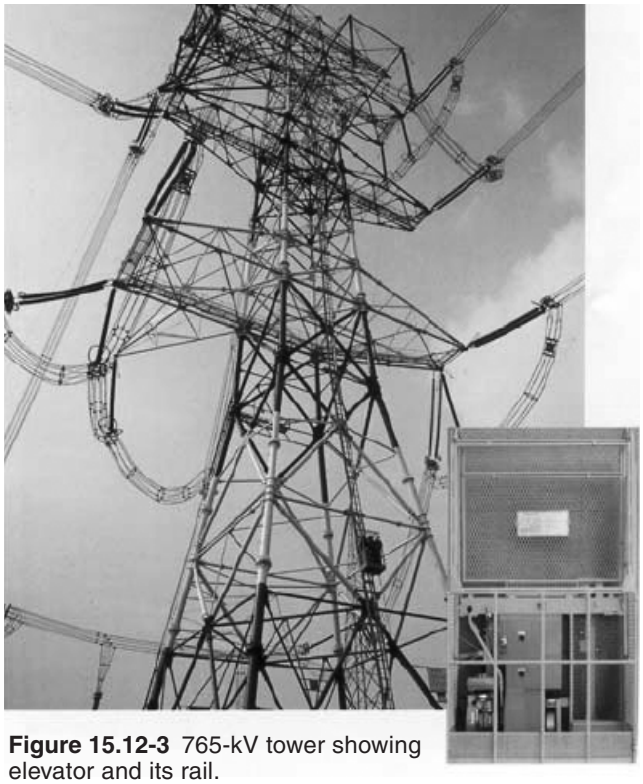


Figure 15.12-3 765-kV tower showing elevator and its rail.

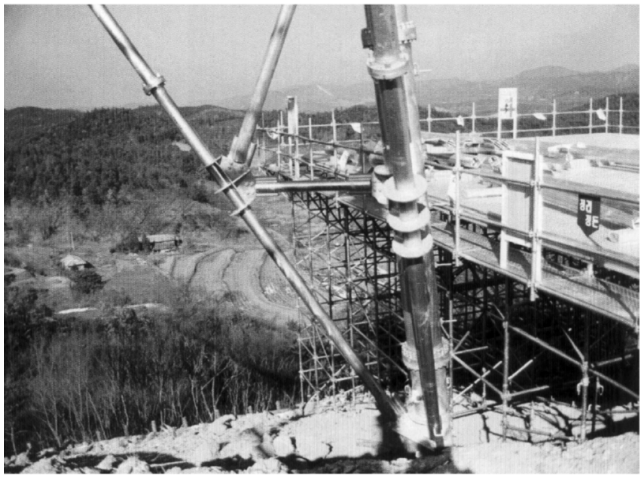


Figure 15.12-4 View of a "work stage" built near one of the 765-kV towers under construction.

To install the conductors, KEPCO used what they called a "semi-prefab wiring method." In conventional wiring method, conductors cut to standard lengths are connected between the towers. Then the conductors are sagged, adjusted, cut, and fitted with compression sleeves. In the semi-prefab method, the required length of wire is calculated beforehand to fit the desired sag.

15.12.4 Operation and Maintenance

Since the KEPCO 765-kV lines have only been in operation for about two years, they do not have a lot of operating and maintenance experience. In fact, the maintenance procedures are still in the development stage.

The 765-kV lines are inspected using a helicopter twice each year. On what are considered important lines or towers that have been classified as being in a dangerous position, linemen climbing the towers do inspections. In the case of the 765-kV lines, the climbing time is shortened by the use of the elevator. Special patrols are sent out after thaws and typhoons. So far, KEPCO has not experienced any outages on the 765-kV lines.

Because large portions of the lines are built in mountainous areas, inspection and maintenance will be done not only on foot but also by helicopter. KEPCO has an ongoing live-line maintenance research program, but at this time does not maintain the 765-kV system live.

The commissioning tests conducted on the 765-kV lines and substations consist of: (1) reviewing the protective schemes; (2) special tests on the 765-kV transformers; (3) special tests on the 765-kV GIS bus, transmission line, meters, and protective relays; (4) end-to-end test; and (5) phase-angle checks on both sides of the transmission line. The majority of these tests were conducted by KEPRI over a four-month period.

The design loadability (theoretical design load) for one of the double-circuit 765-kV lines is 8400 MW, with a 5% voltage drop and 30% stability margin at 250 km. The average operating loads up to 2004 have been between 2000 and 3000 MW. However, the loads are expected to increase chronologically.

KEPCO has received TVI complaints from the public due to ghosting. These complaints were resolved by connecting TVs to cable systems or satellite systems, or through the use of a ghost cancellation TV. Some Koreans still are concerned about EMF from the line, but KEPCO has assured the public that the lines are safe because the EMF values are lower than what is recommended by the World Health Organization (WHO). However, KEPRI is also conducting

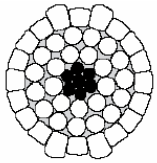
an EMF research project to develop magnetic field reduction techniques if they are ever needed.

KEPCO has had aeolian noise complaints, which are similar to those experienced in Japan. To solve this problem, the utility has installed spiral rods on the conductors on one span of the 765-kV line near the Dangjin Thermal Power Plant. The rods create a drag, which reduces the aeolian noise. Because this could be a prevailing problem, KEPCO will install an LN-Grackle conductor on new lines, depending on the route condition of the aeolian noise. This is a conductor where two of the outer aluminum strands are larger than all of the other outer conductors, as shown in Figure 15.12-5.

Table 15.12-7 shows the specification for the L-N Grackle conductor compared to the Cardinal conductor.

The grounding system for this line uses counterpoise wire (copper-clad steel-stranded cable) and spreading concrete to achieve a ground resistance of 15 ohms or less. Two types of foundations were used: pier foundation for ordinary or mountainous regions, and on-site piling foundation in soft soil.

The Korean Peninsula experiences a variety of wind, snow, and ice conditions. Table 15.12-8 shows the wind and ice loading that the 765-kV system is expected to experience. Data on wind, snow, contamination, temperature, etc. are gathered along the line routes using measurement and



L-N Grackle Conductor

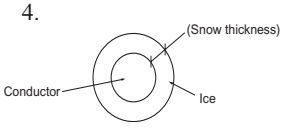
Figure 15.12-5 Cross-section view of a LN-Grackle conductor.

Table 15.12-7 LN-Grackle Conductor Compared to Cardinal Conductor

Conductor	Nominal Area (mm^2)	Stranded		Subconductor Diameter [mm]	Tensile Load (kg)	Max. Use Tension (kg)	Permissible Current (A)
		AL	ST				
Cardinal (480 mm^2)	480	54/3.38 (483)	7/3.38 (62.6)	30.42	15,300	5060	919
LN-Grackle (610 mm^2)	610	20/SB 30/3.8	7/3.38	37.2 (salient) 32.3 (round)	18,350	6110	1,041

Table 15.12-8 Wind and Ice Loading for 765-kV Lines

Description				Area[1] I	II	III	Snow	Heavy Snow
Wind	High Temp.	Speed[2] (m/sec)	Average (10 min.)	40.0	36.6	31.7	31.7	
			Max (3~5sec.)	54.0	50.0	43.7	43.7	
		Pressure[3] (kg/m^2)	Conductor	142	121	92	92	
			Pipe	377	322	245	245	
			L Angle	673	575	437	437	
	Low Temp.	Speed[2] (m/sec)	Average (10 min.)	20.2			20.2	
			Max (3~5sec.)	29.5			26.3	
		Pressure[3] (kg/m^2)	Conductor	46			37	
			Pipe	122			58	
			L Angle	219			115	
Ice	High Temp.	Sleet[4] (mm)		0			0	
		Gravity						
	Low Temp.	Sleet[4] (mm)		6			20	40
		Gravity		0.9			0.6	

1. Area
   I: Island Area.
   II: Seashore or area near sea (about 20~30 km below).
   III: Inland
2. Over ground 10 m reference.
3. Pressure - design load (assuming tower height 100 m).
4. 

meteorological databases. The environment along the line routes has not changed, but that is not surprising given the relative newness of these lines. KEPCO has not yet experienced any line outages due to equipment failure.

To control aeolian vibration, KEPCO has used stockbridge dampers for the ground wire and spacer dampers for the bundle conductor.

Figure 15.12-6 shows one of the spacer dampers used on the 765-kV lines.

As far as emergency restoration procedures are concerned, they are being developed by KEPCO.

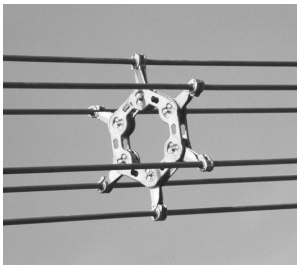


Figure 15.12-6 Six-conductor bundle spacer damper.

15.13 TOKYO ELECTRIC POWER COMPANY (TEPCO) 1000-KV LINES IN JAPAN

Tokyo Electric Power Company (TEPCO) is the largest power company in Japan. The company supplies electric power to more than 40 million people within an area of 39,000 square kilometers, which includes metropolitan Tokyo. Over the years, power demand in the system had been growing at 2 or 3% per year; therefore, in the early 1980s, TEPCO recognized that more bulk-power transmission would eventually be needed. At that time the highest voltage being used in Japan was 500 kV. Working with the Central Research Institute of Electric Power Industry (CRIEPI) and others in Japan, TEPCO started a research program to investigate voltages higher than 500 kV.

To meet the demand of metropolitan Tokyo, which is highly congested, TEPCO has built nuclear power stations and thermal power stations about 300 km from Tokyo. TEPCO has made every effort to provide quality electricity via its 500-kV network, but they have found that it is very difficult to acquire multiple corridors for transmission lines in the land available. Because of this, and the fact that an increased number of 500-kV lines requiring short-circuit capacity countermeasures would be required, TEPCO decided to construct 1000-kV lines having a capacity three to four times greater than conventional 500-kV lines. TEPCO has completed the first 1000-kV link from the Kashiwazaki-Kariwa Nuclear Power Station to the metropolitan region. It was energized at 500 kV in 1992, and the entire line has been operating at 500 kV since that time. Another 250-km branch connecting power sources in the Fukushima area has been constructed. Once the 1000-kV system is operating, it should ensure the stability of long-distance transmission on the TEPCO system and establish the basis for long-distance bulk transmission in the future.

15.13.1 System Planning

Since 1973, much research has been conducted in Japan in order to develop ultra-high-voltage systems. The nominal voltage of 1000 kV was selected after reviewing voltage values between 800 and 1500 kV for technical economical issues and environmental impact.

Before a 1000-kV system could be built, much research needed to be conducted, and this was accomplished by setting up a nationwide research committee, consisting of members of the 10 power companies of the Central Power Council and experts from universities, governmental institutes, and manufacturing companies. The resulting UHV Power Transmission Committee was organized in CRIEPI in November 1978.

To gain experience with this new voltage, CRIEPI built several new facilities. One was a double-circuit full-scale test line at Akagi, which consisted of two 300-m spans and three towers (two deadends and one suspension). To study corona loss, AN, and RI, CRIEPI also built a UHV test cage at the 600-kV Shiobara Testing Laboratory. Also at Shiobara were two impulse generators for full-scale switching impulse tests on phase-to-phase and phase-to-ground air clearances of a mockup of a 1000-kV tower. In addition, CRIEPI also built an impulse generator for conducting tests on snow-covered insulators, and an ac test facility to conduct extensive studies on the characteristics of snow-covered insulator strings under natural conditions. To study the effect of ice and wind, TEPCO built a test line at Takaishiyama, and to test polluted insulators, they built a new fog room. The details on these facilities are discussed in (Power System Planning 1985).

At first, the TNA at CRIEPI was used to determine switching surge overvoltages. After that, digital studies using EMTP have been successfully used to determine the absolute overvoltage levels along the 1000-kV facilities. The maximum phase-to-ground switching surge overvoltage insulation level envisaged for 1000-kV transmission is 1.6 to 1.7 p.u. This level is virtually determined by the level of ground-fault surge overvoltages. To control the switching overvoltages to these levels requires a combination of insertion resistors in the circuit breaker that are used during both opening and closing operations.

The system studies showed that shunt reactors were needed in each substation to: (1) prevent the system voltage from exceeding the specified amount; (2) prevent reactive power from flowing into the generators; (3) prevent voltage fluctuation at secondary and lower systems, which are affected by opening and closing either one of the two circuits of the double-circuit 1000-kV line; (4) keep power frequency temporary overvoltage level and its duration within an acceptable range from the viewpoint of preventing thermal runaway of 1000-kV metal oxide arresters; (5) help reduce switching overvoltages; and (6) prevent resonant overvoltages.

The initial loading of one of the double-circuit 1000-kV lines is 5000 MW, with an ultimate loading of 13,000 MW for some sections.

15.13.2 Electrical Design

Two types of ACSR conductors in a bundle of eight were selected for the 1000-kV system. One conductor has a cross section of 610 mm^2, and the other has a cross section of 810 mm^2. The diameters of these subconductors are 38.4 and 34.2 mm. The 8 x 34.2 mm conductor was installed in mountainous areas where complaints were not expected. The 8 x 38.4 mm conductor is expected to produce AN levels no higher than that of existing 500-kV lines, even though spiral wires will be installed to reduce aeolian noise from the conductors. The diameter of the bundle is about 1 m. The subconductors are arranged in a regular octagon. In the east-west route, a special conductor, which has the same effect as the spiral conductors, was developed and used in sections where whistling noise might be a problem. This special conductor lowered the cost and eliminated the need for the retrofitting process of the spiral rods. Figure 15.13-1 compares the spiral rod conductor with the low-noise conductor.

One of the interference problems anticipated by TEPCO was passive TVI due to television waves being reflected or interrupted by the transmission lines. TEPCO predicted as accurately as possible where this type of TVI would occur and took countermeasures at an early stage, such as adjusting the antenna locations of affected houses and installing high-performance cable television systems.

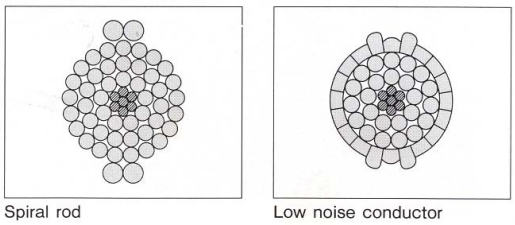


Figure 15.13-1 Comparison of spiral rod and low-noise conductor (Tokyo Electric Power Company 1994).

The overhead ground wires selected for the 1000-kV line are OPGW. Five sets of six optical fibers are housed at the core of the OPGW and are used to send information for maintenance and controlling electric current. Two of these wires are spaced 38 m apart at the top of the tower to provide lightning protection. Each wire is mounted 2.5 m outside of the outermost conductor on each side of the tower for a negative shield angle of 12 degrees.

The L_{50} AN during rain for the 8 x 38.4 mm bundle with spiral wires is expected to be no more than 50 dBA directly below the outermost phase when the maximum voltage of 1100 kV is applied to the line. The RI at 1 MHz in rainy weather directly below the line is expected to be 59 dB. The maximum electric field at ground level in inaccessible areas such as mountainous regions and forests will be 10 kV/m. In accessible areas (places of frequent pedestrian traffic such as agricultural roads serving as routes to schools, etc.), the maximum electric field will be 3 kV/m. The Akagi test site experimented with using underslung ground wires to reduce the electric field to 3 kV/m. This was found to be quite effective, but it is also unattractive. Therefore, Tokyo Electric chose to increase the ground clearance to keep the maximum electric field at 3 kV/m or less in populated areas.

The forecasted value for the rate of lightning failures for the 1000-kV lines is about 0.3 cases/100 km per year, and this is substantially lower than that for 500-kV transmission lines.

The maximum phase-to-ground switching overvoltage for the 1000-kV system will be 1.6 to 1.7 p.u., and the maximum phase-to-phase overvoltage will be 2.6 to 2.8 p.u. The following air gap clearances were envisaged for the maximum overvoltage at an altitude of 1800 m.

6.5 m for conductor-to-tower

6.6 m for conductor-to-arm of tower

6.3 m for horn gap

9.0 m for phase-to-phase

In very lightly contaminated areas (0.01 mg/cm^2), the length of the insulator strings needed to withstand 1.1 p.u. temporary overvoltage on unfaulted phases in case of a ground fault is estimated to be as long as 8 m.

Lightning and switching surge impulse testing was performed by CRIEPI on its full-scale test line. The objective of those tests was to determine the dielectric characteristics of a long air gap needed for designing the 1000-kV transmission line. From those tests, the gap factors were obtained and are shown in Table 15.13-1 and Figure 15.13-2.

The withstand voltages of contaminated long insulator strings were tested in the UHV fog rooms of CRIEPI and NGK. The ac withstand voltages and switching impulse flashover voltages of snow-covered insulator strings for 1000-kV lines were also tested by CRIEPI and NGK at their test sites in cold regions. Artificial snow was used for the most part. From all these tests, it was determined that 40 insulators were needed in the suspension towers. A double set of 33t strength insulators are used for each phase on suspension towers, and quad units are used on tension and deadend structures.

The insulator/conductor assembly for one phase of a suspension tower is shown in Figure 15.13-3.

15.13.3 Mechanical and Tower Design

TEPCO conducted feasibility studies on various kinds of towers, and the self-supporting double-circuit tower was adopted for the following reasons:

- Since guyed-type towers necessitate the additional area for guy-wires and guy-anchors, they are difficult to apply in Japan, where available land is limited. Also, the utility found that securing the anchors in steep mountainous areas is very difficult.
- The self-supporting tower is more economical than any other kind of tower when two circuits are involved.

The structural configuration of the tower is shown in Figure 15.13-4, and a photograph of a tension tower is shown in Figure 15.13-5.

Many of the construction techniques discussed earlier in Section 15.12 on KEPCO's 765-kV line were first used by TEPCO in the construction of the 1000-kV line. These techniques include pier foundations, tower cranes, staging work platforms, and the "engine elevator."

The pier foundations are mainly used in mountainous regions. The ground was excavated to about 20 m and

Table 15.13-1 Gap Factor of Insulator String Assemblies

Gap configuration		Conductor: upper arm[1]	Conductor: upper arm[2]	Conductor: lower arm[3]	
				Triangular configuration	Rectangular configuration
Tension insulator string assemblies	Conductor: under arm edge	1.41	1.24	1.41	1.33
	Conductor: 4m inside from arm edge	1.31		1.34	1.26
Suspension insulator string assemblies	Conductor: under arm edge	—	1.24	1.39	1.28
	Conductor: 4m inside from arm edge	1.19		1.30	1.28
Jumper V-suspension string assemblies	Arm width: 2m	1.29	1.24	—	1.28
	Arm width: 7m	1.19		—	1.24

1. Notes 1, 2, and 3 indicate three kinds of flashover paths, which are illustrated in Figure 15.13-2.

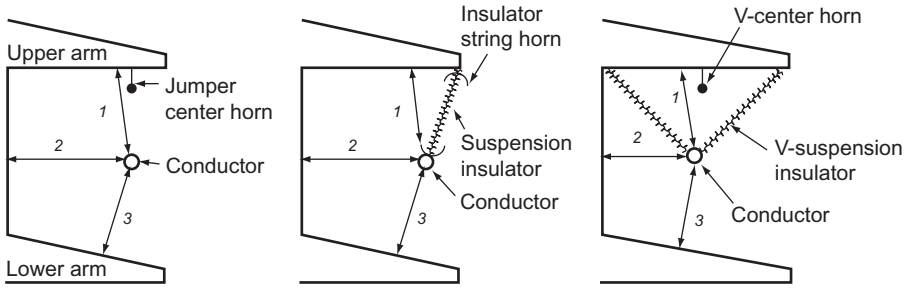


Figure 15.13-2 Illustration of insulator string assemblies (Power System Planning 1985).

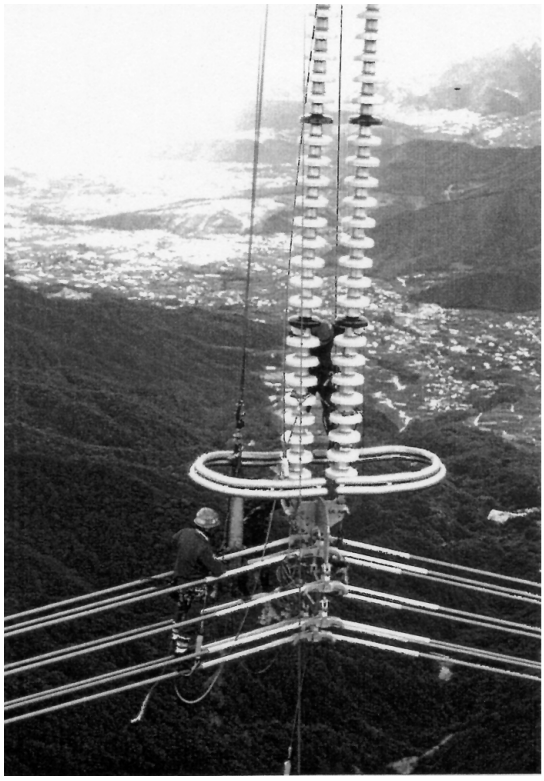


Figure 15.13-3 Tensioning work on a suspension tower (Tokyo Electric Power Company 1994).

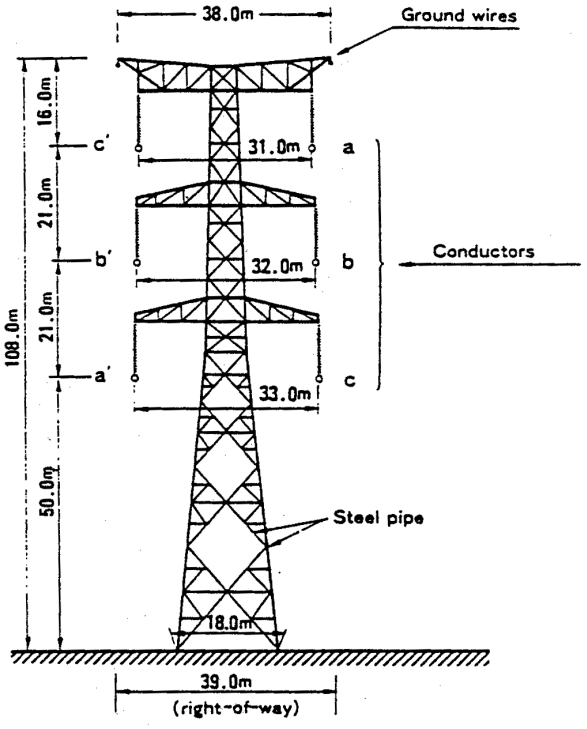


Figure 15.13-4 Structural configuration of a 1000-kV double-circuit tower. (Power System Planning 1985).

solidified with reinforced concrete, with the amount of concrete used per foundation being 1500 tons on average.

The towers are constructed of steel pipes, with each pipe section bolted together. The average weight of a tower is 400 tons, and the diameter of the poles near the surfaces is about 70 cm.

To determine the severity of galloping and subspan oscillation, the eight-conductor bundle with all of the fittings was tested on the Takaishi-yama test line (Power System Planning 1985). From observations up until 1986, there was practically no subspan oscillation, and galloping was not observed on conductors that had galloping control devices. This would indicate that, unlike the lines being built by others with six-conductor bundles, no spacer-dampers were used on the 1000-kV lines. A photograph of an eight-conductor bundle spacer is shown in Figure 15.13-6.

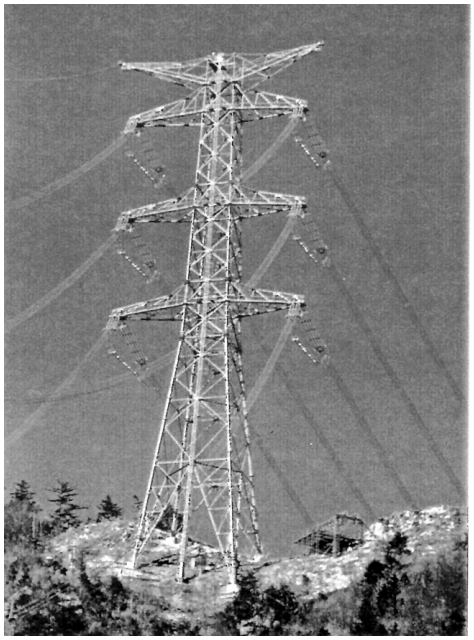


Figure 15.13-5 Photograph of a tension tower. Also seen in this photograph is a staging work platform and the rail used to mount an "engine elevator." (Tokyo Electric Power Company 1994).

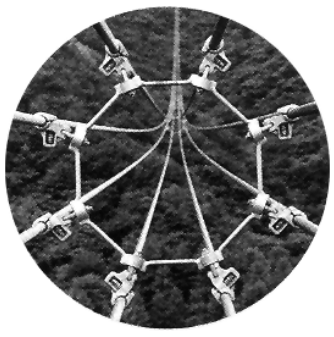


Figure 15.13-6 Spacer used for eight-conductor bundle (Tokyo Electric Power Company 1994).

15.13.4 Operation and Maintenance

As of the writing of this book, the 1000-kV lines in Japan are being operated at 500 kV; therefore, the utility does not have any 1000-kV operating experience as yet.

15.14 SUMMARY

The purpose of this section is to summarize and compare the basic design characteristics of the lines built to operate above 700 kV.

The summary of the line environments is presented in Table 15.14-1. These environments varied from flat to rolling to mountainous. The lines were built at altitudes close to sea level and as high as 1.8 km above sea level. For the most part they were built in pristine environments, but some line portions were built in moderate and heavily contaminated areas.

The number of sub-conductors used in the bundles of each line, along with the sub-conductor diameter, phase spacing, and minimum conductor heights, are presented in Table 15.14-2. All of the 765-kV lines built in the 1960s and 1970s have 4 subconductors. Russian 750-kV lines have 4 and mainly 5 subconductors. The Eskom lines being built at higher altitudes use 6 subconductors, as does the new line being built in the Appalachian Mountains in Virginia by AEP and the double-circuit low-reactance line built by KEPCO in Korea. Both of the lines built to operate above 1000 kV use 8 subconductors. The Russian 1150-kV line operated at that nominal voltage for a few years in the late 1980s and early 1990s, but lately has operated at 500 kV over more than 10 years. The TEPCO 1000-kV lines at this time are energized at 500 kV. Therefore, there are no lines operating anywhere in the world above 1000 kV at the present time.

The electrical environments of the lines operating above 700 kV are summarized in Table 15.14-3. The AN and RI values in this table were obtained by using the BPA empirical models that are described in Chapters 9 and 10. The authors tried to create this table using the design values provided by each electric utility, but this attempt was abandoned for the following reasons: (1) AN was not an issue when the original Hydro-Québec and AEP lines were built; (2) AN levels were calculated by the individual utilities using various empirical formulas under various weather conditions that were available at the time the lines were being designed; and (3) the RI levels were calculated using different formulas for different weather conditions, different frequencies, and different standards using formulas that were available at the time the lines were being designed. The electric field values were provided by the corresponding utility representatives.

For the KEPCO and TEPCO lines, the values in Table 15.14-3 were calculated for populated areas. In the mountainous areas of Korea and Japan with no population, the lines are closer to the ground and the electric fields, as discussed in Sections 15.12 and 15.13, are higher.

The levels in Table 15.14-3 were calculated at the edge of the right-of-way except for Russia. Russia does not have rights-of-way. They have what they call “Security Zones” for their high-voltage lines. The security zone is defined by a

Table 15.14-1 Line Environments

Company/Country	Nominal Voltage (kV)	Terrain	Altitude Range km	Ground Resistivity (Ohms-m)	Contamination Level
Hydro-Québec 1	735	Rolling	<0.3	10–10000	Light
Hydro-Québec 2	735	Rolling	<0.3	10-10000	Light
AEP 1	765	Flat/Rolling/Mountainous	<0.1-1.0	10-10,000	Light
AEP 2	765	Flat/Rolling/Mountainous	<0.1-1.0	10-10,000	Light
AEP 3	765	Rolling/Mountainous	0.5-1.2	10-10,000	Light
NYPA	765	Flat/Rolling	<0.3	10,10000	Light
Eskom	765	Flat/Rolling	1 to 1.8	500-1500	Light
FURNAS	765	Flat	0 to 1.2	1000	Light
EDELCA	765	Plains/Hills	0.3 – 1.0	50 - 2000	Light-Heavy
KEPCO	765	Mountainous	.05 to 1.0	50 - 2000	Light-Heavy
POWERGRID	765	Plains/Hills	0.2–1.0	100 - 600	Light
Russia	750	Plains/Hills	0.1 – 0.5*	200 - 400	Light
Russia	1150	Plains/Hills	0.1 – 0.5*	200 –400	Light
Tokyo Electric	1000	Mountainous			Light-Heavy

* For Russian 750 kV, the insulation of both lines and substations equipment are designated for usage at altitudes up to 1 km, whereas for 1150 kV, the insulation is for lines up to 1 km and for substation equipment up to 0.5 km.

Table 15.14-2 Line Geometries

Company/Country	Nominal Voltage (kV)	No. of Sub-conductors	Cond. Diam. (cm)	Phase Spacing (m)	Min. Conductor Heights* (m)
Hydro-Québec 1	735	4	3.50	15.3	15.3
Hydro-Québec 2	735	4	3.56	12.8	14.1
AEP 1	765	4	2.96	13.7	12.2
AEP 2	765	4	3.52	13.7	12.2/13.7
AEP 3	765	6	2.70	13.7	13.7
NYPA	765	4	3.52	15.2	15.5
Eskom	765	6	2.86	15.8	15.0
FURNAS	765	4	3.20	14.3	13
EDELCA 1 &2	765	4	3.33	15.0	14.7
EDELCA 3	765	4	3.33	13.2	13.7
KEPCO	765	6	3.042	See Note 1	19/28
POWERGRID	765	4	3.50	15.4	15
RUSSIA 1	750	5	2.24	17.5	12
RUSSIA 2	750	4	2.91	19	12
RUSSIA 3	1150	8	2.75	21.5-25	17.5
TEPCO	1000	8	3.42/3.84**	See Note 2	25/35

* Minimum heights in areas frequented by people including agricultural areas.

** Larger conductor used in populated areas; smaller conductor used in mountainous areas.

1. Double-circuit low reactance line: See drawing in Figure 15.12-1.
2. Double-circuit low reactance line: See drawing in Figure 15.13-4.

Table 15.14-3 Line Electrical Environments

Company/Country	Nominal Voltage (kV)	Width of right-of-way (m)	Mean Altitude (m)	Audible Noise (Rain) (dBA)	Radio Noise (Fair) @ 0.5 MHz (dBμV/m	Max. Electric Field* (kV/m)	Electric Field Edge of Right-of-way (kV/m)
Hydro-Québec 1	735	91.5	<300	51.2	43.0	8.7	1.5
Hydro-Québec 2	735	80.0	<300	54.7	46.4	9.3	1.7
AEP 1	765	60.1	<300	59.2	55.4	12.4	4.0
AEP 1	765	60.1	600	61.2	57.4	12.4	4.0
AEP 2	765	60.1	600	57.5	52.8	10.5	4.1
AEP 3	765	91.4	800	54.5	45.8	11.2	4.4
NYPA 1	765	106.7	<300	50.5	42.8	9.2	1.6
Eskom	765	80.0	1500	53	62	10	2.4
FURNAS 1 & 2	765	175**	800	58	42	5/10/15	< 4.2
FURNAS 3	765	94.5	800	58	42	5/10/15	< 4.2
EDELCA 1 & 2	765	120.0	<300	52.2	38.4	9.5	0.7
EDELCA 3	765	90.0	<300	55.0	44.2	10.2	1.3
KEPCO 1	765	37.0	<300	50.0	44.0	3.5/7.0	3.5
POWERGRID	765	85/64	<300	54.3	43.5	10	2.0
RUSSIA 1	750	116.0	<300	50.1	39.7	5/15/20†	1.0
RUSSIA 2	750	116.0	<300	52.3	42.6	5/15/20†	
RUSSIA 3	1150	245.6	<300	51.8	29.4	5/15/20†	
TEPCO	1000	39	<300	46.8	34.9	3.5/7.0	3.5

* Smallest values are for areas frequented by people.

** The transmission lines 1 & 2 are parallel in the same right-of-way.

† 5 kV/m in populated areas. 15 kV/m in unpopulated areas reserved for agriculture; 20 kV/m in areas not accessible by agricultural machinery. No limit for unpopulated in unaccessible areas such as steep slopes, mountains, etc.

Table 15.14-4 Insulation Characteristics of Suspension Towers

Company/Country	Nominal Voltage	Minimum Strike Distance (m)	Insulator Type	No. in string	M&E Rating (kN)	ESDD (mg/cm²)	Creepage (mm/kV)
Hydro-Québec 1	735	4.1	Porcelain	33	110/160	0.03	14
Hydro-Québec 2	735	4.1	Porcelain & Glass	33	110/160	0.03	14
AEP 1	765	4.26	Porcelain	30/32	25/36/50*		15
AEP 2	765	4.26	Porcelain	30/32	25/36/50*		
AEP 3	765	4.26	Polymer	NA	NA		
NYPA	765		Porcelain	35	30		19.8
Eskom 1	765	5.5	Glass	33	300		
Eskom 2	765	5.5	Glass	30			
FURNAS 1	765	5.0/7.0	Glass	30	120		12.55
FURNAS 2 & 3	765	5.0/6.5	Glass	30	160		12.55
EDELCA 1 & 2	765	5.5 no wind 4.0 wind	Porcelain & Glass	37	160/210	0.05 0.24	17.9 26.1
EDELCA 3	765	5.07	Porcelain & Glass	37	160/210	0.05 0.24	17.9 26.1
KEPCO	765	4.9	Porcelain	37/36	300/400	0.03	16.9
POWERGRID	765	5.1 – 5.6 4.4 wind	Porcelain & Glass	40/35	120/210	0.03	16.9
Russia	750	4.1 – 4.5	Glass	41	Mainly** 120/160		15
Russia	1150	6.5	Glass	63/67	Mainly** 210/400		15
Tokyo Electric	1000		Porcelain	40			

* Units are kilopounds (kips).

** Specifications permit the use of insulators from 120 to 400 kN, depending on the load on the I or V strings in either single or double circuit.

boundary on both sides, and construction is not allowed within the zone. For the 750-kV lines, it is 40 m from the outside phase, and for the 1150-kV line it is 100 m. The zone width then is 80 m + 2D for 750-kV lines and 200 m + 2D for the 1150-kV lines, where D is the phase spacing of each line. This creates a very wide "right-of-way" for the Russian lines as compared to the lines in the rest of the world.

Based upon the responses to the questionnaire, it appears that lines built to produce L_{50} rain AN levels less than 55 dBA have experienced few or no complaints, whereas lines that produced AN levels above 55 dBA have had either moderate or scattered complaints. The number of RI and TVI complaints has been quite small, and they have been easily resolved. As would be expected, some of the lines have had complaints about spark-discharges from the electric field, but most of those have been easily resolved through grounding and education.

The insulation characteristics used for all the lines are summarized in Table 15.14-4. The lines utilized either glass or porcelain insulators of various ratings. However, the new AEP line to be built in the Appalachian Mountains in Virginia with a 6-conductor bundle will use nonceramic insulators. This will be the first line that will be fully insulated with NCIs at voltages above 700 kV. Based upon the responses to the questionnaire, none of these lines has had outages due to switching surges. Russia and Venezuela have had outages due to insulator contamination. For the most part, all of the lines were built in pristine environment, which explains the lack of outages due to contamination. However, there have been outages due to lightning, with the frequency of outages corresponding well with the expected outage rate. Some utilities have had outages due to wind and ice causing towers to collapse.

Towers and foundations for each line and the mechanical/structural design criteria used are summarized in Table 15.14-5. All of the single-circuit lines are horizontally configured, although the POWERGRID in India is building new lines with delta configuration. Most of the towers are self-supporting, although Hydro-Québec, Eskom, AEP, and FURNAS have some lines with guyed-V structures. Russia uses almost exclusively guyed support structures. Most of the foundations are the grillage type, but many are the caisson type.

Table 15.14-5 Tower Types, Foundations and Design Loadings

Company/Country	Nominal Voltage (kV)	Tower types	Material	Foundation	Design Wind/Ice Loadings
Hydro-Québec 1	735	SS*	Gal. Steel	Grillage	385 Pa/ 12.7 mm
Hydro-Québec 2	735	SS, Guyed V & Chainette	Gal. Steel	Grillage	300 Pa/ 20 mm (1) 230 Pa/ 10 mm (2)
AEP 1	765	SS & Guyed-V	Gal. Steel & Alum	Grillage/ Caisson	300 Pa/ 25.4 mm
AEP 2	765	SS & Guyed-V	Gal. Steel & Alum	Grillage/ Caisson	300 Pa/ 25.4 mm
AEP 3	765	SS & Guyed-V	Gal. Steel	Grillage	300 Pa/ 25.4 mm
NYPA	765	SS	Gal. Steel	Grillage	190 Pa/ 1.25 mm (8)
Eskom	765	SS & Guyed-V	Gal. Steel Alum.	Caisson	32/45 m/s (3)
FURNAS	765	SS & Guyed-V	Gal. Steel	Grillage	150 km/h (4)
EDELCA	765	SS	Gal. Steel	Spread Footing & Piled	125 km/h (5)
KEPCO	765	SS	Tubular Steel	Caisson	(6)
POWERGRID	765	SS	Steel		47 m/s (7)
Russia	750	Guyed V	Steel	Isolated Footing & Piled	540-640 Pa/ 15-20 mm
Russia	1150	Guyed V	Steel	Caisson	700-800 Pa/ 10-15 mm
TEPCO	1000	SS	Tubular Steel	Caisson	

* SS - self-supporting;

(1) – Southern zone; (2) – Northern zone; (3) – 32 m/s wind on conductors and 45 m/s wind (1.4 gust factor) on the tower; (4) – maximum 30-s duration wind speed at 30 m height and 50-year return period; (5) – maximum 5-s duration wind speed at 10 m height and 200-year return period; (6) – see Table 15.12-8; (7) – maximum wind speed with 150-year return period and also narrow-front wind of 240 km/h; (8) – correspond to NESC Heavy.

Overhead ground wire parameters and grounding systems used for all of the lines, along with the IKL, lightning flash density, and shielding angle are given in Table 15.4-6. As would be expected, the shield angle is much smaller for lines that are in environments with high lightning incidences. Most grounding systems use counterpoise. In Russia, the self-grounding via foundations usually provides grounding resistance close to 15 ohms.

With regard to inspection, all of the utilities have similar programs, which combine ground patrols and tower climbing. Most utilities are using helicopters for line inspection.

A variety of techniques are used to maintain these lines. AEP, for example, today makes every effort to conduct maintenance on de-energized lines even though they were a pioneer in the development of bare-handed techniques. Conducting maintenance on de-energized lines has become the preferred method of most utilities. However, live line work is also being conducted using helicopters, especially for spacer and spacer damper replacements.

Both PLC and microwave have been used by the utilities for communication, with some relying totally on PLC and others totally on microwave. However, OPGW is being incorporated by several utilities.

Lightning detection systems that are correlated with the GPS coordinates of their transmission structures are being used by most of the utilities.

Table 15.14-6 Overhead Ground Wires and Lightning Protection

Company/Country	Nominal Voltage (kV)	Overhead Ground Wire Diameter (cm)	Overhead Ground Wire Spacing (m)	IKL	Lightning Flash Density (Ls-g/km^2/yr)	Shielding Angle (Degrees)	Grounding System	Tower Footing Resistance (Ohms)
Hydro-Québec 1	735	1.27	21.5	20/5	1-2	20	Continuous counterpoise	< 25
Hydro-Québec 2	735	1.27	19.5	20/5	1-2	20	Continuous counterpoise	< 25
AEP 1	765	0.98	22		2-4/km^2/yr	15	Foundation	<10 Target
AEP 2	765	0.98	22		2-4/km^2/yr	15	Foundation	<10 Target
AEP 3	765	0.98	22		2-4/km^2/yr	15	Foundation	<10 Target
NYPA	765	1.159	22.8	30		20	Counterpoise	< 30
Eskom	765		28.2		6-9	2.4		10
FURNAS 1	765	0.914/1.219	27.2	100			Counterpoise	15
FURNAS 2	765	1.219/1.542	27.2	100			Counterpoise	15
FURNAS 3	765	0.914/1.219/ OPGW	27.2	100			Counterpoise	15
EDELCA 1&2	765	0.978	22.5	50/80	6-10	20	Counterpoise	< 20
EDELCA 3	765	0.978	21.3	50/80	6-10	20/0	Counterpoise	< 20
KEPCO	765	1.9	31.0	20		-8.0	Counterpoise	< 15
POWERGRID	765	1.098	22.4	50/60	6-8		Pipe Counterpoise	10
Russia	750	1.54**	15-27		(20-50)*	20/22	Foundation	< 15
Russia	1150	Bundle of two 1.54	35		(20-50)*	20/22	Foundation	< 15
Tokyo Electric	1000		38			-12	Counterpoise	< 15

* Thunderstorm hours/year.

** In Russia, overhead wires are suspended on insulator strings and used for HF relay protection and telecommunication.

APPENDIX 15.1 SURVEY QUESTIONNAIRE

The following questionnaire was prepared and distributed to all the utilities participating in the survey before the Charlotte Workshop. Following discussions at the workshop, a list of supplementary questions was prepared in order to cover some aspects missed in the original questionnaire. This list is shown at the end of the main questionnaire.

System Planning

1. Why was this voltage chosen?
2. How many lines do you have operating at this voltage?
3. How many circuit-kilometers of this line are in operation?
4. What system planning considerations were used in choosing the voltage and the number of lines?
5. What assumptions or philosophy were used in designing the lines?
6. What measures are built into the lines to control overvoltages?
7. Were any power-frequency voltage control considerations (such as use of shunt reactors) involved in designing the lines?
8. Was series compensation used for any of these lines?
9. What type of relaying and protection schemes were used? Is single-pole-reclosing used?
10. What studies were conducted to determine the route(s) for these lines?
11. What difficulties were encountered in siting the line(s)?
12. Was there opposition to the line(s)? If so, where did it come from?

Electrical Design Considerations

1. What are the strike distances for the line(s)? What were the bases for these strike distances?
2. What types of insulators were used? How were they selected? What has been the experience?
3. How was the conductor bundle selected?
4. Were the lines designed to any specific audible noise (AN) or radio interference (RI) limits? If so, what were those limits and where did they come from?
5. Were the line(s) designed to any specific electric field (EF) or magnetic field (MF) limits? If so, what were they and what were the bases?
6. Was contamination a consideration in selecting the insulators?
7. Were overhead ground wires used? If so, what were the reasons for including them and what was the basis for the selection of the conductor size and spacings?
8. What grounding systems are being used and how were they selected?
9. Were losses considered in the selection of the conductor bundle? If so, were both resistive and corona losses considered? If corona losses were considered, how were they calculated?

Tower and Foundations

1. What devices or techniques were employed to control aeolian vibration? What has been the experience in controlling this type of vibration?
2. What types of spacers have been used? What has been the experience?
3. How severe has wind and ice loading for these lines? What has been the experience? Have there been any ice or wind loading failures?
4. What tower types have been used? Why were these tower types selected?
5. What types of foundations have been used? Why were these types selected and has there been any negative experience?
6. What construction techniques have been used to construct the lines? Were any unique or new techniques developed?

Operation and Maintenance

1. How often are the conductors, hardware, insulators, towers and foundations inspected? What techniques are used? What types of failures have occurred? Were any original hardware or insulators replaced because of poor performance? What replacements have been made and for what reasons?
2. What has been the outage experience due to?
    a. Lightning
    b. Switching surges
    c. Contamination
    d. Other
3. Have any outages been responsible for any redesigns?
4. What complaints from the public have there been due to?
    a. Audible noise
    b. Radio interference
    c. Television interference
    d. Electric fields
    e. Magnetic fields
    f. Other
5. How were the complaints resolved?
6. Were the resolutions satisfactory?
7. What mitigation measures have been used? Was anything special developed?

8. What methods are used to maintain the lines?
    a. Sticks
    b. Barehand
    c. Helicopters
    d. Other
    e. Preferred Method
9. What kind of commissioning procedures and tests used before bringing the lines into operation? How were these conducted?
10. How has the operating loads of the line(s) compared with the original design loads for the line(s)

Special Design Considerations

1. What are the minimum, maximum and average altitudes of the lines? How important was altitude in line design?
2. What types of terrain do the lines traverse?
3. What IKL's or other lightning incident indicators are experienced by the line?
4. What types of weather does the line experience? How important was weather in line design?
5. What ground resistances does the line experience?

Physical Characteristics

1. Please provide drawings and photographs of towers.
2. Please provide the electrical characteristics of the line
3. Please provide anything that would be useful in the discussion of line routing

Lines Above 700 kV: Supplementary Questions

1. Were the line(s) transposed? If yes, at what intervals and what were the main reasons for transposition? If not, what were the reasons?
2. Was power line carrier used? If yes, for what purposes? What range of signal frequencies were used and were conducted interferences due to corona and switching taken into account in determining signal to noise ratios and power levels? Please provide details of the carrier current system used.
3. Were ADlash (all dielectric lashed) or ADSS (all dielectric self supporting) types of fiber optic cables used? If yes, what has been the operational experience? Please provide details of the system used.
4. Were optical ground wires (OPGW) used? If yes, what has been the operational experience? Please provide details of the system used.
5. Were ground wires sectionalized and for what purpose? Were the ground wires or sections of ground wires insulated and for what purpose?
6. Were any emergency restoration procedures implemented in case the lines were damaged by natural (tornados, ice storms etc.) or man-made (terrorism) events?
7. Were any lightning location systems (LLS) deployed covering the line routes? If yes, what specific purposes were the systems used for?
8. What were the sources of weather data (particularly, wind, rain, tornados, ice etc.) along the line route? Were any special techniques used, such as for ice accretion? How was the information gathered used in the design, operation and maintenance of the line(s)?
9. How has the environment (such as pollution levels) changed along the line route and how did it affect the operation and maintenance of the line?
10. Have there been any line outages due to equipment failures? If yes, which types of equipment (such as transformers, shunt reactors etc.) were responsible and what were the number of failures corresponding to each type of equipment?

REFERENCES

Abetti, P.A. 1960. "Project E.H.V." CIGRE Paper 406.

Anderson, J. G. and L. O. Barthold. 1968. "Design Challenges of Transmission Lines Above 765 kV." IEEE-EHV Transmission Conference (Publication 68 C 57 – PWR). September 30th to October 2nd. Montreal, Quebec, Canada.

Annestrand, S. A. and G. A. Parks. 1977. "Bonneville Power Administration Prototype 1100/1200 kV Transmission Line Project." *IEEE Transactions on Power Apparatus and Systems.* Vol. PAS- 96. No. 2. pp. 357-366. March/April.

Banks, M. J. J., R. Keitley, and G. C. Stringfellow. 1968. "Radio Noise and Corona Loss Studies at 275/400 and 750 kV on Test and Operational Power Lines." IEE Conference on Progress in Overhead Lines and Cables for 220 kV and Above. p. 306.

Barnes, H. C., A. J. McElroy, D. F. Shankle, and H. M. Smith. 1965. "The Apple Grove 750-kV Project—500-kV Switching Surge and Line Flashover Tests." IEEE PAS-84. pp. 550-560.

Bartenstein, R. 1956. "Measurements of Corona Losses and Interference Levels at the 400 kV Research Station at Mannheim-Rheinau (Germany) with Special Reference to Bundle Conductors." CIGRE Paper 402.

Bartenstein, R., F. Hirsch, and E. Schafer. 1966. "Corona Measurements on a Four-Conductor Bundle for 700 kV Three-Phase Overhead Lines." CIGRE Paper 426.

Beliakov, N. N. et al. 1976. "1150 kV Experimental Installation at Bely Rast Substation." CIGRÉ Report 23-03.

Britten, A. C., E. G. Clarke, and H. E. Konkel. 1987. "Radio Interference, Corona Losses, Audible Noise and Power Frequency Electric Fields as Factors in the Design of ESCOM's 765 kV Lines." Open Conference on EHV Transmission Systems. Eskom Megawatt Park Auditorium. 23 November.

Burgsdorf, V. V., L. V. Egorova, N. P. Emeljanov, and N. N. Tihodeev. 1960. "Corona Investigation on Extra-High Voltage Overhead Lines." CIGRE Paper 413.

Burgsdorf, V. V. et al. 1976. "Design of the EHV (1150 kV) AC Transmission Line." CIGRÉ Report 31-03.

Cahen, F. and R. Pelissier. 1952. "Experience Gained at the 500 kV Test Station of Chevilly during the Period 1950 and 1951." CIGRE Paper 406.

Cassan, J. G. and N. J. McMurtrie. 1960. "The Coldwater 600 kV Experimental Line." CIGRE Paper 408.

Catenacci, G., G. Carrara, G. Furioli, and L. Dellera. 1968. "1500 kV A.C. Lines: A First Look on the Main Electrical Design Problems." IEEE-EHV Transmission Conference (Publication 68 C 57 – PWR). September 30th to October 2nd. Montreal, Quebec, Canada.

CIGRE. 1983. WG 31.04 Report. "Electric Power Transmission at Voltages of 1000 kV and Above: Plans for Future AC and DC Transmission, Data on Technical and Economic Feasibility and on General Design, Information on Testing Facilities and the Research in Progress." *Electra.* No. 91. pp. 83-133.

CIGRE. 1989. WG 38.04 Report. "Electric Power Transmission at Voltages of 1000 kV AC or ±600 kV DC and Above: Network Problems and Solutions Peculiar to UHV AC Transmission." *Electra.* No. 122. pp. 41- 75.

Cladé, J., P. Maréchal, G. Manzoni, L. Paris, and M. Valtorta. 1978. "Factors on Which to Base Comparisons in Choosing the Higher Voltage Level for a Transmission Network." CIGRÉ Report 31-5.

Coney, R.G. 1987. "The Protection of ESKOM's Alpha and Beta 400/765 kV Transmission Lines." Open Conference on EHV Transmission Systems. Eskom Megawatt Park Auditorium. 23 November.

Cretchley, D. H., W. L. Eaterhuizen, and G. M. Ferrero. 1987. "Design and Construction of ESCOM's First 765 kV Transmission Lines." Open Conference on EHV Transmission Systems. Eskom Megawatt Park Auditorium. 23 November.

De Franco, N. and C. A. S. Morissy. 1980. "An Account of Long-Term Transmission System Development in Brazil." CIGRÉ Report 31-13.

EEI. 1968. *EHV Transmission Line Reference Book.* Edison Electric Institute. New York, New York.

EPRI. 1987. *Transmission Line Reference Book: 345 kV and Above*. Second Edition, Revised. EL-2500.

Garrity, T., J. C. Haahr, L. Knudsen, and M. C. Raezer. 1972. "Experience with the AEP 765-kV System – Part V – System Performance." 1972 IEEE/PES Winter Power Meeting. January.

Haas, R. J., J. D. Heiermann, and R.W. Schooley. 1972. "Experience with the AEP 765-kV System – Part IV – Overvoltage and Staged Fault Tests: Analysis." 1972 IEEE/PES Winter Power Meeting. January.

Hauspurg, A., G. S. Vassell, G. I. Stillman, J. H. Charkow, and J. C. Haahr. 1969. "Overvoltages on the AEP 765-kV System." IEEE PAS-88. pp. 1329-1342. September.

Hauspurg, A., V. Caleca, and R. H. Schlomann. 1969. "765-kV Transmission Line Insulation: Testing Program." IEEE PAS-88. pp. 1355-1365. September.

Hylten-Cavallius, N. and D. Train. 1974. "The IREQ Ultra High Voltage Laboratory and Test Facilities." *IEEE Transactions on Power Apparatus and Systems*. Vol. PAS-93. No. 1. pp. 255-263. January/February.

KEPCO. 2003. 765-kV Transmission and Substation. Korea Electric Power Corporation—Power System Construction Office. Seoul, Korea.

Keri, A. J. F., A. Nourai, and J. M. Schneider. 1984. "The Open Loop Scheme: An Effective Method of Ground Wire Loss Reduction." IEEE PAS-103. pp 3615-3624. December.

Kolcio, N., B. J. Ware, R. L. Zagier, V. L. Chartier, and F.M. Dietrich. 1974. "The Apple Grove 750 kV Project: Statistical Analysis of Audible Noise Performance of Conductors at 775 kV." IEEE PAS-93. pp. 831-840. May/June.

Krylov, S. V. 2004. "Design, Mechanical Aspects and Other Subjects of Compact EHV Overhead Line Technology." Presented at Midwest ISO-Expanding Seminar on High Surge Impedance Loading Transmission Line Design and Magnetically Controlled Reactors. St. Paul, Minnesota. September 16.

Le Roux, B. C., A. C. Britten, K. J. Sadurski, and A. W. Chilton. 1987. "A Review of EHV Air-Breakdown Studies in South Africa." Open Conference on EHV Transmission Systems. Eskom Megawatt Park Auditorium. 23 November.

Lee, Dong-I L., J. B. Kim, and K. H. Yang. 1997. "Audible Noise Performance of 6-Rail Conductors on a 765-kV Double Circuit Test Line." IEEE PWRD-12. pp. 1343-1351. July.

Magnien, M., J. Clade, and C. Gary. 1966. "The 'Electricite de France' Test Station for Corona Studies on Future E.H.V. Lines." CIGRE Paper 427.

Nagel, T. J. and G. S. Vassell. 1974. "Development of the American Electric Power System Transmission Network: From 345 kV to 765 kV to UHV." CIGRÉ Report 32-13.

Norman, H. B. 1988. "Why a 765 kV Transmission System?" Elektron. pp. 5-14. January.

Nourse, G. R. 1969. "Development and Trial Installation of an Aluminum Tubing Audible Noise Suppressor for 765 kV Lines." IEEE PAS-97. p. 1009. July/August.

Peixoto, C. A. O. 1980. "Itaipu 6300 MW HVDC Transmission System—Feasibility and Planning Aspects." Symposium on Incorporating HVDC Power Transmission into System Planning. Sponsored by U.S. Department of Energy. Phoenix, Arizona.

Perry, D. E., V. L. Chartier, and G. L. Reiner. 1979. "BPA 1100 kV Transmission Development—Corona and Electric Field Studies." *IEEE Transactions on Power Apparatus and Systems*. Vol. PAS- 98. pp. 1728-1738. September/October.

Pokorny, W. C. and R. W. Flugum. 1975. "UHV Tower Insulation Parameters Defined by Full-Scale Testing." *IEEE Transactions on Power Apparatus and Systems*. Vol. PAS-94. No. 2. pp. 518-529. March/April.

Power System Planning Division of Tokyo Electric Power Company. 1985. "Plan and General Design for 1000-kV Transmission in Japan." Report Presented at the Japanese National Panel of CIGRE WG38-04. June.

Robertson, L. M. and J. K. Dillard. 1961. "Leadville High Altitude EHV Test Project, Part I – Report on 4 Years of Testing" AIEE Transactions on Power Apparatus and Systems, pp. 715-25, December.

Samuelson, A. J., R. L. Retallack, and R. A. Kravitz. 1969. "AEP 765-kV Line Design." IEEE PAS-88, pp. 1366-1371. September.

Sawada, Y. 1965. "Corona Noise Characteristics of Four-Conductor Power Transmission Lines." J. IEE (Japan). Vol. 85. pp. 62-72. January.

Scherer, Jr., H. N. and G. S. Vassell. 1972. "Experience with the AEP 765-kV System – Part I: Overview." 1972 IEEE/PES Winter Power Meeting. January.

Scherer, Jr., H. N., S. H. Horowitz, and R. A. Byron. 1972. "Experience with the AEP 765-kV System – Part III- Construction and Equipment Performance Considerations." 1972 IEEE/PES Winter Power Meeting. January.

Scherer, H. N. et al. 1980. "The AEP-ASEA UHV Project. Results to 1979." CIGRÉ Report 31-04.

Shankle, D. F., S. B. Griscom, E. R. Taylor, Jr., and R. H. Schlomann. 1965. "The Apple Grove 750-kV Project – Equipment Design and Instrumentation." IEEE PAS-84. pp. 541-550. July.

Sporn, P. and A. C. Monteith. 1947. "Transmission of Electric Power at Extra High Voltages." *AIEE Transactions on Power Apparatus and Systems.* Vol. 66. pp. 1571-82.

Tamazov, A. I. 2004. "Corona on Conductors of AC Overhead Transmission Lines." Sputnik Publishing House. Moscow.

Taylor, E. R., W. E. Pakala, and N. Kolcio. 1965. "The Apple Grove 750-kV Project – 515-kV Radio Influence and Corona Loss Investigations." IEEE PAS-84. pp. 561-573. July.

Tokyo Electric Power Company. 1994. "1000 kV Transmission Lines." A Special Publication of the Tokyo Electric Power Company.

Trinh, N. G., P. S. Maruvada, and B. Poirier. 1974. "A Comparative Study of Corona Performance of Conductor Bundles for 1200 kV Transmission Lines." *IEEE Transactions on Power Apparatus and Systems.* Vol. PAS-93. No.3. pp. 940-949. May/June.

Udo, T., M. Yasui, and T. Fujimura. 1980. "An Outline of Testing Facilities for Research of UHV Transmission Lines and Some Test Results in Japan." CIGRÉ Report 31-02.

Vassell, G. S. and R. M. Maliszewski. 1969. "AEP 765-kV System: System Planning Considerations." IEEE PAS-88. pp. 1320-1328.

Vassell, G. S., R. M. Maliszewski, and N. B. Johnsen. 1972. "Experience with the AEP 765-kV System–Part II: System Performance." 1972 IEEE/PES Winter Power Meeting. January.

BIBLIOGRAPHY

Hydro-Québec 735-kV Lines

735 kV – Manicouagan-Montreal. Hydro Quebec Brochure.

Aubin, J., D. McGillis, and J. Parent. 1966. "Composite Insulation Strength of Hydro Quebec's 735 kV Towers." *IEEE Transactions on Power Apparatus and Systems.* June. pp. 633-648.

Baril, G., L. Cahill, A. Dupont, and G. Robert. 1966. "Commissioning of the First Manicouagan-Montreal 735 kV Transmission Lines." CIGRE Paper 429.

Beauchemin, R., A. Dutil, and S. Y. M. Hung. 1979. "Environmental Considerations of Electrical Phenomena in the Design of Hydro Quebec's EHV Systems." Canadian Electrical Association. Halifax, Nova Scotia. October 2-3.

Bernard, S., G. Trudel, and G. Scott. 1996. "A 735 kV Shunt Reactors Automatic Switching System for Hydro Quebec Network." *IEEE Transactions on Power Delivery.* Vol. 11. No. 4. November. pp. 2024-2030.

Breault, S., M. Granger, and A. Dutil. 1985. "Document explicatif relative aux caractéristiques générales normalisées des lignes électriques." Hydro Quebec Report. January.

Bui-Van, Q. and M. Rousseau. "Control of Overvoltages on Hydro Quebec Series Compensated System During a Major Electromechanical Transient Disturbance." (Publication details not available).

Cahill, L. 1964. "La première transmission d'energie électrique à 735 kV: Manicouagan-Montreal." Association Suisse des Electriciens. Zurich. Vol. 55. No. 11. pp. 519-528.

Gagnon, C. and P. Gravel. 1994. "Extensive Evaluation of High Performance Protection Relays for the Hydro Quebec Series Compensated Network." *IEEE Transactions on Power Delivery.* Vol. 9. No. 4. October. pp. 1799-1811.

Ghannoum, E. 1981. "A Rational Approach to Structural Design of Transmission Lines." *IEEE Transactions on Power Apparatus and Systems.* Vol. PAS-100. pp. 3506-3511. July.

Ghannoum, E. 1982. "Hydro Quebec Designs 735 kV Towers." *Transmission & Distribution.* December. pp. 60-62.

Ghannoum, E. and M. Lamarre. 1985. "Hydro Quebec's Experience with the Design and Construction of 1500 km of 735 kV Chainette Transmission Lines." *IEEE Transactions on Power Apparatus and Systems.* Vol. PAS-104. No. 10. October. pp. 2832-2843.

Ghannoum, E., J. P. Chouteau, S. Yaakoub, and K. Yoshida. 1995. "Optical Ground Wire for Hydro Quebec's Telecommunication Network." *IEEE Transactions on Power Delivery.* Vol. 10. No. 4. October. pp. 1724-1730.

Ghannoum, E. and S. J. Yaakoub. 1989. "Optimization of Transmission Towers and Foundations Based on Their Minimum Cost." *IEEE Transactions on Power Delivery.* Vol. 4. No. 1. January. pp. 614-620.

"James Bay Network: Substations and Telecommunications." Hydro Quebec Collection of Papers.

Lacroix, R. and H. Charbonneau. 1968. "Radio Interference from the First 735 kV Lines of Hydro Quebec." *IEEE Transactions on Power Apparatus and Systems.* Vol. PAS-87. No. 4. April. pp. 932-939.

Lajoie, L. G., G. Scott, S. Breault, E. V. Larsen, D. H. Baker, and A. F. Imece. 1990. "Hydro Quebec Multiple SVC Application Control Stability Study." *IEEE Transactions on Power Delivery.* Vol. 5. No. 3. July 1990. pp. 1543-1551.

Lam, L. and R. Morin. 1997. "Specification, Performance, Testing and Qualification of Extra Heavy Duty Connectors for High Voltage Applications." *IEEE Transactions on Power Delivery.* Vol. 12. No. 2. April. pp. 687-693.

Larsen, E. V., D. H. Baker, A. H. Imece, L. Gerin-Lajoie, and G. Scott. 1990. "Basic Aspect of Applying SVC's to Series-Compensated AC Transmission Lines." *IEEE Transactions on Power Delivery.* Vol. 5. No. 3. July. pp. 1466-1473.

Lecomte, D. and P. Meyère. 1980. "Evolution of the Design of 735 kV Lines." CIGRE Report 22-08.

McGillis, D. T. 1964. "Hydro Quebec's 735 kV EHV Project." *Transactions of the American Power Conference.* pp. 836-843.

McGillis, D. 1966. "The Choice of 735 kV Transmission: Economics and System Performance." EHV Symposium. Winnipeg, Manitoba. September.

Normes sur le dégagement électrique des lignes de transport d'énergie. 1981. Hydro Quebec Report NG-003-81-A-(N). September.

Le réseau de transport La Grande: Situation d'ensemble et étude type d'un trace. Hydro Quebec Brochure. 1976.

Souchereau, N., G. Sabourin et al. 1978. "Validation of a Chainette Tower for a 735 kV Line." CIGRE Report No. 22-04.

Trinh, N. G., P. S. Maruvada, J. Flamand, and J. R. Valotaire. 1982. "A Study of the Corona Performance of Hydro Quebec's 735 kV Lines." *IEEE Transactions on Power Apparatus and Systems.* Vol. PAS-101. March. pp. 681-690.

Trudel, G., S. Bernard, and G. Scott. 1999. "Hydro Quebec's Defense Plan Against Extreme Contingencies." *IEEE Transactions on Power Systems.* Vol. 14. No. 3. August. pp. 958-966.

AEP 765-kV Lines

Barnes, H. C. and V. Caleca. 1970. "Initial Experiences on the 765 kV System of the American Electric Power Company." CIGRE Paper #31-06.

Barnes, H. C., V. Caleca, and L. Knudsen. 1972. "Long-Line 765 kV Test Results and Analysis." CIGRE Paper #31-09.

Dietrich, F. M. and N. Kolcio. 1976. "Corona and Electric Field Effects at the Apple Grove Project and an 800-kV Line in the USA." CIGRE Paper #31-08.

DiPlacido, C., H. Shih, and B. J. Ware. 1978. "Analysis of the Proximity Effects in Electric Field Measurements." IEEE-PAS-97. pp. 2167-2177. November/December.

"Experience with the AEP 765-kV System." 1972. Special Publication of the IEEE Power Engineering Society. Six papers presented at the IEEE/PES Winter Meeting and R&D Conference. New York, NY.

Fakheri, A. J. and J. C. Haahr. 1977. "Experience with the AEP 765-kV System." IEEE-PAS-97. pp. 109-117. July/August.

Frydman, M., A. Levy, and S. E. Miller. 1973. "Oxidant Measurements in the Vicinity of Energized 765 kV Lines." IEEE-PAS-92. pp. 1141-1148. May/June.

Frydman, M. and C. H. Shih. 1974. "Effects of the Environment on Oxidants Production in AC Corona." *IEEE Transactions on Power Apparatus and Systems*. Vol. PAS-93. pp. 436-443. January/February.

Horowitz, S. H. and H. T. Seeley. 1969. "Relaying the AEP 765-kV System." IEEE PAS-88. pp. 1382-1389.

Kolcio, N., V. Caleca, S. J. Marmaroff, and W. L. Gregory. 1969. "Radio-Influence and Corona-Loss Aspects of AEP 765-kV Lines." IEEE PAS-88. pp. 1343-1355. September.

Kolcio, N., J. Di Placido, R.J. Haas, and D.K. Nichols. 1979. "Long Term Audible Noise and Radio Noise Performance of American Electric Power's Operating 765 kV Lines." *IEEE PAS-98*. pp. l853-1859. November/December.

Phelps, J. D. M., P. S. Pugh, and J. E. Beehler. 1969. "765-kV Insulation Coordination." IEEE PAS-88. pp. 1377-1382. September.

Popeck, R. A. and R. F. Knapp. 1981. "Measurement and Analysis of Audible Noise from Operating 765 kV Transmission Lines." IEEE-PAS-100. pp. 2138-2148. April.

Scherer, Jr., H. N., C. A. Schwalbe, R. H. Meyer, and J. A. Dibella. 1969. "765-kV Station Design." IEEE PAS-88. pp. 1372-1376. September.

Scherer, Jr., H. N., B. J. Ware, and C. H. Shih. 1973. "Gaseous Effluents due to EHV Transmission Line Corona." IEEE-PAS-92. pp. 1043-1049. May/June.

Scherer, H. N., B. R. Shperling, J. W. Chadwick, N. N. Belyakov, V. S. Rashkes, and K. V. Koetsian. 1985. "Single Phase Switching Tests on 765 kV and 750 kV Transmission Lines." IEEE-PAS-104. pp. 1537-1548. June.

Sebo, S. A, J. T. Heibel, M. Frydman, and C. H. Shih, 1976. "Examination of Ozone Emanating from EHV Transmission Line Corona Discharges." IEEE-PAS-95. pp. 693-703. March/April.

Shperling, B. R., A. J. Fakheri, C. H. Shih, and B. J. Ware. 1981. "Analysis of Single Phase Switching Field Tests on the AEP 765 kV System." IEEE-PAS-100. pp. 1729-1735.

Russian 750-kV and 1150-kV Lines

"110-750 kV Insulator Strings. Technical Requirements and Test Methods", Russian National Standard GOST 26720-85, 1985 *[in Russian]*.

"AC Electric Equipment with Rated Voltage 1150 kV at Switching Overvoltage Suppression to 1.8 p.u. of L-G Voltage. Requirements to Electric Strength of Insulation and Test Methods", Russian Power Industry Standard OST 16.0.800.991-82, 1982 *[in Russian]*.

"AC Electric Installations with Rated Voltage 3-750 kV. Leakage Path Lengths for External Insulation", Russian National Standard GOST 9920-89, 1989 *[in Russian]*.

"AC Electric Equipment with Rated Voltages 1 to 750 kV. Requirements to Electric Strength of Insulation", Russian National Standard GOST 1516.3-96, 1996 *[in Russian]*.

Akopyan, A. A., G. I. Alexandrov, N. P. Emelyanov, Y. I. Lyskov, S. S. Rokotian, and V. P. Fotin. 1972. "Characteristics of UHV 1200 kV Transmission Lines." CIGRE Paper #31-11.

Akopyan, A. A., V. V. Bourgsdorf, et al. 1972. "Switching Overvoltages and the System of Protection against Them in 750 kV Network of the USSR." CIGRE Report 33-07.

Alexandrov, G. N., V. L. Ivanov, V. E. Kizevetter, et al. 1974. "Electric Strength of Typical Air Gaps and Insulator Strings on Overhead Transmission Lines 750 kV." Collection of Papers "Long-Distance 750 kV Transmissions." Vol. 1. Energia Publishing House. Moscow. pp. 131-140. [in Russian].

Alexandrov, G. N., Y. A. Gerasomov, V. L. Ivanov, et al. 1992. "Study of Dielectric Strength of Air Gaps for 1150 kV Lines and Substations." Collection of Papers "1150 kV Transmissions." Volume 2. Energoatomizdat Publishing House. Moscow. pp. 151-184. [in Russian].

Alexandrov, G. N., A. V. Gorelov, V. V. Ershevich, et al. 1993. "Designing EHV Transmission Lines." Energoatomizdat Publishing House. St. Petersburg. 560 pp. [in Russian].

Antemenko, Y., V. Yershevich, Y. Rudenko, et al. 1992. "The USSR United Power Grid: The Experience and Problems of Development." CIGRE Report 37-201.

Antipov, K. M., V. V. Ershevich, G. A Illarionov, and V. D. Shlimovich. 1992. "Development of the USSR Electric Power Industry and the Role of 1150 kV Transmission in Forming the USSR Interconnected Grid." Collection of Papers "1150 kV Transmissions." Vol.1. Energoatomizdat Publishing House. Moscow. pp. 5-28. [in Russian].

Antonova, N. P., N. N. Beliakov, L. L. Glazunova, et al. 1990. "Temporary Overvoltages and Their Influence upon the Insulation Level of the Equipment." CIGRE Report 33-209.

Antonova, N. P., Y. I. Lyskov, V. S. Ljashenko, et al. 1992. "A New Voltage Class of 1150 kV: Basics and Main Technical Decisions Made for the First Transmission." Collection of Papers "1150 kV Transmissions." Vol. 1. Energoatomizdat Publishing House. Moscow. pp. 28-41 [in Russian].

Azernikova, T. I., L. S. Perelman, P. Z. Rokhinson et al. 1980. "Corona-Generated Radio Interference on EHV and UHV Lines." CIGRE Report 36-03.

Baumshtein, I. A. and S. A. Bazhanov, editors. 1989. "Reference Book on High Voltage Electric Installations." Energoatomizdat Publishing House. Moscow. 768 pp. [in Russian]

Belyakov, N. N., V. A. Vershkov, et al. 1976. "1150 kV Experimental Installation at the Bely Rast Substation." CIGRE Report 23-03.

Belyakov, N. N., V. L. Volchek, V. V. Ilyinichnin et al. 1992. "Application of Single-Phase Autoreclosing in a Complex EHV Network Containing 1200 kV Transmission Lines." CIGRE Report 34-207.

Bortnik, I. M. et al. 1988. "1200 kV Transmission Line in the USSR: The First Results of Operation." CIGRE Report 38-09.

Burgsdorf, V. V., N. P. Emelyanov, and L. V. Timashova. 1974. "Choosing Conductors and Phase Design for 750 kV lines on Corona Conditions." Collection of Papers "Long Distance 750 kV Transmissions." Vol. 1. Energia Publishing House. Moscow. pp. 94-109 [in Russian].

Burgsdorf, V. V., N. P. Emeljanov, J. I. Lyskov, V. S. Liashenko, S. S. Rokotian, and B. I. Smirnov. 1976. "Design of the EHV 1150 kV AC Transmission Line." CIGRE Paper #31-03.

Burgsdorf, V. V., D. S. Savvaitov, and V. A. Shkaptsov. 1986. "Dynamics of Conductors on UHV Lines: Control of Vibration and Subspan Oscillations." CIGRE Report 22-15.

Burgsdorf, V. V., N. P. Emelyanov, V. A. Kostjushko et al. 1991. "Validation of 1150 kV Line Design." Collection of Papers "1150 kV Transmissions." Vol. 1. Energoatomizdat Publishing House. Moscow. pp. 178-195 [in Russian].

Dikoy, V. P., Y. M. Koryagin, V. M. Lavrentjev et al. 1992. "Servicing 1150 kV Transmission." Collection of Papers "Electric Transmissions 1150 kV. Vol. 2. Energoatomizdat Publishing House. Moscow. pp. 246-271 [in Russian].

Emelyanov, N. P., V. A. Kostyushko, A. I. Tamazov et al. 1984. "Investigation of Corona Effects on EHV and UHV Transmission Lines." CIGRE Report 36-11.

Ermolenko, V. M. and A. M. Fedoseev 1974. "Relay Protection and Automation in 750 kV Transmission Lines." Collection of Papers "Long Distance 750 kV Transmissions." Vol. 2. Energia Publishing House. Moscow. pp. 183-200 [in Russian].

Ermolenko, V. M., V. I. Kozlov, V. N. Kraseva et al. 1992. "Relay Protection of a 1150 kV Transmission." Collection of Papers "1150 kV Transmissions." Vol. 1. Energoatomizdat Publishing House. Moscow. pp. 231-264 [in Russian].

Glazunova, L. L. and A. K. Lokhanin. 1992. "Requirements to the Electric Strength of AC Electric Equipment with Rated Voltage 1150 kV." Collection of Papers "1150 kV Transmissions." Vol. 2. Energoatomizdat Publishing House. Moscow. pp. 20-28 [in Russian].

Goroshkina, V. A., K. M. Kosareva, F. I. Lyalin et al. 1992. "Main Design Decisions for 1150 kV Transmission Lines." Collection of Papers "1150 kV Transmissions." Vol. 1. Energoatomizdat Publishing House. Moscow. pp. 159-178 [in Russian].

"Guide on Temporary Overvoltages and Protection against Them in 110-750 kV Transmissions." 1991. Article 5.11.16 in the Operational Manual Rules of Operation for Electric Power Plants and Grids. 14th Edition, Revised. USSR Ministry of Electric Power and Electrification/ Energoatomizdat Publishing House. Moscow [in Russian].

Ilyinichnin, V. V., K. V. Khoetzian, V. F. Lachugin et al. 1992. "Service Experience and Field Tests Summarizing. The Protection and Control Devices Improvement in EHV-UHV Transmissions", CIGRE, 1992, Report 34-102.

Ilyinichnin, V. V., V. A. Katunian, V. F. Lachugin et al. 1994. "Existing 110-1150 kV Transmission Line Protection Performance Improvement under Operating Conditions and Network Structure Changes." CIGRE Report 34-202.

Kostjushko, V. A. 1984. "Taking into Account Corona Losses at Changing Voltage on 1150 kV Transmission Lines." VNIIE Proceedings "Overvoltages, Design and Radio Interference in 1150 kV Transmissions." Energoatomizdat Publishing House. Moscow. pp. 31-34 [in Russian].

Levinshtein, M. L. Editor. 1992. "Processes at High-Speed Single-Pole Auto-Reclosure in HV Transmission Lines." Energoatomizdat Publishing House. Moscow. 256 pp. [in Russian].

Levitov, V.I. and V. I. Popkov. 1974. "Energy and Power Corona Losses on Conductors of EHV Transmission Lines." Collection of Papers: Long Distance 750 kV Transmissions. vol. 1. Energia Publishing House. Moscow. pp.114-131 [in Russian].

"Manual on Choosing and Maintaining Insulation in Contaminated Areas." 1975. USSR Ministry of Electric Power and Electrification/ SCNTI. Moscow [in Russian].

"Manual on Ice Melting when Accumulated on Overhead Transmission Lines." 1969. USSR Ministry of Electric Power and Electrification. Printed by SCNTI. Moscow. 96 pp. [in Russian].

"Manual on a Typical Protection against Vibration and Sub-oscillations of Conductors and Shielding Wires on 35-750 kV Overhead Transmission Lines." 1991. USSR Ministry of Electric Power and Electrification. Published by SPO ORGRES. Moscow. [in Russian].

Merkhalev, S. D. and E. A. Solomonik. 1983. "Choosing and Maintenance of Insulation in Areas with Contamination." Energoatomizdat Publishing House. Leningrad. 120 pp. [in Russian].

Popkov, V. I., A. I. Tamazov, and E. V. Kravchenko. 1991. "Corona Losses in 1150 kV Lines." Collection of Papers "1150 kV Transmissions." Vol. 1. Energoatomizdat Publishing House. Moscow. pp. 99-111 [in Russian].

Rashkes, V. S. 1997. "Russian EHV Transmission System." *IEEE Power Engineering Review.* June. pp. 9-12.

Rubtsova, N. B., B. M. Savin, G. G. Putchkov, et al. 1990. "Hygienic Guidelines of Occupational Exposure to Factors Concerning Bare-Hand Live-Line Maintenance. Approaches to Exposure Limits for Industrial Frequency Magnetic Fields." CIGRE Report 36-106.

Scherer, H. N., Jr., B. R. Schperling, N. N. Belyakov, V. S. Rashkes, et al. 1985. "Single-Phase Switching Tests on 765 and 750 kV Transmission Lines." *IEEE Transactions on Power Delivery.* Vol. PAS-104. No. 6. pp. 1537-1548.

Rokotyan, S. S. 1974. "The Place of 750 kV Transmissions in a Modern Power System." Collection of Papers "Long Distance 750 kV Transmissions." Vol. 1. Energia Publishing House. Moscow. pp. 11-21 [in Russian].

"Sanitary Norms of Permissible Audible Noise in Housing Areas and Public Buildings." 1984. #3077-84. Moscow. [in Russian].

"Test Methods for Contaminated External Insulation."1986. Russian National Standard GOST 10390-86 [in Russian].

Timashova, L. V. 1991. "Results of Radio-, TV- and Acoustic Noise Research from EHV Transmission Lines." VNIIE Proceedings "Research and Tests in 750-1150 kV Transmissions." Pp. 141-147 [in Russian].

Yegorova, L. V., N. S. Kislova, and N. N. Tikhodeev. 1974. "Corona Losses on 750 kV Lines." Collection of Papers "Long Distance 750 kV Transmissions." Vol. 1. Energia Publishing House. Moscow. pp.109-113 [in Russian].

Zhehlichenko, A. S., F. I. Lyalin, and I. A. Slyapin. 1974. "Design of 750 kV Overhead Transmission Lines." Collection of Papers "Long Distance 750 kV Transmissions." Vol. 1. Energia Publishing House. Moscow. pp. 157-169 [in Russian].

Zhelichenko, A. S. and B. I. Smirnov. 1981. "[Handbook on] Mechanical Designing of EHV Transmission Lines." Energoizdat Publishing House. Moscow. 336 pp. [in Russian].

EDELCA 765-kV Lines

Alazrachi, A. and J. O. Da Silva. 1983. "Long Distance Transmission Systems." CESI Symposium 83. June.

Aldrovandi, G., C. Carubelli, and G. Furiori (CESI). Aquino, Z., I. J. Gavidia, and M. Millán (CVG EDELCA). 1987. "Measurements of Switching Transients during the Field Tests Performed for the Commissioning of the EDELCA 765 kV System." CIGRE Symposium 05-87.

Aloisantonio, I. and J. González. 1986. "Descripción de los esquemas de protección asociados al Sistema de Transmisión a 800 kV de EDELCA." IV Jornadas Nacionales de Potencia. June.

Aloisantonio, I. and J. González. 1986. "Criterios de coordinación y ajustes de los esquemas de protección asociados al sistema de transmisión a 800 kV de EDELCA." IV Jornadas Nacionales de Potencia. June.

Aloisantonio, S. 1989. "Incorporación de relés ultrarrápidos de onda viajera al sistema de protección asociado a las líneas de transmisión a 765 kV de EDELCA." V Congreso de generación y transmisión de Energía Eléctrica. November.

Artiles, O. and J. Cerdá. 1986. "Recierre monofásico rápido en sistemas de transmisión de extra alta tensión. Parte II. Pruebas de Campo y Experiencias." IV Jornadas Nacionales de Potencia. June.

Bonaguro, D. and L. Morales. "Líneas a 800 kV Guri – Región Central. Diseño de las cadenas de aisladores por contaminación y cargas mecánicas sobre las torres."

Bonaguro, D. (CVG EDELCA), L. Siegert, (USB), and K. Naito. 1982. "Resultados de ensayos eléctricos en las cadenas de aisladores de 800 kV para EDELCA." III Jornadas Nacionales de Potencia. May.

Chacín, E, J. O. Da Silva, and G. Duarte. 1985. "765 kV Lines Carry Hydro Power to Venezuela's Load Centers." 1985 International Power Systems.

Da Silva, J. O., G. Rodríguez, and L. Rugeles. 1986. "Simulación de las pruebas de campo del sistema de transmisión a 765 kV." IV Jornadas Nacionales de Potencia. June.

Ferrín, J. 1993. "Construcción de la línea a 765 kV Nº 3 a través del Parque Nacional Guatopo." XIV Reunión del Subcomité de Ingeniería de Sistemas Eléctricos de la Comisión de Integración Eléctrica Regional. CIER Agosto.

Kelles, J. J. and W. Y. Shield. "Transmitting 7.000 MVA through Five Double Circuits 765 kV Transmission Lines." Harza.

Mogno, A. and J. Pardiñas. 1993. "Selección y diseño de las fundaciones utilizadas por EDELCA en las líneas de transmisión 765 kV." IV Encuentro Latinoamericano de la CIGRE. March.

FURNAS 750-kV Lines

Esmeraldo, P. C. V., L. E. N. Dias, and J. R. Fonseca. 1986. "Calculation of Minimum Safety Distances for Live-Line Maintenance: A Statistical Method Applied to 765 kV AC Itaipu Lines." IEEE-PWRD-1. pp. 264-271. April.

ESKOM 765-kV Lines

Britten, A. C., D. H. Cretchley, K. J. Sadurski, B. Druif, and H. A. Roets. 1991. "The Compaction of Conductor-to-Tower Clearances on ESKOM's 765 kV Transmission Lines." CIGRE Symposium on Compacting Overhead Transmission Lines. June.

Eriksson, A. J. and W. C. van der Merwa. 1987. "Lightning Overvoltage and Insulation Co-ordination in a 765 kV." Open Conference on EHV Transmission Systems. Eskom Megawatt Park Auditorium. 23 November.

Lee, D. I., K. Y. Shin, S. D. Lee, and J. B. Kim. 2000. "Field Test of Semiconducting Glaze Insulators on 765 kV Transmission Test Line in Korea. ICEE.

Lee, D. I., K. Y. Shin, and J. B. Kim. 2001. "Introduction of Korea's 765-kV System Development." Proceedings of the Seventeenth Hungarian-Korean Seminar.

Reynders, J. P. and J. Meppelink. 1987. Characteristics of Disconnect Switch Transients and Control of the Consequent Electromagnetic Interference." Open Conference on EHV Transmission Systems. Eskom Megawatt Park Auditorium. 23 November.

Sadurski, K. J., A. C. Britten and M. P. Van der Merwe. 1987. "Dielectric Strengths and Insulation Coordination of Live-Line Configurations on 765 kV Transmission Lines." Open Conference on EHV Transmission Systems. Eskom Megawatt Park Auditorium. 23 November.

KEPCO 765-kV Lines

Jae, B. M., I. S. Kim, and S. K. Shin.1996. "Long Term Prospect of Electric Power System in Korea." Symposium on 765 kV Transmission Technology. Suanbo, Korea. October.

Jo, S. B. 1996. "Development of the Application Equipment for New Construction Method." Ibid.

Kim, I. D., B.T. Jang, and Y. K. Baek. 1996. "Protection and Control Schemes for 765 kV Power System." Ibid.

Kim, J. B. 1996. "The Research and Development of 765 kV Transmission Technology." Ibid.

Kim, J. B., D. I. Lee, K. Y. Shin, K. H. Yang, H. S. Ahn, and C. H. Oh. 1996. "Environmental Effects from a 765 kV Double Circuit Transmission Line." Ibid.

Kim, J. B., D. I. Lee, K. H. Park, Y. W. Kim, T. D. Park, and J. S. Hwang. 1996. "A Study on the Design and Manufacturing Technique for 765 kV T/L and S/S Pipe Steel Tower." ibid.

Kim, J. B., D. I. Lee, K. Y. Shin, S. B. Jo, H. K. Lee, and H. K. Son. 1996. "Development of Fittings for 765 kV Transmission Lines." Ibid.

Lee, S. K., W. K. Kim, and T. W. Shin. 1996. "765 kV Transmission Line Projects and New Techniques for Line Design." Ibid.

Leem, S. H., J. Y. Hwang, and S. K. Shin. 1996. "Study on the Stability of the Power System with 765 kV T/L." Ibid.

Matsuoka, R., Y. Ozawa, and S. Matsui. 1996. "Design of Insulators and Bushings for the 765 kV Transmission System in Korea." Ibid.

Shim, E. B., J. W. Shim, and J. B. Kim. 1996. "Insulation Coordination and Switching Impulse Test." Ibid.

TEPCO 100-kV Lines

Yamada, T., A. Mochizuki, J. Sawada, E. Zaima, T. Kawamura, A. Ametani, M. Ishii, and S. Kato. "Experimental Evaluation of a UHV Tower Model for Lightning Surge Analysis." IEEE-PWRD-10. pp. 393-402. January.

APPENDIX 1

Base Case Line Configurations

A1.0 INTRODUCTION

Despite the continuing evolution of transmission-line design, certain dimensions remain a characteristic of line voltage, line configuration, and number of circuit. Among specialists, it is often sufficient to refer to a line mentioning these three parameters. For instance, a relatively clear picture is conveyed by referring to a "single-circuit 500-kV line with flat configuration" or to a "double-circuit vertical 345-kV line in a low-reactance configuration." For this reason, it is useful to list commonly used dimensions for a number of configurations called "base cases." Each base case differs from another either because of line voltage, or configuration, or number of circuits, or relative phasing. The performance of an actual line often does not differ significantly from that of the base case with the same line voltage, number of circuits, and configuration of the phases.

The base case configurations considered in this Reference Book include single and double circuits, and flat, delta, and vertical configurations. In total, 24 base case configurations are considered. The geometry of the base cases is listed in Tables A1-1, A1-2, and A1-3. The geometry of the base cases is also provided by Applet BC-1, which is entitled "Base Case Line Configurations and Their Performance." In addition to listing the geometrical parameters of each base case, the applet calculates several basic aspects of performance:

- Surface Gradient
- Corona Loss
- Audible Noise
- Electromagnetic Interference (EMI)
- Surge Impedance
- Electric Field (near ground)
- Magnetic Field (near ground)

The user can select the voltage (230, 345, 500, 765, or 1100 kV), the number of circuits (one or two), and the configuration (flat, delta, single pole triangular, vertical low-reactance, or vertical superbundle). The parameters of the selected base case configuration appear as a default. The user can either accept them or edit them. The results of the calculations made for the selected parameters appear on the screen. The results are given in the form of a brief summary. For greater details, the user is referred to applets specifically created for each individual subject.

Base case line configurations are used in individual chapters to provide examples of performance. Base cases are also considered in four applets that provide tables and graphs describing different aspects of performance for each base case. These applets also perform sensitivity

analyses and show the performance versus the value of any selected geometrical parameter, such as, for instance, the surface gradient versus the conductor diameter. The base case applets are:

- CC-6: Conductor Surface Gradient—Base Case Curves and Effects of Line Parameters
- RN-3: EMI—Base Case Curves and Effects of Line Parameters
- AN-5: Audible Noise—Base Case Curves and Effects of Line Parameters
- CL-2: Corona Loss—Base Case Curves and Effects of Line Parameters

Table A1-1 Base Case Parameters

Voltage		Single Or Double Circuit	Configuration	Subconductors in a Bundle					Span		Height above Ground of Lowest Phase		
Nom.	Max			Number	Diameter		Spacing				Max	Min	Ave
(kV)	(kV)	(S or D)			(in)	(cm)	(in)	(cm)	(ft)	(m)	(m)	(m)	(m)
230	242	S	Flat	1	1.345	3.42			800	244	16	7.5	10.3
		S	Delta	1	1.345	3.42			800	244	16	7.5	10.3
		S	Single Pole Triangular	1	1.345	3.42			800	244	16	7.5	10.3
		S	Vertical	1	1.345	3.42			800	244	16	7.5	10.3
		D	Vertical Low-Reactance	1	1.345	3.42			800	244	16	7.5	10.3
		D	Vertical Superbundle	1	1.345	3.42			800	244	16	7.5	10.3
345	362	S	Flat	2	1.196	3.04	18	45.72	1000	305	18.5	9.5	12.5
		S	Delta	2	1.196	3.04	18	45.72	1000	305	18.5	9.5	12.5
		S	Single Pole Triangular	2	1.196	3.04	18	45.72	900	274	15.5	9.5	11.5
		S	Vertical	2	1.196	3.04	18	45.72	800	244	15.5	9.5	11.5
		D	Vertical Low-Reactance	2	1.196	3.04	18	45.72	800	244	15.5	9.5	11.5
		D	Vertical Superbundle	2	1.196	3.04	18	45.72	800	244	15.5	9.5	11.5
500	550	S	Flat	3	1.165	2.96	18	45.72	1000	305	20	11	14
		S	Delta	3	1.165	2.96	18	45.72	1000	305	20	11	14
		S	Single Pole Triangular	3	1.165	2.96	18	45.72	900	274	18	11	13.3
		S	Vertical	3	1.165	2.96	18	45.72	800	244	17	11	13
		D	Vertical Low-Reactance	3	1.165	2.96	18	45.72	800	244	17	11	13
		D	Vertical Superbundle	3	1.165	2.96	18	45.72	800	244	17	11	13
765	800	S	Flat	4	1.385	3.52	18	45.72	1200	365	27	14.2	18.5
		S	Delta	4	1.385	3.52	18	45.72	1200	365	27	14.2	18.5
		D	Vertical Low-Reactance	4	1.385	3.52	18	45.72	1000	305	25	14.2	17.6
		D	Vertical Superbundle	4	1.385	3.52	18	45.72	1000	305	25	14.2	17.6
1100	1200	S	Flat	8	1.385	3.52	15.3	38.88	1400	426	36	18	24
		S	Delta	8	1.385	3.52	15.3	38.88	1400	426	36	18	24

Table A1-2 Location of Conductors at the Tower for Base Case Lines

Voltage		Single or Double Circuit	Configuration	Phase A		Phase B		Phase C	
				Height	Lateral Dist.	Height	Lateral Dist.	Height	Lateral Dist.
Nom (kV)	Max (kV)	(S or D)		(m)	(m)	(m)	(m)	(m)	(m)
230	242	S	Flat	16	-4.5	16	0	16	4.5
		S	Delta	16	-2.5	20.3	0	16	2.5
		S	Single Pole Triangular	16	-2.5	18	2.5	20	-2.5
		S	Vertical	16	-2.5	18.5	-2.5	21	-2.5
		D	Vertical Low-React.	16	-2.5	18.5	-2.5	21	-2.5
		D	Vertical Superbundle	16	-2.5	18.5	-2.5	21	-2.5
345	362	S	Flat	18.5	-7.5	18.5	0	18.5	7.5
		S	Delta	18.5	-4.5	26.3	0	18.5	4.5
		S	Single Pole Triangular	16.5	-3	20	3	23.5	-3
		S	Vertical	15.5	-3	23	-3	30.5	-3
		D	Vertical Low-React.	15.5	-3	23	-3	30.5	-3
		D	Vertical Superbundle	15.5	-3	23	-3	30.5	-3
500	550	S	Flat	20	-10	20	0	20	10
		S	Delta	20	-5	28.7	0	20	5
		S	Single Pole Triangular	18	-5.1	22	5.1	26	-5.1
		S	Vertical	17	-5.1	26	-5.1	35	-5.1
		D	Vertical Low-React.	17	-5.1	26	-5.1	35	-5.1
		D	Vertical Superbundle	17	-5.1	26	-5.1	35	-5.1
765	800	S	Flat	27	-14	27	0	27	14
		S	Delta	27	-8.4	41.6	0	27	8.4
		D	Vertical Low-React.	25	-7	37	-7	49	-7
		D	Vertical Superbundle	25	-7	37	-7	49	-7
1100	1200	S	Flat	36	-18.5	36	0	36	18.5
		S	Delta	36	-11	55	0	36	11

Table A1-3 Ground Wires for Base Case Lines

Voltage		Single or Double Circuit	Configuration	Ground wires				
				Number and Diameter		Height at Tower	Height At Midspan	Separation
Nom (kV)	Max (kV)	(S or D)			(cm)	(m)	(m)	(m)
230	242	S	Flat	2	0.95	22	16	7.5
		S	Delta	2	0.95	27.4	23.4	4
		S	Single Pole Triangular	1	0.95	27	23	0
		S	Vertical	1	0.95	29	25	0
		D	Vertical Low-React.	2	0.95	29	25	5.5
		D	Vertical Superbundle	2	0.95	29	25	5.5
345	362	S	Flat	2	0.95	25.6	20.5	9.4
		S	Delta	2	0.95	31.1	26	6.8
		S	Single Pole Triangular	1	0.95	33.5	29	0
		S	Vertical	1	0.95	40.5	36.5	0
		D	Vertical Low-React.	2	0.95	40.5	36.5	4
		D	Vertical Superbundle	2	0.95	40.5	36.5	4
500	550	S	Flat	2	0.95	29	22	14.6
		S	Delta	2	0.95	37.7	30.7	7.3
		S	Single Pole Triangular	2	0.95	38	32	6
		S	Vertical	1	0.95	44	39	-2.6
		D	Vertical Low-React.	2	0.95	44	39	6
		D	Vertical Superbundle	2	0.95	44	39	6
765	800	S	Flat	2	0.95	38.1	27	22.1
		S	Delta	2	0.95	52.9	41.8	12.8
		D	Vertical Low-React.	2	0.95	61	52	-9
		D	Vertical Superbundle	2	0.95	61	52	9
1100	1200	S	Flat	2	0.95	50	35	33.8
		S	Delta	2	0.95	68	53	16.8

APPENDIX 2 Applets

A2.1 INTRODUCTION

More than 20 years have passed since the second edition of the Red Book was published. Although the engineering principles of the design handbook have remained constant, new technologies and methods have been developed for transmission-line design. Advances in computer technology have provided the line design engineer with a valuable new tool, the personal computer. Therefore, a key goal of the development of the third edition is to have the Red Book information available in an electronic version to easily and conveniently reference.

In addition to simply converting the paper version to an electronic book version, software applets have also been developed as calculation modules for key design concepts. These software calculation applets provide sample problems and calculation results to illustrate line design parameters. Each applet is a small software routing with transmission-line data input screens, calculation results screens (tabular and/or graphical), and help files.

The applets also contain sample problems that the user can load directly to calculate results. In addition, the user can also enter specific transmission-line information for a particular problem and then calculate specific results for that problem. Transmission-line parameters can also be modified and the results re-calculated, thereby illustrating how the change in a particular line parameter can affect the calculation results. More than fifty different applets have been developed, including calculation modules related to conductor surface gradients, insulator design, switching surges, lightning effects, electric and magnetic fields, radio noise and audible noise generation, and corona loss.

Each applet is a Java-based, stand-alone calculation module. Applets are accessed using the Microsoft Virtual Machine plug-in component of Internet Explorer. These software programs should be included with the Microsoft Windows operating system or Internet Explorer (all users are required to have the Microsoft Virtual Machine plug-in installed; some users may have to install this as a custom option to Internet Explorer).

Each applet is interactive and allows the user to calculate a specific performance parameters for a given transmission-line geometry. Therefore, each applet has its own specific required input data, calculation routines, and output results.

The layout for the applets was designed to be consistent across all of the applets within the Red Book software. Pull-down selection boxes provide data entry for each applet and data input fields that allow the user to select various input parameters and then specify transmission-line design geometry information. Input data can typically be saved to a file, loaded from an existing file, or viewed graphically. Calculation results are typically available in either tabular or graphical formats. Help files for the applets can be accessed individually from each applet and are presented together in the User Manual.

Of particular importance are the Base Cases. They are a set of typical line designs that provide the user with typical parameters of lines of different voltages and, therefore, provide typical ranges of input data. The base cases are discussed in Appendix 1.

The rest of this appendix provides more detailed information on the applets. Table A2-1 lists all the applets. Table A2-2 lists the applets by chapter in the Reference Book. Table A2-3 briefly describes the applets. Table A2-4 is an index of the types of calculation that can be performed by the applets.

Table A2-1 Applets

Applet No.	Applet Name
AN-1	Audible Noise of Transmission Lines (2-D)
AN-2	Audible Noise of Transmission Line (3-D)
AN-3	Bundle Geometry for Minimum Audible Noise
AN-4	Audible Noise, Hum
AN-5	Audible Noise—Base Case Curves and Effect of Line Parameters
AN-6	Audible Noise vs. Rain Rate
BC-1	Base Case Line Configurations and Their Performance
CC-1	Conductor Surface Gradient (2-D)
CC-2	Conductor Surface Gradient (3-D)
CC-3	Surface Gradient on Toroidal Corona Shields
CC-4	Conductor Tables
CC-5	Transmission Line Parameters (Single Circuit)
CC-6	Conductor Surface Gradient—Base Case Curves and Effect of Line Parameters
CC-7	Induction in Parallel De-Energized Lines
CL-1	Transmission Line Corona Loss
CL-2	Corona Loss—Base Case Curves and Effect of Line Parameters
CL-3	Ozone Concentration near Transmission Lines
Co-1	Corona Inception Gradient
EMF-1	Field Ellipse
EMF-2	Electric Field of Transmission Lines (2-D)
EMF-3	Single Conductor Equivalent to a Bundle
EMF-4	Electric Field of Transmission Lines (3-D)
EMF-5	Electric Field Shielding by Grids of Wires (2-D)
EMF-6	Magnetic Field from Sets of Current Carrying Conductors (2-D)
EMF-7	Magnetic Field (3-D)
EMF-8	Magnetic Induction in Wires Parallel to Transmission Lines
EMF-9	Distant Magnetic Field Equations for Transmission Lines
EMF-10	Electric Field Induction on Objects
EMF-11	Magnetic Field Reduction Using Cancellation Loops (3-D)
EMF-12	Magnetic Field Reduction Using 4th-Wire Scheme
G-1	Unit Converter
G-2	World Map of Ground Flash Density and North American Map of Earth Resistivity
I-1	Insulator Equivalent Salt Deposit Density (ESDD) and Parameter Evaluation
I-2	Electric Field Distribution for Polymer Insulators—Effect of Dimensions and Location of Corona Ring
I-3	Statistical Method for Dimensioning Insulators to Meet Contamination Flashover Requirements
IC-1	Insulation Coordination. Comparative Evaluation of Insulation Distance Requirements
IC-2	Risk of Failure (Same as S-2)
L-1	Transmission Line Lightning Performance
L-2	Stoke Attraction Model
L-3	Tower Footing Dynamic Resistance (for Vertical Rods)
L-4	Tower Lightning Flashover Tutorial
L-5	Tower Surge Impedance
L-6	Step and Touch Potential
M-1	Minimum Approach Distance
RN-1	Electromagnetic Interference up to 30 MHz
RN-2	EMI Calculations Using Empirical Method
RN-3	EMI Base Case Curves and Effect of Line Parameters
RN-4	Traditional Radio Noise Calculation Method
S-1	Switching Surge Flashover Model
S-2	Risk of Failure Calculation for Transmission Line Switching Surges
S-3	Calculation of 50% Flashover Voltage and Standard Deviation from a Set of Test Data

Table A2-2 Applets Listed by Chapter

Chapter No.	Applet No.	Applet Name
2	CC-1	Conductor Surface Gradient (2-D)
2	CC-2	Conductor Surface Gradient (3-D)
2	CC-3	Surface Gradient on Toroidal Corona Shields
2	CC-4	Conductor Tables
2	CC-5	Transmission Line Parameters (Single Circuit)
2	CC-6	Conductor Surface Gradient—Base Case Curves and Effect of Line Parameters
2	CC-7	Induction in Parallel De-Energized Lines
3	IC-1	Insulation Coordination. Comparative Evaluation of Insulation Distance Requirements
3	IC-2	Risk of Failure (Same as S-2)
4	I-1	Insulator ESDD and Parameter Evaluation
4	I-2	Electric Field Distribution for Polymer Insulators—Effect of Dimensions and Location of Corona Ring
4	I-3	Statistical Method for Dimensioning Insulators to Meet Contamination Flashover Requirements
5	S-1	Switching Surge Flashover Model
5	S-2	Risk of Failure Calculation for Transmission Line Switching Surges
5	S-3	Calculation of 50% Flashover Voltage and Standard Deviation from a Set of Test Data
6	L-1	Transmission Line Lightning Performance
6	L-2	Stoke Attraction Model
6	L-3	Tower Footing Dynamic Resistance (for Vertical Rods)
6	L-4	Tower Lightning Flashover Tutorial
6	L-5	Tower Surge Impedance
6	L-6	Step and Touch Potential
7	EMF-1	Field Ellipse
7	EMF-2	Electric Field of Transmission Lines (2-D)
7	EMF-3	Single Conductor Equivalent to a Bundle
7	EMF-4	Electric Field of Transmission Lines (3-D)
7	EMF-5	Electric Field Shielding by Grids of Wires (2-D)
7	EMF-6	Magnetic Field from Sets of Current Carrying Conductors (2-D)
7	EMF-7	Magnetic Field (3-D)
7	EMF-8	Magnetic Induction in Wires Parallel to Transmission Lines
7	EMF-9	Distant Magnetic Field Equations for Transmission Lines
7	EMF-10	Electric Field Induction on Objects
7	EMF-11	Magnetic Field Reduction Using Cancellation Loops (3-D)
7	EMF-12	Magnetic Field Reduction Using 4th-Wire Scheme
8	Co-1	Corona Inception Gradient
9	RN-1	Electromagnetic Interference up to 30 MHz
9	RN-2	EMI Calculations Using Empirical Method
9	RN-3	EMI Base Case Curves and Effect of Line Parameters
9	RN-4	Traditional Radio Noise Calculation Method
10	AN-1	Audible Noise of Transmission Lines (2-D)
10	AN-2	Audible Noise of Transmission Line (3-D)
10	AN-3	Bundle Geometry for Minimum Audible Noise
10	AN-4	Audible Noise, Hum
10	AN-5	Audible Noise—Base Case Curves and Effect of Line Parameters
10	AN-6	Audible Noise vs. Rain Rate
11	CL-1	Transmission Line Corona Loss
11	CL-2	Corona Loss—Base Case Curves and Effect of Line Parameters
11	CL-3	Ozone Concentration near Transmission Lines
13	M-1	Minimum Approach Distance
——	G-1	Unit Converter
——	G-2	World Map of Ground Flash Density and North American Map of Earth Resistivity
A1	BC-1	Base Case Line Configurations and Their Performance

Table A2-3 Applet Descriptions

Applet No.	Applet Name and Description
AN-1	***Audible Noise of Transmission Lines (2-D)*** This applet calculates the audible noise caused by corona on high-voltage transmission lines at different distances from the line. The audible noise is calculated as the L_{50} value in rain—i.e., the value exceeded for 50% of the periods during which there is measurable rain. The results are given for both the EPRI and the BPA calculation methods described in Chapter 10. For most lines, the two methods give similar results. The difference between the two sets of values can be used to indicate variations that can be expected between different climates, or different conductor surface conditions (aging). In addition to L_{50} rain, the L_5 rain and the range of possible fair weather values also are given. These are values obtained using the EPRI method. According to the BPA method, the L_5 rain is obtained by adding 3.5 dB to the L_{50} rain, and the L_{50} fair weather value is obtained by subtracting 25 dB from the L_{50} rain value. The fair weather values calculated in this applet are the lower and the upper expected values of the fair weather noise, which is very dependent on season, climate, and particles that may be present in the air. The applet also calculates the generated acoustic power of individual bundles. This gives the user information on which bundle is most responsible for the noise. The applet calculates the noise for any type of bundles, including irregular bundles—i.e., bundles for which the conductors are not placed on the vertices of a regular polygon. The conductors are treated as if they were infinitely long and parallel to a flat conductive earth. The audible noise is calculated at heights of 1.5 m above ground along a user-specified line orthogonal to the line (lateral profile).
AN-2	***Audible Noise of Transmission Line (3-D)*** This applet calculates the audible noise caused by corona on high-voltage transmission lines at different distances from the line. The problem is solved in 3-D. Conductive objects are simulated by sets of cylindrical segments above a conductive flat ground plane. This applet is ideal for conductors that have sags (such as transmission-line conductors), are not parallel to each other (transposition spans), or are at an angle with respect to each other (substation buses). This applet is also ideal to find out the effect of the presence of lattice towers, steel poles, guy wires, and other objects at ground potential that may be well represented by sets of cylindrical segments (see Appendix 7.6). The audible noise is calculated as the L_{50} and L_5 values in rain (i.e., the values exceeded for 50% and 5% of the periods during which there is measurable rain) and the upper limit of expected fair weather values. The noise is calculated using the EPRI calculation method. The applet divides the conductors into a large number of short segments, calculates the surface gradient on each segment using a 3-D electric field program (Applet CC-2), calculates the generated acoustic power for each segment, and finally the noise produced by all segments together at each measuring point. The audible noise is calculated along a line specified by the user.

Table A2-3 Applet Descriptions (Continued)

Applet No.	Applet Name and Description
AN-3	***Bundle Geometry for Minimum Audible Noise*** This applet calculates the optimum bundle geometry corresponding to the minimum audible noise. Only three-phase transmission lines are considered. The bundles of the three phases are all equal. For a given number of subconductors, subconductor diameter, and bundle diameter, there is an optimum arrangement of the individual subconductors on the bundle circumference that produces the lowest audible noise for well-aged conductors in rain. The value calculated is the L_{50} value in rain (i.e., the value exceeded for 50% of the periods during which there is a measurable rain). The calculations are based on the EPRI method to calculate the L_{50} rain value and on the method for bundle geometry optimization described in Section 10.7.2. The experimental data needed to execute the calculations were taken from graphs published in the technical literature, which were digitized for use by this applet. The optimum bundle geometry is given for different bundle diameters. There is a bundle diameter and an optimum subconductor arrangement for which the audible noise reaches an absolute minimum. The applet calculates the audible noise value (at 15 m from the outer phase and 1.5-m height) for regular and optimum bundles and calculates the subconductor location for the optimum bundles. The user is cautioned that the noise performance of an asymmetric bundle is predicted on the basis of laboratory tests. The noise performance of actual lines in natural rain conditions may be degraded by several facts: the water drops do not form exactly at the bottom of the conductors if they are not well-aged or if there is significant wind, the subconductors may have differential sags, the bundle may have some twist, and the water impinging on the upper subconductors may become significant as the rain intensity increases. The best performance of asymmetric bundles over regular bundles is achieved in light rain, drizzle, or fog conditions.
AN-4	***Audible Noise, Hum*** This applet calculates the audible hum at twice the power frequency caused by corona on high-voltage transmission lines at different distances from the line. The hum is a mixture of pure tones, the most significant of which occurs at twice the power frequency. The algorithms for the calculations are described in Chapter 10. The hum is calculated as the L_{50} and the L_5 values in rain (i.e., the values exceeded for 50% and 5%, respectively, of the periods during which there is measurable rain). The rain intensity selected for the L_{50} value is 0.75 mm/h and the rain intensity selected for the L_5 value is 6.5 mm/h. The hum in fair weather is negligible and is not calculated. The hum is calculated for an altitude of 100 m or less above sea level. There is no experimental or other research data to support estimates of the effect of altitude. The applet calculates also the generated acoustic hum power of individual bundles. This gives the user information on which bundle is most responsible for the hum. The applet calculates the hum only for single conductors and regular bundles (i.e., bundles for which the conductors are placed on the vertices of a regular polygon). The conductors are treated as if they were infinitely long and parallel to a flat conductive earth. The hum is calculated at different lateral distances from the center of the line (lateral profile) at a constant height above ground that can be set by the user.

Table A2-3 Applet Descriptions (Continued)

Applet No.	Applet Name and Description
AN-5	***Audible Noise—Base Case Curves and Effect of Line Parameters*** This applet calculates the audible noise for a number of transmission-line configurations considered as base cases from 230 to 1100 kV. The base case configurations include single and double circuits, flat, delta, and vertical configurations. In total, 24 base case configurations are considered. This applet produces tables and graphs, giving the audible noise versus the value of any desired parameter that affects it, such as voltage, phase spacing, height above ground, number of subconductors in a bundle, subconductor diameter, subconductor spacing, ground wire geometrical parameters, and distance from the line. The user can select a base case by choosing the voltage (230, 345, 500, 765, or 1100 kV), the number of circuits (single or double), and the configuration (Flat, Delta, Single Pole Triangular, Vertical Low-Reactance, or Vertical Superbundle). The parameters of the selected base case configuration will appear as a default. The user can either accept them or edit them. For this applet, only parameters that have an effect on the audible noise are listed. Altitude above sea level is assumed to be between 0 and 300 m. The audible noise is calculated at the height of 1.5 m above ground and at a distance specified by the user. Calculations are made for average rain (L_{50} value) according to both EPRI and BPA methods, for heavy rain (L_5 value) according to EPRI method, and for fair weather (range of possible values). The problem is solved in two dimensions (i.e., the conductors are considered straight, infinitely long, and parallel to each other and to the flat surface of a conductive earth). The calculations are made for the parameters selected by the user. In addition, the applet shows how audible noise varies as a specific parameter is varied (Sensitivity Analysis). The user must specify the desired parameter and the range of values between which the parameter is allowed to vary. For any specific case, the results should be identical to those obtained with Applet AN-1.
AN-6	***Audible Noise vs. Rain Rate*** This applet calculates the audible noise caused by corona on high-voltage transmission lines at a specified distance from the line and the noise caused by the rain itself for different rain rates. The calculation of audible noise due to corona versus rain rate is based on the algorithms in Section 10.4.6. The calculation of the noise of rain is based on the algorithms in Appendix 10.2. The applet is useful to determine at which distance from the line and at which rain intensity the noise of rain may mask the noise of the line. The conductors are treated as if they were infinitely long and parallel to a flat conductive earth. The audible noise is calculated for an altitude between 0 and 300 m and for a height of 1.5 m above ground.

Table A2-3 Applet Descriptions (Continued)

Applet No.	Applet Name and Description
BC-1	***Base Case Line Configurations and Their Performance*** This applet shows the geometry of a number of transmission-line configurations considered as base cases from 230 to 1100 kV. The base case configurations include single and double circuits, flat, delta, and vertical configurations. In total, 24 base case configurations are considered. These base cases are considered typical and are referred to by the authors of individual chapters. In addition to listing the geometrical parameters of each base case, the applet calculates several basic aspects of performance: • Surface Gradient • Corona Loss • Audible Noise • Electromagnetic Interference (EMI) • Surge Impedance • Electric Field (near ground) • Magnetic Field (near ground) The user can select a base case by choosing the voltage (230, 345, 500, 765, or 1100 kV), the number of circuits (single or double), and the configuration (Flat, Delta, Single Pole Triangular, Vertical Low-Reactance, or Vertical Superbundle). The parameters of the selected base case configuration will appear as a default. The user can either accept them or edit them. The results of the calculations made for the selected parameters appear on the screen. The results are given in the form of a brief summary. For greater details, the user is referred to applets specifically created for each individual subject.
CC-1	***Conductor Surface Gradient (2-D)*** This applet calculates the electric field at the surface of conductors (*conductor surface gradient*) of high-voltage transmission lines. The problem is solved in two dimensions (i.e., the conductors are considered straight, infinitely long, and parallel to each other and to the flat surface of a conductive earth). The user may input data regarding single conductors, or bundles, or three-phase circuits, or any combination of these elements. The applet can be applied to any number of circuits in a transmission-line corridor. For each conductor, the average surface gradient and the maximum surface gradients are calculated. In the case of a bundle of conductors, the maximum surface gradient is defined as the average of the maximum surface gradients of the individual conductors. The applet calculates also the surface gradient at any point on the surface of a specified conductor. The electric field is calculated only on the surface of the conductors. Calculations do not apply to the electric field away from the conductor surface. To calculate the electric field or the space potential away from the conductor surfaces, use Applet EMF-2. The applet calculates the surface gradient for any type of bundles, including irregular bundles (i.e. bundles for which the conductors are not placed on the vertices of a regular polygon).

Table A2-3 Applet Descriptions (Continued)

Applet No.	Applet Name and Description
CC-2	***Conductor Surface Gradient (3-D)*** This applet calculates the electric field at the surface of conductors (*conductor surface gradient*), either single or regular bundles, of high voltage transmission lines. The problem is solved in 3-D. Conductive objects are simulated by sets of cylindrical segments above a conductive flat ground plane. This applet is ideal for conductors that have sags (such as transmission-line conductors), are not parallel to each other (transposition spans), or are at an angle with respect to each other (substation buses). This applet is also ideal to find out the effect of the presence of lattice towers, steel poles, guy wires, and other objects at ground potential that may be well represented by sets of cylindrical segments (see Appendix 7.6). For each single conductor or bundle, the average surface gradient and the maximum surface gradients are calculated. Only regular bundles are considered (i.e., bundles for which the conductors are placed on the vertices of a regular polygon). The applet does not calculate the surface gradient on conductors that are parts of objects at ground potential, but calculates the gradient only on the surface of energized single conductors or bundles. The electric field is calculated only on the surface of the conductors. Calculations do not apply to the electric field away from the conductor surface. To calculate the electric field or the space potential away from the conductor surfaces, use Applet EMF-4.
CC-3	***Surface Gradient on Toroidal Corona Shields*** This applet calculates the *highest electric field on the surface (maximum surface gradient) of toroids*. Toroids are often used to terminate the high-voltage conductors toward a dead end structure or near the line end of insulator strings to reduce the voltage gradient along the insulators. If the dimensions or the position of the toroid are not appropriate, the electric field may reach unacceptably high values and create a strong corona source. The problem of calculating the surface gradient is solved in 3-D. All conductive objects present (conductors, bundles, tower elements, objects at ground potential) are simulated by sets of cylindrical segments above a conductive flat ground plane. Each toroid is also simulated with a set of 108 cylinders, which provides a very good simulation. The other conductive objects that can be simulated include single or bundled conductors, either straight segments or catenaries and flat plates. The user can build other objects and store them for future use. The maximum surface gradient is calculated only on toroids. A maximum of two toroids is allowed. There is no limitation on other objects.
CC-4	***Conductor Tables*** This applet may be used for the following purposes: 1. Given the name of a conductor, list its properties and show the drawing of its cross-section. 2. Select a conductor with a desired property and look up its other parameters. For instance, the user may want a list of conductors ordered by outside diameter, or by resistance, or by strength and choose a conductor from that list. After selecting the conductor, the user may see the list of its parameters. 3. The user may calculate quantities that are not normally found in a conductor table, such as the resistance at different temperatures and/or different frequencies. All units are both in metric and British units. The applet incorporates tables of common North American Aluminum Conductors Steel Reinforced (ACSR), common British ACSR, ACSR/TW, ACSR-IEC, Single-Layer High-Strength Aluminum Conductors Steel Reinforced (ACSR-EHS), Aluminum Conductors Steel Supported (ACSS), All-Aluminum Conductors (ACC), All-Aluminum-Alloy Conductors (AAAC), Aluminum Conductors Alloy Reinforced (ACAR), Aluminum-Clad Steel Conductors (ALUMOWELD), High-Strength Utility-Grade Steel Conductors (HS), and Extra-High-Strength Utility-Grade Steel Conductors (EHS) (see Chapter 2).

Table A2-3 Applet Descriptions (Continued)

Applet No.	Applet Name and Description
CC-5	***Transmission Line Parameters (Single Circuit)*** This applet calculates the electrical parameters of single-circuit transmission lines with or without ground wires. Calculations require the knowledge of line geometry, conductor electrical characteristics (resistance and geometric mean radius), and earth resistivity. Calculations are made for a specific frequency. The applet calculates: • The series impedance matrix, either full (including the ground wires) or 3 by 3 (after ground wire reduction). Each term of the series impedance matrix is made up of a resistance and a reactance, both given in ohm/km. • The shunt admittance matrix. Each term of the admittance matrix is made up of a conductance, which is zero, and an admittance (μS/km). • The sequence impedance matrix, which expresses the impedances applicable to zero, positive, and negative sequence voltages and currents. Each term of the sequence impedance matrix is made up of a resistance and a reactance, both given in ohm/km. • The surge impedance (ohm). • The surge impedance loading (MW). The applet also calculates the series voltage drop (V/km for each phase) for a given set of line currents and the capacitive currents (A/km for each phase) for a given set of line voltages. Finally, the applet includes a tool that allows passing from phase to sequence quantities and vice versa. The conductors are treated as if they were infinitely long and parallel to a flat conductive earth. The algorithms presented in Chapter 2 are used and expanded as discussed in the Help file of this applet. The maximum number of ground wires that can be considered is two. The frequency can have any value from power frequency up to 100 kHz. The user can input the resistance and the GMR of a conductor directly or input known characteristics of the conductor and let the applet calculate resistance and GMR.
CC-6	***Conductor Surface Gradient—Base Case Curves and Effect of Line Parameters*** This applet calculates the electric field at the surface of conductors for a number of transmission-line configurations considered as base cases from 230 to 1100 kV. The base case configurations include single and double circuits, and flat, delta, and vertical configurations. In total, 24 base case configurations are considered. This applet produces tables and graphs giving the conductor surface gradient of any desired phase or ground wire versus the value of any desired parameter that affects the gradient, such as conductor diameter, phase spacing, height above ground, subconductor spacing, and ground wire geometrical parameters. The user can select a base case by choosing the voltage (230, 345, 500, 765, or 1100 kV), the number of circuits (single or double), and the configuration (Flat, Delta, Single Pole Triangular, Vertical Low-Reactance, or Vertical Superbundle). The parameters of the selected base case configuration will appear as a default. The user can either accept them or edit them. The problem is solved in two dimensions (i.e., the conductors are considered straight, infinitely long, and parallel to each other and to the flat surface of a conductive earth). The voltages are assumed symmetric (i.e., the three phase-to-ground voltages are equal in magnitude and their phase angles differ by 120º). For any specific case, the results should be identical to those obtained with Applet CC-1.

Table A2-3 Applet Descriptions (Continued)

Applet No.	Applet Name and Description
CC-7	***Induction in Parallel De-Energized Lines*** This applet calculates the magnetically or electrically induced voltages and currents on de-energized lines parallel to energized lines. Specifically: 1. The magnetically induced voltages (voltages induced by the currents of the energized circuit) in de-energized lines grounded at one tower and open-circuited at the end of a line section. 2. The electrically induced voltages (voltages induced by the voltages of the energized circuit) in de-energized lines not connected to ground (ungrounded). 3. The electrically induced currents (currents induced by the voltages of the energized circuit) in de-energized lines grounded at one point. The problem is solved in 2-D (i.e., the conductors are considered straight, infinitely long, and parallel to each other and to the flat surface of a conductive earth.) The applet considers only one energized circuit and only one de-energized circuit. Up to four ground wires may be considered. If the user desires to assess the induction on one de-energized wire only (not necessarily a transmission-line conductor), the wire may be considered as phase 1 of the de-energized line, while the parameters of phase 2 and phase 3 of the de-energized line are immaterial.
CL-1	***Transmission Line Corona Loss*** This applet calculates corona loss (W/m) under fair weather and under heavy rain. The loss is calculated for each phase and for the entire line. The applet also calculates the mean annual and maximum corona loss of the line. Corona loss calculations are notoriously inaccurate. Accuracy of empirical formulas for corona effects is generally evaluated by comparing them with good measured data obtained on operating high-voltage transmission lines. Unlike RI and AN, however, sufficient measured data are not available for corona loss from operating lines and, therefore, it is not possible to make a realistic evaluation of the accuracy of corona loss empirical formulas. Different results are obtained using calculation methods developed by different researchers. The difference may be caused by different surface conditions of the conductors tested (particularly the degree of aging), different climates, different rain rates, measurement errors, and approximation in deriving empirical equations. By comparing results obtained with different methods, the user may gather an appreciation for the variability of the phenomenon and the reliability of the data. The various methods are described in Chapter 11. They include: 1. Fair weather loss according to Peterson's equation, which is applicable only for single conductors. 2. Fair weather loss according to Gary and Moreau (EdF). This method is applicable to single conductors and any regular bundle and gives a range of possible fair weather losses. 3. Fair weather loss according to a BPA formula. This method is applicable to single conductors and regular bundles. 4. Heavy rain loss according to a BPA formula. This method is applicable to any regular bundle. 5. Heavy rain loss according to a method developed by Trinh and Maruvada (IREQ). Developed particularly for bundles. 6. Heavy rain loss according to Clade and Gary (EdF). This method is applicable to single conductors and regular bundles. 7. Heavy rain loss according to Comber and Zaffanella (EPRI Red Book, second edition). This method is applicable to single conductors and regular bundles. 8. Loss in rain according to GE's Project EHV (EEI Blue Book). This method was developed for 345-kV to 765-kV lines. Each of these methods is described in Chapter 11. The algorithms are reviewed and described in the Help file of the Applet. Essentially, all methods start with the calculation of the electric field at the surface of the conductors of each phase. The problem is solved in 2-D (i.e., the conductors are considered straight, infinitely long, and parallel to each other and to the flat surface of a conductive earth). For each phase, the surface gradient is calculated. Each method uses empirically derived equations, giving the corona loss as a function of some of the following variables: subconductor diameter, number of subconductors, bundle diameter, rain rate, frequency, and altitude.

Table A2-3 Applet Descriptions (Continued)

Applet No.	Applet Name and Description
CL-2	***Corona Loss—Base Case Curves and Effect of Line Parameters*** This applet calculates the corona loss for a number of transmission-line configurations considered as base cases from 230 to 1100 kV. The base case configurations include single and double circuits, and flat, delta, and vertical configurations. In total, 24 base case configurations are considered. This applet produces tables and graphs, giving the corona loss of any desired phase and the total corona loss of the line versus the value of any desired parameter that affects corona loss, such as conductor diameter, phase spacing, height above ground, subconductor spacing, ground wire geometrical parameters, and rain rate. The user can select a base case by choosing the voltage (230, 345, 500, 765, or 1100 kV), the number of circuits (single or double), and the configuration (Flat, Delta, Single Pole Triangular, Vertical Low-Reactance, or Vertical Superbundle). The parameters of the selected base case configuration will appear as a default. The user can either accept them or edit them. For this applet, only parameters that have an effect on corona loss are listed. They include: voltage, line geometry, bundle geometry, ground wire geometry, frequency, and altitude. The user may choose to calculate the loss for fair weather or for heavy rain (10 mm/min) and the method of calculation: fair weather according to Peterson, fair weather according to EdF, fair weather according to BPA, heavy rain according to BPA, heavy rain according to EdF, heavy rain according to IREQ, heavy rain according to EPRI, and heavy rain according to Project EHV. For the details of how corona loss is calculated according to the various methods, see the Help file of Applet CL-1. For a comparison between methods, exercise Applet CL-1. The applet calculates the corona loss for the selected parameters. In addition, the applet shows how corona loss varies as a specific parameter is varied. The user must specify the desired parameter and the range of values between which the parameter is allowed to vary. For any specific case, the results should be identical to those obtained with Applet CL-1.
CL-3	***Ozone Concentration near Transmission Lines*** This applet calculates the incremental concentration of ozone caused by corona on high-voltage transmission lines at different distances from the line. The amount of ozone is expressed in ppb (parts per billion in terms of weight relative to air). The algorithms for the calculations are described in Chapter 11. Ozone concentration is calculated for fair weather and for rain. In both cases, the most conservative estimates are made. In the case of fair weather, the worst fair weather conditions conducive to corona are assumed. In the case of rain, an intensity of 10 mm/h (heavy rain) is assumed. The generation of ozone is expressed in μg/(m·s). The generation is based on corona loss. For corona loss calculations in fair weather the upper bound values obtained using the EdF method are used. For corona loss calculation in heavy rain the EPRI method, which is generally the most conservative, is used. Corona loss is calculated accounting for frequency and for altitude above sea level. Other than their effect on corona loss, these two variables are assumed not to affect ozone concentration. If the user prefers to calculate the corona loss using other methods, calculations should be made separately (for instance using Applet CL-1), and the user should choose the option of entering the corona loss values for each bundle directly. The applet calculates the lateral profile of ozone concentration and also the ozone generated by individual phases. The user must specify the interval of distances from the line, the number of segments in which this interval is divided, and the height above ground at which ozone concentration is measured. The user must also specify wind speed and direction (parallel or perpendicular to the line), and wind type (stable or unstable). The conductors are treated as if they were infinitely long and parallel to a flat earth.
Co-1	***Corona Inception Gradient*** This applet calculates the corona inception (or corona onset) gradient of conductors for high-voltage lines, as discussed in Chapter 8. The user must enter the conductor diameter, the air temperature, the air pressure (or, alternatively, the altitude above sea level), and the surface irregularity factor. The user may compare the corona onset gradient with the maximum conductor surface gradient calculated with Applet CC-1 (Conductor Surface Gradient – 2D) or Applet CC-2 (Conductor Surface Gradient – 3D).

Table A2-3 Applet Descriptions (Continued)

Applet No.	Applet Name and Description
EMF-1	***Field Ellipse*** This applet shows how the vector representing the instantaneous value of the field (either an electric field or a magnetic field in space) varies in time and direction, describing an ellipse. The user inputs the magnitude and phase angles of the field components along the X, Y, and Z axes. The applet shows the instantaneous values of these components and the resulting vector versus time. The minimum and maximum values of the field components in the plane of the ellipse (ellipse semi-axes) are also calculated.
EMF-2	***Electric Field of Transmission Lines (2-D)*** This applet calculates the electric field and the space potential at power frequency at any point at the ground or in space caused by high-voltage transmission lines or by any set of conductors to which a known voltage may be applied. The conductors are treated as if they were infinitely long and parallel to a flat conductive earth. When three-phase transmission circuits are considered, their voltages are assumed symmetric. The applet can be applied to any number of circuits in a transmission-line corridor. The electric field and the space potential are calculated along a specified line. The space potential may also be calculated on a vertical plane orthogonal to the conductors, and the space potential contour lines may be provided. Calculations, however, do not apply to the field on the conductor surface (surface gradient) or in the immediate vicinity of conductors. Calculation of the conductor surface gradient can be made with Applet CC-1.
EMF-3	***Single Conductor Equivalent to a Bundle*** This applet calculates the diameter of the single-conductor equivalent to a bundle made of two or more subconductors. This is the diameter of a single conductor that would produce the same electric field, away from the bundle, as the field produced by the bundle. Another way of expressing the equivalence is to say that the single conductor holds the same electrical charge and has the same capacitance to ground as the bundle. The calculation assumes that the largest distance between subconductors is small in comparison to the distance between the bundle and ground or to another bundle. This applet applies to any type of bundles, including those that have an irregular geometry (asymmetric bundles). The applet applies also to regular bundles, but for these, the equivalent conductor diameter can be obtained using a simple equation.
EMF-4	***Electric Field of Transmission Lines (3-D)*** This applet calculates the electric field and the potential in space caused by high-voltage transmission lines or any set of conductors to which a voltage may be applied. Conductive objects are simulated by sets of cylindrical segments above a conductive flat ground plane. This applet is ideal for conductors that have sags (such as transmission-line conductors), or are not parallel to each other (transposition spans), or are at an angle with respect to each other (substation buses). This applet is also ideal to find out the effect of the presence of lattice towers, steel poles, guy wires, and other objects at ground potential that may be well represented by sets of cylindrical segments. The algorithms on which this applet is based are described in Appendix 7.6 of Chapter 7. The electric field and space potential can be calculated along a specified line and displayed in both tabular and graphical formats. The electric field and space potential may also be calculated individually on a designated plane orthogonal to one of the coordinate axes (X-Y, X-Z, or Y-Z planes), and contour line maps can be constructed.
EMF-5	***Electric Field Shielding by Grids of Wires (2-D)*** This applet calculates the electric field and space potential caused by high-voltage transmission lines (or any set of conductors to which a voltage may be applied) in the presence of a grid of grounded wires that act as a shield. Both energized and grounded conductors are treated as if they were infinitely long and parallel to a flat conductive earth. If the conductors form catenaries, the height of the conductors above ground should be specified at the location where the field is calculated. Conductor sag is not considered in this calculation. Grounded conductor shielding grids are defined by location and density, and can be either horizontal or vertical grids. The electric field and space potential can be calculated along a specified line, creating a lateral profile plot. Space potential can also be calculated within a rectangular calculation grid in a vertical plane orthogonal to the conductors, with space potential contour lines provided.

Table A2-3 Applet Descriptions (Continued)

Applet No.	Applet Name and Description
EMF-6	***Magnetic Field from Sets of Current Carrying Conductors (2-D)*** This applet calculates the magnetic field at power frequency at any point caused by high-voltage transmission lines or by any set of conductors in which known currents flow. The conductors are treated as if they were infinitely long and parallel to a flat nonmagnetic, nonconductive earth. For the calculation of magnetic field, the current is assumed to be concentrated at the center of each conductor (or conductor bundle). The image currents in the earth are neglected, which is a good approximation for calculation of power frequency magnetic field in proximity to power lines. If the conductors form catenaries, the sag is neglected, and the height of the conductors above ground should be that at the location where the field is calculated. When conductor bundles are considered, they are treated as single conductors with the current concentrated at the center of the bundle. When three-phase transmission circuits are considered, the data for each phase must be entered one at a time. If the transmission line has shield wires for lightning protection, their current must be calculated before exercising this applet. Shield wire currents or currents in any other grounded wires may be calculated using Applet EMF-8. The magnetic field is calculated at points along a specified line or at points of a grid in a vertical plane orthogonal to the conductors, in which case magnetic field contour lines are provided. Calculations, however, do not apply to the field near the conductors of a bundle. If the field in the immediate vicinity of a bundle is desired, the data for each subconductor must be entered separately.
EMF-7	***Magnetic Field (3-D)*** This applet calculates the magnetic field at power frequency at any desired point in space produced by conductors that can be simulated by sets of segments of known starting and ending points and that carry known currents. In addition to conductor segments, the user can enter catenaries just by defining attachment points, sag, and number of segments. This applet is ideal for conductors that have sags (transmission-line conductors), or are not parallel to each other (transposition spans), or are at an angle with each other (substation buses). This applet is also ideal for any three-dimensional arrangement of conductors. The earth is assumed nonconductive and, therefore, the image currents in the earth are neglected, which is a good approximation for calculation of power frequency magnetic field in proximity to power lines. No conductive (other than the specified conductor segments, catenaries, buses, or coils) or magnetic object that may modify the magnetic field is assumed to be present. The magnetic field and space potential can be calculated along a specified line and displayed in both tabular and graphical formats. The magnetic field may also be calculated on a designated plane orthogonal to one of the coordinate axes (X-Y, X-Z, or Y-Z planes), and contour line maps can be constructed.

Table A2-3 Applet Descriptions (Continued)

Applet No.	Applet Name and Description
EMF-8	***Magnetic Induction in Wires Parallel to Transmission Lines*** This applet calculates: • The currents induced in the shield wires when the shield wires are grounded at every tower. The calculations assume that the line is infinitely long in both directions from the point of calculations and that the ground resistance is the same for all towers. In these conditions the current flowing from shield wires to ground at each tower is zero. • The voltages induced between the end of a shield wire section and a tower when the shield wires are sectionalized to avoid current flow. The wires are grounded at one tower and insulated from all the other towers to which the shield wire section is attached. A voltage will exist at the end of the shield wire section between each shield wire and the tower. • The currents induced in shield wires that are grounded at every other tower and isolated and transposed at intermediate towers. A voltage will exist between ground wires and tower at the transposition tower. The calculations assume that the line is infinitely long in both directions from the point of calculations and that the ground resistance is the same for all towers. In these conditions the current flowing from shield wires to ground at each tower is zero. • The voltage induced between ground and the end of a wire strung in the general direction of the transmission line and grounded at the other end. The user must choose which of the above calculations is desired. Calculations are made for the power frequency (50 Hz or 60 Hz). Calculations can be made for any type of line (one or more circuits) in the transmission corridor. Calculations assume all the conductors parallel to each other and to a conductive earth. The earth resistivity must be specified.
EMF-9	***Distant Magnetic Field Equations for Transmission Lines*** This applet calculates the magnitude of the basic elements to which a set of current carrying conductors can be reduced for the purpose of assessing the magnetic field produced. Appendix 2 of Chapter 7 discusses definitions, properties, and methods of calculations of the basic elements: monopole, dipole, and quadrupole. The field produced by each of the basic elements has a different law of decay. For instance, a monopole produces a magnetic field inversely proportional to the distance, equal to $B_M = 2M/R$, where B_M is the magnetic field (mG), M is the magnitude of the monopole (A), and R is the distance from the center of the set of wires to the measuring point (m). A dipole produces a field that decays much faster, being inversely proportional to the square of the distance. The dipole field is $B_D = 2D/R^2$, where D is the magnitude of the dipole (A·m). A quadrupole field decays even faster, the field being equal to $B_Q = 4Q/R^3$, where Q is the magnitude of the quadrupole (A·m^2). These calculations are useful to determine which basic element has the largest effect at a given distance from the line, so that an appropriate field reduction method may be applied. Calculations can be made for any set of parallel current-carrying conductors with a known current (magnitude and phase angle) and location in space. The total magnetic field produced by the set of line currents is equal to the vectorial sum of the field produced by the basic elements (monopole, dipole, and quadrupole). However, the total field is not calculated by the applet, since it depends not only on the distance but also on the direction of the line connecting the point of measurements with the center of the set of line currents. This direction does not affect the magnitudes of the basic elements but affects their relative phase angle and direction in space. The best estimate of the total field is the square root of the sum of the squares of the magnitudes of the fields produced by the basic elements.

Table A2-3 Applet Descriptions (Continued)

Applet No.	Applet Name and Description
EMF-10	***Electric Field Induction in Objects*** This applet calculates the short–circuit current and the capacitance to ground of conductive objects placed in a transmission line environment. These issues are discussed in Section 7.8 of the Reference Book. The short-circuit current is the current that would flow in a zero-resistance connection between object and ground. The capacitance of the object to ground is calculated as if the object were perfectly insulated from ground. The objects may be located in an electric field created by high voltage conductors. In this case the geometry and voltage of these conductors must be specified. The objects may also be placed in an unperturbed (before the introduction of the objects) uniform electric field w/o the need to specify the geometry and voltage of the source of the field. If the electric field is created by energized objects, the short circuit currents and the capacitances to ground will be calculated for all the objects at ground potential ($V = 0$). If the user specifies a uniform electric field, calculations will be performed considering all the objects at ground potential (including those to which a voltage is assigned). Objects are simulated by sets of cylindrical segments at the same potential and the 3-D electric field problem is solved. The charges on each object are calculated and from them short-circuit currents and capacitances. This applet is ideal for three-dimensional objects, for high voltage conductors that have sags (transmission line conductors), or have an irregular geometry (line angles, crossing lines), and when there are other shielding objects present. The most challenging task for the user is the simulation of complex three-dimensional objects using cylindrical segments. This issue is discussed in Section 7.3. Building an object may be a laborious task. The applet provides the tool to save, for future use, the data that define an object.
EMF-11	***Magnetic Field Reduction Using Cancellation Loops (3-D)*** This applet calculates the magnetic field at desired locations before and after the application of conductors arranged to form loops where currents will be induced by field sources such as transmission lines. The induced currents may have the effect of producing a magnetic field that tends to cancel the source field, hence the name "cancellation loop." The source of the field may be one or more transmission lines, or any current carrying conductor, or substation buses, or coils. The cancellation loops are formed by conductor segments that form the so-called "passive network." This applet accepts not only straight conductors, but also conductors that have sags (transmission line conductors), or are not parallel to each other (transposition spans), or are at an angle with each other (substation buses). The magnetic field is calculated along a straight segment or on a plane grid, both with and without the passive network
EMF-12	***Magnetic Field Reduction Using 4th-Wire Scheme*** This applet calculates the magnetic field reduction that can be achieved by adding a fourth wire connected to one of the phases of a thee-phase line. This method of field reduction is discussed in Section 7.17.7 of the Reference Book. Examples of possible geometries for this scheme are shown in the figure of the applet window. The phases are designated as A, B, and C. The fourth wire is connected in parallel to phase A. The applet applies to the field inside a calculation area adjacent to the line. The problem is treated as a 2-D problem. The phase currents are assumed balanced and symmetric.
G-1	***Unit Converter*** This applet allows the user to make conversion of the value of a physical quantity into another—for instance, from milligauss to tesla and vice versa, or from kcmil to square millimeters and vice versa.

Table A2-3 Applet Descriptions (Continued)

Applet No.	Applet Name and Description
G-2	***World Map of Ground Flash Density and North America Map of Earth Resistivity*** This applet provides data on a parameter that is very important for the calculation of lightning performance of transmission lines: the lightning flash density, which is the number of lightning flashes that hit the earth (or objects on the earth) per unit area (one square kilometer) and time (one year). The lightning flash density is provided for the entire world. The applet calculates the lightning flash density from optical transient density data provided by Optical Transient Detectors installed onboard of low-earth orbit satellites. Optical transient detectors measure both inter-cloud and cloud-to-earth lightning. The best estimate of ground flash density is obtained by dividing by 3.0 the density obtained by the optical transient detector. The applet uses data obtained by counting the lightning flashes occurring in cells 0.5° of latitude wide and 0.5° of longitude high over a period of several years in a range of latitudes, from –70 to +80 degrees. A discussion of these data is included in Chapter 6. To smooth the roughness of the original data and to avoid discontinuities, the applet takes an appropriate average of the data for the cell of the selected location and a number of adjacent cells. This applet also provides the earth resistivity for locations in North America. The resistivity data are estimates for the near-surface layer of earth and are useful for the analysis of lightning surges and radio noise signal propagation at frequencies up to 1 MHz. The data cannot be used to estimate the resistivity of the soil near tower footing; this resistivity is affected by local conditions and must be determined by special tests of the soil near each tower. The main purpose of the resistivity map is to indicate the overall resistivity in an area, and in this regard it is better than a map of rock types. The original data from which the applet is based consisted of a limited number of equi-resistivity lines defined as a series of points with given latitudes and longitudes. From these data, the resistivity in all points of a grid with 0.5 X 0.5 degree mesh size was calculated using special software. The applet calculates the resistivity at any specified location by interpolating the data for the four closest nodes of the mesh.
I-1	***Insulator Equivalent Salt Deposit Density (ESDD) and Parameter Evaluation*** This applet calculates the leakage length, surface area, and form factor of an insulator, given its profile. Top and bottom surface parameters can be evaluated separately. The applet also guides the user to the measurements of ESDD and NSDD (Non-Soluble Deposit Density) and their calculation. The recommendations for measurements and calculations are made according to international practice using the methods described in Appendix 1 of the Help file (Leakage Length and Form Factor) and Appendix 2 of the Help file (Measurements And Calculations of Equivalent Salt Deposit Density [ESDD] and Non-Soluble Deposit Density [NSDD]).
I-2	***Electric Field Distribution for Polymer Insulators—Effect of Dimensions and Location of Corona Ring*** This applet calculates the electric field in the space near the end fittings of a polymer insulator. This parameter is important when applying polymer insulators. In fact the electric field needs to be kept below certain limits in order to eliminate corona under dry conditions, reduce corona and arcing under wetting conditions as these aging mechanisms reduce life expectancy, and prevent internal discharges due to defects or voids that may initiate a failure mode. The factor that dominates the application and design of corona rings is the electric field magnitude on the surface of the sheath close to the energized end region. If the electric field in this region exceeds a critical value, excessive corona activity can occur under wetting conditions, resulting in premature degradation of the rubber and reduction in life expectancy. The applet solves the field problem in 3-D. It accounts for a single conductor, which must be sufficiently long so that the end effects do not affect the region near the insulator. Both energized and grounded end fittings can be simulated, as well as the tower truss from which the insulator may be suspended. The corona ring is simulated by a toroid. This applet does not account for the dielectric properties of the rubber or rod, and is intended only as an educational tool for the user. The user may change the position and dimensions of a corona ring and observe how the electric field distribution surrounding the NCI's end fitting is affected.

Table A2-3 Applet Descriptions (Continued)

Applet No.	Applet Name and Description
I-3	***Statistical Method for Dimensioning Insulators to Meet Contamination Flashover Requirements*** This applet applies a statistical method to evaluate the risk of flashover of a specific insulator design at a site with a given contamination severity. As input data, the applet requires the statistical parameters that characterize the contamination severity of the site, the statistical and mathematical parameters that characterize the flashover performance of the insulator selected for the site, and the number of insulators. Based on the risk of flashover, calculated by the applet, the insulator creepage distance can be adjusted until the desired performance is achieved. The algorithms used by the applet are an implementation of statistical method discussed in Section 4.8.5. The input data used in the demonstration example of the applet is the same as was used to derive Figures 4.8-20, 4.8-21, 4.8-22, and 4.8-23.
IC-1	***Insulation Coordination: Comparative Evaluation of Insulation Distance Requirements*** This applet calculates the strike distance at the tower dictated by different requirements. The applet compares the strike distances resulting from design specifications regarding power frequency (insulator contamination), switching surges, lightning, and the U.S. National Electrical Safety Code (NESC). The user may set the design specifications: contamination level, ceramic or polymer insulators, switching surge level, number of towers, admissible switching surge flashover rate, lightning flash density, footing resistance, and admissible lightning flashover rate. The applet will show graphically for maximum system voltages from 200 to 1200 kV the strike distances conductor-to-tower that are required to meet the various specifications. The algorithms used for the calculation of strike distance are described in the Appendix of the Help file of this Applet. This applet uses simple algorithms. The user who desires a more in-depth analysis for a specific stress should refer to the relevant chapters or to more specific and detailed Applets.
IC-2	***Risk of Failure*** This applet calculates the risk of failure of a transmission line due to overvoltages. The risk of failure is defined as the probability of an unwanted flashover of any insulation element of the transmission line when an overvoltage occurs—for instance, as a result of a switching operation. The risk of failure may be expressed as expected flashovers for a given number of operations or as expected number of operations that result in one flashover. Only three-phase lines and only phase-to-ground flashovers are considered. It is implicitly assumed that the risk of phase-to-phase flashover is much lower. The user must input all the parameters that affect the risk of failure, which are: the statistical distribution of the overvoltage amplitudes, the statistical distribution of the overvoltage waveshapes, the statistical distribution of the weather conditions, the strength of each insulation element type, and the number of insulation elements for each type The applet calculates the risk of flashover for the entire line and for each phase and each line section individually. The user may assess the effect of overvoltage waveshape by comparing the results with those obtained if all the overvoltages had critical waveshape.

Table A2-3 Applet Descriptions (Continued)

Applet No.	Applet Name and Description
L-1	***Transmission Line Lightning Performance*** This applet calculates the expected number of transmission line flashovers caused by lightning. The lightning flashover performance is defined as the number of expected flashovers per 100 km of line and per year. Flashovers are divided in two categories: flashovers caused by shielding failures and backflashovers. A shielding failure occurs when the lightning hits a phase conductor without being intercepted by a shield wire. Depending on the magnitude of the lightning current a shielding failure may result in enough voltage on the phase conductor to cause a flashover of the insulators. A backflashover may occur when the lightning hits a shield wire or a tower. The lightning current causes voltages between tower crossarms and phase conductors. These voltages, which occur across insulators and air gaps, may be sufficiently elevated to cause a flashover. This applet calculates also the expected number of flashovers for each individual phase as well as the total number of flashovers. The user must define the geometry of the transmission line phase conductors and shield wires, the characteristics of the tower, and the ground flash density. The characteristics of the tower include the tower surge impedance, tower height, tower footing resistance, and crossarm locations. The tower surge impedance may be calculated using Applet L-5, the footing resistance of some type of ground electrodes may be calculated with Applet L-6. The probability, P, of occurrence of a stroke current with a current magnitude equal or exceeding a given crest value, I (kA), is calculated using the equation: $1/P = 1 + (I/31)^{2.6}$. The chance of a lightning hitting a phase wire or a shield wire is evaluated using the method of maximum heights described in Chapter 6. The applet recommends the strike distance equation $S = Ah^B I^C$ with $A = 10$, $B = 0$, and $C = 0.65$, but gives the user the option to change the coefficients A, B, and C. The strike distance to ground is considered equal to βS, with the coefficient $\beta = 0.95 - 0.0046\ (h\text{-}12)$. The algorithms used to calculate the chance for a backflashover are described in Chapter 6 and, in greater detail, in the Help file of this Applet.
L-2	***Stoke Attraction Model*** This applet graphically shows the randomness of the lightning path and the effect of line geometry on the chances lightning will hit the phase wires rather than the shield wires or the ground. Exercising the applet may help to appreciate the effect of the physical parameters that are at the basis of the lightning model. The user enters line geometry and terrain tilt, and may modify the physical parameters governing lightning initiation, progression, and final jump (unless the proposed default values are accepted). The applet shows the path of lightning in a plane orthogonal to the transmission line from the cloud to the hit point. The user may adjust the starting point horizontal coordinate of the downward leader and the stroke current. The user may run the calculation again and again and obtain a different path each time. Each path will be different from the previous due to the randomness of the lightning process that is modeled by the applet. The randomness of the downward and upward leaders may be eliminated by choosing straight rather than random leader progression. The user can run the applet several times and make a visual assessment of how likely the lightning is to strike any given wire. The applet includes a provision for applying automatically 100 consecutive strokes from the same leader starting point, a provision for varying the downward leader starting point, and a provision for either selecting a fixed crest value of the current or a number of crest values evenly distributed within the range of probability of occurrence. The number of strikes to phase conductors, to shield wires, and to the ground are counted and shown. The applet is based on the model presented in Chapter 6. The following physical parameters are used: • Average Electric Field between cloud and earth at leader initiation. Default value = 15 kV/m • Charge per unit of length of the leader and per crest current. Default value = 15 μC / (m • kA) • Critical gradient at wire corona wall. Default value = 30 kV/cm • Ratio between the velocity of the upward streamer and that of the downward leader. Default = 2. • Critical earth field = 400 kV/m In addition, the user may choose any of three different algorithms for initiation of upward streamers from line conductors.

Table A2-3 Applet Descriptions (Continued)

Applet No.	Applet Name and Description
L-3	***Tower Footing Dynamic Resistance (For Vertical Rods)*** This applet calculates the resistance of ground electrodes of transmission-line towers when lightning currents flow from tower to earth. The resistance is often calculated for low-currents (i.e., currents that are not large enough to cause ionization of the earth near the electrodes). When ionization occurs, the resistivity of earth in the region where ionization occurs changes with time and with current. This applet accounts for earth ionization and calculates the dynamic resistance, so called because it changes with time as the current varies and may exceed values that cause earth ionization. The effect of earth ionization is very complex and is treated differently by different investigators. This applet compares the results obtained by applying the method developed by Liew-Darveniza with that developed by Korsuncev. These issues are described in Chapter 6. The algorithms used are presented in the Help file of this Applet. Only one type of ground electrode is considered: single or multiple interconnected vertical rods of equal or different lengths and diameters. The applet requires as input the current flowing in the ground electrode. The current shape is double exponential with front and tail times that can be set by the user. The user must set the peak value of the current and the resistivity of the soil. Only one-layer soil with uniform resistivity is considered. In addition, the user may set some of the physical parameters that characterize the soil: critical ionization gradient, and earth ionization and de-ionization time constants. The output of the applet is the resistance of the electrode to earth versus time. The input current is plotted together with the resistance calculated with both methods. The voltage between electrode and earth is also calculated and plotted.
L-4	***Tower Lightning Flashover Tutorial*** This applet calculates the currents and voltages that characterize the process of tower insulation flashover due to a lightning stroke that hits the tower. The applet is tutorial in nature, because it allows the user to verify in a friendly graphical way the effect of several physical parameters (Stroke Peak Current, Stroke Waveshape, Maximum Stroke Steepness, Tower Height, Tower Surge Impedance, Shield Wire Surge Impedance, Tower Footing Resistance Characteristics, Location of Phase Conductor in relation to the ground wire hit by lightning, Height of the Crossarm to which the insulators are attached, Insulator String Length, and Span Length) on the currents and voltages (current down the tower, voltage between tower top and earth, voltage between tower base and earth, voltage across the phase insulator) and on the disruptive effect on the insulators (an index that expresses the possibility of insulator flashover). The algorithms used are described in Chapter 6 and, in greater details, in the Help file of this Applet.

Table A2-3 Applet Descriptions (Continued)

Applet No.	Applet Name and Description
L-5	***Tower Surge Impedance*** The purpose of this applet is to determine the equivalent surge impedance of a tower to be used in more simple models for lightning flashover calculations (Applet L-1 and Applet L-4) and to show how this surge impedance depends on the geometry of the tower. This applet calculates in great details the surge response of a transmission tower when a unit current step is injected at the top of the tower where a shield wire is attached. It is assumed that the lightning hits a shield wire and the stroke current comes from the span (horizontal stroke). The surge response for a specified intersection between tower members (node) is defined as the voltage between that node and earth and is expressed in V/A, as if it were impedance. In particular, the applet calculates the surge response for the tower element to which the shield wire hit by lightning is connected (Tower Top) and for the tower element in direct contact with the ground electrode (Tower Base). The applet calculates also the voltage between tower top and tower base. In addition to the response to a step unit current, the applet calculates the response of the tower to a variety of current waveshapes (CIGRE first stroke, Heidler waveshape, and ramp function). In these cases, the tower response is expressed in voltage per peak current (V/A). The tower voltage varies in time because of the propagation of the current surge down the tower and the various reflections and refractions that take place at each discontinuity between tower segments. Given an appropriate description of the tower segments, this applet calculates the tower surge response to a given injected current versus time for the duration of 12 μs. In simple models used for lightning flashover calculations, a tower is characterized by a surge impedance, Z_{tw}, and by the height of the tower top, H_{tw}, above ground. Calculations of voltages are then performed by substituting the tower with an inductance $L_{tw} = Z_{tw} \cdot H_{tw}/c$ (c is the speed of traveling waves = 300 m/μs). The simple models, however, do not give the same answer as the more elaborate model used in this applet. This applet calculates the surge impedance that would give in the simple model the same value of the maximum voltage between tower top and tower base as the elaborate model used in this applet, when the same current waveshape is applied and the same values of shield wire surge impedance and tower footing resistance are used. In reality, the equivalent surge impedance so defined depends a little also on current waveshape, shield wire impedance, and footing resistance. The applet gives the user a chance to see the effect of these parameters. The tower surge impedance and the transfer functions are calculated using a special iterative method for lattice diagrams, discussed in the Help file of this Applet. The impedance of each tower section is estimated based on its size and its height above ground. The problem is approached as if the segments of the tower were laid out horizontally with a horizontal direction of wave propagation as in a transmission line. This is one of the models described in Chapter 6. Reflections from adjacent towers are neglected because they usually do not affect the peak tower top-to-base voltage. Once the transfer function (response to a unit current step) for a tower node is known, the voltage between that node and earth caused by a lightning current of any shape is calculated by convolution of the transfer function with the current wave. The applet performs this operation for some typical waveshape (CIGRE first stroke, Heidler waveshape with any specified maximum steepness of the current wave, and ramp function with any specified ramp steepness). The applet accounts for possible connections to one or more ground wires. The base of the tower is connected to a footing resistance, which may be specified by the user. The footing resistance is assumed constant with time.

Table A2-3 Applet Descriptions (Continued)

Applet No.	Applet Name and Description
L-6	***Step and Touch Potential*** This applet calculates: 1. The low-frequency no-ionization resistance of ground electrodes of transmission-line towers composed of conductive cylindrical wires or rods buried in the ground. 2. The resistance of ground electrodes when ionization is present (dynamic resistance) calculated using Korsuncev method (see Chapter 6). Also calculated is the parameter *S* needed by the Korsuncev method. This resistance is a function of the current. 3. The potential of points on the ground with respect to earth when lightning current flows from tower to earth. The potential is calculated for the no-ionization case and is expressed as a percentage of the tower base-to-earth voltage. 4. The step potential at points on the ground when lightning current flows from tower to earth. The step potential is calculated for the no-ionization case and is expressed as a percentage of the tower base-to-earth voltage. 5. The maximum touch potential for the ground electrode when lightning current flows from tower to earth. The touch potential is calculated for the no-ionization case and is expressed as a percentage of the tower base-to-earth voltage. 6. The step and touch potential reduction factor due to soil ionization. The resistance is first calculated for low frequency (i.e., propagation in the earth is assumed to be faster than the variations of the current) and for low currents (i.e., currents that are not large enough to cause ionization of the earth near the electrodes). When ionization occurs, the earth resistivity in the region where ionization occurs will decrease, and the step and touch potentials will decrease as well. Therefore, the no-ionization assumption results in conservative values of step and touch potentials when they are expressed as a percentage of the tower base voltage. Step and touch potential are defined and described in Chapter 6. Step potential refers to the voltage between two points on the ground distant 1 m from each other. Touch potential refers to the voltage between the electrode and a point at a distance of one meter from the electrode. Potentials and step potential are calculated at any desired point, or along a straight line defined by the user, or in a rectangular area defined by the user. The applet can provide contour maps of the step potential. The basic concepts are discussed in Chapter 6; the algorithms on which this applet is based are presented in the Help file.
M-1	***Minimum Approach Distance*** The Minimum Approach Distance (MAD) is the closest distance that a qualified employee is permitted to approach either an energized or a grounded object, as applicable for the work method being used. The distance is to be measured from the body of the worker including any object directly handled. This applet calculates the minimum approach distance given the maximum overvoltage factor for any set of system voltage and other conditions. Conversely, the applet can be used to calculate the maximum overvoltage factor permissible, given a minimum approach distance. If a Portable Protective Air Gap (PPAG) is used on an adjacent structure, instead of the maximum overvoltage factor, the fifty percent flashover voltage of the PPAG must be provided. The user may perform calculations with either of the following two methods: • IEEE method, as described in IEEE Standard 516-2003. • IEC method, as described in IEC Publication 61472, Second Edition, 2004.

Table A2-3 Applet Descriptions (Continued)

Applet No.	Applet Name and Description
RN-1	***Electromagnetic Interference up to 30 MHz*** This applet calculates the electromagnetic interference (EMI) produced by corona on high-voltage transmission lines. The wideband method of EMI calculation is used. This method does not incorporate the approximations used by the traditional method of radio noise calculations: quasi-TEM modes of propagation, and quasi-static methods of field calculations. Therefore, the results are valid in the entire MF and HF frequency ranges from 300 kHz to 30 MHz. The results consist in the median EMI during measurable rain (L_{50} rain). The EMI is calculated as an electric field (dB above 1 μV/m), read either by a rod or a loop antenna. The location of the measuring point is not confined to points close to the ground as in the traditional radio noise calculation method, but can be also above the conductors. The conductors are treated as if they were infinitely long and parallel to a flat conductive earth. Any number of circuits may be considered, and the voltages do not have to be symmetric. Each phase may have a different bundle, whose geometry must be specified. The conductors are assumed to be ACSR. Ground wires are considered in the calculation of the surface gradient of phase conductors, but are otherwise neglected in the EMI calculation. The applet calculates the excitation function of each phase based on the bundle geometry, the maximum surface gradient, and the altitude above sea level. The excitation function is then used to calculate the EMI accounting for line geometry, measuring frequency, earth resistivity, and earth dielectric constant. The EMI lateral profile is calculated along a specified line orthogonal to the line.
RN-2	***EMI Calculations Using Empirical Method*** This applet calculates the electromagnetic interference (EMI) caused by corona on high-voltage transmission lines at different distances from the line. The EMI is calculated in terms of electric field expressed in decibels above 1 μV/m. The algorithms for the calculations are described in Section 9.5.3 (for frequencies up to 30 MHz) and Section 9.6.3 (for frequencies above 30 MHz). EMI is calculated for fair weather and for rain. In both cases, average values are given. The applet calculates the lateral profile of EMI and also the EMI generated by individual bundles in the reference condition (1MHz, 15 m laterally, quasi-peak detector, 9 kHz bandwidth) so that the bundle that most contributes to the EMI could be assessed. The user must specify the interval of distances from the line, the number of segments in which this interval is divided, and the height above ground at which the antenna measuring EMI is located. The user must also specify the altitude, the ground resistivity, the type of detector (quasi-peak, peak, rms, or average) and its bandwidth. However, for QP only the single bandwidth of 9 kHz is allowed for frequencies from 150 kHz to 30 MHz. From 30 MHz to 1 GHz the QP bandwidth is 120 kHz. These fixed bandwidths are according to CISPR specifications as shown in Table 9.4-1. Any bandwidth can be specified for average, rms and peak detector calculations. The applet calculates EMI for single conductors or regular bundles (i.e., bundles for which the conductors are placed on the vertices of a regular polygon). The conductors are treated as if they were infinitely long and parallel to a flat earth.

Table A2-3 Applet Descriptions (Continued)

Applet No.	Applet Name and Description
RN-3	***EMI Base Case Curves and Effect of Line Parameters*** This applet calculates the Electromagnetic Interference (EMI) level for a number of transmission line configurations considered as base cases from 230 to 1100 kV. The base case configurations include single and double circuits, flat, delta, and vertical configurations. In total, 24 base case configurations are considered. The user can select a base case by choosing the voltage (230, 345, 500, 765, or 1100 kV), the number of circuits (single or double), and the configuration (Flat, Delta, Single Pole Triangular, Vertical Low-Reactance, or Vertical Superbundle). The parameters of the selected base case configuration will appear as a default. The user can either accept them or edit them. They include: voltage, line geometry, bundle geometry, ground wire geometry, measuring point, measuring frequency, and antenna characteristics. Altitude above sea level is assumed to be between 0 and 300 m. The calculated EMI levels are the average value during fair weather and the average value during measurable rain. Calculations are made according to empirical methods (one for measuring frequencies up to 30 MHz, and one for frequencies above 30 MHz) described in Chapter 9 and which can be exercised in more details and for different types of lines with Applet RN-2 (EMI Calculations Using Empirical Method). Calculations giving EMI in fair weather and EMI during rain are made for the parameters selected by the user. In addition, the applet shows how EMI varies as a specific parameter is varied (Sensitivity Analysis). The user must specify the desired parameter and the range of values between which the parameter is allowed to vary.
RN-4	***Traditional Radio Noise Calculation Method*** This applet calculates the radio noise produced by corona on high-voltage transmission lines using the traditional method that has evolved over a period of several decades with contributions and refinements by several researchers. This method incorporates approximations (TEM modes of propagation, quasi-static methods of field calculations) that limit its application to frequencies less than 1.6 MHz, to distances from the line not much greater than a quarter of the wavelength, and to points near ground level. The method is described in the second edition of the Transmission Line Reference Book. All the algorithms are described in detail in the Appendix at the end of the Help file of the applet. In order to overcome the limitations of the traditional method, Dr. Robert Olsen has developed the wideband method of EMI calculations, which is the basis for Applet RN-1. The results of this applet consist in the median Radio Noise during measurable rain (L_{50} rain). The Radio Noise is calculated as an electric field (dB above 1 μV/m) read either by a rod or a loop antenna with a CISPR quasi-peak detector with a 9 kHz bandwidth. The conductors are treated as if they were infinitely long and parallel to a flat conductive earth. Any number of circuits may be considered, and the voltages do not have to be symmetric. Each phase may have a different bundle, whose geometry must be specified. The conductors are assumed to be ACSR. Ground wires are considered for the calculation of the surface gradient of phase conductors and for the propagation of radio noise currents and voltages along the line. The applet calculates the excitation function of each phase based on bundle geometry, surface gradient, frequency, and altitude above sea level. The excitation function is given for a CISPR quasi-peak detector with a 9 kHz bandwidth. The excitation function is then used to calculate the Radio Noise accounting for line geometry, measuring frequency, earth resistivity, and earth dielectric constant. The Radio Noise profile is calculated along a specified horizontal line perpendicular to the transmission line.
S-1	***Switching Surge Flashover Model*** This applet calculates the 50% flashover voltage, V_{50}, of air gaps of complex geometry when stressed with switching impulses of positive polarity and critical time to crest. Chapter 5 reports V_{50} data for several gaps with simple geometry (rod-plane, rod-rod, conductor-plane, conductor-tower truss, etc). This applet extends the calculations to any type of air gap. The algorithms used are described in Chapter 5, Appendix 2 of the Reference Book, and in greater detail in the Help file of this applet.

Table A2-3 Applet Descriptions (Continued)

Applet No.	Applet Name and Description
S-2	***Risk of Failure Calculation for Transmission Line Switching Surges*** This applet calculates the risk of flashover of a transmission line due to switching surges. The risk of flashover is defined as the probability of an unwanted flashover of any insulation element of the transmission line when a switching operation is made. The risk of flashover may be expressed as expected flashovers per number of operations or expected number of operations that result in one flashover. Only three-phase lines are considered. Only phase-to-ground flashovers are considered. It is implicitly assumed that the risk of phase-to-phase flashover is much lower. The user must input all the parameters that affect the risk of flashover are: • The statistical distribution of the surge amplitudes • The statistical distribution of the surge waveshape • The statistical distribution of the weather conditions • The strength of each insulation element type and the number of insulation elements for each type The applet calculates the risk of flashover for the entire line and for each phase and each line section individually. The user may assess the effect of surge waveshape by comparing the results with those obtained if all the surges had critical waveshape.
S-3	***Calculation of 50% Flashover Voltage and Standard Deviation from a Set of Test Data*** This applet calculates the two parameters that characterize the strength of a self-restoring insulation element, such as an insulator string or an air gap, subject to a series of impulses (or, in general, voltage applications), each with a known crest voltage and each resulting either in a withstand or in a flashover. The two characteristic parameters are the 50% flashover voltage, V_{50}, and the standard deviation, σ. V_{50} is the crest voltage of the impulse that has a 50% chance to cause a flashover. σ is the standard deviation of the function, $P(V)$, that defines the probability of flashover versus the crest voltage. These parameters are calculated with the assumption that the function $P(V)$ is Gaussian (see Chapter 5). The input data to the applet are the results of a series of voltage applications (i.e., for each application the crest voltage and the outcome [withstand or flashover]). This applet can be used to evaluate the result of a traditional series of tests (n impulses per level and m levels), or an up and down method (see Chapter 5), or any random sequence of voltage applications. In addition, this applet calculates the lower and upper limits of the 95% confidence intervals of V_{50} and σ. The method used for the calculations is the Method of Maximum Likelihood.

Table A2-4 Index of Applet Calculations

Calculation	Applet	Chapter
AAAC Conductors	CC-4	2
AAC Conductors	CC-4	2
ACAR Conductors	CC-4	2
ACSR Conductors (North America, British, IEC, EHS, TW)	CC-4	2
Altitude Effect on Electromagnetic Interference (EMI)	RN-2	9
Antenna Height Effect on Electromagnetic Interference (EMI)	RN-2	9
Asymmetric Bundles, Audible Noise (dbA)	AN-1	10
Asymmetric Bundles, Optimum Geometry for Minimum Audible Noise (dbA)	AN-3	10
Audible Noise (dbA) of High Voltage Transmission Lines (2-D)	AN-1	10
Audible Noise (dbA) of High Voltage Transmission Lines (3-D)	AN-2	10
Audible Noise (dbA) of High Voltage Transmission Lines versus Rain Rate	AN-6	10
Audible Noise Hum Generated by High Voltage Transmission Lines	AN-4	10
Audible Noise of Base Case Lines	AN-5, BC-1	10, A1
Audible Noise of High Voltage Transmission Lines versus Diameter (of Conductor or Subconductor)	AN-5	10
Audible Noise of High Voltage Transmission Lines versus Ground Wire Parameters	AN-5	10
Audible Noise of High Voltage Transmission Lines versus Height of Conductors above Ground	AN-5	10
Audible Noise of High Voltage Transmission Lines versus Lateral Distance	AN-5	10
Audible Noise of High Voltage Transmission Lines versus Measuring Frequency	AN-5	10
Audible Noise of High Voltage Transmission Lines versus Number of Subconductors	AN-5	10
Audible Noise of High Voltage Transmission Lines versus Subconductor Spacing	AN-5	10
Audible Noise of High Voltage Transmission Lines versus Phase Spacing	AN-5	10
Average Surface Gradient of conductors of High Voltage Transmission Lines in 2-D (or of set of infinitely long parallel overhead energized conductors)	CC-1, RN-4	2, 9
Average Surface Gradient of conductors of High Voltage Transmission Lines in 3-D (including conductors with sag, nonparallel to each other, or near grounded objects)	CC-2	2
Backflashover (Minimum current for a backflashover)	L-1	6
Backflashover (Minimum current for a flashover after a shielding failure)	L-1	6
Backflashover Rate	L-1	6
Bandwidth Effect on Electromagnetic Interference (EMI)	RN-2	9
Base Case Line Electrical Performance	BC-1	A1
Base Case Line Geometry	BC-1	A1
Bundle Diameter, Optimum Bundle Diameter for Minimum Audible Noise (dbA)	AN-3	10
Bundle Geometry for Minimum Audible Noise (dbA)	AN-3	10
Capacitance Matrix	RN-4	9
Capacitance of a conductive object to ground	EMF-10	7
Capacitive Reactance of Conductors	CC-4	2
Characteristic Matrix for Modal Propagation at High Frequency	RN-4	9
Conductor Property Tables (ACSR North America, ACSR British, ACSR IEC, ACSR EHS, ACSR TW, ACAR, AAC, AAAC)	CC-4	2
Conductor Resistance, ac and dc, effect of temperature	CC-4	2
Conductor Surface Gradient for High Voltage Transmission Lines in 2-D (or for set of infinitely long parallel overhead energized conductors)	CC-1, RN-1, RN-2, RN-4, AN-1, AN-4, CL-1,	2, 9, 10, 11
Conductor Surface Gradient for High Voltage Transmission Lines in 3-D (or for set of energized cylindrical segments, including conductors with sag, non-parallel to each other, or near grounded objects)	CC-2	2
Conductor Surface Gradient for High Voltage Transmission Lines versus Diameter (of Conductor or Subconductor)	CC-6	2

Table A2-4 Index of Applet Calculations (Continued)

Calculation	Applet	Chapter
Conductor Surface Gradient for High Voltage Transmission Lines versus Ground Wire Parameters (Diameter, Height above Ground, Separation)	CC-6	2
Conductor Surface Gradient for High Voltage Transmission Lines versus Height above Ground	CC-6	2
Conductor Surface Gradient for High Voltage Transmission Lines versus Phase Spacing (Horizontal or Vertical)	CC-6	2
Conductor Surface Gradient for High Voltage Transmission Lines versus Subconductor Spacing	CC-6	2
Conductor Surface Gradient of Base Case Lines	CC-6, BC-1	2, A1
Contamination Flashover Rate	I-3	4
Contamination Severity Probability	I-3	4
Conversion from one measuring unit to another	G-1	——
Corona Inception Gradient of conductors	Co-1	8
Corona Loss for Base Case Lines	CL-2, BC-1	11, A1
Corona Loss in Fair Weather versus Diameter (of Conductor or Subconductor)	CL-2	11
Corona Loss in Fair Weather versus Ground Wire Parameters	CL-2	11
Corona Loss in Fair Weather versus Height of Conductors above Ground	CL-2	11
Corona Loss in Fair Weather versus Lateral Distance	CL-2	11
Corona Loss in Fair Weather versus Number of Subconductor	CL-2	11
Corona Loss in Fair Weather versus Phase Spacing	CL-2	11
Corona Loss in Fair Weather versus Power Frequency	CL-2	11
Corona Loss in Fair Weather versus Subconductor Spacing	CL-2	11
Corona Loss in Heavy Rain for Base Case High Voltage Transmission Lines	CL-2	11
Corona Loss in Heavy Rain versus Diameter (of Conductor or Subconductor)	CL-2	11
Corona Loss in Heavy Rain versus Ground Wire Parameters	CL-2	11
Corona Loss in Heavy Rain versus Height of Conductors above Ground	CL-2	11
Corona Loss in Heavy Rain versus Lateral Distance	CL-2	11
Corona Loss in Heavy Rain versus Number of Subconductor	CL-2	11
Corona Loss in Heavy Rain versus Phase Spacing	CL-2	11
Corona Loss in Heavy Rain versus Power Frequency	CL-2	11
Corona Loss in Heavy Rain versus Subconductor Spacing	CL-2	11
Corona Loss in Rain versus Rain Rate	CL-2	11
Corona Loss of High Voltage Transmission Lines	CL-1	11
Corona Onset Gradient of conductors	Co-1	8
Creepage Distance versus Contamination Severity	I-3	4
Current in a Wire (grounded at one point) electrically induced by an energized circuit	CC-7	2
Currents in De-Energized Circuit (grounded at one point) electrically induced by an energized circuit	CC-7	2
Currents in Shield Wires of high-voltage transmission lines when the shield wires are grounded at every other tower and insulated and transposed at intermediate towers	EMF-8	7
Currents in Shield Wires of high-voltage transmission lines when the shield wires are grounded at every tower	EMF-8	7
Detector Bandwidth and Type Effects on Electromagnetic Interference (EMI)	RN-2	9
Dipolar Magnetic Field produced by a set of line currents	EMF-9	7
Dipole equivalent to a set of line currents	EMF-9	7
Disruptive Effect when a Lightning Stroke Hits a Shield Wire	L-4	6
Dynamic Resistance of Tower Footing	L-3	6
Earth Resistivity North America Map	G-2	——
Earth Resistivity. Effect of Earth Resistivity on Tower Current, Tower Top Voltage, Tower Base Voltage, Tower Top-to-Base Voltage, Insulator Voltage, Disruptive Effect	L-4	6

Table A2-4 Index of Applet Calculations (Continued)

Calculation	Applet	Chapter
Electric Field (rms) of high-voltage transmission lines in 2-D (or of set of infinitely long parallel overhead energized conductors) along a specified line	EMF-2	7
Electric Field (rms) of high-voltage transmission lines in 3-D (or set of overhead energized conductors) along a specified line or on a specified plane	EMF-4	7
Electric Field near Ground for Base Case Lines	BC-1	——
Electric Field near Polymer Insulators	I-2	3
Electric Field on Corona Shield	CC-3	2
Electric Field on Toroids	CC-3	2
Electric Field Profile along a specified line near a shielding grid, 2-D	EMF-5	7
Electric Field Profile along a specified line, 2-D	EMF-2	7
Electric Field Profile along a specified line, 3-D	EMF-4	7
Electrically Induced Currents in de-energized circuit grounded at one point	CC-7	2
Electrically Induced Voltages in de-energized circuit ungrounded	CC-7	2
Electromagnetic Interference (EMI) below and above 30 MHz using empirical method	RN-2	9
Electromagnetic Interference (EMI) of Base Case High Voltage Transmission Lines	RN-3	9
Electromagnetic Interference (EMI) of High Voltage Transmission Lines versus Diameter (of Conductor or Subconductor)	RN-3	9
Electromagnetic Interference (EMI) of High Voltage Transmission Lines versus Ground Wire Parameters	RN-3	9
Electromagnetic Interference (EMI) of High Voltage Transmission Lines versus Height of Conductors above Ground	RN-3	9
Electromagnetic Interference (EMI) of High Voltage Transmission Lines versus Lateral Distance	RN-3	9
Electromagnetic Interference (EMI) of High Voltage Transmission Lines versus Measuring Frequency	RN-3	9
Electromagnetic Interference (EMI) of High Voltage Transmission Lines versus Phase Spacing	RN-3	9
Electromagnetic Interference (EMI) of High Voltage Transmission Lines versus Subconductor Spacing	RN-3	9
Electromagnetic Interference (EMI) up to 30 MHz	RN-1	9
Ellipse (electric or magnetic field ellipse) parameters, given the orthogonal components	EMF-1	7
EMI of Base Case Lines	BC-1	——
Equivalent Salt Deposit Density (ESDD)	I-1	3
Equivalent Single-Conductor Diameter (diameter of the single conductor with the same capacitance as a bundle)	EMF-3	7
Excitation Function (Radio Noise Excitation Function) of Individual Bundles of High Voltage Transmission Lines	RN-4	9
Fair Weather Corona Loss of High Voltage Transmission Lines	CL-1	11
Fifty Percent Flashover Voltage (V50) from a Set of Test Data	S-3	5
Final Jump of a Lightning Stroke Leader	L-2	6
Flash (chance of lightning flashes hitting a phase wire, a shield wire, the ground)	L-2	6
Flash Density World Map	G-2	——
Flashover Probability versus Contamination Severity	I-3	4
Flashover Rate Due to Shielding Failures	L-1	6
Footing Resistance. Effect of Footing Resistance on Tower Current, Tower Top Voltage, Tower Base Voltage, Tower Top-to-Base Voltage, Insulator Voltage, Disruptive Effect	L-4	6
Form Factor (of an insulator)	I-1	3
Frequency Effect on Electromagnetic Interference (EMI)	RN-2	9
Generated Acoustic Power of Individual Bundles of High Voltage Transmission Lines	AN-1	10
Generated Hum Acoustic Power of Individual Bundles of High Voltage Transmission Lines	AN-4	10
Geometric Mean Radius (GMR) of Conductors	CC-4	2
Ground Electrode Dynamic Resistance	L-3	6

Table A2-4 Index of Applet Calculations (Continued)

Calculation	Applet	Chapter
Ground Electrode Resistance with Soil Ionization	L-3	6
Ground Electrode Resistance, Step and Touch Potential (at low-frequency and for no-ionization)	L-6	6
Ground Flash Density World Map	G-2	——
Ground Resistivity Effect on Electromagnetic Interference (EMI)	RN-2	9
Heavy Rain Corona Loss of High Voltage Transmission Lines	CL-1	11
Impedance (Series impedance, Shunt Impedance, Surge Impedance) of a Transmission (Single Circuit, Power Frequency)	CC-5	2
Induced Voltage in wire parallel to a transmission line and grounded at one point	CC-7	2
Induced Voltages in de-energized line grounded at one tower and parallel to an energized line	CC-7	2
Inductive Reactance of Conductors	CC-4	2
Insulation Coordination, Comparative Evaluation of Insulation Distance Requirements	IC-1	4
Insulation Element Number (Effect of number of insulation elements on the risk of failure of a transmission line)	IC-2	4
Insulation Strength (Effect of insulation strength, V50, on the risk of failure of a transmission line)	IC-2	4
Insulator Surface Area (top and bottom)	I-1	3
Irregular Bundles, Audible Noise (dbA)	AN-1	10
Irregular Bundles, Optimum Geometry for Minimum Audible Noise (dbA)	AN-3	10
Korsuncev's S Dimension of a Ground Electrode	L-6	6
Korsuncev's S Dimension. Effect of Korsuncev's S Dimension on Tower Current, Tower Top Voltage, Tower Base Voltage, Tower Top-to-Base Voltage, Insulator Voltage, Disruptive Effect	L-4	6
Lateral Profile of Audible Noise (dbA) in a Transposition Span or to account for 3-D geometry	AN-2	10
Lateral Profile of Audible Noise (dbA)	AN-1	10
Lateral Profile of Audible Noise Hum	AN-4	10
Lateral Profile of Electromagnetic Interference (EMI) up to 30 MHz	RN-1	9
Lateral profile of Electromagnetic Interference (EMI) using empirical method (for frequencies both below and above 30 MHz)	RN-2	9
Lateral Profile of Radio Noise (up to 1.6 MHz)	RN-4	9
Leader Inception Voltage (during switching impulse flashover process) of Air Gaps with Any Geometry	S-1	5
Leakage Distance (of an insulator)	I-1	3
Lightning Flash Density World Map	G-2	——
Lightning Flashes (number of lightning flashes hitting a phase wire, a shield wire, the ground)	L-2	6
Lightning Path (to a transmission line)	L-2	6
Lightning Performance of a Transmission Line	L-1	6
Lightning, Voltages and Currents when a Lightning Stroke Hits a Shield Wire	L-4	6
Loop Antenna, Electromagnetic Interference (EMI) up to 30 MHz measured with a loop antenna	RN-1	9
Magnetic Field (Bmax, i.e. component along major axis of field ellipse) of high-voltage transmission lines in 2-D (or set of infinitely long parallel overhead energized conductors) along a specified line	EMF-6	7
Magnetic Field (rms, resultant) of high-voltage transmission lines in 2-D (or set of infinitely long parallel overhead energized conductors) along a specified line	EMF-6	7
Magnetic Field (rms, resultant) of high-voltage transmission lines in 3-D (or set of energized conductors) along a specified line or in a specified plane	EMF-7	7
Magnetic Field Components along three orthogonal axes for high-voltage transmission lines in 3-D (or for a set of energized conductors) along a specified line or in a specified plane	EMF-7	7
Magnetic Field Contour Lines in a specified plane, 3-D	EMF-7	7
Magnetic Field Contour Lines in a vertical plane, 2-D	EMF-6	7
Magnetic Field of a bus (three-phase)	EMF-7	7
Magnetic Field of a coil	EMF-7	7
Magnetic Field of Base Case Lines	BC-1	——

Table A2-4 Index of Applet Calculations (Continued)

Calculation	Applet	Chapter
Magnetic Field Profile along a specified line, 2-D	EMF-6	7
Magnetic Field Profile along a specified line, 3-D	EMF-7	7
Magnetic Field Reduction caused by a cancellation loop	EMF-11	7
Magnetic Field Reduction caused by currents induced in a passive network	EMF-11	7
Magnetic Field Reduction using the fourth-wire scheme	EMF-12	7
Magnetically Induced Voltage in wire parallel to a transmission line and grounded at one point	EMF-8, CC-7	7, 2
Magnetically Induced Voltages in de-energized line grounded at one tower	CC-7	2
Maximum Axis of (electric or magnetic) Field Ellipse, given the orthogonal components	EMF-1	7
Maximum Corona Loss of High Voltage Transmission Lines	CL-1	11
Maximum Permissible Overvoltage for a Given Minimum Approach Distance according to IEEE and to IEC	M-1	13
Maximum Surface Gradient for High Voltage Transmission Lines versus Diameter (of Conductor or Subconductor)	CC-6	2
Maximum Surface Gradient for High Voltage Transmission Lines versus Ground Wire Parameters (Diameter, Height above Ground, Separation)	CC-6	2
Maximum Surface Gradient for High Voltage Transmission Lines versus Height above Ground	CC-6	2
Maximum Surface Gradient for High Voltage Transmission Lines versus Phase Spacing (Horizontal or Vertical)	CC-6	2
Maximum Surface Gradient for High Voltage Transmission Lines versus Subconductor Spacing	CC-6	2
Maximum Surface Gradient of conductor bundles of High Voltage Transmission Lines in 3-D (including bundle conductors with sag, non-parallel to each other, or near grounded objects)	CC2	2
Minimum Approach Distance according to IEEE and to IEC	M-1	13
Minimum Axis of (electric or magnetic) Field ellipse, given the orthogonal components	EMF-1	7
Modal Propagation Constant (Attenuation and Velocity) at High Frequency	RN-4	9
Modal Surge Impedance Matrix at High Frequency	RN-4	9
Monopolar Magnetic Field produced by a set of line currents	EMF-9	7
Monopole equivalent to a set of line currents	EMF-9	7
Non Soluble Deposit Density (NSDD)	I-1	3
Nonceramic Insulators (Effect of Corona Rings on Electric Field Distribution)	I-2	3
Nonceramic Insulators (Electric Field Distribution)	I-2	3
Overvoltage Magnitude Distribution (Effect of overvoltage distribution on the risk of failure of a transmission line)	IC-2	4
Overvoltage Profile (Effect of overvoltage profile on the risk of failure of a transmission line)	IC-2	4
Overvoltage Waveshape Distribution (Effect of overvoltage distribution on the risk of failure of a transmission line)	IC-2	4
Ozone Concentration near Transmission Lines	CL-3	11
Ozone Generation Rate of Individual Bundles of High Voltage Transmission Lines	CL-3	11
Phase Admittance Matrix at High Frequencies	RN-4	9
Phase Impedance Matrix at High Frequencies	RN-4	9
Phase Surge Impedance Matrix at High Frequency	RN-4	9
Polymer Insulators (Effect of Corona Rings on Electric Field Distribution)	I-2	4
Polymer Insulators (Electric Field Distribution)	I-2	4
Portable Protective Air Gap (PPAG). Maximum permissible 50% flashover voltage of a PPAG allowed to protect a given minimum approach distance	M-1	13
Potential at the earth surface near the Ground Electrode of a structure hit by lightning	L-6	6
Potential Coefficient Matrix	RN-4	9
Quadrupolar Magnetic Field produced by a set of line currents	EMF-9	7
Quadrupole equivalent to a set of line currents	EMF-9	7

Table A2-4 Index of Applet Calculations (Continued)

Calculation	Applet	Chapter
Radio Noise (up to 1.6 MHz) of High Voltage Transmission Lines	RN-4	9
Rain Noise (dbA) versus Rain Rate	AN-6	10
Reactance of Conductors	CC-4	2
Resistance (Dynamic) of Tower Footing	L-3	6
Resistance of a Ground Electrode (at low-frequency and for no-ionization)	L-6	6
Resistance of Conductors, ac and dc, effect of temperature	CC-4	2
Resistance of Tower Footing with Soil Ionization	L-3	6
Resistivity of the Earth, North America Map	G-2	——
Resultant (electric or magnetic), given the orthogonal components	EMF-1	7
Risk of Failure of a Transmission Line Due to Overvoltages	IC-2	4
Risk of Flashover due to Contamination	I-3	4
Risk of Flashover of a Transmission Line Due to Switching Surges	S-2	5
Rms of electric or magnetic, given the rms values of orthogonal components	EMF-1	7
Rod Antenna, Electromagnetic Interference (EMI) up to 30 MHz measured with a rod antenna	RN-1	9
Sequence Impedance Matrix (Single Circuit, Power Frequency)	CC-5	2
Series Impedance Matrix (Single Circuit, Power Frequency)	CC-5	2
Series Impedance Matrix at High Frequencies	RN-4	9
Shield Wire Currents for high-voltage transmission lines when the shield wires are grounded at every other tower and insulated and transposed at intermediate towers	EMF-8	7
Shield Wire Currents for high-voltage transmission lines when the shield wires are grounded at every tower	EMF-8	7
Shield Wire Impedance. Effect of Shield Wire Impedance on Tower Current, Tower Top Voltage, Tower Base Voltage, Tower Top-to-Base Voltage, Insulator Voltage, Disruptive Effect	L-4	6
Shield Wire Voltage to tower for high-voltage transmission lines with shield wires grounded at every other tower, and insulated and transposed at intermediate towers	EMF-8	7
Shield Wire Voltage to tower for high-voltage transmission lines with shield wires sectionalized, grounded at one tower, and insulated from the others	EMF-8	7
Shielding (of electric field) caused by grids of wires	EMF-5	7
Shielding (of electric field) caused by grounded objects	EMF-10	7
Shielding (of magnetic field) caused by cancellation loops	EMF-11	7
Shielding (of magnetic field) caused by currents induced in passive networks	EMF-11	7
Shielding Failure Rate	L-1	6
Short Circuit Current of a conductive object to ground when the object is in a uniform electric field	EMF-10	7
Short Circuit Current of a conductive object to ground when the object is in an electric field of a transmission line	EMF-10	7
Shunt Admittance Matrix at High Frequencies	RN-4	9
Shunt Impedance Matrix (Single Circuit, Power Frequency)	CC-5	2
Single Conductor Equivalent (same capacitance) of a bundle	EMF-3	7
Space Potential Contour Lines in a specified plane, 3-D	EMF-4	7
Space Potential Contour Lines in a vertical plane near a shielding grid, 2-D	EMF-5	7
Space Potential Contour Lines in a vertical plane, 2-D	EMF-2	7
Space Potential near Nonceramic Insulators	I-2	3
Space Potential of high-voltage transmission lines in 2-D (or set of infinitely long parallel overhead energized conductors) along a specified line or on a vertical plane	EMF-2	7

Table A2-4 Index of Applet Calculations (Continued)

Calculation	Applet	Chapter
Space Potential of high-voltage transmission lines in 3-D (or set of energized conductors) along a specified line or on a specified plane	EMF-4	7
Space Potential Profile along a specified line near a shielding grid, 2D	EMF-5	7
Space Potential Profile along a specified line, 2D	EMF-2	7
Space Potential Profile along a specified line, 3D	EMF-4	7
Standard Deviation of Flashover Voltage from a Set of Test Data	S-3	5
Standard Deviation of Insulation Strength (Effect of standard deviation on the risk of failure of a transmission line)	IC-2	3
Standard Deviation of Switching Impulse Flashover Voltage (Effect of standard deviation on the risk of switching surge flashover of a Transmission Line)	S-2	5
Step Potential near the Ground Electrode of a structure hit by lightning	L-6	6
Strike Distance Required by Lightning, Switching, Insulator Contamination, and Electrical Code	IC-1	4
Stroke Current versus Time for a CIGRE First Stroke, a CIGRE subsequent stroke, Heidler Waveshape, and Ramp Function	L-4	6
Stroke Path (Lightning to a transmission line)	L-2	6
Stroke Peak Current. Effect of Stroke Peak Current on Tower Current, Tower Top Voltage, Tower Base Voltage, Tower Top-to-Base Voltage, Insulator Voltage, Disruptive Effect	L-4	6
Surface Gradient of Conductors. See "Conductor Surface Gradient."	——	——
Surface Gradient of Corona Shield	CC-3	2
Surface Gradient of Toroids	CC-3	2
Surge Impedance (of a transmission line tower)	L-5	6
Surge Impedance of a Transmission Line (Single Circuit)	CC-5	2
Surge Impedance of Base Case Lines	BC-1	——
Switching Impulse Flashover Voltage of Air Gaps with Any Geometry	S-1	5
Switching Surge Magnitude Distribution (Effect of surge distribution on the risk of failure of a transmission line)	S-2	5
Switching Surge Profile (Effect of surge profile on the risk of failure of a Transmission Line)	S-2	5
Switching Surge Strength (Effect of V50, on the risk of flashover of a Transmission Line)	S-2	5
Switching Surge Strength of Air Gaps with Any Geometry	S-1	5
Switching Surge Waveshape Distribution (Effect of surge distribution on the risk of failure of a transmission line)	S-2	5
Touch Potential for the Ground Electrode of a structure hit by lightning	L-6	6
Tower Base Voltage versus Time for a Lightning Stroke Hitting a Shield Wire	L-4	6
Tower Current versus Time for a Lightning Stroke Hitting a Shield Wire	L-4	6
Tower Footing Dynamic Resistance	L-3	6
Tower Footing Resistance versus Time (Dynamic Resistance) for a Lightning Stroke Hitting a Shield Wire	L-4	6
Tower Footing Resistance with Soil Ionization	L-3	6
Tower Footing Resistance, Step and Touch Potential (at low-frequency and for no-ionization)	L-6	6
Tower Height. Effect of Tower Height on Tower Current, Tower Top Voltage, Tower Base Voltage, Tower Top-to-Base Voltage, Insulator Voltage, Disruptive Effect	L-4	6
Tower Node Voltage versus Time	L-5	6
Tower Response to Different Stroke Waveshapes (Top Voltage, Base Voltage, Top-to-Base Voltage)	L-5	6
Tower Strike Distance Required by Lightning, Switching, Insulator Contamination, and Electrical Code	IC-1	3
Tower Surge Impedance	L-5	6
Tower Surge Impedance. Effect of Tower Surge Impedance on Tower Current, Tower Top Voltage, Tower Base Voltage, Tower Top-to-Base Voltage, Insulator Voltage, Disruptive Effect	L-4	6
Tower Top Voltage versus Time for a Lightning Stroke Hitting a Shield Wire	L-4	6

Table A2-4 Index of Applet Calculations (Continued)

Calculation	Applet	Chapter
Transmission Line Parameters (Single Circuit)	CC-5	2
Unit Conversion	G-1	——
V50, Fifty Percent Flashover Voltage from a Set of Test Data	S-3	5
V50, Switching Impulse Flashover Voltage, of Air Gaps with Any Geometry	S-1	5
Voltage between an insulated Wire and Ground electrically induced by a high-voltage transmission line	CC-7	2
Voltage between Shield Wire and tower for high-voltage transmission lines with shield wires grounded at every other tower, and insulated and transposed at intermediate towers	EMF-8	7
Voltage between Shield Wire and tower for high-voltage transmission lines with shield wires sectionalized, grounded at one tower, and insulated from the others	EMF-8	7
Voltage between Wire and Ground for a wire parallel to a high-voltage transmission line, grounded at one end and insulated from ground at the other	EMF-8	7
Voltage on Insulators when a Lightning Stroke Hits a Shield Wire	L-4	7
Voltages in de-energized circuit (ungrounded) electrically induced by an energized circuit	CC-7	2
Wire-to-Ground Voltage for a wire parallel to a high-voltage transmission line, grounded at one end and insulated from ground at the other	CC-7, EMF-8	2, 7
Yearly Average Corona Loss of High Voltage Transmission Lines	CL-1	11

Glossary

AAAC. All Aluminum Alloy Conductor.

ACGIH. American Conference of Governmental Industrial Hygienists.

ACSS. Aluminum Conductor Steel Supported. A stranded conductor made up of fully annealed aluminum strands over a core of steel strands.

Active Loops. System of conductors arranged in a path (loop) and supplying an electric current by an external source for the purpose of magnetic field reduction within a region. The geometry of the loop depends on the magnetic field source geometry. To be effective, an active loop system would utilize an active feedback control system to adjust loop current as the magnetic field within the region of interest changes. *See also* **Cancellation Loops** and **Passive Loops**.

Active Shielding. Magnetic fields can be reduced (shielded) by establishing currents in wires such that the fields produced by those currents oppose the fields to be reduced. Active shielding (or shielding with "active" conductors) refers to any scheme to reduce the magnetic field in certain regions of space by use of conductors with an imposed current whose magnitude, direction, and phase angle create fields in opposition to the ambient fields and thereby reduce the overall magnetic field in a region. *See also* **Passive Shielding**, **Shielding**, and **Shielding Factor**.

Activity Factor (for electric field exposure assessment). Ratio between the electric field exposure during an activity and the electric field exposure that would have been measured in a reference condition for the same exposure time and the same unperturbed electric field. The reference condition consists of body erect with arms at sides, person well grounded through the feet on a conductive, flat ground, and uniform unperturbed electric field. *See also* **Equivalent Electric Field**.

Ac (Alternating Current) Transmission. The transfer of electric energy by alternating current from its source to one or more main receiving stations for subsequent distribution.

Aging of Conductor Surface. The process by which the chemical nature and physical properties of a conductor surface are changed. Over time, the surfaces of conductors lose the grease that is normally present on new conductors. The conductor surface becomes hydrophilic, thereby preventing beading of water during wet weather. Instead, the water flows to the bottom of the conductor where it forms a drip line. The rate of conductor aging and the properties of an aged conductor surface depend on the nature of the newly installed conductor and the prevailing weather and environmental conditions. The rate of conductor aging is accelerated by corona.

Airway Lighting. Lights installed on structures according to Federal Aviation Administration regulations to designate flight hazards during darkness.

Airway Marker Ball (*also* Aviation Marker Ball or Aerial Warning Sphere). A colored ball—usually orange, gloss white, or gloss yellow— attached to the conductors or overhead ground wire on a transmission line to increase their visibility.

Airway Marking. The painting of transmission-line structures according to Federal Aviation Administration regulations to designate flight hazards during daylight.

All-Dielectric Self-Supporting Optical Cable (ADSS). Cable containing optical fibers that includes a non-metallic strength member and is designed to be mounted between power line structures.

Alternating Current. An electric current that reverses direction at regular recurring intervals of times.

Ampacity. Current that will meet the design, security, and safety criteria of a particular line on which the conductor is used.

Ampere-Turn. A term in the MKS (SI) system used to describe the magnetomotive force (mmf) in a closed ring solenoid of a uniform cross section. The ampere-turn is the product of the number of turns of wire (enclosed in a

closed integration path) and the electric current in each turn; it is the magnetomotive force (mmf). (The CGS unit of mmf is the gilbert: $4\pi \times 10^{-1}$ gilbert = 1 ampere-turn.) The ampere-turn per meter (mmf per unit length) is the unit of magnetic field strength in the MKS (SI) system.

Ampère's Law. Ampère's law, including an important extension of it made later by Maxwell, is one of the basic equations of electromagnetic field theory. This law equates the magnetic field integrated around a closed contour or loop to the current through the loop (or integral of the current density over a surface bounded by the loop). The connection between the field and the current is described by Ampère's law: $\oint B \cdot dl = \mu_0 I_{enclosed}$. At first glance one would think that the law is used to determine the current, *I*, by integration (indeed, this principle is how a clamp-on ammeter works to measure the current in a conductor). In practice, the current is usually known, and the law provides a method of finding the magnetic field (for more complex problems, the Biot-Savart law is used). The equation above is true, in general, for any magnetic field configuration, for any assembly of currents, and for any path of integration. (For frequencies much higher than 60 Hz, the equation must be modified if a time-varying electric field is present within the path of integration.) *See also* **Maxwell's Equations** and **Quasistatic**.

AM Radio Broadcast Band. A band of frequencies assigned for amplitude-modulated broadcasting to the general public.

Angular Frequency. The angle (radian) of a sinusoidal quantity per unit of time (second). A quantity that varies sinusoidally with time: $q = Q\sin(\omega t + \varphi)$, has an angular frequency, ω, and a frequency $f = \frac{\omega}{2\pi}$.

Annealing. The process whereby the tensile strength of copper or aluminum wires is reduced and ductility is increased at sustained high temperatures.

Anode. An electrode through which current enters any conductor of the nonmetallic class. Specifically, an electrolytic anode is an electrode at which negative ions are discharged, or positive ions are formed, or at which other oxidizing reactions occur. Current flow is from anode to cathode.

Antenna. *See* **Biconical Antenna**, **Dipole Antenna**, **Log-Periodic Antenna**, **Loop Antenna**, and **Vertical Antenna**.

Arrester. *See* **Transmission Line Surge Arrester.**

ASCR. Aluminum Conductor Steel Reinforced.

ASTM. American Society for Testing and Materials.

ATP. Alternative Transient Program, a free derivative of EMTP.

Attachment Coefficient. The probability that a free electron will attach itself to a neutral molecule when moving a unit distance through the gas in the direction of the applied electric field.

Attractive Radius. A model for the final jump process of lightning, whereby radii, depending on stroke charge, current and height, are centered at the upper extremities of grounded objects. A leader that descends uniquely into the attractive radius of an object will terminate onto that object, with a lightning flash and return stroke(s).

Audible Noise (*also* Acoustic Noise). Any undesired sound. A term associated with noise produced by corona from the conductors on overhead transmission lines.

Average Detector. A detector, the output voltage of which is the average value of the magnitude of the envelope of an applied signal or noise. *Note:* (1) This detector function is often identified on radio noise meters as field intensity (FI). (Field Intensity is deprecated; field strength should be used.) (2) The FI (field strength) setting on some radio noise meters produces a reading proportional to the average value of the logarithmic detector output on the meter scale. (3) Radio noise meters of modern design do not have the detector function identified as "FI" or "Field Intensity." Also, modern radio noise meters have true average detector functions, but a few still have average logarithm (sometimes called "carrier") detector functions.

A-Weighted Network. Network incorporated in the design of audible noise meter to adjust the frequency spectrum of the measured sound pressure in order to better correspond to a measure of annoyance. The term *weighted* is used because some frequencies are given more or less importance, or weight, than other frequencies. The A-weighted network gives more weight to frequencies in the 2 to 4 kHz range and less weight to frequencies below 500 Hz. Other networks are the B-, C-, and D- weighting networks. The A-weighted measurements are the most commonly used for environmental noises, and are used also for transmission-line audible noise. Audible noise is commonly expressed in dBA.

A-Weighted Sound Level. A weighted sound-pressure level obtained by the use of a metering characteristic and the weighting "A" specified in USAS S1.4-1961.

AWG. American Wire Gauge, a measure of wire diameter using $D(AWG) = .005 \cdot 92^{((36\text{-}AWG)/39)}$ for wire diameter in inches, with 2/0 being -1, 3/0 being –2, and 4/0 being -3.

Backflash. A lightning flash hitting a tower or the shield wires and creating overvoltages between the (higher potential) tower and the (lower potential) phase conductors.

Backflashover. A lightning flashover event in which a line supporting structure is driven to a very high voltage by a lightning flash to it or a connected shield wire so that a dielectric breakdown initiates at a phase and travels backwards to the support structure metal.

Backflashover Rate (BFR). The rate of occurrence of backflashovers on a transmission line caused by lightning.

Background Noise. Total of all sources of interference in a system used for the production, detection, measurement, or recording of a signal, independent of the presence of the signal. *Note:* Ambient noise detected, measured, or recorded with the signal becomes part of the background noise.

Balanced Currents. A set of conductors whose currents at any instant in time add up to zero is said to have balanced currents. A three-phase electric power transmission line is said to have balanced currents if it is composed only of positive- and negative-sequence symmetric components, without zero sequence components. If the phase currents are balanced and symmetric, they are equal in magnitude and at 120 electrical degrees with respect to each other.

Bandwidth. The range of frequencies within which performance, with respect to some characteristic, falls within specified limits. *See also* **Impulse Bandwidth** and **Random Noise Bandwidth**.

Baseline Information. Information or data that describe the existing physical, biological, and human conditions in an area that would be affected by a development (e.g., utility) project.

BFR. *See* **Backflashover Rate.**

Biconical Antenna. An antenna consisting of two conical conductors that have a common axis and vertex, and are excited or connected to the receiver of the vertex. When the vertex angle of one of the cones is 180˚, the antenna is called a discone.

Biot-Savart Law. Ampère's law can be used to calculate magnetic fields (or flux density) when the geometry of the current carrying conductors is simple to permit the easy evaluation of the line integral $\oint B \cdot dl$. This requirement limits the usefulness of the law in many practical problems. Another approach to computing the magnetic field at a point for an arbitrary charge distribution is to divide the charge distribution into current elements. The law of Biot and Savart is then used to calculate the field (flux density) contribution, dB, due to each current element at the point in question. The law of Biot and Savart may be written in vector form as: $d\vec{B} = \frac{\mu_0 i\, d\vec{l} \times \vec{r}}{4\pi r^3}$

The resultant field at a point is then found by integrating the field (flux density) contributions for the entire charge distribution as follows:

$$B = \int dB$$

The law of Biot and Savart is used to compute the magnetic field at a point for a system of conductors with complex geometry (e.g., the catenary-shaped conductors of a high-voltage transmission line, substation buswork, etc.). *See also* **Ampère's Law**.

Bird Streamers. The excrement of birds that is typically long and thin, sometimes resulting in phase-to-ground line faults on steel lattice transmission structures.

Body Impedance. The internal electrical resistance of the human body, usually taken as 1000 Ω, used as a series component to calculate the **Fibrillation Current** from **Touch Potential** in electrical safety calculations.

Bonding. Electrical interconnecting of conductive parts, designed to maintain a common electrical potential.

Bonding Connection. Reliable conductor used to make a connection to ensure the proper electrical conductivity between metal parts that are required to be electrically connected.

Bonneville Power Administration (BPA). The federal power marketing agency under the Department of Energy responsible for marketing wholesale electric power from 30 federal dams and one nonfederal nuclear plant throughout Washington, Oregon, Idaho, and western Montana and portions of California, Nevada, Utah, and Wyoming.

Boundary Element Methods. Methods to calculate electric and magnetic fields based on simulating the presence of boundaries between different materials with sets of charges or current distributions that become the unknown quantities to be calculated. For instance, the perturbation of the electric field caused by a conductive object may be simulated by a set of charges placed on or below the surface of the object. The distribution and value of these charges are determined by calculating the known potential on various points of the conductor surface. Similarly, the perturbation of the magnetic field caused by a ferromagnetic object may be simulated by a set of dipole moments.

Boys Camera. A high-speed streak camera used at night with a continuously open shutter to record cloud-earth lightning progression.

BPA. *See* **Bonneville Power Administration.**

BPL. *See* **Broadband Power Line Communication System.**

Breakdown Streamers (*also* **Prebreakdown Streamers***).* Streamers that occur at electric field strengths above those required for onset streamers and positive glow. The discharge appears as a light blue filament with branching extending far into the gap. When appearing as multiple discharges, these streamers are usually referred to as a *plume*. When the plume occurs between an electrode and an airborne particle (snow, rain, aerosols etc.) coming into proximity or impacting on the electrode, it is referred to as an *impingement plume*. When the plume occurs due to the disintegration of water drops resting on the electrode surface, it is referred to as a *spray plume*.

Brittle Fracture (Stress Corrosion Cracking of Fiberglass Rod of Polymer Insulator) A brittle fracture is a mechanical failure of the fiberglass rod—i.e., a complete separation of fiberglass rod.

Features of a brittle fracture are:

- One or more smooth, clean planar surfaces, mainly perpendicular to the axis of the fiberglass rod, giving the appearance of the rod being cut.
- Several planar fracture planes separated by axial delaminations.
- Residual mechanical fracture surfaces—i.e., broomstick.

Broadband Audible Noise. Acoustical noise having a spectrum broad in width as compared to the nominal bandwidth of the measuring instrument and whose spectral components are sufficiently close together and uniform so that the measuring instrument cannot resolve them. Audible noise caused by transmission-line corona has a broadband component and pure tones (hum). The frequency spectrum of the broadband component extends beyond the hearing range of people.

Broadband Power Line Communication System (BPL). A system that uses power lines as a channel for high-speed communications, usually over a frequency range of approximately 2–30 MHz.

Bundle (two-conductor, three-conductor, four-conductor, multiconductor) (*also* **quad-bundle, tri-bundle,** and **twin-bundle).** Circuit phase consisting of more than one conductor. Each conductor of the phase is referred to as a "subconductor." A two-conductor bundle has two subconductors. Similarly, a three-conductor has three subconductors. These usually are arranged in a triangular configuration with the vertex of the triangle up or down. A four-conductor bundle has four subconductors. These normally are arranged in a square configuration. Although other configurations are possible, those listed are the most common.

Bundle (Asymmetric). Set of conductors, not necessarily identical, electrically connected and disposed in a nonregular formation. Asymmetric bundles may be used to optimize some aspect of performance. For instance, asymmetric bundles may produce less audible noise and less corona loss in wet weather than regular bundles with the same number of conductors and the same total cross section.

Bundle (Regular). Set of identical conductors electrically connected and disposed on the vertices of a regular polygon. A bundle of n conductors with a diameter, d, and a bundle diameter, d_b, is denoted as: n x d conductor bundle (d_b diameter).

Bundle Diameter. Diameter of the imaginary circle on which the centers of the conductors of a regular bundle are placed forming a regular polygon.

Bundled Conductor. An assembly of two or more conductors used as a single conductor and employing spacers to maintain a predetermined configuration. The individual conductors are called subconductors.

Burst Corona. Corona mode that occurs just at the onset of positive corona and appears as a bluish film adhering closely to the electrode surface.

Bus. Connection between components of electrical substations such as switchgear, transformers, and exit lines. A bus is generally three-phase, and is composed of flexible or rigid conductor sections mounted on insulators.

Cage. *See* **Test Cage**.

Cancellation Loops. General name given to conductive wires arranged in paths (loops) near transmission or distribution lines (or other magnetic field sources) to reduce magnetic fields within a region of interest. There are two types of cancellation loops: active and passive loops. Passive cancellation loop currents are induced by the source to be shielded, whereas active loop current is supplied by an independent source, and may use a feedback control system to adjust loop current to match magnetic field changes within the region to be shielded due to changes in source current. Sometimes capacitance is added to passive loops to enhance the cancellation effect by inducing larger loop currents to flow, which generates larger cancellation fields. The optimum geometry of the loops depends on the power line geometry. Although the cost of cancellation loops is small compared to the cost of a power line, cancellation loops are expensive to install, they have losses associated with them, magnetic field is reduced in a region but could be increased in another region, and they must be designed and maintained in accordance with the NESC and all applicable safety codes. *See also* **Active Loops** and **Passive Loops**.

Capacitance. Property of a system of conductors to store electric charges. It is expressed as the ratio between an electric charge and a voltage difference (C/V). Its unit is the farad (F).

Categorical Exclusion. A provision under NEPA whereby categories of actions that are judged to have minimal environmental effects are excluded from the requirement to prepare an Environmental Assessment (EA) or Environmental Impact Statement (EIS).

Catenary. Curve assumed by a flexible material (i.e., cable) hanging freely between two supports and loaded uniformly throughout its length.

Cathode. The electrode from which current flows to an external circuit.

Cathode-Ray Tube (CRT). Special kind of funnel-shaped vacuum tube used in test equipment scopes, radar displays, television picture tubes, and computer monitors to present a visual display of information. Inside a sealed, evacuated glass tube, electrons are emitted from a cathode, focused and accelerated by an internal electric field to a high velocity, and brought to converge on a fluorescent screen coating. This screen is the glass face of the tube, and it is usually coated with phosphor dots that glow when bombarded by electrons. The electron beam is moved about over the fluorescent screen in response to an internal deflection system used to guide the beam. Since an electron has a tiny mass (approximately 10^{-27} gram), it has virtually no inertia and thus can be deflected back and forth across the CRT screen at seemingly incredible speeds in response to very weak signals applied to the deflection system. This means the system can be susceptible to interference from relatively low levels of external magnetic fields. In a computer monitor, for example, the electron beam sweeps across the face of the display screen at a speed on the order of 32 km per hour (20,000 miles per hour). Color CRTs use three electron guns, one for each primary color, which scan and stimulate tri-color phosphor dots on the screen to produce color images.

Cathodic Protection. The reduction or prevention of corrosion by making a metal the cathode in a conducting medium by means of a direct electric current (which is either impressed or galvanic).

CFO. *See* **Critical Flashover.**

Charge. *See* **Electric Charge**.

Charge Density. In space, (space charge density) is the electric charge per unit volume (C/m^3). On a surface, (surface charge density) is the electric charge per unit area (C/m^2). The electric field on a conductive surface with charge density σ is given by $E = \sigma/\varepsilon$ (ε is the permittivity of the dielectric medium).

Charge Simulation Method. Method used to calculate electric fields in which charges are placed near or at the surface of electrodes at strategic locations to simulate the effect of the electrodes. Equations are written that relate the voltage at a number of points on the surface of the electrodes (the "potential points") to the charges. If the system can be described with N charges and N potential points are selected, the solution of the N equations provides the value of the charges. Electric fields and space potentials are calculated from the charges so determined. *See also* **Potential Point**.

CIGRE. Acronym from the French: "Conseil International des Grands Réseaux Electriques." In English: "International Council on Large Electric Systems." CIGRE is a permanent nongovernmental and nonprofit international association founded in 1921 and based in France. CIGRE aims at facilitating the development of engineering knowledge and information regarding generation and high-voltage transmission of electricity. Technical work is carried out by several Study Committees. The work of CIGRE is published at a biannual conference in Paris, at periodic symposia around the word on specific subjects, in the CIGRE magazine *Electra*, and in CIGRE special publications. More information can be found at www.cigre.org.

Circular Mil. Area equal to that of a circle with a diameter of 0.001 inch (one mil). It is used to specify the cross section of conductors.

Circulation. Mathematical quantity that is the line-integral of a vector field along a given path.

Clearance Requirements. (1) The distances required between conductors of various voltages and the ground. (2) The distance required between the line and trees, buildings, and other objects on, above, or immediately adjacent to the right-of-way.

CNEL. *See* **Community Noise Equivalent Level.**

Color Purity. Description of the extent to which the correct video signal excites the proper phosphor dot on the screen of a color CRT display. External static (dc) magnetic fields of sufficient intensity and orientation can adversely affect color purity by deflecting the electron beam from its intended target phosphor dot and result in mottled (blotches, streaks) or incorrect colors.

Common Mode. When two parallel conductors are present along with a ground reference conductor, the common mode represents the case for which the two parallel conductors carry the same electrical current or have the same voltage with respect to the ground reference conductor. The sum of the two parallel conductor currents returns to the source through the ground reference conductor.

Community Noise Equivalent Level (CNEL). Energy average A-weighted sound level in decibels integrated over a 24-hour period. A 10-dB penalty is applied to all sound occurring between 10 p.m. and 7 a.m. A 5-dB penalty is applied to all sound occurring between 7 p.m. and 10 p.m.

Compact Line. Power line for which the distances between phases are much less than those used in conventional designs. This is made possible either using special insulators or reducing the overvoltages applied between phases or reducing the flashover reliability of the line.

Compact Multipole. Power line that can be considered a two-dimensional multipole and uses the minimum possible number of conductors. Examples of compact multipoles are given in Figure G-1. The magnetic field produced by a compact multipole is the minimum possible, given the number of conductors and the spacing.

Complex Depth. Location inside the earth in which it is convenient to lump the currents in the earth associated with an infinitely long current-carrying conductor above earth. The complex depth is used to simplify calculations of magnetic fields.

Composite Insulator. *See* **Polymer Insulator.**

Conducted Radio Noise. Radio noise that is propagated by conduction from a source through electrical connections.

Conductive Induction (*also* **Resistive Induction** or **Resistive Coupling**). A mechanism by which current entering the earth from a power line causes currents to flow on other conductors in the earth as part of their path back to their source. These currents, in turn, cause the voltage of these other conductors to be elevated with respect to remote earth.

Conductivity. A conduction current occurs in the presence of an electric field within a conductor. The conductivity (σ) of a material reflects the relative ease with which the current moves through the conductor. Conductivity is the reciprocal of resistivity (ρ), and both are characteristics of a material rather than a particular specimen; it is defined for isotropic materials in units of siemens per meter (S/m) and sometimes in mhos per meter ($1/\Omega m$); like resistivity, conductivity is a function of temperature. *See also* **Resistivity**.

Conductor. Material within which charge is free to move. Metals and electrolytes are conductors; the flow of charge within a metal or electrolyte is governed by Ohm's law at a point: current density is equal to the product of material

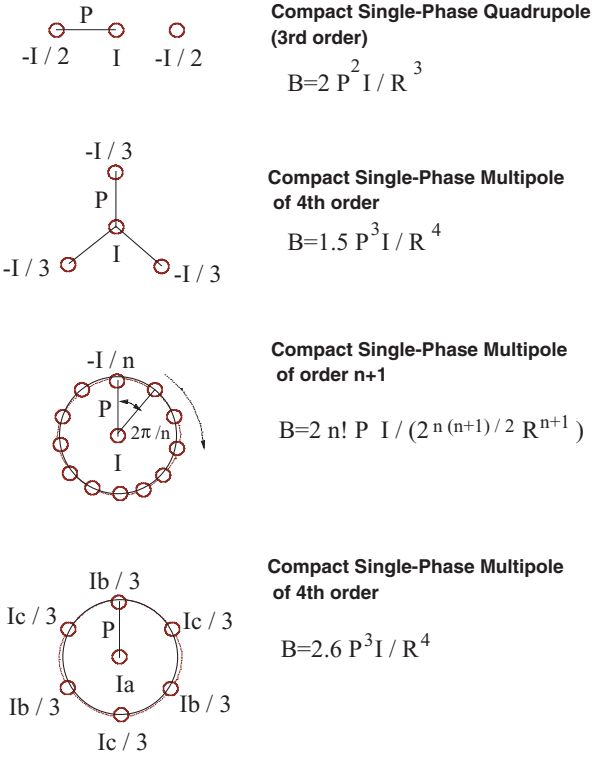


Figure G-1 Examples of compact multipoles.

conductivity and electric field in the material. (*See* equation under **Current Density.**)

Conductor Surface Gradient (*also* **Average Conductor Surface Gradient** and **Maximum Conductor Surface Gradient).** The electric field at the surface of the conductor. The unit is volt per meter (V/m), although for transmission-line conductors, the commonly used unit is kV/cm. For calculating the conductor surface gradient, conductor stranding is generally neglected. For conductors with a circular cross section, the surface gradient varies around the surface and is characterized by an average and a maximum surface gradient. The gradient distribution is well approximated by a sinusoidal function: $E = E_{av}(1 + k\cos(\alpha - \alpha_0))$, where E is the surface gradient at the angle α, E_{av} is the average conductor surface gradient, and $k = E_{\mathrm{m}} / E_{av}$, with E_m being the maximum conductor surface gradient, which occurs at the angle α_0. For a bundle of conductors, the maximum surface gradient is defined as the average of the maximum surface gradients of the individual conductors. The average conductor surface gradient is related to the charge, q, per unit of length by: $E_{av} = q / (\pi\varepsilon d)$, where d is the conductor diameter. For a regular bundle of n conductor, if d_b is the bundle diameter, the ratio between maximum and average surface gradient is given by:

$$k = E_m / E_{av} = 1 + (n-1)d / d_b .$$

Conductor Surface Irregularity Factor. The ratio between the measured corona onset gradient of a practical transmission-line conductor and the corona onset gradient calculated for an ideal smooth cylindrical conductor of the same diameter.

Contact Resistance. The electrical resistance produced by the contact of two surfaces. Also, the difference between the resistance of a grid or ring and the geometric resistance of the metal plate or disc of the same size. *See also* **Geometric Resistance.**

Continuing Current. A long-duration low-amplitude current that flows, usually between subsequent lightning return strokes.

Contour Lines. Set of lines on a plane connecting points where a given quantity has the same values. For instance, lines connecting points with the same magnetic field on the plan view of an area are called "magnetic field contour lines." Similarly, lines connecting points that have the same space potential in a plane perpendicular to a transmission line are called "space potential contour lines."

Core Rod (fiberglass rod) The internal insulating part of a polymer insulator is a fiberglass reinforced plastic (FRP) rod, which is designed to carry the mechanical loading of the insulator. It consists of axially aligned glass fibers that are imbedded by a pultrusion process into a resin matrix to achieve maximum mechanical strength. The fibers are typically 5 to 25 μm in diameter and make up 75–80% of the total weight of the rod.

Corona. Luminous discharge due to ionization of the air surrounding an electrode caused by a voltage gradient exceeding a certain critical value. The electrode may be conductors, hardware, accessories, or insulators.

Corona Attenuation. The specific influence of corona discharges on conductors in decreasing the magnitude of different types of overvoltages as they propagate along a transmission line.

Corona Extinction Gradient. The conductor surface gradient at which continuous corona last persists as the voltage is gradually decreased.

Corona Extinction Voltage. The voltage applied to the conductor to produce the corona extinction gradient. (For the same conductor, corona extinction voltage depends on the actual conductor configuration.)

Corona-Induced Vibrations. During rain and in other wet-weather conditions, when water drops are hanging at the bottom of the conductors and the wind is calm, corona may cause the conductors to vibrate at very low frequency. These corona-induced vibrations are caused by the intermittent space charge produced by corona at the water drops hanging at the bottom of the conductors and by the fact that corona is modulated by the deformation of the water drops during the oscillation cycle itself. This phenomenon is self-excited and results in the conductor vibrating at any of its natural frequencies with increasing amplitude until the deformation of the water drops causes corona out of synchronism with the motion. Corona-induced vibrations do not cause conductor fatigue because the frequency is relatively low (1–5 Hz), and the peak-to-peak amplitude is relatively small (2–10 cm). They cause a modulation of the audible noise, which makes the noise more detectable and distinguishable from the rain noise.

Corona Loss. The power lost due to the occurrence of corona discharges on transmission-line conductors.

Corona Modes. Corona discharges with different physical characteristics. Corona modes are generally classified into two broad categories: streamer and glow. (*See also* **Streamer** and **Glow.**) Their characteristics and occurrence

depend on the polarity of the electrode, the basic ionization characteristics of the ambient air, and the magnitude as well as distribution of the electric field. Corona modes occurring during the positive and negative half cycles of the alternating voltage are essentially similar to those under positive and negative direct voltages. The positive corona modes occurring in the order of increasing electric field strength are: *Burst Corona*, *Onset Streamers*, *Positive Glow, and Breakdown Streamers*. The negative corona modes occurring in the order of increasing electric field strength are: *Trichel Streamer*, *Negative Glow,* and *Negative Streamer*.

Corona Onset Gradient (*also* **Corona Inception Gradient).** The conductor surface gradient at which continuous corona first occurs as the applied voltage is gradually increased.

Corona Onset Voltage. The voltage applied to the conductor to produce the corona onset gradient. (For the same conductor, corona onset voltage depends on the actual conductor configuration.)

Corona Pulse. A voltage or current pulse that occurs at some designated location in a circuit as a result of corona discharge.

Corona Ring (*also* **Grading Ring)**. An electrode of toroidal or similar shape that is placed at the ends of conductors, insulator strings, bushings, etc. in order to grade the electric field and lower the surface gradient on the metallic components and on the dielectric surfaces of insulators. They are often applied on polymer insulators, and may have "horseshoe" shapes to facilitate installation.

Corridor. A long, narrow strip of land, forming a passageway for transportation or utility facilities. *See also* **Joint-Use Corridor** and **Right-of-Way**.

Coulomb. Unit of electric charge named after the French physicist Charles Coulomb (1736-1806). A coulomb is equal to the quantity of electric charge carried by one ampere of current in one second. A coulomb of charge is equal to the charge of 6.25×10^{18} electrons.

Coulomb's Law. The force between two electric charges (or a pair of magnetic poles) is directly proportional to the product of their magnitudes and inversely proportional to the square of the distance between them.

Counterpoise. A buried wire system connected to the footings of towers or poles supporting a transmission line. Used to establish a low-resistance path to earth, usually for managing ac fault currents near stations and sometimes for lightning protection.

Coupling. (1) In general, the association of two or more transmission lines or equipment components in such a manner that power is transferred from one to the other. (2) On a signal transmission system, the effect of an interfering source. (3) In a lightning protection system, the transfer of potential from driven to undriven conductors via a coupling coefficient that reduces insulator voltage stress. *See also* **Coupling Coefficient.**

Coupling Coefficient. An electrical transient flowing in a wire W_1 carries charge with it, and this charge induces a corresponding charge separation in any adjacent isolated conductor W_2. The ratio of the induced voltage V_2 on W_2 to the voltage V_1 on W_1 is called the "coefficient of coupling," and is very important in determining the voltages induced on phase conductors by the flow of lightning surge currents in overhead shield wires. A corona envelope around wire W_1 can form at high voltages, and this increases the coupling to wire W_2 by increasing the capacitance between them and reduces the surge impedance of wire W_1. Corona-modified coupling is nonlinear with voltage.

Covered Conductor. Conductor covered with a dielectric (insulating material) having no rated insulating strength or having a rated insulating strength less than the voltage of the circuit in which the conductor is used.

Creepage Distance. *See* **Leakage Distance.**

Crest (of a wave, surge, or impulse) (*also* **Peak).** Point or part of a wave or a surge or an impulse when the maximum (for positive polarity) or the minimum (for negative polarity) value is attained.

Crest Factor. Ratio of a waveform crest (i.e., peak or maximum) value to its root-mean-square (rms) value. For example, for a purely sinusoidal waveform, the crest factor is: $B_{max}/B_{rms} = \sqrt{2}$. Highly distorted or pulsed waveforms can have much larger crest factors. Some typical crest factors are:

Sine Wave	1.414
Square Wave	1.0
Triangular Wave	1.73
Gaussian Noise	3.0
Rectangular Pulse Train	2-10, or more
50% Duty Cycle	2-10
25% Duty Cycle	4.7

The **Critical Time-to-Crest** is the time-to-crest of the switching impulse that produces the lowest 50% flashover voltage. The **Equivalent Critical Time-to-Crest** is the time-to-crest of the double exponential impulse that produces the lowest 50% flashover voltage.

Crest Value (of a wave, surge, or impulse) (*also* Peak Value). Value at crest.

Critical Current. The first-stroke lightning current to the corona-modified surge impedance of a phase conductor that produces a critical impulse flashover voltage wave. Also, the first negative stroke lightning current to the combined surge impedance of the tower, overhead groundwires, and ground electrodes that just produces a backflashover, based on the volt-time curve or destructive index value of the resulting voltage surge.

Critical 50% Flashover Voltage. The prospective crest value of the impulse voltage with critical time-to-crest that has 50% probability to cause a flashover.

Critical Wave. Double exponential switching impulse with the time-to-crest that produces the lowest 50% flashover voltage.

Cross-Phasing. *See* **Low Reactance Phasing**.

Cross Product (*also* Vector Product). The cross product of a vector $\vec{A}$ and a vector $\vec{B}$ is a vector $\vec{C}$ that has a magnitude obtained by multiplying the magnitudes of $\vec{A}$ and $\vec{B}$ by the sine of the angle between them. The direction of $\vec{C}$ is that traveled by a right-hand screw turning about an axis perpendicular to the plane of $\vec{A}$ and $\vec{B}$, in the sense in which $\vec{A}$ would move into $\vec{B}$ by a rotation of less than 180º. It is assumed that $\vec{A}$ and $\vec{B}$ are drawn from the same point. The vector product is indicated by using a small cross: $\vec{A} \times \vec{B} = \vec{C}$.

Crowfoot Counterpoise. Two or more short buried wires (counterpoise) extending in different directions to form a low-impedance ground electrode.

CRT. *See* **Cathode-Ray Tube.**

Cruciform. *See* **Split Phase**.

Current Density. If an electric current, *I*, is distributed uniformly across a conductor of cross-sectional area, *A*, the magnitude of the current density vector, *J*, for all points on that cross section is: $J = I/A$. The term is used to refer either to conduction-current density or to displacement-current density, or to both. The SI system unit of *J* is ampere per square meter (A/m^2). Current density is proportional to the conductivity (σ) and electric field (E) in a medium (Ohm's Law at a point: $J = \sigma E$). If the current is confined to surface, a surface current density is defined.

Current Uprating. Redesigning a transmission line to operate at a higher current than originally planned. Also known as increasing the line ampacity. Typically, as increasing the current leads to greater conductor temperatures due to resistive losses, current uprating involves a study of the thermal characteristics of a transmission line. Some texts use the term "current upgrading." This handbook has tried to limit use of the term "upgrading" to that of "voltage upgrading" only.

Cycle. Period between two adjacent identical points of a periodic quantity, so that the quantity is completely defined between these two points. The number of cycles per second is the frequency.

Day-Night Sound Level (L_{dn}). Energy average A-weighted sound level, in decibels, integrated over a 24-h period. A 10-dB (A) penalty is applied to all sound occurring between 10 p.m. and 7 a.m. *Notes:* (1) L_{dn} is intended to improve upon the L_{eq} rating by adding a correction for nighttime intrusion because people are more sensitive to such intrusions. (2) The formula to calculate L_{dn} can be found in Chapter 10.

Dc (Direct Current) Transmission. Term applied to both currents and voltages that are nonalternating and change little with time. They may be positive or negative. The transfer or transmission of electric energy by direct current from its source to one or more main receiving stations. *See also* **Direct Current.**

Decibel. Numerical expression of the relative differences between some quantity and a reference level. For a quantity of power (e.g., watts or sound pressure), the decibel (dB) level is equal to 10 times the common logarithm of the ratio of a level to a reference level. For linear quantities (e.g., volts, volts/meter, amps/meter, etc.), the decibel level is 20 times the common logarithm of the ratio of a level to a reference level. For instance, sound-pressure levels are expressed in dB above a reference pressure of 20 μPa ($2 \cdot 10^{-6}$ μB *ar)*. The dB levels corresponding to other pressure levels are: $20\log_{10}\left(\frac{sound\ pressure\ level}{20\,\mu Pa}\right)$. *See also* **Sound-Pressure Level**.

De-energized. Conductor, current-carrying component, or other object that is free from any electrical connection to a source of potential difference. Although de-energized, a conductive object may acquire an electric charge and may have a potential different from that of the earth.

Delta Configuration. Configuration of a single-circuit, three-phase line in which the phases are placed on the vertices of a triangle with the center phase at a greater height above ground than the other two phases. If the middle

phase is lower than the other two, the configuration is called "inverted delta," or by some, "nabla."

Delta Connection. Method of connecting the windings of a transformer in series so that a closed circuit is formed. Delta windings prevent the flow of zero sequence currents.

Destruction of Rod by Discharge Activity (Polymer Insulator). Destruction of the rod by discharge activity is a mechanical failure mode of a polymer insulator. Internal defects or moisture or contaminant ingress may result in internal discharge activity. If the rod becomes carbonized, a larger conductive defect is formed. These discharges degrade the rod until the unit is unable to hold the applied mechanical load and the rod separates.

Detector. Device that performs detection (extraction of signal or noise from a modulated input) and weighting (extraction of a particular characteristic of the signal or noise). *Note:* In a radio noise receiver, the voltage applied to the detector depends on the nature of the noise and the bandwidth of the filter used in the intermediate frequency stages. To furnish calibrations that are independent of the bandwidth and can be made with readily available equipment, an unmodulated carrier is used. With such input, all detectors (peak, quasi-peak, average, or rms) indicate the same value of radio noise. *See also* **Average Detector**, **Peak Detector**, and **Quasi-Peak Detector**.

DGPS. *See* **Differential Global Positioning System.**

Diamagnetism. *See* **Magnetism.**

Dielectric. Term often used to denote an insulating material. A dielectric is so called because it permits the passage of the lines of force of an electric field (electric flux), but does not conduct an electric current. Dielectric materials can therefore store electric charge. *See also* **Permittivity**.

Dielectric Constant. Term used to describe a material's ability (with respect to a vacuum) to store electrostatic energy per unit volume for a unit potential gradient. *See also* **Permittivity**.

Dielectric Flux (*also* **Electric Flux).** Lines of force of an electric field in a dielectric. Dielectric flux is measured in coulomb (C). The dielectric flux, D, is related to electric field, E, by: $D = \varepsilon E$ (ε is the permittivity).

Dielectric Flux Density. *See* **Electric Flux Density.**

Differential Global Positioning System (DGPS). An augmentation to the Global Positioning System using differential correction techniques to improve accuracy. Differential techniques improve radio navigation system accuracy by determining position error at a known location and subsequently transmitting the determined error, or corrective factors, to users of the same radio navigation system, operating in the same area.

Differential Mode. When two parallel conductors are present along with a ground reference conductor, the differential mode represents the case for which the two parallel conductors carry equal and opposite electrical currents, or have equal and opposite voltages with respect to the ground reference conductor. For this mode, no current flows in the ground reference conductor.

Diffusion. Movement of electrons or ions in a gas due to the existence of density gradient of the particles.

Dipolar. Having the property of, or being related to, a dipole. For instance, the field is dipolar, if its structure is the same as that of a field from a dipole.

Dipole. Physical entity consisting of two equal and opposite poles. An electric dipole consists of a positive charge and a negative charge separated by a distance (the distance is usually small compared to other distances being considered). A magnetic dipole is a magnetic system in which the equal (and opposite in character) north and south poles of a magnetic source are separated by a short but definite distance. A magnetic dipole tends to orient itself parallel to an applied magnetic field in the same way an electric dipole does in an electric field. When dealing with two dimensions, an electric dipole consists of two infinitely long, parallel lines of charge (equal but opposite in sign), and a similar magnetic dipole consists of two infinitely long, parallel equal currents in opposite directions. A closed loop of current (either in a plane or along some irregular contour through space) comprises a three-dimensional dipole. Dipoles are sources of fields that attenuate with distance: the field decreases as a function of $1/r^2$ for two-dimensional dipoles (two parallel wires) and $1/r^3$ for three-dimensional dipoles (current loop). *See also* **Dipole Moment**.

Dipole Antenna. Any one of a class of antennas having a radiation pattern approximating that of an elementary electric dipole. *Note:* Common usage considers the dipole antenna to be a metal radiating or receiving structure that supports a line current distribution similar to that of a thin straight wire, a half-wavelength long, so that current has a node at each end of the antenna.

Dipole Moment. Vector used to quantify the size of a dipole. The dipole moment is defined such that its vector cross product with an applied magnetic field gives the

torque that the dipole experiences in the field. For a three-dimensional magnetic dipole (current loop), its dipole moment magnitude is the product of the current and the area enclosed by the loop, and its direction given by a right-hand rule. For a two-dimensional magnetic dipole (long parallel wires with equal and opposite current), the dipole moment is the product of its current and the distance between its two wires. *See also* **Dipole**.

Direct Current. An electric current that flows in one direction. *See also* **dc.**

Discharge. Passage of electricity through gaseous, liquid, or solid insulation.

Disruptive Discharge (*also* Electrical Breakdown). Discharge that completely bridges the insulation under test, reducing the voltage between the electrodes practically to zero.

Disruptive Discharge Probability. Probability that one application of a prospective voltage of a given shape and type will cause a disruptive discharge.

Disruptive Effect. A parameter derived mathematically to determine if a line insulator is likely to flash over when subjected to a lightning stroke voltage having a nonstandard waveshape. A special integration algorithm is used that was originally developed to estimate failure probabilities of power transformers.

Dissipation Factor. The ratio of energy dissipated to the energy stored in a lossy capacitor during one cycle of an alternating voltage. It is also defined as the tangent ($\tan\delta$) of the dielectric loss angle (δ).

Distant Field. Electric or magnetic field in the space located at distances such that the source of the electric or magnetic field can be represented within the desired accuracy by a simple element (e.g., a dipole or a quadrupole). For instance, the "distant" magnetic field, B, of a three-phase line with flat configuration, phase spacing, P, and balanced current, I, is expressed by the "dipole" equation $B = 2\sqrt{3}PI / R^2$ with an accuracy greater than 10% for distances $R > 3.5\ P$. (B in milligauss, I in Ampere, P and R in meter.)

Distant Source. A distant source is located far enough away from an object or a region of interest for its field to be essentially uniform over the spatial region of interest.

DLG. See **Double Line to Ground.**

Dot Product (*also* Scalar Product). The dot product of two vectors is a scalar obtained by multiplying the product of the magnitudes of the two vectors by the cosine of the angle between them. The dot product of the two vectors $\vec{A}$ and $\vec{B}$ is indicated by means of a dot: $\vec{A} \cdot \vec{B}$.

Double-Circuit Lines. Two separate overhead three-phase power lines using the same conductor support structures along some of their length.

Double-Exponential Impulse. Impulse whose waveshape is defined by $v = v_0\left(e^{-t/\tau_1} - e^{-t/\tau_2}\right)$. A double-exponential impulse is more often characterized by a crest value, a time-to-crest, and a time-to-half value.

Double Line to Ground (DLG). Referencing an event involving two phases and ground.

Drift. Movement of electrons or ions in a gas due to the force exerted by the applied electric field.

Dry Arc Distance. The shortest distance in air external to the insulator between those parts that normally have the operating voltage between them.

Dry-Band Arcing. Electrical discharges that occur across the surface of a short band of dry (and hence high electric resistance) dielectric material between two sections of wet (and hence low resistance) dielectric material. These may occur on the jacket of an all-dielectric self-supporting optical cable that is mounted on a power line. In this case, the arc is driven by capacitive coupling between the power line and the optical cable. The discharges may also occur on power line insulators. In this case, the insulator voltage drives the arc.

Earth Surface Potential. V_x is the voltage between a point x on the earth's surface and remote earth.

EC (Grade Aluminum). Electrical conductor grade aluminum. Also called 1350-H19 alloy or A1.

Eddy Currents. When conducting specimens are subjected to a time-varying magnetic field (or motional induction in a static field), currents tend to be induced in the specimen. They flow in closed paths perpendicular to the inducing field in the specimen and are called eddy currents. In accordance with Lenz's law, the eddy current tends to oppose the change in the field inducing it. These induced currents will have a magnetic field associated with them. Eddy currents result in a loss (I^2R) in the conducting specimen. In fact, the technique of induction heating is an application of heat resulting from induced eddy currents.

EGM. *See* **ElectroGeometric Model.**

EHS Steel. Also designated S3. Extra High Strength steel wires for ACSR and shield wire.

EHV. Extra High Voltage. Transmission system voltage between 300 and 800 kV. In the U.S., this includes 345 kV (nominal, 363 kV maximum system voltage), 500 kV (nominal, 550 kV maximum system voltage), and 765 kV (nominal, 800 kV maximum system voltage).

Electric Charge. Quantity of electricity that can be stored on a body. It is measured in coulomb (C), which is the charge flowing in one second in the cross section of a circuit with the current of one ampere. Charges may be either positive or negative. The smallest charge is that of an electron and is equal to about $-1.6 \cdot 10^{-19}$ coulomb.

Electric Field. An electric field exists in the region near electric charges, and the field exerts a force on other electric charges placed in the field. At a given point in space, the ratio of force on a positive test charge (placed at the point) to the magnitude of the test charge, in the limit that the magnitude of the test charge goes to zero is defined as the electric field. The electric field strength (E-field) at a point in space is a vector defined by its space components along three orthogonal axes. For steady-state sinusoidal fields, each space component is a complex number or phasor. The magnitudes of the components are expressed by their rms values in volts per meter (V/m). In a multi-phase environment, such as near a three-phase electric power line, the field is characterized as a vector rotating in a plane where it describes an ellipse whose semi-major axis represents the magnitude and direction of the maximum value of the electric field, and whose semi-minor axis represents the magnitude and direction of the field a quarter cycle later at its minimum value.

Electric-Field Induction (*also* **Capacitive Induction** or **Capacitive Coupling**). A mechanism by which time-varying electric fields in space between a power line and a separate system of conductors cause currents and voltages on the system of conductors.

Electric Field-Vertical Component. The vertical component of the electric field under a transmission line is the rms value of the component of the electric field along the vertical line passing through the point of measurement. This quantity is often used to characterize induction effects in objects close to ground level. *See also* **Electric Field.**

Electric Flux (*also* **Dielectric Flux).** The electric flux through a surface is the integral of the normal component of the electric flux density over the surface.

Electric Flux Density (*also* **Dielectric Flux Density).** The electric flux density, D, is a vector quantity determined by the direction and density of flux lines that emanate from electric charge and follow the direction of the electric field. It is measured in coulomb per square meter. The electric flux, D, is related to electric field, E, by: $D = \varepsilon E$ (ε is the permittivity).

Electrical Breakdown. *See* **Disruptive Discharge**.

Electrical Clearance. The distance between energized conductors and other conductors, buildings, and earth. Minimum clearances are usually specified by regulations.

Electrical Wind. The flow of gas molecules away from a conductor in corona.

Electrode. Conductive element with all its points at the same potential. A voltage can be applied between two electrodes. Related terms include:

> **Energized Electrode**. An electrode whose voltage with respect to ground is greater than zero and that is electrically connected to a power source.
>
> **Floating Electrode**. An electrode that is not connected to a power supply and not connected to ground, and whose potential is not well defined and intermediate between the voltage of the energized electrode and ground.
>
> **Grounded Electrode**. An electrode whose voltage with respect to ground is zero and that is electrically connected to ground through zero impedance.

Electrode Voltage (*also* **Electrode Potential).** V_E is the voltage occurring between the grounding system and reference earth at a given value of the impressed earth current.

ElectroGeometric Model (EGM). A model for the final jump process of lightning, whereby the vertical downward leader reaches a point of discrimination prior to terminating at ground. A radius, depending on stroke charge, current, and height, is centered at the leader tip, and the closest grounded object within this radius is deemed to receive a lightning flash.

Electromagnetic Compatibility. Ability of a device, equipment, or system to function satisfactorily in its electromagnetic environment without introducing intolerable electromagnetic disturbances to anything in that environment.

Electromagnetic Field. Time-varying field, with electric and magnetic field components described by Maxwell's equations.

Electromagnetic Interference (EMI). Degradation of the performance of a device, a piece of equipment, or a system caused by an electromagnetic disturbance. *Note*: The English words "interference" and "disturbance" are often used indiscriminately.

Electromotive Force (EMF). Potential difference (called voltage), indicating the ability to do the work of forcing electrons to move. The term "emf" as an abbreviation of electromotive force is sometimes used for a voltage source or an induced voltage. The unit of emf is the joule/coulomb, which is the volt.

Electron Attachment. The process by which free electrons are captured by the molecules of an electronegative gas.

Electron Avalanche. The cumulative process in which electrons accelerated by an electric field produce additional charged particles through collision with neutral gas atoms or molecules. It is therefore a cascade multiplication of ions.

Electronegative Gas. A gas composed of molecules whose outermost shell is not completely filled in the neutral state, leaving one or two positions readily available to receive free electrons. Examples of electronegative gases are oxygen (O_2), sulfur hexafluoride (SF_6), etc.

Electrostatic. *See* **Quasistatic**.

ELF. Extremely-low-frequency, defined by IEEE as the frequency range from 3 to 3,000 Hz.

EMC. *See* **Electromagnetic Compatibility**.

emf. *See* **Electromotive Force**.

EMF. Nonscientific term in popular use to refer to Electric and Magnetic Fields (or, ElectroMagnetic Fields, and sometimes used to refer only to the magnetic field); not to be confused with the engineering term for electromotive force (emf).

EMI. *See* **Electromagnetic Interference**.

EMTP. Electromagnetic Transient Program.

End Fitting Seal (Polymer Insulator). One of the most vulnerable regions of a polymer insulator is the interface between the end fitting, polymer housing, and the core rod, known as the end fitting seal. Its function is to prevent moisture or contamination from penetrating to the FRP rod, an event that may precipitate a failure.

Energization. Act of applying a voltage to an electrode or to a line or to a network.

Energized. Conductor, current-carrying component, or other object that is electrically connected to a source of potential difference or electrically charged so as to have a potential significantly different from that of nearby earth.

Energy-Equivalent Sound Level (L_{eq}). Energy average of the level (usually A-weighted) of a varying sound over a specified period of time. The term "equivalent" signifies that the average of the fluctuating sound would have the same sound-energy level as a steady sound having the same level. The term "energy" is used because the sound amplitude is averaged on a root-mean-square (rms) pressure-squared basis, and pressure-squared is proportional to energy. The mathematics for calculating L_{eq} can be found in Chapter 10.

Environmental Fields. Types of fields that people are expected to be exposed to in residential, school, work, or other common environments.

Equipotential. Surface (sometimes an imaginary surface in space) that has the same electric potential everywhere on it. Can also be used as an adjective (e.g., "equipotential surface").

Equipotential Zone. A concept that protects workers and the public from hazardous or annoying potentials due to inadvertent energization or induction by ensuring that all equipment, conductors, anchors, and structures within a defined area are electrically connected together, creating a zone of equipotential.

Equivalent Area (for electric field induction). Equivalent area of an object is the area of a flat conductive plate at ground level that has the same short-circuit current as that induced in the object by a uniform electric field.

Equivalent Diameter (for electric field calculations). The equivalent diameter of a bundle of conductors is the diameter of the single conductor that has the same capacitance to ground of the bundle, when placed at the same height above ground.

Equivalent Electric Field (for exposure assessment). Electric field value that would cause a person in a reference condition to experience the same electric field exposure as that occurring in the actual situation. Electric field exposure may be described in terms of currents induced in the upper part of the body, and can be collected, for instance, by a conductive vest. The reference condition consists of body erect with arms at sides, person well grounded through the feet on a conductive, flat ground, and in a uniform unperturbed electric field. *See also* **Activity Factor**.

Exceedance Level. Statistical descriptor often used in expressing levels of quantities. For example, in acoustics, the L_{10} is the A-weighted sound level exceeded for 10% of the time in a specified time period (and for corona noise over a specified weather condition). For the other 90% of the time, the sound level is less than the L_{10}. Similarly, the L_{50} is the sound level exceeded 90% of the time, etc. The concept of exceedance levels can also be used as a statistical term for other corona effects such as radio noise, corona loss, dc fields, and ions. Any exceedance level can be easily obtained from distributions that have been plotted on probability paper.

Excitation. The process by which an atom or molecule receives enough energy (for example, by electron collision) to move an electron in its outermost orbit to a higher energy state. The atom or molecule quickly (in about 10^{-8} seconds) relaxes to its original energy state, releasing the excess energy in the form of a photon.

Exposure. Amount of a chemical or physical agent in the environment with which a person comes into contact over some period of time.

External Insulation. Air insulation and the exposed surface of the solid insulation of a piece of equipment, which are subjected to both electric stress and the effects of atmospheric and other conditions such as contamination, humidity, vermin, etc.

Extra High Voltage. Term applied to ac power system voltage levels that are higher than 230,000 V.

Extreme Value Distribution. Function sometimes used to describe the flashover probability for different voltages. Its density function is: $p(V) = \frac{1}{\beta} \cdot e^{\frac{V-V_0}{\beta}} \cdot e^{-e^{\frac{V-V_0}{\beta}}}$, where V_0 is the voltage corresponding to 63.2% flashover probability. The cumulative probability is: $P(V) = 1 - e^{-e^{\frac{V-V_0}{\beta}}}$.

Extremely-Low-Frequency. *See* **ELF**.

Extruded-Dielectric Cables. Extruded-dielectric cables use either cross-linked polyethylene (XLPE), low- or high-density polyethylene, or ethylene-propylene rubber for insulation. Extruded-dielectric cables are also called solid dielectric or XLPE cables. The reason for use of the extruded dielectric materials for insulation in high-voltage cables is to provide a simple, low-cost, low-maintenance alternative to conventional pipe-type cable systems that use fluid or gas for insulation. These cables are fabricated as single-phase cables and usually placed in a duct with some spacing between the cables, which results in less magnetic field cancellation than if the cables were all placed together. In addition, extruded-dielectric cable construction does not normally have a common shield around all phases, as is the case with the steel pipe in pipe-type cables.

FACTS (Flexible AC Transmission System). Alternating current transmission systems incorporating power electronics-based and other static controllers to enhance controllability and increase power transfer capability.

Fair Weather. Weather condition when the precipitation intensity is zero and the transmission-line conductors are dry. *Note*: This should not be confused with the general connotation of fair weather as descriptive of pleasant weather conditions. Common usage is subject to misinterpretations, for it is purely subjective description. Technically, when this term is used in weather forecasts, it is meant to imply no precipitation; less than 40% sky cover of low clouds; and no other extreme conditions of cloudiness, visibility, or wind.

Fair-Weather Audible Noise (a*lso* Fair-Weather Radio Noise and **Fair-Weather Corona Loss).** In the context of audible noise, radio noise, and corona loss from overhead transmission lines, this term refers to the levels of those phenomena in dry conditions. Therefore, it excludes rain, fog, mist, snow, sleet, and conductor icing, but not conditions of high relative and absolute humidity, and extremes of ambient temperature.

FALLS. Fault Analysis and Lightning Location System. A technology applied to transmission lines that correlates the time (and sometimes distance) of lightning-caused line faults with lightning locations and stroke current magnitude data obtained from the North American Lightning Detection Network. Extremely useful in determining types of transmission-line lightning faults and their locations.

Farad. Unit of electrical capacitance named after the British physicist Michael Faraday (1791-1867). A farad is equal to the capacitance that carries a charge of one coulomb when it is charged by a potential difference of one volt. It is a rather large unit and, in practice, much smaller units such as microfarads (10^{-6} farad) or picofarads (10^{-12} farad) are generally used.

Faraday's Law. Quantitative relationship between the emf (electromotive force) induced in a closed loop and the magnetic field producing the emf. According to this law, the total emf induced in a closed circuit is equal to the time rate of decrease of the total magnetic flux (F) linking the circuit: emf = -df /dt.

Fault. An unintentional short circuit in a power system, due to a breakdown of insulation between a conductor and the ground or between conductors.

Fault Current. An abnormal current flow resulting from a fault.

Ferranti Effect. The phenomenon caused by capacitive charging of lines, and by which the steady voltage at the open end of an uncompensated transmission line is always higher than the voltage at the sending end.

Ferromagnetism. *See* **Magnetism.**

Fiber Optic Cable. Optical fibers incorporated into an assembly of materials that provide tensile strength and external protection, and have handling properties comparable to metallic cables.

Fibrillation Current. A current, typically less than 500 mA for short-duration ac surges from hand to foot, that leads to a significant risk of ventricular fibrillation, an uncoordinated pulsation of the heart that disrupts circulation and leads to death.

Field Ellipse. An electric or magnetic field can have three orthogonal components in space, each of which can vary in time. The instantaneous magnitude and direction of the field at a point in space are defined by these components with proper consideration of the spatial and temporal aspects of each component. The field at a point can be represented in most cases by a field ellipse located in three dimensions. For many practical cases near power lines, the field ellipse throughout a large region can be represented in two dimensions because the component of field parallel to the power line is small. The field ellipse can be characterized by its major and minor axis, the maximum and minimum values obtained by the ellipse (the field is said to be elliptically polarized). The maximum value of the field at a point is simply the value of the semi-major axis (one-half of the major axis dimension), and the minimum value is the semi-minor axis. The resultant field is the square root of the sum of the squares of the semi-major and semi-minor axes. There are two special cases for the field ellipse. In one case the major and minor axes are equal, and the field ellipse becomes a circle; the field is said to be circularly polarized. In the other case, the minor axis goes to zero, and the field is then represented by a space vector, which has a magnitude that varies with time along a straight line; the field is said to be linearly polarized. *See also* **Polarization**.

Field Line. Line in an electric or magnetic field that shows the direction of force exerted by the field. *See also* **Flux**.

Field Management. Application of engineering principles, based on research, to electric and magnetic fields due to power lines or other sources to address or treat situations requiring technical solutions without altering the function for which the system was intended.

Fifty Percent Disruptive Discharge Voltage. Prospective crest value of the test voltage that has a 50% probability of producing a disruptive discharge.

Fifty Percent Flashover Voltage. Prospective crest value of the impulse that has a 50% probability of producing a flashover.

Final Jump. Phase of the flashover process of long air gaps subjected to positive polarity switching impulses. The final jump is the discharge of the air gap between the tip of the leader and the grounded electrode. It occurs very rapidly, practically instantaneously with respect to the other phases of the flashover process, when the streamers at the tip of the leaders reach the grounded electrode. Also used to describe the bidirectional process that closes the gap between a downward lightning leader and a grounded object that initiates an upward connecting leader.

Finite Difference Method. Numerical technique to calculate electric or magnetic fields. The field values are derived from Maxwell differential equations. The method of finite differences applied to the solution of electric field problems solves for the value of the potential at discrete points of a regular mesh placed over the field region. The method is called finite differences because the partial derivative of the potential is replaced by the finite difference between the potentials at adjacent points of the mesh.

Finite Element Method. Numerical technique to calculate electric or magnetic fields based on Maxwell differential equations. The finite element method applied to the solution of electric field problems is based on the principle that the equilibrium distribution of charges present in a closed domain is such as to minimize the electrostatic energy associated with the field. The whole domain is divided into a finite number of sufficiently small elements of simple geometry connected to each other to form a mesh. The electrostatic energy is written as a function of the potentials of the nodes of each element. The minimum energy is obtained by setting the partial derivatives of the total energy with respect to the potential of each node to zero. A system of as many equations as there are node potentials is obtained.

First Corona. First appearance of corona on an electrode stressed with a double-exponential switching impulse.

First Stroke. A lightning flash may consist of several high current strokes traveling down the same channel. The first stroke in a flash is usually considered to be the most severe in creating a line flashover condition, and is the one normally used in lightning simulation programs.

Flash. *See* **Lightning Flash.**

Flashover. Disruptive discharge through air directly or around or over the surface of solid or liquid insulation between electrodes of different potential or polarity, produced by the application of voltage wherein the breakdown path becomes sufficiently ionized to maintain an electric arc.

Flashover Probability. Probability that one application of a prospective voltage of a given shape and type will cause a flashover.

Flashover Voltage. Prospective crest voltage of an impulse of a given shape corresponding to a given flashover probability.

Flashunder (Tracking Along or Through the Fiberglass Rod and the Resulting Flashover of a Polymer Insulator). An electrical failure mode of a polymer insulator. This failure mode occurs when internal discharge activity results in carbonization within or on the surface of the fiberglass rod. Internal discharge activity may occur due to moisture ingress or internal defects—e.g., voids, poor bonding, or conductive defects. Internal tracking grows in or on the rod until a critical distance along the insulator is reached and the applied voltage can no longer be withstood and a flashunder occurs.

Flat Configuration (*also* **Horizontal Configuration Line).** Configuration of a single-circuit, three-phase line in which the three phases are all at the same height above ground.

Flicker. Unintended and perceptible time-dependent fluctuations in brightness or color on the screen of video display terminals due to repetitive variations in background luminance.

Floating Object. Conductive object that is not connected to a power supply and not connected to ground and whose potential is not well defined and intermediate between the voltage of the energized electrode and ground.

Flux. Property of any vector field represented by lines of force that cut through a reference surface. A line of flux is a line so drawn that a tangent to it at any point indicates the direction of the field. There are electric flux lines, which are also called lines of force, and magnetic flux lines, which are sometimes called lines of induction. If a "test" charge were placed in an electric field, or an isolated pole in a magnetic field, the flux lines would describe the direction of force on the test element and hence, its direction of movement within the field. The unit of magnetic flux in the SI system is the weber, and the unit in the CGS system is the maxwell. The number of flux lines per unit cross-sectional area is proportional to the magnitude of the flux density vector (D for electric flux density and B for magnetic flux density). The flux lines give a graphic representation of the way a field varies throughout a certain region of space. Where the flux lines are close together, the field is large, and where they are far apart, the field is small. *See also* **Gauss, Magnetic Flux Density**, **Maxwell**, **Tesla,** and **Weber**.

Flux-Gate Magnetometer. Instrument that uses the flux-gate magnetic sensor technique for measurement of magnetic fields. The flux-gate probe consists of a ferromagnetic core wound with two coils (one for excitation and one for detection). The flux-gate technique utilizes magnetic induction and the hysteresis exhibited by all ferromagnetic materials. A high-purity sinusoidal current is applied to the excitation coil to generate an alternating magnetic field in the core. This excitation current magnetizes the core, continuously driving it in and out of saturation. Because of hysteresis, the magnetic flux through the core will trace a loop if it is plotted against the magnetic field intensity. Changes in the flux density through the core are sensed by the detection coil. As the core is driven into saturation, the reluctance of the core to the external axial magnetic field being measured increases, making it less attractive for the external magnetic field to pass through the core. As the field is repelled, its change in flux density is sensed by the detection coil. When the core comes out of saturation by reducing the current in the excitation coil, the external magnetic field is again attracted to the core, which is again sensed by the detection coil. Thus, alternate attraction and repulsion (gating in and out) cause the magnetic lines of flux to cut the detection coil, and the induced current is converted to a linear voltage, which is proportional to (and used to measure) the external magnetic field.

FM Radio Broadcast Band. Band of frequencies assigned for frequency-modulated broadcasting to the general public.

Fog. Visible aggregate of minute water droplets suspended in the atmosphere near the earth's surface. According to international definition, fog reduces visibility below 1 km. Fog differs from clouds only in that the base of fog is at the earth's surface while clouds are above its surface. When composed of ice crystals, it is termed ice fog. Fog is easily distinguished from haze by its appreciable dampness and gray color. Mist may be considered as intermediate between fog and haze. Mist particles are microscopic in size. Mist is less damp than fog and does not restrict visibility to the same extent. There is not a distinct division, however, between any of these categories. Near industrial

and heavy traffic areas, fog is often mixed with smoke and vehicle exhaust, and this combination is known as smog. *Note:* Under fog or other dew formation conditions, conductors can become wet or dry depending upon the level of the load current in the conductors. Medium- to high-load currents produce enough heat through I^2R (resistance) losses to discourage dew formation. Load current also speeds up the drying process after rain, fog, wet snow, etc.

Form Factor. The form factor of an insulator gives the relationship between the resistivity of a surface layer and the overall resistance of that same surface. This dimensionless ratio is calculated by the integral of the reciprocal value of the insulator circumference over the length of the leakage path.

Foul Weather. Weather condition when there is precipitation or that can cause the transmission-line conductors to be wet. Fog is not a form of precipitation, but it causes conductors to be wet. Dry snow is a form of precipitation, but it may not cause the conductors to be wet.

Foul-Weather Audible Noise (*also* **Foul-Weather Radio Noise** and **Foul-Weather Corona Loss).** In the context of audible noise, radio noise, and corona loss from overhead transmission lines, this term refers to conditions of rain, fog, mist, snow, sleet, and conductor icing.

Free-Body Electric Field Meter. Type of electric field meter where the detector is housed between the two electrodes of the sensor, and the whole assembly is electrically floating in space by means of an insulating handle without any electrical connection to ground.

Frequency Spectrum. Distribution of the amplitude (and sometimes the phase) of the frequency components of a signal, as a function of frequency.

Front (of an impulse). Part of an impulse before it reaches the crest value.

Fundamental-Harmonic. The fundamental of a periodic quantity is a sinusoidal quantity at the same frequency of the periodic quantity, representing the first term of the Fourier expansion of the periodic quantity.

Gamma. Smaller unit of magnetic field strength in the CGS electromagnetic system. One gamma (g) equals 10^{-5} oersted. The earth's magnetic field has sometimes been stated in units of gamma. *See also* **Oersted**.

Gap Discharge (*also* **Microspark).** A spark breakdown occurring in the miniature air gap formed by two conducting or insulating surfaces and sometimes between a conducting and an insulating surface.

Gap Factor. The dimensionless ratio between the 50% flashover voltage of a gap under consideration and the 50% flashover voltage of the rod-plane gap, with the same length and subjected to an impulse of positive polarity and with the critical time-to-crest.

Gap Length (*also* **Gap Spacing** and **Gap Distance).** Shortest distance between energized and grounded electrodes.

Gauss. Unit (in the CGS system) used to describe magnetic flux density (B), or magnetic flux lines (f) per unit of cross-sectional area. The gauss is one maxwell (one flux line) per square centimeter, or 10^{-4} weber per square meter. One gauss equals 10^{-4} tesla (MKS or SI units), and 1 mG equals 0.1 m T. *See also* **Magnetic Flux Density**, **Maxwell**, **Tesla,** and **Weber**.

Gaussian Distribution. *See* **Normal Distribution**.

Generated Acoustic Power. Noise power generated by a conductor or a phase per unit of length. It is expressed in units of W/m. There is a generated acoustic power, A, for the broadband noise and a generated acoustic power, A_h, for the hum.

Generated Corona Loss. A quantity related to the corona loss of a conductor that is a function only of the conductor radius and the electric field distribution near its surface and not on the overall conductor configuration. It is expressed in units of W/m.

Generation Function (for audible noise). Quantity that characterizes the audible noise produced by one conductor or one phase of an overhead transmission line. The generation function is independent on the proximity to ground or to other phases and on the location of the microphone; it depends only on weather and conductor surface conditions, on conductor or bundle dimensions, and on the surface gradient. The generation function for audible noise is the Generated Acoustic Power (W/m).

Geographic Information System (GIS). A computer system capable of storing, analyzing, and displaying data and describing places on the earth's surface.

Geometric Mean Diameter (GMD). Measurement used to characterize a conductor's diameter for inductance calculations. The GMD of various conductors is standard information usually provided by the conductor manufacturer. Chapter 2 of this book provides references to tables of conductor data that include the GMD and also formulas to estimate the GMD for single or bundled configurations. The GMD of a conductor(s) is used in calculations related to active and passive shielding.

Geometric Resistance. The resistance of a solid conducting electrode to remote earth. The difference between the geometric resistance of a wire frame approximation to a solid electrode and its true resistance is given by the contact resistance. *See also* **Contact Resistance.**

GFD. *See* **Ground Flash Density.**

GIS. *See* **Gas-Insulated Substation** or **Geographic Information System.**

GIS (Gas-Insulated Substation). For applications where space requirements are a problem, conventional bus arrangements are replaced with gas-insulated substations. The gas is generally SF_6. Each conductor is placed in the center of an enclosure filled with SF_6, which exhibits excellent dielectric strength and, therefore, allows small distances between the energized conductor and the enclosure, which is at ground potential.

Global Positioning System (GPS). A navigational system involving satellites and computers that can determine the latitude and longitude and elevation of a receiver on earth by computing the time difference for signals from different satellites to reach the receiver.

Glow. A stable, essentially steady discharge of constant luminosity at either positive or negative electrodes.

GMD. *See* **Geometric Mean Diameter.**

GPR. *See* **Ground Potential Rise.**

GPS. *See* **Global Positioning System.**

Gradient. Operator in vector calculus that converts a scalar quantity into a vector quantity whose direction is in the direction of the greatest rate of change of the scalar quantity, and whose magnitude is equal to that rate of change (such as the gradient of the space potential is the electric field). Also sometimes used imprecisely for surface gradient. *See also* **Surface Gradient.**

Grading Ring. *See* **Corona Ring.**

Grounds. Related terms include:

Ground Electrode. A conductor, or a system of interconnected conductors, or other conducting parts acting in the same manner, embedded in the earth and electrically connected to it, or embedded in concrete, which is then in contact with the earth over a large surface area.

Electrical System Grounds. System to limit voltage to ground and give a low impedance path for fault currents. One wire or point of an electrical circuit in an electrical system ground is connected to earth. This connection is usually at the electrical neutral (though not always), and is called the "system ground."

Lightning Grounds. Grounds to safely dissipate lightning currents into the earth. They are part of a lightning protection system (LPS) that usually includes overhead groundwires, down conductors, electrodes, arresters, and other connectors or fittings required for a complete system. A lightning protection system mitigates buildings, their occupants, and contents from the thermal, mechanical, electrical and electromagnetic effects of lightning.

Permanent Grounds. Ground electrodes included in electric power system design to protect system components from unwanted energy flow. Permanent grounds include such components as station grounds and grounding grids, system neutrals, overhead groundwires, wood pole structure downleads, and ground rods, grounding strips, plates, grillages, and buried counterpoise.

Signal Reference Grounds. Grounds that provide a low impedance signal reference system for electronic equipment to minimize higher-frequency noise-induced voltages and thereby reduce equipment malfunctions.

Static Grounds. Grounds that connect a piece of equipment to earth to drain off static or power-frequency capacitive electricity charges before they reach a sparking potential. Static grounding involves connecting large metal objects such as fuel tanks or aircraft to earth through a ground rod. Coupling of energy to the large objects is mainly capacitive, and the source impedance is high, so static bond wires can be too small to provide adequate power system equipment grounding or lighting protection systems.

Temporary Grounds. Grounds used at defined work sites to connect isolated conductors or equipment either to a permanent ground or to an equivalent ground point such as a substation. Portable temporary grounds are assemblies of approved clamps and cables, sized to carry unwanted currents available at the work site from all possible sources.

Grounded. Conductor, current-carrying component, or other object that is intentionally connected to earth through a ground connection or connections of sufficiently low impedance and having sufficient current-carrying capacity to limit the buildup of voltages to levels below that which may result in undue hazard to persons or to connected equipment.

Ground Fault. An insulation fault between a conductor and ground or frame.

Ground Flash Density (GFD). The average number of lightning flashes to the earth per square kilometer per year expected at a specified location.

Grounding (*also* Grounding System). Total of all means and measures by which part of an electrical circuit, accessible conductive parts of electrical equipment (exposed conductive parts) or conductive parts in the vicinity of an electrical installation (extraneous conductive parts) are connected to earth.

Ground Mat. A system of bare connectors, on or below the surface of the earth, connected to a ground or ground grid to provide protection from dangerous touch potentials. *Note:* Plates and gratings of suitable area are common forms of ground mats.

Ground Plane. Geometric plane that is defined to have an electric potential equal to zero everywhere. Usually used to describe the surface of the earth below a transmission line.

Ground Potential Rise (GPR). The difference in electric potential between a location on the ground in proximity to a point of large current injection into the ground and any remote ground point. GPR is usually caused by a short circuit of an energized power conductor to ground, and is the result of an injected current flowing through the impedance of the ground circuit.

Ground Resistance. The ohmic resistance between the grounding electrode and a remote grounding electrode of zero resistance. *Note:* In this context "remote" refers to a distance such that the mutual resistance of the two electrodes is essentially zero.

Ground Resistivity (specific earth resistance). *See* **Resistivity.**

Ground System Impedance. A complex number that is the ratio of the phasor voltage between a grounded conductor (or system of conductors) and remote earth and the phasor current injected into the earth through the conductor. At zero frequency, the ground system impedance reduces to the ground resistance. At high frequency, the ground system impedance is also a function of skin depth. For lightning, the ground system impedance is a function of geometric resistance, contact resistance and ground plane surge impedance. *See also* **Contact Resistance, Geometric Resistance, Ground Resistance, Skin Depth,** and **Surge Impedance.**

Ground Wire. *See* **Grounds.**

GTACSR. Gap-type TAL Aluminum alloy Conductor, Steel Reinforced.

Hall Effect. In 1879, E. H. Hall observed that a small voltage is generated across a conductor carrying current in an external magnetic field. The amount of this "transverse" voltage (or Hall voltage) is directly proportional to the value of magnetic flux density. This means that magnetic flux can be measured by means of the voltage perpendicular to the electric current. Modern instruments (gaussmeters) use sensors, such as Indium-Arsenide probes, that measure the magnetic flux density using the Hall Effect principle.

Harmonic Content. Distortion of a sinusoidal waveform characterized by indication of the magnitude and order of the Fourier series terms describing the wave. For power-frequency fields, the harmonic content of the electric field coincides with that of the line voltage, and the harmonic content of the magnetic field coincides with that of the line current for single-phase systems. For power transmission lines, the harmonic content is small, except during transient conditions, and of little concern for the purpose of field measurements, except at points near large industrial loads such as saturated power transformers, *n*-pulse rectifiers, or aluminum, chlorine, and graphite plants where certain harmonics may reach 10% of the line voltage. Laboratory installations may also have voltage or current sources with significant harmonic content. *See also* **Total Harmonic Distortion.**

Harmonics (*also* Overtones). Integer multiples of a fundamental frequency. The lowest frequency is called the fundamental frequency; for example, the fundamental frequency of the U.S. electric power system is 60 Hz (other countries have a fundamental frequency of 50 Hz). For a 60-Hz fundamental, the second harmonic would be 120 Hz, the third harmonic would be 180 Hz, and so forth.

Helmholtz Coils. Coil system that can produce nearly uniform magnetic fields over a significant volume for calibration purposes. Helmholtz coils have many turns of wire and are identical in construction; the coils can have either circular or rectangular geometry. The pair of coils are placed parallel to each other, spaced at one-half their diameter apart, and are energized by a common source. Careful construction of the coils to ensure accurate dimensions is critical to producing uniform fields. An accurate method of determining the current supplied to the coils is necessary. The measurement of coil current usually employs a precision component or method that is traceable to NIST to guarantee accuracy.

High-Phase-Order Transmission Line. Transmission lines with more than three phases per circuit. The phases are multiples of three. Six-phase and twelve-phase transmission have been the object of several studies and of at least one utility pilot project. They utilize the space more efficiently than three-phase transmission. The space compaction results in reduced electric and magnetic fields.

Hoarfrost. Deposit of interlocking ice crystals (hoar crystals) formed by direct sublimation on objects, usually those of small diameter freely exposed to the air such as tree branches, plant stems and leaf edges, wires, poles, etc. The deposition of hoarfrost on an object is similar to the process by which dew is formed, except that the temperature of the object must be below freezing. It forms when air with a dew point below freezing is brought to saturation by cooling.

Horizontal Scanning Frequency. Frequency that describes how often a video display terminal (CRT-type) draws a single scan line on the display; sometimes called horizontal sync. Horizontal scanning frequencies are many kHz (thousands of lines are drawn each second). For VGA resolution, the horizontal scanning frequency is 31.5 kHz; for Super VGA resolution, the frequency ranges from about 35 to 48 kHz, depending on the vertical refresh rate of the graphics adapter.

HPFF. *See* **Pipe-Type Cable.**

HPGF. *See* **Pipe-Type Cable**.

HPOF. *See* **Pipe-Type Cable.**

HS Steel. Also designated S2. High Strength steel core wires for ACSR.

Hum. Pure tone at a frequency equal to twice the power frequency—i.e., 100 Hz for 50-Hz systems and 120 Hz for 60-Hz systems. This tone is the result of a pressure wave caused by the movement of air ions alternatively attracted to and repelled from the conductors. The pressure variations are not purely sinusoidal and may occur differently during the positive and negative cycles. Therefore, a 50- or 60-Hz component and harmonics of the hum may also be present even though their amplitude is much smaller than the component at 100/120 Hz. Among the harmonics, the second (200/240 Hz) is often measurable above the broadband noise.

HVAC. High Voltage Alternating Current.

HVDC. High Voltage Direct Current. *See* **HVDC Transmission.**

HVDC Transmission (High Voltage Direct Current Transmission). The transfer or transmission of electric energy by direct current from its source to one or more main receiving stations. The use of the term "high voltage" implies that voltages are in excess of 100,000 V (i.e., greater than 100 kV).

Hydrophilic Surfaces. A hydrophilic is characterized by a high surface tension that causes water to form a thin film on the surface. In polluted conditions the surface conductance of a hydrophilic insulator surface increases during wetting conditions, allowing increased leakage currents across the surface of the insulator. Under critical contamination and wetting conditions, the conductivity may become high enough to result in flashover.

Hydrophobic Surfaces. Hydrophobic surfaces have a low surface tension, which causes water to bead when coming into contact with it. In contamination conditions, this provides an advantage for insulator surfaces because a continuous water layer rarely forms on such a surface, which, in turn, reduces leakage currents and the likelihood for flashover.

Hydrophobicity. One of the most important surface characteristics of an insulator is how it interacts with water on its surface. This is normally described in terms of its hydrophobicity. The surface condition may be anything between water-repellent (called *hydrophobic*) to easily wettable (called *hydrophilic*).

I.A.C.S. or **IACS.** International Annealed Copper Standard.

ICNIRP. International Commission on Non-Ionizing Radiation Protection.

IEC. International Electrotechnical Commission.

IEEE. The Institute of Electrical and Electronics Engineers (IEEE) is the world's largest technical professional society. Founded in 1884 by a handful of practitioners of the new electrical engineering discipline, IEEE is comprised of more than 320,000 members who conduct and participate in its activities in approximately 150 countries. The technical objectives of the IEEE focus on advancing the theory and practice of electrical, electronics, and computer engineering and computer science. IEEE promulgates standards that apply to many subjects, including EMF measurements, instrumentation, and calibration.

Image Conductors. An electric field calculation technique consists of replacing the earth or ground plane (modeled as a plane at zero potential) with a set of conductors, called image conductors, which are located as the geometric mirror image of the phase conductors (but with opposite sign charges) below the ground plane. A somewhat similar use

of image conductors can be used for magnetic fields, but since the earth is not a perfect conductor, the location of the currents in the earth is not easily definable. At power frequency and as a practical approximation, the depth of the images below the ground plane is independent of the height of the phase conductors and, for a homogeneous earth, is approximately equal to $600\sqrt{\rho / f}$ (m). For example, for $\rho = 100\ \Omega$ m and f = 60 Hz, the image depth is equal to 852 m.

Immunity. Ability of electronic equipment or systems to perform satisfactorily in the presence of a specified electromagnetic environment.

Impingement Plume. *See* **Breakdown Streamer.**

Impulse. Intentionally applied transient voltage that usually rises rapidly to a peak value and then falls more slowly to zero.

Impulse Bandwidth. Peak values of the responsive envelope divided by the spectrum amplitude of an applied impulse.

Impulse Generator. Electrical equipment used by high-voltage laboratories for the generation of switching and lightning impulses. A conventional impulse generator is composed of capacitors that are first charged and then discharged in a circuit containing the test object.

Impulsive Noise. Noise characterized by transient disturbances separated in time by quiescent intervals. *Notes:* (1) The frequency spectrum of these disturbances is substantially uniform over the useful pass band of the transmission system. (2) The same source may produce impulse noise in one system and random noise in a different system.

Induced Flashover. When lightning strikes near a transmission or distribution line, electromagnetic induction processes can create transient voltages up to several hundred kV on the line phase conductors, even though the line does not sustain a direct strike. If the line insulation levels are low enough, flashover can occur. This is primarily a problem with distribution or subtransmission lines.

Inductive Coordination (electric supply and communication systems). The location, design, construction, operation, and maintenance of systems in conformity with harmoniously adjusted methods that prevent inductive interference.

In-Span Spacers. Insulating spacers located within a span or spans of a power line and installed between phases to maintain adequate mechanical and electrical clearances. These spacers are often used when line phase spacing is to be compacted or to minimize damage due to wind-induced conductor motion.

Insulation Coordination (for a transmission line). The specification of all the dimensions or characteristics of the transmission line that affect its voltage withstand. These dimensions include: strike distance, or clearance between the phase conductor and the grounded tower sides and truss, insulator string length (number and type of insulators), location and number of overhead ground (shield) wires, specification of supplemental tower grounds, phase-phase strike distances, and phase-to-ground clearances at midspan. The goal of line insulation coordination is to specify the above dimensions and characteristics for a specific degree of reliability at minimum cost. Line insulation coordination is achieved through: (1) determining the electrical stress applied to the transmission line, (2) comparing the stress to the insulation characteristics, and (3) applying ameliorating measures such as surge arresters, shield wires, breaker–closing resistors, etc., when the insulation strength requirements are excessive.

Insulation Element. Air gap, or insulator, or a combination of air gaps and insulators that can be considered as a single test object when subjected to a switching impulse.

Ionization. The process by which an atom or molecule receives enough energy (for example, by collision with electrons, photons, etc.) to split it into one or more free electrons and a positive ion.

Ionization Coefficient. The number of electron-ion pairs produced in a gas by a single electron in moving a unit distance in the direction of the applied electric field.

IRPA. International Radiation Protection Agency.

Isolating Joints. Connectors between two sections of pipeline that are constructed of nonconducting material and used to electrically isolate different sections of the pipeline.

Jitter. Undesirable rapid, short-term image movement or distortion on the screen of a video display terminal (CRT type). Image distortion over a longer period of time is called "swim."

Joint-Use Corridor. A corridor occupied by more than one type of utility or transportation system such as pipelines, transmission lines, communication lines, highways, or railroads.

kcmil. A unit of conductor cross section area equal to 1000 times the area of a circle with diameter of 0.001 inch.

Keraunic Level. The expected average number of days per year when thunder will be heard at a specified geographic location. Keraunic level is usually found from "isokeraunic maps" showing contour lines of constant keraunic levels from which the keraunic level at any location can be interpolated. Several equations have been proposed to compute ground flash densities (GFD) from isokeraunic levels.

Kirchhoff's Laws. There are two Kirchhoff's laws that apply to electric networks: (1) The algebraic sum of the currents toward any point in a network is zero, and (2) the algebraic sum of the product of the current and resistance in any closed path in a network is equal to the algebraic sum of the electromotive forces in that path. These laws apply to the instantaneous values of currents and electromotive forces, but may be extended to the phasor equivalent of sinusoidal currents and electromotive forces by replacing the algebraic sum by the phasor sum and by replacing resistance by impedance.

Knee-point Temperature. The conductor temperature above which the aluminum strands of an ACSR conductor have no tension or go into compression.

L_5 Noise Level. Level exceeded 5% of the time. *See* **Exceedance Level**.

L_{10} Noise Level. Level exceeded 10% of the time. *See* **Exceedance Level**.

L_{50} Noise Level. Level exceeded 50% of the time. *See* **Exceedance Level**.

L_{90} Noise Level. Level exceeded 90% of the time. *See* **Exceedance Level**.

L_{95} Noise Level. Level exceeded 95% of the time. *See* **Exceedance Level**.

Lateral Profile. Series of measurements used to evaluate the spatial characteristics of a quantity as a function of distance away from a source. Examples are transmission-line electric or magnetic field lateral profiles, where the field is measured as a function of distance away from a transmission line, usually at equal spacing between measurement points. Typically, the lateral profile is initiated next to the source (or directly underneath a power line) and proceeds away from the source in a direction perpendicular to the source, taking field readings at specific incremental distances. The IEEE standard for measurement procedures for field profiles of ac power lines is IEEE Std. 644-1994.

L_{dn}. *See* **Day-Night Sound Level.**

Leader. Term relevant to the flashover process of long air gaps. The leader is a highly ionized channel that starts at some critical voltage from the stem of the streamers at the positive electrode and proceeds into the gap, often along a crooked path and in irregular fashion, characterized by sudden arrests, dark periods, re-illuminations, and restarts, at an average speed of 1 ~ 2 cm/μs until the negative electrode is at a striking distance, which is suddenly bridged in a "final jump." A **Continuous Leader** is a leader that propagates without steps and that corresponds to the lowest possible flashover voltage.

Leader Progression Model (LPM). An algorithm to simulate the progression of an electrical discharge along an insulating surface or through the air of an air gap prior to breakdown. When the discharge in the form of a leader either bridges the gap or bridges a specified portion of the gap, a breakdown is assumed to take place.

Leakage. Current that flows through or across the surface of insulation and defines the insulation resistance at the specified voltage.

Leakage (*or* Creepage) Distance.The shortest distance over the insulator surface between the end fittings is the leakage creepage distance. Since there is a linear relationship between the contamination flashover strength and leakage distance, the concept of specific leakage distance is commonly used. In the first edition of the IEC 815, the specific creepage distance was defined as the leakage distance divided by the phase-to-phase value of the maximum voltage for the equipment. This definition was based on the assumption that the insulation was installed between phase and ground, which is not always the case. To overcome this deficiency, IEC introduced the "unified specific creepage distance" concept, which is the leakage distance divided by the maximum operating voltage across the insulator. For the same pollution class, the *unified specific creepage distance* is √3 times the *specific creepage distance*. Both are usually expressed in mm/kV.

L_{eq}. *See* **Energy-Equivalent Sound Level**.

Let-Go Current. Largest power frequency current that can flow into the arm of a person contacting an energized electrode while the person is still capable of controlling the muscles of the hand and letting go of the contact.

LFOR. *See* **Lightning Flashover Rate.**

LI. *See* **Lightning Impulse Strength.**

Lightning Flash. The entire process of transporting electrical charge during a lightning event between cloud and earth or between cloud and cloud. This event may consist of several high current strokes as well as one or more gradual discharges between strokes.

Lightning Flashover Rate (LFOR). The rate of occurrence of flashovers on a transmission line caused by lightning, expressed in flashovers per km per year.

Lightning Impulse. A monopolar surge waveform with specified 30-90% equivalent rise time and time to half value—for example, the standard lightning impulse of 1.2/50 μs, or 0.2/10 μs, 4/10 μs, 8/20 μs, and 10/350 μs.

Lightning Impulse Strength (LI). Crest value of the impulse voltage that can be withstood by an insulator.

Lightning Overvoltage. A transient voltage across a line element (e.g., an insulator string) or between a line element and earth (e.g., tower base to deep earth voltage) caused by a lightning stroke.

Lightning Stroke. A momentary high current surge within the channel of a lightning flash, characterized by a rapid current increase to a maximum value, then a gradual decay to zero.

Lightning Stroke Waveshape. The variation of lightning current measured at the ground or apparatus termination during a lightning stroke, characterized by a rapid increase to a maximum value in a few microseconds followed by a slower decay.

Lightning Surge. *See* **Lightning Overvoltage.**

Like Phasing. *See* **Super Bundle Phasing**.

Linearly Polarized. An electric or magnetic field at a given frequency is linearly polarized when the field vector oscillates in time without changing direction. All the space components are in phase with each other. A single high-voltage electrode produces a linearly polarized electric field. A single line current produces a linearly polarized magnetic field. Three-phase electrical installations produce fields that are, in general, not linearly polarized. *See also* **Polarization**.

Line Charge. Electrical charge distributed along a line (usually uniformly along a straight line). Used for calculations of the electric field on conductor surfaces, corona effects, and electric field in proximity of power lines. The unit of measurement is C/m (coulomb per meter). The following equations relate the line charge, q, to the average electric field on the surface of a cylindrical conductor, G, to the electric field, E, and to the space potential, V_{sp}, at a point in space (if no other charges were present).

$G = \frac{q}{2\pi\varepsilon R}$ where R is the conductor radius.

$E = \frac{q}{2\pi\varepsilon R}$ where R is the distance between conductor center and measuring point; the field is directed from the conductor to the measuring point.

$V_{sp} = \frac{q}{2\pi\varepsilon}\ln(R / R_0)$ where R is the distance between conductor center and measuring point and R_o is the distance between conductor center and a reference point where the space potential is set to zero.

Line Current. Current in a straight, infinitely long conductor concentrated at the conductor center. Transmission-line currents are often treated as line currents for the purpose of calculating the magnetic field away from the conductors. The magnetic field, B, at a distance, R, from a single line current, I, is: $B=2I/R$, if B is expressed in milligauss, I in ampere, and R in meter.

Line Surge Arrester. See **TLSA**.

LIS/OTD. Lightning imaging sensors/optical transient detectors. Satellites in low earth orbit continuously operational to detect and report sudden flashes of light from clouds or the earth's surface. Data from these satellites, now operational for many years, provide valuable information on lightning activity around the earth.

Log-Periodic Antenna. Any one of a class of antennas having a structural geometry such that its electrical characteristics repeat periodically as the logarithm of the frequency.

Longitudinal Profile. Profile of a parameter, usually near ground level, measured at a constant lateral distance from the power line and plotted as a function of distance along the line. For example, a longitudinal profile of the vertical component of the electric field strength, of the radio noise field strength, etc.

Loop Antenna. Antenna consisting of one or more turns of a conductor. If the circulatory current is essentially uniform, the antenna will have a radiation pattern approximating that of an elementary dipole. *Note:* The loop antenna responds to the magnetic field component of the electromagnetic wave, in the direction of the loop axis.

Low Reactance Phasing (*also* Cross-Phasing, Reverse Phasing, and **Unlike Phasing).** Multiple electrical circuits arranged in a manner so that the phase sequence for one circuit is placed adjacent to the opposite phase sequence for the other circuit. For example, for a double-circuit vertical configuration line, one circuit may have A-B-C phases arranged top to bottom, and the adjacent circuit would have

C-B-A arranged top to bottom. This method produces lower fields at ground level but somewhat higher conductor surface gradients, with the potential for more corona-related phenomena. Low reactance phasing can be applied to double- or multi-circuit transmission or distribution lines, or transmission lines with a lower voltage underbuild. For magnetic field reduction, the method works best when current flow in the adjacent circuits is equal in magnitude and direction. Any deviation from these conditions lessens the effectiveness of applying low reactance phasing as a field management technique. If the current flow in adjacent circuits is in the opposite direction, the phasing on adjacent circuits should be made similar instead of opposite. *See also* **Super Bundle Phasing**.

LPM. *See* **Leader Progression Model.**

Magnetic Dipole. *See* **Dipole**.

Magnetic Field. Usually referred to as the vector field of magnetic flux density. *See also* **Magnetic Flux Density**.

Magnetic-Field Induction (*also* **Inductive Induction** *or* **Inductive Coupling**). A mechanism by which time-varying magnetic fields in space between a power line and a separate system of conductors cause currents and voltages on the system of conductors.

Magnetic Field Strength. A magnetic field exists in the region near a permanent magnet or current-carrying conductor, and can exert a force on electric currents (or an independent pole) placed in them. The magnetic field strength (H) at a point in space is a vector defined by its space components along three orthogonal axes. For steady-state sinusoidal fields, each space component is a complex number or phasor. The magnitudes of the components are expressed by their rms values of magnetomotive force (mmf) per unit length. In a multi-phase environment, such as near a three-phase electric power line, the field is characterized by a vector rotating in a plane where it describes an ellipse whose semi-major axis represents the magnitude and direction of the maximum value of the magnetic field, and whose semi-minor axis represents the magnitude and direction of the field a quarter cycle later at its minimum value. The unit of magnetic field strength in the SI system is the ampere-turn per meter, or simply, the ampere per meter (A/m), which is mmf per unit length. One ampere-turn per meter is the magnetic field strength in the interior of an elongated, uniformly wound solenoid that is excited with a linear current density in its winding of one ampere per meter of axial distance. (In the CGS system, the oersted is the unit of magnetic field strength: $4\pi\ 10^{-3}$ oersted = 1 A/m.) Sometimes the magnetic field strength (H) is described (incorrectly) using the units of its magnetic flux density (B) with units of tesla (or mT) and CGS units of gauss (or mG). One milligauss equals 0.1 microtesla. Magnetic field and magnetic flux density are related by the permeability of the material or medium in which they are characterized. The ratio of flux density (B) to field strength (H) is the permeability. *See also* **Magnetic Flux Density** and **Permeability**.

Magnetic Flux. Integral of the normal component of the magnetic flux density over a surface.

Magnetic Flux Density. Number of magnetic flux (force) lines per unit of cross-sectional area that permeate a magnetic field. The path of an independent (or isolated) pole in a magnetic field suggests a line of flux. A line of flux is a line so drawn that a tangent to it at any point indicates the direction of the magnetic field. The unit of magnetic flux (F) is the weber (Wb); in the CGS system, the unit of magnetic flux is the maxwell (Mx). One maxwell equals one magnetic flux line, and one weber equals $1 \cdot 10^8$ lines. The lines of flux (F) perpendicular to a specific area (A) in the magnetic field are collectively called the magnetic flux density. Therefore, the magnetic flux density, B, is given by: B = F /A. Magnetic flux density in the SI system is expressed in weber per square meter (Wb/m^2), or tesla (T); in the CGS system, magnetic flux density is expressed in maxwell per square centimeter (Mx/cm^2) or gauss (G). These units have the following equivalence: One tesla equals 10^4 gauss, and 0.1m T = 1mG. The magnetic field strength (H) is related to flux density (B) by the permeability of the medium. (In air, 4π mG equals 1 A/m). *See also* **Flux**, **Gauss**, **Tesla,** and **Weber**. *Note:* According to Maxwell's equations, the net magnetic flux through any closed surface is zero.

Magnetic Materials. Materials that are readily magnetized in a magnetic field. When one considers materials simply as either magnetic or nonmagnetic, this division is really based on the strong magnetic properties of iron. For example, iron, nickel, and cobalt are common examples of magnetic materials, while air, paper, and wood are examples of nonmagnetic materials. However, weak magnetic materials (sometimes called nonmagnetic materials) can be important in some applications. For this reason, a more exact classification includes the following three groups: **Ferromagnetic Materials** include iron, steel, nickel, cobalt, and commercial alloys such as alnico and Permalloy. They become strongly magnetized, in the same direction as the magnetizing field, with high values of permeability from 50 to 50,000. Permalloy has a relative permeability (with respect to air of 1) of 100,000, but is easily saturated at relatively low values of flux density.

Paramagnetic Materials include aluminum, platinum, manganese, and chromium. Their permeability is slightly more than 1. They become very weakly magnetized in the same direction as the magnetizing field. **Diamagnetic Materials** include bismuth, antimony, copper, zinc, mercury, gold, and silver. Their permeability is less than 1. They become very weakly magnetized but in the opposite direction from the magnetizing field.

Magnetic Quadrupole. *See* **Quadrupole**.

Magnetism. Property of materials to be magnetized. A material is magnetized when the orientation of its individual magnetic dipole moments is affected by an externally produced magnetic field. Three types of magnetism are paramagnetism, diamagnetism, and ferromagnetism. Paramagnetic materials, such as aluminum, have individual magnetic dipole moment randomly oriented in the absence of external magnetic field, and the material is unmagnetized. When magnetic field is applied, the individual magnetic moments align themselves with the field. When the field is removed, the magnetic dipoles return to their random orientation. In diamagnetic materials, such as copper, dipole moments are induced in a direction opposite to that of the applied fields. Ferromagnetic materials, such as iron, behave similarly to paramagnetic materials, except that they become much more magnetized than paramagnetic materials with a given applied field and, if the field is removed, many of the magnetic dipoles remain aligned. Paramagnetism and diamagnetism are extremely weak phenomena compared to ferromagnetism. For most practical considerations, they can be completely neglected. It is common practice to refer to ferromagnetic materials as "magnetic" materials. *See also* **Magnetic Materials**.

Magnetization. Vector quantity that quantifies the degree to which a material is magnetized. The magnetization is defined as the net dipole moment per unit volume, or the magnetic dipole density. Just as mass density (kg/m ^{3}) quantifies the degree to which matter is concentrated in materials, magnetization, M, quantifies the degree to which dipole moments are concentrated in materials. Its units are those of dipole moment per unit volume (Am^2/m^3 =A/m), or the same as magnetic field, H, in A/m; its direction is that of the preferred direction of the individual atomic dipoles. The degree to which a material becomes magnetized (the value of M) with a given applied field depends on the properties of the material itself.

Magnetostatic. *See* **Quasistatic**.

Management (EMF management). Prudent use of resources to effectively reduce exposure of people or equipment to power system electric and magnetic fields while maintaining power system reliability, safety, and effectiveness.

Maximum Allowable Conductor Temperature. The highest conductor temperature at which an overhead power line can be safely operated.

Maximum Field. Space component of a power frequency field (electric or magnetic) in the direction where the field is maximum. The maximum electric field is measured by orienting a free-body electric field meter in various ways until the maximum reading is obtained. The maximum magnetic field is measured by orienting a single axis sensor—e.g., a coil—in various ways until the maximum reading is obtained. The measurement of three orthogonal field components is not sufficient for the calculation of the maximum field. The square root of the sum of the squares of three orthogonal field components is the field "resultant." The field resultant coincides with the maximum field only when the field is linearly polarized. Power frequency fields are often elliptically polarized. In these cases, the field resultant is greater than the maximum field, by a factor that can be as large as $\sqrt{2}$.

Maxwell. Unit of magnetic flux in the CGS system. One maxwell (Mx) equals one magnetic line of force (or line of induction). In the SI system, the unit of magnetic flux is the weber. One weber (Wb) equals $1 \cdot 10^8$ lines (or Mx). Since the weber is a large unit for typical fields, the microweber unit can be used (1 μWb = 100 lines or 100 Mx).

Maxwell's Equations. James Clerk Maxwell (1831-1879) put the laws of electromagnetics in the form that we know them today. Maxwell's equations are used constantly and universally in the solution of a wide variety of practical problems. The scope of Maxwell's equations is remarkable, including the fundamental principles of electromagnetic and optical devices. The relations stated by Maxwell, known as Maxwell's equations, consist of four expressions: one derived from Ampère's law, one from Faraday's law, and two from Gauss' law. Maxwell's equations are given

here in general form and for free space. *See also* **Ampère's Law** and **Quasistatic**.

Maxwell's Equations: General Form

Name	Integral Form	(Point) Form
Ampère's Law	$\oint H \cdot dl = \int_S (J_c + \frac{\partial D}{\partial t}) \cdot dS$	$\nabla \times H = \frac{\partial D}{\partial t}$
(extended by Maxwell to describe enclosed current)		
Faraday's Law of Induction	$\oint E \cdot dl = \int_S \frac{\partial B}{\partial t} \cdot dS$	$\nabla \times E = -\frac{\partial B}{\partial t}$
(describes electrical effect of a changing magnetic field)		
Gauss' Law for Electricity	$\oint_S D \cdot dS = \int_V \rho dV$	$\nabla \bullet D = \rho \quad 6$
(describes relation between electric flux and charge)		
Gauss' Law for Magnetism	$\oint_S B \cdot dl = 0 \quad 7$	$\nabla \bullet B = 0 \quad 8$
(describes the nonexistence of a magnetic monopole or isolated pole)		

Notes: J_c = conduction current density and ρ = charge density $\oint$ = closed path integral, $\int_s$ = surface integral, $\oint_s$ = closed surface integral, $\int_v$ = volume integral.

For the special case of free space, where the conduction current density, J_c, and the charge density, ρ, are zero, the equations reduce to the following simpler form:

Maxwell's Equations: Free-Space Set

Name	Integral Form	(Point) Form
Ampère's Law	$\oint H \cdot dl = \int_S \frac{\partial D}{\partial t} \cdot dS$	$\nabla \times H = \frac{\partial D}{\partial t}$
Faraday's Law of Induction	$\oint E \cdot dl = \int_S \frac{\partial B}{\partial t} \cdot dS$	$\nabla \times E = -\frac{\partial B}{\partial t}$
Gauss' Law for Electricity	$\oint_S D \cdot dS = 0$	$\nabla \bullet D = 0 \quad 6$
Gauss' Law for Magnetism	$\oint_S B \cdot dl = 0 \quad 7$	$\nabla \bullet B = 0 \quad 8$

Mean Time Between Failures (MTBF). Basic measure of reliability for repairable systems. It is the mean time expected until the first failure of a piece of equipment. Technically MTBF should be used only in reference to repairable items, while Mean Time to Failure (MTTF) should be used for non-repairable items. However, MTBF is commonly used for both repairable and non-repairable items. *See also* **Mean Time to Failure.**

Mean Time To Failure (MTTF). Basic measure of reliability for non-repairable systems. It is the mean time expected until the first failure of a piece of equipment. MTTF is a statistical value and is meant to be the mean over a long period of time and large number of units. *See also* **Mean Time Between Failures.**

Metal End Fittings (Polymer Insulator). The metal end fittings provide the mechanism by which the fiberglass rod is attached to the structure and conductor hardware. These components are made of hot-dipped, galvanized, forged steel or ductile iron.

Method of Images. Method to calculate electric field and space potential whereby the ground plane (and other conductors) is replaced with fictitious simple charge distributions.

Midspan. Line cross section at the same distance from the two conductor support structures.

Milligauss. Unit in the CGS Systems used to describe magnetic flux density (flux lines per unit of cross-sectional area). It is one thousandth of a gauss (0.001G); it has the following equivalence with the tesla unit of the SI system: 1mG = 0.1m T. *See also* **Gauss**, **Magnetic Flux Density**, and **Tesla**.

MMF. *See* **Magnetomotive Force**.

Mobility. The drift speed of an electron or an ion in a gas per unit electric field strength. Ion mobility depends on the ionic species. In air, several ionic species can exist simultaneously, and therefore ion mobility is represented more appropriately by a statistical distribution, or a *mobility spectrum*, rather than by a single number.

Monopolar. Having the property of, or being related to, a monopole. For instance, the field is monopolar if its structure is the same as that of a field from a monopole.

Monopole. An isolated unit pole of a dipole. In electricity, the isolated (unit) charge, q, is the simplest structure that can exist—it can be called a unit electric pole or monopole. If two such electric charges of opposite sign are placed near each other, they form an electric dipole. In magnetism, isolated magnetic poles (monopoles), which correspond to unit electric charges, apparently do not exist (according to Maxwell's equations, the net magnetic flux through any closed surface is zero). The simplest magnetic structure is the magnetic dipole. All attempts to isolate these poles fail. The fact that iron filings cling mainly to the ends (poles) of a bar magnet does not mean that the

middle region of the magnet is not magnetized. If a magnet is broken, the fragments prove to be dipoles, not isolated poles. However, the fictitious concept of an isolated magnetic pole, or monopole, helps to develop other useful quantitative aspects of magnetism. (For example, a single current-carrying conductor whose return path is located far away is sometimes characterized as a magnetic monopole source). An isolated magnetic pole of unit strength has been defined as one that will repel an equal and similar pole placed 1 cm away (in a vacuum) with a force of 1 dyne. The repulsion or attraction is governed by Coulomb's law. The number of lines of force (flux) emanating from a magnetic pole of unit strength is 4 p maxwells (or 4 p lines). *See also* **Dipole** and **Flux**.

MTBF. *See* **Mean Time Between Failures.**

MTTF. *See* **Mean Time To Failure.**

Multipoles. Any general current distribution can be represented mathematically by a binomial expansion with an infinite number of terms. The first four terms in the series are called the monopole, dipole, quadrupole**,** and octopole terms, respectively. Collectively, they are referred to as multipoles.

NACE. National Association of Corrosion Engineers.

NALDN. North American Lightning Detection Network. An electronic network of lightning sensors located throughout the United States, Canada and Mexico recording magnitude, polarity and location of lightning flashes to earth. Data from this network are used to determine probabilities of stroke current magnitudes, ground flash densities and other stochastic data necessary for evaluating the lightning performance of transmission lines.

National Electrical Code (NEC). Published volume of rules whose purpose is "the practical safeguarding of persons and property from hazards arising from the use of electricity." The NEC states that its rules cover installations of electric conductors and equipment that connect to the supply of electricity, including conductors and equipment within or on public and private buildings or other structures, including mobile homes, recreational vehicles, floating buildings, and other outside premises such as yards, carnival, parking and other lots and industrial substations, installations of optical fiber cable, and installations in buildings used by the electric utility (offices, warehouses, garages, machines shops, etc.). The original code was developed in 1897 as a result of the efforts of various insurance, electrical, architectural, and related interests. The present NEC has been sponsored by the National Fire Protection Association for 87 years (see National Fire Protection Association, http://www.nfpa.org). The NEC is updated and revised, as necessary, on a three-year review cycle. The NEC committee includes representatives from insurance firms, electric utilities, Underwriters Laboratories, OSHA, organized labor, electrical contractors, telecommunications companies, equipment manufacturers, academia, heavy industry, chemical companies, regulatory and inspection organizations, engineering firms, water supply, gas and oil industry, electrical testing firms, cable and wire companies, electronics firms, computer companies, U.S. government agencies, etc. The NEC applies starting at the service point (the electric service meter) and includes facilities within the customer's installation. The NEC does not cover the electric supply system, which is covered by the National Electrical Safety Code. *See also* **National Electrical Safety Code.**

National Electrical Safety Code (NESC). Published volume of rules whose purpose is "the practical safeguarding of persons during the installation, operation, or maintenance of electric supply and communication lines and associated equipment." The NESC states that its rules contain the basic provisions that are considered necessary for the safety of employees and the public, and the NESC is not intended as a design specification or instruction manual. Work on the NESC started 85 years ago at the National Bureau of Standards. The NESC is applied to the electric supply system up to the electric service point of a customer; it does not cover premise wiring. The National Electrical Code (NEC) covers wiring from the electric service or supply point (the electric service meter). The present NESC is an American National Standard (ANSIC2-1997), with IEEE as the administrative secretariat (IEEE standards: http://www.standards.ieee.org). The NESC is revised, as necessary, on a five-year review cycle. The NESC is a consensus document prepared by those substantially concerned with its scope and provisions. The standards committee membership includes representatives, among others, from the electric utility industry, telephone industry, insurance companies, railroads, organized labor, regulatory agencies, contractors, equipment manufacturers, cable TV, and safety council. In some states in the U.S., other codes govern subjects covered by the NESC (e.g., for overhead transmission lines: General Order No. 95 in California and General Order No. 6 in Hawaii). *See also* **National Electrical Code (NEC).**

National Environmental Policy Act of 1969 (NEPA). The legislation that established the basic national policy in the United States for considering the environment effects of agency decisions. It established policy, set goals, and provided requirements for federal agencies to develop implementing regulations that follow the letter and spirit of the Act. Under NEPA, an agency must take a "hard look" at the environmental consequences of its actions and provide for "broad dissemination" of this information to the public.

NEC. *See* **National Electrical Code**.

Negative Glow. Glow corona mode that occurs at electric field strengths above those required for Trichel Streamers.

Negative Sequence. A balanced set of voltages or currents in a symmetrical component analysis corresponding to a phase rotation opposite to the normal rotation of the system.

Negative Sequence Component. *See* **Symmetrical Components**.

Negative Streamers. Streamers occurring at electric field strengths close to breakdown. These streamers appear as a bright filament with very little branching and extend far into the gap. (*Note:* Under alternating voltages, corona onset usually occurs during the negative half-cycle, while breakdown occurs during the positive half-cycle.)

NESC. *See* **National Electrical Safety Code**.

Net Current. When the instantaneous values of all the current-carrying conductors (including neutral conductors) in a circuit do not sum to zero, a net current is said to exist. Net currents are important in field management principles because they attenuate very slowly (with the inverse of distance) and are difficult to cancel with methods commonly used for balanced phase currents. Net currents must always return to the source transformer. Net currents may flow in the neutrals of other circuits, in the earth, or along any other conductive path to return to their source transformer.

Net Current Control Device. Device developed by EPRI that practically reduces to zero the net service drop current when it is inserted in the service drop.

NIEHS. National Institute of Environmental Health Sciences.

NIOSH. National Institute for Occupational Safety and Health.

NIST. The National Institute of Standards and Technology (NIST), formerly the National Bureau of Standards (NBS), was established by Congress in 1901 to support industry, commerce, scientific institutions, and all branches of government. For nearly 100 years the NIST/NBS laboratories have worked with industry and government to advance measurement science and develop standards. NIST maintains measurement and standards laboratories that provide technical leadership for vital components of the nation's technology infrastructure. EMF calibration facilities generally utilize precision components or methods that are traceable to NIST for their accuracy. (NIST: http://www.nist.gov).

Nonceramic Insulator. *See* **Polymer Insulator.**

Normal Distribution (*also* **Gaussian Distribution).** Function sometimes used to describe the flashover probability for different voltages. Its density function is: $p(V) = \frac{1}{\sqrt{2\pi}\sigma} e^{-(V-V_{50})^2/(2\sigma^2)}$. The cumulative probability is given by: $P(V) = \int_{-\infty}^{V} \frac{1}{\sqrt{2\pi}\sigma} e^{-(V-V_{50})^2/(2\sigma^2)}$.

Nuisance Shock. A small electrical discharge passing through a human that is perceptible but not dangerous.

Octave Band (*also* **One-Third** and **One-Tenth Octave Bands).** Term used in reference to measurements of sound-pressure levels. When more detail than can be provided by a simple measure of the noise (e.g., A-weighted) is desired, a complete determination of the frequency spectrum of the noise can be made using frequency analyzers. For field measurements of audible noise from transmission lines, an octave-band filter set is often used. For better definition, narrow-band frequency analyzers with one-third or one-tenth octave filters are also used. One octave is defined as a bandwidth for which the ratio between upper and lower frequency of the band is 2. For the one-third and one-tenth octave bands, the ratios are $2^{1/3}$ and $2^{1/10}$, respectively. As the bandwidth is increased, the pressure level measured for random noise (having a flat spectrum within the band) is proportional to the square root of the bandwidth, whereas for pure tones (e.g., the 120-Hz hum), the measurement is independent of the bandwidth.

Oersted. Unit of magnetic field strength in the CGS electromagnetic system. The oersted is defined as the magnetic field strength in the interior of an elongated, uniformly wound solenoid that is excited with a linear current density in its winding of one abampere (10 amperes) per 4 p centimeters of axial length. The oersted has the following equivalence with the SI unit of magnetic field strength: $4\pi \cdot 10^{-3}$ Oe = 1 A/m. (In air, a 1 oersted magnetic field produces 1 gauss of magnetic flux density.)

OHGW. *See* **Overhead Ground Wire.**

Onset Streamer. Streamer corona that occurs slightly above the positive corona onset and appears as bright blue brushes of increasing length as the voltage is increased.

Open-Circuit Voltage. The open-circuit voltage of an object in an electric field is the voltage between the object and ground after any short-circuit connection to ground has been removed.

OPGW. *See* **Optical Ground Wire.**

Optical Ground Wire (OPGW). Conductor used to shield transmission lines from lightning with its metallic cores replaced with optical fibers.

Outage (*also* **Line Outage).** The state of the line when it is not available to perform its intended function.

Outage Rate. The reliability performance of a transmission line, expressed as the annual number of power outages that result in system fault current, necessitating the operation of a switching device to clear the fault. The **Lightning Outage Rate** is the sum of the **Backflashover Rate** and the **Shielding Failure Flashover Rate**, all expressed in units of tripouts per 100 km per year.

Outside Phase. Arrangement of a support structure consisting of tower elements only partially surrounding the phase conductor and normally consisting of a truss and a tower leg. The **Outside Phase Gap** is defined by the geometry of conductors, hardware (including corona rings), insulators, truss, and tower leg or other tower elements.

Overhead Ground Wire (OHGW). Grounded wire or wires placed above the phase conductors for the purpose of intercepting direct strokes in order to prevent shielding failure flashovers. They may be grounded directly or through short air gaps. *See also* **Shield Wire**.

Parallel Plates. A method used to calibrate free-body electric field meters involves placing the meter between a pair of parallel conductive plates. The parallel plates should have a specific geometry so that there is a 2:1 ratio between plate dimensions and the spacing between them. Typical parallel plates are 1.5 m squares with spacing between the plates of 0.75 m. A variable voltage source is used to apply a potential across the plates, creating a relatively uniform vertical electric field in the central region between the plates. The meter to be calibrated is placed between the plates using the insulating handle that is supplied with this type of instrument. The method requires accurate dimensions for the plates and careful measurement of the applied voltage by use of a precision component or method traceable to NIST to guarantee accuracy.

Paramagnetism. *See* **Magnetism.**

Partial Discharge. Discharge that does not completely bridge the insulation between electrodes and does not reduce the voltage to zero.

Passive Loops. System of conductors arranged in a path (loop) near a transmission or distribution line, or other source, that uses induced currents to reduce the source magnetic field within a region of interest. The magnetic field due to the power line (or other source) induces currents in the conductive loops that, in turn, create another magnetic field that partially cancels the original magnetic field. *See also* **Cancellation Loops.**

Passive Shielding. Magnetic fields can be reduced (shielded) by establishing currents in wires such that the fields produced by those currents oppose the fields to be reduced. Passive shielding (or shielding with "passive" conductors) refers to use of currents induced in conductors by existing (or ambient) magnetic fields to reduce (shield) these fields in a certain region. *See also* **Active Shielding**, **Shielding**, and **Shielding Factor**.

Peak (of a wave, surge, or impulse). *See* **Crest**.

Peak Detector. Detector that indicates an output voltage that is the true peak value of an applied signal or noise.

Peak Value (of a wave, surge, or impulse). *See* **Crest Value**.

Permeability. Property of a material by which it changes the flux density in a magnetic field from the value in air (analogous to permittivity, ε, for electric field). Permeability, μ, is a physical constant (for a given temperature and material density) that reflects a material or medium's ability to "concentrate" magnetic flux lines. It is a function of the magnetic properties of the material (or medium). The permeability of a vacuum, μ_0, is equal to $4\pi\ 10^{-7}$ weber/Am in the SI system (it is $4\pi 10^{-7}$ henry/meter in the CGS system). The permeability of a vacuum and air are very nearly the same (and usually are taken as such). The permeability of diamagnetic materials is slightly less than μ_0, while for paramagnetic materials it is slightly more. Ferromagnetic materials have very large values of permeability. Permeability is the ratio of magnetic flux density (B) to magnetic field (H) in the medium: $B=\mu H$; so that for free space: $B=\mu_0 H$. Therefore, in free space, the conversion between magnetic field (H in A/m) and magnetic flux density (B in gauss or tesla) is as follows: 1mG = 0.1 μT = $(1/4\pi)$ A/m. For ferromagnetic materials, permeability is a nonlinear property. Very frequently in engineering applications, the dimensionless relative permeability (μ_r) is used to quantify a material's permeability (μ) with respect to free space: $\mu = \mu_0 \cdot \mu_r$. Permeability is a function of (among other things), flux density, frequency, and material thickness. *See also* **Relative Permeability**.

Permittivity. Property of a material by which it changes the electric flux density in an electric field from the value in free space (a vacuum) (analogous to permeability, μ, for

magnetic field). Permittivity, ε, is a physical constant (for a given temperature and material density) that reflects a material or medium's ability to "concentrate" electric flux lines. The permittivity of a vacuum, ε_0, is equal to 8.854 x 10^{-12} farad/meter. Permittivity is the ratio of electric flux density (D) to the electric field (E) in the medium: $D = \varepsilon_0 E$; so that for a vacuum $D = \varepsilon_0 E$.

Personal Exposure. Exposure (to electric or magnetic field) measured with an instrument placed on the body of a person or estimated by calculations. *See also* **Exposure**.

Phase. The phase or phase conductor is any conductor (other than the neutral conductor) in an electric power circuit designed to be energized at the nominal system voltage and carry power. In a three-phase power system, there are three phases consisting of one or more conductors per phase. For a balanced and symmetric three-phase electrical system, the phase conductors all have the same magnitude of current and are separated by 120 electrical degrees.

Phase Difference. Time in electrical degrees by which one electrical phase leads or lags another.

Phase Impedance Matrix. A matrix of self and mutual impedances relating the three-phase voltages and currents, as distinguished from the sequence impedance matrix relating sequence voltages and currents in a symmetrical component analysis. The phase impedance matrix can be generalized to higher dimensions to account for shield wires or multiple circuits.

Phase-to-Ground Insulation (or Stress or Strength). Insulation between the conductor of one phase (or any electrode connected to the conductor) and ground or grounded electrodes.

Phase-to-Phase Insulation (or Stress or Strength). Insulation between the conductor of one phase (or any electrode connected to the conductor) and the conductor of another phase (or any electrode connected to the conductor of another phase).

Phasing (of power lines). Order in which different phases of multiphase lines are placed (e.g., two three-phase lines on the same structure, several three-phase cable systems in the same ducts). For double-circuit lines, for instance, there are several possible phasing, such as super-bundle (or same phasing) and low reactance (or reverse phasing).

Phasor. Quantity with a sinusoidal time variation described by a magnitude and an angle (phase angle) in time: $q = Q \cdot \sin(\omega t + \alpha)$.

Pipe-Type Cable. Pressure cable in which the container for the electric conductors and pressurized medium is a rigid metal pipe. The pipe-type system is pressurized, usually with a dielectric liquid, and is commonly called a high-pressure-fluid-filled (HPFF) cable system. This cable system was called high-pressure-oil filled (HPOF) until the 1970s, when synthetic dielectric liquids began to replace the mineral oils that had been used earlier. Pipe-type cables rated up to 138 kV may be pressurized with nitrogen, and then are called high-pressure-gas-filled (HPGF) cables. In general, a cable simply called pipe-type refers to an HPFF cable. The first pipe-type cable system was a 66-kV circuit installed in 1932 by Philadelphia Electric Company. Over 80% of the transmission cable in the United States is HPFF. An excellent reference is the *EPRI Underground Transmission System Reference Book* (EPRI: http://www.epri.com).

PIR. *See* **Preinsertion Resistor.**

Pixel. Contraction of *picture element.* Smallest information building block of an on-screen image on a video display terminal. On a color monitor screen, each pixel is made of one or more triads. Resolution is usually expressed in terms of the number of pixels comprising the width and height of a complete on-screen image. For VGA, the resolution is 640 by 480 pixels; for super VGA, the resolution is 800 by 600 pixels.

PLC. *See* **Power Line Carrier.**

Plume. *See* **Breakdown Streamer.**

Point Source. Source of magnetic field that can be equated to a magnetic dipole (or, rarely, to a higher order element) concentrated at a point. A point source is characterized by a center and by the magnitude and direction of its dipole moment. The magnetic field decays with the third power of the distance from the center of a point source.

Polarity. Electrical state or condition of a quantity (e.g., charge, current, field) with respect to a reference point or condition. For time-invariant (or dc) quantities, the extent to which something is positive or negative describes its polarity. For time-varying (or ac) quantities, the extent to which things have the same instantaneous angular variation with time describes similar polarity. For example, the relative polarity of a transformer is a designation of the relative instantaneous direction of current in its leads (the same principle applies to the polarity of all transformer windings, and their relative polarity can be either additive or subtractive).

Polarization. Angular variation with time of either the electric or the magnetic field vector at a fixed point. If the spatial components of the field are all in phase with each other, the field is said to be linearly polarized (the field vector will oscillate back and forth along a line with time). If, on the other hand, the individual spatial components of the field are not all in phase, the field will be elliptically polarized (the field vector traces out an ellipse with time). An elliptically polarized field can be described by its semi-major axis (or maximum value) and its semi-minor axis (minimum value) a quarter cycle later. The field ellipse is completely specified by its degree of polarization (ratio of minor/major axis) and its orientation (the spatial direction of its major axis). A polarized field with a degree of polarization of unity (major and minor axes are equal) is said to be circularly polarized since its field ellipse will trace out a circle with time.

Polymer Insulator (*also* **Composite or Non-ceramic Insulator [NCI].** An insulator consisting of a fiberglass rod attached to two metal end fittings covered by a rubber weathershed system. The fiberglass rod provides mechanical strength, while the metal end-fittings allow attachment to structures and line hardware. The rubber weathershed system (housing), made up of a sheath and sheds, protects the rod from the environment and provides increased leakage distance.

Polymer Insulator Housing Material. The function of the polymer housing is to hermetically seal the rod from the environment, and to provide sufficient leakage distance to withstand both environmental and electrical stresses to which the insulator may be subjected. The housing typically comprises sheds and sheath (shank) sections. For transmission-line polymer insulators, the housing may be based on either an ethylene propylene rubber (EPR) or a silicone rubber (SIR).

Positive Glow. Glow corona that occurs at positive polarity as the result of a particular combination of rate of creation and removal of positive ions near the electrode and appears as a bright blue luminous sheet adhering closely and uniformly to the electrode. Occurring on thin wires at alternating voltages, this corona mode is also known as *ultra corona*.

Positive Sequence. A balanced set of voltages or currents in a symmetrical component analysis corresponding to normal phase rotation of the system.

Positive Sequence Component. *See* **Symmetrical Components**.

Potential. Functions in space from which vector fields can be obtained by taking spatial derivatives. For instance, the electric field (E) can be obtained by taking the negative gradient of the electric potential (V): $E = -\nabla V$. The above expression defines the potential V (i.e., the electric potential is the scalar function such that its negative gradient is the electric field). Similarly, there is a potential for magnetic fields. However, this potential is a vector function, A, and is defined by: $B = \nabla \times A$ and is called the magnetic vector potential. For the special case of regions of space where there are no currents, there is also a magnetic scalar potential, U, such that: $B = -\mu \nabla U$.

Potential Coefficient. Ratio between the voltage on an electrode not connected to ground (floating) and the charge on another electrode that causes that voltage. For instance, if the charge Q applied to conductor a induces a voltage V on conductor b, the mutual potential coefficient between b and c is: $P_{ba} = \frac{V_b}{Q_a}$.

Potential Point. Point at which the potential is calculated for the solution of electric field problems using the charge simulation method. *See also* **Charge Simulation Method**.

Power Electronic Devices. Systems of nonlinear devices (usually semiconductor) that are used to convert ac currents and voltages to dc currents and voltages and vice versa. Two or more of these systems may be combined to modify the phase or amplitude of ac voltages and currents.

Power Frequency. Frequency of the alternating voltages and currents used for the transmission of electric energy. This frequency is 60 Hz in the U.S., Canada, and Brazil, and 50 Hz in Europe and most other parts of the world.

Power Line Carrier (PLC). System that is connected to power transmission lines, that is operated at a frequency less than approximately 400 kHz, and that can be used for low-speed communication.

Power Quality. Any power problem manifested in voltage, current, or frequency deviations that may result in failure or misoperation of customer equipment.

p-Percent Disruptive Discharge Voltage. Prospective value of the test voltage that has a p-percent probability of producing a disruptive discharge.

p-Percent Flashover Voltage. Prospective value of the test voltage that has a p-percent probability of producing a flashover.

PPG, PPAG. *See* **Protective Gap**.

Pre-insertion Resistor (PIR). Resistor that is briefly inserted in each phase during the opening or closing of a circuit breaker.

Primary Shock. Direct physiological damage to a person caused by an electrical current.

Prospective Crest (of an impulse). Crest that an impulse would have achieved if no disruptive discharge had occurred.

Protective Gap (*also* Portable Gap, Portable Protective Gap [PPG], or Portable Protective Air Gap [PPAG]). Special equipment to be installed between the conductors and a grounded element at a tower adjacent to that on which live line work is performed. The equipment consists of an insulating support and two electrode connected, respectively, to the conductor and to ground. The air gap between the electrodes has a consistent strength, and flashes over if any surge above a given protective level occurs.

Protective Leakage (*or* Creepage) Distance. This is the part of the leakage distance that is not easily accessible to natural cleaning, and it is defined as the part of the creepage distance on the illuminated side of the insulator that would lie in shadow if light were projected on to the insulator at 90° (or 45° in special cases) to the longitudinal axis of the insulator.

Puncture. Electrical breakdown of the solid insulating material of an insulator instead of breakdown through the air around it. Usually the solid material dielectric strength is higher than the air around it, so flashover takes place through the air. However, if a very rapid voltage surge is applied, the air path around the insulator leakage distance can become dielectrically stronger than the solid insulation (volt-time effect) and a puncture of the solid insulation can occur. The dielectric strength of the solid insulation is usually found by testing the insulator immersed in a high-strength insulating liquid such as transformer oil so that dielectric failure can only occur within the solid dielectric.

Quadrupole. System of two equal and oppositely directed dipoles. If the pair of dipoles are two-dimensional (parallel wires), the result is a two-dimensional quadrupole; if they are three-dimensional (current loops), the result is a three-dimensional quadrupole. Similarly, there are even higher order multipoles.

Quasi-Peak (QP) Detector. Detector having a specified electrical time constant that, when regularly repeated pulses of constant amplitude are applied to it, delivers an output voltage that is a fraction of the peak value of the pulses, the fraction increasing toward unity as the pulse repetition rate is increased. *Notes:* (1) The fundamental characteristics of the quasi-peak detector are given in ANSI C63.2-1996. These characteristics, with the exception of the optional 600 ms discharging time constant, are the same as those specified by the International Special Committee on Radio Interference (CISPR Publication 16 [1999]). (2) The QP setting on some older radio noise meters produces a reading proportional to the average value of the quasi-peak output of the logarithmic detector on the meter scale.

Quasistatic. Treatment of a time-varying field as essentially a static field because the frequency has a wavelength much larger than any dimensions under consideration. This is the case of the fields associated with 50/60-Hz electric power (and its harmonics) because these extremely-low-frequency fields (ELF) have a wavelength that is far larger than the maximum dimension of any practical object (the wavelength at 60 Hz is 5000 km, or about 3100 miles; for 50 Hz, it is 6000 km or about 3700 miles). The main characteristic of Maxwell's equations is that the electric field depends on the magnetic field through the time variation of the magnetic field, and that in turn, the magnetic field depends on the electric field through the time variation of the electric field. Thus the fields are mutually coupled, and this is the reason why, in general, we speak of an electromagnetic field, which propagates in space, as Maxwell showed, at the speed of light. This particular form of coupling disappears when the fields are time-invariant (static); the two fields can then be determined, independently of each other, from the free-charge distribution, the free-current distribution, and the properties of the medium. This is why static-field problems are relatively easy to solve. When the dimensions of the system under consideration are much smaller than the wavelength corresponding to the frequency of operation, a quasistatic approximation has sufficient accuracy for most practical purposes. For quasistatic fields (which oscillate relatively slowly), the coupling between fields is disregarded, and both the electric field and the magnetic field are determined as if they were static fields. The reason that quasistatic electric fields can be treated as static fields is that in slowly varying electric fields, the time derivative of the electric flux density (the displacement current density) attains only minor (and insignificant) magnitudes, and the rate-of-change of the displacement current's magnetic field is so small that the electric field induced by it is insignificant. A similar explanation can be presented for the magnetic field to be treated as a static field. Therefore, the electric and magnetic fields effectively do not influence each other at these low frequencies and can be "de-coupled." Fortunately, for slow-varying fields, as any ELF field is, the problem is greatly simplified

by resorting to approximate solutions of Maxwell's equations, which lead to the treatment of quasistatic fields as static fields (i.e., electrostatic and magnetostatic) for most practical purposes. *See also* **Maxwell's Equations**.

Radiated Radio Noise. Radio noise propagated by radiation from a source into space in the form of electromagnetic waves (e.g., the undesired electromagnetic waves generated by corona sources on a transmission line). *Note:* Radiated radio noise includes both the radiation and the induction component of the electromagnetic fields generated by the noise source.

Radio Interference (RI). Degradation of the reception of a wanted signal caused by radio frequency (RF) disturbance. *Note*: Even though the term "radio" covers the entire radio spectrum (up to 3 THz), the term in the electric utility industry has come to be used to mean interference to the AM Broadcast Band.

Radio Navigation Systems. The application of radio frequency electromagnetic waves to determine a position on the earth.

Radio Noise (RN). Electromagnetic noise having components in the radio frequency range. *See also* **Conducted Radio Noise**.

Radio Noise Excitation Function. A quantity related to the radio noise current generated in a conductor by corona discharges and measured using a radio noise meter. This quantity is a function only of the conductor radius and the electric field distribution near its surface and not of the overall conductor configuration. It is expressed in units of $\mu A/m^{1/2}$ for the specific measuring frequency and bandwidth of the radio noise meter.

Railroad Equipment Immunity Level. The amplitude of an electrical signal at the terminals of a piece of railroad equipment below which the equipment operates properly.

Rain. Precipitation in the form of liquid water drops with diameters greater than 0.5 mm, or, if widely scattered, smaller diameters. For observation purposes, the intensity of rainfall at any given time and place may be classified as Very light: scattered drops that do not completely wet an exposed surface regardless of duration; Light: the rate of fall being no more than 2.5 mm/h; Moderate: from 2.6 to 7.6 mm/h, the maximum rate of fall being no more than 0.76 mm in 6 min; Heavy: over 7.7 mm/h. When rain gauge measurements are not readily available to determine the rain intensity, estimates may be made according to a descriptive system set forth in observation manuals. *Notes:* (1) For corona studies, probability distributions for rain are produced from data obtained during "measurable rain" (i.e., rain intensities that can be measured with standard rain counters such as tipping buckets or instantaneous rate meters). (2) For ac lines, heavy rain levels are often considered representative of maximum or L_5 levels. Heavy rain data are often generated by artificial tests on conductors strung in high-voltage test setups. (3) The only other form of liquid precipitation, drizzle, is to be distinguished from rain in the drizzle drops are generally less than 0.5 mm in diameter, are very much more numerous, and reduce visibility much more than does light rain.

Random Noise (*also* Fluctuation Noise). Noise that comprises transient disturbances occurring at random. *Notes:* (1) Random noise is the part of noise that is unpredictable except in a statistical sense. The term is most frequently applied to limiting cases where the number of transient disturbances per unit time is large, so that the spectral characteristics are the same as those of thermal noise. Thermal noise and shot noise are special cases of random noise. (2) A random noise whose instantaneous magnitudes occur according to the Gaussian distribution is called "Gaussian random noise." (3) In power-line noise, "random noise" is a component of the total noise caused by discharges.

Random Noise Bandwidth (*also* Fluctuation Noise Bandwidth). Width in hertz of a rectangle having the same area and maximum amplitude as the square of the amplifier frequency response to a sinusoidal input.

RAPID. Research And Public Information Dissemination program of the NIEHS and Department of Energy to study EMF during the period 1994-1999.

RBS. Rated Breaking Strength of conductor. A calculated value of composite tensile strength, which indicates the minimum test value for stranded bare conductor. Similar terms include Ultimate Tensile Strength (UTS) and Calculated Breaking Load (CBL).

Reduction Factor (*also* Field Reduction Factor). Term sometimes used to qualify shielding effectiveness. It is equal to the reciprocal of the shielding factor.

Reference Earth. That part of the ground, particularly on the earth surface, located outside the sphere of influence of the considered earth electrode. One test (real or conceptual) for sphere of influence is to impress a current through the electrode and to establish the locations where there is no perceptible voltage between two random points resulting from this grounding current flow. The potential of reference earth is always assumed to be zero.

Reflection/Refraction Coefficients. When a traveling wave of current or voltage encounters a discontinuity, a portion of the charge in the transient reflects back in the

opposite direction, and a portion continues to travel in the same direction. Reflection and refraction coefficients determine the resulting voltages and currents flowing in each direction after reaching the discontinuity.

Refresh Rate. *See* **Vertical Scanning Frequency**.

Relative Insulation Stress (RIS). Ratio between the flashover voltage in standard atmospheric conditions (760 mm Hg, 20ºC, 11 g/m^3) and that in actual atmospheric conditions.

Relative Permeability. In engineering applications, the dimensionless ratio of the permeability, μ, of a material or medium with respect to the permeability of free space, μ_0, is sometimes used to quantify the material's magnetic properties. This ratio is called the relative permeability, μ_r, since it is referenced to (or relative) to free space: $\mu_r = \frac{\mu}{\mu_0}$ ($\mu_0 = 4\pi \cdot 10^{-7}$ weber/Am in the SI system and $4\pi \cdot 10^{-7}$ henry/m in the CGS system). *See also* **Permeability**.

Rephase. Changes to power line phase conductor positions on a supporting structure(s). It is usually done to enhance field cancellation between adjacent circuits of a power line. An example of rephasing would be to change the phase positions on a double-circuit transmission line to create opposite or cross-phasing for field management purposes. Rephasing is often done by changing the phase attachment points on the first structure outside substations at each terminus of a line. Sometimes rephasing of an entire power line route is done to achieve a field reduction at one location. Before rephasing a line, consideration is usually given to the initial cost to rephase and to potential impacts on maintenance, emergency repairs, any existing transpositions along the line route, changes in corona performance, different operation of the line in the future such that rephasing advantages disappear, and proximity to other power lines at different locations along a route at which rephasing could potentially increase field levels.

Resistivity. Resistivity of a material, ρ, is the resistance, measured between two opposite faces, of a 1-m cube of earth. Resistivity is the reciprocal of conductivity, σ, and both are characteristics of a material rather than a particular specimen; it is defined for isotropic materials. *See also* **Conductivity.**

Resultant. Square root of the sum of the squared rms values of the three orthogonal components that define an electric or magnetic field. The computed resultant can be larger than the actual maximum value that the field attains. If the field is linearly polarized, the resultant and maximum field values will be the same. However, if the field is elliptically polarized, the resultant will be larger than the maximum field because the resultant algebraically combines field components that do not achieve their maximum individual values at the same time. The largest error occurs for a field with circular polarization, in which case the resultant is about 41% larger than the actual maximum value that the field can attain at any given instant. Many instruments for measurement of magnetic fields report a resultant value obtained from combining the rms value of the three individual components as described above.

Return Stroke. When a downward leader initiating a lightning event reaches the earth, it completes an electrical path between earth and cloud. A strong electrical discharge, called a "return stroke," then travels upward from the earth termination point toward the cloud at a **return stroke velocity** of approximately one-third the velocity of light.

Reverse Phasing. *See* **Low Reactance Phasing**.

RI. *See* **Radio Interference.**

Right-Hand Rule. Method used to determine the direction of a magnetic field around a conductor carrying a current. The conductor is grasped in the right hand with the thumb extending along the conductor pointing in the direction of the current flow. With fingers partly closed, the fingertips point in the direction of the magnetic field.

Right-Of-Way (*also* **Servitude**). Land dedicated to the transmission line; where access is granted for the purpose of constructing, maintaining, and upgrading the line; where constructions and activities that may impair the reliability of the line are not permitted. An easement for a certain purpose over the land of another, such as the strip of land used for a road, electric transmission line, ditch, or pipeline. *See also* **Corridor**.

RIS. *See* **Relative Insulation Stress.**

Risk of Failure. Probability that a transmission line will experience a flashover when subject to a stress of a certain type—e.g., a switching surge caused by line energization or reclosing. For instance: "the risk of failure is one every ten thousand switching operations."

RMS (*also* **rms).** *See* **Root-Mean-Square.**

RN. *See* **Radio Noise.**

Rocket-Triggered Lightning. If a small rocket trailing a grounded wire is launched upward toward a thunder cloud,

the electric field created at the nose of the rocket by the grounded wire can increase until a upward leader initiates off the nose of the rocket to the charged cloud overhead. This completes an electrical path from earth to cloud along the wire, the wire vaporizes and a strong lightning discharge current is created in the wire path simulating a lightning "first stroke," often followed by one or more return strokes down the same path. Rocket-triggered lightning has been frequently used to examine the vulnerability of electrical apparatus to natural lightning damage.

Rod-Plane. Air gap in which the high-voltage electrode is a rod suspended from a distant conductor, and the grounded electrode is the ground plane. The rod may have a square or circular section and has, in general, small dimensions (less than 3 cm).

Rod-Rod. Air gap in which the high-voltage electrode is a rod suspended from a distant conductor, and the grounded electrode is another rod well above the ground plane. The rods may have a square or circular section and have, in general, small dimensions (less than 3 cm).

Rolling Sphere Method. A simplified ElectroGeometric Model (EGM) for calculating lightning striking distances to grounded objects that facilitates effective direct-stroke protection of buildings and substations. *See also* **Electro-Geometric Model.**

Root-Mean-Square. The root-mean-square value of a periodic function is the square root of the squared average value of the function taken throughout one period. Also called the effective value, the rms value of an alternating current is the number of amperes that, in a given resistance, produces heat at the same average rate as that number of amperes of direct current. Most electrical quantities used by electric power engineers and referred to in this handbook are usually given as the rms value (e.g., voltage, current, field strength), unless otherwise stated.

Root-Mean-Square (RMS) Detector. Detector that indicates an output voltage that is the rms value of an applied signal or noise.

RTS (Rated Tensile Strength). The axial mechanical rating of ACSR or other conductors.

Ruling (Effective) Span. Hypothetical level span length where the variation of tension with conductor temperature is the same as in a series of suspension spans.

Sag. Maximum distance, measured vertically, from a span of conductor to the straight line joining its two points of support. Sag of an ACSR conductor (in meters) is approximated by $0.0014(\text{Span})^2/(\%\text{RTS})$ where the span length is also in meters. *See also* **RTS** and **Span.**

Scalar Product. *See* **Dot Product.**

SDC (Self-Damping Conductor). An ACSR conductor with aluminum strands that are trapezoidally shaped and sized such that there is a small gap between layers to allow impact damping of aeolian vibration.

Secondary Ionization. The process by which free electrons are produced either at a conductor surface or in the gas by impact with positive ions or photons produced in the primary discharge process.

Secondary Shock. Person's reaction to the perception of an electrical current that does not cause direct physiological harm. The reaction may cause, however, startle or involuntary movement that may, in some cases, impair the person's safety.

Section Length. The section length refers to the shortest distance between fixing points of the live and earthed metalware, ignoring the presence of any stress control rings, but including intermediate metal parts along the length of the insulator.

Self-Restoring Insulation. Insulation that completely recovers its insulating properties after a disruptive discharge.

Self-Sustaining Discharge. The electrical discharge process that continues to develop even if the source of primary electrons, necessary to initiate the discharge, is removed.

Sensor. Part of an instrument that converts the quantity to be measured into an electrical signal, which is then processed, displayed, or recorded.

Sensor Vest (for electric field exposure measurements). Special vest used to measure human exposure to power frequency electric field. The vest is made of conductive cloth and is connected to a medical electrode on the body of the person through an instrument that detects or records the current induced in the portion of the body covered by the vest. Through calibration, the measurement can provide a record of the "equivalent electric field"—i.e., the field that would cause the same exposure if the person were standing erect and well grounded in a uniform electric field.

Sequence Impedance Matrix. A matrix of self and mutual impedances relating positive, negative, and zero sequence voltages (symmetrical components) to positive, negative, and zero sequence currents.

Shape Factor (for calculations of short-circuit currents induced by the electric field in conductive objects). Ratio between the equivalent area of an object and the area of the object projected on the ground plane. *See also* **Equivalent Area.**

Shape Factor (for calculation of capacitance and resistance). Ratio between the self capacitance of an object and the self capacitance of a sphere with the same surface area.

Sheath. Tubular impervious metallic protective covering applied directly over a cable core.

Shield. Conducting envelope, composed of metal strands, ribbon, or sheet metal that encloses a wire, group of wires, or cable, so constructed that substantially every point on the surface of the underlying insulation or core wrap is at ground potential or at some predetermined potential with respect to ground.

Shield Wire. A grounded wire placed near the phases of a power line for the purposes of: (1) protecting phase conductors from direct lightning strokes, (2) providing redundant parallel paths for a fraction of surge currents, (3) lowering the self-surge impedance of an OHGW system, (4) raising the coupling factor of an OHGW system to the protected phase conductors, (5) reducing induced voltages from external electromagnetic fields, or (6) lowering the external magnetic field of a transmission line.

Shielding. Action using an enclosure, screen, or grounded or energized conductor(s) to reduce the strength of current density or electric or magnetic field in a given region. The materials used for shielding enclosures or screens are always metals, but there is a difference in using good conductors with low resistance or using good magnetic materials with high permeability like soft iron or mu-metal. Energized conductors can also be applied to shielding problems as either active or passive conductors. The effectiveness of a shielding scheme is usually expressed as the shielding factor. *See also* **Active Shielding**, **Coefficient of Coupling, Passive Shielding**, and **Shielding Factor**.

Shielding Angle. The positive or negative angle formed between an overhead groundwire (shield wire) and a protected phase conductor beneath. By convention, if a pair of shield wires are outboard of a set of phase conductors, the shielding angle is negative, and if they are directly above, the shielding angle is zero.

Shielding Effectiveness. Generic term, without a rigorous mathematical definition, that refers to the ability of a shield to reduce field level.

Shielding Efficiency. Ability of a given material or structure(s) to act as a shield against incident fields. *See also* **Shielding Factor**.

Shielding Enclosure. Structure that shields its interior from an external (or exterior) electric or magnetic field, or conversely, shields the surrounding environment from an interior electric or magnetic field source. A high-performance shielding enclosure is generally capable of reducing both the electric and magnetic field strengths by one to seven orders of magnitude, depending on frequency. An enclosure is normally constructed of metal, with provisions for continuous electrical contact between adjoining panels, including doors.

Shielding Factor. Expression used to quantify the degree of magnetic field shielding over a region of space: $SF = \frac{B}{B_0}$. B is the rms value of the magnetic flux density with the shield, B_0 is the rms value of the magnetic flux density without the shield. The shielding factor is a function of position, and in general, can also be a function of frequency, field strength, temperature, etc. Since the shielding factor is the ratio of two magnetic field values, it is a dimensionless quantity. In some literature, the shielding factor (sometimes called the attenuation) is expressed in decibels (dB) of attenuation with respect to the reference value without the shield. $SF_{dB} = 20\log(\frac{B}{B_0})$. Another quantity sometimes used to describe shielding effectiveness is the Shielding Efficiency: SE = (1 - SF) · 100%. *See also* **Active Shielding**, **Passive Shielding,** and **Shielding**.

Shielding Failure. A lightning event characterized by a lightning flash terminating directly on a phase conductor, whether or not one or more shield wires are present to prevent this event. A shielding failure may or may not cause a line insulator flashover, depending on the stroke current magnitude, the surge impedance of the stricken phase, and the dielectric strength of the insulators supporting the phase.

Shielding Failure Flashover Rate. The outage rate caused by the number of shielding failures with first-stroke currents that exceed the critical current of the phase, added to the number of flashovers caused by subsequent strokes that follow the same path as a weak first-stroke current.

Short-Circuit Current (induced in objects by the electric field). Current flowing into a zero resistance connection between a conductive object and a conductive ground, when the object is placed in an electric field.

SI. International System (of units).

SI. *See* **Switching Impulse Strength.**

Signal-to-Interference Ratio (SIR). The ratio of the desired voltage (the signal) to the undesired voltage (the interference) at the input to a receiver. *See also* **Signal-to-Noise Ratio**.

Signal-to-Noise Ratio. Ratio of the value of the signal to that of the noise. *Notes:* (1) This ratio is usually in terms of measured peak values, in the case of impulse noise, and in terms of the root-mean-square (rms), in the case of random noise. (2) Where there is a possibility of ambiguity, definitions of the signal and noise should be associated with this term; as for example, peak signal-to-peak noise ratio, rms signal-to-rms noise ratio, peak-to-peak signal to peak-to-peak noise ratio, etc. In measurements of transmission-line noise in the AM frequency range, the ratio of average station signal level to quasi-peak line noise level is generally used.

Single Line to Ground (SLG). Referencing an event involving one phase and one ground.

Six-Phase Transmission Line. *See* **High-Phase Order Transmission Line**.

Skin Depth. Depth in a material at which the current density (induced by an electromagnetic wave) is attenuated to 1/e (or 36.8%) of its value at the surface of the material. The skin depth is given by: $\delta = \sqrt{\frac{2}{\omega\mu\sigma}}$ $\cdot \omega = 2\pi f$, μ is the permeability, σ is the conductivity. As an example, consider the skin depth of a plane electromagnetic wave incident normally on a good conductor, such as copper ($\mu = 1.26$ μH/m and $\sigma = 58 \cdot 10^{-6}$ siemens/m). The skin depth is 8.5 mm at 60 Hz, 0.066 mm at 1 MHz, and 0.0004 mm at 30 GHz. Thus, a high-frequency field is attenuated as it penetrates a conductor in a shorter distance than a low-frequency field; this phenomenon is often called skin effect. (This phenomenon is analogous to the way in which a rapid temperature variation at the surface of a thermal conductor penetrates a shorter distance than a slow temperature variation.)

Skin Effect. Phenomenon whereby a high-frequency field is attenuated as it penetrates a conductor in a shorter distance than a low-frequency field. It results in the nonuniform distribution of magnetic flux density in the cross section of the material. *See also* **Skin Depth**.

SLG. *See* **Single Line to Ground.**

Snow. Precipitation composed of white or translucent ice crystals, chiefly in complex branched hexagonal form and often agglomerated into snowflakes. For weather classification purposes, the intensity of snow is characterized as: (1) "Very light," when scattered flakes do not completely cover or wet an exposed surface, regardless of duration; (2) "Light," when the visibility is 1.0 km or more; (3) "Moderate," when the visibility is less than 1.0 km but more than 0.5 km; (4) "Heavy," when the visibility is less than 0.5 km. The classification of snowfall according to its intensity is identical to that of rain, where the equivalent amount of water accumulated in millimeters per hour is measured. An easier, but less accurate, approach uses the depth of accumulated snow.

Soil Resistivity. A property of soil that is the ratio of the electric field to the current density at any point in the soil. *See also* **Resistivity.**

Soil-to-Pipe Potential. The voltage difference between a conducting pipe and the adjacent soil. This potential difference could be dangerous when a person touches a conducting part of the pipeline while standing on the earth, or if the difference is sufficient to break down the insulating layer of the pipeline.

Sound-Pressure Level. Rms value of the small variations in air pressure that accompany the passage of a sound wave. It is expressed in N/m^2 or *Pa* (pascal). Since acoustic waves produce very small pressure changes, the sound-pressure levels are often measured in dB above 20 μPa. *See also* **Decibel.**

SOV. *See* **Switching Overvoltage.**

Space Charge. Electrical charges residing in a region of space. In air, under normal conditions, positive and negative charges in the form of air ions are about equal in number. so that the net space charge is zero. The conductor surface gradients of ac transmission lines are calculated assuming that the net space charge is zero—i.e., all the charges reside on the surfaces of the conductors and the ground. Near high-voltage conductors, however, corona produces partial discharges that cause regions with a large imbalance of either positive or negative ions. These space charges have a profound effect on the development of corona (*see* Chapter 8).

Space Potential. The space potential of a point in an electric field is a phasor representing the voltage difference between that point and ground. The unit of space potential is the volt. The space potential is perturbed by the introduction of a conductive object in the field. Unperturbed space potential, which exists if the object is removed, is often used when a space potential value is given.

Span. Distance between contiguous power line support structures.

Spark. A sudden and irreversible transition from a stable corona discharge to a stable arc discharge.

Spark Discharge. Discharges between conductive bodies at different potentials that come into contact in a power frequency electric field. For instance, spark discharges may occur when a person touches a vehicle near a high-voltage transmission line. The discharge occurs in the air gap just before the contact occurs. Often a spark discharge consists of a series of discharges as the arc extinguishes when the alternating voltage between the two bodies passes through zero and is re-established when the voltage increases.

Sparkover. Disruptive discharge between electrodes in a gas or liquid.

Split Phase (Power Line). A single-circuit, three-phase power line in which one or more phases are split into two or more conductors (subphases). The phase current would divide among the subphases and, if the position of the subphases is chosen correctly, the magnetic field at ground level would be significantly reduced. Split-phase lines could have different configurations, as shown in Chapter 7.

Spray Plumes. *See* **Breakdown Streamers.**

SSFOR. *See* **Switching Surge Flashover Rate.**

Stakeholder. A term used in environmental permitting that typically refers to a person, organization, or agency that has a stake or interest in the permitting decisions that are made and in the construction, operation, and maintenance of a development (e.g., utility) project.

Standard Air Density. Air density corresponding to a temperature of 20 ˚C and a pressure of 760 mm Hg, corresponding to 101.3 kPa.

Standard Deviation (of flashover voltage). Difference between the voltages corresponding to 50% and 16% disruptive discharge probabilities, calculated assuming that the curve describing the probability of flashover versus voltage is log-normal.

Standard Humidity (of air). Absolute humidity of 11 g/m^3.

Steady-State. Condition in which voltages and currents in an electrical system do not vary appreciably with time. Voltages and currents may be alternating, in which case the steady-state condition refers to their rms values. The term *steady-state* applies to electric and magnetic fields as well. Intermittents and transients are deviations from the steady-state conditions.

Step Potential. The highest potential difference between two points on the earth's surface separated by a distance of one pace (assumed to be 1 m). This potential difference needs to be coordinated for electrical safety, particularly under ac system fault conditions. *See also* **Fibrillation Current.**

Stoichiometric Mixture. Concerned with, involving, or having the exact proportions for a particular chemical reaction.

Streamer. Repetitive corona discharge characterized by luminous filaments extending into the low electric field region, neither a positive nor a negative electrode, but not completely bridging the gap.

Strength (of an insulation element). Ability of an insulation element to withstand a voltage stress. For switching surges, the strength of an insulation element is expressed by the 50% flashover voltage.

Stress (on an insulation elements). Voltage applied to the insulation element.

Strike Distance. The strike distance is the shortest distance from the energized hardware to the grounded hardware or structure. The strike distance may correspond to the dry arc distance.

Striking Distance. As a charged lightning downward leader approaches a transmission line, it induces strong opposite charges on all the line conductors. If this charge becomes sufficiently large on one or more of the line conductors, an upward streamer can initiate from a conductor and travel toward the approaching downward leader tip. This streamer can ionize and become an upward leader. A critical length of this leader, called the "striking distance," may be sufficient to reach the downward leader tip, closing the circuit and resulting in a completed lightning stroke channel between the downward leader and a wire, characterized as a strike to the wire.

Stroke. *See* **Lightning Stroke.**

Subconductor. Individual conductor of a bundle of conductors used for EHV and UHV transmission lines.

Subsequent Stroke. A stroke in a lightning flash following the initial first stroke, usually characterized by a more rapid rate of current rise, lower crest current, shorter time-to-crest, and shorter tail time than a first stroke.

Super Bundle Phasing (*also* **Like Phasing** or **Similar Phasing).** Multiple electrical circuits arranged in a manner so that the phase sequence for one circuit is placed adjacent to the same phase sequence for the other circuit. For example, for a double-circuit line with vertical configuration, one circuit may have A-B-C phases arranged top to bottom, and the adjacent circuit would also have A-B-C arranged top to bottom. This method produces somewhat higher fields at ground level than low reactance phasing or cross-phasing, but a super bundle configuration has somewhat lower conductor surface gradients with less potential for corona-related phenomena. For the case where current flow in adjacent circuits is in opposite directions, a super bundle will produce lower ground-level magnetic fields than low reactance phasing. *See also* **Low Reactance Phasing**.

Surface Charge. Electric charge distributed over a surface (units of C/m).

Surface Gradient. Magnitude of the electric field (which is the gradient of the space potential) at the surface of an object (e.g., overhead conductor). In general, its magnitude varies around the periphery of transmission conductors. Related terms include:

Average Maximum Bundle Gradient. The average of the maximum surface gradients of the individual subconductors of a conductor bundle.

Maximum Bundle Gradient. Same as *Maximum Surface Gradient*.

Maximum Gradient. Same as *Average Maximum Bundle Gradient*.

Maximum Surface Gradient. For a single conductor, maximum value of the surface gradient around its periphery; for a conductor bundle, maximum of the individual subconductors' maximum surface gradients.

Nominal Surface Gradient. Surface gradient of a transmission-line conductor when treated as a smooth cylinder with diameter equal to its nominal diameter (and in a corona-free environment).

Surge. Transient voltage, which usually rises rapidly to a peak value and then falls more slowly to zero, occurring in electrical equipment or networks in service.

Surge Impedance. Impedance of a load that would cause no net reactive power flow and approximately a flat voltage profile along the length of a transmission line. For a single-phase lossless line, the surge impedance is equal to $Z_S = \sqrt{X_L / Y_C}$, where X_L and Y_C are the series inductance and the shunt admittance per unit of length of the line, respectively. If line losses are neglected, the surge impedance is a pure resistance. The surge impedance loading of a line (*SIL*) is the power carried by the line terminated in its surge impedance: $SIL = \frac{V^2}{Z_S}$, where, for a three-phase line, V is the line voltage. Surge impedance loading is an important parameter affecting the maximum electrical load of a line in stable steady-state conditions.

Surge Impedance. For an individual wire, surge impedance is the ratio of voltage to current created by an electrical transient moving along the wire at the velocity of light in the medium surrounding the wire. The ratio of voltage to current will always be such that the energy stored in the electric field around the wire will be equal to the magnetic field energy stored around the wire. For a transmission-line tower or ground plane, surge impedance is the ratio of lightning surge voltage appearing at the tower top or tower base to the lightning current entering the tower top or tower base, treating the tower as a vertical transmission line and the ground plane as cylindrical waveguide. While tower and ground plane surge impedance is a function of time, average values are usually used to calculate insulator voltages created by lightning.

Surge Impedance Loading. *See* **Surge Impedance**.

Surge Protective Devices (SPD). The generic term used to describe a device by its protective function, regardless of technology, uses ratings, packaging, point of application, etc. An SPD is intended to either limit transient over voltages or divert surge currents or both. It contains at least one linear component. Also called arrester, lightning arrester, surge protector, and surge arrester.

Sustained Discharge. The electrical discharge process that ceases to exist if the source of primary electrons, necessary to initiate the discharge, is removed.

Swing Angle. Angle by which a vertical insulator swings under the action of wind that exercises forces on the conductors.

Switching Impulse. Impulse with a front duration with some tens to thousands of microseconds, used in high-voltage laboratories to simulate a switching surge.

Switching Impulse Strength (SI). Crest value of the switching surge voltage that can be withstood by an insulator.

Switching Overvoltage (SOV). *See* **Switching Surge.**

Switching Surge. Voltage surge resulting from a switching operation.

Switching Surge Flashover Rate (SSFOR). The rate of occurrence of flashovers on a transmission line caused by switching—e.g., expressed in flashovers per km per year.

Symmetrical Components. Mathematical technique developed by C. L. Fortescue (published in 1918) that can be applied to a variety of engineering problems. It is widely used for solving power engineering problems involving unsymmetrical (or unbalanced) power systems. In three-phase power systems, it is applied to current, voltage, and impedance problems. The method is used to transform an unbalanced three-phase system into three sets of balanced three-phase phasors. The method of symmetrical components is one form of a general matrix transformation. In this reference book, the method is applied usually to circuit or load condition issues that could affect EMF levels and attenuation characteristics. In general, an unbalanced system can be resolved into balanced, symmetrical, three-phase or single-phase vector systems (called symmetrical components), and used to obtain solutions to the original unbalanced, nonsymmetrical problem. The unbalanced system is uniquely resolved into three sets of balanced phase-sequence vectors called: positive sequence, negative sequence, and zero sequence components. In the method of symmetrical components, all of the resolved phase-sequence vectors rotate in the positive (counterclockwise) direction. The three vector components of the positive sequence components are equal to each other in magnitude, are 120 electrical degrees apart in phase, and achieve maximum values in the positive phase rotation sequence of A, B, C. The three negative sequence vector components are also equal to each other in magnitude, are 120 electrical degrees apart, and rotate counterclockwise, but in the negative phase sequence of A, C, B. The zero sequence vector components are likewise equal to each other in magnitude, but all three components are in phase (i.e., there is a zero degree angle or zero sequence between the three components). The magnitudes of the components within each of the three phase sequences (positive, negative, zero) are equal, but they may or may not be equal to each other in magnitude. The rotating vectors of each of the three sets of components may be shifted by some electrical angle from a common reference point in the rotating vector diagrams. A physical interpretation of positive sequence components, for example, would be the currents that would occur on a balanced power system; the sum of their instantaneous values is zero. Negative sequence components would exist (along with positive sequence components) in an unbalanced system in which the phase current magnitudes are numerically unequal but still sum to zero. Zero sequence currents exist when there is a net current (i.e., the instantaneous values of the phase currents do not sum to zero). The zero sequence phase currents would flow in the neutral or ground paths.

Symmetric Voltages. Three-phase line voltages are symmetric when the phase angle between them is $2\pi/3$ radian (120 degree). Transmission-line voltages are generally considered symmetric.

T2. Twisted Pair conductor with two ordinary, round, stranded conductors twisted around each other to enhance mechanical stability in wind.

TACIR. TAL Aluminum Alloy Conductor reinforced with an Invar steel core.

TACSR. TAL Aluminum Alloy Conductor reinforced by a conventional stranded steel core.

Tail (of an impulse). Part of an impulse past its peak value.

TAL. ("Thermal-resistant aluminum.") An aluminum zirconium alloy that has stable mechanical and electrical properties after continuous operation at temperatures of up to 150^{o} C.

Television Interference (TVI). Radio interference occurring in the frequency range of television signals.

TEM. Transverse Electro Magnetic. Mode of electrical transient propagation whose electric and magnetic field vectors are both perpendicular to the direction of propagation. No component is in the axial direction. This is the usual transmission-line transient propagation mode assumed for most lightning performance calculations.

Temporary Overvoltage. An oscillatory overvoltage, associated with switching or faults (for example, load rejection, single-phase fault) of relatively long duration and that is undamped or weakly damped.

Tesla. Unit in the SI system used to describe magnetic flux density, *B*, or magnetic flux lines per unit of cross-sectional area. One tesla equals one weber per square meter (or $1 \cdot 10^8$ lines/m^2). One tesla is equal to 10^4 gauss in the CGS system: 0.1 mT = 1mG. *See also* **Flux**, **Magnetic Flux Density,** and **Weber**.

Test Cage. Facility, often present in high-voltage laboratories, for measurement of corona effects of conductors for high-voltage overhead transmission. The conductors are strung in the middle of a tunnel, often of square or cylindrical section with surfaces made of conductive mesh at ground potential. The distance between conductors and cage surfaces is small in comparison to distances between conductors and ground on actual transmission lines. There-

fore, it is possible to obtain the same conductor surface gradients as a phase conductor applying a much smaller voltage. If the same conductor surface gradient is applied, and if the conductor surface has the same property and is subject to the same weather and environmental conditions as the actual phase conductor, then it will have the same corona generation. Through the use of generation quantities such as the radio noise generation function, the audible noise generated acoustic power, and the effective corona loss, it is possible to determine the radio noise, audible noise, and corona loss of ac transmission lines. The length of the cage must be significantly greater than the median distance between corona sources. Thus, in wet weather, when there are several water drops hanging or impinging on the conductor surface, a relatively short test cage may provide accurate results. The test cage used for wet weather corona research at the EPRI laboratory in Lenox, MA, is 15.2-m long and has a square section with a 7.9-m side. The cage has an outer structural frame that supports the cage walls through insulators. This allows the measurements of corona current on the grounded side of the conductor-cage configuration. The test cage at Eskom (South Africa) is cylindrical with an outer diameter of 7 m and a length of 40 m. A test cage may operate in natural weather conditions (rain, fog, snow, frost) or may be equipped with a spray system to simulate various rain conditions. A test cage may have the means to simulate a load current in the conductors in order to study the effect of conductor temperature on corona. Test cages at the EPRI laboratory were used to study visual corona, radio noise, audible noise of bundles and of individual conductors in a bundle, corona loss, methods for reducing audible noise and corona loss, the effect of corona on ice formation on conductors, corona-induced vibrations, and the effect of conductor surface gradient on ignition of gases and fluids.

Thermal Rating. The maximum electrical current that can be safely carried in an overhead transmission line. *See also* **Ampacity**.

Third-party Contractor. A contractor that is hired by an applicant (e.g., utility) but works under the direction of the lead regulatory agency to prepare an Environmental Assessment (EA) or Environmental Impact Statement (EIS) under the provisions of NEPA or a state environmental document under applicable regulations.

Time-to-Crest (of an impulse). Time interval between actual zero and the instant in which the impulse has reached its crest value. The **Equivalent Time-to-Crest** of a switching impulse is the time-to-crest of a double exponential switching impulse that causes the same stress.

Time-to-Half Value (of a double exponential impulse). Time interval between the beginning of the impulse and the instant on the tail when the impulse has decreased to half of the crest value.

TLSA. *See* **Transmission Line Surge Arrester.**

TNA. *See* **Transient Network Analyzer**.

Toroidal Corona Shield. *See* **Corona Ring**.

Total Harmonic Distortion (THD). For a complex waveform, the total harmonic distortion is the ratio of the rms value of the sum of the squared individual harmonic amplitudes to the rms value of the fundamental frequency.

Touch Potential. The highest voltage potential difference between a conductive structure and a point on the earth's surface separated by a distance equal to the normal maximum horizontal reach, approximately 1 m. This voltage potential, applied between hand and foot, can cause a body current in excess of safe levels defined by fibrillation current. *See also* **Fibrillation Current.**

Tower Window. Arrangement of a support structure consisting of tower elements completely surrounding a phase conductor. A tower window gap is defined by the geometry of conductors, hardware (including corona rings), insulators, tower truss, and other tower members.

Transferred Potential. The electrical potential with respect to remote earth on a power system, such as that of a transmission-line tower may also appear at another location if the two are connected by a conductor such as a cable. The potential at the other location is said to be a "transferred potential."

Transient (Magnetic Field Transient). A magnetic field transient occurs during a period of time (e.g., a small fraction of one cycle) when the field has rapid changes in values while passing from one steady-state condition to another. The most important aspect of a transient is the rapidity of the change. A transient is such that the derivative of the magnetic field versus time (db/dt) reaches a peak significantly greater than the peak value of db/dt in the steady-state conditions preceding and following the transients.

Transient Network Analyzer (TNA). Analog test circuit representing a scaled-down version of the pertinent power circuit components, used for a variety of purposes, including analysis of transient overvoltages in networks and of switching surges on transmission lines.

Transient Recovery Voltage (TRV). The transient voltage that occurs across an opening contact—for example, in a circuit breaker.

Transmission Line Surge Arrester (TLSA). A protective device mounted on a transmission structure for limiting surge voltages on transmission-line insulation by discharging or bypassing surge current. A TLSA prevents continued flow of follow current from the power system and is capable of repeating these functions many times.

Transposition. Interchange of a transmission line's phase conductor (and possibly overhead shield wire) positions at selected intervals (often at the one-third points along a line's length or at a specified distance) to compensate for inductive effects.

Trichel Streamer. Streamer corona that occurs at and above the negative corona onset and appears as a small constantly moving purple fan.

Trip (*or* Tripout referred to a line). The opening of the breakers on both sides of the line, causing the disconnection of the line from the network.

Tripout Rate. The average number of tripouts per units of line length and time, usually per 100 km per year.

TRV. *See* **Transient Recovery Voltage.**

TV Broadcast Band. Any one of the frequency bands assigned for the transmission of audio and video signals for television (TV) broadcasting to the general public.

TVI. *See* **Television Interference.**

TW Conductor. A bare overhead stranded conductor with aluminum strands that are trapezoidal in cross-section.

Twelve-Phase Transmission Lines. *See* **High-Phase Order Transmission Line.**

UG. Underground. Referred to underground power lines.

UHV. *See* **Ultra High Voltage.**

Ultra Corona. *See* **Positive Glow.**

Ultra High Voltage. Transmission voltages of 1000 kV or greater. No such voltage exists in the U.S. There is an operating 1100-kV line in Russia. Japan has built sections of lines that may operate at 1100 kV in the future.

Underbuild. Term used in transmission-line engineering to describe lower voltage circuits placed below and on the same structure as the phase conductors of a transmission line.

Uniform Field. A region has a uniform field if, in all points of the region, the magnitude and direction of the field are constant.

Unlike Phasing. *See* **Low Reactance Phasing**.

Unperturbed Field. The field in the vicinity of an object may be perturbed by the presence of the object. The unperturbed field is the field that is present when the object is removed. Because the electric field at, or close to, the surface of an object is generally strongly perturbed, the value of the unperturbed electric field is often used to characterize the field and to evaluate electric field effects of transmission lines and stations. Ac magnetic fields can be perturbed by both ferromagnetic and conductive objects. Dc magnetic fields are perturbed only by ferromagnetic objects.

VDT. Video Display Terminal.

Vector. Quantity that requires both a magnitude and a direction (angle in space) for its complete description.

Vector Product. *See* **Cross Product.**

Vertical Antenna (*also* Monopole Antenna, Rod Antenna, Whip Antenna). Antenna consisting of a vertically arranged conductor.

Vertical Configuration (of a transmission line). Configuration in which the three phases of each three-phase circuit of the line are stacked vertically one above the other (the conductors may not always lie in the same vertical plane due to offsets to reduce the consequence of conductor motion problems caused by sudden ice-drop or wind-induced galloping).

Vertical Refresh Rate. *See* **Vertical Scanning Frequency**.

Vertical Scanning Frequency (*also* Vertical Refresh Rate). How often a video display terminal (CRT-type) paints a complete screen (or refreshes the screen). In some "interlaced" monitor designs, every other line is scanned on one pass and the remaining lines scanned on the next pass. Vertical scanning frequencies ranging from about 56 to 90 Hz (the screen is completely refreshed 56-90 times each second). The rate depends on display design and the graphics card. Higher vertical scanning frequencies are associated with less visual flicker (i.e., the user does not

perceive the screen being refreshed or updated). On many computer monitors, this frequency can be adjusted using the monitor's adjustment buttons or with software. Adjusting the refresh rate is sometimes done to minimize the undesirable effects caused by external power-frequency magnetic fields on image stability.

Very-Low-Frequency. *See* **VLF**.

VLF (Very-Low-Frequency). Defined by IEEE as the frequency range from 3,000 to 30,000 Hz (3-30 kHz).

Volt-Time Curve. The ability of an insulator or air gap to withstand a given voltage depends on how long (microseconds) the voltage is applied. The longer the duration of an applied voltage—above some minimum value—the less the voltage necessary to cause breakdown. A volt-time curve displays instantaneous applied voltage vs. time to breakdown for a specified test voltage waveshape. For breakdown before crest of the applied voltage, the voltage magnitude at the moment of breakdown is plotted vs. time to breakdown. If breakdown occurs after crest of the applied voltage, the crest voltage is usually plotted vs. time to breakdown. The polarity of the applied voltage is important.

Voltage (of a transmission circuit) (*also* **Line-to-Line Voltage** or **Line Voltage).** The greatest rms difference of potential between any two conductors of the circuit.

Voltage Gradient. Vector equal to, and in the direction of, the maximum space rate of change of the voltage at a specified point. Voltage gradient is synonymous with potential gradient and is often referred to simply as "gradient" or "field strength." It has units of volts per meter.

Voltage-Maximum System Voltage. Maximum voltage for which the electrical equipment of the transmission line is designed. Maximum system voltages are standardized by IEC.

Voltage-Nominal. Nominal value assigned to a circuit for the purpose of conveniently designating its voltage class. The actual voltage at which a circuit operates can vary from the nominal within a range specified by the electric utility and that permits satisfactory operation of utility equipment and attached loads.

Voltage-to-Ground (*also* **Line-to-Ground Voltage** or **Line-to-Neutral Voltage).** Rms voltage between a specified conductor and the point or conductor of the circuit that is grounded.

Voltage Upgrading. Redesigning a transmission line to operate at a higher voltage than originally planned.

Wave. Function voltage versus time, describing a transient event occurring in the power system.

Waveshape. Shape of a wave.

Weber. Unit of magnetic flux in the MKS (SI) system. One weber (Wb) equals 1 x 10^8 magnetic lines of force. In the CGS system, the unit of magnetic flux is the maxwell (Mx), and one Mx equals one line. Since the weber is a large unit for typical fields, the microweber unit can be used (1mWb = 100 lines or 100 Mx). *See also* **Flux, Gauss, Magnetic Flux Density**, and **Tesla.**

Weibull Distribution. Function sometimes used to describe the flashover probability for different voltages. Its density function is: $p(V) = \frac{\gamma}{V} \cdot \left(\frac{V}{V_0}\right)^{\gamma} \cdot e^{-\left(\frac{V}{V_0}\right)^{\gamma}}$, where V_0 is the voltage corresponding to 63.2% flashover probability. The cumulative probability is: $P(V) = 1 - e^{-\left(\frac{V}{V_0}\right)^{\gamma}}$.

Weighting Network (for audible noise measurements). Networks incorporated in the design of audible noise meters to adjust the frequency spectrum of the measured sound pressure in order to better correspond to a number of different subjective measures of annoyance. The term "weighted" is used because some frequencies are given more or less importance, or weight, than other frequencies. Instruments incorporate the A-, B-, C-, and D- weighting networks. The most commonly used to characterize environmental noises, including transmission-line audible noise, is the A-weighted network, which gives slightly more weight to frequencies in the 1-8 kHz range and less weight below 1 kHz, particularly below 500 Hz. The 100-120 Hz hum is given a 17-18 dB negative weight. The B-weighting network gives about the same weight to frequencies in the 0.5 to 8 kHz range and less weight (but not as much less as the A-weighted network) to frequencies below 500 Hz. The 100/120 Hz hum is given a 5-6 dB negative weight. Some laboratory experiment has found the B-weighted levels a better measure of annoyance for transmission line noise. Some other experiments have found instead that the D-weighted network is better. The D-weighted network attributes significant more weight to frequencies in the 1.5 to 8 kHz range. The 100-120 Hz hum is given a 7-8 dB negative weight. The C- weighting network has essentially a flat response.

Wet Conductor. Term used extensively in previous editions of the *EPRI Transmission Line Reference Book* to denote a state in which the conductors are saturated with water drops but there are no raindrops falling on the conductors.

This condition was produced with a special procedure in the test cages. The noise produced in this condition was equated to the median noise level during measurable rain. In this edition the term "wet conductor" is not used, and instead the L_{50} rain level is used.

Wet Snow. Deposited snow that contains a great deal of liquid water. If free water entirely fills the air space in the snow, it is classified as "very wet" snow. *Note:* this condition causes water drops similar to rain to form on the conductors and leads to icing-type flashover of dry arc distance on insulators.

White Noise. Noise, either random or impulsive, that has a flat frequency spectrum in the frequency range of interest.

Withstand. Result of an application of a voltage stress that does not cause a disruptive discharge.

Withstand Probability. Probability that one application of a prospective voltage of a given shape and type will not cause a disruptive discharge.

Withstand Voltage. Prospective value of the test voltage that the insulation element under test is capable of withstanding when tested under specified conditions.

"Worst-case" Weather Conditions (for line rating calculation). Weather conditions that yield the maximum or near-maximum value of conductor temperature for a given line current.

WRAP. Similar to ADSS optical cable, but not intended to be self-supporting. Instead it is supported by wrapping it around either a phase conductor (for lower-voltage power lines) or a shield wire (for higher-voltage power lines).

Xplore. An online resource for downloading IEEE technical papers.

Z Ratio. The ratio of intercloud to cloud to ground lightning frequency at a geographic location, used to convert observations of thunder or optical transients into ground flash density.

Zero Sequence. A balanced set of voltages or currents in a symmetrical component analysis corresponding to the average of the phase voltages or currents involving a return path outside the phase conductors.

Zero Sequence Component. *See* **Symmetrical Components**.

ZTACIR. ZTAL aluminum alloy conductor reinforced by an Invar steel core.

ZTAL. ("Super Thermal-resistant aluminum.") An aluminum zirconium alloy that has stable mechanical and electrical properties after continuous operation at temperatures of up to 210° C.

Index

All references are to section or subsection numbers, unless otherwise noted.

A

Accelerated aging tests, polymer insulators, 4.5.1
Ac corona modes, 8.2.4
Acoustic pulse, 8.5.3
Active shielding, 7.16.1
  Of electric field with underbuilt lines, 7.16.16, 12.9
Aging
  Conductor, 8.6.2
  Of ceramic insulators, 4.4.2
  Of conductor surface, effect on audible noise, 10.4.7
  Of conductor surface, effect on EMI, 9.2.1
  Of insulators, 4.4.1
  Of polymer insulators, 4.4.3
Agricultural operations, 12.12
  Biological effects on animals and crops, 7.11, 7.13, 7.15.4, 12.12.1
  Irrigation systems, 12.12.2, 12.12.3
  Shocks from metallic objects: vehicles, fences, etc., 7.8, 7.10, 12.12.1, 12.13, 12.14
Aircraft warning systems, 12.7
  Marking balls, 12.7.3
  Warning lights, 12.7.2
Air density (effect on switching impulse strength), 5.11
All-dielectric self-supporting (ADSS) optical fiber, 12.1.6, 12.5.2, 12.5.5
  Dry-band arcing, 12.5.5
All weather, 8.6.6
Altitude
  Effect on air density, 8.4.1
  Effect on audible noise, 10.4.8
  Effect on CL, 11.6
  Effect on EMI, 9.2.1
  Effect on switching impulse strength, 5.11
AM broadcast
  Band, 9.1
  Re-radiation, 9.7.1
Ambient noise, audible, 10.5.2, A10.1, A10.2
Ampacity, 2.2.9
Ampere's law, 7.2.4
Annoying electrical currents, 7.10.5
Annoying spark discharges, 7.10.5
Anomalous flashover, 5.6.6
Antenna
  Factor, 9.4.4
  For EMI measurements, 9.4.4
  Gain, 9.4.4
Applets. See Table A2-1.
Asset management, 13.2.2
Asymmetric bundle, for audible noise reduction, 10.7.2
Atmospheric air, composition of, 8.2.1
Atmospheric EMI, 9.1
Attachment coefficient, 8.2.1
Audible noise
  Absorption, 10.4.2
  Addition of noise from different conductors, 10.4.2
  All-weather distribution, 10.6.4
  Attenuation, 10.2, 10.4.2
  BPA method for calculations, 10.4.3
  Cage tests, 10.4.2
  Calculations, 10.4
  Design limits for fair weather, 10.6.5
  Design limits for rain, 10.6
  During rain, 10.3.1, 10.4.3, 10.4.6
  Effect of
    Altitude, 10.4.8
    Bundle orientation, 10.4.9
    Conductor aging, 10.4.7
    Conductor diameter, 10.3.2, 10.4.3
    Conductor surface gradient, 10.3.2, 10.4.3
    Fog, 10.3.1
    Frost, 10.3.1
    Ground wires, 10.4.5
    Load current, 10.3.1
    Number of conductors in a bundle, 10.3.2, 10.4.3
    Rain rate, 10.4.6
    Relative air density, 10.3.1, 10.4.8
    Sag, 10.4.5
    Snow, 10.3.1
    Surface gradient, 10.3.2, 10.4.3
    Weather conditions, 10.3.1
  EPRI method for calculations, 10.4.3
  Exceedance levels, 10.5.3
  Frequency spectrum, 10.2
  From fittings, 10.3.3
  From insulators, 10.3.3
  Generation function, 10.4.2

In fair weather, 10.3.1, 10.4.4
Instrumentation, 10.5.5
Lateral profile, 10.2
Measuring techniques, 10.5.6
Propagation, 10.4.2
Pure tones, 10.4.2,10.4.11
Reduction, 10.7
Reflection, 10.4.2
Regulations, 10.6
Results of long-term measurements on three-phase line, 10.4.10
Upgrading existing lines, 14.3, 14.6
Average detector, 9.4.2
Avian interactions with transmission lines (*See* Birds), 12.16
A-weighted audible noise, 10.4.3, 10.5.2
Axial ratio (of a power frequency field), 7.2.3, A7.1

B

Band pass characteristics of EMI meters, 9.4.3
Bandwidth, effect of on EMI measurements, 9.2.2
Bandwidth of audible noise meters, 10.2, 10.5.5
Base Case Line Configurations, A1.0
Biological effects of
Electric fields, 7.11
Magnetic fields, 7.13
Biot-Savart law, 7.2.4, 7.4.4
Bird, 12.16
Collisions, 12.16.3
Electrocutions, 12.16.2
Flashovers, caused by, 12.16.8, 12.16.9
Nesting issues, 1.3.2, 12.16.4, 12.16.5, 12.16.7
Blocking of TV signals, 9.1
Breakdown criterion, 8.2.2
Brittle fracture (stress corrosion cracking) of polymer insulators, 4.4.3
Broadband, audible noise, 10.2, 10.4.2, 10.4.3
Buildings on the right-of-way, 12.14
Bundle gradient, 2.2.1
Bundling, 2.2.1, 2.2.4
Burning
Of dead trees in high electric fields, 7.15.2
Of wood poles in high electric fields, 7.15.1, 12.9

C

Cage tests for audible noise, 10.4.2
Calibration of electric field meters, 7.5.1
Calibration of magnetic field meters, 7.6.1
Cancellation loops (for magnetic field reduction), 7.17.5, 7.17.6
Capacitance
Conductor capacitance matrix, 7.3.1
Object-to-ground, 7.8.2, Table 7.8.2
Of simple geometry, Table 7.2.1
Person-to-ground, Figure 7.10.1
Capacitive coupling or induction (*See* Induction, electric-field)
Carson's earth correction terms, 2.5.2
Cascaded transformer (for switching impulse generation), 5.4.1
Cathodic protection, 12.3.5
Cellular telephones, 12.8.3
Charge-per-length, 2.2.2
Common mode, 12.2.6, 12.2.7
Communications system antennas, 12.6
Community Noise Equivalent Level (CNEL), 10.5.4, 10.6.2
Compact lines for magnetic field reduction, 7.17.3
Condition-based maintenance, 13.2.2
Conductivity, 6.10.5
Applet G-2, 6.1.6, 6.10.5
Inverse of resistivity, 6.10.5
Lightning signal attenuation, 6.10.5
Maps, 6.10.5
Conductor
Air expanded, 2.2.4
Annealing, 2.2.7
Bundle, 2.2.4
Designs, bare stranded
All aluminum, 2.2.0
Aluminum stranded, with steel core, 2.2.0
High temperature, 2.2.0
Shield wires, 2.2.0
Diameter, effect on audible noise, 10.3.2, 10.4.3
Evaluating condition, 14.5
Heating, influence on corona effects, 8.6.5
L-N Gackle, 15.12.3
Low noise, 15.13.3
Maintainability, 13.2.3
Maximum temperature, 2.2.9
Parameters
Area and diameter, 2.2.2
Core magnetization, 2.2.4
Electrical resistance, 2.2.4
Geometric Mean Radius, 2.2.5
Skin effect, 2.2.4
Tables of values, Appendix 2.1
Weight and strength, 2.2.3
Wire choices, 2.2.1
Reactance to 1 ft or m, 2.2.6
Spiral rod, 15.13.3
Surface
Hydrophilic, 8.6.2
Hydrophobic, 8.6.2
Surface gradient. See surface gradient.
Surface irregularity factor, 8.4.1
Conductor-to-bus support (subjected to switching surges), 5.7.3
Conductor-to-conductor (phase-to-phase switching surges), 5.8.3

Conductor-to-ground gaps (subjected to switching surges), 5.6.5
Conductor-to-grounded objects (subjected to switching surges), 5.6
Conductor-to-rod gaps (subjected to switching impulses), 5.5
Conductor-to-tower leg (subjected to switching surges), 5.6.4
Conductor-to-tower, outside phase (subjected to switching surges), 5.6.2
Conductor-to-tower window (subjected to switching surges), 5.6.1
Connection length, insulator (*See* Section length)
Contact resistance, 7.8.5, 12.2
Contaminated insulators
Effect on upgrading line voltage, 14.6
Switching surge performance, 5.12.2
Continuous leader inception voltage, A5.2
Cordless telephones, 12.8.2
Corona
Attenuation, 8.8
Lightning overvoltages, 8.8.1
Switching overvoltages, 8.8.2
Temporary overvoltages, 8.8.3
Causing tree tip damage, 7.5.3
Detection, 8.7.1
Discharge, 8.2.3
Effects, 8.5
Audible noise, 8.5.3
Corona loss, 8.5.1
Electrical wind, 8.5.6
EMI, RI, TVI, 8.5.2, 12.1.4
Light emission, 8.5.5
Of upgrading line voltage, 14.3, 14.6
On polymer insulators, 4.4.3
Other, 8.5.7
Ozone and NO_X, 8.5.4
Vibrations, 8.5.6
Grounded objects, 7.15.4
Induced
Fuel ignition, 7.14.2
Vibrations, 10.2
Loss, 11.1
Effect of altitude, 11.6
Evaluation of, 11.7
Fair weather, 11.4
Foul weather, 11.5
Influence of conductor heating, 11.5.3
Influence of rain rate, 11.5.1
Influence on line design, 11.8
Maximum, 11.7
Mean annual, 11.7
Rain, 11.5.1
Snow, ice and hoarfrost, 11.5.2
Weather modeling, 11.7
Modes, 8.2.4
Non-uniform wetting, on polymer insulators, 4.4.3
Onset, 8.4
Conductors, 8.4.1
Gradient, 8.4.1
Hardware, 8.4.2
Voltage, 8.4.1
Pulse, 8.2.4
Ring, 2.2.5
Insulator, 4.2, 4.9.1
Sources, fair weather, 8.6.1
Testing
Hardware, 8.7.1, A8.1
Test cages, 8.7.1
Test lines, 8.7.1
Water drop on insulators, 4.4.3
Corrective maintenance, 13.2.2
Coulomb's law, 7.2.3
Coupling mechanisms (*See* Induction)
Creep elongation (of conductors), 2.2.8
Creepage distance, insulator string (*See* Leakage distance)
Critical radius of cylinders and spheres (related to switching impulse strength), 5.12.1
Critical time-to-crest (of switching impulse), 5.10
Cumulative distribution, 8.6.6
Current comparator, 11.3
Currents induced by charged particles, A8.1

D

Dead tree burning in high electric fields, 7.15.2
Decibel, unit of measurement of audible noise, 10.5.1
Differential global positioning system (DGPS), 12.10.4
Differential mode, 12.2.6, 12.2.7
Diffusion, 8.2.1
Digital radio mondiale (DRM), 9.3.1
Digital TV and radio, 9.3.1
Dipole (relevant to transmission line magnetic field), A7.2
Direct broadcast satellite (DBS), 9.3.1
Dissipation factor, 11.3
Distribution system, 12.2.5, 12.3.4, 12.6.3
Drift, 8.2.1
Dry-arc distance, Insulator string 4.2.2
Dry-band arcing, 9.1, 12.5.5

E

Edison, Thomas Alva, 1.1.1
Electric and magnetic fields, 1.3.1, Chapter 7
Electric field
Biological effects, 7.11
Boundary surfaces, 7.5.2
Calculations (2-D), 7.3.1
Calculations (3-D), A7.6
Ceramic and glass insulator strings, 4.9.2
Common environments, 7.7
Corona / Grading ring, 4.9.1
Definition, 7.2.3
Double circuit lines, 7.3.5

Effect of
Line bends, 7.3.4
Line configuration, 7.3.4
Line parameters (height, phase spacing, conductor size), 7.3.4
Sag, 7.3.4
Shield wires, 7.3.4
Soil conductivity, 7.3.4
Uneven terrain, 7.3.4
Ellipse, 7.2.3, A7.1
Enhancement on the surface of the body, 7.10.2
Guidelines, A7.3, 12.15.2
Hair stimulation, 7.10.5
Harmonic content, 7.2.3
Lateral profile, 7.3.2
Maximum value at ground near transmission lines, 7.3.3
Measurements, 7.5
Modeling, 4.9.1
Perception, 7.10.5
Polymer Insulators, 4.9.1
Reduction, 7.16
Shielding, 7.16
Shielding by
Horizontal grid, 7.16.2
Mesh, 7.16.4
Objects, 7.16.5
Vertical grid, 7.16.3
Simple geometry, Table 7.2.1
Standards, A7.3, 12.15.2
Substations, 7.3.6
Upgrading existing lines, 14.3, 14.6
Values in common environment, 7.7
Electric flux density, 7.2.3
Electromagnetic compatibility (EMC), 12.1
Electron
Avalanche, 8.2.2
Detachment, 8.2.1
Electron attachment, 8.2.1
Electronegative gas, 8.2.1
EMC
Coupling paths, 12.1.5
Elements of, 12.1.3
Guidelines, 12.1.2
Power line carrier, 12.4
Receptors, 12.1.6
Regulations, 12.1.2
Standards, 12.1.2
Transmission line sources, 12.1.4
Emergency thermal rating, 2.2.10
EMF, Chapter 7
EMI, Chapter 9
All-weather distribution, 9.2
Attenuation, 9.2.1
Canadian limits, 9.3.2
CISPR code of practice, 9.3.2
Czechoslovakia, 9.3.2
Design guidelines, 9.3.2
Due to gap-discharges, 9.2.3
Due to hardware corona, 9.2.2
During rain, 9.2.1
Effect of
Air density, 9.2.1
Altitude, 9.2.1
Conductor diameter, 9.2.1
Conductor surface electric field, 9.2.1
Fog, 9.2.1
Hoarfrost, 9.2.1
Line geometry, 9.2.1
Load current, 9.2.1
Weather, 9.2.1
Weather conditions, 9.2.1
Frequency spectrum, 9.2.1
Gap-discharges, 9.2.3, 12.1.4
Generation function, 9.5.2
In fair weather, 9.2.1
Lateral profiles, 9.2.1
Limits, 9.3.2
Measuring techniques, 9.4
Poland limits, 9.3.2
Propagation, 9.2.1
Radiation patterns above 30 MHz, 9.6.2
Regulations, 9.3.2
Results of long-term measurements on three-phase lines, 9.2.1
Statistical distributions, 9.2.1
Switzerland limits, 9.3.2
Tolerability criteria, 9.3.1
USSR limits, 9.3.2
Zoning criteria for airports, 12.10.2
EMI Calculations
Above 30 MHz, 9.6
Below 30 MHz, 9.5
Below 30 MHz, BPA method, 9.5.3
Below 30 MHz, EPRI quasi-static method, 9.5.2
Below 30 MHz, wide band method, 9.5.2
Environmental Assessment (EA), 1.6.3
Environmental Impact Statement (EIS), 1.6.3
Environmental permitting, 1.6
Communication and coordination, 1.6
Process, 1.6
Review, 1.6
Strategic planning, 1.6.3, 1.6.4
Environmental resource issues, 1.6.3, 1.6.4, 1.6.5
Controversial, 1.6.3
High-profile, 1.6.4
New or expanding, 1.6.5
Equipotential surfaces, 2.2.3
Equivalent charge-collecting area of objects in an electric field, 7.8.2, Tables 7.8.1-2
Equivalent radius, 8.4.2

Equivalent single conductor diameter for electric field calculations, 7.3.1
Equivalent sound level, Leq, 10.5.4, 10.6.2
Excitation, 8.2.1
Excitation function, RN, 8.7.3

F

FACTS facilities, 12.4.1
FACTS, Flexible AC Transmission System, 1.2.1
Fair weather
Audible noise in fair weather, 10.3.1, 10.4.4
Corona sources, 8.6.1
EMI, 9.2.1
Faraday's law of induction, 7.2.4
FCC television service grades, 9.3.1
Ferranti effect, 1.2.2
Fiberglass rod, polymer insulator, 4.2.5
Field ellipse, 7.2, A7.1
Fifty percent flashover voltage (switching impulse strength), 5.2.6, 5.4.2, 5.5-9
Final jump, 5.3, A5.2
Flashover, 6.2
Backflashover, 6.1.6, 6.2, 6.7
Induced flashover, 6.8
Mechanism (for switching impulses), 5.3, A5.2
Midspan flashover, 6.9
Model (for switching impulses), 5.3, A5.2
Shielding failure flashover. See Shielding failure.
Flashunder, of polymer insulator, 4.4.3
Floating objects (for switching impulses), 5.14.4
Fog
Effect on audible noise, 10.3.1
Effect on switching impulse strength, 5.12.1
Form factor, insulator, 2.2.3
Foul weather, corona sources, 8.6.6
Fourth wire scheme for magnetic field reduction, 7.17.7
Free-body electric field meter, 7.5.1
Frequency selective voltmeter for measuring EMI, 9.4.1
Frequency spectrum, audible noise, 10.2
Frost, effect on audible noise, 10.3.1
Fuel ignition by
Corona, 7.14.2
Spark discharges, 7.14.1, 12.13.4, 12.13.5

G

Gap discharge, 8.3, 9.1, 9.2
Gap factor, 5.2.4, 5.5.1, 5.6.1
Generated acoustic power, 10.4.2, 10.4.3, 10.4.11
Generated acoustic power density, 8.7.4
Generated corona loss, 8.7.2
Generation function, for audible noise, 10.4.2
Geometric mean distance (of bundle), 2.4.2, 2.4.3
Geometric mean radius, 2.4.2
Ghosting, TV broadcast band, 9.1, 9.7.2
Global positioning system (GPS), 12.10.3
Gradient, 2.2.1
Grading rings (effect on switching impulse strength), 5.6.1
Ground fault, 12.2.4, 12.2.5, 12.3.3, 12.3.4, 12.3.5, 12.3.6, 12.6.3, 12.14
Ground mats, 12.3.2
Ground plane, 2.2.1
Ground potential rise, 12.3.4, 12.6.3
Ground return (for magnetic field calculations), A7.5
Ground wires, effect on audible noise, 10.4.5
Grounding
Concrete as a conductor, 6.10.14
Dynamic resistance, 6.10.10
Applet L-3, 6.10.10
Ionization gradient, 6.10.10
Korsuncev model, 6.10.13
Liew-Darveniza model, 6.10.12
Equations
Contact resistance, 6.10.4
Dwight and Sunde, 6.10.4
Geometric resistance, 6.10.4
Rod, various authors, 6.10.4
Maintainability, 13.2.3
Surface potential
Applet L-6, 6.1.6, 6.10.10
Step and touch potential, 6.10.17
Surge impedance, 6.4.2
Grounding system, 12.3.2

H

Hardware, maintainability, 13.2.3
Harmonic content of electric field, 7.2.3
Harmonic content of magnetic field, 7.2.4
Harmonic frequency voltages and currents, 12.1.4
Health effects of
Electric fields, 7.11
Magnetic fields, 7.13
High-definition TV (HDTV), 9.3.1
Hoarfrost, EMI during hoarfrost, 9.2.1
Hum, 10.2, 10.4.2, 10.4.11
Humidity (effect on switching impulse strength), 5.11.4
Hybrid (AC and DC) corridors, effect on audible noise, 10.7.3
Hydrophilic, conductor surface, effect on audible noise, 10.3.2
Hydrophobic, conductor surface, effect on audible noise, 10.3.2
Hydrophobicity, 4.2.3
Categorization, 4.2.3
Classification against standard samples, 4.2.3
Definition, 4.2.3
Hydrophobic, 4.2.3
Hydrophilic, 4.2.3
Measurement of contact angle, 4.2.3
Measurement of surface tension, 4.2.3
Polymer insulators, 4.2.3

I

Ice
- Effect on conductor sag, 2.2.8
- Effect on switching impulse strength, 5.12.1
- Ice loading, 1.3.2

IEEE radio noise design guide, 9.3.2
Image depth (in earth), 7.4.1, A7.5
Impedance unbalance, 2.5, 2.5.1, 2.5.2, 2.5.3
Impedance vehicle-to-ground, 7.8.5
Impulse generator, 5.4.1
Induced currents in
- Fences, 7.8.4, 7.9.1
- Human body by electric field, 7.10.1, 7.12
- Human body by magnetic field, 7.12
- Objects by electric field, 7.8
- Vehicles, 7.8, 12.13.2

Induced voltages in
- Fences, 7.8.4, 7.9.1
- Objects by electric field, 2.6, 2.6.1, 7.8
- Parallel wires by transmission line magnetic field, 2.6, 2.6.2, 7.9
- Shield wires, 7.9.1
- Vehicles, 12.13.3

Induction
- Conductive, 12.2.5
- Electric-field, 12.2.3
- Magnetic-field, 12.2.4
- Pipelines, 12.3
- Railroads, 12.2
- Underbuilt distribution lines, 12.9

Inductive coordination, 12.2.1
Inductive coupling or induction (*See* Induction, magnetic-field)
Inspection, 13.2
- Condition rating, 13.2.2
- Frequency of inspections, 13.2.2
- Performance monitoring, 13.2.2
- Prioritization of inspections, 13.2.2
- Rationale for inspection, 13.2.2

Instrumentation for
- Audible noise, 10.5.5
- EMI measurements, 9.4
- RF surveys, 12.6.4

Instrument landing systems (ILS), 12.10.2
Insulated conductors, effect on audible noise, 10.7.3
Insulation
- Applet L-4, 6.1.6
- Disruptive effect (DE) model, 6.5.2, Appendix 6.1
- Leader progression model, 6.5.3
- Lightning impulse strength, 6.1.6
- NESC electrical buffer in live work, 6.9.6
- Puncture, 6.5.4
- Volt-time curve, 6.5.1

Insulators
- Ceramic
  - Degradation, 4.4.2
  - Disc, 4.2.4
  - Failure modes, 4.4.2
- Choice of, 4.8.3
- Classification, 4.2.2
- Configurations, 4.2.2
- Degradation, 4.4.1
- Form factor, 4.2.2
- General terms and types, 4.2.2
- Glass, 4.2.4
  - Degradation, 4.2
  - Failure Modes, 4.4.2
  - History, 4.2.1
- Laboratory Testing, 4.5
- Maintainability, 13.2.3
- Parameters, 4.2.2
- Polymer (also called composite, nonceramic or NCI)
  - Accelerated Aging Tests, 4.5.1
  - Animal Damage, 4.8.3
  - Brittle Fracture (Stress Corrosion Cracking), 4.4.3
  - Components of, 4.2.5
  - Corona Rings, 4.9.1
  - Degradation, 4.4.3
  - Degradation mechanisms, 4.4.3
  - Destruction of rod by discharge activity, 4.4.3
  - E-field, critical values, 4.9.1
  - E-field distribution, 4.9.1
  - E-field grading devices, 4.2.5, 4.9.1
  - E-field magnitudes, 4.9.1
  - E-field modeling, 4.9.1
  - End fitting seal, 4.2.5
  - Ethyl propylene (EP) rubber, 4.2.5
  - Failures, summary of, failure rate, 4.4.3
  - Failure modes, 4.4.3
  - Fiberglass rod, 4.2.5
  - Flashunder, 4.4.3
  - High temp conductors, 4.8.3
  - Housing Core Interface, 4.2.5
  - Housing Material, 4.2.5
  - Hydrophobicity, loss of, 4.4.3
  - Inspection, 4.8.3
  - Live working, 8.3.1
  - Long-term performance tests, 4.5.1
  - Mechanical Failure, 4.4.3
  - Metal End Fitting, 4.2.5
  - Post, 4.2.2
  - Power arc, effect on, 4.4.3, 8.3.1
  - Silicone Rubber, 4.2.5
  - Storing, Transporting and Installing, 4.8.3
  - Suspension, 4.2.2
  - Vandalism, 4.8.3.1
- Puncture, 4.4.2
- Surface area, 4.2.2

Insulator strings
Behavior under switching surges, 5.6.3, 5.7.2, 5.12, 14.3, 14.6
Configuration 4.2.3
Dry-arc distance, 4.2.2
E-field distribution, 4.9
Glass disc, 4.9.2
Polymer, 4.9.1
Porcelain, 4.9.2
Leakage (or creepage) distance, 4.2.2
Protective leakage (or creepage) distance, 4.2.2
Section length, 4.2.2
Insulator swing
Caused by wind; effect on switching surge performance, 5.13.3, A5.1
Upgrading existing lines, 14.3, 14.6
Interference with
Communications receivers, 12.10.11
Monitors (jitter) caused by magnetic fields, A7.4
Optical fiber communications, 12.5
All-dielectric self-supporting (ADSS) cable, 12.5.2,12.5.5
Optical ground wires (OPGW), 12.5.2, 12.5.4
Wrapped around phase conductors (WRAP), 12.5.2, 12.5.3
Power line communications systems, 12.4
High speed (broadband power line) communication, 12.4.2
Power line carrier, 12.4.1
Radionavigation systems, 12.10
Differential global positioning system (DGPS), 12.10.4
Global positioning system (GPS), 12.10.3
Instrument landing systems (ILS), 12.10.2
LORAN-C, 12.10.1
Telephone systems, 12.8
Cellular telephones, 12.8.3
Cordless telephones, 12.8.2
Telephone lines, 12.8.1
Ionization, 8.2.1
Coefficient, 8.2.1
Natural sources of, 8.2.1
Ionizing fields, 7.2.1
Irrigation systems, 12.3.3, 12.12
Isolating joints, 12.3.3, 12.3.5

J

Jitter (monitor interference) caused by magnetic fields, A7.4

L

L_5 rain audible noise, 10.4.3
L_{50} rain audible noise, 10.4.3
Lateral profile
Audible noise, 10.2
Of electric field, 7.3.1, 7.5.1
Of magnetic field, 7.4.1, 7.6.2
L_{dn} sound level, 10.5.4, 10.6.2, 10.6.4
Leader, 5.3, A5.2
Leakage (or creepage) distance, insulator string, 4.2.2
L_{eq}, equivalent sound level, 10.5.4, 10.6.2, 10.6.4
Let-go currents, 7.10.5
Lightning, 1.3.2, Chapter 6, 12.9, 14.6
Attachment process, 6.1.3
Applet L-2, 6.1.6
Attractive radius model, 6.2.7
Electrogeometric model, 6.2.7
Downward leader, 6.2.2
Branching, 6.2.2, 6.6.9
Charge, 6.6.9
Radial gradient, 6.2.2
Velocity, 6.2.2
Voltage, 6.2.5
Electrification process, 6.2.1
Flash (definition), 6.2
Ground flash density, 6.2.6
Location system, 6.1.3, 6.2.6, 6.3, Appendix 6.2
Parameters
Charge, 6.2.10
Continuing current, 6.2.16
Correlations among, 6.2.9
Ground flash density, 6.2.16, 6.3
Optical transient density, 6.3
Peak current, 6.2.9, 6.2.10, 6.2.14
Polarity, 6.2
Rate of current rise, 6.2.9
Thunder observations, 6.3.1
Waveshape, 6.2.8
Return stroke
Continuing current, 6.2.2
Electromagnetic radiation, 6.2.12, Appendix 6.2
First return stroke, 6.2.8
Impedance, 6.2.8
Subsequent return stroke, 6.2.8
Transmission line model, 6.2.8
Velocity of propagation, 6.2.8
Tall structures, 6.2.14, 6.10.14
Upward leader, 6.2.7, 6.2.13
Waveshape, 6.2.8
Live line maintenance
Consideration of switching surges during maintenance, 5.14
Upgrading existing lines, 14.3, 14.6
Load current, effect on audible noise, 10.3.1
LORAN-C, 12.10.1
Low reactance phasing, 2.5.3

M

Magnetic field (of transmission lines), Chapter 7
Magnetic field
- Biological effects, 7.13
- Calculations
  - (2-D), 7.4.1
  - (3-D), 7.4.4
- Common environments, 7.7
- Definition, 7.2.4
- Distant field equations for transmission lines, Table 7.4.3
- Double circuit lines, 7.17.2
- Effect of
  - Line configuration, 7.17.2
  - Line parameters (height, phase spacing, conductor size), 7.17.2
  - Sag, 7.4.4
  - Shield wires, 7.9, 7.17.2
- Ellipse, 7.2.4, A7.1
- Guidelines, A7.3, 12.15.2
- Harmonic content, Table 7.2.2
- Lateral profile, 7.6.2, 7.4.1
- Management, 7.17
- Measurements, 7.6
- Meters, 7.6.1
- Reduction, 7.17
  - By line compaction, 7.17.3
  - By optimization of line parameters, 7.17.2
- Shielding by cancellation loops, 7.17.5
- Simple geometry, Table 7.2.3
- Standards, A7.3, 12.15.2
- Substations, 7.4.4
- Upgrading existing lines, 14.3, 14.6
- Values in common environment, 7.7

Maintainability, 13.2
- Considerations, 13.2.2
- Design examples, 13.2.4
- Designing for maintainability of
  - Conductors, 13.2.3
  - Grounding, 13.2.3
  - Hardware, 13.2.3
  - Insulators, 13.2.3
  - Overhead ground wires, 13.2.3
  - Splices, 13.2.3
  - Structures, 13.2.3
  - Rights-of-way, 13.2.3
- Durability and longevity, 13.2.3

Maintenance, 13.2
- Frequency of maintenance, 13.2.2
- Prioritization of maintenance, 13.2.2
- Rationale for maintenance, 13.2.2
- Types
  - Condition-based maintenance, 13.2.2
  - Corrective maintenance, 13.2.2
  - Preventative maintenance, 13.2.2
  - Reliability-centered maintenance, 13.2.2
  - Scheduled maintenance, 13.2.2

Major axis of field ellipse, A7.1
Maximum gradient (*See* Surface gradient)
Maximum likelihood (applied to switching impulse test results), 5.4.2
Measurements of
- Electric field, 7.5
- Electric field of transmission lines, 7.5.1
- Electric field on boundary surfaces, 7.5.2
- Hydrophobicity, 4.2.3
- Magnetic field, 7.6
- Magnetic field of transmission lines, 7.6.2
- Magnetic field waveform, 7.6.3
- Radio frequency (RF) electromagnetic fields, 12.6.4
- Space potential, 7.5.3
- Transmission line EMI; AM Broadcast band, 9.4.5
- Transmission line EMI; other communication bands, 9.4.5
- Transmission line EMI; TV broadcast band, 9.4.5

Measuring techniques for
- Audible noise, 10.5.6, A10.1
- EMI, 9.4.5
- RF exposure, 12.6.4

Method of images, 2.2.2
Method of successive images, 2.2.3
Mobility, of charged particles, 8.2.1
Monitor interference (jitter) caused by magnetic fields, A7.4
Monopole (relevant to transmission line magnetic field), A7.2

N

NACE design standard for ac current effects, 12.3.3, 12.3.6
National Environmental Policy Act, 1.6.2, 1.6.3
Negative dc corona modes, 8.2.4
Negative sequence, 2.4.1, 2.5, 7.2.4
Nonceramic insulators (see Insulators, polymer)
Nuisance shocks, 12.13.5, 12.14, 12.15
Number of conductors in a bundle, effect on audible noise, 10.3.2, 10.4.3

O

Open-circuit voltage, 12.3.2
Optimization of bundle geometry, for audible noise reduction, 10.7.2
Overhead groundwire
- Applet EMF-8 for induced current, 6.1.6
- Applet L-2 for lightning flash interception, 6.1.6
- Cost versus benefit, 6.1.5
- Maintainability, 13.2.3
- Shield angle, 6.6.4
- Surge impedance, 6.4.1, 6.4.2

Overvoltage, 8.8
- Lightning, 8.8

Switching, 8.8
Temporary, 8.8
Oxides of nitrogen (NO_X), 11.1
Ozone, 11.1
Dispersion, 11.9.3
Levels near transmission lines, 11.9.4
Mechanism of generation, 11.9.1
Rate of generation, 11.9.2
Standards, 11.9.5

P

Parking lots on right-of-way, 12.13.5
Partial discharge, 8.2.3
Passive interference, 9.1, 9.7
Passive shielding of transmission line magnetic field, 7.17.5
Peak detector, 9.4.2
Perception of
Electric currents by people, 7.10.5
Electric fields by people, 7.10.5
Spark discharge by people, 7.10.5
Permitting agencies, 1.6
Authorizing, 1.6.1, 1.6.3, 1.6.4
Cooperating, 1.6.3
Land management, 1.6.1, 1.6.3, 1.6.4
Lead, 1.6.3
Regulatory, 1.6.3, 1.6.4
Permitting communication, 1.6
Permitting report, 1.6.3, 1.6.4
Baseline or existing environment, 1.6.4
Committed protection measures, 1.6.3
Cumulative effects, 1.6.3
Decision record, 1.6.3
Documentation, 1.6.3, 1.6.4
Effects analyses, Section 1.6
Mitigation measures, 1.6.3
Monitoring measures, 1.6.3
Production, 1.6.3
Project alternatives, 1.6.2, 1.6.3
Project scope, 1.6.3
Purpose and need, 1.6.2, 1.6.3, 1.6.4
Phase impedance matrix, 2.5.1, 2.5.2, 2.6.1, 2.6.2
Phase-to-phase switching
Impulse strength, 5.8
Surges, 3.2.3
Surge design, 5.8.6
Photoionization, 8.2.1
Pipelines, 2.3
Cathodic protection, 12.3.5
Conductive induction, 12.3.4
Damage, 12.3.5
Electric-field induction, 12.3.2
Isolating joints, 12.3.3, 12.3.6
Magnetic-field induction, 12.3.4
Shielding, 12.3.3
Soil-to-pipe potential, 12.3.5
Worker safety, 12.3.6
Polarization (of power frequency fields), 7.2.3, A7.1
Polymer insulators (see Insulators, polymer)
Portable Protective Air Gaps (PPAG), 5.14.3, 14.6
Positive dc corona modes, 8.2.4
Positive-polarity streamers, 10.2
Positive sequence, 2.4.1, 2.5, 7.2.4
Reactance, 2.4.2, 2.4.3, 2.5.3
Post-energization EMI measurements, 9.4.6
Potential coefficients
Conductor segments, A7.6
Parallel conductors, 7.3.1
Power electronic devices, 12.1.4
Power line carrier (PLC), 12.4
Voltages and currents, 12.1.4
Power quality
Cost of avoided customer momentary outage, 6.1.5
Momentary outage from lightning, 6.1.5
PPAG. See Portable Protective Air Gaps.
Pre-construction EMI measurements, 9.4.6
Pre-energization EMI measurements, 9.4.6
Preventative maintenance, 13.2.2
Protective leakage (or creepage) distance, 4.2.2
Public permitting involvement, 1.6.3, 1.6.4, 1.6.5
Notice, 1.6.3
Opposition, 1.6.3
Participation, 1.6.1, 1.6.3
Perception, 1.6.3, 1.6.4
Process, 1.6.3
Scoping, 1.6.3
Public use of the right-of-way, 12.15
Commercial activites, 12.15.4
Nuisance shocks, 12.15.3
Parks/recreation areas, 12.15.4
Schools, A7.3, 12.15.4
Trails, 12.15.4
Pulse repetition rate, effect of on EMI measurements, 9.4.6

Q

Quadrupole (relevant to transmission line magnetic field), A7.2
Quasi-peak detector, 9.4.2

R

Radio frequency (RF) electromagnetic fields, 12.6.4
Radio Interference, 9.1
Radio noise, 9.1
EPRI classical method for calculation, 9.5.2
Upgrading existing lines, 14.3, 14.6
Railroads, 12.2
Abnormal equipment operation, 12.2.9
AC interference, 12.2.13
Equipment damage, 12.2.10
Personnel safety, 12.2.11, 12.2.12
Signaling, 12.2.8
Rain
Audible noise during rain, 10.3.1, 10.4.3, 10.4.6

Corona losses in rain, 11.5.1
Effect of rain on switching impulses, 5.2.5, 5.12.1
EMI during rain, 9.2.1
Recombination, 8.2.1
Recombination coefficient, 8.2.1
Regulation, for
Audible noise, 10.6
EMI, 9.3.1
Regulatory framework, 1.6.3
Relative air density
Corona onset gradient, 8.4.1
Effect on audible noise, 10.3.1, 10.4.8
Effect on CL, 11.6
Effect on EMI, 9.2.1
Switching impulse strength, 5.11.3
Reliability-centered maintenance, 13.2.2
Resistive coupling or induction (*See* Conductive induction)
Resistivity
Apparent, 6.10.5
Electrode resistance, 6.10.5
Maps, 6.10.5
Measurement methods, 6.10.5
Right-hand rule, 7.2.4
Rights-of-way, maintainability, 13.2.3
Risk of failure (switching surge design of transmission lines), 5.13
RI tolerability criteria, 9.3.1
Rod-plane gaps (subjected to switching impulses), 5.5.1
Rod-rod gaps (subjected to switching impulses), 5.5.2, 5.5.3, 5.8.2
Root-mean-squared (rms) detector, 9.4.2
Routing, 1.6.2, 1.6.3
Constraints, 1.6.2, 1.6.3, 1.6.5
Opportunities, 1.6.3
Selection, 1.6.3
Siting, 1.6.1, 1.6.2, 1.6.3, 1.6.5

S

Sag
Effect on audible noise, 10.4.5
Effect on voltage upgrading, 14.4
Initial installation, 2.2.8
Sag-tension calculations, 2.2.8
Scheduled maintenance, 13.2.2
Schering bridge, 11.3
Secondary ionization, 8.2.1
Coefficient, 8.2.1
Secondary shock, 7.10.5
Section length, insulator string, 4.2.2
Self-balancing bridge, 11.3
Sequence impedance matrix, 2.5.1, 2.5.2, 2.5.3
Shield wire (*See* Overhead groundwire)
Shield wire currents, 7.9
Shielding electric field, 7.16
Active, 7.16.6
By buildings, 12.14
With horizontal grid, 7.16.2
With mesh, 7.16.4
With objects, 7.16.5
With vertical grid, 7.16.3
Shielding Failure, 6.6
Applet L-2, 6.1.6
Perfect shielding, 6.6.4
Rolling sphere method, 6.6.9
Shielding pipelines, 12.3.3
Shockley-Ramo theorem, A8.2
Short-circuit current, 12.2.11, 12.3.2, 12.13.2
Signal-to-noise ratio, 9.3.1, 12.1.5
Snow
Effect on audible noise, 10.3.1
Effect on switching impulse strength, 5.12.1
Sound pressure level, 10.4.2, 10.4.3, 10.5.1
Space potential
Calculation (2-D), 7.3.1
Calculation (3-D), A7.6
Definition, 7.2.3
Measurements, 7.5.3
Spacer dampers for bundles, 15.5.3, 15.10.3, 15.12.3
Spacers for bundles, 15.6.3, 15.13.3
Spark discharges, 7.8.1, 7.10.3
Annoyance, 7.10.5
Carpet induced, 7.10.3
Causing fuel ignition, 7.14.1
Perception, 7.10.5
Rain gutters, 7.8.2
Vehicles, 7.10.3, 12.13.3
Spectrum analyzer for measuring EMI, 9.4.2
Sphere calibrator, A8.1
Sphere-plane gaps, subjected to switching impulses, 5.5.4
Splice, maintainability, 13.2.3
Split-phase lines, 7.17.4
Stability, 14.2
Standard air density, 5.11.2
Standard deviation (of switching impulse flashover probability), 5.2.6, 5.9
Standard humidity, 5.11.2
Standing waves, 1.2.2
Station post insulators (switching impulse strength), 5.7.3
Statistical distribution, 8.6.6
Statistical maximum switching surge, 5.13.2
Step potential, 12.3.4, 12.3.6
Streamers, 5.3
Stress corrosion cracking (see brittle fracture), 4.4.3
Structure, maintainability, 13.2.3
Subconductors, 2.2.4
Superbundle phasing, 2.5.3
Surface area, insulator, 4.2.2
Surface charge density, 2.2.2

Surface gradient, 2.2.1, 2.2.3, 2.2.7, 2.2.8
Effect on audible noise, 10.3.2, 10.4.3
Surge impedance, 2.4.4, 6.4
Bundle conductor over ground, 6.4.1
Corona-modified, 6.4.1
Coupling coefficient, 6.4.1
Ground plane, 6.4.2
Reflection coefficient, 6.4
Transmission tower
Applet L-5, 6.4.2
Cone and cylinder models, 6.4.2
From capacitance and travel time, 6.4.2
Wire over ground, 6.4.2
Surge impedance loading, 2.4.4, 14.2
Surge protective devices (SPD), 12.2.10
Swimming pools, 12.14
Swing angle (for switching surges), A5.1
Switching impulses, switching surges, Chapter 5
Switching impulse strength, effect of
Air density, 5.11
Altitude, 5.11
Broken insulators, 5.14.2
Conductor size, 5.6.1
Contamination, 5.12.2
Floating objects, 5.14.4
Fog, 5.12.1
Grading rings, 5.6.1
Humidity, 5.11
Ice, 5.12.1
Insulator strings, 5.6.1, 5.6.3, 5.7.2
Insulator swing, 5.13.3, A5.1
Polarity, 5.2.2
Rain, 5.2.5, 5.12.1
Snow, 5.12.1
Time-to-crest, 5.10
Waveshape, 5.2.3, 5.10
Wind, A5.1
Window shape, 5.6.1
Switching surge amplitude distribution, 5.13.2
Symmetrical components, 2.4.1, 2.5

T

Telephone lines, 12.8.1
Television
Broadcast band, 9.1
Interference, Chapter 10
Service grades defined by BPA, 9.3.1
Test methods (for switching impulses), 5.4.2
Thermal rating of line, 2.2.9
Thermal uprating, 14.2, 14.3
Time-to-crest (of switching impulses), 5.2.3, 5.10
Tolerability criteria for other communication systems, 9.3.1
Toroidal corona ring (*See* Corona ring)
Touch potential, 12.3.4, 12.3.6
Transferred potential, 12.3.4
Transient thermal line rating, 2.2.10
Transient voltages and currents, 12.1.4
Transmission lines above 700-kV
AEP 765-kV lines, 15.5
Case Studies, 15.3
EDELCA 765-kV lines, 15.7
Electrical design, 15.1
ESKOM 765-kV lines, 15.10
FURNAS 750-kV lines, 15.8
Hydro-Québec 735-kV lines, 15.4
KEPCO 765-kV lines, 15.12
Mechanical and tower design, 15.1
NYPA 765-kV lines, 15.9
Operation and maintenance, 15.1
POWERGRID 765-kV lines, 15.11
Russian 750-kV and 1150-kV lines, 15.6
Survey Questionnaire, A15.1
System planning, 15.1
TEPCO 1000-kV lines, 15.13
Transmission systems
Blackouts and outages, 1.1.1, 1.4.2
China, 1.1.2
Circuit basics, 1.2.1
Deregulation and planning, 1.4.1, 1.5.1
Environmental considerations, 1.3
European-type systems, 1.1.2
Grid flows, 1.4.2
HVDC, 1.2.1
Increasing power transfer capacity, 1.2.1
Industry trends affecting line design, 1.1.3
Investment in infrastructure, 1.4.2
ISOs, 1.4.2
Japan, 1.1.2
Load growth, 1.4.2
Maintenance, 1.4.2
North American-type systems, 1.1.2
RTOs, 1.4.2
Series reactance, 1.2.1
Standard voltages, 1.1.2
Trading practices, 1.4.2
Transients, 1.2.3
Transmission line voltage 1880–1980, 1.1.1
Voltage, 1.2.1
Transmission towers
Chainette, 15.4.3
Delta 765-kV, 15.11.3
Double-circuit 765-kV horizontal, 15.7.3
Guyed V, 15.5.3, 15.6.3, 15.10.3
Reinforced, 15.4.3, 15.8.3
Self-supporting suspension, 15.4.3, 15.5.3, 15.6.3, 15.9.3
Tubular, 15.4.3
Traveling wave (*See* Surge impedance)
Trees in high electric fields, 7.15
TV broadcast re-radiation, 9.7.2
TVI
BPA method for calculations, 9.6.3

Tolerability criteria, 9.3.1

U

Ultra corona, 8.2.4
Effect on audible noise, 10.7.3
Effect on EMI, 9.2.1
Unbalance factors, 2.5.1, 2.5.2
Up-and-down method, extended up-and-down method, 5.4.2

V

Vehicles, 12.13

W

Water drop corona, 8.6.3
Water drop corona polymer insulators, 4.4.3
Waveshape, of switching impulses and switching surges, 3.2.3, 5.2.3, 5.10
Weather conditions
Effect on audible noise, 10.3.1
Effect on EMI, 9.2.1
For line rating calculation, 2.2.9
Influence on corona performance, 8.6.4
Weighted sound level, 10.5.2
Weighting circuits, EMI, 9.4.2
Weighting networks (A-, B-, C-, D-), for audible noise measurements, 10.5.2
Westinghouse, George, 1.1.1
Wet conductor, audible noise, 10.4.3
Withstand voltage level, for switching surges, 5.9
Wood pole burning caused by high electric fields, 7.15.1
Worker safety, 12.2.6, 12.2.11, 12.2.12, 12.3.2, 12.3.3, 12.3.6, 12.5.4, 12.5.5, 12.6.4, 12.9, 12.16.4

Z

Zero sequence, 2.4.1, 2.5, 2.5.1, 2.5.2, 7.2.4

Export Control Restrictions

Access to and use of EPRI Intellectual Property is granted with the specific understanding and requirement that responsibility for ensuring full compliance with all applicable U.S. and foreign export laws and regulations is being undertaken by you and your company. This includes an obligation to ensure that any individual receiving access hereunder who is not a U.S. citizen or permanent U.S. resident is permitted access under applicable U.S. and foreign export laws and regulations. In the event you are uncertain whether you or your company may lawfully obtain access to this EPRI Intellectual Property, you acknowledge that it is your obligation to consult with your company's legal counsel to determine whether this access is lawful. Although EPRI may make available on a case-by-case basis an informal assessment of the applicable U.S. export classification for specific EPRI Intellectual Property, you and your company acknowledge that this assessment is solely for informational purposes and not for reliance purposes. You and your company acknowledge that it is still the obligation of you and your company to make your own assessment of the applicable U.S. export classification and ensure compliance accordingly. You and your company understand and acknowledge your obligations to make a prompt report to EPRI and the appropriate authorities regarding any access to or use of EPRI Intellectual Property hereunder that may be in violation of applicable U.S. or foreign export laws or regulations.

© 2005 Electric Power Research Institute (EPRI), Inc. All rights reserved. Electric Power Research Institute and EPRI are registered service marks of the Electric Power Research Institute, Inc.

Printed on recycled paper in the United States of America

The Electric Power Research Institute (EPRI)

The Electric Power Research Institute (EPRI), with major locations in Palo Alto, California, and Charlotte, North Carolina, was established in 1973 as an independent, nonprofit center for public interest energy and environmental research. EPRI brings together members, participants, the Institute's scientists and engineers, and other leading experts to work collaboratively on solutions to the challenges of electric power. These solutions span nearly every area of electricity generation, delivery, and use, including health, safety, and environment. EPRI's members represent over 90% of the electricity generated in the United States. International participation represents nearly 15% of EPRI's total research, development, and demonstration program.

Together...Shaping the Future of Electricity

Program:

Overhead Transmission

1011974

ELECTRIC POWER RESEARCH INSTITUTE

3420 Hillview Avenue, Palo Alto, California 94304-1395 • PO Box 10412, Palo Alto, California 94303-0813 USA

800.313.3774 • 650.855.2121 • askepri@epri.com • www.epri.com